ERID-106890

LA-UR-08-06764
October 2008

Los Alamos
NATIONAL LABORATORY
EST.1943

Performance Assessment and Composite Analysis for Los Alamos National Laboratory Technical Area 54, Area G Revision 4

October 2008

Prepared for:
U.S. Department of Energy

LA-UR-08-06764

Approved for public release;
distribution is unlimited.

Title: Performance Assessment and Composite Analysis for Los Alamos National Laboratory Technical Area 54, Area G, Revision 4

Author(s):

Sean French
Rob Shuman
Gregory L. Cole
Kellly J. Crowell
Mark S. Day
Carl W. Gable
Marvin O. Gard
Jeffrey J. Whicker
Daniel G. Levitt
Carl W. Gable
Brent D. Newman
Bruce A. Robinson
Everett Springer
Philip H. Stauffer

Intended for: U.S. Department of Energy

Los Alamos
NATIONAL LABORATORY
EST. 1943

Form 836 (7/06)

Table of Contents

Executive Summary ES-1
List of Figures iv
List of Tables vii
List of Appendices ix
Acronyms and Abbreviations x

1.0 Introduction 1-1
- 1.1 General Approach 1-3
- 1.2 General Facility Description 1-4
- 1.3 Low-Level Radioactive Waste Disposal Facility Life Cycle 1-8
- 1.4 Related Documents 1-10
  - 1.4.1 Site-Wide Environmental Impact Statement 1-10
  - 1.4.2 Environmental Restoration Project Documents 1-10
  - 1.4.3 Land Use Plan 1-11
  - 1.4.4 Groundwater Monitoring Program 1-12
  - 1.4.5 Waste Management Documents 1-12
- 1.5 Performance Criteria 1-14
  - 1.5.1 Public Protection Performance Objectives 1-14
  - 1.5.2 Water Resource Impacts Assessment 1-16
  - 1.5.3 Intruder Analysis 1-17
  - 1.5.4 ALARA Analysis 1-18
  - 1.5.5 Composite Analysis 1-18
  - 1.5.6 Performance Objective Summary 1-19
- 1.6 Summary of Key Assumptions 1-19

2.0 Disposal Facility Characteristics 2-1
- 2.1 Site Characteristics 2-1
  - 2.1.1 Geography and Demography 2-1
  - 2.1.2 Meteorology and Climatology 2-9
  - 2.1.3 Ecology 2-13
  - 2.1.4 Geology, Seismology, and Volcanology 2-20
  - 2.1.5 Hydrology 2-35
  - 2.1.6 Geochemistry 2-46
  - 2.1.7 Natural Resources 2-48
  - 2.1.8 Natural Background Radiation 2-49
- 2.2 Principal Facility Design Features 2-52
  - 2.2.1 Water Infiltration 2-55
  - 2.2.2 Disposal Unit Cover Integrity 2-57
  - 2.2.3 Structural Stability 2-57
  - 2.2.4 Inadvertent Intruder Barrier 2-58
- 2.3 Waste Characteristics 2-59
  - 2.3.1 Background Information 2-59
  - 2.3.2 Performance Assessment Inventory 2-60

Table of Contents (Continued)

2.3.3 Composite Analysis Inventory 2-67
2.3.4 Uncertainty 2-68

3.0 Analysis of Performance 3-1
3.1 Overview of Analysis 3-1
3.1.1 Summary of the Conceptual Model 3-1
3.1.2 Mathematical Models 3-3
3.1.3 Data Quality Objectives Process 3-6
3.2 Conceptual Model of Facility Performance 3-10
3.2.1 Source Term 3-10
3.2.2 Radionuclide Transport 3-17
3.2.3 Exposure Pathways and Scenarios 3-27
3.3 Source Term Modeling 3-37
3.3.1 Representation of Waste Characteristics 3-37
3.3.2 Radionuclide Screening 3-37
3.3.3 Contaminant Release 3-40
3.4 Radionuclide Transport Modeling 3-50
3.4.1 Groundwater Flow and Transport 3-50
3.4.2 Atmospheric Transport 3-56
3.4.3 Surface Erosion 3-64
3.4.4 Vapor- and Gas-Phase Diffusion 3-71
3.5 Dose Assessment 3-72
3.5.1 Exposure Projections 3-73
3.5.2 Alternate-Source Evaluation 3-73
3.5.3 ALARA Analysis 3-74
3.6 Quality Assurance Program 3-76

4.0 Results of Analysis 4-1
4.1 Source Term 4-1
4.1.1 Biotic Intrusion 4-1
4.1.2 Contaminant Leaching 4-3
4.1.3 Vapor- and Gas-Phase Diffusion 4-3
4.2 Environmental Transport of Radionuclides 4-7
4.2.1 Groundwater Transport 4-7
4.2.2 Atmospheric Transport 4-24
4.2.3 Surface Erosion 4-35
4.3 Dose Analysis 4-41
4.3.1 Performance Assessment Projections 4-43
4.3.2 Composite Analysis Projections 4-51
4.4 Uncertainty and Sensitivity Analysis 4-79
4.4.1 Sensitivity Analysis 4-80
4.4.2 Additional Sources of Uncertainty 4-85
4.5 ALARA Analysis 4-92

Table of Contents (Continued)

5.0 Inadvertent Intruder Analysis 5-1
5.1 Exposure Scenarios 5-1
5.2 Modeling Approach and Input Data 5-7
5.3 Intruder Analysis Results 5-10
5.3.1 Exposure Projections 5-10
5.3.2 Intruder-Based Waste Acceptance Criteria 5-16
5.4 Uncertainty and Sensitivity 5-21

6.0 Interpretation of Results 6-1
6.1 Performance Assessment and Composite Analysis 6-1
6.2 Inadvertent Intruder Analysis 6-4

7.0 Performance Evaluation 7-1
7.1 Comparison of Results to Performance Objectives 7-1
7.1.1 Evaluation of Performance Assessment Results 7-1
7.1.2 Evaluation of Composite Analysis Results 7-3
7.1.3 Evaluation of Inadvertent Intruder Analysis Results 7-6
7.2 Use of the Results 7-6
7.2.1 Waste Acceptance Criteria 7-6
7.2.2 Closure Plan 7-7
7.2.3 Monitoring Plan 7-7
7.3 Future Work 7-8
7.3.1 Biotic Intrusion Parameters 7-8
7.3.2 Effects of Elevated Moisture 7-9
7.3.3 Hydrologic Parameter Impacts 7-9
7.3.4 Cliff Retreat 7-9
7.3.5 Sediment Transport 7-10
7.3.6 Subsidence 7-10
7.3.7 Cover Optimization 7-11

8.0 References 8-1

9.0 Preparers 9-1

List of Figures

Figure 1-1 Location of Technical Area 54 at Los Alamos National Laboratory 1-5
Figure 1-2 MDA G and the Zone 4 Expansion Area of Area G 1-7
Figure 1-3 Assumed Area of DOE Control during Passive Institutional Control Period 1-9

Figure 2-1 Locations of Technical Area 54 and Area G 2-2
Figure 2-2 Waste Disposal Units at Material Disposal Area G 2-4
Figure 2-3 Population Data Array Within 80 km Radius of Area 2-6
Figure 2-4 Land Status in Vicinity of LANL 2-8
Figure 2-5 Meteorological Monitoring Towers at LANL 2-10
Figure 2-6 Windroses Illustrating Prevailing Daytime and Nighttime Winds at Mesita del Buey (2002) 2-14
Figure 2-7 Windroses Illustrating Prevailing Daytime and Nighttime Winds at Pajarito Canyon (1998) 2-15
Figure 2-8 Generalized Vegetation Zones of the Pajarito Plateau 2-17
Figure 2-9 Generalized Stratigraphic Relationships of the Pajarito Plateau 2-22
Figure 2-10 Stratigraphic Nomenclature for the Bandelier Tuff 2-23
Figure 2-11 Geology in the Vicinity of Area G 2-26
Figure 2-12 Locations of Regional Characterization Wells R-20, R-21, R-22, R-23, and R-32 2-27
Figure 2-13 Interpretive Geologic Cross Section between Regional Characterization Wells R-21 and R-22 2-28
Figure 2-14 Comparison of 1997 Predicted Stratigraphy to Well Log at Regional Characterization Well R-22 2-29
Figure 2-15 Locations of Major Faults at LANL 2-33
Figure 2-16 Surface Water Drainages on the Pajarito Plateau 2-37
Figure 2-17 Locations of Wells and Generalized Water-Level Contours on the Top of the Regional Aquifer 2-40
Figure 2-18 Proposed Disposal Unit Development at Zone 4 2-53
Figure 2-19 Cross Section of the Conceptual Cover for Area G 2-56

Figure 3-1 Conceptual Model of Area G 3-2
Figure 3-2 Waste Disposal Regions at MDA G 3-7
Figure 3-3 Atmospheric Source Areas at Area G 3-8
Figure 3-4 Root Mass Distributions for Plants with Maximum Rooting Depth of 1.5 m 3-46
Figure 3-5 Burrow Depth Distributions for Animals with Maximum Burrowing Depth of 3 m 3-48
Figure 3-6 Comparison of Modeled Fluxes and Fluxes Based on Chloride Mass Balance Measurements 3-49
Figure 3-7 Three-Dimensional Grid for Area G Model 3-52
Figure 3-8 Model Domain for Near-Field Analysis 3-59
Figure 3-9 Model Domain for Alternate Source Analysis 3-62
Figure 3-10 Model Domain for Far-Field Analysis 3-63

Figure 4-1 Uptake of Selected Radionuclides by Native Vegetation Growing over Waste Disposal Region 8 4-2

List of Figures (Continued)

Figure 4-2 Mean Soil Transport Rates for Burrowing Animals in Waste Disposal Region 8 4-4
Figure 4-3 Mean Groundwater Fluxes from the Bottom of Disposal Units in Waste Disposal Region 8 4-5
Figure 4-4 Mean Diffusive Fluxes from the Top of Waste in Waste Disposal Region 8 4-6
Figure 4-5 Breakthrough Curves for Particles Released from All Waste Disposal Regions (background infiltration of 0.5 mm/yr) 4-8
Figure 4-6 Breakthrough Curves for Particles Released from All Waste Disposal Regions (background infiltration of 10 mm/yr) 4-10
Figure 4-7 Breakthrough Curves for Particles Released from Waste Disposal Region 1 (range of steady-state infiltration rates) 4-11
Figure 4-8 Breakthrough Curves for Particles Released from Waste Disposal Region 5 (range of steady-state infiltration rates) 4-12
Figure 4-9 Early Breakthrough Curves for Particles Released from Waste Disposal Regions 1 and 5 (range of steady-state infiltration rates) 4-13
Figure 4-10 Effect of Permeability Reductions on Subsurface Saturation at Waste Disposal Region 5 4-14
Figure 4-11 Effect of Permeability Reductions on Breakthrough for Releases from Waste Disposal Regions 1 and 5 4-16
Figure 4-12 Effect of Pajarito Canyon Infiltration on Subsurface Saturation at Waste Disposal Region 5 4-17
Figure 4-13 Effect of Pajarito Canyon Infiltration on Breakthrough for Releases from Waste Disposal Regions 1 and 5 4-18
Figure 4-14 Model Sensitivity to Longitudinal Dispersivity at Waste Disposal Region 5 (high- and low-infiltration rates) 4-20
Figure 4-15 Capture Zone for Hypothetical Well with High Pumping Rate 4-21
Figure 4-16 Comparison of Three-Dimensional Particle and One-Dimensional Plume Breakthrough Curves 4-23
Figure 4-17 Relative Air Concentration Contours Predicted by CALPUFF for Releases from Area G Source Area 1 (particle size gdiam 0.48 µm) 4-25
Figure 4-18 Relative Air Concentration Contours Predicted by CALPUFF for Releases from Area G Source Area 2 (particle size gdiam 0.48 µm) 4-26
Figure 4-19 Relative Air Concentration Contours Predicted by CALPUFF for Releases from Area G Source Area 3 (particle size gdiam 0.48 µm) 4-27
Figure 4-20 Relative Air Concentration Contours Predicted by CALPUFF for Releases from Area G Source Area 1 (particle size gdiam 5.0 µm) 4-28
Figure 4-21 Relative Air Concentration Contours Predicted by CALPUFF for Releases from Area G Source Area 2 (particle size gdiam 5.0 µm) 4-29
Figure 4-22 Relative Air Concentration Contours Predicted by CALPUFF for Releases from Area G Source Area 3 (particle size gdiam 5.0 µm) 4-30
Figure 4-23 Air Concentration Contours for Far-Field Analysis 4-33
Figure 4-24 Estimated Vertical Mass Flux Collected during All Sampling Periods (1 m sampling height) 4-36
Figure 4-25 Erosion and Deposition at MDA G for Moderate-Erosion Scenario (as predicted by SIBERIA model after 1,000 years) 4-38

List of Figures (Continued)

Figure 4-26 Erosion and Deposition at MDA G for Low- and High-Erosion Scenarios (as predicted by SIBERIA model after 1,000 years) 4-39
Figure 4-27 Erosion and Deposition at Zone 4 for Moderate-Erosion Scenario (as predicted by SIBERIA model after 1,000 years) 4-40
Figure 4-28 Area G Sediment-Source Areas and Sediment Catchments in Habitable Canyon Bottoms 4-42
Figure 4-29 Deterministic Dose Projections for the Groundwater Resource Protection Scenario 4-45
Figure 4-30 Deterministic Dose Projections for the All Pathways–Groundwater Scenario (performance assessment) 4-46
Figure 4-31 Deterministic Dose Projections for the Atmospheric Scenario (performance assessment) 4-47
Figure 4-32 Probabilistic Dose Projections for the Atmospheric Scenario (performance assessment) 4-49
Figure 4-33 Mean Radionuclide Exposures for the Atmospheric Scenario at the Area G Fence Line Location (performance assessment) 4-50
Figure 4-34 Deterministic Dose Projections for the All Pathways–Canyon Scenarios (performance assessment) 4-52
Figure 4-35 Probabilistic Dose Projections for the All Pathways–Canyon Scenarios (performance assessment) 4-54
Figure 4-36 Mean Radionuclide Doses for the All Pathways–Cañada del Buey Scenario within Catchment CdB2 (performance assessment) 4-55
Figure 4-37 Deterministic Dose Projections for the All Pathways–Groundwater Scenario (composite analysis) 4-56
Figure 4-38 Deterministic Dose Projections for the Atmospheric Scenario (composite analysis) 4-58
Figure 4-39 Probabilistic Dose Projections for the Atmospheric Scenario (composite analysis) 4-59
Figure 4-40 Mean Radionuclide Exposures for the Atmospheric Scenario at the Area G Fence Line Exposure Location (composite analysis) 4-60
Figure 4-41 Deterministic Dose Projections for the All Pathways–Canyon Scenarios (composite analysis) 4-62
Figure 4-42 Probabilistic Dose Projections for the All Pathways–Pajarito Canyon Scenario (composite analysis) 4-64
Figure 4-43 Mean Radionuclide Exposures for the All Pathways–Pajarito Canyon Scenario within Catchment PC5 (composite analysis) 4-65
Figure 4-44 Locations of Alternate Contamination Sources and Generalized Water-Level Contours on the Top of the Regional Aquifer 4-77

List of Tables

Table 1-1 Summary of Performance Objectives Adopted for the Area G Performance Assessment 1-20
Table 1-2 Summary of Performance Objectives Adopted for the Area G Composite Analysis 1-21

Table 2-1 Summary of 12 Years of Meteorological Data at Area G (1993–2004) 2-11
Table 2-2 Plant Rooting Depths Measured on Laboratory Lands 2-19
Table 2-3 Burrow Depth Distributions for Animal Species Encountered or Expected at Area G 2-20
Table 2-4 Lithology of Geologic Units Encountered in Boreholes at Area G 2-24
Table 2-5 Average Hydrologic Characteristics of Los Alamos Area Regional Aquifer 2-39
Table 2-6 Hydrogeologic Characteristics of Area G Vadose Zone Used for Groundwater Pathway Modeling 2-43
Table 2-7 Average Background Concentrations of Radioactivity in the Regional Atmosphere 2-50
Table 2-8 Radionuclide Concentrations Measured in Regional Surface Soils (0 to 5 cm depth), 2001 2-51
Table 2-9 Radiochemical Quality of Surface Water from Off-Site Stations 2-51
Table 2-10 Design Capacities of Zone 4 Development Phases 2-54
Table 2-11 Volumes and Activities for Waste Included in the Area G Performance Assessment and Composite Analysis Inventories 2-61
Table 2-12 Radionuclide, Activation Product, Fission Product, and Material Type Inventories for Waste Included in the Performance Assessment 2-62
Table 2-13 Radionuclide, Activation Product, Fission Product, and Material Type Inventories for Waste Included in the Composite Analysis, Disposal Pits 2-69
Table 2-14 Radionuclide, Activation Product, Fission Product, and Material Type Inventories for Waste Included in the Composite Analysis, Disposal Shafts 2-73

Table 3-1 Off-Site Exposure Scenarios for the Area G Performance Assessment and Composite Analysis 3-29
Table 3-2 Summary of Cover and Production Studies Used to Estimate Aboveground Biomass (early successional stages at Area G) 3-42
Table 3-3 Aboveground Production of Grasses, Forbs, and Shrubs in Mature Piñon-Juniper Woodlands 3-43

Table 4-1 Capture Efficiencies for Waste Disposal Regions 1 through 5 and 8 4-22
Table 4-2 Annual Variability of Particulate Concentrations at Selected Locations North of Area G 4-31
Table 4-3 Ten-Year Average Peak Dry and Wet Deposition Ratios for Source Areas 1, 2, and 3 4-31
Table 4-4 Comparison of Dry Deposition Flux at the LANL Boundary North of Area G 4-31
Table 4-5 Comparison of Air Dispersion Results for Releases from Various Material Disposal Areas 4-32
Table 4-6 Selected Population-Weighted Air Dispersion Values for Source Area 1 4-34
Table 4-7 Summary Statistics for Aerosol Mass Concentration and Vertical Mass Flux at MDA J 4-37

List of Tables (Continued)

Table 4-8 Summary of Sediment Delivery from Area G to Canyon Catchments over 1,000 Years 4-43
Table 4-9 Projected Radon Fluxes for the Eight Waste Disposal Regions 4-48
Table 4-10 Probabilistic Dose Projections for the All Pathways– Canyon Scenarios (performance assessment) 4-53
Table 4-11 Probabilistic Dose Projections for the All Pathways–Canyon Scenarios (composite analysis) 4-63
Table 4-12 Estimates of Radionuclide Inventories at the Material Disposal Areas Included in the Alternate Source Evaluation 4-67
Table 4-13 Estimates of Radionuclide Inventories at Material Disposal Area C 4-69
Table 4-14 Summary of Radionuclide Inventories at the MDAs Included in the Alternate Source Evaluation 4-72
Table 4-15 Comparison of Air Dispersion Results for Releases from Alternate Source Material Disposal Areas 4-75
Table 4-16 Rank Correlation Coefficients for Selected Performance Assessment Exposure Scenarios 4-81
Table 4-17 Rank Correlation Coefficients for Radon Flux from Waste Disposal Region 7 4-82
Table 4-18 Rank Correlation Coefficients for Selected Composite Analysis Exposure Scenarios 4-84
Table 4-19 Field Measurements of Saturated Hydraulic Conductivity at MDA J 4-89
Table 4-20 Collective Doses Estimated for the Area G ALARA Analysis 4-93
Table 4-21 Collective Doses and Closure Strategy Implementation Costs for the Area G ALARA Analysis 4-93

Table 5-1 Inadvertent Intruder Exposure Scenarios Evaluated for Inclusion in the Area G Intruder Assessment 5-2
Table 5-2 Comparison of Intruder Dose Projections with and without the Effects of Radon Diffusion 5-11
Table 5-3 Probabilistic Doses for the Inadvertent Intruder Exposure Scenarios 5-12
Table 5-4 Final Waste Acceptance Criteria for the Disposal Pits and Shafts at MDA G 5-17
Table 5-5 Comparison of the 1997/1999 and 2008 WAC for MDA G 5-22
Table 5-6 Rank Correlation Coefficients for Selected Intruder Exposure Scenarios 5-26

Table 7-1 Comparison of Performance Assessment Results with Performance Objectives 7-2
Table 7-2 Comparison of Composite Analysis Results with Performance Objectives 7-5

List of Appendices

Volume 2

Appendix A Responses to Long-Term Conditions Issued by the Low-Level Waste Federal Review Group

Appendix B Conceptual Design of Zone 4 Disposal Units at Los Alamos National Laboratory Technical Area 54, Material Disposal Area G

Appendix C Assessing Wind Erosion as a Contaminant Transport Mechanism for Los Alamos National Laboratory Technical Area 54, Material Disposal Area G

Appendix D Air Dispersion Analysis for Los Alamos National Laboratory Technical Area 54, Material Disposal Area G

Appendix E Groundwater Pathway Model for the Los Alamos National Laboratory Technical Area 54, Material Disposal Area

Appendix F Spatial Variation in Near-Surface Hydrologic Behavior at Los Alamos National Laboratory Technical Area 54, Material Disposal Area G

Appendix G Modeling of an Evapotranspiration Cover for the Groundwater Pathway at Los Alamos National Laboratory Technical Area 54, Area G

Appendix H Conceptual Design of the Earthen Cover at Los Alamos National Laboratory Technical Area 54, Material Disposal Area G

Appendix I Surface Erosion Modeling for the Repository Waste Cover at Los Alamos National Laboratory TA-54, Material Disposal Area G

Appendix J Radioactive Waste Inventory for Los Alamos National Laboratory Technical Area 54, Area G

Volume 3

Appendix K GoldSim Model Documentation and Data Selection for Los Alamos National Laboratory Technical Area 54, Area G Performance Assessment and Composite Analysis

Appendix L Radiological Dose Assessment for Los Alamos National Laboratory, Technical Area 54, Area G Performance Assessment and Composite Analysis

Appendix M As Low as Reasonably Achievable (ALARA) Analysis for Los Alamos National Laboratory Technical Area 54, Area G Performance Assessment and Composite Analysis

Acronyms and Abbreviations

ALARA	As low as reasonably achievable
ALSM	Airborne laser swath mapping
bgs	Below ground surface
CFR	Code of Federal Regulations
D&D	Decontamination and decommissioning
DEM	Digital elevation Model
DOE	U.S. Department of Energy
DQO	Data quality objectives
EPA	U.S. Environmental Protection Agency
ER	Environmental restoration
FEHM	Finite Element Heat and Mass
gdiam	Geometric mean particle diameter
gsd	Geometric standard deviation
HEM	Hillslope Erosion Model
IWP	Installation work plan
Laboratory	Los Alamos National Laboratory
KINEROS	Kinematic Runoff and Erosion Model
LANL	Los Alamos National Laboratory
LLW	Low-level radioactive waste
Ma	Million years ago
MAP	Mixed-activation products
MDA	Material Disposal Area
MFP	Mixed-fission products
msl	Mean sea level
NAD	North American Datum
NEPA	National Environmental Policy Act
NRC	U.S. Nuclear Regulatory Commission
OU	Operable Unit
PCB	Polychlorinated biphenyl
QA	Quality assurance
QAPjP	Quality Assurance Project Plan
RCRA	Resource Conservation and Recovery Act
RFI	RCRA Facilities Investigation
RTD	Residential time distribution
SWEIS	Site-wide environmental impact statement
TA	Technical Area
TRU	Transuranic
TSCA	Toxic Substances Control Act
USGS	U.S. Geological Survey
UTM	Universal Transverse Mercator
WAC	Waste acceptance criteria
WEPP	Water Erosion Prediction Project (model)
WIPP	Waste Isolation Pilot Plant

Executive Summary

Los Alamos National Laboratory (LANL or the Laboratory) generates radioactive waste as a result of various activities. Most is low-level radioactive waste that is disposed of at Technical Area (TA) 54, Area G. U.S. Department of Energy (DOE) Order 435.1 requires that DOE field sites prepare and maintain site-specific radiological performance assessments and composite analyses for low-level radioactive waste disposal facilities that accept waste after September 26, 1988. This report presents the radiological performance assessment and composite analysis for TA 54, Area G.

The performance assessment and composite analysis model the long-term performance of the Area G disposal facility so that the risk posed by the disposed waste to human health and safety and the environment can be determined. Rates of radionuclide release from the waste and the transport of these releases to locations accessible to humans are evaluated and used to project radiation doses that may be received by exposed persons. The release rates of radon gas from the disposal facility are also estimated. The dose and radon flux projections are compared to the performance objectives provided in DOE M 435.1 to evaluate the ability of the disposal facility to safely isolate the waste.

Disposal Facility Characteristics

Area G is located within TA 54, which lies in the east-central portion of the Laboratory. Annual precipitation averages 34 cm (13 in.) at the site; almost all of the moisture gained through precipitation is lost as a result of evaporation and transpiration. The regional aquifer lies approximately 260 m (850 ft) below the surface of the mesa and rates of recharge are low. The terrain and vegetation characteristics in the vicinity of Area G result in complex patterns of atmospheric transport and dispersion. The canyon and mesa terrain characteristic of the Laboratory provides a variety of habitats for plants and animals.

Waste disposal operations began at Area G in 1957 with the disposal of nonroutine waste; the disposal of routine waste started in 1959 and has continued to the present. The majority of the waste is disposed of in large rectangular pits; disposal shafts are used for selected waste streams because of regulatory requirements or special handling needs. The waste placed in the pits and shafts has assumed a variety of chemical and physical forms. Radionuclide inventories in the waste have been developed in support of the performance assessment and composite analysis.

Waste disposal operations are assumed to continue until 2044, after which the facility will undergo final closure over a 2-year period. An active institutional control period of 100 years, extending from 2047 through 2146, will follow final closure of the facility. Passive institutional control will begin in 2147 and will continue until the disposal facility no longer poses a significant risk to human health and safety and the environment.

Analysis of Performance

The performance assessment and composite analysis were conducted by defining a conceptual model of Area G, creating mathematical models that reflect the characteristics of the conceptual model, and implementing these models to project the long-term performance of the disposal facility. Predominant radionuclide release mechanisms include plant and animal intrusion into the waste, leaching that occurs as water infiltrates through the pits and shafts, and diffusion of vapor- and gas-phase radionuclides from the waste. Surface contamination may be suspended and transported to downwind locations with the prevailing winds or transported into the canyons adjacent to Area G with surface runoff; diffusive releases may also be carried downwind. Contaminants leached from the waste may be transported to the regional aquifer and to locations downgradient of the disposal facility.

Deterministic and probabilistic modeling was conducted using models developed with the GoldSim™ modeling environment or platform; these models simulate radionuclide release and transport to locations accessible to humans and project radionuclide concentrations in environmental media to which human receptors are exposed. Modeling was performed for a number of different scenarios. The Groundwater Resource Protection Scenario estimates exposures for a person living downgradient of the disposal facility who uses the regional aquifer as a source of drinking water; the All Pathways–Groundwater Scenario considers exposures for an individual who uses contaminated groundwater for all domestic needs. Potential exposures received by a person exposed to airborne releases from Area G were assessed using the Atmospheric Scenario; radon fluxes from the disposal site were projected in conjunction with this scenario. Exposures received by persons living in Cañada del Buey and Pajarito Canyon were evaluated using the All Pathways–Canyon Scenario. Doses were also projected for three inadvertent intruder scenarios that represent different levels of disturbance of the buried waste. An “alternate source” evaluation of the potential for significant interactions between releases from Area G and other sources of radioactivity at the Laboratory was conducted, as was an “as low as reasonably achievable” (ALARA) analysis to evaluate the effectiveness of alternative facility closure strategies.

Results of Analysis

The results of the performance assessment and composite analysis provide reasonable assurance of compliance with DOE M 435.1 performance objectives (Table ES-1). No doses are projected to occur over the 1,000-year compliance period for the groundwater pathway scenarios. The peak mean exposures projected for the Atmospheric and All Pathways–Canyon Scenarios are small fractions of the pertinent performance objectives. Radon fluxes averaged over the disposal facility fall within the 20 pCi/m^2/s flux objective.

The probabilistic dose projections provide explicit estimates of the uncertainty associated with the calculated impacts. Sensitivity analyses conducted using these results indicate that the model results are sensitive to the diffusion characteristics of tritium, the depth of cover placed over the disposal units, and the rooting and growth characteristics of plants inhabiting the site. Other potentially important sources of uncertainty include the impacts associated with disposal unit subsidence, hydrologic properties of the materials used to construct the final cover, transient moisture conditions, and sediment transport.

The results of the inadvertent intruder analysis indicate that the doses projected for the waste disposed of in pits from September 27, 1988 through 2010 and from 2011 through 2044 and in shafts from September 27, 1988 through 2015 and from 2016 through 2044 fall within acceptable limits (Table ES-2). The depths at which waste is placed within the disposal shafts have a significant impact on the exposures projected for these units. The ability of the containers used to dispose of high-activity tritium waste to slow the release of tritiated water vapor also plays an important role in the safe disposal of waste in the 2016–2044 shafts.

It appears unlikely that significant interactions will occur between releases from Area G and other sources of radioactivity at the Laboratory. Results of the ALARA analysis indicate that the closure strategy evaluated in the performance assessment and composite analysis yields doses that are ALARA and that less robust cover designs may be more cost-effective.

Table ES-1
Comparison of Performance Assessment and Composite Analysis Results with Performance Objectives

Performance Objective	Exposure Scenario	Projected Impact
Performance Assessment		
All Pathways (25 mrem/yr)	All Pathways–Groundwater	No radionuclides were projected to discharge to the regional aquifer
	All Pathways–Canyon	Peak mean dose of 2.3E+00 mrem/yr for maximally exposed individual
Air Pathway (10 mrem/yr)	Atmospheric	Peak mean dose of 1.8E-01 mrem/yr for maximally exposed individual
Radon Flux (20 pCi/m^2/s)	---	Peak mean flux of 1.4E+01 pCi/m^2/s from waste disposal region 7 Average facility flux of 4.3E-01 pCi/m^2/s
Water Resources Impacts (40 CFR 141 limits)	Groundwater Resources Protection	No radionuclides were projected to discharge to the regional aquifer
Composite Analysis		
All Pathways (30 mrem/yr dose constraint)	All Pathways–Groundwater	No radionuclides were projected to discharge to the regional aquifer
	All Pathways–Canyon	Peak mean dose of 4.4E+00 mrem/yr for maximally exposed individual
Air Pathway (10 mrem/yr)	Atmospheric	Peak mean dose of 6.4E-01 mrem/yr for maximally exposed individual

--- = Radon fluxes are projected in conjunction with the air pathway modeling.

Table ES-2
Comparison of Intruder Analysis Results with Performance Objectives

Performance Objective	Exposure Scenario [a]	Projected Impact
Inadvertent Intruder (500 mrem/yr acute exposure)	Intruder-Construction	
	1988–2010 pits	Peak mean dose of 5.3E-01 mrem/yr
	2011–2044 pits	Peak mean dose of 2.8E-02 mrem/yr
	1988–2015 shafts	Peak mean dose of 5.1E+00 mrem/yr
	2016–2044 shafts	Peak mean dose of 2.5E+00 mrem/yr
Inadvertent Intruder (100 mrem/yr chronic exposure)	Intruder-Agriculture	
	1988–-2010 pits	Peak mean dose of 4.1E+00 mrem/yr
	2011–2044 pits	Peak mean dose of 4.6E-01 mrem/yr
	1988–2015 shafts	Peak mean dose of 8.9E+01 mrem/yr
	2016–2044 shafts	Peak mean dose of 4.9E+01 mrem/yr
Inadvertent Intruder (100 mrem/yr chronic exposure)	Intruder–Post-Drilling	
	1988–2010 pits	Peak mean dose of 3.6E+00 mrem/yr
	2011–2044 pits	Peak mean dose of 6.9E-01 mrem/yr
	1988–2015 shafts	Peak mean dose of 1.1E+01 mrem/yr
	2016–2044 shafts	Peak mean dose of 3.1E+00 mrem/yr

[a] Intruder scenarios were evaluated for waste disposed of in pits from September 27, 1988 through 2010 and from 2011 through 2044 and waste disposed of in shafts from September 27, 1988 through 2015 and from 2016 through 2044.

1.0 Introduction

Los Alamos National Laboratory (LANL or the Laboratory) generates radioactive waste as a result of various activities. Operational waste is generated from a wide variety of research and development activities including nuclear weapons development, energy production, and medical research. Environmental restoration (ER) and decontamination and decommissioning (D&D) waste is generated as contaminated sites and facilities at the Laboratory undergo cleanup or remediation. The majority of this waste is low-level radioactive waste (LLW) and is disposed of at Technical Area (TA) 54, Area G.

U.S. Department of Energy (DOE) Order 435.1 (DOE, 2001a) requires that radioactive waste be managed in a manner that protects worker and public health and safety, and the environment. To comply with this order, DOE field sites must prepare and maintain site-specific radiological performance assessments for LLW disposal facilities that accept waste after September 26, 1988. Furthermore, sites are required to conduct composite analyses for disposal facilities that receive waste after September 26, 1988. These composite analyses account for the cumulative impacts of all waste that has been (or will be) disposed of at the facilities and other sources of radioactive material that may interact with the facilities.

This report presents the radiological performance assessment and composite analysis for the Area G disposal facility. It represents a major revision of the previous performance assessment and composite analysis (Hollis et al., 1997), which was conducted under DOE Order 5820.2A (DOE, 1988), the predecessor to Order 435.1. The report is presented in three volumes. Volume 1 consists of seven major sections, in accordance with the requirements of DOE G 435.1-2 (DOE, 2001b). This introductory section provides an overview of the general approach adopted for the performance assessment and composite analysis (Section 1.1), as well as a brief description of the site (Section 1.2). Section 1.3 discusses the life cycle of the LLW disposal facility. An overview of related documents is presented in Section 1.4, and the performance criteria and key assumptions for the performance assessment and the composite analysis are provided in Sections 1.5 and 1.6, respectively.

Section 2 discusses the natural and man-made characteristics of the disposal facility as well as the characteristics of the waste itself. This section provides the context for the discussion of the pathways, scenarios, and source terms in subsequent sections. The conceptual model that was used to structure the performance assessment and composite analysis and the technical approach used to implement this model are presented in Section 3. Section 4 presents the results of the long-term performance modeling, while Section 5 focuses on the results of the inadvertent intruder analysis. The interpretation of results and a discussion of the sensitivity and uncertainty associated with the modeling are provided in Section 6. Finally, Section 7 presents conclusions

about the evaluation, including a comparison of the results to the performance objectives, a discussion of the results and options analysis, and suggestions for future work. Information about the preparers of this document and a reference list complete Volume 1 of this performance assessment and composite analysis.

The appendices in Volumes 2 and 3 provide the basis for much of the data and analyses presented in Volume 1. Appendix A provides responses to the comments on the previous version of the Area G performance assessment and composite analysis; the remaining appendices summarize technical studies conducted in support of the current analyses. Briefly, these include:

- Appendix B—*Conceptual Design of Zone 4 Disposal Units at Los Alamos National Laboratory Technical Area 54, Material Disposal Area G*—summarizes the planned approach for developing new waste disposal units in the Zone 4 expansion area, just west of the active portion of Area G.

- Appendix C—*Assessing Wind Erosion as a Contaminant Transport Mechanism for Los Alamos National Laboratory Technical Area 54, Material Disposal Area G*—provides estimates of wind erosion and vertical fluxes at Area G and at an analog site considered representative of the postclosure vegetation changes that Area G will experience.

- Appendix D—*Air Dispersion Analysis for Los Alamos National Laboratory Technical Area 54, Material Disposal Area G*—contains the results of atmospheric transport and dispersion modeling performed to evaluate the impacts of airborne releases from Area G on downwind receptors.

- Appendix E—*Groundwater Pathway Model for the Los Alamos National Laboratory Technical Area 54, Material Disposal Area G*—describes the groundwater flow and transport modeling used to estimate impacts from Area G on regional groundwater resources.

- Appendix F—*Spatial Variation in Near-Surface Hydrologic Behavior at Los Alamos National Laboratory Technical Area 54, Material Disposal Area G*—evaluates near-surface moisture flux at specific locations at Area G to determine the effects of site disturbance and ecological succession on water infiltration.

- Appendix G—*Modeling of an Evapotranspiration Cover for the Groundwater Pathway at Los Alamos National Laboratory Technical Area 54, Area G*—presents the approach and results of a study that modeled infiltration through the proposed final waste cover.

- Appendix H—*Conceptual Design of the Earthen Cover at Los Alamos National Laboratory Technical Area 54, Material Disposal Area G*—summarizes the process that was used to develop a conceptual design for a final earthen cover at Area G and presents the results of the design process.

- Appendix I—*Surface Erosion Modeling for the Repository Waste Cover at Los Alamos National Laboratory Technical Area 54, Material Disposal Area G*—reports on modeling conducted to estimate the spatial distribution of depth to waste at Area G following surface erosion and sediment transport.

- Appendix J—*Radioactive Waste Inventory for Los Alamos National Laboratory Technical Area 54, Area G*—characterizes the types of waste that have been and will be disposed of at Area G, describes the disposal methods, and estimates the volumes and activities of the waste.

- Appendix K—*GoldSim Model Documentation and Data Selection for Los Alamos National Laboratory Technical Area 54, Area G Performance Assessment and Composite Analysis*—documents the GoldSim models that were used to conduct the Area G performance assessment and composite analysis and the data that were used to implement these models.

- Appendix L—*Radiological Dose Assessment for Los Alamos National Laboratory Technical Area 54, Area G Performance Assessment and Composite Analysis*—estimates the potential impacts associated with the disposal of waste at Area G including doses received by members of the public and inadvertent human intruders, and radon fluxes from the disposal site.

- Appendix M—*As Low as Reasonably Achievable (ALARA) Analysis for Los Alamos National Laboratory Technical Area 54, Area G Performance Assessment and Composite Analysis*—evaluates waste management options to determine if the projected impacts from the disposal facility are as low as reasonably achievable.

1.1 General Approach

The performance assessment and composite analysis model the long-term performance of the Area G disposal facility so that the risk posed by the disposed waste to human health and safety and the environment can be determined. The modeling includes an estimation of the rates at which radionuclides are released from the waste and the transport of these releases to locations accessible to humans. The projected contaminant concentrations in the soil, air, groundwater, and biota at these locations are used in conjunction with rates of intake and times of exposure to calculate the doses that may be received by exposed persons. Rates of release of radon gas from the disposal facility are also estimated. The dose and radon flux projections are compared to the

performance objectives provided in DOE M 435.1 (DOE, 2001c) to evaluate the ability of the disposal facility to safely isolate the waste. These performance criteria are presented and discussed in Section 1.5.

The performance assessment and composite analysis are limited to radioactive waste that has been, or is expected to be, permanently disposed of at Area G. Significant quantities of transuranic (TRU) waste are currently in storage at the facility, including some waste that has been placed in belowground pits, trenches, and shafts. Current plans call for the retrieval of this waste and subsequent disposal at the Waste Isolation Pilot Plant (WIPP) in southern New Mexico. Therefore, this waste was not included in the facility performance modeling.

Performance assessments and composite analyses are not static processes. Once they have been prepared, they are reviewed, revised, and updated until the facility no longer poses a significant risk to human health and safety and the environment. Consistent with this philosophy, the analyses reported here represent a revision to the performance assessment and composite analysis issued in 1997 (Hollis et al., 1997) under DOE Order 5820.2A (DOE, 1988).

Revision of the 1997 performance assessment and composite analysis was undertaken for several reasons. Changes in disposal operations have occurred since the earlier analyses were conducted, including the increased use of waste containers, changes in the closure schedule for portions of the facility, and modifications to the final cover design. Also, since 1997 a considerable amount of new information has been developed under the Area G Performance Assessment and Composite Analysis Maintenance Program (Shuman et al., 2003). This information has led to more accurate waste inventory projections and more reliable model projections of radionuclide release and transport. Finally, modeling techniques developed under the maintenance program permit a more complete assessment of the projected long-term impacts of the disposal facility.

The revision also addresses the long-term conditions issued by the Low-Level Waste Federal Review Group in conjunction with the review of the 1997 performance assessment and composite analysis. These comments and the manner in which they are addressed by the revised analyses are provided in Appendix A.

1.2 General Facility Description

Area G is located within TA-54, which lies in the east-central portion of the Laboratory (Figure 1-1). It is situated on Mesita del Buey, an east-west trending mesa bounded by Pajarito Canyon to the south and Cañada del Buey to the north. The site was selected for the disposal of radioactive waste generated at LANL on the basis of recommendations made in a survey of the area performed by the U.S. Geological Survey (USGS) in the mid-1950s (Rogers, 1977). The area has functioned as a major waste storage and disposal facility since that time.

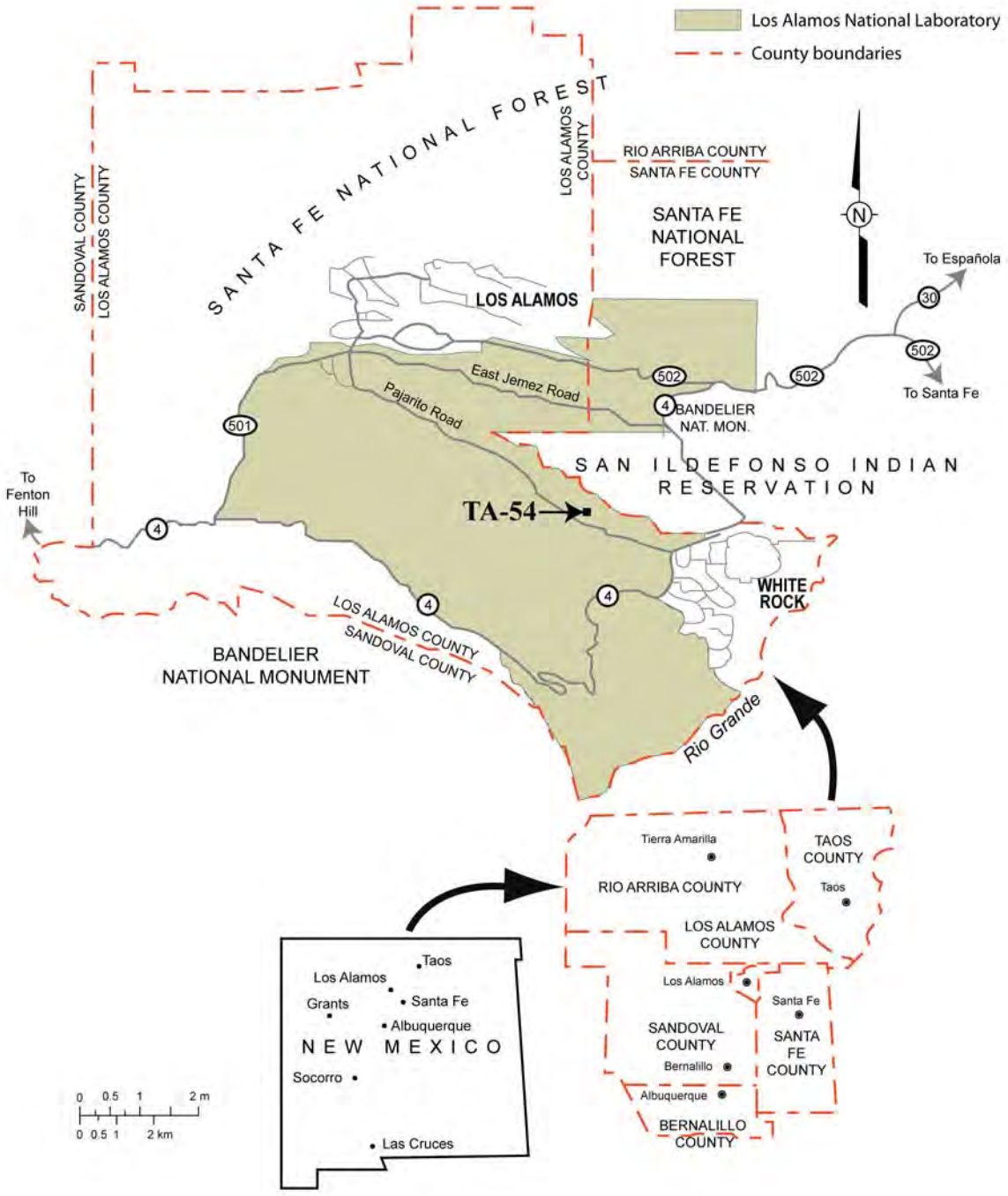

Figure 1-1
Location of Technical Area 54 at Los Alamos National Laboratory

Area G received its first shipment of waste in 1957 and is the only active radioactive waste disposal facility at the Laboratory today. To date, disposal operations have used approximately 26 ha (65 ac) of the 40 ha (100 ac) site. This portion of the facility is referred to as Material Disposal Area (MDA) G. Current plans call for disposal operations to move to an area west of MDA G known as the Zone 4 expansion area (Figure 1-2) when the existing disposal capacity of MDA G has been exhausted.

Waste has been disposed of at Area G in a series of large, generally rectangular pits and circular shafts. The first units developed at the site were pits; these units have continued to receive most of the waste (on a volume basis) disposed of at the facility. First used for disposal in 1966, shafts are designated for waste with high external radiation levels and other unique waste streams.

Prior to the mid-1990s, the waste disposed of in pits was typically placed in lifts; each layer of waste was covered with uncontaminated crushed tuff and compacted by driving heavy equipment over the crushed tuff. Exceptions to this approach occurred primarily when it was thought that the waste might be retrieved at a later date. Current operational procedures require that all waste other than bulk soils and debris be packaged prior to disposal. Bulk materials are placed directly in the disposal pits, and may be used to fill void spaces between and within waste containers. The shafts are drilled using augers and generally range from 0.3 to 6 m (1 to 20 ft) in diameter. Waste packages are lowered into the shafts and stacked on top of one another; crushed tuff may be added as backfill around the waste packages to reduce void spaces in these units.

Current waste management operations at Area G include the permanent disposal of LLW, the temporary storage of TRU waste awaiting final disposal at the WIPP (USAEC, 1970), and the temporary storage of mixed LLW (RCRA, 42 U.S.C. § 6901 et seq.) awaiting final treatment under the Federal Facility Compliance Act (42 U.S.C. § 6961 et seq.). The physical, chemical, and radiological characteristics of all waste sent to Area G for storage or disposal are described by the waste generator on several forms. These forms are reviewed by waste management personnel prior to shipment to ensure that all waste meets applicable acceptance criteria regarding waste form, packaging, chemical content, and radioactivity content. Upon acceptance of the waste, these documents are retained indefinitely.

After the waste arrives at Area G, the shipping packages are inspected and the accompanying documentation is reviewed for consistency and acceptability. If significant discrepancies are identified, the receiving technician issues a nonconformance report describing the problem to the waste generator. The generator is responsible for correcting the problem, either at Area G or, if necessary, after the waste is returned to the generating facility. Nonconformance reports are also permanent quality records. They are reviewed to identify trends that indicate inadequate guidance or surveillance on the part of waste management or recalcitrant waste generators. The documentation, review, approval, and acceptance processes are elements of the Generator Waste Certification Program implemented for LLW (LANL, 1997).

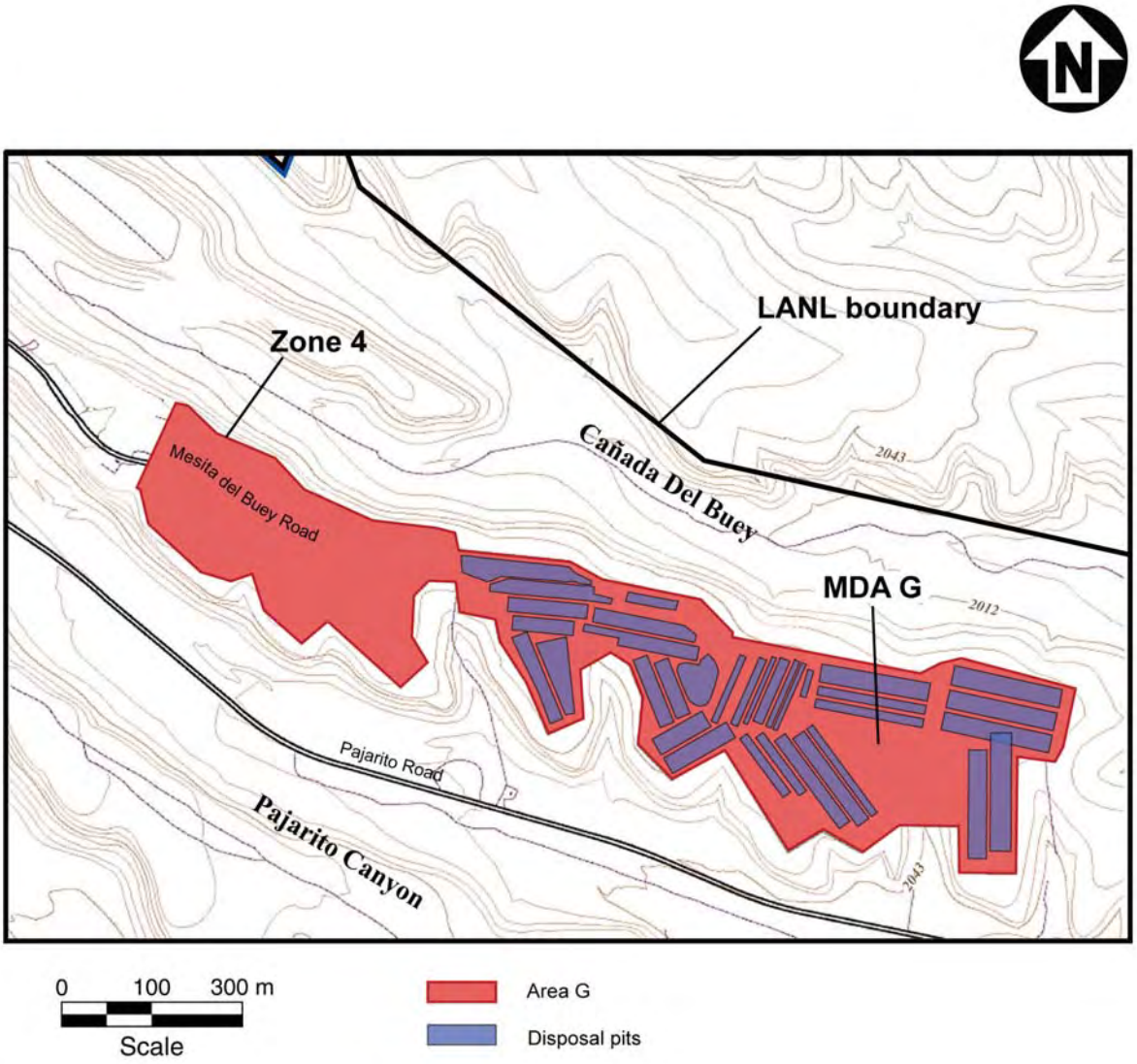

Figure 1-2
MDA G and the Zone 4 Expansion Area of Area G

The residential communities closest to Area G include the town of White Rock, which lies approximately 2 km (1.2 mi) to the east, and the town of Los Alamos, approximately 8 km (5 mi) to the northwest of the disposal facility. The northern and eastern boundaries of the disposal facility coincide with the LANL property boundary. The Pueblo of San Ildefonso owns the land that lies within Cañada del Buey along the north perimeter of the disposal site. A portion of the San Ildefonso land that borders the Laboratory is regarded as sacred hunting grounds. Hunting and gathering activities, as well as use of the canyon stream, occur on land directly adjacent to Area G.

1.3 Low-Level Radioactive Waste Disposal Facility Life Cycle

Waste disposal operations began at Area G in 1957 with the disposal of nonroutine waste in the first pit excavated at the facility. The disposal of routine waste started in 1959 and has continued to the present. Waste disposal in the shafts began in 1966 and has also continued to this day. The disposal capacity of MDA G is nearly exhausted; the majority of the waste requiring disposal in the future will be placed in pits and shafts in Zone 4 (Figure 1-2). For the purposes of conducting the performance assessment and composite analysis, it is assumed that disposal operations at Area G will cease in the year 2044.

The disposal units in MDA G are expected to undergo phased final closure starting in 2010. Current plans call for all pits and shafts within MDA G to be closed by the year 2015 (DOE, 2002). Disposal operations will move to the Zone 4 expansion area once disposal in MDA G is no longer feasible and continue until 2044. It is assumed that it will take 2 years from the time of the last disposal shipment until the closure of the pits and shafts in the expansion area is complete and the cover is in place. Based on this assumption, final closure of the site will be complete in 2046.

An active institutional control period of 100 years, extending from 2047 through 2146, will follow final closure of the facility. During this period, it is assumed that DOE will maintain control over the entire Laboratory, thereby preventing members of the public from entering or otherwise occupying the disposal site. Limited maintenance of the facility is assumed during this period, including actions necessary to prevent the establishment of deep-rooted plants and any actions necessary to prevent significant damage to the cover.

The passive institutional control period will begin in 2147 and will continue until the disposal facility no longer poses a significant risk to human health and safety and the environment. It is assumed that the DOE's control over the entire Laboratory will cease; however, administrative control over individual sites such as Area G is expected to continue. Figure 1-3 indicates the likely area of DOE control during this period of time. The level of control will be sufficient to prevent members of the public from residing over the closed site, but no other maintenance activities are assumed to occur.

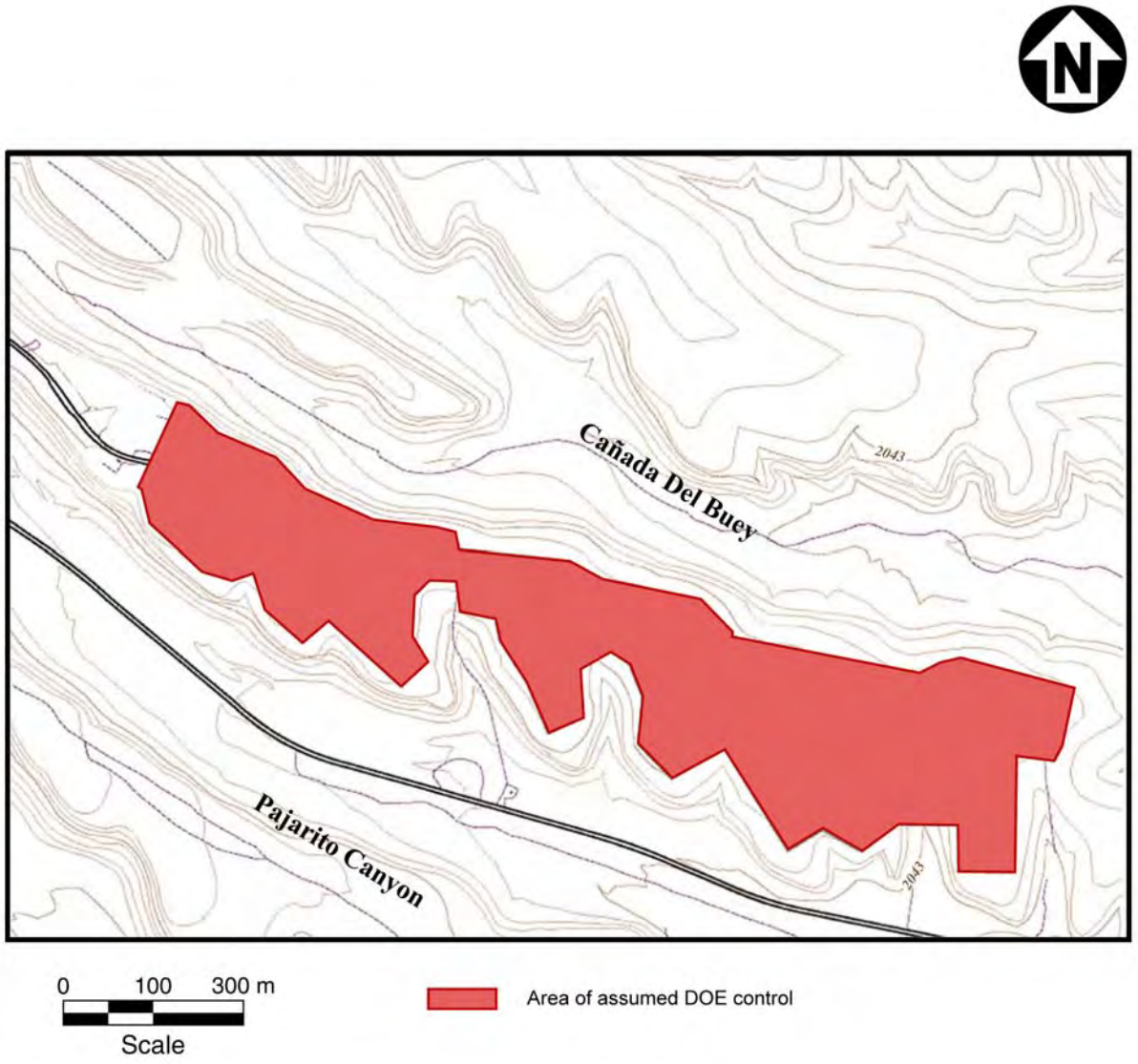

Figure 1-3
Assumed Area of DOE Control during Passive Institutional Control Period

1.4 Related Documents

The results of the performance assessment and composite analysis impact several ongoing programmatic and planning activities at the Laboratory. Likewise, these other programs and activities provide a valuable and dynamic source of information for the performance assessment and composite analysis. The areas of overlap between these activities require interactive, working relationships. These relationships and some of the documents of interest to the performance assessment and composite analysis are described below.

1.4.1 Site-Wide Environmental Impact Statement

In 1999, the DOE issued a site-wide environmental impact statement (SWEIS) (DOE, 1999), pursuant to the National Environmental Policy Act (NEPA, 42 U.S.C. § 4321, et seq). This SWEIS evaluated the potential environmental and economic effects of continued and proposed operations at the Laboratory, including operations at Area G. The performance assessment team and SWEIS personnel coordinated activities to ensure that the analyses related to Area G were approached in a consistent and efficient manner with respect to the following:

- General facility and site description
- Existing waste inventory
- Projected future LLW inventory
- Proposed future disposal unit development
- Disposal unit closure
- Results of transport calculations

LANL issued a revised SWEIS in 2008 (LANL, 2008a); the analyses pertinent to Area G were unaffected by this update.

1.4.2 Environmental Restoration Project Documents

The DOE ER program aims to protect human health and the environment from hazards posed by inactive and surplus DOE facilities and contaminated lands through the cost-efficient and responsible remediation of sites and facilities. The Laboratory's ER Project has many documents that are related to both the performance assessment and composite analysis. Brief descriptions of these documents and their relationship to the Area G analyses are provided below.

1.4.2.1 Installation Work Plan

The installation work plan (IWP) (LANL, 2000a) establishes the regulatory framework, programmatic structure, and life cycle for the Laboratory's ER Project. It also identifies the project scope and schedule for all sites described as solid waste management units, operable units (OUs), and field units under consideration for remediation under the Resource

Conservation and Recovery Act (RCRA). Certain aspects of the IWP are important to the development of the composite analysis. In turn, the results of the composite analysis will provide important information for the implementation of activities described in the work plan. Areas of mutual interest and possible overlap include:

- Radioactively contaminated sites identified in the IWP that may need to be considered in the composite analysis as potentially interacting sources (with Area G)
- Schedules for completing site characterization studies that may impact the maintenance of the composite analysis
- Results of the composite analysis that can be used as a tool to prioritize activities and schedules in the IWP

1.4.2.2 RCRA Facilities Investigations Work Plans

The detailed plans and schedules for individual OUs within the ER Project are described in RCRA Facilities Investigation (RFI) work plan documents. The portion of Area G that contains waste disposed of before 1988 is part of the ER Project's OU 1148 (Krueger, 1992). A later RFI (LANL, 2000b) covers all disposal areas at TA-54. Many activities described in the RFIs are specifically related to the Area G performance assessment and composite analysis. For example, both the work plan and this performance assessment and composite analysis describe natural features of the site, facility uses, and conceptual models for contaminant transport. The RFI work plan describes field investigations to measure releases from historical disposals, while the composite analysis models the same releases. The RFI field investigations have provided a substantial body of data used in the performance assessment and composite analysis. In turn, the results of the composite analysis will be used to evaluate alternative remediation and/or closure options for OU 1148.

Other ER plans describing sites with potentially interacting sources have been useful in developing the composite analysis. The descriptions found in various RFI work plans of the natural setting and the characteristics of various MDAs were used directly to identify, and ultimately to exclude, sources of radioactivity that could interact with projected releases from Area G within a period of 1,000 years (e.g., LANL, 2001). In turn, it is anticipated that the results of the composite analysis will be used to help prioritize field investigations at other sites.

1.4.3 Land Use Plan

The Laboratory's ER Project has developed a site-wide land use plan in cooperation with the New Mexico Environment Department, the U.S. Environmental Protection Agency (EPA), and the DOE. According to Annex E of the land use plan, Area G is designated for eventual industrial use. Access to the site will be limited to workers or authorized visitors and general

facility surveillance will be instituted. Additional institutional controls will be defined and implemented as needed to prevent or limit exposure to contaminants. This Document of Understanding has important implications regarding exposure pathways and scenarios used in the performance assessment and composite analysis to evaluate compliance with specific performance objectives.

1.4.4 Groundwater Monitoring Program

The site-wide hydrogeologic characterization work plan (LANL, 1998a) describes data collection, analysis, and management activities that will be employed to refine the understanding of the hydrology of the Pajarito Plateau (Nylander, 2001). One purpose of the 7-year program described in the work plan is to perform hydrogeologic modeling to answer questions about contaminant pathways and hydrology at ER sites. All of the ER sites considered in the composite analysis are considered in the hydrogeologic work plan. Thus, the results of the performance assessment and composite analysis will be reviewed for consistency with existing conceptual models of the hydrogeology of the LANL site. Furthermore, results will be integrated with any regional analyses to be performed.

1.4.5 Waste Management Documents

In addition to many documents that describe the administrative, programmatic, and/or operational aspects of the LLW management program, the performance assessment is an integral element in the formal configuration of the waste management program. Together, these documents ensure a consistency of approach throughout the facility life cycle. The relationships between the performance assessment and other waste management documents are summarized below.

1.4.5.1 Safety Analysis Report

Area G is identified as a Hazard Category 2 nonreactor nuclear facility due to the presence of TRU waste. A safety analysis report (e.g., LANL, 2003a) is maintained for Area G so that the hazards associated with various facility activities are understood and minimized. The safety analysis describes the natural features of the site and the uses of the facility; it also provides the results of a hazard analysis. This document and the performance assessment contain overlapping information and are considered companion documents that ensure the safety of the facility during the operational and postclosure periods.

1.4.5.2 Waste Acceptance Criteria

The results of the performance assessment are used to set limits on the future waste inventory to provide reasonable assurance that impacts to human health and the environment remain below the applicable performance objectives. These limits are integrated into the Waste Acceptance Criteria (WAC) for the Laboratory's treatment, storage, and disposal facilities (LANL, 2008b).

The acceptance criteria address proper and complete waste characterization, documentation and container requirements, packaging and labeling, and waste form restrictions. Exceptions to the LANL WAC must undergo a formal review process (LANL, 2008c). The relationship between the results of the performance assessment and the WAC is discussed in Section 5 of this report.

1.4.5.3 Waste Certification Program

The requirements for waste characterization as described in the Waste Acceptance and Certification Program are based on the results of the performance assessment. The use of the performance assessment results in this manner is in accordance with the Data Quality Objectives Process endorsed by the EPA and the DOE.

1.4.5.4 Operational Procedures

The performance assessment and composite analysis account for the configuration of the waste in the disposal pits and shafts used at Area G. Procedures have been put in place that govern the design, construction, use, and interim closure of the disposal units in a manner that is consistent with the long-term performance modeling. The LLW Receipt and Disposal procedure (LANL, 2008d) establishes the requirements for the receipt, storage, and disposal of waste at Area G. Most importantly from a disposal standpoint, the procedure specifies the minimum depth at which waste may be disposed of in pits and shafts. The design, construction, and operational closure procedure (LANL, 2007a) imposes restrictions on pit and shaft depth and placement (relative to the edge of the mesa) and the manner in which the disposal units are closed once they are filled.

1.4.5.5 Closure Plan

As discussed in Section 1.3, the disposal pits and shafts in MDA G are scheduled to undergo phased closure between 2010 and 2015 (DOE, 2002); it is assumed that final closure of the disposal units in the Zone 4 expansion area will take place in 2045 and 2046. The closure plan for Area G describes the final conceptual closure design for the site. This configuration of the cover was developed in concert with the surface erosion modeling conducted for the performance assessment and composite analysis.

1.4.5.6 Environmental Monitoring Plan

The environmental monitoring plan (LANL, 2005b) describes activities related to the Area G performance assessment and composite analysis. This plan defines the effluent monitoring and environmental surveillance practices associated with normal operations at Nuclear Waste Infrastructure Services facilities. One of the facilities monitored under this plan is Area G. Annual sampling and analysis of air, sediment, soils, plants, and animals is conducted at and around Area G in support of the Laboratory-wide environmental surveillance program (e.g., LANL, 2007b); these efforts are supplemented with additional field work that specifically supports the performance assessment and composite analysis. As detailed in Section 7 of this

report, additional field investigations are planned to provide information for reducing the uncertainty in the performance assessment and composite analysis evaluations.

1.4.5.7 Storm Water Pollution Prevention Plan

The storm water pollution prevention plan for TA-54 (LANL, 2005c) defines and describes materials and facility activities that are potential sources of pollution. In particular, this plan describes the natural and man-made features that control water runoff from the surface of Area G into the adjacent canyons and the best management practices that have been selected and implemented to prevent pollution. Accordingly, it provides information useful in describing and modeling surface water movement related to the transport of radioactivity both above- and belowground. It also provides information for assessing how the erosive effects of surface water may pose a risk to the long-term ability of the site to contain radioactivity.

1.5 Performance Criteria

In accordance with DOE Order 435.1 (DOE, 2001a), the long-term performance of an LLW disposal facility is evaluated through a series of performance objectives. These criteria, provided in DOE M 435.1 (DOE, 2001c), are designed to:

- Ensure the health and safety of the public
- Protect groundwater resources
- Safeguard persons who may inadvertently intrude into the buried waste
- Maintain radiation doses from DOE facilities at levels that are as low as reasonably achievable (ALARA)

The specific performance objectives adopted for the Area G performance assessment and composite analysis are described below.

1.5.1 Public Protection Performance Objectives

The performance objectives pertinent to the protection of the public, as stated in DOE M 435.1 (DOE, 2001c), include the following:

- Dose to representative members of the public shall not exceed 25 mrem in a year total effective dose equivalent from all exposure pathways, excluding the dose from radon and its progeny in air.

- Dose to representative members of the public via the air pathway shall not exceed 10 mrem in a year total effective dose equivalent, excluding the dose from radon and its progeny.

- Release of radon shall be less than an average flux of 20 pCi/m^2/s at the surface of the disposal facility. Alternatively, a limit of 0.5 pCi/L of radon in air may be applied at the boundary of the facility.

The all pathways performance objective addresses exposures that may be received from any and all modes of exposure, including exposures from airborne contaminants (except radon and its progeny). Compliance with this performance objective is to be demonstrated over a period of 1,000 years following closure of the disposal facility, at the point of maximum exposure that is accessible to members of the public. An evaluation of potential exposures beyond the period of compliance is to be conducted to provide increased confidence in the long-term performance of the disposal facility.

The air pathway performance objective is found in the National Emissions Standards for Hazardous Air Pollutants (40 CFR 61.93, Subpart H [EPA, 2004]). This standard requires that exposures from sources of airborne radioactivity at DOE facilities result in a dose of 10 mrem/yr or less, excluding the contributions of radon and its progeny. Compliance with this criterion is to be demonstrated at the point of maximum exposure that is accessible to members of the public for a period of 1,000 years following facility closure.

Releases of radon gas (i.e., Rn-220 and Rn-222) are subject to requirements in 40 CFR 61, Subpart Q (EPA, 1989), which limit releases to an average flux of 20 pCi/m^2/s at the surface of the disposal facility. An incremental increase in the air concentration of radon of 0.5 pCi/L at the point of assessment may also be used to demonstrate compliance with the radon performance objective. Compliance must be demonstrated for a period of 1,000 years following closure of the disposal facility.

For this performance assessment, a series of four exposure scenarios was used to demonstrate compliance with the DOE public protection performance objectives:

- The *All Pathways–Groundwater Scenario* was used to project doses received by persons living downgradient of Area G who use contaminated groundwater for domestic needs.

- The *All Pathways–Cañada del Buey Scenario* and the *All Pathways–Pajarito Canyon Scenario* were used to project exposures for persons living in either of these two canyons adjacent to Area G.

- The *Atmospheric Scenario* was used to demonstrate compliance with the air pathway performance objective.

Two exposure locations were evaluated for the All Pathways–Groundwater Scenario: the Laboratory boundary near White Rock and a location 100 m (330 ft) downgradient of the Area G fence line. The former location addresses exposures received by persons prior to the loss of active institutional control over the Laboratory, while the location near the fence line considers exposures when DOE control is limited to selected facilities at LANL. The exposure projections focused on the doses received during the 1,000-year compliance period. Two simulations considered potential exposures for a period of 100,000 years after closure to gain additional insight into the potential risk posed by Area G to groundwater users.

The source of contamination for the two all pathways–canyon scenarios is sediment transported from the mesa top by surface runoff. Exposures were projected at nine locations, two of which were in Cañada del Buey and seven in Pajarito Canyon. Exposures to persons at the Cañada del Buey locations were projected starting at the time of facility closure (i.e., during the active institutional control period) because a portion of this canyon lies outside of the Laboratory boundary (Figure 1-2). The portion of Pajarito Canyon that receives sediments from Area G lies within the Laboratory boundary, so it was assumed that no persons will reside in this canyon until the end of the 100-year active institutional control. While the performance assessment modeling was primarily concerned with potential doses during the 1,000-year compliance period, limited evaluations considered exposures over a period of 50,000 years postclosure.

For the Atmospheric Scenario, doses were projected for two receptors. The first was a person living along the LANL boundary downwind of the disposal site. Exposures for this receptor were estimated starting with the placement of waste in the disposal facility. The second receptor was assumed to live immediately outside of the Area G fence line; projections for this receptor were made from the end of the active institutional control period forward. In each case, projections were made for the point of maximum exposure outside of the pertinent boundary (i.e., the LANL boundary or the Area G fence line). The dose projections focused on exposures during the 1,000-year compliance period; however, limited modeling was conducted to investigate facility performance for a period of 50,000 years after facility closure.

Radon fluxes at the surface of the disposal facility were projected for a period of 1,000 years following facility closure. Separate projections were developed for several subsets of the disposal pits and shafts; these subsets generally correspond to different periods of waste disposal at Area G.

1.5.2 Water Resource Impacts Assessment

According to DOE M 435.1 (DOE, 2001c), the performance assessment must include an assessment of impacts to groundwater resources. Potential impacts are to be assessed on a site-specific basis in accordance with a hierarchical set of criteria. In general, these criteria require that the LLW disposal site comply with any applicable state or local law, regulation, or other

legally applicable requirement for water resource protection. Potential impacts are to be evaluated at the point of highest groundwater concentration outside of a 100 m (330 ft) buffer zone for a period of 1,000 years following facility closure.

The performance objectives that were adopted to evaluate potential impacts to groundwater resources are based on the drinking water regulations of New Mexico (NMEIB, 2002), which incorporate the requirements set forth in the Safe Drinking Water Act as codified in 40 CFR 141 (EPA, 2000). The standards in 40 CFR 141 that are relevant to the radiological performance assessment include maximum concentration limits for Ra-226, Ra-228, uranium, and gross alpha activity, and maximum concentration limits for beta particle and photon radioactivity. The specific requirements, as stated in 40 CFR 141, are as follows:

- 141.66(a)—The maximum contaminant level for combined radium-226 and radium-228 is 5 pCi/L.
- 141.66(b)—The maximum contaminant level for gross alpha particle activity (including radium-226 but excluding radon and uranium) is 15 pCi/L.
- 141.66(c)—The average annual concentration of beta particle and photon radioactivity from man-made radionuclides in drinking water must not produce an annual dose equivalent to the total body or any internal organ greater than 4 mrem/yr.
- 141.66(e)—The maximum contaminant level for uranium is 30 µg/L (30 ppb).

The concentrations of radionuclides causing an annual dose equivalent of 4 mrem to the total body or any internal organ have been published in EPA (2002).

For this performance assessment, the Groundwater Resource Protection Scenario was adopted to demonstrate compliance with the water resource impacts objective. Doses were projected for persons living downgradient of Area G at a location 100 m (330 ft) east of the facility fence line. Exposures were estimated from the time waste disposal began to the end of the 1,000-year compliance period; limited modeling was conducted to consider potential impacts to groundwater resources over a period of 100,000 years.

1.5.3 Intruder Analysis

The performance assessment is required to evaluate the potential exposures received by persons who inadvertently intrude into the disposed waste. Institutional controls over the disposal facility are assumed to prevent intrusion from occurring for a minimum of 100 years after facility closure. Projected intruder exposures are subject to chronic and acute dose limits of 100 and 500 mrem/yr, respectively, excluding contributions of radon in air. The results of the intruder analysis are also to be used to develop WAC for the disposal facility.

Three inadvertent intruder scenarios were used to demonstrate compliance with the dose objectives cited above and to establish intruder-based WAC for the disposal units at MDA G. The Intruder-Construction Scenario projects exposures for a person who arrives at the disposal site after active institutional control has ended and constructs a house with a full basement over the closed disposal units. The Intruder-Agriculture Scenario projects doses for a person who lives in that house after it is completed. The Intruder–Post-Drilling Scenario addresses exposures received by a person who resides at the disposal site after active institutional control has ended and has a well drilled though the buried waste to supply domestic water needs. Potential intruder exposures were projected over the 1,000-year compliance period for all three scenarios.

1.5.4 ALARA Analysis

In addition to satisfying the performance objective discussed above, DOE facilities must demonstrate that disposal is conducted in a manner that maintains releases to the environment ALARA. A graded approach is to be used in conducting the ALARA analysis so the rigor of the evaluation is consistent with the magnitude of the risk posed by the disposal facility.

The ALARA analysis conducted in support of the performance assessment and composite analysis considered the relative benefits of three closure strategies. The first of these is the final closure configuration currently proposed for the site. As an alternative, the Extended Control Option considers the effectiveness of maintaining active institutional control over the disposal facility throughout the 1,000-year compliance period. A second alternative, the Biobarrier Option addresses the effectiveness of incorporating a plant and animal intrusion barrier into the final cover design.

1.5.5 Composite Analysis

The performance objective for the composite analysis is to ensure that the DOE's primary dose limit of 100 mrem/yr is met. This limit is intended to apply to radioactivity coming from all radioactive sources at the Laboratory and all exposure pathways (DOE, 1993). A dose constraint of 30 mrem/yr is imposed upon the composite analysis to ensure that any exposures received in conjunction with the disposal facility do not constitute an extraordinary portion of the primary dose limit. Potential exposures are to be evaluated at the point(s) of maximum exposure accessible to members of the public for a period of 1,000 years after facility closure.

Consistent with the National Emissions Standards for Hazardous Air Pollutants in 40 CFR 61 (EPA, 2004), airborne releases from Area G and all other activities at the Laboratory must not result in exposures that are greater than 10 mrem/yr, excluding the contributions of radon and its progeny. Atmospheric pathway exposures are to be evaluated at the point of maximum exposure over the compliance period.

The all pathways (groundwater and canyons) scenarios described in Section 1.5.1 were used to demonstrate compliance with the 100 mrem/yr primary dose limit and the 30 mrem/yr dose constraint. Exposures projected for the Atmospheric Scenario were used to demonstrate compliance with the requirements found in 40 CFR 61. All exposure scenarios were implemented at the exposure locations discussed above over the 1,000-year compliance period. Limited modeling was conducted to investigate the potential impacts to groundwater users for 100,000 years following facility closure; 50,000-year simulations were used to evaluate long-term exposures for the Atmospheric Scenario and canyon receptors.

1.5.6 Performance Objective Summary

Tables 1-1 and 1-2 summarize the performance objectives found in DOE M 435.1-1 (DOE, 2001c) and the exposure scenarios used to demonstrate compliance with those requirements. The requirements associated with the performance assessment are addressed in Table 1-1 and those for the composite analysis are in Table 1-2. For each phase of the disposal facility life cycle, the tables list the performance objectives, the exposure scenarios evaluated to address these criteria, and the point of compliance. A compliance period of 1,000 years following facility closure was adopted for all modeling.

1.6 Summary of Key Assumptions

The performance assessment and composite analysis are based on several assumptions that were adopted to structure and reduce the complexity of the analyses. These assumptions and their potential impact on the conclusions of these evaluations are summarized below. A more thorough consideration of the impacts of these assumptions is provided in Section 6.

The projected impacts for both analyses assume the DOE will maintain control over the entire Laboratory throughout the 100-year active institutional control period; a subsequent period of passive institutional control over Area G is assumed to continue until the site no longer poses an unacceptable risk to human health and safety, and the environment. It is assumed that the level of specified control during the active institutional control period will restrict exposures to members of the public to locations outside of the LANL boundary. Active DOE control will also prevent inadvertent intrusion into the waste, delay the establishment of deep-rooting plants over the disposal units, and limit significant damage to the final cover. During the passive institutional control period, it is assumed that DOE control will be reduced to a point at which it prevents only the long-term occupation of the site by members of the public. The performance assessment considers the consequences of inadvertent intrusion during this period to establish WAC for the disposal facility. If the actual level of control over the Laboratory and Area G is less restrictive than the assumed level, exposures greater than those estimated for the performance assessment and composite analysis could occur.

Table 1-1
Summary of Performance Objectives Adopted for the Area G Performance Assessment

Phase of Facility Life Cycle	Performance Objective	Exposure Scenario	Compliance Point
Operational, Closure, and Active Institutional Control Periods	All pathways (25 mrem/yr)	All Pathways–Groundwater	Point of maximum exposure outside LANL boundary
		All Pathways–Cañada del Buey	Cañada del Buey
	Air pathway (10 mrem/yr)	Atmospheric	Point of maximum exposure outside LANL boundary
	Radon flux (20 pCi/m^2/s)	---	Area G
	Water resources impacts (40 CFR 141 limits)	Groundwater Resource Protection	100 m downgradient of Area G
Passive Institutional Control Period	All pathways (25 mrem/yr)	All Pathways–Groundwater	Point of maximum exposure outside Area G fence line
		All Pathways–Cañada del Buey	Cañada del Buey
		All Pathways–Pajarito Canyon	Pajarito Canyon
	Air pathway (10 mrem/yr)	Atmospheric	Point of maximum exposure outside Area G fence line
	Radon flux (20 pCi/m^2/s)	---	Area G
	Water resources impacts (40 CFR 141 limits)	Groundwater Resource Protection	100 m downgradient of Area G
	Inadvertent intruder (500 mrem/yr acute exposure)	Intruder-Construction	Area G
	Inadvertent intruder (100 mrem/yr chronic exposure)	Intruder-Agriculture	Area G
		Intruder–Post-Drilling	Area G

--- = Radon fluxes are projected in conjunction with the air pathway modeling.

Table 1-2
Summary of Performance Objectives Adopted for the Area G Composite Analysis

Phase of Facility Life Cycle	Performance Objective	Exposure Scenario	Compliance Point
Operational, Closure, and Active Institutional Control Periods	All pathways (100/30 mrem/yr) [a]	All Pathways–Groundwater	Point of maximum exposure outside LANL boundary
		All Pathways–Cañada del Buey	Cañada del Buey
	Air pathway (10 mrem/yr)	Atmospheric	Point of maximum exposure outside LANL boundary
Passive Institutional Control Period	All pathways (100/30 mrem/yr) [a]	All Pathways–Groundwater	Point of maximum exposure outside Area G fence line
		All Pathways–Cañada del Buey	Cañada del Buey
		All Pathways–Pajarito Canyon	Pajarito Canyon
	Air pathway (10 mrem/yr)	Atmospheric	Point of maximum exposure outside Area G fence line

--- = Radon fluxes are projected in conjunction with the air pathway modeling.

[a] The first performance objective (100 mrem/yr) is the DOE's primary limit for the protection of the public; the second performance objective (30 mrem/yr) is the dose constraint imposed on the composite analysis to ensure the disposal facility does not constitute an extraordinary portion of the primary dose limit.

The performance modeling conducted in support of the performance assessment and composite analysis is based on the assumption that climatic conditions in the vicinity of Area G will not change significantly over time. Adoption of this assumption reduces the complexity of modeling groundwater flow and transport, the impacts of biotic intrusion on the facility's ability to safely isolate the waste, and the effects of surface erosion. Long-term changes in climate will affect many of the boundary conditions upon which the modeling is based and, therefore, could alter the impacts projected by these simulations.

Disposal practices in effect prior to the mid-1990s conferred structural stability to the disposal units; the cardboard boxes and plastic bags used to dispose of waste were readily crushed by heavy equipment and the crushed tuff backfill consolidated quickly. Supporting this conclusion is the fact that only infrequent and minor local settlements have been observed at Area G since disposal operations began. The use of metal containers may result in a more efficient use of existing disposal capacity; however, void spaces in the containers may lead to settlement and subsidence when they fail. Although the disposal facility's WAC place stringent requirements on the amount of void space permitted in waste containers, past practices may not have lived up to these standards.

The modeling conducted in support of the performance assessment and composite analysis assumes no significant subsidence of the disposal units at Area G will occur after the facility undergoes final closure. This approach was adopted for two reasons. First, the potential for significant subsidence at Area G has not been fully characterized. Second, options exist for addressing subsidence issues prior to final closure of the facility, including the dynamic compaction of incompletely filled disposal units and the repair of cover failures should they occur during the 100-year active institutional control period.

2.0 Disposal Facility Characteristics

The long-term performance of the Area G disposal facility will depend upon the site conditions, the design features of the facility, and the characteristics of the waste placed in the disposal pits and shafts. Section 2.1 presents the natural and demographic characteristics of the disposal site and surrounding lands that are relevant to the performance assessment and composite analysis. Important design aspects of the disposal facility and their influence on site performance are discussed in Section 2.2, and Section 2.3 presents the characteristics of the waste that has been, or will be, disposed of at Area G. The information presented here forms the basis for the site conceptual model presented later in this report.

2.1 Site Characteristics

The potential risk posed by Area G to human health and safety and the environment is influenced by a number of environmental and demographic variables. For example, environmental characteristics of the disposal site and surrounding lands will affect the rates at which radionuclides are released from the waste and transported to locations accessible to people. The proximity of members of the public to the facility and their anticipated use of potentially contaminated environmental media are also important considerations. This section discusses the characteristics of Area G and the surrounding environs that may influence whether and how radioactive releases from Area G affect human health over the next 1,000 years.

2.1.1 Geography and Demography

Los Alamos National Laboratory is located in Los Alamos County in north-central New Mexico, about 45 km (28 mi) northwest of the state capitol, Santa Fe, and about 100 km (62 mi) north-northeast of Albuquerque, the state's largest city. The DOE controls some 111 km^2 (43 mi^2) of federally owned land occupied by the Laboratory.

2.1.1.1 Disposal Site Location

Area G is located on Mesita del Buey, a finger-like mesa that extends to the southeast from the broad, east-sloping flank of the Jemez Mountains called the Pajarito Plateau. The site lies entirely within TA-54 in the east-southeast portion of the Laboratory complex (Figure 2-1). The northern and eastern borders of TA-54 are coincident with the LANL property boundary. The community of White Rock, about 2 km (1.2 mi) east of Area G, is the closest population center; other nearby communities include Los Alamos, 8 km (5 mi) to the northwest; Española 24 km (15 mi) to the northeast; Santa Fe, 34 km (21 mi) to the southeast; and Albuquerque, 97 km (60 mi) to the south-southwest. The Rio Grande, New Mexico's largest river, passes within 10 km (6 mi) of the site, to the east of White Rock.

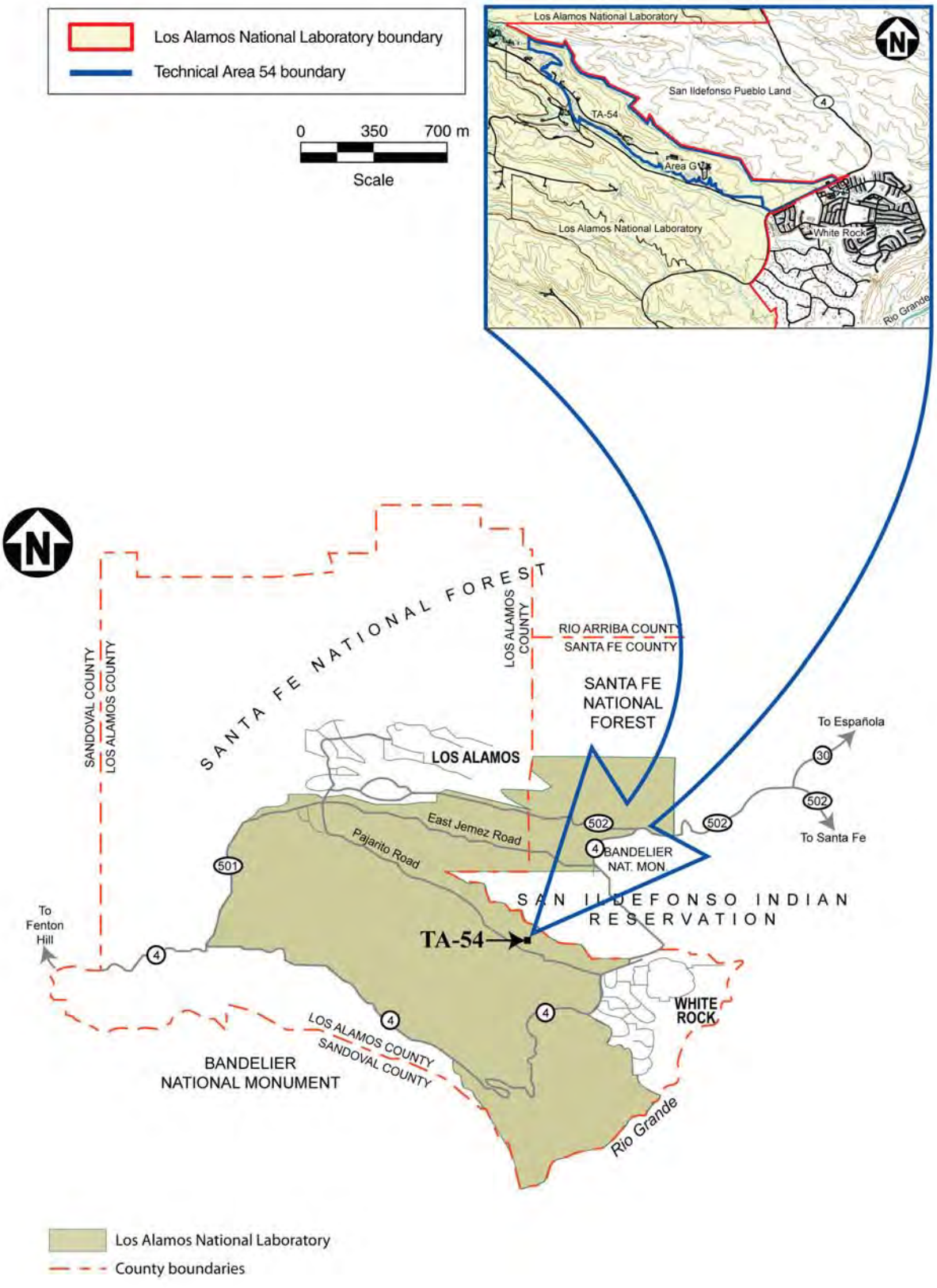

Figure 2-1
Locations of Technical Area 54 and Area G

Mesita del Buey (and most of TA-54) was identified in 1956 by the USGS as a prospective radioactive waste disposal site because of its favorable hydrogeologic properties (see Section 2.1.5). Since 1957, about 26 ha (65 ac) of TA-54 have been used for radioactive waste disposal; the site has served as the primary LLW disposal site for the Laboratory since 1959. The development of disposal units has progressed generally from east to west, in accordance with the pit and shaft construction guidelines in effect at the time of construction. The result has been the construction of 35 disposal pits and more than 200 shafts, the general layout of which is shown in Figure 2-2.

The Area G performance assessment and composite analysis assume that LLW will be disposed of at Area G through the year 2044. However, almost all of the available disposal capacity within MDA G, the portion of the facility that is currently receiving waste, has been exhausted. Preparations have been made to construct additional disposal pits and shafts in a 12 ha (30 ac) area immediately west of the existing disposal units referred to as Zone 4 (Figure 1-2, Section 1). Options for the development of Zone 4 have been evaluated and detailed; a summary of this evaluation is included as *Appendix B* in Volume 2 of this report. Zone 4 is expected to provide more LLW disposal capacity than required to support future Laboratory needs.

It is assumed that the DOE will maintain control of all Laboratory lands throughout the 100-year active institutional control period that begins at the time Area G has undergone final closure. Following this period, it is assumed that DOE's control over the entire Laboratory will cease; however, administrative control over sites such as Area G is expected to continue as long as those facilities pose an unacceptable risk to human health and safety and the environment. Based on these assumptions, the boundary of the controlled land will be reduced from the Laboratory boundary shown in Figure 1-1 to the approximate boundary shown in Figure 1-3 (Section 1).

2.1.1.2 Disposal Site Description

Area G is located on top of Mesita del Buey, a narrow, southeast-trending mesa about 3 km (2 mi) long and 0.4 km (0.25 mi) wide. Mesita del Buey is relatively flat and narrow, sloping gently from an altitude of about 2,100 m (6,900 ft) at its western end to about 2,000 m (6,600 ft) near its eastern end. The mesa has steep sides draining into Cañada del Buey to the north and Pajarito Canyon to the south; the floors of these canyons lie 15 to 30 m (50 to 100 ft) below the surface of the mesa. The northern side of the mesa is more gently sloping than the south faces, which are almost vertical near the rim, becoming more sloped toward the canyon floor. Storm water runoff from Mesita del Buey feeds the streams in both canyons, mostly along the natural drainages evident along the south mesa wall. Pajarito Canyon is a perennial to near-perennial stream, fed by rainfall, snowmelt, and a few springs in the upper reaches of the canyon. Cañada del Buey is much drier than Pajarito Canyon, with a small stream that flows only a few days out of the year.

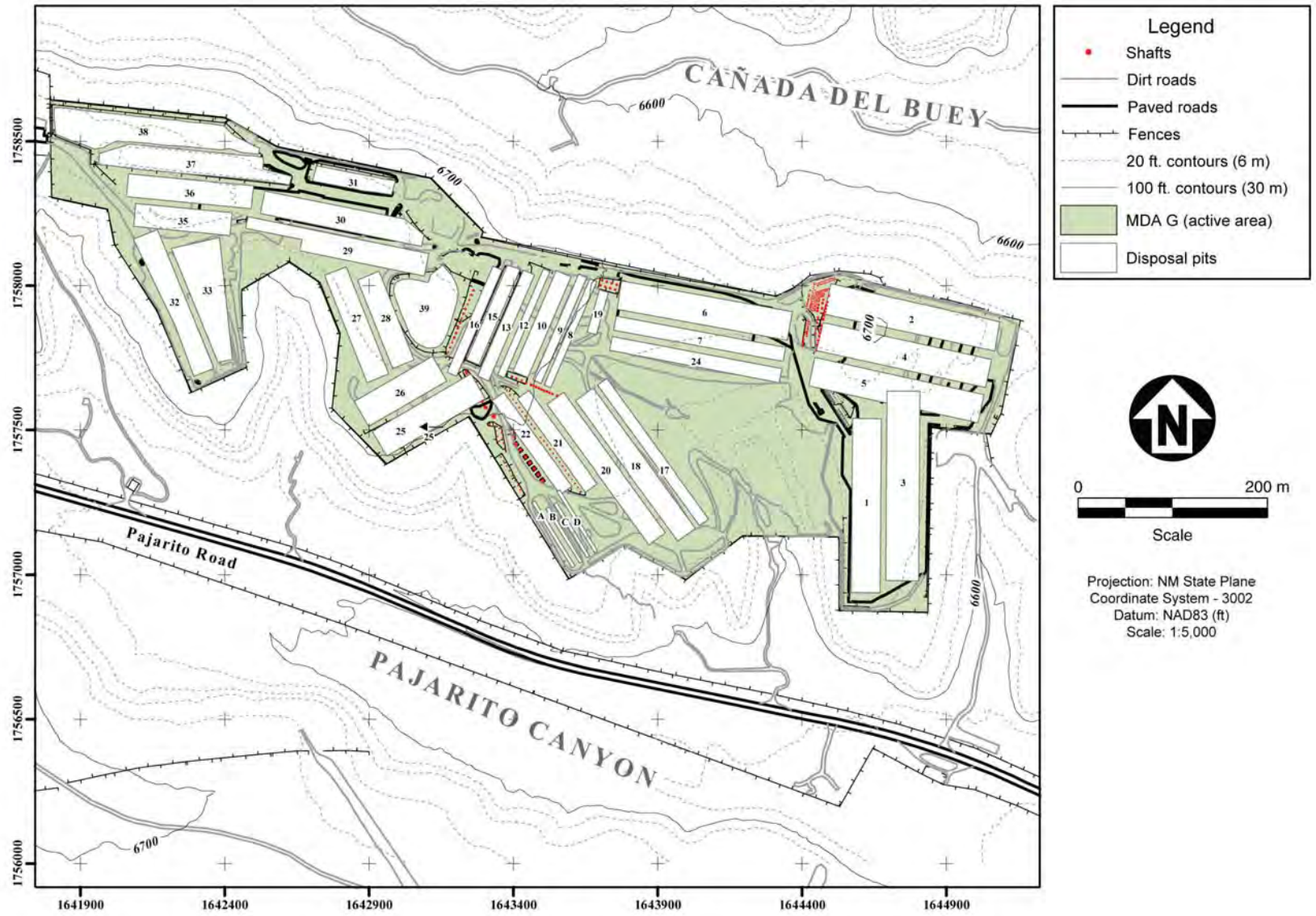

Figure 2-2
Waste Disposal Units at Material Disposal Area G
Source: Apogen Technologies (formerly SEA)
LANL RRES Database, Map ID: 4531.021 (1) Rev. 2

The natural drainage pattern is locally disturbed as a result of waste management activities at Area G. Erosion controls are used to divert water away from waste management activities and disposal units. These controls include graded drainage channels, installed culverts, riprap, silt fences, asphalt channels, asphalt curbing, earthen berms, and weirs. Runoff controls are designed to guide surface water into the natural drainages. Certain surface structures at Area G also alter the natural erosion patterns along the mesa, but only on a local scale. Signs of erosion are identified and mitigation measures are undertaken as a part of the storm water compliance process.

The developed portions of Area G are characterized as grassland, although vegetation is sparse or nonexistent in many areas because of ongoing activities. The vegetation within Zone 4, which has remained relatively undisturbed, is typical of the piñon-juniper woodlands found at similar elevations in northern New Mexico.

Two highway routes provide access to the Laboratory. State Road 502 provides access from Pojoaque, Española, and surrounding areas to the southeast. State Roads 4 and 501 provide access from the Jemez Mountains to the west and southwest. A DOE-owned and controlled roadway (Pajarito Road) passes on the south side of TA-54. This road is not open to the public.

2.1.1.3 Population Distribution

The current and projected population distribution in the vicinity of Area G is an important factor in assessing the potential impacts to human health. The ALARA (as low as reasonably achievable) analysis, which compares the costs and benefits of alternative management scenarios on the basis of population risk, is particularly dependent on this information.

In 1991, Los Alamos County had an estimated population of 18,200 (EPG, 1994). According to 2002 estimates made by the University of New Mexico Bureau of Business and Economic Research (BBER, 2005), the population of Los Alamos County in 2000 was approximately 18,400 and the projected population for the county in 2030 is approximately 20,700. This projection indicates an average annual growth rate of less than half a percent per year.

Two residential and associated commercial areas exist in the county: Los Alamos with a population of 11,400 and White Rock with a population of 6,800 (LANL, 2003a). White Rock borders the LANL boundary to the east, approximately 2 km (1.2 mi) east of Area G. Other major residential population centers within an 80 km (50 mi) radius of the Laboratory include Española to the northeast and Santa Fe to the southeast, as well as portions of greater Albuquerque and Taos (Figure 2-3). Santa Fe, with a population of about 80,000, is expected to remain the major urban center of the region. Approximately 270,000 persons live within an 80 km (50 mi) radius of the Laboratory.

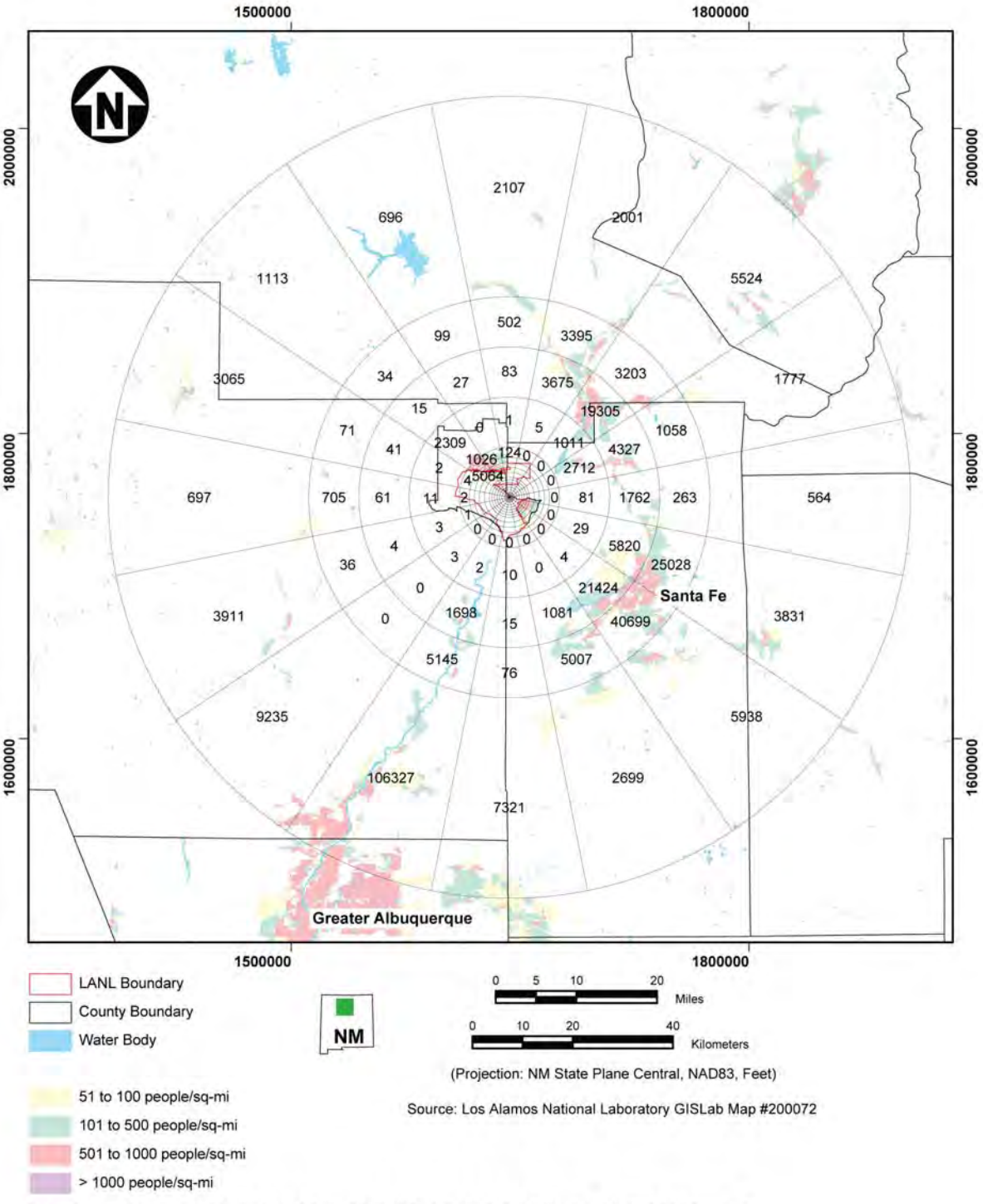

Entire Model Rings at .2, .4, .6, .8, 1, 1.5, 2, 2.5, 3, 3.5, 4, 5, 6, 7, 8, 10, 20, 30, 40, and 80 kilometers.

Note: Populations for grid sectors within first 8 km of Area G not shown because of space; this includes populations for White Rock and some portions of Los Alamos.

Figure 2-3
Population Data Array Within 80 km Radius of Area

In 2003, about 12,350 Laboratory and associated contractor employees worked within the Laboratory's geographic boundaries. Approximately 68 of the Laboratory employees worked at TA-54 (LANL, 2003a).

2.1.1.4 Uses of Adjacent Lands

State and federal government agencies and Indian tribes control most of the land surrounding the Laboratory, as shown in Figure 2-4. Of these, three federal agencies—the U.S. Forest Service, Bureau of Indian Affairs, and Bureau of Land Management—control the majority of land in the area. The Santa Fe National Forest comprises approximately 6.5×10^5 ha (1.6×10^6 ac) of land in several counties. The Española District of the Santa Fe National Forest includes 1.4×10^5 ha (3.5×10^5 ac) that border DOE land to the northwest and southeast. The Bandelier National Monument, managed by the National Park Service, borders the southwest portion of the LANL complex. The monument includes 1.3×10^4 ha (3.3×10^4 ac) of land, 9,400 ha (2.3×10^4 ac) of which are designated wilderness. All access routes to the monument pass through or along Laboratory property.

Thirteen Native American pueblos are located within 80 km (50 mi) of LANL. Each has its own tribal government, with technical and administrative assistance from the Bureau of Indian Affairs. The San Ildefonso Pueblo owns approximately 1.1×10^4 ha (2.6×10^4 ac) of land, a portion of which directly borders Area G within Cañada del Buey to the north of the disposal facility (Figure 2-1). In addition to hunting wildlife for food, pueblo people also harvest the fruit of piñon and juniper trees indigenous to the area. Hunting and gathering activities occur on the land directly adjacent to Mesita del Buey.

Approximately 49 percent of the land in Los Alamos County is vacant. Agriculture in the vicinity of LANL has been declining for the past several decades and is no longer considered an important economic activity in terms of cash income to area residents. Much of the land now occupied by LANL was used historically for grazing. The people of the pueblos in the region continue to graze livestock on their lands near LANL, and numerous private landowners in rural areas keep small numbers of livestock on land that surrounds Los Alamos County. All cattle are range fed in northern New Mexico; livestock forage primarily on native short-grass species. Livestock (primarily cattle) provide nearly 75 percent of the cash revenue from farm commodities in the region; crops (including hay, corn, chile, and apples) provide the remaining 25 percent. Small farms remain an important means of supplemental income and domestic food in the northern New Mexico region. The San Ildefonso Pueblo grows crops such as corn, chile, squash, beans, and tomatoes for domestic consumption and some local marketing.

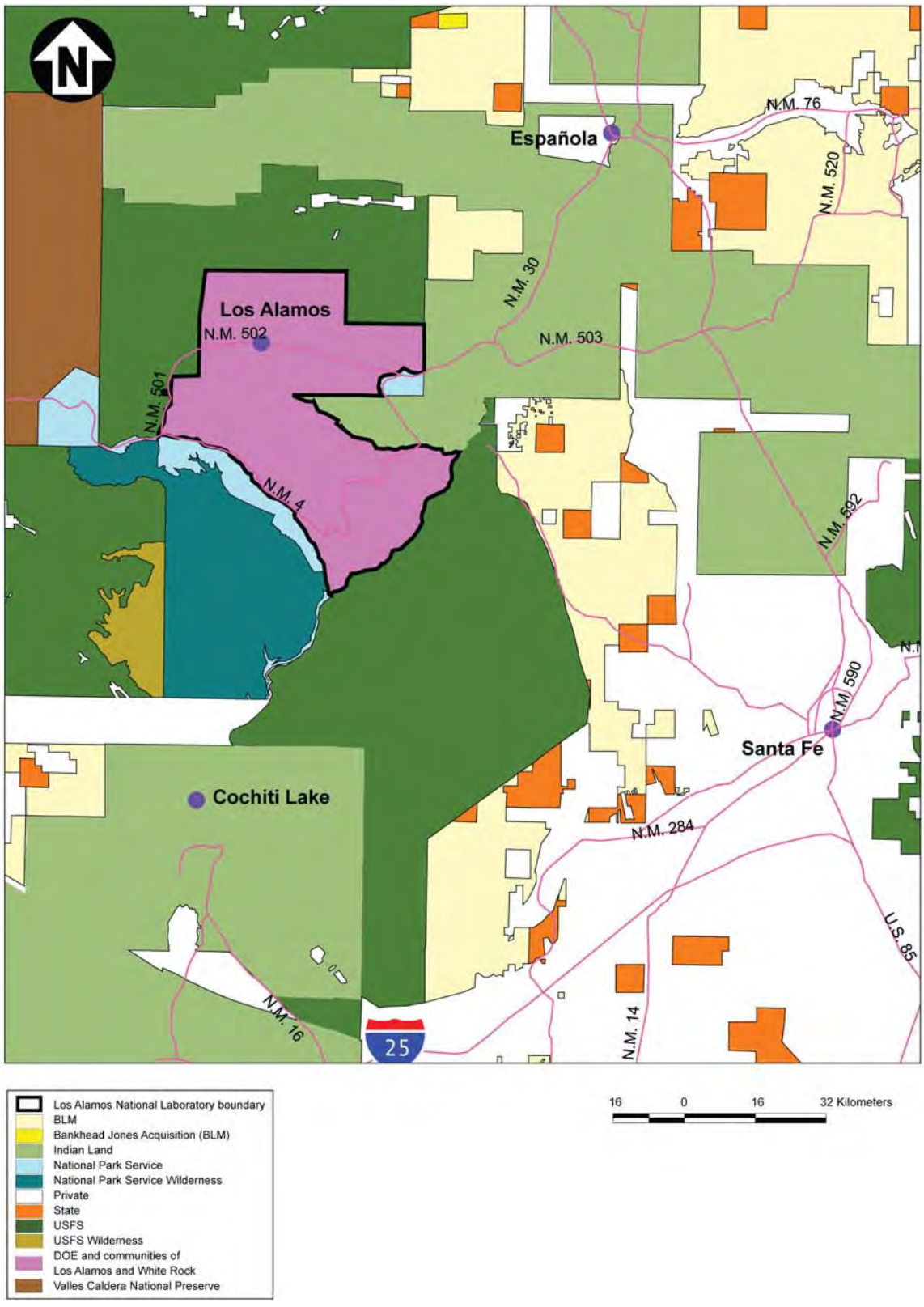

Figure 2-4
Land Status in Vicinity of LANL
Source: DBS&A, 2003

The following points summarize local agricultural activity:

- Only 1 to 2 percent of land is used for growing crops.
- Hay, corn, and chile are the most common crops in Los Alamos, Rio Arriba, and Santa Fe Counties.
- Most agricultural land is irrigated.
- Surface-water irrigation is more common than groundwater irrigation in Sandoval and Rio Arriba Counties; the opposite is true in Santa Fe County.
- Livestock density is low (1 animal per 120 ha [300 ac]).

2.1.2 Meteorology and Climatology

Local and regional atmospheric conditions influence radionuclide transport in several ways. In terms of subsurface transport, water from rain and snow infiltrates into the ground and reaches the saturated zone, thus recharging the aquifer. Runoff from summer rains and spring snowmelt can erode the mesa surface, and has the potential to carry radioactive materials into adjacent canyons. In addition, atmospheric conditions determine the extent to which airborne radioactivity will be transported away from the disposal site.

The semiarid, temperate mountain climate of Los Alamos County has been extensively monitored and described (Bowen, 1990). Five meteorological towers at LANL collect data on precipitation, temperature, humidity, evapotranspiration, and wind speed and direction. The main Los Alamos gauge was initially installed at TA-59, west of and at a higher elevation than TA-54. In 1990, this gauge was moved to TA-6. Additional gauges have been installed at TA-41, TA-49, TA-53, and TA-54 (Figure 2-5); three other sites measure precipitation only. The TA-54 monitoring station operated within the Area G facility boundary from 1980 through 1994; it is presently located at the eastern tip of Mesita del Buey, between the outer boundary of Area G and the community of White Rock. Table 2-1 summarizes pertinent meteorological data measured from 1993 through 2004 at the TA-54 meteorological tower.

2.1.2.1 Precipitation and Evapotranspiration

As shown in Table 2-1, about 32 percent of the annual average precipitation falls during July and August, a period referred to as the monsoon season. Snowfall is greatest from December through March, with annual accumulations of about 150 cm (59 in.). Annual variations in precipitation can be quite large. For the 12-year period shown, the average precipitation is just over 34 cm (13 in.) per year. Evaporation is generally high because of factors such as temperature, humidity, and air movement; the moisture lost through evaporation and transpiration is roughly equivalent to the moisture gained through precipitation. Evapotranspiration is highest in the summer months, when vegetation is lush, temperatures are high, and relative humidity is low.

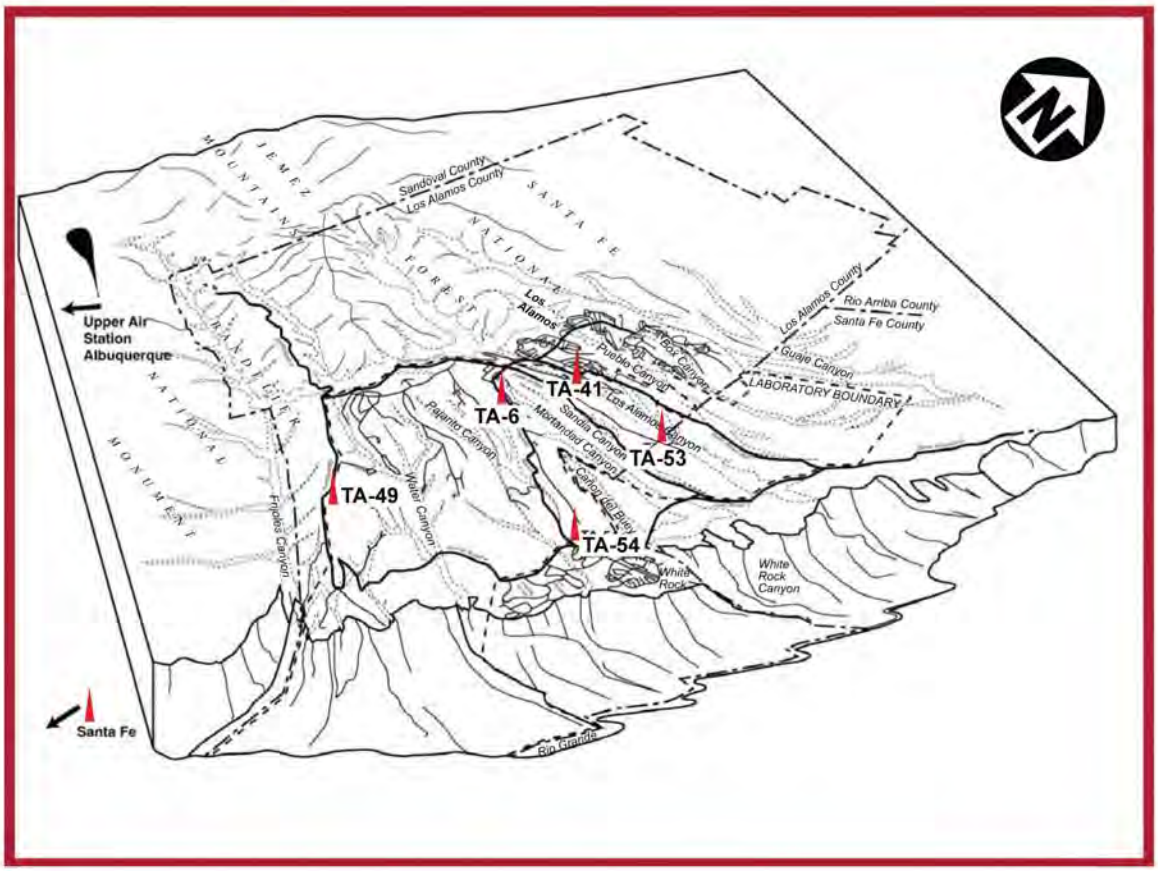

Figure 2-5
Meteorological Monitoring Towers at LANL

Table 2-1
Summary of 12 Years of Meteorological Data at Area G (1993–2004)

Month	Temperature (ºF)		Total Precipitation (cm)	Average Relative Humidity (%)
	Avg. Maximum	Avg. Minimum		
January	43.8	16.2	1.71	60.5
February	47.8	20.1	1.50	56.4
March	56.5	25.7	1.96	49.2
April	63.4	32.0	2.47	42.3
May	75.1	41.1	2.01	35.8
June	84.1	49.1	3.12	34.8
July	86.9	54.5	4.10	46.5
August	83.4	53.4	6.82	55.1
September	77.6	45.6	3.32	50.0
October	65.0	33.8	4.42	52.3
November	51.8	23.3	1.94	57.6
December	43.3	15.4	0.96	60.0

Source: Selected readings from the TA-54 meteorological tower (Jacobson, 2005a)

The average annual precipitation measured over a period of 30 years (1961 through 1990) at the Los Alamos gauge is 46 cm (18 in.) (Nyhan et al., 1989), which is considerably higher than the 34 cm (13 in.) average measured in more recent years at TA-54 (Table 2-1). The 30-year record from the Los Alamos precipitation gauge has been used for predicting annual precipitation in the region, including a 100-year daily rainfall extreme of 6.4 cm (2.5 in.) and a 100-year annual precipitation event for Los Alamos of 84 cm (33 in.) (Nyhan et al., 1989). Daily rainfall extremes of 2.5 cm (1 in.) or more occur in most years.

Additional longer-term evidence of local precipitation history is determined through dendroclimatology, which compares modern meteorological records with contemporaneous tree growth (tree rings) (Schulman, 1951). Semiarid climates exhibit very strong correlation between precipitation and tree-ring width. The best correlations have been found for long-lived coniferous species that survive arid cycles, including ponderosa pine (Abeele and Wheeler, 1981). Although there are no ponderosa pines at Mesita del Buey, this species is abundant at slightly higher elevations on the Pajarito Plateau, including both locales where the Los Alamos weather gauge has been stationed (TA-59 and TA-6). Dendroclimatology has been used to estimate annual precipitation back to the year 1510. The analysis indicates the following precipitation extremes:

- Maximum annual precipitation events were 101 cm (40 in.), 58 cm (23 in.), and 79 cm (31 in.), occurring in 1597, 1794, and 1919, respectively.

- Minimum annual precipitation events were 14 cm (5.5 in.), 11 cm (4.3 in.), and 6 cm (2.4 in.), occurring in 1523, 1585, and 1685, respectively.

These numbers compare well with the estimated maximum precipitation based on pluviometric records. Both suggest that a maximum annual precipitation of about 80 cm (31 in.) can be expected every century. These annual precipitation extremes are based on pluviometric and dendroclimatic records at TA-59 and TA-6, where annual precipitation generally exceeds that at TA-54 by about 10 cm (3.9 in.).

2.1.2.2 Wind Speed and Direction

Wind speed, direction, and stability characteristics are required to model the atmospheric transport of radioactivity from Area G. These factors also affect the rate of wind erosion at the site, a process which could contribute to the transport of contamination from Area G (see *Appendix C,* Volume 2). Wind patterns across the Pajarito Plateau are greatly influenced by the mesa-canyon topography of the area. Winds are generally light, with velocities less than 3 m/s (7 mph). On days with sunshine and light large-scale winds, a deep, thermally driven, upslope wind develops over the Pajarito Plateau (LANL, 2003a). Winds reverse at night, and a shallow, cold-air drainage wind often forms and flows down the plateau on clear nights with large-scale, light wind speeds of 3 to 3.5 m/s (7 to 8 mph). In the Spring, sustained winds in excess of 11 m/s (25 mph) are common and gusts may exceed 22 m/s (50 mph). Wind speeds are greatest from March through June and weakest in December and January (LANL, 2003a).

Wind speed and direction vary with site, height above ground, and time of day. Mean wind speed and direction frequencies have been calculated for day and night at Mesita del Buey and Pajarito Canyon. The frequencies are presented as "wind roses," which show the percentage of time that the wind blows from each of 16 compass points and the distribution of wind speed for each of those directions. Wind data from Mesita del Buey (for 2002) and Pajarito Canyon (for 1998) are shown in Figures 2-6 and 2-7. Winds on the mesa are primarily from the south and southwest during the day and the west and northwest at night (Figure 2-6). Canyon winds are strongly channeled (Figure 2-7), blowing up canyon from the southeast during the day and down canyon at night.

2.1.2.3 Atmospheric Dispersion

The complex terrain and vegetation characteristics at the Laboratory result in complex patterns of atmospheric transport and dispersion, as discussed in more detail in *Appendix D* of this report. These factors create an aerodynamically rough surface, resulting in increased horizontal and vertical turbulence and dispersion (Bowen, 1990). Although the dispersion generally decreases at lower elevations where the terrain becomes smoother and less vegetated, the frequent clear skies

and light winds cause daytime vertical dispersion, especially during the warm season. The daytime heating during the summer can force strong vertical mixing within 1,200 to 2,400 m (4,000 to 8,000 ft) of the ground surface (Bowen, 1990).

Clear skies and light winds have a different effect on dispersion at night, causing strong, shallow surface inversions to form; these inversions severely restrict near-surface vertical and, to a lesser extent, horizontal dispersion. The inversions are especially strong during the winter. Shallow drainage winds fill lower areas with cold air, thereby creating deeper inversions, which are common toward the Rio Grande valley (White Rock) on clear nights with light winds. Canyons also limit dispersion by channeling air flow. Strong, large-scale inversions during the winter can limit vertical mixing to under 3,050 m (10,000 ft) above mean sea level (msl) (Bowen, 1990).

Overall, atmospheric dispersion tends to be greatest in the spring when winds are strongest. However, deep vertical mixing is greatest during summer afternoons when the atmosphere is unstable up to elevations of 1,500 m (5,000 ft) above ground level. Low-level dispersion, when averaged over day and night, is generally smallest during summer and autumn evenings when winds are light. Even though low-level dispersion is generally greater in the winter, intense surface inversions can cause low-level dispersive conditions during nights and early mornings at other times of the year (Bowen, 1990).

2.1.2.4 Severe Weather Events

Thunderstorms are quite common in Los Alamos, with about 58 occurring in an average year. Lightning and hail can be frequent and intense during the thunderstorms (LANL, 2003a). Typically, the hailstones have diameters of about 0.64 cm (0.25 in.), but may be even larger. A thunderstorm on August 11, 1982 dropped about 8 cm (3 in.) of hail near the Los Alamos airport, damaging windshields and vegetation in the area (LANL, 2003a).

No tornado has ever been reported in Los Alamos County, but strong dust devils can produce winds with velocities as great as 34 m/s (75 mph) at isolated spots in the county, especially at lower elevations (Bowen, 1990). According to the DOE publication, *Natural Phenomena Hazards Design and Evaluation Criteria for Department of Energy Facilities* (1996), a design basis tornado need not be considered at Los Alamos because the annual hazard probability of exceedance is smaller than 2×10^{-5}.

2.1.3 Ecology

The ecological setting of Area G is important in modeling the potential for transport and uptake of radioactivity. Animals may burrow into disposal units, disturbing the cover and excavating contaminated material. Plants whose roots extend into the waste may assimilate radionuclides and deposit that contamination on the surface of the disposal facility when they defoliate or die. Plants can also enhance facility performance in two ways. First, they provide surface cover that

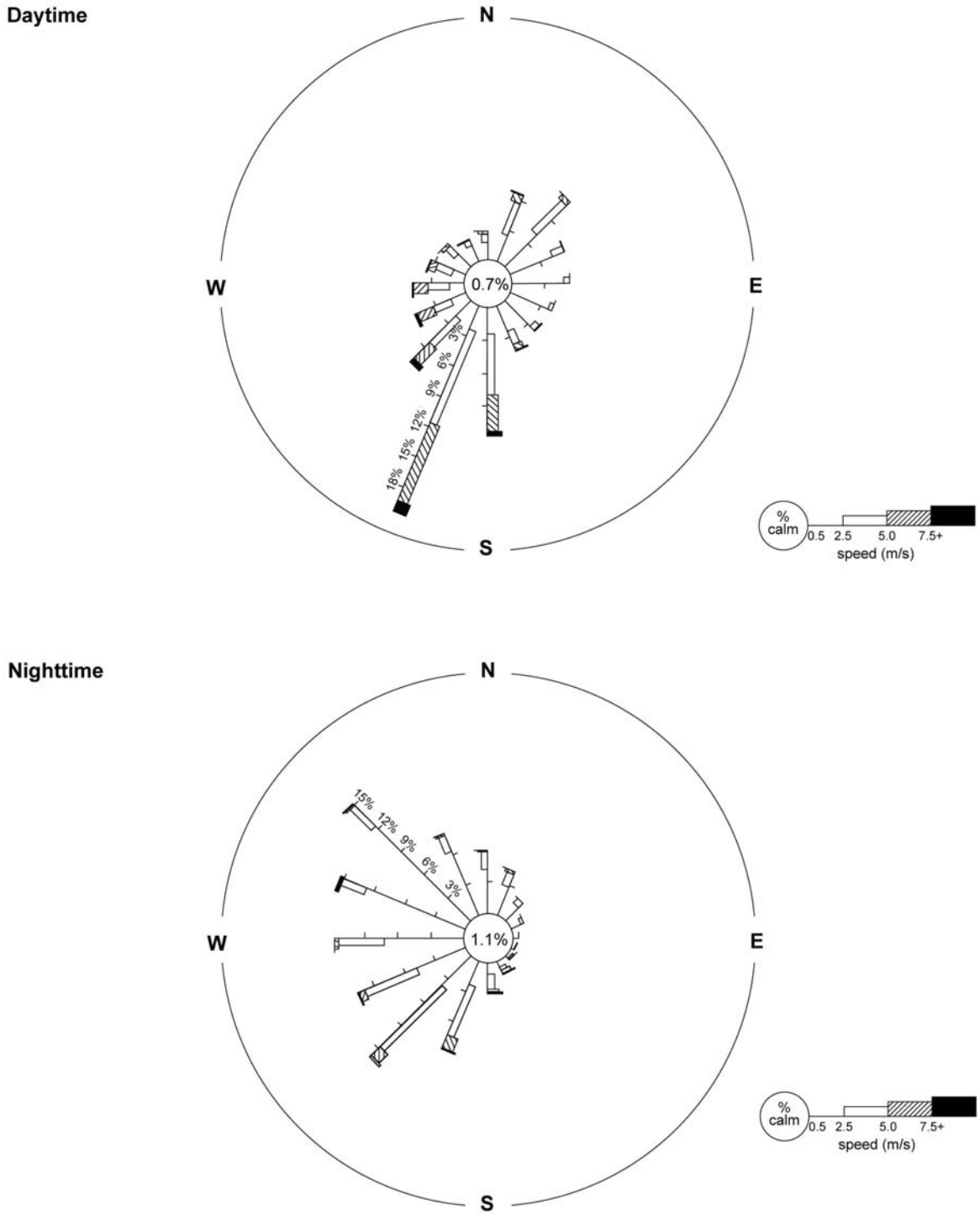

Figure 2-6
Windroses Illustrating Prevailing Daytime and Nighttime Winds at Mesita del Buey (2002)

Source: Jacobson, 2005b

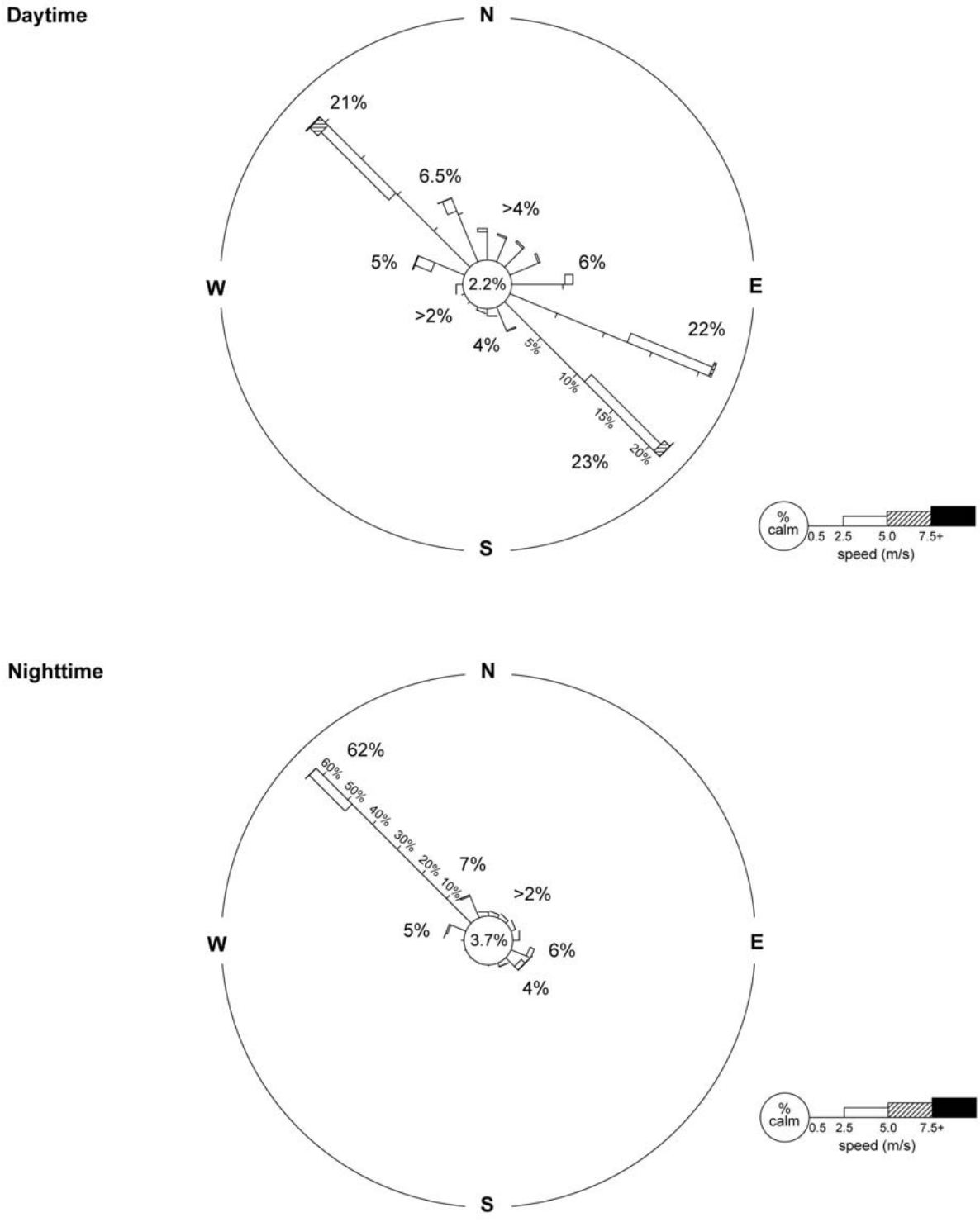

Figure 2-7
Windroses Illustrating Prevailing Daytime and Nighttime Winds at Pajarito Canyon (1998)

Source: LANL, 2001

reduces erosion of disposal unit covers, and second, they remove moisture from the soil that might otherwise be available to percolate into disposal units. The impact of plants on rates of moisture removal is evident in the high evapotranspiration values found in the area.

A diverse array of plants and animals is found in the Los Alamos region. This is due in part to the 1,500 m (4,900 ft) elevation difference between the Rio Grande and the top of the Jemez Mountains (DOE, 1979). The canyon and mesa terrain also contributes to this diversity by providing a variety of habitats.

2.1.3.1 Local Flora

Six major vegetative community types are found in Los Alamos County: juniper-grassland, piñon-juniper, ponderosa pine, mixed conifer, spruce-fir, and subalpine grassland. Juniper-grassland, piñon-juniper, and ponderosa pine communities predominate throughout the Laboratory; a generalized illustration showing the approximate elevations of these communities is provided in Figure 2-8. The juniper-grassland occurs along the Rio Grande and the eastern border of the Pajarito Plateau, extending up to elevations of 1,700 to 1,900 m (5,600 to 6,200 ft) above msl on the south-facing sides of canyons. The piñon-juniper community covers large portions of mesa tops at elevations ranging from about 1,900 to 2,100 m (6,200 to 6,900 ft) above msl. Ponderosa pines are found at elevations ranging from 2,100 to 2,300 m (6,900 to 7,500 ft) above msl in the western portion of the plateau.

Undisturbed areas on Mesita del Buey are dominated by piñon-juniper woodland. Piñon pine (*Pinus edulis*) and one-seed juniper (*Juniperus monosperma*) are the dominant tree species, while common shrub species include big sagebrush (*Artemisia tridentata*), four-wing saltbush (*Atriplex canescens*), currant (*Ribes cereum*), and mountain mahogany (*Cercocarpus montanus*). Blue grama (*Bouteloua gracilis*), cryptogamic soil crust, and prickly pear cactus (*Opuntia polyacantha*) are among the most common understory plants on the mesa top. Others include snakeweed (*Gutierrezia sarothrae*), pingue (*Hymenoxys richardsonii*), wild chrysanthemum (*Bahia dissecta*), leafy golden aster (*Chrysopsis filiosa*), purple horned-toothed moss (*Ceratadon purpureus*), lichen, three-awn grass (*Aristida* spp.), bottlebrush squirreltail (*Sitanion hystrix*), bluegrass (*Poa* spp.), and false tarragon (*Artemisia dracunculus*).

Waste management operations at Area G have replaced a number of the understory plants native to the area. Recently disturbed areas support plants such as goosefoot (*Chenopodium fremontii*), Russian thistle (*Salsola kali*), cutleaf evening primrose (*Oenothera caespitosa*), common sunflower (*Helianthus anuus*), and other colonizing species. Vegetation introduced as disposal pits are closed consists of native grasses, including blue grama, sideoats grama (*Bouteloua curtipendula*), Indian ricegrass (*Oryzopsis hymenoides*), sand dropseed (*Sporobolus cryptandrus*), sheep fescue (*Festuca ovina*), western wheatgrass (*Agropyron smithii*), and forbs such as blue flax (*Linum perenne lewisii*) and prairie coneflower (*Ratibida columnifera*).

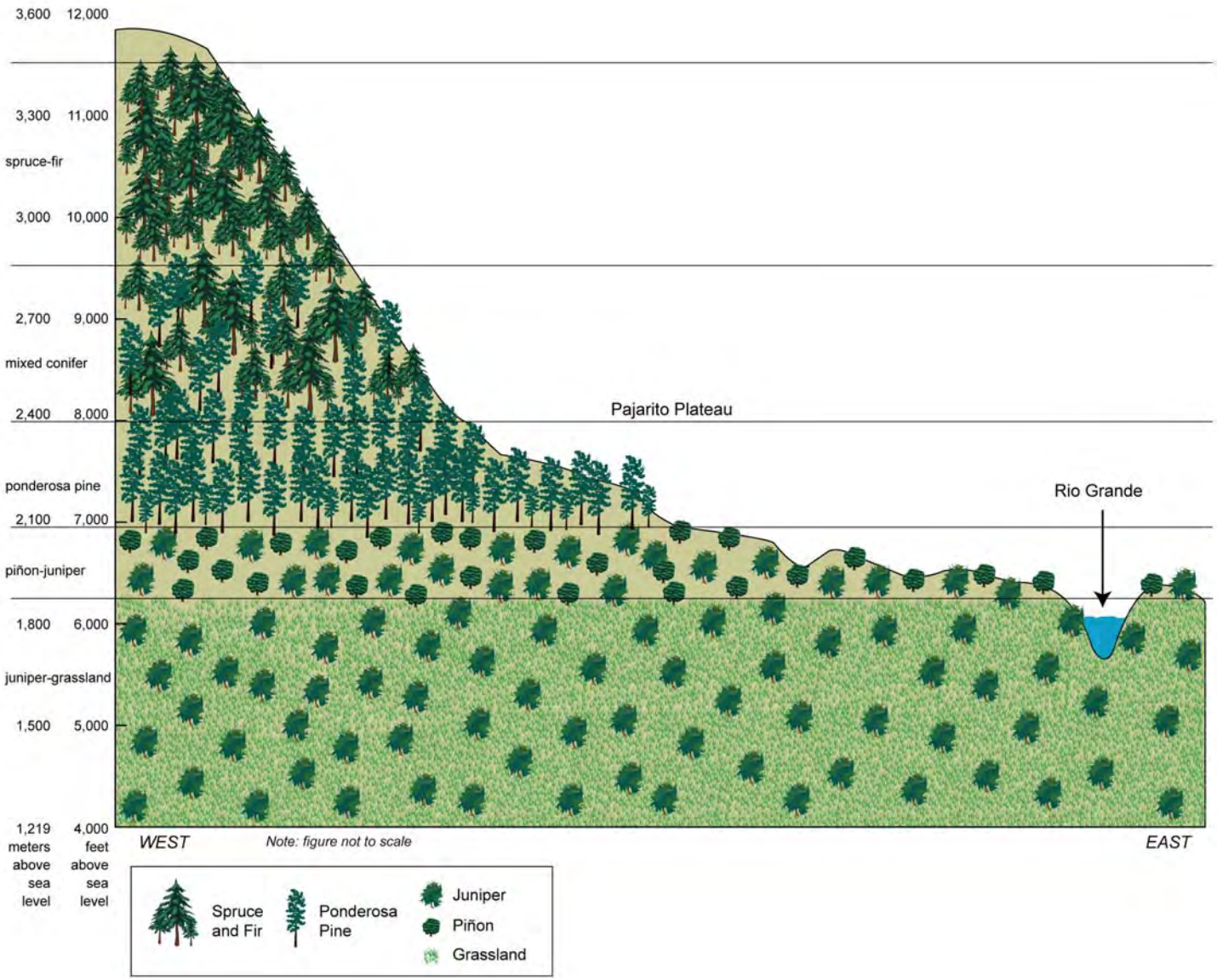

Figure 2-8
Generalized Vegetation Zones of the Pajarito Plateau

The average measured rooting depths for many of the native plants occurring in and around TA-54 are presented in Table 2-2, along with some values obtained from the literature. In a study of 21 species of plants common at LANL, roots were found to be most abundant in the upper 2 m (6.6 ft) of soil (Tierney and Foxx, 1987). Roots of chamisa, apache plume, oak, piñon, and one-seed juniper extended deeper than 2 m (6.6 ft); however, the biomass of plant roots was greatest above this depth.

The operational area at Area G is expected to undergo ecological succession from a disturbed state shortly after facility closure to piñon-juniper woodland that is characteristic of the undisturbed portions of Mesita del Buey. Annual and perennial grasses and forbs will predominate when the site is in its early successional stages, becoming established as covers over disposal units are seeded and as grasses and forbs invade from surrounding areas on the mesa. Over time, shrubs and trees will take hold and become established at the site. While some species of grasses and forbs will die out, others will continue to thrive. Given enough time, it is assumed that a condition approximating the climax piñon-juniper woodland will result.

2.1.3.2 Local Fauna

The plant communities in the LANL region create habitats used by many species of mammals, birds, insects, and reptiles. Of the 60 species of mammals inhabiting the Pajarito Plateau, about 15 are carnivores such as black bear (*Ursus americanus*), mountain lion (*Felis concolor*), bobcat (*Lynx rufus*), gray fox (*Urocyon cinereoargenteus*), and coyote (*Canis latrans*). More common mammals include mice, squirrels (*Citellus* spp., *Sciurus* spp.), gophers (*Thomomys* spp.), chipmunks (*Eutamias* spp.), voles (*Microtus* spp.), porcupines (*Erethizon dorsatum*), elk (*Cervus canadensis*), and mule deer (*Odocoileus hemionus*). Over 100 species of birds breed in Los Alamos County; these include many different songbirds as well as nesting and migrating raptors. Habitats for federally threatened and endangered species such as the bald eagle (*Haliaeetus leucoephalus*), southwestern willow flycatcher (*Empidonax traillii extimus*), and Mexican spotted owl (*Strix occidentalis*) have been identified within the Laboratory (NMED, 2004). Harvester ants (*Pogonomyrmex* spp.) are the most abundant insect at Area G. Common reptiles include fence lizards (*Sceloporus undulatus*), plateau striped whiptails (*Cnemidophorus velox*), gopher snakes (*Pituophis melanoleucus*), and garter snakes (*Thamnophis* spp.).

Burrowing animals are of most concern for the performance assessment and composite analysis because they might disturb the buried waste at Area G. Several species of burrowing animals are currently found at Area G and the area surrounding the site; others may reasonably be expected to inhabit the site after widespread disturbance of the area ceases and as the site undergoes ecological succession to piñon-juniper woodland. The DOE (1979) lists the deer mouse (*Peromyscus maniculatus*), pocket mouse (*Perognathus* spp.), woodrat (*Neotoma* spp.), and mountain cottontail (*Sylvilagus nuttalli*) as inhabitants of juniper grassland within Los Alamos County, while the Colorado chipmunk (*Eutamias quadrivittatus*) is found in conjunction

Table 2-2
Plant Rooting Depths Measured on Laboratory Lands

Growth-Form and Common Name	Scientific Name	Rooting Depth (cm)		
		Range of Measured Values	Range of Estimated Values [a]	Range of Literature Values
Grasses				
Blue Grama	*Bouteloua gracilis*	5.3E+01–5.8E+01	---	3.8E+01–4.0E+02
Forbs				
Mullein	*Verbascum thapsus*	2.8E+01– 4.2E+01	---	NA
Narrowleaf Yucca	*Yucca angustissima*	2.0E+01 [b]	---	4.0E+01–1.5E+02
Prickly Pear	*Opuntia polyacantha*	8.0E+00–2.8E+01	---	2.0E+00–3.7E+02
Sunflower	*Helianthus petiolaris*	4.0E+01–4.5E+01	---	NA
Shrubs and Subshrubs				
Apache Plume	*Fallugia paradoxa*	6.0E+01–1.3E+02	1.7E+02–2.9E+02	NA
Big Sagebrush	*Artemisia tridentata*	1.0E+01–1.5E+02	1.3E+02–1.8E+02	1.1E+02–9.1E+02
Chamisa	*Chrysothamnus nauseosus*	1.0E+02–1.8E+02	1.4E+02–2.1E+02	1.0E+02–4.6E+02
Four-Wing Saltbush	*Atriplex canescens*	6.0E+01–1.1E+02	1.9E+02–2.2E+02	8.0E+01–7.6E+02
Mountain Mahogany	*Cercocarpus montanus*	4.0E+01 [b]	5.0E+01 [b]	4.0E+01–1.5E+02
New Mexico Locust	*Robinia neomexicana*	1.0E+02–1.4E+02	---	NA
Oak	*Quercus* spp.	4.5E+01–1.0E+02	1.5E+02–3.2E+02	8.0E+01–4.0E+02
Snakeweed	*Gutierrezia sarothrae*	6.0E+01–1.3E+02	1.7E+02–2.9E+02	5.1E+01–2.4E+02
Squawberry	*Rhus trilobata*	1.5E+02–1.7E+02	2.1E+02–2.3E+02	NA
Wax Currant	*Ribes cereum*	7.0E+01–1.5E+02	8.0E+01–2.9E+02	NA
Trees				
One-Seed Juniper	*Juniperus monosperma*	1.5E+02 [b]	1.7E+02 [b]	5.8E+02–6.1E+03
Piñon Pine	*Pinus edulis*	3.0E+01–6.0E+01	1.1E+02–1.3E+02	NA
Ponderosa Pine	*Pinus ponderosa*	1.3E+02–1.5E+02	1.5E+02–1.6E+02	1.0E+01–2.4E+03

Source: Tierney and Foxx (1987)

--- = Indicates no root lengths were estimated for the species.

NA = Not applicable; no range in rooting depths was reported.

[a] *Estimated root lengths are provided for roots that broke during excavation and roots that could not be completely excavated due to safety considerations and/or the soil profile.*

[b] *No range is provided either because all root length measurements were the same length or because only a single measurement of root length was collected.*

with these species in piñon-juniper woodland. Harvester ants are routinely sited in recently covered disposal sites and piñon-juniper woodland, pocket gophers have also been observed at Area G. Several species of mice have been routinely trapped at Area G (Biggs et al., 1995, 1997; Bennett et al., 1997, 1998, and 2002).

Relatively little information is available to describe the distribution of animal burrows with depth. McKenzie et al. (1982) conducted a review of the burrowing habits of several species of harvester ants and small mammals, many of which are expected to occur at Area G. As part of that work, they estimated burrow distributions with depth; these estimates are provided in Table 2-3. Reynolds and Laundre (1988) characterized the distribution of deer mouse burrows, finding that none of the 43 burrows examined extended deeper than 50 cm (20 in.).

Table 2-3
Burrow Depth Distributions for Animal Species Encountered or Expected at Area G

Animal Species	Occurrence at Area G	Fraction of Burrow Systems by Depth Interval			
		0–1.0 m	1.0–1.5 m	1.5–2.0 m	> 2.0 m
Harvester Ants	Common in nearby piñon-juniper woodlands; expected to be common after site closure	8.0E-01	1.0E-01	5.0E-02	5.0E-02
Pocket Mice and Kangaroo Rats	Mice are common to juniper-grassland and piñon-juniper woodlands	9.0E-01	5.0E-02	5.0E-02	0.0E+00
Pocket Gophers	Expected to be more common in disturbed areas, diminishing as site progresses to climax vegetation type	1.0E+00	0.0E+00	0.0E+00	0.0E+00
Chipmunks and Ground Squirrels	Anticipated as site transforms to piñon-juniper woodland	8.0E-01	1.5E-01	5.0E-02	0.0E+00

Source: McKenzie et al., 1982

2.1.4 Geology, Seismology, and Volcanology

The geologic setting of Area G has a profound impact on the potential for the release and transport of radionuclides, as discussed in Section 2.1.4.1. Although important from a geological standpoint, the seismology and volcanology of the area are expected to have less impact on site performance during the analysis period (Sections 2.1.4.2 and 2.1.4.3).

2.1.4.1 Regional and Site-Specific Geology and Topography

The Laboratory is located at an average elevation of 2,100 m (6,900 ft) above msl on the Pajarito Plateau, east of the Jemez Mountains. This plateau consists of a series of east-trending finger-like mesas separated by deep erosional canyons. Mesa tops range in elevation from 2,400 m (7,800 ft) above msl on the flank of the Jemez Mountains to approximately 1,900 m (6,200 ft) above msl at the east end of the plateau. The eastern plateau lies 90 to 275 m (300 and 900 ft) above the Rio Grande valley.

Figure 2-9 illustrates the general geologic setting and stratigraphic relationships in the vicinity of Area G. The disposal facility is located near the eastern edge of the Pajarito Plateau; as indicated in Figure 2-9, it sits relatively low in the Bandelier Tuff, which generally thins from its western source (the Jemez Mountains) to its eastern terminus (the Rio Grande valley).

The Pajarito Plateau is formed of consolidated ash (tuff) from two major volcanic eruptions that occurred in the Jemez Mountains about 1.6 and 1.2 million years ago (Ma). These eruptions produced widespread, massive deposits that consolidated into a formation known as the Bandelier Tuff (Spell et al., 1990). The two eruptions produced two deposits with different characteristics which form the Otowi and Tshirege Members of the Bandelier Tuff. Smaller eruptions that occurred between the two major events produced an interbedded sequence of silica-rich (rhyolitic) tuffs and sediments referred to as the Cerro Toledo interval; these deposits occur commonly but not uniformly between the Otowi and Tshirege Members. Figure 2-10 shows the stratigraphic nomenclature for the Bandelier Tuff as used in this report. Table 2-4 summarizes the lithologic characteristics and thicknesses of various units found at Area G based on data from boreholes drilled at the site.

Typically, the older Otowi Member is unwelded to poorly welded and tends to form slopes rather than cliffs in outcrop; the Tshirege Member contains strata that range from strongly welded to unwelded. The Tshirege Member is further subdivided into “cooling units” that represent successive ash-flow deposits separated by periods of inactivity. The properties of the Tshirege Member related to water flow and contaminant migration (e.g., density, porosity, degree of welding, fracture content, and mineralogy) vary both vertically and laterally as a result of localized emplacement temperature, thickness, gas content, and composition. Additional information about the Bandelier Tuff and its units can be found in Broxton and Reneau (1995). Information related to the hydrogeologic properties of the Bandelier Tuff is presented in *Appendix E* (Volume 2) and discussed in Section 2.1.5.

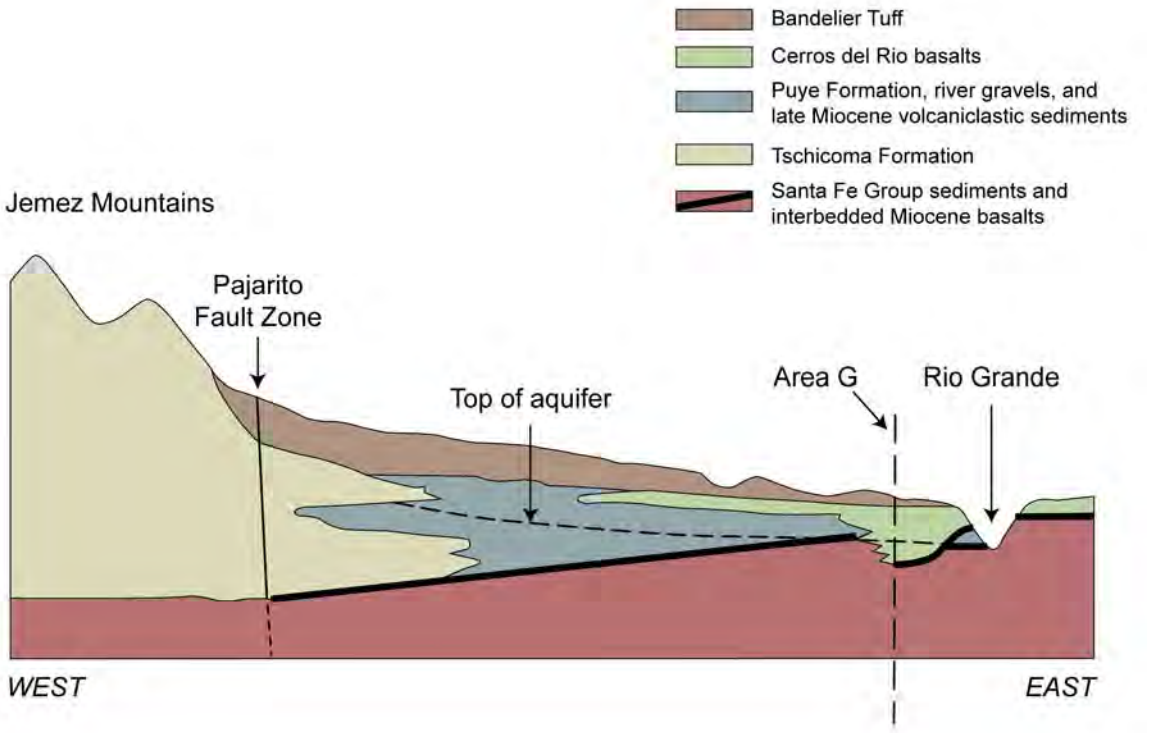

Figure 2-9
Generalized Stratigraphic Relationships of the Pajarito Plateau

Source: Adapted from Hollis et al., (1997) with input from Stauffer (2005) and Broxton (2005)

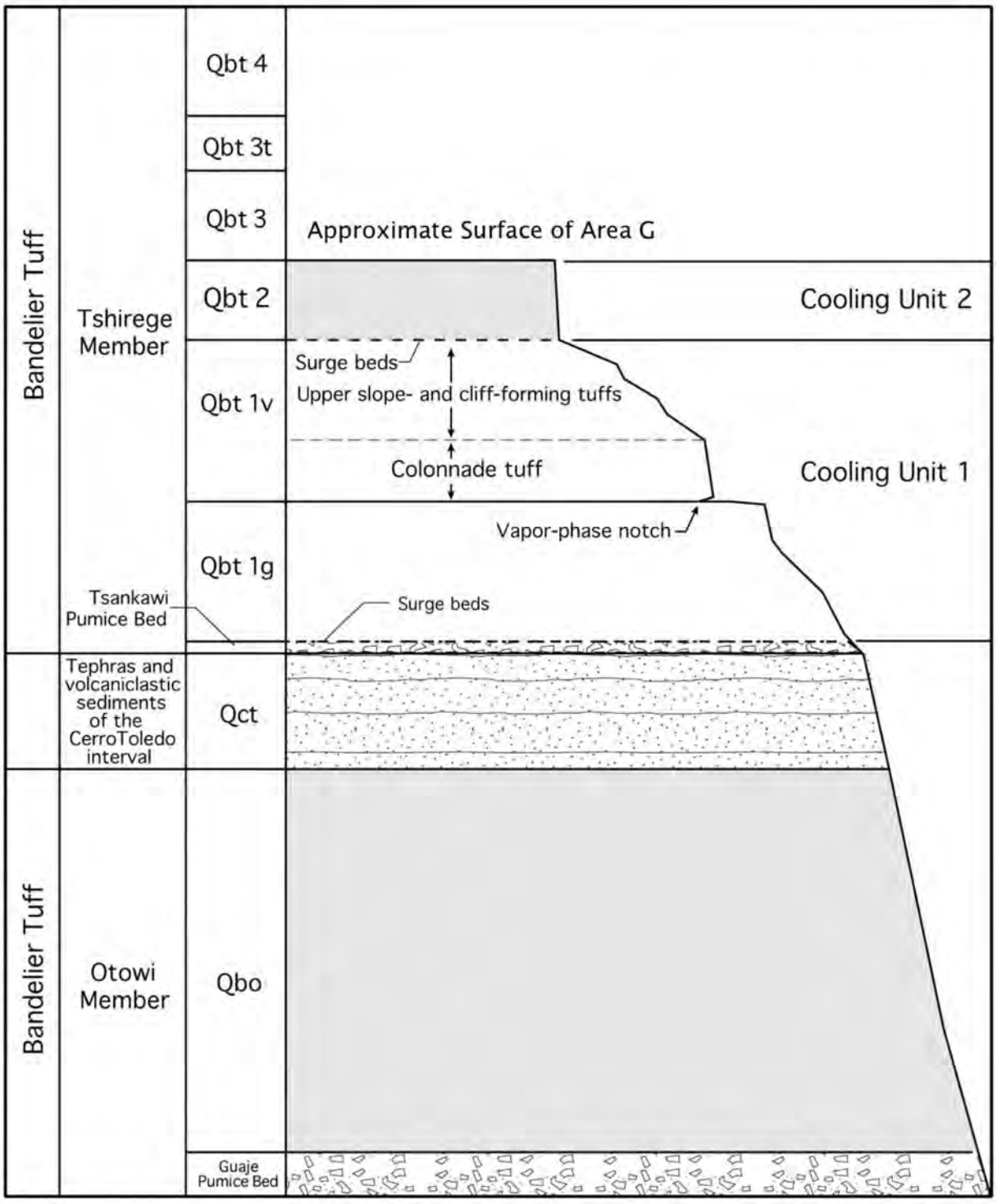

Figure 2-10
Stratigraphic Nomenclature for the Bandelier Tuff
Adapted from Broxton and Reneau (1995)

Table 2-4
Lithology of Geologic Units Encountered in Boreholes at Area G

Geologic Unit	Thickness (m)	Lithology	Fracture		
			Spacing (m)	Median Dip (º) / Aperture (mm)	Fill (%) [a]
Tshirege Member Unit 2	12.2	Massive, crystal-rich, slightly welded tuff; devitrified; vapor-phase altered; pumice swarms; basal surge	1–1.3	87 / 3	72–F 9–P 19–O
Tshirege Member Unit 1vu	13.7	Massive, crystal-rich, nonwelded tuff; devitrified; pumiceous; crystal-rich lapilli	1–1.3	84 / 3	82–F, P 18–O
Tshirege Member Unit 1vc	7.6	Massive, crystal-rich nonwelded tuff; pumiceous; pumice swarms; ash falls; crystal-rich lapilli	Few fractures	ND	---
Tshirege Member Unit 1g	15.2	Massive, nonwelded, nonindurated tuff; vitric; pumiceous; crystal-rich lapilli	Some fractures	ND	---
Tsankawi Pumice/ Cerro Toledo Interval	1.8	Massive air-fall tuff; large white pumice lapilli; topical surge bed of crystals and ash	Rare fractures	ND	---
Otowi Member	36.6	Massive, moderately crystal-rich, nonwelded vitric tuff; ~30% pumice	Few fractures	ND	observed calcite
Guaje Pumice	3.7	Basal nonwelded pumice lapilli bed; vitric	Rare fractures	ND	---
Cerros del Rio Basalts	>36.3 [b]	Dense, fractured, basaltic tondesitic lava flows with flow breccias and conglomerate interbeds	~0.3 (observed)	~5 (observed)	---
Puye Formation	~200 [b]	Fanglomerates and conglomerates; fluviatile and debris-flow deposits; interbedded ash and pumice falls, basalt flows	Poorly developed in outcrop	ND	---

Source: Hollis et al. (1997)

ND = No data; assumed vertical *--- = No data*

[a] *Fracture fill abbreviations: F = filled, P = plated, O = open*

[b] *Regional characterization wells drilled since 1997 indicate that the Cerros del Rio basalts are much thicker and the Puye Formation much thinner in the area of Area G than reflected in this table (see Appendix E, Volume 2)*

The Bandelier Tuff is underlain by interstratified sedimentary and volcanic rock (Broxton and Reneau, 1995 and 1996; Goff et al., 2002). Prominent sedimentary deposits include the Puye Formation, the Totavi Formation, and the Santa Fe Group. Major volcanic rock units include the Tschicoma Formation and the Cerros del Rio basalt. Pre-Bandelier rock units are widely distributed across the

Pajarito Plateau, with the exception of the basalt, which is limited to the eastern and southeastern portions of the plateau. The Puye Formation (deposited from 1.6 to 4 Ma) is a fan-shaped sedimentary deposit (or alluvial fan) consisting of boulders, cobbles, coarse sands, tuff beds, and possibly some andesite and rhyolite components (Goff et al., 2002); it slopes eastward from the Tschicoma volcanic highlands and interfingers with the Santa Fe Group beneath the eastern Pajarito Plateau. The Cerros del Rio basalt, which was deposited from 2.3 to 2.8 Ma (WoldeGabriel et al., 1996), originates from a volcanic ridge east of the Rio Grande and dips westward from the crest of this ridge towards the Rio Grande. Evidence of basaltic vents on trend with the same ridge have been encountered in recent boreholes west of the Rio Grande, suggesting that the entire volcanic ridge from which the Cerros del Rio basalt originated was completely buried by the Bandelier Tuff deposits.

The Otowi Member of the Bandelier Tuff partially filled in and flattened the south-southwest-dipping valley that existed prior to the massive eruption that deposited the Otowi. The tuff accumulated to a thickness of at least 140 m (470 ft) in the northern part of the Laboratory; tuff deposits thinned eastward toward the basaltic ridge (Figure 2-9). At one time, the Otowi Member may have buried the basaltic ridge, but the ridge apparently eroded before the deposition of the later Tshirege Member. This ash flow blanketed most of the area, largely obscuring the former topography (Hollis et al., 1997).

The surface and subsurface geology in the area of Area G is shown in Figure 2-11. The information provided by five new regional characterization wells drilled as part of the ER Project have improved the understanding of the subsurface geology at Area G. The locations of these wells are shown in Figure 2-12. Data collected from the characterization wells shown in this figure have led to improved understanding of the deep subsurface directly beneath Area G and to subsequent modifications in the model used for contaminant transport. New hydrogeologic data sets include an updated compilation and statistical analysis of subsurface material properties of the Bandelier Tuff from TA-54 (Springer, 2005), a statistical analysis of mesa-top infiltration (Springer and Schofield, 2004), and constraints on the properties of vadose-zone, fractured basalt (Stauffer et al., 2005). These new data are discussed in more detail in *Appendix E.*

Figure 2-13 presents an interpretive geologic cross section between two regional characterization wells: R-22, completed in 2000, and R-21, completed in 2003 (Ball et al., 2002; Kleinfelder, 2003). A comparison of the predictions made using the 1996 geologic model (Vaniman et al., 1996) to the actual drilling logs from wells R-22 shows that the stratigraphic contact elevations in the 1996 model were off by 10 m (33 ft) or more in some instances. At R-22, for example, the top of the Cerros del Rio basalt was encountered at an elevation approximately 13 m (42 ft) lower than that predicted using the 1996 model (Figure 2-14). Figure 2-14 also indicates that the Cerros del Rio basalt is considerably thicker at this location than previously thought, while the underlying Puye Formation is considerably thinner. *Appendix E* provides additional discussion of the stratigraphy as it affects the groundwater modeling effort for the performance assessment and composite analysis.

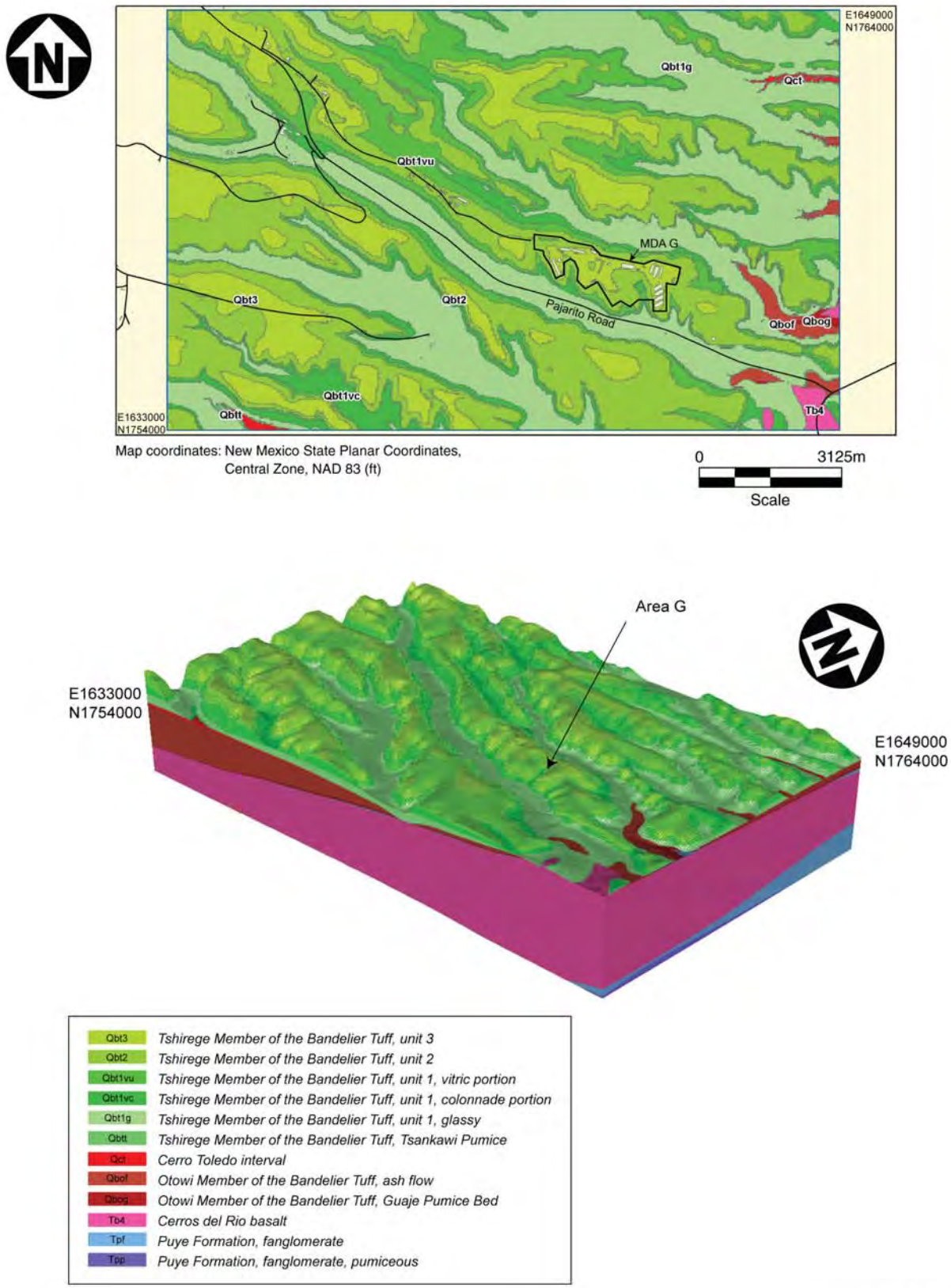

Figure 2-11
Geology in the Vicinity of Area G

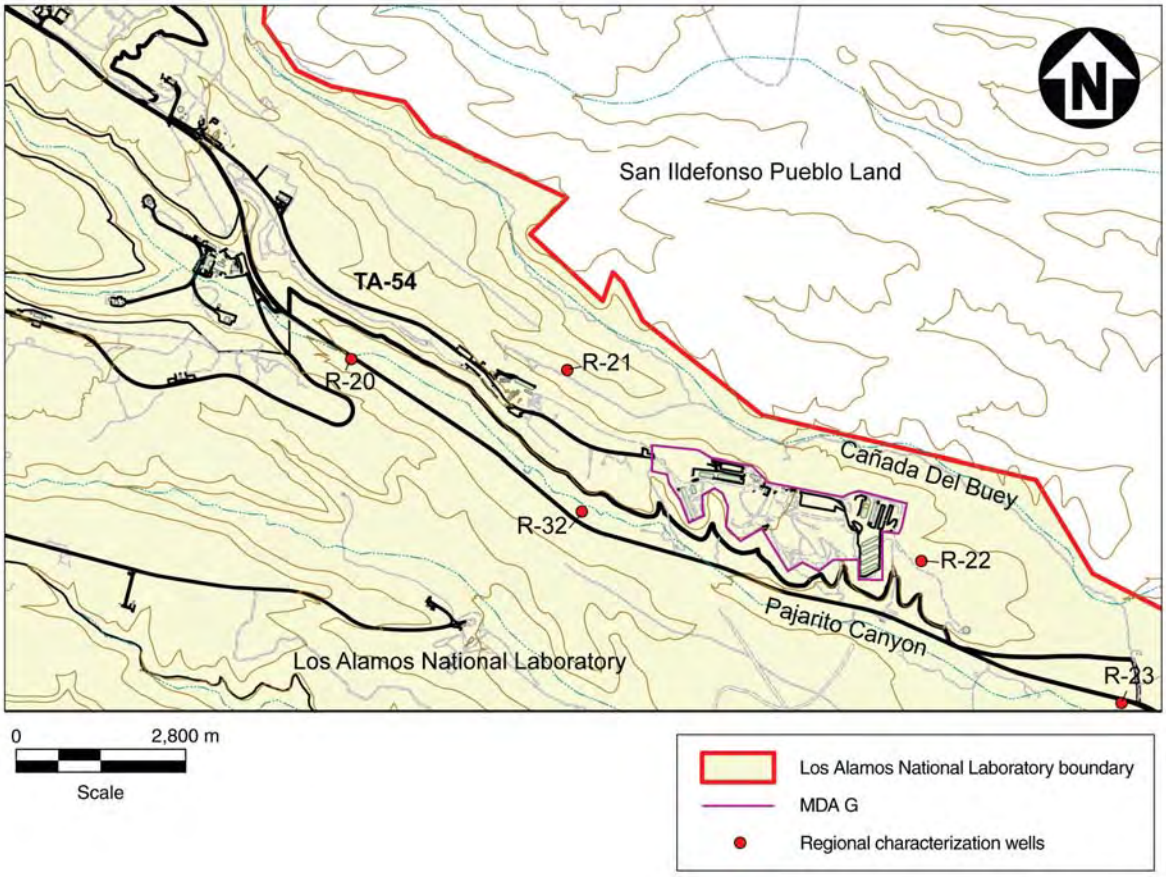

Figure 2-12
Locations of Regional Characterization Wells R-20, R-21, R-22, R-23, and R-32

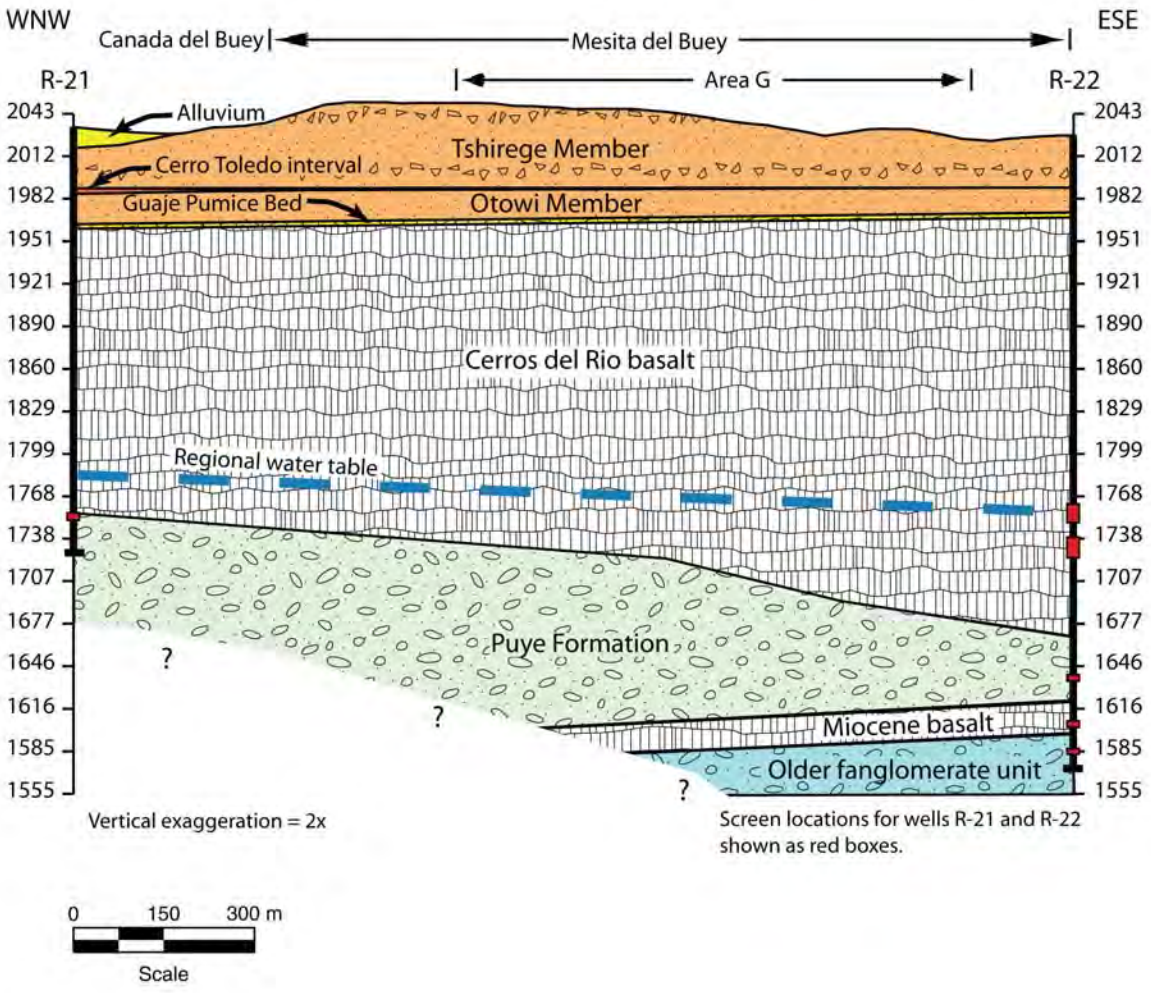

Figure 2-13
Interpretive Geologic Cross Section between Regional Characterization Wells R-21 and R-22

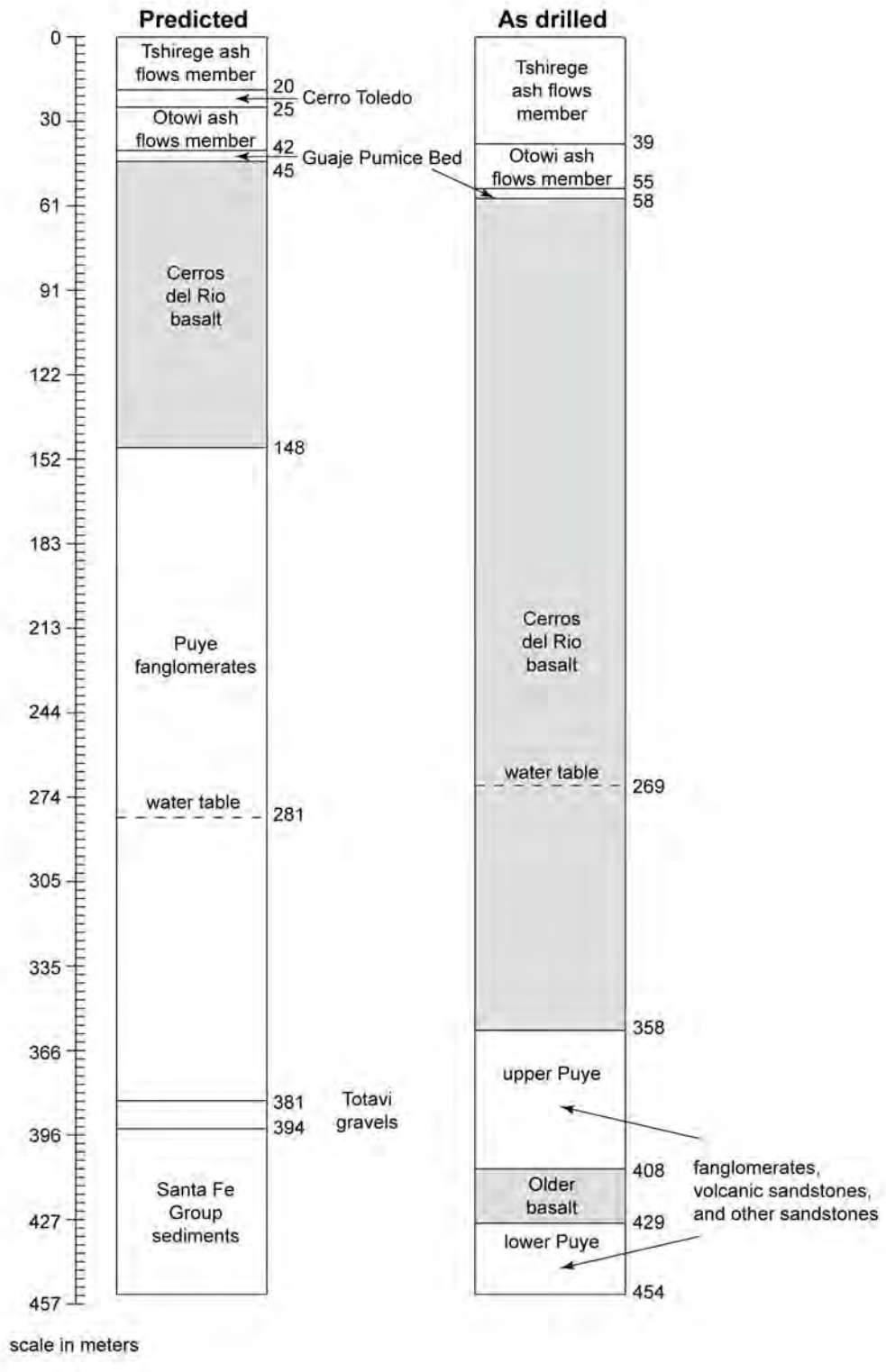

Figure 2-14
Comparison of 1997 Predicted Stratigraphy to Well Log at Regional Characterization Well R-22

Source: Ball et al., 2002

Surface sediments across the Pajarito Plateau are composed of thin soils developed on the mesa top, alluvial (water-transported) and colluvial (gravity-transported) residues on the mesa flanks, and alluvial deposition in the canyon bottoms (Longmire et al., 1996). Typically, colluvium on steep hill slopes is coarser-grained, while that deposited on the flatter mesa tops is fine-grained. Alluvial deposits in the canyons consist of unconsolidated fine and coarse sand composed of quartz, sanidine (volcanic feldspar), and broken pumice fragments that have been weathered and transported from higher areas. The slopes between mesa tops and canyon bottoms often consist of rocky outcrops and patches of undeveloped colluvial soil. The steeper south-facing canyon walls may have no soils at all; north-facing walls generally have areas of very shallow, dark soils. Soils on the Pajarito Plateau have extremely variable physical and chemical properties, including particle size, clay mineralogy, and trace elements. Regionally, the soils are rich in glass and have a high iron content. Thorium and uranium are naturally occurring, and are highly variable in their distribution across the Laboratory complex (Hollis et al., 1997).

The soils on Mesita del Buey, which were mapped by Nyhan et al. in 1978, are the weathering product of the Tshirege Member tuffs and wind-blown sources. On much of the mesa surface, native soils have been disturbed by waste-management operations. In less-disturbed portions of the mesa, native soils are thickest near the center of the mesa and thinner toward the edges. Soils on the flanks of the mesa are developed on Tshirege Member tuffs and colluvium with additional deposits of wind-blown and water-transported material; soils on north-facing slopes are more highly developed and richer in organic matter. Soils tend to be sandy in texture near the surface and more clayey beneath the surface. Soil-forming processes have been identified along fractures in the upper part of the mesa, and the translocation of clay minerals from surface soils into fractures has been described at Area G (Purtymun et al., 1978; Reneau and Vaniman, 1998).

Mesa surfaces erode at a very slow rate as a result of storm water runoff and wind. The long-term accumulation of biomass may compete with erosion, especially along the centerlines of mesas, away from major drainages. Modern drainages, including the steep-sided east-trending canyons that drain the Pajarito Plateau, are eroded into the Tshirege Member. The current surface drainage pattern across the plateau is generally southeast, at an oblique angle to the south-southwest paleochannels, or buried drainages. The pre-Bandelier landscape was apparently exposed for sufficient time to allow for the development of strong soil horizons in many locations, some of which are clay and mineral rich. Geochemical and hydrologic characteristics of these buried soils may have an important impact on the potential for contaminant migration.

In addition to wind and water erosion, mesas erode or “retreat” laterally as a result of mass wasting such as rock falls and larger-scale landslides. Some canyon rims display large-scale mass movement (landslides) in zones determined by a threshold combination of slope gradient and canyon depth (Reneau, 1995a), although most rims retreat as a result of infrequent failures of fractured or jointed tuff blocks. Evidence suggests that blocks may dislodge along cooling joints

or tectonic fractures. Mesita del Buey is a relatively low mesa, ranging from 15 to 30 m (50 to 100 ft) above the adjacent canyons. Although mass wasting does occur on the north and south faces of the mesa, the effects are not nearly as dramatic as those observed along deeper canyons across the Pajarito Plateau.

The rate of mass wasting or cliff retreat is difficult to estimate because it is a discontinuous process. The largest landslides at LANL occur within White Rock Canyon; Reneau et al. (1995) indicate that massive landslides occurred there only after the canyon incised through basalts, exposing a thick section of underlying weak rock units. Massive slope failures within White Rock Canyon correspond to areas where the canyon has cut deeply enough to expose sedimentary units beneath the basalt. Smaller-scale rockfalls or landslides predominate in areas where canyons have incised only into the Bandelier Tuff. Blocks of tuff that extend 15 m (50 ft) or more into the mesa may occur in canyons that are greater than 60 m (200 ft) deep; blocks that extend 0 to 4 m (0 to 13 ft) into the mesa appear to be more typical of shallower canyons.

Reneau (1995b) examined processes and rates of cliff retreat along Los Alamos Canyon and smaller tributary canyons at TA-21. Large landslides in Los Alamos Canyon that extend 15 m (50 ft) or more into the mesa are contrasted with much smaller rockfalls within BV and DP Canyons that typically extend 4 m (13 ft) or less into the mesa. The higher retreat rates in Los Alamos Canyon are attributed to the greater relief of this canyon relative to the others. Based on several techniques for estimating cliff retreat rates, Reneau concludes that maximum average retreat rates over the last million years range from 0.0033 to 0.0079 cm/yr (1.1×10^{-4} to 2.6×10^{-4} ft/yr) in the two tributary canyons. While recognizing the uncertainty associated with these estimates, Reneau states that the removal of 18 m (60 ft) of material at MDA B, enough to expose waste disposed of in units at that site, is unlikely within 10,000 years and could require in excess of 100,000 years.

In conjunction with a proposal to site a mixed waste disposal facility on Pajarito Mesa, Reneau (1995a) examined processes of cliff retreat along Threemile and Pajarito Canyons. The dominant mass-wasting process along the rim of Threemile Canyon, which is a relatively shallow canyon, was shown to be small-scale rock falls. The conclusion is that a 15 m (50 ft) setback, like the one at Area G, should be sufficient to ensure the integrity of proposed disposal pits at Pajarito Mesa for periods exceeding 10,000 years. In contrast, a zone of mass wasting 30 to 60 m (100 to 200 ft) wide has occurred along the rim of deeper Pajarito Canyon; an additional 15 to 30 m (50 to 100 ft) setback from this zone is recommended.

No rates of cliff retreat have been estimated for Area G. However, Pajarito Canyon and Cañada del Buey in the vicinity of Area G are relatively shallow, with only 15 to 30 m (50 to 100 ft) of vertical relief. Consequently, the rates of retreat are expected to resemble those estimated for other, relatively shallow tributary canyons such as BV, DP, and Threemile Canyons as opposed

to the more extreme rates of retreat noted for the deeper parts of White Rock, Los Alamos, and Pajarito Canyons. On this basis, it is unlikely that the integrity of the disposal units at Area G will be threatened by mass wasting within 10,000 years, and possibly much longer.

2.1.4.2 Seismology

The Laboratory is located within the northern Rio Grande rift, a seismically active region undergoing east-west extension. The Pajarito fault zone, a major north-south fault system along the western margin of the Rio Grande rift, lies to the west of Area G (Figure 2-15). Much of the following discussion is taken Hollis et al. (1997) and from the Area G documented safety analysis (LANL, 2003a) and is based on information from Wong et al. (1995) and Olig et al. (1996).

Although microearthquakes are relatively common in the LANL area, only six earthquakes of estimated Richter magnitude 5.0 or greater have occurred in the region. The most significant was the May 18, 1918 Cerrillos earthquake that occurred approximately 50 km (30 mi) southeast of the Laboratory and had an estimated magnitude of 5.5. A number of small-to-moderate earthquakes not associated with mapped faults (background earthquakes) have occurred in north-central New Mexico within the past 100 years. Since 1973, local seismicity has been monitored by the Los Alamos Seismograph Network. Measured events have not exceeded a magnitude of 4, which is relatively weak compared with earthquakes producing damage to buildings and structures (LANL, 2001). There is no physical evidence of seismic motion at Area G.

Wong et al. (1995) identified 26 faults and 5 seismic zones that are potentially significant to the Laboratory in terms of ground shaking. Three faults—the Pajarito, Rendija Canyon, and Guaje Mountain—were the focus of these studies (Figure 2-15). The Pajarito Fault is a 47 km (29 mi) long north-trending, discontinuous fault zone that defines the active western boundary of the Rio Grande rift. Located along the western margin of the Laboratory, it is a normal fault with a down-dropped eastern side and a moderate eastward dip. The 10 km (6 mi) long Rendija Canyon Fault is located 3 km (2 mi) east of the Pajarito Fault and trends north-south across the Laboratory. The nearest of the major system faults to Area G, the Rendija Canyon Fault lies approximately 6 km (3.6 mi) to the west-northwest of the disposal facility. It is a steeply west-dipping normal or oblique slip fault with poorly constrained lateral slip. The 14 km (9 mi) Guaje Mountain Fault is located 1 to 2 km (0.6 to 1.3 mi) east of the Rendija Canyon Fault but does not extend as far south. It is similar to the Rendija Canyon Fault in its orientation, tectonic setting, and probable sense of slip.

The Pajarito Fault is considered active: exploratory trenching has revealed that it has ruptured during multiple surface-faulting events in the past 100,000 to 200,000 years (Wong et al., 1995). The estimated slip rate on the fault during the past 1.1 million years ranges from 0.005 to 0.20 mm/yr (2.0×10^{-4} to 0.0079 in/yr). Although not well constrained, intervals between events

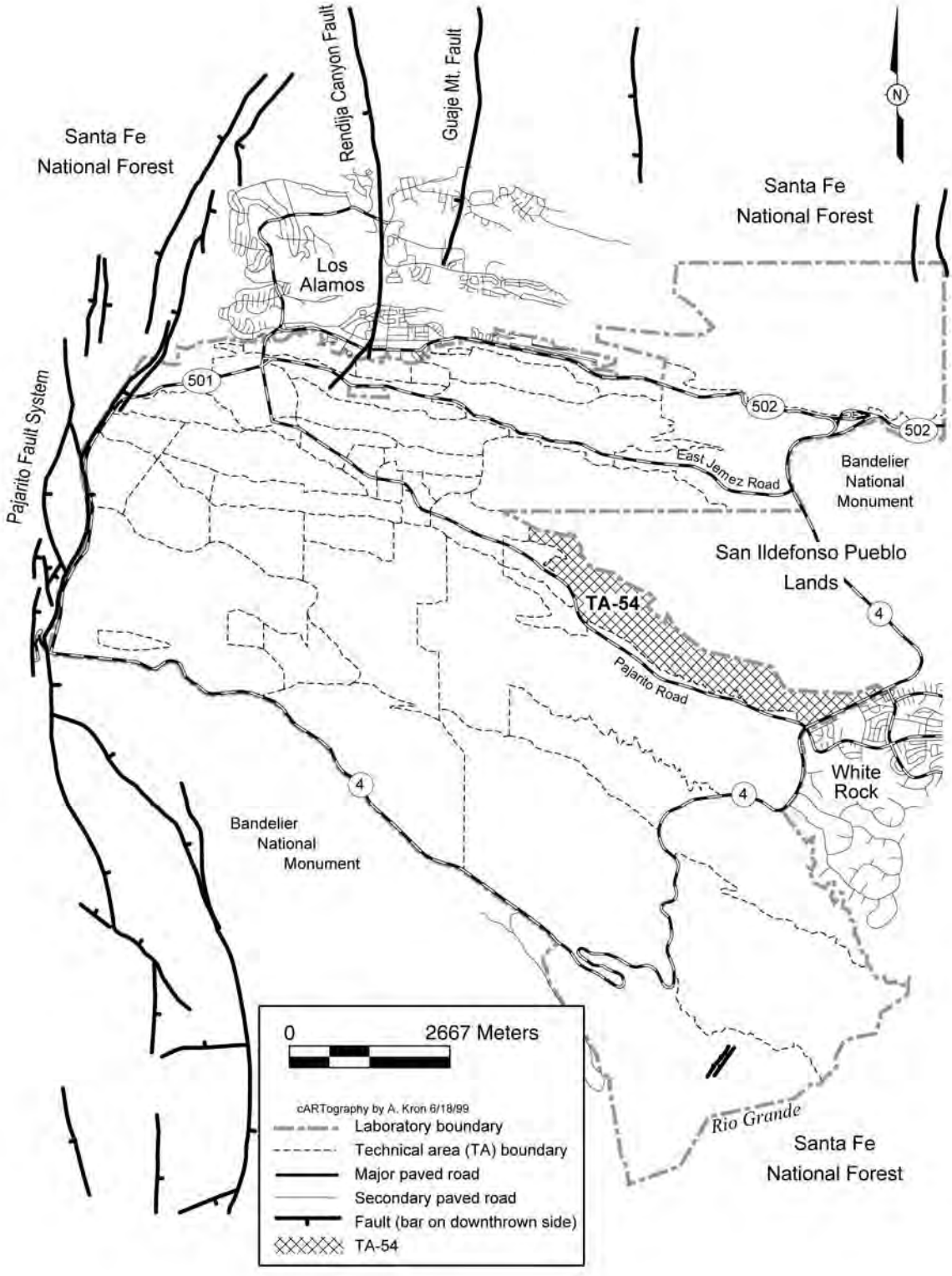

Figure 2-15
Locations of Major Faults at LANL
Source: LANL, 2001

are estimated to range from 10,000 to 40,000 years. Similarly, paleoseismic trenching shows that the Rendija Canyon Fault has ruptured repeatedly during the late Quaternary, with the most recent event occurring about 8,000 to 9,000 years ago. This event did not rupture the southern end of the fault, which is the end nearest to Area G (Hollis et al., 1997). Estimated recurrence intervals on the Rendija Canyon Fault range from 25,000 to 100,000 years, and the slip rate ranges from 0.04 to 0.05 mm/yr (0.0015 to 0.002 in/yr). The Guaje Mountain Fault exhibits evidence of multiple surface ruptures during the past 150,000 to 300,000 years, with the most recent event occurring about 4,000 to 6,000 years ago. Recurrence intervals for this fault are estimated to range from 50,000 to 150,000 years, and the slip rate ranges from 0.01 to 0.03 mm/yr (3.9×10^{-4} to 0.0012 in/yr). The wide range of recurrence intervals for all three local faults demonstrates the considerable uncertainty in the timing of past surface-faulting events.

Maximum magnitudes have been calculated based on estimated rupture lengths and rupture areas for the 26 areal faults (Wong et al., 1995). The source geometry, orientation, sense of slip, slip rate, and recurrence intervals were estimated for each fault considered in the analysis. For the Pajarito, Rendija Canyon, and Guaje Mountain Faults, the maximum magnitudes were estimated at moment magnitude 7, 6.5, and 6.5, respectively, with uncertainties of 0.25 magnitude unit. Several potential rupture scenarios were postulated for the Pajarito Fault.

A seismic hazard evaluation conducted by Olig (1997) indicates that two potential seismic hazards could have possible impacts on the ability of Area G to contain and isolate radioactivity. The first of these is the potential for small displacements or deformation of the disposal unit cover due to surface faulting on minor secondary faults, and the second is the potential disturbance or deformation of the disposal unit cover due to ground shaking. Other potential earthquake hazards are not considered a risk at Area G for a variety of reasons. Most important among these is that the subsurface excavation of disposal units into bedrock precludes the potential for liquifaction of sediments or earthquake-induced slope failures. Although there is a potential for earthquake-induced mass wasting of the cliff walls, there have been no large landslides or other large slope-failures identified near Area G. Should such events occur, the 15 m (50 ft) setback from the edge of the cliffs is judged to provide reasonable protection against loss of integrity of disposal units due to mass wasting.

The Pajarito Fault zone has numerous secondary faults with vertical displacements ranging from 24 to 120 m (80 to 400 ft). In addition, there are 37 known faults within the TA-54 area, but all are minor secondary faults with only 5 to 65 cm (2 to 26 in.) of displacement. There is no evidence of larger-scale offsets along the contacts between Tshirege Member units 2 and 1v (DOE, 2004). The variety of orientations and the very small total offsets in rock that is 1.2 million years old indicate that these faults are not likely seismogenic. Instead, they are thought to be related to cooling of the tuff or to secondary slip triggered by earthquakes occurring in the Pajarito Fault system. If they result from the latter, the average annual slip rate is relatively low: total displacements of 40 to

65 cm (16 to 26 in.) over 1.2 million years yield a slip rate of about 4×10^{-4} mm/yr (1.6×10^{-6} in./yr). Even if the total displacements occurred during a single seismic event, the likelihood of another such event occurring within 1,000 or even 10,000 years is small, given that it has happened only once in the past 1.2 million years (Krier et al., 1997).

2.1.4.3 Volcanology

The 16.5-million year volcanic history of the Pajarito Plateau has been studied extensively (Heiken et al., 1986). Evidence suggests that regional eruptions such as those that deposited the Tshirege and Otowi Members of the Bandelier Tuff have recurred every 200,000 to 500,000 years. The last such event, which deposited the Tshirege Member of the Bandelier Tuff, occurred about 1 Ma. The fact that a million years have passed without a similarly sized eruption suggests that the probability of such an event occurring again in this cycle of volcanism is very small (LANL, 2003a). Small, localized eruptions occurred about 50,000 years ago, but were contained within the Valles Caldera in the Jemez Mountains to the west of the Pajarito Plateau.

2.1.5 Hydrology

The hydrology of the Pajarito Plateau is defined by the geography, geology, and climate of the area (RAC, 2003). Mesas are generally devoid of water, both on the surface and within the rock forming the mesa; Mesita del Buey is one of the drier mesas within the Laboratory. The wet canyons of Pajarito Plateau have perennial or near-perennial streams and may contain groundwater in the canyon-bottom alluvium. The dry canyons of Pajarito Plateau have only intermittent stream flow and lack alluvial groundwater. Pajarito Canyon to the south of Mesita del Buey is one of the wetter canyons at the Laboratory, while Cañada del Buey north of Mesita del Buey is one of the driest. Intermediate perched groundwater occurs beneath the surface of some of the wetter canyons on the Pajarito Plateau at depths ranging from 27 to 135 m (90 to 450 ft) (LANL, 1993, as cited in DOE, 2004) but is not expected to extend beneath the adjacent mesas; no perched water has been found beneath Area G. In general, depths to groundwater below the mesa tops range from about 370 m (1,200 ft) or more along the western margin of the plateau to about 180 m (600 ft) at the eastern margin. (LANL, 2003a). This section discusses the occurrence, distribution, and movement of surface water and groundwater across the Pajarito Plateau in general, and in the vicinity of Area G in particular.

2.1.5.1 Surface Water

Rivers and streams located within 80 km (50 mi) of LANL include the Rio Grande and its tributaries: the Chama, Ojo Caliente, Santa Cruz, Nambe, and Tesuque Rivers to the north and east; the Jemez River and San Antonio Creek to the west; and the Santa Fe and Galisteo Rivers to the south. All surface water from the Pajarito Plateau drains to the Rio Grande. At its closest point, the Rio Grande is 5 km (3.1 mi) hydraulically downgradient from Mesita del Buey. Reservoirs within 80 km (50 mi) include the Cochiti, Abiquiu, Santa Cruz, and Jemez.

The Pajarito Plateau has dramatic erosional topography, the result of greater surface flows in the past. Today, however, only a few streams are perennial or near-perennial; the rest flow only after heavy rains and as a result of snowmelt. Figure 2-16 shows the locations of major surface water drainages on the Pajarito Plateau, including ephemeral, intermittent, and perennial drainages; major wastewater effluent-created reaches; and springs. Pajarito Canyon, one of the wetter canyons, has flow about 8 months out of the year and is fed by a cluster of springs located at TA-9 on the western edge of the Laboratory (RAC, 2003). In contrast, Cañada del Buey is a dry canyon that carries ephemeral flow only after storms or snowmelt (RAC, 2003).

The springs that feed the upper reaches of Pajarito Canyon exist at elevations between 2,400 and 2,700 m (7,870 and 8,850 ft) above msl on the slopes of the Sierra de los Valles to the west of the Pajarito Plateau. The source of these springs is perched water in the Bandelier Tuff and Tschicoma Formations. Typical discharge from these springs is between 7 and 530 L/min (1.8 to 140 gpm), a rate that is sufficient to maintain surface flow only in the upper third of the east-draining canyons of the Pajarito Plateau. Below this, the spring-fed flows are depleted by evaporation and infiltration into the underlying alluvium.

There are no streams on Mesita del Buey; any surface water is a result of storms and snowmelt. Runoff from these events leads to shallow sheet erosion on the relatively flat parts of the mesa, and deeper erosion channels in more sloped areas. After summer storms, runoff reaches a maximum in less than 2 hours and lasts less than 24 hours. In contrast, runoff from spring snowmelt occurs over a period of several weeks at a low discharge rate. In general, more eroded material is transported in summer runoff events than during snowmelt.

Flooding of the disposal facility is not a major concern because excess water typically drains into the canyons on either side of the mesa; however, temporary ponding does occur occasionally within disposal pits. The perimeter of Area G includes nine distinct natural drainage channels, six of which are monitored for potential surface water pollution. In addition, there are a number of areas over which water flows in sheets off the mesa edge after rains.

2.1.5.2 Groundwater

The groundwater system of the Pajarito Plateau, like that of most basins on the margins of the Rio Grande rift, is recharged primarily from adjacent mountains. Within LANL, groundwater occurs (1) in the deep regional aquifer, (2) as moderately deep perched water in bedrock units of the vadose zone, and (3) as shallow groundwater in canyon-floor alluvium (Broxton and Vaniman, 2005). Groundwater flows generally to the east, toward the Rio Grande (RAC, 2003).

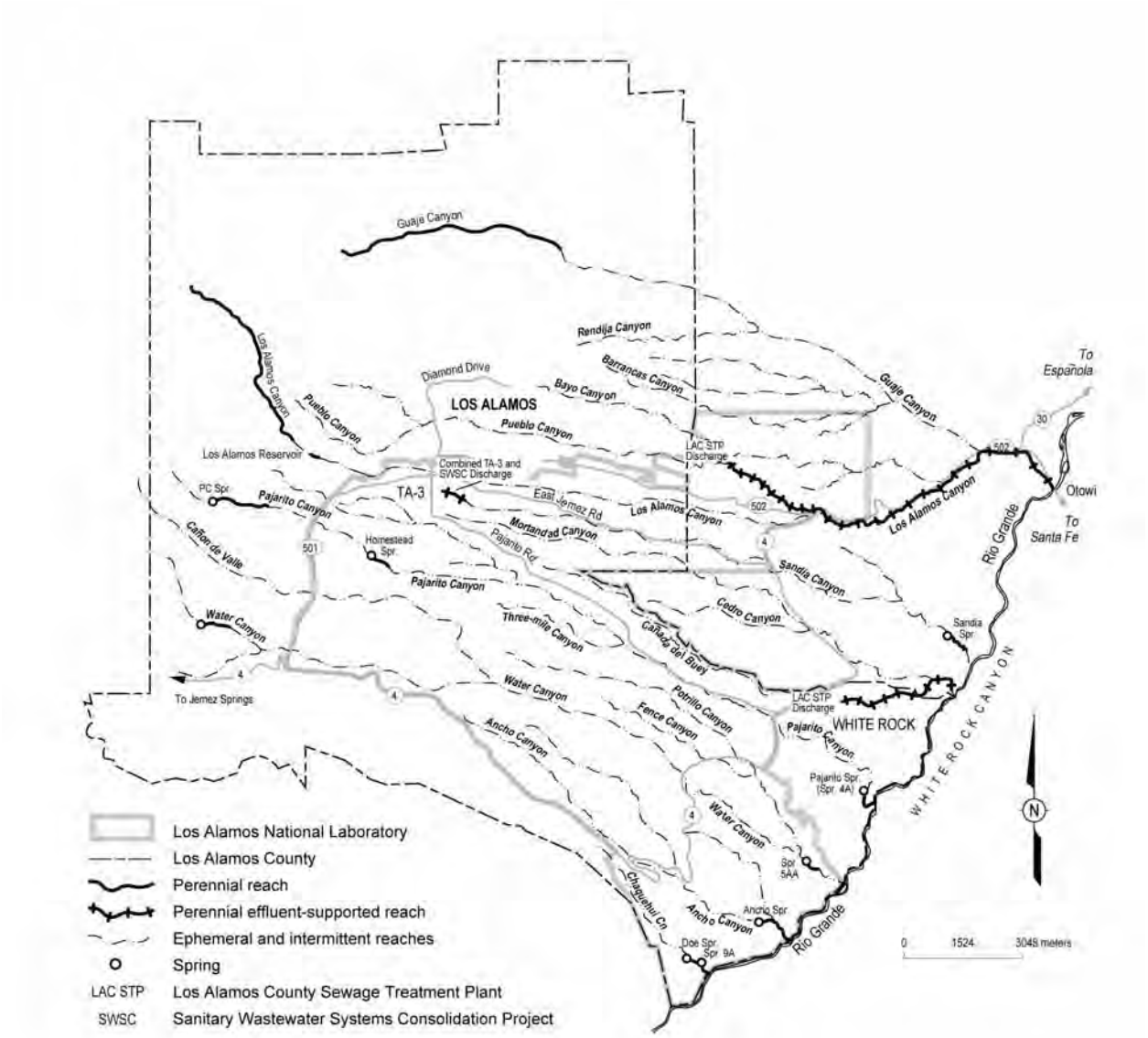

Figure 2-16
Surface Water Drainages on the Pajarito Plateau
Source: LANL, 2001

The only water source capable of serving municipal and industrial water needs is the regional aquifer (Purtymun, 1995), which extends from the mountains west of the Laboratory to the Rio Grande. The surface of the regional aquifer rises westward from the Rio Grande within the Santa Fe Group into the Puye Formation and lower part of the Cerros del Rio basalts (Figure 2-13). Depths to groundwater below the mesa tops range from about 370 m (1,200 ft) or more along the western margin of the plateau to about 180 m (600 ft) at the eastern margin. (LANL, 2003a).

The regional aquifer is separated from the alluvial groundwater and intermediate perched zone groundwater by about 110 to 190 m (350 to 620 ft) of tuff, basalt, and sediments (EPG, 1993). This lack of connection to surface and perched waters implies little possibility of aquifer recharge from these sources; however, as pointed out in a 2003 overview of groundwater issues at LANL (RAC, 2003), a broad characterization of recharge at LANL cannot be made. For example, the basic model for determining the overall water budget is that recharge to the aquifer occurs only from the vadose zone near the Jemez mountains, and that no recharge occurs east of this area. This generalization does not consider minor flows from the surface into the vadose zone within the Laboratory area. Evidence indicates that recharge from the mesa tops is very low, about 1 mm/yr (0.039 in./yr) (Nylander et al., 2003, as cited in RAC, 2003) and that a process of air-drying apparently occurs at middle elevations in the mesa area of the Laboratory (Hollis et al., 1997 as cited in RAC, 2003). However, Laboratory activities can alter the normally dry conditions of the mesa tops in specific areas.

The average hydrologic characteristics of the main aquifer are presented in Table 2-5. Continuously recorded water-level measurements collected in test wells since 1992 indicate that, throughout the plateau, the regional aquifer responds to barometric and earth tide effects in a manner typical of confined aquifers. The hydraulic gradient of the regional aquifer averages about 12 to 15 m/km (60 to 80 ft/mi) within the Puye Formation but increases to 15 to 19 m/km (80 to 100 ft/mi) along the eastern edge of the plateau as the groundwater enters the less permeable sediments of the Santa Fe Group (LANL, 2001). The hydraulic slope of the regional aquifer ranges from 0.011 to 0.015 (Hollis et al., 1997). The flow rate beneath Area G has been estimated at 29 m/yr (95 ft/yr) using data from the Pajarito well field (Abrahams, 1963). This rate is an average over the thickness of the aquifer intercepted by well screens. A portion of the aquifer discharges into the Rio Grande east of the Laboratory; the 18 km (11 mi) reach of the Rio Grande in White Rock Canyon receives about 6.8×10^6 m^3 (5,500 ac-ft) of water annually (LANL, 2001).

The Laboratory and the communities of White Rock and Los Alamos obtain water supplies from the regional aquifer (RAC, 2003), which contains the greatest quantity of stored groundwater in the region. As shown in Figure 2-17, the supply wells are located in four well fields, Los Alamos (7 wells), Guaje (7 wells), Pajarito (5 wells), and Otowi (2 wells). The Los Alamos well field began production in 1947, but was taken out of service for Los Alamos in the early 1990s, when

Table 2-5
Average Hydrologic Characteristics of Los Alamos Area Regional Aquifer

Saturated Location	Thickness (m)	Specific Rate m^3/s	Field Coefficient/ Capacity 10^{-3} m^2/s	Permeability 10^{-6} m/s	Transmissivity m^2/s
Los Alamos Field Tesuque Formation	410	0.0228	0.927	63.2	0.0288
Guaje Field Tesuque Formation and Embedded Basalt	430	0.0235	1.19	92.6	0.0398
Pajarito Field Tesuque Formation and Puye Conglomerate	530	0.0761	6.38	598	0.323
Test Hole TW-4 Tschicoma Formation	12	Data Not Available	0.577	6.77	0.00240
Test Holes DT-5A, DT-9, DT-10 Tesuque Formation and Puye Conglomerate	150	0.00513	3.09	937	0.124
Test Holes TW-1, TW-2, TW-3, and TW-8, Puye Conglomerate	18	0.000495	0.432	1,106	0.0148

Source: LANL, 2003a (Table 1-5)

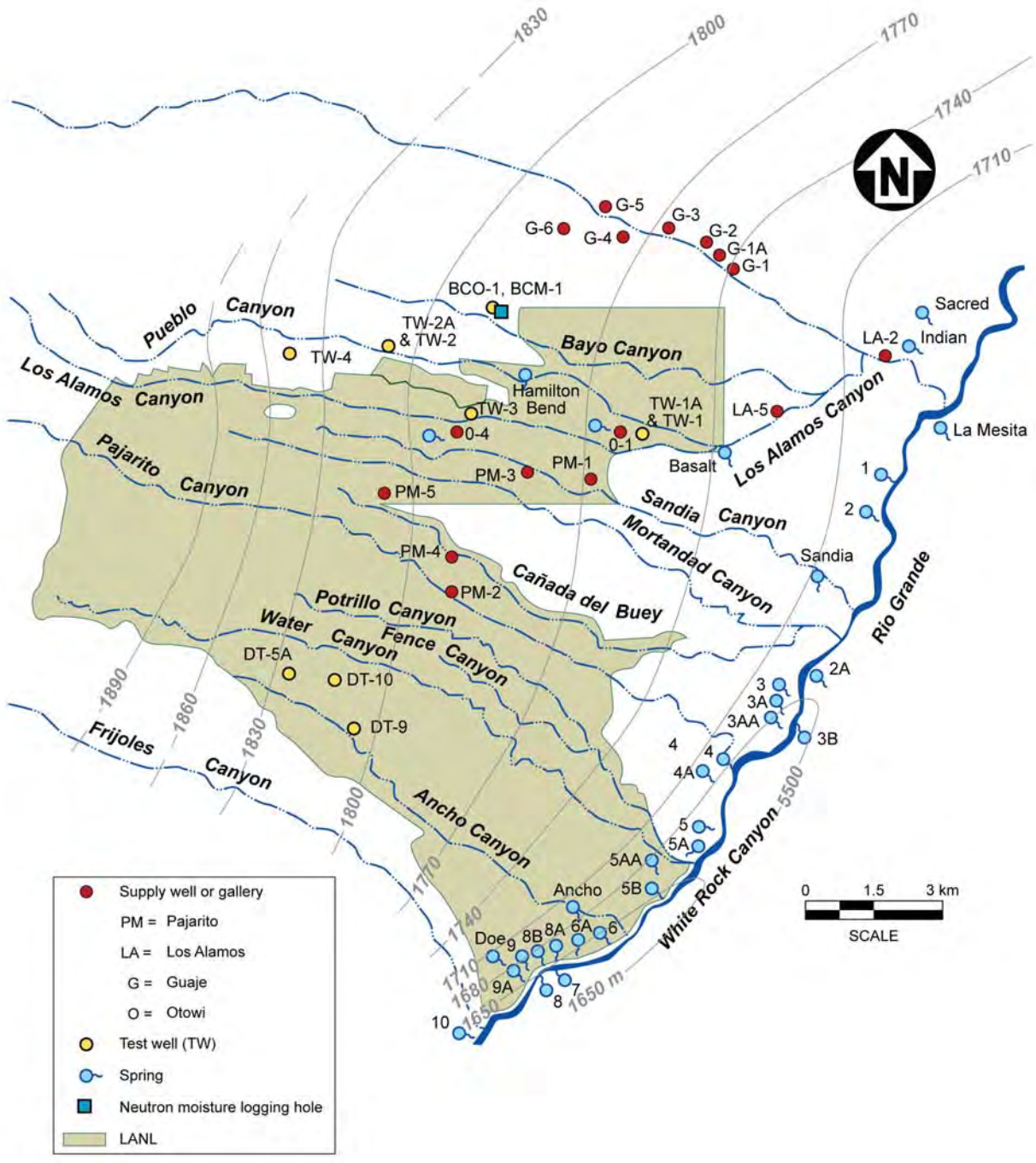

Figure 2-17
Locations of Wells and Generalized Water-Level Contours on the Top of the Regional Aquifer

Sources: Hollis et al., 1997; LANL, 2001; DBS&A, 2003

four of the wells were plugged and the remaining three (LA-1B, LA-2, and LA-5) were transferred to the San Ildefonso Pueblo; only LA-5 currently serves as a water supply well. The Guaje and Otowi well fields primarily serve the community of Los Alamos, while the Pajarito well field serves White Rock and the Laboratory. The Guaje well field began production in 1950 and the Otowi well field was added to the municipal supply system during 1993. The Pajarito field began operating in 1965.

The hydrologic characteristics of the regional aquifer measured at the supply wells and some of the test wells differ due to the geology of the aquifer and the thickness of the region penetrated by the well. The Pajarito Field (the field nearest Area G) contains the most productive supply wells; the aquifer here has an average saturated thickness of about 550 m (1,800 ft).

Vadose-Zone Hydrogeology

The region beneath the mesa surface and above the regional aquifer is referred to as the vadose, or unsaturated, zone. The modeling of radionuclide transport through the vadose zone is a critical aspect of the groundwater protection analysis of the performance assessment and composite analysis and is discussed in detail in *Appendix E*. Many processes and conditions control moisture flow in the vadose zone. Precipitation is the source of moisture in the vadose zone, and any precipitation not removed through the processes of runoff, evaporation, and transpiration moves vertically through the vadose zone toward the water table. As it migrates, this recharge water is influenced by the properties of the vadose zone.

The vadose-zone lithology in the vicinity of Area G consists primarily of various units of the Bandelier Tuff. The extent to which the tuff has been welded or devitrified affects fluid flow through this zone. These properties result from the prolonged presence of residual gases and high temperatures at the time of deposition (and shortly thereafter). Different units of the Bandelier Tuff were deposited at different temperatures and in variable thicknesses over different landscapes; as a result, cooling was not uniform. Consequently, welding varies spatially, both laterally and vertically, even within a single lithological unit.

There are several competing effects that determine moisture content and fluid flux in welded, devitrified tuff. Welded tuffs tend to be more fractured than nonwelded tuffs. Water moves slowly through the unsaturated tuff matrix, and although it can move relatively rapidly through fractured tuff, this occurs only if nearly saturated conditions exist (Abrahams, 1963). Modeling studies indicate that moisture is absorbed into the matrix when fractures disappear at contacts between stratigraphic subunits, when fracture fills are encountered, or when coatings are interrupted. (e.g., Soll and Birdsell, 1998). Thus, fractures may provide conduits for fluid flow, but only in discrete, disconnected intervals of the subsurface. Also, because they are open to the passage of both air and water, fractures can have either wetting or drying effects, depending on the relative abundance of water in the fractures and matrix.

Normally, the Tshirege Member of the Bandelier Tuff, which forms Mesita del Buey, is very dry and does not readily transmit moisture because its small pore spaces have a strong tendency to hold water against gravity by surface-tension forces. Moisture content is generally more variable near the surface of the mesa than at depth as a result of variations in temperature, humidity, and evapotranspiration; near-surface variations are greatest during the monsoons when both precipitation and evapotranspiration are at their highest.

A great deal of information is needed to conceptualize and model moisture flow and contaminant transport in the vadose zone. This includes measurements of basic geologic and hydrologic properties (e.g., porosity, density, fracture patterns, moisture content, hydraulic conductivity, and mineralogy). It also includes knowledge of the complicated relationships describing how fluids move through the rock, attributes that are difficult to establish with certainty in rock with very low moisture content. To support the development of conceptual and mathematical models for flow and transport in the vadose zone, a number of field, laboratory, and analytical studies have been performed (Hollis et al., 1997; Krier et al., 1997; Springer and Schofield, 2004; Springer, 2004 and 2005; Stauffer et al., 2005; Birdsell et al., 2000; also, see *Appendix E)* Much of the following information is summarized from Hollis et al. (1997) and *Appendix E*.

Table 2-6 provides the hydrologic or hydraulic properties used to represent the vadose-zone lithologic units at Area G during modeling. These properties are defined as follows:

- *Bulk density*, the mass of dry soil/rock per unit volume of soil/rock
- *Permeability,* a measure of the ability of soil/rock to transmit fluids
- *Porosity*, the ratio of the air-filled volume to the total volume of the soil/rock
- *Saturated volumetric water content,* the ratio of the water-filled volume of the soil/rock to the total volume of the porous medium when the soil/rock is fully saturated
- *Saturated hydraulic conductivity* (K_s), the rate at which moisture moves through saturated soil/rock when subjected to a hydraulic gradient
- *Residual volumetric water content,* the ratio of the water-filled volume of the soil/rock to the total volume of the porous medium when the flow of liquid water ceases
- *van Genuchten parameters* θ_r, α, and n, derived parameters used to model moisture movement in soil/rock

Table 2-6
Hydrogeologic Characteristics of Area G Vadose Zone Used for Groundwater Pathway Modeling

Geologic Unit	Bulk Density (g/cm^3)	Permeability (m^2)	Porosity	Saturated Vol. Water Content cm^3/cm^3	Saturated Hydraulic Conductivity	Residual Vol. Water Content	van Genuchten Fitting Parameters		
							θ_r	α (m^{-1})	n
Soil	1.5E+00	---	---	4.1E–01	4.7E–06	0.0E+00	---	---	---
Tshirege Member Unit 2	1.4E+00	2.0E–13	4.1E–01	4.1E–01	3.4E–04	1.0E–01	2.4E–02	4.7E–01	2.1E+00
Tshirege Member Unit 1v	1.2E+00	1.2E–13	4.9E–01	4.9E–02	2.4E–04	3.0E–03	6.0E–03	3.6E–01	1.7E+00
Vapor-Phase Notch	1.1E+00	---	---	4.8E–01	9.3E–05	3.0E–03	---	5.E–01	1.6E+00
Tshirege Member Unit 1g	1.2E+00	1.5E–13	4.6E–01	4.6E–01	2.0E–04	1.0E–02	2.2E-02	5.0E-01	1.8E+00
Tsankawi Pumice/Cerro Toledo Interval	1.2E+00	1.8E–13	4.5E–01	4.5E–01	3.4E–04	3.0E–03	7.0E–03	1.3E+00	1.5E+00
Otowi Member above Guaje Pumice	1.2E+00	2.3E–13	4.4E–01	4.4E–01	2.5E–04	1.9E–02	4.3E–02	5.9E–01	1.8E+00
Otowi Member Guaje Pumice	8.0E–01 [c]	1.5E–13 [a]	6.7E–01 [a]	---	---	---	0.0E+00 [a]	8.1E–02 [a]	4.0E+00 [a]
Cerros del Rio Basalts Vadose Zone	2.7E+00	1.0E–12 [b]	1.0E–03 [b]	1.0E–01	2.1E–09	0.0E+00	1.0E–03 [a]	3.8E+00 [a]	1.5E+00 [a]

Source: All data represents mean values from Springer (2005) unless otherwise noted.

Numbers are rounded to two significant digits.

NA = Not applicable

--- = No data available

[a] *Birdsell et al., 1999 and 2000*

[b] *Stauffer et al., 2005*

[c] *Estimated (see Appendix E, Volume 2)*

Variability in vadose-zone flow properties is an important consideration in understanding uncertainty in the travel times of contaminants through the subsurface. Krier et al. (1997) showed that hydraulic conductivity curves were similar for most geologic units found at Area G; the different behavior noted for the Tsankawi Pumice/Cerro Toledo interval was attributed to the highly variable pore sizes in this unit. A recent statistical analysis of the hydrogeologic properties of the vadose zone at TA-54 suggests that the properties of the Tshirege Member units of the Bandelier Tuff do not appear to have any demonstrable differences (*Appendix E, Attachment III*). Although somewhat different, the properties for the Tsankawi Pumice/Cerro Toledo interval and the Otowi Member were still within the range of the means of the Tshirege Member units. The hydrogeologic behavior of the soil unit and the basalt underlying the Bandelier Tuff differs significantly from that of the Tshirege Member; however, this is expected because of the material characteristics and genesis of these layers as opposed to the tuff.

Hydrologic Characteristics of Canyons

The hydrologic characteristics of the canyons bordering Mesita del Buey may influence the hydrology beneath the mesa and thus affect the transport of contamination. To the north, Cañada del Buey contains an intermittent stream. The alluvium is thin and is not saturated year round. Groundwater has been observed and sampled annually in two wells in Cañada del Buey; the saturation appears to be in the underlying tuff rather than the alluvium. As described in Pratt (1998), the lower Pajarito Canyon, just south of Area G, has more subsurface water than Cañada del Buey. Like Cañada del Buey, Pajarito Canyon also contains an intermittent stream, but the larger flow in this canyon supports a perennial groundwater body in the alluvium (Devaurs and Purtymun, 1985).

Pajarito Canyon is relatively wide and has a fairly flat bottom in the vicinity of Area G. Runoff from higher elevations is focused into Pajarito Canyon and creates a transient stream that flows intermittently, sometimes resulting in pooled water in the canyon bottom to the south of Area G (Pratt, 1998). The most recent estimate of average annual infiltration in lower Pajarito Canyon is 18.5 m^3/m (200 ft^3/ft) (Kwicklis et al., 2005, Table 2). This value represents the average infiltration per meter of canyon across the average canyon width between two stream gauges; the upstream gauge is located several kilometers west of Area G and the downstream gauge lies just west of White Rock. The infiltration value does not account for stream losses due to evapotranspiration.

Perched water was encountered at two drillholes in Pajarito Canyon (LANL, 2001); however, this water is confined to the alluvium in the stream channel (Devaurs and Purtymun, 1985, as cited in LANL, 2001). No perched groundwater has been identified beneath Mesita del Buey (LANL, 1998a, as cited in LANL, 2001).

Recharge Beneath Area G

The recharge rate beneath the mesa top is perhaps the most important parameter in modeling the subsurface transport of radioactivity. Recharge largely controls the minimum time required for radioactivity to be transported from Area G through the vadose zone into the regional aquifer, where it may lead to exposures of the general public. The recharge through the undisturbed vadose zone is complex and is complicated further at Area G by man-made disturbances associated with waste management activities.

The infiltration of water from the surface of the mesa through the disposal site is dependent on a number of parameters, including precipitation, evaporation, and transpiration. These factors vary throughout the year. Evaporation, which is highest in the warm summer months, generally occurs within several centimeters of the surface; however, evaporation may be observed at greater depths, especially in fractured or very permeable rock. Transpiration is a result of root uptake and occurs throughout the root zone. Like evaporation, it is greatest in the summer. Natural recharge through the Bandelier Tuff also varies in response to climate and local rock characteristics. The unsaturated upper units of the Bandelier Tuff tend to retain water, which promotes the removal of water through evapotranspiration.

Infiltration rates at Area G have been estimated on a number of occasions. For example, based on an infiltration map for the Los Alamos region developed by Kwicklis et al. (2005), rates of infiltration ranging from about 0 to 10 mm/yr (0 to 0.4 in./yr) are estimated for Mesita del Buey; this range of infiltration rates was also adopted for the modeling conducted in support of the 1997 performance assessment and composite analysis (Hollis et al., 1997). Newman et al. estimated infiltration rates in undisturbed portions of the disposal facility and in areas impacted by disposal operations and found that fluxes were generally on the order of 0.2 mm/yr (0.0079 in./yr) in undisturbed areas and 0 to 10 mm/yr (0 to 0.4 in./yr) in areas impacted by disposal and surface structures (*Appendix F,* Volume 2). Levitt modeled rates of water passage through the proposed final cover, and estimated rates ranging from 1.3×10^{-4} to 7 mm/yr (5.1×10^{-6} to 0.28 in./yr) (*Appendix G,* Volume 2).

Deep infiltration at Area G may or may not result in recharge of the regional aquifer. The presence of cooling joints or fractures within some units of the Tshirege Member of the Bandelier Tuff may dry out portions of the mesa. The driest zone within the mesa generally occurs within the lower portion of Tshirege unit 2 and the upper part of unit 1v, a region that coincides with fractures (Krier et al., 1997). Rogers et al. (1997) note that this region is also generally a zone of high matric suction and a hydraulic head minimum, suggesting that moisture is being mobilized toward this depth, both from above and below, by physical properties of the tuff. The driving force for this movement of water may be evaporation aided by air flow within the fractures or along the surge beds found at the base of unit 2. Chloride and stable isotope

analyses conducted by Newman (1996) support the presence of a dry region within the mesa resulting from deep evaporation.

Birdsell et al. (1997) discuss three distinct moisture content zones within the Bandelier Tuff beneath Area G and indicate that three different recharge rates are necessary to match these moisture conditions. Within unit 2 and the upper portion of unit 1v, a recharge rate of about zero to 0.1 mm/yr (0 to 0.004 in./yr) most closely matches site saturation data, while a range of about 0.1 to 1 mm/yr (0.004 to 0.04 in./yr) is needed to match moisture content data in the lower portion of the Tshirege Member. A recharge rate of about 10 mm/yr (0.4 in./yr) is required to match saturation data for the Cerro Toledo interval and the Otowi Member of the Bandelier Tuff. The vertical disconnects in these estimated recharge rates supports the hypothesis that recharge is not steady state, or that significant moisture sources and sinks exist at depths.

2.1.6 Geochemistry

The geochemical characteristics of the pore water, groundwater, rocks, and soils beneath Area G will have important implications in terms of radionuclide release due to leaching and contaminant transport from the disposal units to the regional aquifer. Rates of leaching will depend largely on the chemistry of the pore water, the physical and chemical forms of the waste, and the sorption behavior of the radionuclides. Contaminant travel times to the aquifer will be directly influenced by the sorption behavior of radionuclides, which itself is a function of the surface area and mineralogy of the porous material and the chemistry of the water in contact with the tuff.

Krier et al. (1997) indicate that rainwater and snowmelt have a low total dissolved solids content and an acidic pH because of low concentrations of bicarbonate, calcium, sodium, and magnesium; storm runoff at Area G may have a higher dissolved solids content and near-neutral pH because of its contact with soils, backfill, and the Bandelier Tuff. Surface water may approach equilibrium with crushed tuff, waste, and associated radionuclides as it infiltrates through the pore spaces of the waste in the disposal units. Geochemical reactions that control contaminant releases will themselves be controlled by pH, oxidation-reduction potential, speciation of the contaminants, temperature, advection, and residence time of the pore water (Krier et al., 1997).

Certain minerals present in the Bandelier Tuff have high sorptive capacity for many radionuclides present in the Area G inventory (Broxton et al., 1995); these minerals include hematite, kaolinite, smectite, and calcite. For example, sources cited by Broxton et al. indicate that smectites are highly selective for cationic radionuclides, and that magnetite and its alteration products (e.g., hematite) have an affinity for uranium and actinide species through surface-complexation. Although these minerals occur only in small quantities at Area G, they are present throughout the entire thickness of the tuff, as fracture linings as well as within the tuff itself. As a result, the aggregate abundance of these minerals and the surface area available for adsorption

are large when the long groundwater flow paths are taken into account. Less important in terms of transport is dissolved organic carbon, which can form soluble complexes with certain radionuclides to form relatively mobile solutes; the organic carbon content of pore water within the Bandelier Tuff is typically less than 1 percent (by weight) (Longmire et al., 1995).

Certain highly sorptive solid phases, including clay minerals, iron oxides, solid organic matter, and carbonate minerals, are known to be present in subsurface soils found across the Laboratory. Calcium carbonate and clay-rich horizons exist beneath Area G at the top of the Cerros del Rio basalts, although they are laterally inconsistent. Calcium carbonate appears as calcrete-like coatings on basalt cobbles and the paleosol above the basalts is clay-rich (LANL, 2005d). Little is known about the effect of clays on the hydrology beneath Area G, but they may be important for sorbing radionuclides. Also, vertical water flow may be inhibited and lateral flow enhanced by clay layers because of their low permeability.

Detailed geochemical modeling was not undertaken for the performance assessment and composite analysis. Geochemical properties of the soil column were used, however, to identify sorption characteristics that are suitable for the performance modeling. Longmire et al. (1996) conducted bench-scale batch experiments to measure sorption under conditions mimicking the vadose zone and saturated zone at Area G. Sorption coefficients were determined for americium, neptunium, plutonium, technetium, and uranium using two pore waters. The first, Water Canyon Gallery groundwater, discharges from the Bandelier Tuff at a pH of 7.3, is relatively oxidizing, and is characterized by a calcium-sodium-bicarbonate ionic composition with a total dissolved solids content of less than 130 mg/L (130 ppm). The second was vadose-zone pore water extracted from the Bandelier Tuff cores collected from beneath Mesita del Buey using an unsaturated/saturated flow apparatus. This pore water is characterized by a sodium-carbonate-bicarbonate solution with a total dissolved solids content greater than 1,300 mg/L (1,300 ppm). The pH values of the pore-water samples range from 9.2 to 9.8 and the solutions are oversaturated with calcite.

The distribution coefficients for radionuclides measured on the Bandelier Tuff, at a pH of 7.3, decrease in the following order: Am(III) >> Pu(V) > U(VI) >> Np(V) > Tc(VII). The coefficients for radionuclides measured on the tuff samples using a synthetic pore water, at a pH of 9.8, decrease in the following order: Am(III) >> Pu(V) > U(VI) > Np(V) > Tc(VII). The distribution coefficients for Tc(VII) were all negative and, therefore, assumed to be zero. The distribution coefficients for Am(III) and Np(V) using the synthetic pore water were higher than the coefficients for these radionuclides using the Water Canyon Gallery groundwater. It was postulated that calcite precipitated from the synthetic pore water enhanced the sorptive capacity of the Bandelier Tuff for these radionuclides.

The results of computer simulations conducted using the geochemical equilibrium speciation model MINTEQA2 indicate that the dominant aqueous complexes of Am(III) and Np(V) will include $Am(CO_3)_3^{3-}$ and $NpO_2(CO_3)_3^{5-}$, respectively (Longmire et al., 1996). The synthetic pore water was predicted to be undersaturated with respect to $Am(OH)_3$(s), $Am(OH)_3$(m), $AmOHCO_3$, NpO_2OH(am), NpO_2OH(aged), $NaNpO_3 \cdot 3.5H_2O$, and $NaNpCO_3$. Enhanced sorption of Am(III) and Np(V) carbonate complexes on calcite is possible through surface exchange with carbonate and bicarbonate functional groups present on the calcite surface.

Krier et al. (1997) conducted a review of literature on sorption and equilibrium solubility in conjunction with the 1997 performance assessment and composite analysis. This review focused on data for devitrified tuff from Yucca Mountain, which are expected to provide reasonable estimates of contaminant behavior at Area G in lieu of site-specific information. Other sources of information were consulted by those investigators as necessary to define the required coefficients. More recent sorption experiments using tuff from Yucca Mountain have been used to estimate distributions of sorption coefficients for selected radionuclides (Bechtel/SAIC 2004).

2.1.7 Natural Resources

An important consideration when projecting the potential for radiological exposures at Area G is the presence of nearby natural resources that may be used in the future. These include geologic resources such as minerals, ores, fossil fuels, and geothermal energy as well as water. The distribution of these resources in the LANL region is discussed in this section.

2.1.7.1 Geologic Resources

There are several mines and quarries in Los Alamos County, none of which is currently active. Small surface mines in Sandoval, Santa Fe, and Rio Arriba Counties near Los Alamos extract pumice. The nearest pumice mine is about 10 km (6 mi) north of Area G. Other active surface mining operations in the region recover sand, gravel, crushed rock, and other fill materials. The nearest of these is located in Santa Fe County, about 10 km (6 mi) east of Area G. Surface mines for volcanic cinders operate approximately 8 km (5 mi) east and 25 km (15 mi) south of the disposal site, and a surface mine for humate (a soil conditioner) operates approximately 55 km (33 mi) west of LANL. Gypsum is also mined at a few locations south of the Laboratory.

Historically, metal deposits (primarily silver, copper, and gold) were mined in the Cochiti (Bland) mining district, about 16 km (10 mi) south of LANL. Mines in the district have been inactive since about 1940, but prospecting and a small amount of production still occur. The closest active metal mines to LANL are located in the San Pedro Mountains, approximately 45 km (27 mi) to the south. Turquoise is also mined 45 km (27 mi) south of the Laboratory.

The natural gas field closest to the Laboratory is approximately 64 km (40 mi) to the northwest in the San Juan Basin. The nearest oil fields are also in the San Juan Basin, with other small

fields located about 70 km (45 mi) west of LANL. The USGS considers the potential for oil and gas discoveries in Los Alamos County area to be poor, although exploration wells have encountered evidence of oil and gas in the Española Basin, a few kilometers northeast of LANL.

The coal fields closest to LANL, located in the San Juan Basin, extend to within 40 km (25 mi) of the northern boundary of LANL. Small coal deposits south of Santa Fe—the Hagen and Cerrillos fields—are located about the same distance to the south of Los Alamos. Relatively small uranium deposits occur in the Nacimiento-Jemez uranium area, about 35 km (20 mi) southwest of LANL. Also, relatively high concentrations of uranium sediments have been found on the southeast flank of the Jemez Mountains.

The USGS has designated portions of the Jemez Mountains as a "Known Geothermal Resource Area." Many of the thermal springs and wells in this area are within 32 km (20 mi) of the Laboratory. To date, test wells installed near Area G show low potential for geothermal resources.

2.1.7.2 Water Resources

Most of the water taken from the Guaje and Otowi well fields (Figure 2-17) serves only the town of Los Alamos. Two of the five wells in the Pajarito field normally serve the town of White Rock and three serve LANL. Under unusual circumstances, water from any well can be routed to any destination. Of the three Los Alamos wells transferred to the San Ildefonso tribe in the early 1990s, only LA-5 is used as a source of drinking water (for San Ildefonso's Totavi gas station and housing complex). Well LA-1B serves as a monitoring well and LA-2 was taken out of service in 1993 (Glasco, 2005). The wells are no longer used for drinking water but do provide nonpotable water for irrigation. In addition, nonpotable industrial water is obtained from the spring gallery in Water Canyon.

The Cochiti reservoir dam is located on the Rio Grande, about 15 km (9.3 mi) from the southernmost point of the LANL boundary. The dam provides flood control, sediment retention, recreation, and fishery development. The permanent pool extends upstream some 12 km (7.4 mi) to a point about 5 km (3.1 mi) from the southernmost point of the LANL boundary. The dam is estimated to trap at least 90 percent of the sediments carried by the Rio Grande.

No municipal water supplies are taken directly from the Rio Grande between LANL and the Cochiti dam. The river along this stretch is used primarily for recreation. Below the dam, irrigation water is taken from the Rio Grande at numerous diversions.

2.1.8 Natural Background Radiation

The total radiation dose from natural background in the vicinity of the Laboratory is 360 mrem/yr. This dose can vary by as much as 10 mrem from year to year (LANL, 2002a).

Naturally occurring radon accounts for nearly half of this total, with the remainder contributed by cosmic and terrestrial radioactivity, and self-irradiation (LANL, 1996b).

The LANL environmental surveillance reports provide information on background concentrations of radionuclides in air and sediments in the greater Los Alamos region. Table 2-7 summarizes regional airborne concentrations of selected radionuclides for 1997 through 2001 (LANL, 2002a). Radionuclide concentrations measured in soils at regional locations are summarized in Table 2-8.

Table 2-7
Average Background Concentrations of Radioactivity in the Regional Atmosphere

Parameter	Units	Annual Averages [a]				
		1997	1998	1999	2000	2001
Gross Alpha	fCi/m^3	0.7	0.8	1.0	1.0	0.8
Gross Beta	fCi/m^3	14.1	12.4	13.4	13.0	13.9
H-3 [b]	pCi/m^3	0.7	0.5	0.5	0.8	-0.1 [c]
Pu-238	aCi/m^3	0.0	0.1	-0.2 [c]	0.0	0.0
Pu-239/240	aCi/m^3	-0.2 [c]	0.4	0.1	0.0	0.1
Am-241	aCi/m^3	0.2	0.3	-0.2 [c]	0.3	-0.2 [c]
U-234	aCi/m^3	14.1	12.9	16.1	17.1	17.9
U-235	aCi/m^3	0.6	0.9	1.2	0.9	1.3
U-238	aCi/m^3	12.2	12.8	15.2	15.9	17.7

Source: LANL, 2002a. Data from regional air sampling stations operated by LANL; sampling locations may vary by year.

[a] *Gross alpha and beta annual averages calculated from gross air concentrations; all others are calculated from net air concentrations.*

[b] *Tritium annual averages have been corrected for the tritium lost to bound water in the silica gel media.*

[c] *Negative values may result because the measured concentration is a sum of the true value and all random errors. As true value approaches zero, measured value approaches the total random errors, which can be negative or positive and overwhelm the true value.*

Surface water samples collected at off-site stations provide baseline information for water quality in the region. Radiochemical quality of water in the Rio Grande upstream from (Embudo sampling station), adjacent to (Otowi sampling station), and downstream from (Cochiti sampling station) the Laboratory are listed in Table 2-9.

Table 2-8
Radionuclide Concentrations Measured in Regional Surface Soils (0 to 5 cm depth), 2001

Radioactivity	Units	Embudo Station	Cochiti Station	Jemez Station
H-3	pCi/mL	0.38 +/- 0.4 [a]	0.94 +/- 0.44	0.26 +/- 0.25
Sr-90	pCi/g dry	0.24 +/- 0.14	0.07 +/- 0.13	0.05 +/- 0.14
Cs-137	pCi/g dry	0.24 +/- 0.04	0.25+/- 0.05	0.13 +/- 0.45
Uranium	µCi/g dry	1.77 +/- 0.13	1.79 +/- 0.13	2.52 +/- 0.19
U-234	pCi/g dry	0.55 +/- 0.04	0.55 +/- 0.04	0.76 +/- 0.06
U-235	pCi/g dry	0.033 +/- 0.005	0.057 +/- 0.007	0.077 +/- 0.009
U-238	pCi/g dry	0.59 +/- 0.04	0.59 +/- 0.04	0.84 +/- 0.06
Pu-238	pCi/g dry	0.003 +/- 0.0001	0.001 +/- 0.001	-0.001 +/- 0.001 [b]
Pu-239/240	pCi/g dry	0.014 +/- 0.003	0.009 +/- 0.002	0.006 +/- 0.002
Am-241	pCi/g dry	0.005 +/- 0.002	0.004 +/- 0.002	0.002 +/- 0.001
Gross Alpha	pCi/g dry	3.9 +/- 0.47	3.7 +/- 0.47	4.2 +/- 0.90
Gross Beta	pCi/g dry	4.4 +/- 0.44	3.7 +/- 0.38	4.5 +/- 0.75
Gross Gamma	pCi/g dry	7.0 +/- 0.3	8.0 +/- 0.3	8.0 +/- 0.3

Source: LANL, 2002a

[a] *+/- 1 counting uncertainty: values are the uncertainty of the analytical results at the 65% confidence level.*

[b] *Measurements of radiochemical samples require that analytical or instrumental backgrounds be subtracted to obtain net values. Because net values may be lower than the minimum detection limit, individual measurements can result in negative values.*

Table 2-9
Radiochemical Quality of Surface Water from Off-Site Stations

Radioactivity	Concentration (pCi/L)		
	Embudo Station	Otowi Station	Cochiti Station
H-3	-99 +/- 45 [a,b]	-105 +/- 47	-82 +/- 54
Sr-90	0.18 +/- 0.12	0.01 +/- 0.07	0.13 +/- 0.09
Cs-137	1.41 +/- 0.82	-3.2 +/- 1.83	-0.81 +/- 0.8
U-234	1.16 +/- 0.098	0.909 +/- 0.077	0.728 +/- 0.069
U-235,236	0.0381 +/- 0.0105	0.0235 +/- 0.0073	0.0838 +/- 0.0169
U-238	0.608 +/- 0.059	0.538 +/- 0.051	0.433 +/- 0.047
Ou-238	0.0 +/- 1.0	0.0 +/- 0.003	0.0 +/- 1.0
Pu-239,240	0.009 +/- 0.007	0.006 +/- 0.006	0.016 +/- 0.007
Am-241	0.021 +/- 0.010	0.014 +/- 0.008	0.012 +/- 0.010

Source: LANL, 2002a

[a] *+/- 1 counting uncertainty; values are the uncertainty of the analytical results at the 65% confidence level.*

[b] *Measurements of radiochemical samples require that analytical or instrumental backgrounds be subtracted to obtain net values. Because net values may be lower than the minimum detection limit, individual measurements can result in negative values.*

2.2 Principal Facility Design Features

In addition to the environmental conditions described in Section 2.1, the long-term performance of Area G depends on a number of engineered or man-made features. These include the depth and configuration of waste units on the mesa and the interim and final covers that are placed over these units. This section discusses the planned expansion of waste disposal into the Zone 4 expansion area and the general characteristics of the final cover for the site, the conceptual design of which has been developed in conjunction with this performance assessment and composite analysis. As discussed in Section 2.2.1, the cover is designed to limit infiltration through the facility, thereby minimizing radionuclide releases due to leaching. The cover also helps minimize the impacts of plant and animal intrusion and protect against surface erosion. Section 2.2.2 discusses the integrity of the proposed final cover with respect to erosion issues. Section 2.2.3 and 2.2.4 discuss other important aspects of the facility design including the structural stability of the facility features and the measures undertaken to prevent or limit intrusion into the waste.

From 1957 through 2007, 35 disposal pits and over 200 shafts have been constructed at MDA G, the currently active portion of the facility. The development of these disposal units has progressed generally from east to west, in accordance with the construction guidelines in effect at the time of construction. Much of the disposal capacity within MDA G has been exhausted (see Figure 1-2, Section 1) and current plans call for a phased closure of this area by 2015. Plans have been made to construct additional disposal pits and shafts in a 12 ha (30 ac) area immediately west of MDA G; this expansion area is referred to as Zone 4.

A phased development approach has been established for Zone 4, as illustrated in Figure 2-18; the design capacities estimated for the different phases are summarized in Table 2-10 for several design options. A detailed description of the phased design may be found in *Appendix B*. As discussed below, it is expected that Zone 4 will provide more than enough LLW disposal capacity to support future Laboratory needs.

Based on inventory projections, approximately 1.2×10^5 m^3 (4.2×10^6 ft^3) of waste is projected to be disposed of in Zone 4. As shown in Table 2-10, this capacity can be realized using several approaches. For example, excavation of all phase 1 pits to a depth of 24 m (80 ft), with or without ramp excavation, would provide the requisite disposal volume. If pits are excavated to a depth of only 18 m (60 ft), some development of the phase 2 area would be needed.

The design of Area G takes advantage of the natural ability of the site to contain radioactivity. The Tshirege Member of the Bandelier Tuff, the bedrock into which the waste units are excavated, is extremely dry and effectively decouples radioactivity in LLW from the main aquifer for hundreds to thousands of years. Crushed tuff removed during excavation is used to

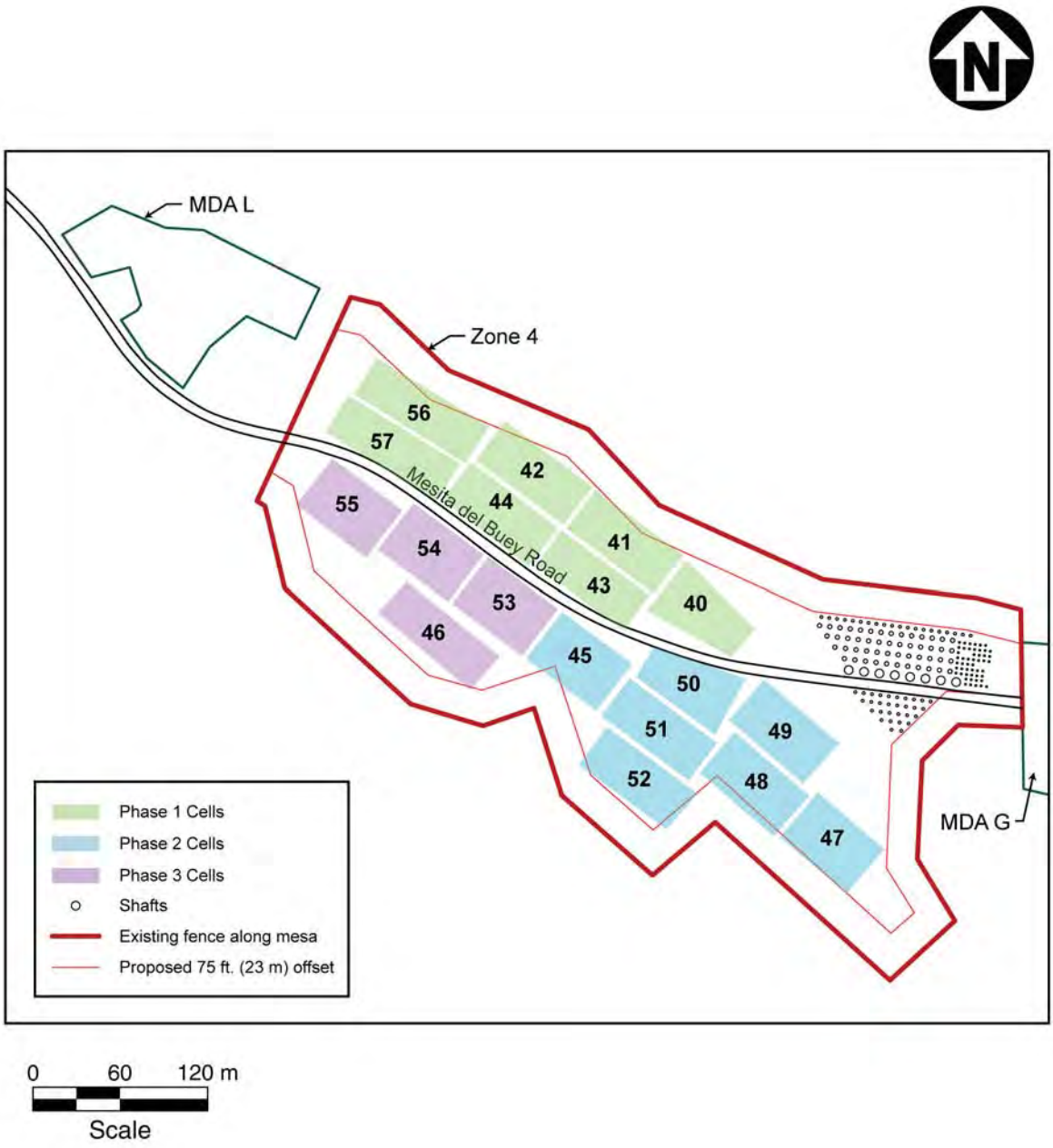

Figure 2-18
Proposed Disposal Unit Development at Zone 4

Source: LANL, 2005b
(after URS 2004a, 2004b, and 2004c)

line and backfill the pits. As a liner, the crushed tuff absorbs moisture and leachate. As backfill, the crushed tuff compacts to stabilize the pits, and also absorbs moisture.

Table 2-10
Design Capacities of Zone 4 Development Phases

Design Options	Design Capacity					
	Phase 1		Phase 1 + Phase 2		Phases 1, 2 and 3	
	Waste Volume (m^3)	Life Expectancy (yr)	Waste Volume (m^3)	Life Expectancy (yr)	Waste Volume (m^3)	Life Expectancy (yr)
18 m Depth, No Ramp Excavation	8.7E+04	31	1.7E+05	60	2.2E+05	77
18 m Depth, 50% Ramp Excavation	1.0E+05	36	2.0E+05	72	2.6E+05	92
24 m Depth, No Ramp Excavation	1.2E+05	43	2.4E+05	83	3.0E+05	106
24 m Depth, 50% Ramp Excavation	1.4E+05	49	2.8E+05	98	3.6E+05	125

When a disposal unit at Area G reaches capacity, it undergoes interim closure. Historically, the interim cover has consisted of 0.6 to 3 m (2.0 to 9.8 ft) of crushed tuff. The cover is designed to minimize radiation exposures received by facility personnel and provide a base for the construction of surface structures used in the management of waste. As a cover, the crushed tuff provides a stable, absorptive barrier, and supports natural vegetation that controls erosion and transpires moisture.

The 1997 performance assessment and composite analysis (Hollis et al., 1997) evaluated the ability of the disposal facility to safely isolate the waste under the condition that only the interim cover was present. Those analyses concluded that the facility satisfied the performance objectives, in part because it was assumed that DOE would be present to maintain the site throughout the 1,000-year compliance period. Since that time, work conducted under the Area G Performance Assessment and Composite Analysis Maintenance Program (Shuman et al., 2003) has indicated that the impacts of biotic intrusion and surface erosion may be more severe than estimated for the 1997 analyses. Furthermore, the position that DOE will be present to ensure proper site functioning throughout the 1,000-year compliance period has been reconsidered. Taken together, these factors suggest the final cover should be capable of performing under much more severe conditions than previously considered. Consequently, it was decided that a more robust cover design will be implemented at the time of final closure to ensure continued protection of human health and the environment.

To develop the final cover design for Area G, preliminary evaluations were conducted to estimate the approximate cover characteristics needed to allow the disposal facility to satisfy DOE performance objectives. These evaluations, described in more detail in *Appendix H* (Volume 2), focused on total cover depth as the primary means of mitigating biotic intrusion into the waste (assuming no engineered biobarriers are present). This is significant because in the 1997 performance assessment and composite analysis, biotic intrusion was the radionuclide release mechanism responsible for the peak exposures projected for persons living downwind of the disposal site and in Pajarito Canyon (Hollis et al., 1997).

The minimum amount of cover required to safely isolate the waste disposed of at Area G was estimated based on the results of Shuman (1999) and preliminary estimates of the impacts of biotic intrusion under what were expected to be conservative estimates of erosion potential. Assuming that the cover would be maintained for a period of 100 years following closure of the disposal facility, it was estimated a minimum cover thickness of 1.5 m (4.9 ft) throughout the 1,000-year compliance period would provide reasonable assurance that the disposal facility would continue to satisfy all performance objectives. On the basis of preliminary estimates of erosion potential that were developed using the SIBERIA erosion model (see *Appendix I*, Volume 2), it was concluded that adopting a minimum initial cover thickness of 2.5 m (8.2 ft) would enable the cover requirement to be met for most, if not all, of the disposal site.

After the minimum initial cover depth was identified, an iterative process was used to evaluate cover designs. The performance of each conceptual design was evaluated for a period of 1,000 years using refinements of the SIBERIA erosion model (*Appendix I*). The cover designs were evaluated to determine their ability to satisfy the minimum cover requirements and to identify areas where projected erosion impacts appeared to be severe. Generally, the erosion modeling indicated that the cover over much of the site performed adequately; however, some elevated rates of erosion were observed in localized areas along mesa edges or adjacent to drainages. These vulnerable locations were fortified using engineered features such as rock armor and the design evaluation process was repeated.

Figure 2-19 shows a profile of the proposed cover for Area G. The following sections discuss important design features of the cover and consider how they affect the long-term performance of the disposal site. *Appendices H* and *I* provide additional information about the cover design process and the surface erosion modeling conducted in support of that effort.

2.2.1 Water Infiltration

Minimizing infiltration through the disposal units will reduce the rates at which radionuclides are leached from the waste and extend the amount of time required for contaminated water to reach the regional aquifer. The final cover at Area G is intended to function as an evapotranspiration cover, which will provide water storage sufficient to contain spring snowmelt within the cover

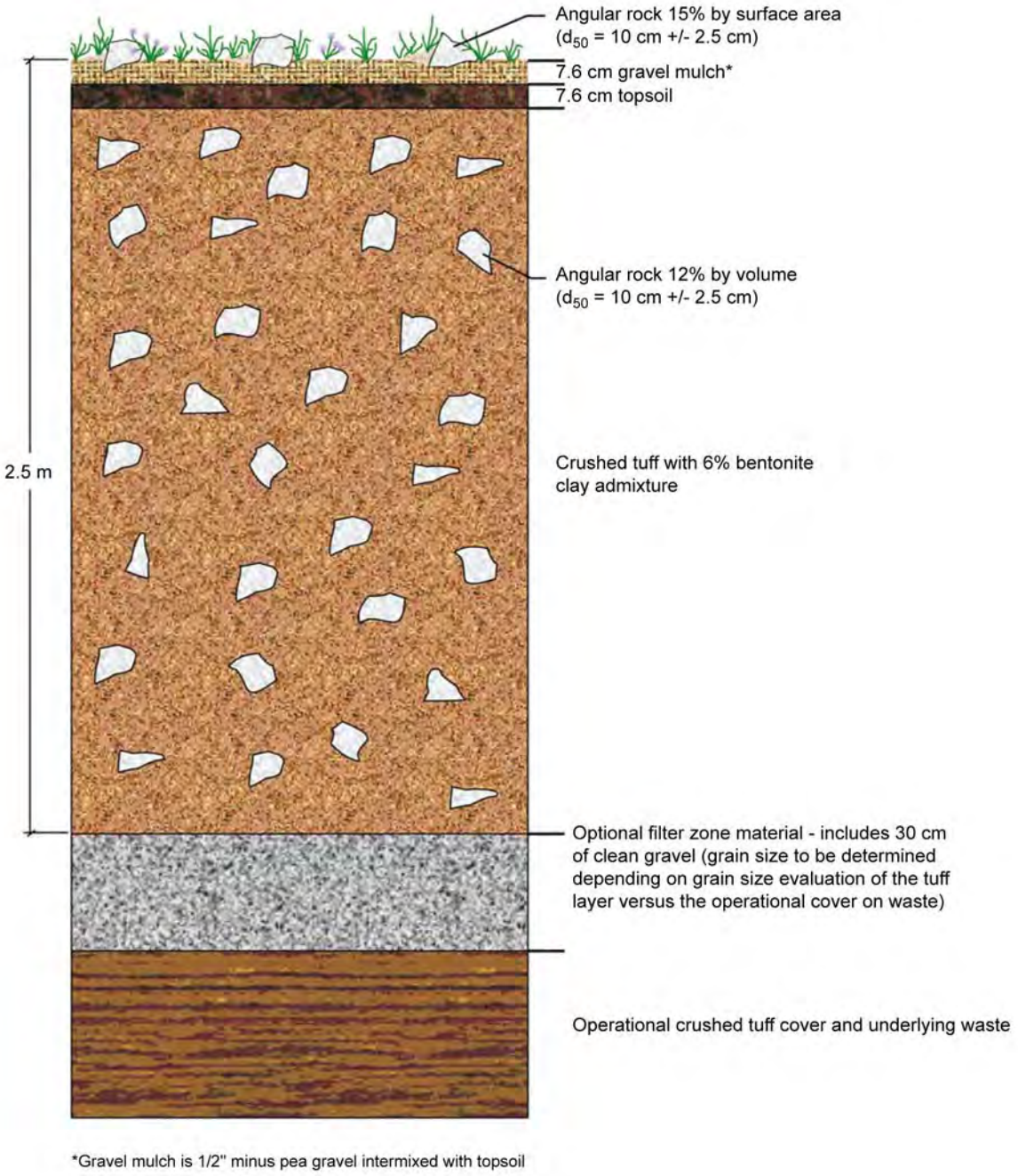

Figure 2-19
Cross Section of the Conceptual Cover for Area G

until it is either used for transpiration by plants or evaporated (Bonaparte et al., 2004; ITRC, 2003; Nyhan, 2005; and Scanlon et al., 2002). The 6 percent bentonite admixture included in the crushed tuff layer (Figure 2-19) will reduce the hydraulic conductivity of the cover, slowing the infiltration of water through the site. The topsoil layer applied at the surface will promote plant growth which will tend to maximize water loss through transpiration.

2.2.2 Disposal Unit Cover Integrity

The long-term integrity of the cover will depend, to a large extent, on its ability to withstand the effects of surface erosion. As discussed earlier, the final cover design was developed using an iterative approach in which successive cover designs underwent long-term erosion analyses using the SIBERIA computer code. This process is addressed in *Appendices H* and *I*. The final, optimized design is expected to meet performance criteria under a range of potential site and climate conditions that could occur over the 1,000-year compliance period.

2.2.3 Structural Stability

On a volume basis, most of the waste at Area G has been placed in the large, generally rectangular pits. Before the mid-1990s, the waste was typically placed in lifts; each layer of waste was covered with uncontaminated crushed tuff and compacted using heavy equipment. Exceptions occurred, primarily when there was a possibility that the waste might be retrieved at a later date. Most waste placed in pits was packaged in plastic bags and cardboard boxes.

The waste packaging requirements and disposal pit operations used prior to the mid-1990s are generally expected to confer structural stability to the pits. Layering waste and crushed tuff and compacting these layers with heavy equipment effectively filled void spaces within the waste and provided an even consolidated surface for the disposal of more waste. The result has been infrequent and minor cases of settlement; no significant subsidence has been observed at Area G.

Although the historical disposal procedures may be an efficient method of ensuring disposal unit stability, these procedures did not ensure efficient use of the available disposal capacity. Estimates developed for the 1997 performance assessment and composite analysis suggest more than 60 percent of the disposal pit capacity consisted of uncontaminated backfill. To more efficiently use the available pit disposal capacity, disposal procedures were modified in the mid-1990s; since that time all waste other than bulk soils and debris is required to be placed in metal containers prior to disposal. The containers used to date have included steel drums, B-25s, compactor boxes, and transportainers. These containers are stacked in the disposal units to maximize usage of the available disposal capacity. Bulk materials are placed directly in the disposal pits, and may be used to fill void spaces between and within waste containers.

The use of containers is expected to reduce the amount of uncontaminated fill needed to ensure waste stability. For example, the conceptual design for the pits in the Zone 4 expansion area is

based on the assumption that 50 percent of the material in the disposal units is waste, taking into account the volume occupied by ramps used to access the units and the sloped walls. The use of containers may, however, increase the potential for subsidence when incompletely filled containers corrode or otherwise fail. To minimize the potential for subsidence following container failure, the waste acceptance criteria for Area G specify the maximum amount of void space that is permissible inside containers of waste. Current requirements call for 95 percent or more of the container to be filled with waste.

The waste disposed of in shafts is generally placed in small metal cans or 0.11 to 0.32 m^3 (30 to 85 gal) drums, depending upon the nature of the waste. The packages are lowered into the disposal units and stacked on top of one another. Crushed tuff may be added as backfill around the waste packages, thereby reducing void spaces in the disposal units. In general, backfilling the disposal shafts is expected to adequately stabilize the waste. However, isolated instances of subsidence near these units have been observed during the 50-year history of the facility.

Significant subsidence of one or more disposal units at Area G may compromise the ability of the site to comply with the performance objectives cited in DOE M 435.1 (DOE, 2001c). If such subsidence were to occur, rates of infiltration through the affected units would likely rise, thus increasing the rates of contaminant release due to leaching and facilitating radionuclide transport to the regional aquifer. Localized failure of the final cover may also provide greater opportunities for plants and animals to penetrate into the waste; the additional contamination deposited on the surface of the site may result in increased exposures to persons living downwind of Area G and in the adjacent canyons. Under extreme conditions, the buried waste may be exposed, elevating rates of release even more.

The ability of the Area G disposal facility to safely isolate the waste is dependent on the absence of any significant subsidence. It is anticipated that measures will be taken prior to the end of the facility's operational period or during the 100-year active institutional control period that will minimize the risks posed by subsidence.

2.2.4 Inadvertent Intruder Barrier

A combination of administrative controls and design features is relied upon to prevent or limit the impacts of inadvertent human intrusion into the disposal facility. As stated earlier, DOE control over the disposal facility is assumed to prevent intrusion throughout the 100-year active institutional control period.

The primary design feature used to limit intruder exposures is the total depth of the cover; no other engineered or structural barriers are incorporated into the final closure configuration. The final cover design includes the placement of a minimum of 2.5 m (8.2 ft) of cover material across all disposal pits and shafts; in actuality, considerably more cover than this exists over the

majority of the site at the time of closure. Taking into account the effects of surface erosion, this design is expected to be capable of maintaining intruder exposures within the acceptable limits.

2.3 Waste Characteristics

The characteristics of the waste—its age, volume and activity, and composition—play an important role in the long-term performance of Area G. The nature of the waste disposed of at the facility and the radionuclide inventories in that waste are summarized in this section. Section 2.3.1 provides a general description of the types of waste that have been disposed of at the facility, including information about the physical and chemical characteristics of the material and the types of packaging that have been used in its disposal. Sections 2.3.2 and 2.3.3 summarize the inventory projections developed for the performance assessment and composite analysis. Sources of uncertainty associated with the inventory projections are discussed in Section 2.3.4.

2.3.1 Background Information

Waste disposed of at Area G includes operational or routine waste, nonroutine waste, and waste from ER and D&D activities at the Laboratory. Operational waste consists of a wide range of materials including compactable trash (e.g., paper, cardboard, and plastic), rubber, glass, disposable protective clothing, solidified powders and ash, animal tissue, and suspect radioactive waste. Nonroutine waste includes classified waste, uranium chips from LANL shops, and pieces of heavy equipment such as dump trucks (Rogers, 1977). Environmental restoration and D&D waste includes equipment and scrap metal, demolition debris, soil, concrete, asphalt, asbestos, and polychlorinated biphenyl (PCB)-contaminated materials. The Area G facility does not accept free liquids for disposal.

The nature of the waste disposed of at MDA G has changed over the facility's lifetime. Waste that, under current definitions, is considered to be TRU was disposed of at the facility through 1970. Since then, the vast majority of TRU waste generated at the Laboratory has been segregated and retrievably stored for permanent disposal at WIPP (the Waste Isolation Pilot Plant), although small amounts of TRU waste were disposed of at Area G between 1971 and 1979. Most of the TRU waste awaiting disposal at WIPP is stored at Area G under large domes that have been placed on asphalt pads. Some of the TRU waste is stored in below-grade retrievable arrays, including material placed in pits 9 and 29, trenches A–D, and shafts 200–232, 235–243, 246–253, 262–266, and 302–306.

Waste that, under current definitions, qualifies as mixed LLW was placed in Area G pits and shafts through 1985. Mixed TRU waste was routinely disposed of at Area G prior to 1971; smaller quantities of mixed TRU waste were disposed of between 1971 and 1979. Since 1986, when the EPA affirmed its authority over the regulation of the hazardous component of mixed LLW, the vast majority of mixed LLW has been segregated from LLW and sent off-site for treatment and/or

disposal. Small amounts of mixed LLW were inadvertently placed in a single pit and shaft between 1986 and 1990; no mixed waste has been disposed of at Area G since 1990. In addition to LLW, Area G is permitted to accept low-level Toxic Substances Control Act (TSCA) waste (i.e., asbestos and PCBs). Solid LLW is currently the only waste type disposed of at Area G.

As discussed in Section 2.2.3, a variety of waste packages have been used to dispose of waste at Area G. Waste was disposed of in the pits using cardboard boxes and plastic boxes before the mid-1990s. Since that time, all waste except bulk materials has been put in metal containers prior to placement in these units. Bulk soil and debris is placed around and within these containers. Metal containers have been used for almost all waste that has been disposed of in the shafts.

The radionuclides included in the radioactive waste disposed of at Area G have radioactive half-lives ranging from seconds to millions of years. Many of the short-lived isotopes will decay to negligible levels by the end of the 100-year active institutional control period. Exceptions to this will include radionuclides that are daughters of parents with much longer half-lives; these isotopes will effectively assume the half-lives of their parents.

The Area G inventory was simplified by eliminating short-lived radionuclides that will decay to negligible levels by the end of the 100-year active institutional control period. All radionuclides disposed of in the pits and shafts were reviewed in terms of their modes of decay; radionuclides with half-lives of 5 years or less were generally excluded from the inventory projections. The primary exception to this is radionuclides that are daughters of parents with half-lives greater than 5 years. Several radionuclides found in the Area G inventory have half-lives of 5 years or less but decay to form daughter products with much longer half-lives. These contaminants were excluded from the final inventory projections on the basis that the activities associated with the long-lived isotopes will be negligible. A screening evaluation was conducted to ensure that eliminating the long-lived daughters and their short-lived precursors would not compromise the doses projected for the performance assessment and composite analysis. A complete description of the methods used to eliminate radionuclides from the inventory on the basis of decay characteristics is provided in *Appendix J* (Volume 2).

2.3.2 Performance Assessment Inventory

Separate performance assessment inventories were developed for waste disposed of from September 27, 1988 through 2007 and material placed in the pits and shafts from 2008 through 2044. Estimates of the total volumes and activities of waste disposed of during each period and the radionuclide-specific inventories in the waste were prepared. The 1988–2007 radionuclide inventories were assigned to specific disposal pits and shafts.

Characterization of the waste disposed of through 2007 was based on disposal data maintained by the Laboratory in its LLW disposal database. The types and quantities of LLW disposed of at

Area G are recorded on shipment manifests and entered into this database on a per-package basis. Disposal records have been maintained in this manner since the early 1970s.

Inventory projections for the waste disposed of from 2008 through 2044 were based largely on an extrapolation process. It was generally assumed that the waste requiring disposal in the future would resemble that disposed of from 2000 through 2007, with the exception of several waste streams that were considered unlikely to reoccur; average annual volumes and activities and radionuclide concentrations in the material were calculated and used to determine rates of disposal over the remaining years of the facility's lifetime. Information collected through interviews with Laboratory personnel was used to estimate future inventories of high-activity tritium waste. Radionuclide concentrations in the ER and D&D waste that was disposed of at Area G from 2000 through 2007 were used in conjunction with ER and D&D waste volume projections to estimate future inventories associated with waste generated by cleanup efforts at the Laboratory.

The inventory projections for the performance assessment are summarized in Tables 2-11 and 2-12. Table 2-11 summarizes the total volumes and activities for waste disposed of from September 27, 1988 through 2044; separate totals are provided for the pits and shafts that were used from 1988 through 2007 and that are projected to receive waste from 2008 through 2044. Radionuclide-specific inventories of the disposal pits and shafts are provided in Table 2-12. The activities listed in these tables represent as-disposed activities; radionuclides that were eliminated from the inventory on the basis of half-life are not included. Additional details about the performance assessment inventory projections may be found in *Appendix J*.

Table 2-11
Volumes and Activities for Waste Included in the Area G Performance Assessment and Composite Analysis Inventories

	Disposal Pits		Disposal Shafts	
Analysis and Period of Disposal	Volume (m^3)	Activity (Ci)	Volume (m^3)	Activity (Ci)
Performance Assessment				
September 27, 1988–2007	8.9E+04	3.5E+03	5.2E+02	1.7E+06
2008–2044	1.6E+05	3.9E+02	1.0E+03	9.8E+05
Total	2.5E+05	3.9E+03	1.6E+03	2.7E+06
Composite Analysis				
Pre-1971	4.9E+04	1.8E+04	4.8E+01	6.4E+04
1971–September 26, 1988	9.9E+04	4.3E+04	9.2E+02	8.2E+05
September 27, 1988–2007	8.9E+04	3.5E+03	5.2E+02	1.7E+06
2008–2044	1.6E+05	3.9E+02	1.0E+03	9.8E+05
Total	4.0E+05	6.5E+04	2.5E+03	3.6E+06

Table 2-12
Radionuclide, Activation Product, Fission Product, and Material Type Inventories for Waste Included in the Performance Assessment

Constituent	Activity (Ci)					
	Disposal Pits			Disposal Shafts		
	September 26, 1988–2007 Waste	2008–2044 Waste	Total	September 26, 1988–2007 Waste	2008–2044 Waste	Total
Ac-227	1.8E-05	6.6E-05	8.4E-05	5.3E-07	---	5.3E-07
Ag-108m	1.7E-04	5.8E-05	2.3E-04	4.4E+00	4.2E-08	4.4E+00
Al-26	2.6E-04	1.2E-06	2.6E-04	---	---	---
Am-241	8.1E+00	1.5E+01	2.3E+01	3.2E-01	1.2E-03	3.2E-01
Am-243	8.6E-03	3.8E-02	4.7E-02	1.0E-09	---	1.0E-09
Ba-133	6.9E-01	3.2E+00	3.9E+00	2.8E-03	---	3.7E-03
Be-10	4.6E-03	---	4.6E-03	---	---	---
Bi-207	1.5E-02	7.0E-02	8.6E-02	6.0E-05	7.3E-06	6.8E-05
Bk-247	2.8E-07	---	2.8E-07	---	---	---
C-14	3.3E+00	1.2E-02	3.3E+00	1.6E+01	3.5E-01	1.6E+01
Ca-41	2.7E-01	---	2.7E-01	---	---	---
Cf-249	1.0E-04	4.7E-04	5.7E-04	---	---	---
Cf-252	2.0E-05	---	2.0E-05	9.6E-06	3.6E-05	4.5E-05
Cl-36	1.8E-02	---	1.8E-02	2.5E-04	---	2.5E-04
Cm-243	4.2E-05	5.1E-05	9.2E-05	---	---	---
Cm-244	2.8E-03	1.3E-02	1.6E-02	2.2E-03	9.3E-03	1.1E-02

-- = None

Table 2-12 (Continued)
Radionuclide, Activation Product, Fission Product, and Material Type Inventories for Waste Included in the Performance Assessment

Constituent	Activity (Ci)					
	Disposal Pits			Disposal Shafts		
	September 26, 1988–2007 Waste	2008–2044 Waste	Total	September 26, 1988–2007 Waste	2008–2044 Waste	Total
Cm-245	4.6E-05	2.1E-04	2.6E-04	---	---	---
Cm-248	4.5E-07	2.1E-06	2.5E-06	---	---	---
Co-60	4.5E+01	7.5E+01	1.2E+02	3.1E+03	3.8E+01	3.1E+03
Cs-135	1.3E-04	7.5E-06	1.4E-04	4.5E-06	---	4.5E-06
Cs-137	5.8E+00	4.8E+00	1.1E+01	8.3E+01	1.9E+00	8.5E+01
D38	4.0E+00	4.3E+00	8.3E+00	2.4E+00	7.0E+00	9.4E+00
Eu-152	4.4E-01	2.0E-01	6.4E-01	1.1E-02	3.0E-03	1.4E-02
Eu-154	5.2E-02	3.1E-03	5.5E-02	9.8E-02	---	9.8E-02
Gd-148	1.0E-05	---	1.0E-05	7.7E-09	---	7.7E-09
H-3	3.1E+03	1.9E+01	3.2E+03	1.7E+06	9.7E+05	2.7E+06
Ho-163	9.1E-01	---	9.1E-01	7.0E-02	---	7.0E-02
Ho-166m	1.4E-03	6.6E-03	8.0E-03	---	---	---
I-129	3.1E-05	1.4E-04	1.7E-04	3.0E-08	---	3.0E-08
K-40	2.7E-01	8.5E-01	1.1E+00	4.3E-07	2.0E-06	2.4E-06
Kr-85	4.6E-02	4.6E-04	4.7E-02	8.9E-03	3.7E-02	4.6E-02
Lu-176	1.7E-06	---	1.7E-06	---	---	---
MAP	1.3E+01	---	1.3E+01	5.6E+03	---	5.6E+03

-- = None

Table 2-12 (Continued)
Radionuclide, Activation Product, Fission Product, and Material Type Inventories for Waste Included in the Performance Assessment

Constituent	Activity (Ci)					
	Disposal Pits			Disposal Shafts		
	September 26, 1988–2007 Waste	2008–2044 Waste	Total	September 26, 1988–2007 Waste	2008–2044 Waste	Total
MFP	1.8E+01	---	1.8E+01	6.0E+01	---	6.0E+01
Mo-93	2.0E-05	9.3E-05	1.1E-04	1.3E-02	---	6.8E-02
Nb-91	1.2E-05	5.3E-05	6.5E-05	9.4E-03	4.3E-02	5.3E-02
Nb-92	3.0E-06	1.4E-05	1.7E-05	4.0E-03	---	4.0E-03
Nb-93m	1.0E-03	4.8E-03	5.8E-03	2.2E+00	1.0E+01	1.3E+01
Nb-94	4.0E-02	6.9E-02	1.1E-01	1.3E-04	---	1.3E-04
Nd-144	1.0E-08	4.6E-08	5.6E-08	---	---	---
Ni-59	6.3E-03	3.3E-05	6.3E-03	2.6E+00	---	1.4E+01
Ni-63	2.0E+00	9.5E-01	2.9E+00	1.2E+03	4.6E+01	1.2E+03
Np-237	4.9E-03	2.0E-02	2.4E-02	3.1E-08	1.4E-07	1.7E-07
Os-194	1.3E-07	6.0E-07	7.3E-07	---	---	---
Pa-231	4.2E-05	1.1E-04	1.5E-04	2.7E-03	2.3E-07	2.7E-03
Pb-210	2.7E-01	8.5E-02	3.5E-01	2.9E-08	1.2E-07	1.5E-07
Pm-145	1.1E-01	4.6E-08	1.1E-01	---	---	---
Pu-236	1.0E-09	4.6E-09	5.6E-09	---	---	---
Pu-238	1.4E+01	2.2E+01	3.6E+01	2.6E-01	3.5E-02	3.0E-01
Pu-239	1.6E+01	1.8E+01	3.4E+01	7.6E-02	3.2E-02	1.1E-01

-- = None

Table 2-12 (Continued)
Radionuclide, Activation Product, Fission Product, and Material Type Inventories for Waste Included in the Performance Assessment

Constituent	Activity (Ci)					
	Disposal Pits			Disposal Shafts		
	September 26, 1988–2007 Waste	2008–2044 Waste	Total	September 26, 1988–2007 Waste	2008–2044 Waste	Total
Pu-240	5.3E-01	1.3E+00	1.8E+00	1.2E-03	---	1.2E-03
Pu-241	2.8E+00	4.9E+00	7.6E+00	3.7E-02	---	3.7E-02
Pu-242	6.3E-03	2.6E-02	3.2E-02	2.0E-06	---	2.0E-06
Pu-244	3.5E-06	1.6E-05	2.0E-05	---	---	---
PU52	5.1E+00	---	5.1E+00	5.7E-02	---	5.7E-02
Ra-226	1.2E-01	3.2E-01	4.4E-01	7.8E-01	8.4E-05	7.8E-01
Ra-228	3.4E-02	1.1E-01	1.5E-01	---	---	---
Si-32	2.7E-05	7.7E-05	1.0E-04	---	---	---
Sm-151	3.4E-09	1.4E-08	1.8E-08	---	---	---
Sn-126	2.7E-06	---	2.7E-06	2.4E-02	---	2.4E-02
Sr-90	2.8E+00	9.8E+00	1.3E+01	8.7E+01	1.8E+00	8.8E+01
Tb-157	4.5E-08	2.1E-07	2.5E-07	---	---	---
Tc-97	2.1E-06	9.2E-08	2.2E-06	---	---	---
Tc-99	3.2E-01	2.8E-01	6.0E-01	1.2E-05	---	1.2E-05
Th-228	2.2E-03	3.0E-03	5.2E-03	6.9E-04	3.2E-03	3.9E-03
Th-229	3.8E-04	1.4E-03	1.8E-03	5.4E-08	---	5.4E-08
Th-230	1.2E-03	4.2E-04	1.6E-03	1.6E-08	---	1.6E-08

-- = None

Table 2-12 (Continued)
Radionuclide, Activation Product, Fission Product, and Material Type Inventories for Waste Included in the Performance Assessment

Constituent	Activity (Ci)					
	Disposal Pits			Disposal Shafts		
	September 26, 1988–2007 Waste	2008–2044 Waste	Total	September 26, 1988–2007 Waste	2008–2044 Waste	Total
Th-232	3.2E-01	8.1E-03	3.3E-01	1.9E-01	6.0E-02	2.5E-01
TH88	3.7E-02	---	3.7E-02	---	---	---
Ti-44	2.6E-03	1.2E-02	1.5E-02	2.0E-02	9.0E-02	1.1E-01
U(DEP)	5.3E+00	2.4E+01	3.0E+01	4.4E-05	2.0E-04	2.5E-04
U(NAT)	6.4E-05	2.9E-04	3.6E-04	1.8E-01	8.3E-01	1.0E+00
U11	8.7E-06	---	8.7E-06	---	---	---
U-232	8.8E-04	1.7E-04	1.1E-03	2.0E-04	---	2.0E-04
U-233	7.3E-02	2.4E-01	3.1E-01	5.8E-04	---	5.8E-04
U-234	1.1E+00	1.6E+00	2.6E+00	5.0E-01	2.3E+00	2.8E+00
U-235	8.7E-01	1.0E-01	9.7E-01	2.8E-02	1.3E-01	1.5E-01
U-236	3.7E-03	1.1E-02	1.5E-02	3.8E-06	1.8E-05	2.1E-05
U-238	1.2E+01	2.6E+00	1.4E+01	4.5E-01	1.1E+00	1.6E+00
U38	5.0E-02	---	5.0E-02	---	---	---
U39	3.1E-03	---	3.1E-03	---	---	---
U81	5.7E-04	---	5.7E-04	---	---	---
Zr-93	2.0E-08	---	2.0E-08	---	---	---

-- = None

2.3.3 Composite Analysis Inventory

The composite analysis inventory includes all waste disposed of at Area G from the start of disposal operations through 2044. Separate inventories were developed for waste disposed of from the start of operations through 1970, from 1971 through September 26, 1988, from September 27, 1988 through 2007, and from 2008 through 2044. Estimates of the total volumes and activities of waste disposed of during each period and the radionuclide-specific inventories in the waste were prepared. Separate inventories were generated for the disposal pits and shafts.

The pre-1971 pit inventories were estimated using an extrapolation process that accounted for unique disposals that occurred during this period or the period from which data were drawn to estimate the characteristics of the waste. In general, waste data from 1971 through 1977 were used to estimate annual disposal volumes and radionuclide concentrations; these results were used to develop estimates of the rates of disposal from 1959 (the time at which the disposal of routine waste began at Area G) through 1970. The dataset used in the extrapolation process was evaluated to identify disposals during this period that would not have occurred prior to 1971; the data representing these wastes were removed prior to estimating the pre-1971 pit inventory.

The data used to estimate the pre-1971 pit inventories include information for the LLW disposed of from 1971 through 1977 as well as TRU waste placed in storage or irretrievably disposed of during this period. Waste that, under current definitions, is considered to be TRU was disposed of at the facility through 1970. Since then, the vast majority of TRU waste generated at the Laboratory has been segregated and retrievably stored for permanent disposal at WIPP. As mentioned earlier, small amounts of TRU waste were disposed of at Area G between 1971 and 1979.

Typically, the extrapolation process used to estimate the pre-1971 pit inventories does not capture nonroutine or unique disposals that occurred between the start of disposal operations and 1970. Although it is practically impossible to identify all unique disposal events that took place at Area G before 1971, Warren (1980) identified several nonroutine events that involved large quantities of specific radionuclides. On the basis of this information, waste was added to the totals estimated through extrapolation.

Inventory projections for the waste disposed of in shafts prior to 1971 and for all waste placed in pits and shafts from 1971 through September 26, 1988 were developed using disposal data. Pre-1971 disposal data summarized by Rogers (1977) were used to characterize the shaft waste that was disposed of from 1966, when shaft disposal at Area G began, through 1970. Data taken from the LLW disposal and TRU waste databases were used to directly estimate the inventories for pit and shaft waste disposed of from 1971 through September 26, 1988. The TRU waste included in these projections includes the small amount of waste that was irretrievably disposed of between 1971 and 1979. Transuranic waste that is currently being stored underground in several pits,

trenches, and shafts was not included in the inventory projections because this material is expected to be retrieved and shipped to WIPP.

The inventories for the waste disposed of at Area G from September 27, 1988 through 2044 are the same as those developed for the performance assessment. The methods used to characterize this waste have been summarized above.

The inventory projections for the composite analysis are summarized in Tables 2-11, 2-13, and 2-14. The total volumes and activities of waste projected to be disposed of from the start of disposal operations through 2044 are included in Table 2-11 for the pits and shafts. Radionuclide-specific inventories in the disposal pits and shafts are provided in Tables 2-13 and 2-14, respectively. The listed activities represent as-disposed activities; radionuclides that were eliminated from the inventory on the basis of half-life are not included. Additional details about the composite analysis inventory projections may be found in *Appendix J*.

2.3.4 Uncertainty

The inventories developed for the performance assessment and composite analysis are estimates of the quantities of the radioactive materials that were, or will be, disposed of in the pits and shafts at Area G. These projections are subject to uncertainty introduced by the assumptions made in developing the inventories and the data upon which the estimates are based. Potentially important sources of uncertainty associated with the inventory projections are discussed below. Additional details can be found in *Appendix J*.

The primary sources of uncertainty associated with the Area G inventory projections depend, in part, upon the segment of the inventory under consideration. Perhaps the most basic source of uncertainty, and one that applies to all of the waste disposed of at Area G, is the measurement or estimation of radionuclide activities in the waste. The accuracy of the activity measurements and estimation techniques used to characterize Area G waste is influenced by the radionuclides under consideration and the time at which disposal occurred. Specific radionuclides may affect characterization efforts in two distinct ways. First, the radiation types and energies emitted by the isotopes may make measurement more or less difficult. For example, high-energy gamma emissions from a radionuclide, such as Co-60, are generally more readily detected than low-energy beta emissions from tritium. Second, accountability requirements for some radionuclides are such that greater effort has been invested in measuring or estimating activities associated with a portion of the waste packages.

Timing of waste disposal is also an important factor affecting the accuracy of the activity estimates. Area G has been in operation for over 50 years, during which time changes in technology and focus have significantly impacted the accuracy of the inventory estimates. In general, detection equipment has improved over the years, as have efforts to more accurately characterize the material placed in the disposal facility.

Table 2-13
Radionuclide, Activation Product, Fission Product, and Material Type Inventories for Waste Included in the Composite Analysis, Disposal Pits

Constituent	Activity (Ci)				
	Pre-1971 Waste	1971–September 26, 1988 Waste	September 26, 1988–2007 Waste	2008–2044 Waste	Total
Ac-227	8.6E-01	7.0E-02	1.8E-05	6.6E-05	9.3E-01
Ag-108m	---	---	1.7E-04	5.8E-05	2.3E-04
Al-26	---	---	2.6E-04	1.2E-06	2.6E-04
Am-241	2.4E+03	2.4E+01	8.1E+00	1.5E+01	2.4E+03
Am-243	---	---	8.6E-03	3.8E-02	4.7E-02
Ba-133	---	---	6.9E-01	3.2E+00	3.9E+00
Be-10	---	---	4.6E-03	---	4.6E-03
Bi-207	---	---	1.5E-02	7.0E-02	8.6E-02
Bk-247	---	---	2.8E-07	---	2.8E-07
C-14	---	2.3E-01	3.3E+00	1.2E-02	3.6E+00
Ca-41	---	---	2.7E-01	---	2.7E-01
Cf-249	2.4E-03	4.1E-04	1.0E-04	4.7E-04	3.4E-03
Cf-251	2.7E-03	1.6E-03	---	---	4.3E-03
Cf-252	1.5E-02	8.6E-03	2.0E-05	---	2.3E-02
Cl-36	---	---	1.8E-02	---	1.8E-02
Cm242	1.8E-03	---	---	---	1.8E-03
Cm-243	---	---	4.2E-05	5.1E-05	9.2E-05
Cm-244	1.7E-03	---	2.8E-03	1.3E-02	1.7E-02
Cm-245	---	---	4.6E-05	2.1E-04	2.6E-04
Cm-248	---	---	4.5E-07	2.1E-06	2.5E-06
Co-60	---	1.3E+03	4.5E+01	7.5E+01	1.4E+03
Cs-135	---	---	1.3E-04	7.5E-06	1.4E-04
Cs-137	2.6E-01	1.1E+03	5.8E+00	4.8E+00	1.1E+03
D38	---	---	4.0E+00	4.3E+00	8.3E+00
Eu-152	---	---	4.4E-01	2.0E-01	6.4E-01
Eu-154	---	---	5.2E-02	3.1E-03	5.5E-02
Gd-148	---	---	1.0E-05	---	1.0E-05
H-3	2.7E+00	7.5E+03	3.1E+03	1.9E+01	1.1E+04

--- = None

Table 2-13 (Continued)
Radionuclide, Activation Product, Fission Product, and Material Type Inventories for Waste Included in the in the Composite Analysis, Disposal Pits

Constituent	Activity (Ci)				
	Pre-1971 Waste	1971–September 26, 1988 Waste	September 26, 1988–2007 Waste	2008–2044 Waste	Total
Ho-163	---	---	9.1E-01	---	9.1E-01
Ho-166m	---	---	1.4E-03	6.6E-03	8.0E-03
I-129	---	---	3.1E-05	1.4E-04	1.7E-04
K-40	---	---	2.7E-01	8.5E-01	1.1E+00
Kr-85	1.7E-03	1.0E-03	4.6E-02	4.6E-04	4.9E-02
Lu-176	---	---	1.7E-06	---	1.7E-06
MAP	3.6E-01	1.2E+03	1.3E+01	---	1.2E+03
MFP	1.0E+03	6.5E+02	1.8E+01	---	1.7E+03
Mo-93	---	---	2.0E-05	9.3E-05	1.1E-04
Nb-91	---	---	1.2E-05	5.3E-05	6.5E-05
Nb-92	---	---	3.0E-06	1.4E-05	1.7E-05
Nb-93m	---	---	1.0E-03	4.8E-03	5.8E-03
Nb-94	---	8.0E-06	4.0E-02	6.9E-02	1.1E-01
Nd-144	---	---	1.0E-08	4.6E-08	5.6E-08
Ni-59	---	---	6.3E-03	3.3E-05	6.3E-03
Ni-63	---	---	2.0E+00	9.5E-01	2.9E+00
Np-237	4.0E-03	7.0E-07	4.9E-03	2.0E-02	2.8E-02
Os-194	---	---	1.3E-07	6.0E-07	7.3E-07
Pa-231	---	---	4.2E-05	1.1E-04	1.5E-04
Pb-210	---	---	2.7E-01	8.5E-02	3.5E-01
Pm-145	---	---	1.1E-01	4.6E-08	1.1E-01
Pu-236	---	---	1.0E-09	4.6E-09	5.6E-09
Pu-238	3.8E+03	4.9E+02	1.4E+01	2.2E+01	4.3E+03
Pu-239	1.7E+02	2.3E+01	1.6E+01	1.8E+01	2.2E+02
Pu-240	4.0E+00	2.8E-05	5.3E-01	1.3E+00	5.8E+00
Pu-241	---	5.8E-06	2.8E+00	4.9E+00	7.6E+00
Pu-242	---	7.8E-06	6.3E-03	2.6E-02	3.2E-02
Pu-244	---	---	3.5E-06	1.6E-05	2.0E-05
PU51	1.6E+00	---	---	---	1.6E+00
PU52	7.7E+03	2.3E+00	5.1E+00	---	7.7E+03

--- = None

Table 2-13 (Continued)
Radionuclide, Activation Product, Fission Product, and Material Type Inventories for Waste Included in the in the Composite Analysis, Disposal Pits

Constituent	Activity (Ci)				
	Pre-1971 Waste	1971–September 26, 1988 Waste	September 26, 1988–2007 Waste	2008–2044 Waste	Total
PU53	2.5E+02	3.7E-04	---	---	2.5E+02
PU54	1.1E+03	1.5E-01	---	---	1.1E+03
PU55	6.8E+01	---	---	---	6.8E+01
PU56	1.2E+03	---	---	---	1.2E+03
PU57	7.1E+01	---	---	---	7.1E+01
PU83	5.0E+02	1.5E-02	---	---	5.0E+02
Ra-226	---	2.0E-01	1.2E-01	3.2E-01	6.4E-01
Ra-228	---	2.1E-01	3.4E-02	1.1E-01	3.6E-01
Si-32	---	---	2.7E-05	7.7E-05	1.0E-04
Sm-151	---	---	3.4E-09	1.4E-08	1.8E-08
Sn-126	---	---	2.7E-06	---	1.5E-05
Sr-90	2.9E-01	1.4E+03	2.8E+00	9.8E+00	1.4E+03
Tb-157	---	---	4.5E-08	2.1E-07	2.5E-07
Tc-97	---	---	2.1E-06	9.2E-08	2.2E-06
Tc-99	---	---	3.2E-01	2.8E-01	6.0E-01
Th-228	---	---	2.2E-03	3.0E-03	5.2E-03
Th-229	---	---	3.8E-04	1.4E-03	1.8E-03
Th-230	1.6E+01	9.5E+00	1.2E-03	4.2E-04	2.6E+01
Th-232	---	1.4E-03	3.2E-01	8.1E-03	3.3E-01
TH88	1.9E-03	2.7E-02	3.7E-02		6.6E-02
Ti-44	---	---	2.6E-03	1.2E-02	1.5E-02
U(DEP)	---	---	5.3E+00	2.4E+01	3.0E+01
U(NAT)	---	---	6.4E-05	2.9E-04	3.6E-04
U10	8.8E-01	5.1E-01	---	---	1.4E+00
U11	---	1.5E-01	8.7E-06	---	1.5E-01
U12	7.9E+00	5.8E+00	---	---	1.4E+01
U-232	---	---	8.8E-04	1.7E-04	1.1E-03
U-233	6.1E+00	1.9E-02	7.3E-02	2.4E-01	6.4E+00
U-234	---	---	1.1E+00	1.6E+00	2.6E+00
U-235	3.7E-01	7.1E-01	8.7E-01	1.0E-01	2.1E+00

--- = None

Table 2-13 (Continued)
Radionuclide, Activation Product, Fission Product, and Material Type Inventories for Waste Included in the in the Composite Analysis, Disposal Pits

Constituent	Activity (Ci)				
	Pre-1971 Waste	1971–September 26, 1988 Waste	September 26, 1988–2007 Waste	2008–2044 Waste	Total
U-236	---	6.3E-08	3.7E-03	1.1E-02	1.5E-02
U-238	4.3E+00	1.1E+01	1.2E+01	2.6E+00	2.9E+01
U35	---	4.9E-04	---	---	4.9E-04
U36	---	2.2E-05	---	---	2.2E-05
U38	2.3E-02	4.5E-02	5.0E-02	---	1.2E-01
U39	---	---	3.1E-03	---	3.1E-03
U81	4.7E-03	2.8E-03	5.7E-04	---	8.1E-03
Zr-93	---	---	2.0E-08	---	2.0E-08

--- = None

Table 2-2-14
Radionuclide, Activation Product, Fission Product, and Material Type Inventories for Waste Included in the Composite Analysis, Disposal Shafts

Constituent	Activity (Ci)				
	Pre-1971 Waste	1971-September 26, 1988 Waste	September 26, 1988-2007 Waste	2008-2044 Waste	Total
Ac-227	---	---	5.3E-07	---	5.3E-07
Ag-108m	---	---	4.4E+00	4.2E-08	4.4E+00
Am-241	---	4.0E-02	3.2E-01	1.2E-03	3.6E-01
Am-243	2.0E-02	1.1E-05	1.0E-09	---	2.0E-02
Ba-133	---	---	2.8E-03	---	2.8E-03
Bi-207	---	---	6.0E-05	7.3E-06	6.8E-05
C-14	---	1.1E+00	1.6E+01	3.5E-01	1.7E+01
Cf-252	4.0E+00	5.5E+01	9.6E-06	3.6E-05	5.9E+01
Cl-36	---	---	2.5E-04	---	2.5E-04
Cm-244	2.3E-04	1.9E-01	2.2E-03	9.3E-03	2.0E-01
Co-60	1.8E+01	2.8E+03	3.1E+03	3.8E+01	5.9E+03
Cs-135	---	---	4.5E-06	---	4.5E-06
Cs-137	6.3E-01	4.2E+01	8.3E+01	1.9E+00	1.3E+02
D38	6.2E-05	---	2.4E+00	7.0E+00	9.4E+00
Eu-152	1.2E-01	---	1.1E-02	3.0E-03	1.4E-01
Eu-154	---	---	9.8E-02	---	9.8E-02
Gd-148	---	---	7.7E-09	---	7.7E-09
H-3	6.1E+04	8.0E+05	1.7E+06	9.7E+05	3.5E+06
Ho-163	---	---	7.0E-02	---	7.0E-02
I-129	---	---	3.0E-08	---	3.0E-08
K-40	---	---	4.3E-07	2.0E-06	2.4E-06
Kr-85	---	4.5E-04	8.9E-03	3.7E-02	4.6E-02
MAP	8.0E+01	1.4E+04	5.6E+03	---	1.9E+04
MFP	2.7E+03	7.4E+03	6.0E+01	---	1.0E+04
Mo-93	---	---	1.3E-02	---	1.3E-02
Nb-91	---	---	9.4E-03	4.3E-02	5.3E-02
Nb-92	---	---	4.0E-03	---	4.0E-03
Nb-93m	---	---	2.2E+00	1.0E+01	1.3E+01

--- = None

Table 2-14 (Continued)
Radionuclide, Activation Product, Fission Product, and Material Type Inventories for Waste Included in the Composite Analysis, Disposal Shafts

Constituent	Activity (Ci)				
	Pre-1971 Waste	1971-September 26, 1988 Waste	September 26, 1988-2007 Waste	2008-2044 Waste	Total
Nb-94	---	---	1.3E-04	---	1.3E-04
Ni-59	---	---	2.6E+00	---	2.6E+00
Ni-63	---	4.3E-03	1.2E+03	4.6E+01	1.2E+03
Np-237	1.4E-04	7.8E-05	3.1E-08	1.4E-07	2.2E-04
Pa-231	---	---	2.7E-03	2.3E-07	2.7E-03
Pb-210	---	---	2.9E-08	1.2E-07	1.5E-07
Pu-238	5.6E+00	9.7E-01	2.6E-01	3.5E-02	6.9E+00
Pu-239	2.1E+01	8.3E+01	7.6E-02	3.2E-02	1.0E+02
Pu-240	3.4E-02	---	1.2E-03	---	3.6E-02
Pu-241	5.4E-03	7.3E-01	3.7E-02	---	7.7E-01
Pu-242	1.2E-04	3.1E-07	2.0E-06	---	1.2E-04
PU52	---	7.5E+01	5.7E-02	---	7.6E+01
PU54	---	2.0E-08	---	---	2.0E-08
Ra-226	1.0E-01	2.5E+00	7.8E-01	8.4E-05	3.4E+00
Sn-126	---	---	2.4E-02	---	2.4E-02
Sr-90	1.1E+00	9.5E-02	8.7E+01	1.8E+00	9.0E+01
Tc-99	---	---	1.2E-05	---	1.2E-05
Th-228	---	---	6.9E-04	3.2E-03	3.9E-03
Th-229	---	---	5.4E-08	---	5.4E-08
Th-230	5.7E-04	---	1.6E-08	---	5.7E-04
Th-232	1.7E-05	1.5E-02	1.9E-01	6.0E-02	2.7E-01
Th-88	---	4.0E-03	---	---	4.0E-03
Ti-44	---	---	2.0E-02	9.0E-02	1.1E-01
U(DEP)	---	---	4.4E-05	2.0E-04	2.5E-04
U(NAT)	---	---	1.8E-01	8.3E-01	1.0E+00
U10	---	3.0E-03	---	---	3.0E-03
U12	---	1.7E+00	---	---	1.7E+00
U-232	---	2.1E-01	2.0E-04	---	2.1E-01

--- = None

Table 2-14 (Continued)
Radionuclide, Activation Product, Fission Product, and Material Type Inventories for Waste Included in the Composite Analysis, Disposal Shafts

Constituent	Activity (Ci)				
	Pre-1971 Waste	1971-September 26, 1988 Waste	September 26, 1988-2007 Waste	2008-2044 Waste	Total
U-233	1.5E+00	4.0E+00	5.8E-04	---	5.5E+00
U-234	7.8E-06	4.9E-06	5.0E-01	2.3E+00	2.8E+00
U-235	1.3E-02	9.8E-01	2.8E-02	1.3E-01	1.1E+00
U-236	1.2E-07	2.5E-05	3.8E-06	1.8E-05	4.7E-05
U-238	1.3E-06	9.5E+00	4.5E-01	1.1E+00	1.1E+01
U38	---	3.9E-02	---	---	3.9E-02
U81	---	2.3E-02	---	---	2.3E-02

--- = None

The measurement errors associated with the activities listed in the LLW and TRU waste databases cannot be determined with a high degree of accuracy, but some generalities can be drawn about this source of uncertainty (Myers, 2004). The greatest uncertainties are expected to be associated with the measurement of the activities of pure beta emitters. The low energy and penetrating power of beta radiation are such that detailed separation techniques must be performed before accurate assessments of the waste activity can be conducted. Characterization efforts at the Laboratory rarely, if ever, include these analyses for this class of waste. As a result, the activities associated with these radionuclides are expected to be accurate only to within one order of magnitude.

In theory, the higher energy emissions associated with many gamma emitters should make accurate characterization an easier task. Nevertheless, gamma waste disposed of prior to the 1990s is expected to have a level of accuracy similar to that discussed for the beta emitters. The magnitude of the errors associated with the gamma emitters decreased during the 1990s to the extent that errors are currently on the order of $\pm$25 percent to $\pm$100 percent, depending upon the size and composition of the waste package.

Greater effort has generally been expended on the characterization of waste contaminated with uranium and transuranics because of accountability issues. However, the concentrations of americium, plutonium, and uranium in the waste have a significant impact on the accuracy of the measured activities. Activities of these radionuclides have probably been overestimated in LLW because concentrations in this waste are low and the measurement techniques formerly used did not have very low detection limits. Drums and boxes with detectable quantities of plutonium (i.e., approximately 0.50 g [0.001 lb] or more per package) are likely to have errors of around 20 to 30 percent for measurements conducted in the 1970s and 1980s; errors of about 10 to 20 percent are typical for more recent measurements. Errors may also result even if the measurement error is small, as in the case of misapplying scaling factors to estimate isotopic distributions in waste.

The ability to accurately measure the quantities of uranium isotopes depends, in part, on the isotopic quantities in the waste package. For example, U-235 has gone undetected during the assay of drums of TRU waste that contain a few grams or less of the isotope; errors of this sort may occur in a small proportion of the drums. Generators are usually aware of drums that contain greater quantities of U-235 (e.g., 10 g [0.022 lb] or more) and measure the packages directly to determine the waste activity. Waste containing depleted uranium is usually measured with errors of $\pm$25 percent to $\pm$100 percent, depending upon the size and composition of the package.

Although tritium is a pure beta emitter, it is considered separately from the other beta emitters because of its generation pattern at the Laboratory. Low-activity tritium waste is expected to have uncertainties associated with its characterization similar to those discussed for the pure beta

emitters. However, high-activity tritium waste receives greater scrutiny. Measurement errors associated with high-activity tritium waste disposed of prior to the 1990s are expected to be around ±100 percent. Improvements since that time have reduced these errors to values that are expected to be about ±25 percent.

An extrapolation process was used to estimate the quantities of waste disposed of in pits prior to 1971 and in pits and shafts from 2008 through 2044. The pre-1971 pit inventory was estimated, in part, on the basis of waste disposed of from 1971 through 1977; the 2008–2044 pit and shaft inventories were based on the characteristics of the material disposed of from 2000 through 2007. In each case, it was implicitly assumed that the waste disposed of during the extrapolation period was similar to that emplaced during the period of interest.

It is unlikely that the nature of the waste that was disposed of in pits during the early to mid-1970s extrapolation period was exactly the same as material emplaced from 1959 through 1970. Some insight into the error introduced by using the extrapolation approach as a means for estimating the inventory for this waste is provided by the results of the pre-1971 disposal record review (Pollard and Shuman, 1999). The analysis indicated that the americium and plutonium activities estimated for the concrete and sludge disposed of in pits prior to 1971 agreed with available historical disposal data. The majority of this waste, however, was included in the inventory estimates on the basis of information about unique disposals during the period. The Pu-238 sludge inventory included in the pre-1971 waste was based on the extrapolation process and generally agrees with the inventory estimated using the historical sludge disposal data.

Radionuclide inventories estimated for the pre-1971 nonsludge waste streams on the basis of the extrapolation approach do not compare favorably with estimates developed using historical data records. For all radionuclides examined, the total activity estimates developed for the 1997 composite analysis readily exceed the activities indicated by the disposal data. It is unclear if this finding signifies that the extrapolation process is inappropriate or if the historical data are incomplete in terms of this waste.

Dissimilarities between the future waste (to be emplaced from 2008 through 2044) and the 2000–2007 extrapolation data used to estimate future pit and shaft inventories may also be expected. Changes in LANL operations may result in shifts in the relative proportions of the operational and ER and D&D waste disposed of at Area G. Given that the radiological characteristics of the two types of waste differ, any such shifts will affect the estimated inventories. Considerable quantities of ER and D&D waste have been generated in recent years and similar quantities are expected over the next few years. The precise nature of how cleanup activities and operations change over time will determine the accuracy of the extrapolated future inventories.

Many of the waste packages disposed of at Area G contain activation- and fission-product waste; in many instances the radionuclides in these packages were simply listed in terms of total activities of MAP and MFP. These activities were allocated to specific radionuclides using the methods described in *Appendix J*. Several sources of uncertainty are associated with the allocation of the MFP activities to specific radionuclides:

- Nature of the fission reactions that generate the fission products
- Age of the MFP waste
- Impacts of daughter ingrowth

The identity of the fissile materials that led to the generation of the MFP appears to be clear. Pu-239 and U-235 are common fissile materials and are associated with a large number of the waste packages that contain the MFP. However, the proportion of this waste that was generated by Pu-239 fission as opposed to reactions involving U-235 is not clear, nor is it clear what proportion of the waste resulted from interactions with thermal and fast neutrons.

The short-lived nature of the majority of the fission products requires that an accurate assessment be made of the age of the waste at the time of disposal. The composition of the waste changes rapidly as radionuclides with very short half-lives decay. The error introduced into the inventory projections by uncertainties in the age of the MFP waste may be significant. For example, the activity allocation fractions for Cs-137, averaged over the thermal and fast neutron yields for Pu-239 and U-235, increase from about 0.14 to 0.73 as the age of the MFP waste increases from 1 to 10 years. Thus, changing the age of the waste by an order of magnitude results in a five-fold change in the projected Cs-137 inventory.

Most radionuclides associated with MFP waste are very short-lived and decay to negligible levels within a matter of days or weeks. The daughter products generated by the decay process may, in some instances, be longer-lived than their parents and, as a result, contribute to estimated MFP waste activities beyond the time of generation. Due to the very large number of short-lived daughter products, however, the contributions of long-lived daughter products were not taken into account in the current inventory update. This simplification will underestimate the activities of any long-lived daughters that were overlooked and overestimate the activities of the radionuclides that were carried forward in the analysis.

The allocation of the listed MAP activities to specific radionuclides was based on information provided by the Los Alamos Neutron Science Center (formerly the Los Alamos Meson Physics Facility) at TA-53, a major generator of MAP waste. This facility generates three major waste streams of activated waste: trash, beam-line inserts, and targets. The activity allocation factors adopted for the inventory update are based on a characterization of the trash. While similar

activated materials may occur in all three waste streams, it is unclear if the allocation factors developed for the trash accurately represent the targets and beam-line inserts.

Many of the radionuclides in the MAP waste are short-lived and will undergo significant decay between the time of generation and disposal. In a manner similar to the situation noted for the MFP waste, the decay dynamics of the waste will have a significant impact on the fractional abundances of the radionuclides in the material. Both the age of the waste at the time the allocation factors were developed and the age of the waste at the time it was disposed of at Area G are unknown.

A number of material types have been used to refer to specific radionuclide compositions; the majority of these have been used to identify isotopic mixtures of uranium and plutonium isotopes. The Area G pit and shaft inventory update includes approximately 1.1×10^4 Ci of activity reported using these material types; about 98 percent of the material type activity included in the inventory is represented by plutonium material types PU52, PU53, PU54, PU56, and PU83.

The Laboratory's LLW and TRU waste databases use point estimates of radionuclide abundances to assign material type waste to specific isotopes. In fact, ranges of radionuclide abundances are observed for these wastes. Information generated by Veilleux (2005) provides insight into the distributions of radionuclide activities associated with the major plutonium material types.

3.0 Analysis of Performance

The technical approach used to conduct the Area G performance assessment and composite analysis is described in this section. An overview of this approach is provided in Section 3.1. Section 3.2 describes the conceptual model of the facility upon which the modeling for the performance assessment and composite analysis is based; this model considers the mechanisms through which radionuclides may be released from the pits and shafts, the transport pathways responsible for the movement of contaminants from the point(s) of release to the exposure locations, and the pathways through which exposures may occur at these locations. A description of the mathematical models that were used to implement the conceptual model is provided in Sections 3.3 through 3.5; these sections describe the models for the source term, radionuclide transport, and the dose assessment, respectively. Section 3.6 summarizes the quality assurance program that was instituted in support of the Area G performance assessment and composite analysis revision effort.

3.1 Overview of Analysis

The performance assessment and composite analysis were conducted by defining a conceptual model of Area G, creating mathematical models that reflect the characteristics of the conceptual model, and implementing these models to project the long-term performance of the disposal facility. The conceptual model integrates the site characteristics, facility design features, and waste characteristics provided in Section 2 to identify radionuclide release mechanisms and transport pathways through which the waste disposed of at Area G may pose a risk to members of the public. A brief summary of the conceptual model is provided in Section 3.1.1. Section 3.1.2 provides background information on the mathematical models that were used to represent the conceptual model. The planning and implementation of the composite analysis is to be conducted using the data quality objectives (DQO) process (DOE, 2001b). The manner in which the DQO process was applied to the Area G composite analysis is described in Section 3.1.3.

3.1.1 Summary of the Conceptual Model

The conceptual model upon which the Area G performance assessment and composite analysis are based is shown in Figure 3-1. The diagram illustrates:

- The topographic setting of Area G on Mesita del Buey, which is bounded by Cañada del Buey to the north and Pajarito Canyon to the south. The mesa-canyon topography of the region has significant impacts on the manner in which radionuclides are transported by the prevailing winds, by surface water, and through the vadose zone.
- The geologic setting of Area G, consisting of volcanic deposits including units of the Tshirege and Otowi Members of the Bandelier Tuff and the Cerros del Rio basal, the geohydrologic characteristics of which greatly affect subsurface contaminant transport.

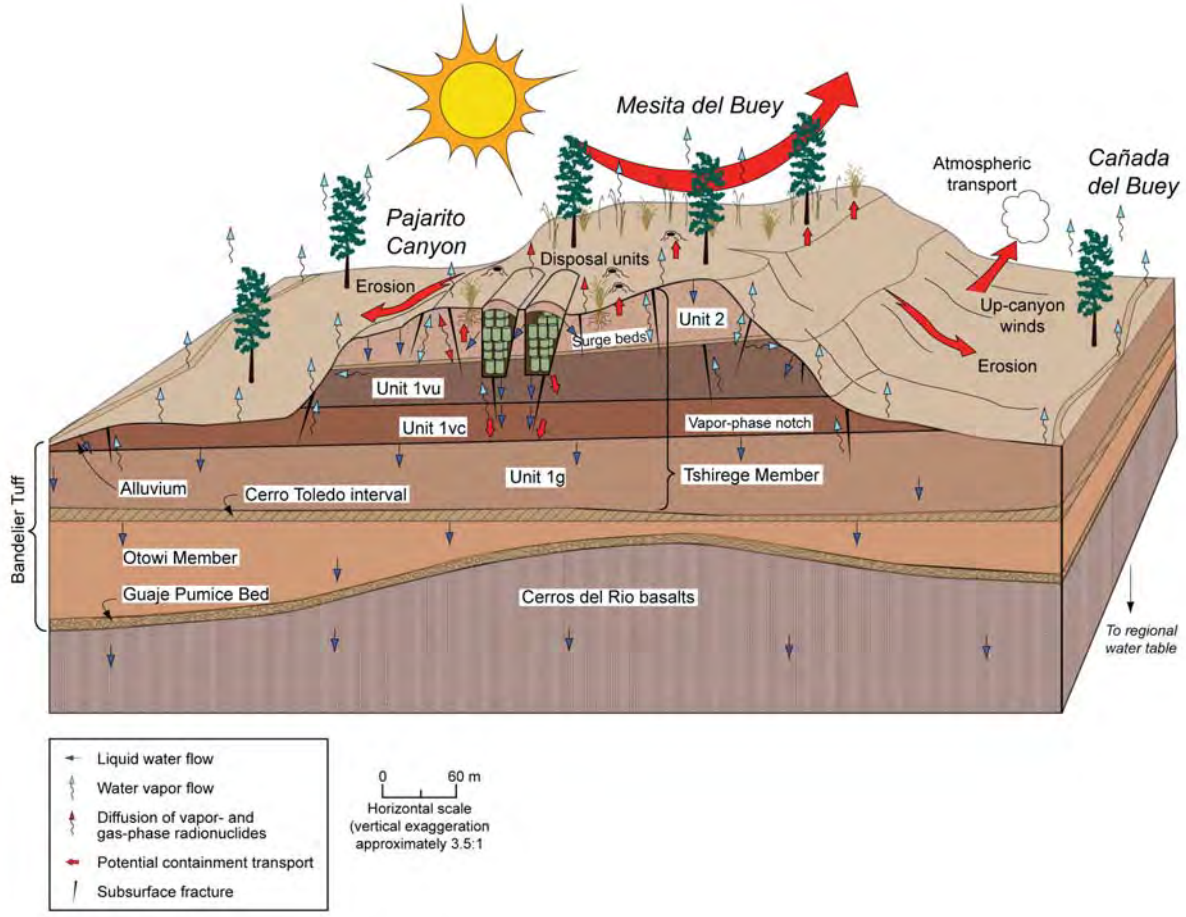

Figure 3-1
Conceptual Model of Area G
Source: Adapted from Hollis et al., 1997

- *The hydrologic setting of Area G*. This includes intermittent surface streams in Cañada del Buey and Pajarito Canyon, as well as the infiltration and evapotranspiration of water and water vapor in the subsurface along pathways defined by interstitial pores, fractures, or geologic contacts.

The figure does not illustrate the locations at which exposures may occur.

Figure 3-1 depicts the movement of water and contamination using a series of arrows. The straight blue arrows represent the infiltration of water through the disposal facility and vertical movement downward through the vadose zone, while the serpentine blue arrows represent the evaporation of water from the mesa and canyons and the transpiration of water from plants. Contaminant releases and transport are represented using red arrows. The small, straight red arrows originating from the disposal units represent the release of contaminants due to leaching as water infiltrates through the site and the deposition of contamination on the surface of the disposal facility by plants and animals intruding into the waste. Small, straight red arrows extending upward from the surface of the disposal facility represent the resuspension of contaminated particulates from the surface of the facility, while the serpentine red arrows signify the diffusion of vapor- and gas-phase radionuclides. Finally, the large red arrows that run from the mesa top to the adjacent canyons and to the atmosphere represent the transport of contamination due to water and wind erosion.

Contaminant releases from Area G may be transported to locations accessible to members of the public through a variety of processes. Radionuclides resuspended from the surface of the disposal facility in the form of particulates or contaminants diffusing from the site may be transported to locations downwind of the disposal facility and the Laboratory by the prevailing winds. Radionuclides leached from the waste may be transported through the vadose zone, discharged to the regional aquifer, and transported off-site. Finally, surface contamination at Area G may be transported into the canyons adjacent to the disposal facility due to the effects of wind and water erosion. Each of these potential exposure locations is addressed in the performance assessment and composite analysis modeling.

The primary focus of the performance assessment and composite analysis is to evaluate the potential risks posed by Area G to human health and the environment. The composite analysis also evaluates potential risks posed by other sources of radioactivity at the Laboratory. The modes of contaminant release, transport, and exposure that are pertinent to these facilities are generally consistent with the processes depicted in Figure 3-1.

3.1.2 Mathematical Models

The Area G Site Model was used to simulate the release of radionuclides from Area G, to transport these releases to locations accessible to members of the public, and to estimate the

potential exposures received by these receptors. This model was developed using the GoldSim™ modeling environment or platform (GoldSim, 2007a, 2007b, and 2007c). A second model, the Area G Inventory Model, was used to calculate initial radionuclide inventories for the site model.

The Area G Site Model integrates the radionuclide release, transport, and exposure models required to estimate the potential impacts associated with the disposal of radioactive waste at Area G. The technical bases of the release, transport, and exposure models and how they are implemented using GoldSim are discussed in Sections 3.3 through 3.5. The following discussion provides information needed to understand how the site model operates and how it was configured to represent the site. Complete details of the site and inventory models may be found in *Appendix K* (Volume 3).

The site model represents the system being modeled using objects known as elements. These elements are used to input data into the model, perform calculations using defined inputs, and physically represent the system being modeled. To model a facility such as Area G, the species or radionuclides of interest are defined and their properties are specified. The physical components of the system (e.g., the disposal units, the atmosphere, the regional aquifer, and exposure locations) are represented using transport pathway elements. The system is reflected by the geometry of these transport pathway elements, and the environmental media (e.g., soil, water, and air) that comprise the pathway elements. The transport pathway elements are connected to one another using mass-flux links, which define the rates at which radionuclides move from one physical compartment to another. The result is a dynamic simulation of the movement of radionuclides from the disposal units to locations that are accessible to human receptors. Contaminant concentrations projected for the various environmental media at the exposure locations form the basis for calculating rates of radionuclide intake for the receptors and the consequent doses.

Most physical components of the disposal system are represented in the site model using elements called cells. For example, the waste disposed of in the pits and shafts at Area G and the overlying cover are represented using cells. These elements are mathematically equivalent to mixing cells; contamination introduced into a cell is instantaneously and completely mixed throughout the element. Each cell is defined in terms of the environmental media of which it is composed (e.g., soil and water); distribution coefficients and solubility limits are used to partition radionuclides among these media.

The accuracy of the GoldSim model projections is influenced by the manner in which the cells are used to represent the disposal units at Area G. Specifically, discretization—or dividing the waste and overlying cover into a series of layers, each represented by a cell—generally results in more accurate estimates of the quantities of radionuclides released and transported from the disposal units. This can be illustrated by considering the impacts of plant intrusion on a disposal

facility. Assume contamination is deposited on the surface of the facility by plants whose roots extend into the waste. This contamination will initially reside within a shallow layer of soil at the surface of the disposal facility; using a cell to represent this thin layer will yield reasonable approximations of the actual radionuclide concentrations. However, if the entire cover is represented using a single mixing cell, the GoldSim model would mix the contamination throughout the total thickness of the cover. The result would be projected radionuclide concentrations that are significantly smaller than expected.

The level of discretization of the waste and cover required to yield accurate model projections depends upon the processes being modeled. For example, reasonably accurate projections of diffusive transport typically require that the waste and cover be more finely divided than do projections of the impacts of biotic intrusion. The site model divides the cover into a thin surface soil layer, 16 cap layers, and 20 waste layers. Although this level of discretization is not necessary to model the impacts of biotic intrusion, it is needed to accurately project rates of vapor- and gas-diffusion through these materials. Using fewer layers to represent the cover and waste will tend to artificially increase rates of transport through the disposal system, while using an excessive number of layers complicates the model and slows execution. The analyses that were conducted to identify a suitable degree of discretization for the site model are discussed in *Appendix K*.

The Area G Site Model is probabilistic in nature. As applied here, this means that input parameters are defined using stochastic distributions to reflect the variability in the properties, characteristics, or processes they represent. These distributions are sampled repeatedly and used to conduct multiple model realizations to project the long-term performance of the disposal facility under multiple sets of conditions. The output of the modeling consists of distributions of projected contaminant release rates, environmental concentrations, and exposures. These results represent the variability, and uncertainty, in the projected quantities based on the input parameter distributions used to represent the disposal system.

Area G is a large, complex site. Many aspects of the facility's long-term performance are spatially dependent in response to local variations in topography and geohydrology. To more accurately model long-term performance, the disposal site was divided, or discretized, into several areas. An understanding of how this was done is critical to the discussions about the mathematical models.

The primary subdivisions of the facility are referred to as waste disposal regions; each region includes a subset of the disposal pits and/or shafts at Area G. The waste disposal regions were defined (1) on the basis of changes in groundwater transport properties from east to west across the facility and (2) to capture differences in the depths at which waste has been disposed of in the pits and shafts. Material Disposal Area G was divided into seven disposal regions as shown in

Figure 3-2. Disposal regions 1 and 6 each include some of the shafts in the shaft field west of pits 2 and 4, consequently the boundaries of these regions overlap. Disposal region 7 includes numerous shafts scattered among the units that make up disposal region 3 (i.e., pits 8 through 22), and thus the boundaries of these two regions also overlap. An eighth waste disposal region is used to represent the Zone 4 expansion area; this region is not shown in Figure 3-2.

The waste facility was also compartmentalized to enable more accurate atmospheric transport modeling. The patterns of transport and dispersal of radionuclides in the form of suspended particulates, gases, or vapors by prevailing winds depend, in part, upon the portion of the facility from which these releases originate. To better account for these dependencies, the disposal site was divided into three atmospheric source areas, as shown in Figure 3-3. Each source area consists of one or more of the eight waste disposal regions discussed above.

3.1.3 Data Quality Objectives Process

Planning and implementation of the Area G composite analysis was conducted using the U.S. EPA's DQO process (EPA, 2006). This process consists of the seven steps listed below.

1. State the problem.
2. Identify the goal of the study.
3. Identify information inputs.
4. Define the boundaries of the problem.
5. Develop the analytic approach.
6. Specify performance or acceptance criteria.
7. Develop the plan for obtaining the data.

The DQO process is recommended as a means of using data for environmental decision-making. It is used to develop performance and acceptance criteria (data quality objectives), define appropriate types of data, and specify tolerable levels of potential decision errors. Thus, the process forms the basis for determining the quality and quantity of data needed to support decisions.

The composite analysis is primarily a modeling exercise, as opposed to a data collection effort. Given this, Step 6, which is concerned with the quality of the collected data, and Step 7, which addresses data collection plans, are not directly applicable to the assessment. Therefore, only the first five steps of the DQO process were applied to the composite analysis. The application of the process to the Area G composite analysis is shown below.

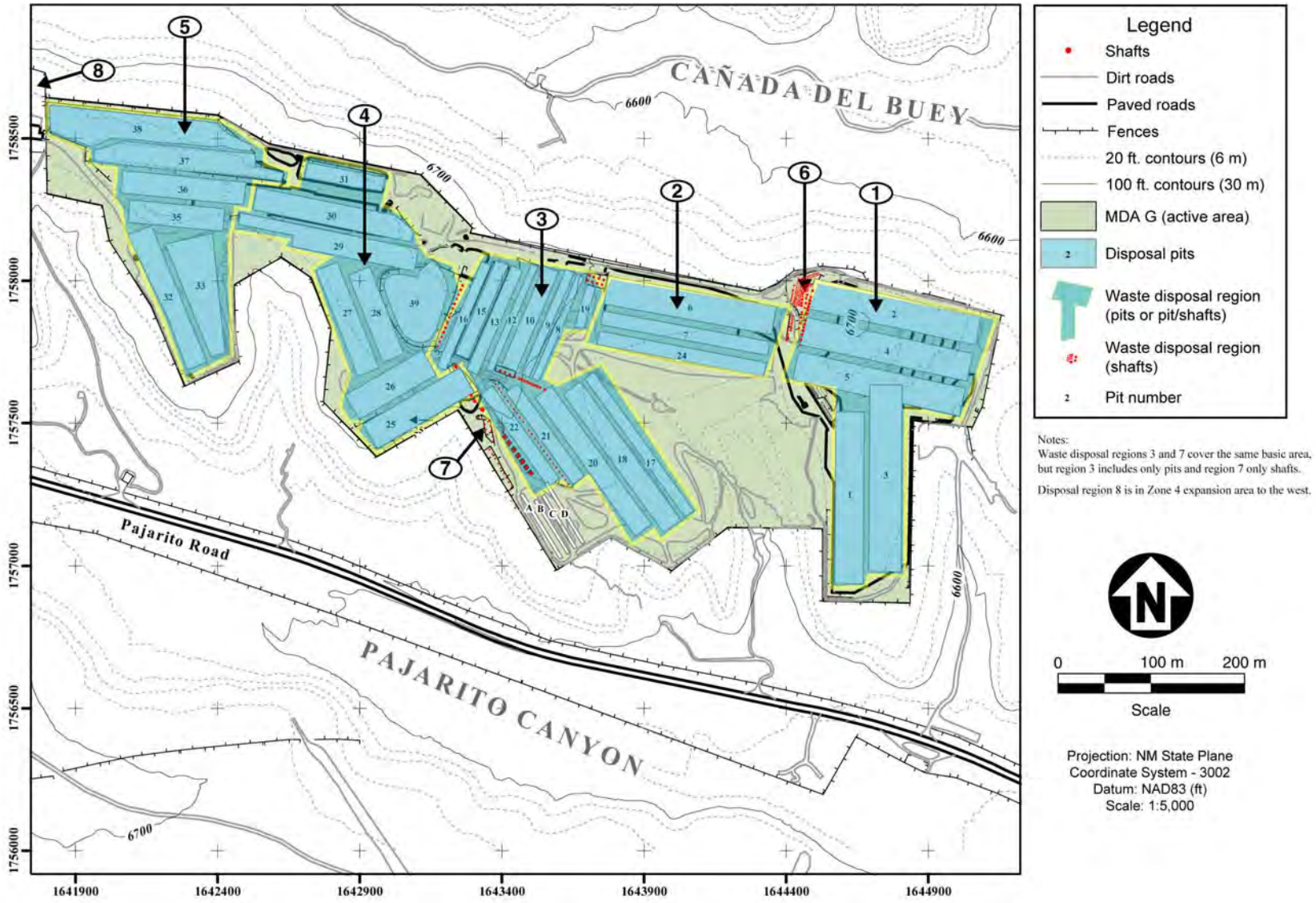

Figure 3-2
Waste Disposal Regions at MDA G

Source: Apogen Technologies (formerly SEA)
LANL RRES Database, Map ID: 4531.021 (1) Rev. 2

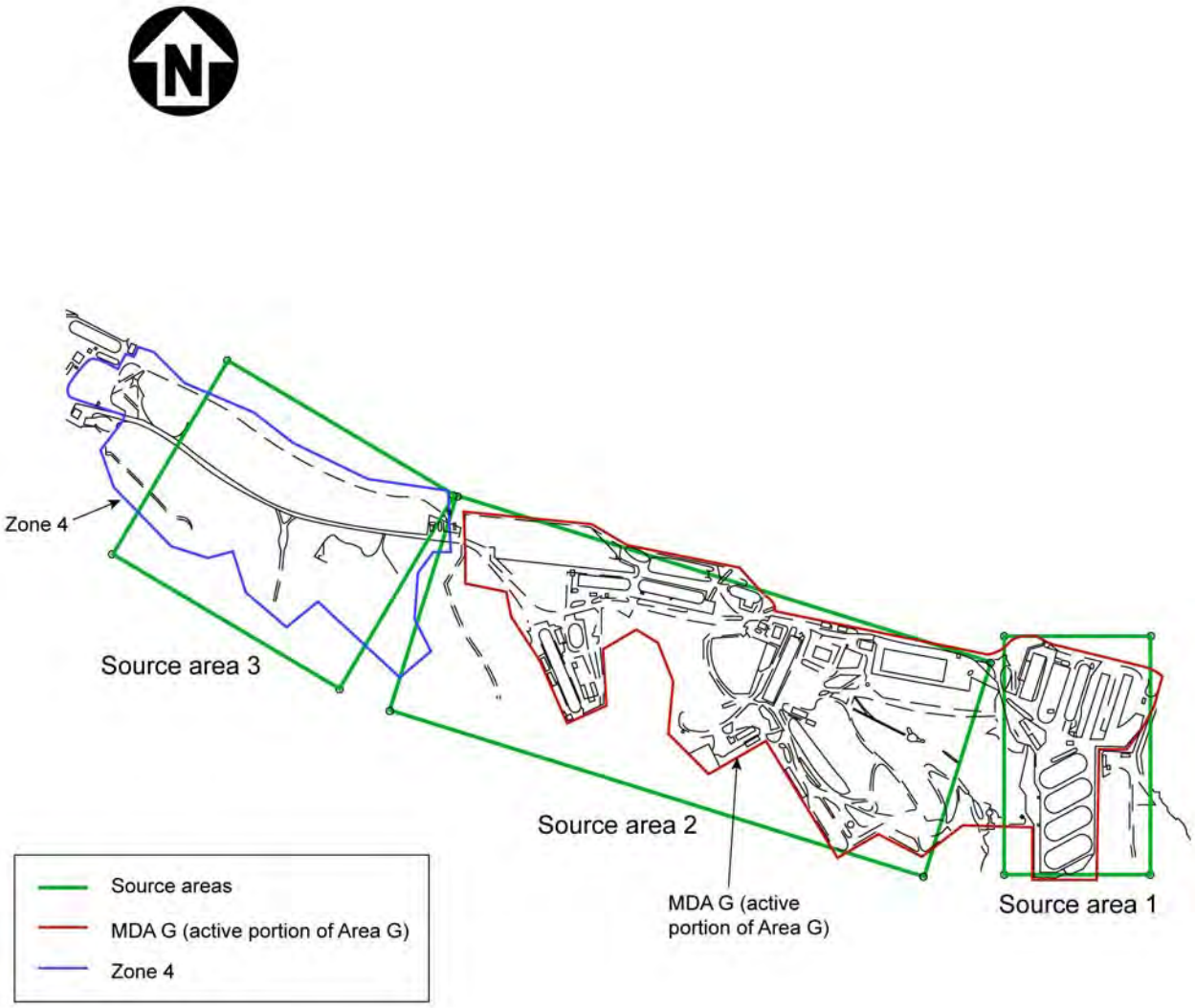

Figure 3-3
Atmospheric Source Areas at Area G

1. *State the problem.* Radionuclides released from Area G may be transported to downwind and downgradient locations where members of the public may be exposed to radiation. Releases of radionuclides from other sources at LANL may be transported through similar means and interact with the releases from Area G, adding to the exposures received by the receptors. Reasonable assurance that the cumulative exposures experienced by the receptors do not exceed acceptable levels must be provided.

2. *Identify the goal of the study.* The goal of the composite analysis is to estimate the cumulative exposures for receptors exposed to radionuclide releases from Area G and all other sources of radioactive material at LANL that may interact with Area G contaminants. While cumulative exposures in excess of acceptable limits are not anticipated, any such finding will require that actions be taken to reduce these impacts. Such actions will depend upon the facilities contributing to the cumulative exposures and their relative contributions, but may include the collection of data to improve the accuracy of the performance modeling, identification of closure options that better isolate the sources of radiation at the various sites, revision of the Area G waste acceptance criteria (WAC), and remediation of contamination at one or more sources.

3. *Identify information inputs.* An indication of the cumulative radiation doses received by persons exposed to releases from Area G and all interacting sources is required to evaluate the acceptability of waste disposal at Area G. Estimates of exposure for releases from Area G take into account the site and disposal facility characteristics and radiological inventory presented in Section 2 of this report and the results of the modeling analyses described in the following sections. Projections of exposures from other sources of radioactive material at the Laboratory are based on information about the nature of these facilities, the quantities of waste contained therein, and the modes and rates of contaminant release and transport from these sources.

4. *Define the boundaries of the problem.* The composite analysis addresses potential interactions between releases from Area G and other sources of radioactive material at LANL. Cumulative radiological impacts will be evaluated at the locations where exposures to releases from Area G result in the greatest potential doses. Four such exposure locations exist: (1) 100 m downgradient of the Area G fence line (for groundwater pathway exposures), (2) along the facility fence line (for atmospheric exposures), (3) Cañada del Buey adjacent to Area G, and (4) Pajarito Canyon adjacent to Area G. The cumulative impacts of source interaction will be considered for a period of 1,000 years following final closure of Area G.

5. *Develop the analytic approach.* The cumulative doses projected for the Area G composite analysis must be less than or equal to 10 mrem/yr for airborne radioactivity and less than or equal to 100 mrem/yr for all pathways exposures to contaminated groundwater and canyon

sediments. If there is reasonable assurance that the projected impacts exceed these limits, actions will be taken to better understand the potential risk and ensure compliance with the exposure limits. If there is reasonable assurance that the projected exposures fall within the dose objectives, consideration will be given to actions that may reduce doses further, consistent with the "as low as reasonably achievable" (ALARA) philosophy.

3.2 Conceptual Model of Facility Performance

The different components of the conceptual model shown in Figure 3-1 are described below. Section 3.2.1 considers the inventories included in the performance assessment and composite analysis and discusses the mechanisms through which radionuclides in the waste may be released from the disposal units; these aspects of the conceptual model are collectively referred to as the source term. Section 3.2.2 considers the processes through which radionuclides may be transported from the point(s) of release to locations accessible to persons living in the vicinity of Area G. Section 3.2.3 describes the means through which people may be exposed to contaminated environmental media at these locations.

3.2.1 Source Term

The conceptual model of the source term addresses the waste disposed of in the pits and shafts at Area G and the mechanisms through which radionuclides in that waste may be released from these units. Section 3.2.1.1 discusses characteristics of the waste that are relevant to the release of the radionuclides contained therein. The contaminant release mechanisms depicted in Figure 3-1 are addressed in Section 3.2.1.2.

3.2.1.1 Waste Characteristics

The types and quantities of waste that have been, or are projected to be, disposed of at Area G are reported in *Appendix J*; a summary of the inventory is provided in Section 2.3 of this volume. Characteristics of the waste that may influence the rates at which radionuclides are released from the disposal units are discussed here.

The physical form of the waste and the packaging used to dispose of the material may have strong implications in terms of radionuclide release within the pits and shafts. For example, the leaching of contamination from activated metal or sealed sources will be limited by the rate of corrosion of the steel or metal jacket. Packaging used in the disposal of the waste may further limit access to the waste by water percolating through the disposal units. The waste form and packaging may also limit the amount of contamination that can be assimilated by plants growing into the waste and the quantity of waste that can be moved to the surface of the site by burrowing animals.

As discussed in Section 2.3, the waste disposed of at Area G has assumed a wide variety of forms. The leachability of these waste forms will be determined, in part, by the distribution of contamination within the material. Surface contamination may be removed or rinsed quickly

from the waste as water passes through the disposal units. In contrast, releases from contaminated soils, concrete, and sludges will likely be controlled by the sorption characteristics of the radionuclides within those matrices.

Prior to the mid-1990s, bulk waste was placed directly in the disposal units and other waste was generally disposed of in plastic bags and cardboard boxes. The integrity of these containers was compromised by the periodic use of heavy equipment to compress the waste and apply lifts of clean backfill. Metal drums and wooden boxes were used to dispose of waste for which the possibility of future retrieval existed. Since the mid-1990s most of the nonbulk waste has been placed in metal containers prior to disposal.

As long as they retain their integrity, metal containers may provide an advantage by limiting the contact of water with the waste, preventing intrusion into the waste by plants and animals, and, possibly, limiting diffusive releases. Realization of these benefits will depend, in part, on the construction of the containers and their final configuration in the disposal units. Metal containers may lose integrity as a result of corrosion. Containers that are crushed as intermediate layers of fill or covers are applied will be less likely to isolate the waste regardless of their material characteristics.

The range of waste forms disposed of at Area G and the packages used to dispose of the material complicates the task of modeling contaminant releases. The different waste forms found at the disposal facility and the wide variety of packaging that has been used to date are such that detailed, spatially dependent modeling would be required to model potential releases within the pits and shafts with a high degree of accuracy. To simplify the matter, all waste was conservatively assumed to be in a form that did not prevent or slow the release of radionuclides due to leaching, vapor- and gas-phase diffusion, or biotic intrusion. Furthermore, packaging was not assumed to prevent or otherwise impede the release of contaminants from the waste.

3.2.1.2 Contaminant Release Mechanisms

Radionuclides disposed of at Area G may be displaced by plants and animals intruding into the waste, or leached from the waste by water infiltrating through the disposal units. Vapor- and gas-phase contaminants may diffuse from the disposed material. Under extreme conditions, the waste may be exposed as a result of surface erosion or cliff retreat. The conceptual models of these release mechanisms are described in the following sections.

Biotic Intrusion

Radionuclides disposed of at Area G may be transported to the surface of the disposal facility by plants whose roots penetrate into the waste and animals whose burrows extend into the zone of contamination. While biotic intrusion will result in the transport of contaminants to the surface of

the site, it is discussed here as a mechanism of release. The description of the conceptual model that follows is based on information included in *Appendix K*.

The amount of contamination deposited on the ground surface by plants is a function of the radionuclide concentrations in plant litter and the quantity of litter generated by the plants. Radionuclide concentrations in the litter depend upon the distribution of root mass with depth and the efficiency with which radionuclides are extracted from contaminated soils by plant roots. Rates of litter production are estimated on the basis of aboveground plant yields and the fractions of these yields that fall as litter in any given year. Plant yields and litter generation fractions are specific to the plant growth forms under consideration; yields may vary over time as the disposal site undergoes ecological succession.

Animals constructing burrows for cover or as a means of foraging may penetrate into the buried waste and bring waste contaminants to the surface of the site. This contamination is mixed with clean soil excavated from the portions of the burrows that lie above the waste, and spread over the ground surface. Over time, the burrows excavated by animals will settle or collapse, resulting in the gradual downward movement of contamination brought to the surface by animals and deposited on the ground by plants. Vertical transport of the surface contamination will be enhanced as radionuclides are transported downward with water infiltrating through the site.

The amount of contaminated soil brought to the surface by burrowing animals will depend upon the distribution of burrows relative to the waste and the soil removal rates of the various species or taxa of animals. Burrow distributions are used to estimate rates of soil removal with depth; the total quantities of excavated soil are calculated using information about animal densities and life spans, burrow volumes, and burrow renewal fractions. Many of these parameters may change over time as the composition of the animal community shifts in response to the changes in the plant community.

The potential impact of biotic intrusion upon the long-term integrity of the disposal facility will depend, in part, on the ecological characteristics of the site and, hence, on the plant and animal species that can reasonably be expected to inhabit the closed facility. As discussed in Section 2.1.3, a diverse array of plants and animals is found in the Los Alamos region, owing to the 1,500 m (5,900 ft) elevational gradient between the Rio Grande and the Jemez Mountains, and to the canyon and mesa terrain (DOE, 1979). Undisturbed areas on Mesita del Buey, the mesa on which Area G is located, are dominated by piñon-juniper woodland, while portions of the site that have been disturbed by disposal operations are dominated by native and introduced grasses and forbs. Plants used to revegetate the site after the disposal units are closed will introduce additional species of grasses and forbs. Once final closure is complete, it is assumed the site will undergo ecological succession from a disturbed state to a piñon-juniper woodland climax condition, which is characteristic of the undisturbed portions of Mesita del Buey.

Although the general nature of the vegetative cover at Area G can be predicted for the early successional stages and climax condition, predicting the species-specific plant composition with any degree of accuracy is essentially impossible. Given this, the biotic intrusion modeling identifies the plant communities present at the site in terms of the general growth forms present under each set of conditions, rather than on a species-specific basis. Four growth forms were identified: annual and perennial grasses, annual and perennial forbs, shrubs (including subshrubs), and trees. The impacts of grasses, forbs, and shrubs are simulated during the early stages of site succession. Grasses and forbs are expected to be early colonizers at the site; shrubs will likely begin to colonize within a few years after closure and are therefore included in the simulation of the site. Simulation of the disposal site as it passes to piñon-juniper woodland considers the impacts of trees in addition to grasses, forbs, and shrubs.

The predominant plant communities at Area G will have a direct influence on the species of burrowing animals that occur at the site following facility closure. Several species of burrowing animals are currently found at Area G and the area surrounding the site; others may reasonably be expected to inhabit the site after widespread disturbance of the area ceases and the site undergoes ecological succession to piñon-juniper woodland.

As with plants, predicting the specific animal communities that may inhabit the disposal site after the facility is closed is difficult at best. However, it is possible to estimate major groups or categories of burrowing animals that are likely to occur at Area G as the site passes from grassland to woodland. Using data specific to Area G and information from the literature, four taxa of burrowing animals were selected to simulate the impacts of animal intrusion: harvester ants, mice, pocket gophers, and chipmunks and ground squirrels. The impacts of harvester ants and mice are considered during the early successional stages at Area G and after the site has transitioned to piñon-juniper woodland. Pocket gophers are not expected to inhabit the woodland site and, conversely, chipmunks and ground squirrels are not expected in the grassland community. Consequently, the impacts of these taxa will be greatest in the early successional and woodland communities, respectively.

Identification of the animals likely to be present at the closed disposal site on the basis of taxa is expected to be more accurate than projecting the presence of specific species. Although the process is still prone to uncertainty, the animals selected for the biotic intrusion modeling are expected to reasonably capture the range of actual species that will be present at Area G after closure, thus enabling fairly accurate projections of the potential impacts of animal intrusion. Other burrowing animals (e.g., voles, woodrats, and rabbits) may occur at the site at various points in time, but the potential for these species to cause significant disruption of the waste is expected to be small.

Contaminant Leaching

Rates of contaminant leaching from the disposal pits and shafts will depend upon the amount of water passing through the disposal units and the physical and chemical characteristics of the waste. The rate at which water infiltrates through the disposal units is a function of natural site characteristics and the long-term performance of the cover placed over the disposal units.

As discussed in Section 2.1.2, Area G receives approximately 34 cm (13 in.) of precipitation annually. Under natural conditions, the vast majority of this precipitation is lost through evaporation and transpiration, resulting in low rates of infiltration through undisturbed portions of the site. Nyhan et al. (1990) found that evapotranspiration accounted for the removal of almost 90 percent of the precipitation from two control plots over a 3-year period, while information cited in a LANL report (LANL, 2003b) indicates that the ratio of potential evapotranspiration to precipitation is greater than 6 to 1. The effects of evapotranspiration on infiltration rates are apparent from work done by Newman et al. (*Appendix F*), who estimated long-term moisture fluxes in piñon-juniper woodland just west of MDA G on the basis of pore-water chloride concentrations. Samples were collected from 1 to 2 m (3.3 to 6.6 ft) deep boreholes underneath tree canopies and in intercanopy spaces. The fluxes estimated for these areas were generally around 0.1 to 0.4 mm/yr (3.9×10^{-4} to 0.016 in./yr), a small fraction of current-day rates of precipitation.

Rates of infiltration through the disposal units will generally be greater than those observed in undisturbed areas prior to closure of the pits and shafts, primarily because of the lack of vegetation and associated transpiration. Higher rates of infiltration through the active units are suggested by moisture content measurements that have shown elevated water contents within several pits at Area G relative to adjacent, undisturbed areas (Loaiza and Vold, 1995). The amount of water percolating through the waste will likely decrease after the interim cover is placed over the disposal units, but rates of water loss due to evapotranspiration are still expected to be less than those found in undisturbed areas.

One function of the final cover placed over Area G will be to limit rates of infiltration through the disposal units. The proposed cover will function as an evapotranspiration cover system, employing vegetated soil layers to retain the water until it is removed through evaporation or plant transpiration. The top layers of the cover are to be installed at relatively low compaction levels, which will help plants become established. The bulk of the cover consists of crushed tuff with a 6 percent bentonite admixture. The clay helps increase the compactibility of the soil and is also expected to play a role in reducing rates of water infiltration (*Appendix G*).

Rates of infiltration through the disposal units were estimated on the basis of flux measurements conducted by Newman et al. and model simulations performed by Levitt, as reported in *Appendices F* and *G*, respectively. Steady-state flow conditions were assumed to exist throughout the model simulations. The data needed to establish the moisture characteristics of

the disposal units with a reasonable level of accuracy were not available; thus, the source term modeling did not account for the effects that elevated moisture contents within the pits and shafts may have on rates of water passage through the waste.

Rates of leaching within the disposal units will depend upon several factors, among them the chemistry of the water, the physical and chemical forms of the waste, and the packaging used to dispose of the waste. Krier et al. (1997) indicate that rainwater and snowmelt will have a low total dissolved solids content and an acidic pH because of low concentrations of bicarbonate, calcium, sodium, and magnesium. Storm runoff may have a higher dissolved solids content and near-neutral pH because of its contact with soils, backfill, and Bandelier Tuff. Surface water entering the pore spaces of the waste may approach equilibrium with crushed tuff, waste, and the radionuclides contained therein. Geochemical reactions that control contaminant releases will be controlled by pH, oxidation-reduction potential, speciation of the contaminants, temperature, advection, and the residence time of the pore water (Krier et al., 1997). As discussed earlier, the physical forms of the waste disposed of at Area G and the types of packaging used at the facility will affect the availability of the waste for leaching and the modes of leaching observed.

The information needed to model radionuclide releases due to leaching from the waste forms disposed of at Area G with a high degree of accuracy is unavailable. Furthermore, it is not clear how metal containers will affect the infiltration rate in disposal units where these packages were used. Thus, the conceptual model adopts a simplified, conservative approach to estimate radionuclide releases due to leaching. This approach assumes that all radionuclides disposed of at Area G are in equilibrium with the crushed tuff backfill used in the disposal units, regardless of the form of the waste and the containers in which they reside. Contaminants are assumed to partition between the solid tuff and the fluid in the pore spaces in proportion to their distribution coefficients. Radionuclides within the liquid phase are transported by water percolating through the site and “released” from the disposal pits and shafts.

Based on the conceptual model outlined above, the rates of radionuclide leaching from the waste will depend upon the pore-water chemistry and the solubility and sorption behavior of the contaminants. Longmire et al. (1996) conducted batch sorption tests to estimate sorption coefficients for selected radionuclides. Krier et al. (1997) conducted a review of literature on sorption and equilibrium solubility in conjunction with the 1997 performance assessment and composite analysis. This review focused on data for devitrified tuff from Yucca Mountain, which are expected to provide reasonable estimates of contaminant behavior for radionuclides in the absence of site-specific data. A more recent compilation of data for Yucca Mountain tuffs may be found in Bechtel/SAIC (2004).

Vapor- and Gas-Phase Diffusion

A small number of the contaminants included in the performance assessment and composite analysis exist in the vapor or gas phase: these include tritiated water vapor, C-14 gas, and isotopes of krypton and radon. Such radionuclides may diffuse upward from the buried waste and exit from the surface of the facility. Vapor- and gas-phase diffusion is addressed here as a release mechanism.

The disposal of large quantities of tritium at Area G has occurred in the past and is expected to continue in the future. The vast majority of this waste is in the form of tritiated water in a solid matrix (e.g., molecular sieves). This tritium will partition between vapor and liquid phases in proportion to its vapor pressure; vapor-phase contamination will diffuse through the air-filled pore spaces. Although high-activity tritium waste is disposed of in metal drums, these containers were not assumed to influence rates of diffusion from the disposal units.

C-14 gas is assumed to be generated as a result of the biodegradation of organic waste, and exists either as carbon dioxide (CO_2) or methane (CH_4). The quantities of gases generated will depend upon how much of the waste consists of organic matrices and the rate at which that waste degrades. Kr-85 and radon are noble gases that will exist almost entirely in the air-filled pore spaces. Although the waste disposed of at Area G contains Kr-85, the isotopes of radon gas diffusing from the disposal units will originate with the decay of their parent radionuclides. Thus, the radon diffusion modeling estimates the rate of generation of Rn-220 and Rn-222 as a result of radioactive decay.

Only a portion of the radon generated from radioactive decay will enter the air-filled pore spaces of the waste and diffuse from the disposal units. The radon emanation coefficient, or the fraction of the radon gas generated by radioactive decay that enters the pore spaces, is a function of many factors including the recoil energy of the radon isotope under consideration, and the pore structure and moisture content of the medium in which the gas is generated. The radon diffusion modeling accounts for the net amount of gas that enters the air spaces in the waste.

Surface Erosion and Cliff Retreat

Surface erosion may serve as a release mechanism if it results in complete removal of the cover over portions of the site, thereby exposing the underlying waste. Under these conditions, contaminants may be resuspended directly into the atmosphere and transported into the adjacent canyons by wind and water. For the most part, however, surface erosion will result in a gradual thinning of the cover over extended periods of time and eroded sediments will be transported into the adjacent canyons. A conceptual discussion of surface erosion as a transport mechanism is provided in Section 3.2.2.

The topographical features of Area G make it susceptible to cliff retreat, wherein portions of the mesa walls collapse into the adjacent canyons. Over extended periods of time, cliff retreat may result in the exposure of waste disposed of in the pits and shafts located near the edges of the mesa. The time required for exposure of the waste to occur will depend upon the rate of cliff retreat and the distance the disposal units are set back from the edges of Mesita del Buey.

Information summarized in Section 2.1.4.1 indicates that it is unlikely cliff retreat will threaten the integrity of the disposal units at Area G in the near term. Data collected by Reneau (1995b) suggest that it would take more than 10,000 years, and possibly more than 100,000 years, to expose waste disposed of at MDA B, where disposal units lie approximately 18 m (60 ft) from the edge of the mesa. Cliff retreat is expected to pose a similar risk to the disposal units at Area G, based on the general characteristics of Cañada del Buey and Pajarito Canyon and the layout of the pits and shafts at this facility. On this basis, the effects of cliff retreat were not included in the performance assessment and composite analysis modeling.

3.2.2 Radionuclide Transport

Contaminant releases from the disposal pits and shafts at Area G may be (1) transported to and discharged into the regional aquifer by water percolating through the facility, (2) carried by the prevailing winds to downwind locations, and (3) transported into adjacent canyons by water and wind action. Each of these transport pathways plays a potentially important role at Area G. The conceptual model of radionuclide transport is described below.

3.2.2.1 Groundwater Transport

Rates of contaminant transport to locations that are accessible to members of the public are a function of groundwater travel times through the vadose and saturated zones. In general, travel times to downgradient wells are controlled by rates of flow within the vadose zone; while groundwater travel times within the aquifer are poorly understood, they are expected to be much shorter than those in the vadose zone. Thus, the following discussion of the groundwater conceptual model focuses on processes that affect vadose zone transport. These include the hydrologic processes that occur within the Bandelier Tuff and alluvium of the mesas and canyons of the Pajarito Plateau as well as the processes that occur in the vadose zone beneath the Bandelier Tuff. An overview of factors affecting saturated zone travel is also included. The section concludes with a brief discussion of geochemical interactions.

These discussions rely heavily upon the conceptual model for groundwater transport at Area G that was developed in conjunction with the 1997 performance assessment and composite analysis (Rogers et al., 1997). Information published since 1997 is included where appropriate, including work conducted by Stauffer et al. in support of the performance assessment and composite analysis effort (*Appendix E*).

Mesa Hydrologic Processes

A predominant feature of the Laboratory is its mesa-canyon topography. From a hydrologic perspective, the mesas in the eastern portion of the Laboratory, where Area G is located, tend to be dry. When undisturbed, relatively small amounts of water infiltrate into and pass through these mesas because of low rainfall, high evaporation, and the efficient use of water by plants. This low natural rate of infiltration is significant because infiltration is the primary determinant of the rates at which radionuclides are leached from the waste disposed of at Area G and transported to the regional aquifer.

Abeele et al. (1981, as cited in Rogers et al., 1997) collected neutron-probe moisture measurements from several holes at Area G. The data revealed that seasonal fluctuations in moisture were primarily confined to the top 4 m (13 ft) of holes drilled in undisturbed tuff within a shaft field; the essentially constant moisture content below this depth was concluded to be indicative of steady state conditions. On the basis of the Abeele et al. findings, Rogers et al. (1997) conclude that low liquid water fluxes of about 10^{-11} cm/s (3.9×10^{-12} in./s) occur below 4 or 5 m (13 or 16 ft).

Newman (1996) used pore-water chloride measurements from samples collected from four wells at Area G to estimate water fluxes as a function of depth. At depths ranging from about 3 to 40 m (3 to 140 ft), the chloride profiles indicate at least three intervals with different infiltration characteristics. Water fluxes were lowest in the middle interval, at depths ranging from about 6 to 25 m (20 and 80 ft). Fluxes above and below this interval were similar to one another, ranging from 0.1 to 6 mm/yr (0.0039 to 0.24 in./yr); these fluxes were five or more times greater than the fluxes estimated for the middle segment. The fluxes estimated by Newman were generally higher than those simulated by Birdsell et al. (1995). Variations between the two studies were attributed to differences in the moisture contents adopted for the modeling and the chloride analyses.

As indicated earlier, rates of infiltration may be higher in disturbed regions of the mesa. The disposal units at Area G are generally excavated close to the base of unit 2 of the Tshirege Member of the Bandelier Tuff. Rogers et al. (1997) cite studies that found elevated moisture contents within the pit fill, which may be indicative of higher rates of infiltration. Loaiza and Vold (1995) report measurements collected from a series of vertical boreholes located across Area G including boreholes located within disposal units or in otherwise disturbed tuff, and in areas undisturbed by disposal operations. Data for the boreholes in undisturbed areas indicate near-surface moisture contents ranging from 5 to 7 percent; water contents typically decrease to 1 to 2 percent at depths of 3.5 m (12 ft) or more. Moisture contents measured at disturbed locations were higher, generally ranging from 7.5 to 14 percent near the surface.

Birdsell et al. (2005) cite borehole monitoring results from Mesita del Buey that illustrate the potential impacts of operations on rates of infiltration rates. Runoff in the vicinity of the borehole was focused by an asphalt pad and resulted in a transient ponded condition around the hole. Periodic monitoring of the borehole revealed increasing water contents to a depth of 24 m (80 ft) over the 10 years since the borehole was established.

Newman et al. (*Appendix F*) compare moisture contents in boreholes drilled into and adjacent to disposal pit covers but report no statistically significant differences. However, moisture fluxes in MDA G were about an order of magnitude higher than fluxes estimated within piñon-juniper woodland next to the disposal facility. Moisture contents and fluxes in paved portions of MDA G were found to be significantly higher than those in unpaved portions of the active site.

Elevated moisture near the surface of Area G may or may not translate into higher water contents at depth. That is because atmospheric evaporation extends within the mesas, drying the mesa interior and further limiting the downward movement of moisture. Cooling joints or fractures within some units of the Tshirege Member of the Bandelier Tuff may help dry out portions of the mesa. The driest zone within the mesa generally occurs within the lower portion of Tshirege unit 2 and the upper part of unit 1v, a region that coincides with fractures reported by Krier et al. (1997). Rogers et al. (1997) note that this region is also generally a zone of high matric suction and a hydraulic head minimum, suggesting that moisture is being drawn toward this depth from above and below. The driving force for this movement of water may be evaporation aided by air flow within the fractures or along the surge beds found at the base of unit 2.

Data collected and evaluated by Newman (1996) support the presence of a dry region within the mesa resulting from deep evaporation. Measurements of chloride concentrations in pore water were collected from core samples that were taken from four wells at depths ranging from 3 to 40 m (3 to 140 ft); stable isotope measurements were collected from samples for one of these wells. Chloride concentrations at depths of approximately 6 to 25 m (20 to 80 ft) were elevated relative to those measured in shallower and deeper zones; this is considered likely evidence of a zone of evaporation and vapor phase transport. Stable isotope data indicate the removal of water from the system at depths that are unaffected by surface evaporation. This drying is expected to pose as a significant barrier to recharge passing through the mesa under natural conditions. The chloride data suggest that the age of water at depths of 20 to 45 m (65 to 145 ft) range from 1,300 to more than 17,000 years.

In addition to helping dry out the interior of the mesa, the fractures beneath Area G could also function as conduits for the rapid movement of water. The conditions observed at Area G, however, indicate that infiltrating water is likely absorbed into the surrounding dry rock. Several studies suggest that fracture flow within the Bandelier Tuff beneath Area G is unlikely.

Soll and Birdsell (1998) conducted work in support of the 1997 performance assessment and composite analysis to evaluate the likelihood of fracture flow beneath the disposal facility. This work modeled the effects of fracture coatings and fills on the potential for flow under two boundary conditions: a constant flux of 5 cm/d (2 in./d) for 100 days and a ponded condition for half a day. Both conditions were applied at the top of the fracture. The simulations conducted by Soll and Birdsell indicate that flow in fractures located in porous, unwelded to moderately welded tuff is likely to occur only during the most extreme infiltration events. Even under extremely high infiltration conditions, fractures lacking coatings or fills were unable to transmit water very far; the saturation front resembled that observed in a nonfractured system with point injection. Simulations in which a 1 m (3.3 ft) cap was placed across the entire fracture-matrix system and held at saturation levels of 50 to 90 percent failed to generate fracture flow.

In their description of the conceptual model for vadose-zone flow and transport beneath the Pajarito Plateau, Birdsell et al. (2005) cite work conducted by Robinson et al. (2005) that supports the notion that fracture flow under Area G is unlikely. Robinson et al. modeled a vadose-zone, wellbore injection test performed on Mesita del Buey, west of MDA G, using several conceptual models of fracture flow behavior. The results of these simulations indicate that the observed moisture distribution was consistent with a continuum model without fractures. For those conceptual models that included fractures, the fracture-matrix interaction had to be muted in the models (i.e., little flow into the fracture) to match the observations.

Moisture contents that are 10 to 20 percent (by volume) higher than those in surrounding geologic units have been observed across the Laboratory in the vapor-phase notch at the base of Tshirege Member unit 1v (see Figure 2-10, Section 2). These higher water contents occur regardless of elevation or relationship of the vapor-phase notch to geographic features such as canyon bottoms (Turin, 1995), and are probably the result of changes in hydraulic properties related to vapor-phase alteration (Rogers et al., 1997). It is conceivable that the high moisture contents are generated from lateral flow beneath the mesa; however, data provided in Rogers et al. (1997) suggest otherwise. For example, no evidence of saturation was noted near the mesa walls in wells drilled along the base of the mesa in Pajarito Canyon (Devaurs and Purtymun, 1985).

Based on a review of the existing information, Rogers et al. (1997) conclude that no recharge is taking place beneath the mesa at Area G, and that such recharge may have not occurred for thousands of years. Most moisture profiles observed beneath Area G and MDA L to the west have displayed three moisture content zones. Three rates of recharge are needed to explain the presence of these zones, which suggests that there are significant sources or sinks of moisture at different depths. These sources and sinks, however, are not fully understood.

The lack of data about the sources and sinks needed to explain the variation in moisture contents with depth limits the ability to prescribe recharge variations with depth in the transport modeling

(Rogers et al., 1997). Furthermore, it is not clear what effect the flow conditions within the disposal units will have upon rates of recharge at greater depths. In lieu of this information, the conceptual groundwater model assumes a vertical recharge rate that is constant with depth; this rate is estimated on the basis of expected moisture flux boundary conditions at the surface of the disposal facility. Rates of infiltration were assumed to be the same for portions of the site occupied by disposal units and undisturbed areas; this approach is consistent with the findings of Newman et al. (*Appendix F*), which indicated no significant differences in fluxes for boreholes located within and immediately adjacent to disposal pits.

Several surface structures, including asphalt pads, have been constructed at MDA G in support of waste management activities. These paved areas may result in elevated moisture contents in the underlying soils and focus runoff, both of which could translate into higher rates of water infiltration through the disposal pits and shafts. The effects of these pads were noted in recent work conducted by Newman et al. (*Appendix F*), who found that moisture contents and fluxes were significantly higher in paved portions of MDA G than in unpaved portions. The long-term impacts of elevated moisture contents resulting from asphalt pads will depend on the amount of additional water that is present and how long these conditions last. Some asphalt pads have been in place at MDA G for several decades, others are expected to be in place for much shorter periods of time before they are removed in conjunction with final closure of the disposal units. Once the pads are removed, moisture conditions are expected to gradually return to natural or background conditions. However, this may require several years.

It is not entirely clear which disposal units may be affected by the elevated moisture conditions caused by the placement of asphalt pads at MDA G or how much additional water may be in contact with the waste as a result of these pads. Furthermore, while elevated moisture may be present in some of the pits and shafts, information discussed earlier suggests these moisture conditions may not persist at depth. Based on this lack of information, the conceptual model does not assume that groundwater contaminant transport is affected by any additional moisture introduced by the presence of the asphalt pads.

Canyon Hydrologic Processes

The canyons at the Laboratory may be wet or dry; the wet canyons contain ephemeral streams and groundwater in the canyon bottom alluvium. Liquid discharges to these canyons and natural runoff reaching the stream channel may maintain shallow bodies of water in the alluvium; these waters typically reach their highest levels in response to runoff from late spring snowmelt and late summer thunderstorms. Shallow alluvial groundwater serves as a source of infiltration to the underlying unsaturated zone; this infiltration may recharge deeper zones of perched groundwater and the regional aquifer. Dry canyons have less stream flow and may lack alluvial groundwater altogether. They generally contribute little recharge under natural conditions. However, prolonged discharges of effluent to dry canyons may result in enhanced recharge to the deeper unsaturated zone.

The canyons adjacent to Area G include Cañada del Buey to the north and Pajarito Canyon to the south. Cañada del Buey is one of the drier canyons at the Laboratory; the alluvium in this canyon is thin and contains no perennial saturation (Purtymun and Kennedy, 1971; Devaurs and Purtymun, 1985). Pajarito Canyon also contains an intermittent stream but the larger flows observed in this canyon support a perennial groundwater body in the alluvium (Devaurs and Purtymun, 1985).

Intermediate zones of groundwater occur beneath the major canyon systems at the Laboratory, particularly those that originate in the Jemez Mountains to the west. The locations of these zones depend upon the availability of water from overlying alluvium as well as the hydrogeologic characteristics of subsurface units. The locations of perched zones are determined by the presence of sufficient recharge, permeability variations, and geologic structure and may occur at several depths. The perched zones do not generally extend laterally beneath the mesas, although some lateral spreading of the perched groundwater may occur if the course of the canyon and dip of the perched water do not coincide.

High rates of recharge in the canyons may influence the transport of contaminants leached from the disposal units at Area G. While it is highly unlikely that rates of water infiltration beneath Cañada del Buey are great enough to impact the disposal facility, this is less clear with respect to Pajarito Canyon. As part of the groundwater transport modeling conducted in support of the performance assessment and composite analysis, Stauffer et al. (*Appendix E*) examined the impacts of a range of Pajarito Canyon infiltration rates on the times required for contaminants to travel between the disposal units and the underlying regional aquifer. The results of this modeling indicated that contaminant transport is insensitive to increased recharge from the canyon for realistic values of infiltration rate and canyon width along Pajarito Canyon.

Vadose-Zone Hydrologic Processes Below the Bandelier Tuff

The Cerros del Rio basalts lie between the Guaje Pumice Bed and the Puye Formation; the lower portion of the basalts lies below the surface of the water table. While numerous studies have provided large-scale measurements of saturated conductivity within the basalts, large-scale unsaturated properties are generally unknown (Rogers et al., 1997). The basalts are highly variable in texture and contain joints and vesicles; these flows include interflow deposits and sections of scoria, which may or may not contain deposits of secondary minerals. Large spatial variations in texture can be expected to lead to large variations in unsaturated hydrologic properties.

Evidence for fracture flow and transport in the Cerros del Rio basalts is cited by Stauffer and Stone (2005). Ponded water that accumulated at the top of the basalts in lower Los Alamos Canyon quickly advanced several tens of meters within 10 to 14 days of the first ponding event; this rapid advance suggests flow through the fractures. While a large supply of water was required to promote fracture flow, bodies of perched water in some wet canyons may be capable

of supplying the necessary water. Model calibration to the observed data yielded high permeability and low effective porosity, consistent with fracture transport.

Groundwater modeling conducted in support of the 1997 performance assessment and composite analysis (Hollis et al., 1997) described the basalts using an equivalent continuum approximation with media properties that produced rapid fracture transport. A similar approach was adopted for the current analyses using ranges for permeability and porosity values derived by Stauffer and Stone (2005). The high permeability and low porosity assigned to the material under this approach ensure high rates of travel through this formation.

Lateral flow may occur at dipping lithologic interfaces when there are large contrasts in permeability and flow retention properties (Rogers et al., 1997); several such interfaces may occur beneath Area G. These include the vapor-phase notch, the Cerro Toledo interval, and the Guaje Pumice Bed. The lateral diversion of flow could significantly alter groundwater flow paths and, as a result, change contaminant transport behavior at the site.

As discussed in *Appendix E*, Robinson et al. (1999) conducted simulations which demonstrated that changes in material properties can lead to reduced permeability across interfaces. Those investigators report that perched water was projected to occur at the top of the Cerros del Rio basalts with a reduction in the interface permeability on the order of 0.001. The groundwater flow and transport modeling conducted in support of the performance assessment and composite analysis imposed permeability reductions at the top of the basalts and at the base of Tshirege Member unit 1g to address the potential impacts of permeability reductions on flow patterns beneath the disposal facility.

Saturated Zone Transport

The aquifer beneath the Laboratory lies within the fractured Cerros del Rio basalts and the sedimentary rocks of the Puye Formation (Keating et al., 2005) (see Figure 2-9, Section 2). The water table is located at depths of approximately 360 m (1,200 ft) along the western edge of the Pajarito Plateau and 180 m (600 ft) along the eastern edge. Water in the aquifer flows in an east-southeasterly direction toward the Rio Grande (Purtymun, 1984); available data indicate that flow has been in this direction for several thousand years (Keating et al., 2005). While flow within the aquifer is primarily horizontal, water and solutes may also move vertically in response to the pumping of water supply wells in the area. Travel times within the aquifer are poorly understood.

The Rio Grande is the main discharge area for the aquifer. The largest component of aquifer recharge occurs as underflow of water from the Sierra de los Valles, west of the Pajarito Plateau. Recharge from the larger canyons on the Pajarito Plateau is a secondary source of recharge to the aquifer.

Contaminant travel times within the regional aquifer are poorly understood because of the lack of tracer tests and in situ measurements of effective porosity (Keating et al., 2005). Radiocarbon ages for groundwater reported by Rogers et al. (1996, as cited in Keating et al., 2005) range from about 1,000 to 6,000 years beneath the Pajarito Plateau to several tens of thousands of years near the Rio Grande. The presence of tritium in the aquifer beneath the Laboratory demonstrates that young waters are present as well.

The groundwater transport modeling conducted in support of the performance assessment and composite analysis did not explicitly model flow and transport within the regional aquifer. Also, the effects that pumping at water supply wells may have on contaminant transport were not considered in the modeling. An average gradient to the Rio Grande was defined based on head measurements at regional wells. This approach results in rapid transport of contaminants from the locations where contaminants are discharged to the aquifer beneath Area G to the compliance boundary; travel times are on the order of a few to several years.

Geochemical Interactions

Rates of contaminant transport from the disposal units at Area G to the regional aquifer will depend upon rates of recharge through the vadose zone, as discussed below. They will also depend on geochemical interactions between the radionuclides and the Bandelier Tuff (Longmire et al., 1996). The sorption of radionuclides on the tuff is a function of the surface area and mineralogy of the material and the chemistry of the water in contact with the tuff. As discussed with respect to contaminant leaching, Longmire et al. conducted batch sorption experiments to estimate the sorption behavior of radionuclides disposed of at Area G. Krier et al. (1997) and Bechtel/SAIC (2004) have compiled sorption coefficients for some of the elements that are of concern at Area G, including data for devitrified tuff from Yucca Mountain; the Bandelier Tuff is expected to have similar sorption capacities as this material.

3.2.2.2 Atmospheric Transport

Contaminants deposited on the surface of the disposal facility as a result of plant and animal intrusion and vapor- and gas-phase radionuclides diffusing from the site may be transported off-site by the prevailing winds. Rates of particulate resuspension will depend upon the characteristics of the soil (e.g., particle size distribution, cohesiveness, and moisture content), surface conditions (e.g., plant cover, ground surface roughness, and topography), and site meteorological conditions (e.g., wind velocity and turbulence). From an exposure standpoint, particles greater than 50 μm (0.002 in.) in diameter will pose little risk to persons living downwind of Area G because of their large settling velocities. Smaller particles may remain airborne long enough to be transported significant distances downwind. Cover conditions will change over time as the site transitions from a grassland-dominated landscape shortly after facility closure to piñon-juniper woodland. As

discussed in Section 2.1.2, the complex terrain and vegetation characteristics at the Laboratory result in complex wind conditions at sites such as Area G.

The atmospheric dispersion conditions described in Section 2.1.2.3 will ultimately determine airborne contaminant concentrations downwind of Area G. Dispersion patterns change dramatically in response to wind conditions. In a tracer study conducted by Archuleta et al. (1978), 3 μm (1.2×10^{-4} in.) diameter particles released in Los Alamos Canyon under stable nocturnal conditions were transported down the canyon by the drainage winds. In contrast, particles released at TA-50 (to the west of Area G) under daytime cross-canyon wind conditions were transported in a northwesterly direction. Modeling conducted by Costigan and Bossert (1996) suggested that releases from Area G under daytime conditions would also be transported to the north and west.

As shown in Figure 2-6 (Section 2), mesa-top winds are predominantly from the northwest under nighttime conditions, mirroring conditions in Pajarito Canyon (Figure 2-7, Section 2). On this basis and the results of the tracer experiment discussed above, airborne contaminants will be transported in a southeasterly direction toward the town of White Rock during the night. Under daytime conditions, any releases from the site are likely to be transported to the north and east with the prevailing southwesterly winds (Figure 2-6, Section 2).

Particulates suspended from Area G will undergo dry and wet deposition as they are transported to downwind locations. As was the case for particulate resuspension, rates of dry deposition will depend on a variety of particle, surface, and meteorological characteristics. In terms of wet deposition, particulates may be removed by in-cloud scavenging (rainout) and below-cloud scavenging (washout). Particulate deposition is taken into account in the atmospheric transport modeling. No deposition of the vapor- and gas-phase contaminants included in the performance assessment and composite analysis is assumed to occur.

3.2.2.3 Surface Erosion

Contamination deposited on the surface of the disposal facility may be transported into the adjacent canyons through the effects of surface erosion. Under extreme conditions, or over extended periods of time, complete loss of cover over portions of the disposal site may result in the direct transport of waste off the mesa. Sediments may be transported from the disposal facility with surface runoff or as a result of winds.

Although most erosion studies of landfill covers have focused on water erosion, recent studies in semiarid landscapes have shown that the effects of wind on erosion and contaminant transport may be substantial (Whicker et al., 2002; Breshears et al., 2003). In fact, Breshears et al. note that soil loss due to wind erosion may exceed that due to water erosion in some systems. Thus, wind erosion could affect the long-term integrity of landfill covers and be an important

mechanism for the redistribution of any surficial contamination at a landfill site (Anspaugh et al., 1975; Sehmel, 1980; Arimoto et al., 2002).

As discussed by Whicker and Breshears in *Appendix C*, wind-driven soil movement can be thought of as having two directional components. Mass horizontal transport is a process in which larger soil particles (generally greater than 50 μm [0.002 in.] in diameter) are transported in a horizontal direction by saltation. The particles remain close to the ground (e.g., at a height of less than 1 m [3.3 ft]) and the process is generally indicative of local soil redistribution (Stout and Zobeck, 1996; Gillette et al., 1997). Mass vertical transport refers to the movement of smaller soil particles (generally less than 50 μm [0.002 in.] in diameter) at heights of 1 m (3.3 ft) or more over extended distances. These particles can be transported into an area (deposition) or removed from an area (resuspension).

Although wind erosion may play an important role in contaminant transport, the data needed to quantify these effects are limited. In recognition of this, Whicker and Breshears (*Appendix C*) collected data to provide initial estimates of wind erosion for Area G. Data were collected at grassland and piñon-juniper woodland settings located west of the disposal facility; these sites were considered to be reasonable analogs for the disposal site shortly after facility closure and after the site transitions to woodland, respectively. Horizontal particulate flux measurements were conducted at both sites, while vertical fluxes were measured at the grassland location.

Horizontal fluxes 1 m (3.3 ft) above the ground at the grassland site were significantly greater than fluxes measured in the woodland setting. This difference was likely the result of higher ground-level wind velocities at the grass-covered site. However, measurements of fluxes entering and exiting the circular study plots at both sites indicated no net loss of soil from either area. Vertical flux measurements at a height of 2 m (6.6 ft) indicate little, if any, net loss of soil from the grassland study site.

On the basis of the work conducted by Whicker and Breshears (*Appendix C*), it appears that little or no net loss of cover will occur at Area G as a result of wind erosion. This study was not designed to investigate the manner in which soils may be redistributed across the disposal site, however, and these findings do not rule out potentially significant impacts of wind in terms of contaminant transport. That is, contaminated soils at the surface of the disposal facility may be transported vertically and horizontally, only to be replaced by uncontaminated soils from upwind locations. Because the information needed to model this aspect of wind erosion was not available, the horizontal transport of surface contamination by wind was not included in the radionuclide transport modeling conducted in support of the performance assessment and composite analysis. As discussed elsewhere, the vertical flux measurements collected by the investigators were used to estimates rates of particulate resuspension from Area G.

Spatial and temporal patterns of surface erosion due to runoff are a complex function of many factors, including the design features of the cover placed over the disposal units and site ecological and meteorological conditions. Important cover design features include the manner in which the cover is sloped and contoured in response to the topography of the site, the physical properties of the materials used in its construction, and the presence of any engineered features. The plants and animals inhabiting the site will influence the water balance of site soils, affect cover conditions at the site, and shape the development of soil structure over time. The quantities and intensities of precipitation falling on the site as well as the thermal regime will have strong impacts on the generation of surface runoff and, hence, rates and patterns of erosion.

Sediment transport from the mesa top will include runoff-driven or advective processes and gravity-driven (diffusion) processes. The intensity of runoff-driven sediment transport at a given location is a function of the area that drains through that location and the slope of the surrounding landscape; runoff-driven erosion will be moderated by several factors including vegetation cover, the degree of soil disturbance, and soil type. Diffusive transport includes processes such as rainsplash (sediment particles ejected from the surface by raindrop impacts), tree-throw (sediment tumbled downslope when the root ball of a fallen tree is exposed at the surface), and the establishment of animal burrow mounds.

3.2.3 Exposure Pathways and Scenarios

The means through which humans may be exposed to radioactive materials are called exposure pathways. Each exposure pathway includes a source or release from a source, a transport or exposure medium, a location at which the exposure occurs, and an exposure route. The actual exposure pathways that may lead to human exposures will depend upon the patterns of human activity at, and adjacent to, the disposal site. Patterns of human activity may be specified by using a collection of appropriate exposure pathways, which is generally referred to as an exposure scenario.

The level of control exerted by the DOE over the Laboratory and Area G is assumed to change over the facility's lifetime; these changes will play a role in determining the relevant exposure pathways and scenarios. As discussed in Section 1.3, it is assumed that the DOE will retain control over the entire Laboratory throughout the operational, closure, and active institutional control periods. During these periods, the exposure locations closest to Area G will be downwind or downgradient of the Laboratory. Control over the entire Laboratory is assumed to cease at the end of the active institutional control period; however, it is expected that the DOE will continue to exercise administrative control over individual sites such as Area G. Thus, receptors may move nearer to the closed disposal facility during the passive institutional control period, perhaps as close as immediately outside of the Area G boundary or fence line.

The exposure pathways and scenarios included in the performance assessment and composite analysis are based on the level of DOE control outlined above. These pathways and scenarios are described in Section 3.2.3.1 for the operational, closure, and active institutional control periods, and in Section 3.2.3.2 for the passive institutional control period. Releases from other sources of radioactivity at LANL may add to the exposures projected for these scenarios. Any interactions between Area G and these other sources must be taken into account for the composite analysis; a conceptual discussion of the potential for source interaction is provided in Section 3.2.3.3.

3.2.3.1 Operational, Closure, and Active Institutional Control Periods

The sources of contamination that may result in human exposure will change as the site passes from the operational period to the active institutional control period. Plants and animals may root or burrow into the buried waste and bring contamination to the surface of the disposal facility during all phases; however, the quantities of contamination deposited on the surface during the operational and closure periods will tend to be small. The establishment of plant and animal communities at the site will be slowed or prevented by ongoing operations and closure activities, and any signs of significant intrusion into the waste will be remedied quickly. Radionuclides may be leached from the buried waste by water infiltrating through the site and be transported to the regional aquifer, exposing persons who use this water downgradient of the Laboratory to contamination. Similarly, vapor- or gas-phase contaminants may diffuse from the waste and enter the atmosphere, exposing persons living downwind of LANL to airborne contaminants that have been transported by the prevailing winds.

Although steps will be taken to ensure proper facility functioning during the active institutional control period, these may not prevent plant roots and animal burrows from penetrating the waste and depositing contamination on the surface. Contamination may be suspended and transported by prevailing winds to locations downwind of the Laboratory and transported to canyons adjacent to Area G by surface runoff. Receptors in areas downwind of the Laboratory or in Cañada del Buey, part of which lies outside the Laboratory, may be exposed to radiation. Members of the public living outside the Laboratory boundary may continue to be exposed to radionuclides discharged to the regional aquifer and to vapor- and gas-phase contaminants diffusing from the disposal facility.

The exposure scenarios selected for the performance assessment and composite analysis take into account the sources of contamination discussed above; these scenarios are summarized in Table 3-1. The Groundwater Resource Protection Scenario is implemented at a location 100 m (330 ft) downgradient of Area G; projected exposures are limited to the ingestion of contaminated groundwater and are used to assess compliance with the groundwater protection standards discussed in Section 1.5.2. The scenario is implemented on restricted Laboratory lands because it is designed to ensure protection of the groundwater resource, regardless of whether members of the public can access the water.

Table 3-1
Off-Site Exposure Scenarios for the Area G Performance Assessment and Composite Analysis

Period and Exposure Scenario	Exposure Pathways and Routes	Point of Exposure
Operational, Closure, and Active Institutional Control Periods		
Groundwater Resource Protection [a]	Ingestion of drinking water	100 m downgradient of Area G
All Pathways–Groundwater	• Ingestion of drinking water • Ingestion of food crops grown in contaminated soils and irrigated with well water • Ingestion of animal products from animals raised by the receptor • Ingestion of contaminated soil • Inhalation of airborne radionuclides • Direct radiation from airborne radionuclides • Direct radiation from contaminated soils	LANL boundary near White Rock
Atmospheric	• Ingestion of food crops grown in contaminated soils and contaminated by airborne radionuclides • Ingestion of animal products from animals raised by the receptor • Ingestion of contaminated soil • Inhalation of airborne radionuclides • Direct radiation from airborne radionuclides • Direct radiation from contaminated soils	Point of maximum exposure outside of LANL boundary
All Pathways–Cañada del Buey	• Ingestion of food crops grown in contaminated soils • Ingestion of animal products from animals raised by the receptor • Ingestion of contaminated soil • Inhalation of airborne radionuclides • Direct radiation from airborne radionuclides • Direct radiation from contaminated soils	Cañada del Buey adjacent to Area G

[a] *This scenario was evaluated only for the performance assessment.*

Table 3-1 (Continued)
Off-Site Exposure Scenarios for the MDA G Performance Assessment and Composite Analysis

Period and Exposure Scenario	Exposure Pathways and Routes	Point of Exposure
Passive Institutional Control Period		
Groundwater Resource Protection [a]	Ingestion of drinking water	100 m downgradient of Area G
All Pathways–Groundwater	• Ingestion of drinking water • Ingestion of food crops grown in contaminated soils and irrigated with well water • Ingestion of animal products from animals raised by the receptor • Ingestion of contaminated soil • Inhalation of airborne radionuclides • Direct radiation from airborne radionuclides • Direct radiation from contaminated soils	100 m downgradient of Area G
Atmospheric	• Ingestion of food crops grown in contaminated soils and contaminated by airborne radionuclides • Ingestion of animal products from animals raised by the receptor • Ingestion of contaminated soil • Inhalation of airborne radionuclides • Direct radiation from airborne radionuclides • Direct radiation from contaminated soils	Point of maximum exposure outside of Area G boundary
All Pathways–Cañada del Buey	• Ingestion of food crops grown in contaminated soils • Ingestion of animal products from animals raised by the receptor • Ingestion of contaminated soil • Inhalation of airborne radionuclides • Direct radiation from airborne radionuclides • Direct radiation from contaminated soils	Cañada del Buey adjacent to Area G

[a] *This scenario was evaluated only for the performance assessment.*

Table 3-1 (Continued)
Off-Site Exposure Scenarios for the MDA G Performance Assessment and Composite Analysis

Period and Exposure Scenario	Exposure Pathways and Routes	Point of Exposure
All Pathways–Pajarito Canyon	• Ingestion of food crops grown in contaminated soils • Ingestion of animal products from animals raised by the receptor • Ingestion of contaminated soil • Inhalation of airborne radionuclides • Direct radiation from airborne radionuclides • Direct radiation from contaminated soils	Pajarito Canyon adjacent to Area G

[a] *This scenario was evaluated only for the performance assessment.*

The All Pathways–Groundwater Scenario is implemented at the Laboratory boundary near the town of White Rock. The receptor is assumed to receive exposures from the inhalation and ingestion of radioactivity, and from direct radiation. Radionuclides deposited on the surface soil with irrigation water are suspended and inhaled by the individual during time spent at home. Ingestion doses result from the consumption of crops irrigated with contaminated water, animal products (e.g., beef and milk or chicken and eggs) from animals raised on location, soil, and drinking water. Exposures to direct radiation from airborne contamination at the homestead and radioactivity deposited on the soil add to internal exposures.

The Atmospheric Scenario is implemented at the point of maximum atmospheric exposure outside of the Laboratory's boundaries. During the operational and closure periods, the receptor inhales radioactive gases (excluding radon and its progeny, which are modeled separately); following closure, contaminated particulates resuspended from the surface of Area G and transported with the prevailing winds add to these exposures. The deposition of airborne radionuclides contaminates crops grown by the individual and surface soils at the exposure location. Doses are received through the ingestion of contaminated vegetables, animal products, and soil. External exposures are received from contaminated soil surfaces and airborne radioactivity. Radon fluxes from the disposal site are projected separately.

The All Pathways–Cañada del Buey Scenario estimates potential doses resulting from the transport of contamination from Mesita del Buey to the canyon due to surface runoff and erosion. A person residing in the canyon is assumed to be exposed to radiation as a result of inhaling particulates suspended from contaminated soil surfaces and by way of ingesting contaminated crops, animal products, and soil. Exposures to direct radiation from airborne contamination at the homestead and radioactivity deposited over the resident's lot add to the internal exposures.

The locations used to project doses for the off-site exposure scenarios are consistent with DOE restrictions on public access, hydrologic and atmospheric conditions, and land use patterns in the vicinity of Area G. Because the DOE is expected to retain control of the entire Laboratory during the operational, closure, and active institutional control periods, the nearest location that a residence or well could be established during this time would be in Cañada del Buey to the north of Area G or the area immediately adjacent to White Rock. The area around White Rock lies along the prevailing groundwater flow path and is the first location at which groundwater contaminated by releases from Area G could be used while restrictions on Laboratory access are in place.

The exposures modeled at the point of maximum atmospheric exposure account for the prevailing meteorological conditions, the complex terrain, and the demographics in the vicinity of Area G. The receptor location in Cañada del Buey is the closest point to the disposal facility where members of the public can take up residence while DOE maintains control over the

Laboratory. While no residences currently exist in the canyon, inclusion of the All Pathways–Cañada del Buey Scenario addresses this future possibility.

The assessment of exposures to members of the public at the locations identified in Table 3-1 is expected to provide reasonably conservative estimates of potential exposures during the operational, closure, and active institutional control periods. As stated earlier, the location near White Rock is the first point where regular usage of water drawn from the regional aquifer is possible. Consequently, any exposures from the use of contaminated groundwater are expected to be greatest at this location. Groundwater pathway doses at locations farther downgradient of Area G will diminish as the concentrations of groundwater contamination abate due to dilution and dispersion. By definition, the location of the point of maximum atmospheric exposure will bound doses to off-site individuals following airborne releases from the disposal facility. Finally, during the operational, closure, and active institutional control periods, Cañada del Buey will be the closest receptor location subject to potential impacts from contamination transported by surface runoff from Area G.

Groundwater may occur at the Laboratory in the alluvium in canyon bottoms, as zones of perched groundwater, and in the regional aquifer. The source of water used by an off-site resident will directly influence the magnitude of any doses received from contaminated groundwater. Therefore, the water source selected for the performance assessment and composite analysis is a significant aspect of the dose assessment.

The groundwater source used to estimate groundwater pathway exposures must meet three conditions. First, the potential for the groundwater source to be contaminated by radionuclides leached from the disposal facility must exist. Second, the groundwater must be of adequate quality and quantity to meet the user's needs. Finally, the source must be accessible to the individual during the operational, closure, and active institutional control periods.

The majority of the water percolating through the disposal facility is expected to flow vertically until it contacts the regional aquifer. Alluvial water in Pajarito Canyon and Cañada del Buey may become contaminated if radionuclides deposited on the surface of the disposal facility are transported into the canyons with surface runoff. No contamination of canyon alluvial waters is anticipated from radionuclides leached from the waste and transported downward with the water percolating through the disposal site. Zones of perched water may be present in the canyons and may become contaminated as radioactivity in the alluvium is transported downward; perched groundwater has not been observed below the surface of Mesita del Buey (LANL, 1998a, as cited in LANL, 2001).

In terms of water quality and supply characteristics, there is no evidence that zones of perched water in the vicinity of Area G are capable of meeting an individual's water needs. Similarly, the

alluvial waters in Pajarito Canyon and Cañada del Buey are not expected to be capable of supporting average household use. The alluvial water in Pajarito Canyon, which is a more substantial source of water than Cañada del Buey, would generally be pumped dry by a household well during most seasons of the year. Adequate water may be available in the canyons for short periods of time following spring snowmelt and in summer thunderstorms. However, the only reliable source of water capable of meeting the quality and quantity needs of a resident is the regional aquifer.

During the operational, closure, and active institutional control periods, off-site residents would have limited access to groundwater from alluvial and perched zone sources. Any such sources within Pajarito Canyon near Area G will be inaccessible because of DOE land use restrictions; access may be available near the town of White Rock, approximately 2 km (1.2 mi.) downstream. The limited quantity of alluvial and perched groundwater within Cañada del Buey would be accessible to individuals throughout these periods because the border of LANL and San Ildefonso lands cuts through this canyon.

On the basis of the information presented above, the regional aquifer was selected as the source of water for the Groundwater Resource Protection and All Pathways–Groundwater Scenarios. While alluvial and perched groundwater in Cañada del Buey is accessible in some areas and may be contaminated with radionuclides transported with surface runoff, it is not capable of meeting year-round household water needs. The regional aquifer may be contaminated by releases from Area G, is capable of meeting the off-site receptor's water needs, and is accessible to members of the public during the operational, closure, and active institutional control periods.

The potential exists for a member of the public to be exposed to radionuclides released from Area G to surface waters adjacent to, and downgradient of, Mesita del Buey. Surface runoff from the mesa may result in contaminated flows in Pajarito Canyon and Cañada del Buey. Separately, contaminated groundwater in the regional aquifer may eventually discharge to the Rio Grande, approximately 5 km (3.1 mi) downgradient of Area G.

Exposures resulting from the use of contaminated surface water during the operational, closure, and active institutional control periods were not considered in the Area G dose assessment. Surface flows within Cañada del Buey will be infrequent at best, and involve small amounts of water. Furthermore, active controls over the disposal site during these periods are expected to prevent significant transfers of contamination into the canyon via surface runoff. Projected exposures resulting from the use of contaminated surface water from the Rio Grande will be bounded by doses resulting from the use of contaminated water drawn from the regional aquifer. Radionuclide concentrations in the river will be lower than concentrations in the aquifer because of dispersive effects that occur within the aquifer during transport and because releases will be

diluted in the river. Consequently, the potential doses resulting from the use of surface water will be lower than the exposures received by using groundwater closer to the disposal facility.

3.2.3.2 Passive Institutional Control Period

Radionuclide releases to groundwater and the atmosphere, and any subsequent human exposures, may continue following the end of active institutional control. The loss of DOE control over the entire Laboratory may result in people residing immediately outside of the Area G fence line. Exposures to these potential receptors during the passive institutional control period are projected using the exposure scenarios listed in the latter portion of Table 3-1. The groundwater and atmospheric scenarios are functionally the same as those evaluated for the operational, closure, and active institutional control periods. The Groundwater Resource Protection and All Pathways–Groundwater Scenarios are implemented 100 m (330 ft) downgradient of Area G. The Atmospheric Scenario is implemented at the point of maximum exposure outside of the Area G boundary; radon fluxes from the disposal site are projected separately.

The All Pathways–Cañada del Buey Scenario is the same as that evaluated during the active institutional control period. In addition, the loss of control over the entire Laboratory provides an opportunity for persons to reside in Pajarito Canyon, to the south of Area G. Potential exposures received by a person residing in this canyon are evaluated using the All Pathways–Pajarito Canyon Scenario. Contamination transported into the canyon with surface runoff is assumed to lead to exposures of the canyon resident via the same pathways described for the scenario in Cañada del Buey.

The source of groundwater for the Groundwater Resource Protection and All Pathways–Groundwater Scenarios was assumed to be the regional aquifer. While Pajarito Canyon is a much wetter canyon than Cañada del Buey, the alluvial groundwater is still not plentiful enough to meet domestic household needs. Exposures resulting from the use of contaminated surface water during the passive institutional control period were not considered. Concentrations of soluble radionuclides in the stream in Pajarito Canyon are expected to be small and flow within the stream is not sufficient to supply water needs on a permanent basis. Radionuclide concentrations in the regional aquifer are expected to exceed those encountered in the Rio Grande for the reasons discussed above.

3.2.3.3 Alternate Source Contributions

The potential for significant interactions between alternate sources of radioactive contamination at the Laboratory and releases from Area G will depend upon three factors:

- The magnitude of the radionuclide inventories at the other sources
- The potential for and the magnitude of contaminant release rates from these sources

- The potential for the transport of significant quantities of contamination to the exposure locations included in the Area G composite analysis during the 1,000-year compliance period

Potentially significant quantities of radioactive waste have been disposed of at several locations across the Laboratory. Several MDAs have been used for the disposal of radioactive waste since the Laboratory began operations in 1943; the more prominent ones include MDAs A, B, C, and T. Some of these facilities were the primary radioactive waste disposal sites in their day, much as Area G is today. Another disposal area, MDA AB, was used in the early 1960s to conduct belowground hydronuclear experiments, which resulted in the contamination of crushed tuff surrounding the test chambers. Liquid wastes have been discharged to many of the canyons found at LANL, including Cañada del Buey and Pajarito Canyon; although these discharges have decreased over the years, significant quantities of radioactivity were disposed of in some canyons.

The potential for the release of contaminants from other sources of radioactivity at the Laboratory varies by site. Waste at the MDAs mentioned above is buried beneath varying thicknesses of cover material. As a result, releases from these facilities are most likely to occur as a result of biotic intrusion into the waste or groundwater leaching; also, vapor- or gas-phase radionuclides may diffuse from the waste. The magnitudes of any such releases will depend on the characteristics of the repository covers, the plant and animal communities inhabiting the sites, and the amount of water percolating through the waste, among other factors.

Radionuclides leached from the waste at the alternate source MDAs may be transported through the vadose zone and discharged to the regional aquifer; contaminant plumes from these facilities could intersect releases at the base of Area G and pose a higher cumulative risk to groundwater users than that estimated for Area G alone. Contaminants deposited at the surface of an alternate source MDA may be resuspended and carried with the prevailing winds to locations that are affected by atmospheric releases from Area G; radionuclides diffusing from another site may also be transported to these locations. Radionuclides discharged to canyons may migrate downstream with normal stream flow and floods, be transported to the regional aquifer, or be resuspended and transported by the prevailing winds.

Cumulative exposures from all sources of radioactivity at the Laboratory are evaluated over the 1,000-year compliance period. Contaminant releases from other MDAs or the canyons must be transported to the exposure locations impacted by Area G within this period in order for interactions to occur between these sources. Although any radionuclides that become airborne from MDAs will be transported to downwind locations quickly, releases to groundwater may require hundreds or thousands of years to reach the regional aquifer. Thus, groundwater releases that may occur from other sources are not likely to interact with Area G groundwater releases during the compliance period.

3.3 Source Term Modeling

The source term modeling conducted in support of the Area G performance assessment and composite analysis is described below. The manner in which the waste inventory was represented is discussed in Section 3.3.1, and screening evaluations conducted to limit the scope of the modeling to those radionuclides that may pose a significant risk to human health and the environment are described in Section 3.3.2. The approaches used to model the release mechanisms discussed in Section 3.2 are addressed in Section 3.3.3.

3.3.1 Representation of Waste Characteristics

The performance assessment and composite analysis inventories are summarized in Section 2.3; complete details of these inventories are provided in *Appendix J*. As described in Section 2.3.4, several sources of uncertainty are associated with the projected waste inventories; these include the techniques used to estimate radionuclide activities in waste packages; the allocation of MAP, MFP, and material type waste to specific radionuclides; and the use of extrapolation methods to estimate pre-1970 and post-2003 inventories. Distributions were used to describe the errors associated with activity estimation techniques and the allocation of MFP and material type waste to specific radionuclides (*Appendix K*). The information needed to quantify the errors associated with the allocation of MAP waste to specific radionuclides and those introduced by the use of extrapolation techniques was unavailable.

The waste disposal units within each waste disposal region are represented in the GoldSim models as a mixture of waste and crushed tuff backfill. Radionuclide inventories are introduced into the units over the period of time that the units were, or will be, active; all units within a waste disposal region are assigned to the same disposal period. Rates of addition are assumed to be linear throughout the disposal period. The introduced waste is partitioned between the waste/backfill and the air and water-filled pore spaces within these media.

As discussed above, the site model represents the buried waste as 20 discrete layers. The use of multiple layers requires that the inventories be allocated among the different layers. This is done on the basis of the volume of waste within each layer, resulting in homogeneous radionuclide concentrations throughout the disposal units.

3.3.2 Radionuclide Screening

Disposal records indicate that more than 240 radionuclides have been disposed of in the pits and shafts at Area G; however, many of these contaminants pose little or no risk to human health and the environment. To minimize the complexity of the models and to streamline model computations, screening evaluations were conducted to identify low-risk radionuclides. These radionuclides were subsequently excluded from the performance assessment and composite analysis.

As discussed in Section 2.3.1, some radionuclides were excluded from the performance assessment and composite analysis inventories on the basis of their half-lives. All radionuclides disposed of in the pits and shafts were reviewed in terms of their modes of decay and those with half-lives of 5 years or less were generally excluded from the inventory projections. The primary exception was for radionuclides that are daughters of parents with half-lives greater than 5 years. A complete description of the methods used to eliminate radionuclides from the inventory on the basis of decay characteristics is provided in *Appendix J*.

Most of the radionuclides included in the performance assessment and composite analysis will not pose a health threat to persons using water contaminated by Area G releases because they will be present in the regional aquifer in negligible quantities, if at all. A screening evaluation was conducted to identify these radionuclides, which were then eliminated from the groundwater transport modeling. The two-step process took into account the risk posed by the contaminants under conservative release conditions and radionuclide travel times to a well immediately downgradient of Area G. A detailed description of the screening evaluation is provided in *Appendix L* (Volume 3).

The first groundwater pathway screen examined the potential for unacceptable impacts under conservative release conditions. For this screen, it was assumed that all radionuclides present in the waste entered into the soil moisture and were transported immediately to the regional aquifer. Further, it was assumed that the leachate was diluted in the regional aquifer and that water drawn from the aquifer was consumed by a hypothetical receptor at the rate of 2 L/d (0.53 gal/d). Radionuclide-specific doses were estimated for the receptor and compared to a dose limit of 4 mrem/yr, the dose standard included in 40 CFR 191 for beta and photon emitters (Section 1.5.2). Radionuclides with an estimated dose of less than 4 mrem/yr were eliminated from the groundwater transport modeling; contaminants with doses greater than 4 mrem/yr were carried forward in the screening process.

The maximum leachate concentrations were calculated as the quotient of the radionuclide concentrations in the buried waste and the volume of moisture in the pit and shaft waste. The radionuclide inventories used in these calculations were those estimated for the composite analysis, which represent all waste that has been or will be disposed of at Area G. The volume of water in which these inventories were dissolved was estimated by multiplying the total waste volume by the volume-based moisture content of the material. Leachate discharged to the regional aquifer will be diluted with clean water prior to the withdrawal of the contaminated water via a hypothetical domestic well. This dilution volume was estimated as the product of the area of the disposal units in which the waste is disposed of at Area G and the assumed casing length of the domestic well.

Several radionuclides included in the Area G inventory are parents of radioactive decay chains. To project drinking water doses for these radionuclides it was necessary to make assumptions about the extent to which daughter ingrowth occurred for these constituents. Consequently, all short-lived daughters of long-lived parents were assumed to be in secular equilibrium with their parents. Long-lived daughters of short-lived parents were assumed to be present at a fraction of the parent's inventory that was equal to the ratio of the parent's and daughter's half-lives. Long-lived daughters of long-lived parents were assumed to be present at the maximum activity achieved during 10,000 years of ingrowth.

The second step of the groundwater pathway screening evaluation considered the time required for radionuclides leached from the waste to reach the regional aquifer. Modeling conducted by Stauffer et al. (*Appendix E*) indicates that groundwater travel times to the aquifer range from hundreds to thousands of years. Many of the radionuclides leached from the waste will decay to negligible levels by the time they discharge to the aquifer, rendering them harmless to persons using the water. Given this, the radionuclides that were not excluded from the groundwater pathway modeling on the basis of the first screen were evaluated to determine their decay characteristics relative to the time required to transport releases from the pits and shafts to the aquifer.

The potential for radionuclide release to the aquifer was evaluated using a two-step process. First, the estimated time needed for groundwater to travel from the base of the disposal units to the aquifer was compared to the half-life of each radionuclide. If the ratio of groundwater travel time to half-life was greater than 10, the contaminant was excluded from further consideration. The second step compared contaminant travel times to radionuclide half-lives; if the ratios of the contaminant travel times and half-lives were equal to or greater than 10, the constituents were excluded from the performance assessment and composite analysis groundwater modeling.

Particle tracking to estimate the groundwater travel times was performed with the Finite Element Heat and Mass (FEHM) model. As discussed in detail in *Appendix E*, FEHM was used to estimate rates of contaminant transport vertically through the unsaturated zone and horizontally within the regional aquifer. Travel times will depend upon the rate at which water infiltrates through the disposal site. For screening purposes, an infiltration rate of 0.1 mm/yr (0.039 in./yr) was assumed; this rate functionally bounds the infiltration rates projected for the final cover configuration that was adopted for the performance assessment and composite analysis. Based on this infiltration rate, a distribution of travel times ranging from approximately 23,000 to 100,000 years was projected; a travel time of 23,000 years was adopted for screening purposes.

The contaminant travel time is given by the following equation:

$$CT_i = \frac{GT \times Kd_i \times \rho}{p} \qquad 3\text{-}1$$

Where

CT_i = contaminant travel time for radionuclide *i* (yr)
GT = groundwater travel time (yr)
Kd_i = distribution coefficient for radionuclide *i* (m^3/kg)
ρ = bulk density of unsaturated zone (kg/m^3)
p = effective porosity of unsaturated zone

The unsaturated zone distribution coefficients that were used to estimate contaminant travel times were selected on the basis of several sources of information about devitrified tuffs and, when necessary, other soils. The minimum values found in these sources were used to conduct the groundwater pathway screening. A bulk density of 1,400 kg/m^3 (87 lb/ft^3) and an effective porosity of 0.4 were adopted for the contaminant travel time calculations; these data are consistent with hydrogeologic data provided in Table 2-6 (Section 2).

3.3.3 Contaminant Release

As discussed in Section 3.2.1.2, contaminants may be released from the waste stored at Area G through biotic intrusion, leaching, diffusion, and erosion. The models for each of these release mechanisms are described in detail below.

3.3.3.1 Biotic Intrusion

Intrusion into the waste by plants and animals inhabiting the closed disposal site may result in the transport of radionuclides to the surface of the facility. Consistent with the discussion in Section 3.2.1.2, biotic intrusion is considered here as a mechanism of release. Complete details of the biotic intrusion modeling may be found in *Appendix K*.

Plant Intrusion

Radionuclides taken up by plant roots will be deposited on the surface of the disposal facility when the plant sheds leaves or dies; contaminants will enter the surface soil as that litter decomposes. The rate of litter production is estimated as the product of the aboveground biomass of the plant and the litter production factor, which describes the annual fraction of the standing biomass that contributes to litterfall. The aboveground biomass densities and litter production factors differ among the four plant growth forms included in the modeling (i.e., grasses, forbs, shrubs, and trees), thus, rates of litter production are specific to the growth form under consideration.

The aboveground biomass densities of the four plant growth forms will change over time as the site transitions from grassland-dominated landscape shortly after closure to piñon-juniper woodland. Estimates of understory biomass for the early successional stages at Area G were based on information from several different sites. These sites included piñon-juniper woodlands that had been disturbed by fire or physical means, piñon-juniper grasslands, and areas adjacent to mature woodlands. Although the conditions at Area G are not expected to coincide exactly with the

conditions at any one of these sites, understory production data obtained from these communities provide reasonable estimates of conditions at the disposal site. A summary of the studies used to estimate aboveground biomass densities for early successional stages is provided in Table 3-2.

Biomass estimates for grasses, forbs, and shrubs in the mature piñon-juniper woodland were developed in a manner similar to that described above for the disturbed site. The data used to generate these estimates are summarized in Table 3-3, which includes a description of the investigated sites and a summary of the production and cover information provided in the literature. Some of the cited studies provide direct estimates of understory production in the mature woodland.

Limited information exists with respect to the aboveground biomass of trees in piñon-juniper woodlands. Grier et al. (1992) estimated aboveground biomass and net productivity for 90- and 350-year-old piñon-juniper communities in northern Arizona. Tree biomass was estimated using regression equations developed from destructive analysis of the two tree species, taking into account the full diameter range of trees found at the study sites. Net productivity was estimated as the sum of the annual biomass increment and litterfall. Though limited in nature, this information was used to estimate the aboveground biomass for trees.

The litter production rate is defined as the fraction of the aboveground biomass that dies and falls to the ground surface on an annual basis. With respect to grasses and forbs, several studies indicate that annual production rates typically range from 0.3 to 1.0 (Grier et al., 1992; Cox, 1984; Sims and Singh, 1978; and Scurlock et al., 2003). Rates of shrub litter production appear to be less than those observed in many grassland areas. Strojan et al. (1979) found 7 to 83 percent of live aboveground biomass was shed annually by six species of shrubs in the northern Mojave Desert; other estimates tend to range from 6 to 63 percent (e.g., Charley and Cowling, 1968; West, 1985; Parmenter et al., (1987); and Whittaker, 1975). Rates of tree litter production were estimated using data collected by Grier et al. (1992), which suggest litterfall is 0.1 percent of the aboveground biomass estimates for the two piñon-juniper woodlands examined. Other estimates tend to be higher and suggest 1 to 10 percent of the tree biomass is shed annually as litter (Hinesley et al., 1991; Strojan et al., 1979; and Whittaker, 1975).

The data cited above allow estimation of the litter production rates for the early successional stages at Area G and the piñon-juniper woodland. Rates of litterfall between these end points were estimated by assuming a linear transition from grassland and woodland. It was assumed that the successional transition started at the end of the 100-year active institutional control period and ended when the climax woodland was assumed to exist. The time required to attain the climax condition was defined on the basis of data collected in piñon-juniper woodlands in the southwestern U.S. by several investigators.

Table 3-2
Summary of Cover and Production Studies Used to Estimate Aboveground Biomass (early successional stages at Area G)

Community Characteristics	Reference	Cover (%)			Aboveground Production (kg/ha)		
		Grasses	Forbs	Shrubs	Grasses	Forbs	Shrubs
Piñon-Juniper Woodland in Central Utah (4 sites)	Clary, 1989	---	---	---	2.9E+02–7.7E+02	0–1.0E+02	7.9E+00–1.8E+02
Piñon-Juniper Woodland in Northern Arizona (4 plots, 4–11 years after cabling and seeding)	Clary, 1971	---	---	---	2.5E+02 (avg.)	4.8E+02 (avg.)	3.8E+02 (avg.)
Piñon-Juniper Woodland in Arizona (22 plots)	Clary and Jameson, 1981	---	---	---	1.1E+03 (avg.)	2.8E+02 (avg.)	1.1E+02 (avg.)
Piñon-Juniper Rangeland in South-Central New Mexico (3 transects)	Dwyer and Pieper, 1967	1.3E+01–2.7E+01	1.7E-01–8.7E-01	NA	8.1E+02–1.0E+03	7.1E+02–2.4E+03	NA
Piñon-Juniper Rangeland in South-Central New Mexico (2 ungrazed sites)	Pieper, 1968	7.6E+00–1.1E+01, (basal cover)	3.0E-01–1.8E+00	NA	6.8E+02 and 7.3E+02 (total herbage)		
(2 grazed sites)		9.2E+00–1.4E+01 (basal cover)			3.3E+02 and 6.2E+03 (total herbage)		
Piñon-Juniper Woodland in Northern Arizona	O'Rourke and Ogden, 1969	1.4E+01–2.4E+01 (perennial basal cover) 1.0E+00–1.4E+01 (annual basal cover)	1.2E+00–5.6E+00	Statistically similar to cover for woodland (3.0E-01–2.1E+00)	2.8E+01–3.9E+03 (perennial grasses)	NA	NA
Grasslands Surrounding Piñon-Juniper Woodlands in Arizona (sites without trees)	Arnold et al., 1964	3.7E+00 (mean basal cover)	5.0E-01 (mean basal cover)	3.9E+00 (mean canopy cover)	7.0E+02		
Piñon-Juniper Rangeland in South-Central New Mexico	Pieper, 1990	---	---	---	9.0E+02–1.1E+03 (areas with 10% tree cover; three species of grass accounted for 7.0E+02–8.5E+02 kg/ha of this amount)		
Piñon-Juniper Woodland Sites Converted to Grassland (5 sites)	Aro, 1971	---	---	---	5.6E+02–1.5E+03	NA	NA

--- = Measurements were not performed.

NA = Not applicable; growth form was not considered in the study.

Table 3-3
Aboveground Production of Grasses, Forbs, and Shrubs in Mature Piñon-Juniper Woodlands

Study	Aboveground Production (kg/ha, dry weight)		
	Grasses	Forbs	Shrubs
Clary, 1971	7.1E+01	7.7E+01	1.0E+02
Clary, 1989			
Church Hills Site—1980	4.7E+01	4.5E+01	5.7E+01
Church Hills Site—1982	1.4E+02	1.6E+01	1.3E+02
Church Hills Site—1985	7.7E+01	3.5E+01	7.2E+01
Clay Springs Site—1980	2.0E+01	1.0E+01	3.0E+01
Clary and Jameson, 1981	1.0E+02	4.6E+01	7.0E+01
Pieper, 1968	6.2E+02	1.1E+01	---
O'Rourke and Ogden, 1969			
Boundary Site—1961	2.5E+02	---	---
Boundary Site—1962	1.7E+02	---	---
Ryan Site—1961	9.8E+01	---	---
Ryan Site—1962	2.1E+02	---	---
Second Site—1961	1.0E+02	---	---
Second Site—1962	6.7E+01	---	---
Chevelon Site—1961	1.6E+02	---	---
Chevelon Site—1962	9.4E+01	---	---
Aro, 1971			
Colorado Site	2.8E+01	---	---
Fire Site No. 1	1.1E+02	---	---
Fire Site No. 2	1.1E+02	---	---
Fire Site No. 3	2.2E+02	---	---

--- = No production measurements were conducted for the indicated growth form.

Radionuclides in litter that falls to the ground enter the soil as the plant material decomposes. Several sources discuss litter decay in terms of the decomposition half-life, or the time required for half of the original dry mass of litter to decompose. Half-lives for litter in grasslands, boreal conifer forests, and temperate deciduous forests were estimated at 2.8, 7.0, and 1.0 years, respectively (Whittaker, 1975). Other estimates typically range from 1 to 6 years, depending

upon the climatic conditions and plant material under consideration (e.g., Koukoura et al., 2003; Shariff et al., 1994; and Murphy et al., 1998). Longer half-lives may be anticipated for the more substantial woody litter from mature shrubs and trees.

Radionuclide concentrations in litter deposited on the surface of Area G will be proportional to radionuclide concentrations in the soil where the plant that produced the litter grew. The plant intrusion model assumes that litter is generated in proportion to the root mass found in each layer of the disposal system (i.e., the surface soil, cap, and waste layers). For example, if 50 percent of the root mass for a given growth form occurred in a given layer of the cap, 50 percent of the total litter production is assumed to have radionuclide concentrations proportional to the contaminant concentrations within that layer. Total radionuclide concentrations in the litter, then, represent the contaminant concentrations calculated for each layer of the disposal system, weighted by the root mass in each layer.

Limited information exists regarding root mass distributions with depth. Foxx et al. (1984) conducted a comprehensive review of rooting data for species of plants that grow at Laboratory disposal sites and used the collected data to develop root frequencies with depth for individual plant species. Distributions of rooting depth were developed for 12 species or genera of grasses, 10 species or genera of forbs, 2 species or genera of shrubs, and a single species of tree. Rooting information for additional species of shrubs is reported by Tierney and Foxx (1987).

The rooting depth distributions discussed above represent the frequencies with which plant roots penetrate to specified depths below the ground surface. As discussed earlier, plant uptake of radionuclides is assumed to be proportional to the root mass in a given layer or segment of the waste and cover. Rooting depth frequencies and root mass distributions may be highly correlative; however, data found in the literature suggest otherwise. For example, on the basis of a literature review on root biomass distributions with depth, Jackson et al. (1996) estimated that 53, 83, and 52 percent of the total root biomass in deserts, temperate grasslands, and temperate coniferous forests, respectively, occurs within 30 cm (1 ft) of the soil surface. An examination of plant growth forms across all biomes except tundra indicated that 75 percent of the root mass of grasses occurs in the top 30 cm (1 ft) of soil; the corresponding figures for shrubs and trees are 47 and 60 percent. In contrast, data collected by Foxx et al. (1984) and Tierney and Foxx (1987) suggest that 20 percent or less of the root mass of grasses, forbs, and shrubs lie within 30 cm (1 ft) of the ground surface.

The information needed to accurately characterize the distribution of root mass with depth for the grasses, forbs, shrubs, and trees that inhabit Area G is unavailable. Consequently, a series of functions was adopted to represent the distribution of root mass between the ground surface and the maximum rooting depth. This modeling was conducted using beta functions, the parameters for which were selected to evaluate a range of root distribution patterns.

An example of the series of root mass distributions generated using the beta functions is presented in Figure 3-4. This figure shows the distribution curves for a plant growth form with a maximum rooting depth of 1.5 m (4.9 ft). Similar curves are generated for alternate values of maximum rooting depth. In general, the root mass distributions estimated using this approach span the range of distributions suggested by the rooting depth frequencies discussed above and the findings of Jackson et al. (1996).

The radionuclide concentrations in the layer-specific litter fractions are determined by the rate at which plants extract contamination from the soil or waste via their roots. Rates of contaminant uptake are proportional to element-specific root uptake factors. While authors such as Baes et al. (1984) suggest applying plant uptake factors for leafy vegetables to fresh forage such as grass, other information indicates that plant uptake factors for native plants may be greater than those observed for agricultural crops. Given that there are relatively few data available to characterize plant uptake for native species, the plant uptake factors provided in the National Council on Radiation Protection and Measurements Report 129 (NCRP, 1999) for grass and fodder were adopted for the biotic intrusion modeling; uptake factors for leafy vegetables were generally used for elements that were not included in the NCRP report. In adopting this approach, it was assumed that patterns of plant uptake in grasses will more nearly approximate those in native vegetation, relative to agricultural crops. In fact, these factors are typically larger than those adopted for agricultural crops and generally agree with the native plant uptake factors reported by Wirth (1999) for selected elements.

Animal Intrusion

The animal intrusion model simulates the transport of contamination to the surface of Area G by harvester ants, pocket gophers, mice, and chipmunks and ground squirrels. The amount of contamination transported by these species is proportional to the quantity of material excavated from the surface soil, cap, and waste layers and the radionuclide concentrations in each layer. The amounts of material excavated by the different species or taxa depend, in part, upon the renewal rate of the burrows. The annual burrow renewal rate is set to 1.0 in the first year following final closure of the disposal facility. For harvester ants, this fraction is estimated in subsequent years as the inverse of the harvester any colony lifespan. Data presented in McKenzie et al. (1982) were used to define renewal rates for the other animals in subsequent years.

The soil removal rates calculated for the animals are allocated among the cover and waste layers that comprise the disposal facility using burrow depth distribution functions. Relatively little information is available to describe the distribution of animal burrows with depth. Because the information required to accurately define these distributions for the animals at Area G was lacking, a series of burrow depth distributions was developed using beta functions. The parameters for these functions were selected to evaluate a range of burrow distribution patterns.

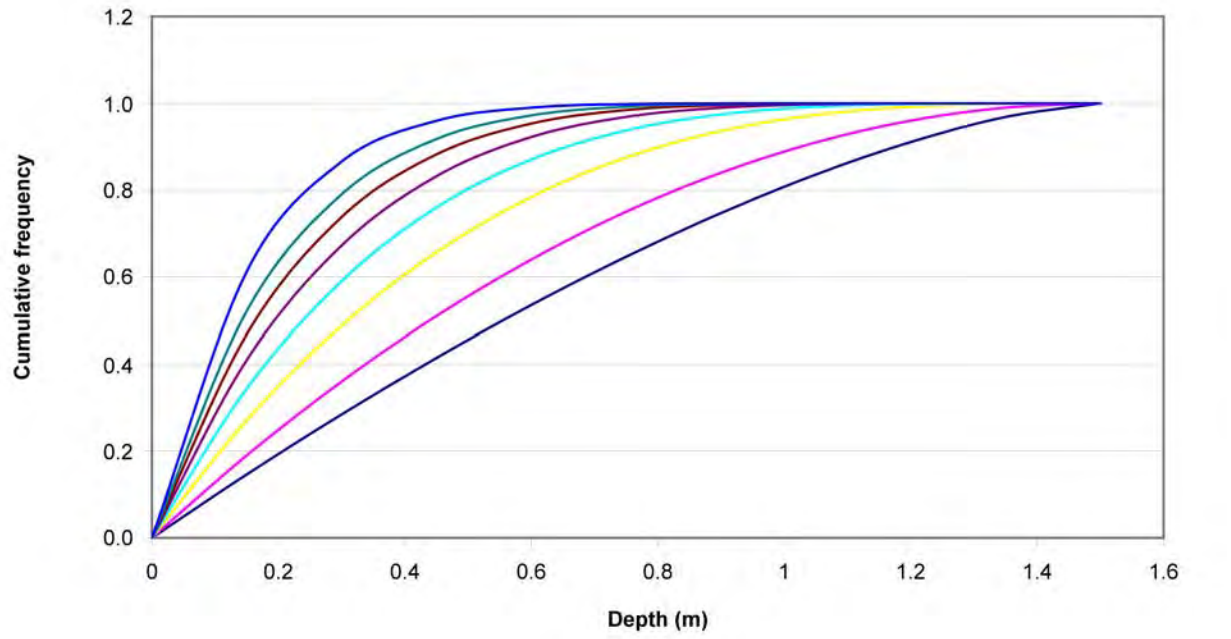

Figure 3-4
Root Mass Distributions for Plants with Maximum Rooting Depth of 1.5 m

An example of the series of burrow depth distributions generated using the beta functions is shown in Figure 3-5. This figure presents the distribution curves for an animal species with a maximum burrowing depth of 3 m (10 ft). Similar curves are generated for alternate values of maximum burrowing depth.

Multiplying the soil or waste removal rate for a given animal species by the fractions of the burrow system within the cap and waste layers yields layer-specific bulk removal rates for that material. The site model differentiates between radionuclides contained in the solid phase of the soil (or waste) and the moisture occupying the pores of the material. The calculated soil (or waste) and water removal rates are summed across animal species to yield layer-specific soil (or waste) and water transport rates for each waste disposal region.

As discussed in Section 3.2.1, the animal community inhabiting Area G is expected to change as the site transitions from grassland-dominated landscape to piñon-juniper woodland. Rates of soil excavation between the early successional and woodland end points are estimated as a linear function of the animal burrow density present at the two end points. The successional transition was assumed to start at the end of the 100-year active institutional control period and end when the climax woodland was assumed to exist.

3.3.3.2 Contaminant Leaching

Rates of radionuclide leaching within the disposal units are controlled by the sorption characteristics assigned to the waste and crushed tuff backfill and the rate of infiltration through the pits and shafts. The information needed to differentiate between the properties of the waste and backfill were unavailable, so all material in the disposal units was assigned properties characteristic of crushed tuff. Several sources were used to estimate the sorption characteristics of crushed tuff. These include the site-specific sorption data collected Longmire et al. (1996), the data compiled by Krier et al. (1997) in their review of the literature, and recent compilations of data for Yucca Mountain tuffs (Bechtel/SAIC, 2004).

Steady-state flow conditions were assumed to prevail in the disposal units throughout the simulation period. Rates of infiltration were estimated on the basis of chloride flux measurements developed by Newman et al. and infiltration model simulations conducted using HYDRUS by Levitt; these efforts are discussed in *Appendices F* and *G* (Volume 2), respectively. Levitt compared the fluxes estimated on the basis of these two approaches; Figure 3-6 shows the distribution of these approximations. As indicated, the fluxes projected using HYDRUS bound those estimated using the chloride-based approach; modeled infiltration rates tended to be less than those measured under vegetated conditions and greater than the chloride-based fluxes under unvegetated conditions. In any event, it should be noted that the chloride-based fluxes represent long-term average values for current conditions at Area G and do not account for the addition of the proposed final cover design.

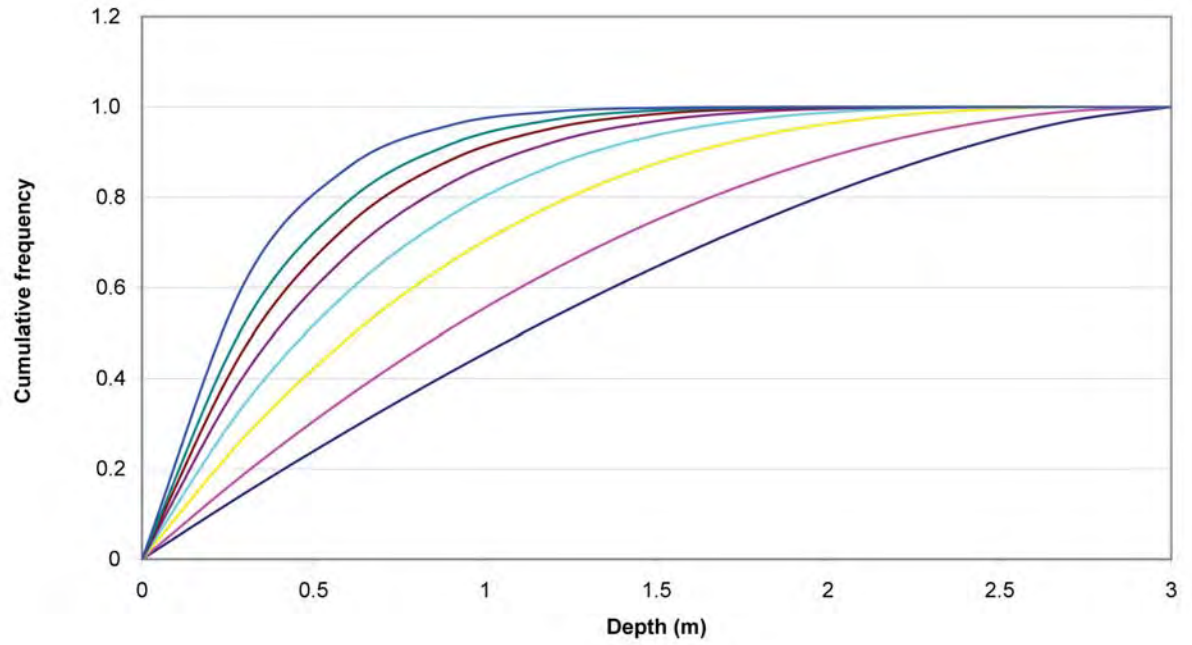

Figure 3-5
Burrow Depth Distributions for Animals with Maximum Burrowing Depth of 3 m

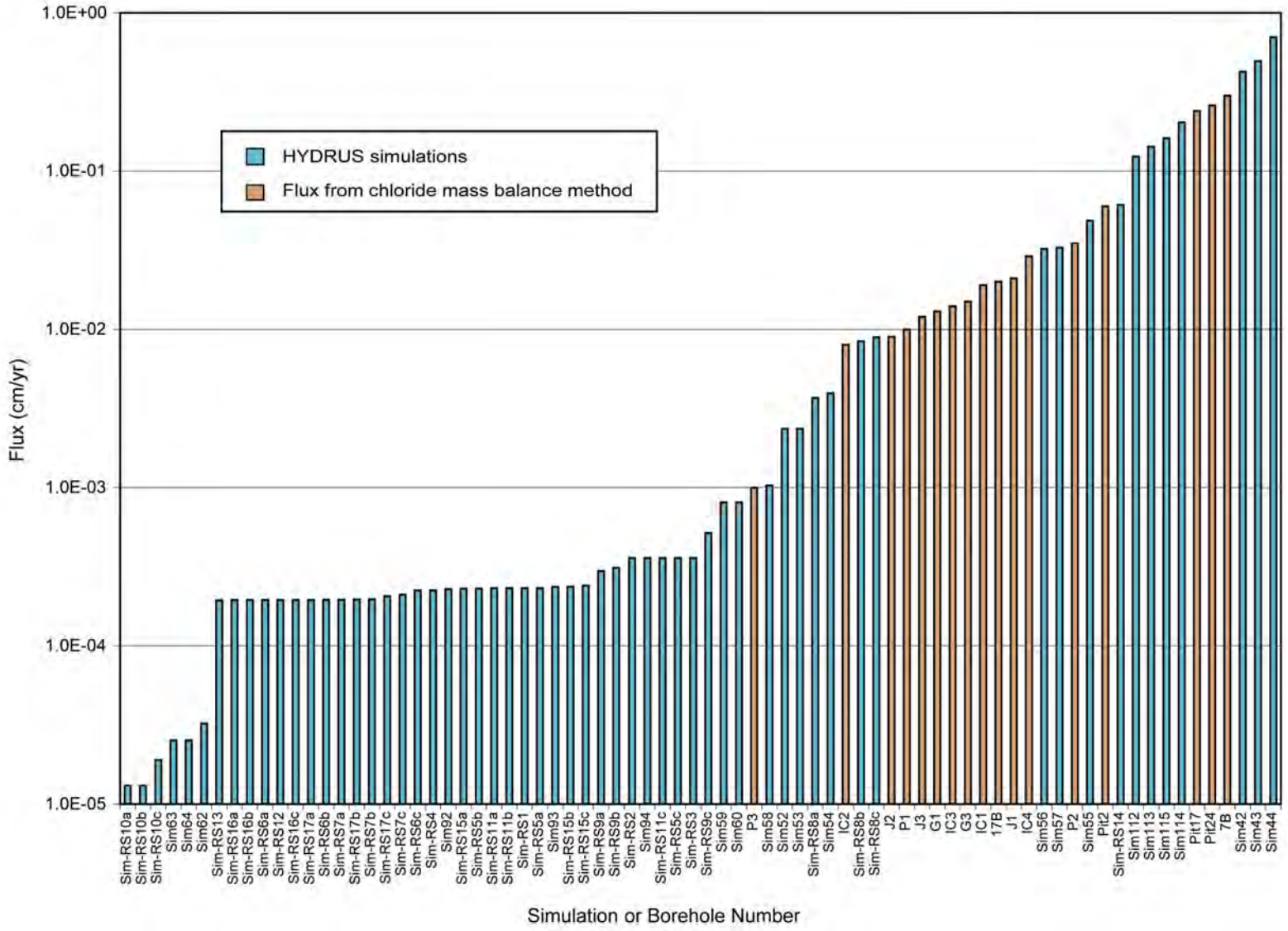

Figure 3-6
Comparison of Modeled Fluxes and Fluxes based on Chloride-Mass Balance Measurements

3.3.3.3 Surface Erosion

As discussed in Section 3.2.2.3, surface erosion may expose waste buried in disposal pits and shafts and thus initiate the release of radionuclides. More typically, however, release mechanisms such as biotic intrusion will expose radionuclide-contaminated sediments to the action of wind and water. Therefore, the discussion of the modeling done to address erosive impacts is found under transport mechanisms in Section 3.4.

3.4 Radionuclide Transport Modeling

The modeling approaches used to simulate the transport of radionuclides to locations accessible to members of the public are described below. Section 3.4.1 addresses the groundwater transport modeling conducted in support of the performance assessment and composite analysis. Atmospheric transport of radionuclides released to the air above the site is considered in Section 3.4.2, while Section 3.4.3 describes the surface erosion modeling that was used in the design of the final cover and to estimate rates of sediment transport from the mesa top. The manner in which the results of these modeling efforts were incorporated into the GoldSim models is also described.

3.4.1 Groundwater Flow and Transport

Groundwater flow and transport modeling was conducted to simulate the movement of radionuclides leached from the disposal units to exposure locations downgradient of Area G. The modeling effort included the development of a three-dimensional (3-D) model capable of simulating the transport of water-soluble radionuclides released from the pits and shafts at Area G. As was the case for the 1997 performance assessment and composite analysis, the 3-D modeling was conducted using the process-level, multidimensional, finite-element porous flow and transport simulator known as FEHM (Zyvoloski et al., 1995a and 1995b).

The potential impacts of releases from Area G on regional groundwater supplies were modeled within GoldSim in a probabilistic fashion. Stochastic modeling of groundwater transport can, potentially, require thousands of simulations. Given the computer-resource-intensive nature of FEHM, one-dimensional (1-D) abstractions of the 3-D model were developed for use in these probabilistic analyses. The Area G Site Model controls these 1-D model abstractions, allowing the bulk transport properties of the subsurface for all radionuclides undergoing groundwater transport to be modified as desired.

The groundwater flow and transport modeling effort is summarized below. The configuration of the 3-D FEHM model and the input data used in the modeling are addressed in Section 3.4.1.1, while Section 3.4.1.2 discusses the initial and boundary conditions used in the evaluation. The 3-D model simulations conducted to evaluate the potential groundwater impacts are discussed in Section 3.4.1.3. Section 3.4.1.4 concludes the discussion with a consideration of the model abstraction process. A complete description of the groundwater modeling effort is provided in *Appendix E*.

3.4.1.1 Model Configuration and Input Data

The first stage of the groundwater pathway modeling effort was to develop the 3-D model using FEHM. Since the completion of the last performance assessment and composite analysis (Hollis et al., 1997), new information and techniques have become available that were used to update and refine the models used to conduct this evaluation. The 3-D grid upon which this modeling is based incorporates a new mesh refinement technique that provides high resolution near the Area G disposal units and lower resolution away from the Area G fence line. The new 3-D grid has approximately 10 times as many nodes and a resolution in the area of the disposal units that is 6 times greater than the resolution of the previous vadose-zone grid (Birdsell et al., 1999). Furthermore, the new grid spans an area of nearly 15 km^2 (5.8 mi^2), which is large enough to avoid edge effects that led to nonphysical flow in previous transport simulations. The grid extends well below the water table and is used to follow contaminant pathways from the surface of the disposal facility through the vadose zone, into the saturated zone, and to the compliance boundary. The footprint of the grid was designed to encompass several regional characterization and supply wells that are located in the vicinity of Area G. A depiction of the grid is provided in Figure 3-7.

The 3-D grid relies on a 2003 update of the vadose-zone geologic model of Area G and the surrounding area. This update represents the third major revision of the 3-D LANL site-wide geologic model since it was developed in 1996 and incorporates information collected from regional characterization wells that were drilled in the vicinity of Area G from 2000 through 2003 (the locations of these wells are shown in Figure 2-12 [Section 2]). As a result, it is expected to more accurately represent actual geologic conditions than previous versions of the geologic model. Comparisons of predictions made using the 1996 geologic model (Vaniman et al., 1996) to the actual drilling logs from characterization wells R-21 and R-22 show that the elevations at which unit contacts occur differ by 10 m (33 ft) or more in some instances. These differences may lead to projected contaminant travel times that are shorter than those previously estimated.

The 3-D site-scale model is used to trace the travel times of particles released from Area G and to generate conservative breakthrough curves, otherwise known as residence time distribution functions (RTDs). These RTDs vary with the location at which radionuclides are released from Area G and the rates of infiltration through the disposal units. To maintain the complexity of the model at a reasonable level, simplifying assumptions were made to address these dependencies.

Particle travel times will vary across Area G because (1) the thickness of the Bandelier Tuff, which largely determines particle breakthrough behavior, increases from east to west, and (2) the differences in the depths of the disposal units influence particle travel time to the compliance boundary. As discussed earlier, the disposal facility was divided into eight waste disposal regions to capture these spatial dependencies; each region represents an area where flow and contaminant transport behavior will be different. These disposal regions are shown in Figure 3-2 at the beginning of this section.

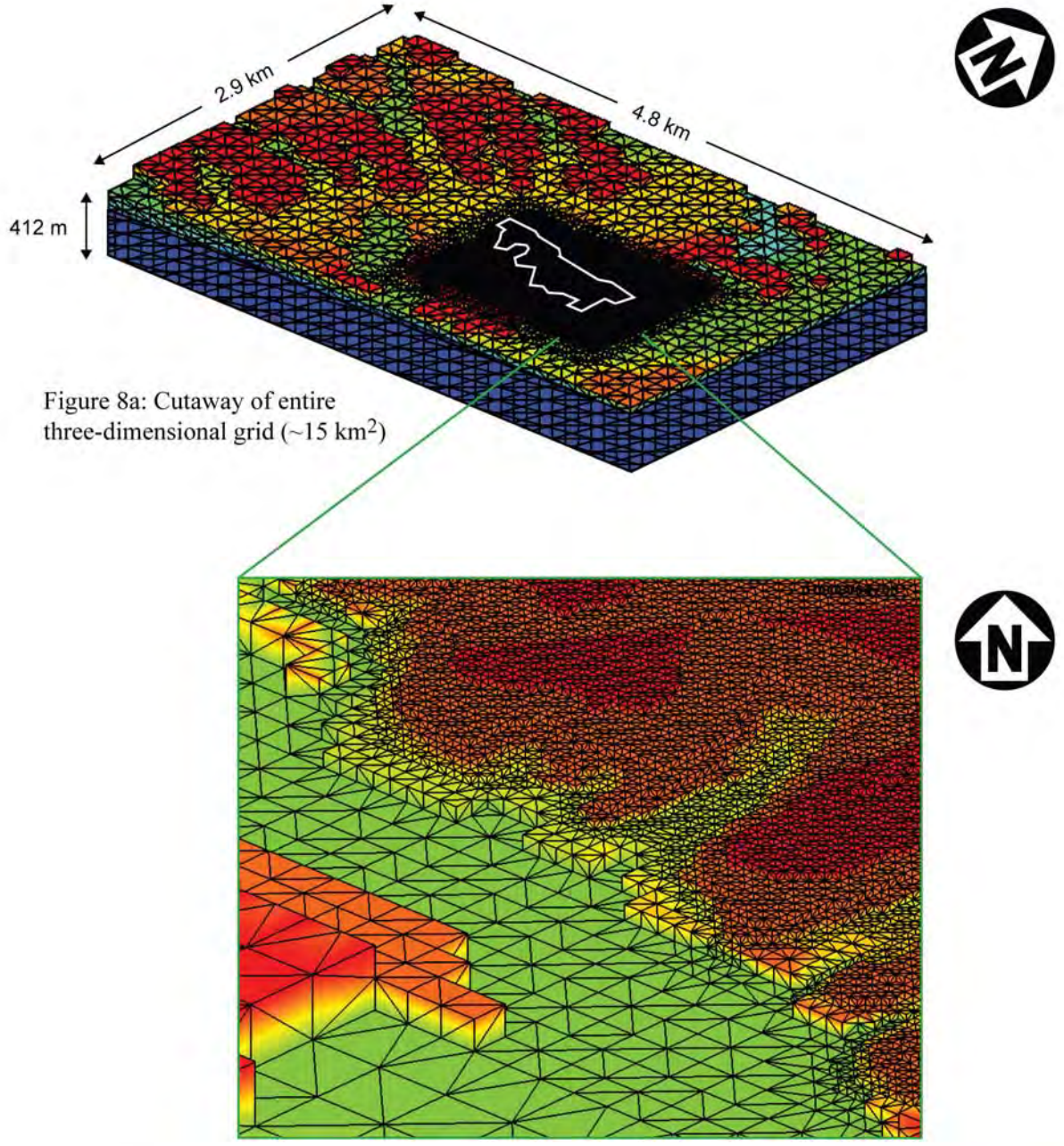

Figure 8a: Cutaway of entire three-dimensional grid (~15 km^2)

Figure 8b: Magnified view of southeastern portion of Area G. The largest grid squares (lower left) are 125 m x 125 m.

Figure 3-7
Three-Dimensional Grid for Area G Model

Disposal regions 1 and 8 contain aggregates of pits and shafts with similar depths, while the remaining disposal regions contain either all pits or all shafts. Although the shafts in disposal region 6 are immediately adjacent to the shafts included in disposal region 1, region 6 was modeled separately because its shafts are significantly deeper than those in region 1. Similarly, the shafts in waste disposal region 7 are interspersed among the pits in region 3, but were modeled separately because of differences in depth. Particles were released from the entire extent of disposal regions 1 through 5; release points for regions 6 and 7 coincide with areas where large numbers of shafts are located. The particle release locations used for disposal region 8 represent reasonably conservative release points for the future disposal units that will be constructed in Zone 4. All of the waste disposal regions fall within the high-resolution portions of the 3-D model grid.

Residence time distribution functions were developed for 10 discrete infiltration rates within each waste disposal region. The infiltration rates used to generate these RTDs are based on data compiled by Springer and Schofield (2004), and span the approximate range of infiltration rates observed for relatively undisturbed mesa-top locations. This resulted in the creation of 80 unique breakthrough curves that can be sampled from within GoldSim and used to generate the 1-D pipe pathways needed for calculating contaminant migration to the compliance boundary. In this approach, GoldSim samples the actual, continuous infiltration rate distribution adopted for the performance assessment and composite analysis and selects the breakthrough curve that most closely corresponds to this rate within the waste disposal region under consideration. The discretization of the infiltration distribution in the manner described above provides a mechanism for considering the effects of variable infiltration rates on facility performance while maintaining model complexity at a reasonable level.

3.4.1.2 Initial and Boundary Conditions

A number of initial and boundary conditions were used to constrain the groundwater transport modeling. Birdsell et al. (1999) showed that evaporation could cause extremely high capillary forces resulting in the flow of water toward the surge bed. Although this hypothesis is supported by some data (Rogers et al., 1996) the result of implementing an internal evaporative boundary at the base of Tshirege Member unit 2 would be to stop transport below this horizon. This “dry barrier” hypothesis was not considered in the current performance assessment and composite analysis modeling because the extent of this phenomenon has not been adequately addressed.

All lateral boundaries in the vadose zone were assumed to be no-flow boundaries; that is, no mass could enter or leave the system via these boundaries. Lateral gradients on these boundaries were not considered for two reasons. First, the simulation domain boundaries are located more than a kilometer away from the Area G fence line. Second, previous modeling studies of the Pajarito Plateau found the magnitude of lateral gradients in the unsaturated zone to be generally quite small (Birdsell et al., 1999; Stauffer et al., 2000).

Saturated flow in all simulations was assumed to be from west to east following the water table gradient in the area. The gradient was fixed for all simulations and was based on a water table elevation of 1,798 m (5,900 ft) along the western model boundary and 1,737 m (5,700 ft) to the east. These elevations yield an average gradient across the domain of approximately 0.013 m/m (0.042 ft/ft) toward the Rio Grande. This gradient, based on data from Stone et al. (1999) and more recent data from Keating et al. (2003), is expected to capture the general trend of flow near the water table.

Saturated zone pressure was fixed along both east and west boundaries such that a constant head is maintained on each of these faces. The northern and southern boundaries in the saturated zone are no-flow boundaries. This method ignores data reported by Keating et al. (2003) that indicate there may be downward vertical gradients as high as 0.10 m/m (0.33 ft/ft). Some controversy surrounds these data: one interpretation is that the gradients are caused by groundwater pumping while another postulates that deeper flow in the aquifer is confined with respect to flow near the water table. After discussions with Keating and other coauthors of the 2003 study, the second interpretation was adopted for this study, and no downward gradients were prescribed in the simulations. This is a conservative assumption because downward gradients would lead to increased mixing and lower concentrations in the saturated zone near any pumping well.

The hydrogeologic properties used in the groundwater modeling are generally the same as those shown in Table 2.6 (Section 2); values for some of these properties were estimated because of an absence of reported values in the literature. The hydrogeologic properties adopted for the groundwater modeling differ somewhat from the properties used in earlier modeling efforts (Birdsell et al., 1995, 1999, and 2000). However, the overall characteristics of the geologic units remain the same. For example, the vadose-zone basalt permeability and porosity values used for the model were adopted from Stauffer et al. (2005), and are conservative estimates that yield the fastest travel times. These new properties are more defensible than those used previously, but the general behavior of this rock unit is unchanged.

3.4.1.3 Model Simulations

The 3-D site-scale model was used to trace the travel times of particles released from Area G and to generate conservative breakthrough curves. Because each particle has a random component that determines its pathway through the complex 3-D grid, thousands of particles must be released at the same time and at the same surface location to create an RTD. The RTD basically shows the probability that a given particle will arrive at the compliance boundary in a given amount of time. Particle tracer simulations were also run to determine appropriate dispersivity values and to predict how contaminants might be captured by a nearby groundwater well. All simulations of contaminant transport assumed steady-state flow throughout the domain. To generate a steady-state flow field, simulations were run with constant boundary conditions for 2.5 million years.

High rates of infiltration in the canyons adjacent to Area G may influence contaminant breakthrough times. Consequently, modeling was performed to determine how infiltration from nearby Pajarito Canyon—the wettest canyon in the vicinity of Area G—should be considered in the groundwater pathway model. Multiple simulations were conducted using canyon infiltration rates that were bound by conditions observed in Pajarito Canyon; varying rates of infiltration were used over the rest of the model surface. The results of these simulations were compared to model projections based on infiltration rates that were constant across the entire model surface, including Pajarito Canyon.

The groundwater-pathway modeling estimates the contaminant-specific mass that crosses the compliance boundary downgradient of the Area G fence line. This boundary was assumed to be located 100 m (330 ft) downgradient (east) of Area G for the Groundwater Resource Protection Scenario. For the All Pathways–Groundwater Scenario, the compliance boundary was assumed to be located near the town of White Rock until the end of the active institutional control period and 100 m (330 ft) downgradient of Area G thereafter. However, given that contaminated groundwater was not projected to reach the regional aquifer within 100 years of facility closure, the detailed groundwater modeling considered only the 100 m (330 ft) compliance well. Only a portion of the mass that crosses this boundary would, in fact, be captured by a domestic well and contribute to the exposure projected for the individual using the well. Simulations were performed to estimate the size of the capture zone and, in so doing, the capture efficiencies for a hypothetical nearby well.

It was assumed that the hypothetical well would serve a single household; the well radius was set at 0.125 m (0.41 ft) and the screen interval was assumed to extend downward 37.5 m (123 ft) from the top of the water table. A range of pumping rates was used to estimate the size of the well's capture region; these rates were 50, 600, 1,200, and 2,500 m^3/yr (1.3×10^4, 1.6×10^5, 3.2×10^5, and 6.6×10^5 gal/yr). An infiltration rate of 10 mm/yr (0.39 in./yr) was assumed and a steady-state flow field was established with the pumping well in place. The radius of influence of the well was estimated by introducing particles along a line source that was situated 100 m (330 ft) upgradient of the well and at an elevation corresponding to the midpoint of the well screen interval. Capture efficiencies, or the fraction of contaminant released from the disposal facility that is intercepted by the well, were estimated for each waste disposal region.

3.4.1.4 Model Abstraction

The ability to conduct probabilistic analyses of groundwater transport is hampered by the fact that the 3-D site-scale model takes significant time and computer memory to run. The use of 1-D abstractions of the 3-D model overcomes this difficulty while retaining the overall characteristics of the transport simulations. The theory of micromixing (Robinson and Viswanathan, 2003) was used to reduce complex 3-D simulations to 1-D abstractions. These abstractions recreate particle

breakthrough at the compliance boundary while retaining the ability to modify the bulk transport properties of the subsurface for all radionuclides undergoing groundwater transport. The development of these 1-D abstractions provided the means for incorporating the groundwater pathway model directly into the GoldSim site model that was used to project long-term performance of the disposal facility.

To support the development of the 1-D abstractions, the FEHM model was modified so that GoldSim controls the contaminant mass flux, the specified surface infiltration, and the bulk transport properties (i.e., sorption parameters) used in the groundwater pathway modeling. As implemented for the performance assessment and composite analysis, the FEHM model recreates an approximation of the complex 3-D RTD on a simple 1,000-node, 1-D grid. GoldSim calls eight separate FEHM simulations, each of which corresponds to a waste disposal region, and passes the appropriate data to FEHM. Using these data, FEHM calculates the mass of each radionuclide crossing the compliance boundary as a function of time, and passes the results back to GoldSim.

The 1-D abstraction grid uses the advection-dispersion formulation of the transport equations (Zyvoloski et al., 1995a) to simulate tracer movement. This allows simulation of both sorption and radioactive decay, processes that are important for estimating the breakthrough of the multiple species that may be released into groundwater from the pits and shafts at Area G.

3.4.2 Atmospheric Transport

The transport of airborne releases from Area G to downwind locations was conducted using the CALPUFF modeling package; details of this effort are provided in *Appendix D*. This package or system has three major components: (1) CALMET, a meteorological model with both diagnostic and prognostic wind-field generators, (2) CALPUFF, a nonsteady-state dispersion model, and (3) CALPOST, a postprocessing program. CALMET performs a number of analyses to generate 3-D wind fields and information about the types and durations of the releases; these data are used by the CALPUFF model to conduct the transport modeling. Output from CALPUFF is processed in CALPOST and graphics packages for presentation.

The CALPUFF package was developed by Earth Tech, Inc. for regulatory use in air quality programs, and has been approved by the U.S. Environmental Protection Agency (EPA, 2003) for use in demonstrating regulatory compliance. The package, considered suitable for complex and rugged terrain conditions, is a nonsteady-state or puff trajectory model that applies hourly averages of wind speed and direction to generate air-concentration values (ASG, 2005; Scire et al., 2000a and 2000b).

Three atmospheric modeling efforts were conducted in support of the Area G performance assessment and composite analysis. The first of these, referred to as the near-field analysis, focused on transport phenomenon within a few kilometers of the disposal facility; these model

projections were used in the site model to estimate exposures for the Atmospheric Scenario. The second analysis evaluated the potential contributions made by airborne releases from other waste disposal sites at LANL to the impacts attributed to Area G. This analysis directly supports the composite analysis and is referred to as the alternate-source analysis. The final analysis, referred to here as the far-field analysis, projected air concentrations and deposition rates up to 80 km (50 mi.) from the disposal facility. The results of this modeling were used to conduct an ALARA analysis. The input data used in these analyses are presented in Section 3.4.2.1. This is followed by a description of the different approaches adopted for the three modeling efforts (Sections 3.4.2.2 through 3.4.2.4).

3.4.2.1 Input Data

The major types or categories of input information required to conduct the CALPUFF analyses include meteorological data and terrain and land use information. The meteorological data describe atmospheric conditions at and in the vicinity of Area G; they include local, surface meteorological data and regional, upper-air data. The local, surface meteorological data were obtained from a network of meteorological towers located within the Laboratory; these towers include stations at TA-6, TA-49, TA-53, and TA-54, the locations of which are shown in Figure 2-5 (Section 2). One of these towers, the station at TA-54, is located less than 2 km (1.2 mi) from Area G. The upper-air data are used to complete the construction of wind fields in the vertical direction; data from the Albuquerque International Airport, the closest site to LANL that collects the upper-air data, were used in the modeling.

Terrain data are used to describe the topography of the model domains used in the CALPUFF modeling. Digital elevation model data for the terrain were obtained from the USGS. Land use data describe the vegetation, water, natural surface, and cultural features of the land surface, and are the basis for defining several geophysical parameters that are used in the air dispersion modeling. Land use is defined within CALPUFF using one of 14 land use types. The modeling conducted in support of the Area G performance assessment and composite analysis considered two land use types: rangeland, which was used to represent site conditions shortly after closure, and forest, used to represent the site after its transition to piñon-juniper woodland. Both land uses were modeled for the near-field analysis: in one case, the land use was set to rangeland for all grid locations, and in the other it was set to forest. All alternate-source and far-field simulations were performed using a land use type of rangeland.

The atmospheric transport modeling considered two particle size distributions to evaluate how particle characteristics affect deposition rates. The first is based on a geometric mean particle diameter (gdiam) of 0.48 μm (1.9×10^{-5} in.) with a geometric standard deviation (gsd) of 2.0; these are the CALPUFF default values. The second considers particles with a gdiam of 5 μm (2.0×10^{-4} in.) and a gsd of 2.0. This second distribution is expected to be more representative of soil particles undergoing resuspension at Area G and formed the basis of the modeling results

used to estimate exposures for the Atmospheric Scenario. The transport analyses for vapor- and gas-phase radionuclides assumed that there was no deposition of airborne contamination.

3.4.2.2 Near-Field Analysis

The near-field analysis model domain includes the portion of LANL surrounding Area G, the western portion of White Rock, and the southern portion of San Ildefonso tribal lands (Figure 3-8). The model domain is 3.5 km (2.2 mi) in the east-west direction by 2.1 km (1.3 mi) in the north-south direction and includes the TA-54 meteorological tower. The analysis used the highest resolution that CALPUFF could read for the terrain grid spacing. This corresponds to the 30 m (98 ft) grid resolution typical of the USGS 7.5-minute quadrangle maps.

The disposal facility was divided into three atmospheric source areas to conduct the near-field transport modeling. These areas, shown in Figure 3-3 roughly coincide with the pits and shafts used to dispose of waste prior to 1971 (source area 1), from 1971 through 2004 (source area 2), and from 2005 through 2044 (source area 3). The surface areas of source areas 1, 2, and 3 are approximately 7.5, 27, and 13 ha (19, 67, and 32 ac), respectively.

The near-field analysis evaluated the potential impacts of particulate releases and radionuclides diffusing from the site in the form of vapors or gases. A unit emission (release) rate (1 g/m^2/s [6.2×10^{-5} lb/ft^2/s]) for both particulate and vapor/gas releases was assigned to each source area and air concentrations and particulate deposition fluxes were projected for all locations within the model domain. The transport and dispersion of particulate releases were evaluated using the meteorological data for 1992 through 2001 and the rangeland and forest land use types discussed above. The model simulations for vapor- and gas-phase radionuclides used the same meteorological data, but projected downwind concentrations for the rangeland land use only.

The dispersion factors and deposition rates for the identified points of maximum exposure were used in the site model to estimate doses for the Atmospheric Scenario. The points of maximum exposure prior to, and following, active institutional control were identified using a screening evaluation. A location screening value was calculated for each grid of the near-field model domain as follows:

$$LSV_x = \sum_{i=1}^{3} \left[\frac{\chi}{Q_{i,x}} \times DSF_i \right] \qquad 3\text{-}2$$

Where

LSV_x = location screening value for grid location x

$\frac{\chi}{Q_{i,x}}$ = air dispersion factor for source area i at grid location x (s/m^3)

DSF_i = dose screening factor for source area i (mrem-m^3/yr)

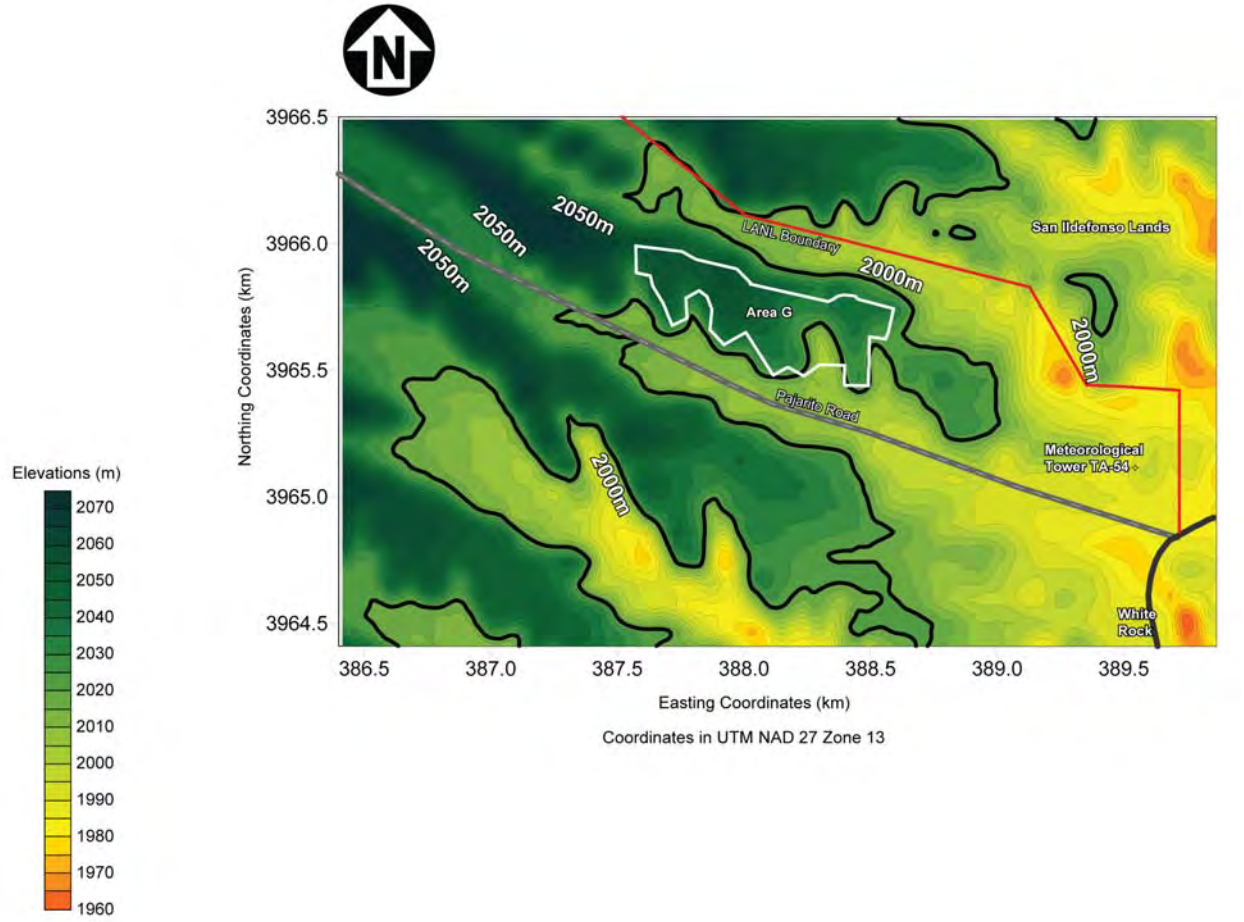

Figure 3-8
Model Domain for Near-Field Analysis

In Equation 3-2, the dispersion and dose screening factors corresponding to each source area are multiplied and the products are summed to yield an overall screening value for the exposure location under consideration. The dose screening factor is given by the following expression:

$$DSF_i = \sum_{j=1}^{n} \left[DCF_{inh,j} \times A_{j,i} \right] \qquad 3\text{-}3$$

Where

$DCF_{inh,j}$ = inhalation dose conversion factor for radionuclide j (mrem/yr per Ci/m^3)

$A_{j,i}$ = inventory of radionuclide j in source area i (Ci)

Location screening values were calculated using Equations 3-2 and 3-3 for all grid or exposure locations outside the Laboratory boundary and outside the Area G fence line. The location with the greatest screening value outside each boundary represents the point of maximum exposure.

Separate screening calculations were conducted for the performance assessment and composite analysis, and for particulate releases and vapor- and gas-phase radionuclides diffusing from the site. The screening used the appropriate inventory for all radionuclides. Location screening values for particulate releases were calculated for the rangeland and forest land uses, while the screening for vapor- and gas-phase contaminants considered only the rangeland land use. The screening for vapor- and gas-phase contaminants was restricted to exposures from tritium, C-14, and Kr-85; radon was not considered because doses from this radionuclide are not addressed by the Atmospheric Scenario.

The dispersion factors and deposition rates for the identified points of maximum exposure were input into the site model to estimate doses for the Atmospheric Scenario. The atmospheric modeling projections for the rangeland and forest land uses were assumed to pertain to the disposal site at the time of facility closure and after the site transitioned to piñon-juniper woodland, respectively. For intermediate times, dispersion factors and particulate deposition rates were assumed to change in a linear fashion between the two defined end points. For example, dispersion factors and deposition rates halfway between those projected for rangeland and forest were assumed to apply when the site had achieved 50 percent of the transition from grassland to woodland.

3.4.2.3 Alternate Source Analysis

The alternate-source analysis considers how other significant sources of contamination at the Laboratory may affect the anticipated exposure levels for persons living downwind of Area G. The atmospheric transport modeling conducted in support of this evaluation used a model domain consisting of an 8 × 8 km (5 × 5 mi) grid with a mesh size, or receptor spacing, of 200 m (660 ft). This domain, shown in Figure 3-9, includes several significant material disposal areas at LANL including MDAs A, AB, B, C, and T. An atmospheric source area was used to represent releases

from each MDA, and a unit release rate was applied. Figure 3-9 shows the source areas used to represent the MDAs; a single source area was used to represent MDAs A, B, and T, which are located close to one another. Air concentrations at receptor locations downwind of Area G were projected for releases from these facilities. Meteorological data collected in 2001 were used for the alternate-source analysis and a land use type of rangeland was applied over the entire model domain.

The air concentrations projected for the alternate-source analysis were used to estimate the degree to which airborne releases from the MDAs could interact with releases from Area G. Simply, the air concentrations projected by CALPUFF for unit releases from the alternate MDAs were compared to the air concentrations projected under the same release conditions for Area G. These comparisons examined representative exposure locations downwind of Area G.

3.4.2.4 Far-Field Analysis

The far-field analysis, which models air concentrations up to 80 km (50 mi) from Area G, was conducted to evaluate potential population exposures to airborne releases from Area G. The model domain for this analysis was centered at a point on the east end of Area G (Zone 13 388460 E 3965620 N, Universal Transverse Mercator [UTM], North American Datum [NAD] 27). This point also served as the grid origin. The elevation contours of the model domain are shown in Figure 3-10, along with the approximate location of Area G. A grid size of 160 × 160 km (100 × 100 mi) with a mesh size or receptor spacing of 4 km (2.5 mi) was used. Unit releases from the three Area G atmospheric source areas used in the near-field analysis were used to project air concentrations and dispersion factors for each grid of the model domain. The far-field analysis was conducted using meteorological data collected in 2001, and the rangeland land use type was applied over the entire model domain.

The population data used to conduct the far-field analysis are summarized in Figure 2-3 (Section 2). The model domain for the far-field analysis includes all of Los Alamos County and portions of Bernalillo, Mora, Rio Arriba, Sandoval, San Miguel, Santa Fe, and Taos Counties. The domain also encompasses all or part of the pueblos of Santa Clara, Picuris, San Juan, San Ildefonso, Pojoaque, Nambe, Tesuque, San Felipe, Cochiti, Santo Domingo, Santa Ana, Zia, Jemez, and Taos. Other significant population centers included in the model domain are the townships of Santa Fe, Española, and Los Alamos as well as the southwestern edge of the City of Taos and the northern portion of the Albuquerque metropolitan area.

The results of the far-field atmospheric modeling were used to model air and surface soil concentrations at discrete population centers across the model domain. These projections were used to calculate the collective population doses needed to conduct the ALARA analysis (*Appendix M*).

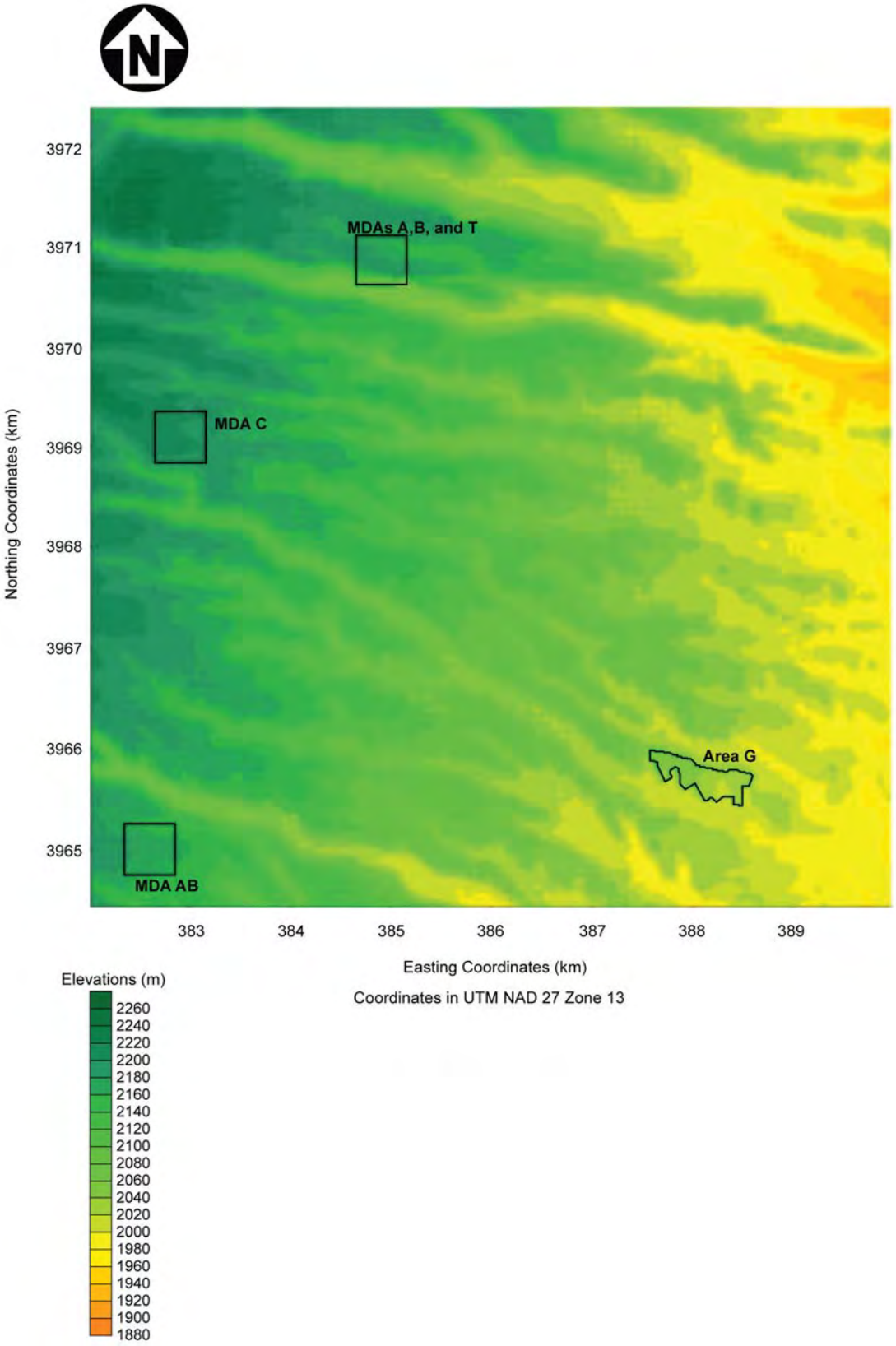

Figure 3-9
Model Domain for Alternate Source Analysis

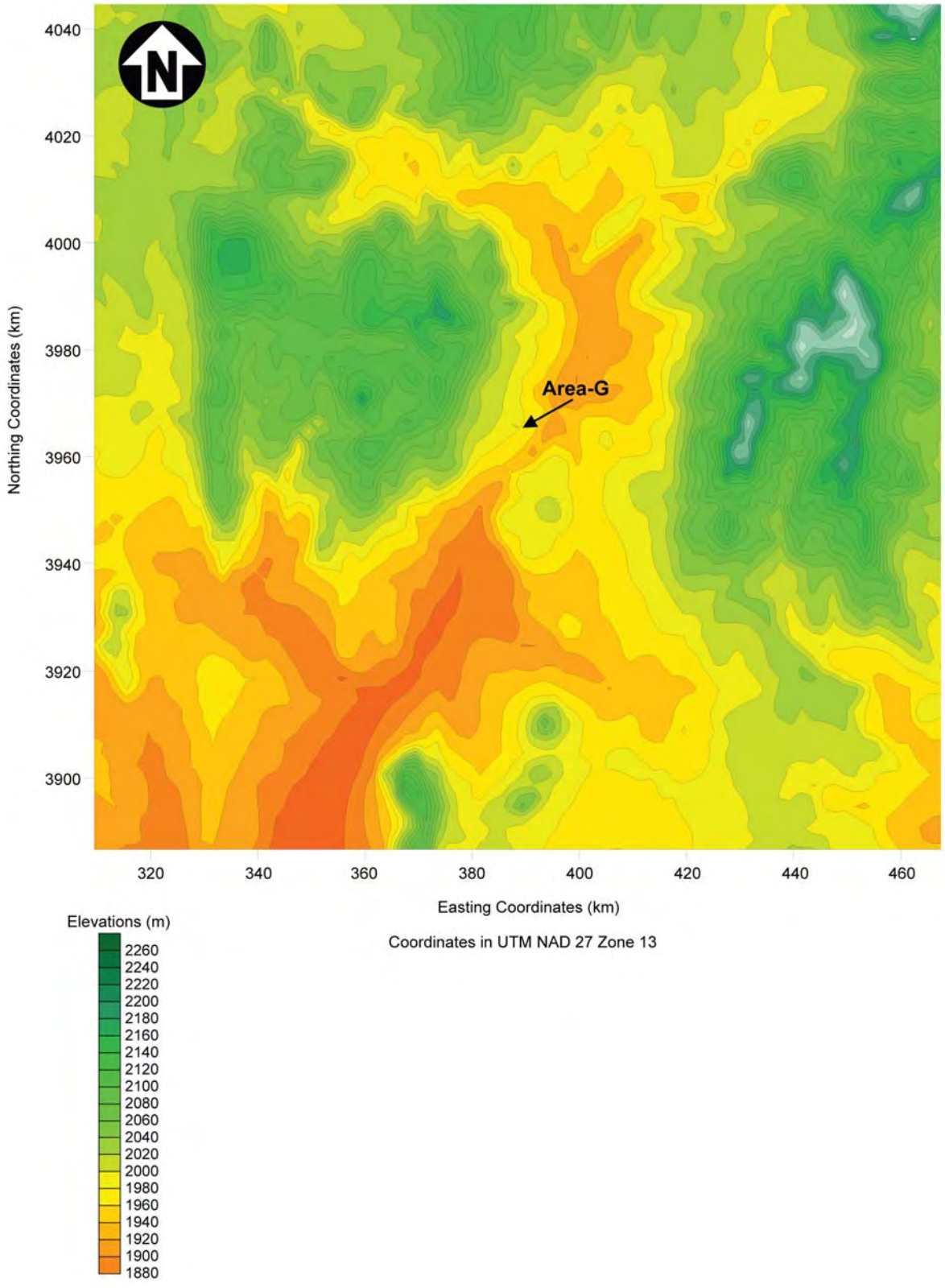

Figure 3-10
Model Domain for Far-Field Analysis

3.4.3 Surface Erosion

Given a long enough period of time, the final cover placed over the disposal units at Area G will be compromised by the effects of surface erosion due to runoff. Surface erosion conducted using the SIBERIA model was conducted to evaluate these impacts. The details of this modeling effort are provided in *Appendix I* of this report, a summary of this information is presented in Section 3.4.3.1.

Surface erosion modeling was conducted with two objectives in mind. First, erosion modeling was used in an iterative approach to help design a final cover capable of minimizing the impacts of erosion over the long term. Second, SIBERIA was used to model the performance of the adopted cover design for periods of up to 50,000 years. The efforts involved in these two phases are discussed in Sections 3.4.3.2 and 3.4.3.3.

3.4.3.1 Model Configuration and Input Data

The SIBERIA model (Willgoose and Riley, 1998) was selected for the surface erosion modeling because it is a well-tested version of a new class of erosion models developed to predict long-term landscape evolution. Like well-known hillslope-based erosion models such as the Water Erosion Prediction Project (WEPP) (Laflen et al., 1991) and the Kinematic Runoff and Erosion (KINEROS) (Smith et al., 1995) models, SIBERIA predicts sediment transport derived from shallow sheet and rill processes for a range of soil, runoff, vegetation cover, and hillslope properties. Unlike other models, SIBERIA predicts the spatial distribution of deformation across complex, 3-D topography over thousands of years. This includes the lowering of ridges, the incision or infilling of valleys and hollows, and the development of gullies and fans.

The erosion model predicts steady-state erosion and sediment transport across a landscape that is represented as elevations in a gridded digital elevation model (DEM). The DEM is adjusted at each time step (typically 1 year) to account for any change in surface elevation that occurred from erosion or deposition since the last time step. The governing equation for the SIBERIA model is:

$$Q_s = BA^m S^n + D_z S \qquad 3\text{-}4$$

Where

Q_s = the annual sediment flux through a grid cell (kg per meter width)
B = a coefficient that represents all factors that moderate runoff-driven erosion in the grid cell, except slope and runoff
$A^m S^n$ = the relationship between contributing area (A), slope (S), and sediment yield
D_z = a diffusion coefficient
S = the terrain gradient (slope) (%)

Equation 3-4 includes sediment transport terms for both runoff-driven (advective) processes and gravity-driven (diffusion) processes. The intensity of runoff-driven sediment transport is given

by the first term (BA^mS^n). The coefficient B accounts for all factors (e.g., vegetation cover, degree of soil disturbance, and soil type) that moderate runoff-driven erosion in the grid cell, except for slope and runoff. The amount of runoff in a grid cell increases as the area that contributes runoff to that cell increases (i.e., a bigger contributing area feeding into a grid cell equates to a greater runoff volume flowing through the grid cell) and as the gradient of the cell increases. The exponents m and n determine how sediment yield depends on contributing area and slope for a given site, and can be determined empirically (where data are plentiful) or through an optimization process using other hillslope-based models. Diffusive transport, represented by the second term in Equation 3-4, includes processes such as rainsplash (sediment particles ejected from the surface by raindrop impacts), tree-throw (sediment tumbled downslope when the root ball of a fallen tree is exposed at the surface), and the establishment of animal burrow mounds. The diffusion coefficient D_z captures the intensity of these gravity-driven sediment transport processes.

Within the SIBERIA model, Equation 3-4 represents sediment-transport processes at all scales. In addition, the sediment yield, Q_s, when applied to each time step over long periods of time, is equivalent to the average annual sediment that would result from large and small events of all return periods. Equation 3-4 is solved for every grid cell in the SIBERIA model domain for each time step. Every grid cell has an upslope contributing area (A) and a slope (S). In any given grid cell the values of A and S may change through time as the landscape deforms; thus, these values are recalculated for each time step. The values of B, m, n and D_z are considered inherent material and site properties for soil and bedrock; for this modeling effort they were held constant over time for specific soil and bedrock layers.

Developing the parameters required to conduct the Area G SIBERIA modeling proved challenging. The typical approach for developing values for the SIBERIA parameters B, m, n and D_z is to calibrate the model to one or more standard hillslope-runoff erosion models. In principle, SIBERIA can be parameterized directly using long-term rainfall, runoff, and sediment yield data. However, to derive the relationship for runoff-driven transport (BA^mS^n) empirically, data must exist for a range of hillslope and watershed gradients, S, at a range of area scales, A (hillslope, subwatershed, and watershed); such data are rare.

While multiple rainfall, runoff, and sediment data sets exist for Mesita del Buey at a range of scales (experimental measurement plot, hillslope, and watershed scales), these data are neither continuous over time nor of the uniform quality required for direct determination of SIBERIA parameter values. Consequently, the rainfall-runoff model IRS9 (Stone et al., 1992) and the runoff-sediment yield Hillslope Erosion Model (HEM) (Lane et al., 2001) were used to develop parameter values for the advective transport term in SIBERIA.

Determining the diffusion term for the SIBERIA model is considered an art. Research by Heimsath et al. (1997) has significantly advanced the quantitative determination of diffusion in equilibrium landscapes. Unfortunately, Mesita del Buey is a poor candidate for the application of these techniques because soil geochronology suggests that the local soils are aeolian and may have been emplaced rapidly about 10,000 years ago. Given this, the diffusivity was constrained by estimating a match between SIBERIA-generated topography and direct observations of headwater drainage lines using data from the field and from airborne laser swath mapping (ALSM) digital topographic maps. For example, if a SIBERIA run predicted that observed well-defined drainage lines at Area G aggraded (filled-in with sediment) significantly over 1,000 years, then the value used for the diffusion coefficient in that run was likely set too high. If many new drainage lines appeared across the site, then the diffusion coefficient was likely too low.

A final challenge in parameterizing SIBERIA is developing steady-state values for *B, m,* and *n* such that application of the model on an annual time step reproduces nature's highly dynamic runoff and erosion rates. In nature, landscape-forming runoff events occur sporadically, perhaps once every 10, 20, or 1,000 years, rather than every year. Analysis of long-term data sets shows that the cumulative effect of a few "large" runoff events over the monitoring period is greater than the cumulative effect of the smaller runoff events that occur every year. Because SIBERIA is a steady-state model, the user must determine the return period of a landscape-forming event that can be applied annually in the model domain to predict the same long-term sediment yield that would be generated through periodic large events.

Given the difficulties outlined above, the parameterization of the SIBERIA model for application at Area G required a multistep approach, as described below and detailed in *Appendix I.*

Step 1: *Collect, collate, and evaluate precipitation, runoff, and sediment-yield data for Mesita del Buey.* These data were used to parameterize the rainfall-runoff ISR9 model and the runoff-erosion HEM, as well as to test SIBERIA results.

Step 2: *Evaluate long-term runoff and sediment-yield data sets to estimate the return period for landscape-forming events.* Because no long-term, coupled rainfall, runoff, and erosion data sets exist for LANL or nearby areas, data from an analog site, the semiarid Santa Rita Experimental Range (in Arizona), were used to estimate the return period for landscape-forming events. An evaluation of these data showed that the average annual sediment yield for a period of approximately 16 years fell within the range of the sediment yield values from events with return periods of 2 and 5 years. Consequently, return periods of 2 and 5 years were adopted for the erosion modeling.

Step 3: *Develop rainfall-runoff relationships for Area G using the selected return periods for the landscape-forming events.* Apply the ISR9 model using Area G soil and vegetation

properties and precipitation amounts for events with 2- and 5-year return periods for Area G. The excess runoff values predicted by ISR9 for the 2- and 5-year events were used as input to the HEM.

Step 4: *Apply the HEM to predict sediment yield for hillslopes using a range of slopes and areas*. This model calculates the erosion or deposition in each hillslope segment as a function of the segment runoff, gradient, ground cover, canopy cover, and soil type. Simulations were run to generate sediment yield values over a wide range of hillslope lengths and gradients; three combinations of these parameters were selected to represent low-, medium-, and high-erosion scenarios at Area G.

Step 5: Apply a simulated multiparameter regression annealing technique (Crowell et al., 2004) to obtain values for B, m, and n. The simulated-annealing algorithm was used to minimize the difference between the HEM-predicted target yields and the SIBERIA sediment yields for trial sets of *B, m, n* and D_z values. The optimal set of *B, m,* and *n* values shows a minimal difference between HEM and SIBERIA sediment yields for all hillslope length and gradient combinations of interest.

Step 6: Estimate D_z by matching SIBERIA results to present-day topography. To determine a site-specific D_z value, SIBERIA runs were made using a range of D_z values. The resulting topography was visually inspected and compared to the current topography as represented by the DEM derived from ALSM. The comparison focused on gullies and hollows; if SIBERIA predicted the development of deep colluvial fills in the hollows, it was assumed that diffusion was too high relative to the advective processes (fluvial transport), whereas if SIBERIA predicted excessive gullying, diffusion was considered too low relative to the advective processes.

The SIBERIA model domain is represented by a DEM that consists of current topography from the LANL 2000 ALSM survey (Carey and Cole, 2002) and the elevations of the final cover. The domain has two layers. The top layer is composed of cover material and extends from the surface of the final cover, through the interim cover, to bedrock. The proposed final cover material is moderately compacted crushed tuff, augmented with bentonite and angular gravel, overlain with a topsoil and pea gravel mixture approximately 5 mm (0.2 in.) thick (see *Appendix H*). The gravel admixtures are used to aid in the establishment of vegetation during the active institutional control period and will help increase soil surface cover and reduce erosion. The second layer is composed of the mesa bedrock material. This layer also includes armoring material (i.e., riprap) emplaced around the edges of the cover, where the transition from mesa top to cliff occurs. This armoring is included to reduce erosion at the cover-cliff boundary, slow runoff, and capture sediment eroded from the cover.

The current version of SIBERIA does not automatically track the depth of a given layer, though it does account for the spatial extent of a material type that is exposed at the surface of the model domain. In nature, the rate of downcutting in a gully slows once the base of the gully reaches bedrock. To simulate this situation, SIBERIA was run in a "start-stop-start" mode. The model was stopped after every 20 years of simulated time and each cell was checked to determine if its elevation had dropped below the bedrock surface. Cells that had reached bedrock were relabeled as such so that erosion would proceed at a slower rate, and the model was restarted.

The disposal facility was divided into two model regions: MDA G and the Zone 4 expansion area (Figure 1-2, Section 1). The same SIBERIA parameter values for erosion were used for both areas; however, the cover size and depth and pit configurations are quite different between the two sites.

The erosion modeling was used to estimate the spatial distribution of depth to waste at Area G after 1,000 years of erosion and sediment transport. Any such estimates are uncertain due to potential variations in climate, soil properties, evolution of the vegetation structure, and other factors over the 1,000-year time frame. To help constrain the uncertainty, three erosion scenarios were developed that are expected to result in low, moderate, and high rates of erosion at the site. The low-erosion scenario assumes that the soil will have the erosion and runoff properties of a sandy loam (crushed tuff and gravel with no clay admixture) with high infiltration capacity, a thick vegetation cover of native grasses (canopy cover of 70 percent, ground cover of 70 percent), and an annual design runoff of 2.6 mm (1.0 in.). The moderate-erosion scenario considers a sandy loam with mixed-grass and shrub vegetation cover similar to the current, relatively undisturbed conditions that exist in Zone 4 and at the eastern end of Mesita del Buey (i.e., canopy cover of 30 percent, ground cover of 70 percent). The annual design runoff for the moderate scenario is 7.0 mm (0.28 in.). The high-erosion scenario assumes a loam soil (crushed tuff and gravel mixed with bentonite), a sparse vegetation cover within the range of conditions found on Mesita del Buey (i.e., canopy cover of 30 percent, ground cover of 30 percent), and an annual design runoff of 12 mm (0.48 in.).

3.4.3.2 Model Simulations

Surface erosion modeling was conducted to support the development of the final cover design upon which the performance assessment and composite analysis are based, to model rates of cover loss over the 1,000-year compliance period and beyond, and to project patterns and rates of sediment transport. The simulations conducted in support of these objectives are described below.

Cover Design Evaluation

The 1997 performance assessment and composite analysis (Hollis et al., 1997) evaluated the long-term performance of Area G in its interim closure condition, and concluded that the facility would satisfy the performance requirements with only 1 to 2 m (3.3 to 6.6 ft) of cover over the disposal pits and shafts. However, those analyses assumed very low rates of surface erosion

based on modeling conducted at the time, and assumed that active maintenance of the site over the 1,000-year compliance period would limit the impacts of biotic intrusion. Since that time, work conducted under the Area G Performance Assessment and Composite Analysis Maintenance Program has indicated that the impacts of surface erosion may be more severe than estimated in 1997. Furthermore, the position that the DOE will be present to actively maintain the site throughout the compliance period has been reconsidered. Taken together, these factors suggest the final cover should be capable of performing under much more severe conditions than previously considered.

The need to address more severe long-term impacts on cover performance and the key role the cover plays in limiting risks to humans and the environment led to consideration of a more robust final cover design for Area G. Toward this end, preliminary evaluations were conducted to estimate the approximate cover characteristics needed to allow the disposal facility to satisfy the DOE Order 435.1 performance objectives (DOE, 2001a). Once these minimum criteria were identified, an iterative design process was undertaken until a configuration capable of meeting these criteria was developed. This process is described more fully in *Appendix H.*

The evaluation of minimum cover requirements focused on total cover depth because, in the absence of engineered biobarriers, cover depth is the primary factor affecting the degree to which biotic intrusion will impact the site. This is significant because biotic intrusion was the radionuclide release mechanism responsible for the peak atmospheric pathway exposure estimated for the 1997 composite analysis and the peak performance assessment dose projected for a receptor living adjacent to Area G in Pajarito Canyon.

The minimum amount of cover required to safely isolate the waste disposed of at Area G was estimated based on the results of biotic intrusion modeling conducted by Shuman (1999) and preliminary estimates of the impacts of biotic intrusion under what were expected to be conservative estimates of erosion potential. Assuming that the cover would be maintained for a period of 100 years following closure of the disposal facility, it was estimated that maintaining at least 1.5 m (4.9 ft) of cover over the site throughout the compliance period would provide reasonable assurance that the disposal facility would meet all performance objectives. On the basis of preliminary estimates of erosion potential developed using the SIBERIA erosion model (*Appendix I*), it was concluded that adopting a minimum initial cover thickness of 2.5 m (8.2 ft) would enable the cover requirement to be met for most, if not all, of the disposal site.

After the minimum initial cover depth was identified, an iterative process was used to evaluate cover designs. The performance of each conceptual design was evaluated for a period of 1,000 years using refinements of the SIBERIA erosion model (*Appendix I*). Successive cover designs were evaluated to determine their ability to satisfy the minimum cover requirements and to identify areas where projected erosion impacts appeared to be severe. Generally, the erosion modeling

indicated that the cover over much of the site performed adequately; however, some elevated rates of erosion were observed in localized areas along mesa edges or adjacent to drainages. These vulnerable locations were fortified using engineered features such as rock armor and the design evaluation process was repeated until a satisfactory final cover design was achieved.

Long-Term Performance Modeling

SIBERIA simulations were conducted using the final cover design to project rates of soil loss across MDA G and the Zone 4 expansion area. Simulations were used to determine the remaining cover at all grid locations within the model domain at selected times following closure; separate simulations were conducted for the low-, moderate-, and high-erosion scenarios. The surface erosion modeling considered cover performance over periods ranging from 1,000 to 50,000 years following the closure of Area G.

The SIBERIA modeling was also used to assign the sediments that are transported by surface runoff from the mesa top to the different catchments in Cañada del Buey and Pajarito Canyon. These calculations assumed that the sediments eroded from the disposal site would be transported to the canyon floors when they reached the edge of the mesa. The deposition location of the sediment was assumed to be the catchment directly below the point of departure at the mesa edge. Rates of sediment transport to the catchments were averaged over 20-year time steps.

The SIBERIA modeling represented the disposal facility, including the disposal units and the intervening areas, using over 70,000 nodes; rates of cover loss versus time were projected for each of these nodes. The results of the SIBERIA modeling are used in the site model to project rates of cover loss at Area G. To illustrate, consider the disposal units in waste disposal region 1. The pits and shafts in this region are represented by approximately 4,000 nodes in the SIBERIA modeling. One of these nodes is randomly selected in the first realization of the probabilistic simulation; the initial cover thickness at that location and the projected rate at which the material is eroded are assumed to apply to all nodes within the disposal region and the performance of the facility over the 1,000-year compliance period is projected on this basis. Successive realizations are performed in which other nodes are selected to represent the disposal region and the process is repeated.

As discussed above, the SIBERIA modeling evaluated rates of cover loss for three scenarios under which erosional pressures were expected to vary. The erosion modeling conducted within the site model takes the results for these scenarios into account by assigning a likelihood of occurrence to each scenario. This distribution is sampled for each realization of the probabilistic simulation and used to determine which set of cover loss projections is adopted for each node. For example, assume moderate erosion conditions persist 80 percent of the time, while conditions conducive to low and high erosion pressures each exist 10 percent of the time. In this case, the distribution of cover loss projections for the moderate erosion scenario is sampled in 80

percent of the realizations, while cover loss projections for each of the other scenarios are sampled in 10 percent of the realizations.

The erosion modeling estimates the cumulative soil loss within each waste disposal region throughout the model simulations; these losses are used to update the thickness of the surface soil, cap, and waste layers for each zone. The erosion model calculations yield the cumulative depths from the ground surface to the bottoms of the different layers, and the thickness of each layer. A series of adjustments is made within the GoldSim models to prevent the complete removal of one or more layers of the cover, as this can lead to instability in the models. A complete description of these adjustments is provided in *Appendix K*.

Two 50,000-year simulations were conducted to gain insight into the impacts of surface erosion on Area G for periods of time well in excess of the 1,000-year compliance period; these deterministic simulations were conducted using the performance assessment and composite analysis inventories. Both simulations used the SIBERIA erosion modeling results for the node in each waste disposal region that had the median initial cover thickness.

3.4.4 Vapor- and Gas-Phase Diffusion

The Area G Site Model estimates the rates of generation of vapor- and gas-phase radionuclides, and simulates these radionuclides' movement upward from the buried waste; the radionuclides for which diffusion modeling was conducted include tritium, C-14 as CO_2 and CH_4, Kr-85, and radon. Contamination is transported from the waste to the air above the disposal facility. The mathematical model used by GoldSim to simulate vapor- and gas-phase diffusion is discussed in the user's manual for the contaminant transport module (GoldSim, 2007c).

As explained in Section 3.1, the site model divides the cap into 16 layers and the waste into 20 layers to ensure accurate estimates of the diffusion rates through these materials. The model simulates the movement of tritiated water vapor, C-14 gas, krypton, and radon through the disposal system. Gas-to-water partition coefficients are calculated within the model to describe how these species are allocated between their vapor or gas phase and the water occupying the pores of the cover and waste. The partition coefficient for tritium is a function of its vapor pressure; the partition coefficients for carbon dioxide, methane, Kr-85, and radon are estimated using the appropriate Henry's Law constant.

The diffusion coefficients used in the diffusion modeling are calculated using the empirical relationship developed by Millington (1959) shown below:

$$D_e = D_o \times \frac{p_a^{10/3}}{p^2} \qquad 3\text{-}5$$

Where

D_e = pore diffusion coefficient (m^2/s)
D_o = gas diffusion coefficient in free air (m^2/s)
p_a = air-filled porosity
p = effective porosity

Separate diffusion coefficients were calculated for the waste in the disposal units and the cap. The cap and waste diffusion coefficients calculated for tritium were multiplied by a thermal gradient factor to account for the effect of thermal gradients in these materials upon the apparent rate of diffusion (Philip and DeVries, 1957).

The amount of C-14 available for diffusion as C-14 gas is given by the product of the C-14 inventory and the organic fraction of the waste. The organic waste inventory is multiplied by a gas generation rate constant that describes the rate at which the waste biodegrades. As mentioned earlier, the gas generated as a result of biodegradation is allocated to carbon dioxide and methane. All Kr-85 was assumed to be available for immediate diffusion from the waste.

Radon will be generated by the decay of its long-lived parent radionuclides. Only a portion of the gas generated will be available for diffusion; the rest will remain trapped within the solid waste until it decays to negligible levels. Radon gas generation rates are represented by modifying the decay characteristics of the parents of Rn-220 and Rn-222. Specifically, the fraction of time the parents of the radon isotopes decay to form radon gas is set equal to the radon emanation coefficient; during the remainder of the time, the decay of the parents forms daughters of Rn-220 and Rn-222. The form of the waste and the packaging used to dispose of the material are not assumed to prevent or limit the diffusion of radon.

The diffusion modeling projected fluxes of radon for the performance assessment inventory. Flux estimates were developed for each of the eight waste disposal regions; these region-specific results were used to calculate a facility-wide flux.

3.5 Dose Assessment

The radiological dose assessment estimates the potential impacts that may result from the disposal of radioactive waste at Area G. These impacts are characterized in terms of the exposures received by persons coming into contact with the radioactive waste placed in the disposal facility and radon fluxes from the disposal site. Section 3.5.1 discusses the technical approach used to estimate these doses and fluxes. Section 3.5.2 describes the approach used to assess the potential for interactions between releases from Area G and other sources of radioactivity at the Laboratory. The approach used to conduct the ALARA analysis is described in Section 3.5.3.

3.5.1 Exposure Projections

Several exposure scenarios were used to evaluate the risk posed by the disposal of radioactive waste at Area G to members of the public. These scenarios and the exposure pathways included in each have been provided in Section 2.2 and are summarized in Table 3-1. The models and data used to estimate the potential exposures are described by Shuman (*Appendix L*).

The site model was implemented in deterministic and probabilistic fashions to project potential exposures for members of the public. Deterministic simulations were conducted to gain insight into the performance of the disposal facility well beyond the 1,000-year compliance period. These simulations were conducted using a simulation period of 100,000 years for the groundwater pathway-based scenarios and 50,000 years for the Atmospheric and All Pathways–Canyon Scenarios. The probabilistic modeling was used to simulate facility performance and project potential exposures over the 1,000-year compliance period.

Preliminary modeling of the groundwater pathway exposures indicated that most radionuclides included in the Area G inventory arrive at the downgradient well long after the 1,000-year compliance period. Consequently, the number of radionuclides included in the probabilistic simulations was reduced from the number of contaminants that were initially identified for the groundwater modeling to those posing a potentially significant risk to groundwater users. The radionuclides selected for exclusion were identified using a 50-realization probabilistic simulation; potential doses were projected for the All Pathways–Groundwater Scenario over the 1,000-year compliance period using the composite analysis inventory. Contaminants contributing less than 1 percent of the mean peak dose over the simulation period were excluded from the final probabilistic analysis.

3.5.2 Alternate-Source Evaluation

The composite analysis must consider alternate sources of contamination that may add to exposures resulting from Area G releases. The first step in the alternate source analysis was to locate other sources of contamination at the Laboratory that could potentially interact with releases from Area G. Alternate sources were considered viable candidates for inclusion in the analysis if the quantities of radionuclides associated with those sources are similar in scale to the radionuclide inventories at Area G, or if the source is near Area G or the area affected by potential releases from Area G.

Once the alternate sources of contamination were identified, the potential for significant interaction between these sources and releases from Area G was evaluated. In most cases, interaction requires the release of contaminants from the alternate sources to the atmosphere or groundwater and the subsequent transport of this contamination to locations downwind or downgradient of Area G. Radionuclides released to, or otherwise present in, Cañada del Buey

and Pajarito Canyon may also interact with releases from the disposal facility if they are discharged or transported to locations adjacent to Area G.

Modeling conducted in support of the performance assessment and composite analysis was used to estimate the potential for interaction between contaminants released to the atmosphere or groundwater at the alternate sources and the releases from Area G. Atmospheric transport modeling, as described in Section 3.4.2 and detailed in *Appendix D*, considered whether airborne releases from alternate sources might add to the exposures estimated for members of the public living downwind of Area G. The groundwater flow and transport modeling conducted by Stauffer et al. (*Appendix E*) and described in Section 3.4.1, provided information that was used to assess the potential for significant interaction from a groundwater pathway perspective. The potential significance of interactions between canyon contamination from other sources and releases to Cañada del Buey and Pajarito Canyon from Area G was evaluated using information about the types of discharges that enter the canyons and sampling results for canyon sediments.

3.5.3 ALARA Analysis

The ALARA analysis conducted in support of the performance assessment and composite analysis evaluates the effectiveness of three closure strategies. The Base-Case Scenario considers the facility in the configuration upon which the performance assessment and composite analysis modeling is based. The first closure alternative, referred to as the Extended Control Option, is similar to the base-case condition insofar as it assumes that the same cover configuration exists at the time of closure. The option differs, however, in that it assumes that active maintenance of the site persists throughout the 1,000-year compliance period. During this time, the establishment of all shrubs and trees is prevented through annual mowing of the site. Furthermore, inhabitance of the site by burrowing animals is discouraged as a result of periodic trapping campaigns, poisoning, and destruction of surface manifestations of burrows.

The second alternative closure strategy is referred to as the Biobarrier Option. As its name implies, this option evaluates the impacts of incorporating a biobarrier into the final cover placed over the pits and shafts. This option evaluates the effectiveness of using a biobarrier to minimize biotic intrusion into the waste relative to reliance on total cover depth. The level of DOE control over the site is assumed to be the same as that described for the Base-Case Scenario.

The period over which the collective dose is integrated will have a profound effect on the results of the ALARA analysis. While the exposure period for short-term releases may be readily defined, this period is much harder to define for a situation in which long-lived radionuclides are released into the environment over hundreds to thousands of years. Under these conditions, exposures may occur over several generations, during which population densities and distributions may change substantially. In its draft guidance on the ALARA process (DOE, 1997), the DOE states that quantitative comparisons should typically consider periods of a few

hundred years or less, and that periods of more than 1,000 years should not be used. This guidance document also discusses how the probability of occurrence of exposure scenarios can be used to determine the integration of doses over time. For example, it may be reasonable to weight near-term doses more heavily than those that are projected far into the future.

Another complicating factor associated with activities that pose long-term risks to members of the public is the issue of discounting the costs of reducing health detriments that are projected to occur hundreds or thousands of years in the future. Draft DOE guidance (DOE, 1997) notes that it is rational, from an economics standpoint, to discount cost estimates for projected health effects that are centuries in the future. However, using any finite discounting will cause the present worth to be a very small fraction of the cost of the future impact. Because of this and the level of uncertainty associated with long-range dose projections, the DOE concludes that quantitative ALARA analyses should be limited to a few hundred years.

The nature of the risks posed by the waste disposed at Area G requires that hard decisions be made regarding the period of integration and the issue of cost discounting. Modeling of the facility in the base-case condition indicates that risks posed by the site increase throughout the 1,000-year compliance period due to the release of long-lived radionuclides. Thus, limiting the ALARA analysis to the first few hundred years, as suggested by the draft DOE guidance, will fail to capture the greatest potential risks posed by the disposal facility. On the other hand, it is not prudent to assume that doses hundreds of years into the future are as certain as those projected for times shortly after Area G is closed.

The preceding discussion suggests that any approach used to deal with integration periods and cost discounting is open to criticism. A moderate period of integration (300 years) and no cost discounting were selected for use in conducting the ALARA analysis for the Area G performance assessment and composite analysis. Although this approach does not address the most severe risks posed by the site, it also does not weight the importance of future exposures through considerations of scenario probability and cost discounting. Overall, this approach is generally consistent with DOE guidance on the matter.

A complete description of the modeling conducted in support of the ALARA analysis is provided in *Appendix M*. Briefly, the assessment estimated total costs associated with each closure strategy on the basis of the Atmospheric, All Pathways–Cañada del Buey, and All Pathways–Pajarito Canyon Scenarios. The alternative closure options are not expected to influence rates of contaminant leaching and transport to the aquifer or releases of vapor- and gas-phase radionuclides to the atmosphere. Because the collective impact of groundwater and diffusive releases will not be a discriminating factor among the closure options, the ALARA analysis does not address the collective exposure of groundwater users or persons exposed to tritiated water vapor, C-14 gas, and Kr-85. The inadvertent intruder scenarios are conducted primarily to

establish WAC, as opposed to projecting health detriment. Consequently, these scenarios are also excluded from the ALARA analysis.

The models used to conduct the Area G ALARA analysis are substantially the same as the site model used to estimate individual doses for the performance assessment and composite analysis. Modifications were made to permit consideration of the collective dose to persons living within 80 km (50 mi) of Area G for the Atmospheric Scenario. This was accomplished by assigning the population surrounding the disposal facility to a discrete number of locations. The GoldSim model estimates radionuclide concentrations in air and surface soils at each location; these concentrations are weighted by the location-specific populations and used to estimate the collective dose. In terms of the All Pathways–Canyon Scenario, the only difference between the ALARA analysis and site model is the fact that the individual doses estimated by the site model are multiplied by the canyon population and integrated over time.

The rates at which radionuclides are released and transported from Area G will be influenced by the closure strategy implemented at the facility. Modifications are made to the base-case condition models to estimate these impacts for the ALARA analysis. For the Extended Control Option, all shrubs and trees are assumed to be absent from the closed disposal site. Pest control efforts are assumed to rid the site of 70 to 90 percent of the burrowing species. The effects of incorporating a biobarrier in the final cover is approximated by adjusting input values of plant biomass, animal density, and burrow density; the barrier is assumed to exclude 70 to 90 percent of roots and burrows from the waste. Successional changes in the plant and animal communities at the site are assumed to proceed unimpeded for the Biobarrier Option.

The cost estimates take into account the projected health detriment and the implementation costs associated with each option. Health detriment costs are based on DOE guidance (DOE, 1997), which adopts a monetary equivalent value of collective dose ranging from $1,000 to $6,000 per person-rem. Implementation costs are estimated on the basis of cost data for the closure of the MDA G and maintenance costs associated with MDA J, a disposal site located to the west of Area G that recently underwent final closure.

3.6 Quality Assurance Program

A formal quality assurance program was established to guide the revision of the Area G performance assessment and composite analysis. This program is summarized in the following paragraphs. Complete details of the program may be found in Beckman and French (2007).

The Quality Assurance (QA) requirements for the revision implement the requirements of 10 Code of Federal Regulations (CFR) Part, 830, *Nuclear Safety Management*, Subpart A. *ASME Nuclear Quality Assurance-1*, (NQA-1) requirements have been adopted by the Laboratory to implement 10 CFR 830, Subpart A. These requirements are implemented in the Quality

Assurance Project Plan (QAPjP), a copy of which is included in Beckman and French (2007) as Appendix I.

This revision effort is designated as a management level 2 project per the QAPjP. The Project Leader delegated the review of design items to appropriate independent subject matter experts. The results of these independent technical reviews were documented and submitted to provide objective evidence that the assumptions, calculations, and modeling meet the QA requirements for the project. The independent technical reviews and the objective evidence were reviewed against the QA requirements in *AP-WFM-044, QAP 3.0, NQA-1 Requirement 3: Design Control*.

The following components of the performance assessment and composite analysis underwent independent technical reviews.

- Appendix C—LA-UR-05-5371, *Assessing Wind Erosion as a Contaminant Transport Mechanism for Los Alamos National Laboratory Technical Area 54, Material Disposal Area G*
- Appendix D—LA-UR-05-7232, *Air Dispersion Analysis for Los Alamos National Laboratory Technical Area 54, Material Disposal Area G*
- Appendix E—LA-UR-05-7393, *Groundwater Pathway Model for the Los Alamos National Laboratory Technical Area 54, Material Disposal Area G*
- Appendix F—LA-UR-05-6898, *Spatial Variation in Near-Surface Hydrologic Behavior at Los Alamos National Laboratory Technical Area 54, Material Disposal Area G*
- Appendix G—LA-UR-08-5468, *Modeling of an Evapotranspiration Cover for the Groundwater Pathway at Los Alamos National Laboratory Technical Area 54, Area G*
- Appendix H—LA-UR-05-7394, *Conceptual Design of the Earthen Cover at Los Alamos National Laboratory Technical Area 54, Material Disposal Area G*
- Appendix I—LA-UR-05-7771, *Surface Erosion Modeling for the Repository Waste Cover at Los Alamos National Laboratory Technical Area 54, Material Disposal Area G*
- Appendix J—*Radioactive Waste Inventory for Los Alamos National Laboratory TA-54, Area G*

- Appendix K—*GoldSim Model Documentation and Data Selection for Los Alamos National Laboratory Technical Area 54, Area G Performance Assessment and Composite Analysis*

- Appendix L—*Radiological Dose Assessment for Los Alamos National Laboratory Technical Area 54, Area G Performance Assessment and Composite Analysis*

- Appendix M—*As Low As Reasonably Achievable (ALARA) Analysis for Los Alamos National Laboratory Technical Area 54, Area G Performance Assessment and Composite Analysis*

Appendices A and B of the performance assessment and composite analysis report were not reviewed. Appendix A of the report contains responses to comments submitted by DOE on the 1997 performance assessment and composite analysis and is included as information in revised report. Appendix B of the updated report contains a summary of the conceptual design report for the Zone 4 expansion area, where the disposal of future waste is expected to occur. It, too, is provided for informational purposes only.

4.0 Results of Analysis

The results of the modeling conducted in support of the performance assessment and composite analysis are presented here. Section 4.1 provides some sample results of the source term modeling; a more extensive discussion of the transport modeling results may be found in Section 4.2. Results of these modeling efforts are used to project potential impacts to human health and safety; the results of the dose assessment can be found in Section 4.3. A discussion of the uncertainties associated with the model projections is provided in Section 4.4 and the results of the ALARA analysis are presented and discussed in Section 4.5.

4.1 Source Term

Radionuclides may be released from the disposal pits and shafts at Area G as a result of biotic intrusion, contaminant leaching, and the diffusion of vapor- and gas-phase contaminants. Projected rates of release via these mechanisms are discussed in the following sections.

4.1.1 Biotic Intrusion

The rates at which radionuclides are deposited on the surface of the disposal facility as a result of plant intrusion depend on the plants' rooting characteristics and rates of radionuclide uptake, the thickness of the cover, and the contaminant inventories in the disposal units. Examples of this are seen in Figure 4-1, which shows the activity of C-14, Sr-90, and Pu-239 in native vegetation growing over the units in waste disposal region 8. These radionuclides were selected to provide a sample of the behaviors projected by the GoldSim models; actual rates of uptake will vary depending upon the radionuclide and waste disposal region under consideration. The results for C-14 and Pu-239 are shown using log scales to capture the range of the model projections.

Radionuclide uptake by native vegetation growing over the disposal units increases rapidly shortly after facility closure in response to the establishment of grasses, forbs, and shrubs over the site. The quantities of C-14 and Pu-239 assimilated by the plants stabilize for several years before rising again, approximately 100 years after facility closure. Sr-90 activities in the native vegetation drop quickly after the initial increase, in response to radioactive decay, but increase 100 years after facility closure as well. The increases in plant activities seen at 100 years postclosure reflect the end of active institutional control and subsequent colonization of the closed site by trees. The roots of these plants extend deeper into the buried waste and assimilate greater amounts of contamination than the grasses, forbs, and shrubs that colonize the site during active institutional control. Eventually, the activities of C-14 and Sr-90 decrease as the radionuclides decay. The activity of very long-lived Pu-239 in plants increases throughout the simulation period, an indication of the fact that a greater proportion of the roots of trees penetrate into the waste as the cover erodes.

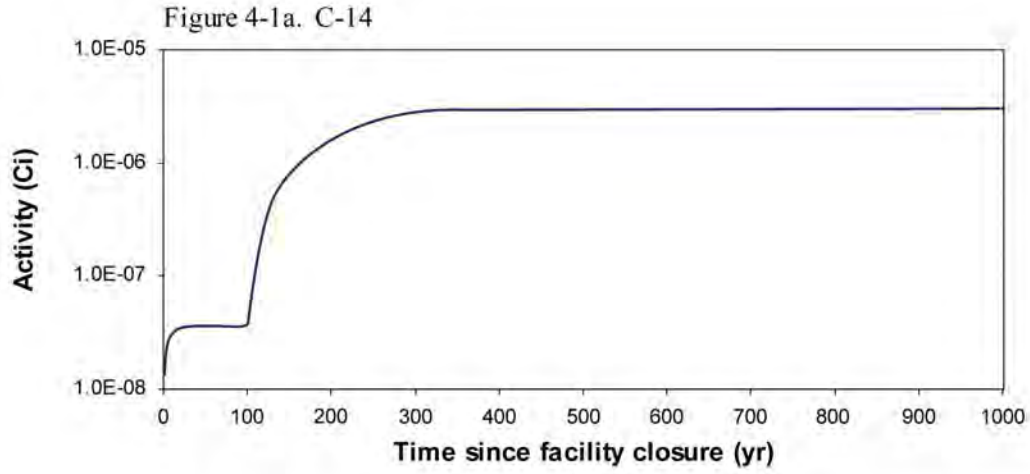

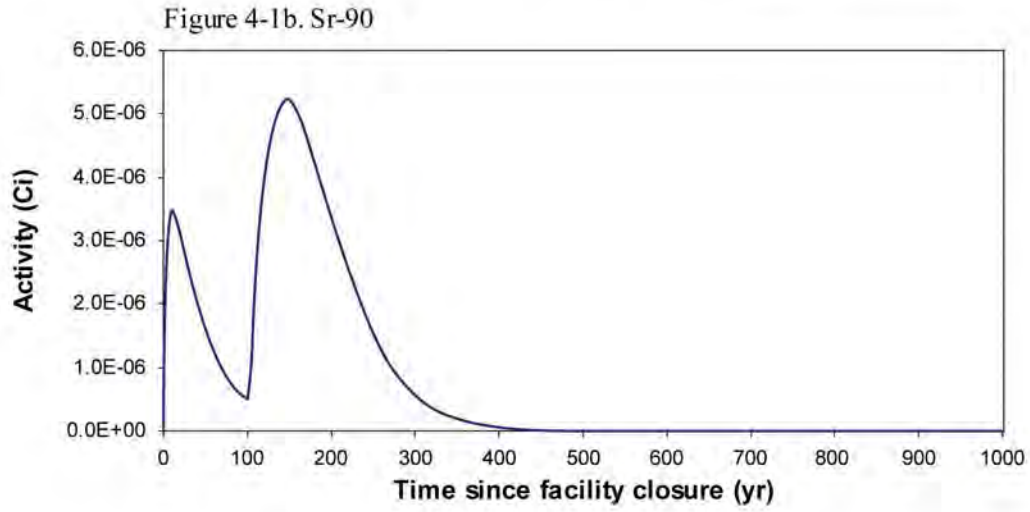

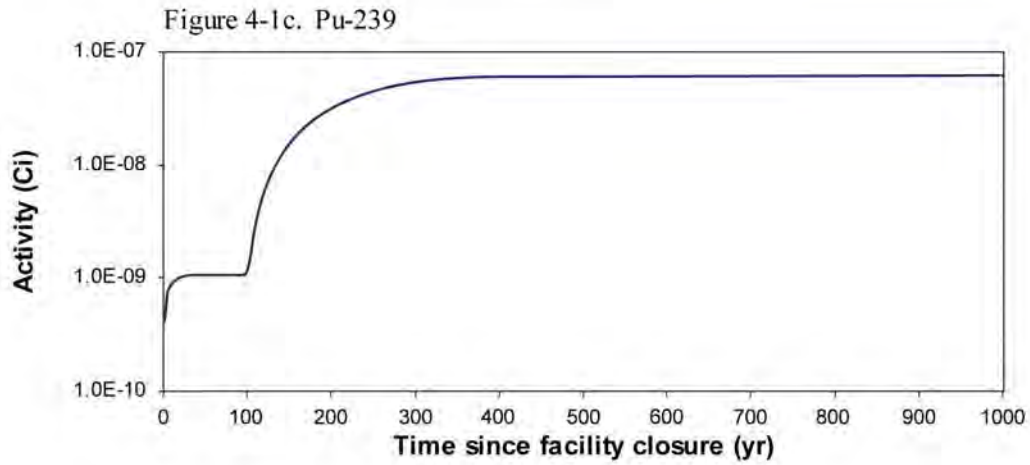

Figure 4-1
Uptake of Selected Radionuclides by Native Vegetation
Growing over Waste Disposal Region 8

The amount of contamination brought to the surface by burrowing animals is proportional to the quantity of soil these animals excavate. Figure 4-2 shows excavation rates for selected layers of the cap and the waste. Soil is excavated from the cap layers at a relatively constant rate during the 100-year active institutional control period. The site does not begin its transition to piñon-juniper woodland while under active control, and thus the types and numbers of animals inhabiting the site remain constant. Only small quantities of material are excavated from the top waste layer within 100 years of facility closure.

Rates of soil excavation in the uppermost portions of the cover decrease after the end of active institutional control as the site transitions to piñon-juniper woodland. Pocket gophers, which are prolific burrowers within 2 m (6.6 ft) of the surface, decrease in abundance and rates of excavation in this region decline. After a period of decline, rates of excavation in all cap layers stabilize or start to increase as the thickness of the overlying layer(s) decreases in response to surface erosion. Greater penetration into the waste occurs, causing increased rates of contaminant deposition on the surface of the disposal facility.

4.1.2 Contaminant Leaching

Radionuclides are leached from the waste at rates determined by the amount of water passing through the disposal units and the contaminants' sorption coefficients. Mean fluxes of H-3, C-14, and U-238 leaving the bottom of the disposal units in waste disposal region 8 are shown in Figure 4-3, from the start of facility operations to the end of the 1,000-year compliance period. Rates of release increase rapidly during the period of time that the units in this disposal region receive waste. Releases decrease at different rates following closure in response to each radionuclide's half-life and sorption properties. The rate of decrease is greatest for short-lived tritium. Because of its highly mobile nature, the inventory of C-14 is depleted relatively quickly; the distribution coefficient of C-14 is assumed to be zero, indicating that it does not sorb to the solid phase of the material in the disposal units. Rates of release are constant for U-238, reflecting the long half-life of the radionuclide and the fact that it sorbs to the crushed tuff/waste mixture in the disposal units.

4.1.3 Vapor- and Gas-Phase Diffusion

Vapor- and gas-phase radionuclides are projected to diffuse upward from the waste and exit from the facility surface. Mean fluxes from the top waste layer into the overlying cap are shown in Figure 4-4 for H-3, CH_4, and Rn-222 in waste disposal region 8. The fluxes of all three radionuclides increase rapidly while waste is placed in the disposal units. Projected fluxes of tritium (Figure 4-4a) fall rapidly thereafter as this radionuclide is depleted due to diffusion and radioactive decay. The diffusion of C-14 is more prolonged, as the biodegradation of the organic C-14 waste generates CH_4 (Figure 4-4b). As shown in Figure 4-4c, fluxes of Rn-222 decrease relatively slowly throughout the simulation period as the decay of its long-lived parent, Ra-226, provides a continuing supply of the isotope.

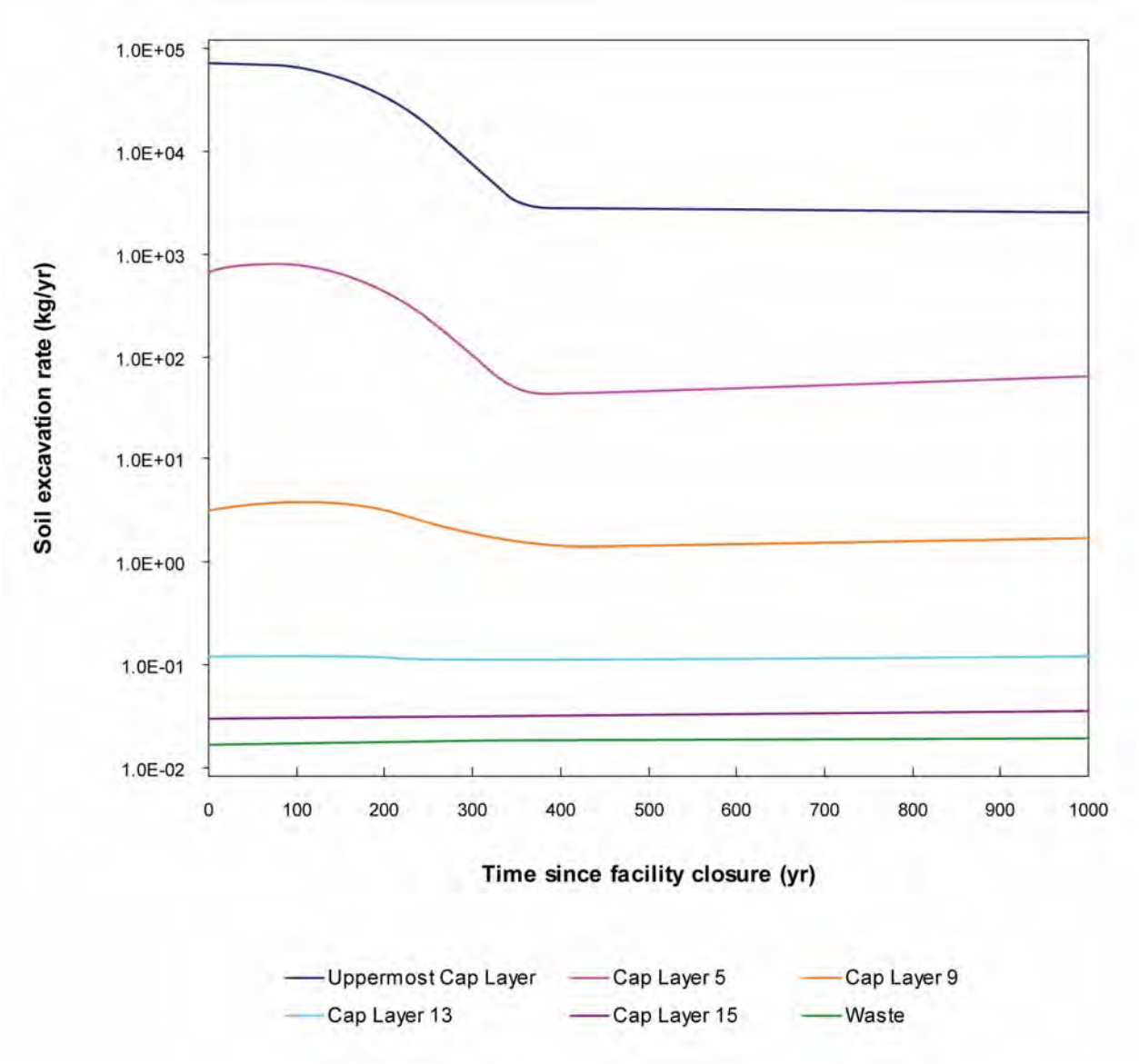

Figure 4-2
Mean Soil Transport Rates for Burrowing Animals in Waste Disposal Region 8

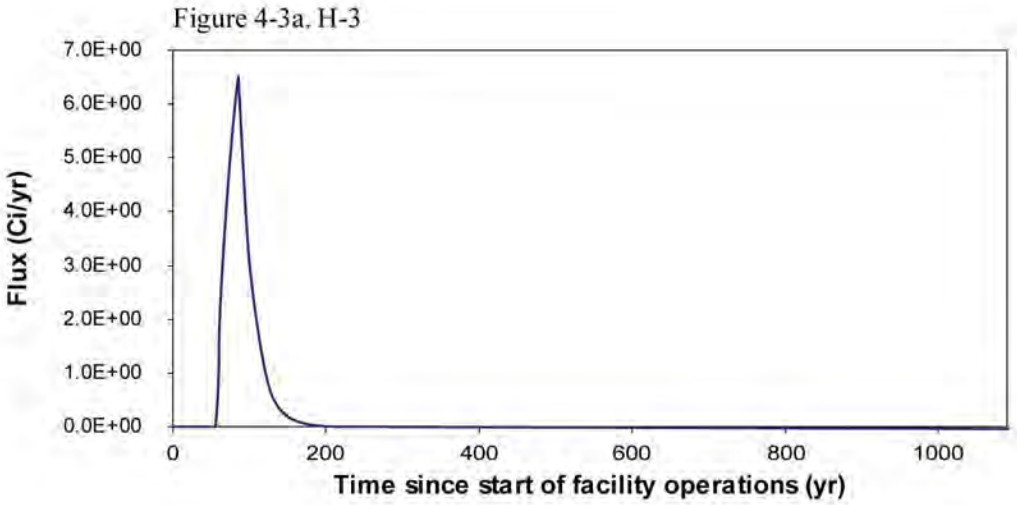

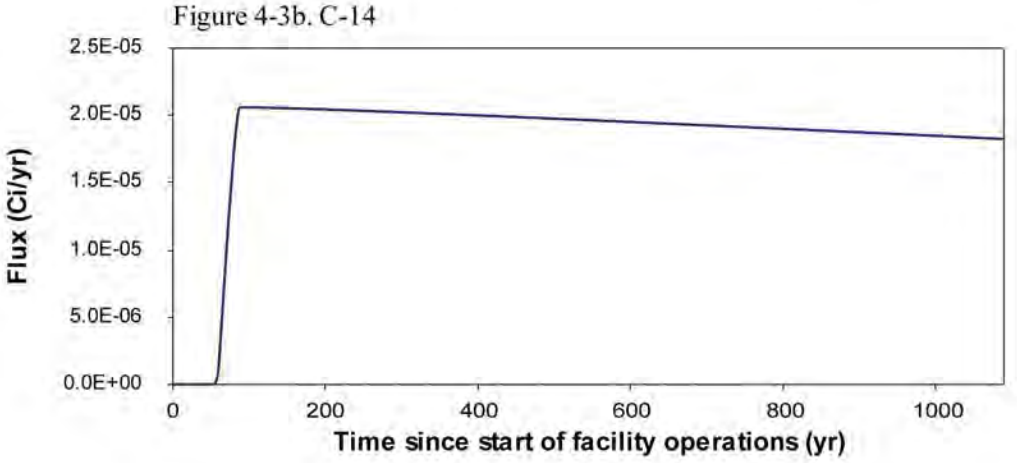

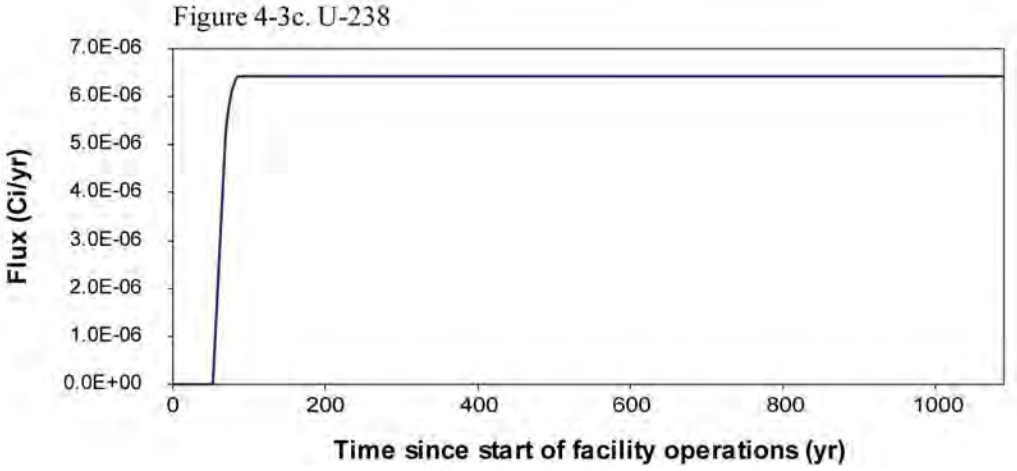

Figure 4-3
Mean Groundwater Fluxes from the Bottom of Disposal Units in Waste Disposal Region 8

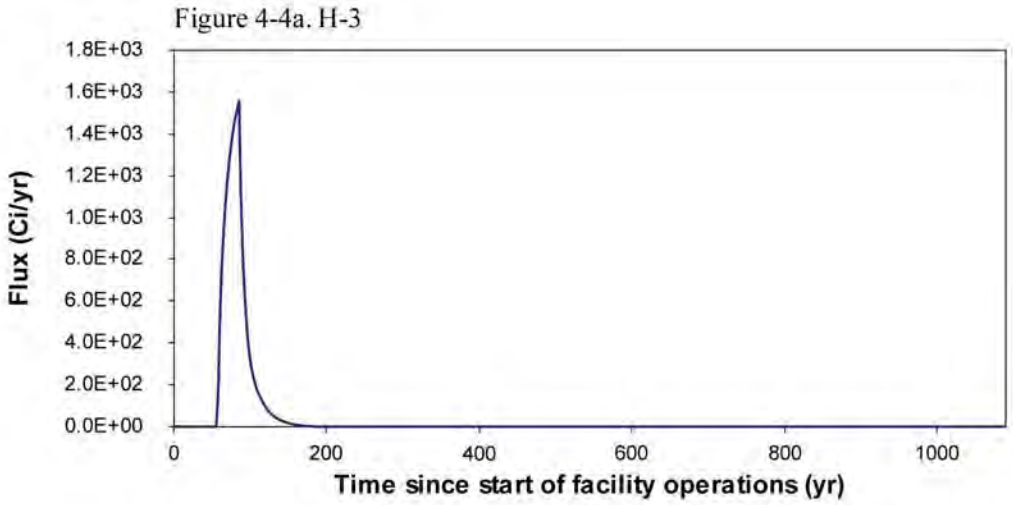

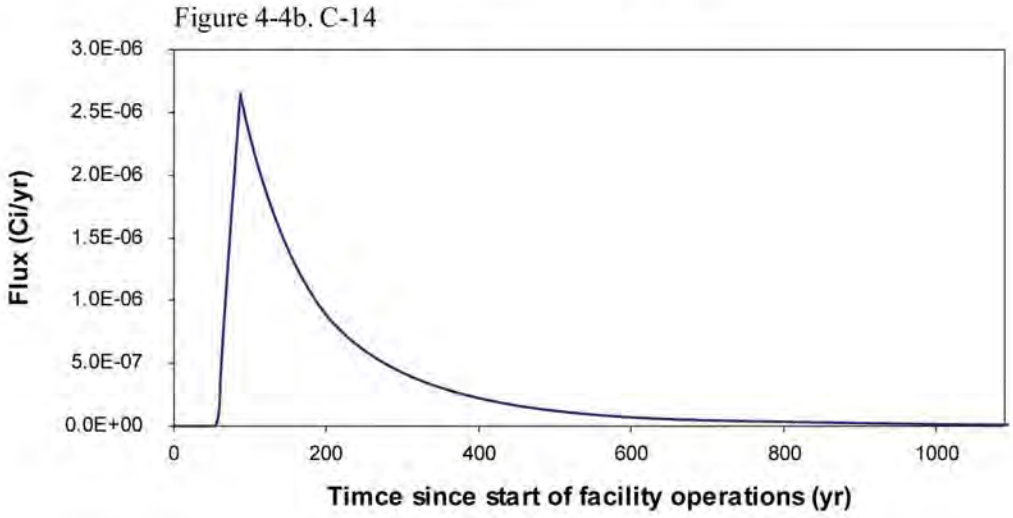

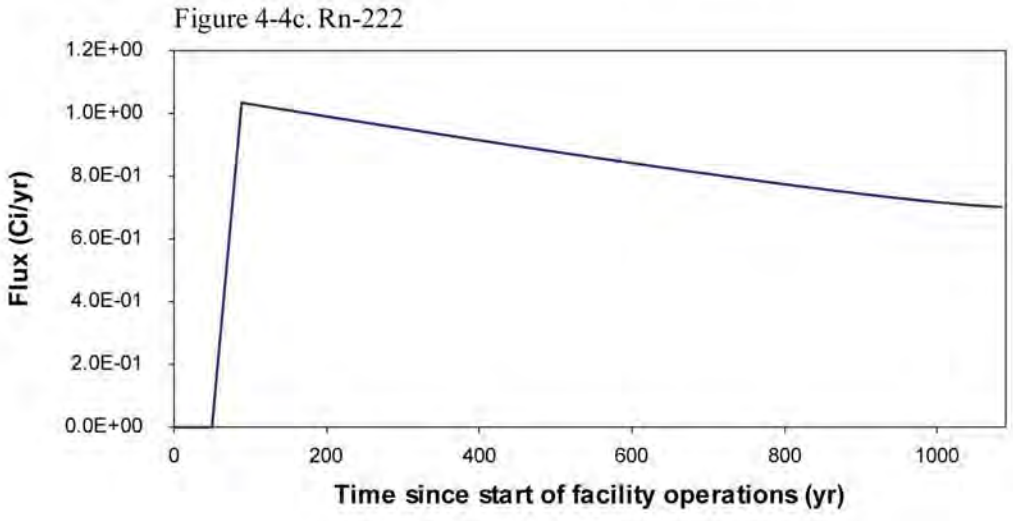

Figure 4-4
Mean Diffusive Fluxes from the Top of Waste in Waste Disposal Region 8

4.2 Environmental Transport of Radionuclides

The results of the radionuclide transport modeling are presented below. Section 4.2.1 discusses the findings of the groundwater transport modeling conducted by Stauffer et al. (*Appendix E*). The results of the atmospheric dispersion modeling undertaken by Jacobson (*Appendix D*) are addressed in Section 4.2.2; this section also discusses the vertical flux measurements that were collected by Whicker and Breshears (*Appendix C*) and used to define rates of resuspension for the atmospheric pathway. The results of the surface erosion modeling conducted using SIBERIA (*Appendix I*) are provided in Section 4.2.3, along with the findings of the wind erosion study performed by Whicker and Breshears.

4.2.1 Groundwater Transport

Contaminants leached from the waste are transported by water infiltrating through the site to the regional aquifer. The risk posed by these contaminants to groundwater users downgradient of the disposal facility will depend upon the magnitude of the release and the decay characteristics of the radionuclides relative to the amount of time required to reach the compliance well. Modeling conducted by Stauffer et al. (*Appendix E*) was used to characterize groundwater travel times to downgradient locations and to develop groundwater transport models that could be implemented within the Area G Site Model. The results of this modeling effort are presented in the following sections.

The groundwater transport modeling conducted using FEHM projected groundwater travel times in terms of particle breakthrough times for each of the eight waste disposal regions at Area G. Several plots of these results are presented below; all of these figures show normalized breakthrough. To generate these results, the number of particles crossing the compliance boundary during a given time interval was divided by both the time increment and the total number of particles that reach the boundary, such that the integral of the area under the curve is 1 for all plots.

4.2.1.1 Particle Breakthrough

Groundwater travel times to the 100 m (330 ft) compliance well will be influenced by the rate of infiltration through the site and the waste disposal region under consideration. To illustrate, Figure 4-5 shows conservative breakthrough curves at the compliance boundary for particles released from each of the eight disposal regions. The background infiltration rate for this example is 0.5 mm/yr (0.02 in./yr). Waste disposal region 6, which consists of a cluster of deep shafts near the eastern boundary of Area G, has the fastest breakthrough, beginning at 5,000 years after the release of the particles and peaking at around 13,000 years. The arrival of releases from disposal region 1 is slightly slower than that observed for region 6 because of the higher elevation of the release points within this region. Disposal regions 5 and 8, located to the west, have longer breakthrough times, beginning at around 9,500 years after the release of the particles and peaking at about 18,000 years.

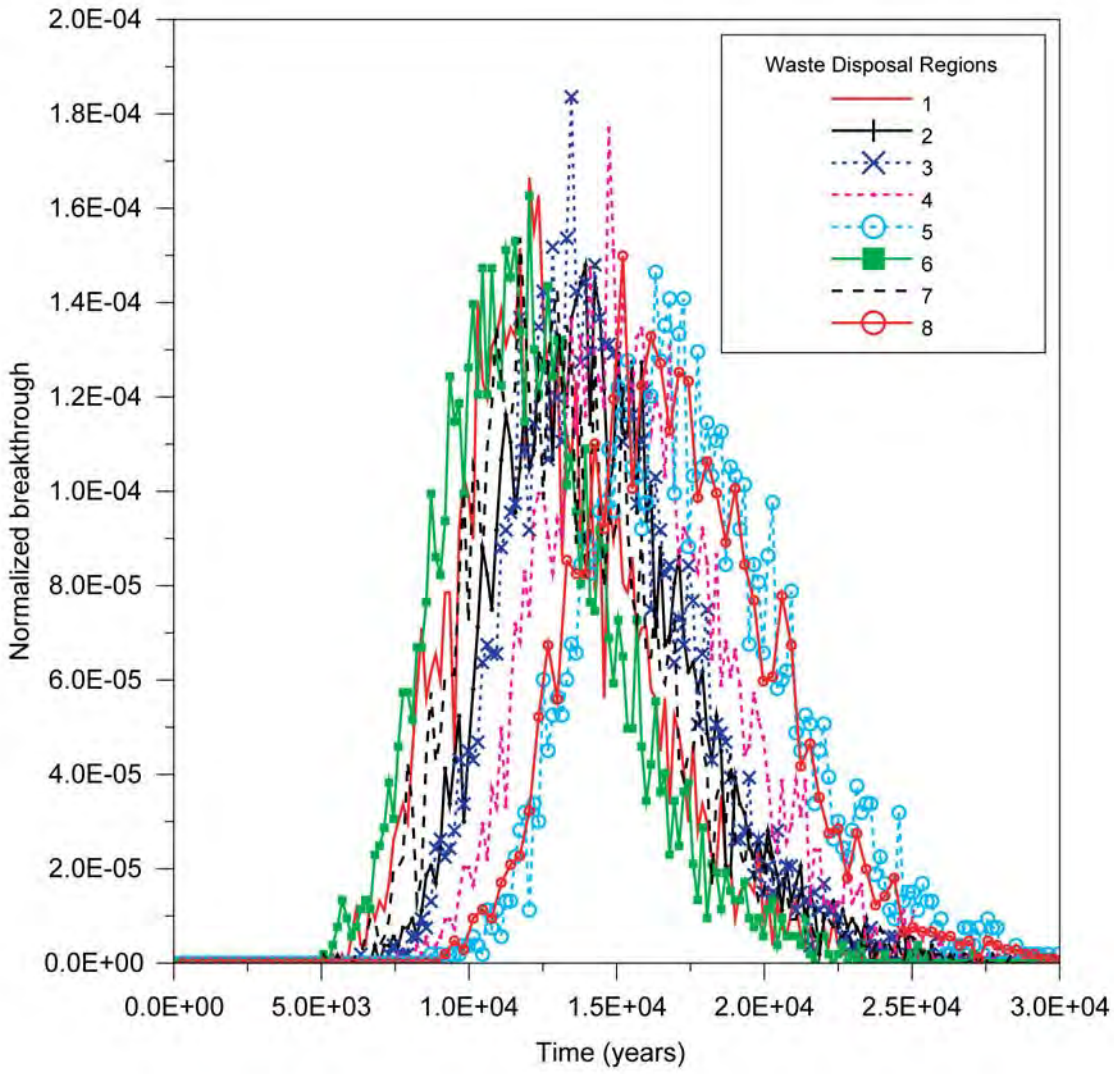

Figure 4-5
Breakthrough Curves for Particles Released from All Waste Disposal Regions (background infiltration of 0.5 mm/yr)

Releases from the disposal regions in the central portion of Area G generally show increased time to breakthrough as the distance from the compliance boundary to the disposal region increases. However, the observed breakthrough times are almost exclusively determined by travel times within the vadose zone; travel times from the points of discharge below the waste disposal regions and the compliance boundary range from about 2 to 15 years.

Higher rates of infiltration through the disposal facility will result in shorter groundwater travel times to the compliance well. To illustrate, conservative breakthrough curves for releases from the eight disposal regions at a background infiltration rate of 10 mm/yr (0.39 in./yr) are shown in Figure 4-6. The relative breakthrough for the different regions at this infiltration rate is similar to that noted at a rate of 0.5 mm/yr (0.02 in./yr); however, at the higher infiltration rate, the first breakthrough occurs for disposal region 6 within 500 years of particle release, with peak breakthrough at about 750 years.

Greater insight into the effects of the rate of infiltration on groundwater travel times is provided by Figures 4-7 through 4-9. These figures show particle breakthrough curves for releases from waste disposal regions 1 and 5 for the range of infiltration rates considered in the FEHM modeling. They show breakthrough curves for three time spans: 80,000 years, 20,000 years, and 5,000 years; breakthrough curves corresponding to some of the lower infiltration rates do not fall within the shorter time spans. As discussed above, breakthrough occurs more quickly for releases on the east end of Area G (disposal region 1) at a given infiltration rate than for more westerly locations (disposal region 5). Breakthrough for releases from disposal region 5 typically takes about 1.5 times as long as for region 1. Thus, peak breakthrough with a 0.25 mm/yr (9.8×10^{-9} in./yr) background infiltration rate occurs for disposal region 1 at approximately 20,000 years after particle release while the corresponding peak breakthrough for disposal region 5 occurs at approximately 30,000 years.

As discussed in Section 3.2.2.1, groundwater travel times may be influenced by permeability reductions between geologic units and elevated infiltration rates within Pajarito Canyon; these effects were evaluated in conjunction with the groundwater modeling. Figure 4-10 shows how interface permeability reductions affect subsurface saturations; a high infiltration rate of 10 mm/yr (0.39 in./yr) was chosen to more clearly demonstrate the effect. The permeability reduction at the base of unit 1g results in an increase in saturation of 10 percent in the lower part of unit 1g, while the permeability reduction at the top of the basalt yields an increase in saturation of only 2 percent in the lower few meters of the Otowi Member of the Bandelier Tuff.

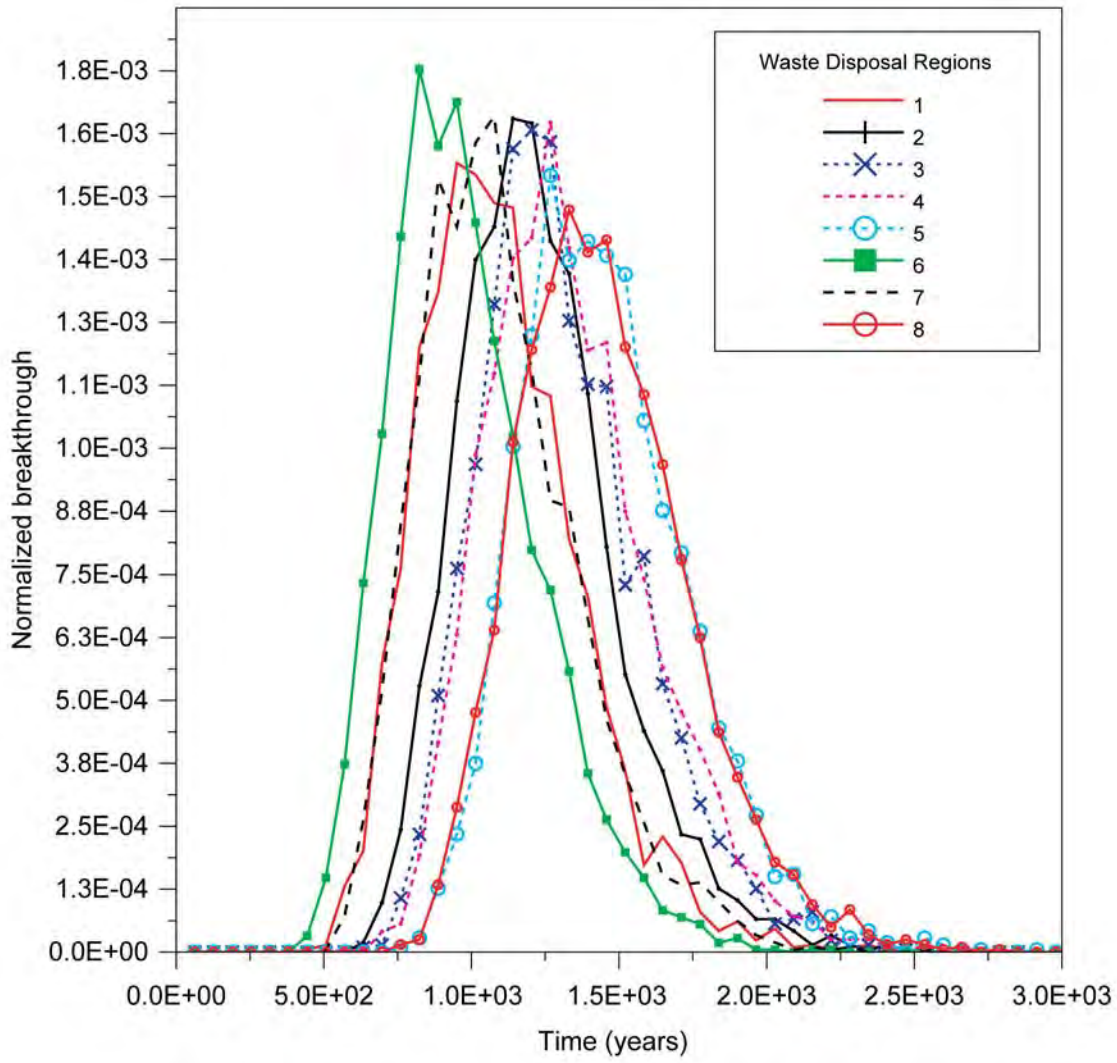

Figure 4-6
Breakthrough Curves for Particles Released from All Waste Disposal Regions (background infiltration of 10 mm/yr)

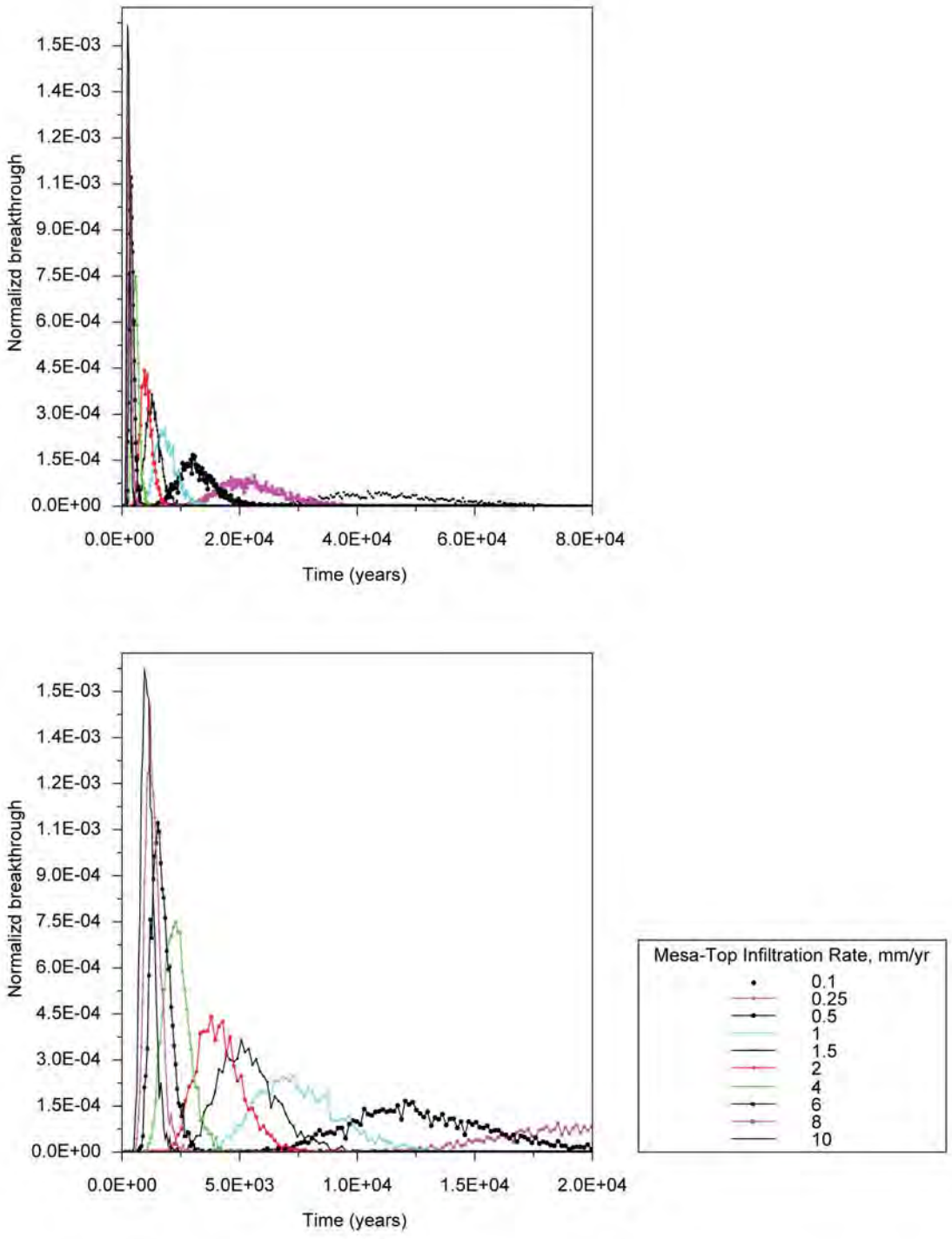

Figure 4-7
Breakthrough Curves for Particles Released from Waste Disposal Region 1 (range of steady-state infiltration rates)

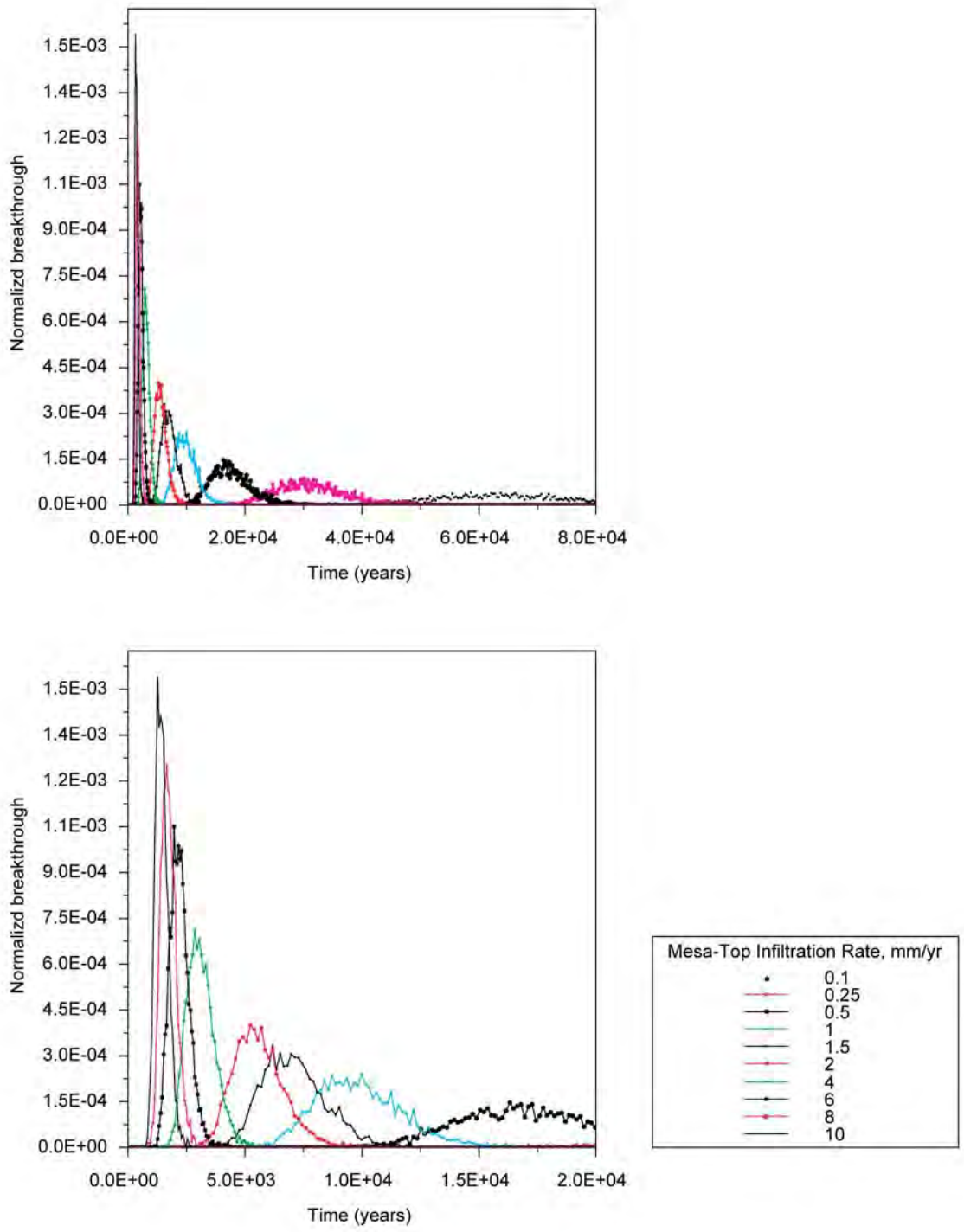

Figure 4-8
Breakthrough Curves for Particles Released from Waste Disposal Region 5 (range of steady-state infiltration rates)

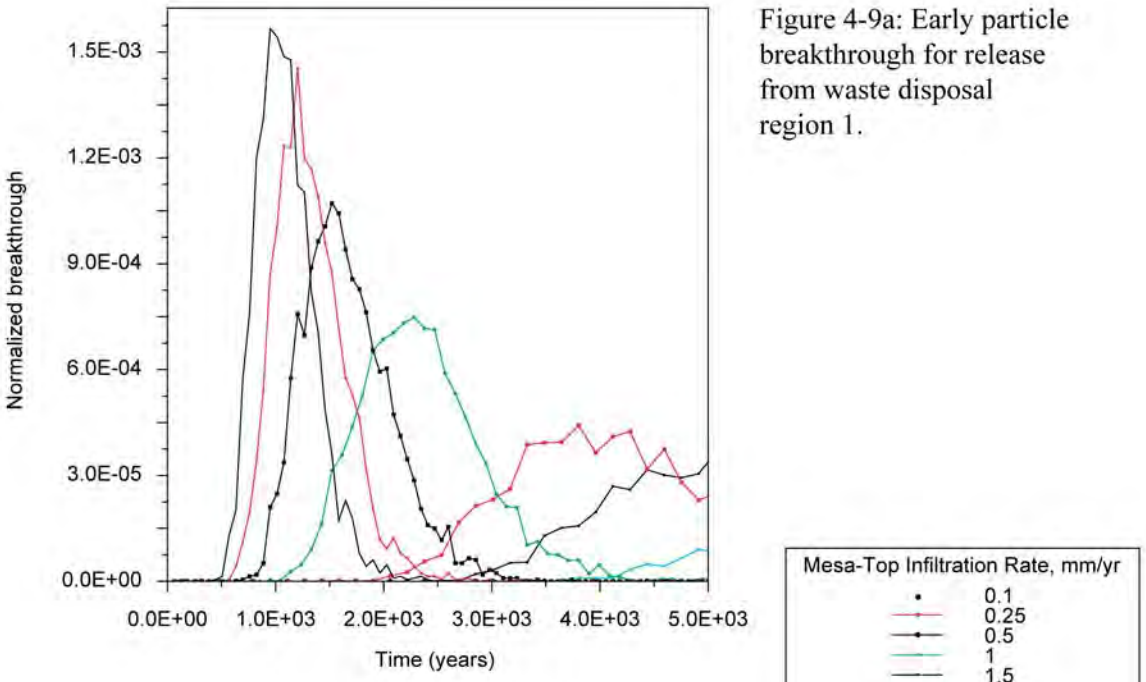

Figure 4-9a: Early particle breakthrough for release from waste disposal region 1.

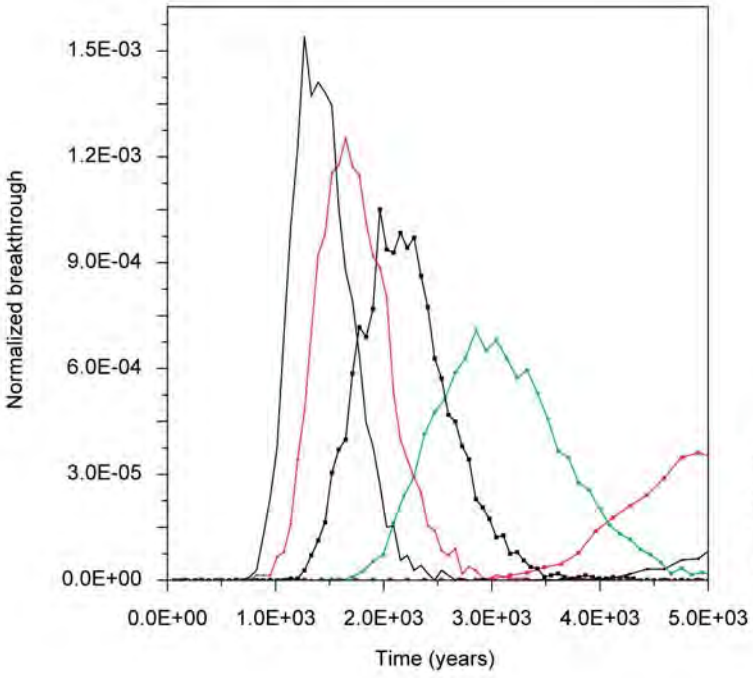

Figure 4-9b: Early particle breakthrough for release from waste disposal region 5.

Figure 4-9
Early Breakthrough Curves for Particles Released from Waste Disposal Regions 1 and 5 (range of steady-state infiltration rates)

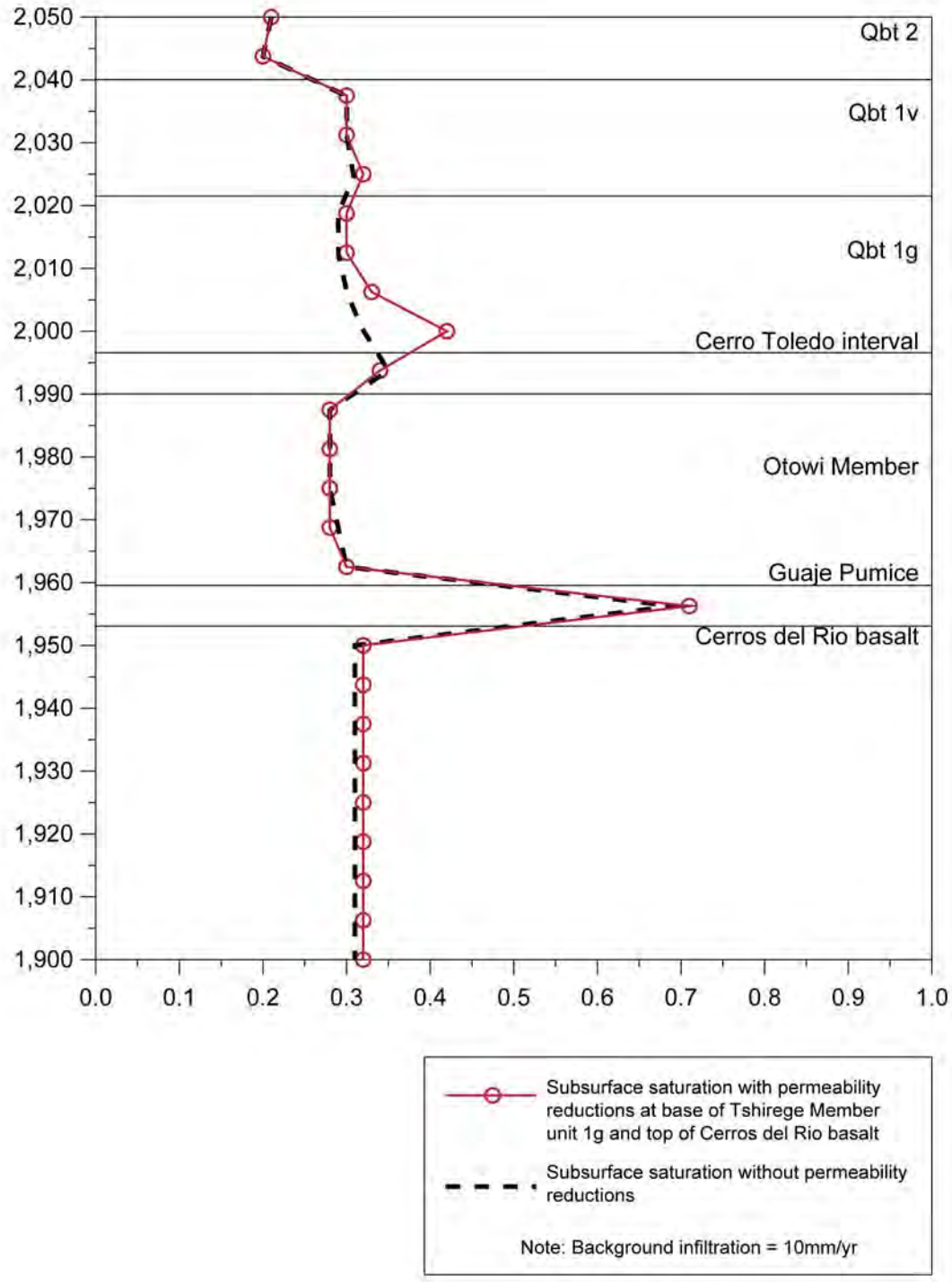

Figure 4-10
Effect of Permeability Reductions on Subsurface Saturation at Waste Disposal Region 5

Figure 4-11 shows how the reduced permeability interfaces impact conservative tracer breakthrough at the compliance boundary for particle releases from waste disposal regions 1 and 5. The assumed background infiltration for the results shown in this figure is 10 mm/yr (0.39 in./yr) and the assumed infiltration rate in Pajarito Canyon is 100 mm/yr (3.9 in./yr). These results indicate that particle breakthrough from disposal region 1 is slightly faster at a reduced permeability. This occurs because the 3-D geometry causes variable subsurface fluxes, despite an average infiltration rate throughout the domain of 10 mm/yr (0.39 in./yr). Particles released from disposal region 5 behaved as expected, with the reduced permeability scenario leading to a slightly retarded breakthrough. Interface permeability reductions had fairly minor impacts on predicted travel times and were included in all model simulations.

Steady-state saturation profiles beneath waste disposal region 5 illustrate the effect of increased annual Pajarito Canyon infiltration of 6 m^3/m (65 ft^3/ft) for two different assumed background infiltration levels (Figure 4-12). When the rate of infiltration on the surrounding mesas and canyons is low (0.1 mm/yr [0.0039 in./yr]), an infiltration rate of 100 mm/yr (3.9 in./yr) across a 60 m (200 ft) channel clearly affects saturations in the Guaje Pumice. However, saturation levels change very little when the background infiltration rate in areas surrounding Pajarito Canyon is increased to 0.5 mm/yr (0.02 in./yr).

The effect of 6 m^3/m (65 ft^3/ft) annual infiltration in Pajarito Canyon on breakthrough time was evaluated under steady-state conditions for tracer particles released from waste disposal regions 1 and 5. As shown in Figure 4-13, at an assumed background infiltration rate of 0.1 mm/yr (0.0039 in./yr), the particles released from disposal regions 1 and 5 behaved nearly identically with and without increased Pajarito Canyon infiltration. These results demonstrate that transport is insensitive to increased recharge from the canyon for realistic values of Pajarito Canyon infiltration and channel width.

Setting the Pajarito Canyon infiltration rate to 100 mm/yr (3.9 in/yr) over a 240 m (790 ft) wide channel causes water to spread axially from the canyon when it encounters the permeability reduction interface at the top of the basalt, forcing flow northward under Area G. Because of this northward component of flow in the Guaje Pumice, tracer particles migrate up to 100 m (330 ft) to the north before they pass into the basalt and down to the water table. Although this behavior has been suggested as a possible mechanism for the transference of contaminants from Pajarito Canyon to wells drilled under Cañada del Buey, the net effect on breakthrough at the compliance boundary is not significant. Furthermore, because the effect of increased saturation in the Guaje Pumice is to spread the particles laterally, it is concluded that the most conservative numerical representation of Pajarito Canyon includes no increased infiltration. Therefore rates of infiltration in Pajarito Canyon were assumed to be the same as the mesa-top, or background, rates when calculating breakthrough from the waste disposal units.

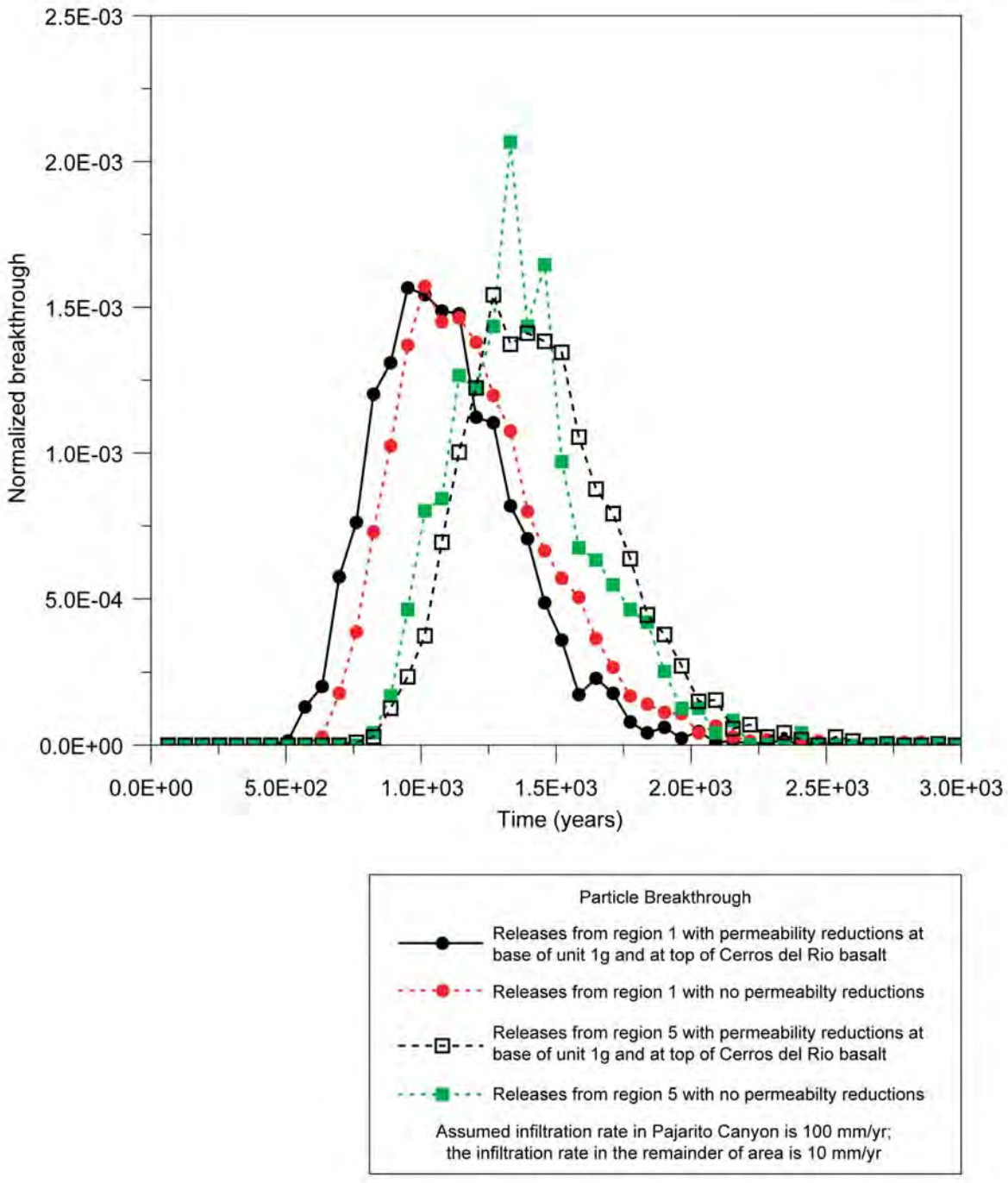

Figure 4-11
Effect of Permeability Reductions on Breakthrough for Releases from Waste Disposal Regions 1 and 5

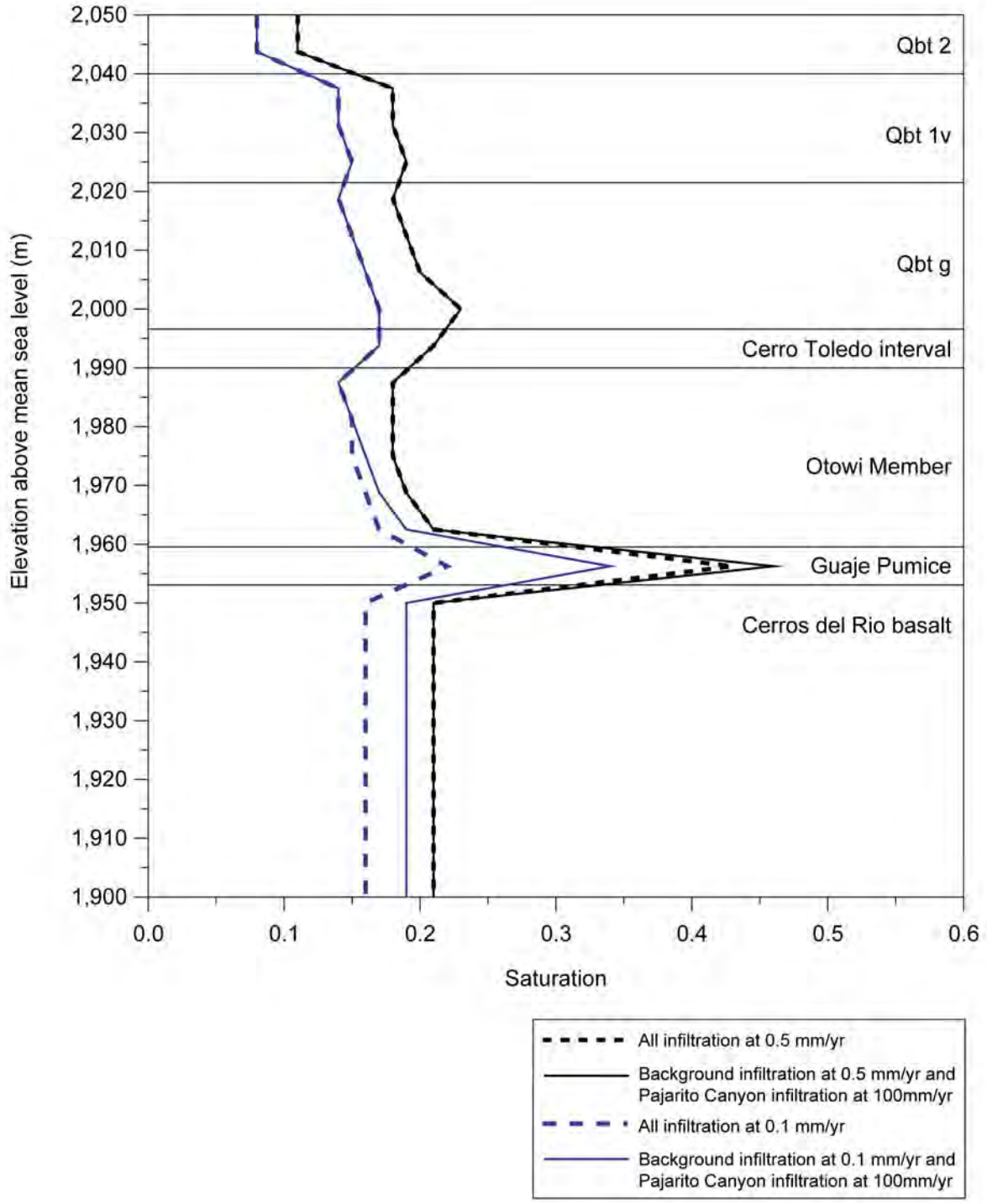

Figure 4-12
Effect of Pajarito Canyon Infiltration on Subsurface Saturation at Waste Disposal Region 5

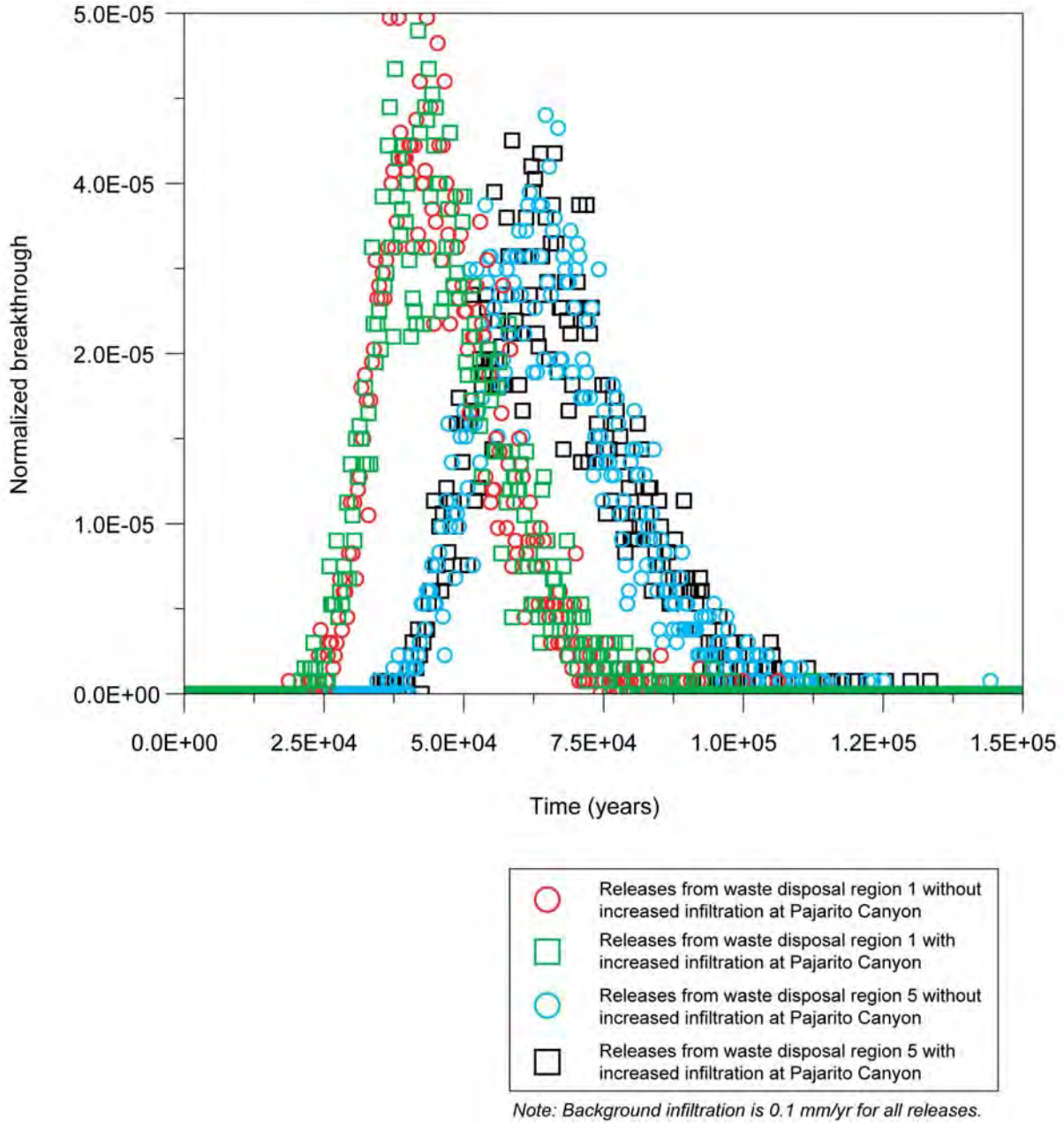

Note: Background infiltration is 0.1 mm/yr for all releases.

Figure 4-13
Effect of Pajarito Canyon Infiltration on Breakthrough for Releases from Waste Disposal Regions 1 and 5

Projected particle breakthrough times from waste disposal region 5 were relatively insensitive to the vadose-zone longitudinal dispersivity at mesa-top infiltration rates of 0.1 mm/yr and 10 mm/yr (0.039 and 0.39 in./yr). However, higher vadose-zone longitudinal dispersivities cause the width of the breakthrough curve to increase while the peak value falls. Examples of this are shown in Figure 4-14. The groundwater transport modeling was conducted using a longitudinal dispersivity in the vadose zone of 2 m (7 ft). This value was chosen because it is intermediate in what is considered to be a reasonable range of possible values.

4.2.1.2 Well Capture

Radionuclides discharged to the regional aquifer will disperse as they are transported to locations downgradient of Area G; only a portion of the contaminant plume will be intersected by the compliance well and contribute to the exposures of the groundwater user. To account for this effect, well capture simulations were conducted to determine the capture zone radius and the capture efficiency of a hypothetical nearby pumping well. Because the background gradient in the aquifer is fairly high, the well capture simulations project relatively narrow capture zones for the pumping rates considered. The capture radius ranged from 0.4 m (1.3 ft) for the 50 m^3/yr (13,000 gal/yr) pumping rate to 5.7 m (19 ft) for a pumping rate of 2,500 m^3 (6.6×10^5 gal/yr). Figure 4-15 shows the capture zone for a pumping rate of 1,200 m^3/yr (3.2×10^5 gal/yr). Table 4-1 summarizes the well capture efficiencies calculated using the 3-D particle tracer simulations. Capture efficiency is highly dependent on the transverse dispersivity, decreasing most rapidly between dispersivities of 0 and 2 m (0 and 6.6 ft). These capture efficiencies are expected to be conservative for reasons discussed in *Appendix E*.

4.2.1.3 Model Abstraction

The 3-D modeling conducted using FEHM produced the particle breakthrough curves shown above. The results of this modeling were used to develop 1-D abstractions that could be implemented within the Area G Site Model. Comparisons of breakthrough from the 3-D simulations and the 1-D abstractions show that the abstractions recreate the breakthrough curves of the complex 3-D simulations. Although the input RTDs from the 3-D model are more finely detailed than the 1-D abstraction RTDs, the peak breakthrough times and standard deviations are similar. Thus, simulations performed using either set of projections will lead to the same conclusions.

Similarities in peak breakthrough times for releases from waste disposal regions 1 and 3 can be seen in Figure 4-16. The fits between the 1-D abstraction breakthrough curves and the 3-D particle breakthrough distributions are quite good when the sorption coefficient (K_d) is low. As the distribution coefficient increases, the scatter in the 3-D breakthrough distribution becomes more pronounced and the fit is less accurate. The algorithm used to create the 1-D abstraction leads to some smoothing of the scattered data and approximations of the shape and peak value of the 3-D data. Although the fits appear less good at longer times, these times fall well beyond the 1,000-year

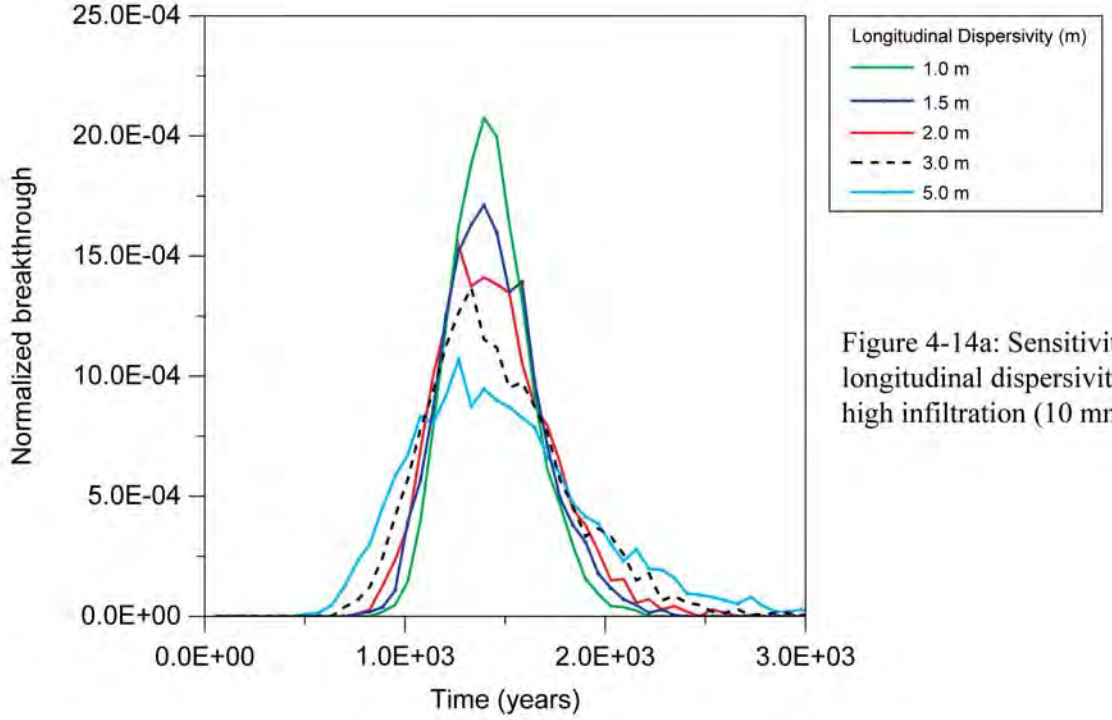

Figure 4-14a: Sensitivity to longitudinal dispersivity at high infiltration (10 mm/yr)

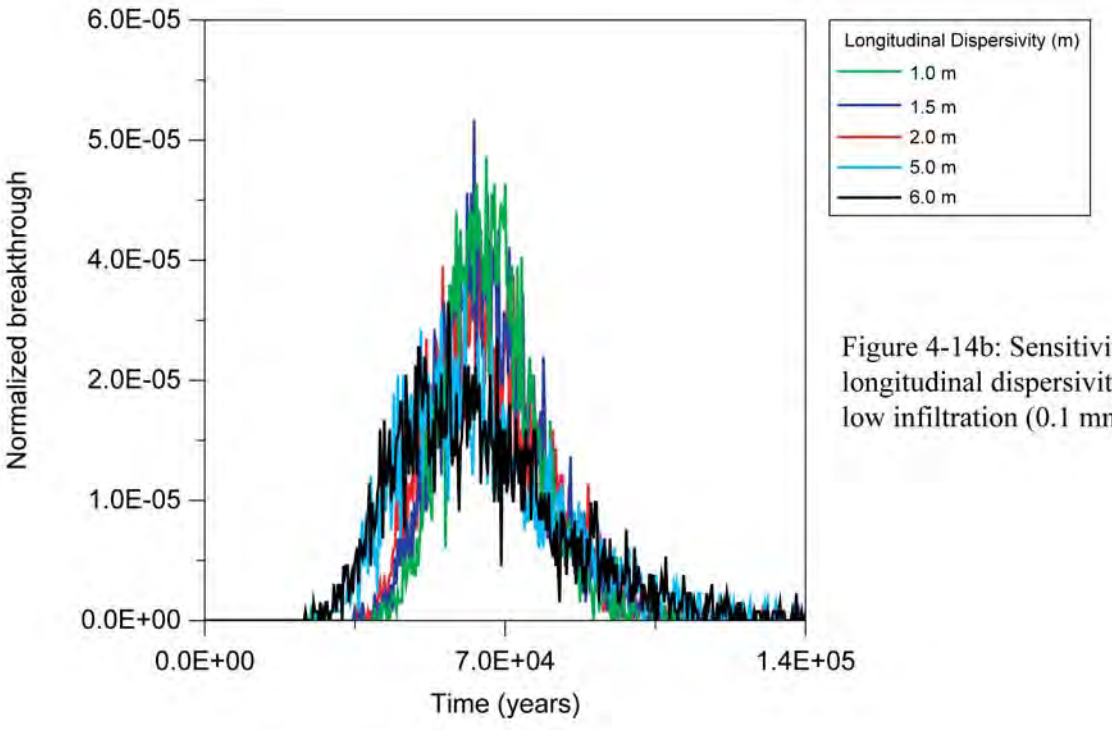

Figure 4-14b: Sensitivity to longitudinal dispersivity at low infiltration (0.1 mm/yr)

Figure 4-14
Model Sensitivity to Longitudinal Dispersivity at Waste Disposal Region 5 (high- and low-infiltration rates)

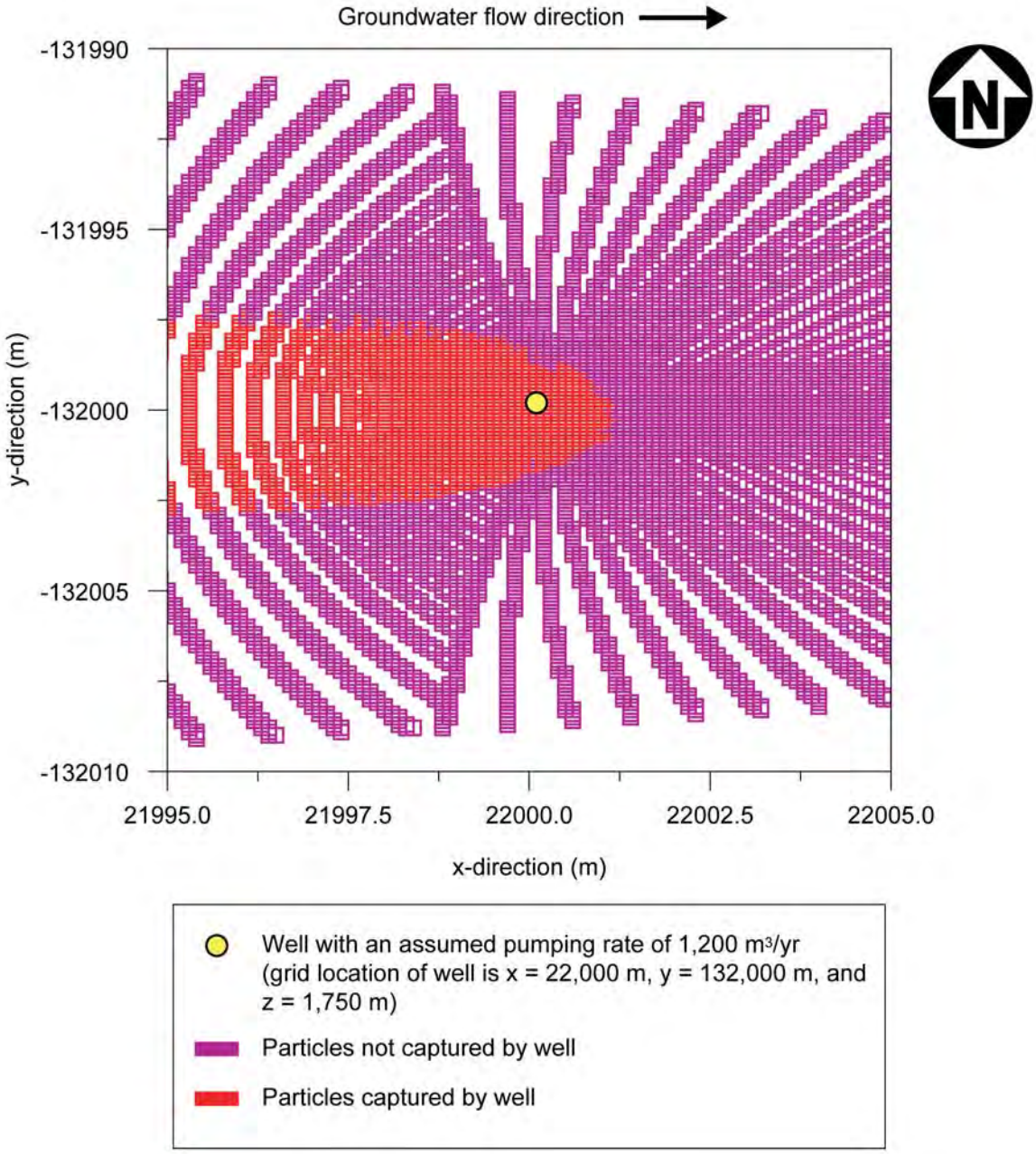

Figure 4-15
Capture Zone for Hypothetical Well with High Pumping Rate

Table 4-1
Capture Efficiencies for Waste Disposal Regions 1 through 5 and 8

Waste Disposal Region	Transverse Dispersivity (m)	Well Pumping Rates (m^3/yr)			
		50	600	1,200	2,500
1	0	4.1E–02	4.1E–02	4.1E–02	4.1E–02
	1	1.7E–03	9.9E–03	1.9E–02	3.1E–02
	2	1.5E–03	9.2E–03	1.5E–02	2.6E–02
	5	2.0E–03	5.3E–03	1.3E–02	2.0E–02
2	0	1.1E–01	1.1E–01	1.1E–01	1.1E–01
	1	6.7E–03	2.3E–02	3.9E–02	7.1E–02
	2	5.3E–03	8.6E–03	2.2E–02	4.7E–02
	5	7.3E–04	6.7E–03	1.2E–02	2.7E–02
3	0	3.6E–02	3.6E–02	3.6E–02	3.6E–02
	1	1.2E–03	5.4E–03	9.7E–03	2.4E–03
	2	3.1E–03	2.8E–03	6.8E–03	1.4E–02
	5	3.0E–04	4.1E–03	4.2E–03	7.7E–03
4	0	3.6E–02	3.6E–02	3.6E–02	3.6E–02
	1	5.6E–04	5.0E–03	5.9E–03	1.7E–02
	2	0.0E+00 [a]	1.6E–03	5.5E–03	1.1E–02
	5	2.6E–04	2.1E–03	2.7E–03	4.8E–03
5	0	5.8E–02	5.8E–02	5.8E–02	5.8E–02
	1	1.5E–03	9.2E–03	9.3E–03	1.9E–02
	2	5.8E–04	2.0E–03	5.5E–03	1.3E–02
	5	2.8E–04	2.2E–03	1.4E–03	3.9E–03
	10	0.0E+00 [a]	2.8E–04	8.3E–04	2.7E–03
8	0	2.7E–02	2.7E–02	3.2E–02	8.1E–02
	1	1.7E–03	7.3E–03	8.0E–03	2.1E–02
	2	0.0E+00 [a]	4.1E–03	4.9E–03	1.2E–02
	5	2.6E–04	1.3E–03	3.9E–03	5.1E–03
	10	2.5E–04	1.3E–03	1.8E–03	2.3E–03

[a] *No particles were captured under the indicated conditions.*

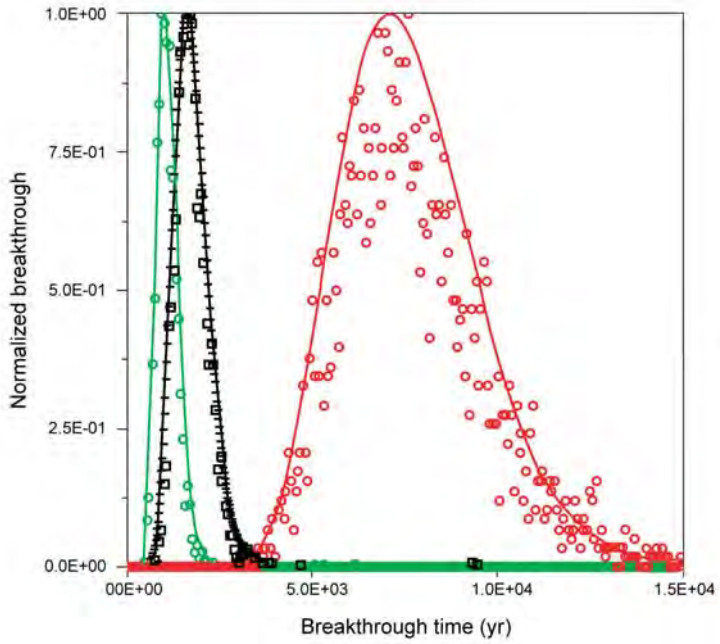

Figure 4-16a: Waste disposal region 3, infiltration rate = 4 mm/yr

Model Used	Distribution Coefficient (Kd)
3-D particle	0
1-D plume	0
3-D particle	0.1
1-D plume	0.096
3-D particle	1.0
1-D plume	0.96

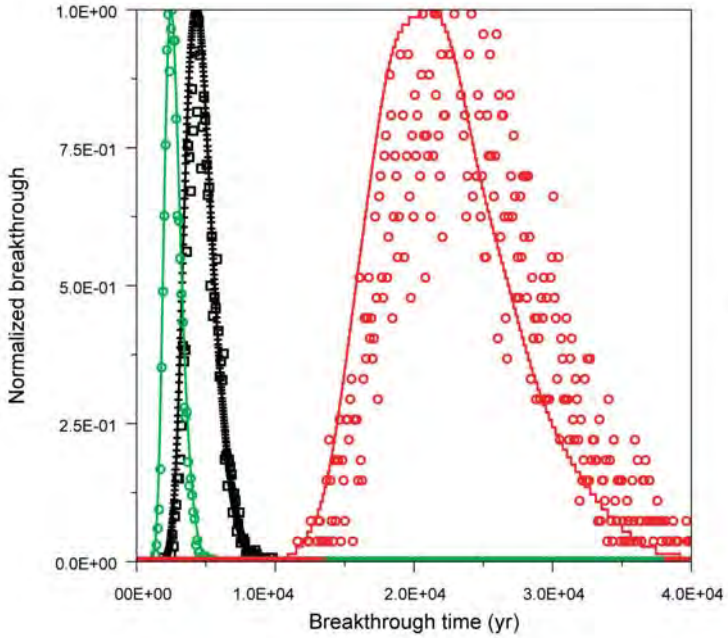

Figure 4-16b: Waste disposal region 1, infiltration rate = 10 mm/yr

Figure 4-16
Comparison of Three-Dimensional Particle and One-Dimensional Plume Breakthrough Curves

compliance period and the approximate fit is considered acceptable for the groundwater pathway modeling. More importantly, the results for times less than 5,000 years match well and provide confidence that the 1-D abstraction retains the information embedded in the 3-D model.

4.2.2 Atmospheric Transport

The atmospheric transport modeling results are provided below. Section 4.2.2.1 addresses the near-field analysis, the results of which were used to estimate exposures for the Atmospheric Scenario. Results of the atmospheric transport modeling conducted to evaluate the potential for interaction between releases from Area G and alternate sources of radioactivity at the Laboratory are addressed in Section 4.2.2.2. The far-field analysis was used to estimate population-scale impacts of atmospheric releases from Area G, in support of the ALARA analysis, these results are discussed in Section 4.2.2.3. Results of the vertical flux measurements conducted in support of the performance assessment and composite analysis are discussed in Section 4.2.2.4.

4.2.2.1 Near-Field Analysis

Particulate concentrations in air were projected using CALPUFF for the 10-year period from 1992 through 2001. Projections were made for all grid or exposure locations included in the model domain (Figure 3-8, Section 3). Figures 4-17 through 4-19 show air concentration contours for particulates with a geometric mean diameter of 0.48 μm (1.9×10^{-5} in.) from atmospheric source areas 1 through 3, respectively. Figures 4-20 through 4-22 show the corresponding results for particulates with a geometric mean diameter of 5 μm (2.0×10^{-4} in.). All results shown in these figures were projected using 2001 meteorological data.

The results shown in Figures 4-17 through 4-22 indicate the tendency for contaminants to be transported in an easterly direction, towards the town of White Rock. Airborne releases disperse to the north and south while in transit. The smaller particulates demonstrate greater rates of dispersal; rates of dispersal for a given particle size tend to increase as the point of release moves westward up the mesa. Table 4-2 provides typical air-concentration values resulting from releases from atmospheric source area 1 for an area to the north of Area G. As seen from these results and the figures, the area to the north of Area G is characterized by some of the highest air concentrations projected by the model for locations outside of the Area G fence line.

Deposition fluxes were also determined using CALPUFF. Dry deposition fluxes are a function of particulate concentrations in air and the deposition velocity; the deposition velocity is a function of particle size. Because a distribution of particle sizes was used in the modeling, a distribution of deposition velocities is generated by CALPUFF and used to estimate the dry deposition flux. CALPUFF calculates wet deposition fluxes based on the calculated air concentration and scavenging coefficients. Table 4-3 provides dry and wet deposition fluxes for each of the three source areas shown in Figure 3-3 (Section 3). These flux values represent the 10-year average of the maximum flux at a location along the LANL/San Ildefonso border to the north of Area G.

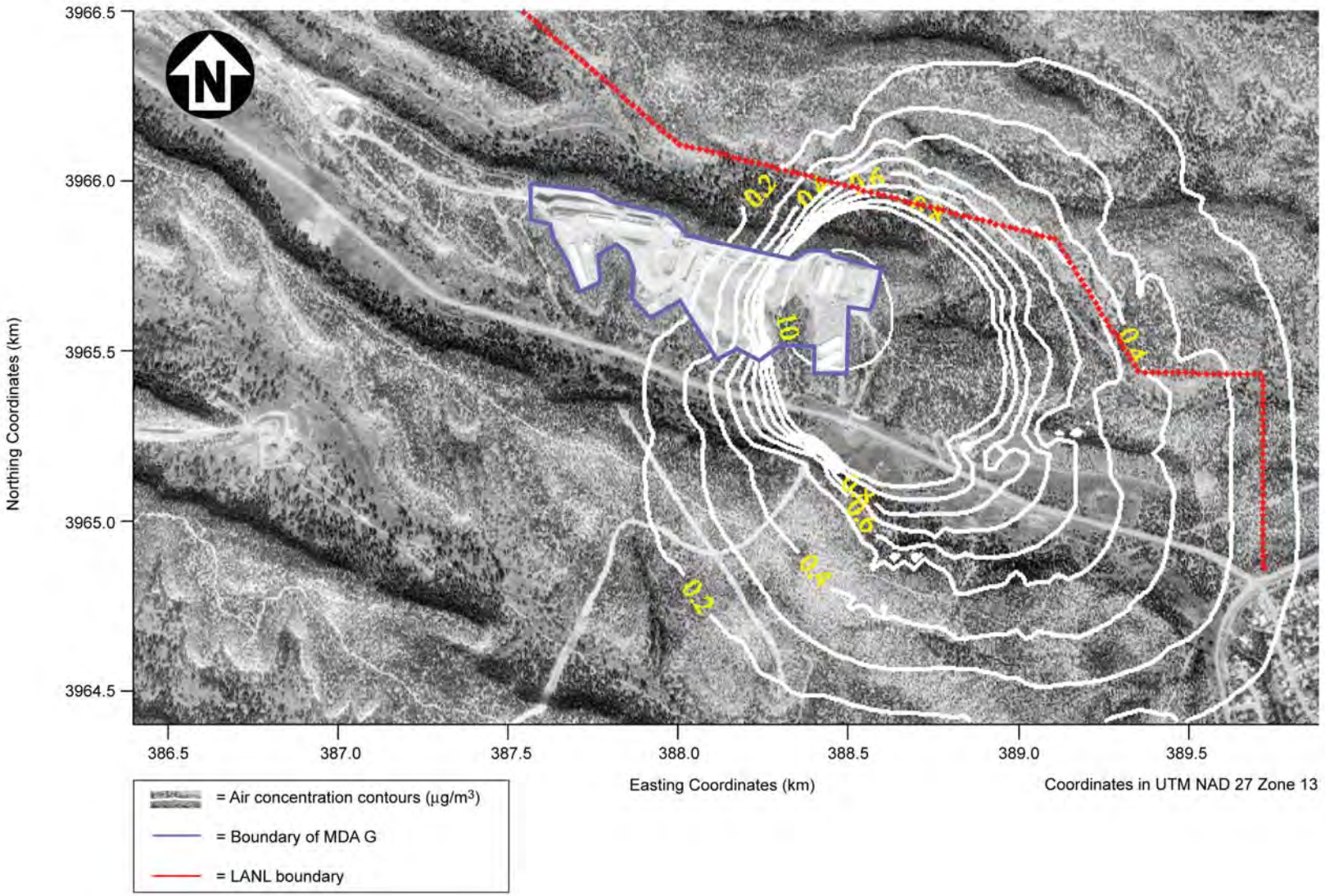

Figure 4-17
Relative Air Concentration Contours Predicted by CALPUFF for Releases from Area G Source Area 1 (particle size gdiam 0.48 µm)

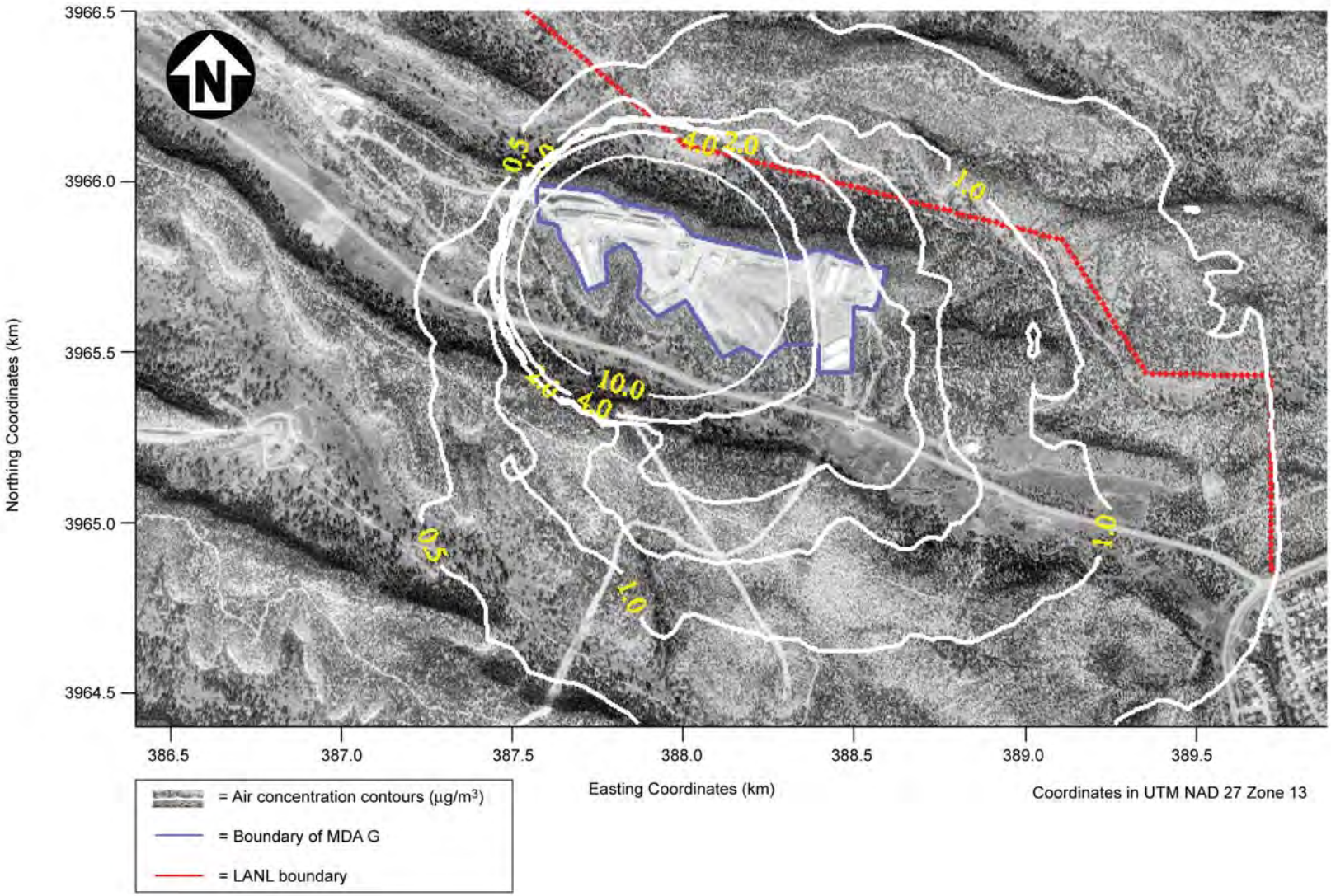

Figure 4-18
Relative Air Concentration Contours Predicted by CALPUFF for Releases from Area G Source Area 2 (particle size gdiam 0.48 µm)

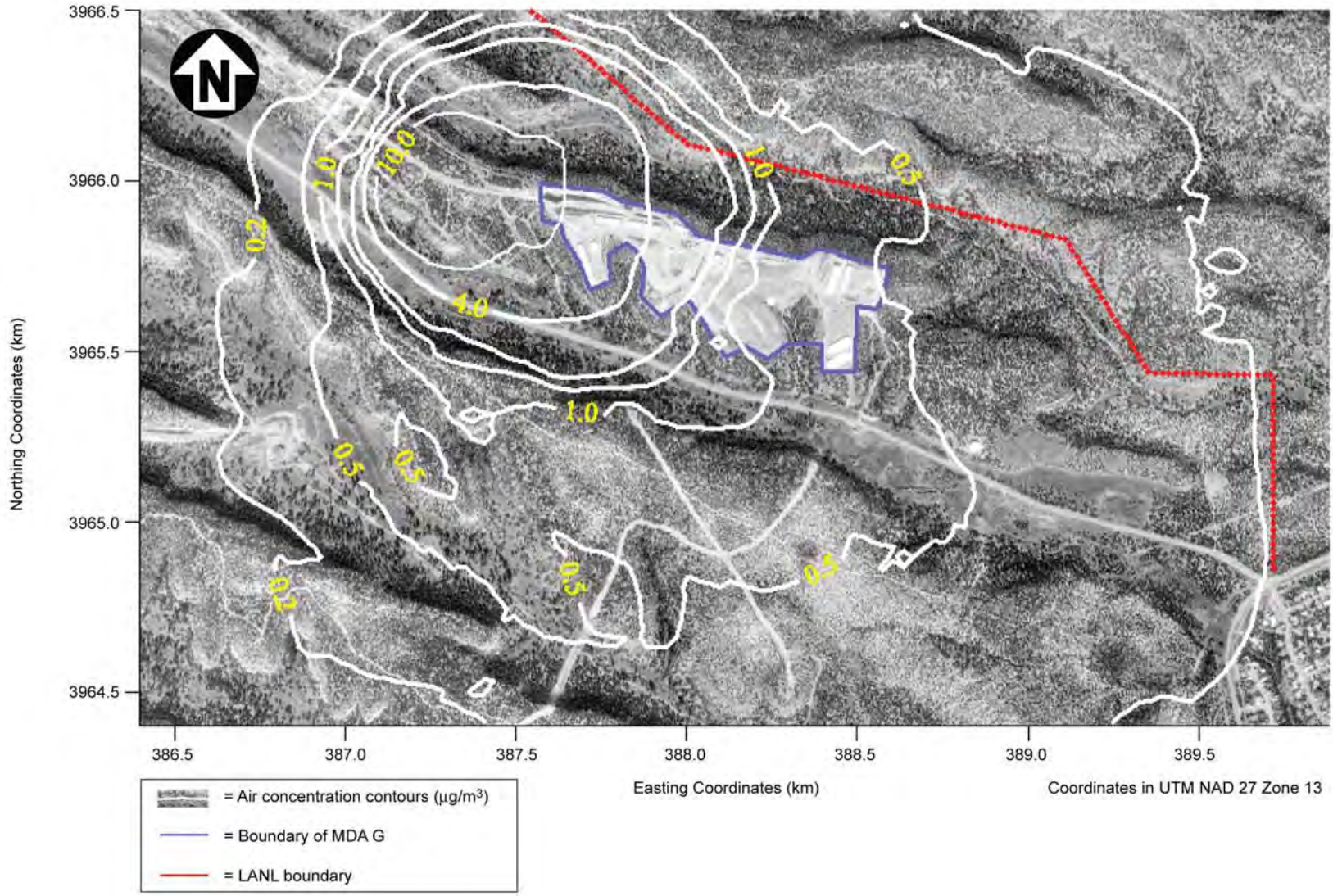

Figure 4-19
Relative Air Concentration Contours Predicted by CALPUFF for Releases from Area G Source Area 3 (particle size gdiam 0.48 µm)

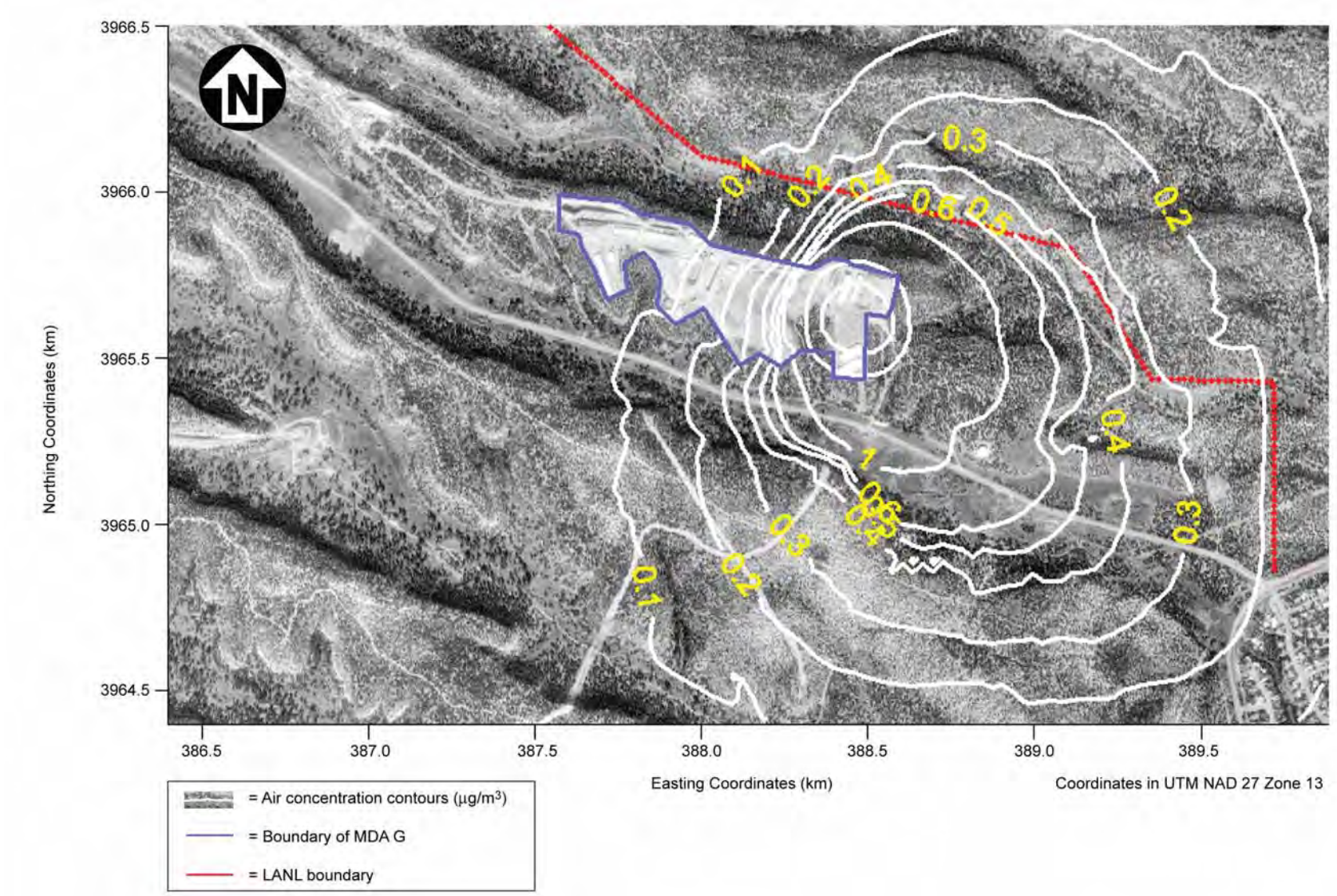

Figure 4-20
Relative Air Concentration Contours Predicted by CALPUFF for Releases from Area G Source Area 1 (particle size gdiam 5.0 µm)

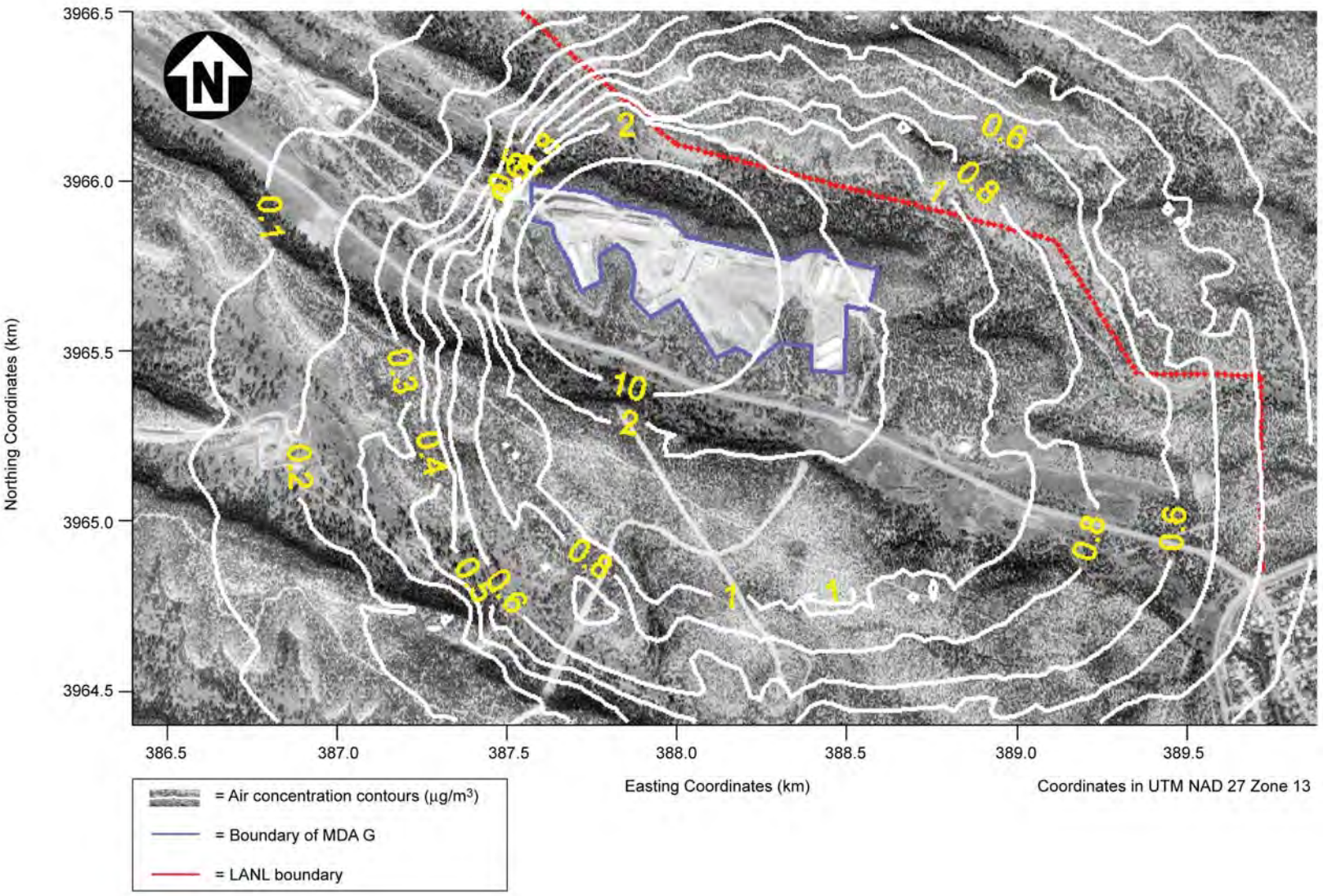

Figure 4-21
Relative Air Concentration Contours Predicted by CALPUFF for Releases from Area G Source Area 2 (particle size gdiam 5.0 µm)

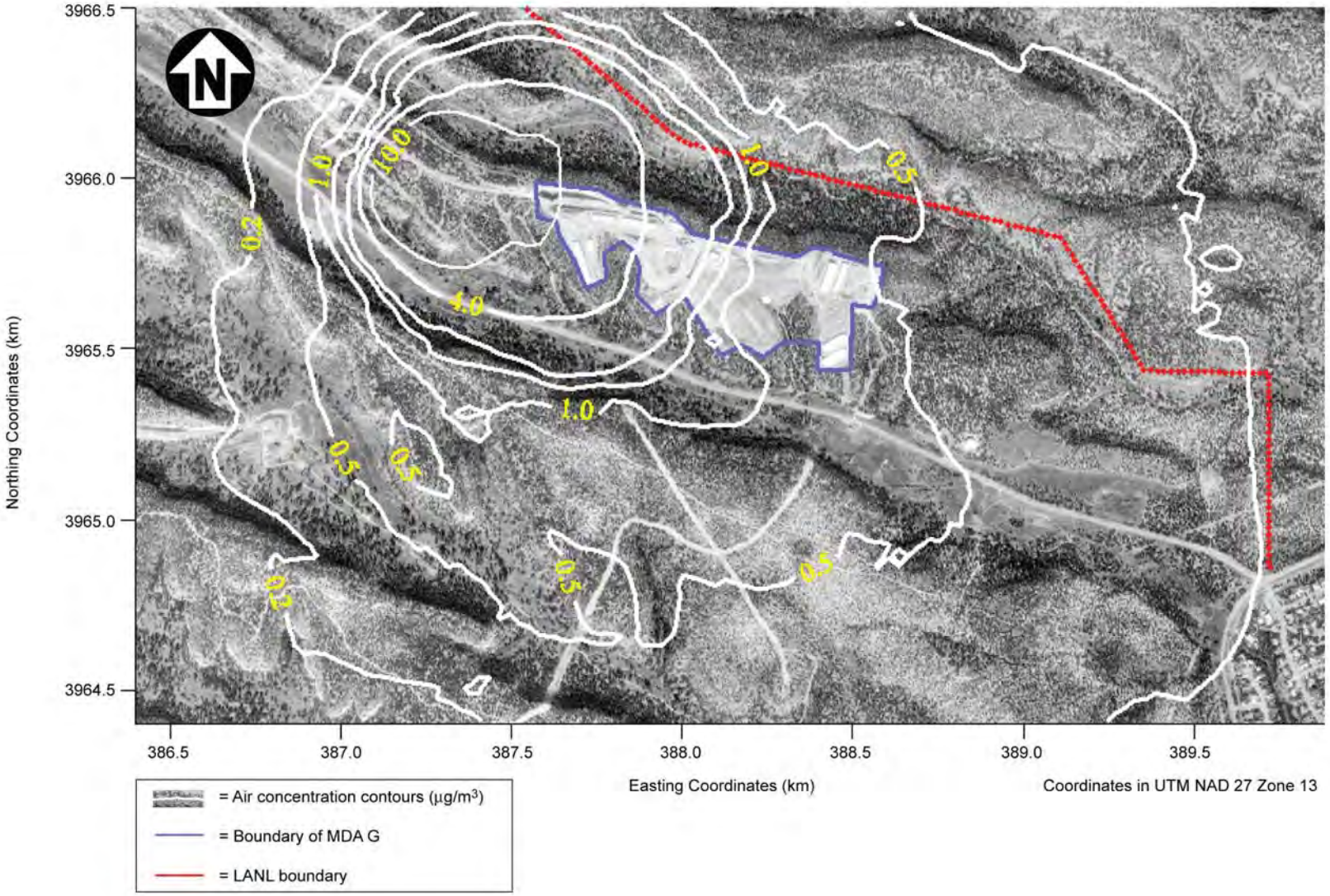

Figure 4-22
Relative Air Concentration Contours Predicted by CALPUFF for Releases from Area G Source Area 3 (particle size gdiam 5.0 µm)

Table 4-2
Annual Variability of Particulate Concentrations at Selected Locations North of Area G

UTM Grid Coordinates (m)		Average Annual Particulate Concentration (μg/m³)									
E	N	1992	1993	1994	1995	1996	1997	1998	1999	2000	2001
Particles with Geometric Mean Diameter of 0.48 μm											
388545	3965975	7.1E-01	7.7E-01	7.5E-01	7.4E-01	6.9E-01	7.4E-01	7.4E-01	6.1E-01	7.6E-01	7.0E-01
388605	3965945	8.4E-01	9.2E-01	9.0E-01	8.6E-01	8.4E-01	9.0E-01	8.9E-01	7.3E-01	9.1E-01	8.6E-01
388665	3965945	7.8E-01	8.5E-01	8.3E-01	7.8E-01	7.8E-01	8.4E-01	8.4E-01	6.8E-01	8.4E-01	8.0E-01
Particles with Geometric Mean Diameter of 5.0 μm											
388545	3965975	6.4E-01	7.0E-01	6.8E-01	6.8E-01	6.3E-01	6.7E-01	6.7E-01	5.6E-01	6.9E-01	6.2E-01
388605	3965945	7.6E-01	8.4E-01	8.2E-01	7.8E-01	7.7E-01	8.2E-01	8.1E-01	6.7E-01	8.3E-01	7.6E-01
388665	3965945	7.0E-01	7.7E-01	7.6E-01	7.5E-01	7.1E-01	7.6E-01	7.6E-01	6.2E-01	7.7E-01	7.1E-01

UTM = Universal Transverse Mercator *E = Easting* *N = Northing*

Table 4-3
Ten-Year Average Peak Dry and Wet Deposition Ratios for Source Areas 1, 2, and 3

Source Area	Dry Deposition Flux (g/m²/s)	Coefficient of Variation (%)	Wet Deposition Flux (g/m²/s)	Coefficient of Variation (%)
1	5.8E-5	5	8.2E-5	38
2	2.7E-4	10.	1.9E-4	30
3	1.3E-4	5	8.2E-5	28

The values shown in Table 4-3 are for the distribution of particles with a gdiam of 0.48 μm (1.9×10^{-5} in.). Table 4-4 provides a comparison of dry deposition flux for the two different particle size distributions used in the near-field analysis (for atmospheric source area 1). As expected, the deposition flux for the larger particles was considerably greater, owing to the order-of-magnitude difference in deposition velocity between particles with a gdiam of 0.48 μm (1.9×10^{-5} in.) and those with a gdiam of 5.0 μm (2.0×10^{-4} in.).

Table 4-4
Comparison of Dry Deposition Flux at the LANL Boundary North of Area G

Particle Size (gdiam, μm)	Dry Deposition Flux, by Year (g/m²/s)									
	1992	1993	1994	1995	1996	1997	1998	1999	2000	2001
0.48	1.8E-5	1.9E-5	2.0E-5	1.9E-5	1.9E-5	1.9E-5	2.0E-5	1.8E-5	2.0E-5	1.9E-5
5.0	7.1E-4	7.6E-4	7.6E-4	7.5E-4	7.6E-4	7.6E-4	7.9E-4	7.3E-4	7.7E-4	9.7E-4

4.2.2.2 Alternate Source Analysis

The alternate source analysis evaluated how potential contributions from MDAs at the Laboratory may impact the exposure conditions for persons living downwind of Area G. Table 4-5 shows the air dispersion factors for releases originating at Area G (atmospheric source area 1) and various MDAs; results are shown for 10 selected receptor locations. The air dispersion factors for the MDAs are less than 1 percent of those projected for releases from source area 1 at Area G.

Table 4-5
Comparison of Air Dispersion Results for Releases from Various Material Disposal Areas

UTM Grid Coordinates (m)		Air Dispersion Results for Various Sources (s/m^3)			
Easting	Northing	Source Area 1 Area G	MDAs A,B,T	MDA C	MDA AB
388567	3965965	8.9E-06	6.7E-08	6.0E-08	5.1E-08
388586	3965960	9.3E-06	6.7E-08	5.9E-08	5.0E-08
388606	3965955	9.7E-06	6.6E-08	5.9E-08	5.0E-08
388625	3965950	9.6E-06	6.6E-08	5.8E-08	5.0E-08
388644	3965945	9.9E-06	6.5E-08	5.8E-08	4.9E-08
388664	3965940	9.5E-06	6.4E-08	5.7E-08	4.9E-08
388683	3965935	9.6E-06	6.4E-08	5.7E-08	4.9E-08
388703	3965931	9.4E-06	6.3E-08	5.7E-08	4.8E-08
388722	3965926	9.4E-06	6.3E-08	5.6E-08	4.8E-08
388741	3965921	9.1E-06	6.2E-08	5.6E-08	4.7E-08

UTM = Universal Transverse Mercator

4.2.2.3 Far-Field Analysis

The far-field analysis evaluated the potential impact of airborne releases from Area G on persons living within 80 km (50 mi) of the disposal facility. The results of the analysis are summarized in Figure 4-23, which shows air concentration contours within the transport model domain. Projected concentrations are generally greatest immediately to the north and south of Area G, decreasing by a factor of 100 or more near the edges of the model domain.

Annual average air concentrations at the center of each of the polar grid cells were calculated by CALPUFF. These air concentrations were used to determine a population-weighted air dispersion value for each grid cell. A selection of some of the weighted values obtained in this manner is provided in Table 4-6.

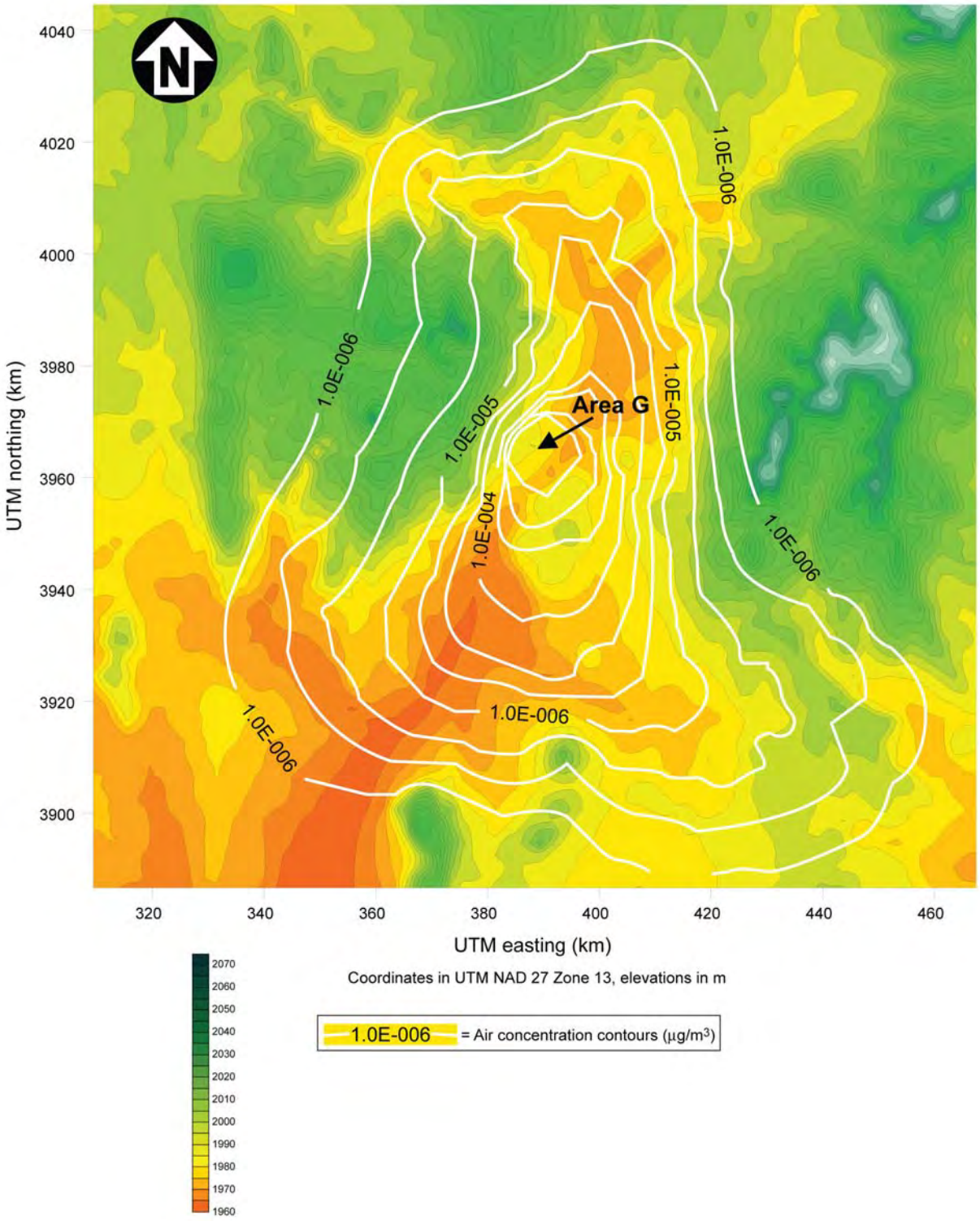

Figure 4-23
Air Concentration Contours for Far-Field Analysis

Table 4-6
Selected Population-Weighted Air Dispersion Values for Source Area 1

General Description	Direction from Area G	Radial Distance (km)	Grid Cell Population	Air concentration (g/m^3)	X/Q (s/m^3)	Population-weighted X/Q ($person\text{-}s/m^3$)
Los Alamos Western Area	NW	8.0 to 10	5.0E+03	4.3E-04	5.7E-09	2.9E-05
		10 to 20	2.3E+03	1.8E-04	2.3E-09	5.4E-06
Los Alamos North Mesa	NNW	7.0 to 8.0	8.9E+02	2.6E-04	3.5E-09	3.1E-06
White Rock ESE	ESE	2.0 to 2.5	2.6E+02	5.2E-03	6.9E-08	1.8E-05
		3.0 to 3.5	6.9E+02	1.2E-03	1.5E-08	1.1E-05
		4.0 to 5.0	1.7E+03	4.3E-04	5.7E-09	9.4E-06
Espanola Area	NE	20 to 30	1.9E+04	2.5E-06	3.3E-11	6.4E-07
Pojoaque Area	ENE	20 to 30	4.3E+03	2.5E-06	3.3E-11	1.4E-07
Santa Fe Area	ESE	20 to 30	5.8E+03	5.1E-06	6.8E-11	4.0E-07
		30 to 40	2.5E+04	2.5E+04	3.3E-01	8.3E+03
	SE	20 to 30	2.1E+04	2.2E-05	2.9E-10	6.2E-06
		30 to 40	4.1E+04	9.5E-06	1.3E-10	5.2E-06
North Edge of Albuquerque	SSW	40 to 80	1.1E+05	6.6E-06	8.8E-11	9.4E-06

4.2.2.4 Vertical Flux Measurements

Vertical flux measurements conducted at TA-54 were used to characterize particulate resuspension rates for the GoldSim modeling. Figure 4-24 shows the range of measured values for the vertical flux. Note that positive numbers represent upward flux (removal from the area) and negative numbers represent downward net flux (deposition within the area). Table 4-7 shows the summary statistics for aerosol mass concentrations and the vertical flux measurement data. Overall, the average vertical flux at 2 m (6.6 ft) above the soil surface was 2.6 ± 12.3 g/m^2/yr ($5.4 \times 10^{-4} \pm 3.0 \times 10^{-3}$ lb/ft^2/yr) or 0.03 ± 0.12 T/ha/yr (0.013 ± 0.054 t/ac/yr), which suggests little, if any, net loss of soil from the area.

4.2.3 Surface Erosion

Surface erosion modeling was used in an iterative fashion to aid in the design of the final cover that serves as the basis for the performance assessment and composite analysis modeling. Results of the SIBERIA simulations for the final conceptual cover are shown in Figures 4-25 through 4-27. These figures show the remaining cover depths, 1,000 years after closure of Area G, over portions of the facility occupied—either now or in the future—by pits and shafts. An orange-green color scale indicates how well the cover performs over the pits. Green and yellow shades indicate depth to waste values in excess of 2.5 m (8.2 ft), whereas dark orange indicates that the cover is approaching a thickness of only 1 m (3.3 ft). The blue-red color scale on these figures shows the cumulative change in elevation across the site at the end of the 1,000-year simulation period. Blue shows deposition (net accumulation) and red shows net erosion.

Examination of Figure 4-25 reveals that, for the moderate-erosion scenario, 2.5 m (8.2 ft) or more of cover remains over the majority of the disposal units at MDA G 1,000 years after facility closure. Away from the disposal units, areas of erosion and deposition are observed. Gully formation is seen in areas marked by long slope lengths (e.g., in the vicinity of pits 20, 21, and 22) and along the edges of the mesa. Figures 4-26a and 4-26b show similar results for the low- and high-erosion scenarios at MDA G. While greater erosion is noted in some portions of the facility under high-erosion conditions, a minimum of 1.75 m (5.7 ft) of cover appears to exist over most, if not all, of the disposal units. Figure 4-27 shows the depth-to-waste results for the moderate-erosion scenario at the Zone 4 expansion area. Results from all three scenarios show that a minimum of 1.75 m (5.7 ft) of cover exists across this portion of Area G at the end of the 1,000-year simulation period.

Although Figures 4-25 through 4-27 show results for the end of the 1,000-year simulation period, SIBERIA allows the user to track depth-to-waste and sediment-yield information at all points across the facility through time. Depth-to-waste values, which were saved every 20 years for the whole facility, were used to estimate the effects of cover loss on the rate at which radionuclides were deposited on the surface of Area G as a result of plant and animal intrusion.

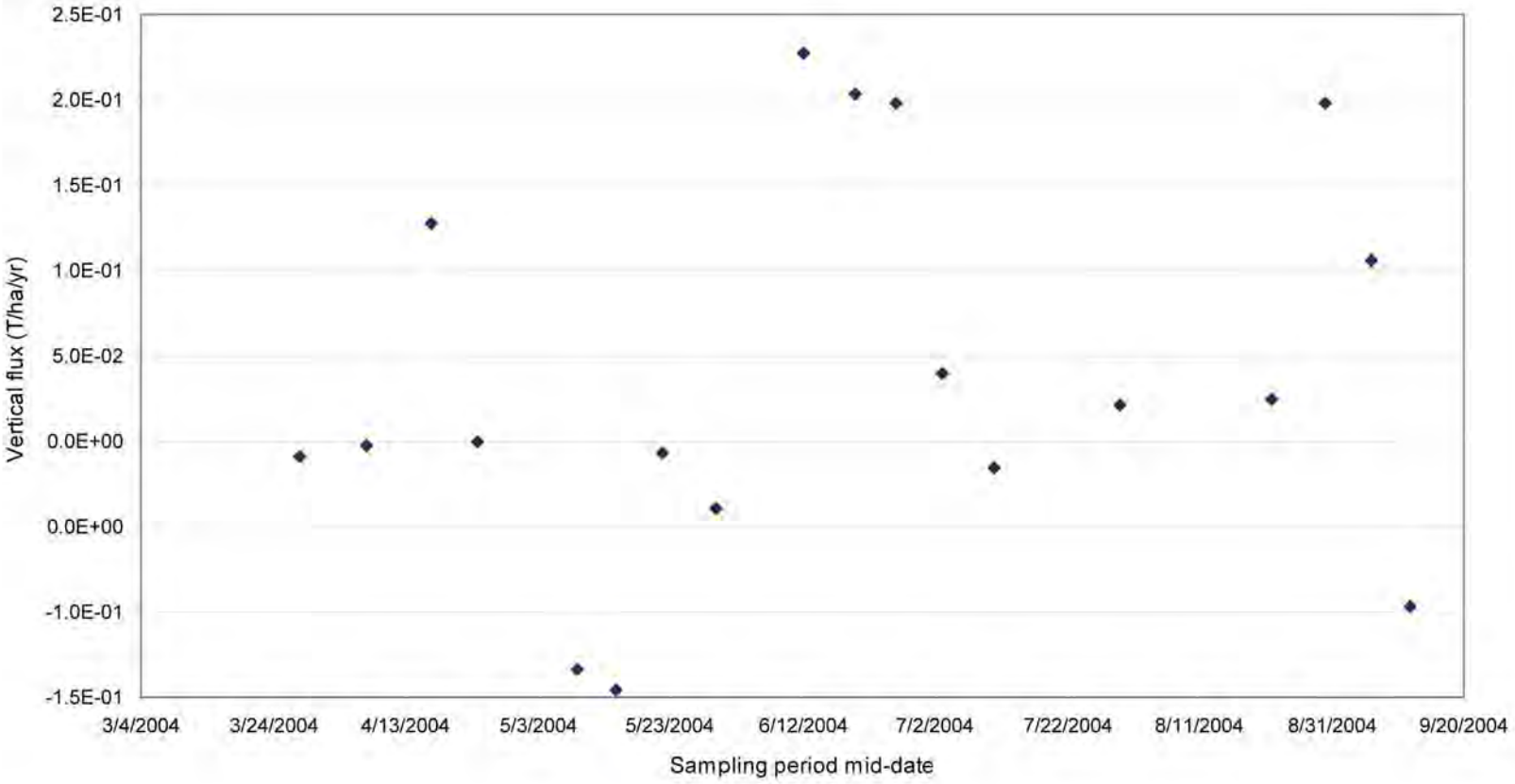

Figure 4-24
Estimated Vertical Mass Flux Collected during All Sampling Periods (1 m sampling height)

Table 4-7
Summary Statistics for Aerosol Mass Concentration and Vertical Mass Flux at MDA J

Summary Statistic	Mass Concentration ($\mu g/m^3$) [a]	Vertical Mass Flux ($g/m^2/yr$)	Vertical Mass Flux (T/ha/yr)
Average	1.1E+01	2.6E+00	3.0E–02
Standard Deviation	1.7E+01	1.2E+01	1.2E–01
Median	1.0E+01	0.0E+00	0.0E+00
Minimum	3.5E+00	–2.0E+01	–2.0E–01
Maximum	2.7E+01	2.3E+01	2.3E–01
Range	2.4E+01	4.3E+01	4.3E–01

[a] *Measurements for aerosol mass concentration averaged over 1 m and 3 m sampling heights for a total of 19 samples.*

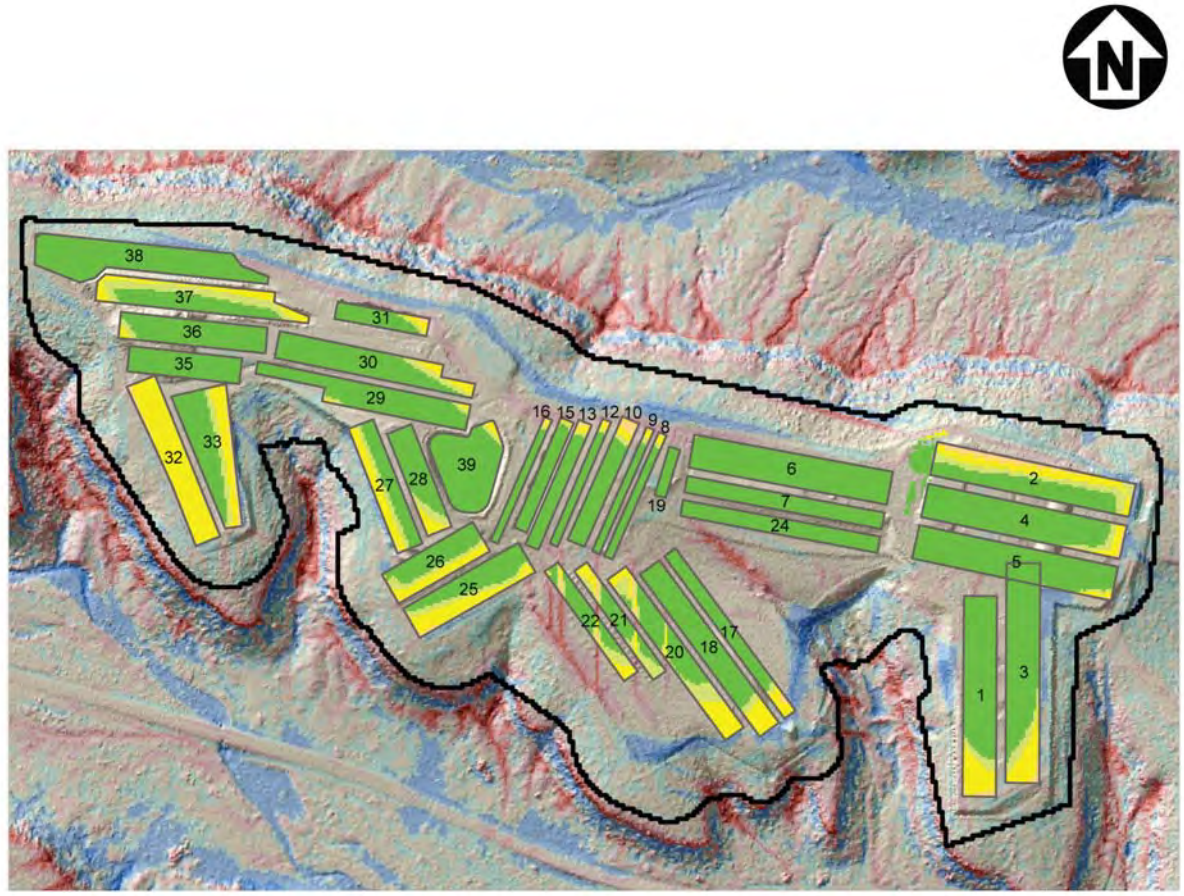

Figure 4-25
Erosion and Deposition at MDA G for Moderate-Erosion Scenario (as predicted by SIBERIA model after 1,000 years)

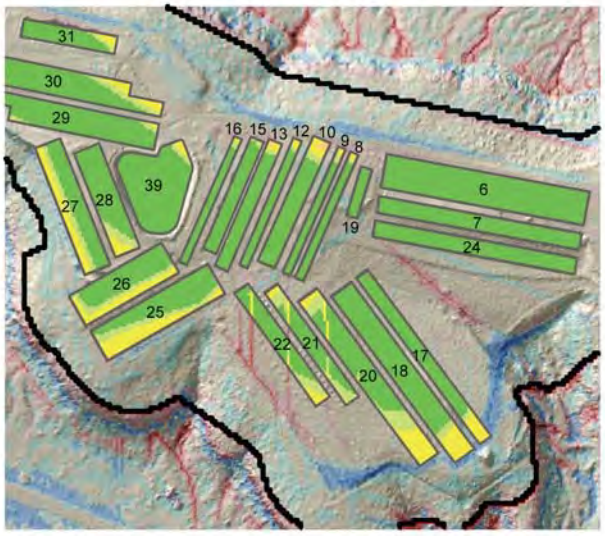

Figure 4-26a.
Low-erosion scenario (70% canopy cover, 70% ground cover, sandy loam soil, 2-year runoff event [2.6 mm], and diffusion coefficient of 1.0×10^{-4}.

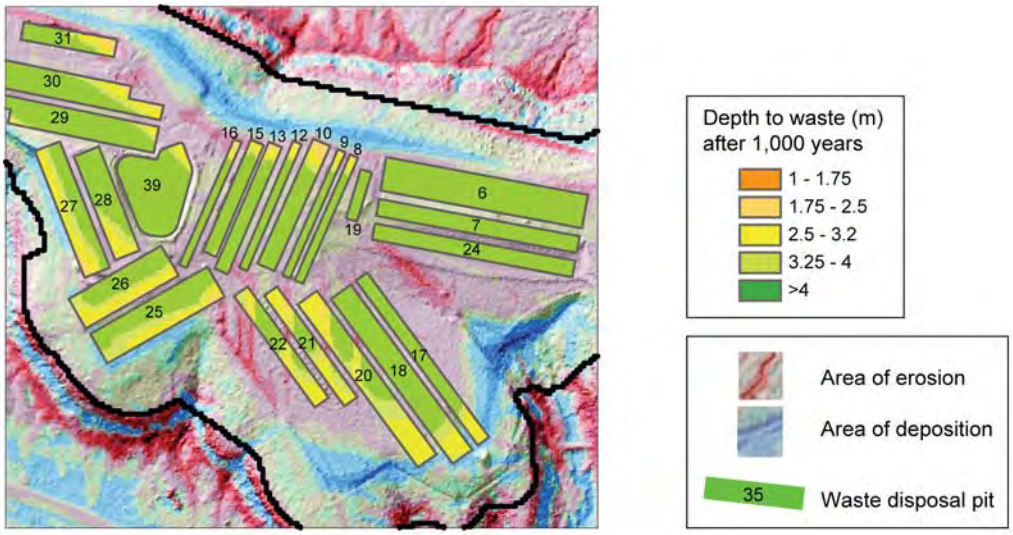

Figure 4-26b.
High-erosion scenario (30% canopy cover, 30% ground cover, sandy loam soil, 5-year runoff event [12 mm], and diffusion coefficient of 2.5×10^{-3}.

Figure 4-26
Erosion and Deposition at MDA G for Low- and High-Erosion Scenarios (as predicted by SIBERIA model after 1,000 years)

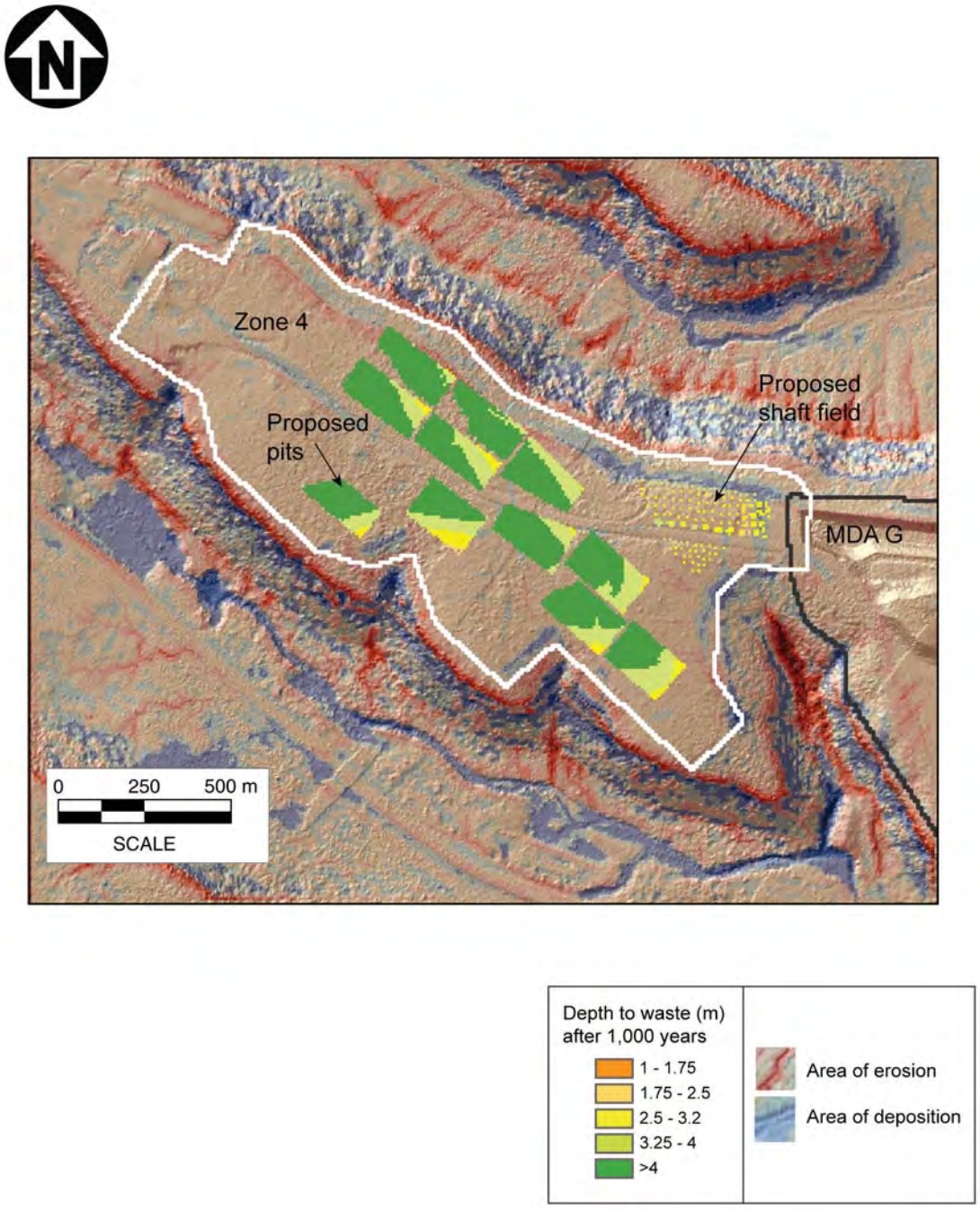

Figure 4-27
Erosion and Deposition at Zone 4 for Moderate-Erosion Scenario (as predicted by SIBERIA model after 1,000 years)

The surface erosion modeling was also used to estimate time-dependent sediment-yield values from the portions of the cover located over the pits and shafts and from other portions of the disposal facility. The time-dependent sediment-yield values were used to determine how much potentially contaminated sediment may be delivered to different parts of the Cañada del Buey and Pajarito Canyon floodplains. Figure 4-28 shows how the surface of Area G was divided into sediment source areas (indicated by the divisions of the mesa top) that drain into catchments within each canyon. The boundaries of the catchments were estimated on the basis of visual inspection of the topographic features along the edges of Mesita del Buey and the water drop diagram developed in conjunction with the cover design effort (see *Appendix H*, Figure 4).

Table 4-8 summarizes the delivery of sediment to each of the catchments shown in Figure 4-28 for the moderate-erosion scenario. The yields listed in the table represent the total quantities of sediment transported to each catchment over a 1,000-year period; a distinction is made between sediment from uncontaminated areas and the portions of the site overlying the disposal pits and shafts. Examination of these results indicates that a relatively small proportion of the total sediment delivered to a catchment originates from above the disposal units. For example, over the 1,000-year period, Pajarito Canyon catchment PC2 was projected to receive 8,995 T (9,915 t) of sediment from uncontaminated portions of Area G and 766 T (844 t) from portions of the site overlying disposal units; thus, sediment from the disposal units represents 8 percent of the total sediment delivered from the mesa to PC2.

The boundaries of the sediment source areas may shift over time. For example, from zero to 100 years, the eroded cover material from a given pit may be transported into catchment PC2, but from 100 to 200 years, some or all of the sediment originating over that pit may spill into another drainage and be deposited in another catchment. These shifts in sediment yield were tracked.

4.3 Dose Analysis

The dose projections for members of the public living in the vicinity of Area G are presented below. Section 4.3.1 presents and discusses the doses projected using the Area G performance assessment inventory, and exposure estimates for the composite analysis are presented in Section 4.3.2. Both deterministic and probabilistic dose projections are provided. The deterministic modeling was conducted to provide general insight into the performance of the disposal facility well past the 1,000-year compliance period. Results of the deterministic modeling will provide an indication of the spatial and temporal aspects of radionuclide release and transport over the simulation periods shown, but the magnitudes of the projected exposures should be used with caution. The input data used in this modeling generally represent the medians of the distributions adopted for stochastic parameters. Exposures projected on the basis of these data do not necessarily represent the most likely doses, nor do they necessarily bound likely exposures. Full probabilistic modeling is required to estimate doses that are statistically meaningful.

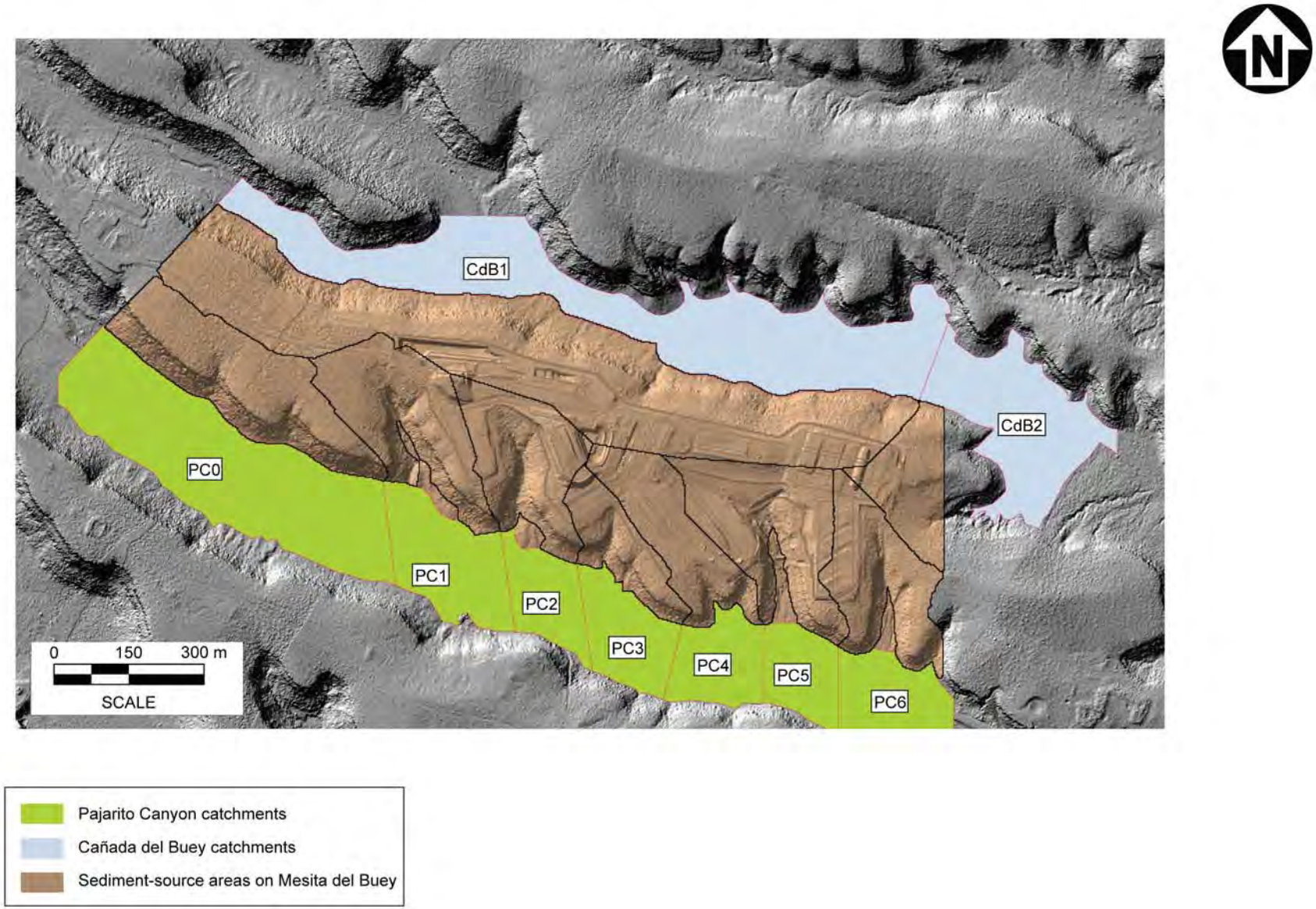

Figure 4-28
Area G Sediment-Source Areas and Sediment Catchments in Habitable Canyon Bottoms

Table 4-8
Summary of Sediment Delivery from Area G to Canyon Catchments over 1,000 Years

Canyon Catchment Number	Mass of Sediment Delivered (T)		Sediment Overlying Disposal Units as % of Total Sediment
	Clean Sediment	Sediment Overlying Disposal Units	
PC0	5,644	767	12
PC1	16,987	580	3
PC2	8,995	766	8
PC3	8,823	1,251	12
PC4	5,405	1,400	21
PC5	6,549	1,340	17
PC6	5,435	478	8
CdB1	39,930	3,482	8
CdB2	1,005	153	13

PC = Pajarito Canyon catchment *CdB = Cañada del Buey catchment*

The probabilistic modeling results are provided in terms of distributions of dose. These distributions may be highly skewed and yield arithmetic means that do not provide an accurate estimate of central tendency. Consequently, information is presented throughout the following discussion to provide an indication of the nature of the projected distributions.

4.3.1 Performance Assessment Projections

The exposure scenarios adopted for the performance assessment address potential exposures received by persons living downgradient of the disposal facility, at the point(s) of maximum atmospheric exposure, and in the canyons adjacent to Area G. The dose projections for the performance assessment are organized in terms of these exposure locations. Sections 4.3.1.1 and 4.3.1.2 present and discuss dose estimates for the Groundwater Resource Protection and All Pathways–Groundwater Scenarios, respectively. Section 4.3.1.2 addresses the exposures estimated for the Atmospheric Scenario and the projected radon fluxes for the facility. The dose projections for persons living in Cañada del Buey and Pajarito Canyon are presented in Section 4.3.1.4.

4.3.1.1 Groundwater Resource Protection Scenario

Deterministic and probabilistic analyses were conducted to estimate the potential impacts of radionuclides discharged to the regional aquifer on persons who rely upon that aquifer as a source of drinking water. The deterministic analysis simulated facility performance over a period

of 100,000 years to provide insight into facility performance well beyond the 1,000-year compliance period. The results of the deterministic simulations are shown in Figure 4-29.

The doses shown in Figure 4-29 correspond to the point of maximum groundwater exposure 100 m (330 ft) east of the Area G fence line. Annual doses at the point of maximum exposure peak about 46,000 years after facility closure, reaching a maximum of 0.0058 mrem/yr; C-14 is the sole contributor to this exposure. No other radionuclides are projected to reach the receptor's well during the 100,000-year period.

A screening analysis was conducted to limit the number of radionuclides included in the probabilistic modeling to those that would make a meaningful contribution to exposures during the 1,000-year compliance period. The results of this 50-realization probabilistic evaluation indicated that no radionuclides would reach the well located 100 m (330 ft) east of Area G during this period. Consequently, a probabilistic assessment of the exposures for the groundwater protection scenario was not conducted.

4.3.1.2 All Pathways–Groundwater Scenario

The deterministic modeling results for the All Pathways–Groundwater Scenario are shown in Figure 4-30. The doses shown in the figure correspond to the point of maximum groundwater exposure 100 m (330 ft) east of the Area G fence line. The receptor near the town of White Rock was not projected to be exposed to contaminated groundwater during the operational, closure, and active institutional control periods because of very long groundwater travel times to this location. The projected peak exposure, which occurs 46,000 years after facility closure, is 0.0062 mrem/yr; C-14 concentrations in the regional aquifer decline thereafter. No other radionuclides are projected to discharge to the regional aquifer within 100,000 years of facility closure. The doses are dominated by the ingestion of contaminated crops and animal products raised by the receptor, with the ingestion of contaminated drinking water making a smaller contribution. The screening analysis indicated that no radionuclides will reach the receptor's well during the 1,000-year compliance period. Therefore, no probabilistic modeling results are provided for this scenario.

4.3.1.3 Atmospheric Scenario

The deterministic modeling results for the Atmospheric Scenario are shown in Figure 4-31 for 50,000 years following site closure, the period for which surface erosion modeling was conducted. The projected downwind exposures at the LANL boundary are greatest early in the simulation period and are the result of tritiated water vapor diffusing from the disposal facility. A peak exposure of 0.25 mrem/yr is projected to occur and results almost entirely from inhaling airborne tritium. The exposures projected for the Area G fence line exposure location increase throughout most of the simulation. The peak exposure of 0.032 mrem/yr is dominated by exposures to Ac-227, K-40, Pa-231, Pb-210, Ra-226, and U-238; the projected exposures result primarily from the ingestion of crops grown in contaminated soils and direct radiation from these soils.

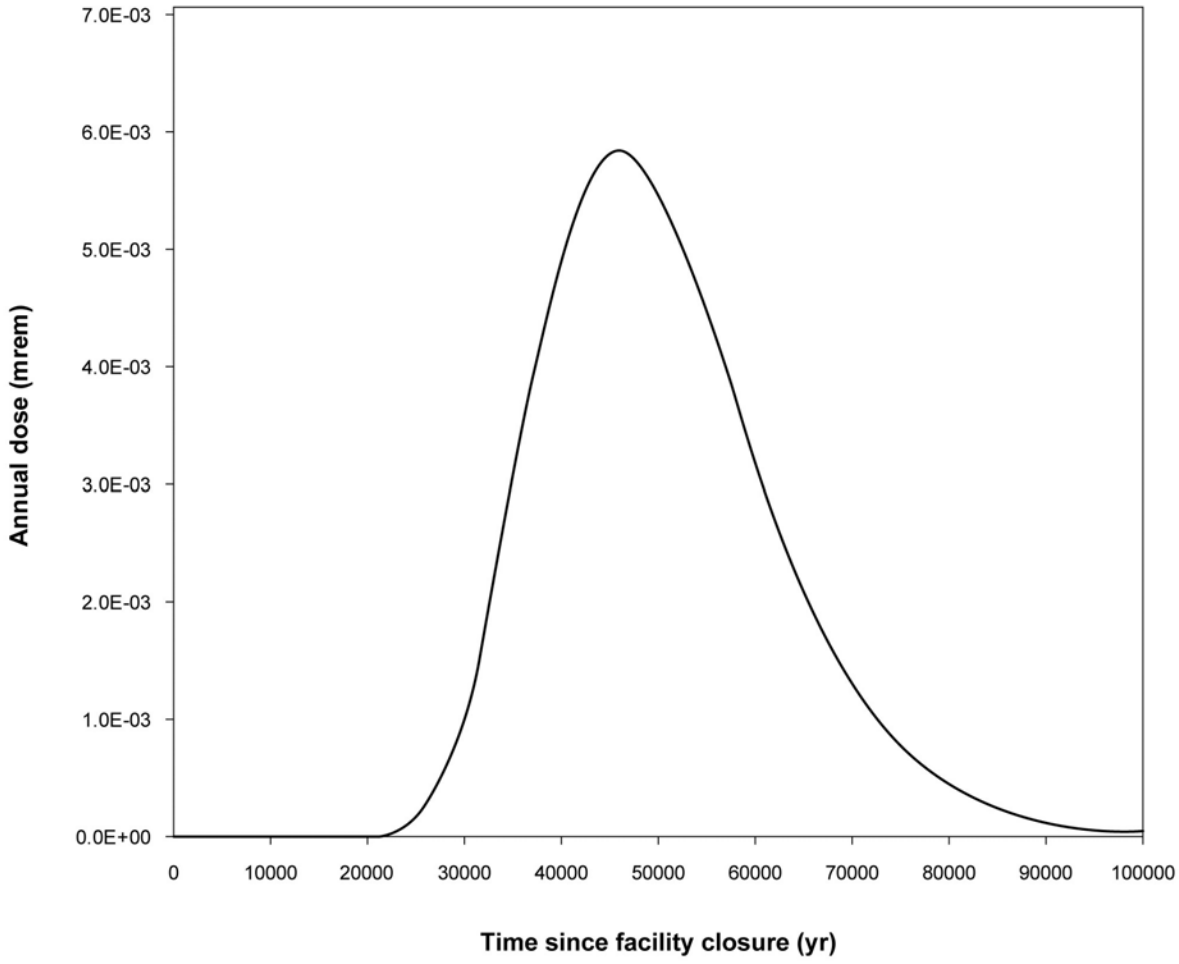

Figure 4-29
Deterministic Dose Projections for the Groundwater Resource Protection Scenario

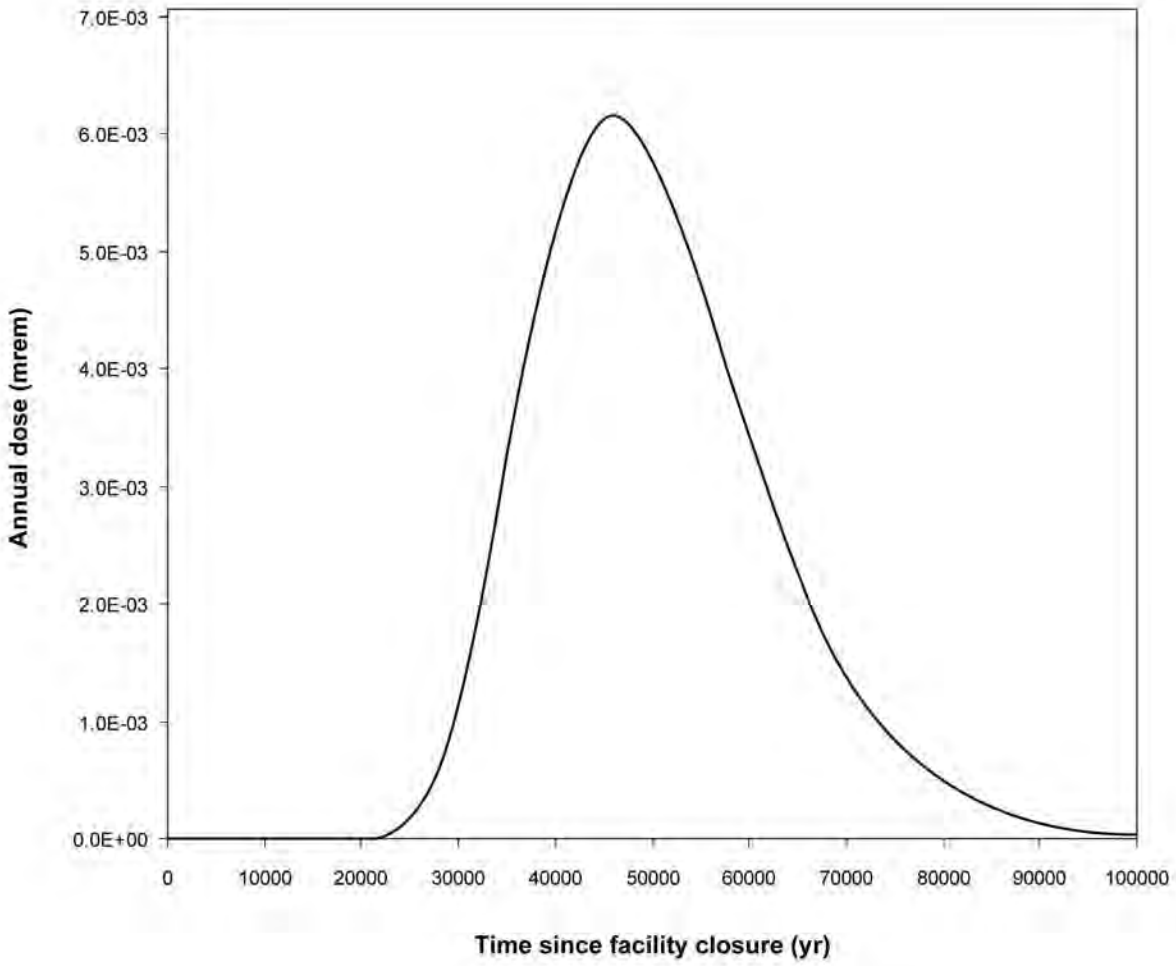

Figure 4-30
Deterministic Dose Projections for the All Pathways–Groundwater Scenario (performance assessment)

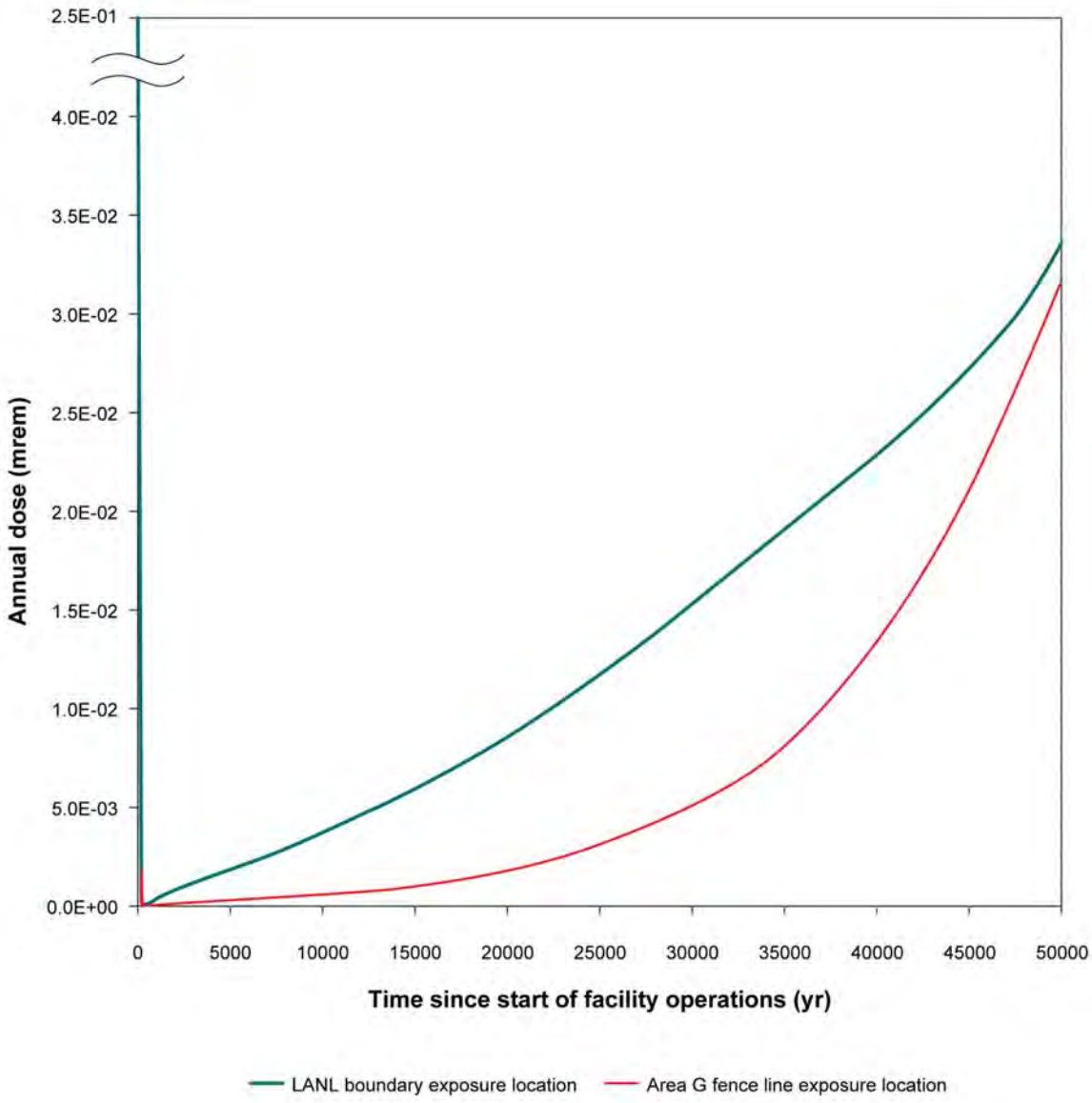

Figure 4-31
Deterministic Dose Projections for the Atmospheric Scenario (performance assessment)

Figure 4-32 shows probabilistic model projections for the Atmospheric Scenario. The doses projected for the receptor at the LANL boundary reach a maximum of 0.18 mrem/yr about 60 years after the start of disposal operations at Area G (Figure 4-32a). This exposure is due to the inhalation of tritiated water vapor that diffuses upward from the site and is transported with the prevailing winds. The exposures to tritium decrease rapidly as the inventory of the radionuclide is depleted and the isotope undergoes radioactive decay. The exposures projected for the other radionuclides in the waste increase slowly over the time, reaching a peak mean exposure of 0.0055 mrem/yr at the end of the 1,000-year compliance period. The exposures projected for the LANL boundary receptor are less than the 10 mrem/yr performance objective that applies to all airborne releases from the Laboratory.

The exposures projected for the receptor at the Area G fence line (Figure 4-32b) decrease initially as exposures from vapor- and gas-phase radionuclides wane. The projected doses increase throughout the latter portion of the compliance period, however, reaching a peak mean dose of 0.014 mrem/yr at the end of the period. The radionuclides that make major contributions to the projected exposures are shown in Figure 4-33. K-40 is responsible for 79 percent of the projected peak mean exposure; Pb-210, U-234, and U-238 contribute another 16 percent of the total. The primary exposure pathways for the fence line receptor are the ingestion of contaminated crops and animal products, and direct radiation from soils; these account for about 90 percent of the peak mean exposure. All of the projected mean exposures are much less than the 10 mrem/yr performance objective that applies to airborne releases.

The radon fluxes projected for the eight waste disposal regions are summarized in Table 4-9. The peak mean fluxes range from about 1.8×10^{-6} pCi/m^2/s for disposal region 1 to 14 pCi/m^2/s for region 7; fluxes for all disposal regions are less than the flux objective of 20 pCi/m^2/s. The radon fluxes projected for the different waste disposal regions yield a site-wide peak mean flux of 0.43 pCi/m^2/s; this peak occurs at about the time that waste disposal at Area G ceases.

Table 4-9
Projected Radon Fluxes for the Eight Waste Disposal Regions

Waste Disposal Region	Projected Radon Flux (pCi/m^2/s)		
	Mean	5th Percentile	95th Percentile
1	1.8E-06	3.3E-13	7.3E-06
2	---	---	---
3	3.5E-01	3.6E-02	1.0E+00
4	3.9E-02	2.1E-03	1.2E-01
5	5.0E-01	5.1E-02	1.5E+00
6	3.5E-03	6.8E-11	1.4E-02
7	1.4E+01	1.1E+00	4.3E+01
8	3.3E-01	4.5E-02	9.4E-01

--- = None of the performance assessment inventory was disposed of in this waste disposal region.

Figure 4-32a. LANL boundary exposure location

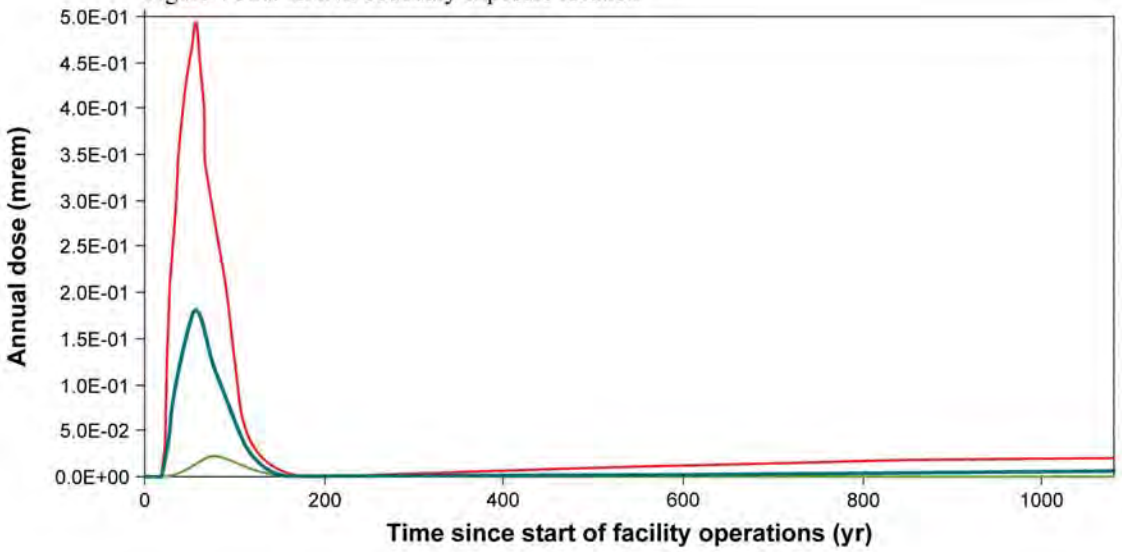

Figure 4-32b. Area G fence line exposure location

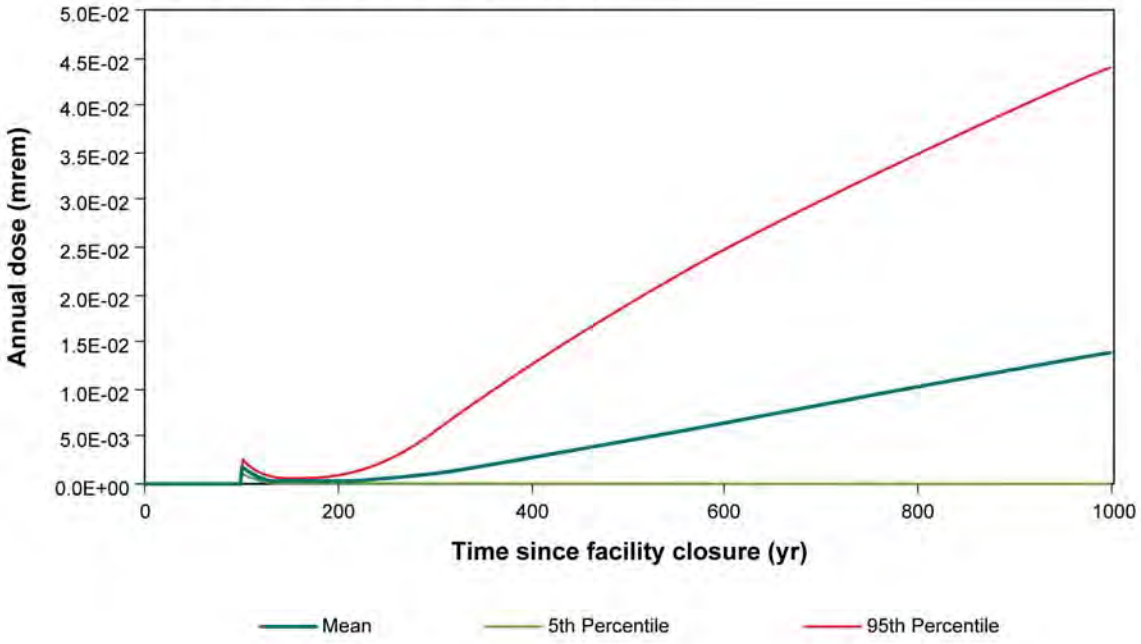

Figure 4-32
Probabilistic Dose Projections for the Atmospheric Scenario (performance assessment)

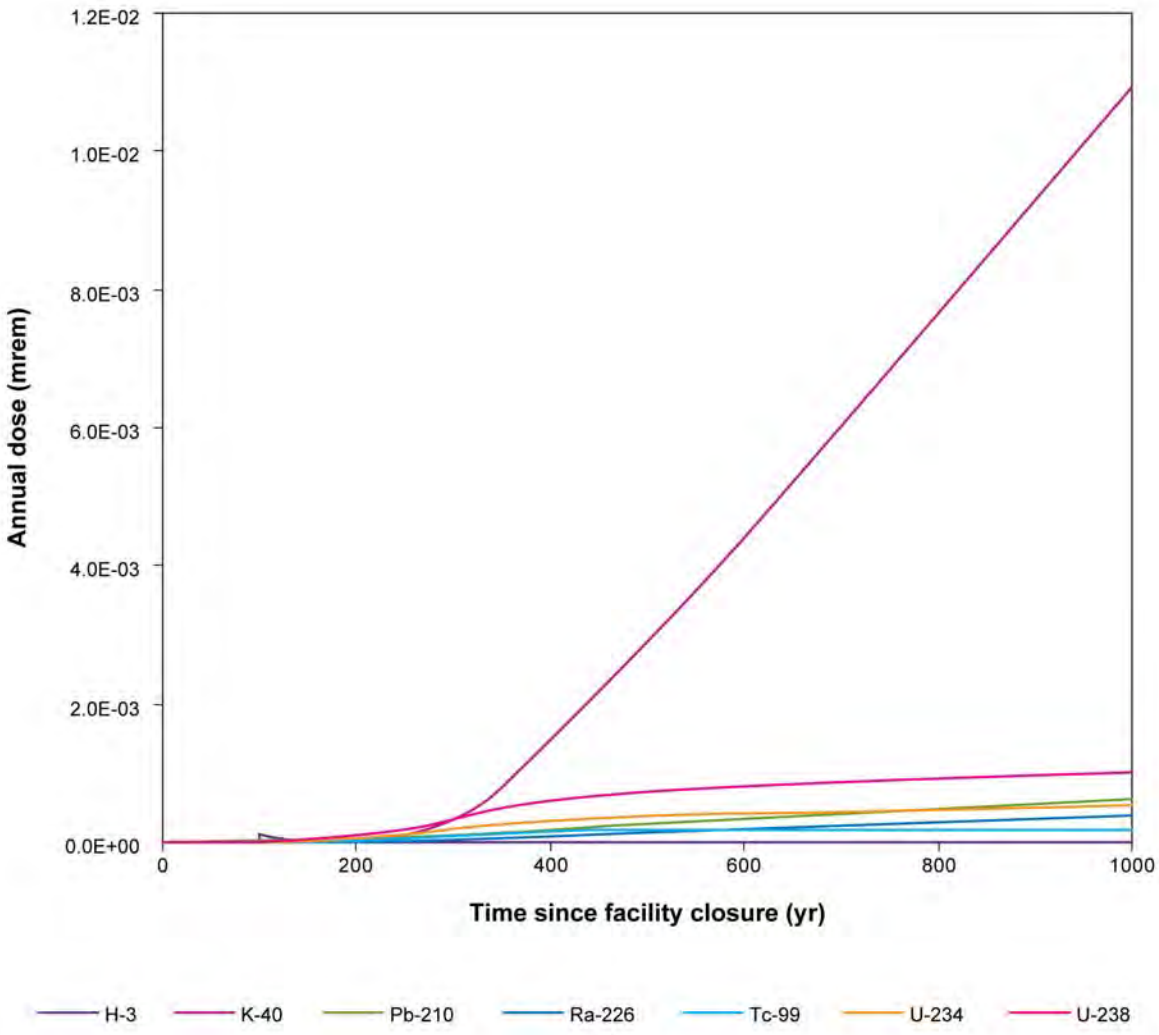

Figure 4-33
Mean Radionuclide Exposures for the Atmospheric Scenario at the Area G Fence Line Location (performance assessment)

4.3.1.4 All Pathways–Canyon Scenarios

Doses received by persons residing in the canyons adjacent to Area G were projected for two locations in Cañada del Buey and seven locations in Pajarito Canyon. Figure 4-34 shows the deterministic modeling results for these locations over 50,000 years, the period for which surface erosion modeling was conducted. The doses projected for all locations behave similarly, reaching maximum values at the end of the simulation period. Peak annual doses range from 0.013 to 0.35 mrem among the nine receptor locations. Ac-227, K-40, Pa-231, Pb-210, Ra-226, and U-238 make significant contributions to the projected exposures for one or more exposure locations. Important exposure pathways include the ingestion of contaminated crops and direct radiation from radionuclides in the canyon soils.

The probabilistic doses for the canyon scenario are summarized in Table 4-10. The projected doses for catchments CdB1 and CdB2 are shown in Figure 4-35; these catchments yielded the highest peak mean doses among the nine canyon locations, with exposures projected at approximately 20 and 1,000 years after facility closure, respectively. Tritium is responsible for the peak mean exposure projected for catchment CdB1. In this case, tritiated water vapor diffuses upward from the waste and contaminates surface soils at Area G; the contaminated soils are subsequently transported into Cañada del Buey. The radionuclides that make significant contributions to the doses projected for the receptor in catchment CdB2 are Cl-36, K-40, Pb-210, Ra-226, and U-238; these isotopes account for about 90 percent of the peak exposure. Radionuclide-specific contributions to the mean dose over time are shown for catchment CdB2 in Figure 4-36. Important exposure pathways include the ingestion of crops, beef, and milk at CdB1; these same pathways and direct radiation from contaminated soils account for the major portion of the peak dose at catchment CdB2. The peak mean doses projected for the canyon residents are 0.05 to 9 percent of the 25 mrem/yr all-pathways performance objective.

4.3.2 Composite Analysis Projections

The dose projections for the composite analysis are presented below, organized in terms of the exposure scenarios. Section 4.3.2.1 presents and discusses the dose estimates for the All Pathways–Groundwater Scenario, and Section 4.3.2.2 considers the exposures projected for the Atmospheric Scenario. The exposures projected for persons residing in Cañada del Buey and Pajarito Canyon are discussed in Section 4.3.2.3. The potential impacts of alternate sources of contamination on the receptors represented using these exposure scenarios are discussed in Section 4.3.2.4.

4.3.2.1 All Pathways–Groundwater Scenario

The deterministic modeling results for the All Pathways–Groundwater Scenario are shown in Figure 4-37. Doses peak at 0.025 mrem/yr approximately 43,000 years after facility closure; exposures at this time are due solely to C-14 leached from the waste and transported to the compliance well. The ingestion of crops and animal products raised by the receptor make the largest contributions to the peak dose in terms of exposure pathways. No other radionuclides are projected to discharge to the regional aquifer within 100,000 years of facility closure.

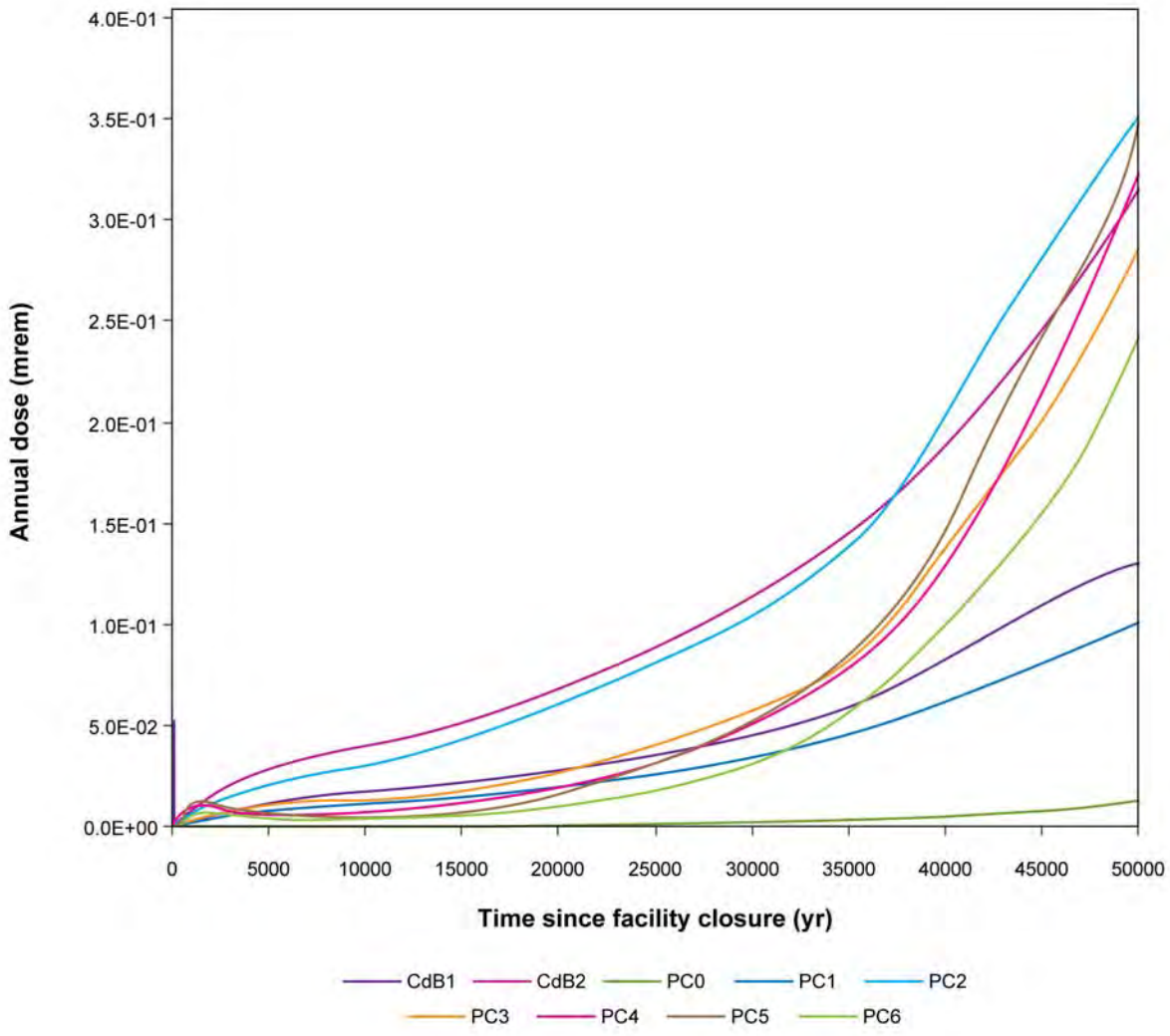

Figure 4-34
Deterministic Dose Projections for the All Pathways–Canyon Scenarios (performance assessment)

Table 4-10
Probabilistic Dose Projections for the All Pathways–
Canyon Scenarios (performance assessment)

Exposure Location (Catchment)	Projected Dose (mrem/yr)			Time of Peak Exposure (yr post closure)
	Mean	5th Percentile	95th Percentile	
CdB1	2.3E+00	8.3E-04	1.3E+01	20
CdB2	4.1E-01	8.1E-05	1.3E+00	1,000
PC0	1.3E-02	9.9E-07	3.3E-02	808
PC1	8.8E-02	2.2E-05	2.7E-01	868
PC2	1.9E-01	3.4E-05	6.8E-01	960
PC3	1.1E-01	7.9E-05	5.0E-01	1,000
PC4	3.3E-01	2.5E-04	1.5E+00	904
PC5	3.6E-01	1.2E-04	1.6E+00	1,000
PC6	1.9E-01	1.9E-05	8.2E-01	1,000

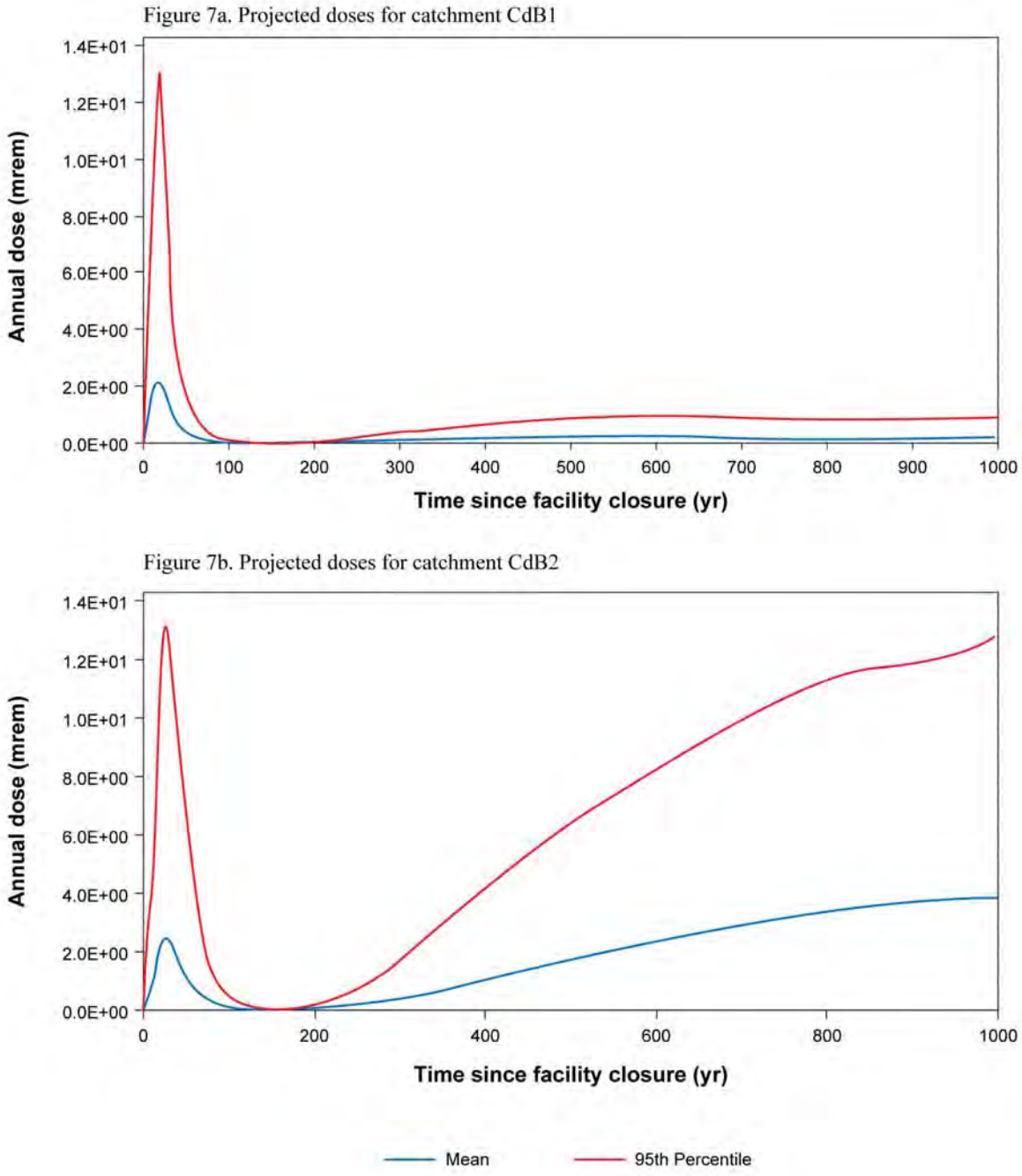

Figure 4-35
Probabilistic Dose Projections for the All Pathways–Canyon Scenarios (performance assessment)

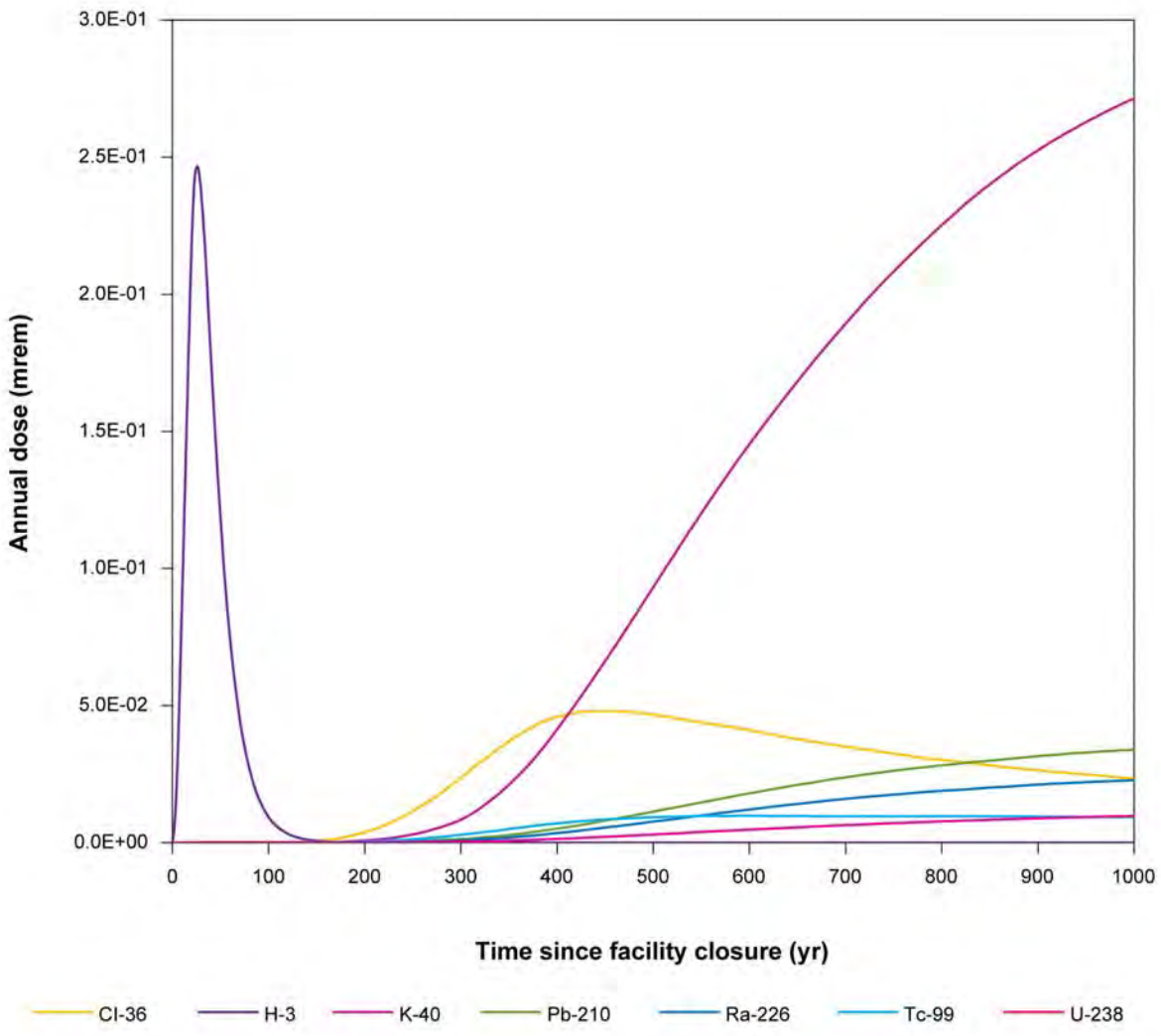

Figure 4-36
Mean Radionuclide Doses for the All Pathways–Cañada del Buey Scenario within Catchment CdB2 (performance assessment)

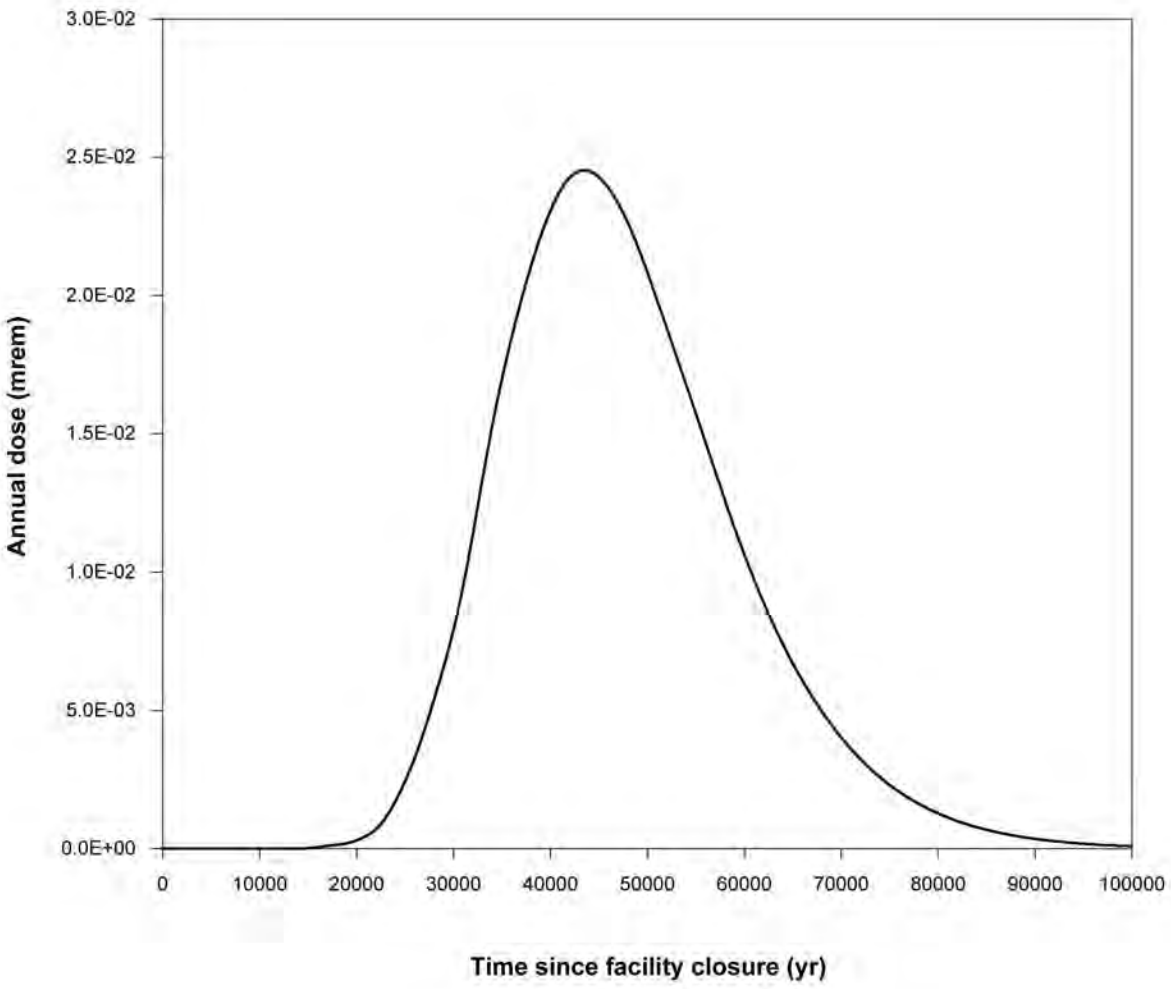

Figure 4-37
Deterministic Dose Projections for the All Pathways–Groundwater Scenario (composite analysis)

The probabilistic modeling projected that no radionuclides would discharge to the regional aquifer during the 1,000-year compliance period. Therefore, no exposures were projected for the individual residing 100 m (330 ft) downgradient of the Area G fence line.

4.3.2.2 Atmospheric Scenario

Figure 4-38 shows the composite analysis doses for the Atmospheric Scenario based on the deterministic modeling. The results shown in this figure are for receptors residing at the LANL boundary (Figure 4-38a) and the Area G fence line (Figure 4-38b). The peak exposure for the receptor at the LANL boundary is projected to occur while the facility is still receiving waste; tritiated water vapor diffusing from the site is responsible for the 0.28 mrem/yr dose. Exposures from the other radionuclides in the inventory increase slowly throughout the 50,000-year period as the cover thins and plants and animals inhabiting the site gain greater access to the waste. The exposures projected for the fence line receptor increase throughout much of the 50,000-year period, reaching a maximum of 0.70 mrem/yr. Ac-227, Pa-231, Pb-210, Pu-239, Ra-226, and Sn-126 are among the major contributors to the peak dose; the exposures for this receptor are due largely to the ingestion of contaminated crops, inhalation, and direct radiation from soils.

The probabilistic model projections for the Atmospheric Scenario are shown in Figure 4-39. The peak mean dose for the receptor at the LANL boundary is 0.23 mrem/yr (Figure 4-39a); it is due entirely to tritium vapor diffusing from the surface of the disposal facility and traveling downwind with the prevailing winds. The peak exposure is projected to occur in about 2015, while the disposal facility is still in its operational phase. Much smaller doses are projected to occur later, in response to the resuspension of contaminated soils from the surface of Area G; particulate releases yield a dose of 0.0081 mrem/yr at the end of the 1,000-year compliance period. All of the projected mean exposures are much less than the 10 mrem/yr performance objective that applies to airborne releases.

The exposures projected for the receptor at the Area G fence line increase throughout much of the compliance period, reaching a peak mean dose of 0.64 mrem/yr (Figure 4-39b). Two important contributors to the exposures projected for this location are Pb-210 and Ra-226, which account for 42 and 22 percent of the peak mean dose, respectively. Together, Am-241, Pu-239, and Pu-240 contribute about 32 percent of the peak mean exposure. Figure 4-40 illustrates the contributions made by various radionuclides to the projected receptor exposures at the fence line location. The primary exposure pathways for the fence line receptor are the ingestion of contaminated crops, inhalation, and direct radiation from soils; these account for 63, 14, and 13 percent of the peak mean exposures, respectively. The peak mean dose projected for the fence line receptor is about 6 percent of the 10 mrem/yr performance objective.

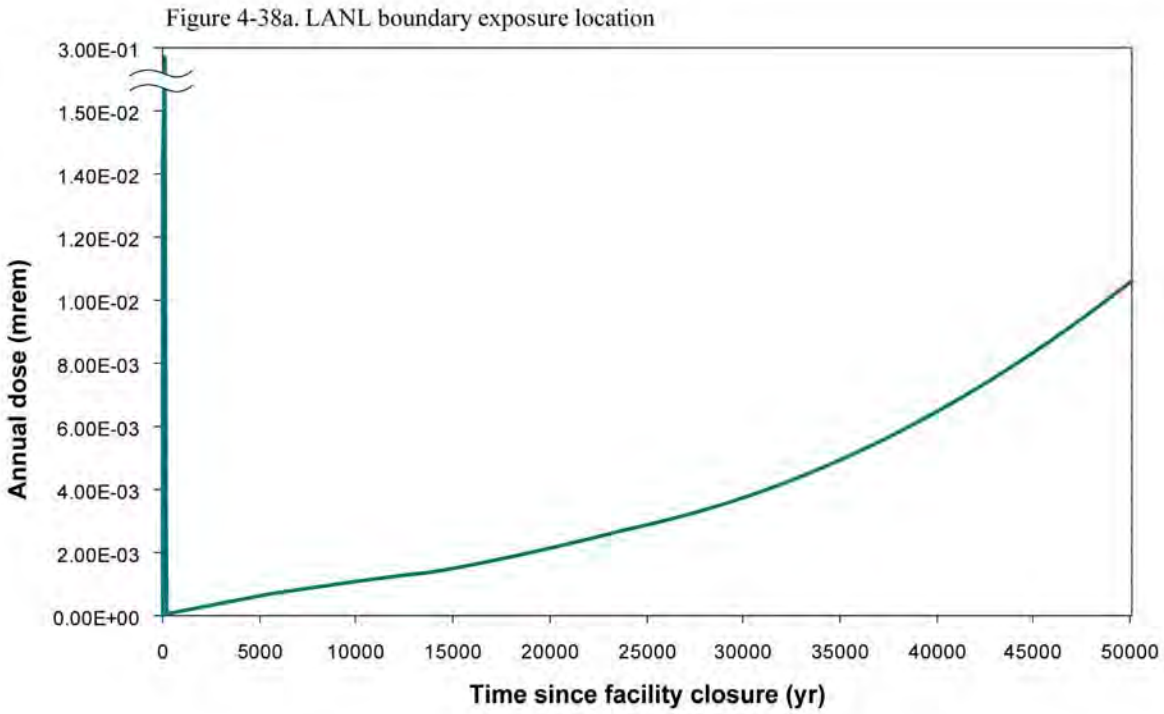

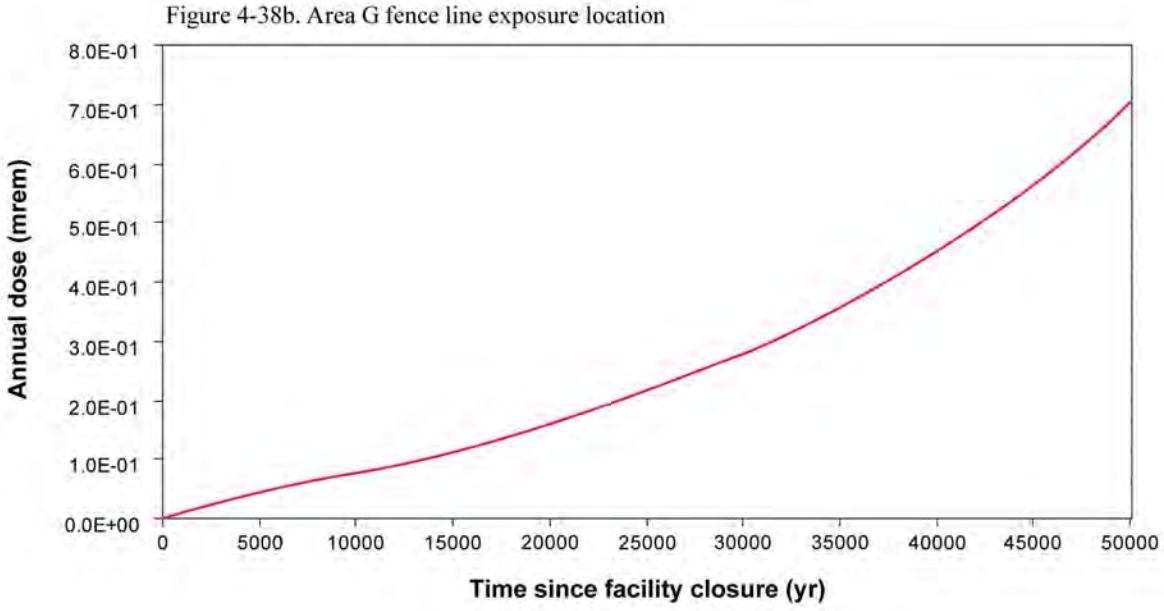

Figure 4-38
Deterministic Dose Projections for the Atmospheric Scenario (composite analysis)

Figure 4-39a. LANL boundary exposure location

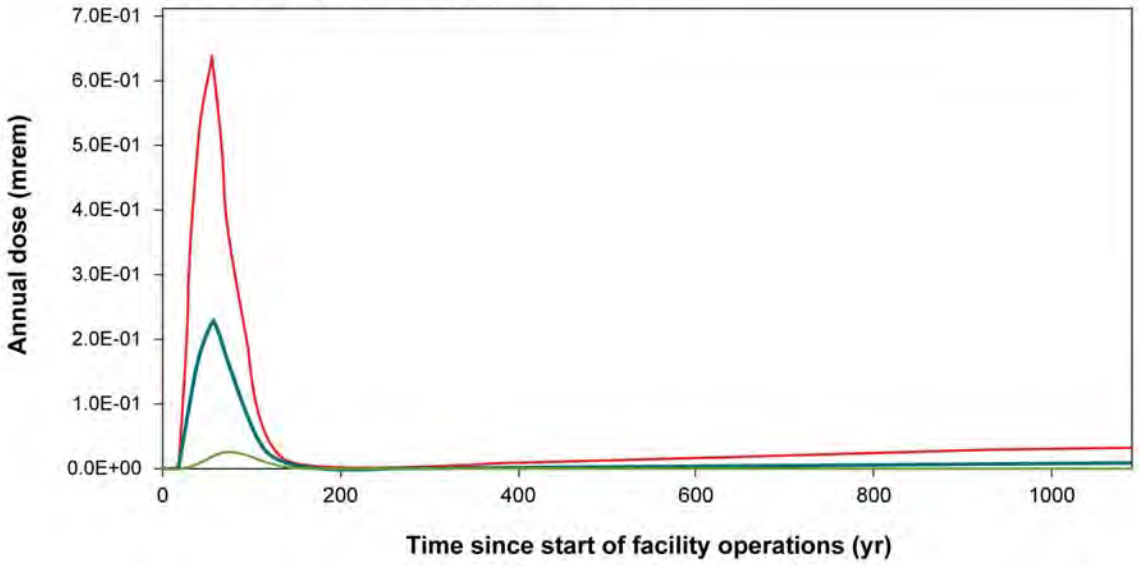

Figure 4-39b. Area G fence line exposure location

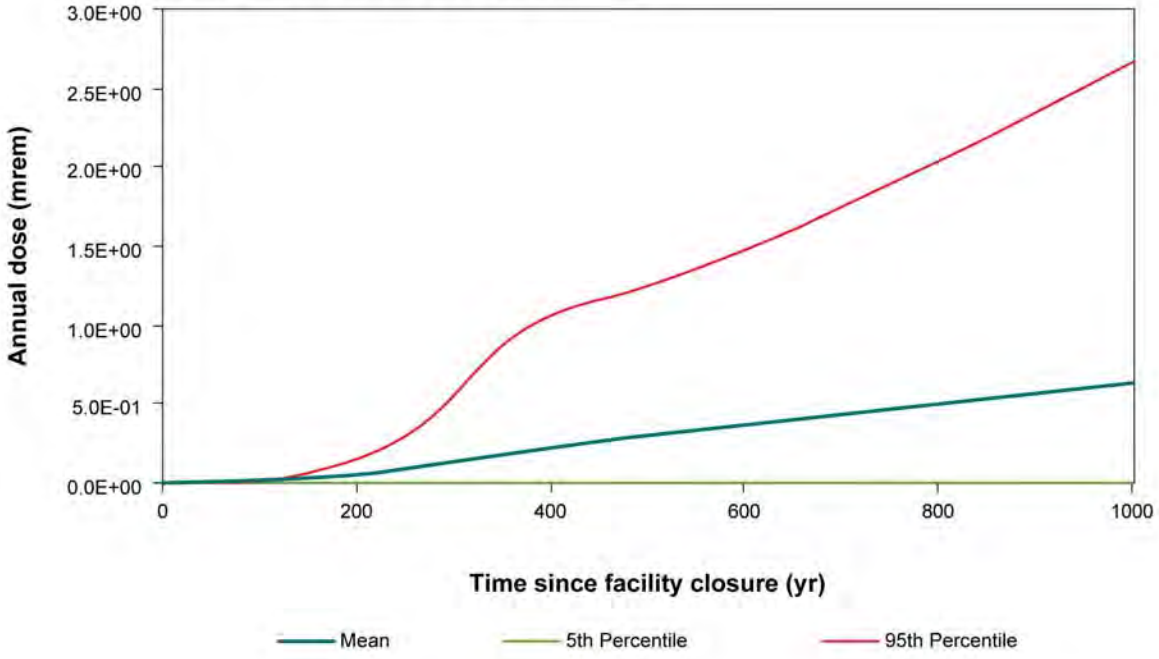

Figure 4-39
Probabilistic Dose Projections for the Atmospheric Scenario (composite analysis)

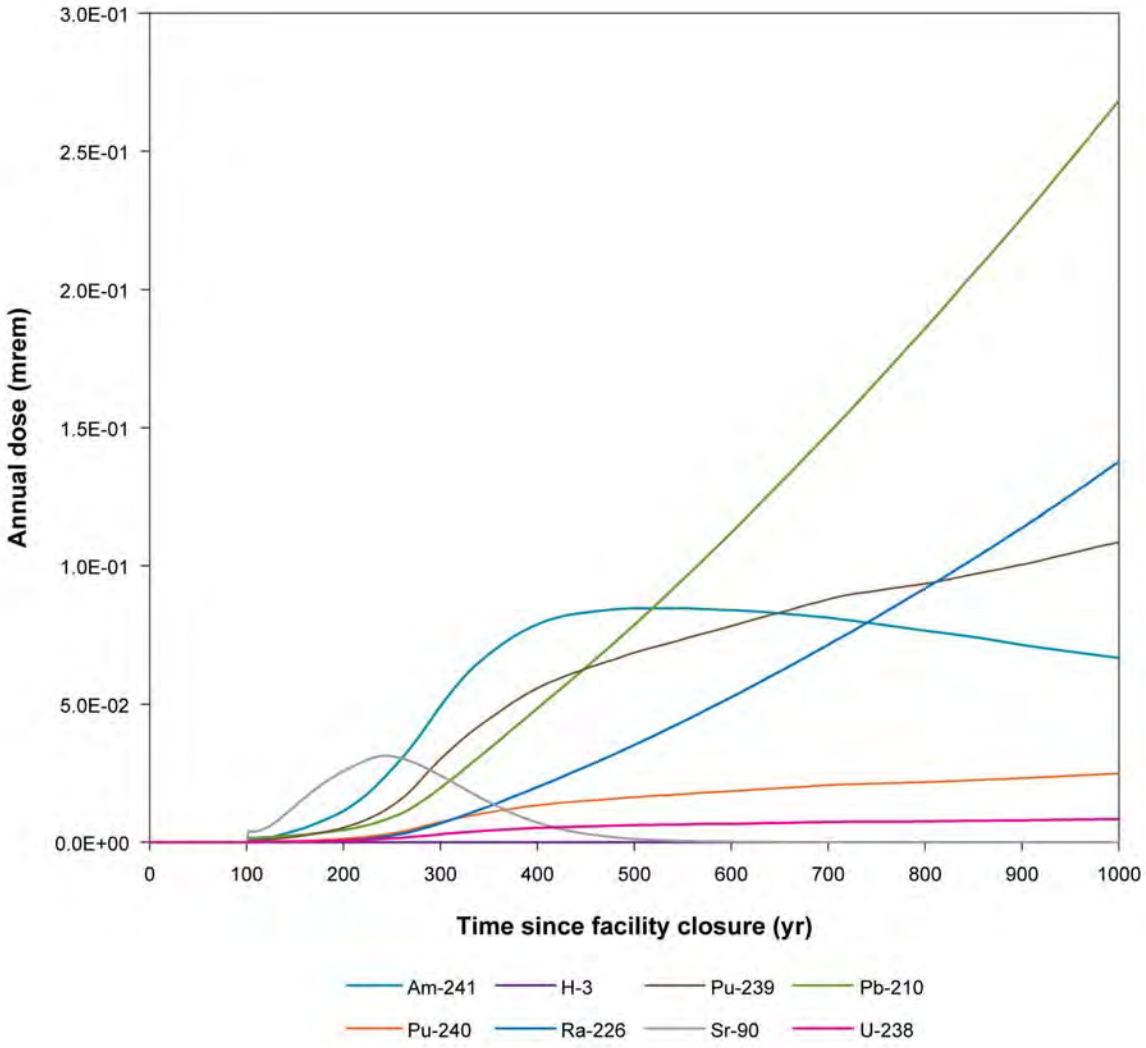

Figure 4-40
Mean Radionuclide Exposures for the Atmospheric Scenario at the Area G Fence Line Exposure Location (composite analysis)

4.3.2.3 All Pathways–Canyon Scenario

The deterministic composite analysis doses projected for the Cañada del Buey and Pajarito Canyon receptors over a 50,000-year period are shown in Figure 4-41. The doses projected for the nine exposure locations behave similarly, reaching maxima at the end of the simulation period. Peak annual doses range from 0.017 to 1.2 mrem among the nine receptor locations. Ac-227, K-40, Pa-231, Pb-210, Pu-239, Ra-226, and U-238 make significant contributions to the projected exposures for one or more exposure locations; the ingestion of contaminated crops and direct radiation from contaminated soils make significant contributions to the peak mean doses.

The probabilistic doses for the canyon scenario are summarized in Table 4-11. The projected doses for catchments PC5 and PC6 are shown in Figure 4-42; these catchments yielded the highest peak mean doses among the nine canyon locations. The mean dose at the former location reaches a peak value about 230 years after Area G undergoes final closure (Figure 4-42a) ; the mean dose for catchment PC6 displays an intermediate peak about 230 years after facility closure but reaches a maximum at the end of the compliance period (Figure 15b). Sr-90 accounts for more than 97 percent of the peak mean exposure projected for catchment PC5. Pb-210 and Ra-226 account for 78 percent of the peak mean dose projected for catchment PC6; a total of 17 percent of the projected exposure comes from Pu-239 and Am-241. Changes in radionuclide contributions to the projected exposures over time are shown in Figure 4-43 for catchment PC5; a similar pattern is seen for catchment PC6. The peak mean exposure estimated for the receptor in catchment PC5 is due almost entirely to the ingestion of contaminated crops, beef, and milk; the ingestion of vegetables grown in, and direct radiation from, contaminated soils account for about 84 percent of the peak mean dose projected for catchment PC6. The peak mean exposures projected for all nine canyon exposure locations are less than the 100 mrem/yr primary dose limit and the 30 mrem/yr dose constraint.

Examination of Figure 42 reveals that the mean doses projected for catchments PC5 and PC6 exceed the 95^{th} percentile exposures for a period of about 200 years following facility closure. This behavior is an outcome of the distribution selected to model Sr-90 uptake by native vegetation growing over the closed disposal facility. Large values are sampled from the distribution in a small fraction of the model realizations, yielding large Sr-90 concentrations in the surface soils at Area G and large exposures for the canyon residents. These doses are great enough to significantly elevate the mean exposure estimated for all 1,000 realizations.

4.3.2.4 Alternate Source Evaluation

Several sources of contamination at the Laboratory were identified for consideration in the alternate source analysis. These sources include MDAs A, AB, B, C, H, J, L, and T, as well as Cañada del Buey and Pajarito Canyon. The MDAs were included either because they were used to dispose of potentially large quantities of radioactive waste, are highly contaminated, or are located near Area G. All of these facilities are located on mesas. The two canyons were included

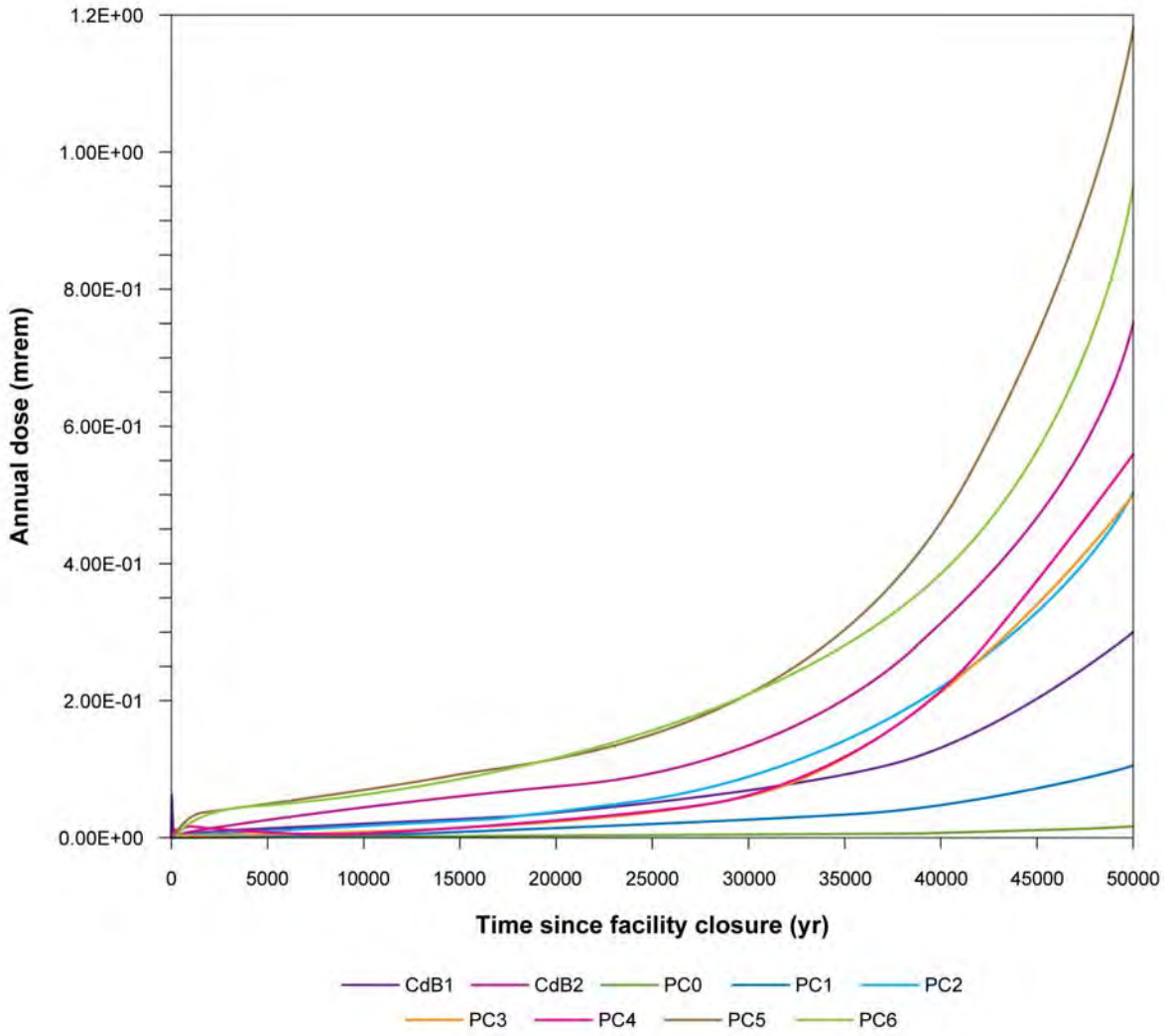

Figure 4-41
Deterministic Dose Projections for the All Pathways–Canyon Scenarios (composite analysis)

Table 4-11
Probabilistic Dose Projections for the All Pathways–Canyon Scenarios (composite analysis)

Catchment	Projected Dose (mrem/yr)			Time of Peak Exposure (yr post closure)
	Mean	5th Percentile	95th Percentile	
CdB1	2.2E+00	2.7E-03	1.4E+01	20
CdB2	2.1E+00	1.7E-03	1.0E+01	1,000
PC0	1.4E-02	7.9E-07	3.4E-02	700
PC1	9.3E-02	2.3E-05	2.6E-01	724
PC2	4.4E-01	4.3E-05	2.8E-01	196
PC3	4.2E-01	8.4E-05	2.0E-01	196
PC4	1.2E+00	2.4E-04	4.4E-01	196
PC5	4.4E+00	7.9E-04	8.7E-01	232
PC6	3.6E+00	1.4E-03	1.5E+01	1,000

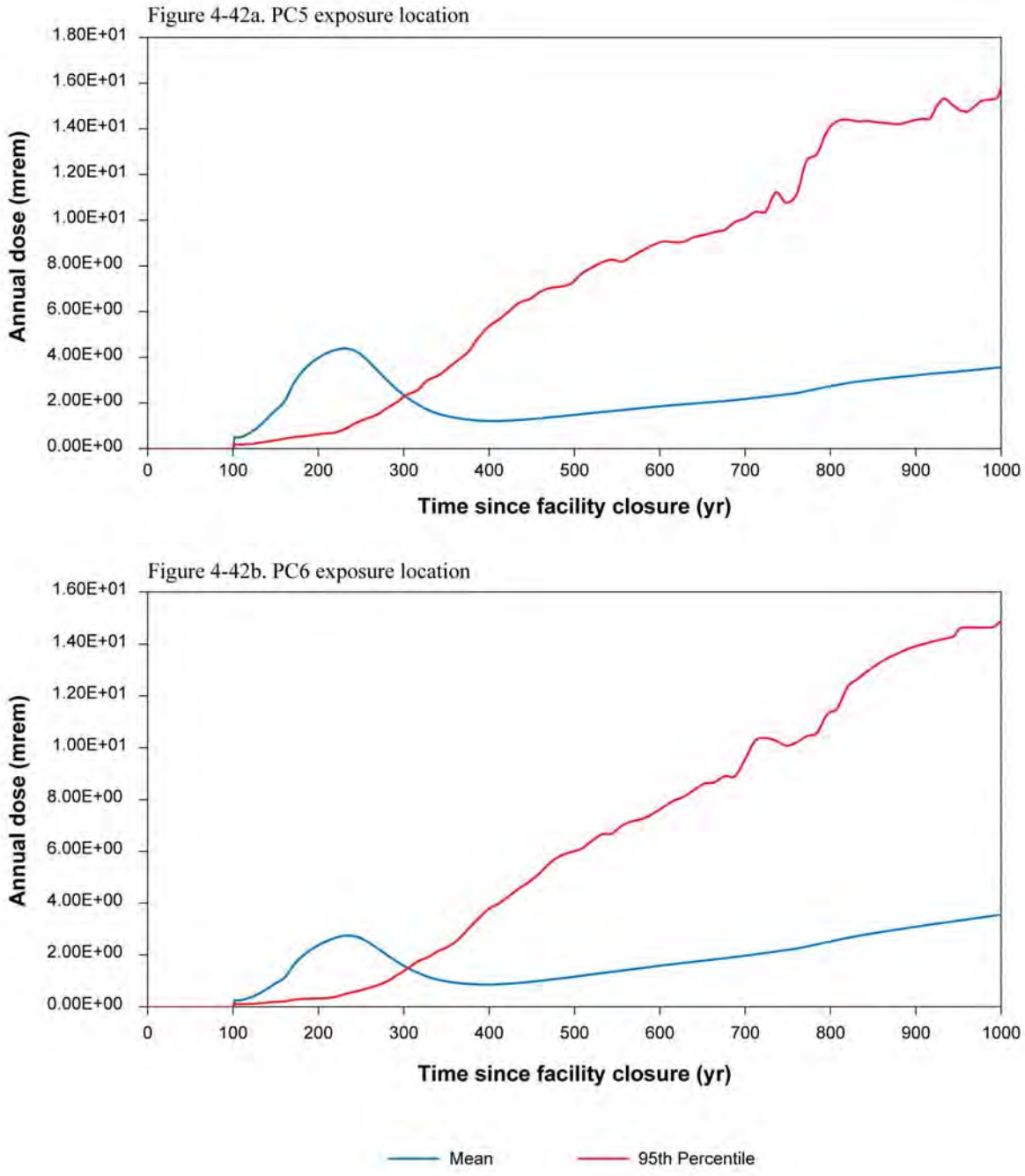

Figure 4-42
Probabilistic Dose Projections for the All Pathways–Pajarito Canyon Scenario (composite analysis)

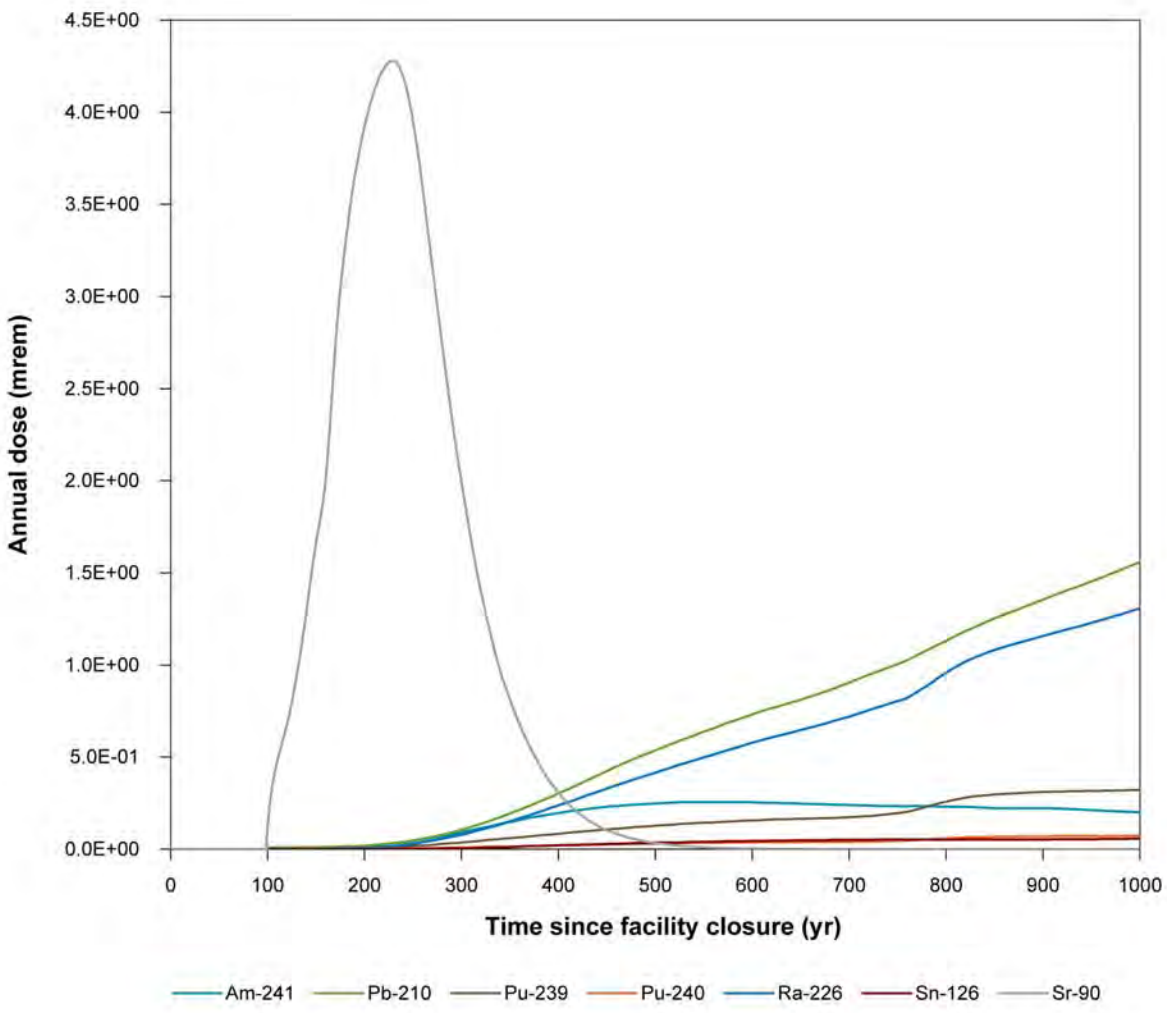

Figure 4-43
Mean Radionuclide Exposures for the All Pathways–Pajarito Canyon Scenario within Catchment PC5 (composite analysis)

in the alternate source evaluation because they are adjacent to Area G and have received discharges of waste in the past or are otherwise contaminated. Brief descriptions of these alternate sources are provided below, followed by an assessment of the potential for interaction between these sources of radioactivity and releases from Area G.

Alternate Source Descriptions

Material Disposal Area A. This disposal area is located at TA-21, approximately 6.7 km (4.2 mi) north-northwest of Area G, and occupies 5,060 m^2 (1.25 ac). Pits were excavated to a depth of about 4 m (13 ft) at the east end of the facility in late 1944 or early 1945 and used to dispose of solid waste with alpha contamination and small amounts of beta and gamma contamination. Two underground tanks were built in 1945 and used to store approximately 185 m^3 (4.9×10^4 gal) of a sodium hydroxide solution containing 334 g (0.74 lb) of Pu-239 (approximately 21 Ci) at the time of emplacement in or about 1947 (LANL, 1971a). The liquid from these tanks was later recovered, treated, and solidified in cement in 1975. Estimates of the residual radionuclide inventories in the two tanks are provided in the LANL Documented Safety Analysis (DSA) (LANL, 2007c); these estimates are included in Table 4-12.

In 1969, a 9 m (30 ft) deep pit was excavated at MDA A for the disposal of U-235, Pu-238, and Pu-239-contaminated building debris from demolition work at TA-21. Estimates of the inventories in this pit are unavailable but are expected to be significantly smaller than the corresponding activities at Area G.

Material Disposal Area AB. Material Disposal Area AB is located at TA-49, which is about 5 km (3 mi) west-southwest of Area G. It was used for belowground hydronuclear experiments in 1960 and 1961. Experiments were conducted in shafts and chambers at depths between 18 and 24 m (60 and 80 ft). The total volume of contaminated tuff has been estimated at about 3×10^4 m^3 (1×10^6 ft^3) (LANL, 1995). Estimates of the radiological inventories at MDA AB are included in Table 4-12.

Material Disposal Area B. Like MDA A, this disposal area is located at TA-21. It occupies approximately 2.4×10^4 m^2 (6.0 ac), and was probably the first common solid waste burial ground for the Laboratory (Rogers, 1977). Engineering drawings show that a single large pit comprises MDA B, but there is evidence that a series of pits was excavated. Solid waste was disposed of at MDA B between 1947 and 1950. The radiological inventory includes "plutonium, polonium, uranium, americium, curium, RaLa [radioactive lanthanum], (and) actinium" (LANL, 1952). The disposal capacity of the MDA B pits is estimated to be about 2.1×10^4 m^3 (7.6×10^5 ft^3); the LANL DSA (LANL, 2007c) estimates of the radionuclide inventories at MDA B are included in Table 4-12.

Table 4-12
Estimates of Radionuclide Inventories at the Material Disposal Areas Included in the Alternate Source Evaluation

Material Disposal Area	Radionuclide	Inventory (Ci)
MDA A	Am-241	6.1E+00
	Pu-238	2.7E-01
	Pu-239	5.4E+01
	Pu-241	7.9E+01
	U-235	1.4E-03
MDA AB	Am-241	5.3E+02
	Pu-239	2.4E+03
	Pu-240	5.1E+02
	Pu-241	2.5E+03
	U-235	2.0E-01
	U-238	5.7E-02
MDA B	Cs-134	5.5E-03
	Pu-239	6.2E+00
	Sr-90	2.9E-01
	Th-228	1.8E-01
MDA H	Am-241	5.0E-06
	H-3	2.4E+02
	Pu (total)	---
	Pu-238	2.5E-02
	Pu-240	1.6E-03
	Pu-241	5.0E-05
	U (total)	---
	U-234	2.6E+01
	U-235	1.4E+01
	U-236	5.7E-01
	U-238	3.5E+01
MDA T	Am-241	3.7E+03
	H-3	---
	MFP	---
	Pu (undifferentiated)	9.8E+00
	Pu-238	3.1E+01
	Pu-239	1.5E+02
	Pu-241	3.7E+04
	U-233	6.9E+00

--- = No inventory included for this radionuclide. *MFP = Mixed-fission products*

Source: LANL, 2007c

Material Disposal Area C. Located at TA-50 on a mesa about 6.7 km (4 mi) northwest of Area G, MDA C occupies about 4.9×10^4 m^2 (12 ac). Radioactive and hazardous waste was disposed of in 6 pits and 107 shafts at MDA C between 1948 and 1965. The average depth of the disposal pits is 6 m (20 ft), while the average depth of the shafts is about 5 m (16 ft). The pits were filled between 1948 and 1959, and the shafts were filled between 1958 and 1965.

Estimates of the total radiological inventory at MDA C are 196 Ci in pits and 4.9×10^4 Ci in shafts. Rogers (1977) provides preliminary estimates of radionuclide-specific inventories decay corrected to January 1, 1973. The pits contain 25 Ci of uranium (including U-234, U-235, U-236, and U-238), 26 Ci of Pu-239, and 149 Ci of Am-241. The shafts are estimated to contain 4.9×10^4 Ci of H-3, 40 Ci of Na-22, 20 Ci of Co-60, 31 Ci of Sr-90/Y-90, 1 Ci of Ra-226, 5 Ci of U-233, less than 0.1 Ci of uranium (including U-234, U-235, U-236, and U-238), 50 Ci of fission products, and 200 Ci of induced activity.

Estimates of the radionuclide inventories disposed of at MDA C were developed in conjunction with the investigation report issued in 2006 (LANL, 2006); these updated inventory estimates are presented in Table 4-13 along with the inventories for this MDA that were included in the LANL DSA (LANL, 2007c). The 2006 investigation report lists inventories for several radionuclides that are not included in the DSA inventory for this MDA. The 2006 investigation report inventories are typically higher than the DSA inventories for radionuclides that are common to both efforts; exceptions include the inventories for Am-241 and Ra-226.

Material Disposal Area H. Material Disposal Area H is located at TA-54, approximately 2 km (1.2 mi) northwest of Area G; the site is approximately 1,300 m^2 (0.3 ac) and contains nine inactive shafts. The facility served as the Laboratory's primary disposal area for solid-classified waste from 1960 to 1986. The waste in all but one shaft is covered with 0.9 m (3 ft) of concrete placed over 0.9 m (3 ft) of crushed tuff; the waste in the remaining shaft is covered with 1.8 m (6 ft) of concrete. The majority of the waste disposed of at MDA H was nonhazardous classified waste; estimates of the radiological inventory are reported in LANL (2003b) and include 3.5 to 106 Ci of H-3, as much as 284.5 Ci of uranium (best estimate is 94.2 Ci), and a maximum of 0.014 Ci of plutonium. More recently, estimates of the radionuclide inventories at MDA H were published in the LANL DSA; these inventories are included in Table 4-12.

Material Disposal Area J. This site is located west of Area G at TA-54, between MDAs H and L. The 1.1×10^4 m^2 (2.7 ac) facility was used for the disposal of administratively controlled waste, for surface storage of nonfriable asbestos, and for land-farming (aeration) of petroleum-contaminated soils (LANL, 1999). No radioactive waste was disposed of at MDA J (LANL, 2002b).

Material Disposal Area L. Located immediately west of Area G at TA-54, this 1.0×10^4 m^2 (2.5 ac) site was used for the disposal of Laboratory-generated hazardous (nonradioactive).

Table 4-13
Estimates of Radionuclide Inventories at Material Disposal Area C

Radionuclide	Inventory (Ci)	
	Investigation Report (LANL, 2006)	LANL DSA (LANL, 2007c)
Ac-227	1.8E+00	---
Al-26	1.4E+02	---
Am-241	4.5E+01	1.5E+02
Cf-249	6.4E-04	---
Cf-251	2.5E-03	---
Cf-252	1.3E-02	---
Cl-36	5.0E-02	---
Co-60	1.9E+02	2.4E+00
Cs-137	1.5E+03	---
Eu-154	5.9E-02	---
H-3	6.1E+04	2.0E+04
Kr-85	2.1E+02	---
Na-22	---	5.8E-01
Np-237	2.9E-04	---
Pu-238	4.0E+03	2.6E+01
Pu-239	1.7E+03	---
Pu-240	4.3E+02	---
Pu-241	7.5E+03	1.5E+03
Pu-242	4.5E-02	---
Ra-226	7.0E-01	1.0E+00
Sm-151	7.9E-03	---
Sn-121m	4.9E-01	---
Sn-126	5.6E-02	---
Sr-90	1.1E+03	2.1E+01
Tc-99	7.1E-05	---
Th-230	1.5E+01	---
Th-232	7.5E-01	---
U (total)	1.2E+02[g]	2.5E+01
U-233	7.0E+00	5.0E+00
U-234	1.9E+01	---
U-235	8.1E+01	---
U-236	2.5E-01	---
U-238	1.2E+01	---
Zr-93	1.3E-01	---

--- = No inventory included for this radionuclide.

wastes until 1985. It is presently used for RCRA-permitted hazardous waste storage and treatment, and for mixed waste storage under interim status authority. Waste was disposed of in 1 pit, 3 surface impoundments, and 34 shafts; all of these units were used for the disposal of uncontained or packaged liquid wastes. No radioactive contaminants are included in the disposal records for MDA L (LANL, 2005e)

Material Disposal Area T. This facility is located at TA-21, along with MDAs A and B. Material Disposal Area T includes four 1.2 m (3.9 ft) deep absorption beds where radioactively contaminated liquid waste from the plutonium processing laboratories at TA-21 was disposed of between 1945 and 1952; these beds continued to receive relatively small quantities of LLW until 1967. The absorption beds contained 4 Ci of H-3 and 10 Ci of Pu-239 as of January 1973 (Rogers, 1977). Between 1968 and 1975, treated liquid waste was mixed with cement and pumped into 4.6 to 19.8 m (15 to 65 ft) deep shafts at MDA T for disposal. After 1975, the cement paste was poured into corrugated metal pipes, and retrievably buried at MDA T. Rogers (1977) reported that the disposal shafts contained 7 Ci of U-233, 47 Ci of Pu-238, 191 Ci of Pu-239, 3,761 Ci of Am-241, and 3 Ci of mixed fission products as of January 1973. Estimates of radionuclide inventories at MDA T taken from the LANL DSA (LANL, 2007c) are summarized in Table 4-12; all but the undifferentiated plutonium was disposed of in the shafts.

Cañada del Buey. This canyon has been used as a buffer zone for MDAs at TA-54, including Area G, and, to a lesser extent for liquid waste disposal. The earliest discharges to the canyon were associated with outfalls, surface runoff, and dispersion from firing sites located at former TA-4, which is now located partially within the boundaries of TA-52 (LANL, 1999). Additional discharges began with the expansion of Laboratory operations to new sites from the 1950s through the 1990s, specifically at TA-46, TA-51, TA-52, and TA-54. Elevated levels of Am-241, Cs-137, Pu-238, Pu-239/240, U-234, U-235, U-238, and Th-230 have been detected in soils at various locations in the canyon, including several sites associated with TA-54.

Pajarito Canyon. The primary use of Pajarito Canyon has been as the location of the Los Alamos Critical Experiments Facility at TA-18; areas within this watershed have also been used for surface and subsurface disposal areas and as a buffer zone for mesa-top firing activities (LANL, 1998b). The canyon has been used for liquid waste disposal since the Laboratory began operation in 1943. Soil samples have been collected at multiple locations along the canyon, including several in the vicinity of Area G. Elevated levels of Am-241, Cs-137, Co-60, H-3, Pu-238, Pu-239/240, Po-210, Sr-90/Y-90, Tc-99, and U-235 have been detected; the source of this material is expected to be Area G.

Other canyons. In addition to Cañada del Buey and Pajarito Canyon, other canyons have been contaminated as a result of Laboratory operations. These include Pueblo and Los Alamos Canyons, which have received liquid effluent discharges from nuclear materials processing, and

Mortandad Canyon, which has been contaminated in conjunction with liquid waste treatment activities. In general, the probability that contaminants discharged to canyons other than Cañada del Buey and Pajarito Canyon will interact with releases from Area G is low. However, groundwater transport modeling has indicated that, under some water supply well pumping scenarios, small portions of discharges to Mortandad Canyon that reach the regional aquifer could migrate towards Area G and possibly interact with groundwater releases from the disposal facility (Birdsell, 2005).

Alternate Source Interactions

The potential for significant interactions between alternate sources of radioactive contamination at the Laboratory and releases from Area G were evaluated using three criteria:

- The magnitude of radionuclide inventories
- The potential for and the magnitude of contaminant release rates
- The potential for the transport of significant quantities of contamination to the exposure locations included in the Area G composite analysis during the 1,000-year compliance period

If radionuclide inventories or contaminant release rates for the alternate sources are low compared to those projected for Area G, there is little likelihood that significant interactions will occur. The risk posed by alternate sources to the receptors included in the composite analysis will also be low if contaminants released from the other sources are not transported to the exposure locations associated with Area G or undergo significant dilution before reaching these locations.

Table 4-14 compares the radiological inventory estimates provided for the MDAs in the LANL DSA (LANL, 2007c) to the radionuclide inventories projected for the Area G composite analysis; short-lived radionuclides are excluded from the table. Generally speaking, the Area G radionuclide inventories are substantially greater than the inventories listed for the MDAs. Exceptions are as follows:

- MDA AB Pu-239 and Pu-240 inventories are 11 to 14 percent greater than their Area G counterparts.
- MDA B Th-228 inventory is about 20 times that projected for Area G.
- MDA H U-234, U-235 and U-236 inventories are 1.1, 3.3, and 38 times the corresponding Area G inventories.
- MDA T Am-241 and Pu-241 inventories are 54 percent and 4.5 times greater than the Area G activities.

Also, although the DSA inventory estimates for MDA C are less than the corresponding Area G activities, the inventories projected for U-235 and U-236 in the MDA C investigation report are about 20 and 16 times greater than the corresponding Area G inventories.

Table 4-14
Summary of Radionuclide Inventories at the MDAs Included in the Alternate Source Evaluation

	Disposal Area [a]						
Radionuclide	Area G [b]	MDA A	MDA AB	MDA B	MDA C [b]	MDA H	MDA T [b]
Am-241	2.4E+03	6.1E+00	5.3E+02	---	1.5E+02	5.0E-06	3.7E+03
Co-60	8.0E+03 [c]	---	---	---	2.4E+00	---	---
H-3	3.5E+06	---	---	---	2.0E+04	2.4E+02	
Pu (undifferentiated)	1.6E+04 [d,e]	---	---	---	---		9.8E+00
Pu-238	4.9E+03 [e]	2.7E-01	---	---		2.5E-02	3.1E+01
Pu-239	2.1E+03 [e]	5.4E+01	2.4E+03	6.2E+00	---	---	1.5E+02
Pu-240	4.6E+02 [e]		5.1E+02			1.6E-03	
Pu-241	8.2E+03 [e]	7.9E+01	2.5E+03		1.5E+03	5.0E-05	3.7E+04
Ra-226	4.0E+00	---	---	---	1.0E+00	---	---
Sr-90	3.3E+03 [f]	---	---	2.9E-01	2.1E+01	---	---
Th-228	9.1E-03			1.8E-01			
U	1.3E+02 [e,g]	---	---	---	2.5E+01		---
U-233	1.2E+01	---	---	---	5.0E+00	---	6.9E+00
U-234	2.4E+01 [e]					2.6E+01	
U-235	4.0E+00 [e]	1.4E-03	2.0E-01	---	---	1.4E+01	---
U-236	1.6E-02 [e]					5.7E-01	
U-238	8.6E+01 [e]		5.7E-02			3.5E+01	

--- None reported

Source: LANL (2007c)

[a] *No radioactive waste inventories are expected to reside in MDAs J and L.*

[b] *Includes pit and shaft waste inventories.*

[c] *Listed activity includes the MAP waste assigned to Co-60.*

[d] *Includes total activity of all plutonium isotopes.*

[e] *Listed activity includes the material type waste activity assigned to isotope.*

[f] *Listed activity includes the MFP waste activity assigned to Sr-90.*

[g] *Includes total activity of all uranium isotopes.*

On the basis of the comparison of the LANL DSA and Area G activities, all disposal areas except MDAs AB, H, and T were excluded from further consideration in the alternate source analysis. Although the Th-228 inventory for MDA B was greater than that for Area G, this radionuclide has a short half-life (1.9 yr) and, therefore, has little impact on the long-term performance of the disposal facilities. The inventory estimates provided in the MDA C investigation report are expected to be approximate at best. Nevertheless, this MDA was added to the list of MDAs carried through the alternate source evaluation.

The primary release mechanisms for radionuclides disposed of at MDAs AB, H, and T are similar to those evaluated for Area G. Plants whose roots penetrate into the buried waste or zone of contamination may deposit radionuclides on the surface of the facility following litterfall and decay. Similarly, animals whose burrows extend into the contamination may transport contamination to the ground surface. Water infiltrating through the disposal areas may leach radionuclides and transport them to the regional aquifer. Finally, vapor- and gas-phase radionuclides may diffuse upward from the waste, exiting from the surface of the facility.

The potential for releases to occur as a result of biotic intrusion is primarily a function of the depth of the cover over the waste or zone of contamination and the presence of barriers to root and burrow penetration. Based on the manner in which the disposal units at MDAs C and T were closed, the transport of contamination to the surface of the facility by plants and animals cannot be ruled out. However, the shafts at MDA C were closed by filling the units with crushed tuff and concrete**,** and the majority of the waste (on an activity basis) disposed of at MDA T exists as a cement paste. The use of concrete for shaft closure and the cement waste form could minimize plant and animal interactions with the material at these facilities. Biotic intrusion is not generally expected to provide a viable release mechanism for the contamination at MDA AB or the waste disposed of at MDA H. The zone of contamination at the former site is 18 to 24 m (60 and 80 ft) bgs, well below the maximum plant rooting and animal burrowing depths identified for the Area G composite analysis. The disposal shafts at MDA H have been covered with 1.8 m (6.6 ft) of cover material, including 0.9 to 1.8 m (3 to 6 ft) of concrete; the facility is expected to receive more cover at final closure. The presence of concrete and the total thickness of the cover suggest intrusion pressures will be small.

The potential for releases of radionuclides due to leaching at MDAs AB, C, H, and T may or may not resemble that projected for Area G. Wet conditions have existed at MDA AB in the past because portions of the site were paved with asphalt; the elevated asphalt pad inhibited evapotranspiration and caused surface water to accumulate because of damming. Monitoring at MDA AB in areas affected by the asphalt pad revealed elevated moisture to depths of about 18 m (60 ft) (Birdsell et al., 2005). However, the pad at MDA AB has been removed and moisture contents are projected to return to background levels over several years. Elevated moisture contents may persist for some time at depths of 12 to 18 m (40 to 60 ft), but it is unclear whether

this additional moisture will result in more rapid leaching of the contamination found at depths of 18 to 24 m (60 to 80 ft).

The hydrologic conditions at Area G and MDA H are expected to be similar; wetter conditions may exist at MDA C due to moderately higher rates of precipitation. Hydrologic conditions at MDA T are expected to be more severe than those at Area G for two reasons. First, MDA T receives higher annual average precipitation. Second, rates of water infiltration through the absorption beds at MDA T were considerably higher than background or natural rates during the 22 years that liquid waste was disposed of at this facility. However, the Am-241 and Pu-241 that have been identified as the critical radionuclides at this facility were disposed of in shafts, which did not receive liquid waste. Birdsell et al. (2005) note that data collected beneath the absorption beds show evidence of fracture flow, while data collected from boreholes adjacent to the beds do not. These results suggest the effects of liquid discharges may have been reasonably contained within the absorption beds.

Although the potential for vapor- and gas-phase radionuclides to diffuse from the waste disposed of at the alternate MDAs exists, the magnitude of any such release is expected to be small. None of the critical radionuclides at MDAs AB, C, H, and T (Table 4-14) exist as a vapor or gas. Although radon gas may be generated from the uranium disposed of at MDA H, the amount of radon that will be generated over the 1,000-year compliance period will be small because the half-lives of the uranium isotopes are large, leading to small generation rates of radon. Therefore, any diffusive releases from these facilities will be low compared to those from Area G.

Releases from the alternate source MDAs must be transported to locations downwind and downgradient of Area G in order to significantly contribute to the exposures estimated in Section 4.3.2. Atmospheric transport modeling by Jacobson (*Appendix D*) projected particulate air concentrations at locations downwind of Area G for releases from MDAs A, AB, B, C, and T. Model simulations were conducted using meteorological data for 2001 and a land use type of "rangeland" across the model domain. A complete description of the modeling effort is available in *Appendix D*.

The results of the atmospheric transport modeling are summarized in Table 4-15 for MDAs AB, C, and T. This table compares the projected air dispersion factors for unit releases from Area G and the alternate source MDAs at receptor locations in the vicinity of Area G. Examination of these results reveals that the air dispersion factors for MDAs AB, C, and T are less than 1 percent of those estimated for releases from Area G. In other words, for a given release rate, concentrations of airborne contaminants originating at the alternate source MDAs will be less than 1 percent of those resulting from the same releases at Area G.

Table 4-15
Comparison of Air Dispersion Results for
Releases from Alternate Source Material Disposal Areas

UTM Grid Coordinates (m) of Exposure Location		Air Dispersion Factor by Release Location (s/m^3)			
Easting	Northing	Source Area 1 Area G	MDA AB	MDA C	MDA T
388567	3965965	8.9E-06	5.1E-08	6.0E-08	6.7E-08
388586	3965960	9.3E-06	5.0E-08	5.9E-08	6.7E-08
388606	3965955	9.7E-06	5.0E-08	5.9E-08	6.6E-08
388625	3965950	9.6E-06	5.0E-08	5.8E-08	6.6E-08
388644	3965945	9.9E-06	4.9E-08	5.8E-08	6.5E-08
388664	3965940	9.5E-06	4.9E-08	5.7E-08	6.4E-08
388683	3965935	9.6E-06	4.9E-08	5.7E-08	6.4E-08
388703	3965931	9.4E-06	4.8E-08	5.7E-08	6.3E-08
388722	3965926	9.4E-06	4.8E-08	5.6E-08	6.3E-08
388741	3965921	9.1E-06	4.7E-08	5.6E-08	6.2E-08

UTM = Universal Transverse Mercator

Atmospheric transport modeling of the alternate source MDAs did not consider the dispersion characteristics of particulate releases from MDA H or the characteristics of vapor- and gas-phase releases from any of the MDAs. For a given release, downwind concentrations of particulates originating at MDA H should be approximately similar to those estimated for releases from Area G. The relative dispersion characteristics of vapor- and gas-phase releases from the various MDAs are generally expected to resemble those shown in Table 4-15 for particulate releases.

Modeling of the transport of groundwater contaminants from the alternate source MDAs to locations downgradient of Area G was not conducted. However, various lines of evidence were used to estimate the potential for interactions between contaminant plumes from these facilities and releases from Area G during the compliance period.

Interactions between groundwater contaminant plumes originating at MDAs AB, C, H, and T and releases from Area G may occur during the compliance period if two conditions are satisfied. First, radionuclides released from the MDAs must discharge to the regional aquifer within 1,000 years of the closure of Area G. Second, the groundwater flowpaths in the aquifer beneath the alternate source MDAs must intersect with contaminant plumes from Area G.

The FEHM groundwater flow and transport modeling conducted in support of the performance assessment and composite analysis (*Appendix E,* Volume 2) projected groundwater travel times

to a domestic well 100 m (330 ft) downgradient of Area G. These times ranged from about 1,000 years to more than 10,000 years, depending upon the infiltration rate and location of the disposal units where the release occurs. Using the infiltration rate estimated for the final cover at Area G, the probabilistic modeling conducted using the Area G Site Model projected that no radionuclides will arrive at the compliance well within the 1,000-year compliance period.

The groundwater travel times (to the compliance well) estimated using FEHM are heavily influenced by the rate at which water passes through the Bandelier Tuff; travel times through the Cerros del Rio basalts are relatively rapid and do not add significantly to the overall travel time. Stratigraphic comparisons across the Laboratory indicate that the thickness of the Bandelier Tuff generally increases from east to west; Figure 2-9 (Section 2) illustrates this trend. This suggests that groundwater travel times at MDAs AB, C, and T may be greater than those estimated for Area G. Given the proximity of Area G and MDA H, relatively little difference in travel time is expected for groundwater contamination from these facilities.

The comparison of relative travel times to the aquifer, based on stratigraphy, is expected to be valid if the hydrologic conditions, most notably rates of infiltration through the disposal units, are similar at the various facilities. Rates of infiltration at MDA H are generally expected to be similar to those modeled by Stauffer et al. (2005). As discussed earlier, this may not be the case with respect to MDAs AB, C, and T. However, although wet conditions have prevailed at MDA AB in the past, it is not clear that the additional moisture observed at depths of 12 to 18 m (40 to 60 ft) bgs will yield faster rates of contaminant travel to the regional aquifer now that the pads have been removed. Although the average precipitation rate at MDA C may be moderately higher than that at Area G, the two locations are not expected to have significantly different infiltration rates. Neither disposal facility received liquid waste during its operational history or was otherwise exposed to long periods of elevated moisture. In terms of MDA T, the effects of liquid discharges to the absorption beds do not appear to have affected the disposal shafts that received the large quantities of Am-241 and Pu-241.

Based on the preceding discussion, no significant releases of uranium from MDA H are expected to discharge to the regional aquifer during the 1,000-year compliance period. Deterministic modeling for Area G suggests that radionuclides other than C-14 will require more than 100,000 years to reach the aquifer beneath the disposal facility. Available data also indicate that releases from MDAs AB, C, and T are unlikely to reach the aquifer during the composite analysis compliance period. If the infiltration rates at MDAs AB, C, and T are at all similar to those at Area G, the critical radionuclides at these sites will require thousands or tens of thousands of years to reach the regional aquifer.

Radionuclides discharged to the regional aquifer from MDAs AB, C, H, and T may or may not intersect with contaminant plumes from Area G. Figure 4-44 indicates the general flowpaths of the regional aquifer and the approximate locations of MDAs AB, C, H, and T and Area G. Based

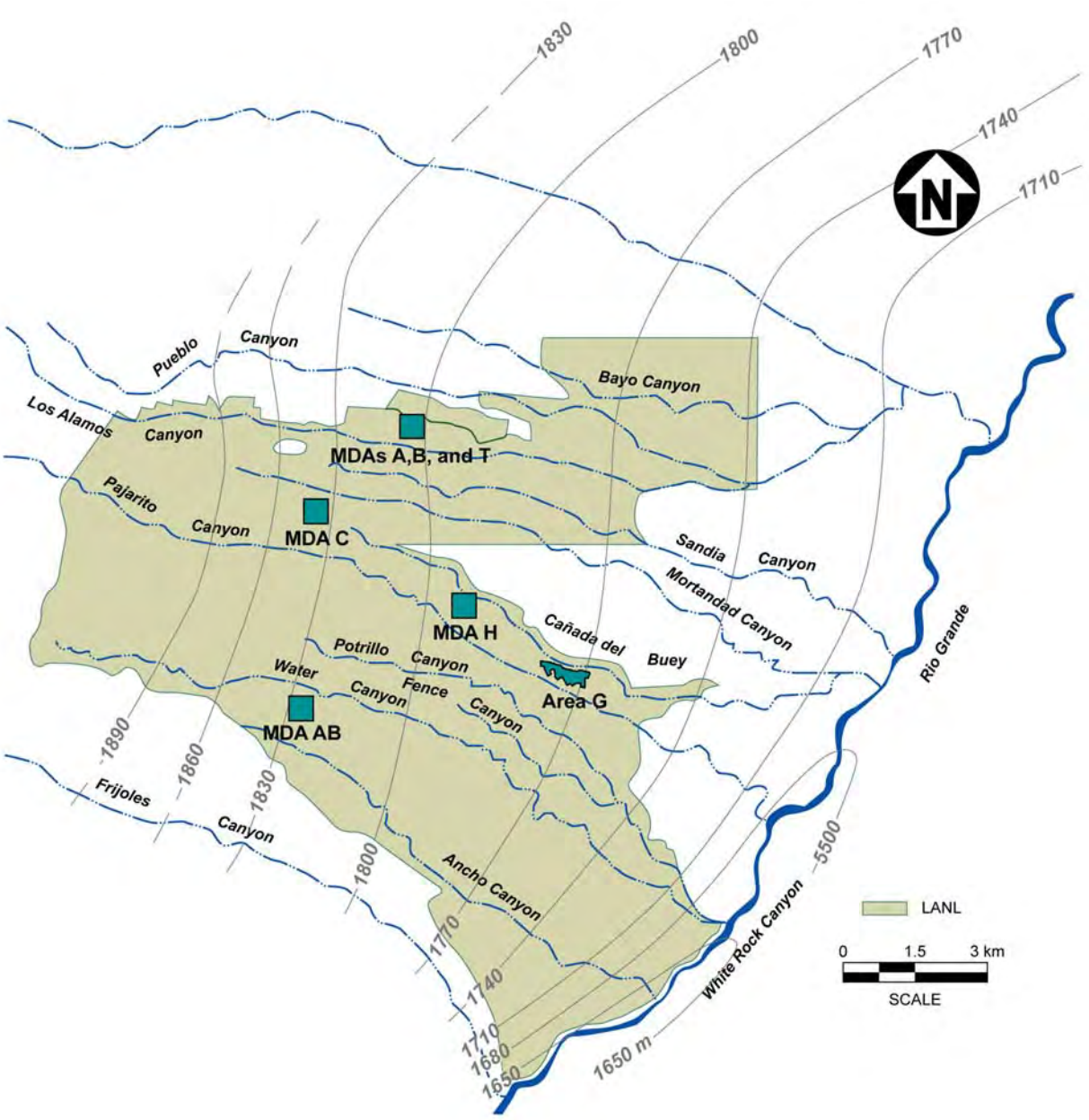

Figure 4-44
Locations of Alternate Contamination Sources and Generalized Water-Level Contours on the Top of the Regional Aquifer

on the information provided in this figure, the aquifer flow paths beneath MDAs AB, C, and T appear to parallel the flow path below Area G. MDA H lies on the same aquifer flow path as Area G, and any contaminant discharges to the aquifer from MDA H are expected to interact directly with releases from Area G.

Existing sampling data suggests that Area G is the primary source of contamination in the portions of Cañada del Buey and Pajarito Canyon that could interact with the receptors considered in the performance assessment and composite analysis. Radionuclides detected in the canyon sediments are thought to be related to residual contamination rather than releases from the pits and shafts. The release of residual contamination to Cañada del Buey and Pajarito Canyon should decrease as Area G undergoes closure and the final cover is applied across the facility. After closure, any contamination in the canyons is expected to result primarily from releases from the disposal facility. Thus, no significant interactions between canyon contamination from other sources at the Laboratory and Area G are anticipated. This conclusion may change if unforeseen releases to the canyons occur.

Some groundwater transport modeling has indicated that, under certain supply well pumping scenarios, small amounts of contamination released to Mortandad Canyon could discharge to the regional aquifer and intersect groundwater releases from Area G (Birdsell, 2005). Although theoretically possible, the likelihood of such interaction is small because water-supply pumping has had very little effect on water levels to date. Any contaminants that arrive at the aquifer will tend to follow the water table gradient; this gradient is almost due east below Mortandad Canyon and to the southeast at Area G.

In summary, the findings of the alternate source evaluation are as follows:

- Radionuclide inventories at most MDAs are significantly smaller than the corresponding inventories at Area G. Possible exceptions include Pu-239 and Pu-240 at MDA AB; U-235 and U-236 at MDA C; U-234, U-235, and U-236 at MDA H; and Am-241 and Pu-241 at MDA T. On a radionuclide-specific basis, this means that potential exposures resulting from releases at the MDAs will generally be much smaller than the contaminant-specific exposures projected for Area G. Divergences between the exposures projected for the alternate source MDAs and Area G will be even greater when cumulative exposures from all radionuclides are considered because Area G is the only source under consideration that has large inventories of several radionuclides.

- The likelihood of radionuclide releases due to biotic intrusion at MDAs AB and H is expected to be smaller than that at Area G; the impacts of biotic intrusion on the waste disposed of at MDA C and in the shafts at MDA T may be similar to those projected for Area G. Elevated moisture contents that could result in increased leaching have been observed at MDAs AB and T in the past, but it is not clear that

these conditions will affect the waste containing the critical radionuclides at these sites. Hydrologic conditions at Area G and MDAs C and H are probably similar.

- On a relative basis, airborne concentrations of contaminants released from MDAs AB, C, and T will be diluted by a factor of 100 or more at the exposure locations downwind of Area G. Contaminant releases from Area G and MDA H are expected to disperse in a similar manner.

- Releases of critical radionuclides from MDAs AB, C, H, and T are generally expected to discharge to the regional aquifer long after the 1,000-year compliance period. It is not clear that contaminants discharged to the aquifer below MDAs AB, C, and T will intersect contaminant plumes that originate at Area G.

- The major source of contamination in the canyons adjacent to Area G is expected to be the disposal facility itself.

Based on these findings, the potential for significant interaction between the releases from Area G and discharges from other facilities at the Laboratory is expected to be low. This conclusion should be verified as further information about alternate sources of radioactivity at the Laboratory becomes available.

The alternate source evaluation does not address releases from facilities that are currently operating at LANL. The composite analysis focuses on the long-term performance of Area G after the facility undergoes final closure. It is assumed that the facilities that are currently operating and that may pose a current-day risk to human health and safety will not be operating over most, if not all, of the 1,000-year compliance period that starts when the final closure of Area G is complete. The impacts of present-day radionuclide releases on persons living in the vicinity of LANL are evaluated as part of the Laboratory's ongoing environmental surveillance program; results such as those presented in LANL (2007b) indicate that the Laboratory's current operations pose little or no risk to members of the public.

4.4 Uncertainty and Sensitivity Analysis

Several sources of uncertainty associated with the performance assessment and composite analysis modeling are discussed below. The probabilistic modeling conducted using the GoldSim models provides insight into the uncertainties introduced by parameter variability. These results may be used to identify the site characteristics and processes to which the long-term performance of the disposal facility is most responsive. Toward this end, sensitivity analyses were conducted; the results of these analyses are provided in Section 4.4.1. Several other sources of uncertainty were not explicitly represented in the modeling; some of these are discussed in Section 4.4.2.

4.4.1 Sensitivity Analysis

Separate sensitivity analyses were conducted for the performance assessment and composite analysis. The results of these evaluations are presented in Section 4.4.1.1 and 4.4.1.2, below.

4.4.1.1 Performance Assessment

Model sensitivities were evaluated for the Atmospheric Scenario and the All Pathways–Cañada del Buey Scenario within catchments CdB1 and CdB2. An additional analysis examined the sensitivity of the projected radon fluxes in waste disposal region 7. The fact that no exposures were projected to occur for the Groundwater Resource Protection and All Pathways–Groundwater Scenarios eliminated the need to evaluate model sensitivities for these scenarios.

Sensitivity analysis results for the two exposure scenarios are summarized in Table 4-16. This table includes the five parameters that had the highest absolute values of the Spearman rank correlation coefficient. The rank correlation coefficient is a nonparametric method to delineate relationships between random variables, in this case the projected doses and the stochastic parameters used in their estimation.

The sensitivity analysis results for the Atmospheric Scenario indicate that the parameters to which the projected peak mean doses are correlated differ between the two exposure locations. The peak exposure projected for the receptor at the LANL boundary is due almost entirely to tritium diffusing from the disposal site. The first three parameters listed in Table 4-16 for this scenario affect the magnitude of the diffusion coefficient of the water vapor and, therefore, the rates at which the contaminant is released to the atmosphere. The moisture contents of the crushed tuff and waste are inversely correlated to the projected exposure because the diffusion coefficient of water vapor decreases as more of the pore space of these media is occupied by water. The diffusion coefficient of vapor-phase tritium is multiplied by the thermal gradient factor to account for the effects of thermal gradients in the waste and cover on rates of diffusion. The indoor exposure time is directly proportional to how long the receptor is exposed to the airborne vapor at the LANL boundary. The dispersion factor affects the concentration of tritiated water vapor at the exposure location; a higher factor implies a higher concentration of airborne tritium. The dispersion factor for atmospheric source area 2 is important because a major portion of the tritium inventory resides in this part of Area G.

All of the parameters listed in Table 4-16 for the Atmospheric Scenario at the Area G fence line influence the rates at which contaminants are either deposited on the surface by plants growing over the disposal facility or resuspended for transport downwind of the site. Three of the parameters (the beta-shape factor used to describe root mass distributions with depth, the maximum rooting depth of trees, and the aboveground biomass density of trees) influence the degree to which plant roots

penetrate into the waste and deposit contamination on the soil surface. Doses are inversely proportional to the shape factor because larger values of the parameter predict that a greater proportion of the total root mass lies close to the surface; fewer roots are likely to extend into the waste as a result. The plant-uptake factor for potassium in native vegetation controls the rate of K-40 assimilation by plants; this isotope is one of the major contributors to the peak mean dose. Finally, the projected exposures are sensitive to the particulate resuspension flux as this parameter determines the rate at which contamination deposited on the surface of Area G is entrained by the prevailing winds.

Table 4-16
Rank Correlation Coefficients for Selected Performance Assessment Exposure Scenarios

Exposure Scenario	Exposure Location	Model Parameter	Rank Correlation Coefficient
Atmospheric	LANL boundary	Moisture content of crushed tuff	-4.6E-01
		Moisture content of waste	-4.6E-01
		Thermal gradient factor	4.3E-01
		Indoor exposure time	2.6E-01
		Dispersion factor for atmospheric source area 2	2.0E-01
	Area G fence line	Maximum rooting depth of trees	5.4E-01
		Root-mass-distribution beta-shape factor	-4.8E-01
		Particulate resuspension flux	2.6E-01
		Aboveground biomass density of trees in piñon-juniper woodland	1.5E-01
		Plant-uptake factor of potassium in native vegetation	1.3E-01
All Pathways–Cañada del Buey	Catchment CdB1	Surface erosion scenario	4.8E-01
		Sediment dispersal factor	-1.9E-01
		Moisture content of crushed tuff	-1.8E-01
		Moisture content of waste	-1.8E-01
		Thermal gradient factor	1.5E-01
	Catchment CdB2	Maximum rooting depth of trees	5.6E-01
		Root-mass-distribution beta-shape factor	-4.9E-01
		Plant litter production factor for trees	1.7E-01
		Aboveground biomass density of trees in piñon-juniper woodland	1.7E-01
		Plant-uptake factor of potassium in native vegetation	1.5E-01

The peak mean dose projected for the All Pathways–Canyon Scenario within catchment CdB1 is dominated by exposures to tritium; a portion of the tritium diffusing upward from the waste partitions into the liquid phase of the surface soils and acts as a source of contamination for the canyon resident. Three of the parameters included in Table 4-16 affect the rates at which tritiated water vapor diffuses from the waste and, therefore, the level of contamination in the surface soils. The erosion scenario is a parameter used in the GoldSim modeling to evaluate the impacts of low, moderate, and high erosion on facility performance. As the scenario index increases so too does the rate of erosion, causing greater cover loss and, ultimately, increased exposures to the canyon resident. The sediment dispersal factor is used to control the area over which the sediments eroded from Area G are dispersed within catchment CdB1; the dispersal area increases as the value of the factor rises, yielding lower soil concentrations of tritium and smaller exposures.

The results of the sensitivity analysis for the exposures projected for the canyon resident in catchment CdB2 indicate the importance of plant intrusion into the waste. Four of the five parameters relate to the distribution of tree roots with depth and the plants' litter production capacity. The plant-uptake factor for potassium influences the degree to which K-40 is assimilated by plants growing over the disposal site; K-40 is a major contributor to the doses projected for the resident in catchment CdB2.

The sensitivity of radon flux to the site diffusion model input parameters was evaluated using the model projections for waste disposal region 7, the region yielding the highest flux for the performance assessment inventory. Table 4-17 shows the results of this analysis, which indicate that the fluxes are most sensitive to the inventory of Ra-226. The radon-emanation coefficient specifies how much of the generated radon enters the air-filled pore spaces within the waste and, therefore, the amount of gas available for diffusion. The moisture contents of the crushed tuff and waste influence the magnitude of the radon diffusion coefficients used in the modeling.

Table 4-17
Rank Correlation Coefficients
for Radon Flux from Waste Disposal Region 7

Model Parameter	Rank Correlation Coefficient
Ra-226 Inventory	7.1E-01
Radon Emanation Coefficient	3.8E-01
Moisture Content of Crushed Tuff	-1.5E-01
Moisture Content of Waste	-1.5E-01
Cover Node	-7.5E-02

The final parameter listed in Table 4-17, the cover node, highlights the relationship between cover thickness and radon flux. The surface erosion modeling conducted in support of the performance assessment and composite analysis divided or discretized the cover overlying the disposal units into a series of 6.25-m^2 (67-ft^2) nodes. Each node is characterized by an initial cover thickness and soil loss function. The site model randomly selects a node at the start of each realization of the probabilistic simulation and uses the corresponding cover thickness and cover loss function to project facility performance over the 1,000-year compliance period. Selecting a cover node that has a relatively high initial cover thickness and a slow erosion rate will tend to yield lower radon fluxes than will a node with a thin initial cover and high rate of erosion.

The nodes used to represent the disposal site are sequentially numbered; the cover node element identified in the sensitivity analysis is simply a distribution of those numbers. The numbers of the nodes are assigned in a random manner, and do not systematically increase or decrease with the initial cover thickness. Because of this, the correlation between the peak mean dose and the cover node is low.

Several parameters that have no apparent effect on the radon fluxes projected for waste disposal region 7 were identified as potentially important by the sensitivity analysis. Examples include plant uptake factors and transfer factors for various radionuclides, plant biomass and animal burrow characteristics at Area G, and sediment transport rates for selected contaminants. These parameters do not affect the rates of generation of radon or the diffusion characteristics of the gas and, therefore, the projected fluxes. Consequently, these results are considered spurious and are not included in Table 4-17.

4.4.1.2 Composite Analysis

Sensitivity analyses were conducted using the site model results for the Atmospheric and All Pathways–Canyon Scenarios. The analysis for the All Pathways–Canyon Scenario considered the exposures for the receptors within catchments PC5 and PC6, the locations with the highest peak mean doses of the nine canyon locations included in the dose assessment. The results of the sensitivity analysis are summarized in Table 4-18. This table includes the five parameters with the highest absolute values of the Spearman rank correlation coefficient.

The results of the sensitivity analysis for the Atmospheric Scenario receptor at the LANL boundary are the same as those discussed above for the performance assessment. Three of the five parameters control rates of tritium diffusion from the site, while the other two define the length of exposure and airborne concentrations over the receptor's residence. In terms of the exposures projected for the individual at the Area G fence line, it is clear that trees play a major role in the release of contamination to the surface environment. Three of the listed parameters influence the degree to which tree roots penetrate into the waste and deposit contaminated litter on the surface of the disposal site. The resuspension flux at Area G affects the rate at which contamination deposited

on the surface of the facility is released to the atmosphere and transported downwind. The initial inventory of Th-230 in the pre-1971 disposal pits is important because it is a source of Ra-226 and Pb-210, two of the major contributors to the peak mean exposure.

Table 4-18
Rank Correlation Coefficients for Selected Composite Analysis Exposure Scenarios

Exposure Scenario	Exposure Location	Model Parameter	Rank Correlation Coefficient
Atmospheric	LANL boundary	Moisture content of crushed tuff	-4.6E-01
		Moisture content of waste	-4.6E-01
		Thermal gradient factor	4.3E-01
		Indoor exposure time	2.6E-01
		Dispersion factor for atmospheric source area 2	2.0E-01
	Area G fence line	Root-mass-distribution beta-shape factor	-4.7E-01
		Maximum rooting depth of trees	4.6E-01
		Particulate resuspension flux	3.0E-01
		Initial inventory of Th-230 in pre-1971 disposal pits	1.7E-01
		Aboveground biomass density of trees in piñon-juniper woodland	1.5E-01
All Pathways–Pajarito Canyon	Catchment PC5	Root-mass-distribution beta-shape factor	-3.7E-01
		Maximum rooting depth of trees	3.4E-01
		Erosion scenario	2.9E-01
		Plant-uptake factor of strontium in native vegetation	1.9E-01
		Ingestion rate of grain	1.5E-01
	Catchment PC6	Maximum rooting depth of trees	5.0E-01
		Root-mass-distribution beta-shape factor	-4.1E-01
		Plant-uptake factor of radium in native vegetation	2.2E-01
		Initial inventory of Th-230 in pre-1971 disposal pits	1.7E-01
		Erosion scenario	1.7E-01

--- = Site diffusion model was not used to evaluate sensitivities for the exposure scenario.

Four of the parameters to which the canyon exposures in catchments PC5 and PC6 are most sensitive influence the amount of contamination taken up by deep-rooting trees. Two of these affect the distribution of root mass with depth, while the plant uptake factors control the rates of Sr-90 and Ra-226 assimilation by plants; these radionuclides are major contributors to the peak mean exposures projected for the different catchments. The dose projections for the two locations are also sensitive to the erosion scenario, because of the effect this parameter has on the rate of soil loss. The ingestion rate of grain is important for catchment PC5 because this exposure

route is an important contributor to the projected doses. The initial Th-230 inventory in the pre-1971 disposal pits is important for catchment PC6 because it is a source of Ra-226 and Pb-210, the two radionuclides that make the greatest contributions to the projected peak mean dose.

4.4.2 Additional Sources of Uncertainty

The sensitivity analyses conducted in support of the performance assessment and composite analysis are useful for evaluating the effects of parameter variability on the dose and radon flux projections. However, several additional sources of uncertainty are associated with the results provided in this report. Some of these are discussed in the following sections.

4.4.2.1 Key Assumptions

The performance assessment and composite analysis are based on several key assumptions. The first of these pertains to the level of control exerted over the disposal facility after final closure. The analyses assume that the DOE will actively maintain the disposal facility for a period of 100 years following closure, during which time efforts will be made to prevent the establishment of deep-rooting trees and to limit significant erosion of the cover placed over the disposal units.

The doses projected for the Atmospheric Scenario at the Area G fence line and for the All Pathways–Canyon Scenarios at most exposure locations are dominated by exposures to contaminated soils that are suspended from the disposal site and transported with the prevailing winds, and to contaminated sediments transported with surface runoff into Cañada del Buey and Pajarito Canyon. In many cases, the contamination responsible for these exposures is deposited on the surface of the disposal facility by plants and animals intruding into the waste. Logically, then, any controls on the establishment of deep-rooting plants at the site could be viewed as having a potentially significant impact on the exposures projected for these scenarios. This hypothesis is supported by the results of the sensitivity analysis, which indicate that the doses projected for many receptor locations are highly correlated with the abundance and rooting characteristics of trees.

Nevertheless, modeling results suggest that the control of deep-rooting species of plants by the DOE during the active institutional control period will have a limited impact on the doses projected for the downwind and canyon receptors. For example, the composite analysis exposures projected for the fence line location increase slowly over the latter portions of the compliance period, with the highest doses occurring at the end of the 1,000-year compliance period. Earlier establishment of deep-rooted trees at the closed facility will cause exposures to increase sooner. However, the rate of increase during the latter stages of the compliance period is expected to be similar to that indicated by the GoldSim modeling. If this is the case, the peak mean exposures will likely increase 10 to 15 percent if the DOE fails to prevent the site from transitioning to piñon-juniper woodland during the active institutional control period.

A similar pattern is observed for the exposures projected for the canyon residents in catchments CdB2, PC0, PC1, and PC6. In each case, the projected exposures for most radionuclides increase slowly over long periods of time suggesting the earlier presence of trees will only cause moderate increases in dose. In some cases, Sr-90 taken up by plants and deposited on the surface of the disposal facility makes an important contribution to the exposures projected for the canyon receptors. Sr-90 has a relatively short half-life and is, therefore, more influenced by the time required for deep-rooted vegetation to become established at the closed site. Earlier establishment of trees could result in significantly higher doses from this isotope, perhaps as much as three times higher. That said, the total exposures received by the receptors are expected to remain well within the 30 mrem/yr dose constraint that applies to the canyon scenario.

It is also assumed that the DOE will prevent any significant erosion of the closed site during the active institutional control period. However, the surface erosion rate modeling did not project any significant rates of soil loss during this period and erosion was allowed to proceed unimpeded. Although prevention of all soil loss for a period of 100 years would help minimize plant root penetration of the waste, any resulting reductions in projected exposures are expected to be less than 10 percent. That aside, it is unrealistic to expect that all soil loss could be prevented.

The long-term performance modeling is based on the assumption that there will be no significant climatic changes during the period of performance. Should climatic changes occur, many aspects of the facility's performance could be affected. A wetter climate would likely result in increased rates of infiltration through the disposal units with subsequent elevated rates of radionuclide leaching from the waste and reduced groundwater travel times to the regional aquifer; both of these effects would increase the exposures projected for persons who use groundwater resources downgradient of Area G. Additional moisture could result in different plant and animal communities at the site, possibly altering the impacts of biotic intrusion on facility performance. On the other hand, drier conditions would likely result in reduced rates of contaminant leaching and longer groundwater travel times, ensuring little or no risk of exposure to groundwater users. Again, shifts in the plant and animal communities may occur, influencing the degree to which biotic intrusion impacts the site.

Subsidence of incompletely filled disposal units is not explicitly modeled nor is it assumed to impact the long-term performance of the disposal facility. While the potential for subsidence may be real, it is assumed that efforts will be taken to minimize or eliminate this potential by the time the facility undergoes final closure. Potential impacts on facility performance if subsidence does occur will depend upon what disposal units are impacted and the degree to which the integrity of the affected pits and shafts is undermined. In general, however, subsidence could lead to greater rates of infiltration through the waste, faster contaminant travel times to the regional aquifer, and increased access to the waste by plants and animals inhabiting the site; waste could, conceivably, be exposed under extreme circumstances.

Isolated incidences of subsidence have been observed at Area G. Most of these have consisted of small holes developing next to several disposal shafts. However, more significant subsidence events have been also been observed. In 2004, a 1 to 1.5 m (3.3 to 5 ft) diameter hole of unknown depth developed in a portion of pit 15. Pit 15 was dedicated to the disposal of waste packaged in metal and wood containers of various proportions; comparisons of the volumes of waste placed in these containers and the capacities of the packages suggest that many of these containers were incompletely filled. Also in 2004, a 1 to 1.5 m (3.3 to 5 ft) diameter hole of unknown depth developed between pits 32 and 33; these pits received mostly uncontainerized waste in the mid-1980s. In 2005, subsidence occurred over an area of approximately 50 m^2 (500 ft^2) within pit 9; the maximum depth of the depression was about 0.6 m (2 ft). This pit contains retrievably stored transuranic waste that was packaged in wooden boxes and metal drums to facilitate its retrieval. Finally, a 1 to 1.5 m (3.3 to 5 ft) diameter hole of unknown depth developed in pit 31 in 2005. This pit, which underwent interim closure in 2005, received both containerized and bulk (uncontainerized) waste (French, 2005).

Inspections are conducted annually to identify and correct the impacts of any subsidence events. Other options have also been considered by Laboratory personnel for addressing subsidence issues at Area G, including dynamic compaction of selected disposal units. To the extent that these or other options are successful, the long-term performance of Area G is not expected to be substantially undermined by subsidence. It is on this basis that the long-term performance modeling was conducted.

4.4.2.2 Saturated Hydraulic Conductivity

The material properties of the cover and bedrock are critical in terms of the long-term erosion and infiltration behavior of the final cover. An important parameter for both processes is the saturated hydraulic conductivity of the bentonite/crushed tuff layer. The surface erosion and infiltration modeling relied on different literature-based estimates of this parameter. The SIBERIA modeling (*Appendix I,* Volume 2) adopted a saturated hydraulic conductivity of 11 mm/hr (0.43 in./hr); this value is significantly greater than the value of 0.065 mm/hr (0.0026 in./hr) adopted as the base-case condition for the infiltration modeling (*Appendix G,* Volume 2).

The hydraulic conductivity values used in the surface erosion modeling were taken from literature values (Nyhan et al., 1993; Charman and Murphy, 1992) for actual soils with the same texture (i.e., the same proportions of sand, silt and clay) as that for the proposed cover. The infiltration calculations used an estimated hydraulic conductivity for a 6 percent bentonite/crushed tuff mixture; this estimate was based on a linear regression fit between the measured hydraulic conductivity of pure crushed tuff and the value reported in Nyhan et al. (1997) for a 10 percent bentonite/tuff mixture. Both sets of values have limitations. The values representing actual soils reflect the fact that these soils have developed, over a long period of time, a structure with a hierarchy of pores and water pathways. This type of soil structure may

develop at Area G, but it may require many years after the placement of the final cover to do so. On the other hand, the hydraulic conductivity of crushed tuff/bentonite that was used for the infiltration modeling assumes the material is homogeneous, with none of the characteristics that may develop near the surface of the disposal site as a result of biotic activities such as root growth or the burrowing activities of insects or animals.

The uncertainty about the saturated hydraulic conductivity characteristics of the cover material is a potentially significant source of error in the surface erosion modeling. If the actual hydraulic conductivity values are lower than the values adopted for the modeling, the SIBERIA runoff rates—and subsequent erosion—will be higher than predicted; rates of infiltration will tend to decline. Given higher saturated hydraulic conductivities, rates of erosion will decrease while the amount of water passing through the disposal units will rise. As discussed earlier, increases in rates of infiltration may result in greater leaching of the waste and faster contaminant travel times to the compliance well.

Field and laboratory data provide additional insight into the values used to characterize the saturated hydraulic conductivity of the cover material at Area G. Field measurements of saturated hydraulic conductivity were collected as a function of depth below the surface at MDA J, a disposal site located 2 km (1.2 mi) west of Area G that underwent final closure in 2002 (Apogen, 2006). At each of three locations, measurements were collected at the soil surface, at 15 cm (6 in.) bgs, and at the top of a bentonite/tuff infiltration layer found at depths ranging from 23 to 28 cm (9 to 11 in.) bgs. Although the cover at MDA J differs from that assumed for Area G, the properties of the surface soils and bentonite/tuff layers are expected to be similar. The results of the field measurements are summarized in Table 4-19.

The field measurements at MDA J indicate that the saturated hydraulic conductivity decreases with depth from the topsoil layer to the bentonite/tuff infiltration layer. The average conductivity for the surface and at a 15 cm (6 in.) depth in sample hole 1 is about 180 times that measured in the infiltration layer, while the average conductivities measured at the surface and at a depth of 15 cm (6 in.) in holes 2 and 3 are 62 and 9 times greater than the corresponding infiltration layer values. The mean conductivity for all three sample holes at the surface and at a 15 cm (6 in.) depth is 6.8 mm/hr (0.27 in./hr), or about 45 times the mean conductivity of 0.15 mm/hr (0.0059 in./hr) found for the infiltration layer.

The decrease in saturated conductivity with depth observed at MDA J is a direct reflection of the materials comprising the surface and infiltration layers of the final cover. The topsoil layer is much less compacted than the bentonite/tuff infiltration layer and, therefore, is more permeable to water. The presence of plant roots and insect and animal burrows in the cover may enhance the conductivity of the cover. Although these effects may reasonably be expected to be greatest

near the surface of the site, measurements needed to differentiate between the relative influence of roots and burrows on the two layers were not collected.

Table 4-19
Field Measurements of Saturated Hydraulic Conductivity at MDA J

Sample Hole	Sample Depth	Saturated Hydraulic Conductivity (mm/hr)
1	Surface	9.3E+00
	15 cm	8.5E+00
	25 cm [a]	4.9E-02
2	Surface	1.0E+01
	15 cm	8.1E+00
	28 cm [a]	1.5E-01
3	Surface	2.4E+00
	15 cm	2.4E+00
	23 cm [a]	2.6E-01

Source: Apogen, 2006

[a] *Sample was collected at the top of the bentonite/crushed tuff infiltration layer.*

On the basis of the findings at MDA J, the saturated hydraulic conductivity used for the erosion modeling should be representative of the surface of the cover at Area G. The conductivity measurements for the surface of MDA J average 7.3 mm/hr (0.29 in./hr); the measurements at 15 cm (6 in.) bgs are functionally the same and average 6.3 mm/hr (0.25 in./hr) across the three holes. These measurements compare favorably with the value of 11 mm/hr (0.43 in./hr) used in the SIBERIA modeling. In terms of infiltration characteristics, the 6 percent bentonite/tuff layer included in the final cover design for Area G is generally expected to have the greatest impact on rates of infiltration through the disposal units. The average saturated hydraulic conductivity measured for the infiltration layer at MDA J is 0.15 mm/hr (0.0059 in./hr); this value is similar to the average conductivity of 0.14 mm/hr (0.0055 in./hr) measured in four holes in 2003 (LANL, 2003c), shortly after the cover was placed over the disposal facility. These values are 2.1 to 2.3 times greater than the value of 0.065 mm/hr (0.0026 in./hr) adopted for the base-case HYDRUS simulations.

Laboratory measurements of hydraulic conductivity were conducted on replicate samples of crushed tuff with 6 and 8 percent bentonite (DBS&A, 2006). The average saturated hydraulic conductivity of the two 6 percent bentonite/tuff samples was 0.099 mm/hr (0.0039 in./hr); the corresponding value for the two 8 percent bentonite/tuff samples was 0.038 mm/hr (0.0015 in./hr). The mean conductivity for the 6 percent mixture is 1.5 times greater than the

value used for the HYDRUS modeling, while the mean for the 8 percent mixture is about 60 percent of the value used in HYDRUS. The fact that the conductivity measured for the 6 percent mixture is higher than the modeled value may result, in part, from the fact that the laboratory samples were less compacted than the samples upon which the HYDRUS model value was based. The mean bulk density of all four laboratory samples was 1,250 kg/m^3 (78 lb/ft^3), or about 90 percent of the 1,400 kg/m^3 (87 lb/ft^3) bulk density typical of the mixtures upon which the conductivity used in the HYDRUS infiltration modeling was based.

Based on the preceding discussion, the use of two distinct saturated hydraulic conductivities for the erosion and infiltration modeling appears warranted. The higher value used for the SIBERIA modeling addresses the properties of the surface soils expected at Area G and is consistent with measurements conducted for surface soil at MDA J. It remains to be seen, however, if the conductivity of the bentonite/tuff layer at Area G will increase over time as the surface soil erodes and plant roots and insect and animal burrows penetrate further into the material. The measurements collected at MDA J indicate that no significant changes in the conductivity of the bentonite/tuff layer have occurred since the disposal site was covered, but only 4 years had passed between the time the cover was applied and the time the measurements were taken.

The use of a much lower hydraulic conductivity for the infiltration modeling is consistent with the expectation that the bentonite/tuff layer will exert a major influence on rates of water infiltration through the cover at Area G. The values used in the HYDRUS modeling are generally consistent with the values measured at MDA J and in the laboratory.

4.4.2.3 Sediment Transport and Canyon Interactions

The exposures projected for the All Pathways–Cañada del Buey and All Pathways–Pajarito Canyon Scenarios result from the transport of contaminated sediments into the canyons adjacent to Area G. Sediments transported to the edge of the mesa were allocated among several drainages or catchments within the two canyons in an attempt to more accurately estimate contaminant concentrations on the canyon floors. Nevertheless, the projected sediment paths and radionuclide concentrations are subject to a large amount of uncertainty.

The SIBERIA model does not allow particle tracking or sediment-packet tracking, which means the model cannot determine if contaminated particles reaching the edge of the mesa will become trapped within the rock armor or migrate over the mesa edge to a downhill location. Because of this limitation, the modeling conducted in support of the performance assessment and composite analysis assumed that all sediments reaching the edge of the mesa were transported over the edge and migrated immediately to the canyon floors. This approach is expected to be conservative in terms of the exposures received by persons living in the canyon because a portion of the sediments would probably require longer periods of time to reach the canyon floors.

Sediments transported from the mesa top will disperse over some portion of the canyon floor in Cañada del Buey and Pajarito Canyon. Lacking specific information about how sediment dispersal will evolve, it was assumed that the material would spread over 10 to 50 percent of the area of a given catchment. Dispersal over smaller areas will result in doses that are larger than projected; the reverse will be true if the area of dispersal is larger.

As modeled, the sediments reaching the canyon floors are assumed to be slowly transported down Cañada del Buey and Pajarito Canyon in response to flooding events. Information has been collected about sediment transport rates within some canyons at the Laboratory, but no direct estimates of sediment transport within Cañada del Buey and Pajarito Canyon exist. Although rates of transport were assumed to be slow within these canyons, the 200-year residence time upon which the modeled rates are based is still highly uncertain. Shorter residence times will result in lower exposures than those projected for the canyon residents. If however, sediment transport rates are substantially lower than assumed, exposures could rise significantly over long periods of time.

4.4.2.4 Short-Term Moisture Conditions

Several surface structures have been constructed at Area G in support of waste management operations at that facility. These structures include asphalt pads, the presence of which has been shown to result in elevated moisture contents in nearby areas and subsurface soils. These pads inhibit removal of water through evapotranspiration and often focus runoff to small portions of the site. The result is increased fluxes of water; Newman et al. (*Appendix F,* Volume 2) compared moisture contents in boreholes drilled in paved and unpaved portions of Area G and found that moisture contents and fluxes in the former were significantly higher than those in unpaved portions of the site. Birdsell et al. (2005) found that runoff focused by an asphalt pad at Area G resulted in a transient ponded condition near a borehole. Periodic monitoring of water content in the borehole revealed increasing water contents to a depth of 24 m (80 ft) within 10 years of when the borehole was established.

Elevated moisture conditions and corresponding increases in rates of infiltration that persist over time will have obvious effects on the rates at which contaminants are leached from the waste and transported to the regional aquifer. However, evidence from MDA AB suggests that moisture contents will gradually return to natural levels once the asphalt pads are removed (Birdsell et al., 2005). Thus, the long-term impacts of these pads will depend on the length of time they are in place as well as flow conditions specific to each pad.

4.4.2.5 Effects of Waste-Form and Packaging

The waste disposed of at Area G has assumed a wide variety of chemical and physical forms. Packaging of this waste has ranged from nonexistent to metal containers. Despite this, the modeling conducted in support of the performance assessment and composite analysis is based

on the simplifying assumption that all waste radionuclides are in equilibrium with the crushed tuff backfill as soon as the waste is placed in the disposal units.

Simplifying the effects of waste form and packaging in this manner may provide estimates of radionuclide release in excess of what will actually occur. For example, plants will be unable to assimilate contaminants in solidified waste (e.g., concrete), sealed sources, and activated metals until those matrices degrade. The radionuclides in these wastes will also be resistant to transport to the surface of the facility by burrowing animals and contaminant leaching. Likewise, as long as metal containers remain intact, the impacts of biotic intrusion and contaminant leaching may be limited. Understanding the overall effect of waste form and packaging on the doses projected for the performance assessment and composite analysis will require a detailed investigation of the distributions of the critical radionuclides among the various forms and package types.

4.4.2.6 Spatial Dependencies of Long-Term Performance

Several aspects of the long-term performance modeling conducted in support of the performance assessment and composite analysis are spatially variable across the facility. In response to this, the facility was divided into eight waste disposal regions to account for variations in groundwater flow and transport behavior. The erosion modeling estimates rates of cover loss taking into account the locations of the disposal units and variations in cover thickness and slope. Accounting for the spatial variability in site conditions is expected to provide a more accurate representation of facility performance.

The spatial dependencies of facility performance make it clear that the manner in which the facility is operated, maintained, and closed need to be carefully considered. As an example, the groundwater transport modeling conducted by Stauffer et al. (*Appendix E,* Volume 2) indicates that groundwater travel times to the compliance well generally increase from the eastern edge of Area G to the western boundary; travel times for releases from waste disposal regions 1 and 8 may differ by hundreds to thousands of years depending upon the rate at which water infiltrates through the site. In this instance, the placement of large inventories of highly mobile radionuclides in the easternmost disposal units could have more serious consequences than placing the same waste in pits and shafts in the western portion of the facility. Alternatively, the surface erosion modeling conducted using SIBERIA (*Appendix I*) generally indicates more severe erosion pressures exist along the edges of the mesa; information of this nature should be used to intelligently site future disposal units.

4.5 ALARA Analysis

The results of the ALARA analysis are summarized in Tables 4-20 and 4-21. Table 4-20 summarizes the mean collective population doses for the Atmospheric and All Pathways–Canyon Scenarios, integrated over 300 years. The doses listed for the canyon scenario include all

persons living in both canyons. Table 4-21 summarizes the costs associated with the projected health impacts and implementation of each closure strategy.

Table 4-20
Collective Doses Estimated for the Area G ALARA Analysis

Closure Strategy	Mean Collective Dose (person-rem)	
	Atmospheric Scenario	All Pathways–Canyon Scenario
Base-Case Scenario	1.1E-01	2.9E+00
Extended Control Option	3.2E-02	2.3E+00
Biobarrier Option	4.6E-02	2.2E+00

Table 4-21
Collective Doses and Closure Strategy
Implementation Costs for the Area G ALARA Analysis

Exposure Scenario and Closure Strategy	Mean Cost ($)		
	Health Detriment	Strategy Implementation	Total
Atmospheric Scenario			
Base-Case Scenario	3.3E+02	6.9E+07	6.9E+07
Extended Control Option	1.1E+02	2.4E+08	2.4E+08
Biobarrier Option	1.4E+02	6.9E+07	6.9E+07
All Pathways–Canyon Scenario			
Base-Case Scenario	7.1E+03	6.9E+07	6.9E+07
Extended Control Option	5.0E+03	2.4E+08	2.4E+08
Biobarrier Option	4.8E+03	6.9E+07	6.9E+07

The results in Table 4-20 indicate that the collective doses over the 300-year integration period are low and similar among the three closure strategies. Although the exposed population for the Atmospheric Scenario is orders of magnitude greater than the total canyon population, the collective dose for the latter is larger. The costs associated with the projected doses are low compared to the costs associated with implementing the three closure alternatives (Table 4-21). For example, the health detriment costs for the Base-Case Scenario are about 0.01 percent of the total implementation cost for the All Pathways–Canyon Scenario.

The costs associated with the Base-Case Scenario and the Biobarrier Option are essentially the same, reflecting the small cost of installing a biobarrier during facility closure. The mean cost of the Extended Control Option is significantly higher than the others because of the expense of continued active maintenance of the site.

The results shown in Table 4-20 indicate that the collective doses projected for the Atmospheric and All Pathways–Canyon Scenarios are very low. For the three closure strategies examined here, these doses are ALARA insofar as the implementation costs of these strategies far exceed the costs associated with the health detriments (Table 4-21). This conclusion is consistent with the guidance offered by the DOE on ALARA analyses (DOE, 1997).

The fact that the total cost of the Base-Case Scenario closure strategy is dominated by implementation expenses suggests that an evaluation of more cost-effective ways of closing the disposal facility may be in order. That is, from an ALARA standpoint, the development of less expensive strategies may be appropriate if the collective health impacts from such strategies are not substantially greater than those estimated here. Any such strategy will, of course, need to comply with all individual dose limits, no matter what the cost.

The ALARA analysis performed here was conducted using an integration period of 300 years and did not discount costs or consider the probability of scenarios occurring far in the future. Although different sets of assumptions regarding these aspects of the analysis would yield different results, the costs associated with health detriment are expected to remain a small proportion of the total closure strategy cost. Furthermore, the relative cost-effectiveness of the three strategies is not expected to change. Finally, the same general trends noted here are expected to apply if the performance assessment inventory is substituted for the composite analysis inventory used in the ALARA analysis.

5.0 Inadvertent Intruder Analysis

The DOE is assumed to retain control over the entire Laboratory throughout the operational, closure, and active institutional control periods. As discussed in Section 2, it is assumed that members of the public will be prevented from entering the disposal facility during this time. Although control over the entire Laboratory is assumed to cease at the end of the active institutional control period, it is expected that the DOE will continue to exercise administrative control over individual sites such as Area G. It is generally expected that all persons will be excluded from the site during the passive institutional control period; however, it is conceivable that a temporary lapse in control could provide an opportunity for persons to arrive at the disposal site and inadvertently intrude into the disposed waste. It is on this basis that the inadvertent intruder analysis is conducted.

The intruder analysis estimates the exposures that may be received by inadvertent intruders from the waste disposed of in pits from September 27, 1988 through 2010 and from 2011 through 2044, and material placed in shafts from September 27, 1988 through 2015 and from 2016 through 2044. The primary objective of the analysis, however, is to establish WAC for the safe disposal of waste at MDA G, the portion of the facility currently receiving waste.

The exposure scenarios upon which the inadvertent intruder analysis is based are discussed in Section 5.1; a general discussion of the modeling approach is provided in Section 5.2. The results of the intruder analysis are presented in Section 5.3, followed by a discussion of the uncertainties associated with these projections in Section 5.4.

5.1 Exposure Scenarios

Five intruder exposure scenarios were evaluated for inclusion in the intruder dose assessment; these are summarized in Table 5-1. This table briefly discusses the activities that are assumed to occur, lists the period of time each intruder is exposed to radioactivity, and summarizes the potential routes of exposure. These exposure scenarios are the same as those evaluated for the 1997 Area G performance assessment and generally resemble those used by the NRC in support of 10 CFR Part 61 (NRC, 1986).

The Intruder-Construction and Intruder-Agriculture Scenarios are based on the assumption that an individual arrives at Area G and decides to establish a residence over one or more of the closed disposal units. The house includes a full basement, which extends to a depth of 3 m 9.8 ft) bgs. Any waste brought to the surface during basement excavation is spread over the homeowner's lot. The Intruder-Construction Scenario projects exposures received by the builder during construction, while the Intruder-Agriculture Scenario estimates the doses for a person living in the completed house.

Table 5-1
Inadvertent Intruder Exposure Scenarios Evaluated for Inclusion in the Area G Intruder Assessment

Exposure Scenario	Scenario Description	Period of Exposure (hr/yr)	Exposure Routes
Intruder-Construction	An individual arrives at the disposal site and constructs a house over the closed disposal units. Radioactivity brought to the surface during basement excavation is spread over the house lot.	500	• Inhalation of airborne radionuclides • Ingestion of contaminated soils • Direct radiation from airborne contaminants, contaminated soils, and buried waste
Intruder-Agriculture	The intruder resides in a house constructed over the closed disposal units. The person works away from the house during the day and spends some spare time raising crops and animals to provide foodstuffs for personal consumption. Crops and forage crops for animals are grown in contamination brought to the surface during basement excavation.	7,100 [a]	• Ingestion of contaminated crops, animal products (e.g., milk and beef or chicken and eggs), and soil • Inhalation of airborne contaminants • Direct radiation from airborne radionuclides, contaminated soils, and buried waste
Intruder–Post-Drilling	An individual resides in a house constructed over the closed disposal units. The person works away from the house during the day and spends some spare time raising crops and animals to provide foodstuffs for personal consumption. Crops and forage crops for animals are grown in contamination brought to the surface during well drilling.	7,100 [a]	• Ingestion of contaminated crops, animal products (e.g., milk and beef or chicken and eggs), and soil • Inhalation of airborne contaminants • Direct radiation from airborne radionuclides, contaminated soils, and buried waste
Intruder-Drilling	A local well driller is contracted to drill a well through the closed disposal units. Radioactivity brought to the surface with the drill cuttings is spread over a limited area around the drill rig.	100 or less [b]	• Inhalation of airborne radionuclides • Ingestion of contaminated soils • Direct radiation from air immersion and contaminated drill cuttings
Intruder-Discovery	An individual arrives at the disposal site to construct a house. The person encounters an intact barrier, stabilized waste, or a waste package in the course of excavating a basement; determines that the site was used for radioactive waste disposal; and abandons all efforts.	6	• Inhalation of airborne radionuclides • Ingestion of contaminated soils • Direct radiation from airborne contaminants, contaminated soils, and waste

[a] *A distribution of exposure times is used in the intruder analysis; the value listed is approximately equal to the sum of the mean indoor and outdoor exposure times.*

[b] *The time required to drill the well is specific to the area geology and depth of the well.*

The homebuilder may be exposed to contamination through several exposure routes. Contaminated soils suspended during construction may be inhaled by the worker; vapor- and gas-phase radionuclides diffusing upward from the waste may also be inhaled. The individual is assumed to inadvertently ingest contaminated soils during the construction process. Finally, the worker is subject to direct radiation from airborne radionuclides, the waste excavated during construction, and the waste that remains buried in the pits and shafts. The magnitude of the exposures received will depend, in part, on the length of time the receptor spends in the excavation, on the surface of the disposal site, and inside the house.

Several exposure routes may contribute to the doses received by the agricultural intruder. Radionuclides suspended from the surface of the intruder's lot and contaminants diffusing from the surface of the site or into the receptor's home may result in inhalation exposures. The individual is assumed to raise vegetable crops for home consumption, and to raise forage crops for animals that supply the household with beef and milk or chicken and eggs. The dose received by the intake of contaminated soil will add to the ingestion exposure. Finally, the intruder is subject to direct radiation from the contaminated soils spread over his or her lot, from the buried waste, and from airborne radionuclides.

The Intruder–Post-Drilling Scenario also considers the exposures received by a person who lives in a house built over the disposal facility. Unlike the agricultural intruder scenario, however, the house is assumed to be built at grade on a concrete slab, rather than on a full foundation. While this construction technique avoids the excavation of disposed waste, it is assumed that contamination is brought to the surface in the course of drilling a well for domestic use. This contamination is assumed to be spread over the homeowner's lot. Routes of exposure for this intruder are the same as those outlined above for the Intruder-Agriculture Scenario.

The Intruder-Drilling Scenario evaluates the potential exposures received by a member of the crew responsible for drilling a domestic well through the closed disposal units. Contaminated cuttings brought to the surface during drilling may result in exposures to the crew. The Intruder-Discovery Scenario represents an aborted attempt to build a house over the closed disposal units. For this scenario, it is assumed that an individual arrives at the site to begin construction, but abandons efforts when stabilized waste or a waste package is encountered.

The routes through which members of a drilling crew or a prospective homebuilder may be exposed to radiation are limited to the inhalation of airborne radionuclides (i.e., suspended particulates, vapors, and gases), the incidental ingestion of contaminated soil or waste, and direct radiation from the air and contaminated soil or waste. The exposures received by the drilling crew member may be moderated because of the high moisture content of the drill cuttings. The moisture may reduce the rate at which radionuclides are resuspended and thereby limit driller exposure from inhalation, air immersion, and possibly soil ingestion.

The intruder scenario with the greatest risk for high doses will result in the most restrictive radionuclide concentration limits. Although all the scenarios listed in Table 5-1 could be included in the intruder assessment, it is more efficient to eliminate scenarios that clearly do not result in significant exposures. Toward this end, the intruder scenarios were evaluated in terms of their expected impact, and the scenarios expected to yield the greatest potential doses were identified.

The magnitude of the exposure received by an intruder is a function of the period of exposure to the contaminated media, the radionuclide concentrations in these media, and the extent to which the individual uses the contaminated resources. The two scenarios for residents—the Intruder–Post-Drilling and Intruder-Agriculture Scenarios—assume the same period of exposure for the receptors. The homebuilder in the Intruder-Construction Scenario is assumed to be exposed to contamination for a significantly longer period of time than the receptors for the Intruder-Discovery and Intruder-Drilling Scenarios. However, the times of exposure for all three of these intruders are much smaller than those associated with the resident intruder scenarios.

The two resident intruder scenarios differ in terms of the radionuclide concentrations in the media contacted by the individuals. If the depth of the basement excavation exceeds the thickness of the cover placed over the waste, the quantities of waste brought to the surface during basement excavation will generally exceed those brought to the surface with drill cuttings. Under these conditions, the agricultural intruder will be exposed to higher radionuclide concentrations in surface soils. If, however, the thickness of the cover at the time of intrusion is greater than the assumed basement depth of 3 m (10 ft), no waste will be brought to the surface during construction of the agricultural intruder's house. Under these conditions, radionuclide concentrations in surface soils will be greater for the postdrilling intruder. Concentrations of vapor- and gas-phase radionuclides in the agricultural intruder's house may be greater than those projected for the postdrilling intruder because the distance these contaminants must diffuse before entering the house is shorter.

The radionuclide concentrations encountered by the homebuilder, the intruder who abandons construction when waste is encountered, and members of the drilling crew may be greater than those encountered by the resident intruders, at least for a portion of the exposure time. The homebuilder may come into contact with undiluted waste during the time spent in the basement excavation if the depth of the basement excavation exceeds the cover depth; contaminant concentrations during the time spent on the surface are assumed to be the same as those used to model exposures for the agricultural intruder. The receptor for the Intruder-Discovery Scenario may contact the waste during exploratory activities, while the drilling crew will come in contact with undiluted waste.

The resource utilization patterns are identical for the agricultural and postdrilling intruder scenarios. Rates of resource utilization for both of these receptors are higher than the rates corresponding to the homebuilder, the person who abandons construction efforts, and the well driller.

When the concentrations of radioactivity encountered, the periods of exposure, and the level of resource utilization are taken into consideration, potential exposures are expected to be greatest for the agricultural intruder in those cases where the excavated basement intersects the waste. Consequently, this scenario was included in the intruder analysis. The period of time the construction worker is exposed to contamination is much shorter than the agricultural intruder's exposure period; however, it was not clear whether closer contact with the waste, during the time spent in the basement excavation, might result in higher exposures of the homebuilder in some situations. Thus, the Intruder-Construction Scenario was also included in the intruder assessment.

From all appearances, the exposures received by the postdrilling intruder should be significantly smaller than those estimated for the agricultural intruder, and possibly less than those estimated for the construction worker. However, if the waste remains undisturbed by the construction of the agricultural intruder's house, potential exposures will be greater for the postdrilling intruder than for the agricultural intruder. The Intruder–Post-Drilling Scenario was also included in the inadvertent intruder analysis because neither the Intruder-Agriculture nor Intruder-Construction Scenarios adequately address the potential risk posed by waste disposed of at depth.

The Intruder-Discovery and Intruder-Drilling Scenarios were excluded from the intruder analysis. The receptor for the discovery scenario has the shortest exposure time of all the intruders and will contact contaminant concentrations similar to those encountered by the construction worker during basement excavation. Since the potential exposures will be greater for the construction worker (and will lead to more restrictive WAC), the Intruder-Discovery Scenario was not evaluated.

The radionuclide concentrations to which members of the drilling crew may be exposed will probably be greater than those encountered by the postdrilling resident. However, because the maximum exposure time for the well driller is about 3 percent of the exposure time for the postdrilling intruder, the driller is expected to receive much smaller exposures than the postdrilling intruder. In addition, the saturated nature of the drill cuttings will tend to minimize the potential for exposure of the crew. On this basis, then, the Intruder-Drilling Scenario was excluded from the intruder analysis.

The time at which a particular intruder scenario occurs may have significant effects on the projected doses. In general, intrusion into the waste is considered feasible at any time following the 100-year active institutional control period as long as the waste has decomposed sufficiently to resemble ordinary soil and no barriers to intrusion are present. If the intruder encounters intact

waste packages, stabilized waste (e.g., grout), or engineered barriers (e.g., concrete caps on disposal shafts), it was assumed that the person would stop all intrusive activities and leave the site.

It was assumed that, beyond the 100-year active institutional control period, conditions will not prevent intrusion into the disposal pits and shafts. The waste disposed of at Area G generally consists of routine operational waste and bulk material generated from remediation and decommissioning efforts at the Laboratory; operational waste destined for the pits has been placed in metal containers since the mid-1990s, and almost all waste placed in shafts since 1988 has been containerized. No impediments to intrusion into the bulk waste exist. While intact, the metal containers used in the disposal of routine operational waste may resist intrusion attempts, but their actual lifetimes under the disposal conditions at Area G are not known. Consequently, it was assumed that these containers do not limit the potential for intrusion into the waste. In terms of waste form, metals and stabilized waste may be recognizable after 100 years of burial. Once again, however, the rate at which these materials will degrade to forms that are indistinguishable from the remainder of the material in the disposal units is unknown. Lacking this information, it was conservatively assumed that these waste forms will not prevent intrusion. The other forms of waste disposed of in the pits and shafts (e.g., cellulosics, sludges, animal tissues, and filters) may be totally unrecognizable as waste within 100 years of closure of the disposal facility. Intrusion into the disposal pits and shafts was not assumed to be limited by the presence of engineered barriers because no such features are included in the facility's final closure configuration.

As discussed earlier, the basis for projecting intruder exposures and establishing intruder-based WAC is that the DOE may experience a temporary lapse in control that allows persons to arrive at the disposal site and inadvertently intrude into the disposed waste. The period of time that hypothetical intruders occupy the site must be established in order to compare the projected exposures to the appropriate intruder performance objectives and to calculate radionuclide concentration limits. The NRC defines acute exposure events as those that occur for less than 1 year (NRC, 1986). On this basis, then, the Intruder-Construction Scenario constitutes an acute exposure, and is subject to the acute intruder dose limit of 500 mrem/yr. Although it is unclear how long a temporary lapse in the DOE's control over the site may last, it was assumed that the resident intruders will occupy the site for a year or more. Consequently, these scenarios constitute chronic exposures that are subject to the chronic intruder performance objective of 100 mrem/yr.

The intruder exposure scenarios used to develop WAC should be placed in proper perspective with respect to current land use patterns and the need to demonstrate compliance with DOE performance objectives. The exposure scenarios were selected to provide reasonably conservative estimates of the potential exposures that may result from the waste disposed of at Area G in the event that DOE control over the facility lapses for a brief period of time. To the extent that the scenarios represent more intensive use of potentially contaminated resources than

might actually occur, the calculated doses are expected to provide additional assurance that the disposal system will perform at least as well as projected.

5.2 Modeling Approach and Input Data

Two models developed using the GoldSim modeling environment or platform (GoldSim, 2007a, 2007b, and 2007c) were used to evaluate the risks posed by Area G to inadvertent intruders. The Area G Intruder Model was used to project doses and estimate intruder-based WAC for all radionuclides except vapor- and gas-phase isotopes and some parent radionuclides that decay to form such. The Area G Intruder Diffusion Model projects doses and estimates WAC for radionuclides whose impacts are affected by diffusive release and transport. A third model, the Area G Inventory Model, was used to estimate the initial radionuclide inventories that are used to conduct the intruder analysis. The intruder and intruder diffusion models resemble the site model in many aspects; primary differences relate to modeling the impacts of human intrusion into the buried waste and the diffusion of vapor- and gas-phase radionuclides into the basement excavation and resident intruder's house. A complete description of the intruder models and the data used to implement them is provided in *Appendix K*.

The intruder analysis considers four subsets of the performance assessment inventory, including the waste disposed of in pits from September 27, 1988 through 2010 and from 2011 through 2044, and the waste disposed of in shafts from September 27, 1988 through 2015 and from 2016 through 2044. The waste placed in pits and shafts through 2010 and 2015, respectively, is assumed to be placed in units located in MDA G; waste disposed of after these dates will be placed in the Zone 4 expansion area. The disposal units in these areas are physically separated; dividing the inventory into these segments allows consideration of the exposures that may occur for each set of units. Modeling subsets of the inventory also facilitates the development of WAC specific to MDA G.

The inventories in the disposal pits were assumed to be uniformly distributed throughout the units for the intruder analysis; the same approach was adopted for the shafts that are projected to receive waste from 2016 through 2044. Preliminary modeling indicated that the projected exposures for the 1988–2015 shafts under the agricultural intruder scenario would be approximately equal to or greater than the 100 mrem/yr chronic dose objective if the radionuclides in the waste were homogeneously mixed throughout the disposal units. Consequently, the depth at which critical radionuclides were disposed of within these units was evaluated to ensure that the projected inventory for these units has been, and will be, disposed of in a safe manner. The approach used to conduct the depth-of-disposal evaluation is described in *Appendix K* (Volume 3); the results of the analysis were used to model the exposures that may result from intrusion into the 1988–2015 shafts.

The disposal facility is assumed to function in the manner projected by the site model prior to the arrival of the intruder. Releases of radionuclides will occur as a result of plants and animals penetrating into the waste, contaminant leaching by water passing through the pits and shafts, and vapor- and gas-phase radionuclides diffusing upward from the waste. Contamination deposited on, or diffusing from, the surface of the facility will be transported to off-site locations with the prevailing winds, and into Cañada del Buey and Pajarito Canyon with surface runoff. Radionuclides released and transported via these processes will affect the amounts of contamination brought to the surface by the intruder and contaminant concentrations in the surface soils to which the intruder is exposed.

With one exception, the rates of release via the mechanisms outlined above were assumed to be unaffected by the presence of waste containers or the form of the waste (e.g., activated metals or other bulk-contaminated media). This approach overlooks the fact that intact containers may limit contact between the waste and plants, animals, and infiltrating water, and may slow the release of vapor- or gas-phase radionuclides. The potential impact of container performance on vapor-phase tritium releases was investigated as part of the intruder analysis for the disposal shafts. The containers used to dispose of high-activity tritium waste in these units are subject to WAC that prescribe maximum off-gas rates (LANL, 2008b); exposures for the intruders were evaluated taking these release limits into account.

The amount of contaminated material brought to the surface of the disposal facility as a result of human intrusion depends upon the intruder scenario under consideration and the thickness of the cover at the time of intrusion. The Intruder-Construction and Intruder-Agriculture Scenarios are based on the assumption that a 10×20 m (33×66 ft) basement is excavated to a depth of 3 m (9.8 ft) below the surface of the disposal facility; a 1:1 slope is assumed for all walls of the excavation. Excavation of the basement will transport waste to the surface of the facility only if the depth of the basement exceeds the cover thickness. However, contaminants present in the cover due to the effects of biotic intrusion and the diffusion of vapor- and gas-phase radionuclides from the waste may be transported to the surface even if the cover thickness exceeds the depth of the basement. Establishment of a domestic well at the site brings waste to the surface regardless of the cover depth.

The material deposited on the surface during basement excavation is assumed to be thoroughly mixed. Approximately one-third of the total is used to backfill around the perimeter of the foundation of the house. The remainder is spread uniformly across the intruder's 2,300 m^2 (0.6 ac) lot, less the area occupied by a 10×20 m (33×66 ft) house. No mixing of this material in the existing surface soils is assumed to occur.

The amount of material excavated during well drilling is calculated as the product of the well diameter and the depth to the bottom of the waste disposal units. The well will also pass through

the strata that lie between the bottom of the disposal units and the regional aquifer. While this material will also be brought to the surface, it is ignored in terms of determining radionuclide concentrations in the surface soils to which the intruder is exposed. All contamination brought to the surface is assumed to be spread over the intruder's 2,300 m^2 (0.6 ac) lot, less the area occupied by the house; contamination is assumed to be mixed to a depth of 15 cm (6 in.).

The exposures projected for the inadvertent intruders are influenced by the location of the pits and shafts within the disposal facility. This is due, in large part, to variations in the amount of cover placed over the site at the time of final closure and the spatial variability in the rates of erosion across the site. These factors ultimately determine how much cover exists over the disposal units at the time of human intrusion and, therefore, how much of the waste is disturbed by the intrusive activities.

The waste disposed of in pits since 1988 has been placed in units 15, 30, 31, and 36 through 39; these units are located in waste disposal regions 3, 4, and 5 (Figure 3-2, Section 3). Waste placed in pits through 2010 is expected to be disposed of in MDA G; for modeling purposes, this waste was assumed to be placed in pit 38. The intruder analysis for the 1988–2010 waste was conducted using the initial cover thicknesses and erosion rates estimated for the specific pits in which the waste was placed. Waste disposed of in pits from 2011 through 2044 is expected to be placed in the Zone 4 expansion area; the cover and erosion characteristics of waste disposal region 8 were used to model intruder exposures for this waste.

Waste disposed of in shafts since 1988 has been placed in units located in disposal region 6 (Figure 3-2, Section 3), near the east end of the facility, and in region 7, in the center of MDA G; most waste has been placed in shafts located in disposal region 7. Shaft waste disposal is expected to continue in MDA G through 2015; waste disposed of from 2016 through 2044 will be placed in Zone 4. The cover thicknesses and erosion rates projected for waste disposal region 7 formed the basis of the intruder modeling for the 1988–2015 shaft waste; the Zone 4 cover and erosion characteristics were used to evaluate the 2016 through 2044 waste.

Preliminary modeling was conducted to determine if the redistribution of radionuclides resulting from radon diffusion had any impacts on the exposures estimated for the three intruder scenarios. A series of 50-realization probabilistic simulations was conducted in which intruder doses were calculated with and without the effects of radon diffusion; all four subsets of the performance assessment inventory were addressed. The results of this modeling were used to configure the full probabilistic assessment of intruder doses.

The intruder and intruder diffusion models were used to calculate WAC for all radionuclides that were encountered in the development of the performance assessment inventory, except for those eliminated on the basis of half-life. This modeling yielded distributions of radionuclide-specific doses for the disposal units under consideration; using those results, the corresponding WAC

were calculated. The final concentration limits adopted for the disposal units represent the means or medians of the distributions corresponding to the most restrictive exposure conditions.

5.3 Intruder Analysis Results

The results of the inadvertent intruder analysis are discussed below. Section 5.3.1 presents the exposures projected for the different subsets of the performance assessment inventory. The intruder-based WAC calculated using the intruder and intruder diffusion models are provided in Section 5.3.2.

5.3.1 Exposure Projections

As discussed above, preliminary modeling was conducted to determine the need for considering the effects of radon diffusion when estimating the total intruder exposures from the different subsets of waste. The results of this analysis are summarized in Table 5-2, which shows projected exposures for selected radionuclides that eventually decay to form Rn-220 or Rn-222. Two sets of results are provided—one that includes the effects of diffusion and one that excludes these effects. The table shows the peak mean exposures projected for each radionuclide, assuming intrusion occurs at the end of the 100-year active institutional control period.

The results shown in Table 5-2 indicate that the diffusion of Rn-220 has little or no effect on the doses projected for its longer-lived parents (i.e., Th-232, Ra-228, and Th-228); projected doses are the same whether or not diffusion is included. These results are not surprising because Rn-220 is very short-lived and decays to form very short-lived daughters.

In contrast, the effects of radon diffusion on intruder exposures are apparent for some radionuclides that decay to form Rn-222. For example, depending upon the disposal units and intruder scenario under consideration, the peak mean Ra-226 dose estimated for the agricultural intruder increases by a factor of 1.1 to 14 when the effects of radon diffusion are included. The peak mean exposures projected for Th-230 tend to be affected by diffusion in a similar fashion as Ra-226, but these effects are negligible from the perspective of overall intruder exposures because the projected doses from this radionuclide are small. The projected exposures for U-234 are little affected by radon diffusion. Based on these results, the intruder exposures for tritium, C-14, Kr-85, and Ra-226 were projected using the intruder diffusion model, while doses for all remaining radionuclides were modeled using the intruder model.

The projected dose distributions for the Intruder-Construction, Intruder-Agriculture, and Intruder–Post-Drilling exposure scenarios are summarized in Table 5-3; exposures are provided for each subset of the performance assessment inventory discussed earlier. The distributional information shown in the table includes the mean, fifth percentile, and ninety-fifth percentile exposures; results for nondiffusive contaminants and radionuclides whose impacts are influenced by the effects of diffusion (i.e., tritium, C-14, Kr-85, and Ra-226) are provided for each exposure scenario.

Table 5-2
Comparison of Intruder Dose Projections with and without the Effects of Radon Diffusion

Parent Radionuclide by Exposure Scenario	Peak Mean Dose (mrem/yr)							
	Diffusive Effects Included				Diffusive Effects Excluded			
	1988–2010 Pits	2011–2044 Pits	1988–2015 Shafts	2016–2044 Shafts	1988–2010 Pits	2011–2044 Pits	1988–2015 Shafts	2016–2044 Shafts
Postdrilling Intruder								
U-234	6.7E-04	8.5E-04	3.7E-02	4.8E-02	6.6E-04	8.5E-04	3.7E-02	4.8E-02
Th-230	1.6E-05	1.6E-06	4.9E-09	---	2.3E-06	3.2E-07	3.9E-09	---
Ra-226	5.4E-02	2.4E-02	2.6E+00	3.9E-04	4.0E-03	2.6E-03	2.0E+00	2.3E-04
Th-232	4.2E-03	5.9E-05	4.1E-01	1.2E-01	4.2E-03	5.9E-05	4.1E-01	1.2E-01
Ra-228	2.4E-11	6.8E-10	---	---	2.4E-11	6.8E-10	---	---
Th-228	9.2E-23	1.1E-22	1.5E-20	3.8E-20	9.2E-23	1.1E-22	1.5E-20	3.8E-20
Agricultural Intruder								
U-234	8.2E-04	2.5E-04	7.7E-02	8.1E-01	8.1E-04	2.5E-04	7.6E-02	8.1E-01
Th-230	1.8E-04	1.0E-05	6.4E-08	---	1.5E-04	9.1E-06	5.3E-08	---
Ra-226	5.3E-01	1.9E-01	7.0E-01	1.8E-02	4.9E-01	1.7E-01	4.0E-01	1.6E-02
Th-232	6.5E-01	7.0E-03	8.0E+01	1.5E+01	6.5E-01	7.0E-03	8.0E+01	1.5E+01
Ra-228	7.5E-09	5.4E-08	---	---	7.5E-09	5.4E-08	---	---
Th-228	3.0E-20	8.7E-21	5.7E-19	7.3E-18	3.0E-20	8.7E-21	5.7E-19	7.3E-18
Construction Intruder								
U-234	6.3E-04	6.4E-04	3.6E-02	1.8E-01	6.3E-04	6.4E-04	3.6E-02	1.8E-01
Th-230	7.0E-06	8.6E-07	7.5E-09	---	4.6E-06	5.7E-07	6.7E-09	---
Ra-226	2.1E-02	1.1E-02	4.7E-01	9.0E-04	1.3E-02	7.7E-03	3.3E-02	7.7E-04
Th-232	1.8E-02	3.2E-04	5.7E+00	7.6E-01	1.8E-02	3.2E-04	5.7E+00	7.6E-01
Ra-228	1.9E-10	2.0E-09	---	---	1.9E-10	2.0E-09	---	---
Th-228	7.6E-22	3.4E-22	2.9E-20	3.2E-19	7.6E-22	3.4E-22	2.9E-20	3.2E-19

--- = Radionuclide was not included in the inventory.

Table 5-3
Probabilistic Doses for the Inadvertent Intruder Exposure Scenarios

Disposal Units	Exposure Scenario	Projected Dose (mrem/yr)					
		Mean		5th Percentile		95th Percentile	
		Nondiffusive Radionuclides	Diffusive Radionuclides	Nondiffusive Radionuclides	Diffusive Radionuclides	Nondiffusive Radionuclides	Diffusive Radionuclides
1988–2010 Pits	Construction	4.9E-01	4.0E-02	1.5E-09	5.6E-04	2.6E+00	1.7E-01
	Agriculture	3.7E+00	4.7E-01	1.5E-05	3.4E-03	2.1E+01	3.5E+00
	Postdrilling	3.3E+00	2.5E-01	1.8E-01	4.8E-03	1.2E+01	1.1E+00
2011–2044 Pits	Construction	2.1E-02	6.9E-03	3.5E-12	1.3E-04	2.7E-02	2.7E-02
	Agriculture	3.6E-01	9.7E-02	2.1E-10	8.8E-04	1.4E+00	2.3E-01
	Postdrilling	6.0E-01	9.2E-02	8.7E-02	1.7E-03	1.5E+00	2.4E-01
1988–2015 Shafts	Construction	4.5E+00	5.2E-01	5.0E-17	1.1E-02	3.0E+01	2.1E+00
	Agriculture	8.4E+01	5.8E+00	1.4E-15	3.0E-01	5.5E+02	1.9E+01
	Postdrilling	6.4E+00	4.5E+00	1.7E+00	1.5E+00	1.8E+01	9.6E+00
2016–2044 Shafts	Construction	1.5E+00	9.7E-01	6.4E-04	1.9E-01	5.2E+00	2.3E+00
	Agriculture	2.6E+01	2.3E+01	3.7E-02	5.9E+00	8.6E+01	5.6E+01
	Postdrilling	4.3E-01	2.7E+00	1.3E-01	1.2E+00	1.0E+00	4.8E+00

The peak mean doses for the 1988–2010 disposal pits range from 0.49 to 3.7 mrem/yr for the radionuclides that are unaffected by diffusive releases; the exposures projected for H-3, C-14, Kr-85, and Ra-226 range from 0.04 to 0.47 mrem/yr. The corresponding ranges for the 2011–2044 pits are 0.021 to 0.60 mrem/yr and 0.0069 to 0.097 mrem/yr. The radionuclides making significant contributions to the doses projected for the three receptors include Cl-36, K-40, Pu-239, Ra-226, Tc-99, and U-238, depending upon the disposal units and exposure scenario under consideration. The exposures projected for the agricultural and postdrilling intruders are largely the result of the ingestion of contaminated crops and animal products and direct radiation from contaminated soils; the exposures for the homebuilder result primarily from the ingestion of soil, inhalation, and direct radiation from contaminated soils.

The exposures projected for the disposal pits under the three intruder scenarios are of a similar magnitude, despite the fact that excavation of the basement brings significantly more material to the surface than does well drilling. This is because of the thickness of the cover placed over the disposal units relative to the depth of disturbance associated with the different intruder scenarios. The initial cover thickness over the 1988–2010 disposal pits ranges from 2.5 to 6 m (8.2 to 19.6 ft) and has a median value of 4.2 m (13.7 ft); the initial cover thickness is greater than 3 m (9.8 ft) for 92 percent of the nodes used to represent the pits. Setting aside the effects of surface erosion for a moment, this means that in more than 90 percent of the model realizations the waste is undisturbed by the excavation of a 3 m (9.8 ft) basement and no contamination is brought to the surface as a result of human activities. A similar set of circumstances is seen for the 2011–2044 pits; the initial cover thickness over these units is less than 3 m (9.8 ft) in only 2 percent of the model realizations. In contrast, drilling a well through the pits brings contamination to the surface of the facility in all model realizations.

Projected exposures change over time in response to the decay of shorter-lived radionuclides, continued penetration into the waste by plants and animals inhabiting the site, and thinning of the cover due to erosion. In terms of the 1988–2010 pits, the peak mean exposures projected for the construction, agricultural, and postdrilling scenarios occur 100, 740, and 620 years after facility closure. The peak exposures for all three scenarios occur at the end of the 1,000-year compliance period for the 2011–2044 disposal pits.

The agricultural intruder doses shown in Table 5-3 for waste disposed of in pits from 1988 through 2010 and from 2011 through 2044 are less than the exposures projected for the historical and future pits in conjunction with the 1997 performance assessment (Hollis et al., 1997). The 1997 analysis projected peak agricultural intruder doses of about 30 mrem/yr for both the 1988–1995 and 1996–2044 pits. Several differences exist between the earlier, deterministic modeling and the current intruder dose assessment; however, the decrease in the projected exposures for the agricultural intruder is primarily a reflection of the placement of additional cover over the

disposal units. The 1997 assessment included 1 to 2 m (3.3 to 6.6 ft) of cover over the pits; 2.5 m (8.2 ft) or more exists over the 1988–2010 and 2011–2044 pits, as modeled here.

The 1997 performance assessment did not estimate the exposures received by the construction and postdrilling intruders following disturbance of the disposal pits. Dose projections for the postdrilling scenario were, however, estimated by Shuman (1999). The peak mean dose projected for the postdrilling intruder living over the 2005–2044 pits is greater than the dose of 0.3 mrem/yr projected for the 1996–2044 pits by Shuman. This increase is due to differences in the models and data used in the two analyses.

The peak mean exposures calculated for the waste disposed of in shafts from 1988 through 2015 range from 4.5 to 84 mrem/yr for radionuclides that are unaffected by diffusion and 0.52 to 5.8 mrem/yr for H-3, C-14, Kr-85, and Ra-226. Total peak mean doses representing the sum of these results range from 5.1 to 89 mrem/yr. Th-232 accounts for 92 and 87 percent of the peak mean doses for the construction and agricultural intruders, respectively; Ra-226 is the other major contributor to the projected exposures for these intruders. Important radionuclides for the postdrilling scenario include Ag-108m, C-14, Cs-137, H-3, Ni-63, Ra-226, and Sr-90; these isotopes account for almost 95 percent of the peak exposure. The ingestion of crops and animal products, and direct radiation from contaminated soils are the exposure pathways that contribute most to the postdrilling intruder dose; the ingestion of crops and direct radiation from contaminated soils are the major contributors to the projected agricultural intruder dose. Inhalation, the ingestion of contaminated soils, and direct radiation are the pathways making the largest contributions to the peak mean dose for the construction worker.

The peak mean exposures projected for the waste disposed of in shafts from 2016 through 2044 range from 0.43 to 26 mrem/yr for radionuclides that are unaffected by diffusion and from 0.97 to 23 mrem/yr for tritium, C-14, Kr-85, and Ra-226; summing these results yields total peak mean doses of 2.5 to 49 mrem/yr. Tritium accounts for 39 to 86 percent of the peak mean doses projected for the three intruder scenarios; the sum of the exposures estimated for Sr-90 and Th-232 account for 9 and 43 percent of the postdrilling and agricultural doses, respectively; Cs-137, Th-232, U-234, and U-238 account for 57 percent of the construction intruder's peak dose. Inhalation of tritium, and the ingestion of crops and animal products are the major exposure pathways for the postdrilling intruder; the same pathways plus direct radiation from contaminated soils play a major role in the exposures estimated for the agricultural intruder. The inhalation of resuspended soil and tritium, direct radiation from contaminated soils, and ingestion of soil all make significant contributions to the peak mean dose projected for the construction intruder.

The dose projections provided in Table 5-3 for the 1988–2015 and 2016–2044 shafts take into account the packaging requirements for containers of high-activity tritium waste. Waste acceptance criteria for tritium disposal at Area G impose off-gas limits on the containers used to

dispose of the waste (LANL, 2008b). For waste packages with a tritium concentration of 10 Ci/m^3 of waste to 500 Ci per package, the stainless steel containers in which the waste is placed must limit the annual off-gas rate to 0.01/yr or less; containers with 500 to 100,000 Ci of tritium per package must meet an off-gas requirement of no more than 1×10^{-4}/yr. Based on these requirements, the effects of limiting off-gas rates to 0.01/yr were simulated in the modeling for the 1988–2015 and 2016–2044 shafts.

The use of the higher of the two off-gas rates is expected to yield conservative results in terms of the overall release of tritium. That is because most of the high-activity tritium waste packages disposed of to date have contained more than 500 Ci of the isotope, making them subject to the more restrictive off-gas limits. For example, about 96 percent of the tritium waste activity disposed of in shafts from September 27, 1988 through 2007 was packaged in containers that contained at least 500 Ci. It is anticipated that a similar pattern of disposal will occur in the future.

The magnitude of the tritium container off-gas rate has a significant impact on the doses projected for the 2016–2044 disposal shafts. Tritium contributes about 47 percent (23 mrem) to the peak annual dose (49 mrem) calculated for these units under the agricultural intruder scenario when an off-gas rate of 0.01/yr is assumed. If this rate is decreased to 0.0001/yr, the peak mean tritium dose drops to less than 0.5 mrem/yr. On this basis alone, the peak mean dose for the scenario declines approximately 50 percent if the more restrictive off-gas rate is applied. Tritium did not make a significant contribution to the peak mean dose calculated for the 1988–2015 shafts under the agricultural intruder scenario. Therefore, the off-gas rate used in the modeling is less important for these disposal units.

The projected doses for the disposal shafts are significantly higher than those estimated for the pits. This is because higher activity waste has been placed in the shafts and because the average cover thickness over the shafts is less than that of the pits.

The agricultural intruder doses projected for the waste disposed of in shafts are substantially higher than those estimated in conjunction with the 1997 performance assessment. In the earlier assessment, a peak dose of 22 mrem/yr was estimated for the disposal units that were active from 1988 through 1995. This is about 24 percent of the total dose determined by the GoldSim modeling for the 1988–2015 shafts. Much of the reason these estimates differ is because of the Th-232 inventories used in the two analyses. The 1997 modeling was based on a Th-232 inventory of 4.1×10^{-4} Ci, which was assumed to be distributed uniformly throughout the disposal shafts. In contrast, the current intruder analysis uses a mean Th-232 inventory of 0.74 Ci and assumes that more than half of the inventory is in the upper 1.5 m (4.9 ft) of the waste profile. As a result, higher concentrations of Th-232 are brought to the surface during basement excavation, leading to higher exposures for the receptor.

The peak agricultural intruder dose projected for waste disposed of in the 2016–2044 shafts is about 4 times greater than the peak dose of 12 mrem/yr that was estimated in 1997 for waste disposed of from 1996 through 2044. Part of the difference in these doses stems from different assumptions about when intrusion might occur: the 1997 modeling assumed that concrete caps placed over the disposal shafts would prevent intrusion into the waste for 300 years after facility closure, but the current assessment assumes intrusion could take place any time after the 100-year active institutional control period ends. The extra 200-year delay in intrusion assumed for the 1997 modeling allows for additional decay; if this delay had been assumed in the current modeling it would have decreased the peak mean dose for the agricultural intruder by about 57 percent. Other factors that contribute to the disparity between the two modeling efforts include differences in the radionuclide inventories used, the closure configuration of the disposal facility, and the projected impacts of biotic intrusion and surface erosion on the disposal units.

The peak postdrilling dose estimated for the 2016-2044 shafts is about 10 percent of the peak dose projected for the 1996–2044 waste by Shuman (1999) using the 1997 performance assessment methodology; both of these doses pertain to intrusion at the end of the 100-year active institutional control period. Differences in inventories and assumptions about off-gas rates are major factors contributing to this disparity.

All of the peak intruder doses projected by the current modeling effort for the disposal pits and shafts at Area G are lower than the chronic and acute intruder performance objectives (100 and 500 mrem/yr, respectively). In terms of the pits, none of the peak mean exposures exceeds 4.1 percent of the respective limits. The peak mean doses projected for the shafts under the construction scenario are 1 percent or less of the 500 mrem/yr acute dose limit, while the exposures projected for the postdrilling intruder range from 3 to 11 percent of the chronic limit. Finally, the peak mean doses received by the agricultural intruder from waste disposed of in the 1988–2015 and 2016–2044 shafts are 89 and 49 percent of the dose objective, respectively.

5.3.2 Intruder-Based Waste Acceptance Criteria

Intruder-based WAC were developed for the disposal pits and shafts in MDA G; separate criteria were developed for the three intruder scenarios. The most restrictive of these scenario-specific limits represent the final intruder-based WAC for MDA G. These limits are provided in Table 5-4. Limits were estimated for radionuclides that may exist in a vapor or gas phase, or give rise to such, using the intruder and intruder diffusion models (i.e., with and without the effects of diffusion taken into account). With the exception of Kr-85, which exists only as a gas, the smaller of the limits calculated for each radionuclide was adopted as the final criterion for that contaminant. The limits listed in the table have not been adjusted to reflect or account for the specific activities of the isotopes.

Table 5-4
Final Waste Acceptance Criteria for the Disposal Pits and Shafts at MDA G

	Disposal Pits		Disposal Shafts	
Radionuclide	Limit (Ci/m^3)	Limiting Scenario	Limit (Ci/m^3)	Limiting Scenario
Ac-227	1.8E+00	Post-Drilling	2.1E+01	Post-Drilling
Ag-108m	6.8E-02	Post-Drilling	8.7E-01	Post-Drilling
Al-26	3.1E-02	Post-Drilling	4.2E-01	Post-Drilling
Am-241	1.2E-01	Post-Drilling	1.4E+00	Post-Drilling
Am-243	7.9E-02	Post-Drilling	9.8E-01	Post-Drilling
Ba-133	4.2E+03	Post-Drilling	4.2E+04	Post-Drilling
Be-10	4.8E+01	Post-Drilling	6.4E+02	Post-Drilling
Bi-207	1.4E+00	Post-Drilling	1.6E+01	Post-Drilling
Bk-247	7.2E-02	Post-Drilling	8.8E-01	Post-Drilling
C-14	1.3E+00	Post-Drilling	2.2E+01	Post-Drilling
Ca-41	2.2E+00	Post-Drilling	6.9E+01	Post-Drilling
Cf-249	7.6E-02	Post-Drilling	9.2E-01	Post-Drilling
Cf-251	7.2E-02	Post-Drilling	8.9E-01	Post-Drilling
Cf-252	3.2E+03	Post-Drilling	4.0E+04	Post-Drilling
Cl-36	1.2E-03	Post-Drilling	1.2E-01	Post-Drilling
Cm-243	3.7E+00	Post-Drilling	4.3E+01	Post-Drilling
Cm-244	2.0E+01	Post-Drilling	2.3E+02	Post-Drilling
Cm-245	8.4E-02	Post-Drilling	1.0E+00	Post-Drilling
Co-60	6.1E+06	Post-Drilling	4.8E+07	Post-Drilling
Cs-135	4.4E+00	Post-Drilling	6.8E+01	Post-Drilling
Cs-137	3.9E+00	Post-Drilling	4.4E+01	Post-Drilling
Eu-152	1.6E+02	Post-Drilling	1.6E+03	Post-Drilling
Eu-154	9.8E+03	Post-Drilling	9.1E+04	Post-Drilling
Gd-148	1.8E+00	Post-Drilling	2.2E+01	Post-Drilling
H-3	4.9E+02	Agriculture	4.5E+04	Agricultural
Ho-163	---	---	---	---
Ho-166m	5.7E-02	Post-Drilling	7.3E-01	Post-Drilling
I-129	1.8E-01	Post-Drilling	2.5E+00	Post-Drilling

--- = Concentration limits could not be calculated because no dose conversion factor was found for the radionuclide.

Table 5-4 (Continued)
Final Waste Acceptance Criteria for the Disposal Pits and Shafts at MDA G

	Disposal Pits		Disposal Shafts	
Radionuclide	Limit (Ci/m^3)	Limiting Scenario	Limit (Ci/m^3)	Limiting Scenario
K-40	6.3E-02	Post-Drilling	2.0E+00	Post-Drilling
Kr-85	2.2E+15	Post-Drilling	4.6E+06	Post-Drilling
Lu-176	1.9E-01	Post-Drilling	2.5E+00	Post-Drilling
Mo-93	3.7E+00	Post-Drilling	6.2E+01	Post-Drilling
Nb-91	---	---	---	---
Nb-92	---	---	---	---
Nb-93m	1.3E+05	Post-Drilling	1.4E+06	Post-Drilling
Nb-94	4.9E-02	Post-Drilling	7.0E-01	Post-Drilling
Nd-144	---	---	---	---
Ni-59	1.0E+02	Post-Drilling	2.3E+03	Post-Drilling
Ni-63	2.0E+02	Post-Drilling	2.7E+03	Post-Drilling
Np-237	3.6E-02	Post-Drilling	5.3E-01	Post-Drilling
Os-194	1.3E+07	Post-Drilling	1.0E+08	Post-Drilling
Pa-231	9.9E-03	Post-Drilling	1.3E-01	Post-Drilling
Pb-210	3.2E+00	Post-Drilling	3.6E+01	Post-Drilling
Pm-145	5.1E+03	Post-Drilling	5.5E+04	Post-Drilling
Pu-236	1.7E+00	Post-Drilling	1.8E+00	Post-Drilling
Pu-238	3.4E-01	Post-Drilling	4.0E+00	Post-Drilling
Pu-239	9.5E-02	Post-Drilling	1.2E+00	Post-Drilling
Pu-240	9.6E-02	Post-Drilling	1.2E+00	Post-Drilling
Pu-241	3.4E+00	Post-Drilling	4.1E+01	Post-Drilling
Pu-242	9.9E-02	Post-Drilling	1.2E+00	Post-Drilling
Pu-244	6.7E-02	Post-Drilling	8.3E-01	Post-Drilling
Ra-226	1.6E-02	Post-Drilling	9.2E-02	Agricultural
Ra-228	7.7E+05	Post-Drilling	6.1E+06	Post-Drilling
Si-32	8.6E+00	Post-Drilling	1.1E+02	Post-Drilling
Sm-146	5.7E-01	Post-Drilling	7.9E+00	Post-Drilling
Sm-151	1.2E+03	Post-Drilling	1.4E+04	Post-Drilling

--- = Concentration limits could not be calculated because no dose conversion factor was found for the radionuclide.

Table 5-4 (Continued)
Final Waste Acceptance Criteria for the Disposal Pits and Shafts at MDA G

	Disposal Pits		Disposal Shafts	
Radionuclide	Limit (Ci/m^3)	Limiting Scenario	Limit (Ci/m^3)	Limiting Scenario
Sn-121m	5.0E+02	Post-Drilling	6.1E+03	Post-Drilling
Sn-126	8.1E-01	Post-Drilling	1.9E+01	Post-Drilling
Sr-90	2.2E+00	Post-Drilling	2.6E+01	Post-Drilling
Tb-157	6.3E+02	Post-Drilling	7.6E+03	Post-Drilling
Tc-97	7.6E-01	Post-Drilling	5.2E+01	Post-Drilling
Tc-99	9.1E-02	Post-Drilling	6.2E+00	Post-Drilling
Th-228	5.4E+20	Post-Drilling	1.3E+21	Post-Drilling
Th-229	5.5E-02	Post-Drilling	6.8E-01	Post-Drilling
Th-230	3.5E-02	Post-Drilling	2.3E-01	Agricultural
Th-232	2.0E-02	Post-Drilling	2.5E-01	Post-Drilling
Ti-44	2.4E-01	Post-Drilling	2.8E+00	Post-Drilling
U-232	1.6E-01	Post-Drilling	1.9E+00	Post-Drilling
U-233	2.7E-01	Post-Drilling	3.7E+00	Post-Drilling
U-234	5.3E-01	Post-Drilling	7.6E+00	Post-Drilling
U-235	1.8E-01	Post-Drilling	2.5E+00	Post-Drilling
U-236	6.2E-01	Post-Drilling	8.9E+00	Post-Drilling
U-238	5.3E-01	Post-Drilling	7.5E+00	Post-Drilling
Zr-93	8.6E+01	Post-Drilling	1.1E+03	Post-Drilling

--- = Concentration limits could not be calculated because no dose conversion factor was found for the radionuclide.

The limits included in Table 5-4 are the lesser of the medians and means of the estimated distributions; since projected distributions of the WAC are generally skewed to the right, the median values tend to be the most limiting. Four of the radionuclides included in the table do not have concentration limits; dose conversions factors for these isotopes were unavailable in federal guidance reports 11 and 12 (EPA, 1988 and 1993).

As is evident from earlier discussions, the depth at which waste is placed in the disposal pits and shafts will have a significant effect on the magnitude of the projected intruder doses and, therefore, the WAC. The WAC calculated for the pits in MDA G are based on the assumption that waste will be uniformly distributed throughout the waste profile, consistent with disposal practices in MDA G. The surface erosion modeling estimated the top of the waste profile, or waste elevation, for the disposal shafts in MDA G. The WAC for the 1988–2015 shafts assume the waste placed in these units is an additional 1.5 m (4.9 ft) below the waste elevation established for the erosion modeling. Placing additional restrictions on the minimum depth of disposal allows the disposal of waste with higher radionuclide concentrations.

Table 5-5 compares the final WAC presented in Table 5-4 to the WAC developed in conjunction with the 1997 performance assessment; only those radionuclides common to the two efforts are included. Separate comparisons are provided for the pits and shafts. The 1997 pit limits represent the most restrictive criteria estimated on the basis of the Intruder–Post-Drilling and Intruder-Agriculture Scenarios; the former limits are provided in Shuman (1999) while the limits for the agricultural intruder are taken from Hollis et al. (1997). The 1997 limits for the shafts include two sets of criteria to address different depths of disposal.

The 2008 intruder-based WAC for the disposal pits are significantly higher than the limits calculated in conjunction with the 1997 performance assessment for all radionuclides except tritium. Although several differences exist in the models and data used to calculate the two sets of WAC, the primary reason for this difference is the amount of cover placed over the disposal units. Whereas the earlier limits are based on an initial cover thickness of 2 m (8 ft), the 2008 analysis considers initial cover depths ranging from 2.5 to 6.0 m (8.2 to 20 ft), with a median thickness of 4.2 m (14 ft). The additional cover all but eliminates contact with the waste during basement excavation, resulting in small exposures to the intruder and larger WAC. The much lower concentration limit calculated for tritium in the 2008 analysis is due, in large measure, to differences in diffusion models.

The WAC calculated in 2008 for the disposal shafts are greater than the 1997 disposal-at-any-depth limits for some radionuclides and lower for others. In most cases, the radionuclides with 2008 limits that are much lower than, or similar to, the 1997 limits are short-lived. The 2008 limits for these radionuclides would be substantially higher if it was assumed that intrusion occurred 300 years after facility closure, as it was for the 1997 analysis. The 2008 limits for most long-lived radionuclides are significantly greater than their 1997 counterparts, reflecting

differences in the initial cover thickness placed over the disposal units and the distribution of waste within the units. The 2008 limit for H-3 is much lower than the 1997 limit due to differences in the time of intrusion and differences in diffusion models.

The 2008 WAC for the disposal shafts are lower than about half of the disposal-at-depth limits calculated in conjunction with the 1997 performance assessment (Table 5-5). The limits for 22 of the 28 radionuclides that are common to both sets of criteria differ by a factor of 5 or less. Many of these disparities, as well as those noted earlier, result from differences in the models and data used to project intruder exposures in 1997 and 2008.. A number of these differences are addressed by a benchmarking analysis, the results of which may be found in *Appendix L*.

5.4 Uncertainty and Sensitivity

The intruder exposures reported here, and the WAC developed on the basis of these exposures, are subject to several sources of uncertainty. Some of the more important of these are discussed below, followed by a sensitivity analysis for selected intruder exposure scenarios.

The distributional information shown in Table 5-3 provides insight into the uncertainty associated with the projected doses. In terms of the doses for radionuclides that are unaffected by diffusion, the variability associated with the construction and agricultural intruder exposures is significantly greater than that observed for the postdrilling intruder doses. The greater variability noted for the former scenarios is an indication of the impact that the thickness of the cover placed over the pits and shafts has upon the projected impacts. As discussed earlier, the distributions of initial cover thickness over the disposal units are such that the excavation of a basement is not projected to contact the waste in a large number of model realizations. In terms of the two sets of disposal pits, the waste would remain undisturbed by basement excavation in more than 90 percent of the realizations. Contact with the 1988–2015 shaft waste during basement excavation will occur about 10 percent of the time and contact with the 2016–2044 shaft waste will occur about 50 percent of the time.

Failure to contact the waste during basement excavation does not prevent exposures of the construction and agricultural intruders; plants and animals may transport contaminants to portions of the cover that are disturbed during excavation, and vapor- and gas-phase radionuclides may diffuse upward. However, the intruders are exposed to significantly smaller concentrations of contamination under these conditions, relative to the contaminant concentrations encountered when the basement extends into the waste. Because of this, a wide range in the projected exposures is observed, as witnessed by the statistics shown in Table 5-3. The variability in the exposures projected for the postdrilling intruder is much smaller because contact with the waste occurs in all model realizations. In this situation, similar amounts of waste are brought to the surface in all realizations, resulting in narrower distributions of dose.

Table 5-5
Comparison of the 1997/1999 and 2008 WAC for MDA G

Radionuclide	Disposal Pits		Disposal Shafts		
			1997 WAC		
	1997 WAC [a]	2008 WAC	Disposal at any Depth [a,b]	Disposal at Depth [c]	2008 WAC
Ac-227	5.1E-03	1.8E+00	---	---	2.1E+01
Ag-108m	3.5E-04	6.8E-02	---	---	8.7E-01
Al-26	1.0E-04	3.1E-02	---	---	4.2E-01
Am-241	2.3E-03	1.2E-01	3.7E-02	2.7E+00	1.4E+00
Am-243	1.1E-03	7.9E-02	---	---	9.8E-01
Ba-133	7.3E+01	4.2E+03	1.9E+11	9.2E+04	4.2E+04
Bi-207	3.3E-03	1.4E+00	3.7E+00	4.4E+00	1.6E+01
Bk-247	2.7E-03	7.2E-02	---	---	8.8E-01
C-14	2.8E-03	1.3E+00	2.1E-01	2.1E+01	2.2E+01
Cf-252	1.1E+02	3.2E+03	8.8E+02	8.7E+04	4.0E+04
Cl-36	1.3E-04	1.2E-03	---	---	1.2E-01
Co-60	5.1E+02	6.1E+06	1.6E+15	6.9E+05	4.8E+07
Cs-135	1.2E-01	4.4E+00	2.3E+00	2.3E+02	6.8E+01
Cs-137	9.2E-03	3.9E+00	1.1E+01	1.2E+01	4.4E+01
Eu-152	2.0E-01	1.6E+02	1.2E+05	2.7E+02	1.6E+03
Eu-154	4.4E-02	9.8E+03	2.9E+03	5.9E+01	9.1E+04
Gd-148	1.3E-02	1.8E+00	---	---	2.2E+01
H-3	3.4E+04	4.9E+02	1.2E+09	1.6E+04	4.5E+04

--- = Not included in the 1999 shaft WAC effort

[a] Source: Hollis et al., 1997

[b] Corresponds to the concentration limits developed on the basis of the Intruder-Agriculture Scenario.

[c] Corresponds to the concentration limits developed on the basis of the Intruder–Post-Drilling Scenario (Shuman, 1999).

Table 5-5 (Continued)
Comparison of the 1997/1999 and 2006 Waste Acceptance Criteria for MDA G

	Disposal Pits		Disposal Shafts		
			1997 WAC		
Radionuclide	1997 WAC [a]	2008 WAC	Disposal at any Depth [a,b]	Disposal at Depth [c]	2008 WAC
I-129	1.8E-03	1.8E-01	---	---	2.5E+00
K-40	1.1E-03	6.3E-02	---	---	2.0E+00
Kr-85	3.1E+02	2.2E+15	1.3E+09	4.0E+05	4.6E+06
Mo-93	1.2E-01	3.7E+00	---	---	6.2E+01
Nb-92	1.8E-04	---	2.0E-03	2.4E-01	---
Nb-94	1.8E-04	4.9E-02	---	---	7.0E-01
Ni59	2.3E+00	1.0E+02	---	---	2.3E+03
Ni-63	2.2E+00	2.0E+02	1.6E+03	3.5E+04	2.7E+03
Np-237	3.7E-04	3.6E-02	---	---	5.3E-01
Pa-231	1.4E-04	9.9E-03	---	---	1.3E-01
Pb-210	2.5E-02	3.2E+00	4.0E+02	4.4E+01	3.6E+01
Pm-145	3.8E+00	5.1E+03	1.5E+05	5.8E+03	5.5E+04
Pu-238	6.8E-03	3.4E-01	3.7E-01	7.5E+00	4.0E+00
Pu-239	2.2E-03	9.5E-02	2.6E-02	2.5E+00	1.2E+00
Pu-240	2.3E-03	9.6E-02	2.6E-02	2.5E+00	1.2E+00
Pu-241	7.4E-02	3.4E+00	1.0E+00	7.5E+01	4.1E+01
Pu-242	2.3E-03	9.9E-02	2.7E-02	2.7E+00	1.2E+00
Ra-226	1.2E-04	1.6E-02	1.7E-03	1.7E-01	9.2E-02

--- = Not included in the 1999 shaft WAC effort

[a] Source: Hollis et al., 1997

[b] Corresponds to the concentration limits developed on the basis of the Intruder-Agriculture Scenario.

[c] Corresponds to the concentration limits developed on the basis of the Intruder–Post-Drilling Scenario (Shuman, 1999).

Table 5-5 (Continued)
Comparison of the 1997/1999 and 2006 Waste Acceptance Criteria for MDA G

	Disposal Pits		Disposal Shafts		
			1997 WAC		
Radionuclide	1997 WAC [a]	2008 WAC	Disposal at any Depth [a,b]	Disposal at Depth [c]	2008 WAC
Sm-146	1.3E-02	5.7E-01	---	---	7.9E+00
Sm-151	3.1E+01	1.2E+03	---	---	1.4E+04
Sr-90	1.5E-02	2.2E+00	3.9E+01	2.6E+01	2.6E+01
Tb-157	5.0E-01	6.3E+02	---	---	7.6E+03
Tc-97	7.2E-02	7.6E-01	---	---	5.2E+01
Tc-99	1.3E-02	9.1E-02	---	---	6.2E+00
Th-229	4.8E-04	5.5E-02	5.6E-03	5.7E-01	6.8E-01
Th-230	3.1E-04	3.5E-02	---	---	2.3E-01
Th-232	9.9E-05	2.0E-02	1.1E-03	1.3E-01	2.5E-01
Ti-44	8.8E-04	2.4E-01	---	---	2.8E+00
U-232	5.5E-04	1.6E-01	---	---	1.9E+00
U-233	3.2E-03	2.7E-01	---	---	3.7E+00
U-234	7.4E-03	5.3E-01	9.5E-02	9.5E+00	7.6E+00
U-235	1.5E-03	1.8E-01	1.7E-02	1.8E+00	2.5E+00
U-236	8.8E-03	6.2E-01	1.2E-01	1.1E+01	8.9E+00
U-238	5.7E-03	5.3E-01	7.0E-02	7.4E+00	7.5E+00
Zr-93	8.5E-01	8.6E+01	---	---	1.1E+03

--- = Not included in the 1999 shaft WAC effort

[a] Source: Hollis et al., 1997

[b] Corresponds to the concentration limits developed on the basis of the Intruder-Agriculture Scenario.

[c] Corresponds to the concentration limits developed on the basis of the Intruder–Post-Drilling Scenario (Shuman, 1999).

The variability inherent in the doses projected for vapor- and gas-phase radionuclides tends to be less than that for contaminants that are unaffected by diffusion. Diffusion through the cover and waste makes vapor- and gas-phase contaminants accessible to the intruders over the range of cover depths modeled. More stable contaminant concentrations result between model realizations, leading to less variable dose estimates.

The inadvertent intruder exposures projected for the disposal pits are based on average radionuclide concentrations in the buried waste. Radionuclide concentrations are averaged over the units used from September 27, 1988 through 2010 and from 2011 through 2044. Depth-dependent inventories are used to model exposures from the 1988–2015 shafts, but these inventories are averaged over discrete depth intervals; the waste in the 2016–2044 shafts is uniformly distributed throughout the disposal units. Radionuclide concentrations in all shafts are further modified to account for the discrete nature of these units and their spatial distribution within the shaft fields. Using spatially averaged inventories all but ensures that the projected doses will not equal the doses received if human intrusion actually occurred. However, this approach takes into account the fact that a person arriving at the site could excavate a basement or drill a well at countless locations at the site. Using average waste concentrations functionally weights the likelihood that the individual will decide to intrude into waste that contains higher or lower than average radionuclide concentrations.

It is assumed that intrusion may occur at any time following the end of active institutional control over the site. This assumption, in conjunction with the degree of disturbance assumed, is expected to result in reasonably conservative estimates of potential intruder impacts. Use of the site for nonresidential uses (e.g., hunting or other forms of recreation) would result in little or no disruption of the waste and, consequently, significantly smaller exposures. As shown by the results of the agricultural and postdrilling intruder scenarios, impacts may vary significantly for resident intruders, depending upon the type of construction undertaken.

Sensitivity analyses were conducted for the agricultural and postdrilling intruder scenarios in conjunction with the 1988–2010 pits and 1988–2015 shafts. These scenarios address two distinct types or degrees of intrusion into the waste, one in which large quantities of material are excavated from shallow depths (basement excavation) and one in which smaller amounts of material are removed from the cover and waste profile (well drilling). These disposal units were chosen for consideration because they yielded higher doses than the pits and shafts in the Zone 4 expansion area.

The results of the sensitivity analysis are summarized in Table 5-6. This table includes the five parameters that had the highest absolute values of the Spearman rank correlation coefficient. For the 1988–2010 disposal pits, the doses projected for the agricultural intruder using the intruder model are correlated with two parameters that determine the degree to which plants intrude into the waste prior

Table 5-6
Rank Correlation Coefficients for Selected Intruder Exposure Scenarios

Waste Disposal Units and Exposure Scenario	Intruder Model		Intruder Diffusion Model	
	Model Parameter	Rank Correlation Coefficient	Model Parameter	Rank Correlation Coefficient
1988–2010 Disposal Pits				
Intruder-Agriculture Scenario	Maximum rooting depth of trees	4.2E-01	Ra-226 waste inventory in 1988–2015 pits	3.6E-01
	Root-mass-distribution beta-shape factor	-3.1E-01	Cover node	-2.3E-01
	Cover node	-2.4E-01	Radon emanation coefficient	1.6E-01
	Plant uptake factor of chloride in native vegetation	1.5E-01	Root-mass-distribution beta-shape factor	-1.5E-01
	Milk transfer factor for plutonium	1.1E-01	Maximum rooting depth of trees	1.5E-01
Intruder–Post-Drilling Scenario	Maximum rooting depth of trees	4.3E-01	Ra-226 waste inventory in 1988–2015 pits	4.2E-01
	Root-mass-distribution beta-shape factor	-4.1E-01	Root-mass-distribution beta-shape factor	3.9E-01
	Ingestion rate of grain	2.2E-01	Maximum rooting depth of trees	3.3E-01
	Plant uptake factor of chloride in native vegetation	1.6E-01	Ingestion rate of grain	2.0E-01
	Fractions of vegetables grown by intruder	1.2E-01	Cover node	-1.7E-01
1988–2015 Disposal Shafts				
Intruder-Agriculture Scenario	Cover node	-1.9E-01	Ra-226 waste inventory in 1988–2015 shafts	5.8E-01
	Maximum rooting depth of trees	1.4E-01	Radon-emanation coefficient	3.0E-01
	Indoor exposure time	8.6E-02	Ingestion rate of grain	2.1E-01
	Dry-to-wet weight fraction for produce	-8.3E-02	Fraction of vegetables grown by intruder	1.4E-01
	Root-mass-distribution beta-shape factor	-8.0E-02	Plant-uptake factor of lead in grain	1.4E-01
Intruder–Post-Drilling Scenario	Animals raised	-4.4E-01	Ra-226 waste inventory in 1988–2015 shafts	6.5E-01
	Sr-90 waste inventory in 2005–2044 shafts	3.4E-01	Ingestion rate of grain	3.4E-01
	Plant-uptake factor of strontium in grain	2.7E-01	Fraction of vegetables grown by intruder	2.4E-01
	Ingestion rate of grain	2.1E-01	Animals raised by intruder	-2.4E-01
	Plant-uptake factor of strontium in pasture grass and native vegetation	2.1E-01	Plant-uptake factor of carbon in grain	1.6E-01

--- = Sensitivity analysis did not address intruder diffusion dose projections for the exposure scenario

to the intruder's arrival: root depth and the beta shape factor for root-mass distribution. Greater penetration of the waste occurs as the maximum root depth of the trees increases; the trees deposit higher radionuclide activities on the surface of the facility prior to the arrival of the intruder and radionuclide concentrations in the material brought to the surface during basement excavation increase. The intruder doses are inversely proportional to the shape factor. Larger values of the parameter predict that a greater proportion of the total root mass lies close to the surface; less contamination is brought to the surface as a result. The third parameter listed in Table 5-6, the cover node, relates to the initial cover thicknesses and erosion loss functions that are used in the modeling. In addition to affecting how deeply tree roots extend into the waste, these factors determine how far the basement of the intruder's house extends into the waste and, therefore, how much contamination is brought to the surface. The last two parameters in the table affect how much Cl-36 is assimilated by trees growing over the closed disposal site and to what degree the milk consumed by the intruder is contaminated with Pu-239. Both of these radionuclides are important contributors to the projected peak mean dose.

The sensitivity analysis for the intruder diffusion model indicates that the peak mean dose estimated for the agricultural intruder who accesses waste in the 1988–2010 pits is most sensitive to the Ra-226 inventory in these pits. Similar to the intruder model, two parameters control the distribution of tree roots in the waste: the maximum rooting depth of trees and the beta shape factor. The cover node parameter reflects the importance of the initial cover thickness over the waste and the rate at which the cover is eroded over extended periods of time. The peak mean dose is also sensitive to the radon emanation coefficient. Pb-210, a daughter of Ra-226, is a major contributor to the peak exposure projected for the intruder. The surface soils over the intruder's lot become contaminated with Pb-210 following the diffusion of Rn-222 upward from the waste; the magnitude of the projected radon flux is determined, in part, by the radon-emanation coefficient.

The sensitivity analysis results for the postdrilling intruder with respect to the 1988–2010 pits are similar to those for the agricultural intruder. The intruder model projections are sensitive to the root-mass distribution of trees with depth and the rate at which Cl-36 is assimilated by the trees. The quantity of the intruder's diet that comes from growing crops on the receptor's lot and the rate at which grain is consumed also affect the results for this model; the ingestion of crops makes a significant contribution to the peak mean dose projected for the intruder. The peak mean dose projected by the intruder diffusion model for the postdrilling scenario is most sensitive to the Ra-226 inventory in the disposal pits. Three parameters control the distribution of tree roots in the waste; these include the maximum rooting depth of trees, the beta shape factor, and the cover node parameter. The ingestion rate of grain influences how much contaminated food is consumed by the intruder.

The agricultural intruder exposures projected in conjunction with the 1988–2015 shafts using the intruder model are correlated with three parameters that determine the extent to which plant roots

penetrate the buried waste: the cover node parameter, the maximum rooting depth of trees, and the beta-shape factor. The indoor exposure time and the wet-to-dry weight fraction for produce affect the magnitudes of the exposures received through direct radiation and crop ingestion; these exposure pathways are responsible for most of the projected peak mean dose. The sensitivity analysis identified two spurious parameters that are used to model radionuclide concentrations in crops for two isotopes that did not contribute to the projected exposures; these parameters are excluded from the table.

The agricultural intruder diffusion model projections for the 1988–2015 shafts are highly correlated to the inventory of Ra-226 and the radon-emanation coefficient. The remaining parameters listed in Table 5-6 relate to the intake of vegetables contaminated with Pb-210; the ingestion of contaminated crops is an important contributor to the peak mean exposure. The parameters specify how much grain is consumed by the individual, the fraction of the receptor's crops raised in contaminated soils, and the rate at which lead is assimilated by food crops.

The postdrilling intruder doses projected by the intruder model in conjunction with the 1988–2015 shafts are strongly correlated to the inventory of Sr-90, the parameters that determine Sr-90 concentrations in various foodstuffs, and the quantity of food consumed. The correlation between the projected exposures and the type of animal raised by the intruder reflects the fact that much larger Sr-90 doses result from the consumption of beef and milk than from the ingestion of chicken and eggs. The doses projected for this scenario using the intruder diffusion model are sensitive to the Ra-226 inventory in the shafts and to several factors that determine the types and amounts of contaminated foodstuffs that are consumed by the receptor. These parameters include how much grain is consumed, the fraction of the intruder's food that is grown on site, the types of animal products consumed by the intruder (i.e., beef and milk or chicken and eggs), and the plant uptake factor for carbon in grain.

6.0 Interpretation of Results

An interpretation of the performance assessment and composite analysis results presented in Sections 4 and 5 of this report is provided below. Section 6.1 addresses the modeling conducted to project doses for members of the public and to estimate radon fluxes from the undisturbed facility. The results of the inadvertent intruder analysis are addressed in Section 6.2.

6.1 Performance Assessment and Composite Analysis

The potential risks posed by the disposal of radioactive waste at Area G were evaluated in terms of individuals who (1) use groundwater contaminated by releases from the disposal facility, (2) live downwind of the facility, or (3) live in Cañada del Buey and Pajarito Canyon. These results, the associated uncertainty, and the parameters and processes that significantly influence these exposures are discussed in Section 4.

No radionuclides were projected to discharge to the regional aquifer during the 1,000-year compliance period. Therefore, no exposures were projected for the Groundwater Resource Protection and All Pathways–Groundwater Scenarios. The time it takes for radionuclides to discharge to the aquifer and the concentrations they attain in groundwater is significantly impacted by the rate at which water infiltrates through the disposal facility. The long-term average infiltration rate for Area G used in the groundwater modeling is based on fluxes estimated from infiltration modeling conducted using HYDRUS. The estimated fluxes are generally consistent with those estimated from empirical studies.

The groundwater transport modeling upon which the groundwater pathway projections are based is expected to more accurately represent the hydrogeologic conditions at Area G than did the modeling conducted in support of the 1997 analyses (Hollis et al., 1997). A significant amount of new information has become available since the earlier analysis was conducted, allowing the development of a more accurate representation of subsurface conditions at the site. Improvements in modeling techniques since the mid-1990s have permitted explicit consideration of many of the uncertainties associated with projecting groundwater impacts.

The deposition of contamination on the surface of the disposal facility by plants and animals inhabiting the site represents a potentially significant mode of release. The actual impacts of biotic intrusion on facility performance depend upon the plant and animal communities inhabiting the site and important facility design features. As modeled, the plants and animals found at Area G are assumed to change over time as the site transitions from grassland-dominated landscape to piñon-juniper woodland. These end points are consistent with the conditions found at recently closed disposal sites such as MDA J, located 2 km (1.2 mi) west of Area G, and undisturbed portions of Mesita del Buey, respectively.

The principal design feature used to ensure the long-term performance of Area G is the total depth of cover placed over the disposal facility at final closure. Although the cover design is based on a minimum thickness of 2.5 m (8 ft) of material over all disposal units, the actual cover thickness placed over the majority of the site exceeds 3 m (10 ft); additional material was put in place to ensure satisfactory slopes and contours. This additional cover further restricts the ability of plants and animals to penetrate into the waste, limiting releases to the surface of the facility.

Most of the plants and animals projected to inhabit the closed site do not root or burrow deep enough to contact the waste during the 1,000-year compliance period. As indicated by the sensitivity analysis results, the establishment of deep-rooting trees after the end of active institutional control leads to the highest releases of radionuclides to the surface of Area G; the doses projected for several individuals living downwind of Area G and in the adjacent canyons are strongly correlated to the root mass distribution and biomass density of trees. Among the animals, only harvester ants are projected to penetrate into the waste to a significant degree during the compliance period; the pocket gophers, mice, chipmunks, and ground squirrels that inhabit the site at one time or another are excluded from the waste over the vast majority of the facility.

The diffusion of vapor- and gas-phase radionuclides upward from the waste is another potentially important contaminant release mechanism at Area G. The performance assessment and composite analysis consider the impacts of surface erosion on contaminant release rates and explicitly model many sources of uncertainty associated with vapor- and gas-phase diffusion. Overall, the diffusion modeling is expected to more accurately simulate the diffusion of contaminants upward from the waste than did the analytical expressions that were used for the 1997 performance assessment and composite analysis.

The releases of contamination to the surface that result from biotic intrusion and diffusion yield peak mean doses for the Atmospheric and All Pathways–Canyon Scenarios that fall well within the pertinent performance objectives. Particulate releases yield performance assessment and composite analysis doses for the Atmospheric Scenario ranging from 1.8 to 6.4 percent of the 10 mrem/yr performance objective that applies to all airborne releases at the Laboratory. The peak mean exposures projected for the maximally exposed canyon receptors are 9.2 and 15 percent of the performance assessment and composite analysis performance objectives, respectively. Rates of release of radon gas from the performance assessment inventory are less than the 20 $pCi/m^2/s$ flux objective; the peak mean flux averaged over all disposal units is 2 percent of the flux limit.

The exposures projected for the Atmospheric Scenario take into account the complex air dispersion patterns observed across the Laboratory and, as such, are considered to be a reasonable representation of actual conditions and a vast improvement over the modeling conducted in support of the 1997 performance assessment and composite analysis. The majority

of the meteorological data used in the atmospheric transport modeling are specific to Area G and the Laboratory. Assumptions made about land use are generally consistent with the conditions that are expected to prevail at Area G.

Contamination deposited on the surface of Area G by plants and animals is transported with surface water runoff into the adjacent canyons. The surface erosion modeling conducted using SIBERIA was used in the development of the final cover design and to estimate spatially variable rates of soil loss across the site. Projected rates of soil loss are moderate over the 1,000-year compliance period, consistent with the fact that design features of the cover were adjusted until satisfactory rates of cover loss were attained.

The exposures projected for individuals in Cañada del Buey and Pajarito Canyon are determined by the rates of contaminant deposition on the surface of the disposal facility by plants and animals and the rates and patterns of sediment transport from the mesa top. Although the modeling conducted to estimate radionuclides in canyon soils is a significant improvement on that conducted in 1997 (Hollis et al., 1997), it is still subject to simplifying assumptions. These assumptions pertain to how sediment is transported down the slopes of the mesa, disperses upon reaching the canyon floor, and migrates within the canyons.

The migration paths of sediments that are transported down the mesa slopes and onto the canyon floor were not modeled. Sediments reaching the edge of the mesa were assumed to be transported immediately to the canyon floor; lacking more accurate information, the area of dispersal was assumed to be a fraction of the canyon floor in the catchment receiving the material. As a result, the radionuclide concentrations projected for the canyon soils are subject to a fair degree of uncertainty and may not represent actual exposure conditions. Similarly, although the transport of sediments down the canyons as a result of periodic flooding was modeled, the sediment residence times within Cañada del Buey and Pajarito Canyon were estimated using a limited amount of information. Consequently, it would not be surprising to find that actual rates of transport differ from the projected rates.

In general, the modeling conducted in support of the performance assessment and composite analysis is expected to adequately address the potential risks posed by the site to members of the public. Although the adoption of several simplifying assumptions will reduce the accuracy with which actual site conditions are represented, the models capture the major modes of radionuclide release, transport, and exposure that are relevant to the site over the 1,000-year compliance period. Improvements can, and will, be made to the data and models used here; however, the analyses presented in this report are considered reasonable representations of the current state of knowledge about Area G.

The alternate source evaluation conducted in support of the composite analysis revealed little likelihood that releases from other facilities at the Laboratory will interact significantly with releases from Area G. Although some of the MDAs have inventories of specific radionuclides in excess of those projected to reside at Area G, releases from these sites are expected either to exist in small concentrations at exposure locations near Area G or to fail to reach these locations during the 1,000-year compliance period. These conclusions are based on existing information about contaminant inventories, site-specific information about geologic conditions, and atmospheric and groundwater transport modeling conducted in support of the performance assessment and composite analysis. Contaminant discharges to Cañada del Buey and Pajarito Canyon have occurred, but the existing levels of contamination near Area G appear to have resulted from the transport of contaminants from the disposal facility with surface runoff.

Collective doses from particulate releases are projected to be low for persons living downwind of the disposal facility and in the canyons adjacent to Area G. Releases to the atmosphere disperse quickly as they are transported with the prevailing winds to distant locations, resulting in very low concentrations of airborne contaminants at most exposure locations within 80 km (50 mi) of Area G. Contaminant concentrations in the canyons may be more substantial, but only a few people can inhabit Cañada del Buey and Pajarito Canyon, which limits the total collective dose.

The final cover evaluated for the performance assessment and composite analysis is reasonably robust and will cost a considerable sum of money to install. This cost, in conjunction with the results of the dose assessment and ALARA analysis, suggests there may be opportunities to develop a more cost-effective strategy for closing Area G. For example, reducing the minimum cover requirements for the disposal facility could result in significant reductions in closure expenses with only small increases in the radiological impact to members of the public and the collective population. The collective doses estimated by the ALARA analysis were similar for the Base-Case Scenario, which assumed installation of the proposed final cover, and the Biobarrier Option, which assumed the addition of an engineered biobarrier. From an ALARA perspective, the benefit of using a biobarrier may be more substantial if the total thickness of the cover is modified in concert with the incorporation of the barrier in the final cover design. For example, given that the costs for including a biobarrier are relatively low, the application of a thinner cover with a biobarrier may prove to be an optimal closure strategy.

6.2 Inadvertent Intruder Analysis

The doses projected for the inadvertent intruder scenarios are expected to be reasonably conservative estimates of exposures that could occur if the DOE's administrative control over the facility lapses for a brief period of time. For example, the assumed land uses are generally more intensive than were pre-Laboratory uses. Furthermore, the probability that a person will arrive at the site during a lapse in control and intrude into the waste is not taken into account.

The magnitude of the exposures projected for the construction worker and the agricultural intruder are correlated to the thickness of the cover placed over the disposal units. The cover placed over the 1988–2010 pits, the 2011–2044 pits, and the 2016-2044 shafts is sufficient to maintain exposures at acceptable levels. For the 1988–2015 shafts, greater attention to the depth at which waste containing critical radionuclides is disposed provides the level of protection required for the inadvertent intruder and helps maximize the quantities of waste that can be safely disposed of within these units.

7.0 Performance Evaluation

The results of the performance assessment and composite analysis are presented in Sections 4 and 5, and discussed in Section 6. In Section 7.1, these results are compared to the performance objectives to determine if Area G satisfies the established requirements with a reasonable level of assurance. Section 7.2 discusses how the results of the performance assessment and composite analysis will be applied in the management of LLW at LANL. A discussion of informational needs that could be addressed by future studies is provided in Section 7.3 as the conclusion to the report.

7.1 Comparison of Results to Performance Objectives

The purpose of the performance assessment and composite analysis is to provide a reasonable level of assurance that the disposal of radioactive waste at Area G can be accomplished in a manner that protects human health and safety and the environment. This assurance is provided by projecting the long-term impacts of the facility and comparing those projections to the performance objectives provided in Section 1.5. Doses and radon fluxes projected for the performance assessment are compared to the performance objectives in Section 7.1.1, while the composite analysis projections are compared against objectives in Section 7.1.2. A comparison of the projected intruder exposures and the acute and chronic performance objectives for these receptors may be found in Section 7.1.3.

7.1.1 Evaluation of Performance Assessment Results

The performance assessment projected exposures for the Groundwater Resource Protection, All Pathways–Groundwater, Atmospheric, and All Pathways–Canyon Scenarios; radon fluxes from the undisturbed site were estimated in conjunction with the Atmospheric Scenario. The following discussion compares the projected impacts for these scenarios to the performance objectives; a summary of this comparison is provided in Table 7-1.

7.1.1.1 Groundwater Resource Protection and All Pathways–Groundwater Scenarios

The performance objective for the resource protection scenario varies depending upon the radionuclide under consideration; the performance objective for the all pathways scenario is 25 mrem/yr at the point of maximum exposure. Exposures for the former scenario were projected for a point 100 m (330 ft) downgradient of the Area G fence line. The potential doses received by the all pathways receptor were projected for two locations, near the town of White Rock (prior to the end of active institutional control) and at a hypothetical well 100 m (330 ft) downgradient of Area G.

The groundwater pathway modeling conducted in support of the performance assessment projected that no radionuclides would discharge to the regional aquifer during the 1,000-year compliance period. Therefore, no exposures were projected for the Groundwater Resource Protection and All Pathways–Groundwater Scenarios.

Table 7-1
Comparison of Performance Assessment Results with Performance Objectives

Performance Objective	Exposure Scenario	Projected Impact
All Pathways (25 mrem/yr)	All Pathways–Groundwater	No radionuclides were projected to discharge to the regional aquifer
	All Pathways–Canyon	Peak mean dose of 2.3E+00 mrem/yr for maximally exposed individual
Air Pathway (10 mrem/yr)	Atmospheric	Peak mean dose of 1.8E-01 mrem/yr for maximally exposed individual
Radon Flux (20 pCi/m^2/s)	---	Peak mean flux of 1.4E+01 pCi/m^2/s from waste disposal region 7 Average facility flux of 4.3E-01 pCi/m^2/s
Water Resources Impacts (40 CFR 141 limits)	Groundwater Resources Protection	No radionuclides were projected to discharge to the regional aquifer
Inadvertent Intruder (500 mrem/yr acute exposure)	Intruder-Construction	
	1988–2010 pits	Peak mean dose of 5.3E-01 mrem/yr [a]
	2011–2044 pits	Peak mean dose of 2.8E-02 mrem/yr [a]
	1988–2015 shafts	Peak mean dose of 5.1E+00 mrem/yr [a]
	2016–2044 shafts	Peak mean dose of 2.5E+00 mrem/yr [a]
Inadvertent Intruder (100 mrem/yr chronic exposure)	Intruder-Agriculture	
	1988–2010 pits	Peak mean dose of 4.1E+00 mrem/yr [a]
	2011–2044 pits	Peak mean dose of 4.6E-01 mrem/yr [a]
	1988–2015 shafts	Peak mean dose of 8.9E+01 mrem/yr [a]
	2016–2044 shafts	Peak mean dose of 4.9E+01 mrem/yr [a]
	Intruder–Post-Drilling	
	1988–2010 pits	Peak mean dose of 3.6E+00 mrem/yr [a]
	2011–2044 pits	Peak mean dose of 6.9E-01 mrem/yr [a]
	1988–2015 shafts	Peak mean dose of 1.1E+01 mrem/yr [a]
	2016–2044 shafts	Peak mean dose of 3.1E+00 mrem/yr [a]

--- = Radon fluxes are projected in conjunction with the air pathway modeling.

[a] Dose represents the sum of the peak mean exposures for diffusive and nondiffusive releases.

7.1.1.2 Atmospheric Scenario and Radon Analysis

The dose objective for the Atmospheric Scenario is 10 mrem/yr for all sources of airborne radioactivity at the Laboratory. Exposures were projected for receptors residing at the points of maximum exposure along the LANL boundary and the Area G fence line. Fluxes of radon from the surface of the disposal facility must not exceed an average value of 20 pCi/m^2/s or result in an incremental increase in the air concentration of radon of more than 0.5 pCi/L at the boundary of the disposal facility. Radon fluxes and air concentrations were projected in conjunction with the Atmospheric Scenario modeling.

The peak mean exposures projected for the receptors at the LANL boundary and Area G fence line are 0.18 and 0.014 mrem/yr, respectively. These doses are small fractions of the LANL limit of 10 mrem/yr. The 2003 environmental surveillance report (LANL, 2004) reports an annual dose of 0.65 mrem for the maximally exposed individual due to airborne releases from LANL. This exposure and those projected for Area G occur at different times and, therefore, are not additive. However, the magnitudes of these doses suggest that LANL will readily comply with the performance objective.

The peak mean radon fluxes projected for the eight waste disposal regions shown in Figure 3-2 are summarized in Table 4-9; the radon concentrations at the facility boundary that correspond to these fluxes are included as well. All projected fluxes and air concentrations fall within the 20 pCi/m^2/s performance objectives. A facility-wide average flux of 0.43 pCi/m^2/s is estimated on the basis of these results.

7.1.1.3 All Pathways–Canyon Scenario

The performance objective for the All Pathways–Canyon Scenario is 25 mrem/yr at the point of maximum exposure. Doses were projected for nine exposure locations within Cañada del Buey and Pajarito Canyon. The receptors in Cañada del Buey were assumed to receive exposures starting at the time of facility closure, while receptors were assumed to arrive in Pajarito Canyon at the end of the active institutional control period.

Canyon receptors at two locations in Cañada del Buey were projected to receive peak mean exposures of 2.3 and 0.41 mrem/yr; doses for the receptors in Pajarito Canyon were smaller than these exposures. All dose projections fall well within the 25 mrem/yr performance objective.

7.1.2 Evaluation of Composite Analysis Results

The composite analysis projected exposures for the All Pathways–Groundwater, Atmospheric, and All Pathways–Canyon Scenarios; radon fluxes from the disposal site were estimated in conjunction with the Atmospheric Scenario. Additionally, the potential for releases from other facilities at the Laboratory to significantly interact with releases from Area G was evaluated. Finally, an analysis was conducted to evaluate whether releases from Area G were ALARA and

to evaluate the effectiveness of alternative closure strategies. The following discussion compares the projected impacts for these scenarios to the performance objectives; Table 7-2 summarizes this comparison for the individual dose and radon flux projections.

7.1.2.1 All Pathways–Groundwater Scenario

The performance objective for the All Pathways–Groundwater Scenario is the primary DOE dose limit of 100 mrem/yr; the 30 mrem/yr dose constraint is used to evaluate the exposures projected for Area G. Exposures were projected for a groundwater user near the town of White Rock (prior to the end of active institutional control), and for the user of a hypothetical well 100 m (330 ft) downgradient of Area G. The modeling conducted in support of the composite analysis projected that no radionuclides would discharge to the regional aquifer during the 1,000-year compliance period. Therefore, no exposures were projected for the Groundwater Resource Protection and All Pathways–Groundwater Scenarios.

7.1.2.2 Atmospheric Scenario and Radon Analysis

The dose objective for the Atmospheric Scenario is 10 mrem/yr for all sources of airborne radioactivity at the Laboratory. Exposures were projected for receptors residing at the points of maximum exposure along the LANL boundary and the Area G fence line.

The peak mean exposure projected for the receptor at the LANL boundary is 0.23 mrem/yr; the corresponding exposure for the fence line resident is 0.64 mrem/yr. These exposures are small fractions of the Laboratory limit of 10 mrem/yr. The environmental surveillance report for 2003 (LANL, 2004) reports an annual dose of 0.65 mrem for the maximally exposed individual due to airborne releases from the Laboratory. This dose and those projected for Area G occur at different times and, therefore, are not additive. However, the magnitudes of these exposures suggest that the Laboratory will readily comply with the performance objective.

7.1.2.3 All Pathways–Canyon Scenario

The performance objective for the All Pathways–Canyon Scenario is the DOE primary dose limit of 100 mrem/yr and the corresponding 30 mrem/yr dose constraint. The composite analysis projected exposures for persons residing within nine catchments in Cañada del Buey and Pajarito Canyon (Figure 4-28). Canyon receptors within catchments PC5 and PC6, near the east end of Area G, were projected to receive peak mean exposures of 4.4 and 3.6 mrem/yr, respectively; doses projected for the other locations within Pajarito Canyon and the two locations in Canada del Buey were lower. These dose projections are less than the 100 mrem/yr performance objective and the 30 mrem/yr dose constraint.

Table 7-2
Comparison of Composite Analysis Results with Performance Objectives

Performance Objective	Exposure Scenario	Projected Impact
All Pathways (30 mrem/yr dose constraint)	All Pathways–Groundwater	No radionuclides were projected to discharge to the regional aquifer
	All Pathways–Canyon	Peak mean dose of 4.4E+00 mrem/yr for maximally exposed individual
Air Pathway (10 mrem/yr)	Atmospheric	Peak mean dose of 6.4E-01 mrem/yr for maximally exposed individual

7.1.2.4 Alternate Source Evaluation

The DOE primary dose limit of 100 mrem/yr applies to all sources of radioactivity at the Laboratory. An evaluation of the potential for significant interaction between releases from other facilities at LANL and those projected to occur at Area G was conducted. On the basis of this evaluation, the potential for any such interaction is considered negligible at this time.

7.1.2.5 ALARA Analysis

Field sites are required to conduct waste disposal in a manner that maintains releases to the environment ALARA. An evaluation of the collective impacts of releases from Area G under the closure configuration adopted for the performance assessment and composite analysis indicates that this is the case.

7.1.3 Evaluation of Inadvertent Intruder Analysis Results

The chronic and acute performance objectives for the inadvertent intruder are 100 and 500 mrem/yr, respectively. The intruder analysis projected exposures for the Intruder-Construction, Intruder-Agriculture, and Intruder–Post-Drilling Scenarios. Separate exposures were projected for the disposal pits used from September 27, 1988 through 2010 and those used from 2011 through 2044; the exposure estimates for the shafts distinguished between the units used from September 27, 1988 through 2015 and those used from 2016 through 2944. The following discussion compares the projected intruder impacts to the performance objectives; Table 7-1 summarizes this comparison.

All of the peak intruder doses projected for the disposal pits and shafts are lower than the 100 mrem/yr chronic and 500 mrem/yr acute intruder performance objectives. The peak mean doses projected for the 1988-2015 shafts are sensitive to the depths at which packages containing critical radionuclides are placed; the ability of the containers used to dispose of high-activity tritium waste to limit vapor-phase releases is an important consideration for the 2016–2044 shafts.

7.2 Use of the Results

The results of the performance assessment and composite analysis provide information important to the effective management of LLW at the Laboratory. The ways in which these results will be applied are discussed below.

7.2.1 Waste Acceptance Criteria

The results of the performance assessment were used to set limits on the amount of radioactivity that may be disposed of at Area G. Radionuclide concentration limits were calculated for the disposal units in MDA G on the basis of the three inadvertent intruder scenarios; these limits are discussed in Section 5 of this report. Table 5-4 presents the final WAC for the disposal units at MDA G.

The radionuclide concentration limits estimated on the basis of the intruder scenarios are isotope specific. The disposal of waste with several radionuclides requires consideration of the cumulative impacts of all sources of radioactivity within that material. In this case, the sum-of-fractions rule is applied. The concentration of each radionuclide in the waste is divided by that isotope's concentration limit; the resulting fractions are subsequently summed for all radionuclides present. If the sum of these fractions is 1.0 or less, the waste qualifies for safe disposal in the appropriate disposal units at Area G. Waste that yields a sum-of-fractions value greater than 1.0 will need to be evaluated for disposal on a case-by-case basis.

The intruder-based WAC represent limits on the average radionuclide concentrations in the waste placed in the disposal pits and shafts. Packages with contaminant concentrations in excess of these limits may be disposed of as long as the average concentrations remain at acceptable levels. However, acceptance of waste in excess of the limits on a routine basis will require that total disposal unit inventories be tracked to provide assurance that these average concentration limits are not violated.

It is possible to estimate facility inventory limits for Area G using the results of the performance assessment and composite analysis modeling. Any such limits, however, will be specific to the portion of Area G in which the waste is disposed, because rates of contaminant release and transport vary across the disposal facility. For example, differences in cover depths and erosion pressures among the waste disposal regions may allow greater quantities of waste to be safely disposed of in one portion of the facility relative to another.

7.2.2 Closure Plan

The final cover design upon which the performance assessment and composite analysis are based has changed dramatically from that considered in the 1997 analyses (Hollis et al., 1997). The modeling results suggest the updated design will prove capable in terms of limiting the amount of water that infiltrates through the waste, controlling the impacts of biotic intrusion, and maintaining releases of vapor- and gas-phase radionuclides at acceptable levels.

The closure plan for Area G has been updated to reflect the final cover design proposed for the disposal facility. However, as discussed in Section 7.3.7, an opportunity for optimizing this design to provide a safe, more cost-effective solution to facility closure exists. The findings of any such evaluations will be used to update the closure plan, performance assessment, and composite analysis as appropriate.

7.2.3 Monitoring Plan

The performance assessment and composite analysis identify parameters and processes of possible importance in terms of the long-term performance of the disposal facility. This information may be used to identify environmental monitoring and surveillance activities that

address potentially important modes of radionuclide release and transport. Information generated by these activities may subsequently be used to refine the performance modeling.

Careful planning is needed to integrate the performance assessment and composite analysis with the environmental monitoring effort at Area G so that maximum benefit can be gained from the monitoring activities. Most monitoring efforts conducted at Area G address operational releases. As a result, little of the information collected from these activities provides insight into release conditions that may prevail after the site has undergone final closure. With thought, however, it should be possible to design monitoring activities that address operational needs as well as issues pertinent to long-term facility performance.

7.3 Future Work

The performance assessment and composite analysis have been, and will continue to be, maintained under the Area G Performance Assessment and Composite Analysis Maintenance Program. Past activities conducted under this program have been used to improve knowledge about the site, develop new modeling techniques, and generally reduce the uncertainty associated with projections of the long-term performance of the disposal facility. Many of these efforts are detailed in the appendices contained in Volumes 2 and 3 of this report.

A considerable amount of progress has been made through efforts conducted under the maintenance program; more work remains to be done. For example, the uncertainty and sensitivity analyses conducted in support of the performance assessment and composite analysis identified several areas in need of further investigation. Some of the assumptions upon which the modeling was based highlight additional informational needs. The following discussion focuses on some of the key areas that would benefit from additional study.

7.3.1 Biotic Intrusion Parameters

The deposition of contamination on the surface of Area G resulting from the intrusion of plants and animals into the waste is an important mechanism of radionuclide release at the disposal facility. Given the amount of cover placed over the waste during interim and final closure, the rooting and growth characteristics of trees within the piñon-juniper woodland climax condition had significant impacts on the amount of contamination brought to the surface during modeling. Animal intrusion had a smaller impact on facility performance.

The biotic intrusion modeling relied heavily on data from the literature to characterize the four plant growth forms in terms of their rooting characteristics, biomass densities, and litter production rates. Given the relative importance of plant intrusion, it is reasonable to pursue investigations at the Laboratory that provide more site-specific data concerning these parameters and their variability. Although the root mass distributions of deep-rooted species such as trees are difficult to establish, estimates of biomass production and litter production are more readily obtained.

7.3.2 Effects of Elevated Moisture

Chloride measurements and infiltration modeling suggest rates of infiltration through the closed disposal facility will be low, but elevated moisture contents have been observed in active pits at Area G. Furthermore, the placement of surface structures such as asphalt pads has resulted in elevated moisture contents and focused runoff in some portions of the site. Increases in soil moisture may cause infiltration rates through the disposal units to rise, resulting in higher releases of mobile radionuclides and shorter travel times to the regional aquifer. It is not clear, however, how long elevated moisture contents will persist once the source of the additional water is removed. Evidence from other sites at the Laboratory suggests that moisture contents will return to natural conditions, but may require several years to do so depending upon the source-specific factors.

Plans are being made to evaluate the effects that variations in initial moisture contents may have upon projected rates of infiltration through the site. This work will build upon the infiltration modeling that was conducted in support of the performance assessment and composite analysis using HYDRUS (*Appendix G*, Volume 2*)*.

7.3.3 Hydrologic Parameter Impacts

The discussion of uncertainty and sensitivity in Section 4 highlights the fact that widely differing values of saturated hydraulic conductivity were used in the infiltration and surface erosion modeling. While initially this may appear contradictory, information collected since those modeling efforts were completed supports the values selected for use. Questions remain, however, such as how the conductivities of subsurface soils will evolve over time as they are penetrated by plant roots and animal burrows and exposed by erosion. Given that the infiltration and erosion model projections are expected to be quite sensitive to the hydraulic properties of the cover, it is worth pursuing these issues.

7.3.4 Cliff Retreat

The long-term impacts of cliff retreat on the performance of Area G were not evaluated in the performance assessment and composite analysis; work conducted at the Laboratory suggests any detrimental effects on the disposal pits and shafts are unlikely within 10,000—and possibly 100,000—years. However, cliff retreat continues to pose a risk, albeit a very long-term one, to the integrity of the disposal units.

No data are available to assess rates of cliff retreat with any degree of accuracy; studies designed to provide this information would represent a significant improvement in the knowledge base regarding this phenomenon. The development of estimates of cliff retreat rates requires the collection and processing of a statistically meaningful set of samples to determine the distribution of cliff face ages at Mesita del Buey using cosmogenic radionuclides. A thorough

investigation of cliff retreat rates and processes will help reduce uncertainty about the impacts of this phenomenon.

7.3.5 Sediment Transport

The exposures projected for the individuals residing in Cañada del Buey and Pajarito Canyon are proportional to the rate of contaminant deposition on the surface of the facility following biotic intrusion and the rate at which contaminated sediments are transported into the canyons. The surface erosion modeling conducted using SIBERIA estimated rates of sediment transport to the edge of the mesa, but did not track the movement of sediment down the sides of the mesa and onto the canyon floors. Without this information, it was necessary to make simplifying assumptions to estimate where and how the sediments were dispersed.

Since the surface erosion modeling was conducted, improvements have been made to the SIBERIA model. These improvements will allow more careful consideration of sediment transport from the mesa top, including dispersion during and after transport to the canyon floors. These increased modeling capabilities provide an opportunity to reduce the uncertainty associated with the simplifying assumptions that were used to estimate exposure concentrations for the All Pathways–Canyon Scenario.

Rates of sediment transport within Cañada del Buey and Pajarito Canyon are largely unknown. While canyon sediment residence times have been estimated for other locations at the Laboratory, it is unlikely that the implied transport rates apply to the canyons adjacent to Area G. The rates of sediment transport applied in the performance assessment and composite analysis modeling may be conservative, but actual measurements are needed to confirm this. Such information is important because less rapid rates of sediment transport may result in significantly higher exposures within the canyons, especially over very long periods of time.

The characterization of wind erosion conducted in support of the performance assessment and composite analysis implied no net loss of soil due to the actions of wind; simply put, the quantities of particulates entering and leaving an area were approximately equal. These results do not, however, indicate to what degree contaminated sediments may be redistributed across the site as a result of the horizontal movement of soil particles. The wind erosion work conducted in 2005 was not designed to address contaminant redistribution due to wind, but future work in this area may be warranted.

7.3.6 Subsidence

One of the key assumptions upon which the performance assessment and composite analysis are based is that subsidence will have no long-term impact on the performance of the disposal facility. This assumption is based on the supposition that actions will be taken over the remainder

of the facility's operational period and the100-year active institutional control period to correct any subsidence issues. It also presumes that such corrective actions will be effective.

Although the methods to dispose of waste are generally expected to minimize the potential for subsidence, the increased use of containers in the past 10 years has probably increased the likelihood of subsidence. Inspections of the disposal facility have indicated isolated incidences of subsidence near several shafts and larger impacts have been observed in conjunction with pits 9 and 15. Both of these pits have been used to store or dispose of waste placed in wooden and metal containers. It is unclear how these issues will be resolved in the future to avoid long-term impacts on facility performance, but it is evident that a course of action must be developed to address this issue.

7.3.7 Cover Optimization

The results of the performance assessment and composite analysis modeling suggest that the final cover design will effectively protect against the release of radionuclides from biotic intrusion into the waste. While the design specifications call for a minimum of 2.5 m (8.2 ft) of cover over all disposal units, significantly more material exists over the vast majority of the facility. This material is the primary defense against plant roots and burrowing animals.

Rough estimates suggest the design and application of the final cover over Area G could cost upwards of $70 million. This high cost, combined with the level of performance projected for the disposal facility, suggests an opportunity for cover design optimization. Effectively performed, optimization could reduce the costs associated with facility closure while safeguarding human health and safety and the environment. The modeling tools developed in support of the performance assessment and composite analysis will aid in any such optimization effort.

8.0 References

Abeele, W.V. and M.L. Wheeler, 1981, *Geohydrology of Bandelier Tuff,* Los Alamos Scientific Laboratory Report LA-8962-MS.

Abrahams, J.H. 1963, *Physical Properties of and Movement of Water in the Bandelier Tuff, Los Alamos and Santa Fe Counties, New Mexico,* U.S. Geological Survey Admin. Report.

Anspaugh, L.R., J.H. Shinn, P.L. Phelps, and N.C. Kennedy, 1975, "Resuspension and Redistribution of Plutonium in Soils," *Health Physics*, Vol. 29, pp. 571–582.

Apogen (Apogen Technologies), 2006, *Field Saturated Hydraulic Conductivity Investigation of Engineered Pit Cover Soils at Los Alamos National Laboratory, Material Disposal Area J,* Los Alamos report LA-UR-06-8746, November.

Archuleta, J., S. Barr, W.E. Clements, T. Gedayloo, and S.K. Wilson, 1978, *Some Atmospheric Tracer Experiments in Complex Terrain at LASL*, Los Alamos National Laboratory Report LA-7198-MS, Vol. 1, March.

Arimoto R., T.B. Kirchner, J. Webb, M. Conley, B. Stewart, D. Schoep, and M. Walthall, 2002, "$^{239, 240}$Pu and Inorganic Substances in Aerosols from the Vicinity of the Waste Isolation Pilot Plant: The Importance of Resuspension," *Health Physics*, Vol. 83, pp. 456–470.

Arnold, J. F., D.A. Jameson, and E.H. Reid, 1964, *The Pinyon-Juniper Type of Arizona: Effects of Grazing, Fire, and Tree Control,* U.S. Department of Agriculture, Forest Service, Production Research Report No. 84, September.

Aro, R.S., 1971, "Evaluation of Piñon-Juniper Conversion to Grassland," *J. Range Manage.*, Vol. 24, 188–197.

ASG, 2005, ASG (Atmospheric Study Group) at Earth Tech: Official CALPUFF Web Site, CALPUFF Modeling, updated July 7, 2005 <http://www.src.com/calpuff/calpuff1.htm>.

Baes, C.F. III, R.D. Sharp, A.L. Sjoreen, and R.W. Shor, 1984, *A Review and Analysis of Parameters for Assessing Transport of Environmentally Released Radionuclides through Agriculture,* Oak Ridge National Laboratory, ORNL-5786, September.

Ball, T., M. Everett, P. Longmire, D. Vaniman, W. Stone, D. Larssen, K. Greene, N. Clayton, and S. McLin, 2002, *Characterization Well R-22 Completion Report*, Groundwater Investigations Focus Area, Los Alamos National Laboratory Report LA-13893-MS, ER2001-0960, February.

BBER, 2005, "Data Bases on our Web Site," The Bureau of Business and Economic Research, University of New Mexico, <www.unm.edu/~bber/demo/table2.xls>.

Bechtel/SAIC, 2004, *Radionuclide Transport Models Under Ambient Conditions*, prepared for U.S. Department of Energy, Office of Civilian Radioactive Waste Management, by Bechtel SAIC Company, DOC.20041101.0002, October.

Bennett, K., J. Biggs, and P. Fresquez, 1997, *Radionuclide Contaminant Analysis of Small Mammals at Area G, TA-54, Los Alamos National Laboratory, 1995*, Los Alamos National Laboratory Report LA-13242-MS, January.

Bennett, K., J. Biggs, and P. Fresquez, 1998, *Radionuclide Contaminant Analysis of Small Mammals at Area G, Technical Area 54, G 1997 (with cumulative summary 1994-1997)*, Los Alamos National Laboratory Report LA-13517-MS, December.

Bennett, K.D., R.J. Robinson, and P.R. Fresquez, 2002, *Radionuclide Contaminant Analysis of Small Mammals at Area G, Technical Area 54, 1998 (with cumulative summary 1994-1998)*, Los Alamos National Laboratory Report LA-13874-MS, January.

Biggs, J.R., K.D. Bennett, and P.R. Fresquez, 1995, *Radionuclide Contaminant Analysis of Small Mammals at Area G, TA-54, 1994*, Los Alamos National Laboratory Report LA-13015-MS, September.

Biggs, J.R., K.D. Bennett, and P.R. Fresquez, 1997, *Radionuclide Contaminant Analysis of Small Mammals at Area G, Technical Area 54, 1996 (with cumulative summary for 1994-1995)*, Los Alamos National Laboratory Report LA-13345-MS, July.

Birdsell, K., 2005, Personal communication from Kay Birdsell, Los Alamos National Laboratory EES-6, to Rob Shuman, URS Corporation, October 26.

Birdsell, K.H., W.E. Soll, N.D. Rosenberg, and B.A. Robinson, 1995, *Numerical Modeling of Unsaturated Groundwater Flow and Radionuclide Transport at MDA G*, Los Alamos National Laboratory Report LA-UR-95-2735.

Birdsell, K.H., W.E. Soll, K.M. Bower, A.V. Wolfsberg, T.W. Orr, and T.A. Cherry, 1997, *Simulations of Groundwater Flow and Radionuclide Transport in the Vadose and Saturated Zones beneath Area G, Los Alamos National Laboratory*, Los Alamos National Laboratory Report LA-UR-97-157.

Birdsell, K., K. Bower, A. Wolfsberg, W. Soll, T. Cherry, and T. Orr, 1999, *Simulations of Groundwater Flow and Radionuclide Transport in the Vadose and Saturated Zones beneath Area G, Los Alamos National Laboratory*, Los Alamos National Laboratory Report LA-13299-MS.

Birdsell, K.H., A.V. Wolfsberg, D.H. Hollis, T.A. Cherry, and K.M. Bower, 2000, "Groundwater Flow And Radionuclide Transport Calculations for a Performance Assessment of a Low-Level Waste Site," *J. Contaminant Hydrology*, 46, pp. 99-129.

Birdsell, K.H., B.D. Newman, D.E. Broxton, and B.A. Robinson, 2005, "Conceptual Models of Vadose Zone Flow and Transport beneath the Pajarito Plateau, Los Alamos, New Mexico," *Vadose Zone Journal*, Vol. 4, pp. 620–636.

Bonaparte, R., B.A. Gross, D.E. Daniel, R.M. Koerner, and S.F. Dwyer, 2004, *Draft Technical Guidance For RCRA/CERCLA Final Covers*, U.S. Environmental Protection Agency, Office of Solid Waste and Emergency Response, Washington D.C.

Bowen, B.M., 1990, *Los Alamos Climatology*, Los Alamos National Laboratory Report LA-11735-MS.

Breshears, D.D., J.J. Whicker, M.P. Johansen, and J.E. Pinder, 2003, "Wind and Water Erosion and Transport in Semi-Arid Shrubland, Grassland, and Forest Ecosystems: Quantifying Dominance of Horizontal Wind-Driven Transport," *Earth Surface Processes and Landforms*, Vol. 28, pp. 1,189–1,209.

Broxton, D.E., 2005, Personal communication between Dave Broxton, LANL EES-6, and Phil Stauffer, LANL EES-6, October.

Broxton, D.E. and D.T. Vaniman, 2005, "Geologic Framework of a Groundwater System on the Margin of a Rift Basin, Pajarito Plateau, North-Central New Mexico," *Vadose Zone Journal*, Vol. 4, pp. 522–550.

Broxton, D.E., G. Heiken, S.J. Chipera, and F.M. Byers, Jr., 1995, "Stratigraphy, Petrography, and Mineralogy of Bandelier Tuff and Cerro Toledo Deposits" In *Earth Science Investigations for Environmental Restoration—Los Alamos National Laboratory, Technical Area 21*, Broxton, D.E. and P.G. Eller, eds., Los Alamos National Laboratory Report LA-12934-MS.

Broxton, D.E. and S.L. Reneau, 1995, *Stratigraphic Nomenclature of the Bandelier Tuff for the Environmental Restoration Project at Los Alamos National Laboratory*, Los Alamos National Laboratory Report, LA-13010-MS.

Broxton, D.E. and S.L. Reneau, 1996, "Buried Early Pleistocene Landscapes beneath the Pajarito Plateau, Northern New Mexico," *1996 New Mexico Geologic Society Field Trip Guidebook.*

Carey, J.W. and G. Cole, 2002, *Description of the Cerro Grande Fire Laser-Altimetry (LIDAR) Data Set*, Los Alamos National Laboratory, Report LA-13892-MS, 57pp. plus appendices.

Charley, J.L. and S.W. Cowling, 1968, "Changes in Soil Nutrient Status Resulting from Overgrazing and their Consequences in Plant Communities of Semiarid Areas," *Proceedings of the Ecological Society of Australia*, Vol 3, pp. 28–38.

Charman, P.E.V. and B.W. Murphy, 1992, *Soils—Their Properties and Management, A Soil Conservation Handbook for New South Wales*, Sydney University Press, ISBN 042 4001837, 363 pp.

Clary, W.P., 1971, "Effects of Utah Juniper Removal on Herbage Yields from Springerville Soils," *J. Range Manage.*, Vol. 24, pp. 373–378.

Clary, W.P., 1989, *Test of RPA Production Coefficients and Local Assumptions for the Pinyon-Juniper Ecosystem in Central Utah*," U.S. Forest Service, Intermountain Research Station, Research Paper INT-403, May.

Clary, W.P. and D.A. Jameson, 1981, "Herbage Production Following Tree and Shrub Removal in the Piñon-Juniper Type of Arizona," *J. Range Manage.*, Vol. 34, No. 2, pp. 109–113.

Costigan, K.R. and J.E. Bossert, 1996, "Three-Dimensional Modeling Study of Atmospheric Circulations and Dispersion at TA-54," Los Alamos National Laboratory Report LAUR-96-4793.

Cox, J.R., 1984, "Shoot Production and Biomass Transfer of Big Sacaton [*Sporobolus wrightii*]," *J. Range Manage.*, Vol. 34, No. 7, pp. 377–380.

Crowell, K.J., C.J. Wilson, and L.J. Lane, 2004, "Constraining Uncertainty in the Application of a Landscape Evolution Model to Predict 1000 Years of Erosion at a Mesa-Top Waste Repository", presented at American Geophysical Union Fall Meeting, 13–17 December, San Francisco, CA, Poster H51C-1142.

DBS&A (Daniel B. Stephens & Associates), 2003, *Jemez y Sangre Regional Water Plan*, Prepared for Jemez y Sangre Water Planning Council by Daniel B. Stephens & Associates in association with Amy Lewis, Albuquerque, New Mexico, March.

DBS&A, 2006 Laboratory Report for Los Alamos National Laboratory, Request No. 4526S, April 25.

Devaurs, M. and W. D. Purtymun 1985, "Hydrologic Characteristics of the Alluvial Aquifers in Mortandad, Cañada del Buey, and Pajarito Canyons," Los Alamos National Laboratory Report LA-UR-85-4002, Los Alamos, NM.

DOE, 1979, "Final Environmental Impact Statement, Los Alamos National Laboratory Site, Los Alamos, New Mexico," U.S. Department of Energy Report DOE/EIS-0018, December 1979.

DOE, 1988, *Radioactive Waste Management*, U.S. Department of Energy Order DOE O 5820.2A, September 26.

DOE, 1993, *Radiation Protection of the Public and the Environment*, U.S. Department of Energy Order 5400.5, Change 2, January 7.

DOE, 1996, *Natural Phenomena Hazards Design and Evaluation Criteria for Department of Energy Facilities*, DOE-STD-1020-94 (Change notice #1, January 1996) U.S. Department of Energy, Washington, D.C.

DOE, 1997, *Applying the ALARA Process for Radiation Protection of the Public and Environmental Compliance with 10 CFR Part 834 and DOE 5400.5 ALARA Program Requirements, Volume 1 – Discussion*, U.S. Department of Energy, DOE-STD-ALARA1 Draft, April.

DOE, 1999, *Site-Wide Environmental Impact Statement for Continued Operation of the Los Alamos National Laboratory*, U.S. Department of Energy, Albuquerque Operations Office, DOE/EIS – 0238, Albuquerque, NM, January.

DOE, 2001a, *Radioactive Waste Management*, U.S. Department of Energy Order DOE O 435.1 (change 1 to document issued July 9, 1999), August 28.

DOE, 2001b, *Implementation Guide for use with DOE M 435.1-2: Format and Content Guide for U.S. Department of Energy Low-Level Waste Disposal Facility Performance Assessments and Composite Analyses*, U.S. Department of Energy DOE G 435.1-2, January 10.

DOE, 2001c, *Radioactive Waste Management Manual*, U.S. Department of Energy Report DOE M 435.1-1 (change 1 to document approved on July 9, 1999), June 19.

DOE, 2002, *Los Alamos National Laboratory–Performance Management Plan for Accelerating Cleanup*, U.S. Department of Energy, July.

DOE, 2004, *Environmental Assessment for Proposed Corrective Measures at Material Disposal Area H within Technical Area 54 at Los Alamos National Laboratory, Los Alamos, New Mexico*, DOE/EA-1464, Department of Energy National Nuclear Security Administration, Los Alamos, June 14, <http://www.eh.doe.gov/nepa/pub_ea_toc.html>.

Dwyer, D.D. and R.D. Pieper, 1967, "Fire Effects on Blue Grama-Piñon-Juniper Rangeland in New Mexico," *J. Range Manage.*, Vol. 20, pp. 359–362.

EPA, 1988, *Limiting Values of Radionuclide Intake and Air Concentration and Dose Conversion Factors for Inhalation, Submersion, and Ingestion*, U.S. Environmental Protection Agency Federal Guidance Report 11, EPA 520/1-88-020, September.

EPA, 1989, Code of Federal Regulations, 40 CFR 61.192 Subpart Q, *National Emission Standards for Radon Emissions from Department of Energy Facilities*, (from Federal Register Vol. 54, p. 51701, December 15 1989 as amended by Vol. 65, p. 62158, October 17, 2000) <http://www.access.gpo.gov/nara/cfr/waisidx_04/40cfr61_04.html>).

EPA, 1993, *External Exposure to Radionuclides in Air, Water, and Soil*, U.S. Environmental Protection Agency Federal Guidance Report 12, EPA 402-R-93-081, September.

EPA, 2000, "Part II, Environmental Protection Agency, 40 CFR Parts 9, 141, and 142, National Primary Drinking Water Regulations; Radionuclides; Final Rule," Federal Register, Vol. 65, No. 236, pp. 76708–76753, December 7, <http://www.epa.gov/fedrgstr/EPA-GENERAL/2000/December/Day-07/g30421.pdf>.

EPA, 2002, *Final Implementation Guidance for Radionuclides*, United States Environmental Protection Agency, EPA 816-F-00-002, March.

EPA, 2003, "Part III, Environmental Protection Agency, 40 CFR Part 51, Revision to the Guideline on Air Quality Models: Adoption of a Preferred Long Range Transport Model and Other Revisions; Final Rule," *Federal Register*, Vol. 68, No. 72, pp. 18440–18482, April 15, <http://www.epa.gov/fedrgstr/EPA-AIR/2003/April/Day-15/a8542.pdf>

EPA, 2004, Code of Federal Regulations, 40 CFR 61.93 Subpart H, "National Emission Standards for Hazardous Air Pollutants; National Emission Standards for Emissions of

Radionuclides Other than Radon from Department of Energy Facilities," *Federal Register,* Vol. 69, No. 116, p. 33865, June 2004, <http://www.epa.gov/fedrgstr/EPA-AIR/2004/June/Day-17/a13679.htm>.

EPA, 2006, *Guidance on Systematic Planning Using the Data Quality Objectives Process*, U.S. EPA report EPA/240/B-06/001, February.

EPG (Environmental Protection Group), 1993, *Environmental Surveillance at Los Alamos During 1991*, Los Alamos National Laboratory Report LA-12572-ENV, August.

EPG, 1994, *Environmental Surveillance at Los Alamos during 1992*, Los Alamos, New Mexico, Los Alamos National Laboratory Report LA-12764-MS, UC-902, 192 p.

Federal Facility Compliance Act of 1992, 42 U.S.C. § 6961, et seq.

Foxx, T.S., G.D. Tierney, and J.M. Williams, 1984, *Rooting Depths of Plants on Low-Level Waste Disposal Sites*, Los Alamos National Laboratory Report LA-10253-MS, November.

French, S.B., 2005, Personal communication between Sean French, Los Alamos National Laboratory, and Rob Shuman, URS Corporation, October 24.

Gillette, D.A, D.W. Fryrear, J.B. Xiao, P. Stockton, D. Ono, P.J. Helm, T.E. Gill, and T. Ley, 1997, "Large-Scale Variability of Wind Erosion Mass Flux Rates at Owens Lake: Vertical Profiles of Horizontal Mass Fluxes of Wind-Eroded Particles with Diameter Greater than 50 μm," *J. Geophys. Res.,* Vol. 102(D22), pp. 25,977–25,987.

Glasco, T., 2005, E-mail from Timothy Glasco, Los Alamos County Water Utility, to Konnie Andrews, Shaw Environmental, Subject: "Re: Verification of LA Well Field Info," October 5.

Goff, F. J.N. Gardner, and S.L. Reneau, 2002, *Geology of the Frijoles 7.5-minute Quadrangle Los Alamos and Sandoval Counties, New Mexico*, New Mexico Bureau of Mines and Mineral Resources Open-file Digital Geologic Map OF-GM 42, Scale 1:24,000, Socorro, NM, June.

GoldSim, 2007a, *User's Guide — GoldSim Probabilistic Simulation Environment,Volume 1 of 2, Version 9.60*, GoldSim Technology Group, March.

GoldSim, 2007b, *User's Guide — GoldSim Probabilistic Simulation Environment,Volume 2 of 2, Version 9.60*, GoldSim Technology Group, March.

GoldSim, 2007c, *User's Guide — GoldSim Contaminant Transport Module, Version 4.20*, GoldSim Technology Group, March.

Grier, C.C., K.J. Elliott, and D.G. McCullough, 1992, "Biomass Distribution and Productivity of *Pinus edulis-Juniperus monosperma* Woodlands of North-Central Arizona," *Forest Ecology and Management*, Vol. 50, pp. 331–350.

Heiken, G., F. Goff, J. Stix, S. Tamanyu, M. Shafiqullah, S. Garcia, and R.C. Hagan, 1986, "Intracaldera Volcanic Activity, Toledo Caldera and Embayment, Jemez Mountains, New Mexico," *J. Geophys. Res*., Vol. 91, pp. 1799–1816.

Heimsath, A.M., W.E. Dietrich, K. Nishiizumi, and R.C. Finkel, 1997, "The Soil Production Function and Landscape Equilibrium," *Nature*, Vol. 388, pp. 358–361.

Hinesley, L.E., L.E. Nelson, and G.L. Switzer, 1991, "Weight and Nutrient Content of Litter During Secondary Succession on Well-Drained Uplands of the East Gulf Coastal Plain in Mississippi," *Can. J. For. Res.*, Vol. 21, pp. 848–857.

Hollis, D., E. Vold, R. Shuman, K. Birdsell, K. Bower, W. Hansen, D. Krier, P. Longmire, B. Newman, D. Rogers, E. Springer, 1997, *Performance Assessment and Composite Analysis for the Los Alamos National Laboratory Disposal Area G*, Los Alamos National Laboratory Report LA-UR-97-85, Report-54G-013, March.

ITRC, 2003, *Technical and Regulatory Guidance for Design, Installation, and Monitoring of Alternative Final Landfill Covers, ALT-2*, Interstate Technology & Regulatory Council Alternative Landfill Technologies Team, Washington, D.C.

Jackson, R.B., J. Canadell, J.R. Ehleringer, H.A. Mooney, O.E. Sala, and E.D. Schulze, 1996, "A Global Analysis of Root Distributions for Terrestrial Biomes," *Oecologia*, Vol. 108, pp. 389–411.

Jacobson, K.W., 2005a, E-mail from Keith Jacobson, Meteorology and Air Quality Group, Los Alamos National Laboratory, to Konnie Andrews, Shaw Environmental, "Met data from TA-54 tower" with attached Excel file "TA_monthly_summaries.xls," September 29.

Jacobson, K.W., 2005b, E-mail from Keith Jacobson, Meteorology and Air Quality Group, Los Alamos National Laboratory, to Konnie Andrews, Shaw Environmental, "Re: Met data from TA-54 tower" with attached GIF files "wr_day_2002.gif" and "wr_night_2002.gif."

Keating, E.H., V.V. Vesselinov, E. Kwicklis, and Z. Lu, 2003, "Coupling Basin- and Local-Scale Inverse Models of the Española Basin," *Ground Water*, Vol. 4, No. 2, pp. 200–211.

Keating, E.H., B.A. Robinson, and V.V. Vesselinov, 2005, "Development and Application of Numerical Models to Estimate Fluxes through the Regional Aquifer beneath the Pajarito Plateau," *Vadose Zone Journal*, Vol. 4, pp. 653–671.

Kleinfelder, Inc., 2003, *Characterization Well R-21 Los Alamos National Laboratory, Los Alamos, New Mexico*, Prepared for the United States Department of Energy and the National Nuclear Security Administration through the United States Army Corps of Engineers, Sacramento District, June 6.

Koukoura, Z., A.P. Mamolos, and K.L. Kalburtji, 2003, "Decomposition of Dominant Plant Species Litter in a Semiarid Grassland," *Applied Soil Ecology*, Vol. 23, pp. 13–23.

Krier, D., P.A. Longmire, R.H. Gilkeson, and H.J. Turin, 1997, *Geologic, Geohydrologic, and Geochemical Data Summary of Material Disposal Area G, Technical Area 54, Los Alamos National Laboratory*, Los Alamos National Laboratory Report LAUR-95-2696, February.

Krueger, J.W., 1992, *RFI Work Plan for Operable Unit 1148: Environmental Restoration Program*, Los Alamos National Laboratory Report LA-UR-92-855, May.

Kwicklis, E., M. Witkowski, K. Birdsell, B. Newman and D. Walther, 2005, "Development of an Infiltration Map for the Los Alamos Area, New Mexico," *Vadose Zone Journal*, Vol. 4, pp. 672–693.

Laflen, J.M., L.J. Lane, and G.R. Foster, 1991, "WEPP- A New Generation of Erosion Prediction Technology," *J of Soil and Water Conservation* Vol. 46, No. 1, pp. 34-38.

Lane, L.J., M.H. Nichols, L.R. Levick, and M.R. Kidwell, 2001, "A Simulation Model for Erosion and Sediment Yield at the Hillslope Scale," Chapter 8 (pp. 201–237) in *Landscape Erosion and Evolution Modeling*,(Harmon, R.S. and W.W. Doe, III, eds., Kluwer Academic/ Plenum Publishers, New York.

LANL, 1952, Los Alamos National Laboratory Internal Memorandum from Dean Meyer to Salvatore Russo, Subject: "Location of Contaminated Waste Burial Pits," January 31.

LANL, 1971a, Los Alamos Scientific Laboratory internal memorandum from W.B. Gibson to W.J. Maramam, Subject: General's Tanks – Memo from Dean D. Meyer, December 3.

LANL, 1993, *Installation Work Plan for Environmental Restoration*, Revision 3, Los Alamos National Laboratory Report LA-UR-93-3987, Los Alamos, NM. November.

LANL, 1995, *Installation Work Plan for Environmental Restoration*, Los Alamos National Laboratory ER Project Report LA-UR-95-4048.

LANL 1996b, *Environmental Surveillance at Los Alamos during 1994*, Los Alamos National Laboratory Report LA-13047-ENV, Los Alamos, NM.

LANL, 1997, *Waste Acceptance, Characterization, and Certification Program*, Los Alamos National Laboratory Interim Laboratory Implementation Requirements ILIR404-00-01.0, January.

LANL, 1998a, *Hydrogeologic Workplan Los Alamos National Laboratory*, Los Alamos National Laboratory Report, May 22.

LANL, 1998b, *Work Plan for Pajarito Canyon: Environmental Restoration Project*, Los Alamos National Laboratory Report LA-UR-98-2550, September.

LANL, 1999, *Work Plan for Sandia Canyon and Cañada del Buey: Environmental Restoration Project September 1999*, Los Alamos National Laboratory Report LA-UR-99-3610, September.

LANL, 2000a, *Installation Work Plan for Environmental Restoration Project, Revision 8, Regulatory Compliance Focus Area*, Los Alamos National Laboratory Report LA-UR-00-1336, March.

LANL, 2000b, *Resource Conservation and Recovery Act (RCRA) Facility Investigation (RFI) for Material Disposal Areas (MDAs) G, H, and L at Technical Area 54 (TA-54)*, March 21.

LANL, 2001, *RFI Report for Material Disposal Area H at Technical Area 54*, Los Alamos National Laboratory Report LA-UR-01-1208, May.

LANL, 2002a, *Environmental Surveillance at Los Alamos during 2001*, LA-13979-ENV, September.

LANL, 2002b, *TA-54 Area J Closure Certification Report*, Los Alamos National Laboratory Report LA-UR-02-6548.

LANL, 2003a, *TA-54 Area G Documented Safety Analysis*, written by Nuclear Waste Infrastructure Services Nuclear Assurance Group at the Los Alamos National Laboratory, Report No. ABD-WFM-001, April.

LANL, 2003b, Corrective Measures Study Report for Material Disposal Area H, Solid Waste Management Unit 54-004, at Technical Area 54, LANL Report LA-UR-03-3354, May.

LANL, 2003c, *Measurements of Field Saturated Hydraulic Conductivity of an Engineered Soil at Los Alamos National Laboratory's Technical Area 54, Material Disposal Area J*, Los Alamos National Laboratory report LA-UR-04-0325.

LANL, 2004, *Environmental Surveillance at Los Alamos During 2003*, Los Alamos National Laboratory Report LA-14162-ENV, September.

LANL, 2005b, *NWIS Environmental Monitoring Plan for 2005*, Los Alamos National Laboratory Report LA-UR-05-7154, August 1.

LANL, 2005c, *Storm Water Pollution Prevention Plan*, Los Alamos DIV-PLAN-0404, May 5.

LANL, 2005d, Investigation Report for Materials Disposal Area G, Consolidated Unit 54-013(b)-99, at Technical Area 54, Los Alamos National Laboratory Report LA-UR-05-6398.

LANL, 2005e, *Investigation Report for MDA L*, Los Alamos National Laboratory Report LA-UR-05-5777, September.

LANL, 2006, *Investigation Report for Material Disposal Area C, Solid Waste Management Unit 50-009, at Technical Area 50*, Los Alamos National Laboratory Report LA-UR-06-8096, December.

LANL, 2007a, *Pit and Shaft Design, Construction, and Operational Closure*, Los Alamos National Laboratory Procedure AP-2201, R.0, December.

LANL, 2007b *Environmental Surveillance at Los Alamos During 2006*, Los Alamos National Laboratory Report LA-14341-ENV, September.

LANL, 2007d, *Documented Safety Analysis for Surveillance and Maintenance of Nuclear Environmental Sites at Los Alamos National Laboratory, Los Alamos National Laboratory Report NES-ABD-0101*, Revision 1.0, June.

LANL, 2008a, Final Site-Wide Environmental Impace Statement for Continued Operation of Los Alamos National Laboratory, Los Alamos, New Mexico (SWEIS) (DOE/EIS-0380), Responsible Agency: U.S. Department of Energy, National Nuclear Security Administration, prepared at Los Alamos Site Office, May.

LANL, 2008b, *LANL Waste Acceptance Criteria*, Los Alamos National Laboratory Procedure No. P930-1, Rev. 0, Issued June 5.

LANL, 2008c, *Processing Waste Acceptance Criteria Exception Forms*, Los Alamos National Laboratory Procedure, SOP-5186, May.

LANL, 2008d, *LLW Receipt and Disposal*, Los Alamos National Laboratory Procedure, EP-DOP-2201, R.0, March.

Loaiza, D. and E. Vold, 1995, *Moisture Profiles Measured in Subsurface Monitor Holes at the Los Alamos LLRW Disposal Site*, Los Alamos National Laboratory Report LA-UR-95-1922.

Longmire, P.A., S.L. Reneau, P.M. Watt, L.D. McFadden, J. Gardner, C.J. Duffy, and R.T. Ryti, 1995, *Natural Background Geochemistry, Geomorphology, and Pedogenesis of Selected Soil Profiles and Bandelier Tuff, Los Alamos, New Mexico*, Los Alamos National Laboratory Report LA-12913-MS.

Longmire, P.A., C.R. Cotter, I.R. Triay, J.J. Kitten, C. Hall, J. Bentley, D. Hollis, and A.I. Adams, 1996, *Batch Sorption Results for Americium, Neptunium, Plutonium, Technetium, and Uranium Transport through the Bandelier Tuff, Los Alamos, New Mexico*, Los Alamos National Laboratory Report LA-UR-96-4716.

McKenzie, D.H., L.L. Cadwell, L.E. Eberhardt, W.E. Kennedy, Jr., R.A. Peloquin, and M.A. Simmons, M.A., 1982, *Relevance of Biotic Pathways to the Long-Term Regulation of Nuclear Waste Disposal*, prepared by Pacific Northwest Laboratory for the U.S. Nuclear Regulatory Commission, NUREG/CR-2675, Volume 2, October.

Millington, R.J., 1959, "Gas Diffusion in Porous Media," *Science*, Vol. 130, pp.100–102.

Murphy, K.L., J.M. Klopatek, and C.C. Klopatek, 1998, "The Effects of Litter Quality and Climate on Decomposition Along an Elevational Gradient," *Ecological Applications*, Vol. 8, No. 4, pp. 1,061–1,071.

Myers, S., 2004, E-mail from Steve Myers, LANL Nuclear Waste and Infrastructure Services – Solid Waste Operations, to Rob Shuman, URS Corporation, regarding measurement errors, June 15.

NCRP, 1999, *Recommended Screening Limits for Contaminated Surface Soil and Review of Factors Relevant to Site-Specific Studies*, National Council on Radiation Protection and Measurements, Report No. 129.

NEPA, National Environmental Policy Act, as amended, 42 U.S.C. § 4321, et seq.

Newman, B., 1996, *Vadose Zone Water Movement at Area G, Los Alamos National Laboratory, TA-54: Interpretations Based on Chloride and Stable Isotope Profiles*, Los Alamos National Laboratory Report LA-UR-96-4682.

NMED (New Mexico Environment Department), 2004, "Fact Sheet: Proposed Order on Consent under Section 74-4-10 of the New Mexico Hazardous Waste Act and Section 74-9-36(D) of the New Mexico Solid Waste Act, Issued to the United States Department of Energy, and the Regents of University of California for the Los Alamos National Laboratory, Los Alamos, New Mexico," EPA ID Number NM0890010515, State of New Mexico Environment Department, Hazardous Waste Bureau, Santa Fe, September, <http://www.nmenv.state.nm.us/HWB/pubnotice.html>.

NMEIB, 2002, *Drinking Water*, New Mexico Environmental Improvement Board, 20.7.10 NMAC (12/4/02 as amended through 9/1/2005).

NRC, 1986, *Update of Part 61 Impacts Analysis Methodology, Methodology Report*, U.S. Nuclear Regulatory Commission, NUREG/CR-4370, Vol. 1, January.

Nyhan, J.W., 2005, "A Seven-Year Water Balance Study of an Evapotranspiration Landfill Cover Varying in Slope for Semiarid Regions," *Vadose Zone Journal*, Vol. 4, pp. 466–480.

Nyhan, J., L. Hacker, T. Calhoun, and D. Young, 1978, *Soil Survey of Los Alamos County, New Mexico*, Los Alamos Scientific Laboratory Report LA-6779-MS, June.

Nyhan, J., B. Drennon, T.E. Hakonson, 1989, *Field Evaluation of Two Shallow Land Burial Trench Cap Designs for Long-Term Stabilization and Closure of Waste Repositories at Los Alamos, New Mexico*, Los Alamos National Laboratory Report LA-11281-MS.89.12.

Nyhan, J.W., T.E. Hakonson, and B.J. Drennon, 1990, "A Water Balance Study of Two Landfill Cover Designs for Semiarid Regions," *J. Environ. Qual.*, Vol. 19, p. 281–288.

Nyhan, J.W., G.J. Langhorst, C.E. Martin, J.L. Martinez, and T.G. Schofield, 1993, "Field Studies of Engineered Barriers for Closure of Low Level Radioactive Waste Landfills at Los Alamos, New Mexico, USA," In *Proceedings of the International Conf. on Nuclear Waste Management and Environmental Restoration*, Ahlstroem, P.E., C.C. Chapman, R. Kohout, and J. Marek, eds., Am. Soc. of Mechanical Engineers, pp. 255–266.

Nyhan, J.W., T.G. Schofield, and R.H. Starmer, 1997, "A Water Balance Study of Four Landfill Cover Designs Varying in Slope for Semiarid Regions," *J. Environ. Qual.*, Vol. 26, pp. 1385–1392.

Nylander, C.L., 2001, *Groundwater Monitoring Program at Los Alamos National Laboratory*, Los Alamos National Laboratory Report LA-UR-01-2054.

Nylander, C.L, K. A. Bitner, G. Cole, E. H. Keating, S. Kinkead, P. Longmire, B. Robinson, D. B. Rogers, and D. Vaniman, 2003, *Groundwater Annual Status Report for Fiscal Year 2002*, Los Alamos National Laboratory Report LA-UR-03-0244.

O'Rourke, J.T. and P.R. Ogden, 1969, "Vegetative Response Following Piñon-Juniper Control in Arizona," *J. Range Manage.*, Vol. 22, No. 6, pp. 416–418.

Olig, S.S. 1997, Letter-report to D. Hollis, LANL, from S. Olig, Senior Project Seismologist, Woodward-Clyde Federal Services, March 21, 1997, Oakland, CA.

Olig, S.S., K.I. Kelson, J.N. Gardner, S.L. Reneau, and M. Hemphill-Haley, 1996, "The Earthquake Potential of the Pajarito Fault System," In *The Jemez Mountains Region: New Mexico Geological Society Forty-Seventh Annual Field Conference Guidebook,* Goff, F., B.S. Kues, M.A. Rogers, L.D. McFadden, and J.N. Gardner, eds., pp. 143–151.

Parmenter, R.R., M.R. Mesch, and J.A. Macmahon, 1987, "Shrub Litter Production in a Sagebrush-Steppe Ecosystem: Rodent Population Cycles as a Regulating Factor," *J. Range Manage.*, Vol. 40, No. 1, pp. 50–54.

Philip, J.R. and D.A. DeVries, 1957, "Moisture Movement in Porous Materials under Temperature Gradients," Trans., *Amer. Geophys. Union*, Vol. 38, No. 2, pp. 222–232.

Pieper, R.D., 1968, "Comparison of Vegetation on Grazed and Ungrazed Piñon-Juniper Grassland Sites in Southcentral New Mexico," *J. Range Manage.*, Vol. 21, pp.51–53.

Pieper, R.D., 1990, "Overstory-Understory Relations in Piñon-Juniper Woodlands in New Mexico," *J. Range Manage.*, Vol. 43, No. 5, pp. 413–415.

Pollard, C.G. and R. Shuman, 1999, *Evaluation of Pre-1971 Radioactive Waste Disposal Data for TA-54 MDA G*, Rogers and Associates Engineering Corporation Report RAE-9629/3005-3, December.

Pratt, A.R., 1998, *Work Plan for Pajarito Canyon: Environmental Restoration Project*, Los Alamos National Laboratory Report LA-UR-98-2550.

Purtymun, W.D., 1984, *Hydrogeologic Characteristics of the Main Aquifer in the Los Alamos Area: Development of Ground Water Supplies*, Los Alamos National Laboratory Report LA-9957-MS.

Purtymun, W.D., 1995, *Geologic and Hydrologic Records of Observation Wells, Test Holes, Test Wells, Supply Wells, Springs, and Surface Water Stations in the Los Alamos Area*, Los Alamos National Laboratory Report LA-12883-MS.

Purtymun, W.D. and Kennedy, W.R., 1971, *Geology and Hydrology of Mesita del Buey*, Los Alamos Scientific Laboratory Report LA-4660.

Purtymun, W. D., M.L. Wheeler, and M. Rogers, 1978, *Geologic Description of Cores from Holes P-3 MH-1 through P-3 MH-5, Area G, Technical Area 54*, Los Alamos Scientific Laboratory Report LA-7308-MS.

RAC (Risk Asessment Corporation), 2003, *Risk Analysis, Communication, Evaluation, and Reduction at LANL: Overview of Groundwater Issues at Los Alamos National Laboratory, Draft Report*, submitted to Colorado State University in partial fulfillment of contract no.CSU G-3959-1, August 18.

RCRA, *Resource Conservation and Recovery Act (Solid Waste Disposal Act) as amended*, 42 U.S.C. § 6901, et seq.

Reneau, S.L., 1995a, "Potential Mesa-Edge Instability at Pajarito Mesa," In *Geological Site Characterization for the Proposed Mixed Waste Disposal Facility,* Reneau, S.L. and R. Raymond Jr., eds., Los Alamos National Laboratory Report LA-13089-MS, pp. 87–100.

Reneau, S.L. 1995b, "Geomorphic Studies at DP Mesa and Vicinity," In *Earth Science Investigations for Environmental Restoration—Los Alamos National Laboratory Technical Area 21*, Broxton, D.E. and P.G. Eller, eds., Los Alamos National Laboratory Report LA-12934-MS, pp. 65–92.

Reneau, S.L., D.P. Dethier, and J.S. Carney, 1995, *Landslides and Other Mass Movements near Technical Area 33,* Los Alamos National Laboratory Report LA-12955-MS, June.

Reneau, S.L. and D.L. Vaniman, 1998, *Fracture Characteristics in a Disposal Pit on Mesita del Buey*, Los Alamos National Laboratory Report LA-13539-MS.

Reynolds, T.D. and J.W. Laundre, 1988, "Vertical Distribution of Soil Removed by Four Species of Burrowing Rodents in Disturbed and Undisturbed Soils," *Health Physics*, Vol. 54, No. 4, pp. 445–450.

Robinson, B.A., M. Witkowski, C. J. Elliot, L. Dale, and R. Koch, 1999, *Numerical Model of Flow and Transport for Los Alamos Canyon*, Los Alamos National Laboratory (contact author at robinson@lanl.gov for an electronic copy).

Robinson, B.A. and H. Viswanathan, 2003, "Application of the Theory of Micromixing to Groundwater Reactive Transport Models," *Water Resources Res*., Vol. 39, No. 11.

Robinson, B.A., S.G. McLin, and H.S. Viswanathan, 2005, "*Hydrologic Behavior of Unsaturated, Fractured Tuff: Interpretation and Modeling of a Wellbore Injection Test*," *Vadose Zone Journal*, Vol. 4, pp. 694–707.

Rogers, D.B., B.M. Gallaher, E.L. Vold, 1996, *Vadose Zone Infiltration Beneath the Pajarito Plateau at Los Alamos National Laboratory*, Los Alamos National Laboratory Report LA-UR-96–485.

Rogers, D.B., P. Longmire, B.D. Newman, K. H. Birdsell, W.E. Soll, E.L. Vold, 1997, *Conceptual Model for Subsurface Transport at MDA G*, Los Alamos National Laboratory Report LA-UR-97-179, January.

Rogers, M.A., 1977, *History and Environmental Setting of LASL Near-Surface Land Disposal Facilities for Radioactive Wastes (Areas A, B, C, D, E, F, G, and T)*, Los Alamos Scientific Laboratory Report LA-6848-MN, Vol. 1, June.

Scanlon, B.R., M. Christman, R.C. Reedy, I. Porro, J. Simunek, and G.N. Flerchinger, 2002, "Intercode Comparisons for Simulating Water Balance of Surficial Sediments in Semiarid Regions," *Water Resources Research* Vol. 38, p. 1323 [doi:10.1029/2001WR001233].

Schulman, E., 1951, "Tree-Ring Indices of Rainfall, Temperature, and River Flow," in T.F. Malone, ed., *Compendium of Meteorology*, American Meteorological Society, pp. 1024–1029, Boston MA.

Scire, J.S., D. G. Stimanitis., and R.J. Yamartino, 2000a, *A Users Guide for the CALPUFF Dispersion Mode (Version 5)*, Earth Tech. Inc., Concord, Massachusetts, January.

Scire, J.S., F.R. Robe, M.E. Fernau and R.J. Yamartino, 2000b, *A User's Guide for the CALMET Meteorological* Model (Version 5), Earth Tech, Inc., Concord, Massachusetts.

Scurlock, J.M.O., K.R. Johnson, and R.J. Olson, 2003, *NPP Grassland: NPP Estimates from Biomass Dynamics for 31 Sites, 1948-1994*, Data set available on-line [http://www.daac.ornl.gov] from Oak Ridge National Laboratory Distributed Active Archive Center, Oak Ridge, TN.

Sehmel, G.A., 1980, "Particle Resuspension: A Review," *Environment International*, Vol. 4, pp. 107–127.

Shariff, A.R., M.E. Biondini, and C.E. Grygiel, 1994, "Grazing Intensity Effects on Litter Decomposition and Soil Nitrogen Mineralization," *J. Range Manage.*, Vol. 47, No. 6, pp. 444–449.

Shuman, R., 1999, *An Evaluation of the Potential Impacts of Plant and Animal Intrusion into Disposed Waste at TA-54, MDA G*, Rogers and Associates Engineering Corporation, RAE-9629/3005-1, April.

Shuman, R., S. French, and C. Pollard, 2003, *Performance Assessment and Composite Analysis Maintenance Program Plan for MDA G—2003*, Los Alamos National Laboratory Report LA-UR-03-3472.

Sims, P.L. and J.S. Singh, 1978, "The Structure and Function of Ten Western North American Grasslands; IV Compartmental Transfers and Energy Flow Within the Ecosystem," *J. Ecology*, Vol. 66, pp. 983–1,009.

Smith, R.E., D.C. Goodrich, D.A. Woolhiser, and C.L. Unkrich, 1995, "Chapter 20: KINEROS – a Kinematic Runoff and Erosion Model," in *Computer Models of Watershed Hydrology*, Singh, V.P.(ed.), Water Resources Publications, Highlands Ranch, Colorado, pp. 697–732.

Soll, W. and K. Birdsell, 1998, "The Influence of Coatings and Fills on Flow in Fractured, Unsaturated Tuff Porous Media System," *Water Resour. Res*., Vol. 34, pp. 193–202.

Spell, T.L., T.M. Harrison, and J.A. Wolff, 1990, "40Ar/39Ar Dating of the Bandelier Tuff and San Diego Canyon Ignimbrites, Jemez Mountains, New Mexico: Temporal Constraints on Magmatic Evolution," *J. Volcan. and Geothermal Research*, V. 43.

Springer, E.P., 2004, *Statistical Exploration of Matrix Hydrologic Properties for the Bandelier Tuff, Los Alamos, New Mexico*, Los Alamos National Laboratory Report LA-UR-04-2830.

Springer, E.P., 2005, "Statistical Exploration of Matrix Hydrologic Properties for the Bandelier Tuff, Los Alamos, New Mexico," submitted to *Vadose Zone Journal*.

Springer, E.P and T.G. Schofield, 2004, *Statistical Analyses of Mesa-Top Percolation Rates at Los Alamos National Laboratory, New Mexico*, Los Alamos National Laboratory Report LA-UR-04-7801.

Stauffer, P.H., 2005, Personal communication from Phil Stauffer, LANL EES-6, to Konnie Andrews, Shaw Environmental, October 13.

Stauffer, P.H., B.A. Robinson, and K.H. Birdsell, 2000, *Modeling Transport in Los Alamos Canyon: Effects of Hypothetical Increased Infiltration after the Cerro Grande Fire*, Los Alamos National Laboratory Report LA-UR-00-5923.

Stauffer, P.H., K Birdsell, M.S. Witkowski, and J.K. Hopkins, 2005, "Vadose Zone Transport of 1,1,1-Trichloroethane: Conceptual Model Validation through Numerical Simulation," *Vadose Zone Journal*, Vol. 4, pp. 760–773.

Stauffer, P.H. and W.J. Stone, 2005, "The Los Alamos Canyon Weir Site: Part 2. Modeling of Tracer Test Results," *Vadose Zone Journal*, Vol. 4, pp. 718–728

Stone, J.J., L.J Lane, and E.D. Shirley, 1992, "Infiltration and Runoff Simulation on a Plane," *Transactions of the American Society of Agricultural Engineers*, Vol. 35, pp. 161–170.

Stone, W.J., G.L. Cole, and M.A. Jones, 1999, *Documentation for the Preliminary Hydrogeologic Atlas for Los Alamos National Laboratory*, Los Alamos National Laboratory Report LA-UR-99-4619.

Stout, J.E. and T.M. Zobeck, 1996, "The Wolfforth Field Experiment: A Wind Erosion Study," *Soil Science*, Vol. 161, pp. 616–632.

Strojan, C.L., F.B. Turner, and R. Castetter, 1979, "Litter Fall from Shrubs in the Northern Mojave Desert," *Ecology*, Vol. 60, No. 5, pp. 891–900.

Tierney, G.D. and T.S. Foxx, 1987, *Root Lengths of Plants on Los Alamos National Laboratory Lands*, Los Alamos National Laboratory Report LA-10865-MS, January.

Turin, H. J., 1995, *Subsurface Transport Beneath MDA G: A Conceptual Model*, Los Alamos National Laboratory Report LA-UR 95-1663.

URS Corporation, 2004a, *TA-54 Zone 4 Conceptual Design Report*, Draft document, URS-24342406-00004-0, prepared for Los Alamos National Laboratory, Basic Agreement 13567-000-00-FT, Task Order No. 73, Salt Lake City, UT, September.

URS Corporation, 2004b, *TA-54 Zone 4 Disposal Cell Excavation and Waste Capacity Calculation*, Draft document, URS-24342406-00004-0, prepared for Los Alamos National Laboratory, Basic Agreement 13567-000-00-FT, Task Order No. 73, Salt Lake City, UT, September.

URS Corporation, 2004c, *TA-54 LLRW Operations Relocation (MDA G) Preliminary Design*, URS-24342406-00004-0, prepared for Los Alamos National Laboratory, Basic Agreement 13567-000-00-FT, Task Order No. 73, Salt Lake City, UT, September.

USAEC, 1970, "Policy Statement Regarding Solid Waste Burial," U.S. Atomic Energy Commission, Immediate Action Directive (IAD) 0511-21, March 20.

Vaniman, D., G. Cole, J. Gardner, J. Conaway, D. Broxton, S. Reneau, M. Rice, G. WoldeGabriel, J. Blossom, and F. Goff, 1996, *Development of a Site-Wide Geologic Model for Los Alamos National Laboratory*, Los Alamos National Laboratory Report LA-UR-96-2059.

Veilleux, J.M., 2005, *Determination of Plutonium Mass Fractions and Uncertainties from Waste Assay Measurements*, Los Alamos National Laboratory Report LA-UR-05-8922, November.

Warren, J.L., 1980, Memorandum from J.L. Warren to W. Hansen, Los Alamos Scientific Laboratory, *Program Status Report: Review of Past Waste Disposal Records*, January 2.

West, N.E., 1985, "Aboveground Litter Production of Three Temperate Semidesert Shrubs," *American Midland Naturalist*, Vol. 113, No. 1, pp. 158–169.

Whicker, J.J., D.D. Breshears, P.T. Wasiolek, T.B. Kirchner, R.A. Tavani, D. Schoop, and J. Rodgers, 2002, "Temporal and Spatial Variation of Episodic Wind Erosion in Unburned and Burned Shrubland," *J. Environ. Qual.*, Vol. 31, pp. 599–612.

Whittaker, R.H., 1975, *Communities and Ecosystems*, MacMillan Publishing Co., New York.

Willgoose, G.R. and S. Riley, 1998, "The Long Term Stability of Engineered Landforms of the Ranger Uranium Mine, Northern Territory, Australia: Application of a Catchment Evolution Model," *Earth Surf. Process. Landf.*, Vol. 23, No. 3, pp. 237–259.

Wirth, S., 1999, *Modeling the Potential Biological Effects on the Performance of TRU Waste Buried in GCD Boreholes at the Nevada Test Site*, IT Corporation Report, February.

WoldeGabriel, G., A. Laughlin, D. Dethier, and M. Heizler, 1996, "Temporal and Geochemical Trends of Lavas in White Rock Canyon and the Pajarito Plateau, Jemez Volcanic Field, New Mexico, USA," Goff, F., B. Kues, M. Rogers, L. McFadden, and G. Gardner, eds, *The Jemez Mountains Region, New Mexico Geologic Society Forty-Seventh Annual Field Conference*, pp. 251–261.

Wong, I., K. Kelson, S. Olig, S., T. Kolbe, M. Hemphill-Haley, J. Bott, R. Green, H. Kanakari, J. Sawyer, W. Silva, C. Stark, C. Haraden, C. Fenton, J. Unruh, J. Gardner, S. Reneau, and L. House, 1995, *Seismic Hazards Evaluation of the Los Alamos National Laboratory: Final Report.*

Zyvoloski, G.A., B.A. Robinson, Z.V. Dash, and L.L. Trease, 1995a, *Models and Methods Summary for the FEHMN Application*, Los Alamos National Laboratory Report LA-UR-94-3787, Rev. 1.

Zyvoloski, G.A., B.A. Robinson, Z.V. Dash, and L.L. Trease, 1995b, *User's Manual for the FEHMN Application*, Los Alamos National Laboratory Report LA-UR-94-3788, Rev. 1.

9.0 Preparers

The investigations conducted in support of the Area G performance assessment and composite analysis were performed by subject-matter experts. This section identifies the members of the team and provides information about their qualifications and contributions.

Greg Cole

Staff Scientist, Earth and Environmental Science Division, Los Alamos National Laboratory
B.A., M.S., Ph.D. Geological Sciences

Greg and coworkers developed the three-dimensional geological model used in the subsurface transport modeling. He is the author of *Update of the Vadose-Zone Geologic Model,* which serves as Attachment II to *Appendix E, Groundwater Pathway Model for Los Alamos National Laboratory Technical Area 54, Material Disposal Area G* (Volume 2).

Greg has 30 years of experience in geological data integration and analysis. He led the development of the initial three-dimensional geologic model of the Pajarito Plateau and, with coworkers, has continued to update and upgrade the model over the past 10 years. He also provides geologic models and visualizations for a number of other projects, both domestic and foreign.

Kelly Crowell

Postdoctoral Research Associate, Los Alamos National Laboratory
B.S., M.S. Electrical Engineering
M.S., PhD. Geography

Kelly implemented the SIBERIA landscape evolution model to evaluate surface erosion as described in *Appendix I, Surface Erosion Modeling for the Repository Waste Cover at Los Alamos National Laboratory Technical Area 54, Material Disposal Area G* (Volume 2). He also participated in obtaining field data used to calibrate the model.

Kelly has 10 years of experience in environmental remote sensing and geographical information systems (GIS). He most recently provided GIS support for modeling sediment and contaminant transport in a canyon stream following the Cerro Grande fire.

Mark S. Day

Principal Scientist, Senior Program Manager, URS Corporation
B.S. Civil and Environmental Engineering

Mark led the conceptual design effort for the final cover of the Area G repository, working closely with the team that implemented the surface erosion modeling. The final conceptual design is documented in *Appendix H, Conceptual Design of the Earthen Cover at Los Alamos National Laboratory Technical Area 54, Material Disposal Area G* (Volume 2).

Mark has 30 years of experience working as an engineer and has been a practicing professional engineer for 26 years. He has been in charge of multimillion dollar construction contracts from preliminary engineering through design to construction. He worked for 10 years in the Superfund program cleaning up large hazardous waste sites and for 7 years in the Radiation Control program, where he served as the Uranium Mill Tailings Remedial Action (UMTRA) project manager.

Carl W. Gable

Technical Staff Member, Hydrology Geochemistry and Geology Group (EES-6), Earth and Environmental Sciences Division, Los Alamos National Laboratory
A.B. Geophysics
M.S. Applied Physics
Ph.D. Geophysics

Carl designed and built the computation grids used in the flow and transport modeling as described in *Generation of the Three-Dimensional Numerical Grid*, which serves as Attachment I to *Appendix E, Groundwater Pathway M*odel *for Los Alamos National Laboratory Technical Area 54, Material Disposal Area G* (Volume 2). He also developed software tools to carry out the grid generation work.

For the past 15 years, Carl has been the LANL lead in all grid generation work for applications including the Yucca Mountain Project hydrology, Nevada Test Site hydrology, and Los Alamos ER hydrology. In addition, he works in the field of computational fluid dynamics with applications to plate tectonics and mantle convection and modeling heat and mass transport in hydrothermal systems.

Marvin O. Gard

Senior Technician, Earth & Environmental Sciences Division, Los Alamos National Laboratory
B.S. Agricultural Economics

Marvin helped prepare the chloride-based flux estimates and chloride and nitrate inventories as well as the statistical analyses for *Appendix F, Spatial Variation in Near-Surface Hydrologic*

Behavior at Los Alamos National Laboratory Technical Area 54, Material Disposal Area G (Volume 2). Marvin has 13 years of experience in data collection, analysis, and modeling.

Keith W. Jacobson

Technical Staff Member, Meteorology and Air Quality Group, Los Alamos National Laboratory
B.S. Environmental Science
M.S. Health Physics

Keith performed the atmospheric transport and dispersion modeling which calculated off-site air concentrations and ground deposition rates for the various radionuclide release scenarios used in the performance assessment and composite analysis. This modeling is described in *Appendix D, Air Dispersion Analysis for Los Alamos National Laboratory Technical Area 54, Material Disposal Area G* (Volume 2).

Keith has 20 years of experience in environmental monitoring, environmental assessments, and regulatory compliance work. In addition, he has 14 years of experience in various areas related to air transport and air-dispersion modeling.

Daniel G. Levitt

Technical Staff Member, Hydrology Geochemistry and Geology Group (EES-6), Earth and Environmental Sciences Division, Los Alamos National Laboratory
B.A. Geology
M.S. Soil Science
Ph.D. Soil Science

Dan was the principal investigator in the HYDRUS modeling efforts discussed in *Appendix G, Modeling of an Evapotranspiration Cover for the Groundwater Pathway at Los Alamos National Laboratory Technical Area 54, Area G.*

Dan has 16 years of experience in vadose zone hydrology and broad experience in numerical modeling and field and lab measurements. This experience includes 8 years supporting performance assessment work for the Nevada Test Site low-level radioactive and transuranic waste sites, 8 years supporting performance assessment work for Yucca Mountain Project, and his current work on the Area G performance assessment and composite analysis.

Brent D. Newman

Technical Staff Member, Earth & Environmental Sciences Division, Los Alamos National Laboratory
B.S., M.S. Geology
Ph.D. Geochemistry

Brent was principal investigator and lead author for *Appendix F, Spatial Variation in Near-Surface Hydrologic Behavior at Los Alamos National Laboratory Technical Area 54, Material Disposal Area G* (Volume 2).

Brent has been involved with the Area G performance assessment since 1996, and has over 15 years of experience working on landfill cover performance and radioactive waste site characterization issues. He has published papers on near-surface/vadose zone hydrology in journals such as *Hydrological Processes*, *Journal of Hydrology*, *Science*, *Vadose Zone Journal*, and *Water Resources Research.*

Bruce A. Robinson

Deputy Group Leader (acting), Hydrology, Geology, and Geochemistry Group, Earth and Environmental Sciences Division, Los Alamos National Laboratory
Ph.D. Chemical Engineering

Bruce assisted in the development of the simplified abstraction model used to compute the transport through the vadose zone and regional aquifer for the performance assessment model. This model is documented in *Incorporation of Sorption in the Micromixing Model* which serves as Attachment IV to *Appendix E, Groundwater Pathway M*odel *for Los Alamos National Laboratory Technical Area 54, Material Disposal Area G* (Volume 2).

Bruce has over 20 years of experience in flow and transport modeling in unsaturated and saturated media, developing models and performing analyses for the Yucca Mountain Project and the LANL Groundwater Protection Program. He has been project leader for the interpretation and analysis portion of the Yucca Mountain Project for the past 3 years.

Rob Shuman

Principal Scientist, URS Corporation
B.S. Zoology
M.S. Health Physics/Radioecology

Rob designed and implemented the GoldSim probabilistic modeling used in the performance assessment and composite analysis for Area G, as described in *Appendix K, GoldSim Model Documentation and Data Selection for Los Alamos National Laboratory Technical Area 54, Area G Performance Assessment and Composite Analysis* (Volume 3). In addition, he prepared

the waste inventory and characterization used in the source term modeling, which is described in *Appendix J, Radioactive Waste Inventory for Los Alamos National Laboratory Technical Area 54, Area G* (Volume 2). He conducted and documented the dose assessment *(Appendix L, Radiological Dose Assessment for Los Alamos National Laboratory Technical Area 54, Area G Performance Assessment and Composite Analysis)* and the as low as reasonably achievable (ALARA) analysis (*Appendix M, ALARA analysis for Los Alamos National Laboratory Technical Area 54, Area G Performance Assessment and Composite Analysis),* both of which are contained in Volume 3. Rob was the author of Volume 1 of this report.

Rob has more than 20 years of experience in radioactive waste management, having focused on human health and ecological risk assessment over this period. He has been involved with the Area G performance assessment and composite analysis since the mid-1990s and has participated in the reviews of such analyses for other DOE sites.

Everett Springer

Technical Staff Member, Atmospheric, Climate and Environmental Dynamics Group, Earth and Environmental Sciences Division, Los Alamos National Laboratory
B.S., Ph.D. Watershed Science

Everett performed statistical analyses of the unsaturated zone hydrologic properties for Technical Area 54 for use in modeling the subsurface pathway. He is the author of *Attachment III, Statistical Description of Vadose-Zone Hydrologic Properties for the Los Alamos National Laboratory TA-54, Material Disposal Area G Groundwater Pathway Model,* which is included with Appendix E in Volume 2.

Everett has many years of experience in simulation and assessment of surface and subsurface arid and semiarid hydrologic systems. He is working on a coupled atmospheric, surface water, and subsurface model of the Rio Grande basin to examine the impacts of climate variability and land use change.

Philip H. Stauffer

Staff Scientist, Hydrology, Geochemistry and Geology Group, Earth and Environmental Sciences Division, Los Alamos National Laboratory
B.S. Physics
Ph.D. Geophysics

Phil was the principal investigator for *Appendix E, Groundwater Pathway Model for the Los Alamos National Laboratory Technical Area 54, Material Disposal Area G* (Volume 2). This task involved integrating scientific input from Everett Springer, Carl Gable, and Greg Cole into a three-dimensional numerical model of flow and transport in the subsurface at Area G. Phil

worked with Bruce Robinson and Hari Viswanathan to abstract the three-dimensional model to one-dimensional pathways and was the technical lead on coupling the one-dimensional pathways to GoldSim, working closely with Rob Shuman to ensure compatibility with the performance assessment system model. In addition, Phil worked with Rob Shuman on the development, implementation, and interpretation of all aspects of the groundwater pathway modeling. He was responsible for writing Appendix E.

Phil has 14 years of experience in simulation and assessment of subsurface arid and semiarid hydrologic systems in the Los Alamos area. He has 10 years of experience simulating subsurface transport at MDA L, which is immediately adjacent to Area G and shares many of the same subsurface characteristics.

Hari S. Viswanathan
Technical Staff Member, Hydrology, Geochemistry and Geology Group (EES-6), Earth and Environmental Sciences Division, Los Alamos National Laboratory
B.S. Chemical Engineering
M.S., Ph.D. Environmental Engineering

Hari helped develop the GoldSim transport abstraction model, as documented in *Incorporation of Sorption in the Micromixing Model* which serves as Attachment IV to *Appendix E, Groundwater Pathway M*odel *for Los Alamos National Laboratory Technical Area 54, Material Disposal Area G* (Volume 2). The work included developing the interface between FEHM, the flow and transport code, and the GoldSim performance assessment model. Hari also coauthored *Details on the Coupling of GoldSim and the Finite Element Heat and Mass (FEHM) Transfer Code for the Los Alamos National Laboratory TA-54, Material Disposal Area G* (Attachment V to Appendix E).

For the past five years, Hari has been working in the area of contaminant transport modeling for both the Yucca Mountain and Nevada Test Site programs. He was the lead investigator for the Yucca Mountain colloid work, which studied the transport of colloids through the saturated zone. For the Nevada Test Site, Hari studies the colloid-facilitated transport of radionuclides such as plutonium. He also works in the area of CO_2 sequestration on the Zert Emission Research and Technology Program. This work involves developing a performance assessment model for possible sites that could be used for CO_2 sequestration.

Jeff Whicker

Technical Staff Member, Los Alamos National Laboratory
M.S. Health Physics
Ph.D. Radioecology

Jeff was the lead researcher and principal author of *Assessing Wind Erosion as a Contaminant Transport Mechanism at Los Alamos National Laboratory Technical Area 54, Material Disposal Area G.* This study is included as Appendix C in Volume 2 of this report.

Jeff has over 17 years of experience in operational and environmental health physics, and his research has resulted in over 60 scientific publications, reports, and presentations. Jeff's research in outdoor air quality has focused on aerosol transport through wind-driven resuspension of contaminated soil and the effects of ecosystem disturbance on environmental transport rates through wind erosion.

Cathy Wilson

Technical Staff Member, Earth and Environmental Sciences, Los Alamos National Laboratory
B.A. Mathematics
Ph.D. Geology

Cathy was the technical lead on the 2003–2005 study that dealt with the long-term erosion performance of the closure cover for Area G. Cathy developed and managed the work plan for parameterizing, applying, and testing the SIBERIA model at TA-54. This included overseeing the collation and analysis of relevant field data, development of SIBERIA input data to account for uncertainty, and assessment of SIBERIA results in relation to published long-term sediment yields. Cathy wrote *Appendix I, Surface Erosion Modeling for the Repository Waste Cover at Los Alamos National Laboratory Technical Area 54, Material Disposal Area G*, which is included in Volume 2 of this report.

Cathy's research includes theoretical and experimental hydrology and geomorphology with an emphasis on understanding and predicting contaminant transport processes in natural and engineered systems. She has 16 years of project management and environmental modeling experience.

LA-UR-08-06097

Approved for public release;
distribution is unlimited.

Title:	Responses to Long-Term Conditions Issued by the Low-Level Waste Federal Review Group
Author(s):	Rob Shuman Sean French
Intended for:	U.S. Department of Energy

Form 836 (7/06)

The 1997 Area G performance assessment and composite analysis were reviewed by the Low-Level Waste Federal Review Group (LFRG) and accepted with conditions (DOE, 1998). A series of short-term conditions requested clarification on several aspects of the analyses, a response to these conditions was sent in late 1998 (LANL, 1998). The long-term conditions were to be addressed by activities conducted under the Area G Performance Assessment and Composite Analysis Maintenance Program. Those conditions are provided below along with a discussion of how the revised performance assessment and composite analysis addresses them.

1.0 Land Use, Closure, and Institutional Control

The site assumes that the disposal facility cover remains unchanged (e.g., gravel covered and lush grasses) for the entire 1,000-year compliance period.

Condition: The site must include a plan in the Performance Assessment/Composite Analysis to ensure that the cover is maintained as assumed. There must be a process in place to ensure that the closure plans for the facility are consistent with long-term use. LANL is to provide more detailed plans for control of the cover as part of the Performance Assessment/Composite Analysis maintenance plan.

Response: The assumption that the DOE will actively maintain the closed disposal facility throughout the 1,000-year compliance period has been reconsidered. The revised performance assessment and composite analysis assume active institutional control is maintained over Area G for a period of 100 years following facility closure. During this time, the site is assumed to be maintained to prevent the establishment of deep-rooted trees, to prevent severe localized erosion, and to exclude members of the public from the site. Passive institutional control is assumed for the remainder of the compliance period; while members of the public are prevented from entering the site during this period; no other maintenance activities are performed. In conjunction with changes in assumptions about future control of the disposal facility, a more robust final cover design has been developed that is expected to provide adequate isolation of the waste over the 1,000-year compliance period. Given these changes and improvements, no plans for control or maintenance of the cover following the active institutional control period were developed.

Condition: The site should continue to collect additional data (environmental transport, chloride, and stable isotope) and perform studies (surface water runoff, erosion, and water balance) as necessary (described in Appendix E of the Review Team's Report) to ensure that the uncertainty is minimized and that the projected doses are adequately protective. This activity should be included in the site documentation of the Performance Assessment/Composite Analysis maintenance plan.

Response: Several investigations have been conducted under the Area G Performance Assessment and Composite Analysis Maintenance Program since the 1997 performance assessment and composite analysis were issued; many of these address the uncertainty associated with the long-term performance projections developed for the facility. The results of these efforts may be found in the other appendices to this report. The studies directly pertinent to the condition provided above include the collection of chloride and stable isotope data that were used to establish subsurface moisture conditions at the facility and estimate moisture fluxes; the conduct of infiltration modeling to estimate rates of infiltration through the final cover; characterization of the wind erosion potential for site conditions expected after facility closure; and three-dimensional surface erosion modeling conducted to estimate rates of cover loss and patterns of sediment dispersal.

2.0 Subsidence

Use of B-25 boxes and Land/Sea containers in the trenches in the past few years (based on a DNFSB recommendation) has led to a situation where wastes are not being compacted.

Condition: The policy described above should be re-examined in light of the evaluation provided to the LFRG and the LFRG is to be notified of any potential impacts. Policy and operational changes are to be addressed in the Performance Assessment Maintenance Plan and in the relevant operational procedures.

Response: Waste containers have continued to be used for the disposal of waste, save for bulk contaminated materials such as soils and debris. The use of containers is expected to result in more efficient use of the available disposal capacity. More restrictive container fill requirements have been developed to minimize the void spaces in the containers to 5 percent or less of the container volume; compaction of the waste within the containers also minimizes the void paces in the packages.

Disposal units at Area G have received incompletely filled containers of waste in the past; this may be the cause of some of the subsidence events observed in recent years. Recognizing the potential for subsidence, options for minimizing the impacts of such have been considered, ranging from repairing damage as it occurs over the facility's operational period and the 100-year active institutional control period to dynamic compaction of selected disposal units. No final decisions have been made with respect to how the potential for subsidence will be addressed.

3.0 Air Pathway Analysis

The upper end of the range of doses reported in the uncertainty analysis for the Composite Analysis resulting from resuspension of contaminated soils exceeds the performance objective.

Condition: Uncertainties associated with the dose resulting from the resuspension of contaminated soils need to be addressed in terms of source contribution; additional actions to be taken with regard to cover stability. These actions can be addressed in the Performance Assessment Maintenance Program through the appropriate data collection and re-evaluation.

Response: The potential for airborne releases of contaminated soils and the transport of airborne contaminants to locations downwind of the disposal facility have been re-evaluated. The biotic intrusion modeling has been updated to consider a suite of plants and burrowing animals that may penetrate into the buried waste. Estimates of the rates at which surface contamination will be suspended from the site have been improved based on field studies conducted at the Laboratory. Finally, complex terrain atmospheric transport modeling has been conducted to provide more reliable estimates of contaminant concentrations at downwind exposure locations.

4.0 ALARA Analysis

The ALARA evaluation presented in the Performance Assessment/Composite Analysis does not lead to a clear conclusion.

Condition: LANL is to develop, based on the ALARA rationale submitted as a short term condition, a comprehensive approach for making decisions with respect to operations, closure, and post-closure care of the facility as part of the development and implementation of the Performance Assessment Maintenance Plan.

Response: An ALARA analysis was conducted to evaluate the relative effectiveness of the closure strategy upon which the performance assessment and composite analysis were based and two closure alternatives. The results of these analyses were used to conclude if current closure plans are consistent with maintaining doses ALARA and to determine if the other strategies provide more cost-effective alternatives to facility closure. The level of detail of the analysis was commensurate with the collective risk posed by releases from the disposal facility.

5.0 Closure and Postclosure Care (RCRA/CERCLA)

Although not necessarily evident from the Performance Assessment, there are ancillary data that suggest there is an urgent need to integrate activities performed under RCRA and CERCLA to ensure that the facility is operated and maintained in accordance with requirements and that potential impacts from programmatic and regulatory changes are evaluated prior to implementation.

Condition: LANL is to address long term RCRA / CERCLA integration issues in the Performance Assessment Maintenance Program and specific commitments must be provided to ensure that integration efforts are effective.

Response: Regulatory authority for closure of MDA G is shared by both the New Mexico Environment Department and the Department of Energy. LANL's Environmental Division (ENV) is responsible for actual closure of the site in accordance with Resource Conservation and Recovery Act regulations and DOE Order 435.1. LANL's Nuclear Waste Facilities Division (NWIS) is responsible for management and maintenance of the Area G performance assessment and composite analysis, and for continually assessing the long-term performance of the site to ensure adequacy of the analyses.

As recognized by the DOE in Section 5.2 of its authorization for continued disposal of low-level waste at Area G, the complex network of authorities and responsibilities for closure of MDA G necessitates integration among the various entities responsible for planning and executing closure of MDA G. To this end, in 2003 the responsibility for management and maintenance of the Performance Assessment was transferred to the LANL Nuclear Waste Facilities Operations Support Group (NWIS-OS). NWIS-OS is directly responsible for environmental management at NWIS facilities (including Area G). By combining institutional responsibility for environmental compliance at Area G and management of the Area G performance assessment into a single organization, LANL helps to ensure RCRA closure requirements are integrated with those of DOE Order 435.1. In addition to this effort, the following initiatives are also in place to integrate closure and post-closure care strategies between LANL's ENV and NWIS Divisions:

- NWIS-OS personnel have been assigned as standing review members for LANL ENV project documents related to final closure and care of MDA G, as well as ongoing characterization activities at the site
- NWIS has established a Facility Operations Review Committee (FORC) which reviews and approves activities occurring within NWIS facilities (including Area G). All ENV activities proposed for MDA G must be approved through the established FORC process. An environmental specialist familiar with the Area G performance

assessment is a member of the FORC review team, which promotes integration of ENV activities with current and long-term NWIS plans for the facility.

- LANL Readiness in Technical Basis and Facilities (RTBF) and Environmental Management (EM) Program Managers responsible for defining funding for ongoing work at NWIS facilities work closely to ensure adequate and appropriate allocation of funds for operations and closure at MDA G. This partnership between EM and RTBF funding leads to integrated planning of closure and post-closure care at MDA G.

As evidence of the success of these integration efforts, note that the final closure alternative that LANL's ENV Division intends to propose to the New Mexico Environment Department will be based on the conceptual cover design developed by NWIS Division as part of recent efforts to revise the Area G performance assessment and composite analysis.

6.0 References

DOE, 1998, Department of Energy Memorandum from James Fiore, Acting Deputy Assistant Secretary for Environmental Restoration, and Mark W. Frei, Acting Deputy Assistant Secretary for Waste Management to William John Arthur III, Assistant Manager, Office of Environment and Project Management, Albuquerque Operations Office, regarding Disposal Authorization for the Los Alamos National Laboratory Low-Level Waste Disposal Area G, October 2.

LANL, 1998, Memorandum from Dennis L. Newell, EM-SWO, Los Alamos National Laboratory, to Jim Orban, U.S. Department of Energy, Albuquerque Operations Office, regarding LFRG Short Term Conditions for Disposal Authorization at Area G, December 15.

LA-UR-05-6899

Approved for public release;
distribution is unlimited.

Title: CONCEPTUAL DESIGN OF ZONE 4 DISPOSAL UNITS AT LOS ALAMOS NATIONAL LABORATORY TECHNICAL AREA 54, MATERIAL DISPOSAL AREA G

Author(s): Sean French

Submitted to: U.S. Department of Energy

Form 836 (8/00)

Table of Contents

List of Figures i
List of Tables i
Acronyms and Abbreviations ii

1.0 Introduction 1
2.0 Description of Zone 4 3
3.0 Design Approach 5
3.1 Document Review 5
3.2 Archeological Evaluation 5
3.3 Volatile Organic Compound Plume Evaluation 6
3.4 Operational Needs Assessment 6
3.5 Preliminary Layouts and Designs 6
4.0 Conceptual Design 7
4.1 Design Criteria and Parameters 7
4.2 Conceptual Design 9
4.2.1 Phased Development Approach 9
4.2.2 Conceptual Layout 10
4.2.2.1 Pit Details and Ramps 10
4.2.2.2 Disposal Pit Calculations 11
5.0 Differences between the Preliminary and Final Conceptual Designs 13
6.0 References 15

List of Figures

Figure 1 Active Portion of Material Disposal Area G and Location of Zone 4 2
Figure 2 Topography of Zone 4 Area 4
Figure 3 Proposed Disposal Cell Development in Zone 4 8

List of Tables

Table 1 Design Capacities of Zone 4 Development Phases 11
Table 2 Differences in Phased Pit Development for Preliminary and Final Conceptual Designs 13

Acronyms and Abbreviations

LANL	Los Alamos National Laboratory
LLW	Low-level waste
MDA	Material disposal area
PCB	Polychlorinated biphenyl

1.0 Introduction

Material Disposal Area (MDA) G at Technical Area (TA-) 54 has served as the primary low-level radioactive waste disposal site for the Los Alamos National Laboratory (LANL or the Laboratory) since 1959. During that time, the development of disposal units has progressed generally from east to west, in accordance with the pit and shaft construction guidelines in effect at the time of construction. The result has been the construction of 35 disposal pits and more than 200 shafts. Figure 1 shows the general layout of the disposal pits in the active portion of MDA G.

The MDA G performance assessment and composite analysis are based on the assumption that low-level waste (LLW) will be disposed of at MDA G through the year 2044. By the end of 2004, however, almost all of the available disposal capacity within the active footprint of MDA G had been exhausted. Preparations have been made to construct additional disposal pits and shafts in the area immediately west of the existing disposal units, in an undeveloped area referred to as Zone 4 (Figure 1). Several options for the development of Zone 4 have been evaluated; these options are detailed in the LANL Zone 4 development report (2005b).

Most of the LLW requiring disposal after 2004 will be placed in disposal units that will be constructed in Zone 4. The assessment of the long-term performance of these pits and shafts requires an understanding of the spatial arrangement and construction of the units as well as the procedures that will be followed for their closure. Thus, the design plans for Zone 4 are an integral component of the performance assessment and composite analysis.

This report presents the design characteristics of Zone 4 pertinent to the MDA G performance assessment and composite analysis. Nearly all of the information presented is summarized from the development report for Zone 4 (LANL, 2005b), which contains a more in-depth discussion of the proposed design of future disposal units. Section 2 discusses the physical characteristics of the site and Section 3 presents the general approach adopted for the design process. Section 4 summarizes the conceptual design, aspects of which directly affect the modeling conducted in support of the MDA G performance assessment and composite analysis. Because the performance assessment and composite analysis modeling was underway before the conceptual design of Zone 4 was finalized, some of the design characteristics used for the modeling differ slightly from those presented in the development report (LANL, 2005b). Section 5 addresses the differences between the conceptual design summarized in Section 4 (the final conceptual design) and the preliminary design on which the performance assessment and composite analysis are based.

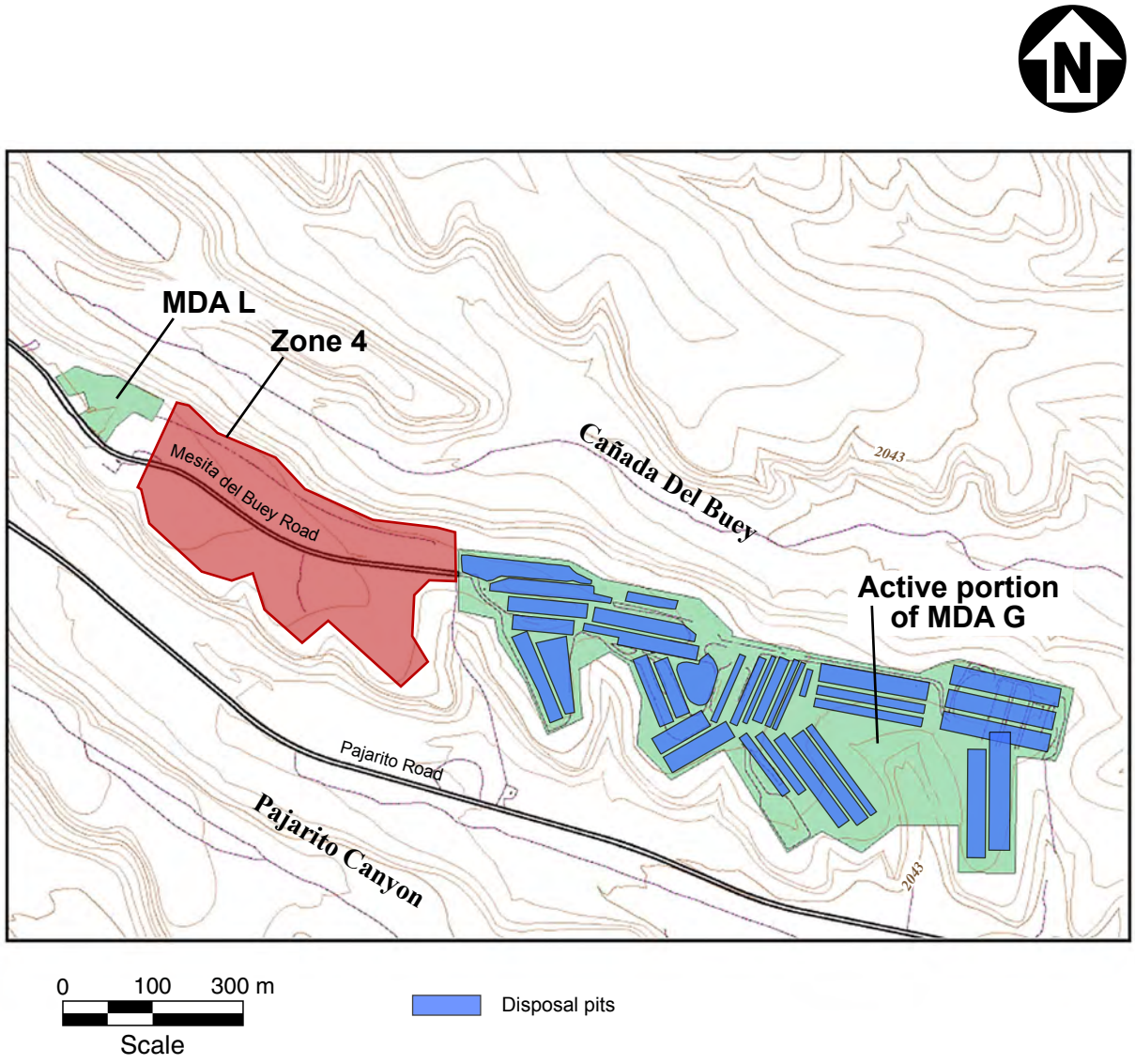

Figure 1
Active Portion of Material Disposal Area G and Location of Zone 4

2.0 Description of Zone 4

Zone 4, as identified in the site-wide environmental impact statement (DOE, 1999), is located on Mesita del Buey, within TA-54. Encompassing slightly more than 12 ha (30 acres), it extends from MDA L eastward to the footprint of the active disposal area of MDA G. The Mesita del Buey Road, which bisects Zone 4, allows traffic to flow east and west along the axis of the mesa and divides Zone 4 into "north" and "south" sides (Figure 2).

Within Zone 4, the top of the mesa slopes about 3.5 percent in a northwest to southwest direction; slopes near the mesa edge and beyond are considerably steeper, ranging from 20 to 200 percent to near vertical in a few localized areas. Drainage generally follows the direction of the 3.5 percent slope. At least four pronounced erosional features, the result of surface water drainage and cliff retreat, cut into the south edge of the mesa (Figure 2). No major erosional features exist on the north edge of the mesa, as only minor channels transport water off of the mesa in this direction.

The surface and upper portion of Mesita del Buey consists of Bandelier Tuff, volcanic ash that has been compacted and cemented over time. The tuff is relatively soft and readily removed by excavation, as evidenced by the pits and shafts located in the active area of MDA G. The thickness of the Bandelier Tuff is assumed to be relatively consistent across Mesita del Buey.

Several archeological sites containing the remains of prehistoric Native American habitation have been identified within Zone 4. All but one of these sites are on the south side of the road. Other archeological features associated with Zone 4 include *cavates*, which are small caves carved or hollowed into the face of the south mesa cliff.

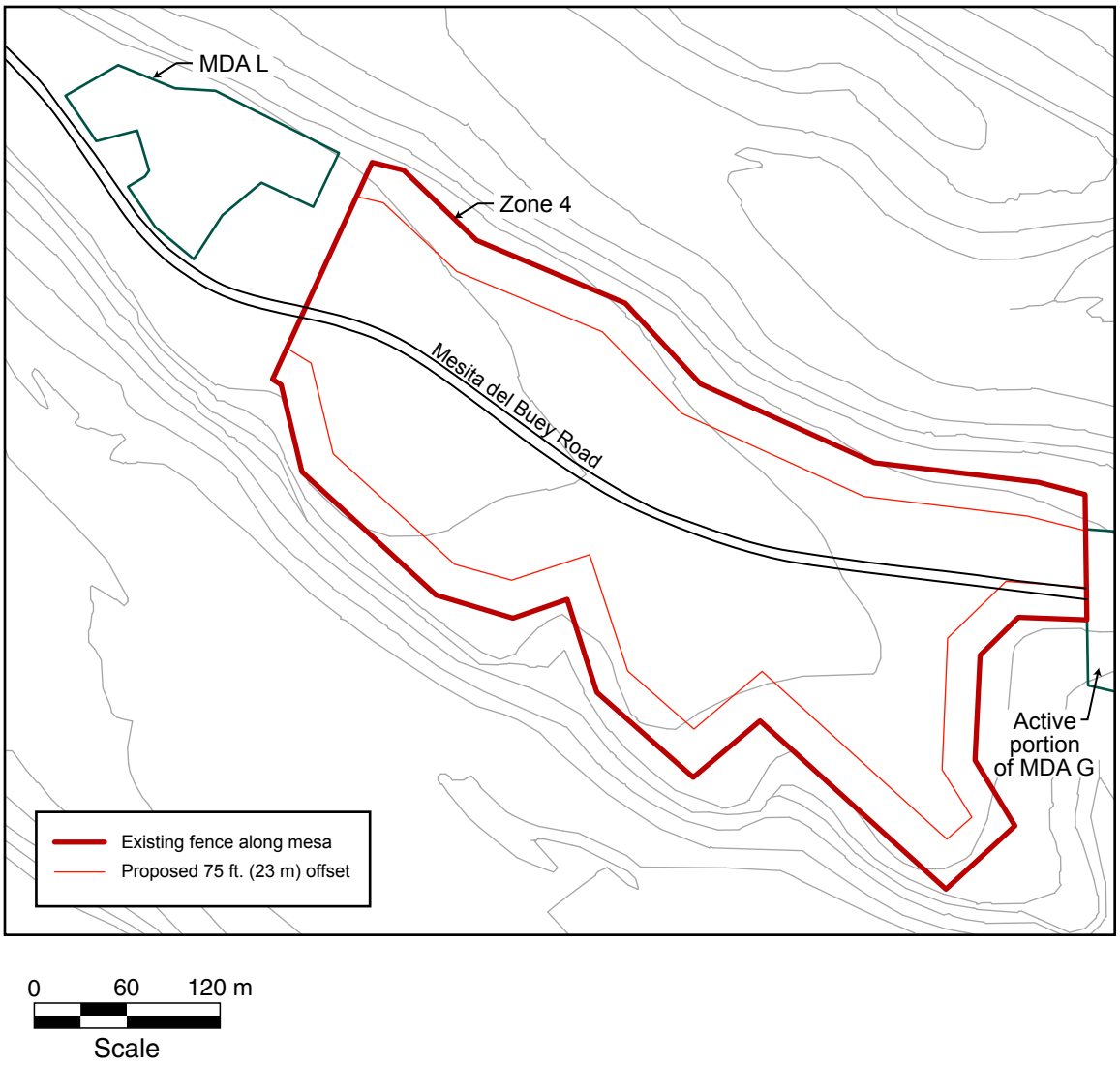

Figure 2
Topography of Zone 4 Area

Source: LANL, 2005b
(after URS 2004a, 2004b, 2004c)

3.0 Design Approach

The Zone 4 development effort included the collection and evaluation of information to establish input parameters, design criteria, and functional requirements relevant to disposal and support operations. This information was used to develop site layouts, preliminary design details, and volume calculations (where appropriate) for Zone 4. The specific activities undertaken during the development effort are discussed below.

3.1 Document Review

A document review was conducted to determine the applicability and relevance of existing documentation related to development of Zone 4. This documentation included, but was not limited to, the following:

- *Site-Wide Environmental Impact Statement for the Continued Operation of the Los Alamos National Laboratory* (DOE, 1999)
- *Performance Assessment and Composite Analysis for Los Alamos National Laboratory Material Disposal Area G* (Hollis, et al., 1997)
- *Investigation Work Plan for Material Disposal Area L, Solid Waste Management Unit 54-006 at Technical Area 54* (LANL, 2004)
- *Work Plan for the Implementation of an In Situ Soil-Vapor Extraction Pilot Study at Technical Area 54, Material Disposal Area L, Los Alamos National Laboratory* (draft) (LANL, 2005a)
- Waste volume forecasts (White et al., 2003 and Bachmeier and James, 2004)
- *An Evaluation of LANL Post Legacy TRU Waste Management* (Vance, 2004)

3.2 Archeological Evaluation

An archaeological site evaluation examined the impacts of expansion activities on the known archeological sites within Zone 4. The two expansion options presented in the site-wide environmental impact statement (DOE, 1999) were evaluated in terms of their potential impact on these sites; the first option called for development of the area located to the north of Mesita del Buey Road and the second for development of both the north and south sides of the road. Consideration was also given to protection of the *cavates* along the face of the mesa.

3.3 Volatile Organic Compound Plume Evaluation

A known volatile organic compound (VOC) plume originates at MDA L, an area just west of Zone 4 that was used for the disposal of VOCs in the past. Extensive monitoring efforts (e.g., LANL, 2005a) indicate that a portion of the plume extends into the western portion of Zone 4, primarily to the north of Mesita del Buey Road. An evaluation was made to characterize the advisability and feasibility of expanding disposal activities into the portions of Zone 4 that have been impacted by the plume.

3.4 Operational Needs Assessment

A needs assessment was conducted to identify input parameters and design criteria that are relevant to the development of Zone 4 and continued operation of the facility. These include information about current disposal pits and shafts (e.g., disposal efficiency and the depths and orientations of disposal units), regulatory compliance concerns and requirements (e.g., stormwater management, the MDA G performance assessment and composite analysis, and the disposal authorization basis), and the need for continued access to operations in other parts of MDA G. An evaluation of LLW support operations that will need to be relocated or removed from MDA G as closure activities in the active portion of the facility progress was also included in this activity.

3.5 Preliminary Layouts and Designs

Using the information gathered in the activities described above, preliminary designs and layouts were developed for the Zone 4 disposal pits and support operations. The layouts, preliminary design details, and calculations were completed by a LANL contractor (URS 2004a, 2004b, and 2004c) and modified by LANL personnel (LANL, 2005b) to reflect the intended development approach.

4.0 Conceptual Design

This section presents the conceptual design of the disposal units in Zone 4. Section 4.1 summarizes the design criteria and parameters that were selected on the basis of the activities described above, and Section 4.2 presents the phased approach and layout for developing Zone 4. All material presented in this section is summarized from the Zone 4 development report (LANL, 2005b).

4.1 Design Criteria and Parameters

Based on the results of the activities described in Section 3, a list of input parameters and design criteria was compiled to guide the development of the conceptual site layout and design details for disposal operations in Zone 4. Although none of the investigations described in Section 3 indicated that the development of disposal units in Zone 4 would be inadvisable, they did highlight factors to be considered during the design and implementation activities. The archeological site evaluation indicated that a phased excavation approach would be most suitable in the southern portion of Zone 4 due to the number of sites located in this area; this approach is incorporated into the input parameters and design criteria presented below and is described in more detail in Section 4.2. In response to the concern about the protection of the *cavates*, the design criteria indicate that disposal units will be set back from the mesa edge. The VOC plume evaluation determined that the construction of disposal units in the northern portion of Zone 4 will not impact the ability to investigate, monitor, or implement a remedy for the VOC plume emanating from MDA L. However, as disposal units are developed, health and safety plans will be required to evaluate the effect of any subsurface VOCs on workers.

A list of input parameters and design criteria for Zone 4 was compiled on the basis of the considerations discussed above and the operational needs assessment. An overall goal of the design process was to position pits and shafts in an efficient manner that disturbed the mesa top as little as possible while maintaining adequate access, safety, and staging areas. Key input parameters and design criteria include the following:

- A setback of 23 m (75 ft) from the mesa edge (see Figure 3) to protect *cavates*, address cliff retreat concerns, provide access to site utilities and security fences, and serve as a buffer zone for personnel and equipment.
- A shaft field containing eight 4.9- to 6.1-m (16- to 20-ft) diameter shafts and three groups of 50 shafts with diameters of 1.2, 1.8, and 2.4 m (4, 6, and 8 ft) to accommodate waste streams requiring additional administrative controls (e.g., wastes containing biological hazards, polychlorinated biphenyls [PCBs], and beryllium).

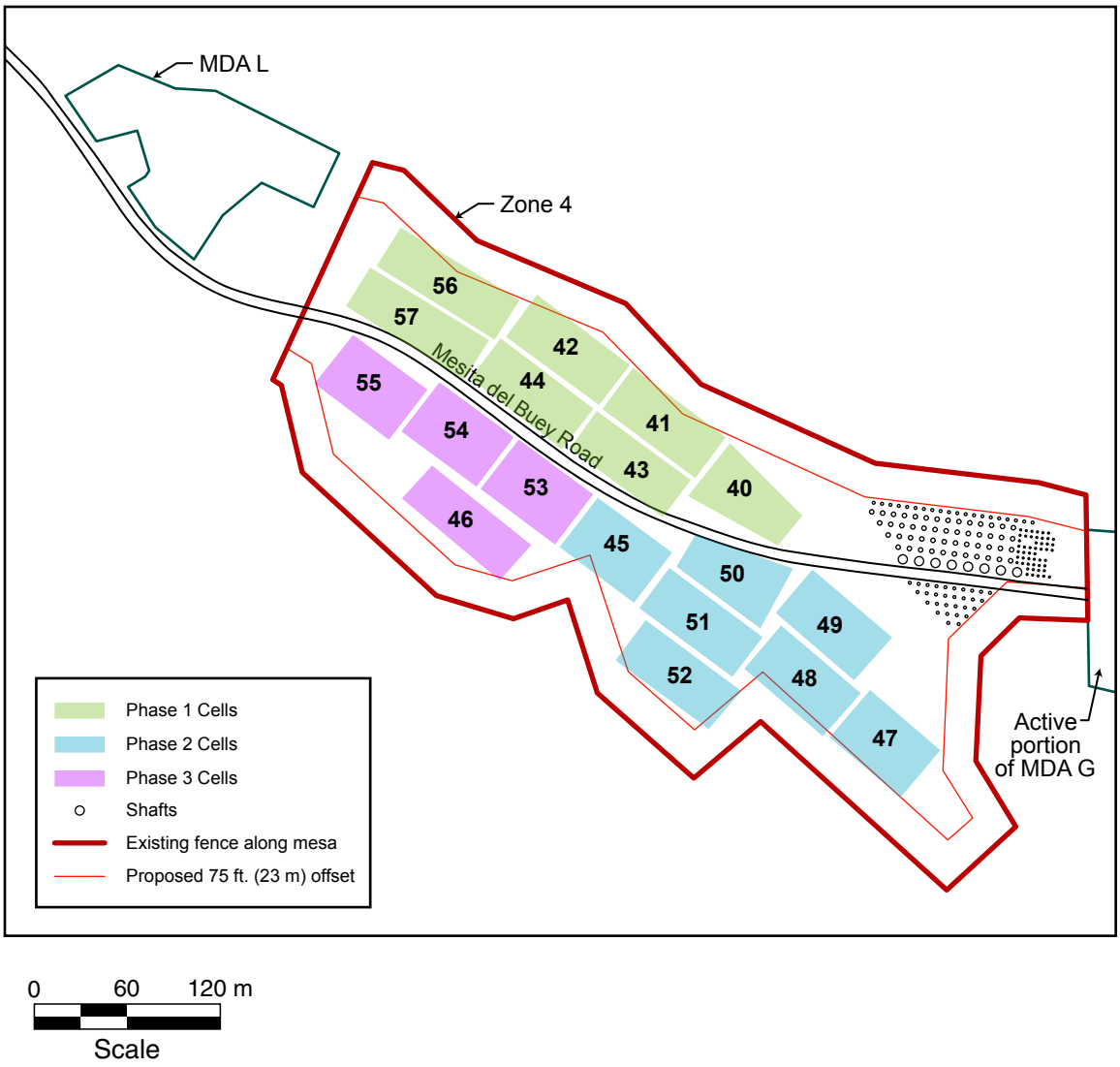

Figure 3
Proposed Disposal Cell Development in Zone 4

Source: LANL, 2005b
(after URS 2004a, 2004b, 2004c)

- Positioning the long axis of the disposal pits parallel to the long axis of the mesa to reduce fracturing and resultant rock spalling.
- Disposal pits sized for a life expectancy of about 5 years to minimize storm water infiltration.
- Avoidance of existing high-voltage transmission lines (if possible) to minimize infrastructure modifications needed for development.
- A total waste disposal capacity equivalent to at least 40 years to match the requirements of the performance assessment and composite analysis and the waste disposal forecast of 2,850 m^3 (3,728 yd^3) per year (White et al., 2003).
- Maximum pit and shaft depths of 18 and 24 m (60 and 80 ft); the disposal units are not to extend below a plane projected from the floors of the adjacent canyons.
- An assumed waste emplacement efficiency of 50 percent.
- A 3-m (10-ft) freeboard area, where no waste is placed, at the top of pits and shafts so that the final cover can be placed at or near the original ground surface.
- Vehicle entry to Zone 4 and continued access to the currently active portion of MDA G for ongoing and closure activities.
- Ramp access to the disposal pits that allows for the safe and efficient ingress and egress of a semitrailer-truck type vehicle in the WB-50 class.

4.2 Conceptual Design

The initial conceptual design developed by URS Corporation (2004a, 2004b, and 2004c) consisted of a disposal unit layout, preliminary design details, and waste volume calculations. Laboratory personnel modified the number of disposal pits and associated calculations in the initial design to reflect the intended approach to site development. This section provides an overview of the conceptual design including the proposed three-phase approach and the layout of disposal pits for each phase.

4.2.1 Phased Development Approach

A phased approach will be implemented for the development and use of Zone 4. This approach, which consists of three distinct phases, is expected to result in the most efficient usage of the available area for disposal operations:

- During *phase 1* disposal units will be developed on the north side of Mesita del Buey Road. Excavation and pit placement will occur in the vicinity of the subsurface VOC

plume area (in the northwest portion of Zone 4), but will not impact the sole archeological site located on the north side of the road.

- Development of disposal units will begin on the south side of Mesita del Buey Road at the east end of Zone 4 during *phase 2*. Several archeological sites will be excavated to clear the southeastern portion of Zone 4 at this time.

- *Phase 3* will involve the development of disposal pits on the south side of Mesita del Buey Road at the west end of Zone 4. During this phase, the remaining archeological sites on the south side of the road will be excavated and/or removed.

At present, the need for expansion into the portion of Zone 4 addressed by phase 3 is considered unlikely.

4.2.2 Conceptual Layout

Multiple disposal pits will be constructed for each phase of Zone 4 development. The pit layouts for phases 1, 2, and 3 are shown in Figure 3. The conceptual layout for each phase is as follows:

- Phase 1 area (north side of Mesita del Buey Road) contains pits 40 – 44, 56, and 57. Six pits are rectangular and one is trapezoidal.

- Phase 2 area (east end of the south side of Mesita del Buey Road) contains pits 45, and 47 – 52. Six pits are rectangular and one is trapezoidal.

- Phase 3 area (west end of the south side of Mesita del Buey Road) contains disposal pits 46 and 53 – 55. These four pits are rectangular.

The completion of all three phases will involve excavating, operating, maintaining, and closing 18 disposal pits. However, as mentioned above, it is doubtful that expansion into the phase 3 area will be needed.

All disposal shafts will be arranged in a single shaft field located immediately west of the active portion of MDA G and east of the power transmission lines that traverse Zone 4. The field layout includes shafts on both sides of the road, providing for access to multiple active shafts at any given time.

4.2.2.1 Pit Details and Ramps

Disposal pit cross sections, access ramp details, and calculations supporting the general layout and feasibility of the conceptual design for both 18- and 24-m (60- and 80-ft) deep units are presented in the Zone 4 development report (LANL, 2005b). To simplify design and construction, all disposal pits, regardless of depth, will have similar side slopes and access ramp

widths. All pits will be designed with horizontal-to-vertical side slopes of 1:7 and will be separated by 3 m (10 ft) to provide safe access for workers. Reinforcement will be used in the near-vertical side walls and will be maintained as needed to minimize sloughing or spalling of rock along fractures.

Pit access ramps for the ingress and egress of waste transport and construction equipment will have a grade of 12 percent, or about 8:1 (horizontal to vertical). The ramp will be 6.1-m (20-ft) wide along the length of the disposal pit, increasing to 9.1-m (30-ft) wide along the pit width and through the turns. The turns or curves will have an outside front radius of 15 m (50 ft) and an inside rear radius of 6.1 m (20 ft). The access ramps will be oriented to convey loaded trucks downward in a counterclockwise direction to provide maximum visibility and protection of personnel and equipment. The pit floor layout incorporates space for multipoint backing so that vehicles can turn around before exiting the disposal unit.

4.2.2.2 Disposal Pit Calculations

The disposal pit volumes, waste disposal capacity, and life expectancy of the pits were calculated for each of the three phases (LANL, 2005b). The calculations accounted for the slopes of the pit walls and volumes occupied by the access ramps and assumed a 50 percent waste emplacement efficiency and a waste receipt rate of 2,850 m^3/yr (3,730 yd^3/yr). Two different pit depths were considered and calculations were performed to examine the effects of leaving the access ramp in place versus excavating 50 percent of the volume occupied by the ramps. A summary of these calculations is presented in Table 1.

Table 1
Design Capacities of Zone 4 Development Phases

Design Options	Design Capacity					
	Phase 1 (Pits 40 – 44, 56, and 57)		Phase 2 (Phase 1 plus Pits 45 and 47 – 52)		Phase 3 (Phase 2 plus Pits 46 and 53 – 55)	
	Waste Volume (m^3)	Life Expectancy (yr)	Waste Volume (m^3)	Life Expectancy (yr)	Waste Volume (m^3)	Life Expectancy (yr)
18-m depth, no ramp excavation	8.7E+04	31	1.7E+05	60	2.2E+05	77
18-m depth, 50% ramp excavation	1.0E+05	36	2.0E+05	72	2.6E+05	92
24-m depth, no ramp excavation	1.2E+05	43	2.4E+05	83	3.0E+05	106
24-m depth, 50% ramp excavation	1.4E+05	49	2.8E+05	98	3.6E+05	125

The disposal capacity required to accommodate 2,850 m^3 (3,730 yd^3) of waste through 2044 is 1.1×10^5 m^3 (1.5×10^5 yd^3). As shown in Table 1, this capacity can be realized using several approaches. For example, excavation of all phase 1 pits to a depth of 24 m (80 ft), with or without ramp excavation, would provide the requisite disposal volume. If pits are excavated to a depth of only 18 m (60 ft), some development of the phase 2 area would be needed.

5.0 Differences between the Preliminary and Final Conceptual Designs

The conceptual design of Zone 4 directly affects the long-term performance modeling conducted in support of the MDA G performance assessment and composite analysis. For example, the dimensions and placement of the disposal pits and shafts influence the rates of projected surface erosion. Among other parameters, assumptions about waste emplacement efficiency and the spacing of the disposal shafts influence the calculation of inadvertent intruder-based waste acceptance criteria for the disposal facility.

Several aspects of the modeling conducted in support of the performance assessment and composite analysis were completed before the Zone 4 conceptual design was finalized. As a result, the modeling relied on preliminary design specifications (URS 2004a, 2004b, and 2004c). Although most of the preliminary design data was incorporated into the final conceptual design, some aspects were changed to reflect the intended usage of Zone 4. Consequently, in some cases the modeling is based on specifications that differ slightly from those summarized in Section 4.0 and in the development report (LANL, 2005b). The primary differences between the preliminary and final conceptual designs relate to the phased development of pits at Zone 4. These differences are summarized in Table 2 and described below.

Table 2
Differences in Phased Pit Development for Preliminary and Final Conceptual Designs

Development Phase	Pits to Be Developed	
	Preliminary Design	Final Design
Phase 1	40, 41, 42, 43, 44, 45, 46	40, 41, 42, 43, 44, 56, 57
Phase 2	47, 48, 49	45, 47, 48, 49, 50, 51, 52
Phase 3	50, 51, 52	46, 53, 54, 55
Phase 4	53, 54, 55, 56, 57	N/A

The preliminary design adopted a four-phase approach to disposal pit development while the final design considers three phases. Although both designs include the development of seven pits during phase 1, the preliminary design included the development of disposal units south of Mesita del Buey Road while the final design does not. The two designs call for the development of different numbers of disposal pits for the remaining phases.

The performance assessment and composite analysis modeling assumed that all disposal pits in Zone 4 would be 18-m (60-ft) deep and that access ramps would be left intact. Based on these assumptions and the information shown in Table 1, all the pits included in the final design

phase 1, and two of the units developed in the final design phase 2, would be required to meet the projected waste disposal needs through the year 2044. Assuming the pits within a phase are excavated in ascending order, this means that pits 40 – 45, 47, 56, and 57 would require excavation. In contrast, based on the preliminary design (and making the same assumption about sequential excavation), pits 40 – 50 would require excavation to meet the projected waste disposal needs.

The shaft field shown in Figure 3 is the same as that included in the preliminary design. Therefore, the locations and numbers of shafts upon which the performance assessment and composite analysis modeling is based are consistent with the Zone 4 conceptual design adopted by the Laboratory.

6.0 References

Bachmeier C.L. and J. Scott, 2004, *Waste Volume Forecast, Revision 1*, Los Alamos National Laboratory Report LA-UR-04-6682, Los Alamos, NM, September.

DOE, 1999, *Site-Wide Environmental Impact Statement for Continued Operation of the Los Alamos National Laboratory*, U.S. Department of Energy, Albuquerque Operations Office,. DOE/EIS – 0238, Albuquerque, NM, January.

Hollis, D., E. Vold, R. Shuman, K. Birdsell, K. Bower, W. Hansen, D. Krier, P. Longmire, B. Newman, D. Rogers, E. Springer, 1997, *Performance Assessment and Composite Analysis for the Los Alamos National Laboratory Disposal Area G*, Los Alamos National Laboratory Report LA-UR-97-85, Report-54G-013, March.

LANL, 2004, *Investigation Work Plan for Material Disposal Area L, Solid Waste Management Unit 54-006 at Technical Area 54*, Los Alamos National Laboratory Report LA-UR-04-8245.

LANL, 2005a, *Work Plan for the Implementation of an In Situ Soil-Vapor Extraction Pilot Study at Technical Area 54, Material Disposal Area L, Los Alamos National Laboratory*, Los Alamos National Laboratory Interim Draft Report LA-UR-05-0633, ER2005-0XXX, February.

LANL, 2005b, *Development of Zone 4, Area G, Technical Area 54,* Los Alamos National Laboratory Report DIV-REPORT-0201, R.0, April.

URS Corporation, 2004a, *TA-54 Zone 4 Conceptual Design Report*, Draft document, URS-24342406-00004-0, prepared for Los Alamos National Laboratory, Basic Agreement 13567-000-00-FT, Task Order No. 73, Salt Lake City, UT, September.

URS Corporation, 2004b, *TA-54 Zone 4 Disposal Cell Excavation and Waste Capacity Calculation*, Draft document, URS-24342406-00004-0, prepared for Los Alamos National Laboratory, Basic Agreement 13567-000-00-FT, Task Order No. 73, Salt Lake City, UT, September.

URS Corporation, 2004c, *TA-54 LLRW Operations Relocation (MDA G) Preliminary Design*, URS-24342406-00004-0, prepared for Los Alamos National Laboratory, Basic Agreement 13567-000-00-FT, Task Order No. 73, Salt Lake City, UT, September.

Vance, J. (Vance and Associates), 2004, *An Evaluation of LANL Post Legacy TRU Waste Management*, Los Alamos National Laboratory Report LA-UR-04-7125, submitted to C. Bachmeier (RTBF Program), October.

White, A., C.L. Bachmeier, and J. Scott, 2003, *Waste Volume Forecast*, Los Alamos National Laboratory Report LA-UR-03-4009, June.

LA-UR-05-5371

Approved for public release; distribution is unlimited.

Title: ASSESSING WIND EROSION AS A CONTAMINANT TRANSPORT MECHANISM AT LOS ALAMOS NATIONAL LABORATORY TECHNICAL AREA 54, MATERIAL DISPOSAL AREA G

Author(s): Jeffrey J. Whicker
David D. Breshears

Submitted to: U.S. Department of Energy

Table of Contents

List of Figures i
List of Tables ii
Acronyms and Abbreviations iii
Acknowledgements iv

1.0 Introduction 1
2.0 Methods 3
2.1 Selection of Measurement Sites 3
2.2 Measurements 3
2.2.1 Horizontal Mass Flux Measurements 6
2.2.2 Vertical Mass Flux Measurements 9
2.3 Statistical Analyses 11
3.0 Results 12
4.0 Discussion 22
4.1 Significance of Results 22
4.2 Qualifications 23
5.0 References 27

List of Figures

Figure 1 Grass and Forb Cover at MDA J Analog Site 4
Figure 2 Piñon-Juniper Cover at TA-51 Analog Site 5
Figure 3 Field Dust Collector with Rotating Samplers at Three Heights 7
Figure 4 Circular Arrangement of Field Dust Samplers 8
Figure 5 Sonic Anemometer for Measuring Wind Velocity 10
Figure 6 Horizontal Mass Flux at Grassland and Woodland Analog Sites over Time (1 m sampling height) 15
Figure 7 Horizontal Mass Flux at Grassland and Woodland Analog Sites (all sampling heights) 16
Figure 8 Wind Velocities at Grassland and Woodland Analog Sites (1 m sampling height) 17
Figure 9 Horizontal Mass Flux at Inward- and Outward-Facing Samplers at Both Analog Sites 18
Figure 10 Estimated Vertical Mass Flux Collected during All Sampling Periods (1 m sampling height) 20
Figure 11 Pre- and Post-Thinning Dust Concentrations at TA-54 Meteorological Station 25
Figure 12 Weekly Flux Gradient Measurements at TA-54 before and after Nearby Thinning Operations 26

List of Tables

Table 1 Summary Statistics for Horizontal Mass Flux Measurements from All Sampling Periods 13
Table 2 Summary Statistics for Horizontal Mass Flux Measurements from Periods without Precipitation 14
Table 3 Summary Statistics for Aerosol Mass Concentration and Vertical Mass Flux at MDA J..... 21

Acronyms and Abbreviations

BSNE	Big Spring Number Eight (dust sampler)
LANL	Los Alamos National Laboratory
MDA	Material Disposal Area
TA	Technical Area
TSP	Total suspended particulate

Acknowledgements

The authors would like to acknowledge the able field assistance of Johnny Salazar, Marvin Gard, and Leo Martinez. They overcame many obstacles to get the job done.

1.0 Introduction

Recent evaluations of landfill performance at Material Disposal Area (MDA) G at Los Alamos National Laboratory (LANL) have highlighted the need to more rigorously consider erosional processes that could impact landfill covers through time. Wind erosion at MDA G is of particular concern for both operational and long-term performance issues associated with covers. Nevertheless, there is a lack of site-specific wind erosion data needed to estimate and project soil loss and contaminant transport rates.

Landfill covers in semiarid settings may be particularly vulnerable to surface erosion because, in general, the limited amount of precipitation does not allow a homogeneous vegetation cover to develop. Hence, these areas often have significant patches of unprotected or bare soil, which are subject to increased soil erosion. Most erosion studies of landfill covers have focused on water erosion. However, recent studies in semiarid landscapes have shown that wind erosion and transport can be substantial (Whicker et al., 2002; Breshears et al., 2003). For example, in a study of three different semiarid ecosystems (shrubland, woodland, and grassland), Breshears et al. (2003) note that long-term wind erosion rates exceeded water erosion rates by approximately 33 times at the shrubland site and 5 times at the woodland site, although water erosion rates at the grassland site were about 3 times greater than wind erosion rates because of the high clay content of the soils. The results of the Breshears et al. study also show that horizontal transport by wind was greater than that by water for all three ecosystems, especially for the shrubland environment. These and other results indicate that wind erosion could affect the long-term integrity of landfill covers and be an important mechanism for the redistribution of surficial contamination at a landfill site (Anspaugh et al., 1975; Sehmel, 1980; Arimoto et al., 2002).

In a broad sense, wind-driven soil movement can be thought of as having two directional components:

- *Mass horizontal transport* is a process in which larger soil particles (generally greater than 50 μm [2.0×10^{-3} in.] in diameter) are transported in a horizontal direction by saltation. The particles remain close to the ground (e.g., at a height of less than 1 m [3.3 ft]) and the process is generally indicative of local soil redistribution (Stout and Zobeck, 1996; Gillette et al., 1997).

- *Mass vertical transport* (e.g., vertical dust movement at a height of more than 1 m [3.3 ft]) suggests long-distance transport of smaller soil particles (generally less than 50 μm [2.0×10^{-3} in.] in diameter). These small particles can be transported into an area (deposition) or removed from an area (net loss).

Vegetation changes through time are important considerations in assessing future wind erosion rates. First, vegetation cover on landfills is likely to undergo successional processes resulting in changes in cover type, coverage, and structure. These changes are expected to impact wind erosion rates; therefore, it is important to quantify the influence of vegetation changes on wind erosion. Second, in addition to the effect of normal vegetation succession, it is important to consider environmental disturbances that may reduce vegetation cover and thus result in significantly increased soil erosion (Fryrear, 1985). Decreases in the amount of ground cover can be particularly dramatic following disturbances such as drought and fire, and can lead to increased wind and water erosion (Davenport et al., 1998; Whicker et al., 2002).

The objective of this study was to provide initial estimates of wind erosion for MDA G through (1) the installation of equipment and collection of wind erosion data at two analog study sites and (2) the development of site-specific wind erosion projections based on collected data. The two analog sites are on Mesita del Buey, to the west of MDA G. The first, located at MDA J, was selected for study because it is representative of the surface soil and vegetative conditions that are expected to prevail at MDA G immediately following closure of the facility. The second site, a piñon-juniper woodland located at Technical Area (TA) 51, was selected because it is expected to represent the type of vegetation that will be present at MDA G after the site has undergone successional changes. Measurements were taken at these two analog sites, rather than directly at MDA G, because ongoing operations at MDA G (such as soil transportation and heavy truck use) would likely mask any wind erosion that would occur in the absence of these activities.

Detailed wind erosion measurements at MDA J included evaluations of vertical and horizontal flux as a function of micrometeorological conditions and particle-size distribution. Horizontal flux measurements were made at TA-51 to address the effects that successional changes in vegetation and soil cover may have on erosional processes at MDA G. This report provides the methodology used to conduct and analyze the measurements, the results obtained from both analog sites (MDA J and TA-51), and projections of annual wind erosion rates.

2.0 Methods

Specific tasks covered by this study included the selection of analog sites, installation of measuring devices and collection of samples, and analysis of field data. This section describes the methodology used to perform these tasks. Section 2.1 focuses on why and how measurement sites were selected, Section 2.2 explains how measurements were made, and Section 2.3 describes how the statistical analysis was performed.

2.1 Selection of Measurement Sites

Erosion measurements were conducted at two surrogate or analog sampling sites located near (i.e., within a couple of kilometers of) MDA G. The first site, MDA J, is characterized as grassland (Figure 1), which is likely to be the first successional stage experienced by MDA G immediately following closure. The second site, located at TA-51 (Figure 2), is a piñon-juniper woodland, which represents a later possible successional state for MDA G. To limit spatial variability in the dust flux measurements, each of the sampling sites was located on top of the same mesa as MDA G and at a similar elevation.

Site selection was based on several important criteria. First, both sites were relatively flat (slopes less than 10 percent) with vegetative cover that was relatively homogeneous in all directions for at least 50 m (160 ft), especially in the prevailing upwind directions. Second, the sites were as far away as possible from roads or other recently disturbed soil surfaces that could produce unusual amount of dust. Third, these sites were expected to be reasonably representative of the likely ground cover that MDA G will experience during early and late stages of succession following its closure and final remediation.

2.2 Measurements

Once representative analog sites were selected, measurements were obtained to quantify the horizontal mass flux of wind-driven dust at both the MDA J and TA-51 sites. Measurements were also obtained at the MDA J site to quantify the vertical dust flux. Sections 2.2.1 and 2.2.2 discuss how horizontal and vertical mass flux measurements were obtained.

Figure 1
Grass and Forb Cover at MDA J Analog Site

Figure 2
Piñon-Juniper Cover at TA-51 Analog Site

2.2.1 Horizontal Mass Flux Measurements

Wind erosion rates at the two sites were quantified using numerous Big Spring Number Eight (BSNE) samplers (Figure 3). These samplers are passive collectors of airborne dust that have been extensively tested and show good sampling efficiency for soils with higher fractions of sand and silt (Fryrear, 1986; Goossens and Offer, 2000) such as those that are abundant at LANL (Nyhan et al., 1978). These samplers can be assembled easily and inexpensively from interchangeable parts and do not require electricity to operate; thus, numerous samplers can be employed and great flexibility can be used in their placement. Because of this, it was possible to obtain continuous measurements using multiple samplers at multiple sites.

As shown in Figure 3, a fully rotating BSNE sampling station has three samplers operating at heights of 25 cm, 50 cm, and 1 m (10, 20, and 39 in.). This configuration provided measures of integrated resuspension that were generally collected over one- to two-week sampling intervals. The horizontal mass flux was calculated as follows:

$$F_H = \frac{m}{t \times a} \qquad 1$$

Where

F_H = horizontal mass flux ($g/m^2/d$)
m = mass of the material collected during sampling (g)
t = number of sampling days
a = sampling area (10 cm^2 [1.6 $in.^2$])

Big Spring Number Eight samplers are designed to rotate 360^o to allow them to sample wind-blown dust from any direction. This provides a measure of dust flux integrated over all sampling directions. The arrangement of BSNE samplers for this study is shown in Figure 4. To measure total dust flux, four rotating BSNE sampling stations were placed 20 m (65 ft) apart along the east-west and north-south axes of each sampling area.

The net horizontal dust flux was determined at each measurement site by using eight pairs of BSNE samplers positioned 20 m (65 ft) from the center of a circular sampling area at a height of 50 cm (20 in.) (Figure 4); the range of movement of these samplers was restricted to 45^o. Each pair consisted of one sampler facing toward the center of the circle and one facing 180^o in the opposite direction, away from the center of the circle. Because the collection efficiency of the BSNE samplers is less than 10 percent for off-angle sampling (Fryrear, 1986), each of the eight pairs of motion-restricted collectors sampled wind-blown dust for a different 45° angle from the center point (yielding a combined total of 360° for all eight pairs of inward- and outward-facing samplers). Using these measurements, the net dust flux in the sampling area was calculated as the difference in the amount of dust collected in the inward- versus the outward-facing samplers.

Figure 3
Field Dust Collector with Rotating Samplers at Three Heights

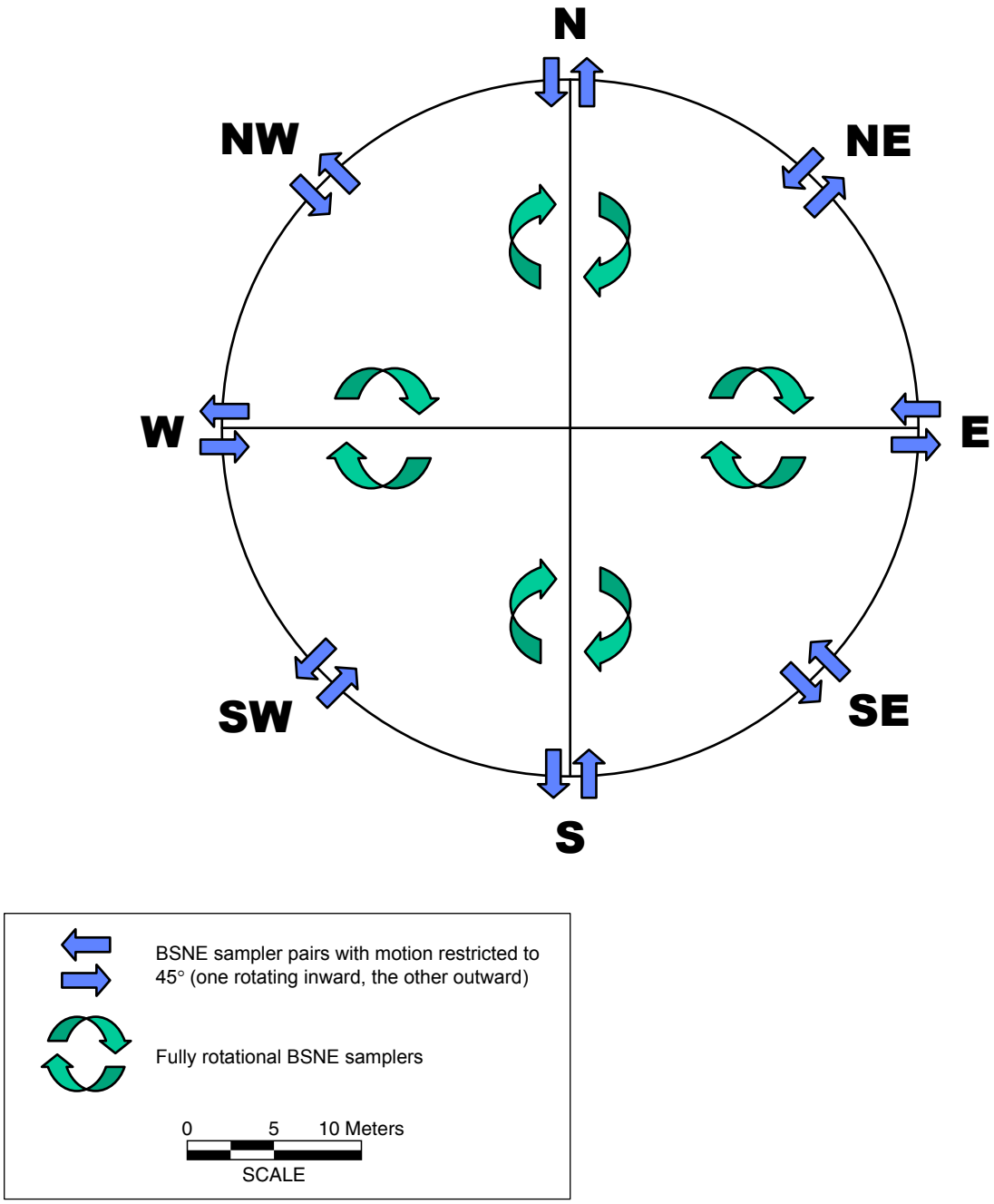

Figure 4
Circular Arrangement of Field Dust Samplers

2.2.2 Vertical Mass Flux Measurements

Vertical flux measurements are primarily a measure of the suspended mass of particles passing through the sampled area during the given sampling time. Resuspension rates are estimated using the meteorological flux gradient method (Stull, 1988):

$$F = K_z \frac{d\chi}{dz} \qquad 2$$

Where

F = vertical mass flux
K_z = eddy diffusivity coefficient
$d\chi/dz$ = differential mass air concentration (χ) with height (z)

The eddy diffusivity coefficient is a linear function of the friction velocity (u_*). The friction velocity is a measure of the boundary shear created as winds pass over vegetation and soils. The friction velocity for a given terrain and wind velocity can be obtained by measuring the wind velocity profile with height (Bagnold, 1941) or it can be determined with highly frequent three-dimensional measurements of wind velocities (Stull, 1988) using Equation 3:

$$u_*^2 = \left[\overline{u'w'}^2 + \overline{v'w'}^2 \right]^{\frac{1}{2}} \qquad 3$$

Where

u' = instantaneous wind velocity component in horizontal direction x (m/s)
v' = instantaneous wind velocity component in horizontal direction y (m/s)
w' = instantaneous wind velocity component in vertical direction z (m/s)

The instantaneous wind velocity components were measured using a sonic anemometer (Campbell Scientific Model CSAT3) (Figure 5), and used to calculate an average friction velocity for each sampling period. In addition, data for the wind profiles with height (as well as other meteorological conditions) were obtained from meteorological stations that were approximately centered within the sampling plots. Once the vertical mass flux (F) was determined, the resuspension rate was calculated by dividing that flux by the density of the local soil and the depth of the resuspendable soil (e.g., 3 mm [0.12 in.]) (Webb et al., 1997).

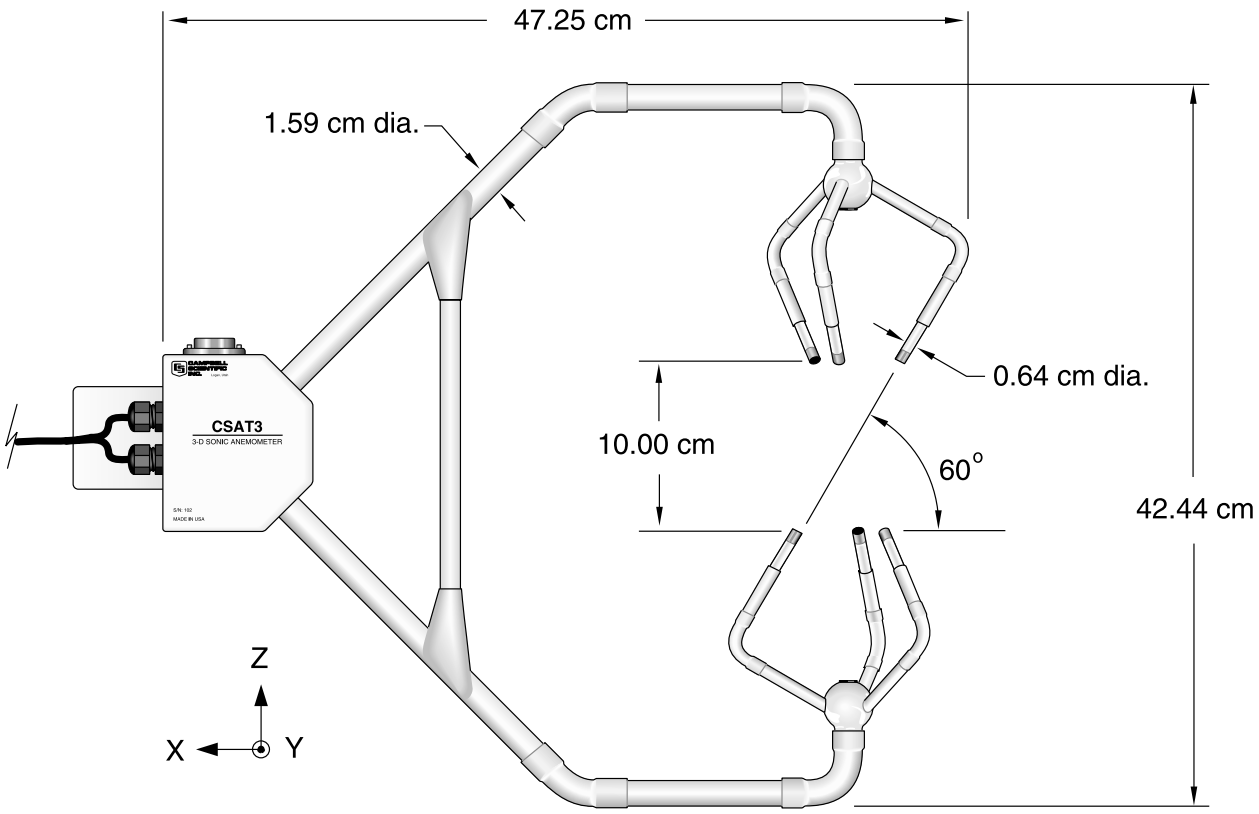

Figure 5
Sonic Anemometer for Measuring Wind Velocity

Source: Campbell Scientific, 2004

To determine the concentration gradient with height ($d\chi/dz$), which is needed for resuspension rate measurements, total suspended particulate (TSP) measurements were made each week. Samplers were placed at heights of 1 and 3 m (3.3 and 9.8 ft) to measure the concentration gradients. The concentration difference ($d\chi$) was calculated as the difference between the mass concentrations at 1 and 3 m (3.3 and 9.8 ft), and the height (dz) was the 2 m (6.6 ft) vertical separation between samplers. The sampling inlet on the TSP air samplers used for this study is slightly modified from the inlet in the sampler described by Liu and Pui (1981), which had an aspiration efficiency of 100 percent (±10 percent) for particles with aerodynamic diameters of 8.5 and 11 μm (3.0×10^{-4} and 4.0×10^{-4} in.) and wind speeds up to 2.5 m/s (8.2 ft/s). While these wind speeds are typical velocities measured at LANL, measurements of resuspension at higher velocities were also needed. Because of this, and the fact that the original Liu and Pui inlet design was for sampling particulate matter with diameters of 10μm (4.0×10^{-4} in.) or less, modifications were made that included placing the filter close to the bottom plate and adding a coarse wire screen to keep insects out of the filter. These changes to the inlet allow sampling without directional dependence, and permit accurate sampling over a wider range of wind velocities and particulate size.

Rodgers et al. (2000) tested the sampler with the modified inlet at wind velocities of 12, 15, and 17 m/s (39, 49, and 56 ft/s), for aerodynamic particle diameters of 5, 10, and 30 μm (2.0×10^{-5}, 3.0×10^{-5}, and 1.0×10^{-4} in.) to determine sampling efficiencies at higher wind velocities. Results of this study suggested that the collection efficiency of the modified inlet was more affected by particle size than by wind velocity. For example, the collection efficiency for the 5-μm (2.0×10^{-5}-in.) diameter particles was about 120 percent (20 percent over sampling, on average) while the collection efficiency dropped to around 50 percent for both the 10- and 30-μm (3.0×10^{-5} and 1.0×10^{-4}-in.) diameter particles.

2.3 Statistical Analyses

Parametric and nonparametric summary statistics for horizontal and vertical fluxes were calculated using SYSTAT® software. The nonparametric Mann-Whitney test was used to test for statistical differences in horizontal flux between grassland and woodland sites and also between inward and outward directional fluxes within each sampling site. Statistical testing for differences between the two sites was performed separately for each sampling height. Attempts were made to limit the potential for soil collection in the BSNE samplers from rainsplash by collecting most of the samples at heights greater than 50 cm (20 in.); even so, the data suggested that rainsplash slightly increased the soil mass collected in our samplers. To compensate, statistical analyses were performed for periods with and without precipitation. Including fluxes measured during periods of precipitation provided higher (more conservative) estimates of mean and standard deviations, but did not change the conclusions of the statistical analyses.

3.0 Results

The summary statistics for the horizontal flux measurements made during sampling periods with and without precipitation are shown in Tables 1 and 2, respectively. A Mann-Whitney test of the differences between these data sets showed that both the grassland and woodland sites had significant increases in horizontal mass flux during periods with precipitation at the sampling height closest to the ground (25 cm [10 in.]). This increase was not seen at the 50 cm and 1 m (20 and 39 in.) sampling heights. These results suggest that rainsplash does contribute to the amount of soil collected in the BSNE samplers, but that these effects are greatest at the lowest sampling heights; rainsplash does not appear to significantly affect the results at sampling heights of 50 cm (20 in.) and above.

Figure 6 shows the measured horizontal mass flux at a 1 m (39 in.) height for all sampling periods at the MDA J grass-covered site (Figure 6a) and at the TA-51 piñon-juniper woodland site (Figure 6b). The horizontal mass flux appears to increase through the spring and early summer months, with more variability in the later summer months. A visual comparison of the graphs indicates that the horizontal mass flux seems to be greater at the grass-covered site than at the woodland site.

Figure 7 compares the horizontal mass flux results by sampling height. The data used in Figure 7 were collected during sampling periods with no precipitation because of the impact of rainsplash on measured dust flux at 25 cm (10 in.). Thus, the figure reflects only the differences in wind-driven dust flux between the grass and woodland cover. Statistical comparisons between the two sites show the horizontal mass flux at the grass-covered site was significantly greater than at the woodland site. This difference in dust flux was likely the result of higher ground-level wind velocities at the grass-covered site. The difference in wind velocities is shown in Figure 8; the average and maximum gust velocities at 1 m (39 in.) above the ground are about two times greater at the more open grass-covered site than at the woodland site.

Figure 9 compares the horizontal mass flux measured by the motion-restricted BSNE samplers facing inward and outward relative to the center of the circular plot. Statistical comparisons of the inward and outward fluxes show no significant difference, regardless of whether precipitation occurred during the sampling period. Thus, the quantity of dust entering the circular sample site was equal to that leaving the sampling site, which suggests no net loss of soil from the area. These findings were consistent at both the grass-covered and woodland sites.

Table 1
Summary Statistics for Horizontal Mass Flux Measurements from All Sampling Periods

Sampling Location	Summary Statistics ($g/m^2/yr$)					No. of Samples
	Mean	Standard Deviation	Median	Minimum	Maximum	
Grass-Covered Site (MDA J)						
Fully Rotating Samplers						
All Heights	1.3E+03	2.9E+03	4.6E+02	0E+00	2.7E+04	324
25 cm	2.5E+03	4.6E+03	7.0E+02	2.9E+01	2.7E+04	108
50 cm	8.3E+02	1.0E+03	4.9E+02	1.8E+01	4.8E+03	108
1 m	4.7E+02	4.9E+02	3.6E+02	0E+00	4.3E+03	108
Motion-Restricted (45°) Samplers						
Inward-Facing	5.8E+02	8.4E+02	3.0E+02	1.1E+01	7.1E+03	216
Outward-Facing	5.1E+02	8.3E+02	2.5E+02	–1.3E+03	6.1E+03	216
Woodland Site (TA-51)						
Fully Rotating Samplers						
All Heights	1.2E+03	5.3E+03	2.7E+02	–4.0E+00	6.8E+04	336
25 cm	2.7E+03	8.9E+03	3.3E+02	–4.0E+00	6.8E+04	112
50 cm	5.9E+02	1.2E+03	2.8E+02	–3.3E+01	9.5E+03	112
1 m	3.0E+02	3.0E+02	2.5E+02	–3.7E+01	2.6E+03	112
Motion-Restricted (45°) Samplers						
Inward-Facing	4.6E+02	9.0E+02	2.4E+02	–2.6E+03	7.0E+03	224
Outward-Facing	4.5E+02	8.5E+02	2.3E+02	–1.2E+01	8.3E+03	224

Table 2
Summary Statistics for Horizontal Mass Flux Measurements from Periods without Precipitation

Sampling Location	Summary Statistics ($g/m^2/yr$)					No. of Samples
	Mean	Standard Deviation	Median	Minimum	Maximum	
Grass-Covered Site (MDA J)						
Fully Rotating Samplers						
All Heights	5.3E+02	3.3E+02	4.4E+02	7.3E+01	2.3E+03	120
25 cm	5.6E+02	3.6E+02	4.6E+02	1.3E+02	1.7E+03	40
50 cm	5.2E+02	2.4E+02	4.5E+02	1.5E+02	1.1E+03	40
1 m	5.0E+02	3.7E+02	3.7E+02	7.3E+01	2.3E+03	40
Motion-Restricted (45°) Samplers						
Inward-Facing	2.8E+02	1.3E+02	2.4E+02	9.5E+01	6.4E+02	80
Outward-Facing	3.2E+02	6.7E+02	2.1E+02	7.7E+01	6.1E+03	80
Woodland Site (TA-51)						
Fully Rotating Samplers						
All Heights	3.9E+02	3.0E+02	3.1E+02	7.3E+01	2.3E+03	76
25 cm	3.3E+02	2.2E+02	2.5E+02	1.6E+02	1.2E+03	36
50 cm	2.6E+02	9.7E+01	2.4E+02	7.3E+01	5.8E+02	36
1 m	2.6E+02	7.8E+01	2.5E+02	1.4E+02	4.3E+02	36
Motion-Restricted (45°) Samplers						
Inward-Facing	2.5E+02	2.6E+02	2.0E+02	7.7E+01	2.3E+03	72
Outward-Facing	2.2E+02	9.3E+01	2.0E+02	–1.2E+02	4.6E+02	72

Figure 6a
Horizontal Mass Flux at MDA J Grassland Site

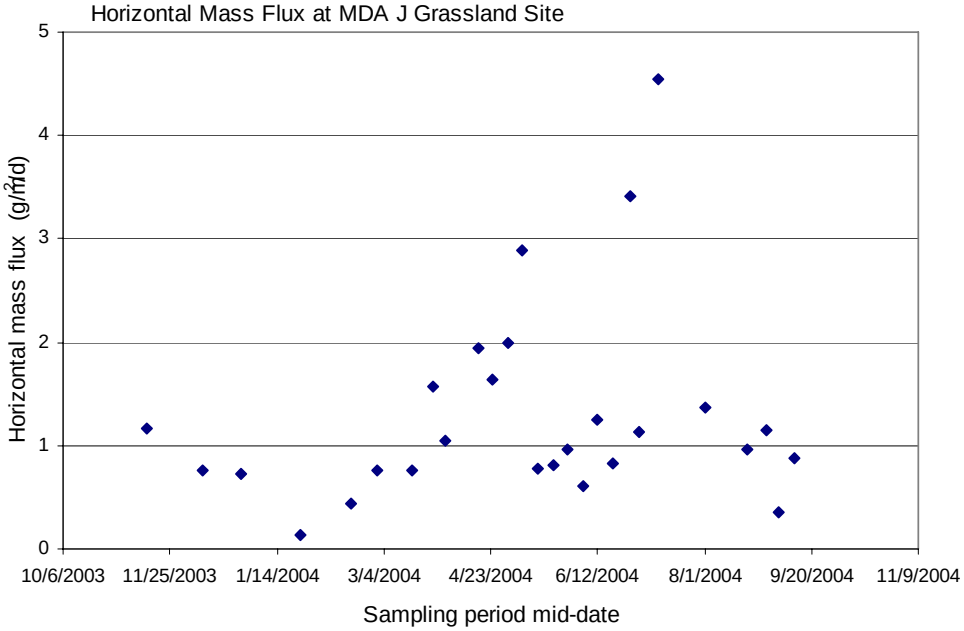

Figure 6b
Horizontal Mass Flux at TA-51 Woodland Site

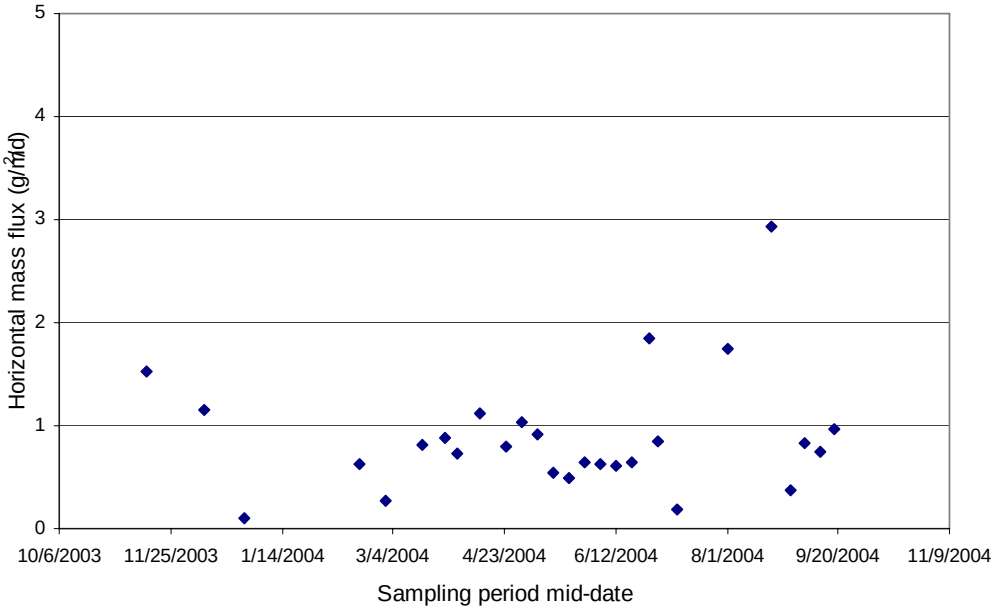

Figure 6
Horizontal Mass Flux at Grassland and Woodland Analog Sites over Time (1 m sampling height)

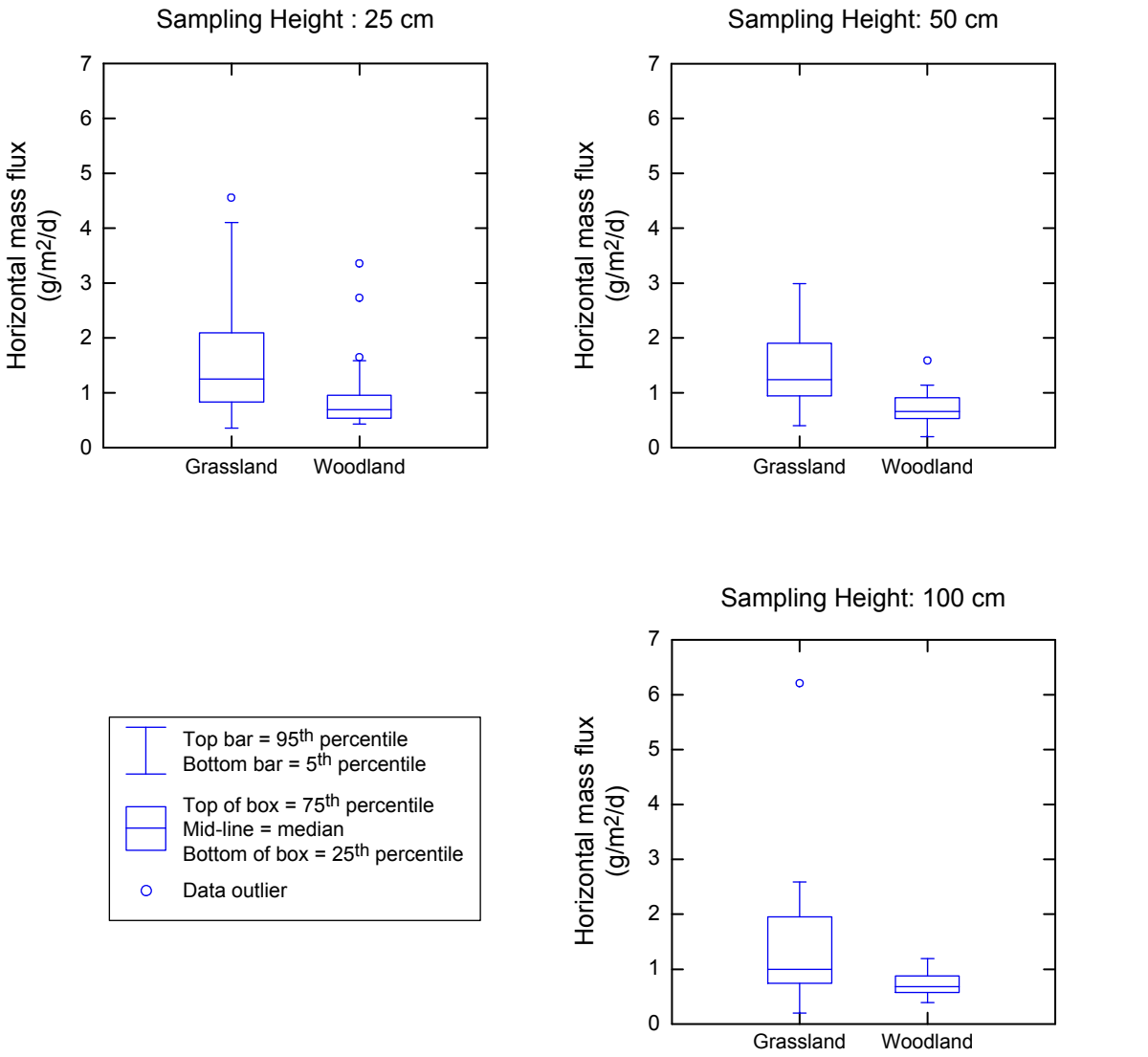

Figure 7
Horizontal Mass Flux at Grassland and Woodland Analog Sites (all sampling heights)

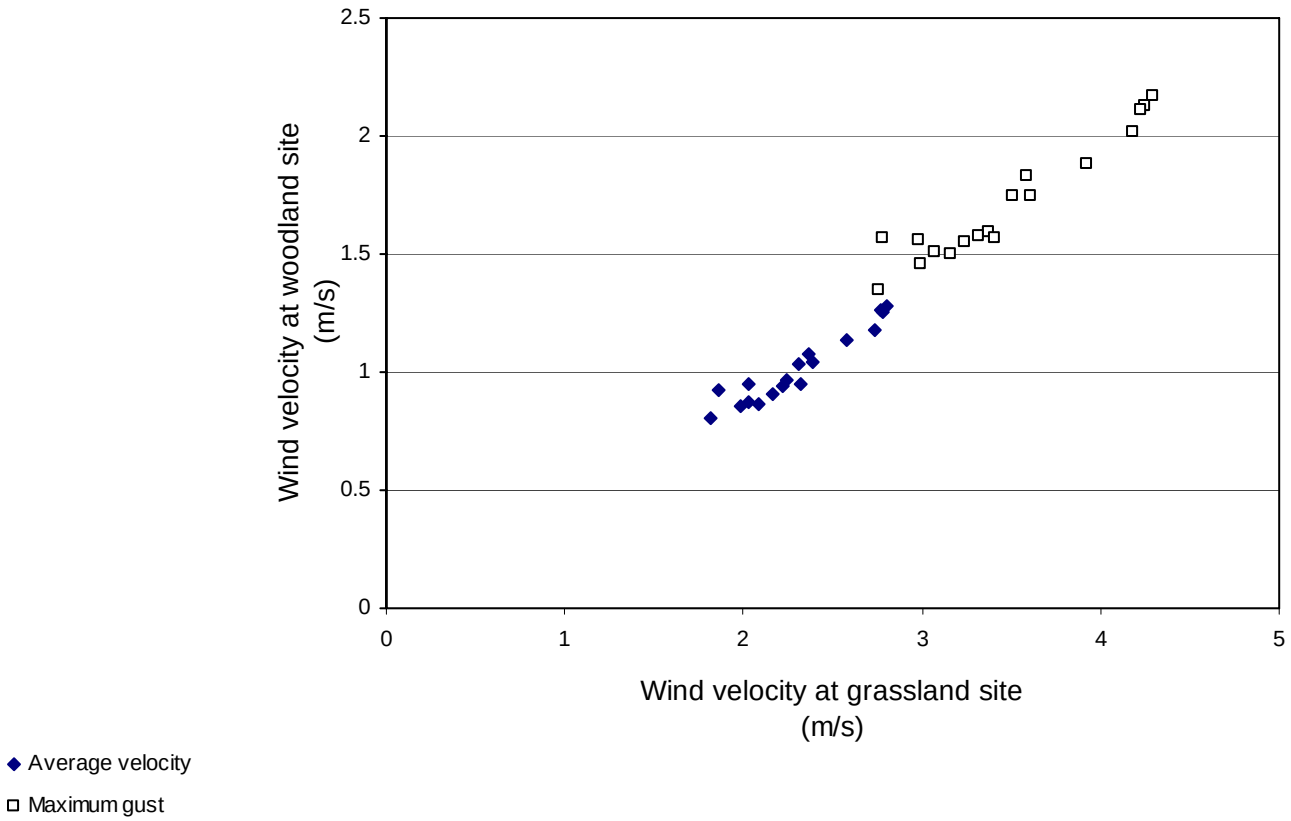

Figure 8
Wind Velocities at Grassland and Woodland Analog Sites
(1 m sampling height)

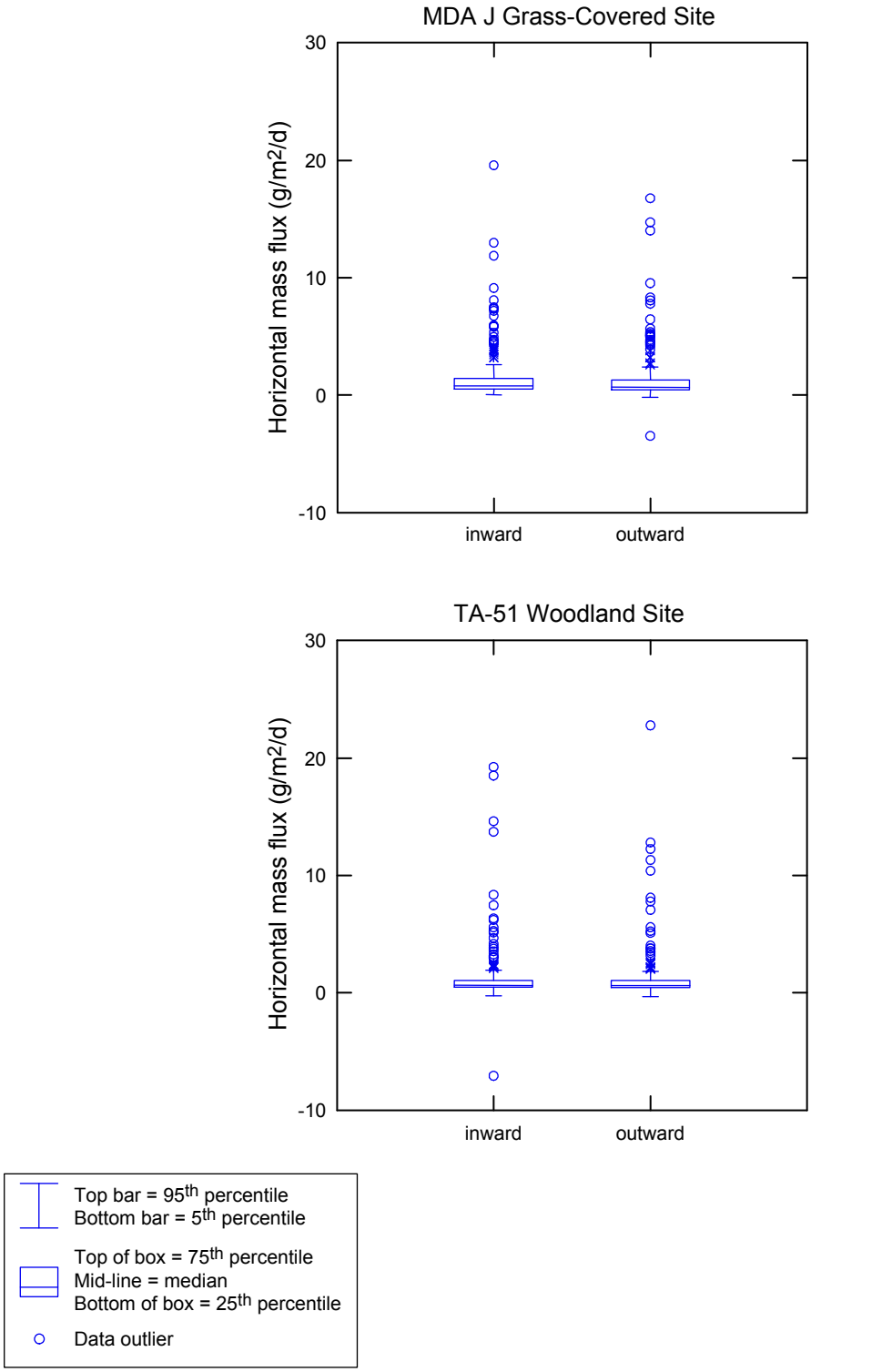

Figure 9
Horizontal Mass Flux at Inward- and Outward-Facing Samplers at Both Analog Sites

While horizontal flux describes saltating dust moving horizontally through an area at lower heights, vertical flux describes dust moving up and down. The particles described by vertical flux are typically smaller in diameter and can be transported for long distances; accordingly, these particles present an off-site risk. Figure 10 shows the range of measured values for the vertical flux. Note that positive numbers represent upward flux (removal from the area) and negative numbers represent downward net flux (deposition within the area). Table 3 shows the summary statistics for aerosol mass concentrations and the vertical flux measurement data. Overall, the average vertical flux at 2 m (6.6 ft) above the soil surface was 2.6 ± 12.3 g/m^2/yr ($5.4 \times 10^{-4} \pm 3.0 \times 10^{-3}$ lb/ft^2/yr) or 0.03 ± 0.12 T/ha/yr (0.013 ± 0.054 t/ac/yr), which suggests little, if any, net loss from the area from suspended soils.

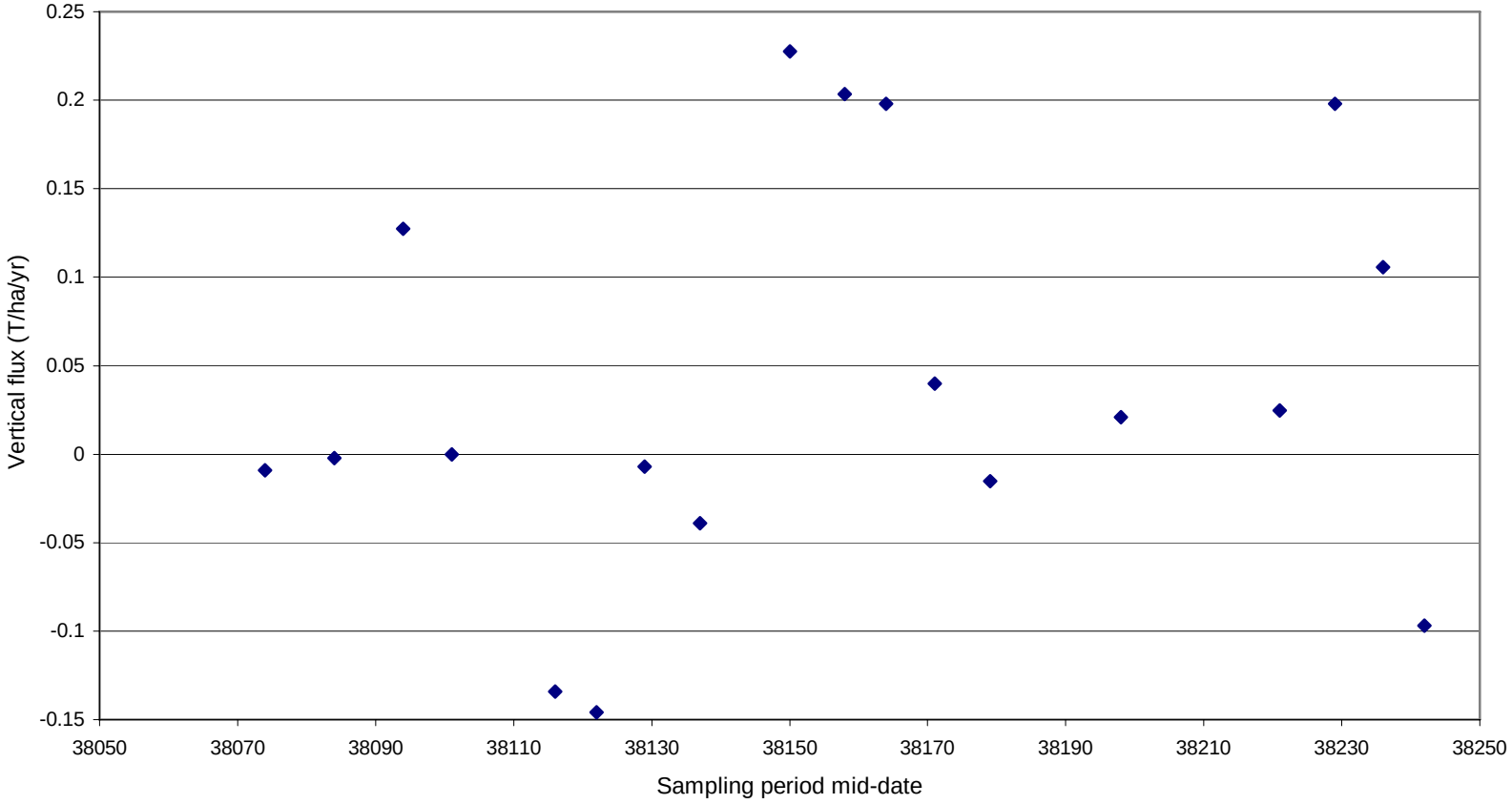

Figure 10
Estimated Vertical Mass Flux Collected during All Sampling Periods (1 m sampling height)

Table 3
Summary Statistics for Aerosol Mass Concentration and Vertical Mass Flux at MDA J

Summary Statistic	Mass Concentration ($\mu g/m^3$) [a]	Vertical Mass Flux ($g/m^2/yr$)	Vertical Mass Flux (T/ha/yr)
Average	1.1E+01	2.6E+00	3.0E–02
Standard Deviation	1.7E+01	1.2E+01	1.2E–01
Median	1.0E+01	0.0E+00	0.0E+00
Minimum	3.5E+00	–2.0E+01	–2.0E–01
Maximum	2.7E+01	2.3E+01	2.3E–01
Range	2.4E+01	4.3E+01	4.3E–01

[a] *Measurements for aerosol mass concentration averaged over 1 m and 3 m sampling heights for a total of 19 samples.*

4.0 Discussion

This study provides the first known set of wind erosion measurements on a landfill cover. No previous assessment has estimated the effect of wind erosion using data, site-specific or otherwise, on long-term cover performance and associated risks. In fact, there are few data sets on wind erosion for semiarid ecosystems dominated by grass cover, the results for short-grass steppe adjacent to Rocky Flats in Colorado (Breshears et al., 2003) being the one noteworthy exception.

The horizontal transport component of wind erosion was quantified using rotating BSNE samplers. Transport, as noted above, relates to the local movement and redistribution of soil, but does not necessarily reflect net erosion. That is, significant amounts of soil can move into and out of an area, and previous estimates have reflected only relative differences in total horizontal mass flux, not net erosion (Breshears et al., 2003). The study design adopted here used motion-restricted samplers that allowed directional measurements for analysis of net loss due to horizontal transport.

The estimates of vertical flux provide the most direct measurements of wind erosion and suggest a small net loss of soil from the sampling sites over the period studied. The flux measurements presented here are similar to those reported by Breshears et al. (2003), who measured a mean vertical flux of 3.0 $g/m^2/yr$ (0.071 $lb/ft^2/yr$) at a grassland near Denver, Colorado. As seen in previous studies (Whicker et al., 2002; Breshears et al., 2003), wind erosion is highly variable temporally within the one- to two-week intervals studied. The results of this study provide distributions that describe this temporal variability for the period studied.

4.1 Significance of Results

As seen in previous studies (Breshears et al., 2003), horizontal wind transport greatly exceeds net soil loss, by more than two orders of magnitude for some conditions and heights. The results of the current study suggest that horizontal wind-driven dust flux is frequently moving material into and out of the area, resulting in a small net erosional loss accumulated over the course of the study. The additional data from the circular design reinforce this interpretation: the net flux into and out of the circular area were not significantly different. Because this study quantifies all three components of dust-flux, it provides a higher degree of confidence about interpreting wind-driven processes than is feasible with less robust studies.

The wind-driven transport and erosion data set in the woodland site is also unique. Only a few measurements of soil erosion have been reported for a woodland setting (Baker and Jemison, 1991), and those data estimate only horizontal transport rates; they do not provide information on site conditions or estimates of uncertainty or variance. Not surprisingly, the present study

showed that horizontal wind-driven dust fluxes in the woodland site (TA-51) were lower than those at the grass-covered (MDA J) site. This is consistent with the findings of Breshears et al. (2003), who found horizontal fluxes in grassland were about an order of magnitude greater than those in woodlands. In each case, the rough, heterogeneous canopy structure associated with the woodland has a major effect on the boundary layer and surface roughness, and these factors, in turn, affect wind dynamics and associated soil transport and erosion. In addition, data from the circular sampling area at the woodland site indicate no significant net gain or loss of soil (i.e., the amounts of dust being deposited into and removed from the study area are essentially the same). Again, this indicates that, despite the fairly substantial amount of transport occurring at the site, overall net loss of soil cover is relatively low.

The data collected in this study can be used to provide parameters for models used to assess long-term cover performance and associated risks. Also, the wind erosion estimates can be compared against the estimates of water erosion being developed for MDA G to assess the relative magnitude of the two processes.

Wind erosion is important at MDA G in two contexts, both of which should be considered. First, wind erosion should be factored into estimations of long-term cover integrity. Second, even if water erosion proves to be the dominant force for degradation of the landfill, wind-driven transport may be the most important risk pathway for any exposed contamination. Such contamination might result from erosional loss of the cover or from biological intrusion into the waste caused by burrowing animals or plant root uptake.

4.2 Qualifications

Although the results reported above are useful for assessing the long-term performance of MDA G, a number of qualifications apply to the findings:

1. The data reported here cover only part of a year. Improved estimates would be obtained if the measurements were made over a minimum of a full year. Year-to-year variation is also of concern (Breshears et al., 2003) and multiyear estimates would provide even more confidence for longer-term extrapolations.

2. Correlation of wind transport and erosion to wind conditions is currently limited to one- to two-week intervals because of limits imposed by the need to collect and weigh dust. However, new automated systems for measuring dust flux could provide a basis for developing more predictive relationships between wind distributions and wind erosion.

3. Two vegetation scenarios were evaluated in this study: MDA J as an analog for immediate postclosure conditions at MDA G and the TA-51 woodland site as a later

successional analog. There is, however, considerable uncertainty about the actual ecological trajectory that vegetation will follow at MDA G. This trajectory will, of course, be influenced by climate. Periods of drought could lead to loss of ground cover through mortality and fire. Indeed, such changes have driven the dominant vegetation and soil erosion dynamics around Los Alamos for the past several decades, most notably through the 1950s drought, the Cerro Grande Fire of 2000, and the tree-killing drought of the new millennium (2000 to 2004) (Breshears and Allen, 2002; Allen and Breshears, 1998; Davenport et al., 1998). Disturbances such as fire result in major increases in wind and water erosion and associated contaminant transport (Whicker et al., 2002, Johansen et al., 2001a, 2001b, 2003). The estimates presented here do not account for such probable events, which are of increased likelihood due to global change (Breshears and Allen, 2002).

Anthropogenic disturbances can also have tremendous impacts on soil erosion. For example, Figures 11 and 12 illustrate how wind erosion at a site just east of MDA G, but within the TA-54 boundary, increased following tree-thinning operations in the nearby piñon-juniper woodland. Figure 11 shows aerosol mass concentrations before and after tree thinning and Figure 12 shows that the flux gradient changed from neutral (no net loss) to one of sustained soil loss following tree thinning. Clearly, ecosystem disturbance through anthropogenic management of the vegetation cover can dramatically alter soil erosion rates over short periods of time; the effects of these disturbances may persist over longer periods of time, depending on how long it takes the ecosystem to recover.

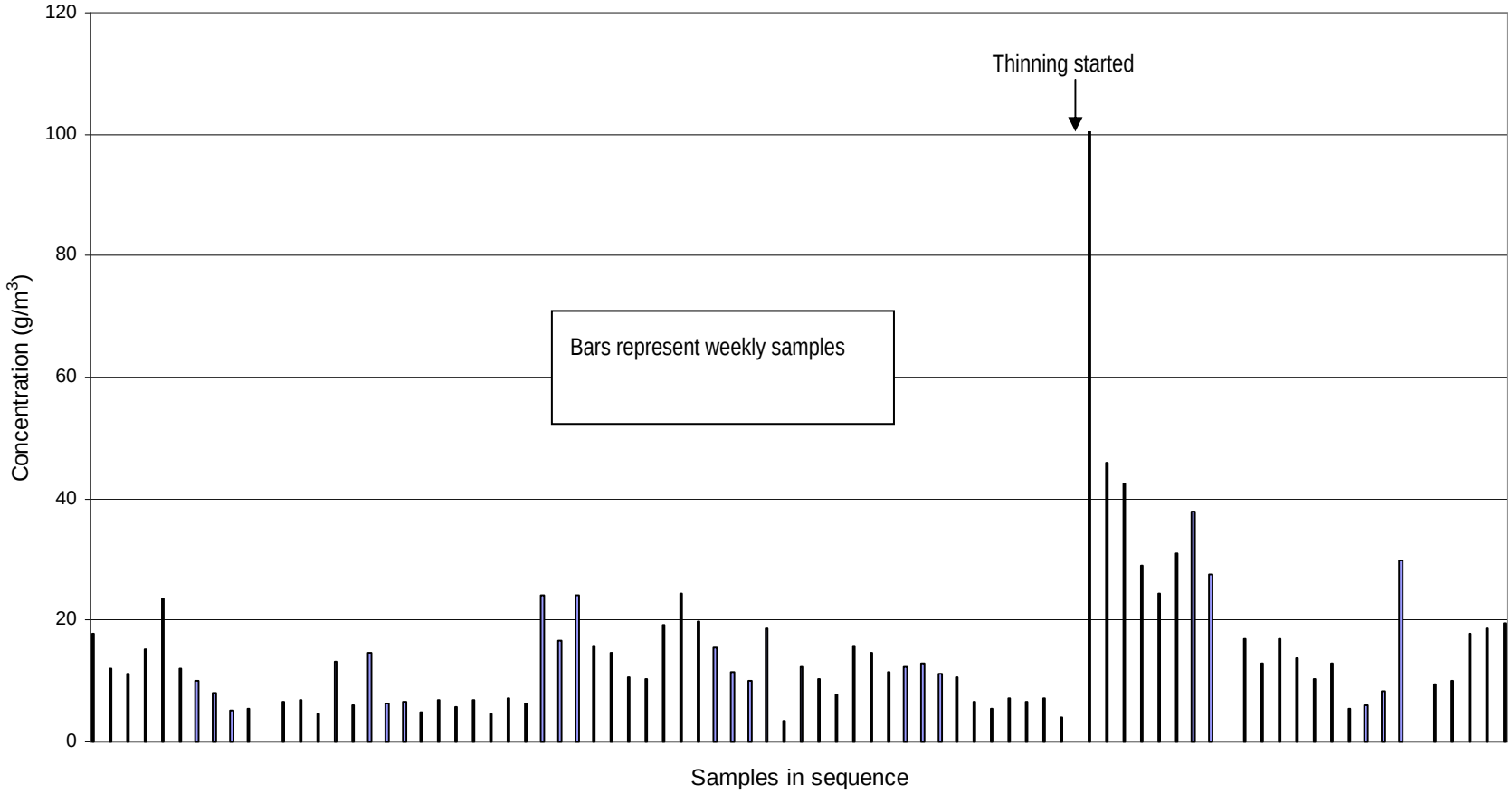

Figure 11
Pre- and Post-Thinning Dust Concentrations at TA-54 Meteorological Station

Source: Whicker et al., 2003

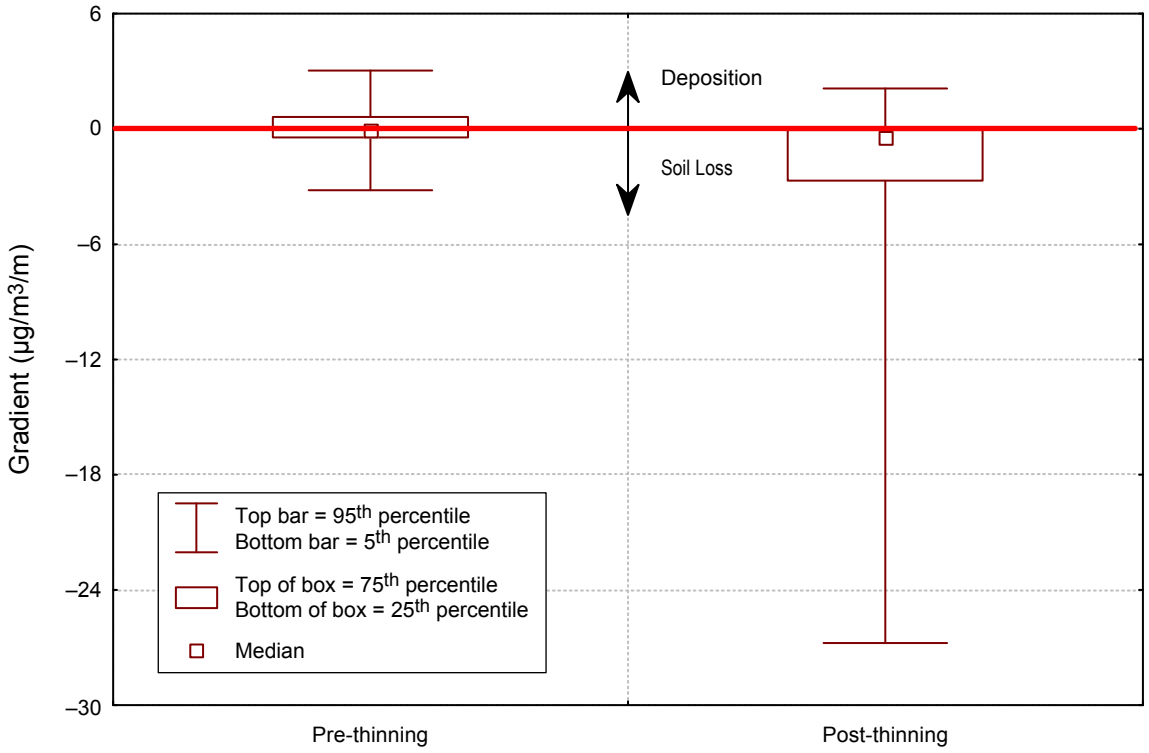

Figure 12
Weekly Flux Gradient Measurements at TA-54 before and after Nearby Thinning Operations

Source: Whicker et al., 2003

5.0 References

Allen, C.D., and D.D. Breshears, 1998, "Drought-Induced Shift of a Forest-Woodland Ecotone: Rapid Landscape Response to Climate Variation," *Proceedings of the National Academy of Sciences USA,* Vol. 95, pp. 14,839–14,842.

Anspaugh, L.R., J.H. Shinn, P.L. Phelps, and N.C. Kennedy, 1975, "Resuspension and Redistribution of Plutonium in Soils," *Health Physics*, Vol. 29, pp. 571–582.

Arimoto R., T.B. Kirchner, J. Webb, M. Conley, B. Stewart, D. Schoep, and M. Walthall. 2002. "239, 240Pu and Inorganic Substances in Aerosols from the Vicinity of the Waste Isolation Pilot Plant: The Importance of Resuspension," *Health Physics*, Vol. 83, pp. 456–470.

Bagnold, R.A., 1941, *The Physics of Blown Sand and Desert Dunes,* Chapman and Hall Ltd., London.

Baker M.B. Jr., R.L. Jemison, 1991, "Soil Loss—Key to Understanding Site Productivity," *Proceedings of 36th Annual New Mexico Water Conference–Agencies and Science Working for the Future, 1991 November 7–8,* New Mexico Water Resources Research Institute Report No. 265, New Mexico Water Resources Research Institute, Las Cruces, New Mexico.

Breshears, D.D., C.D. Allen, 2002, "The Importance of Rapid, Disturbance-Induced Losses in Carbon Management and Sequestration," *Global Ecology and Biogeography*, Vol. 11, pp. 1–5.

Breshears, D.D., J.J. Whicker, M.P. Johansen, and J.E. Pinder, 2003, "Wind and Water Erosion and Transport in Semi-Arid Shrubland, Grassland, and Forest Ecosystems: Quantifying Dominance of Horizontal Wind-Driven Transport," *Earth Surface Processes and Landforms,* Vol. 28, pp. 1,189–1,209.

Campbell Scientific Canada Corp., 2004, *3-D Sonic Anemometer, Model CSAT3,* Brochure printed January 2004. <http://www.campbellsci.ca/CampbellScientific/Catalogue/CSAT3-_Br.pdf>.

Davenport, D.W., D.D. Breshears, B.P. Wilcox, and C.D. Allen, 1998, "Viewpoint: Sustainability on Piñon-Juniper Ecosystems: A Unifying Perspective on Soil Erosion Thresholds," *Journal of Range Management,* Vol. 51, pp. 231–240.

Fryrear, D.W., 1985, "Soil Cover and Wind Erosion," *Transactions of ASAE,* Vol. 28, pp. 781–784.

Fryrear, D.W., 1986, "A Field Dust Sampler," *Journal of Soil and Water Conservation,* Vol. 41, pp. 117–120.

Gillette, D.A, D.W. Fryrear, J.B. Xiao, P. Stockton, D. Ono, P.J. Helm, T.E. Gill, and T. Ley, 1997, "Large-Scale Variability of Wind Erosion Mass Flux Rates at Owens Lake: Vertical Profiles of Horizontal Mass Fluxes of Wind-Eroded Particles with Diameter Greater than 50 μm," *Journal of Geophysical Research,* Vol. 102(D22), pp. 25,977–25,987.

Goossens, D. and Z.Y. Offer, 2000, "Wind Tunnel and Field Calibration of Six Aeolian Dust Samplers," *Atmospheric Environment*, Vol. 34, pp. 1,043–1,057.

Johansen, M.P., T.E. Hakonson, and D.D. Breshears, 2001a, "Post-Fire Runoff and Erosion from Rainfall Simulation: Contrasting Forests with Shrublands and Grasslands, *Hydrologic Processes*, Vol. 15, pp. 2,953–2,965.

Johansen, M.P., T.E. Hakonson, F.W. Whicker, and D.D. Breshears, 2003, "Pulsed Redistribution of a Contaminant Following Forest Fire: Cs-137 in Runoff," *Journal of Environmental Quality*, in press.

Johansen, M.P., T.E. Hakonson, F.W. Whicker, R.J. Simanton, and J.J. Stone, 2001b, "Hydrologic Response and Radionuclide Transport Following Fire at Semiarid Sites," *Journal of Environmental Quality*, Vol. 30(6), pp. 2,010–2,017.

Liu, B.Y.H. and Y.H. Pui, 1981, "Aerosol Sampling Inlets and Inhalable Particles," *Atmospheric Environment*, Vol. 15, pp. 589–600.

Nyhan, J.W., L.W. Hacker, T.E. Calhoun, and D.L. Young, 1978, *Soil Survey of Los Alamos County, New Mexico*, Los Alamos National Laboratory Report LA-677-MS.

Rodgers, J.C., P.T. Wasiolek, J.J. Whicker, C. Eberhart, K. Saxton, and D. Chandler, 2000, *Performance Evaluation of LANL Environmental Radiological Air Monitoring Inlets at High Wind Velocities Associated with Resuspension*, Los Alamos National Laboratory Report LA-UR-00-3091.

Sehmel, G.A., 1980, "Particle Resuspension: A Review," *Environment International*, Vol. 4, pp. 107–127.

Stout, J.E. and T.M. Zobeck, 1996, "The Wolfforth Field Experiment: A Wind Erosion Study," *Soil Science*, Vol. 161, pp. 616–632.

Stull, R.B., 1988, *An Introduction to Boundary Layer Meteorology*, Kluwer Academic Publishers, The Netherlands.

Webb, S.B., S.A. Ibrahim, and F.W. Whicker, 1997, "A Three-Dimensional Spatial Model of Plutonium in Soil Near Rocky Flats, Colorado," *Health Physics*, Vol. 73(2), pp. 340–349.

Whicker J.J., J.E. Pinder, and D.D. Breshears, 2003, "Increased Contaminant Transport Following Wildfire," presented at the Annual Health Physics Society, *Health Physics* Vol. 84, p. S206.

Whicker, J.J., D.D. Breshears, P.T. Wasiolek, T.B. Kirchner, R.A. Tavani, D. Schoop, and J. Rodgers, 2002, "Temporal and Spatial Variation of Episodic Wind Erosion in Unburned and Burned Shrubland," *Journal of Environmental Quality*, Vol. 31, pp. 599–612.

LA-UR-05-7232

Approved for public release;
distribution is unlimited.

Title: AIR DISPERSION ANALYSIS FOR
LOS ALAMOS NATIONAL LABORATORY
TECHNICAL AREA 54, MATERIAL DISPOSAL AREA G

Author(s): Keith W. Jacobson

Submitted to: U.S. Department of Energy

Form 836 (8/00)

Table of Contents

List of Figures i
List of Tables ii
Acronyms and Abbreviations iii
1.0 Introduction 1
2.0 Methods 2
2.1 Input Data 2
2.1.1 Meteorological Data 4
2.1.2 Terrain Elevation and Land Use Data 6
2.2 Modeling Approach 6
2.2.1 Near-Field Analysis 6
2.2.2 Alternate-Source Analysis 11
2.2.3 Far-Field Analysis 11
2.3 CALMET Processing 16
2.4 CALPUFF Modeling 18
2.4.1 Particle Size and Dry Deposition 18
2.4.2 Scavenging Coefficient 22
2.4.3 Miscellaneous Parameters 22
2.5 CALPOST Processing 24
3.0 Results 25
3.1 Near-Field Air Concentrations 25
3.2 Alternate-Source Analysis 34
3.3 Far-Field Analysis 36
4.0 Discussion of Air Dispersion Modeling Uncertainty 39
5.0 References 41

List of Figures

Figure 1 Major Inputs, Steps, and Outputs in the CALPUFF Air Dispersion Analysis 3
Figure 2 Meteorological Towers Used for Air Dispersion Analysis 5
Figure 3 Model Domain for Near-Field Analysis 7
Figure 4 Digital Orthophotograph Superimposed on Terrain Data 9
Figure 5 Source Areas Used in Near-Field Analysis 10
Figure 6 Model Domain for the Alternate-Source Analysis 12
Figure 7 Model Domain for Far-Field Analysis 13
Figure 8 Population Data Array for 80-Mile Radius from Material Disposal Area G 14
Figure 9 Dry Depletion Rate vs. Particle Size 20
Figure 10 Frequency Distribution for Various Particle Sizes 21
Figure 11 Wet Deposition Rate vs. Scavenging Coefficient 23
Figure 12 Relative Air Concentration Contours Predicted by CALPUFF for Releases from MDA G Source Area 1 (particle size gdiam 0.48 µm) 26

Figure 13 Relative Air Concentration Contours Predicted by CALPUFF for Releases from MDA G Source Area 2 (particle size gdiam 0.48 µm) 27
Figure 14 Relative Air Concentration Contours Predicted by CALPUFF for Releases from MDA G Source Area 3 (particle size gdiam 0.48 µm) 28
Figure 15 Relative Air Concentration Contours Predicted by CALPUFF for Releases from MDA G Source Area 1 (particle size gdiam 5.0 µm) 29
Figure 16 Relative Air Concentration Contours Predicted by CALPUFF for Releases from MDA G Source Area 2 (particle size gdiam 5.0 µm) 30
Figure 17 Relative Air Concentration Contours Predicted by CALPUFF for Releases from MDA G Source Area 3 (particle size gdiam 5.0 µm) 31
Figure 18 Average Air Concentration vs. Particle Size (dry deposition over a range of 1 to 5 km) 35
Figure 19 Air Concentration Contours for Far-Field Analysis 37

List of Tables

Table 1 2002 Population Data by Polar Grid Sector for Circular Area with 80-km Radius 15
Table 2 Comparative Influence of Surface Meteorological Station Data Used for MDA G Dispersion Analyses 17
Table 3 Bias Settings for Upper-Air Wind Observations Used in Air Dispersion Analysis 18
Table 4 Parameter Values Selected for CALMET and CALPUFF Models through Trial Runs 24
Table 5 Annual Variability of Particulate Concentrations at Selected Locations North of MDA G 25
Table 6 Projected Air Concentrations along Border between LANL and San Ildefonso Pueblo, by Source 32
Table 7 Ten-Year Average Peak Dry and Wet Deposition Ratios for Source Areas 1, 2, and 3 33
Table 8 Comparison of Dry Deposition Flux at the LANL Boundary North of MDA G 33
Table 9 Comparison of Air Dispersion Results for Releases from Various Material Disposal Sites 34
Table 10 Selected Population-Weighted Air Dispersion Values for Source Area 1 38

Acronyms and Abbreviations

3-D	Three-dimensional
ALARA	As low as reasonably achievable
DEM	Digital elevation model
gdiam	Geometric mean diameter
gsd	Geometric standard deviation
LANL	Los Alamos National Laboratory
LULC	Land use/land coverage
MDA	Material Disposal Area
NAD 27	North American Datum 1927
TA	Technical Area
USGS	U.S. Geological Survey
UTM	Universal Transverse Mercator

1.0 Introduction

This report summarizes air dispersion analyses used to model the atmospheric transport and dispersion of contaminants released from Material Disposal Area (MDA) G. These analyses were performed as part of an effort to update the 1997 performance assessment and composite analysis for MDA G (Hollis et al., 1997). The 1997 study evaluated the potential impacts of airborne releases to persons living downwind of the disposal facility using the results of a simple atmospheric dispersion model, which was adjusted in an attempt to account for the effects of complex terrain on contaminant transport.

Los Alamos surface winds often vary dramatically with time of day, location, and height above ground due to the influence of the terrain (Bowen, 1990) and these winds, in turn, have varying effects on the atmospheric transport characteristics of releases from the facility. Since 1997, efforts have been made to explicitly model the effects of the mesa and canyon topography on the transport of airborne contaminants to locations downwind of MDA G. Toward this end, the Meteorology Air Quality Group of the Los Alamos National Laboratory (LANL or the Laboratory) has applied CALPUFF®, an advanced meteorological and air quality modeling package, to simulate atmospheric transport and dispersion of hypothetical radionuclide releases from MDA G. The CALPUFF package was developed by Earth Tech, Inc. for regulatory use in air quality programs, and is an officially approved model for regulatory compliance by the U.S. Environmental Protection Agency (EPA, 2003). The package, considered suitable for complex and rugged terrain conditions, is a nonsteady-state or puff trajectory model that applies hourly averages of wind speed and direction to generate air-concentration values (ASG, 2005; Scire et al., 2000a and 2000b).

Following this brief introduction, Section 2 describes the methods used in applying the CALPUFF modeling system; the results of the modeling are presented in Section 3. Section 4 discusses the uncertainties involved in using the CALPUFF package and the impact of these on the MDA G air dispersion analysis.

2.0 Methods

The CALPUFF computer-modeling package or system has three major components: (1) CALMET, a meteorological model with both diagnostic and prognostic wind-field generators, (2) CALPUFF, a nonsteady state dispersion model, and (3) CALPOST, a postprocessing program. CALMET performs a number of analyses to generate three-dimensional (3-D) wind fields and information about the types and durations of the releases; these data are used by the CALPUFF model to conduct the transport modeling. Output from CALPUFF is processed in CALPOST and graphics packages such as Surfer (Golden, 2002 and 2005) for presentation. Figure 1 shows the relationship between the three system components and the corresponding information flows. A complete description of the modeling package is provided in the CALPUFF user's manual (Scire et al., 2000a).

Three separate modeling efforts were conducted in support of the MDA G performance assessment and composite analysis. The first of these, referred to as the near-field analysis, focused on transport phenomenon within a few kilometers of the disposal facility; these model projections were used to estimate exposures for persons located immediately downwind of MDA G. The second analysis evaluated the potential contributions made by airborne releases from other waste disposal sites at the LANL to the impacts attributed to MDA G. This analysis directly supports the composite analysis and is referred to as the alternate-source analysis in this report. The final analysis, referred to here as the far-field analysis, projected air concentrations and deposition rates up to 80 km (50 mi) from the disposal facility. The results of this modeling were used to conduct an ALARA (as low as reasonably achievable) analysis.

The following sections discuss the data and modeling approaches used to conduct the three atmospheric modeling efforts. Sections 2.1 and 2.2 describe the input data and the modeling approach used in the analyses. Details of the CALMET, CALPUFF, and CALPOST processing are discussed in Sections 2.3, 2.4, and 2.5, respectively.

2.1 Input Data

The major categories of input parameters used in the CALPUFF analyses include meteorological data, which describe atmospheric conditions at and in the vicinity of MDA G, and terrain and land use information. The terrain data characterize the topography of the landscape while the land use data specify vegetational characteristics and other surface conditions. This section discusses these parameters in more detail and identifies the sources of data used to characterize them.

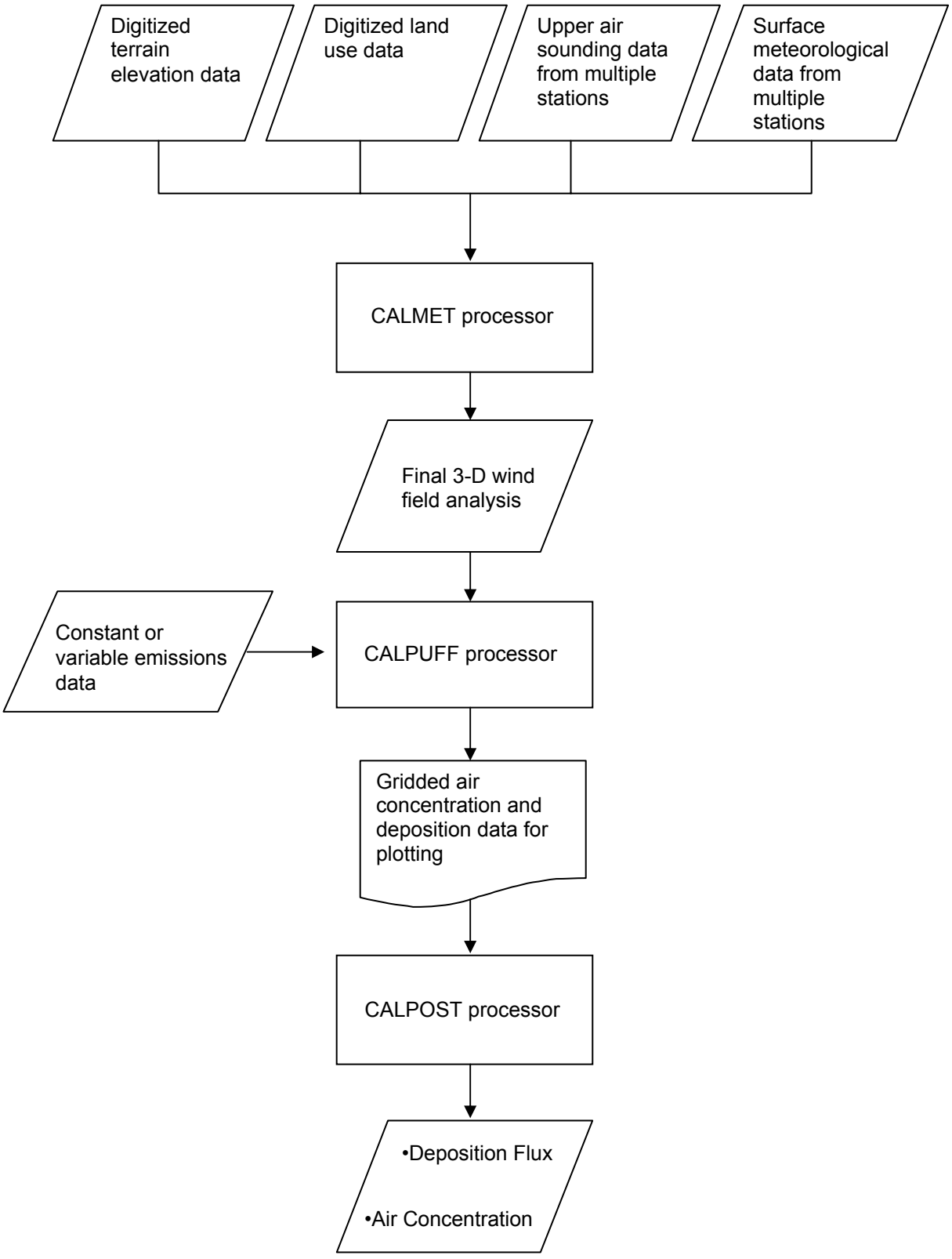

Figure 1
Major Inputs, Steps, and Outputs in the CALPUFF Air Dispersion Analysis

2.1.1 Meteorological Data

The meteorological data used in the atmospheric transport modeling include local, surface meteorological data gathered by the Meteorology Air Quality Group monitoring network at LANL and regional, upper-air data from nearby National Weather Service monitoring sites such as Santa Fe and Albuquerque. Local surface meteorological data were obtained from a network of meteorological towers located within the Laboratory. These towers include stations at Technical Area (TA)-6, TA-49, TA-53, and TA-54, the locations of which are shown in Figure 2. One of these towers, the station at TA-54, is located less than 2 km (1.2 mi) from MDA G. Data obtained from these stations consist of 15-minute average readings for a number of meteorological parameters:

- Wind speed
- Wind direction
- Air temperature
- Relative humidity
- Cloud cover
- Ceiling height
- Pressure
- Precipitation

These data were merged into one-hour average readings using the preprocessing program SMERGE, which is included in the CALPUFF modeling package. Since four towers were used in this study, there are four records for each hour run in the CALMET model. The hourly meteorological dataset was developed using measurements collected continuously over a 10-year period, from 1992 through 2001.

To complete the construction of wind fields in the vertical direction, the CALPUFF package requires upper-air, or rawinsonde, data from at least one nearby station. Upper-air data become increasingly important for modeling of larger domains and in long-range transport analyses, and data from multiple stations is often used in these cases. For this analysis, however, data from one nearby station was judged sufficient, as the primary focus was the near field dispersion analysis for which upper-air data are not critical. The closest rawinsonde site to LANL, Albuquerque International Airport, was used as the source for upper-air data. Los Alamos is located about 85 km (53 mi) from Albuquerque, thus the upper wind data should be fairly representative for Los Alamos. These sounding data consist of measurements such as temperature and wind speed and direction at various heights, or sounding levels, above ground. The CALMET processing program requires sounding levels up to a 300 mb (4.4 psi) pressure level, which corresponds to about 9,500 m (3.2×10^4 ft) above mean sea level in Albuquerque.

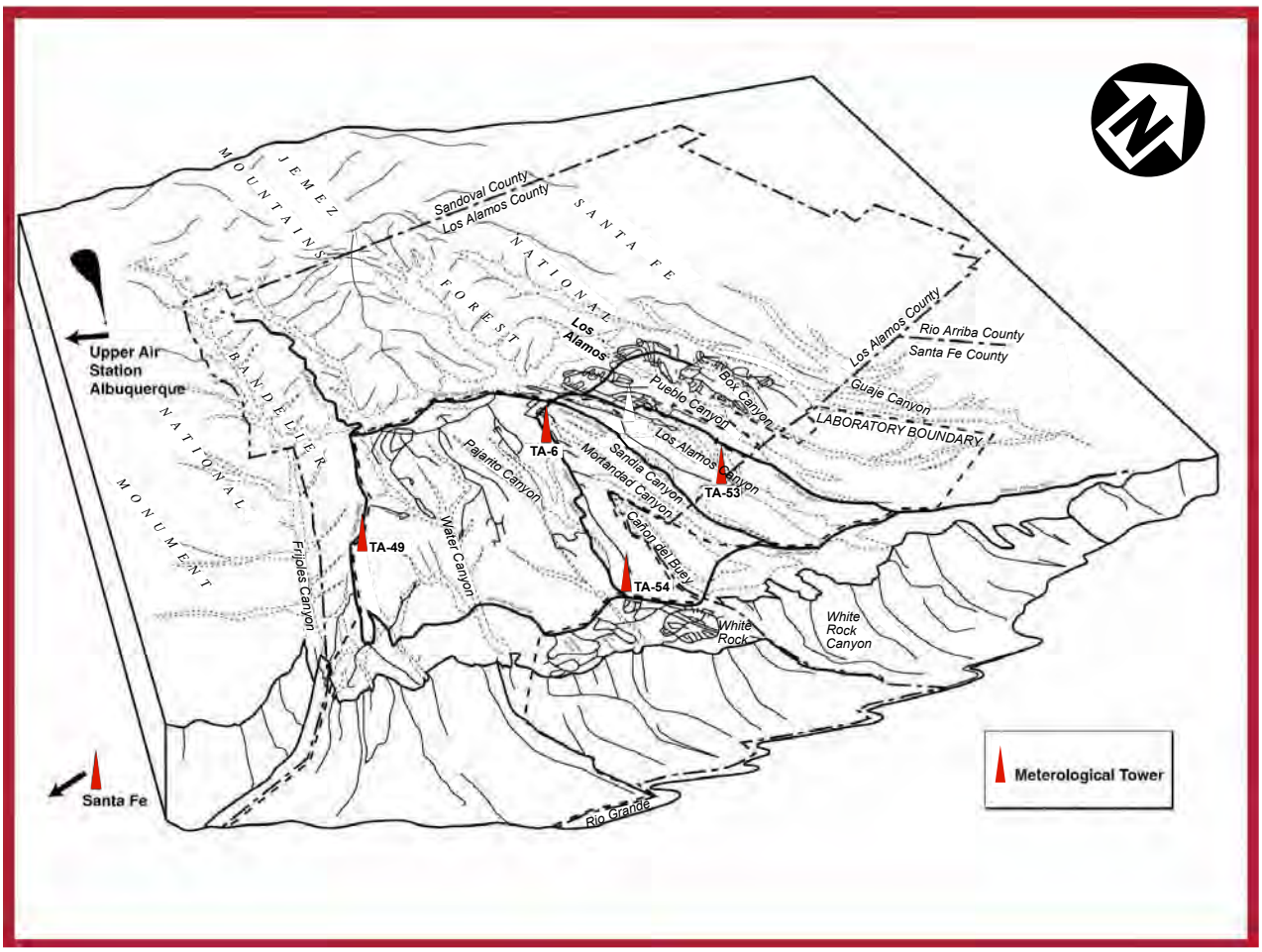

Figure 2
Meteorological Towers Used for Air Dispersion Analysis

2.1.2 Terrain Elevation and Land Use Data

Digital elevation model (DEM) data define the topography of the model domains used in the CALPUFF modeling. The land use/land coverage (LULC) data describe the vegetation, water, natural surface, and cultural features of the land surface, and are the basis for defining several geophysical parameters (e.g., surface roughness, albedo, the Bowen ratio, and leaf area index) that are used in the air dispersion modeling. Both DEM and LULC data were obtained directly from the USGS and are projected in a "modified" Universal Transverse Mercator (UTM) system. The CALPUFF package includes a preprocessor, the MAKEGEO program, that processes both the terrain elevation and LULC data to create the modeling grids for CALMET and CALPUFF. All coordinates used in the analysis were converted to the UTM North American Datum 1927 (NAD 27) to correspond to the USGS data.

Land use is defined for each grid location using one of 14 land use types. The modeling conducted in support of the MDA G performance assessment and composite analysis considered two land use types: rangeland, which was used to represent site conditions shortly after closure, and forest, used to represent the site after its transition to a piñon-juniper woodland. Two sets of simulations were run for the near-field analysis, one in which the land use was set to rangeland for all grid locations, and one in which it was set to forest. All alternate-source and far-field simulations were performed using a land use type of rangeland.

2.2 Modeling Approach

As discussed earlier, the atmospheric transport modeling evaluated transport characteristics for three separate analyses, referred to as the near-field, alternate-source, and far-field analyses. The modeling approach, including the model domains, grid definition, and source areas used to conduct these analyses, is described below.

2.2.1 Near-Field Analysis

The near-field analysis model domain includes the portion of LANL surrounding MDA G, the western portion of White Rock, and the southern portion of San Ildefonso tribal lands (Figure 3). The model domain is 3.5 km (2.2 mi) in the east-west direction by 2.1 km (1.3 mi) in the north-south direction and includes the TA-54 meteorological tower. The grid origin is Zone 13 386400 E and 3964400 N (UTM NAD 27).

A major consideration of the air transport modeling is to incorporate the effects of terrain on air dispersion; thus, the near-field analysis used the highest resolution that CALPUFF could read for the terrain grid spacing. This matched the 30-m (98-ft) grid resolution typical of USGS 7.5-minute quadrangle maps, and resulted in 116 points along the east-west direction and 70 points in the north-south direction. Because the fine-grid analysis requires considerable run time, a coarser grid spacing of 100 m (330 ft) was used for preliminary evaluations. The coarse grid allowed for rapid testing and validation of meteorological input files as they were constructed.

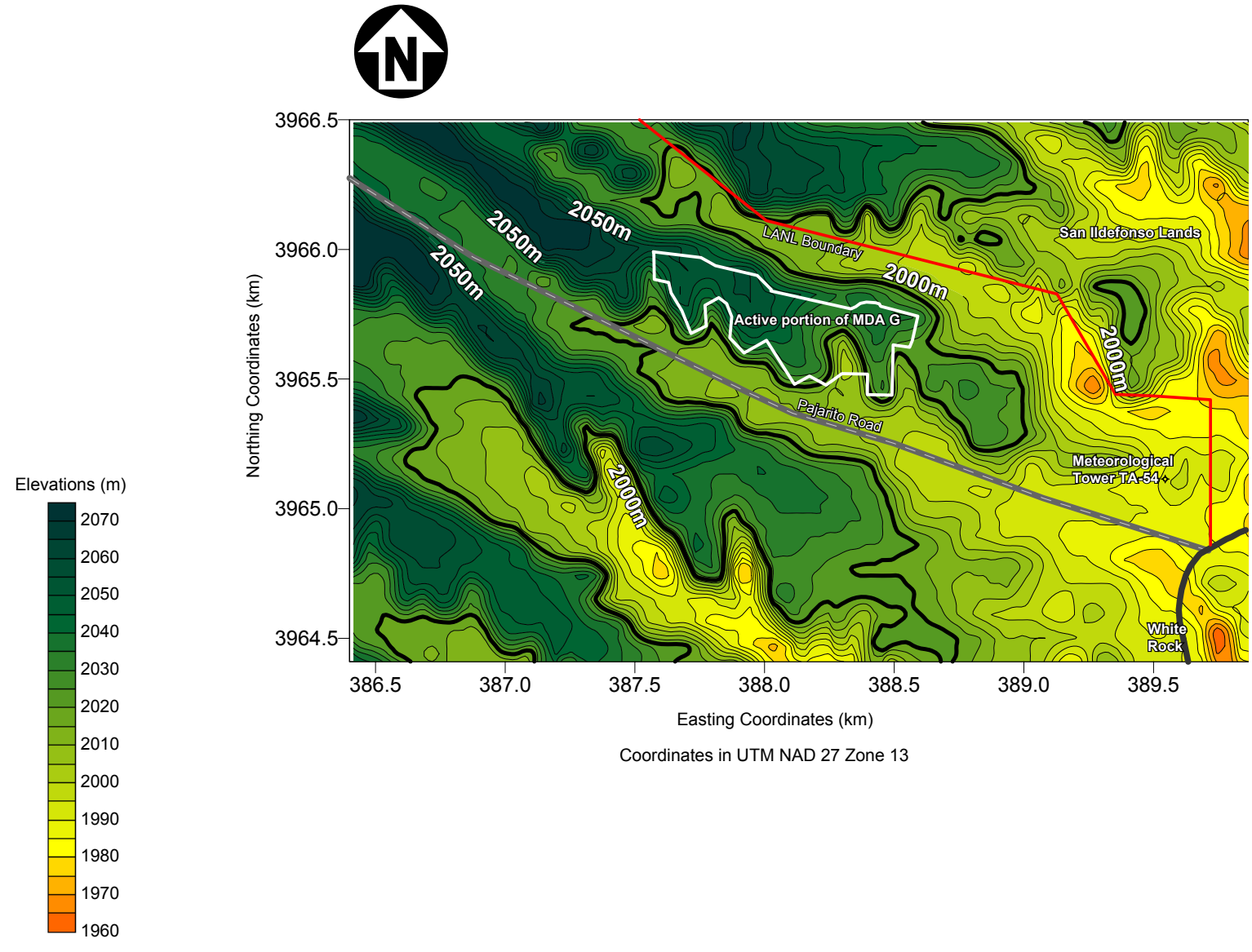

Figure 3
Model Domain for Near-Field Analysis

Once the grid was defined, an output grid file was loaded into Surfer and a contour plot was generated using the terrain and land use data that had been input into CALMET. Additional features such as the LANL boundary, the boundary of the active portion of MDA G, and White Rock were included. Figure 3 is a contour plot of the model domain showing the results of the terrain processing overlain with local landmarks. To verify that the map attributes were correctly matched to the elevation data, a draped map was created which shows, in an exaggerated manner, the terrain of MDA G and the surrounding area (Figure 4). A visual inspection of Figure 4, in which mesa tops are shaded grayish green and lower elevations such as the canyon floor are shaded yellow, showed that the elevation data were handled correctly in the model.

The disposal facility was divided into three atmospheric source areas to conduct the near-field transport modeling (Figure 5). These areas roughly coincide with the pits and shafts used to dispose of waste prior to 1971 (source area 1), from 1971 through 2004 (source area 2), and from 2005 through 2044 (source area 3). The surface areas of source areas 1, 2, and 3 are approximately 7.5, 27, and 13 ha (19, 67, and 32 ac), respectively.

The near-field analysis evaluated the potential impacts of particulate releases and radionuclides diffusing from the site in the form of vapors or gases. A unit emission (release) rate (1 $g/m^2/s$ [6.2×10^{-5} $lb/ft^2/s$]) for both particulate and vapor/gas releases was assigned to each source area and air concentrations and particulate deposition fluxes were projected for all locations within the model domain. The projected air concentrations were used to calculate air dispersion factors as follows:

$$\frac{X}{Q} = \left(\frac{X}{R \times A} \right) \qquad 1$$

Where

$\frac{X}{Q}$ = the air dispersion factor (s/m^3)

X = the air concentration (g/m^3)

R = the release rate ($g/m^2/s$)

A = the source area (m^2)

The transport and dispersion of particulate releases were evaluated using the meteorological data for 1992 through 2001 and the land use types discussed in section 2.1.2. The model simulations for vapor and gas-phase radionuclides used the same meteorological data, but projected downwind concentrations for the rangeland land use only.

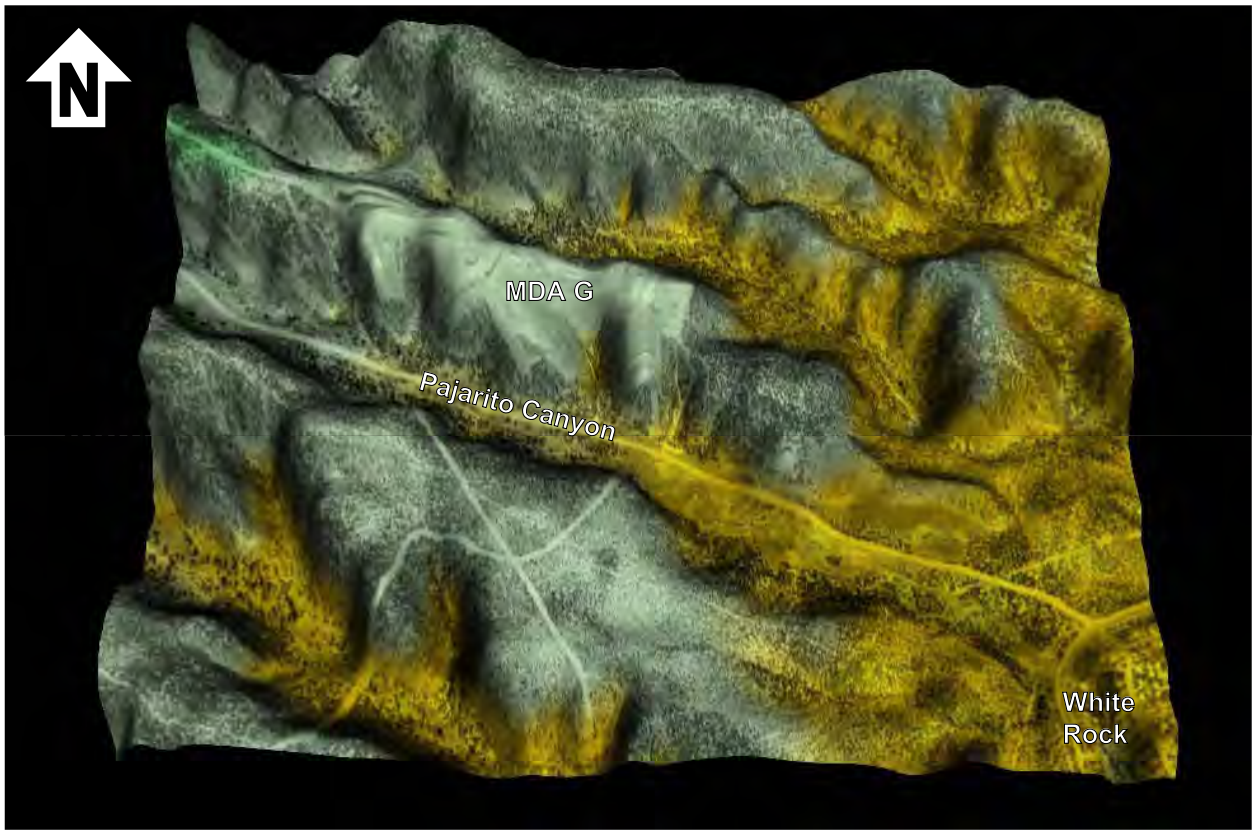

Figure 4
Digital Orthophotograph Superimposed on Terrain Data

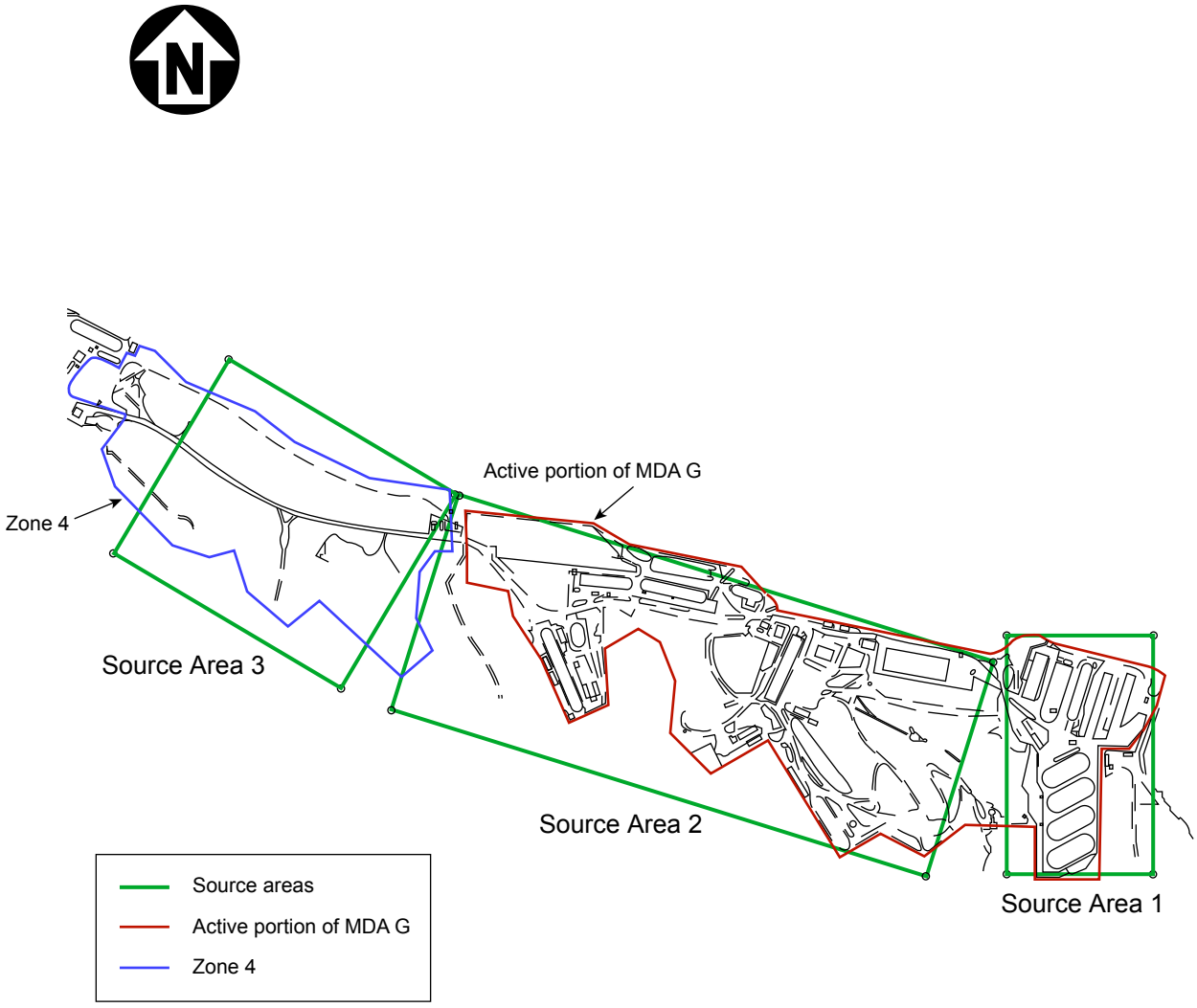

Figure 5
Source Areas Used in Near-Field Analysis

2.2.2 Alternate-Source Analysis

The alternate-source analysis considers how other significant sources of contamination at the Laboratory may affect the anticipated exposure levels for persons living downwind of MDA G. The atmospheric transport modeling conducted in support of this evaluation used a model domain consisting of an 8 × 8 km (5 × 5 mi) grid with a mesh size, or receptor spacing, of 200 m (660 ft). This domain, shown in Figure 6, includes several significant material disposal areas at LANL including MDAs A, AB, B, C, and T. Terrain elevation and land use data were obtained from the USGS and processed for this scenario in the manner described for the near-field analysis. Meteorological data collected in 2001 were used for the alternate-source analysis and a land use type of rangeland was applied over the entire model domain.

As with the near-field analysis, an atmospheric source area represented the release from each MDA, and a unit release rate was applied; the source areas are indicated in Figure 6. Material Disposal Areas A, B, and T lie sufficiently close to one another that they were represented using a single source area for the transport modeling. To determine how releases from other LANL MDAs compare to potential future releases from MDA G, air concentrations were projected and dispersion factors calculated for potential receptor locations in the vicinity of MDA G.

2.2.3 Far-Field Analysis

The far-field analysis, which models air concentrations up to 80 km (50 mi) from MDA G, was conducted to evaluate potential population exposures to airborne releases from MDA G. The model domain for this analysis was centered at a point on the east end of MDA G (Zone 13 388460 E 3965620 N), which was also used as the grid origin. The elevation contours of the model domain are shown in Figure 7, along with the approximate location of MDA G. A grid size of 160 × 160 km (100 × 100 mi) with a mesh size or receptor spacing of 4 km (2.5 mi) was used.

Terrain elevation and land use data were obtained from the USGS and processed as described for the other analyses. Unit releases from the three MDA G atmospheric source areas used in the near-field analysis were used to project air concentrations and dispersion factors for each grid of the model domain. The far-field analysis was conducted using meteorological data collected in 2001, and the rangeland land use type was applied over the entire model domain.

The population data adopted for the far-field analysis are shown in Figure 8. Table 1 shows the population totals in tabular form. Population data are provided for individual cells in a 16-sector polar-type array at multiple radial distances. The coordinates for the center point and grid divisions are in the New Mexico State Plane (NAD 27) coordinate system.

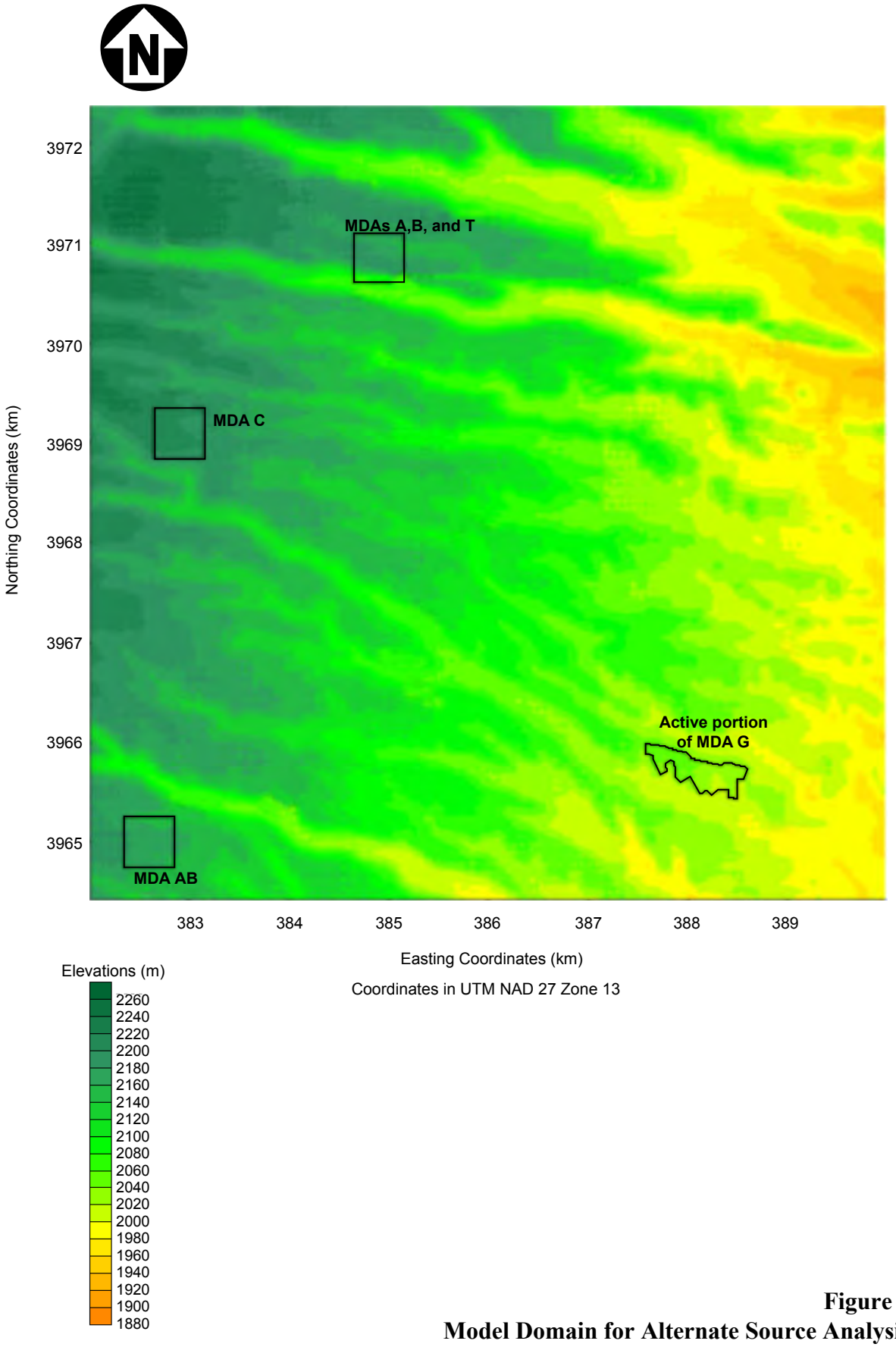

Figure 6
Model Domain for Alternate Source Analysis

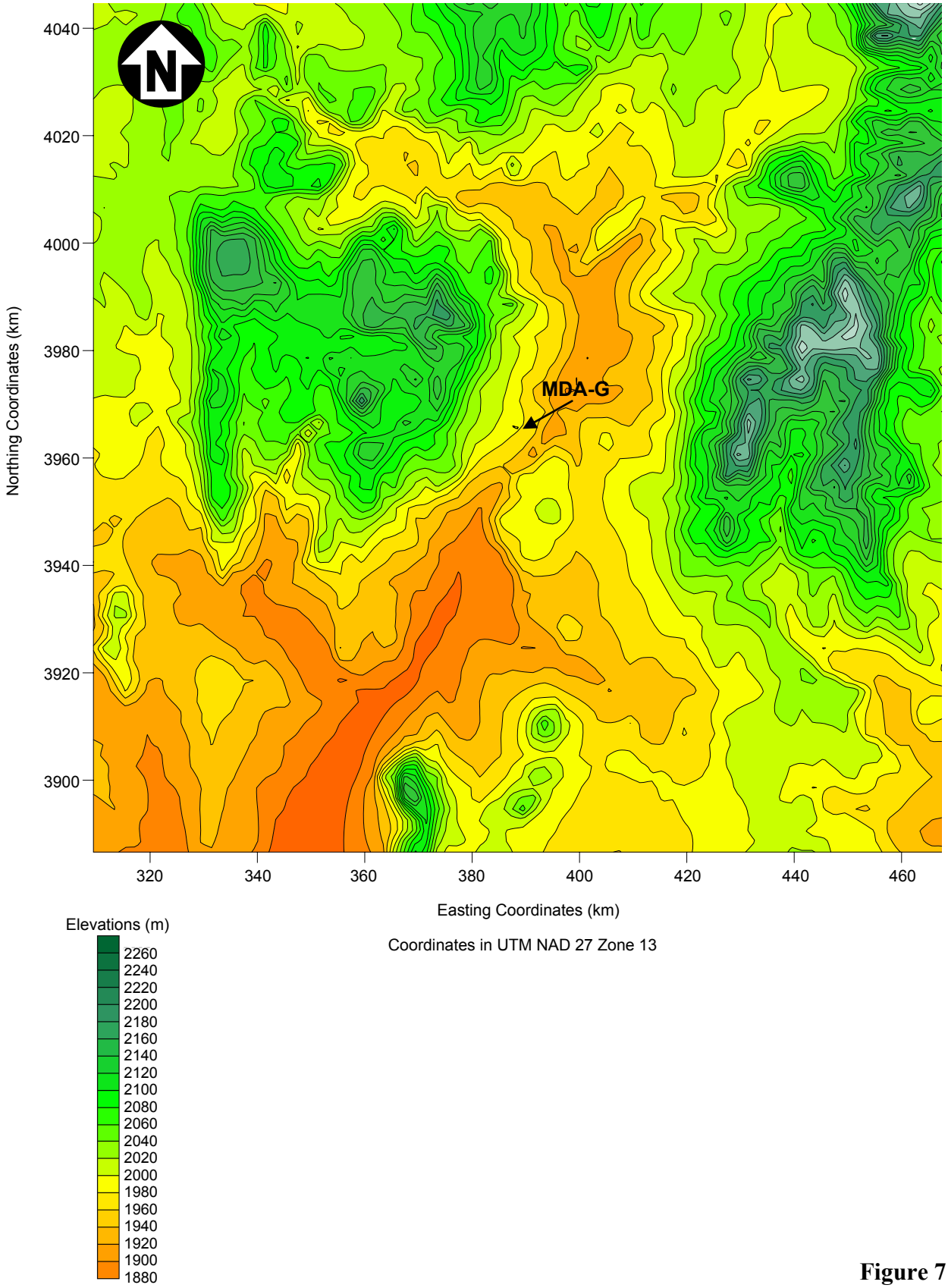

Figure 7
Model Domain for Far-Field Analysis

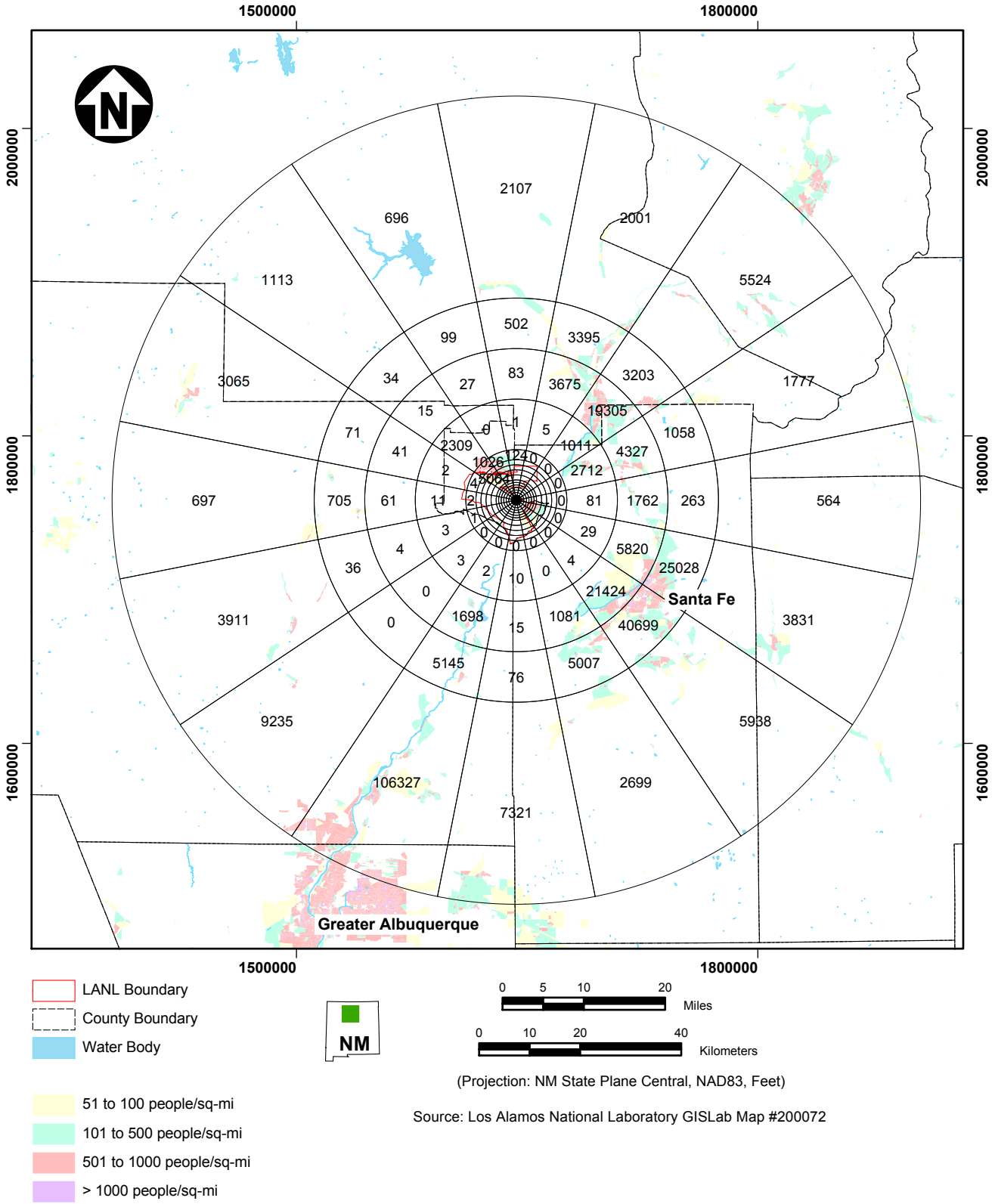

Entire Model Rings at .2, .4, .6, .8, 1, 1.5, 2, 2.5, 3, 3.5, 4, 5, 6, 7, 8, 10, 20, 30, 40, and 80 kilometers.

Figure 8
Population Data Array for 80-mile Radius from Material Disposal Area G

Table 1
2002 Population Data by Polar Grid Sector for Circular Area with 80-km Radius

Direction	Population by Distance (km) and Direction from MDA G (km)												
	0 – 2.5	2.5 – 3.0	3.0 – 3.5	3.5 – 4.0	4.0 – 5.0	5.0 – 6.0	6.0 – 7.0	7.0 – 8.0	8.0 – 10	10 – 20	20 – 30	30 – 40	40 – 80
N	0E+00	0E+00	0E+00	0E+00	1.0E+01	7.3E+01	7.2E+01	1.5E+02	1.2E+02	1.0E+00	8.3E+01	5.0E+02	2.1E+03
NNW	0E+00	0E+00	0E+00	0E+00	4.6E+01	1.4E+02	7.0E+03	8.9E+02	1.0E+03	0E+00	2.7E+01	9.9E+01	7.0E+02
NW	0E+00	0E+00	0E+00	0E+00	0E+00	0E+00	2.3E+02	1.8E+03	5.0E+03	2.3E+03	1.5E+01	3.4E+01	1.1E+03
WNW	0E+00	0E+00	0E+00	0E+00	0E+00	0E+00	0E+00	0E+00	0E+00	3.0E+00	4.1E+01	7.1E+01	3.1E+03
W	0E+00	0E+00	0E+00	0E+00	0E+00	0E+00	0E+00	1E+00	2E+01	1.0E+01	6.1E+01	7.1E+03	7.0E+02
WSW	0E+00	0E+00	0E+00	0E+00	0E+00	0E+00	0E+00	1E+00	1E+01	3E+00	4E+00	3.6E+01	3.9E+03
SW	0E+00	0E+00	0E+00	0E+00	0E+00	0E+00	0E+00	0E+00	0E+00	3E+00	0E+00	0E+00	9.2E+03
SSW	0E+00	0E+00	0E+00	0E+00	0E+00	1.3E+01	9E+00	1.0E+00	0E+00	2E+00	1.7E+03	5.2E+03	1.1E+05
S	0E+00	0E+00	0E+00	0E+00	0E+00	0E+00	0E+00	0E+00	0E+00	1.0E+01	1.5E+01	7.6E+01	7.3E+03
SSE	3E+00	1.6E+01	2.1E+01	2.6E+01	5.6E+01	4.3E+01	2.7E+01	0E+00	0E+00	0E+00	1.1E+03	5.0E+03	2.7E+03
SE	1.1E+02	1.6E+02	1.3E+02	1.4E+02	2.0E+02	8.1E+01	9E+00	0E+00	0E+00	4E+00	2.1E+04	4.1E+04	5.9E+03
ESE	2.6E+02	4.4E+02	6.9E+02	1.3E+03	1.7+03	1.2E+03	3E+00	0E+00	0E+00	3E+00	5.8E+03	2.5E+04	3.8E+03
E	0E+00	5E+00	1.8E+02	2.6E+03	6.0E+02	5.2E+01	6E+00	0E+00	0E+00	8.1E+01	1.8E+03	2.6E+02	5.6E+02
ENE	0E+00	0E+00	0E+00	0E+00	0E+00	0E+00	0E+00	0E+00	0E+00	2.7E+03	4.3E+03	1.1E+03	1.8E+03
NE	0E+00	0E+00	0E+00	0E+00	0E+00	0E+00	0E+00	1E+00	0E+00	1.0E+03	1.9E+04	3.2E+03	5.5E+03
NNE	0E+00	0E+00	0E+00	0E+00	0E+00	0E+00	0E+00	0E+00	0E+00	5E+00	3.7E+03	3.4E+03	2.0E+03

[a] *The 2000 Census showed no persons living at a distance of 0 – 2.0 km from MDA G.*

The population model domain for the far-field analysis includes all of Los Alamos County and portions of Bernalillo, Mora, Rio Arriba, Sandoval, San Miguel, Santa Fe, and Taos Counties. The domain also encompasses all or part of the pueblos of Santa Clara, Picuris, San Juan, San Ildefonso, Pojoaque, Nambe, Tesuque, San Felipe, Cochiti, Santo Domingo, Santa Ana, Zia, Jemez, and Taos. Other significant areas of inhabitation included in the model domain are the townships of Santa Fe, Española, and Los Alamos as well as southwestern edge of the City of Taos and the northern portion of the Albuquerque metropolitan area.

The atmospheric transport modeling results were used in conjunction with the population data to estimate the impacts of releases from MDA G on surrounding populations. The center of each of the population grid units defined by the intersection of the 16 sectors in the polar grid and 13 radial rings was calculated. This yielded 208 discrete locations, each of which was assigned the population of its surrounding grid unit. Air concentrations were estimated for the 208 locations and multiplied by the corresponding population estimates to yield population-scale results.

2.3 CALMET Processing

CALMET generates a 3-D set of meteorological data, such as wind speed and direction, over the extent of the model domain at user-specified sampling locations and elevations. A postprocessing program (PRTMET) allows the user to plot wind vectors over the model domain for any of the vertical layers specified by the user. The plotting of 3-D wind fields allows the user to verify model output against expected results (Scire et al., 2000b). The meteorological data used for the near-field analysis were developed using a sampling grid of 30×30 m (98×98 ft); the alternate source and far-field analyses used sampling grids of 200×200 m (660×660 ft) and 4×4 km (2.5×2.5 mi), respectively. The near-field and alternate source analyses used three vertical layers, while five layers were used for the far-field analysis. The additional layers used in the far-field analysis were required to account for increased vertical dispersion that would occur at greater distances.

The wind field generated by CALMET is developed in a two-step process. In the first step, the program estimates a wind field using information about the terrain of the model domain as specified using DEM data. Meteorological surface data for the region being modeled are used to refine the wind field in the second step. Surface data from multiple towers are used in an inverse-distance squared interpolation scheme to develop the wind field at each sampling location within the model domain. In this scheme, data collected by the meteorological station nearest to the emissions source, which for this study was tower TA-54, receives greater weighting in the dispersion calculations than the towers located farther away.

Characterization of the wind field using multiple meteorological sampling locations (i.e., towers) was important for several reasons. First, multiple towers provide backup data, an important

consideration because each tower averages approximately 5 percent missing data per year. Also, due to surrounding terrain characteristics, data from some towers are more representative of conditions at the receptor locations than others. CALMET takes this into consideration by allowing the user to input weighting values for various meteorological stations. Table 2 provides the distance and approximate weighting value used for each of the LANL meteorological towers included in the MDA G atmospheric transport modeling.

Table 2
Comparative Influence of Surface Meteorological Station Data Used for MDA G Dispersion Analyses

Meteorological Tower	Distance to MDA G (km)	CALMET Weighting Factor
TA-54	1.8	0.77
TA-53	4.5	0.12
TA-49	5.6	0.08
TA-06	7.8	0.04

Wind fields are generated for each vertical layer used in the modeling. CALMET allows the user to specify one of three methods to extrapolate surface meteorological data to estimate initial conditions above the surface layer. These methods include a simple power law extrapolation, an inverse-distance squared weighting of surface and upper-air data, and the recommended approach, which relies on the Monin-Obukhov similarity theory. The Monin-Obukhov similarity theory method was used in this analysis.

The near-field analysis considered the effect of variable meteorological conditions on atmospheric transport in the vicinity of MDA G. Toward that end, CALMET was used to construct meteorological data files that spanned the 10-year period from 1992 through 2001.

The CALMET model allows the user to specify the amount of influence upper-air data have on the construction of the final meteorological dataset used for the dispersion modeling. For each vertical layer specified in the CALMET input, the user can specify the bias or influence of the upper-air data to the surface air data. Each specified bias value can range from “no influence of upper-air observations” (-1) to “no influence of surface observations” (+1). Table 3 shows the data and bias values used for each layer in the near-field, alternate-source, and far-field analyses. Use of the upper-air observations becomes increasingly important for longer range transport scenarios of more than 50 km (31 mi). The values adopted for this analysis were selected on the basis of their suitability for dispersion modeling in complex terrain.

Table 3
Bias Settings for Upper-Air Wind Observations Used in Air Dispersion Analysis

Layer Number	Near-Field Analysis		Alternate-Source Analysis		Far-Field Analysis	
	Layer Depth (m)	Upper-Air-Observation Bias [a]	Layer Depth (m)	Upper-Air-Observation Bias	Layer Depth (m)	Upper-Air-Observation Bias
1	0 – 20	–1.0	0 – 20	–1.0	0 – 20	–1.0
2	20 – 40	–0.8	20 – 40	–0.8	20 – 40	–0.8
3	40 – 80	–0.5	40 – 80	–0.5	40 – 80	–0.5
4	NA	NA	NA	NA	80 – 160	–0.2
5	NA	NA	NA	NA	160 – 320	0

NA = Not applicable

[a] A value of –1.0 indicates that complete weight (bias) is given to surface data and zero weight is given to upper-air data; a value of 0 indicates that equal weight is given to surface and upper-air data.

2.4 CALPUFF Modeling

CALPUFF was used to conduct the atmospheric transport modeling for the near-field, alternate-source, and far-field analyses. The CALMET-generated meteorological data files for 1992 through 2001 were input into the CALPUFF model and used to project air concentrations across the near-field model domain for each of the 10 years. The annual simulations were divided into three parts because of operating system limits on file space. Output files generated by CALPUFF for each year were concatenated using the APPEND processor (included in the CALPUFF modeling package), and these concatenated files were imported into CALPOST for final processing. The air dispersion modeling conducted in support of the alternate source and far-field analyses was based on meteorological data for 2001 only.

A number of modeling evaluations were undertaken to define the input data that were used in the atmospheric transport modeling. These evaluations are described below, organized by the input parameter that was being estimated or established.

2.4.1 Particle Size and Dry Deposition

The CALPUFF modeling accounted for dry and wet deposition of the material contained in the plume of airborne contaminants. Because downwind exposures are typically dominated by the inhalation pathway, most modeling applications conservatively ignore plume deposition and depletion. Realistically, however, some of the airborne contamination will deposit on surface soil and plant surfaces downwind of the point of release. Consequently, these depositional mechanisms were accounted for in the modeling.

The rate of particulate deposition determines the rate of contamination of the ground surface and the rate at which contaminant plumes are depleted as they travel with the prevailing winds. Plume depletion is not a linear process and is normally insignificant when the distance from the source to receptor is small, as is the case in the near-field and alternate-source analyses. Only when the travel distance is 10 km (6.2 mi) or greater does plume depletion become an important factor in calculating downwind air concentrations. Miller (1978) showed that plume depletion is insensitive to changes in the deposition velocity for distances less than 10 km (6.2 mi).

Rates of deposition are highly dependent on the physical characteristics of the contaminants. Sehmel and Hodgson (1978) note that "particle and gaseous removal rates are a nonsteady-state process dependent upon the delivery capability of the upper atmosphere as well as surface mass transfer resistance within the cm adjacent to the deposition surface." Rates of deposition for particulates can range over three orders of magnitude (Sehmel and Hodgson, 1976; Hoffman, 1977; Miller, 1978); those for gases can range over four orders of magnitude (Sehmel, 1980).

Dry deposition rates of particulates depend partly on the physical characteristics of the particles, most notably their size. CALPUFF's full-resistance model generates a range of deposition velocities based on the input median particle diameter and the corresponding particle size distribution. Specifically, the user supplies a geometric mean diameter (gdiam) and geometric standard deviation (gsd) for the particles of interest. CALPUFF sets up particle-size intervals ranging from $-4 \times$ gsd to $+4 \times$ gsd based on the user-supplied gdiam, and performs calculation loops over these size intervals, calculating the gravitational-settling velocity for nine particle-size groups. The deposition velocity for a specific size interval is calculated as a function of gravitational-settling velocity, aerodynamic resistance, and deposition layer resistance. Finally, a mass-weighted particle-deposition velocity is calculated for the user-supplied distribution.

Sehmel's review (1980) of particle deposition studies concluded that the minimum deposition velocity occurs for particles with diameters ranging from 0.1 to 1 μm (3.9×10^{-6} to 3.9×10^{-5} in.). To investigate this further, CALPUFF simulations were conducted to determine how different particle-size distributions would affect the dry deposition rate. The results indicate that the deposition flux can vary by about an order of magnitude for different mean particle sizes (Figure 9). Rates of deposition show considerable variation with different particle-size distributions, as indicated by the curves for the different geometric standard deviations.

The atmospheric transport modeling considered two particle size distributions to evaluate the impacts of particle characteristics on deposition rates. The first is based on a geometric mean particle diameter of 0.48 μm (1.9×10^{-5} in.) and 2.0 for the gsd, the CALPUFF default values (Figure 10a). The second considers particles with a gdiam of 5 μm (2.0×10^{-4} in.) and a gsd of 2. This distribution, shown in Figure 10b, is expected to be more representative of soil particles undergoing resuspension at MDA G.

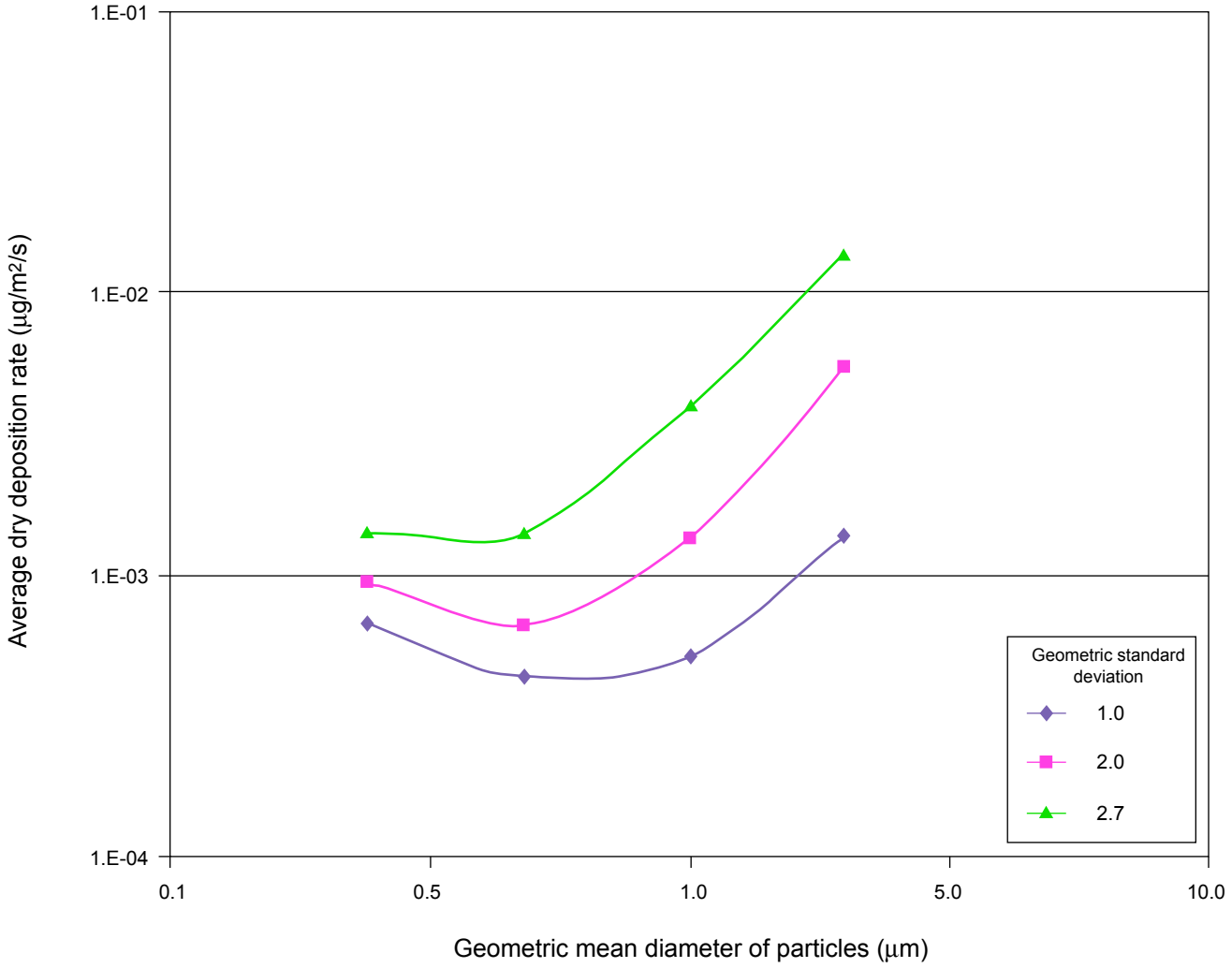

Figure 9
Dry Deposition Rate vs. Particle Size

Figure 10a
Distribution for particles with gdiam = 0.48 µm (gsd =2)

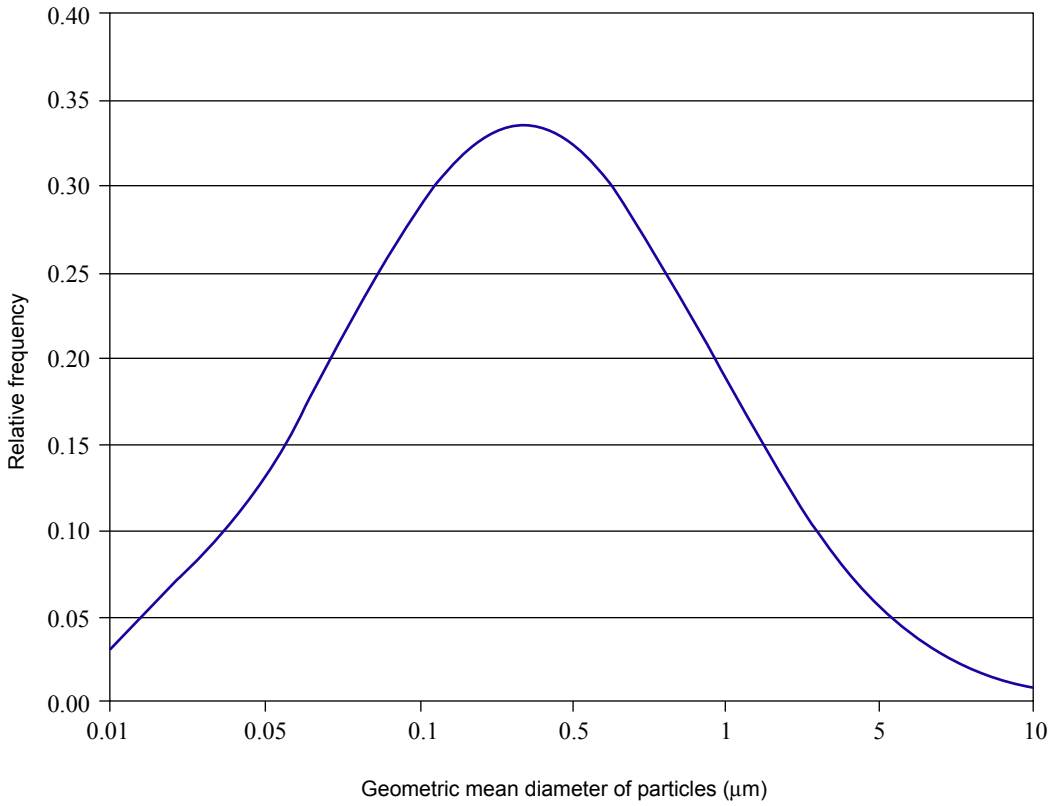

Figure 10b
Distribution for particles with gdiam = 5.0 µm (gsd =2)

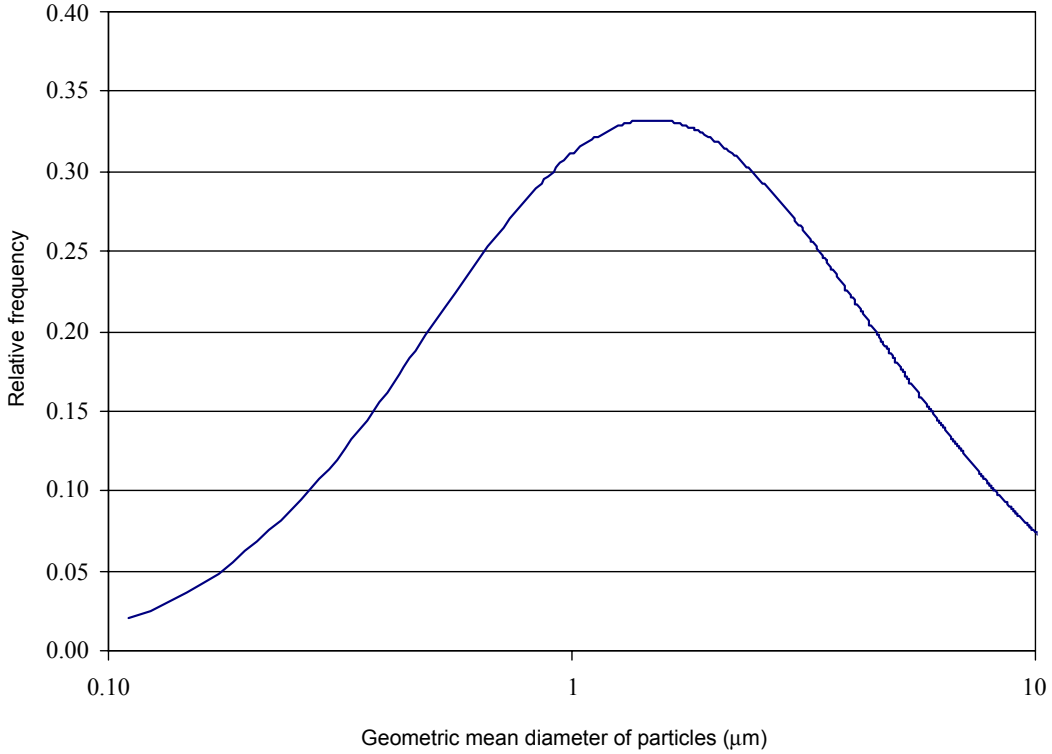

Figure 10
Frequency Distribution of Various Particle Sizes

Transport analyses were also conducted to project air concentrations of vapor or gas-phase radionuclides downwind of MDA G. These simulations used the gaseous dispersion option of CALPUFF. Under this option, no deposition of airborne contamination is assumed to occur.

2.4.2 Scavenging Coefficient

Depending on the type of pollutant involved, a number of physical and chemical processes can affect the depletion of contaminant plumes due to wet depositional processes. The two most important processes involved in particulate deposition are in-cloud scavenging by cloud droplets and below-cloud scavenging by raindrops.

CALPUFF relies on a user-selected empirical scavenging coefficient to estimate losses due to wet deposition. For particulate matter, aerosols, and gases, the typical range of values for the scavenging coefficient is 1×10^{-5} to 1×10^{-3} per second (PNL, 1970; Slinn, 1977; Pruppacher et al., 1982). A number of simulations were conducted to determine how variations in the scavenging coefficient affected rates of wet deposition; the results of these analyses are summarized in Figure 11. These results show a linear dependence between the deposition rate and the scavenging coefficient.

As specified in CALPUFF, the scavenging coefficient includes a wet (rain) scavenging component and a frozen-precipitation scavenging component. Coefficients of 1×10^{-4} and 3×10^{-5} per second were adopted for these parameters, respectively; these are the default values included in CALPUFF.

2.4.3 Miscellaneous Parameters

Several parameters are used to configure the simulations conducted by CALPUFF and CALMET. A full description of these options is provided in the CALPUFF user's manual (Scire et al., 2000a). Briefly, they affect or control the following:

- Dispersion coefficients based on turbulence, as computed by meteorological data analysis
- CALPUFF terrain adjustments applied to the receptor grid
- Gaussian vertical distribution in the near-field model domain
- Integrated puff algorithm

Simulations were conducted in which the values of these parameters were varied (on a case-by-case basis). The results of the modeling were compared to the expected results at MDA G and the final values, shown in Table 4, were selected on the basis of how well the simulation results matched the anticipated results.

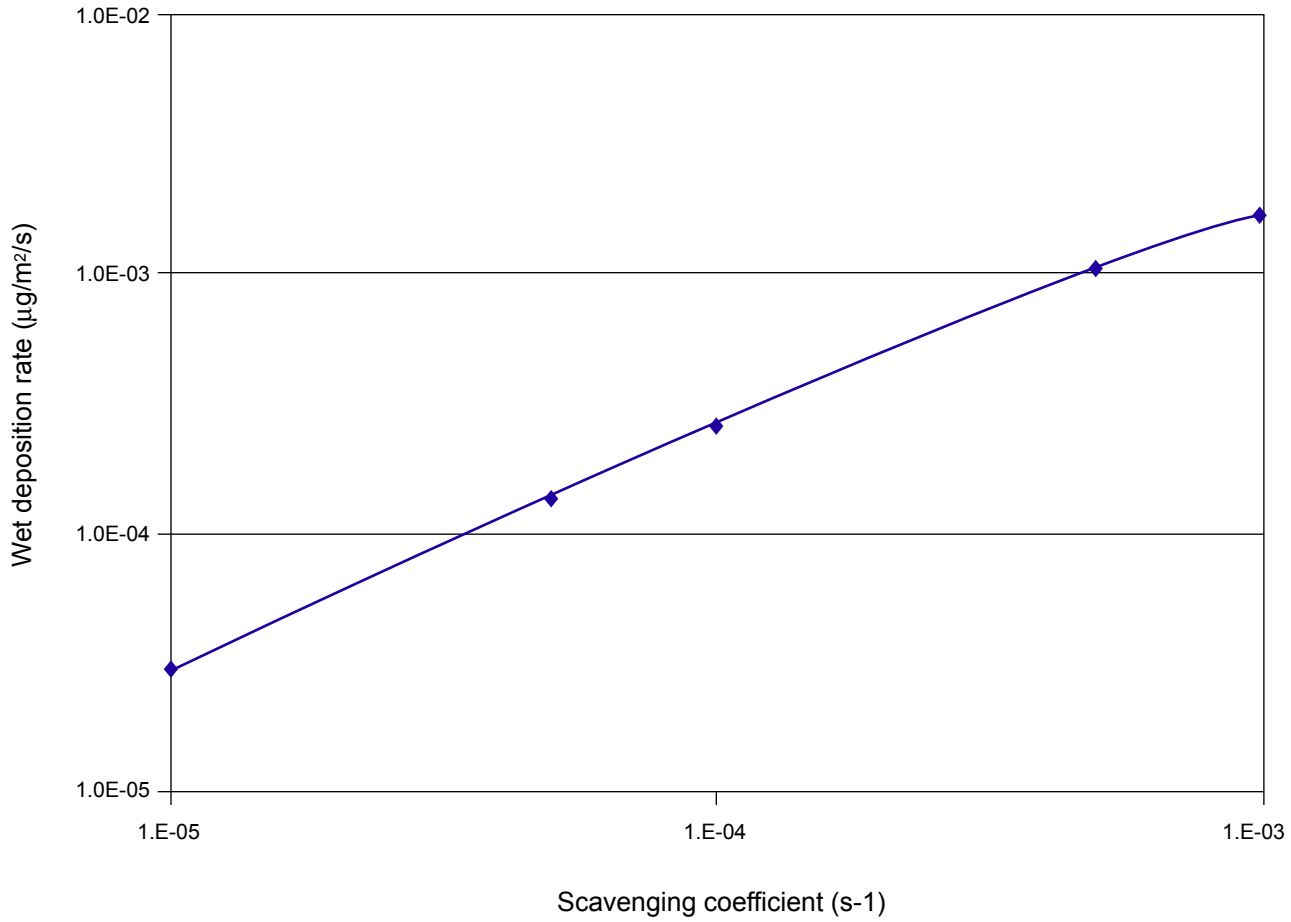

Figure 11
Wet Deposition Rate vs. Scavenging Coefficient

Table 4
Parameter Values Selected for CALMET and CALPUFF Models through Trial Runs

Input Parameter	Units	Value	Affects or Specifies...
IKINE	NA	1	Computation of kinematic effects
ISLOPE	NA	1	Calculation of slope flows
IEXTRAP	NA	-4	Extrapolation of surface winds using similarity theory
TERRAD	km	0.5	Radius of influence of terrain features
RMAX1	km	5.0	Maximum radius of influence for observations vs. interpolated values
R1	NA	1.0	Weighting of the first estimate of wind-field components to the actual observed values
MCTADJ	NA	2	CALPUFF type terrain adjustment
MDISP	NA	2	Micrometeorological variables used to determine dispersion coefficients

NA = Not applicable

Vold (1996) noted that mesa-top and canyon winds near MDA G often have quite different characteristics. Consequently, one of the modeling goals of the current study was to determine the influences that local topography may have on the wind field (and hence, dispersion patterns) near and around MDA G. Three key parameters shown in Table 4 — TERRAD, RMAX1, and R1 — were identified as primary parameters or options that govern how topography affects dispersion within the CALMET model. To determine the effects these parameters might have on wind patterns, multiple sets of modeling runs were used to vary the values for each of these parameters over the potential range, while other parameters were held constant. From these simulations, hourly snapshots of the surface level wind field were made with the CALMET postprocessor PRTMET, which generates a wind vector at each grid point in the model. Visual comparisons were made of the resultant wind fields. The modeling parameters associated with the results that most closely matched observations presented by Vold (1996) and information in Bowen (1990) were selected as the final values for the MDA G air dispersion model.

2.5 CALPOST Processing

Output from CALPUFF and air concentration contours generated from this output were passed to CALPOST for final processing. The result was annual average air concentrations and particulate deposition rates for each location within the model domain. Output grid files were generated and used by Surfer (Golden, 2002 and 2005) to create air concentration maps for viewing and validating modeling results. Also, to allow comparisons of results between modeling runs, a postprocessing program was created to extract air concentration data along the LANL boundary with San Ildefonso tribal lands.

3.0 Results

This section presents the findings of the atmospheric transport modeling analyses. The results of the near-field analysis, including projected air concentrations and deposition fluxes, are presented in Section 3.1. The results of the alternate-source analysis conducted in support of the composite analysis and the far-field analysis used to estimate population doses from MDA G contaminant releases are described in Sections 3.2 and 3.3, respectively.

3.1 Near-Field Air Concentrations

Particulate concentrations in air were projected using CALPUFF for the 10-year period from 1992 through 2001. Projections were made for all grid or exposure locations included in the model domain. Figures 12 through 14 show air concentration contours for particulates with a geometric mean diameter of 0.48 μm from source areas 1 through 3, respectively. Figures 15 through 17 show contours for particulates with a gdiam of 5 μm. All results shown in these figures represent 2001 meteorological data.

Table 5 provides typical air-concentration values resulting from releases from atmospheric source area 1 for an area to the north of MDA G. As seen in Figures 12 and 15, the area to the north of MDA G is characterized by some of the highest air concentrations projected by the model for locations outside of the MDA G fence line. Results are shown for particles with a gdiam of 0.48 μm (1.5×10^{-5} in.) and with a gdiam of 5.0 μm (2.0×10^{-7} in.).

Table 5
Annual Variability of Particulate Concentrations at Selected Locations North of MDA G

UTM Grid Coordinates (m)		Average Annual Particulate Concentration (μg/m³)									
E	N	1992	1993	1994	1995	1996	1997	1998	1999	2000	2001
Particles with geometric mean diameter of 0.48 μm											
388545	3965975	7.1E-01	7.7E-01	7.5E-01	7.4E-01	6.9E-01	7.4E-01	7.4E-01	6.1E-01	7.6E-01	7.0E-01
388605	3965945	8.4E-01	9.2E-01	9.0E-01	8.6E-01	8.4E-01	9.0E-01	8.9E-01	7.3E-01	9.1E-01	8.6E-01
388665	3965945	7.8E-01	8.5E-01	8.3E-01	7.8E-01	7.8E-01	8.4E-01	8.4E-01	6.8E-01	8.4E-01	8.0E-01
Particles with geometric mean diameter of 5.0 μm											
388545	3965975	6.4E-01	7.0E-01	6.8E-01	6.8E-01	6.3E-01	6.7E-01	6.7E-01	5.6E-01	6.9E-01	6.2E-01
388605	3965945	7.6E-01	8.4E-01	8.2E-01	7.8E-01	7.7E-01	8.2E-01	8.1E-01	6.7E-01	8.3E-01	7.6E-01
388665	3965945	7.0E-01	7.7E-01	7.6E-01	7.5E-01	7.1E-01	7.6E-01	7.6E-01	6.2E-01	7.7E-01	7.1E-01

UTM = Universal Transverse Mercator *E = Easting* *N = Northing*

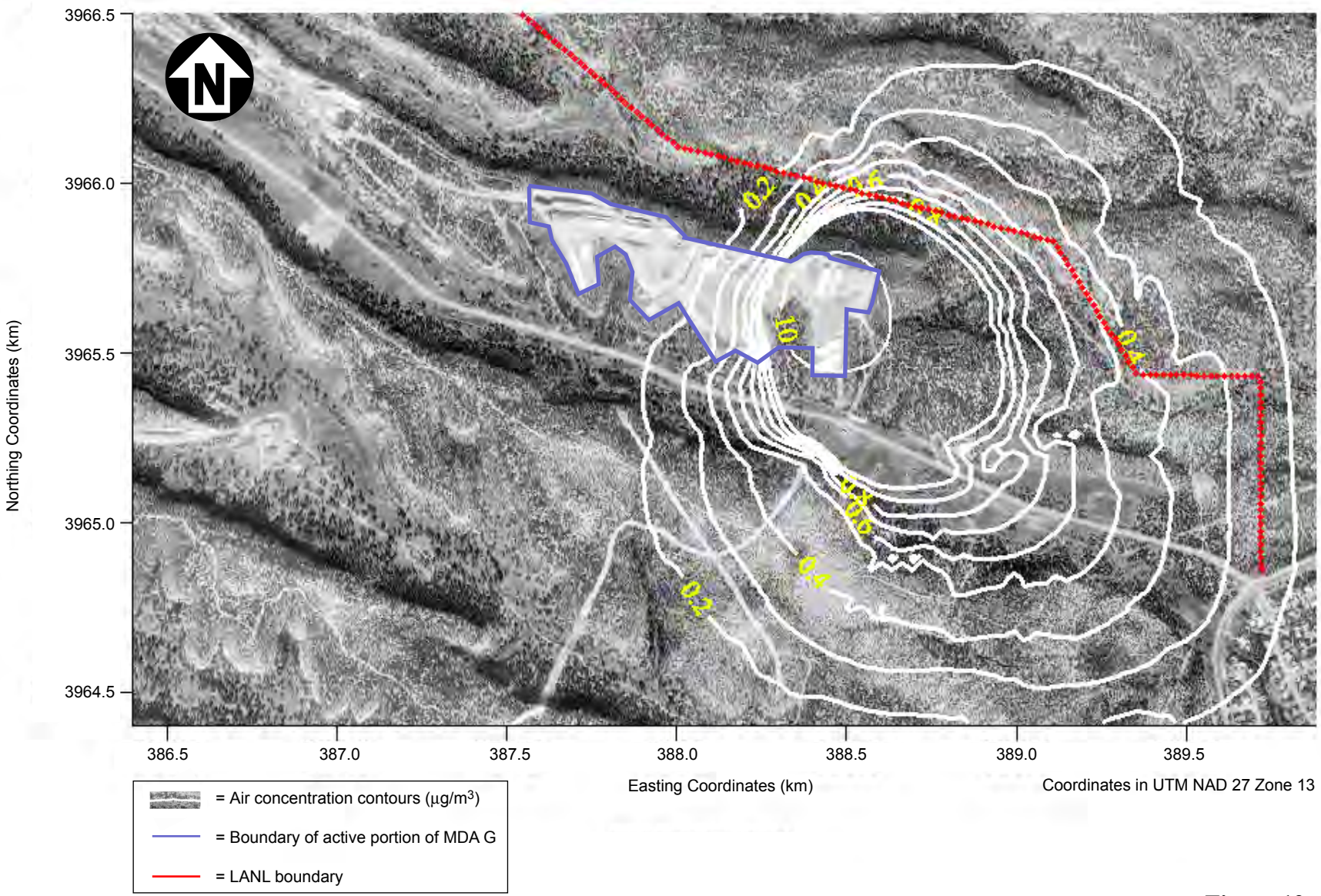

Figure 12
Relative Air Concentration Contours Predicted by CALPUFF for Releases from MDA G Source Area 1 (particle size gdiam 0.48 µm)

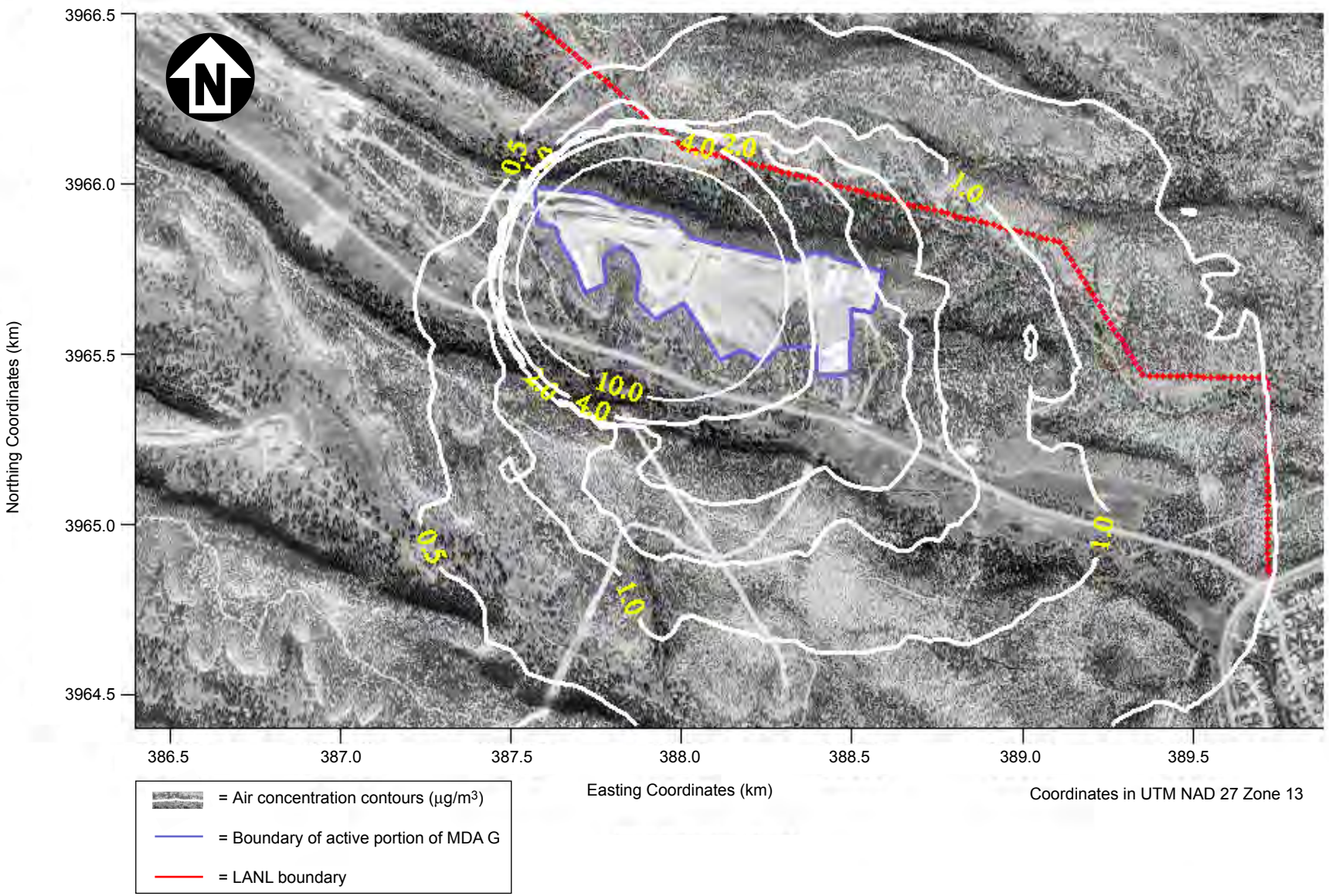

Figure 13
Relative Air Concentration Contours Predicted by CALPUFF for Releases from MDA G Source Area 2 (particle size gdiam 0.48 µm)

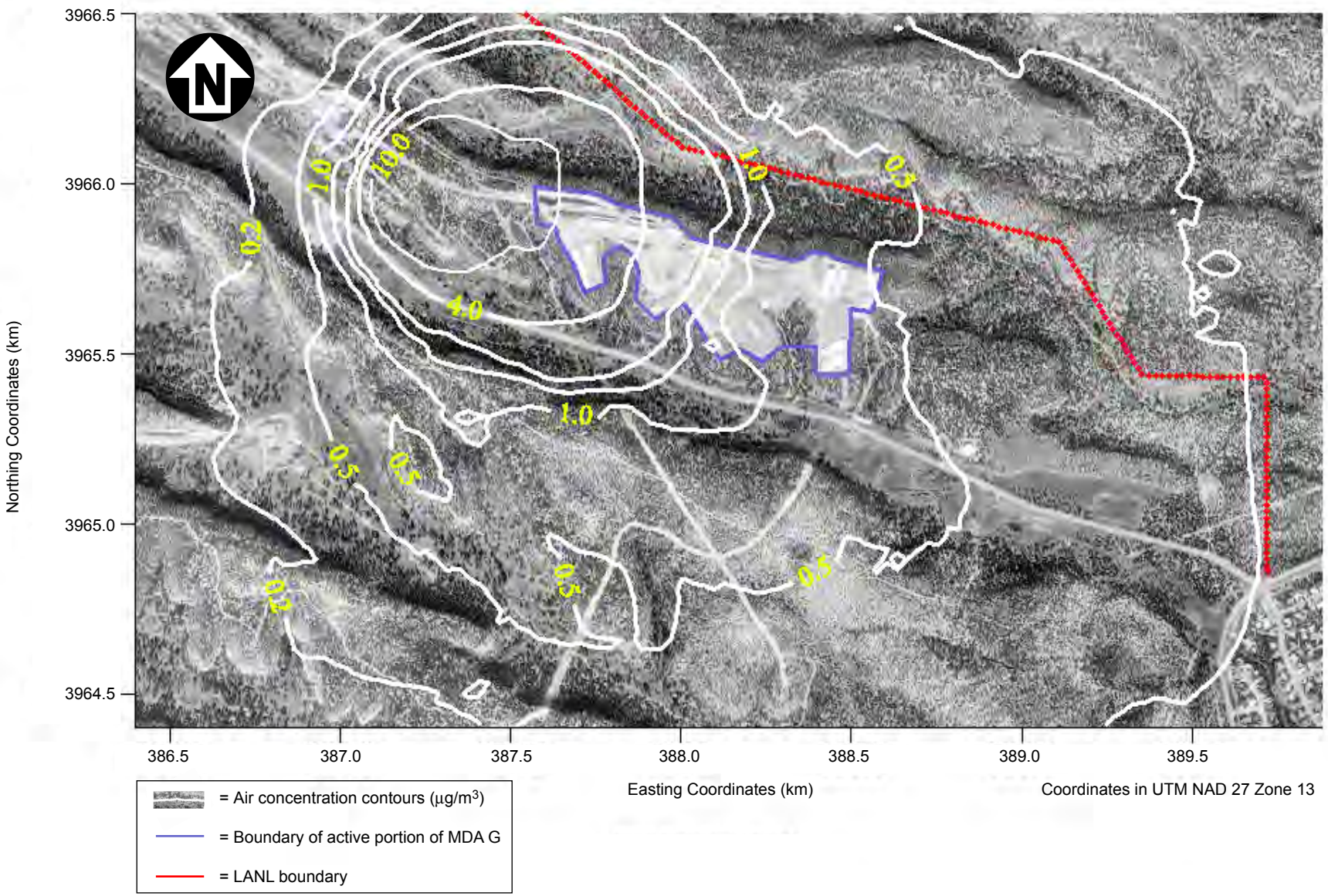

Figure 14
Relative Air Concentration Contours Predicted by CALPUFF for Releases from MDA G Source Area 3 (particle size gdiam 0.48 µm)

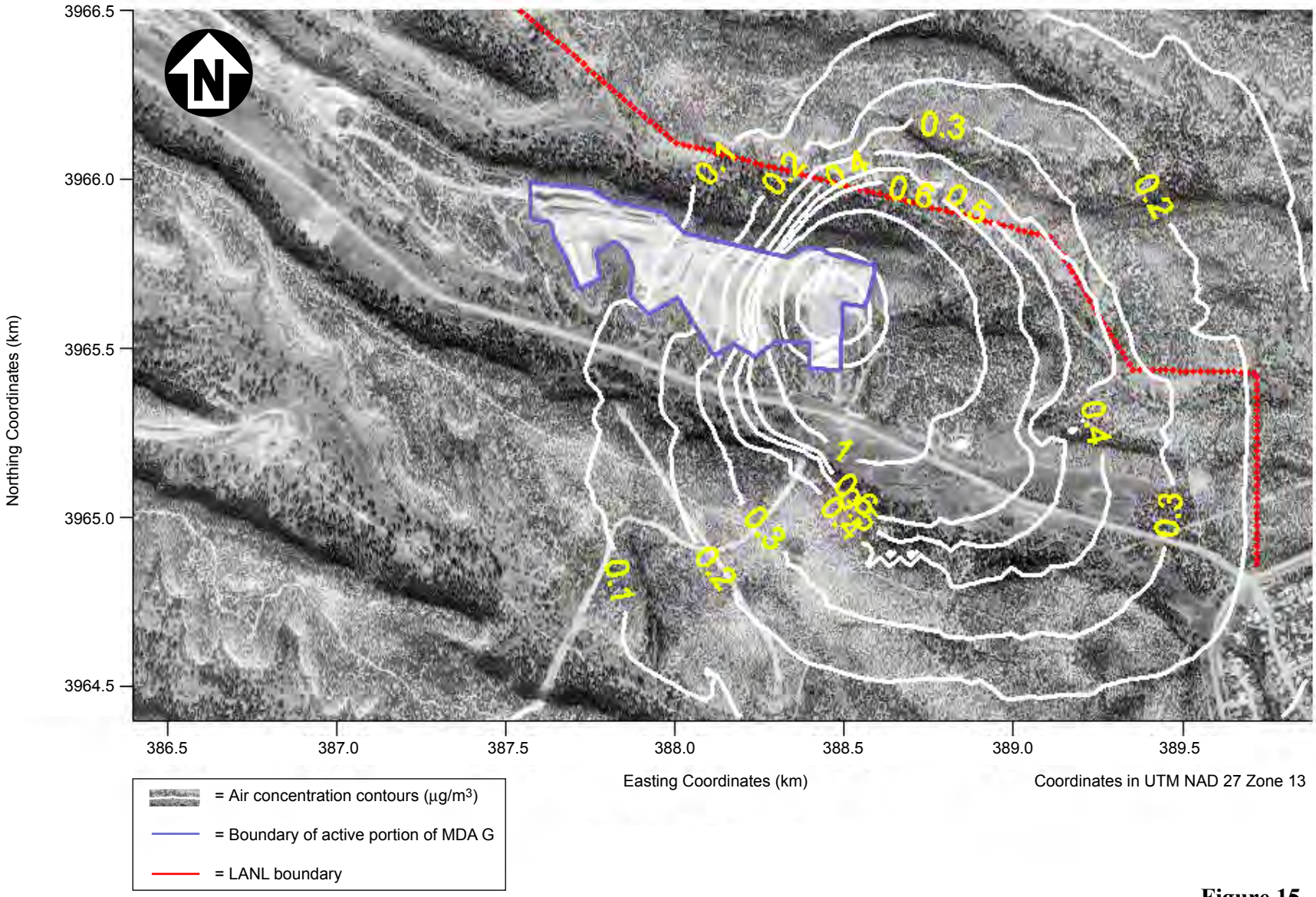

Figure 15
Relative Air Concentration Contours Predicted by CALPUFF for Releases from MDA G Source Area 1 (particle size gdiam 5.0 µm)

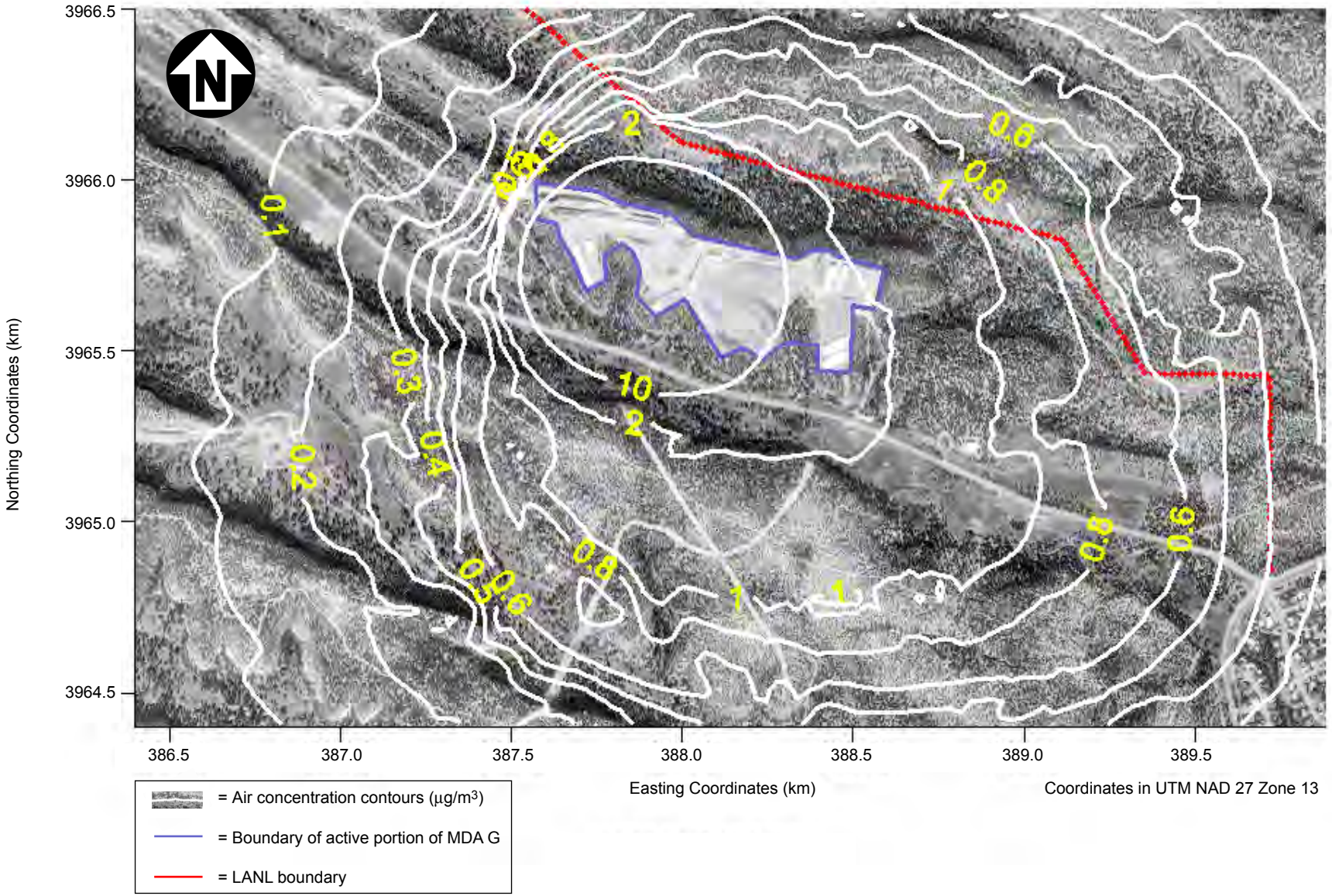

Figure 16
Relative Air Concentration Contours Predicted by CALPUFF for Releases from MDA G Source Area 2 (particle size gdiam 5.0 µm)

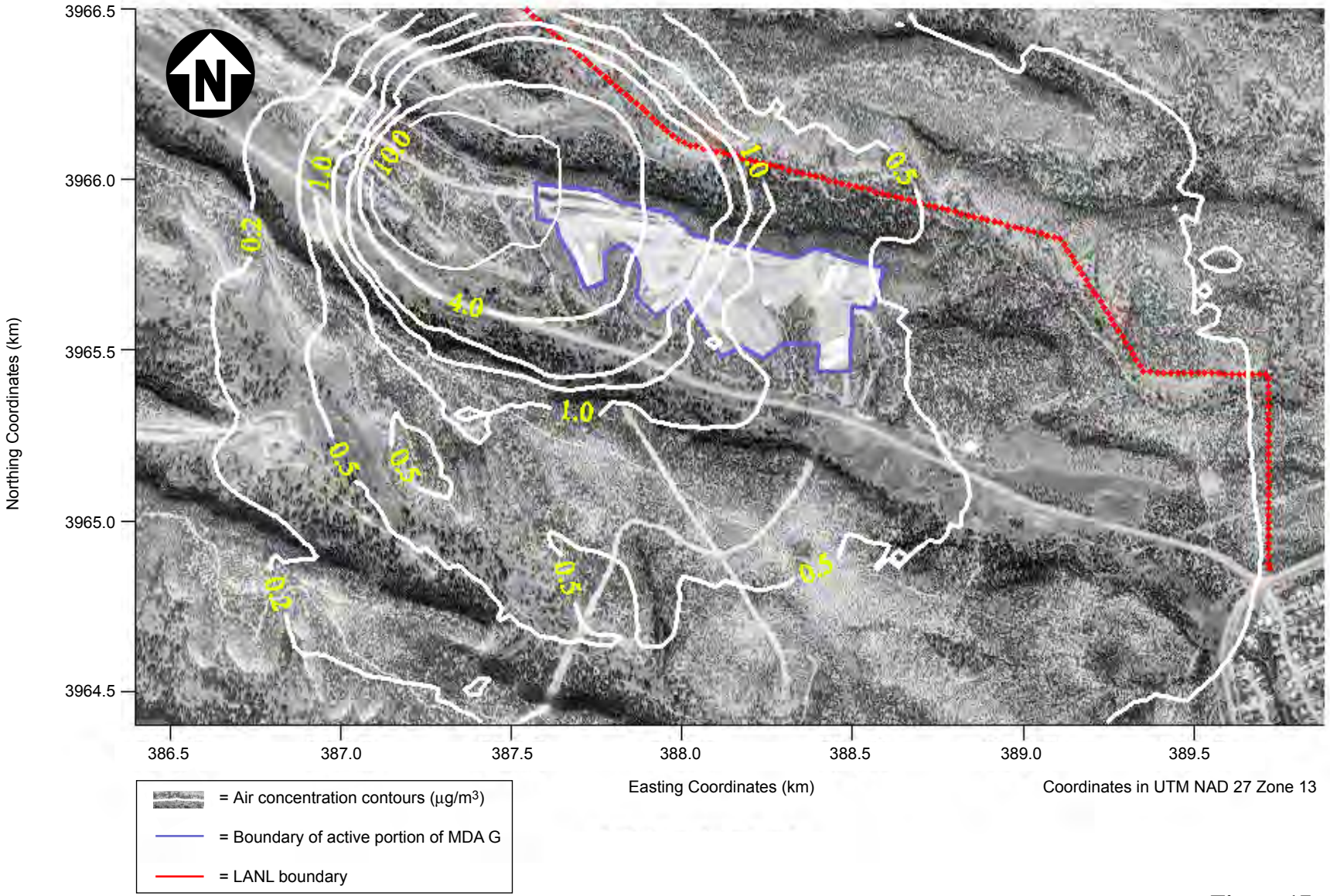

Figure 17
Relative Air Concentration Contours Predicted by CALPUFF for Releases from MDA G Source Area 3 (particle size gdiam 5.0 µm)

Model results for the three source areas were used to identify peak concentrations along the boundary between LANL and the San Ildefonso tribal lands. Table 6, which shows these concentrations over a 10-year period for particulate diameters of 0.48 and 5 μm (1.5×10^{-5} and 2.0×10^{-4} in.), and for vapors and gases, indicates the potential variability in the CALPUFF output. The location at which exposures from airborne contaminants will be greatest is a function of the projected airborne concentrations, such as those included in the table, and the magnitudes of the releases from the source areas.

Table 6
Projected Air Concentrations along Border between LANL and San Ildefonso Pueblo, by Source

Source Area	Average Annual Concentration (μg/m³)									
	1992	1993	1994	1995	1996	1997	1998	1999	2000	2001
Particles with geometric mean diameter of 0.48 μm										
1	8.2E-01	8.9E-01	8.8E-01	8.3E-01	8.2E-01	8.8E-01	8.8E-01	7.2E-01	8.9E-01	8.4E-01
2	5.9E+00	5.8E+00	5.4E+00	5.3E+00	5.0E+00	5.3E+00	5.3E+00	5.0E+00	5.3E+00	5.4E+00
3	2.7E+00	2.5E+00	2.5E+00	2.7E+00	2.5E+00	3.0E+00	2.6E+00	2.7E+00	2.7E+00	2.9E+00
Particles with geometric mean diameter of 5.0 μm										
1	7.4E-01	8.1E-01	8.0E-01	7.5E-01	7.5E-01	8.0E-01	7.9E-01	6.5E-01	8.1E-01	7.4E-01
2	5.6E+00	5.5E+00	5.1E+00	5.0E+00	4.8E+00	5.0E+00	5.0E+00	4.8E+00	5.0E+00	5.1E+00
3	1.3E+00	1.4E+00	1.4E+00	1.3E+00	8.4E-01	8.2E-01	8.5E-01	7.5E-01	8.6E-01	8.3E-01
Vapors and Gases										
1	8.2E-01	9.0E-01	8.8E-01	8.3E-01	8.2E-01	8.8E-01	8.8E-01	7.2E-01	8.9E-01	8.4E-01
2	5.9E+00	5.8E+00	5.4E+00	5.3E+00	5.0E+00	5.3E+00	5.3E+00	5.0E+00	5.3E+00	5.1E+00
3	3.0E+00	2.8E+00	2.7E+00	2.7E+00	2.5E+00	3.0E+00	2.6E+00	2.7E+00	2.7E+00	2.9E+00

The CALPUFF air concentration projections were used to calculate air dispersion factors for the performance assessment and composite analysis modeling. To illustrate, the results shown in Table 6 for source area 1 indicate an average peak concentration of 0.77 μg/m^3 (4.8×10^{-11} lb/ft^3) for particulates with a gdiam of 5 μm (2.0×10^{-4} in.). Equation 1 is used to calculate an air dispersion value of 1.0×10^{-5} s/m^3 (2.9×10^{-7} s/ft^3). The coefficient of variation among the 10 annual values is about 6 percent. Air dispersion values for source areas 2 and 3, calculated using Equation 1, are 1.9×10^{-5} s/m^3 (5.3×10^{-7} s/ft^3) and 8.0×10^{-6} s/m^3 (2.3×10^{-7} s/ft^3), respectively; coefficients of variation for these areas are 6 and 4 percent.

Deposition fluxes were also determined using CALPUFF. Dry deposition fluxes are a function of particulate concentrations in air and the deposition velocity; as discussed earlier, the deposition velocity is a function of particle size. Because a distribution of particle sizes was used in the modeling, a distribution of deposition velocities is generated by CALPUFF and used to estimate the dry deposition flux. CALPUFF calculates wet deposition fluxes based on the calculated air concentration and scavenging coefficients. Table 7 provides dry and wet deposition fluxes for each of the three source areas shown in Figure 5. These flux values represent the 10-year average of the maximum flux at a location along the LANL/San Ildefonso border to the north of MDA G.

Table 7
Ten-Year Average Peak Dry and Wet Deposition Ratios for Source Areas 1, 2, and 3

Source Area	Dry Deposition Flux ($g/m^2/s$)	Coefficient of Variation (%)	Wet Deposition Flux ($g/m^2/s$)	Coefficient of Variation (%)
1	5.8E-5	5	8.2E-5	38
2	2.7E-4	10.	1.9E-4	30
3	1.3E-4	5	8.2E-5	28

The values shown in Table 7 are for the distribution of particles with a gdiam of 0.48 μm (1.5×10^{-5} in.). Table 8 provides a comparison of dry deposition flux for the two different particle size distributions used in the near-field analysis (for source area 1). As expected, the deposition flux for the larger particles was considerably greater, owing to the order-of-magnitude difference in deposition velocity between particles with a gdiam of 0.48 μm (1.5×10^{-5} in.) and those with a gdiam of 5.0 μm (2.0×10^{-4} in.).

Table 8
Comparison of Dry Deposition Flux at the LANL Boundary North of MDA G

Particle Size (gdiam, μm)	Dry Deposition Flux, by Year ($g/m^2/s$)									
	1992	1993	1994	1995	1996	1997	1998	1999	2000	2001
0.48	1.8E-5	1.9E-5	2.0E-5	1.9E-5	1.9E-5	1.9E-5	2.0E-5	1.8E-5	2.0E-5	1.9E-5
5.0	7.1E-4	7.6E-4	7.6E-4	7.5E-4	7.6E-4	7.6E-4	7.9E-4	7.3E-4	7.7E-4	9.7E-4

The effect of changes in the input deposition rate (as determined by different particle size distributions) on the downwind air concentrations projected by CALPUFF was analyzed. Air concentrations were estimated for a series of particle sizes along the LANL/San Ildefonso boundary, at distances of 1 to 5 km (0.62 to 3.1 mi) from MDA G. The results are shown in Figure 18, which represents the projected concentrations averaged over the distances included in the modeling. These results confirm that, over these distances, variations in particle size have little effect on the projected air concentrations. The same analysis conducted using different values of precipitation scavenging showed negligible change in air concentrations for all cases with respect to the values used for this study. Thus, for the near-field and alternate-source analyses, the projected air concentrations are relatively insensitive to depositional characteristics**.**

3.2 Alternate-Source Analysis

The alternate source analysis evaluated how potential contributions from other Laboratory MDAs may impact the exposure conditions for persons living downwind of MDA G. Table 9 shows the air dispersion factors for releases originating at MDA G (source area 1) and other MDAs; results are shown for 10 selected receptor locations. The air dispersion factors for the other sites are less than 1 percent of those for source area 1 at MDA G.

Table 9
Comparison of Air Dispersion Results for Releases from Various Material Disposal Sites

UTM Grid Coordinates (m)		Air Dispersion Results for Various Sources (s/m^3)			
Easting	Northing	Source Area 1 MDA G	MDAs A,B,T	MDA C	MDA AB
388567	3965965	8.9E-06	6.7E-08	6.0E-08	5.1E-08
388586	3965960	9.3E-06	6.7E-08	5.9E-08	5.0E-08
388606	3965955	9.7E-06	6.6E-08	5.9E-08	5.0E-08
388625	3965950	9.6E-06	6.6E-08	5.8E-08	5.0E-08
388644	3965945	9.9E-06	6.5E-08	5.8E-08	4.9E-08
388664	3965940	9.5E-06	6.4E-08	5.7E-08	4.9E-08
388683	3965935	9.6E-06	6.4E-08	5.7E-08	4.9E-08
388703	3965931	9.4E-06	6.3E-08	5.7E-08	4.8E-08
388722	3965926	9.4E-06	6.3E-08	5.6E-08	4.8E-08
388741	3965921	9.1E-06	6.2E-08	5.6E-08	4.7E-08

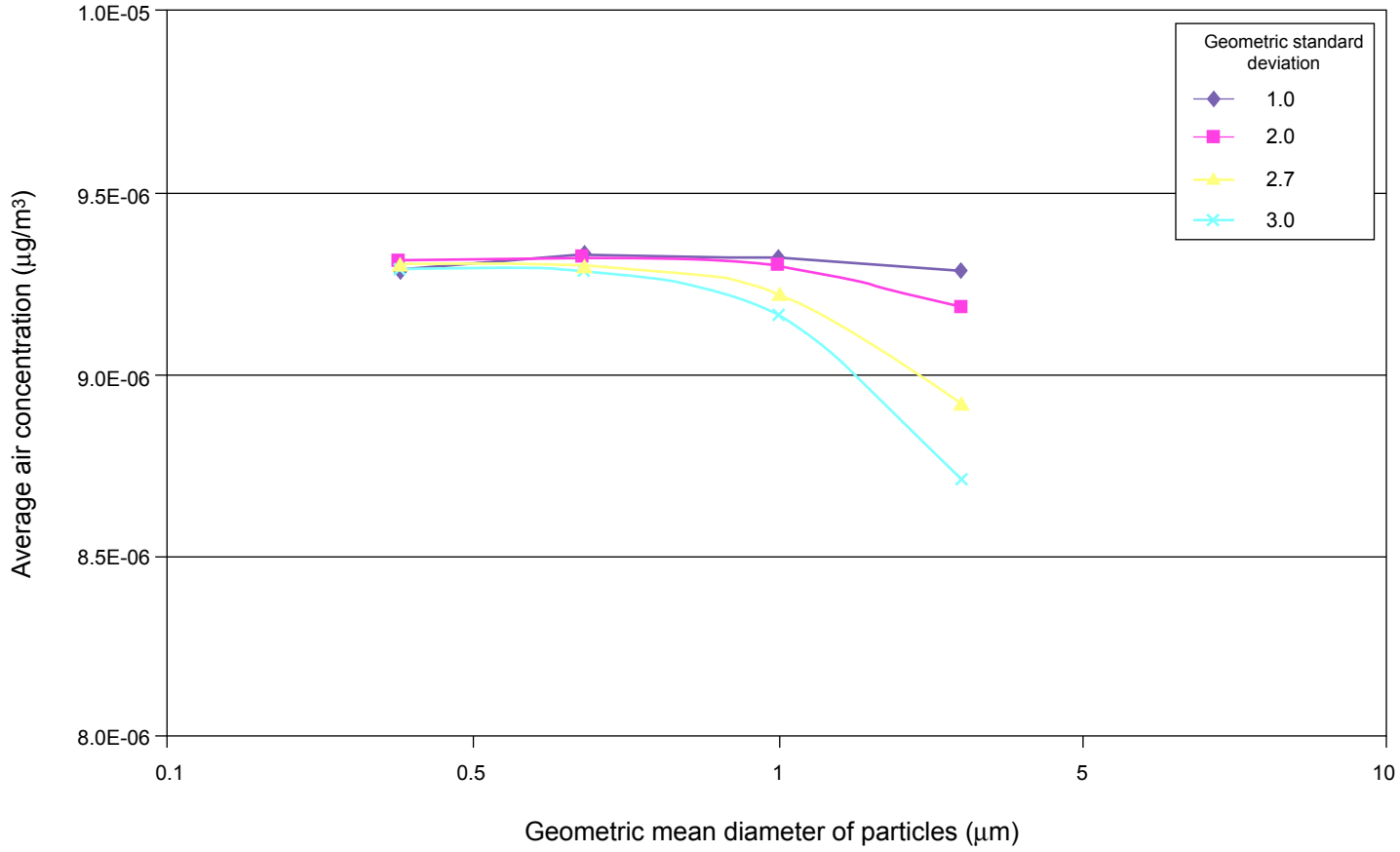

Figure 18
Average Air Concentration vs. Particle Size
(dry deposition over range of 1 to 5 km)

3.3 Far-Field Analysis

The far-field analysis evaluated the potential impact of airborne releases from MDA G on persons living within 80 km (50 mi) of the disposal facility. The results of the analysis are summarized in Figure 19, which shows air concentration contours within the transport model domain. Projected concentrations are generally greatest immediately to the north and south of MDA G, decreasing by a factor of 100 or more near the edges of the model domain.

Annual average air concentrations at the center of each of the polar grid cells were calculated by CALPUFF. These air concentrations were used to determine a population-weighted air dispersion value for each grid cell. A selection of some of the weighted values obtained in this manner is provided in Table 10.

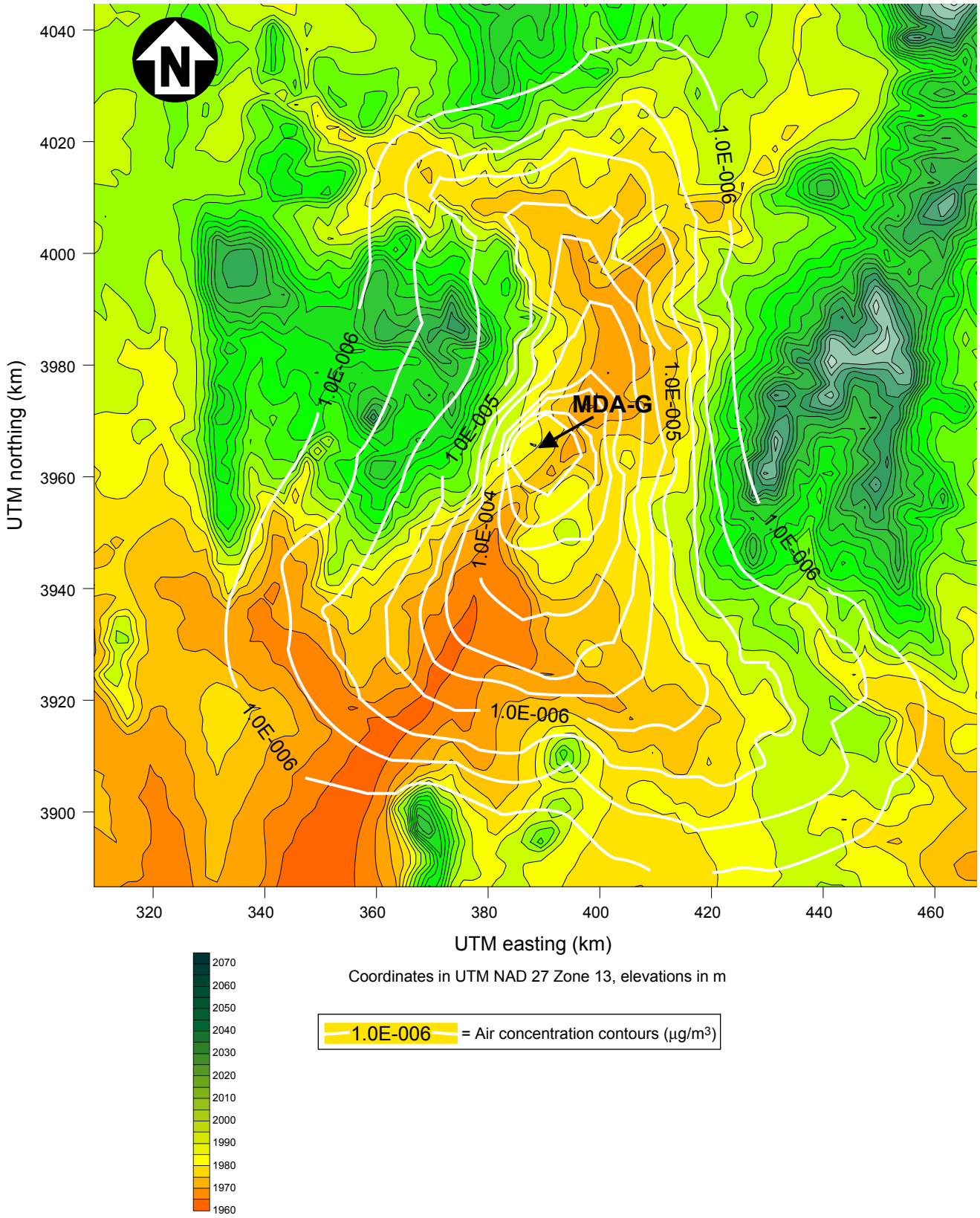

Figure 19
Air Concentration Contours for Far-Field Analysis

Table 10
Selected Population-Weighted Air Dispersion Values for Source Area 1

General Description	Direction from MDA G	Radial Distance (km)	Grid Cell Population	Air concentration (g/m^3)	X/Q (s/m^3)	Population-weighted X/Q ($person\text{-}s/m^3$)
Los Alamos Western Area	NW	8.0 to 10	5.0E+03	4.3E-04	5.7E-09	2.9E-05
Los Alamos Western Area	NW	10 to 20	2.3E+03	1.8E-04	2.3E-09	5.4E-06
Los Alamos North Mesa	NNW	7.0 to 8.0	8.9E+02	2.6E-04	3.5E-09	3.1E-06
White Rock ESE	ESE	2.0 to 2.5	2.6E+02	5.2E-03	6.9E-08	1.8E-05
White Rock ESE	ESE	3.0 to 3.5	6.9E+02	1.2E-03	1.5E-08	1.1E-05
White Rock ESE	ESE	4.0 to 5.0	1.7E+03	4.3E-04	5.7E-09	9.4E-06
Espanola Area	NE	20 to 30	1.9E+04	2.5E-06	3.3E-11	6.4E-07
Pojoaque Area	ENE	20 to 30	4.3E+03	2.5E-06	3.3E-11	1.4E-07
Santa Fe area	ESE	20 to 30	5.8E+03	5.1E-06	6.8E-11	4.0E-07
Santa Fe Area	ESE	30 to 40	2.5E+04	2.5E+04	3.3E-01	8.3E+03
Santa Fe Area	SE	20 to 30	2.1E+04	2.2E-05	2.9E-10	6.2E-06
Santa Fe Area	SE	30 to 40	4.1E+04	9.5E-06	1.3E-10	5.2E-06
North Edge of Albuquerque	SSW	40 to 80	1.1E+05	6.6E-06	8.8E-11	9.4E-06

4.0 Discussion of Air Dispersion Modeling Uncertainty

The level of uncertainty in modeling results affects the level of uncertainty associated with predicting future impacts at a site such as MDA G. The CALPUFF model has recently been promulgated by the U.S. Environmental Protection Agency (EPA) as a "guideline" or approved model for air-dispersion analysis. This means CALPUFF has been through a substantial amount of scientific peer review, performance evaluation, and analysis. Some of these performance evaluations were conducted using data obtained in field trials; the results of these evaluations demonstrate how well the model simulates the average temporal and spatial conditions for the site(s) under consideration. Other supportive analyses have included diagnostic evaluations (designed to determine the ability of the model to simulate certain processes), code verification, and uncertainty analysis.

There are three general areas of uncertainty associated with air-dispersion modeling: the supplied meteorological data, the magnitude and characteristics of releases to the atmosphere, and the model physics and procedures. Validation of air-dispersion modeling normally involves comparing model projections with measured concentrations, a process that also can have bias and uncertainty involved. Even when known accurate meteorological site conditions are supplied to the dispersion model, there will be unknown conditions that cannot be accounted for, such as eddies and vorticity in the wind field (collectively known as turbulence). For this discussion, it has been assumed that the supplied source term information and meteorological data are "perfect" and that any uncertainty relates to the model physics and formulation.

Topographic features in the modeling domain cause turbulence, which is difficult to simulate with a model due to its random nature and the dispersive effects associated with it. Because random events are unpredictable, air dispersion models can only incorporate these events by representing conditions averaged over space and time. Although the use of average conditions to model dispersion does introduce uncertainty into the modeling process, the magnitude of this uncertainty typically decreases as the length of the period being modeled increases. In other words, air-dispersion models are more reliable for estimating long-term concentrations (e.g., annual averages) than short-term concentrations. Most compliance-type air-dispersion models such as CALPUFF are reliable in predicting the magnitude of the maximum air concentration within the modeling domain, even if the location of the maximum concentration is not correctly predicted; model projections have generally been found to fall within 10 to 40 percent of the actual peak concentrations (EPA, 2003).

A number of tracer studies have sought to validate or test modeling results by releasing tracer material from a source and using an array of field collectors to characterize dispersion. Many such studies have been used to evaluate the results of the CALPUFF model. For example, data

from the "Kincaid SF_6" tracer study were used to evaluate CALPUFF (Stimanitis et al., 1998) and the comparison of predicted to observed or measured values was very good. The overall observed mean and standard deviation of the observed X/Q values were about 54 ns/m^3 and 40 ns/m^3 (1.5 ns/ft^3 and 1.1 ns/ft^3), respectively, while the values predicted by CALPUFF for the same variables were 54 ns/m^3 and 53 ns/m^3 (1.5 ns/ft^3 and 1.5 ns/ft^3). Stimanitis et al. (1998) also used data from the "Lovet SO_2" study, a tracer study conducted in complex terrain, to evaluate CALPUFF. Again, there was good agreement; the mean and standard deviation for measured concentrations were 14 ± 24 μg/m^3 ($8.8 \times 10^{-10} \pm 1.5 \times 10^{-9}$ lb/ft^3), those for CALPUFF-predicted concentrations were 11 ± 36 μg/m^3 ($6.7 \times 10^{-10} \pm 2.2 \times 10^{-9}$ lb/ft^3).

Irwin (1997) presented a detailed evaluation of CALPUFF using data from the "1977 INEL SO_2, perfluorocarbon" tracer study. Irwin's evaluation focused on the suitability of puff (vs. plume) modeling for this short-term tracer release. CALPUFF seemed to overpredict concentrations that were closer to the release source as compared to sampling locations farther away. Irwin speculates that this could be due to plume mixing or puff lifting sooner than expected, but concludes that "there does not appear to be any ready explanation." Comparisons between actual and CALPUFF-predicted values for concentrations farther from the source were typical of other tracer experiments in that the CALPUFF-predicted maximum concentrations were within a factor of two of the field-measured concentrations. Irwin notes that when multiple meteorological observation sites (rather than one station) are used, agreement between observed and simulated concentrations improved.

The EPA compared CALPUFF modeling results to the "1975 Savannah River Laboratory SF_6" and "1981 Great Plains perfluorocarbon" tracer study results (Paumier, 1998 and EPA, 1998). In each case, there was overall agreement between the observed and modeled plumes in terms of transport time and direction, and the modeled plume concentrations were within a factor of two of those for the observed plumes. This EPA study also compared CALPUFF to an advanced Lagrangian particle-dispersion model and found that the models performed similarly.

The current study focused on a near-field analysis that calculated annual average concentrations within a 1- to 3-km (0.62- to 1.9-mi) range of the source area. On the basis of the reviews of CALPUFF's performance and the uncertainty of air dispersion modeling in general, it is expected that any single or individual concentration estimate at a specific receptor point will be accurate to within a factor of two or better. The highest concentration predicted by CALPUFF along a boundary and/or in an off-site area is probably accurate to about 20 percent of the maximum that would actually occur somewhere within the model domain.

5.0 References

ASG, 2005, ASG (Atmospheric Study Group) at Earth Tech: Official CALPUFF Web Site, The CALPUFF Modeling, updated July 7, 2005 <http://www.src.com/calpuff/calpuff1.htm>.

Bowen, B.M., 1990, *Los Alamos Climatology*, Los Alamos National Laboratory Report LA-11735-MS.

EPA, 1998, *A Comparison of CALPUFF Modeling Results to Two Tracer Field Experiments*, U.S. Environmental Protection Agency Report EPA-454/R-98-009, Office of Air Quality Planning and Standards Emission, Monitoring, and Analysis Division, Research Triangle Park, NC, June.

EPA, 2003, "Part III, Environmental Protection Agency, 40 CFR Part 51, Revision to the Guideline on Air Quality Models: Adoption of a Preferred Long Range Transport Model and Other Revisions; Final Rule," *Federal Register*, Vol. 68, No. 72, April 15

Golden Software, 2002, "Surfer 8 Users Guide", Golden Software Inc., February.

Golden Software, 2005, "Golden Software: Makers of Strater, Surfer, Grapher, MapViewer and Didger Software," Copyright 1997 -2004, Golden Software, Inc., August.

Hoffman F.O., 1977, "A Reassessment of the Deposition Velocity in the Prediction of the Environmental Transport of Radioiodine from Air to Milk," *Health Physics* Vol. 32, p. 437. Pergamon Press Ltd. 1977

Irwin, J.S., 1997, "A Comparison of CALPUFF Modeling Results with 1977 INEL Field Results," *Twenty-second NATO/CCMS International Technical Meeting on Air Pollution Modeling and its Application,* Clermont-Ferrand, France, June 2–6.

Miller C.W. 1978, "The Importance of Variations in the Deposition Velocity Assumed from the Assessment of Airborne Radionuclide Releases," *Heath Physics* Vol. 35, No. 6, pp. 730 – 734, Pergamon Press Ltd, June.

PNL, 1970, "Precipitation Scavenging" Proceedings of a symposium held at Richland, Washington, June 2-4, 1970. Engelmann, R. J., Slinn G.N., editors, Pacific Northwest Laboratory, U.S. Atomic Energy Commission, Division of Technical Information; Oak Ridge Tennessee.

Paumier, J.O. and R.W. Brode, 1998, "Comparison of CALPUFF Modeling Results with Tracer Data", *10th Joint Conference on the Applications of Air Pollution Meteorology with the A&WMA*; American Meteorological Society.

Pruppacher, H.R., R.G. Semonin, W.G.N. Slinn., eds., 1982, "Precipitation Scavenging, Dry Deposition, and Resuspension," *Proceedings of the Fourth International Conference, Santa Monica, California*, 29 November–3 December, Elsevier Science Publishing Company Inc.

Scire, J.S., D. G. Stimanitis., and R.J. Yamartino, 2000a, *A Users Guide for the CALPUFF Dispersion Mode (Version 5)*, Earth Tech. Inc., Concord, Massachusetts, January.

Scire, J.S., F.R. Robe, M.E. Fernau and R.J. Yamartino, 2000b, *A User's Guide for the CALMET Meteorological Model (Version 5)*, Earth Tech, Inc., Concord, Massachusetts.

Sehmel G.A. and W.H. Hodgson, 1976, "Predicted Deposition Velocities," in Proceedings, *Atmosphere-Surface Exchange of Particulate and Gaseous Pollutants*, ERDA Symposium Series 38, CONF-740921.

Sehmel G.A. and W.H. Hodgson, 1978, *A Model for Predicting Dry Deposition of Particles and Gases to Environmental Surfaces*, Pacific Northwest Laboratory Report PNL-SA-6721, January.

Sehmel, G.A. 1980, "Particle and Gas Dry Deposition: A Review," *Atmospheric Environment*, Vol. 14, pp. 983-1101, Pergamon Press Ltd.

Slinn W.G.N., 1977, "Some Approximations for the Wet and Dry Removal of Particles and Gases from the Atmosphere," *Air and Soil Pollution*, Vol. 7, pp. 513-543.

Stimanitis D.G., J.S. Scire, and J.C. Chang, 1998, "Evaluation of the CALPUFF Dispersion Model with Two Power Plant Data Sets," *10th Joint Conference on the Applications of Air Pollution Meteorology*, January 11-16, Phoenix, AZ.

Vold, E.L., M.C. Vold, and L. Sanders, 1996, "Preliminary Results from the Los Alamos TA54 Complex Terrain Atmospheric Transport Study (ATS)," Presented at the *AMS 9th Joint Conference on Applications of Air Pollution Meteorology* with the Air and Waste Management Association, Jan. 28 – Feb. 2, Atlanta, GA.

LA-UR-05-7393

Approved for public release;
distribution is unlimited.

Title: GROUNDWATER PATHWAY MODEL FOR THE LOS ALAMOS NATIONAL LABORATORY TECHNICAL AREA 54, MATERIAL DISPOSAL AREA G

Author(s):
Philip H. Stauffer
Hari S. Viswanathan
Bruce A. Robinson
Carl W. Gable
Greg L. Cole
Dave E. Broxton
Everett P. Springer and Tracy G. Schofield

Submitted to: U. S. Department of Energy

Form 836 (8/00)

Table of Contents

List of Figures i
List of Tables iii
List of Attachments iii
Acronyms and Abbreviations iv

1.0 Introduction 1
2.0 Background 2
2.1 Site Description 2
2.2 Previous Investigations 9
3.0 Methods 13
3.1 Three-Dimensional Model Development 13
3.1.1 Grid Development 13
3.1.2 Model Configuration and Boundary Conditions 19
3.1.2.1 Infiltration 21
3.1.2.2 Initial and Boundary Conditions 24
3.1.3 Hydrogeologic Input Data 25
3.1.4 Model Simulations 27
3.1.4.1 Conservative Breakthrough Curves 28
3.1.4.2 Longitudinal Dispersivity 28
3.1.4.3 Well Capture 30
3.2 Model Abstraction 34
4.0 Results 35
4.1 Breakthrough at the Compliance Boundary 35
4.1.1 Effects of Changes in Permeability and Infiltration 37
4.1.2 Effects of Changes in Dispersivity 47
4.2 Well Capture 47
4.3 Comparison of Three-Dimensional and One-Dimensional Breakthrough Curves 54
5.0 References 56

List of Figures

Figure 1 Locations of Material Disposal Area G and Model Area 3
Figure 2 Aerial Photograph of Material Disposal Area G Looking West Toward Jemez Mountains 4
Figure 3 Waste Disposal Pits and Shafts at Material Disposal Area G 5
Figure 4 Interpretive Geologic Cross Section Between Regional Characterization Wells R-21 and R-22 7
Figure 5 Stratigraphic Nomenclature for the Bandelier Tuff 8
Figure 6 Locations of Regional Characterization Wells R-20, R-21, R-22, R-23, and R-32 10
Figure 7 Digital Elevation Model for the Domain of the Numerical Grid 15
Figure 8 Horizontal Resolution of Numerical Grid Digital Elevation Model 16
Figure 9 Comparison of Predicted to As-Drilled Stratigraphy at Regional Characterization Well R-22 18

Figure 10 Waste Disposal Pits and Waste Disposal Regions Superimposed on the Numerical Grid 20
Figure 11 Normalized Histogram of Mesa-Top Infiltration Rates 23
Figure 12 Sensitivity Analysis of Particle Breakthrough to Size of Release Area at Waste Disposal Region 5 29
Figure 13 Distribution of Particle Release Points for Waste Disposal Region 5 (well capture simulation) 31
Figure 14 Cross Section of Numerical Grid Showing Vertical Steps in Water Table 33
Figure 15 Two-Dimensional Views of Pathways for Particles Released from Waste Disposal Region 5 (high- and low-infiltration rates) 36
Figure 16 Breakthrough Curves for Particles Released from All Waste Disposal Regions (background infiltration of 0.5 mm/yr) 38
Figure 17 Breakthrough Curves for Particles Released from All Waste Disposal Regions (background infiltration of 10 mm/yr) 39
Figure 18 Effect of Permeability Reductions on Subsurface Saturation at Waste Disposal Region 5 40
Figure 19 Effect of Permeability Reductions on Breakthrough for Releases from Waste Disposal Regions 1 and 5 41
Figure 20 Subsurface Saturations at Waste Disposal Region 5 for Range of Steady-State Infiltration Rates (without increased Pajarito Canyon infiltration) 43
Figure 21 Simulated Surface Saturation with Increased Pajarito Canyon Infiltration 44
Figure 22 Effect of Pajarito Canyon Infiltration on Subsurface Saturation at Waste Disposal Region 5 45
Figure 23 Effect of Pajarito Canyon Infiltration on Breakthrough for Releases from Waste Disposal Regions 1 and 5 46
Figure 24 Breakthrough Curves for Particles Released from Waste Disposal Region 1 (range of steady-state infiltration rates) 48
Figure 25 Breakthrough Curves for Particles Released from Waste Disposal Region 5 (range of steady-state infiltration rates) 49
Figure 26 Early Breakthrough Curves for Particles Released from Waste Disposal Regions 1 and 5 (range of steady-state infiltration rates) 50
Figure 27 Model Sensitivity to Longitudinal Dispersivity at Waste Disposal Region 5 (high- and low-infiltration rates) 51
Figure 28 Capture Zone for Hypothetical Well with High Pumping Rate 52
Figure 29 Comparison of Three-Dimensional Particle and One-Dimensional Plume Breakthrough Curves 55

List of Tables

Table 1 Depths and Elevations of Material Disposal Area G Pits 6
Table 2 Comparison of As-Drilled Stratigraphy from Regional Characterization Well R-22 to Three-Dimensional Model Predictions 19
Table 3 Particle Release Point Locations Representing the Eight Waste Disposal Regions 21
Table 4 Hydrogeologic Properties Used for the Three-Dimensional Model 26
Table 5 Transformed Values for Shift of Tracer Particle Release Points [a] 32
Table 6 Capture Efficiencies for Waste Disposal Regions 1 through 5 and 8 53

List of Attachments

Attachment I Generation of the Three-Dimensional Numerical Grid
Attachment II Update of the Vadose-Zone Geologic Model
Attachment III Statistical Description of Vadose-Zone Hydrologic Properties
Attachment IV Incorporation of Sorption in the Micromixing Model
Attachment V Details on the Coupling of GoldSim and the Finite Element Heat and Mass (FEHM) Transfer Code
Attachment VI Summary of Pre- and Post- Processing Codes

Acronyms and Abbreviations

1-D	One-dimensional
3-D	Three-dimensional
DEM	Digital elevation model
FEHM	Finite Element Heat and Mass (transfer code)
LANL	Los Alamos National Laboratory
MDA	Material Disposal Area
msl	Mean sea level
OMR	Octree mesh refinement
RTD	Residence time distribution functions

1.0 Introduction

This report describes the groundwater flow and transport modeling conducted in support of the Los Alamos National Laboratory (LANL or the Laboratory) Material Disposal Area (MDA) G performance assessment and composite analysis. The MDA G performance assessment and composite analysis use models created with GoldSim™ (Golder, 2005a and 2005b), a system-level modeling tool that allows the integration of numerous process-level models and provides the tools needed to conduct probabilistic assessments of long-term facility performance. The groundwater transport model detailed in this report is one of several process models incorporated into the performance assessment and composite analysis model.

The groundwater transport modeling effort builds on the knowledge gained through previous studies at MDA G and is augmented by the use of new data, modeling tools, and computer simulations. The approach combines geologic, hydrologic, and topographic data into a three-dimensional (3-D) site-scale model. Mathematical models are used to simulate the transport of radionuclides from the surface through a deep vadose (unsaturated) zone, into the saturated zone, and finally to a compliance boundary located 100 m (330 ft) east of MDA G. Although the compliance period for the performance assessment and composite analysis is 1,000 years, the simulations are designed to be robust and can be used to estimate groundwater impacts well past the regulatory timeframe to provide insight into possible long-term issues.

This report consists of four major sections, including this introductory section. Section 2 provides an overview of previous investigations related to the development of the current site-scale model. The methods and data used to develop the 3-D groundwater model and the techniques used to distill that model into a form suitable for use in the GoldSim models are discussed in Section 3. Section 4 presents the results of the model development effort and discusses some of the uncertainties involved. Six attachments that provide details about the components and data used in this groundwater pathway model are also included with this report.

2.0 Background

Material Disposal Area G, the only active low-level waste repository for the Laboratory, has been in operation since 1957. The location, topography, and general stratigraphy of MDA G are described briefly in Section 2.1. Section 2.2 summarizes some of the details of previous geologic and groundwater transport studies relevant to this study of groundwater transport of contaminants from MDA G disposal units.

2.1 Site Description

As shown in Figure 1, MDA G is located on the eastern edge of the Laboratory in Technical Area (TA) 54, approximately 2 km (1.2 mi) west of the town of White Rock and about 5 km (3.1 mi) west of the Rio Grande. The site lies on Mesita del Buey, which is bounded to the north by Cañada del Buey and to the south by Pajarito Canyon (Figure 2). The surface of MDA G slopes to the east from an elevation of 2,070 m (6,790 ft) above mean sea level (msl) in the expansion area near MDA L, to an elevation of approximately 2,033 m (6,670 ft) above msl at the eastern end of MDA G.

The site has been in operation since 1957, during which time radioactive waste generated at the Laboratory has been disposed of in pits (Figure 3) and shafts. Table 1 lists the depth and average surface and bottom elevations of each of the waste disposal pits. The shafts range in depth from approximately 8 to 20 m (26 to 66 ft) and are typically 0.5 to 1.0 m (1.6 to 3.3 ft) in diameter. Operational plans call for expansion of MDA G to the west into Zone 4, toward the boundary with MDA L (Figure 2).

Subsurface information about the basic stratigraphy beneath MDA G, obtained from regional characterization wells, is shown in cross section in Figure 4. The nomenclature for the Bandelier Tuff units discussed in this report (Figure 5) follows the usage of Broxton and Reneau (1995), who provide a detailed description of this formation. The disposal pits and shafts at MDA G have been excavated into unit 2 and unit 1v of the Tshirege Member of the Bandelier Tuff, which extends below the ground surface to approximately 1,970 m (6,463 ft) above msl in the vicinity of MDA G. The Cerro Toledo interval (Qct) lies below the Tshirege Member and above the Otowi Member of the Bandelier Tuff. Although the Cerro Toledo interval is technically not a part of the Bandelier Tuff, its material properties are more similar to the tuff than to the Cerros del Rio basalt. As shown in Figure 4, the thickness of the Bandelier Tuff increases from east to west in the vicinity of MDA G. The Cerros del Rio basalt lies beneath the Bandelier Tuff; the lower portion of the basalt extends below the surface of the regional water table, along with several deeper formations such as the Puye Formation (Figure 4).

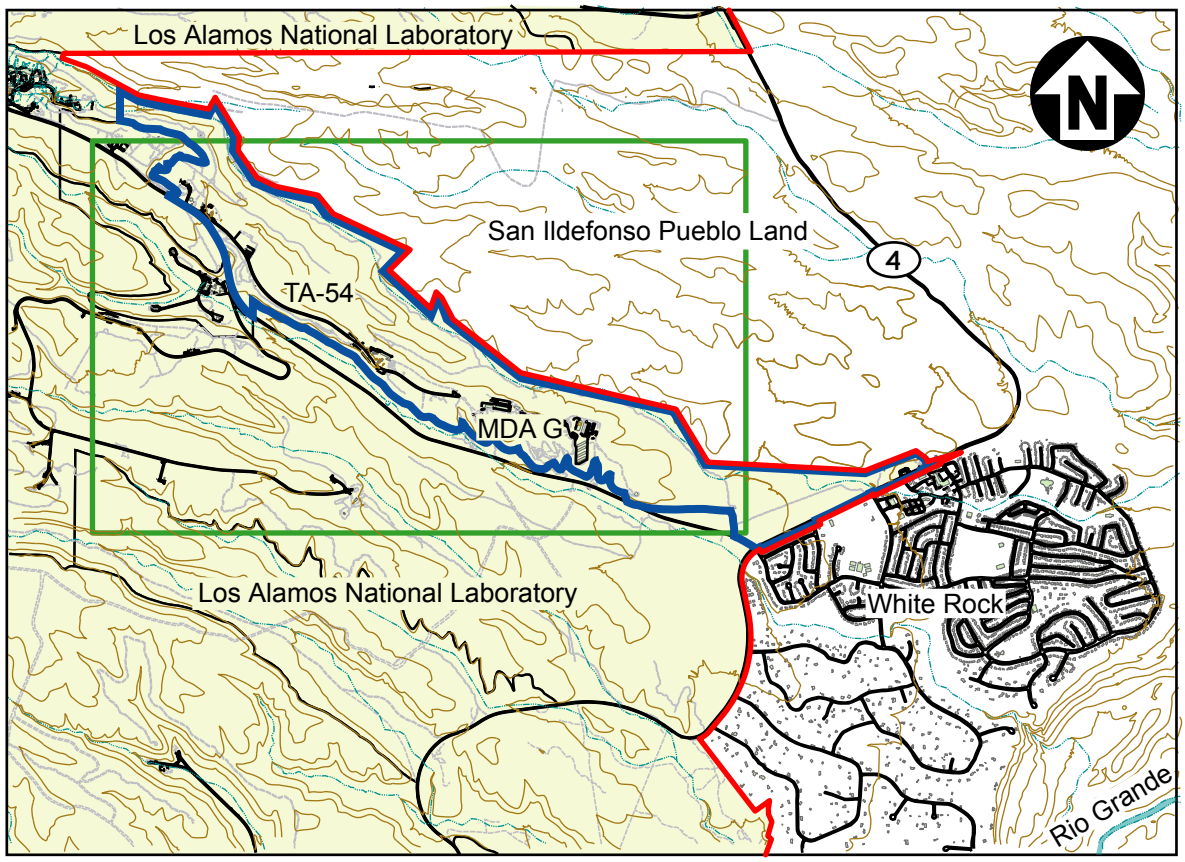

Figure 1
Locations of Material Disposal Area G and Model Area

Figure 2
Aerial Photograph of Material Disposal Area G
Looking West Toward Jemez Mountains

Source: Apogen Technologies (formerly SEA)

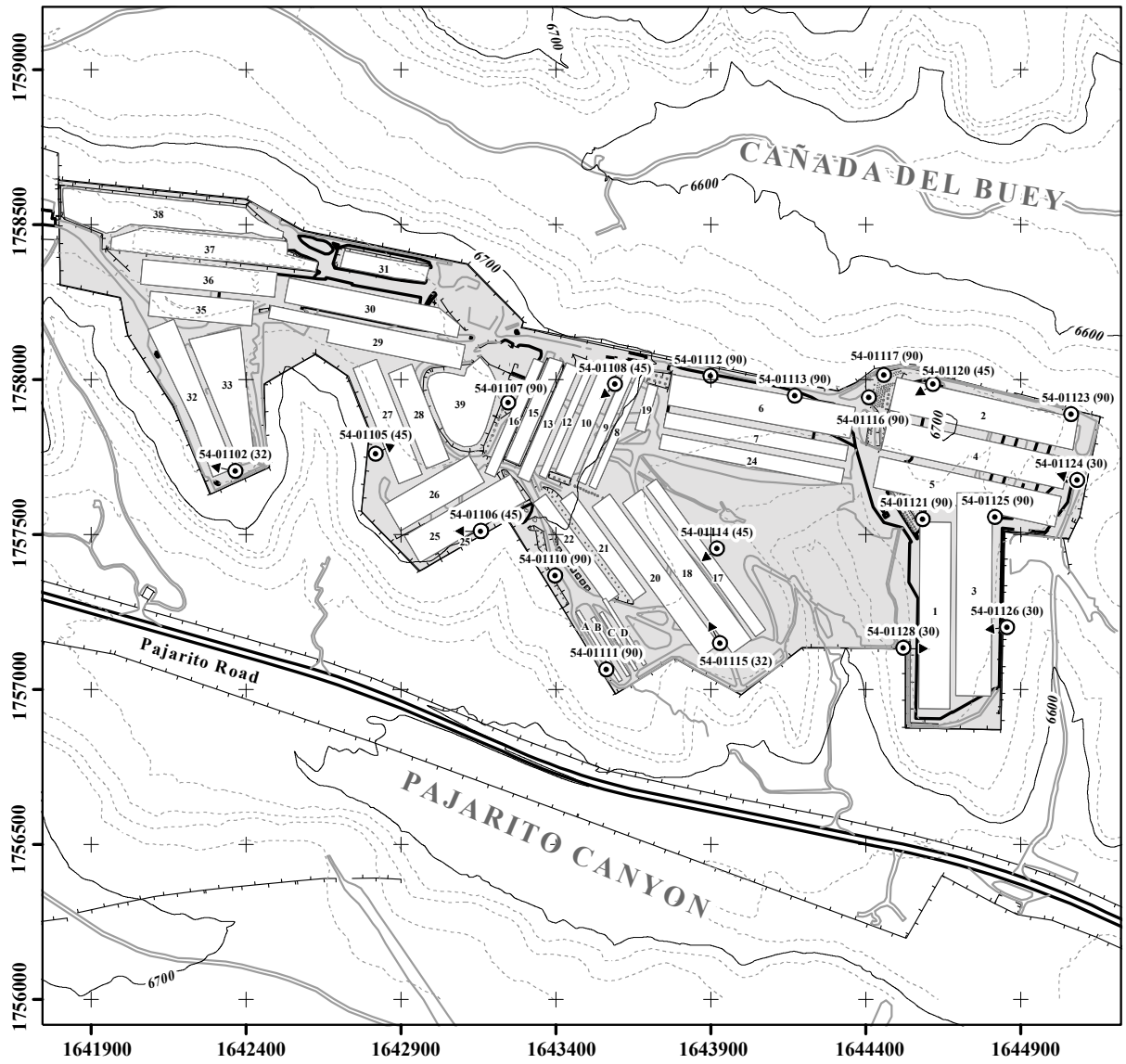

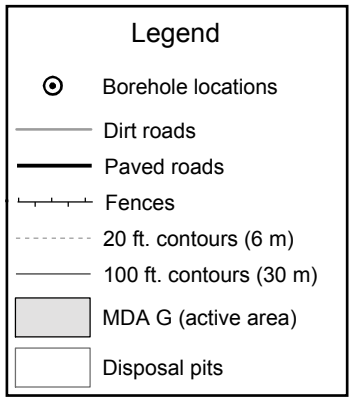

Note: Arrows indicate boring direction; numbers in parantheses adjacent to location IDs indicate inclination from horizontal.

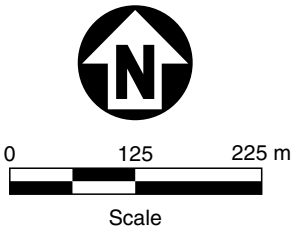

Projection: NM State Plane
Coordinate System - 3002
Datum: NAD83 (ft)
Scale: 1:5,000

Figure 3
Waste Disposal Pits at Material Disposal Area G
Source: Apogen Technologies (formerly SEA), LANL RRES Database, Map ID: 4531.021 (1) Rev. 2

Table 1
Depths and Elevations of Material Disposal Area G Pits

Pit Number	Depth (m)	Elevation above Mean Sea Level (m)	
		Surface	Bottom of Pit
1	6	2,034	2,028
2	8	2,037	2,029
3	10	2,034	2,024
4	10	2,036	2,026
5	9	2,034	2,025
6	8	2,039	2,031
7	9	2,039	2,030
8	8	2,042	2,034
9	6	2,043	2,037
10	8	2,044	2,036
12	8	2,047	2,039
13	9	2,047	2,038
15	9	2,047	2,038
16	8	2,047	2,039
17	7	2,034	2,027
18	12	2,035	2,023
19	5	2,042	2,037
20	11	2,038	2,027
21	8	2,041	2,033
22	10	2,042	2,032
24	9	2,033	2,024
25	12	2,044	2,032
26	11	2,050	2,039
27	14	2,055	2,041
28	12	2,047	2,035
29	15	2,050	2,035
30	11	2,050	2,039
31	8	2,043	2,035
32	16	2,051	2,035
33	12	2,052	2,040
35	12	2,052	2,040
36	13	2,052	2,039
37	19	2,052	2,033
38	18	2,055	2,037
39	14	2,047	2,033

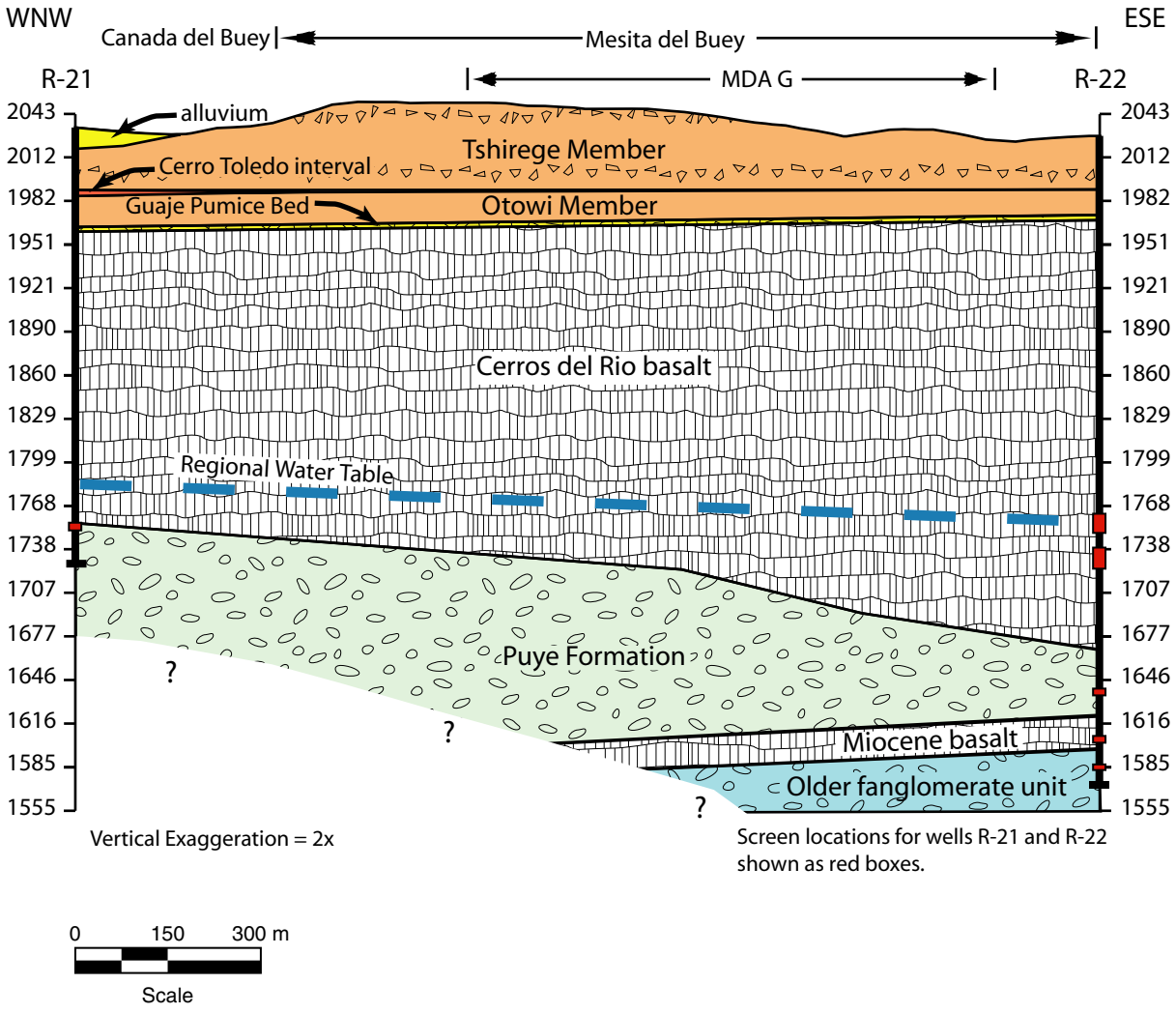

Figure 4
Interpretive Geologic Cross Section Between Regional Characterization Wells R-21 and R-22

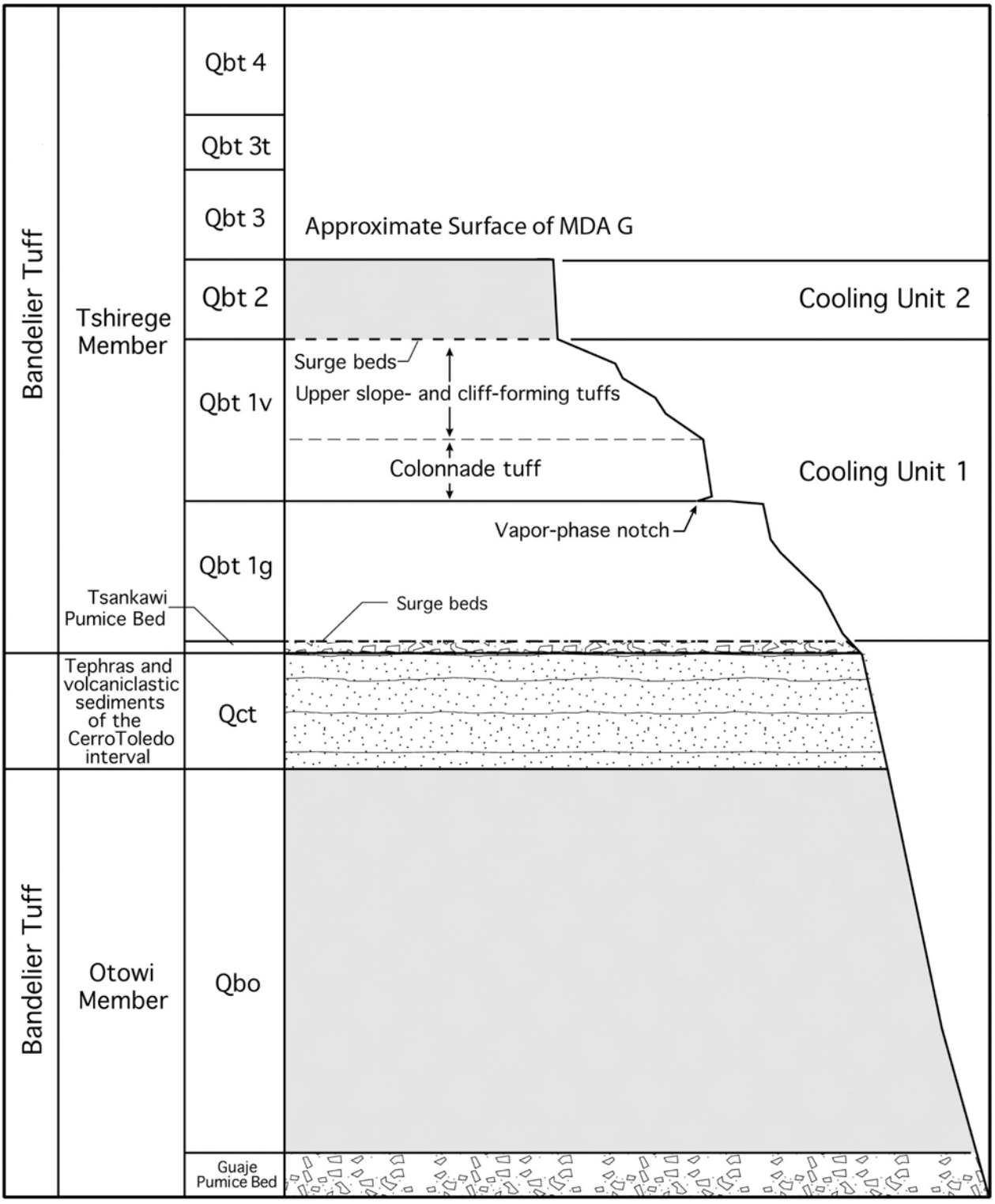

Figure 5
Stratigraphic Nomenclature for the Bandelier Tuff

Source: Adapted from Broxton and Reneau (1995)

2.2 Previous Investigations

The groundwater pathway modeling presented in this report builds upon the findings and information provided by a number of earlier investigations. A solid foundation was provided by data compiled in support of the 1997 performance assessment and composite analysis (Hollis et al., 1997); this includes geologic information (Vaniman et al., 1996) and hydrologic parameters for MDA G (Krier et al., 1996; Rogers and Gallaher, 1995). Information developed since the completion of the 1997 performance assessment and composite analysis also played a key role in this groundwater transport analysis.

The new model incorporates a high resolution digital elevation model (DEM) of the surface topography (Carey and Cole, 2002). Also, a more accurate 3-D representation of the site was developed using a new geologic model that incorporates increased stratigraphic control from five regional characterization wells (R-20, R-21, R-22, R-23, and R-32) drilled in the vicinity of MDA G between 2000 and 2003. Figure 6 shows the location of these characterization wells.

Data collected from the characterization wells shown in Figure 6 have led to improved understanding of the deep subsurface directly beneath MDA G and to subsequent modifications in the model used for contaminant transport. New hydrogeologic datasets include an updated compilation and statistical analysis of subsurface material properties of the Bandelier Tuff from TA-54 (Springer, 2005), a statistical analysis of mesa-top infiltration (Springer and Schofield, 2004), and constraints on the properties of vadose-zone, fractured basalt (Stauffer et al., 2005). These new data, discussed below, are important inputs to the groundwater pathway model.

Springer (2005) examined geographical differences among vadose-zone hydrologic properties across the Laboratory as a means of estimating vadose-zone model parameters for the Bandelier Tuff. Hydrologic properties included measured properties such as bulk density, saturated water content, and saturated hydraulic conductivity, and fitted parameters such as the van Genuchten equation parameters (α and n) and residual water content. Nonparametric analyses were used to identify differences among the measured hydrologic properties for (1) lithologic units within a LANL technical area (2) at different TAs (3) in mesa-top versus canyon settings, and (4) across lithologic units. Most hydrologic properties were similar within lithologic units at a TA. No consistent relationships were found among TA, except for the residual water content, which was essentially zero at all locations. Hydrologic properties of the Tshirege Member unit 1g were somewhat similar at mesa-top and canyon settings, but this was not true of the Otowi Member. Hydrologic properties for Tshirege units 1v and 1g were essentially the same.

Stauffer et al. (2005) used data from a bromide tracer test at the Los Alamos Canyon low-head weir to constrain basalt material properties in the unsaturated zone. This study showed that, under ponded conditions, the Cerros del Rio basalt behaves like a very low-porosity, high-permeability system.

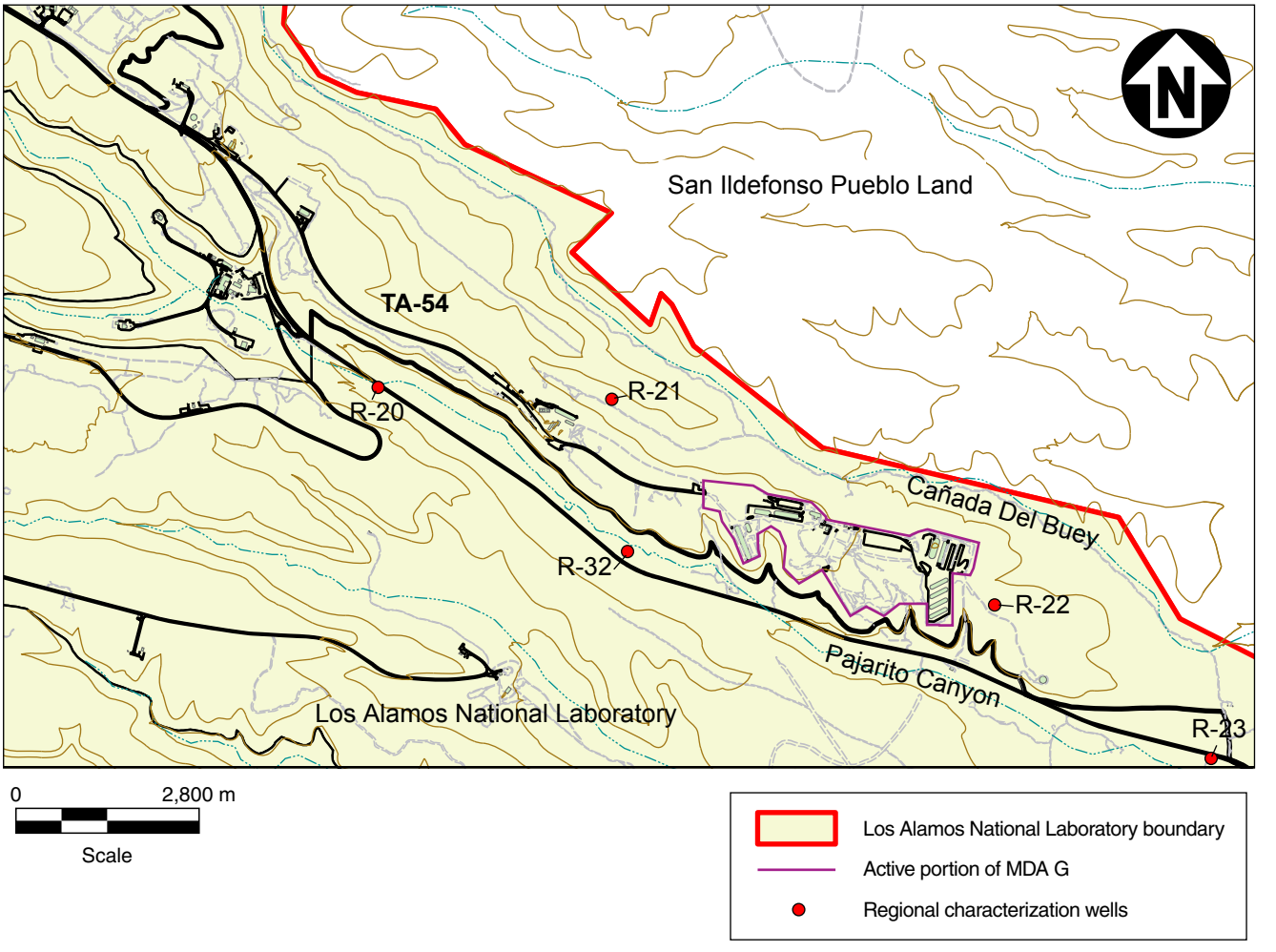

Figure 6
Locations of Regional Characterization Wells
R-20, R-21, R-22, R-23, and R-32

Previous groundwater transport investigations at MDA G (Birdsell et al., 1995, 1999, and 2000; Hollis et al., 1997; Soll, 1995) provide a wealth of insight into the local transport of radionuclides; these studies relied on the process-level, multidimensional, finite-element porous flow and transport simulator known as FEHM (Finite Element Heat and Mass) (Zyvoloski et al., 1995a and 1995b) to model the movement of water-soluble radionuclides from the disposal pits and shafts at MDA G to a drinking water compliance point. Summaries of pertinent aspects of these studies, which guided the current effort, are provided below.

Birdsell et al. (1999) conducted investigations into specific flow processes that are relevant to the modeling approach adopted for this study. To determine the effect of transient pulses of moisture on radionuclide transport in the MDA G area, Birdsell et al. ran 1-D and 2-D models of liquid-phase C-14 transport through the Bandelier Tuff. Four scenarios were evaluated. These scenarios had nearly identical long-term infiltration rates of 5.5 mm/yr (0.22 in./yr); however, infiltration rates for individual years varied greatly (from zero to over 100 mm/yr [3.9 in./yr]), and the four selected scenarios had different temporal distributions. Simulations were run for 5,000 years, and the results of the C-14 transport modeling were compared to a simulation using the long-term average infiltration rate. This study showed that a steady-state flow assumption is valid within the range of likely infiltration rates for MDA G and the surrounding area because the transient pulses were damped out as they propagated downward through the system.

Other modeling examined the effect that fractures in the tuff may have on water flow, examining possible scenarios where significant fracture flow may occur (Birdsell et al., 1999; Soll and Birdsell, 1998). In this study, the effects of fracture coatings and fills, locations of fractures with respect to the waste, and interactions between fractures and the surrounding matrix were examined. High-infiltration rates were assigned to the top of the simulated fracture systems to ensure that “worst case” conditions were achieved. The results showed that limited fracture flow was activated only during extreme events such as surface ponding of water. The authors concluded that, in most cases, fractures at MDA G are not a major conduit for the movement of water from the surface to the water table.

Birdsell et al. (1999) also examined how evaporation from the surge bed at the base of Tshirege Member unit 2 (see Figure 5) might affect vadose-zone flow. Their results show that evaporation could cause extremely high capillary forces resulting in the flow of water toward the surge bed.

Modeling by Robinson et al. (1999) showed that changes in hydrologic properties at the subgrid scale can lead to reduced permeability across unit interfaces. Saturation data from regional characterization well R-32, located to the west of MDA G, indicates that reductions in permeability occur at two interfaces, one at the base of Tshirege Member unit 1g and the other at the top of the Cerros del Rio basalt. Robinson et al. (1999) reported that perched water at the top of the basalt occurs with a reduction of interface permeability of about 1,000.

Another consideration for the groundwater pathway modeling is the effect that increased infiltration in nearby canyons may have on the transport of contaminants from MDA G. As described in Pratt (1998), the lower Pajarito Canyon, just south of MDA G, has more subsurface water than Cañada del Buey and thus is more likely to have an impact on modeling results. Pajarito Canyon is relatively wide and has a fairly flat bottom in the area near MDA G, as seen in Figure 2. Shallow wells located along the canyon bottom between TA-18 to the west of MDA G and White Rock to the east indicate the presence of alluvial groundwater, which is attributed to the fact that this section of Pajarito Canyon is a major drainage between the Pajarito Mountains and the Rio Grande (Pratt, 1998). The section of Pajarito Canyon just south of MDA G is hydrologically similar to other major drainages at the Laboratory**,** such as lower Los Alamos Canyon (Nylander et al., 2003). Runoff from higher elevations is focused into Pajarito Canyon and creates a transient stream that flows intermittently, sometimes resulting in pooled water in the canyon bottom to the south of MDA G (Pratt, 1998). The most recent estimate of average annual infiltration in lower Pajarito Canyon is 18.5 m^3/m (200 ft^3/ft) (Kwicklis et al., 2005, Table 2). This value represents the average infiltration per meter of canyon across the average canyon width between two stream gauges; the upstream gauge is located several kilometers west of MDA G and the downstream gauge lies just west of White Rock. The infiltration value does not account for stream losses due to evapotranspiration.

3.0 Methods

The MDA G groundwater pathway modeling effort included (1) the development of a 3-D model capable of simulating the transport of water-soluble radionuclides released from the pits and shafts at MDA G and (2) the abstraction of this complex model to a 1-D form suitable for implementation within GoldSim. As was the case for the 1997 performance assessment and composite analysis, the 3-D modeling was conducted using the process-level, multidimensional, finite-element porous flow and transport simulator known as FEHM (Finite Element Heat and Mass) (Zyvoloski et al., 1995a and 1995b). Stochastic modeling of groundwater transport can, potentially, require thousands of simulations. Given the computer-resource-intensive nature of FEHM, 1-D abstractions of the 3-D model were developed for use in the probabilistic analyses (see Section 3.2). The GoldSim model controls these 1-D model abstractions, allowing the bulk transport properties of the subsurface for all radionuclides undergoing groundwater transport to be modified as desired.

The 3-D modeling requires a numerical grid that represents the topography and geology of MDA G and the surrounding area. Section 3.1 describes how the grid was developed and the 3-D model was configured to enable more realistic simulations of flow and transport. Section 3.2 describes how the resultant 3-D breakthrough curves were abstracted to a series of 1-D models that recreate particle breakthrough at the compliance boundary.

3.1 Three-Dimensional Model Development

Since the completion of the last performance assessment and composite analysis (Hollis et al., 1997), new information and techniques have become available to update and refine the models used to conduct groundwater pathway modeling. Section 3.1.1 discusses the development of a new 3-D topographic and geologic grid, Section 3.1.2 explains how the model was configured to simulate actual conditions, and Section 3.1.3 presents the hydrogeologic input data used to populate the model. Descriptions of the simulations that were conducted in support of the groundwater modeling effort are presented in Section 3.1.4.

3.1.1 Grid Development

The 3-D grid used to conduct the groundwater modeling was designed to meet several conditions:

- Continuity and correlation with the Española basin site-scale regional aquifer computational model (Keating et al., 2003)
- Resolution adequate to accurately locate features such as waste pits, truncated material layers along the mesa, fence boundaries, and the compliance boundary

- Incorporation of the latest 3-D geologic model to define the hydrogeologic layers
- Adequate hydrogeologic layer resolution to provide accurate streamline-particle-tracking solutions

The grid incorporates a new mesh refinement technique that provides high resolution near the MDA G waste pits and lower resolution away from the MDA G fence line. The new 3-D grid has approximately 10 times as many nodes and a resolution in the area of the disposal pits that is 6 times greater than that of the previous vadose-zone grid (Birdsell et al., 1999). Furthermore, the new grid spans an area of nearly 15 km^2 (5.8 mi^2), which is large enough to avoid edge effects that led to nonphysical flow in previous transport simulations. The grid extends well below the water table and is used to follow contaminant pathways from the surface of the disposal facility through the vadose zone, into the saturated zone, and finally to the compliance boundary. A metric-based polar stereographic coordinate system used in the Española basin site-scale regional aquifer computational model (Keating et al., 2003) was applied to the new grid. The use of this coordinate system allows flow in the saturated section of the MDA G model to be easily validated against the calibrated regional model. A complete description of the grid generation process is presented in *Attachment 1*.

The numerical grid measures 4,750 m (3 mi) from east to west and 2,875 km (1.8 mi) from north to south (Figure 1). The footprint of the grid was designed to encompass several important wells, including regional characterization wells R-20, R-21, R-22, R-23, and R-32 (Figure 6), and water supply well PM-2, to the northwest of well R-20.

The surface elevation of the grid was interpolated from a high-resolution DEM (Carey and Cole, 2002) that ranges from 2,150 m (7,055 ft) above msl in the northwest to approximately 2,000 m (6,560 ft) above msl in the southeast; this model is shown in Figure 7. As discussed earlier, the grid resolution decreases with distance from MDA G, yielding the most accurate representation of the surface topography near the disposal pits. This can be seen in Figure 8, where the well-defined topography on Mesita del Buey (MDA G) contrasts with the blocky appearance of the mesa to the south. The grid spacing between nodes in the horizontal direction reaches a minimum of 7.8 m (26 ft) in the vicinity of the pits and shafts and is coarsest (125 m [410 ft]) in the regions farthest from MDA G. The high-resolution section extends more than 100 m (330 ft) beyond the boundary of MDA G to ensure that lateral transport issues can be adequately addressed.

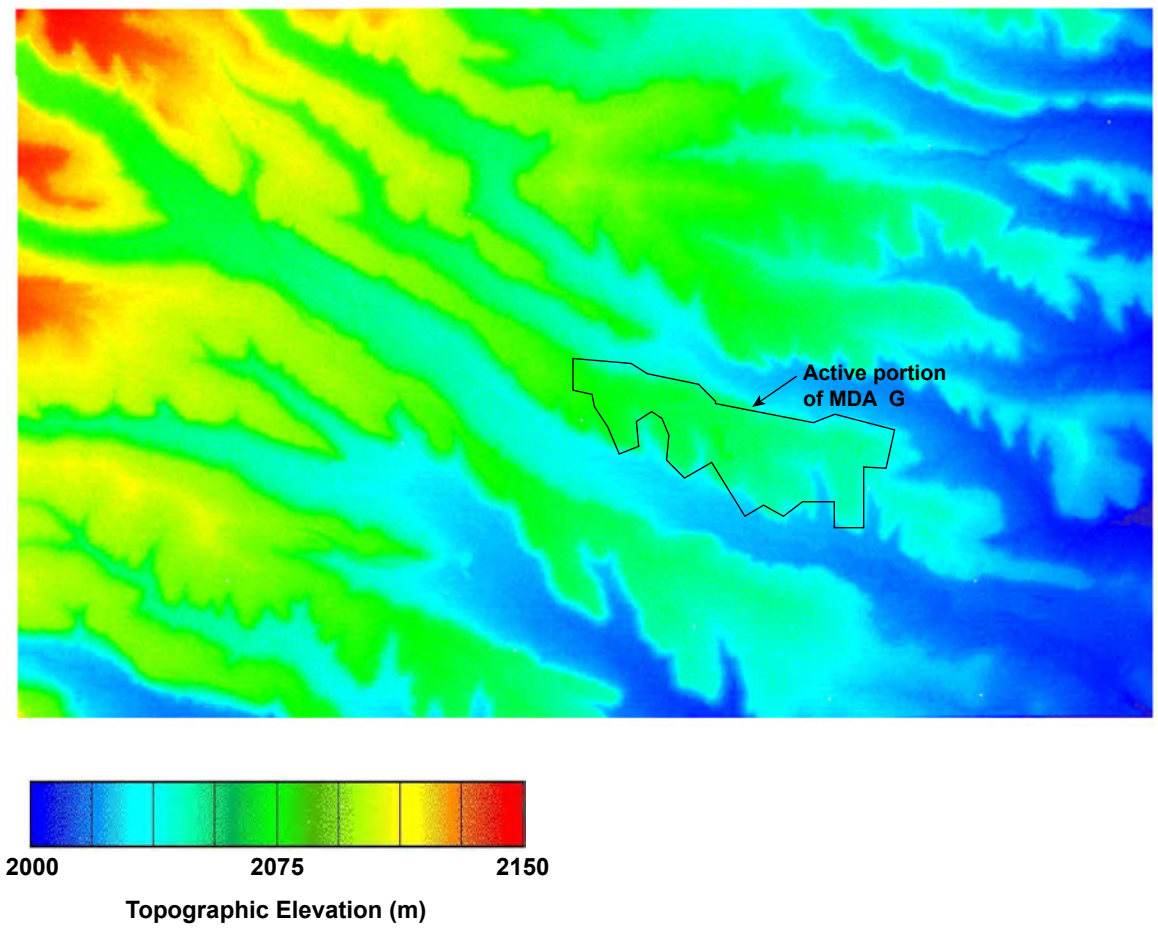

Figure 7
Digital Elevation Model for the Domain of the Numerical Grid

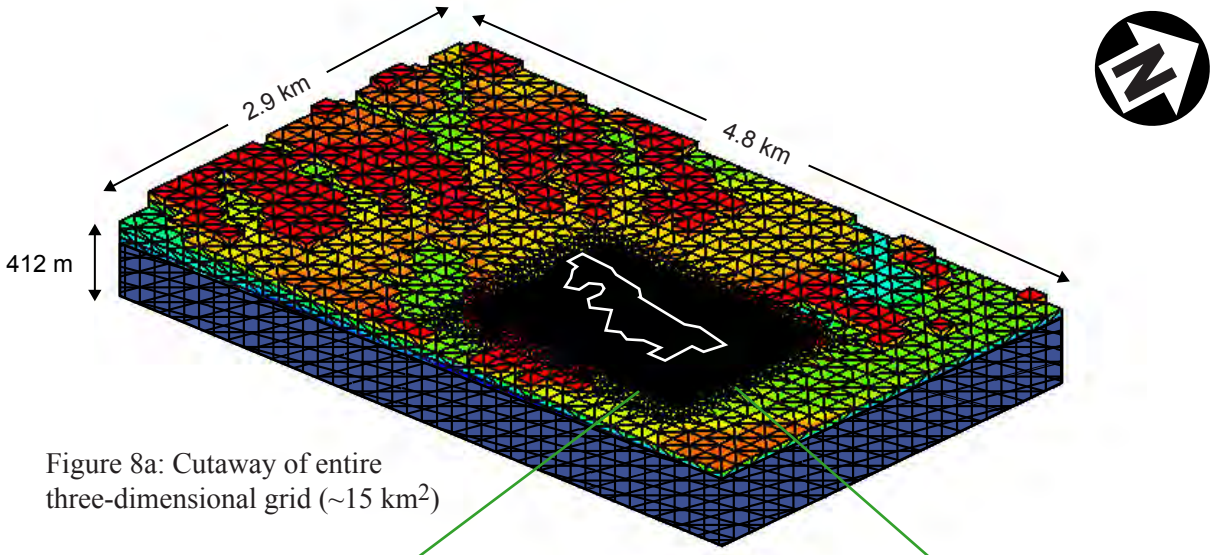

Figure 8a: Cutaway of entire three-dimensional grid (~15 km^2)

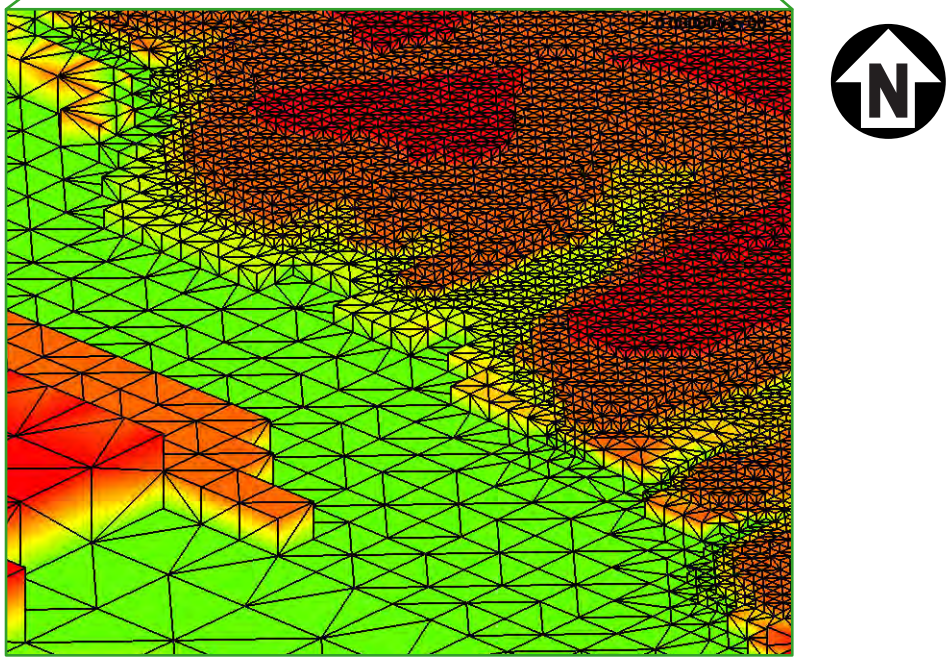

Figure 8b: Magnified view of southeastern portion of Material Disposal Area G. The largest grid squares (lower left) are 125 m x 125 m.

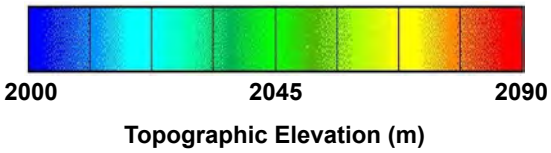

Figure 8
Horizontal Resolution of Numerical Grid Digital Elevation Model

The vertical resolution of the grid varies; the resolution is greatest in the vadose-zone and upper parts of the saturated zone where most contaminant transport is expected to occur, and decreases with depth below ground surface. In the vicinity of MDA G, a vertical resolution of 6.25 m (20.5 ft) is used to represent the Bandelier Tuff and the uppermost 50 to 70 m (160 to 230 ft) of the basalt. Below this, a two-step transition is applied, resulting in a vertical grid spacing of 37.5 m (123 ft) from the bottom of the high resolution region to approximately 1,000 m (3,300 ft) below ground surface, and a 150 m (490 ft) grid spacing at greater depths. To minimize boundary effects, the grid extends to an elevation of 100 m (330 ft) above msl. This is far below the surface of the water table, which lies at an elevation of 1,740 to 1,800 m (5,700 to 5,900 ft) above msl.

The 3-D grid relies on a 2003 update of the vadose-zone geologic model of MDA G and the surrounding area (see *Attachment II* for a complete description of the vadose-zone geologic model). This update represents the third major revision of the 3-D LANL site-wide geologic model since it was developed in 1996 and incorporates information collected from regional characterization wells that were drilled in the vicinity of MDA G from 2000 through 2003 (Figure 6). As a result, it is expected to more accurately represent actual geologic conditions. To illustrate, comparisons of predictions made using the 1996 geologic model (Vaniman et al., 1996) to the actual drilling logs from wells R-21 and R-22 show that the elevations at which unit contacts occur differ by 10 m (33 ft) or more in some instances. At R-22, for example, the top of the Cerros del Rio basalt was encountered approximately 13 m (42 ft) lower than that predicted using the 1996 model (Figure 9).

The updates to the geologic model have varied effects on the projected contaminant travel times near MDA G. The increased thickness of the Bandelier Tuff in the vicinity of MDA G (Figure 9), may imply longer travel times than predicted by the 1996 model. For a given infiltration rate, water moving through the tuff has a relatively long travel time when compared to the underlying basalt; thus, contaminants released in the vicinity of R-22 will reach the basalt more slowly than previously thought. On the other hand, unlike the 1996 model, the new geologic model does not include Puye fanglomerates, but does include a basalt layer that is 209 m (686 ft) thicker than in the previous model. Rates of contaminant transport within the basalt are expected to be rapid due its highly fractured nature. Because of this, the overall contaminant travel time to the regional aquifer may be shorter.

Table 2 compares the 3-D grid to actual data from well R-22, the only regional characterization well that lies within the high resolution section of the grid (6.25 m [20.5 ft] vertical resolution). The model stratigraphy and well data are good matches within this region, and within the 7.6 m (25 ft) resolution of the MDA G vadose-zone geologic model used to define the layer stratigraphy.

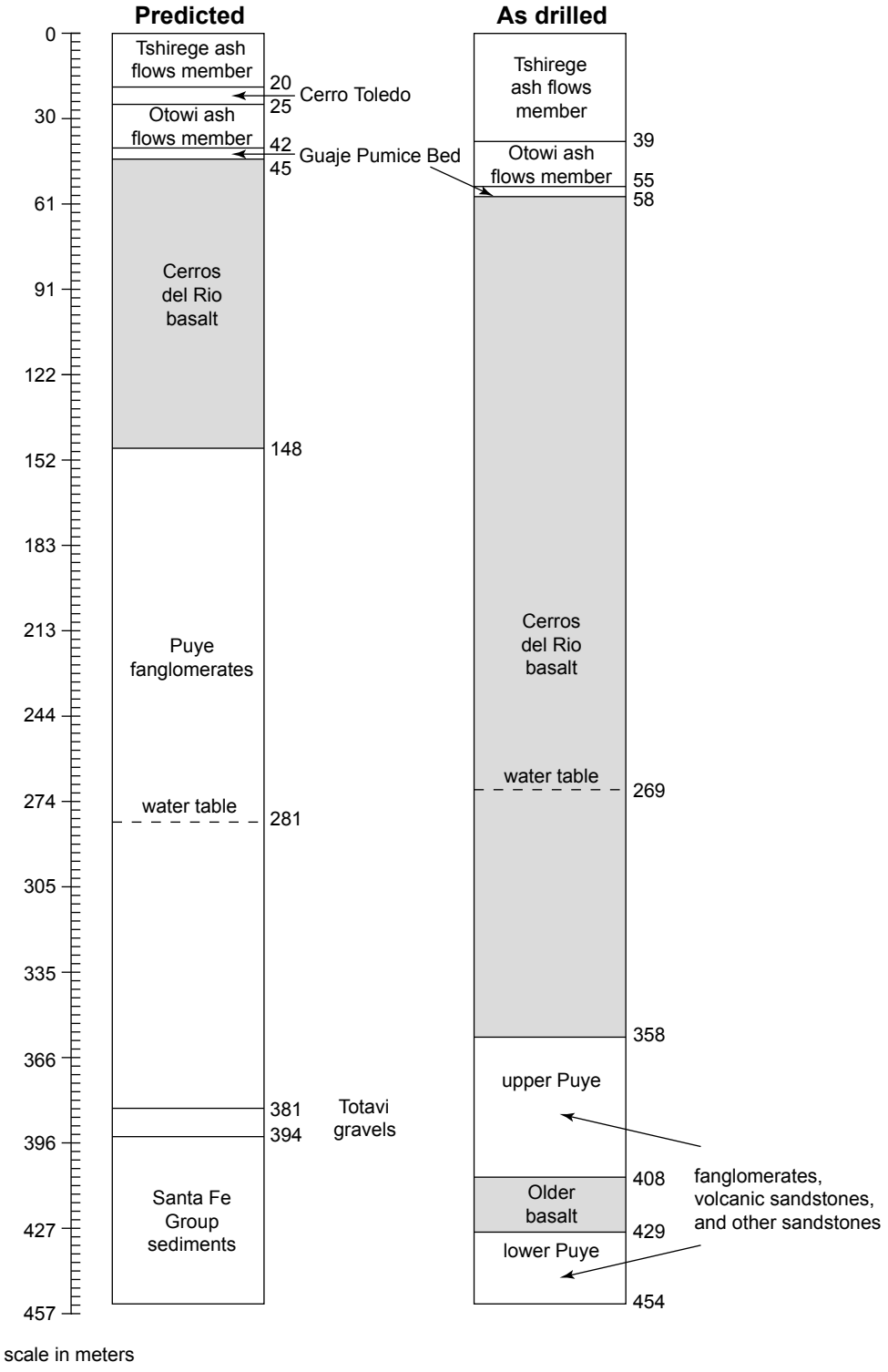

Figure 9
Comparison of Predicted to As-Drilled Stratigraphy at Regional Characterization Well R-22

Source: Ball et al. (2002)

Table 2
Comparison of As-Drilled Stratigraphy from Regional Characterization Well R-22 to Three-Dimensional Model Predictions

Geologic Unit Contact	Elevation above msl (m)		Difference (m) [a]
	As-Drilled	3-D Model	
Surface	2,027	2,025	2
Contacts within Bandelier Tuff			
Tshirege Member unit 2 and unit 1v	2,014	2,009	4
Tshirege Member unit 1v and 1g	2,004	2,003	1
Tshirege Member unit 1g and uppermost Otowi Member	1,988	1,984	4
Uppermost Otowi Member and Guaje Pumice	1,973	1,972	1
Contacts below Bandelier Tuff			
Guaje Pumice and Cerros del Rio basalt	1,969	1,966	4

msl = Mean sea level

[a] *Numbers shown in this column may vary from calculated differences between numbers shown in first two columns because of rounding.*

3.1.2 Model Configuration and Boundary Conditions

The 3-D site-scale model is used to trace the travel times of particles released from MDA G and to generate conservative breakthrough curves, otherwise known as residence time distribution functions (RTDs). Because the RTDs vary with release location and infiltration rate, the complexity of the model is reduced by adopting a number of assumptions and boundary conditions that constrain the groundwater transport model and simplify the modeling task.

To account for variations in particle travel times across MDA G, the facility was divided into eight discrete waste disposal regions, each representing an area where flow and contaminant transport behavior will be different. These variations occur because (1) the thickness of the Bandelier Tuff, which largely determines particle breakthrough behavior, increases from east to west, and (2) the differences in the depths of the disposal units influence particle travel time to the compliance boundary. Figure 10 shows the location of the waste disposal regions. Disposal regions 1 and 8 contain aggregates of pits and shafts with similar depths, while the remaining disposal regions contain either all pits or all shafts. Although the shafts in disposal region 6 are immediately adjacent to the shafts included in disposal region 1, region 6 is modeled separately because its shafts are significantly deeper than those in region 1. Similarly, the shafts in waste disposal region 7 are interspersed among the pits in region 3, but are modeled separately because of differences in depth. Figure 10 shows the approximate areas where large numbers of the region 6 and 7 shafts are located. Disposal region 8, west of the active portion of the disposal facility, is within the expansion area of MDA G referred to as Zone 4. The location shown in the figure for the disposal units in this region represents a reasonably conservative release point for the poorly constrained future contaminant releases from this site.

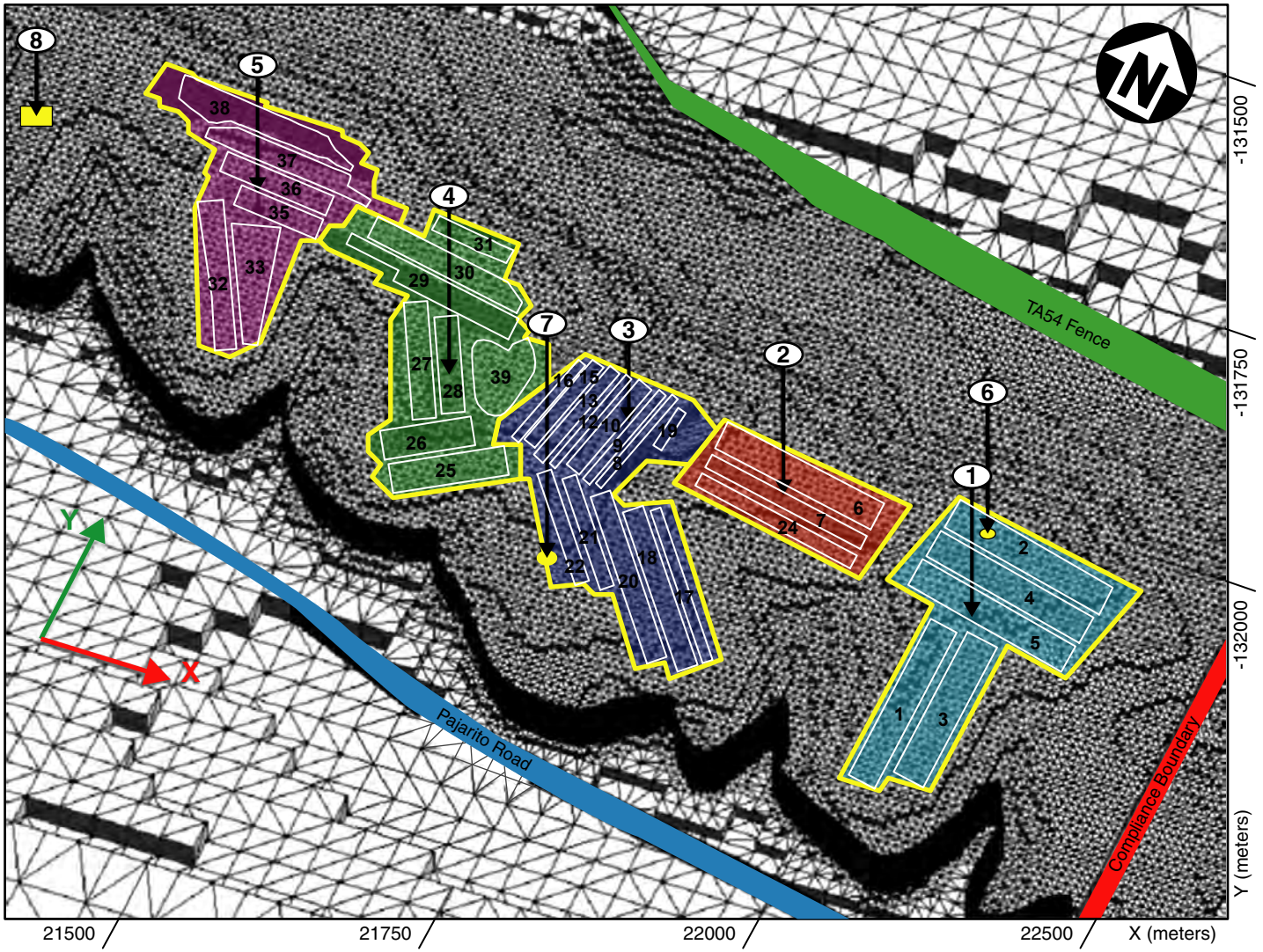

Figure 10
Waste Disposal Pits and Waste Disposal Regions Superimposed on the Numerical Grid

All of the waste disposal regions fall within the high-resolution portions of the 3-D model grid. This is shown in Figure 10, where each square in the figure corresponds to one node on the surface of the grid and the transition from high resolution to low resolution is apparent.

Table 3 provides the model coordinates for and a brief description of the pits and shafts included in each waste disposal region. The average bottom elevation of the disposal units in each region was calculated and used as the point of entry into the groundwater model for radionuclides leached from the waste. The controlling GoldSim model was responsible for estimating contaminant mass fluxes exiting from the bottom of each waste disposal region.

Particle breakthrough was specified relative to a vertical plane approximately 100 m (330 ft) east of the MDA G fence line. Figure 10 shows the compliance boundary plane in map view with respect to the numerical grid and the locations of the disposal pits.

Table 3
Particle Release Point Locations Representing the Eight Waste Disposal Regions

Waste Disposal Region	Grid Location Coordinates (m) [a]			Description
	East-West Axis (x-coordinate)	North-South Axis (y-coordinate)	Elevation above msl (z-coordinate)	
1	22,023	–132,148	2,024	Pits 1–5, shallow shafts near pit 2
2	21,820	-132,086	2,028	Pits 6,7,24
3	21,688	-132,125	2,032	Pits 8 through 22
4	21,500	-132,063	2,036	Pits 25 through 31, 39
5	21,281	-131,961	2,037	Pits 32 through 38
6	22,000	-132,047	2,015	Deep shafts near pit 2
7	21,656	-132,218	2,020	Deep shafts among pits 8 – 22
8	21,063	-131,938	2,038	Zone 4 pits and shafts

msl = Mean sea level

[a] Grid coordinates based on metric polar stereographic coordinates used in Española site-scale basin model (Keating, et al., 2003)

3.1.2.1 Infiltration

Long-term infiltration on the mesa is one of the primary uncertainties in simulations of contaminant transport from MDA G to the compliance boundary. For this study, it was assumed that MDA G will remain hydrologically similar to an undisturbed mesa-top site, especially after final closure. To capture the uncertainty in transport travel times through the unsaturated zone, a probability distribution that spans a reasonable range of infiltration rates was used. This distribution was based on data compiled in Springer and Schofield (2004), as described below.

Another uncertainty identified at the outset of this study was the effect of elevated infiltration in nearby canyons on the transport of contaminants from MDA G. The modeling performed to evaluate the potential impacts of canyon infiltration on the MDA G groundwater modeling is discussed at the end of this section.

Springer and Schofield (2004) compiled almost 200 mesa-top infiltration estimates from various modeling, field experiment, and chloride mass balance studies to estimate rates of infiltration. Their statistical analysis shows that the data are trimodal, with modal values around 0, 15, and 60 mm/yr (0, 0.59, and 2.4 in./yr) (Springer and Schofield, 2004, Fig. 4). In their analysis, Springer and Schofield indicated that infiltration rates greater than 10 mm/yr (0.39 in./yr) were typically associated with disturbed sites.

It is anticipated that the landfill cover designed for MDA G will behave at least as well as the undisturbed mesa top. Consequently, the probability distribution of infiltration rates adopted for the groundwater transport modeling considers infiltration values of 10 mm/yr (0.39 in./yr) or less. Figure 11 shows a normalized histogram of infiltration for undisturbed mesa tops in the general area of MDA G. This histogram was generated with the Springer and Schofield (2004) data by dividing the total samples in a given infiltration increment by the size of the increment. For example, there are 37 estimates in the 0 to 0.1 mm/yr (0 to 0.0039 in./yr) increment (yielding a normalized probability of about 0.37) and only 8 estimates in the 8 to 10 mm/yr (0.32 to 0.39 in./yr) interval (yielding a normalized probability of approximately 0.004).

This preliminary estimate of the probability distribution function for infiltration was used to determine the range of likely MDA G infiltration values. Ten infiltration rates spanning this range were identified and used to create a series of 3-D RTD breakthrough curves for releases from the 8 waste disposal regions. This resulted in the creation of 80 unique breakthrough curves that can be sampled from within GoldSim and used to generate the 1-D pipe pathways needed for calculating contaminant migration to the compliance boundary. In this approach, GoldSim samples the actual, continuous infiltration rate distribution during model simulations and selects the breakthrough curve that most closely corresponds to this rate within the waste disposal region under consideration. The discretization of the infiltration distribution in the manner described above provides a mechanism for considering the effects of variable infiltration rates on facility performance while maintaining model complexity at a reasonable level.

Potential groundwater-pathway risks are expected to be small during the 1,000-year compliance period at low rates of infiltration. However, at infiltration rates of 2 to 10 mm/yr (0.079 to 0.39 in./yr), the possibility for significant exposures within the compliance period increases substantially. Thus, although the infiltration probability distribution is heavily weighted toward values below 2 mm/yr (0.079 in./yr), an effort was made to include several discrete infiltration values at the upper end of the infiltration distribution because of the associated higher risk.

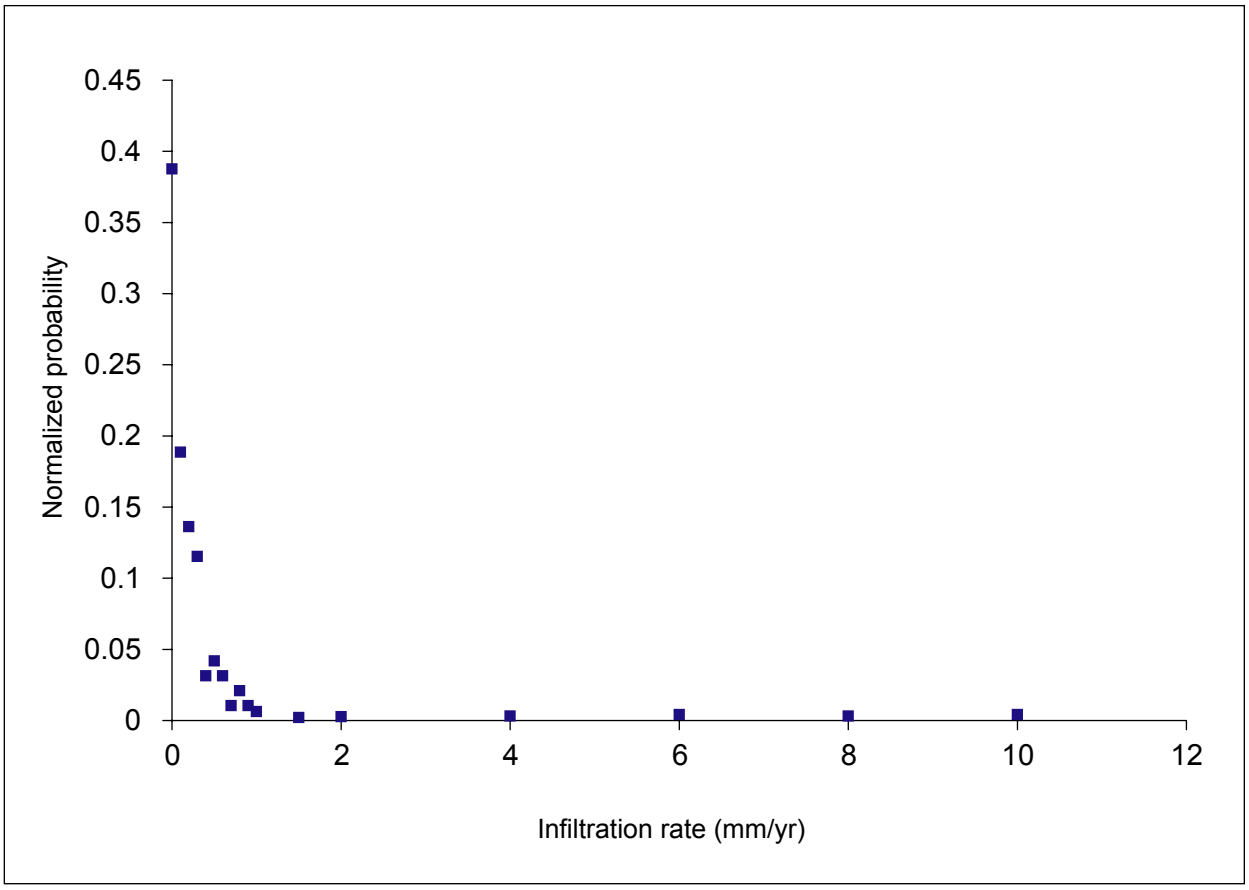

Figure 11
Normalized Histogram of Mesa-Top Infiltration Rates

Each infiltration, or mass flow, value (kg/yr) was assigned to every surface node within the numerical model. This value represents the product of the desired infiltration rate (mm/yr), the surface area over which infiltration occurs (m^2), and the density of water (1,000 kg/m^3 [62 lb/ft^3]). For example, if a node has a surface area of 1.0 m^2 (11 ft^2) and the desired infiltration rate is 1.0 mm/yr (0.039 in./yr), the infiltration value would be 1.0 kg/yr (2.2 lb/yr) or 3.2×10^{-8} kg/s (7.0×10^{-8} lb/yr). If a node was located along the edge of Mesita del Buey, only the area on top of the mesa was used to calculate infiltration; the mesa sides were assumed to have zero net infiltration.

High rates of infiltration in the canyons adjacent to MDA G may influence contaminant breakthrough times. Consequently, modeling was performed to determine how infiltration from nearby Pajarito Canyon — the wettest canyon in the vicinity of MDA G — should be considered in the groundwater pathway model. Kwicklis et al. (2005) estimated annual infiltration of 18.5 m^3/m (200 ft^3/ft) in the lower Pajarito Canyon. Using the Kwicklis et al. estimate as a guide, two cases were developed. The first case uses an annual infiltration of 6 m^3/m (65 ft^3/ft), which is based on an infiltration rate of 100 mm/yr (3.9 in./yr) over a 60-m (200-ft) wide, 3-km (1.9-mi) long stream channel). This case represents infiltration under conditions of high evapotranspiration, conditions that are expected to prevail in the canyon and that were not taken into account by the infiltration estimate provided by Kwicklis et al. (2005). The second case assumes no evapotranspiration and an annual infiltration of 24 m^3/m (260 ft^3/ft), based on an infiltration rate of 100 mm/yr (3.9 in./yr) over a channel width of 240 m (790 ft). For both cases, simulations were run using varied rates of infiltration over the rest of the model surface (i.e., "background" infiltration rates). The results of these simulations were compared to model projections based on infiltration rates that were constant across the entire model surface, including Pajarito Canyon.

3.1.2.2 Initial and Boundary Conditions

High capillary forces within the Bandelier Tuff lead to very low flow rates at the low-to-moderate saturations typical of the subsurface beneath mesas on the Pajarito Plateau. As discussed in Section 2.2, Birdsell et al. (1999) showed that evaporation could cause extremely high capillary forces resulting in the flow of water toward the surge bed. Although this hypothesis is supported by some data (Rogers et al., 1996) the result of implementing an internal evaporative boundary at the base of Tshirege Member unit 2 would be to stop transport below this horizon. This "dry barrier" hypothesis was not considered in the current study because the extent of this phenomenon has not been adequately addressed.

All lateral boundaries in the vadose zone were assumed to be no-flow boundaries, that is, no mass could enter or leave the system via these boundaries. Lateral gradients on these boundaries were not considered for two reasons. First, the simulation domain boundaries are located more

than a kilometer away from the MDA G fence line. Second, previous modeling studies of the Pajarito Plateau found the magnitude of lateral gradients in the unsaturated zone to be generally quite small (Birdsell et al., 1999; Stauffer et al., 2000).

Groundwater flow in all simulations was assumed to be from west to east following the water table gradient in the area. The gradient was fixed for all simulations and was based on a water table elevation of 1,798 m (5,900 ft) along the western boundary and 1,737 m (5,700 ft) to the east. These elevations yield an average gradient across the domain of approximately 0.013 m/m (0.042 ft/ft) toward the Rio Grande. This gradient, based on data from Stone et al. (1999) and more recent data from Keating et al. (2003), is expected to capture the general trend of flow near the water table.

Saturated zone pressure was fixed along both east and west boundaries such that a constant head is maintained on each of these faces. The northern and southern boundaries in the saturated zone are no-flow boundaries. This method ignores data reported by Keating et al. (2003) that indicates there may be downward vertical gradients as high as 0.10 m/m (0.33 ft/ft). Some controversy surrounds these data; one interpretation is that the gradients are caused by groundwater pumping while another postulates that deeper flow in the aquifer is confined with respect to flow near the water table. After discussions with Keating and other co-authors of the 2003 study, the second interpretation was adopted for this study, and no downward gradients were prescribed in the simulations. This is a conservative assumption because downward gradients would lead to increased mixing and lower concentrations in the saturated zone near any pumping well.

All groundwater flow simulations were performed at 20°C. This assumption assured that density and viscosity changes due to temperature were negligible.

3.1.3 Hydrogeologic Input Data

The hydrogeologic properties used in the modeling are presented in Table 4. These values are based on data from Springer (2005), Stauffer et al. (2005), and Birdsell et al. (1999 and 2000). The results of Springer's analysis (2005), described in Section 2.2, were used to identify the hydrologic properties for the Bandelier Tuff. Springer found that most hydrologic properties were not different for a given TA and hydrogeologic unit, which indicates that the values can be pooled within a TA. No consistent relationships were found among technical areas except for the residual water content, the value of which was essentially zero. Properties compared for mesa-top and canyon settings revealed limited consistencies in the Tshirege Member unit 1g and no consistency in the Otowi Member. A comparison of properties among hydrogeologic units showed that the hydrologic properties of Tshirege units 1v and 1g were essentially the same. On the basis of Springer's analysis, the hydrologic properties for the Bandelier Tuff used in this study are based only on measured data from TA-54.

Table 4
Hydrogeologic Properties Used for the Three-Dimensional Model

Geologic Unit	Bulk Density (kg/m^3)	Permeability (m^2)	Porosity	van Genuchten Parameters		
				s_r	α (m^{-1})	n
Tshirege Member unit 2	1.4E+03	2.0E–13	4.1E–01	2.4E–02	4.7E–01	2.1E+00
Tshirege Member unit 1v	1.2E+03	1.2E–13	4.9E–01	6.0E–03	3.6E–01	1.7E+00
Tshirege Member unit 1g	1.2E+03	1.5E–13	4.6E–01	2.2E–02	5.E–01	1.8E+00
Cerro Toledo interval	1.2E+03	1.8E–13	4.5E–01	7.0E–03	1.3E+00	1.5E+00
Otowi Member above Guaje Pumice	1.2E+03	2.3E–13	4.4E–01	4.3E–02	5.9E–01	1.8E+00
Otowi Member Guaje Pumice	8.0E+02 [c]	1.5E–13 [a]	6.7E–01 [a]	0.0E+00 [a]	8.1E–02 [a]	4.0E+00 [a]
Cerros del Rio basalts vadose zone	2.7E+03	1.0E–12 [b]	1.0E–03 [b]	1.0E–03 [a]	3.8E+00 [a]	1.5E+00 [a]
Cerros del Rio basalts saturated zone	2.7E+03	1.0E–12 [b]	5.0E–02 [c]	NA	NA	NA

SOURCE: All data represents mean values from Springer (2005) unless otherwise noted

Numbers are rounded to two significant digits

NA = Not applicable

[a] *Birdsell, et al., 1999 and 2000* [b] *Stauffer, 2005* [c] *Estimated in this report*

The Springer data represent mean values determined through the statistical analysis described in *Attachment III*, in which Springer calculated descriptive statistics and correlation properties for geologic units and all data. Retention data by geologic unit and across the Bandelier Tuff were pooled and fitted to Equation 1 in *Attachment III* to provide additional estimates of the hydrologic parameters. In some cases the values used in model simulations are slightly different than those listed in *Attachment III* because the modeling was performed before the final draft of the statistical analysis was completed.

The hydrogeologic properties adopted for the groundwater modeling differ somewhat from the properties used in earlier modeling efforts (Birdsell et al., 1995, 1999, and 2000). However, the overall characteristics of the geologic units remain the same. For example, the vadose-zone basalt permeability and porosity values used for the model were adopted from Stauffer et al. (2005), and are conservative estimates that yield the fastest travel times. These new properties are more defensible than those used previously; however, the general behavior of this rock unit is unchanged. Travel times through the basalt remain quite low, and this unit has little impact on the total travel times of contaminants from the source region to the groundwater pathway compliance boundary.

A permeability reduction factor of 0.01 was set at the top of the basalt. This permeability reduction factor is not as low as that set by Robinson et al. (1999) (see Section 2.2) because

R-22, the deep borehole drilled just to the east of MDA G, showed no perched water at this location (perched water was noted at the location studied by Robinson et al.). Thus, the higher value was selected because it yielded increased saturations in the overlying few meters of the Bandelier Tuff, but did not result in ponding during the simulations. Also, a permeability reduction of 0.1 was included at the base of the Tshirege Member unit 1g unit after examining data from borehole R-32. This reduction allows increased saturations when infiltration is high, for example, in wetter canyon bottoms.

Values for some of the hydrogeologic properties used in the modeling were estimated because of an absence of reported values in the literature. The Guaje Pumice is a high-silica basal pumice within the Otowi Member of the Bandelier Tuff (Broxton and Reneau, 1995). The bulk density of this unit was estimated to be 890 kg/m^3 (56 lb/ft^3) using a grain density for the silica of approximately 2,700 kg/m^3 (170 lb/ft^3) and a reported mean porosity of 0.667 (Birdsell et al., 1999 and 2000). The effective porosity of the basalt below the water table is expected to be greater than that in the vadose zone (i.e., the water in the saturated zone encounters more flow paths). The basalt within this region was assigned a porosity of 0.05 based on massive basalt porosity values found in the literature (Doughty, 2000) and discussions with Dr. V. Vesselinov at LANL (2004), whose unpublished work, conducted in conjunction with the work by Keating et al. (2003), supports this value.

The groundwater pathway modeling adopted an approximate mean value of the longitudinal dispersivity for modeling flow and transport within the vadose zone. A dispersivity of 2 m (7 ft) was used throughout the model domain except for a section of the basalt in which the vertical resolution of the grid changes (see *Attachment I*). Dispersivity in the octree mesh refinement (OMR) grid area was set to zero because, at the time the modeling was performed, coding limitations precluded the application of dispersion across OMR sections (this code limitation has since been corrected). Setting dispersivity to zero in the OMR section will have little impact on the breakthrough times at the compliance boundary because particle velocities in the basalt are high and travel times are very low through this part of the grid.

3.1.4 Model Simulations

The 3-D site-scale model was used to trace the travel times of particles released from MDA G and to generate conservative breakthrough curves. Because each particle has a random component that determines its pathway through the complex 3-D grid, thousands of particles must be released at the same time and at the same surface location to create an RTD (see Section 3.1.2 for a discussion of the selected release points). The RTD basically shows the probability that a given particle will arrive at the compliance boundary in a given amount of time. Particle tracer simulations were also run to determine appropriate dispersivity values and to predict how contaminants might be captured by a nearby groundwater well. All simulations of contaminant

transport assumed steady-state flow throughout the domain. To generate a steady-state flow field, simulations were run with constant boundary conditions for 2.5 million years.

3.1.4.1 Conservative Breakthrough Curves

Conservative RTDs of particle breakthrough at the compliance boundary were generated for each waste disposal region by releasing over 3,000 particles instantaneously from eight 1-m^3 (35-ft^3) volumes. The volumes were centered on each of the release locations listed in Table 3. A sensitivity analysis was performed to ensure that the size of the release area centered on a given disposal region did not affect the RTD. The results of this analysis, shown in Figure 12, indicate that there was little difference in RTD values even when the size of the release area was increased by a factor of 4.

Previous simulations of transport beneath MDA G used the advection-dispersion equation to solve for tracer concentrations and were strongly affected by numerical dispersion (Birdsell et al., 1999). For the 3-D simulations presented in this study, particles were chosen to simulate transport because they are not affected by numerical dispersion (Lichtner et al., 2002). Another benefit associated with using particles is that their exact position in the numerical grid is known at all times, allowing very accurate tracer pathways to be analyzed. Particle tracking is also much faster than the traditional finite-element implementation of the advection-dispersion solution. Particle-tracking simulations were implemented using the *sptr* macro in FEHM (Dash, 2003).

3.1.4.2 Longitudinal Dispersivity

Several simulations were conducted to estimate suitable values of longitudinal dispersivity within the vadose zone. Disposal region 5, the westernmost waste disposal region in the active portion of MDA G, was chosen as the release point because particles released there must travel a greater distance to the compliance boundary than those from most other regions. As a result, particles from region 5 should be more prone to dispersivity effects.

The range of longitudinal dispersivities considered in the evaluation was selected on the basis of work conducted by Neuman (1990) and Gelhar et al. (1992) that shows longitudinal dispersivity increasing with the length of the flow path. Gelhar et al. found that the maximum expected longitudinal dispersivity is approximately one-tenth the total flow path length. Although the Gelhar et al. results pertained to saturated systems, they were applied to this study because there are no similar vadose-zone dispersion studies. Particle breakthrough at MDA G is controlled by the travel time through the Bandelier Tuff because flow in the basalt is very rapid relative to flow in the tuff. This means that the expected flow path length is approximately 60 m (200 ft). Since dispersivity is generally expected to be lower in the vadose zone than in the saturated zone, 6 m (20 ft), or one-tenth of the 60 m (200 ft) flow path length, was used as an upper limit for vadose-zone longitudinal dispersivity. On this basis, the sensitivity analysis explored how changes in dispersivity ranging from 1 m to 6 m (3.3 to 20 ft) affected model behavior.

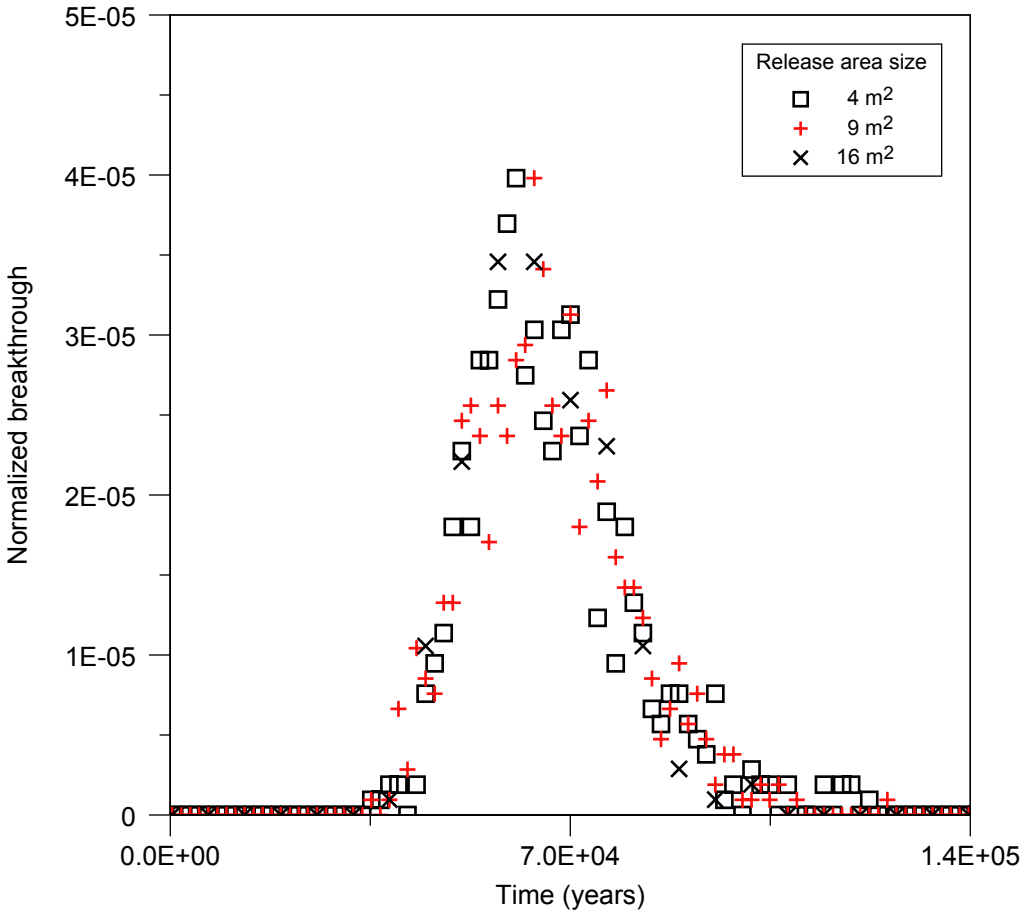

Figure 12
Sensitivity Analysis of Particle Breakthrough to Size of Release Area at Waste Disposal Region 5 (0.1 mm/yr background infiltration)

3.1.4.3 Well Capture

The groundwater-pathway modeling estimates the contaminant-specific mass that crosses the compliance boundary 100 m (330 ft) downgradient of the MDA G fence line. Only a portion of the mass that crosses this boundary would, in fact, be captured by a domestic well and contribute to the exposure projected for the individual using the well. Simulations were performed to estimate the size of the capture zone and, in so doing, the capture efficiencies for a hypothetical nearby well.

The hypothetical well, which was assumed to supply a single household, was assumed to be located at the compliance boundary, 100 m (330 ft) directly downgradient (east) of MDA G. The radius was set at 0.125 m (0.41 ft) and the screen interval was assumed to extend downward 37.5 m (123 ft) from the top of the water table. A range of pumping rates was used to estimate the size of the well's capture region; these rates were 50, 600, 1,200, and 2,500 m^3/yr (1.3×10^4, 1.6×10^5, 3.2×10^5, and 6.6×10^5 gal/yr). An infiltration rate of 10 mm/yr (0.39 in./yr) was assumed and a steady-state flow field was established with the pumping well in place.

To determine the radius of influence, simulations introduced particles along a line source that was situated 100 m (330 ft) upgradient of the well and at an elevation corresponding to the midpoint of the well screen interval, or nearly 19 m (62 ft) below the top of the water table. The particles were released at a closer spacing than the pit node distribution so that the well radius of influence could be determined to within hundredths of a meter.

Capture efficiencies, or the fraction of contaminant released from the disposal facility that is intercepted by the well, were also estimated for each waste disposal region. The pumping well was fixed for all simulations at approximate grid coordinates of x = 22,000 m, y = –132,000 m, and z = 1,750 m. Ten particles were introduced at every x-y grid location corresponding to a disposal unit node. Because the capture efficiency relies mainly on the number of particles coming from directly upgradient of the well, the disposal units were shifted along the y-direction so that the maximum east-west point density was aligned with the pumping well. To do this, the release points from each disposal region were first binned into groups with the same north-south (y) coordinate, then the east-west (x) section with the most points was shifted to align with the pumping well. The locations were mapped vertically to the midpoint of the pumping well (i.e., 19 m [62 ft] below the water table) and the effect of transverse dispersivity (the amount of spread perpendicular to the direction of travel**)** on particle capture was evaluated using dispersivities ranging from 0 to 10 m (0 to 33 ft). Figure 13 shows the adjusted alignment for the release from waste disposal region 5. Capture efficiencies were calculated separately for all waste disposal regions except regions 6 and 7, to account for the regions' unique geometries. Regions 6 and 7 were assumed to have capture efficiencies equal to those of regions 2 and 3, respectively.

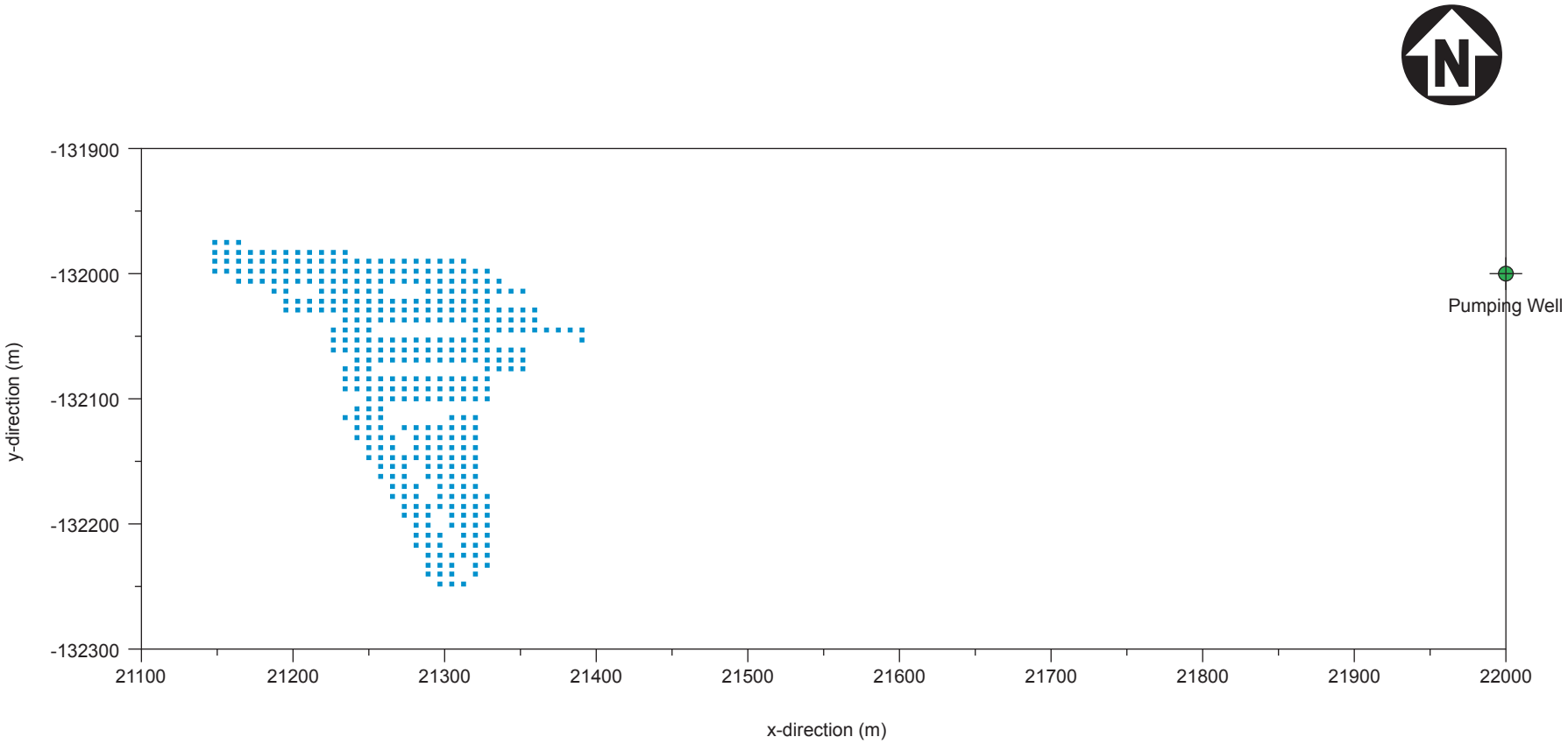

■ = Node within disposal unit

Note: Well location is fixed for all simulations at x=22,000 m, y= -132,000 m, and z = 1,750 m; release points have been shifted so that the maximum east-west point density is directly west of the pumping well. Release points are approximately 19 m below the water table surface.

Grid coordinates (m) based on polar stereographic projection used for Española basin site-scale model (Keating et al., 2003)

Figure 13
Distribution of Particle Release Points for Waste Disposal Region 5 (well capture simulation)

The finite vertical resolution of the 3-D numerical grid causes two vertical steps in the grid cells that represent the water table (shown in Figure 14). The easternmost step occurs just past the compliance boundary and causes the particles to dive deeper into the saturated zone in an unrealistic fashion near the hypothetical well. Because the well's screened interval extends only 37.5 m (123 ft) downward from the top of the water table, this discontinuity in the water level can lead to low calculated capture efficiencies. The shift in the x-direction was made to ensure that the step in the simulated water table did not reduce the well capture efficiency. This shift does not affect the analysis because all nodes below the water table are in homogeneous basalt and the gradient used for the analysis is fixed and linear from west to east.

Table 5 presents the transformed values for both the x-direction (east-west) and y-direction (north-south) shifts that were applied to every particle from a given disposal region. As explained, the north-south shift was made to ensure that the well was aligned with the greatest density of particles along the line source. The shift from east to west was made to ensure that the step in the grid due to the change in vertical resolution did not reduce the well capture efficiency.

Table 5
Transformed Values for Shift of Tracer Particle Release Points [a]

	Horizontal Shift (m) [b]		Path Length to Well (m) from Region	
Waste Disposal Region	X-Direction	Y-Direction	Shortest (from eastern boundary)	Longest (from western boundary)
1	–250	94	109	304
2	–250	62.5	328	515
3	–250	203	421	680
4	–250	–23.5	656	900
5	–250	–125	855	1101
8	–250	–57	1120	1468

[a] *All particles were released at an elevation of 1,750 m above mean sea level*

[b] *Represents change from original x or y coordinate; a negative change in the x-direction represents a shift to the west and a negative change in the y-direction represents a shift to the south.*

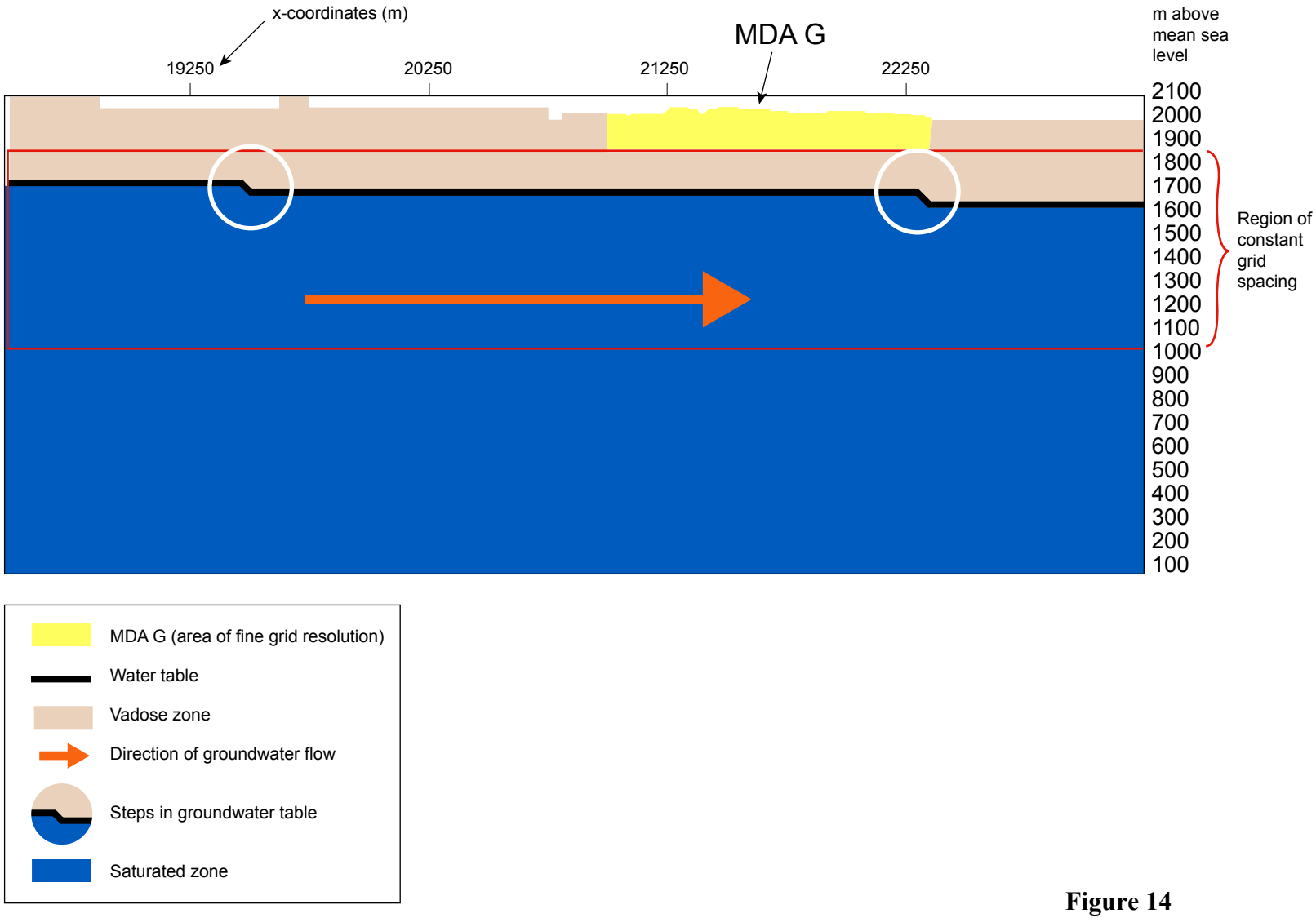

Figure 14
Cross Section of Numerical Grid Showing Vertical Steps in Water Table

3.2 Model Abstraction

The 3-D site-scale model takes significant time and computer memory to run. Consequently, an approach was developed to reduce the FEHM model complexity while retaining the overall characteristics of the transport simulations. The theory of micromixing (Robinson and Viswanathan, 2003) was used to reduce complex 3-D simulations to 1-D abstractions that recreate particle breakthrough at the compliance boundary, while retaining the ability to modify the bulk transport properties of the subsurface for all radionuclides undergoing groundwater transport. The development of these 1-D abstractions provided the means for incorporating the groundwater pathway model directly into the GoldSim model that was used to project long-term performance of the disposal facility.

To support the development of the 1-D abstractions, the FEHM model was modified so that GoldSim controls the contaminant mass flux, the specified surface infiltration, and the bulk transport properties (i.e., sorption parameters) used in the groundwater pathway modeling. As implemented for the performance assessment and composite analysis, the FEHM model recreates an approximation of the complex 3-D RTD on a simple 1,000-node, 1-D grid using the algorithm described in *Attachment IV*. GoldSim calls eight separate FEHM simulations, each of which corresponds to a waste disposal region, and passes the appropriate data to FEHM. Using these data, FEHM calculates the mass of each radionuclide crossing the compliance boundary as a function of time, and passes the results back to GoldSim. Details of the coupling between GoldSim and FEHM, with information about the directory structure and examples of input structure and code, are included in *Attachment V*. Specialized codes used to create the 1-D abstraction are described in more detail in *Attachment VI*.

The 1-D abstraction grid uses the advection-dispersion formulation of the transport equations (Zyvoloski et al., 1995a) to simulate tracer movement. As explained in *Attachment IV*, this allows simulation of both sorption and radioactive decay, processes that are important for estimating the breakthrough of the multiple species that may be released into groundwater from the pits and shafts at MDA G.

To mimic the instantaneous release of particles used in the 3-D simulations, many small time steps, each with a single pulse input of tracer mass, must be used by GoldSim for the 1-D simulations. It was found that a time step equal to one one-thousandth of the simulation period results in convergence between the 3-D and 1-D breakthrough curves. Thus, for a 5,000-year simulation, a GoldSim time step of 5 years is used to recreate an instantaneous release of particles moving from the mesa top to the compliance boundary.

4.0 Results

This section presents the results of the groundwater modeling efforts. Section 4.1 summarizes breakthrough at the compliance boundary and Section 4.2 describes the results of well capture simulations. The overall results obtained from the 1-D and 3-D models are compared in Section 4.3.

4.1 Breakthrough at the Compliance Boundary

All breakthrough plots presented in this report show normalized breakthrough. Thus, the number of particles crossing the compliance boundary during a given time interval is divided by both the time increment and the total number of particles that reach the boundary, such that the integral of the area under the curve is 1 for all plots. Figure 15 shows typical particle pathways through the complex 3-D model domain for contaminants released from waste disposal region 5; pathways are shown in the z (vertical), x (east-west), and y (north-south) directions. Results for high- (10 mm/yr [0.39 in./yr]) and low- (0.1 mm/yr [0.039 in./yr]) infiltration cases are included.

Particles move downward from the bottom of the disposal units to the regional aquifer; as seen in Figures 15a and 15b, the particles do not move far in the x-direction (eastward) during this transit. Once in the aquifer, the particles move eastward toward the compliance boundary. Because lateral transport in the vadose zone is relatively minor, any particles that cross the boundary do so in the saturated zone. The particles appear to drop suddenly just east of the compliance boundary because the grid spacing at this elevation creates a step in the surface of the water table. However, all transport to the compliance boundary occurs before this step. Also, once the particles reach the saturated zone, they travel more quickly and the extra drop in elevation does not add significant travel time.

Figures 15c and 15d show that, for both high- and low-infiltration cases, particles are diverted to the south within the Guaje Pumice, which lies directly over the basalt at an elevation of about 1,960 m (6,420 ft) above msl. For the low-infiltration case (Figure 15d), the particles disperse more than 100 m (330 ft) laterally by the time they reach the water table. The southward spreading in the vadose zone occurs when the particles enter the water pooled at the top of the Cerros del Rio basalt at a depth of approximately 1,960 m (6,430 ft). The particles then take a variety of pathways following the water flow, which lead south. Once they drop through the zone of permeability reduction, the particles travel downward to the water table then eastward to the compliance boundary. Figures 15e and 15f provide a view of particle movement in both horizontal directions (x,y) for high- and low-infiltration cases.

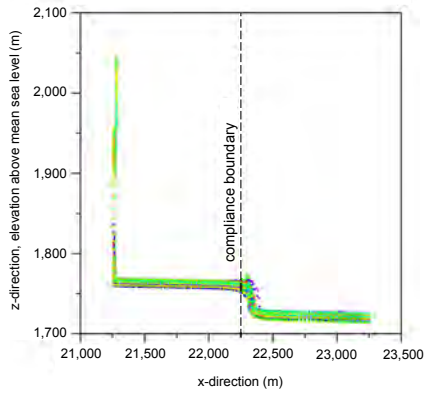

Figure 15a: Movement in x and z directions with high infiltration (10 mm/yr)

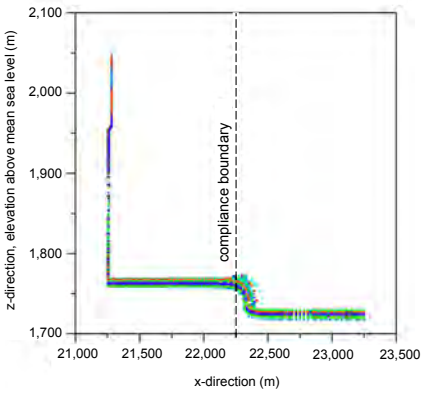

Figure 15b: Movement in x and z directions with low infiltration (0.1 mm/yr)

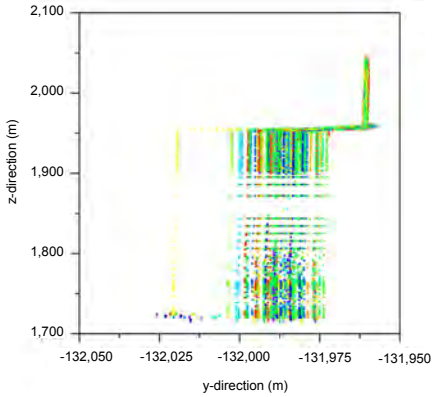

Figure 15c: Movement in y and z directions with high infiltration (10 mm/yr)

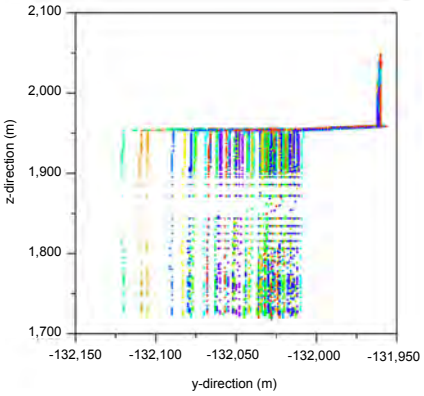

Figure 15d: Movement in y and z directions with low infiltration (0.1 mm/yr)

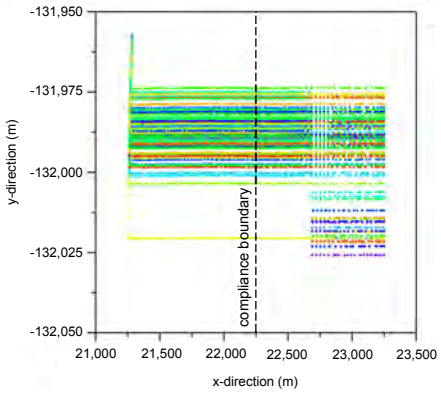

Figure 15e: Movement in x and y directions with high infiltration (10 mm/yr)

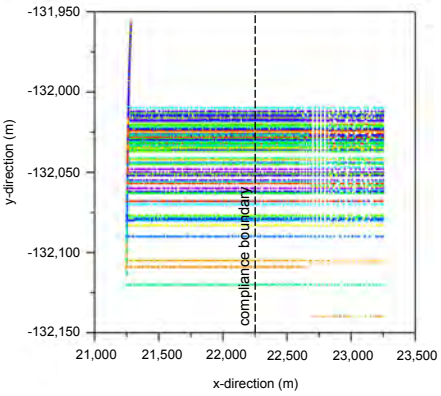

Figure 15f: Movement in x and y directions with low infiltration (0.1 mm/yr)

Grid Coordinates based on polar stereographic projection
used for Española basin
site-scale model (Keating et al., 2003)

Figure 15
Two-Dimensional Views of Pathways for Particles Released from Waste Disposal Region 5 (high- and low-infiltration rates)

Figure 16 shows conservative breakthrough curves at the compliance boundary for particles released from each of the eight disposal regions. The background infiltration rate for this example is 0.5 mm/yr (0.2 in./yr). Waste disposal region 6, consisting of a cluster of deep shafts located near the eastern boundary of MDA G, has the fastest breakthrough, beginning at 5,000 years and peaking at around 1.25×10^4 years. The arrival of releases from disposal region 1 is slightly slower, which is to be expected because of the higher elevation of the release points within this region (Table 3). Disposal regions 5 and 8, located to the west, show much slower breakthrough times, beginning at around 9,500 years and peaking at about 1.8×10^4 years. Releases from the disposal regions in the central portion of MDA G generally show increased time to breakthrough as the distance from the compliance boundary to the disposal region increases.

Figure 17 shows the conservative breakthrough curves for releases from the eight disposal regions at a background infiltration rate of 10 mm/yr (0.39 in./yr); this infiltration rate is the upper limit of the probability distribution used for infiltration (as shown in Figure 11). The relative breakthrough for the different regions is similar to the situation noted above for an infiltration rate of 0.5 mm/yr (0.2 in./yr); however, at the higher infiltration rate, the first breakthrough occurs for disposal region 6 in less than 500 years, with peak breakthrough at about 750 years. Travel time within the saturated zone is brief compared to travel time in the vadose zone. Assuming an aquifer velocity of 70 m/yr (230 ft/yr), the travel time from the point at which particles discharge to the aquifer to the compliance boundary is approximately 2 years.

4.1.1 Effects of Changes in Permeability and Infiltration

Figure 18 shows how interface permeability reductions affect subsurface saturations; a high infiltration rate of 10 mm/yr (0.39 in./yr) was chosen to more clearly demonstrate the effect. The permeability reduction at the base of unit 1g results in an increase in saturation of 10 percent in the lower part of unit 1g, while the permeability reduction at the top of the basalt yields an increase in saturation of only 2 percent in the lower few meters of the Otowi Member of the Bandelier Tuff. Figure 19 shows how the reduced permeability interfaces impact conservative tracer breakthrough at the compliance boundary for particle releases from waste disposal regions 1 and 5 at an assumed background infiltration of 10 mm/yr (0.39 in./yr). For this figure, the assumed infiltration rate in Pajarito Canyon is 100 mm/yr (3.9 in./yr).

Interestingly, breakthrough from disposal region 1 was slightly faster at a reduced permeability. This is because the 3-D geometry causes variable subsurface fluxes, despite an average infiltration rate throughout the domain of 10 mm/yr (0.39 in./yr). Particles released from disposal region 5 behaved as expected, with the reduced permeability scenario leading to a slightly retarded breakthrough. Interface permeability reductions had fairly minor impacts on predicted travel times and were included in all subsequent simulations.

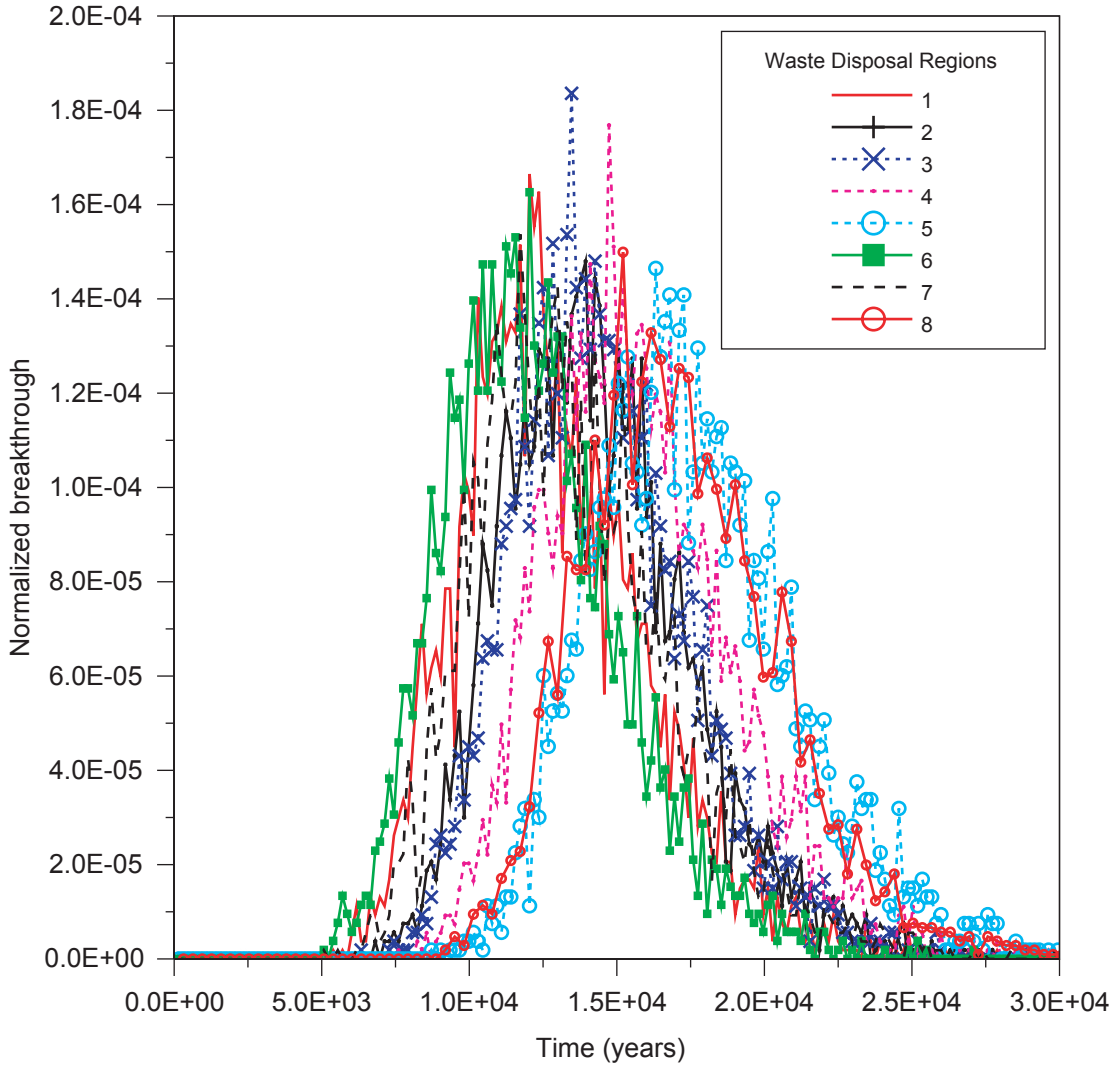

Figure 16
Breakthrough Curves for Particles Released from All Waste Disposal Regions (background infiltration of 0.5 mm/yr)

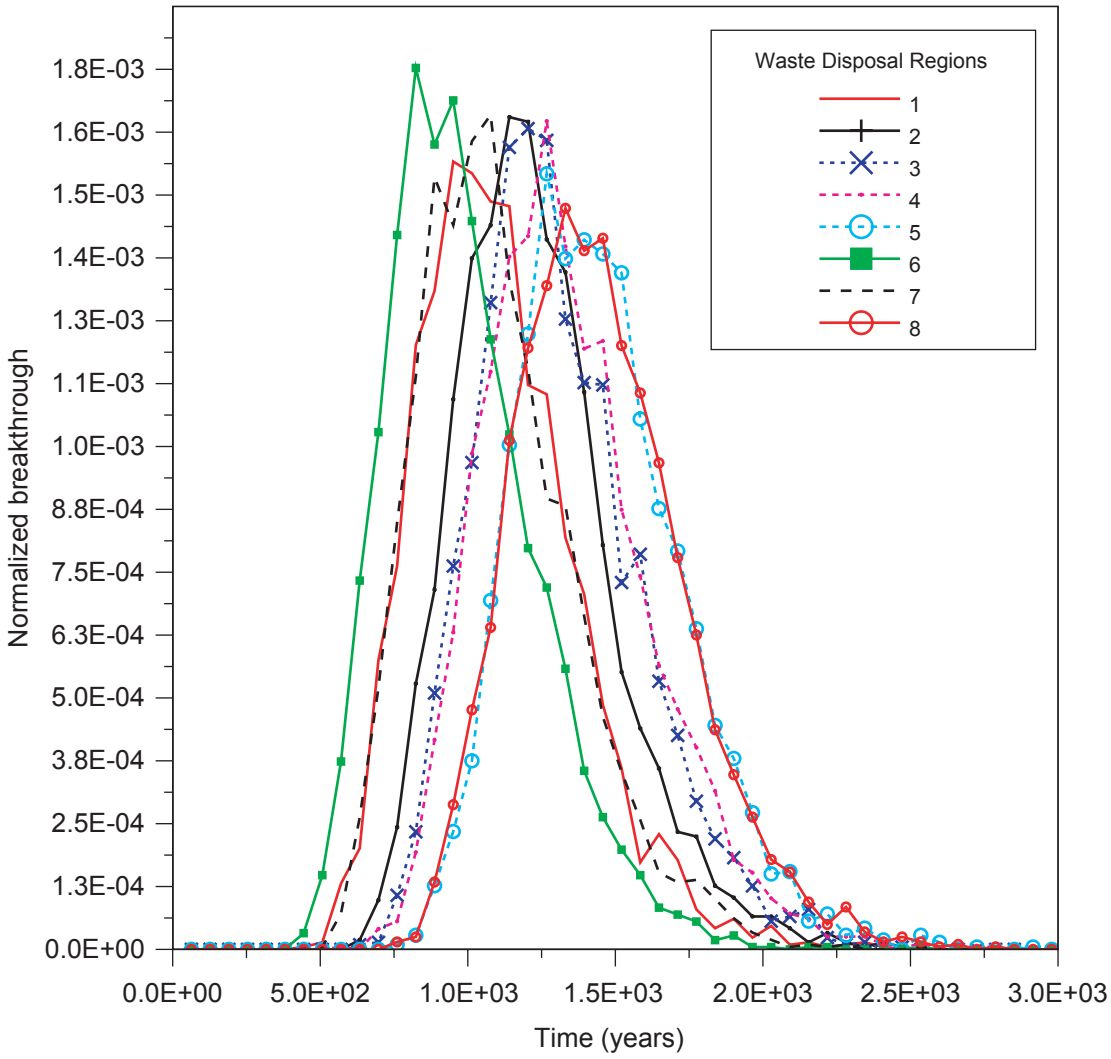

Figure 17
Breakthrough Curves for Particles Released from All Waste Disposal Regions (background infiltration of 10 mm/yr)

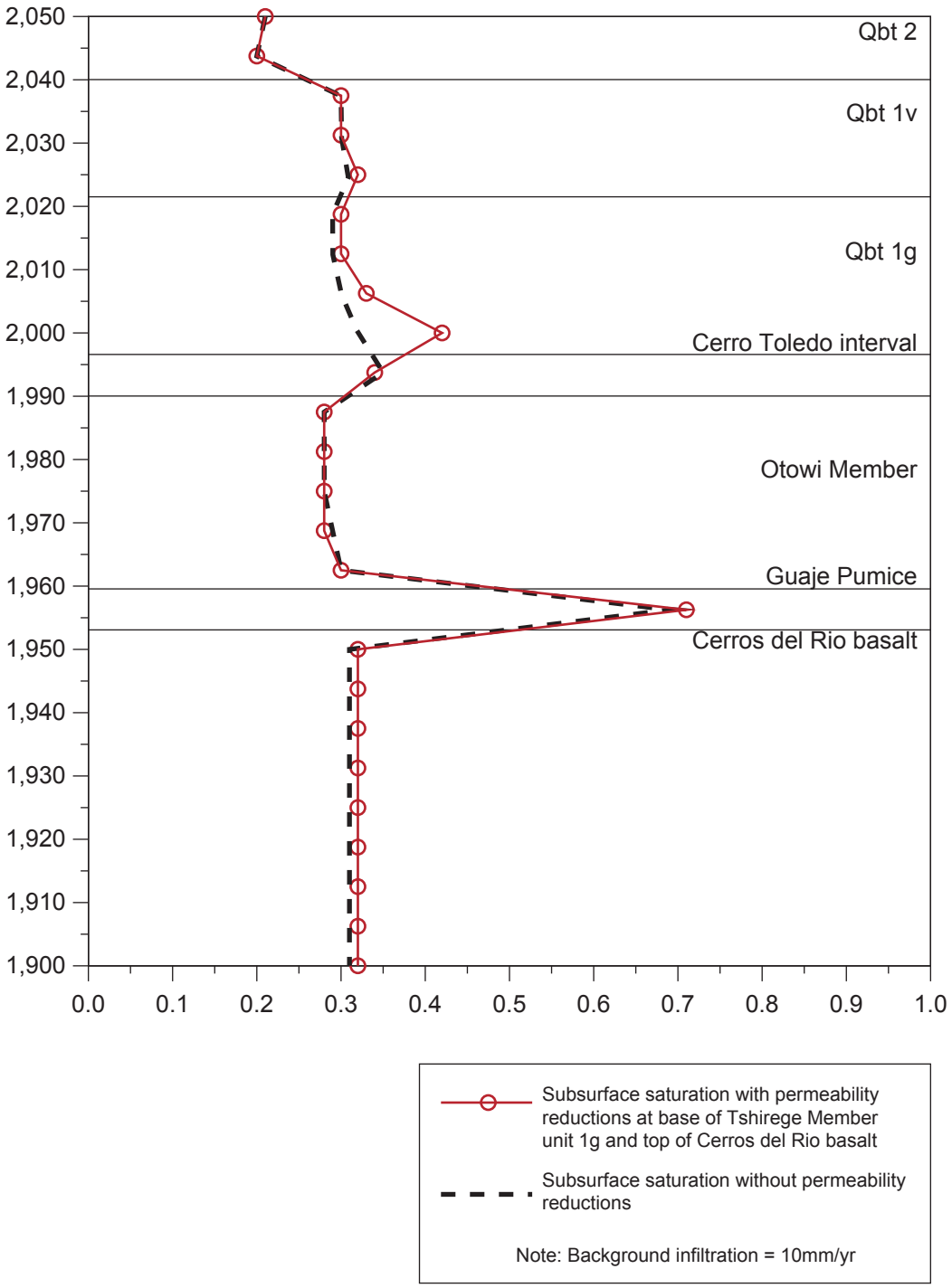

Figure 18
Effect of Permeability Reductions on Subsurface Saturation at Waste Disposal Region 5

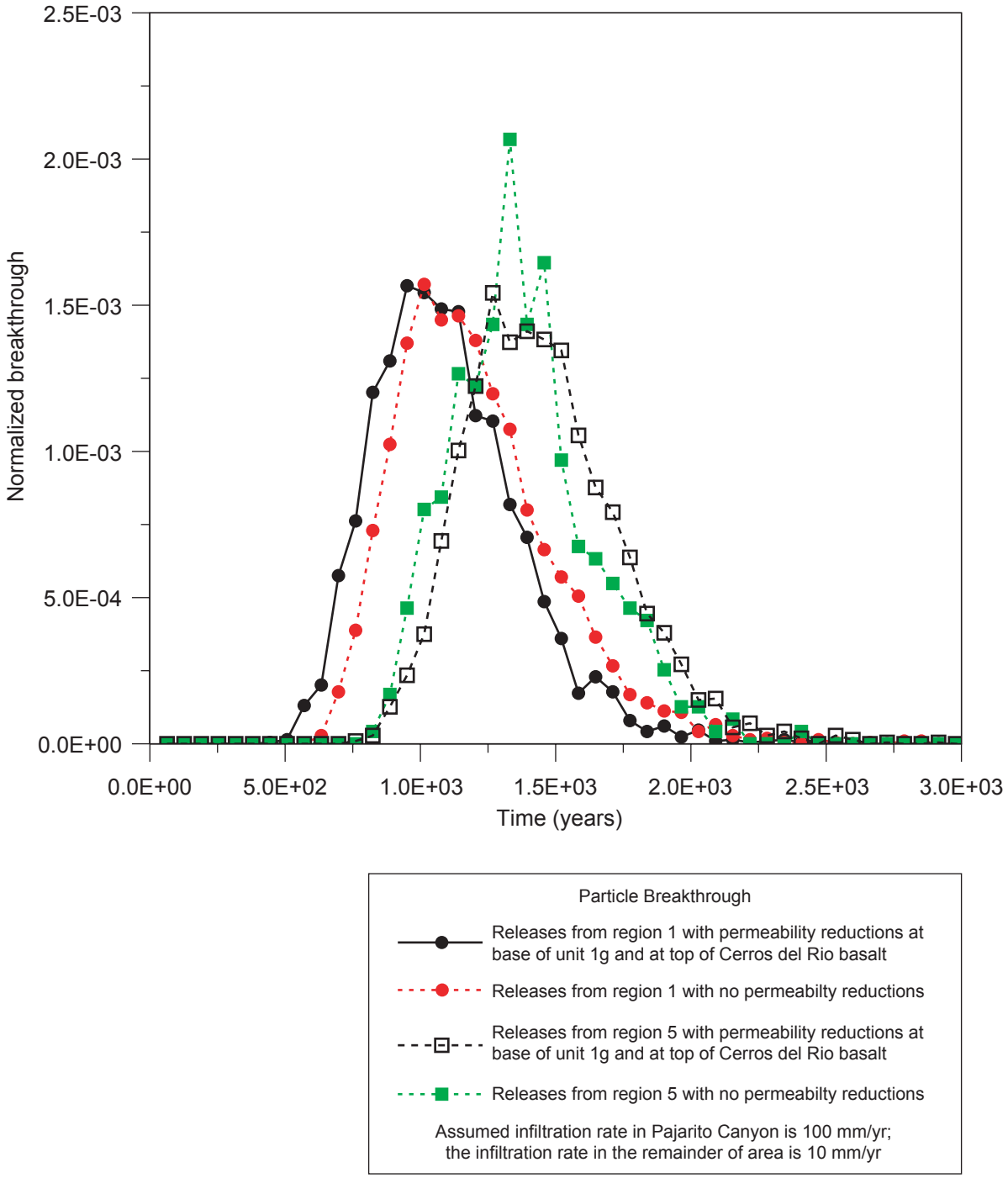

Figure 19
Effect of Permeability Reductions on Breakthrough for Releases from Waste Disposal Regions 1 and 5

As seen in Figure 20, an increase in the rate of infiltration yields higher in-situ saturation. At a net infiltration of zero, saturations beneath MDA G are below 10 percent in all units. As infiltration increases to 10 mm/yr (0.39 in./yr), the effect of the permeability reduction at the base of unit 1g is seen. Also, because of its material properties, the Guaje Pumice accumulates more water as infiltration increases. The behavior seen in these simulations spans the range of in-situ saturations reported in Birdsell et al. (1999), who also report that no single infiltration rate can reproduce moisture content data from individual boreholes. Birdsell et al. (1999) suggest that mesa-top infiltration has changed over time, perhaps in response to climate and rainfall changes.

Figure 21 shows the steady-state simulated surface saturation for increased Pajarito Canyon infiltration of 6 m^3/m (65 ft^3/ft) over a width of 60 m (200 ft) (see Section 3.1.2.1). Steady-state saturation profiles beneath waste disposal region 5 illustrating the effect of increased annual Pajarito Canyon infiltration of 6 m^3/m (65 ft^3/ft) for two different assumed background infiltration levels are shown in Figure 22. When the rate of infiltration on the surrounding mesas and canyons is low (0.1 mm/yr [0.0039 in./yr]), an infiltration rate of 100 mm/yr (3.9 in./yr) across a 60-m (200-ft) channel clearly affects saturations in the Guaje Pumice. However, saturation levels change very little when the background infiltration rate in areas surrounding Pajarito Canyon is increased to 0.5 mm/yr (0.02 in./yr).

The effect of 6 m^3/m (65 ft^3/ft) annual infiltration in Pajarito Canyon on breakthrough time was evaluated under steady-state conditions for tracer particles released from waste disposal regions 1 and 5. As shown in Figure 23, at an assumed background infiltration rate of 0.1 mm/yr (0.0039 in./yr), the particles released from disposal regions 1 and 5 behaved nearly identically with and without increased Pajarito Canyon infiltration. These results demonstrate that transport is insensitive to increased recharge from the canyon for realistic values of Pajarito Canyon infiltration and channel width.

Setting the Pajarito Canyon infiltration rate to 100 mm/yr (3.9 in/yr) over a 240-m (190-ft) wide channel causes water to spread axially from the canyon when it encounters the permeability reduction interface at the top of the basalt, forcing flow northward under MDA G. Because of this northward component of flow in the Guaje Pumice, tracer particles migrate up to 100 m (330 ft) northward before they pass into the basalt and down to the water table. Although this behavior has been suggested as a possible mechanism for the transference of contaminants from Pajarito Canyon to wells drilled under Cañada del Buey, the net effect on breakthrough at the compliance boundary is not significant. Furthermore, because the effect of increased saturation in the Guaje Pumice is to spread the particles laterally, it is concluded that the most conservative numerical representation of Pajarito Canyon includes no increased infiltration. Therefore rates of infiltration in Pajarito Canyon were assumed to be the same as the mesa-top, or background, rates when calculating breakthrough from the waste disposal units.

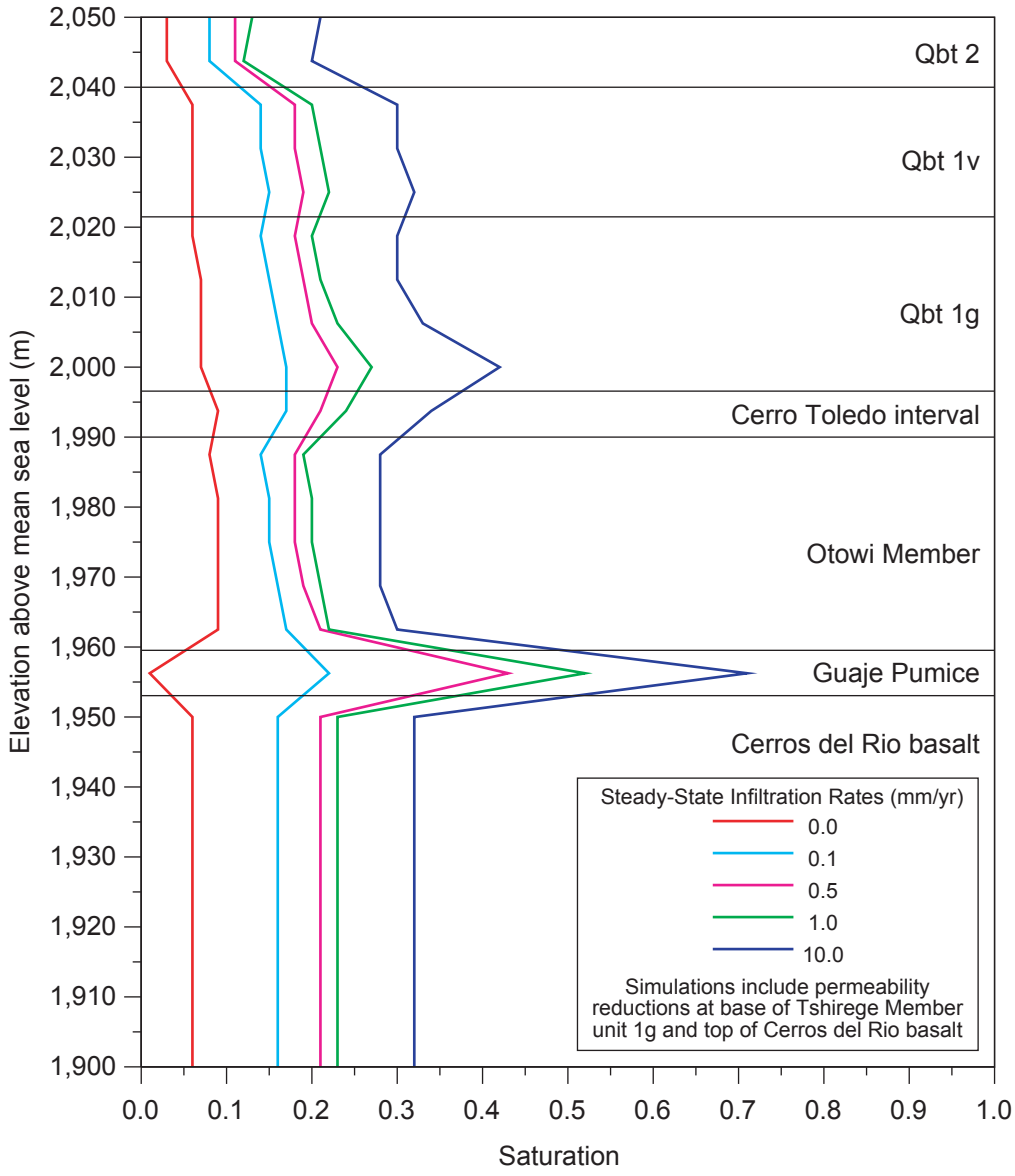

Figure 20
Subsurface Saturations at Waste Disposal Region 5 for Range of Steady-State Infiltration Rates (without increased Pajarito Canyon infiltration)

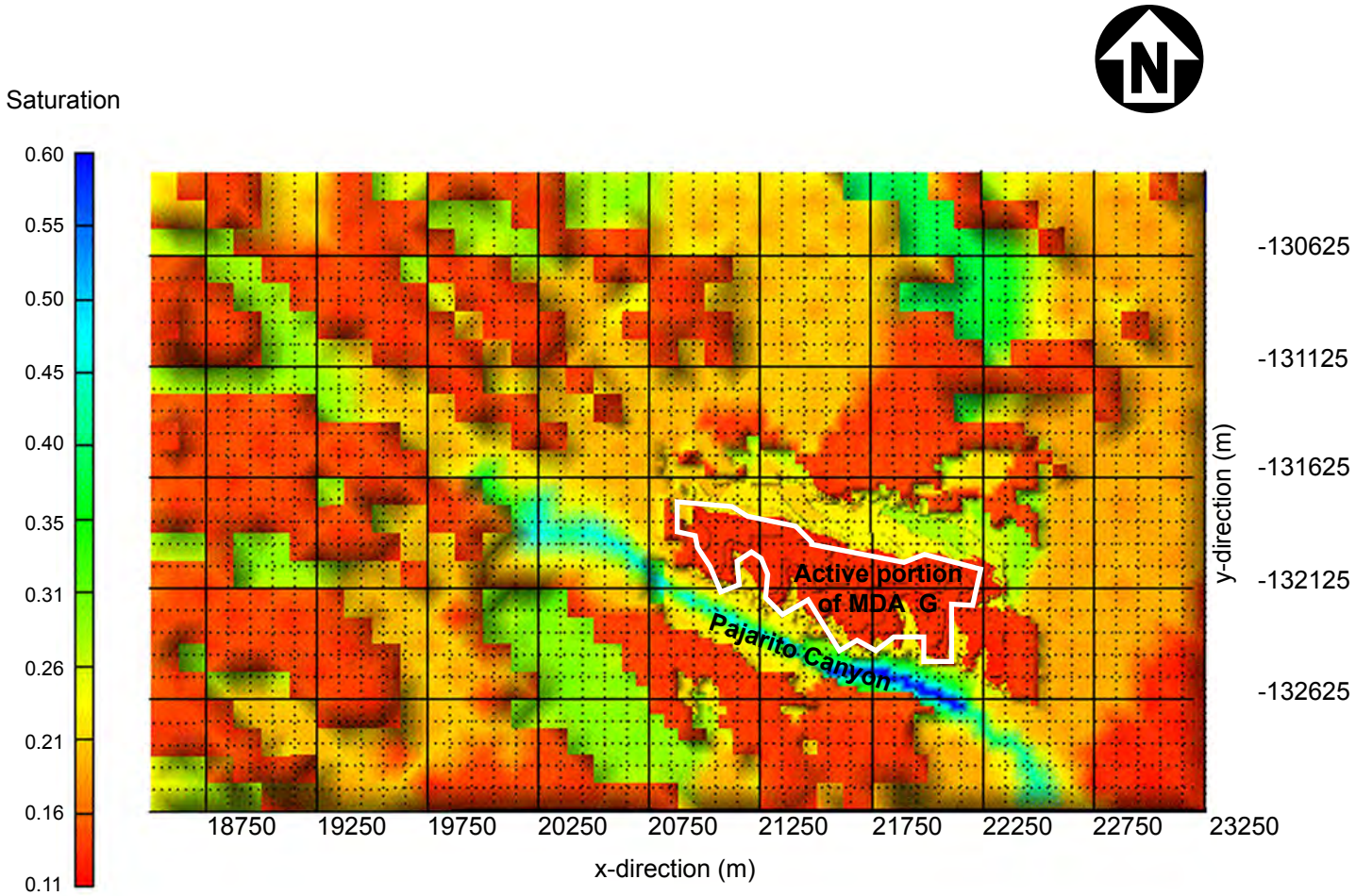

Grid coordinates based on polar stereographic projection used for Española basin site-scale model (Keating et al., 2003)

Figure 21
Simulated Surface Saturation with Increased Pajarito Canyon Infiltration

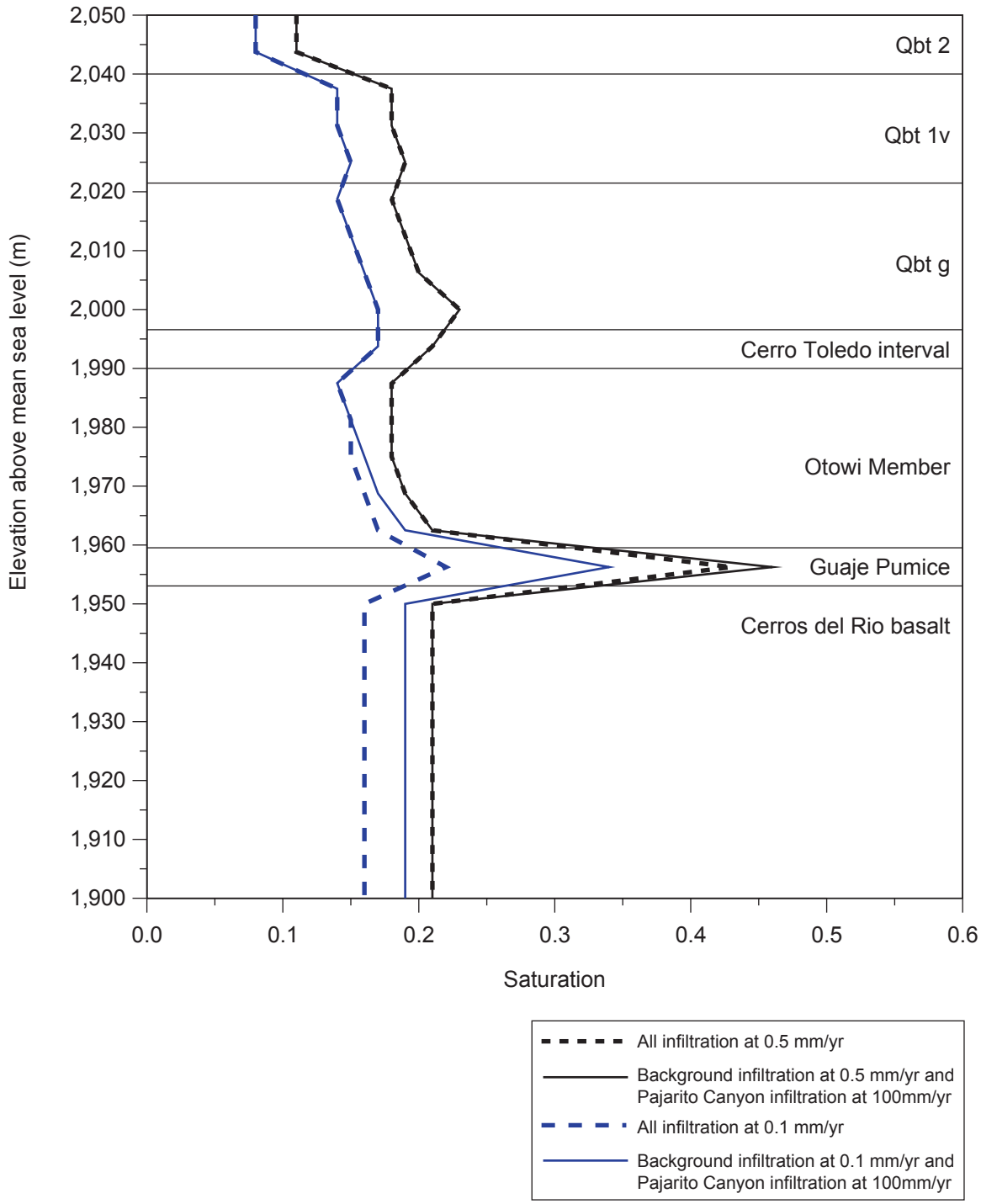

Figure 22
Effect of Pajarito Canyon Infiltration on Subsurface Saturation at Waste Disposal Region 5

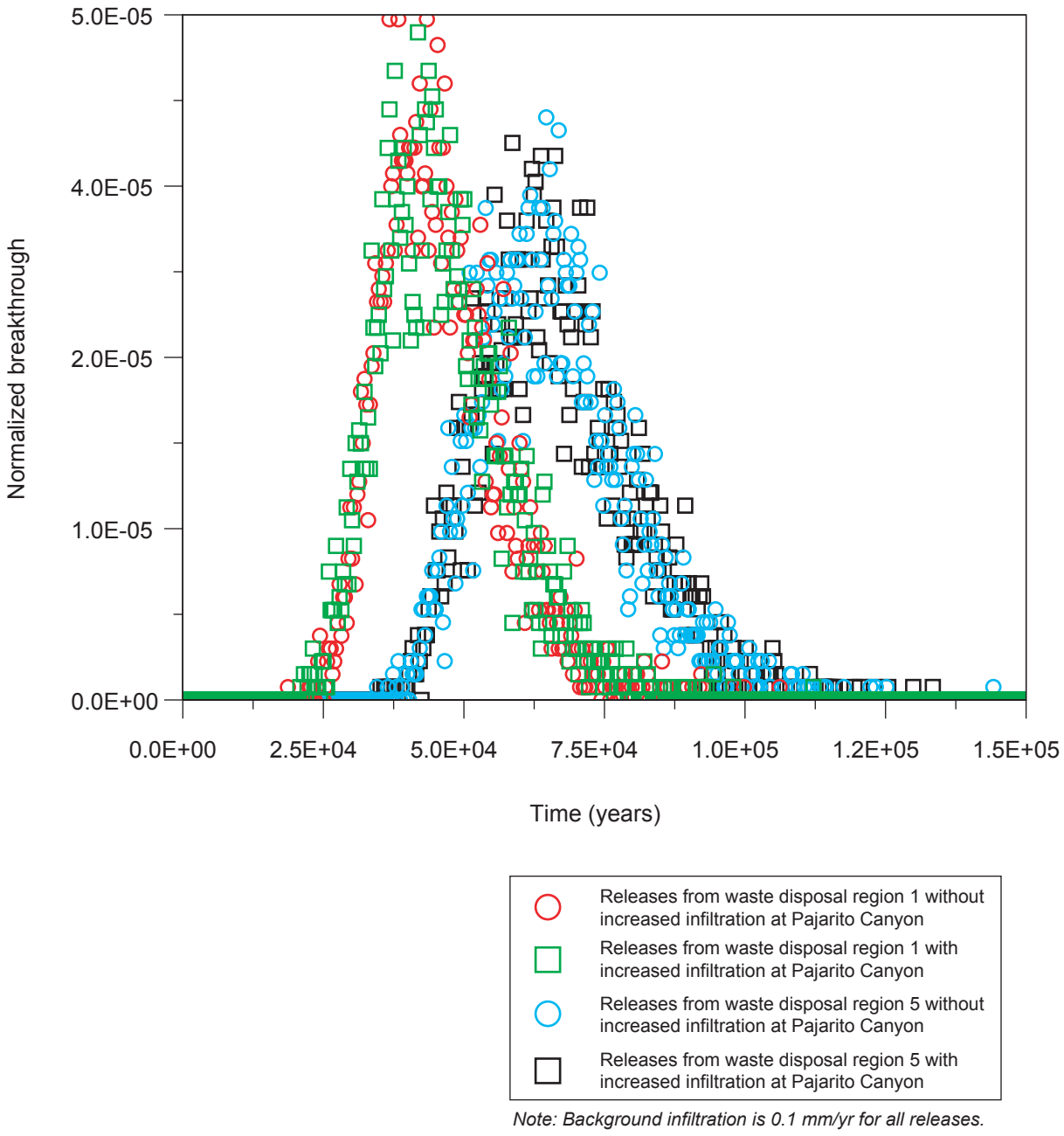

Note: Background infiltration is 0.1 mm/yr for all releases.

Figure 23
Effect of Pajarito Canyon Infiltration on Breakthrough for Releases from Waste Disposal Regions 1 and 5

Figures 24, 25, and 26 show breakthrough curves for waste disposal regions 1 and 5 at the 10 infiltration rates chosen as representative of the expected range of behavior. These figures show the curves for three time spans: 8×10^4 years, 2×10^4 years, and 5,000 years; breakthrough curves corresponding to some of the lower infiltration rates do not fall within the shorter time spans. As previously described, breakthrough occurs more quickly for releases on the east end of MDA G (disposal region 1) at a given infiltration rate than for more westerly locations (disposal region 5). Breakthrough for disposal region 5 typically takes about 1.5 times as long as for region 1. Thus, peak breakthrough with a 0.25 mm/yr (9.8×10^{-9} in./yr) background infiltration rate occurs for disposal region 1 at approximately 2×10^4 years while the corresponding peak breakthrough for disposal region 5 occurs at approximately 3×10^4 years.

4.1.2 Effects of Changes in Dispersivity

Figure 27 shows model sensitivity for particles released from waste disposal region 5 for a range of vadose-zone longitudinal dispersivities at both high- (10 mm/yr [0.39 in./yr]) and low- (0.1 mm/yr [0.039 in./yr]) infiltration rates. Changes in longitudinal dispersivity in the vadose zone cause little change in the peak breakthrough time for either high- or low-flow examples. However, higher vadose-zone longitudinal dispersivities cause the width of the breakthrough curve to increase while the peak value is decreased. This behavior is consistent with the theory of dispersion and confirms that the model is functioning as expected (Fetter, 1999). Because vadose-zone longitudinal dispersivity is expected to be smaller than one-tenth of the flow path length (see discussion in Section 3.1.4.2), longitudinal dispersivity in the vadose zone was fixed at 2 m (7 ft) for all simulations. This value was chosen because it is intermediate in what is considered to be a reasonable range of possible values. For a fixed vadose-zone longitudinal dispersivity value of 2 m (7 ft), a change in the saturated zone longitudinal dispersivity from 2 m (7 ft) to 20 m (66 ft) has little impact on breakthrough. This can be seen in Figure 27 where the red line represents 2 m dispersivity and the red dots 20 m dispersivity.

4.2 Well Capture

The well capture simulations were used to determine both the capture zone radius and the capture efficiency of a hypothetical nearby pumping well. Because the background gradient in the aquifer is fairly high, the well capture simulations project relatively narrow capture zones for the pumping rates considered. The capture radius ranged from 0.4 m (1.3 ft) for the 50 m^3/yr (1,300 gal/yr) pumping rate to 5.7 m (19 ft) for a pumping rate of 2,500 m^3 (6.6×10^5 gal/yr). Figure 28 shows the capture zone for a pumping rate of 1,200 m^3/yr (3.2×10^5 gal/yr). Table 6 summarizes the well capture efficiencies calculated using the 3-D particle tracer simulations. Capture efficiency is highly dependent on the transverse dispersivity, decreasing most rapidly between dispersivities of 0 and 2 m (0 and 6.6 ft).

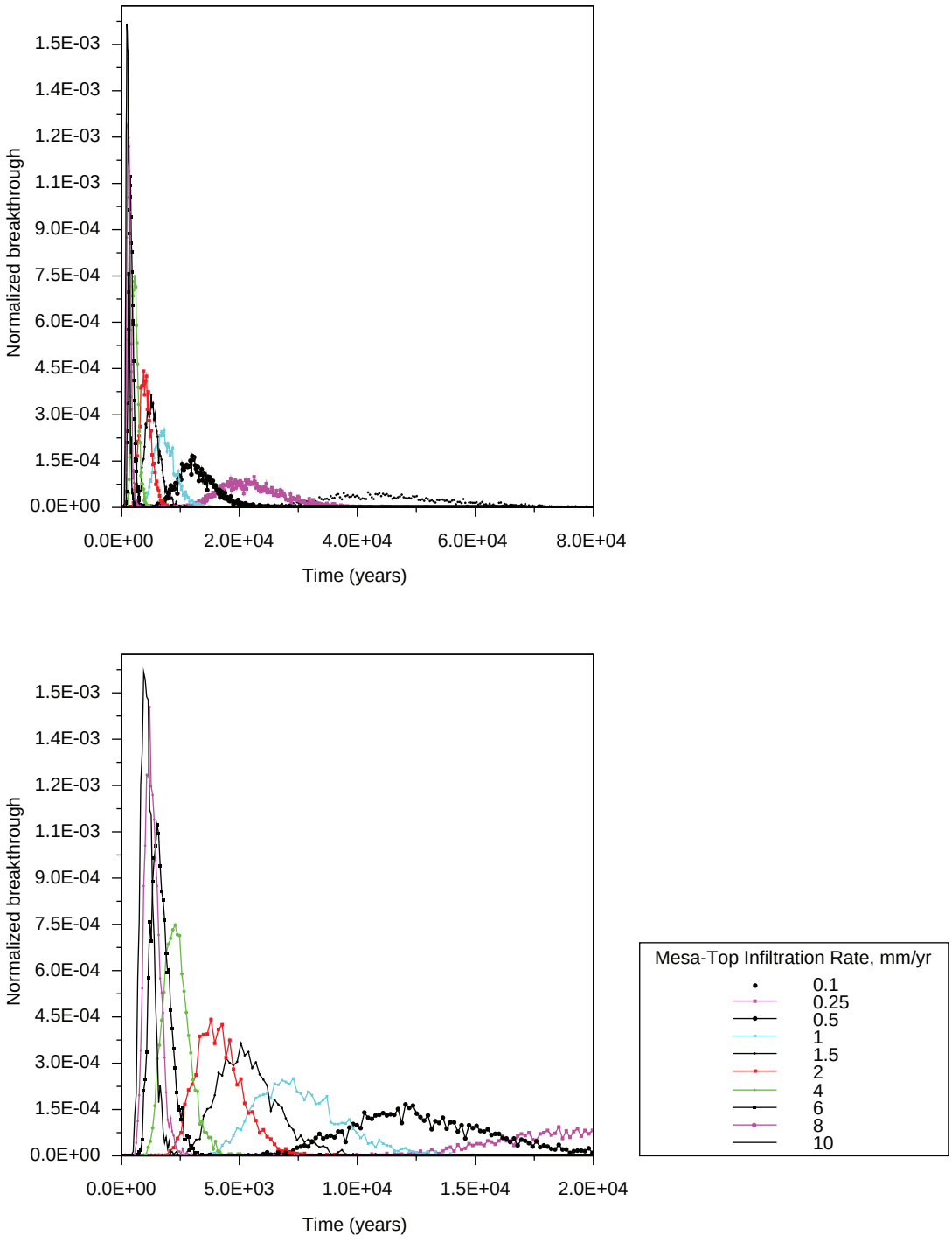

Figure 24
Breakthrough Curves for Particles Released from Waste Disposal Region 1 (range of steady-state infiltration rates)

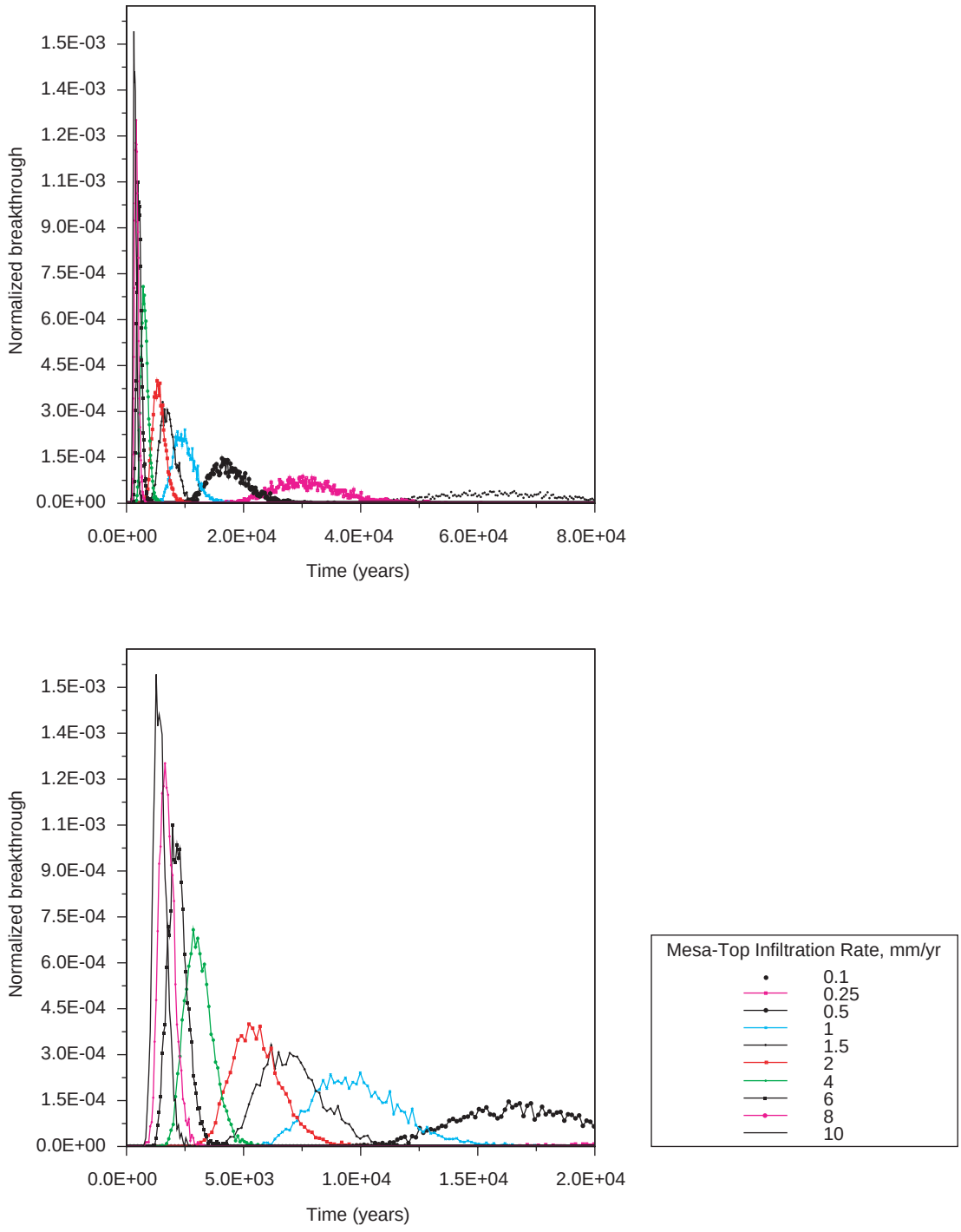

Figure 25
Breakthrough Curves for Particles Released from Waste Disposal Region 5 (range of steady-state infiltration rates)

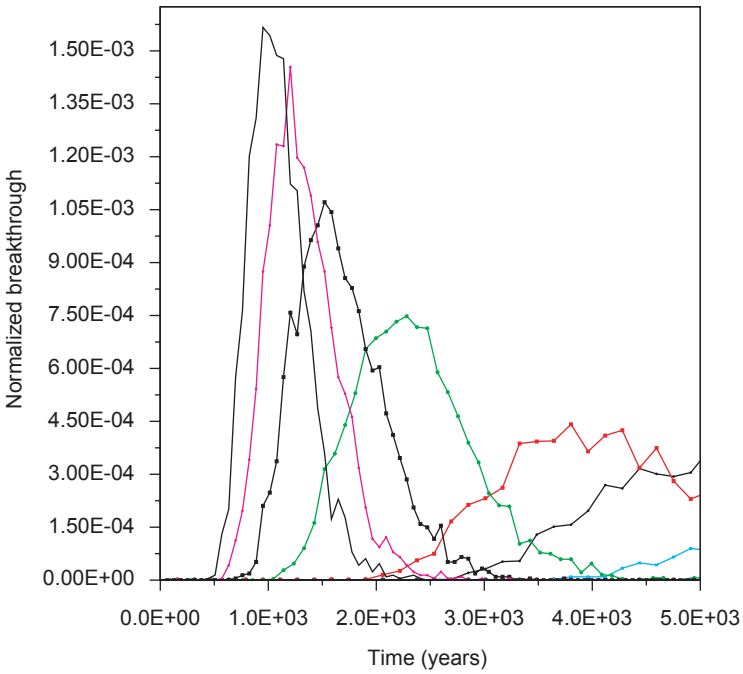

Figure 26a: Early particle breakthrough for release from waste disposal region 1.

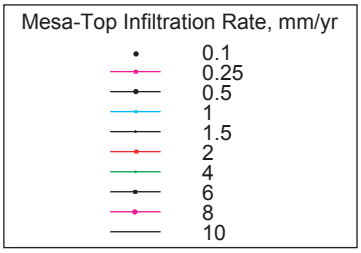

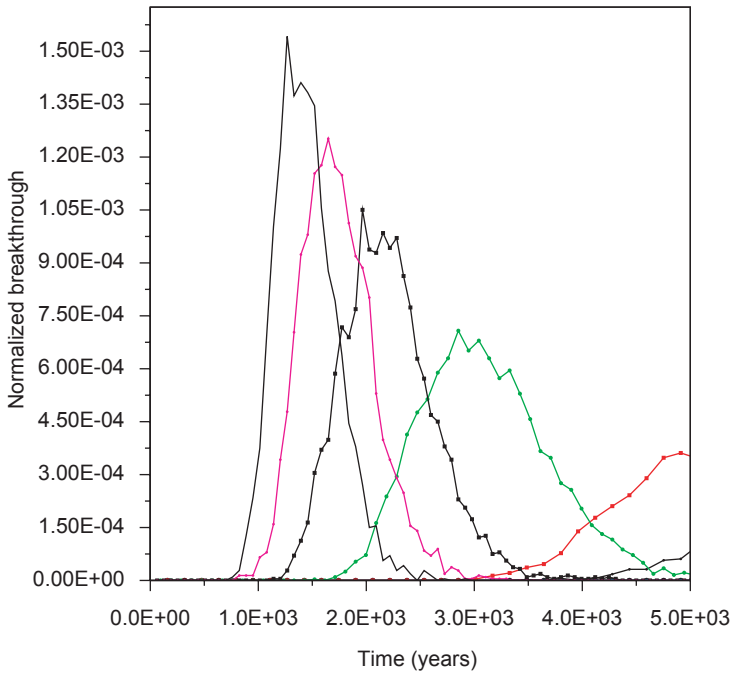

Figure 26b: Early particle breakthrough for release from waste disposal region 5.

Figure 26
Early Breakthrough Curves for Particles Released from Waste Disposal Regions 1 and 5 (range of steady-state infiltration rates)

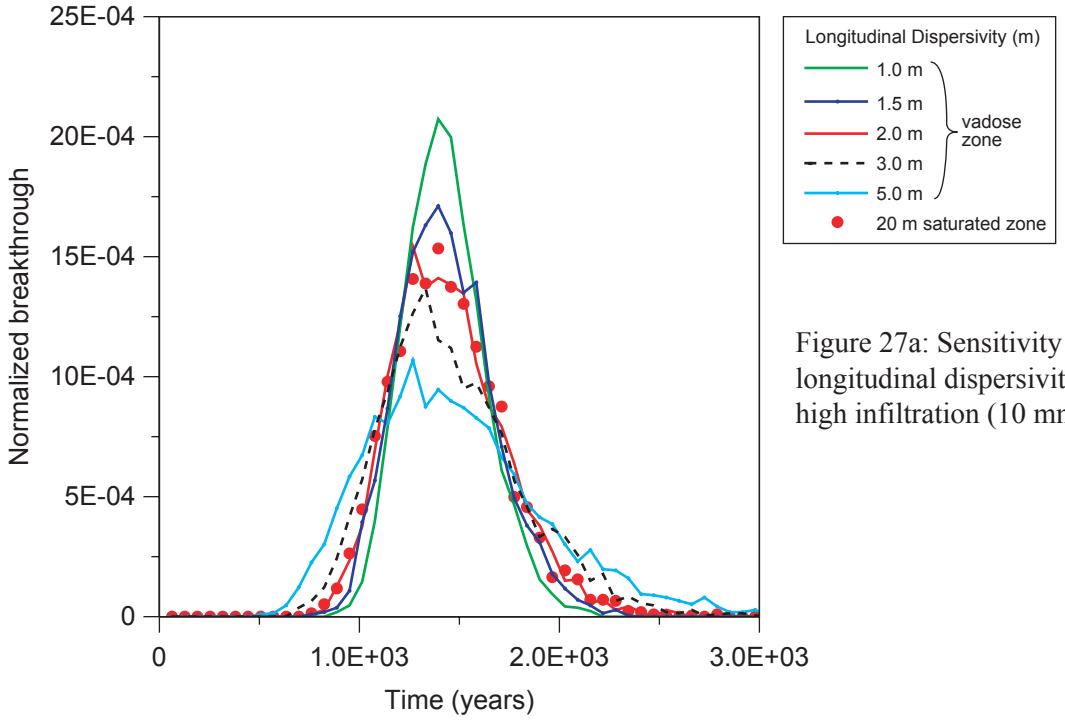

Figure 27a: Sensitivity to longitudinal dispersivity at high infiltration (10 mm/yr)

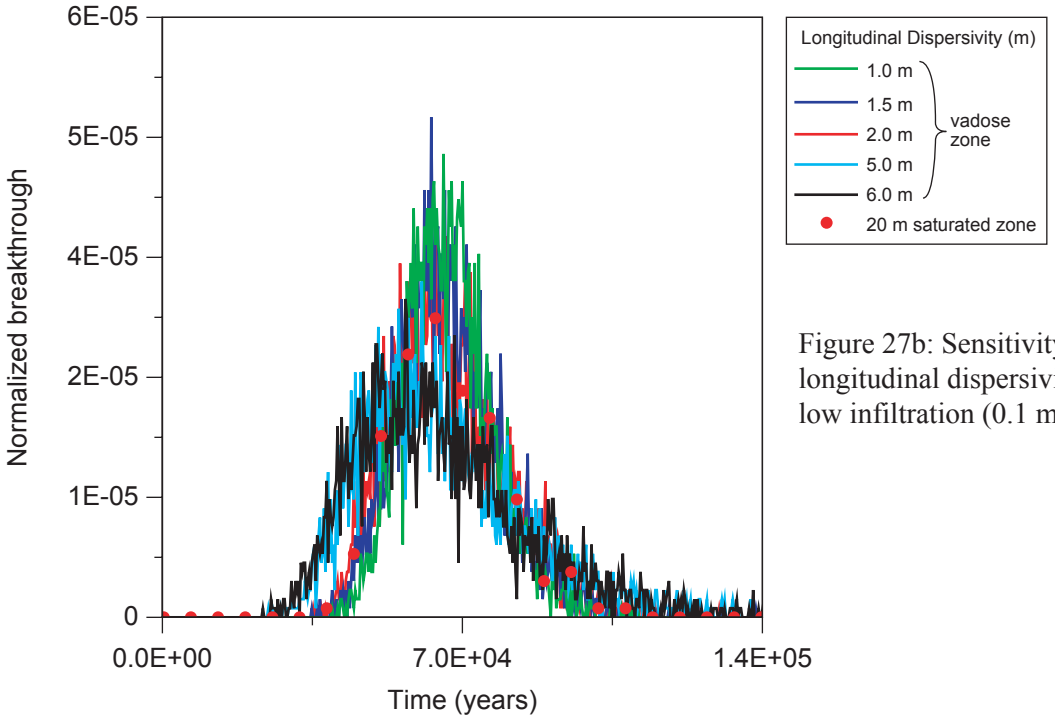

Figure 27b: Sensitivity to longitudinal dispersivity at low infiltration (0.1 mm/yr)

Figure 27
Model Sensitivity to Longitudinal Dispersivity at Waste Disposal Region 5 (high- and low-infltration rates)

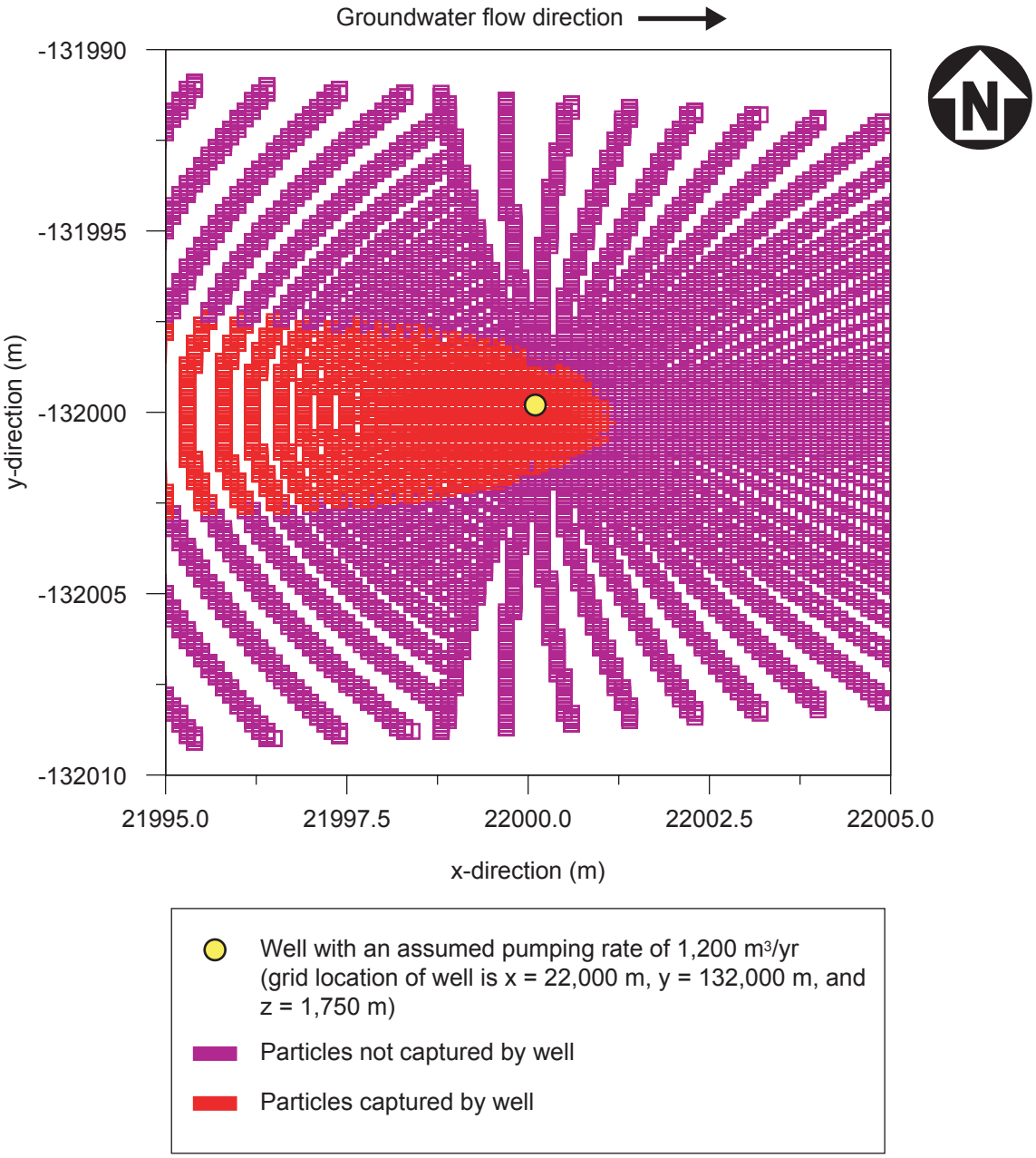

Figure 28
Capture Zone for Hypothetical Well with High Pumping Rate

Table 6
Capture Efficiencies for Waste Disposal Regions 1 through 5 and 8

Waste Disposal Region	Transverse Dispersivity (m)	Well Pumping Rates (m3/yr)			
		50	600	1,200	2,500
1	0	4.1E–02	4.1E–02	4.1E–02	4.1E–02
	1	1.7E–03	9.9E–03	1.9E–02	3.1E–02
	2	1.5E–03	9.2E–03	1.5E–02	2.6E–02
	5	2.0E–03	5.3E–03	1.3E–02	2.0E–02
2	0	1.1E–01	1.1E–01	1.1E–01	1.1E–01
	1	6.7E–03	2.3E–02	3.9E–02	7.1E–02
	2	5.3E–03	8.6E–03	2.2E–02	4.7E–02
	5	7.3E–04	6.7E–03	1.2E–02	2.7E–02
3	0	3.6E–02	3.6E–02	3.6E–02	3.6E–02
	1	1.2E–03	5.4E–03	9.7E–03	2.4E–03
	2	3.1E–03	2.8E–03	6.8E–03	1.4E–02
	5	3.0E–04	4.1E–03	4.2E–03	7.7E–03
4	0	3.6E–02	3.6E–02	3.6E–02	3.6E–02
	1	5.6E–04	5.0E–03	5.9E–03	1.7E–02
	2	0.0E+00 [a]	1.6E–03	5.5E–03	1.1E–02
	5	2.6E–04	2.1E–03	2.7E–03	4.8E–03
5	0	5.8E–02	5.8E–02	5.8E–02	5.8E–02
	1	1.5E–03	9.2E–03	9.3E–03	1.9E–02
	2	5.8E–04	2.0E–03	5.5E–03	1.3E–02
	5	2.8E–04	2.2E–03	1.4E–03	3.9E–03
	10	0.0E+00 [a]	2.8E–04	8.3E–04	2.7E–03
8	0	2.7E–02	2.7E–02	3.2E–02	8.1E–02
	1	1.7E–03	7.3E–03	8.0E–03	2.1E–02
	2	0.0E+00 [a]	4.1E–03	4.9E–03	1.2E–02
	5	2.6E–04	1.3E–03	3.9E–03	5.1E–03
	10	2.5E–04	1.3E–03	1.8E–03	2.3E–03

[a] *No particles were captured under the indicated conditions.*

The capture efficiencies estimated for the waste disposal regions are expected to be conservative. As discussed earlier, the efficiencies for each region were estimated by aligning the maximum particle densities with the well and then releasing the particles directly within the aquifer. This approach does not consider the north-south spatial distribution of the different disposal regions or the lateral spreading of contaminants at material contacts within the vadose zone. Taking these aspects into account, it is expected that a single well would be capable of intercepting maximum radionuclide releases from only one disposal region, capturing only fractions of the peak releases from the other disposal regions.

4.3 Comparison of Three-Dimensional and One-Dimensional Breakthrough Curves

The complex 3-D model produced the breakthrough curves described in Section 4.1. Comparisons of breakthrough from the 3-D simulations and the 1-D abstractions (*Attachment IV*) show that the 1-D abstractions recreate the breakthrough curves of the complex 3-D simulations. Although the input RTDs from the 3-D model are more finely detailed than the 1-D abstraction RTDs, the peak breakthrough times and standard deviations are similar. Thus, simulations performed on either grid will lead to the same conclusions.

Similarities in peak breakthrough times for releases from waste disposal regions 1 and 3 can be seen in Figure 29. The fits between the 1-D abstraction breakthrough curves and the 3-D particle breakthrough distributions are quite good when the sorption distribution coefficient (K_d) is low. As the distribution coefficient increases, the scatter in the 3-D breakthrough becomes more pronounced and the fit is not as accurate. The algorithm used to create the 1-D abstraction leads to some smoothing of the scattered data and approximations of the shape and peak value of the 3-D data. Although the fits appear less good at longer times, these times fall well beyond the 1,000-year compliance period and the approximate fit is acceptable for the analysis. More importantly, the 1-D and 3-D results for times less than 5,000 years match well and provide confidence that the 1-D abstraction retains the information embedded in the 3-D model. Results for the low end of the infiltration distribution or for higher distribution coefficients were not included because the breakthrough times are quite long for these cases and lie well beyond the compliance period.

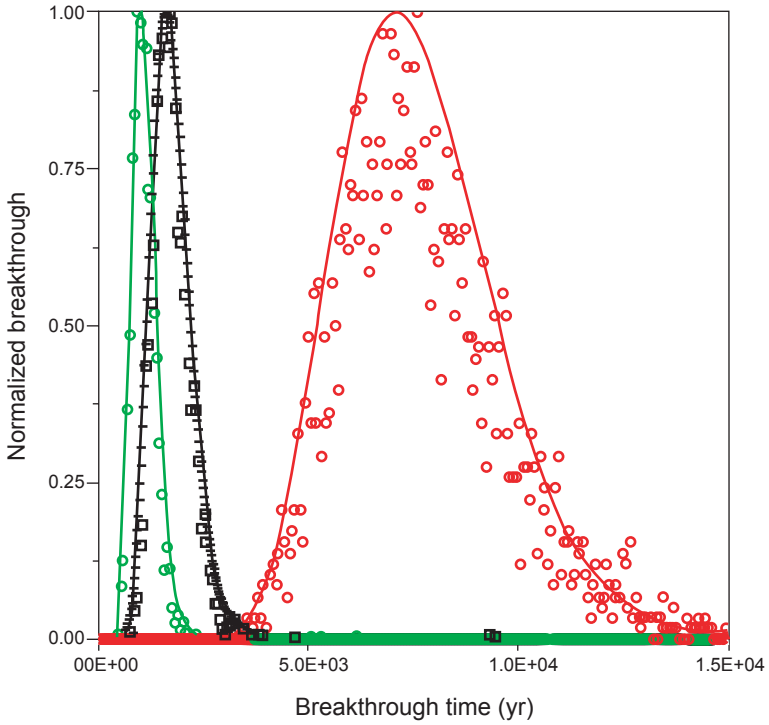

Figure 29a: Waste disposal region 3, infiltration rate = 4 mm/yr

Model Used	Distribution Coefficient (Kd)
3-D particle	0
1-D plume	0
3-D particle	0.1
1-D plume	0.096
3-D particle	1.0
1-D plume	0.96

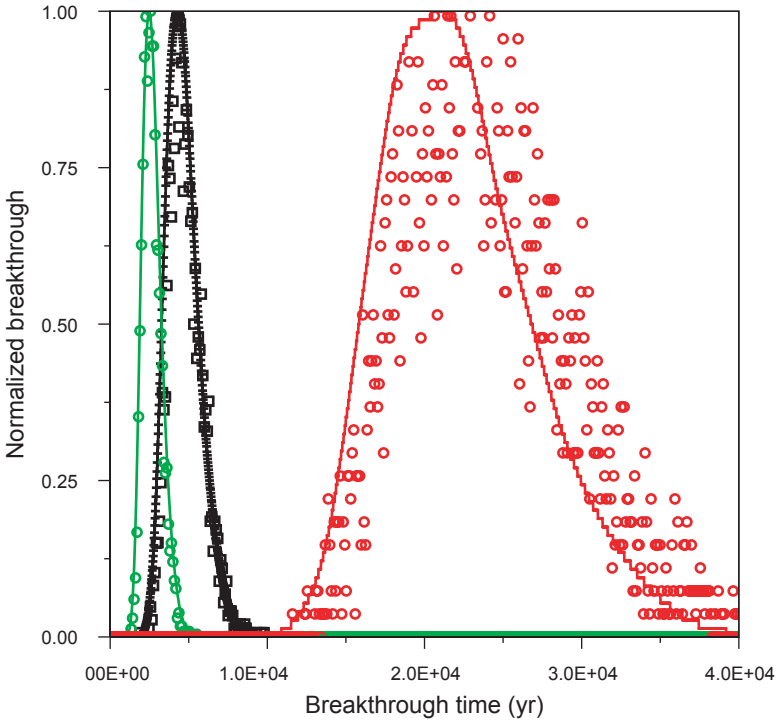

Figure 29b: Waste disposal region 1, infiltration rate = 10 mm/yr

Figure 29
Comparison of Three-Dimensional Particle and One-Dimensional Plume Breakthrough Curves

5.0 References

Ball, T., M. Everett, P. Longmire, D. Vaniman, W. Stone, D. Larssen, K. Greene, N. Clayton, and S. McLin, 2002, *Characterization Well R-22 Completion Report*, Los Alamos National Laboratory Report LA-13893-MS.

Birdsell, K.H., W.E. Soll, N.D. Rosenberg, and B.A. Robinson, 1995, *Numerical Modeling of Unsaturated Groundwater Flow and Radionuclide Transport at MDA G*, Los Alamos National Laboratory Report LA-UR-95-2735.

Birdsell, K., K. Bower, A. Wolfsberg, W. Soll, T. Cherry, and T. Orr, 1999, *Simulations of Groundwater Flow and Radionuclide Transport in the Vadose and Saturated Zones beneath Area G, Los Alamos National Laboratory*, Los Alamos National Laboratory Report LA-13299-MS.

Birdsell, K.H., A.V. Wolfsberg, D.H. Hollis, T.A. Cherry, K.M. Bower, 2000, "Groundwater Flow And Radionuclide Transport Calculations for a Performance Assessment of a Low-Level Waste Site," *J. Contaminant Hydrology*, 46, pp. 99-129.

Broxton D.E., 2001, *Geology of the Pajarito Plateau and Vicinity, North-Central New Mexico*, Los Alamos National Laboratory Report LA-UR-01-2055.

Broxton, D.E. and S.L. Reneau, 1995, *Stratigraphic Nomenclature of the Bandelier Tuff for the Environmental Restoration Project at Los Alamos National Laboratory*, Los Alamos National Laboratory Report, LA-13010-MS.

Carey, J.W. and Cole, G., 2002, *Description of the Cerro Grande Fire Laser-Altimetry (LIDAR) Data Set*, Los Alamos National Laboratory, Report LA-13892-MS, 57pp. plus appendices.

Dash, Z.V., 2003, *Software Users Manual (UM) for the FEHM Application Version 2.22*, Los Alamos National Laboratory Document 10086-UM-2.22-00.

Doughty, C., 2000, "Numerical Model of Water Flow in a Fractured Basalt Vadose Zone: Box Canyon site, Idaho," *Water Resources Research*, Vol.36, No.12, pp. 3,521-3534.

Fetter, C.W., 1999, *Contaminant Hydrogeology*, Prentice-Hall: NJ, USA.

Gable, C.W., T. Cherry, H. Trease, and G. A. Zyvoloski, 1995, *GEOMESH Grid Generation*, Los Alamos National Laboratory Report LA-UR-95-4143.

Gelhar, LW; C. Welty, and K.R. Rehfeldt, 1992, "A Critical-Review of Data on Field-Scale Dispersion in Aquifers," *Water Resources Research*, Vol. 28, No. 7.

Golder, 2005a, *User's Guide – GoldSim – Probabilistic Simulation Environment, Version 8.02.3*, GoldSim Technology Group, January.

Golder, 2005b, *User's Guide – GoldSim Contaminant Transport Module, Version 2.22.2*, GoldSim Technology Group, January.

Hollis, D., E. Vold, R. Shuman, K. Birdsell, K. Bower, W. Hansen, D. Krier, P. Longmire, B. Newman, D. Rogers, E. Springer, 1997, *Performance Assessment and Composite Analysis for the Los Alamos National Laboratory Disposal Area G*, Los Alamos National Laboratory Report LA-UR-97-85, Report-54G-013, March.

Keating, E.H., V.V. Vesselinov, E. Kwicklis, and Z. Lu, 2003, "Coupling Basin- and Local-Scale Inverse Models of the Española Basin," *Ground Water*, Vol. 41, No. 2, pp. 200-211.

Krier, D., R. Longmire, and H.J. Turin, 1996, *Geologic, Geohydrologic and Geochemical Data Summary of MDA G, TA-54, Los Alamos National Laboratory*, Los Alamos National Laboratory Report LA-UR-95-2696.

Kwicklis, E., M. Witkowski, B. Newman, and K. Birdsell, 2005, "Characterization and Mapping of Deep Infiltration on the Pajarito Plateau, New Mexico," *Vadose Zone Journal*, in press.

Lichtner P.C., S. Kelkar, and B.A. Robinson, 2002,"New Form of Dispersion Tensor for Axisymmetric Porous Media with Implementation in Particle Tracking," *Water Resour. Res.*, Vol. 38, No. 8.

Longmire, P., C.R. Cotter, I.R. Triay, J.J. Kitten, C. Hall, J. Bentley, D. Hollis, and A.I. Adams, 1996, *Batch Sorption Results for Americium, Neptunium, Plutonium, Technetium, and Uranium Transport through the Bandelier Tuff, Los Alamos, New Mexico*, Los Alamos National Laboratory Report LA-UR-96-4716.

Neuman, S.P., 1990, "Universal Scaling of Hydraulic Conductivities and Dispersivities in Geologic Media", *Water Resources Research*, Vol. 26, No. 8.

Newman, B.D and T.G. Schofield, 2005, *Modeling of an Evapotranspiration Cover for the Groundwater Pathway at Los Alamos National Laboratory Technical Area 54, Material Disposal Area G*, Los Alamos National Laboratory Report, September.

Nylander, C.L, K. A. Bitner, G. Cole, E. H. Keating, S. Kinkead, P. Longmire, B. Robinson, D. B. Rogers, and D. Vaniman, 2003, *Groundwater Annual Status Report for Fiscal Year 2002*, Los Alamos National Laboratory Report LA-UR-03-0244.

Pratt, A.R., 1998, Work *Plan for Pajarito Canyon: Environmental Restoration Project*, Los Alamos National Laboratory Report LA-UR-98-2550.

Reneau, S.L., D.E. Broxton, J.S. Carney, and C. LaDelfe, 1998, *Structure of the Tshirege Member of the Bandelier Tuff at Mesita del Buey, Technical Area 54, Los Alamos National Laboratory*, Los Alamos National Laboratory Report LA-13538-MS.

Robinson, B.A. and H. Viswanathan, 2003 "Application of the Theory of Micromixing to Groundwater Reactive Transport Models," *Water Resources Res.*, Vol. 39, No. 11.

Robinson, B.A., M. Witkowski, C. J. Elliot, L. Dale, and R. Koch, 1999, *Numerical Model of Flow and Transport for Los Alamos Canyon*, Los Alamos National Laboratory (contact author at robinson@lanl.gov for an electronic copy).

Rogers, D.B. and B.M. Gallaher, 1995, *The Unsaturated Hydraulic Characteristics of the Bandelier Tuff*, Los Alamos National Laboratory Report LA-12968-MS, September.

Rogers, D.B., E.L. Vold, and B.M Gallaher, 1996, "Bandelier Tuff Hydraulic Characteristics from Los Alamos National Laboratory Borehole G-5 at MDA G, TA-54", New Mexico Geologic Society Guidebook, 47th Field Conference, The Jemez Mountains Region, pp. 413-420.

Rogers, D.B., B.M. Gallaher, E.L. Vold, 1996, *Vadose Zone Infiltration Beneath the Pajarito Plateau at Los Alamos National Laboratory*, Los Alamos National Laboratory Report LA-UR-96-485.

Rogers, D.B., P. Longmire, B.D. Newman, K.H. Birdsell, W.E. Soll, and E.L. Vold, 1997, *Conceptual Model for Subsurface Transport at MDA G*, Los Alamos National Laboratory Report LA-UR-97-179.

Rosenberg, N.D., W.E. Soll, and H.J. Turin, 1993, *Potential Transport of PCBs Through Fractured Tuff at Area G*, Los Alamos National Laboratory Report LA-UR-94-28.

Soll, W.E., 1995, *Influence of Fracture Fills and Fracture Coatings on Flow in Bandelier Tuff*, Los Alamos National Laboratory Report LA-UR-95-2695.

Soll, W. and K. Birdsell, 1998, "The Influence of Coatings and Fills on Flow in Fractured, Unsaturated Tuff Porous Media System," *Water Resour. Res.*, Vol. 34, pp. 193 –202.

Springer, E.P., 2005 , "Statistical Exploration of Matrix Hydrologic Properties for the Bandelier Tuff, Los Alamos, New Mexico", submitted to *Vadose Zone Journal*.

Springer, E.P and T.G. Schofield, 2004, *Statistical Analyses of Mesa-Top Percolation Rates at Los Alamos National Laboratory, New Mexico*, Los Alamos National Laboratory Report LA-UR-04-7801.

Stauffer, P.H., 2003, *Modeling the Los Alamos Canyon Weir Bromide Tracer Experiment*, Los Alamos National Laboratory Report LA-UR-03-82448.

Stauffer, P.H., B.A. Robinson, and K.H. Birdsell, 2000, *Modeling Transport in Los Alamos Canyon: Effects of Hypothetical Increased Infiltration after the Cerro Grande Fire*, Los Alamos National Laboratory Report LA-UR-00-5923.

Stauffer, P.H., K Birdsell, M.S. Witkowski, and J.K. Hopkins, 2005," Vadose Zone Transport of 1,1,1-Trichloroethane: Conceptual Model Validation through Numerical Simulation," *Vadose Zone Journal*, In press.

Stone, W.J., G.L. Cole, and M.A. Jones, 1999, *Documentation for the Preliminary Hydrogeologic Atlas for Los Alamos National Laboratory*, Los Alamos National Laboratory Report LA-UR-99-4619.

Turin, H. J., 1995, *Subsurface Transport Beneath MDA G: A Conceptual Model*, Los Alamos National Laboratory Report LA-UR 95-1663.

Vaniman, D., G. Cole, J. Gardner, J. Conaway, D. Broxton, S. Reneau, M. Rice, G. WoldeGabriel, J. Blossom, and F. Goff, 1996, *Development of a Site-Wide Geologic Model for Los Alamos National Laboratory*, Los Alamos National Laboratory Report LA-UR-96-2059.

Zyvoloski, G. A., B. A. Robinson, Z. V. Dash, and L. L. Trease, 1995a, *Models and Methods Summary for the FEHMN Application*, Los Alamos National Laboratory Report LA-UR-94-3787, Rev. 1.

Zyvoloski, G. A., B. A. Robinson, Z. V. Dash, and L. L. Trease, 1995b, *User's Manual for the FEHMN Application*, Los Alamos National Laboratory Report LA-UR-94-3788, Rev. 1.

Attachment I
Generation of the Three-Dimensional Numerical Grid for the Los Alamos National Laboratory Technical Area 54, Material Disposal Area G Groundwater Pathway Model

Authors:
Carl W. Gable
Terry A. Miller

I.1 Introduction

The groundwater pathway modeling conducted in support of the Material Disposal Area (MDA) G performance assessment and composite analysis requires various input data, including water level and head distributions, hydrogeologic unit definitions, recharge flux and lateral flux distribution into the model domain, geographic information system (GIS) feature locations, and boundary conditions. Incorporation of these data into the Finite Element Heat and Mass (FEHM) model used for the modeling first requires the generation of a geologic framework model and a three-dimensional (3-D) computational grid. The grid represents the physical features of the disposal site, underlying vadose zone, and regional aquifer using a series of nodes or elements. Each node is assigned properties consistent with the feature it represents. This report describes the process used to develop the computational grid used in the 3-D groundwater modeling.

I.2 Methods and Input Data

The 3-D grid was developed to meet specific criteria, including consistency with regional groundwater models, adequate resolution, and up-to-date geologic information. Various input data used to develop the computational grid include hydrogeologic units and properties, GIS data, water table definition data, and grid coordinates. The nature of these data and the sources of information used to construct the grid are discussed below.

I.2.1 Criteria for Grid

Four criteria were adopted to guide the development of the 3-D computational grid. These criteria are as follows:

- The grid must use the latest geologic framework model — in this case, the vadose-zone geologic model for MDA G — to define the hydrogeologic layers of the model.
- Grid resolution must capture the ground topography accurately enough to locate features within the model domain. Features of interest include waste pits, truncated material layers along the mesa, fence boundaries, and the compliance boundary.
- The grid must coincide horizontally with the Española basin site-scale regional aquifer computational model (Keating et al., 2003).
- The grid must be either a uniform, orthogonal finite difference grid or a balanced octree grid. The grid must have adequate hydrogeologic layer resolution to permit accurate streamline-particle-tracking using the FEHM groundwater code.

The various inputs used to create the 3-D grid and the efforts to meet these criteria are described in the following sections.

I.2.2 MDA G Vadose-Zone Geologic Model

The hydrogeologic units for the flow and transport grid are defined by surface data that represent the elevation of the bottom of each geologic unit on a regularly-spaced grid. The local geologic framework used to define these units is referred to in this report as the MDA G vadose-zone geologic model. This geologic model is the result of a 2003 study that investigated the 3-D geometry of the unsaturated-zone geology for the portion of Los Alamos National Laboratory encompassing MDA G and Mortandad Canyon. The MDA geologic model study area is rectangular in shape, extending approximately 4,880 m (1.6×10^4 ft) in the east-west direction and approximately 3,050 m (1.0×10^4 ft) in the north-south direction**.** The vertical domain extends about 410 m (1,350 ft) from the interpreted topographic surface to the top of the saturated zone. Surface grids for 14 geologic units as well as the surface topography and the top of the saturated zone (water table) are included in the geologic model. The grid for the MDA G vadose-zone geologic model consists of a rectangular array of nodes with a horizontal spacing of 7.6 m (25 ft). The coordinates are expressed in feet according to the New Mexico State Plane system (North American Datum [NAD] 83).

The geometry of the MDA G geologic model is defined in Stratamodel™ Framework files which characterize a 3-D geocellular model of the study area encompassing MDA G and Mortandad Canyon. The framework stratigraphy is formed through a process that uses data to create gridded contours with uniform horizontal spacing and variable vertical spacing. The final unit volumes are defined by the set of surfaces, a top and a bottom, that truncate against one another but do not intersect or cross. This representation coarsens the available data near the model area and extrapolates from widely spaced data in other areas of the model domain. A full description of the MDA G vadose-zone geologic model is provided in *Attachment II* of this report. Figure II-2 (*Attachment II*) shows the surface geology of the model area and provides a color key representing the various formations present in the area.

The unit surfaces defined by the MDA G geologic framework model are used to identify zones of node properties for the 3-D computational grid. The stratigraphic surfaces are used to identify material zones and the topographic surfaces are used to truncate the top of the grid at the ground surface. Because the MDA G geologic model is larger than the area being modeled using FEHM, some of the units included in the geologic model are not incorporated into the computational grid. Table I-1 shows the correlation between the hydrogeologic units in the MDA G geologic model and the units included in the flow and transport model grid. Figure I-1 presents a map view of the geologic model (Figure I-1a) and the grid in the area around MDA G (Figure I-1b).

Table I-1
Correlation of Hydrogeologic Units Used in the MDA G Vadose-Zone Geologic Model and the 3-D Computational Grid

Hydrogeologic Unit in the MDA G Geologic Model	Flow and Transport Model Grid Unit		
	ID No.	Name	Number of Nodes/Unit [a]
Bandelier Tuff (Tshirege Member) unit 3	9	Qbt2	
Bandelier Tuff (Tshirege Member) unit 2			20,063
Bandelier Tuff (Tshirege Member) unit 1, vitric portion	8	Qbt1vu	16,023
Bandelier Tuff (Tshirege Member) unit 1, colonnade portion	7	Qbt1vc	10,078
Bandelier Tuff (Tshirege Member) unit 1, glassy	6	Qbt1g	427,55
Bandelier Tuff (Tshirege), Unit 1, Tsankawi Pumice	5	Qbtt	1,065
Cerro Toledo interval	4	Qct	6,518
Bandelier Tuff (Otowi Member), ash flow	3	Qbof	63,522
Bandelier Tuff (Otowi Member), Guaje Pumice Bed	2	Qbog	11,471
Cerros del Rio basalts	1		
Puye Formation, fanglomerate		basalts	203,956
Puye Formation, fanglomerate, pumiceous		Nodes below water table: 44,489	
Puye Formation, river gravels, "Totavi Lentil"			
Tschicoma Formation, lower flows			
Total nodes			375,451

Figure 1a. Surface geology of area around MDA G (source: Attachment II, Figure 2)

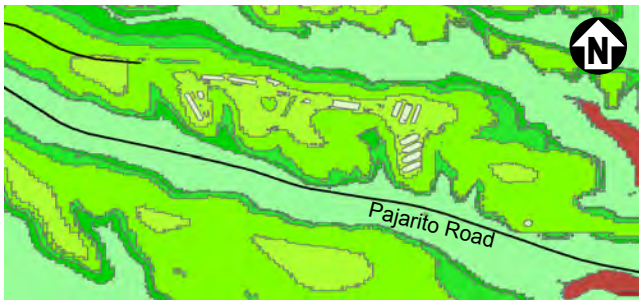

Figure 1b. Top surface of the 3-D grid viewed from southwest.

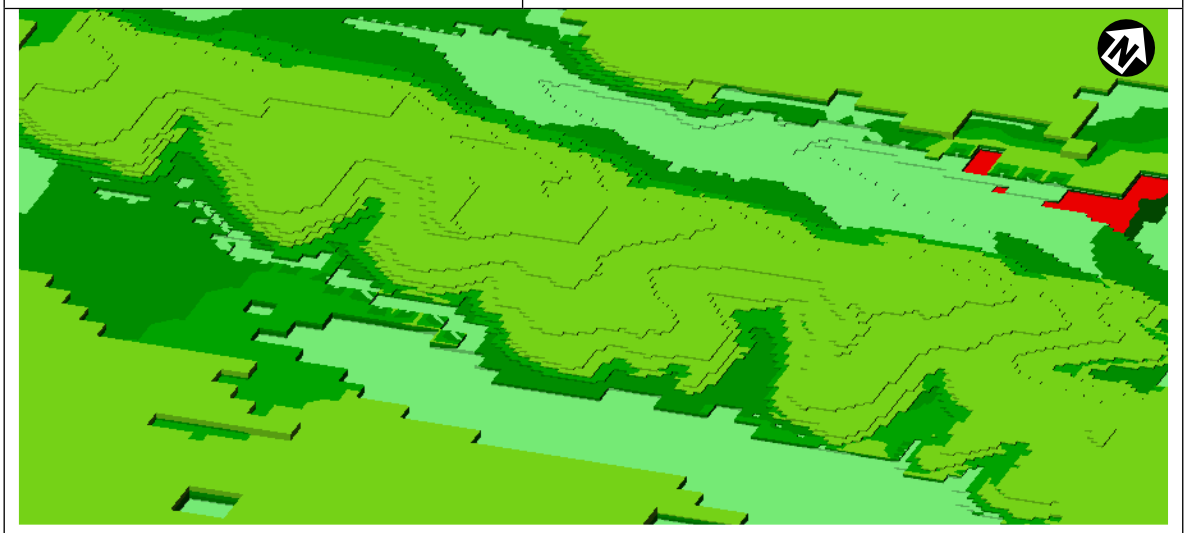

Unit Color	Geologic Unit Description	Grid Unit	Unit Name
Qbt3	Bandelier Tuff (Tshirege Member), unit 3	9	Qbt2
Qbt2	Bandelier Tuff (Tshirege Member), unit 2		
Qbt1vu	Bandelier Tuff (Tshirege Member), unit 1, vitric portion	8	Qbt1vu
Qbt1vc	Bandelier Tuff (Tshirege Member), unit 1, colonnade portion	7	Qbt1vc
Qbt1g	Bandelier Tuff (Tshirege Member), unit 1, glassy	6	Qbt1g
Qbtt	Bandelier Tuff (Tshirege), unit 1, Tsankawi Pumice	5	Qbtt
Qct	Cerro Toledo interval	4	Qct
Qbof	Bandelier Tuff (Otowi Member), ash flow	3	Qbof
Qbog	Bandelier Tuff (Otowi Member), Guaje Pumice Bed	2	Qbog
Tb4	Cerros del Rio basalts		
Tpf	Puye Formation, fanglomerate	1	basalts
Tpp	Puye Formation, fanglomerate, pumiceous		
Tpt	Puye Formation, river gravels, “Totavi Lentil”		
Tt1	Tschicoma Formation, lower flows		

Figure I-1
Images Showing Correlation of Geologic Framework Model to Flow and Transport Grid

I.2.3 Geographic Information System Data

Data describing the location of waste disposal units, the boundaries of Technical Area (TA) 54, and the position of Pajarito Road were extracted from the LANL geographic information system (GIS) database and used as input. Pit locations are defined by closed polygons. Locations of other features such as TA boundaries and roads are defined by open polylines. These data have no elevation coordinates and are used to identify features on the grid where the polygons and polylines intersect the top of the grid representing the ground surface. Figure 10 of the main groundwater pathway model report shows some of these surface features relative to the grid.

I.2.4 Water Table

The water table is defined by a regular grid of elevations, z(x,y), that form a surface of quadrilaterals. This surface is also equivalent to the bottom of the vadose zone and matches that used in the Española basin site-scale regional aquifer computational model (Keating et al., 2003).

I.2.5 Coordinate System

The computational grid is based on polar stereographic projections and follows the coordinate system used in the Española basin site-scale regional aquifer computational model (Keating et al. 2003). Various attempts to ensure that all data would reside in the same coordinate system were made. The GIS data reside in Universal Transverse Mercator (UTM) coordinate system (metric), the MDA G geologic model data follow the New Mexico State Plane Coordinate System (English), and the Española basin site-scale regional aquifer computational model resides in polar stereographic coordinates (metric). Conversions between UTM and NM state plane coordinates presented no difficulties or changes in accuracy, but conversions from state plane to polar stereographic coordinates yielded slightly different values depending upon the computer code used to conduct these operations. The result was that data converted with different programs did not align exactly. Although the differences were small, generally less than 10 m (33 ft), the errors were large enough to cause problems. The final solution was to ensure that all state plane data were converted to polar stereographic coordinates using the same conversion program. This approach maintained the relative position of features.

Another issue involved the geologic model data. Conversion of the stratigraphic surface grids from state plane coordinates to polar stereographic coordinates was first done using an ESRI software package. Instead of simply converting the horizontal (x,y) coordinates of the surfaces, this program defined a regular grid in polar stereographic coordinates and interpolated the elevations from the state plane grids. This resulted in problems with layer inversion and an inability to maintain the position of the zero isopach contour. In general, the converted stratigraphic model was not usable. The solution was to convert only the x,y coordinates of the surfaces and to leave the elevation coordinates unchanged.

I.3 Grid Generation Process

The computational grid for the MDA G flow and transport model was developed using the Los Alamos Grid Generation software package (LaGriT) (George, 1997). LaGriT contains a comprehensive set of software macros that uses hydrogeological, GIS, and geometrical data to build and optimize computational grids. LaGriT is also used for grid analysis and visualization work.

I.3.1 Grid Selection

A structured grid using orthogonal hexahedral elements was chosen for the MDA G flow and transport model. The principal reason structured grids are used for this work is to allow for the use of the streamline-particle-tracking transport capability of FEHM Version 2.20. Although structured grids are not as flexible as unstructured grids in terms of representing complex geometries, tests have shown that they provide accurate solutions as long as there is adequate resolution to represent the geometries of the different materials in each hydrogeologic layer (Bower et al., 2004). Moreover, there must be sufficient resolution to account for any large gradients present in the flow or transport model. Therefore, the grid needs appropriate resolution along the expected particle paths. Accuracy and higher resolution at the ground surface is needed to correctly locate features such as waste disposal pits.

I.3.2 Grid Extents

The first step in building the computational grid was to extract a subset of the Española basin site-scale regional aquifer computational model representing the regional aquifer beneath MDA G. The boundaries of the MDA G subset are listed in Table I-2.

Table I-2
Boundary Coordinates for MDA G Computational Grid

Direction	Grid Extent (m) [a]		
	Minimum	Maximum	Difference
East-West (x)	18,500	23,250	4,750
North-South (y)	-133,125	-130,250	2,875
Vertical (z)	100	2,050	1,950

[a] *Coordinates based on polar stereographic projections used in the Española basin site-scale model (Keating et al., 2003)*

I.3.3 Grid Resolution

The MDA G portion of the Española basin site-scale regional aquifer computational model, shown in Figure I-2, does not cross any boundaries where the horizontal resolution of the grid changes; it lies entirely within the high-resolution portion of the Española basin model, where nodes have regular orthogonal horizontal spacing of 125 m (410 ft). Thus, the "base" grid for the MDA G 3-D computational model is a regular mesh with horizontal node spacing of 125 m (410 ft) and variable vertical node spacing.

The vertical grid resolution is important for adequately representing groundwater flow and transport in the model. Each layer in the structured grid is horizontal, but the layers of the physical hydrogeologic units are gently sloping. Therefore, a finer, nonuniform grid resolution was used in the vertical dimension to capture the geometry of the hydrogeologic units. The vertical grid spacing was selected to accurately represent flow and transport along critical flow and transport pathways in the model domain. A finer resolution is used to represent shallower portions of the modeled region with progressively coarser resolutions for deeper portions. The vertical grid spacing ranges from 6.25 m (21 ft) at the mesa top to 150 m (490 ft) at the bottom of the model domain. The structure of the grid's vertical layering is summarized in Table I-3, which shows the vertical spacing of the base grid and the final refined area of the grid. Grid nodes are extended at the bottom of the MDA G grid to a 150-m (490-ft) layer spacing and a base grid spacing of 100 m (330 ft) to preserve octree refinement in the critical areas while maintaining the same number of grid nodes. Figure I-3 shows a close-up view of the horizontal and vertical resolution in the grid, where vertical spacing is reduced from 37.5 m (120 ft) to 6.25 m (21 ft). The grid east of regional characterization well R-22 was removed to better show the resolutions used to represent the disposal facility.

Table I-3
Vertical Grid Spacing of the MDA G Computational Grid

Elevation of Spacing Layers (m above mean sea level)	Vertical Grid Spacing (m)	
	Base Grid	Refined Area
Truncated top of grid (2,150)		
2075.00	50.00	50.00
2,062.50		12.50
1900.00		6.25
1881.25		9.38
1,862.50		18.75
925.00	37.50	37.50
850.00	75.00	75.00
100.00 (bottom)	150.00	150.00

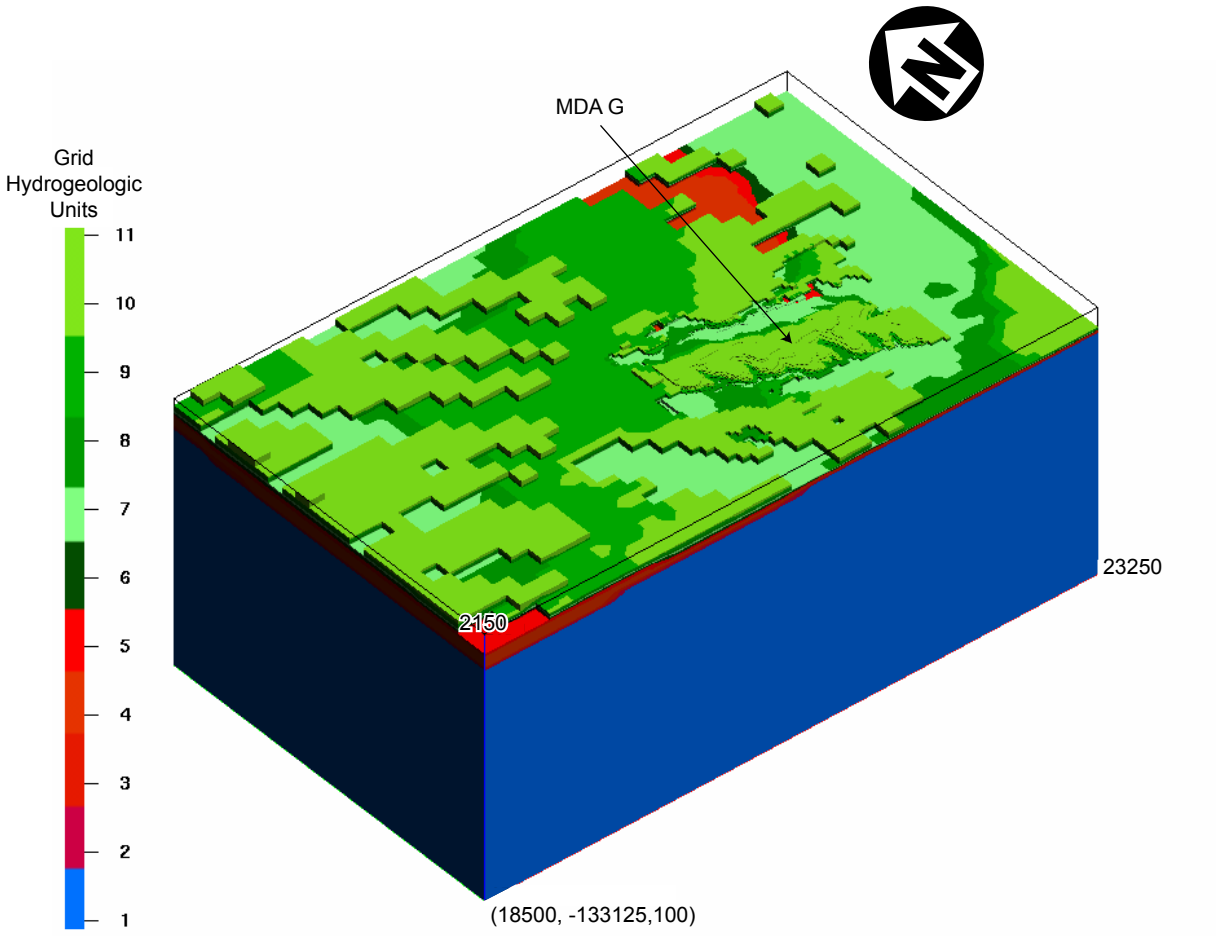

Grid coordinates (m) based on polar stereographic projections used for Española basin site-scale model (Keating et al., 2003)

Figure I-2
Final MDA G Computational Grid Truncated by Topology, Extended Vertically below Water Table, and Refined near MDA G

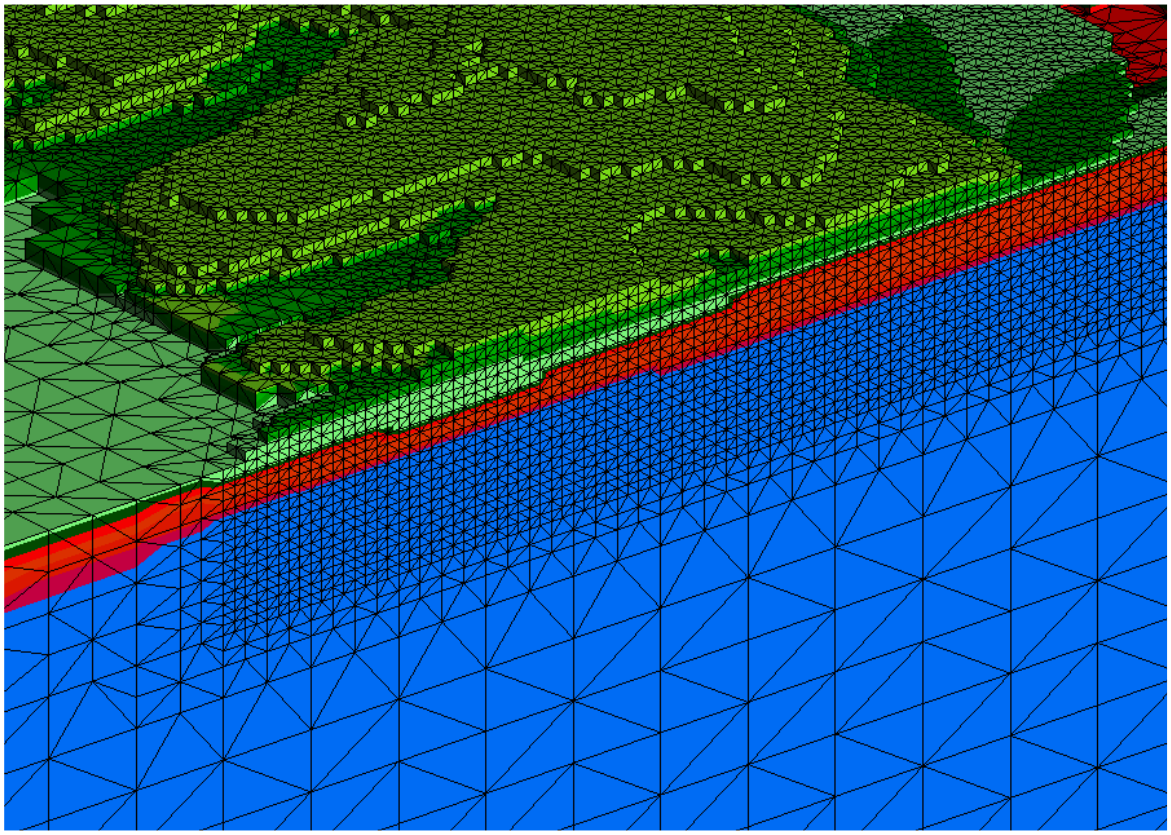

Note: Slice is N-S along Easting coordinate = 22248.4 (Well R-22 is at 22255.3E, 132532N)
Grid coordinates (m) based on polar stereographic projection for Española basin site-scale model (Keating et. al, 2003)

- *Tshirege Member of the Bandelier Tuff, unit 3*
- *Tshirege Member of the Bandelier Tuff, unit 2*
- *Tshirege Member of the Bandelier Tuff, unit 1, vitric portion*
- *Tshirege Member of the Bandelier Tuff, unit 1, colonnade portion*
- *Tshirege Member of the Bandelier Tuff, unit 1, glassy*
- *Tshirege Member of the Bandelier Tuff, Tsankawi Pumice*
- *Cerro Toledo interval*
- *Otowi Member of the Bandelier Tuff, ash flow*
- *Otowi Member of the Bandelier Tuff, Guaje Pumice Bed*
- *Basalts beneath Bandelier Tuff*

Figure I-3
Cutaway Revealing Refined Area of the Grid near MDA G and Transition to Coarser Spacing of Outer Grid

The general criteria used for grid refinement of the horizontal resolution are geometric. A polygon that outlines the TA-54 boundary was created (Figure I-4), partly from the GIS dataset that defines the southern fence line of TA-54 and partly by manual digitization. The horizontal grid spacing was refined in the area around MDA G by repeatedly splitting the grid cells by a factor of two until the finest grid spacing of exactly 7.8125 m (~26 ft) was attained in the vicinity of the active disposal area. Figure I-5 illustrates the horizontal transition from the low-resolution (125-m [410-ft]) base grid to the high-resolution (7.81-m [26-ft]) refined grid around MDA G. The grid resolution in the transition area (Figure 5) changes from 62.5 to 31.25 to 15.625 m (205 to 103 to 51 ft).

The top surface of the grid is an irregular stair-stepped surface created by the removal of any element located above the site surface, as represented using a digital elevation model (DEM). Since the top surface will not exactly match the elevations provided by the DEM a decision was made to use the following procedure:

- Remove any elements whose centroid (i.e., the average value of the eight corner nodes of a hexahedral element) is above the DEM.
- Check ground surface elevations to ensure that they allow for accurate locations of features such as the waste pits and adjust as needed.

The final truncated grid has a stair-stepped top surface with some nodes above the DEM. Figure I-6 illustrates how topography is represented by the grid in plan view.

I.3.4 Grid Properties

After the grid was constructed, the appropriate physical hydrogeologic unit was assigned to each node. The MDA G geologic model Stratamodel surface files represent the bottom surface of each hydrogeologic layer. The structured grid and the hydrogeologic surfaces were imported into LaGriT and were used to identify the hydrogeologic layer designation for each node and cell of the computational grid. Nodes were also identified as being above or below the water table, and association with any of the 35 geometrically defined pits was noted.

I.3.5 Grid Quality

The node distribution created by the refinement and removal of the top surface (see Section I.3.3) was connected to form a Delaunay tetrahedral grid. This is required because FEHM does not support direct import of an octree-refined hexahedral grid.

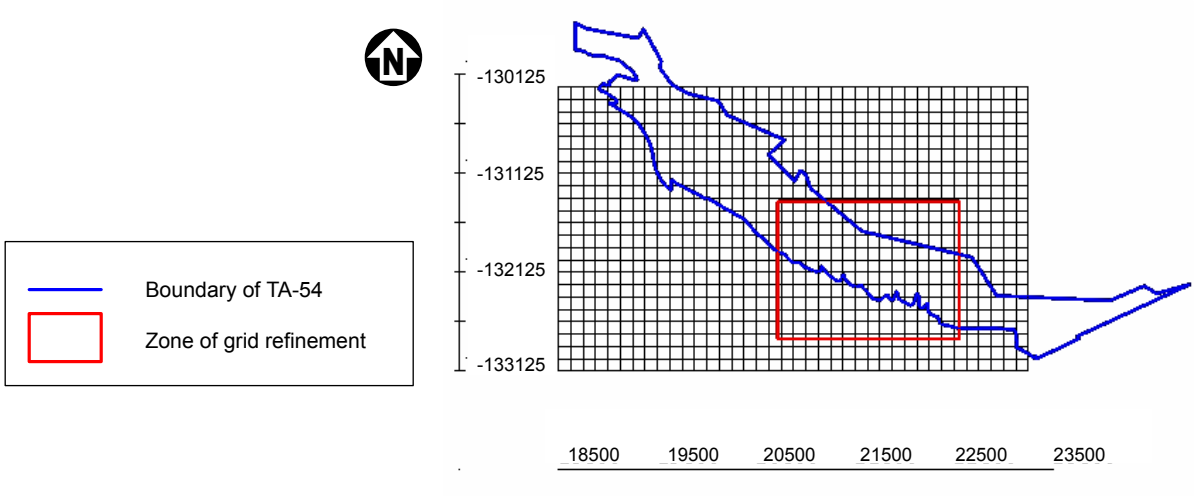

Figure I-4
Extent of Grid as Defined by Subset of the Española Basin Site-Scale Regional Aquifer Computational Model

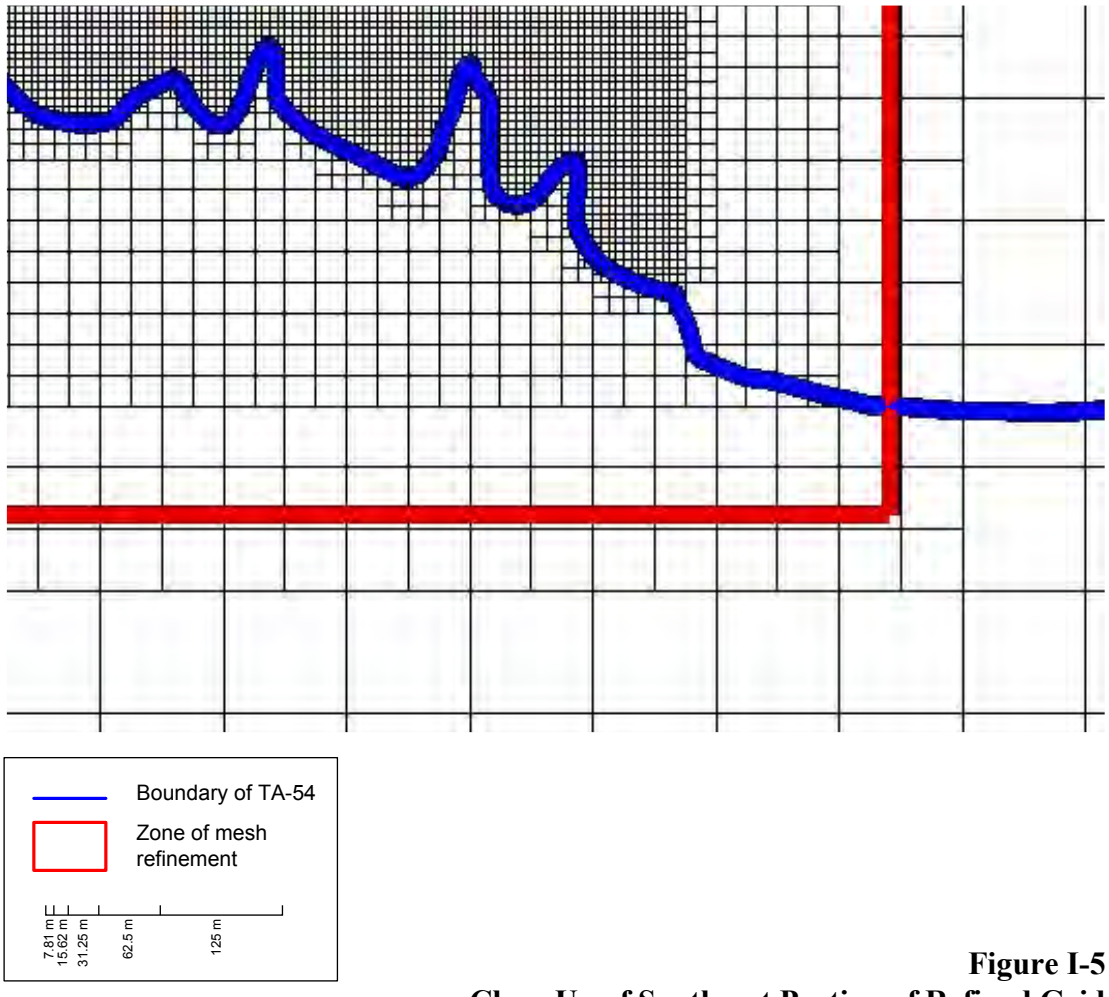

Figure I-5
Close-Up of Southeast Portion of Refined Grid Illustrating Grid Resolution Transition

Grid coordinates (m) based on polar stereographic projection for Española basin site-scale model (Keating et al., 2003)

Figure I-6
Surface Elevation of the Computational Grid

Quality checks were performed to ensure that the final grid is correct; these included isopach checks to ensure accurate thickness of the hydrogeologic surfaces units. All nodes were automatically and visually checked to ensure that they were assigned the correct material identification corresponding to the input data from the geologic model. Lists of the number of nodes associated with each material were compared to confirm that the hydrogeologic units were identified correctly. Feature locations were checked against the geologic model and area maps. Slices through the grid were compared to slices through the geologic model.

As expected, the accuracy of the representations of the hydrogeologic units is related to the grid spacing. The amount of error within the refined area is less than the grid block size of approximately 7.81 m (26 ft). Away from the refined area, and beyond the region that influences particle pathways, the grid blocks are larger and represent the units only coarsely. Some reasonable grid simplifications were made. For example, there is no Bandelier Tuff Tshirege Member unit 3 (Qbt3) material in the modeled area, therefore the few nodes tagged as Qbt3 during the unit identification process were reassigned to Tshirege Member unit 2 (Qbt2). Material unit designations below the Bandelier Tuff are not needed for the groundwater modeling; consequently, all layers below the Otowi Member of the Bandelier Tuff (Qbog) were assigned to a single basalt material.

I.3.6 Output

After the grid quality was checked and the geometry was determined to conform to the geologic model, the FEHM input files were generated. The FEHM software uses the control-volume finite element (CVFE) method to obtain numerical solutions to the groundwater flow equation over the model domain. LaGriT is designed to produce these CVFE grids by translating the coordinate and grid attribute information into a form that is valid for input into FEHM. Grid tetrahedral elements were divided into volumes associated with Voronoi control volumes and areas associated with Voronoi control volume faces. The control volumes are the Voronoi volumes associated with each node of the grid.

LaGriT was used to write the FEHM files listed in Table I-4. The files include the grid geometry, lists of nodes along external boundaries, and node lists sorted by hydrogeologic unit. The number of nodes assigned to each hydrogeologic unit is included in Table I-1.

Table I-4
Grid Generation Output Files for Finite Element Heat and Mass (FEHM) Modeling

Output File	Description
areag_lev4b_rsz_material.zone areag_lev5b_rsz_material.zone	FEHM zone list format for each hydrostratigraphic unit
areag_lev4b_rsz_outside.zone areag_lev5b_rsz_outside.zone	FEHM zone list format for each face of the model (top, bottom, N, S, E, W)
areag_lev4b_rsz_outside.area areag_lev5b_rsz_outside.area	FEHM area format file with the vector area associated with each exterior node
areag_lev4b_rsz.fehmn areag_lev5b_rsz.fehmn	FEHM 'cord' and 'elem' information for node coordinates and element connectivity
areag_lev4b_rsz.stor areag_lev5b_rsz.stor	FEHM sparse matrix coefficients
areag_lev4b_rsz.inp areag_lev5b_rsz.inp	AVS (Advanced Visual Systems) format graphic file
areag_lev4b_rsz.gmv areag_lev5b_rsz.gmv	GMV (General Grid Viewer) format graphics file

I.4 References

K. M. Bower, K.M, C.W. Gable, G.A. Zyvoloski, 2005, "Grid resolution study of ground water flow and transport", *Ground Water*, V 43, No. 1, pp. 122-132.

Keating, E.H., V.V. Vesselinov, E. Kwicklis, and Z. Lu, 2003, "Coupling Basin- and Local-Scale Inverse Models of the Española Basin," *Ground Water*, Vol. 4, No. 2, pp. 200-211.

George, D., 1997, "Unstructured 3D Grid Toolbox for Modeling and Simulation," Los Alamos National Laboratory Report LA-UR-97-3052, presented at the 1997 Workshop on Computational Electronics and Nanoelectronics, Urbana, Illinois, October 20-22, 1997.

Attachment II
Update of the Vadose-Zone Geologic Model for the Los Alamos National Laboratory TA-54, Material Disposal Area G Groundwater Pathway Model

Author:
Greg Cole

II.1 Geologic Model Update

The groundwater pathway modeling conducted in support of the Material Disposal Area (MDA) G performance assessment and composite analysis requires a variety of input data, including a geologic model of the region under consideration. A study performed in early 2003 investigated the three-dimensional (3-D) geometry of the vadose-zone geology for the portion of Los Alamos National Laboratory (LANL) that encompasses MDA G and Mortandad Canyon. As shown in Figure II-1, this area was enlarged by a buffer zone to include surrounding deep drill holes in all directions, thus ensuring regional continuity with the site-wide geology. This report describes the portion of the 2003 model that pertains to the groundwater modeling for the MDA G performance assessment and composite analysis (the MDA G geologic model area).

Figure II-1 shows the location of the MDA G geologic model area relative to the larger 2003 study area and the LANL boundary. The MDA G model area is rectangular in shape, extending approximately 4,880 m (1.6×10^4 ft) from east to west, and 3,050 m (1.0×10^4 ft) from north to south. The corner coordinates of the MDA G geologic model area are 1633000 E 1754000 N and 1649000 E 1764000 N (ft) using the New Mexico State Plane Coordinate System (NM SPCS) North America Datum (NAD) 83 system (approximately 3927471 E 421225 N and 3932308 E 424333 N in the Universal Transverse Mercator system [UTM], NAD 83, Zone 13).

The vertical range of the MDA G geologic model area is approximately 412 m (1,350 ft). It is defined by the topography in the northwest part of the model area, at approximately 2,140 m (7,025 ft) above mean sea level (msl), and the top of the saturated zone in the southeast, at approximately 1,730 m (5,675 ft) above msl. The model consists of top and bottom surface grids (where appropriate) for 14 geologic units and subunits, as well as grids for surface topography and the top of the saturated zone (water table). Each surface unit or subunit representation consists of a grid with 601 columns (east-west, or x-direction) and 401 rows (north-south, or y-direction) of elevation values at a 7.6-m (25-ft) spacing, with the lower left grid point at 1633000 E 175400 N NMSP (3927471 E 421225 N UTM, NAD 83, Zone 13). The surface geology, geology at the top of the saturated zone, and three-dimensional geology are shown in Figures II-2, II-3, and II-4, respectively, for the MDA G geologic model area.

There are no major faults within the MDA G geologic model, thus, the model is defined by the depositional and erosional geometry of the stratigraphic units. The stratigraphic nomenclature used generally follows that of Broxton and Reneau (1995). The youngest unit is unit 3 of the Tshirege Member of the Bandelier Tuff (Qbt 3), which crops out in topographic highs throughout most of the area, predominantly in the west (Figure II-2). The oldest unit, pumiceous Puye Formation (Tpp) of Tertiary age, occurs at the depth of the water table in the east (Figure II-3). Totavi Lentil axial river gravels (Tpt), and older Tschicoma Formation dacite lavas (Tt1) also lie within the central and western portions of the modeled block, below the water table.

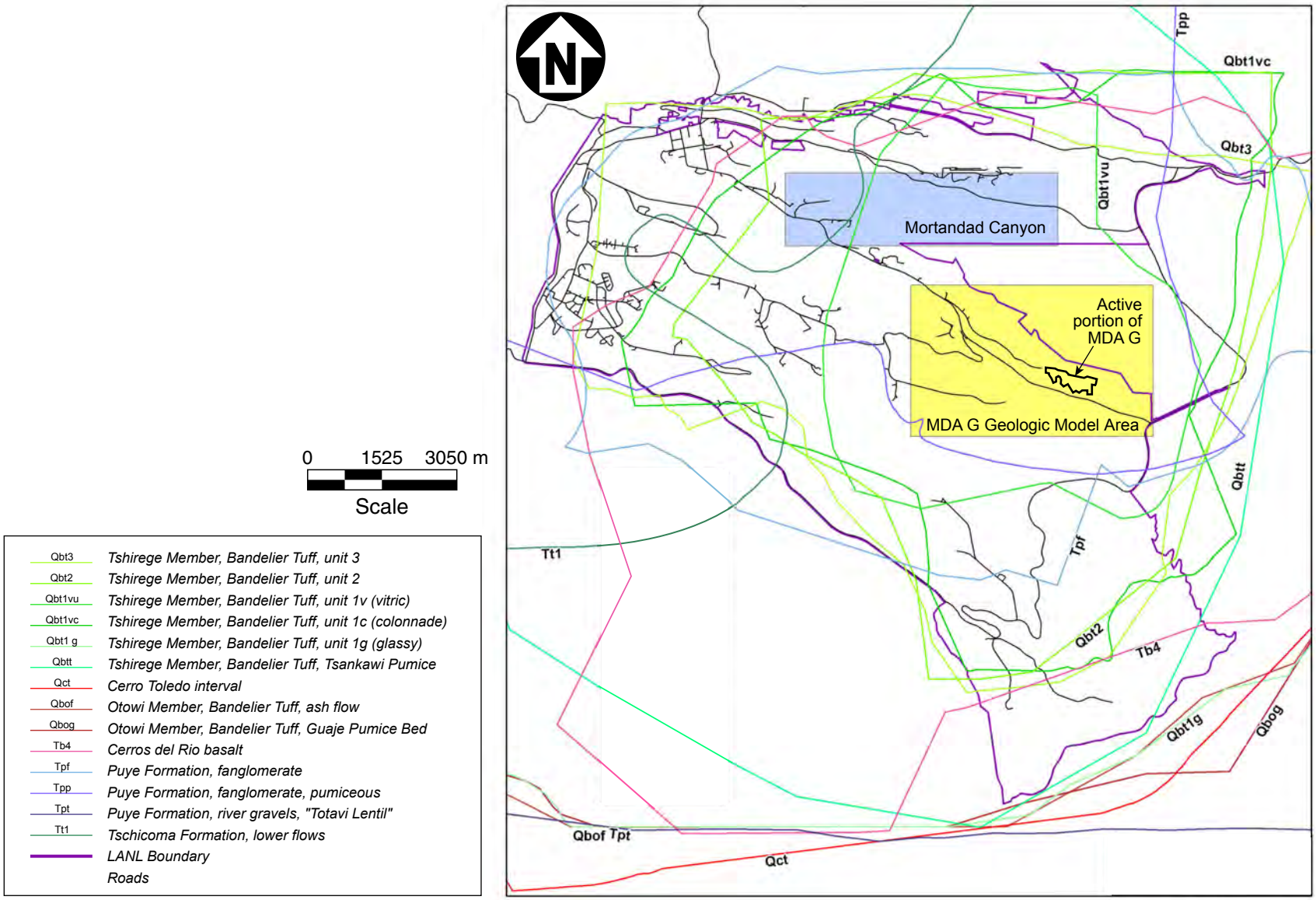

Figure II-1
MDA Geologic Model Area and Limits of 2003 Detailed Study Area for Each Geologic Unit

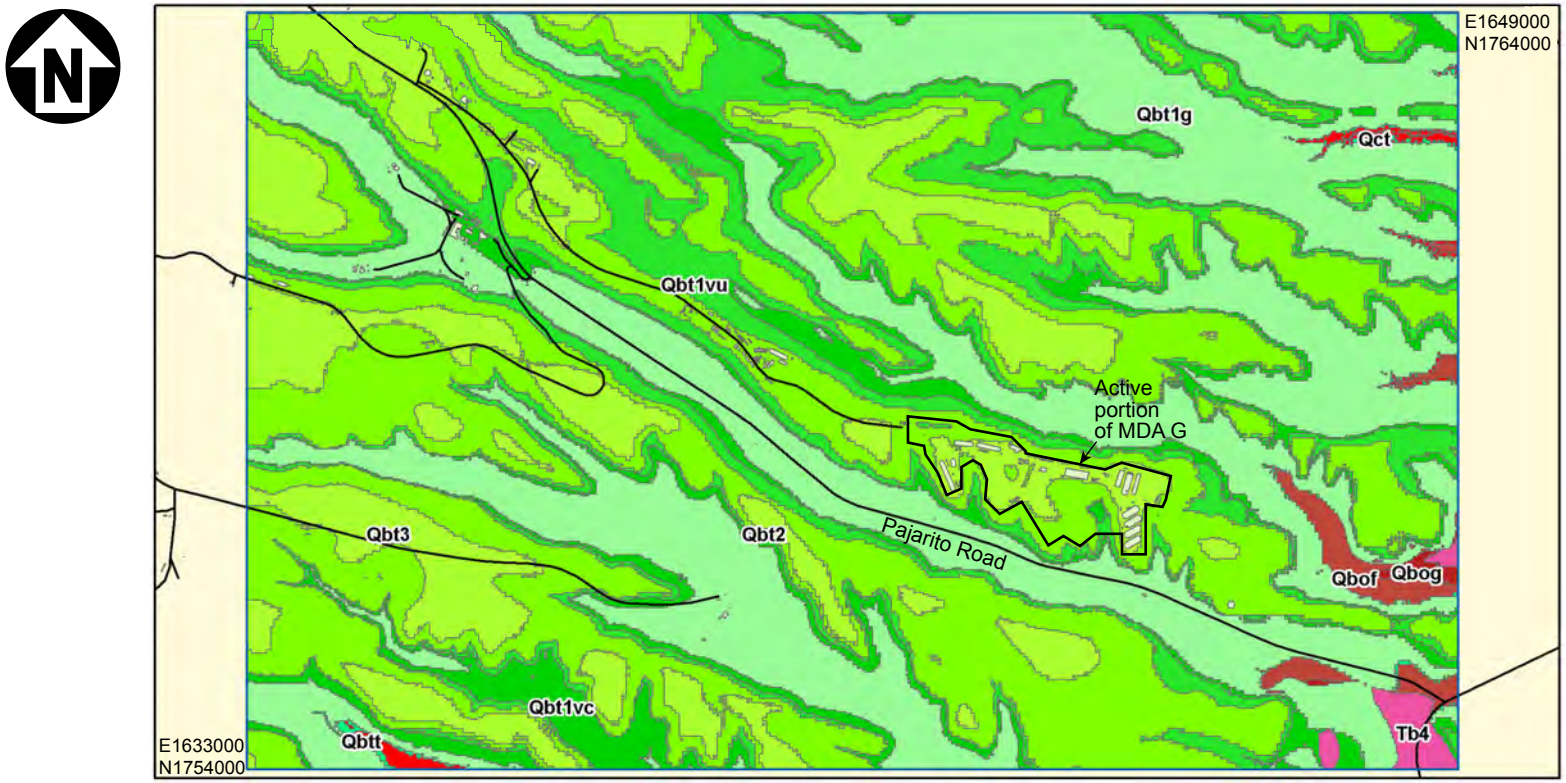

Qbt3	*Tshirege Member of the Bandelier Tuff, unit 3*
Qbt2	*Tshirege Member of the Bandelier Tuff, unit 2*
Qbt1vu	*Tshirege Member of the Bandelier Tuff, unit 1, vitric portion*
Qbt1vc	*Tshirege Member of the Bandelier Tuff, unit 1, colonnade portion*
Qbt1g	*Tshirege Member of the Bandelier Tuff, unit 1, glassy*
Qbtt	*Tshirege Member of the Bandelier Tuff, Tsankawi Pumice*
Qct	*Cerro Toledo interval*
Qbof	*Otowi Member of the Bandelier Tuff, ash flow*
Qbog	*Otowi Member of the Bandelier Tuff, Guaje Pumice Bed*
Tb4	*Cerros del Rio basalt*

0 1250 2500m

Scale

Map coordinates: New Mexico State Planar Coordinates, Central Zone, NAD 83 (ft)

Figure II-2
Surface Geology of MDA G Geologic Model

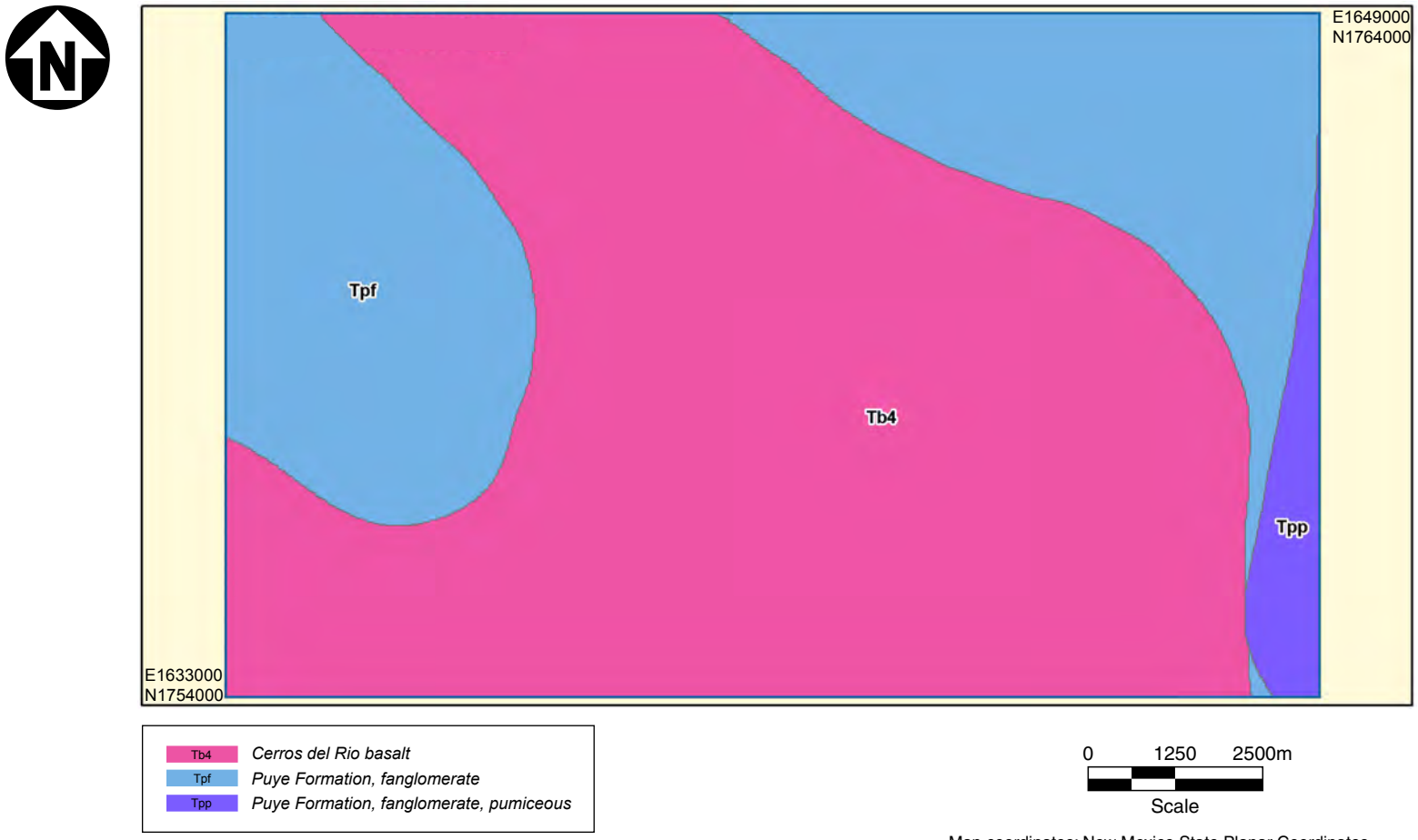

Figure II-3
Geology at Top of Saturated Zone for MDA G Geologic Model

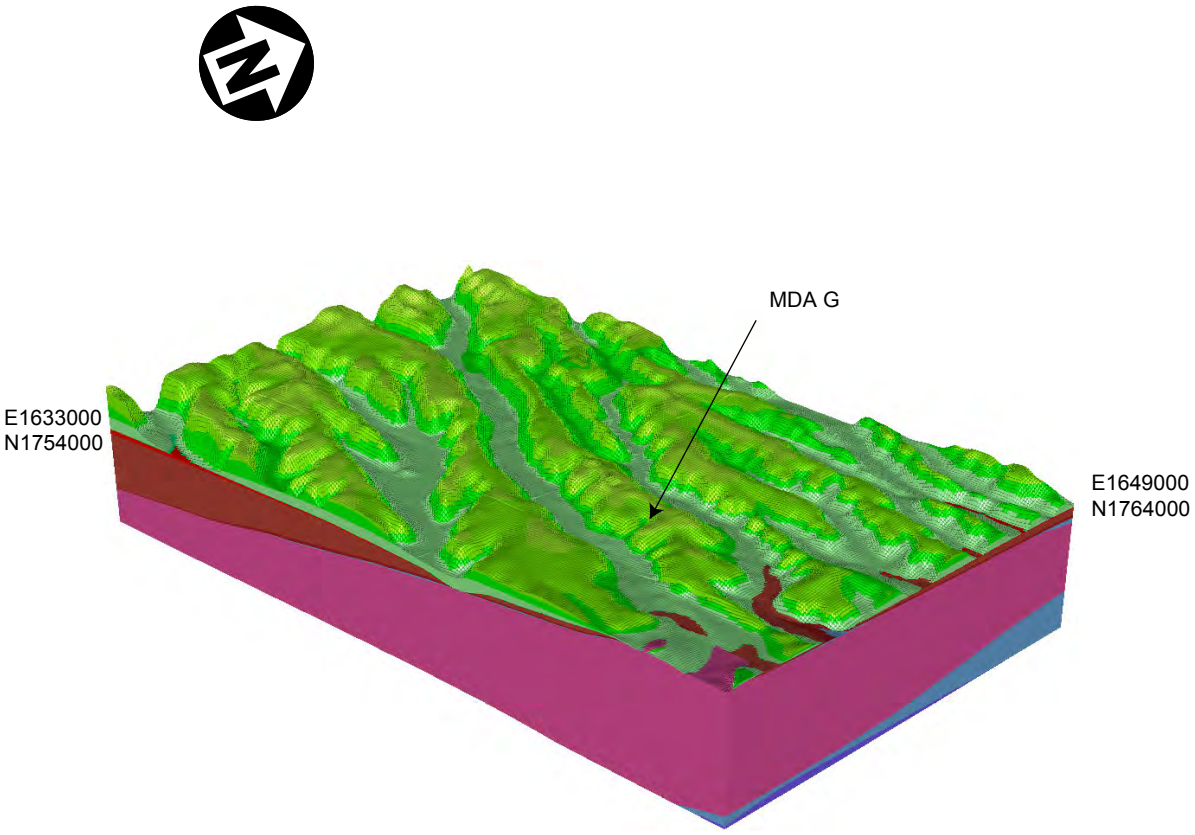

Qbt3	*Tshirege Member of the Bandelier Tuff, unit 3*
Qbt2	*Tshirege Member of the Bandelier Tuff, unit 2*
Qbt1vu	*Tshirege Member of the Bandelier Tuff, unit 1, vitric portion*
Qbt1vc	*Tshirege Member of the Bandelier Tuff, unit 1, colonnade portion*
Qbt1g	*Tshirege Member of the Bandelier Tuff, unit 1, glassy*
Qbtt	*Tshirege Member of the Bandelier Tuff, Tsankawi Pumice*
Qct	*Cerro Toledo interval*
Qbof	*Otowi Member of the Bandelier Tuff, ash flow*
Qbog	*Otowi Member of the Bandelier Tuff, Guaje Pumice Bed*
Tb4	*Cerros del Rio basalt*
Tpf	*Puye Formation, fanglomerate*
Tpp	*Puye Formation, fanglomerate, pumiceous*

Figure II-4
Three-Dimensional Geology of MDA G Geologic Model

The principal sources of data for the geologic model are mapped contacts in canyon walls and stratigraphic data obtained from drill cores. Figure II-5 is a visualization of the subsurface data control provided by the array of drill holes within the survey area. Contact elevations and depths below ground surfaces of the various geologic units, as obtained from drill holes, are tabulated in Tables II-1 and II-2, respectively. Drill holes outside of the MDA G geologic model area that were also used to constrain the contact surface positions are not shown. The distribution of drill hole, surface contact elevation (or thickness), and geological interpretation constraints for individual surfaces are provided in Figures II-6 through II-13. Individual contact surfaces were obtained through a three-step process that included the following:

- Creation of plots showing measured contact/isopach locations and other controls indicating the presence or absence of the unit
- Hand-contouring of data by geologists, guided by the data plot(s) and the conceptual geologic model
- Computer gridding of contact positions and the geologist-generated contours, using a minimum curvature and minimum surface sink algorithm, ANUDEM, developed at the University of Australia (ANU, 2004)

The set of surfaces was then examined to resolve conflicts such as inappropriate intersections between units or unrealistic thicknesses of individual units. The final unit volumes were defined by the set of surfaces (and model boundaries) that truncated, but did not intersect, one other.

The stratigraphy of the MDA G geologic model area is illustrated through a set of cross sections. Figure II-14 shows the locations of these cross sections. Figure II-15 is a cross section of the 3-D geologic model along the NW–SE trending mesa, incorporating subsurface data from regional characterization wells R-20, R-21, R-22, and R-23. Figures II-16 through II-19 provide cross sections that span the mesa from north to south, each passing through a single characterization well (wells R-20, R-21, R-22, and R-23, respectively). Detailed descriptions of stratigraphic units can be obtained from the characterization well reports (Ball et al., 2002; LANL, 2003a, 2003b, 2003c; Kleinfelder, 2003).

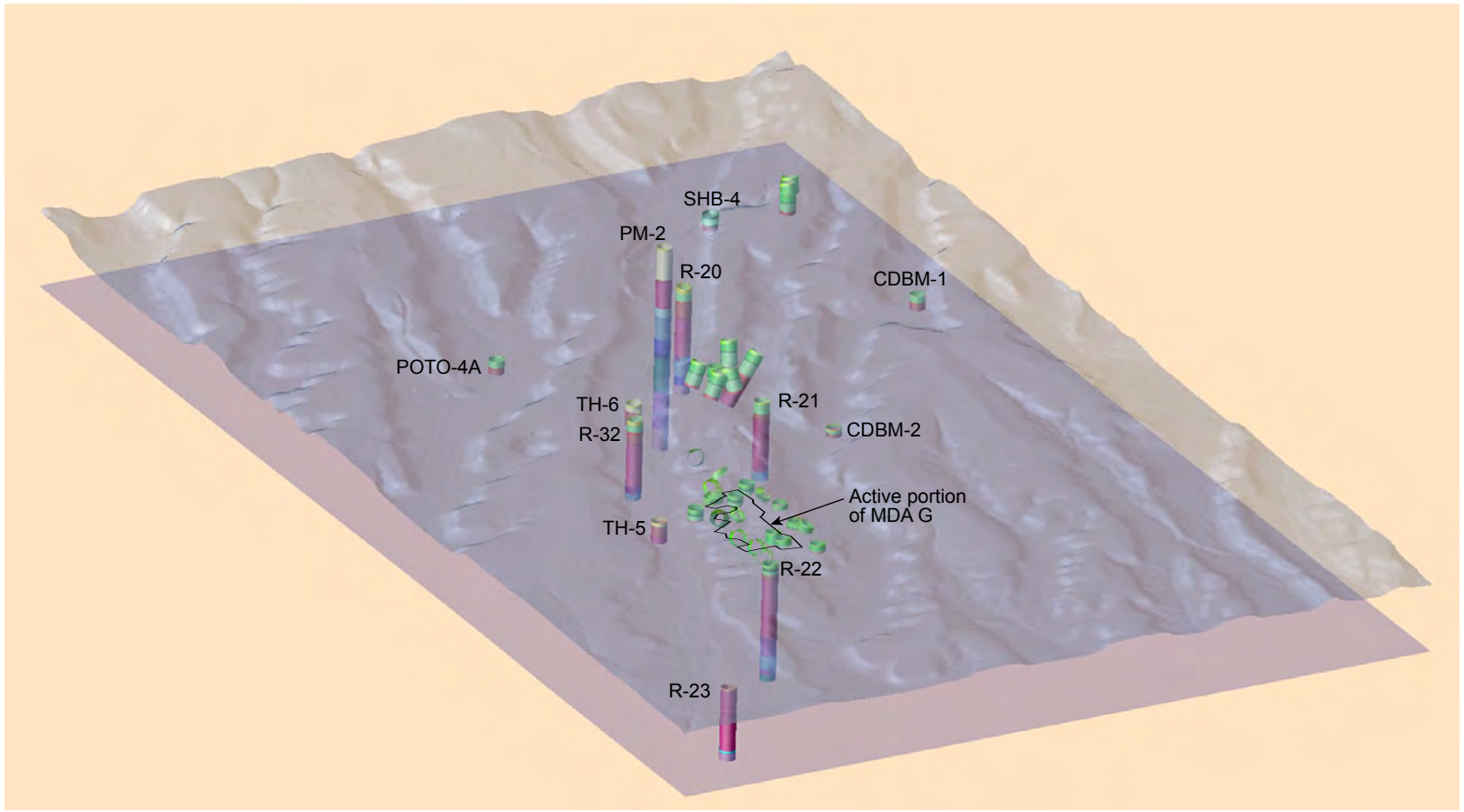

Figure II-5
Stratigraphy of Drill Holes in and around MDA G Geologic Model Area

Table II-1
Elevations of Basal Contacts of Geologic Units as Encountered by Drill Holes

Drill Hole	Elevation of Basal Contact (m above mean sea level)												
	Qbt 3	Qbt 2	Qbt 1vu	Qbt 1vc	Qbt 1g	Qbtt	Qct	Qbof	Qbog	Tb4	Tpf	Tpp	Tpt
54-1001	---	2,055.6	2,035.1	2,028.7	1,989.7	1,989.4	1,981.2	---	---	---	---	---	---
54-1002	---	2,056.5	2,033.9	2,028.7	1,990.3	1,989.7	1,981.2	---	---	---	---	---	---
54-1003	---	2,058.0	2,035.5	2,029.4	1,990.3	1,989.4	1,979.1	---	---	---	---	---	---
54-1004	---	2,057.7	2,037.0	2,029.1	1,984.6	1,983.6	1,979.1	1,965.4	---	---	---	---	---
54-1005	---	2,056.2	2,038.2	2,028.1	1,992.8	1,990.6	1,983.3	---	---	---	---	---	---
54-1006	---	2,058.6	2,037.6	2,030.3	1,991.0	1,990.6	1,981.2	---	---	---	---	---	---
54-1007	---	2,058.3	2,035.8	2,029.7	2,023.9	---	---	---	---	---	---	---	---
54-1008	---	2,059.8	2,038.8	2,032.1	2,026.0	---	---	---	---	---	---	---	---
54-1009	---	2,059.5	2,036.7	2,030.3	2,024.5	---	---	---	---	---	---	---	---
54-1010	---	2,057.4	2,056.8	---	---	---	---	---	---	---	---	---	---
54-1011	---	2,058.9	2,057.7	---	---	---	---	---	---	---	---	---	---
54-1012	---	2,058.9	2,058.0	---	---	---	---	---	---	---	---	---	---
54-1013	---	2,059.8	2,058.3	---	---	---	---	---	---	---	---	---	---
54-1014	---	2,059.8	2,058.3	---	---	---	---	---	---	---	---	---	---
54-1015	---	---	---	2,033.0	1,994.9	1,994.0	1,983.6	1,953.8	1,950.4	1,902.6	1,948.3	---	---
54-1016	---	---	---	2,032.4	1,994.0	1,993.1	1,978.5	1,960.8	1,958.3	1,882.7	---	---	---
54-1018	---	2,056.8	2,037.0	2,029.1	1,990.3	1,990.0	1,978.2	1,969.0	---	---	---	---	---
54-1023	---	2,087.6	2,058.9	2,053.7	2,020.8	2,020.2	2,019.0	---	---	---	---	---	---
54-1024	---	2,087.3	2,071.1	---	---	---	---	---	---	---	---	---	---
54-1025	---	2,089.4	2,072.6	---	---	---	---	---	---	---	---	---	---

--- = Not encountered

Table II-1 (Continued)
Elevations of Basal Contacts of Geologic Units as Encountered by Drill Holes

Drill Hole	Elevation of Basal Contact (m above mean sea level)												
	Qbt 3	Qbt 2	Qbt 1vu	Qbt 1vc	Qbt 1g	Qbtt	Qct	Qbof	Qbog	Tb4	Tpf	Tpp	Tpt
54-1026	---	2,089.4	2,072.6	---	---	---	---	---	---	---	---	---	---
54-1102	---	2,035.5	2,028.7	---	---	---	---	---	---	---	---	---	---
54-1105	---	617.6	---	---	---	---	---	---	---	---	---	---	---
54-1106	---	618.8	---	---	---	---	---	---	---	---	---	---	---
54-1107	---	2,030.3	2,020.2	2,016.6	2,008.0	---	---	---	---	---	---	---	---
54-1108	---	2,030.3	2,026.6	---	---	---	---	---	---	---	---	---	---
54-1110(G-3)	---	2,024.8	2,018.1	2,013.5	2,008.0	---	---	---	---	---	---	---	---
54-1111(G-4)	---	2,022.3	2,016.6	2,010.2	1,992.5	1,991.9	1,987.9	---	---	---	---	---	---
54-1112	---	2,028.4	2,021.7	---	---	---	---	---	---	---	---	---	---
54-1114	---	2,024.2	2,019.6	---	---	---	---	---	---	---	---	---	---
54-1115	---	2,021.1	2,013.8	2,012.0	---	---	---	---	---	---	---	---	---
54-1116	---	2,025.4	2,015.9	2,009.9	---	---	---	---	---	---	---	---	---
54-1117	---	2,026.9	2,015.9	2,011.4	2,007.7	---	---	---	---	---	---	---	---
54-1120	---	2,027.2	2,023.6	---	---	---	---	---	---	---	---	---	---
54-1121	---	2,026.9	2,014.1	2,010.5	1,997.7	---	1,990.6	1,989.1	---	---	---	---	---
54-1123	---	2,023.0	2,012.6	2,011.1	2,004.4	---	2,001.0	---	---	---	---	---	---
54-1124	---	2,013.2	2,011.1	---	---	---	---	---	---	---	---	---	---
54-1125	---	2,021.1	2,013.5	---	---	---	---	---	---	---	---	---	---
54-1126	---	2,020.2	2,013.8	2,013.2	---	---	---	---	---	---	---	---	---

--- = Not encountered

Table II-1 (Continued)
Elevations of Basal Contacts of Geologic Units as Encountered by Drill Holes

Drill Hole	Elevation of Basal Contact (m above mean sea level)												
	Qbt 3	Qbt 2	Qbt 1vu	Qbt 1vc	Qbt 1g	Qbtt	Qct	Qbof	Qbog	Tb4	Tpf	Tpp	Tpt
54-1128	---	2,021.7	2,015.3	---	---	---	---	---	---	---	---	---	---
54-15462	---	2,085.7	2,057.4	2,052.5	2,019.3	---	2,016.3	2,005.6	---	---	---	---	---
54-G-2	---	2,024.5	2,024.5	2,014.1	2,009.2	---	---	---	---	---	---	---	---
54-G-5	---	2,025.1	2,025.1	2,012.9	2,007.4	---	---	---	---	---	---	---	---
CDBM-1	---	---	---	---	2,023.9	2,023.0	2,019.9	1,991.3	---	---	---	---	---
CDBM-2	---	---	---	---	2,006.8	2,006.2	2,005.6	1,991.9	---	---	---	---	---
PM-2	---	---	---	---	---	---	---	---	1,914.1	1,811.1	1,689.8	1,637.4	1,616.0
POTO-4A	---	---	---	---	1,992.8	1,991.9	1,986.7	1,965.4	---	---	---	---	---
R20	---	---	---	---	1,990.0	---	1,984.9	1,926.6	1,921.2	1,756.6	1,697.1	1,662.1	---
R21	---	---	---	---	1,987.0	1,986.1	1,983.9	1,966.0	1,960.8	1,758.7	1,726.7	---	---
R22	---	2,013.5	2,013.5	2,003.5	1,987.9	---	---	1,972.4	1,968.4	1,669.4	1,619.1	---	---
R23	---	---	---	---	---	---	---	1,977.8	1,976.0	1,744.7	---	---	---
R32	---	---	---	---	1,980.0	---	1,969.0	1,937.6	1,934.6	1,740.7	1,714.2	---	---
SHB-4	---	---	---	2,044.6	2,021.1	2,020.2	---	1,995.8	---	---	---	---	---
TH-5	---	---	---	---	---	---	---	1,960.2	1,956.8	1,928.8	---	---	---
TH-6	---	---	---	---	---	---	---	1,944.0	1,937.9	---	1,933.3	---	---

--- = Not encountered

Table II-2
Depths of Basal Contacts of Geologic Units Encountered by Drill Holes

Drill Hole	Depth of Basal Contact (m below ground surface)													
	Qbt 3	Qbt 2	Qbt 1vu	Qbt 1vc	Qbt 1g	Qbtt	Qct	Qbof	Qbog	Tb4	Tpf	Tpp	Tpt	Tt1
54-1001	---	11.6	32.0	38.1	77.4	77.7	86.0	---	---	---	---	---	---	---
54-1002	---	12.8	35.7	40.5	78.9	79.6	88.1	---	---	---	---	---	---	---
54-1003	---	12.2	34.7	40.8	79.9	80.8	91.1	---	---	---	---	---	---	---
54-1004	---	11.6	32.0	39.9	84.7	85.3	89.9	103.6	---	---	---	---	---	---
54-1005	---	10.1	28.0	37.8	73.5	75.3	82.9	---	---	---	---	---	---	---
54-1006	---	11.0	32.0	39.3	78.6	79.2	88.4	---	---	---	---	---	---	---
54-1007	---	11.3	33.8	39.9	45.7	---	---	---	---	---	---	---	---	---
54-1008	---	11.9	32.9	39.6	45.7	---	---	---	---	---	---	---	---	---
54-1009	---	10.7	33.5	40.2	45.7	---	---	---	---	---	---	---	---	---
54-1010	---	12.5	12.8	---	---	---	---	---	---	---	---	---	---	---
54-1011	---	11.6	12.5	---	---	---	---	---	---	---	---	---	---	---
54-1012	---	11.6	12.5	---	---	---	---	---	---	---	---	---	---	---
54-1013	---	11.0	12.5	---	---	---	---	---	---	---	---	---	---	---
54-1014	---	11.0	12.5	---	---	---	---	---	---	---	---	---	---	---
54-1015	---	---	---	11.6	50.0	50.6	61.0	90.8	94.2	142.0	96.3	---	---	---
54-1016	---	---	---	9.8	48.5	49.1	63.7	81.4	83.8	159.4	---	---	---	---
54-1018	---	12.2	32.0	39.9	78.6	78.9	90.8	100.0	---	---	---	---	---	---
54-1023	---	10.7	39.3	44.5	77.7	78.0	79.2	---	---	---	---	---	---	---
54-1024	---	11.3	27.4	---	---	---	---	---	---	---	---	---	---	---
54-1025	---	10.7	27.4	---	---	---	---	---	---	---	---	---	---	---

--- = Not encountered

Table II-2 (Continued)
Depths of Basal Contacts of Geologic Units Encountered by Drill Holes

Drill Hole	Depth of Basal Contact (m below ground surface)													
	Qbt 3	Qbt 2	Qbt 1vu	Qbt 1vc	Qbt 1g	Qbtt	Qct	Qbof	Qbog	Tb4	Tpf	Tpp	Tpt	Tt1
54-1026	---	10.4	27.4	---	---	---	---	---	---	---	---	---	---	---
54-1102	---	13.1	19.5	---	---	---	---	---	---	---	---	---	---	---
54-1105	---	14.6	---	---	---	---	---	---	---	---	---	---	---	---
54-1106	---	15.8	---	---	---	---	---	---	---	---	---	---	---	---
54-1107	---	17.4	27.4	31.1	39.6	---	---	---	---	---	---	---	---	---
54-1108	---	12.2	15.8	---	---	---	---	---	---	---	---	---	---	---
54-1110 (G-3)	---	14.6	21.3	25.9	31.4	---	---	---	---	---	---	---	---	---
54-1111 (G-4)	---	12.2	18.0	24.4	42.1	42.7	46.6	---	---	---	---	---	---	---
54-1112	---	11.6	18.6	---	---	---	---	---	---	---	---	---	---	---
54-1114	---	7.9	12.8	---	---	---	---	---	---	---	---	---	---	---
54-1115	---	12.5	19.8	21.9	---	---	---	---	---	---	---	---	---	---
54-1116	---	11.6	21.3	27.4	---	---	---	---	---	---	---	---	---	---
54-1117	---	9.1	20.1	24.7	28.3	---	---	---	---	---	---	---	---	---
54-1120	---	11.6	15.2	---	---	---	---	---	---	---	---	---	---	---
54-1121	---	7.3	20.1	23.8	36.6	---	43.6	45.1	---	---	---	---	---	---
54-1123	---	8.5	19.2	20.7	27.4	---	30.5	---	---	---	---	---	---	---
54-1124	---	9.4	11.9	---	---	---	---	---	---	---	---	---	---	---
54-1125	---	11.6	19.5	---	---	---	---	---	---	---	---	---	---	---
54-1126	---	8.5	14.9	15.5	---	---	---	---	---	---	---	---	---	---

--- = Not encountered

Table II-2 (Continued)
Depths of Basal Contacts of Geologic Units Encountered by Drill Holes

Drill Hole	Depth of Basal Contact (m below ground surface)													
	Qbt 3	Qbt 2	Qbt 1vu	Qbt 1vc	Qbt 1g	Qbtt	Qct	Qbof	Qbog	Tb4	Tpf	Tpp	Tpt	Tt1
54-1128	---	6.1	12.5	---	---	---	---	---	---	---	---	---	---	---
54-15462	---	11.3	39.6	44.5	77.7	---	80.8	91.4	---	---	---	---	---	---
54-G-2	---	15.8	15.8	26.5	31.1	---	---	---	---	---	---	---	---	---
54-G-5	---	16.8	16.8	29.0	34.4	---	---	---	---	---	---	---	---	---
CDBM-1	---	---	---	---	25.0	25.9	29.0	57.6	---	---	---	---	---	---
CDBM-2	---	---	---	---	15.5	16.2	16.8	30.2	---	---	---	---	---	---
PM-2	---	---	---	---	---	---	---	---	131.7	234.7	356.0	408.4	429.8	---
POTO-4A	---	---	---	---	25.6	26.5	31.7	53.0	---	---	---	---	---	---
R-20	---	---	---	---	50.6	---	55.8	114.0	119.5	284.1	343.5	378.6	---	---
R-21	---	---	---	---	43.0	44.2	46.0	64.0	69.2	271.3	303.3	---	---	---
R-22	---	13.4	13.4	23.5	39.0	---	---	54.6	58.5	357.5	407.8	---	---	---
R-23	---	---	---	---	---	---	---	9.1	11.0	242.3	---	---	---	---
R-32	---	---	---	---	42.1	---	53.0	84.4	87.5	281.3	307.8	---	---	---
SHB-4	---	---	---	12.2	35.7	36.6	---	61.0	---	---	---	---	---	---
TH-5	---	---	---	---	---	---	---	48.8	52.1	80.2	---	---	---	---
TH-6	---	---	---	---	---	---	---	80.8	86.9	---	91.4	---	---	---

--- = Not encountered

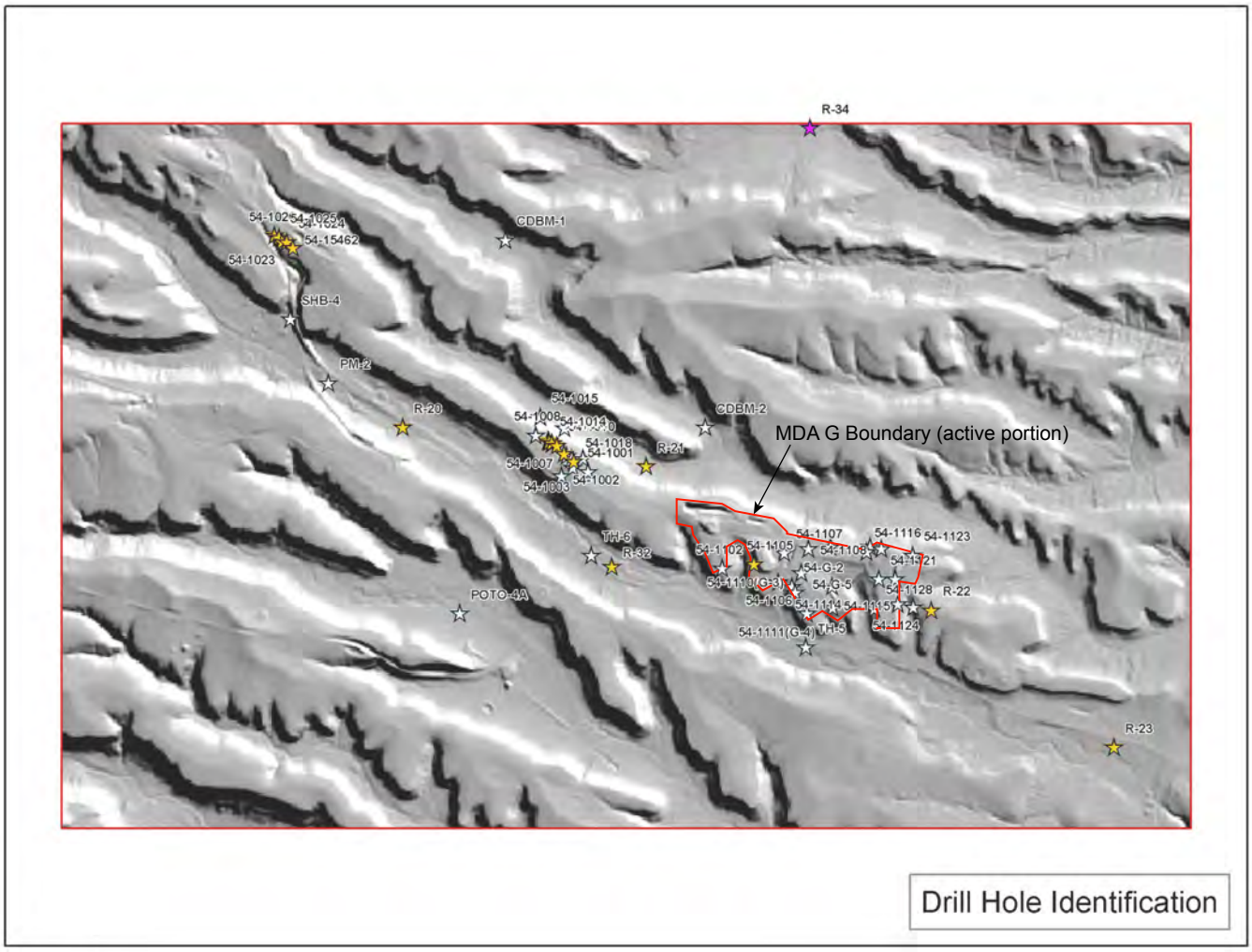

☆ Drill hole data from Birdsell et al. (1999)

★ New drill hole data incorporated into 2003 model

★ Drill hole data (from regional characterization well R-34) generated after 2003 modeling activities

0 1250 2500m

Scale

Figure II-6
Drill Hole Locations in and around MDA G Geologic Model

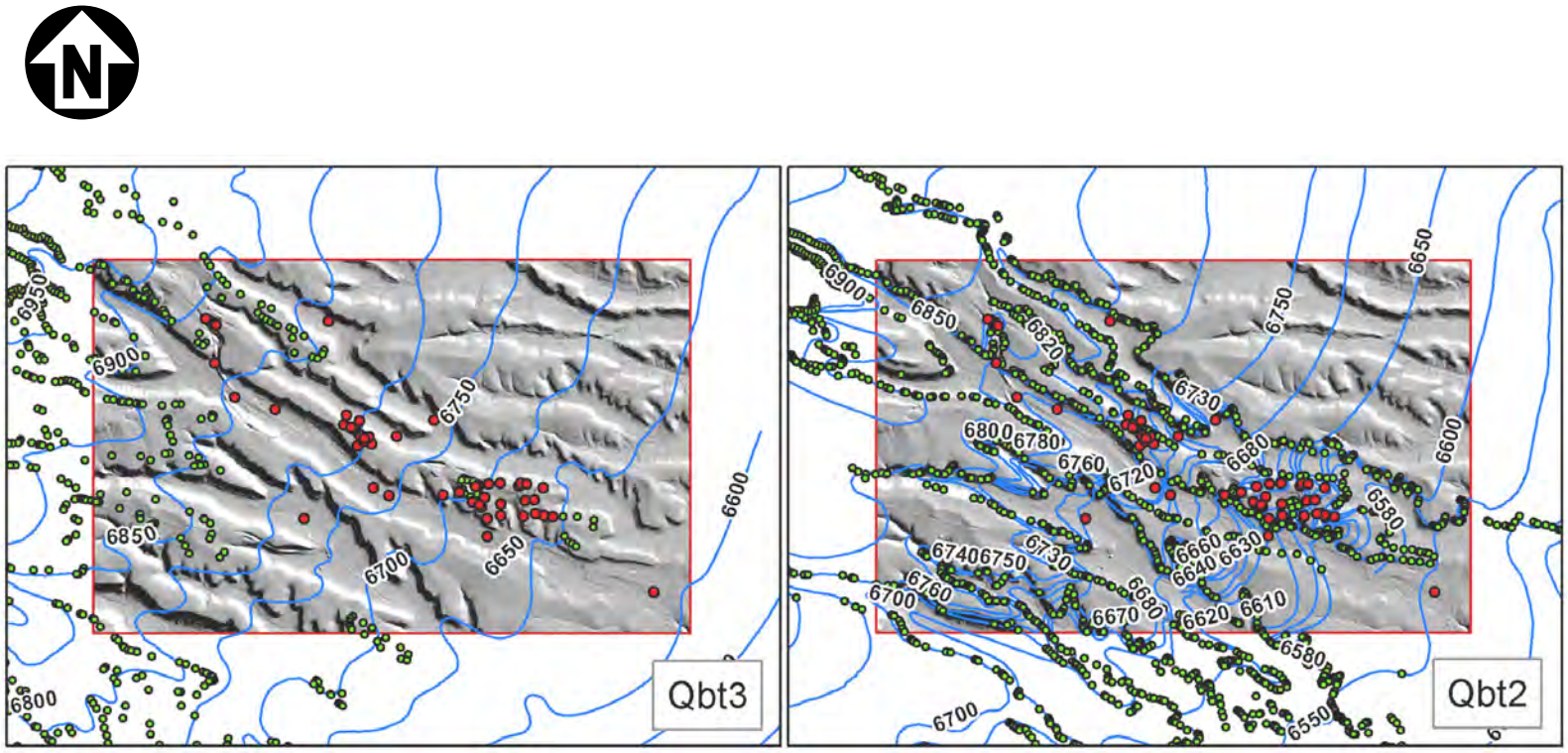

Figure II-7
Surface, Subsurface, and Interpretive Controls for Base of Bandelier Tuff Units 2 and 3

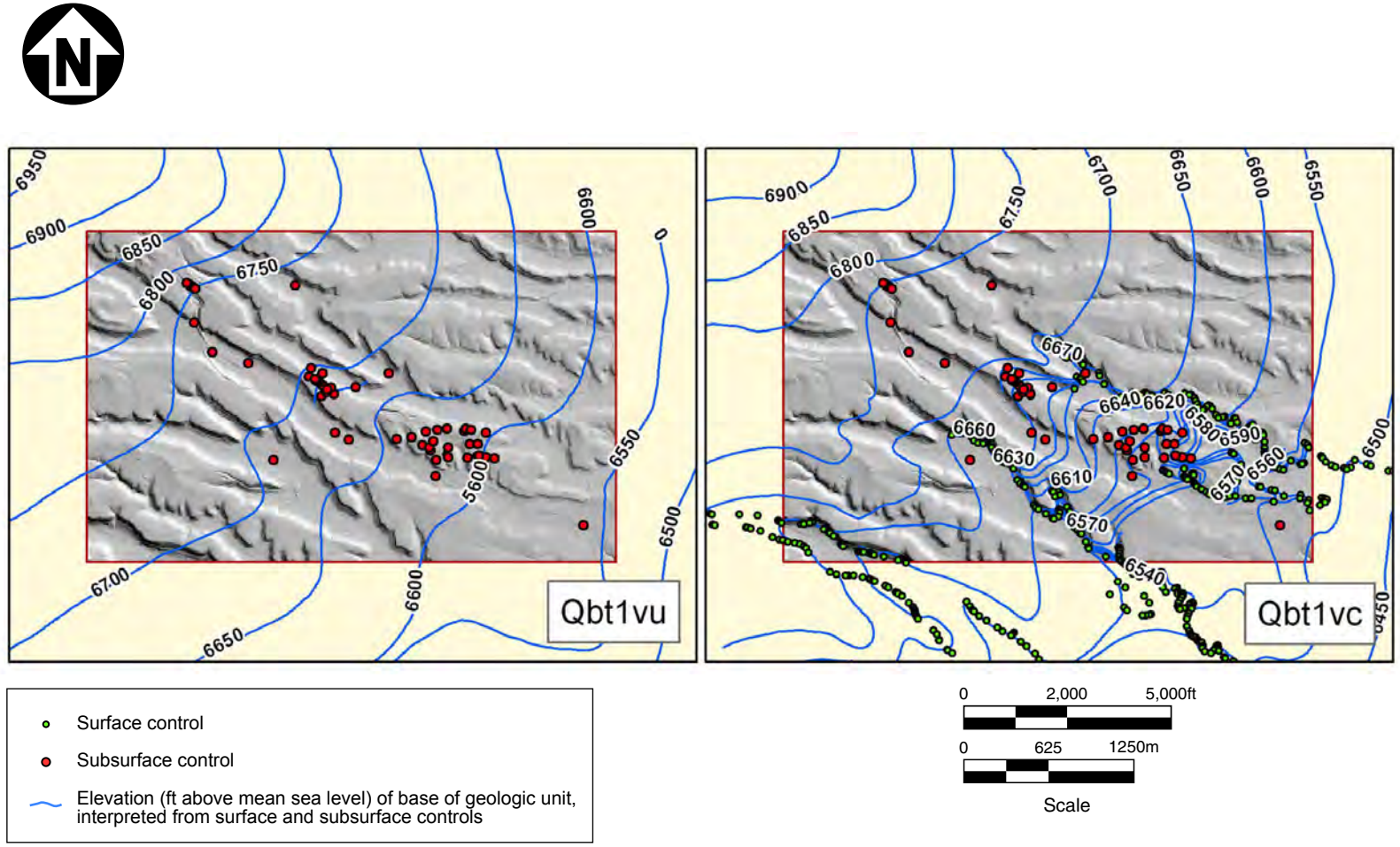

Figure II-8
Surface, Subsurface, and Interpretive Controls for Base of Bandelier Tuff Units 1v and 1vc

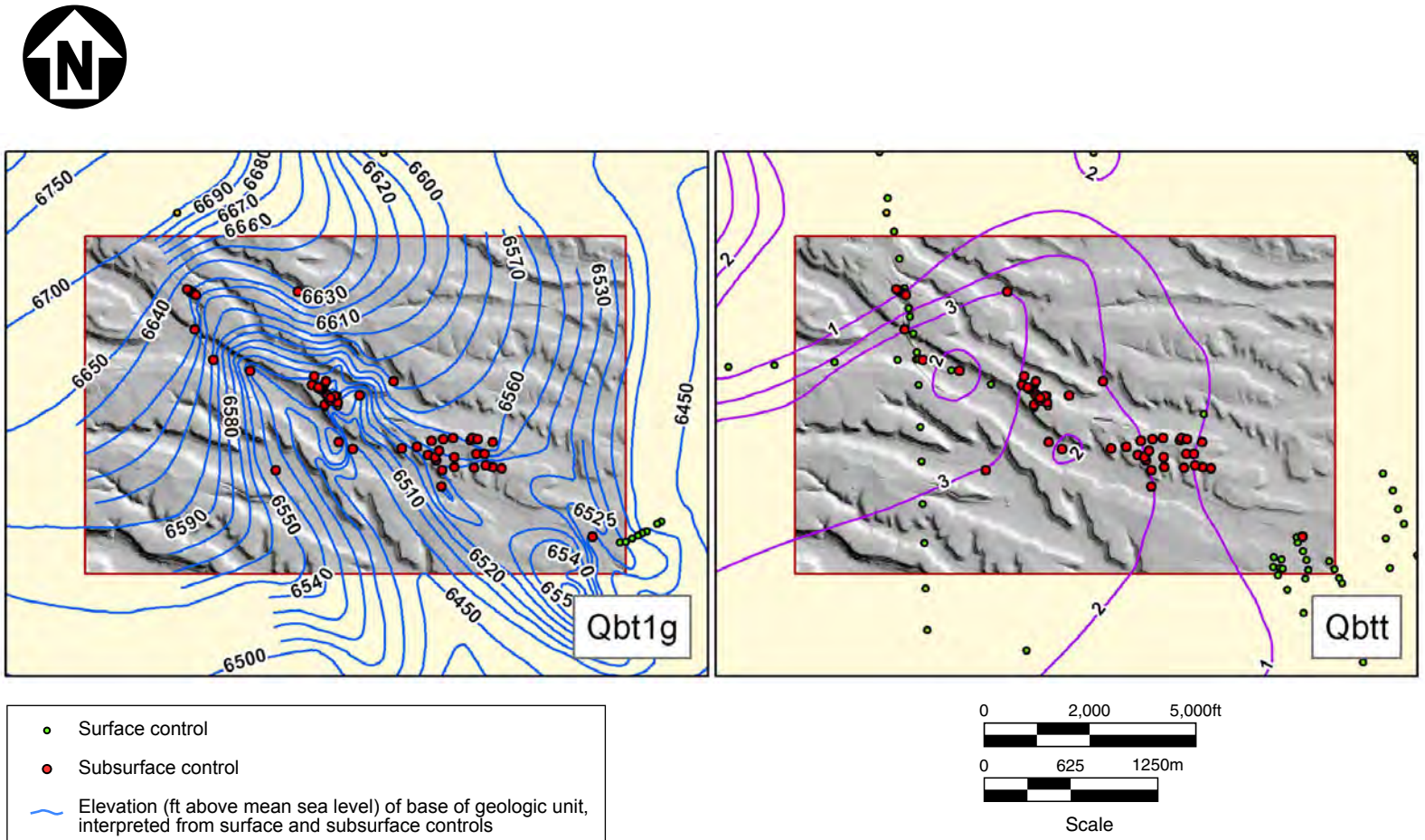

Figure II-9
Surface, Subsurface, and Interpretive Controls for Base of Bandelier Tuff Units 1g and Tsankawi Pumice

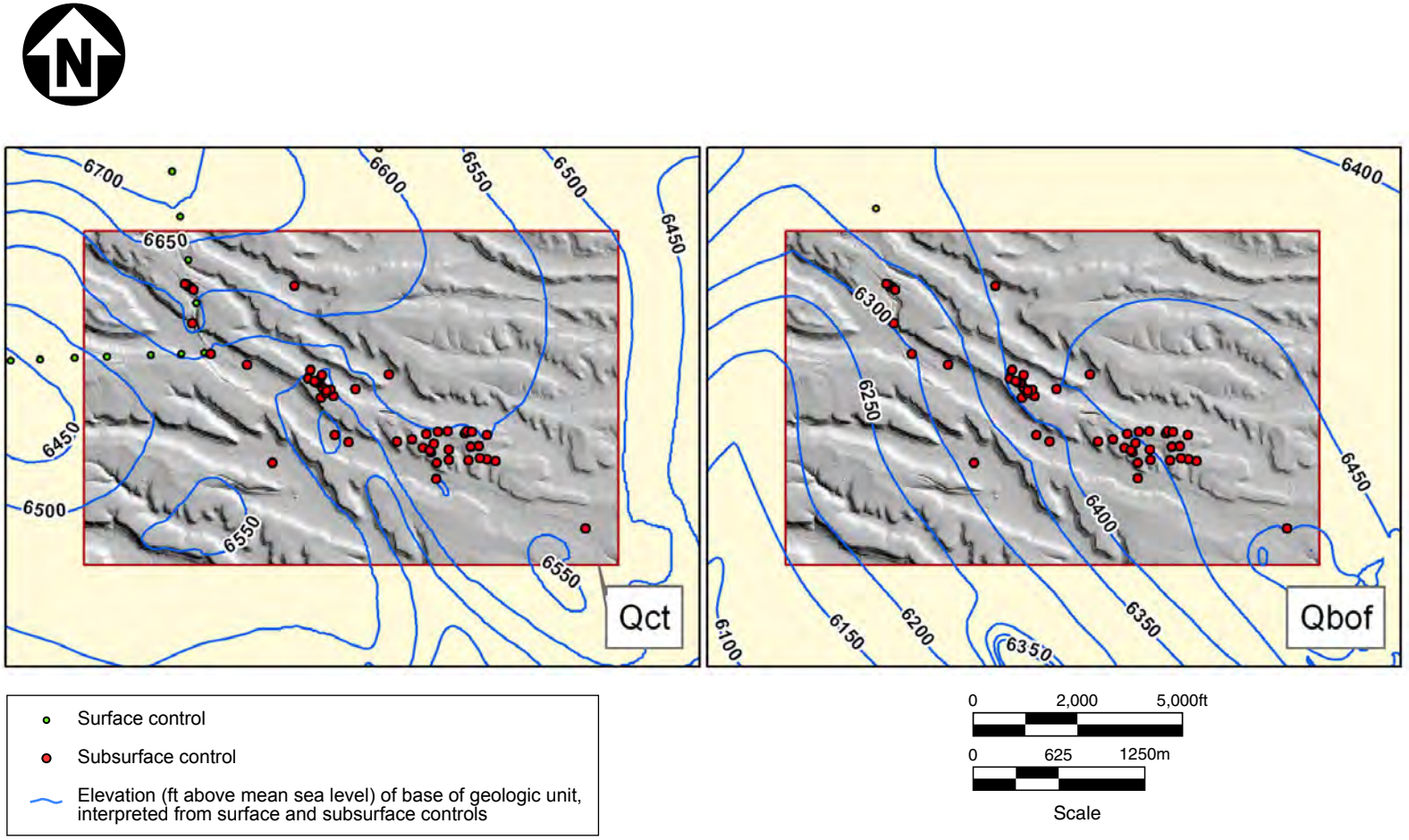

Figure II-10
Surface, Subsurface, and Interpretive Controls for Base of Cerro Toledo Interval and Bandelier Tuff Otowi Member Ash Flow

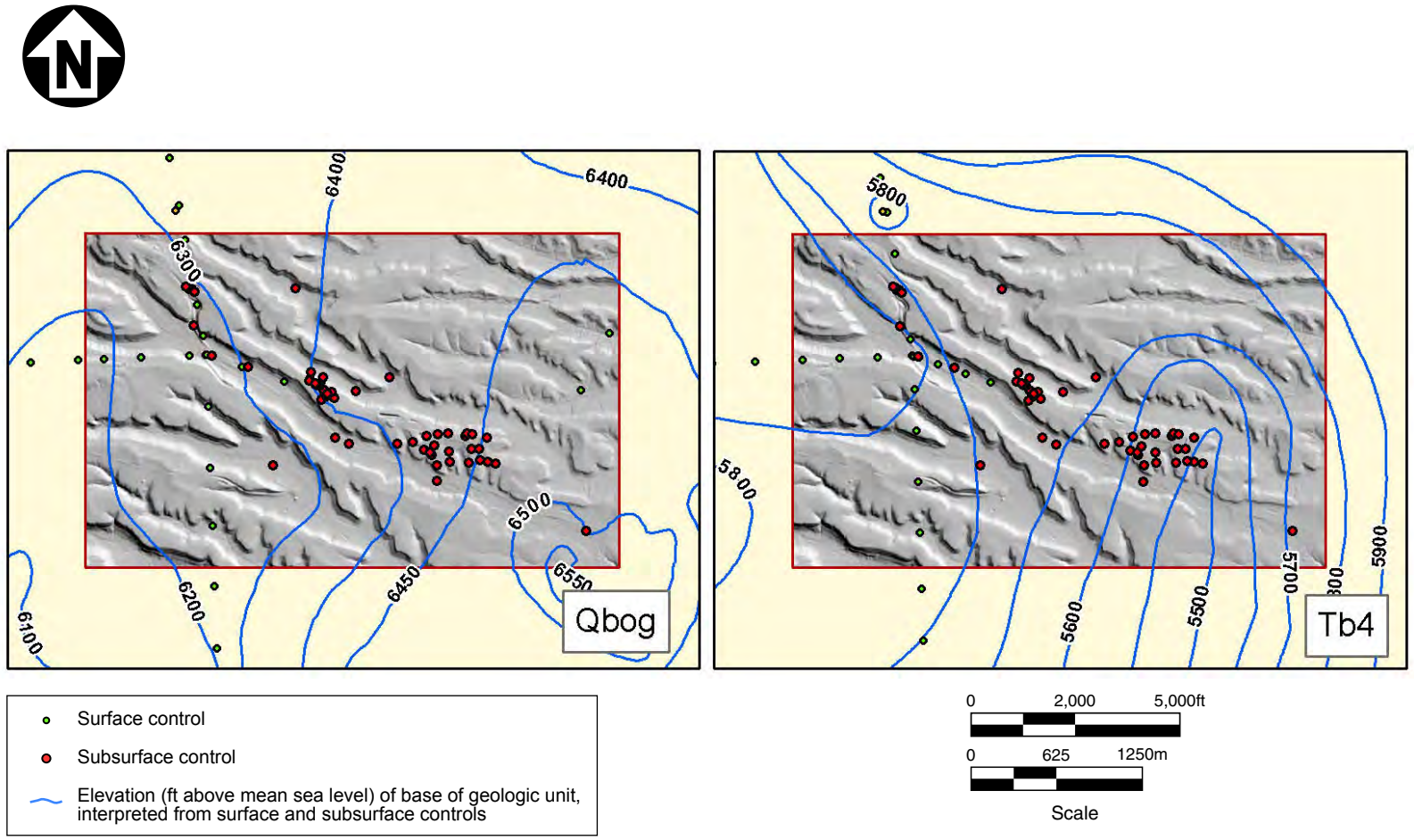

Figure II-11
Surface, Subsurface, and Interpretive Controls for Base of Bandelier Tuff Otowi Member Guaje Pumice Bed and Cerros del Rio Basalt

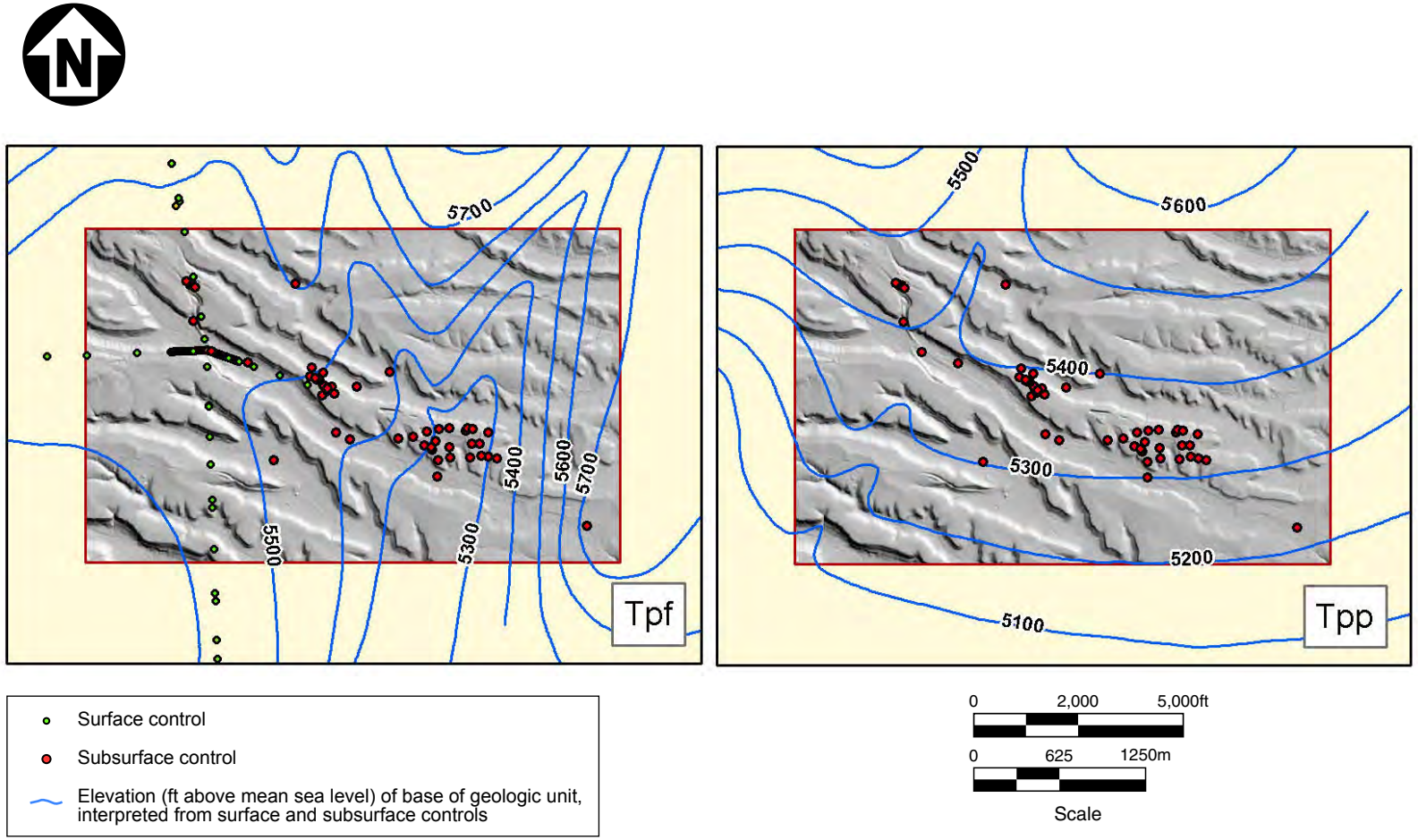

Figure II-12
Surface, Subsurface, and Interpretive Controls for Base of Puye Formation Fanglomerate and Puye Formation Fanglomerate and Pumiceous Units

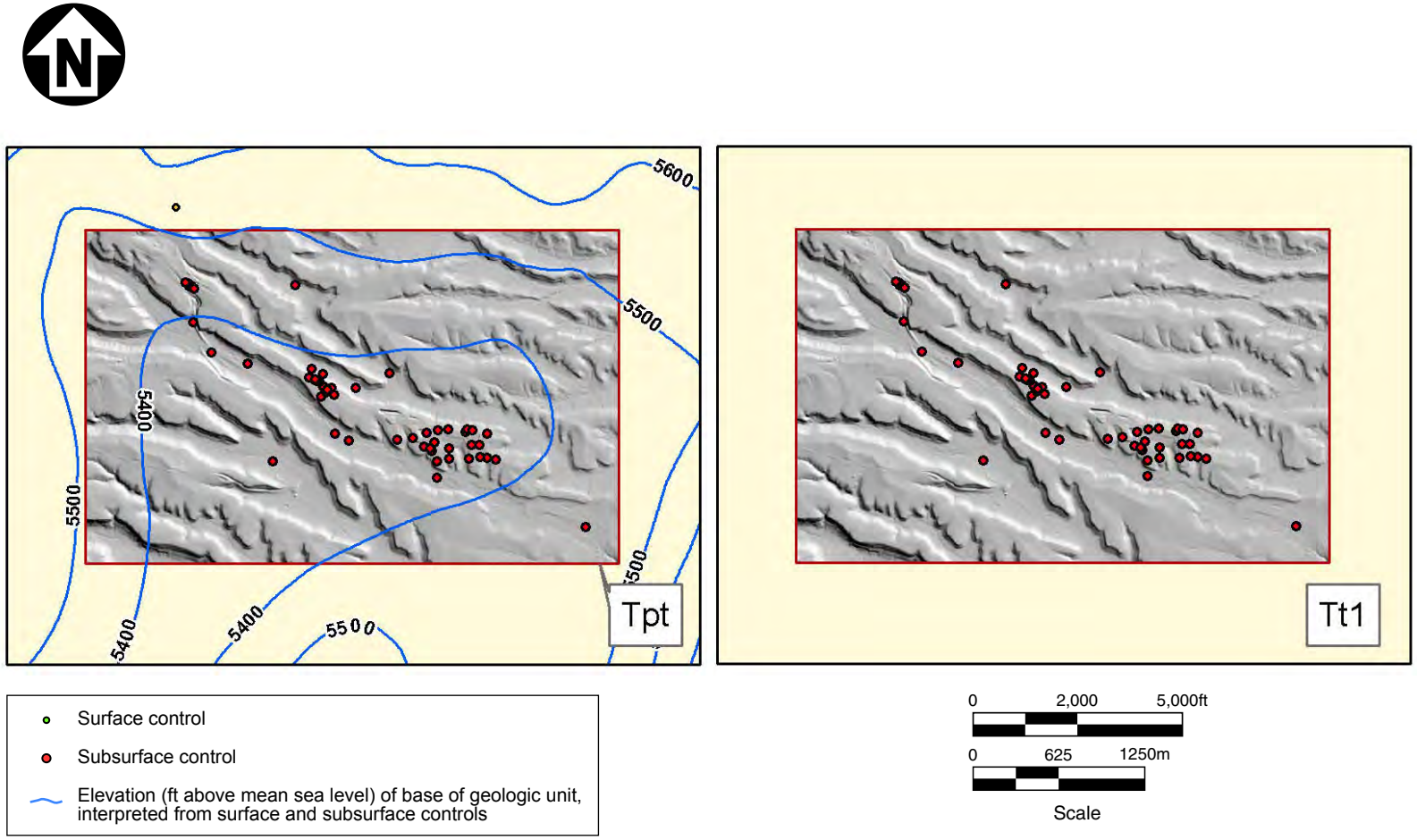

Figure II-13
Surface, Subsurface, and Interpretive Controls for Base of Puye Formation Totavi Lentil and Puye Formation Lower Flows

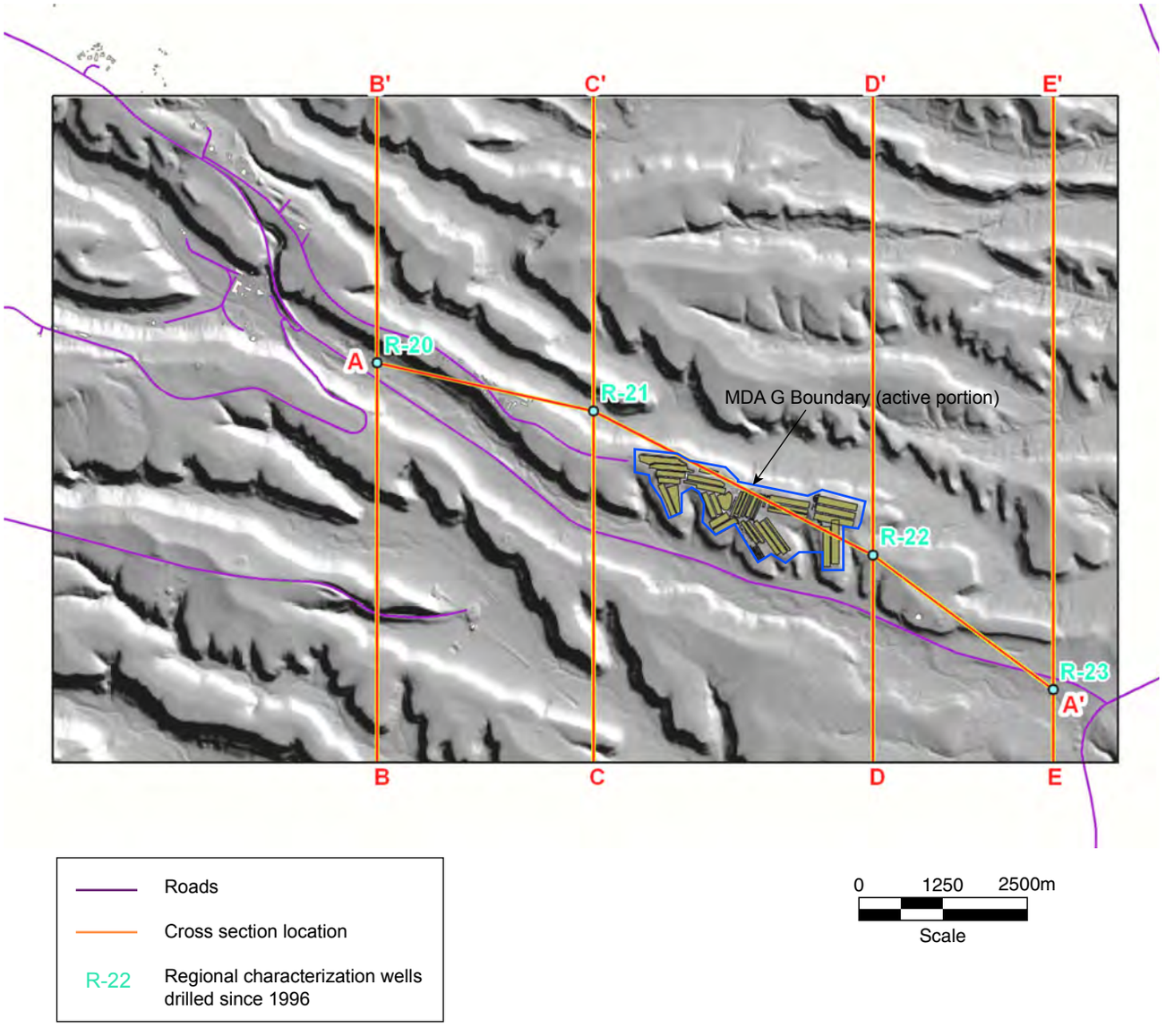

Figure II-14
Location of Cross Sections Representative of MDA G Vadose-Zone Geologic Model

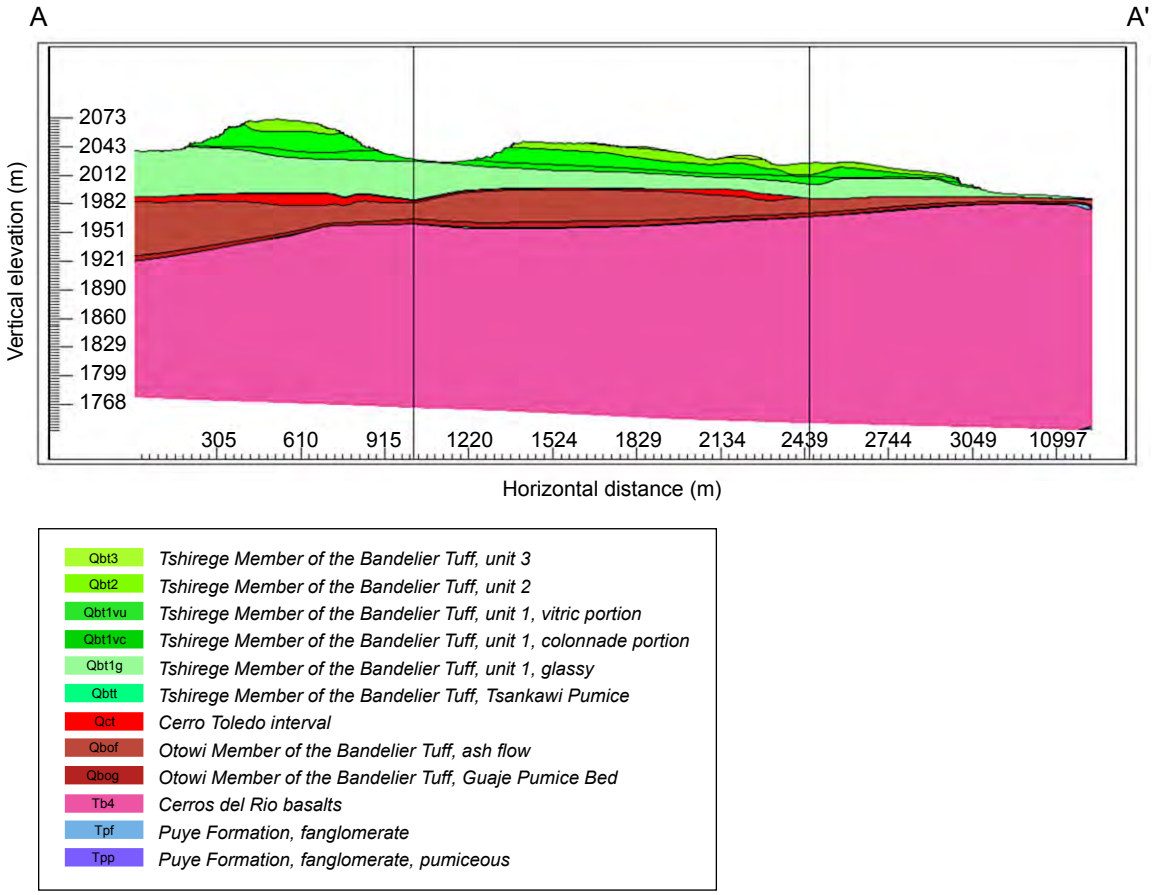

Figure II-15
East-Southwest Cross Section along Mesa Top from Characterization Well R-20 to Well R-23 (cross section A-A')

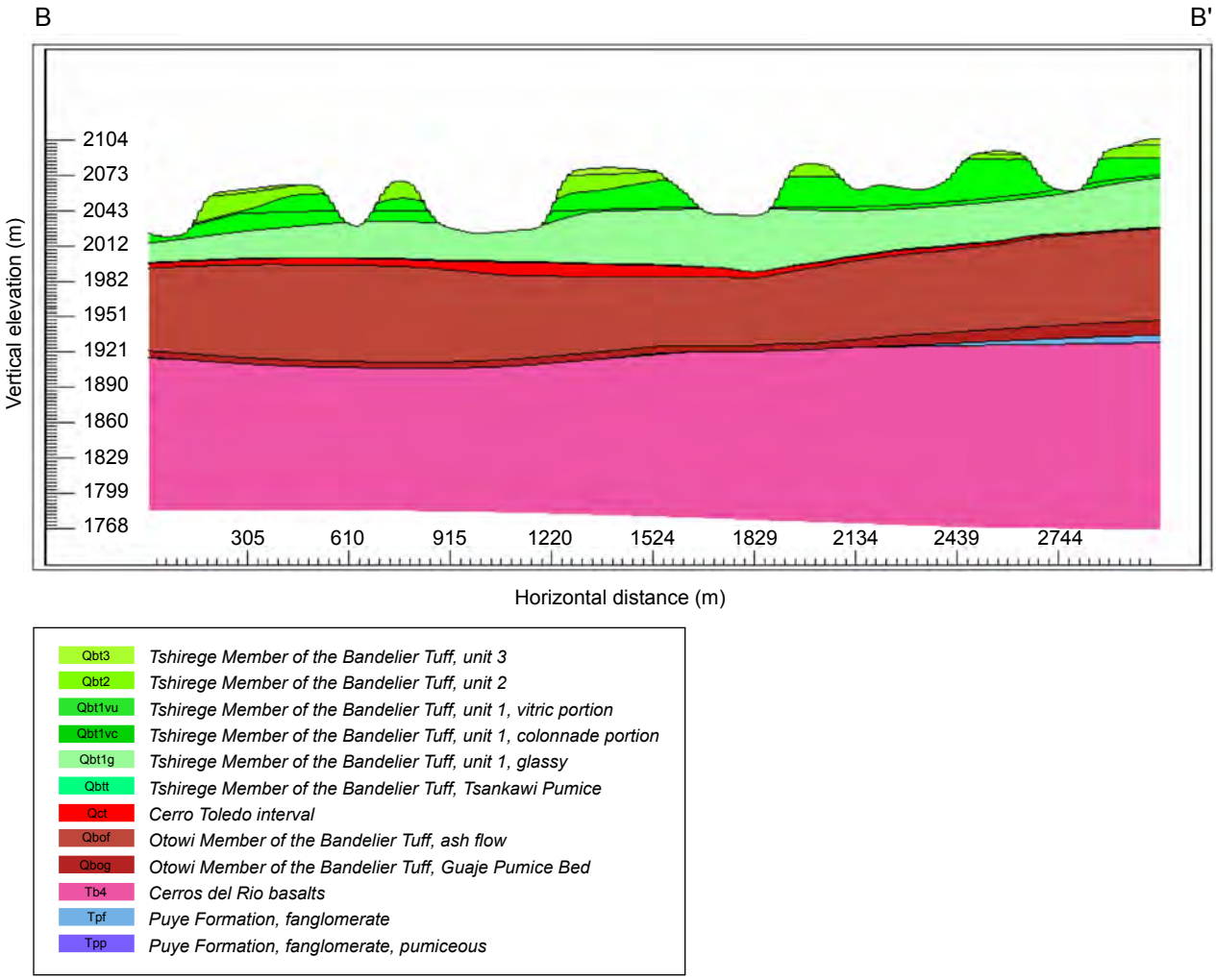

Figure II-16
North-South Cross Section through Characterization Well R-20 (cross section B'-B)

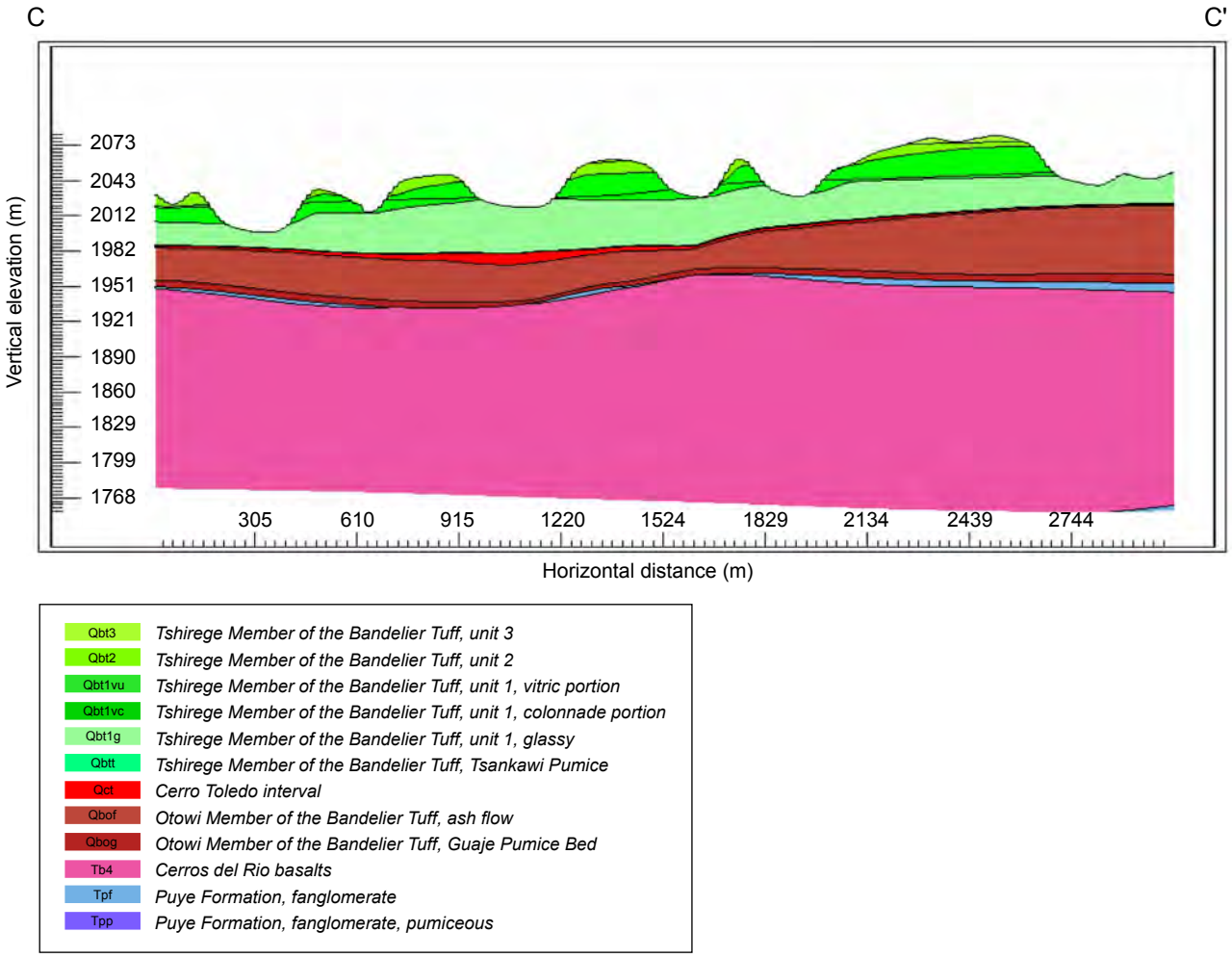

Figure II-17
North-South Cross Section through Characterization Well R-21 (cross section C'-C)

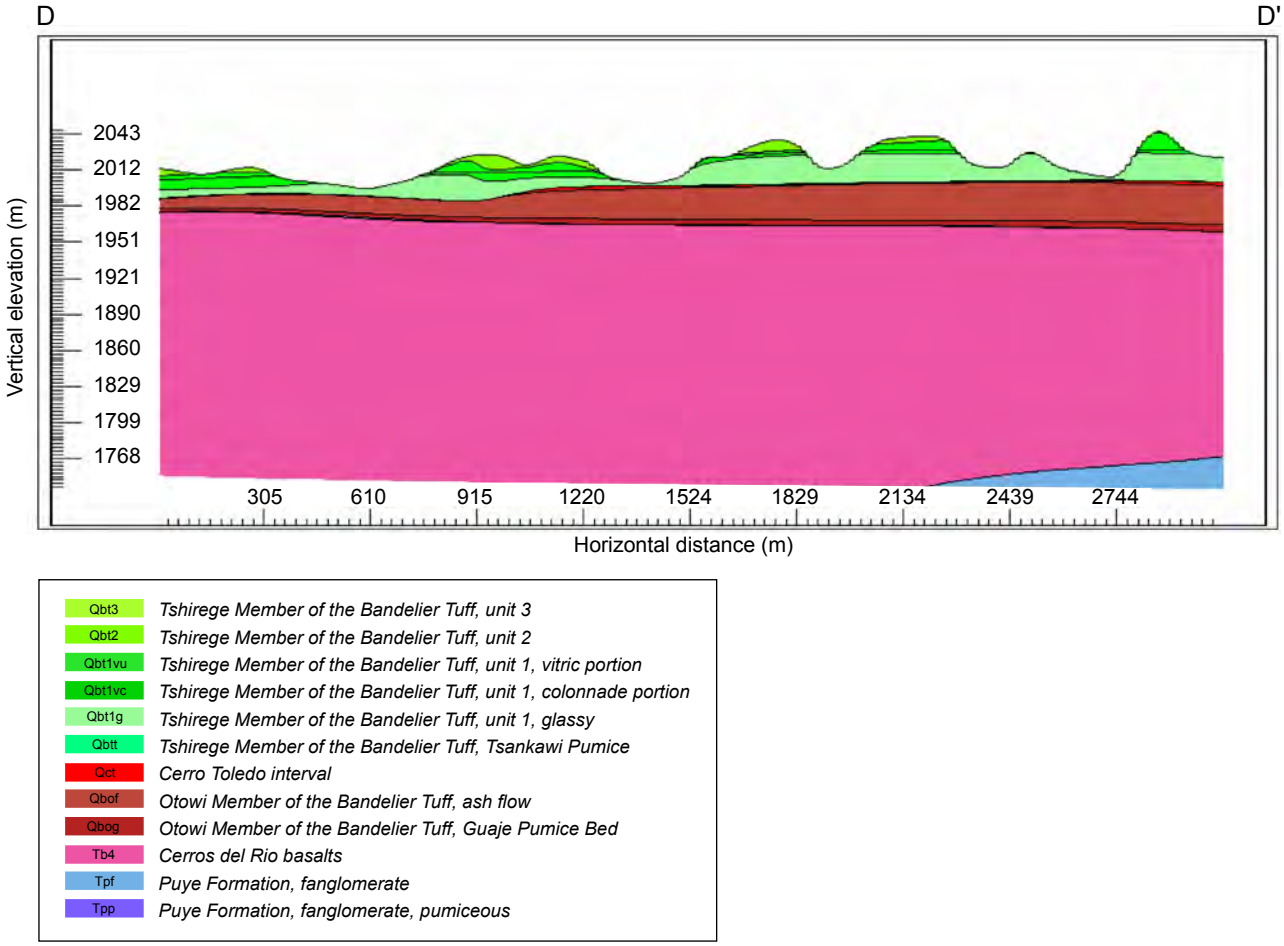

Figure II-18
North-South Cross Section through Characterization Well R-22 (cross section D'-D)

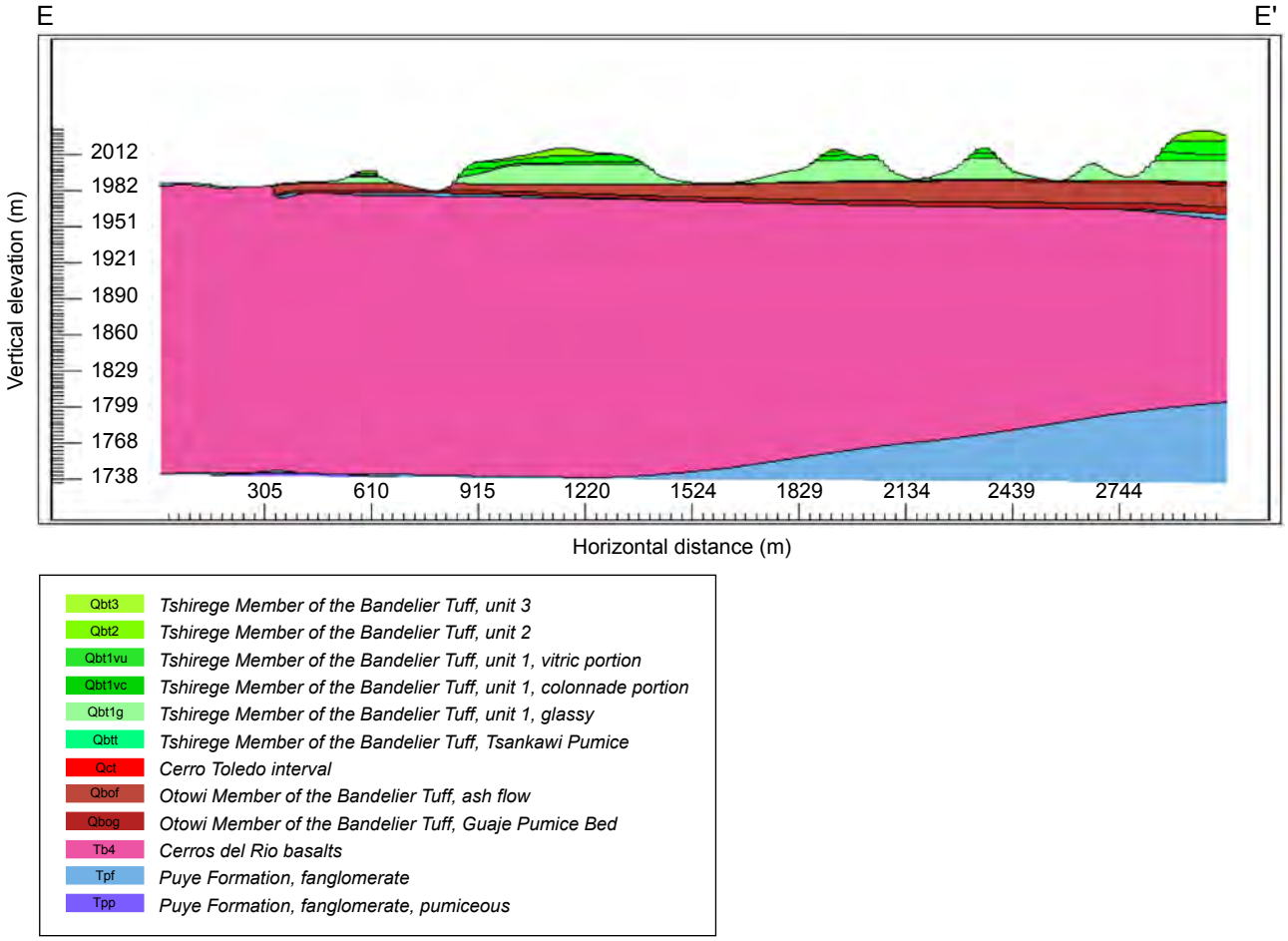

Figure II-19
North-South Cross Section through Characterization Well R-23 (cross section E'-E)

II.2 Model Quality

This new vadose-zone geologic model is the third major revision of the 3-D LANL site-wide geologic model that was first developed in 1996. Tables II-3 and II-4 provide statistics on the differences in contact elevations and unit thicknesses between the 1996 model and the current model. The differences are based on a summary of the individual cell values of the gridded contact surfaces. Because these differences in elevation and thickness can be either positive or negative, the average differences tend to be relatively small. To more adequately portray model variations, statistics for the absolute values of the differences are also provided in these tables; the absolute differences may be up to 8 times greater than the average differences. Table II-4 provides an average unit thickness, which can be used to calculate a relative thickness difference/uncertainty. This measure of absolute values would correlate directly to differences in the hydraulic transmissivity, if the hydraulic conductivity were isotropic. It was calculated using the average of the absolute values of the thickness differences to provide a conservative (maximum) uncertainty. In actuality, offsetting positive and negative thickness values may more closely reflect reality, so that the uncertainty may be better calculated using the actual differences rather than the absolute values of such.

Other approaches could be used to compare model differences. Because the calculated differences in contact elevation and thickness are based on the addition or subtraction of smoothly curving surfaces, results are highly correlated to the x,y locations. Thus, a set of 2-D plots of the model differences may be used for analyzing model differences and their effect on the hydrologic modeling. However, although both the statistical approach (Table II-4) and the graphical approach define model differences, neither actually quantifies the quality of the current model. Examining differences with intermediate models may help identify a trend in the differences, allowing a prediction about model quality. The best way to provide "hard" data to quantify the model quality is to compare the current model against actual drilling results.

Only one new characterization well, R-34 (shown in the northeast quadrant of Figure II-6) has been completed within the MDA G geologic model area since the generation of the 2003 model described in this report. This well is located on lands of the San Ildefonso Pueblo at the northern edge of the study area, and is a considerable distance from other subsurface control. Preliminary results from this well provide a dataset for a very approximate quantification of the model quality. Differences in the elevations of the stratigraphic contacts predicted by the geologic model and those measured at characterization well R-34 are shown in Table II-5. These results should be coupled with the unit hydrologic properties to adequately assess the groundwater model's sensitivities to the geologic uncertainties.

Table II-3
Statistical Differences in Geologic Contact Elevations and Unit Thicknesses between 1996 and 2003 Models

	Statistical Differences Between Models (m) [a]													
	Difference in Contact Elevation (2003 model – 1996 model)							Difference in Unit Thickness (2003 model – 1996 model)						
	Average Difference		Standard Deviation		Minimum and Maximum			Average Difference		Standard Deviation		Minimum and Maximum		
Unit	Avg.	Abs. Avg.	SD	Abs. SD	Min.	Max.	Abs. Max.	Avg.	Abs. Avg.	SD	Abs. SD	Min.	Max.	Abs. Max.
Qbt 3	-0.4	2.8	3.3	1.8	-9.6	7.9	9.6	0.4	2.8	3.3	1.8	-7.9	9.6	9.6
Qbt 2	2.4	3.5	4.0	3.1	-10.1	24.1	24.1	-2.9	4.5	5.2	3.8	-30.4	11.1	30.4
Qbt 1v	9.7	10.2	8.0	7.3	-10.4	25.9	25.9	-7.6	9.1	8.6	7.1	-30.6	21.1	30.6
Qbt 1g	2.5	6.1	7.9	5.6	-15.9	19.7	19.7	6.3	8.4	7.5	5.1	-22.1	25.0	25.0
Qct	-2.9	9.5	11.6	7.3	-37.0	19.1	37.0	5.9	8.4	11.9	10.4	-11.0	48.3	48.3
Qbof	-10.6	29.1	35.2	22.4	-87.2	53.6	87.2	23.7	27.4	26.7	22.8	-31.6	93.0	93.0
Qbog	-7.0	8.6	8.4	6.7	-32.8	18.0	32.8	-3.0	26.1	32.0	18.7	-71.8	50.6	71.8

[a] The 1996 model is based on surface mapping and drilling completed by 1996 and described by Birdsell et al. (1999). The 2003 model includes data available at the start of 2003.

Table II-4
Percent Error in Relative Thickness Measurements of Geologic Units

Unit	Average Thickness (m)	Percent Error in Unit Thickness Statistics (Absolute Values)		
		Average	Standard Deviation	Maximum
Qbt 2	19.7	2.3E+01	9.0E+00	4.9E+01
Qbt 1v	20.8	4.4E+01	1.9E+01	1.5E+02
Qbt 1g	25.4	3.3E+01	2.8E+01	1.2E+02
Qct	18.2	4.6E+01	2.8E+01	1.4E+02
Qbof	74.5	3.7E+01	1.4E+01	6.5E+01
Qbog	160.8	1.6E+01	1.4E+01	5.8E+01

Table II-5
Comparison of Predictions from 2003 Geologic Model to Preliminary As-Drilled Results for Well R-34

Geologic Unit	Elevation above Mean Sea Level (m)		
	Actual [a]	Predicted	Difference
Qbt 1g	1998.8	2013.1	-14.3
Qbof	1986.3	1965.2	21.0
Qbog	1982.9	1960.1	22.9
Tb4 (top)	1982.9	1957.3	25.6
Tb4 (bottom)	1814.6	1763.1	51.5
Tpp	1707.9	1697.0	11.0
Water Table	1785.7	1748.9	36.8

[a] *These preliminary drilling results from well R-34 were not available until after 2003.*

II.3 References

ANU, 2004, The Australian National University, *ANU-CRES Centre for Resource and Environmental Studies, ANUDEM Version 5.1*, <http://cres.anu.edu.au/outputs/anudem.php>, Canberra, Australia, (Accessed on August 2005).

Ball, T., M. Everett, P. Longmire, D. Vaniman, W. Stone, D. Larssen, K. Greene, N. Clayton, and S. McLin, 2002, *Characterization Well R-22 Completion Report*, Groundwater Investigations Focus Area, Los Alamos National Laboratory Report LA-13893-MS, ER2001-0960, February.

Birdsell, K., K. Bower, A. Wolfsberg, W. Soll, T. Cherry, and T. Orr, 1999, *Simulations of Groundwater Flow and Radionuclide Transport in the Vadose and Saturated Zones beneath Area G, Los Alamos National Laboratory*, Los Alamos National Laboratory Report LA-13299-MS.

Broxton, D.E. and S.L. Reneau, 1995, *Stratigraphic Nomenclature of the Bandelier Tuff for the Environmental Restoration Project at Los Alamos National Laboratory*, Los Alamos National Laboratory Report, LA-13010-MS.

Kleinfelder, Inc., 2003, *Characterization Well R-21 Los Alamos National Laboratory, Los Alamos, New Mexico*, Prepared for the United States Department of Energy and the National Nuclear Security Administration through the United States Army Corps of Engineers, Sacramento District, June 6.

LANL, 2003a, *Characterization Well R-20 Completion Report*, Groundwater Protection Program, Risk Reduction & Environmental Stewardship Division, Los Alamos National Laboratory Report LA-UR-03-1839, ER2003-0199, GPP-03-032, June.

LANL, 2003b, *Characterization Well R-23 Completion Report*, Groundwater Protection Program, Risk Reduction & Environmental Stewardship Division, Los Alamos National Laboratory Report LA-UR-03-2059, ER2003-0235, GPP-03-042, June.

LANL, 2003c, *Characterization Well R-32 Completion Report*, Groundwater Protection Program, Risk Reduction & Environmental Stewardship Division, Los Alamos National Laboratory Report LA-UR-03-3984, ER2003-0415, GPP-03-0712, June.

Attachment III
Statistical Description of Vadose-Zone Hydrologic Properties for the Los Alamos National Laboratory TA-54, Material Disposal Area G Groundwater Pathway Model

Author:
Everett P. Springer

III.1 Introduction

Variability in unsaturated-zone flow properties is an important consideration in understanding uncertainty in the travel times of contaminants through the subsurface. Simulation is the most readily available approach to assess flow and transport of contaminants in the unsaturated zone at TA-54 because flow processes are slow and large events are episodic, both of which make measurement difficult. This analysis provides statistical descriptions of the unsaturated-zone hydrologic properties at Technical Area (TA) 54 at Los Alamos National Laboratory (the Laboratory or LANL), using available data to support MDA G groundwater modeling efforts.

III.2 Methods

The methodology used to conduct the statistical analysis of TA-54 hydrologic properties is presented below. Section III.2.1 discusses the sources of data used in the investigation and Section III.2.2 describes the data analyses undertaken.

III.2.1 Data Sources

The data used in the TA-54 investigation were obtained from two sources. The first was a detailed study by Rogers and Gallaher (1995) on the hydrologic properties of Bandelier Tuff found at TA-54 and across the Laboratory. The second source was data from boreholes sampled at TA-54 after the Rogers and Gallaher (1995) report was completed. These data were reported by D.B. Stephens & Associates, Inc. (DBS&A) in two reports. The first report (DBS&A, 1995) presented data for borehole TA-54-G-5 (G-5), while the second (DBS&A, 1996) presented data for boreholes 54-501, 54-502, 54-503, 54-504, 54-1015, 54-1107, 54-1121, G-P38-HH3, and samples from an outcrop of the vapor-phase notch in Mortandad Canyon. The stratigraphy of borehole G-P38-HH3, a horizontal hole drilled from Pit 38, is provided in Puglisi and Vold (1995).

The Broxton and Reneau (1995) nomenclature was used to define the geologic units for the Bandelier Tuff. The stratigraphic correlation provided by Broxton and Reneau was used to map the parameters from Rogers and Gallaher (1995) onto the geologic units.

III.2.2 Data Analysis

The water content and pressure head (retention) data for the boreholes listed above were fitted to the moisture characteristic equation developed by van Genuchten (1980) using the Retention Curve (RETC) computer code (van Genuchten et al., 1991). The water retention relation is described as follows:

$$S_e = \frac{\theta - \theta_r}{\theta_s - \theta_r} = \frac{1}{\left[1 + (\alpha h)^n\right]^m} \qquad 1$$

Where

S_e = effective saturation
θ = volumetric water content (cm^3/cm^3)
θ_r = residual volumetric water content (cm^3/cm^3)
θ_s = saturated volumetric water content (cm^3/cm^3)
h = pressure head (cm)
α = fitting parameter (cm^{-1})
n, m = fitting parameters with $m = 1 - 1/n$

Parameters for Equation 1 were estimated from parameter fitting using the RETC computer code, with the exception of the saturated water content (θ_s). Measured values were used for this parameter because of the limited number of data points for each retention curve. Parameters determined by Rogers and Gallaher (1995) using Equation 1 are included in this report. For a listing of all hydrologic properties and parameter values used for statistical analyses, by geologic unit and borehole, see *Annex IIIa***.**

The hydrologic parameters for a geologic unit can also be estimated by the RETC computer code, by pooling data from the given geologic unit. This approach was used to produce the alternative estimates reported in Section III.3.4.

III.3 Results

This section provides the results of the statistical analysis. Section III.3.1 describes the distributions for parameters used for the Bandelier Tuff, Section III.3.2 provides descriptive statistics, and Section III.3.3 discusses correlation among the various parameters.

III.3.1 Distributions of Hydraulic Parameters

Figures III-1 through III-8 are normal probability plots for the saturated water content, residual water content, saturated hydraulic conductivity, and the van Genuchten fitting parameters α and n for unit 1v of the Tshirege Member of the Bandelier Tuff (Qbt 1v). This geologic unit has the largest number of samples so it was used to identify distributions of the unsaturated-zone parameters. By inference, the distributions identified for Qbt 1v should be used in combination with statistical parameters for the other geologic units.

The saturated water content of the Bandelier Tuff appears to follow a normal distribution (Figure III-1), as confirmed by the descriptive statistics presented in Section III.3.2. The

distribution for residual water content, shown on Figure III-2, is discussed in Section III.3.2. The *n* parameter (Figure III-3) appears to follow a normal distribution except for some tailing in the lower values. The α plot (Figure III-4) illustrates how a single value may affect a distribution. The value of α estimated on the basis of the sample taken at a 30-m (99-ft) depth from borehole 54-1107 is 0.29/cm, which is two orders of magnitude greater than the other values of this parameter. The moisture retention data for this sample differed substantially from the other samples, yielding a moisture retention curve that was essentially inverted. When this sample is removed from the analysis, the distribution of the remaining α values is skewed (Figure III-5). Figure III-6 shows the logarithmic transformation of α values (without the sample from borehole 54-1107), which appears to follow a normal distribution. A lognormal distribution has been suggested for saturated hydraulic conductivity (Nielsen et al. 1973; Freeze 1975). The application of a logarithmic transformation to this parameter (Figure III-7) resulted in a normal distribution (Figure III-8).

III.3.2 Descriptive Statistics

The geologic column included in the unsaturated zone beneath TA-54 consists primarily of the Bandelier Tuff and a portion of the underlying Cerros del Rio basalt. The Bandelier Tuff units that occur at TA-54 include the Tshirege Member (consisting here of units 2, 1v, the vapor-phase notch, and unit 1g), Tsankawi Pumice, Cerro Toledo interval, and Otowi Member. Samples from the surface soil and basalt layers at TA-54 are included in this analysis. Tables III-1 through III-8 present statistics for each unit, beginning with the surface soil.

The distribution statistics, skew and kurtosis, are included in the last two columns of Tables III-1 through III-8. Skewness is a measure of the symmetry of the distribution relative to a normal distribution (which has zero skewness). Kurtosis describes the peakedness or flatness of a distribution relative to a normal curve. The kurtosis value for a normal distribution is 3. Distributions with kurtosis values greater than 3 have a relatively greater concentration of the probability near the mean than a normal distribution. Conversely, distributions with a kurtosis less than 3 are flat with a greater portion of the probability away from the mean than a normal distribution. When the number of samples is limited (i.e., when there are fewer than 30 samples), these statistics do not provide very good estimates. For this study, unit 1v (Table III-3) is the only unit with more than 30 samples.

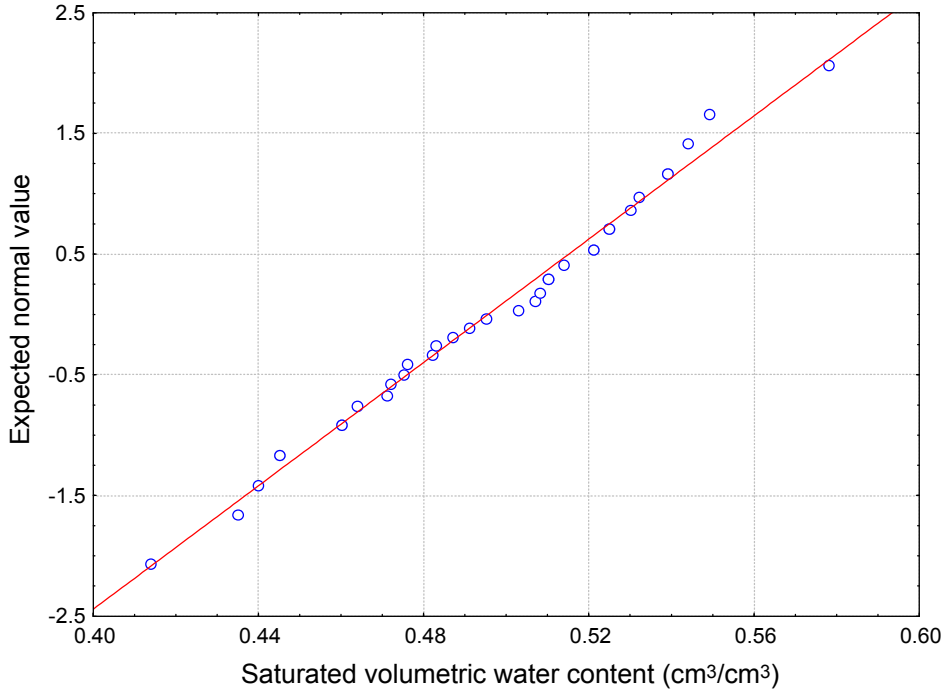

Figure III-1
Normal Probability Plot of Saturated Volumetric Water Content for Bandelier Tuff Tshirege Member Unit 1v

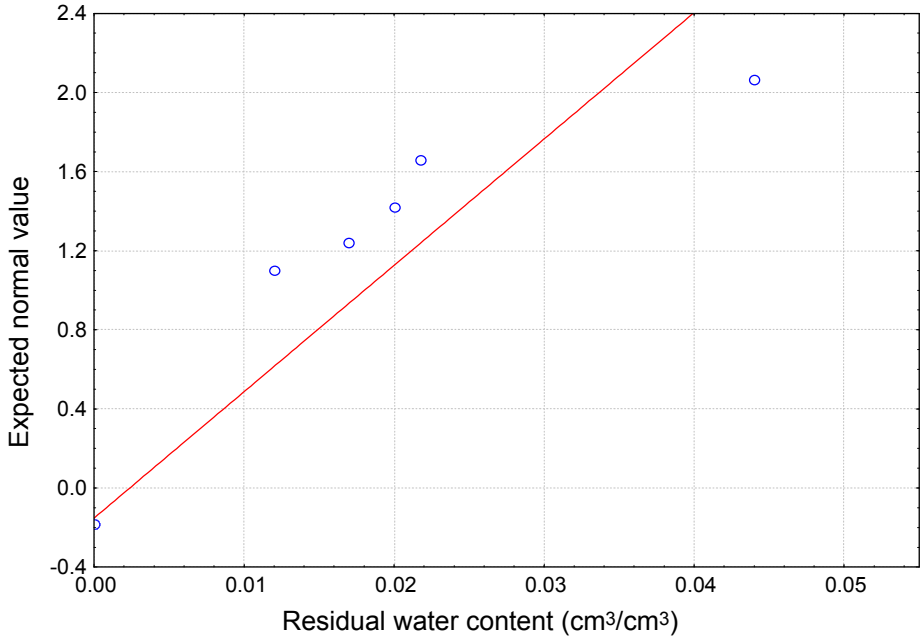

Figure III-2
Normal Probability Plot of Residual Volumetric Water Content for Bandelier Tuff Tshirege Member Unit 1v

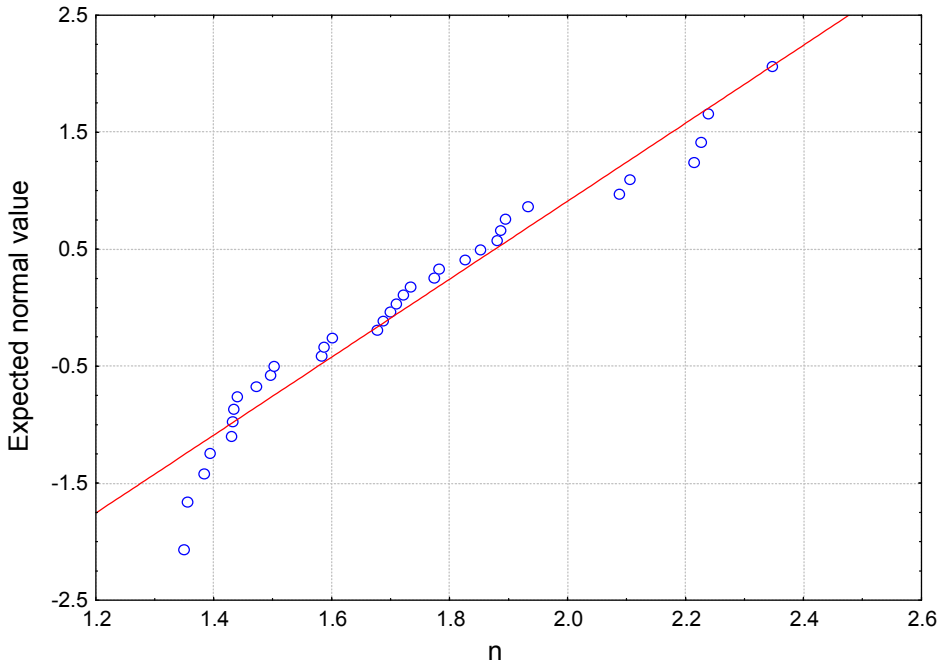

Figure III-3
Normal Probability Plot of van Genuchten *n* Parameter
for Bandelier Tuff Tshirege Member Unit 1v

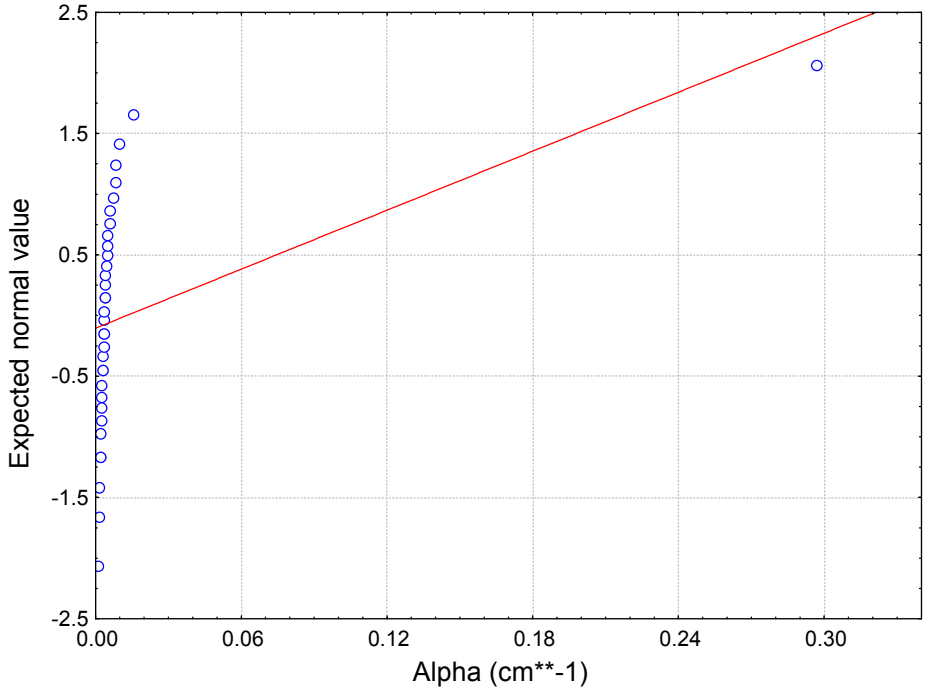

Figure III-4
Normal Probability Plot of van Genuchten α Parameter
for Bandelier Tuff Tshirege Member Unit 1v

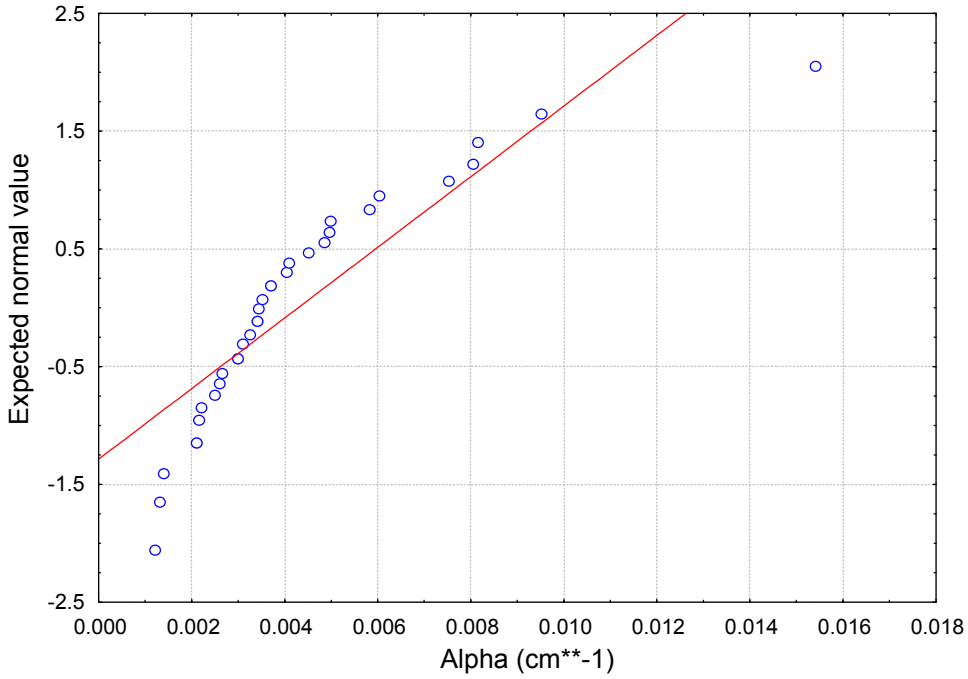

Figure III-5
Normal Probability Plot of van Genuchten α Parameter for Bandelier Tuff Tshirege Member Unit 1v without Data from Borehole 54-1107 (30-m depth)

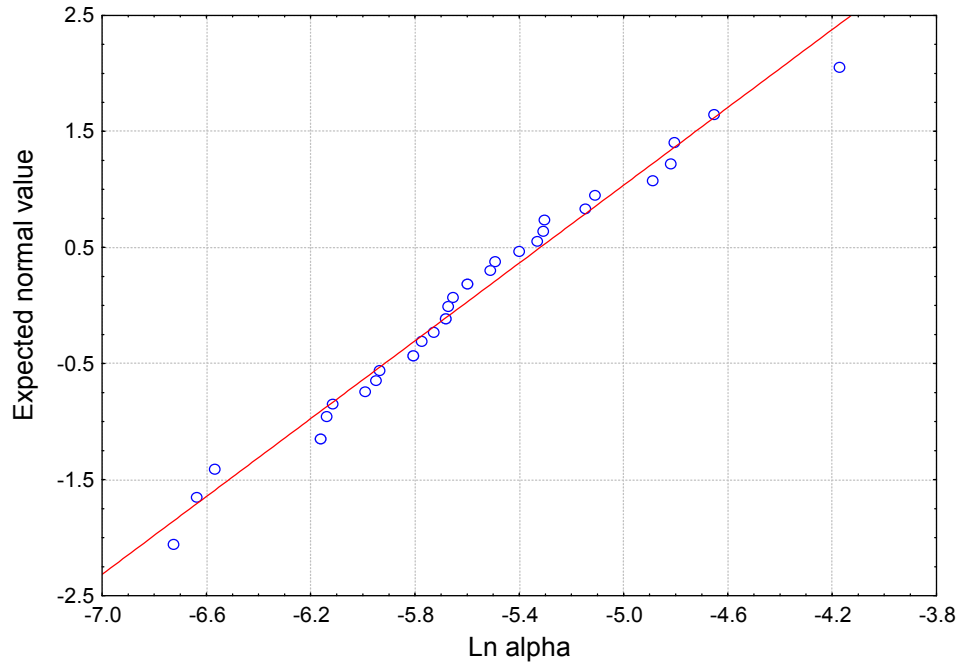

Figure III-6
Normal Probability Plot of Natural-Logarithm-Transformed van Genuchten α Parameter for Bandelier Tuff Tshirege Member Unit 1v without Data from Borehole 54-1107 (30-m depth)

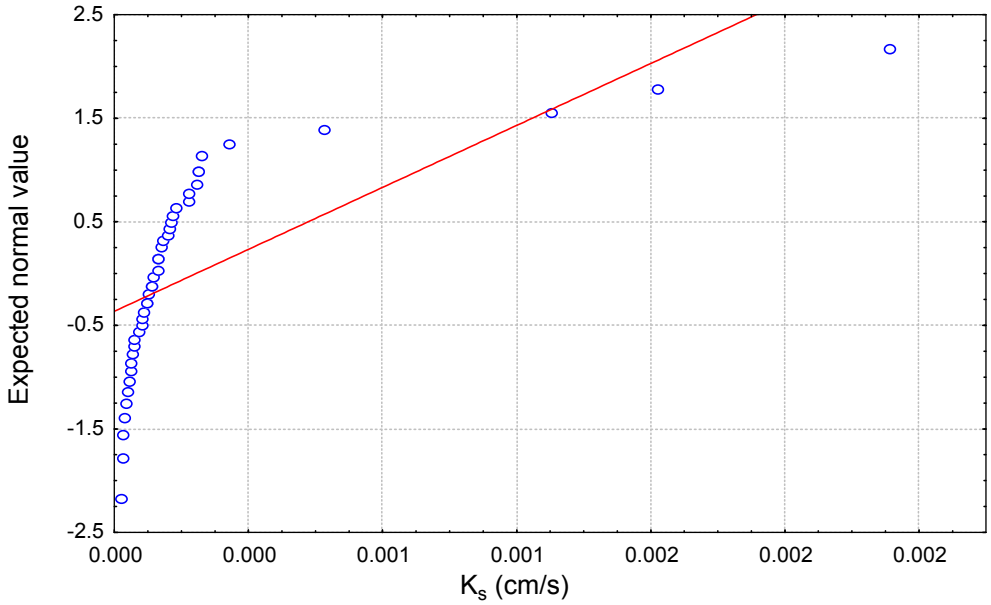

Figure III-7
Normal Probability Plot of Saturated Hydraulic Conductivity for Bandelier Tuff Tshirege Member Unit 1v

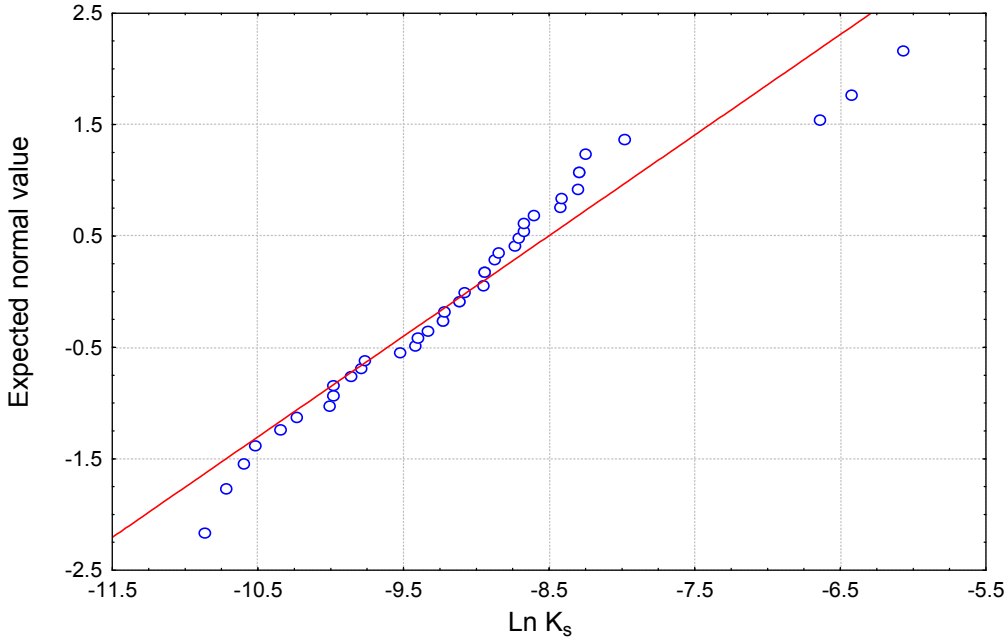

Figure III-8
Normal Probability Plot of Natural-Logarithm-Transformed Saturated Hydraulic Conductivity for Bandelier Tuff Tshirege Member Unit 1v

Table III-1
Statistics for Unsaturated Hydraulic Properties for Soil Unit

Variable	Unit	N	Mean	Standard Deviation	Median	Maximum	Minimum	Skew	Kurtosis
Bulk Density (ρ_b)	g/cm^3	4	1.5E+00	2.4E–02	1.5E+00	1.5E+00	1.4E+00	0.0E+00	–4.3E+00
Saturated Volumetric Water Content (θ_s)	cm^3/cm^3	4	4.1E–01	1,5E–02	4.1E–01	4.3E–01	4.0E–01	2.8E–01	–4.3E+00
Saturated Hydraulic Conductivity (K_s)	cm/s	4	4.7E–06	2.3E–06	5.4E–06	6.5E–06	1.4E–06	–1.7E+00	3.2E+00
Lognormal Saturated Hydraulic Conductivity (Ln K_s)	NA	4	–1.2E+01	7.2E–01	–1.2E+01	–1.2E+01	–1.4E+01	–1.9E+00	3.7E+00
Residual Volumetric Water Content (θ_r)	cm^3/cm^3	4	0.0E+00	0.0E+00	0.0E+00	0.0E+00	0.0E+00	---	---
van Genuchten Fitting Parameter *n*	NA	4	1.2E+00	1.9E–02	1.2E+00	1.3E+00	1.2E+00	–7.4E–01	1.8E+00
van Genuchten Fitting Parameter α	cm^{-1}	4	1.3E–02	4.0E–03	1.2E–02	2.0E–02	9.6E–03	7.6E–01	–1.8E+00
Lognormal α	NA	4	–4.4E+00	3.1E–01	–4.4E+00	–4.0E+00	–4.7E+00	5.3E–01	–3.0E+00

N = Number (of samples) *NA = Not applicable* *--- = Not estimated*

Table III-2
Statistics for Unsaturated Hydraulic Properties for Bandelier Tuff Tshirege Member Unit 2

Variable	Unit	N	Mean	Standard Deviation	Median	Maximum	Minimum	Skew	Kurtosis
Bulk Density (ρ_b)	g/cm^3	8	1.4E+00	7.0E–02	1.4E+00	1.5E+00	1.3E+00	–2.0E–02	–1.9E+00
Saturated Volumetric Water Content (θ_s)	cm^3/cm^3	8	4.1E–01	4.0E–02	4.2E–01	4.6E–01	3.7E–01	2.1E+00	5.8+00
Saturated Hydraulic Conductivity (K_s)	cm/s	17	3.4E–04	3.8E–04	2.2E–04	1.6E–03	2.7E–05	2.6E+00	8.4E+00
Lognormal Saturated Hydraulic Conductivity (Ln K_s)	NA	17	–8.5E+00	1.1E+00	–8.4E+00	–6.4E+00	–1.1E+01	–3.0E–01	–4.8E–01
Residual Volumetric Water Content (θ_r)	cm^3/cm^3	8	1.0E–01	1.3E–02	6.0E–03	3.8–02	0.0E+00	1.4E+00	1.9E+00
van Genuchten Fitting Parameter *n*	NA	8	2.1E+00	5.1E–01	2.0E+00	3.0E+00	1.5E+00	0.8E+00	–3.8E–01
van Genuchten Fitting Parameter α	cm^{-1}	8	6.0E–03	4.0E–03	6.0E–03	1.5E–02	1.9E–03	1.5E+00	3.0E+00
Lognormal α	NA	8	–5.4E+00	7.0E–01	–5.1E+00	–4.2E+00	–6.3E+00	0.01E+00	–6.9–01

N = Number (of samples) *NA = Not applicable*

Table III-3
Statistics for Unsaturated Hydraulic Properties for Bandelier Tuff Tshirege Member Unit 1v

Variable	Unit	N	Mean	Standard Deviation	Median	Maximum	Minimum	Skew	Kurtosis
Bulk Density (ρ_b)	g/cm^3	36	1.17E+00	9.0E–02	1.18E+00	1.32E+00	9.3E–01	–7.0E–01	1.3E–01
Saturated Volumetric Water Content (θ_s)	cm^3/cm^3	33	4.9E–02	4.0E–02	5.0E–01	5.8E–01	4.1E–01	–6.0E–02	–4.5E–01
Saturated Hydraulic Conductivity (K_s)	cm/s	43	2.35E–04	4.40E–04	1.13E–04	2.31E–03	1.90E–05	3.73E+00	1.409E+01
Lognormal Saturated Hydraulic Conductivity (Ln K_s)	NA	43	–9.06E+00	1.04E+00	–9.09E+00	–6.07E+00	–1.087E+01	8.3E–01	1.50E+00
Residual Volumetric Water Content (θ_r)	cm^3/cm^3	33	3.0E–03	9.0E–03	0.0E+00	4.0E–02	0.0E+00	3.74E+00	1.52E+01
van Genuchten Fitting Parameter n	NA	33	1.74E+00	2.8E–01	1.71E+00	2.35E+00	1.35E+00	5.6E–01	–5.6E–01
van Genuchten Fitting Parameter α	cm^{-1}	33	4.0E–03	3.0E–03	3.0E–03	1.5E–02	1.0E–03	2.18E+00	6.31E+00
Lognormal α	NA	33	–5.62E+00	5.7E–01	–5.68E+00	–4.17E+00	–6.73E+00	2.9E–01	3.3E–01

N = Number (of samples) *NA = Not applicable*

Table III-4
Statistics for Unsaturated Hydraulic Properties for Vapor-Phase Notch of the Bandelier Tuff (including values from Mortandad Canyon outcrop)

Variable	Unit	N	Mean	Standard Deviation	Median	Maximum	Minimum	Skew	Kurtosis
Bulk Density (ρ_b)	g/cm^3	5	1.1E+00	5.0E–02	1.1E+00	1.2E+00	1.0E+00	–1.2E+00	1.7E+00
Saturated Volumetric Water Content (θ_s)	cm^3/cm^3	5	4.8E–01	5.0E–02	4.5E–01	5.3E–01	4.3E–01	5.9E–01	–3.2E+00
Saturated Hydraulic Conductivity (K_s)	cm/s	5	9.3E–05	1.4E–04	4.5E–05	3.3E–04	4.8E–06	2.1E+00	4.3E+00
Lognormal Saturated Hydraulic Conductivity (Ln K_s)	NA	5	–1.0E+01	1.6E+00	–1.0E+01	–8.0E+00	–1.2E+01	1.0E–01	–3.0E–02
Residual Volumetric Water Content (θ_r)	cm^3/cm^3	5	3.0E–03	7.0E–03	0.0E+00	2.0E–02	0.0E+00	2.2E+00	5.0E+00
van Genuchten Fitting Parameter *n*	NA	5	1.6E+00	1.6E–01	1.7E+00	1.8E+00	1.4E+00	–5.4E–01	–1.5E+00
van Genuchten Fitting Parameter α	cm^{-1}	5	5.0E–03	5.0E–01	4.0E–03	1.5E–02	2.0E–03	2.1E+00	4.5E+00
Lognormal α	NA	5	–5.6E+00	8.3E–01	–5.6E+00	–4.2E+00	–6.4E+00	1.2E+00	2.4E+00

N = Number (of samples) *NA = Not applicable*

Table III-5
Statistics for Unsaturated Hydraulic Properties for Bandelier Tuff Tshirege Member Unit 1g

Variable	Unit	N	Mean	Standard Deviation	Median	Maximum	Minimum	Skew	Kurtosis
Bulk Density (ρ_b)	g/cm^3	20	1.2E+00	7.0E–02	1.1E+00	1.3E+00	9.4E–01	–5.7E–01	3.2E+00
Saturated Volumetric Water Content (θ_s)	cm^3/cm^3	16	4.6E–01	4.0E–02	4.5E–01	5.2E–01	3.9E–01	–2.9E–01	–7.0E–01
Saturated Hydraulic Conductivity (K_s)	cm/s	24	2.0E–04	1.9E–04	1.4E–04	8.5E–04	3.1E–05	2.2E+00	5.4E+00
Lognormal Saturated Hydraulic Conductivity (Ln K_s)	NA	24	–8.8E+00	8.1E–01	–8.9E+00	–7.1E+00	–1.0E+01	1.6E–01	–1.0E–01
Residual Volumetric Water Content (θ_r)	cm^3/cm^3	16	1.0E–02	2.0E–02	0.0E+00	5.0E–02	0.0E+00	1.5E+00	1.2E+00
van Genuchten Fitting Parameter *n*	NA	16	1.8E+00	1.8E–01	1.8E+00	2.2E+00	1.4E+00	5.1E–01	8.5E–01
van Genuchten Fitting Parameter α	cm^{-1}	16	6.0E–03	6.0E–03	5.0E–03	2.8E–02	3.0E–03	3.6E+00	1.42E+01
Lognormal α	NA	16	–5.3E+00	5.7E–01	–5.3E+00	–3.6E+00	–6.0E+00	1.9E+00	5.5E+00

N = Number (of samples) *NA = Not applicable*

Table III-6
Statistics for Unsaturated Hydraulic Properties for Bandelier Tuff Tsankawi Pumice/Cerro Toledo Interval

Variable	Unit	N	Mean	Standard Deviation	Median	Maximum	Minimum	Skew	Kurtosis
Bulk Density (ρ_b)	g/cm^3	7	1.2E+00	7.0E–02	1.2E+00	1.3E+00	1.1E+00	–1.8E+00	4.2E+00
Saturated Volumetric Water Content (θ_s)	cm^3/cm^3	7	4.5E–01	4.0E–02	4.4E–01	5.0E–01	4.0E–01	2.5E–01	–1.3E+00
Saturated Hydraulic Conductivity (K_s)	cm/s	7	3.4E–04	5.2E–04	1.3E–04	1.5E–03	6.0E–05	2.5E–01	6.5E+00
Lognormal Saturated Hydraulic Conductivity (Ln K_s)	NA	7	–8.6E+00	1.1E+00	–9.0E+00	–6.5E+00	–9.8E+00	1.3E–01	2.2E+00
Residual Volumetric Water Content (θ_r)	cm^3/cm^3	7	3.0E–03	6.0E–03	0.0E+00	1.6E–02	0.0E+00	2.1E+00	4.5E+00
van Genuchten Fitting Parameter n	NA	7	1.5E+00	9.0E–02	1.5E+00	1.6E+00	1.4E+00	4.3E–01	–1.3E+00
van Genuchten Fitting Parameter α	cm^{-1}	7	2.0E–02	7.0E–03	1.3E–02	2.5E–02	7.1E–03	4.3E–01	–1.6E+00
Lognormal α	NA	7	–4.3E+00	5.0E–01	–4.3E+00	–3.7E+00	–5.0E+00	–6.0E–02	1.6E+00

N = Number (of samples) *NA = Not applicable*

Table III-7
Statistics for Unsaturated Hydraulic Properties for Bandelier Tuff Otowi Member

Variable	Unit	N	Mean	Standard Deviation	Median	Maximum	Minimum	Skew	Kurtosis
Bulk Density (ρ_b)	g/cm^3	12	1.2E+00	6.0E–02	1.20E+00	1.3E+00	1.1E+00	1.5E–01	–1.0E–02
Saturated Volumetric Water Content (θ_s)	cm^3/cm^3	12	4.4E–01	1.0E–02	4.4E–01	4.5E–01	4.1E–01	–8.3E–02	–5.4E–01
Saturated Hydraulic Conductivity (K_s)	cm/s	12	2.5E–04	1.2E–04	2.2E–04	5.0E–04	1.0E–04	1.1E+00	7.7E–02
Lognormal Saturated Hydraulic Conductivity (Ln K_s)	NA	12	–8.4E+00	4.5E–01	–8.4E+00	–7.6E+00	–9.2E+00	1.1E–01	–7.0E–02
Residual Volumetric Water Content (θ_r)	cm^3/cm^3	12	1.9E–02	2.0E–02	2.0E–02	4.0E–02	0.0E+00	5.0E–02	–1.3E+00
van Genuchten Fitting Parameter *n*	NA	12	1.8E+00	2.5E–01	1.7E+00	2.3E+00	1.5E+00	7.7E–01	4.7E–01
van Genuchten Fitting Parameter α	cm^{-1}	12	6.0E–03	1.3E–03	6.0E–03	8.0E–03	3.9E–03	6.0E–01	5.8E–01
Lognormal α	NA	12	–5.1E+00	2.1E–01	–5.1E+00	–4.8E+00	–5.6E+00	–4.0E–02	5.8E–01

N = Number (of samples) *NA = Not applicable*

Table III-8
Statistics for Unsaturated Hydraulic Properties for Cerros del Rio Basalt

Variable	Unit	N	Mean	Standard Deviation	Median	Maximum	Minimum	Skew	Kurtosis
Bulk Density (ρ_b)	g/cm^3	4	2.7E+00	3.1E–01	2.8E+00	2.8E+00	2.2E+00	–2.0E+00	3.8E+00
Saturated Volumetric Water Content (θ_s)	cm^3/cm^3	4	1.0E–01	5.0E–02	1.0E–01	1.6E–01	5.0E–02	4.4E–01	9.5E–01
Saturated Hydraulic Conductivity (K_s)	cm/s	4	2.1E–09	1.6E–09	2.2E–09	3.8E–09	8.7E–11	–5.3E–01	2.8E–01
Lognormal Saturated Hydraulic Conductivity (Ln K_s)	NA	4	–2.1E+01	1.7E+00	–2.0E+01	–1.9E+01	–2.3E+01	–1.8E+00	3.4E+00
Residual Volumetric Water Content (θ_r)	cm^3/cm^3	4	0.0E+00	0.0E+00	0.0E+00	0.0E+00	0.0E+00	---	---
van Genuchten Fitting Parameter *n*	NA	4	1.3E+00	9.0E–02	1.2E+00	1.4E+00	1.2E+00	1.1E+00	1.1E+00
van Genuchten Fitting Parameter α	cm^{-1}	4	3.3E–02	3.5E–2	2.4E–02	8.0E–02	1.0E–03	1.4E+00	2.6E+00
Lognormal α	NA	4	–4.1E+00	1.8E+00	–3.7E+00	–2.5E+00	–6.6E+00	–1.3E+00	2.5E+00

N = Number (of samples) *NA = Not applicable* *--- Not estimated*

The skewness statistics for residual water content, the van Genuchten fitting parameter α, and saturated hydraulic conductivity for unit 1v (Table III-3) indicate that the distributions for these parameters are not normal for unit 1v; this is also seen in the normal probability plots for these parameters (Figures III-2, III-5, and III-7, respectively). A logarithmic transformation was applied to the saturated hydraulic conductivity and α; however, the residual water content was not transformed because its skewness is a result of the fitting by the RETC code, which sets the parameter to zero when its value is below 0.001. The rationale for setting this limit on the residual water content is that this is a fitting parameter and its physical meaning is not clear. For unit 1v, 29 of the 34 total samples had residual water contents equal to zero (Table III-3). A mixed distribution (Yevjevich, 1972) with a probability spike at zero could be used for residual water content, but the analysis for this type of distribution was not performed.

The properties for the Tshirege Member units of the Bandelier Tuff (Tables III-2 through III-5) do not appear to show any demonstrable differences; the properties for the Tsankawi Pumice/Cerro Toledo interval (Table III-6) and the Otowi Member (Table III-7) are also within the range of the means of the other units. The obvious differences between the soil unit (Table III-1) and basalt (Table III-8) properties and the Bandelier Tuff properties are expected because of the material and genesis of these layers as opposed to the tuff.

III.3.3 Correlation

Consideration of the correlation between parameters is important because sampling distributions may not be independent. Correlation may also be used to estimate parameters using more easily measured variables such as soil texture. Correlation matrices were calculated for the aggregated hydraulic parameters for all geologic units at TA-54 (Table III-9) and for each geologic unit (Tables III-10 through 17).

Some of correlations shown in Table III-9 are expected because of functional relationships; these include correlations between saturated conductivity and log-transformed saturated conductivity; α and n; and α and log-transformed α. The RETC code generates a correlation matrix during the fitting process, and α and n are usually highly correlated. Other correlations such as that between the log-transformed saturated conductivity and the saturated water content (θ_s) need to be considered when developing the stochastic simulation for TA-54, as these linear dependencies can affect sampling from distributions when performing Monte Carlo analyses.

Correlations vary among geologic units (Tables III-10 through III-17), as does the number of significant correlations. Again, sample size must be considered when using the correlation coefficients.

Table III-9
Correlation Matrix for Unsaturated Zone Hydraulic Parameters for All Geologic Units

Variable	ρ_b	θ_s	K_s	Ln K_s	θ_r	n	α	Ln α
Bulk Density (ρ_b)	1.0E+00	–8.8E–01	–1.6E–01	–8.6E–01	–1.2E–01	–2.1E–01	1.3E–01	2.3E–01
Saturated Volumetric Water Content (θ_s)	–8.8E–01	1.0E+00	2.1E–01	8.3E–01	4.0E–02	1.6E–01	–7.0E–02	–2.1E–01
Saturated Hydraulic Conductivity (K_s)	–1.6E–01	2.1E–01	1.0E+00	4.6E–01	3.8E–01	4.0E–02	1.9E–01	2.8E–01
Lognormal Saturated Hydraulic Conductivity (Ln K_s)	–8.6E–01	8.3E–01	4.6E–01	1.0E+00	2.0E–01	3.2E–01	–6.0E–02	–1.6E–01
Residual Volumetric Water Content (θ_r)	–1.2E–01	4.0E–02	3.8E–01	2.0E–01	1.0E+00	2.6E–01	1.2E–01	9.0E–02
van Genuchten Fitting Parameter *n*	–2.1E–01	1.6E–01	4.0E–02	3.2E–01	2.6E–01	1.0E+00	–2.5E–01	–6.0E–01
van Genuchten Fitting Parameter α	1.3E–01	–7.0E–02	1.9E–01	–6.0E–02	1.2E–01	–2.5E–01	1.0E+00	6.8E–01
Lognormal α	2.3E–01	–2.1E–01	2.8E–01	–1.6E–01	9.0E–02	–6.0E–01	6.8E–01	1.0E+00

Bold *= Correlation is significant at $p < 0.05$, $N = 90$*

Table III-10
Correlation Matrix for Unsaturated Zone Hydraulic Parameters for Soil Layer

Variable	ρ_b	θ_s	K_s	Ln K_s	θ_r	n	α	Ln α
Bulk Density (ρ_b)	1.0E+00	–3.6E–01	4.8E–01	4.5E–01	---	6.5E–01	1.9E–01	1.5E–01
Saturated Volumetric Water Content (θ_s)	–3.6E–01	1.0E+00	6.2E–01	6.2E–01	---	1.9E–01	6.0E–02	1.0E–02
Saturated Hydraulic Conductivity (K_s)	4.8E–01	6.2E–01	1.0E+00	**9.9E–01**	---	8.2E–01	2.0E–02	–5.0E–02
Lognormal Saturated Hydraulic Conductivity (Ln K_s)	4.5E–01	6.2E–01	**9.9E–01**	1.0E+00	---	8.6E–01	–8.0E–02	–1.6E–01
Residual Volumetric Water Content (θ_r)	---	---	---	---	1.0E+00	---	---	---
van Genuchten Fitting Parameter *n*	6.5E–01	1.9E–01	8.2E–01	8.6E–01	---	1.0E+00	–4.0E–01	–4.7E–01
van Genuchten Fitting Parameter α	1.9E–01	6.0E–02	2.0E–02	–8.0E–02	---	–4.0E–01	1.0E+00	**1.0E+00**
Lognormal α	1.5E–01	1.0E–02	–5.0E–02	–1.6E–01	---	–4.7E–01	**1.0E+00**	1.0E+00

Bold *= Correlation is significant at p < 0.05, N = 4* *--- = Not estimated*

Table III-11
Correlation Matrix for Unsaturated Zone Hydraulic Parameters for Bandelier Tuff Tshirege Member Unit 2

Variable	ρ_b	θ_s	K_s	Ln K_s	θ_r	n	α	Ln α
Bulk Density (ρ_b)	1.0E+00	–4.5E–01	1.0E–01	–4.1E–01	6.9E–01	6.0E–01	–5.8E–01	–6.8E–01
Saturated Volumetric Water Content (θ_s)	–4.5E–01	1.0E+00	7.4E–01	9.3E–01	7.0E–02	–6.3E–01	3.1E–01	5.7E–01
Saturated Hydraulic Conductivity (K_s)	1.0E–01	7.4E–01	1.0E+00	8.4E–01	6.7E–01	–1.9E–01	1.5E–01	3.2E–01
Lognormal Saturated Hydraulic Conductivity (Ln K_s)	–4.1E–01	9.3E–01	8.4E–01	1.0E+00	1.9E–01	–5.5E–01	4.9E–01	6.9E–01
Residual Volumetric Water Content (θ_r)	6.9E–01	7.0E–02	6.7E–01	1.9E–01	1.0E+00	5.0E–01	–3.8E–01	–3.6E–01
van Genuchten Fitting Parameter *n*	6.0E–01	–6.3E–01	–1.9E–01	–5.5E–01	5.0E–01	1.0E+00	–7.3E–01	–8.2E–01
van Genuchten Fitting Parameter α	–5.8E–01	3.1E–01	1.5E–01	4.9E–01	–3.8E–01	–7.3E–01	1.0E+00	9.4E–01
Lognormal α	–6.8E–01	5.7E–01	3.2E–01	6.9E–01	–3.6E–01	–8.2E–01	9.4E–01	1.0E+00

***Bold** = Correlation is significant at $p < 0.05$, $N = 8$*

Table III-12
Correlation Matrix for Unsaturated Zone Hydraulic Parameters for Bandelier Tuff Tshirege Member Unit 1v

Variable	ρ_b	θ_s	K_s	Ln K_s	θ_r	n	α	Ln α
Bulk Density (ρ_b)	1.0E+00	–1.7E–01	–5.0E–02	9.0E–02	–2.4E–01	**6.0E–01**	–1.1E–01	–2.9E–01
Saturated Volumetric Water Content (θ_s)	–1.7E–01	1.0E+00	**4.3E–01**	**4.6E–01**	**1.3E–01**	–3.1E–01	**1.4E–01**	**3.1E–01**
Saturated Hydraulic Conductivity (K_s)	–5.0E–02	**4.3E–01**	1.0E+00	**8.7E–01**	**5.0E–02**	–1.5E–01	**7.5E–01**	**6.8E–01**
Lognormal Saturated Hydraulic Conductivity (Ln K_s)	**9.0E–02**	**4.6E–01**	**8.7E–01**	1.0E+00	–2.5E–01	**2.0E–02**	**4.0E–01**	**4.2E–01**
Residual Volumetric Water Content (θ_r)	–2.4E–01	**1.3E–01**	**5.0E–02**	–2.5E–01	1.0E+00	–7.0E–02	**3.5E–01**	**2.6E–01**
van Genuchten Fitting Parameter *n*	**6.0E–01**	–3.1E–01	–1.5E–01	**2.0E–02**	–7.0E–02	1.0E+00	–2.7E–01	–5.9E–01
van Genuchten Fitting Parameter α	–1.1E–01	**1.4E–01**	**7.5E–01**	**4.0E–01**	**3.5E–01**	–2.7E–01	1.0E+00	**8.3E–01**
Lognormal α	–2.9E–01	**3.1E–01**	**6.8E–01**	**4.2E–01**	**2.6E–01**	–5.9E–01	**8.3E–01**	1.0E+00

Bold *= Correlation is significant at p < 0.05, N = 33*

Table III-13
Correlation Matrix for Unsaturated Zone Hydraulic Parameters for Bandelier Tuff Vapor-Phase Notch

Variable	ρ_b	θ_s	K_s	Ln K_s	θ_r	n	α	Ln α
Bulk Density (ρ_b)	1.0E+00	2.5E–01	–1.1E–01	–3.6E–01	5.6E–01	–8.1E–01	5.8E–01	5.4E–01
Saturated Volumetric Water Content (θ_s)	2.5E–01	1.0E+00	7.5E–01	7.9E–01	–3.4E–01	–4.9E–01	–1.9E–01	4.0E–02
Saturated Hydraulic Conductivity (K_s)	–1.1E–01	7.5E–01	1.0E+00	8.6E–01	–3.6E–01	1.1E–01	–2.4E–01	–6.0E–02
Lognormal Saturated Hydraulic Conductivity (Ln K_s)	–3.6E–01	7.9E–01	8.6E–01	1.0E+00	–7.2E–01	1.3E–01	–6.1E–01	–3.9E–01
Residual Volumetric Water Content (θ_r)	5.6E–01	–3.4E–01	–3.6E–01	–7.2E–01	1.0E+00	–3.7E–01	9.9E–01	9.0E–01
van Genuchten Fitting Parameter *n*	–8.1E–01	–4.9E–01	1.1E–01	1.3E–01	–3.7E–01	1.0E+00	–4.4E–01	–5.2E–01
van Genuchten Fitting Parameter α	5.8E–01	–1.9E–01	–2.4E–01	–6.1E–01	9.9E–01	–4.4E–01	1.0E+00	9.6E–01
Lognormal α	5.4E–01	4.0E–02	–6.0E–02	–3.9E–01	9.0E–01	–5.2E–01	9.6E–01	1.0E+00

***Bold** = Correlation is significant at $p < 0.05$, $N = 5$*

Table III-14
Correlation Matrix for Unsaturated Zone Hydraulic Parameters for Bandelier Tuff Tshirege Member Unit 1g

Variable	ρ_b	θ_s	K_s	Ln K_s	θ_r	n	α	Ln α
Bulk Density (ρ_b)	1.0E+00	–1.9E–01	–2.7E–01	–4.0E–01	–4.0E–02	–4.0E–02	5.0E–02	–1.0E–01
Saturated Volumetric Water Content (θ_s)	–1.9E–01	1.0E+00	3.5E–01	3.4E–01	8.0E–02	–1.0E–02	1.4E–01	8.0E–02
Saturated Hydraulic Conductivity (K_s)	–2.7E–01	3.5E–01	1.0E+00	9.2E–01	4.5E–01	–6.0E–01	8.4E–01	8.6E–01
Lognormal Saturated Hydraulic Conductivity (Ln K_s)	–4.0E–01	3.4E–01	**9.2E–01**	1.0E+00	2.1E–01	**–6.8E–01**	6.6E–01	8.1E–01
Residual Volumetric Water Content (θ_r)	–4.0E–02	8.0E–02	4.5E–01	2.1E–01	1.0E+00	–2.7E–01	6.1E–01	4.8E–01
van Genuchten Fitting Parameter *n*	–4.0E–02	–1.0E–02	**–6.0E–01**	**–6.8E–01**	–2.7E–01	1.0E+00	**–6.2E–01**	**–8.0E–01**
van Genuchten Fitting Parameter α	5.0E–02	1.4E–01	**8.4E–01**	**6.6E–01**	**6.1E–01**	**–6.2E–01**	1.0E+00	**9.3E–01**
Lognormal α	–1.0E–01	8.0E–02	**8.6E–01**	**8.1E–01**	4.8E–01	**–8.0E–01**	**9.3E–01**	1.0E+00

***Bold** = Correlation is significant at $p < 0.05$, $N = 16$*

Table III-15
Correlation Matrix for Unsaturated Zone Hydraulic Parameters for Tsankawi Pumice/ Cerro Toledo Interval

Variable	ρ_b	θ_s	K_s	Ln K_s	θ_r	n	α	Ln α
Bulk Density (ρ_b)	1.0E+00	–7.5E–01	**–9.3E–01**	**–8.9E–01**	**–7.6E–01**	–1.0E–01	–4.0E–01	–4.8E–01
Saturated Volumetric Water Content (θ_s)	–7.5E–01	1.0E+00	5.7E–01	4.1E–01	5.5E–01	4.0E–02	**7.7E–01**	**7.8E–01**
Saturated Hydraulic Conductivity (K_s)	**–9.3E–01**	5.7E–01	1.0E+00	**9.3E–01**	**9.1E–01**	3.3E–01	1.1E–01	2.0E–01
Lognormal Saturated Hydraulic Conductivity (Ln K_s)	**–8.9E–01**	4.1E–01	**9.3E–01**	1.0E+00	7.0E–01	1.9E–01	6.0E–02	1.8E–01
Residual Volumetric Water Content (θ_r)	**–7.6E–01**	5.5E–01	**9.1E–01**	7.0E–01	1.0E+00	4.9E–01	0.0E+00	7.0E–02
van Genuchten Fitting Parameter *n*	–1.0E–01	4.0E–02	3.3E–01	1.9E–01	4.9E–01	1.0E+00	–4.8E–01	–5.3E–01
van Genuchten Fitting Parameter α	–4.0E–01	**7.7E–01**	1.1E–01	6.0E–02	0.0E+00	–4.8E–01	1.0E+00	**9.9E–01**
Lognormal α	–4.8E–01	**7.8E–01**	2.0E–01	1.8E–01	7.0E–02	–5.3E–01	**9.9E–01**	1.0E+00

***Bold** = Correlation is significant at $p < 0.05$, $N = 7$*

Table III-16
Correlation Matrix for Unsaturated Zone Hydraulic Parameters for Bandelier Tuff Otowi Member

Variable	ρ_b	θ_s	K_s	Ln K_s	θ_r	n	α	Ln α
Bulk Density (ρ_b)	1.0E+00	2.0E–02	–6.9E–01	–7.7E–01	1.7E–01	7.0E–02	–7.6E–01	–7.9E–01
Saturated Volumetric Water Content (θ_s)	2.0E–02	1.0E+00	2.3E–01	2.8E–01	–3.5E–01	–4.3E–01	4.3E–01	4.5E–01
Saturated Hydraulic Conductivity (K_s)	–6.9E–01	2.3E–01	1.0E+00	9.7E–01	2.4E–01	2.2E–01	6.8E–01	6.7E–01
Lognormal Saturated Hydraulic Conductivity (Ln K_s)	–7.7E–01	2.8E–01	9.7E–01	1.0E+00	1.9E–01	1.8E–01	7.2E–01	7.4E–01
Residual Volumetric Water Content (θ_r)	1.7E–01	–3.5E–01	2.4E–01	1.9E–01	1.0E+00	9.5E–01	–4.4E–01	–4.4E–01
van Genuchten Fitting Parameter *n*	7.0E–02	–4.3E–01	2.2E–01	1.8E–01	9.5E–01	1.0E+00	–5.0E–01	–4.8E–01
van Genuchten Fitting Parameter α	–7.6E–01	4.3E–01	6.8E–01	7.2E–01	–4.4E–01	–5.0E–01	1.0E+00	9.9E–01
Lognormal α	–7.9E–01	4.5E–01	6.7E–01	7.4E–01	–4.4E–01	–4.8E–01	9.9E–01	1.0E+00

***Bold** = Correlation is significant at $p < 0.05$, $N = 12$*

Table III-17
Correlation Matrix for Unsaturated Zone Hydraulic Parameters for Cerros del Rio Basalt

Variable	ρ_b	θ_s	K_s	Ln K_s	θ_r	n	α	Ln α
Bulk Density (ρ_b)	1.0E+00	–8.2E–01	1.8E–01	–1.0E–01	---	5.0E–02	1.6E–01	–2.1E–01
Saturated Volumetric Water Content (θ_s)	–8.2E–01	1.0E+00	4.1E–01	6.6E–01	---	2.3E–01	1.0E–01	1.6E–01
Saturated Hydraulic Conductivity (K_s)	1.8E–01	4.1E–01	1.0E+00	9.3E–01	---	3.8E–01	5.1E–01	4.0E–02
Lognormal Saturated Hydraulic Conductivity (Ln K_s)	–1.0E–01	6.6E–01	9.3E–01	1.0E+00	---	5.7E–01	2.7E–01	–1.3E–01
Residual Volumetric Water Content (θ_r)	---	---	---	---	1.0E+00	---	---	---
van Genuchten Fitting Parameter *n*	5.0E–02	2.3E–01	3.8E–01	5.7E–01	---	1.0E+00	–6.0E–01	–8.8E–01
van Genuchten Fitting Parameter α	1.6E–01	1.0E–01	5.1E–01	2.7E–01	---	–6.0E–01	1.0E+00	8.4E–01
Lognormal α	–2.1E–01	1.6E–01	4.0E–02	–1.3E–01	---	–8.8E–01	8.4E–01	1.0E+00

Bold *= Correlation is significant at p < 0.05, N = 4* *--- = Not estimated*

III.3.4 Alternative Estimates

An alternative approach to provide parameter estimates for a geologic unit is to combine the retention data for the geologic unit and obtain a single set of parameter estimates using the RETC code. The RETC geologic unit fitted curve for Tshirege Member unit 2 is shown in Figure III-9. The saturated volumetric water content (θ_s) was a fitting parameter for this curve. Figure III-9 also shows curves for Tshirege Member unit 2 using mean and median parameter values from Table III-2. The curves for mean and median parameter values appear similar, but both diverge from the geologic unit fitted curve over the range of 100 cm to 1.0×10^4 cm (39 to 3,900 in.).

The RETC code generates statistics including 95 percent confidence intervals for fitted parameters; Table III-18 lists these statistics for Tshirege Member unit 2. A comparison of the estimated parameters in Table III-18 to the mean and median estimates in Table III-2 shows that both the saturated volumetric water content (θ_s) and α fall inside the 95 percent confidence intervals, but the mean and median estimates for n (Table III-2) lie outside the 95 percent confidence limits given in Table III-18. The limited sample size for unit 2 makes it virtually impossible to determine which set of parameters is more appropriate for unit 2; however, the values in Table III-18 provide another estimate that can be used in Monte Carlo analyses of flow and transport at TA-54.

Table III-18
Parameter Estimates and Statistics for RETC Fit to All Retention Data for Bandelier Tuff Tshirege Member Unit 2

Parameter	Value	Standard Error of Coefficient	95% Confidence Limit	
			Lower	Upper
Saturated Volumetric Water Content (θ_s)	4.1E–01	1.0E–02	3.9E–01	4.3E–01
van Genuchten Fitting Parameter α	5.0E–03	1.0E–03	3.0E–03	7.0E–03
van Genuchten Fitting Parameter n	1.7E+00	9.0E–02	1.5E+00	1.9E+00

The alternative estimates of hydrologic parameters developed for unit 1v are provided in Figure III-10 and Table III-19. Figure III-10 shows an obvious bias for the saturated volumetric water volume (θ_s) estimated from all the data; this bias results from setting the zero-pressure values in the data to 0.10 cm. These initial data values are weighted heavily in fitting the saturated volumetric water content values. Comparison of the all-data parameter estimates shown in Table III-19 with the mean and median estimates in Table III-3 reveal the bias in saturated volumetric water content; the median values for both α and n lie within the 95 percent confidence intervals. The mean values for α and n from Table III-3 lie at the upper range of the 95 percent confidence limit for these parameters (Table III-19).

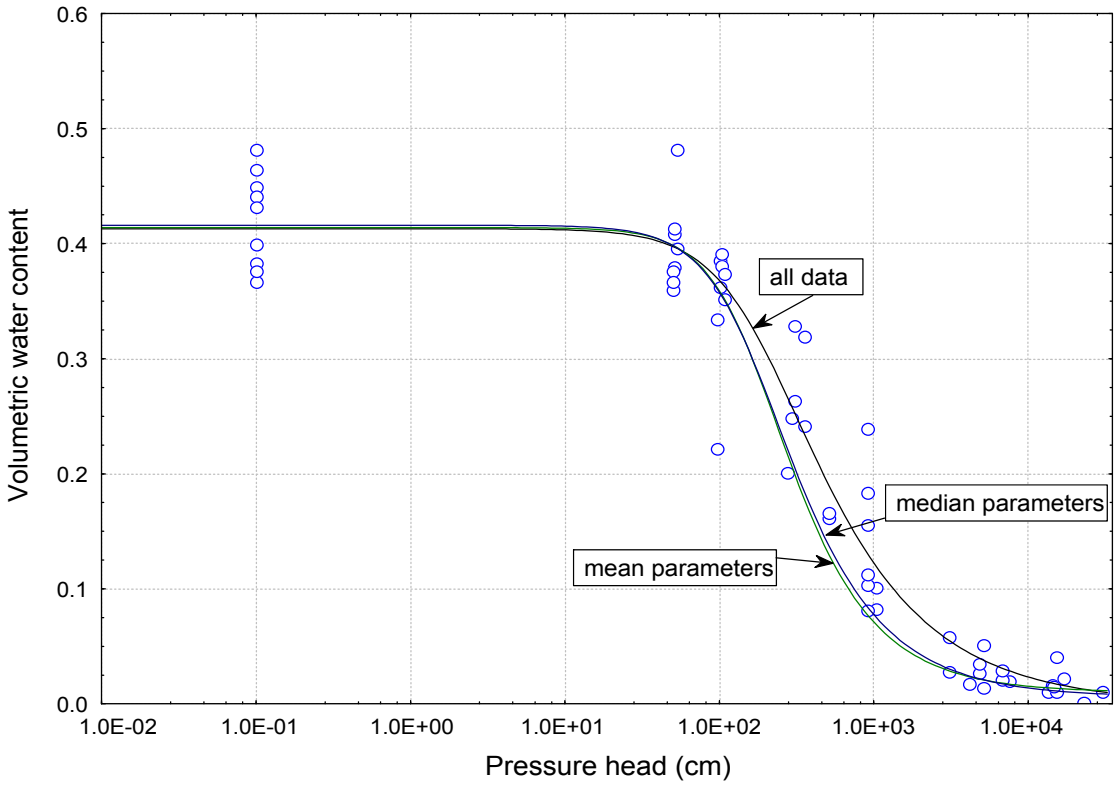

Figure III-9
Comparison of van Genuchten Retention Curve Fits for Bandelier Tuff Tshirege Member Unit 2: Curves for All Retention Data, Mean Values, and Median Values

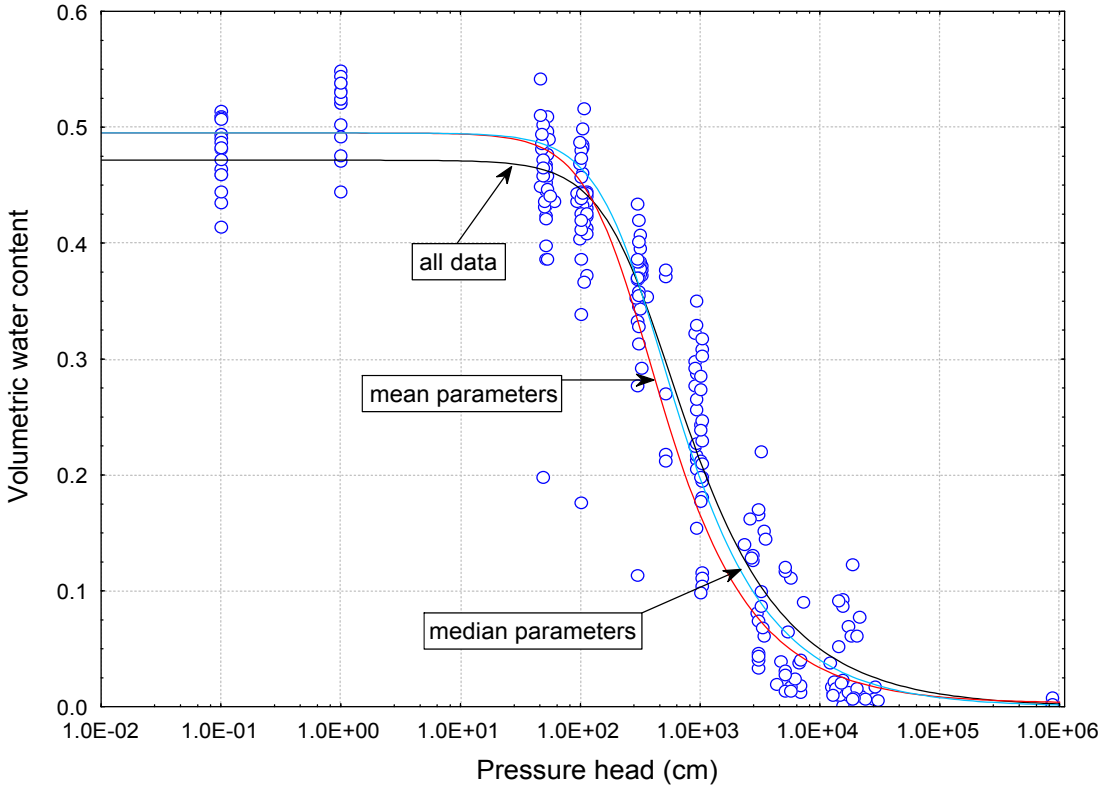

Figure III-10
Comparison of van Genuchten Retention Curve Fits for Bandelier Tuff Tshirege Member Unit 1v: Curves for All Retention Data, Mean Values, and Median Values

Table III-19
Parameter Estimates and Statistics for RETC Fit to All Retention Data for Bandelier Tuff Tshirege Member Unit 1v

Parameter	Value	Standard Error of Coefficient	95% Confidence Limit	
			Lower	Upper
Saturated Volumetric Water Content (θ_s)	4.7E–01	1.0E–02	4.6E–01	4.8E–01
van Genuchten Fitting Parameter α	3.0E–03	3.0E–04	3.0E–03	4.0E–03
van Genuchten Fitting Parameter *n*	1.7E+00	4.0E–02	1.6E+00	1.7E+00

Tables III-20 and III-21 and Figures III-11 and III-12 present results of the all-data RETC-fitted curve for unit 1g and the Otowi Member, respectively. Again, comparisons can be made with the mean and median estimates for these units (Tables III-5 and III-7). For Tshirege Member unit 1g, mean and median *n* parameter values exceed the upper 95 percent confidence limits of the parameters fitted to all retention values. Mean and median parameter values for the Otowi Member (Table III-7) are within the 95 percent confidence interval of the parameters fitted to all retention data (Table III-21).

Table III-20
Parameter Estimates and Statistics for RETC Fit to All Retention Data for Bandelier Tuff Tshirege Member Unit 1g

Parameter	Value	Standard Error of Coefficient	95% Confidence Limits	
			Lower	Upper
Saturated Volumetric Water Content (θ_s)	4.6E–01	1.0E–02	4.4E–01	4.7E–01
van Genuchten Fitting Parameter α	5.0E–03	5.0E–04	4.0E–03	6.0E–03
van Genuchten Fitting Parameter *n*	1.7E+00	4.0E–02	1.6E+00	1.7E+00

Table III-21
Parameter Estimates and Statistics for RETC Fit to All Retention Data for Bandelier Tuff Otowi Member

Parameter	Value	Standard Error of Coefficient	95% Confidence Limits	
			Lower	Upper
Residual Volumetric Water Content (θ_r)	1.6E–02	8.0E–03	1.0E–03	3.1E–02
Saturated Volumetric Water Content (θ_s)	4.3E–01	4.0E–03	4.2E–01	4.4E–01
van Genuchten Fitting Parameter α	6.0E–03	4.0E–04	5.0E–03	7.0E–03
van Genuchten Fitting Parameter *n*	1.7E+00	6.0E–02	1.6E+00	1.8E+00

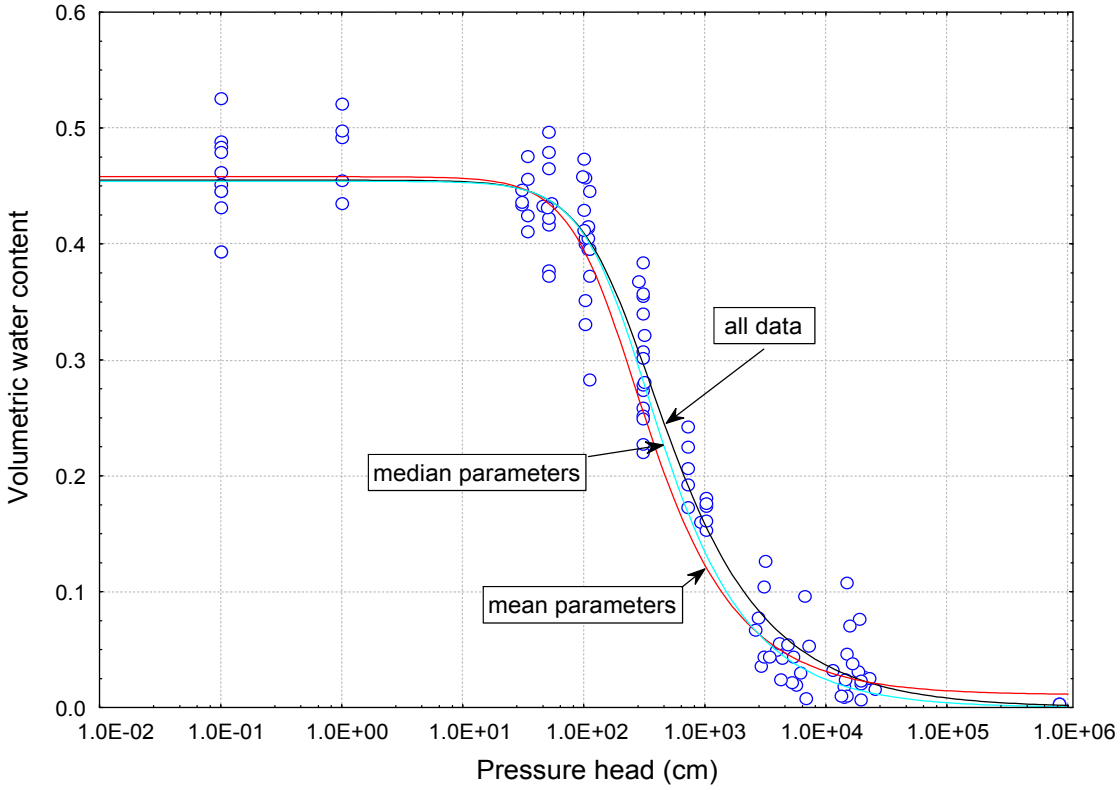

Figure III-11
Comparison of van Genuchten Retention Curve Fits for Bandelier Tuff Tshirege Member Unit 1g : Curves for All Retention Data, Mean Values, and Median Values

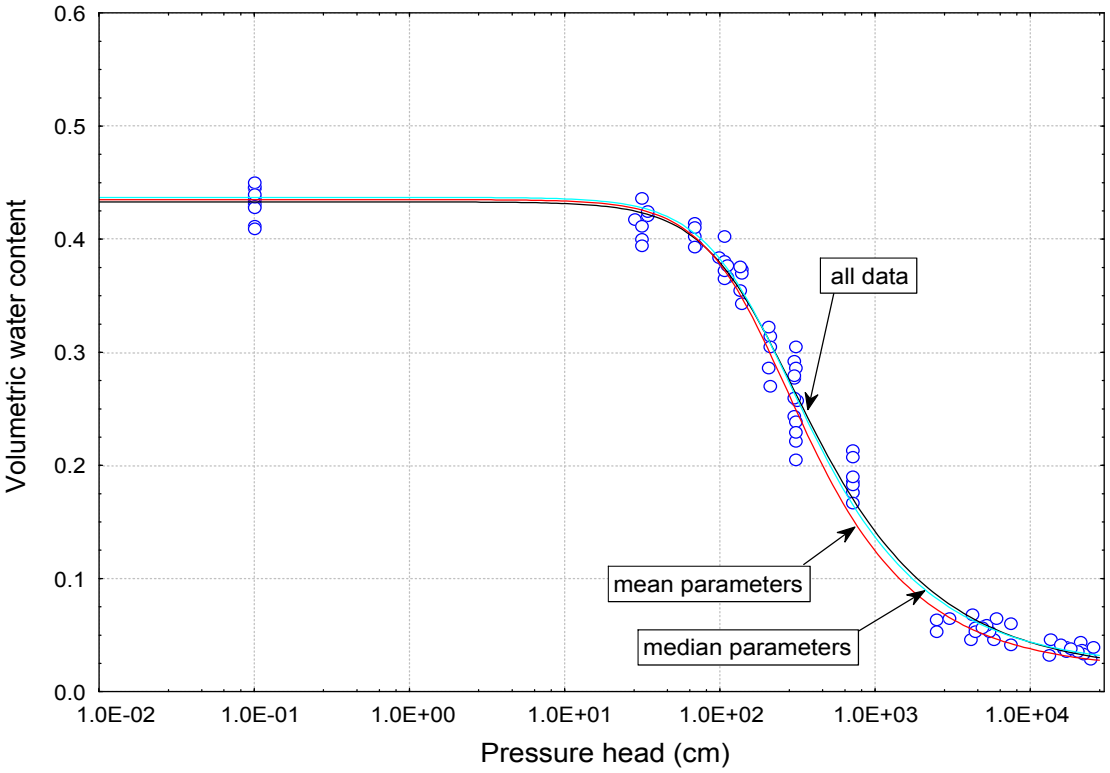

Figure III-12
Comparison of van Genuchten Retention Curve Fits for Bandelier Tuff Otowi Member: Curves for All Retention Data, Mean Values, and Median Values

III.4 Summary and Conclusions

This study provided a statistical analysis of hydrologic properties of geologic units from TA-54 to estimate parameters for stochastic analyses of groundwater flow and transport. Descriptive statistics and correlation properties were calculated both by geologic unit and for the aggregated data. Distribution plots and the skew statistic indicated that saturated hydraulic conductivity and the van Genuchten α parameter were not described by a normal distribution; consequently, natural logarithmic transformations were performed on these two parameters. Correlation analyses revealed some linear relationships between parameters that are important when generating distributions for Monte Carlo analysis. Retention data were pooled and fitted to Equation 1 by geologic unit to provide additional estimates of the hydrologic parameters.

The parameters estimated in this report pertain to core samples that represent matrix properties of the materials. At high saturation, features such as fractures or macropores can change hydrologic behavior substantially. The parameters presented in this study will not accurately represent these features at high saturation conditions.

There were a limited number of samples for the geologic units included in this study, which prevents meaningful comparative analyses among units and makes it difficult to define statistics such as parameter correlation within a single unit. The lack of spatial correlation data, in both the vertical and lateral directions, is also a limiting factor in terms of using this information for flow and transport simulation.

III.5 References

Broxton, D.E. and S.L. Reneau, 1995, *Stratigraphic Nomenclature of the Bandelier Tuff for the Environmental Restoration Project at Los Alamos National Laboratory*, Los Alamos National Laboratory Report, LA-13010-MS.

DBS&A, 1995, *Laboratory Analysis of Soil Hydraulic Properties of G-5 Soil Samples*, Daniel B. Stephens & Associates, Inc., Contract completion Report to Los Alamos National Laboratory, January.

DBS&A, 1996, *Hydraulic Properties of Los Alamos National Laboratory Soil Samples*, Contract completion Report to Los Alamos National Laboratory, October.

Freeze, R.A., 1975, "A Stochastic-Conceptual Analysis of One-Dimensional Groundwater Flow in Nonuniform Homogeneous Media," *Water Resources Res.*, Vol. 11, pp. 725–741.

Nielsen, D. R., J.W. Biggar, and K.T. Erh, 1973, "Spatial Variability of Field-Measured Soil-Water Properties," *Hilgardia*, Vol. 42, pp. 215–259.

Puglisi, C.V. and E.L. Vold, 1995, "Low-Impact Sampling under an Active Solid Low-Level Radioactive Waste Disposal Unit Using Horizontal Drilling Technology," *Symposium on the Scientific Basis for Nuclear Waste Management*, Materials Research Society, Boston, MA, November 27, 1995.

Rogers, D.B. and B.M. Gallaher, 1995, *The Unsaturated Hydraulic Characteristics of the Bandelier Tuff*, Los Alamos National Laboratory Report LA-12968-MS, September.

van Genuchten, M.Th., 1980, "A Closed Form Equation for Predicting the Hydraulic Conductivity of Unsaturated Soil," *Soil Science Soc. Am. J.*, Vol. 44, pp. 892–898.

van Genuchten, M.Th., F.J. Leij, and S.R. Yates, 1991, *The RETC Code for Quantifying the Hydraulic Functions of Unsaturated Soils*, U.S. Environmental Protection Agency Rep. No. EPA/600/2-91/065, 85p.

Yevjevich, V.M., 1972, "Probability and Statistics in Hydrology," *Water Resources Publication*, Fort Collins, Co. 276p.

Annex IIIa
Parameters and Data Used for Statistical Analyses

The following table contains the parameters and other data used for the statistical analyses reported above. Values have been rounded to three significant digits (except for sampling depths).

Annex IIIa:
Parameters and Data Used for Statistical Analyses

Unit	Borehole	Depth (ft)	Depth (m)	ρ_b (g/cm^3)	θ_s (cm^3/cm^3)	Porosity (cm^3/cm^3)	K_s (cm/s)	Ln K_s	θ_r (cm^3/cm^3)	n	α (cm^{-1})	Ln α
soil	54-501 [a]	0	0.0	1.47E+00	4.00E–01	4.44E–01	5.45E–06	–1.21E+01	0.00E+00	1.26E+00	9.58E–03	–4.65E+00
	54-502 [a]	0	0.0	1.42E+00	4.29E–01	4.66E–01	5.43E–06	–1.21E+01	0.00E+00	1.24E+00	9.73E–03	–4.63E+00
	54-503 [a]	0	0.0	1.46E+00	4.20E–01	4.51E–01	6.52E–06	–1.19E+01	0.00E+00	1.24E+00	1.83E–02	–4.00E+00
	54-504 [a]	0	0.0	1.43E+00	3.98E–01	4.62E–01	1.39E–06	–1.35E+01	0.00E+00	1.21E+00	1.42E–02	–4.26E+00
2	54-1006[d]	42	12.8	1.28E+00	4.49E–01		4.10E–04	–7.80E+00	0.00E+00	1.76E+00	6.40E–03	–5.05E+00
	TA-54-G-5 [b]	9	2.7	1.35E+00	3.99E–01	4.74E–01	2.10E–04	–8.47E+00	0.00E+00	1.56E+00	1.46E–02	–4.23E+00
		21.5	6.6	1.37E+00	4.32E–01	4.67E–01	1.30E–04	–8.95E+00	0.00E+00	1.49E+00	6.84E–03	–4.99E+00
		32.5	9.9	1.45E+00	3.67E–01	4.37E–01	3.10E–05	–1.04E+01	1.22E–02	2.63E+00	2.85E–03	–5.86E+00
		42.5	13.0	1.49E+00	3.83E–01	4.20E–01	2.70E–05	–1.05E+01	1.22E–02	2.19E+00	1.86E–03	–6.29E+00
		52.5	16.0	1.43E+00	3.76E–01	4.43E–01	4.00E–05	–1.01E+01	1.85E–02	2.95E+00	2.04E–03	–6.20E+00
	LGM-85-06 [d]	29	8.8		4.25E–01		4.80E–04	–7.64E+00				
		51	15.5		4.02E–01		8.40E–05	–9.39E+00				
	LGM-85-11 [d]	3	0.9		5.40E–01	5.40E–01	5.40E–04	–7.52E+00				
		30	9.1		5.15E–01	5.15E–01	2.80E–04	–8.18E+00				
	LLC-85-14 [d]	30	9.1	1.37E+00	4.41E–01		4.20E–04	–7.78E+00	0.00E+00	1.89E+00	6.00E–03	–5.12E+00
	LLC-85-15 [d]	10.5	3.2	1.46E+00	4.64E–01		1.60E–03	–6.44E+00	3.80E–02	2.04E+00	6.00E–03	–5.12E+00
	LLM-85-01 [d]	30	9.1		3.96E–01	3.96E–01	1.10E–04	–9.12E+00				

vpn= Vapor-phase notch

[a] *Parameters for these boreholes obtained and/or calculated from data in DBS&A (1996).*

[b] *Parameters for this borehole obtained and/or calculated from data in DBS&A (1995).*

[c] *Parameters for this borehole obtained and/or calculated from data in DBS&A (1996); stratigraphy from Puglisi and Vold (1995)*

[d] *Parameters from Rogers and Gallaher (1995)*

Annex IIIa: (Continued)
Parameters and Data Used for Statistical Analyses for

Unit	Borehole	Depth (ft)	Depth (m)	ρ_b (g/cm³)	θ_s (cm³/cm³)	Porosity (cm³/cm³)	K_s (cm/s)	Ln K_s	θ_r (cm³/cm³)	n	α (cm^{-1})	Ln α
2 (cont.)	LLM-85-02 [d]	7	2.1		4.15E–01	4.15E–01	4.40E–04	–7.73E+00				
		36	11.0		4.65E–01	4.65E–01	1.20E–04	–9.03E+00				
	LLM-85-05 [d]	15	4.6		5.26E–01	5.26E–01	5.60E–04	–7.49E+00				
		36	11.0		7.36E–01	7.36E–01	2.20E–04	–8.42E+00				
1v	54-1001 [d]	68	20.7	1.20E+00	4.14E–01		1.30E–04	–8.95E+00	0.00E+00	1.89E+00	3.40E–03	–5.68E+00
		83	25.3	1.25E+00	4.60E–01		1.10E–04	–9.12E+00	0.00E+00	2.23E+00	2.20E–03	–6.12E+00
		102	31.1	1.19E+00	5.14E–01		1.60E–04	–8.74E+00	0.00E+00	1.78E+00	3.40E–03	–5.68E+00
		122	37.2	1.18E+00	4.64E–01		2.20E–05	–1.07E+01	0.00E+00	1.58E+00	4.10E–03	–5.50E+00
		142	43.3	1.20E+00	4.82E–01		8.20E–05	–9.41E+00	0.00E+00	1.43E+00	3.70E–03	–5.60E+00
	54-1002 [d]	92.5	28.2	1.26E+00	4.60E–01		8.10E–05	–9.42E+00	0.00E+00	2.21E+00	1.20E–03	–6.73E+00
		122	37.2	1.23E+00	4.95E–01		4.60E–05	–9.99E+00	0.00E+00	1.77E+00	3.10E–03	–5.78E+00
		142.5	43.4	1.19E+00	4.91E–01		2.50E–05	–1.06E+01	1.70E–02	1.39E+00	1.54E–02	–4.17E+00
	54-1003 [d]	102	31.1	1.22E+00	5.10E–01		1.30E–04	–8.95E+00	0.00E+00	1.73E+00	3.00E–03	–5.81E+00
		119.5	36.4	1.22E+00			9.90E–05	–9.22E+00				
	54-1006 [d]	76.9	23.4	1.28E+00	4.45E–01		9.80E–05	–9.23E+00	0.00E+00	1.88E+00	3.00E–03	–5.81E+00
		124.5	38.0	1.22E+00	4.35E–01		4.50E–05	–1.00E+01	0.00E+00	2.09E+00	3.50E–03	–5.66E+00
		136.7	41.7	1.28E+00	4.72E–01		5.70E–05	–9.77E+00	0.00E+00		1.40E–03	–6.57E+00
	54-1107 [a]	93.2	28.4	1.16E+00	5.49E–01	4.98E–01	1.29E–04	–8.96E+00	0.00E+00	1.47E+00	6.02E–03	–5.11E+00

vpn= Vapor-phase notch

[a] *Parameters for these boreholes obtained and/or calculated from data in DBS&A (1996).*

[b] *Parameters for this borehole obtained and/or calculated from data in DBS&A (1995).*

[c] *Parameters for this borehole obtained and/or calculated from data in DBS&A (1996); stratigraphy from Puglisi and Vold (1995)*

[d] *Parameters from Rogers and Gallaher (1995)*

Annex IIIa: (Continued)
Parameters and Data Used for Statistical Analyses for

Unit	Borehole	Depth (ft)	Depth (m)	ρ_b (g/cm³)	θ_s (cm³/cm³)	Porosity (cm³/cm³)	K_s (cm/s)	Ln K_s	θ_r (cm³/cm³)	n	α (cm^{-1})	Ln α
1v (cont.)	54-1107 [a] (cont.)	96.25	29.3	1.18E+00	5.21E–01	4.89E–01	1.13E–04	–9.09E+00	0.00E+00	1.35E+00	9.51E–03	–4.66E+00
		98.2	29.9	9.30E–01	4.45E–01	6.01E–01	4.61E–05	–9.99E+00	0.00E+00	1.43E+00	5.82E–03	–5.15E+00
		99.2	30.2	1.13E+00	5.21E–01	5.11E–01	6.25E–04	–7.38E+00	2.18E–02	1.35E+00	2.97E–01	–1.21E+00
		101.3	30.9	1.20E+00	5.03E–01	4.83E–01	3.20E–05	–1.04E+01	0.00E+00	1.43E+00	2.64E–03	–5.94E+00
	54-1121 [a]	64.25	19.6	1.09E+00	5.32E–01	5.30E–01	2.21E–04	–8.42E+00	0.00E+00	1.50E+00	7.52E–03	–4.89E+00
		67.75	20.7	1.18E+00	5.44E–01	4.89E–01	1.64E–04	–8.72E+00	0.00E+00	1.70E+00	4.04E–03	–5.51E+00
		70.25	21.4	1.07E+00	5.25E–01	5.39E–01	1.43E–04	–8.85E+00	0.00E+00	1.44E+00	8.05E–03	–4.82E+00
		75.25	22.9	1.20E+00	4.71E–01	4.83E–01	7.32E–05	–9.52E+00	0.00E+00	1.68E+00	3.24E–03	–5.73E+00
		77.75	23.7	1.08E+00	5.39E–01	5.32E–01	1.71E–04	–8.67E+00	0.00E+00	1.38E+00	8.16E–03	–4.81E+00
	TA-54-G-5 [b]	60.5	18.4	1.17E+00	5.78E–01	5.42E–01	2.20E–04	–8.42E+00	0.00E+00	1.85E+00	4.97E–03	–5.30E+00
		70	21.3	1.17E+00	4.75E–01	5.45E–01	8.80E–05	–9.34E+00	0.00E+00	2.10E+00	1.31E–03	–6.64E+00
		82.5	25.2	1.18E+00	4.40E–01	5.43E–01	3.60E–05	–1.02E+01	0.00E+00	1.83E+00	2.15E–03	–6.14E+00
	G-P38-HH3 [c]	70.25	21.4	1.03E+00		5.58E–01	1.62E–03	–6.43E+00				
		122.25	37.3	1.02E+00		5.59E–01	2.31E–03	–6.07E+00				
		129.25	39.4	1.32E+00	5.39E–01	4.32E–01	2.47E–04	–8.31E+00	0.00E+00	1.89E+00	2.49E–03	–6.00E+00
		144.25	44.0	1.06E+00	5.25E–01	5.42E–01	3.42E–04	–7.98E+00	0.00E+00	1.69E+00	3.43E–03	–5.68E+00
		204.25	62.3	1.17E+00	5.30E–01	4.95E–01	1.82E–04	–8.61E+00	0.00E+00	1.49E+00	4.84E–03	–5.33E+00
		257.27	78.4	1.09E+00	4.76E–01	5.32E–01	5.58E–05	–9.79E+00	0.00E+00	1.60E+00	4.94E–03	–5.31E+00

vpn= Vapor-phase notch

[a] *Parameters for these boreholes obtained and/or calculated from data in DBS&A (1996).*

[b] *Parameters for this borehole obtained and/or calculated from data in DBS&A (1995).*

[c] *Parameters for this borehole obtained and/or calculated from data in DBS&A (1996); stratigraphy from Puglisi and Vold (1995)*

[d] *Parameters from Rogers and Gallaher (1995)*

Annex IIIa: (Continued)
Parameters and Data Used for Statistical Analyses for

Unit	Borehole	Depth (ft)	Depth (m)	ρ_b (g/cm³)	θ_s (cm³/cm³)	Porosity (cm³/cm³)	K_s (cm/s)	Ln K_s	θ_r (cm³/cm³)	n	α (cm^{-1})	Ln α
1v (cont.)	LGM-85-06 [d]	99	30.2		5.26E–01		1.30E–03	–6.65E+00				
	LGM-85-11 [d]	94	28.7		6.43E–01	6.43E–01	1.10E–04	–9.12E+00				
	LLC-86-22 [d]	54.5	16.6	1.26E+00	5.10E–01		5.20E–05	–9.86E+00	2.00E–02	2.24E+00	3.70E–03	–5.60E+00
		54.5	16.6	1.26E+00	4.83E–01		2.50E–04	–8.29E+00	0.00E+00	1.93E+00	4.50E–03	–5.40E+00
		65	19.8	1.27E+00	4.87E–01		1.40E–04	–8.87E+00	0.00E+00	2.35E+00	2.60E–03	–5.95E+00
		131.5	40.1	1.05E+00	5.07E–01		1.90E–05	–1.09E+01	1.20E–02	1.59E+00	2.10E–03	–6.17E+00
		131.5	40.1	1.05E+00	5.08E–01		2.70E–05	–1.05E+01	4.40E–02	1.71E+00	2.10E–03	–6.17E+00
	LLM-85-01 [d]	52	15.9		6.44E–01	6.44E–01	2.60E–04	–8.26E+00				
		101	30.8		6.21E–01	6.21E–01	2.50E–04	–8.29E+00				
	LLM-85-02 [d]	67	20.4		4.33E–01	4.33E–01	9.80E–05	–9.23E+00				
		117	35.7		4.85E–01	4.85E–01	1.70E–04	–8.68E+00				
		76	23.2		7.42E–01	7.42E–01	1.30E–04	–8.95E+00				
vpn	TA-54-G-5 [b]	92.5	28.2	1.13E+00	5.25E–01	5.58E–01	6.80E–05	–9.60E+00	0.00E+00	1.40E+00	3.54E–03	–5.64E+00
	MC-1 [a]		0.0	1.09E+00	5.33E–01	5.31E–01	3.29E–04	–8.02E+00	0.00E+00	1.67E+00	3.96E–03	–5.53E+00
	MC-2 [a]		0.0	1.01E+00	4.39E–01	5.65E–01	4.54E–05	–1.00E+01	0.00E+00	1.80E+00	2.72E–03	–5.91E+00
	MC-4 [a]		0.0	1.15E+00	4.45E–01	5.03E–01	4.77E–06	–1.23E+01	1.48E–02	1.52E+00	1.48E–02	–4.21E+00
	MC-5 [a]		0.0	1.10E+00	4.33E–01	5.27E–01	1.54E–05	–1.11E+01	0.00E+00	1.73E+00	1.59E–03	–6.44E+00
1g	54-1002 [d]	179.3	54.7	1.16E+00	3.93E–01		6.50E–05	–9.64E+00	0.00E+00	1.82E+00	4.30E–03	–5.45E+00

vpn= Vapor-phase notch

[a] *Parameters for these boreholes obtained and/or calculated from data in DBS&A (1996).*

[b] *Parameters for this borehole obtained and/or calculated from data in DBS&A (1995).*

[c] *Parameters for this borehole obtained and/or calculated from data in DBS&A (1996); stratigraphy from Puglisi and Vold (1995)*

[d] *Parameters from Rogers and Gallaher (1995)*

Annex IIIa: (Continued)
Parameters and Data Used for Statistical Analyses for

Unit	Borehole	Depth (ft)	Depth (m)	ρ_b (g/cm³)	θ_s (cm³/cm³)	Porosity (cm³/cm³)	K_s (cm/s)	Ln K_s	θ_r (cm³/cm³)	n	α (cm^{-1})	Ln α
1g (cont.)	54-1002 [d] (cont.)	244	74.4	1.14E+00	3.93E–01		1.70E–04	–8.68E+00	0.00E+00	1.75E+00	6.20E–03	–5.08E+00
	54-1003 [d]	157	47.9	1.14E+00	4.32E–01		1.30E–04	–8.95E+00	2.50E–02	1.77E+00	4.00E–03	–5.52E+00
		207	63.1	1.18E+00	4.28E–01		1.50E–04	–8.81E+00				
		261	79.6	1.11E+00	4.88E–01		2.70E–04	–8.22E+00				
		271.5	82.8	1.31E+00	4.10E–01		2.60E–04	–8.26E+00				
	54-1006 [d]	161	49.1	1.13E+00	5.26E–01		1.20E–04	–9.03E+00				
	54-1107 [a]	104.3	31.8	1.13E+00	4.92E–01	5.12E–01	8.06E–05	–9.43E+00	0.00E+00	2.00E+00	2.64E–03	–5.94E+00
		108.25	33.0	1.15E+00	5.21E–01	5.05E–01	4.61E–04	–7.68E+00	0.00E+00	1.77E+00	4.61E–03	–5.38E+00
	54-1121 [a]	80.25	24.5	1.18E+00	4.35E–01	4.93E–01	3.71E–05	–1.02E+01	4.31E–02	1.80E+00	3.04E–03	–5.80E+00
		82.75	25.2	1.14E+00	4.98E–01	5.09E–01	1.22E–04	–9.01E+00	1.59E–02	1.59E+00	5.94E–03	–5.13E+00
		87.75	26.8	1.14E+00	4.55E–01	5.10E–01	1.02E–04	–9.19E+00	0.00E+00	1.67E+00	5.06E–03	–5.29E+00
	CDBM-1 [d]	24	7.3	1.17E+00	4.88E–01		6.20E–05	–9.69E+00	0.00E+00	1.94E+00	2.90E–03	–5.84E+00
		34	10.4	1.07E+00	4.62E–01		2.20E–04	–8.42E+00	0.00E+00	1.63E+00	5.50E–03	–5.20E+00
		44	13.4	1.26E+00	4.45E–01		7.00E–05	–9.57E+00	0.00E+00	1.68E+00	4.10E–03	–5.50E+00
		54	16.5	1.09E+00	4.46E–01		4.60E–04	–7.68E+00	0.00E+00	1.52E+00	7.00E–03	–4.96E+00
		64	19.5	1.23E+00	4.51E–01		1.20E–04	–9.03E+00	5.00E–03	1.72E+00	5.30E–03	–5.24E+00
	CDBM-2 [d]	28	8.5	1.19E+00	4.79E–01		8.50E–04	–7.07E+00	5.10E–02	1.43E+00	2.81E–02	–3.57E+00
		38	11.6	9.40E–01	4.84E–01		4.50E–04	–7.71E+00	2.60E–02	1.79E+00	7.10E–03	–4.95E+00

vpn= Vapor-phase notch

[a] *Parameters for these boreholes obtained and/or calculated from data in DBS&A (1996).*

[b] *Parameters for this borehole obtained and/or calculated from data in DBS&A (1995).*

[c] *Parameters for this borehole obtained and/or calculated from data in DBS&A (1996); stratigraphy from Puglisi and Vold (1995)*

[d] *Parameters from Rogers and Gallaher (1995)*

Annex IIIa: (Continued)
Parameters and Data Used for Statistical Analyses for

Unit	Borehole	Depth (ft)	Depth (m)	ρ_b (g/cm³)	θ_s (cm³/cm³)	Porosity (cm³/cm³)	K_s (cm/s)	Ln K_s	θ_r (cm³/cm³)	n	α (cm^{-1})	Ln α
1g (cont.)	TA-54-G-5 [b]	102.5	31.3	1.14E+00	4.52E–01	5.30E–01	3.10E–05	–1.04E+01	8.25E–03	2.16E+00	2.60E–03	–5.95E+00
	LGM-85-06 [d]	115	35.1		5.63E–01		9.10E–05	–9.31E+00				
	LGM-85-11 [d]	115	35.1		6.01E–01	6.01E–01	1.80E–04	–8.62E+00				
	LLM-85-01 [d]	124	37.8		4.89E–01	4.89E–01	2.20E–04	–8.42E+00				
	LLM-85-05 [d]	123	37.5		6.56E–01	6.56E–01	1.60E–04	–8.74E+00				
Tsankawi	54-1121 [a]	121.25	37.0	1.21E+00	4.86E–01	4.69E–01	1.16E–04	–9.06E+00	0.00E+00	1.52E+00	2.46E–02	–3.70E+00
	54-1123 [a]	89.25	27.2	1.20E+00	4.64E–01	4.63E–01	8.30E–05	–9.40E+00	0.00E+00	1.36E+00	2.39E–02	–3.74E+00
	CDBM-1 [d]	89	27.1	1.20E+00	4.42E–01		2.30E–04	–8.38E+00	0.00E+00	1.43E+00	1.31E–02	–4.34E+00
		94	28.7	1.05E+00	5.03E–01		1.50E–03	–6.50E+00	1.60E–02	1.59E+00	1.73E–02	–4.06E+00
Cerro Toledo	54-1121 [a]	124.75	38.0	1.28E+00	4.26E–01	4.74E–01	5.60E–05	–9.79E+00	5.41E–03	1.57E+00	8.05E–03	–4.82E+00
		134.75	41.1	1.24E+00	4.15E–01	4.72E–01	1.25E–04	–8.99E+00	0.00E+00	1.61E+00	6.86E–03	–4.98E+00
	54-1123 [a]	91.75	28.0	1.23E+00	3.98E–01	4.73E–01	2.77E–04	–8.19E+00	0.00E+00	1.45E+00	1.10E–02	–4.51E+00
Otowi	CDBM-1 [d]	104	31.7	1.20E+00	4.46E–01		2.30E–04	–8.38E+00	0.00E+00	1.49E+00	6.40E–03	–5.05E+00
		114	34.8	1.29E+00	4.51E–01		1.60E–04	–8.74E+00	2.50E–02	1.78E+00	4.50E–03	–5.40E+00
		124	37.8	1.10E+00	4.37E–01		2.90E–04	–8.15E+00	0.00E+00	1.45E+00	8.20E–03	–4.80E+00
		134	40.9	1.24E+00	4.47E–01		1.60E–04	–8.74E+00	1.20E–02	1.65E+00	5.70E–03	–5.17E+00
		144	43.9	1.14E+00	4.28E–01		4.20E–04	–7.78E+00	4.20E–02	2.31E+00	5.50E–03	–5.20E+00
		154	47.0	1.29E+00	4.10E–01		1.00E–04	–9.21E+00	2.70E–02	1.89E+00	3.90E–03	–5.55E+00

vpn= Vapor-phase notch

[a] *Parameters for these boreholes obtained and/or calculated from data in DBS&A (1996).*

[b] *Parameters for this borehole obtained and/or calculated from data in DBS&A (1995).*

[c] *Parameters for this borehole obtained and/or calculated from data in DBS&A (1996); stratigraphy from Puglisi and Vold (1995)*

[d] *Parameters from Rogers and Gallaher (1995)*

Annex IIIa: (Continued)
Parameters and Data Used for Statistical Analyses for

Unit	Borehole	Depth (ft)	Depth (m)	ρ_b (g/cm³)	θ_s (cm³/cm³)	Porosity (cm³/cm³)	K_s (cm/s)	Ln K_s	θ_r (cm³/cm³)	n	α (cm^{-1})	Ln α
Otowi (cont.)	CDBM-1 [d] (cont.)	164	50.0	1.21E+00	4.36E–01		1.70E–04	–8.68E+00	0.00E+00	1.49E+00	6.10E–03	–5.10E+00
		174	53.0	1.18E+00	4.12E–01		2.10E–04	–8.47E+00	3.00E–02	1.90E+00	5.30E–03	–5.24E+00
		184	56.1	1.18E+00	4.32E–01		3.00E–04	–8.11E+00	2.60E–02	1.89E+00	6.20E–03	–5.08E+00
		189	57.6	1.19E+00	4.30E–01		1.80E–04	–8.62E+00	8.00E–03	1.65E+00	5.70E–03	–5.17E+00
	CDBM-2 [d]	67	20.4	1.16E+00	4.46E–01		5.00E–04	–7.60E+00	1.70E–02	1.60E+00	8.40E–03	–4.78E+00
		68	20.7	1.22E+00	4.40E–01		2.70E–04	–8.22E+00	3.90E–02	1.99E+00	6.00E–03	–5.12E+00
Basalt	54-1015 [a]	384.65	117.3	2.19E+00	1.62E–01	2.52E–01	1.80E–09	–2.01E+01	0.00E+00	1.26E+00	2.37E–02	–3.74E+00
		464.25	141.5	2.77E+00	4.50E–02	5.50E–02	8.74E–11	–2.32E+01	0.00E+00	1.17E+00	2.52E–02	–3.68E+00
		465.75	142.0	2.84E+00	8.70E–02	3.00E–02	2.65E–09	–1.97E+01	0.00E+00	1.38E+00	1.31E–03	–6.64E+00
		521.25	158.9	2.81E+00	1.05E–01	4.20E–02	3.75E–09	–1.94E+01	0.00E+00	1.21E+00	8.25E–02	–2.50E+00

vpn= Vapor-phase notch

[a] *Parameters for these boreholes obtained and/or calculated from data in DBS&A (1996).*

[b] *Parameters for this borehole obtained and/or calculated from data in DBS&A (1995).*

[c] *Parameters for this borehole obtained and/or calculated from data in DBS&A (1996); stratigraphy from Puglisi and Vold (1995)*

[d] *Parameters from Rogers and Gallaher (1995)*

Attachment IV
Incorporation of Sorption in the Micromixing Model for the Los Alamos National Laboratory Technical Area-54, Material Disposal Area G Groundwater Pathway Model

Prepared by
Bruce Robinson
Hari Viswanathan
Phil Stauffer

IV.1 Introduction

In a complex numerical model such as the groundwater transport model for Material Disposal Area (MDA) G, spatial variability in hydrologic and transport properties and nonpoint-source regions over which contaminants enter the system give rise to a distribution of reactive travel times, t_r, through the system. Particle-tracking calculations provide a straightforward means for representing this variability for a simple source term such as a pulse. However, for more complex sources for a given particle path, or for reactions such as chemical transformations, sorption, or decay, particle-tracking approaches become cumbersome.

A simplified approach has been developed for obtaining a solute mass-flux model for reactive chemical species using particle-tracking results obtained from a groundwater flow and transport model of arbitrary complexity. Information extracted from particle-tracking simulations using the complex, multidimensional model are used to construct a simplified model that reproduces the residence time distribution (RTD) of a conservative solute using the theory introduced by Robinson and Viswanathan (2003). For conservative solutes or solutes with reactions that do not vary spatially, this mixing model can be used directly to simulate time-dependent solute-release functions or sorption and kinetic parameters. This model, called an abstracted or reduced model, can be run at a small fraction of the computational burden of the original groundwater flow model. When reactions possess spatially dependent properties, the situation becomes more complex. However, by treating the particle-tracking information statistically, reasonable abstraction models can be constructed for those situations as well.

IV.2 Numerical Formulation

The micromixing model of Robinson and Viswanathan (2003) may be used to simulate a solute molecule traveling through a system with a conservative (nonreactive) travel time of t_p. This molecule is subject to advective and dispersive transport so that, in general, there is a distribution of arrival times at a downstream location for an ensemble of particles released from a source. The micromixing model constructs a simple one-dimensional (1-D) pathway that reproduces an arbitrary RTD for this conservative transport situation. This simplified model can be used in

place of the original model to reproduce the distribution of travel times, while incorporating arbitrary source terms and chemical reactions. The goal of this study, which extends the 2003 work of Robinson and Viswanathan, is to incorporate sorption into the model in a manner that reproduces the original model's sorption behavior.

For a particle traveling with a conservative travel time of t_p, the corresponding reactive travel time (t_r) for a species undergoing equilibrium, linear sorption (the so-called K_d model) can be expressed as follows:

$$t_r = \int_0^t R(t')dt' \qquad 1$$

Where

t_r = the reactive travel time
$R(t')$ = the path-dependent retardation factor (i.e., the local retardation factor for the portion of the flow path between times t' and $t' + dt'$)

In terms of reproducing a given transit time of a particle, the final arrival time is all that matters. Therefore, one approach is to define an effective retardation factor R_p for a particle as follows:

$$R_p = t_r / t_p = \int_0^t R(t')dt' / t_p \qquad 2$$

Where

t_p = the conservative (nonreactive) travel time
R_p = the effective retardation factor

These expressions divide the particle path into discrete intervals (at the resolution of the numerical model) of computed travel times to obtain an average retardation factor. Numerically, the integral in Equation 2 is computed as follows:

$$t_r = \int_0^t R(t')dt' = \sum_{i=1}^{N} R_i(t_{p,i} - t_{p,i-1}) \qquad 3$$

Where

i = the i^{th} segment of the particle path
R_i = the local retardation factor along that the i^{th} segment

The time difference included in this equation represents the conservative travel time along a given segment.

Equation 4, below, can be used to calculate the local retardation factor for segment *i*:

$$R_i = 1 + \frac{\rho_i K_{d,i}}{\theta_i} \qquad 4$$

Where

ρ_i = the bulk rock density
$K_{d,i}$ = the sorption coefficient
θ_i = the volumetric water content

While the development above holds for a single particle, complications arise when an ensemble of particles of different travel times are considered. The complications arise from the fact that all paths of conservative residence time t_p need not possess the same sorbing travel time because the paths may not have equivalent R_p. Therefore, in the most general sense, the transport times of conservative and sorbing species must be described using a joint probability distribution function. Using this approach, the following relations apply:

$$\int_0^\infty h(t_p, t_r)dt_r = f(t_p)dt_p \qquad 5$$

and

$$\int_0^\infty h(t_p, t_r)dt_p = g(t_r)dt_r \qquad 6$$

Where

$h(t_p, t_r)dt_p dt_r$ = the fraction of the particle trajectories with conservative residence times between t_p and $t_p + dt_p$ and sorbing residence times between t_r and $t_r + dt_r$

$f(t_p)dt_p$ = the fraction of conservative particles leaving the system with residence times between t_p and $t_p + dt_p$

$g(t_r)dt_r$ = the fraction of sorbing particles leaving the system with residence times between t_r and $t_r + dt_r$

As discussed earlier, particle-tracking information from a complex model provides the means for determining $h(t_p, t_r)$, as each particle passing through a model possesses a unique t_p and t_r. To proceed from this information to a simplified mixing model that includes sorption, it is recognized that the exact order in which the sorption takes place within the mixing reactor is relatively unimportant, as long as the appropriate RTDs are reproduced. Furthermore, for linear, equilibrium sorption, Robinson and Viswanathan (2003) showed that both early and late mixing models yield an identical result. In the present study, the reduced model is assembled on the basis of the maximum mixedness model developed in Robinson and Viswanathan (2003), but it is recognized that the minimum mixedness model would yield the same results. The goal is to populate the maximum mixedness model with a variable sorption coefficient along the flow path in a manner that approximates the behavior of the complex model.

Because all particles of a given conservative travel time do not necessarily have the same sorptive travel time, it is impossible in a single mixing model such as this to exactly replicate the behavior of the complex system. However, reasonable approximations are possible, and these can be verified simply by performing a comparison to the results from the original model. In this study, the approximation is to define $\bar{t}_r(t_p)$, the mean sorptive travel time for a given conservative travel time t_p, so as to yield a reasonable average sorptive travel time that applies for a given t_p:

$$\bar{t}_r(t_p) = \int_0^\infty \frac{t_r h(t_p, t_r)}{f(t_p)} dt_r \qquad 7$$

Where

$\bar{t}_r(t_p)$ = the mean sorptive travel time for a given conservative travel time t_p

Equation 7 prescribes that the arithmetic average of the t_r values be used for all particles of conservative travel time t_p (i.e., values between t_p and $t_p + dt_p$). Subject to checks using the original model, this travel time abstraction is postulated to yield a reactive RTD that is close to that of the original model.

Next, the function $\bar{t}_r(t_p)$ is used to populate the maximum mixedness model with sorption parameters along its length. Because the internal flow in the model is plug flow, the sorption parameters at all locations less than $x(t_p)$ must be accounted for when the value is assigned at the corresponding location in order to reproduce $\bar{t}_r(t_p)$ for a particular travel time t_p. In other words, the local retardation factor that yields the proper reactive travel time must be incrementally determined. The following expressions from Robinson and Viswanathan (2003) describe the construction of the mixedness model:

$$x(t_p) = \frac{Q}{\theta A_x} \int_0^{t_p} [1 - F(t_p)] dt_p \qquad 8$$

and

$$q(t_p) = Qf(t_p) dt_p \qquad 9$$

Where

$x(t_p)$ = the location along the model associated with residence time t_p
Q = the volumetric flow rate in the mixing model
θ = the volumetric water content (assumed constant along the model)
A_x = the cross-sectional area
$F(t_p)$ = the cumulative RTD, and
$q(t_p)$ = the incremental flow rate entering the model at the location corresponding to time t_p

One way to approach this problem is to compute a spatially dependent retardation factor $R_f(t_p)$ as the local retardation factor for the interval within the model corresponding to residence times between t_p and $t_p + dt_p$ using the following expression:

$$\bar{t}_r(t_p) = \int_0^{t_p} R(t_p)dt_p \qquad 10$$

Numerically, this integration can be carried out along the model. Starting at $t_p = 0$ (the model outlet), the following is assigned: $R(t_p \le t_{p,\min}) = \bar{t}_r(t_{p,\min})/t_{p,\min}$. This allows the desired sorptive travel time for the mass arriving at the outlet to be achieved with the absolute shortest conservative travel time. Then, for each successive interval in the mixing model,

$$R(t_p + dt_p) = \frac{\bar{t}_r(t_p + dt_p) - \bar{t}_r(t_p)}{dt_p} \qquad 11$$

Equation 11 prescribes the incremental sorbing travel time needed to attain the "correct" overall retardation factor and travel time for the mass entering the system at the location corresponding to $t_p + dt_p$.

The above approach takes advantage of a simplifying assumption to facilitate the construction of the mixing model for sorption, namely that the distribution of t_r values at a given t_p be used to compute an average sorptive travel time function $\bar{t}_r(t_p)$, as shown in Equation 7. Nevertheless, this approach still requires the cell-by-cell definition of the retardation factor to reproduce this function in the model. A further simplification may be possible that allows the entire model to be reduced to a uniform retardation factor. For systems in which the function $\bar{t}_r(t_p)$ versus t_p is a straight line, it is observed that the slope of the straight line is an effective retardation factor that would apply for all travel times, and therefore a uniform retardation factor throughout the mixing model would be applicable.

The validity of each of these successively more restrictive approximations must be evaluated on a case-by-case basis. To evaluate a particular flow field and transport scenario, particle-tracking

runs can be conducted in which, for each particle trajectory, t_p and t_r are computed, and a scatter plot of t_r and t_p is produced. If the series of points follows a relatively tight, confined curve (all particles of time t_p have approximately the same value of t_r), then the mixing model can be assigned retardation factors along its length using Equation 11. If that curve is a straight line, then the retardation factor that applies throughout the entire mixing model is computed as t_r / t_p.

IV.3 Transformation of Sorption Parameters to 1-D Abstractions

This section presents an analysis that demonstrates the relationship between sorption parameters in the three-dimensional (3-D) site-scale MDA G model and sorption parameters in the 1-D abstraction models. Sorption of radionuclides in the 3-D site-scale model is limited to the Bandelier Tuff, and thus a single sorption distribution coefficient, K_d, is assigned to all units above the Cerros del Rio basalt. The relationship between K_d and the amount of retardation experienced by a radionuclide in the system is given by the following equation:

$$R_f = 1 + \frac{K_d \rho_b}{s\phi} \qquad 12$$

Where

R_f = the retardation factor
K_d = the distribution coefficient
ρ_b = bulk rock density
s = saturation
ϕ = porosity

In the 3-D model, s, ρ_b, ϕ, and K_d may vary spatially throughout the model. An equivalent retardation factor for a given infiltration rate, release location, and K_d can be estimated by fitting a line to a scatter plot of retarded versus conservative breakthrough times developed using the 3-D model. For example, Figures IV-1 and IV-2 show a best-fit line through approximately 3,400 particles for two values of K_d; the slope of each line is equivalent to the effective R_f for

the 3-D simulation. Differences between the particle travel times and the best-fit line occur because each particle travels a slightly different pathway through the system; each of these pathways is characterized by a different set of saturation, porosity, and bulk density values.

The effective 3-D R_f is used to calculate an equivalent K_d that will recreate the correct amount of retardation in the 1-D abstraction, based on the assumption that all 80 of the 1-D models (i.e., 8 waste disposal regions × 10 infiltration rates) use the same value for saturation, porosity, and bulk density. The 3-D K_d is divided by the 1-D K_d to calculate a transformation factor (Table IV-1); this factor is used to transform the stochastic K_d chosen by the GoldSim® software for each realization and species into the correct 1-D K_d for input into the FEHM abstraction model. The transformation factor calculated for a given infiltration rate and release location is not sensitive to the value of K_d, allowing the 80 values presented in Table IV-1 to be applied to all values of K_d that may be used in the stochastic GoldSim simulations.

Table IV-1
Transformation Matrix for Converting the Distribution Coefficient for the GoldSim One-Dimensional Abstraction Models

Infiltration (mm/yr)	FFindex	Distribution Coefficient Value by Waste Disposal Region [a]							
		1	2	3	4	5	6	7	8
1.0E+01	10	9.1E-01	9.2E-01	9.3E-01	9.9E-01	1.1E+00	8.5E-01	1.1E+00	1.1E+00
8.0E+00	9	9.9E-01	9.8E-01	9.5E-01	1.0E+00	1.1E+00	8.9E-01	1.1E+00	1.1E+00
6.0E+00	8	9.6E-01	1.0E+00	9.9E-01	1.1E+00	1.2E+.00	9.3E-01	1.2E+00	1.2E+00
4.0E+00	7	9.7E-01	1.1E+00	1.1E+00	1.2E+00	1.3E+00	9.7E-01	1.3E+00	1.3E+00
2.0E+00	6	1.1E+00	1.2E+00	1.3E+00	1.4E+00	1.4E+00	1.1E+00	1.4E+00	1.5E+00
1.5E+00	5	1.2E+00	1.3E+00	1.4E+00	1.5E+00	1.5E+00	1.1E+00	1.5E+00	1.6E+00
1.0E+00	4	1.2E+00	1.4E+00	1.5E+00	1.5E+00	1.7E+00	1.3E+00	1.6E+00	1.7E+00
5.0E-01	3	1.4E+00	1.7E+00	1.8E+00	1.8E+00	1.9E+00	1.5E+00	1.8E+00	1.9E+00
2.5E-01	2	1.7E+00	2.0E+00	2.1E+00	2.1E+00	2.1E+00	1.7E+00	2.0E+00	2.1E+00
1.0E-01	1	2.1E+00	2.4E+00	2.5E+00	2.5E+00	2.4E+00	2.2E+00	2.3E+00	2.5E+00

FFindex = An index used by GoldSim to select the 10 different infiltration scenarios

[a] Numbers are rounded to two significant digits.

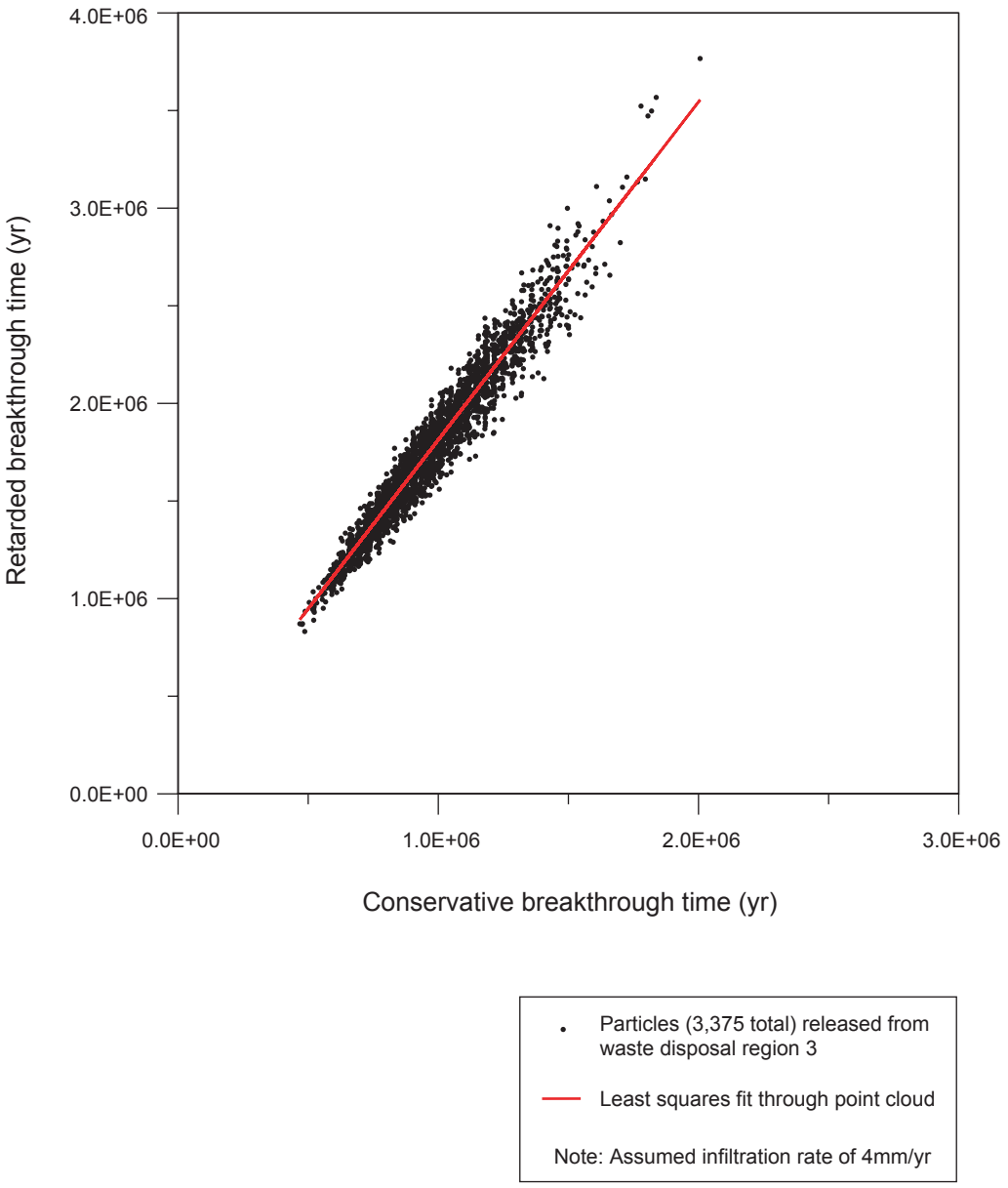

Figure IV-1
Retarded vs. Conservative Breakthrough Times for Particles Released from Waste Disposal Region 3 (distribution coefficient = 0.1)

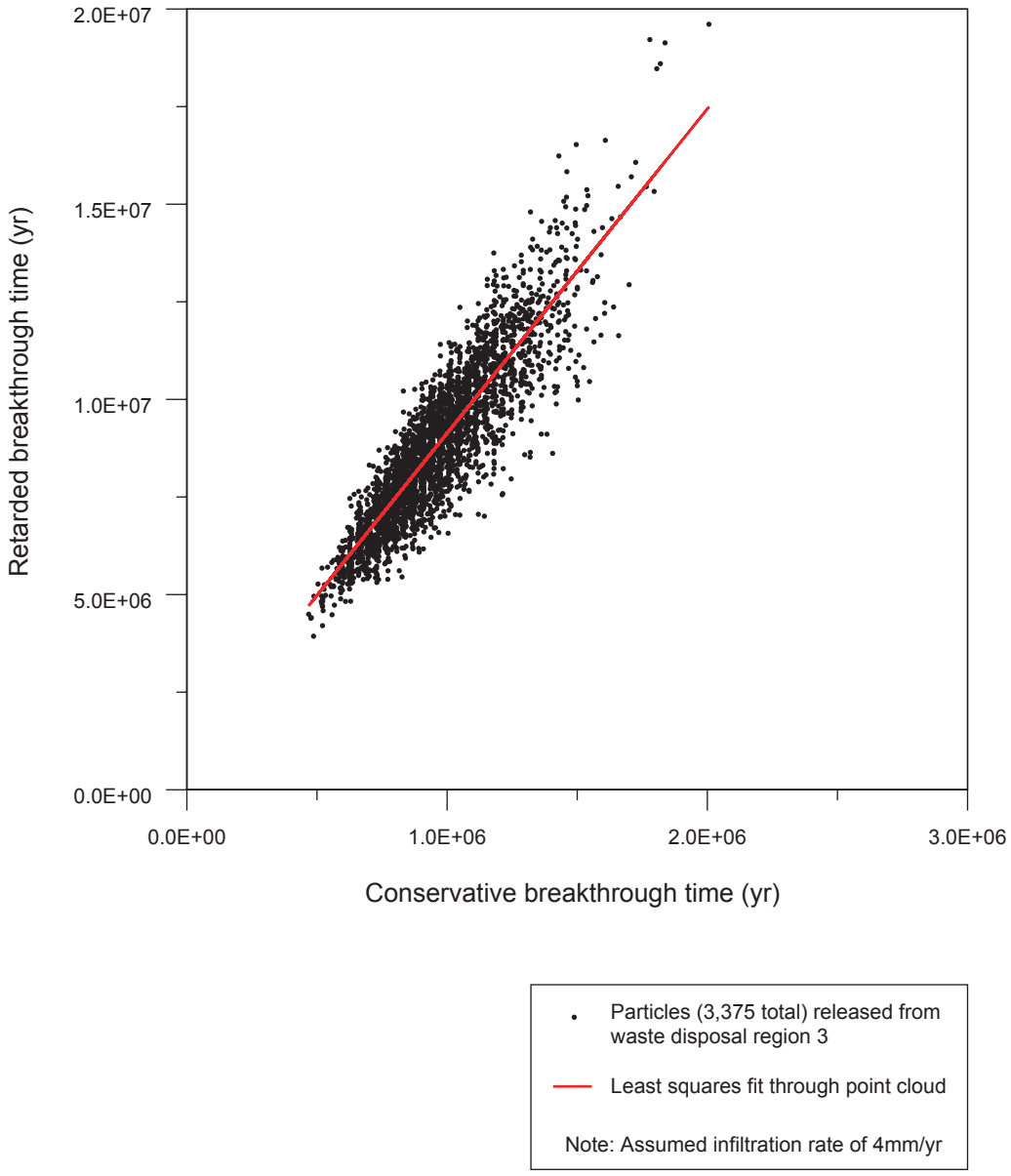

Figure IV-2
Retarded vs. Conservative Breakthrough Times for Particles Released from Waste Disposal Region 3 (distribution coefficient = 1.0)

This simplification is not exact because many of the variables in Equation 12 are not constant among the 1-D models. The tighter cloud of particles shown in Figure IV-1 (as compared to the looser cloud of particles in Figure IV-2) leads to a better match between breakthrough from the 1-D abstraction calculations, which use the advection/dispersion equation, and breakthrough from the full 3-D model, which uses particle tracking. This can be seen in Figures IV-3 and IV-4 where the conservative and K_d = 0.1 cases are very good matches while there is quite a bit of scatter in the K_d = 1.0 cases, especially for the lower infiltration example shown in Figure IV-3. Low K_d and higher infiltration rates lead to tighter particle clouds and better matches between the 3-D and 1-D models.

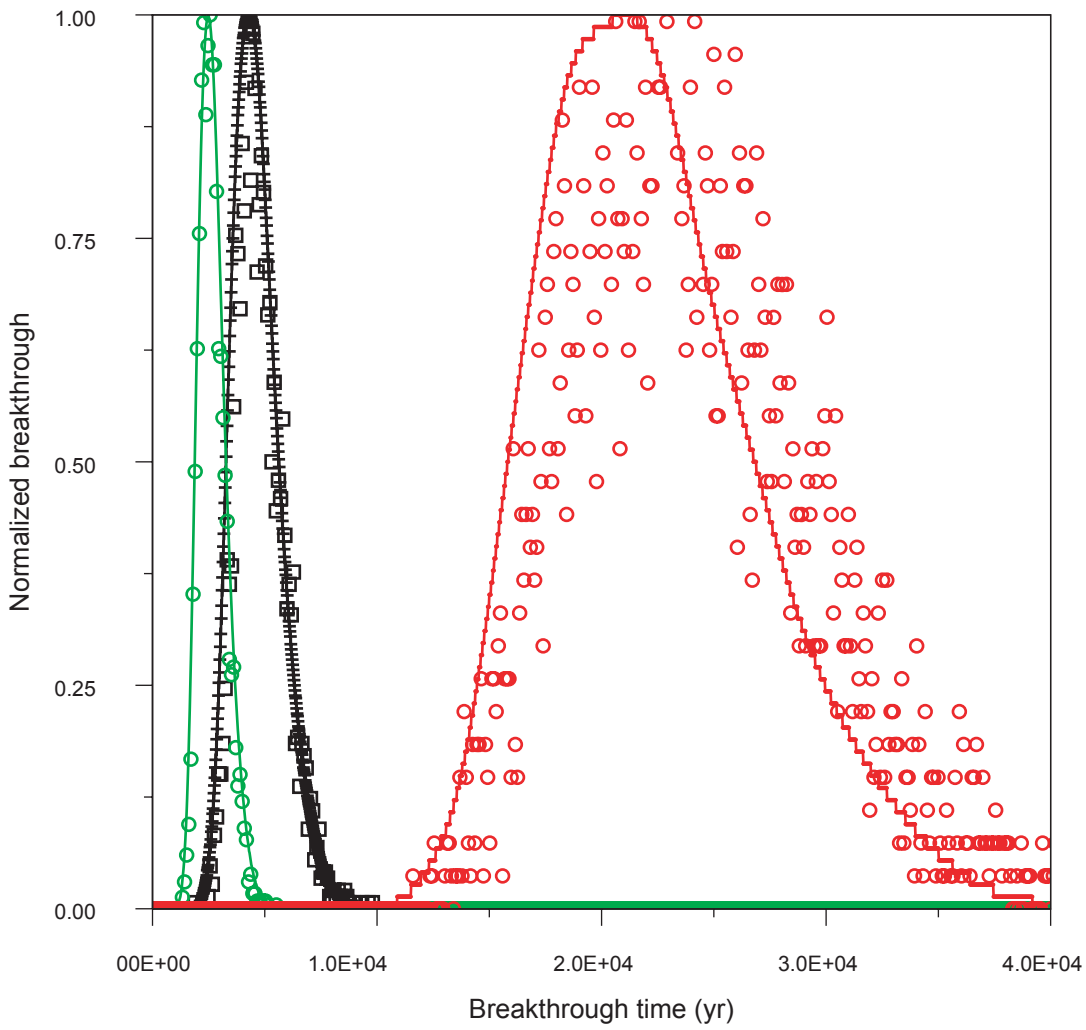

Figure IV-3
Comparison of Three-Dimensional Particle and One-Dimensional Plume Breakthrough Curves for Waste Disposal Region 3 (infiltration rate = 4 mm/yr)

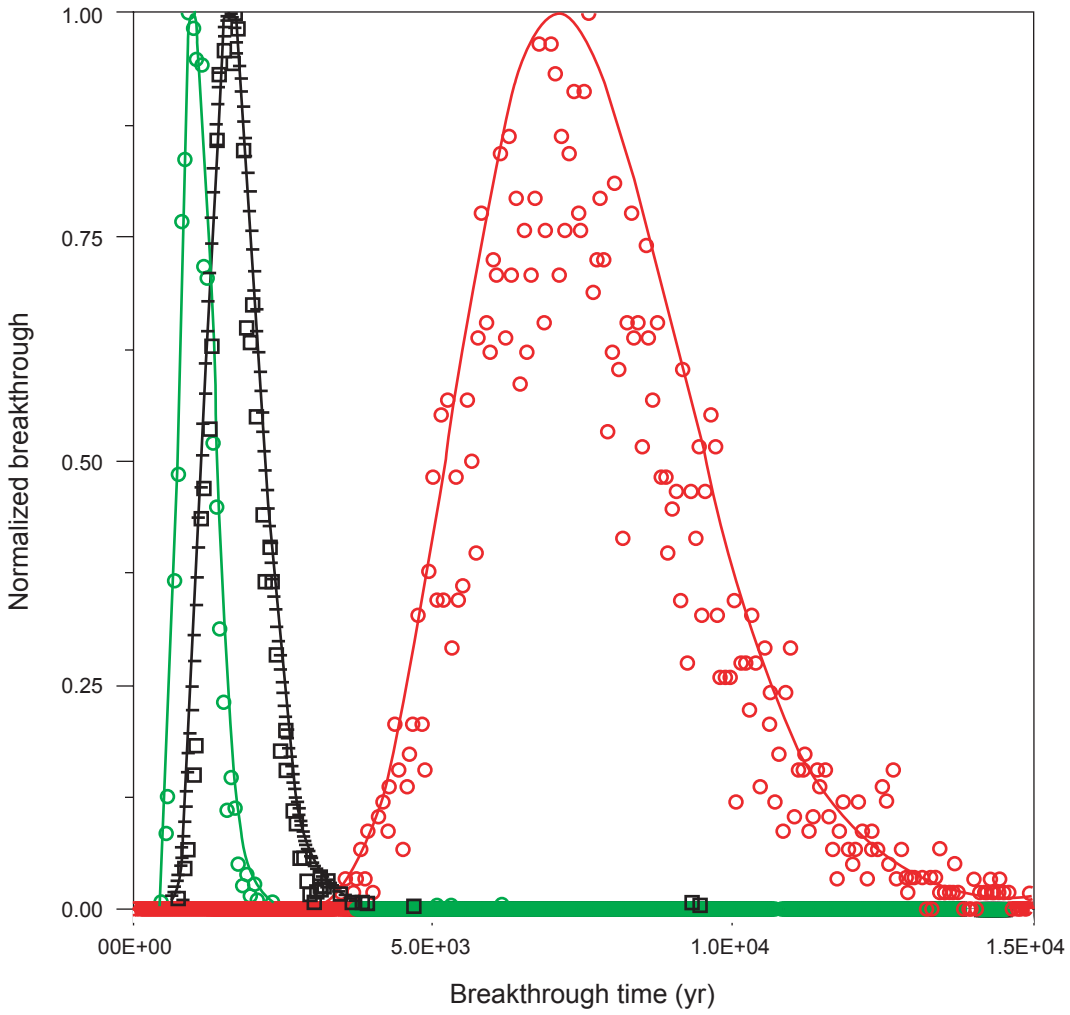

Figure IV-4
Comparison of Three-Dimensional Particle and One-Dimensional Plume Breakthrough Curves for Waste Disposal Region 1 (infiltration rate = 10 mm/yr)

IV.4 References

Robinson, B.A. and H. Viswanathan, 2003, "Application of the Theory of Micromixing to Groundwater Reactive Transport Models," *Water Resources Res*., Vol. 39, No. 11.

Attachment V
Details on the Coupling of GoldSim and the Finite Element Heat and Mass (FEHM) Transfer Code for the Los Alamos National Laboratory TA-54, Material Disposal Area G Groundwater Pathway Model

Authors:
Philip Stauffer
Hari Viswanathan

V.1 Introduction

This attachment describes the manner in which the system-level GoldSim® model of Material Disposal Area (MDA) G is coupled with the process-level Finite Element Heat and Mass (FEHM) model of the groundwater pathway. Section V-2 provides background information on how the personal computer environment is configured to run the coupled models. Section V-3 describes the parameters that are passed from the GoldSim model to FEHM to control the groundwater simulations and to maintain compatibility with the logic structure embedded in FEHM. Details about the FEHM data file that are specific to the MDA G model are presented in Section V-4. Finally, Section V-5 provides pieces of the FEHM source code that have been modified and describe how these changes allow FEHM and GoldSim to communicate. Throughout this report, the GoldSim working directory refers to the directory that contains the GoldSim MDA G performance assessment and composite analysis model.

V.2 Directory Structure and File Requirements for the GoldSim Coupling

The GoldSim model calls FEHM eight times simultaneously during the model simulations. Several modifications were made to FEHM to ensure that file-sharing violations and memory management errors do not occur. The first step was to develop a subdirectory structure that organizes the parameter files associated with each possible combination of waste disposal region and flow-field index. The structure consists of eight subdirectories (clusters 1 through 8) located in the GoldSim working directory; these subdirectories correspond to the eight waste disposal regions. Each subdirectory contains 10 *Flowfield index* subdirectories (A through J). Starting with directory A, these correspond to infiltration rates of 0.1, 0.25, 0.5, 1.0, 1.5, 2.0, 4.0, 6.0, 8.0, and 10 mm/yr (0.0039, 0.0098, 0.02, 0.039, 0.059, 0.079, 0.16, 0.24, 0.32, and 0.39 in./yr). These directories and the FEHM input files they contain were built using a shell script and two FORTRAN codes (see Attachment VI). Each of the 80 individual subdirectories located within the GoldSim working directory contains three files required to set up and run a single FEHM simulation (i.e., fehmn.files, goldfehm.dat, and areag.rtd).

To avoid memory management errors, a copy of the FEHM executable (i.e., fehm_01.dll through fehm_08.dll) must be located in each of the eight cluster subdirectories. The process has been automated from within FEHM so that a single copy of the executable located in the GoldSim working directory (Bruce1_fehm04.dll) is copied into the correct location. This is done when FEHM calls the batch file copy_dll.bat, which must be located in the GoldSim working directory. The batch file approach to copying the executable to subdirectories was chosen to allow flexibility in naming the FEHM executable without having to recompile the source code.

The coupling between GoldSim and FEHM allows the user to specify how many parameters are passed to each FEHM simulation from the GoldSim model. This is done using the file fehmn.gold. The first number in this file is the total number of user-specified inputs found in the GoldSim model. These inputs are specified in the FEHM external pathway element in GoldSim; the values of these parameters are explained in the next section.

The output from the eight simultaneous FEHM simulations is written to a single file, goldfehm.out. This file is located in the GoldSim working directory.

V.3 Parameter-Sharing between GoldSim and FEHM

GoldSim passes a string of variables to FEHM to initialize each simulation and at each time step of the system-level simulation. These variables include *time*, *Flowfield index*, *cluster*, the *number of species* that FEHM will be simulating, the K_d sorption parameter for each species, and the *amount of mass* entering the groundwater pathway from each waste disposal region (Table V-1). The GoldSim MDA G performance assessment model uses a stochastic variable called *flowfield* to pick an infiltration scenario for each realization. This value is passed to FEHM, which then sets up and runs the correct residence time distribution (RTD) function from the subdirectories cluster 1 through cluster 8 and the 10 infiltration subdirectories A through J. This process is repeated eight times, corresponding to the eight waste disposal regions, to activate the eight FEHM pipe pathways in the system model; each pipe pathway contains a call to the FEHM dynamic link library (dll).

Once the appropriate files for the randomly chosen *Flowfield index* have been assembled by FEHM, GoldSim initializes the simulation by passing the first time increment to FEHM. In each simultaneous FEHM simulation, GoldSim passes into FEHM the amount of mass arriving into the groundwater pathway for a given waste disposal region. FEHM accepts the incoming mass and adds it to the ongoing calculation of transport through the subsurface to the compliance boundary using the abstraction model described in *Attachment IV*. Within each of the eight simultaneous FEHM simulations, the cumulative transport of each species is modeled, taking into account sorption, radioactive decay, and ingrowth. FEHM takes many small time steps for each GoldSim time step to ensure that the tracer transport solution converges to the correct answer. At the end of each GoldSim time step, FEHM passes any mass reaching the compliance boundary back to GoldSim. Mass reaching the compliance boundary represents radionuclides that have migrated from the waste inventory or daughter products formed as a result of ingrowth during transport along the groundwater pathway. Simulations performed to test the GoldSim coupling included radioactive decay, ingrowth, and sorption.

Table V-1
Variables Passed from GoldSim to FEHM during System-Level Simulations

IN Array Index	GoldSim Variable	Range of Values	FEHM Variable	Comments
1	*Etime*	0 to final time	in(1)	---
2	*Flowfield index*	1 to 10; generated within GoldSim from a stochastic distribution	in(2)	---
3	Not Used	---	in(3)	---
4	Not Used	---	in(4)	---
5	Not Used	---	in(5)	---
6	User input	5 to 12	in(6)	Cluster index plus 4
7	User input	Currently fixed at 19	in(7)	Number of FEHM species
8 to (8 + in(7) -1)	GoldSim Species number for each of the 19 FEHM species	1 to the total number of GoldSim species	in(8) through in(8 + in(7) -1)	Species in FEHM are numbered 1 to 19
(8 + in(7)) to (8 +2*in(7) -1)	Sorption parameter K_d for each FEHM species	Generated within GoldSim from stochastic distributions	in(8 + in(7)) through in(8 +2*in(7) -1)	---
(8+2*in(7))	Number of GoldSim species	Set within GoldSim (80+)	in(8+2*in(7))	Value provided directly by GoldSim.
(8+2*in(7) +1)	Mass input flag	---	in(1)	Not used
(8+2*in(7) +2)	# input buffer	---	in(1)	Not used
(8+2*in(7) +3)	# output buffer	---	in(1)	Not used
(8+2*in(7) +4) through (8+2*in(7) +	Mass of each GoldSim species entering the groundwater pathway	---	in(1)	Value provided directly by GoldSim.

--- = None

The number of radionuclides or species included in the FEHM modeling is much smaller than the total number of contaminants included in the performance assessment and composite analysis. Screening calculations were performed to remove radionuclides that do not pose a risk by means of groundwater pathway exposures.

Although parameters are shared by GoldSim and FEHM, there are no files common to both programs. The parameters passed to FEHM from GoldSim via the IN array described in Table V-1 contain all the necessary information to instruct FEHM to set up a 1-D pipe pathway representative of the conditions specified for a particular GoldSim realization. Continued parameter sharing through the IN array during a realization allows mass to be moved from

GoldSim to FEHM. Finally, the OUT array, which is also passed between GoldSim and FEHM at each time step, allows mass to move back to GoldSim from FEHM.

V.4 FEHM Data File Modifications

Each data file (areag.dat) created by the Datamaker.f program (see *Attachment VI*) contains a path to the correct RTD for a given pipe with a given *Flowfield index*. The only other changes to the areag.dat file specific to the MDA G performance assessment and composite analysis model are found in the TRAC macro. First, after the keyword "trac" a line has been added that contains the keyword "rip" to tell FEHM that this is a simulation controlled by GoldSim. Second, when the first number in Group 12 of the TRAC macro is set to 66, FEHM recognizes that GoldSim will provide the K_d for each species as part of the IN array that GoldSim passes into FEHM.

V.4.1 Example FEHM Data File

An example of a FEHM data file is shown in Table V-2. This particular file pertains to *cluster 5* and *Flowfield index F*. Experienced FEHM users will notice a new macro for residence time distribution (RTDM) that is currently being documented for inclusion in the next version of the user's manual. The RTDM macro instructs FEHM to set up and use a one-dimensional (1-D) abstraction model to recreate a conservative RTD breakthrough curve. This RTD curve can be specified either through statistical parameters (e.g., mean, standard deviation) or the RTD can be read in from a file. For the MDA G modeling, the RTD is read from a file called cluster5/F/areag.rtd. The following example has 19 species in FEHM; this number is listed just before the beginning of the TRAC macro in a comment section.

Several parameters are common to all of the 1-D abstraction simulations. The water saturation in the entire domain is set to 1 (fully saturated), the permeability is fixed at 1×10^{-10} m^2 (1.1×10^{-9} ft^2), porosity is fixed at 0.3, rock density is fixed at 2,000 kg/m^3 (125 lb/ft^3) and the entire domain is fixed at 20°C (68ºF). The tracer concentration in the entire domain is initially zero, and the first number in Unit 12 of TRAC is fixed to 66 for all species to indicate that GoldSim is controlling the K_d. Also, although the input deck appears to assign an injection for each species over all nodes for the entire simulation (1 0 0 1 0. 1.e9), FEHM has been changed to inject the incoming mass (passed through the IN array) into only the first node of the 1-D abstraction pathway. The mass flux conversion from the IN array is performed in the FEHM subroutine USERC.f (see Section V.4.3).

Table V-2
Example FEHM Data File for Cluster 5 and Flowfield Index F

```
Bruce test1
cond
1 0 0 2.7 2.7 2.7
init
1. 20 20 0 1000 20 0 0
node
3
1 10 50
perm
1 0 0 1.e-10 1.e-10 1.e-10
rock
1 0 0 2000.0 0.1E+31 0.3000
sol
1 -1
time
1.0e9 1.0e9 1000 1 92 11 0.
ctrl
50 1e-6 8
1 0 0 1
1 0 0.5
25 2. 1 1.e20
1 1
rflo
rest
rtdm
min
0.3   1000.
file
cluster5\F\areag.rtd
#-------------------------------------------------
# 19 species,
#      Species   Half-Life (yr)
# 1   Pu-242    3.750e5
# 2   Pu-240    6.560e3
# 3   Pu-239    2.410e4
# 4   Np-237    2.140e6
# 5   U-238     4.470e9
# 6   U-236     2.342e7
# 7   U-235     7.040e8
# 8   U-234     2.460e5
# 9   U-233     1.592e5
# 10 Pa-231    3.280e4
# 11 Th-232    1.400e10
# 12 Th-230    7.540e4
# 13 Th-229    7.300e3
# 14 Th-228    1.912
# 15 Ra-228    5.760
# 16 Ra-226    1.599e3
# 17 Ac-227    2.177e1
```

```
# 18 Pb-210    2.230e1
# 19 C-14      5.715e3
trac
rip
1
0 1 1.e-6 1.
0. 1.e20 1.e20 1.e20
50 2.0 2000. 73000.
19
1
 66 0. 0. 1. 1.e-30 1.e-30 1.e-30 1.e-30
1 0 0 1
1 0 0 0.
1 0 0 1. 0. 1.e9
1
 66 0. 0. 1. 1.e-30 1.e-30 1.e-30 1.e-30
1 0 0 1
1 0 0 0.
1 0 0 1. 0. 1.e9
1
 66 0. 0. 1. 1.e-30 1.e-30 1.e-30 1.e-30
1 0 0 1
1 0 0 0.
1 0 0 1. 0. 1.e9
1
 66 0. 0. 1. 1.e-30 1.e-30 1.e-30 1.e-30
1 0 0 1
1 0 0 0.
1 0 0 1. 0. 1.e9
1
 66 0. 0. 1. 1.e-30 1.e-30 1.e-30 1.e-30
1 0 0 1
1 0 0 0.
1 0 0 1. 0. 1.e9
1
 66 0. 0. 1. 1.e-30 1.e-30 1.e-30 1.e-30
1 0 0 1
1 0 0 0.
1 0 0 1. 0. 1.e9
1
 66 0. 0. 1. 1.e-30 1.e-30 1.e-30 1.e-30
1 0 0 1
1 0 0 0.
1 0 0 1. 0. 1.e9
```

```
1
 66 0. 0. 1. 1.e-30 1.e-30 1.e-30 1.e-30
1 0 0 1
1 0 0 0.
1 0 0 1. 0. 1.e9
1
 66 0. 0. 1. 1.e-30 1.e-30 1.e-30 1.e-30
1 0 0 1
1 0 0 0.
1 0 0 1. 0. 1.e9
1
 66 0. 0. 1. 1.e-30 1.e-30 1.e-30 1.e-30
1 0 0 1
1 0 0 0.
1 0 0 1. 0. 1.e9
1
 66 0. 0. 1. 1.e-30 1.e-30 1.e-30 1.e-30
1 0 0 1
1 0 0 0.
1 0 0 1. 0. 1.e9
1
 66 0. 0. 1. 1.e-30 1.e-30 1.e-30 1.e-30
1 0 0 1
1 0 0 0.
1 0 0 1. 0. 1.e9
1
 66 0. 0. 1. 1.e-30 1.e-30 1.e-30 1.e-30
1 0 0 1
1 0 0 0.
1 0 0 1. 0. 1.e9
1
 66 0. 0. 1. 1.e-30 1.e-30 1.e-30 1.e-30
1 0 0 1
1 0 0 0.
1 0 0 1. 0. 1.e9
1
 66 0. 0. 1. 1.e-30 1.e-30 1.e-30 1.e-30
1 0 0 1
1 0 0 0.
1 0 0 1. 0. 1.e9
1
```

```
 66 0. 0. 1. 1.e-30 1.e-30 1.e-30 1.e-30
1 0 0 1
1 0 0 0.
1 0 0 1. 0. 1.e9
1
 66 0. 0. 1. 1.e-30 1.e-30 1.e-30 1.e-30
1 0 0 1
1 0 0 0.
1 0 0 1. 0. 1.e9
1
 66 0. 0. 1. 1.e-30 1.e-30 1.e-30 1.e-30
1 0 0 1
1 0 0 0.
1 0 0 1. 0. 1.e9
1
 66 0. 0. 1. 1.e-30 1.e-30 1.e-30 1.e-30
1 0 0 1
1 0 0 0.
1 0 0 1. 0. 1.e9
rxn
** NCPLX, NUMRXN
0, 19
** Coupling of the aqueous components for computing efficency(dRi/dUj)
19
1 0 0 0 0 0 0 0 0 0 0 0 0 0 0 0 0 0 0
0 1 0 0 0 0 0 0 0 0 0 0 0 0 0 0 0 0 0
0 0 1 0 0 0 0 0 0 0 0 0 0 0 0 0 0 0 0
0 0 0 1 0 0 0 0 0 0 0 0 0 0 0 0 0 0 0
0 0 0 0 1 0 0 0 0 0 0 0 0 0 0 0 0 0 0
0 0 0 0 0 1 0 0 0 0 0 0 0 0 0 0 0 0 0
0 0 0 0 0 0 1 0 0 0 0 0 0 0 0 0 0 0 0
0 0 0 0 0 0 0 1 0 0 0 0 0 0 0 0 0 0 0
0 0 0 0 0 0 0 0 1 0 0 0 0 0 0 0 0 0 0
0 0 0 0 0 0 0 0 0 1 0 0 0 0 0 0 0 0 0
0 0 0 0 0 0 0 0 0 0 1 0 0 0 0 0 0 0 0
0 0 0 0 0 0 0 0 0 0 0 1 0 0 0 0 0 0 0
0 0 0 0 0 0 0 0 0 0 0 0 1 0 0 0 0 0 0
0 0 0 0 0 0 0 0 0 0 0 0 0 1 0 0 0 0 0
0 0 0 0 0 0 0 0 0 0 0 0 0 0 1 0 0 0 0
0 0 0 0 0 0 0 0 0 0 0 0 0 0 0 1 0 0 0
0 0 0 0 0 0 0 0 0 0 0 0 0 0 0 0 1 0 0
0 0 0 0 0 0 0 0 0 0 0 0 0 0 0 0 0 1 0
0 0 0 0 0 0 0 0 0 0 0 0 0 0 0 0 0 0 1
** IDCPNT(IC),CPNTNAM(IC),IFXCONC(IC),CPNTPRT(IC),CPNTGS
      1    Pu-242     0    0   1e-9
      2    Pu-240     0    0   1e-9
      3    Pu-239     0    0   1e-9
      4    Np-237     0    0   1e-9
```

```
      5    U-238      0    0   1e-9
      6    U-236      0    0   1e-9
      7    U-234      0    0   1e-9
      8    U-233      0    0   1e-9
      9    U-232      0    0   1e-9
      10   Pa-231     0    0   1e-9
      11   Th-232     0    0   1e-9
      12   Th-230     0    0   1e-9
      13   Th-229     0    0   1e-9
      14   Th-228     0    0   1e-9
      15   Ra-228     0    0   1e-9
      16   Ra-226     0    0   1e-9
      17   Ac-227     0    0   1e-9
      18   Pb-229     0    0   1e-9
      19   C-14       0    0    1e-9
** Aqueous Complex Identification: IDCPLX(IX), CPLXNAM(IX),CPLXPRT(IX)
** Immobile Compoenet Identification:  IDIMM(IM), IMMNAM(IM),IMMPRT(IM):
** IDVAP(IV), VAPNAM(IM), VAPPRT(IV) (ID # and name of vapor spec, NVAP rows)
** skip nodes? for chemical speciation calculation
  0
** RSDMAX tolerance for equil. speciation calculation
  1.0e-8
******  Chemical reaction information group 9-11 omitted if NCPLX=0 *******
** Group 9  LOGKEQ (=0 if stability constants are given as K, =1 if given as log
** Group 10 CKEQ(IX) (Stability constants, NCPLX rows)
** Group 11 STOIC(IX,IC) (Stoichiometric coeff: NCPLX rows, NCPNT columns)
**=========================================================
      5
** Group 13 Where does the reaction take place? **
  1 0 0
** GROUP 14   HALF LIFE (years)       1    **  Pu242 to U238
3.75e5
** Group 15 RXNTYPE
1
** GROUP 16  Parent Daughter
   1     5
**=========================================================
      5
** Group 13 Where does the reaction take place? **
  1 0 0
** GROUP 14   HALF LIFE (years)       2    **  U238 to U234
4.47e9
** Group 15 RXNTYPE
1
** GROUP 16  Parent Daughter
   5     8
**=========================================================
      5
** Group 13 Where does the reaction take place? **
  1 0 0
** GROUP 14   HALF LIFE (years)       3    **  U234 to Th230
2.46e5
** Group 15 RXNTYPE
1
```

```
** GROUP 16  Parent Daughter
   8     12
**=========================================================
       5
** Group 13 Where does the reaction take place? **
  1 0 0
** GROUP 14   HALF LIFE (years)        4    **  Th230 to Ra226
7.54e4
** Group 15 RXNTYPE
1
** GROUP 16  Parent Daughter
   12     16
**=========================================================
       5
** Group 13 Where does the reaction take place? **
  1 0 0
** GROUP 14   HALF LIFE (years)        5    **  Ra226 to Pb210
1.599e3
** Group 15 RXNTYPE
1
** GROUP 16  Parent Daughter
   16   18
**=========================================================
       5
** Group 13 Where does the reaction take place? **
  1 0 0
** GROUP 14   HALF LIFE (years)        6    **  Pb210 to Dummy
22.3
** Group 15 RXNTYPE                        END OF Pu242 Chain
1
** GROUP 16  Parent Daughter
   18    0
**=========================================================
       5
** Group 13 Where does the reaction take place? **
  1 0 0
** GROUP 14   HALF LIFE (years)        7    ** Pu240 tto U236
6.56e3
** Group 15 RXNTYPE
1
** GROUP 16  Parent Daughter
   2      6
**=========================================================
       5
** Group 13 Where does the reaction take place? **
  1 0 0
** GROUP 14   HALF LIFE (years)        8    **  U236 to Th232
2.342e7
** Group 15 RXNTYPE
1
** GROUP 16  Parent Daughter
   6      11
**=========================================================
```

```
      5
** Group 13 Where does the reaction take place? **
  1 0 0
** GROUP 14   HALF LIFE (years)        9    **  Th232 to Ra228
1.4e10
** Group 15 RXNTYPE
1
** GROUP 16  Parent Daughter
   11     15
**=========================================================
      5
** Group 13 Where does the reaction take place? **
  1 0 0
** GROUP 14   HALF LIFE (years)        10   ** Ra228 to Th228
5.76
** Group 15 RXNTYPE
1
** GROUP 16  Parent Daughter
   15    14
**=========================================================
      5
** Group 13 Where does the reaction take place? **
  1 0 0
** GROUP 14   HALF LIFE (years)        11   **  Th228 to Dummy
1.912
** Group 15 RXNTYPE
1
** GROUP 16  Parent Daughter              END of Pu240 Chain
  14  0
**=========================================================
      5
** Group 13 Where does the reaction take place? **
  1 0 0
** GROUP 14   HALF LIFE (years)        12   **  Pu239 to U235
2.41e4
** Group 15 RXNTYPE
1
** GROUP 16  Parent Daughter
   3  7
**=========================================================
      5
** Group 13 Where does the reaction take place? **
  1 0 0
** GROUP 14   HALF LIFE (years)        13   **  U235 to Pa231
7.04e8
** Group 15 RXNTYPE
1
** GROUP 16  Parent Daughter
   7     10
**=========================================================
      5
** Group 13 Where does the reaction take place? **
  1 0 0
```

```
** GROUP 14   HALF LIFE (years)        14   **  Pa231 to Ac227
3.28e4
** Group 15 RXNTYPE
1
** GROUP 16  Parent Daughter
   10   17
**============================================================
       5
** Group 13 Where does the reaction take place? **
  1 0 0
** GROUP 14   HALF LIFE (years)        15   ** Ac227 to Dummy
21.77
** Group 15 RXNTYPE
1
** GROUP 16  Parent Daughter              END of Pu239 Chain
   17     0
**============================================================
       5
** Group 13 Where does the reaction take place? **
  1 0 0
** GROUP 14   HALF LIFE (years)        16   **  Np237 to U233
2.14e6
** Group 15 RXNTYPE
1
** GROUP 16  Parent Daughter
   4     9
**============================================================
       5
** Group 13 Where does the reaction take place? **
  1 0 0
** GROUP 14   HALF LIFE (years)        17   **  U233 Th229
1.592e5
** Group 15 RXNTYPE
1
** GROUP 16  Parent Daughter
   9    13
**============================================================
       5
** Group 13 Where does the reaction take place? **
  1 0 0
** GROUP 14   HALF LIFE (years)        18   **  Th229 to Dummy
7.3e3
** Group 15 RXNTYPE
1
** GROUP 16  Parent Daughter              END of Np237 Chain
   13   0
**============================================================
       5
** Group 13 Where does the reaction take place? **
  1 0 0
** GROUP 14   HALF LIFE (years)        19   **  C14 to Dummy
5.715e3
```

```
** Group 15 RXNTYPE
1
** GROUP 16  Parent Daughter
  19   0
stop
```

V.4.2 FEHM Code Modifications

Modifications of the FEHM code were needed to allow the GoldSim system model to communicate with FEHM. These changes are outlined in the following

V.4.2.1 Modifications to fehmn.f

Integer method_dum has been introduced to allow multiple simultaneous realizations to be run. qcout_old was added to correctly output the mass leaving the system during a GoldSim time increment. At the end of each GoldSim time increment, the mass arriving at the compliance boundary is qcout – qcout_old.

```
integer dum_iread , method_dum
    save qcout_old, in3_old
```

File 66 is the debugging file that was used before the team learned how to debug FEHM from within the GoldSim environment.

```
    inquire(unit=66,opened=it_is_open)
CHari PHS  6/17/2004
    if (method.eq.3)then
            in3_old = 1.0
    if(it_is_open.EQ..false.) then
      open(66,file = 'a_in_array.text')
      call system ('copy_dll')
             end if
            endif
c--9-14-04-------- PHS FIX Multiple Realizations
            if (method.EQ.1) then
              if(in(3).EQ.(in3_old+1.0)) then
                method_dum = 0
                qcout_old = 0.0
                in3_old = in(3)
              end if
            end if
```

The following subroutine in fehmn.f uses the indexing scheme presented in Table V-1 to determine the mass flux returning to GoldSim

```
cHari compute conc values to pass back to goldsim
    implicit none
    real*8, allocatable :: out_save(:)
    real*8, allocatable :: time_dump(:)
    integer ispecies
    integer number_of_species
    integer ns2,izones, sflag
    integer nflow_frac, number_of_zones,indexout,indexmzone
    integer add_spots, add_spots2
    real*8 cur_time, prev_time, del_time
     real*8 :: cur_time_save = 0.
    save out_save, time_dump, cur_time_save
c     index_in_species= 4 + 6 +
c     number_of_species = int(in(index_in_species))
c     Changing SUPER INDEX CHANGE  9/28/04 in(8+in(7)*2))
     write(66,*) 'loadoutarray ',in(8+in(7)*2)
            do jjj = 1, in(8+in(7)*2)
              out(jjj) = 0.0
            end do

            do sflag = 1, in(7)
              out(in(7+sflag)) = qcout(sflag) - qcout_old(sflag)
    qcout_old(sflag) = qcout(sflag)
              write(66,*) 'out',sflag,int(in(7+sflag)),out(in(7+sflag))
            end do
            return
            end subroutine loadoutarray_trac
```

The following subroutine in fehm.f copies the correct fehmn.files file into the GoldSim working directory to initialize each of the eight simultaneous FEHM simulations. For a given stochastic *Flowfield index*, FEHM calls the following:

```
subroutine inreal
 implicit none

integer ncase

    open(dum_iread,file = 'fehmn_real.bat')
    select case(int(in(6)))
     case (5)
            select case(int(in(2)))
    case (1)
            write(dum_iread,*)
```

```
  2                              ' copy cluster1\A\fehmn_1.files fehmn.files '
case (2)
        write(dum_iread,*)
  2                              ' copy cluster1\B\fehmn_1.files fehmn.files '
 case (3)
         write(dum_iread,*)
  2                              ' copy cluster1\C\fehmn_1.files fehmn.files '
case (4)
         write(dum_iread,*)
  2                              ' copy cluster1\D\fehmn_1.files fehmn.files '
case (5)
        write(dum_iread,*)
  2                              ' copy cluster1\E\fehmn_1.files fehmn.files '
 case (6)
         write(dum_iread,*)
  2                               ' copy cluster1\F\fehmn_1.files fehmn.files '
case (7)
        write(dum_iread,*)
  2                              ' copy cluster1\G\fehmn_1.files fehmn.files '
case (8)
         write(dum_iread,*)
  2                              ' copy cluster1\H\fehmn_1.files fehmn.files '
case (9)
        write(dum_iread,*)
  2                               ' copy cluster1\I\fehmn_1.files fehmn.files '
case (10)
         write(dum_iread,*)
  2                               ' copy cluster1\J\fehmn_1.files fehmn.files '
end select
      case (6)
        select case(int(in(2)))
case (1)
        write(dum_iread,*)
  2                              ' copy cluster2\A\fehmn_2.files fehmn.files '
case (2)
        write(dum_iread,*)
  2                              ' copy cluster2\B\fehmn_2.files fehmn.files '
case (3)
    write(dum_iread,*)
  2                              ' copy cluster2\C\fehmn_2.files fehmn.files '
case (4)
        write(dum_iread,*)
  2                              ' copy cluster2\D\fehmn_2.files fehmn.files '
case (5)
```

```
        write(dum_iread,*)
  2                          ' copy cluster2\E\fehmn_2.files fehmn.files '
case (6)
        write(dum_iread,*)
  2                          ' copy cluster2\F\fehmn_2.files fehmn.files '
case (7)
        write(dum_iread,*)
  2                          ' copy cluster2\G\fehmn_2.files fehmn.files '
case (8)
        write(dum_iread,*)
  2                          ' copy cluster2\H\fehmn_2.files fehmn.files '
case (9)
        write(dum_iread,*)
  2                          ' copy cluster2\I\fehmn_2.files fehmn.files '
case (10)
        write(dum_iread,*)
  2                          ' copy cluster2\J\fehmn_2.files fehmn.files '
end select
     case (7)
        select case(int(in(2)))
 case (1)
        write(dum_iread,*)
  2                          ' copy cluster3\A\fehmn_3.files fehmn.files '
case (2)
        write(dum_iread,*)
  2                          ' copy cluster3\B\fehmn_3.files fehmn.files '
case (3)
        write(dum_iread,*)
  2                          ' copy cluster3\C\fehmn_3.files fehmn.files '
case (4)
        write(dum_iread,*)
  2                          ' copy cluster3\D\fehmn_3.files fehmn.files '
case (5)
        write(dum_iread,*)
  2                          ' copy cluster3\E\fehmn_3.files fehmn.files '
 case (6)
        write(dum_iread,*)
  2                          ' copy cluster3\F\fehmn_3.files fehmn.files '
case (7)
        write(dum_iread,*)
  2                          ' copy cluster3\G\fehmn_3.files fehmn.files '
case (8)
        write(dum_iread,*)
  2                          ' copy cluster3\H\fehmn_3.files fehmn.files '
```

```
      case (9)
            write(dum_iread,*)
     2                          ' copy cluster3\I\fehmn_3.files fehmn.files '
      case (10)
            write(dum_iread,*)
     2                  ' copy cluster3\J\fehmn_3.files fehmn.files '
      end select
          case (8)
c              write(66,*)'in(2)', in(2)
               select case(int(in(2)))
      case (1)
            write(dum_iread,*)
     2                          ' copy cluster4\A\fehmn_4.files fehmn.files '
      case (2)
            write(dum_iread,*)
     2                          ' copy cluster4\B\fehmn_4.files fehmn.files '
      case (3)
            write(dum_iread,*)
     2                          ' copy cluster4\C\fehmn_4.files fehmn.files '
      case (4)
            write(dum_iread,*)
     2                          ' copy cluster4\D\fehmn_4.files fehmn.files '
      case (5)
            write(dum_iread,*)
     2                          ' copy cluster4\E\fehmn_4.files fehmn.files '
      case (6)
            write(dum_iread,*)
     2                          ' copy cluster4\F\fehmn_4.files fehmn.files '
      case (7)
            write(dum_iread,*)
     2                          ' copy cluster4\G\fehmn_4.files fehmn.files '
      case (8)
            write(dum_iread,*)
     2                          ' copy cluster4\H\fehmn_4.files fehmn.files '
      case (9)
            write(dum_iread,*)
     2                          ' copy cluster4\I\fehmn_4.files fehmn.files '
      case (10)
            write(dum_iread,*)
     2                          ' copy cluster4\J\fehmn_4.files fehmn.files '
      end select
          case (9)
            select case(int(in(2)))
      case (1)
```

```
        write(dum_iread,*)
  2                ' copy cluster5\A\fehmn_5.files fehmn.files '
case (2)
        write(dum_iread,*)
  2                ' copy cluster5\B\fehmn_5.files fehmn.files '
case (3)
        write(dum_iread,*)
  2                ' copy cluster5\C\fehmn_5.files fehmn.files '
case (4)
        write(dum_iread,*)
  2                ' copy cluster5\D\fehmn_5.files fehmn.files '
case (5)
        write(dum_iread,*)
  2                ' copy cluster5\E\fehmn_5.files fehmn.files '
case (6)
        write(dum_iread,*)
  2                ' copy cluster5\F\fehmn_5.files fehmn.files '
case (7)
        write(dum_iread,*)
  2                ' copy cluster5\G\fehmn_5.files fehmn.files '
case (8)
        write(dum_iread,*)
  2                ' copy cluster5\H\fehmn_5.files fehmn.files '
case (9)
        write(dum_iread,*)
  2                ' copy cluster5\I\fehmn_5.files fehmn.files '
case (10)
        write(dum_iread,*)
  2                ' copy cluster5\J\fehmn_5.files fehmn.files '
end select
     case (10)
        select case(int(in(2)))
case (1)
        write(dum_iread,*)
  2                ' copy cluster6\A\fehmn_6.files fehmn.files '
case (2)
        write(dum_iread,*)
  2                ' copy cluster6\B\fehmn_6.files fehmn.files '
case (3)
        write(dum_iread,*)
  2                ' copy cluster6\C\fehmn_6.files fehmn.files '
case (4)
        write(dum_iread,*)
  2                ' copy cluster6\D\fehmn_6.files fehmn.files '
```

```
    case (5)
          write(dum_iread,*)
      2                          ' copy cluster6\E\fehmn_6.files fehmn.files '
    case (6)
          write(dum_iread,*)
      2                          ' copy cluster6\F\fehmn_6.files fehmn.files '
    case (7)
          write(dum_iread,*)
      2                          ' copy cluster6\G\fehmn_6.files fehmn.files '
    case (8)
          write(dum_iread,*)
      2                          ' copy cluster6\H\fehmn_6.files fehmn.files '
    case (9)
          write(dum_iread,*)
      2                          ' copy cluster6\I\fehmn_6.files fehmn.files '
    case (10)
          write(dum_iread,*)
      2                          ' copy cluster6\J\fehmn_6.files fehmn.files '
    end select
        case (11)
          select case(int(in(2)))
case (1)
          write(dum_iread,*)
      2                          ' copy cluster7\A\fehmn_7.files fehmn.files '
    case (2)
          write(dum_iread,*)
      2                          ' copy cluster7\B\fehmn_7.files fehmn.files '
    case (3)
          write(dum_iread,*)
      2                          ' copy cluster7\C\fehmn_7.files fehmn.files '
    case (4)
          write(dum_iread,*)
      2                          ' copy cluster7\D\fehmn_7.files fehmn.files '
    case (5)
          write(dum_iread,*)
      2                          ' copy cluster7\E\fehmn_7.files fehmn.files '
    case (6)
          write(dum_iread,*)
      2                          ' copy cluster7\F\fehmn_7.files fehmn.files '
    case (7)
          write(dum_iread,*)
      2                          ' copy cluster7\G\fehmn_7.files fehmn.files '
    case (8)
          write(dum_iread,*)
```

```
  2                          ' copy cluster7\H\fehmn_7.files fehmn.files '
 case (9)
        write(dum_iread,*)
  2                          ' copy cluster7\I\fehmn_7.files fehmn.files '
 case (10)
        write(dum_iread,*)
  2                          ' copy cluster7\J\fehmn_7.files fehmn.files '
 end select
     case (12)
       select case(int(in(2)))
 case (1)
        write(dum_iread,*)
  2                          ' copy cluster8\A\fehmn_8.files fehmn.files '
 case (2)
        write(dum_iread,*)
  2                          ' copy cluster8\B\fehmn_8.files fehmn.files '
 case (3)
        write(dum_iread,*)
  2                          ' copy cluster8\C\fehmn_8.files fehmn.files '
 case (4)
        write(dum_iread,*)
  2                          ' copy cluster8\D\fehmn_8.files fehmn.files '
 case (5)
        write(dum_iread,*)
  2                          ' copy cluster8\E\fehmn_8.files fehmn.files '
 case (6)
        write(dum_iread,*)
  2                          ' copy cluster8\F\fehmn_8.files fehmn.files '
 case (7)
        write(dum_iread,*)
  2                          ' copy cluster8\G\fehmn_8.files fehmn.files '
 case (8)
        write(dum_iread,*)
  2                          ' copy cluster8\H\fehmn_8.files fehmn.files '
 case (9)
        write(dum_iread,*)
  2                          ' copy cluster8\I\fehmn_8.files fehmn.files '
 case (10)
        write(dum_iread,*)
  2                          ' copy cluster8\J\fehmn_8.files fehmn.files '
 end select
        end select
close(dum_iread)
```

```
return
end subroutine inreal
```

V.4.3 Modifications to userc.f

Code changes to this part of FEHM allow the K_d to be set by GoldSim and convert the radionuclide masses supplied by GoldSim to the correct units. This section is hard-wired to input mass only into the first node (1), and assumes that the mixing model is of the minimum-mixedness variety described in *Attachment IV*.

```
c-------------------------------------------------------
c   Phil and Hari  6/2004 - 9/2004
c   This section is for Tracer transport coupled
c   with Goldsim.  The input flux is calculated from
c   the mass/time
Ci  also, feed in kd from in(*) array
c   AND check to see if deltat is negative and reset
c   meaning that a new realization is underway!
c-------------------------------------------------------

      if((i.eq.1).AND.(in(1).GT.0)) then

c         write(66,*)'nspeci', nspeci, nsp
c---   Changes to SUPER INDEXING  9 28 04  IN(8+in(7)-1+nsp)
         if(in3_old.NE.in(3)) kdflag = 0
            if((iadsfl(nsp,1).eq.66).and.(kdflag.ne.1))then
               a1adfl(nsp,1) = in(8+in(7)-1+nsp)
             if(nsp.eq.nspeci) then
               kdflag = 1
              in3_old = in(3)
            end if
c           write(66,*) 'iadsfl', iadsfl(nsp,1), 'a1adfl', a1adfl(nsp,1)
         endif

         deltat = (in(1) - in1save)*3600.*24.*365.25

c-------- 9-14-2004  PHS reset deltat when new realization
         if(deltat.LE.0.0) then
           in1save = 0.0
      deltat = (in(1) - in1save)*3600.*24.*365.25
         end if

c       ispecies = 1 + npn/n0
c   PHS Hari changing to reflect nspeci+nsp = current spec
c       in the in(xx) array there are 4 things after
```

```
      sflag = in(7+nsp)
c       getflux = in(11+2*nspeci+sflag)/deltat
      getflux = in(11+2*nspeci+sflag)/deltat
c           write(66,*) int(in(6)),nsp,i, days
c                   write(66,*) 'USERC deltat ',deltat
c            write(66,*) 'userc', (in(j), j=1,18)

      rc_ss   = -getflux
      drc_ss  = 0.
c               write(66,*) getflux, 'getflux'
c               write(66,*) ' getflux i ', getflux, in(1), i,nsp
    endif
      endif
```

Attachment VI
Summary of Pre- and Post-Processing Codes for the Los Alamos National Laboratory TA-54, Material Disposal Area G Groundwater Pathway Model

Author:
Philip H. Stauffer

VI.1 Introduction

This attachment lists the source code for the pre- and postprocessor codes that were used in conjunction with the Material Disposal Area (MDA) G groundwater pathway model. Section VI.2 presents the preprocessor codes gwtable.f, points.f, run_directory_builder, FILEmaker.f, and Datmaker.f. The postprocessor codes histo.f, satchopg.f, and well.f are provided in Section VI.3. Brief descriptors are given for each code with explanations of input and output so a future user can recreate the analysis using the same logic.

VI.2 Preprocessing Codes

Five preprocessor codes were used to conduct the groundwater pathway modeling. Listings of these codes are provided below.

VI.2.1. gwtable.f

```
program gwtable

c------------------
c     code to take the  xyz coordinates
c     work with the xyz coordinates
c     and assign macro to create a water
c     table set that lies below the plane
c     with z = 5900 W  to z = 5700. E
c
c     Also creates the E and W boundaries
c     flow macros
c-----------------------------------------

      implicit none

      integer nd,i

      real*8 x, y,z, pg
      real*8 pres, heade, headw, rol, tope, topw
      real*8 topn, xdum , xe, xw, rolt, rolb, depth

c--------------------  Head on east and west boundary
```

```
      heade = 5700. * .3048
      headw = 5900. * .3048

c------------------------------ density of water
c                              gage pressure
      rolt = 998.6023
      rolb = 1007.235
      pg  = 0.08

c--------------  elevation of gw

      topw = 5900. * .3048
      tope = 5700. * .3048

      xe = 23250.
      xw = 18500.
c------------

      open(unit=7,file='areag.10001_geo')
      open(unit=16,file='gwpres_try2.macro')
      open(unit=17,file='gwflow_try2.macro')
      open(unit=18,file='gw_above2.zone')
      open(unit=19,file='gw_below2.zone')

      write(16,329)
      write(17,328)
      write(18,327)
      write(19,327)

c------   Read in the Geo file

      read(7,*)

c------------   Decide if node is below
c                water table plane: set to correct P

      do i=1 , 375451
        read(7,*) nd,x,y,z
        xdum = x - xw
        topn = topw - (topw-tope)*(xdum/4750.)
        if(topn.GT.z) then
          depth = topn - z
          rol = rolt + 0.5*(depth/1698.)*(rolb-rolt)
          pres = pg + (depth*rol*9.81 / 1.e6)
```

```
          write(16,330)  nd,nd, pres
          write(19,*) nd
          if((x.EQ.xe).OR.(x.EQ.xw)) then
            write(17,331)  nd,nd, pres
          end if
        else
          write(18,*) nd
        endif
      enddo

      write(16,*)
      write(17,*)
      write(18,*)
      write(18,332)
      write(19,*)
      write(19,332)

c-----------------------------------------
       close(7)
       close(8)
       close(16)

 327   format('zone')
 328   format('flow')
 329   format('pres')
 330   format(2x,I10,2x,I10,'  1  ',e16.9,2x,' 15.00  1')
 331   format(2x,I10,2x,I10,' 1 ',e16.9,2x,' -15.00 1000')
 332   format('stop')

      end
```

VI.2.2. points.f

```
      program points

c------------------
c     code to  distribute points at each pit node
c     for each cluster for input to the sptr macro.
C     Used in the Well Capture Analysis
c-----------------------------------------

      implicit none

      character*24 filein
```

```
      character*12 fileout

      integer index, npart, i, j, k , n, pnum(40), numn
      integer pnode, count, nybin, bin(1000), flag
      integer pit_node(66,2000), pit(40), npits , dum
      integer m1,m2

      real*8  x(400000), y(400000), zdum,  zfix, z(400000)
      real*8  xmin, xmax, ymin, ymax
      real*8  ybin(1000) , xshift, yshift

c--------------------------------------
c     pit_node(pit_number,node number)
c--------------------------------------
      write(6,*) 'what is the input file '
      read(5,*) filein

      fileout = 'points_x.out'

      fileout(8:8) = filein(9:9)

      open(unit=7,file=
     2 '/scratch/fwo/stauffer/G/Grid/areag_lev4b_pits_RENUMBERD.zone')
      open(unit=8,file='/scratch/fwo/stauffer/G/Grid/areag.10001_geo')
      open(unit=9,file=filein)
      open(unit=17,file=fileout)
      open(unit=18,file='points_bin.out')

c-------------------------------------------------------
c   read in the geo file and store nodal x,y information
c-------------------------------------------------------

      read(8,*) numn
      do i = 1, numn
        read(8,*) dum, x(i), y(i), z(i)
      end do

c--------------------------------------
c    read in the pit_node(pit_number,node number)
c    and
c    pnum(n) which are the number of nodes in pit n
c    and
c    remove any duplicate x,y points (take only the second)
c    set the bad node to node = zero
```

```
c-----------------------------------------------------

      flag = 0
      read(7,*)
      do i = 1,36
       read(7,*) j
       read(7,*)
       read(7,*) pnum(j)
       read(7,*) (pit_node(j,k) , k=1,pnum(j))

       do k = 1,pnum(j)-2
         m1 = pit_node(j,k)
         if(m1.NE.0) then
          do n = k+1 , pnum(j)
           m2 = pit_node(j,n)
           if((x(m1).EQ.x(m2)).AND.(y(m1).EQ.y(m2))) then
            pit_node(j,n) = 0
           end if
          end do
         end if
       end do
      end do

c-----------------------------------------------------
c   assign variables
c   npart = number of particles per node
c   pit(n) = pit# of the nth pit
c   pnode = node number of the nth node in a given pit
c   pit_node(pit_number,node number)
c   xshift yshift to set center of cluster on well
c-----------------------------------------------------

c   THINGS TO  READ IN DEPENDING ON CLUSTER
c    set in   file=9   cluster_info.in
c-----------------------------------------------

      read(9,*)
      read(9,*)
      read(9,*)

      read(9,*) npart
      read(9,*) npits
      do i = 1,npits
        read(9,*) pit(i)
```

```
      end do

      read(9,*)

      read(9,*) xshift
      read(9,*) yshift
      read(9,*) zfix
c-----------------------------------------

      count = 0

      xmin=1.e6
      xmax=0.
      ymin=0.
      ymax=-140000.

      do i = 1, npits
        index = pit(i)
        do j = 1,pnum(index)
          pnode = pit_node(index,j)
          if(pnode.NE.0) then
           do k = 1,npart
             write(17,666) count,x(pnode)+xshift,
     2                     y(pnode)+yshift,zfix
            count = count + 1
           end do
           if(x(pnode).LT.xmin) xmin = x(pnode)
           if(x(pnode).GT.xmax) xmax = x(pnode)
           if(y(pnode).LT.ymin) ymin = y(pnode)
           if(y(pnode).GT.ymax) ymax = y(pnode)
          end if
        end do
      end do

      write(6,*) 'surface nodes in cluster ', count
      write(6,*) 'Min dist to well ', 22000. - (xmax+xshift)
      write(6,*) 'Max dist to well ', 22000. - (xmin+xshift)
      write(6,*) 'xmax ymax ', xmax,ymax
      write(6,*) 'xmin ymin ', xmin,ymin

c-----------------------------------------------------
c   search pnode's y values and place into ybin(1..nybin)
c   then add a number to the bin(1..nybin)
c-----------------------------------------------------
```

```
      write(6,*) xmin, xmax, ymin, ymax
      do i = 1,200
       bin(i) = 0
       ybin(i) = 0
      end do

      count = 0
      nybin = 1
      ybin(1) = ymin

      do i = 1, npits
        index = pit(i)
        do j = 1,pnum(index)
          pnode = pit_node(index,j)
         if(pnode.NE.0) then
          flag = 0
          do k = 1,nybin
            if(y(pnode).EQ.ybin(k)) flag = 1
          end do
          if(flag.NE.1) then
            nybin = nybin + 1
            ybin(nybin) = y(pnode)
          end if
          do k = 1,nybin
            if(y(pnode).EQ.ybin(k)) then
              bin(k) = bin(k) + 1
              n = k
              count = count + 1
            end if
          end do
         end if
        end do
      end do

      write(6,*) count, nybin, (bin(n), n=1,nybin)

c-------------------------------------------------
c  write out the x for each bin and the number of
c  particles per bin
c-------------------------------------------------
      count = 0
      do i = 1,nybin
        write(18,667)  ybin(i), bin(i)
```

```
      count = count + bin(i)
    end do
      write(6,*) 'Surface nodes in cluster ', count

666  format(i6,x,F9.1,x,F12.1,x,F8.1)
667  format(F12.1, x, I5)

    End
```

Example input for this program for Cluster 5:

==========

points to write at each node

number of pits in cluster

pits 1 - n

10

6

32

33

35

36

37

38

Shift in x and y

-250.

-125.

1750.

VI.2.3. Run_directory_builder

This shell script creates a directory called Cluster_Directories then fills it with the 80 subdirectories necessary for use in the GoldSim system-level model. Once the directory structure is built, each of the 80 subdirectories gets an fehmn.files file, an goldfehm.dat file, and an areag.rtd file. The two FORTRAN code that follow this script (FILEmaker.f and Datmaker) are used to change characters in the fehmn.files and goldfehm.dat files so that thy have the correct information regarding pathways to the data files and correct rtd files for a given cluster at a given flow-rate. The shell script below is designed to be run from /scratch/fwo/stauffer/G/Filemaker and requires the FILEmaker.f, Datmaker.f, goldfehm.dat. The FILEmaker.f program is set up to create the directory structure that Rob Shuman requires for GoldSim on his PC.

```
cd /scratch/fwo/stauffer/G

rm -r Cluster_Directories
mkdir Cluster_Directories
cd Cluster_Directories

mkdir cluster1
```

```
mkdir cluster2
mkdir cluster3
mkdir cluster4
mkdir cluster5
mkdir cluster6
mkdir cluster7
mkdir cluster8

cd cluster1
mkdir A
mkdir B
mkdir C
mkdir D
mkdir E
mkdir F
mkdir G
mkdir H
mkdir I
mkdir J
cd ../cluster2
mkdir A
mkdir B
mkdir C
mkdir D
mkdir E
mkdir F
mkdir G
mkdir H
mkdir I
mkdir J
cd ../cluster3
mkdir A
mkdir B
mkdir C
mkdir D
mkdir E
mkdir F
mkdir G
mkdir H
mkdir I
mkdir J
cd ../cluster4
mkdir A
mkdir B
```

```
mkdir C
mkdir D
mkdir E
mkdir F
mkdir G
mkdir H
mkdir I
mkdir J
cd ../cluster5
mkdir A
mkdir B
mkdir C
mkdir D
mkdir E
mkdir F
mkdir G
mkdir H
mkdir I
mkdir J
cd ../cluster6
mkdir A
mkdir B
mkdir C
mkdir D
mkdir E
mkdir F
mkdir G
mkdir H
mkdir I
mkdir J
cd ../cluster7
mkdir A
mkdir B
mkdir C
mkdir D
mkdir E
mkdir F
mkdir G
mkdir H
mkdir I
mkdir J
cd ../cluster8
mkdir A
mkdir B
```

```
mkdir C
mkdir D
mkdir E
mkdir F
mkdir G
mkdir H
mkdir I
mkdir J

cp /scratch/fwo/stauffer/G/bg0.1/cluster1/areag.rtd /scratch/fwo/stauffer/G/Cluster_Directories/cluster1/A/.
cp /scratch/fwo/stauffer/G/bg0.1/cluster2/areag.rtd /scratch/fwo/stauffer/G/Cluster_Directories/cluster2/A/.
cp /scratch/fwo/stauffer/G/bg0.1/cluster3/areag.rtd /scratch/fwo/stauffer/G/Cluster_Directories/cluster3/A/.
cp /scratch/fwo/stauffer/G/bg0.1/cluster4/areag.rtd /scratch/fwo/stauffer/G/Cluster_Directories/cluster4/A/.
cp /scratch/fwo/stauffer/G/bg0.1/cluster5/areag.rtd /scratch/fwo/stauffer/G/Cluster_Directories/cluster5/A/.
cp /scratch/fwo/stauffer/G/bg0.1/cluster6/areag.rtd /scratch/fwo/stauffer/G/Cluster_Directories/cluster6/A/.
cp /scratch/fwo/stauffer/G/bg0.1/cluster7/areag.rtd /scratch/fwo/stauffer/G/Cluster_Directories/cluster7/A/.
cp /scratch/fwo/stauffer/G/bg0.1/cluster8/areag.rtd /scratch/fwo/stauffer/G/Cluster_Directories/cluster8/A/.

cp /scratch/fwo/stauffer/G/bg0.25/cluster1/areag.rtd /scratch/fwo/stauffer/G/Cluster_Directories/cluster1/B/.
cp /scratch/fwo/stauffer/G/bg0.25/cluster2/areag.rtd /scratch/fwo/stauffer/G/Cluster_Directories/cluster2/B/.
cp /scratch/fwo/stauffer/G/bg0.25/cluster3/areag.rtd /scratch/fwo/stauffer/G/Cluster_Directories/cluster3/B/.
cp /scratch/fwo/stauffer/G/bg0.25/cluster4/areag.rtd /scratch/fwo/stauffer/G/Cluster_Directories/cluster4/B/.
cp /scratch/fwo/stauffer/G/bg0.25/cluster5/areag.rtd /scratch/fwo/stauffer/G/Cluster_Directories/cluster5/B/.
cp /scratch/fwo/stauffer/G/bg0.25/cluster6/areag.rtd /scratch/fwo/stauffer/G/Cluster_Directories/cluster6/B/.
cp /scratch/fwo/stauffer/G/bg0.25/cluster7/areag.rtd /scratch/fwo/stauffer/G/Cluster_Directories/cluster7/B/.
cp /scratch/fwo/stauffer/G/bg0.25/cluster8/areag.rtd /scratch/fwo/stauffer/G/Cluster_Directories/cluster8/B/.

cp /scratch/fwo/stauffer/G/bg0.5/cluster1/areag.rtd /scratch/fwo/stauffer/G/Cluster_Directories/cluster1/C/.
cp /scratch/fwo/stauffer/G/bg0.5/cluster2/areag.rtd /scratch/fwo/stauffer/G/Cluster_Directories/cluster2/C/.
cp /scratch/fwo/stauffer/G/bg0.5/cluster3/areag.rtd /scratch/fwo/stauffer/G/Cluster_Directories/cluster3/C/.
cp /scratch/fwo/stauffer/G/bg0.5/cluster4/areag.rtd /scratch/fwo/stauffer/G/Cluster_Directories/cluster4/C/.
cp /scratch/fwo/stauffer/G/bg0.5/cluster5/areag.rtd /scratch/fwo/stauffer/G/Cluster_Directories/cluster5/C/.
cp /scratch/fwo/stauffer/G/bg0.5/cluster6/areag.rtd /scratch/fwo/stauffer/G/Cluster_Directories/cluster6/C/.
cp /scratch/fwo/stauffer/G/bg0.5/cluster7/areag.rtd /scratch/fwo/stauffer/G/Cluster_Directories/cluster7/C/.
cp /scratch/fwo/stauffer/G/bg0.5/cluster8/areag.rtd /scratch/fwo/stauffer/G/Cluster_Directories/cluster8/C/.

cp /scratch/fwo/stauffer/G/bg1/cluster1/areag.rtd /scratch/fwo/stauffer/G/Cluster_Directories/cluster1/D/.
cp /scratch/fwo/stauffer/G/bg1/cluster2/areag.rtd /scratch/fwo/stauffer/G/Cluster_Directories/cluster2/D/.
cp /scratch/fwo/stauffer/G/bg1/cluster3/areag.rtd /scratch/fwo/stauffer/G/Cluster_Directories/cluster3/D/.
cp /scratch/fwo/stauffer/G/bg1/cluster4/areag.rtd /scratch/fwo/stauffer/G/Cluster_Directories/cluster4/D/.
cp /scratch/fwo/stauffer/G/bg1/cluster5/areag.rtd /scratch/fwo/stauffer/G/Cluster_Directories/cluster5/D/.
cp /scratch/fwo/stauffer/G/bg1/cluster6/areag.rtd /scratch/fwo/stauffer/G/Cluster_Directories/cluster6/D/.
cp /scratch/fwo/stauffer/G/bg1/cluster7/areag.rtd /scratch/fwo/stauffer/G/Cluster_Directories/cluster7/D/.
cp /scratch/fwo/stauffer/G/bg1/cluster8/areag.rtd /scratch/fwo/stauffer/G/Cluster_Directories/cluster8/D/.
```

```
cp /scratch/fwo/stauffer/G/bg1.5/cluster1/areag.rtd /scratch/fwo/stauffer/G/Cluster_Directories/cluster1/E/.
cp /scratch/fwo/stauffer/G/bg1.5/cluster2/areag.rtd /scratch/fwo/stauffer/G/Cluster_Directories/cluster2/E/.
cp /scratch/fwo/stauffer/G/bg1.5/cluster3/areag.rtd /scratch/fwo/stauffer/G/Cluster_Directories/cluster3/E/.
cp /scratch/fwo/stauffer/G/bg1.5/cluster4/areag.rtd /scratch/fwo/stauffer/G/Cluster_Directories/cluster4/E/.
cp /scratch/fwo/stauffer/G/bg1.5/cluster5/areag.rtd /scratch/fwo/stauffer/G/Cluster_Directories/cluster5/E/.
cp /scratch/fwo/stauffer/G/bg1.5/cluster6/areag.rtd /scratch/fwo/stauffer/G/Cluster_Directories/cluster6/E/.
cp /scratch/fwo/stauffer/G/bg1.5/cluster7/areag.rtd /scratch/fwo/stauffer/G/Cluster_Directories/cluster7/E/.
cp /scratch/fwo/stauffer/G/bg1.5/cluster8/areag.rtd /scratch/fwo/stauffer/G/Cluster_Directories/cluster8/E/.

cp /scratch/fwo/stauffer/G/bg2/cluster1/areag.rtd /scratch/fwo/stauffer/G/Cluster_Directories/cluster1/F/.
cp /scratch/fwo/stauffer/G/bg2/cluster2/areag.rtd /scratch/fwo/stauffer/G/Cluster_Directories/cluster2/F/.
cp /scratch/fwo/stauffer/G/bg2/cluster3/areag.rtd /scratch/fwo/stauffer/G/Cluster_Directories/cluster3/F/.
cp /scratch/fwo/stauffer/G/bg2/cluster4/areag.rtd /scratch/fwo/stauffer/G/Cluster_Directories/cluster4/F/.
cp /scratch/fwo/stauffer/G/bg2/cluster5/areag.rtd /scratch/fwo/stauffer/G/Cluster_Directories/cluster5/F/.
cp /scratch/fwo/stauffer/G/bg2/cluster6/areag.rtd /scratch/fwo/stauffer/G/Cluster_Directories/cluster6/F/.
cp /scratch/fwo/stauffer/G/bg2/cluster7/areag.rtd /scratch/fwo/stauffer/G/Cluster_Directories/cluster7/F/.
cp /scratch/fwo/stauffer/G/bg2/cluster8/areag.rtd /scratch/fwo/stauffer/G/Cluster_Directories/cluster8/F/.

cp /scratch/fwo/stauffer/G/bg4/cluster1/areag.rtd /scratch/fwo/stauffer/G/Cluster_Directories/cluster1/G/.
cp /scratch/fwo/stauffer/G/bg4/cluster2/areag.rtd /scratch/fwo/stauffer/G/Cluster_Directories/cluster2/G/.
cp /scratch/fwo/stauffer/G/bg4/cluster3/areag.rtd /scratch/fwo/stauffer/G/Cluster_Directories/cluster3/G/.
cp /scratch/fwo/stauffer/G/bg4/cluster4/areag.rtd /scratch/fwo/stauffer/G/Cluster_Directories/cluster4/G/.
cp /scratch/fwo/stauffer/G/bg4/cluster5/areag.rtd /scratch/fwo/stauffer/G/Cluster_Directories/cluster5/G/.
cp /scratch/fwo/stauffer/G/bg4/cluster6/areag.rtd /scratch/fwo/stauffer/G/Cluster_Directories/cluster6/G/.
cp /scratch/fwo/stauffer/G/bg4/cluster7/areag.rtd /scratch/fwo/stauffer/G/Cluster_Directories/cluster7/G/.
cp /scratch/fwo/stauffer/G/bg4/cluster8/areag.rtd /scratch/fwo/stauffer/G/Cluster_Directories/cluster8/G/.

cp /scratch/fwo/stauffer/G/bg6/cluster1/areag.rtd /scratch/fwo/stauffer/G/Cluster_Directories/cluster1/H/.
cp /scratch/fwo/stauffer/G/bg6/cluster2/areag.rtd /scratch/fwo/stauffer/G/Cluster_Directories/cluster2/H/.
cp /scratch/fwo/stauffer/G/bg6/cluster3/areag.rtd /scratch/fwo/stauffer/G/Cluster_Directories/cluster3/H/.
cp /scratch/fwo/stauffer/G/bg6/cluster4/areag.rtd /scratch/fwo/stauffer/G/Cluster_Directories/cluster4/H/.
cp /scratch/fwo/stauffer/G/bg6/cluster5/areag.rtd /scratch/fwo/stauffer/G/Cluster_Directories/cluster5/H/.
cp /scratch/fwo/stauffer/G/bg6/cluster6/areag.rtd /scratch/fwo/stauffer/G/Cluster_Directories/cluster6/H/.
cp /scratch/fwo/stauffer/G/bg6/cluster7/areag.rtd /scratch/fwo/stauffer/G/Cluster_Directories/cluster7/H/.
cp /scratch/fwo/stauffer/G/bg6/cluster8/areag.rtd /scratch/fwo/stauffer/G/Cluster_Directories/cluster8/H/.

cp /scratch/fwo/stauffer/G/bg8/cluster1/areag.rtd /scratch/fwo/stauffer/G/Cluster_Directories/cluster1/I/.
cp /scratch/fwo/stauffer/G/bg8/cluster2/areag.rtd /scratch/fwo/stauffer/G/Cluster_Directories/cluster2/I/.
cp /scratch/fwo/stauffer/G/bg8/cluster3/areag.rtd /scratch/fwo/stauffer/G/Cluster_Directories/cluster3/I/.
cp /scratch/fwo/stauffer/G/bg8/cluster4/areag.rtd /scratch/fwo/stauffer/G/Cluster_Directories/cluster4/I/.
cp /scratch/fwo/stauffer/G/bg8/cluster5/areag.rtd /scratch/fwo/stauffer/G/Cluster_Directories/cluster5/I/.
cp /scratch/fwo/stauffer/G/bg8/cluster6/areag.rtd /scratch/fwo/stauffer/G/Cluster_Directories/cluster6/I/.
cp /scratch/fwo/stauffer/G/bg8/cluster7/areag.rtd /scratch/fwo/stauffer/G/Cluster_Directories/cluster7/I/.
cp /scratch/fwo/stauffer/G/bg8/cluster8/areag.rtd /scratch/fwo/stauffer/G/Cluster_Directories/cluster8/I/.
```

```
cp /scratch/fwo/stauffer/G/bg10/cluster1/areag.rtd /scratch/fwo/stauffer/G/Cluster_Directories/cluster1/J/.
cp /scratch/fwo/stauffer/G/bg10/cluster2/areag.rtd /scratch/fwo/stauffer/G/Cluster_Directories/cluster2/J/.
cp /scratch/fwo/stauffer/G/bg10/cluster3/areag.rtd /scratch/fwo/stauffer/G/Cluster_Directories/cluster3/J/.
cp /scratch/fwo/stauffer/G/bg10/cluster4/areag.rtd /scratch/fwo/stauffer/G/Cluster_Directories/cluster4/J/.
cp /scratch/fwo/stauffer/G/bg10/cluster5/areag.rtd /scratch/fwo/stauffer/G/Cluster_Directories/cluster5/J/.
cp /scratch/fwo/stauffer/G/bg10/cluster6/areag.rtd /scratch/fwo/stauffer/G/Cluster_Directories/cluster6/J/.
cp /scratch/fwo/stauffer/G/bg10/cluster7/areag.rtd /scratch/fwo/stauffer/G/Cluster_Directories/cluster7/J/.
cp /scratch/fwo/stauffer/G/bg10/cluster8/areag.rtd /scratch/fwo/stauffer/G/Cluster_Directories/cluster8/J/.

cd /scratch/fwo/stauffer/G/Filemaker

FILEmaker

Datmaker
```

VI.2.3.1 FILEmaker.f

```
c- --- - - - ------------------------------------------------------------------
c-------- program to  make the fehmn.files files for all
c-------- 80 subdirectories in the MDA G GoldSim Model..
c- --- - - - ------------------------------------------------------------------

      program filemaker

      implicit none

    character*1  cluster(8), infil(10), slash
      character*74 zzout
    integer   i,   j, k

      infil(1) = 'A'
      infil(2) = 'B'
      infil(3) = 'C'
      infil(4) = 'D'
      infil(5) = 'E'
      infil(6) = 'F'
      infil(7) = 'G'
      infil(8) = 'H'
      infil(9) = 'I'
      infil(10) = 'J'

      cluster(1) = '1'
      cluster(2) = '2'
```

```
      cluster(3) = '3'
      cluster(4) = '4'
      cluster(5) = '5'
      cluster(6) = '6'
      cluster(7) = '7'
      cluster(8) = '8'

c ----------------------------  44 characters plus  24 characters
c  1234567890         2         3         4
c  /scratch/fwo/stauffer/G/Cluster_Directories/
c  ------- character 52=cluster  54=infil  62=cluster
c-----------------------------------------------------------------

      zzout(1:44)  = '/scratch/fwo/stauffer/G/Cluster_Directories/'
      zzout(45:68) = 'cluster1/A/fehmn_1.files'
      slash = '/'

     do i = 1,8
       zzout(52:52) = cluster(i)
       zzout(62:62) = cluster(i)
       do j = 1,10
         zzout(54:54) = infil(j)
         open(11,file=zzout)

         write(11,20) cluster(i),slash,infil(j)
         write(11,21)
         write(11,20) cluster(i),slash,infil(j)
         write(11,22)
           do k=1,6
             write(11,*)
           end do
         write(11,23)
         write(11,24)
         write(11,25)
         write(11,26)
         write(11,*)

         close(11)
       end do
     end do


c--------0---------2---------3---------4---------5---------6---------7--
```

```
 20    format("c:/Program Files/GTG/GoldSim/MDA G PA-CA Model/cluster",
   x       A1,A1,A1, "/goldfehm.dat")
 21    format("c:/Program Files/GTG/GoldSim/MDA G PA-CA Model/",
   x        "grid/grid.fehmn")
 22    format('goldfehm.out')
 23    format("c:/Program Files/GTG/GoldSim/MDA G PA-CA Model/",
   x        "grid/grid.stor")
 24    format('goldfehm.chk')
 25    format('none')
 26    format('0')
   END
```

VI.2.3.2 Datmaker.f

```
c- --- - - - -------------------------------------------
c-------- program to change the .dat file for each case
c-------- 80 subdirectories in the MDA G GoldSim model.
c---------  independent of pc directory pathway
c           uses only clusterX/Y/*.dat subdirectories
c- --- - - - -------------------------------------------

      program filemaker

      implicit none

    character*1  cluster(8), infil(10), slash
       character*80 dumchar
       character*67 zzout
    integer   i,   j, k

       infil(1) = 'A'
       infil(2) = 'B'
       infil(3) = 'C'
       infil(4) = 'D'
       infil(5) = 'E'
       infil(6) = 'F'
       infil(7) = 'G'
       infil(8) = 'H'
       infil(9) = 'I'
       infil(10) = 'J'

       cluster(1) = '1'
       cluster(2) = '2'
       cluster(3) = '3'
```

```
      cluster(4) = '4'
      cluster(5) = '5'
      cluster(6) = '6'
      cluster(7) = '7'
      cluster(8) = '8'

      open(12,file='/scratch/fwo/stauffer/G/Filemaker/goldfehm.dat')

c ----------------------------  44 characters plus  23 characters
c  ------- character 52=cluster  54=infil
c-----------------------------------------------------------------

      zzout(1:44)  = '/scratch/fwo/stauffer/G/Cluster_Directories/'
      zzout(45:67) = 'cluster1/A/goldfehm.dat'
      slash = '/'

     do i = 1,8
       zzout(52:52) = cluster(i)
       do j = 1,10
         zzout(54:54) = infil(j)
         open(11,file=zzout)
         rewind(12)
           do k = 1,1000
             read(12,20,end=81,err=81) dumchar
             if(dumchar(1:4).EQ.'clus') then
               dumchar(8:8) = cluster(i)
               dumchar(10:10) = infil(j)
             end if
           write(11,20) dumchar
         end do
 81        continue
         close(11)
       end do
     end do


c--------0---------2---------3---------4---------5---------6---------7--

  20    format(A80)

     END
```

VI.3 Postprocessing Codes

Three postprocessing codes were used in conjunction with the groundwater pathway model. The codes are listed below.

VI.3.1. histo.f

This program creates the rtd file (areag.rtd) for input to the 1-D abstraction model used in GoldSim. Also created are two files containing histogram information for particle breakthrough.

```
      program histo

c------------------
c     code to take the sptr 3  file and
c     and convert the output to a histogram
c     of breakthrough in a series of bins.
c----------------------------------------

      implicit none

      integer part(25000),index, partTot
      integer i, flag, sump ,  bindex, dp

      real*8 time(25000), dtdum, sumt, normp(25000), partr
      real*8 maxc

c---------------------------------------
c   partr = ratio of particles to total particles
c   normp = partr normalized to the size of dtdum
c------------

      open(unit=7,file='areag.sptr3')
      open(unit=16,file='areag.rtd')
      open(unit=17,file='areag.hist3')
      open(unit=18,file='areag.hist_norm')

c------  read in particles and times
      read(7,*)
      read(7,*)
      read(7,*)

      index = 1
      do while(flag.NE.1)
```

```
      read(7,*,err=100) time(index), part(index)
      partTot = part(index)
      index = index + 1
     end do

 100  continue
c--------------------  Write particles per bin

     bindex = 1
     flag = 0
     sump = 0
     sumt = 0.

     write(6,*) ' Total Particles ' , partTot
c     write(16,*) 'Time(s)   part/(partTot*dt)    '
     write(17,*) 'Time(yrs)   particles bin  dT(days)'
     write(18,*) 'Time(s) Time(yrs) Norm1 part/(partTot*dt)  '

     maxc = 0.
     do i=2, index - 1
      dtdum = time(i) - time(i-1)
      dp = part(i) - part(i-1)
      partr = dreal(dp)/dreal(partTot)
      normp(i) = partr / (dtdum/365.25)
      write(16,*) time(i)*86400., normp(i)
      write(17,*) time(i)/365.25, dp, i-1, dtdum
      if(normp(i).GT.maxc) maxc = normp(i)
      sump = sump + dp
      sumt = sumt + dtdum
     end do

     do i=2, index - 1
      write(18,*) time(i)*86400.,time(i)/365.25,normp(i)/maxc,normp(i)
     end do

     write(16,*)
c-----------------------------------------

      close(7)
      close(16)
      close(17)

     end
```

VI.3.2. satchopg.f

```
c-------- program to take data from  '.sca'  file and put
c---------   depth vs  sat  for R20,  R21 R32, 1121,1107, and pit 36
,
     program schop

    character*80  zzin
    integer  node(1000,6),  i, nn(6),  n
    real*8   x,y,z(1000,6),sat, x1,x2,x3,x5
      write(6,*) 'What is the name of the file to format'
      read *, zzin

      open(16,file=zzin)
      open(18,file='/scratch/fwo/stauffer/G/Grid/1121_borehole.zone')
      open(19,file='/scratch/fwo/stauffer/G/Grid/R20_borehole.zone')
      open(20,file='/scratch/fwo/stauffer/G/Grid/R21_borehole.zone')
      open(21,file='/scratch/fwo/stauffer/G/Grid/R32_borehole.zone')
      open(22,file='/scratch/fwo/stauffer/G/Grid/1107_borehole.zone')
      open(23,file='/scratch/fwo/stauffer/G/Grid/Pit36_borehole.zone')
      open(24,file='zzSat_1121')
      open(25,file='zzSat_R20')
      open(26,file='zzSat_R21')
      open(27,file='zzSat_R32')
      open(28,file='zzSat_1107')
      open(29,file='zzSat_Pit36')
      open(30,file='zzSat_Hari')

      read(18,*)
      read(18,*) nn(4)
      read(19,*)
      read(19,*) nn(1)
      read(20,*)
      read(20,*) nn(2)
      read(21,*)
      read(21,*) nn(3)
      read(22,*)
      read(22,*) nn(5)
      read(23,*)
      read(23,*) nn(6)

      do i = 1,nn(1)
       read(19,*)  node(i,1) , x, y, z(i,1)
      end do
      do i = 1,nn(2)
```

```
 read(20,*)  node(i,2) , x, y, z(i,2)
end do
do i = 1,nn(3)
 read(21,*)  node(i,3) , x, y, z(i,3)
end do
do i = 1,nn(4)
 read(18,*)  node(i,4) , x, y, z(i,4)
end do
do i = 1,nn(5)
 read(22,*)  node(i,5) , x, y, z(i,5)
end do
do i = 1,nn(6)
 read(23,*)  node(i,6) , x, y, z(i,6)
end do

write(6,*) nn(1)  , x, y
write(6,*) nn(2)  , x, y
write(6,*) nn(3)  , x, y
write(6,*) nn(4)  , x, y
write(6,*) nn(5)  , x, y
write(6,*) nn(6)  , x, y

  read(16,*)

write(24,*) 'Node1121 Elev(m) Elev(ft) Sat1121 '
write(25,*) 'NodeR20 Elev(m) Elev(ft) SatR20 '
write(26,*) 'NodeR21 Elev(m) Elev(ft) SatR21 '
write(27,*) 'NodeR32 Elev(m) Elev(ft) SatR32 '
write(28,*) 'Node1107 Elev(m) Elev(ft) Sat1107 '
write(29,*) 'NodePit36 Elev(m) Elev(ft) SatPit36 '

s1  = 1
s2  = 1
s3  = 1
s4 =  1
s5  = 1
s6 =  1

do i = 1,  375451
  read(16,665) n,x1, x2, x3, sat
  write(30,*) sat

  if(i.EQ.node(s1,1)) then
    zd = z(s1,1)
```

```
      write(25,20) node(s1,1), zd, zd/.3048, sat
      s1 = s1 + 1
    end if

    if(i.EQ.node(s2,2)) then
      zd = z(s2,2)
      write(26,20) node(s2,2), zd, zd/.3048, sat
      s2 = s2 + 1
    end if

    if(i.EQ.node(s3,3)) then
      zd = z(s3,3)
      write(27,20) node(s3,3), zd, zd/.3048, sat
      s3 = s3 + 1
    end if

    if(i.EQ.node(s4,4)) then
      zd = z(s4,4)
      write(24,20) node(s4,4), zd, zd/.3048, sat
      s4 = s4 + 1
    end if

    if(i.EQ.node(s5,5)) then
      zd = z(s5,5)
      write(28,20) node(s5,5), zd, zd/.3048, sat
      s5 = s5 + 1
    end if

    if(i.EQ.node(s6,6)) then
      zd = z(s6,6)
      write(29,20) node(s6,6), zd, zd/.3048, sat
      s6 = s6 + 1
    end if

  end do

 10    format(i8,1x,6g13.4)
 20    format(i10,f10.3,1x,f10.3,1x,f8.2)
665    format(i10.10,2x,4(' : ',e16.9,x))
666    format(i10.10,5(' : ',e16.9))


    close(16)
    close(25)
```

```
      close(26)
    close(27)
      close(30)


    END
```

Example input for this code is the list of nodes in the approximate x-y location of Borehole 1121. The header line is for reference, the second line is the number of nodes in the file and the next 23 nodes are the numerical representation of the well.

```
=====================================================
Borehole 1121   top at 6685 ft
23
0000062729     0.219843750E+05  -0.132164062E+06   0.190000000E+04
0000077832     0.219843750E+05  -0.132164062E+06   0.190625000E+04
0000091771     0.219843750E+05  -0.132164062E+06   0.191250000E+04
0000105758     0.219843750E+05  -0.132164062E+06   0.191875000E+04
0000120315     0.219843750E+05  -0.132164062E+06   0.192500000E+04
0000134792     0.219843750E+05  -0.132164062E+06   0.193125000E+04
0000148731     0.219843750E+05  -0.132164062E+06   0.193750000E+04
0000162718     0.219843750E+05  -0.132164062E+06   0.194375000E+04
0000177629     0.219843750E+05  -0.132164062E+06   0.195000000E+04
0000192732     0.219843750E+05  -0.132164062E+06   0.195625000E+04
0000206671     0.219843750E+05  -0.132164062E+06   0.196250001E+04
0000220658     0.219843750E+05  -0.132164062E+06   0.196875001E+04
0000235215     0.219843750E+05  -0.132164062E+06   0.197500001E+04
0000249692     0.219843750E+05  -0.132164062E+06   0.198125001E+04
0000263631     0.219843750E+05  -0.132164062E+06   0.198750001E+04
0000277618     0.219843750E+05  -0.132164062E+06   0.199375001E+04
0000292529     0.219843750E+05  -0.132164062E+06   0.200000001E+04
0000307631     0.219843750E+05  -0.132164062E+06   0.200625001E+04
0000321290     0.219843750E+05  -0.132164062E+06   0.201250001E+04
0000333891     0.219843750E+05  -0.132164062E+06   0.201875001E+04
0000345275     0.219843750E+05  -0.132164062E+06   0.202500001E+04
0000354487     0.219843750E+05  -0.132164062E+06   0.203125001E+04
0000361096     0.219843750E+05  -0.132164062E+06   0.203750001E+04
```

VI.3.3. well.f

```
      program well

c------------------
c    Code to take the sptr 2  file and
c    find the particles entering the well, output to areag.wellout.
```

```
c    All particles last points are output to the file areag.allout.
c    Also creates areag.sptr2_capture file that
c    contains a flag so the particles pathways can be colored
c    from the release point to the well.
c----------------------------------------

      implicit none

      integer part,zone,old,new, flag, index, count
      integer numpart, i, partn(50000), parts(50000)
      integer capt(50000)

      real*8 x,y,z,time
      real*8 xs(50000), ys(50000), zs(50000),times(50000)
c--------------------------------------

      open(unit=7,file='areag.sptr2')
      open(unit=17,file='areag.wellout')
      open(unit=18,file='areag.allout')
      open(unit=19,file='areag.sptr2_capture')

      write(17,*) 'part x y z time zone old new'
      write(19,*) 'part x y z t zone old new capture'
c------  read in particles and other info
      read(7,*)
      read(7,*)
      read(7,*)

      do while(flag.NE.1)
       read(7,*,err=100) part,x,y,z,time,zone,old,new
       if(time.EQ.0.0) numpart = numpart + 1
       partn(part) = new
       xs(part) = x
       ys(part) = y
       zs(part) = z
       times(part) = time
       parts(part) = part

       if(new.EQ.0) index = index + 1
      end do

 100  continue

      write(6,*) numpart
```

```
      do i = 1,numpart
         capt(i) = -1
         write(6,555) parts(i),xs(i),ys(i),zs(i),times(i),partn(i)
         write(18,555) parts(i),xs(i),ys(i),zs(i),times(i),partn(i)
         if(partn(i).LT.0) then
         write(17,555) parts(i),xs(i),ys(i),zs(i),times(i),partn(i)
         count = count + 1
         capt(i) = 1
       end if
      end do

      index = index + count

      write(17,*) count, index , dreal(count)/dreal(index)
      write(6,*) count, index , dreal(count)/dreal(index)

c-----------------------------------------
c     WRite out new sptr2 file with the capture flag set +1 -1

c       rewind(7)
c       read(7,*)
c       read(7,*)
c       read(7,*)

c       do while(flag.NE.1)
c         read(7,*,err=101) part,x,y,z,time,zone,old,new
c         write(19,556) part,x,y,z,time,zone,old,new,capt(part)
c       end do

c 101   continue

c---------------------------------------

     close(7)
       close(17)

 555  format(I5,x,F12.1,xF9.1,x,F6.1,x,F9.1,x,I6,x,I6,x,I6)
 556  format(I5,x,F12.1,xF9.1,x,F6.1,x,F9.1,4(x,I6))

      end
```

LA-UR-05-6898

Approved for public release; distribution is unlimited.

Title: SPATIAL VARIATION IN NEAR-SURFACE HYDROLOGIC BEHAVIOR AT LOS ALAMOS NATIONAL LABORATORY TECHNICAL AREA 54, MATERIAL DISPOSAL AREA G

Author(s):
Brent Newman
Dale Counce
Emily Kluk
Leo Martinez
Dennis Newell
Johnny Salazar

Submitted to: U.S. Department of Energy

Form 836 (8/00)

Table of Contents

List of Figures i
List of Tables ii
Acronyms and Abbreviations iii
Acknowledgements iv
1.0 Introduction 1
2.0 Methods 3
2.1 Borehole Drilling 3
2.2 Chloride and Nitrate Analyses 7
2.3 Chloride Mass Balance Approach 7
2.4 Stable Isotope Analyses 9
2.5 Pressure Head Analyses 10
2.6 Statistical Analyses 10
3.0 Results 11
3.1 Water Content 11
3.2 Chloride Profiles and Flux Estimates 11
3.3 Stable Isotopes 20
3.4 Pressure Head 30
3.5 Statistical Analyses 30
4.0 Discussion 42
4.1 Comparative Hydrology of Pit Covers and Adjacent Unexcavated Areas 42
4.2 Comparative Hydrology of Paved and Unpaved Areas 44
4.3 Comparative Hydrology of Active Area and Zone 4 47
5.0 References 51

List of Figures

Figure 1 Location of 1999 and 2002 Boreholes in Active Part of Material Disposal Area G 5
Figure 2 Location of 2002 Boreholes within Zone 4 at Material Disposal Area G 6
Figure 3 Water Content and Chloride Profiles of 1999 Boreholes Drilled into Pit Covers 12
Figure 4 Water Content and Chloride Profiles of 1999 Boreholes Drilled Adjacent to Pits 13
Figure 5 Water Content and Chloride Profiles of 1999 Boreholes Drilled through Asphalt Pads 14
Figure 6 Water Content and Chloride Profiles of 2002 Boreholes Drilled through Asphalt Pads 15
Figure 7 Water Content and Chloride Profiles of 2002 Boreholes Drilled in Unpaved Areas 16
Figure 8 Water Content and Chloride Profiles of 2002 Boreholes Drilled in Piñon Canopy Locations within Zone 4 17
Figure 9 Water Content and Chloride Profiles of 2002 Boreholes Drilled in Juniper Canopy Locations within Zone 4 18
Figure 10 Water Content and Chloride Profiles of 2002 Boreholes Drilled in Intercanopy Locations within Zone 4 19
Figure 11 Stable Isotope Ratios in Pore Water of 1999 Boreholes Drilled Into Pit Covers 22
Figure 12 Stable Isotope Ratios in Pore Water of 1999 Boreholes Drilled Adjacent to Pits 23

Figure 13 Stable Isotope Ratios in Pore Water of 2002 Boreholes Drilled in Unpaved Areas 24
Figure 14 Stable Isotope Ratios in Pore Water of 2002 Boreholes Drilled in Piñon Canopy Locations within Zone 4 25
Figure 15 Stable Isotope Ratios in Pore Water of 2002 Boreholes Drilled in Juniper Canopy Locations within Zone 4 26
Figure 16 Stable Isotope Ratios in Pore Water of 2002 Boreholes Drilled in Intercanopy Locations within Zone 4 27
Figure 17 Stable Isotope Ratios in Pore Water of 1999 Boreholes Drilled through Asphalt Pads 28
Figure 18 Stable Isotope Ratios in Pore Water of 2002 Boreholes Drilled through Asphalt Pads 29
Figure 19 Comparison of Isotopic Ratios in 1999 Boreholes Drilled in Paved and Unpaved Areas 31
Figure 20 Pressure Head Measurements for 1999 Boreholes Drilled into Pit Covers 32
Figure 21 Pressure Head Measurements for 1999 Boreholes Drilled Adjacent to Pits 33
Figure 22 Pressure Head Measurements for 1999 Boreholes Drilled through Asphalt Pads 34
Figure 23 Comparison of Downward Flux in 1999 Boreholes Drilled into Pit Covers and Areas Adjacent to Pits 43
Figure 24 Comparison of Average Water Content in Boreholes Drilled in Paved and Unpaved Areas 45
Figure 25 Comparison of Maximum Delta Deuterium Values in Boreholes Drilled in Paved and Unpaved Areas 46
Figure 26 Comparison of Downward Flux in Unpaved Parts of Active Area and Zone 4 48
Figure 27 Comparison of Maximum Delta Deuterium Values in Canopy and Intercanopy Locations within Zone 4 50

List of Tables

Table 1 Shallow Boreholes Drilled within Material Disposal Area G 4
Table 2 Chloride-Based Flux Estimates 21
Table 3 Comparison of T-Test Results for Pit Covers and Unexcavated Locations Adjacent to Pits 35
Table 4 Comparison of T-Test Results for Paved and Unpaved Locations 36
Table 5 Comparison of T-Test Results for Unpaved Portions of Active Disposal Area and Zone 4 38
Table 6 Comparison of T-Test Results for Zone 4 Canopy and Intercanopy Locations 40

Attachments

Attachment 1 Hydrographic Properties of Shallow Boreholes at Material Disposal Area G

Acronyms and Abbreviations

$\delta^{18}O$	Delta value (ratio) of oxygen-18 (heavy oxygen)
δD	Delta value (ratio) of deuterium
θg	Water content
Laboratory	Los Alamos National Laboratory
LANL	Los Alamos National Laboratory
MDA	Material Disposal Area
TA	Technical Area

Acknowledgements

Support for this study was provided through the Material Disposal Area G performance assessment maintenance project. The contributions of Andrew Campbell, Richard Cardellino, Sean French, Mel Garcia, Phil Fresquez, Eli Ludwig, Stephanie Maez, Rob Shuman, Tracy Schofield, and Mark Vaneeckhout are appreciated.

1.0 Introduction

This report describes two studies undertaken in 1999 and 2002 as part of the Los Alamos National Laboratory Low-Level Radioactive Waste Disposal Performance Assessment Maintenance Program. The studies were completed to reduce uncertainties relative to near-surface hydrologic conditions at Los Alamos National Laboratory (LANL or the Laboratory) Material Disposal Area (MDA) G, a low-level radioactive waste disposal site. Both studies analyzed data (i.e., water content, pore water chloride, and stable isotopes) from shallow (< 2 m [6.6 ft]) cores collected at MDA G. The specific objectives of the studies were to (1) determine the appropriateness of using a uniform horizontal near-surface flux boundary condition for hydrological modeling of the groundwater pathway, (2) assess potential impacts of asphalt paving on site performance, and (3) evaluate potential effects of post-institutional control changes in site vegetation on near-surface hydrology. Each of these objectives is described in more detail below.

One of the assumptions of the 1997 MDA G performance assessment (Hollis et al., 1997) was that the MDA G site, located on Mesita del Buey, had a crushed tuff cover that was assumed to have uniform hydrologic properties. This assumption allowed the use of a uniform-flux near-surface boundary condition for modeling the groundwater pathway. The 1999 near-surface hydrologic behavior study was undertaken to test this assumption. Specifically, near-surface hydrologic behavior was examined to compare similarities and differences between pit covers and adjacent areas that still retained part or all of the in situ soil or tuff materials. The term "near-surface" is used to indicate the upper 1 to 2 m (3.3 to 6.6 ft) of the mesa top, which includes the soil zone and either crushed tuff backfill (i.e., over the disposal units) or the top of the intact Tshirege Member of the Bandelier Tuff. Core samples were collected from borings into pit covers and into the adjacent areas that still retained in situ near-surface material. To evaluate hydrologic behavior, measurements of water content, pressure head, and naturally occurring chloride and stable oxygen and hydrogen isotope tracers were made. This suite of evaluations provides data for both a qualitative and quantitative assessment of the variation in the near-surface vadose-zone hydrology at MDA G.

An additional objective of the 1999 study was to examine the hydrologic effects of asphalt paving at MDA G. Since the initial performance assessment was completed, substantial areas of the mesa top have been paved with asphalt. To determine how the paving affects near-surface hydrologic behavior, an effort was made to compare water content, chloride concentrations, and stable isotope data from core samples taken in the unpaved areas to core samples from three paved locations. Four additional cores from paved areas were collected in 2002 to supplement the 1999 data.

An objective of the 2002 study was to assess the impact of plant succession on the near-surface hydrology of the site. It is likely that MDA G will transition from a grassland to a piñon-juniper woodland after closure and the cessation of active management. To evaluate how this conversion may affect near-surface hydrologic behavior, 10 cores were collected in a portion of MDA G referred to in the LANL site-wide environmental impact statement as Zone 4 (DOE, 1999). This area, which extends westward from the active disposal area of MDA G to MDA L, contains a relatively undisturbed piñon-juniper woodland (i.e., no waste pit excavations have been made, and no thinning had taken place prior to sampling). Given its proximity to the active disposal area, Zone 4 is an excellent natural analog for likely post-institutional control conditions. Pore water chloride, water content, and stable isotope data collected from Zone 4 were compared to similar data collected from the active part of MDA G in 1999 and from an additional 3 cores collected from unpaved locations in the active area during 2002.

Following this introductory section, Section 2 of this report describes the methods used for obtaining and analyzing the borehole samples. Chloride and water content data were used to quantify differences in percolation fluxes across the major surface and near-surface conditions at MDA G (e.g., paved vs. unpaved, trees vs. no trees). Stable isotope values were used to examine variations in evaporation, which is a critical control on percolation rates. Finally, pressure head and nitrate data were used as additional characterization information to understand processes and differences in near-surface hydrologic behavior at MDA G. Section 3 discusses the results of the analyses and Section 4 presents a discussion of the significance of the findings, focusing on the objectives described above.

2.0 Methods

This section describes how samples were collected and analyzed for the 1999 and 2002 investigations of near-surface hydrologic behavior. Section 2.1 provides information about the drilling of 26 boreholes in the active and currently undeveloped portions of MDA G. The methods used to determine chloride content, stable isotope ratios, and pressure head are described in Sections 2.2 through 2.5, and Section 2.6 discusses how statistical analyses were performed.

2.1 Borehole Drilling

Nine boreholes were cored at MDA G on July 1 and 2, 1999 and an additional 17 boreholes were drilled in August 2002 (Table 1). The 1999 boreholes, shown in Figure 1, were drilled in the active part of MDA G using a CME-45 hollow-stem auger system. Three boreholes — designated Pit2, Pit17, and Pit24 — were drilled into existing crushed tuff pit covers and range from 0.9 to 1 m (3.0 to 3.3 ft) deep; the depths of these boreholes were limited to prevent drilling into waste. Boreholes 7B, 17B, and 21B are located next to deep boreholes 1107, 1117, and 1121, respectively, and are 1.9 to 2 m (6.2 to 6.6 ft) deep. Boreholes BT2, BT21, and BT30 are drilled into paved areas and are 1 to 2 m (3.3 to 6.6 ft) deep. At each of these boreholes, the core barrel was split and the core was quickly screened for tritium and volatile organic carbon contamination (none was found) using handheld survey instruments. Immediately after screening, samples were collected for water content, pressure head, chloride, and stable isotope analyses.

Sampling during the 2002 study was conducted using a trailer-mounted, hollow-stem auger rig manufactured by SIMCO Drilling Equipment, Inc. All 2002 boreholes were drilled between 1 and 2 m (3.3 and 6.6 ft) deep. Ten of the boreholes were drilled in Zone 4; these boreholes are shown in Figure 2. Boreholes IC1, IC2, IC3, and IC4 were located in intercanopy spaces in Zone 4 that had some sparse grass, but also a large amount of bare ground. Boreholes J1, J2, and J3 were drilled beneath juniper (*Juniperus monosperma*) canopies, approximately half the distance between the main trunk and the drip line. Boreholes P1, P2, and P3 were drilled underneath piñon (*Pinus edulis*) canopies in the same manner as the juniper boreholes. This approach allowed data to be collected from the three main vegetation-cover conditions present in typical piñon-juniper woodlands on the Pajarito Plateau. In addition to the boreholes drilled in Zone 4, seven boreholes were drilled in the active part of MDA G in 2002; the locations of these boreholes are shown in Figure 1. Boreholes G1, G2, and G3 were drilled in unpaved areas and boreholes AS1, AS2, AS3, and AS4 were drilled in paved areas. Details of the sampling and analytical procedures are provided below.

Table 1
Shallow Boreholes Drilled within Material Disposal Area G

Year Drilled	Borehole	Depth (m)	Description
1999	Pit2	0.9 –1	Drilled into existing crushed pit covers in active part of MDA G
	Pit 17		
	Pit24		
	7B	1.9 – 2	Drilled into intact tuff between pits near deep borehole 1107
	17B		Drilled into intact tuff between pits near deep borehole 1117
	21B		Drilled into intact tuff between pits near deep borehole 1121
	BT2	1 – 2	Drilled through asphalt pads in active part of MDA G
	BT21		
	BT30		
2002	IC1	1 – 2	Drilled in intercanopy spaces in Zone 4
	IC2		
	IC3		
	IC4		
	J1		Drilled beneath juniper canopy in Zone 4
	J2		
	J3		
	P1		Drilled beneath piñon canopy in Zone 4
	P2		
	P3		
	G1		Drilled in unpaved location in active part of MDA G
	G2		Drilled in unpaved location (but adjacent to pavement) in active part of MDA G
	G3		Drilled in unpaved location in active part of MDA G
	AS1		Drilled through asphalt pads in active part of MDA G
	AS2		
	AS3		
	AS4		

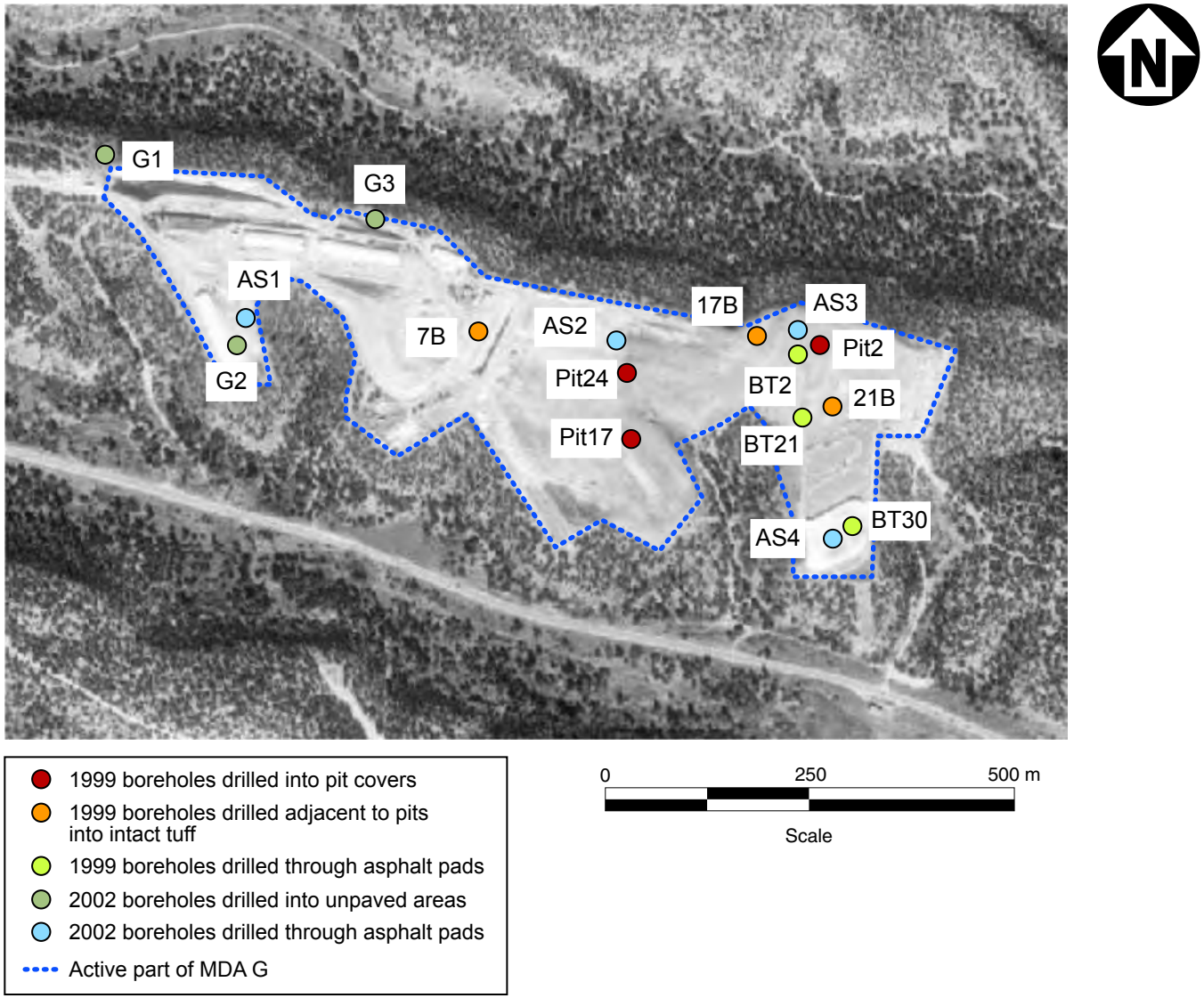

Figure 1
Location of 1999 and 2002 Boreholes in Active Part of Material Disposal Area G

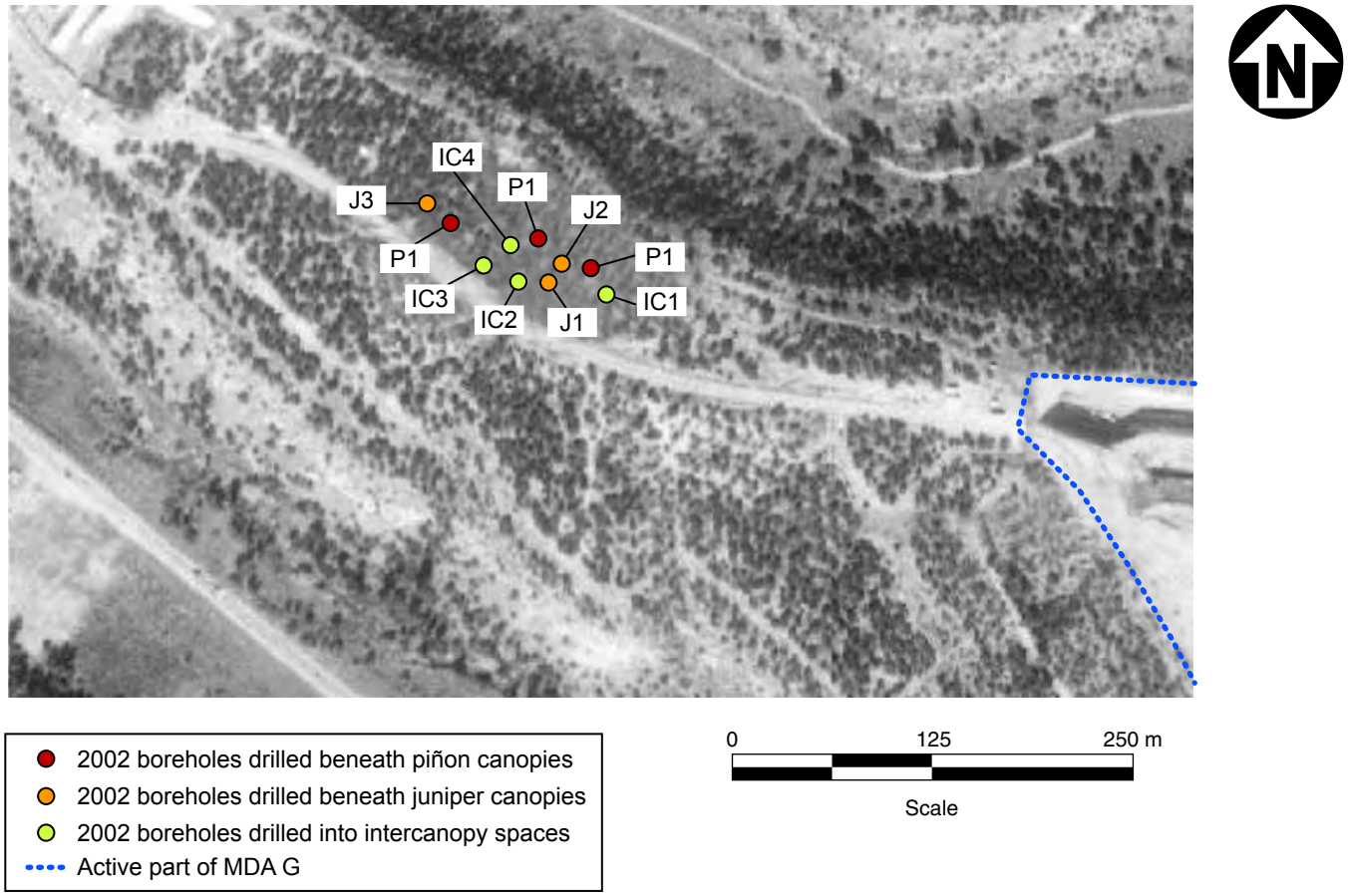

Figure 2
Location of 2002 Boreholes within Zone 4 at Material Disposal Area G

2.2 Chloride and Nitrate Analyses

Pore water chloride concentrations are increasingly used as tracers of hydrologic behavior in arid and semiarid environments. Using a mass balance approach, pore water chloride concentrations can be used to estimate long-term average percolation fluxes in the vadose zone. This section describes the sampling and analytical methods used to determine pore-water chloride concentrations; Section 2.3 describes the mass balance approach used to estimate flux.

In addition to chloride concentrations, pore-water nitrate concentrations were measured. Nitrate is subject to a variety of biogeochemical processes that are often related to the presence of reducing or oxidizing conditions. Thus, nitrate levels can be a good qualitative indicator of the local biogeochemical conditions. This is especially true in Zone 4, where the presence of trees may result in different types and rates of biogeochemical cycling than occur in the adjacent grassy or bare intercanopy spaces. Local differences in nitrate content can provide insight into the spatial distributions and transport of radionuclides that may be translocated to the near-surface. Nitrate sampling and analysis was identical to that of chloride, and was performed on the same leachate samples used for the chloride analyses.

Chloride and nitrate profiles were determined for all of the boreholes shown in Figures 1 and 2. Samples were collected every 0.1 m (3.9 in.), stored in pretared amber glass jars with Teflon-lined lids, and oven dried to determine gravimetric water content according to ASTM International's method D2216-90. Chloride and nitrate concentrations were determined following the procedure in Newman et al. (1997), except that samples were leached by combining approximately 50 g (0.11 lb) of dried soil or tuff with approximately 75 g (0.17 lb) of deionized water. The samples were agitated for 24 hours using a rotary shaker, the solid material was allowed to settle, and the supernatant was filtered and analyzed using a Dionex Ion Chromatograph at the LANL Earth & Environmental Sciences Geochemistry Laboratory. The analytical precision of the ion chromatograph is better than 5 percent.

Pore-water chloride and nitrate concentrations were calculated using leachate concentrations, gravimetric water contents, and bulk densities. A bulk density of 1.40 g/cm^3 (87 lb/ft^3) was used for soils and crushed tuff on the basis of values reported in DBS&A (1994). For intact tuff, a value of 1.37 g/cm^3 (86 lb/ft^3) was adopted from Rogers and Gallaher (1995), who reported this as the mean value for Bandelier Tuff Tshirege Member unit 2. These two bulk density values were also used to calculate volumetric water contents.

2.3 Chloride Mass Balance Approach

The pore-water chloride concentrations were used in the chloride mass balance approach to estimate long-term average percolation fluxes and the corresponding vadose-water residence times. This approach, which involves measuring chloride concentrations in vadose-zone water

with depth, is particularly useful for estimating vadose-zone fluxes in semiarid and arid environments (Allison et al., 1985; Newman et al., 1997; Phillips, 1994; Scanlon, 2000). Chloride concentrations serve as indicators of downward flux and water age. The downward flux is inversely proportional to the amount of chloride accumulation: high chloride concentrations indicate a low flux that represents many years of meteoric chloride accumulation coupled with the removal of water through evapotranspiration. Relatively low chloride contents indicate a high downward flux, or water that is able to move through the vadose zone at a fast enough rate to minimize evapotranspiration effects.

The chloride mass balance method is based on the following assumptions: (1) flow occurs largely in a downward piston-like fashion, (2) there is little dispersive mixing of water and chloride, (3) atmospheric chloride deposition has remained relatively constant over many thousands of years and is the sole source of chloride to the system, and (4) chloride uptake by plants is negligible.

If vadose-zone chloride concentrations are constant, the average annual flux can be estimated using the following equation:

$$R = \frac{P \times Cl_p}{Cl_{sw}} \qquad 1$$

Where

R = flux (m/yr)
P = the average annual precipitation rate (m/yr)
Cl_p = the average concentration of chloride in bulk precipitation (g/m^3)
Cl_{sw} = the chloride concentration in vadose-zone water (g/m^3)

However, chloride concentrations in profiles are not always constant (i.e., fluxes can change over time as a result of changes in climate, land use, or other factors). In this case, plots of cumulative chloride as a function of cumulative water in the profile can be used to determine changes in fluxes. Approximately linear segments on these water-versus-chloride-content plots indicate zones of constant flux. The flux for a segment is determined as follows:

$$R = \frac{P \times Cl_p}{Cl_{seg}} \qquad 2$$

Where

Cl_{seg} = average chloride content of the samples represented by the segment (g/m^3)

A value of 0.37 m/yr (15 in./yr) was used for the average annual precipitation (P) on the basis of data in Bowen (1990). A value of 0.29 g/m^3 (18 lb/ft^3) was used for the average concentration of chloride in bulk precipitation (Cl_p), as reported in Anderholm (1994).

2.4 Stable Isotope Analyses

Samples for pore water stable isotope analyses were collected over 0.02-m (0.79-in.) intervals for the first 0.1 m (3.9 in.) and every 0.1 m (3.9 in.) thereafter; higher resolution sampling was implemented above 0.1 m (3.9 in.) to better define the effect of evaporation. Upon removal from the core barrel, the samples were placed immediately in glass mason jars, the mouths of which were coated with vacuum grease, and screw-on lids were applied. This procedure reduces the chance that pore water will evaporate during the period between sampling and analysis, thus altering the isotopic composition of the water.

The stable-isotope analyses were carried out at the stable isotope laboratory at the New Mexico Institute of Mining and Technology. All samples taken from the top 1 m (3.3 ft.) were analyzed, but only one-quarter to one-half of the samples collected at depths greater than 1 m (3.3 ft) were analyzed (approximately one sample from each 0.2- to 0.4-m [7.9- to 16-in.] interval). Soil water was extracted by high-temperature vacuum distillation following methods reported by Shurbaji et al. (1995). The samples were analyzed with a Finnegan Mat Delta-E stable-isotope-ratio mass spectrometer using gas standards from the Oztech Trading Corporation. The isotopic values are expressed in delta (δ) notation as per mil (parts per thousand [‰]) differences relative to the Vienna Standard Mean Ocean Water (V-SMOW) isotope standard:

$$\delta^{18}O \text{ or } \delta D = \frac{R_{sample} - R_{V-SMOW}}{R_{V-SMOW}} \times 1{,}000 \qquad 3$$

Where

R_{sample}	= the isotope ratio of the sample (^{18}O:^{16}O or D:H)
$R_{V\text{-}SMOW}$	= the isotope ratio of the V-SMOW standard
1,000	= a constant used to allow delta values to be expressed as per mil (‰)

The value of $\delta^{18}O$ was measured from extractions made using the carbon dioxide equilibration technique of Socki et al. (1992). For the δD analyses, hydrogen was extracted using the zinc method of Kendall and Coplen (1985). The analytical precision for the $\delta^{18}O$ and δD analyses by mass spectroscopy is better than ±0.2 ‰ and ±2 ‰, respectively. However, some of the 2002 distillations did not yield sufficient water for analyses, especially for the $\delta^{18}O$ analyses, because the samples were too dry.

2.5 Pressure Head Analyses

Pressure head analyses were conducted only for the 1999 samples. These analyses were made on samples of approximately 100 g (0.22 lb) taken at 0.1-m intervals from each borehole. Each sample was placed in a resealable plastic bag that was folded over and encapsulated in packaging tape to prevent the loss or gain of water that might alter the results. Analyses were conducted in duplicate using an AquaLab model CX2 chilled-mirror psychrometer following methods in Gee et al. (1992). All runs were bracketed by measurements of distilled water and salt solution standards. Analytical precision was better than 0.003 water activity units based on the distilled water standard.

2.6 Statistical Analyses

Statistical analyses were performed using version 7.0 of the STATISTICA® software package (StatSoft, 2005). T-tests were used to compare data representing different site conditions (e.g., paved vs. unpaved areas or grassland vs. woodland vegetation). The tests included up to 28 hydrological variables obtained from the borehole analyses. A probability (p) value of 0.05 was used for all tests.

3.0 Results

This section provides the results of the hydrologic analyses. Sections 3.1 and 3.2 summarize the results of the water content and chloride profile determinations, Section 3.3 provides results for the stable isotope analyses, and Section 3.4 describes the pressure head findings, and Section 3.5 presents a statistical comparison of the hydrological characteristics of the different boreholes. *Attachment I* provides specific water content, pressure head, chloride, and stable isotope data.

3.1 Water Content

Gravimetric water content (θg) profiles for the various boreholes are shown in Figures 3 – 10. Water content profiles for pit cover boreholes collected in 1999 range from approximately 2 to 14 percent. Profiles from pits 17 and 24 are consistently below 10 percent, with pit 2 having some values in the low teens (Figure 3). Water content profiles for unexcavated areas adjacent to pits collected in 1999 range from 2 to 24 percent (Figure 4). The water contents from borehole 21b are the highest because of its proximity to a paved area.

The 1999 water content profiles from paved areas range from about 4 to 18 percent (Figure 5); 2002 profiles from paved areas range from about 3 to 16 percent (Figure 6). Water content profiles measured during 2002 in unpaved areas in the active part of MDA G range from nearly zero to about 19 percent (Figure 7). The profiles of boreholes G1 and G3 are substantially drier than that of G2. Borehole G2 was located next to a building suspected of having a leaky sump system; the reason this borehole was drilled was to help determine the extent of leakage.

The samples from boreholes located in the piñon-juniper canopy of Zone 4 have water contents ranging from nearly zero to 16 percent (Figures 8 and 9). Similarly, water contents for the boreholes in the Zone 4 intercanopy areas have a lower bound of approximately zero, but these boreholes are drier overall, with a maximum water content of about 9 percent (Figure 10).

3.2 Chloride Profiles and Flux Estimates

Chloride profiles for each of the boreholes are shown in Figures 3 – 10. Samples from the 1999 boreholes drilled into pit covers yielded variable chloride contents (Figure 3) that are generally lower than for the 2002 boreholes (see *Attachment I*). Boreholes collected adjacent to pits in 1999 (Figure 4) have even more variability than the boreholes drilled within pits. Borehole 17B, for example, shows a substantial spike in chloride concentration of over 1,000 mg/L (1,000 ppm) at a depth of about 1.4 m (4.6 ft). Borehole 17B was drilled adjacent to deep borehole 1117, which was also found to have high chloride concentrations, although at greater depths (Newman, 1996). Borehole 21B has low chloride concentrations consistent with the high water contents.

Figure 3a
Borehole Pit2

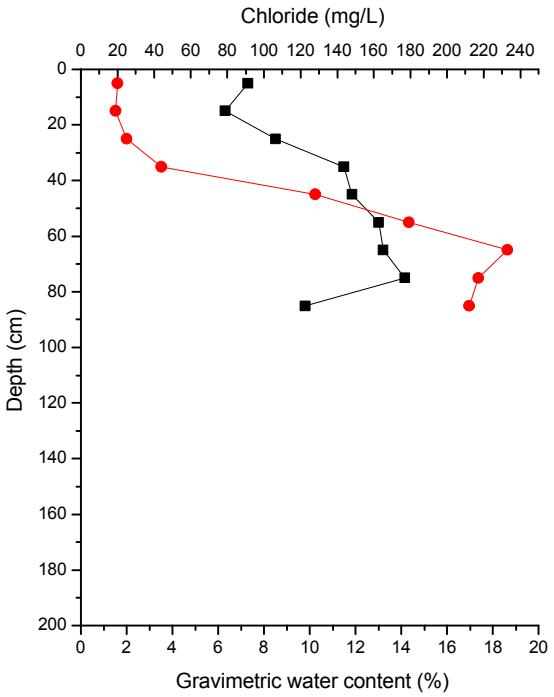

Figure 3b
Borehole Pit17

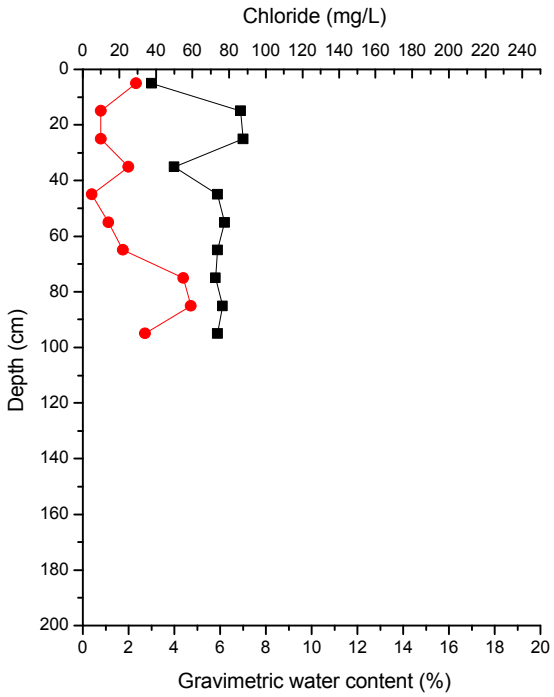

Figure 3c
Borehole Pit24

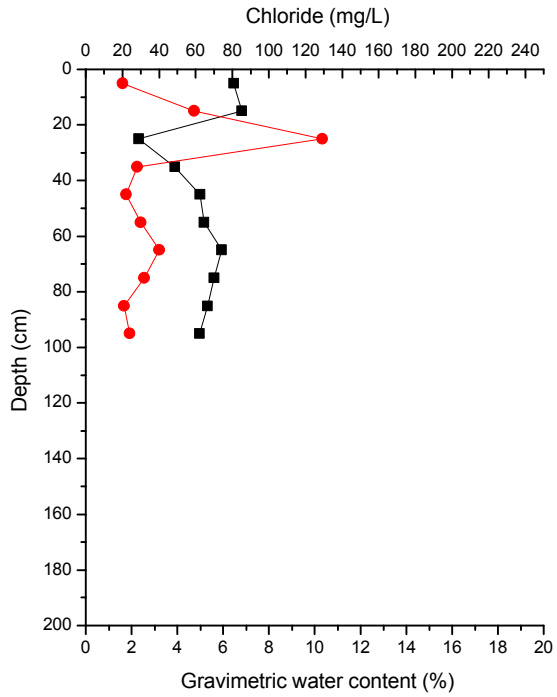

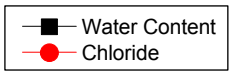

Figure 3
Water Content and Chloride Profiles of 1999 Boreholes Drilled into Pit Covers

Figure 4a
Borehole 7B

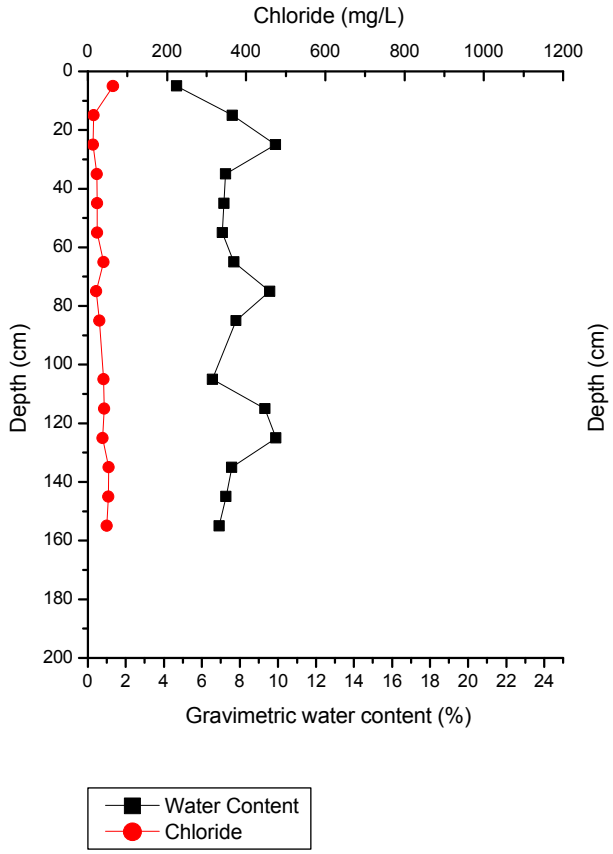

Figure 4b
Borehole 17B

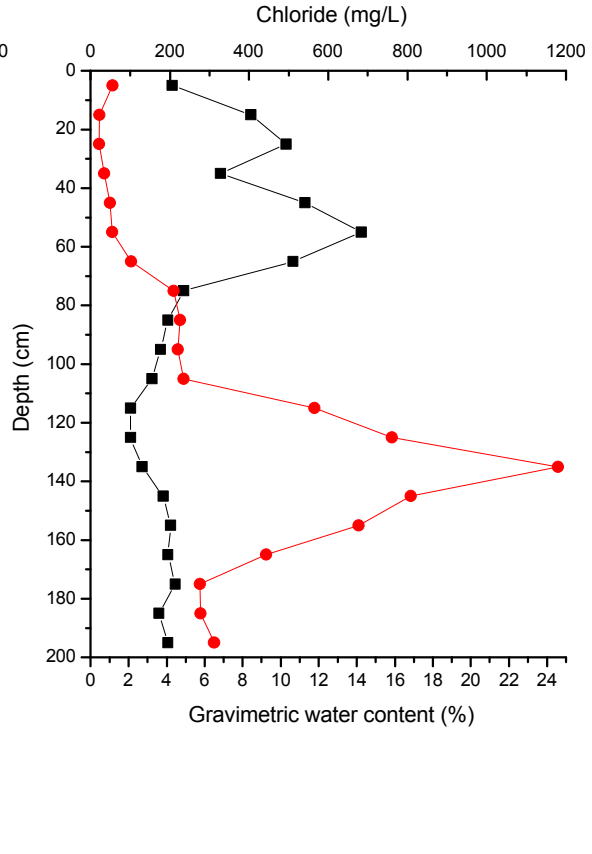

Figure 4c
Borehole 21B

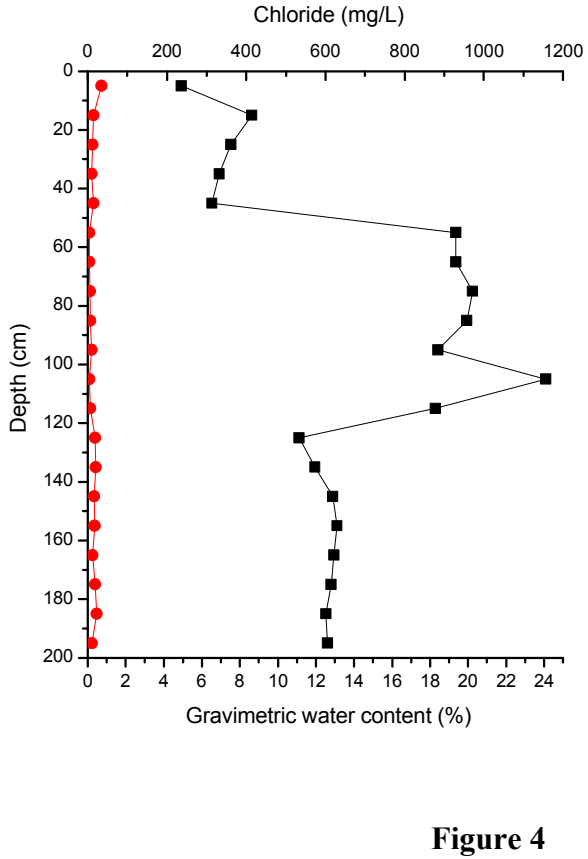

Figure 4
Water Content and Chloride Profiles of 1999 Boreholes Drilled Adjacent to Pits

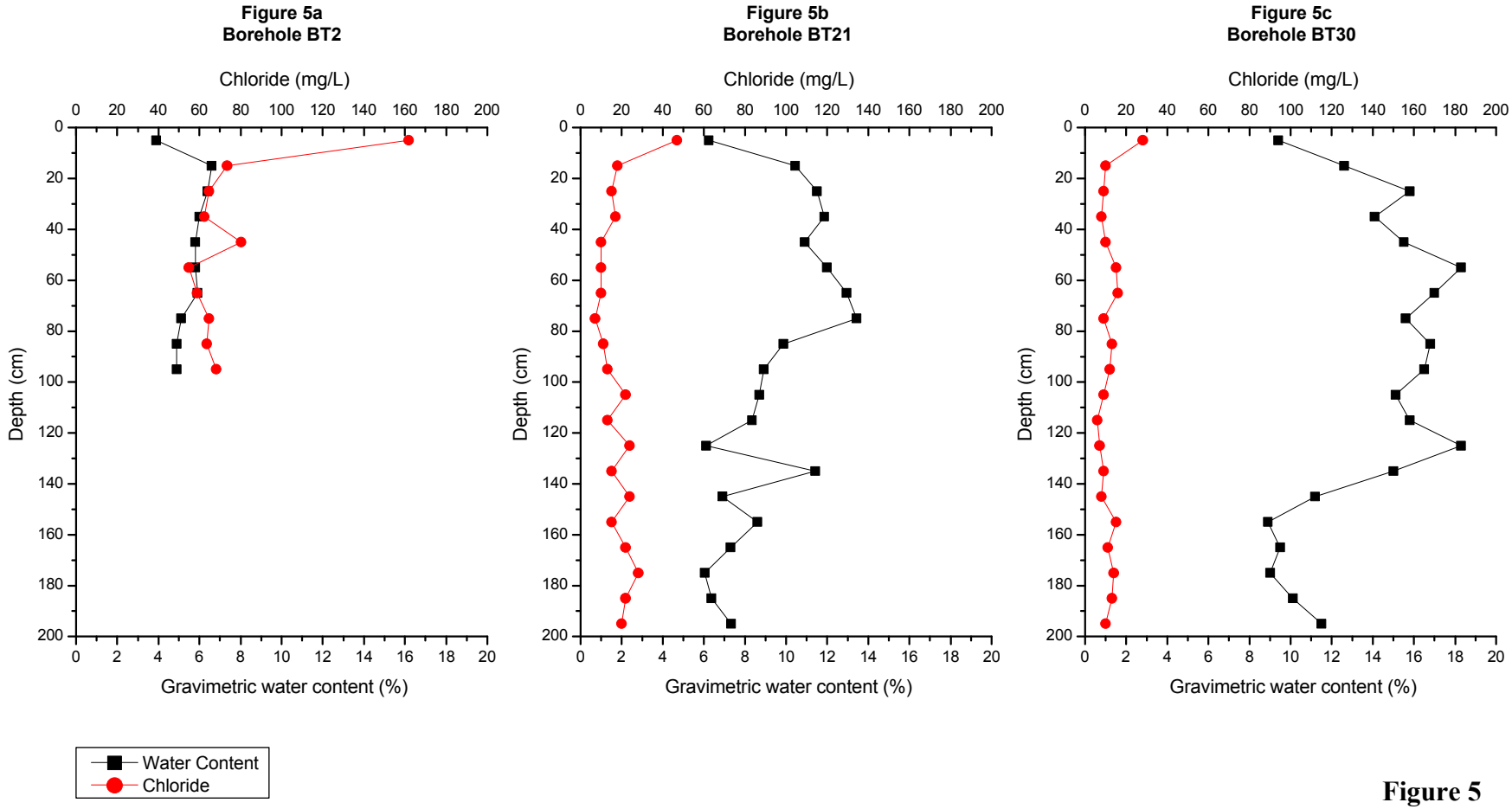

Figure 5
Water Content and Chloride Profiles of 1999 Boreholes Drilled through Asphalt Pads

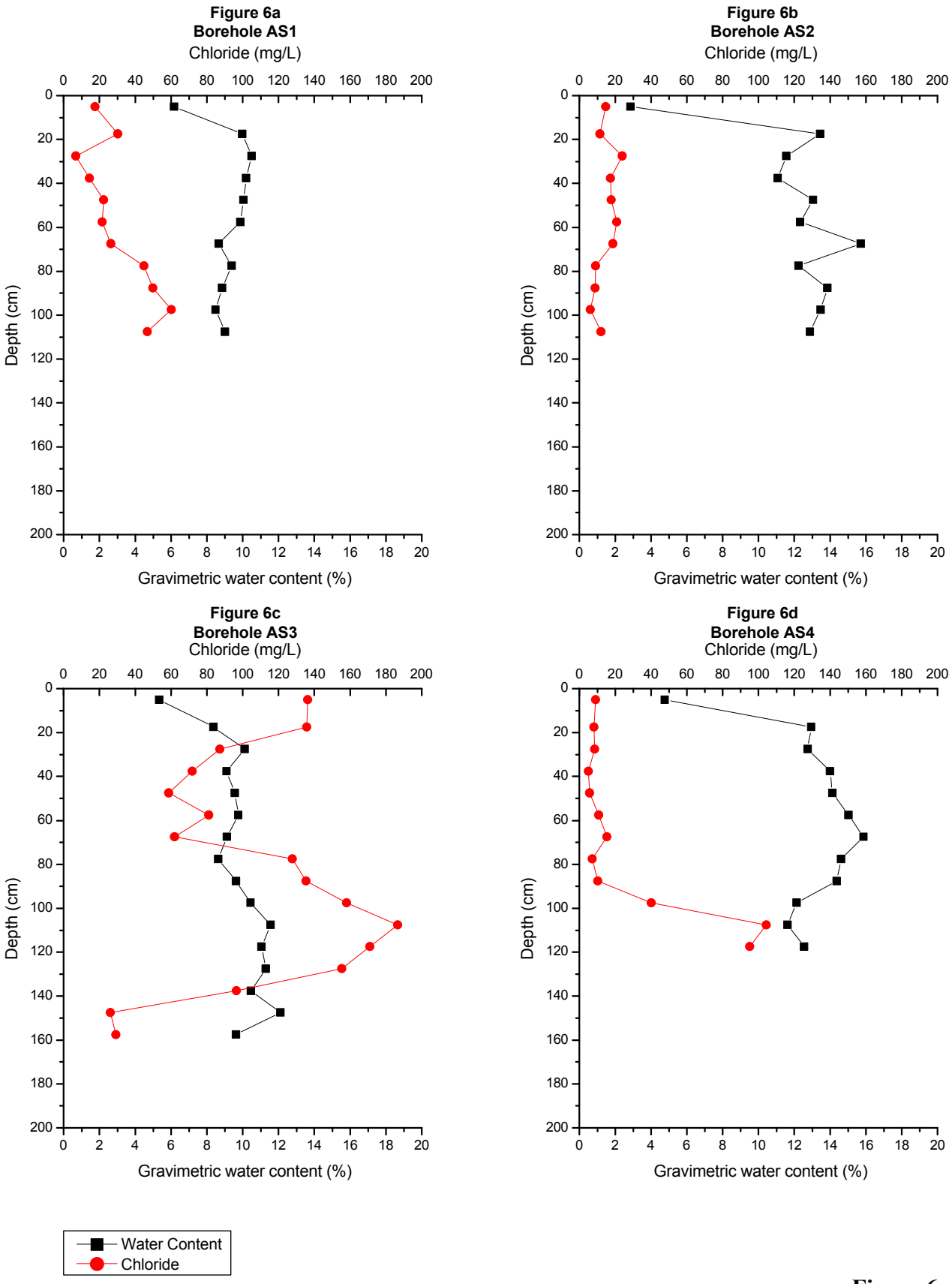

Figure 6
Water Content and Chloride Profiles of 2002 Boreholes Drilled through Asphalt Pads

Figure 7a
Borehole G1

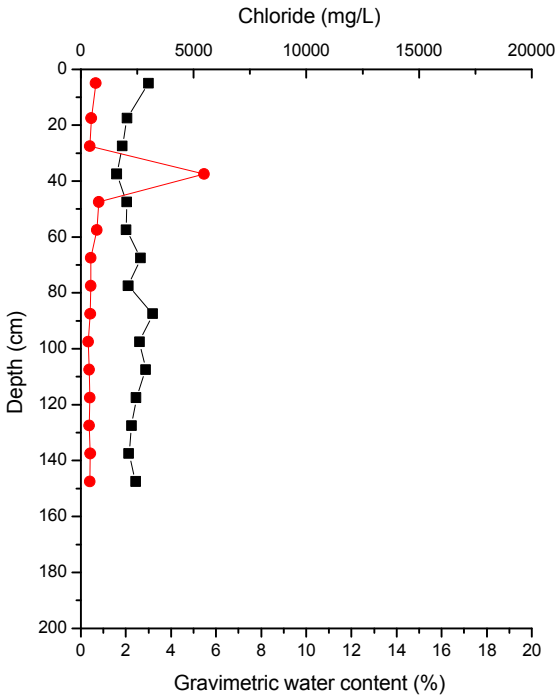

Figure 7b
Borehole G2

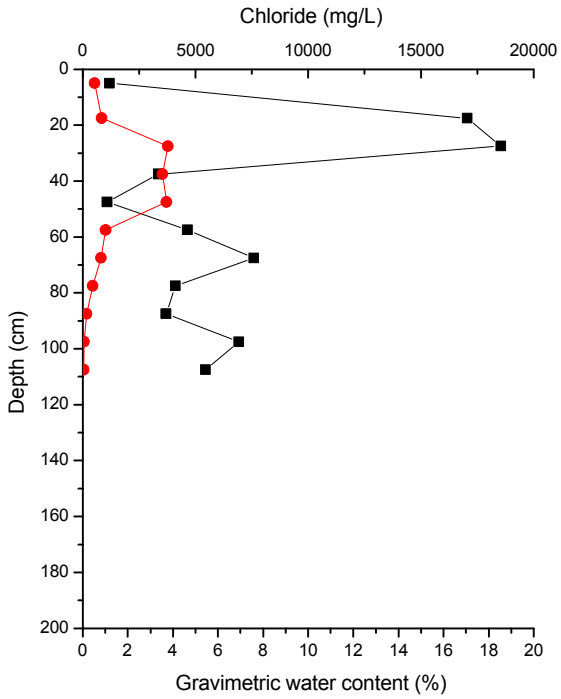

Figure 7c
Borehole G3

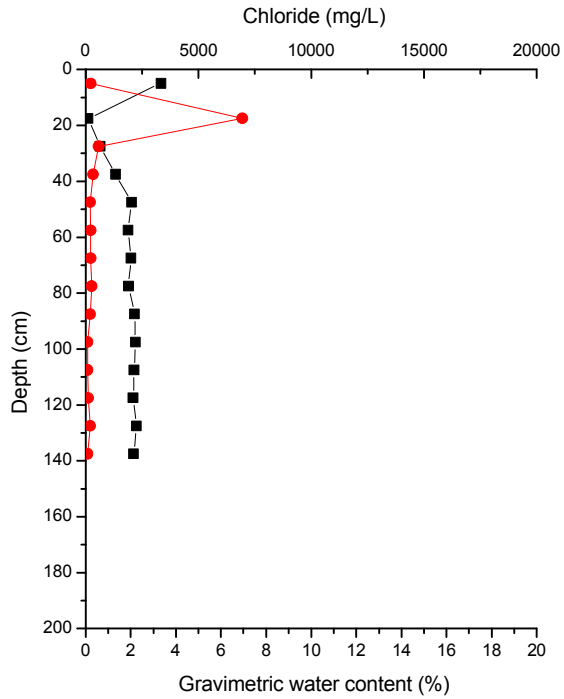

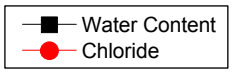

Figure 7
Water Content and Chloride Profiles of 2002 Boreholes Drilled in Unpaved Areas

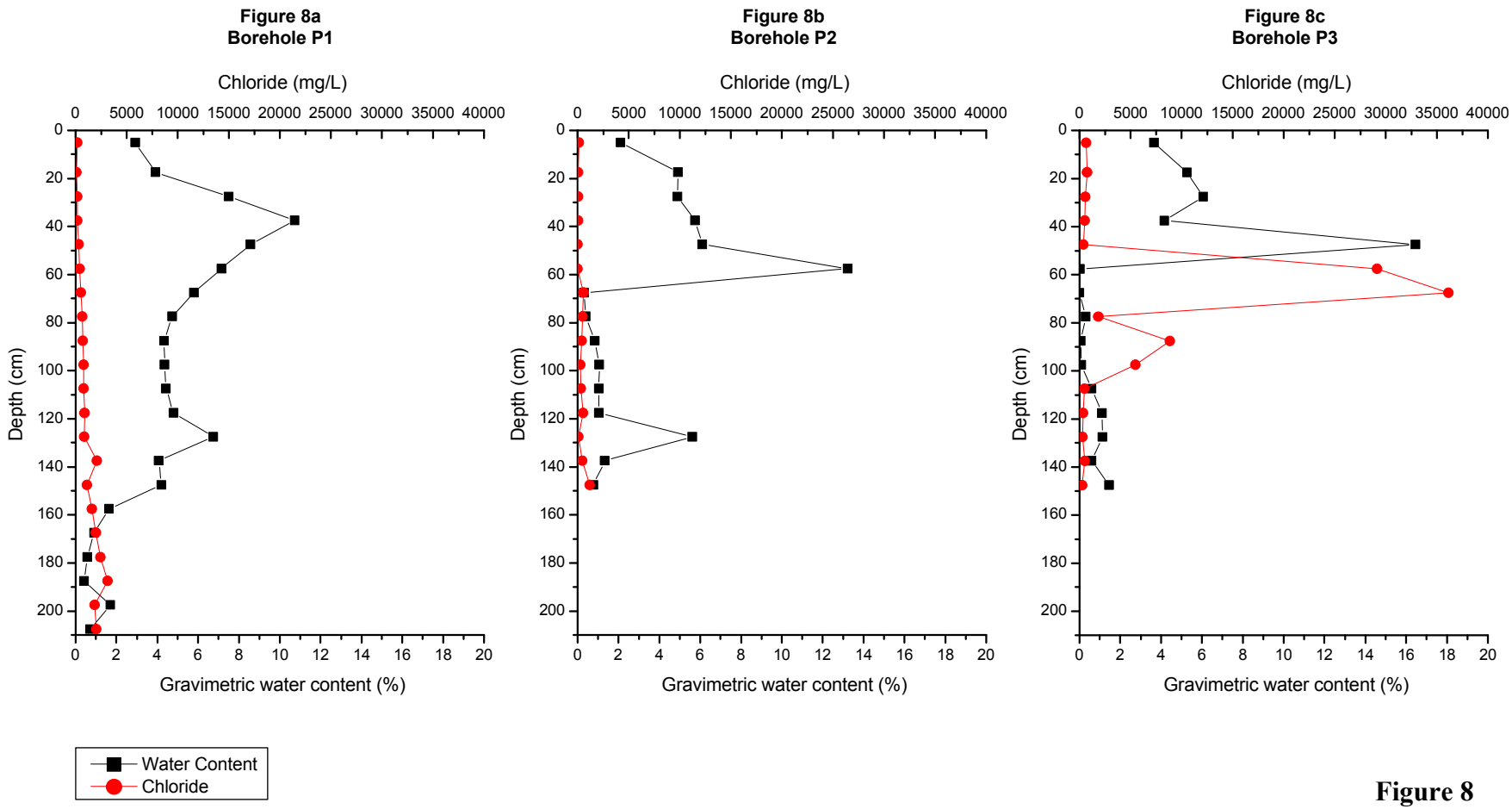

Figure 8
Water Content and Chloride Profiles of 2002 Boreholes Drilled in Piñon Canopy Locations within Zone 4

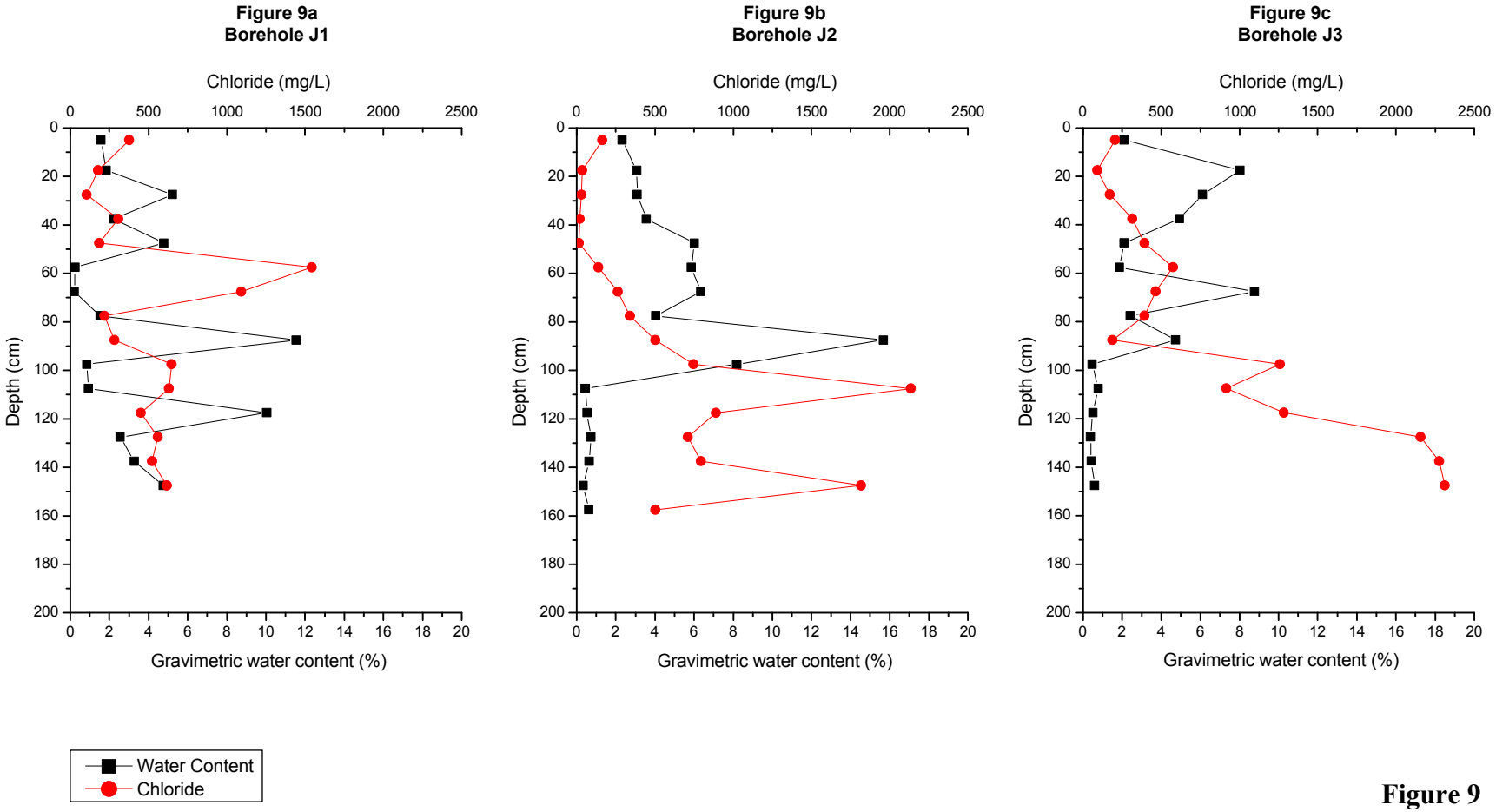

Figure 9
Water Content and Chloride Profiles of 2002 Boreholes Drilled in Juniper Canopy Locations within Zone 4

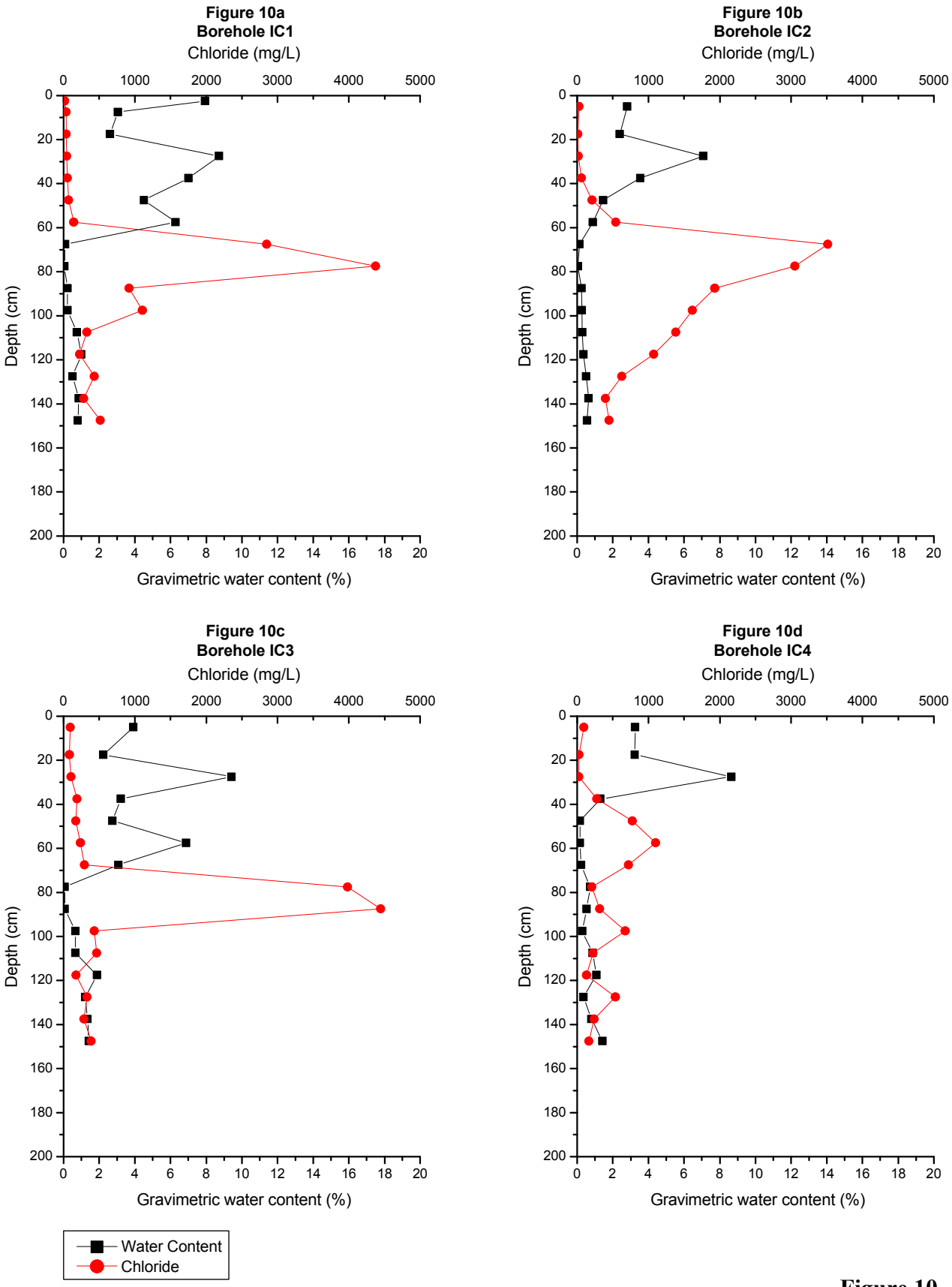

Figure 10
Water Content and Chloride Profiles of 2002 Boreholes Drilled in Intercanopy Locations within Zone 4

Boreholes drilled in paved areas (Figures 5 and 6) have fairly constant chloride profiles (except AS3 and the bottom of AS4). None of these boreholes have chloride concentrations greater than 200 mg/L (200 ppm). Boreholes BT2 and AS3 have the highest chloride concentrations and greatest chloride inventories of all the boreholes drilled in paved areas, which suggests that they are the least affected by paving. Both of these boreholes are on the eastern edge of MDA G. Below 0.1 m (0.33 ft), boreholes BT21, BT30, and AS2 have chloride concentrations of less than 25 mg/L (25 ppm), which is relatively low. Low chloride concentrations are consistent with the relatively high water contents observed for these three boreholes.

Chloride profiles for samples collected from unpaved areas of MDA G in 2002 (Figure 7) have higher concentrations than most of the samples collected from unpaved areas in 1999. All three of the 2002 boreholes drilled in unpaved areas have chloride concentrations greater than 1,000 mg/L (1,000 ppm). Even borehole G2, which has relatively high water content, has high chloride concentrations. Likewise, the chloride profiles of samples from Zone 4 — whether from piñon canopy (Figure 8), juniper canopy (Figure 9), or intercanopy areas (Figure 10) — all have concentrations of more than 1,000 mg/L (1,000 ppm); some depth intervals have extremely high concentrations of more than 1×10^4 mg/L (1×10^4 ppm).

The chloride mass balance method was used to calculate residual (percolation) fluxes for each borehole. The cumulative water and chloride data indicate that the fluxes vary with depth in eight of the boreholes, as shown in Table 2. This type of behavior is not unusual, especially in the root zone (Newman et al., 1997).

3.3 Stable Isotopes

Stable isotope data for boreholes drilled in unpaved areas are fairly similar in that all show well-defined evaporation zones (i.e., heavier or more positive isotopic values) in the top 0.1 m (0.33 ft) (Figures 11 – 16). Stable isotope data for all boreholes drilled through asphalt show that the release of water vapor into the atmosphere by evaporation is either muted or nonexistent (Figures 17 and 18).

Except for boreholes drilled beneath piñon canopy, all shallow 2002 samples from unpaved areas have maximum δD values greater than –20 ‰; in contrast, δD values for samples from 1999 boreholes in unpaved areas are typically less than –20 ‰. The heavier 2002 values likely reflect the high evaporation conditions during the multiyear drought between 2000 and 2002. Boreholes located within the piñon canopy have maximum δD values similar to the 1999 samples, probably because of the canopy shading effects (piñon canopies are generally fuller than juniper canopies, which reduces evaporation).

Table 2
Chloride-Based Flux Estimates

Borehole	Flux 1 Depth Interval (m)	Flux (cm/yr)	Flux 2 Depth Interval (m)	Flux (cm/yr)	Flux 3 Depth Interval (m)	Flux (cm/yr)
7B	0 – 1.6	3.0E-01	---	---	---	---
17B	0 – 0.6	3.0E-01	0.65 – 2	2.0E-02	---	---
21B	0 – 2	9.0E-01	---	---	---	---
Pit2	0 – 0.35	4.0E-01	0.35 – 1	6.0E-02	---	---
Pit17	0 – 0.7	6.0E-01	0.7 – 1	2.0E-01	---	---
Pit24	0 – 1	3.0E-01	---	---	---	---
G1	0 – 1.5	1.0E-02	---	---	---	---
G2 [a]	0 – 0.7	1.0E-02	0.7 – 1.1	3.0E-02	---	---
G3	0 – 1.4	2.0E-02	---	---	---	---
BT2 [a]	0 – 1	1.0E-01	---	---	---	---
BT21 [a]	0 – 2	6.0E-01	---	---	---	---
BT30 [a]	0 – 2	9.0E-01	---	---	---	---
AS1 [a]	0 – 1.1	4.0E-01	---	---	---	---
AS2 [a]	0 – 1.1	7.4E-01	---	---	---	---
AS3 [a]	0 – 1.6	1.0E-01	---	---	---	---
AS4 [a]	0 – 0.9	1.2E+00	0.9 – 1.2	2.0E-01	---	---
P1	0 – 2.1	1.0E-02	---	---	---	---
P2	0 – 1.5	4.0E-02	---	---	---	---
P3	0 – 0.5	2.0E-02	0.5 – 1.5	1.0E-03	---	---
J1	0 – 1.5	2.0E-02	---	---	---	---
J2	0 – 0.5	2.0E-02	0.5 – 1.0	3.2E-02	1.0 – 1.5	1.0E-02
J3	0 – 1.5	1.0E-02	---	---	---	---
IC1	0 – 1.5	2.0E-02	---	---	---	---
IC2	0 – 0.3	2.8E-01	0.3 – 1.5	1.0E-02	---	---
IC3	0 – 1.5	1.0E-02	---	---	---	---
IC4	0 – 1.5	3.0E-02	---	---	---	---

--- = Not applicable

[a] Flux estimates for the boreholes drilled through asphalt and for G2 are highly uncertain.

Figure 11a
Borehole Pit2

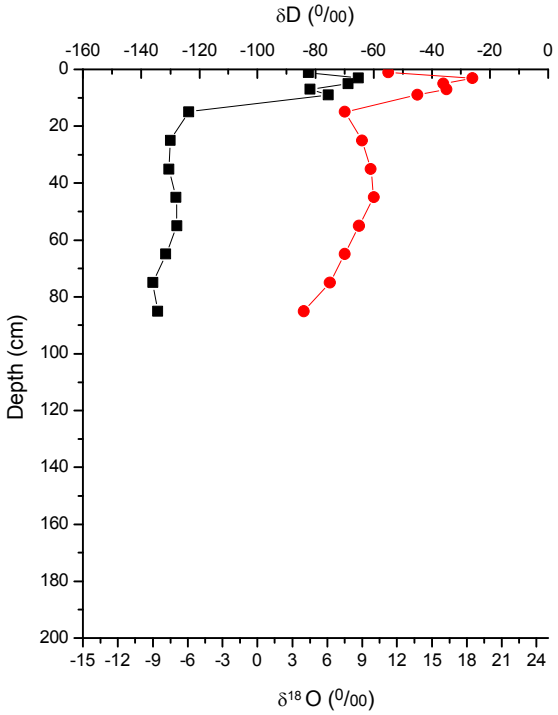

Figure 11b
Borehole Pit17

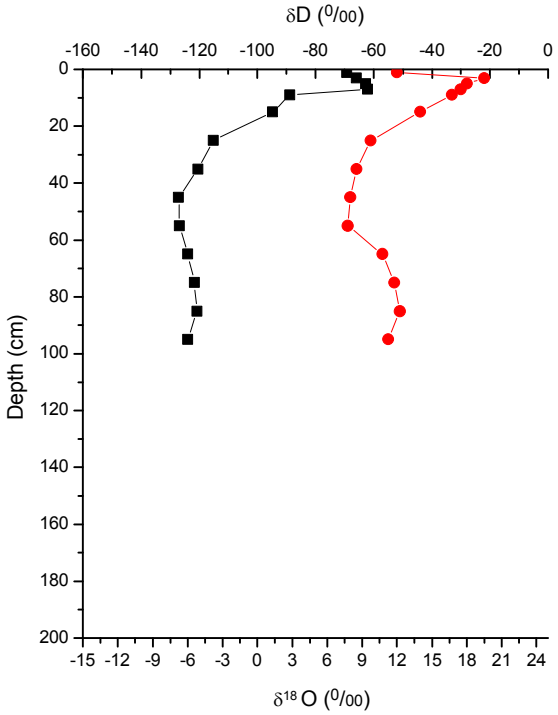

Figure 11c
Borehole Pit24

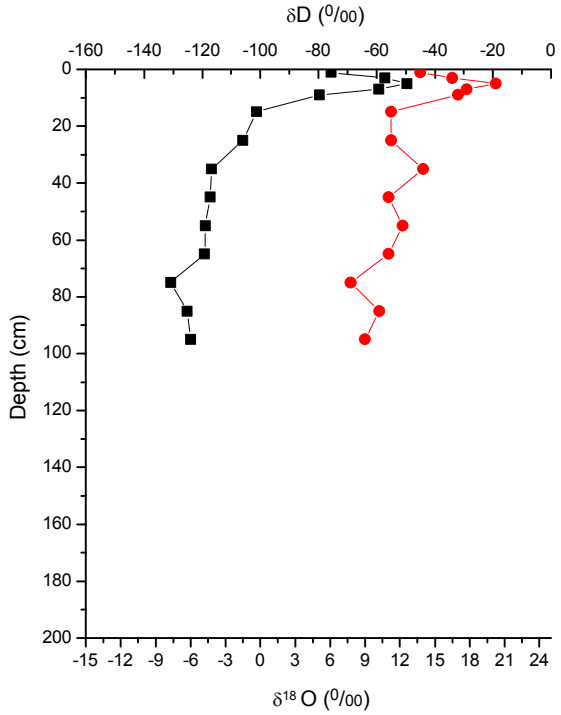

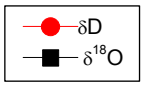

Figure 11
Stable Isotope Ratios in Pore Water of 1999 Boreholes Drilled Into Pit Covers

Figure 12a
Borehole 7B

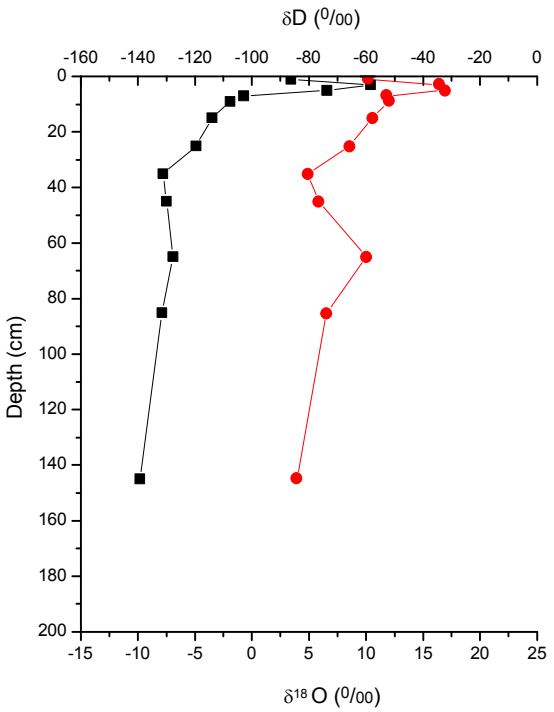

Figure 12b
Borehole 17B

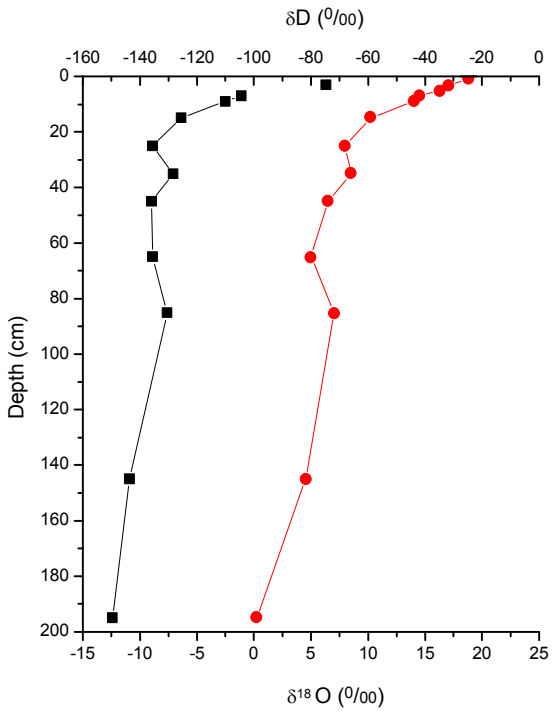

Figure 12c
Borehole 21B

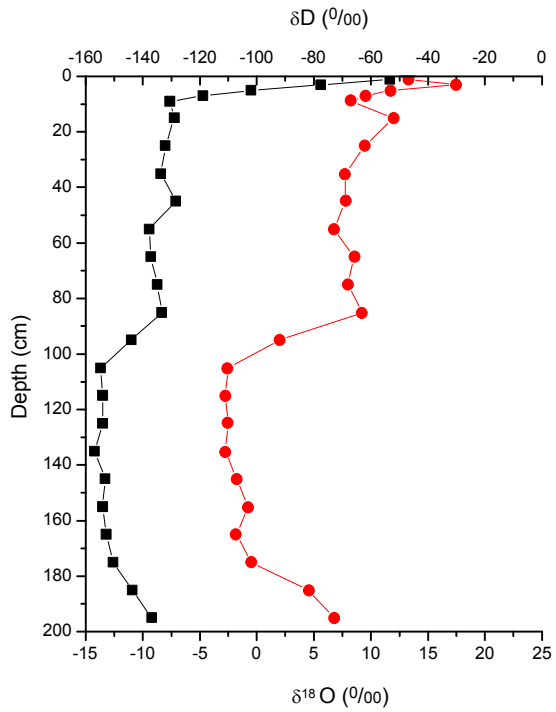

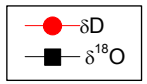

Figure 12
Stable Isotope Ratios in Pore Water of 1999 Boreholes Drilled Adjacent to Pits

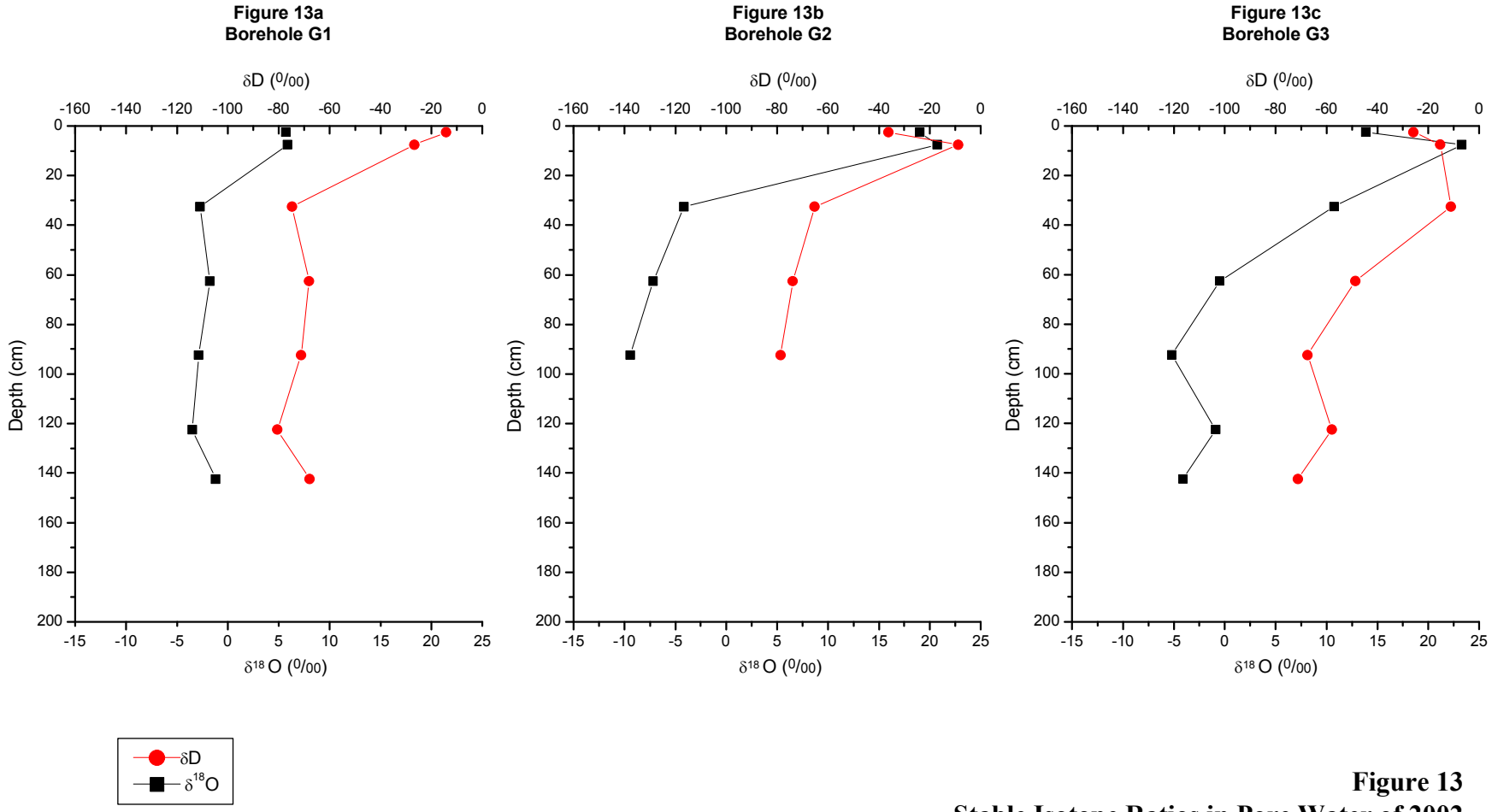

Figure 13
Stable Isotope Ratios in Pore Water of 2002 Boreholes Drilled in Unpaved Areas

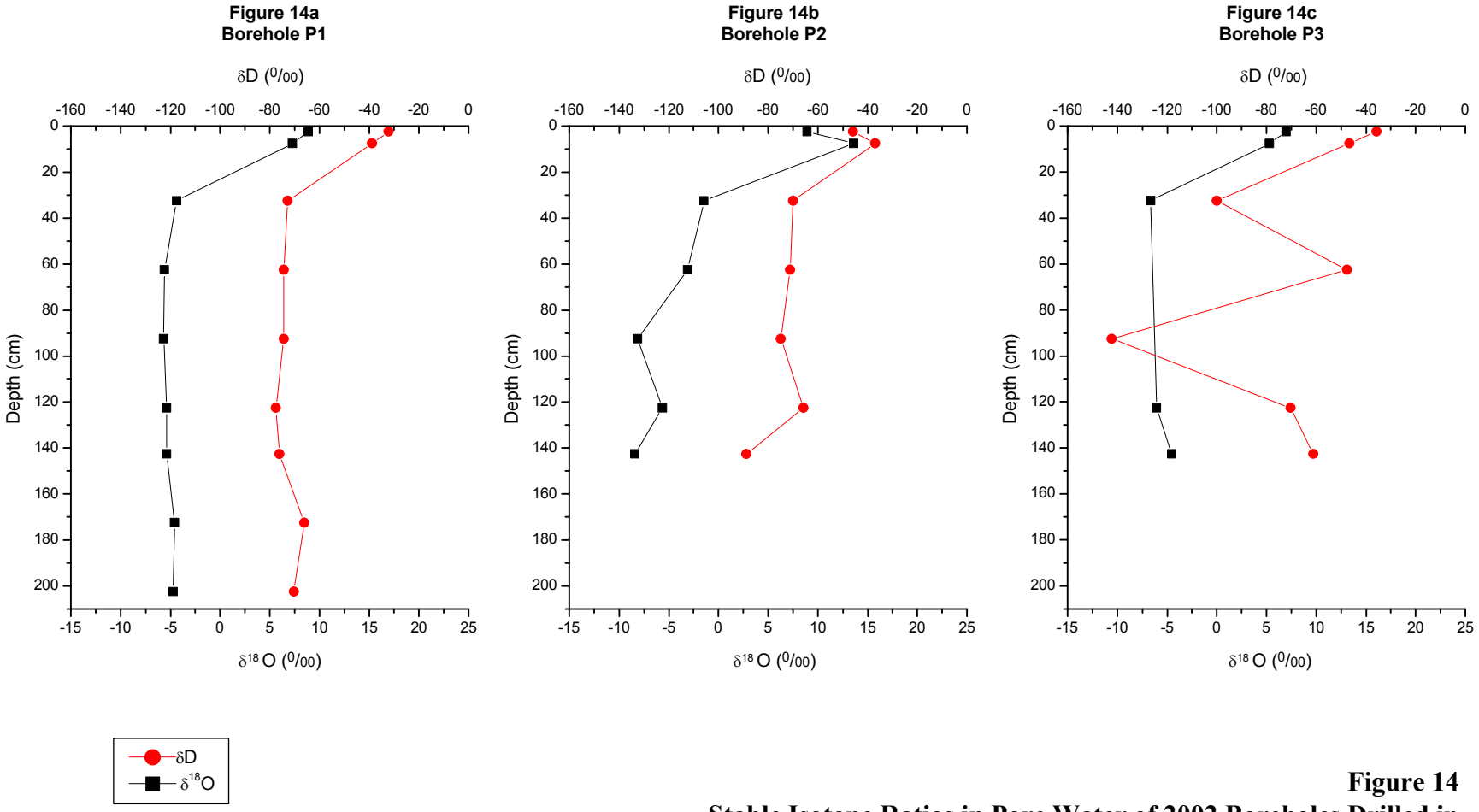

Figure 14
Stable Isotope Ratios in Pore Water of 2002 Boreholes Drilled in Piñon Canopy Locations at Woodland Analog Site within Zone 4

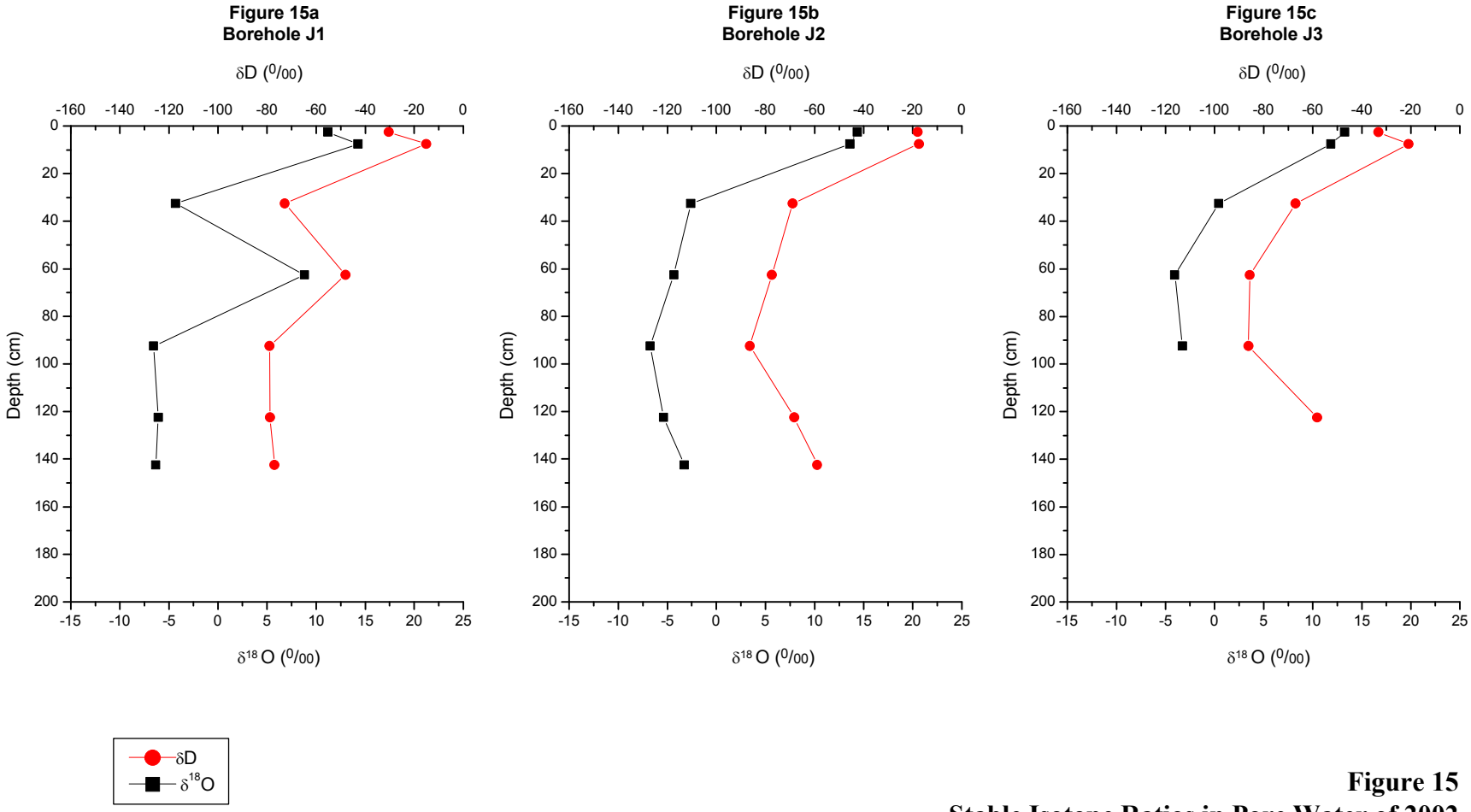

Figure 15
Stable Isotope Ratios in Pore Water of 2002
Boreholes Drilled in Juniper Canopy Locations within Zone 4

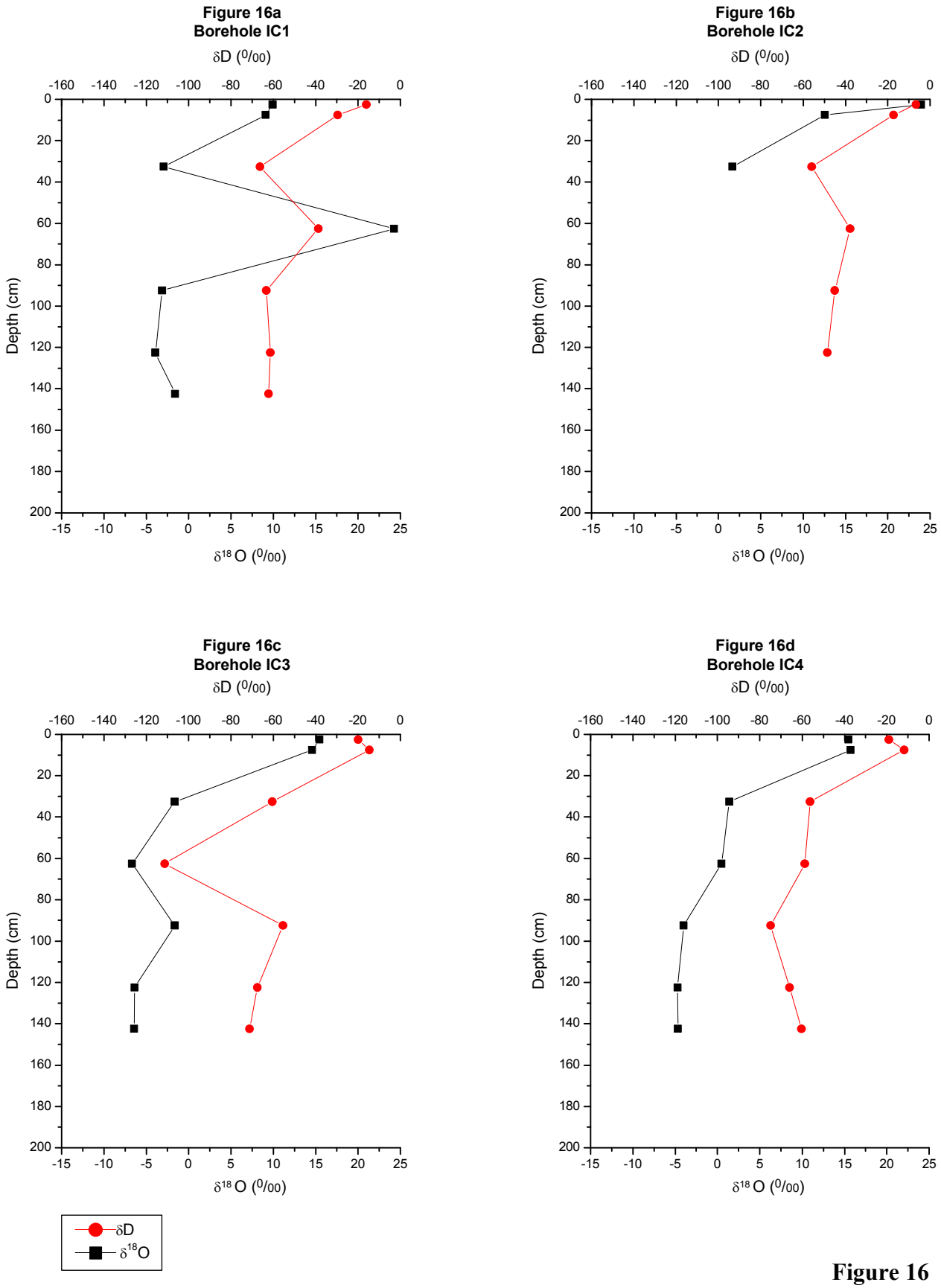

Figure 16
Stable Isotope Ratios in Pore Water of 2002 Boreholes Drilled in Intercanopy Locations within Zone 4

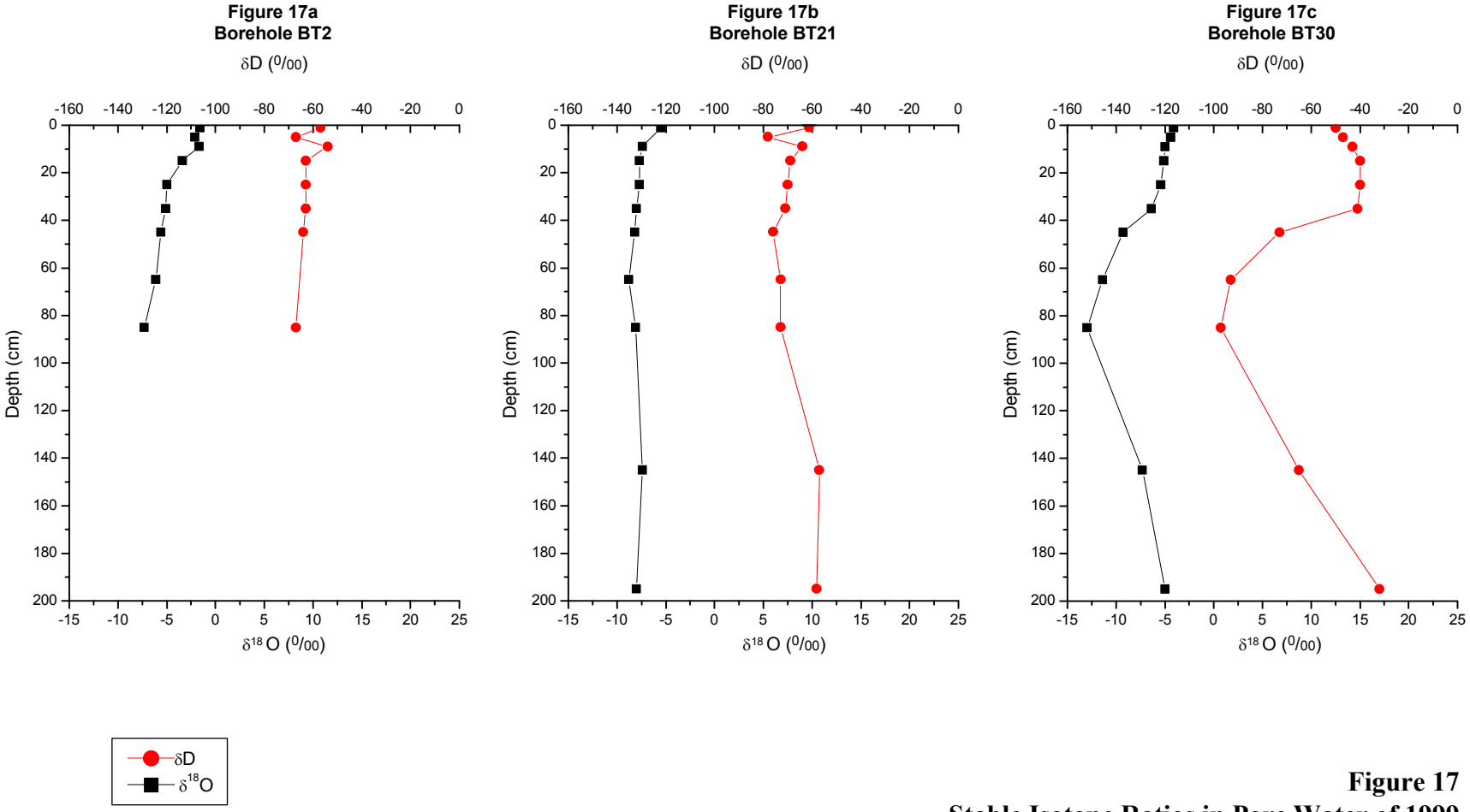

Figure 17
Stable Isotope Ratios in Pore Water of 1999 Boreholes Drilled through Asphalt Pads

Figure 18a
Borehole AS1

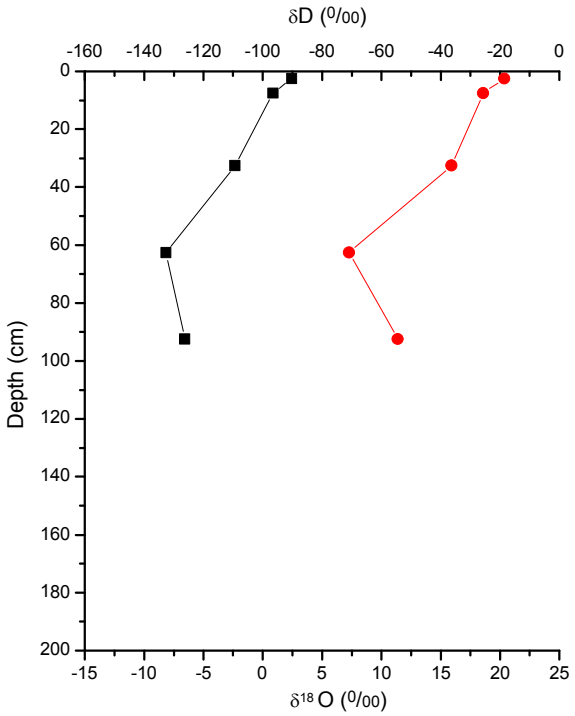

Figure 18b
Borehole AS2

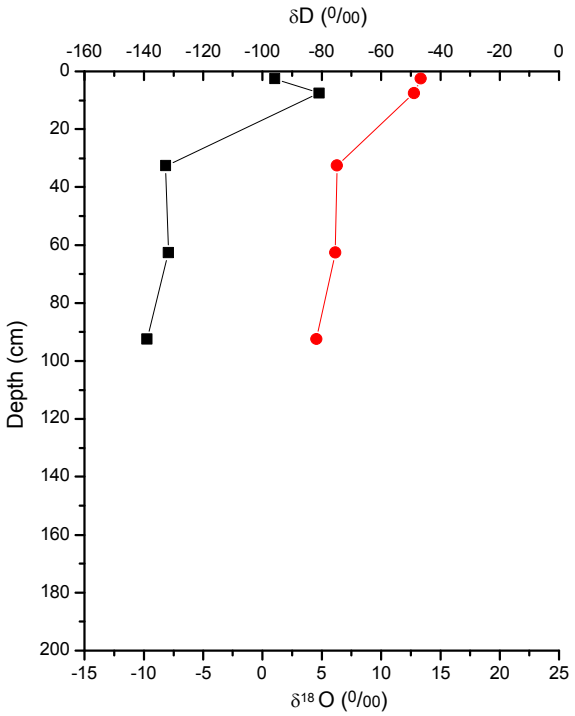

Figure 18c
Borehole AS3

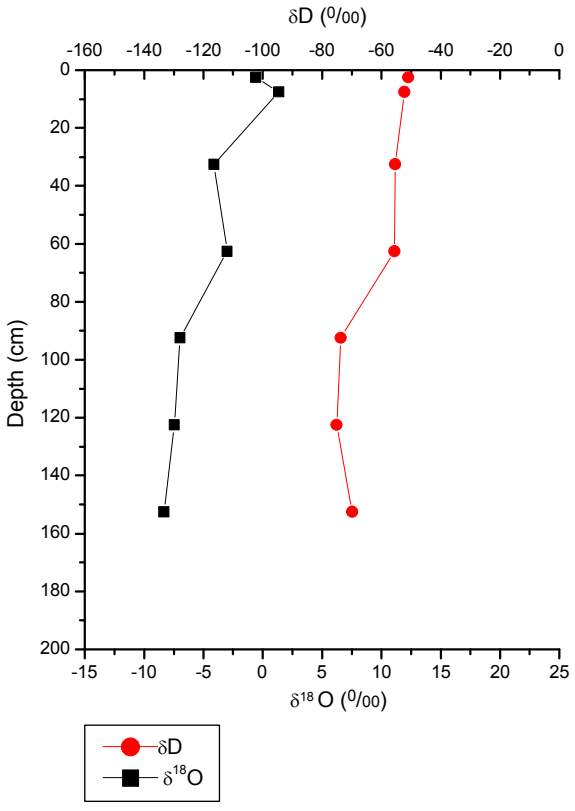

Figure 18d
Borehole AS4

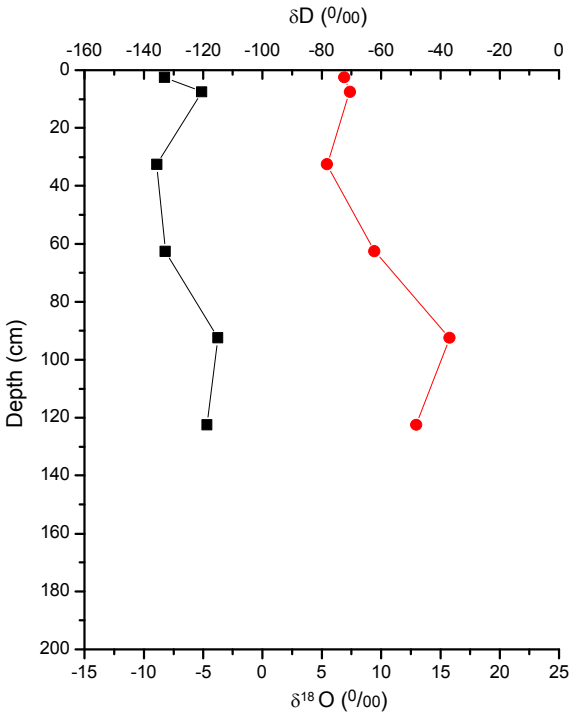

Figure 18
Stable Isotope Ratios in Pore Water of 2002 Boreholes Drilled through Asphalt Pads

Stable isotope profiles for boreholes in active-area unpaved locations (Figures 11 – 16) typically have profiles with shallow, isotopically heavy evaporation bulges that are quite different from the profiles of boreholes drilled through pavement (Figures 17 and 18). This is shown in Figure 19, a meteoric water diagram on which isotopic values from the 1999 boreholes drilled through pit covers and asphalt are plotted against the local meteoric water line of Vuataz and Goff (1986). The local meteoric water line, a benchmark for evaluating evaporation, represents the isotopic composition of precipitation in the Los Alamos area. Isotopic compositions vary along this line because of temperature and other effects. When evaporation occurs, isotopic values increase and fall to the right of the meteoric water line; the difference between the measured values and the meteoric water line indicates the degree of evaporation. Samples from unpaved locations at MDA G plot well to the right of the meteoric water line, which indicates substantial evaporation. Samples from paved locations, however, show little evaporative effect.

3.4 Pressure Head

Most samples used in the 1999 pressure head analyses were too wet for the chilled mirror method and yielded unreliable results; consequently, pressure head was not measured in 2002. The minimum pressure head that can be measured using the chilled-mirror method is about 4,100 cm (1,600 in.). This is indicated as a red dotted line in Figures 20 – 22, which show the pressure head values for the 1999 boreholes. Note that the red line appears at different locations on each of these figures because of the difference in scale.

Because of the wetness of the samples, the only reliable measurements for boreholes drilled into pit covers were from depths of 0.5 m (1.6 ft) or less (Figure 20 and *Attachment I*), where evapotranspiration had depleted the water. Borehole 7B, drilled into unexcavated ground adjacent to pits, showed a similar high-suction (low-water-content) zone near the surface, but boreholes 17B and 21B, also drilled in unexcavated areas, did not. Below 0.8 m (2.6 ft), borehole 17B had pressure heads of around 1×10^4 cm (3,900 in.), which correspond to decreased water content and increased chloride. Borehole 21B was too wet throughout its entire profile to accurately measure the pressure head. Other than thin zones in the top 0.1 m (3.9 in.) of the profiles (and one zone at around 0.45 m [1.5 ft] in borehole BT2), all of the boreholes in paved areas were too wet to reliably determine pressure heads using the chilled mirror method.

3.5 Statistical Analyses

T-tests were used to compare hydrological variables measured (1) in pit covers versus intact adjacent tuff, (2) at paved versus unpaved locations, and (3) under current versus potential postclosure vegetative conditions. Results for the variables used to compare the performance of pit covers and intact tuff are shown in Table 3. Similar statistics for paved and unpaved locations and for the active disposal area and Zone 4 are shown in Tables 4 and 5. Statistical comparisons of samples taken from canopy and intercanopy locations within Zone 4 are shown in Table 6.

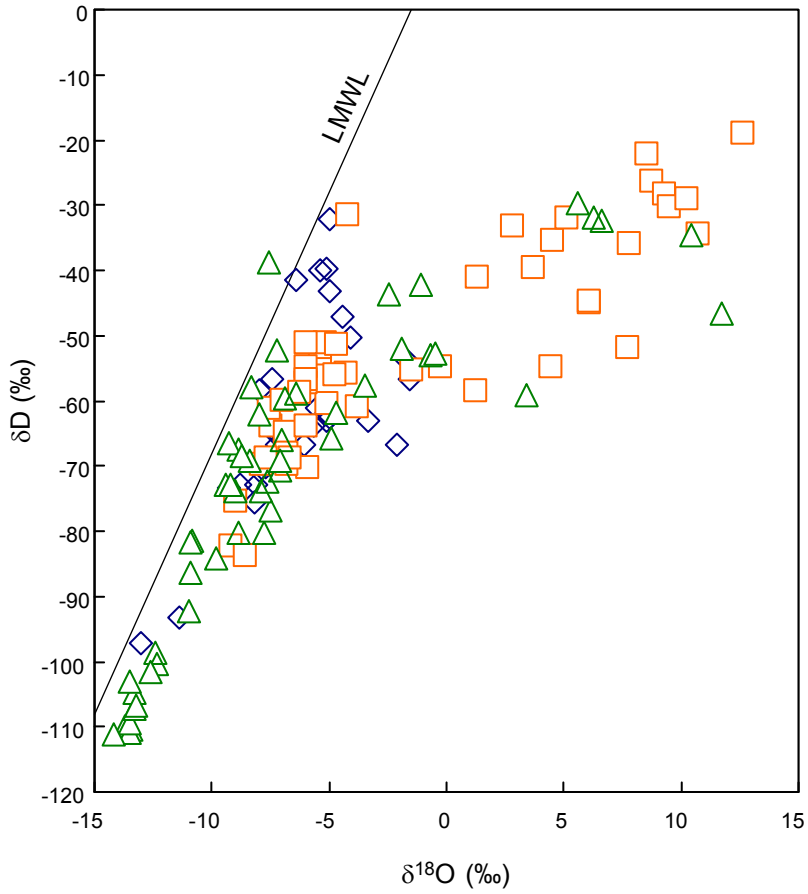

Figure 19
Comparison of Isotopic Ratios in 1999 Boreholes Drilled in Paved and Unpaved Areas

Figure 20a
Borehole Pit2

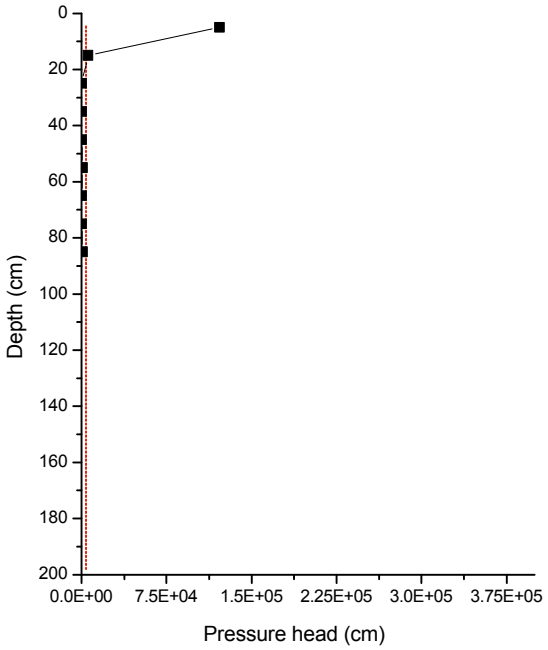

Figure 20b
Borehole Pit17

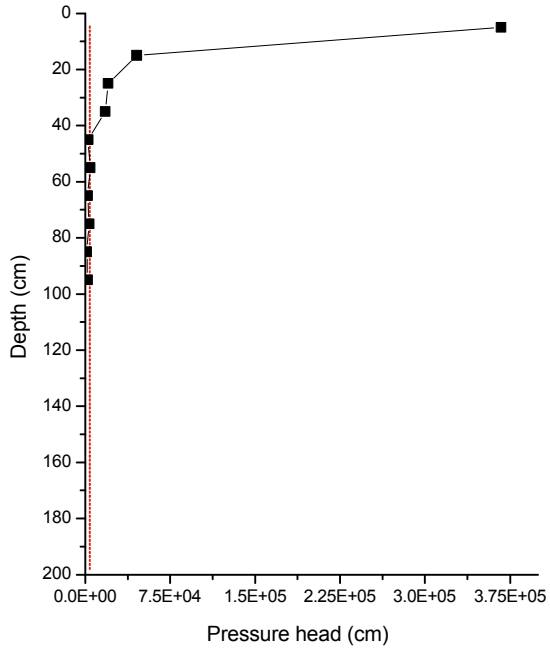

Figure 20c
Borehole Pit24

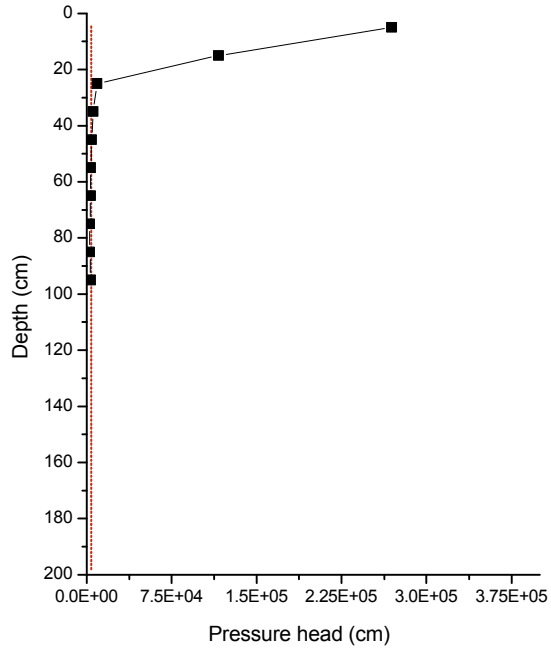

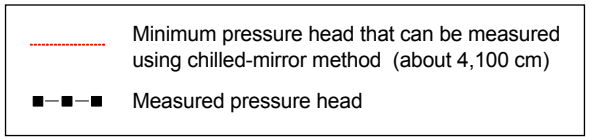

Figure 20
Pressure Head Measurements for 1999 Boreholes Drilled into Pit Covers

Figure 21a
Borehole 7B

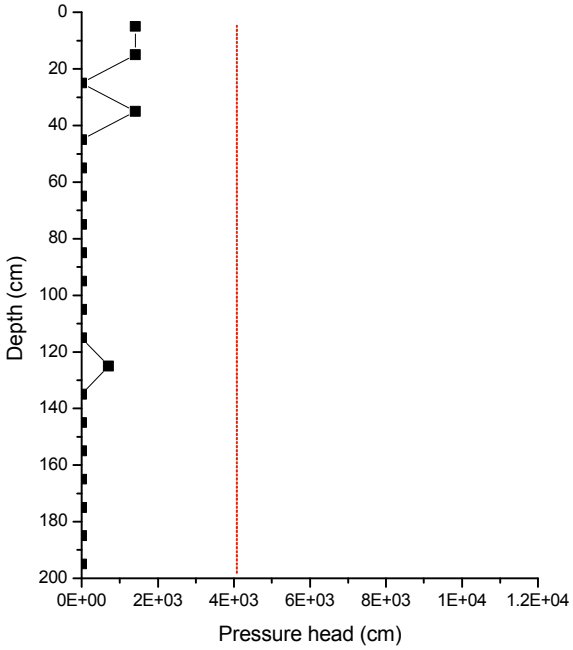

Figure 21b
Borehole 17B

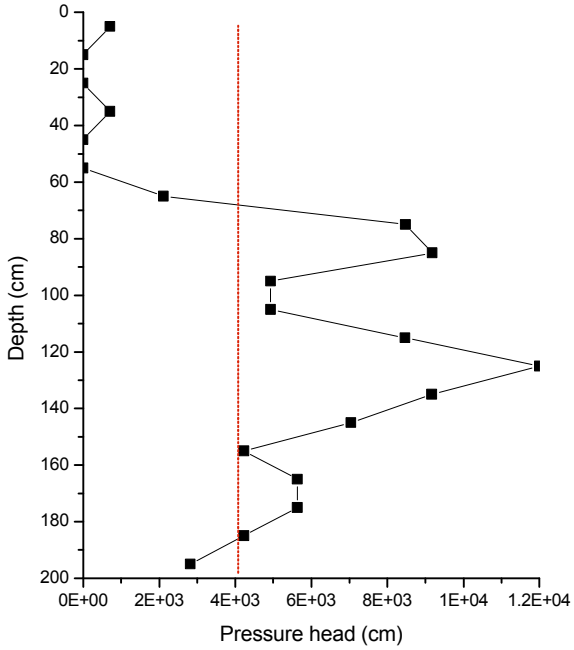

Figure 21c
Borehole 21B

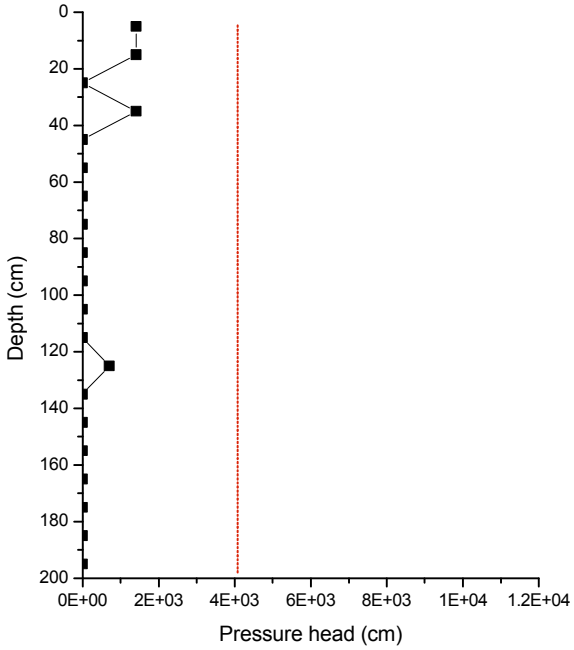

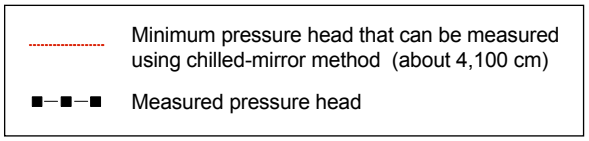

Figure 21
Pressure Head Measurements for 1999 Boreholes Drilled Adjacent to Pits

Figure 22a
Borehole BT2

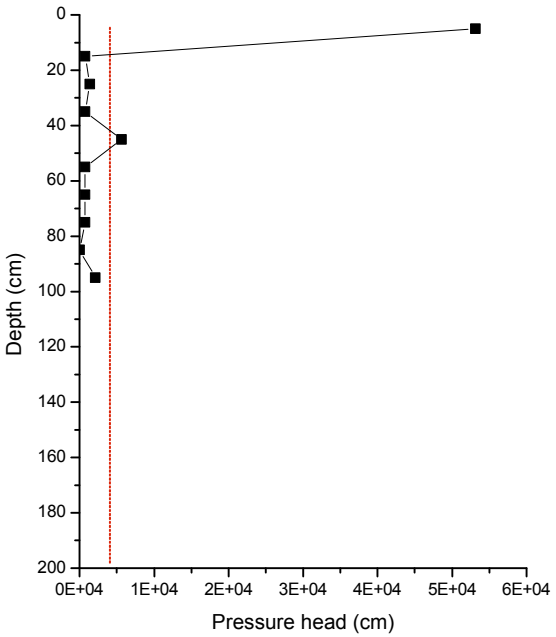

Figure 22b
Borehole BT21

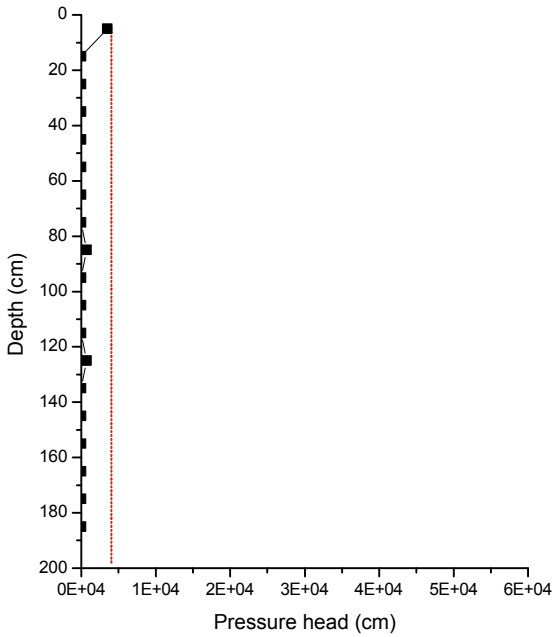

Figure 22c
Borehole BT30

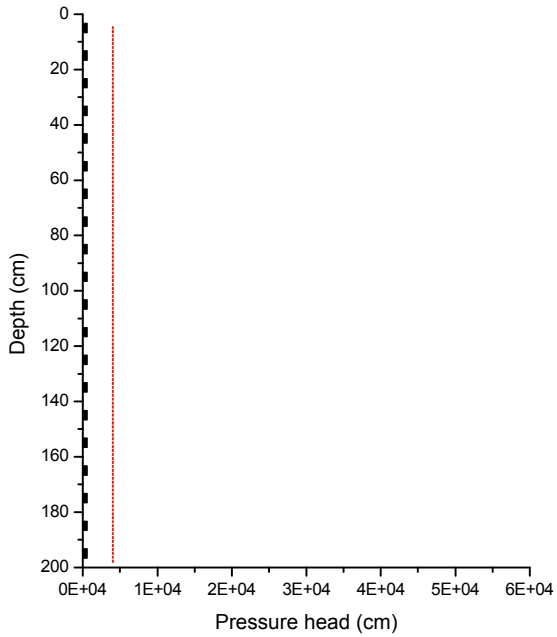

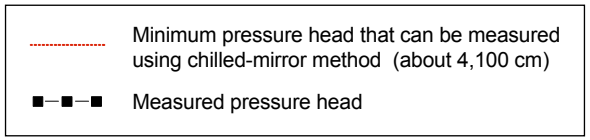

Figure 22
Pressure Head Measurements for 1999 Boreholes Drilled through Asphalt Pads

Table 3
Comparison of T-Test Results for Pit Covers and Unexcavated Locations Adjacent to Pits

Hydrological Variable	Mean Value		T-Test Statistic	Degrees of Freedom	p [a]	Number of Samples [b]		Standard Deviation	
	Adjacent to Pit	Pit				Adjacent to Pit	Pit	Adjacent to Pit	Pit
Water Residence Time at 1-m depth (yr)	5.0E+01	7.0E+01	-3.0E-01	3.0E+00	7.8E-01	2	3	3.9E+01	8.7E+01
Cumulative Water Content at 1-m depth	1.1E-01	4.8E-02	1.9E+00	3.0E+00	1.5E-01	2	3	1.0E-03	4.2E-02
Total Flux (cm/yr) [c]	1.7E-01	2.5E-01	-5.3E-01	3.0E+00	6.3E-01	2	3	2.0E-01	1.6E-01
Flux 1 (cm/yr) [c]	2.9E-01	4.4E-01	-1.0E+00	3.0E+00	3.9E-01	2	3	2.8E-02	2.0E-01
Flux 2 (cm/yr) [c]	1.7E-01	1.9E-01	-1.9E-01	3.0E+00	8.6E-01	2	3	2.0E-01	1.1E-01
Flux 3 (cm/yr) [c]	1.7E-01	1.9E-01	-1.9E-01	3.0E+00	8.6E-01	2	3	2.0E-01	1.1E-01
Average Chloride Content in Top 1 m (mg/L)	6.4E+01	6.2E+01	4.6E-02	3.0E+00	9.7E-01	2	3	5.0E+01	5.0E+01
Maximum Chloride Content in Top 1 m (mg/L)	1.4E+02	1.4E+02	4.7E-02	3.0E+00	9.7E-01	2	3	1.1E+02	8.7E+01
Average Nitrate Content in Top 1 m (mg/L)	6.4E+01	5.8E+01	8.5E-02	3.0E+00	9.4E-01	2	3	8.6E+01	8.9E+01
Maximum Nitrate Content in Top 1 m (mg/L)	2.7E+02	3.1E+02	-8.4E-02	3.0E+00	9.4E-01	2	3	3.6E+02	4.9E+02
Average $\delta^{18}O$ in Top 1 m (‰)	-3.4E+00	-7.7E-01	-1.8E+00	3.0E+00	1.8E-01	2	3	2.2E+00	1.3E+00
Maximum $\delta^{18}O$ in Top 1 m (‰)	8.3E+00	1.0E+01	-8.9E-01	3.0E+00	4.4E-01	2	3	2.9E+00	2.1E+00
Average δD in Top 1 m (‰)	-5.6E+01	-5.1E+01	-1.2E+00	3.0E+00	3.2E-01	2	3	3.1E+00	5.2E+00
Maximum δD in Top 1 m (‰)	-2.9E+01	-2.2E+01	-1.7E+00	3.0E+00	1.9E-01	2	3	5.0E+00	3.6E+00
Average θg in Top 1 m (%)	7.7E+00	7.1E+00	2.4E-01	3.0E+00	8.2E-01	2	3	2.4E-01	3.0E+00
Maximum θg in Top 1 m (%)	1.2E+01	9.3E+00	7.7E-01	3.0E+00	5.0E-01	2	3	3.1E+00	4.2E+00

$\delta^{18}O$= Delta oxygen-18 value δD= Delta deuterium value θg = Gravimetric water content

[a] Probability value used in the T-test approach to determine significance of differences
[b] Samples from borehole 21B were not considered valid because of excessive water content due to its location near an asphalt pad.

[c] Total flux represents the average chloride content from the entire borehole. For boreholes that displayed varying flux with depth (see Table 2), Flux 1 refers to the flux in the shallow region, Flux 2 refers to the flux in the intermediate region, and Flux 3 refers to the flux in the deepest region .

Table 4
Comparison of T-Test Results for Paved and Unpaved Locations

Hydrological Variable	Mean Value		T-Test Statistic	Degrees of Freedom	p [a]	Number of Samples [b]		Standard Deviation	
	Paved	Unpaved				Paved	Unpaved	Paved	Unpaved
Water Residence Time at 1-m depth (yr)	4.2E+01	2.0E+02	-1.1E+00	2.3E+01	2.6E-01	7	18	3.7E+01	3.5E+02
Water Residence Time 1 at 5-m depth (yr)	9.3E+01	2.0E+02	-1.0E+00	1.5E+01	3.4E-01	3	14	1.1E+02	1.7E+02
Cumulative Water Content at 1-m depth	1.5E-01	5.9E-02	5.8E+00	2.3E+01	0.0E+00	7	18	4.4E-02	3.0E-02
Cumulative Water Content at 1.5-m depth	2.4E-01	7.4E-02	6.3E+00	1.5E+01	0.0E+00	3	14	5.8E-02	3.9E-02
Total Flux (cm/yr) [c]	4.6E-01	7.3E-02	4.7E+00	2.3E+01	0.0E+00	7	18	3.0E-01	1.2E-01
Flux 1 (cm/yr) [c]	5.8E-01	1.6E-01	3.6E+00	2.3E+01	2.0E-03	7	18	4.1E-01	1.8E-01
Flux 2 (cm/yr) [c]	4.5E-01	6.4E-02	4.8E+00	2.3E+01	0.0E+00	7	18	3.1E-01	9.9E-02
Flux 3 (cm/yr) [c]	4.5E-01	6.2E-02	4.8E+00	2.3E+01	0.0E+00	7	18	3.1E-01	1.0E-01
Average Chloride Content in Top 1 m (mg/L)	3.8E+01	9.7E+02	-1.3E+00	2.3E+01	2.2E-01	7	18	3.7E+01	1.9E+03
Average Chloride Content in Top 1.5 m (mg/L)	4.7E+01	9.8E+02	-1.1E+00	1.5E+01	2.9E-01	3	14	5.7E+01	1.4E+03
Maximum Chloride Content in Top 1 m (mg/L)	7.4E+01	3.9E+03	-1.2E+00	2.3E+01	2.4E-01	7	18	6.0E+01	8.3E+03
Maximum Chloride Content in Top 1.5 m (mg/L)	8.7E+01	5.1E+03	-9.3E-01	1.5E+01	3.7E-01	3	14	8.7E+01	9.1E+03
Average Nitrate Content in Top 1 m (mg/L)	8.6E+01	8.2E+01	5.1E-02	2.3E+01	9.6E-01	7	18	1.1E+02	2.2E+02
Average Nitrate Content in Top 1.5 m (mg/L)	7.2E+01	7.0E+01	1.7E-02	1.5E+01	9.9E-01	3	14	6.0E+01	1.8E+02
Maximum Nitrate Content in Top 1 m (mg/L)	1.6E+02	6.6E+02	-6.0E-01	2.3E+01	5.6E-01	7	18	1.8E+02	2.2E+03
Maximum Nitrate Content in Top 1.5 m (mg/L)	1.8E+02	7.8E+02	-4.0E-01	1.5E+01	6.9E-01	3	14	1.7E+02	2.5E+03

$\delta^{18}O$= Delta oxygen-18 value δD= Delta deuterium value θg = Gravimetric water content

[a] Probability value used in the T-test approach to determine significance of differences

[b] Samples from borehole 21B were not considered valid because of excessive water content due to its location near an asphalt pad.

[c] Total flux represents the average chloride content from the entire borehole. For boreholes that displayed varying flux with depth (see Table 2), Flux 1 refers to the flux in the shallow region, Flux 2 refers tp the flux in the intermediate region, and Flux 3 refers to the flux in the deepest region.

***Bold** indicates variables are significantly different.*

Table 4 (Continued)
Comparison of T-Test Results for Paved and Unpaved Locations

Hydrological Variable	Mean Value		T-Test Statistic	Degrees of Freedom	p [a]	Number of Samples [b]		Standard Deviation	
	Paved	Unpaved				Paved	Unpaved	Paved	Unpaved
Average $\delta^{18}O$ in Top 1 m (‰)	-5.0E+00	2.2E+00	-4.5E+00	2.3E+01	0.0E+00	7	18	2.1E+00	4.0E+00
Average $\delta^{18}O$ in Top 1.5 m (‰)	-6.3E+00	1.3E+00	-3.0E+00	1.5E+01	1.0E-02	3	14	1.9E+00	4.3E+00
Maximum $\delta^{18}O$ in Top 1 m (‰)	-9.1E-01	1.3E+01	-6.6E+00	2.3E+01	0.0E+00	7	18	3.8E+00	5.1E+00
Maximum $\delta^{18}O$ in Top 1.5 m (‰)	-2.8E+00	1.3E+01	-5.0E+00	1.5E+01	0.0E+00	3	14	3.6E+00	5.2E+00
Average δD in Top 1 m (‰)	-6.0E+01	-5.2E+01	-1.6E+00	2.3E+01	1.3E-01	7	18	9.2E+00	1.1E+01
Average δD in Top 1.5 m (‰)	-6.3E+01	-5.4E+01	-1.2E+00	1.5E+01	2.6E-01	3	14	5.2E+00	1.3E+01
Maximum δD in Top 1 m (‰)	-4.4E+01	-1.6E+01	-3.0E+00	2.3E+01	7.0E-03	7	18	1.4E+01	2.3E+01
Maximum δD in Top 1.5 m (‰)	-4.9E+01	-1.5E+01	-2.2E+00	1.5E+01	4.7E-02	3	14	8.6E+00	2.7E+01
Average θg in Top 1 m (%)	1.1E+01	4.7E+00	5.1E+00	2.3E+01	0.0E+00	7	18	3.1E+00	2.4E+00
Average θg in Top 1.5 m (%)	1.2E+01	3.5E+00	6.2E+00	1.5E+01	0.0E+00	3	14	3.0E+00	1.9E+00
Maximum θg in Top 1 m (%)	1.3E+01	1.0E+01	1.4E+00	2.3E+01	1.9E-01	7	18	4.0E+00	4.3E+00
Maximum θg in Top 1.5 m (%)	1.5E+01	1.0E+01	1.8E+00	1.5E+01	8.9E-02	3	14	3.2E+00	4.0E+00

$\delta^{18}O$= Delta oxygen-18 value δD= Delta deuterium value θg = Gravimetric water content

[a] *Probability value used in the T-test approach to determine significance of differences*

[b] *Samples from borehole 21B were not considered valid because of excessive water content due to its location near an asphalt pad.*

[c] Total flux represents the average chloride content from the entire borehole. For boreholes that displayed varying flux with depth (see Table 2), Flux 1 refers to the flux in the shallow region, Flux 2 refers to the flux in the intermediate region, and Flux 3 refers to the flux in the deepest region.

Bold *indicates variables are significantly different.*

Table 5
Comparison of T-Test Results for Unpaved Portions of Active Disposal Area and Zone 4

Hydrological Variable	Mean Value		T-Test Statistic	Degrees of Freedom	p [a]	Number of Valid Samples [b]		Standard Deviation	
	Active Area	Zone 4				Active Area	Zone 4	Active Area	Zone 4
Water Residence Time at 1-m depth (yr)	2.8E+02	1.4E+02	8.3E-01	1.6E+01	4.2E-01	8	10	5.2E+02	1.1E+02
Water Residence Time at 1.5-m depth (yr)	1.6E+02	2.1E+02	-4.4E-01	1.2E+01	6.7E-01	4	10	1.3E+02	1.9E+02
Cumulative Water Content at 1-m depth	6.5E-02	5.4E-02	7.7E-01	1.6E+01	4.5E-01	8	10	4.1E-02	2.0E-02
Cumulative Water Content at 1.5-m depth	9.5E-02	6.5E-02	1.3E+00	1.2E+01	2.2E-01	4	10	6.1E-02	2.7E-02
Total Flux (cm/yr) [c]	1.4E-01	1.7E-02	2.5E+00	1.6E+01	2.4E-02	8	10	1.6E-01	1.0E-02
Flux 1 (cm/yr) [c]	2.4E-01	9.8E-02	1.8E+00	1.6E+01	8.9E-02	8	10	2.3E-01	9.9E-02
Flux 2 (cm/yr) [c]	1.2E-01	1.8E-02	2.6E+00	1.6E+01	2.0E-02	8	10	1.3E-01	1.0E-02
Flux 3 (cm/yr) [c]	1.2E-01	1.4E-02	2.7E+00	1.6E+01	1.7E-02	8	10	1.3E-01	1.0E-02
Average Chloride Content in Top 1 m (mg/L)	4.7E+02	1.4E+03	-9.8E-01	1.6E+01	3.4E-01	8	10	5.8E+02	2.5E+03
Average Chloride Content Top 1.5 m (mg/L)	4.6E+02	1.2E+03	-8.5E-01	1.2E+01	4.1E-01	4	10	3.6E+02	1.6E+03
Maximum Chloride Content in Top 1 m (mg/L)	2.1E+03	5.4E+03	-8.2E-01	1.6E+01	4.2E-01	8	10	2.8E+03	1.1E+04
Maximum Chloride Content in Top 1.5 m (mg/L)	3.4E+03	5.8E+03	-4.3E-01	1.2E+01	6.7E-01	4	10	3.3E+03	1.1E+04
Average Nitrate Content in Top 1 m (mg/L)	1.7E+02	1.0E+01	1.6E+00	1.6E+01	1.4E-01	8	10	3.3E+02	1.3E+01
Average Nitrate Content in Top 1.5 m (mg/L)	2.2E+02	9.6E+00	2.3E+00	1.2E+01	4.3E-02	4	10	3.2E+02	1.1E+01
Maximum Nitrate Content in Top 1 m (mg/L)	1.4E+03	5.1E+01	1.3E+00	1.6E+01	2.0E-01	8	10	3.3E+03	6.1E+01
Maximum Nitrate Content in Top 1.5 m (mg/L)	2.6E+03	5.5E+01	1.9E+00	1.2E+01	8.6E-02	4	10	4.6E+03	6.0E+01

$\delta^{18}O$= Delta oxygen-18 value δD= Delta deuterium value θg = Gravimetric water content

[a] *Probability value used in the T-test approach to determine significance of differences*

[b] *Samples from borehole 21B were not considered valid because of excessive water content due to its location near an asphalt pad.*

[c] Total flux represents the average chloride content from the entire borehole. For boreholes that displayed varying flux with depth (see Table 2), Flux 1 indicates the flux in the shallow region, Flux 2 indicates the flux in the intermediate region, and Flux 3 indicates flux in the deepest region.

***Bold** indicates variables are significantly different.*

Table 5 (Continued)
Comparison of T-Test Results for Unpaved Portions of Active Disposal Area and Zone 4

Hydrological Variable	Mean Value		T-Test Statistic	Degrees of Freedom	p [a]	Number of Valid Samples [b]		Standard Deviation	
	Active Area	Zone 4				Active Area	Zone 4	Active Area	Zone 4
Average $\delta^{18}O$ in Top 1 m (‰)	6.0E-01	3.6E+00	-1.6E+00	1.6E+01	1.2E-01	8	10	4.1E+00	3.6E+00
Average $\delta^{18}O$ in Top 1.5 m (‰)	-7.4E-01	2.1E+00	-1.1E+00	1.2E+01	2.8E-01	4	10	4.6E+00	4.1E+00
Maximum $\delta^{18}O$ in Top 1 m (‰)	1.3E+01	1.4E+01	-2.9E-01	1.6E+01	7.7E-01	8	10	6.0E+00	4.7E+00
Maximum $\delta^{18}O$ in Top 1.5 m (‰)	1.3E+01	1.4E+01	-2.2E-01	1.2E+01	8.3E-01	4	10	7.3E+00	4.7E+00
Average δD in Top 1 m (‰)	-4.9E+01	-5.5E+01	1.2E+00	1.6E+01	2.6E-01	8	10	1.2E+01	9.6E+00
Average δD in Top 1.5 m (‰)	-4.9E+01	-5.7E+01	9.8E-01	1.2E+01	3.5E-01	4	10	1.8E+01	1.0E+01
Maximum δD in Top 1 m (‰)	-9.6E+00	-2.1E+01	1.0E+00	1.6E+01	3.3E-01	8	10	3.3E+01	1.1E+01
Maximum δD in Top 1.5 m (‰)	-1.6E-01	-2.1E+01	1.4E+00	1.2E+01	2.0E-01	4	10	4.8E+01	1.1E+01
Average θg in Top 1 m (%)	6.0E+00	3.8E+00	2.1E+00	1.6E+01	5.1E-02	8	10	2.9E+00	1.4E+00
Average θg in Top 1.5 m (%)	4.6E+00	3.1E+00	1.4E+00	1.2E+01	1.8E-01	4	10	2.9E+00	1.2E+00
Maximum θg in Top 1 m (%)	9.6E+00	1.1E+01	-6.7E-01	1.6E+01	5.2E-01	8	10	5.6E+00	3.2E+00
Maximum θg in Top 1.5 m (%)	7.7E+00	1.1E+01	-1.5E+00	1.2E+01	1.7E-01	4	10	5.4E+00	3.2E+00

$\delta^{18}O$= Delta oxygen-18 value δD= Delta deuterium value θg = Gravimetric water content

[a] *Probability value used in the T-test approach to determine significance of differences*

[b] *Samples from borehole 21B were not considered valid because of excessive water content due to its location near an asphalt pad.*

[c] Total flux represents the average chloride content from the entire borehole. For boreholes that displayed varying flux with depth (see Table 2), Flux 1 refers to the flux in the shallow region, Flux 2 refers to the flux in the intermediate region, and Flux 3 refers to the flux in the deepest region.

Bold *indicates variables are significantly different.*

Table 6
Comparison of T-Test Results for Zone 4 Canopy and Intercanopy Locations

Hydrological Variable	Mean		T-Test Statistic	Degrees of Freedom	p [a]	Number of Valid Samples [b]		Standard Deviation	
	Inter-canopy	Canopy				Inter-canopy	Canopy	Inter-canopy	Canopy
Water Residence Time at 1-m depth (yr)	4.9E+01	1.9E+02	-2.5E+00	8.0E+00	3.8E-02	4	6	2.4E+01	1.1E+02
Water Residence Time at 1.5-m depth (yr)	7.1E+01	3.0E+02	-2.3E+00	8.0E+00	5.3E-02	4	6	3.1E+01	2.0E+02
Cumulative Water Content at 1-m depth	3.8E-02	6.4E-02	-2.6E+00	8.0E+00	3.4E-02	4	6	1.3E-02	1.7E-02
Cumulative Water Content at 1.5-m depth	4.4E-02	7.9E-02	-2.6E+00	8.0E+00	3.2E-02	4	6	1.4E-02	2.4E-02
Total Flux (cm/yr) [c]	1.7E-02	1.6E-02	1.4E-01	8.0E+00	8.9E-01	4	6	9.0E-03	1.1E-02
Flux 1 (cm/yr) [c]	1.1E-01	8.7E-02	3.8E-01	8.0E+00	7.1E-01	4	6	1.2E-01	9.2E-02
Flux 2 (cm/yr) [c]	1.7E-02	1.8E-02	-1.7E-01	8.0E+00	8.7E-01	4	6	1.0E-02	1.1E-02
Flux 3 (cm/yr) [c]	1.6E-02	1.3E-02	4.7E-01	8.0E+00	6.5E-01	4	6	1.1E-02	1.0E-02
Average Chloride Content in Top 1 m (mg/L)	8.8E+02	1.7E+03	-4.8E-01	8.0E+00	6.4E-01	4	6	4.7E+02	3.3E+03
Average Chloride Content Top 1.5 m (mg/L)	7.8E+02	1.4E+03	-6.0E-01	8.0E+00	5.6E-01	4	6	4.6E+02	2.1E+03
Maximum Chloride Content in Top 1 m (mg/L)	3.2E+03	6.8E+03	-5.0E-01	8.0E+00	6.3E-01	4	6	1.7E+03	1.4E+04
Maximum Chloride Content in Top 1.5 m (mg/L)	3.2E+03	7.6E+03	-6.1E-01	8.0E+00	5.6E-01	4	6	1.7E+03	1.4E+04
Average Nitrate Content in Top 1 m (mg/L)	2.2E+01	2.5E+00	3.9E+00	8.0E+00	4.0E-03	4	6	1.2E+01	2.3E+00
Average Nitrate Content in Top 1.5 m (mg/L)	2.0E+01	2.6E+00	3.8E+00	8.0E+00	5.0E-03	4	6	1.1E+01	1.9E+00
Maximum Nitrate Content in Top 1 m (mg/L)	1.1E+02	1.0E+01	5.0E+00	8.0E+00	1.0E-03	4	6	5.1E+01	7.8E+00
Maximum Nitrate Content in Top 1.5 m (mg/L)	1.2E+02	1.3E+01	5.7E+00	8.0E+00	0.0E+00	4	6	4.5E+01	6.6E+00

$\delta^{18}O$= Delta oxygen-18 value δD= Delta deuterium value θg = Gravimetric water content

[a] *Probability value used in the T-test approach to determine significance of differences*

[b] *Samples from borehole 21B were not considered valid because of excessive water content due to its location near an asphalt pad.*

[c] Total flux represents the average chloride content from the entire borehole. For boreholes that displayed varying flux with depth (see Table 2), Flux 1 refers to the flux in the shallow region, Flux 2 refers to the flux in the intermediate region, and Flux 3 refers to the flux in the deepest region.

Bold *indicates variables are significantly different.*

Table 6 (Continued)
Comparison of T-Test Results for Zone 4 Canopy and Intercanopy Locations

Hydrological Variable	Mean		T-Test Statistic	Degrees of Freedom	p [a]	Number of Valid Samples [b]		Standard Deviation	
	Inter-canopy	Canopy				Inter-canopy	Canopy	Inter-canopy	Canopy
Average $\delta^{18}O$ in Top 1 m (‰)	6.1E+00	1.9E+00	2.1E+00	8.0E+00	6.6E-02	4	6	4.7E+00	1.3E+00
Average $\delta^{18}O$ in Top 1.5 m (‰)	4.5E+00	4.9E-01	1.6E+00	8.0E+00	1.4E-01	4	6	5.6E+00	1.9E+00
Maximum $\delta^{18}O$ in Top 1 m (‰)	1.6E+01	1.2E+01	1.6E+00	8.0E+00	1.6E-01	4	6	5.8E+00	3.2E+00
Maximum $\delta^{18}O$ in Top 1.5 m (‰)	1.6E+01	1.2E+01	1.6E+00	8.0E+00	1.6E-01	4	6	5.8E+00	3.2E+00
Average δD in Top 1 m (‰)	-4.7E+01	-6.0E+01	2.6E+00	8.0E+00	3.1E-02	4	6	9.1E+00	6.3E+00
Average δD in Top 1.5 m (‰)	-4.8E+01	-6.2E+01	3.0E+00	8.0E+00	1.7E-02	4	6	9.2E+00	6.0E+00
Maximum δD in Top 1 m (‰)	-1.2E+01	-2.6E+01	2.7E+00	8.0E+00	2.6E-02	4	6	4.1E+00	9.7E+00
Maximum δD in Top 1.5 m (‰)	-1.2E+01	-2.6E+01	2.7E+00	8.0E+00	2.6E-02	4	6	4.1E+00	9.7E+00
Average θg in Top 1 m (%)	2.8E+00	4.4E+00	-2.2E+00	8.0E+00	5.7E-02	4	6	1.1E+00	1.2E+00
Average θg in Top 1.5 m (%)	2.1E+00	3.7E+00	-2.6E+00	8.0E+00	3.4E-02	4	6	7.5E-01	1.1E+00
Maximum θg in Top 1 m (%)	8.5E+00	1.3E+01	-2.7E+00	8.0E+00	2.6E-02	4	6	9.9E-01	3.0E+00
Maximum θg in Top 1.5 m (%)	8.5E+00	1.3E+01	-2.7E+00	8.0E+00	2.6E-02	4	6	9.9E-01	3.0E+00

$\delta^{18}O$= Delta oxygen-18 value δD= Delta deuterium value θg = Gravimetric water content

[a] *Probability value used in the T-test approach to determine significance of differences*

[b] *Samples from borehole 21B were not considered valid because of excessive water content due to its location near an asphalt pad.*

[c] Total flux represents the average chloride content from the entire borehole. For boreholes that displayed varying flux with depth (see Table 2), Flux 1 refers to the flux in the shallow region, Flux 2 refers to the flux in the intermediate region, and Flux 3 refers to the flux in the deepest region.

Bold *indicates variables are significantly different.*

4.0 Discussion

This section discusses the findings as they relate to the three primary objectives of the study: (1) determining if the assumption of a uniform near-surface vadose-zone flux at MDA G is appropriate, (2) gauging the effect of asphalt paving at the site, and (3) assessing the impact of vegetative succession on the near-surface hydrology of the site. Section 4.1 compares pit covers to adjacent unexcavated areas, Section 4.2 compares paved to unpaved areas, and Section 4.3 compares the active portion of MDA G to Zone 4, the analog site for postclosure conditions.

4.1 Comparative Hydrology of Pit Covers and Adjacent Unexcavated Areas

The T-test results shown in Table 3 reveal no significant differences between pit covers and adjacent areas for any of the 16 hydrologic variables examined. There appears to be as much variation in water content values, chloride profiles, and stable isotope data within the pit covers and adjacent unexcavated areas as there is between the two types of sites. The downward fluxes at the two location types are similar, as shown in the box-and-whisker plot provided in Figure 23.

Chloride-based fluxes suggest that both the pit covers and unexcavated areas have fluxes in the soil zone ranging from about 0.3 to 0.9 cm/yr (0.1 to 0.4 in./yr). Below the soil zone, fluxes are more variable, ranging from 0.02 to 0.9 cm/yr (7.9×10^{-3} to 0.4 in./yr). The similarity in the range of chloride-based fluxes suggests that, if a conservative upper flux condition is used in numerical models of subsurface flow and transport, a uniform value appears justified. This finding indicates that the 1997 performance assessment assumption of a uniform flux across pit covers and adjacent unexcavated areas appears to be reasonable, especially since the flux used in the 1997 modeling was conservative (i.e., greater than the highest chloride-based flux identified in this study).

One limitation of the data used to draw this conclusion is the small number of boreholes, which results in low statistical power. (For reasons explained in Section 4.2, the data from borehole 21B, which was located in an adjacent area, were not used in the statistical T-test analyses.) Even so, the mean values for many of the variables (e.g., fluxes and water contents) in Table 3 show little difference between the pit and unexcavated areas, indicating qualitative support for the statistical conclusion. Finally, although there are no significant hydrological differences between pits and adjacent areas, there appears to be at least an order of magnitude variability in near-surface fluxes across the mesa (Table 2), and it may be important to consider this variability in stochastic models of the site.

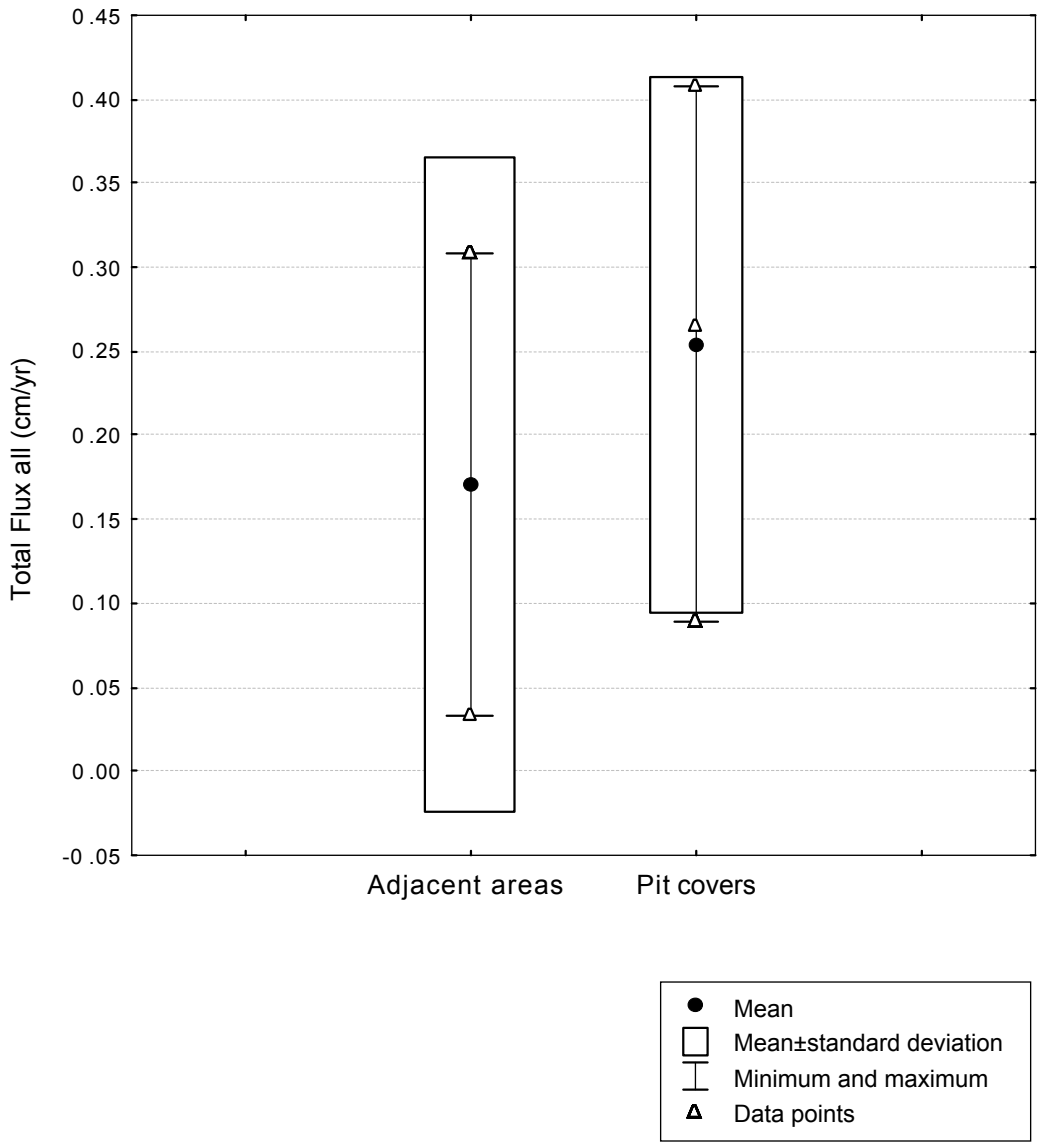

Note: Total flux represents the average chloride content from the entire borehole.

Figure 23
Comparison of Downward Flux in 1999 Boreholes Drilled into Pit Covers and Areas Adjacent to Pits

4.2 Comparative Hydrology of Paved and Unpaved Areas

One of the more distinct differences between the boreholes at the paved and unpaved locations is the lack of well-developed isotopically heavy bulges in the top 0.1 m (0.33 ft) of the profiles (Figures 17 and 18). This result and the meteoric water line plot shown in Figure 19 indicate that evaporation of water is minimal under the asphalt. Because no plants grow through the asphalt, transpiration in paved areas is also minimal, except perhaps along the margins of the pads. The substantially lower level of evaporation and transpiration at the paved locations is an important hydrological difference that is reflected in the water content and flux data.

Comparative T-test results show significant differences between cores from paved and unpaved areas for 14 of the 28 hydrological variables examined (Table 4). The estimated flux and water content values of paved areas were higher than those observed at the unpaved locations and the isotopic values were lower. This indicates that water is accumulating beneath some paved areas. The differences in water content and stable isotope values between the paved and unpaved areas are shown in Figures 24 and 25. Over the long term, the lack of an evaporative (and transpirative) release of water can create an accumulation of water beneath the asphalt, which will increase percolation. This is demonstrated by the high apparent flux shown in Table 2 for borehole BT30, which was drilled in an asphalt-covered area.

The long-term impacts of the asphalt pads on site hydrology are not clear for two reasons. First, the downward extent of the elevated moisture conditions is unknown because of the limited sampling depths. Second, the period of time the asphalt pads will remain in place is unknown. If fluxes remain relatively low at depth and the pads are removed as currently planned, there may be no significant long-term effects from the pavement. However, the asphalt pads could cause increased fluxes through the waste zone, which may accelerate waste container degradation and rates of radionuclide release and transport.

Compared to other areas at the Laboratory where water accumulation has occurred under asphalt, the paved areas at MDA G are still relatively dry. Data from the former pad at MDA AB within TA-49 (Rofer et al., 1999) and from a TA-3 parking lot (Newman, 1998) show that saturated conditions can eventually develop under pavement. Thus, over time, differences between paved and unpaved areas at MDA G may increase. If the pavement becomes cracked or perforated, water accumulation will likely accelerate.

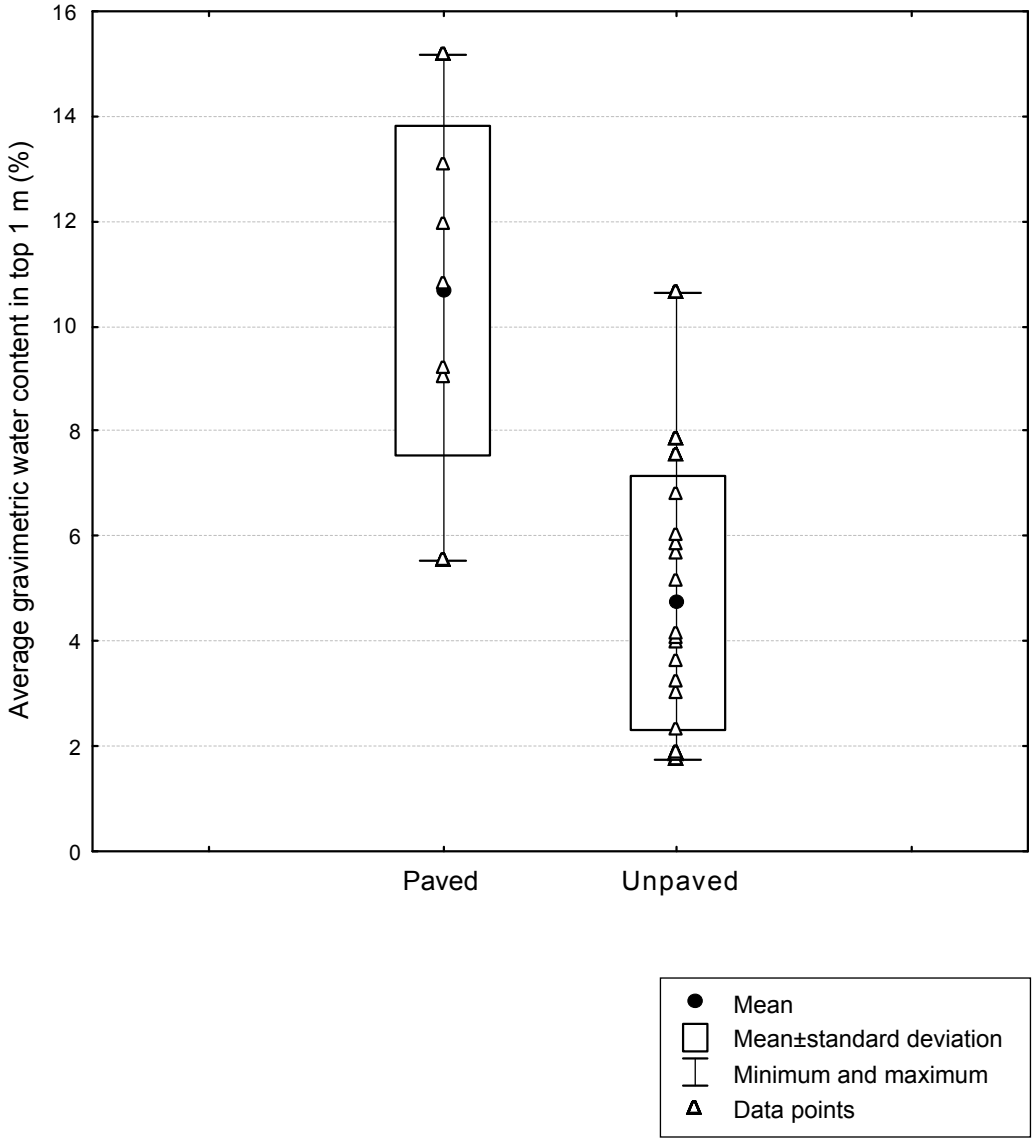

Figure 24
Comparison of Average Water Content in Boreholes Drilled in Paved and Unpaved Areas

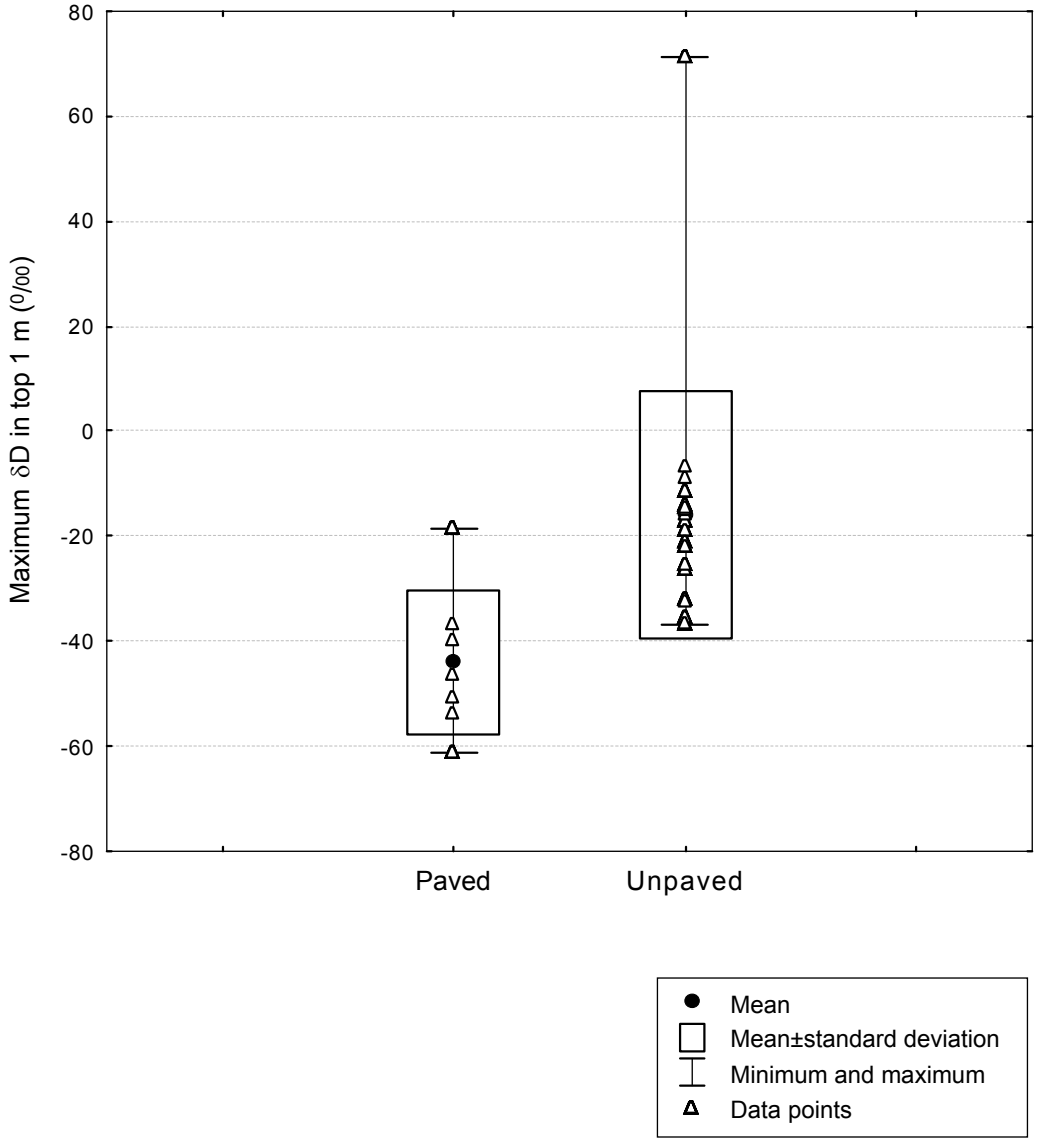

Figure 25
Comparison of Maximum Delta Deuterium Values in Boreholes Drilled in Paved and Unpaved Areas

The data from borehole 21B demonstrates an additional impact of paving. The area around this borehole received runoff from a paved area, which led to wetter near-surface conditions and a relatively high apparent flux (Table 2). The added runoff increases the uncertainty about the chloride-based flux estimate, but the relatively low chloride content and wetter conditions are also consistent with an elevated flux. Additional evidence for a relatively high flux in the vicinity of borehole 21B is provided by neutron probe surveys of deep borehole 1121, adjacent to borehole 21B. Data from deep borehole 1121 show increases in volumetric water content, over time, that occur as deep as 24 m (78 ft) (Newell, 1999). Thus, focused runoff from asphalt pavement near boreholes 21B and 1121 has had an apparently substantial impact on the movement of water into the subsurface. Since the boreholes were drilled, this problem has been remedied by directing asphalt runoff away from the area.

Some flux estimates presented in this section are more uncertain than others. The presence of pavement violates some assumptions associated with the chloride method (e.g., that flow is downward and piston-like). Thus, the estimated fluxes for boreholes drilled through asphalt covers and for borehole 21B (located adjacent to an asphalt area) must be viewed as highly uncertain. Leakage from a nearby building increases the uncertainty of the flux estimate for borehole G2. Although uncertain, these fluxes are presented in Table 2 for comparison to the fluxes from the unaffected boreholes. Prior to paving, each of these borehole locations probably had chloride contents similar to those observed at the borehole locations in unpaved areas. Therefore, any differences in chloride concentrations and resultant fluxes are likely to be related to changes that have occurred since the areas were paved.

4.3 Comparative Hydrology of Active Area and Zone 4

T-test results comparing 28 hydrological variables from the active (unpaved) disposal area and the Zone 4 site show significant differences for only 4 variables, 3 of which are downward flux estimates (Table 5). A box-and-whisker diagram comparing downward flux is shown in Figure 26. Flux differences may be related, in part, to the extreme drought conditions between the 1999 and 2002 sampling events. If these differences are not drought related, the transition from a grass- and forb-covered area to a mature piñon-juniper woodland may lead to drier near-surface conditions and a decrease in the downward flux of as much as an order of magnitude.

Differences between canopy and intercanopy conditions in the piñon-juniper analog area were also examined. T-tests on hydrologic variables obtained from canopy and intercanopy borehole samples indicate significant differences for 14 of 28 variables (Table 6). Most differences were related to nitrate concentrations or to δD values. The nitrate data suggest that there may be higher nitrate use under the canopy. These data also indicate that there may be variations in biogeochemical conditions at the canopy-intercanopy-scale that could affect the spatial distributions and transport of radionuclides that are translocated to the near-surface.

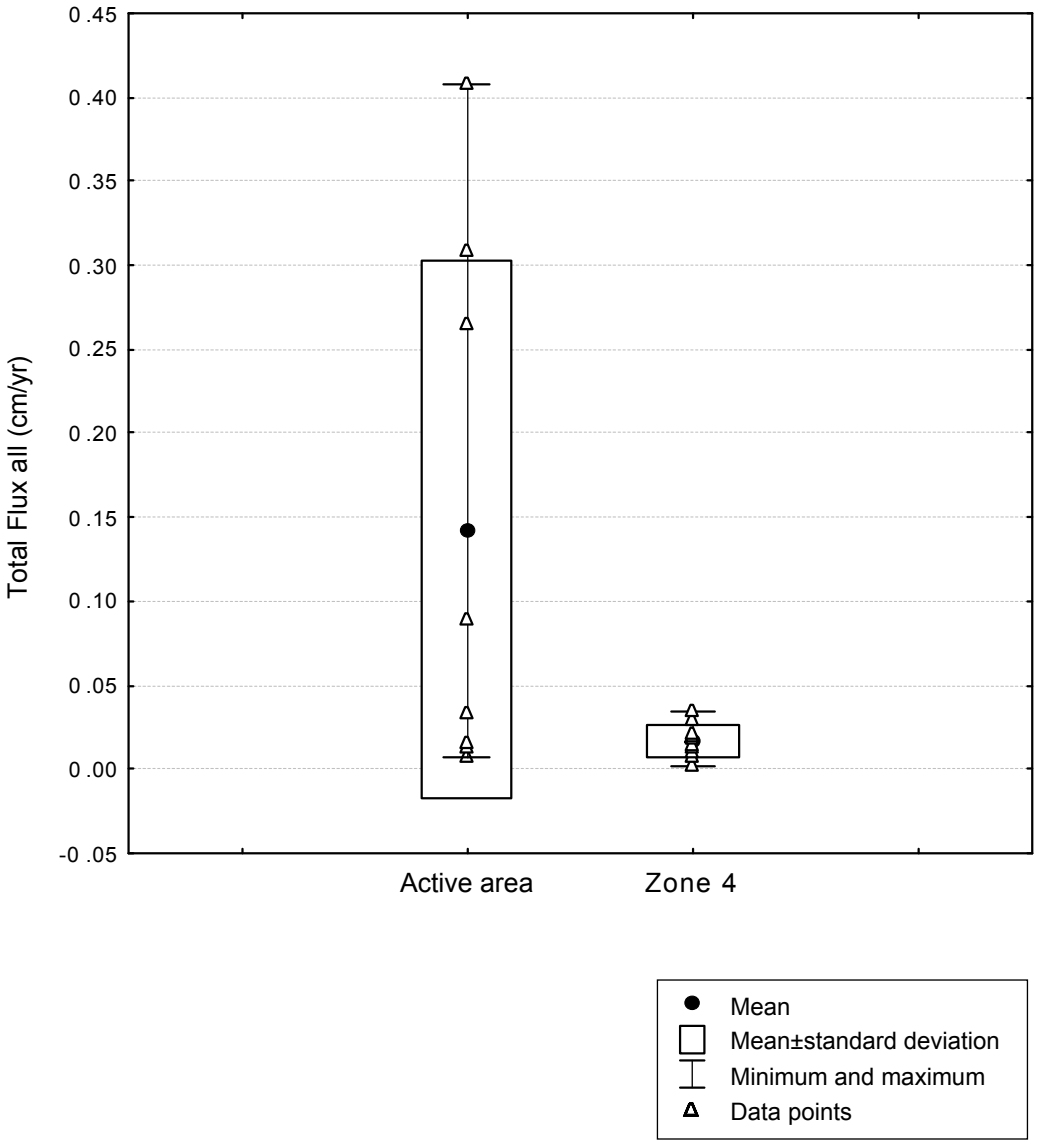

Note: Total flux represents the average chloride content from the entire borehole.

Figure 26
Comparison of Downward Flux in Unpaved Parts of Active Area and Zone 4

The δD data shows generally heavier (more positive) values in the intercanopy areas (Figure 27). This suggests that more evaporation occurs in the intercanopy spaces; the δ^{18}O data are consistent with this interpretation but show no significant difference. The lack of significance among δ^{18}O data may be related to the dryness of many of the samples. Some samples were too dry to use for the δ^{18}O analyses, thereby reducing the statistical power of the T-test; others yielded so little water that the accuracy of the δ^{18}O data was relatively poor.

Interestingly, there are no significant differences in the chloride mass balance flux values for the canopy and intercanopy boreholes, despite the differences in evaporation at these locations. This suggests that increased transpiration under the tree canopies may balance out the lower evaporation values, resulting in total evapotranspiration values that are similar for the canopy and intercanopy spaces. However, this assumes that differences in interception and infiltration between the canopy and intercanopy areas also offset each other (i.e., higher interception in the intercanopy areas is offset by higher infiltration in the canopies). In terms of modeling post-institutional control conditions at MDA G, these results suggest that it may not be necessary to use different downward fluxes for canopy and intercanopy areas.

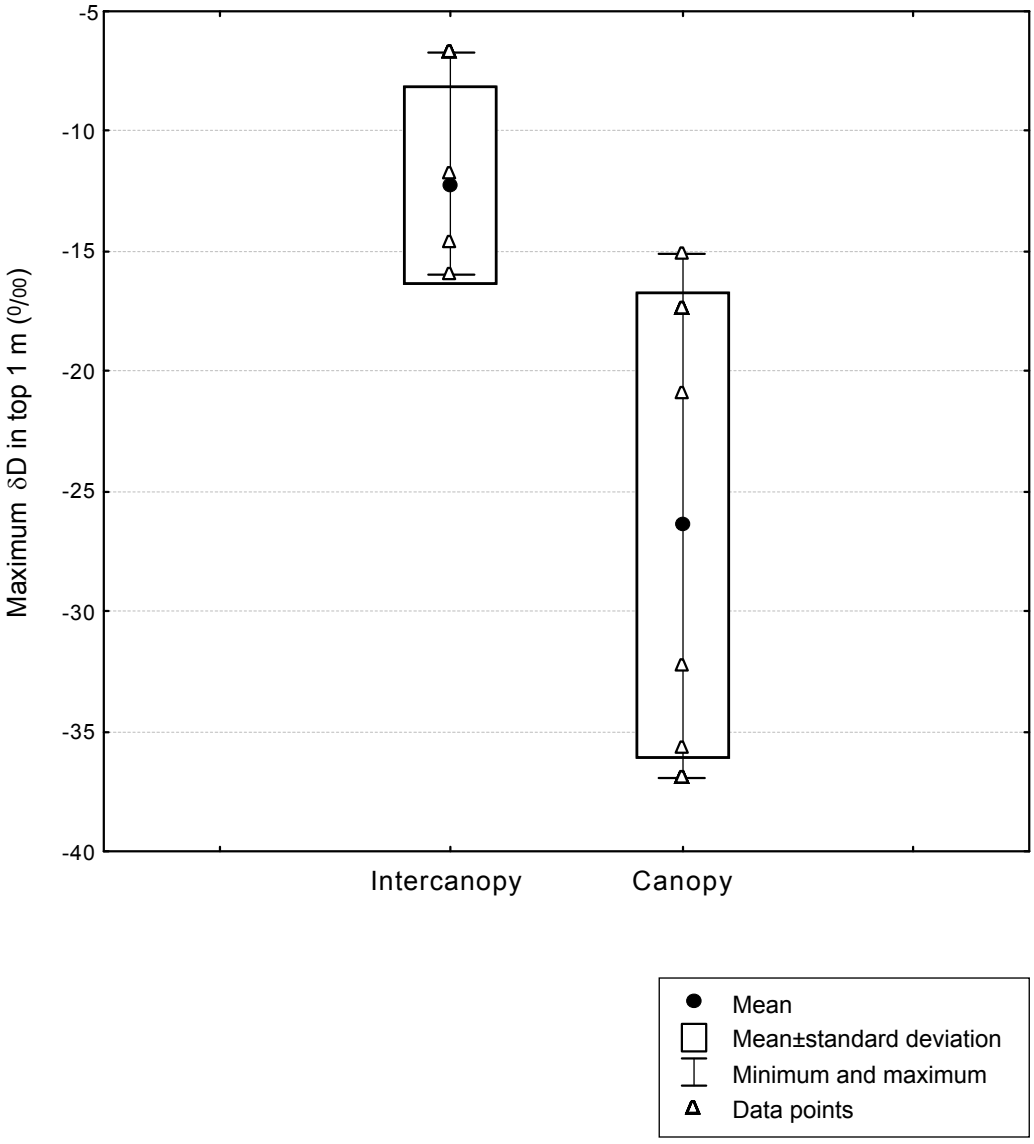

Figure 27
Comparison of Maximum Delta Deuterium Values in Canopy and Intercanopy Locations at Zone 4

5.0 References

Allison, G.B., W.J. Stone, and M.W. Hughes, 1985, "Recharge in Karst and Dune Elements of a Semi-Arid Landscape as Indicated by Natural Isotopes and Chloride," *Journal of Hydrology*, Vol. 76, pp. 1–25.

Anderholm, S.K, 1994, *Ground-Water Recharge Near Santa Fe, North-Central New Mexico*, USGS Water Res. Invest. Rep. 94-4078.

Bowen, B.M., 1990, *Los Alamos Climatology*, Los Alamos National Laboratory Report LA-11735-MS.

DBS&A, 1994, *Laboratory Analysis of Soil Hydraulic Properties of Protective Barrier Landfill Cover Demonstration Samples*, Daniel B. Stephens & Associates, Inc. LANL\RPT494, April

DOE, 1999, *Site-Wide Environmental Impact Statement for Continued Operation of the Los Alamos National Laboratory*, U.S. Department of Energy, Albuquerque Operations Office,. DOE/EIS – 0238, Albuquerque, NM, January.

Gee, G.W., G.S. Campbell, and J.H. Campbell, 1992, "Rapid Measurement of Soil Water Potentials Using a Water Activity Meter," *Soil Science Society of America Journal*, Vol. 56, pp. 1068–1070.

Hollis, D., E. Vold, R. Shuman, K. Birdsell, K. Bower, W. Hansen, D. Krier, P. Longmire, B. Newman, D. Rogers, E. Springer, 1997, *Performance Assessment and Composite Analysis for the Los Alamos National Laboratory Disposal Area G*, Los Alamos National Laboratory Report LA-UR-97-85, Report-54G-013, March.

Kendall, C., and T.B. Coplen, 1985, "Multisample Conversion of Water to Hydrogen by Zinc for Stable Isotope Determination," *Analytical Chemistry*, Vol. 57, pp. 1437–1446.

Newell, D, 1999, *Neutron Probe Water Content Data from Borehole 1121 at MDA G*, Los Alamos National Laboratory unpublished report.

Newman, B.D., 1996, "Vadose Zone Water Movement at Area G, Los Alamos National Laboratory, TA-54: Interpretations Based on Chloride and Stable Isotope Profiles," in D. Hollis et al., *Performance Assessment and Composite Analysis for Los Alamos National Laboratory Material Disposal Area G*.

Newman, B.D, 1998, *Water Content Data Below a TA-3 Parking Lot*, Los Alamos National Laboratory unpublished report.

Newman, B.D., A.R. Campbell, and B.P. Wilcox, 1997, "Tracer-Based Studies of Soil Water Movement in Semi-Arid Forests of New Mexico," *Journal of Hydrology*, Vol. 196, pp. 251–270.

Phillips, F.M, 1994, "Environmental Tracers for Water Movement in Desert Soils of the American Southwest," *Soil Science Society of America Journal*, Vol. 58, p. 1994.

Rofer, C.K., B.A. Martinez, G.K. Bayhurst, and I.R. Triay, 1999, "Moisture Accumulation under Asphalt Cover at a Radioactive Waste-Burial Site," *Practice Periodical of Hazardous, Toxic, and Radioactive Waste Management*, Vol. 3, pp. 10–16.

Rogers, D.B. and B.M. Gallaher, 1995, *The Unsaturated Hydraulic Characteristics of the Bandelier Tuff*, Los Alamos National Laboratory Report LA-12968-MS, September.

Scanlon, B.R, 2000, "Uncertainties in Estimating Water Fluxes and Residence Times Using Environmental Tracers in an Arid Unsaturated Zone," *Water Resources Research*, Vol. 36, pp. 395–409.

Shurbaji, A.-R.M., F.M. Phillips, A.R. Campbell, and R.G. Knowlton, 1995, "Application of a Numerical Model for Simulating Groundwater Flow, Isotope Transport, and Heat Transfer in the Unsaturated Zone," *Journal of Hydrology*, Vol. 171, pp. 143–163.

Socki, R.A., H.R. Karlsson, and E.K. Gibson, 1992, "Extraction Technique for the Determination of Oxygen-18 in Water Using Preevacuated Glass Vials," *Analytical Chemistry*, Vol. 64, pp. 829–831.

StatSoft, 2005, "Statistica – Data Mining, Data Analysis, Quality Control, and Web Analytics Software," http://www.statsoft.com (August 2005).

Vuataz, F.D., and F. Goff, 1986, "Isotope Chemistry of Thermal and Nonthermal Waters in the Valles Caldera, Jemez Mountains, Northern New Mexico," *Journal of Geophysical Research*, Vol. 91, No. B2, pp. 1835–1853.

Attachment I
Hydrographic Properties of Shallow Boreholes at Material Disposal Area G

This attachment contains the hydrographic properties for the shallow boreholes drilled at Material Disposal Area G, Technical Area 54 during 1999 and 2002. A separate table is provided for each borehole; the locations of these boreholes are described in the main report.

Borehole Pit2

Sample Depth (cm)	Gravimetric Water Content (%)	Chloride Content (mg/L)	Pressure Head (cm)	Isotope Sample Depth (cm)	Delta Oxygen-18 (‰)	Delta Deuterium (‰)
5	7.3E+00	2.0E+01	1.2E+05	1	4.4E+00	-5.5E+01
15	6.3E+00	1.9E+01	5.6E+03	3	8.7E+00	-2.6E+01
25	8.5E+00	2.5E+01	1.0E+00	5	7.8E+00	-3.6E+01
35	1.1E+01	4.4E+01	1.0E+00	7	4.5E+00	-3.5E+01
45	1.2E+01	1.3E+02	1.0E+00	9	6.1E+00	-4.5E+01
55	1.3E+01	1.8E+02	7.1E+02	15	-5.9E+00	-7.0E+01
65	1.3E+01	2.3E+02	1.0E+00	25	-7.5E+00	-6.4E+01
75	1.4E+01	2.2E+02	1.0E+00	35	-7.6E+00	-6.1E+01
85	9.8E+00	2.1E+02	7.1E+02	45	-7.0E+00	-6.0E+01
---	---	---	---	55	-6.9E+00	-6.5E+01
---	---	---	---	65	-7.9E+00	-7.0E+01
---	---	---	---	75	-9.0E+00	-7.5E+01
---	---	---	---	85	-8.6E+00	-8.4E+01

Borehole Pit17

Sample Depth (cm)	Gravimetric Water Content (%)	Chloride Content (mg/L)	Pressure Head (cm)	Isotope Sample Depth (cm)	Delta Oxygen-18 (‰)	Delta Deuterium (‰)
5	3.0E+00	2.9E+01	3.7E+05	1	7.7E+00	-5.2E+01
15	6.9E+00	1.0E+01	4.6E+04	3	8.5E+00	-2.2E+01
25	7.0E+00	1.0E+01	2.1E+04	5	9.3E+00	-2.8E+01
35	4.0E+00	2.5E+01	1.8E+04	7	9.5E+00	-3.0E+01
45	5.9E+00	5.0E+00	2.8E+03	9	2.8E+00	-3.3E+01
55	6.2E+00	1.4E+01	4.2E+03	15	1.3E+00	-4.4E+01
65	5.9E+00	2.2E+01	2.1E+03	25	-3.8E+00	-6.1E+01
75	5.8E+00	5.5E+01	3.5E+03	35	-5.1E+00	-6.6E+01
85	6.1E+00	5.9E+01	1.4E+03	45	-6.8E+00	-6.8E+01
95	5.9E+00	3.4E+01	2.1E+03	55	-6.7E+00	-6.9E+01
---	---	---	---	65	-6.0E+00	-5.7E+01
---	---	---	---	75	-5.4E+00	-5.3E+01
---	---	---	---	85	-5.2E+00	-5.1E+01
---	---	---	---	95	-6.0E+00	-5.5E+01

--- = Not sampled *NM = Not measured*

Borehole Pit24

Sample Depth (cm)	Gravimetric Water Content (%)	Chloride Content (mg/L)	Pressure Head (cm)	Isotope Sample Depth (cm)	Delta Oxygen-18 (‰)	Delta Deuterium (‰)
5	6.5E+00	2.0E+01	2.7E+05	1	6.1E+00	-4.5E+01
15	6.8E+00	5.9E+01	1.2E+05	3	1.1E+01	-3.4E+01
25	2.3E+00	1.3E+02	9.2E+03	5	1.3E+01	-1.9E+01
35	3.9E+00	2.8E+01	5.6E+03	7	1.0E+01	-2.9E+01
45	5.0E+00	2.2E+01	4.2E+03	9	5.1E+00	-3.2E+01
55	5.2E+00	3.0E+01	3.5E+03	15	-3.0E-01	-5.5E+01
65	5.9E+00	4.0E+01	3.5E+03	25	-1.5E+00	-5.5E+01
75	5.6E+00	3.2E+01	2.8E+03	35	-4.2E+00	-4.4E+01
85	5.3E+00	2.1E+01	2.8E+03	45	-4.3E+00	-5.6E+01
95	5.0E+00	2.4E+01	3.5E+03	55	-4.7E+00	-5.1E+01
---	---	---	---	65	-4.8E+00	-5.6E+01
---	---	---	---	75	-7.7E+00	-6.9E+01
---	---	---	---	85	-6.3E+00	-5.9E+01
---	---	---	---	95	-6.0E+00	-6.4E+01

Borehole 7B

Sample Depth (cm)	Gravimetric Water Content (%)	Chloride Content (mg/L)	Pressure Head (cm)	Isotope Sample Depth (cm)	Delta Oxygen-18 (‰)	Delta Deuterium (‰)
5	4.7E+00	6.4E+01	5.1E+05	1	3.4E+00	-5.9E+01
15	7.6E+00	1.4E+01	2.5E+04	3	1.0E+01	-3.5E+01
25	9.9E+00	1.3E+01	4.2E+03	5	6.6E+00	-3.2E+01
35	7.3E+00	2.2E+01	2.1E+03	7	-7.0E-01	-5.3E+01
45	7.2E+00	2.4E+01	1.4E+03	9	-1.9E+00	-5.2E+01
55	7.1E+00	2.4E+01	1.4E+03	15	-3.5E+00	-5.8E+01
65	7.7E+00	4.0E+01	2.1E+03	25	-4.9E+00	-6.6E+01
75	9.6E+00	2.1E+01	2.1E+03	35	-7.8E+00	-8.0E+01
85	7.8E+00	2.9E+01	5.7E+03	45	-7.5E+00	-7.7E+01
105	6.6E+00	3.9E+01	2.1E+03	65	-6.9E+00	-6.0E+01
115	9.3E+00	4.1E+01	1.0E+00	85	-7.9E+00	-7.4E+01
125	9.9E+00	3.7E+01	2.1E+03	145	-9.8E+00	-8.4E+01
135	7.6E+00	5.3E+01	1.4E+03	---	---	---
145	7.3E+00	5.2E+01	1.0E+00	---	---	---
155	6.9E+00	4.7E+01	1.4E+03	---	---	---

--- = Not sampled *NM = Not measured*

Borehole 17B

Sample Depth (cm)	Gravimetric Water Content (%)	Chloride Content (mg/L)	Pressure Head (cm)	Isotope Sample Depth (cm)	Delta Oxygen-18 (‰)	Delta Deuterium (‰)
5	4.3E+00	5.6E+01	7.0E+02	1	NM	-2.5E+01
15	8.4E+00	2.2E+01	1.0E+00	3	6.3E+00	-3.2E+01
25	1.0E+01	2.1E+01	1.0E+00	5	NM	-3.5E+01
35	6.8E+00	3.5E+01	7.0E+02	7	-1.1E+00	-4.2E+01
45	1.1E+01	5.0E+01	1.0E+00	9	-2.5E+00	-4.4E+01
55	1.4E+01	5.5E+01	1.0E+00	15	-6.4E+00	-5.9E+01
65	1.1E+01	1.0E+02	2.1E+03	25	-8.9E+00	-6.8E+01
75	4.9E+00	2.1E+02	8.5E+03	35	-7.1E+00	-6.6E+01
85	4.1E+00	2.3E+02	9.2E+03	45	-9.0E+00	-7.4E+01
95	3.7E+00	2.2E+02	4.9E+03	65	-8.9E+00	-8.0E+01
105	3.2E+00	2.4E+02	4.9E+03	85	-7.6E+00	-7.2E+01
115	2.1E+00	5.7E+02	8.5E+03	145	-1.1E+01	-8.2E+01
125	2.1E+00	7.6E+02	1.2E+04	195	-1.2E+01	-9.9E+01
135	2.7E+00	1.2E+03	9.2E+03	---	---	---
145	3.8E+00	8.1E+02	7.0E+03	---	---	---
155	4.2E+00	6.8E+02	4.2E+03	---	---	---
165	4.1E+00	4.4E+02	5.6E+03	---	---	---
175	4.5E+00	2.8E+02	5.6E+03	---	---	---
185	3.6E+00	2.8E+02	4.2E+03	---	---	---
195	4.1E+00	3.1E+02	2.8E+03	---	---	---

--- = Not sampled *NM = Not measured*

Borehole 21B

Sample Depth (cm)	Gravimetric Water Content (%)	Chloride Content (mg/L)	Pressure Head (cm)	Isotope Sample Depth (cm)	Delta Oxygen-18 (‰)	Delta Deuterium (‰)
5	4.9E+00	3.4E+01	1.4E+03	1	1.2E+01	-4.7E+01
15	8.6E+00	1.4E+01	1.4E+03	3	5.6E+00	-3.0E+01
25	7.5E+00	1.2E+01	1.0E+00	5	-5.0E-01	-5.3E+01
35	6.9E+00	9.3E+00	1.4E+03	7	-4.7E+00	-6.2E+01
45	6.5E+00	1.4E+01	1.0E+00	9	-7.6E+00	-6.7E+01
55	1.9E+01	4.1E+00	1.0E+00	15	-7.2E+00	-5.2E+01
65	1.9E+01	4.3E+00	1.0E+00	25	-8.0E+00	-6.2E+01
75	2.0E+01	4.7E+00	1.0E+00	35	-8.4E+00	-6.9E+01
85	2.0E+01	6.3E+00	1.0E+00	45	-7.1E+00	-6.9E+01
95	1.8E+01	9.5E+00	1.0E+00	55	-9.4E+00	-7.3E+01
105	2.4E+01	4.4E+00	1.0E+00	65	-9.3E+00	-6.6E+01
115	1.8E+01	7.1E+00	1.0E+00	75	-8.7E+00	-6.8E+01
125	1.1E+01	1.8E+01	7.1E+02	85	-8.3E+00	-6.3E+01
135	1.2E+01	1.9E+01	1.0E+00	95	-1.1E+01	-9.2E+01
145	1.3E+01	1.6E+01	1.0E+00	105	-1.4E+01	-1.1E+02
155	1.3E+01	1.7E+01	1.0E+00	115	-1.4E+01	-1.1E+02
165	1.3E+01	1.2E+01	1.0E+00	125	-1.4E+01	-1.1E+02
175	1.3E+01	1.9E+01	1.0E+00	135	-1.4E+01	-1.1E+02
185	1.3E+01	2.3E+01	1.0E+00	145	-1.3E+01	-1.1E+02
195	1.3E+01	1.1E+01	1.0E+00	155	-1.4E+01	-1.0E+02
---	---	---	---	165	-1.3E+01	-1.1E+02
---	---	---	---	175	-1.3E+01	-1.0E+02
---	---	---	---	185	-1.1E+01	-8.2E+01
---	---	---	---	195	-9.2E+00	-7.3E+01

--- = Not sampled *NM = Not measured*

Borehole BT2

Sample Depth (cm)	Gravimetric Water Content (%)	Chloride Content (mg/L)	Pressure Head (cm)	Isotope Sample Depth (cm)	Delta Oxygen-18 (‰)	Delta Deuterium (‰)
5	3.9E+00	1.6E+02	5.3E+04	1	-1.6E+00	-5.7E+01
15	6.6E+00	7.4E+01	7.0E+02	5	-2.1E+00	-6.7E+01
25	6.4E+00	6.5E+01	1.4E+03	9	-1.7E+00	-5.4E+01
35	6.0E+00	6.2E+01	7.0E+02	15	-3.4E+00	-6.3E+01
45	5.8E+00	8.0E+01	5.6E+03	25	-5.0E+00	-6.3E+01
55	5.8E+00	5.5E+01	7.0E+02	35	-5.1E+00	-6.3E+01
65	5.9E+00	5.9E+01	7.0E+02	45	-5.6E+00	-6.4E+01
75	5.1E+00	6.5E+01	7.0E+02	65	-6.1E+00	
85	4.9E+00	6.4E+01	1.0E+00	85	-7.3E+00	-6.7E+01
95	4.9E+00	6.8E+01	2.1E+03	---	---	---

Borehole BT21

Sample Depth (cm)	Gravimetric Water Content (%)	Chloride Content (mg/L)	Pressure Head (cm)	Isotope Sample Depth (cm)	Delta Oxygen-18 (‰)	Delta Deuterium (‰)
5	6.2E+00	4.7E+01	3.5E+03	1	-5.5E+00	-6.1E+01
15	1.0E+01	1.8E+01	1.0E+00	5	NM	-7.8E+01
25	1.2E+01	1.5E+01	1.0E+00	9	-7.4E+00	-6.4E+01
35	1.2E+01	1.7E+01	1.0E+00	15	-7.7E+00	-6.9E+01
45	1.1E+01	1.0E+01	1.0E+00	25	-7.7E+00	-7.0E+01
55	1.2E+01	1.0E+01	1.0E+00	35	-8.0E+00	-7.1E+01
65	1.3E+01	1.0E+01	1.0E+00	45	-8.2E+00	-7.6E+01
75	1.3E+01	7.0E+00	1.0E+00	65	-8.8E+00	-7.3E+01
85	9.9E+00	1.1E+01	7.1E+02	85	-8.1E+00	-7.3E+01
95	8.9E+00	1.3E+01	1.0E+00	145	-7.4E+00	-5.7E+01
105	8.7E+00	2.2E+01	1.0E+00	195	-8.0E+00	-5.8E+01
115	8.3E+00	1.3E+01	1.0E+00	---	---	---
125	6.1E+00	2.4E+01	7.0E+02	---	---	---
135	1.1E+01	1.5E+01	1.0E+00	---	---	---
145	6.9E+00	2.4E+01	1.0E+00	---	---	---
155	8.6E+00	1.5E+01	1.0E+00	---	---	---
165	7.3E+00	2.2E+01	1.0E+00	---	---	---
175	6.0E+00	2.8E+01	1.0E+00	---	---	---
185	6.4E+00	2.2E+01	1.0E+00	---	---	---
195	7.3E+00	2.0E+01	NM	---	---	---

--- = Not sampled *NM = Not measured*

Borehole BT30

Sample Depth (cm)	Gravimetric Water Content (%)	Chloride Content (mg/L)	Pressure Head (cm)	Isotope Sample Depth (cm)	Delta Oxygen-18 (‰)	Delta Deuterium (‰)
5	9.4E+00	2.8E+01	1.0E+00	1	-4.1E+00	-5.0E+01
15	1.3E+01	1.0E+01	1.0E+00	5	-4.4E+00	-4.7E+01
25	1.6E+01	9.0E+00	1.0E+00	9	-5.0E+00	-4.3E+01
35	1.4E+01	8.0E+00	1.0E+00	15	-5.1E+00	-4.0E+01
45	1.6E+01	1.0E+01	1.0E+00	25	-5.4E+00	-4.0E+01
55	1.8E+01	1.5E+01	1.0E+00	35	-6.4E+00	-4.1E+01
65	1.7E+01	1.6E+01	1.0E+00	45	-9.3E+00	-7.3E+01
75	1.6E+01	9.0E+00	1.0E+00	65	-1.1E+01	-9.3E+01
85	1.7E+01	1.3E+01	1.0E+00	85	-1.3E+01	-9.7E+01
95	1.7E+01	1.2E+01	1.0E+00	145	-7.3E+00	-6.5E+01
105	1.5E+01	9.0E+00	1.0E+00	195	-5.0E+00	-3.2E+01
115	1.6E+01	6.0E+00	1.0E+00	---	---	---
125	1.8E+01	7.0E+00	1.0E+00	---	---	---
135	1.5E+01	9.0E+00	1.0E+00	---	---	---
145	1.1E+01	8.0E+00	1.0E+00	---	---	---
155	8.9E+00	1.5E+01	1.0E+00	---	---	---
165	9.5E+00	1.1E+01	1.0E+00	---	---	---
175	9.0E+00	1.4E+01	1.0E+00	---	---	---
185	1.0E+01	1.3E+01	1.0E+00	---	---	---
195	1.2E+01	1.0E+01	1.0E+00	---	---	---

--- = Not sampled *NM = Not measured*

Borehole AS1

Sample Depth (cm)	Gravimetric Water Content (%)	Chloride Content (mg/L)	Pressure Head (cm)	Isotope Sample Depth (cm)	Delta Oxygen-18 (‰)	Delta Deuterium (‰)
5	6.2E+00	1.8E+01	NM	2.5	2.5E+00	-1.9E+01
17.5	1.0E+01	3.0E+01	NM	7.5	8.8E-01	-2.6E+01
27.5	1.1E+01	6.9E+00	NM	32.5	-2.3E+00	-3.6E+01
37.5	1.0E+01	1.4E+01	NM	62.5	-8.1E+00	-7.1E+01
47.5	1.0E+01	2.2E+01	NM	92.5	-6.5E+00	-5.5E+01
57.5	9.9E+00	2.2E+01	NM	---	---	---
67.5	8.7E+00	2.6E+01	NM	---	---	---
77.5	9.4E+00	4.5E+01	NM	---	---	---
87.5	8.9E+00	5.0E+01	NM	---	---	---
97.5	8.5E+00	6.0E+01	NM	---	---	---
107.5	9.0E+00	4.7E+01	NM	---	---	---

Borehole AS2

Sample Depth (cm)	Gravimetric Water Content (%)	Chloride Content (mg/L)	Pressure Head (cm)	Isotope Sample Depth (cm)	Delta Oxygen-18 (‰)	Delta Deuterium (‰)
5	2.9E+00	1.5E+01	NM	2.5	1.0E+00	-4.7E+01
17.5	1.3E+01	1.1E+01	NM	7.5	4.8E+00	-4.9E+01
27.5	1.2E+01	2.4E+01	NM	32.5	-8.1E+00	-7.5E+01
37.5	1.1E+01	1.7E+01	NM	62.5	-7.9E+00	-7.5E+01
47.5	1.3E+01	1.8E+01	NM	92.5	-9.7E+00	-8.2E+01
57.5	1.2E+01	2.1E+01	NM	---	---	---
67.5	1.6E+01	1.9E+01	NM	---	---	---
77.5	1.2E+01	9.1E+00	NM	---	---	---
87.5	1.4E+01	8.8E+00	NM	---	---	---
97.5	1.3E+01	6.1E+00	NM	---	---	---
107.5	1.3E+01	1.2E+01	NM	---	---	---

--- = Not sampled *NM = Not measured*

Borehole AS3

Sample Depth (cm)	Gravimetric Water Content (%)	Chloride Content (mg/L)	Pressure Head (cm)	Isotope Sample Depth (cm)	Delta Oxygen-18 (‰)	Delta Deuterium (‰)
5	5.3E+00	1.4E+02	NM	2.5	-6.0E-01	-5.1E+01
17.5	8.4E+00	1.4E+02	NM	7.5	1.3E+00	-5.2E+01
27.5	1.0E+01	8.7E+01	NM	32.5	-4.1E+00	-5.5E+01
37.5	9.1E+00	7.2E+01	NM	62.5	-3.0E+00	-5.6E+01
47.5	9.6E+00	5.9E+01	NM	92.5	-6.9E+00	-7.4E+01
57.5	9.8E+00	8.1E+01	NM	122.5	-7.4E+00	-7.5E+01
67.5	9.1E+00	6.2E+01	NM	152.5	-8.3E+00	-7.0E+01
77.5	8.6E+00	1.3E+02	NM	---	---	---
87.5	9.6E+00	1.4E+02	NM	---	---	---
97.5	1.0E+01	1.6E+02	NM	---	---	---
107.5	1.2E+01	1.9E+02	NM	---	---	---
117.5	1.1E+01	1.7E+02	NM	---	---	---
127.5	1.1E+01	1.6E+02	NM	---	---	---
137.5	1.0E+01	9.7E+01	NM	---	---	---
147.5	1.2E+01	2.6E+01	NM	---	---	---
157.5	9.6E+00	2.9E+01	NM	---	---	---

Borehole AS4

Sample Depth (cm)	Gravimetric Water Content (%)	Chloride Content (mg/L)	Pressure Head (cm)	Isotope Sample Depth (cm)	Delta Oxygen-18 (‰)	Delta Deuterium (‰)
5	4.8E+00	9.1E+00	NM	2.5	-8.2E+00	-7.3E+01
17.5	1.3E+01	8.2E+00	NM	7.5	-5.1E+00	-7.0E+01
27.5	1.3E+01	8.5E+00	NM	32.5	-8.9E+00	-7.8E+01
37.5	1.4E+01	5.2E+00	NM	62.5	-8.2E+00	-6.2E+01
47.5	1.4E+01	5.6E+00	NM	92.5	-3.8E+00	-3.7E+01
57.5	1.5E+01	1.1E+01	NM	122.5	-4.7E+00	-4.8E+01
67.5	1.6E+01	1.5E+01	NM	---	---	---
77.5	1.5E+01	7.2E+00	NM	---	---	---
87.5	1.4E+01	1.0E+01	NM	---	---	---
97.5	1.2E+01	4.0E+01	NM	---	---	---
107.5	1.2E+01	1.0E+02	NM	---	---	---
117.5	1.3E+01	9.5E+01	NM	---	---	---

--- = Not sampled *NM = Not measured*

Borehole G1

Sample Depth (cm)	Gravimetric Water Content (%)	Chloride Content (mg/L)	Pressure Head (cm)	Isotope Sample Depth (cm)	Delta Oxygen-18 (‰)	Delta Deuterium (‰)
5	3.0E+00	6.5E+02	NM	2.5	1.1E+01	-1.4E+01
17.5	2.1E+00	4.6E+02	NM	7.5	1.2E+01	-2.7E+01
27.5	1.8E+00	3.9E+02	NM	32.5	-5.5E+00	-7.5E+01
37.5	1.6E+00	5.5E+03	NM	62.5	-3.5E+00	-6.8E+01
47.5	2.0E+00	8.0E+02	NM	92.5	-5.8E+00	-7.1E+01
57.5	2.0E+00	7.1E+02	NM	122.5	-7.0E+00	-8.1E+01
67.5	2.7E+00	4.4E+02	NM	---	---	---
77.5	2.1E+00	4.5E+02	NM	---	---	---
87.5	3.2E+00	4.2E+02	NM	---	---	---
97.5	2.6E+00	3.3E+02	NM	---	---	---
107.5	2.9E+00	3.7E+02	NM	---	---	---
117.5	2.5E+00	4.1E+02	NM	---	---	---
127.5	2.3E+00	3.9E+02	NM	---	---	---
137.5	2.1E+00	4.3E+02	NM	---	---	---
147.5	2.4E+00	4.0E+02	NM	---	---	---

Borehole G2

Sample Depth (cm)	Gravimetric Water Content (%)	Chloride Content (mg/L)	Pressure Head (cm)	Isotope Sample Depth (cm)	Delta Oxygen-18 (‰)	Delta Deuterium (‰)
5	1.2E+00	5.2E+02	NM	2.5	1.9E+01	-3.6E+01
17.5	1.7E+01	8.4E+02	NM	7.5	2.1E+01	-8.7E+00
27.5	1.9E+01	3.8E+03	NM	32.5	-4.2E+00	-6.5E+01
37.5	3.4E+00	3.5E+03	NM	62.5	-7.2E+00	-7.4E+01
47.5	1.1E+00	3.7E+03	NM	92.5	-9.4E+00	-7.9E+01
57.5	4.7E+00	1.0E+03	NM	---	---	---
67.5	7.6E+00	8.3E+02	NM	---	---	---
77.5	4.1E+00	4.5E+02	NM	---	---	---
87.5	3.7E+00	1.8E+02	NM	---	---	---
97.5	6.9E+00	5.7E+01	NM	---	---	---
107.5	5.4E+00	4.6E+01	NM	---	---	---

--- = Not sampled *NM = Not measured*

Borehole G3

Sample Depth (cm)	Gravimetric Water Content (%)	Chloride Content (mg/L)	Pressure Head (cm)	Isotope Sample Depth (cm)	Delta Oxygen-18 (‰)	Delta Deuterium (‰)
5	3.3E+00	2.3E+02	NM	2.5	1.4E+01	-2.6E+01
17.5	1.1E-01	7.0E+03	NM	7.5	2.3E+01	-1.5E+01
27.5	3.3E+00	2.3E+02	NM	32.5	1.1E+01	-1.1E+01
37.5	1.1E-01	7.0E+03	NM	62.5	-4.9E-01	-4.9E+01
47.5	6.5E-01	5.8E+02	NM	92.5	-5.2E+00	-6.7E+01
57.5	1.3E+00	3.3E+02	NM	122.5	-8.8E-01	-5.8E+01
67.5	2.0E+00	2.0E+02	NM	142.5	-4.1E+00	-7.1E+01
77.5	1.9E+00	2.3E+02	NM			
87.5	2.0E+00	2.3E+02	NM	---	---	---
97.5	1.9E+00	2.7E+02	NM	---	---	---
107.5	2.2E+00	1.9E+02	NM	---	---	---
117.5	2.2E+00	9.5E+01	NM	---	---	---
127.5	2.2E+00	9.3E+01	NM	---	---	---
137.5	2.1E+00	1.2E+02	NM	---	---	---

--- = Not sampled *NM = Not measured*

Borehole P1

Sample Depth (cm)	Gravimetric Water Content (%)	Chloride Content (mg/L)	Pressure Head (cm)	Isotope Sample Depth (cm)	Delta Oxygen-18 (‰)	Delta Deuterium (‰)
5	2.9E+00	1.8E+02	NM	2.5	8.9E+00	-3.2E+01
17.5	3.9E+00	1.1E+02	NM	7.5	7.3E+00	-3.9E+01
27.5	7.5E+00	1.9E+02	NM	32.5	-4.4E+00	-7.3E+01
37.5	1.1E+01	1.8E+02	NM	62.5	-5.6E+00	-7.4E+01
47.5	8.6E+00	2.9E+02	NM	92.5	-5.7E+00	-7.4E+01
57.5	7.2E+00	4.2E+02	NM	122.5	-5.4E+00	-7.8E+01
67.5	5.8E+00	5.2E+02	NM	142.5	-5.4E+00	-7.6E+01
77.5	4.7E+00	6.8E+02	NM	172.5	-4.6E+00	-6.6E+01
87.5	4.3E+00	7.2E+02	NM	202.5	-4.7E+00	-7.0E+01
97.5	4.4E+00	7.9E+02	NM	---	---	---
107.5	4.4E+00	8.0E+02	NM	---	---	---
117.5	4.8E+00	8.7E+02	NM	---	---	---
127.5	6.7E+00	8.5E+02	NM	---	---	---
137.5	4.1E+00	2.1E+03	NM	---	---	---
147.5	4.2E+00	1.1E+03	NM	---	---	---
157.5	1.6E+00	1.6E+03	NM	---	---	---
167.5	9.1E-01	2.0E+03	NM	---	---	---
177.5	5.8E-01	2.4E+03	NM	---	---	---
187.5	4.2E-01	3.1E+03	NM	---	---	---
197.5	1.7E+00	1.9E+03	NM	---	---	---
207.5	7.0E-01	2.0E+03	NM	---	---	---

--- = Not sampled *NM = Not measured*

Borehole P2

Sample Depth (cm)	Gravimetric Water Content (%)	Chloride Content (mg/L)	Pressure Head (cm)	Isotope Sample Depth (cm)	Delta Oxygen-18 (‰)	Delta Deuterium (‰)
5	2.1E+00	1.4E+02	NM	2.5	8.9E+00	-4.6E+01
17.5	4.9E+00	5.3E+01	NM	7.5	1.4E+01	-3.7E+01
27.5	4.9E+00	3.9E+01	NM	32.5	-1.5E+00	-7.0E+01
37.5	5.8E+00	2.2E+01	NM	62.5	-3.1E+00	-7.1E+01
47.5	6.1E+00	1.1E+01	NM	92.5	-8.2E+00	-7.5E+01
57.5	1.3E+01	1.5E+01	NM	122.5	-5.6E+00	-6.6E+01
67.5	3.2E-01	5.7E+02	NM	142.5	-8.4E+00	-8.9E+01
77.5	3.9E-01	4.8E+02	NM	2.5	8.9E+00	-4.6E+01
87.5	8.5E-01	4.2E+02	NM	7.5	1.4E+01	-3.7E+01
97.5	1.1E+00	2.8E+02	NM	---	---	---
107.5	1.0E+00	3.2E+02	NM	---	---	---
117.5	1.0E+00	5.3E+02	NM	---	---	---
127.5	5.6E+00	9.4E+01	NM	---	---	---
137.5	1.3E+00	4.6E+02	NM	---	---	---
147.5	7.8E-01	1.2E+03	NM	---	---	---

--- = Not sampled *NM = Not measured*

Borehole P3

Sample Depth (cm)	Gravimetric Water Content (%)	Chloride Content (mg/L)	Pressure Head (cm)	Isotope Sample Depth (cm)	Delta Oxygen-18 (‰)	Delta Deuterium (‰)
5	3.7E+00	6.8E+02	NM	2.5	7.0E+00	-3.6E+01
17.5	5.3E+00	7.6E+02	NM	7.5	5.3E+00	-4.7E+01
27.5	6.1E+00	5.9E+02	NM	32.5	-6.6E+00	-1.0E+02
37.5	4.2E+00	5.3E+02	NM	122.5	---	-4.8E+01
47.5	1.6E+01	4.2E+02	NM	142.5	---	-1.4E+02
57.5	2.0E-02	2.9E+04	NM	2.5	-6.1E+00	-7.0E+01
67.5	1.0E-02	3.6E+04	NM	7.5	-4.5E+00	-6.1E+01
77.5	3.2E-01	1.8E+03	NM	---	---	---
87.5	7.0E-02	8.8E+03	NM	---	---	---
97.5	9.0E-02	5.5E+03	NM	---	---	---
107.5	5.9E-01	4.9E+02	NM	---	---	---
117.5	1.1E+00	3.3E+02	NM	---	---	---
127.5	1.1E+00	3.2E+02	NM	---	---	---
137.5	6.0E-01	5.5E+02	NM	---	---	---
147.5	1.5E+00	2.7E+02	NM	---	---	---

Borehole J1

Sample Depth (cm)	Gravimetric Water Content (%)	Chloride Content (mg/L)	Pressure Head (cm)	Isotope Sample Depth (cm)	Delta Oxygen-18 (‰)	Delta Deuterium (‰)
5.0	1.6E+00	3.7E+02	NM	2.5	1.1E+01	-3.0E+01
17.5	1.8E+00	1.8E+02	NM	7.5	1.4E+01	-1.5E+01
27.5	5.2E+00	1.1E+02	NM	32.5	-4.3E+00	-7.3E+01
37.5	2.2E+00	3.1E+02	NM	62.5	8.8E+00	-4.8E+01
47.5	4.8E+00	1.9E+02	NM	92.5	-6.6E+00	-7.9E+01
57.5	2.4E-01	1.5E+03	NM	122.5	-6.1E+00	-7.9E+01
67.5	2.0E-01	1.1E+03	NM	142.5	-6.4E+00	-7.7E+01
77.5	1.5E+00	2.2E+02	NM	---	---	---
87.5	1.2E+01	2.8E+02	NM	---	---	---
97.5	8.3E-01	6.5E+02	NM	---	---	---
107.5	9.2E-01	6.3E+02	NM	---	---	---
117.5	1.0E+01	4.5E+02	NM	---	---	---
127.5	2.6E+00	5.6E+02	NM	---	---	---
137.5	3.3E+00	5.2E+02	NM	---	---	---
147.5	4.8E+00	6.2E+02	NM	---	---	---

--- = Not sampled *NM = Not measured*

Borehole J2

Sample Depth (cm)	Gravimetric Water Content (%)	Chloride Content (mg/L)	Pressure Head (cm)	Isotope Sample Depth (cm)	Delta Oxygen-18 (‰)	Delta Deuterium (‰)
2.5	2.3E+00	1.6E+02	NM	2.5	1.4E+01	-1.8E+01
7.5	3.1E+00	3.6E+01	NM	7.5	1.4E+01	-1.7E+01
32.5	3.1E+00	3.0E+01	NM	32.5	-2.6E+00	-6.9E+01
62.5	3.6E+00	2.0E+01	NM	62.5	-4.3E+00	-7.7E+01
92.5	6.0E+00	1.4E+01	NM	92.5	-6.7E+00	-8.6E+01
122.5	5.9E+00	1.4E+02	NM	122.5	-5.4E+00	-6.8E+01
142.5	6.4E+00	2.6E+02	NM	142.5	-3.3E+00	-5.9E+01
2.5	4.1E+00	3.4E+02	NM	---	---	---
7.5	1.6E+01	5.0E+02	NM	---	---	---
32.5	8.2E+00	7.5E+02	NM	---	---	---
62.5	4.4E-01	2.1E+03	NM	---	---	---
92.5	5.3E-01	8.9E+02	NM	---	---	---
122.5	7.4E-01	7.1E+02	NM	---	---	---
142.5	6.4E-01	7.9E+02	NM	---	---	---
2.5	3.3E-01	1.8E+03	NM	---	---	---
7.5	6.3E-01	5.0E+02	NM	---	---	---

--- = Not sampled *NM = Not measured*

Borehole J3

Sample Depth (cm)	Gravimetric Water Content (%)	Chloride Content (mg/L)	Pressure Head (cm)	Isotope Sample Depth (cm)	Delta Oxygen-18 (‰)	Delta Deuterium (‰)
5	2.1E+00	2.0E+02	NM	2.5	1.3E+01	-3.3E+01
17.5	8.0E+00	9.1E+01	NM	7.5	1.2E+01	-2.1E+01
27.5	6.1E+00	1.7E+02	NM	32.5	4.5E-01	-6.7E+01
37.5	4.9E+00	3.2E+02	NM	62.5	-4.1E+00	-8.6E+01
47.5	2.1E+00	3.9E+02	NM	92.5	-3.3E+00	-8.6E+01
57.5	1.9E+00	5.8E+02	NM	122.5	---	-5.8E+01
67.5	8.8E+00	4.7E+02	NM	---	---	
77.5	2.4E+00	3.9E+02	NM	---	---	
87.5	4.7E+00	1.9E+02	NM	---	---	
97.5	4.7E-01	1.3E+03	NM	---	---	---
107.5	7.7E-01	9.2E+02	NM	---	---	---
117.5	5.1E-01	1.3E+03	NM	---	---	---
127.5	3.8E-01	2.2E+03	NM	---	---	---
137.5	4.2E-01	2.3E+03	NM	---	---	---
147.5	6.0E-01	2.3E+03	NM	---	---	---

Borehole IC1

Sample Depth (cm)	Gravimetric Water Content (%)	Chloride Content (mg/L)	Pressure Head (cm)	Isotope Sample Depth (cm)	Delta Oxygen-18 (‰)	Delta Deuterium (‰)
2.5	7.9E+00	1.8E+01	NM	2.5	9.9E+00	-1.6E+01
7.5	3.1E+00	4.0E+01	NM	7.5	9.1E+00	-3.0E+01
17.5	2.6E+00	3.7E+01	NM	32.5	-3.0E+00	-6.6E+01
27.5	8.7E+00	4.2E+01	NM	62.5	2.4E+01	-3.9E+01
37.5	7.0E+00	5.4E+01	NM	92.5	-3.1E+00	-6.3E+01
47.5	4.5E+00	7.0E+01	NM	122.5	-3.9E+00	-6.1E+01
57.5	6.3E+00	1.5E+02	NM	142.5	-1.6E+00	-6.2E+01
67.5	9.0E-02	2.8E+03	NM	---	---	---
77.5	5.0E-02	4.4E+03	NM	---	---	---
87.5	2.3E-01	9.2E+02	NM	---	---	---
97.5	2.2E-01	1.1E+03	NM	---	---	---
107.5	7.6E-01	3.2E+02	NM	---	---	---
117.5	1.0E+00	2.2E+02	NM	---	---	---
127.5	5.0E-01	4.3E+02	NM	---	---	---
137.5	8.7E-01	2.8E+02	NM	---	---	---
147.5	7.9E-01	5.1E+02	NM	---	---	---

--- = Not sampled *NM = Not measured*

Borehole IC2

Sample Depth (cm)	Gravimetric Water Content (%)	Chloride Content (mg/L)	Pressure Head (cm)	Isotope Sample Depth (cm)	Delta Oxygen-18 (‰)	Delta Deuterium (‰)
5	2.8E+00	2.5E+01	NM	2.5	2.4E+01	-6.7E+00
17.5	2.4E+00	1.3E+01	NM	7.5	1.3E+01	-1.7E+01
27.5	7.1E+00	1.8E+01	NM	32.5	1.7E+00	-5.6E+01
37.5	3.6E+00	5.9E+01	NM	62.5	---	-3.8E+01
47.5	1.5E+00	2.1E+02	NM	92.5	---	-4.5E+01
57.5	8.9E-01	5.4E+02	NM	122.5	---	-4.9E+01
67.5	1.4E-01	3.5E+03	NM	---	---	---
77.5	5.0E-02	3.1E+03	NM	---	---	---
87.5	2.4E-01	1.9E+03	NM	---	---	---
97.5	2.7E-01	1.6E+03	NM	---	---	---
107.5	2.9E-01	1.4E+03	NM	---	---	---
117.5	3.6E-01	1.1E+03	NM	---	---	---
127.5	5.0E-01	6.3E+02	NM	---	---	---
137.5	6.4E-01	4.0E+02	NM	---	---	---
147.5	5.5E-01	4.5E+02	NM	---	---	---

Borehole IC3

Sample Depth (cm)	Gravimetric Water Content (%)	Chloride Content (mg/L)	Pressure Head (cm)	Isotope Sample Depth (cm)	Delta Oxygen-18 (‰)	Delta Deuterium (‰)
5	3.9E+00	9.1E+01	NM	2.5	1.5E+01	-2.0E+01
17.5	2.2E+00	8.4E+01	NM	7.5	1.5E+01	-1.5E+01
27.5	9.4E+00	1.0E+02	NM	32.5	-1.7E+00	-6.0E+01
37.5	3.2E+00	1.9E+02	NM	62.5	-6.7E+00	-1.1E+02
47.5	2.7E+00	1.7E+02	NM	92.5	-1.7E+00	-5.5E+01
57.5	6.9E+00	2.4E+02	NM	122.5	-6.4E+00	-6.7E+01
67.5	3.1E+00	2.9E+02	NM	142.5	-6.4E+00	-7.1E+01
77.5	6.0E-02	4.0E+03	NM	---	---	---
87.5	6.0E-02	4.4E+03	NM	---	---	---
97.5	6.7E-01	4.3E+02	NM	---	---	---
107.5	6.7E-01	4.7E+02	NM	---	---	---
117.5	1.9E+00	1.7E+02	NM	---	---	---
127.5	1.2E+00	3.3E+02	NM	---	---	---
137.5	1.3E+00	2.9E+02	NM	---	---	---
147.5	1.4E+00	3.9E+02	NM	---	---	---

--- = Not sampled *NM = Not measured*

Borehole IC4

Sample Depth (cm)	Gravimetric Water Content (%)	Chloride Content (mg/L)	Pressure Head (cm)	Isotope Sample Depth (cm)	Delta Oxygen-18 (‰)	Delta Deuterium (‰)
5	3.3E+00	9.4E+01	NM	2.5	1.5E+01	-1.9E+01
17.5	3.2E+00	3.0E+01	NM	7.5	1.6E+01	-1.2E+01
27.5	8.6E+00	2.4E+01	NM	32.5	1.4E+00	-5.6E+01
37.5	1.3E+00	2.8E+02	NM	62.5	4.8E-01	-5.9E+01
47.5	1.5E-01	7.7E+02	NM	92.5	-4.0E+00	-7.5E+01
57.5	1.5E-01	1.1E+03	NM	122.5	-4.7E+00	-6.6E+01
67.5	2.3E-01	7.2E+02	NM	142.5	-4.7E+00	-6.0E+01
77.5	7.4E-01	2.1E+02	NM	---	---	---
87.5	5.4E-01	3.2E+02	NM	---	---	---
97.5	2.8E-01	6.8E+02	NM	---	---	---
107.5	8.6E-01	2.2E+02	NM	---	---	---
117.5	1.1E+00	1.3E+02	NM	---	---	---
127.5	3.5E-01	5.4E+02	NM	---	---	---
137.5	8.0E-01	2.4E+02	NM	---	---	---
147.5	1.4E+00	1.7E+02	NM	---	---	---

--- = Not sampled *NM = Not measured*

LA-UR-08-5468

Approved for public release;
distribution is unlimited.

Title:	Modeling of an Evapotranspiration Cover for the Groundwater Pathway at Los Alamos National Laboratory Technical Area 54, Area G
Author(s):	Daniel G. Levitt
Intended for:	U.S. Department of Energy

Form 836 (7/06)

Table of Contents

List of Figures ii
List of Tables ii
Acronyms and Abbreviations iii

1.0 Introduction 1
2.0 Methods 3
2.1 Selection of the HYDRUS Model 3
2.2 Input Data 4
2.2.1 Atmospheric Input Data 4
2.2.2 Hydraulic Properties 5
2.3 Model Calibration 9
2.4 Model Settings 16
2.5 Simulations Using Variable Conditions 17
3.0 Results and Discussion 23
3.1 Cover Thickness 23
3.2 Hydraulic Properties 29
3.3 Vegetation 29
3.4 Elevated Precipitation 31
3.5 Runoff 31
3.6 Long-Term Simulations 31
3.7 Modeling Uncertainties 34
4.0 Conclusions 39
5.0 References 40

List of Figures

Figure 1 Cross Section of Proposed Evapotranspiration Cover for Area G 2
Figure 2 Calculated Potential Evapotranspiration and Measured Precipitation Based on Data Collected at the TA-54 Weather Station 6
Figure 3 Cover Design from ITP Experiment (Nyhan, 2005) Used for Model Calibration 10
Figure 4 Precipitation Measured at the TA-54 Weather Station and the ITP Site, 1992 Through 1997 12
Figure 5 Water Content and Precipitation from ITP Experiment, 5% Slope Cover 13
Figure 6 HYDRUS Simulations of Soil Water Storage from ITP Experiment, 5% Slope Cover 14
Figure 7 HYDRUS Simulations of Soil Water Content from ITP Experiment, 5% Slope Cover 15
Figure 8 Root Mass Distribution Functions Used in HYDRUS Simulations 22
Figure 9 Cumulative Distribution of Average Annual Drainage Results 26
Figure 10 HYDRUS Projections of Drainage versus Cover Thickness, All Simulations 27
Figure 11 HYDRUS Projections of Drainage versus Cover Thickness, Selected Simulations 28
Figure 12 Cumulative Drainage Results for HYDRUS Simulations 112, 113, and 114 32
Figure 13 Water Storage Results for HYDRUS Simulations 112, 113, and 114 33
Figure 14 Distribution of Annual Precipitation for 1,000-Year Period at MDA H, Estimated Using WGEN 35
Figure 15 Volumetric Water Content at Eight Depths for HYDRUS Simulation 112 36
Figure 16 Comparison of HYDRUS Flux Estimates and Chloride Mass Balance Estimates for Area G 38

List of Tables

Table 1 Summary of Hydraulic Properties Compiled for this Study 7
Table 2 Summary of the 59 HYDRUS-1D Simulations 18
Table 3 Average Annual Drainage and Runoff from All 59 HYDRUS Simulations 24

Acronyms and Abbreviations

1-D	One-dimensional
2-D	Two-dimensional
3-D	Three-dimensional
EPA	U. S. Environmental Protection Agency
ET	Evapotranspiration
GIS	Geographic information system
HELP	Hydrologic Evaluation of Landfill Performance
ITP	Integrated Test Plots
ITRC	Interstate Technology & Regulatory Council
Ksat	Saturated hydraulic conductivity
LANL	Los Alamos National Laboratory
MDA	Material Disposal Area
PE	Potential evaporation
PET	Potential evapotranspiration
PT	Potential transpiration
RCRA	Resource Conservation and Recovery Act
TA	Technical Area
WGEN	Weather GENerator

Acknowledgements

The author would like to thank Rob Shuman, Kay Birdsell, and Mike Sully for their helpful reviews of this work, Jack Nyhan for collecting invaluable datasets for model calibration, and Gary Langhorst for his assistance in locating and providing those datasets. In addition, he would like to acknowledge the work performed by Brent D. Newman and Tracy G. Schofield, which served as the foundation for this modeling effort.

1.0 Introduction

A landfill cover design is being considered for installation as part of the closure process at the Area G Low-Level Radioactive Waste Site, Technical Area (TA) 54, Los Alamos National Laboratory (LANL). Landfill covers are one of the most common management approaches for reducing risks from buried waste sites. Covers serve two primary risk reduction roles. First, they serve as a barrier between the waste and the surface environment, thus reducing the potential for waste exposure by erosion and transport of wastes to the surface by flora and fauna. Second, landfill covers reduce the downward movement of water into and below the waste zone. This decrease in downward flux is expected to reduce the rate of waste container degradation and downward transport of contaminants to the groundwater system. The modeling analysis presented in this report focuses on estimating the downward flux of water through the cover and into the waste zone. Downward flux from the bottom boundary of the waste cover is referred to as drainage in this report and is synonymous with seepage, recharge, or net infiltration.

This assessment evaluates the performance of the Area G evapotranspiration (ET) cover described in Day et al. (2005) (Figure 1). ET covers are intended to provide water storage sufficient to contain spring snowmelt within the cover until it is used through ET later in the year. The cover design proposed for Area G has a variable thickness and is composed of crushed Bandelier Tuff mixed with 6 percent bentonite and 12 percent angular cobbles, and has a shallow surface zone designed to promote plant growth. Additional information on the general performance of ET covers can be found in Bonaparte et al. (2004), Interstate Technology and Regulatory Council (ITRC) (2003), Nyhan (2005), and Scanlon et al. (2002 and 2005).

The remainder of this report describes the approach, results, and discussion of this study. An overview of the HYDRUS software package selected for the modeling and a description of the methods used to conduct the model simulations are provided in Section 2. The results of the modeling, including consideration of modeling uncertainties, are presented and discussed in Section 3.

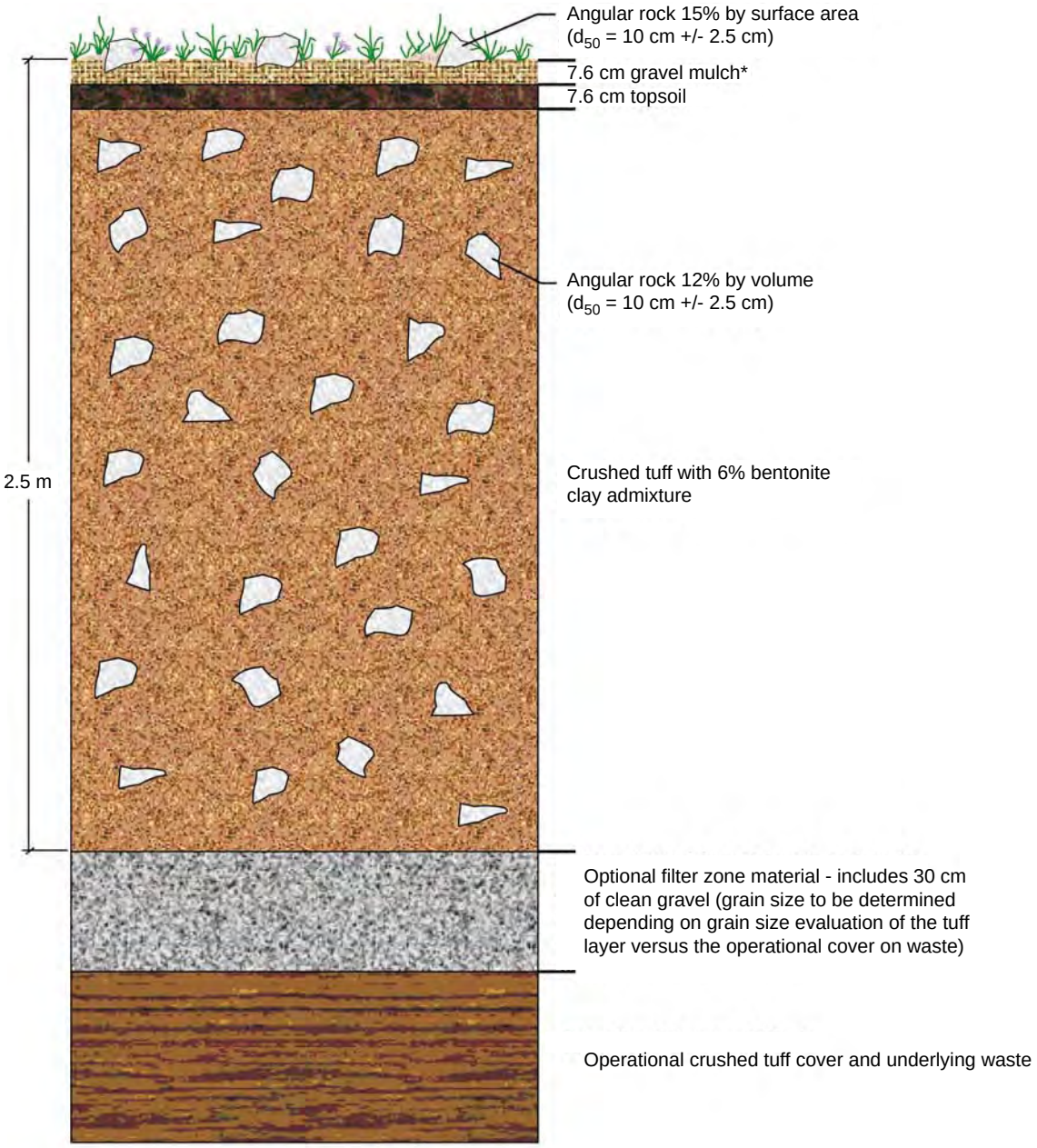

Figure 1
Cross Section of Proposed Evapotranspiration Cover for Area G

2.0 Methods

Three major considerations for this study were the selection of an appropriate modeling package, the selection of representative input datasets, and the sensitivity of the model to variations in conditions such as cover thickness and hydraulic properties. This section explains why HYDRUS was selected to conduct the modeling, details the types of input data required to implement HYDRUS and the values used for the modeling, and describes the simulations used to characterize the performance of the ET cover.

2.1 Selection of the HYDRUS Model

All of the modeling work undertaken to evaluate cover performance at Area G was conducted with HYDRUS-1D, version 3.0 (Šimůnek et al., 2005). The HYDRUS model is based on Richards' equation (the theoretical equation for vertical unsaturated flow) and allows for the analysis of water flow and solute transport in variably saturated porous media. HYDRUS-1D uses a finite-element approach for simulating the one-dimensional (1-D) movement of water, heat, and multiple solutes in variably saturated media. Consequently, it is used extensively to address a wide variety of waste disposal and other hydrologic applications that require consideration of variably saturated porous media. HYDRUS numerically solves the Richards' equation for saturated-unsaturated water flow and Fickian based advection-dispersion equations for heat and solute transport. The water flow part of the model, which was the feature of HYDRUS used specifically for this study, can address constant or time-varying prescribed head or flux boundaries, boundaries controlled by atmospheric conditions, and free-drainage boundary conditions. Unsaturated soil hydraulic properties can be described using a variety of analytical functions (e.g., van Genuchten-type parameters) and both evaporation and root water uptake (transpiration) can be modeled. The HYDRUS package has been extensively tested, used for regulatory-based assessments, and used for research. Additional information on the HYDRUS modeling package can be found in the HYDRUS-1D manual (Šimůnek et al., 2005).

Other landfill performance models based on the Richards' equation (e.g., UNSAT-H) could have been selected for this study; however, using HYDRUS offered several advantages. First, two-dimensional (2-D) and three-dimensional (3-D) versions of HYDRUS (HYDRUS-2D and HYDRUS-3D) are available (Šimůnek et al., 1999), and future studies at Area G may require 2-D or 3-D modeling. Second, models are more easily developed and implemented using HYDRUS because of its graphical interface. Finally, recent versions of the code have received excellent reviews by the scientific community (Selker, 2004).

The Hydrologic Evaluation of Landfill Performance (HELP) model (Schroeder et al., 1994) is often used for landfill cover modeling. However, recent literature (Albright et al., 2002; Scanlon

et al., 2002), the draft U.S. Environmental Protection Agency (EPA) alternative cover guidance (Bonaparte et al., 2004), and ITRC cover guidance (2003) all indicate that HELP is a poor choice for modeling ET and capillary-barrier covers, especially in semiarid environments. This is mainly because the HELP model is not based on Richard's equation and thus cannot properly represent the dynamics of water content changes and fluxes, particularly under dry climate conditions. Also, HELP is limited to 1-D or pseudo 2-D modeling.

2.2 Input Data

The HYDRUS model requires various input parameters to define the atmospheric boundary conditions for the simulations and to specify the hydraulic properties of the cover materials. This section discusses the data selected to characterize these parameters. A total of 59 model simulations were conducted to evaluate the ranges of input data discussed below.

2.2.1 Atmospheric Input Data

The atmospheric input data (e.g., site-specific precipitation and potential ET time-series values) are important controls on how well a landfill cover model actually represents cover performance (Bonaparte et al., 2004; ITRC, 2003). These data can be a key source of uncertainty, especially in semiarid environments where the ET and precipitation are of similar magnitudes, and precipitation is highly variable in time and space. Because of the importance of the atmospheric input data to the modeling, substantial effort was spent in determining the best approach for constraining the atmospheric boundary in HYDRUS. The objective of this effort was to develop input data that accurately represent the site under current climatic conditions. The paramount concern in developing atmospheric input data was to constrain ET, as this is often where the greatest uncertainty exists. Overestimation of ET leads to underprediction of downward fluxes (drainage) and vice versa.

Potential ET (PET), the driving force for ET that represents the climatic demand for water, was calculated using the method of Doorenbos and Pruitt (1977) described in Jensen et al. (1990). This PET calculation method is a solar radiation method and was selected to complement the meteorological data available from TA-54 (LANL, 2008). Data inputs required for this method include daily maximum and minimum air temperature, average relative humidity, average wind speed, average barometric pressure, and daily incoming solar radiation. A near-complete data record of these parameters for the 15-year period from January 1, 1993 through December 31, 2007 is available for a weather station at TA-54. Sporadic missing data were replaced with the previous day's value, or with zero for precipitation.

The average PET for this 15-year period was calculated to be 1,736 mm/yr (68 in./yr) using the Doorenbos and Pruitt (1977) method. Considering that different PET calculation methods will yield somewhat different PET estimates, this value compares reasonably well with the average value of 1,996 mm/yr (79 in./yr) calculated using the TA-54 data for 1992 to 2001 and reported in LANL

(2003, Section 2.1.3.1). Calculated PET and measured precipitation from the TA-54 weather station are shown in Figure 2 for the 15-year period from January 1, 1993 through December 31, 2007.

HYDRUS-1D requires the separation of daily PET into inputs of potential evaporation (PE) and potential transpiration (PT). In the case of an unvegetated cover, PT is zero for all days, and PE is equal to some fraction of PET. In the case of a fully vegetated cover, PE is generally set to zero, and PT is equal to PET or some fraction of PET. The fraction of PET used depends on many factors, and this fraction (f) can be used as a model calibration variable. In this study, PE (PE = PET × f) was estimated as part of the model calibration effort described in Section 2.3, using data collected for unvegetated covers. Potential transpiration was subsequently bounded to address the effects of vegetation on water balance; a range of values (0.1 to 0.5) of f was used to estimate PT (PT = PET × f) because the Area G vegetation is not expected to be a full cover, even under climax conditions.

2.2.2 Hydraulic Properties

The hydraulic properties (e.g., saturated hydraulic conductivity [Ksat] and the van Genuchten parameters) of the materials used in the cover have a major effect on the rate at which water flows through the waste cover. Two cover materials were the focus of the modeling conducted in this study: a top layer that consists of crushed tuff with 6 percent bentonite, and a lower layer that consists solely of crushed tuff. The lower, crushed tuff layer was included to represent the operational cover placed over disposal units during interim closure (Figure 1).

The hydraulic properties of crushed tuff from TA-53, compiled from several sources, are presented in Table 1. Material 1, reported in van Genuchten et al. (1987, Table 2), has a Ksat that is intermediate to the other Ksats reported for crushed tuff. Because of this, the hydraulic properties for material 1 were selected for most of the simulations. However, some simulations used the properties for crushed tuff materials 2 and 4 (Table 1) to investigate the effects of different crushed tuff properties.

Unfortunately, no hydraulic measurements are available for the 6-percent bentonite/crushed tuff mixture used in the Area G cover design. When crushed tuff is mixed with small percentages of bentonite, the Ksat decreases dramatically. For example, the addition of 10 percent bentonite can cause the Ksat to decrease by four orders of magnitude (Nyhan et al., 1997). In fact, a 10-percent bentonite addition reduces conductivity to such an extent that the resultant crushed tuff/bentonite material is equivalent to the “impermeable” clay layer used in the EPA Resource Conservation and Recovery Act (RCRA) cover design (Nyhan et al., 1997).

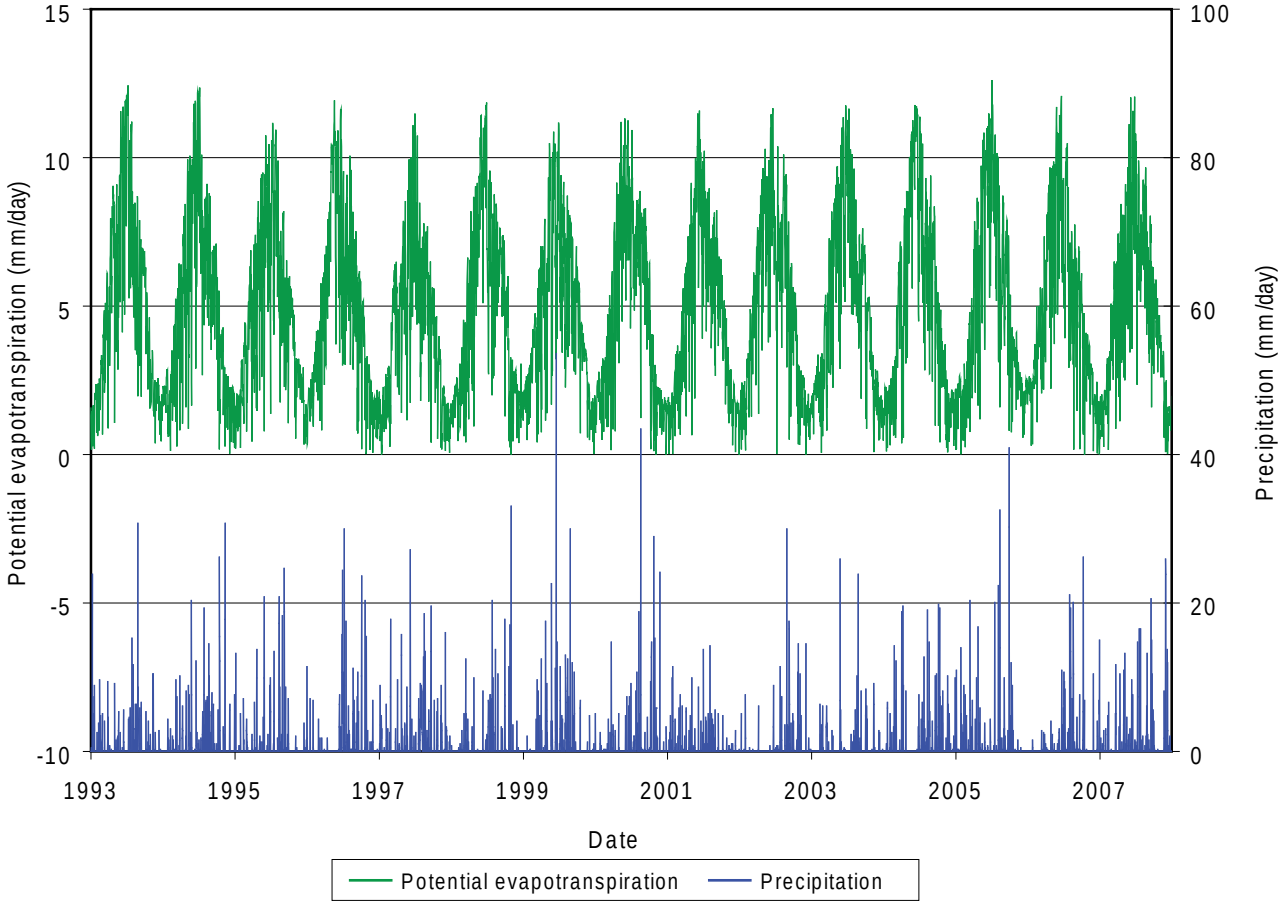

Figure 2
Calculated Potential Evapotranspiration and Measured Precipitation Based on Data Collected at the TA-54 Weather Station

Table 1
Summary of Hydraulic Properties Compiled for this Study

Material		Residual Water Content	Saturated Water Content	van Genuchten Parameters		Saturated Hydraulic Conductivity		Source
No.	Description			***α*** (1/m)	*n*	m/d	cm/s	
1	Crushed tuff	1.0E-02	3.3E-01	1.43E+00	1.5E+00	2.5E-01	2.9E-04	van Genuchten et al., 1987, Table 2.
2	Crushed tuff	3.1E-03	4.1E-01	1.04E+00	1.7E+00	7.1E-01	8.2E-04	Nyhan et al., 1997, Table 1.
3	Crushed tuff	0.0E+00	3.8E-01	8.3E-01	1.8E+00	7.1E-01	8.2E-04	Rogers and Gallaher, 1995, Table B1, Stephens data
4	Crushed tuff	0.0E+00	4.0E-01	4.49E+00	1.38E+00	8.0E-02	9.2E-05	Rogers and Gallaher, 1995, Abeele 1979 data
5	Crushed tuff	---	4.0E-01	---	---	1.2E-01	1.4E-04	Rogers and Gallaher, 1995, Table B1, Abeele 1984 data
6	Crushed tuff with 6% bentonite	4.0E-03	4.0E-01	8.8E-02	3.0E+00	1.6E-03	1.8E-06	Linear interpolation between materials 1 and 12.
7	Crushed tuff with 4–6% bentonite, MDA J, surface layer	---	---	---	---	3.3E-03	3.8E-06	Wald-Hopkins, 2004, Table 8.
8	Crushed tuff with 4–6% bentonite, MDA J, surface layer	---	---	---	---	1.5E-01	1.7E-04	Cocina, 2006, Table 5-1
9	Crushed tuff with 4–6% bentonite, MDA J, 15-cm depth	---	---	---	---	1.3E-01	1.5E-04	Cocina, 2006, Table 5-1
10	Crushed tuff with 4–6% bentonite, MDA J, 25-cm depth	---	---	---	---	3.0E-03	3. 5E-06	Cocina, 2006, Table 5-1
11	Crushed tuff with 6% bentonite	---	---	---	---	2.2E-03 – 2.4E-05	2.5E-06 – 2.8E-08	Abeele, 1984, Table III.
12	Crushed tuff with 10% bentonite	0.0E+00	4.4E-01	1.4E-02	4.0E+00	5.4E-05	6.30E-08	Nyhan et al., 1997, Table 1.

--- = Not measured or not provided in original source.

Table 1 also includes published values of Ksats for crushed tuff mixed with various percentages of bentonite. Two reports (Wald-Hopkins, 2004 and Cocina, 2006) provide Ksat values for crushed tuff and 4-to-6-percent bentonite/crushed tuff mixtures from measurements at LANL Material Disposal Area (MDA) J. The highest published Ksat value for a crushed tuff and 4- to 6-percent bentonite mixture is 1.7×10^{-4} cm/s (5.6×10^{-6} ft/s) (Cocina, 2006). Abeele (1984) conducted a laboratory and modeling study of crushed tuff mixtures with various proportions of bentonite and presents methods for predicting Ksat at various compactions for a given percentage of bentonite. When used to estimate Ksat for the 6-percent bentonite admixture, these models yielded values ranging from 2.5×10^{-6} to 2.8×10^{-8} cm/s (8.2×10^{-8} to 9.2×10^{-10} ft/s) (using Table III in Abeele, 1984). Nyhan et al. (1997) reported a Ksat of 6.3×10^{-8} cm/s (2.1×10^{-9} ft/s) for a 10-percent bentonite/crushed tuff mixture.

The hydraulic conductivity of the 6-percent bentonite/crushed tuff mixture was estimated by interpolating between the properties of crushed tuff and the 10-percent bentonite mixture reported in Nyhan et al. (1997). The crushed tuff properties used in this calculation are those reported by van Genuchten (1987, Table 2). The estimated Ksat for the 6-percent bentonite/crushed tuff mixture was 1.8×10^{-6} cm/s (5.9×10^{-8} ft/s); this value is within the range reported by Abeele (1984) and similar to two of the four MDA J Ksat measurements. Different hydraulic properties were not calculated for the crushed tuff/bentonite mixture in conjunction with the use of crushed tuff materials 2 and 4. This is because the uncertainty in Ksat as a result of the interpolation method is probably greater than the variability of crushed tuff hydraulic properties. However, high and low Ksat values for the crushed tuff/bentonite mixture were included among the 59 model simulations.

The linear interpolation approach was also used to estimate the water content at saturation, the residual water content, and the van Genuchten α (in log space) and n parameters. These parameters are used to estimate unsaturated hydraulic conductivities under varying water content conditions. The linear interpolation approach was pragmatic, given that there were data for only two crushed tuff/bentonite mixtures and that all of these properties are highly nonlinear. The approach was discussed with Rien van Genuchten from the George E. Brown, Jr. Salinity Laboratory (operated by the U.S. Department of Agriculture), who concurred that estimation using linear interpolation was probably the best available approach given the lack of measurements (van Genuchten, 2004). However, the hydraulic properties developed for the crushed tuff/bentonite layer are highly uncertain, the impacts of which are discussed in Section 3.

Topsoil and gravel mulch layers are also shown in Figure 1; these features were excluded from all but 3 of the 59 HYDRUS simulations. It was anticipated that these layers would have little impact on the overall performance of the cover. This approach was consistent with the surface erosion modeling conducted in support of the Area G performance assessment and composite

analysis (Wilson et al., 2005), which also did not explicitly consider these layers. In addition, an optional gravel filter zone is shown in Figure 1. This layer was not included in any simulations because the performance assessment and composite analysis do not assume it is present in the final cover configuration.

2.3 Model Calibration

Model calibration was undertaken using HYDRUS for two reasons. First, it helped identify suitable values for some of the input parameters required to conduct the simulations. Second, it provided an opportunity to observe how well model projections resembled the actual behavior of engineered covers. The scope of this effort and the results of the modeling are described below.

Although ET cover monitoring data that could be used for model calibration (or validation) do not yet exist for the proposed Area G cover design, a nearby research site at TA-54 known as the Integrated Test Plot (ITP) experiment has collected long-term water balance datasets for a variety of landfill cover designs. Nyhan et al. (1990) describe the performance of two landfill cover designs at the ITP site: a conventional topsoil and crushed tuff design, and a capillary barrier design. Nyhan et al. (1997) describe the performance of four landfill cover designs with varied slopes. The four designs represent a conventional cover, an EPA recommended cover, and two capillary barrier designs. Nyhan (2005) describes the performance of an unvegetated landfill cover design (a conventional design of topsoil and crushed tuff) with slopes of 5, 10, 15, and 20 percent. Figure 3 shows the cover design from Nyhan (2005).

Water balance monitoring data are available for December 1, 1991 through December 31, 1997 from the Nyhan (2005) experiment. These data include precipitation, drainage, runoff, and interflow as well as the change in soil water content at three depths within each unvegetated cover. Nyhan et al. (1997) provide the hydraulic properties for the cover materials described in Nyhan (2005). Together, the data from Nyhan (2005) and Nyhan et al. (1997) provide water balance data and hydraulic properties that can be used for model calibration. Given the nature of the data from Nyhan (2005) and Nyhan et al. (1997), the basis of the model calibration is to compare simulated to measured water contents within the unvegetated cover described by Nyhan (2005), and to make appropriate adjustments to improve the comparison. These same adjustments may then be applied to the Area G cover simulations, as appropriate.

A HYDRUS simulation was set up to match the cover design shown in Figure 3 (from ground surface to the geotextile layer) and described in Nyhan (2005). The 5-percent slope cover was selected for model calibration since it most closely matches the slope range of 2 to 10 percent that is used in the Area G cover design (Day et al., 2005). Drainage from the cover was set as a boundary condition in the modeling; the interflow measured by Nyhan et al., (2005) was added to the measured drainage because interflow occurred at the geotextile layer and HYDRUS 1D does not account for lateral flow. Runoff measured for the cover design was subtracted from the

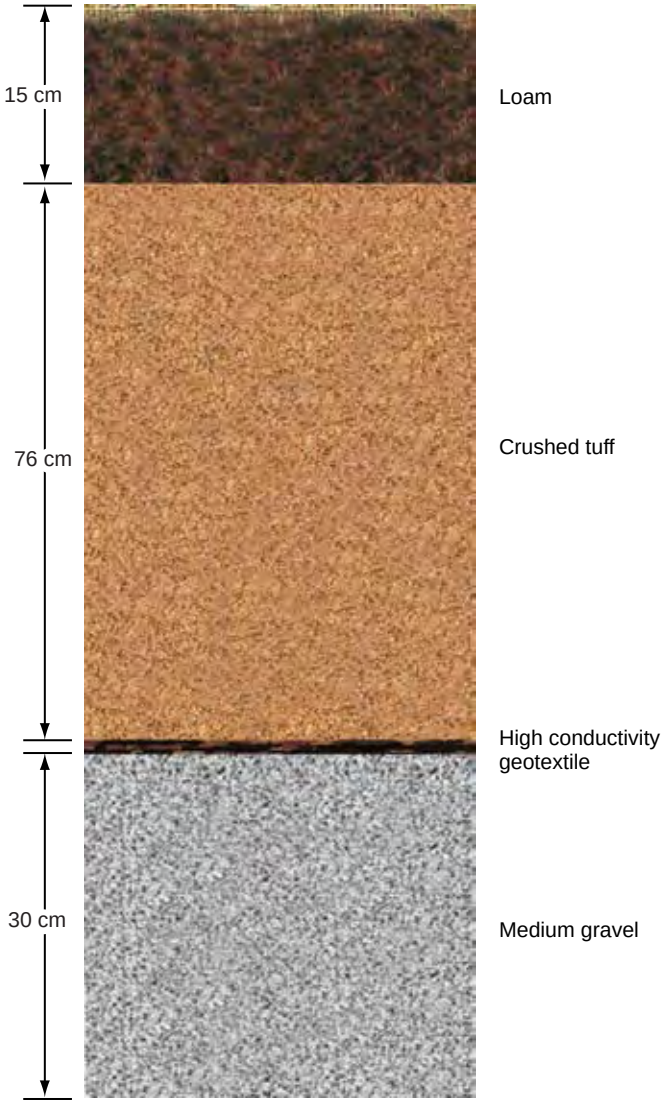

Figure 3
Cover Design from ITP Experiment (Nyhan, 2005)
Used for Model Calibration

Source*: Nyhan (2005), Figure 2*

total precipitation input to HYDRUS because HYDRUS-1D did not calculate any runoff for the model calibration simulations. The lack of projected runoff resulted from the use of daily time steps (since only daily precipitation data were available); higher resolution data are generally needed to obtain projections of overland flow.

The Nyhan datasets do not include the data necessary to calculate PET, so weather data from the TA-54 weather station (LANL, 2008) were used to calculate PET, using the approach described previously. Because the TA-54 weather station dataset begins on January 29, 1992, the model calibration runs used atmospheric data inputs from January 29, 1992 through December 31, 1997 (5.9 years). Precipitation data measured at the ITP site were used rather than the precipitation record from the TA-54 weather station. The precipitation records from the ITP experiment and from the TA-54 weather station are surprisingly different. Average annual precipitation for the 5.9-year period was 462 and 380 mm/yr (18.2 and 15.0 in./yr) for the ITP and TA-54 datasets, respectively. The ITP dataset was assumed to be more appropriate for the model calibration since it represented the precipitation conditions to which the cover was exposed. Annual precipitation values measured at TA-54 and the ITP site are shown in Figure 4.

Total drainage, runoff, and interflow measured for the 5-percent slope cover were 28, 36, and 99 mm (1.1, 1.4, and 3.9 inches), respectively (Nyhan et al., 2005); Figure 5 shows the measured precipitation and water content data for the cover. Numerous HYDRUS simulations were conducted to try to reproduce the water contents shown in the figure, adjusting the PE multiplier and some hydraulic properties to improve the comparison. For the initial calibration, referred to as the nominal fit, the PE multiplier was set to 0.25 (PE = PET × 0.25); no other model input parameters were varied. The results of the calibration are shown in Figures 6 and 7. Figure 6 compares the measured and simulated total water storage; Figure 7 compares measured and simulated water contents at three locations within the cover profile. As shown in Figure 7, the nominal fit tends to overestimate the water contents in the topsoil and underestimate water contents in the lowest portion of the profile (75 to 91 cm [2.5 to 3.0 feet]).

A second calibration was conducted in which the PE multiplier was set to 0.25, the residual water content of the topsoil was reduced (from 0.07 to 0.0), and the saturated water content within the 75 to 91 cm (2.5 to 3.0 feet) interval was increased (from 0.41 to 0.5). Referred to as the adjusted fit, this simulation was conducted to try to improve upon the fit between the data and the model projections; this calibration effort also addressed some data discrepancies noted between the measured water contents and the hydraulic parameters presented in Nyhan et al. (1997). The results for the adjusted fit are also shown in Figures 6 and 7 and indicate that the water contents projected by the model tended to improve within the topsoil and deep cover intervals.

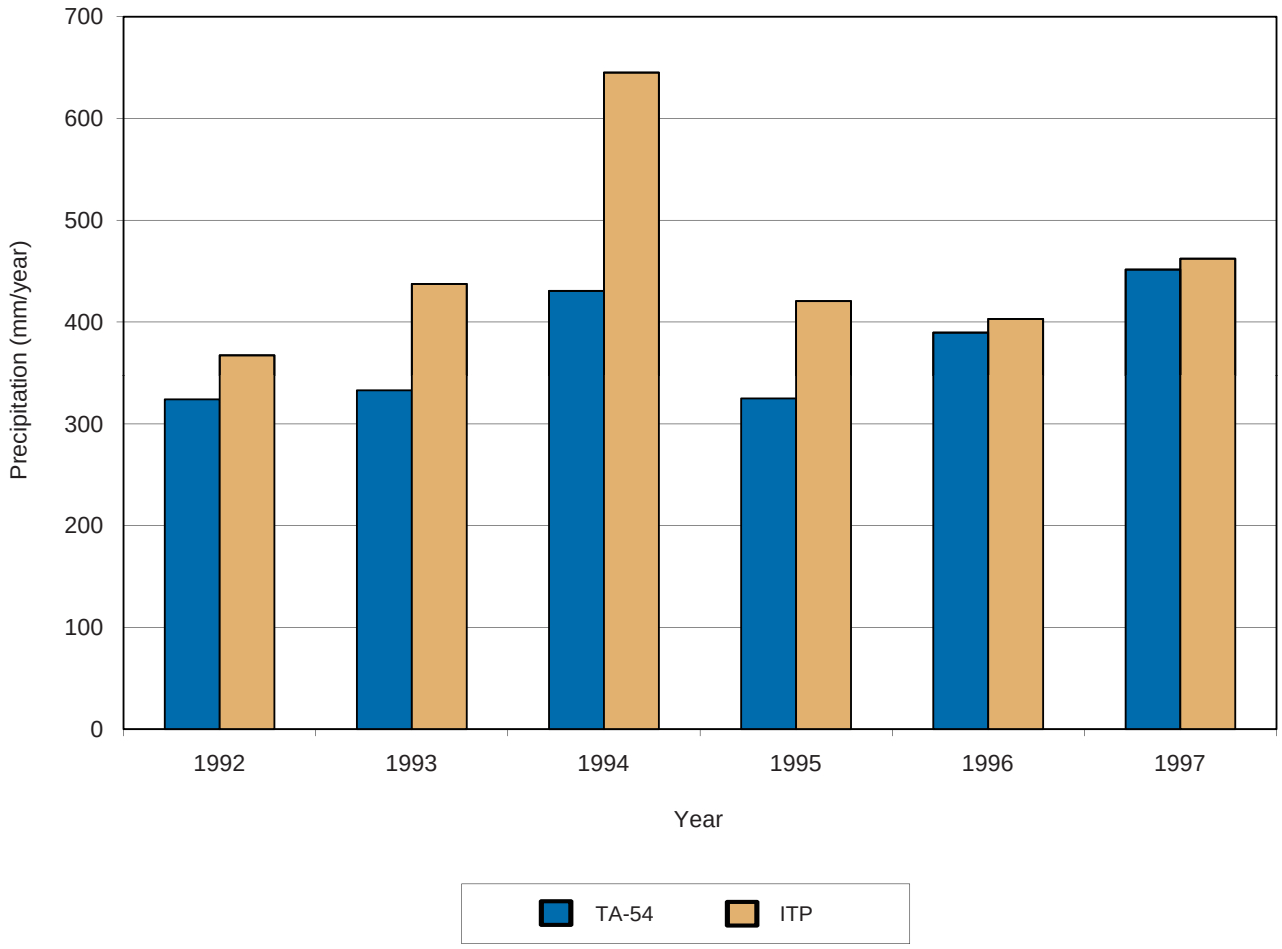

Figure 4
Precipitation Measured at the TA-54 Weather Station and the ITP Site, 1992 Through 1997

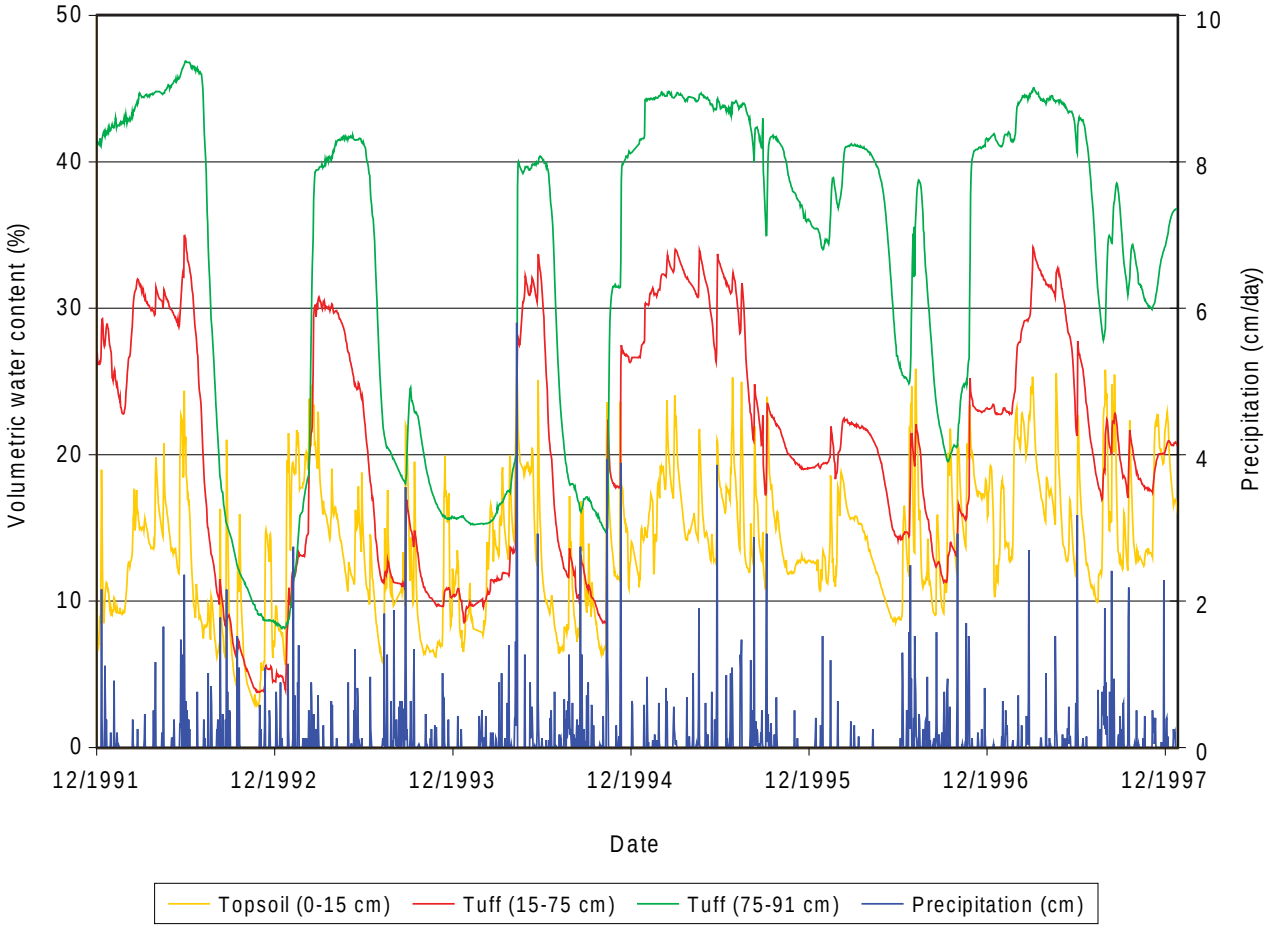

Figure 5
Water Content and Precipitation from ITP Experiment, 5% Slope Cover

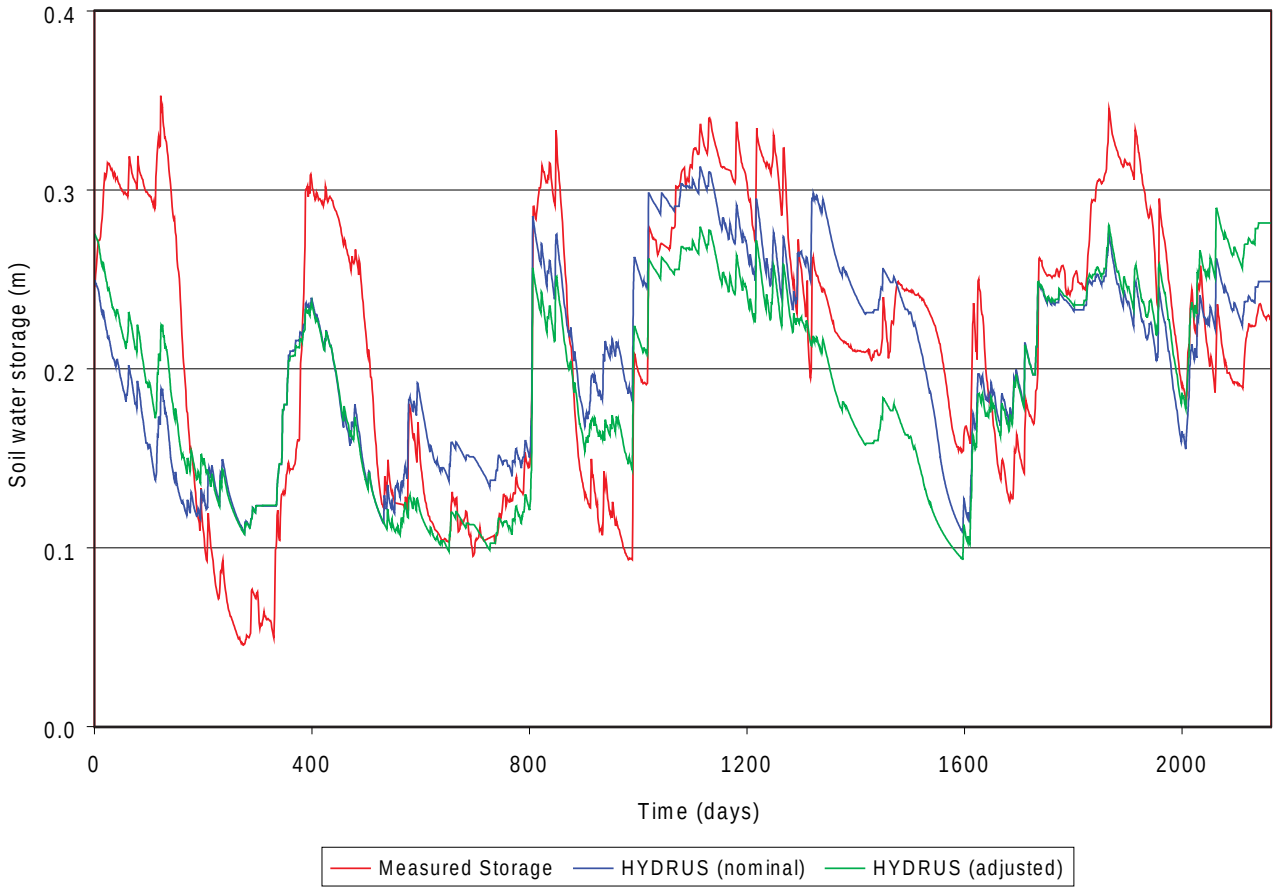

Figure 6
HYDRUS Simulations of Soil Water Storage from ITP Experiment, 5% Slope Cover

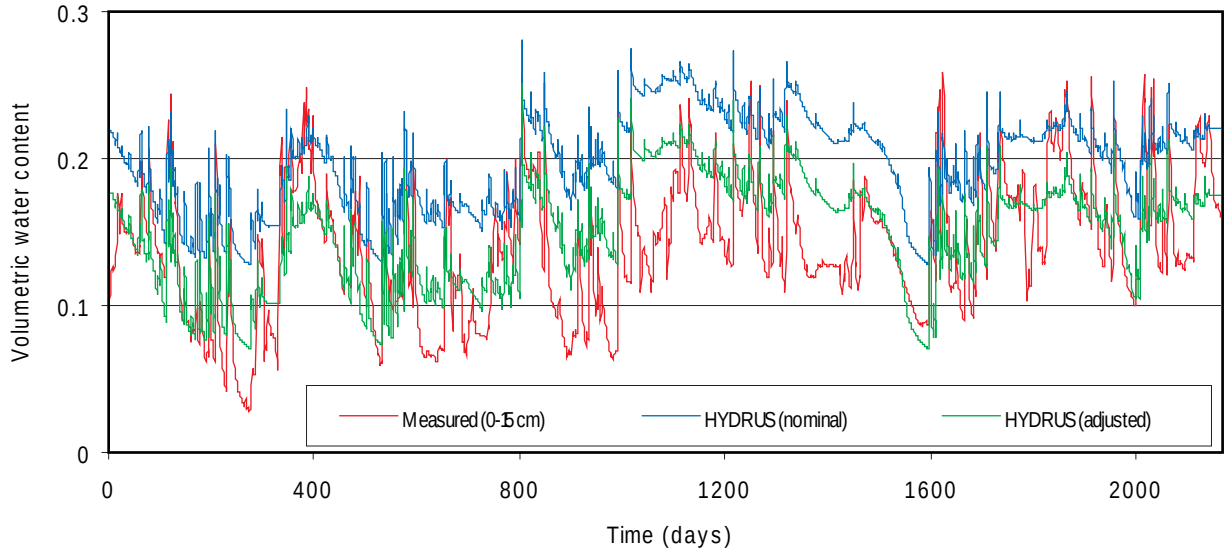

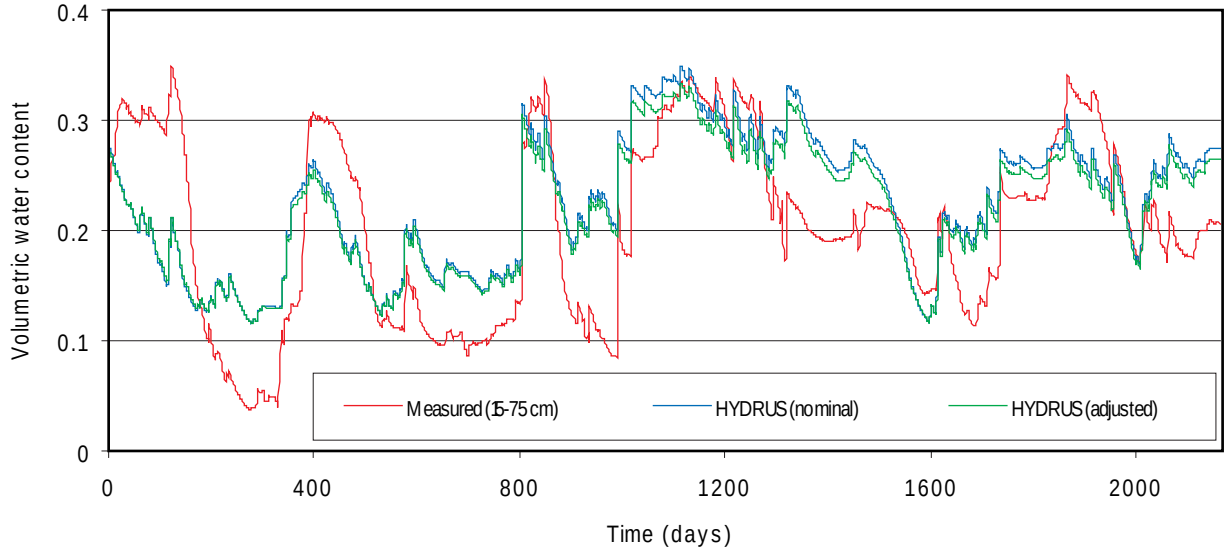

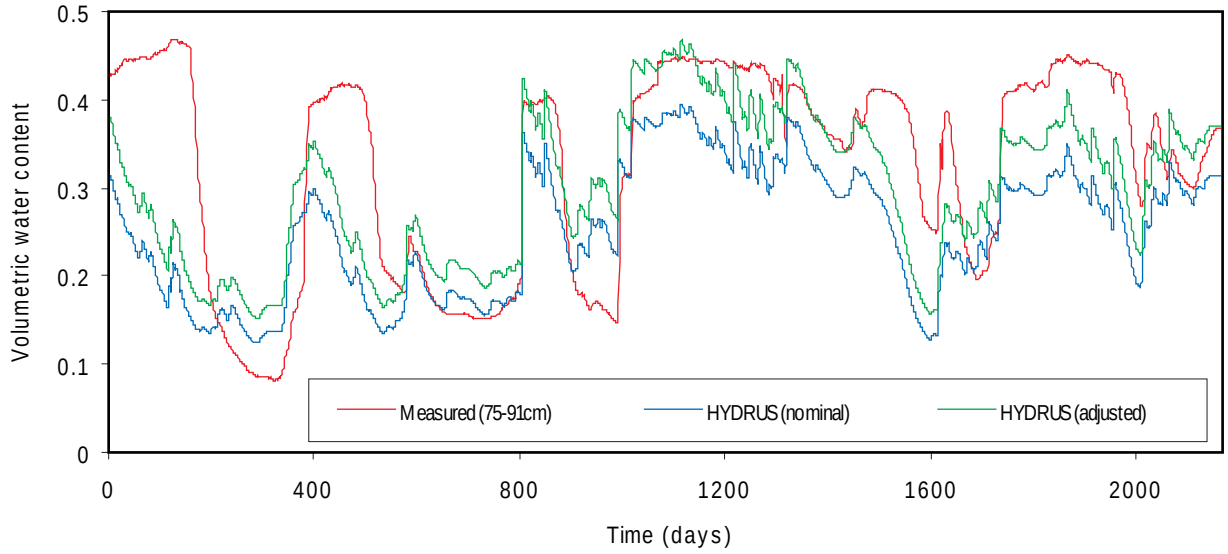

Figure 7
HYDRUS Simulations of Soil Water Content from ITP Experiment, 5% Slope Cover

That the model did not accurately predict the field conditions is not surprising, given the uncertainty and heterogeneity inherent in the hydraulic properties of the crushed tuff/. Nevertheless, it is clear from the results provided in Figures 6 and 7 that HYDRUS captures the overall trends in water content observed by Nyhan et al. (2005) Additional calibration will likely improve upon the level of agreement between the measured and modeled values.

The results of the calibration effort helped define the PE multiplier used in the Area G cover performance modeling. Daily evaporation is estimated as PE = PET × 0.25 for all HYDRUS simulations of the Area G cover. The changes to the hydraulic parameters made for the adjusted fit were not applied to the Area G cover simulations because the hydraulic properties of the cover characterized by Nyhan et al. (1997) and the Area G cover are not the same.

2.4 Model Settings

A series of 59 HYDRUS model simulations was conducted to characterize the performance of the Area G ET cover depicted in Figure 1. The model settings used to conduct these simulations are described below.

Heat flow: All HYDRUS simulations were run with heat flow set to simulate snow hydrology. Air temperature data were obtained from the TA-54 weather station dataset. Thermal properties were taken from HYDRUS pull-down menus, with clay and sand properties used for the first and second layers of the Area G cover, respectively.

Snow: All HYDRUS simulations were run with snow hydrology simulated. One HYDRUS input for snow is the snowmelt constant, which was set to 2 mm/day (0.079 in./day) snowmelt per °C increase above 2°C (36°F). This value is consistent with the range of snowmelt coefficients in Maidment (1993, p. 7.24). HYDRUS results are not sensitive to this parameter.

HcritA: This is the minimum allowed pressure head at the soil surface, which was set to –150 m tension (–15 bars or –218 PSI) for all simulations. HYDRUS results are not sensitive to this parameter.

Gridding: Model grid spacing varied from simulation to simulation. In general, the number of nodes approximately matched the model depth in centimeters, plus one (i.e., a 200-cm [79-inch] deep profile was simulated with 201 grids). The lower grid density was set to 0.5 which generated nonuniform grid spacings of approximately 0.6 cm (0.24 inch) at the ground surface to 1.3 cm (0.51 inch) at the lower boundary.

Boundary Conditions: The bottom boundary condition for all 59 simulations was set to free drainage. The top boundary condition for all 59 simulations was set to an atmospheric boundary condition with surface water runoff.

Initial Conditions: Initial conditions varied from simulation to simulation. The initial pressure head conditions for every simulation were varied until equilibrium pressure head and water content conditions were established. For example, if initial conditions were too wet, then water contents over 15 years displayed a decreasing trend and drainage was overestimated. If initial conditions were too dry, then water contents displayed an increasing trend and drainage was underestimated. In some cases, the initial conditions were adequately approximated using a single value of pressure head for a layer, but in most cases a pressure head gradient was used for the initial conditions (i.e., for most of the vegetated simulations). This approach ensures that the simulated profiles are stable and not in a long-term wetting or draining status.

2.5 Simulations Using Variable Conditions

Simulations were varied to explore the effects of changes in total cover thickness, hydraulic properties, and vegetation properties. In addition, several simulations were run with elevated precipitation. Table 2 describes general aspects of the 59 model simulations that were run. All 59 simulations were run using the 15-year daily atmospheric boundary data measured at the TA-54 weather station, and all simulations used PE = PET × 0.25.

Cover thickness: The effects of cover thickness were evaluated for nearly every model scenario listed in Table 2, using total cover thicknesses of 2, 3, and 4 m (6.6, 9.8, and 13 feet). The thickness of the crushed tuff/bentonite layer (referred to as the tuff+clay or T+C layer) was variable while the underlying crushed tuff layer was nearly always 1-m (3.3-feet) thick. In simulations 115 and RS2, the T+C and crushed tuff layers were each 2-m (6.6 feet) thick.

Hydraulic properties: All 59 model simulations used the van Genuchten–Mualem hydraulic property model, with no hysteresis. The nominal hydraulic properties used for the crushed tuff layer and the crushed tuff/bentonite layer are described in Section 2.2.2 and shown in Table 1 as materials 1 and 6. Many simulations were run to test the effects of different hydraulic properties. Simulations 55, 56, and 57 tested the effects of a high-Ksat T+C layer (material 8 in Table 1) while simulations 58, 59, 60, 62, 63, 64, RS10a, RS10b, and RS10c tested the effects of a low-Ksat T+C layer (material 12 in Table 1). Simulations 42, 43, 44, 55, 56, 57, 58, 59, 60, RS9a, RS9b, RS9c, and RS14 tested the effects of a high-Ksat crushed tuff layer (material 2 in Table 1) while simulations 52, 53, 54, 62, 63, 64, RS10a, RS10b, and RS10c tested the effects of a low-Ksat tuff layer (material 4 in Table 1). Finally, simulations 92, 93, and 94 include the gravel mulch and topsoil layers shown in Figure 1. Hydraulic properties for these layers were taken from the HYDRUS pull-down menu by selecting loam for both the topsoil and gravel layers (because the gravel layer includes topsoil), and then reducing the gravel layer saturated water content from 0.43 to 0.33, reducing the gravel layer residual water content from 0.08 to 0.01, and increasing the gravel layer Ksat from 0.2 to 2 m/day (0.66 to 6.6 ft/day) to adjust for the gravel.

Table 2
Summary of the 59 HYDRUS-1D Simulations

Simulation No.	Cover Thickness (m)			Plants	Initial Head (m)		Model Scenario
	Layer 1	Layer 2	Total		Layer 1	Layer 2	
112	1	1	2	No	–12		T+C; Tuff1 (base case)
113	2	1	3	No	–12		
114	3	1	4	No	–11	–12	
115	2	2	4	No	–11	–12	T+C (2 m); Tuff1 (2 m)
42	1	1	2	No	–12		T+C; Tuff2 (high Ksat)
43	2	1	3	No	–12		
44	3	1	4	No	–11	–12	
52	1	1	2	No	–12		T+C; Tuff4 (low Ksat)
53	2	1	3	No	–12		
54	3	1	4	No	–11	–12	
55	1	1	2	No	–20		T+C (high Ksat); Tuff2 (high Ksat)
56	2	1	3	No	–22		
57	3	1	4	No	–23		
58	1	1	2	No	–55		T+C (low Ksat); Tuff2 (high Ksat)
59	2	1	3	No	–60		
60	3	1	4	No	–60		
62	1	1	2	No	–55		T+C (low Ksat); Tuff4 (low Ksat)
63	2	1	3	No	–60		
64	3	1	4	No	–60		

T+C = tuff + clay (bentonite)
Tuff1 = Material 1 as described in Table 1
Tuff2 = Material 2 as described in Table 1
Ksat = Saturated hydraulic conductivity
Tuff4 = Material 4 as described in Table 1
PT = Potential transpiration

[a] *A range of numbers implies a gradient.*

Table 2 (Continued)
Summary of the 59 HYDRUS-1D Simulations

Simulation No.	Cover Thickness (m)			Plants	Initial Head (m)		Model Scenario
	Layer 1	Layer 2	Total		Layer 1	Layer 2	
RS4	1	1	2	Yes	–80 to –75		T+C; Tuff1; Grass; 2 m curvilinear roots (base case)
RS1	2	1	3	Yes	–80 to –60		
RS3	3	1	4	Yes	–80 to –65		
RS2	2	2	4	Yes	–80 to –65		T+C (2 m); Tuff1 (2 m); Grass; 2 m curvilinear roots
RS5a	1	1	2	Yes	–80 to –75		T+C; Tuff1; Grass; 1 m curvilinear roots
RS5b	2	1	3	Yes	–80 to –60		
RS5c	3	1	4	Yes	–80 to –65		
RS6a	1	1	2	Yes	–80 to –75		T+C; Tuff1; Trees; 6 m curvilinear roots
RS6b	2	1	3	Yes	–80 to –60		
RS6c	3	1	4	Yes	–80 to –65		
RS7a	1	1	2	Yes	–80 to –75		T+C; Tuff1; Grass; 2 m linear roots
RS7b	2	1	3	Yes	–80 to –60		
RS7c	3	1	4	Yes	–80 to –65		
RS8a	1	1	2	Yes	–30		T+C; Tuff1; Grass; 2 m curvilinear roots; low PT
RS8b	2	1	3	Yes	–25		
RS8c	3	1	4	Yes	–25		
RS9a	1	1	2	Yes	–80 to –75		T+C; Tuff2 (high Ksat); Grass; 2 m curvilinear roots
RS9b	2	1	3	Yes	–80 to –60		
RS9c	3	1	4	Yes	–80 to –65		
RS10a	1	1	2	Yes	–80 to –75		T+C (low Ksat); Tuff4 (low Ksat); Grass; 2 m curvilinear roots
RS10b	2	1	3	Yes	–80 to –60		

T+C = tuff + clay (bentonite)
Tuff1 = Material 1 as described in Table 1
Tuff2 = Material 2 as described in Table 1
Ksat = Saturated hydraulic conductivity
Tuff4 = Material 4 as described in Table 1
PT = Potential transpiration

[a] *A range of numbers implies a gradient.*

Table 2 (Continued)
Summary of the 59 HYDRUS-1D Simulations

Simulation No.	Cover Thickness (m)			Plants	Initial Head (m)		Model Scenario
	Layer 1	Layer 2	Total		Layer 1	Layer 2	
RS10c	3	1	4	Yes	–80 to –65		
RS11a	1	1	2	Yes	–80 to –75		Vegetated base case; precipitation × 2
RS11b	2	1	3	Yes	–80 to –60		
RS11c	3	1	4	Yes	–80 to –65		
92	1	1	2	Yes	–75		Vegetated base case + gravel + topsoil layers
93	2	1	3	Yes	–75		
94	3	1	4	Yes	–80 to –65		
RS12	1	1	2	Yes	–20 to –80		T+C; Tuff1; Trees; 6 m curvilinear roots; low PT; 2 m cover
RS13	1	1	2	Yes	–40 to –80		T+C; Tuff1; Trees; 6 m curvilinear roots; high PT; 2 m cover
RS14	1	1	2	Yes	–20 to –40		T+C; Tuff2; Grass; 1 m curvilinear roots; low PT; 2 m cover
RS15a	1	1	2	Yes	–60	–75	T+C; Tuff1; Grass; 2 m curvilinear roots; medium PT
RS15b	2	1	3	Yes	–60 to –75	–75	
RS15c	3	1	4	Yes	–60 to –75	–75	
RS16a	1	1	2	Yes	–60	–75	T+C; Tuff1; Trees; 6 m linear roots
RS16b	2	1	3	Yes	–60	–75	
RS16c	3	1	4	Yes	–60	–75	
RS17a	1	1	2	Yes	–60	–75	T+C; Tuff1; Trees; 6 m curvilinear roots; medium PT
RS17b	2	1	3	Yes	–60	–75	
RS17c	3	1	4	Yes	–60 to –75	–75	

T+C = tuff + clay (bentonite)
Tuff1 = Material 1 as described in Table 1
Tuff2 = Material 2 as described in Table 1
Ksat = Saturated hydraulic conductivity
Tuff4 = Material 4 as described in Table 1
PT = Potential transpiration

[a] *A range of numbers implies a gradient.*

Vegetation: Many simulations were run to investigate the effects of vegetation properties including the PT multiplier, rooting depths, and root mass density functions. Of the 59 model simulations described in this report, 40 simulated a vegetated cover. For all 40 vegetated simulations, the Feddes root uptake model was used. This root uptake model was recommended by J. Šimůnek (Šimůnek, 2005) over the S-shaped model (the other root uptake model included in HYDRUS) (Šimůnek et al., 2005). As discussed in Section 2.3, all simulations used PE = PET × 0.25. However, PT was estimated using a range of multipliers from 0.1 to 0.5. A value of PE = PET × 0.25 and PT = PET × 0.5 indicates that actual ET is approximately equal to PET × 0.75 (i.e., under saturated or near-saturated conditions).

Rooting depths were set to 1, 2, or 6 m (3.3, 6.6, or 20 feet). Root mass distribution functions were usually simulated using a curvilinear beta distribution with beta = 5 and alpha = 1. Simulations RS7a, RS7b, RS7c, RS16a, RS16b, and RS16c used a linear distribution such that the relative weight was 1 at ground surface, and zero at the maximum rooting depth. Root mass distribution functions used in this study are shown in Figure 8. Root growth with growing season was not simulated, but rather, established vegetation scenarios were simulated using root uptake options.

Elevated precipitation: Three simulations (RS11a, RS11b, and RS11c) were run with daily precipitation multiplied by two. These simulations were included to simulate extraordinarily wet periods, potential future glacial-transition, or full-glacial climates for cover thicknesses of 2, 3, and 4 m (6.6, 9.8, and 13 feet).

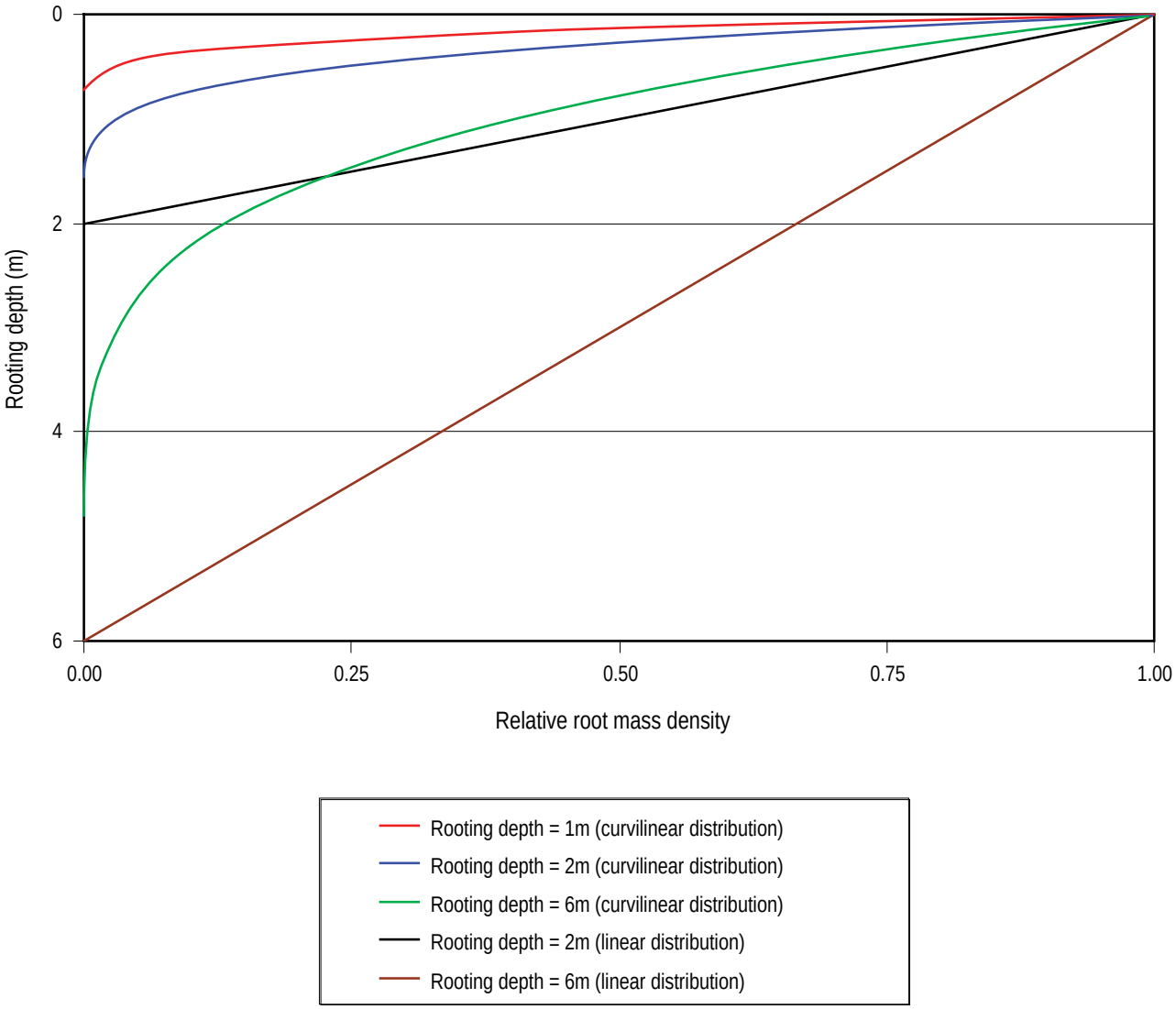

Figure 8
Root Mass Distribution Functions Used in HYDRUS Simulations

3.0 Results and Discussion

The results of the HYDRUS model simulations are summarized in Table 3; the average annual drainage and runoff projections shown in the table represent the average annual values over the 15-year simulation period. Overall, average annual drainage ranged from 2.5×10^{-4} to 7.0 mm/yr (9.8×10^{-6} to 0.28 ft/yr) and average annual runoff ranged from zero to 16.8 mm/yr (0.63 in./yr) for unvegetated covers. Annual drainage ranged from 1.3×10^{-4} to 0.61 mm/yr (5.1×10^{-6} to 0.02 in./yr) and annual runoff ranged from 0 to 11.6 mm/yr (0 to 0.46 in./yr) for vegetated covers. Six of the 59 simulations resulted in average annual drainage rates of less than 0.001 mm/yr (3.9×10^{-5} in./yr) and 17 of the 59 simulations resulted in drainage rates greater than 0.01 mm/yr (3.9×10^{-4} in./yr) . More than 60 percent of the 59 model simulations (36) resulted in average annual drainage rates from 0.001 to 0.01 mm/yr (3.9×10^{-5} to 3.9×10^{-4} in./yr). Figure 9 is a cumulative distribution function plot showing drainage results for all 59 simulations.

The 59 HYDRUS simulations evaluated the sensitivity of the drainage projections to a variety of conditions. The results of this effort are discussed in the following sections.

3.1 Cover Thickness

Nearly every model scenario described in Tables 2 and 3 was evaluated over a range of cover thicknesses. Figure 10 illustrates average annual drainage as a function of cover thickness; Figure 11 also shows drainage versus cover thickness, but focuses on the drainage values between 0.0015 and 0.004 mm/yr (0.0049 and 0.013 ft/yr) because many drainage values occurred in this range. Results indicate that drainage and runoff were generally quite similar for 2-, 3-, and 4-m (6.6-, 9.8-, and 13-foot) thick covers (Table 3). In some cases, drainage slightly increased as cover thickness increased, and in other cases, drainage decreased slightly as cover thickness increased. Although one might expect drainage to simply decrease with increasing cover thickness, the behavior of the crushed tuff/bentonite layer with the underlying tuff layer is complex due to the high water holding capacity of the former. In addition, drainage results are also affected by variations in the initial pressure head conditions used in the simulations (Table 2; Section 2.3).

Simulations 112, 113, and 114 are considered to be base-case simulations for unvegetated conditions. Drainage for these simulations range from 1.2 to 2.0 mm/yr (0.047 to 0.079 in./yr). Simulation 115 was identical to 114 in total cover thickness, but with different layer thicknesses. Simulation 115 drainage was 1.6 mm/yr (0.063 in./yr). The vegetated base-case simulations are RS1, RS3, and RS4. Drainage for these vegetated simulations range from 0.0022 to 0.0036 mm/yr (8.7×10^{-5} to 1.4×10^{-4} in./yr). A fourth simulation, RS2, was identical to RS3 in overall cover thickness, but had different layer thicknesses; the drainage for this simulation is the same as that projected for RS3.

Table 3
Average Annual Drainage and Runoff from all 59 HYDRUS Simulations

Simulation No.	Depth (m)	Plants	Drainage (mm/yr)	Runoff (mm/yr)	Model Scenario
112	2	No	1.2E+00	3.3E-01	T+C; Tuff1 (base case)
113	3	No	1.4E+00	3.6E-01	
114	4	No	2.0E+00	3.4E-01	
115	4	No	1.6E+00	3.7E-01	T+C (2 m); Tuff1 (2 m)
42	2	No	4.2E+00	3.2E-01	T+C; Tuff2 (high Ksat)
43	3	No	5.0E+00	3.3E-01	
44	4	No	7.0E+00	3.2E-01	
52	2	No	2.4E-02	3.4E-01	T+C; Tuff4 (low Ksat)
53	3	No	2.4E-02	3.8E-01	
54	4	No	3.9E-02	3.6E-01	
55	2	No	4.9E-01	0.0E+00	T+C (high Ksat); Tuff2 (high Ksat)
56	3	No	3.2E-01	0.0E+00	
57	4	No	3.4E-01	0.0E+00	
58	2	No	1.0E-02	1.7E+01	T+C (low Ksat); Tuff2 (high Ksat)
59	3	No	8.1E-03	1.7E+01	
60	4	No	8.1E-03	1.6E+01	
62	2	No	3.2E-4	1.7E+01	T+C (low Ksat); Tuff4 (low Ksat)
63	3	No	2.5E-4	1.7E+01	
64	4	No	2.5E-4	1.6E+01	
RS4	2	Yes	2.2E-03	2.2E-02	T+C; Tuff1; Grass; 2 m curvilinear roots (base case)
RS1	3	Yes	2.3E-03	1.0E-02	
RS3	4	Yes	3.6E-03	2.2E-02	
RS2	4	Yes	3.6E-03	2.2E-02	T+C (2 m); Tuff1 (2 m); Grass; 2-m curvilinear roots
RS5a	2	Yes	2.3E-03	6.1E-02	T+C; Tuff1; Grass; 1 m curvilinear roots
RS5b	3	Yes	2.3E-03	4.5E-02	
RS5c	4	Yes	3.6E-03	5.9E-02	
RS6a	2	Yes	1.9E-03	1.0E-03	T+C; Tuff1; Trees; 6 m curvilinear roots
RS6b	3	Yes	2.0E-03	0.00E+00	
RS6c	4	Yes	2.2E-03	0.00E+00	

T+C = tuff + clay (bentonite)
Tuff1 = Material 1 as described in Table 1
Tuff2 = Material 2 as described in Table 1
Ksat = Saturated hydraulic conductivity
Tuff4 = Material 4 as described in Table 1
PT = Potential transpiration

Table 3 (Continued)
Average Annual Drainage and Runoff from All 59 HYDRUS Simulations

Simulation No.	Depth (m)	Plants	Drainage (mm/yr)	Runoff (mm/yr)	Model Scenario
RS7a	2	Yes	2.0E-03	0.00E+00	T+C; Tuff1; Grass; 2 m linear roots
RS7b	3	Yes	2.0E-03	0.00E+00	
RS7c	4	Yes	2.1E-03	0.00E+00	
RS8a	2	Yes	3.7E-02	3.0E-03	T+C; Tuff1; Grass; 2 m curvilinear roots; low PT
RS8b	3	Yes	8.4E-02	3.0E-03	
RS8c	4	Yes	8.9E-02	3.0E-03	
RS9a	2	Yes	3.0E-03	2.2E-02	T+C; Tuff2 (high Ksat); Grass; 2 m curvilinear roots
RS9b	3	Yes	3.1E-03	1.0E-02	
RS9c	4	Yes	5.2E-03	2.2E-02	
RS10a	2	Yes	1.3E-04	8.131E+00	T+C (low Ksat); Tuff4 (low Ksat); Grass; 2 m curvilinear roots
RS10b	3	Yes	1.3E-04	8.334E+00	
RS10c	4	Yes	1.9E-04	8.141E+00	
RS11a	2	Yes	2.3E-03	9.746E+00	Vegetated base case; precipitation × 2
RS11b	3	Yes	2.3E-03	1.1614E+01	
RS11c	4	Yes	3.6E-03	9.755E+00	
92	2	Yes	2.3E-03	1.5E-02	Vegetated base case + gravel + topsoil layers
93	3	Yes	2.4E-03	9.0E-03	
94	4	Yes	3.6E-03	1.5E-02	
RS12	2	Yes	1.9E-03	2.3E-02	T+C; Tuff1; Trees; 6 m curvilinear roots; low PT; 2 m cover
RS13	2	Yes	1.9E-03	1.0E-03	T+C; Tuff1; Trees; 6 m curvilinear roots; high PT; 2 m cover
RS14	2	Yes	6.1E-01	5.0E-03	T+C; Tuff2; Grass; 1 m curvilinear roots; low PT; 2 m cover
RS15a	2	Yes	2.3E-03	9.2E-03	T+C; Tuff1; Grass; 2 m curvilinear roots; medium PT
RS15b	3	Yes	2.4E-03	2.0E-03	
RS15c	4	Yes	2.4E-03	9.2E-03	
RS16a	2	Yes	1.9E-03	0.00E+00	T+C; Tuff1; Trees; 6 m linear roots
RS16b	3	Yes	1.9E-03	1.2E-03	
RS16c	4	Yes	1.9E-03	4.1E-03	
RS17a	2	Yes	1.9E-03	7E-04	T+C; Tuff1; Trees; 6 m curvilinear roots; medium PT
RS17b	3	Yes	2.0E-03	2.0E-03	
RS17c	4	Yes	2.1E-03	2.3E-03	

T+C = tuff + clay (bentonite)
Tuff1 = Material 1 as described in Table 1
Tuff2 = Material 2 as described in Table 1
Ksat = Saturated hydraulic conductivity
Tuff4 = Material 4 as described in Table 1
PT = Potential transpiration

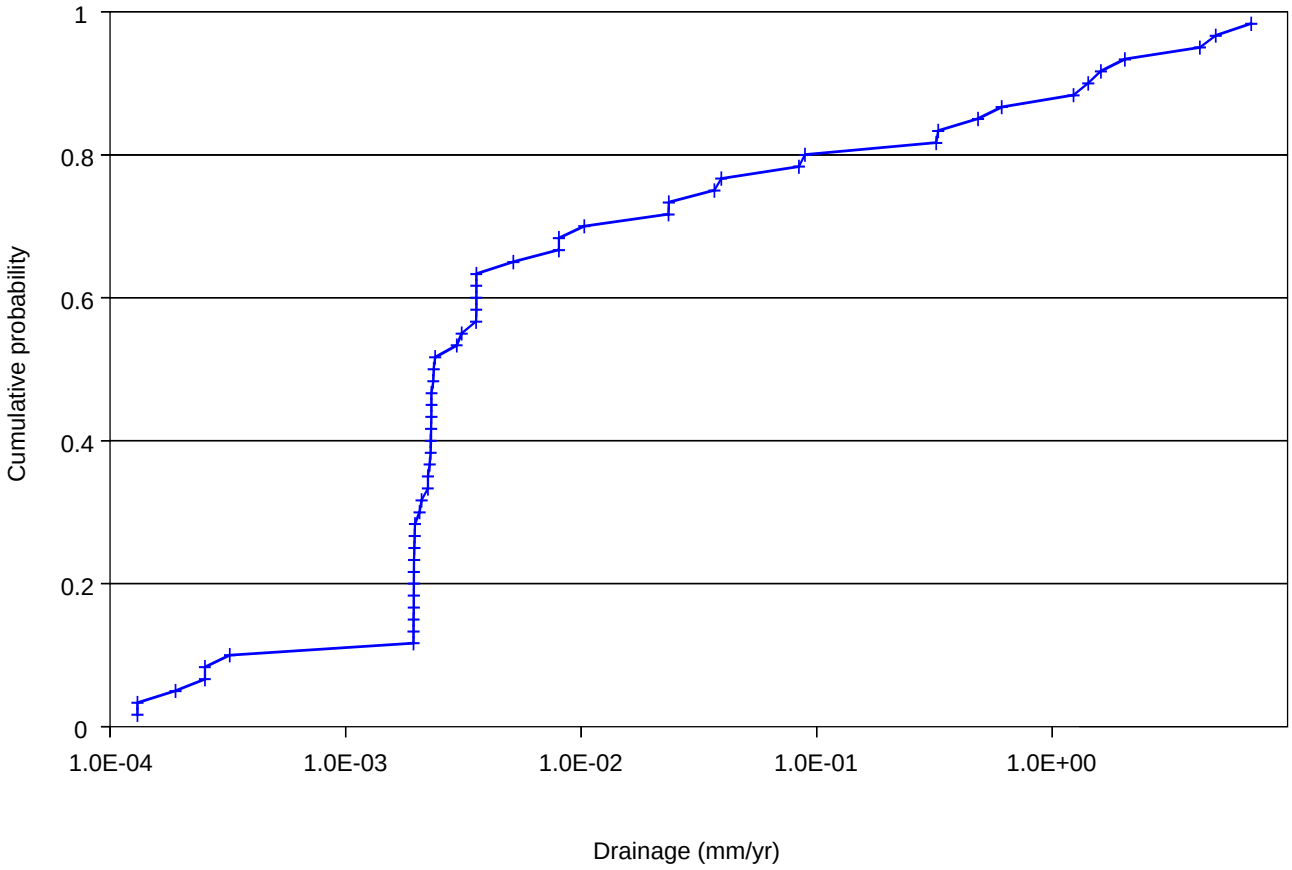

Figure 9
Cumulative Distribution of Average Annual Drainage Results

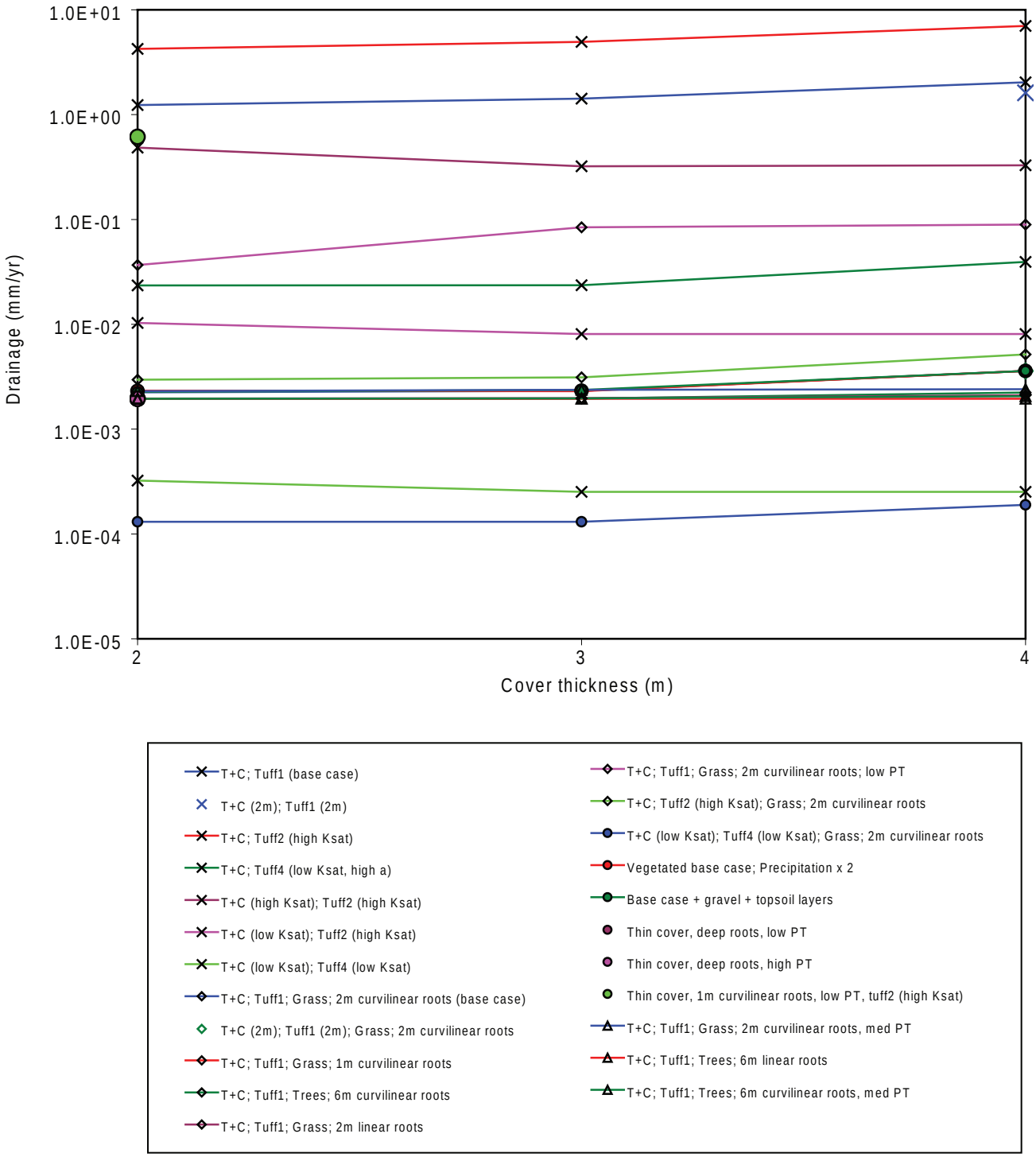

Figure 10
HYDRUS Projections of Drainage versus Cover Thickness, All Simulations

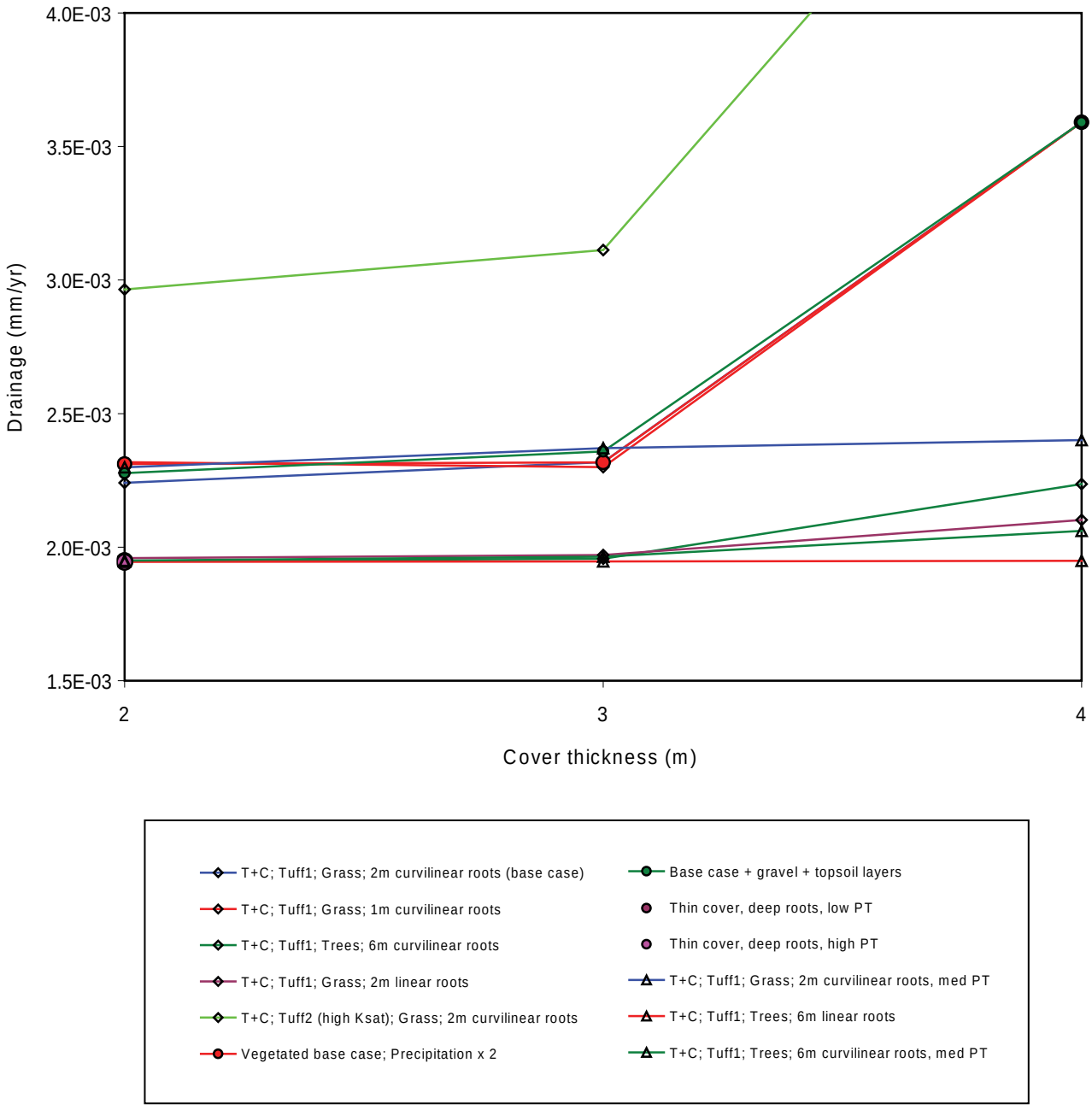

Figure 11
HYDRUS Projections of Drainage versus Cover Thickness, Selected Simulations

3.2 Hydraulic Properties

Model results were extremely sensitive to changes in hydraulic properties. The unvegetated base-case results (simulations 112, 113, and 114) are quite different from results for simulations 42, 43, and 44, which used the high-Ksat crushed tuff properties (material 2 in Table 1). Drainage for simulations 42, 43, and 44 ranged from 4.2 to 7.0 mm/yr (0.17 to 0.28 in./yr), the highest drainage of all 59 simulations. Simulations 55, 56, and 57 used high-Ksat crushed tuff/bentonite (layer 1) and crushed tuff (layer 2) properties, but drainage for these simulations was surprisingly low, ranging from 0.49 to 0.33 mm/yr (0.019 to 0.013 in./yr); in these cases the higher Ksat of layer 1 allowed higher rates of evaporation from this layer. Simulations 52, 53, and 54 used low-Ksat layer 2 properties (material 4 in Table 1), and drainage decreased significantly to between 0.02 and 0.04 mm/yr (7.9×10^{-4} and 0.0016 in./yr). When simulations 58, 59, 60, 62, 63, and 64 used low-Ksat layer 1 properties (material 12 in Table 1) with either low or high-Ksat layer 2 properties, then drainage decreased to between 0.01 to 2.5×10^{-4} mm/yr (3.9×10^{-4} to 9.8×10^{-6} in./yr), the drainage values for simulations 62, 63, and 64 are the lowest projected for unvegetated conditions.

The base-case drainage for the vegetated simulations (RS1, RS3, and RS4) ranged from 0.0022 to 0.0036 mm/yr (8.7×10^{-5} to 1.5×10^{-4} in./yr). When high-Ksat layer 2 properties were used in simulations RS9a, RS9b, and RS9c, drainage remained essentially the same. When low-Ksat layer 1 and 2 properties were used in simulations RS10a, RS10b, and RS10c, drainage values decreased to 1.3×10^{-4} to 1.9×10^{-4} mm/yr (5.1×10^{-6} to 7.5×10^{-6} in./yr), which are the lowest drainage values for vegetated conditions.

Simulations 92, 93, and 94 included the gravel and topsoil layers shown in Figure 1. Values of drainage for these simulations are essentially the same as those projected for the base-case vegetated simulations.

3.3 Vegetation

Results of the vegetated cover simulations indicate that the presence of vegetation tends to lower drainage significantly. Drainage from the base-case vegetated cover simulations (RS1, RS3, and RS4) ranged from 0.0022 to 0.0036 mm/yr (9.1×10^{-5} to 1.4×10^{-4} in./yr). The base-case simulations assumed a 50 percent grass cover such that PT = PET × 0.5. Rooting depth was 2 m (6.6 feet) with a curvilinear beta distribution root mass density. Simulations RS5a, RS5b, and RS5c were identical to the base-case simulations, except that the rooting depth was reduced to 1 m (3.3 feet). Drainage values for these simulations were the same as those projected for the base-case simulations. In simulations RS6a, RS6b, and RS6c, rooting depth was increased to 6 m (20 feet), and drainage decreased to between 0.0019 and 0.0022 mm/yr (7.5×10^{-5} and 8.7×10^{-5} in./yr). These results indicate that drainage is fairly insensitive to rooting depths between 1 and 2 m (3.3 and 6.6 feet); increases in rooting depth to 6 m (20 ft) results in reduced

drainage, most notably in thicker covers. In simulations RS7a, RS7b, and RS7c, the root mass distribution was changed from 2-m (6.6-foot) deep curvilinear to 2-m (6.6-foot) deep linear. Drainage for these simulations was less than that projected for the base-case vegetated simulations (RS1, RS3, and RS4), especially for the thicker covers. The linear root depth distribution results in a greater proportion of roots deeper within the cover, resulting in greater extraction of water through transpiration. This effect is less obvious when the root mass distribution of trees was changed from curvilinear (RS6a, RS6b, and RS6c) to linear (RS16a, RS16b, and RS16c); only moderate declines in drainage were noted in these cases.

The effects of variations in PT are evident in several simulations. Simulations RS8a, RS8b, and RS8c used base-case conditions except that PT was set to PET × 0.1, approximating a 10 percent vegetative cover. Drainage for these simulations ranged from 0.037 to 0.089 mm/yr (1.5×10^{-3} to 3.5×10^{-3} in./yr). In simulations RS15a, RS15b, and RS15c, base-case conditions were used, except that PT was set at a moderate value (PET × 0.3), approximating a 30 percent vegetative cover. Drainage for these simulations ranged from 0.0023 to 0.0024 mm/yr (9.1×10^{-5} to 9.5×10^{-5} in./yr). These results suggest that increased drainage will result if vegetative cover is poor (simulations RS8a, RS8b, and RS8c). The fact that the drainage values for simulations RS15a, RS15b, and RS51c are lower than the base-case results (RS1, RS3, and RS4) appears contradictory, given the fact that PT for the former simulations are less than that for the base-case simulations. This discrepancy is the result of slightly different initial pressure head conditions. The use of varying initial pressure head conditions for many simulations facilitated steady-state conditions, but it occasionally made it difficult to compare model results when drainage values were very small (i.e., 0.002 mm/yr), as was typical for vegetated conditions.

Simulations RS16a, RS16b, and RS16c used a rooting depth of 6 m (20 feet) with a linear root mass distribution. Simulations RS17a, RS17b, and RS17c used the same rooting depth with curvilinear root mass distribution, and PT was set to PET × 0.3. Drainage values from the two sets of simulations are nearly identical. Results from both sets of simulations are nearly the same as those from simulations RS6a, RS6b, and RS6c, which assumed 6 m deep roots, a curvilinear root mass distribution, and PT = PET × 0.5.

For simulations RS12 and RS13, a thin (2-m [6.6-foot] thick) cover was simulated, with a 6-m (20-foot) deep root function (truncated at 2 m [6.6 feet] deep). Simulation RS12 had a low PT (PET × 0.1) and RS13 had a high PT (PET × 0.5). Despite the differences in PT rates, drainage for these two simulations was identical at 0.0019 mm/yr (7.5×10^{-5} in./yr) because of the substantial root mass density throughout the profiles. These results indicate that the presence of deep, dense roots will significantly minimize drainage, even at low rates of PT.

In simulation RS14, a thin (2-m [6.6-foot]) cover was again simulated, but with 1-m (3.3-foot) deep roots, low PT (PET × 0.1), and high-Ksat layer 2 properties. This simulation is considered

to be a worst-case scenario for vegetated cover. Drainage for this simulation was 0.61 mm/yr (0.024 in./yr), which is the highest drainage of any vegetated cover simulation, but is still considerably less than the maximum drainage value for the unvegetated cover.

3.4 Elevated Precipitation

In simulations RS11a, RS11b, and RS11c daily precipitation was doubled. Drainage for these simulations ranged from 0.0023 to 0.0036 mm/yr (9.1×10^{-5} to 1.4×10^{-4} in./yr), which is nearly identical to the base-case drainage results. However, runoff results increased significantly for these simulations, to between 9.7 and 12 mm/yr (0.38 and 4.7 in./yr). These results illustrate the efficiency of vegetation in removing water by root uptake and transpiration.

3.5 Runoff

Average annual runoff for all simulations (except for the low-Ksat layer 1 and elevated precipitation simulations) was less than 0.4 mm/yr (0.016 in./yr) and is considered to be insignificant to these simulations; this observation is surprising because runoff is an important component of the water balance for Area G. The reason for these results is expected to lie in the temporal resolution of the atmospheric data used in the HYDRUS modeling. As discussed earlier, the atmospheric boundary condition datasets used for this work include daily precipitation totals and daily total PET. Local thunderstorms often result in short, intense rainfall; thus, if hourly or 15-minute datasets can be acquired for future modeling, runoff may become a much larger component of the model simulations. Alternatively, daily precipitation can be used with assumed storm durations of less than one day to simulate runoff from brief rainfall events. It is important to note, however, that underestimating runoff results in overestimating infiltration and drainage and thus provides conservative results for groundwater pathway migration.

3.6 Long-Term Simulations

Long-term (i.e., 1,000-year) simulations were not conducted in this study. The meteorological data required to conduct long-term simulations are not available. Although these simulations could be conducted by repeating the 15-year dataset used in the study, doing so is not expected to generate significantly different annual drainage amounts. Initial pressure head conditions were adjusted for all simulations until a relatively steady-state equilibrium was achieved. Under steady-state conditions, the modeled performance of the cover will tend to oscillate about a central behavior regardless of how many times the weather data are repeated. To illustrate, plots of cumulative drainage and total water storage are provided in Figures 12 and 13, respectively, for simulations 112, 113, and 114 (the unvegetated base-case simulations). Because the model is operating under near steady-state conditions, the cumulative drainage curves (Figure 12) are generally linear over the 15-year simulation period and the total water storage data (Figure 13) vary about central values.

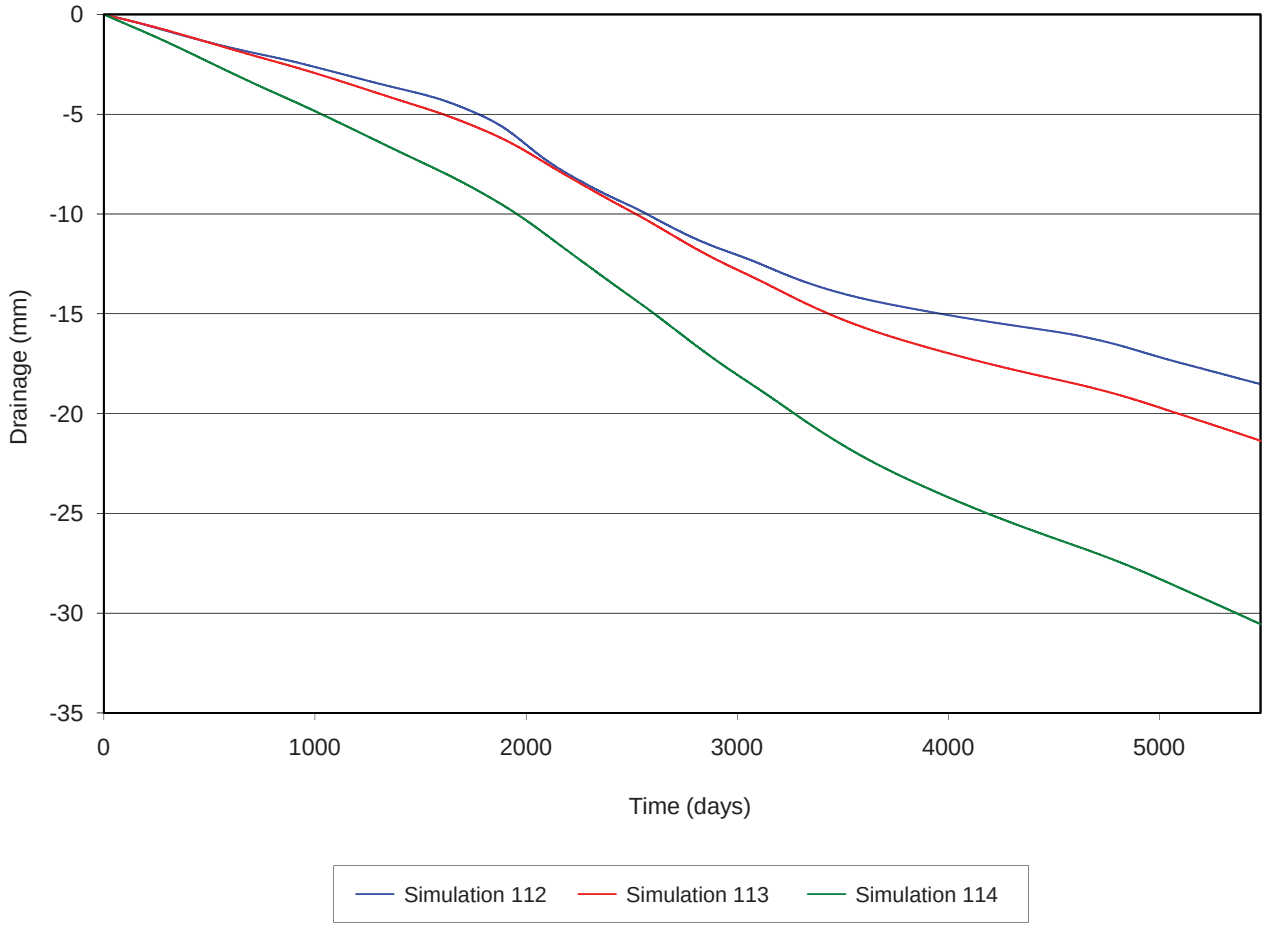

Figure 12
Cumulative Drainage Results for HYDRUS Simulations 112, 113, and 114

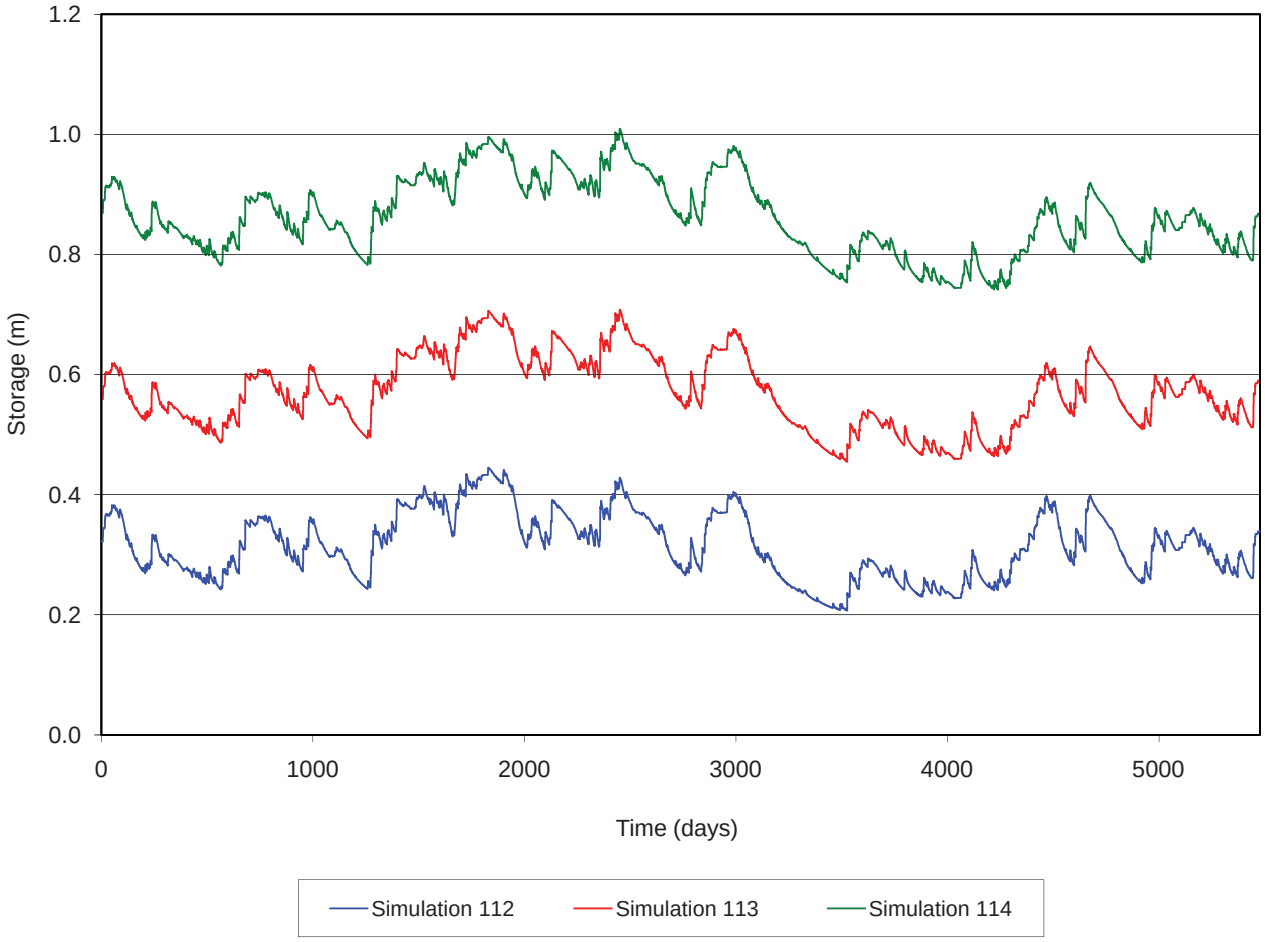

Figure 13
Water Storage Results for HYDRUS Simulations 112, 113, and 114

Long-term weather inputs can also be generated using stochastic methods such as the Weather GENerator (WGEN) method described in Appendix G of LANL (2003). The WGEN results provided in LANL (2003; Figure G-1.2-1) indicate that the low-probability, maximum annual precipitation for a 1,000-year record is less than 95 cm/yr (37 in./yr) at MDA H, which is located 2 km [1.3 mi] west of Area G. This amount is not much greater than the average annual precipitation of about 70 cm (28 in./yr) used in the elevated precipitation simulations (RS11a, RS11b, and RS11c). As shown in Figure 14, the median annual precipitation over the 1,000-year period was between 45 and 50 cm (18 and 20 in.), considerably less than the 70 cm/yr (28 in./yr) used in the RS11 simulations. Although long-term precipitation datasets may include sustained periods of high precipitation, the results of the RS11 simulations, which showed no change in average annual drainage compared to base-case vegetated conditions, suggest that the use of long-term precipitation records is not expected to significantly increase drainage for a vegetated cover.

3.7 Modeling Uncertainties

A number of significant modeling uncertainties in this study should be acknowledged. As explained in Section 2, the atmospheric-boundary-condition time series (e.g., precipitation and ET) is a critically important aspect of the cover modeling. This study used weather data collected at the TA-54 weather station. Although these data represent short-term-average conditions, they do not capture the wide variations in long-term climatic conditions. One means of addressing this variation would be to model a 1,000-year, stochastically generated time series as was done for MDA H (LANL, 2003). As indicated above, however, it is not expected that doing so would result in drainage values that differ significantly from those presented in this report.

The hydraulic properties of the crushed tuff/bentonite mixture are highly uncertain given that they were estimated by linear interpolation using the properties of two measured materials: 100 percent crushed tuff and a 10-percent bentonite/crushed tuff mixture Future work should include a thorough hydraulic property analysis of the materials to be used in the construction of the final cover at Area G.

The HYDRUS simulations showed a marked contrast in water contents at the contact between the crushed tuff/bentonite layer and the underlying crushed tuff/waste at a depth between 1 and 1.25 m (3.3 and 4.1 feet) in simulation 112 (Figure 15). Given the large differences in hydraulic properties between these two layers, this cover design acts as a capillary barrier. Future work might include the use of HYDRUS-2D or possibly HYDRUS-3D simulations to examine capillary barrier effects and possible generation of interflow. Examination of slope length effects would also need to be considered. A capillary barrier is often viewed as a design asset and is intentionally incorporated into some cover designs. However, it is important to determine if interflow will occur, because engineering controls may be needed to manage this water and route it away from the site.

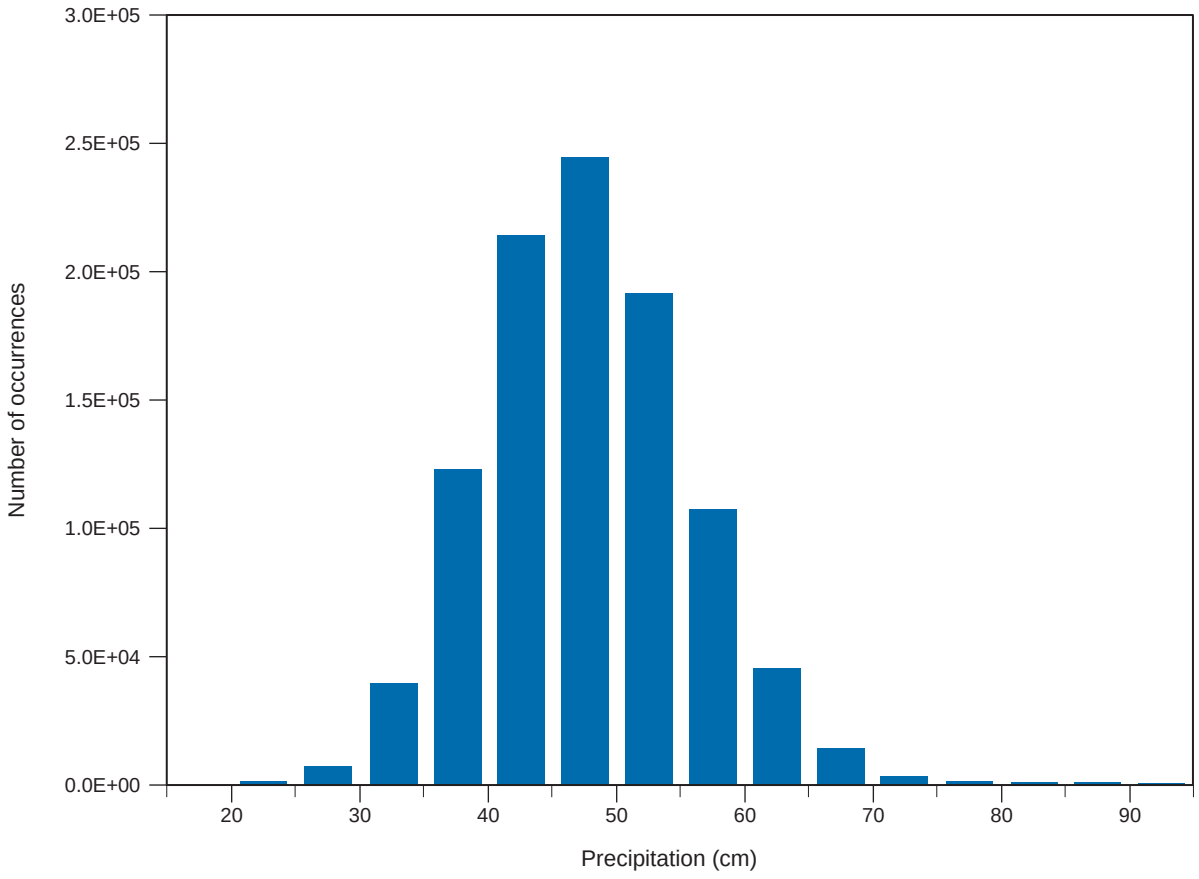

Figure 14
Distribution of Annual Precipitation for 1,000-Year Period at MDA H, Estimated Using WGEN

Source: *LANL (2003), Figure G-1.2-1*

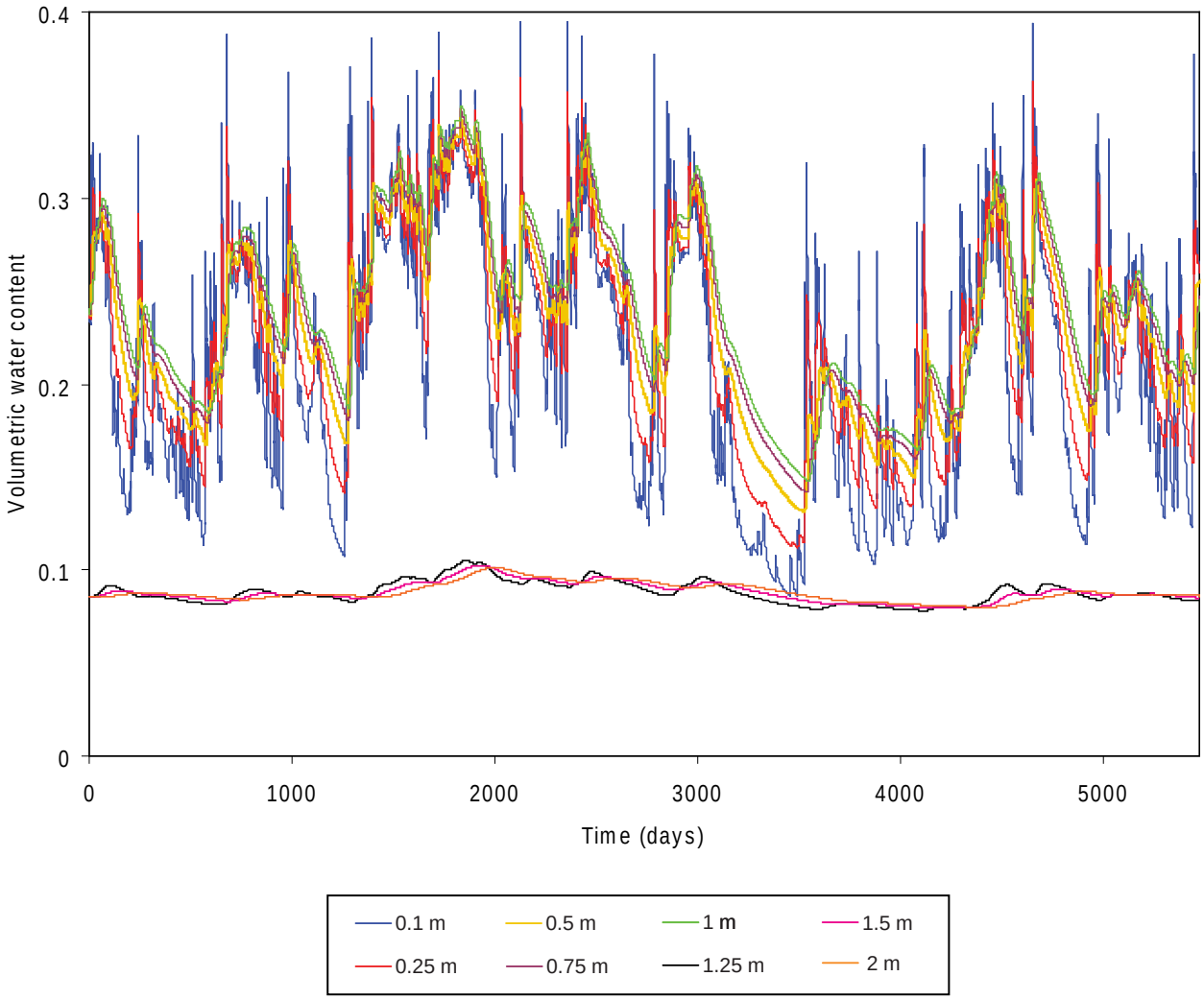

Figure 15
Volumetric Water Content at Eight Depths for HYDRUS Simulation 112

There is considerable uncertainty in the multipliers used to allocate PET to PT and PE, and in the use of vegetation parameters. For these simulations, a PE multiplier of 0.25 (PE = PET × 0.25) was used for the HYDRUS simulations, based on the results of the model calibration discussed in Section 2.3; the PT multiplier varied from 0.1 to 0.5. A generic grass or tree cover was simulated with rooting depths of 1, 2, and 6 m (3.3, 6.6, and 20 feet), and with linear and curvilinear root density functions. Although there is considerable uncertainty in the vegetation properties used to represent the cover at Area G, these simulations included a broad range of rooting depths, root mass density functions, and vegetation cover densities; thus the drainage results are expected to encompass the actual cover drainage amounts.

One additional uncertainty that may require future assessment is the issue of preferential flow. The modeling presented here assumed porous media (matrix) type flow and did not assume any cover evolution or degradation. However, the addition of bentonite may make the cover prone to cracking, which has been a significant failure route in RCRA-type clay-layer covers. The percentage of clay may be low enough to prevent cracking, but the possibility should be assessed because cracks can route water quickly through a cover. In addition, the potential for tree invasion indicates that stemflow and macropore flow in root channels may be important preferential flow considerations. HYDRUS-2D has been used to examine ponderosa pine root channel preferential flow (Guan, 2005); a similar analysis could be conducted for Area G.

Finally, it should be noted that field experiments and studies could be performed to support or complement future HYDRUS modeling. This applies not only to preferential flow questions, but to the testing of cover materials. Small- or intermediate-scale field experiments would be very useful in terms of testing expected behaviors and performance and would help identify unanticipated effects and build confidence in model calibration and model results.

Given the variety of uncertainties, an important question is whether the HYDRUS-predicted fluxes obtained in this study are reasonable. To examine this question, the distribution of HYDRUS fluxes (59 values) were plotted against fluxes estimated independently at Area G using the chloride mass-balance approach (17 values) described in Newman et al. (2005). This plot, shown in Figure 16, indicates that the HYDRUS results bound the chloride-based fluxes, and consequently, that the HYDRUS results are reasonable values for the Area G environment. It should be noted, however, that the chloride-based fluxes represent long-term average values for current conditions at Area G and do not account for the addition of the proposed cover design modeled here. Nevertheless, the comparison is useful for evaluation purposes.

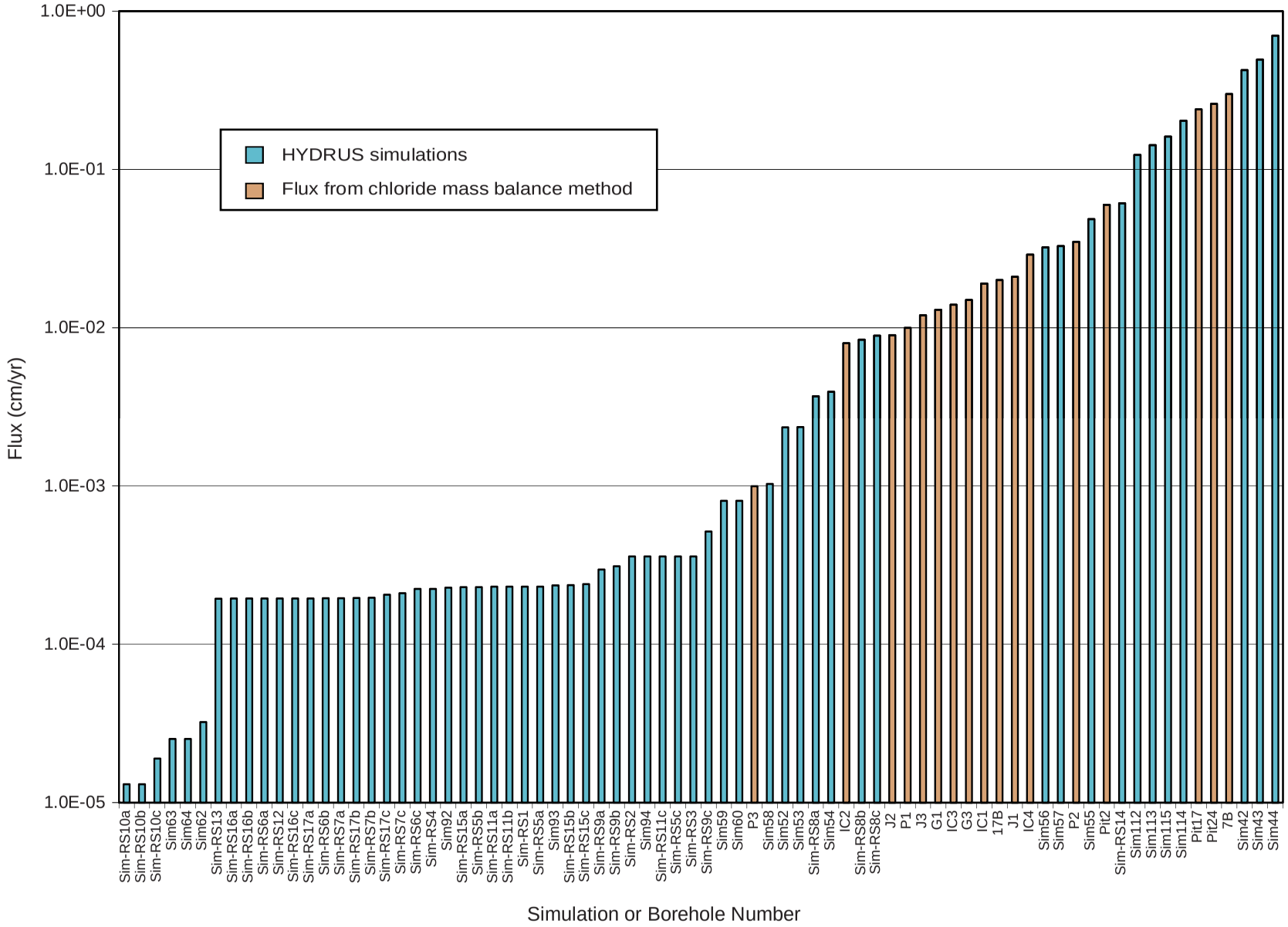

Figure 16
Comparison of HYDRUS Flux Estimates and Chloride Mass Balance Estimates for Area G

4.0 Conclusions

Results of the 59 HYDRUS-1D simulations described in this report indicate that the ET cover design described in Day et al. (2005) will perform as expected by storing large amounts of infiltrated water, and evaporating or transpiring back to the atmosphere at least 98 percent of precipitation. In most simulations, average annual drainage ranged from 0.001 to 0.01 mm/yr (3.9×10^{-5} to 3.9×10^{-4} in./yr) compared to the average annual precipitation of 350 mm/yr (14 in./yr) measured at the TA-54 weather station for the 15-year period (1993 through 2007) that was simulated.

A variety of simulations were run to explore the effects of variations in total cover thickness, variations in layer thicknesses, hydraulic properties, and vegetation properties. In addition, several simulations were run with elevated precipitation. Model results indicate that average annual drainage through the simulated ET covers ranged from 2.5×10^{-4} to 7.0 mm/yr (9.8×10^{-6} to 0.28 in./yr) for unvegetated covers, and from 1.3×10^{-4} to 0.61 mm/yr (5.1×10^{-6} to 0.02 in./yr) for vegetated covers. Model results were sensitive to initial pressure head conditions, especially for unvegetated conditions, as well as to hydraulic properties. Model results indicate that vegetation, even at low density and with shallow rooting depths, substantially reduced drainage. Doubling the amount of daily precipitation had virtually no effect on drainage under vegetated conditions, although runoff increased significantly. Of the 59 model simulations, 6 simulations resulted in average annual drainage rates of less than 0.001 mm/yr (3.9×10^{-5} in./yr) and 17 resulted in average annual drainage rates greater than 0.01 mm/yr (3.9×10^{-4} in./yr). Thirty-six of the 59 simulations resulted in average annual drainage rates ranging from 0.001 to 0.01 mm/yr (3.9×10^{-5} to 3.9×10^{-4} in./yr). The HYDRUS model projections are generally consistent with the net infiltration fluxes calculated for Area G using the chloride mass-balance method (Newman et al. (2005). Although the cover configurations addressed by the HYDRUS simulations and chloride measurements differ, the consistency of the two sets of results builds further confidence in the model projections.

5.0 References

Abeele, W.V., 1984, *Geotechnical Characteristics of Bentonite/Sandy Silt Mixes for Use in Waste Disposal Sites*, Los Alamos National Laboratory Report LA-10101-MS.

Albright, W.H., G.W. Gee, G.V. Wilson, and M.J. Fayer, 2002, *Alternative Cover Assessment Project Phase I Report*, DRI Report #41183, Desert Research Institute, University of Nevada, Las Vegas.

Bonaparte, R., B.A. Gross, D.E. Daniel, R.M. Koerner, and S.F. Dwyer, 2004, *Draft Technical Guidance For RCRA/CERCLA Final Covers*, U.S. Environmental Protection Agency, Office of Solid Waste and Emergency Response, Washington D.C.

Cocina, F., 2006, *Field Saturated Hydraulic Conductivity Investigation of Engineered Pit Cover Soils at Los Alamos National Laboratory, Material Disposal Area J*, Los Alamos National Laboratory Report LA-UR-06-8746.

Day, M.S., C.K. Anderson, and C.D. Pedersen, 2005, *Conceptual Design of the Earthen Cover for Los Alamos National Laboratory Technical Area 54, Material Disposal Area G*, URS Corporation Report to LANL, September.

Doorenbos, J., and W.O. Pruitt, 1977, *Guidelines for Predicting Crop Water Requirements*, FAO Irrigation and Drainage Paper 24.

Guan, H., 2005, Ph.D. dissertation in progress, Department of Earth and Environmental Science, New Mexico Institute of Mining and Technology, Socorro, NM.

Interstate Technology & Regulatory Council (ITRC), 2003, *Technical and Regulatory Guidance for Design, Installation, and Monitoring of Alternative Final Landfill Covers*, *ALT-2*, Interstate Technology & Regulatory Council Alternative Landfill Technologies Team, Washington, D.C.

Jensen, M.E., R.D. Burman, and R.G. Allen, Eds., 1990, *Evapotranspiration and Irrigation Water Requirements*, ASCE Manuals and Reports on Engineering Practice No. 70, American Society of Civil Engineers, New York, New York.

Los Alamos National Laboratory (LANL), 2003, *Corrective Measures Study Report for Material Disposal Area H (Solid Waste Management Unit 54-004) at Technical Area 54*, Los Alamos National Laboratory Report LA-UR-02-4587, ER2003-0121.

LANL, 2008, The Weather Machine, Los Alamos National Laboratory, site updated hourly, <http://weather.lanl.gov> (March 11, 2008)

Maidment, D.R., Ed., 1993, *Handbook of Hydrology*, McGraw-Hill, New York, New York.

Newman, B.D., M.O. Gard, D.A. Counce, E.C. Kluk, J.L. Martinez, D. Newell, and J. Salazar, 2005, *Spatial Variation in Near-Surface Hydrologic Behavior at TA-54, MDA G*, Los Alamos National Laboratory Report LA-UR-05-4632, September.

Nyhan, J.W., 2005, "A Seven-Year Water Balance Study of an Evapotranspiration Landfill Cover Varying in Slope for Semiarid Regions," *Vadose Zone Journal*, Vol. 4, pp. 466 – 480.

Nyhan, J.W., T.E. Hakonson, and B.J. Drennon, 1990, "A Water Balance Study of Two Landfill Cover Designs for Semiarid Regions," *Journal of Environmental Quality,* Vol. 19, pp. 281 – 288.

Nyhan, J.W., T.G. Schofield, and R.H. Starmer, 1997, "A Water Balance Study of Four Landfill Cover Designs Varying in Slope for Semiarid Regions," *Journal of Environmental Quality,* Vol. 26, pp. 1385 – 1392.

Rogers, D.B., and B.M. Gallaher, 1995, *The Unsaturated Hydraulic Characteristics of the Bandelier Tuff*, Los Alamos National Laboratory Report LA-12968-MS.

Scanlon, B.R., M. Christman, R.C. Reedy, I. Porro, J. Šimůnek, and G.N. Flerchinger, 2002, "Intercode Comparisons for Simulating Water Balance of Surficial Sediments in Semiarid Regions," *Water Resources Research,* Vol. 38, p. 1323 [doi:10.1029/2001WR001233].

Scanlon, B.R., R.C. Reedy, K.E. Keese, and S.F. Dwyer, 2005. "Evaluation of Evapotranspirative Covers for Waste Containment in Arid and Semiarid Regions in the Southwestern USA", *Vadose Zone Journal*, Vol. 4:55-71.

Schroeder, P.R., C.M. Lloyd, and P.A. Zappi, 1994, *The Hydrologic Evaluation of Landfill Performance (HELP) Model: User's Guide for Version 3*, EPA/600/R-94/168a, U.S. Environmental Protection Agency, Risk Reduction Engineering Laboratory, Cincinnati, OH.

Selker, J. 2004, "Modeling Variably Saturated Flow with HYDRUS-2D," *Vadose Zone Journal*, Vol. 3, p. 725.

Shaw Environmental Inc., 2006, *Geotechnical and Hydraulic Characterization at the Technical Area 61 Borrow Area, Los Alamos, New Mexico*, ERID-091368.

Šimůnek, J., M. Sejna, and M.T. van Genuchten, 1999, *The HYDRUS-2D Software Package for Simulating the Two-Dimensional Movement of Water, Heat, and Multiple Solutes in Variably Saturated Media, Version 2.0*, IGWMC-TPS53, International Groundwater Modeling Center.

Šimůnek, J., 2005, Personal communication between J. Šimůnek, Research hydrologist, Department of Soil and Environmental Sciences, University of California, and Brent Newman, LANL.

Šimůnek, J., M. Th. van Genuchten, and M. Šejna, 2005, *The HYDRUS-1D Software Package for Simulating the One-Dimensional Movement of Water, Heat, and Multiple Solutes in Variably Saturated Media, Version 3.0*, Department of Environmental Sciences, University of California Riverside, Riverside, California.

van Genuchten, M.T., J.C. Parker, and J.B. Kool, 1987, "Analysis and Prediction of Water and Solute Transport in a Large Lysimeter," p. 242 in (E.P. Springer and H.R. Fuentes, eds.) *Modeling Study of Solute Transport in the Unsaturated Zone*, Vol. 2, NUREG/CR-4615, LA-10730-MS ed. U.S. Nuclear Regulatory Commission.

van Genuchten, R., 2004, Personal communication between Rien van Genuchten, Soil physicist, USDA, ARS George E. Brown Jr. Salinity Lab, and Brent Newman, LANL.

Wald-Hopkins, M., 2004, *Measurements of Field Saturated Hydraulic Conductivity of an Engineered Soil at Los Alamos National Laboratory's Technical Area 54, Material Disposal Area J*, Los Alamos National Laboratory Report LA-UR-04-0325.

Wilson, J.C.J., Crowell, K.J., and Lane, L.J., 2005, *Surface Erosion Modeling for the Repository Waste Cover at Los Alamos National Laboratory Technical Area 54, Material Disposal Area G*, Los Alamos National Laboratory Report, September.

LA-UR-05-7394

Approved for public release;
distribution is unlimited.

Title: CONCEPTUAL DESIGN OF THE EARTHEN COVER AT LOS ALAMOS NATIONAL LABORATORY TECHNICAL AREA 54, MATERIAL DISPOSAL AREA G

Author(s): Mark S. Day
C. K. Anderson
C. D. Pedersen

Submitted to: U.S. Department of Energy

Form 836 (8/00)

Table of Contents

List of Figures i
Acronyms and Abbreviations ii

1.0 Introduction 1
2.0 Conceptual Design Process 3
2.1 Design Considerations and Approach 3
2.2 Design Criteria 4
2.3 Input Data and Assumptions 6
2.4 Design Process 8
3.0 Conceptual Design 18
4.0 References 23

List of Figures

Figure 1 Establishment of Cover Edge Line 10
Figure 2 Establishment of Cover Ridge Line 11
Figure 3 Interior Slopes 12
Figure 4 Determination of Water Pathways 13
Figure 5 Establishment of Cover Edge Slopes 14
Figure 6 Detail of Grid Point Elevations for Cover Design 16
Figure 7 Final Cover Design for Active Portion of MDA G 19
Figure 8 Final Cover Contours for Active Portion of MDA G 20
Figure 9 Cross Section of Conceptual Cover for MDA G 21
Figure 10 Placement of Rock Armor around Cover Edge 22

Acronyms and Abbreviations

DOE	U.S. Department of Energy
LANL	Los Alamos National Laboratory
LIDAR	Light Detection and Ranging
LLW	Low-level (radioactive) waste
MDA	Material Disposal Area
TA	Technical Area

1.0 Introduction

The Los Alamos National Laboratory (LANL) generates low-level radioactive waste (LLW) and disposes of that material at Technical Area (TA) 54, Material Disposal Area (MDA) G. U.S. Department of Energy (DOE) Order 435.1 (DOE, 1999) requires that this waste be managed in a manner that protects the health and safety of workers and the public, and that protects the environment. To comply with this order, DOE field sites must prepare and maintain site-specific radiological performance assessments and composite analyses for LLW disposal facilities that accepted waste after September 26, 1988. In compliance with DOE Order 5820.2A (DOE, 1988), the predecessor to Order 435.1, LANL issued the *Performance Assessment and Composite Analysis for Los Alamos National Laboratory Material Disposal Area G* in 1997 (Hollis et al., 1997). The performance assessment and composite analysis are currently undergoing revision to address changes in operational procedures, incorporate new knowledge about the disposal facility and site, and update the modeling approaches used to project the long-term performance of the disposal facility.

The long-term performance of MDA G and its ability to safely isolate the waste from the environment is strongly dependent upon the final cover placed over the disposal pits and shafts. The cover is designed to limit infiltration through the disposal facility, thereby minimizing radionuclide releases due to leaching. The cover also plays an important role in minimizing the impacts of plant and animal intrusion into the waste. Finally, the cover provides long-term protection against surface erosion.

As the disposal units at MDA G reach their capacity, they undergo interim closure. Historically, the interim cover has consisted of 0.6 to 2 m (2.0 to 6.6 ft) of crushed tuff. The cover is designed to minimize radiation exposures received by facility personnel and provide a base for the construction of surface structures used in the management of waste.

The 1997 performance assessment and composite analysis (Hollis et al., 1997) assumed that only the interim cover was present and evaluated the long-term performance of the disposal facility on that basis. The interim cover was assumed to range from 1 to 2 m (3.3 to 6.6 ft) in total thickness, including a 10-cm (4–in.) vegetated topsoil layer placed over the crushed tuff. It was also assumed that gravel mulch was placed over the cover to reduce the erodibility of the cover.

The conclusion of the 1997 performance assessment and composite analysis was that the interim cover was capable of safely isolating the waste at MDA G. However, investigations undertaken since those analyses were issued have concluded that the impacts of biotic intrusion and surface erosion on the long-term performance of the facility may be more severe than previously

estimated. Consequently, it was decided that a more robust cover design will be implemented at the time of final closure to ensure continued protection of human health and the environment.

This report documents the conceptual design of the final cover for the disposal pits and shafts at MDA G. The general considerations, design criteria, and input data and assumptions that guided the design process are discussed in Section 2. The conceptual design itself is presented and discussed in Section 3.

2.0 Conceptual Design Process

This section discusses the approach and data upon which the conceptual design of the final MDA G cover is based. Section 2.1 provides a brief narrative of the general constraints that guided the design process. Section 2.2 discusses the design criteria that were considered in developing the cover; Section 2.3 describes the data and assumptions upon which the design is based. Finally, Section 2.4 details the design process itself.

2.1 Design Considerations and Approach

The long-term performance of the cover placed over MDA G will exert a significant influence on the facility's ability to satisfy the performance objectives listed in DOE Order 435.1. The thickness of the cover and the presence of engineered barriers will play an important role in limiting disturbance of the waste by plants and animals. The cover configuration and the hydraulic properties of materials used in its construction will influence the rate at which water infiltrates through the waste and, hence, the rates at which radionuclides will be leached from the pits and shafts. Finally, the erosion characteristics of the cover will affect the rate at which surface contamination is transported into the canyons adjacent to MDA G.

The 1997 performance assessment and composite analysis (Hollis et al., 1997) assumed very low rates of surface erosion, based on modeling conducted in support of those analyses and the assumption that active maintenance of the site would be exercised, as necessary, throughout the 1,000-year compliance period. Since that time, work conducted under the MDA G Performance Assessment and Composite Analysis Maintenance Program has indicated that the impacts of surface erosion may be more severe than estimated in 1997. Furthermore, the position that DOE will be present to actively maintain the site throughout the 1,000-year compliance period has been reconsidered. Taken together, these factors suggest the final cover should be capable of performing under much more severe conditions than previously considered.

The need to address more severe long-term impacts on cover performance and the key role the cover plays in limiting risks to humans and the environment led to consideration of a more robust final cover design for MDA G. Toward this end, preliminary evaluations were conducted to estimate the approximate cover characteristics needed to allow the disposal facility to satisfy the DOE Order 435.1 performance objectives. Once these minimum criteria were identified, an iterative design process was undertaken until a configuration capable of meeting these criteria was developed.

The evaluation of minimum cover requirements focused on total cover depth. This approach was adopted because, assuming there are no engineered bio-barriers present, depth is the primary cover characteristic that determines the degree to which biotic intrusion will impact the site. This

is significant because biotic intrusion was the radionuclide release mechanism responsible for the peak atmospheric pathway exposure estimated for the 1997 composite analysis and the peak performance assessment dose projected for a receptor living adjacent to MDA G in Pajarito Canyon.

The 1997 performance assessment and composite analysis concluded that 1 to 2 m (3.3 to 6.6 ft) of cover provided adequate protection against biotic intrusion. A later report documenting improvements in the biotic intrusion model indicated impacts may be greater when a comprehensive suite of plants and animals is considered (Shuman, 1999). Although Shuman concluded that 1 to 2 m (3.3 to 6.6 ft) of initial cover would probably be adequate under conditions characterized by very small rates of surface erosion, it was noted that additional cover might be necessary if rates of erosion at the site were significantly greater than originally estimated.

The minimum amount of cover required to safely isolate the waste disposed of at MDA G was estimated based on the results of Shuman (1999) and preliminary estimates of the impacts of biotic intrusion under what were expected to be conservative estimates of erosion potential. Assuming that the cover would be maintained for a period of 100 years following closure of the disposal facility, it was estimated that maintaining at least 1.5 m (4.9 ft) of cover over the site throughout the compliance period would provide reasonable assurance that the disposal facility would continue to satisfy all performance objectives. On the basis of preliminary estimates of erosion potential that were developed using the SIBERIA erosion model (Wilson et al., 2005), it was concluded that adopting a minimum initial cover thickness of 2.5 m (8.2 ft) would enable the cover requirement to be met for most, if not all, of the disposal site.

After the minimum initial cover depth was identified, an iterative process was used to evaluate cover designs. The performance of each conceptual design was evaluated for a period of 1,000 years using refinements of the SIBERIA erosion model (Wilson et al., 2005). The cover designs were evaluated to determine their ability to satisfy the minimum cover requirements and to identify areas where projected erosion impacts appeared to be severe. Generally, the erosion modeling indicated that the cover over much of the site performed adequately; however, some elevated rates of erosion were observed in localized areas along mesa edges or adjacent to drainages. These vulnerable locations were fortified using engineered features such as rock armor and the design evaluation process was repeated.

2.2 Design Criteria

The primary criterion that guided the design process was the maintenance of at least 1.5 m (4.9 ft) of cover over most of the disposal facility throughout the 1,000-year compliance period. Other criteria were also considered while designing the conceptual cover. The first designs assumed that all slopes would be 5 percent or less to limit runoff and the subsequent formation of

rills and gullies. The constraints imposed by the unique topography of the site, however, led to the adoption of a less stringent slope requirement of 2 to 10 percent. Another design criterion was that the cover function as an evapotranspiration cover system, employing vegetated soil layers to retain the water until it is removed through evaporation or plant transpiration. This type of design minimizes the amount of water percolating through the underlying waste and provides the greatest assurance that the cover will perform adequately for hundreds to thousands of years. The specific criteria that guided the design process are provided below.

- *Gas emissions* – One of the principal objectives of the cover is to limit the escape of gases generated by the waste. The thickness and air permeability of the cover shall be such that gas flux performance objectives and doses arising from exposure to vapor or gas-phase contaminants remain within allowable limits.

- *Water infiltration* – An important role of the cover is to limit the amount of water contacting the waste. The hydraulic properties of the materials used to construct the cover shall limit infiltration, thereby maintaining groundwater pathway exposures within allowable limits.

- *Design term* – The cover must be capable of fulfilling its design functions for a minimum of 1,000 years, the compliance period imposed by DOE Order 435.1. Maintenance of the cover was assumed to occur for the first 100 years of this period.

- *Wind and water erosion resistance* – The cover must resist erosive impacts, thereby limiting biotic intrusion into the waste, minimizing rates of water percolation through the waste, and limiting the transport of contamination into adjacent canyons.

- *Slope* – All cover slopes shall range from 2 to 10 percent to limit generation of runoff and, hence, the potential for rill and gully formation.

- *Intruder control* – The cover must limit inadvertent human intrusion and biotic intrusion into the disposed waste.

- *Surface water control* – The profile, slope, and grading of the cover must be completed in a manner that limits rill and gully formation following rainfall and snowmelt events.

- *Vegetation support* – The cover shall be designed to support vegetation native to the semiarid environment of northern New Mexico. The vegetative cover will be relied upon to remove water through transpiration and to stabilize surface soils, thereby resisting erosive forces.

- *Settlement resistance* – The cover shall be installed to eliminate voids and areas of low density, thereby limiting the potential for settlement of the cover.

- *Engineering controls* – Engineering controls such as rock armor or slope stabilization techniques shall be used as necessary to maintain the integrity of the cover in critical portions of the site.

- *Rock hardness* – Rock incorporated into the cover design shall be capable of resisting weathering and other forces of nature during the design term.

- *Seismic event* – The cover design shall consider resistance to the effects of seismic events. Parameters of concern include, but are not limited to, seismic magnitude, on-site peak horizontal acceleration, the distances to and lengths of capable faults, and the types of capable faults and associated displacement.

- *Reactive materials* – The materials used in cover construction shall be limited to natural materials that support the longevity of the cover over the design term. Aggregates or other materials that are known to be reactive shall not be used.

- *Soil strength* – The cover must have the internal soil strength to remain in place for the entire design term. Weaker soils such as crushed tuff shall be amended with other materials to enhance internal strength and compactability.

In general, the design process was undertaken with the goal of developing a cover with characteristics resembling those of natural landscapes in the vicinity of the disposal facility. This approach is expected to provide the greatest assurance that the facility will safely contain the waste over extended periods of time.

2.3 Input Data and Assumptions

Various types of information were used in the design of the conceptual cover for MDA G. These include the following:

- Record drawings ("as-builts") of the pits upon completion of excavation. The drawings for a given unit were developed at the time of pit excavation and prior to the placement of any waste. They were established using first-order land surveying methods and equipment available at the time of pit development.

- Aerial photography completed in the year 2000 was used to locate existing surface features and to establish the physical location of the cover.

- Light Detection and Ranging (LIDAR) images generated in 2000 were relied upon for ground surface views and to better define the locations of existing site features.

The elevations of the waste in the disposal pits and shafts must be known to ensure that the minimum cover depth requirements are satisfied. Unfortunately, surveys of the final waste elevations have not generally been conducted. Lacking these data, information found in specifications and memoranda that addressed general disposal requirements at MDA G were used to estimate the required elevations.

Disposal pits 1 through 4 were constructed using Materials Waste Pits Standard Specifications, Engineering Drawing ENG-C 18463 (Rogers, 1977). Although the Rogers' specifications provided maximum dimensions for the disposal units, information about the minimum cover depth was not included. According to the notes on the drawing, decisions regarding the thickness of the cover and the covering schedule were to be made by the custodial representative.

Formalized guidelines for disposal unit construction and closure were proposed by the U.S. Geological Survey in 1965 (Koopman, 1965), and subsequently adopted by the Laboratory. The guidelines specified that the disposal pits were to be filled with waste to within 0.6 m (2 ft) of the land surface. The seal material, or tuff, overlying the waste was to range in thickness from 1.8 to 2.4 m (6 to 8 ft); the surface of the seal material was to be slightly rounded. Pit 5 was the first disposal unit constructed and closed using these guidelines and the new standard pit specifications.

The disposal of waste in the shafts at MDA G began in 1966. The disposal guidelines proposed by the U.S. Geological Survey in 1965 (Koopman, 1965) did not address these units as they were not yet in use. Nevertheless, it is expected that pertinent parts of those guidelines were applied to these units once they were placed in operation. Specifically, it is expected that waste was disposed of to within 0.6 m (2 ft) of the ground surface.

An internal LANL memorandum issued in 1975 formalized disposal operations further, modifying some of the guidelines proposed by the earlier U.S. Geological Survey memorandum (Koopman, 1965). With respect to waste elevation and cover thickness, these guidelines specified that pits and shafts be filled with waste to a minimum depth of 0.9 m (3 ft) below the spill point, or the lowest point on the rim of the disposal unit. The final cover of a pit was specified as crushed tuff, overlain by topsoil, at a minimum of 0.6 m (2 ft) above the original land surface at the edge of the pit. The cover was to extend beyond the edges of the pit at least 0.9 m (3 ft) and to be slightly rounded to allow surface drainage without excessive erosion.

The guidelines for the design, construction, and closure of disposal pits and shafts at MDA G were updated in 1998 (LANL, 1998). In general, these draft guidelines adhere to the 1975 memorandum. However, some changes were implemented to address practical considerations and to implement procedural improvements. Most significantly, the requirement that waste be placed at a minimum depth of 0.9 m (3 ft) below the "spill point" of the pits was changed; the

new requirement was that waste be 3 m (9.8 ft) below the disposal unit rim. According to the 1998 guidelines, exceptions to this requirement were acceptable as long as the MDA G Waste Acceptance Criteria were met and the waste was a minimum of 2 m (6.6 ft) below the rim of the disposal unit.

For the conceptual design, the waste elevations of each pit were estimated using the information summarized above, based on the assumption that all waste disposal operations abided by these requirements. First, the elevations of the pits at grade were established. The record drawings were used to establish the elevations of the rim of each pit along the longitudinal centerline of the unit (i.e., at the midpoint of each end of the pit). The elevations of the corners at each end of the pit were set equal to the nearest centerline elevation, resulting in the same elevation for both corners at each end of the pit. Having established the corner elevations, the surface of the pit was estimated as a plane intersecting the four corners of the pit. Lacking shaft-specific construction details, it was assumed that the surface elevations of these units were the same as the spill points of the nearest pits. The waste elevations in the pits and shafts were subsequently calculated by subtracting the freeboard (i.e., the distance between the top of the waste and the spill point) specified in the disposal guidelines from the pit surface elevations.

2.4 Design Process

As discussed earlier, the conceptual cover for MDA G was designed using an iterative approach. Each design was evaluated and the process was repeated until a design expected to be capable of meeting the minimum cover requirements was identified. The specific process differed slightly depending on whether the portion of the facility under consideration was the area with established disposal units (the "active" portion of MDA G) or the portion of MDA G referred to as Zone 4, which is an area designated for future development. The initial design process for the active portion of MDA G included the following procedures:

- *Identifying the completion year of each disposal unit*. The completion year shown on the record drawings was used to classify each pit and shaft by construction year. The freeboard distance pertaining to a specific unit could then be established by referring to the disposal guidelines in force at that time.

- *Determining the waste elevation within the disposal unit*. The pertinent freeboard distance, as determined in step 1, was subtracted from the elevation of the spill point for each pit. The spill point was established using the assumptions discussed above.

- *Designing the cover*. Once the waste elevations were established, Geographical Information System (GIS) software was used to determine the cover location and establish initial lines and grades. The output of this effort was transferred to

Autodesk® Land Desktop 2004 to establish the final surface of the cover using the basic steps outlined below.

1. *Establish the edge line of the cover*. This boundary was established by identifying the perimeters of the pits and shafts closest to the edges of the mesa and joining these points with a continuous line, as shown in Figure 1. A cover elevation of 2.5 m (8.2 ft) was placed along the edge line once it was located to ensure that the minimum cover requirement was satisfied along the outer extent of the waste.

2. *Set the ridge lines*. The initial approximation of the surface of the cover was established as shown in Figure 2 by joining the ridge lines to the edge line. This allowed identification of the peaks, valleys, and slopes of the cover (Figure 3). The contours shown on these figures are the ultimate result of computer-modeling enhancements that occurred throughout the iterative design process. For this reason, some of the ridge breaks are not readily apparent.

3. *Examine the cover slopes for grade and flow concentrations*. Slopes were maintained between 2 and 10 percent to promote moderate sheet flow and minimize flow concentration. Sheet flow was checked using a feature in the Land Desktop design software called "Water Drop." Figure 4 shows consistent uniform path lines indicating sheet flow. Dramatic convergence of flow lines would indicate concentrated flow and would require that the surface of the cover be recontoured or smoothed to correct this condition. Through an iterative process, areas of abrupt grade change were adjusted and smoothed, and elevations were modified to approach the desired profile. The cover elevations over the waste were checked to ensure that a minimum of 2.5 m (8.2 ft) of cover material was present across the site.

4. *Establish the slopes from the cover edge line to the existing ground surface at the edge of the mesa.* These edge slopes, shown in Figure 5 were kept to a minimum where physically possible. Once the edge slopes were established, the contours were examined for areas marked by sharp valleys or ridges and these areas were smoothed and adjusted as necessary.

The cover design process for the Zone 4 expansion area took advantage of the fact that disposal unit construction had not yet begun. Restrictions were placed on waste placement and elevation, specifying that waste would be placed to within 3 m (10 ft) of the ground surface in all pits and shafts. This restriction allows the 2.5 m (8.2 ft) minimum cover to be placed within the footprints of the disposal units.

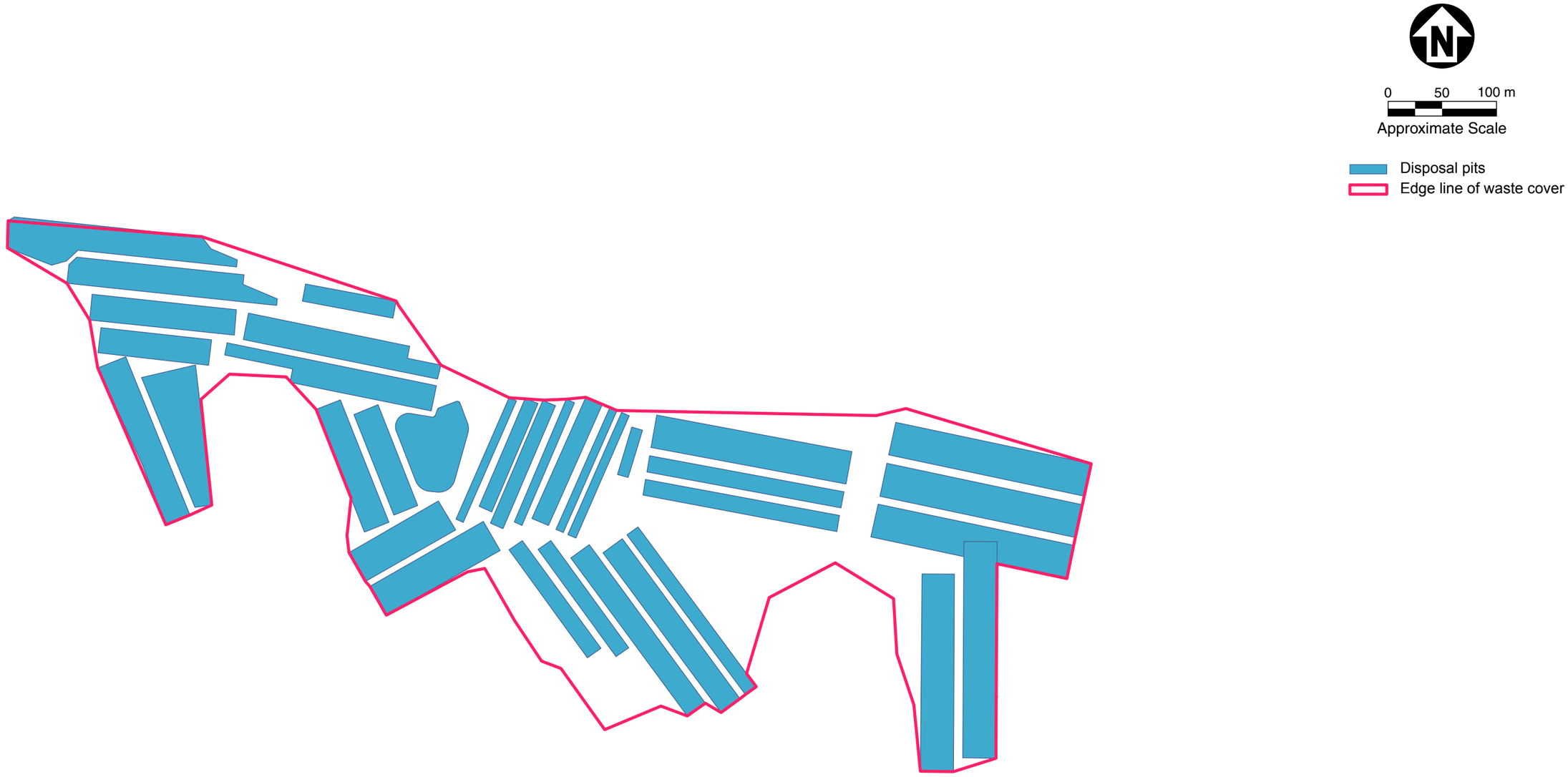

Figure 1
Establishment of Cover Edge Line

Source: URS Corporation, Salt Lake City, 2005

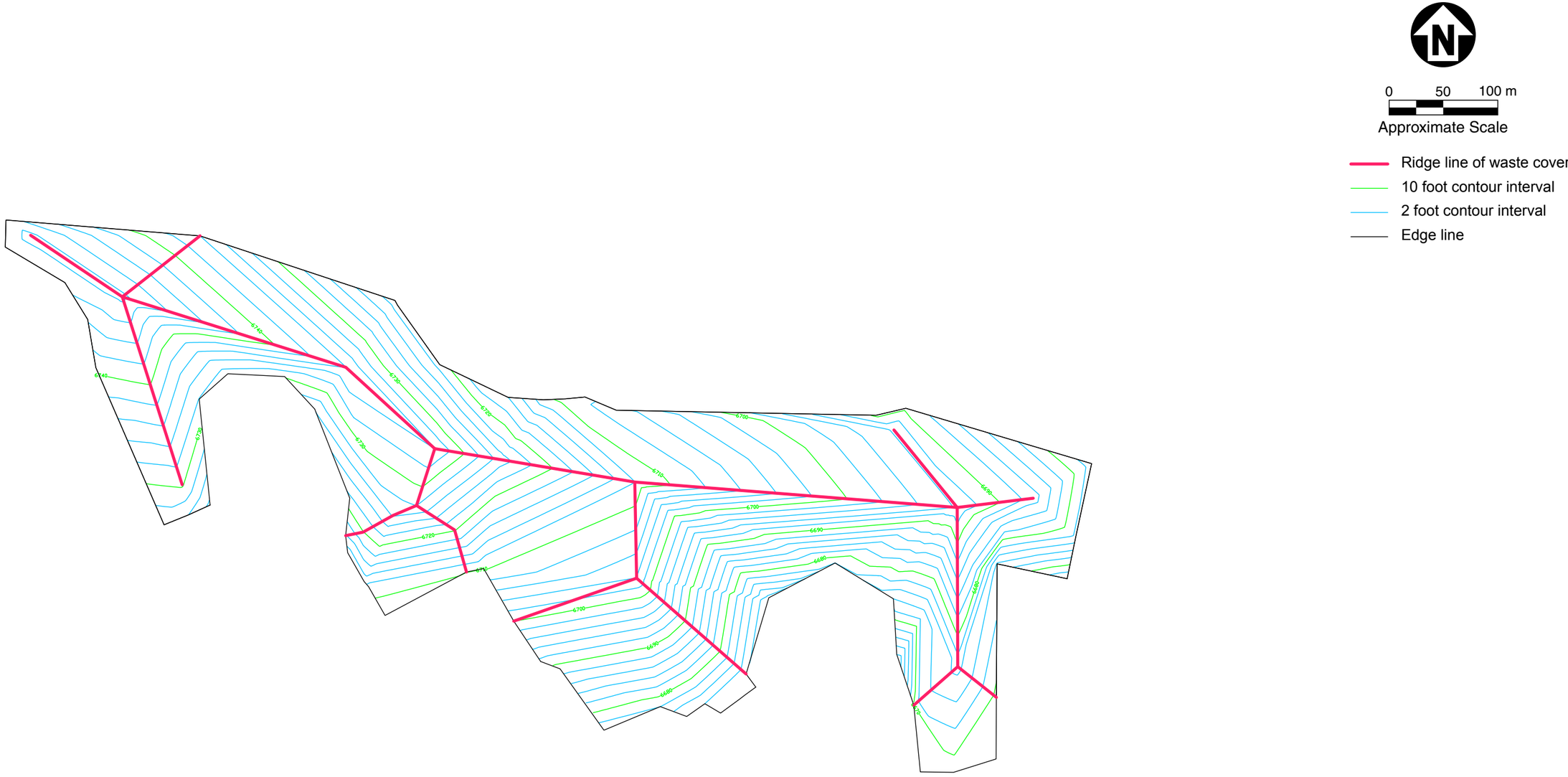

Figure 2
Establishment of Cover Ridge Line

Source: URS Corporation, Salt Lake City, 2005

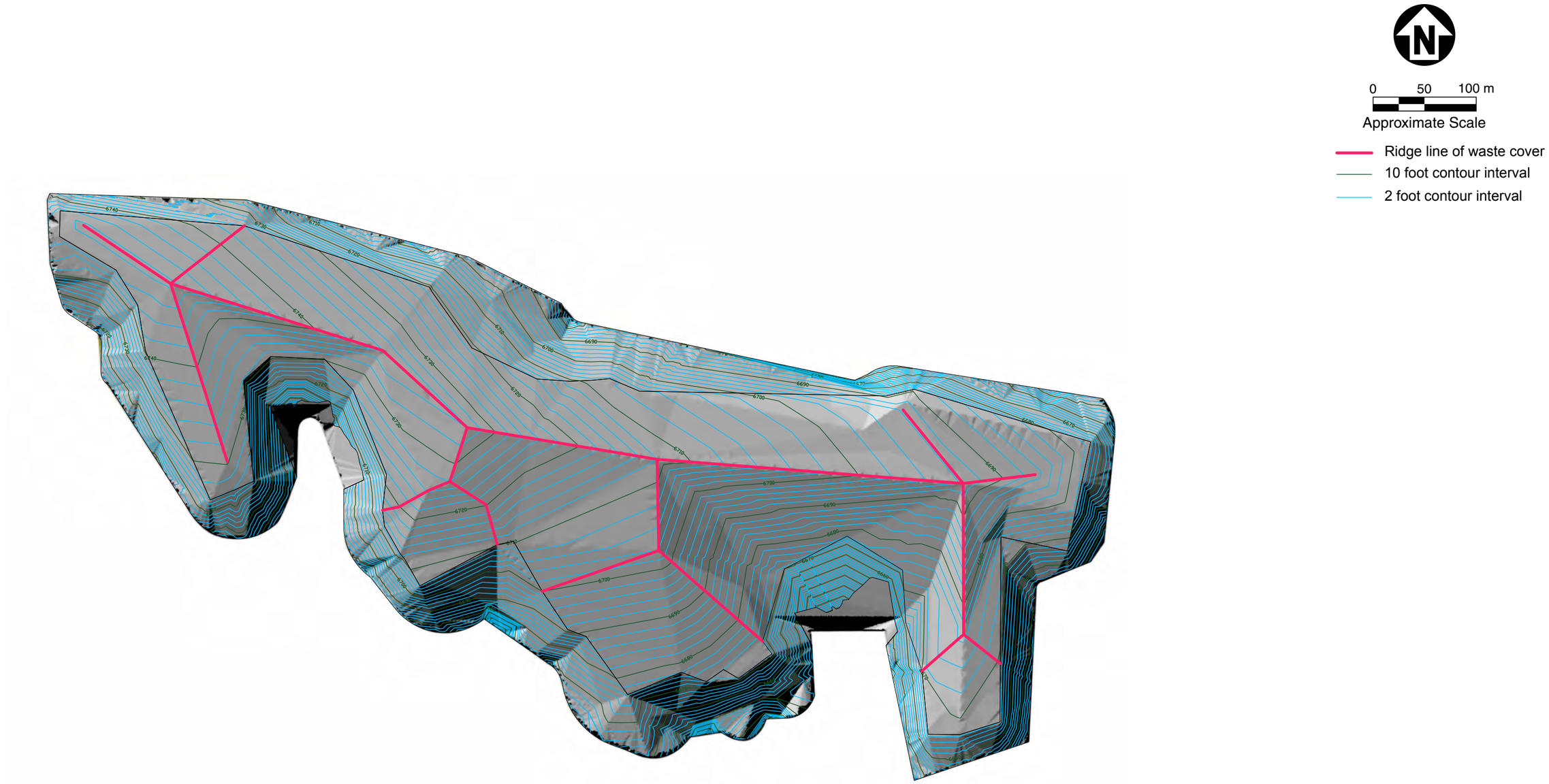

Figure 3
Interior Slopes

Source: URS Corporation, Salt Lake City, 2005

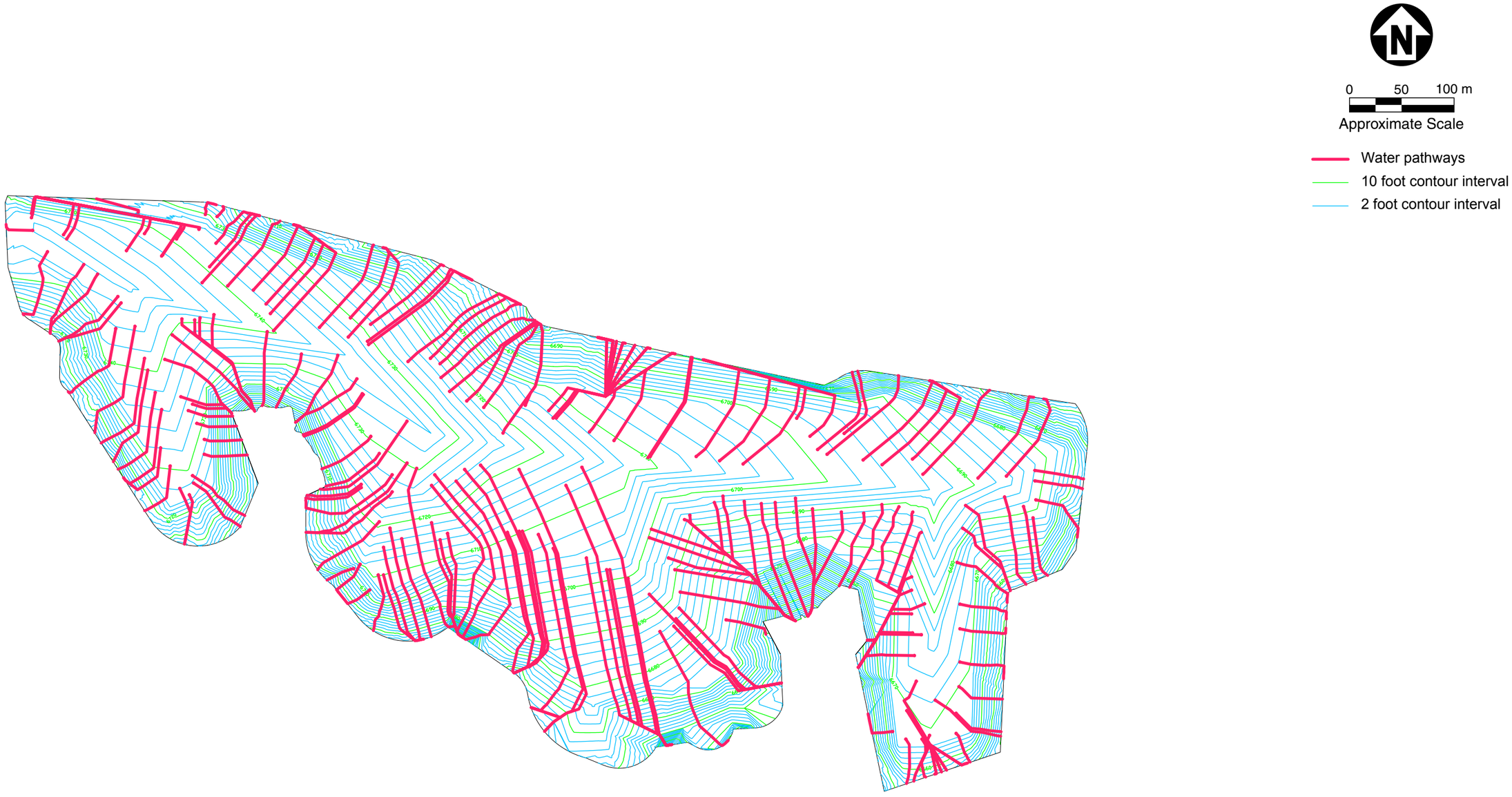

Figure 4
Determination of Water Pathways

Source: URS Corporation, Salt Lake City, 2005

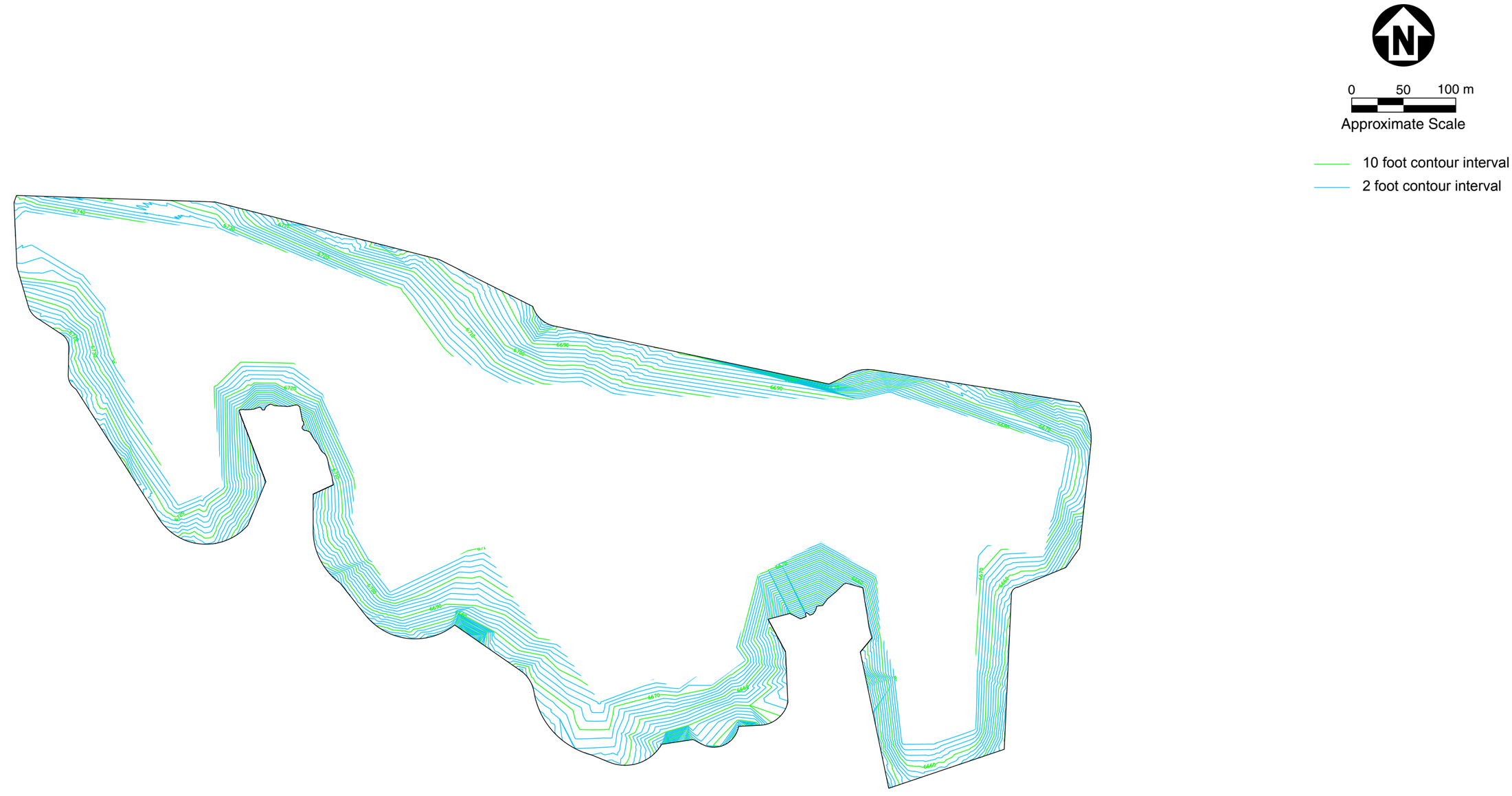

Figure 5
Establishment of Cover Edge Slopes

Source: URS Corporation, Salt Lake City, 2005

With the waste elevations in Zone 4 established, the remainder of the design process was similar to that described for the active portion of MDA G. The final surface of the cover was established using points around the perimeter of the expansion area and points along a centerline that represented the ridge-line of the cover. The elevation of the ridge line was established using slopes of 2 to 5 percent. Finally, the cover over Zone 4 was graded so it matched the contour lines of the cover over the active portion of the disposal site.

After the initial design for the entire disposal facility was completed, the cover elevations were used to create a three-dimensional grid of the surface of the disposal facility using LandDesktop 2004. Elevations were assigned using a 9.3 m^2 (100 ft^2) grid (Figure 6) and these data were used in the SIBERIA surface erosion modeling (Wilson et al., 2005).

The SIBERIA modeling was used to project remaining cover depths across the disposal facility after a 1,000-year period. These simulations indicated that the minimum cover requirements were generally satisfied over much of the site throughout the 1,000-year compliance period. Nevertheless, higher rates of erosion were observed over small portions of the site; these areas generally occurred where the cover and the original grade met along the edges of the mesa and adjacent to drainages. The cover was redesigned and enhanced as necessary to address these critical areas. The design considerations and modifications that went into this process included the following:

- Various engineering controls were considered in the development of the cover design. One such control was an increase in the footprint of the cover to achieve gentler slopes along the edges of the mesa and to provide greater quantities of sacrificial material that could be eroded without compromising the minimum cover requirement.

- The use of earth-filled dams was considered as a means for increasing the footprint of the cover. This technique was used in initial iterations but was later discarded because of concerns about subsurface water collection in the areas behind these dams. This subsurface water could contact the waste in nearby disposal units and leach radionuclides from the pits and shafts.

- Rock armor was applied along edge slopes to limit erosion along the edges of the mesa. Other engineering controls, such as retaining walls and rock bolt reinforcements, were found to be less effective than rock armor.

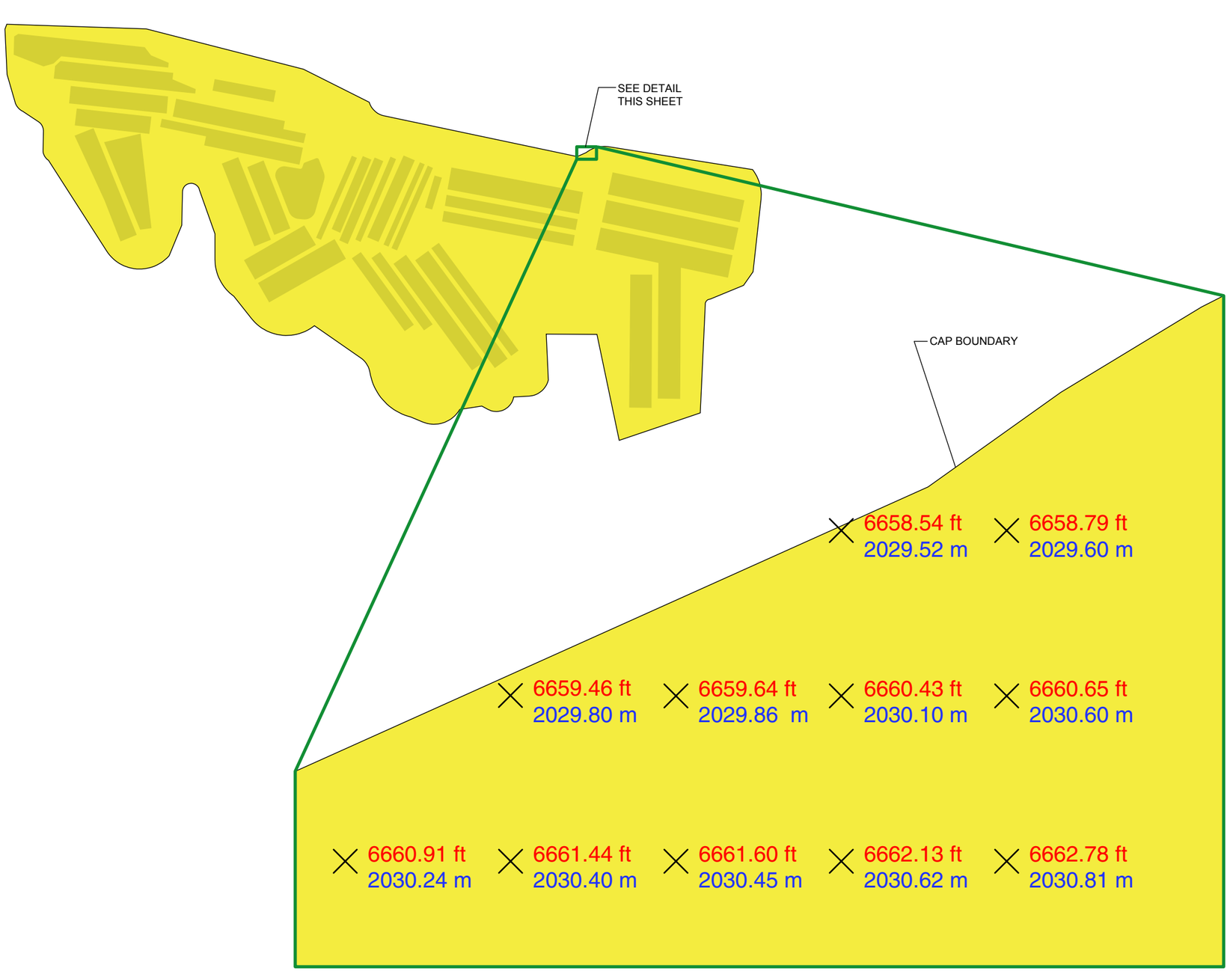

DETAIL

Figure 6
Detail of Grid Point Elevations for Cover Design

Source: URS Corporation, Salt Lake City, 2005

- The peaks and valleys and some of the rough edges shown on the contour of the cover design were smoothed digitally in order to more accurately represent the constructed cover. This smoothing reduced the tendency of the erosion model to artificially initiate erosion at the valleys, ridges, and some edges.

- Pea gravel was mixed into the upper 7.5 cm (3 in.) of topsoil to promote the establishment and growth of vegetation over the site. Angular rock with a diameter of 10-cm (4-in.) was randomly placed on the surface of the cover; these rocks help trap nutrients and provide a stable growth surface, thus promoting the development of a vigorous plant community.

- The predominant soil available for cover construction at TA-54 consists of the crushed tuff borrow from excavations and available "bank-run" sources. Crushed tuff is a friable, low-strength material that is difficult to form into an earthen embankment without admixtures. Clay was combined with the crushed tuff to increase the compactability of the soil, thereby enhancing cover stability; rock was included to increase the strength of the cover.

3.0 Conceptual Design

The conceptual design of the final cover for the active portion of MDA G is depicted in Figures 7 and 8. The three-dimensional perspective of the cover shown in Figure 7 accentuates the ridges, slopes, and valleys to highlight their locations. During construction, transitional areas such as edges, ridges, and valleys will be smoothed to minimize erosion potential. The final contours of the cover are displayed in Figure 8. The gentle slopes characteristic of the majority of the cover contrast with the relatively steep slopes required to transition from the cover to the edges of the mesa.

The final cover configuration for the Zone 4 expansion area (not shown) is generally less complex than the cover over the active portion of MDA G. As discussed in Section 2.4, the minimum cover requirements for the units in Zone 4 will be met because all waste will be placed at least 3 m (9.8 ft) beneath the ground surface. Consequently, development of the final cover consists primarily of contouring the land surface so the cover transitions smoothly with the edges of the mesa and the cover over the active portion of MDA G.

A cross section of the final cover design is provided in Figure 9. This figure shows the general configuration of the cover, including the gravel mulch and topsoil layers at the surface and the crushed tuff/clay layer that forms the bulk of the cover. The top layers of the cover are to be installed at relatively low compaction levels, which will help promote the establishment of plants. The optional layer shown above the interim cover is designed to serve as a capillary break. This layer enhances the water-carrying capacity of the soil above and therefore promotes and sustains vegetation growth.

Figure 10 shows the location of the rock armor along the edges of critical portions of the mesa. The thickness of the rock armor will be specified to be at least six times the average diameter of the rock material. In other words, if material with a diameter of 10 cm (4 in) is used, the rock armor layer will be designed to be at least 60 cm (2 ft) thick. The final grain diameter will be determined during the final design.

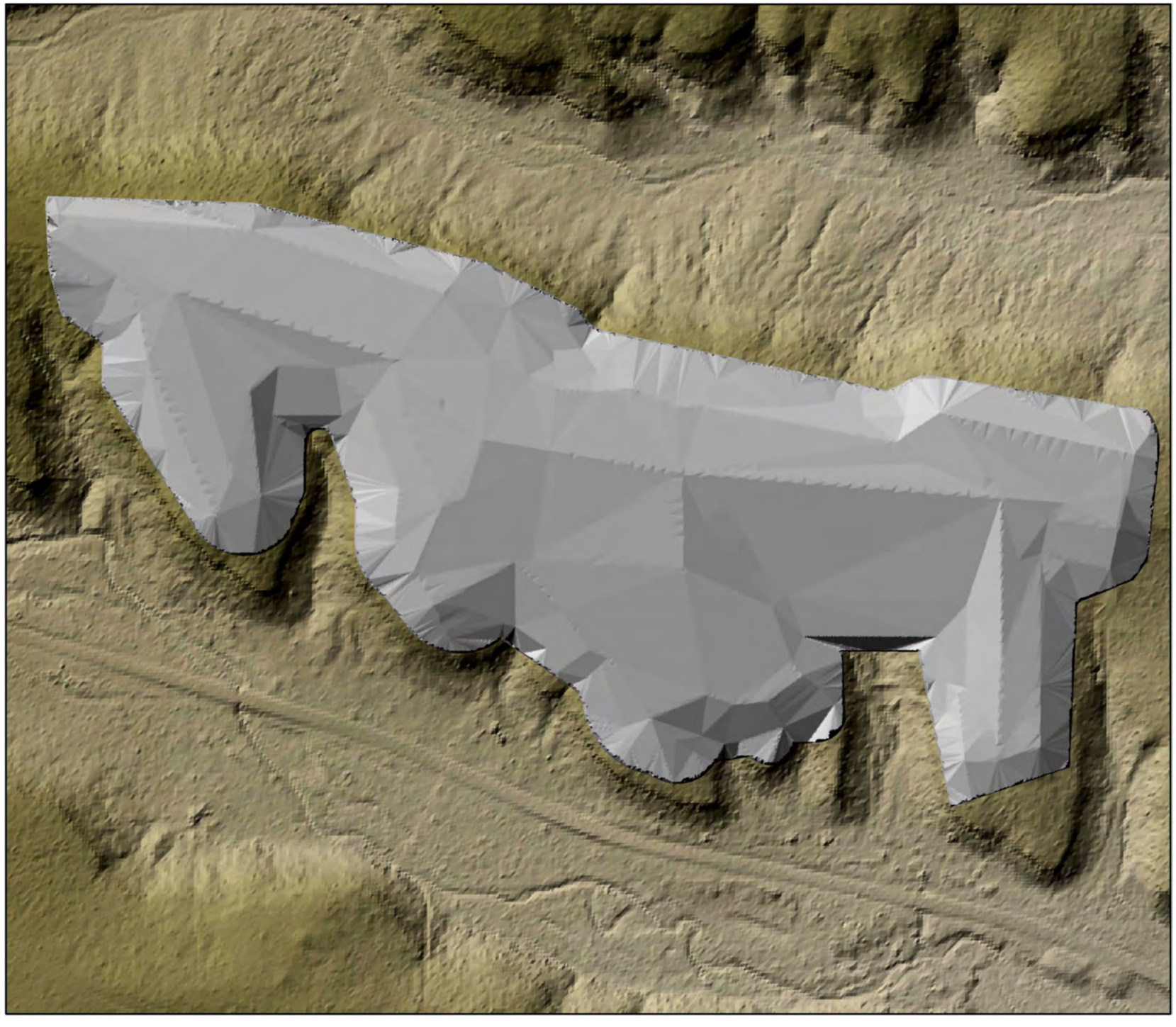

Figure 7
Final Cover Design for Active Portion of MDA G

Source: URS Corporation, Salt Lake City, 2005

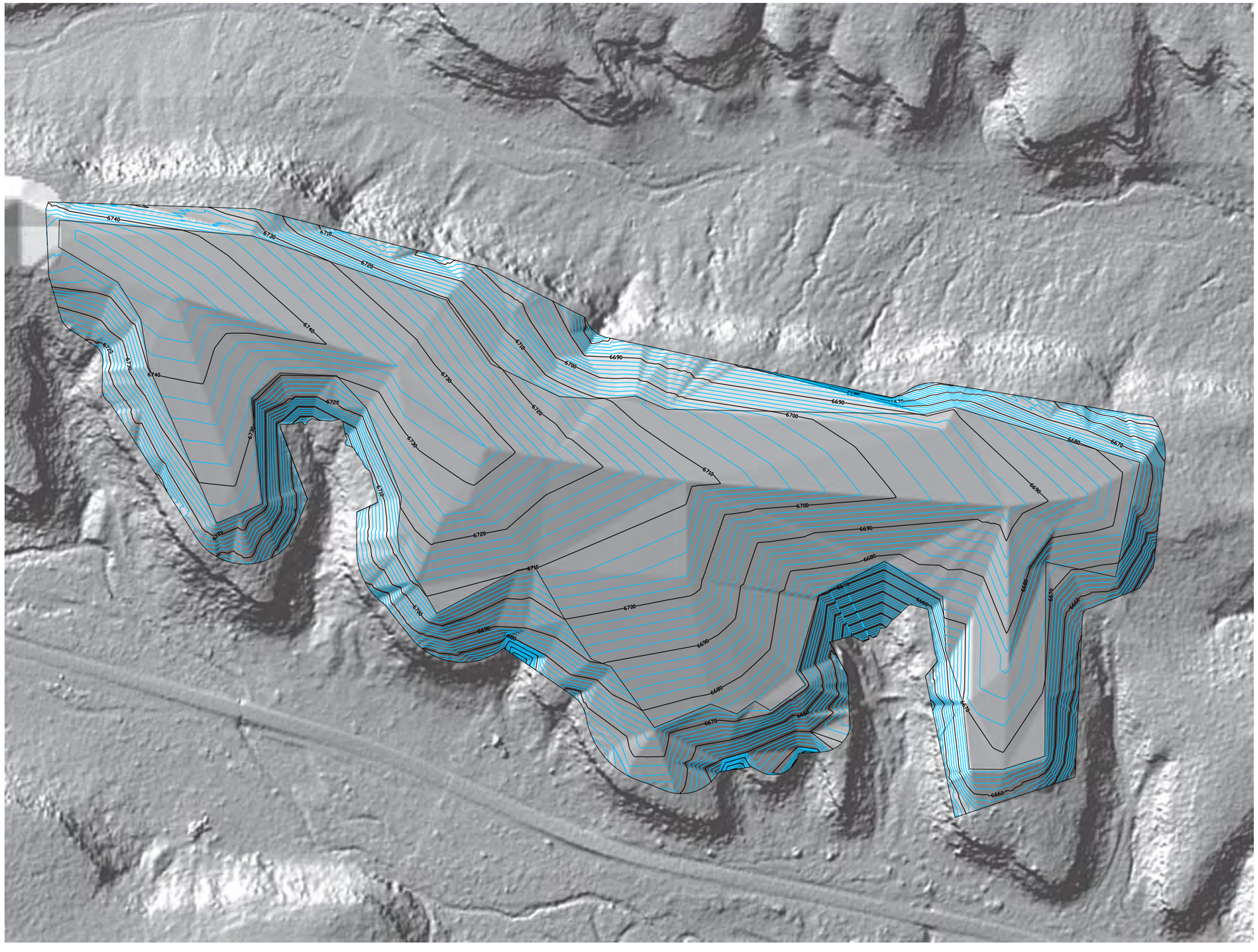

Figure 8
Final Cover Design for Active Portion of MDA G

Source: URS Corporation, Salt Lake City, 2005

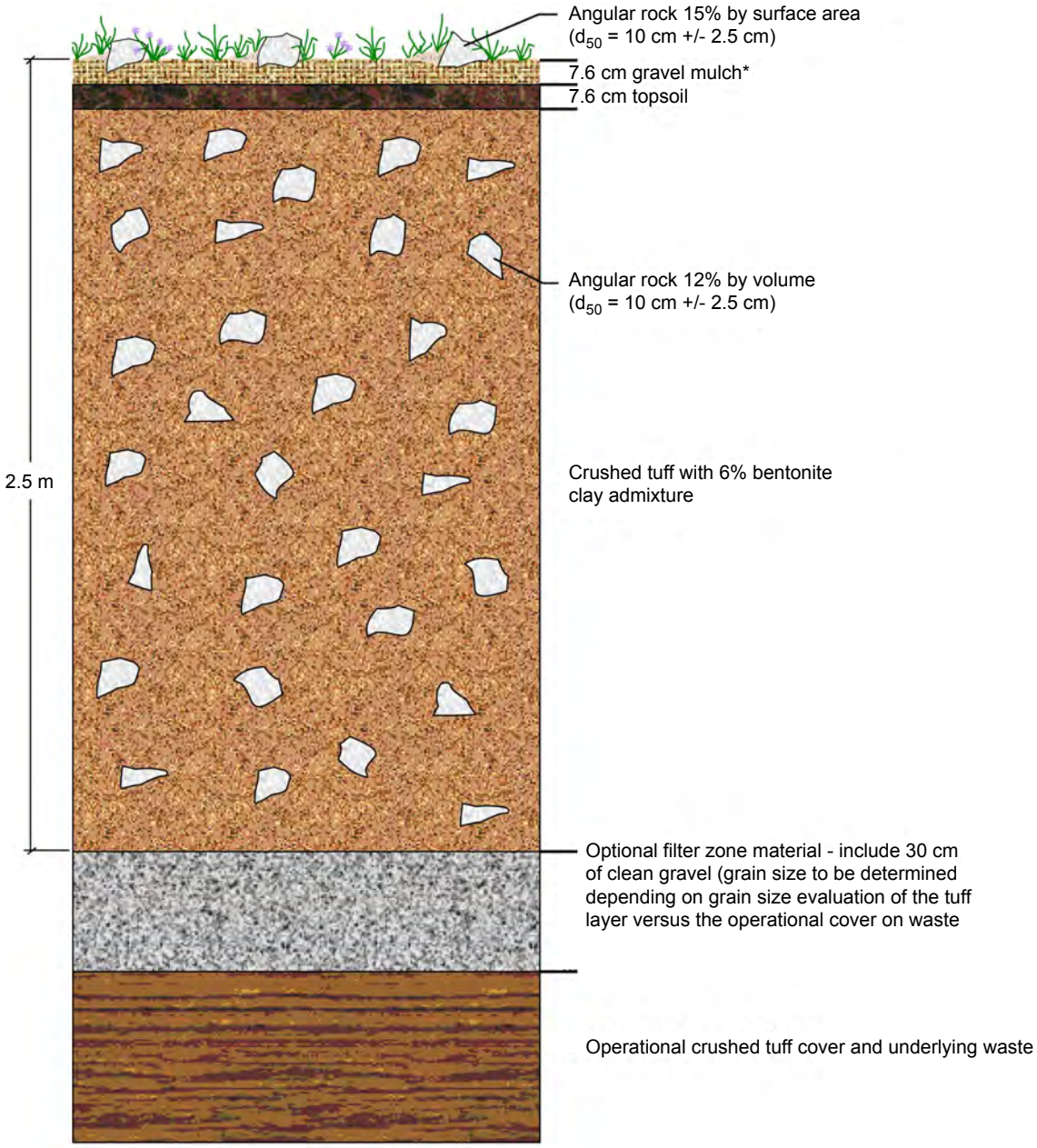

Figure 9
Cross Section of the Conceptual Cover for MDA G
Source: Day et al., 2005

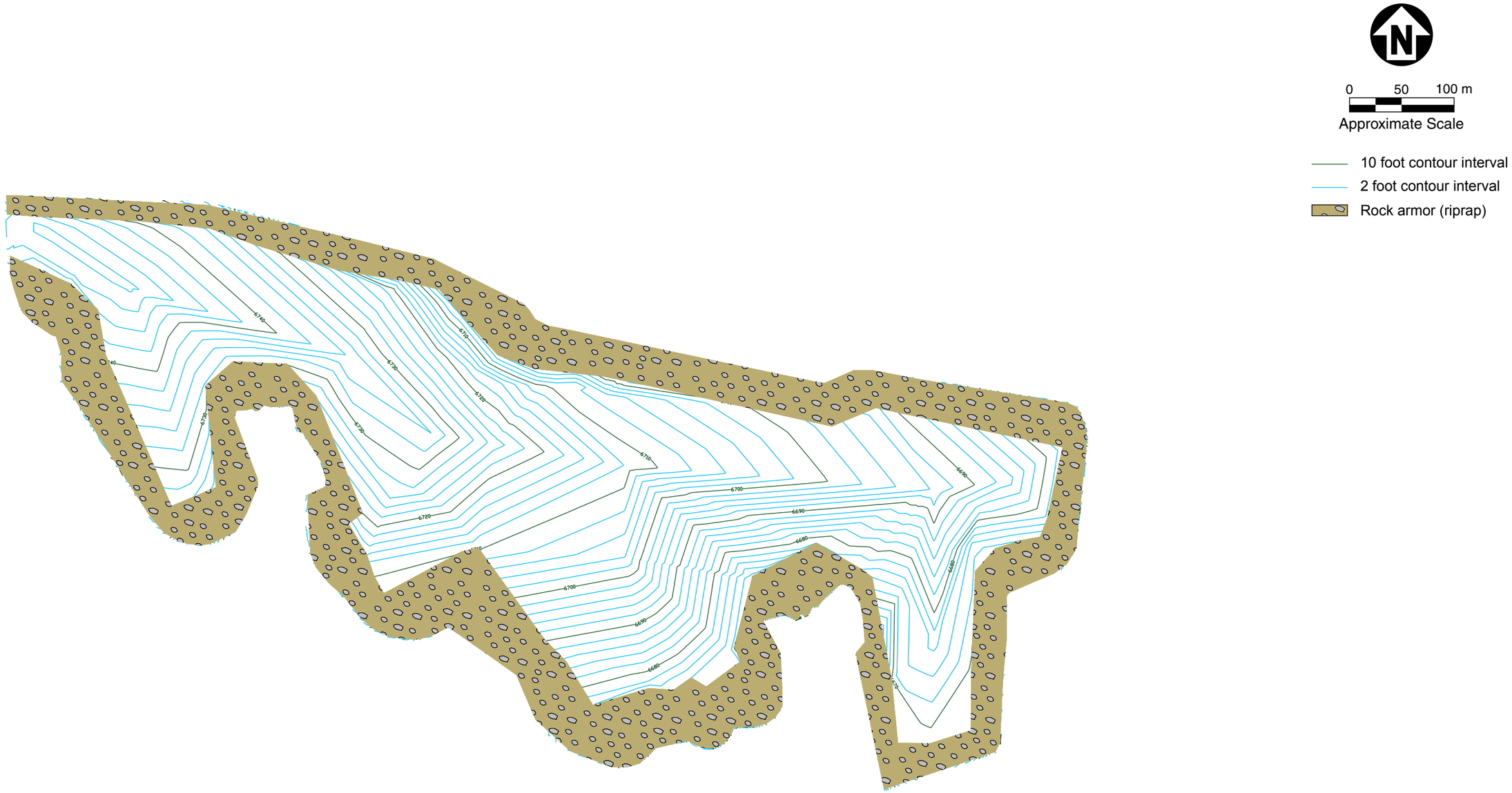

Figure 10
Placement of Rock Armor around Cover Edge

Source: URS Corporation, Salt Lake City, 2005

4.0 References

DOE, 1988, *Radioactive Waste Management*, U.S. Department of Energy Order DOE O 5820.2A, September 26.

DOE, 1999, *Radioactive Waste Management*, U.S. Department of Energy Order 435.1, July 9.

Hollis, D., E. Vold, R. Shuman, K. Birdsell, K. Bower, W. Hansen, D. Krier, P. Longmire, B. Newman, D. Rogers, E. Springer, 1997, *Performance Assessment and Composite Analysis for the Los Alamos National Laboratory Disposal Area G*, Los Alamos National Laboratory Report LA-UR-97-85, Report-54G-013, March.

Koopman, 1965, Memorandum from F.C. Koopman of the US Dept of the Interior, Geological Survey, to Salvatore E. Russo, Engineering 3, LASL, June 30, 1965.

LANL, 1975, Memorandum "Solid Radioactive Waste Disposal Guidelines" from L.J. Johnson, H8-WM-461 at LASL, to Distribution. April 24, 1975.

LANL, 1998, *Material Disposal Unit Design, Construction, Use, and Closure*, Los Alamos National Laboratory Report, Draft DOP-54G-013, Rev. 1, August.

Rogers, M.A., 1977, *History and Environmental Setting of LASL Near-Surface Land Disposal Facilities for Radioactive Wastes (Areas A, B, C, D, E, F, G, and T)*, Los Alamos Scientific Laboratory Report LA-6848-MN, Vol. 1, June.

Shuman, R., 1999, *An Evaluation of the Potential Impacts of Plant and Animal Intrusion into Disposed Waste at TA-54, MDA G*, Rogers and Associates Engineering Corporation, RAE-9629/3005-1, April.

Wilson, J.C.J., Crowell, K.J., and Lane, L.J., 2005, *Surface Erosion Modeling for the Repository Waste Cover at Los Alamos National Laboratory Technical Area 54, Material Disposal Area G*, Los Alamos National Laboratory Report, September.

LA-UR-05-7771

Approved for public release; distribution is unlimited.

Title: SURFACE EROSION MODELING FOR THE REPOSITORY WASTE COVER AT LOS ALAMOS NATIONAL LABORATORY TECHNICAL AREA 54, MATERIAL DISPOSAL AREA G

Author(s): Cathy J. Wilson
Kelly J. Crowell
Leonard J. Lane

Submitted to: U. S. Department of Energy

Table of Contents

1.0 Introduction 1
2.0 Methods 4
2.1 Development of SIBERIA Parameters for Material Disposal Area G 5
2.1.1 Local Data Analysis 6
2.1.2 Definition of a Steady-State Landscape-Forming Event 9
2.1.3 Estimation of Runoff and Erosion 9
2.1.4 Sediment Yield Predictions 12
2.1.5 Optimization of SIBERIA Advective Transport Parameters 17
2.1.6 Estimation of the Diffusion Coefficient 20
2.2 SIBERIA Model Domain Configuration 21
2.3 Model Scenarios 21
3.0 Results 23
4.0 Discussion and Qualifications 30
4.1 Model Limitations 30
4.2 Data Limitations 32
4.3 Comparison of SIBERIA Results to Field-Collected Data 34
5.0 References 35

List of Figures

Figure 1 Aerial Photograph of Material Disposal Area G 2
Figure 2 Proposed Configuration of Cover for Material Disposal Area G 3
Figure 3 Sediment Concentration Data for Runoff Plots, Small Watersheds, and Cañada del Buey 8
Figure 4 Locations of 17 Hillslope Profiles in Vicinity of Material Disposal Area G 10
Figure 5 Photographs Showing Expected Range in Canopy and Ground Cover after Site Closure 14
Figure 6 Mean Excess Runoff Values and Ranges for Soil-Type/Return-Period Pairs 15
Figure 7 Artificial Surface Showing HEM Profiles and SIBERIA Flow Paths Used during Simulated Annealing 18
Figure 8 Correlation in Sediment Yield between the HEM and the SIBERIA Model for a Range of Slopes and Hillslope Lengths (low-erosion scenario) 19
Figure 9 Erosion and Deposition at MDA G for Moderate-Erosion Scenario (as predicted by SIBERIA model after 1,000 years) 24
Figure 10 Erosion and Deposition at MDA G for Low- and High-Erosion Scenarios (as predicted by SIBERIA model after 1,000 years) 25
Figure 11 Erosion and Deposition at Zone 4 for Moderate-Erosion Scenario (as predicted by SIBERIA model after 1,000 years) 26
Figure 12 MDA G Sediment-Source Areas and Sediment Catchments in Habitable Canyon Bottoms 28

List of Tables

Table 1	Characteristics of Four Small Watersheds within the Santa Rita Experimental Range near Tucson, Arizona (analog site)	11
Table 2	Summary of Rainfall-Runoff Simulation Results for Hillslope Profiles at TA-54	13
Table 3	Summarized Input and Output for the Three Erosion Scenarios Used in SIBERIA Model	16
Table 4	Summary of Sediment Delivery from MDA G to Canyon Catchments over 1,000 Years	29
Table 5	Estimated Sediment Yield for Mesita del Buey Sites from Events with 2- and 5-Year Return Periods	34

Acronyms and Abbreviations

ALSM	Airborne laser swath mapping
CREAMS	Chemicals, Runoff, and Erosion from Agricultural Management Systems
DEM	Digital elevation model
HEM	Hillslope Erosion Model
LANL	Los Alamos National Laboratory
MDA	Material Disposal Area
NOAA	National Oceanic & Atmospheric Administration
TA	Technical Area
WEPP	Water Erosion Prediction Project

Acknowledgements

Technical assistance and review for SIBERIA parameterization was provided by the author of SIBERIA, Garry Willgoose, at the School of Geography, University of Leeds. Sean French, at the Nuclear Waste Operations at Los Alamos National Laboratory, provided expertise on Material Disposal Area G, project oversight, and logistical and funding support. Rob Shuman, at URS Corporation, provided guidance on project requirements, site information, and a review of the model results. Mark Day and Garth Weber, also at URS Corporation, developed the cover design datasets. Ricki Sheldon analyzed the runoff and erosion data for Mesita del Buey. This work was funded through the U.S. Department of Energy.

1.0 Introduction

Low-level radioactive waste from operations at Los Alamos National Laboratory (LANL or the Laboratory) is currently disposed of in pits excavated into the mesa top at Material Disposal Area (MDA) G of Technical Area (TA) 54. One requirement for the operation of this repository is to limit releases of radioactive material to the environment for a period of 1,000 years or more following the facility's closure. The Laboratory is required to demonstrate that the repository can be successfully closed, which includes showing that the waste pits will not be excavated by long-term surface erosion processes such as rilling and gullying. Toward that end, surface erosion modeling was conducted to estimate the spatial distribution of depth to waste at MDA G after 1,000 years of erosion and sediment transport.

Material Disposal Area G is located on a slender finger mesa, Mesita del Buey, which has complex topography and a challenging layout of legacy waste pits located close to the edge of the mesa and natural drainage features (Figure 1). As a result, the closure cover has a complex topography, and the performance of the cover must be assessed as a three-dimensional unit. The SIBERIA model (Willgoose and Riley, 1998) was selected for the erosion evaluation because it is a well-tested version of a new class of erosion models developed to predict long-term landscape evolution. Like well-known hillslope-based erosion models such as the Water Erosion Prediction Project (WEPP) (Laflen et al., 1995) and KINEROS (Smith et al., 1995), SIBERIA predicts sediment transport derived from shallow sheet and rill processes for a range of soil, runoff, vegetation cover, and hillslope properties. Unlike WEPP and KINEROS, SIBERIA predicts the spatial distribution of deformation across complex, three-dimensional topography over hundreds to thousands of years. This includes the lowering of ridges, the incision or infilling of valleys and hollows, and the development of gullies and fans.

Scientists at LANL worked with cover design engineers at URS Corporation in an iterative process to develop a stable closure cover design (Figure 2). The SIBERIA modeling results described in this report demonstrate that the final, optimized design meets performance criteria across the site for a wide range of potential site and climate conditions that could occur over the 1,000-year compliance period. Section 2 of this report describes the principles behind the SIBERIA model and the methods for defining parameters and running the model. The results of the model simulations are provided in Section 3, and Section 4 discusses these results and some of the uncertainties associated with the modeling.

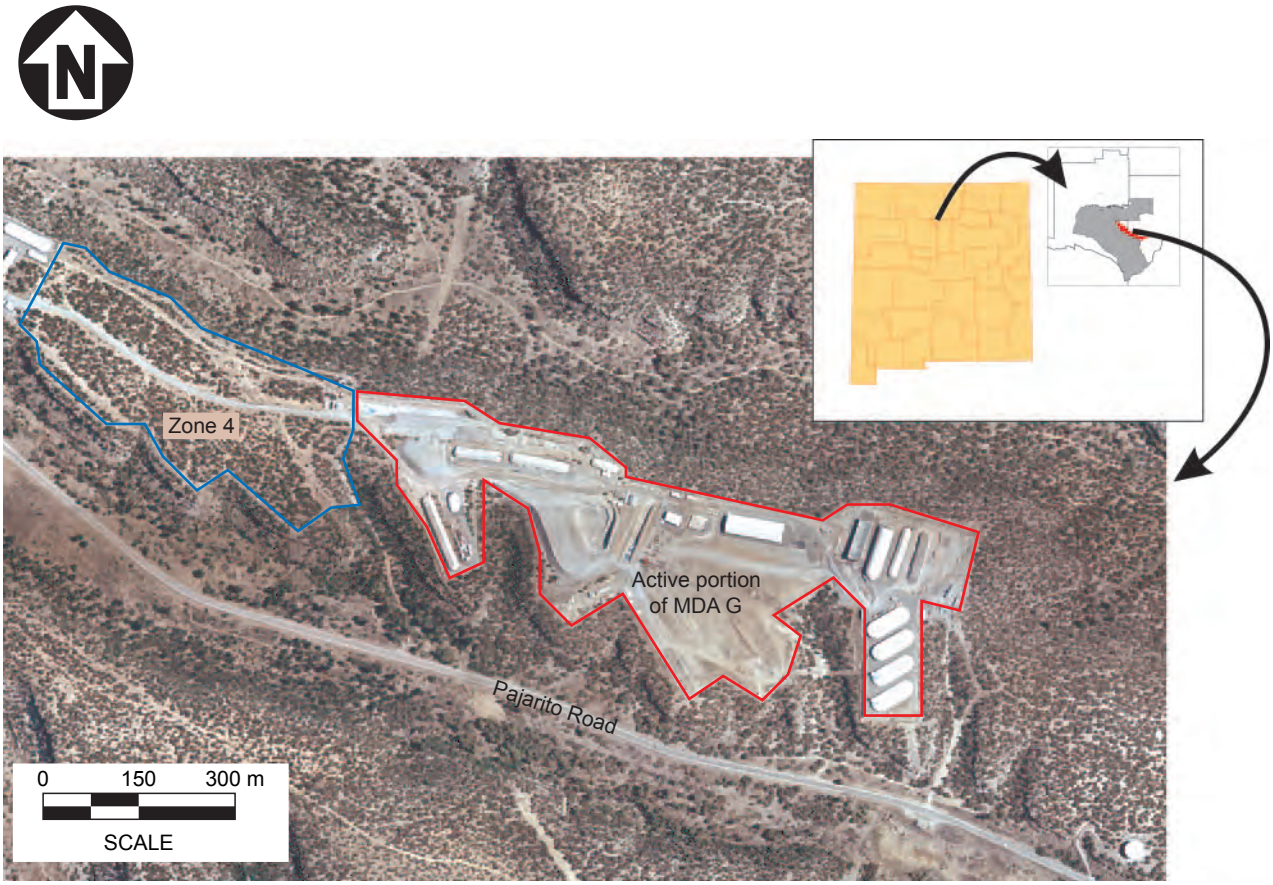

Figure 1
Aerial Photograph of Material Disposal Area G

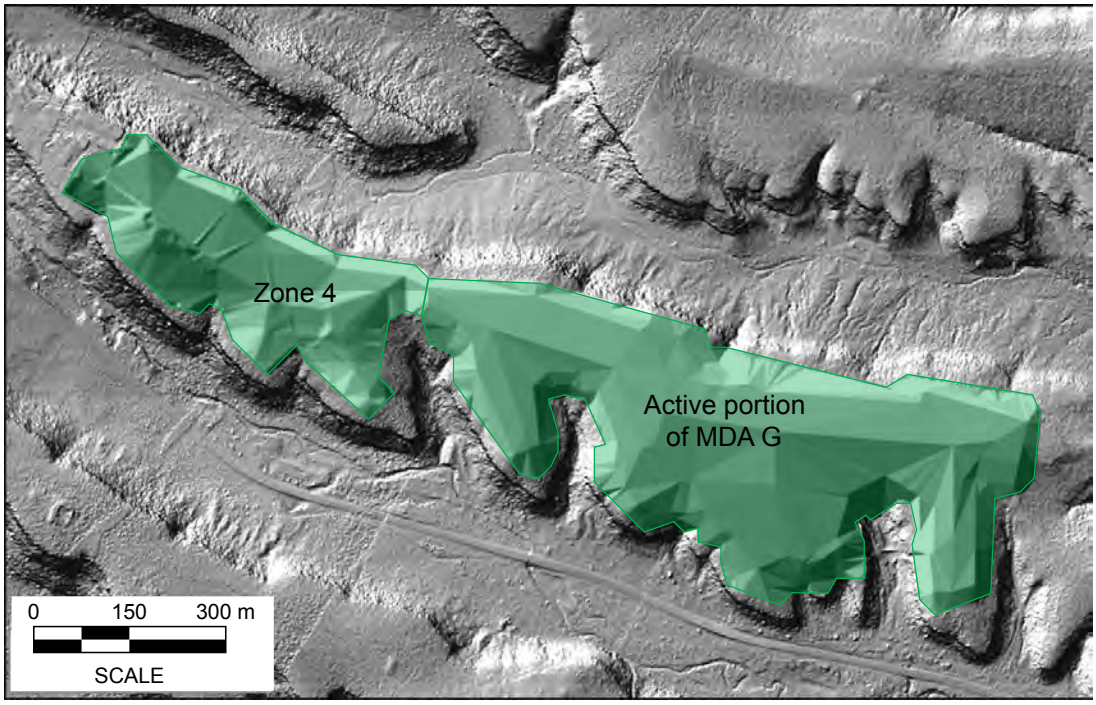

Figure 2
Proposed Configuration of Cover
for Material Disposal Area G

2.0 Methods

The long-term erosion assessment at MDA G was performed using the SIBERIA landscape evolution model (Willgoose et al., 1991a, 1991b). This model predicts steady-state erosion and sediment transport across a landscape that is represented as elevations in a gridded digital elevation model (DEM). The DEM is adjusted each time step (typically 1 year) to account for any change in surface elevation that occurred from erosion or deposition since the last time step. The governing equation for the SIBERIA model is:

$$Q_s = B A^m S^n + D_z S \qquad 1$$

Where

Q_s	=	the annual sediment flux through a grid cell (kg per meter width)
B	=	a coefficient that represents all factors that moderate runoff-driven erosion in the grid cell, except slope and runoff
$A^m S^n$	=	the relationship between contributing area (*A*), slope (*S*), and sediment yield
D_z	=	a diffusion coefficient
S	=	the terrain gradient (slope) (%)

Thus, Equation 1 includes sediment transport terms for both runoff-driven (advective) processes ($B A^m$) and gravity-driven (diffusion) processes. The intensity of runoff-driven sediment transport is given by $B A^m S^n$. The coefficient B accounts for all factors (e.g., vegetation cover, degree of soil disturbance, and soil type) that moderate runoff-driven erosion in the grid cell, except for slope and runoff. The $A^m S^n$ value increases as the catchment area above a grid cell increases (i.e., a bigger catchment area feeding into a grid cell equates to a greater runoff volume flowing through the grid cell) and as the gradient of the cell increases. The exponents m and n determine how sediment yield depends on contributing area and slope for a given site, and can be determined empirically (where data are plentiful) or through an optimization process using other hillslope-based models. Diffusive transport includes processes such as rainsplash (sediment particles ejected from the surface by raindrop impacts), tree-throw (sediment tumbled downslope when the root ball of a fallen tree is exposed at the surface), and animal burrow mounds. The diffusion coefficient D_z captures the intensity of these gravity-driven sediment transport processes.

Within the SIBERIA model, Equation 1 represents sediment-transport processes at all scales. In addition, the sediment yield, Q_s, when applied to each time step over long periods of time, is equivalent to the average annual sediment that would result from large and small events of all return periods. Equation 1 is solved for every grid cell in the SIBERIA model domain for each

time step. Every grid cell has an upslope contributing area, A, and a slope, S. In any given grid cell the values of A and S may change through time as the landscape deforms; thus, these values are recalculated for each time step. The values of B, m, n and D_z are considered inherent material and site properties for soil and bedrock, even though they may change slowly or catastrophically as a result of long-term soil development or fire. The user may change these values in time through a start-and-stop process. However, because it is virtually impossible to project how time will affect these values at MDA G, in this study they were held constant over time for specific soil and bedrock layers.

2.1 Development of SIBERIA Parameters for Material Disposal Area G

The typical approach for developing values for the SIBERIA parameters B, m, n, and D_z is to calibrate SIBERIA to one or more standard hillslope-runoff erosion models. In principle, SIBERIA can be parameterized directly using long-term rainfall, runoff, and sediment yield data, but these datasets are rare. To derive the relationship for runoff-driven transport ($B A^m S^n$) empirically, data must exist for a range of hillslope and watershed gradients, S, at a range of area scales, A (hillslope, subwatershed, and watershed).

Multiple rainfall, runoff, and sediment datasets do exist for Mesita del Buey at a range of scales (experimental measurement plot, hillslope, and watershed scales), but these data are neither continuous over time nor of the uniform quality required for direct determination of SIBERIA parameter values. They were, however, sufficient for parameterizing the rainfall-runoff model IRS9 (Stone et al., 1992) and the runoff-sediment yield Hillslope Erosion Model (HEM) (Lane et al., 2001). Both the IRS9 model and the HEM were used to develop parameter values for the advective transport term in SIBERIA.

Although a quantitative path exists for developing the advective term in SIBERIA, determining the diffusion term is still an art. Research by Heimsath et al. (1997) has significantly advanced the quantitative determination of diffusion in equilibrium landscapes. Unfortunately, Mesita del Buey is a poor candidate for the application of these techniques because soil geochronology suggests that the local soils are aeolian and may have been emplaced rapidly about 10,000 years ago. Given this, the diffusivity was constrained by estimating a match between SIBERIA-generated topography and direct observations of headwater drainage lines using data from the field and from airborne laser swath mapping (ALSM) digital topographic maps. For example, if a SIBERIA run predicted that observed well-defined drainage lines at MDA G aggraded (filled-in with sediment) significantly over 1,000 years, then the value used for the diffusion coefficient in that run was probably set too high. If many new drainage lines appeared across the site, then the diffusion coefficient was probably too low.

A final challenge in parameterizing SIBERIA is developing steady-state values for B, m, and n such that the application of Equation 1 on an annual time step in the model domain reproduces

nature's highly dynamic runoff and erosion rates. In nature, landscape-forming runoff events occur sporadically, perhaps once every 10, 20, or 1,000 years, rather than every year. Analysis of long-term datasets shows that the cumulative effect of a few "large" runoff events over the monitoring period is greater than the cumulative effect of the smaller runoff events that occur every year. Because SIBERIA is a steady-state model, the user must determine the size (return period) of a landscape-forming event that can be applied annually in the model domain to predict the same long-term sediment yield that would be generated through periodic large events.

Thus, the parameterization of the SIBERIA model for application at MDA G required a multistep approach. This approach, which is explained in more detail in the following sections, consisted of six major steps:

1. Collect, collate, and evaluate precipitation, runoff, and sediment-yield data for Mesita del Buey. These data were used to parameterize the rainfall-runoff ISR9 model and the runoff-erosion HEM, as well as to test SIBERIA results.

2. Evaluate long-term runoff and sediment-yield datasets from an analog site, the semiarid Santa Rita Experimental Range (in Arizona), to estimate the return period for landscape-forming events.

3. Develop rainfall-runoff relationships for MDA G using the selected return period for the landscape-forming events, as determined from data collected at the Santa Rita Experimental Range. Apply the ISR9 model using MDA G soil and vegetation properties and precipitation amounts for events with 2- and 5-year return periods for MDA G. The excess runoff values predicted by ISR9 for the 2- and 5-year events were used as input to the HEM.

4. Apply the HEM to predict sediment yield for hillslopes using a range of slopes and areas.

5. Apply a simulated multiparameter regression annealing technique (Crowell et al., 2004) to obtain values for *B*, *m*, and *n* that minimize the difference between sediment yields predicted by HEM and SIBERIA for the same set of test hillslopes.

6. Estimate D_z by matching SIBERIA results to present-day topography.

2.1.1 Local Data Analysis

A number of rainfall, runoff, and erosion datasets have been collected at LANL over the past five decades. Several long-term precipitation records for LANL (available at <http://weather.lanl.gov/>) were analyzed in relation to data posted for Mesita del Buey in the National Oceanic & Atmospheric Administration's Atlas 14 (NOAA, 2004) and were found to

have similar rainfall frequency characteristics. For reproducibility and ease of analysis, the NOAA Atlas 14 rainfall frequency data were used for all analyses reported in this study; these data were generated from NOAA Atlas 14 for the rain gauge located at the LANL water quality monitoring site E247 (35.83° N 106.24° W). This site lies between the Zone 4 expansion area and the active portion of MDA G, immediately south of Mesita del Buey.

There are also a number of runoff and sediment-yield datasets for Mesita del Buey, which are of varying duration and quality. The two datasets determined to be of the most use for parameterizing ISR9 and assessing the HEM and SIBERIA results are (1) TA-51 runoff plots and (2) runoff and sediment-concentration data from eight small watersheds draining TA-54 and from two water quality monitoring stations on Cañada del Buey (E218 and E230). The first dataset contains runoff and erosion data for 52 runoff events; these data were collected from six 3×10 m $(9.8 \times 30$ ft) plots located at TA-51. The second provides runoff and sediment concentration data for watersheds ranging in size from 1 ha to 10 km^2 (2.5 ac to 3.9 mi^2) and includes data for 141 runoff events. Both datasets were preconditioned to remove obviously poor data. Only those events for which rainfall, runoff, and sediment values could be matched, and for which rainfall was greater than runoff, were included.

Sediment concentration data for the TA-51, TA-54, and Cañada del Buey sites are summarized in Figure 3. In order to show both datasets in equivalent units (mg/l), sediment concentration values for the runoff plots were calculated by dividing the amount of sediment eroded during an event by the runoff volume for the same event. For the second dataset (representing the small watersheds at TA-54 and the Cañada del Buey monitoring stations), sediment concentration data were derived from total suspended solids samples collected with an ISCO automated sampler during storm runoff.

It was hoped that the data shown in Figure 3 would enable the estimation of the values of *m* and *n* in the $A^m S^n$ term (Equation 1). However, the variation in sediment concentration between subwatersheds appears to be more a result of site conditions (e.g., paving, soil disturbance, and drainage pipes) than a difference in watershed area or gradient, *S*. In addition, the event data are not equivalent for all sites. Consequently, it was determined that using these data to directly parameterize the SIBERIA model was inappropriate. These data were, however, used as one means of verifying SIBERIA model output.

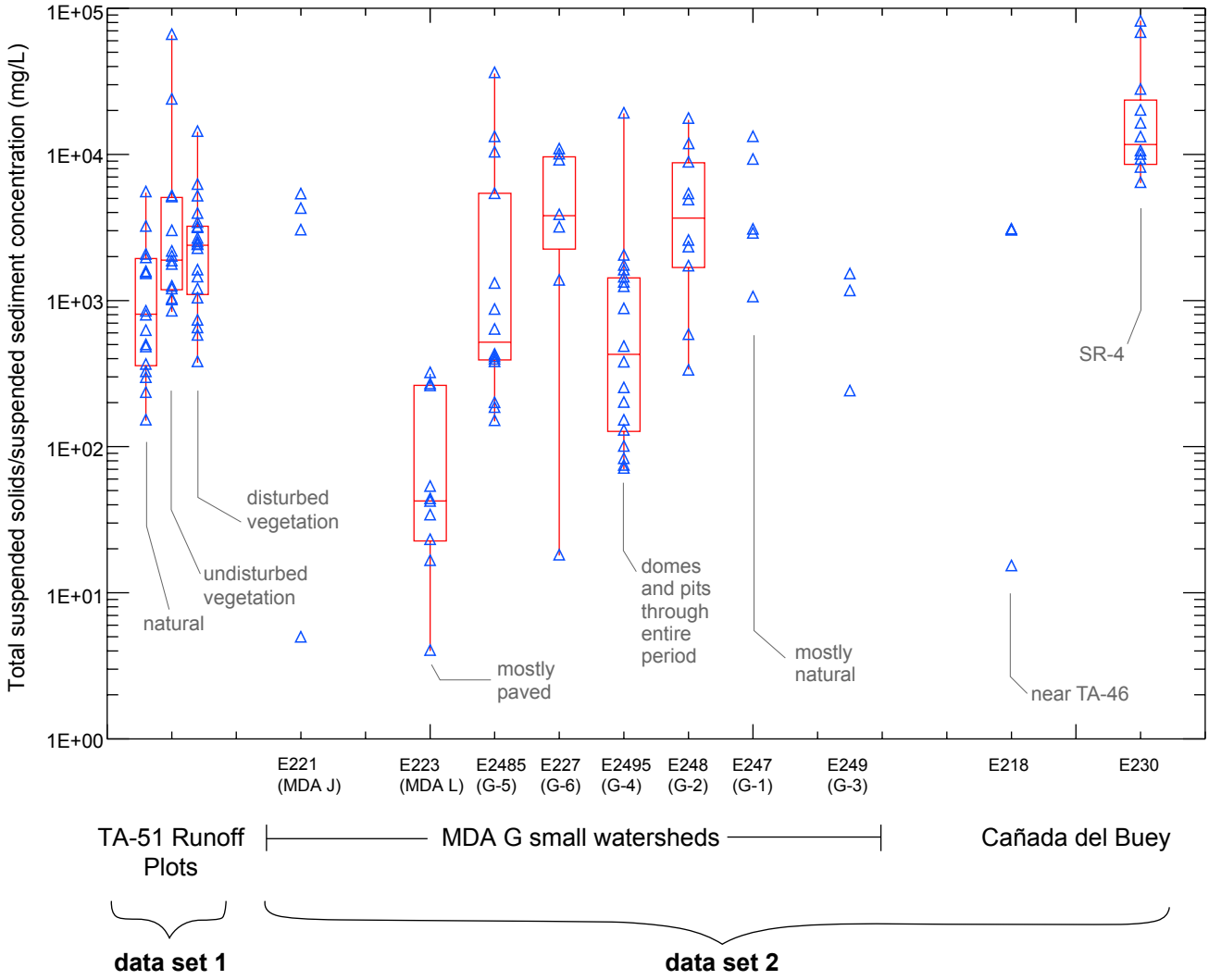

= Mean and variation of sediment concentration data

= Sediment concentration values (calculated from measured event-sediment volume divided by event-runoff volume)

Sediment concentrations measured using EPA method 160.2
E numbers indicate number of New Mexico surveillance program gauging station
G- numbers indicate TA-54 gauge number

Figure 3
Sediment Concentration Data for Runoff Plots, Small Watersheds, and Cañada del Buey

Hillslope topography and vegetation cover profile data were collected specifically for this project (Lane et al., 2002) and used in the ISR9 analysis to develop excess runoff values (with uncertainty) for the range of conditions expected after closure of the disposal facility. The profiles were located in areas with varying degrees of disturbance and rehabilitation. Data defining the shape of the hillslope as well as canopy and ground cover were collected at 1 m (3.3 ft) intervals along each of the 17 profiles shown in Figure 4.

2.1.2 Definition of a Steady-State Landscape-Forming Event

No long-term, coupled rainfall, runoff, and erosion datasets exist for LANL or nearby areas. As an analog, the long-term record of runoff and sediment-yield data from the Santa Rita Experimental Range in Southern Arizona was analyzed to determine the return period for a steady-state landscape-forming event in a semiarid environment. The analysis of these data showed that the average annual sediment yield for a period of approximately 16 years fell within the range of the sediment yield values from events with return periods of 2 and 5 years (Table 1). This is in agreement with the return period recommended by SIBERIA's author of about 2.3 years, which was based on his analysis of a long-term dataset from Europe (Willgoose, 2004). Rather than choose a single return period for the landscape-forming event, SIBERIA runs were performed for both the 2-and 5-year events. The assumption was that the two events would provide low and high estimates of sediment yield over the 1,000-year time frame of the model, and would account for the uncertainty in using data from an analog site to determine the landscape-forming event for MDA G.

2.1.3 Estimation of Runoff and Erosion

The IRS9 infiltration and runoff model (Stone et al., 1992) was used to estimate runoff volumes. Precipitation data for Los Alamos, New Mexico were taken from the NOAA Atlas 14 for events with 2- and 5-year return periods. The IRS9 model was applied to the 17 hillslope profiles shown in Figure 4 for two soil types, sandy loam and loam. These soil types bound the expected soil texture for the MDA G cover as given in the cover design specifications (Day et al., 2005). It is important to note that, although this cover is composed of multiple layers with different admixture materials, SIBERIA assumes the cover is a single homogenous layer of either loam or sandy loam. The loam cover consists of crushed tuff with a 6 percent admixture of bentonite, and the sandy loam assumes a cover composed of crushed tuff with no bentonite. Both covers include an admixture of 12 percent, by volume, of angular rock. The bentonite adds strength to the cover, inhibiting soil mass wasting on the steeper parts of the cover, but decreasing soil hydraulic conductivity, which in turn increases the amount of runoff available to drive erosion. The angular rock provides protection from surface erosion. As the cover erodes more rock is exposed at the surface, reducing the amount of soil surface exposed to erosion.

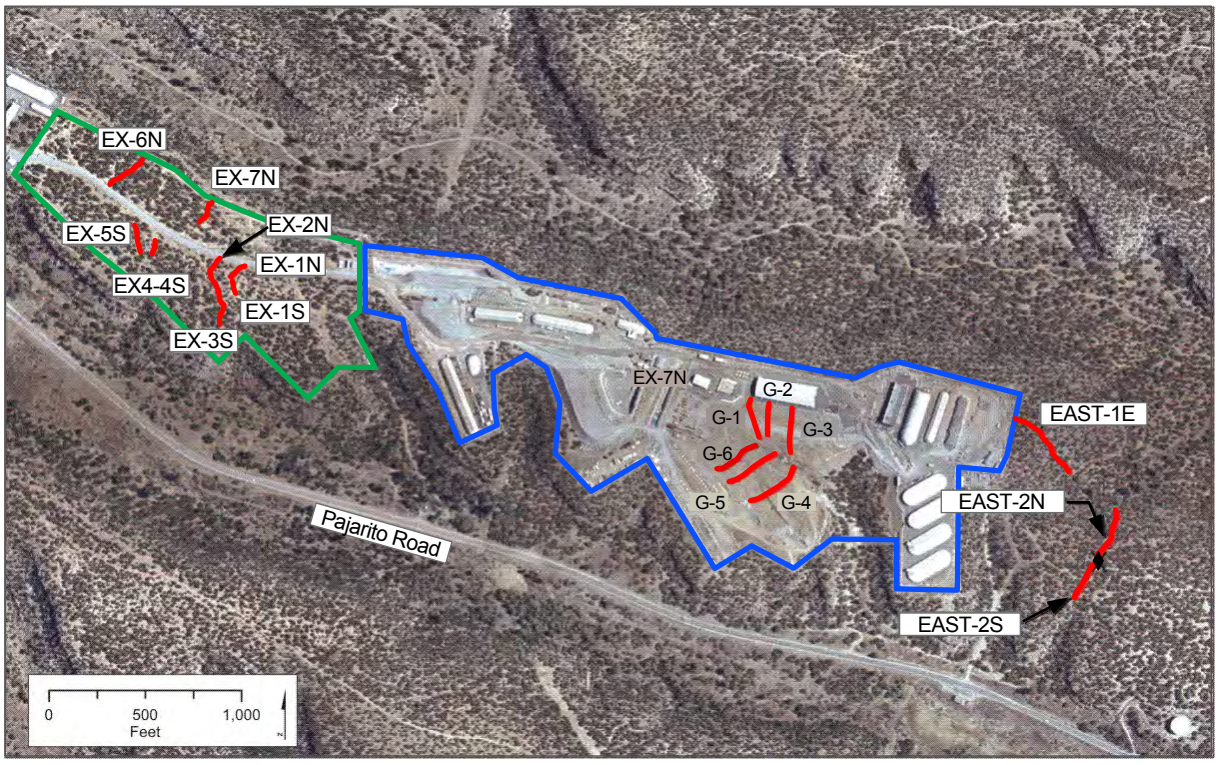

Figure 4
Location of 17 Hillslope Profiles in Vicinity of Material Disposal Area G

Table 1
Characteristics of Four Small Watersheds within the Santa Rita Experimental Range near Tucson, Arizona (analog site)

Watershed ID	Drainage Area (ha)	Grazing System	Vegetation Type	Soil Type	Event Runoff [a] (mm)			Sediment Yield (T/ha)	
					2-Year Event	5-Year Event	16-Year Mean [b]	2-Year Event	5-Year Event
5	4.0E+00	Rotation	Mesquite and grass [c]	Sasabe sandy loam	9.5E+00	2.7E+01	1.7E+01	2.9E+00	6.2E+00
6 [d]	3.1E+00	Rotation	Grass	Diaspar loamy sand	1.3E+00	3.8E+00	1.6E+00	5.4E-02	1.2E-01
7	1.1E+00	Year long	Grass	Sasabe sandy loam	1.6E+01	3.9E+01	2.5E+01	7.8E-01	2.8E+00
8	1.1E+00	Year long	Mesquite and grass [c]	Sasabe sandy loam	2.3E+01	5.1E+01	3.0E+01	1.9E+00	8.0E+00

[a] Sixteen years of hydrologic data (1976 – 1991) were used in this analysis

[b] Mean annual runoff for all runoff events that occurred during the 16-year observation period

[c] Mesquite trees (Prosopis velutina (woot.)) and Lehmann lovegrass (Eragrostis lehmanniana (Nees)) as well as lesser amounts of other shrubs and desert grasses

[d] Watershed 6 has predominantly loamy sand of the Diaspar soil series and thus its runoff and sediment yield are significantly lower than from the sandy loam of the Sasabe soil series.

The hydraulic properties of the cover material determine the amount of runoff associated with the two landscape-forming events. A saturated hydraulic conductivity value of 11 mm/hr (0.43 in./hr) was assigned to the sandy loam in accordance with the value provided by Nyhan et al. (1993) for crushed tuff. A value of 6.5 mm/hr (0.26 in./hr) was used for the loam soil; this is about half the value for sandy loam and is a typical value from the literature (Lane, 2004). These hydraulic conductivity values were used in the IRS9 model to calculate runoff values for the rain events with 2- and 5-year return periods. As discussed in more detail in Section 4.2, the values used for saturated hydraulic conductivity are highly uncertain.

Table 2 shows the results of the ISR9 simulations, including mean runoff values and ranges for each of the soil-type/return-period pairs (Lane, 2004). The percent canopy and ground cover vary significantly among the 17 hillslope profiles; these data can be compared to the range of cover values expected to exist after the closure of MDA G (Figure 5). The effect of cover variation on runoff is evident from the results listed in Table 2. These results also indicate that the average runoff from an annual landscape-forming event is likely to range from about 1 to 18 mm/yr (0.039 to 0.71 in/yr) depending on the soil type, hillslope topography, and cover properties at the site.

2.1.4 Sediment Yield Predictions

The excess runoff estimates calculated by the ISR9 model were used as input to the HEM (Lane et al. 2001) to estimate hillslope erosion resulting from the 2- and 5-year runoff events for both soil types. The HEM is an erosion and sediment transport model that analytically solves the kinematic wave equation for sediment transport on a series of connected hillslope segments. The model calculates the erosion or deposition in each hillslope segment as a function of the segment runoff, gradient, ground cover, canopy cover and soil type. The HEM is well tested and calibrated to hundreds of rainfall simulator experiments performed for the WEPP model calibration. A primary advantage of the HEM over the WEPP and other hillslope erosion models is its ease of use, including the availability of an online version for rapid evaluation of erosion.

For this study, the online version of HEM (USDA, 2002) was modified to run in a batch mode to generate sediment yield values over a wide range of hillslope lengths and gradients for the combinations of soil type and excess runoff shown in Figure 6 and Table 3. Three combinations were selected to represent low-, medium-, and high-erosion scenarios at MDA G; these are described in more detail in Section 2.3. In brief, the low-erosion scenario assumed that the closure cover was composed of sandy loam, the ground and canopy cover were high, and the runoff event had an associated value of 2.6 mm (0.1 in.). The moderate-erosion scenario assumed a sandy loam soil, moderate cover conditions, and a runoff event of 7 mm (0.28 in.). The high-erosion scenario assumed a loam soil, low ground and canopy cover, and a runoff event of 12.4 mm (0.49 in.).

Table 2
Summary of Rainfall-Runoff Simulation Results for Hillslope Profiles at TA-54

Hillslope Profile ID	Amount of Cover (%) [a]		Estimated Runoff (mm) [b]			
	Canopy	Ground	2-Year, 6-Hour Storm		5-Year, 6-Hour Storm	
			Sandy Loam [c]	Loam [d]	Sandy Loam [c]	Loam [d]
Area G-1 SE	6.1E+01	2.3E+01	1.1E+00	5.0E+00	4.8E+00	1.0E+01
Area G-2 S	6.4E+01	2.4E+01	8.0E-01	4.7E+00	4.3E+00	9.7E+00
Area G-3 S	6.3E+01	2.2E+01	1.0E+00	5.0E+00	4.6E+00	1.0E+01
Area G-4 NE	2.0E+01	3.3E+01	3.4E+00	7.6E+00	8.3E+00	1.4E+01
Area G-5 NE	2.4E+01	4.6E+01	2.2E+00	6.4E+00	6.8E+00	1.2E+01
Area G-6 NE	2.6E+01	4.1E+01	2.4E+00	6.6E+00	7.0E+00	1.3E+01
EX-1N NE	8.0E+00	2.7E+01	5.0E+00	9.3E+00	1.0E+01	1.6E+01
EX-1S SE	2.9E+00	7.9E+00	6.7E+00	1.1E+01	1.3E+01	1.8E+01
EX-2N NE	1.5E+01	4.4E+01	3.0E+00	7.2E+00	7.9E+00	1.4E+01
EX-3S SE	2.6E+01	4.0E+01	2.4E+00	6.7E+00	7.1E+00	1.3E+01
EX-4S S	1.2E+01	3.2E+01	4.3E+00	8.5E+00	9.2E+00	1.5E+01
EX-5S S	6.9E+00	1.7E+01	5.8E+00	1.0E+01	1.1E+01	1.7E+01
EX-6N NE	3.2E+01	6.1E+01	8.0E-01	4.7E+00	4.3E+00	9.7E+00
EX-7N NE	2.7E+01	5.7E+01	1.4E+00	5.4E+00	5.4E+00	1.1E+01
East-1E SE	2.9E+01	7.2E+01	5.0E-01	4.2E+00	3.6E+00	9.1E+00
East-2N N	2.9E+01	6.9E+01	6.0E-01	4.4E+00	3.8E+00	9.3E+00
East-2S SW	1.8E+01	5.4E+01	2.2E+00	6.4E+00	6.7E+00	1.2E+01
Statistical Summary of Hillslope Profile Values						
Mean	2.7E+01	3.9E+01	2.6E+00	6.7E+00	7.0E+00	1.2E+01
Standard Deviation (SD)	1.9E+01	1.9E+01	1.9E+00	2.1E+00	2.7E+00	2.6E+00
Coefficient of Variation	7.0E-01	5.0E-01	7.0E-01	3.0E-01	4.0E-01	2.0E-01
Mean – SD	8.0E+00	2.0E+01	7.0E-01	4.6E+00	4.3E+00	9.8E+00
Mean + SD	4.6E+01	5.8E+01	4.5E+00	8.8E+00	9.7E+00	1.5E+01

[a] *All data were collected in July and August 2002.*

[b] *The initial soil water condition was assumed to be wet (tension of approximately 0.33 bar).*

[c] *Sandy loam was used to simulate crushed tuff.*

[d] *Loam was used to simulate a mixture of crushed tuff and 6 percent clay admixture.*

Figure 5a
Example of highest ground
and canopy cover conditions in area
(90% ground cover, 90% canopy cover).

Figure 5b
Example of well-established
ground cover following rehabilitation
(30% ground cover, 90% canopy cover).

Figure 5
Photographs Showing Expected Range in Canopy and Ground Cover after Site Closure

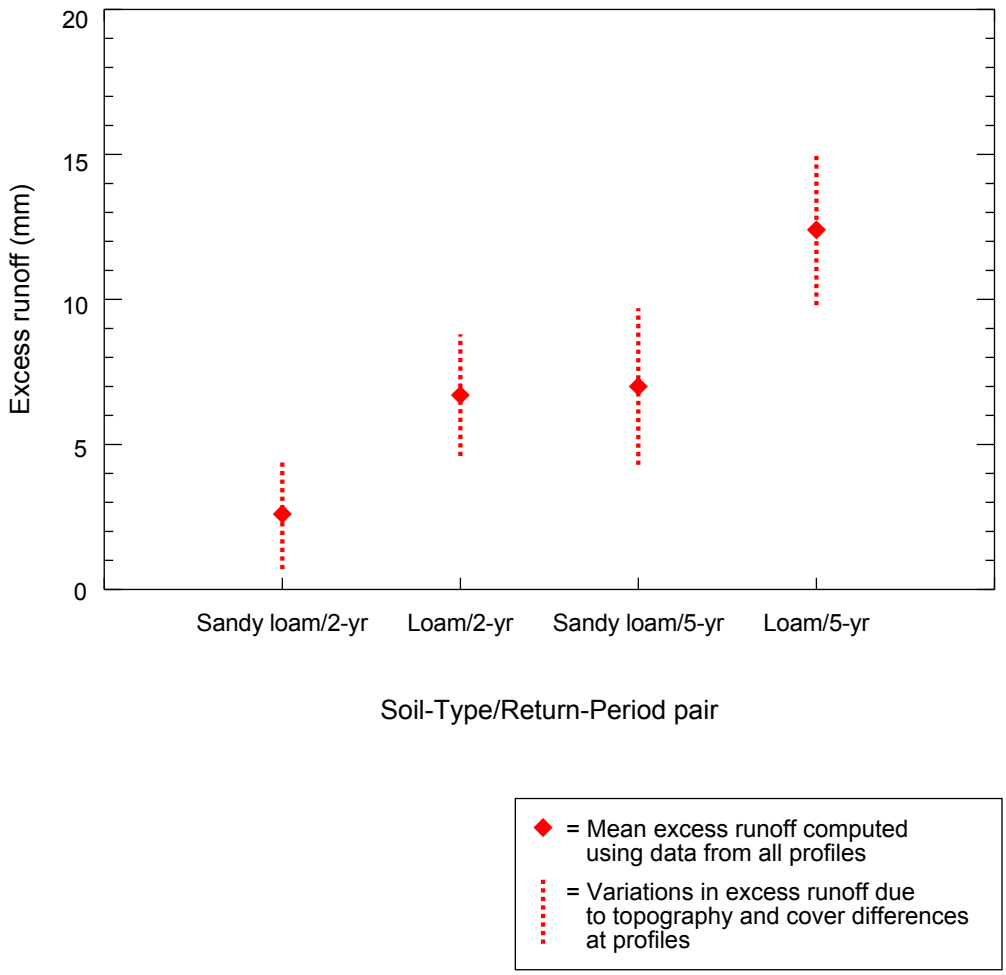

Figure 6
Mean Excess Runoff Values and Ranges for Soil-Type/Return-Period Pairs

Table 3
Summarized Input and Output for the Three Erosion Scenarios Used in SIBERIA Model

Model Parameters	Erosion Scenarios over 1,000-Year Period		
	Low	Moderate	High
Hillslope Erosion Model Parameters			
Soil Texture	Sandy Loam	Sandy Loam	Loam
Canopy Cover / Ground Cover (%)	70 / 70	30 / 70	30 / 30
Landscape-Forming Event (return period in years)	2	5	5
Excess Runoff (mm)	2.6	7	1.2
SIBERIA Model Parameters			
B	9.4E-06	4.2E-05	6.8E-04
m	1.6E+00	1.6E+00	1.3E+00
n	8.6E-01	8.7E-01	8.6E-01
D_z	1.0E-03	2.5E-03	5.0E-03
SIBERIA Model Sediment Yield (T/ha/yr)			
100 years	5.0E-01	1.3E+00	3.2E+00
500 years	4.0E-01	1.1E+00	2.5E+00
1000 years	4.0E-01	1.0E+00	2.3E+00

The HEM runs were performed for the low-, moderate-, and high-erosion parameter sets shown in Table 3 on eight artificial hillslopes. The hillslopes, which were constructed to represent the range of lengths and gradients found on the proposed MDA G closure cover, are shown in Figure 7. The hillslope sediment yields from each set of HEM runs (low, moderate, and high erosion) were then compared to sediment yields from three sets of SIBERIA runs (low, moderate, and high erosion) performed on the same artificial hillslopes. An optimization routine was applied to find the SIBERIA parameters that minimized the difference in sediment yield predicted by the two models for the same profiles. This optimization process is described below.

2.1.5 Optimization of SIBERIA Advective Transport Parameters

The SIBERIA parameter values for the advective transport term $B\ A^m\ S^n$ (Equation 1) were developed using an optimization process called simulated annealing (Press et al., 1996). The process requires the user to specify a set of target values and an equation that, when solved with the right parameter values, will match the target values. In this analysis, the HEM sediment yields from the artificial hillslopes shown in Figure 7 were the target values and Equation 1 was the equation of interest. The simulated-annealing algorithm was used to minimize the difference between the HEM-predicted target yields and the SIBERIA sediment yields for trial sets of *B*, *m*, *n* and D_z values. The optimal set of *B*, *m*, and *n* values shows a minimal difference between HEM and SIBERIA sediment yields for all hillslope length and gradient combinations of interest.

For a given profile, the HEM provides total sediment flux (kg), runoff volume (m^3), mean sediment concentration (%), and inter-rill and rill detachment and deposition rates (kg/m) on a per-meter-width basis. The SIBERIA model provides outputs allowing an equivalent total mass flux to be calculated along a flow path identical to the HEM profiles. Parameters *B*, *m*, *n*, and D_z were varied by the simulated-annealing code to minimize an objective function that is formulated as an "energy" in constraining a randomized exploration of the parameter space. The objective function used was the sum of the squared differences between the net sediment fluxes that were calculated by the two models along the artificial planar hillslopes. The simulated-annealing code calculation was evaluated for low-, moderate- and high-erosion scenarios on length-and-slope combinations derived from the artificial hillslopes shown in Figure 7. Lengths ranged from 30 to 130 m (98 to 430 ft) and were sampled every meter, while gradients ranged from 2 to 16 percent at 2 percent intervals. This yielded 808 hillslope cases (101 slope lengths times 8 gradients). The upper length was chosen to avoid edge effects at the hillslope profile ends. The shortest hillslope length was chosen to limit effects due to differences in how diffusion is calculated for short slope lengths in the HEM and SIBERIA models. Figure 8 shows the correlation between the sediment yields predicted by HEM and SIBERIA for the optimal set of values selected for *B*, *m*, *n*, and D_z by the simulated-annealing algorithm for the low-erosion scenario case; a similarly good match was seen for the moderate and high erosion scenarios. Table 3 summarizes the optimized SIBERIA parameter values for all three erosion scenarios.

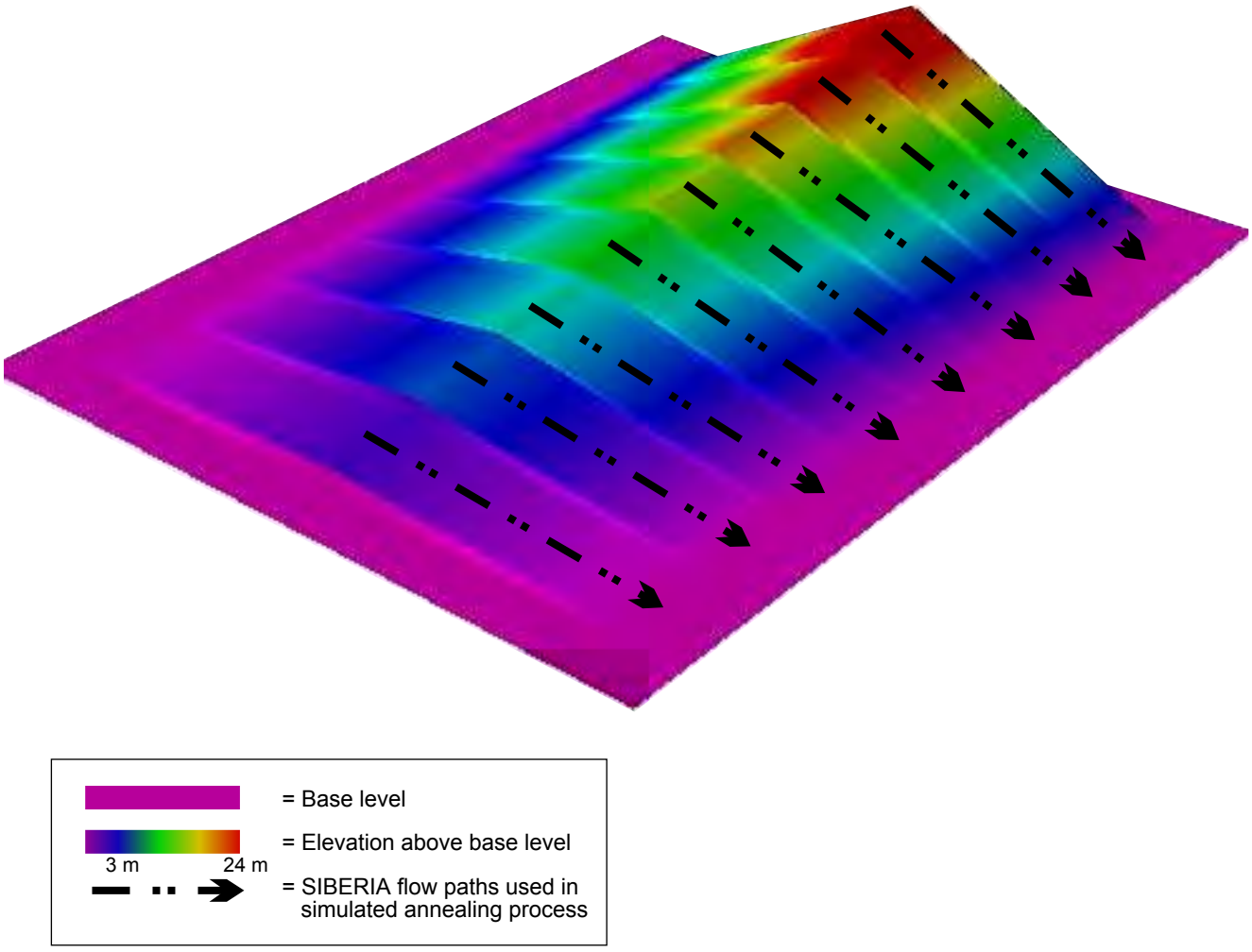

Figure 7
Artificial Surface Showing HEM Profiles and SIBERIA Flow Paths Used during Simulated Annealing

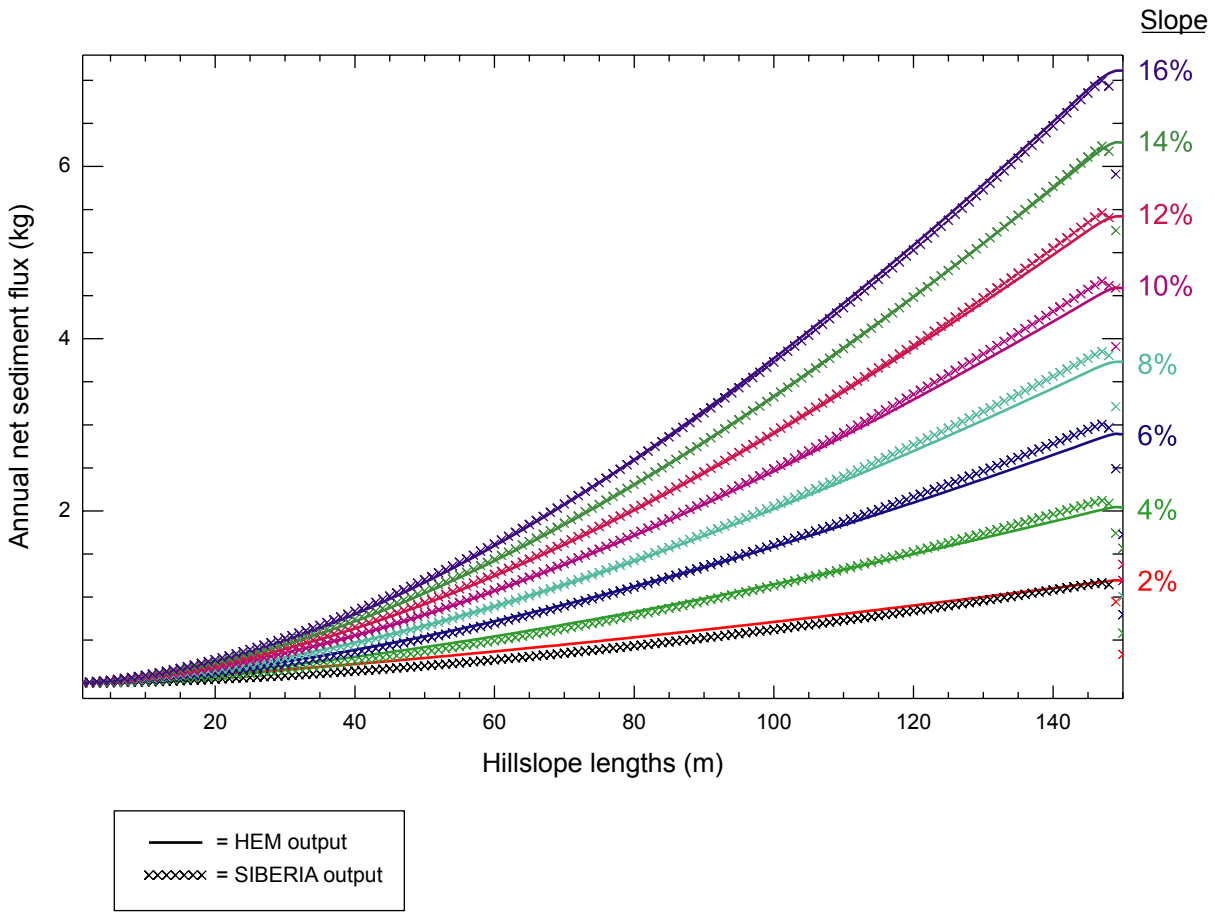

Figure 8
Correlation in Sediment Yield between the HEM and SIBERIA Model for a Range of Slopes and Hillslope Lengths (low-erosion scenario)

2.1.6 Estimation of the Diffusion Coefficient

Within the SIBERIA model, diffusion is added to advective transport as the product of the diffusion coefficient, D_z, and the hillslope gradient, S. Advective and diffusive processes are thought to be largely in balance in the undisturbed portions of Mesita del Buey because there are no well-developed, deep gullies or deep colluvial fills in headwater regions on the mesa. Values given for D_z in the literature range over several orders of magnitude; it was not possible to select a meaningful value among these for the specific site conditions. Although the simulated-annealing procedure found D_z values for the three erosion scenarios, these values do not include the full range of diffusion processes represented by SIBERIA because the HEM includes only that component of diffusion caused by rainsplash. In reality, biotic and other processes contribute significantly to diffusion in the landscape over long time scales and must be considered.

To determine a site-specific D_z value, SIBERIA runs were made using a range of D_z values. The resulting topography was visually inspected and compared to current topography as represented by the DEM derived from ALSM. The comparison focused on gullies and hollows; if SIBERIA predicted the development of deep colluvial fills in the hollows, it was assumed that diffusion was too high relative to advective processes (fluvial transport), whereas if SIBERIA predicted excessive gullying, diffusion was considered too low relative to advective processes. For this analysis, D_z values of 1.0×10^{-4}, 0.0025, and 0.005 were used as input to the moderate-erosion scenario to assess the impact of diffusion on the landscape over 1,000 years of erosion.

The low D_z value of 1.0×10^{-4} led to the development of a highly dissected gully network, which currently does not exist at TA-54. As a result, this value was rejected as being too low for the current model. The middle D_z value of 0.0025 resulted in a landscape with more of the characteristics of the current landscape, whereas the high D_z value resulted in a landscape that looked much more rounded than the current landscape. Because the results associated with the middle value seemed to best represent conditions at MDA G, and because no better method for estimating the D_z was available, the value of 0.0025 was chosen as the moderate-erosion D_z value and the best value for MDA G.

A D_z value of 0.001 was chosen for the low-erosion scenario. This value was selected because a low diffusion rate coupled with a low advective-erosion rate should yield the correct balance between the two processes and result in a landscape that looks somewhat similar to the current landscape; this diffusion rate would also result in slower overall erosion than the moderate- and high-erosion scenarios. Similarly, a D_z value of 0.005 was used in combination with a high erosion rate for the high-erosion scenario. A more rigorous test of the effect of D_z on landscape form is desirable, but experts in the field of landscape evolution modeling suggest that this approach was reasonable given the state of the science (Dietrich, 2004; Willgoose, 2004; Bras, 2004).

2.2 SIBERIA Model Domain Configuration

The SIBERIA model domain is represented by a DEM that consists of current topography from the LANL 2000 ALSM survey (Carey and Cole, 2002) and the proposed cover elevations supplied by URS Corporation personnel. The domain has two layers. The top layer is composed of cover material and extends from the surface of the final cover, through the interim cover, to bedrock. The cover material proposed by Day et al. (2005) is moderately compacted crushed tuff, augmented with bentonite and angular gravel, overlain with a topsoil and pea gravel mixture approximately 5-mm (0.2-in.) thick. The gravel admixtures are used to aid in the establishment of vegetation during the active institutional control period and will help increase soil surface cover and reduce erosion. The second layer is composed of the mesa bedrock material. This layer also includes armoring material (i.e., riprap) emplaced around the edges of the cover, where the transition from mesa-top to cliff occurs. The armoring is included to reduce erosion at the cover-cliff boundary, slow runoff, and capture sediment eroded from the cover.

The current version of SIBERIA does not automatically track the depth of a given layer, though it does account for the spatial extent of a material type that is exposed at the surface of the model domain. In nature, the rate of downcutting in a gully slows once the base of the gully reaches bedrock. To simulate this situation, SIBERIA was run in a "start-stop-start" mode. The model was stopped after every 20 years of simulated time and each cell was checked to determine if its elevation had dropped below the bedrock surface. Cells that had reached bedrock were relabeled as such so that erosion would proceed at a slower rate, and the model was restarted.

The disposal facility was divided into two model regions: the active portion of MDA G and the Zone 4 expansion area (Figure 1). The same SIBERIA parameter values for erosion were used for both areas; however, the cover size and depth and pit configurations are quite different between the two sites

2.3 Model Scenarios

The objective of the erosion modeling was to estimate the spatial distribution of depth to waste at MDA G after 1,000 years of erosion and sediment transport. Any such estimates are uncertain due to potential variations in climate, soil properties, evolution of the vegetation structure, and other factors over the 1,000-year time frame. To help constrain the uncertainty, three scenarios were developed that are expected to result in low, moderate, and high rates of erosion at the site. Each of the long-term outcomes is plausible on the basis of long-term erosion rates reported in the literature (Kirchner et al., 2001) and local current observations. The parameter values for each scenario were developed from soil, vegetation, rainfall, runoff, erosion, and sediment-yield data collected over a range of time frames at the Laboratory and at an analog site (Santa Rita Experimental Watershed, AZ), as described above. Soil properties for the simulations are based on material specifications provided by the cover design engineers (Day et al., 2005).

The low-erosion scenario assumes that the soil will have the erosion and runoff properties of a sandy loam (crushed tuff and gravel with no clay admixture) with high infiltration capacity, a thick vegetation cover of native grasses (canopy cover of 70 percent, ground cover of 70 percent), and an annual design runoff of 2.6 mm (1.0 in.). The moderate-erosion scenario represents an estimate of the average conditions that currently exist at the site. This scenario also assumes a sandy loam with mixed-grass and shrub vegetation cover similar to the current, relatively undisturbed conditions that exist in Zone 4 at TA-54 and at the eastern end of Mesita del Buey (i.e., canopy cover of 30 percent, ground cover of 70 percent). The annual design runoff for the moderate scenario is 7.0 mm (0.28 in.). The high-erosion scenario assumes a loam soil (crushed tuff and gravel mixed with bentonite), a sparse vegetation cover within the range of conditions found on Mesita del Buey (i.e., canopy cover of 30 percent, ground cover of 30 percent), and an annual design runoff of 12 mm (0.48 in.). These scenario parameters are summarized in Table 3.

3.0 Results

The SIBERIA simulations were performed for a range of different cover designs in an iterative process that involved close coordination with the cover designers at URS Corporation. The process enabled the development of an optimized design that was expected to satisfy the performance criteria. Results of the SIBERIA simulations for the final conceptual cover are shown in Figures 9, 10 and 11. These figures show the remaining cover depths, after 1,000 years, over portions of the facility occupied (now and in the future) by pits and shafts. An orange–green color scale indicates how well the cover performs over the pits. Green and yellow shades indicate depth to waste values in excess of 2.5 m (8.2 ft), whereas dark orange indicates that the cover is approaching a thickness of only 1 m (3.3 ft). The blue–red color scale on these figures shows the cumulative change in elevation across the site at the end of the 1,000-year-simulation period. Blue shows deposition (net accumulation) and red shows net erosion.

Examination of Figure 9 reveals that, for the moderate-erosion scenario, 2.5 m (8.2 ft) or more of cover remains over the majority of the disposal units at MDA G 1,000 years after facility closure. Away from the disposal units, areas of erosion and deposition are observed. Gully formation is seen in areas marked by long slope lengths (e.g., in the vicinity of pits 20, 21, and 22) and along the edges of the mesa. Figures 10a and 10b show similar results for the low- and high-erosion scenarios at MDA G. While greater erosion is noted in some portions of the facility under high erosion conditions, a minimum of 1.75 m (5.7 ft) of cover appears to exist over most, if not all, of the disposal units. Figure 11 shows the depth-to-waste results for the moderate-erosion scenario at the Zone 4 expansion area. Results from all three scenarios show that a minimum of 1.75 m (5.7 ft) of cover exists across the site at the end of the 1,000-year simulation period.

Although Figures 9 through 11 show results at the end of the 1,000-year simulation period, SIBERIA allows the user to track depth-to-waste and sediment-yield information at all points across the facility through time. Depth-to-waste values, which were saved every 20 years for the whole facility, are the basis for determining the rate at which waste may be brought to the surface by means of biologic mechanisms such as root uptake and leaf drop. In addition, time-dependent sediment-yield values from the portions of the cover located over the pits and shafts were tracked independently of areas that were located away from waste, such as cliff faces. In the following discussion, these two sediment source areas are loosely referred to as pit-affected and clean-sediment contributing areas, respectively.

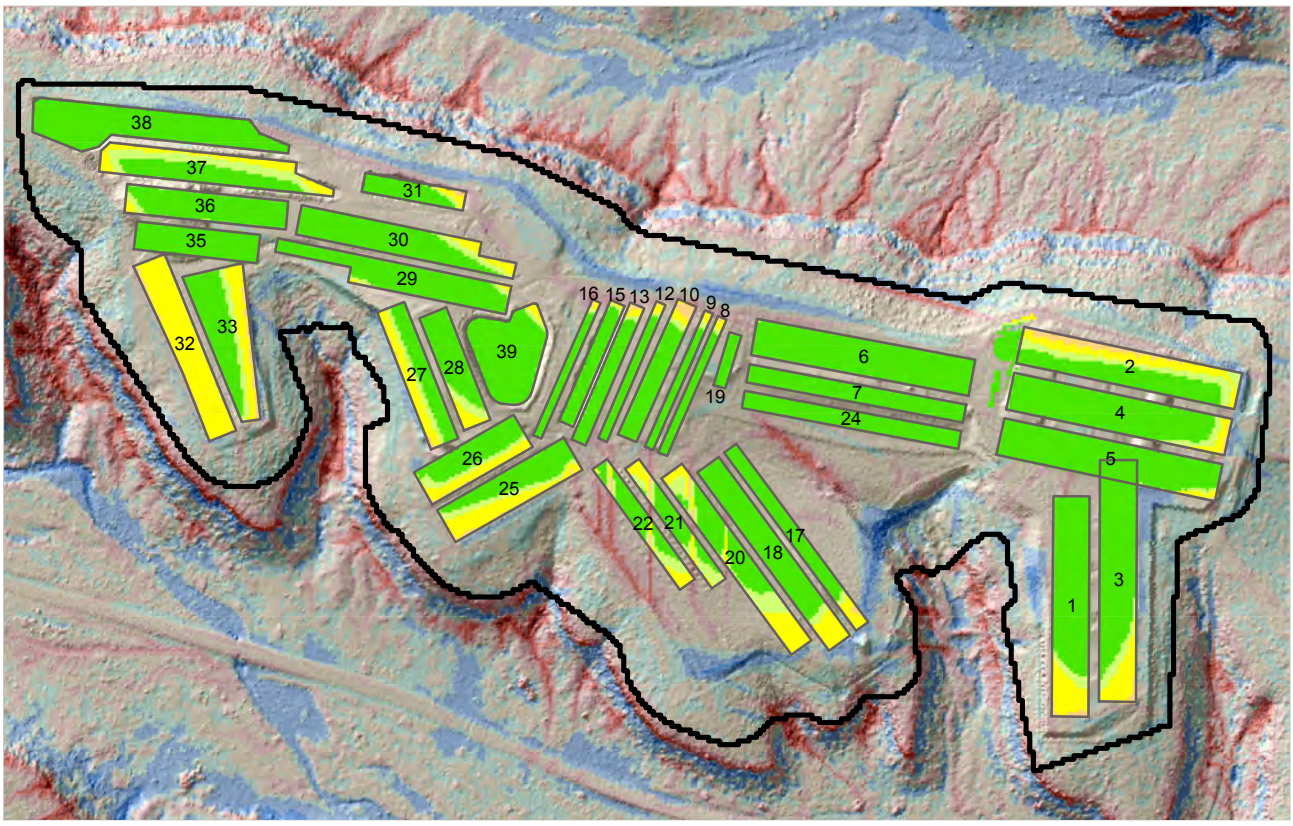

0 80 160 m

Scale

Site conditions:
Canopy cover = 30%
Ground cover = 70%
Soil = Sandy Loam
Runoff event = 5 years (7 mm)
Diffusion coefficient = 2.5 x 10^{-3}

Depth to waste (m) after 1,000 years
- 1 - 1.75
- 1.75 - 2.5
- 2.5 - 3.2
- 3.25 - 4
- >4

Area of erosion

Area of deposition

35 Waste disposal pit

Figure 9
Erosion and Deposition at MDA G for Moderate-Erosion Scenario (as predicted by SIBERIA model after 1,000 years)

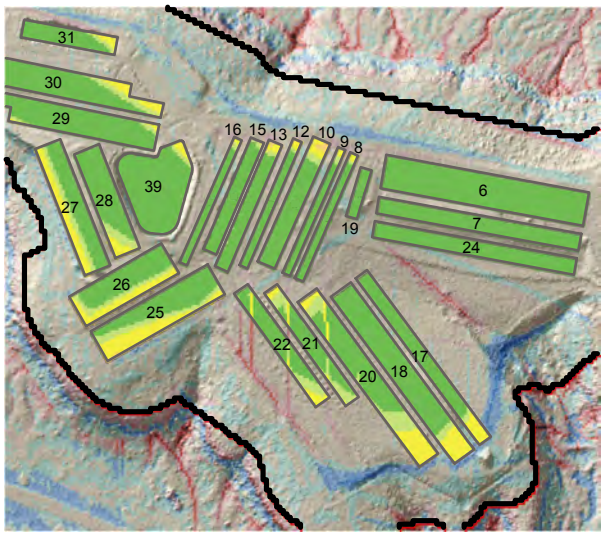

Figure 10a.
Low-erosion scenario (70% canopy cover, 70% ground cover, sandy loam soil, 2-year runoff event [2.6 mm], and diffusion coefficient of 1.0×10^{-4}.

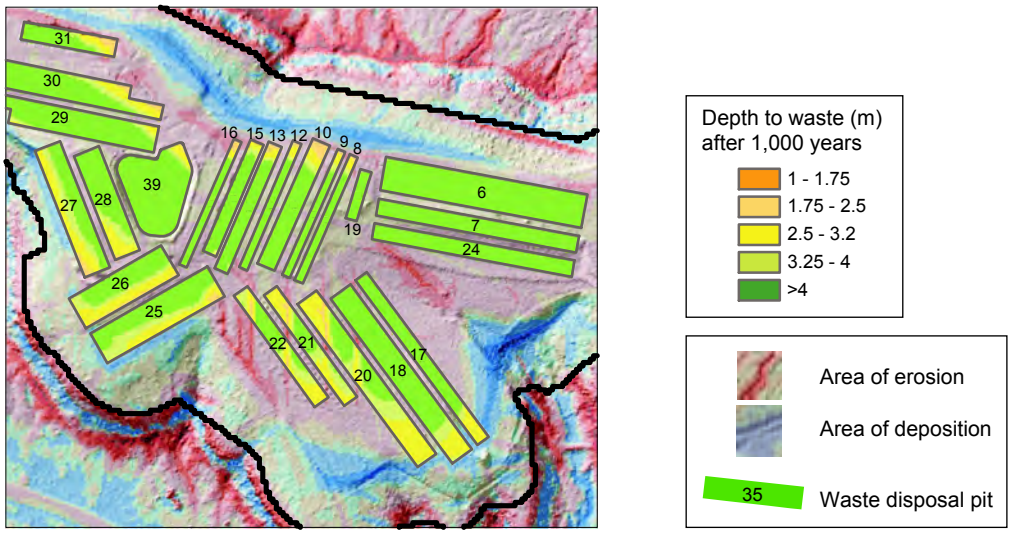

Figure 10b.
High-erosion scenario (30% canopy cover, 30% ground cover, sandy loam soil, 5-year runoff event [12 mm], and diffusion coefficient of 2.5×10^{-3}.

Figure 10
Erosion and Deposition at MDA G for Low- and High-Erosion Scenarios (as predicted by SIBERIA after 1,000 years)

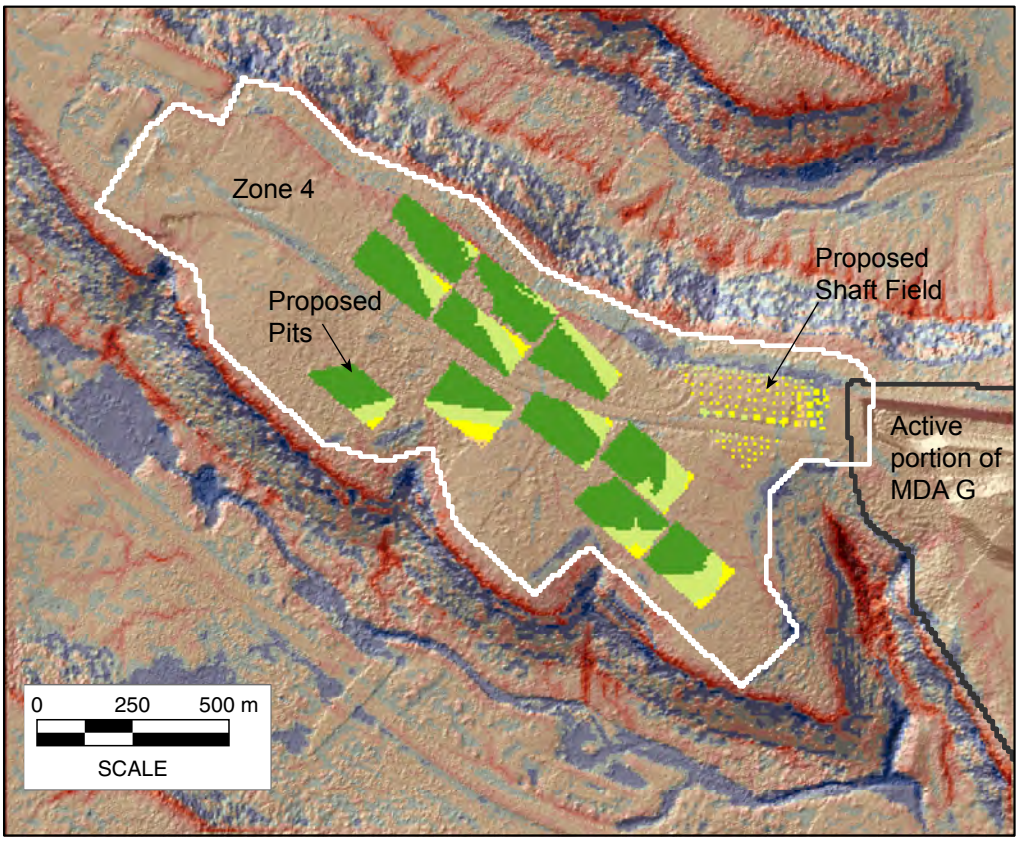

Figure 11
Erosion and Deposition at Zone 4 for Moderate-Erosion Scenario
(as predicted by SIBERIA model after 1,000 years)

The time-dependent sediment-yield values can be used to determine how much potentially contaminated sediment may be delivered to different parts of the Cañada del Buey and Pajarito Canyon floodplains. Figure 12 shows how the surface of MDA G is divided into sediment source areas (indicated by the divisions of the mesa-top) that drain into catchments within each canyon. The boundaries of the catchments were estimated on the basis of visual inspection of the topographic features along the edges of Mesita del Buey and the water drop diagram developed in conjunction with the cover design effort (Day et al., 2005, Figure 4).

Pit-affected sediment eroded from a grid cell over a given disposal unit within a drainage is assigned the disposal unit and drainage name, and is transferred across the lower boundary of the drainage into the corresponding catchment in the canyon. In this manner the total amount of potentially contaminated sediment, as well as the type and concentration of the contaminated sediment delivered to the canyon can be tracked through time. Table 4 summarizes the delivery of sediment to each of the catchments shown in Figure 12 for the moderate-erosion scenario. Although the data have been stored as a function of time and disposal unit, Table 4 shows the total sediment yield into each catchment for the 1,000-year time frame. For example, over the 1,000-year period, Pajarito Canyon catchment PC2 was projected to receive 8,995 T (9,915 t) of sediment from uncontaminated portions of MDA G and 766 T (844 t) from pit-affected areas; thus, the pit-affected sediment is 8 percent of the total sediment delivered from the mesa to PC2. Note that the drainage boundaries may change through time. For example, between 0 and 100 years the cover over a given pit may spill sediment to PC2, but from 100 to 200 years, some or all of the cover over that pit may spill into another drainage, and therefore be deposited in another catchment. These shifts in sediment yield are also tracked.

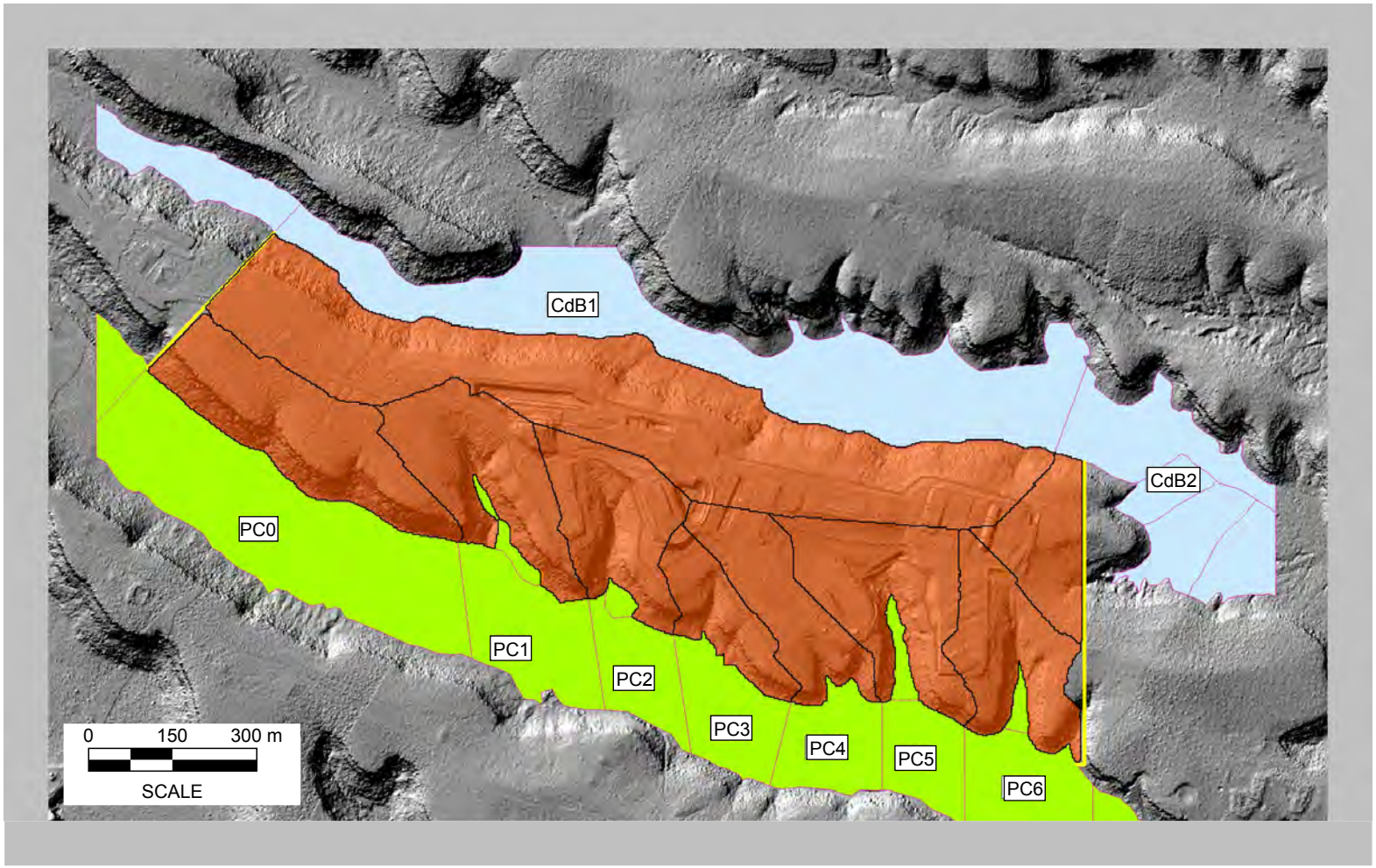

Figure 12
MDA G Sediment-Source Areas and Sediment Catchments in Habitable Canyon Bottoms

Table 4
Summary of Sediment Delivery from MDA G to Canyon Catchments over 1,000 Years

Canyon Catchment Number	Mass of Sediment Delivered (T)		Pit-Affected Sediment as % of Total Sediment
	Clean Sediment	Pit-Affected Sediment	
PC0	5,644	767	12
PC1	16,987	580	3
PC2	8,995	766	8
PC3	8,823	1,251	12
PC4	5,405	1,400	21
PC5	6,549	1,340	17
PC6	5,435	478	8
CdB1	39,930	3,482	8
CdB2	1,005	153	13

PC = Pajarito Canyon catchment *CdB = Cañada del Buey catchment*

4.0 Discussion and Qualifications

The SIBERIA simulations represent a significant step forward in cover-performance modeling, as they allow the feedback between erosion and the shape of the repository cover to be explored over a highly complex topography. This work represents a robust application of SIBERIA and reflects the opinion of the authors that landscape evolution models provide the best current option for assessing the performance of a cover exposed to long-term erosion. Nevertheless, significant uncertainty exists in the predictions. These uncertainties are the result of both model structure, as discussed in Section 4.1, and lack of adequate data for model parameterization, as discussed in Section 4.2. Even with these uncertainties, however, the SIBERIA sediment-yield predictions were in line with long-term values cited in the literature as well as with data from Mesita del Buey, as discussed in Section 4.3.

4.1 Model Limitations

The SIBERIA model was chosen because it was the only landscape evolution model that had been applied to and validated for critical environmental problems constrained by regulations such as mine reclamation and tailing pile remediation. The model version used for this study, however, had four potential drawbacks. First, it did not automatically modify material properties in cells when erosion cut into a new layer. Second, the sediment-transport-capacity equation may cause spurious deposition to occur when there was a change in material type along a flow path from a material with higher transport capacity (e.g., the cover) to one with lower transport capacity (e.g., bedrock). In addition, the model does not allow particle tracking or sediment-packet tracking through the landscape, hence it is impossible to determine if the sediment that eroded from the cover over a given pit was trapped permanently in the rock armor, or eventually made its way to the stream bottom. Third, it is likely that a dynamic climate will give a different result than the steady-state climate the user is forced to adopt by the SIBERIA model. And fourth, the model did not include an explicit cliff-retreat algorithm. A new version of SIBERIA is currently being tested that addresses all but the fourth of these issues.

Each of the model limitations noted above introduces uncertainty in the model results. The fact that the version of SIBERIA used for this study did not automatically update material properties as erosion progressed to a new layer was not a major problem since this study modeled only two materials, a homogeneous cover material and bedrock. Even so, an effort was made to minimize the effect that this limitation had on modeling results. During the simulations performed for this study, the model was manually stopped every 20 years to determine if the amount of erosion or the change in elevation in a given grid cell had caused the cell to move below the cover layer boundary. If it had, the cell type was changed from “cover” to “bedrock” and the model was restarted. Because there was no way of knowing when the boundary between the cover and

bedrock had been reached during the 20-year interval, the affected cell was also reassigned a cell elevation of the original bedrock surface. This approach is not expected to introduce much error into the model projections because rates of erosion within the bedrock are small.

A seemingly more difficult problem arises from the use of the sediment-transport-capacity equation to predict both erosion and transport. The amount of eroded sediment transported out of a grid cell depends on the gradient of the cell, its material composition, and the size of the upslope area contributing to the cell. A problem may arise when a grid cell with a material type of "cover" is upslope from a cell with material type "bedrock"; because of the rock armor, this situation occurs around the entire edge of the cover. Under natural conditions, sediment undergoing transport from a more erodible upslope area would stay in suspension and travel across the downslope bedrock area. In the model, however, if the two cells have the same gradient and the same approximate upslope area, the dramatic change in erodibility between the upslope cover cell and downslope bedrock cell causes the sediment transport capacity to drop significantly. This results in sediment deposition at the transition between the cells and could pose a nonquantifiable error in the results, since the deposition around the edge of the cover suppresses erosion at the edge of the cover. For the cover design at MDA G, however, the proposed placement of rock armor at the MDA G cover edge would, in fact, cause deposition of sediment due to frictional resistance and water loss between boulders. Because the rock armor is assigned a material type of "bedrock," the model behavior in this situation is expected to be similar to the actual conditions that will occur at MDA G. Thus, the model limitation noted above probably does not strongly affect the predicted cover performance.

The other aspect of the second model limitation mentioned above is that the model does not allow particle tracking or sediment-packet tracking. This means the model cannot determine if contaminated particles will remain trapped in the rock armor or migrate to a downhill location. Application of the new version of SIBERIA, which replaces the sediment-transport-capacity equation with grain-size-explicit-erosion and sediment-transport equations, would enable particle tracking through the landscape and thus increase understanding of how contaminants will redistribute through the landscape over time. It would also solve the issue of sediment dropping out of suspension at boundaries between upslope cover and lower bedrock cells.

The third model limitation, the fact that SIBERIA uses a steady-state landscape-forming event to drive erosion, is likely to have a significant impact on the predicted cover performance. In nature, many storms of different durations and intensities occur throughout a single year; over a period of 1,000 years the climate may become significantly wetter or drier. Even if the mean annual precipitation remains the same, rain may come in fewer but larger events that would result in more erosion per event. In this analysis, the uncertainty introduced by climate variability over the 1,000-year simulation period is only partially addressed. An attempt was made to bracket the impact of climate on cover performance by using both a 2- and 5-year runoff event,

with the 5-year event representing a wet and highly erosive condition over the 1,000 year time frame and the 2-year event representing a more moderate climate over that same period. The choice of the 2- and 5-year landscape-forming events was based on data from the Santa Rita Experimental Watershed in southern Arizona and is supported by analyses for climates as diverse as Australia and England (Willgoose and Riley, 1998; Willgoose et al., 1991b). However, the impacts of climate variability and extreme events on long-term cover performance should probably be considered in greater detail. The new version of SIBERIA allows consideration of an event-based climate series; the application of this version to MDA G may be appropriate.

The fourth limitation of the model used in this analysis is that it does not include the process of cliff retreat. While including a stochastic rockfall algorithm in SIBERIA would not be difficult, calibrating such a model would be difficult without better quantification of the actual processes. Data limitation issues related to modeling cliff retreat are discussed below.

4.2 Data Limitations

In some cases, uncertainties were introduced because of the lack of adequate data for model parameterization. Areas of particular concern include the characterization of the hydraulic and erosional properties of the proposed cover, the role of climate variability and extreme events in cover performance, and the impact of various ongoing geomorphic processes on cover performance at MDA G.

The material properties of the cover and bedrock are critical data for determining the predicted performance of the cover in relation to both erosion processes and infiltration (Newman and Schofield, 2005). A critical parameter for both processes is saturated hydraulic conductivity. The SIBERIA analysis was performed before the results of hydraulic conductivity measurements performed on samples of the proposed cover material were available. In the absence of a measured value, Newman and Schofield (2005) estimated a saturated hydraulic conductivity of 0.039 mm/hr (1.3×10^{-4} in./hr) for the proposed cover material. This value is almost 300 times less than the value of 11 mm/hr (4.3×10^{-1} in./hr) used in ISR9 to compute runoff for the 2- and 5-year events used in SIBERIA.

The hydraulic conductivity values used in the ISR9 modeling were taken from literature values (Nyhan et al., 1993; Charman and Murphy, 1992) for actual soils with the same texture (i.e., the same proportions of sand, silt and clay) as that for the proposed cover. The Newman and Schofield (2005) infiltration calculations used estimated hydraulic conductivities for a 6 percent bentonite/crushed tuff mixture. These estimates were based on a linear regression fit between the measured hydraulic conductivity of pure crushed tuff and the value reported in Nyhan et al. (1997) for a 10 percent bentonite/tuff mixture. Both sets of values have limitations. The values

representing actual soils reflect the fact that these soils have developed, over a long period of time, a structure with a hierarchy of pores and water pathways. The samples of crushed tuff/bentonite used for the Newman and Schofield estimate were homogeneous with none of the characteristics that will develop as a result of biotic activities such as root growth or the burrowing activities of insects or animals. In all likelihood, the actual value for the saturated hydraulic conductivity of the cover lies somewhere between the Newman and Schofield value and the value used for the SIBERIA modeling.

The uncertainty in the saturated hydraulic conductivity of the cover material is a potentially significant source of error in the surface erosion modeling. If the actual hydraulic conductivity values are lower than the values adopted for the modeling, the SIBERIA runoff rates, and subsequent erosion, will be higher than predicted. As mentioned, samples of the proposed cover material have been submitted for analysis; the results of this testing should provide additional insight into this critical property of the cover.

Rainfall simulator experiments carried out on test plots at a hillslope scale (including flow in drainage lines) would help to fully characterize the infiltration, runoff, erosion, and transport characteristics of the cover over a wide range of event intensities. Such experiments would significantly reduce the main source of uncertainty in the performance assessment — the hydraulic properties of the cover. They would also provide data about the amount of runoff and erosion associated with the wide range of rainfall events expected under actual variable climate conditions, which is critical to running SIBERIA with a climate series rather than a steady-state landscape-forming event. The development of a set of potential future climate series to be used as input to the new version of SIBERIA would help to lower uncertainty related to climate and provide a better understanding of the uncertainty associated with the timing and size of extreme events.

Currently, it is not known which of the ongoing geomorphic processes at MDA G pose the greatest risk to the long-term integrity of the waste disposal units. Although rough estimates exist for fluvial and wind erosion, no data are available to assess rates of cliff retreat or sediment-diffusion processes. Studies to determine the rates of cliff retreat, fluvial erosion, wind erosion, soil development, and diffusion at Mesita del Buey would improve knowledge in this area. The development of cliff retreat rates requires the collection and processing of a statistically meaningful set of samples to determine the distribution of cliff face ages at Mesita del Buey using cosmogenic radionuclides. Similar techniques can be used to assess diffusion and soil development rates. Observations suggest that the cliff faces at Mesita del Buey are eroding through mass wasting (block falls), wind erosion, and fluvial erosion but no useful data exist about the erosion rates. A thorough investigation of cliff retreat rates and processes, including time for collecting and processing enough samples to be statistically meaningful, would help to lower uncertainty in this area.

4.3 Comparison of SIBERIA Results to Field-Collected Data

In spite of the sources of error and uncertainty in the parameterization of the model and the model structure, a comparison of annual sediment yield predicted by SIBERIA and that estimated from mean sediment concentrations collected at experimental plots and gauging stations on Mesita del Buey suggest that SIBERIA performed well. Table 5 shows sediment yield values derived from these sites range from 0.2 to 1 T/ha (0.089 to 0.45 t/ac) per landscape-forming event; this is close to the range of predicted values of 0.4 to 3.2 T/ha (0.16 to 1.3 t/ac) per event. The fact that the values derived for Mesita del Buey are lower than the SIBERIA values could be a result of the relatively short data-collection periods, which did not include large events. In contrast, the SIBERIA analysis was based on 16 years of data from the Santa Rita Experimental Watershed which included several large erosional events.

Table 5
Estimated Sediment Yield for Mesita del Buey Sites from Events with 2- and 5-Year Return Periods [a]

Observation Site	Drainage Area (m^2)	Return Period Runoff Volumes [b] (m^3)		Mean Sediment Concentration (mg/L)	Sediment Yield [c] (T/ha)	
		2-Year Event	5-Year Event		2-Year Event	5-Year Event
TA-51 Runoff Plots	3.3E+01	3.0E-01	5.0E-01	2.3E+03	1.9E-01	3.6E-01
Small catchments draining TA-54						
E221	4.1E+03	5.2E+01	8.3E+01	4.1E+03	5.2E-01	8.3E-01
E227	1.7E+04	2.1E+02	3.4E+02	5.0E+03	6.3E-01	1.0E+00
E247	5.0E+04	3.2E+02	5.4E+02	4.1E+03	2.7E-01	4.4E-01

[a] *All values from actual site data, except as noted*

[b] *Calculated using the Chemicals, Runoff, and Erosion from Agricultural Management Systems (CREAMS) model*

[c] *Calculated by multiplying the mean concentration from observed events by the calculated runoff volume. These yields compare favorably with those predicted by SIBERIA for the annual landscape-forming event, as shown in Table 3.*

5.0 References

Bras, R., 2004, Personal Communication, December.

Carey, J.W. and Cole, G., 2002, *Description of the Cerro Grande Fire Laser-Altimetry (LIDAR) Data Set*, Los Alamos National Laboratory, Report LA-13892-MS, 57pp. plus appendices.

Charman, P.E.V., B.W. Murphy, 1992, *Soils—Their Properties and Management, A Soil Conservation Handbook for New South Wales*, Sydney University Press, ISBN 042 4001837, 363 pp.

Crowell, K.J., C.J. Wilson, and L.J. Lane, 2004, "Constraining Uncertainty in the Application of a Landscape Evolution Model to Predict 1000 Years of Erosion at a Mesa-Top Waste Repository", presented at American Geophysical Union Fall Meeting, 13 – 17 December, San Francisco, CA, Poster H51C-1142.

Day, M.S., C.K. Anderson, and C.D. Pedersen, 2005, *Conceptual Design of the Earthen Cover for at Los Alamos National Laboratory Technical Area 54, Material Disposal Area G*, Los Alamos National Laboratory Report LA-UR-05-7394, September.

Dietrich, W., 2004, Personal Communication, December.

Heimsath, A.M., W.E. Dietrich, K. Nishiizumi, and R.C. Finkel, 1997, "The Soil Production Function and Landscape Equilibrium," *Nature*, Vol. 388, pp. 358 – 361.

Kirchner, J.W., R.C. Finkel, C.S. Riebe, D.E. Granger, J.L. Clayton, J.G. King, and W.F. Megahan, 2001, "Mountain Erosion over 10 yr, 10 k.y. and 10 m.y. Time Scales," *Geology;* Vol. 29, No. 7, pp. 591 – 594, Geological Society of America.

Laflen, J.M., L.J. Lane, and G.R. Foster, 1991, "WEPP- A New Generation of Erosion Prediction Technology," J of Soil and Water Conservation, Vol. 46, No. 1, pp. 34-38.

Lane, L.J., M.H. Nichols, L.R. Levick, and M.R. Kidwell, 2001, "A Simulation Model for Erosion and Sediment Yield at the Hillslope Scale," Chapter 8 (pp. 201 – 237) in *Landscape Erosion and Evolution Modeling* (Harmon, R. S. and Doe, W. W.,III, eds.), Kluwer Academic/Plenum Publishers, New York.

Lane, L.J., C.J. Wilson, and E.P. Springer, 2002, *Field Data and Analysis of Event Based Surface Erosion: Initial Calibration of the 1000 Year Erosion Model for TA-54, MDA G*, Los Alamos National Laboratory Report LA-UR-02-6257.

Lane, L.J., 2004, Estimation of Runoff Volumes for Erosion Prediction in Support of Landscape Evolution Modeling at MDA G, Interim Report No. 3, Memo to LANL, August, 8pp.

NOAA (National Oceanic & Atmospheric Administration), 2004, Precipitation Frequency Data Server, http://hdsc.nws.noaa.gov/hdsc/pfds (August 4, 2004).

Newman, B.D and T.G. Schofield, 2005, *Modeling of an Evapotranspiration Cover for the Groundwater Pathway at Los Alamos National Laboratory TA-54, Material Disposal Area G*, Los Alamos National Laboratory Report LA-UR-05-7094, September.

Nyhan, J.W., G.J. Langhorst, C.E. Martin, J.L. Martinez, and T.G. Schofield, 1993, "Field Studies of Engineered Barriers for Closure of Low Level Radioactive Waste Landfills at Los Alamos, New Mexico, USA," *Proceedings of the International Conf. on Nuclear Waste Management and Environmental Restoration*, (P.E. Ahlstroem, C.C. Chapman, R. Kohout, and J. Marek, eds.), Am. Soc. of Mechanical Engineers, pp. 255 – 266.

Nyhan, J.W., T.G. Schofield, and R.H. Starmer, 1997, "A Water Balance Study of Four Landfill Cover Designs Varying in Slope for Semiarid Regions," *Journal of Environmental Quality*, Vol. 26, pp. 1385 – 1392.

Press, W., S. Teukolsky, W. Vetterling, and B. Flannery, 1996, *Numerical Recipes in C: the Art of Scientific Computing*. 2nd ed., Cambridge University Press, pp. 451 – 455.

Smith, R.E., Goodrich, D.C., Woolhiser, D.A.,and Unkrich, C.L., 1995, "Chapter 20: KINEROS – a kinematic runoff and erosion model," in *Computer Models of Watershed Hydrology*, Singh, V.P.(ed.), Water Resources Publications, Highlands Ranch, Colorado, pp. 697–732.

Stone, J.J., L.J Lane, and E.D. Shirley, 1992, "Infiltration and Runoff Simulation on a Plane," *Transactions of the American Society of Agricultural Engineers*, Vol. 35, pp. 161 – 170.

USDA, 2002, *Hillslope Erosion Model*, Engineered Information Systems for Natural Resources, USDA-ARS Southwest Watershed Research Center, Tucson, AZ, <http://eisnr.tucson.ars.ag.gov/hillslopeerosionmodel/>.

Willgoose, G.R. and S. Riley, 1998, "The Long Term Stability of Engineered Landforms of the Ranger Uranium Mine, Northern Territory, Australia: Application of a Catchment Evolution Model," *Earth Surf. Process. Landf.*, Vol. 23, No. 3, pp. 237-259.

Willgoose, G.R., R.L. Bras, and I. Rodriguez-Iturbe, 1991a, "A Physically Based Coupled Network Growth and Hillslope Evolution Model: 1 Theory," *Water Res. Res.*, Vol. 27, No. 7, pp. 1671-1684.

Willgoose, G.R., R.L. Bras, and I. Rodriguez-Iturbe, 1991b, "A Physically Based Coupled Network Growth and Hillslope Evolution Model: 2 Applications," *Water Res. Res.*, Vol. 27, No. 7, pp. 1685-1696.

Willgoose, G., 2000, *User manual for SIBERIA (Version 8.10)*, The University of Newcastle and Landtech Landform Technologies (a division of TUNRA), July, 91 pp.

Willgoose, G., 2004, Personal Communication, November.

Wilson, C.J., K.J. Crowell, L.J. Lane, 2004, "Challenges in Parameterizing a Landscape Evolution Model to Predict 1000 Years of Erosion on a Mesa-Top Waste Repository," presented at American Geophysical Union Fall Meeting, 13 – 17 December, San Francisco, CA, Poster H51C-1141.

LA-UR-08-06107

Approved for public release;
distribution is unlimited.

Title:	Radioactive Waste Inventory for Los Alamos National Laboratory Technical Area 54, Area G
Author(s):	Rob Shuman
Intended for:	U.S. Department of Energy

Form 836 (7/06)

Table of Contents

Table of Contents i
List of Tables i
List of Attachments iii
Acronyms and Abbreviations iv

1.0 Introduction 1
2.0 Background: Waste Characteristics and Disposal Technologies 3
3.0 Methods Used for Inventory Projections 25
3.1 Historical Inventory Projections 25
3.2 Future Inventory Projections 34
4.0 Area G Inventory Projections 39
4.1 Historical Inventory Projections 39
4.1.1 Pre-1971 Waste Inventory 39
4.1.1.1 Historical Disposal Data Evaluation 40
4.1.1.2 Pit and Shaft Inventory Estimates 55
4.1.2 Waste Inventory for 1971 Through September 26, 1988 69
4.1.3 Waste Inventory for September 27, 1988 Through 2007 78
4.2 Future Inventory Projections 83
4.3 Uncertainty Analysis 87
4.4 Summary of the Area G Radioactive Waste Inventory 93
5.0 References 108

List of Tables

Table 1 Historical Use and General Characteristics of Disposal Pits at Area G 5
Table 2 Historical Use and General Characteristics of Disposal Shafts at Area G 9
Table 3 Material Type Allocations for the Area G Inventory 29
Table 4 Volume Projections for ER and D&D Waste 35
Table 5 Waste Disposal Volume and Activity Based on Disposal Memoranda 42
Table 6 Annual Los Alamos National Laboratory Radioactive Waste Disposal Volume, 1959–1969 43
Table 7 Annual Los Alamos National Laboratory Radioactive Waste Stream Volume and Activity, 1959–1970 44
Table 8 Area G Inventory Estimates Developed by Workman and Wheeler 45
Table 9 Estimated Radionuclide Inventory for Area G Pits and Shafts, January 1976 46
Table 10 Summary of Area G Disposal Data Provided by Warren (1980) 47
Table 11 Pre-1971 Inventory Projections for Area G Based on Disposal Memoranda 48
Table 12 Comparison of Pre-1971 Inventory Projections Based on Disposal Memoranda and Laboratory-Wide Disposal Data with the 1997 Composite Analysis Inventory 49
Table 13 Comparison of Pu-Equivalent Waste Inventories, 1959 Through 1970 50
Table 14 Pre-1971 Radionuclide-Specific Inventories Projected for Sludge 52

List of Tables (Continued)

Table 15 Comparison of Pre-1971 Radionuclide Inventories in Nonsludge Waste Streams 54
Table 16 Extrapolation-Based Disposal Volumes and Activities, Pre-1971 Waste 58
Table 17 Extrapolation-Based Radionuclide, Activation Product, Fission Product, and Material Type Inventories for Pits, Pre-1971 Waste 59
Table 18 Additions to Extrapolation-Based Inventory Projections for Pits, Pre-1971 Waste 61
Table 19 Disposal Volumes and Activities for Pits, Pre-1971 Waste 61
Table 20 Radionuclide, Activation Product, Fission Product, and Material Type Inventories for Pits, Pre-1971 Waste 62
Table 21 Comparison of Pre-1971 Radionuclide, Activation Product, and Fission Product Inventories for Shafts Projected from Extrapolation Datasets and Pre-1971 Disposal Data 65
Table 22 Comparison of Various Pre-1971 Radionuclide, Activation Product, and Fission Product Inventories for Shafts 66
Table 23 Shaft-Specific Disposal Volumes and Activities, Pre-1971 Waste 70
Table 24 Unit-Specific Disposal Volumes and Activities, 1971 Through 2007 Waste 71
Table 25 Unit-Specific Disposal Volumes and Activities of Transuranic Waste, 1971 Through September 26, 1988 79
Table 26 Unit-Specific Radionuclide, Fission Product, and Material Type Inventories of Transuranic Waste, 1971 Through September 26, 1988 81
Table 27 Disposal Volumes and Activities for Pits and Shafts, 2008 Through 2044 Waste 83
Table 28 Radionuclide and Material Type Inventories, 2008 Through 2044 Waste 84
Table 29 Projected Tritium Waste Inventory Generated by Weapons Engineering Test Facility 87
Table 30 Criteria for Assigning Waste to Selected Plutonium Material Types 92
Table 31 Mass Fractions and Uncertainties for Selected Plutonium Material Types 93
Table 32 Volumes and Activities for Waste Included in the Area G Performance Assessment Inventory 94
Table 33 Radionuclide, Activation Product, Fission Product, and Material Type Inventories for Waste Included in the Performance Assessment 95
Table 34 Radionuclide, Activation Product, Fission Product, and Material Type Inventories for Waste Included in the Composite Analysis, Disposal Pits 100
Table 35 Radionuclide, Activation Product, Fission Product, and Material Type Inventories for Waste Included in the Composite Analysis, Disposal Shafts 104

List of Attachments

Attachment I Methodology for Estimating Radionuclide-Specific Activities for Mixed-Fission and Mixed-Activation Product Waste .....

Attachment II Bases For Radionuclide Inclusion in the Area G Inventory

Attachment III Pit-Specific Radionuclide, Activation Product, Fission Product, and Material Type Inventories for Area G

Attachment IV Pre-1971 Shaft Disposal Records for Area G .....

Attachment V Shaft-Specific Radionuclide, Activation Product, Fission Product, and Material Type Inventories for Area G

Acronyms and Abbreviations

CMP	Corrugated metal pipe
CMPAC	Corrugated metal pipe, asphalt coated
D&D	Decontamination and decommissioning
DOE	U.S. Department of Energy
DU	Depleted uranium
EBR	Experimental Breeder Reactor
EPA	U.S. Environmental Protection Agency
ER	Environmental restoration
HEPA	High efficiency particulate air (filter)
Laboratory	Los Alamos National Laboratory
LAMPF	Los Alamos Meson Physics Facility
LAMPRE	Los Alamos Molten Plutonium Reactor Experiment
LANL	Los Alamos National Laboratory
LLW	Low-level (radioactive) waste
MAP	Mixed-activation products
MDA	Material Disposal Area
MFP	Mixed-fission products
PCB	Polychlorinated biphenyl
SPI	Steel pipe insert
SRL	Size Reduction Lab
TA	Technical Area
TREAT	Transient Reactor Test
TRU	Transuranic
TSCA	Toxic Substances Control Act
TSFF	Tritium Science and Fabrication Facility
TSTA	Tritium Systems Test Assembly
UHTREX	Ultra-high temperature reactor experiment
UL	Unlined
WETF	Weapons Engineering Tritium Facility
WIPP	Waste Isolation Pilot Plant

1.0 Introduction

Los Alamos National Laboratory (LANL or the Laboratory) generates radioactive waste as a result of various activities. Operational waste is generated at the Laboratory from a wide variety of research and development activities including nuclear weapons development, energy production, and medical research. Environmental restoration (ER) and decontamination and decommissioning (D&D) waste is generated as contaminated sites and facilities at the Laboratory undergo cleanup or remediation. The majority of this waste is low-level radioactive waste (LLW) and is disposed of at the Technical Area (TA) 54, Area G disposal facility.

U.S. Department of Energy (DOE) Order 435.1 (DOE, 2001) requires that radioactive waste is managed in a manner that protects worker and public health and safety, and the environment. To comply with this order, DOE field sites must prepare and maintain site-specific radiological performance assessments for LLW disposal facilities that accept waste after September 26, 1988. Furthermore, sites are required to conduct composite analyses for disposal facilities that receive waste after September 26, 1988. These composite analyses account for cumulative impacts of all waste that has been (or will be) disposed of at the facilities and other sources of radioactive material that may interact with the facilities.

In compliance with DOE Order 5820.2A (DOE, 1988), the predecessor to Order 435.1, the Laboratory issued the Area G performance assessment and composite analysis in 1997 (Hollis et al., 1997). The 1997 analyses are being revised and reissued to incorporate new knowledge about the Area G facility and site, and to update the modeling approaches used to project the long-term performance of the disposal facility. The inventory characterization has been updated in support of the performance assessment and composite analysis revisions; this report documents the latest radiological inventory for the disposal facility.

The waste projections developed through this inventory characterization will be input directly into the models used to revise the performance assessment and composite analysis. In terms of the performance assessment, the inventory includes all LLW that has been disposed of at Area G since September 27, 1988 as well as the LLW that will require disposal until the facility closes in 2044. The waste inventory for the composite analysis includes all radioactive waste disposed of at Area G since the facility opened in 1957 as well as the projected LLW that will require disposal through 2044. In brief, this characterization effort:

- Establishes the types of waste that have been, or will be, disposed of at Area G
- Briefly describes the methods used to dispose of the waste

- Estimates the total volume and activity of the waste as well as the radionuclide-specific inventories present in the material

Following this brief introduction (Section 1), Section 2 of this report summarizes the types of waste that have been disposed of at Area G, describes the disposal units used to contain the waste, and considers the operational practices used to place and isolate the waste. The methods used to estimate the waste inventories for the performance assessment and composite analysis are described in Section 3. Inventory projections are presented in Section 4, along with a discussion of the uncertainties associated with these estimates. In addition, there are five attachments to this report: *Attachment I* provides additional details regarding the methodology used for estimating radionuclide-specific activities, *Attachment II* establishes the bases for eliminating specific radionuclides from the inventory, *Attachment III* provides tables with pit-specific waste activity estimates, *Attachment IV* presents pre-1971 disposal records for Area G shafts, and *Attachment V* provides shaft-specific waste activity estimates.

2.0 Background: Waste Characteristics and Disposal Technologies

The types of waste disposed of at Area G and the methods used to isolate the waste from the environment have influenced the approach adopted to develop the performance assessment and composite analysis inventory projections. This section provides background information including a general description of the waste and the disposal technologies and operational procedures used at the site.

Waste disposed of at Area G includes operational or routine waste, nonroutine waste, and waste from ER and D&D activities at the Laboratory. Operational waste consists of a wide range of materials including compactable trash (e.g., paper, cardboard, and plastic), rubber, glass, disposable protective clothing, solidified powders and ash, animal tissue, and suspect radioactive waste. Nonroutine waste includes classified waste, uranium chips from LANL shops, and pieces of heavy equipment such as dump trucks (Rogers, 1977). Environmental restoration and D&D waste includes equipment and scrap metal, demolition debris, soil, concrete, asphalt, asbestos, and polychlorinated biphenyl (PCB)-contaminated materials. The Area G facility does not accept free liquids for disposal.

The nature of the waste disposed of at Area G has changed over the facility's lifetime. Waste that, under current definitions, is considered to be transuranic (TRU) was disposed of at the facility through 1970. Since then, the vast majority of TRU waste generated at the Laboratory has been segregated and retrievably stored for permanent disposal at the Waste Isolation Pilot Plant (WIPP), although small amounts of TRU waste were disposed of at Area G between 1971 and 1979. Most of the TRU waste awaiting disposal at the WIPP is stored at Area G under large domes that have been placed on asphalt pads. Some of the TRU waste is stored in below-grade retrievable arrays, including material placed in pits 9 and 29, trenches A–D, and shafts 200–232, 235–243, 246–253, 262–266, and 302–306.

Waste that, under current definitions, qualifies as mixed LLW was placed in Area G pits and shafts through 1985. Mixed TRU waste was routinely disposed of at Area G prior to 1971; smaller quantities of mixed TRU waste were disposed of between 1971 and 1979. Since 1986, when the U.S. Environmental Protection Agency (EPA) affirmed its authority over the regulation of the hazardous component of mixed LLW, the vast majority of the mixed LLW has been segregated from LLW and sent off site for treatment and/or disposal. Small amounts of mixed LLW were inadvertently placed in a single pit and shaft between 1986 and 1990; no mixed waste has been disposed of at Area G since 1990. In addition to LLW, Area G is permitted to accept low-level Toxic Substances Control Act (TSCA) waste (i.e., asbestos and PCBs). Solid LLW is currently the only type of waste disposed of at Area G.

Two major types of disposal units are used at Area G: pits and shafts. Routine LLW (e.g., operational, ER, and D&D waste) is typically placed in disposal pits; these large, generally rectangular units are excavated using heavy equipment. Disposal pits are set back at least 15 m (50 ft) from the nearest canyon rim and are dug no deeper than 3 m (10 ft) above the canyon floor. To date, no pits are deeper than 19 m (60 ft). Pit disposal began in the second quarter of 1957, when nonroutine waste was placed in pit 1 (Rogers, 1977). The disposal of routine radioactive waste began in January 1959.

Prior to the mid-1990s, waste disposed of in pits was typically placed in lifts; each layer of waste was covered with uncontaminated crushed tuff and compacted by driving heavy equipment over the crushed tuff. Exceptions to this approach occurred, predominantly when the possibility existed that the waste might be retrieved at a later date. Current operational procedures require that waste other than bulk soils and debris be packaged prior to disposal. Bulk materials are placed directly in the disposal pits, and may be used to fill void spaces between and within waste containers.

Shafts were first used for waste disposal at Area G in April 1966 (Rogers, 1977). A regulatory requirement for some types of waste, disposal shafts are used to provide additional shielding of waste with high external radiation levels, to facilitate placement using remote handling techniques, and to accommodate special packaging requirements. The shafts are drilled using augers and, like the pits, are set back at least 15 m (50 ft) from the nearest canyon rim, and are dug no deeper than 3 m (10 ft) above the adjacent canyon floor. Shaft diameters generally range from 0.3 to 6 m (1 to 20 ft). Waste packages are lowered into the shafts and stacked on top of one another. Crushed tuff may be added as backfill around the waste packages, thereby reducing void spaces in the disposal units.

From 1957 through December 31, 2007, 35 pits and over 200 shafts were used for the disposal of radioactive waste at Area G. Table 1 provides the periods of operation, dimensions, and types of waste that have been placed in the 35 pits during this time period; Table 2 provides similar information for the disposal shafts. Three of the 35 disposal pits—pits 15, 37, and 38—were open and receiving waste in early 2008; another, pit 39, may receive additional waste before it undergoes operational closure. These pits are used for the disposal of operational, ER, and D&D waste generated at the Laboratory. Approximately 20 shafts were open and had remaining disposal capacity in early 2008.

Table 1
Historical Use and General Characteristics of Disposal Pits at Area G

Pit No.	Operational Period	Length × Width × Depth (m)	Field Measured Pit Volume (m^3)	Waste Volume (m^3)	Waste Description
1	Jan. 1959–April 1961	188 x 34 x 6	2.8E+04	4.2E+03	Wing tanks from Kirtland Air Force Base, dry boxes, and "normal trash."
2	April 1961–July 1963	188 x 32 x 8	3.3E+04	4.9E+03	Classified Bendix waste, 0.21 m^3 (55 gal) drums, equipment, DU, and soil.
3	June 1963–March 1966	200 x 35 x 10	4.3E+04	7.2E+03	Miscellaneous material, lumber, pipe, 0.21 m^3 (55 gal) drums, D&D waste, DU, Bendix classified waste, and soil from TA-10.
4	Jan. 1966–Dec. 1967	183 x 34 x 10	3.4E+04	6.3E+03	D&D waste, graphite, wooden boxes, DU, 0.21 m^3 (55 gal) drums, classified Bendix waste, and equipment.
5	Jan. 1967–Dec. 1973	183 x 30 x 9	3.2E+04	5.1E+03	Scrap material, D&D waste, graphite hoppers, sludge drums (possibly aqueous solution from TA-50), and equipment.
6	Jan. 1970–Aug. 1972	183 x 34 x 8	3.4E+04	5.1E+03	Miscellaneous scrap, wood, and D&D waste; covered with topsoil from TA-1 with up to 20 pCi/g plutonium contamination.
7	March 1974–Dec. 1975	183 x 15 x 9	1.3E+04	3.3E+03	Low-level TRU waste; replaced pit 17 for low-level TRU waste in 1974. Covered with topsoil from TA-1 with up to 20 pCi/g plutonium contamination.
8	Sept. 1971–March 1974	122 x 8 x 8	5.0E+03	1.8E+03	0.21 m^3 (55 gal) drums of sludge, nonretrievable TRU waste, and drums from TA-50 (aqueous and nonretrievable TRU waste).
9	Oct. 1971–Nov. 1979	122 x 9 x 6	6.9E+03	4.8E+00 [a]	Drums and fiberglass crates containing retrievable TRU waste (>10 nCi/g Pu-239 or U-233 or >100 nCi/g Pu-238).
10	April 1979–May 1980	116 x 17 x 8	1.2E+04	3.1E+03	Building debris, lab wastes, and sludge drums (from TA-50 dewatering, possibly aqueous waste).

Source: LANL, 2003, adapted from Table B-1

DU = Depleted uranium
TRU = Transuranic
--- = No waste volume listed; more material is expected to be placed in the pit.
D&D = Decontamination and decommissioning
MFP = Mixed-fission products
PCB = Polychlorinated biphenyl
TA = Technical Area (e.g., TA-10)
MAP = Mixed-activation products
UHTREX = Ultra-high temperature reactor experiment

[a] *The listed waste volume for pit 9 represents LLW; this pit was used primarily for the retrievable storage of TRU waste.*

[b] *"Present" indicates early 2008.*

Table 1 (Continued)
Historical Use and General Characteristics of Disposal Pits at Area G

Pit No.	Operational Period	Length × Width × Depth (m)	Field Measured Pit Volume (m^3)	Waste Volume (m^3)	Waste Description
11	Never excavated				
12	June 1972–Nov. 1975	122 x 8 x 8	5.6E+03	1.8E+03	Non-retrievable TRU waste; contained 30 0.21 m^3 (55 gal) drums of retrievable TRU waste that were later transferred to pit 9.
13	Nov. 1976–Sept. 1977	122 x 13 x 9	9.3E+03	1.5E+03	Uranium, MFP, and MAP.
14	Never excavated				
15	June 1997–Present [b]	107 x 15 x 9	9.0E+03	---	Lab trash, building debris, scrap metal, and filter media waste; operational as of 2008.
16	June 1972–July 1975	122 x 8 x 8	6.2E+03	1.7E+03	Crates and drums containing uranium-contaminated wastes.
17	Aug. 1972–March 1974	183 x 14 x 7	1.3E+04	3.8E+03	Low-level plutonium TRU waste, misc. scrap wastes, crates, and filter plenum.
18	Feb. 1978–Aug. 1979	183 x 23 x 12	3.6E+04	9.6E+03	Contaminated dirt, lab wastes, noncompactable waste, D&D waste, and drums.
19	Nov. 1975–Aug. 1979	47 x 9 x 5	1.0E+03	5.5E+01	Asbestos and carcinogens.
20	Nov. 1975–Oct. 1977	183 x 22 x 11	2.9E+04	1.1E+04	Lab waste, oil, sludge drums, trash, and contaminated dirt.
21	Aug. 1972–Dec. 1974	123 x 17 x 8	1.0E+04	2.8E+03	Uranium, classified material, boxes, drums, and scrap metal.
22	Dec. 1976–March 1978	126 x 17 x 10	1.4E+04	2.9E+03	Filter plenum, sludge drums (possibly aqueous waste from TA-50), lab waste, graphite fuel rods, and contaminated soil.
23	Never excavated				
24	July 1975–Nov. 1976	183 x 18 x 9	1.8E+04	5.6E+03	Graphite, lab wastes, and 22 truckloads of soil; uranium, tritium, MFP, and MAP.

Source: LANL, 2003, adapted from Table B-1

DU = Depleted uranium
TRU = Transuranic
--- = No waste volume listed; more material is expected to be placed in the pit.
D&D = Decontamination and decommissioning
MFP = Mixed-fission products
PCB = Polychlorinated biphenyl
TA = Technical Area (e.g., TA-10)
MAP = Mixed-activation products
UHTREX = Ultra-high temperature reactor experiment

[a] *The listed waste volume for pit 9 represents LLW; this pit was used primarily for the retrievable storage of TRU waste.*

[b] *"Present" indicates late 2008.*

Table 1 (Continued)
Historical Use and General Characteristics of Disposal Pits at Area G

Pit No.	Operational Period	Length × Width × Depth (m)	Field Measured Pit Volume (m^3)	Waste Volume (m^3)	Waste Description
25	Dec. 1979–June 1981	120 x 31 x 12	3.6E+04	4.6E+03	Reactor control rods, D&D waste, scrap drums, lab wastes, test drums, and PCB-contaminated waste.
26	Feb. 1984–Feb. 1985	94 x 30 x 11	1.7E+04	3.8E+03	Building debris, TRU waste culverts, asbestos, alpha box soil, lumber, and PCBs.
27	May 1981–Aug. 1982	122 x 24 x 14	2.1E+04	6.1E+03	Lab waste, contaminated soil and pipe, D&D waste, PCBs, and unknown chemical waste.
28	Dec. 1981–April 1983	101 x 25 x 12	1.6E+04	3.6E+03	Barium nitrate, PCB-contaminated soil, lab waste, equipment, transformers, clay pipes, building debris, and uranium graphite.
29	Aug. 1984–Oct. 1986	201 x 24 x 15	3.5E+04	8.0E+03	TRU cement paste (retrievable), D&D soil, glove boxes, plywood boxes, asbestos, PCBs, and unknown chemical waste.
30	Oct. 1988–Sept. 2001	173 x 12 x 11	3.3E+04	1.0E+04	Asbestos, PCBs, and unknown chemical waste.
31	Sept. 1990–Oct. 2004	85 x 16 x 8	7.2E+03	3.7E+03	Asbestos, asbestos-contaminated debris, and contaminated soil; operational as of 2004.
32	Nov. 1985–Sept. 1987	158 x 23 x 16	2.8E+04	4.8E+03	PCB-contaminated asphalt, transformers, contaminated soil, glove boxes, plywood boxes, capacitors, and building debris.
33	Nov. 1982–July 1984	130 x 35 x 12	4.6E+04	6.6E+03	Beryllium in stainless steel, lab waste, building debris, asbestos, Noncombustible trash, PCBs, and unknown chemical waste.
34	Never excavated				
35	June 1987–April 1988	111 x 25 x 12	1.6E+04	2.9E+03	Compactable trash, plywood boxes, asbestos, lab waste, PCBs, and unknown chemical waste.
36	Jan. 1988–Dec. 1988	133 x 25 x 13	2.1E+04	4.1E+03	Plywood boxes, compactable trash, rubble, building waste, beryllium, and PCB-contaminated soil.

Source: LANL, 2003, adapted from Table B-1

DU = Depleted uranium
TRU = Transuranic
--- = No waste volume listed; more material is expected to be placed in the pit.
D&D = Decontamination and decommissioning
MFP = Mixed-fission products
PCB = Polychlorinated biphenyl
TA = Technical Area (e.g., TA-10)
MAP = Mixed-activation products
UHTREX = Ultra-high temperature reactor experiment

[a] *The listed waste volume for pit 9 represents LLW; this pit was used primarily for the retrievable storage of TRU waste.*

[b] *"Present" indicates late 2008.*

Table 1 (Continued)
Historical Use and General Characteristics of Disposal Pits at Area G

Pit No.	Operational Period	Length × Width × Depth (m)	Field Measured Pit Volume (m^3)	Waste Volume (m^3)	Waste Description
37	April 1990–Present [b]	223 x 25 x 19	4.4E+04	---	UHTREX reactor vessel and stack, asbestos, PCBs, and unknown chemical waste; operational as of 2008
38	Sept. 1994–Present [b]	219 x 40 x 18	5.6E+04	---	Lab trash, contaminated soil, building debris, scrap metal, and filter media waste; operational as of 2008.
39	Aug. 1993–Present [b]	88 x 69 x 14	2.9E+04	---	Lab trash, contaminated soil, building debris, and scrap metal; operational as of 2008.

Source: LANL, 2003, adapted from Table B-1.

DU = Depleted uranium
TRU = Transuranic
--- = No waste volume listed; more material is expected to be placed in the pit.
D&D = Decontamination and decommissioning
MFP = Mixed-fission products
PCB = Polychlorinated biphenyl
TA = Technical Area (e.g., TA-10)
MAP = Mixed-activation products
UHTREX = Ultra-high temperature reactor experiment

[a] *The listed waste volume for pit 9 represents LLW; this pit was used primarily for the retrievable storage of TRU waste.*
[b] *"Present" indicates early 2008*

Table 2
Historical Use and General Characteristics of Disposal Shafts at Area G

Shaft No.	Operational Period	Diameter/Depth (m)	Liner	Shaft Volume (m^3)	Waste Volume (m^3) [a]	Waste Description
1	1966–1967	0.61 / 8	UL	2.2E+00	1.8E+00	Cell trash, irradiated metal, and animal tissue
2	1966–1967	0.61 / 8	UL	2.2E+00	1.2E+00	DU chips, animal tissue, and irradiated plutonium cell waste
3	1967	0.61 / 8	UL	2.2E+00	1.1E+00	Plutonium-contaminated Na and metal, and neutron generators
4	1967	0.61 / 8	UL	2.2E+00	1.3E+00	Uranium-contaminated metal, U-238 samples, and DU
5	1967	0.61 / 8	UL	2.2E+00	8.4E-01	DU, tritium-contaminated materials, and U-238 contaminated metal
6	1967–1968	0.61 / 8	UL	2.2E+00	5.8E-01	Tritium contaminated materials and U-235
7	1968	0.61 / 8	UL	2.2E+00	1.6E+00	Animal tissue, plasma thermocouple waste, and tritium DU
8	1968	0.61 / 8	UL	2.2E+00	3.0E+00	Plutonium cell waste, animal tissue, and end boxes
9	1968–1969	0.61 / 8	UL	2.2E+00	2.0E+00	Hot cell waste, plutonium cell waste, EBR-II waste, and fuel elements
10	1969	0.61 / 8	UL	2.2E+00	1.5E+00	Animal tissue, Pu-239 waste, and uranium-contaminated chemicals
11	1969	0.91 / 8	UL	5.0E+00	2.0E+00	Pee Wee waste and trash, U-235 cell waste, and graphite

Source: LANL, 2003, adapted from Table B-3

UL = Unlined
CMP = Corrugated metal pipe
MAP = Mixed-activation products
CMPAC = Corrugated metal pipe, asphalt coated
LLW = Low-level waste
DU = Depleted uranium
LAMPRE = Los Alamos Molten Plutonium Reactor Experiment
SRL = Size Reduction Lab
LAMPF = Los Alamos Meson Physics Facility
PCB = Polychlorinated biphenyl
EBR = Experimental Breeder Reactor
MFP = Mixed-fission products
HEPA = High efficiency particulate air
SPI = Steel pipe insert

[a] *The listed waste volumes represent the sum of the LLW and transuranic (TRU) waste placed in the shafts; LLW disposal and TRU waste databases were used to estimate post-1970 volumes while pre-1971 volumes were adopted from Rogers (1977). In some case the listed volume exceeds the shaft volume; the sources of these errors were not evident.*

[b] *"Present" indicates early 2008.*

Table 2 (Continued)
Historical Use and General Characteristics of Disposal Shafts at Area G

Shaft No.	Operational Period	Diameter/Depth (m)	Liner	Shaft Volume (m^3)	Waste Volume (m^3) [a]	Waste Description
12	1969–1970	0.91 / 8	UL	5.0E+00	2.3E+00	Cell waste, rover waste, and tritium
13	1969–1970	0.91 / 8	UL	5.0E+00	3.4E+00	Animal tissue, EBR hardware, and reactor parts
14	1968–1969	0.3 / 8	CMP	5.6E-01	7.6E-01	U-235 contaminated vermiculite and neutralized solution HCL+U-235
15	1969–1970	0.3 / 8	CMP	5.6E-01	1.4E-01	Tritium in H_3PO_4 and hot cell waste
16	1969	0.3 / 8	CMP	5.6E-01	1.1E-01	Tritium
17	1970–1974	0.3 / 8	CMP	5.6E-01	1.8E-01	Tritium pump and U-235 in Na
18	1970–1979	0.3 / 8	CMP	5.6E-01	3.3E-01	Neutralized Na and Cs-137+Ba-140
19	1971–1974	0.3 / 8	CMP	5.6E-01	7.6E-02	Pu-239 solution and reacted Pu-239
20	1974–1975	0.3 / 8	CMP	5.6E-01	7.6E-02	Sorbed Pu-239 solution
21	1985	0.3 / 8	CMP	5.6E-01	3.8E-03	Radioactive sources
22	1980–1993	0.3 / 8	CMP	5.6E-01	1.9E-01	Radioactive sources
23	1980	0.3 / 8	CMP	5.6E-01	2.8E-02	Radioactive sources
24	1969–1972	0.61 / 8	UL	2.2E+00	1.9E+00	Animal tissue, DU, and unloaded fuel elements
25	1969–1971	0.61 / 8	UL	2.2E+00	1.2E+00	DU, U-238 residue, and U-238 contaminated metal
26	1969–1970	0.61 / 8	UL	2.2E+00	1.6E+00	Hot cell trash, fuel elements, and DU-contaminated metal

Source: LANL, 2003, adapted from Table B-3

UL = Unlined
CMP = Corrugated metal pipe
MAP = Mixed-activation products
CMPAC = Corrugated metal pipe, asphalt coated
LLW = Low-level waste
DU = Depleted uranium
LAMPRE = Los Alamos Molten Plutonium Reactor Experiment
SRL = Size Reduction Lab
LAMPF = Los Alamos Meson Physics Facility
PCB = Polychlorinated biphenyl
EBR = Experimental Breeder Reactor
MFP = Mixed-fission products
HEPA = High efficiency particulate air
SPI = Steel pipe insert

[a] *The listed waste volumes represent the sum of the LLW and transuranic (TRU) waste placed in the shafts; LLW disposal and TRU waste databases were used to estimate post-1970 volumes while pre-1971 volumes were adopted from Rogers (1977). In some case the listed volume exceeds the shaft volume; the sources of these errors were not evident.*

[b] *"Present" indicates early 2008.*

Table 2 (Continued)
Historical Use and General Characteristics of Disposal Shafts at Area G

Shaft No.	Operational Period	Diameter/Depth (m)	Liner	Shaft Volume (m^3)	Waste Volume (m^3) [a]	Waste Description
27	1970	0.61 / 8	UL	2.2E+00	3.6E-01	Irradiated material and DU-contaminated material
28	1970	0.61 / 8	UL	2.2E+00	8.4E-01	Los Alamos notebooks and U-235 residues
29	1970–1971	0.61 / 8	UL	2.2E+00	7.6E-01	Thermocouple waste and U-235 residues
30	1970–1985	0.61 / 8	UL	2.2E+00	5.0E-01	Animal tissue and Pu-239 hot cell waste
31	1970–1971	0.61 / 8	UL	2.2E+00	1.3E+00	DU
32	1970–1971	0.61 / 8	UL	2.2E+00	1.6E+00	LAMPRE-II lines and valves, animal tissue, and irradiated stainless steel
33	1970–1971	0.61 / 8	UL	2.2E+00	5.1E-01	Pu-239 hot cell waste
34	1971–1972	1.8 / 18	UL	4.8E+01	2.6E+01	U-contaminated oil
35	1971–1985	0.91 / 12	UL	8.0E+00	2.7E+00	Hot cell wastes, animal tissues, herbicide containers, and fission products
36	1970–1985	0.91 / 12	UL	8.0E+00	2.6E+00	Hot cell wastes and spallation products
37	1970–1985	0.91 / 12	UL	8.0E+00	5.6E+00	Animal and chemical wastes
38	1970–1974	0.91 / 12	UL	8.0E+00	1.9E+00	Rover reactor parts and LAMPRE-II tank
39	1970–1973	1.8 / 18	UL	4.8E+01	1.6E+01	Tritium-contaminated equipment
40	1971	0.61 / 8	UL	2.2E+00	1.1E+00	Animal tissue
41	1971–1972	0.61 / 8	UL	2.2E+00	2.3E+00	Animal tissue and graphite
42	1971–1972	0.61 / 8	UL	2.2E+00	1.8E+00	Animal tissue and uranium-contaminated metal

Source: LANL, 2003, adapted from Table B-3

UL = Unlined
CMP = Corrugated metal pipe
MAP = Mixed-activation products
CMPAC = Corrugated metal pipe, asphalt coated
LLW = Low-level waste
DU = Depleted uranium
LAMPRE = Los Alamos Molten Plutonium Reactor Experiment
SRL = Size Reduction Lab
LAMPF = Los Alamos Meson Physics Facility
PCB = Polychlorinated biphenyl
EBR = Experimental Breeder Reactor
MFP = Mixed-fission products
HEPA = High efficiency particulate air
SPI = Steel pipe insert

[a] *The listed waste volumes represent the sum of the LLW and transuranic (TRU) waste placed in the shafts; LLW disposal and TRU waste databases were used to estimate post-1970 volumes while pre-1971 volumes were adopted from Rogers (1977). In some case the listed volume exceeds the shaft volume; the sources of these errors were not evident.*

[b] *"Present" indicates early 2008.*

Table 2 (Continued)
Historical Use and General Characteristics of Disposal Shafts at Area G

Shaft No.	Operational Period	Diameter/Depth (m)	Liner	Shaft Volume (m^3)	Waste Volume (m^3) [a]	Waste Description
43	1971–1972	0.61 / 8	UL	2.2E+00	1.5E+00	Uranium-contaminated metal and DU
44	1971–1972	0.61 / 8	UL	2.2E+00	1.7E+00	Animal tissue, Pu-239 contaminated vermiculite, and DU with graphite
45	1971–1972	0.61 / 8	UL	2.2E+00	1.8E+00	Plutonium-contaminated steel and U-235 residues
46	1972	0.61 / 8	UL	2.2E+00	1.8E+00	Animal tissue and Pu-239 contaminated steel
47	1972	0.61 / 8	UL	2.2E+00	1.0E+00	Animal tissue, contaminated metal, and fuel waste
48	1972	0.61 / 8	UL	2.2E+00	1.1E+00	Hot cell trash and fuel waste
49	1972	0.61 / 8	UL	2.2E+00	7.9E-01	Animal tissue
50	1974–1976	1.8 / 18	UL	4.8E+01	1.9E+01	Tritium
51	1975	0.61 / 8	UL	2.2E+00	3.6E-01	Hot cell waste
52	1975–1976	0.61 / 8	UL	2.2E+00	3.1E-01	Plutonium, uranium, MFP, MAP, and hot cell wastes
53	1975–1976	0.61 / 8	UL	2.2E+00	8.3E-01	MFP, cell wastes, Pu-239, and U-235
54	1976	0.61 / 8	UL	2.2E+00	4.5E-01	MFP and cell trash
55	1976–1977	0.61 / 8	UL	2.2E+00	1.4E+00	Hot cell trash
56	1977	0.61 / 8	UL	2.2E+00	7.5E-01	Cell waste and contaminated parts from SRL
57	1977	0.61 / 8	UL	2.2E+00	3.1E-01	Hot cell waste
58	1972–1973	0.91 / 8	UL	5.0E+00	3.6E+00	Hot cell waste and DU

Source: LANL, 2003, adapted from Table B-3

UL = Unlined
CMP = Corrugated metal pipe
MAP = Mixed-activation products
CMPAC = Corrugated metal pipe, asphalt coated
LLW = Low-level waste
DU = Depleted uranium
LAMPRE = Los Alamos Molten Plutonium Reactor Experiment
SRL = Size Reduction Lab
LAMPF = Los Alamos Meson Physics Facility
PCB = Polychlorinated biphenyl
EBR = Experimental Breeder Reactor
MFP = Mixed-fission products
HEPA = High efficiency particulate air
SPI = Steel pipe insert

[a] *The listed waste volumes represent the sum of the LLW and transuranic (TRU) waste placed in the shafts; LLW disposal and TRU waste databases were used to estimate post-1970 volumes while pre-1971 volumes were adopted from Rogers (1977). In some case the listed volume exceeds the shaft volume; the sources of these errors were not evident.*

[b] *"Present" indicates early 2008.*

Table 2 (Continued)
Historical Use and General Characteristics of Disposal Shafts at Area G

Shaft No.	Operational Period	Diameter/Depth (m)	Liner	Shaft Volume (m^3)	Waste Volume (m^3) [a]	Waste Description
59	1972–1974	1.8 / 18	UL	4.8E+01	5.4E+00	Tritium-contaminated steel, tools, and waste
60	1972–1974	0.91 / 8	UL	5.0E+00	3.2E+01	Oil-contaminated with U-235 and Pu-239
61	1973–1974	0.91 / 8	UL	5.0E+00	4.4E+00	Beryllium waste, U-238 contaminated metal, and animal tissue
62	1974 - 1976	0.91 / 8	UL	5.0E+00	3.5E+00	Animal tissue, Pu-238, and P-32
63	1976	0.91 / 8	UL	5.0E+00	2.3E+00	DU and residues
64	1976–1977	0.91 / 8	UL	5.0E+00	1.1E+00	Animal wastes and U-235
65	1976–1977	0.91 / 8	UL	5.0E+00	3.9E+00	Classified U wastes, targets, and animal tissue
66	1976	0.91 / 8	UL	5.0E+00	6.5E-01	Animal tissue
67	1977	0.61 / 8	UL	5.0E+00	1.3E+00	Targets and cell trash
68	1977	0.61 / 8	UL	5.0E+00	9.0E-01	Cell trash and classified notebooks
69	1977	0.61 / 8	UL	5.0E+00	5.7E-01	Parts from recovery
70	1975–1976	1.8 / 18	UL	4.8E+01	2.6E+01	Contaminated oil
71	1978	0.91 / 8	UL	5.0E+00	8.8E-01	No description
72	1972–1973	0.61 / 8	UL	2.2E+00	2.8E+00	Irradiated stainless steel and hot cell waste trash
73	1973	0.61 / 8	UL	2.2E+00	3.4E-01	Hot cell trash
74	1973	0.61 / 8	UL	2.2E+00	9.3E-01	Pu-239 waste

Source: LANL, 2003, adapted from Table B-3

UL = Unlined
CMP = Corrugated metal pipe
MAP = Mixed-activation products
CMPAC = Corrugated metal pipe, asphalt coated
LLW = Low-level waste
DU = Depleted uranium
LAMPRE = Los Alamos Molten Plutonium Reactor Experiment
SRL = Size Reduction Lab
LAMPF = Los Alamos Meson Physics Facility
PCB = Polychlorinated biphenyl
EBR = Experimental Breeder Reactor
MFP = Mixed-fission products
HEPA = High efficiency particulate air
SPI = Steel pipe insert

[a] *The listed waste volumes represent the sum of the LLW and transuranic (TRU) waste placed in the shafts; LLW disposal and TRU waste databases were used to estimate post-1970 volumes while pre-1971 volumes were adopted from Rogers (1977). In some case the listed volume exceeds the shaft volume; the sources of these errors were not evident.*

[b] *"Present" indicates early 2008.*

Table 2 (Continued)
Historical Use and General Characteristics of Disposal Shafts at Area G

Shaft No.	Operational Period	Diameter/Depth (m)	Liner	Shaft Volume (m^3)	Waste Volume (m^3) [a]	Waste Description
75	1973	0.61 / 8	UL	2.2E+00	9.2E-01	Pu-238 waste and cell trash
76	1973–1974	0.61 / 8	UL	2.2E+00	8.1E-01	Hot cell trash
77	1974	0.61 / 8	UL	2.2E+00	3.4E-01	Hot cell trash and Pu-239 hot cell trash
78	1974–1975	0.61 / 8	UL	2.2E+00	1.3E+00	Cell wastes, reactor wastes, and irradiated box ends
79	1974–1975	0.61 / 8	UL	2.2E+00	3.4E-01	Hot cell waste and irradiated metal
80	1975–1976	0.61 / 8	UL	2.2E+00	1.2E+00	Sodalime, Ta-182 chips, and animal tissue
81	1975–1976	0.61 / 8	UL	2.2E+00	9.9E-01	Animal tissue
82	1978	0.91 / 8	UL	5.0E+00	6.9E-01	Trash and chemical wastes
83	1978	0.91 / 8	UL	5.0E+00	1.3E+00	Animal tissue and DU
84	1978	0.91 / 8	UL	5.0E+00	4.9E-01	Trash from SRL and cell trash
85	1978	0.91 / 8	UL	5.0E+00	5.1E-01	Neutralized Na Dowanol and cell trash
86	1977	0.91 / 8	UL	5.0E+00	6.2E-01	Spallation products and classified materials
87	1977	0.61 / 8	UL	2.2E+00	6.1E-01	Cell wastes
88	1977	0.61 / 8	UL	2.2E+00	5.0E-01	Cell wastes
89	1977–1978	0.61 / 8	UL	2.2E+00	8.1E-01	Animal tissue and cell waste
90	1978	0.61 / 8	UL	2.2E+00	9.1E-01	DU and hot cell trash

Source: LANL, 2003, adapted from Table B-3

UL = Unlined
CMP = Corrugated metal pipe
MAP = Mixed-activation products
CMPAC = Corrugated metal pipe, asphalt coated
LLW = Low-level waste
DU = Depleted uranium
LAMPRE = Los Alamos Molten Plutonium Reactor Experiment
SRL = Size Reduction Lab
LAMPF = Los Alamos Meson Physics Facility
PCB = Polychlorinated biphenyl
EBR = Experimental Breeder Reactor
MFP = Mixed-fission products
HEPA = High efficiency particulate air
SPI = Steel pipe insert

[a] *The listed waste volumes represent the sum of the LLW and transuranic (TRU) waste placed in the shafts; LLW disposal and TRU waste databases were used to estimate post-1970 volumes while pre-1971 volumes were adopted from Rogers (1977). In some case the listed volume exceeds the shaft volume; the sources of these errors were not evident.*

[b] *"Present" indicates early 2008.*

Table 2 (Continued)
Historical Use and General Characteristics of Disposal Shafts at Area G

Shaft No.	Operational Period	Diameter/Depth (m)	Liner	Shaft Volume (m^3)	Waste Volume (m^3) [a]	Waste Description
91	1977–1978	0.81 / 15	UL	1.0E+01	2.1E+00	Spallation products, animal waste, cell trash, and trash cans
92	1977–1978	0.81 / 15	UL	1.0E+01	3.7E+00	Spallation products and uranyl-nitrate in HNO_3
93	1978–1984	0.91 / 15	UL	1.0E+01	7.5E+00	Spallation products, fuel elements, cell waste, and animal tissues
94	1978–1984	0.91 / 15	UL	1.0E+01	2.7E+00	Hot cell waste, DU, and control rods
95	1984	0.91 / 15	UL	1.0E+01	4.1E+00	Cell wastes and animal tissues
96	1977–1979	1.8 / 15	UL	4.0E+01	1.2E+01	Uranium-contaminated oil, niobium, zirconium, chlorides, and aluminum shell
97	1978–1984	0.91 / 18	UL	1.2E+01	6.8E+00	Uranium chips and turnings, vials, and animal waste
99	1983–1984	0.91 / 18	UL	1.2E+01	5.6E+00	Hot cell wastes, animal tissue, and machine parts
100	1983	0.91 / 18	UL	1.2E+01	1.7E+00	Hot cell waste, and target/stinger
101	1980–1981	0.91 / 18	UL	1.2E+01	2.5E+00	Spallation products and hot cell waste
102	1982–1983	0.91 / 18	UL	1.2E+01	5.2E+00	No description
103	1981–1982	0.91 / 18	UL	1.2E+01	4.8E+00	Hot cell waste and spent fuel elements
104	1982	0.91 / 18	UL	1.2E+01	4.3E+00	Uranium chips and scrap metal
105	1982–1983	0.91 / 18	UL	1.2E+01	5.6E+00	Animal tissue

Source: LANL, 2003, adapted from Table B-3

UL = Unlined
CMP = Corrugated metal pipe
MAP = Mixed-activation products
CMPAC = Corrugated metal pipe, asphalt coated
LLW = Low-level waste
DU = Depleted uranium
LAMPRE = Los Alamos Molten Plutonium Reactor Experiment
SRL = Size Reduction Lab
LAMPF = Los Alamos Meson Physics Facility
PCB = Polychlorinated biphenyl
EBR = Experimental Breeder Reactor
MFP = Mixed-fission products
HEPA = High efficiency particulate air
SPI = Steel pipe insert

[a] *The listed waste volumes represent the sum of the LLW and transuranic (TRU) waste placed in the shafts; LLW disposal and TRU waste databases were used to estimate post-1970 volumes while pre-1971 volumes were adopted from Rogers (1977). In some case the listed volume exceeds the shaft volume; the sources of these errors were not evident.*

[b] *"Present" indicates early 2008.*

Table 2 (Continued)
Historical Use and General Characteristics of Disposal Shafts at Area G

Shaft No.	Operational Period	Diameter/Depth (m)	Liner	Shaft Volume (m^3)	Waste Volume (m^3) [a]	Waste Description
106	1980–1981	0.91 / 18	UL	1.2E+01	2.1E+00	Spallation products and hot cell waste
107	1978–1981	0.91 / 18	UL	1.2E+01	1.4E+00	Hot trash, animal tissue, and chemical waste
108	1980–1982	0.91 / 18	UL	1.2E+01	6.5E+00	Spallation products, solvent, and animal tissue
109	1980	0.61 / 18	UL	5.3E+00	2.3E+00	Spallation products and trash cans
110	1979	0.91 / 18	UL	1.2E+01	3.6E+00	Spallation products, animal tissue, and mixed combustible trash
111	1979–1980	0.61 / 18	UL	5.3E+00	3.8E+00	Cell waste, spallation products, and niobium and tantalum perchloride
112	1978–1979	0.91 / 18	UL	1.2E+01	4.2E+00	Classified pieces, animal waste, cell waste, and spallation products
114	1979–1982	1.8 / 18	UL	4.8E+01	2.8E+01	Shielding blocks and graphite design assembly
115	1979–1982	1.8 / 18	UL	4.8E+01	1.5E+01	Hot trash and tritium scrap
118	1983–1984	2.4 / 20	UL	9.3E+01	1.3E+01	Vials
119	1983	2.4 / 19	UL	8.8E+01	1.6E+01	DU chips, hydrocarbons, and HF leach solids
120	1983–1984	2.4 / 19	UL	9.0E+01	1.5E+01	Shielding blocks and graphite design assembly
121	1984–1985	1.2 / 18	UL	2.1E+01	6.9E+00	Animal tissue and cell trash
122	1984–1985	1.2 / 18	UL	2.1E+01	7.3E+00	Hot cell waste and waste cans
123	1984	1.8 / 18	UL	4.8E+01	1.5E+01	DU chips and turnings, and firing residue

Source: LANL, 2003, adapted from Table B-3

UL = Unlined
CMP = Corrugated metal pipe
MAP = Mixed-activation products
CMPAC = Corrugated metal pipe, asphalt coated
LLW = Low-level waste
DU = Depleted uranium
LAMPRE = Los Alamos Molten Plutonium Reactor Experiment
SRL = Size Reduction Lab
LAMPF = Los Alamos Meson Physics Facility
PCB = Polychlorinated biphenyl
EBR = Experimental Breeder Reactor
MFP = Mixed-fission products
HEPA = High efficiency particulate air
SPI = Steel pipe insert

[a] *The listed waste volumes represent the sum of the LLW and transuranic (TRU) waste placed in the shafts; LLW disposal and TRU waste databases were used to estimate post-1970 volumes while pre-1971 volumes were adopted from Rogers (1977). In some case the listed volume exceeds the shaft volume; the sources of these errors were not evident.*

[b] *"Present" indicates early 2008.*

Table 2 (Continued)
Historical Use and General Characteristics of Disposal Shafts at Area G

Shaft No.	Operational Period	Diameter/Depth (m)	Liner	Shaft Volume (m^3)	Waste Volume (m^3) [a]	Waste Description
124	1984–1991	1.8 / 20	UL	5.2E+01	1.4E+01	Vials, organics
125	1984	1.8 / 20	UL	5.2E+01	1.7E+01	DU chips and turnings
126	1985–1987	1.8 / 20	UL	5.2E+01	2.2E+01	Meson and hot cell waste
127	1985	1.8 / 20	UL	5.2E+01	1.4E+01	DU chips and turnings and U3 08 oil and wax
128	1985–1986	1.8 / 20	UL	5.2E+01	1.2E+01	Animal tissue and mustargem
129	1986	0.91 / 20	UL	1.3E+01	3.8E+00	Mixed spallation products
130	1986–1987	1.8 / 20	UL	5.2E+01	3.1E+01	DU chips and metal trash
131	1987–1998	1.8 / 20	CMP	5.2E+01	1.3E+01	Activated shielding
132	1987–1993	1.8 / 20	UL	5.2E+01	1.8E+01	Classified material
133	1986–1987	1.2 / 20	UL	2.3E+01	2.7E+00	Spallation products and hot cell waste
134	1986	0.91 / 20	UL	1.3E+01	6.8E+00	Animal tissue
135	1986–1987	0.91 / 20	UL	1.3E+01	6.2E+00	Animal tissue
136	1986–1996	1.8 / 20	UL	5.2E+01	9.3E+00	Low-level tritium
137	1987–1996	1.8 / 20	UL	5.2E+01	1.9E+01	Low-level tritium
138	1987	1.2 / 18	UL	2.1E+01	5.4E+00	Animal tissue
139	1987–1999	1.2 / 18	UL	2.1E+01	8.8E+00	Hot cell waste
140	1987–1991	1.8 / 19	UL	4.9E+01	2.5E+01	Animal tissue

Source: LANL, 2003, adapted from Table B-3

UL = Unlined
CMP = Corrugated metal pipe
MAP = Mixed-activation products
CMPAC = Corrugated metal pipe, asphalt coated
LLW = Low-level waste
DU = Depleted uranium
LAMPRE = Los Alamos Molten Plutonium Reactor Experiment
SRL = Size Reduction Lab
LAMPF = Los Alamos Meson Physics Facility
PCB = Polychlorinated biphenyl
EBR = Experimental Breeder Reactor
MFP = Mixed-fission products
HEPA = High efficiency particulate air
SPI = Steel pipe insert

[a] *The listed waste volumes represent the sum of the LLW and transuranic (TRU) waste placed in the shafts; LLW disposal and TRU waste databases were used to estimate post-1970 volumes while pre-1971 volumes were adopted from Rogers (1977). In some case the listed volume exceeds the shaft volume; the sources of these errors were not evident.*

[b] *"Present" indicates early 2008.*

Table 2 (Continued)
Historical Use and General Characteristics of Disposal Shafts at Area G

Shaft No.	Operational Period	Diameter/Depth (m)	Liner	Shaft Volume (m^3)	Waste Volume (m^3) [a]	Waste Description
141	1988–1991	1.8 / 18	UL	4.8E+01	9.2E+00	Hot cell waste and reactor parts
142	1991	1.2 / 18	UL	2.1E+01	3.2E+00	Hot cell waste
143	1991–1995	1.8 / 19	UL	5.0E+01	9.4E+00	Hot cell waste
144	1994–1998	1.8 / 20	UL	5.2E+01	8.8E+00	Animal tissue
147	1991–1999	1.8 / 20	UL	5.2E+01	9.5E+00	Graphite
148	1991–1993	1.2 / 20	UL	2.3E+01	7.9E+00	HEPA filter shaft
149	1991–1994	1.2 / 20	UL	2.3E+01	9.1E+00	HEPA filter shaft
150	1976–1979	1.8 / 18	CMPAC	4.8E+01	1.8E+01	Low-level tritium
151	1979–1986	0.91 / 18	CMPAC	1.2E+01	2.0E+01	Low-level tritium
152	1980–1983	0.91 / 18	CMPAC	1.2E+01	4.2E+00	Tritium scrap, tubing, and hardware
153	1983–1984	0.91 / 18	CMPAC	1.2E+01	3.1E+00	Contaminated pump and equipment
154	1984–1986	0.91 / 20	CMPAC	1.3E+01	5.5E+00	High-level tritium, molecular sieves
155	1988–1989	0.91 / 20	CMPAC	1.3E+01	3.8E+00	High-level tritium
156	1986–1987	0.91 / 14	CMPAC	9.0E+00	1.7E+00	Dry box trash and molecular sieves
157	1987–1988	0.91 / 14	CMPAC	9.0E+00	2.5E+00	Tritium
158	1989–1993	0.61 / 14	CMPAC	4.0E+00	2.2E+00	High-level tritium
159	1989–Present [b]	0.61 / 14	CMPAC	4.0E+00	3.2E-01	High-level tritium; operational as of 2008

Source: LANL, 2003, adapted from Table B-3

UL = Unlined
CMP = Corrugated metal pipe
MAP = Mixed-activation products
CMPAC = Corrugated metal pipe, asphalt coated
LLW = Low-level waste
DU = Depleted uranium
LAMPRE = Los Alamos Molten Plutonium Reactor Experiment
SRL = Size Reduction Lab
LAMPF = Los Alamos Meson Physics Facility
PCB = Polychlorinated biphenyl
EBR = Experimental Breeder Reactor
MFP = Mixed-fission products
HEPA = High efficiency particulate air
SPI = Steel pipe insert

[a] *The listed waste volumes represent the sum of the LLW and transuranic (TRU) waste placed in the shafts; LLW disposal and TRU waste databases were used to estimate post-1970 volumes while pre-1971 volumes were adopted from Rogers (1977). In some case the listed volume exceeds the shaft volume; the sources of these errors were not evident.*

[b] *"Present" indicates early 2008.*

Table 2 (Continued)
Historical Use and General Characteristics of Disposal Shafts at Area G

Shaft No.	Operational Period	Diameter/Depth (m)	Liner	Shaft Volume (m^3)	Waste Volume (m^3) [a]	Waste Description
160	1990–1993	0.61 / 14	CMPAC	4.0E+00	2.5E+00	High-level tritium
161	1993–2001	0.91 / 18	CMPAC	1.2E+01	3.7E+00	High-level tritium
162	1995	0.91 / 18	CMPAC	1.2E+01	1.6E+00	High-level tritium
163	1999	0.91 / 18	CMP	1.2E+01	3.5E+00	High-level tritium
164	1999	0.91 / 18	CMP	1.2E+01	3.4E+00	High-level tritium
165	1999–Present [b]	0.91 / 18	CMP	1.2E+01	2.7E+00	High-level tritium; operational as of 2008
166	2001	0.91 / 18	CMP	1.2E+01	2.6E+00	High-level tritium
167	2001	0.91 / 18	CMP	1.2E+01	2.4E+00	High-level tritium
168	2001	0.91 / 18	CMP	1.2E+01	2.4E+00	High-level tritium
169	1999–Present [b]	0.91 / 18	CMP	1.2E+01	1.7E+00	High-level tritium; operational as of 2008
170	2001–Present [b]	0.91 / 18	CMP	1.2E+01	9.5E-01	High-level tritium; operational as of 2008
171	1995	1.8 / 20	CMPAC	5.2E+01	5.0E+00	Hydrocarbon oil, absorbed, no free liquid; lab trash
172	1995	1.8 / 20	CMPAC	5.2E+01	8.3+00	Chemical treatment sludge and noncombustibles
173	1995–2000	1.8 / 20	CMPAC	5.2E+01	3.7E+00	Contaminated soil, animal tissue, and cement paste
174	1995	1.8 / 20	CMPAC	5.2E+01	6.2E+00	Contaminated soil and chemical treatment sludge
175	1995	1.8 / 20	CMPAC	5.2E+01	2.3E+00	Chemical treatment sludge

Source: LANL, 2003, adapted from Table B-3

UL = Unlined
CMP = Corrugated metal pipe
MAP = Mixed-activation products
CMPAC = Corrugated metal pipe, asphalt coated
LLW = Low-level waste
DU = Depleted uranium
LAMPRE = Los Alamos Molten Plutonium Reactor Experiment
SRL = Size Reduction Lab
LAMPF = Los Alamos Meson Physics Facility
PCB = Polychlorinated biphenyl
EBR = Experimental Breeder Reactor
MFP = Mixed-fission products
HEPA = High efficiency particulate air
SPI = Steel pipe insert

[a] *The listed waste volumes represent the sum of the LLW and transuranic (TRU) waste placed in the shafts; LLW disposal and TRU waste databases were used to estimate post-1970 volumes while pre-1971 volumes were adopted from Rogers (1977). In some case the listed volume exceeds the shaft volume; the sources of these errors were not evident.*

[b] *"Present" indicates early 2008.*

Table 2 (Continued)
Historical Use and General Characteristics of Disposal Shafts at Area G

Shaft No.	Operational Period	Diameter/Depth (m)	Liner	Shaft Volume (m^3)	Waste Volume (m^3) [a]	Waste Description
176	1995	1.8 / 20	CMPAC	5.2E+01	6.0E+00	Hydrocarbon oil, chemical treatment sludge, and equipment
177	1995	1.8 / 20	CMPAC	5.2E+01	9.4E+00	Chemical treatment sludge
189	1987–1988	4.9 / 20	UL	3.7E+02	4.9E+01	LAMPF activated shielding
190	1983–1984	4.9 / 20	UL	3.7E+02	3.1E+01	Scrap metal
191	1984–1986	4.9 / 20	UL	3.7E+02	3.9E+01	LAMPF scrap metal and graphite target
192	1984–1987	4.9 / 20	UL	3.7E+02	4.4E+01	LAMPF scrap metal
196	1989–1993	4.9 / 16	UL	3.0E+02	5.8E+01	LAMPF inserts
197	1993–1999	4.9 / 18	UL	3.4E+02	4.0E+01	Hot cell waste, trash, and trash cans
206	1980	0.61 / 5	SPI	1.6E+00	4.5E-01	Cell trash and fuel sample
300	2004–Present [b]	2.4 / 7	CMP	3.1E+01	7.1E-01	Lab trash; operational as of 2008
301	1992–Present [b]	2.4 / 7	CMP	3.1E+01	6.4E-01	Irradiation sources; operational as of 2008
307	1992–1994	0.61 / 15	UL	4.4E+00	3.4E+00	Control rods
308	1992–1998	1.5 / 20	SPI	3.6E+01	2.9E+00	Beryllium-contaminated debris and scrap metal
309	2006–2007	1.2 / 20	SPI	2.3E+01	2.0E+00	Scrap metal, molecular sieves, and hot-cell waste
311	2006	1.2 / 20	SPI	2.3E+01	3.4E+00	Lab trash, beryllium-contaminated debris, and hot-cell waste

Source: LANL, 2003, adapted from Table B-3

UL = Unlined
CMP = Corrugated metal pipe
MAP = Mixed-activation products
CMPAC = Corrugated metal pipe, asphalt coated
LLW = Low-level waste
DU = Depleted uranium
LAMPRE = Los Alamos Molten Plutonium Reactor Experiment
SRL = Size Reduction Lab
LAMPF = Los Alamos Meson Physics Facility
PCB = Polychlorinated biphenyl
EBR = Experimental Breeder Reactor
MFP = Mixed-fission products
HEPA = High efficiency particulate air
SPI = Steel pipe insert

[a] *The listed waste volumes represent the sum of the LLW and transuranic (TRU) waste placed in the shafts; LLW disposal and TRU waste databases were used to estimate post-1970 volumes while pre-1971 volumes were adopted from Rogers (1977). In some case the listed volume exceeds the shaft volume; the sources of these errors were not evident.*

[b] *"Present" indicates early 2008.*

Table 2 (Continued)
Historical Use and General Characteristics of Disposal Shafts at Area G

Shaft No.	Operational Period	Diameter/Depth (m)	Liner	Shaft Volume (m^3)	Waste Volume (m^3) [a]	Waste Description
313	2005–2006	1.2 / 20	SPI	2.3E+01	4.3E+00	Lab trash, beryllium-contaminated debris, and hot-cell waste
315	2005	1.2 / 20	SPI	2.3E+01	3.1E+00	Lab trash, beryllium-contaminated debris, and hot-cell waste
317	2005	1.2 / 20	SPI	2.3E+01	3.2E+00	Lab trash, irradiation sources, and hot-cell waste
319	2005	1.2 / 20	SPI	2.3E+01	8.0E+00	Molecular sieves
321	2005	1.2 / 20	SPI	2.3E+01	2.7E+00	Lab trash, beryllium-contaminated debris, and hot-cell waste
323	2004–2005	1.2 / 20	SPI	2.3E+01	3.1E+00	Lab trash, beryllium-contaminated debris, and molecular sieves
325	2004	1.2 / 20	SPI	2.3E+01	2.1E+00	Lab trash
327	2003–2004	1.2 / 20	SPI	2.3E+01	4.9E+00	Beryllium-contaminated debris, molecular sieves, and scrap metal
329	2003	1.2 / 20	SPI	2.3E+01	3.7E+00	Lab trash and scrap metal
331	2003–2005	1.2 / 20	SPI	2.3E+01	2.9E+00	Beryllium-contaminated debris, scrap metal, lab trash, and hot-cell waste
333	2003–2007	1.2 / 20	SPI	2.3E+01	2.5E+00	Lab trash and molecular sieves
335	2003–Present [b]	1.2 / 20	SPI	2.3E+01	1.4E+00	Molecular sieves and hot-cell waste; operational as of 2008

Source: LANL, 2003, adapted from Table B-3

UL = Unlined
CMP = Corrugated metal pipe
MAP = Mixed-activation products
CMPAC = Corrugated metal pipe, asphalt coated
LLW = Low-level waste
DU = Depleted uranium
LAMPRE = Los Alamos Molten Plutonium Reactor Experiment
SRL = Size Reduction Lab
LAMPF = Los Alamos Meson Physics Facility
PCB = Polychlorinated biphenyl
EBR = Experimental Breeder Reactor
MFP = Mixed-fission products
HEPA = High efficiency particulate air
SPI = Steel pipe insert

[a] *The listed waste volumes represent the sum of the LLW and transuranic (TRU) waste placed in the shafts; LLW disposal and TRU waste databases were used to estimate post-1970 volumes while pre-1971 volumes were adopted from Rogers (1977). In some case the listed volume exceeds the shaft volume; the sources of these errors were not evident.*

[b] *"Present" indicates early 2008.*

Table 2 (Continued)
Historical Use and General Characteristics of Disposal Shafts at Area G

Shaft No.	Operational Period	Diameter/Depth (m)	Liner	Shaft Volume (m^3)	Waste Volume (m^3) [a]	Waste Description
339	1997–2002	1.2 / 20	SPI	2.3E+01	5.4E+00	Lab trash, animal tissue, and radioactive sources
341	2003	1.2 / 20	SPI	2.3E+01	6.2E+00	Beryllium-contaminated debris, scrap metal, and lab trash
343	2002–2003	1.2 / 20	SPI	2.3E+01	6.0E+00	Lab trash, animal tissue, and scrap metal
345	2002	1.2 / 20	SPI	2.3E+01	4.1E+00	Lab trash and animal tissue
347	2001–2005	1.2 / 20	SPI	2.3E+01	3.8E+00	Molecular sieves
349	2000	1.2 / 20	SPI	2.3E+01	5.0E+00	Lab trash, molecular sieves, and scrap metal
351	1999–2002	1.2 / 20	SPI	2.3E+01	6.8E+00	Lab trash, molecular sieves, and skull and oxide
355	2001–2002	1.2 / 20	SPI	2.3E+01	4.9E+00	Lab trash, animal tissue, and scrap metal
357	1999–2001	1.2 / 20	SPI	2.3E+01	5.5E+00	Lab trash and radioactive sources
360	2003	1.8 / 19	UL	5.0E+01	1.9E+01	Beryllium-contaminated debris and other building debris
361	2003–2005	1.8 / 19	UL	5.0E+01	2.4E+01	Lab trash and building debris
362	2003–Present [b]	1.8 / 19	UL	5.0E+01	2.2E+01	Lab trash; operational as of 2008
363	2003–Present [b]	1.8 / 19	UL	5.0E+01	3.4E+00	Lab trash; operational as of 2008
364	2003–Present [b]	1.8 / 19	UL	5.0E+01	6.2E+00	Lab trash; operational as of 2008
365	2003–Present [b]	1.8 / 19	UL	5.0E+01	3.1E+00	Lab trash and scrap metal; operational as of 2008
366	2003–Present [b]	1.8 / 19	UL	5.0E+01	8.2E+00	Beryllium; operational as of 2008

Source: LANL, 2003, adapted from Table B-3

UL = Unlined
CMP = Corrugated metal pipe
MAP = Mixed-activation products
CMPAC = Corrugated metal pipe, asphalt coated
LLW = Low-level waste
DU = Depleted uranium
LAMPRE = Los Alamos Molten Plutonium Reactor Experiment
SRL = Size Reduction Lab
LAMPF = Los Alamos Meson Physics Facility
PCB = Polychlorinated biphenyl
EBR = Experimental Breeder Reactor
MFP = Mixed-fission products
HEPA = High efficiency particulate air
SPI = Steel pipe insert

[a] *The listed waste volumes represent the sum of the LLW and transuranic (TRU) waste placed in the shafts; LLW disposal and TRU waste databases were used to estimate post-1970 volumes while pre-1971 volumes were adopted from Rogers (1977). In some case the listed volume exceeds the shaft volume; the sources of these errors were not evident.*

[b] *"Present" indicates early 2008.*

Table 2 (Continued)
Historical Use and General Characteristics of Disposal Shafts at Area G

Shaft No.	Operational Period	Diameter/Depth (m)	Liner	Shaft Volume (m^3)	Waste Volume (m^3) [a]	Waste Description
367	2003–Present [b]	1.8 / 19	UL	5.0E+01	1.2E+01	Lab trash, molecular sieves, scrap metal; operational as of 2008
370	1999–Present [b]	4.9 / 18	UL	3.4E+02	5.0E-01	Scrap metal; operational as of 2008
C1	1980	1.8 / 18	UL	4.8E+01	6.2E+00	PCBs
C2	1981	1.8 / 18	UL	4.8E+01	1.0E+01	PCBs
C3	1981	1.8 / 18	UL	4.8E+01	9.6E+00	PCBs
C4	1981	1.8 / 18	UL	4.8E+01	1.1E+01	PCBs
C5	1981	1.8 / 18	UL	4.8E+01	7.3E+00	PCBs
C6	1981	1.8 / 18	UL	4.8E+01	1.3E+01	PCBs
C7	1981	1.8 / 18	UL	4.8E+01	1.4E+01	PCBs
C8	1981–1982	1.8 / 18	UL	4.8E+01	1.4E+01	PCBs
C9	1982–1984	1.8 / 18	UL	4.8E+01	1.1E+01	PCBs
C10	1984–1985	1.8 / 18	UL	4.8E+01	1.5E+01	PCBs
C11	1985–1992	1.8 / 18	UL	4.8E+01	1.4E+01	PCBs
C12	1986–1990	1.8 / 18	UL	4.8E+01	1.7E+01	PCBs
C13	1987–Present [b]	1.8 / 20	CMP	5.2E+01	3.1E+01	PCBs; operational as of 2008
C14	1992–Present [b]	1.8 / 20	UL	5.2E+01	2.4E+00	PCBs; operational as of 2008

Source: LANL, 2003, adapted from Table B-3

UL = Unlined
CMP = Corrugated metal pipe
MAP = Mixed-activation products
CMPAC = Corrugated metal pipe, asphalt coated
LLW = Low-level waste
DU = Depleted uranium
LAMPRE = Los Alamos Molten Plutonium Reactor Experiment
SRL = Size Reduction Lab
LAMPF = Los Alamos Meson Physics Facility
PCB = Polychlorinated biphenyl
EBR = Experimental Breeder Reactor
MFP = Mixed-fission products
HEPA = High efficiency particulate air
SPI = Steel pipe insert

[a] *The listed waste volumes represent the sum of the LLW and transuranic (TRU) waste placed in the shafts; LLW disposal and TRU waste databases were used to estimate post-1970 volumes while pre-1971 volumes were adopted from Rogers (1977). In some case the listed volume exceeds the shaft volume; the sources of these errors were not evident.*

[b] *"Present" indicates early 2008.*

The Area G disposal facility includes Material Disposal Area G (MDA G), the portion of the facility that is currently receiving waste, and the Zone 4 expansion area located immediately west of MDA G. The performance assessment and composite analysis issued in 1997 (Hollis et al., 1997) assumed that the disposal facility would accept LLW through 2044 and undergo final closure during the subsequent two years. The closure schedule for the facility has changed since that analysis was completed. Current plans call for all pits and shafts within MDA G to be closed by the year 2015; phased closure of the site is expected to begin by about 2010 (DOE, 2002). Additional LLW disposal capacity will be needed during and following this phased closure. Consequently, plans call for the establishment of new pits and shafts in the Zone 4 expansion area; it is assumed that disposal will continue within this expansion area until 2044.

As mentioned, quantities of TRU waste were retrievably placed in pits 9 and 29, trenches A–D, and several shafts. Analyses have been conducted to determine if the retrieval and subsequent shipment of the waste in these units to WIPP is the best management strategy for this material. Current plans call for the retrieval of all of this waste.

3.0 Methods Used for Inventory Projections

This section describes the methodology used to develop the inventory projections. The methodology discussion is divided into two major parts: determining the inventory for the *historical* waste disposed of at Area G from 1957 through the end of 2007 (Section 3.1) and determining the inventory for the *future* waste projected to require disposal from 2008 until the closure of the disposal facility in 2044 (Section 3.2).

3.1 Historical Inventory Projections

The historical inventory, as the term is applied in this report, refers to all waste disposed of at Area G since the facility opened in 1957 through the end of 2007. Currently, the types and quantities of LLW disposed of at Area G are recorded on shipment manifests and entered into the LANL LLW disposal database on a per-package basis. Disposal records from 1971 through the present day have been maintained in this database. Compiled information includes the waste form, volume, and total activity of the waste package, and radionuclide activities in the waste. Records for waste disposed of before 1971 were generally maintained in handwritten logbooks; the information recorded in these logbooks tends to be considerably less detailed than the disposal database records.

The records for TRU waste disposed of at Area G prior to 1971 are also included in handwritten logbooks. Since 1971, almost all TRU waste generated at the Laboratory has been segregated and placed in retrievable storage, although small quantities of TRU waste were nonretrievably disposed of in pits and shafts through 1979. Since 1971, the types and quantities of TRU waste placed in storage or disposed of have been recorded on shipment manifests and entered into the TRU waste database.

Because records for radioactive waste disposed of prior to 1971 are incomplete, an alternate means of characterizing pre-1971 waste was needed. The pre-1971 portion of the historical inventory was estimated for the 1997 composite analysis (Hollis et al., 1997) through an extrapolation process that assumed the characteristics of waste disposed of from 1971 through 1977 could be applied to pre-1971 waste. The estimated pit and shaft inventories were adjusted to account for unique or nonroutine disposals that were overlooked by the extrapolation process.

The pre-1971 waste was a significant contributor to the doses projected for the 1997 composite analysis. Consequently, the inventory projections for this period were reexamined with the aim of reducing the uncertainty inherent in these estimates. A comprehensive evaluation of the disposal records maintained from 1957 through 1970 was conducted, focusing on Am-241 and several isotopes of plutonium, which were the radionuclides that resulted in the greatest potential

doses in the 1997 composite analysis. The methods used to conduct this evaluation are summarized below; Pollard and Shuman (1999) provide a complete description of the effort.

The first step in the pre-1971 waste evaluation effort was to identify the types of records available for characterizing the waste. Toward this end, all information available for the January through June 1965 period was assembled and reviewed; the period from which records were reviewed was extended (to provide a larger dataset) for some types of disposal records. Sources of information were evaluated in terms of their relevance to the development of radionuclide-specific inventories and a subset of the sources was identified for inclusion in the comprehensive data evaluation. All pre-1971 data found in the selected sources were extracted and entered into databases; these data were subsequently used to project inventories for 1959 through 1970, the period during which routine waste was disposed of at Area G. Section 4.1.1 provides a description of the types of records reviewed and those used to estimate inventories.

A comparison of the extrapolation approach used in the 1997 composite analysis inventory and the inventory estimates developed using data extracted from actual disposal records revealed similarities for some waste streams and significant differences for others. Because of these mixed results, the 1997 extrapolation approach was also considered for use in the updated inventory characterization. This approach is described in the following paragraphs.

The extrapolation approach characterizes waste from a post-1970 period (which had more complete disposal records) and applies these characteristics to the pre-1971 material. The first step was to identify the period(s) to be used as the basis for the extrapolation. The selection of these periods for the 1997 composite analysis and the current Area G inventory update was based on an examination of the LLW and TRU waste disposal databases, combined with additional information about the Laboratory. After suitable extrapolation periods were identified, average annual disposal volumes and activities were calculated for the pits and shafts, and multiplied by the number of years the facility accepted waste for disposal in the respective disposal units. For example, the average annual pit inventories were multiplied by 12 years because the disposal facility began accepting routine contaminated waste on January 2, 1959; only nonroutine waste was disposed of in 1957 and 1958. The average annual disposal quantities disposed of in shafts were multiplied by 5 years, consistent with the fact that these units began accepting waste in April 1966.

The extrapolation approach outlined above is based on the assumption that the waste disposed of during the selected extrapolation periods was similar to the 1959–1970 wastes. While this is generally expected to be the case, some types of wastes generated before and after the end of 1970 were unique to those periods. Laboratory personnel familiar with historical operations at the Laboratory were asked to identify wastes unique to pre-1971 and to the extrapolation periods selected for the pits and shafts. Based on this information, waste that was unique to the 1957–

1970 period was added to the inventories estimated using the extrapolation approach. Conversely, waste that was generated during the extrapolation periods under conditions that did not exist prior to 1971 was removed from the datasets used to estimate the earlier inventories.

The inventory characterization approach used to estimate the 1997 composite analysis inventory was reviewed by J. L. Warren, a former LANL employee, prior to its implementation. Two suggestions for refining the inventory estimates for the pre-1971 disposal shafts emerged from that review (Warren, 1996). First, Warren suggested that the shaft inventory might be better estimated using actual disposal records for 1966 through 1970 rather than assigning waste properties based on the extrapolation approach. This was recommended because, in general, the pre-1971 shaft disposal records are believed to be relatively complete (in contrast to the pre-1971 pit records). A second alternative suggested by Warren was to increase the length of the period from which data were drawn to extrapolate shaft waste characteristics. Specifically, Warren was of the opinion that using waste data from 1971 through 1977 might result in a more accurate estimate of the shaft inventory than limiting data to the 1971–1975 period, which had been chosen as the shaft extrapolation period. Although Warren's recommendations were not adopted for the 1997 performance assessment and composite analysis, their impacts on shaft inventory projections were considered during the current characterization effort.

The Area G historical waste inventory for 1971 through 2007 was estimated using the data in both the LANL LLW disposal and TRU waste databases. Most of the inventory for this period was derived from the LLW disposal records. The TRU waste that was nonretrievably disposed of in pits and shafts from 1971 through 1979 was added to the LLW inventory to determine the total inventory for the period. The TRU waste component includes material that was placed in pits 6–8, 20, and 22, and shafts 17–110. It was assumed that all TRU waste that has been retrievably placed in pits 9 and 29, trenches A–D, and shafts 200–232, 235–243, 246–253, 262–266, and 302–306 will be removed from Area G and shipped for off-site disposal. Consequently, this waste is not included in the inventory projections.

The physical and chemical forms of the waste disposed of in the pits and shafts may play an important role in determining how, and at what magnitude, radionuclides are released to the environment from the disposal units. For example, surface contamination on glass may be quickly rinsed from the waste as water percolates through the disposal units, whereas radionuclides sorbed to soils or concrete may be released gradually over time. The release characteristics of different waste forms were taken into account in the 1997 performance assessment and composite analysis (Hollis et al., 1997). The inventory characterization categorized or grouped the various waste streams disposed of at Area G into four waste forms in support of that effort; these forms included surface-contaminated waste, soil, concrete and sludge, and bulk waste. Modeling conducted in support of the performance assessment and composite analysis since 1997 has been based on the assumption that the form of the waste has

no effect on the rates at which radionuclides become available for transport away from the disposal pits and shafts. As a result, no effort has been made to differentiate between waste forms in the current inventory characterization effort.

With some exceptions, inventory projections were developed for each Area G waste unit that received waste between the start of operations and the end of 2007; these projections include total volumes, total activities, and radionuclide-specific activities. Unit-specific inventories could not be developed for pits 1 through 4 because these units were active prior to 1971, the first year for which detailed pit-specific disposal data exist. Pits 5 and 6 were active prior to and following the end of 1970. Waste disposed of in these units after 1970 was assigned to the specific pits; the characteristics of the waste that was disposed of in these units prior to 1971 were estimated using the extrapolation approach and generally assigned to pits 1 through 5.

The performance assessment and composite analysis modeling combines the unit-specific inventories to yield the inventories needed to conduct those analyses. For example, the performance assessment addresses only the waste that was disposed of after September 26, 1988. Thus, the inventories for disposal units that were active after September 26, 1988 are used to project potential future impacts for this assessment. In contrast, inventories for all disposal units at Area G are summed to arrive at the composite analysis inventory.

In the past, material types that refer to specific radionuclide compositions have been used to describe the LLW and TRU waste shipped to Area G for disposal or storage; these material types and the activity-based radionuclide abundances that they represent are listed in Table 3. This report presents the inventories for the affected waste in terms of the material types; the inventory modeling conducted in support of the performance assessment and composite analysis (Shuman, 2008) uses the abundances provided in the table and information about the uncertainty associated with these abundances to estimate radionuclide-specific activities associated with the material types. A small portion of the waste included in the historical inventory was characterized using material types for which there were no definitions (i.e., GAMMA, GRALPH, GRBETA, and TRU); this waste was not included in the inventory projections.

A portion of the waste disposed of at Area G is listed in the LLW and TRU waste databases as mixed-fission products (MFP) and mixed-activation products (MAP). This report provides the activities associated with LLW and TRU wastes in terms of MFP and MAP. Inventory modeling conducted in support of the performance assessment and composite analysis allocates these activities to specific radionuclides using the approaches described in *Attachment I*.

Table 3
Material Type Allocations for the Area G Inventory

Material Type	Isotope	Fractional Abundance [a]
AM44	Am-241	1.0E+00
AM45	Am-243	1.0E+00
BK47	Bk-249	1.0E+00
CF48	Cf-252	1.0E+00
CM46	Cm-246	1.0E+00
D38	U-234	2.9E-01
	U-235	1.3E-02
	U-238	6.9E-01
NP82	Np-237	1.0E+00
PU42	Pu-238	6.2E-02
	Pu-239	3.2E-04
	Pu-240	6.5E-03
	Pu-241	9.3E-01
	Pu-242	2.1E-03
	Pu-244	2.0E-09
PU51	Pu-238	7.0E-03
	Pu-239	4.1E-01
	Pu-240	4.9E-02
	Pu-241	5.4E-01
	Pu-242	4.8E-06
PU52	Pu-238	6.1E-03
	Pu-239	2.1E-01
	Pu-240	4.9E-02
	Pu-241	7.4E-01
	Pu-242	2.8E-06
PU53	Pu-238	1.1E-02
	Pu-239	1.2E-01
	Pu-240	4.2E-02
	Pu-241	8.2E-01
	Pu-242	6.1E-06
PU54	Pu-238	8.5E-03
	Pu-239	5.9E-02
	Pu-240	2.8E-02

[a] *Fractional abundance is given on an activity basis.*

Table 3 (Continued)
Material Type Allocations for the Area G Inventory

Material Type	Isotope	Fractional Abundance [a]
PU54 (Cont.)	Pu-241	9.0E-01
	Pu-242	9.4E-06
PU55	Pu-238	8.9E-03
	Pu-239	4.5E-02
	Pu-240	2.9E-02
	Pu-241	9.2E-01
	Pu-242	1.0E-05
PU56	Pu-238	8.0E-03
	Pu-239	3.9E-02
	Pu-240	2.9E-02
	Pu-241	9.3E-01
	Pu-242	1.1E-05
PU57	Pu-238	2.7E-02
	Pu-239	1.7E-02
	Pu-240	1.7E-02
	Pu-241	9.4E-01
	Pu-242	2.4E-05
PU83	Pu-238	9.9E-01
	Pu-239	5.0E-04
	Pu-240	1.9E-04
	Pu-241	1.2E-02
	Pu-242	1.4E-07
TH88	Th-232	1.0E+00
U(DEP)	U-234	2.9E-01
	U-235	1.3E-02
	U-238	6.9E-01
U(NAT)	U-234	4.9E-01
	U-235	2.3E-02
	U-238	4.8E-01
U10	U-238	1.0E+00
U11	U-234	2.2E-01
	U-235	5.2E-03
	U-238	7.7E-01

[a] *Fractional abundance is given on an activity basis.*

Table 3 (Continued)
Material Type Allocations for the Area G Inventory

Material Type	Isotope	Fractional Abundance [a]
U12	U-234	2.7E-01
	U-235	1.0E-02
	U-238	7.2E-01
U13	U-234	2.8E-01
	U-235	1.2E-02
	U-238	7.1E-01
U14	U-234	2.8E-01
	U-235	1.2E-02
	U-238	7.0E-01
U15	U-234	2.9E-01
	U-235	1.3E-02
	U-238	6.9E-01
U16	U-234	3.3E-01
	U-235	1.7E-02
	U-238	6.5E-01
U17	U-234	3.8E-01
	U-235	2.1E-02
	U-238	6.0E-01
U18	U-234	4.1E-01
	U-235	2.4E-02
	U-238	5.6E-01
U21	U-234	4.6E-01
	U-235	2.7E-02
	U-238	5.2E-01
U22	U-234	5.1E-01
	U-235	3.1E-02
	U-236	1.6E-03
	U-238	4.6E-01
U23	U-234	5.7E-01
	U-235	3.5E-02
	U-236	4.1E-03
	U-238	3.9E-01
U24	U-234	6.3E-01
	U-235	3.8E-02

[a] *Fractional abundance is given on an activity basis.*

Table 3 (Continued)
Material Type Allocations for the Area G Inventory

Material Type	Isotope	Fractional Abundance [a]
U24 (Cont.)	U-236	6.1E-03
	U-238	3.3E-01
U25	U-234	6.8E-01
	U-235	4.1E-02
	U-236	7.7E-03
	U-238	2.7E-01
U26	U-234	7.2E-01
	U-235	4.2E-02
	U-236	8.5E-03
	U-238	2.3E-01
U27	U-234	7.3E-01
	U-235	4.3E-02
	U-236	8.9E-03
	U-238	2.2E-01
U28	U-234	7.5E-01
	U-235	4.3E-02
	U-236	9.2E-03
	U-238	2.0E-01
U29	U-234	7.7E-01
	U-235	4.4E-02
	U-236	9.5E-03
	U-238	1.8E-01
U30	U-234	7.8E-01
	U-235	4.4E-02
	U-236	9.7E-03
	U-238	1.6E-01
U31	U-234	8.0E-01
	U-235	4.4E-02
	U-236	1.0E-02
	U-238	1.5E-01
U32	U-234	8.6E-01
	U-235	4.4E-02
	U-236	1.0E-02

[a] *Fractional abundance is given on an activity basis.*

Table 3 (Continued)
Material Type Allocations for the Area G Inventory

Material Type	Isotope	Fractional Abundance [a]
	U-238	8.4E-02
U33	U-234	9.1E-01
	U-235	4.1E-02
	U-236	9.1E-03
	U-238	3.6E-02
U34	U-234	9.4E-01
	U-235	3.7E-02
	U-236	7.5E-03
	U-238	1.5E-02
U35	U-234	9.5E-01
	U-235	3.5E-02
	U-236	6.5E-03
	U-238	8.2E-03
U36	U-234	9.6E-01
	U-235	3.3E-02
	U-236	5.2E-03
	U-238	3.0E-03
U37	U-234	9.6E-01
	U-235	3.1E-02
	U-236	4.3E-03
	U-238	7.0E-04
U38	U-234	9.7E-01
	U-235	3.0E-02
	U-236	4.1E-03
	U-238	2.8E-04
U39	U-234	9.7E-01
	U-235	3.0E-02
	U-236	4.0E-03
	U-238	7.2E-05
U70	U-233	1.0E+00
U81	U-234	5.1E-01
	U-235	2.2E-02
	U-238	4.7E-01

[a] *Fractional abundance is given on an activity basis.*

Active institutional control will be maintained over Area G for a minimum of 100 years after final closure of the disposal facility. During this period, people will be prevented from intruding onto the site for extended periods of time and steps will be taken to ensure proper facility functioning. The effect of these measures will be to minimize any impacts to human health and the environment from the buried waste during this period.

The radionuclides included in the LLW and TRU waste disposed of at Area G have radioactive half-lives ranging from seconds to millions of years. Many of the short-lived isotopes will decay to negligible levels by the end of the 100-year active institutional control period. Exceptions to this will include radionuclides that are daughters of parents with much longer half-lives; these isotopes will effectively assume the half-lives of their parents.

The Area G inventory was simplified by eliminating short-lived radionuclides that will decay to negligible levels by the end of the 100-year institutional control period. All radionuclides disposed of in the pits and shafts were reviewed in terms of their modes of decay; radionuclides with half-lives of 5 years or less were generally excluded from the inventory projections. A description of the methods used to eliminate short-lived radionuclides from the inventory is provided in *Attachment II*.

3.2 Future Inventory Projections

The waste that has been or will be disposed of at Area G between 2008 and the closure of the site includes operational waste and material generated by ER and D&D activities. As with the 1997 performance assessment and composite analysis (Hollis et al., 1997), it was assumed that waste will be disposed of through 2044, at which point the facility will undergo final closure. Current plans call for the closure of MDA G by the year 2015; a phased closure approach is expected to be implemented starting in 2010. Disposal operations at the facility will expand into the Zone 4 expansion area, immediately west of the existing pits and shafts, as disposal operations in MDA G come to an end.

The disposal capacity remaining in MDA G is fast declining; efforts are being made to make the most efficient use of the remaining capacity and, therefore, to delay moving disposal operations into the Zone 4 expansion area. In years past, the Laboratory planned to limit the amount of low-activity ER and D&D waste that was disposed of at Area G with the intent of preserving the remaining capacity for the higher activity operational waste. Since that time, however, a decision has been made to dispose of all LANL waste at Area G as long as disposal capacity remains.

The disposal capacity remaining at MDA G is estimated annually. These estimates are used in conjunction with estimates of new capacity realized by the construction of new disposal units within MDA G and projections of operational and ER/D&D waste generation rates to estimate the amount of time before it will be necessary to move disposal operations to the Zone 4

expansion area. The evaluation conducted in 2007 projected the ER and D&D waste volumes shown in Table 4. Large amounts of waste are anticipated in the coming years as major ER and D&D projects are completed; a nominal amount of non-operational waste is anticipated after the ER effort ends in 2015.

Table 4
Volume Projections for ER and D&D Waste

Fiscal Year	Annual Volume (m^3)
2008	10,816
2009	16,527
2010	13,514
2011	6,000
2012	6,000
2013	6,000
2014	6,000
2015	6,000
2016–2044	1,520

Based on these projections and information about operational waste generation rates, it is estimated that waste generated through 2010 can be disposed of in pits within MDA G; pit disposal operations will be required to move to the Zone 4 expansion area in 2011. Current expectations are that the disposal of waste in shafts will not be limited by capacity considerations prior to the closure of MDA G. Therefore, it is assumed that all shaft waste will be placed at MDA G through 2015.

Future operational and ER/D&D waste inventories were prepared as separate projections. Estimates of the volumes and activities of the operational waste were based on the assumption that future operations at the Laboratory will resemble those of the recent past. On this basis, future pit and shaft inventories were projected using an extrapolation approach. Operational waste data drawn from 2000 through 2007 were used to develop average annual disposal volumes and activities (total and radionuclide-specific) for the pits and shafts; these averages were multiplied by 37 years to yield the 2008–2044 operational waste inventories for the two sets of units.

The 2000–2007 waste data found in the LANL LLW database include material generated during routine operations and waste generated as a result of ER and D&D activities; it was necessary to

distinguish between these waste types to conduct the extrapolation. This was done on the basis of the waste codes assigned to the waste packages in the LLW disposal database. Specifically, 11 waste codes or waste streams were assumed to result largely from ER and D&D efforts:

- Petroleum-contaminated soil (waste code 22)
- Combustible building debris (waste code 35)
- Noncombustible building debris (waste code 36)
- Asbestos (waste code 68)
- Asbestos-contaminated debris (waste code 69)
- Beryllium-contaminated debris (waste code 72)
- PCB-contaminated materials (waste code 77)
- PCB-contaminated equipment (waste code 78)
- PCB-contaminated soil (waste code 79)
- PCB-contaminated concrete (waste code 791)
- Radioactively contaminated soil (waste code 90)

All other waste streams were assumed to be generated by normal LANL operations.

Several sites at LANL are currently undergoing remediation. Large quantities of ER and D&D waste have been generated in recent years and, as shown in Table 4, these quantities are expected to continue through at least 2010. No comprehensive estimates of the radionuclide inventories in the future ER and D&D waste have been developed.

Given the information summarized above and the lack of radiological characterization, the future inventory of ER and D&D waste was estimated using a hybrid approach. The volumes of waste requiring disposal were assumed to be those provided in Table 4. Radionuclide inventories in the waste were estimated using the average contaminant concentrations in the ER and D&D waste that was disposed of at Area G from 2000 through 2007. The radionuclide concentrations used in these calculations correspond to the ER and D&D waste codes listed above.

Although the extrapolation approach is expected to provide reasonable estimates of future generation trends for most operational wastes, it is not expected to adequately characterize some waste streams. The first of these is the high-activity tritium waste generated at LANL. Although this waste is routinely generated at the Laboratory, it has been disposed of on a sporadic basis. In the early 1990s, the disposal of this waste was discontinued for several years until the adequacy of its packaging could be evaluated and options for recovering the tritium from the waste were explored. Although the Laboratory initially intended to recover tritium, ultimately the decision

was made to dispose of it. In 1999, generators of tritium waste were advised to send their stored tritium waste for disposal.

The decision to forego the tritium recovery option has had a significant impact on the rate at which high-activity tritium waste has been sent to Area G for disposal. The activities disposed of in 1999 and 2000 were significantly greater than those disposed of in 7 of the 9 years previous to this decision; elevated disposal activities were also observed in 2001 and 2003. Many of the high-activity tritium packages disposed of from 1999 through 2003 contain waste that was held for recovery.

The disposal history of tritium waste was further complicated when two major tritium facilities at TA-21 were closed. Stabilization and shutdown of the Tritium Systems Test Assembly (TSTA) facility was completed in 2003, while shutdown activities at the Tritium Science and Fabrication Facility (TSFF) were completed in 2006. Ongoing Laboratory operations that were conducted at these facilities were transferred to the Weapons Engineering Tritium Facility (WETF). These changes affected the quantities of high-activity tritium waste that required disposal during this period. More recently, there has been discussion of moving tritium operations from LANL to another DOE Laboratory; this would have obvious impacts on the amount of tritium requiring disposal at Area G.

The storage of high-activity tritium waste for recovery and changes in tritium operations at the Laboratory limit the usefulness of the 2000–2007 disposal data in terms of extrapolating the future tritium inventory. Consequently, this inventory was projected on the basis of data collected from WETF personnel at TA-16. It is not clear if tritium operations will, in fact, move to another DOE Laboratory. Consequently, it was assumed that operations at WETF will continue for the foreseeable future and that all waste generated by the facility will be disposed of at Area G. Given that the future tritium inventory was estimated directly, all tritium waste generated by TAs 16 and 21 was excluded from the 2000–2007 dataset used in the extrapolation process; the generation of tritium by other facilities at LANL was assumed to continue at the rates observed from 2000 through 2007.

The inventory characterization effort conducted in support of the 1997 performance assessment and composite analysis (Hollis et al., 1997) concluded that the extrapolation approach would also fall short in terms of accurately projecting the amounts of uranium chips and turnings that will require disposal at Area G. Although this waste stream continues to be generated at the Laboratory, a decision has been made to ship all uranium chips and turnings off site for treatment and disposal. Therefore, the waste stream no longer enters into the future inventory characterization effort.

In the past, waste packages containing high activities of specific radionuclides were occasionally disposed of at Area G. Because the disposal of similar materials at Area G is not expected to occur in the future, the disposal data for these wastes, described in the following list, were removed from the extrapolation dataset.

- Several containers of waste containing high activities of C-14, Co-60, Fe-55, H-3, and Ni-63 were generated in 2003 in conjunction with reactor D&D at TA-2; the activities of all but tritium were among the highest shipped for disposal at Area G. Only a minor amount of low-activity waste has been shipped from TA-2 since 2003; this material was generated in the course of determining the nature and extent of any remaining contamination at the site. No other significant quantities of waste are anticipated from the facility in the future. Consequently, all disposal records for waste generated at TA-2 from 2000 through 2007 were removed from the extrapolation dataset.

- A relatively large amount of waste contaminated with Th-232 was shipped to Area G for disposal in 2004; the activity of this waste is about 5 percent greater than all other Th-232 waste disposed of at Area G from 1971 through 2007. Generated during cleanup activities at TA-18, waste of this type is not expected to require disposal in the future; the data for this material were deleted from the extrapolation dataset.

- Waste generated from research reactors at Brookhaven National Laboratory was shipped for disposal at Area G in 2005 and 2006. This waste will no longer be shipped to LANL so the disposal records for this waste were removed from the extrapolation dataset.

In summary, future inventory projections were developed for the waste expected to be disposed of in the Area G pits and shafts from 2008 through 2044. In general, future inventories of operational waste were estimated by extrapolating from 2000–2007 disposal records; selected waste streams were removed from the extrapolation dataset because these wastes are not anticipated to require disposal at Area G in the future. Information collected through interviews with Laboratory personnel was used to estimate future inventories of high-activity tritium waste. Radionuclide concentrations in the ER and D&D waste that was disposed of at Area G from 2000 through 2007 were used in conjunction with ER and D&D waste volume projections to estimate future inventories associated with waste generated by cleanup efforts at the Laboratory.

4.0 Area G Inventory Projections

This section presents the Area G inventory projections developed using the methodology discussed in Sections 3.1 and 3.2. Inventory projections for the historical waste, which was disposed of from the beginning of operations at Area G through 2007, are provided in 4.1. Projected future inventories for waste disposed of from 2008 through 2044 are presented in Section 4.2. Section 4.3 provides a discussion of the uncertainties associated with the inventory projections. The performance assessment and composite analysis inventories are summarized in Section 4.4.

4.1 Historical Inventory Projections

The historical Area G inventory is presented for three waste disposal periods:

- From the start of operations at the disposal facility through 1970
- From the beginning of 1971 through September 26, 1988
- From September 27, 1988 through the end of 2007

Separate inventories were developed for these periods for two reasons. First, the amount of detailed data available for characterizing the waste disposed of prior to 1971 is less than that for the post-1970 periods. As a result, different approaches must be taken to estimate radionuclide inventories. Maintaining the identities of the pre-1971 and post-1970 inventories also permits evaluation of the uncertainties inherent in each inventory. Second, the performance objectives upon which the performance assessment is based are specific to waste that is disposed of after September 26, 1988. Consequently, separate inventories were developed for waste disposed of through September 26, 1988 and waste disposed of after this date to demonstrate compliance with these objectives.

Section 4.1.1 presents the results of the inventory characterization for waste disposed of from the start of operations at Area G through 1970. Sections 4.1.2 and 4.1.3 present the inventories for 1971 through September 26, 1988 and September 27, 1988 through 2007, respectively.

4.1.1 Pre-1971 Waste Inventory

The development of the pre-1971 pit and shaft inventories was based on information from a variety of sources. The comprehensive evaluation of the 1959–1970 Area G disposal records conducted by Pollard and Shuman (1999) provided insight into the accuracy of the inventories develop for the 1997 composite analysis (Hollis et al., 1997) and helped identify a suitable approach for conducting this inventory update. The results of the data evaluation are discussed in Section 4.1.1.1. Following this discussion, the methods adopted for estimating the pre-1971 pit

and shaft inventories for the current inventory update are described and the results presented (Section 4.1.1.2).

4.1.1.1 Historical Disposal Data Evaluation

The pre-1971 data evaluation focused on the radionuclides that made the greatest contributions to the doses projected for the 1997 composite analysis: Am-241 and several isotopes of plutonium. A summary of the results of the 1997 analysis is provided below. Pollard and Shuman (1999) provide a detailed description of the 1997 evaluation.

A review of the 1959–1970 disposal records for Area G revealed the following sources of information that documented the waste disposed of at the facility:

- Handwritten, bound logbooks with detailed entries describing the burial of each waste shipment
- Handwritten spreadsheets that list LANL-wide radioactive waste disposals during the 1960s
- Disposal memoranda that summarize radioactive waste disposals at the Laboratory
- Sludge disposal records that document the disposal of sludge between 1960 and the mid-1970s
- Miscellaneous disposal records

The information in the bound logbooks includes the disposal date for each waste shipment, the location of the waste in the disposal pits (i.e., pit, layer, and post number), the volume of waste, the type of packaging, the LANL waste generator, and a physical description of the waste. Neither radionuclide identities nor quantities are provided for any shipments. Tables included in the logbooks summarize routine LANL waste shipments disposed of at Area G. These tables list the number of plastic bags, cardboard boxes, and drums that were disposed of and the disposal locations, but do not provide any information about the radionuclide contents of these packages.

The handwritten spreadsheets were developed by the Laboratory in response to a 1960 Atomic Energy Commission request to report radioactive waste disposals at each federal facility in the U.S. (Johnson, 1960). These spreadsheets provide the dates of disposal, waste generators, physical descriptions of the waste, types and numbers of packages, and waste volumes; the need for shielding of the waste was also specified. The identities of specific radionuclides and activity estimates are provided for some of the waste shipments. The radioactivity level for each shipment is given as low (up to 350 Ci/m^3 [10 Ci/ft^3]), intermediate (350 to 3.5×10^4 Ci/m^3 [10 to 1,000 Ci/ft^3]), or high (greater than 3.5×10^4 Ci/m^3 [1,000 Ci/ft^3]).

Disposal memoranda authored by Dean Meyer, H-1 Group Leader, summarize radioactive waste disposals at the Laboratory from 1960 through 1968 (Meyer, 1960–1969). It appears these memoranda were developed from the handwritten spreadsheets, as they include all radionuclide-specific information from those spreadsheets. Neither the handwritten spreadsheets nor the memoranda specify where the waste shipments were disposed of at the Laboratory. Three radioactive waste disposal sites were used to dispose of waste during the 1959–1969 period addressed by the spreadsheets and memoranda: MDA C, Area G, and MDA T.

The sludge disposal records describe waste disposed of from October 1960 through the mid-1970s and include information on the waste generators, physical forms, and radionuclide contents. Starting in July 1968, the records also specify disposal location (i.e., Area G or MDA T). The miscellaneous disposal records include a variety of documents found in the course of searching the waste records (e.g., Enders, 1969 and 1970; Warren, 1980).

The various sources of information about the pre-1971 waste were reviewed in terms of their relevance to the development of radionuclide-specific inventories. Based on this review, it was decided that the disposal memoranda, sludge disposal records, and several of the miscellaneous records provided the most value. The logbook information was of marginal use in the development of inventory estimates because of the lack of information about specific radionuclides and because data from the logbooks were also available in Meyer's disposal memoranda. The handwritten spreadsheets and the disposal memoranda contain much duplicate information; it was concluded that the disposal memoranda sufficiently summarized the relevant disposal data. More detailed information about waste volumes and generators was provided in the spreadsheets, but this information was not needed to develop estimates of radionuclide-specific inventories.

All of the pre-1971 disposal memoranda written by Meyer were located and reviewed, and the data contained in these memoranda were tabulated. These memoranda provide detailed information for mid-1960 through December 1961 and for July 1964 through December 1968. No data were found in the Meyer disposal memoranda for 1959, the first half of 1960, January 1962 through June 1964, 1969, or 1970. A memorandum from Enders (1970) provides information about the annual volumes of waste that were shipped for disposal prior to 1970.

As discussed, in most cases the disposal memoranda do not specify the waste disposal locations. Consequently, the waste documented in these memoranda was assigned to specific disposal facilities using several assumptions. First, it was assumed that all large volumes of low-activity waste listed in the memoranda were disposed of in the pits at Area G. This assumption was adopted because solid waste disposal operations at MDA C were slowing down in the early 1960s, while Area G was receiving more and more of this waste. The waste disposed of at the third disposal site, MDA T, was primarily liquid waste. Comparisons of the MDA C shaft

disposal records and the memoranda data indicate that most high-activity, low-volume waste was disposed of at MDA C through 1966. Three waste shipments were reported to have been disposed of at MDA C in 1967, but it was not possible to clearly identify these shipments. Therefore, it was assumed that all low-volume, high-activity waste disposed of from 1967 through 1970 was placed in the shafts at Area G.

Table 5 summarizes the total waste volumes and activities that were disposed of at Area G based on the disposal memoranda. The three identified categories of waste are tritium-contaminated waste, waste contaminated with fission products, and all other waste. The third category of waste includes material contaminated with plutonium and Pu-equivalents and is referred to as Pu-equivalent waste in the following discussion. The term Pu-equivalent refers to various alpha-emitting radionuclides such as isotopes of plutonium and Am-241. The Pu-equivalent waste includes sludge that was disposed of during the 1960s; sludge accounts for approximately 3,000 m^3 (1.1×10^5 ft^3) and 1,500 Ci of the totals listed in Table 5 for Pu-equivalent waste.

Table 5
Waste Disposal Volume and Activity Based on Disposal Memoranda

Waste Type	Total Volume (m^3)	Total Activity (Ci)
Tritium-Contaminated Waste	5.1E–01	4.3E+04
Fission-Product Waste	9.6E–01	3.5E+02
Pu-Equivalent Waste	4.0E+04	1.7E+03
Total	4.0E+04	4.5E+04

Source: Meyer, 1960 –1969

All existing sludge disposal records for the pre-1971 period were located and the data contained therein tabulated. Records began in October 1960 and extended into the mid 1970s; no records were found for 1963 or 1970. As stated earlier, the records included the disposal location starting in mid-1968. It was assumed that all waste disposed of prior to this time was sent to Area G. Waste disposed of at TA-21 (MDA T) was excluded from the data evaluation.

The sludge disposal record evaluation indicates that more than 15,000 drums, with capacities of 0.11 and 0.21 m^3 (30 and 55 gal) were disposed of at Area G. This amounts to approximately 2,000 m^3 (7.1×10^4 ft^3) of waste. The records provide radionuclide contents in terms of mass; the masses of Am-241, Pu-239, and Pu-equivalents in the waste are 470, 530, and 2.6×10^4 g (1.0, 1.2, and 57 lb), respectively. Converting these masses to activities yields an Am-241 activity of 1,600 Ci, Pu-239 activity of 33 Ci, and Pu-equivalents activity of 160 Ci; the specific activity used to convert the Pu-equivalents mass to activity was 0.062 Ci/g (1.4×10^{-4} Ci/lb) as reported in Enders (1969).

The mass of Pu-equivalents listed in the sludge disposal records includes the Am-241 and Pu-239 masses that were listed separately as well as any Pu-238 and U-235 present in the waste. The total mass of Pu-238 and U-235 may be estimated by taking the difference between the Pu-equivalent mass and the sum of the Am-241 and Pu-239 masses; the result is 2.5×10^4 g (55 lb). Note that this method does not work for determining activities, as the sum of the Am-241 and Pu-239 activities is greater than the total activity calculated for the Pu-equivalents.

In general, the quantities of sludge estimated by the disposal memoranda and the sludge disposal records concur. The disposal memoranda indicate approximately 3,000 m^3 (1.1×10^5 ft^3) of this waste, while the sludge disposal records indicate 2,000 m^3 (7.1×10^4 ft^3) of material. The Pu-equivalent mass of 2.5×10^4 g (55 lb) listed in the disposal memoranda is in close agreement with the mass of 2.6×10^4 g (57 lb) listed in the sludge disposal records.

A number of miscellaneous waste records that were found in the course of searching the pre-1971 Area G disposal records contain information relevant to the inventory characterization effort. As discussed, an office memorandum from Enders (Enders, 1970) lists the annual volumes of radioactive waste disposed of at the Laboratory; data for the 1959–1969 period are summarized in Table 6. A spreadsheet with total Laboratory disposal volumes and activities for 1944 through 1978 was found, though there was no reference for this information. The information contained in this spreadsheet for the 1959–1970 period is summarized in Table 7. The volumes listed in Tables 6 and 7 generally fall within 5 percent of one another.

Table 6
Annual Los Alamos National Laboratory Radioactive Waste Disposal Volume, 1959–1969

Year	Disposal Volume (m^3)
1959	3.7E+03
1960	4.4E+03
1961	5.5E+03
1962	5.5E+03
1963	6.0E+03
1964	7.7E+03
1965	5.0E+03
1966	6.3E+03
1967	6.8E+03
1968	6.3E+03
1969	5.3E+03
Total	6.3E+04

Source: Enders, 1970

Table 7
Annual Los Alamos National Laboratory Radioactive Waste Stream Volume and Activity, 1959–1970

Waste Stream	Waste Disposal by Year											
	1959	1960	1961	1962	1963	1964	1965	1966	1967	1968	1969	1970
Volume (m^3)												
Stored/Buried TRU Waste (> 10 nCi/g)	2.0E+02	3.4E+02	3.6E+02	3.5E+02	3.9E+02	4.1E+02	4.0E+02	5.0E+02	5.4E+02	6.6E+02	5.6E+02	6.7E+02
U/Th Waste	1.3E+03	1.4E+03	1.4E+03	1.4E+03	1.6E+03	4.4E+03	1.6E+03	2.0E+03	2.2E+03	1.9E+03	1.6E+03	1.9E+03
Fission Products	1.0E+01	1.0E+01	1.0E+03	1.0E+03	1.0E+03	1.0E+01	1.0E+01	1.5E+01	1.5E+01	1.5E+01	1.0E+01	1.5E+01
Induced Activity	1.5E+01	2.0E+01	2.0E+01	2.0E+01	2.0E+01	2.0E+01	2.0E+01	2.5E+01	3.0E+01	2.5E+01	2.0E+01	2.5E+01
Tritium Waste	4.0E+01	5.0E+01	5.0E+01	5.0E+01	5.5E+01	6.0E+01	6.0E+01	7.0E+01	8.0E+01	7.0E+01	6.0E+01	7.5E+01
Beta/Gamma Emitters in TRU Waste	---	---	5.0E+00	5.0E+00	5.0E+00	5.0E+00	5.0E+00	5.0E+00	5.0E+00	5.0E+00	5.0E+00	5.0E+00
Buried TRU Waste (< 10 nCi/g)	2.4E+03	2.7E+03	2.9E+03	2.8E+03	3.2E+03	3.3E+03	3.2E+03	4.0E+03	4.3E+03	3.9E+03	3.3E+03	4.0E+03
Total	4.0E+03	4.5E+03	5.8E+03	5.7E+03	6.2E+03	8.3E+03	5.3E+03	6.6E+03	7.1E+03	6.6E+03	5.6E+03	6.7E+03
Activity (Ci)												
Stored/Buried TRU Waste (> 10 nCi/g)	1.0E+02	2.0E+02	2.0E+02	2.0E+02	2.0E+02	2.0E+02	2.0E+02	2.0E+02	2.0E+02	3.0E+02	4.5E+02	6.0E+02
U/Th Waste	2.8E+00	2.8E+00	2.8E+00	2.8E+00	2.8E+00	2.8E+00	2.8E+00	2.8E+00	2.8E+00	2.8E+00	2.8E+00	2.8E+00
Fission Products	3.0E+02	3.0E+02	1.9E+03	1.9E+03	1.9E+03	3.0E+02	3.0E+02	3.0E+02	3.0E+02	3.0E+02	3.0E+02	3.0E+02
Induced Activity	1.5E+02	1.5E+02	1.5E+02	1.5E+02	1.5E+02	1.5E+02	1.5E+02	1.5E+02	1.5E+02	1.5E+02	1.5E+02	1.5E+02
Tritium Waste	4.0E+02	6.6E+02	8.5E+01	1.0E+00	3.0E+01	1.8E+03	5.9E+02	5.1E+04	6.3E+03	2.0E+04	3.0E+04	3.4E+04
Beta/Gamma Emitters in TRU Waste	---	---	1.0E+02	1.0E+02	1.0E+02	1.0E+02	1.0E+02	1.0E+02	1.0E+02	1.0E+02	1.0E+02	1.0E+02
Buried TRU Waste (< 10 nCi/g)	7.0E+00	1.0E+01	1.0E+01	1.0E+01	1.0E+01	1.0E+01	1.0E+01	1.0E+01	1.0E+01	1.0E+01	1.0E+01	1.0E+01
Total	9.6E+02	1.3E+03	2.4E+03	2.4E+03	2.4E+03	2.6E+03	1.3E+03	5.2E+04	7.0E+03	2.0E+04	3.1E+04	3.5E+04

TRU = Transuranic *--- = Not applicable*

Various Area G inventory estimates were found during the record search. Unreferenced handwritten calculations dated 1963 through December 22, 1969 indicate a total of 860 and 7,300 g (1.9 and 16 lb) of Pu-239 and U-235, respectively. A draft report entitled "Area G" that describes facility operations from the initial area survey in 1956 through 1972 was also found. The report discusses inventory estimates prepared by Wilbur Workman in 1970 and Wheeler (1974); Table 8 summarizes these data. Another estimate of the Area G inventory is provided in Rogers (1977); the Rogers information is reproduced in Table 9. Finally, Warren (1980) provides quantities of selected radionuclides that were disposed of at the Laboratory through 1978; these data include waste placed in MDAs B, C, and T, and in Area G. The information pertinent to waste disposal at Area G is summarized in Table 10.

Table 8
Area G Inventory Estimates Developed by Workman and Wheeler

Constituent	Workman Inventory [a] (g)	Wheeler Inventory (Ci) [b]	
		Pits	Shafts
Am-241	---	2.1E+03	---
Co-60	---	---	2.3E+02
Cs-137	---	---	6.0E+00
D-38	2.3E+07	---	---
Fission Products	---	---	7.7E+01
H-3	< 1.0E+01 [c]	---	7.8E+04 [d]
Induced Activity	---	---	2.5E+03
Na-22	---	---	4.6E+01
Pu-238	2.0E-01	1.5E+01	---
Pu-239	1.1E+03	3.3E+02	---
Sr-90/Y-90	---	4.0E+03	7.5E+02
U-233	---	---	5.0E+00
U-235	9.0E+03	---	---
U [e]	---	4.8E+01	---

--- = Not listed in the inventory

[a] Inventory as of December 18, 1970

[b] Listed activities are decay-corrected to December 31, 1972

[c] Total inventory for Material Disposal Area C and Area G

[d] The tritium inventory was listed as 9.8×10^4 Ci in the report titled "Area G"; an office memorandum later issued by Wheeler (1974) corrected it to the value listed here.

[e] Includes U-234, U-235, U-236, and U-238

Table 9
Estimated Radionuclide Inventory for Area G Pits and Shafts, January 1976

Constituent	Inventory (Ci) [a]	
	Pits (1959–1975)	Shafts (1965–1975)
H-3	---	9.2E+04
Na-22	---	2.0E+01
Co-60	---	1.5E+02
Sr-90/Y-90	2.8E+03	2.8E+02
Cs-137	---	6.0E+00
U-233	---	5.0E+00
U [b]	5.4E+01	< 1.0E+00
Pu-238	4.4E+01	4.0E+00
Pu-239 [c]	3.7E+02	4.6E+01
Am-241	2.1E+03	---
Fission Products	---	2.0E+02
Induced Activity	---	6.6E+02

Source: Rogers, 1977

--- = Not listed in the inventory

[a] *Listed activities are decay-corrected to January 1976.*

[b] *Includes U-234, U-235, U-236, and U-238*

[c] *Mostly weapons-grade Pu (94 wt. % Pu-239, 6 wt. % Pu-240); curie value based upon 0.072 Ci (alpha)/g*

Table 10
Summary of Area G Disposal Data Provided by Warren (1980)

Disposal Date	Disposal Area	Disposal Unit	Mass (g)				Notes
			Pu	Am-241	U-233	Other	
1951–1963	MDA C, Area G	Pits	NA	NA	NA	NA	Sludges in 0.21-m^3 drums; generated by the TA-45 treatment plant
1952–1967	MDA C, Area G	Pits	3.4E+02	---	---	5.8E+02 (equivalent Pu) [a]	Over 3,000 0.21-m^3 drums of weapons-grade Pu disposed of as sludge; generated by the TA-21 treatment plant.
1959–1968	MDA C, Area G	Pits	7.4E+02	6.6E+02	6.5E+02	---	Approximately 11,800 0.21-m^3 drums of weapons-grade material disposed of as cement paste.
1960	Area G	Pit 1	6.0E+02	---	---	---	Approximately 30 to 40 0.11-m^3 drums containing sand from TA-21 decontamination activities.
1963–1971	MDA C, Area G	Pits	NA	NA	NA	NA	Sludge in 0.21-m^3 drums
1967–1978	Area G	Shafts	2.1E+03	---	---	Additional Pu, U, and MFP	Recorded values for all waste disposed of in shafts; primarily hot cell waste.
1972–1978	Area G	Pits 7, 8, 12, 13, 17, 18, 20, and 22	1.3E+02	---	---	Additional Pu, U, MFP, MAP, and H-3	

Source: Warren, 1980

MDA = Material Disposal Area *NA = No radionuclide content data provided* *--- = Not listed in the inventory*

MFP = Mixed-fission products *MAP = Mixed-activation products*

[a] *This waste has a specific activity of 0.073 Ci/g*

The disposal memoranda, sludge disposal records, and miscellaneous records were used to estimate radiological inventories for the waste disposed of at Area G prior to 1971. As discussed, the disposal memoranda that were found during the investigation did not include detailed data for waste disposed of in 1959, the first half of 1960, January 1962 through June 1964, 1969, and 1970. The properties of the waste disposed of during the periods for which limited information was available were estimated through extrapolation. For example, late 1960 and 1961 waste data were used to estimate the characteristics of the waste disposed of during 1959 and the first half of 1960. The properties of the waste disposed of between January 1962 and June 1964 were estimated using disposal data for 1961 and from July 1964 through December 1965; waste data from mid-1968 through 1969 were used to characterize the waste disposed of in 1970. The projections developed using the disposal memoranda are summarized in Table 11.

Table 11
Pre-1971 Inventory Projections for Area G
Based on Disposal Memoranda

Waste Stream	Volume (m^3)	Activity (Ci)
Pu-Equivalent Waste	5.4E+04	2.7E+03
Sludge [a]	4.8E+03	2.4E+03
All Waste [b]	5.4E+04	5.6E+04

Source: Meyer, 1960–1969

[a] Sludge waste is a subset of the Pu-equivalent waste.

[b] All waste includes the Pu-equivalent waste, tritium waste, and fission products.

Sludge disposal records could not be found for 1959 through September 1960, 1963, and 1970. The characteristics of the waste disposed of during the first of these periods were extrapolated from waste data for October 1960 through December 1961, while the properties of the 1963 waste were estimated using 1962 and 1964 disposal records. Sludge disposal data for waste disposed of from July 1968 through December 1969 were used to estimate the characteristics of the 1970 waste; this period excludes waste that was generated and disposed of at TA-21 (MDA T) starting in mid-1968. These calculations yielded a total waste volume of 2,800 m^3 (9.9×10^4 ft^3); activities associated with the waste include 1,800, 40, and 2,300 Ci of Am-241, Pu-239, and Pu-equivalents, respectively.

The handwritten calculations for the 1963 through December 22, 1969 period were used to estimate total inventories of Pu-239 and U-235. These calculations indicate that 53 Ci of Pu-239 were disposed of at Area G over this period; if similar generation rates are assumed for the missing portions of the 1959–1970 period, a total inventory of 91 Ci is estimated for all waste

emplaced at Area G. In a similar fashion, the handwritten calculations were used to obtain a total U-235 inventory of 0.027 Ci for the 1959–1970 timeframe.

The inventory projections developed using the disposal memoranda, sludge disposal records, and miscellaneous records were compared to the inventory projections developed for the 1997 composite analysis (Hollis et al., 1997). Table 12 compares the total volume and activity projections developed using the disposal memoranda and the two sets of LANL-wide disposal data (Tables 6 and 7) to the composite analysis inventory. The Area G disposal volume projected using the Area G data from the 1960–1969 Meyer memoranda is consistent with the volume projected for the 1997 composite analysis. Both of these estimates are less than the LANL-wide estimates; this is logical due to the fact that radioactive waste was being disposed of at facilities other than Area G. The total activity projected using the Area G disposal memoranda data is in close agreement with the activity estimated for the composite analysis. The LANL-wide disposal activity is about three times greater than the Area G total, reflective of the fact that low-volume, high-activity waste was disposed of at other facilities prior to 1967.

Table 12
Comparison of Pre-1971 Inventory Projections Based on Disposal Memoranda and Laboratory-Wide Disposal Data with the 1997 Composite Analysis Inventory

Source of Inventory Projections	Volume (m^3)	Activity (Ci)
Disposal Memoranda (Meyer, 1960–1969)	5.4E+04	5.6E+04
LANL Annual Disposal Data (Enders, 1970)	6.3E+04 [a]	---
LANL-Wide Spreadsheet Data	7.2E+04	1.6E+05
1997 Composite Analysis (Hollis et al., 1997)	5.6E+04 [b]	5.5E+04 [b]

LANL = Los Alamos National Laboratory *--- = Data source did not include waste activity.*

[a] Total excludes waste disposed of in 1970. *[b] Entries represent the sum of the projected pit and shaft inventories.*

The volumes and activities of Am-241 and plutonium-contaminated waste projected using the disposal memoranda (Meyer, 1960–1969) and the sludge disposal records were compared to the 1997 composite analysis estimates for this waste. The results of this comparison are summarized in Table 13. The Pu-equivalent waste shown in this table includes all material containing plutonium and other alpha-emitting radionuclides; the sludge waste information from the disposal memoranda is a subset of the Pu-equivalent material. The composite analysis waste projections are divided into three waste streams.

A comparison of the waste projections shown in Table 13 is complicated by the fact that a large portion of the surface-contaminated waste included in the 1997 composite analysis is expected to be free of any alpha contamination. Perhaps the most reliable comparison involves the sludge

data from the disposal memoranda, the totals developed from the sludge disposal records, and the concrete and sludge inventory estimated for the composite analysis. These data are expected to generally represent the same waste and, as such, provide three estimates of the volumes and activities of sludge disposed of at Area G prior to 1971. As shown in Table 13, the 1997 composite analysis volume projection is 1.5 to 2.6 times greater than the volume projections developed using the disposal memoranda and sludge disposal records. The projected activities for all estimates, however, fall within 20 percent of one another. In terms of nonsludge waste, the composite analysis inventory includes a large Pu-equivalent component associated with the surface-contaminated waste. The total activity of this waste is significantly greater than the activities projected using the historical waste disposal records.

Table 13
Comparison of Pu-Equivalent Waste Inventories, 1959 Through 1970

Source of Inventory Projections	Volume (m^3)	Activity (Ci)
Disposal Memoranda (Meyer, 1960–1969)		
Pu-Equivalent Waste	5.4E+04	2.7E+03
Sludge Waste	4.8E+03	2.4E+03
Sludge Disposal Records	2.8E+03	2.3E+03
Composite Analysis Projections (Hollis et al., 1997)		
Surface-Contaminated Waste	4.2E+04 [a]	1.5E+04 [b]
Soil	6.1E+03 [a]	3.9E+01 [b]
Concrete and Sludge	7.5E+03 [a]	2.8E+03 [b]

[a] *The quantities of waste contaminated with Am-241 and plutonium could not be separated from the waste without these radionuclides. Thus, listed volumes represent all waste projected for a waste stream; the entries represent the sum of pit and shaft inventories.*

[b] *The listed activities represent the sum of the activities of Am-241 and isotopes of plutonium and uranium; entries represent the sum of pit and shaft inventories.*

Historical disposal records were used to estimate radionuclide-specific inventories that were subsequently compared to the activities developed for the 1997 composite analysis. The development of these inventories from historical data was complicated by data availability issues. Pu-equivalent, Pu-239, and Am-241 inventories were provided for the sludge waste; however, the other waste streams had only Pu-equivalent inventories. No detailed information about Pu-238, Pu-240, or Pu-241 inventories was found in the historical data.

The key to estimating radionuclide-specific activities lies in the ability to accurately allocate the Pu-equivalent inventories. Information to perform this allocation was found in the course of the data evaluation. Enders (1969) provides a specific activity of 0.062 Ci/g (28 Ci/lb) for Pu-equivalent waste. A note found in the miscellaneous records indicates that activities for

Pu-238 and Pu-239 occur in a ratio of about 9:1. Finally, the LANL sludge disposal records indicate that the main contributors to Pu-equivalent activities are Pu-238, Pu-239, Am-241, and U-235.

The information cited above was used in a three-step process to estimate radionuclide-specific activities for the waste included in the sludge disposal records. First, the total masses of Am-241 and Pu-239 in the waste were converted to activities using the specific activities of the two isotopes. Second, the activity of Pu-238 in the waste was estimated by multiplying the Pu-239 activity by 9, consistent with the 9:1 activity ratio discussed above. Finally, the mass of Pu-equivalent not accounted for by the Am-241, Pu-238, and Pu-239 assignments was assumed to be U-235; the specific activity of U-235 was used to convert that mass to an activity. Although other alpha-emitting radionuclides may have been present in the waste disposed of during this period, they were assumed to have made negligible contributions to the total mass.

Data from Warren (1980), summarized in Table 10, were also used to develop radionuclide-specific inventories for the sludge. In developing these estimates, it was assumed that 1,500 of the 0.21-m^3 (55-gal) drums of sludge disposed of from 1952 through 1967 were buried at Area G; the other 1,500 drums were assumed to have been sent to MDA C. It was also assumed that all 11,800 of the 0.21-m^3 (55-gal) drums disposed of from 1959 through 1968 went to Area G. The sand disposed of in 1960 and the hot cell waste were not included in the sludge waste inventory calculations.

Based on the preceding assumptions, it was estimated that the sludge disposed of at Area G prior to 1971 contained 910 g (2 lb) of plutonium, 660 g (1.5 lb) of Am-241, and 290 g (0.64 lb) of Pu-equivalents. It appears that the majority of the plutonium in the waste is Pu-239. The sludge waste disposed of from 1952 through 1967 and the cement paste buried from 1959 through 1968 is weapons-grade material (Warren, 1980); the specific activity given for the 1952–1967 waste is 0.73 Ci/g (330 Ci/lb), which is similar to the specific activity of Pu-239 (i.e., 0.62 Ci/g [280 Ci/lb]). Additionally, Warren (1980) indicates that very little Pu-238 was disposed of at Area G prior to 1979. Assuming that all of the plutonium is, indeed, Pu-239, then the 910 g (2 lb) represents an activity of 58 Ci; the 660 g (1.5 lb) of Am-241 corresponds to an activity of about 2.1×10^3 Ci.

The 290 g (0.64 lb) of Pu-equivalents included in the Warren data (1980) was converted to radionuclide-specific activities using the same three-step process outlined for the sludge disposal records. Using this approach, 0.1, 1.7, 1.4, and 96.8 percent of the total mass of Pu-equivalents in the sludge is Pu-238, Pu-239, Am-241, and U-235, respectively. Applying these percentages to the 290 g (0.64 lb) of Pu-equivalents listed in Warren and converting the masses to activities yields 4.5, 0.3, 14, and 0.006 Ci of Pu-238, Pu-239, Am-241, and U-235, respectively.

The radionuclide-specific inventories estimated from various sources for the sludge waste are summarized in Table 14. The radionuclide-specific activities estimated using the sludge disposal records, the handwritten spreadsheet calculations, and the Warren data (1980) generally agree with the 1997 composite analysis inventory estimates. The composite analysis inventory for Pu-239 is similar to estimates based on the Warren data, handwritten calculations, and Workman data, while the Am-241 inventory estimates are similar across the board. The similarity between the 1997 composite analysis estimates and those based on the Warren data is expected because data from Warren (1980) formed the basis for supplementing the composite analysis inventory to account for waste that was not captured by the extrapolation process. In contrast, the majority of the Pu-238 that is included in the composite analysis inventory was estimated through the extrapolation process and differs markedly from the activity estimated for this radionuclide using the Warren data. The Pu-238 activity projection developed using the sludge disposal data is most similar to the composite analysis inventory for this radionuclide, although the two estimates still differ by approximately 200 Ci.

Table 14
Pre-1971 Radionuclide-Specific Inventories Projected for Sludge

	Activity (Ci)				
Source of Inventory Projections	Pu-equiv.	Pu-238	Pu-239	Am-241	U-235
Sludge disposal records	2.3E+03	3.6E+02	4.0E+01	1.8E+03	7.7E-02
Miscellaneous records					
Warren (1980)	2.2E+03 [a]	4.5E+00	5.8E+01	2.1E+03	6.0E-03
Handwritten Spreadsheet Calculations [b]	---	---	9.1E+01	---	2.7E-02
Workman [b]	---	3.5E+00	6.7E+01	---	1.9E-02
Wheeler [b] (1974)	---	1.5E+01	3.3E+02	2.1E+03	---
Rogers (1977)	---	4.8E+01	4.2E+02	2.1E+03	---
Composite Analysis (Hollis et al., 1997)	2.8E+03 [c, d]	5.7E+02 [c]	8.0E+01 [c]	2.2E+03 [c]	3.5E-03 [c]

--- = None

[a] *Estimated as the sum of the radionuclide-specific activities.*

[b] *Listed activities are for all waste, not just sludge.*

[c] *Entries represent the concrete and sludge inventory disposed of in the pits.*

[d] *Pu-equivalent activity was not calculated for the composite analysis; it is estimated here as the sum of the activities of Am-241 and isotopes of plutonium and uranium.*

Caution needs to be exercised when interpreting the inventory projections provided in Table 14. As pointed out, the handwritten spreadsheet calculations, the Workman and Wheeler data, and the estimates from the Rogers report include all waste, not just the sludge component.

Furthermore, although the Workman data generally coincide with the pre-1971 period of interest, the Wheeler data represent inventories through much of 1972 and the Rogers data address waste disposed of through 1975. Finally, the Wheeler and Rogers data are decay-corrected whereas other activities included in the table are not.

As discussed, the inventory developed for the 1997 composite analysis includes large inventories of plutonium-contaminated waste other than sludge. Information about radionuclide activities in nonsludge waste is scarce in the historical disposal records; the historical information that was found is compared to the composite analysis inventory in Table 15. Sources of historical data used in this analysis include the disposal memoranda (Meyer, 1960–1969) for nonsludge waste, the handwritten spreadsheet calculations, and the Workman and Wheeler (1974) data. The disposal memoranda data included in Table 15 represent the Pu-equivalent data found in these records minus the portion of the waste represented by sludge. The handwritten calculations, Workman data, and Wheeler data address all waste disposed of at Area G, including sludge. The composite analysis inventories are provided for two nonsludge waste streams (i.e., surface-contaminated waste and soil).

It is apparent from Table 15 that the different sources of information do not agree with respect to the nonsludge radionuclide-specific inventories. Using Pu-equivalent activities as a guide, the total activity represented by the composite analysis inventory (Hollis et al., 1997) is about 50 times greater than the total activity estimated from the disposal memoranda. Although the disposal memoranda data have not been allocated to individual radionuclides, it is clear that the isotope-specific activities listed for the composite analysis will be much greater than those that might be estimated from the disposal records. The Pu-238 inventories estimated by Workman and Wheeler are less than 1 percent of the composite analysis inventory for this isotope; Pu-239 inventories estimated using the historical information are 4 to 18 percent of the composite analysis inventory.

The pre-1971 disposal data evaluation effort showed that portions of the 1997 composite analysis inventory are in reasonable agreement with available historical data, while other portions are not. The composite analysis projections for the sludge disposed of at Area G are in general agreement with the historical sludge data. However, the composite analysis inventory for the nonsludge waste includes total and radionuclide-specific activities that are significantly higher than the activities indicated by the historical data.

Table 15
Comparison of Pre-1971 Radionuclide Inventories in Nonsludge Waste Streams

Source of Inventory Projections	Activity (Ci)						
	Pu-equiv.	Pu-238	Pu-239	Pu-240	Pu-241	Pu-242	Am-241
Disposal Memoranda–Nonsludge Waste (Meyer, 1960-1969)	3.0E+02	---	---	---	---	---	---
Handwritten Spreadsheet Calculations	---	---	9.1E+01	---	---	---	---
Workman	---	3.5E+00	6.7E+01	---	---	---	---
Wheeler (1974)	---	1.5E+01	3.3E+02	---	---	---	2.1E+03
Composite Analysis (Hollis et al., 1997)	---	---	---	---	---	---	---
Surface-Contaminated Waste [a]	1.5E+04 [b]	4.2E+03	1.8E+03	4.5E+02	8.2E+03	4.9E-02	4.4E+01
Soil	3.7E+01 [b]	3.1E-01	3.7E+01	---	---	---	---

--- = None

[a] Entries represent the sum of pit and shaft inventories, although the vast majority of the waste was assumed to be disposed of in pits.

[b] Pu-equivalent activity was not calculated for the composite analysis; it is estimated here as the sum of the activities of Am-241 and isotopes of plutonium and uranium.

The source of the discrepancy for the nonsludge waste streams is unclear. The activities listed in the 1997 composite analysis for the nonsludge waste were projected almost entirely by assuming the waste disposed of prior to 1971 resembled waste disposed of during the early to mid-1970s. If the pre-1971 waste records are deemed to be relatively complete, it would appear the extrapolation approach is inappropriate or that the waste characteristics that were extrapolated back in time are not representative of the material disposed of prior to 1971. However, if the historical disposal records do not represent all the waste disposed of at Area G, the extrapolation approach used for the composite analysis inventory may, in fact, be more appropriate.

Although available information is inconclusive, it appears likely that the historical disposal data are incomplete with respect to the nonsludge waste streams disposed of at Area G. Technical Area 21 was the primary generator of the plutonium isotopes included in Table 15 for the nonsludge waste streams. This facility was the site of plutonium operations from 1945 to 1978, a period that encompasses the 1971–1977 extrapolation period used in the 1997 composite analysis. There is no compelling reason to think the waste generated from 1971 through 1977 was unique or dissimilar to material generated prior to 1971.

Based on these considerations, it was decided that an extrapolation approach similar to the one used for the 1997 composite analysis would generate more appropriate estimates of the pre-1971 pit inventory. This approach appears to generate reliable inventory estimates for radionuclides in the sludge waste and is expected to provide better estimates of the radionuclides found in the nonsludge waste.

The historical records included in the pre-1971 data evaluation did not provide sufficient detail to estimate the shaft inventory. Therefore, extrapolation methods and alternative sources of information were investigated to develop the inventory for those units.

4.1.1.2 Pit and Shaft Inventory Estimates

The extrapolation process that is used to estimate the pre-1971 pit inventory relies upon post-1970 data from the LLW disposal and TRU waste databases to estimate the characteristics of the earlier waste. The period from which the extrapolation disposal data are drawn strongly influences the resulting inventory projections. Thus, the selected data need to be as representative of the 1957–1970 period as possible. Under ideal conditions, the operations generating waste would be identical for both periods. As the amount of elapsed time between the two time periods increases, however, the likelihood of satisfying this condition decreases. This is because the role of the Laboratory evolves over time, resulting in the phase out of some operations and the start up of new ones.

The 1997 composite analysis (Hollis et al., 1997) used LLW and TRU waste data for the 1971–1977 period to extrapolate pre-1971 pit inventories. This period was selected partly on the basis

of the types and quantities of waste disposed of or placed in storage at Area G from 1971 forward. Waste generated in 1971 is expected to closely resemble material generated prior to that year. The year 1977 was selected as the end of the extrapolation period because the nature of the LLW and TRU waste generated at the Laboratory changed shortly after that point in time. Although LLW pit disposal volumes and activities were relatively constant until 1978, there was a large increase in the activity of the LLW placed in these units in 1979. Similarly, the quantities of TRU waste placed in storage, and the radionuclide activities in that waste, increased substantially in the late 1970s and early 1980s. On the basis of these findings, the extrapolation period was ended in 1977 to minimize divergences between the extrapolated LLW and TRU waste inventories and the actual waste disposed of prior to 1971.

Conveniently, the 1971–1977 extrapolation period also excludes a number of unique waste streams associated with D&D and startup activities at the Laboratory, including those generated during the decommissioning of the TA-21 plutonium facility and the startup of TA-55. In addition, this period generally predates a number of changes in disposal operations at Area G, including the implementation of waste compaction in 1977 and the end of mixed LLW disposal in the mid-1980s.

The 1971–1977 extrapolation period adopted by the 1997 composite analysis for the disposal pits was used in the inventory characterization update as well. The data for this period were examined to identify, to the extent possible, any nonroutine or special case waste that would not have been disposed of prior to 1971. As a result, the following wastes were eliminated from the LLW and TRU waste data used to estimate the pre-1971 inventories.

- All waste generated at TA-53, which was referred to as the Los Alamos Meson Physics Facility during the 1970s. This waste was excluded because the facility began operations in June 1972.
- All LLW and small amounts of TRU waste generated by the town site (TA-1) cleanup activities that took place in the mid-1970s. This waste was excluded because no similar activities occurred prior to 1971.
- Radioactively contaminated soil generated at TA-0 and TA-43 in 1977 in conjunction with the removal of the acid sewer system. This waste was excluded because similar activities did not occur prior to 1971.
- High-activity Pu-238 and U-233 waste generated at TA-21 and stored in trenches A-C. The Pu-238 waste was shipped to the Savannah River Site for disposal prior to 1974. When that site stopped accepting such waste, it was retrievably stored in the Area G trenches. The Laboratory did not receive approval to dispose of the U-233

waste until after 1971. Because these wastes were retrievably stored or sent off site prior to 1971, they were excluded from the inventory estimates.

After the dataset to be used for the extrapolation was identified, the inventory for the pre-1971 pits was developed. With the exceptions noted above, all waste types disposed of in pits from 1971 through 1977 were assumed to have been placed in pits prior to 1971. A few TRU waste shipments included in the extrapolation process were placed in storage domes at Area G; waste similar to this was assumed to have been disposed of in the pits prior to 1971. The total volumes and activities of waste projected for the disposal pits are summarized in Table 16. The extrapolation-based, contaminant-specific inventories estimated for the pre-1971 disposal pits are summarized in Table 17. Volumes and activities of waste estimated on the basis of the LLW disposal data and the TRU waste data are provided separately in each table. The MAP, MFP, and material type waste is not allocated among radionuclides in Table 17; assignments of these wastes to specific isotopes are conducted in the performance assessment and composite analysis modeling. The listed activities represent as-disposed activities; the inventories do not include the radionuclides eliminated on the basis of decay characteristics (see *Attachment II*).

Using the 1971–1977 pit waste data to infer the quantities and characteristics of the waste placed in Area G prior to 1971 does not account for all material that was disposed of during the pre-1971 period. It is practically impossible to identify all unique disposal events that took place at Area G before 1971. However, Warren (1980) identified several events that involved large quantities of specific radionuclides; these were not captured by the extrapolation process. Table 10 indicates the nature of the waste generated by these events.

Based on the information presented in Table 10, waste was added to the extrapolation-based pit inventory projections. The waste form, total volume and activity, and radiological characteristics of the waste represented by these additions are listed in Table 18. These additions were based on a number of assumptions. The sludge generated from 1952 through 1967 was assumed to be disposed of at MDA C and Area G in equal amounts because the Area G pits did not receive routine operational waste until the late 1950s. The masses listed for plutonium were assumed to be Pu-239 (Warren, 1996); the 590 g (1.3 lb) of Pu-equivalents were assumed to be 94 and 6 percent Pu-239 and Pu-240 (by weight), respectively, based on information contained in Warren (1980) and Rogers (1977). All of the cement paste disposed of from 1959 through 1968 was assumed to be placed in pits at Area G, although small quantities of it were probably placed in pits at MDA C.

Table 16
Extrapolation-Based Disposal Volumes and Activities, Pre-1971 Waste

Waste Form by Disposal Unit	LLW		TRU Waste		All Waste	
	Volume (m^3)	Activity (Ci)	Volume (m^3)	Activity (Ci)	Volume (m^3)	Activity (Ci)
Pit Waste (estimates based on 1971–1977 data)	4.5E+04	7.7E+02	1.9E+03	1.5E+04	4.7E+04	1.6E+04
Shaft Waste (estimates based on 1971–1975 data)	1.4E+02	3.5E+04	1.2E+00	8.3E+02	1.5E+02	3.6E+04
Shaft Waste (estimates based on 1971–1977 data)	1.3E+02	8.2E+04	1.7E+00	1.6E+03	1.3E+02	8.3E+04

LLW = Low-level waste *TRU = Transuranic*

Table 17
Extrapolation-Based Radionuclide, Activation Product, Fission Product, and Material Type Inventories for Pits, Pre-1971 Waste

Constituent	Activity (Ci)		
	LLW	TRU Waste	All Waste
Ac-227	1.2E-01	7.4E-01	8.6E-01
Am-241	7.2E-01	8.1E+01	8.2E+01
Bk-249	---	1.6E-03	1.6E-03
Cf-249	7.0E-04	1.7E-03	2.4E-03
Cf-251	---	2.7E-03	2.7E-03
Cf-252	1.5E-02	---	1.5E-02
Cm-242	---	1.8E-03	1.8E-03
Cm-244	---	1.7E-03	1.7E-03
Cs-137	2.6E-01	---	2.6E-01
H-3	2.7E+00	---	2.7E+00
Kr-85	1.7E-03	---	1.7E-03
MAP	3.6E-01	---	3.6E-01
MFP	7.7E-01	1.0E+03	1.0E+03
Np-237	---	4.0E-03	4.0E-03
Po-210	1.9E-03	---	1.9E-03
Pu-238	7.3E+02	3.0E+03	3.8E+03
Pu-239	5.4E+00	5.0E+01	5.5E+01
PU51	---	1.6E+00	1.6E+00
PU52	6.2E-02	7.7E+03	7.7E+03
PU53	---	2.5E+02	2.5E+02
PU54	---	1.1E+03	1.1E+03
PU55	---	6.8E+01	6.8E+01
PU56	---	1.2E+03	1.2E+03
PU57	---	7.1E+01	7.1E+01
PU83	1.5E-02	5.0E+02	5.0E+02
Sr-90	2.9E-01	---	2.9E-01
Th-230	1.6E+01	---	1.6E+01
TH88	1.9E-03	---	1.9E-03
U10	8.8E-01	---	8.8E-01
U12	7.9E+00	---	7.9E+00
U-235	3.7E-01	3.2E-04	3.7E-01
U-238	4.3E+00	---	4.3E+00
U38	2.3E-02	---	2.3E-02
U81	4.7E-03	---	4.7E-03

LLW = Low-level waste *TRU = Transuranic* *--- = None*

Adjustments to the pre-1971 pit inventories could not be made or were unnecessary for three entries in Table 10. Data needed to estimate radionuclide activities were unavailable for sludge generated at TA-45 from 1951 through 1963 and for sludge disposed of in pits from 1963 through 1971. Additions to the inventories to account for the waste placed in selected pits from 1972 through 1978 were not needed. The quantities and nature of the waste disposed of during this period were estimated using actual disposal data that capture the information summarized by Warren (1980).

The total pre-1971 pit inventory combines the extrapolation-based inventory summarized in Tables 16 and 17, and the waste included to account for nonroutine or unique disposals (Table 18). The total volumes and activities of the pre-1971 pit waste are summarized in Table 19, and the contaminant-specific inventories in this waste are listed in Table 20. Pit-specific inventories for pre-1971 waste are provided in *Attachment III.* All activities represent as-disposed activities; inventories are not listed for the radionuclides that were eliminated on the basis of decay characteristics.

The pre-1971 inventory that was disposed of at Area G was placed in pits 1 through 6. Approximately 10 percent of the waste in pit 5 was emplaced after 1970; this waste is addressed in the 1971 through September 26, 1988 inventory projections discussed in Section 4.1.2. Approximately 10 percent of the waste in pit 6 was disposed of prior to 1971; this waste was assigned to the pits 1–5 inventory as it could not be differentiated from other pre-1971 waste. The material disposed of in pit 6 after 1970 is also addressed in Section 4.1.2.

The 1997 composite analysis shaft inventory was estimated through an extrapolation process that used 1971–1975 waste data. As discussed in Section 3.1, Warren (1996) suggested alternative methods for estimating this inventory, including the use of pre-1971 disposal records. This suggestion was made because the quality of pre-1971 shaft data was expected to be similar to the quality of the 1971–1975 shaft data. Use of the 1971–1977 dataset as the basis for estimating the characteristics of the pre-1971 waste through extrapolation was also mentioned by Warren, because the overall quality of these data may be greater than that seen for the 1971–1975 data. Both of these approaches were evaluated as part of the inventory characterization update.

The shaft waste inventories projected using the extrapolation approach are included in Table 16. The projected volumes of shaft waste are similar for both extrapolation datasets (1971–1975 and 1971–1977). However, the total activity projected using the 1971–1977 data is significantly higher than that calculated using the 1971–1975 data. In both cases, the majority of the projected activity is estimated on the basis of LLW disposal data.

Table 18
Additions to Extrapolation-Based Inventory Projections for Pits, Pre-1971 Waste

Waste	Waste Form	Total Volume (m^3)	Total Activity (Ci)	Radionuclide	Radionuclide Activity (Ci)
1952–1967 Sludge	Concrete/Sludge	3.1E+02	3.1E+01	Pu-239	2.7E+01
				Pu-240	4.0E+00
1959–1968 Cement Paste	Concrete/Sludge	2.5E+03	2.3E+03	Am-241	2.3E+03
				Pu-239	4.6E+01
				U-233	6.1E+00
1960 Soil	Soil	4.5E+00	3.7E+01	Pu-239	3.7E+01

Source: Warren (1980)

Table 19
Disposal Volumes and Activities for Pits, Pre-1971 Waste

Waste Type	Volume (m^3)	Activity (Ci)
LLW	4.5E+04	7.7E+02
TRU Waste	4.7E+03	1.7E+04
All Waste	4.9E+04	1.8E+04

LLW = Low-level waste *TRU = Transuranic*

Table 20
Radionuclide, Activation Product, Fission Product, and Material Type Inventories for Pits, Pre-1971 Waste

Constituent	Activity (Ci)		
	LLW	TRU Waste	All Waste
Ac-227	1.2E-01	7.4E-01	8.6E-01
Am-241	7.2E-01	2.4E+03	2.4E+03
Cf-249	7.0E-04	1.7E-03	2.4E-03
Cf-251	---	2.7E-03	2.7E-03
Cf-252	1.5E-02	---	1.5E-02
Cm-242	---	1.8E-03	1.8E-03
Cm-244	---	1.7E-03	1.7E-03
Cs-137	2.6E-01	---	2.6E-01
H-3	2.7E+00	---	2.7E+00
Kr-85	1.7E-03	---	1.7E-03
MAP	3.6E-01	---	3.6E-01
MFP	7.7E-01	1.0E+03	1.0E+03
Np-237	---	4.0E-03	4.0E-03
Po-210	1.9E-03	---	1.9E-03
Pu-238	7.3E+02	3.0E+03	3.8E+03
Pu-239	5.4E+00	1.6E+02	1.7E+02
Pu-240	---	4.0E+00	4.0E+00
PU51	---	1.6E+00	1.6E+00
PU52	6.2E-02	7.7E+03	7.7E+03
PU53	---	2.5E+02	2.5E+02
PU54	---	1.1E+03	1.1E+03
PU55	---	6.8E+01	6.8E+01
PU56	---	1.2E+03	1.2E+03
PU57	---	7.1E+01	7.1E+01
PU83	1.5E-02	5.0E+02	5.0E+02
Sr-90	2.9E-01	---	2.9E-01
Th-230	1.6E+01	---	1.6E+01
TH88	1.9E-03	---	1.9E-03
U10	8.8E-01	---	8.8E-01
U12	7.9E+00	---	7.9E+00
U-233	---	6.1E+00	6.1E+00
U-235	3.7E-01	3.2E-04	3.7E-01
U-238	4.3E+00	---	4.3E+00
U38	2.3E-02	---	2.3E-02
U81	4.7E-03	---	4.7E-03

LLW = Low-level waste *TRU = Transuranic* *--- = None*

Rogers (1977) summarizes the Area G shaft disposal data for waste placed in these units from 1966 through early 1976. A subset of these data (1966 through December 1970) was used to estimate the pre-1971 shaft inventory directly, as suggested by Warren (1996); this subset is referred to as the *historical shaft data* or *historical disposal records* in the following discussion. The data used in this analysis are provided in *Attachment IV*. Table IV-1 provides disposal information for all pre-1971 shipments that include estimates of radionuclide mass or activity. Numerous records included in Rogers provide estimates of disposal volumes but no indication of contaminant quantity. The volumes were extracted from these records to estimate the total volumes of waste disposed of in shafts prior to 1971; these volumes are summarized in Table IV-2.

The pre-1971 historical shaft data in Rogers (1977) provide estimates of radionuclide content in terms of mass for some wastes and in terms of activity for others. The conversion of mass to activity and the assignment of activities to specific radionuclides for this inventory update were based on several assumptions, including:

- The masses listed for TRU waste were assigned to the radionuclides indicated in the waste description; listed activities were divided equally among all listed radionuclides. All plutonium waste was assumed to be Pu-239 unless otherwise indicated. The masses listed for TRU waste that did not have any radionuclide identifier were assumed to represent Pu-239.

- The masses listed for the uranium waste were assigned to the radionuclides included in the waste description; listed activities were divided equally among all listed isotopes. All uranium was assumed to be U-235 unless otherwise indicated. The masses listed for waste packages that did not have any radionuclide identifier were assumed to be U-235.

- MAP and MFP activities were assigned to specific radionuclides when the necessary information was provided in the disposal records; listed activities were divided equally among all listed radionuclides.

- The activation-product activities were assigned to specific radionuclides when the necessary information was provided in the disposal records; specific isotopes were not defined for the tantalum activities.

- The radium sources listed under the “Other” category were assumed to be Ra-226, while the thorium waste was assumed to be Th-232; masses listed for silver and platinum were not accounted for in the activity calculations because it was not clear what isotopes were present in the waste.

The historical disposal records for the shafts indicate that 48 m^3 (160 ft^3) of waste was disposed of prior to 1970; the material had a total activity of 6.4×10^4 Ci (Rogers, 1977). This is about one-third of the volume projected using the extrapolation approach (Table 16). Overall, the total volume of waste disposed of in shafts that were active prior to 1971 is about 80 m^3 (280 ft^3) or about 45 percent of the disposal capacity. This emplacement efficiency fraction is similar to that seen for other shafts at Area G. Emplacement efficiencies calculated using the extrapolated volumes of shaft waste are on the order of 70 to 80 percent. These efficiencies are higher than normal and suggest that the extrapolation approach overestimates actual waste volumes. The total activity of the waste that was estimated using the historical disposal records is intermediate between the activities calculated using the 1971–1975 and 1971–1977 extrapolation datasets.

The inventories estimated using the two extrapolation datasets and the historical shaft data (Rogers, 1977) are provided in Table 21. The material type waste inventories projected through extrapolation have been assigned to their component radionuclides to facilitate comparison of the three sets of data; MAP and MFP waste has not been assigned to specific contaminants. Examination of the results in the table indicates that the constituent-specific activities estimated using the 1971–1977 extrapolation dataset are generally similar to, or greater than, those estimated using the 1971–1975 dataset. Radionuclide-specific activities estimated using the pre-1971 disposal records are similar to or less than those projected using the extrapolation approach for the plutonium and uranium isotopes; the tritium inventory projected using the actual disposal data falls between the two extrapolation-based estimates. The inventory projections based on the historical shaft data yield the lowest activity of MAP waste, but the greatest activity of MFP waste.

The inventory projections developed for the shafts using the historical disposal records and the extrapolation approach were evaluated to determine which estimates should be used in the updated inventory. Bases of comparison included total waste volume and projected radionuclide-specific activities. From the perspective of waste volume, the inventory projections based on the pre-1971 historical disposal records appear most reasonable. As discussed earlier, the emplacement efficiency indicated by the projected waste volume is consistent with historical patterns of shaft usage; the volumes of waste projected through the extrapolation process imply emplacement efficiencies that appear to be unrealistic.

The radionuclide, MAP, and MFP inventories projected using the historical shaft data and the extrapolation approach were compared to inventory estimates reported by Rogers (1977); this comparison is shown in Table 22. The table lists as-disposed activities for the inventories developed using the pre-1971 disposal records and the extrapolation approach. The inventory provided by Rogers includes waste disposed of in shafts through 1975; the listed activities are decay-corrected to January 1976.

Table 21
Comparison of Pre-1971 Radionuclide, Activation Product, and Fission Product Inventories for Shafts Projected from Extrapolation Datasets and Pre-1971 Disposal Data

Constituent	Projected Activity (Ci)		
	1971–1975 Extrapolation Dataset	1971–1977 Extrapolation Dataset	Pre-1971 Shaft Data [a]
Am-241	3.4E-08	2.7E-02	---
Am-243	---	7.7E-06	2.0E-02
Be-7	1.2E+02	8.3E+01	---
C-14	1.0E-02	7.1E-03	---
Ce-137	---	---	5.0E-01
Cf-252	5.5E+01	3.9E+01	8.0E+00
Cm-244	1.9E-01	1.3E-01	2.3E-04
Co-57	1.0E-03	7.1E-04	5.0E-01
Co-60	1.0E+00	7.3E-01	1.8E+01
Cs-134	---	---	1.2E-01
Cs-137	5.0E-03	3.6E-03	6.3E-01
Eu-152	---	---	1.2E-01
H-3	3.4E+04	8.0E+04	6.1E+04
MAP	3.7E+02	2.6E+02	8.0E+01
MFP	1.7E+03	2.4E+03	2.7E+03
Np-237	7.0E-05	5.0E-05	1.4E-04
Po-210	2.0E-02	1.8E-02	1.0E-01
Pu-238	1.1E+00	8.5E-01	5.6E+00
Pu-239	5.0E+01	5.1E+01	2.1E+01
Pu-240	1.0E+00	1.2E+00	3.4E-02
Pu-241	1.6E+01	1.9E+01	5.4E-03
Pu-242	5.8E-05	7.2E-05	1.2E-04
Ra-226	---	2.6E-04	1.0E-01
Sr-90	4.9E-08	3.5E-08	1.1E+00
Th-232	1.1E-02	1.0E-02	3.1E+00
U-232	2.1E-01	1.5E-01	---
U-233	4.0E+00	2.8E+00	1.5E+00
U-234	4.8E-02	8.0E-02	2.3E-01
U-235	8.3E-03	9.3E-03	1.3E-02
U-236	1.8E-04	1.3E-04	1.2E-07
U-238	4.4E+00	3.4E+00	3.1E-05
Y-88	---	3.6E-03	---
Zn-65	---	---	1.2E-01

--- = None *MAP = Mixed-activation products* *MFP = Mixed-fission products*

[a] *From Rogers, 1977*

Table 22
Comparison of Various Pre-1971 Radionuclide, Activation Product, and Fission Product Inventories for Shafts

	Projected Activity (Ci) [a]			
		Extrapolation Approach		
Constituent	Pre-1971 Shaft Data [b]	1971–1975 Dataset	1971–1977 Dataset	Rogers Inventory [c]
Am-241	---	3.4E-08	2.7E-02	---
Am-243	2.0E-02	---	7.7E-06	---
Be-7	---	1.2E+02	8.3E+01	---
C-14	---	1.0E-02	7.1E-03	
Ce-137	5.0E-01	---	---	---
Cf-252	8.0E+00	5.5E+01	3.9E+01	---
Cm-244	2.3E-04	1.9E-01	1.3E-01	---
Co-57	5.0E-01	1.0E-03	7.1E-04	---
Co-60	1.8E+01	1.0E+00	7.3E-01	1.5E+02
Cs-134	1.2E-01	---	---	---
Cs-137	6.3E-01	5.0E-03	3.6E-03	6.0E+00
Eu-152	1.2E-01	---	---	---
H-3	6.1E+04	3.4E+04	8.0E+04	9.2E+04
MAP	8.0E+01	3.7E+02	2.6E+02	6.6E+02
MFP	2.7E+03	1.7E+03	2.4E+03	2.0E+02
Na-22	---	---	---	2.0E+01
Np-237	1.4E-04	7.0E-05	5.0E-05	---
Po-210	1.0E-01	2.0E-02	1.8E-02	---
Pu-238	5.6E+00	1.1E+00	8.5E-01	4.0E+00
Pu-239	2.1E+01	5.0E+01	5.1E+01	4.6E+01
Pu-240	3.4E-02	1.0E+00	1.2E+00	---
Pu-241	5.4E-03	1.6E+01	1.9E+01	---
Pu-242	1.2E-04	5.8E-05	7.2E-05	---
Ra-226	1.0E-01	---	2.6E-04	---
Sr-90	1.1E+00	4.9E-08	3.5E-08	2.8E+02
Th-232	3.1E+00	1.1E-02	1.0E-02	---
U [d]	---	---	---	< 1.0E+00

--- = None *MAP = Mixed-activation products* *MFP = Mixed-fission products*

[a] The inventory projections based on the historical data and the extrapolation approach are as-disposed activities for the 1966 to 1970 period; the radionuclide activities listed for the Rogers report pertain to the 1965 to 1975 period and are decay-corrected to January 1976.

[b] Based on historical shaft data from Rogers (1977) *[c] From data summarized in Rogers (1977, Table G-IV)*

[d] Includes U-234, U-235, U-236, and U-238

Table 22 (Continued)
Comparison of Various Pre-1971 Radionuclide, Activation Product, and Fission Product Inventories for Shafts

Constituent	Projected Activity (Ci) [a]			
		Extrapolation Approach		
	Pre-1971 Shaft Data [b]	1971–1975 Dataset	1971–1977 Dataset	Rogers Inventory [c]
U-232	---	2.1E-01	1.5E-01	---
U-233	1.5E+00	4.0E+00	2.8E+00	5.0E+00
U-234	2.3E-01	4.8E-02	8.0E-02	---
U-235	1.3E-02	8.3E-03	9.3E-03	---
U-236	1.2E-07	1.8E-04	1.3E-04	---
U-238	3.1E-05	4.4E+00	3.4E+00	---
Y-88	---	---	3.6E-03	---
Zn-65	1.2E-01	---	---	---

--- = None *MAP = Mixed-activation products* *MFP = Mixed-fission products*

[a] The inventory projections based on the historical data and the extrapolation approach are as-disposed activities for the 1966 to 1970 period; the radionuclide activities listed for the Rogers report pertain to the 1965 to 1975 period and are decay-corrected to January 1976.

[b] Based on historical shaft data from Rogers (1977) *[c] From data summarized in Rogers (1977, Table G-IV)*

[d] Includes U-234, U-235, U-236, and U-238

Among the radionuclides common to the four inventories (Table 22), the activities of several radionuclides projected using the pre-1971 historical disposal data tend to be greater than those estimated using the extrapolation approach. Examples include Co-60, Cs-137, and Sr-90. However, the activities based on both the historical shaft data and extrapolation approaches are much less than the activities reported by Rogers. Although some of this discrepancy is doubtless introduced by the fact that the Rogers activities pertain to waste disposed of through 1975, it is not clear that the observed differences are fully explained by this factor.

The tritium activities listed in Table 22 must be adjusted before the different sets of inventory projections can be compared. Toward this end, the tritium activities projected using the historical data and the extrapolation approach were decayed to January 1976 and the waste disposed of after 1970 was excluded from the Rogers inventory. The activity estimated by the historical data records was decayed to January 1976 using the dates of disposal listed in the disposal records. The extrapolation-based activities were decayed based on the assumption that the tritium waste was placed in the shafts at a uniform rate between the time of the first shaft disposal in 1966 and the end of 1970. The post-1970 tritium waste disposals listed in Rogers were decayed to 1976 and subtracted from the total tritium inventory listed in the Rogers report. The decay-corrected tritium activities estimated using the historical data, the 1971–1975 extrapolation dataset, and the 1971–1977 extrapolation dataset are 4.4×10^4, 2.3×10^4, and 5.4×10^4 Ci, respectively. Subtracting the post-1970 disposals from the Rogers inventory of 9.2×10^4 Ci yields a tritium inventory of 6.2×10^4 Ci.

The tritium activity projected using the historical data is intermediate between the two extrapolation-based estimates, and about 70 percent of the corresponding inventory listed in the Rogers report. The extrapolation process using the 1971–1975 dataset appears to significantly underestimate the tritium inventory. The extrapolation-based estimate developed using the 1971–1977 dataset falls within 13 percent of the Rogers inventory.

The activity estimated for Pu-238 using the historical data generally agrees with the Rogers inventory. The Pu-239 inventory developed using the historical data is approximately 50 percent of the corresponding activity listed by Rogers. However, a large portion of the activity listed in the Rogers report was disposed of from 1971 through 1975. When these disposals are accounted for, it appears the activity estimates based on the historical data and the Rogers inventory will both be much smaller than the 50 Ci inventories projected using the extrapolation process.

The U-233 activity projected using the historical shaft data is lower than the activity listed by Rogers. Approximately 4 Ci of this isotope's inventory was disposed of from 1971 through 1975. When this activity is subtracted from the inventory cited by, the result is essentially the same as that projected using the historical shaft data, but still less than the extrapolation-based activities estimated for this radionuclide. The sum of the U-234, U-235, U-236, and U-238 activities estimated using the

historical data is less than 1 Ci, consistent with the Rogers uranium inventory. The extrapolation-based approach estimates a total activity for these isotopes that is greater than 1 Ci.

The activities of MAP and MFP waste projected using historical data and the extrapolation approach all differ significantly from the activities reported by Rogers (Table 22). The projected activities of the MAP waste are less than the Rogers inventory, while much higher activities are projected for the MFP waste relative to the Rogers data. The differences observed for the MAP waste may be due, in part, to the longer period of disposal addressed by the Rogers data. The fact that the MFP inventories listed in Rogers are decayed to January 1976 and the other estimates are not also helps explain the differences because many fission products are very short-lived, leading to significant changes in the activity of the waste over relatively short periods of time.

The shaft inventory estimated using the historical pre-1971 disposal records from Rogers (1977) was adopted for the inventory characterization update on the basis of the comparison described above. The historical data appear to estimate more realistic volumes of waste for the pre-1971 period. Furthermore, the use of these data is expected to result in inventories of plutonium and uranium isotopes that are more accurate than the extrapolation-based inventories. Although discrepancies exist between the adopted inventory and the Rogers inventory for several other radionuclides, it is not clear that the extrapolation-based inventories are consistently more accurate than the inventory estimated using the historical data.

The pre-1971 shaft inventory is summarized in Tables 23 and in *Attachment V*. Table 23 provides total waste volumes and activities for each shaft active during this period; the radionuclide, MAP, MFP, and material type activities projected for each shaft are provided in *Attachment V*. Some of the shafts included in the tables continued to receive waste after 1970; this waste is not included in Table 23. The activities listed in both tables represent as-disposed activities; the radionuclides included in *Attachment V* are those remaining after the half-life screen described in *Attachment II* is applied.

4.1.2 Waste Inventory for 1971 Through September 26, 1988

Twenty-five pits and over 140 shafts were used to dispose of waste at Area G from the beginning of 1971 through September 26, 1988. The total volumes and activities of waste placed in these units during this period are included in Table 24; individual totals are reported for all pits and shafts that received waste during this period.

Table 23
Shaft-Specific Disposal Volumes and Activities, Pre-1971 Waste

Shaft	Volume (m^3)	Activity (Ci)
1	1.8E+00	3.2E+02
2	1.2E+00	1.2E+03
3	1.1E+00	2.2E+02
4	1.3E+00	1.1E+01
5	8.4E-01	2.5E+01
6	5.8E-01	3.0E+02
7	1.6E+00	5.2E+03
8	3.0E+00	3.0E+00
9	2.0E+00	5.6E+00
10	1.5E+00	1.0E+00
11	2.0E+00	3.1E+00
12	2.3E+00	5.6E+01
13	3.4E+00	5.0E+01
14	7.6E-01	5.9E+00
15	1.4E-01	1.8E+04
16	1.1E-01	1.8E+04
17	1.5E-01	2.1E+04
18	1.5E-01	5.2E+01
24	1.2E+00	2.6E+00
25	9.6E-01	4.4E+01
26	1.6E+00	2.8E+00
27	3.6E-01	1.0E+02
28	8.4E-01	2.7E+02
29	6.7E-01	2.5E+01
30	2.4E-01	7.3E+01
31	5.4E-01	7.5E-03
32	2.8E-01	6.2E-03
33	2.7E-01	7.4E+01
34	1.1E+01	---
36	1.8E+00	---
37	1.8E+00	---
38	1.8E+00	---
39	9.3E-01	5.7E+02

--- = None

Table 24
Unit-Specific Disposal Volumes and Activities, 1971 Through 2007 Waste

	1971 Through September 26, 1988		September 27, 1988 Through 2007	
Disposal Unit	Volume (m^3)	Activity (Ci)	Volume (m^3)	Activity (Ci)
Pit 5	5.6E+02	2.6E+02	---	---
Pit 6	5.5E+03	1.9E+02	---	---
Pit 7	3.3E+03	2.1E+01	---	---
Pit 8	1.8E+03	2.1E+01	---	---
Pit 9	4.8E+00	1.2E+00	---	---
Pit 10	3.1E+03	6.8E+03	---	---
Pit 12	1.8E+03	3.5E-01	---	---
Pit 13	1.5E+03	2.1E+00	---	---
Pit 15	---	---	6.6E+03	2.1E+02
Pit 16	1.7E+03	1.9E+00	---	---
Pit 17	3.8E+03	7.0E-02	---	---
Pit 18	9.6E+03	3.0E+04	---	---
Pit 19	5.5E+01	3.0E-01	---	---
Pit 20	1.1E+04	6.4E+00	---	---
Pit 21	2.8E+03	5.5E-01	---	---
Pit 22	2.9E+03	6.0E+02	---	---
Pit 24	5.6E+03	1.4E+01	---	---
Pit 25	4.6E+03	3.7E+02	---	---
Pit 26	3.8E+03	1.2E+02	---	---
Pit 27	6.1E+03	1.9E+02	---	---
Pit 28	3.6E+03	1.3E+03	---	---
Pit 29	8.0E+03	2.3E+03	---	---
Pit 30	---	---	1.0E+04	3.7E+01
Pit 31	---	---	3.7E+03	8.5E-01
Pit 32	4.8E+03	1.6E+02	8.5E+00	0.0E+00
Pit 33	6.6E+03	5.3E+01	---	---
Pit 35	2.9E+03	8.0E+01	---	---
Pit 36	3.0E+03	3.7E+01	1.1E+03	1.9E+00
Pit 37	---	---	2.2E+04	8.9E+02
Pit 38	---	---	2.0E+04	2.3E+03
Pit 39	---	---	2.5E+04	2.3E+01
Shaft 17	2.9E-02	4.9E+00	---	---
Shaft 18	1.7E-01	3.8E+01	---	---
Shaft 19	7.6E-02	1.5E-01	---	---

--- = *None*

Table 24 (Continued)
Unit-Specific Disposal Volumes and Activities, 1971 Through 2007 Waste

	1971 Through September 26, 1988		September 27, 1988 Through 2007	
Disposal Unit	Volume (m^3)	Activity (Ci)	Volume (m^3)	Activity (Ci)
Shaft 20	7.6E-02	3.2E-02	---	---
Shaft 21	3.8E-03	9.5E-06	---	---
Shaft 22	6.4E-02	4.9E+02	1.3E-01	1.5E+00
Shaft 23	2.8E-02	5.6E+02	---	---
Shaft 24	6.2E-01	0.0E+00	---	---
Shaft 25	2.8E-01	0.0E+00	---	---
Shaft 29	8.8E-02	2.5E-02	---	---
Shaft 30	2.6E-01	1.0E+01	---	---
Shaft 31	7.9E-01	4.3E+00	---	---
Shaft 32	1.4E+00	1.7E+00	---	---
Shaft 33	2.4E-01	1.7E+01	---	---
Shaft 34	1.5E+01	0.0E+00	---	---
Shaft 35	2.7E+00	3.5E+01	---	---
Shaft 36	7.9E-01	1.2E+02	---	---
Shaft 37	3.8E+00	0.0E+00	---	---
Shaft 38	1.1E-01	1.2E-02	---	---
Shaft 39	1.5E+01	8.2E+03	---	---
Shaft 40	1.1E+00	2.1E+01	---	---
Shaft 41	2.3E+00	3.0E+01	---	---
Shaft 42	1.8E+00	1.3E+01	---	---
Shaft 43	1.5E+00	1.3E+01	---	---
Shaft 44	1.7E+00	4.7E+01	---	---
Shaft 45	1.8E+00	1.2E+02	---	---
Shaft 46	1.8E+00	2.9E+00	---	---
Shaft 47	1.0E+00	1.1E+01	---	---
Shaft 48	1.1E+00	2.0E+01	---	---
Shaft 49	7.9E-01	2.9E+00	---	---
Shaft 50	1.9E+01	2.9E+04	---	---
Shaft 51	3.6E-01	3.6E+02	---	---
Shaft 52	3.1E-01	1.6E+02	---	---
Shaft 53	8.3E-01	1.1E+02	---	---
Shaft 54	4.5E-01	1.9E+02	---	---
Shaft 55	1.4E+00	5.1E+01	---	---
Shaft 56	7.5E-01	2.7E+01	---	---
Shaft 57	3.1E-01	7.5E+00	---	---
Shaft 58	3.6E+00	2.3E+02	---	---

--- = *None*

Table 24 (Continued)
Unit-Specific Disposal Volumes and Activities, 1971 Through 2007 Waste

	1971 Through September 26, 1988		September 27, 1988 Through 2007	
Disposal Unit	Volume (m^3)	Activity (Ci)	Volume (m^3)	Activity (Ci)
Shaft 59	5.4E+00	2.3E+03	---	---
Shaft 60	3.2E+01	0.0E+00	---	---
Shaft 61	4.4E+00	5.0E+00	---	---
Shaft 62	3.5E+00	1.0E-03	---	---
Shaft 63	2.3E+00	2.0E-01	---	---
Shaft 64	1.1E+00	1.9E-02	---	---
Shaft 65	3.9E+00	1.6E+01	---	---
Shaft 66	6.5E-01	2.0E-03	---	---
Shaft 67	1.3E+00	4.4E+01	---	---
Shaft 68	9.0E-01	1.0E+02	---	---
Shaft 69	5.7E-01	2.1E-03	---	---
Shaft 70	2.6E+01	0.0E+00	---	---
Shaft 71	8.8E-01	5.2E+01	---	---
Shaft 72	2.8E+00	4.8E+01	---	---
Shaft 73	3.4E-01	1.5E+02	---	---
Shaft 74	9.3E-01	1.6E+02	---	---
Shaft 75	9.2E-01	7.9E+01	---	---
Shaft 76	8.1E-01	1.4E+02	---	---
Shaft 77	3.4E-01	4.7E+02	---	---
Shaft 78	1.3E+00	4.7E+01	---	---
Shaft 79	3.4E-01	1.9E+02	---	---
Shaft 80	1.2E+00	3.1E+01	---	---
Shaft 81	9.9E-01	3.0E-03	---	---
Shaft 82	6.9E-01	3.7E+01	---	---
Shaft 83	1.3E+00	1.7E+01	---	---
Shaft 84	4.9E-01	5.5E+01	---	---
Shaft 85	5.1E-01	5.8E+01	---	---
Shaft 86	6.2E-01	1.0E+03	---	---
Shaft 87	6.1E-01	8.8E+01	---	---
Shaft 88	5.0E-01	4.1E+01	---	---
Shaft 89	8.1E-01	1.9E+01	---	---
Shaft 90	9.1E-01	3.5E+02	---	---
Shaft 91	2.1E+00	3.2E+01	---	---
Shaft 92	3.7E+00	3.9E+01	---	---
Shaft 93	7.5E+00	6.3E+02	---	---
Shaft 94	2.7E+00	3.5E+03	---	---

--- = *None*

Table 24 (Continued)
Unit-Specific Disposal Volumes and Activities, 1971 Through 2007 Waste

	1971 Through September 26, 1988		September 27, 1988 Through 2007	
Disposal Unit	Volume (m^3)	Activity (Ci)	Volume (m^3)	Activity (Ci)
Shaft 95	4.1E+00	2.1E+02	---	---
Shaft 96	1.2E+01	4.4E+00	---	---
Shaft 97	6.8E+00	1.4E+02	---	---
Shaft 99	5.6E+00	1.4E+01	---	---
Shaft 100	1.7E+00	3.7E+02	---	---
Shaft 101	2.5E+00	1.2E+01	---	---
Shaft 102	5.2E+00	3.4E+02	---	---
Shaft 103	4.8E+00	5.2E+01	---	---
Shaft 104	4.3E+00	1.8E-01	---	---
Shaft 105	5.6E+00	1.8E-03	---	---
Shaft 106	2.1E+00	9.4E+01	---	---
Shaft 107	1.4E+00	7.4E+02	---	---
Shaft 108	6.5E+00	4.3E+02	---	---
Shaft 109	2.3E+00	2.1E+01	---	---
Shaft 110	3.6E+00	4.6E+02	---	---
Shaft 111	3.8E+00	5.8E+01	---	---
Shaft 112	4.2E+00	2.6E+02	---	---
Shaft 114	2.8E+01	5.3E+02	---	---
Shaft 115	1.5E+01	9.2E-01	---	---
Shaft 118	1.3E+01	0.0E+00	---	---
Shaft 119	1.6E+01	1.4E+00	---	---
Shaft 120	1.5E+01	6.3E+02	---	---
Shaft 121	6.9E+00	4.1E-04	---	---
Shaft 122	7.3E+00	2.6E+03	---	---
Shaft 123	1.5E+01	9.3E-01	---	---
Shaft 124	1.1E+01	1.1E-02	3.0E+00	1.0E+00
Shaft 125	1.7E+01	1.2E+01	---	---
Shaft 126	2.2E+01	7.0E+02	---	---
Shaft 127	1.4E+01	1.3E+00	---	---
Shaft 128	1.2E+01	4.5E-03	---	---
Shaft 129	3.8E+00	9.3E+02	---	---
Shaft 130	3.1E+01	3.6E+01	---	---
Shaft 131	3.6E+00	1.9E+01	9.0E+00	2.1E+03
Shaft 132	4.5E+00	4.3E-05	1.3E+01	1.0E-05
Shaft 133	2.7E+00	3.4E+03	---	---
Shaft 134	6.8E+00	2.5E+00	---	---

--- = *None*

Table 24 (Continued)
Unit-Specific Disposal Volumes and Activities, 1971 Through 2007 Waste

	1971 Through September 26, 1988		September 27, 1988 Through 2007	
Disposal Unit	Volume (m^3)	Activity (Ci)	Volume (m^3)	Activity (Ci)
Shaft 135	6.2E+00	0.0E+00	---	---
Shaft 136	6.1E+00	3.7E+03	3.2E+00	1.8E+03
Shaft 137	3.8E+00	1.5E+00	1.5E+01	6.8E+01
Shaft 138	5.4E+00	0.0E+00	---	---
Shaft 139	8.0E+00	8.7E+02	7.9E-01	6.0E+01
Shaft 140	8.9E+00	1.0E-03	1.6E+01	0.0E+00
Shaft 141	---	---	9.2E+00	1.8E+03
Shaft 142	---	---	3.2E+00	3.8E+02
Shaft 143	---	---	9.4E+00	3.2E+03
Shaft 144	---	---	8.8E+00	6.0E+03
Shaft 147	---	---	9.5E+00	1.9E+01
Shaft 148	---	---	7.9E+00	3.0E-02
Shaft 149	---	---	9.1E+00	2.0E+03
Shaft 150	1.8E+01	1.6E+05	---	---
Shaft 151	2.0E+01	1.4E+05	---	---
Shaft 152	4.2E+00	4.3E+04	---	---
Shaft 153	3.1E+00	2.6E+04	---	---
Shaft 154	5.5E+00	3.2E+05	---	---
Shaft 155	1.0E+00	5.5E+03	2.7E+00	5.7E+04
Shaft 156	1.7E+00	3.7E+04	---	---
Shaft 157	2.5E+00	2.4E+04	---	---
Shaft 158	---	---	2.2E+00	1.2E+04
Shaft 159	---	---	3.2E-01	8.6E+00
Shaft 160	---	---	2.5E+00	7.0E+02
Shaft 161	---	---	3.7E+00	4.6E+03
Shaft 162	---	---	1.6E+00	3.6E+05
Shaft 163	---	---	3.5E+00	4.8E+03
Shaft 164	---	---	3.4E+00	3.8E+03
Shaft 165	---	---	2.7E+00	6.0E+03
Shaft 166	---	---	2.6E+00	1.5E+05
Shaft 167	---	---	2.4E+00	1.5E+05
Shaft 168	---	---	2.4E+00	9.5E+04
Shaft 169	---	---	1.7E+00	3.2E+03
Shaft 170	---	---	9.5E-01	9.4E+04
Shaft 171	---	---	5.0E+00	1.7E-03
Shaft 172	---	---	8.3E+00	3.5E-02

--- = *None*

Table 24 (Continued)
Unit-Specific Disposal Volumes and Activities, 1971 Through 2007 Waste

	1971 Through September 26, 1988		September 27, 1988 Through 2007	
Disposal Unit	Volume (m^3)	Activity (Ci)	Volume (m^3)	Activity (Ci)
Shaft 173	---	---	3.7E+00	1.2E-06
Shaft 174	---	---	6.2E+00	9.1E-02
Shaft 175	---	---	2.3E+00	0.0E+00
Shaft 176	---	---	6.0E+00	7.1E-02
Shaft 177	---	---	9.4E+00	1.7E-01
Shaft 189	4.9E+01	1.0E+02	---	---
Shaft 190	3.1E+01	8.8E+02	---	---
Shaft 191	3.9E+01	1.4E+02	---	---
Shaft 192	4.4E+01	7.8E+02	---	---
Shaft 196	---	---	5.8E+01	2.7E+03
Shaft 197	---	---	4.0E+01	2.2E+04
Shaft 206	4.5E-01	4.5E-05	---	---
Shaft 301	---	---	6.4E-01	1.8E+02
Shaft 307	---	---	3.4E+00	1.9E+02
Shaft 308	---	---	2.9E+00	6.7E-02
Shaft 309	---	---	2.0E+00	5.4E+04
Shaft 311	---	---	3.4E+00	5.1E+04
Shaft 313	---	---	4.3E+00	4.6E+03
Shaft 315	---	---	3.1E+00	5.4E+01
Shaft 317	---	---	3.2E+00	2.2E+03
Shaft 319	---	---	8.0E+00	1.5E+05
Shaft 321	---	---	2.7E+00	1.7E+03
Shaft 323	---	---	3.1E+00	1.0E+03
Shaft 325	---	---	2.1E+00	3.1E-05
Shaft 327	---	---	4.9E+00	9.6E+02
Shaft 329	---	---	3.7E+00	5.1E+03
Shaft 331	---	---	2.9E+00	1.7E+03
Shaft 333	---	---	2.5E+00	1.9E+05
Shaft 335	---	---	1.4E+00	2.3E+04
Shaft 339	---	---	5.4E+00	1.3E+05
Shaft 341	---	---	6.2E+00	3.9E+03
Shaft 343	---	---	6.0E+00	1.5E+03
Shaft 345	---	---	4.1E+00	2.4E+03
Shaft 347	---	---	3.8E+00	1.8E+03
Shaft 349	---	---	5.0E+00	1.2E+04
Shaft 351	---	---	6.8E+00	1.9E+04

--- = *None*

Table 24 (Continued)
Unit-Specific Disposal Volumes and Activities, 1971 Through 2007 Waste

	1971 Through September 26, 1988		September 27, 1988 Through 2007	
Disposal Unit	Volume (m^3)	Activity (Ci)	Volume (m^3)	Activity (Ci)
Shaft 355	---	---	4.9E+00	1.9E+02
Shaft 357	---	---	5.5E+00	4.7E+02
Shaft 360	---	---	1.9E+01	1.1E+03
Shaft 361	---	---	2.4E+01	5.6E+02
Shaft 362	---	---	2.2E+01	4.5E+02
Shaft 363	---	---	3.4E+00	4.9E+04
Shaft 364	---	---	6.2E+00	3.7E+02
Shaft 365	---	---	3.1E+00	1.8E+02
Shaft 366	---	---	8.2E+00	1.0E+04
Shaft 367	---	---	1.2E+01	5.5E+04
Shaft 370	---	---	5.0E-01	1.1E+01
Shaft C01	6.2E+00	0.0E+00	---	---
Shaft C02	1.0E+01	0.0E+00	---	---
Shaft C03	9.6E+00	0.0E+00	---	---
Shaft C04	1.1E+01	0.0E+00	---	---
Shaft C05	7.3E+00	0.0E+00	---	---
Shaft C06	1.3E+01	0.0E+00	---	---
Shaft C07	1.4E+01	0.0E+00	---	---
Shaft C08	1.4E+01	0.0E+00	---	---
Shaft C09	1.1E+01	0.0E+00	---	---
Shaft C10	1.5E+01	0.0E+00	---	---
Shaft C11	1.3E+01	0.0E+00	1.0E+00	0.0E+00
Shaft C12	1.6E+01	0.0E+00	3.7E-01	0.0E+00
Shaft C13	2.9E+00	0.0E+00	2.8E+01	1.5E-02
Shaft C14	---	---	2.4E+00	9.2E-04

--- = *None*

Waste was disposed of in pit 6 before and after the start of 1971. The waste placed in this pit prior to 1971 is addressed by the pre-1971 inventory projections provided in Section 4.1.1.2. Pit 9 was used for the disposal of small amounts of LLW and the retrievable storage of TRU waste. Although the LLW will probably be removed during the retrieval of the TRU waste, it was included in the Area G inventory.

The radionuclide, MAP, MFP, and material type inventories in the 1971 through September 26, 1988 waste are included in *Attachments III* and *V* for the pits and shafts, respectively. Individual inventories are provided for each disposal unit; the listed activities represent as-disposed activities. The radionuclides included in the table do not include those that were eliminated on the basis of decay characteristics as described in *Attachment II*.

Transuranic waste was nonretrievably disposed of in pits 6, 7, 8, 20, and 22 and in several shafts from 1971 through 1979. Table 25 lists the total volumes and activities of TRU waste in each disposal unit; radionuclide, fission product, and material type specific inventories for the waste are listed in Table 26. In each case, individual totals are reported for the affected pits, while inventory data are summed over the shafts. These TRU waste data are also included in the radionuclide inventories shown in Table 24 and *Attachments III* and *V*.

4.1.3 Waste Inventory for September 27, 1988 Through 2007

The LLW disposed of at MDA G from September 27, 1988 through the end of 2007 was placed in 8 pits and almost 80 shafts; the total volumes and activities of waste placed in these units are included in Table 24. Individual totals are reported for all pits and shafts that received waste during this period.

The inventories of radionuclides, MAP and MFP waste, and material type waste disposed of from September 27, 1988 through 2007 waste are included in *Attachments III* and *V* for the pits and shafts, respectively. The listed activities represent as-disposed activities; radionuclides that were eliminated on the basis of their decay characteristics, as described in *Attachment II*, are not included in the tables.

Table 25
Unit-Specific Disposal Volumes and Activities of Transuranic Waste, 1971 Through September 26, 1988

Disposal Unit	Disposal Volume (m^3)	Disposal Activity (Ci)
Pit 6	1.9E+01	6.0E+01
Pit 7	1.9E+00	6.5E-02
Pit 8	5.8E+01	7.1E+00
Pit 20	8.5E-02	1.6E-03
Pit 22	1.1E+01	6.0E+02
Shaft 17	7.6E-03	5.1E-01
Shaft 33	5.3E-02	1.7E+01
Shaft 42	7.6E-03	8.1E+00
Shaft 43	1.5E-02	3.5E+00
Shaft 44	1.5E-02	1.9E+01
Shaft 45	1.5E-02	1.7E+01
Shaft 47	4.0E-02	5.9E+00
Shaft 48	3.0E-02	3.8E+00
Shaft 49	1.9E-02	1.9E+00
Shaft 51	1.6E-01	2.2E+02
Shaft 52	3.8E-02	6.4E+01
Shaft 53	1.3E-01	3.9E+01
Shaft 54	8.9E-02	1.4E+02
Shaft 55	3.0E-01	4.3E+01
Shaft 56	1.7E-01	1.5E+01
Shaft 58	1.9E-02	2.7E+00
Shaft 64	1.7E-01	3.0E-03
Shaft 65	1.9E-03	2.3E-04
Shaft 67	5.7E-02	3.3E+01
Shaft 68	1.7E-01	8.8E+01
Shaft 71	4.5E-01	2.3E+01
Shaft 72	6.5E-02	3.6E+01
Shaft 73	1.1E-01	3.9E+01
Shaft 74	1.5E-01	1.2E+02
Shaft 75	1.1E-01	6.3E+01

Table 25 (Continued)
Unit-Specific Disposal Volumes and Activities of Transuranic Waste, 1971 Through September 26, 1988

Disposal Unit	Disposal Volume (m^3)	Disposal Activity (Ci)
Shaft 76	1.3E-01	5.5E+01
Shaft 77	3.0E-02	7.8E+01
Shaft 78	7.6E-02	1.2E+01
Shaft 79	5.7E-02	8.4E+01
Shaft 82	3.5E-01	3.3E+01
Shaft 83	5.3E-02	1.7E+01
Shaft 84	4.7E-01	4.1E+01
Shaft 85	7.6E-03	5.2E+01
Shaft 86	5.7E-02	1.0E+03
Shaft 87	7.6E-03	1.1E+01
Shaft 88	5.7E-02	1.4E+01
Shaft 89	7.6E-03	6.7E+00
Shaft 90	2.5E-01	3.5E+02
Shaft 91	4.2E-01	7.3E+00
Shaft 110	7.6E-03	5.6E+00

Table 26
Unit-Specific Radionuclide, Fission Product, and Material Type Inventories of Transuranic Waste, 1971 Through September 26, 1988

	Constituent													
Disposal Unit	Am-241	Cf-251	Cm-244	MFP	Np-237	Po-210	Pu-238	Pu-239	PU52	U12	U-233	U-235	U-238	U38
Pit 6	---	---	---	---	---	---	5.6E+01	3.6E+00	---	---	---	---	---	---
Pit 7	---	---	---	---	---	---	6.2E-02	3.8E-03	---	---	---	5.6E-05	---	---
Pit 8	9.3E-01	---	---	---	---	---	3.6E+00	2.6E+00	---	---	---	---	---	---
Pit 20	---	1.6E-03	---	---	---	---	---	---	---	---	---	---	---	---
Pit 22	3.4E-03	---	---	6.0E+02	---	---	---	9.3E-01	---	---	---	1.1E-04	---	---
Shaft 17	---	---	---	3.3E-01	---	---	---	1.8E-01	---	---	---	2.3E-05	---	---
Shaft 33	---	---	---	1.6E+01	---	---	---	9.6E-01	---	---	---	1.7E-05	---	---
Shaft 42	---	---	---	8.0E+00	---	---	---	6.2E-02	---	---	---	---	---	---
Shaft 43	---	---	---	3.3E+00	---	---	---	2.5E-01	---	---	---	---	---	---
Shaft 44	---	---	---	1.3E+01	---	---	---	5.7E+00	---	---	---	---	---	---
Shaft 45	---	---	---	1.2E+01	---	---	---	4.1E+00	---	---	---	---	---	---
Shaft 47	---	---	---	5.6E+00	---	---	---	3.2E-01	---	---	---	1.5E-05	---	---
Shaft 48	---	---	---	3.4E+00	---	---	---	3.8E-01	---	---	---	---	---	---
Shaft 49	---	---	---	1.2E+00	---	---	---	6.7E-01	---	---	---	---	---	---
Shaft 51	---	---	---	2.1E+02	---	---	---	9.7E+00	---	---	---	1.7E-03	---	---
Shaft 52	---	---	---	6.1E+01	---	---	---	3.2E+00	---	---	---	7.4E-05	---	---
Shaft 53	---	---	---	3.7E+01	---	---	---	1.8E+00	---	---	---	2.8E-04	---	---
Shaft 54	3.4E-03	---	---	1.3E+02	---	---	---	4.5E+00	---	---	---	6.0E-04	---	---
Shaft 55	---	---	---	4.2E+01	---	---	---	1.0E+00	---	---	---	1.2E-04	---	---
Shaft 56	---	---	---		---	---	---	---	1.5E+01	---	---	---	---	---
Shaft 58	---	---	---	2.6E+00	---	---	---	6.9E-02	---	---	---	---	---	---
Shaft 64	---	---	---	---	---	9.9E-04	9.8E-04	1.0E-03	---	---	---	---	---	---
Shaft 65	---	---	2.3E-04		---	---	---	---	---	---	---	---	---	---

--- = None

Table 26 (Continued)
Unit-Specific Radionuclide, Activation Product, Fission Product, and Material Type Inventories of Transuranic Waste, 1971 Through September 26, 1988

	Constituent													
Disposal Unit	Am-241	Cf-251	Cm-244	MFP	Np-237	Po-210	Pu-238	Pu-239	PU52	U12	U-233	U-235	U-238	U38
Shaft 67	---	---	---	3.0E+01	---	---	---	2.7E+00	---	---	---	2.4E-05	---	---
Shaft 68	---	---	---	8.4E+01	---	---	---	3.5E+00	---	---	---	3.8E-04	---	---
Shaft 71	---	---	---	1.6E+01	---	---	---	3.8E+00	3.8E+00	---	---	5.7E-05	---	---
Shaft 72	---	---	---	3.6E+01	---	---	---	2.3E-01	---	---	---	---	---	---
Shaft 73	---	---	---	3.8E+01	---	---	---	1.3E+00	---	---	---	8.4E-05	---	---
Shaft 74	---	---	---	1.2E+02	---	---	---	1.9E+00	---	---	---	1.1E-04	---	---
Shaft 75	---	---	---	6.1E+01	---	---	---	1.4E+00	---	---	---	7.7E-06	---	---
Shaft 76	---	---	---	4.5E+01	---	---	---	1.0E+01	---	---	---	---	---	---
Shaft 77	---	---	---	7.7E+01	---	---	---	6.5E-01	---	---	---	8.8E-05	---	---
Shaft 78	---	---	---	1.1E+01	---	---	---	1.4E+00	---	---	---	1.7E-04	---	---
Shaft 79	---	---	---	6.1E+01	---	---	1.7E-01	2.5E+00	2.1E+01	---	---	2.3E-04	---	2.1E-02
Shaft 82	---	---	---	1.0E+01	---	---	---	4.3E+00	1.9E+01	---	---	4.0E-08	---	---
Shaft 83	---	---	---	1.0E+01	7.1E-06	---	---	6.7E+00	---	---	9.7E-04	6.9E-04	6.8E-05	---
Shaft 84	---	---	---	2.9E+01	---	---	---	1.5E+00	9.7E+00	---	---	1.5E-04	---	---
Shaft 85	---	---	---	5.0E+01	---	---	---	1.9E+00	---	---	---	9.9E-05	---	---
Shaft 86	---	---	---	1.0E+03	---	---	---	1.1E+00	---	---	---	1.6E-04	---	---
Shaft 87	---	---	---	1.1E+01	---	---	---	6.2E-02	---	---	---	8.8E-06	---	---
Shaft 88	---	---	---	1.1E+01	---	---	---	2.6E+00	---	---	---	2.8E-07	---	---
Shaft 89	---	---	---	6.5E+00	---	---	---	1.6E-01	---	---	---	2.2E-05	---	---
Shaft 90	---	---	---	3.5E+02	---	---	---	9.3E-02	3.1E-01	2.8E-03	---	1.3E-05	---	---
Shaft 91	---	---	---	---	---	---	---	---	7.3E+00	---	---	---	---	---
Shaft 110	---	---	---	5.5E+00	---	---	---	6.2E-02	---	---	---	8.8E-06	---	---

--- = None

4.2 Future Inventory Projections

Table 27 provides the future inventory projections for Area G, addressing the waste that is expected to require disposal from 2008 through 2044; separate inventories are provided for pits and shafts. The table shows contributions made to the inventory by the extrapolated volumes and activities and tritium waste. Radionuclide and material type inventories for the pits and shafts are provided in Table 28. The listed activities represent as-disposed activities; radionuclides that were eliminated on the basis of their decay characteristics (see *Attachment II*) are not shown in the tables.

Table 27
Disposal Volumes and Activities for Pits and Shafts, 2008 Through 2044 Waste

Disposal Unit	Extrapolation-Based Inventory [a]		Tritium Waste [b]		Total Future Waste	
	Volume (m^3)	Activity (Ci)	Volume (m^3)	Activity (Ci)	Volume (m^3)	Activity (Ci)
Pits	1.6E+05	3.9E+02	---	---	1.6E+05	3.9E+02
Shafts	4.3E+02	1.3E+04	6.0E+02	9.6E+05	1.0E+03	9.8E+05

--- = None

[a] Based on data from Los Alamos National Laboratory low-level waste (LLW) databases.

[b] Estimated from data collected from TA-16 personnel.

The information used to estimate the quantities of tritium waste that will be shipped to Area G for disposal by the WETF is summarized in Table 29. As shown, it is assumed that 2,000 Ci of compactable and noncompactable waste will require disposal each year for the remaining lifetime of the disposal facility. Shipments of 5.0×10^4 Ci are projected for each of the next five years, after which an annual disposal activity of 2.0×10^4 Ci is estimated. In total, the WETF is projected to send 9.6×10^5 Ci of high-activity tritium waste to Area G for disposal by 2044; all of this waste is expected to be disposed of in shafts. Additional tritium waste will be generated in conjunction with the D&D of the tritium facilities (TSTA and TSFF). The waste that will be generated in conjunction with TSFF is estimated to contain approximately 1,500 Ci of tritium, decay-corrected to 2007; a 2006 estimate of the tritium remaining at the TSFF was less than 65 Ci (Madonia, 2008). Together, these activities are less than 0.1 percent of tritium inventories estimated through extrapolation and interviews with WETF personnel and were not specifically included in the inventory update.

Table 28
Radionuclide and Material Type
Inventories, 2008 Through 2044 Waste

Radionuclide	Activity (Ci)			
	Pit Inventory	Shaft Inventory		
		Extrapolation-Based Inventory	High-Activity Tritium Waste	All Future Waste
Ac-227	6.6E-05	---	---	---
Ag-108m	5.8E-05	4.2E-08	---	4.2E-08
Al-26	1.2E-06	---	---	---
Am-241	1.5E+01	1.2E-03	---	1.2E-03
Am-243	3.8E-02	---	---	---
Ba-133	3.2E+00	---	---	---
Bi-207	7.0E-02	7.3E-06	---	7.3E-06
C-14	1.2E-02	3.5E-01	---	3.5E-01
Cf-249	4.7E-04	---	---	---
Cf-252	---	3.6E-05	---	3.6E-05
Cm-243	5.1E-05	---	---	---
Cm-244	1.3E-02	9.3E-03	---	9.3E-03
Cm-245	2.1E-04	---	---	---
Cm-248	2.1E-06	---	---	---
Co-60	7.5E+01	3.8E+01	---	3.8E+01
Cs-135	7.5E-06	---	---	
Cs-137	4.8E+00	1.9E+00	---	1.9E+00
D38	4.3E+00	7.0E+00	---	7.0E+00
Eu-152	2.0E-01	3.0E-03	---	3.0E-03
Eu-154	3.1E-03	---	---	---
H-3	1.9E+01	9.1E+03	9.6E+05	9.7E+05
Ho-166m	6.6E-03	---	---	---
I-129	1.4E-04	---	---	---
K-40	8.5E-01	2.0E-06	---	2.0E-06
Kr-85	4.6E-04	3.7E-02	---	3.7E-02
Mo-93	9.3E-05	---	---	---
Nb-91	5.3E-05	4.3E-02	---	4.3E-02

--- = *None*

Table 28 (Continued)
Radionuclide and Material Type
Inventories, 2008 Through 2044 Waste

Radionuclide	Activity (Ci)			
	Pit Inventory	Shaft Inventory		
		Extrapolation-Based Inventory	High-Activity Tritium Waste	All Future Waste
Nb-92	1.4E-05	---	---	---
Nb-93m	4.8E-03	1.0E+01	---	1.0E+01
Nb-94	6.9E-02	---	---	---
Nd-144	4.6E-08	---	---	---
Ni-59	3.3E-05	---	---	---
Ni-63	9.5E-01	4.6E+01	---	4.6E+01
Np-237	2.0E-02	1.4E-07	---	1.4E-07
Os-194	6.0E-07	---	---	---
Pa-231	1.1E-04	2.3E-07	---	2.3E-07
Pb-210	8.5E-02	1.2E-07	---	1.2E-07
Pm-145	4.6E-08	---	---	---
Pu-236	4.6E-09	---	---	---
Pu-238	2.2E+01	3.5E-02	---	3.5E-02
Pu-239	1.8E+01	3.2E-02	---	3.2E-02
Pu-240	1.3E+00	---	---	---
Pu-241	4.9E+00	---	---	---
Pu-242	2.6E-02	---	---	---
Pu-244	1.6E-05	---	---	---
Ra-226	3.2E-01	8.4E-05	---	8.4E-05
Ra-228	1.1E-01	---	---	---
Si-32	7.7E-05	---	---	---
Sm-151	1.4E-08	---	---	---
Sr-90	9.8E+00	1.8E+00	---	1.8E+00
Tb-157	2.1E-07	---	---	---
Tc-97	9.2E-08	---	---	---
Tc-99	2.8E-01	---	---	---
Th-228	3.0E-03	3.2E-03	---	3.2E-03
Th-229	1.4E-03	---	---	---

--- = *None*

Table 28 (Continued)
Radionuclide and Material Type
Inventories, 2008 Through 2044 Waste

Radionuclide	Activity (Ci)			
	Pit Inventory	Shaft Inventory		
		Extrapolation-Based Inventory	High-Activity Tritium Waste	All Future Waste
Th-230	4.2E-04	---	---	---
Th-232	8.1E-03	6.0E-02	---	6.0E-02
Ti-44	1.2E-02	9.0E-02	---	9.0E-02
U(DEP)	2.4E+01	2.0E-04	---	2.0E-04
U(NAT)	2.9E-04	8.3E-01	---	8.3E-01
U-232	1.7E-04	---	---	---
U-233	2.4E-01	---	---	---
U-234	1.6E+00	2.3E+00	---	2.3E+00
U-235	1.0E-01	1.3E-01	---	1.3E-01
U-236	1.1E-02	1.8E-05	---	1.8E-05
U-238	2.6E+00	1.1E+00	---	1.1E+00

--- = *None*

Table 29
Projected Tritium Waste Inventory Generated by Weapons Engineering Test Facility

Tritium Waste Stream	Container Type	Annual Waste Volume	Tritium Activity (Ci)		
			Annual		
			2008–2012	2013–2044	Total (2008–2044)
Compactable and Noncompactable Waste	Various	15 m^3	2.0E+03	2.0E+03	7.4E+04
Overpack Waste	Stainless steel	1.25-m^3 [a]	5.0E+04	2.0E+04	8.9E+05

[a] *Projected waste volume is based on the shipment of one container per year; the annual waste volume will increase if the waste must be shipped in more containers in order to comply with waste acceptance criteria for tritium waste.*

4.3 Uncertainty Analysis

The inventories presented in this report are estimates of the quantities of the radioactive materials that were, or will be, disposed of in the pits and shafts at Area G. These projections are subject to uncertainty introduced by the assumptions made in developing the inventories and the data upon which the estimates are based. Potentially important sources of uncertainty associated with the inventory projections are discussed below.

The primary sources of uncertainty associated with the Area G inventory projections depend, in part, upon the segment of the inventory under consideration. Perhaps the most basic source of uncertainty, and one that applies to all of the waste disposed of at Area G, is the measurement or estimation of radionuclide activities in the waste. The accuracy of the activity measurements and estimation techniques used to characterize Area G waste is influenced by the radionuclides under consideration and the time at which disposal occurred. Specific radionuclides may affect characterization efforts in two distinct ways. First, the radiation types and energies emitted by the isotopes may make measurement more or less difficult. For example, high-energy gamma emissions from a radionuclide such as Co-60 are generally more readily detected than low-energy beta emissions from tritium. Second, accountability requirements for some radionuclides are such that greater effort has been invested in measuring or estimating activities associated with the waste packages.

Timing of waste disposal is also an important factor affecting the accuracy of the activity estimates. In general, detection equipment has improved over the years, as have efforts to more accurately characterize the material placed in the disposal facility. Area G has been in operation for over 50 years, during which time changes in technology and focus have significantly impacted the accuracy of the inventory estimates.

The measurement errors associated with the activities listed in the LLW and TRU waste databases cannot be determined with a high degree of accuracy, but some generalities can be drawn about this source of uncertainty. The information summarized below is based on discussions with LANL personnel experienced in radiation characterization procedures and measurement techniques (Myers, 2004).

The radionuclides included in the Area G inventory have been divided into a number of classes or groups to simplify this discussion about uncertainty. These classes include pure beta emitters such as C-14, Ni-63, Sr-90 and Tc-99; gamma emitters such as Co-60 and Cs-137; alpha emitters such as americium, plutonium, and uranium; and tritium. The greatest uncertainties are expected to be associated with the measurement of the activities of the pure beta emitters. The low energy and penetrating power of beta radiation are such that detailed separation techniques must be performed before accurate assessments of the waste activity can be conducted. Characterization efforts at the Laboratory rarely, if ever, include these analyses for this class of waste. As a result, the activities associated with these radionuclides are expected to be accurate only to within one order of magnitude.

In theory, the higher energy emissions associated with many gamma emitters should make accurate characterization an easier task. Nevertheless, gamma waste disposed of prior to the 1990s is expected to have a similar level of accuracy as that discussed for the beta emitters. The magnitude of the errors associated with the gamma emitters decreased during the 1990s to the extent that errors are currently on the order of $\pm$25 percent to $\pm$100 percent, depending upon the size and composition of the waste package.

Greater effort has generally been expended on the characterization of waste contaminated with uranium and transuranics because of accountability issues. However, the concentrations of americium, plutonium, and uranium in the waste have a significant impact on the accuracy of the measured activities. Activities of these radionuclides have probably been overestimated in LLW because concentrations in this waste are low and the former measurement techniques used did not have very low detection limits. Drums and boxes with detectable quantities of plutonium (i.e., on the order of 0.50 g [0.001 lb] or more per package) are likely to have errors on the order of 20 to 30 percent for measurements conducted in the 1970s and 1980s; errors on the order of 10 to 20 percent are typical for more recent measurements.

The errors estimated for the uranium and transuranic waste may not always be realized. For example, some waste generators measured drums of TRU waste using neutron counters and used scaling factors to estimate isotopic distributions. Inappropriately applied scaling factors have resulted in overestimates of some isotopes' activities and underestimates of others. For example, Am-241 activities have been underestimated by an order of magnitude or more in a small proportion of TRU waste drums because of the misapplication of scaling factors.

The ability to accurately measure the quantities of uranium isotopes depends, in part, on the isotopic quantities in the waste package. For example, U-235 has gone undetected during the assay of drums of TRU waste that contain a few grams or less of the isotope; errors of this sort may occur in a small proportion of the drums. Generators are usually aware of drums that contain greater quantities of U-235 (e.g., 10 g [0.022 lb] or more) and measure the packages directly to determine the waste activity. Waste containing depleted uranium is usually measured with errors of $\underline{+}$25 percent to $\underline{+}$100 percent, depending upon the size and composition of the package.

Although tritium is a pure beta emitter, it is considered separately from the other beta emitters because of its generation pattern at the Laboratory. Low-activity tritium waste is expected to have uncertainties associated with its characterization similar to those discussed for the pure beta emitters. However, high-activity tritium waste receives greater scrutiny. Measurement errors associated with high-activity tritium waste disposed of prior to the 1990s are expected to be on the order of ±100 percent. Improvements since that time have reduced these errors to values that are expected to be on the order of $\underline{+}$25 percent.

An extrapolation process was used to estimate the quantities of waste disposed of in pits prior to 1971 and in pits and shafts from 2008 through 2044. The pre-1971 pit inventory was estimated, in part, on the basis of waste disposed of from 1971 through 1977; the 2008–2044 pit and shaft inventories were based, in large part, on the characteristics of the material disposed of from 2000 through 2007. In each case, it was implicitly assumed that the waste disposed of during the extrapolation period was similar to that emplaced during the period of interest.

It is unlikely that the nature of the waste that was disposed of in pits during the early to mid-1970s extrapolation period was exactly the same as material emplaced from 1959 through 1970. Some insight into the error introduced by using the extrapolation approach as a means for estimating the inventory for this waste may be gained by examining the results of the pre-1971 disposal record review (Pollard and Shuman, 1999); this evaluation is described in Sections 3.1 and 4.1.1.

In general, the americium and plutonium activities included in the 1997 composite analysis inventory for the concrete and sludge disposed of in pits prior to 1971 agreed with available historical disposal data (Table 14). However, the majority of the Am-241 and Pu-239 activities included in the 1997 composite analysis and in the inventory update are based on data published by Warren (1980); the extrapolation process had little to do with these projections. The Pu-238 sludge inventory estimated in 1997 and updated in this study was based on the extrapolation process and generally agrees with the inventory estimated using the historical sludge disposal data.

Radionuclide inventories estimated for the pre-1971 nonsludge waste streams on the basis of the extrapolation approach do not compare favorably with estimates developed using historical data records. For all radionuclides examined, the total activity estimates developed for the 1997 composite analysis readily exceed the activities indicated by the disposal data. As discussed earlier, it is unclear if this finding signifies that the extrapolation process is inappropriate or if the historical data are incomplete in terms of this waste.

Dissimilarities between the future waste (to be emplaced from 2008 through 2044) and the 2000–2007 extrapolation data used to estimate future pit and shaft inventories may also be expected. As discussed earlier, considerable quantities of ER and D&D waste have been generated in recent years and similar quantities are expected over the next few years. The large volumes of low-activity waste generated by these cleanup activities will greatly affect the overall nature of the waste disposed of at Area G, but this impact will be reduced after 2015. The nature of the operational waste shipped to Area G will also change as programs at the Laboratory evolve over time. The precise nature of how cleanup activities and operations change over time will determine the accuracy of the extrapolated future inventories.

Many of the waste packages disposed of at Area G contained activation- and fission-product waste; typically, the radionuclides in these packages were simply listed in terms of total activities of MAP and MFP. These activities are allocated to specific radionuclides in conjunction with the performance assessment and composite analysis modeling using the methods described in *Attachment I*. Several sources of uncertainty are associated with the allocation of the MFP activities to specific radionuclides:

- Nature of the fission reactions that generate the fission products
- Age of the MFP waste
- Impacts of daughter ingrowth

These sources of uncertainty are discussed below.

The identity of the fissile materials that led to the generation of the MFP appears to be clear. Pu-239 and U-235 are common fissile materials and are associated with many of the waste packages that contain MFP. However, the proportion of this waste that was generated by Pu-239 fission as opposed to reactions involving U-235 is not clear, nor is it clear what proportion of the waste resulted from interactions with thermal and fast neutrons.

Fission yields and, hence, the radionuclides assigned to the MFP waste, will vary depending upon the fissile material and the neutron energy. This is illustrated by the fission yields that are listed in Table I-2 (*Attachment I*). The effect that these differences in yield may have on the radionuclide allocations is more apparent through an examination of Table I-3, which shows that

the minimum and maximum activity fractions for a given radionuclide may differ by a factor of two or more, and commonly by more than an order of magnitude.

The short-lived nature of the majority of the fission products requires that an accurate assessment be made of the age of the waste at the time of disposal. The composition of the waste changes rapidly as radionuclides with very short half-lives decay. The effects of decay on waste composition are apparent from a comparison of the number of radionuclides included in the waste at the time the material is generated (*Attachment I*, Table I-2) and the number of radionuclides present when the waste is 1 or more years old (*Attachment I*, Table I-3).

The error introduced into the inventory projections by uncertainties in the age of the MFP waste may be significant. For example, the activity allocation fractions for Cs-137, averaged over the thermal and fast neutron yields for Pu-239 and U-235, increase from about 0.14 to 0.73 as the age of the MFP waste increases from 1 to 10 years. Thus, changing the waste age by an order of magnitude causes a five-fold change in the projected Cs-137 inventory.

Most radionuclides associated with MFP waste are very short-lived and decay to negligible levels within a matter of days or weeks. The daughter products generated by the decay process may, in some instances, be longer-lived than their parents and, as a result, contribute to estimated MFP waste activities beyond the time of generation. Due to the very large number of short-lived fission products, however, the contributions of any long-lived daughter products are not taken into account when assigning the MFP waste to specific radionuclides. This simplification will underestimate the activities of any long-lived daughters that were overlooked and overestimate the activities of the radionuclides that were carried forward in the analysis.

The allocation of the listed MAP activities to specific radionuclides was based on information provided by the Los Alamos Neutron Science Center (formerly the Los Alamos Meson Physics Facility) at TA-53, a major generator of MAP waste. This facility generates three major waste streams of activated waste including trash, beam-line inserts, and targets; the activity allocation factors adopted for the inventory update are based on a characterization of the trash. While similar activated materials may occur in all three waste streams, it is unclear if the allocation factors developed for the trash accurately represent the targets and beam-line inserts.

Many of the radionuclides in the MAP waste are short-lived and will undergo significant decay between the time of generation and disposal. Similar to the situation noted for the MFP waste, the decay dynamics of the waste will have a significant impact on the fractional abundances of the radionuclides in the material. Both the age of the waste at the time the allocation factors were developed and the age of the waste at the time it was disposed of at Area G are unknown. Lacking this information, it was assumed these two ages were the same. If this is not the case, the relative activities of the radionuclides in the waste will be different.

A number of material types have been used to refer to specific radionuclide compositions; the majority of these have been used to identify isotopic mixtures of uranium and plutonium isotopes. The Area G pit and shaft inventory update includes approximately 1.1×10^4 Ci of activity reported using these material types; about 98 percent of the material type activity included in the inventory is represented by plutonium material types PU52, PU53, PU54, PU56, and PU83.

Waste generated at the Laboratory was assigned to a material type on the basis of the mass content of specific radionuclides in the waste. Table 30 shows the criteria used to assign waste to the dominant plutonium material types. Four of these material types are assigned waste on the basis of Pu-240 content; PU83 is the material type for waste that is essentially all Pu-238. The LLW and TRU waste databases use point estimates to assign the material types to specific radionuclides; these factors, converted to an activity basis, are provided in Table 3.

Table 30
Criteria for Assigning Waste to Selected Plutonium Material Types

Plutonium Material Type	Type Description [a]
PU52	4.0 to < 7.0 % Pu-240
PU53	7.0 to < 10.0 % Pu-240
PU54	10.0 to < 13.0 % Pu-240
PU56	16.0 to < 20.0 % Pu-240
PU83	Total Pu-238

[a] *Fractional amounts are mass-based.*

As indicated in Table 30, waste with a range of radionuclide contents may be assigned to a specific material type. Consequently, using the point estimates adopted for the databases to assign material type activities to specific radionuclides will introduce uncertainty into the inventory projections for the affected waste. The errors introduced by these uncertainties are examined below for the plutonium material types that dominated this category of waste.

Veilleux (2005) used spectral data collected with a high-purity germanium detector to estimate distributions of the radionuclide-specific mass contents of several plutonium material types. By evaluating detection results for almost 3,300 drums, he was able to calculate the mean, standard deviation, and median of the mass fractions of Pu-238, Pu-239, Pu-240, Pu-241, Pu-242, and Am-241 included in each type of waste. A summary of the evaluation conducted by Veilleux is presented in Table 31; the table lists the mean radionuclide abundances and relative standard deviations (or coefficients of variation) for the major plutonium material types. The results for material types PU52, PU53, PU54, and PU83 were taken directly from Veilleux (2005, Table 9; rounded to two significant digits); the results for material type PU56 were calculated using data

presented by Veilleux. It is clear from these results that the actual quantities of radionuclides in the material type waste may be quite variable.

Table 31
Mass Fractions and Uncertainties for Selected Plutonium Material Types

	Mass Fraction by Material Type									
	PU52		PU53		PU54		PU56		PU83	
Radionuclide	Mean	RSD (%)	Mean	RSD (%)	Mean	RSD (%)	Mean	RSD (%)	Mean	RSD (%)
Pu-238	2.1E-04	79	2.3E-04	38	3.3E-04	69	4.5E-04	22	7.8E-01	8.5
Pu-239	9.3E-01	1.0	9.1E-01	2.5	9.1E-01	3.0	8.6E-01	3.0	2.0E-01	31
Pu-240	6.5E-02	15	8.8E-02	25	8.6E-02	31	1.3E-01	19	2.0E-02	68
Pu-241	1.4E-03	20	2.1E-03	42	2.2E-03	53	4.4E-03	19	1.7E-03	12
Pu-242	9.9E-05	23	2.5E-04	68	3.0E-04	78	8.0E-04	33	9.2E-04	67
Am-241	6.1E-03	85	7.8E-03	53	1.4E-02	116	5.2E-02	54	2.5E-03	61

RSD = Relative standard deviation

As discussed earlier, definitions were unavailable for several material types including GAMMA, GRALPH, GRBETA, and TRU. Lacking these definitions, waste assigned to these material types was excluded from the inventory characterization. This is not expected to introduce significant error into the final inventory projections because the total activity associated with all of these material types is approximately 1.5 Ci.

4.4 Summary of the Area G Radioactive Waste Inventory

The Area G performance assessment addresses the LLW disposed of since September 26, 1988 and the waste expected to require disposal over the remainder of the facility's lifetime (through 2044). The characteristics of this waste are detailed in Sections 4.1.3 and 4.2 of this report. The inventory developed for the composite analysis includes all waste that has been disposed of at Area G since the facility opened in 1957 and the waste expected to require disposal over the remainder of the facility's lifetime. Estimated quantities and radiological characteristics of this waste are presented and discussed in Sections 4.1 and 4.2 of this report.

The total volumes and activities of waste projected for the Area G performance assessment and composite analysis are listed in listed in Table 32; separate inventories are provided for disposal pits and shafts. The projected radionuclide, MAP, MFP, and material type activities associated with the performance assessment inventory are provided in Table 33; again, separate inventories are provided for the pits and shafts. The contaminant-specific inventories for the composite analysis are provided in Tables 34 and 35 for the disposal pit and shafts, respectively. All

activities listed in Tables 32 through 35 are as-disposed activities. Radionuclides that were eliminated on the basis of their decay characteristics, as described in *Attachment II*, are not included in Tables 33 through 35.

Table 32
Volumes and Activities for Waste Included in the Area G Performance Assessment and Composite Analysis Inventory

	Disposal Pits		Disposal Shafts	
Analysis and Period of Disposal	Volume (m^3)	Activity (Ci)	Volume (m^3)	Activity (Ci)
Performance Assessment				
September 27, 1988–2007	8.9E+04	3.5E+03	5.2E+02	1.7E+06
2008 –2044	1.6E+05	3.9E+02	1.0E+03	9.8E+05
Total	2.5E+05	3.9E+03	1.6E+03	2.7E+06
Composite Analysis				
Pre-1971	4.9E+04	1.8E+04	4.8E+01	6.4E+04
1971-September 26, 1988	9.9E+04	4.3E+04	9.2E+02	8.2E+05
September 27, 1988–2007	8.9E+04	3.5E+03	5.2E+02	1.7E+06
2008–2044	1.6E+05	3.9E+02	1.0E+03	9.8E+05
Total	4.0E+05	6.5E+04	2.5E+03	3.6E+06

Table 33
Radionuclide, Activation Product, Fission Product, and Material Type Inventories for Waste Included in the Performance Assessment

Constituent	Activity (Ci)					
	Disposal Pits			Disposal Shafts		
	September 26, 1988–2007 Waste	2008–2044 Waste	Total	September 26, 1988–2007 Waste	2008–2044 Waste	Total
Ac-227	1.8E-05	6.6E-05	8.4E-05	5.3E-07	---	5.3E-07
Ag-108m	1.7E-04	5.8E-05	2.3E-04	4.4E+00	4.2E-08	4.4E+00
Al-26	2.6E-04	1.2E-06	2.6E-04	---	---	---
Am-241	8.1E+00	1.5E+01	2.3E+01	3.2E-01	1.2E-03	3.2E-01
Am-243	8.6E-03	3.8E-02	4.7E-02	1.0E-09	---	1.0E-09
Ba-133	6.9E-01	3.2E+00	3.9E+00	2.8E-03	---	3.7E-03
Be-10	4.6E-03	---	4.6E-03	---	---	---
Bi-207	1.5E-02	7.0E-02	8.6E-02	6.0E-05	7.3E-06	6.8E-05
Bk-247	2.8E-07	---	2.8E-07	---	---	---
C-14	3.3E+00	1.2E-02	3.3E+00	1.6E+01	3.5E-01	1.6E+01
Ca-41	2.7E-01	---	2.7E-01	---	---	---
Cf-249	1.0E-04	4.7E-04	5.7E-04	---	---	---
Cf-252	2.0E-05	---	2.0E-05	9.6E-06	3.6E-05	4.5E-05
Cl-36	1.8E-02	---	1.8E-02	2.5E-04	---	2.5E-04
Cm-243	4.2E-05	5.1E-05	9.2E-05	---	---	---
Cm-244	2.8E-03	1.3E-02	1.6E-02	2.2E-03	9.3E-03	1.1E-02
Cm-245	4.6E-05	2.1E-04	2.6E-04	---	---	---
Cm-248	4.5E-07	2.1E-06	2.5E-06	---	---	---

-- = None

Table 33 (Continued)
Radionuclide, Activation Product, Fission Product, and Material Type Inventories for Waste Included in the Performance Assessment

Constituent	Activity (Ci)					
	Disposal Pits			Disposal Shafts		
	September 26, 1988–2007 Waste	2008–2044 Waste	Total	September 26, 1988–2007 Waste	2008–2044 Waste	Total
Co-60	4.5E+01	7.5E+01	1.2E+02	3.1E+03	3.8E+01	3.1E+03
Cs-135	1.3E-04	7.5E-06	1.4E-04	4.5E-06	---	4.5E-06
Cs-137	5.8E+00	4.8E+00	1.1E+01	8.3E+01	1.9E+00	8.5E+01
D38	4.0E+00	4.3E+00	8.3E+00	2.4E+00	7.0E+00	9.4E+00
Eu-152	4.4E-01	2.0E-01	6.4E-01	1.1E-02	3.0E-03	1.4E-02
Eu-154	5.2E-02	3.1E-03	5.5E-02	9.8E-02	---	9.8E-02
Gd-148	1.0E-05	---	1.0E-05	7.7E-09	---	7.7E-09
H-3	3.1E+03	1.9E+01	3.2E+03	1.7E+06	9.7E+05	2.7E+06
Ho-163	9.1E-01	---	9.1E-01	7.0E-02	---	7.0E-02
Ho-166m	1.4E-03	6.6E-03	8.0E-03	---	---	---
I-129	3.1E-05	1.4E-04	1.7E-04	3.0E-08	---	3.0E-08
K-40	2.7E-01	8.5E-01	1.1E+00	4.3E-07	2.0E-06	2.4E-06
Kr-85	4.6E-02	4.6E-04	4.7E-02	8.9E-03	3.7E-02	4.6E-02
Lu-176	1.7E-06	---	1.7E-06	---	---	---
MAP	1.3E+01	---	1.3E+01	5.6E+03	---	5.6E+03
MFP	1.8E+01	---	1.8E+01	6.0E+01	---	6.0E+01
Mo-93	2.0E-05	9.3E-05	1.1E-04	1.3E-02	---	6.8E-02
Nb-91	1.2E-05	5.3E-05	6.5E-05	9.4E-03	4.3E-02	5.3E-02
Nb-92	3.0E-06	1.4E-05	1.7E-05	4.0E-03	---	4.0E-03

-- = None

Table 33 (Continued)
Radionuclide, Activation Product, Fission Product, and Material Type Inventories for Waste Included in the Performance Assessment

Constituent	Activity (Ci)					
	Disposal Pits			Disposal Shafts		
	September 26, 1988–2007 Waste	2008–2044 Waste	Total	September 26, 1988–2007 Waste	2008–2044 Waste	Total
Nb-93m	1.0E-03	4.8E-03	5.8E-03	2.2E+00	1.0E+01	1.3E+01
Nb-94	4.0E-02	6.9E-02	1.1E-01	1.3E-04	---	1.3E-04
Nd-144	1.0E-08	4.6E-08	5.6E-08	---	---	---
Ni-59	6.3E-03	3.3E-05	6.3E-03	2.6E+00	---	1.4E+01
Ni-63	2.0E+00	9.5E-01	2.9E+00	1.2E+03	4.6E+01	1.2E+03
Np-237	4.9E-03	2.0E-02	2.4E-02	3.1E-08	1.4E-07	1.7E-07
Os-194	1.3E-07	6.0E-07	7.3E-07	---	---	---
Pa-231	4.2E-05	1.1E-04	1.5E-04	2.7E-03	2.3E-07	2.7E-03
Pb-210	2.7E-01	8.5E-02	3.5E-01	2.9E-08	1.2E-07	1.5E-07
Pm-145	1.1E-01	4.6E-08	1.1E-01	---	---	---
Pu-236	1.0E-09	4.6E-09	5.6E-09	---	---	---
Pu-238	1.4E+01	2.2E+01	3.6E+01	2.6E-01	3.5E-02	3.0E-01
Pu-239	1.6E+01	1.8E+01	3.4E+01	7.6E-02	3.2E-02	1.1E-01
Pu-240	5.3E-01	1.3E+00	1.8E+00	1.2E-03	---	1.2E-03
Pu-241	2.8E+00	4.9E+00	7.6E+00	3.7E-02	---	3.7E-02
Pu-242	6.3E-03	2.6E-02	3.2E-02	2.0E-06	---	2.0E-06
Pu-244	3.5E-06	1.6E-05	2.0E-05	---	---	---
PU52	5.1E+00	---	5.1E+00	5.7E-02	---	5.7E-02
Ra-226	1.2E-01	3.2E-01	4.4E-01	7.8E-01	8.4E-05	7.8E-01

-- = None

Table 33 (Continued)
Radionuclide, Activation Product, Fission Product, and Material Type Inventories for Waste Included in the Performance Assessment

Constituent	Activity (Ci)					
	Disposal Pits			Disposal Shafts		
	September 26, 1988–2007 Waste	2008–2044 Waste	Total	September 26, 1988–2007 Waste	2008–2044 Waste	Total
Ra-228	3.4E-02	1.1E-01	1.5E-01	---	---	---
Si-32	2.7E-05	7.7E-05	1.0E-04	---	---	---
Sm-151	3.4E-09	1.4E-08	1.8E-08	---	---	---
Sn-126	2.7E-06	---	2.7E-06	2.4E-02	---	2.4E-02
Sr-90	2.8E+00	9.8E+00	1.3E+01	8.7E+01	1.8E+00	8.8E+01
Tb-157	4.5E-08	2.1E-07	2.5E-07	---	---	---
Tc-97	2.1E-06	9.2E-08	2.2E-06	---	---	---
Tc-99	3.2E-01	2.8E-01	6.0E-01	1.2E-05	---	1.2E-05
Th-228	2.2E-03	3.0E-03	5.2E-03	6.9E-04	3.2E-03	3.9E-03
Th-229	3.8E-04	1.4E-03	1.8E-03	5.4E-08	---	5.4E-08
Th-230	1.2E-03	4.2E-04	1.6E-03	1.6E-08	---	1.6E-08
Th-232	3.2E-01	8.1E-03	3.3E-01	1.9E-01	6.0E-02	2.5E-01
TH88	3.7E-02	---	3.7E-02	---	---	---
Ti-44	2.6E-03	1.2E-02	1.5E-02	2.0E-02	9.0E-02	1.1E-01
U(DEP)	5.3E+00	2.4E+01	3.0E+01	4.4E-05	2.0E-04	2.5E-04
U(NAT)	6.4E-05	2.9E-04	3.6E-04	1.8E-01	8.3E-01	1.0E+00
U11	8.7E-06	---	8.7E-06	---	---	---
U-232	8.8E-04	1.7E-04	1.1E-03	2.0E-04	---	2.0E-04
U-233	7.3E-02	2.4E-01	3.1E-01	5.8E-04	---	5.8E-04

-- = None

Table 33 (Continued)
Radionuclide, Activation Product, Fission Product, and Material Type Inventories for Waste Included in the Performance Assessment

Constituent	Activity (Ci)					
	Disposal Pits			Disposal Shafts		
	September 26, 1988–2007 Waste	2008–2044 Waste	Total	September 26, 1988–2007 Waste	2008–2044 Waste	Total
U-234	1.1E+00	1.6E+00	2.6E+00	5.0E-01	2.3E+00	2.8E+00
U-235	8.7E-01	1.0E-01	9.7E-01	2.8E-02	1.3E-01	1.5E-01
U-236	3.7E-03	1.1E-02	1.5E-02	3.8E-06	1.8E-05	2.1E-05
U-238	1.2E+01	2.6E+00	1.4E+01	4.5E-01	1.1E+00	1.6E+00
U38	5.0E-02	---	5.0E-02	---	---	---
U39	3.1E-03	---	3.1E-03	---	---	---
U81	5.7E-04	---	5.7E-04	---	---	---
Zr-93	2.0E-08	---	2.0E-08	---	---	---

-- = None

Table 34
Radionuclide, Activation Product, Fission Product, and Material Type Inventories for Waste Included in the Composite Analysis, Disposal Pits

Constituent	Activity (Ci)				
	Pre-1971 Waste	1971–September 26, 1988 Waste	September 26, 1988–2007 Waste	2008–2044 Waste	Total
Ac-227	8.6E-01	7.0E-02	1.8E-05	6.6E-05	9.3E-01
Ag-108m	---	---	1.7E-04	5.8E-05	2.3E-04
Al-26	---	---	2.6E-04	1.2E-06	2.6E-04
Am-241	2.4E+03	2.4E+01	8.1E+00	1.5E+01	2.4E+03
Am-243	---	---	8.6E-03	3.8E-02	4.7E-02
Ba-133	---	---	6.9E-01	3.2E+00	3.9E+00
Be-10	---	---	4.6E-03	---	4.6E-03
Bi-207	---	---	1.5E-02	7.0E-02	8.6E-02
Bk-247	---	---	2.8E-07	---	2.8E-07
C-14	---	2.3E-01	3.3E+00	1.2E-02	3.6E+00
Ca-41	---	---	2.7E-01	---	2.7E-01
Cf-249	2.4E-03	4.1E-04	1.0E-04	4.7E-04	3.4E-03
Cf-251	2.7E-03	1.6E-03	---	---	4.3E-03
Cf-252	1.5E-02	8.6E-03	2.0E-05	---	2.3E-02
Cl-36	---	---	1.8E-02	---	1.8E-02
Cm242	1.8E-03	---	---	---	1.8E-03
Cm-243	---	---	4.2E-05	5.1E-05	9.2E-05
Cm-244	1.7E-03	---	2.8E-03	1.3E-02	1.7E-02
Cm-245	---	---	4.6E-05	2.1E-04	2.6E-04
Cm-248	---	---	4.5E-07	2.1E-06	2.5E-06
Co-60	---	1.3E+03	4.5E+01	7.5E+01	1.4E+03
Cs-135	---	---	1.3E-04	7.5E-06	1.4E-04
Cs-137	2.6E-01	1.1E+03	5.8E+00	4.8E+00	1.1E+03
D38	---	---	4.0E+00	4.3E+00	8.3E+00
Eu-152	---	---	4.4E-01	2.0E-01	6.4E-01
Eu-154	---	---	5.2E-02	3.1E-03	5.5E-02
Gd-148	---	---	1.0E-05	---	1.0E-05
H-3	2.7E+00	7.5E+03	3.1E+03	1.9E+01	1.1E+04

-- = None

Table 34 (Continued)
Radionuclide, Activation Product, Fission Product, and Material Type Inventories for Waste Included in the in the Composite Analysis, Disposal Pits

Constituent	Activity (Ci)				
	Pre-1971 Waste	1971–September 26, 1988 Waste	September 26, 1988–2007 Waste	2008–2044 Waste	Total
Ho-163	---	---	9.1E-01	---	9.1E-01
Ho-166m	---	---	1.4E-03	6.6E-03	8.0E-03
I-129	---	---	3.1E-05	1.4E-04	1.7E-04
K-40	---	---	2.7E-01	8.5E-01	1.1E+00
Kr-85	1.7E-03	1.0E-03	4.6E-02	4.6E-04	4.9E-02
Lu-176	---	---	1.7E-06	---	1.7E-06
MAP	3.6E-01	1.2E+03	1.3E+01	---	1.2E+03
MFP	1.0E+03	6.5E+02	1.8E+01	---	1.7E+03
Mo-93	---	---	2.0E-05	9.3E-05	1.1E-04
Nb-91	---	---	1.2E-05	5.3E-05	6.5E-05
Nb-92	---	---	3.0E-06	1.4E-05	1.7E-05
Nb-93m	---	---	1.0E-03	4.8E-03	5.8E-03
Nb-94	---	8.0E-06	4.0E-02	6.9E-02	1.1E-01
Nd-144	---	---	1.0E-08	4.6E-08	5.6E-08
Ni-59	---	---	6.3E-03	3.3E-05	6.3E-03
Ni-63	---	---	2.0E+00	9.5E-01	2.9E+00
Np-237	4.0E-03	7.0E-07	4.9E-03	2.0E-02	2.8E-02
Os-194	---	---	1.3E-07	6.0E-07	7.3E-07
Pa-231	---	---	4.2E-05	1.1E-04	1.5E-04
Pb-210	---	---	2.7E-01	8.5E-02	3.5E-01
Pm-145	---	---	1.1E-01	4.6E-08	1.1E-01
Pu-236	---	---	1.0E-09	4.6E-09	5.6E-09
Pu-238	3.8E+03	4.9E+02	1.4E+01	2.2E+01	4.3E+03
Pu-239	1.7E+02	2.3E+01	1.6E+01	1.8E+01	2.2E+02
Pu-240	4.0E+00	2.8E-05	5.3E-01	1.3E+00	5.8E+00
Pu-241	---	5.8E-06	2.8E+00	4.9E+00	7.6E+00
Pu-242	---	7.8E-06	6.3E-03	2.6E-02	3.2E-02
Pu-244	---	---	3.5E-06	1.6E-05	2.0E-05
PU51	1.6E+00	---	---	---	1.6E+00

-- = None

Table 34 (Continued)
Radionuclide, Activation Product, Fission Product, and Material Type Inventories for Waste Included in the in the Composite Analysis, Disposal Pits

Constituent	Activity (Ci)				
	Pre-1971 Waste	1971–September 26, 1988 Waste	September 26, 1988–2007 Waste	2008–2044 Waste	Total
PU52	7.7E+03	2.3E+00	5.1E+00	---	7.7E+03
PU53	2.5E+02	3.7E-04	---	---	2.5E+02
PU54	1.1E+03	1.5E-01	---	---	1.1E+03
PU55	6.8E+01	---	---	---	6.8E+01
PU56	1.2E+03	---	---	---	1.2E+03
PU57	7.1E+01	---	---	---	7.1E+01
PU83	5.0E+02	1.5E-02	---	---	5.0E+02
Ra-226	---	2.0E-01	1.2E-01	3.2E-01	6.4E-01
Ra-228	---	2.1E-01	3.4E-02	1.1E-01	3.6E-01
Si-32	---	---	2.7E-05	7.7E-05	1.0E-04
Sm-151	---	---	3.4E-09	1.4E-08	1.8E-08
Sn-126	---	---	2.7E-06	---	1.5E-05
Sr-90	2.9E-01	1.4E+03	2.8E+00	9.8E+00	1.4E+03
Tb-157	---	---	4.5E-08	2.1E-07	2.5E-07
Tc-97	---	---	2.1E-06	9.2E-08	2.2E-06
Tc-99	---	---	3.2E-01	2.8E-01	6.0E-01
Th-228	---	---	2.2E-03	3.0E-03	5.2E-03
Th-229	---	---	3.8E-04	1.4E-03	1.8E-03
Th-230	1.6E+01	9.5E+00	1.2E-03	4.2E-04	2.6E+01
Th-232	---	1.4E-03	3.2E-01	8.1E-03	3.3E-01
TH88	1.9E-03	2.7E-02	3.7E-02		6.6E-02
Ti-44	---	---	2.6E-03	1.2E-02	1.5E-02
U(DEP)	---	---	5.3E+00	2.4E+01	3.0E+01
U(NAT)	---	---	6.4E-05	2.9E-04	3.6E-04
U10	8.8E-01	5.1E-01	---	---	1.4E+00
U11	---	1.5E-01	8.7E-06	---	1.5E-01
U12	7.9E+00	5.8E+00	---	---	1.4E+01
U-232	---	---	8.8E-04	1.7E-04	1.1E-03
U-233	6.1E+00	1.9E-02	7.3E-02	2.4E-01	6.4E+00

-- = None

Table 34 (Continued)
Radionuclide, Activation Product, Fission Product, and Material Type Inventories for Waste Included in the in the Composite Analysis, Disposal Pits

Constituent	Activity (Ci)				
	Pre-1971 Waste	1971–September 26, 1988 Waste	September 26, 1988–2007 Waste	2008–2044 Waste	Total
U-234	---	---	1.1E+00	1.6E+00	2.6E+00
U-235	3.7E-01	7.1E-01	8.7E-01	1.0E-01	2.1E+00
U-236	---	6.3E-08	3.7E-03	1.1E-02	1.5E-02
U-238	4.3E+00	1.1E+01	1.2E+01	2.6E+00	2.9E+01
U35	---	4.9E-04	---	---	4.9E-04
U36	---	2.2E-05	---	---	2.2E-05
U38	2.3E-02	4.5E-02	5.0E-02	---	1.2E-01
U39	---	---	3.1E-03	---	3.1E-03
U81	4.7E-03	2.8E-03	5.7E-04	---	8.1E-03
Zr-93	---	---	2.0E-08	---	2.0E-08

-- = None

Table 35
Radionuclide, Activation Product, Fission Product, and Material Type Inventories for Waste Included in the Composite Analysis, Disposal Shafts

Constituent	Activity (Ci)				
	Pre-1971 Waste	1971-September 26, 1988 Waste	September 26, 1988-2007 Waste	2008-2044 Waste	Total
Ac-227	---	---	5.3E-07	---	5.3E-07
Ag-108m	---	---	4.4E+00	4.2E-08	4.4E+00
Am-241	---	4.0E-02	3.2E-01	1.2E-03	3.6E-01
Am-243	2.0E-02	1.1E-05	1.0E-09	---	2.0E-02
Ba-133	---	---	2.8E-03	---	2.8E-03
Bi-207	---	---	6.0E-05	7.3E-06	6.8E-05
C-14	---	1.1E+00	1.6E+01	3.5E-01	1.7E+01
Cf-252	4.0E+00	5.5E+01	9.6E-06	3.6E-05	5.9E+01
Cl-36	---	---	2.5E-04	---	2.5E-04
Cm-244	2.3E-04	1.9E-01	2.2E-03	9.3E-03	2.0E-01
Co-60	1.8E+01	2.8E+03	3.1E+03	3.8E+01	5.9E+03
Cs-135	---	---	4.5E-06	---	4.5E-06
Cs-137	6.3E-01	4.2E+01	8.3E+01	1.9E+00	1.3E+02
D38	6.2E-05	---	2.4E+00	7.0E+00	9.4E+00
Eu-152	1.2E-01	---	1.1E-02	3.0E-03	1.4E-01
Eu-154	---	---	9.8E-02	---	9.8E-02
Gd-148	---	---	7.7E-09	---	7.7E-09
H-3	6.1E+04	8.0E+05	1.7E+06	9.7E+05	3.5E+06
Ho-163	---	---	7.0E-02	---	7.0E-02

--- = None

Table 35 (Continued)
Radionuclide, Activation Product, Fission Product, and Material Type Inventories for Waste Included in the in the Composite Analysis, Disposal Shafts

Constituent	Activity (Ci)				
	Pre-1971 Waste	1971-September 26, 1988 Waste	September 26, 1988-2007 Waste	2008-2044 Waste	Total
I-129	---	---	3.0E-08	---	3.0E-08
K-40	---	---	4.3E-07	2.0E-06	2.4E-06
Kr-85	---	4.5E-04	8.9E-03	3.7E-02	4.6E-02
MAP	8.0E+01	1.4E+04	5.6E+03	---	1.9E+04
MFP	2.7E+03	7.4E+03	6.0E+01	---	1.0E+04
Mo-93	---	---	1.3E-02	---	1.3E-02
Nb-91	---	---	9.4E-03	4.3E-02	5.3E-02
Nb-92	---	---	4.0E-03	---	4.0E-03
Nb-93m	---	---	2.2E+00	1.0E+01	1.3E+01
Nb-94	---	---	1.3E-04	---	1.3E-04
Ni-59	---	---	2.6E+00	---	2.6E+00
Ni-63	---	4.3E-03	1.2E+03	4.6E+01	1.2E+03
Np-237	1.4E-04	7.8E-05	3.1E-08	1.4E-07	2.2E-04
Pa-231	---	---	2.7E-03	2.3E-07	2.7E-03
Pb-210	---	---	2.9E-08	1.2E-07	1.5E-07
Pu-238	5.6E+00	9.7E-01	2.6E-01	3.5E-02	6.9E+00
Pu-239	2.1E+01	8.3E+01	7.6E-02	3.2E-02	1.0E+02
Pu-240	3.4E-02	---	1.2E-03	---	3.6E-02
Pu-241	5.4E-03	7.3E-01	3.7E-02	---	7.7E-01

--- = None

Table 35 (Continued)
Radionuclide, Activation Product, Fission Product, and Material Type Inventories for Waste Included in the in the Composite Analysis, Disposal Shafts

Constituent	Activity (Ci)				
	Pre-1971 Waste	1971-September 26, 1988 Waste	September 26, 1988-2007 Waste	2008-2044 Waste	Total
Pu-242	1.2E-04	3.1E-07	2.0E-06	---	1.2E-04
PU52	---	7.5E+01	5.7E-02	---	7.6E+01
PU54	---	2.0E-08	---	---	2.0E-08
Ra-226	1.0E-01	2.5E+00	7.8E-01	8.4E-05	3.4E+00
Sn-126	---	---	2.4E-02	---	2.4E-02
Sr-90	1.1E+00	9.5E-02	8.7E+01	1.8E+00	9.0E+01
Tc-99	---	---	1.2E-05	---	1.2E-05
Th-228	---	---	6.9E-04	3.2E-03	3.9E-03
Th-229	---	---	5.4E-08	---	5.4E-08
Th-230	5.7E-04	---	1.6E-08	---	5.7E-04
Th-232	1.7E-05	1.5E-02	1.9E-01	6.0E-02	2.7E-01
Th-88	---	4.0E-03	---	---	4.0E-03
Ti-44	---	---	2.0E-02	9.0E-02	1.1E-01
U(DEP)	---	---	4.4E-05	2.0E-04	2.5E-04
U(NAT)	---	---	1.8E-01	8.3E-01	1.0E+00
U10	---	3.0E-03	---	---	3.0E-03
U12	---	1.7E+00	---	---	1.7E+00
U-232	---	2.1E-01	2.0E-04	---	2.1E-01
U-233	1.5E+00	4.0E+00	5.8E-04	---	5.5E+00

--- = None

Table 35 (Continued)
Radionuclide, Activation Product, Fission Product, and Material Type Inventories for Waste Included in the in the Composite Analysis, Disposal Shafts

Constituent	Activity (Ci)				
	Pre-1971 Waste	1971-September 26, 1988 Waste	September 26, 1988-2007 Waste	2008-2044 Waste	Total
U-234	7.8E-06	4.9E-06	5.0E-01	2.3E+00	2.8E+00
U-235	1.3E-02	9.8E-01	2.8E-02	1.3E-01	1.1E+00
U-236	1.2E-07	2.5E-05	3.8E-06	1.8E-05	4.7E-05
U-238	1.3E-06	9.5E+00	4.5E-01	1.1E+00	1.1E+01
U38	---	3.9E-02	---	---	3.9E-02
U81	---	2.3E-02	---	---	2.3E-02

--- = *None*

5.0 References

DOE (U.S. Department of Energy), 1988, *Radioactive Waste Management*, U.S. Department of Energy Order 5820.2A, September 26.

DOE, 2001, *Radioactive Waste Management*, U.S. Department of Energy Order 435.1 (change 1 to document issued July 9, 1999), August 28.

DOE, 2002, *Los Alamos National Laboratory—Performance Management Plan for Accelerating Cleanup*, U.S. Department of Energy, July 24.

Enders, J., 1969, Handwritten calculation note from J. Enders to Wilbur, July 9.

Enders, J., 1970, Memorandum from John Enders, H-1, to Dean Meyer, Group Leader, H-1, *1969 Annual Report on Disposal of Solid Radioactive Waste*, January 27.

Hollis, D., E. Vold, R. Shuman, K. Birdsell, K. Bower, W. Hansen, D. Krier, P. Longmire, B. Newman, D. Rogers, and E. Springer, 1997, *Performance Assessment and Composite Analysis for Los Alamos National Laboratory Material Disposal Area G*, Los Alamos National Laboratory Report-54G-013, March.

Johnson, R.P., 1960, Memorandum from Ralph P. Johnson, Assistant Manager for Administration and Construction, ALO, to Paul A. Wilson, Area Manager, LAAO, *Reports on Disposal of Radioactive Wastes*, November 2.

LANL, 2003, *Investigation Work Plan for Material Disposal Area G, at Technical Area 54*, Los Alamos National Laboratory Report LA-UR-03-6491, September.

Madonia, M., 2008, E-mails from Mike Madonia, Los Alamos National Laboratory, to Rob Shuman, URS Corporation, regarding radiological data for TA-21 ER/D&D waste, May 29 and June 2,

Meyer, D.D., 1960–1969 Memoranda from Dean Meyer, H-1, to Edwin Wingfield, Administrative Branch, LAAO, *Disposal of Radioactive Wastes*, November 18, 1960 through January 20.

Myers, S., 2004, E-mail from Steve Myers, LANL Nuclear Waste and Infrastructure Services – Solid Waste Operations, to Rob Shuman, URS Corporation, regarding measurement errors, June 15.

Pollard, C.G., and R. Shuman, 1999, *Evaluation of Pre-1971 Radioactive Waste Disposal Data for TA-54 MDA G*, Rogers and Associates Engineering Corporation report RAE-9629/3005-3, December.

Rogers, M.A., 1977, *History and Environmental Setting of LASL Near-Surface Land Disposal Facilities for Radioactive Wastes (Areas A, B, C, D, E, F, G, and T),* Los Alamos Scientific Laboratory Report LA-6848-MN, Vol. 1, June.

Shuman, R., 2008, GoldSim Model Documentation and Data Selection for Los Alamos National Laboratory Technical Area 54, Area G Performance Assessment and Composite Analysis, Los Alamos National Laboratory Report, September.

Veilleux, J.M., 2005, *Determination of Plutonium Mass Fractions and Uncertainties from Waste Assay Measurements*, Los Alamos National Laboratory Report LA-UR-05-8922, November.

Warren, J.L., 1980, Memorandum from J.L. Warren to W. Hansen, Los Alamos Scientific Laboratory, *Program Status Report: Review of Past Waste Disposal Records*, January 2.

Warren, J.L., 1996, "Report on Review of Proposed Method for Characterizing 1959-1971 MDA-G Disposal Inventory," prepared for the Los Alamos National Laboratory, CST-14, July.

Wheeler, M., 1974, Memorandum from M. Wheeler to Distribution, Los Alamos Scientific Laboratory, *Tritium Content of Disposal Areas*, October 7.

Attachment I
Methodology for Estimating Radionuclide-Specific Activities for Mixed-Fission and Mixed-Activation Product Waste

I.1 Introduction

A portion of the waste included in the low-level waste (LLW) disposal database and the transuranic (TRU) waste database at Los Alamos National Laboratory (LANL or the Laboratory) is referred to as mixed-fission products (MFP) and mixed-activation products (MAP). The radionuclide-specific activities associated with these materials were estimated as part of the inventory characterization effort. The methods used to develop these activities for the MFP waste are described below, followed by a discussion of the approach used to estimate isotope-specific activities for the MAP waste.

I.2 Mixed-Fission Product Waste

Approximately 8,100 Ci of MFP waste was generated at LANL, and disposed of at Area G, from 1971 through 2007. The major generators of the disposed waste were Technical Areas (TAs) 2, 3, 21, and 48; the volumes and activities of waste sent for disposal by these facilities are summarized in Table I-1. On an activity basis, TA-3 accounts for 85 percent of the MFP waste that has been disposed of at Area G; TA-2, TA-21, and TA-48 account for 3 to 8 percent of the total. Approximately 60 percent of the total activity associated with the MFP waste was associated with LLW.

Table I-1 Mixed-Fission Waste Characteristics, by Waste Generator

Technical Area Generating MFP Wastes	Waste Volume (m^3)	Waste Activity (Ci)
2	3.2E+02	3.3E+02
3	2.9E+03	6.9E+03
21	6.8E+02	2.4E+02
48	3.1E+03	6.6E+02

The radionuclides present in MFP waste depend on the fissionable materials that led to the generation of the waste. An examination of the LLW and TRU waste data indicated that Pu-239 and U-235, both of which are fissile materials, were frequently associated with the MFP waste. A total of 178 packages of TRU waste include MFP with a listed activity greater than zero. All of these packages contain Pu-239 and 48 percent of the containers include U-235. An examination of the MFP waste included in the LLW disposal database shows that Pu-239 occurred in about 25 percent of the packages while U-235 occurred in 9 percent; neither radionuclide was listed in the majority of the MFP waste containers.

Insight into the nature of the fission events is also provided by historical reviews of reactor operations at the Laboratory. Bunker (1983) and Widner et al. (2004) indicate that most reactors in operation during the time Area G accepted MFP waste were fueled by enriched uranium; this

suggests the majority of the fission products were the result of neutron interactions with U-235. Nevertheless, the presence of plutonium fission products is also expected because one reactor in operation during the period of interest accepted molten plutonium as fuel. Furthermore, plutonium fission products occur in waste from uranium-based reactors as a result of interactions between fast neutrons and U-238. These plutonium fissions may represent a significant proportion of the total fission events; they account for one-third or more of the total fission events during the latter stages of commercial reactor operations.

Based on the evaluation of the waste records and historical information, it was assumed that the MFP waste was generated by neutron interactions with Pu-239 and U-235. England and Rider (1994) have compiled fission-product yields for U-235 and Pu-239; these data are provided in Table I-2. This table lists the radionuclides generated by U-235 and Pu-239 fission for thermal and fast neutrons, the fission products' half-lives, and the corresponding yields. The listed yields represent the abundance of each radionuclide per 100 fissions of the listed radionuclide and neutron energy. The fission yields may be expressed in terms of activity by multiplying the data by the decay constants of the various radionuclides. Normalizing these activities by the total MFP activity yields radionuclide-specific activity fractions that may be used to allocate the listed MFP activities to specific isotopes. These calculations are included in the table.

Although it was clear that the MFP waste was generated by Pu-239 and U-235 fission events, the information needed to determine the actual proportion of the waste generated by each radionuclide was unavailable. The probabilistic inventory modeling conducted in support of the performance assessment and composite analysis (Shuman, 2008) assumes that 0 to 30 percent of the waste was generated by Pu-239 fissions, with the remainder coming from U-235 fission events. All fission events were assumed to result from interactions with thermal neutrons. While some fission products will form as a result of interactions with fast neutrons, the majority will be generated by thermal fission.

The yields and activity fractions shown in Table I-2 correspond to the time at which fission occurs. Given the very short half-lives of most of the fission products, the radionuclide abundances in the waste will change significantly as the age of the waste increases and radioactive decay occurs. The effects that the age of the waste has on radionuclide abundances are shown in Table I-3; this table lists radionuclide activity fractions for radionuclides in MFP waste with ages of 1, 2, 5, and 10 years. For simplicity, all radionuclides with activity fractions less than 1.0×10^{-6} have been excluded from the table. Approximately 400 radionuclides have activity fractions equal to or greater than 1.0×10^{-6} at the time of fission. This number drops to 24 radionuclides at the end of the first year after waste generation; only 11 radionuclides have activity fractions of 1.0×10^{-6} or more 10 years after the MFP waste is generated.

Table I-2
Fission Product Yields and Activity Fractions for Mixed-Fission Product Waste at the Time of Generation

Isotope	Half-Life (yr) [a]	Fission Yields (yield/100 fissions)				Fractional Abundance (activity basis)			
		U-235		Pu-239		U-235		Pu-239	
		Thermal Neutrons	Fast Neutrons	Thermal Neutrons	Fast Neutrons	Thermal Neutrons	Fast Neutrons	Thermal Neutrons	Fast Neutrons
Cr-66	4.8E-15	2.4E-12	4.0E-11	0.0E+00	8.9E-12	5.8E-08	5.2E-06	0.0E+00	1.9E-06
Mn-66	2.1E-09	7.2E-10	9.4E-09	3.7E-10	4.0E-09	3.9E-11	2.7E-09	1.7E-10	1.9E-09
Fe-66	1.4E-06	3.8E-08	4.0E-07	3.6E-08	2.4E-07	3.1E-12	1.7E-10	2.5E-11	1.7E-10
Co-66	6.0E-09	2.8E-08	2.7E-07	1.2E-07	4.6E-07	5.4E-10	2.7E-08	1.8E-08	7.5E-08
Ni-66	6.2E-03	5.8E-09	5.0E-08	6.8E-08	1.7E-07	1.1E-16	4.9E-15	1.0E-14	2.7E-14
Cu-66	9.7E-06	1.4E-11	1.1E-10	1.4E-09	2.1E-09	1.7E-16	7.2E-15	1.4E-13	2.1E-13
Zn-66	NA	0.0E+00	0.0E+00	3.5E-12	3.1E-12	0.0E+00	0.0E+00	0.0E+00	0.0E+00
Cr-67	---	0.0E+00	4.9E-12	0.0E+00	0.0E+00	0.0E+00	0.0E+00	0.0E+00	0.0E+00
Mn-67	1.3E-09	5.4E-10	5.3E-09	7.6E-11	1.6E-09	4.6E-11	2.5E-09	5.4E-11	1.2E-09
Fe-67	1.5E-08	6.9E-08	5.1E-07	1.8E-08	2.3E-07	5.2E-10	2.1E-08	1.1E-09	1.5E-08
Co-67	1.4E-08	2.0E-07	1.3E-06	1.9E-07	1.4E-06	1.7E-09	5.9E-08	1.3E-08	1.0E-07
Ni-67	6.7E-07	9.0E-08	5.0E-07	2.3E-07	1.2E-06	1.6E-11	4.6E-10	3.3E-10	1.7E-09
Cu-67	7.1E-03	9.7E-10	5.1E-09	1.6E-08	4.8E-08	1.6E-17	4.4E-16	2.1E-15	6.7E-15
Zn-67	NA	0.0E+00	4.5E-12	9.9E-11	1.9E-10	0.0E+00	0.0E+00	0.0E+00	0.0E+00
Mn-68	8.9E-10	6.7E-11	6.7E-10	1.6E-11	3.1E-10	8.6E-12	4.6E-10	1.7E-11	3.5E-10
Fe-68	4.1E-09	3.9E-08	2.9E-07	1.4E-08	1.6E-07	1.1E-09	4.3E-08	3.1E-09	3.9E-08
Co-68	4.1E-08	2.5E-07	1.5E-06	3.1E-07	2.2E-06	6.9E-10	2.3E-08	7.2E-09	5.4E-08

NA = Not applicable; no half-life or fractional abundances are provided because the isotope is stable.

--- = No half-life was found for the radionuclide; the isotope was not included in the fission product allocation.

[a] The primary source of radionuclide half-lives was KAPL (2002). Alternate sources include England and Rider (1994) and NNDC (2004).

Table I-2 (Continued)
Fission Product Yields and Activity Fractions for Mixed-Fission Product Waste at the Time of Generation

Isotope	Half-Life (yr) [a]	Fission Yields (yield/100 fissions)				Fractional Abundance (activity basis)			
		U-235		Pu-239		U-235		Pu-239	
		Thermal Neutrons	Fast Neutrons	Thermal Neutrons	Fast Neutrons	Thermal Neutrons	Fast Neutrons	Thermal Neutrons	Fast Neutrons
Ni-68	9.2E-07	4.2E-07	2.2E-06	1.1E-06	5.5E-06	5.2E-11	1.5E-09	1.2E-09	6.0E-09
Cu-68m	7.2E-06	7.4E-09	3.7E-08	1.2E-07	3.8E-07	1.2E-13	3.2E-12	1.5E-11	5.2E-11
Cu-68	9.8E-07	3.2E-09	1.4E-08	5.0E-08	1.4E-07	3.7E-13	8.6E-12	4.8E-11	1.4E-10
Zn-68	NA	4.7E-11	2.1E-10	3.7E-09	7.3E-09	0.0E+00	0.0E+00	0.0E+00	0.0E+00
Ga-68	1.3E-04	0.0E+00	0.0E+00	2.0E-12	2.4E-12	0.0E+00	0.0E+00	1.5E-17	1.9E-17
Mn-69	4.4E-10	8.0E-12	8.9E-11	2.7E-12	6.3E-11	2.1E-12	1.2E-10	5.8E-12	1.4E-10
Fe-69	5.4E-09	1.2E-08	9.6E-08	5.9E-09	8.5E-08	2.6E-10	1.1E-08	1.0E-09	1.6E-08
Co-69	7.0E-09	3.3E-07	2.1E-06	4.7E-07	3.9E-06	5.3E-09	1.8E-07	6.4E-08	5.6E-07
Ni-69	3.6E-07	1.1E-06	6.0E-06	3.7E-06	2.1E-05	3.6E-10	1.0E-08	9.7E-09	5.8E-08
Cu-69	5.4E-06	1.1E-07	5.6E-07	1.7E-06	6.0E-06	2.4E-12	6.3E-11	2.9E-10	1.1E-09
Zn-69m	1.6E-03	1.1E-09	4.8E-09	7.0E-08	1.7E-07	7.7E-17	1.9E-15	4.3E-14	1.1E-13
Zn-69	1.1E-04	2.5E-10	9.8E-10	1.6E-08	3.5E-08	2.7E-16	5.7E-15	1.5E-13	3.3E-13
Ga-69	NA	0.0E+00	1.1E-12	1.8E-10	2.5E-10	0.0E+00	0.0E+00	0.0E+00	0.0E+00
Mn-70	---	0.0E+00	5.8E-12	0.0E+00	5.3E-12	0.0E+00	0.0E+00	0.0E+00	0.0E+00
Fe-70	4.8E-15	3.2E-09	2.8E-08	1.8E-09	2.6E-08	7.8E-05	3.6E-03	3.7E-04	5.5E-03
Co-70	4.1E-09	2.1E-07	1.4E-06	3.6E-07	3.0E-06	5.8E-09	2.1E-07	8.4E-08	7.3E-07
Ni-70	1.9E-07	2.8E-06	1.5E-05	9.3E-06	5.0E-05	1.7E-09	4.7E-08	4.7E-08	2.6E-07
Cu-70m	1.5E-06	4.5E-07	2.2E-06	6.6E-06	2.4E-05	3.4E-11	8.9E-10	4.2E-09	1.6E-08
Cu-70	1.6E-07	1.5E-07	6.1E-07	2.2E-06	6.7E-06	1.1E-10	2.3E-09	1.3E-08	4.2E-08

NA = Not applicable; no half-life or fractional abundances are provided because the isotope is stable.

--- = No half-life was found for the radionuclide; the isotope was not included in the fission product allocation.

[a] The primary source of radionuclide half-lives was KAPL (2002). Alternate sources include England and Rider (1994) and NNDC (2004).

Table I-2 (Continued)
Fission Product Yields and Activity Fractions for Mixed-Fission Product Waste at the Time of Generation

Isotope	Half-Life (yr) [a]	Fission Yields (yield/100 fissions)				Fractional Abundance (activity basis)			
		U-235		Pu-239		U-235		Pu-239	
		Thermal Neutrons	Fast Neutrons	Thermal Neutrons	Fast Neutrons	Thermal Neutrons	Fast Neutrons	Thermal Neutrons	Fast Neutrons
Zn-70	NA	3.0E-08	1.2E-07	1.5E-06	3.5E-06	0.0E+00	0.0E+00	0.0E+00	0.0E+00
Ga-70	4.0E-05	1.5E-11	5.7E-11	7.8E-09	1.1E-08	4.2E-17	8.6E-16	1.8E-13	2.7E-13
Fe-71	4.8E-15	4.9E-10	5.2E-09	1.8E-10	3.9E-09	1.2E-05	6.7E-04	3.7E-05	8.0E-04
Co-71	6.7E-09	1.5E-07	1.1E-06	1.3E-07	1.6E-06	2.6E-09	1.1E-07	1.9E-08	2.4E-07
Ni-71	8.1E-08	4.4E-06	2.6E-05	7.5E-06	6.1E-05	6.1E-09	1.9E-07	8.8E-08	7.5E-07
Cu-71	6.3E-07	3.5E-06	1.8E-05	2.1E-05	1.1E-04	6.3E-10	1.7E-08	3.2E-08	1.7E-07
Zn-71m	4.5E-04	3.3E-07	1.5E-06	6.2E-06	2.4E-05	8.3E-14	2.0E-12	1.3E-11	5.2E-11
Zn-71	4.6E-06	7.7E-08	3.0E-07	1.5E-06	4.8E-06	1.9E-12	4.1E-11	3.1E-10	1.0E-09
Ga-71	NA	9.4E-10	3.8E-09	1.4E-07	3.1E-07	0.0E+00	0.0E+00	0.0E+00	0.0E+00
Ge-71m	3.1E-02	0.0E+00	0.0E+00	1.0E-10	1.5E-10	0.0E+00	0.0E+00	3.1E-18	4.8E-18
Fe-72	4.8E-15	7.2E-11	1.1E-09	2.3E-11	4.6E-10	1.7E-06	1.4E-04	4.6E-06	9.5E-05
Co-72	2.9E-09	5.8E-08	6.0E-07	4.1E-08	4.9E-07	2.3E-09	1.3E-07	1.4E-08	1.7E-07
Ni-72	5.1E-08	7.6E-06	5.6E-05	8.5E-06	6.4E-05	1.7E-08	6.8E-07	1.6E-07	1.3E-06
Cu-72	2.1E-07	1.3E-05	7.8E-05	5.2E-05	2.5E-04	7.0E-09	2.3E-07	2.4E-07	1.2E-06
Zn-72	5.3E-03	6.1E-06	3.1E-05	5.8E-05	2.0E-04	1.3E-13	3.5E-12	1.0E-11	3.7E-11
Ga-72	1.6E-03	3.9E-08	1.6E-07	2.4E-06	5.2E-06	2.8E-15	6.2E-14	1.4E-12	3.2E-12
Ge-72	NA	3.6E-11	1.4E-10	1.3E-08	1.8E-08	0.0E+00	0.0E+00	0.0E+00	0.0E+00
As-72	3.0E-03	0.0E+00	0.0E+00	1.7E-12	1.5E-12	0.0E+00	0.0E+00	5.3E-19	4.9E-19
Fe-73	---	5.5E-12	8.3E-11	0.0E+00	1.5E-11	0.0E+00	0.0E+00	0.0E+00	0.0E+00

NA = Not applicable; no half-life or fractional abundances are provided because the isotope is stable.

--- = No half-life was found for the radionuclide; the isotope was not included in the fission product allocation.

[a] The primary source of radionuclide half-lives was KAPL (2002). Alternate sources include England and Rider (1994) and NNDC (2004).

Table I-2 (Continued)
Fission Product Yields and Activity Fractions for Mixed-Fission Product Waste at the Time of Generation

Isotope	Half-Life (yr) [a]	Fission Yields (yield/100 fissions)				Fractional Abundance (activity basis)			
		U-235		Pu-239		U-235		Pu-239	
		Thermal Neutrons	Fast Neutrons	Thermal Neutrons	Fast Neutrons	Thermal Neutrons	Fast Neutrons	Thermal Neutrons	Fast Neutrons
Co-73	4.1E-09	2.2E-08	2.2E-07	6.8E-09	6.0E-08	6.2E-10	3.3E-08	1.6E-09	1.4E-08
Ni-73	1.9E-08	7.1E-06	5.0E-05	3.5E-06	2.0E-05	4.3E-08	1.6E-06	1.8E-07	1.0E-06
Cu-73	1.3E-07	4.7E-05	2.6E-04	7.1E-05	2.5E-04	4.1E-08	1.2E-06	5.1E-07	1.8E-06
Zn-73	7.6E-07	4.6E-05	2.1E-04	1.7E-04	4.1E-04	7.0E-09	1.7E-07	2.1E-07	5.3E-07
Ga-73	5.6E-04	1.2E-06	4.8E-06	2.2E-05	3.5E-05	2.5E-13	5.3E-12	3.8E-11	6.2E-11
Ge-73m	1.7E-08	5.6E-10	1.7E-09	5.6E-08	5.3E-08	3.8E-12	6.4E-11	3.2E-09	3.1E-09
Ge-73	NA	2.4E-09	8.5E-09	2.4E-07	2.6E-07	0.0E+00	0.0E+00	0.0E+00	0.0E+00
As-73	2.2E-01	0.0E+00	0.0E+00	1.4E-10	9.1E-11	0.0E+00	0.0E+00	6.2E-19	4.1E-19
Fe-74	---	0.0E+00	3.5E-12	0.0E+00	0.0E+00	0.0E+00	0.0E+00	0.0E+00	0.0E+00
Co-74	2.9E-09	3.0E-09	2.4E-08	7.3E-10	7.2E-09	1.2E-10	5.1E-09	2.4E-10	2.4E-09
Ni-74	2.2E-08	4.6E-06	2.5E-05	1.4E-06	8.5E-06	2.4E-08	6.9E-07	5.8E-08	3.8E-07
Cu-74	5.1E-08	6.8E-05	2.9E-04	6.3E-05	2.5E-04	1.5E-07	3.5E-06	1.2E-06	4.9E-06
Zn-74	3.0E-06	2.5E-04	8.4E-04	4.4E-04	1.2E-03	9.5E-09	1.7E-07	1.4E-07	4.0E-07
Ga-74	1.5E-05	1.5E-05	4.2E-05	1.2E-04	2.3E-04	1.1E-10	1.7E-09	7.7E-09	1.5E-08
Ge-74	NA	1.7E-07	4.2E-07	5.6E-06	7.2E-06	0.0E+00	0.0E+00	0.0E+00	0.0E+00
As-74m	2.5E-07	1.2E-11	3.0E-11	4.7E-09	4.1E-09	5.2E-15	7.2E-14	1.8E-11	1.6E-11
As-74	4.9E-02	5.0E-12	1.1E-11	2.0E-09	1.5E-09	1.2E-20	1.4E-19	4.0E-17	3.1E-17
Co-75	2.6E-09	3.8E-10	3.4E-09	5.5E-11	4.0E-10	1.7E-11	8.1E-10	2.0E-11	1.5E-10
Ni-75	1.9E-08	1.5E-06	8.9E-06	2.6E-07	1.3E-06	9.2E-09	2.9E-07	1.3E-08	6.6E-08

NA = Not applicable; no half-life or fractional abundances are provided because the isotope is stable.

--- = No half-life was found for the radionuclide; the isotope was not included in the fission product allocation.

[a] The primary source of radionuclide half-lives was KAPL (2002). Alternate sources include England and Rider (1994) and NNDC (2004).

Table I-2 (Continued)
Fission Product Yields and Activity Fractions for Mixed-Fission Product Waste at the Time of Generation

Isotope	Half-Life (yr) [a]	Fission Yields (yield/100 fissions)				Fractional Abundance (activity basis)			
		U-235		Pu-239		U-235		Pu-239	
		Thermal Neutrons	Fast Neutrons	Thermal Neutrons	Fast Neutrons	Thermal Neutrons	Fast Neutrons	Thermal Neutrons	Fast Neutrons
Cu-75	3.9E-08	1.0E-04	4.4E-04	4.4E-05	1.3E-04	3.0E-07	6.9E-06	1.1E-06	3.4E-06
Zn-75	3.2E-07	7.7E-04	2.6E-03	6.8E-04	1.5E-03	2.7E-07	4.9E-06	2.0E-06	4.6E-06
Ga-75	4.0E-06	1.9E-04	5.0E-04	5.8E-04	8.6E-04	5.5E-09	7.7E-08	1.4E-07	2.1E-07
Ge-75m	1.5E-06	4.6E-06	1.1E-05	5.3E-05	5.7E-05	3.4E-10	4.2E-09	3.3E-08	3.7E-08
Ge-75	1.6E-04	6.8E-07	1.4E-06	7.9E-06	7.8E-06	5.0E-13	5.6E-12	4.8E-11	4.9E-11
As-75	NA	2.6E-09	5.5E-09	2.7E-07	1.9E-07	0.0E+00	0.0E+00	0.0E+00	0.0E+00
Se-75	3.3E-01	0.0E+00	0.0E+00	9.1E-11	4.5E-11	0.0E+00	0.0E+00	2.6E-19	1.3E-19
Co-76	---	2.5E-11	3.5E-10	2.2E-12	2.0E-11	0.0E+00	0.0E+00	0.0E+00	0.0E+00
Ni-76	6.3E-09	5.0E-07	4.4E-06	3.9E-08	2.4E-07	9.1E-09	4.2E-07	5.9E-09	3.7E-08
Cu-76	2.0E-08	8.3E-05	5.2E-04	1.7E-05	6.3E-05	4.7E-07	1.6E-05	7.8E-07	3.1E-06
Zn-76	1.8E-07	1.8E-03	1.2E-02	8.6E-04	2.3E-03	1.2E-06	4.1E-05	4.6E-06	1.2E-05
Ga-76	9.2E-07	1.1E-03	4.7E-03	1.5E-03	2.8E-03	1.3E-07	3.1E-06	1.6E-06	3.0E-06
Ge-76	NA	1.3E-04	4.7E-04	5.1E-04	6.7E-04	0.0E+00	0.0E+00	0.0E+00	0.0E+00
As-76	3.0E-03	1.7E-07	5.5E-07	5.5E-06	4.8E-06	6.3E-15	1.1E-13	1.8E-12	1.6E-12
Se-76	NA	3.0E-11	9.4E-11	7.1E-09	4.3E-09	0.0E+00	0.0E+00	0.0E+00	0.0E+00
Ni-77	3.3E-09	5.6E-08	4.1E-07	3.5E-09	2.1E-08	2.0E-09	7.7E-08	1.0E-09	6.3E-09
Cu-77	1.5E-08	4.5E-05	2.2E-04	5.4E-06	2.1E-05	3.4E-07	9.2E-06	3.5E-07	1.4E-06
Zn-77	6.7E-08	3.1E-03	1.2E-02	6.8E-04	1.8E-03	5.4E-06	1.1E-04	9.7E-06	2.7E-05
Ga-77	4.1E-07	4.1E-03	1.7E-02	3.8E-03	7.0E-03	1.1E-06	2.5E-05	8.8E-06	1.7E-05

NA = Not applicable; no half-life or fractional abundances are provided because the isotope is stable.

--- = No half-life was found for the radionuclide; the isotope was not included in the fission product allocation.

[a] The primary source of radionuclide half-lives was KAPL (2002). Alternate sources include England and Rider (1994) and NNDC (2004).

Table I-2 (Continued)
Fission Product Yields and Activity Fractions for Mixed-Fission Product Waste at the Time of Generation

Isotope	Half-Life (yr) [a]	Fission Yields (yield/100 fissions)				Fractional Abundance (activity basis)			
		U-235		Pu-239		U-235		Pu-239	
		Thermal Neutrons	Fast Neutrons	Thermal Neutrons	Fast Neutrons	Thermal Neutrons	Fast Neutrons	Thermal Neutrons	Fast Neutrons
Ge-77m	1.7E-06	8.9E-05	4.3E-04	3.5E-04	4.5E-04	6.1E-09	1.6E-07	2.0E-07	2.7E-07
Ge-77	1.3E-03	6.0E-04	3.2E-03	2.3E-03	3.3E-03	5.3E-11	1.5E-09	1.7E-09	2.5E-09
As-77	4.4E-03	4.3E-06	1.9E-05	9.9E-05	9.4E-05	1.1E-13	2.6E-12	2.1E-11	2.1E-11
Se-77m	5.5E-07	1.8E-09	7.5E-09	2.6E-07	2.2E-07	3.8E-13	8.3E-12	4.5E-10	4.0E-10
Se-77	NA	2.8E-10	1.0E-09	3.9E-08	3.0E-08	0.0E+00	0.0E+00	0.0E+00	0.0E+00
Ni-78	4.2E-09	5.0E-09	2.6E-08	2.4E-10	1.2E-09	1.4E-10	3.8E-09	5.4E-11	2.8E-10
Cu-78	1.1E-08	1.1E-05	3.8E-05	9.8E-07	3.1E-06	1.2E-07	2.1E-06	8.7E-08	2.8E-07
Zn-78	4.8E-08	3.6E-03	8.6E-03	4.4E-04	9.5E-04	8.6E-06	1.1E-04	8.9E-06	2.0E-05
Ga-78	1.6E-07	1.0E-02	2.6E-02	5.5E-03	8.2E-03	7.3E-06	9.9E-05	3.3E-05	5.0E-05
Ge-78	1.7E-04	6.9E-03	2.2E-02	1.2E-02	1.3E-02	4.8E-09	8.2E-08	6.8E-08	7.8E-08
As-78	1.7E-04	1.3E-04	2.9E-04	9.9E-04	7.7E-04	8.6E-11	1.0E-09	5.5E-09	4.4E-09
Se-78	NA	2.5E-07	6.2E-07	1.2E-05	6.5E-06	0.0E+00	0.0E+00	0.0E+00	0.0E+00
Cu-79	6.0E-09	0.0E+00	4.7E-06	1.1E-07	4.9E-07	0.0E+00	4.8E-07	1.8E-08	8.1E-08
Zn-79	3.2E-08	1.6E-03	2.6E-03	1.3E-04	4.0E-04	5.9E-06	5.1E-05	3.9E-06	1.3E-05
Ga-79	9.0E-08	1.7E-02	3.2E-02	5.5E-03	1.2E-02	2.2E-05	2.2E-04	5.8E-05	1.3E-04
Ge-79	6.0E-07	2.3E-02	5.4E-02	3.0E-02	4.1E-02	4.4E-06	5.5E-05	4.7E-05	6.7E-05
As-79	1.7E-05	2.7E-03	2.9E-03	8.0E-03	7.7E-03	1.8E-08	1.0E-07	4.5E-07	4.4E-07
Se-79m	7.5E-06	1.7E-06	1.9E-06	3.0E-05	2.0E-05	2.5E-11	1.6E-10	3.8E-09	2.6E-09
Se-79	2.9E+05	1.1E-05	1.4E-05	2.0E-04	1.5E-04	4.4E-21	2.9E-20	6.6E-19	5.0E-19

NA = Not applicable; no half-life or fractional abundances are provided because the isotope is stable.

--- = No half-life was found for the radionuclide; the isotope was not included in the fission product allocation.

[a] *The primary source of radionuclide half-lives was KAPL (2002). Alternate sources include England and Rider (1994) and NNDC (2004).*

Table I-2 (Continued)
Fission Product Yields and Activity Fractions for Mixed-Fission Product Waste at the Time of Generation

Isotope	Half-Life (yr) [a]	Fission Yields (yield/100 fissions)				Fractional Abundance (activity basis)			
		U-235		Pu-239		U-235		Pu-239	
		Thermal Neutrons	Fast Neutrons	Thermal Neutrons	Fast Neutrons	Thermal Neutrons	Fast Neutrons	Thermal Neutrons	Fast Neutrons
Br-79m	1.5E-07	1.0E-09	1.2E-09	1.9E-07	9.7E-08	7.7E-13	4.8E-12	1.2E-09	6.2E-10
Ni-80	---	1.6E-12	1.3E-11	0.0E+00	0.0E+00	0.0E+00	0.0E+00	0.0E+00	0.0E+00
Cu-80	2.9E-09	5.3E-08	2.5E-07	7.2E-09	2.7E-08	2.1E-09	5.5E-08	2.4E-09	9.3E-09
Zn-80	1.7E-08	2.4E-04	7.1E-04	3.3E-05	8.0E-05	1.6E-06	2.5E-05	1.8E-06	4.6E-06
Ga-80	5.4E-08	1.2E-02	2.1E-02	3.6E-03	5.6E-03	2.5E-05	2.4E-04	6.4E-05	1.0E-04
Ge-80	9.4E-07	1.0E-01	1.4E-01	5.5E-02	6.0E-02	1.3E-05	9.0E-05	5.6E-05	6.4E-05
As-80	5.1E-07	1.4E-02	1.6E-02	3.2E-02	2.5E-02	3.1E-06	2.0E-05	6.0E-05	4.8E-05
Se-80	NA	4.9E-04	4.3E-04	3.3E-03	1.8E-03	0.0E+00	0.0E+00	0.0E+00	0.0E+00
Br-80m	5.0E-04	1.1E-07	9.0E-08	1.1E-06	2.6E-06	2.5E-14	1.1E-13	2.1E-12	5.2E-12
Cu-81	2.3E-09	0.0E+00	9.4E-09	2.8E-10	1.1E-09	0.0E+00	2.5E-09	1.1E-10	4.6E-10
Zn-81	9.2E-09	0.0E+00	7.2E-05	3.6E-06	8.9E-06	0.0E+00	4.8E-06	3.7E-07	9.6E-07
Ga-81	3.9E-08	8.2E-03	1.0E-02	1.5E-03	2.3E-03	2.4E-05	1.6E-04	3.7E-05	5.9E-05
Ge-81	2.4E-07	1.3E-01	1.5E-01	5.5E-02	5.7E-02	6.0E-05	3.7E-04	2.2E-04	2.4E-04
As-81	1.0E-06	6.1E-02	6.8E-02	1.0E-01	7.1E-02	6.7E-06	4.0E-05	9.4E-05	6.7E-05
Se-81m	1.1E-04	6.9E-03	3.9E-03	2.1E-02	1.1E-02	7.3E-09	2.2E-08	1.9E-07	9.6E-08
Se-81	3.5E-05	1.0E-03	5.3E-04	3.2E-03	1.4E-03	3.4E-09	9.2E-09	8.6E-08	4.0E-08
Br-81	NA	8.9E-06	5.9E-06	2.7E-04	8.3E-05	0.0E+00	0.0E+00	0.0E+00	0.0E+00
Cu-82	---	1.5E-10	1.6E-10	3.4E-12	2.0E-11	0.0E+00	0.0E+00	0.0E+00	0.0E+00
Zn-82	4.0E-09	1.1E-05	6.4E-06	1.8E-07	6.5E-07	3.1E-07	9.8E-07	4.2E-08	1.6E-07

NA = Not applicable; no half-life or fractional abundances are provided because the isotope is stable.

--- = No half-life was found for the radionuclide; the isotope was not included in the fission product allocation.

[a] The primary source of radionuclide half-lives was KAPL (2002). Alternate sources include England and Rider (1994) and NNDC (2004).

Table I-2 (Continued)
Fission Product Yields and Activity Fractions for Mixed-Fission Product Waste at the Time of Generation

Isotope	Half-Life (yr) [a]	Fission Yields (yield/100 fissions)				Fractional Abundance (activity basis)			
		U-235		Pu-239		U-235		Pu-239	
		Thermal Neutrons	Fast Neutrons	Thermal Neutrons	Fast Neutrons	Thermal Neutrons	Fast Neutrons	Thermal Neutrons	Fast Neutrons
Ga-82	1.9E-08	6.3E-03	2.4E-03	2.0E-04	4.6E-04	3.8E-05	7.7E-05	1.0E-05	2.4E-05
Ge-82	1.5E-07	1.3E-01	1.5E-01	2.7E-02	4.1E-02	9.9E-05	6.3E-04	1.8E-04	2.8E-04
As-82m	4.3E-07	2.7E-02	7.4E-02	5.7E-02	5.7E-02	7.2E-06	1.0E-04	1.3E-04	1.3E-04
As-82	6.0E-07	1.3E-01	7.4E-02	5.7E-02	5.7E-02	2.5E-05	7.5E-05	9.0E-05	9.4E-05
Se-82	NA	3.7E-02	4.0E-02	8.8E-02	6.2E-02	0.0E+00	0.0E+00	0.0E+00	0.0E+00
Zn-83	2.7E-09	6.3E-08	2.5E-07	4.9E-09	2.2E-08	2.7E-09	5.7E-08	1.8E-09	8.3E-09
Ga-83	9.8E-09	1.9E-04	4.7E-04	2.3E-05	6.1E-05	2.2E-06	2.9E-05	2.2E-06	6.2E-06
Ge-83	6.0E-08	4.8E-02	7.7E-02	8.0E-03	1.4E-02	9.1E-05	7.8E-04	1.3E-04	2.4E-04
As-83	4.2E-07	2.9E-01	3.1E-01	1.2E-01	1.3E-01	7.9E-05	4.4E-04	2.6E-04	3.1E-04
Se-83m	2.2E-06	3.4E-02	3.2E-02	3.7E-02	2.7E-02	1.7E-06	8.8E-06	1.6E-05	1.2E-05
Se-83	4.2E-05	1.4E-01	1.6E-01	1.2E-01	1.3E-01	3.9E-07	2.3E-06	2.7E-06	3.1E-06
Br-83	2.7E-04	2.0E-02	3.2E-03	1.7E-02	1.0E-02	8.2E-09	7.1E-09	6.0E-08	3.6E-08
Kr-83m	2.1E-04	1.6E-06	8.5E-07	2.9E-05	1.1E-05	8.4E-13	2.5E-12	1.3E-10	5.1E-11
Zn-84	---	1.2E-06	7.2E-09	1.0E-10	5.8E-10	0.0E+00	0.0E+00	0.0E+00	0.0E+00
Ga-84	2.9E-09	1.1E-02	3.8E-05	1.4E-06	4.5E-06	4.5E-04	8.3E-06	4.5E-07	1.6E-06
Ge-84	3.0E-08	1.9E-02	3.0E-02	1.9E-03	4.0E-03	7.2E-05	6.1E-04	5.8E-05	1.3E-04
As-84	1.3E-07	2.0E-01	2.8E-01	6.6E-02	9.0E-02	1.8E-04	1.3E-03	5.0E-04	7.0E-04
Se-84	6.1E-06	6.3E-01	5.9E-01	3.3E-01	3.3E-01	1.2E-05	6.0E-05	5.1E-05	5.4E-05
Br-84m	1.1E-05	1.7E-02	1.8E-02	4.9E-02	3.5E-02	1.7E-07	9.6E-07	4.1E-06	3.0E-06

NA = Not applicable; no half-life or fractional abundances are provided because the isotope is stable.

--- = No half-life was found for the radionuclide; the isotope was not included in the fission product allocation.

[a] The primary source of radionuclide half-lives was KAPL (2002). Alternate sources include England and Rider (1994) and NNDC (2004).

Table I-2 (Continued)
Fission Product Yields and Activity Fractions for Mixed-Fission Product Waste at the Time of Generation

Isotope	Half-Life (yr) [a]	Fission Yields (yield/100 fissions)				Fractional Abundance (activity basis)			
		U-235		Pu-239		U-235		Pu-239	
		Thermal Neutrons	Fast Neutrons	Thermal Neutrons	Fast Neutrons	Thermal Neutrons	Fast Neutrons	Thermal Neutrons	Fast Neutrons
Br-84	6.1E-05	1.9E-02	8.4E-03	2.7E-02	1.6E-02	3.5E-08	8.6E-08	4.3E-07	2.7E-07
Ga-85	2.8E-09	5.9E-07	2.2E-06	2.9E-08	2.0E-07	2.4E-08	5.0E-07	9.9E-09	7.1E-08
Ge-85	1.7E-08	2.1E-03	4.9E-03	1.1E-04	5.0E-04	1.4E-05	1.8E-04	6.0E-06	2.9E-05
As-85	6.4E-08	1.2E-01	2.1E-01	1.4E-02	4.2E-02	2.2E-04	2.0E-03	2.1E-04	6.5E-04
Se-85m	6.0E-07	4.5E-01	5.3E-01	2.0E-01	1.9E-01	8.5E-05	5.4E-04	3.2E-04	3.1E-04
Se-85	1.0E-06	4.5E-01	5.3E-01	2.1E-01	1.9E-01	5.1E-05	3.2E-04	1.9E-04	1.9E-04
Br-85	5.5E-06	2.4E-01	1.8E-01	1.5E-01	1.9E-01	4.9E-06	2.1E-05	2.6E-05	3.5E-05
Kr-85m	5.1E-04	5.9E-03	6.3E-04	2.4E-03	1.9E-03	1.3E-09	7.6E-10	4.4E-09	3.8E-09
Kr-85	1.1E+01	2.6E-02	3.1E-03	1.0E-02	9.5E-03	2.7E-13	1.8E-13	8.9E-13	8.7E-13
Zn-86	---	2.3E-10	0.0E+00	0.0E+00	0.0E+00	0.0E+00	0.0E+00	0.0E+00	0.0E+00
Ga-86	4.8E-15	3.3E-05	4.9E-08	1.2E-09	4.4E-09	7.9E-01	6.3E-03	2.4E-04	9.3E-04
Ge-86	7.8E-09	6.3E-01	5.4E-04	1.8E-05	4.5E-05	9.2E-03	4.3E-05	2.1E-06	5.7E-06
As-86	2.9E-08	2.0E-02	5.9E-02	6.0E-03	1.1E-02	8.0E-05	1.3E-03	2.0E-04	3.7E-04
Se-86	4.8E-07	8.4E-01	1.2E+00	2.9E-01	3.3E-01	2.0E-04	1.6E-03	5.9E-04	6.8E-04
Br-86m	1.4E-07	2.3E-01	2.2E-01	1.9E-01	1.8E-01	1.8E-04	9.7E-04	1.3E-03	1.2E-03
Br-86	1.8E-06	2.3E-01	2.3E-01	1.9E-01	1.8E-01	1.5E-05	7.9E-05	1.0E-04	9.9E-05
Ge-87	4.2E-09	2.2E-03	3.2E-05	9.3E-07	2.6E-06	5.9E-05	4.6E-06	2.1E-07	6.0E-07
As-87	1.9E-08	5.1E-02	1.7E-02	1.3E-03	2.3E-03	3.0E-04	5.4E-04	6.4E-05	1.2E-04
Se-87	1.8E-07	7.3E-01	6.8E-01	1.4E-01	1.8E-01	4.6E-04	2.3E-03	7.1E-04	9.7E-04

NA = Not applicable; no half-life or fractional abundances are provided because the isotope is stable.

--- = No half-life was found for the radionuclide; the isotope was not included in the fission product allocation.

[a] The primary source of radionuclide half-lives was KAPL (2002). Alternate sources include England and Rider (1994) and NNDC (2004).

Table I-2 (Continued)
Fission Product Yields and Activity Fractions for Mixed-Fission Product Waste at the Time of Generation

Isotope	Half-Life (yr) [a]	Fission Yields (yield/100 fissions)				Fractional Abundance (activity basis)			
		U-235		Pu-239		U-235		Pu-239	
		Thermal Neutrons	Fast Neutrons	Thermal Neutrons	Fast Neutrons	Thermal Neutrons	Fast Neutrons	Thermal Neutrons	Fast Neutrons
Br-87	1.8E-06	1.3E+00	1.4E+00	5.5E-01	6.2E-01	8.2E-05	5.0E-04	3.0E-04	3.5E-04
Kr-87	1.4E-04	4.6E-01	3.5E-01	2.8E-01	2.2E-01	3.7E-07	1.5E-06	1.9E-06	1.5E-06
Rb-87	4.9E10	2.5E-03	1.3E-03	1.5E-02	6.5E-03	5.9E-24	1.7E-23	2.9E-22	1.3E-22
Sr-87m	3.2E-04	2.5E-07	9.8E-08	5.8E-06	2.3E-06	9.0E-14	1.9E-13	1.7E-11	7.3E-12
Ge-88	4.1E-09	5.2E-05	1.4E-06	2.7E-08	7.6E-08	1.5E-06	2.1E-07	6.4E-09	1.8E-08
As-88	4.3E-09	1.2E-01	2.0E-03	1.0E-04	1.9E-04	3.3E-03	2.9E-04	2.3E-05	4.5E-05
Se-88	4.8E-08	2.7E-01	4.5E-01	4.2E-02	5.8E-02	6.5E-04	5.8E-03	8.5E-04	1.2E-03
Br-88	5.2E-07	1.4E+00	1.7E+00	4.7E-01	4.9E-01	3.1E-04	2.0E-03	8.6E-04	9.3E-04
Kr-88	3.2E-04	1.7E+00	1.3E+00	7.5E-01	7.3E-01	6.1E-07	2.4E-06	2.2E-06	2.2E-06
Rb-88	3.4E-05	2.2E-02	5.5E-02	5.7E-02	4.1E-02	7.6E-08	1.0E-06	1.6E-06	1.2E-06
Sr-88	NA	7.7E-05	3.6E-05	6.8E-04	3.4E-04	0.0E+00	0.0E+00	0.0E+00	0.0E+00
As-89	3.8E-09	1.5E-04	2.1E-04	4.6E-06	1.3E-05	4.6E-06	3.4E-05	1.1E-06	3.3E-06
Se-89	1.3E-08	4.9E-02	1.2E-01	5.0E-03	1.1E-02	4.3E-04	5.8E-03	3.7E-04	8.3E-04
Br-89	1.4E-07	1.0E+00	1.3E+00	3.4E-01	3.2E-01	8.6E-04	5.9E-03	2.4E-03	2.3E-03
Kr-89	6.0E-06	3.4E+00	2.6E+00	1.1E+00	1.1E+00	6.6E-05	2.6E-04	1.8E-04	1.9E-04
Rb-89	2.9E-05	2.1E-01	3.9E-01	2.6E-01	2.7E-01	8.0E-07	8.2E-06	8.3E-06	9.1E-06
Sr-89	1.4E-01	1.8E-02	8.3E-04	1.5E-02	5.1E-03	1.5E-11	3.7E-12	1.0E-10	3.6E-11
Y-89m	5.0E-07	1.9E-07	6.7E-08	7.0E-06	3.1E-06	4.3E-11	8.3E-11	1.3E-08	6.2E-09
Se-90	1.4E-08	1.3E-02	2.4E-02	1.2E-03	1.5E-03	1.1E-04	1.1E-03	8.6E-05	1.1E-04

NA = Not applicable; no half-life or fractional abundances are provided because the isotope is stable.

--- = No half-life was found for the radionuclide; the isotope was not included in the fission product allocation.

[a] The primary source of radionuclide half-lives was KAPL (2002). Alternate sources include England and Rider (1994) and NNDC (2004).

Table I-2 (Continued)
Fission Product Yields and Activity Fractions for Mixed-Fission Product Waste at the Time of Generation

Isotope	Half-Life (yr) [a]	Fission Yields (yield/100 fissions)				Fractional Abundance (activity basis)			
		U-235		Pu-239		U-235		Pu-239	
		Thermal Neutrons	Fast Neutrons	Thermal Neutrons	Fast Neutrons	Thermal Neutrons	Fast Neutrons	Thermal Neutrons	Fast Neutrons
Br-90	6.0E-08	5.5E-01	7.3E-01	2.1E-01	1.2E-01	1.1E-03	7.4E-03	3.4E-03	1.9E-03
Kr-90	1.0E-06	4.4E+00	4.0E+00	1.1E+00	1.3E+00	4.9E-04	2.4E-03	1.0E-03	1.3E-03
Rb-90m	8.2E-06	7.1E-01	6.9E-01	6.0E-01	4.8E-01	9.9E-06	5.2E-05	7.1E-05	5.9E-05
Rb-90	4.9E-06	1.4E-01	1.3E-01	1.4E-01	9.9E-02	3.2E-06	1.6E-05	2.7E-05	2.0E-05
Sr-90	2.9E+01	7.4E-02	3.4E-02	9.7E-02	4.5E-02	2.9E-13	7.3E-13	3.2E-12	1.6E-12
Y-90	7.3E-03	9.0E-06	4.6E-06	1.9E-04	9.7E-05	1.4E-13	3.9E-13	2.5E-11	1.3E-11
Se-91	8.6E-09	6.7E-04	9.6E-04	0.0E+00	1.1E-04	8.9E-06	6.9E-05	0.0E+00	1.3E-05
Br-91	1.7E-08	2.2E-01	1.4E-01	2.0E-02	3.3E-02	1.5E-03	4.9E-03	1.1E-03	1.9E-03
Kr-91	2.7E-07	3.2E+00	2.9E+00	7.0E-01	9.4E-01	1.3E-03	6.6E-03	2.4E-03	3.4E-03
Rb-91	1.8E-06	2.2E+00	2.0E+00	1.4E+00	1.3E+00	1.4E-04	6.7E-04	7.2E-04	7.0E-04
Sr-91	1.1E-03	2.5E-01	6.9E-01	3.9E-01	2.5E-01	2.7E-08	3.9E-07	3.4E-07	2.3E-07
Y-91	1.6E-01	3.3E-04	1.7E-04	2.5E-03	2.0E-03	2.4E-13	6.6E-13	1.5E-11	1.2E-11
Se-92	5.3E-09	4.2E-05	5.5E-05	2.3E-06	5.8E-06	9.0E-07	6.4E-06	4.1E-07	1.1E-06
Br-92	1.1E-08	2.7E-02	2.1E-02	2.5E-03	4.8E-03	2.9E-04	1.2E-03	2.2E-04	4.4E-04
Kr-92	5.8E-08	1.7E+00	1.4E+00	3.1E-01	4.9E-01	3.3E-03	1.4E-02	5.1E-03	8.3E-03
Rb-92	1.4E-07	3.1E+00	2.8E+00	1.6E+00	1.5E+00	2.5E-03	1.2E-02	1.1E-02	1.1E-02
Sr-92	3.1E-04	1.1E+00	1.6E+00	1.0E+00	9.6E-01	4.0E-07	3.2E-06	3.2E-06	3.1E-06
Y-92	4.0E-04	7.2E-02	2.9E-03	4.5E-02	2.0E-02	2.0E-08	4.4E-09	1.1E-07	4.9E-08
Br-93	3.2E-09	3.1E-03	6.4E-02	6.6E-03	4.9E-04	1.1E-04	1.2E-02	2.0E-03	1.5E-04

NA = Not applicable; no half-life or fractional abundances are provided because the isotope is stable.

--- = No half-life was found for the radionuclide; the isotope was not included in the fission product allocation.

[a] The primary source of radionuclide half-lives was KAPL (2002). Alternate sources include England and Rider (1994) and NNDC (2004).

Table I-2 (Continued)
Fission Product Yields and Activity Fractions for Mixed-Fission Product Waste at the Time of Generation

Isotope	Half-Life (yr) [a]	Fission Yields (yield/100 fissions)				Fractional Abundance (activity basis)			
		U-235		Pu-239		U-235		Pu-239	
		Thermal Neutrons	Fast Neutrons	Thermal Neutrons	Fast Neutrons	Thermal Neutrons	Fast Neutrons	Thermal Neutrons	Fast Neutrons
Kr-93	4.1E-08	4.9E-01	3.1E-01	6.4E-02	1.4E-01	1.4E-03	4.6E-03	1.5E-03	3.3E-03
Rb-93	1.9E-07	3.1E+00	3.4E+00	1.4E+00	1.5E+00	1.9E-03	1.1E-02	7.0E-03	7.8E-03
Sr-93	1.4E-05	2.6E+00	2.1E+00	2.1E+00	2.0E+00	2.1E-05	9.3E-05	1.5E-04	1.4E-04
Y-93	1.2E-03	1.1E-01	2.1E-01	1.7E-01	1.5E-01	1.1E-08	1.1E-07	1.4E-07	1.3E-07
Zr-93	1.5E+06	1.4E-04	4.9E-05	1.7E-03	1.2E-03	1.0E-20	2.0E-20	1.1E-18	7.6E-19
Nb-93m	1.6E+01	8.5E-10	2.1E-10	9.9E-08	4.8E-08	6.1E-21	8.1E-21	5.9E-18	3.0E-18
Se-94	4.8E-15	1.7E-08	1.6E-08	2.3E-07	2.5E-09	4.1E-04	2.0E-03	4.6E-02	5.1E-04
Br-94	2.2E-09	1.7E-04	8.1E-05	2.7E-03	2.3E-05	8.6E-06	2.3E-05	1.2E-03	1.0E-05
Kr-94	6.7E-09	8.7E-02	6.2E-02	2.2E-02	2.4E-02	1.5E-03	5.7E-03	3.1E-03	3.6E-03
Rb-94	8.6E-08	1.6E+00	1.9E+00	7.0E-01	6.5E-01	2.1E-03	1.4E-02	7.8E-03	7.5E-03
Sr-94	2.4E-06	4.5E+00	3.8E+00	2.9E+00	2.9E+00	2.2E-04	9.8E-04	1.2E-03	1.2E-03
Y-94	3.6E-05	3.9E-01	6.8E-01	6.8E-01	7.3E-01	1.3E-06	1.2E-05	1.8E-05	2.0E-05
Zr-94	NA	2.0E-02	1.3E-03	3.0E-02	1.5E-02	0.0E+00	0.0E+00	0.0E+00	0.0E+00
Kr-95	2.5E-08	7.2E-03	2.3E-02	1.1E-03	3.1E-03	3.3E-05	5.6E-04	4.3E-05	1.2E-04
Rb-95	1.2E-08	7.6E-01	9.0E-01	4.3E-01	2.9E-01	7.3E-03	4.6E-02	3.5E-02	2.4E-02
Sr-95	8.0E-07	4.5E+00	4.4E+00	2.6E+00	2.9E+00	6.5E-04	3.4E-03	3.1E-03	3.6E-03
Y-95	2.0E-05	1.1E+00	1.2E+00	1.7E+00	1.4E+00	6.5E-06	3.7E-05	8.2E-05	7.1E-05
Zr-95	1.8E-01	1.3E-01	1.5E-02	1.3E-01	9.3E-02	8.3E-11	5.2E-11	6.8E-10	5.3E-10
Nb-95m	9.9E-03	2.5E-05	9.1E-07	1.3E-04	3.9E-05	2.9E-13	5.6E-14	1.3E-11	4.0E-12

NA = Not applicable; no half-life or fractional abundances are provided because the isotope is stable.

--- = No half-life was found for the radionuclide; the isotope was not included in the fission product allocation.

[a] The primary source of radionuclide half-lives was KAPL (2002). Alternate sources include England and Rider (1994) and NNDC (2004).

Table I-2 (Continued)
Fission Product Yields and Activity Fractions for Mixed-Fission Product Waste at the Time of Generation

Isotope	Half-Life (yr) [a]	Fission Yields (yield/100 fissions)				Fractional Abundance (activity basis)			
		U-235		Pu-239		U-235		Pu-239	
		Thermal Neutrons	Fast Neutrons	Thermal Neutrons	Fast Neutrons	Thermal Neutrons	Fast Neutrons	Thermal Neutrons	Fast Neutrons
Nb-95	9.6E-02	1.1E-04	4.4E-06	5.7E-04	1.9E-04	1.3E-13	2.8E-14	5.6E-12	2.0E-12
Mo-95	NA	4.9E-10	1.5E-10	9.3E-08	4.9E-08	0.0E+00	0.0E+00	0.0E+00	0.0E+00
Se-96	---	1.3E-11	3.1E-12	4.8E-12	0.0E+00	0.0E+00	0.0E+00	0.0E+00	0.0E+00
Br-96	2.8E-09	1.9E-06	2.3E-07	6.2E-07	2.3E-08	7.8E-08	5.0E-08	2.1E-07	8.0E-09
Kr-96	9.3E-09	3.8E-02	2.3E-03	8.2E-03	2.5E-04	4.7E-04	1.5E-04	8.4E-04	2.6E-05
Rb-96	6.3E-09	1.7E-01	2.3E-01	3.9E-02	6.0E-02	3.1E-03	2.2E-02	5.9E-03	9.5E-03
Sr-96	3.4E-08	3.6E+00	4.4E+00	1.8E+00	2.0E+00	1.2E-02	7.9E-02	5.1E-02	5.8E-02
Y-96m	3.0E-07	2.0E+00	1.4E+00	2.2E+00	2.1E+00	7.6E-04	2.7E-03	7.0E-03	6.8E-03
Y-96m	1.7E-07	2.2E-01	1.3E-01	2.5E-01	2.1E-01	1.5E-04	4.9E-04	1.4E-03	1.2E-03
Kr-97	3.2E-09	3.0E-05	1.2E-04	1.6E-03	1.2E-05	1.1E-06	2.2E-05	4.9E-04	3.8E-06
Rb-97	5.4E-09	3.8E-02	5.4E-02	5.4E-03	1.1E-02	8.1E-04	6.2E-03	9.6E-04	2.0E-03
Sr-97	1.4E-08	1.7E+00	2.4E+00	7.9E-01	8.6E-01	1.4E-02	1.1E-01	5.5E-02	6.2E-02
Y-97	1.2E-07	3.1E+00	3.0E+00	3.0E+00	3.0E+00	3.0E-03	1.6E-02	2.4E-02	2.5E-02
Zr-97	1.9E-03	1.1E+00	5.6E-01	1.6E+00	1.4E+00	6.5E-08	1.8E-07	7.9E-07	7.5E-07
Nb-97m	1.7E-06	2.5E-03	4.4E-04	1.5E-02	5.3E-03	1.7E-07	1.6E-07	8.7E-06	3.1E-06
Nb-97	1.4E-04	1.1E-02	2.2E-03	6.5E-02	2.6E-02	8.8E-09	9.5E-09	4.4E-07	1.8E-07
Kr-98	5.1E-09	1.6E-03	4.3E-06	2.2E-07	3.9E-07	3.7E-05	5.2E-07	4.2E-08	7.5E-08
Rb-98	3.4E-09	2.4E-03	5.4E-03	6.8E-04	9.3E-04	8.0E-05	9.7E-04	1.9E-04	2.7E-04
Sr-98	2.1E-08	8.1E-01	1.0E+00	3.3E-01	2.6E-01	4.5E-03	3.1E-02	1.5E-02	1.3E-02

NA = Not applicable; no half-life or fractional abundances are provided because the isotope is stable.

--- = No half-life was found for the radionuclide; the isotope was not included in the fission product allocation.

[a] The primary source of radionuclide half-lives was KAPL (2002). Alternate sources include England and Rider (1994) and NNDC (2004).

Table I-2 (Continued)
Fission Product Yields and Activity Fractions for Mixed-Fission Product Waste at the Time of Generation

Isotope	Half-Life (yr) [a]	Fission Yields (yield/100 fissions)				Fractional Abundance (activity basis)			
		U-235		Pu-239		U-235		Pu-239	
		Thermal Neutrons	Fast Neutrons	Thermal Neutrons	Fast Neutrons	Thermal Neutrons	Fast Neutrons	Thermal Neutrons	Fast Neutrons
Y-98m	6.7E-08	1.1E+00	1.4E+00	1.2E+00	1.1E+00	1.9E-03	1.3E-02	1.7E-02	1.6E-02
Y-98	1.9E-08	1.1E+00	1.4E+00	1.2E+00	1.1E+00	6.8E-03	4.6E-02	6.1E-02	5.6E-02
Zr-98	9.7E-07	2.6E+00	2.0E+00	2.9E+00	3.1E+00	3.0E-04	1.3E-03	2.9E-03	3.2E-03
Nb-98m	9.7E-05	3.9E-02	5.0E-03	4.5E-02	3.7E-02	4.6E-08	3.2E-08	4.4E-07	3.8E-07
Nb-98	9.2E-08	1.2E-01	1.8E-02	1.3E-01	1.3E-01	1.4E-04	1.2E-04	1.4E-03	1.4E-03
Sr-99	8.5E-09	1.3E-01	2.2E-01	3.8E-02	4.9E-02	1.8E-03	1.6E-02	4.2E-03	5.7E-03
Y-99	4.7E-08	2.0E+00	2.3E+00	1.4E+00	1.3E+00	4.8E-03	3.0E-02	3.0E-02	2.7E-02
Zr-99	7.0E-08	3.6E+00	3.4E+00	3.8E+00	4.0E+00	5.9E-03	3.0E-02	5.2E-02	5.7E-02
Nb-99m	4.9E-06	4.1E-01	1.4E-01	8.8E-01	6.3E-01	9.4E-06	1.8E-05	1.7E-04	1.3E-04
Nb-99	4.8E-07	3.0E-02	1.2E-02	7.5E-02	5.4E-02	7.2E-06	1.6E-05	1.5E-04	1.1E-04
Mo-99	7.5E-03	4.3E-02	7.2E-04	3.8E-02	1.3E-02	6.5E-10	5.9E-11	4.8E-09	1.7E-09
Tc-99m	6.9E-04	2.9E-08	9.9E-09	2.8E-06	1.5E-06	4.8E-15	8.9E-15	3.9E-12	2.2E-12
Tc-99	2.1E+05	1.2E-07	4.9E-08	1.2E-05	7.3E-06	6.6E-23	1.4E-22	5.4E-20	3.4E-20
Kr-100	4.8E-15	1.2E-06	9.6E-10	6.5E-11	1.0E-10	2.8E-02	1.2E-04	1.3E-05	2.1E-05
Rb-100	1.7E-09	3.5E-02	1.6E-05	2.1E-06	2.5E-06	2.4E-03	5.7E-06	1.2E-06	1.5E-06
Sr-100	6.4E-09	8.2E-03	3.6E-02	6.8E-03	6.7E-03	1.5E-04	3.4E-03	1.0E-03	1.1E-03
Y-100	2.3E-08	5.7E-01	8.7E-01	3.5E-01	4.4E-01	2.8E-03	2.3E-02	1.4E-02	1.9E-02
Zr-100	2.3E-07	5.0E+00	4.9E+00	4.8E+00	4.4E+00	2.5E-03	1.3E-02	2.0E-02	1.9E-02
Nb-100m	9.5E-08	3.2E-01	2.5E-01	7.5E-01	8.2E-01	3.8E-04	1.6E-03	7.5E-03	8.6E-03

NA = Not applicable; no half-life or fractional abundances are provided because the isotope is stable.

--- = No half-life was found for the radionuclide; the isotope was not included in the fission product allocation.

[a] The primary source of radionuclide half-lives was KAPL (2002). Alternate sources include England and Rider (1994) and NNDC (2004).

Table I-2 (Continued)
Fission Product Yields and Activity Fractions for Mixed-Fission Product Waste at the Time of Generation

Isotope	Half-Life (yr) [a]	Fission Yields (yield/100 fissions)				Fractional Abundance (activity basis)			
		U-235		Pu-239		U-235		Pu-239	
		Thermal Neutrons	Fast Neutrons	Thermal Neutrons	Fast Neutrons	Thermal Neutrons	Fast Neutrons	Thermal Neutrons	Fast Neutrons
Nb-100	4.8E-08	3.2E-01	2.5E-01	7.5E-01	8.2E-01	7.7E-04	3.2E-03	1.5E-02	1.7E-02
Mo-100	NA	7.3E-02	1.1E-02	1.4E-01	1.1E-01	0.0E+00	0.0E+00	0.0E+00	0.0E+00
Tc-100	5.0E-07	5.6E-06	2.4E-06	3.1E-04	1.9E-04	1.3E-09	2.9E-09	5.9E-07	3.8E-07
Sr-101	3.7E-09	4.5E-03	2.6E-03	2.9E-04	4.7E-04	1.4E-04	4.3E-04	7.5E-05	1.3E-04
Y-101	1.4E-08	2.8E-01	2.8E-01	8.4E-02	1.1E-01	2.3E-03	1.3E-02	5.9E-03	8.2E-03
Zr-101	7.6E-08	2.8E+00	3.4E+00	2.3E+00	2.7E+00	4.2E-03	2.8E-02	2.9E-02	3.5E-02
Nb-101	2.3E-07	1.9E+00	1.4E+00	3.5E+00	3.3E+00	9.8E-04	3.7E-03	1.5E-02	1.4E-02
Mo-101	2.8E-05	1.9E-01	6.9E-02	1.4E-01	5.7E-01	7.7E-07	1.5E-06	4.8E-06	2.0E-05
Tc-101	2.7E-05	1.6E-04	7.6E-05	1.2E-02	3.7E-03	6.8E-10	1.7E-09	4.4E-07	1.4E-07
Ru-101	NA	1.6E-08	6.4E-09	2.4E-06	2.0E-06	0.0E+00	0.0E+00	0.0E+00	0.0E+00
Rh-101m	1.2E-02	0.0E+00	0.0E+00	3.8E-11	2.9E-11	0.0E+00	0.0E+00	3.1E-18	2.4E-18
Rh-101	3.3E+00	3.3E-11	0.0E+00	9.0E-12	5.9E-12	1.1E-21	0.0E+00	2.6E-21	1.8E-21
Sr-102	2.2E-09	1.7E-04	1.7E-04	8.0E-06	2.4E-05	9.2E-06	4.8E-05	3.6E-06	1.1E-05
Y-102	1.1E-08	2.7E-01	4.6E-02	6.1E-03	1.6E-02	2.7E-03	2.5E-03	5.1E-04	1.4E-03
Zr-102	9.2E-08	1.8E+00	2.2E+00	1.2E+00	1.3E+00	2.2E-03	1.5E-02	1.3E-02	1.4E-02
Nb-102	4.1E-08	1.6E+00	1.7E+00	3.1E+00	3.5E+00	4.4E-03	2.6E-02	7.2E-02	8.5E-02
Mo-102	2.1E-05	6.5E-01	3.7E-01	1.8E+00	1.8E+00	3.5E-06	1.0E-05	7.8E-05	8.5E-05
Tc-102m	8.4E-06	9.6E-03	4.9E-04	3.4E-02	1.6E-02	1.3E-07	3.6E-08	3.9E-06	1.9E-06
Tc-102	1.7E-07	9.6E-03	4.9E-04	3.4E-02	1.6E-02	6.5E-06	1.8E-06	1.9E-04	9.3E-05

NA = Not applicable; no half-life or fractional abundances are provided because the isotope is stable.

--- = No half-life was found for the radionuclide; the isotope was not included in the fission product allocation.

[a] The primary source of radionuclide half-lives was KAPL (2002). Alternate sources include England and Rider (1994) and NNDC (2004).

Table I-2 (Continued)
Fission Product Yields and Activity Fractions for Mixed-Fission Product Waste at the Time of Generation

Isotope	Half-Life (yr) [a]	Fission Yields (yield/100 fissions)				Fractional Abundance (activity basis)			
		U-235		Pu-239		U-235		Pu-239	
		Thermal Neutrons	Fast Neutrons	Thermal Neutrons	Fast Neutrons	Thermal Neutrons	Fast Neutrons	Thermal Neutrons	Fast Neutrons
Ru-102	NA	9.8E-07	4.0E-07	7.7E-05	6.9E-05	0.0E+00	0.0E+00	0.0E+00	0.0E+00
Y-103	7.0E-09	2.6E-03	5.6E-03	1.0E-03	1.4E-03	4.2E-05	4.9E-04	1.4E-04	2.0E-04
Zr-103	4.1E-08	5.0E-01	6.3E-01	2.2E-01	3.2E-01	1.4E-03	9.3E-03	5.2E-03	7.8E-03
Nb-103	4.8E-08	1.4E+00	1.8E+00	2.7E+00	2.9E+00	3.4E-03	2.3E-02	5.4E-02	6.0E-02
Mo-103	2.1E-06	1.0E+00	8.0E-01	3.8E+00	3.4E+00	5.6E-05	2.3E-04	1.7E-03	1.6E-03
Tc-103	1.7E-06	8.2E-02	9.4E-03	2.5E-01	2.1E-01	5.5E-06	3.4E-06	1.4E-04	1.2E-04
Ru-103	1.1E-01	2.4E-05	9.9E-06	1.3E-03	1.3E-03	2.5E-14	5.7E-14	1.1E-11	1.2E-11
Rh-103m	1.1E-04	4.3E-10	1.5E-10	2.2E-07	2.2E-07	4.6E-16	8.6E-16	2.0E-12	2.1E-12
Sr-104	5.2E-09	1.3E-07	6.9E-08	9.4E-09	8.6E-09	2.9E-09	8.2E-09	1.7E-09	1.7E-09
Y-104	6.3E-09	5.7E-04	2.3E-04	7.3E-05	6.5E-05	1.0E-05	2.3E-05	1.1E-05	1.0E-05
Zr-104	3.8E-08	8.3E-02	1.2E-01	6.1E-02	5.6E-02	2.5E-04	1.9E-03	1.5E-03	1.5E-03
Nb-104	1.6E-07	5.7E-01	7.1E-01	1.2E+00	1.2E+00	4.2E-04	2.8E-03	7.1E-03	7.9E-03
Mo-104	1.9E-06	1.1E+00	1.2E+00	4.3E+00	4.6E+00	6.8E-05	3.9E-04	2.2E-03	2.4E-03
Tc-104	3.5E-05	9.3E-02	3.2E-02	5.4E-01	6.7E-01	3.1E-07	5.6E-07	1.5E-05	1.9E-05
Ru-104	NA	3.3E-04	1.6E-04	2.4E-02	1.5E-02	0.0E+00	0.0E+00	0.0E+00	0.0E+00
Zr-105	1.9E-08	1.2E-01	5.5E-04	6.4E-03	4.9E-03	7.0E-04	1.8E-05	3.2E-04	2.6E-04
Nb-105	9.2E-08	1.4E-01	2.8E-01	4.9E-01	3.9E-01	1.7E-04	1.9E-03	5.1E-03	4.2E-03
Mo-105	1.1E-06	6.7E-01	9.2E-01	3.5E+00	3.4E+00	6.7E-05	4.9E-04	2.9E-03	2.9E-03
Tc-105	1.4E-05	4.9E-02	7.5E-03	1.6E+00	1.5E+00	3.8E-07	3.2E-07	1.1E-04	1.0E-04

NA = Not applicable; no half-life or fractional abundances are provided because the isotope is stable.

--- = No half-life was found for the radionuclide; the isotope was not included in the fission product allocation.

[a] The primary source of radionuclide half-lives was KAPL (2002). Alternate sources include England and Rider (1994) and NNDC (2004).

Table I-2 (Continued)
Fission Product Yields and Activity Fractions for Mixed-Fission Product Waste at the Time of Generation

Isotope	Half-Life (yr) [a]	Fission Yields (yield/100 fissions)				Fractional Abundance (activity basis)			
		U-235		Pu-239		U-235		Pu-239	
		Thermal Neutrons	Fast Neutrons	Thermal Neutrons	Fast Neutrons	Thermal Neutrons	Fast Neutrons	Thermal Neutrons	Fast Neutrons
Ru-105	5.1E-04	1.1E-07	1.0E-07	4.5E-02	8.9E-02	2.5E-14	1.2E-13	8.6E-08	1.7E-07
Rh-105m	1.4E-06	0.0E+00	8.4E-09	2.1E-05	2.2E-05	0.0E+00	3.8E-12	1.5E-08	1.6E-08
Rh-105	4.0E-03	0.0E+00	6.2E-08	1.4E-04	1.6E-04	0.0E+00	9.4E-15	3.3E-11	4.0E-11
Pd-105	NA	0.0E+00	0.0E+00	2.4E-08	3.3E-08	0.0E+00	0.0E+00	0.0E+00	0.0E+00
Zr-106	2.9E-08	1.7E-06	2.7E-05	1.8E-04	3.2E-04	6.7E-09	5.9E-07	6.1E-06	1.1E-05
Nb-106	2.9E-08	1.6E-02	4.4E-02	3.5E-02	6.7E-02	6.2E-05	9.2E-04	1.1E-03	2.3E-03
Mo-106	2.8E-07	3.6E-01	4.8E-01	2.2E+00	1.9E+00	1.5E-04	1.1E-03	7.5E-03	7.0E-03
Tc-106	1.1E-06	2.7E-02	1.0E-02	1.8E+00	2.0E+00	2.7E-06	5.6E-06	1.5E-03	1.7E-03
Ru-106	1.0E+00	9.1E-07	8.7E-07	3.2E-01	3.9E-01	1.0E-16	5.2E-16	3.0E-10	3.8E-10
Rh-106m	2.5E-04	0.0E+00	0.0E+00	2.2E-04	1.1E-03	0.0E+00	0.0E+00	8.5E-10	4.4E-09
Rh-106	9.5E-07	0.0E+00	0.0E+00	2.2E-04	1.1E-03	0.0E+00	0.0E+00	2.2E-07	1.2E-06
Pd-106	NA	0.0E+00	0.0E+00	9.2E-07	1.5E-06	0.0E+00	0.0E+00	0.0E+00	0.0E+00
Ag-106m	2.3E-02	0.0E+00	0.0E+00	8.1E-12	1.7E-11	0.0E+00	0.0E+00	3.4E-19	7.3E-19
Nb-107	9.8E-09	2.3E-03	1.0E-02	9.8E-03	7.7E-03	2.7E-05	6.4E-04	9.5E-04	7.8E-04
Mo-107	1.1E-07	1.2E-01	2.7E-01	5.9E-01	5.6E-01	1.3E-04	1.5E-03	5.1E-03	5.0E-03
Tc-107	6.7E-07	2.2E-02	2.6E-02	1.8E+00	1.8E+00	3.8E-06	2.4E-05	2.6E-03	2.7E-03
Ru-107	7.2E-06	4.9E-06	8.4E-06	8.4E-01	8.2E-01	7.8E-11	7.2E-10	1.1E-04	1.1E-04
Rh-107	4.1E-05	0.0E+00	0.0E+00	7.6E-02	1.7E-02	0.0E+00	0.0E+00	1.8E-06	4.1E-07
Pd-107m	6.6E-07	0.0E+00	0.0E+00	1.3E-05	2.3E-05	0.0E+00	0.0E+00	1.8E-08	3.4E-08

NA = Not applicable; no half-life or fractional abundances are provided because the isotope is stable.

--- = No half-life was found for the radionuclide; the isotope was not included in the fission product allocation.

[a] The primary source of radionuclide half-lives was KAPL (2002). Alternate sources include England and Rider (1994) and NNDC (2004).

Table I-2 (Continued)
Fission Product Yields and Activity Fractions for Mixed-Fission Product Waste at the Time of Generation

Isotope	Half-Life (yr) [a]	Fission Yields (yield/100 fissions)				Fractional Abundance (activity basis)			
		U-235		Pu-239		U-235		Pu-239	
		Thermal Neutrons	Fast Neutrons	Thermal Neutrons	Fast Neutrons	Thermal Neutrons	Fast Neutrons	Thermal Neutrons	Fast Neutrons
Pd-107	6.5E+06	0.0E+00	0.0E+00	6.8E-06	1.0E-05	0.0E+00	0.0E+00	1.0E-21	1.5E-21
Ag-107m	1.4E-06	0.0E+00	0.0E+00	8.4E-10	1.8E-09	0.0E+00	0.0E+00	5.8E-13	1.3E-12
Ag-107	NA	0.0E+00	0.0E+00	1.3E-10	2.5E-10	0.0E+00	0.0E+00	0.0E+00	0.0E+00
Zr-108	1.2E-08	3.1E-10	1.9E-08	4.6E-07	1.5E-07	3.0E-12	9.5E-10	3.6E-08	1.3E-08
Nb-108	6.0E-09	9.0E-05	8.2E-04	9.3E-04	3.5E-04	1.7E-06	8.4E-05	1.5E-04	5.8E-05
Mo-108	3.5E-08	3.0E-02	1.1E-01	2.2E-01	9.7E-02	1.0E-04	1.9E-03	6.0E-03	2.8E-03
Tc-108	1.6E-07	2.4E-02	2.2E-02	6.3E-01	7.6E-01	1.7E-05	8.5E-05	3.7E-03	4.6E-03
Ru-108	8.6E-06	1.7E-05	4.9E-05	1.3E+00	1.1E+00	2.2E-10	3.5E-09	1.4E-04	1.3E-04
Rh-108m	1.1E-05	0.0E+00	6.8E-12	2.0E-02	2.9E-02	0.0E+00	3.7E-16	1.7E-06	2.5E-06
Rh-108	5.4E-07	0.0E+00	6.8E-12	2.0E-02	2.9E-02	0.0E+00	7.8E-15	3.5E-05	5.3E-05
Nb-109	6.0E-09	4.8E-04	1.6E-03	1.8E-09	4.0E-11	9.2E-06	1.6E-04	2.8E-10	6.6E-12
Mo-109	1.6E-08	1.6E-02	4.2E-02	5.9E-03	1.6E-04	1.1E-04	1.6E-03	3.6E-04	1.0E-05
Tc-109	2.8E-08	1.3E-02	3.4E-02	4.0E-01	1.9E-01	5.6E-05	7.6E-04	1.4E-02	6.9E-03
Ru-109	1.1E-06	1.7E-03	4.0E-03	1.0E+00	8.3E-01	1.8E-07	2.2E-06	8.7E-04	7.5E-04
Rh-109m	1.6E-06	2.1E-06	5.3E-06	3.6E-02	7.6E-03	1.5E-10	2.0E-09	2.2E-05	4.7E-06
Rh-109	2.5E-06	2.1E-06	5.3E-06	3.6E-02	7.6E-03	9.3E-11	1.3E-09	1.4E-05	2.9E-06
Pd-109m	8.9E-06	5.5E-10	1.6E-09	2.6E-07	2.6E-07	7.0E-15	1.1E-13	2.8E-11	2.9E-11
Pd-109	1.5E-03	2.9E-10	7.0E-10	1.4E-07	1.2E-07	2.2E-17	2.8E-16	8.8E-14	7.6E-14
Zr-110	4.8E-15	9.3E-09	4.3E-08	0.0E+00	0.0E+00	2.2E-04	5.6E-03	0.0E+00	0.0E+00

NA = Not applicable; no half-life or fractional abundances are provided because the isotope is stable.

--- = No half-life was found for the radionuclide; the isotope was not included in the fission product allocation.

[a] The primary source of radionuclide half-lives was KAPL (2002). Alternate sources include England and Rider (1994) and NNDC (2004).

Table I-2 (Continued)
Fission Product Yields and Activity Fractions for Mixed-Fission Product Waste at the Time of Generation

Isotope	Half-Life (yr) [a]	Fission Yields (yield/100 fissions)				Fractional Abundance (activity basis)			
		U-235		Pu-239		U-235		Pu-239	
		Thermal Neutrons	Fast Neutrons	Thermal Neutrons	Fast Neutrons	Thermal Neutrons	Fast Neutrons	Thermal Neutrons	Fast Neutrons
Nb-110	5.4E-09	1.5E-05	5.5E-05	0.0E+00	0.0E+00	3.3E-07	6.3E-06	0.0E+00	0.0E+00
Mo-110	9.5E-09	3.9E-03	1.1E-02	8.3E-06	9.5E-06	4.7E-05	7.2E-04	8.4E-07	1.0E-06
Tc-110	2.8E-08	1.2E-02	3.1E-02	4.0E-02	4.2E-02	4.8E-05	6.8E-04	1.4E-03	1.5E-03
Ru-110	3.8E-07	9.9E-03	2.3E-02	5.7E-01	5.8E-01	3.0E-06	3.8E-05	1.4E-03	1.5E-03
Rh-110m	9.2E-07	5.7E-05	1.3E-04	1.5E-02	1.4E-02	7.1E-09	8.9E-08	1.6E-05	1.6E-05
Rh-110	9.8E-08	5.7E-05	1.3E-04	1.5E-02	1.4E-02	6.6E-08	8.3E-07	1.5E-04	1.5E-04
Pd-110	NA	2.2E-07	5.1E-07	4.4E-06	3.9E-06	0.0E+00	0.0E+00	0.0E+00	0.0E+00
Ag-110m	6.8E-01	2.3E-12	6.5E-12	0.0E+00	0.0E+00	3.8E-22	5.8E-21	0.0E+00	0.0E+00
Mo-111	1.5E-08	2.3E-04	7.0E-04	2.5E-07	3.1E-07	1.8E-06	2.9E-05	1.6E-08	2.1E-08
Tc-111	9.5E-09	4.5E-03	1.2E-02	6.7E-03	7.9E-03	5.4E-05	7.8E-04	6.7E-04	8.2E-04
Ru-111	6.7E-08	1.2E-02	2.8E-02	2.5E-01	3.0E-01	2.0E-05	2.6E-04	3.5E-03	4.4E-03
Rh-111	3.5E-07	8.8E-04	2.1E-03	4.4E-02	5.2E-02	2.9E-07	3.7E-06	1.2E-04	1.5E-04
Pd-111m	6.3E-04	4.7E-06	1.2E-05	1.5E-05	2.0E-05	8.6E-13	1.1E-11	2.3E-11	3.1E-11
Pd-111	4.5E-05	2.5E-06	5.2E-06	8.1E-06	8.8E-06	6.5E-12	7.1E-11	1.7E-10	2.0E-10
Ag-111m	2.1E-06	8.3E-10	2.1E-09	3.3E-12	3.8E-12	4.6E-14	6.3E-13	1.5E-15	1.9E-15
Ag-111	2.0E-02	1.2E-10	2.9E-10	0.0E+00	0.0E+00	7.0E-19	8.7E-18	0.0E+00	0.0E+00
Mo-112	3.1E-08	9.7E-06	4.4E-05	6.0E-09	1.0E-08	3.6E-08	8.8E-07	1.8E-10	3.3E-10
Tc-112	8.2E-09	6.9E-04	2.5E-03	6.1E-04	9.4E-04	9.5E-06	1.8E-04	7.1E-05	1.1E-04
Ru-112	5.7E-08	9.9E-03	2.9E-02	9.2E-02	1.4E-01	2.0E-05	3.1E-04	1.5E-03	2.4E-03

NA = Not applicable; no half-life or fractional abundances are provided because the isotope is stable.

--- = No half-life was found for the radionuclide; the isotope was not included in the fission product allocation.

[a] The primary source of radionuclide half-lives was KAPL (2002). Alternate sources include England and Rider (1994) and NNDC (2004).

Table I-2 (Continued)
Fission Product Yields and Activity Fractions for Mixed-Fission Product Waste at the Time of Generation

Isotope	Half-Life (yr) [a]	Fission Yields (yield/100 fissions)				Fractional Abundance (activity basis)			
		U-235		Pu-239		U-235		Pu-239	
		Thermal Neutrons	Fast Neutrons	Thermal Neutrons	Fast Neutrons	Thermal Neutrons	Fast Neutrons	Thermal Neutrons	Fast Neutrons
Rh-112	2.2E-07	2.3E-03	6.1E-03	3.6E-02	4.9E-02	1.2E-06	1.7E-05	1.6E-04	2.3E-04
Pd-112	2.4E-03	1.3E-04	3.0E-04	9.5E-05	1.2E-04	6.1E-12	7.6E-11	3.8E-11	5.1E-11
Ag-112	3.6E-04	8.3E-07	1.5E-07	5.9E-11	7.6E-11	2.7E-13	2.6E-13	1.6E-16	2.1E-16
Cd-112	NA	1.1E-09	1.2E-11	0.0E+00	0.0E+00	0.0E+00	0.0E+00	0.0E+00	0.0E+00
Tc-113	4.8E-09	1.4E-04	4.9E-04	7.9E-05	1.3E-04	3.4E-06	6.3E-05	1.6E-05	2.8E-05
Ru-113	1.6E-08	6.1E-03	1.6E-02	3.8E-02	6.2E-02	4.3E-05	5.9E-04	2.2E-03	3.8E-03
Rh-113	8.9E-08	6.8E-03	1.5E-02	4.4E-02	6.5E-02	8.8E-06	1.0E-04	4.7E-04	7.3E-04
Pd-113	2.9E-06	1.2E-03	2.0E-03	3.7E-04	5.5E-04	4.6E-08	4.3E-07	1.2E-07	1.9E-07
Ag-113m	2.2E-06	3.6E-06	5.7E-06	1.2E-09	1.6E-09	1.9E-10	1.6E-09	5.3E-13	7.2E-13
Ag-113	6.1E-04	5.4E-07	7.8E-07	1.8E-10	2.2E-10	1.0E-13	7.9E-13	2.9E-16	3.5E-16
Cd-113m	1.4E+01	8.7E-10	1.4E-09	0.0E+00	0.0E+00	7.1E-21	5.9E-20	0.0E+00	0.0E+00
Cd-113	7.7E15	2.6E-10	3.6E-10	0.0E+00	0.0E+00	3.9E-36	2.9E-35	0.0E+00	0.0E+00
Mo-114	1.2E-08	4.4E-09	4.6E-08	5.4E-07	5.1E-07	4.2E-11	2.4E-09	4.4E-08	4.2E-08
Tc-114	4.8E-09	7.0E-06	4.5E-05	2.7E-04	2.9E-04	1.7E-07	5.8E-06	5.3E-05	6.1E-05
Ru-114	1.8E-08	1.7E-03	7.1E-03	1.6E-02	2.1E-02	1.1E-05	2.4E-04	8.4E-04	1.2E-03
Rh-114	5.7E-08	5.0E-03	1.6E-02	3.2E-02	5.0E-02	1.0E-05	1.7E-04	5.4E-04	8.7E-04
Pd-114	4.7E-06	4.2E-03	9.6E-03	1.2E-02	2.3E-02	1.0E-07	1.2E-06	2.5E-06	4.8E-06
Ag-114	1.5E-07	9.2E-04	8.6E-05	1.5E-04	3.4E-04	7.2E-07	3.6E-07	9.8E-07	2.3E-06
Cd-114	NA	7.7E-08	1.3E-07	2.2E-07	6.5E-07	0.0E+00	0.0E+00	0.0E+00	0.0E+00

NA = Not applicable; no half-life or fractional abundances are provided because the isotope is stable.

--- = No half-life was found for the radionuclide; the isotope was not included in the fission product allocation.

[a] The primary source of radionuclide half-lives was KAPL (2002). Alternate sources include England and Rider (1994) and NNDC (2004).

Table I-2 (Continued)
Fission Product Yields and Activity Fractions for Mixed-Fission Product Waste at the Time of Generation

Isotope	Half-Life (yr) [a]	Fission Yields (yield/100 fissions)				Fractional Abundance (activity basis)			
		U-235		Pu-239		U-235		Pu-239	
		Thermal Neutrons	Fast Neutrons	Thermal Neutrons	Fast Neutrons	Thermal Neutrons	Fast Neutrons	Thermal Neutrons	Fast Neutrons
In-114m	1.4E-01	0.0E+00	1.3E-12	5.6E-12	2.1E-11	0.0E+00	5.9E-21	3.9E-20	1.6E-19
In-114	2.3E-06	0.0E+00	0.0E+00	1.9E-12	6.0E-12	0.0E+00	0.0E+00	7.8E-16	2.6E-15
Ru-115	2.3E-08	2.6E-04	1.5E-03	1.8E-03	2.9E-03	1.3E-06	3.8E-05	7.3E-05	1.2E-04
Rh-115	2.3E-08	3.6E-03	1.4E-02	1.8E-02	3.1E-02	1.8E-05	3.5E-04	7.3E-04	1.3E-03
Pd-115	1.6E-06	7.1E-03	1.8E-02	2.2E-02	4.4E-02	5.2E-07	7.1E-06	1.3E-05	2.8E-05
Ag-115m	5.9E-07	1.4E-03	3.7E-04	7.2E-04	1.6E-03	2.7E-07	3.9E-07	1.2E-06	2.7E-06
Ag-115	3.8E-05	1.9E-04	3.7E-04	7.2E-04	1.6E-03	5.8E-10	6.0E-09	1.8E-08	4.2E-08
Cd-115m	1.2E-01	5.5E-06	2.4E-06	6.8E-06	1.9E-05	5.2E-15	1.2E-14	5.3E-14	1.6E-13
Cd-115	6.1E-03	9.0E-07	6.4E-07	2.0E-06	5.1E-06	1.7E-14	6.5E-14	3.2E-13	8.3E-13
In-115m	5.1E-04	3.8E-11	3.7E-11	3.3E-10	1.0E-09	8.6E-18	4.5E-17	6.2E-16	2.0E-15
In-115	4.4E+14	1.6E-10	1.8E-10	1.4E-09	5.0E-09	4.3E-35	2.5E-34	3.1E-33	1.1E-32
Mo-116	---	0.0E+00	5.9E-12	1.2E-11	1.2E-11	0.0E+00	0.0E+00	0.0E+00	0.0E+00
Tc-116	3.6E-09	6.3E-09	9.2E-08	1.5E-07	1.5E-07	2.0E-10	1.5E-08	3.8E-08	4.1E-08
Ru-116	5.4E-08	2.5E-05	2.0E-04	2.0E-04	2.1E-04	5.2E-08	2.3E-06	3.5E-06	3.9E-06
Rh-116	2.2E-08	8.7E-04	4.8E-03	6.7E-03	7.5E-03	4.5E-06	1.3E-04	2.9E-04	3.4E-04
Pd-116	3.8E-07	6.8E-03	2.6E-02	3.6E-02	4.3E-02	2.1E-06	4.3E-05	9.0E-05	1.1E-04
Ag-116m	2.9E-07	7.7E-04	1.3E-03	3.8E-03	4.7E-03	3.1E-07	2.8E-06	1.3E-05	1.6E-05
Ag-116	5.1E-06	4.7E-03	1.3E-03	3.8E-03	4.7E-03	1.1E-07	1.6E-07	7.2E-07	9.2E-07
Cd-116	NA	3.0E-05	5.5E-05	2.6E-04	3.4E-04	0.0E+00	0.0E+00	0.0E+00	0.0E+00

NA = Not applicable; no half-life or fractional abundances are provided because the isotope is stable.

--- = No half-life was found for the radionuclide; the isotope was not included in the fission product allocation.

[a] The primary source of radionuclide half-lives was KAPL (2002). Alternate sources include England and Rider (1994) and NNDC (2004).

Table I-2 (Continued)
Fission Product Yields and Activity Fractions for Mixed-Fission Product Waste at the Time of Generation

Isotope	Half-Life (yr) [a]	Fission Yields (yield/100 fissions)				Fractional Abundance (activity basis)			
		U-235		Pu-239		U-235		Pu-239	
		Thermal Neutrons	Fast Neutrons	Thermal Neutrons	Fast Neutrons	Thermal Neutrons	Fast Neutrons	Thermal Neutrons	Fast Neutrons
In-116m	1.0E-04	3.9E-09	5.8E-09	1.1E-07	1.6E-07	4.3E-15	3.5E-14	1.0E-12	1.5E-12
Ru-117	1.1E-08	2.5E-06	1.5E-05	8.6E-06	1.2E-05	2.7E-08	8.6E-07	7.5E-07	1.1E-06
Rh-117	1.4E-08	4.7E-04	1.9E-03	1.4E-03	2.1E-03	3.8E-06	8.2E-05	9.8E-05	1.5E-04
Pd-117	1.4E-07	8.8E-03	2.4E-02	2.2E-02	3.5E-02	7.2E-06	1.1E-04	1.5E-04	2.5E-04
Ag-117m	1.7E-07	1.5E-03	5.1E-03	9.5E-03	1.5E-02	1.0E-06	1.9E-05	5.4E-05	8.7E-05
Ag-117	2.3E-06	1.5E-03	5.1E-03	9.5E-03	1.5E-02	7.5E-08	1.3E-06	3.9E-06	6.3E-06
Cd-117m	3.9E-04	3.7E-04	4.6E-04	1.5E-03	2.7E-03	1.1E-10	7.3E-10	3.7E-09	6.9E-09
Cd-117	2.8E-04	1.1E-04	1.2E-04	4.5E-04	7.2E-04	4.5E-11	2.6E-10	1.5E-09	2.5E-09
In-117m	2.2E-04	8.6E-08	1.2E-07	1.7E-06	2.6E-06	4.5E-14	3.2E-13	7.1E-12	1.2E-11
In-117	8.4E-05	3.7E-07	5.7E-07	7.0E-06	1.3E-05	5.0E-13	4.2E-12	8.0E-11	1.5E-10
Ru-118	2.1E-08	6.9E-08	6.9E-07	2.2E-07	3.5E-07	3.8E-10	2.0E-08	1.0E-08	1.7E-08
Rh-118	9.5E-09	3.6E-05	2.5E-04	1.3E-04	2.0E-04	4.4E-07	1.6E-05	1.3E-05	2.0E-05
Pd-118	6.7E-08	3.2E-03	1.5E-02	8.6E-03	1.4E-02	5.5E-06	1.4E-04	1.2E-04	2.1E-04
Ag-118m	7.6E-08	3.0E-03	7.2E-03	9.9E-03	1.6E-02	4.5E-06	5.8E-05	1.2E-04	2.1E-04
Ag-118	1.3E-07	3.4E-03	7.2E-03	9.9E-03	1.6E-02	3.1E-06	3.5E-05	7.5E-05	1.2E-04
Cd-118	9.6E-05	1.7E-03	3.8E-03	3.9E-03	1.4E-02	2.1E-09	2.5E-08	3.9E-08	1.5E-07
In-118m	8.4E-06	1.7E-06	2.9E-06	1.9E-05	4.5E-05	2.3E-11	2.1E-10	2.2E-09	5.4E-09
In-118	1.6E-07	5.1E-06	1.0E-05	5.8E-05	1.6E-04	3.7E-09	4.0E-08	3.5E-07	1.0E-06
Sn-118	NA	4.1E-09	7.0E-09	1.3E-07	3.8E-07	0.0E+00	0.0E+00	0.0E+00	0.0E+00

NA = Not applicable; no half-life or fractional abundances are provided because the isotope is stable.

--- = No half-life was found for the radionuclide; the isotope was not included in the fission product allocation.

[a] The primary source of radionuclide half-lives was KAPL (2002). Alternate sources include England and Rider (1994) and NNDC (2004).

Table I-2 (Continued)
Fission Product Yields and Activity Fractions for Mixed-Fission Product Waste at the Time of Generation

Isotope	Half-Life (yr) [a]	Fission Yields (yield/100 fissions)				Fractional Abundance (activity basis)			
		U-235		Pu-239		U-235		Pu-239	
		Thermal Neutrons	Fast Neutrons	Thermal Neutrons	Fast Neutrons	Thermal Neutrons	Fast Neutrons	Thermal Neutrons	Fast Neutrons
Ru-119	6.2E-09	6.6E-10	1.4E-08	3.1E-09	5.2E-09	1.2E-11	1.4E-09	4.8E-10	8.3E-10
Rh-119	1.5E-08	1.9E-06	2.7E-05	8.2E-06	1.3E-05	1.4E-08	1.1E-06	5.3E-07	8.8E-07
Pd-119	2.9E-08	4.4E-04	4.5E-03	1.7E-03	2.8E-03	1.7E-06	9.7E-05	5.5E-05	9.7E-05
Ag-119	6.7E-08	7.3E-03	1.9E-02	1.4E-02	2.4E-02	1.2E-05	1.7E-04	2.1E-04	3.5E-04
Cd-119m	4.2E-06	2.3E-03	5.8E-03	7.7E-03	1.4E-02	6.2E-08	8.6E-07	1.8E-06	3.2E-06
Cd-119	5.1E-06	2.5E-03	5.8E-03	7.7E-03	1.4E-02	5.5E-08	7.0E-07	1.4E-06	2.6E-06
In-119m	3.4E-05	1.6E-05	3.5E-05	1.7E-04	2.7E-04	5.4E-11	6.3E-10	4.8E-09	7.7E-09
In-119	4.4E-06	4.7E-04	1.7E-04	7.2E-04	1.3E-03	1.2E-08	2.4E-08	1.6E-07	2.9E-07
Sn-119m	8.0E-01	1.1E-07	2.6E-07	3.7E-06	7.2E-06	1.6E-17	2.0E-16	4.4E-15	8.9E-15
Ru-120	1.1E-08	3.0E-10	1.8E-10	3.3E-11	5.3E-11	3.1E-12	1.0E-11	2.9E-12	4.7E-12
Rh-120	5.5E-09	2.4E-06	1.1E-06	2.8E-07	4.4E-07	5.0E-08	1.2E-07	4.8E-08	8.0E-08
Pd-120	1.6E-08	2.7E-03	9.4E-04	2.4E-04	4.1E-04	2.0E-05	3.6E-05	1.5E-05	2.6E-05
Ag-120	3.9E-08	8.8E-04	9.4E-03	5.7E-03	9.8E-03	2.6E-06	1.5E-04	1.4E-04	2.5E-04
Cd-120	1.6E-06	8.4E-03	2.4E-02	2.1E-02	3.9E-02	6.0E-07	9.1E-06	1.3E-05	2.4E-05
In-120m	1.5E-06	3.2E-04	5.3E-04	1.6E-03	3.1E-03	2.4E-08	2.2E-07	1.0E-06	2.0E-06
In-120	9.8E-08	3.2E-04	5.3E-04	1.6E-03	3.1E-03	3.7E-07	3.3E-06	1.6E-05	3.1E-05
Sn-120	NA	3.0E-06	8.9E-06	7.3E-05	1.5E-04	0.0E+00	0.0E+00	0.0E+00	0.0E+00
Sb-120m	1.6E-02	1.3E-10	4.6E-10	2.5E-08	5.8E-08	9.5E-19	1.8E-17	1.5E-15	3.7E-15
Rh-121	7.9E-09	1.4E-08	4.3E-08	9.1E-09	1.2E-08	2.1E-10	3.3E-09	1.1E-09	1.5E-09

NA = Not applicable; no half-life or fractional abundances are provided because the isotope is stable.

--- = No half-life was found for the radionuclide; the isotope was not included in the fission product allocation.

[a] The primary source of radionuclide half-lives was KAPL (2002). Alternate sources include England and Rider (1994) and NNDC (2004).

Table I-2 (Continued)
Fission Product Yields and Activity Fractions for Mixed-Fission Product Waste at the Time of Generation

Isotope	Half-Life (yr) [a]	Fission Yields (yield/100 fissions)				Fractional Abundance (activity basis)			
		U-235		Pu-239		U-235		Pu-239	
		Thermal Neutrons	Fast Neutrons	Thermal Neutrons	Fast Neutrons	Thermal Neutrons	Fast Neutrons	Thermal Neutrons	Fast Neutrons
Pd-121	2.0E-08	4.7E-05	1.0E-04	2.5E-05	3.6E-05	2.7E-07	3.1E-06	1.2E-06	1.7E-06
Ag-121	2.5E-08	2.6E-03	4.8E-03	2.4E-03	3.5E-03	1.2E-05	1.2E-04	9.2E-05	1.4E-04
Cd-121	4.3E-07	7.2E-03	2.7E-02	2.3E-02	3.7E-02	1.9E-06	3.9E-05	5.0E-05	8.7E-05
In-121m	7.2E-06	3.2E-04	8.4E-04	2.3E-03	3.5E-03	5.1E-09	7.2E-08	3.0E-07	4.8E-07
In-121	7.3E-07	2.5E-03	4.1E-03	9.8E-03	1.7E-02	3.9E-07	3.5E-06	1.3E-05	2.3E-05
Sn-121m	4.4E+01	2.8E-05	8.2E-05	5.4E-04	1.1E-03	7.3E-17	1.2E-15	1.2E-14	2.5E-14
Sn-121	3.1E-03	3.6E-04	2.9E-05	2.2E-04	3.9E-04	1.3E-11	5.8E-12	6.8E-11	1.2E-10
Rh-122	3.4E-09	2.9E-10	8.1E-10	1.3E-10	1.6E-10	9.6E-12	1.5E-10	3.7E-11	4.6E-11
Pd-122	4.5E-08	4.8E-06	1.0E-05	1.6E-06	2.1E-06	1.2E-08	1.4E-07	3.5E-08	4.7E-08
Ag-122	1.7E-08	6.7E-04	1.2E-03	4.7E-04	6.4E-04	4.6E-06	4.4E-05	2.6E-05	3.8E-05
Cd-122	1.7E-07	1.2E-02	2.7E-02	1.7E-02	2.5E-02	8.1E-06	1.0E-04	9.6E-05	1.5E-04
In-122m	3.4E-07	1.3E-03	5.4E-03	1.1E-02	1.7E-02	4.2E-07	9.7E-06	3.1E-05	5.0E-05
In-122	4.8E-08	1.3E-03	5.4E-03	1.1E-02	1.7E-02	3.0E-06	7.0E-05	2.2E-04	3.6E-04
Sn-122	NA	3.7E-04	1.1E-03	5.3E-03	9.2E-03	0.0E+00	0.0E+00	0.0E+00	0.0E+00
Rh-123	4.2E-09	8.5E-12	1.4E-11	0.0E+00	1.3E-12	2.3E-13	2.0E-12	0.0E+00	3.0E-13
Pd-123	9.5E-09	4.0E-07	4.8E-07	3.6E-08	5.7E-08	4.8E-09	3.1E-08	3.6E-09	5.9E-09
Ag-123	9.5E-09	2.8E-04	2.8E-04	4.8E-05	7.4E-05	3.3E-06	1.8E-05	4.8E-06	7.7E-06
Cd-123	6.7E-08	1.0E-02	1.5E-02	5.0E-03	8.4E-03	1.7E-05	1.4E-04	7.2E-05	1.3E-04
In-123m	1.5E-06	2.5E-04	3.9E-03	4.6E-03	6.9E-03	1.9E-08	1.6E-06	2.9E-06	4.6E-06

NA = Not applicable; no half-life or fractional abundances are provided because the isotope is stable.

--- = No half-life was found for the radionuclide; the isotope was not included in the fission product allocation.

[a] The primary source of radionuclide half-lives was KAPL (2002). Alternate sources include England and Rider (1994) and NNDC (2004).

Table I-2 (Continued)
Fission Product Yields and Activity Fractions for Mixed-Fission Product Waste at the Time of Generation

Isotope	Half-Life (yr) [a]	Fission Yields (yield/100 fissions)				Fractional Abundance (activity basis)			
		U-235		Pu-239		U-235		Pu-239	
		Thermal Neutrons	Fast Neutrons	Thermal Neutrons	Fast Neutrons	Thermal Neutrons	Fast Neutrons	Thermal Neutrons	Fast Neutrons
In-123	1.9E-07	3.9E-03	1.9E-02	1.9E-02	3.4E-02	2.4E-06	6.2E-05	9.8E-05	1.7E-04
Sn-123m	7.6E-05	3.1E-04	1.4E-03	4.2E-03	7.0E-03	4.7E-10	1.1E-08	5.3E-08	9.2E-08
Sn-123	3.5E-01	8.0E-04	4.0E-03	1.0E-02	2.0E-02	2.6E-13	6.9E-12	2.8E-11	5.6E-11
Sb-123	NA	5.2E-06	3.0E-05	4.6E-04	8.7E-04	0.0E+00	0.0E+00	0.0E+00	0.0E+00
Rh-124	---	1.0E-12	0.0E+00	0.0E+00	0.0E+00	0.0E+00	0.0E+00	0.0E+00	0.0E+00
Pd-124	1.6E-08	2.7E-07	2.3E-08	0.0E+00	0.0E+00	1.9E-09	8.8E-10	0.0E+00	0.0E+00
Ag-124	5.4E-09	5.5E-04	3.7E-05	6.2E-10	9.4E-10	1.2E-05	4.2E-06	1.1E-10	1.7E-10
Cd-124	3.9E-08	1.2E-02	8.9E-03	2.7E-04	4.3E-04	3.5E-05	1.4E-04	6.7E-06	1.1E-05
In-124	1.0E-07	3.4E-03	2.9E-02	3.5E-02	5.3E-02	3.9E-06	1.7E-04	3.3E-04	5.2E-04
Sn-124	NA	1.1E-02	2.6E-02	4.4E-02	6.8E-02	0.0E+00	0.0E+00	0.0E+00	0.0E+00
Sb-124m	3.8E-05	2.4E-06	1.8E-04	5.0E-05	7.6E-05	7.2E-12	2.8E-09	1.2E-09	2.0E-09
Sb-124	1.6E-01	7.6E-06	1.8E-04	5.0E-05	7.6E-05	5.3E-15	6.5E-13	2.9E-13	4.6E-13
Ag-125	5.4E-09	1.7E-09	2.4E-09	5.0E-11	9.3E-11	3.5E-11	2.7E-10	8.8E-12	1.7E-11
Cd-125	2.2E-08	5.6E-03	5.2E-04	7.0E-05	1.3E-04	3.0E-05	1.5E-05	3.1E-06	5.8E-06
In-125m	3.9E-07	4.7E-03	1.8E-02	1.7E-02	2.7E-02	1.4E-06	2.9E-05	4.2E-05	7.0E-05
In-125	7.5E-08	4.7E-03	1.8E-02	1.7E-02	2.7E-02	7.2E-06	1.5E-04	2.2E-04	3.6E-04
Sn-125m	1.8E-05	1.1E-02	8.0E-03	2.2E-02	3.2E-02	6.7E-08	2.7E-07	1.2E-06	1.7E-06
Sn-125	2.6E-02	8.5E-03	2.3E-02	5.5E-02	9.1E-02	3.7E-11	5.3E-10	2.0E-09	3.4E-09
Sb-125	2.8E+00	2.7E-05	3.8E-05	6.6E-04	9.4E-04	1.1E-15	8.5E-15	2.3E-13	3.4E-13

NA = Not applicable; no half-life or fractional abundances are provided because the isotope is stable.

--- = No half-life was found for the radionuclide; the isotope was not included in the fission product allocation.

[a] The primary source of radionuclide half-lives was KAPL (2002). Alternate sources include England and Rider (1994) and NNDC (2004).

Table I-2 (Continued)
Fission Product Yields and Activity Fractions for Mixed-Fission Product Waste at the Time of Generation

Isotope	Half-Life (yr) [a]	Fission Yields (yield/100 fissions)				Fractional Abundance (activity basis)			
		U-235		Pu-239		U-235		Pu-239	
		Thermal Neutrons	Fast Neutrons	Thermal Neutrons	Fast Neutrons	Thermal Neutrons	Fast Neutrons	Thermal Neutrons	Fast Neutrons
Te-125m	1.6E-01	2.3E-11	4.1E-11	4.8E-09	6.2E-09	1.7E-20	1.6E-19	2.9E-17	3.9E-17
Ag-126	5.4E-09	4.8E-10	1.9E-10	3.9E-12	6.2E-12	1.0E-11	2.1E-11	6.9E-13	1.1E-12
Cd-126	1.6E-08	8.1E-03	1.9E-04	2.3E-05	3.4E-05	5.6E-05	7.2E-06	1.3E-06	2.1E-06
In-126	5.2E-08	3.3E-03	2.9E-02	2.9E-02	4.0E-02	7.3E-06	3.5E-04	5.4E-04	7.7E-04
Sn-126	2.3E+05	4.5E-02	6.8E-02	1.7E-01	2.2E-01	2.2E-17	1.8E-16	7.0E-16	9.6E-16
Sb-126m	3.5E-07	1.7E-03	1.1E-04	2.3E-03	2.0E-03	5.7E-07	1.9E-07	6.4E-06	5.6E-06
Sb-126	3.4E-02	6.5E-04	7.9E-05	1.4E-03	1.4E-03	2.2E-12	1.4E-12	3.9E-11	4.2E-11
Te-126	NA	8.3E-10	1.3E-09	1.4E-07	1.2E-07	0.0E+00	0.0E+00	0.0E+00	0.0E+00
Ag-127	2.5E-09	1.6E-10	3.9E-11	0.0E+00	0.0E+00	7.2E-12	9.6E-12	0.0E+00	0.0E+00
Cd-127	1.3E-08	8.2E-03	1.1E-04	8.9E-06	9.3E-06	7.4E-05	5.1E-06	6.7E-07	7.3E-07
In-127m	1.2E-07	6.3E-03	3.3E-02	2.4E-02	2.1E-02	6.1E-06	1.7E-04	1.9E-04	1.7E-04
In-127	3.6E-08	4.1E-02	3.3E-02	2.4E-02	2.1E-02	1.3E-04	5.6E-04	6.4E-04	5.7E-04
Sn-127m	7.9E-06	7.9E-03	6.2E-02	1.3E-01	1.1E-01	1.2E-07	4.8E-06	1.5E-05	1.4E-05
Sn-127	2.4E-04	8.7E-02	1.8E-01	3.0E-01	3.2E-01	4.1E-08	4.5E-07	1.2E-06	1.3E-06
Sb-127	1.1E-02	7.1E-03	2.5E-03	2.8E-02	2.3E-02	7.7E-11	1.4E-10	2.5E-09	2.2E-09
Te-127m	3.0E-01	2.4E-08	3.1E-08	1.8E-06	1.7E-06	9.3E-18	6.4E-17	5.8E-15	5.6E-15
Te-127	1.1E-03	9.9E-09	1.1E-08	7.4E-07	5.9E-07	1.1E-15	6.3E-15	6.6E-13	5.5E-13
Pd-128	---	1.3E-12	0.0E+00	0.0E+00	0.0E+00	0.0E+00	0.0E+00	0.0E+00	0.0E+00
Ag-128	1.9E-09	1.1E-11	1.5E-12	0.0E+00	0.0E+00	6.8E-13	4.9E-13	0.0E+00	0.0E+00

NA = Not applicable; no half-life or fractional abundances are provided because the isotope is stable.

--- = No half-life was found for the radionuclide; the isotope was not included in the fission product allocation.

[a] The primary source of radionuclide half-lives was KAPL (2002). Alternate sources include England and Rider (1994) and NNDC (2004).

Table I-2 (Continued)
Fission Product Yields and Activity Fractions for Mixed-Fission Product Waste at the Time of Generation

Isotope	Half-Life (yr) [a]	Fission Yields (yield/100 fissions)				Fractional Abundance (activity basis)			
		U-235		Pu-239		U-235		Pu-239	
		Thermal Neutrons	Fast Neutrons	Thermal Neutrons	Fast Neutrons	Thermal Neutrons	Fast Neutrons	Thermal Neutrons	Fast Neutrons
Cd-128	8.9E-09	3.6E-03	2.3E-05	4.0E-06	1.6E-06	4.6E-05	1.6E-06	4.3E-07	1.8E-07
In-128	2.5E-08	2.6E-02	3.9E-02	6.9E-02	2.3E-02	1.2E-04	9.5E-04	2.6E-03	9.0E-04
Sn-128	1.1E-04	3.0E-01	4.5E-01	5.5E-01	7.7E-01	3.1E-07	2.5E-06	4.6E-06	6.8E-06
Sb-128m	1.9E-05	6.4E-03	6.0E-03	5.7E-02	5.1E-02	3.8E-08	1.9E-07	2.9E-06	2.6E-06
Sb-128	1.0E-03	1.1E-02	4.4E-03	6.2E-02	3.7E-02	1.2E-09	2.6E-09	5.7E-08	3.5E-08
Te-128	NA	1.7E-04	9.5E-07	4.3E-05	3.9E-05	0.0E+00	0.0E+00	0.0E+00	0.0E+00
Cd-129	8.6E-09	7.2E-07	3.8E-06	1.1E-07	1.9E-07	9.7E-09	2.7E-07	1.3E-08	2.2E-08
In-129m	3.9E-08	2.5E-02	1.7E-02	5.1E-03	6.4E-03	7.4E-05	2.6E-04	1.3E-04	1.6E-04
In-129	2.0E-08	2.8E-02	1.7E-02	5.1E-03	6.4E-03	1.6E-04	5.1E-04	2.5E-04	3.2E-04
Sn-129m	1.3E-05	2.0E-01	1.9E-01	2.9E-01	2.8E-01	1.7E-06	9.0E-06	2.1E-05	2.1E-05
Sn-129	4.6E-06	2.3E-01	5.5E-01	6.9E-01	8.0E-01	5.8E-06	7.4E-05	1.4E-04	1.7E-04
Sb-129	5.0E-04	6.4E-02	6.1E-02	3.8E-01	3.6E-01	1.5E-08	7.4E-08	7.3E-07	7.1E-07
Te-129m	9.2E-02	1.4E-05	1.2E-05	4.8E-04	3.9E-04	1.7E-14	7.9E-14	5.0E-12	4.2E-12
Te-129	1.3E-04	5.7E-06	4.1E-06	2.0E-04	1.4E-04	5.0E-12	1.9E-11	1.4E-09	1.0E-09
I-129	1.6E+07	0.0E+00	0.0E+00	3.9E-10	2.3E-10	0.0E+00	0.0E+00	2.3E-26	1.4E-26
Pd-130	---	6.8E-11	2.6E-12	0.0E+00	0.0E+00	0.0E+00	0.0E+00	0.0E+00	0.0E+00
Ag-130	1.6E-09	6.7E-06	1.5E-07	1.7E-08	2.3E-08	4.8E-07	5.6E-08	1.0E-08	1.4E-08
Cd-130	5.1E-09	8.8E-02	1.1E-03	1.6E-04	2.0E-04	2.0E-03	1.4E-04	2.9E-05	3.9E-05
In-130	9.2E-09	9.4E-03	8.6E-02	3.3E-02	4.0E-02	1.2E-04	5.7E-03	3.5E-03	4.3E-03

NA = Not applicable; no half-life or fractional abundances are provided because the isotope is stable.

--- = No half-life was found for the radionuclide; the isotope was not included in the fission product allocation.

[a] The primary source of radionuclide half-lives was KAPL (2002). Alternate sources include England and Rider (1994) and NNDC (2004).

Table I-2 (Continued)
Fission Product Yields and Activity Fractions for Mixed-Fission Product Waste at the Time of Generation

Isotope	Half-Life (yr) [a]	Fission Yields (yield/100 fissions)				Fractional Abundance (activity basis)			
		U-235		Pu-239		U-235		Pu-239	
		Thermal Neutrons	Fast Neutrons	Thermal Neutrons	Fast Neutrons	Thermal Neutrons	Fast Neutrons	Thermal Neutrons	Fast Neutrons
Sn-130	7.1E-06	1.1E+00	1.3E+00	9.4E-01	1.1E+00	1.8E-05	1.1E-04	1.3E-04	1.5E-04
Sb-130m	1.2E-05	3.6E-01	2.1E-01	5.9E-01	6.9E-01	3.4E-06	1.1E-05	4.7E-05	5.7E-05
Sb-130	7.5E-05	2.2E-01	1.5E-01	5.9E-01	4.4E-01	3.3E-07	1.2E-06	7.5E-06	5.9E-06
Te-130	NA	5.8E-02	2.4E-02	2.1E-01	2.0E-01	0.0E+00	0.0E+00	0.0E+00	0.0E+00
Cd-131	2.2E-09	1.4E-02	9.8E-05	9.4E-06	1.2E-05	7.3E-04	2.8E-05	4.1E-06	5.3E-06
In-131	8.9E-09	1.1E-02	3.8E-02	8.4E-03	9.4E-03	1.4E-04	2.6E-03	9.0E-04	1.0E-03
Sn-131	1.8E-06	8.8E-01	1.4E+00	6.1E-01	6.9E-01	5.7E-05	4.8E-04	3.3E-04	3.8E-04
Sb-131	4.4E-05	1.7E+00	1.5E+00	1.9E+00	2.2E+00	4.3E-06	2.1E-05	4.2E-05	5.0E-05
Te-131m	3.7E-03	2.3E-01	2.2E-01	8.7E-01	7.1E-01	7.2E-09	3.7E-08	2.3E-07	1.9E-07
Te-131	4.8E-05	9.7E-02	7.5E-02	4.5E-01	2.5E-01	2.3E-07	9.8E-07	9.1E-06	5.2E-06
I-131	2.2E-02	3.9E-03	1.1E-03	2.3E-02	2.0E-02	2.0E-11	3.0E-11	1.0E-09	9.1E-10
Xe-133m	3.3E-02	3.5E-07	2.4E-07	3.0E-05	2.7E-05	1.2E-15	4.5E-15	8.8E-13	8.1E-13
Cd-132	3.2E-10	0.0E+00	1.6E-06	5.7E-07	3.0E-07	0.0E+00	3.1E-06	1.7E-06	9.4E-07
In-132	6.3E-09	6.2E-03	1.8E-03	1.6E-03	7.7E-04	1.1E-04	1.8E-04	2.4E-04	1.2E-04
Sn-132	1.3E-06	5.9E-01	3.2E-01	4.8E-01	2.3E-01	5.4E-05	1.6E-04	3.7E-04	1.8E-04
-m-132	5.3E-06	8.6E-01	1.5E+00	5.5E-01	9.1E-01	1.9E-05	1.8E-04	9.8E-05	1.7E-04
Sb-132	8.0E-06	1.3E+00	1.7E+00	1.9E+00	1.0E+00	1.9E-05	1.3E-04	2.2E-04	1.3E-04
Te-132	8.8E-03	1.5E+00	1.1E+00	2.3E+00	3.0E+00	2.0E-08	7.5E-08	2.5E-07	3.4E-07
I-132	2.6E-04	1.8E-02	1.0E-02	2.7E-01	1.7E-01	8.1E-09	2.4E-08	9.8E-07	6.6E-07

NA = Not applicable; no half-life or fractional abundances are provided because the isotope is stable.

--- = No half-life was found for the radionuclide; the isotope was not included in the fission product allocation.

[a] The primary source of radionuclide half-lives was KAPL (2002). Alternate sources include England and Rider (1994) and NNDC (2004).

Table I-2 (Continued)
Fission Product Yields and Activity Fractions for Mixed-Fission Product Waste at the Time of Generation

Isotope	Half-Life (yr) [a]	Fission Yields (yield/100 fissions)				Fractional Abundance (activity basis)			
		U-235		Pu-239		U-235		Pu-239	
		Thermal Neutrons	Fast Neutrons	Thermal Neutrons	Fast Neutrons	Thermal Neutrons	Fast Neutrons	Thermal Neutrons	Fast Neutrons
Xe-132	NA	4.2E-05	1.7E-05	1.5E-03	1.4E-03	0.0E+00	0.0E+00	0.0E+00	0.0E+00
Cs-132	1.8E-02	7.4E-08	2.6E-10	3.0E-07	2.6E-07	4.8E-16	9.1E-18	1.6E-14	1.5E-14
In-133	5.2E-09	1.7E-04	2.7E-04	3.8E-05	3.8E-05	3.8E-06	3.2E-05	7.0E-06	7.2E-06
Sn-133	4.6E-08	1.4E-01	1.4E-01	3.4E-02	3.6E-02	3.5E-04	1.9E-03	7.2E-04	7.8E-04
Sb-133	4.8E-06	2.3E+00	1.5E+00	1.2E+00	1.2E+00	5.5E-05	2.0E-04	2.4E-04	2.5E-04
Te-133m	1.1E-04	3.0E+00	2.1E+00	2.9E+00	3.2E+00	3.3E-06	1.2E-05	2.6E-05	3.0E-05
Te-133	2.4E-05	1.2E+00	2.6E+00	1.8E+00	1.2E+00	5.6E-06	6.8E-05	7.2E-05	5.2E-05
I-133	2.4E-03	1.7E-01	3.8E-01	1.1E+00	1.3E+00	8.0E-09	1.0E-07	4.5E-07	5.4E-07
Xe-133m	6.0E-03	1.9E-03	4.2E-03	3.4E-02	4.7E-02	3.6E-11	4.3E-10	5.4E-09	7.7E-09
Xe-133	1.4E-02	6.7E-04	1.5E-03	9.5E-03	1.6E-02	5.3E-12	6.3E-11	6.3E-10	1.1E-09
Cd-134	---	9.3E-11	3.0E-10	2.1E-11	1.8E-11	0.0E+00	0.0E+00	0.0E+00	0.0E+00
In-134	4.4E-09	3.5E-06	6.0E-06	9.0E-07	7.2E-07	9.0E-08	8.3E-07	1.9E-07	1.6E-07
Sn-134	3.3E-08	1.8E-02	1.7E-02	3.8E-03	3.1E-03	6.2E-05	3.1E-04	1.1E-04	9.3E-05
Sb-134	2.5E-08	7.2E-01	4.9E-01	4.0E-01	3.1E-01	3.2E-03	1.2E-02	1.5E-02	1.2E-02
Te-134	8.0E-05	6.2E+00	6.0E+00	4.4E+00	4.5E+00	8.9E-06	4.6E-05	5.3E-05	5.6E-05
I-134m	7.0E-06	3.6E-01	3.4E-01	1.2E+00	1.2E+00	5.9E-06	3.0E-05	1.6E-04	1.6E-04
I-134	1.0E-04	5.0E-01	7.5E-01	1.4E+00	1.2E+00	5.7E-07	4.6E-06	1.4E-05	1.2E-05
Xe-134m	9.2E-09	2.5E-02	1.4E-02	1.7E-01	1.8E-01	3.1E-04	9.2E-04	1.8E-02	1.9E-02
Sn-135	1.7E-08	6.3E-04	1.6E-03	1.4E-04	1.3E-04	4.3E-06	5.9E-05	8.1E-06	7.4E-06

NA = Not applicable; no half-life or fractional abundances are provided because the isotope is stable.

--- = No half-life was found for the radionuclide; the isotope was not included in the fission product allocation.

[a] The primary source of radionuclide half-lives was KAPL (2002). Alternate sources include England and Rider (1994) and NNDC (2004).

Table I-2 (Continued)
Fission Product Yields and Activity Fractions for Mixed-Fission Product Waste at the Time of Generation

Isotope	Half-Life (yr) [a]	Fission Yields (yield/100 fissions)				Fractional Abundance (activity basis)			
		U-235		Pu-239		U-235		Pu-239	
		Thermal Neutrons	Fast Neutrons	Thermal Neutrons	Fast Neutrons	Thermal Neutrons	Fast Neutrons	Thermal Neutrons	Fast Neutrons
Sb-135	5.4E-08	1.5E-01	2.5E-01	6.7E-02	5.3E-02	3.1E-04	2.8E-03	1.2E-03	9.7E-04
Te-135	6.0E-07	3.2E+00	2.5E+00	2.2E+00	2.1E+00	6.1E-04	2.5E-03	3.5E-03	3.5E-03
I-135	7.5E-04	2.9E+00	3.6E+00	4.3E+00	3.9E+00	4.5E-07	3.0E-06	5.5E-06	5.2E-06
Xe-135m	2.9E-05	1.8E-01	1.9E-01	7.5E-01	8.5E-01	7.0E-07	3.9E-06	2.5E-05	2.9E-05
Xe-135	1.0E-03	7.9E-02	1.2E-01	3.1E-01	6.1E-01	8.7E-09	7.1E-08	2.9E-07	5.9E-07
Cs-135	2.3E+06	4.9E-04	2.1E-04	1.3E-02	1.3E-02	2.4E-20	5.5E-20	5.2E-18	5.4E-18
In-136	---	1.7E-10	6.9E-10	2.8E-11	5.2E-11	0.0E+00	0.0E+00	0.0E+00	0.0E+00
Sn-136	8.2E-09	1.6E-05	3.2E-05	1.9E-06	3.2E-06	2.2E-07	2.4E-06	2.2E-07	3.9E-07
Sb-136	2.9E-08	1.2E-02	1.4E-02	2.9E-03	4.2E-03	4.5E-05	3.0E-04	9.6E-05	1.4E-04
Te-136	5.5E-07	1.3E+00	1.0E+00	5.1E-01	6.8E-01	2.7E-04	1.1E-03	8.7E-04	1.2E-03
I-136m	1.5E-06	1.3E+00	1.5E+00	1.6E+00	1.6E+00	9.6E-05	6.0E-04	1.1E-03	1.1E-03
I-136	2.6E-06	1.3E+00	1.9E+00	1.3E+00	1.6E+00	5.7E-05	4.3E-04	4.5E-04	6.0E-04
Sn-137	7.6E-09	1.9E-05	3.7E-07	4.4E-08	4.9E-08	2.8E-07	3.0E-08	5.5E-09	6.4E-09
Sb-137	2.9E-08	7.4E-02	8.4E-04	2.8E-04	2.6E-04	3.0E-04	1.8E-05	9.2E-06	9.1E-06
Te-137	7.9E-08	3.9E-01	1.6E-01	1.3E-01	1.2E-01	5.7E-04	1.2E-03	1.6E-03	1.4E-03
I-137	7.8E-07	2.6E+00	2.4E+00	2.3E+00	1.9E+00	3.9E-04	1.9E-03	2.8E-03	2.4E-03
Xe-137	7.3E-06	3.2E+00	3.5E+00	3.7E+00	3.7E+00	5.0E-05	3.0E-04	4.8E-04	5.0E-04
Cs-137	3.0E+01	6.0E-02	2.3E-01	6.0E-01	1.0E+00	2.3E-13	4.7E-12	1.9E-11	3.3E-11
Ba-137m	4.9E-06	1.3E-04	6.3E-05	4.5E-03	4.1E-03	3.1E-09	8.0E-09	8.9E-07	8.3E-07

NA = Not applicable; no half-life or fractional abundances are provided because the isotope is stable.

--- = No half-life was found for the radionuclide; the isotope was not included in the fission product allocation.

[a] The primary source of radionuclide half-lives was KAPL (2002). Alternate sources include England and Rider (1994) and NNDC (2004).

Table I-2 (Continued)
Fission Product Yields and Activity Fractions for Mixed-Fission Product Waste at the Time of Generation

Isotope	Half-Life (yr) [a]	Fission Yields (yield/100 fissions)				Fractional Abundance (activity basis)			
		U-235		Pu-239		U-235		Pu-239	
		Thermal Neutrons	Fast Neutrons	Thermal Neutrons	Fast Neutrons	Thermal Neutrons	Fast Neutrons	Thermal Neutrons	Fast Neutrons
Sn-138	---	3.3E-09	1.8E-08	3.8E-10	9.7E-10	0.0E+00	0.0E+00	0.0E+00	0.0E+00
Sb-138	5.5E-09	3.9E-05	1.1E-04	6.5E-06	1.5E-05	8.2E-07	1.3E-05	1.1E-06	2.7E-06
Te-138	4.4E-08	6.6E-02	1.1E-01	1.2E-02	2.5E-02	1.7E-04	1.5E-03	2.5E-04	5.6E-04
I-138	2.1E-07	1.4E+00	1.3E+00	1.3E+00	1.0E+00	7.9E-04	3.7E-03	5.9E-03	4.9E-03
Xe-138	2.7E-05	4.8E+00	4.7E+00	3.9E+00	3.7E+00	2.1E-05	1.1E-04	1.4E-04	1.4E-04
Cs-138m	5.5E-06	2.2E-01	1.2E-01	5.9E-01	6.8E-01	4.6E-06	1.3E-05	1.0E-04	1.2E-04
Cs-138	6.1E-05	2.4E-01	5.5E-01	3.1E-01	6.8E-01	4.6E-07	5.6E-06	4.8E-06	1.1E-05
Sb-139	6.9E-09	1.4E-06	3.9E-06	1.7E-07	2.8E-07	2.3E-08	3.5E-07	2.4E-08	4.1E-08
Te-139	1.8E-08	6.7E-03	9.8E-03	8.1E-04	1.3E-03	4.2E-05	3.3E-04	4.2E-05	7.0E-05
I-139	7.3E-08	7.7E-01	4.6E-01	3.2E-01	1.9E-01	1.2E-03	3.9E-03	4.2E-03	2.6E-03
Xe-139	1.3E-06	4.3E+00	3.8E+00	2.8E+00	2.9E+00	3.9E-04	1.9E-03	2.1E-03	2.3E-03
Cs-139	1.8E-05	1.3E+00	2.1E+00	2.3E+00	2.3E+00	8.5E-06	7.3E-05	1.3E-04	1.3E-04
Ba-139	1.6E-04	6.9E-02	2.0E-02	2.3E-01	2.4E-01	5.0E-08	7.8E-08	1.4E-06	1.5E-06
La-139	NA	2.3E-05	8.9E-06	1.0E-03	9.5E-04	0.0E+00	0.0E+00	0.0E+00	0.0E+00
Ce-139m	1.8E-06	7.0E-10	2.3E-10	2.4E-07	2.4E-07	4.5E-14	7.7E-14	1.3E-10	1.3E-10
Te-140	2.8E-08	1.7E-02	9.0E-04	1.4E-04	8.1E-05	6.8E-05	2.0E-05	4.8E-06	2.8E-06
I-140	2.7E-08	1.4E-01	1.1E-01	5.9E-02	3.2E-02	5.8E-04	2.5E-03	2.1E-03	1.2E-03
Xe-140	4.3E-07	3.5E+00	2.6E+00	1.5E+00	1.6E+00	9.3E-04	3.7E-03	3.4E-03	3.7E-03
Cs-140	2.0E-06	2.1E+00	3.1E+00	2.3E+00	2.8E+00	1.2E-04	9.3E-04	1.1E-03	1.4E-03

NA = Not applicable; no half-life or fractional abundances are provided because the isotope is stable.

--- = No half-life was found for the radionuclide; the isotope was not included in the fission product allocation.

[a] The primary source of radionuclide half-lives was KAPL (2002). Alternate sources include England and Rider (1994) and NNDC (2004).

Table I-2 (Continued)
Fission Product Yields and Activity Fractions for Mixed-Fission Product Waste at the Time of Generation

Isotope	Half-Life (yr) [a]	Fission Yields (yield/100 fissions)				Fractional Abundance (activity basis)			
		U-235		Pu-239		U-235		Pu-239	
		Thermal Neutrons	Fast Neutrons	Thermal Neutrons	Fast Neutrons	Thermal Neutrons	Fast Neutrons	Thermal Neutrons	Fast Neutrons
Ba-140	3.5E-02	4.9E-01	2.4E-01	1.5E+00	9.2E-01	1.6E-09	4.2E-09	4.1E-08	2.6E-08
La-140	4.6E-03	5.2E-03	2.0E-04	1.0E-02	9.9E-03	1.3E-10	2.7E-11	2.1E-09	2.1E-09
I-141	1.4E-08	4.1E-02	1.7E-02	7.0E-03	3.6E-03	3.3E-04	7.3E-04	4.7E-04	2.5E-04
Xe-141	5.5E-08	1.2E+00	8.8E-01	4.7E-01	4.8E-01	2.6E-03	9.9E-03	8.3E-03	8.7E-03
Cs-141	7.9E-07	2.9E+00	3.5E+00	2.9E+00	2.6E+00	4.2E-04	2.7E-03	3.5E-03	3.3E-03
Ba-141	3.5E-05	1.7E+00	1.6E+00	1.8E+00	2.0E+00	5.5E-06	2.8E-05	5.0E-05	5.6E-05
La-141	4.5E-04	1.9E-02	4.7E-03	7.2E-02	6.9E-02	4.8E-09	6.4E-09	1.5E-07	1.5E-07
Ce-141	8.9E-02	5.0E-06	3.2E-05	2.3E-04	2.5E-04	6.4E-15	2.2E-13	2.5E-12	2.7E-12
Te-142	1.9E-08	2.1E-06	1.4E-06	5.7E-07	4.6E-08	1.3E-08	4.6E-08	2.9E-08	2.4E-09
I-142	6.3E-09	5.9E-03	2.3E-03	2.5E-03	2.0E-04	1.1E-04	2.2E-04	3.7E-04	3.1E-05
Xe-142	3.9E-08	4.3E-01	5.7E-01	1.4E-01	9.7E-02	1.3E-03	9.0E-03	3.5E-03	2.5E-03
Cs-142	5.7E-08	2.3E+00	2.3E+00	1.4E+00	1.3E+00	4.6E-03	2.4E-02	2.3E-02	2.2E-02
Ba-142	2.0E-05	3.0E+00	2.7E+00	3.1E+00	3.1E+00	1.7E-05	8.0E-05	1.4E-04	1.5E-04
La-142	1.8E-04	9.7E-02	3.0E-02	3.0E-01	2.7E-01	6.3E-08	1.0E-07	1.6E-06	1.5E-06
Ce-142	5.0E+16	1.8E-04	7.1E-05	3.6E-03	3.7E-03	4.0E-31	8.8E-31	6.8E-29	7.3E-29
Xe-143	9.5E-09	5.3E-02	6.4E-02	1.2E-02	1.2E-02	6.4E-04	4.1E-03	1.2E-03	1.2E-03
Cs-143	5.6E-08	1.4E+00	1.2E+00	6.8E-01	5.5E-01	2.8E-03	1.3E-02	1.2E-02	9.6E-03
Ba-143	4.5E-07	4.1E+00	3.6E+00	2.9E+00	2.9E+00	1.0E-03	4.9E-03	6.1E-03	6.4E-03
La-143	2.7E-05	3.8E-01	8.7E-01	8.2E-01	8.4E-01	1.6E-06	2.0E-05	2.9E-05	3.1E-05

NA = Not applicable; no half-life or fractional abundances are provided because the isotope is stable.

--- = No half-life was found for the radionuclide; the isotope was not included in the fission product allocation.

[a] The primary source of radionuclide half-lives was KAPL (2002). Alternate sources include England and Rider (1994) and NNDC (2004).

Table I-2 (Continued)
Fission Product Yields and Activity Fractions for Mixed-Fission Product Waste at the Time of Generation

Isotope	Half-Life (yr) [a]	Fission Yields (yield/100 fissions)				Fractional Abundance (activity basis)			
		U-235		Pu-239		U-235		Pu-239	
		Thermal Neutrons	Fast Neutrons	Thermal Neutrons	Fast Neutrons	Thermal Neutrons	Fast Neutrons	Thermal Neutrons	Fast Neutrons
Ce-143	3.8E-03	3.1E-02	1.4E-03	2.7E-02	2.9E-02	9.5E-10	2.3E-10	6.8E-09	7.6E-09
Pr-143	3.7E-02	4.5E-07	1.6E-07	3.4E-05	3.6E-05	1.4E-15	2.7E-15	8.6E-13	9.5E-13
Nd-143	NA	4.8E-12	1.4E-12	2.9E-09	3.5E-09	0.0E+00	0.0E+00	0.0E+00	0.0E+00
Xe-144	3.8E-08	6.1E-03	0.0E+00	7.4E-04	9.1E-04	1.8E-05	0.0E+00	1.9E-05	2.4E-05
Cs-144	3.2E-08	4.2E-01	3.8E-01	1.6E-01	1.1E-01	1.5E-03	7.3E-03	4.7E-03	3.5E-03
Ba-144	3.6E-07	4.0E+00	3.0E+00	2.2E+00	2.0E+00	1.3E-03	5.1E-03	5.7E-03	5.6E-03
La-144	1.3E-06	1.1E+00	1.9E+00	1.3E+00	1.4E+00	9.5E-05	8.8E-04	9.7E-04	1.0E-03
Ce-144	7.8E-01	3.5E-02	1.7E-02	1.2E-01	1.6E-01	5.1E-12	1.3E-11	1.4E-10	2.1E-10
Pr-144m	1.4E-05	1.3E-05	4.9E-06	3.3E-04	5.2E-04	1.1E-10	2.2E-10	2.3E-08	3.7E-08
Pr-144	3.3E-05	1.4E-06	4.8E-07	3.7E-05	5.1E-05	5.0E-12	9.0E-12	1.1E-09	1.5E-09
Nd-144	2.38E15	9.6E-09	1.3E-08	1.4E-07	5.7E-08	4.6E-34	3.3E-33	5.5E-32	2.4E-32
Xe-145	2.9E-08	7.2E-05	8.5E-04	5.7E-05	3.6E-05	2.9E-07	1.8E-05	1.9E-06	1.2E-06
Cs-145	1.9E-08	7.6E-02	1.4E-01	2.8E-02	1.8E-02	4.6E-04	4.5E-03	1.4E-03	9.3E-04
Ba-145	1.3E-07	1.9E+00	2.3E+00	8.0E-01	8.0E-01	1.7E-03	1.1E-02	6.1E-03	6.3E-03
La-145	7.6E-07	1.9E+00	1.2E+00	1.7E+00	1.7E+00	2.9E-04	1.0E-03	2.1E-03	2.2E-03
Ce-145	5.7E-06	8.5E-02	9.2E-02	4.6E-01	5.0E-01	1.7E-06	9.9E-06	7.6E-05	8.7E-05
Pr-145	6.8E-04	3.3E-04	1.5E-04	5.8E-03	6.5E-03	5.6E-11	1.3E-10	8.1E-09	9.4E-09
Nd-145	NA	5.6E-08	1.8E-08	5.9E-06	7.5E-06	0.0E+00	0.0E+00	0.0E+00	0.0E+00
Pm-145	1.8E+01	0.0E+00	0.0E+00	2.0E-10	2.7E-10	0.0E+00	0.0E+00	1.1E-20	1.5E-20

NA = Not applicable; no half-life or fractional abundances are provided because the isotope is stable.

--- = No half-life was found for the radionuclide; the isotope was not included in the fission product allocation.

[a] The primary source of radionuclide half-lives was KAPL (2002). Alternate sources include England and Rider (1994) and NNDC (2004).

Table I-2 (Continued)
Fission Product Yields and Activity Fractions for Mixed-Fission Product Waste at the Time of Generation

Isotope	Half-Life (yr) [a]	Fission Yields (yield/100 fissions)				Fractional Abundance (activity basis)			
		U-235		Pu-239		U-235		Pu-239	
		Thermal Neutrons	Fast Neutrons	Thermal Neutrons	Fast Neutrons	Thermal Neutrons	Fast Neutrons	Thermal Neutrons	Fast Neutrons
Xe-146	1.8E-08	1.1E-05	3.4E-05	1.5E-06	9.5E-07	6.8E-08	1.2E-06	8.2E-08	5.3E-08
Cs-146	1.0E-08	7.6E-03	1.5E-02	2.1E-03	1.3E-03	8.6E-05	9.2E-04	2.0E-04	1.3E-04
Ba-146	7.0E-08	9.1E-01	1.2E+00	2.4E-01	2.2E-01	1.5E-03	1.0E-02	3.3E-03	3.2E-03
La-146	2.0E-07	1.5E+00	1.3E+00	1.2E+00	1.1E+00	8.6E-04	4.1E-03	5.6E-03	5.6E-03
Ce-146	2.6E-05	5.8E-01	4.3E-01	1.0E+00	1.1E+00	2.6E-06	1.0E-05	3.9E-05	4.2E-05
Pr-146	4.6E-05	3.6E-03	1.8E-03	2.0E-02	3.6E-02	9.0E-09	2.4E-08	4.1E-07	7.8E-07
Nd-146	NA	3.2E-06	1.2E-06	8.1E-05	1.7E-04	0.0E+00	0.0E+00	0.0E+00	0.0E+00
Pm-146	5.5E+00	4.5E-10	7.2E-12	7.9E-09	1.7E-08	9.3E-21	8.0E-22	1.4E-18	3.1E-18
Ba-147	2.8E-08	2.5E-01	2.4E-01	3.5E-02	3.4E-02	1.0E-03	5.3E-03	1.2E-03	1.2E-03
La-147	1.3E-07	6.4E-01	1.1E+00	6.1E-01	5.8E-01	5.8E-04	5.4E-03	4.6E-03	4.5E-03
Ce-147	1.8E-06	1.0E+00	7.7E-01	1.2E+00	1.2E+00	6.4E-05	2.7E-04	6.6E-04	6.9E-04
Pr-147	2.5E-05	3.6E-01	1.5E-02	1.4E-01	1.4E-01	1.6E-06	3.7E-07	5.2E-06	5.5E-06
Nd-147	3.0E-02	6.7E-05	2.8E-05	1.6E-03	1.7E-03	2.6E-13	5.7E-13	5.1E-11	5.7E-11
Pm-147	2.6E+00	2.5E-09	8.6E-10	6.5E-07	7.0E-07	1.1E-19	2.0E-19	2.4E-16	2.7E-16
Sm-147	1.1E+11	0.0E+00	0.0E+00	1.8E-11	2.3E-11	0.0E+00	0.0E+00	1.7E-31	2.1E-31
Xe-148	---	1.1E-09	6.2E-09	9.1E-11	1.5E-10	0.0E+00	0.0E+00	0.0E+00	0.0E+00
Cs-148	4.8E-09	1.3E-05	4.1E-05	1.5E-06	2.3E-06	3.2E-07	5.3E-06	3.0E-07	4.8E-07
Ba-148	2.0E-08	2.2E-02	3.9E-02	2.6E-03	4.0E-03	1.3E-04	1.2E-03	1.2E-04	2.0E-04
La-148	3.5E-08	3.4E-01	4.2E-01	1.2E-01	1.7E-01	1.1E-03	7.4E-03	3.2E-03	4.9E-03

NA = Not applicable; no half-life or fractional abundances are provided because the isotope is stable.

--- = No half-life was found for the radionuclide; the isotope was not included in the fission product allocation.

[a] The primary source of radionuclide half-lives was KAPL (2002). Alternate sources include England and Rider (1994) and NNDC (2004).

Table I-2 (Continued)
Fission Product Yields and Activity Fractions for Mixed-Fission Product Waste at the Time of Generation

Isotope	Half-Life (yr) [a]	Fission Yields (yield/100 fissions)				Fractional Abundance (activity basis)			
		U-235		Pu-239		U-235		Pu-239	
		Thermal Neutrons	Fast Neutrons	Thermal Neutrons	Fast Neutrons	Thermal Neutrons	Fast Neutrons	Thermal Neutrons	Fast Neutrons
Ce-148	1.8E-06	1.2E+00	1.2E+00	8.9E-01	1.2E+00	8.0E-05	4.0E-04	4.8E-04	6.5E-04
Pr-148	4.3E-06	7.8E-02	5.6E-02	6.2E-01	3.1E-01	2.1E-06	8.0E-06	1.4E-04	7.0E-05
Nd-148	NA	9.9E-04	5.2E-04	1.4E-02	1.4E-02	0.0E+00	0.0E+00	0.0E+00	0.0E+00
Ba-149	1.1E-08	1.0E-03	2.6E-03	2.2E-04	2.4E-04	1.1E-05	1.5E-04	1.9E-05	2.2E-05
La-149	3.3E-08	8.0E-02	1.3E-01	3.6E-02	3.9E-02	2.8E-04	2.3E-03	1.0E-03	1.2E-03
Ce-149	1.6E-07	7.0E-01	7.6E-01	5.6E-01	6.4E-01	4.9E-04	2.8E-03	3.3E-03	3.9E-03
Pr-149	4.4E-06	3.0E-01	1.5E-01	5.7E-01	5.0E-01	7.8E-06	2.1E-05	1.2E-04	1.1E-04
Nd-149	2.0E-04	6.8E-03	3.5E-03	5.0E-02	6.0E-02	4.0E-09	1.1E-08	2.4E-07	3.0E-07
Pm-149	6.1E-03	3.9E-06	1.6E-06	2.4E-04	2.5E-04	7.3E-14	1.7E-13	3.8E-11	4.1E-11
Sm-149	1.0E+16	1.7E-10	5.7E-11	8.2E-08	9.4E-08	2.0E-36	3.5E-36	7.8E-33	9.4E-33
Cs-150	3.9E-09	2.0E-09	1.1E-08	6.3E-10	5.6E-10	5.8E-11	1.8E-09	1.5E-10	1.4E-10
Ba-150	9.5E-09	5.0E-05	1.5E-04	1.2E-05	1.1E-05	6.1E-07	9.6E-06	1.2E-06	1.2E-06
La-150	1.6E-08	1.0E-02	1.9E-02	5.2E-03	4.9E-03	7.4E-05	7.2E-04	3.1E-04	3.0E-04
Ce-150	1.4E-07	3.9E-01	4.6E-01	2.8E-01	2.8E-01	3.2E-04	2.0E-03	1.9E-03	2.0E-03
Pr-150	2.0E-07	2.2E-01	1.9E-01	5.1E-01	5.2E-01	1.3E-04	5.9E-04	2.5E-03	2.6E-03
Nd-150	NA	3.3E-02	2.0E-02	1.7E-01	1.9E-01	0.0E+00	0.0E+00	0.0E+00	0.0E+00
Pm-150	3.1E-04	3.0E-05	2.5E-05	1.2E-03	2.2E-03	1.1E-11	5.0E-11	3.6E-09	7.2E-09
Sm-150	NA	1.2E-08	4.6E-09	2.5E-06	3.2E-06	0.0E+00	0.0E+00	0.0E+00	0.0E+00
La-151	2.3E-08	1.0E-03	2.4E-03	4.8E-04	4.2E-04	5.2E-06	6.4E-05	2.0E-05	1.8E-05

NA = Not applicable; no half-life or fractional abundances are provided because the isotope is stable.

--- = No half-life was found for the radionuclide; the isotope was not included in the fission product allocation.

[a] The primary source of radionuclide half-lives was KAPL (2002). Alternate sources include England and Rider (1994) and NNDC (2004).

Table I-2 (Continued)
Fission Product Yields and Activity Fractions for Mixed-Fission Product Waste at the Time of Generation

Isotope	Half-Life (yr) [a]	Fission Yields (yield/100 fissions)				Fractional Abundance (activity basis)			
		U-235		Pu-239		U-235		Pu-239	
		Thermal Neutrons	Fast Neutrons	Thermal Neutrons	Fast Neutrons	Thermal Neutrons	Fast Neutrons	Thermal Neutrons	Fast Neutrons
Ce-151	3.2E-08	9.9E-02	1.4E-01	6.3E-02	6.2E-02	3.6E-04	2.7E-03	1.9E-03	1.9E-03
Pr-151	6.0E-07	2.4E-01	2.2E-01	3.7E-01	3.7E-01	4.6E-05	2.2E-04	5.9E-04	6.2E-04
Nd-151	2.4E-05	8.0E-02	5.4E-02	2.9E-01	3.4E-01	3.9E-07	1.4E-06	1.2E-05	1.4E-05
Pm-151	3.2E-03	6.4E-04	3.2E-04	1.1E-02	1.3E-02	2.3E-11	6.1E-11	3.2E-09	3.9E-09
Sm-151	9.0E+01	4.8E-07	1.6E-07	3.9E-05	5.4E-05	6.1E-19	1.1E-18	4.1E-16	5.9E-16
Eu-151	NA	2.5E-10	9.6E-10	4.6E-09	6.8E-09	0.0E+00	0.0E+00	0.0E+00	0.0E+00
Ba-152	1.3E-08	1.5E-08	8.2E-08	5.4E-09	4.1E-09	1.3E-10	3.8E-09	3.9E-10	3.1E-10
La-152	9.0E-09	4.5E-05	1.4E-04	2.4E-05	2.0E-05	5.8E-07	9.3E-06	2.6E-06	2.2E-06
Ce-152	4.4E-08	2.1E-02	3.5E-02	1.2E-02	1.1E-02	5.3E-05	4.9E-04	2.5E-04	2.4E-04
Pr-152	1.0E-07	1.0E-01	1.2E-01	1.6E-01	1.6E-01	1.2E-04	7.3E-04	1.5E-03	1.6E-03
Nd-152	2.2E-05	1.4E-01	1.1E-01	3.7E-01	4.1E-01	7.5E-07	3.2E-06	1.6E-05	1.9E-05
Pm-152m	2.6E-05	1.4E-03	8.3E-04	1.7E-02	2.0E-02	6.1E-09	1.9E-08	6.1E-07	7.7E-07
Pm-152	7.8E-06	1.4E-03	8.3E-04	1.7E-02	2.0E-02	2.0E-08	6.5E-08	2.0E-06	2.6E-06
Sm-152	NA	9.7E-06	4.1E-06	4.3E-04	6.1E-04	0.0E+00	0.0E+00	0.0E+00	0.0E+00
Eu-152m	1.8E-04	1.4E-10	4.7E-11	6.8E-08	1.1E-07	8.5E-17	1.6E-16	3.6E-13	5.9E-13
La-153	1.0E-08	1.4E-06	6.0E-06	8.5E-07	6.3E-07	1.6E-08	3.5E-07	7.9E-08	6.1E-08
Ce-153	4.7E-08	1.7E-03	3.9E-03	1.1E-03	9.6E-04	4.2E-06	5.2E-05	2.2E-05	2.0E-05
Pr-153	1.4E-07	3.7E-02	5.5E-02	4.9E-02	5.0E-02	3.1E-05	2.5E-04	3.5E-04	3.6E-04
Nd-153	1.0E-06	1.1E-01	1.0E-01	2.4E-01	2.8E-01	1.3E-05	6.2E-05	2.3E-04	2.7E-04

NA = Not applicable; no half-life or fractional abundances are provided because the isotope is stable.

--- = No half-life was found for the radionuclide; the isotope was not included in the fission product allocation.

[a] The primary source of radionuclide half-lives was KAPL (2002). Alternate sources include England and Rider (1994) and NNDC (2004).

Table I-2 (Continued)
Fission Product Yields and Activity Fractions for Mixed-Fission Product Waste at the Time of Generation

Isotope	Half-Life (yr) [a]	Fission Yields (yield/100 fissions)				Fractional Abundance (activity basis)			
		U-235		Pu-239		U-235		Pu-239	
		Thermal Neutrons	Fast Neutrons	Thermal Neutrons	Fast Neutrons	Thermal Neutrons	Fast Neutrons	Thermal Neutrons	Fast Neutrons
Pm-153	1.0E-05	8.8E-03	6.5E-03	6.8E-02	9.3E-02	9.8E-08	3.9E-07	6.4E-06	8.9E-06
Sm-153	5.3E-03	8.0E-05	4.2E-05	2.1E-03	3.6E-03	1.7E-12	4.9E-12	3.8E-10	6.7E-10
Eu-153	NA	2.3E-07	4.6E-09	2.5E-06	4.5E-06	0.0E+00	0.0E+00	0.0E+00	0.0E+00
Gd-153	6.6E-01	0.0E+00	0.0E+00	2.2E-10	5.0E-10	0.0E+00	0.0E+00	3.1E-19	7.5E-19
Ba-154	---	0.0E+00	3.7E-12	0.0E+00	0.0E+00	0.0E+00	0.0E+00	0.0E+00	0.0E+00
La-154	4.7E-09	1.5E-08	8.0E-08	1.8E-08	1.0E-08	3.5E-10	1.0E-08	3.7E-09	2.1E-09
Ce-154	6.4E-08	9.1E-05	2.5E-04	8.6E-05	5.8E-05	1.6E-07	2.4E-06	1.3E-06	9.0E-07
Pr-154	7.3E-08	5.0E-03	7.9E-03	9.7E-03	7.7E-03	7.9E-06	6.7E-05	1.3E-04	1.1E-04
Nd-154	8.2E-07	5.8E-02	5.7E-02	1.5E-01	1.5E-01	8.1E-06	4.2E-05	1.8E-04	1.8E-04
Pm-154m	5.1E-06	5.4E-03	3.7E-03	4.5E-02	5.0E-02	1.2E-07	4.4E-07	8.4E-06	9.7E-06
Pm-154	3.2E-06	5.4E-03	3.7E-03	4.5E-02	5.0E-02	1.9E-07	7.0E-07	1.3E-05	1.5E-05
Sm-154	NA	4.7E-04	2.1E-04	9.4E-03	1.3E-02	0.0E+00	0.0E+00	0.0E+00	0.0E+00
Eu-154	8.6E+00	1.9E-07	6.2E-08	2.8E-05	4.7E-05	2.6E-18	4.4E-18	3.1E-15	5.5E-15
Ce-155	1.7E-08	2.6E-06	1.2E-05	3.5E-06	2.5E-06	1.7E-08	4.3E-07	2.0E-07	1.5E-07
Pr-155	3.6E-08	6.7E-04	1.7E-03	1.4E-03	1.2E-03	2.2E-06	2.9E-05	3.9E-05	3.4E-05
Nd-155	2.8E-07	1.8E-02	2.5E-02	5.1E-02	5.6E-02	7.1E-06	5.5E-05	1.7E-04	2.0E-04
Pm-155	1.3E-06	1.3E-02	1.2E-02	9.2E-02	1.2E-01	1.1E-06	5.5E-06	6.6E-05	8.7E-05
Sm-155	4.2E-05	1.3E-03	7.9E-04	2.1E-02	3.5E-02	3.6E-09	1.2E-08	4.8E-07	8.2E-07
Eu-155	4.8E+00	2.6E-06	1.1E-06	1.9E-04	4.5E-04	6.4E-17	1.4E-16	3.9E-14	9.4E-14

NA = Not applicable; no half-life or fractional abundances are provided because the isotope is stable.

--- = No half-life was found for the radionuclide; the isotope was not included in the fission product allocation.

[a] The primary source of radionuclide half-lives was KAPL (2002). Alternate sources include England and Rider (1994) and NNDC (2004).

Table I-2 (Continued)
Fission Product Yields and Activity Fractions for Mixed-Fission Product Waste at the Time of Generation

Isotope	Half-Life (yr) [a]	Fission Yields (yield/100 fissions)				Fractional Abundance (activity basis)			
		U-235		Pu-239		U-235		Pu-239	
		Thermal Neutrons	Fast Neutrons	Thermal Neutrons	Fast Neutrons	Thermal Neutrons	Fast Neutrons	Thermal Neutrons	Fast Neutrons
Gd-155	NA	4.1E-10	1.3E-10	1.7E-07	5.2E-07	0.0E+00	0.0E+00	0.0E+00	0.0E+00
Tb-155	1.5E-02	0.0E+00	0.0E+00	4.7E-12	1.9E-11	0.0E+00	0.0E+00	3.1E-19	1.3E-18
Ce-156	1.9E-08	5.7E-08	4.2E-07	1.2E-07	7.9E-08	3.5E-10	1.4E-08	6.2E-09	4.1E-09
Pr-156	1.2E-08	4.1E-05	1.5E-04	1.3E-04	1.0E-04	3.9E-07	7.6E-06	1.0E-05	8.3E-06
Nd-156	1.7E-07	4.7E-03	9.1E-03	1.6E-02	1.6E-02	3.1E-06	3.2E-05	8.8E-05	8.9E-05
Pm-156	8.5E-07	7.1E-03	8.7E-03	6.2E-02	7.3E-02	9.6E-07	6.3E-06	7.0E-05	8.5E-05
Sm-156	1.1E-03	3.0E-03	2.3E-03	4.5E-02	6.5E-02	3.2E-10	1.3E-09	4.0E-08	6.0E-08
Eu-156	4.2E-02	1.6E-05	8.3E-06	1.2E-03	2.0E-03	4.5E-14	1.2E-13	2.7E-11	4.8E-11
Gd-156	NA	1.4E-08	3.9E-09	3.9E-06	1.3E-06	0.0E+00	0.0E+00	0.0E+00	0.0E+00
Tb-156m	6.1E-04	0.0E+00	0.0E+00	2.9E-11	7.7E-11	0.0E+00	0.0E+00	4.6E-17	1.3E-16
Tb-156	1.5E-02	0.0E+00	0.0E+00	2.6E-10	7.7E-10	0.0E+00	0.0E+00	1.7E-17	5.3E-17
Ce-157	6.8E-09	4.6E-10	6.6E-09	1.8E-09	1.2E-09	7.8E-12	6.0E-10	2.5E-10	1.8E-10
Pr-157	1.2E-08	1.7E-06	1.1E-05	7.2E-06	5.8E-06	1.6E-08	5.7E-07	5.7E-07	4.8E-07
Nd-157	7.9E-08	4.9E-04	1.6E-03	2.2E-03	2.3E-03	7.1E-07	1.3E-05	2.7E-05	2.9E-05
Pm-157	3.5E-07	2.9E-03	5.8E-03	2.7E-02	3.4E-02	9.7E-07	1.0E-05	7.6E-05	9.7E-05
Sm-157	1.5E-05	2.7E-03	3.2E-03	4.1E-02	6.4E-02	2.0E-08	1.3E-07	2.6E-06	4.2E-06
Eu-157	1.7E-03	6.4E-05	4.7E-05	3.5E-03	6.4E-03	4.2E-12	1.7E-11	1.9E-09	3.6E-09
Gd-157	NA	1.5E-07	6.5E-08	2.9E-05	6.9E-05	0.0E+00	0.0E+00	0.0E+00	0.0E+00
Tb-157	7.0E+01	4.9E-12	1.5E-12	8.2E-09	2.4E-08	8.1E-24	1.3E-23	1.1E-19	3.4E-19

NA = Not applicable; no half-life or fractional abundances are provided because the isotope is stable.

--- = No half-life was found for the radionuclide; the isotope was not included in the fission product allocation.

[a] The primary source of radionuclide half-lives was KAPL (2002). Alternate sources include England and Rider (1994) and NNDC (2004).

Table I-2 (Continued)
Fission Product Yields and Activity Fractions for Mixed-Fission Product Waste at the Time of Generation

Isotope	Half-Life (yr) [a]	Fission Yields (yield/100 fissions)				Fractional Abundance (activity basis)			
		U-235		Pu-239		U-235		Pu-239	
		Thermal Neutrons	Fast Neutrons	Thermal Neutrons	Fast Neutrons	Thermal Neutrons	Fast Neutrons	Thermal Neutrons	Fast Neutrons
Ce-158	---	3.9E-12	9.3E-11	1.9E-11	1.3E-11	0.0E+00	0.0E+00	0.0E+00	0.0E+00
Pr-158	5.4E-09	3.8E-08	4.0E-07	2.0E-07	1.7E-07	8.0E-10	4.6E-08	3.5E-08	3.1E-08
Nd-158	8.5E-08	5.2E-05	2.6E-04	2.2E-04	2.3E-04	7.0E-08	1.9E-06	2.5E-06	2.7E-06
Pm-158	1.6E-07	7.1E-04	2.0E-03	6.4E-03	8.2E-03	5.1E-07	7.8E-06	3.9E-05	5.1E-05
Sm-158	1.0E-05	2.4E-03	4.1E-03	2.9E-02	4.7E-02	2.7E-08	2.5E-07	2.8E-06	4.6E-06
Eu-158	8.7E-05	1.3E-04	1.4E-04	5.4E-03	1.0E-02	1.7E-10	9.8E-10	5.9E-08	1.2E-07
Gd-158	NA	1.5E-06	8.8E-07	1.5E-04	3.7E-04	0.0E+00	0.0E+00	0.0E+00	0.0E+00
Tb-158m	3.3E-07	1.3E-11	4.8E-12	1.1E-08	3.1E-08	4.6E-15	8.8E-15	3.2E-11	9.3E-11
Tb-158	1.8E+02	1.2E-10	4.8E-11	1.0E-07	3.1E-07	7.6E-23	1.7E-22	5.3E-19	1.7E-18
Pr-159	5.7E-09	4.9E-10	1.0E-08	4.1E-09	3.8E-09	9.8E-12	1.1E-09	6.9E-10	6.5E-10
Nd-159	2.0E-08	1.8E-06	1.7E-05	1.2E-05	1.4E-05	1.0E-08	5.0E-07	5.6E-07	6.8E-07
Pm-159	6.3E-08	1.1E-04	5.3E-04	1.2E-03	1.7E-03	1.9E-07	5.2E-06	1.8E-05	2.7E-05
Sm-159	3.6E-07	7.4E-04	2.2E-03	1.2E-02	2.2E-02	2.4E-07	3.7E-06	3.2E-05	5.9E-05
Eu-159	3.4E-05	1.6E-04	2.9E-04	6.8E-03	1.4E-02	5.2E-10	5.2E-09	1.9E-07	4.1E-07
Gd-159	2.1E-03	3.7E-06	4.5E-06	4.5E-04	1.2E-03	2.0E-13	1.3E-12	2.1E-10	5.7E-10
Tb-159	NA	1.7E-09	1.3E-09	1.3E-06	4.0E-06	0.0E+00	0.0E+00	0.0E+00	0.0E+00
Dy-159	4.0E-01	0.0E+00	0.0E+00	2.6E-10	1.1E-09	0.0E+00	0.0E+00	6.3E-19	2.8E-18
Pr-160	---	2.8E-12	9.1E-11	4.8E-11	3.3E-11	0.0E+00	0.0E+00	0.0E+00	0.0E+00
Nd-160	2.5E-08	5.0E-08	7.1E-07	5.1E-07	4.5E-07	2.3E-10	1.7E-08	1.9E-08	1.8E-08

NA = Not applicable; no half-life or fractional abundances are provided because the isotope is stable.

--- = No half-life was found for the radionuclide; the isotope was not included in the fission product allocation.

[a] The primary source of radionuclide half-lives was KAPL (2002). Alternate sources include England and Rider (1994) and NNDC (2004).

Table I-2 (Continued)
Fission Product Yields and Activity Fractions for Mixed-Fission Product Waste at the Time of Generation

Isotope	Half-Life (yr) [a]	Fission Yields (yield/100 fissions)				Fractional Abundance (activity basis)			
		U-235		Pu-239		U-235		Pu-239	
		Thermal Neutrons	Fast Neutrons	Thermal Neutrons	Fast Neutrons	Thermal Neutrons	Fast Neutrons	Thermal Neutrons	Fast Neutrons
Pm-160	2.3E-08	7.6E-06	5.4E-05	1.3E-04	1.4E-04	3.7E-08	1.4E-06	5.2E-06	6.0E-06
Sm-160	3.0E-07	2.1E-04	8.3E-04	4.0E-03	5.7E-03	8.0E-08	1.7E-06	1.3E-05	1.9E-05
Eu-160	1.2E-06	9.0E-05	2.3E-04	4.6E-03	8.0E-03	8.6E-09	1.2E-07	3.6E-06	6.6E-06
Gd-160	NA	1.0E-05	1.5E-05	9.7E-04	2.2E-03	0.0E+00	0.0E+00	0.0E+00	0.0E+00
Tb-160	2.0E-01	2.8E-08	1.1E-08	6.3E-06	1.8E-05	1.6E-17	3.5E-17	3.0E-14	9.1E-14
Dy-160	NA	1.9E-12	1.2E-12	4.7E-09	1.8E-08	0.0E+00	0.0E+00	0.0E+00	0.0E+00
Nd-161	9.9E-09	6.2E-10	1.3E-08	1.1E-08	9.9E-09	7.2E-12	8.1E-10	1.1E-09	1.0E-09
Pm-161	2.5E-08	4.4E-07	4.5E-06	1.0E-05	1.1E-05	2.0E-09	1.1E-07	4.0E-07	4.4E-07
Sm-161	1.6E-07	2.8E-05	1.5E-04	7.8E-04	1.1E-03	2.0E-08	5.9E-07	4.7E-06	7.0E-06
Eu-161	8.2E-07	4.5E-05	1.5E-04	2.8E-03	4.7E-03	6.3E-09	1.1E-07	3.2E-06	5.6E-06
Gd-161	7.0E-06	1.1E-05	2.3E-05	1.3E-03	2.8E-03	1.8E-10	2.0E-09	1.7E-07	4.0E-07
Tb-161	1.9E-02	6.0E-08	7.7E-08	2.9E-05	7.8E-05	3.6E-16	2.5E-15	1.4E-12	4.1E-12
Dy-161	NA	2.5E-11	2.2E-11	5.5E-08	2.8E-07	0.0E+00	0.0E+00	0.0E+00	0.0E+00
Ho-161m	2.2E-07	0.0E+00	0.0E+00	0.0E+00	2.8E-12	0.0E+00	0.0E+00	0.0E+00	1.3E-14
Ho-161	2.8E-04	0.0E+00	0.0E+00	3.1E-12	2.0E-11	0.0E+00	0.0E+00	1.0E-17	7.1E-17
Nd-162	---	3.5E-12	1.1E-10	1.8E-10	2.1E-10	0.0E+00	0.0E+00	0.0E+00	0.0E+00
Pm-162	1.0E-08	6.8E-09	9.6E-08	4.2E-07	6.2E-07	7.6E-11	5.8E-09	3.9E-08	6.0E-08
Sm-162	1.7E-07	2.0E-06	1.4E-05	1.1E-04	2.2E-04	1.4E-09	5.1E-08	6.4E-07	1.3E-06
Eu-162	3.5E-07	7.0E-06	2.8E-05	8.6E-04	2.1E-03	2.3E-09	4.9E-08	2.4E-06	5.9E-06

NA = Not applicable; no half-life or fractional abundances are provided because the isotope is stable.

--- = No half-life was found for the radionuclide; the isotope was not included in the fission product allocation.

[a] The primary source of radionuclide half-lives was KAPL (2002). Alternate sources include England and Rider (1994) and NNDC (2004).

Table I-2 (Continued)
Fission Product Yields and Activity Fractions for Mixed-Fission Product Waste at the Time of Generation

Isotope	Half-Life (yr) [a]	Fission Yields (yield/100 fissions)				Fractional Abundance (activity basis)			
		U-235		Pu-239		U-235		Pu-239	
		Thermal Neutrons	Fast Neutrons	Thermal Neutrons	Fast Neutrons	Thermal Neutrons	Fast Neutrons	Thermal Neutrons	Fast Neutrons
Gd-162	1.6E-05	6.8E-06	1.6E-05	1.2E-03	3.6E-03	4.9E-11	6.1E-10	7.1E-08	2.3E-07
Tb-162m	2.5E-04	4.5E-08	6.5E-08	3.1E-05	1.2E-04	2.0E-14	1.6E-13	1.2E-10	4.6E-10
Tb-162	1.4E-05	4.5E-08	6.5E-08	3.1E-05	1.2E-04	3.6E-13	2.8E-12	2.1E-09	8.1E-09
Dy-162	NA	2.0E-10	1.7E-10	4.4E-07	2.2E-06	0.0E+00	0.0E+00	0.0E+00	0.0E+00
Ho-162m	1.3E-04	0.0E+00	0.0E+00	5.2E-11	3.6E-10	0.0E+00	0.0E+00	3.9E-16	2.8E-15
Nd-163	---	0.0E+00	0.0E+00	1.3E-12	1.6E-12	0.0E+00	0.0E+00	0.0E+00	0.0E+00
Pm-163	---	1.8E-10	1.6E-09	1.2E-08	1.9E-08	0.0E+00	0.0E+00	0.0E+00	0.0E+00
Sm-163	4.0E-08	1.4E-07	5.5E-07	8.0E-06	1.7E-05	3.9E-10	8.4E-09	1.9E-07	4.2E-07
Eu-163	2.4E-07	1.9E-06	4.2E-06	2.1E-04	5.5E-04	9.2E-10	1.1E-08	8.2E-07	2.3E-06
Gd-163	2.1E-06	3.8E-06	4.7E-06	6.0E-04	2.1E-03	2.0E-10	1.3E-09	2.7E-07	9.8E-07
Tb-163	3.7E-05	2.1E-07	1.6E-07	1.0E-04	4.4E-04	6.6E-13	2.6E-12	2.6E-09	1.2E-08
Dy-163	NA	1.2E-09	5.2E-10	1.7E-06	1.1E-05	0.0E+00	0.0E+00	0.0E+00	0.0E+00
Ho-163m	3.5E-08	0.0E+00	0.0E+00	1.4E-10	1.1E-09	0.0E+00	0.0E+00	4.0E-12	3.1E-11
Ho-163	4.6E+03	0.0E+00	0.0E+00	9.6E-10	7.8E-09	0.0E+00	0.0E+00	2.0E-22	1.7E-21
Pm-164	---	1.7E-12	4.0E-11	1.7E-10	3.6E-10	0.0E+00	0.0E+00	0.0E+00	0.0E+00
Sm-164	4.4E-08	6.0E-09	6.2E-08	4.2E-07	1.2E-06	1.6E-11	8.7E-10	9.1E-09	2.7E-08
Eu-164	5.0E-08	2.0E-07	1.1E-06	2.5E-05	9.7E-05	4.6E-10	1.3E-08	4.8E-07	1.9E-06
Gd-164	1.4E-06	1.5E-06	4.3E-06	2.2E-04	1.1E-03	1.2E-10	1.9E-09	1.5E-07	7.9E-07
Tb-164	5.7E-06	1.8E-07	3.2E-07	7.8E-05	5.1E-04	3.6E-12	3.4E-11	1.3E-08	8.9E-08

NA = Not applicable; no half-life or fractional abundances are provided because the isotope is stable.

--- = No half-life was found for the radionuclide; the isotope was not included in the fission product allocation.

[a] The primary source of radionuclide half-lives was KAPL (2002). Alternate sources include England and Rider (1994) and NNDC (2004).

Table I-2 (Continued)
Fission Product Yields and Activity Fractions for Mixed-Fission Product Waste at the Time of Generation

Isotope	Half-Life (yr) [a]	Fission Yields (yield/100 fissions)				Fractional Abundance (activity basis)			
		U-235		Pu-239		U-235		Pu-239	
		Thermal Neutrons	Fast Neutrons	Thermal Neutrons	Fast Neutrons	Thermal Neutrons	Fast Neutrons	Thermal Neutrons	Fast Neutrons
Dy-164	NA	4.8E-09	4.7E-09	4.5E-06	4.1E-05	0.0E+00	0.0E+00	0.0E+00	0.0E+00
Ho-164m	7.2E-05	0.0E+00	0.0E+00	4.9E-09	6.5E-08	0.0E+00	0.0E+00	6.5E-14	8.9E-13
Ho-164	5.5E-05	0.0E+00	0.0E+00	2.1E-09	2.4E-08	0.0E+00	0.0E+00	3.7E-14	4.3E-13
Pm-165	---	0.0E+00	0.0E+00	2.2E-12	5.1E-12	0.0E+00	0.0E+00	0.0E+00	0.0E+00
Sm-165	1.4E-08	2.6E-10	2.7E-09	1.4E-08	4.5E-08	2.0E-12	1.1E-10	9.3E-10	3.1E-09
Eu-165	4.3E-08	3.9E-08	2.0E-07	3.0E-06	1.3E-05	1.0E-10	2.8E-09	6.8E-08	2.9E-07
Gd-165	3.2E-07	6.1E-07	1.6E-06	6.0E-05	3.4E-04	2.2E-10	3.2E-09	1.8E-07	1.1E-06
Tb-165	4.0E-06	2.8E-07	4.5E-07	6.3E-05	4.6E-04	8.1E-12	7.0E-11	1.5E-08	1.1E-07
Dy-165m	2.4E-06	2.3E-09	1.9E-09	1.1E-06	1.0E-05	1.1E-13	5.0E-13	4.3E-10	4.1E-09
Dy-165	2.7E-04	1.5E-08	1.4E-08	7.2E-06	7.4E-05	6.6E-15	3.3E-14	2.6E-11	2.7E-10
Ho-165	NA	2.1E-11	1.1E-11	4.8E-08	6.4E-07	0.0E+00	0.0E+00	0.0E+00	0.0E+00
Er-165	1.2E-03	0.0E+00	0.0E+00	2.1E-11	4.2E-10	0.0E+00	0.0E+00	1.7E-17	3.5E-16
Sm-166	---	6.4E-12	9.6E-11	4.4E-10	1.7E-09	0.0E+00	0.0E+00	0.0E+00	0.0E+00
Eu-166	---	2.5E-09	1.7E-08	2.4E-07	1.3E-06	0.0E+00	0.0E+00	0.0E+00	0.0E+00
Gd-166	---	1.7E-07	5.8E-07	1.6E-05	1.2E-04	0.0E+00	0.0E+00	0.0E+00	0.0E+00
Tb-166	6.3E-07	1.5E-07	3.2E-07	3.6E-05	3.3E-04	2.8E-11	3.1E-10	5.4E-08	5.2E-07
Dy-166	9.3E-03	4.0E-08	4.7E-08	1.5E-05	1.9E-04	4.9E-16	3.1E-15	1.5E-12	2.0E-11
Ho-166m	1.2E+03	9.4E-11	6.0E-11	1.3E-07	2.5E-06	9.0E-24	3.1E-23	1.1E-19	2.1E-18
Ho-166	3.1E-03	4.0E-11	2.2E-11	5.6E-08	9.3E-07	1.5E-18	4.5E-18	1.8E-14	3.0E-13

NA = Not applicable; no half-life or fractional abundances are provided because the isotope is stable.

--- = No half-life was found for the radionuclide; the isotope was not included in the fission product allocation.

[a] The primary source of radionuclide half-lives was KAPL (2002). Alternate sources include England and Rider (1994) and NNDC (2004).

Table I-2 (Continued)
Fission Product Yields and Activity Fractions for Mixed-Fission Product Waste at the Time of Generation

Isotope	Half-Life (yr) [a]	Fission Yields (yield/100 fissions)				Fractional Abundance (activity basis)			
		U-235		Pu-239		U-235		Pu-239	
		Thermal Neutrons	Fast Neutrons	Thermal Neutrons	Fast Neutrons	Thermal Neutrons	Fast Neutrons	Thermal Neutrons	Fast Neutrons
Er-166	NA	0.0E+00	0.0E+00	3.1E-10	8.3E-09	0.0E+00	0.0E+00	0.0E+00	0.0E+00
Sm-167	---	0.0E+00	1.6E-12	3.5E-12	2.1E-11	0.0E+00	0.0E+00	0.0E+00	0.0E+00
Eu-167	---	2.2E-10	1.4E-09	6.9E-09	5.6E-08	0.0E+00	0.0E+00	0.0E+00	0.0E+00
Gd-167	---	3.7E-08	1.0E-07	1.1E-06	1.3E-05	0.0E+00	0.0E+00	0.0E+00	0.0E+00
Tb-167	6.0E-07	1.3E-07	2.1E-07	7.5E-06	1.1E-04	2.6E-11	2.2E-10	1.2E-08	1.8E-07
Dy-167	1.2E-05	7.5E-08	6.6E-08	6.4E-06	1.3E-04	7.3E-13	3.5E-12	5.2E-10	1.1E-08
Ho-167	3.5E-04	1.0E-09	5.2E-10	2.9E-07	8.2E-06	3.3E-16	9.1E-16	7.9E-13	2.3E-11
Er-167m	7.2E-08	0.0E+00	0.0E+00	1.6E-10	6.1E-09	0.0E+00	0.0E+00	2.1E-12	8.4E-11
Er-167	NA	1.1E-12	0.0E+00	1.1E-09	4.5E-08	0.0E+00	0.0E+00	0.0E+00	0.0E+00
Tm-167	2.5E-02	0.0E+00	0.0E+00	0.0E+00	1.0E-11	0.0E+00	0.0E+00	0.0E+00	4.0E-19
Eu-168	NA	2.9E-12	2.8E-11	1.2E-10	8.9E-10	0.0E+00	0.0E+00	0.0E+00	0.0E+00
Gd-168	---	2.2E-09	9.4E-09	7.0E-08	7.2E-07	0.0E+00	0.0E+00	0.0E+00	0.0E+00
Tb-168	2.5E-07	1.7E-08	4.0E-08	1.1E-06	1.5E-05	7.8E-12	9.6E-11	4.1E-09	5.9E-08
Dy-168	1.7E-05	3.6E-08	4.6E-08	2.8E-06	5.3E-05	2.5E-13	1.7E-12	1.6E-10	3.2E-09
Ho-168	5.7E-06	1.2E-09	8.5E-10	2.9E-07	7.3E-06	2.3E-14	9.2E-14	4.9E-11	1.3E-09
Er-168	---	6.8E-12	2.7E-12	4.3E-09	1.6E-07	0.0E+00	0.0E+00	0.0E+00	0.0E+00
Tm-168	2.6E-01	0.0E+00	0.0E+00	1.6E-12	8.3E-11	0.0E+00	0.0E+00	5.9E-21	3.2E-19
Eu-169	---	0.0E+00	1.1E-12	2.3E-12	1.4E-11	0.0E+00	0.0E+00	0.0E+00	0.0E+00
Gd-169	---	1.2E-10	9.5E-10	3.3E-09	3.0E-08	0.0E+00	0.0E+00	0.0E+00	0.0E+00

NA = Not applicable; no half-life or fractional abundances are provided because the isotope is stable.

--- = No half-life was found for the radionuclide; the isotope was not included in the fission product allocation.

[a] The primary source of radionuclide half-lives was KAPL (2002). Alternate sources include England and Rider (1994) and NNDC (2004).

Table I-2 (Continued)
Fission Product Yields and Activity Fractions for Mixed-Fission Product Waste at the Time of Generation

Isotope	Half-Life (yr) [a]	Fission Yields (yield/100 fissions)				Fractional Abundance (activity basis)			
		U-235		Pu-239		U-235		Pu-239	
		Thermal Neutrons	Fast Neutrons	Thermal Neutrons	Fast Neutrons	Thermal Neutrons	Fast Neutrons	Thermal Neutrons	Fast Neutrons
Tb-169	---	4.1E-09	1.6E-08	1.8E-07	2.1E-06	0.0E+00	0.0E+00	0.0E+00	0.0E+00
Dy-169	1.2E-06	1.7E-08	3.8E-08	9.7E-07	1.7E-05	1.6E-12	1.9E-11	7.5E-10	1.3E-08
Ho-169	8.9E-06	2.2E-09	2.8E-09	3.1E-07	6.8E-06	2.9E-14	1.9E-13	3.3E-11	7.6E-10
Er-169	2.6E-02	3.3E-11	2.3E-11	1.1E-08	3.5E-07	1.5E-19	5.4E-19	4.1E-16	1.4E-14
Tm-169	NA	0.0E+00	0.0E+00	1.5E-11	6.7E-10	0.0E+00	0.0E+00	0.0E+00	0.0E+00
Gd-170	---	2.7E-12	4.4E-11	8.1E-11	8.5E-10	0.0E+00	0.0E+00	0.0E+00	0.0E+00
Tb-170	---	2.2E-10	1.7E-09	1.0E-08	1.5E-07	0.0E+00	0.0E+00	0.0E+00	0.0E+00
Dy-170	---	3.7E-09	1.5E-08	1.8E-07	3.7E-06	0.0E+00	0.0E+00	0.0E+00	0.0E+00
Ho-170m	1.4E-06	4.9E-10	1.2E-09	5.8E-08	1.6E-06	4.1E-14	5.3E-13	4.1E-11	1.2E-09
Ho-170	5.3E-06	4.9E-10	1.2E-09	5.8E-08	1.6E-06	1.1E-14	1.4E-13	1.0E-11	3.0E-10
Er-170	NA	6.4E-11	8.3E-11	1.4E-08	5.5E-07	0.0E+00	0.0E+00	0.0E+00	0.0E+00
Tm-170	3.5E-01	0.0E+00	0.0E+00	4.5E-11	2.6E-09	0.0E+00	0.0E+00	1.2E-19	7.4E-18
Gd-171	---	0.0E+00	1.2E-12	2.4E-12	1.5E-11	0.0E+00	0.0E+00	0.0E+00	0.0E+00
Tb-171	---	2.9E-11	2.2E-10	1.1E-09	9.5E-09	0.0E+00	0.0E+00	0.0E+00	0.0E+00
Dy-171	---	1.1E-09	4.0E-09	4.4E-08	5.6E-07	0.0E+00	0.0E+00	0.0E+00	0.0E+00
Ho-171	1.7E-06	1.1E-09	2.3E-09	8.9E-08	1.5E-06	7.3E-14	8.5E-13	5.1E-11	8.6E-10
Er-171	8.6E-04	1.6E-10	1.9E-10	2.3E-08	5.4E-07	2.1E-17	1.3E-16	2.5E-14	6.3E-13
Tm-171	1.9E+00	0.0E+00	0.0E+00	2.7E-10	9.0E-09	0.0E+00	0.0E+00	1.4E-19	4.7E-18
Yb-171	NA	0.0E+00	0.0E+00	0.0E+00	1.4E-11	0.0E+00	0.0E+00	0.0E+00	0.0E+00

NA = Not applicable; no half-life or fractional abundances are provided because the isotope is stable.

--- = No half-life was found for the radionuclide; the isotope was not included in the fission product allocation.

[a] The primary source of radionuclide half-lives was KAPL (2002). Alternate sources include England and Rider (1994) and NNDC (2004).

Table I-2 (Continued)
Fission Product Yields and Activity Fractions for Mixed-Fission Product Waste at the Time of Generation

Isotope	Half-Life (yr) [a]	Fission Yields (yield/100 fissions)				Fractional Abundance (activity basis)			
		U-235		Pu-239		U-235		Pu-239	
		Thermal Neutrons	Fast Neutrons	Thermal Neutrons	Fast Neutrons	Thermal Neutrons	Fast Neutrons	Thermal Neutrons	Fast Neutrons
Tb-172	---	1.1E-12	1.1E-11	4.1E-11	2.8E-10	0.0E+00	0.0E+00	0.0E+00	0.0E+00
Dy-172	---	1.8E-10	7.7E-10	5.6E-09	5.7E-08	0.0E+00	0.0E+00	0.0E+00	0.0E+00
Ho-172	7.9E-07	3.7E-10	8.7E-10	2.4E-08	3.3E-07	5.3E-14	6.7E-13	2.9E-11	4.1E-10
Er-172	5.6E-03	2.2E-10	2.7E-10	1.9E-08	3.7E-07	4.5E-18	3.0E-17	3.3E-15	6.5E-14
Tm-172	7.3E-03	1.7E-12	1.1E-12	5.4E-10	1.5E-08	2.7E-20	9.6E-20	7.1E-17	2.0E-15
Yb-172	NA	0.0E+00	0.0E+00	1.9E-12	7.9E-11	0.0E+00	0.0E+00	0.0E+00	0.0E+00

--- = No half-life was found for the radionuclide; the isotope was not included in the fission product allocation.

NA = No half-life or fractional abundances are provided because the isotope is stable.

[a] The primary source of radionuclide half-lives was KAPL (2002). Alternate sources include England and Rider (1994) and NNDC (2004).

Table I-3
Radionuclide Activity Fractions for Mixed-Fission Product Waste as a Function of the Age of the Waste

Radionuclide	Activity Fractions							
	Waste Age = 1 yr				Waste Age = 2 yr			
	U-235 Fission		Pu-239 Fission		U-235 Fission		Pu-239 Fission	
	Thermal Neutrons	Fast Neutrons	Thermal Neutrons	Fast Neutrons	Thermal Neutrons	Fast Neutrons	Thermal Neutrons	Fast Neutrons
Kr-85	5.6E-02	1.3E-02	3.3E-03	2.5E-03	1.5E-01	2.0E-02	6.2E-03	4.6E-03
Sr-89	2.1E-02	1.9E-03	2.8E-03	7.4E-04	4.0E-04	2.1E-05	3.7E-05	9.7E-06
Sr-90	6.3E-02	5.5E-02	1.2E-02	4.6E-03	1.7E-01	9.1E-02	2.5E-02	8.9E-03
Y-91	6.8E-04	6.8E-04	7.7E-04	4.9E-04	2.5E-05	1.5E-05	2.1E-05	1.3E-05
Nb-95	2.0E-05	1.6E-06	1.6E-05	4.4E-06	---	---	---	---
Zr-95	3.5E-01	7.7E-02	5.2E-02	3.1E-02	1.9E-02	2.5E-03	2.0E-03	1.2E-03
Ru-103	8.7E-06	7.0E-06	7.0E-05	5.8E-05	---	---	---	---
Ru-106	1.1E-05	2.1E-05	6.1E-01	5.8E-01	1.6E-05	1.7E-05	6.2E-01	5.8E-01
Cd-115m	3.9E-06	3.2E-06	---	1.6E-06	---	---	---	---
Sn-119m	1.5E-06	6.5E-06	7.3E-06	1.1E-05	1.8E-06	4.6E-06	6.2E-06	9.5E-06
Sn-121m	1.6E-05	8.8E-05	4.6E-05	7.4E-05	4.3E-05	1.4E-04	9.1E-05	1.4E-04
Sn-123	8.0E-03	7.5E-02	1.6E-02	2.4E-02	3.2E-03	1.8E-02	4.5E-03	6.7E-03
Sb-124	1.7E-05	7.6E-04	1.7E-05	2.1E-05	---	1.9E-05	---	---
Sb-125	1.9E-04	5.1E-04	7.0E-04	8.0E-04	4.2E-04	6.6E-04	1.1E-03	1.2E-03
Sn-126	4.8E-06	1.4E-05	2.8E-06	2.9E-06	1.4E-05	2.4E-05	5.6E-06	5.8E-06
Te-127m	---	---	2.2E-06	1.7E-06	---	---	---	---
Te-129m	2.0E-06	3.3E-06	1.1E-05	6.9E-06	---	---	---	---

--- = Indicates the radionuclide is not generated by the specified fission event or is present at a radionuclide activity fraction of less than 1.0×10^{-6} due to radioactive decay.

Table I-3 (Continued)
Radionuclide Activity Fractions for Mixed-Fission Product Waste as a Function of the Age of the Waste

	Activity Fractions							
	Waste Age = 1 yr				Waste Age = 2 yr			
	U-235 Fission		Pu-239 Fission		U-235 Fission		Pu-239 Fission	
Radionuclide	Thermal Neutrons	Fast Neutrons	Thermal Neutrons	Fast Neutrons	Thermal Neutrons	Fast Neutrons	Thermal Neutrons	Fast Neutrons
Cs-137	4.9E-02	3.5E-01	7.3E-02	9.8E-02	1.3E-01	5.8E-01	1.4E-01	1.9E-01
Ce-141	---	7.2E-06	4.0E-06	3.5E-06	---	---	---	---
Ce-144	4.5E-01	4.2E-01	2.3E-01	2.6E-01	5.3E-01	2.9E-01	1.9E-01	2.1E-01
Pm-147	---	---	---	---	---	---	1.1E-06	
Sm-151	---	---	1.6E-06	1.8E-06	---	---	3.2E-06	3.5E-06
Eu-154	---	---	1.1E-05	1.5E-05	1.3E-06	---	2.1E-05	2.8E-05
Eu-155	1.2E-05	9.5E-06	1.3E-04	2.5E-04	2.9E-05	1.4E-05	2.3E-04	4.2E-04
Tb-160	---	---	3.6E-06	8.3E-06	---	---	---	---

--- = Indicates the radionuclide is not generated by the specified fission event or is present at a radionuclide activity fraction of less than 1.0×10^{-6} due to radioactive decay.

Table I-3 (Continued)
Radionuclide Activity Fractions for Mixed-Fission Product Waste as a Function of the Age of the Waste

	Activity Fractions							
	Waste Age = 5 yr				Waste Age = 10 yr			
	U-235 Fission		Pu-239 Fission		U-235 Fission		Pu-239 Fission	
Radionuclide	Thermal Neutrons	Fast Neutrons	Thermal Neutrons	Fast Neutrons	Thermal Neutrons	Fast Neutrons	Thermal Neutrons	Fast Neutrons
Kr-85	2.7E-01	2.5E-02	2.0E-02	1.4E-02	2.6E-01	2.1E-02	2.5E-02	1.6E-02
Sr-89	---	---	---	---	---	---	---	---
Sr-90	3.6E-01	1.3E-01	8.8E-02	3.0E-02	4.2E-01	1.3E-01	1.4E-01	4.3E-02
Y-91	---	---	---	---	---	---	---	---
Nb-95	---	---	---	---	---	---	---	---
Zr-95	---	---	---	---	---	---	---	---
Ru-103	---	---	---	---	---	---	---	---
Ru-106	4.7E-06	3.4E-06	3.1E-01	2.7E-01	---	---	1.8E-02	1.5E-02
Cd-115m	---	---	---	---	---	---	---	---
Sn-119m	---	---	1.8E-06	2.5E-06	---	---	---	---
Sn-121m	9.3E-05	2.1E-04	3.4E-04	4.9E-04	1.1E-04	2.2E-04	5.4E-04	7.5E-04
Sn-123	2.0E-05	7.6E-05	4.9E-05	6.7E-05	---	---	---	---
Sb-124	---	---	---	---	---	---	---	---
Sb-125	4.5E-04	4.7E-04	2.0E-03	2.1E-03	1.7E-04	1.6E-04	1.0E-04	9.6E-04
Sn-126	3.1E-05	3.6E-05	2.2E-05	2.1E-05	4.0E-05	4.1E-05	3.8E-05	3.4E-05
Te-127m	---	---	---	---	---	---	---	---
Te-129m	---	---	---	---	---	---	---	---
Cs-137	2.8E-01	8.2E-01	5.2E-01	6.3E-01	3.3E-01	8.5E-01	8.2E-01	9.2E-01

--- = Indicates the radionuclide is not generated by the specified fission event or is present at a radionuclide activity fraction of less than 1.0×10^{-6} due to radioactive decay.

Table I-3 (Continued)
Radionuclide Activity Fractions for Mixed-Fission Product Waste as a Function of the Age of the Waste

	Activity Fractions							
	Waste Age = 5 yr				Waste Age = 10 yr			
	U-235 Fission		Pu-239 Fission		U-235 Fission		Pu-239 Fission	
Radionuclide	Thermal Neutrons	Fast Neutrons	Thermal Neutrons	Fast Neutrons	Thermal Neutrons	Fast Neutrons	Thermal Neutrons	Fast Neutrons
Ce-141	---	---	---	---	---	---	---	---
Ce-144	8.3E-02	3.1E-02	5.2E-02	5.3E-02	1.3E-03	4.2E-04	1.1E-03	1.0E-03
Pm-147	---	---	2.0E-06	1.5E-06	---	---	---	---
Sm-151	---	---	1.2E-05	1.2E-05	1.0E-06	---	2.1E-05	1.9E-05
Eu-154	2.4E-06	0.0E+00	6.4E-05	7.8E-05	2.1E-06	---	7.5E-05	8.6E-05
Eu-155	4.2E-05	1.3E-05	5.8E-04	9.7E-04	2.7E-05	7.6E-06	4.9E-04	7.7E-04
Tb-160	---	---	---	---	---	---	---	---

--- = Indicates the radionuclide is not generated by the specified fission event or is present at a radionuclide activity fraction of less than $1.0x10^{-6}$ due to radioactive decay.

--- = Indicates the radionuclide is not generated by the specified fission event or is present at a radionuclide activity fraction of less than 1.0×10^{-6} due to radioactive decay.

It is virtually impossible to predict the time lapse between the generation of the fission-product waste and the characterization of the material for disposal for each of the numerous packages of waste that were shipped to Area G. The inventory modeling estimates radionuclide abundances for waste ranging in age from 1 to 10 years.

I.3 Mixed-Activation Product Waste

More than 2.0×10^4 Ci of MAP waste were disposed of at Area G from 1971–1996. Waste shipped from TA-48 accounted for 62 percent of the total activity and waste shipped from TA-53 accounted for another 34 percent. A large portion of the waste shipped by TA-48 originated at TA-53. All of the MAP waste shipped for disposal was LLW.

The MAP waste was allocated to specific radionuclides using information collected for the 1997 performance assessment and composite analysis (Hollis et al., 1997). Conversations with TA-53 staff indicated that the Los Alamos Meson Physics Facility at TA-53 (now referred to as the Los Alamos Neutron Science Center) generated three activated waste streams: trash, beam-line inserts, and targets (Hollis et al., 1997, Appendix 2f). Similar materials—such as steel, aluminum, and graphite—may occur in all three waste streams. The radionuclide abundances in the trash waste stream were established and these abundances were assumed to apply to all of the MAP waste that has been shipped for disposal.

The radionuclide abundances for the MAP waste are provided in Table I-4 in terms of mass fractions. Corresponding activity fractions were calculated by multiplying the mass fractions by the radionuclides' specific activities and normalizing these products by the sum of these activities. Many of the radionuclides included in the MAP waste have very short half-lives. Consequently, the radionuclide abundances in the waste will change significantly as the age of the waste increases and radioactive decay occurs. It was assumed that the age of the waste when it was shipped for disposal and the age of the material used to establish the radiological profile shown in Table I-4 were the same.

Table I-4
Radionuclide Mass and Activity Fractions for Mixed-Activation Product Waste

Radionuclide	Mass Fraction	Activity Fraction
Be-7	3.0E-02	7.0E-01
Na-22	1.0E-01	4.1E-02
Mn-54	1.8E-01	9.2E-02
Co-57	1.2E-01	6.7E-02
Co-60	4.4E-01	3.3E-02
Zn-65	1.3E-01	7.1E-02

References

Bunker, M.E., 1983, "Early Reactors", *Los Alamos Science*, Vol. Winter/Spring.

England, T.R., and B.F. Rider, 1994, *Evaluation and Compilation of Fission Product Yields 1993*, Los Alamos National Laboratory Report LA-UR-94-3106, October.

Hollis, D., E. Vold, R. Shuman, K. Birdsell, K. Bower, W. Hansen, D. Krier, P. Longmire, B. Newman, D. Rogers, and E. Springer, 1997, *Performance Assessment and Composite Analysis for Los Alamos National Laboratory Material Disposal Area G,* Los Alamos National Laboratory Report-54G-013, March.

KAPL, 2002, *Nuclides and Isotopes, Chart of the Nuclides, 16th Edition*, Knolls Atomic Power Laboratory, Eds. E.M. Baum, H.D. Knox, and T.R. Miller.

National Nuclear Data Center (NNDC), 2004, "Evaluated Nuclear Structure Data File," <http://www.nndc.bnl.gov/-ensdf/index.jsp>, (June 7).

Shuman, R., 2008, GoldSim Model Documentation and Data Selection for Los Alamos National Laboratory Technical Area 54, Area G Performance Assessment and Composite Analysis, Los Alamos National Laboratory Report, September.

Widner, T., J. Shonka, S. Flack, J. O'Brien, R. Burns, J. Buddenbaum, D. Shonka, et al., 2004, *Draft Interim Report of the Los Alamos Historical Document Retrieval and Assessment (LAHDRA) Project,* prepared by individuals from ENSR Corporation, Shonka Research Associates, Inc., and ChemRisk, Inc. for the Centers for Disease Control and Prevention, March 21.

Attachment II
Bases for Radionuclide Inclusion in the Area G Inventory

Active institutional control will be exercised over Area G for a period of 100 years following the end of disposal operations. During this period, persons will be prevented from intruding onto the site for extended periods of time and measures will be taken to ensure proper facility function. As a result of these actions, there will be little or no potential for exposures from radionuclides with extremely short half-lives.

Because of this, most radionuclides with half-lives of 5 years or less were excluded from the Area G inventory. The primary exception to this is radionuclides that are daughters of parents with half-lives greater than 5 years. Table II-1 lists all radionuclides that were encountered in the inventory characterization update and their half-lives, briefly describes their decay characteristics, and specifies whether, or in what manner, the constituents were included in the final inventory.

The radionuclides listed in the table are referred to as either short or long-lived. For the purpose of presenting the decay information, short-lived refers to isotopes with half-lives of less than 1 year, while radionuclides with half-lives of 1 year or more are referred to as long-lived.

Several radionuclides in Table II-1 have half-lives of 5 years or less but decay to form daughter products with much longer half-lives. The potential exists for these long-lived daughter products to make significant contributions to the long-term risks posed by the disposal facility to human health and safety. These contributions were expected to be negligible because of the very small activities associated with the longer-lived isotopes. Nevertheless, screening calculations were conducted to ensure that eliminating the long-lived daughters and their short-lived precursors would not compromise the doses projected for the performance assessment and composite analysis.

The screening evaluation modeled the decay of the short-lived daughters under consideration and the ingrowth of their long-lived daughter products. These calculations were conducted using the composite analysis inventory projections, summed over all disposal units that have been or will be used for the disposal of waste at Area G. The decay and ingrowth calculations were performed over a 1,000-year period and used, in conjunction with the total waste volume, to estimate radionuclide concentrations in the waste as a function of time. The projected concentrations were used to conservatively estimate exposures to a hypothetical person who ingested small quantities of waste, inhaled suspended contamination, and received direct radiation from the waste.

The exposure parameters that were used to conduct the screening evaluation are summarized in Table II-2. The internal and external dose conversion factors used in the assessment were taken from Federal Guidance Reports 11 and 12, respectively (EPA, 1988 and 1993). Direct radiation dose conversion factors for soil contaminated to an infinite depth were selected for the analysis.

Table II-1
Radionuclide Decay Characteristics and Bases for Inclusion in the Area G Inventory

Radionuclide	Half-Life (yr) [a]	Decay Chain Characteristics and Assumptions
Ac-227	2.2E+01	Decays to form short-lived Fr-223 and Th-227; daughter of long-lived Pa-231. Included in final inventory.
Ac-228	7.0E-04	Decays to form long-lived Th-228; daughter of long-lived Ra-228. Included in final inventory as a short-lived daughter of Ra-228.
Ag-105	1.1E-01	Decays to form stable Pd-105; daughter of short-lived Ag-105m and Cd-105. Excluded from final inventory.
Ag-108m	4.2E+02	Decays to form short-lived Ag-108 and stable Pd-108; included in final inventory.
Ag-110m	6.8E-01	Decays to form short-lived Ag-110 and stable Cd-110; excluded from final inventory.
Ag-111	2.0E-02	Decays to form stable Cd-111; daughter of short-lived Pd-111. Excluded from final inventory.
Al-26	7.1E+05	Decays to form stable Mg-26; daughter of short-lived Si-26. Included in final inventory.
Am-240	5.8E-03	Decays to form long-lived Np-236 and Pu-240; inventory of long-lived daughters expected to be negligible. Excluded from final inventory.
Am-241	4.3E+02	Decays to form long-lived Np-237; daughter of long-lived Pu-241. Included in final inventory.
Am-242	1.8E-03	Decays to form short-lived Cm-242 and long-lived Pu-242; daughter of long-lived Am-242m. Inventory of long-lived daughter expected to be negligible; included in final inventory as a short-lived daughter of Am-242m.
Am-243	7.4E+03	Decays to form short-lived Np-239; daughter of long-lived Cm-243 and short-lived Pu-243. Included in final inventory.
As-72	3.0E-03	Decays to form stable Ge-72; daughter of short-lived Se-72. Excluded from final inventory.
As-73	2.2E-01	Decays to form stable Ge-73; daughter of short-lived Se-73. Excluded from final inventory.
As-74	4.9E-02	Decays to form stable Ga-74 and Se-74; excluded from final inventory.
Au-194	4.3E-03	Decays to form stable Pt-194; daughter of long-lived Hg-194. Included in final inventory as a short-lived daughter of Hg-194.
Au-195	5.1E-01	Decays to form stable Pt-195; daughter of short-lived Hg-195m. Excluded from final inventory.
Ba-133	1.1E+01	Decays to form stable Cs-133; daughter of short-lived Ba-133m. Included in final inventory.
Ba-137m	4.9E-06	Decays to form stable Ba-137; daughter of long-lived Cs-137. Included in final inventory as a short-lived daughter of Cs-137.
Ba-139	1.6E-04	Decays to form stable La-139; daughter of short-lived Ce-139. Excluded from final inventory.

[a] *Primary source of radionuclide half-lives was KAPL (2002). Alternate sources include England and Rider (1994) and NNDC (2004).*

Table II-1 (Continued)
Radionuclide Decay Characteristics and Bases for Inclusion in the Area G Inventory

Radionuclide	Half-Life (yr) [a]	Decay Chain Characteristics and Assumptions
Ba-140	3.5E-02	Decays to form short-lived La-140; daughter of short-lived Cs-140. Excluded from final inventory.
Be-7	1.5E-01	Decays to form stable Li-7; excluded from final inventory.
Be-10	1.5E+06	Decays to form stable B-10; included in final inventory.
Bi-207	3.2E+01	Decays to form stable Pb-207; daughter of short-lived At-211. Included in final inventory.
Bi-210	1.4E-02	Decays to form short-lived Po-210; daughter of long-lived Pb-210. Included in final inventory as a short-lived daughter of Pb-210.
Bi-211	4.1E-06	Decays to form short-lived Po-211 and Tl-207; daughter of short-lived Pb-211. Included in final inventory as a short-lived daughter of Ac-227.
Bi-212	1.2E-04	Decays to form short-lived Po-212 and Tl-208; daughter of short-lived Pb-212. Included in final inventory as a short-lived daughter of Th-228.
Bi-214	3.8E-05	Decays to form short-lived Po-214; daughter of short-lived Pb-214. Included in final inventory as a short-lived daughter of Ra-226.
Bk-247	1.4E+03	Decays to form long-lived Am-243; included in final inventory.
Bk-249	9.0E-01	Decays to form long-lived Cf-249; inventory of long-lived daughter expected to be negligible. Excluded from final inventory.
Br-76	1.8E-03	Decays to form stable Se-76; daughter of short-lived Kr-76. Excluded from final inventory.
Br-77	6.5E-03	Decays to form stable Se-77; daughter of short-lived Kr-77. Excluded from final inventory.
Br-82	4.0E-03	Decays to form stable Kr-82; daughter of short-lived Br-82m. Excluded from final inventory.
C-14	5.7E+03	Decays to form stable N-14; included in final inventory.
Ca-41	1.0E+05	Decays to form stable K-41; daughter of short-lived Sc-41. Included in final inventory.
Ca-45	4.5E-01	Decays to form stable Sc-45; daughter of short-lived K-45. Excluded from final inventory.
Cd-109	1.3E+00	Decays to form short-lived Ag-109m and stable Ag-109; daughter of short-lived In-109. Excluded from final inventory.
Cd-113m	1.4E+01	Decays to form long-lived Cd-113 and stable In-113; daughter of short-lived Ag-113. Included in final inventory.
Cd-115	6.1E-03	Decays to form short-lived In-115m and long-lived In-115; daughter of short-lived Ag-115. Inventory of long-lived daughter expected to be negligible; excluded from final inventory.
Ce-137	1.0E-03	Decays to form long-lived La-137; daughter of short-lived Ce-137m. Inventory of long-lived daughter expected to be negligible; excluded from final inventory.
Ce-139	3.8E-01	Decays to form stable La-139; daughter of short-lived Ce-139m. Excluded from final inventory.

[a] *Primary source of radionuclide half-lives was KAPL (2002). Alternate sources include England and Rider (1994) and NNDC (2004).*

Table II-1 (Continued)
Radionuclide Decay Characteristics and Bases for Inclusion in the Area G Inventory

Radionuclide	Half-Life (yr) [a]	Decay Chain Characteristics and Assumptions
Ce-141	8.9E-02	Decays to form stable Pr-141; daughter of short-lived La-141. Excluded from final inventory.
Ce-144	7.8E-01	Decays to form short-lived Pr-144; daughter of short-lived La-144. Excluded from final inventory.
Cf-249	3.5E+02	Decays to form long-lived Cm-245; daughter of short-lived Bk-249. Included in final inventory.
Cf-251	9.0E+02	Decays to form long-lived Cm-247; daughter of short-lived Bk-241 and Fm-255. Included in final inventory.
Cf-252	2.6E+00	Decays to form long-lived Cm-248; daughter of short-lived Fm-256. Included in final inventory.
Cl-36	3.0E+05	Decays to form stable Ar-36 and S-36; included in final inventory.
Cm-242	4.5E-01	Decays to form long-lived Pu-238; daughter of short-lived Am-242. Inventory of long-lived daughter expected to be negligible; excluded from final inventory.
Cm-243	2.9E+01	Decays to form long-lived Pu-239; included in final inventory.
Cm-244	1.8E+01	Decays to form long-lived Pu-240; daughter of short-lived Am-244 and Cf-248. Included in final inventory.
Cm-245	8.5E+03	Decays to form long-lived Pu-241; daughter of short-lived Am-245 and long-lived Cf-249. Included in final inventory.
Cm-248	3.4E+05	Decays to form long-lived Pu-244; included in final inventory.
Co-56	2.1E-01	Decays to form stable Fe-56; daughter of short-lived Ni-56. Excluded from final inventory.
Co-57	7.4E-01	Decays to form stable Fe-57; daughter of short-lived Ni-57. Excluded from final inventory.
Co-58	1.9E-01	Decays to form stable Fe-58; excluded from final inventory.
Co-60	5.3E+00	Decays to form stable Ni-60; daughter of long-lived Fe-60. Included in final inventory.
Cr-51	7.6E-02	Decays to form stable V-51; daughter of short-lived Mn-51. Excluded from final inventory.
Cs-134	2.1E+00	Decays to form stable Ba-134 and Xe-134; excluded from final inventory.
Cs-135	2.3E+06	Decays to form stable Ba-135; daughter of short-lived Xe-135. Included in final inventory.
Cs-136	3.6E-02	Decays to form stable Ba-136; excluded from final inventory.
Cs-137	3.0E+01	Decays to form short-lived Ba-137m; daughter of short-lived Xe-133. Included in final inventory.
Cu-67	7.1E-03	Decays to form stable Zn-67; daughter of short-lived Ni-67. Excluded from final inventory.

[a] *Primary source of radionuclide half-lives was KAPL (2002). Alternate sources include England and Rider (1994) and NNDC (2004).*

Table II-1 (Continued)
Radionuclide Decay Characteristics and Bases for Inclusion in the Area G Inventory

Radionuclide	Half-Life (yr) [a]	Decay Chain Characteristics and Assumptions
Dy-154	3.0E+06	Decays to form long-lived Gd-150; daughter of short-lived Ho-154m. Included in final inventory.
Dy-159	4.0E-01	Decays to form stable Tb-159; daughter of short-lived Ho-159. Excluded from final inventory.
Eu-149	2.6E-01	Decays to form stable Sm-149; daughter of short-lived Gd-149. Excluded from final inventory.
Eu-150	3.6E+01	Decays to form stable Sm-150; included in final inventory.
Eu-152	1.4E+01	Decays to form long-lived Gd-152 and stable Sm-152; daughter of short-lived Eu-152m. Included in final inventory.
Eu-154	8.6E+00	Decays to form stable Gd-154 and stable Sm-154; daughter of short-lived Eu-154m. Included in final inventory.
Eu-155	4.8E+00	Decays to form stable Gd-155; daughter of short-lived Sm-155. Excluded from final inventory.
Eu-156	4.2E-02	Decays to form stable Gd-156; daughter of short-lived Sm-146. Excluded from final inventory.
Eu-158	8.7E-05	Decays to form stable Gd-158; daughter of short-lived Sm-158. Excluded from final inventory.
Fe-52	9.5E-04	Decays to form short-lived Mn-52 and Mn-52m; daughter of short-lived Co-52. Excluded from final inventory.
Fe-55	2.7E+00	Decays to form stable Mn-55; daughter of short-lived Co-55. Excluded from final inventory.
Fe-59	1.2E-01	Decays to form stable Co-59; daughter of short-lived Mn-59. Excluded from final inventory.
Ga-68	1.3E-04	Decays to form stable Zn-68; daughter of short-lived Ge-68. Excluded from final inventory.
Ga-72	1.6E-03	Decays to form stable Ge-72; daughter of short-lived Zn-72. Excluded from final inventory.
Gd-146	1.3E-01	Decays to form short-lived Eu-146 and, ultimately, long-lived Sm-146; daughter of short-lived Tb-146. Inventory of long-lived daughter expected to be negligible; excluded from final inventory.
Gd-148	7.5E+01	Decays to form stable Sm-144; daughter of short-lived Tb-148. Included in final inventory.
Gd-150	1.8E+06	Decays to form long-lived Sm-146; daughter of short-lived Tb-150. Included in final inventory.
Gd-151	3.4E-01	Decays to form stable Eu-151 and long-lived Sm-147; daughter of short-lived Tb-151. Inventory of long-lived daughter expected to be negligible; excluded from final inventory.
Gd-152	1.1E+14	Decays to form long-lived Sm-148; daughter of short-lived Tb-152. Included in final inventory.

[a] *Primary source of radionuclide half-lives was KAPL (2002). Alternate sources include England and Rider (1994) and NNDC (2004).*

Table II-1 (Continued)
Radionuclide Decay Characteristics and Bases for Inclusion in the Area G Inventory

Radionuclide	Half-Life (yr) [a]	Decay Chain Characteristics and Assumptions
Gd-153	6.6E-01	Decays to form stable Eu-153; daughter of short-lived Tb-153. Excluded from final inventory.
Ge-68	7.4E-01	Decays to form short-lived Ga-68; daughter of short-lived As-68. Excluded from final inventory.
H-3	1.2E+01	Decays to form stable He-3; included in final inventory.
Hf-172	1.9E+00	Decays to form short-lived Lu-172; daughter of short-lived Ta-172. Excluded from final inventory.
Hf-175	1.9E-01	Decays to form stable Lu-175; daughter of short-lived Ta-175. Excluded from final inventory.
Hf-178m	3.1E+01	Decays to form stable Hf-178; excluded from final inventory.
Hf-181	1.2E-01	Decays to form stable Ta-181; daughter of short-lived Lu-181. Excluded from final inventory.
Hg-203	1.3E-01	Decays to form stable Tl-203; daughter of short-lived Au-203. Excluded from final inventory.
Ho-163	4.6E+03	Decays to form stable Dy-163; daughter of short-lived Er-173. Included in final inventory.
Ho-166	3.1E-03	Decays to form stable Er-166; daughter of short-lived Dy-166. Excluded from final inventory.
Ho-166m	1.2E+03	Decays to form stable Er-166; included in final inventory.
I-125	1.6E-01	Decays to form stable Te-125; daughter of short-lived Xe-125. Excluded from final inventory.
I-129	1.6E+07	Decays to form stable Xe-129; daughter of short-lived Te-129. Included in final inventory.
I-131	2.2E-02	Decays to form stable Xe-131 and short-lived Xe-131m; daughter of short-lived Te-125. Excluded from final inventory.
I-133	2.4E-03	Decays to form short-lived Xe-133 and Xe-133m; daughter of short-lived Te-133 and Te-133m. Excluded from final inventory.
In-114m	1.4E-01	Decays to form stable Cd-114 and short-lived In-114; excluded from final inventory.
In-115m	5.1E-04	Decays to form long-lived In-115 and stable Sn-115; inventory of long-lived daughter expected to be negligible. Excluded from final inventory.
Ir-192	2.0E-01	Decays to form stable Os-194 and Pt-194; daughter of short-lived Ir-192m. Excluded from final inventory.
Ir-194	2.2E-03	Decays to form stable Pt-194; daughter of short-lived Ir-194m and long-lived Os-194. Included in final inventory as a short-lived daughter of Os-194.
K-40	1.3E+09	Decays to form stable Ar-40 and stable Ca-40; included in final inventory.

[a] *Primary source of radionuclide half-lives was KAPL (2002). Alternate sources include England and Rider (1994) and NNDC (2004).*

Table II-1 (Continued)
Radionuclide Decay Characteristics and Bases for Inclusion in the Area G Inventory

Radionuclide	Half-Life (yr) [a]	Decay Chain Characteristics and Assumptions
Kr-81	2.3E+05	Decays to form stable Br-81; daughter of short-lived Rb-81. Included in final inventory.
Kr-85	1.1E+01	Decays to form stable Rb-85; daughter of Kr-85m. Included in final inventory.
La-137	6.0E+04	Decays to form stable Ba-137; daughter of short-lived Ce-137. Included in final inventory.
La-140	1.7E+00	Decays to form stable Ce-140; daughter of short-lived Ba-140. Excluded from final inventory.
Lu-172	1.8E-02	Decays to form stable Yb-172; daughter of short-lived Hf-172. Excluded from final inventory.
Lu-172m	7.0E-06	Decays to form short-lived Lu-172; excluded from final inventory.
Lu-173	1.4E+00	Decays to form stable Yb-173; daughter of short-lived Hf-173. Excluded from final inventory.
Lu-174	3.3E+00	Decays to form stable Yb-174; daughter of short-lived Lu-174m. Excluded from final inventory.
Lu-176	3.8E+10	Decays to form stable Hf-176; included in final inventory.
Lu-177	1.8E-02	Decays to form stable Hf-177; daughter of short-lived Yb-177. Excluded from final inventory.
Mn-52	1.5E-02	Decays to form stable Cr-52; daughter of short-lived Fe-52. Excluded from inventory.
Mn-52m	4.0E-05	Decays to form stable Cr-52 and short-lived Mn-52; daughter of short-lived Fe-52. Excluded from final inventory.
Mn-54	8.6E-01	Decays to form stable Cr-54 and stable Fe-54; excluded from final inventory.
Mn-56	2.9E-04	Decays to form stable Fe-56; daughter of short-lived Cr-56. Excluded from final inventory.
Mo-93	3.5E+03	Decays to form stable Nb-93; daughter of short-lived Tc-93. Included in final inventory.
Mo-99	7.5E-03	Decays to form long-lived Tc-99 and short-lived Tc-99m; daughter of short-lived Nb-99. Inventory of long-lived daughter expected to be negligible; excluded from final inventory.
Na-22	2.6E+00	Decays to form stable Ne-22; daughter of short-lived Mg-22. Excluded from final inventory.
Na-24	1.7E-03	Decays to form stable Mg-24; daughter of short-lived Ne-24. Excluded from final inventory.
Nb-91	7.0E+02	Decays to form stable Zr-91; daughter of short-lived Mo-91 and Nb-91m. Included in final inventory.
Nb-91m	1.7E-01	Decays to form long-lived Nb-91 and stable Zr-91; daughter of short-lived Mo-91. Inventory of long-lived daughter expected to be negligible; excluded from final inventory.
Nb-92	3.5E+07	Decays to form stable Zr-92; included in final inventory.
Nb-92m	2.8E-02	Decays to form stable Zr-92; excluded from final inventory.

[a] *Primary source of radionuclide half-lives was KAPL (2002). Alternate sources include England and Rider (1994) and NNDC (2004).*

Table II-1 (Continued)
Radionuclide Decay Characteristics and Bases for Inclusion in the Area G Inventory

Radionuclide	Half-Life (yr) [a]	Decay Chain Characteristics and Assumptions
Nb-93m	1.6E+01	Decays to form stable Nb-93; included in final inventory.
Nb-94	2.0E+04	Decays to stable Mo-94; included in final inventory.
Nb-95	9.6E-02	Decays to form stable Mo-95; daughter of short-lived Zr-95. Excluded from final inventory.
Nd-144	2.4E+15	Decays to stable Ce-140; daughter of short-lived Pm-144, Pr-144, and Pr-144m. Included in final inventory.
Nd-147	3.0E-02	Decays to form short-lived Pm-147 and, ultimately, long-lived Sm-147; daughter of short-lived Pr-147. Inventory of long-lived daughter expected to be negligible; excluded from final inventory.
Ni-56	1.6E-02	Decays to form short-lived Co-56; excluded from final inventory.
Ni-57	4.1E-03	Decays to form short-lived Co-57; daughter of short-lived Cu-57. Excluded from final inventory.
Ni-59	7.6E+04	Decays to form stable Co-59; daughter of short-lived Cu-59. Included in final inventory.
Ni-63	1.0E+02	Decays to form stable Cu-63; daughter of short-lived Co-63. Included in final inventory.
Ni-65	2.9E-04	Decays to form stable Cu-65; daughter of short-lived Co-65. Excluded from final inventory.
Np-235	1.1E+00	Decays to form long-lived U-235; inventory of long-lived daughter expected to be negligible. Excluded from final inventory.
Np-237	2.1E+06	Decays to form short-lived Pa-233; daughter of long-lived Am-241. Included in final inventory.
Np-239	6.5E-03	Decays to form long-lived Pu-239; daughter of long-lived Am-243. Included in final inventory as a short-lived daughter of Am-243.
Np-242	1.0E-05	Decays to form long-lived Pu-242; inventory of long-lived daughter expected to be negligible. Excluded from final inventory.
Os-194	6.0E+00	Decays to form short-lived Ir-194; included in final inventory.
P-32	3.9E-02	Decays to stable S-32; daughter of long-lived Si-32. Included in final inventory as a short-lived daughter of Si-32.
P-33	6.9E-02	Decays to form stable S-33; daughter of short-lived Si-33. Excluded from final inventory.
Pa-231	3.3E+04	Decays to form long-lived Ac-227; daughter of short-lived Th-231. Included in final inventory.
Pa-233	7.4E-02	Decays to form long-lived U-233; daughter of long-lived Np-237. Included in final inventory as a short-lived daughter of Np-237.
Pa-234	7.6E-04	Decays to form long-lived U-234; daughter of short-lived Pa-234m. Included in final inventory as a short-lived daughter of U-238.

[a] *Primary source of radionuclide half-lives was KAPL (2002). Alternate sources include England and Rider (1994) and NNDC (2004).*

Table II-1 (Continued)
Radionuclide Decay Characteristics and Bases for Inclusion in the Area G Inventory

Radionuclide	Half-Life (yr) [a]	Decay Chain Characteristics and Assumptions
Pa-234m	2.2E-06	Decays to form long-lived U-234; daughter of short-lived Th-234. Included in final inventory as a short-lived daughter of U-238.
Pb-203	5.9E-03	Decays to form stable Tl-203; daughter of short-lived Bi-203. Excluded from final inventory.
Pb-210	2.2E+01	Decays to form short-lived Bi-210; daughter of short-lived Po-214. Included in final inventory.
Pb-211	6.9E-05	Decays to form short-lived Bi-211; daughter of short-lived Po-211. Included in final inventory as a short-lived daughter of Ac-227.
Pb-212	1.2E-03	Decays to form short-lived Bi-212; daughter of short-lived Po-216. Included in final inventory as a short-lived daughter of Th-228.
Pb-214	5.1E-05	Decays to form short-lived Bi-214; daughter of short-lived Po-218. Included in final inventory as a short-lived daughter of Ra-226.
Pd-107	6.5E+06	Decays to form stable Ag-107; daughter of short-lived Rh-107. Included in final inventory.
Pm-143	7.3E-01	Decays to form stable Nd-143; daughter of short-lived Sm-143. Excluded from final inventory.
Pm-145	1.8E+01	Decays to form stable Nd-145 and stable Pr-141; daughter of short-lived Sm-145. Included in final inventory.
Pm-146	5.5E+00	Decays to form stable Nd-146 and long-lived Sm-146. Included in final inventory.
Pm-147	2.6E+00	Decays to form long-lived Sm-147; daughter of short-lived Nd-147. Inventory of long-lived daughter expected to be negligible; excluded from final inventory.
Po-208	2.9E+00	Decays to form stable Pb-204 and long-lived Bi-208; inventory of long-lived daughter expected to be negligible. Excluded from final inventory.
Po-209	1.0E+02	Decays to form long-lived Pb-205 and stable Bi-209; inventory of long-lived daughter expected to be negligible. Excluded from final inventory.
Po-210	3.8E-01	Decays to form stable Pb-206; daughter of short-lived Bi-210. Included in final inventory as a short-lived daughter of Pb-210.
Pu-233	4.0E-05	Decays to form short-lived Np-233 and U-229, and ultimately forms long-lived U-233; inventory of long-lived daughter expected to be negligible. Excluded from final inventory.
Pu-234	1.0E-03	Decays to form short-lived Np-234 and U-230; the Np-234 decays to form long-lived U-234 while the U-230 ultimately forms long-lived Pb-210. Inventory of long-lived daughters expected to be negligible; excluded from final inventory.
Pu-236	2.9E+00	Decays to form long-lived U-232; included in final inventory.
Pu-238	8.8E+01	Decays to form long-lived U-234; daughter of short-lived Cm-242. Included in final inventory.

[a] *Primary source of radionuclide half-lives was KAPL (2002). Alternate sources include England and Rider (1994) and NNDC (2004).*

Table II-1 (Continued)
Radionuclide Decay Characteristics and Bases for Inclusion in the Area G Inventory

Radionuclide	Half-Life (yr) [a]	Decay Chain Characteristics and Assumptions
Pu-239	2.4E+04	Decays to form long-lived U-235; daughter of long-lived Cm-243 and short-lived Np-239. Included in final inventory.
Pu-240	6.6E+03	Decays to form long-lived U-236; daughter of long-lived Cm-244 and short-lived Np-240 and Np-240m. Included in final inventory.
Pu-241	1.4E+01	Decays to form long-lived Am-241; daughter of long-lived Cm-245. Included in final inventory.
Pu-242	3.8E+05	Decays to form long-lived U-238; daughter of long-lived Cm-246 and short-lived Am-242. Included in final inventory.
Pu-244	8.0E+07	Decays to form short-lived U-240; daughter of long-lived Cm-248. Included in final inventory.
Ra-223	3.1E-02	Decays to form short-lived Rn-219; daughter of short-lived Fr-223 and Th-227. Included in final inventory as a short-lived daughter of Ac-227.
Ra-224	1.0E-02	Decays to form short-lived Rn-220; daughter of long-lived Th-228. Included in final inventory as a short-lived daughter of Th-228.
Ra-226	1.6E+03	Decays to form short-lived Rn-222; daughter of long-lived Th-230. Included in final inventory.
Ra-228	5.8E+00	Decays to form short-lived Ac-228; daughter of long-lived Th-232. Included in final inventory.
Rb-82	2.4E-06	Decays to form stable Kr-82; daughter of short-lived Sr-82. Excluded from final inventory.
Rb-83	2.4E-01	Decays to form short-lived Kr-83m and stable Kr-83; daughter of short-lived Sr-83. Excluded from final inventory.
Rb-84	9.0E-02	Decays to form stable Kr-84 and Sr-84; excluded from final inventory.
Rb-86	5.1E-02	Decays to form stable Kr-86 and Sr-86; excluded from final inventory.
Re-183	1.9E-01	Decays to form stable; daughter of short-lived Os-183. Excluded from final inventory.
Re-184	1.0E-01	Decays to form stable W-184; daughter of short-lived Re-184m. Excluded from final inventory.
Re-184m	1.8E-01	Decays to form short-lived Re-184 and stable W-184; excluded from final inventory.
Re-188	1.9E-03	Decays to form stable Os-188; daughter of short-lived W-188. Excluded from final inventory.
Rh-97	5.9E-05	Decays to form short-lived Ru-97 and, ultimately, long-lived Tc-97; daughter of short-lived Pd-97. Inventory of long-lived daughter expected to be negligible; excluded from final inventory.
Rh-99	4.4E-02	Decays to form stable Ru-99; daughter of short-lived Pd-99. Excluded from final inventory.

[a] *Primary source of radionuclide half-lives was KAPL (2002). Alternate sources include England and Rider (1994) and NNDC (2004).*

Table II-1 (Continued)
Radionuclide Decay Characteristics and Bases for Inclusion in the Area G Inventory

Radionuclide	Half-Life (yr) [a]	Decay Chain Characteristics and Assumptions
Rh-101	3.3E+00	Decays to form stable Ru-101; daughter of short-lived Rh-101m. Excluded from final inventory.
Rh-102	5.7E-01	Decays to form stable Pd-102 and Ru-102; daughter of short-lived Rh-102m. Excluded from final inventory.
Rh-102m	3.7E+00	Decays to form stable Ru-102 and short-lived Rh-102; excluded from final inventory.
Rh-106	9.5E-07	Decays to form stable Pd-106; daughter of short-lived Ru-106. Excluded from final inventory.
Rn-219	1.3E-07	Decays to form short-lived Po-215; daughter of short-lived Ra-223. Included in final inventory as a short-lived daughter of Ac-227.
Ru-103	1.1E-01	Decays to form stable Rh-103; daughter of short-lived Ru-103m and Tc-103. Excluded from final inventory.
Ru-106	1.0E+00	Decays to form short-lived Rh-106; daughter of Tc-106. Excluded from final inventory.
S-35	2.4E-01	Decays to form stable Cl-35; daughter of short-lived P-35. Excluded from final inventory.
Sb-124	1.6E-01	Decays to form stable Te-124; daughter of short-lived Sb-124m. Excluded from final inventory.
Sb-125	2.8E+00	Decays to form short-lived Te-125m and stable Te-125; daughter of short-lived Sn-125. Excluded from final inventory.
Sb-126	3.4E-02	Decays to form stable Te-126; daughter of long-lived Sn-126 and short-lived Sb-126m. Included in final inventory as a short-lived daughter of Sn-126.
Sc-43	4.5E-04	Decays to form stable Ca-43; daughter of short-lived Ti-43. Excluded from final inventory.
Sc-44	4.5E-04	Decays to form stable Ca-44; daughter of long-lived Ti-44. Included in final inventory as a short-lived daughter of Ti-44.
Sc-46	2.3E-01	Decays to form stable Ti-46; daughter of short-lived Sc-46m. Excluded from final inventory.
Sc-48	4.2E-04	Decays to form stable Ti-48; excluded from final inventory
Se-73	8.1E-04	Decays to form short-lived As-73; daughter of short-lived Br-73. Excluded from final inventory.
Se-75	3.3E-01	Decays to form stable As-75; daughter of short-lived Br-75. Excluded from final inventory.
Se-79	2.9E+05	Decays to form stable Br-79; daughter of short-lived As-79. Included in final inventory.
Si-32	1.6E+02	Decays to form short-lived P-32; daughter of short-lived Al-32. Included in final inventory.
Sm-145	9.3E-01	Decays to form long-lived Pm-145; daughter of short-lived Eu-145. Inventory of long-lived daughter expected to be negligible; excluded from final inventory.
Sm-151	9.0E+01	Decays to form stable Eu-150; daughter of short-lived Pm-151. Included in final inventory.

[a] *Primary source of radionuclide half-lives was KAPL (2002). Alternate sources include England and Rider (1994) and NNDC (2004).*

Table II-1 (Continued)
Radionuclide Decay Characteristics and Bases for Inclusion in the Area G Inventory

Radionuclide	Half-Life (yr) [a]	Decay Chain Characteristics and Assumptions
Sn-113	3.2E-01	Decays to form short-lived In-113m and stable In-113; daughter of short-lived Sb-113. Excluded from final inventory.
Sn-119m	8.0E-01	Decays to form stable Sn-119; daughter of short-lived In-119. Excluded from final inventory.
Sn-121	3.1E-03	Decays to form stable Sb-121; daughter of short-lived In-121 and Sn-121m. Excluded from final inventory.
Sn-121m	4.4E+01	Decays to form stable Sb-121 and short-lived Sn-121; daughter of short-lived In-121. Included in final inventory.
Sn-123	3.5E-01	Decays to form stable Sb-123; daughter of short-lived In-123. Excluded from final inventory.
Sn-126	2.3E+05	Decays to form short-lived Sb-126 and Sb-126m; daughter of short-lived In-126. Included in final inventory.
Sr-82	6.9E-02	Decays to form short-lived Rb-82; daughter of short-lived Y-82. Excluded from final inventory.
Sr-85	1.8E-01	Decays to form stable Rb-85; daughter of short-lived Y-85. Excluded from final inventory.
Sr-89	1.4E-01	Decays to form short-lived Y-89m and stable Y-89; daughter of short-lived Rb-89. Excluded from final inventory.
Sr-90	2.9E+01	Decays to form short-lived Y-90; daughter of short-lived Rb-90. Included in final inventory.
Ta-179	1.8E+00	Decays to form stable Hf-179; daughter of short-lived W-179. Excluded from final inventory.
Ta-182	3.1E-01	Decays to form stable W-182; daughter of long-lived Hf-182. Excluded from final inventory because of the absence of Hf-182.
Ta-183	1.4E-02	Decays to form stable W-183; daughter of short-lived Hf-183. Excluded from final inventory.
Tb-157	7.0E+01	Decays to form stable Gd-157; daughter of short-lived Dy-157. Included in final inventory.
Tb-158	1.8E+02	Decays to form stable Dy-158 and Gd-158; included in final inventory.
Tb-160	2.0E-01	Decays to form stable Dy-160; excluded from final inventory.
Tc-95	2.3E-03	Decays to form stable Mo-95; daughter of short-lived Ru-95 and Tc-95m. Excluded from final inventory.
Tc-95m	1.7E-01	Decays to form stable Mo-95 and short-lived Tc-95; daughter of short-lived Ru-95. Excluded from final inventory.
Tc-97	4.2E+06	Decays to form stable Mo-97; daughter of short-lived Tc-97m. Included in final inventory.
Tc-99	2.1E+05	Decays to form stable Ru-99; daughter of short-lived Mo-99 and Tc-99m. Included in final inventory.

[a] *Primary source of radionuclide half-lives was KAPL (2002). Alternate sources include England and Rider (1994) and NNDC (2004).*

Table II-1 (Continued)
Radionuclide Decay Characteristics and Bases for Inclusion in the Area G Inventory

Radionuclide	Half-Life (yr) [a]	Decay Chain Characteristics and Assumptions
Tc-99m	6.9E-04	Decays to form stable Ru-99 and long-lived Tc-99; daughter of short-lived Mo-99. Inventory of long-lived daughter expected to be negligible; excluded from final inventory.
Te-125m	1.6E-01	Decays to form stable Te-125; excluded from final inventory.
Te-129m	9.2E-02	Decays to form long-lived I-129 and short-livedTe-129; daughter of short-lived Sb-129. Inventory of long-lived daughter expected to be negligible; excluded from final inventory.
Th-227	5.1E-02	Decays to form short-lived Ra-223; daughter of long-lived Ac-227. Included as a short-lived daughter of Ac-227.
Th-228	1.9E+00	Decays to form short-lived Ra-224; daughter of short-lived Ac-228. Included in final inventory.
Th-229	7.3E+03	Decays to form short-lived Ra-225; daughter of long-lived U-233. Included in final inventory.
Th-230	7.5E+04	Decays to form long-lived Ra-226; daughter of long-lived U-234. Included in final inventory.
Th-231	2.9E-03	Decays to form long-lived Pa-231; daughter of long-lived U-235. Included in final inventory as a short-lived daughter of U-235.
Th-232	1.4E+10	Decays to form long-lived Ra-228; daughter of long-lived U-236. Included in final inventory.
Th-234	6.6E-02	Decays to form short-lived Pa-234m; daughter of long-lived U-238. Included in final inventory as a short-lived daughter of U-238.
Ti-44	6.0E+01	Decays to form short-lived Sc-44; daughter of short-lived V-44. Included in final inventory.
Tl-204	3.8E+00	Decays to form stable Hg-204 and stable Pb-204; excluded from final inventory.
Tl-208	5.8E-06	Decays to form stable Pb-208; daughter of short-lived Bi-212. Included in final inventory as a short-lived daughter of Th-228.
Tm-170	3.5E-01	Decays to form stable Er-170 and Yb-170; excluded from final inventory.
Tm-171	1.9E+00	Decays to form stable Yb-171; daughter of short-lived Er-171. Excluded from final inventory.
U-232	7.0E+01	Decays to form long-lived Th-228; daughter of long-lived Pu-236. Included in final inventory.
U-233	1.6E+05	Decays to form long-lived Th-229; daughter of short-lived Pa-233. Included in final inventory.
U-234	2.5E+05	Decays to form long-lived Th-230; daughter of short-lived Pa-234 and Pa-234m and long-lived Pu-238. Included in final inventory.
U-235	7.0E+08	Decays to form short-lived Th-231; daughter of long-lived Pu-239. Included in final inventory.

[a] *Primary source of radionuclide half-lives was KAPL (2002). Alternate sources include England and Rider (1994) and NNDC (2004).*

Table II-1 (Continued)
Radionuclide Decay Characteristics and Bases for Inclusion in the Area G Inventory

Radionuclide	Half-Life (yr) [a]	Decay Chain Characteristics and Assumptions
U-236	2.3E+07	Decays to form long-lived Th-232; daughter of long-lived Pu-240. Included in final inventory.
U-237	2.1E-03	Decays to form long-lived Np-237; inventory of long-lived daughter expected to be negligible. Excluded from final inventory.
U-238	4.5E+09	Decays to form short-lived Th-234; daughter of long-lived Pu-242. Included in final inventory.
U-239	4.5E-05	Decays to form short-lived Np-239 and, ultimately, long-lived Pu-239; inventory of long-lived daughter expected to be negligible. Excluded from final inventory.
V-48	4.4E-02	Decays to form stable Ti-48; daughter of short-lived Cr-48. Excluded from final inventory.
V-49	9.1E-01	Decays to form stable Ti-49; daughter of short-lived Cr-49. Excluded from final inventory.
V-52	1.4E-06	Decays to form stable Cr-52; daughter of short-lived Ti-52. Excluded from final inventory.
W-181	3.3E-01	Decays to form stable Ta-181; daughter of short-lived Re-181. Excluded from final inventory.
W-185	2.0E-01	Decays to form stable Re-185; daughter of short-lived Ta-185. Excluded from final inventory.
Xe-133	1.4E-02	Decays to form stable Cs-133; daughter of short-lived I-133. Excluded from final inventory.
Y-88	2.9E-01	Decays to form stable Sr-88; daughter of short-lived Zr-88. Excluded from final inventory.
Y-90	7.3E-03	Decays to form stable Zr-90; daughter of long-lived Sr-90. Included in final inventory as a short-lived daughter of Sr-90.
Y-91	1.6E-01	Decays to form stable Zr-91; daughter of short-lived Sr-91. Excluded from final inventory.
Yb-169	8.8E-02	Decays to form stable Tm-169; daughter of short-lived Lu-169. Excluded from final inventory.
Zn-65	6.7E-01	Decays to form stable Cu-65; daughter of short-lived Ga-65. Excluded from final inventory.
Zn-69m	1.6E-03	Decays to form stable Ga-69 and short-lived Zn-69; excluded from final inventory.
Zn-72	7.4E-04	Decays to form short-lived Ga-72; daughter of short-lived Cu-72. Excluded from final inventory.
Zr-88	2.3E-01	Decays to form short-lived Y-88; daughter of short-lived Nb-88. Excluded from final inventory.
Zr-93	1.5E+06	Decays to form stable Nb-93; daughter of short-lived Y-93. Included in final inventory.
Zr-95	1.8E-01	Decays to form short-lived Nb-95 and Nb-95m; daughter of short-lived Y-95. Excluded from final inventory.

[a] *Primary source of radionuclide half-lives was KAPL (2002). Alternate sources include England and Rider (1994) and NNDC (2004).*

Table II-2
Exposure Parameters Used to Conduct the Screening Evaluation

Parameter	Units	Screening Value
Soil Ingestion Rate	mg/d	2.0E+02
Inhalation Rate	m^3/d	2.2E+01
Dust Loading	kg/m^3	1.0E-07
Site Occupancy Fraction	---	1.0E+00

The parameter values adopted for the screening evaluation were selected in a conservative manner. The soil ingestion rate of 200 mg/d (4.4×10^{-4} lb/d) exceeds the central estimate of 50 mg/d (1.1×10^{-4} lb/d) cited by the U.S. Environmental Protection Agency (EPA, 1997) and the range of 50 to 100 mg/d (1.1×10^{-4} to 2.2×10^{4} lb/d) adopted by the National Council on Radiation Protection and Measurements (NCRP, 1999) for screening evaluations. However, 200 mg/d (4.4×10^{-4} lb/d) is equal to the soil ingestion rate cited by Simon (1998) for a rural lifestyle in a sparsely vegetated area. An inhalation rate of 22 m^3/d (77 ft^3/d) falls outside of the 10 to 20 m^3/d (35 to 70 ft^3/d) range provided as a long-term average for adult males by the EPA (1997), and is almost 50 percent greater than the average inhalation rate adopted by the Agency. The dust-loading factor used to estimate airborne radionuclide concentrations directly above the waste exceeds the value of 8.0×10^{-8} kg/m^3 (6.2×10^{-6} lb/ft^3) adopted by the NCRP (1999) to conduct screening assessments for residential scenarios. It is equal to the default value suggested by Anspaugh et al. (1975) in lieu of site-specific data. Dust loadings cited by Baes et al. (1984), the NCRP (1984), INEEL (1994), and DOE (1995) for various locations in the U.S. are all less than 1.0×10^{-7} kg/m^3 (7.8×10^{-6} lb/ft^3). Finally, it was conservatively assumed that the hypothetical receptor was present at the site 100 percent of the time.

The doses projected for the screening assessment decline from a peak exposure of 0.78 mrem/yr at the beginning of the simulation to 2.9×10^{-6} mrem/yr by the end of the 1,000-year period. Direct radiation from the waste is the primary contributor to the projected peak dose. All doses fall well within the performance objectives for the atmospheric pathway and all pathways exposure scenarios, 10 and 25 mrem/yr, respectively.

The doses calculated for the screening assessment are considered to be extremely conservative estimates of actual exposures for several reasons, some of which are considered here. First, the calculations assume the receptor is located directly above the disposal units at Area G when, in fact, controls over the site will preclude long-term occupation of the site. Any such controls would force the receptor to occupy locations downwind of the site, where exposures would be

orders of magnitude smaller. Second, the screening evaluation assumes there is no cover material placed over the waste and therefore does not consider the isolation of the waste afforded by the cover. With a cover in place, the amount of contamination available for direct ingestion and inhalation would be significantly smaller, limited to only that contamination deposited on the surface of the site by plants and animals penetrating into the waste. Additionally, the cover would shield the receptor from direct radiation emitted from the waste, reducing the projected exposures from that pathway by orders of magnitude. Third, the manner in which the screening assessment was conducted implicitly assumes that all waste was placed in the disposal units at the beginning of the 1,000-year simulation period. In fact, this waste was, or will be, disposed of over a period of several years during the disposal facility's operational period. Accounting for the decay and ingrowth of the radionuclides during the portion of the operational period that the waste resides at Area G would result in smaller doses than those estimated by the screening assessment.

All told, the elimination of several short-lived radionuclides with long-lived daughters is not expected to compromise the performance assessment and composite analysis. Conservative estimates of the doses resulting from these isotopes are much less than acceptable limits and will be lower still under more realistic exposure conditions. On this basis, these radionuclides were excluded from the Area G inventory.

Many of the radionuclides in Table II-1 are short-lived daughters of long-lived parents and, as such, are expected to be in secular equilibrium with said parents. Examples of these radionuclides include Ac-228, Ba-137m, and Bi-214. These short-lived isotopes are not listed in the tables provided in the main report, but will be included at the appropriate activities in the performance assessment and composite analysis modeling. An indication to this effect is provided in Table II-1.

References

Anspaugh, L.R., J.H. Shinn, P.L. Phelps, and N.C. Kennedy, 1975, "Resuspension and Redistribution of Plutonium in Soils," *Health Physics* Vol. 29, p. 571.

Baes, C.F. III, R.D. Sharp, A.L. Sjoreen, and R.W. Shor, 1984, *A Review and Analysis of Parameters for Assessing Transport of Environmentally Released Radionuclides through Agriculture,* Oak Ridge National Laboratory, ORNL-5786, September.

DOE, 1995, *Cost/Risk/Benefit Analysis of Alternative Cleanup Requirements for Plutonium-Contaminated Soils On and Near the Nevada Test Site*, U.S. Department of Energy Report DOE/NV-399, May.

England, T.R., and B.F. Rider, 1994, *Evaluation and Compilation of Fission Product Yields 1993*, Los Alamos National Laboratory Report LA-UR-94-3106, October.

EPA, 1988, *Limiting Values of Radionuclide Intake and Air Concentration and Dose Conversion Factors for Inhalation, Submersion, and Ingestion*, U.S. Environmental Protection Agency Federal Guidance Report 11, EPA 520/1-88-020, September.

EPA, 1993, *External Exposure to Radionuclides in Air, Water, and Soil*, U.S. Environmental Protection Agency Federal Guidance Report 12, EPA 402-R-93-081, September.

EPA, 1997, *Exposure Factors Handbook,* U.S. Environmental Protection Agency, EPA/600/P-95/002Fa, August.

INEEL, 1994, *Radioactive Waste Management Complex Low-Level Waste Radiological Performance Assessment*, Idaho National Engineering and Environmental Laboratory Report EGG-WM-8773, May.

KAPL, 2002, *Nuclides and Isotopes, Chart of the Nuclides, 16th Edition*, Knolls Atomic Power Laboratory, Eds. E.M. Baum, H.D. Knox, and T.R. Miller.

NCRP, 1984, *Radiological Assessment: Predicting the Transport, Bioaccumulation, and Uptake by Man of Radionuclides Released to the Environment*, National Council on Radiation Protection and Measurements, Report No. 76, March.

NCRP, 1999, *Recommended Screening Limits for Contaminated Surface Soil and Review of Factors Relevant to Site-Specific Studies*, National Council on Radiation Protection and Measurements, Report No. 129.

National Nuclear Data Center (NNDC), 2004, "Evaluated Nuclear Structure Data File," <http://www.nndc.bnl.gov/ensdf/index .jsp>, June.

Simon, S.L., 1998, "Soil Ingestion by Humans: A Review of History, Data, and Etiology with Application to Risk Assessment of Radioactively Contaminated Soil," *Health Physics,* Vol. 74, No. 6, pp. 647–672.

Attachment III
Pit-Specific Radionuclide, Activation Product, Fission Product, and Material Type Inventories for Area G

This attachment summarizes the unit-specific radionuclide inventories for the disposal pits at Area G; the listed inventories address waste disposed of through 2007. The information needed to assign the waste disposed of prior to 1971 to specific units was unavailable; this waste is listed in the column for pits 1 through 5 as these units received most of the pre-1971 material. The manner in which these inventories were estimated is discussed in the main report.

Table III-1
Pit-Specific Radionuclide, Activation Product, Fission Product, and Material Type Inventories

Constituent [a]	Waste Inventory by Disposal Pit and Period of Disposal (Ci)											
	1–5	5	6	7	8	9	10	12	13	15	16	17
	Pre-1971	1971–1988 [b]	1971–1988	1971–1988	1971–1988	1971–1988	1971–1988	1971–1988	1971–1988	1988–2007 [c]	1971–1988	1971–1988
Ac-227	8.6E-01	---	---	---	---	---	---	---	---	---	---	7.0E-02
Ag-108m	---	---	---	---	---	---	---	---	---	1.1E-04	---	---
Am-241	2.4E+03	---	---	1.3E-01	9.7E-01	---	1.0E-03	---	---	1.7E-01	---	---
Am-243	---	---	---	---	---	---	---	---	---	1.3E-05	---	---
Ba-133	---	---	---	---	---	---	---	---	---	6.2E-06	---	---
Bk-249	1.6E-03	---	---	---	---	---	---	---	---	---	---	---
C-14	---	---	---	---	---	---	9.0E-07	---	---	5.2E-07	---	---
Cf-249	2.4E-03	---	---	---	---	---	---	---	---	4.3E-07	---	---
Cf-251	2.7E-03	---	---	---	---	---	---	---	---	---	---	---
Cf-252	1.5E-02	---	---	8.6E-03	---	---	8.0E-06	---	---	---	---	---
Cm-242	1.8E-03	---	---	---	---	---	---	---	---	---	---	---
Cm-243	---	---	---	---	---	---	---	---	---	7.2E-07	---	---
Cm-244	1.7E-03	---	---	---	---	---	---	---	---	---	---	---
Co-60	---	---	---	---	---	---	1.6E-02	---	---	2.4E+00	---	---
Cs-135	---	---	---	---	---	---	---	---	---	5.9E-07	---	---
Cs-137	2.6E-01	---	---	---	---	---	1.5E-03	---	---	1.0E+00	---	---
D38	---	---	---	---	---	---	---	---	---	4.1E-01	---	---
Eu-152	---	---	---	---	---	---	---	---	---	2.7E-03	---	---
Eu-154	---	---	---	---	---	---	---	---	---	2.1E-06	---	---
H-3	2.7E+00	---	---	---	---	---	6.1E+03	---	5.0E-01	1.5E+02	---	---
Ho-166m	---	---	---	---	---	---	---	---	---	6.2E-06	---	---

--- = None

[a] This column includes radionuclides, material types, mixed-activation products (MAP), and mixed-fission products (MFP).

[b] Refers to waste disposed of from 1971 through September 26, 1988.

[c] Refers to waste disposed of from September 27, 1988 through 2007.

Table III-1 (Continued)
Pit-Specific Radionuclide, Activation Product, Fission Product, and Material Type Inventories

	Waste Inventory by Disposal Pit and Period of Disposal (Ci)											
	1–5	5	6	7	8	9	10	12	13	15	16	17
Constituent [a]	Pre-1971	1971–1988 [b]	1971–1988	1971–1988	1971–1988	1971–1988	1971–1988	1971–1988	1971–1988	1988–2007 [c]	1971–1988	1971–1988
I-129	---	---	---	---	---	---	---	---	---	1.0E-06	---	---
K-40	---	---	---	---	---	---	---	---	---	3.3E-04	---	---
Kr-85	1.7E-03	---	---	---	---	---	---	---	---	2.2E-06	---	---
MAP	3.6E-01	---	---	5.4E-02	---	---	7.6E+02	---	3.6E-02	---	1.2E-01	---
MFP	1.0E+03	---	---	4.7E-02	---	1.0E+00	5.1E-02	8.0E-03	1.5E-02	---	---	---
Nb-94	---	---	---	---	---	---	---	---	---	1.7E-05	---	---
Ni-59	---	---	---	---	---	---	---	---	---	6.1E-06	---	---
Ni-63	---	---	---	---	---	---	---	---	---	5.5E-04	---	---
Np-237	4.0E-03	---	---	---	---	---	---	---	---	1.1E-04	---	---
Pa-231	---	---	---	---	---	---	---	---	---	1.0E-09	---	---
Po-210	1.9E-03	---	---	---	---	---	---	---	---	1.6E-01	---	---
Pu-238	3.8E+03	2.6E+02	1.8E+02	2.0E+01	1.6E+01	1.8E-01	2.2E-02	2.7E-01	---	1.2E+00	---	---
Pu-239	1.7E+02	---	3.8E+00	4.3E-01	3.5E+00	---	5.2E-02	7.1E-02	---	9.7E-01	---	---
Pu-240	4.0E+00	---	---	---	---	---	---	---	---	6.9E-02	---	---
Pu-241	---	---	---	---	---	---	---	---	---	1.2E+00	---	---
Pu-242	---	---	---	---	---	---	---	---	---	5.1E-04	---	---
Pu51	1.6E+00	---	---	---	---	---	---	---	---	---	---	---
PU52	7.7E+03	---	---	2.4E-03	---	---	1.3E-02	2.1E-04	---	---	---	---
PU53	2.5E+02	---	---	---	---	---	---	---	---	---	---	---
PU54	1.1E+03	---	---	---	---	---	---	---	---	---	---	---
PU55	6.8E+01	---	---	---	---	---	---	---	---	---	---	---
PU56	1.2E+03	---	---	---	---	---	---	---	---	---	---	---

--- = None

[a] *This column includes radionuclides, material types, mixed-activation products (MAP), and mixed-fission products (MAP).*

[b] *Refers to waste disposed of from 1971 through September 26, 1988.*

[c] *Refers to waste disposed of from September 27, 1988 through 2007.*

Table III-1 (Continued)
Pit-Specific Radionuclide, Activation Product, Fission Product, and Material Type Inventories

	Waste Inventory by Disposal Pit and Period of Disposal (Ci)											
	1–5	5	6	7	8	9	10	12	13	15	16	17
Constituent [a]	Pre-1971	1971–1988 [b]	1971–1988	1971–1988	1971–1988	1971–1988	1971–1988	1971–1988	1971–1988	1988–2007 [c]	1971–1988	1971–1988
PU57	7.1E+01	---	---	---	---	---	---	---	---	---	---	---
PU83	5.0E+02	---	---	---	---	---	2.0E-04	---	---	---	---	---
Ra-226	---	---	---	---	---	---	9.9E-02	---	---	7.7E-02	---	---
Ra-228	---	---	---	---	---	---	---	---	---	1.9E-04	---	---
Si-32	---	---	---	---	---	---	---	---	---	1.2E-05	---	---
Sm-151	---	---	---	---	---	---	---	---	---	---	---	---
Sn-126	---	---	---	---	---	---	---	---	---	1.9E-06	---	---
Sr-90	2.9E-01	---	---	---	---	---	2.1E-01	---	---	5.1E-02	---	---
Tb-157	---	---	---	---	---	---	---	---	---	4.5E-08	---	---
Tc-99	---	---	---	---	---	---	---	---	---	9.9E-03	---	---
Th-228	---	---	---	---	---	---	---	---	---	4.9E-04	---	---
Th-229	---	---	---	---	---	---	---	---	---	6.9E-05	---	---
Th-230	1.6E+01	---	---	---	---	---	---	---	---	2.2E-08	---	---
Th-232	---	---	---	---	---	---	4.4E-04	---	---	1.6E-02	---	---
TH88	1.9E-03	---	---	---	3.3E-05	---	---	---	---	---	6.5E-04	---
Ti-44	---	---	---	---	---	---	---	---	---	3.8E-04	---	---
U10	8.8E-01	---	---	---	---	---	---	---	---	---	5.1E-01	---
U12	7.9E+00	---	---	---	---	---	3.0E-01	---	4.6E-01	---	4.3E-01	---
U-232	---	---	---	---	---	---	---	---	---	1.8E-08	---	---
U-233	6.1E+00	---	---	---	---	---	1.9E-05	---	---	7.5E-03	---	---
U-234	---	---	---	---	---	---	---	---	---	1.4E-01	---	---
U-235	3.7E-01	4.9E-03	---	1.6E-03	---	---	7.9E-03	---	1.1E-05	1.6E-02	3.9E-02	---

--- = None

[a] *This column includes radionuclides, material types, mixed-activation products (MAP), and mixed-fission products (MAP).*

[b] *Refers to waste disposed of from 1971 through September 26, 1988.*

[c] *Refers to waste disposed of from September 27, 1988 through 2007.*

Table III-1 (Continued)
Pit-Specific Radionuclide, Activation Product, Fission Product, and Material Type Inventories

	Waste Inventory by Disposal Pit and Period of Disposal (Ci)											
	1–5	5	6	7	8	9	10	12	13	15	16	17
Constituent [a]	Pre-1971	1971–1988 [b]	1971–1988	1971–1988	1971–1988	1971–1988	1971–1988	1971–1988	1971–1988	1988–2007 [c]	1971–1988	1971–1988
U-236	---	---	---	---	---	---	6.3E-08	---	---	3.2E-05	---	---
U-238	4.3E+00	1.6E-04	---	---	---	---	1.5E+00	---	1.1E+00	5.5E+00	8.0E-01	---
U38	2.3E-02	---	---	---	---	---	---	---	---	---	1.3E-02	---
U81	4.7E-03	---	---	---	---	---	---	---	---	---	---	---
Zr-93	---	---	---	---	---	---	---	---	---	2.0E-08	---	---

--- = None

[a] This column includes radionuclides, material types, mixed-activation products (MAP), and mixed-fission products (MAP).

[b] Refers to waste disposed of from 1971 through September 26, 1988.

[c] Refers to waste disposed of from September 27, 1988 through 2007.

Table III-1 (Continued)
Pit-Specific Radionuclide, Activation Product, Fission Product, and Material Type Inventories

	Waste Inventory by Disposal Pit and Period of Disposal (Ci)										
	18	19	20	21	22	24	25	26	27	28	29
Constituent [a]	1971–1988 [b]	1971–1988	1971–1988	1971–1988	1971–1988	1971–1988	1971–1988	1971–1988	1971–1988	1971–1988	1971–1988
Am-241	3.3E-01	---	1.0E-01	---	1.7E-01	---	3.1E-03	1.4E+01	8.6E-06	3.0E-06	3.2E+00
C-14	2.0E-06	---	---	---	---	---	---	---	---	---	2.1E-01
Cf-249	---	---	4.1E-04	---	---	---	---	---	---	---	---
Cf-251	---	---	1.6E-03	---	---	---	---	---	---	---	---
Co-60	1.1E+03	---	---	---	---	2.0E-03	1.2E+02	1.0E+00	2.0E-03	---	8.0E-03
Cs-135	---	---	---	---	---	---	---	---	---	---	---
Cs-137	---	---	---	---	---	1.5E-01	2.0E+02	---	2.0E-06	---	8.8E+02
H-3	1.0E+01	---	6.0E-01	---	5.0E-05	5.0E-01	5.0E+01	3.0E-03	1.1E+02	1.2E+03	5.8E-01
Kr-85	---	---	---	---	1.0E-03						
MAP	5.2E+00	---	---	---	3.2E-01	8.3E-01	1.0E+00	9.6E+01	8.0E+01	1.3E+02	4.8E+00
MFP	1.2E+00	3.0E-01	6.5E-02	---	6.0E+02	---	1.2E+00	5.7E-01	3.2E-02	---	1.7E+01
Np-237	---	---	---	---	---	---	---	---	---	---	7.0E-07
Pu-238	1.2E+00	---	4.4E+00	---	4.5E-01	---	1.2E-03	8.2E-01	4.8E-02	3.2E-01	1.5E+00
Pu-239	1.0E+00	---	1.2E+00	---	1.3E+00	---	5.3E-02	2.7E+00	5.7E-01	2.4E-01	5.7E-01
Pu-240	---	---	---	---	---	---	5.0E-07	---	---	---	---
Pu-241	---	---	---	---	---	---	---	---	---	---	5.8E-06
PU52	4.1E-02	---	1.1E-02	---	2.5E-02	---	9.5E-03	2.8E-01	1.4E-02	1.3E-02	6.8E-01
PU53	---	---	---	---	---	---	---	---	---	---	3.7E-04
PU54	---	---	---	---	---	---	---	---	---	---	1.3E-01
PU83	4.9E-04	---	3.5E-03	---	5.3E-03	---	3.8E-04	3.0E-05	1.6E-03	7.1E-05	2.1E-03

--- = None

[a] This column includes radionuclides, material types, mixed-activation products (MAP), and mixed-fission products (MFP).

[b] Refers to waste disposed of from 1971 through September 26, 1988.

[c] Refers to waste disposed of from September 27, 1988 through 2007.

Table III-1 (Continued)
Pit-Specific Radionuclide, Activation Product, Fission Product, and Material Type Inventories

	Waste Inventory by Disposal Pit and Period of Disposal (Ci)										
	18	19	20	21	22	24	25	26	27	28	29
Constituent [a]	1971–1988 [b]	1971–1988	1971–1988	1971–1988	1971–1988	1971–1988	1971–1988	1971–1988	1971–1988	1971–1988	1971–1988
Ra-226	---	---	---	---	---	---	---	---	9.7E-02	---	---
Sr-90	1.0E+00	---	---	---	---	1.7E-01	1.1E-02	1.0E-01	2.1E-03	---	1.4E+03
Th-230	---	---	---	---	---	9.5E+00	---	---	---	---	---
Th-232	8.7E-04	---	---	---	---	---	---	---	---	---	4.9E-05
TH88	---	---	---	---	---	4.4E-04	---	---	---	2.3E-02	---
U10	---	---	---	---	---	5.0E-09	---	---	---	---	---
U11	---	---	---	---	---	---	---	---	---	---	1.3E-01
U12	5.7E-01	---	---	3.8E-01	1.8E-01	3.2E+00	1.0E-01	---	1.7E-01	---	---
U-233	---	---	---	---	---	---	---	---	---	---	1.9E-02
U-235	9.4E-03	---	4.7E-04	1.7E-01	5.8E-04	1.9E-03	9.9E-03	1.5E-01	6.1E-03	8.0E-03	2.4E-01
U-238	1.9E+00	---	---	1.8E-03	4.7E-01	1.1E-01	1.2E+00	1.1E-01	7.4E-01	5.2E-01	8.2E-01
U35	---	---	---	---	---	---	---	---	4.9E-04	---	---
U36	---	---	---	---	---	---	---	---	2.2E-05	---	---
U38	1.3E-03	---	---	---	---	7.5E-04	---	---	1.5E-03	---	1.1E-02
U81	---	---	---	---	2.8E-03	---	---	---	---	---	---

--- = None

[a] This column includes radionuclides, material types, mixed-activation products (MAP), and mixed-fission products (MAP).

[b] Refers to waste disposed of from 1971 through September 26, 1988.

[c] Refers to waste disposed of from September 27, 1988 through 2007.

Table III-1 (Continued)
Pit-Specific Radionuclide, Activation Product, Fission Product, and Material Type Inventories

	Waste Inventory by Disposal Pit and Period of Disposal (Ci)										
	30	31	32		33	35	36		37	38	39
Constituent [a]	1988–2007 [c]	1988–2007	1971–1988 [b]	1988–2007	1971–1988	1971–1988	1971–1988	1988–2007	1988–2007	1988–2007	1988–2007
Ac-227	---	---	---	---	---	---	---	---	3.7E-06	1.4E-05	---
Ag-108m	---	---	---	---	---	---	---	---	---	1.3E-05	4.9E-05
Al-26	---	---	---	---	---	---	---	---	2.6E-04	2.7E-07	---
Am-241	2.7E-02	1.3E-01	2.2E+00	---	1.9E+00	4.3E-01	1.3E-01	1.2E-04	3.7E-01	6.6E+00	7.3E-01
Am-243	---	---	---	---	---	---	---	---	2.5E-05	8.5E-03	1.3E-06
Ba-133	---	---	---	---	---	---	---	---	1.3E-03	6.9E-01	1.6E-06
Be-10	---	---	---	---	---	---	---	---	---	4.6E-03	---
Bi-207	---	---	---	---	---	---	---	---	2.0E-05	1.5E-02	7.4E-05
Bk-247	---	---	---	---	---	---	---	---	5.4E-08	2.3E-07	---
C-14	2.0E-09	6.8E-09	1.5E-06	---	1.5E-02	---	---	---	1.7E-02	3.3E+00	4.8E-05
Ca-41	---	---	---	---	---	---	---	---	---	2.7E-01	---
Cf-249	---	---	---	---	---	---	---	---	---	1.0E-04	---
Cf-252	---	---	---	---	---	---	---	---	1.4E-05	5.6E-06	---
Cl-36	---	---	---	---	---	---	---	---	3.7E-04	1.8E-02	---
Cm-243	---	---	---	---	---	---	---	---	---	4.1E-05	---
Cm-244	---	---	---	---	---	---	---	---	---	2.8E-03	---
Cm-245	---	---	---	---	---	---	---	---	---	4.6E-05	---
Cm-248	---	---	---	---	---	---	---	---	---	4.5E-07	---
Co-60	7.5E-01	3.7E-05	1.0E-02	---	5.0E-02	---	1.0E-04	3.2E-01	6.9E+00	2.8E+01	6.0E+00
Cs-135	---	---	---	---	---	---	---	---	7.0E-08	3.2E-05	1.0E-04
Cs-137	1.7E+00	2.8E-01	7.2E-03	---	1.5E+00	---	1.4E-03	3.0E-01	4.0E-01	1.9E+00	2.2E-01
D38	---	6.6E-03	---	---	---	---	---	---	3.0E-02	8.7E+00	1.9E-01

--- = None

[a] This column includes radionuclides, material types, mixed-activation products (MAP), and mixed-fission products (MFP).

[b] Refers to waste disposed of from 1971 through September 26, 1988.

[c] Refers to waste disposed of from September 27, 1988 through 2007.

Table III-1 (Continued)
Pit-Specific Radionuclide, Activation Product, Fission Product, and Material Type Inventories

	Waste Inventory by Disposal Pit and Period of Disposal (Ci)										
	30	31	32		33	35	36		37	38	39
Constituent [a]	1988–2007 [c]	1988–2007	1971–1988 [b]	1988–2007	1971–1988	1971–1988	1971–1988	1988–2007	1988–2007	1988–2007	1988–2007
Eu-152	---	---	---	---	---	---	---	2.9E-02	5.8E-07	3.9E-01	1.2E-02
Eu-154	---	---	---	---	---	---	---	---	1.0E-06	5.2E-02	1.2E-04
Gd-148	---	---	---	---	---	---	---	---	---	---	1.0E-05
H-3	8.6E-01	1.8E-02	1.5E+00	---	4.0E+00	1.2E+00	3.0E+01	2.9E-01	7.5E+02	2.2E+03	4.1E+00
Ho-163	---	---	---	---	---	---	---	---	8.3E-01	8.3E-02	---
Ho-166m	---	---	---	---	---	---	---	---	---	1.4E-03	---
I-129	---	---	---	---	---	---	---	---	---	2.9E-05	1.1E-06
K-40	---	1.5E-03	---	---	---	---	---	---	1.5E-01	1.2E-01	2.4E-04
Kr-85	4.3E-02	---	---	---	---	---	1.4E-06	---	6.7E-04	2.9E-03	5.7E-08
Lu-176	---	---	---	---	---	---	---	---	---	1.7E-06	---
MAP	7.9E+00	1.0E-07	2.0E+01	---	3.0E+01	6.8E+01	4.0E+00	8.8E-01	4.1E+00	---	---
MFP	1.7E+01	1.9E-05	2.1E+00	---	1.2E+01	8.6E+00	1.2E+00	1.0E-02	6.1E-01	---	---
Mo-93	---	---	---	---	---	---	---	---	---	2.0E-05	---
Nb-91	---	---	---	---	---	---	---	---	---	1.2E-05	---
Nb-92	---	---	---	---	---	---	---	---	---	3.0E-06	---
Nb-93m	---	---	---	---	---	---	---	---	---	1.0E-03	---
Nb-94	---	---	---	---	---	---	8.0E-06	---	2.5E-02	1.5E-02	1.0E-05
Nd-144	---	---	---	---	---	---	---	---	---	---	1.0E-08
Ni-59	---	---	---	---	---	---	---	---	2.1E-03	1.8E-03	2.4E-03
Ni-63	1.0E-05	---	---	---	---	---	---	---	5.6E-03	2.0E+00	5.1E-04
Np-237	---	---	---	---	---	---	---	---	1.1E-05	4.2E-03	6.3E-04
Os-194	---	---	---	---	---	---	---	---	---	1.3E-07	---

--- = None

[a] This column includes radionuclides, material types, mixed-activation products (MAP), and mixed-fission products (MAP).

[b] Refers to waste disposed of from 1971 through September 26, 1988.

[c] Refers to waste disposed of from September 27, 1988 through 2007.

Table III-1 (Continued)
Pit-Specific Radionuclide, Activation Product, Fission Product, and Material Type Inventories

	Waste Inventory by Disposal Pit and Period of Disposal (Ci)										
	30	31	32		33	35	36		37	38	39
Constituent [a]	1988–2007 [c]	1988–2007	1971–1988 [b]	1988–2007	1971–1988	1971–1988	1971–1988	1988–2007	1988–2007	1988–2007	1988–2007
Pa-231	---	---	---	---	---	---	---	---	1.0E-08	2.4E-05	1.8E-05
Pb-210	---	2.8E-03	---	---	---	---	---	---	9.6E-03	3.3E-03	9.0E-02
Pm-145	---	---	---	---	---	---	---	---	1.0E-01	1.0E-02	---
Pu-236	---	---	---	---	---	---	---	---	---	1.0E-09	---
Pu-238	1.7E+00	3.5E-02	1.5E+00	---	5.9E-02	3.1E-01	8.5E-02	1.0E-09	1.1E+00	8.6E+00	1.9E+00
Pu-239	1.6E-01	2.0E-01	3.6E+00	---	2.2E+00	9.3E-01	3.9E-01	3.8E-03	3.1E+00	1.0E+01	1.5E+00
Pu-240	---	4.3E-03	2.7E-05	---	---	---	---	---	2.4E-02	1.7E-01	2.6E-01
Pu-241	---	5.6E-02	---	---	---	---	---	---	2.9E-01	6.1E-01	6.1E-01
Pu-242	---	2.3E-07	---	---	---	---	7.8E-06	---	8.0E-07	5.8E-03	7.2E-06
Pu-244	---	---	---	---	---	---	---	---	---	3.5E-06	---
PU52	5.9E-01	---	1.6E-01	---	1.1E-01	5.1E-01	4.1E-01	4.4E-02	4.4E+00	---	1.6E-01
PU53	---	---	---	---	---	---	---	---	---	---	---
PU54	---	---	2.0E-02	---	---	---	---	---	---	---	---
PU83	---	---	1.1E-05	---	1.3E-03	1.3E-04	---	---	---	---	---
Ra-226	1.0E-03	2.3E-03	1.0E-05	---	---	---	---	---	2.8E-02	1.5E-02	1.3E-03
Ra-228	---	3.7E-03	---	---	2.1E-01	---	---	---	5.9E-03	7.5E-03	1.7E-02
Si-32	---	---	---	---	---	---	---	---	---	1.6E-05	1.1E-07
Sm-151	---	9.0E-10	---	---	---	---	---	---	---	2.5E-09	---
Sn-126	---	---	---	---	---	---	---	---	---	---	8.5E-07
Sr-90	1.3E-01	1.0E-01	1.3E-03	---	1.2E-01	---	---	---	1.2E-01	2.3E+00	7.8E-02
Tc-97	---	---	---	---	---	---	---	---	2.1E-06	2.0E-08	7.0E-09
Tc-99	8.3E-09	9.6E-06	---	---	---	---	---	---	9.9E-03	2.8E-01	2.8E-02

--- = None

[a] This column includes radionuclides, material types, mixed-activation products (MAP), and mixed-fission products (MAP).

[b] Refers to waste disposed of from 1971 through September 26, 1988.

[c] Refers to waste disposed of from September 27, 1988 through 2007.

Table III-1 (Continued)
Pit-Specific Radionuclide, Activation Product, Fission Product, and Material Type Inventories

	Waste Inventory by Disposal Pit and Period of Disposal (Ci)										
	30	31	32		33	35	36		37	38	39
Constituent [a]	1988–2007 [c]	1988–2007	1971–1988 [b]	1988–2007	1971–1988	1971–1988	1971–1988	1988–2007	1988–2007	1988–2007	1988–2007
Th-228	1.0E-06	3.3E-07	---	---	---	---	---	---	1.1E-03	5.7E-04	4.4E-05
Th-229	---	---	---	---	---	---	---	---	4.0E-05	2.7E-04	4.8E-07
Th-230	---	---	2.6E-09	---	---	---	---	---	5.0E-07	1.2E-03	5.2E-07
Th-232	1.1E-05	3.0E-06	1.0E-09	---	---	---	---	---	1.6E-02	2.9E-01	1.4E-03
TH88	3.7E-02	---	---	---	2.6E-03	---	---	---	2.0E-09	---	---
Ti-44	---	---	---	---	---	---	---	---	3.0E-05	2.2E-03	---
U(NAT)	---	---	---	---	---	---	---	---	---	6.4E-05	---
U11	---	---	2.4E-02	---	---	---	---	---	8.7E-06	---	---
U12	---	---	---	---	2.4E-03	---	---	---	---	---	---
U-232	---	---	---	---	---	---	---	---	3.4E-05	3.2E-04	5.2E-04
U-233	---	---	---	---	---	---	---	---	2.3E-03	6.2E-02	5.4E-04
U-234	1.5E-04	1.2E-03	---	---	---	---	---	---	3.5E-01	2.7E-01	2.9E-01
U-235	5.1E-01	7.2E-04	2.9E-03	---	1.1E-02	1.2E-03	4.8E-02	4.2E-09	2.9E-01	2.8E-02	1.9E-02
U-236	---	---	---	---	---	---	---	---	3.1E-05	3.6E-03	1.3E-07
U-238	3.5E+00	1.7E-03	3.9E-01	---	7.6E-01	1.6E-01	3.1E-03	6.5E-02	9.6E-01	9.1E-01	8.3E-01
U38	3.0E-02	---	1.6E-02	---	---	---	8.2E-04	---	2.0E-02	---	---
U39	---	---	---	---	---	---	---	---	3.1E-03	---	---
U81	3.5E-06	---	---	---	---	---	---	---	5.7E-04	---	---

--- = None

[a] This column includes radionuclides, material types, mixed-activation products (MAP), and mixed-fission products (MAP).

[b] Refers to waste disposed of from 1971 through September 26, 1988.

[c] Refers to waste disposed of from September 27, 1988 through 2007.

Attachment IV
Pre-1971 Shaft Disposal Records for
Area G

This attachment summarizes the disposal records used to estimate the pre-1971 shaft inventories for the Area G inventory characterization update. Table IV-1 provides the date of disposal for each waste package, describes the waste, lists the radionuclide mass or activity associated with each package, and specifies the dimensions of the disposal shafts. Data are provided for waste that was placed in the shafts prior to 1971 and for which estimates of contaminant mass or volume were provided; some of the shafts were used for waste disposal after 1970. Table IV-2 lists the total volumes of waste placed in the shafts that were active prior to 1971. All data provided in the tables were taken from Rogers (1977).

Table III-1
Pre-1971 Shaft Disposal Records [a]

Shaft No.	Disposal Date	Waste Description	Radionuclide Content				
			MFP (Ci)	MAP (Ci)	Transuranics (g)	Tritium (Ci)	Uranium (g)
1	8/2/1966	Cell filters	1.0E+00	---	---	---	---
	8/10/1966	Irradiated Ta	---	---	3.0E+00	---	---
	8/15/1966	Cell trash	2.0E+00	---	---	---	---
	8/24/1966	Sr-90 waste	1.0E+00	---	---	---	---
	8/24/1966	Pu trash	1.0E+00	---	---	---	---
	8/25/1966	Irradiated Pu trash	2.5E+00	---	---	---	---
	9/14/1966	Np-237 foil	---	---	---	2.0E-01	---
	9/14/1966	Irradiated Pu	---	---	---	1.0E+00	---
	9/16/1966	Pu, Ce, Co waste	1.5E+00	---	---	---	---
	9/22/1966	Co-60	---	---	4.0E+00	---	---
	9/22/1966	Ce-137	---	---	5.0E-01	---	---
	9/27/1966	Irradiated Pu	1.5E+02	---	---	---	---
	10/7/1966	Cell waste	1.0E+00	---	---	---	---
	10/25/1966	Irradiated metal	---	1.0E+00	---	---	---
	10/27/1966	Irradiated metal	1.0E+00	---	---	---	---
	11/7/1966	Cell filter	1.0E+00	---	---	---	---

Source: Rogers, 1977

MFP = Mixed-fission product *MAP = Mixed-activation product* *--- = No data*

PTC = Plasma thermocouple *FP = Fission products* *OWREX = Omega West Reactor Experiment*

GETR = General Electric Test Reactor *SS = Stainless steel* *LAMPRE = Los Alamos Molten Plutonium Reactor Experiment*

[a] The table includes only those disposal records for which there were estimates of radionuclide mass or activity.

Table IV-1 (Continued)
Pre-1971 Shaft Disposal Records [a]

Shaft No.	Disposal Date	Waste Description	Radionuclide Content				
			MFP (Ci)	MAP (Ci)	Transuranics (g)	Tritium (Ci)	Uranium (g)
1 (Cont.)	11/8/1966	Irradiated Al	---	1.0E+00	---	---	---
	11/9/1966	H-3 waste	---	---	---	---	1.5E+02
	1/18/1967	Co-60 source	---	---	2.0E+00	---	---
	1/20/1967	U-235 metal	---	---	---	---	---
2	6/15/1966	Irradiated Pu cell waste	1.4E+01	---	---	---	---
	9/27/1966	Irradiated Pu cell waste	1.1E+03	---	---	---	---
	12/8/1966	Irradiated metal	1.0E+00	---	---	---	---
	12/20/1966	U-233 and U-235	---	---	---	---	---
	1/17/1967	PTC waste	6.1E+01	---	---	---	---
	1/18/1967	Co-60 waste	---	---	4.0E+00	---	---
	1/18/1967	Vacuum filter	2.5E+00	---		---	---
	1/19/1967	Irradiated metal	1.0E+00	---		---	---
	3/7/1967	Po-210 sources	---	---	1.0E-01	---	---
	3/10/1967	Co-60 source	---	---	4.5E+00	---	---
	4/14/1967	Co-60 sources	---	---	5.0E-01	---	---
	4/17/1967	U-235 and FP waste	1.0E+00	---	---	---	---
	5/15/1967	Co-57, La waste	---	1.0E+00	---	---	---

Source: Rogers, 1977

MFP = Mixed-fission product *MAP = Mixed-activation product* *--- = No data*

PTC = Plasma thermocouple *FP = Fission products* *OWREX = Omega West Reactor Experiment*

GETR = General Electric Test Reactor *SS = Stainless steel* *LAMPRE = Los Alamos Molten Plutonium Reactor Experiment*

[a] *The table includes only those disposal records for which there were estimates of radionuclide mass or activity.*

Table IV-1 (Continued)
Pre-1971 Shaft Disposal Records [a]

Shaft No.	Disposal Date	Waste Description	Radionuclide Content				
			MFP (Ci)	MAP (Ci)	Transuranics (g)	Tritium (Ci)	Uranium (g)
3	1/31/1967	Pu-contaminated Na	2.0E+02	---	---	---	---
	1/31/1967	Pu-contaminated Na	8.0E+00	---	---	---	---
	3/30/1967	Pu-239 contaminated squibbs	---	---	---	1.5E+02	---
	4/12/1967	Irradiated thermocouple	---	8.0E-01	---	---	---
	5/11/1967	Irradiated metal	2.0E+00	---	---	---	---
	8/15/1967	Irradiated Ta	---	---	5.0E-01	---	---
	8/23/1967	Cell waste - U-235 and FP	5.0E+00	---	---	---	---
	11/1/1967	D-38 and U-235	---	---	---	---	---
	11/9/1967	Irradiated metal	1.0E-02	---	---	---	---
4	4/5/1967	Control rods	---	6.0E+00	---	---	---
	6/7/1967	Pu and Ta cell trash	1.0E+00	---	---	---	---
	6/21/1967	Pu contaminated cell waste	1.0E+00	---	---	---	---
	7/19/1967	Co-60, Cs-137, U-233- and U-235 sources	1.0E+00	---	---	---	---
	7/26/1967	Pu, U, Cm, Np and Th sources	1.0E+00	---	---	---	---
	---	Pu-239	---	---	---	1.1E-01	---
	---	Pu-240	---	---	---	3.0E-03	---

Source: Rogers, 1977

MFP = Mixed-fission product *MAP = Mixed-activation product* *--- = No data*

PTC = Plasma thermocouple *FP = Fission products* *OWREX = Omega West Reactor Experiment*

GETR = General Electric Test Reactor *SS = Stainless steel* *LAMPRE = Los Alamos Molten Plutonium Reactor Experiment*

[a] The table includes only those disposal records for which there were estimates of radionuclide mass or activity.

Table IV-1 (Continued)
Pre-1971 Shaft Disposal Records [a]

Shaft No.	Disposal Date	Waste Description	Radionuclide Content				
			MFP (Ci)	MAP (Ci)	Transuranics (g)	Tritium (Ci)	Uranium (g)
4 (Cont.)	---	Pu-241	---	---	---	5.0E-05	---
	---	Np-237	---	---	---	6.0E-03	---
	---	Cm-244	---	---	---	2.9E-06	---
	---	U-233	---	---	---	---	---
	---	U-234	---	---	---	---	---
	---	U-236	---	---	---	---	---
	---	Th-230	---	---	---	---	---
	8/11/1967	Pu-239 contaminated U-235	---	---	---	---	---
	9/14/1967	End boxes	---	1.0E+00	---	---	---
5	8/7/1967	Cell trash	---	---	---	5.0E-01	---
	10/2/1967	U-235	---	---	---	---	---
	10/30/1967	Sample elements	1.0E+01	---	---	---	---
	10/37/67	Sample elements	1.0E+01	---	---	---	---
	11/1/1967	Sample elements	5.0E+00	---	---	---	---
	11/29/1967	U-235 contaminated BF3 chambers	---	---	---	---	---
	11/29/1967	Pu foils	---	---	---	1.0E-03	---

Source: Rogers, 1977

MFP = Mixed-fission product *MAP = Mixed-activation product* *--- = No data*

PTC = Plasma thermocouple *FP = Fission products* *OWREX = Omega West Reactor Experiment*

GETR = General Electric Test Reactor *SS = Stainless steel* *LAMPRE = Los Alamos Molten Plutonium Reactor Experiment*

[a] The table includes only those disposal records for which there were estimates of radionuclide mass or activity.

Table IV-1 (Continued)
Pre-1971 Shaft Disposal Records [a]

Shaft No.	Disposal Date	Waste Description	Radionuclide Content				
			MFP (Ci)	MAP (Ci)	Transuranics (g)	Tritium (Ci)	Uranium (g)
5 (Cont.)	12/11/1967	H-3 waste	---	---	---	---	1.0E-01
6	10/25/1967	U-235 samples	---	---	---	---	---
	1/18/1967	U-235 samples	---	---	---	---	---
	2/8/1968	H-3 trap	---	---	---	---	3.0E+02
7	5/6/1968	OWREX waste	1.0E+01	---	---	---	---
	5/8/1968	PTC waste	1.1E-02	---	---	---	---
	5/8/1968	PTC waste	9.0E+00	---	---	---	---
	5/8/1968	U-235, U-233, Pu-239, and Cf 252 sources	7.0E-02	---	---	3.0E-02	---
	5/23/1968	H-3 contaminated pump	---	---	---	---	5.2E+03
	7/15/1968	Fuel pins	---	---	---	---	---
	7/23/1968	Pu-238 foils	---	---	---	2.3E-03	---
8	7/1/1968	End boxes	---	1.0E+00	---	---	---
	8/13/1968	End boxes	---	1.0E+00	---	---	---
	9/12/1968	End boxes	---	1.0E+00	---	---	---
	11/25/1968	Th waste	---	---	---	---	---
9	12/31/1968	Irradiated Al and graphite	---	5.0E+00	---	---	---

Source: Rogers, 1977

MFP = Mixed-fission product *MAP = Mixed-activation product* *--- = No data*

PTC = Plasma thermocouple *FP = Fission products* *OWREX = Omega West Reactor Experiment*

GETR = General Electric Test Reactor *SS = Stainless steel* *LAMPRE = Los Alamos Molten Plutonium Reactor Experiment*

[a] *The table includes only those disposal records for which there were estimates of radionuclide mass or activity.*

Table IV-1 (Continued)
Pre-1971 Shaft Disposal Records [a]

Shaft No.	Disposal Date	Waste Description	Radionuclide Content				
			MFP (Ci)	MAP (Ci)	Transuranics (g)	Tritium (Ci)	Uranium (g)
9 (Cont.)	1/28/1969	Co-60, Cs-134, Cs-137, Eu-152, Pa-231, Zn-65, Pu-239, Pu-240, Pu-241, U-233, U-235, U-238 sources	6.1E-01	---	---	---	---
	---	Pu-239	---	---	---	8.3E-03	---
	---	Pu-240	---	---	---	5.8E-04	---
	---	Pu-241	---	---	---	2.0E-06	---
	---	U-233	---	---	---	---	---
	---	U-235	---	---	---	---	---
	---	U-236	---	---	---	---	---
10	3/27/1969	U-235 waste	---	---	---	---	---
	4/11/1969	Pu-239 cell waste	1.0E+00	---	---	---	---
	4/16/1969	U-235 contaminated chemicals	---	---	---	---	---
	5/20/1969	Pu-contaminated Ag	---	---	---	---	---
	---	Ag	---	---	---	---	---
	---	Ag 82%	---	---	---	---	---
	---	Ag 71.9%	---	---	---	---	---
11	4/21/1969	Pu, U sample vials	---	---	---	2.0E+00	---

Source: Rogers, 1977

MFP = Mixed-fission product *MAP = Mixed-activation product* *--- = No data*

PTC = Plasma thermocouple *FP = Fission products* *OWREX = Omega West Reactor Experiment*

GETR = General Electric Test Reactor *SS = Stainless steel* *LAMPRE = Los Alamos Molten Plutonium Reactor Experiment*

[a] *The table includes only those disposal records for which there were estimates of radionuclide mass or activity.*

Table IV-1 (Continued)
Pre-1971 Shaft Disposal Records [a]

Shaft No.	Disposal Date	Waste Description	Radionuclide Content				
			MFP (Ci)	MAP (Ci)	Transuranics (g)	Tritium (Ci)	Uranium (g)
11 (Cont.)	5/1/1969	Irradiated U-235 sample	---	---	---	---	---
	6/25/1969	U-235 residues	---	---	---	---	---
	7/1/1969	End boxes	---	1.0E+00	---	---	---
	7/2/1969	Rover waste	1.0E+00	---	---	---	---
	8/15/1969	Sample holders	---	1.0E+00	---	---	---
12	5/16/1969	U-235 residues	---	---	---	---	---
	6/16/1969	Pu cell waste	3.0E+01	---	---	---	---
	7/2/1969	Rover waste	1.0E+00	---	---	---	---
	8/20/1969	U-235 residues	---	---	---	---	---
	9/16/1967	Al sample holders	---	5.0E+00	---	---	---
	9/24/1969	H-3 waste	---	---	---	---	5.0E+00
	10/8/1969	H-3 containers	---	---	---	---	9.5E+00
	10/8/1969	H-3 cylinder	---	---	---	---	4.5E+00
	11/4/1969	Cm-243, Cm-244, Am-243	---	---	---	---	---
	---	Am-243	---	---	---	1.0E-01	---
	1/15/1970	End boxes	---	1.0E+00	---	---	---
	2/20/1970	Pu lab waste	---	---	---	1.0E-03	---

Source: Rogers, 1977

MFP = Mixed-fission product
MAP = Mixed-activation product
--- = No data
PTC = Plasma thermocouple
FP = Fission products
OWREX = Omega West Reactor Experiment
GETR = General Electric Test Reactor
SS = Stainless steel
LAMPRE = Los Alamos Molten Plutonium Reactor Experiment

[a] The table includes only those disposal records for which there were estimates of radionuclide mass or activity.

Table IV-1 (Continued)
Pre-1971 Shaft Disposal Records [a]

Shaft No.	Disposal Date	Waste Description	Radionuclide Content				
			MFP (Ci)	MAP (Ci)	Transuranics (g)	Tritium (Ci)	Uranium (g)
12 (Cont.)	2/26/1970	Lab waste	---	---	---	1.0E-02	---
	3/4/1970	Pu-240	---	---	---	1.5E-01	---
13	8/29/1969	Pu, H-3 contamination, U-235	---	---	---	---	---
	10/10/1969	U-235 residues	---	---	---	---	---
	1/20/1970	Pu-239 contaminated waste	3.1E-01	---	---	---	---
	1/20/1970	Irradiated SS	---	5.5E-01	---	---	---
	1/22/1970	Irradiated concrete and iron	---	3.0E-01	---	---	---
	1/22/1970	U-235 metallographic samples	2.0E+00	---	---	---	---
	1/26/1970	Pu-238 waste	---	---	---	2.5E-02	---
	1/27/1970	U-235 cell waste	---	---	---	---	---
	1/29/1970	Hot cell waste	2.0E+00	---	---	---	---
	1/30/1970	Pu-239 contaminated waste	2.8E+00	---	---	---	---
	2/2/1970	Pu-239 contaminated waste	---	---	---	7.0E+00	---
	2/2/1970	Irradiated U-235 fuel	---	---	---	---	---
	2/4/1970	End boxes	---	3.0E-01		---	---
	2/4/1970	Hot cell waste	5.7E+00	---	---	3.0E+00	---
	2/13/1970	Pu-contaminated waste	1.0E-02	---	---	---	---

Source: Rogers, 1977

MFP = Mixed-fission product *MAP = Mixed-activation product* *--- = No data*

PTC = Plasma thermocouple *FP = Fission products* *OWREX = Omega West Reactor Experiment*

GETR = General Electric Test Reactor *SS = Stainless steel* *LAMPRE = Los Alamos Molten Plutonium Reactor Experiment*

[a] *The table includes only those disposal records for which there were estimates of radionuclide mass or activity.*

Table IV-1 (Continued)
Pre-1971 Shaft Disposal Records [a]

Shaft No.	Disposal Date	Waste Description	Radionuclide Content				
			MFP (Ci)	MAP (Ci)	Transuranics (g)	Tritium (Ci)	Uranium (g)
13 (Cont.)	3/3/1970	Pu-239 contaminated trash	1.2E+01	---	---	---	---
	3/3/1970	Ra source	---	---	---	---	---
	3/5/1970	End boxes	---	1.0E-01	---	---	---
	3/9/1970	Metallographic samples	3.5E+00	---	---	4.0E+00	---
	3/18/1970	D-38 with H-3	---	---	---	---	8.7E-04
	3/18/1970	Hot cell waste	5.0E+00	---	---	---	---
	3/18/1970	Hot cell waste	8.0E+00	---	---	---	---
	3/19/1970	Hot cell waste	1.0E+00	---	---	---	---
	3/19/1970	Hot cell waste	3.0E+00	---	---	---	---
	5/7/1970	Co-60 source	---	---	2.2E+00	---	---
14	5/8/1968	Neut. acids and NaOH	5.3E-01	---	---	---	---
	5/8/1968	Neut. acids and NaOH	5.4E+00	---	---	---	---
	5/14/1968	U-235 solution in vermiculite	---	---	---	---	---
	11/13/1968	U-235 solution in vermiculite	---	---	---	---	---
	8/6/1969	U-235 precipitate in vermiculite	---	---	---	---	---
	9/10/1969	Neut. solution HCL and U-235	---	---	---	---	---
15	11/25/1969	H-3 in H_3PO_4	---	---	---	---	1.8E+04

Source: Rogers, 1977

MFP = Mixed-fission product *MAP = Mixed-activation product* *--- = No data*

PTC = Plasma thermocouple *FP = Fission products* *OWREX = Omega West Reactor Experiment*

GETR = General Electric Test Reactor *SS = Stainless steel* *LAMPRE = Los Alamos Molten Plutonium Reactor Experiment*

[a] *The table includes only those disposal records for which there were estimates of radionuclide mass or activity.*

Table IV-1 (Continued)
Pre-1971 Shaft Disposal Records [a]

Shaft No.	Disposal Date	Waste Description	Radionuclide Content				
			MFP (Ci)	MAP (Ci)	Transuranics (g)	Tritium (Ci)	Uranium (g)
15 (Cont.)	6/16/1970	Hot cell waste	4.0E+00	---	---	---	---
16	11/25/1969	H-3	---	---	---	---	1.8E+04
17	3/30/1970	H-3 pump	---	---	---	---	2.0E+04
	7/9/1970	Neut. acids	---	---	---	---	---
	7/10/1970	U-235 neut. acids	---	---	---	---	---
	8/13/1970	Ra-226 contaminated Pt	---	---	---	---	---
	9/28/1970	U-235 in Na	1.2E-01	---	---	---	---
	9/29/1970	U-235 in Na	4.0E+02	---	---	---	---
18	7/13/1970	Neut. Na	2.2E+01	---	---	---	---
	10/26/1970	Neut. Na	1.0E-01	---	---	---	---
	11/25/1970	Neut. Na	---	3.0E+01	---	---	---
24	9/3/1969	U-235 (52%)	---	---	---	---	---
	6/23/1970	Irradiated thermocouple	---	2.0E+00	---	---	---
	6/23/1970	U-235 residues	1.0E-01	---	---	---	---
	10/14/1970	End boxes	---	4.0E-01	---	---	---
	10/16/1970	Pu-contaminated metal	6.7E-02	---	---	---	---
25	9/29/1969	D-38 and U-235 (3%)	---	---	---	---	---

Source: Rogers, 1977

MFP = Mixed-fission product *MAP = Mixed-activation product* *--- = No data*

PTC = Plasma thermocouple *FP = Fission products* *OWREX = Omega West Reactor Experiment*

GETR = General Electric Test Reactor *SS = Stainless steel* *LAMPRE = Los Alamos Molten Plutonium Reactor Experiment*

[a] *The table includes only those disposal records for which there were estimates of radionuclide mass or activity.*

Table IV-1 (Continued)
Pre-1971 Shaft Disposal Records [a]

Shaft No.	Disposal Date	Waste Description	Radionuclide Content				
			MFP (Ci)	MAP (Ci)	Transuranics (g)	Tritium (Ci)	Uranium (g)
25 (Cont.)	12/8/1969	Pu-238 contaminated Pt	---	---	---	---	---
	1/6/1970	U-233 foil	---	---	---	---	---
	3/23/1970	Irradiated SS tube	---	5.0E+00	---	---	---
	3/25/1970	End boxes	---	2.4E-01	---	---	---
	4/1/1970	Fuel elements, U-235 and FP	1.0E+00	---	---	---	---
	4/1/1970	Fuel elements, U-235 and FP	2.5E+00	---	---	---	---
	4/6/1970	U-235 residues	---	---	---	---	---
	4/7/1970	Hot cell waste	3.5E+01	---	---	---	---
	6/10/1970	U residue	---	---	---	---	---
	6/23/1970	U-235 residues	1.0E-01	---	---	---	---
	11/25/1970	End boxes	---	4.5E-01	---	---	---
26	12/10/1969	U-235 fuel element chips	1.0E+00	---	---	---	---
	4/15/1970	U-235 and D-38	---	---	---	---	---
	4/29/1970	Na, Cs-137, Pu contaminated pipe	1.0E-02	---	---	---	---
	5/1/1970	Cs-137, Sr-90 sources and rat bones	1.0E-03	---	---	---	---
	5/4/1970	Hot cell waste	1.0E+00	---	---	---	---

Source: Rogers, 1977

MFP = Mixed-fission product *MAP = Mixed-activation product* *--- = No data*

PTC = Plasma thermocouple *FP = Fission products* *OWREX = Omega West Reactor Experiment*

GETR = General Electric Test Reactor *SS = Stainless steel* *LAMPRE = Los Alamos Molten Plutonium Reactor Experiment*

[a] The table includes only those disposal records for which there were estimates of radionuclide mass or activity.

Table IV-1 (Continued)
Pre-1971 Shaft Disposal Records [a]

Shaft No.	Disposal Date	Waste Description	Radionuclide Content				
			MFP (Ci)	MAP (Ci)	Transuranics (g)	Tritium (Ci)	Uranium (g)
26 (Cont.)	5/5/1970	Hot cell waste	1.5E-02	---	---	---	---
	5/6/1970	U-235 hot cell trash	5.0E-01	---	---	---	---
	6/12/1970	U-235 and Pu-242	1.2E-01	---	---	3.0E-02	---
	5/20/1970	Old sources	---	---	---	---	---
	6/2/1970	Sr-90 waste	1.0E-01	---	---	---	---
	6/23/1970	U-235 residues	---	---	---	---	---
	5/6/1970	Irradiated metal	1.0E-02	---	---	---	---
27	5/22/1970	U-235, Pu-239 reactor fuel	5.0E+00	---	---	3.4E+00	---
	5/22/1970	U, Pu, Co, Ce lab waste	2.0E-01	---	---	1.1E+01	---
	5/22/1970	Pu-239 hot cell waste	3.2E+01	---	---	---	---
	5/25/1970	Pu-239, U-235 hot cell waste	2.2E+01	---	---	5.8E+01	---
	5/27/1970	Pu-239 and FP	7.0E-01	---	---	1.0E+00	---
	6/1/1970	Manipulator booties	1.0E-01	---	---		---
	6/4/1970	Hot cell waste	3.5E+01	---	---	2.1E+01	---
	8/25/1970	End boxes		2.0E-01	---	---	---
28	6/23/1970	Hot cell waste	6.5E+01	---	---	---	---
	6/25/1970	Hot cell waste	7.9E+01	---	---	---	---

Source: Rogers, 1977

MFP = Mixed-fission product *MAP = Mixed-activation product* *--- = No data*

PTC = Plasma thermocouple *FP = Fission products* *OWREX = Omega West Reactor Experiment*

GETR = General Electric Test Reactor *SS = Stainless steel* *LAMPRE = Los Alamos Molten Plutonium Reactor Experiment*

[a] The table includes only those disposal records for which there were estimates of radionuclide mass or activity.

Table IV-1 (Continued)
Pre-1971 Shaft Disposal Records [a]

Shaft No.	Disposal Date	Waste Description	Radionuclide Content				
			MFP (Ci)	MAP (Ci)	Transuranics (g)	Tritium (Ci)	Uranium (g)
28 (Cont.)	7/1/1970	Irradiated sample holders	---	1.4E+01	---	---	---
	7/13/1970	GETR hardware	1.2E+02	---	---	---	---
	7/17/1970	U-235 residues	---	---	---	---	---
29	7/9/1970	Thermocouple waste	1.9E+01	---	---	---	---
	7/15/1970	U-235 thermocouple waste	2.5E+00	---	---	---	---
	7/22/1970	Pu-239 residue	2.0E-03	---	---	---	---
	7/29/1970	U-235 residues		---	---	---	---
	7/29/1970	U-235 cell filter (charcoal)	1.5E+00	---	---	---	---
	7/29/1970	U-235 hot cell waste	2.0E+00	---	---	---	---
30	7/28/1970	Pu-239 hot cell waste	4.1E+01	---	---	---	---
	8/24/1970	Irradiated SS pipe	---	1.0E-01	---	---	---
	9/8/1970	Pu-239 hot cell waste	2.0E+00	---	---	---	---
	9/8/1970	Pu-239 hot cell waste	4.5E+00	---	---	---	---
	9/15/1970	Pu-239 hot cell waste	2.4E+01	---	---	5.0E+00	---
	9/16/1970	Pu-239 hot cell waste	3.3E-01	---	---	5.3E-01	---
	10/13/1970	Irradiated Al	4.0E-01	---	---	---	---
	2/26/1970	End boxes	4.0E-01	---	---	---	---
31	9/24/1970	U-235 residues	---	---	---	---	---

Source: Rogers, 1977

MFP = Mixed-fission product
MAP = Mixed-activation product
--- = No data
PTC = Plasma thermocouple
FP = Fission products
OWREX = Omega West Reactor Experiment
GETR = General Electric Test Reactor
SS = Stainless steel
LAMPRE = Los Alamos Molten Plutonium Reactor Experiment

[a] *The table includes only those disposal records for which there were estimates of radionuclide mass or activity.*

Table IV-1 (Continued)
Pre-1971 Shaft Disposal Records [a]

Shaft No.	Disposal Date	Waste Description	Radionuclide Content				
			MFP (Ci)	MAP (Ci)	Transuranics (g)	Tritium (Ci)	Uranium (g)
31 (Cont.)	10/1/1970	U-235 and U-238 residue	---	---	---	---	---
	11/13/1970	U-235 residue and D-38	---	---	---	---	---
32	5/27/1970	LAMPRE-II lines and valves	---	---	---	1.0E-01	---
33	10/23/1970	Pu-239 hot cell waste	5.0E+00	---	---	---	---
	10/26/1970	Pu-239 hot cell waste	9.0E-01	---	---	---	---
	10/26/1970	Pu-239 hot cell waste	2.8E+00	---	---	---	---
	10/26/1970	Pu-239 metallographic samples	3.1E+01	---	---	2.5E+01	---
	10/28/1970	Pu-239 hot cell waste	2.2E+00	---	---	---	---
	10/30/1970	Pu-239 hot cell waste	1.3E+00	---	---	---	---
	11/2/1970	Pu-239 hot cell waste	4.0E+00	---	---	4.5E+01	---
	11/17/1970	Pu-238 lab waste	5.8E-02	---	---		---
	---	Pu-238	---	---	---	3.0E-01	---
	12/10/1970	Hot cell waste	1.3E+01	---	---	---	---
	12/10/1970	Pu-239 hot cell waste	5.0E+00	---	---	---	---
39	11/30/1970	Be and steel	---	2.0E-03	---	---	---
	12/28/1970	H-3 waste	---	---	---	---	5.7E+02

Source: Rogers, 1977

MFP = Mixed-fission product *MAP = Mixed-activation product* *--- = No data*

PTC = Plasma thermocouple *FP = Fission products* *OWREX = Omega West Reactor Experiment*

GETR = General Electric Test Reactor *SS = Stainless steel* *LAMPRE = Los Alamos Molten Plutonium Reactor Experiment*

[a] *The table includes only those disposal records for which there were estimates of radionuclide mass or activity.*

Table IV-2
Pre-1971 Shaft Waste Volumes

Shaft No.	Shaft Dimensions (diameter, depth in m)	Waste Volume (m^3)
1	6.1E-01, 7.6E+00	1.8E+00
2	6.1E-01, 7.6E+00	1.2E+00
3	6.1E-01, 7.6E+00	1.1E+00
4	6.1E-01, 7.6E+00	1.3E+00
5	6.1E-01, 7.6E+00	8.4E-01
6	6.1E-01, 7.6E+00	5.8E-01
7	6.1E-01, 7.6E+00	1.6E+00
8	6.1E-01, 7.6E+00	3.0E+00
9	6.1E-01, 7.6E+00	2.0E+00
10	6.1E-01, 7.6E+00	1.5E+00
11	9.1E-01, 7.6E+00	2.0E+00
12	9.1E-01, 7.6E+00	2.3E+00
13	9.1E-01, 7.6E+00	3.4E+00
14	3.0E-01, 7.6E+00	7.6E-01
15	3.0E-01, 7.6E+00	1.4E-01
16	3.0E-01, 7.6E+00	1.1E-01
17	3.0E-01, 7.6E+00	1.5E-01
18	3.0E-01, 7.6E+00	1.5E-01
24	3.0E-01, 7.6E+00	1.2E+00
25	6.1E-01, 7.6E+00	9.6E-01
26	6.1E-01, 7.6E+00	1.6E+00
27	6.1E-01, 7.6E+00	3.6E-01
28	6.1E-01, 7.6E+00	8.4E-01
29	6.1E-01, 7.6E+00	6.7E-01
30	6.1E-01, 7.6E+00	2.4E-01
31	6.1E-01, 7.6E+00	5.4E-01
32	6.1E-01, 7.6E+00	2.8E-01
33	6.1E-01, 7.6E+00	2.7E-01
34	1.8E+00, 1.8E+01	1.1E+01
36	9.1E-01, 1.2E+01	1.8E+00
37	9.1E-01, 1.2E+01	1.8E+00
38	9.1E-01, 1.2E+01	1.8E+00
39	1.8E+00, 1.8E+01	9.3E-01

Source: Rogers, 1977

References

Rogers, M.A., 1977, *History and Environmental Setting of LASL Near-Surface Land Disposal Facilities for Radioactive Wastes (Areas A, B, C, D, E, F, G, and T)*, Los Alamos Scientific Laboratory Report LA-6848-MN, Vol. 1, June.

Attachment V
Shaft-Specific Radionuclide, Activation Product, Fission Product, and Material Type Inventories for Area G

This attachment summarizes the unit-specific radionuclide inventories for the disposal shafts at Area G; the listed inventories address waste disposed of through 2007. The manner in which these inventories were estimated is discussed in the main report.

Table V-1
Shaft-Specific Radionuclide, Activation Product, Fission Product, and Material Type Inventories

	Waste Inventory by Disposal Shaft and Period of Disposal (Ci)											
	1	2	3	4	5	6	7	8	9	10	11	12
Constituent [a]	Pre-1971	Pre-1971	Pre-1971	Pre-1971	Pre-1971	Pre-1971	Pre-1971	Pre-1971	Pre-1971	Pre-1971	Pre-1971	Pre-1971
Am-243	---	---	---	---	---	---	---	---	---	---	---	2.0E-02
Cf-252	---	---	---	---	---	---	4.0E+00	---	---	---	---	---
Cm-244	---	---	---	2.3E-04	---	---	---	---	---	---	---	---
Co-60	6.0E+00	9.0E+00	---	5.0E-01	---	---	---	---	1.2E-01	---	---	---
Cs-137	---	---	---	5.0E-01	---	---	---	---	1.2E-01	---	---	---
D38	---	---	1.1E-05	---	---	---	---	---	---	---	---	---
Eu-152	---	---	---	---	---	---	---	---	1.2E-01	---	---	---
H-3	1.5E+02	---	---	---	1.0E-01	3.0E+02	5.2E+03	---	---	---	---	1.9E+01
MAP	2.0E+00	5.0E-01	8.0E-01	7.0E+00	---	---	---	3.0E+00	5.0E+00	---	2.0E+00	6.0E+00
MFP	1.6E+02	1.2E+03	2.2E+02	3.0E+00	2.5E+01	---	1.9E+01	---	---	1.0E+00	1.0E+00	3.1E+01
Np-237	1.4E-04	---	---	4.2E-06	---	---	---	---	---	---	---	---
Pu-238	---	---	---	---	---	---	3.9E-02	---	---	---	---	---
Pu-239	6.2E-02	---	9.1E+00	6.5E-03	3.1E-02	---	4.7E-04	---	5.1E-04	---	1.2E-01	6.8E-04
Pu-240	---	---	---	6.7E-04	---	---	---	---	1.3E-04	---	---	3.4E-02
Pu-241	---	---	---	5.2E-03	---	---	---	---	2.1E-04	---	---	---
Sr-90	1.0E+00	---	---	---	---	---	---	---	---	---	---	---
Th-230	---	---	---	5.7E-04	---	---	---	---	---	---	---	---
Th-232	---	---	---	---	---	---	---	1.7E-05	---	---	---	---
U-233	---	1.5E+00	---	3.1E-03	---	---	7.2E-05	---	1.3E-06	---	---	---
U-234	---	---	---	7.8E-06	---	---	---	---	---	---	---	---
U-235	5.5E-04	3.3E-04	5.0E-05	1.0E-03	1.1E-06	2.0E-03	5.0E-06	---	4.0E-08	2.8E-04	9.7E-04	1.4E-03
U-236	---	---	---	9.7E-08	---	---	---	---	2.1E-08	---	---	---

--- = None

[a] *This column includes radionuclides, material types, mixed activation products (MAP), and mixed fission products (MFP).*

Table V-1 (Continued)
Shaft-Specific Radionuclide, Activation Product, Fission Product, and Material Type Inventories

	Waste Inventory by Disposal Shaft and Period of Disposal (Ci)										
	13	14	15	16	17		18		19	20	21
Constituent [a]	Pre-1971	Pre-1971	Pre-1971	Pre-1971	Pre-1971	1971–1988 [b]	Pre-1971	1971–1988	1971–1988	1971–1988	1971–1988
Cf-252	---	---	---	---	---	---	---	---	---	---	9.5E-06
Co-60	2.2E+00	---	---	---	---	---	---	---	---	---	---
H-3	8.7E-04	---	1.8E+04	1.8E+04	2.0E+04	---	---	---	---	---	---
MAP	1.3E+00	---	---	---	---	---	3.0E+01	5.0E-02	---	---	---
MFP	4.5E+01	5.9E+00	4.0E+00	---	4.0E+02	7.7E-01	2.2E+01	3.7E+01	1.5E-01	3.2E-02	---
Pu-238	4.3E-01	---	---	---	---	---	---	2.4E-01	---	---	---
Pu-239	8.7E-01	---	---	---	---	1.9E-01	---	6.1E-07	---	---	---
Ra-226	1.0E-01	---	---	---	---	---	---	---	---	---	---
U-233	---	---	---	---	---	4.0E+00	---	---	---	---	---
U-235	2.3E-03	3.5E-05	---	---	6.3E-07	2.3E-05	---	---	2.3E-05	---	---
U-238	---	---	---	---	---	---	---	3.3E-04	---	---	---

--- = None

[a] This column includes radionuclides, material types, mixed activation products (MAP), and mixed fission products (MFP).

[b] Refers to waste disposed of from 1971 through September 26, 1988.

[c] Refers to waste disposed of from September 27, 1988 through 2007.

Table V-1 (Continued)
Shaft-Specific Radionuclide, Activation Product, Fission Product, and Material Type Inventories

Constituent [a]	Waste Inventory by Disposal Shaft and Period of Disposal (Ci)											
	22		23	24	25	26	27	28	29		30	
	1971–1988 [b]	1988–2007 [c]	1971–1988	Pre-1971	Pre-1971	Pre-1971	Pre-1971	Pre-1971	Pre-1971	1971–1988	Pre-1971	1971–1988
Am-241	---	5.0E-07	---	---	---	---	---	---	---	---	---	---
Ba-133	---	2.5E-04	---	---	---	---	---	---	---	---	---	---
C-14	---	2.7E-09	---	---	---	---	---	---	---	---	---	---
Co-60	4.9E+02	1.5E+00	5.2E+02	---	---	---	---	---	---	---	---	---
Cs-137	---	9.0E-04	4.2E+01	---	---	5.5E-03	---	---	---	---	---	---
D38	---	---	---	---	2.4E-05	2.4E-05	---	---	---	---	---	---
Eu-152	---	7.5E-09	---	---	---	---	---	---	---	---	---	---
Kr-85	---	1.0E-03	---	---	---	---	---	---	---	---	---	---
MAP	---	---	---	2.4E+00	5.7E+00	---	2.0E-01	1.4E+01	---	2.5E-02	1.0E-01	2.0E-01
MFP	---	---	---	1.7E-01	3.9E+01	2.7E+00	9.5E+01	2.6E+02	2.5E+01	---	7.2E+01	1.0E+01
Ni-63	---	3.0E-05	---	---	---	---	---	---	---	---	---	---
Pb-210	---	2.3E-09	---	---	---	---	---	---	---	---	---	---
Pu-239	---	4.1E-05	---	---	---	---	5.9E+00	---	---	---	3.4E-01	---
Pu-242	---	---	---	---	---	1.2E-04	---	---	---	---	---	---
Sr-90	---	7.3E-04	---	---	---	1.0E-01	---	---	---	---	---	---
Th-232	---	2.2E-06	---	---	---	---	---	---	---	---	---	---
U-233	---	---	---	---	1.9E-05	---	---	---	---	---	---	---
U-235	---	5.2E-05	---	1.1E-03	9.1E-04	4.4E-04	---	5.7E-04	6.1E-04	---	---	---
U-238	---	5.0E-07	---	---	---	---	---	---	---	---	---	---

--- = None

[a] This column includes radionuclides, material types, mixed activation products (MAP), and mixed fission products (MFP).

[b] Refers to waste disposed of from 1971 through September 26, 1988.

[c] Refers to waste disposed of from September 27, 1988 through 2007.

Table V-1 (Continued)
Shaft-Specific Radionuclide, Activation Product, Fission Product, and Material Type Inventories

Constituent [a]	Waste Inventory by Disposal Shaft and Period of Disposal (Ci)											
	31		32		33		35	36	38	39		40
	Pre-1971	1971–1988 [b]	Pre-1971	1971–1988	Pre-1971	1971–1988	1971–1988	1971–1988	1971–1988	Pre-1971	1971–1988	1971–1988
D38	1.9E-06	---	---	---	---	---	---	---	---	---	---	---
H-3	---	---	---	---	---	---	3.9E-02	---	---	5.7E+02	8.2E+03	---
MAP	---	---	---	5.6E-01	---	---	---	---	1.2E-02	2.0E-03	---	4.8E-01
MFP	1.0E-03	---	---	1.1E+00	6.4E+01	1.6E+01	3.5E+01	1.2E+02	---	---	---	2.0E+01
Pu-238	---	---	---	---	5.1E+00	---	---	---	---	---	---	---
Pu-239	6.2E-03	---	6.2E-03	9.1E-03	4.3E+00	9.6E-01	---	---	---	---	---	---
Th-232	---	---	---	1.0E-02	---	---	---	---	---	---	---	---
U-235	3.2E-04	---	---	2.4E-05	2.7E-05	1.7E-05	---	---	---	---	---	---
U-238	1.3E-06	4.3E+00	---	1.0E-04	---	---	---	---	---	---	---	5.4E-02

--- = None

[a] This column includes radionuclides, material types, mixed activation products (MAP), and mixed fission products (MFP).

[b] Refers to waste disposed of from 1971 through September 26, 1988.

[c] Refers to waste disposed of from September 27, 1988 through 2007.

Table V-1 (Continued)
Shaft-Specific Radionuclide, Activation Product, Fission Product, and Material Type Inventories

Constituent [a]	Waste Inventory by Disposal Shaft and Period of Disposal (Ci)											
	41	42	43	44	45	46	47	48	49	50	51	52
	1971–1988 [b]	1971–1988	1971–1988	1971–1988	1971–1988	1971–1988	1971–1988	1971–1988	1971–1988	1971–1988	1971–1988	1971–1988
Cf-252	---	---	---	---	5.4E+01	---	1.6E+00	---	---	---	4.7E-05	---
Co-60	---	---	---	---	---	---	---	---	---	---	---	1.5E-02
H-3	1.0E+01	---	7.0E+00	3.0E-03	3.7E-02	---	1.4E+00	---	---	2.9E+04	---	---
MAP	2.0E+01	4.4E-01	4.1E-01	---	2.0E+01	5.0E-01	1.0E-03	1.2E+01	1.0E+00	1.5E+01	1.1E-01	4.0E-02
MFP	---	1.2E+01	4.4E+00	4.0E+01	4.0E+01	1.8E+00	7.2E+00	7.7E+00	1.2E+00	1.5E-01	2.3E+02	1.5E+02
Pu-238	---	---	3.0E-04	---	---	5.4E-01	---	---	---	---	---	---
Pu-239	---	6.2E-02	2.5E-01	6.6E+00	4.1E+00	4.7E-02	3.2E-01	5.1E-01	6.7E-01	---	9.7E+00	3.4E+00
Pu-241	---	---	7.3E-01	---	---	---	---	---	---	---	---	---
U10	---	---	---	---	---	---	---	---	---	---	1.8E-05	---
U12	---	---	---	---	---	---	---	5.6E-05	5.6E-05	4.6E-02	---	---
U-232	---	---	---	---	---	---	---	---	---	---	---	2.1E-01
U-233	---	---	6.2E-05	---	---	---	---	---	---	---	---	---
U-234	---	---	---	---	---	---	---	---	---	---	---	---
U-235	2.2E-03	---	4.6E-04	2.4E-04	1.2E-04	---	1.5E-05	1.5E-05	---	---	1.7E-03	7.6E-05
U-236	---	---	---	---	---	---	---	---	---	---	2.5E-05	---
U-238	---	1.7E-05	9.8E-04	2.4E-04	8.2E-04	---	---	---	---	5.1E-05	1.0E-05	3.3E-04

--- = None

[a] This column includes radionuclides, material types, mixed activation products (MAP), and mixed fission products (MFP).

[b] Refers to waste disposed of from 1971 through September 26, 1988.

[c] Refers to waste disposed of from September 27, 1988 through 2007.

Table V-1 (Continued)
Shaft-Specific Radionuclide, Activation Product, Fission Product, and Material Type Inventories

	Waste Inventory by Disposal Shaft and Period of Disposal (Ci)											
	53	54	55	56	57	58	59	61	62	63	64	65
Constituent [a]	1971–1988 [b]	1971–1988	1971–1988	1971–1988	1971–1988	1971–1988	1971–1988	1971–1988	1971–1988	1971–1988	1971–1988	1971–1988
Am-241	---	3.4E-03	---	---	3.5E-02	---	---	---	---	---	---	---
Am-243	---	---	---	---	---	---	---	---	---	---	---	1.1E-05
Cm-244	---	---	---	---	---	---	---	---	---	---	---	2.3E-04
H-3	2.0E+00	---	---	---	---	---	2.3E+03	---	---	---	---	---
MAP	5.0E-04	---	---	---	1.2E-04	2.3E+02	---	---	---	---	---	2.4E-02
MFP	1.1E+02	1.9E+02	5.0E+01	1.1E+01	7.5E+00	2.8E+00	---	5.0E+00	---	---	---	1.6E+01
Pu-238	---	---	---	---	---	---	---	---	1.0E-03	---	2.0E-03	4.1E-03
Pu-239	1.8E+00	4.5E+00	1.0E+00	---	---	6.9E-02	---	6.1E-06	6.1E-08	---	2.0E-03	1.1E-03
Pu-242	---	---	---	---	---	---	---	---	---	---	---	3.1E-07
PU52	---	---	---	1.5E+01	---	---	---	---	---	---	---	---
Ra-226	---	3.6E-04	---	---	---	---	---	---	---	---	---	---
Th-232	---	---	---	---	---	---	---	4.7E-04	---	---	---	---
U12	---	---	---	---	---	---	---	---	---	1.9E-01	1.3E-02	---
U-233	1.9E-02	---	---	---	---	---	---	---	---	---	---	---
U-234	---	---	---	---	---	---	---	---	---	---	---	1.4E-06
U-235	2.8E-04	6.4E-04	1.3E-04	---	---	3.1E-04	---	---	---	5.0E-04	---	3.5E-04
U-238	5.7E-06	4.5E-04	3.0E-04	---	---	2.3E-03	---	---	---	1.0E-06	1.7E-04	2.1E-01
U81	---	---	---	---	---	---	---	---	---	1.8E-02	---	---

--- = None

[a] This column includes radionuclides, material types, mixed activation products (MAP), and mixed fission products (MFP).

[b] Refers to waste disposed of from 1971 through September 26, 1988.

[c] Refers to waste disposed of from September 27, 1988 through 2007.

Table V-1 (Continued)
Shaft-Specific Radionuclide, Activation Product, Fission Product, and Material Type Inventories

Constituent [a]	Waste Inventory by Disposal Shaft and Period of Disposal (Ci)											
	66	67	68	69	71	72	73	74	75	76	77	78
	1971–1988 [b]	1971–1988	1971–1988	1971–1988	1971–1988	1971–1988	1971–1988	1971–1988	1971–1988	1971–1988	1971–1988	1971–1988
Am-241	---	---	---	---	---	---	---	---	---	3.4E-08	---	---
Cf-252	---	---	---	---	---	---	---	---	---	2.7E-07	---	1.1E-06
Cm-244	---	---	---	---	---	---	---	---	3.0E-03	---	---	---
Co-60	---	---	---	---	---	1.0E+00	---	---	---	---	---	---
H-3	---	1.0E-02	---	---	---	1.0E-01	---	---	---	---	---	---
MAP	---	4.7E-04	8.3E-02	---	5.0E-01	4.0E-01	2.0E-01	1.3E+01	1.7E+00	1.4E+01	4.4E+01	2.0E-01
MFP	---	4.1E+01	1.0E+02	---	4.4E+01	4.6E+01	1.5E+02	1.5E+02	7.6E+01	1.1E+02	4.3E+02	4.5E+01
Np-237	---	---	---	---	---	---	---	---	---	7.0E-05	---	---
Pu-238	1.0E-03	---	---	---	1.0E-07	5.0E-03	---	---	---	---	---	---
Pu-239	---	2.7E+00	3.5E+00	---	3.8E+00	2.3E-01	1.3E+00	1.9E+00	1.4E+00	1.0E+01	6.5E-01	1.4E+00
PU52	---	---	---	---	3.8E+00	---	---	---	---	---	---	---
U10	---	---	---	---	---	---	---	---	---	---	---	3.0E-03
U12	---	---	---	2.0E-06	---	---	---	---	---	---	---	---
U-233	---	---	---	---	---	2.0E-03	---	---	---	---	---	---
U-234	---	---	---	---	---	---	---	---	---	4.3E-07	---	---
U-235	---	2.4E-05	3.8E-04	---	5.7E-05	4.6E-05	1.8E-04	3.3E-04	4.6E-05	5.8E-05	1.5E-04	1.7E-04
U-238	---	---	1.5E-06	---	---	---	---	---	---	8.0E-05	---	8.3E-04
U38	---	---	---	2.1E-03	---	7.6E-03	7.6E-03	2.0E-07	---	---	---	---
U81	---	---	---	---	---	---	---	1.5E-04	---	---	---	---

--- = None

[a] This column includes radionuclides, material types, mixed activation products (MAP), and mixed fission products (MFP).

[b] Refers to waste disposed of from 1971 through September 26, 1988.

[c] Refers to waste disposed of from September 27, 1988 through 2007.

Table V-1 (Continued)
Shaft-Specific Radionuclide, Activation Product, Fission Product, and Material Type Inventories

	Waste Inventory by Disposal Shaft and Period of Disposal (Ci)											
	79	80	81	82	83	84	85	86	87	88	89	90
Constituent [a]	1971–1988 [b]	1971–1988	1971–1988	1971–1988	1971–1988	1971–1988	1971–1988	1971–1988	1971–1988	1971–1988	1971–1988	1971–1988
C-14	---	1.0E-02	---	---	---	---	---	---	---	---	---	---
Cm-244	---	1.8E-01	---	---	---	---	---	---	---	---	---	---
Co-60	1.0E-03	2.9E-03	---	---	---	---	---	---	---	---	---	---
Cs-137	---	5.0E-03	---	---	---	---	---	---	---	---	---	---
H-3	---	---	---	---	5.0E-07	---	---	---	---	---	---	---
Kr-85	---	---	---	---	---	---	---	---	---	---	---	---
MAP	1.0E+01	---	---	---	---	---	---	2.0E-01	---	---	---	---
MFP	1.5E+02	---	---	1.4E+01	1.0E+01	4.4E+01	5.6E+01	1.0E+03	8.8E+01	3.8E+01	1.9E+01	3.5E+02
Np-237	---	---	---	---	7.1E-06	---	---	---	---	---	---	---
Pu-238	1.7E-01	---	3.0E-03	---	1.0E-03	---	---	---	1.0E-03	1.0E-04	1.1E-04	1.0E-04
Pu-239	2.5E+00	---	---	4.3E+00	6.7E+00	1.5E+00	1.9E+00	1.1E+00	6.3E-02	2.6E+00	1.6E-01	9.3E-02
PU52	2.1E+01	---	---	1.9E+01	---	9.7E+00	---	---	---	---	---	3.1E-01
Sr-90	4.9E-08	---	---	---	---	---	---	---	---	---	---	---
Th-88	---	3.3E-03	---	---	---	---	---	---	---	---	---	---
U12	---	---	---	---	---	---	---	6.7E-04	---	---	---	2.8E-03
U-233	---	---	---	---	9.7E-04	---	---	---	---	---	---	---
U-234	3.1E-06	---	---	---	---	---	---	---	---	---	---	---
U-235	2.3E-04	8.1E-06	---	4.0E-08	6.9E-04	1.5E-04	9.9E-05	1.6E-04	8.8E-06	2.8E-07	2.3E-05	1.3E-05
U-238	7.5E-04	9.3E-06	3.3E-05	3.3E-05	6.8E-05	---	---	---	---	---	---	---
U38	2.1E-02	---	---	---	---	---	---	3.9E-06	---	---	---	---

--- = None

[a] This column includes radionuclides, material types, mixed activation products (MAP), and mixed fission products (MFP).

[b] Refers to waste disposed of from 1971 through September 26, 1988.

[c] Refers to waste disposed of from September 27, 1988 through 2007.

Table V-1 (Continued)
Shaft-Specific Radionuclide, Activation Product, Fission Product, and Material Type Inventories

	Waste Inventory by Disposal Shaft and Period of Disposal (Ci)											
	91	92	93	94	95	96	97	99	100	101	102	103
Constituent [a]	1971–1988 [b]	1971–1988	1971–1988	1971–1988	1971–1988	1971–1988	1971–1988	1971–1988	1971–1988	1971–1988	1971–1988	1971–1988
Am-241	---	---	---	1.0E-04	---	---	1.0E-06	---	---	---	---	1.2E-05
C-14	---	---	---	---	---	---	---	---	---	---	---	5.0E-04
Co-60	---	---	1.0E-03	1.5E+02	---	---	1.0E+02	1.2E+01	---	---	3.3E+02	3.0E-06
Cs-137	---	---	---	2.0E-03	---	---	1.0E-04	---	---	---	1.0E-03	8.7E-08
H-3	---	---	1.0E-06	---	---	---	1.0E+01	---	---	---	---	---
MAP	---	3.3E+00	2.1E+01	3.4E+03	---	4.0E+00	2.5E-01	2.0E+00	3.7E+02	---	8.0E-01	5.2E+01
MFP	2.5E+01	3.6E+01	6.1E+02	4.4E+01	2.1E+02	2.5E-01	2.6E+01	---	---	1.2E+01	7.0E+00	---
Pu-238	2.0E-04	3.0E-05	6.0E-05	3.0E-05	7.5E-05	---	7.5E-05	2.1E-04	---	6.0E-05	1.5E-05	---
Pu-239	2.6E-04	3.0E-05	6.0E-05	3.0E-05	7.5E-05	---	1.1E-03	2.1E-04	---	6.0E-05	1.5E-05	---
PU52	7.3E+00	---	---	---	---	---	---	---	---	---	---	---
Ra-226	---	---	4.4E-05	---	---	---	2.0E-03	---	---	---	2.5E+00	---
Sr-90	---	---	---	5.0E-02	---	---	---	---	---	---	---	---
Th-232	---	3.7E-03	---	---	---	---	---	---	---	---	---	---
U12	---	5.4E-03	1.0E-01	---	---	---	---	---	---	---	6.0E-06	---
U-235	---	5.6E-02	---	---	---	1.0E-09	---	---	---	3.0E-05	3.6E-04	1.3E-03
U-238	2.2E-04	---	2.2E-02	---	---	1.0E-01	1.8E-03	2.0E-03	---	1.3E-04	---	3.3E-07

--- = None

[a] This column includes radionuclides, material types, mixed activation products (MAP), and mixed fission products (MFP).

[b] Refers to waste disposed of from 1971 through September 26, 1988.

[c] Refers to waste disposed of from September 27, 1988 through 2007.

Table V-1 (Continued)
Shaft-Specific Radionuclide, Activation Product, Fission Product, and Material Type Inventories

Constituent [a]	Waste Inventory by Disposal Shaft and Period of Disposal (Ci)											
	104	105	106	107	108	109	110	111	112	114	115	119
	1971–1988 [b]	1971–1988	1971–1988	1971–1988	1971–1988	1971–1988	1971–1988	1971–1988	1971–1988	1971–1988	1971–1988	1971–1988
Am-241	---	1.0E-03	---	---	---	---	---	---	---	---	---	---
C-14	1.1E-01	---	---	---	1.0E-03	---	---	1.0E-06	---	1.0E+00	---	---
Cf-252	---	---	---	---	---	---	---	---	5.6E-04	---	---	---
Cm-244	---	---	---	---	---	---	---	---	5.0E-05	---	---	---
Co-60	---	---	---	---	4.3E+02	---	---	---	---	---	---	---
Cs-137	---	---	---	---	---	---	1.1E-02	---	5.0E-06	---	---	---
H-3	---	---	---	1.0E-06	1.0E-03	---	1.0E-09	---	---	5.1E-01	4.0E-01	---
Kr-85	---	---	---	---	---	---	---	---	---	9.0E-05	---	---
MAP	---	---	---	---	---	5.0E-01	1.0E-09	2.5E+00	---	5.3E+02	---	---
MFP	---	---	9.4E+01	7.4E+02	---	2.0E+01	4.6E+02	5.5E+01	2.6E+02	---	---	---
Ni-63	---	---	---	---	---	---	---	---	---	3.2E-04	---	---
Pu-238	---	2.4E-04	6.0E-05	3.0E-05	1.5E-04	6.0E-05	6.0E-05	1.0E-04	6.0E-05	1.5E-05	---	---
Pu-239	---	2.4E-04	5.5E-05	3.0E-05	1.5E-04	6.0E-05	6.2E-02	1.1E-04	6.0E-05	1.5E-05	---	---
Ra-226	---	---	---	---	---	---	1.0E-04	---	---	---	---	---
Sr-90	---	---	1.0E-03	---	2.0E-03	---	---	---	4.2E-02	---	---	---
Th-232	---	---	---	---	---	---	---	---	---	---	6.5E-04	2.2E-04
Th-88	---	---	---	---	---	---	---	---	---	---	---	2.7E-06
U12	6.4E-02	---	---	---	---	---	---	---	---	---	---	8.0E-01
U-235	---	---	---	---	1.1E-05	---	8.8E-06	4.0E-06	2.1E-07	1.0E-09	---	1.8E-03
U-238	---	---	---	6.7E-04	---	---	6.7E-03	4.3E-03	2.4E-02	1.0E-03	5.2E-01	6.3E-01
U81	---	---	---	---	---	---	---	---	---	---	4.5E-03	---

--- = None

[a] This column includes radionuclides, material types, mixed activation products (MAP), and mixed fission products (MFP).

[b] Refers to waste disposed of from 1971 through September 26, 1988.

[c] Refers to waste disposed of from September 27, 1988 through 2007.

Table V-1 (Continued)
Shaft-Specific Radionuclide, Activation Product, Fission Product, and Material Type Inventories

	Waste Inventory by Disposal Shaft and Period of Disposal (Ci)											
	120	121	122	123	124		125	126	127	128	129	130
Constituent [a]	1971–1988 [b]	1971–1988	1971–1988	1971–1988	1971–1988	1988–2007 [c]	1971–1988	1971–1988	1971–1988	1971–1988	1971–1988	1971–1988
Am-241	2.6E-04	---	---	---	---	---	---	---	---	---	---	---
Co-60	---	---	2.3E+02	---	1.1E-02	---	---	5.1E-01	---	---	8.1E+01	---
Cs-137	1.5E-02	---	5.0E-03	---	---	---	---	---	---	---	---	---
H-3	1.3E+01	---	---	---	3.0E-07	---	---	---	---	---	---	---
Kr-85	3.6E-04	---	---	---	---	---	---	---	---	---	---	---
MAP	6.2E+02	---	2.0E+03	---	---	1.0E+00	1.1E+01	6.2E+02	---	---	1.4E+02	3.4E+01
MFP	---	---	3.5E+02	---	---	---	---	7.1E+01	---	---	2.2E+02	---
Ni-63	1.5E-07	---	---	---	---	---	---	---	---	---	---	---
Pu-238	---	1.0E-04	6.0E-05	---	---	---	---	---	---	1.7E-05	---	---
Pu-239	---	1.0E-04	7.3E-05	---	---	---	---	---	---	6.1E-08	---	5.8E-08
PU54	---	---	---	---	2.0E-08	---	---	---	---	---	---	---
Ra-226	5.1E-03	---	---	---	---	---	---	---	---	---	---	---
Sr-90	1.8E-04	---	---	---	---	---	---	---	---	---	---	---
Th-232	---	---	---	---	---	4.0E-04	---	---	---	---	---	---
Th-88	---	---	2.1E-06	---	---	---	7.6E-04	---	---	---	---	---
U12	---	---	---	6.4E-02	---	---	3.8E-01	---	---	---	---	---
U-235	---	3.0E-06	2.1E-06	---	---	1.0E-05	---	3.2E-12	---	---	---	9.1E-01
U-238	---	9.5E-05	4.0E-05	8.7E-01	---	---	5.7E-01	9.8E-02	1.3E+00	---	---	8.5E-01

--- = None

[a] This column includes radionuclides, material types, mixed activation products (MAP), and mixed fission products (MFP).

[b] Refers to waste disposed of from 1971 through September 26, 1988.

[c] Refers to waste disposed of from September 27, 1988 through 2007.

Table V-1 (Continued)
Shaft-Specific Radionuclide, Activation Product, Fission Product, and Material Type Inventories

Constituent [a]	Waste Inventory by Disposal Shaft and Period of Disposal (Ci)											
	131		132		133	134	136		137		139	
	1971–1988 [b]	1988–2007 [c]	1971–1988	1988–2007	1971–1988	1971–1988	1971–1988	1988–2007	1971–1988	1988–2007	1971–1988	1988–2007
Co-60	---	7.6E+01	---	---	2.2E+02	---	---	---	---	---	2.6E+02	6.0E-02
Cs-137	---	1.5E+01	---	---	---	---	---	---	---	---	---	---
Eu-152	---	1.9E-03	---	---	---	---	---	---	---	---	---	---
Eu-154	---	9.7E-02	---	---	---	---	---	---	---	---	---	---
H-3	---	---	---	---	---	---	3.7E+03	1.8E+03	1.5E+00	6.8E+01	---	---
MAP	1.9E+01	1.0E-02	---	---	3.1E+03	---	---	---	---	---	5.3E+02	2.0E+00
MFP	---	---	---	---	8.3E+01	2.5E+00	---	---	---	---	1.0E+01	5.8E+01
Nb-92	---	4.0E-03	---	---	---	---	---	---	---	---	---	---
Pu-238	---	---	---	1.0E-05	---	---	---	---	---	---	---	---
Pu-239	---	---	---	2.0E-09	---	---	---	---	---	---	---	---
Sn-126	---	2.4E-02	---	---	---	---	---	---	---	---	---	---
U-238	3.3E-07	---	4.3E-05	1.0E-09	---	---	---	---	---	---	---	---

--- = None

[a] This column includes radionuclides, material types, mixed activation products (MAP), and mixed fission products (MFP).

[b] Refers to waste disposed of from 1971 through September 26, 1988.

[c] Refers to waste disposed of from September 27, 1988 through 2007.

Table V-1 (Continued)
Shaft-Specific Radionuclide, Activation Product, Fission Product, and Material Type Inventories

Constituent [a]	Waste Inventory by Disposal Shaft and Period of Disposal (Ci)											
	140	141	142	143	144	147	148	149	150	151	152	153
	1971–1988 [b]	1988–2007 [c]	1988–2007	1988–2007	1988–2007	1988–2007	1988–2007	1988–2007	1971–1988	1971–1988	1971–1988	1971–1988
Ag-108m	---	---	---	---	4.9E-03	---	---	---	---	---	---	---
Am-241	---	---	---	6.7E-04	2.1E-03	6.0E-06	---	3.6E-04	---	---	---	---
Am-243	---	---	---	---	1.0E-09	---	---	---	---	---	---	---
Ba-133	---	---	---	---	---	1.3E-03	---	---	---	---	---	---
Bi-207	---	---	---	---	5.0E-05	---	---	---	---	---	---	---
Cf-252	---	---	---	---	2.7E-08	---	---	---	---	---	---	---
Cm-244	---	---	---	---	---	4.0E-09	---	---	---	---	---	---
Co-60	---	4.7E+01	4.1E+01	4.0E+01	1.2E+01	6.0E-02	---	6.3E-01	---	---	---	---
Cs-137	---	1.1E-02	---	---	1.8E-01	1.5E-05	---	---	---	1.0E-03	---	---
D38	---	---	---	---	2.9E-04	---	---	---	---	---	---	---
Eu-152	---	---	---	---	6.4E-05	5.5E-08	---	---	---	---	---	---
H-3	---	---	---	---	1.0E-09	3.2E-02	---	---	1.6E+05	1.4E+05	4.3E+04	2.6E+04
MAP	1.0E-03	1.7E+03	1.4E+02	1.2E+03	---	---	1.0E-07	5.5E+02	---	1.0E-03	---	---
MFP	---	2.1E+00	---	---	---	---	---	---	---	---	---	---
Ni-63	---	---	---	---	---	---	---	---	---	4.0E-03	---	---
Np-237	---	---	---	---	1.0E-09	---	---	---	---	---	---	---
Pu-238	---	---	---	6.7E-04	1.8E-02	---	---	3.6E-04	---	---	---	---
Pu-239	---	---	---	6.7E-04	8.8E-04	1.1E-06	2.2E-05	3.6E-04	---	---	---	---
Pu-240	---	---	---	---	9.3E-04	---	---	---	---	---	---	---
Pu-241	---	---	---	---	3.7E-02	---	---	---	---	---	---	---
Pu-242	---	---	---	---	1.0E-09	---	---	---	---	---	---	---

--- = None

[a] This column includes radionuclides, material types, mixed activation products (MAP), and mixed fission products (MFP).

[b] Refers to waste disposed of from 1971 through September 26, 1988.

[c] Refers to waste disposed of from September 27, 1988 through 2007.

Table V-1 (Continued)
Shaft-Specific Radionuclide, Activation Product, Fission Product, and Material Type Inventories

	Waste Inventory by Disposal Shaft and Period of Disposal (Ci)											
	140	141	142	143	144	147	148	149	150	151	152	153
Constituent [a]	1971–1988 [b]	1988–2007 [c]	1988–2007	1988–2007	1988–2007	1988–2007	1988–2007	1988–2007	1971–1988	1971–1988	1971–1988	1971–1988
PU52	---	---	---	---	---	---	---	---	---	5.4E-09	---	---
Ra-226	---	1.5E-05	---	---	5.0E-02	---	---	---	---	---	---	---
Sr-90	---	5.0E+00	---	---	5.6E+01	---	---	---	---	---	---	---
Th-232	---	---	---	---	1.0E-09	1.1E-05	---	---	---	---	---	---
U-233	---	---	---	---	---	1.6E-06	---	---	---	---	---	---
U-234	---	---	---	---	2.8E-07	1.4E-02	---	---	---	---	---	---
U-235	---	---	---	6.7E-04	1.0E-09	1.2E-04	---	3.6E-04	---	---	---	---
U-238	1.0E-06	---	9.5E-02	6.7E-04	1.0E-09	8.3E-02	---	3.6E-04	---	---	1.5E-05	---

--- = None

[a] This column includes radionuclides, material types, mixed activation products (MAP), and mixed fission products (MFP).

[b] Refers to waste disposed of from 1971 through September 26, 1988.

[c] Refers to waste disposed of from September 27, 1988 through 2007.

Table V-1 (Continued)
Shaft-Specific Radionuclide, Activation Product, Fission Product, and Material Type Inventories

Constituent [a]	Waste Inventory by Disposal Shaft and Period of Disposal (Ci)											
	154	155		156	157	158	159	160	161	162	163	164
	1971–1988 [b]	1971–1988	1988–2007 [c]	1971–1988	1971–1988	1988–2007	1988–2007	1988–2007	1988–2007	1988–2007	1988–2007	1988–2007
C-14	---	---	8.9E-03	---	---	---	---	---	---	---	---	---
H-3	3.2E+05	5.5E+03	5.7E+04	3.7E+04	2.4E+04	1.2E+04	8.6E+00	7.0E+02	4.6E+03	3.6E+05	4.8E+03	3.8E+03
Pu-239	---	---	---	---	---	---	---	---	---	---	4.6E-07	---
PU52	---	---	---	---	---	5.7E-02	---	---	---	---	---	---

--- = None

[a] This column includes radionuclides, material types, mixed activation products (MAP), and mixed fission products (MFP).

[b] Refers to waste disposed of from 1971 through September 26, 1988.

[c] Refers to waste disposed of from September 27, 1988 through 2007.

Table V-1 (Continued)
Shaft-Specific Radionuclide, Activation Product, Fission Product, and Material Type Inventories

	Waste Inventory by Disposal Shaft and Period of Disposal (Ci)											
	165	166	167	168	169	170	171	172	173	174	176	177
Constituent [a]	1988–2007 [c]	1988–2007	1988–2007	1988–2007	1988–2007	1988–2007	1988–2007	1988–2007	1988–2007	1988–2007	1988–2007	1988–2007
Am-241	---	---	---	---	---	---	---	2.3E-02	1.9E-08	1.0E-02	8.3E-03	2.8E-02
H-3	6.0E+03	1.5E+05	1.5E+05	9.5E+04	3.2E+03	9.4E+04	1.2E-03	---	---	---	---	---
Pu-238	---	---	---	---	---	---	---	3.8E-03	6.4E-09	6.8E-02	5.0E-02	1.1E-01
Pu-239	---	---	---	---	---	---	---	8.2E-03	1.7E-08	1.2E-02	1.3E-02	3.1E-02
U-235	---	---	---	---	---	---	---	6.0E-05	1.8E-07	2.1E-05	5.1E-06	4.2E-05
U-238	---	---	---	---	---	---	1.7E-05	2.0E-09	1.0E-06	---	---	3.8E-07

--- = None

[a] This column includes radionuclides, material types, mixed activation products (MAP), and mixed fission products (MFP).

[b] Refers to waste disposed of from 1971 through September 26, 1988.

[c] Refers to waste disposed of from September 27, 1988 through 2007.

Table V-1 (Continued)
Shaft-Specific Radionuclide, Activation Product, Fission Product, and Material Type Inventories

Constituent [a]	Waste Inventory by Disposal Shaft and Period of Disposal (Ci)										
	189	190	191	192	196	197	206	301	307	308	309
	1971–1988 [b]	1971–1988	1971–1988	1971–1988	1988–2007 [c]	1988–2007	1971–1988	1988–2007	1988–2007	1988–2007	1988–2007
Am-241	---	---	---	---	---	---	---	1.0E-05	---	---	1.0E-04
Ba-133	---	---	---	---	---	---	---	2.6E-06	---	---	---
Bi-207	---	---	---	---	---	---	---	4.0E-06	---	---	---
Cf-252	---	---	---	---	---	---	---	4.5E-08	---	---	---
Co-60	---	1.1E-05	---	---	1.6E+02	3.6E+02	---	1.2E+02	1.7E+02	---	---
Cs-135	---	---	---	---	---	4.5E-06	---	---	---	---	---
Cs-137	---	---	---	---	---	4.5E-01	---	6.7E+01	---	---	---
D38	---	---	---	---	---	4.4E-01	---	---	---	4.5E-07	---
Eu-152	---	---	---	---	---	---	---	3.4E-04	---	---	---
Eu-154	---	---	---	---	---	---	---	5.5E-10	---	---	---
H-3	---	---	---	---	---	---	---	---	---	---	5.3E+04
Ho-163	---	---	---	---	---	7.0E-02	---	---	---	---	---
MAP	1.0E+02	8.8E+02	1.4E+02	7.8E+02	2.0E+03	---	---	---	---	---	---
Pu-238	---	---	---	---	---	---	1.5E-05	---	---	---	---
Pu-239	---	---	---	---	---	---	1.5E-05	---	---	---	6.0E-04
Ra-226	---	---	---	---	---	---	---	5.5E-01	---	8.2E-09	---
Sr-90	---	---	---	---	---	---	---	1.9E-01	---	---	---
Th-228	---	---	---	---	---	---	---	---	---	1.3E-09	---
Th-229	---	---	---	---	---	---	---	5.4E-08	---	---	---
Th-232	---	---	---	---	---	1.1E-01	---	---	---	6.7E-02	---

--- = None

[a] This column includes radionuclides, material types, mixed activation products (MAP), and mixed fission products (MFP).

[b] Refers to waste disposed of from 1971 through September 26, 1988.

[c] Refers to waste disposed of from September 27, 1988 through 2007.

Table V-1 (Continued)
Shaft-Specific Radionuclide, Activation Product, Fission Product, and Material Type Inventories

	Waste Inventory by Disposal Shaft and Period of Disposal (Ci)										
	189	190	191	192	196	197	206	301	307	308	309
Constituent [a]	1971–1988 [b]	1971–1988	1971–1988	1971–1988	1988–2007 [c]	1988–2007	1971–1988	1988–2007	1988–2007	1988–2007	1988–2007
U-235	---	---	---	---	---	---	---	---	---	1.4E-09	1.1E-05
U-238	---	---	---	---	2.5E-02	---	---	---	---	8.9E-07	1.0E-03

--- = None

[a] This column includes radionuclides, material types, mixed activation products (MAP), and mixed fission products (MFP).

[b] Refers to waste disposed of from 1971 through September 26, 1988.

[c] Refers to waste disposed of from September 27, 1988 through 2007.

Table V-1 (Continued)
Shaft-Specific Radionuclide, Activation Product, Fission Product, and Material Type Inventories

Constituent [a]	Waste Inventory by Disposal Shaft and Period of Disposal (Ci)											
	311	313	315	317	319	321	323	325	327	329	331	333
	1988–2007 [c]	1988–2007	1988–2007	1988–2007	1988–2007	1988–2007	1988–2007	1988–2007	1988–2007	1988–2007	1988–2007	1988–2007
Ag-108m	---	---	---	2.0E-05	---	---	---	---	---	---	---	---
Am-241	---	---	1.1E-07	9.0E-05	---	3.0E-07	2.6E-07	9.4E-08	2.1E-06	---	3.3E-06	---
Ba-133	---	---	---	5.8E-06	---	5.1E-10	---	---	5.3E-06	---	---	---
C-14	---	---	---	9.1E-07	---	---	---	---	---	---	---	---
Cf-252	---	---	---	1.8E-06	---	---	---	---	---	---	---	---
Cl-36	---	---	---	1.0E-08	---	---	---	---	---	---	---	---
Co-60	---	6.1E-03	8.8E-01	6.2E+00	---	---	1.7E-02	---	1.4E-06	---	7.8E-03	---
Cs-137	---	---	7.1E-02	1.4E-01	---	4.0E-08	3.4E-08	---	---	---	---	---
D38	---	---	---	---	5.0E-02	---	3.8E-09	---	---	---	7.0E-05	---
Eu-152	---	---	---	1.0E-05	---	---	---	---	---	---	---	---
H-3	5.1E+04	4.6E+03	2.1E-04	2.1E+03	1.5E+05	1.6E+03	1.0E+03	---	9.6E+02	5.1E+03	1.6E+03	1.9E+05
I-129	---	---	---	3.0E-08	---	---	---	---	---	---	---	---
Kr-85	---	---	5.4E-03	---	---	---	---	---	---	---	---	---
Nb-91	---	9.4E-03	---	---	---	---	---	---	---	---	---	---
Nb-93m	---	---	---	2.2E+00	---	---	---	---	---	---	---	---
Nb-94	---	---	---	9.2E-07	---	---	---	---	---	---	---	---
Ni-59	---	---	---	2.0E-07	---	---	---	---	---	---	---	---
Ni-63	---	---	---	9.9E+00	---	---	---	---	---	---	---	---
Pa-231	---	---	---	2.7E-03	---	---	---	---	---	---	---	---
Pu-238	---	---	1.2E-04	2.0E-08	---	7.1E-05	2.1E-04	---	1.1E-03	---	1.2E-03	---

--- = None

[a] This column includes radionuclides, material types, mixed activation products (MAP), and mixed fission products (MFP).

[b] Refers to waste disposed of from 1971 through September 26, 1988.

[c] Refers to waste disposed of from September 27, 1988 through 2007.

Table V-1 (Continued)
Shaft-Specific Radionuclide, Activation Product, Fission Product, and Material Type Inventories

Constituent [a]	Waste Inventory by Disposal Shaft and Period of Disposal (Ci)											
	311	313	315	317	319	321	323	325	327	329	331	333
	1988–2007 [c]	1988–2007	1988–2007	1988–2007	1988–2007	1988–2007	1988–2007	1988–2007	1988–2007	1988–2007	1988–2007	1988–2007
Pu-239	---	---	1.5E-04	3.0E-07	---	6.5E-05	1.9E-04	3.1E-05	8.6E-04	---	9.1E-04	---
Ra-226	---	---	---	9.6E-03	---	---	---	---	---	---	---	---
Sr-90	---	8.0E-06	6.9E-02	1.0E-03	---	---	---	---	---	---	---	---
Tc-99	---	---	---	3.0E-08	---	---	---	---	---	---	---	---
Th-228	---	---	---	5.7E-08	---	---	---	---	---	---	---	---
Th-230	---	---	---	1.1E-08	---	---	---	---	---	---	---	---
Ti-44	---	---	2.0E-02	---	---	---	---	---	---	---	---	---
U-234	---	---	4.9E-01	---	---	---	---	---	---	---	---	---
U-235	---	3.8E-07	2.7E-02	---	---	4.1E-08	1.9E-08	---	8.5E-08	---	7.7E-08	---
U-238	4.4E-04	1.0E-05	2.2E-02	1.7E-05	---	1.0E-04	8.3E-07	---	6.1E-06	---	6.8E-03	---

--- = None

[a] This column includes radionuclides, material types, mixed activation products (MAP), and mixed fission products (MFP).

[b] Refers to waste disposed of from 1971 through September 26, 1988.

[c] Refers to waste disposed of from September 27, 1988 through 2007.

Table V-1 (Continued)
Shaft-Specific Radionuclide, Activation Product, Fission Product, and Material Type Inventories

	Waste Inventory by Disposal Shaft and Period of Disposal (Ci)											
	335	339	341	343	345	347	349	351	355	357	360	361
Constituent [a]	1988–2007 [c]	1988–2007	1988–2007	1988–2007	1988–2007	1988–2007	1988–2007	1988–2007	1988–2007	1988–2007	1988–2007	1988–2007
Ac-227	---	5.3E-07	---	---	---	---	---	---	---	---	---	---
Am-241	---	3.7E-08	7.2E-06	1.1E-06	9.3E-08	---	---	---	2.3E-07	5.6E-07	---	1.2E-06
Ba-133	---	6.6E-06	---	---	---	---	---	---	---	---	---	---
C-14	---	1.1E-06	---	7.6E-02	---	---	---	---	---	---	1.1E-02	1.7E-03
Cl-36	---	9.9E-09	---	---	---	---	---	---	---	---	---	---
Co-60	---	1.2E-02	---	1.5E-02	1.5E-04	8.4E-01	---	---	6.5E-01	1.8E+02	4.7E+02	7.3E+01
Cs-137	---	8.9E-04	---	---	---	---	---	---	2.4E-03	3.2E-01	---	---
D38	---	---	1.3E-02	1.6E-01	6.0E-02	---	---	4.8E-01	6.7E-01	5.6E-01	---	---
Eu-152	---	5.1E-07	---	---	---	---	---	---	---	---	---	---
Eu-154	---	1.2E-06	---	---	---	---	---	---	---	---	---	---
Gd-148	---	7.7E-09	---	---	---	---	---	---	---	---	---	---
H-3	2.3E+04	1.3E+05	3.9E+03	1.5E+03	2.4E+03	1.8E+03	1.2E+04	1.9E+04	1.6E+02	2.8E+02	---	---
Mo-93	---	---	---	---	---	---	---	---	---	---	5.1E-03	---
Ni-59	---	---	---	---	---	---	---	---	---	---	2.5E+00	
Ni-63	---	---	---	---	---	---	---	---	---	---	3.8E+02	7.6E+01
Pu-238	---	3.6E-11	2.6E-03	8.0E-04	---	---	---	---	3.4E-06	3.9E-04	---	---
Pu-239	---	5.2E-07	2.0E-03	7.2E-04	---	---	---	---	1.7E-07	9.6E-04	---	1.8E-06
Ra-226	---	1.7E-01	---	---	---	---	---	---	---	---	---	---
Sr-90	---	6.2E-03	---	---	---	---	---	---	---	3.2E-01	---	---
Tc-99	---	1.0E-08	---	---	---	---	---	---	---	---	---	---

--- = None

[a] This column includes radionuclides, material types, mixed activation products (MAP), and mixed fission products (MFP).

[b] Refers to waste disposed of from 1971 through September 26, 1988.

[c] Refers to waste disposed of from September 27, 1988 through 2007.

Table V-1 (Continued)
Shaft-Specific Radionuclide, Activation Product, Fission Product, and Material Type Inventories

	Waste Inventory by Disposal Shaft and Period of Disposal (Ci)											
	335	339	341	343	345	347	349	351	355	357	360	361
Constituent [a]	1988–2007 [c]	1988–2007	1988–2007	1988–2007	1988–2007	1988–2007	1988–2007	1988–2007	1988–2007	1988–2007	1988–2007	1988–2007
Th-228	---	1.5E-06	2.5E-05	---	---	---	---	---	---	---	---	---
Th-230	---	5.3E-09	---	---	---	---	---	---	---	---	---	---
Th-232	---	4.5E-07	4.8E-05	---	4.0E-08	---	---	---	---	---	---	---
U(NAT)	---	---	---	---	---	---	---	1.8E-01	---	---	---	---
U-233	---	5.8E-04	---	---	---	---	---	---	---	---	---	---
U-234	---	---	---	---	---	---	---	---	3.7E-08	2.0E-03	---	---
U-235	---	---	1.5E-07	6.3E-08	---	---	---	4.4E-07	3.5E-09	6.0E-05	---	---
U-236	---	---	---	---	---	---	---	---	---	3.8E-06	---	---
U-238	---	7.7E-06	1.0E-02	3.8E-06	5.0E-06	---	---	2.7E-05	2.0E-01	1.1E-06	---	---

--- = None

[a] This column includes radionuclides, material types, mixed activation products (MAP), and mixed fission products (MFP).

[b] Refers to waste disposed of from 1971 through September 26, 1988.

[c] Refers to waste disposed of from September 27, 1988 through 2007.

Table V-1 (Continued)
Shaft-Specific Radionuclide, Activation Product, Fission Product, and Material Type Inventories

	Waste Inventory by Disposal Shaft and Period of Disposal (Ci)								
	362	363	364	365	366	367	370	C13	C14
Constituent [a]	1988–2007 [c]	1988–2007	1988–2007	1988–2007	1988–2007	1988–2007	1988–2007	1988–2007	1988–2007
Ag-108m	---	---	---	---	4.4E+00	9.8E-05	---	---	9.0E-09
Am-241	1.2E-06	---	2.0E-06	---	---	2.4E-01	---	8.6E-05	1.5E-04
Am-243	---	---	---	---	---	---	---	1.0E-18	---
Ba-133	1.0E-03	---	1.0E-06	---	---	2.4E-04	---	---	---
Bi-207	---	---	1.6E-06	---	---	4.8E-06	---	---	---
C-14	9.1E-03	1.6E+01	7.4E-03	---	8.9E-05	4.4E-03	---	---	---
Cf-252	---	---	7.7E-06	---	---	---	---	---	---
Cl-36	1.9E-04	---	---	---	---	6.5E-05	---	---	---
Cm-244	---	---	2.0E-03	---	---	1.6E-04	---	---	---
Co-60	1.8E+02	1.1E+02	1.6E+02	7.9E+01	7.7E+02	1.7E+01	4.2E+00	---	3.1E-06
Cs-137	5.4E-02	---	2.2E-07	---	---	1.8E-01	---	2.6E-05	4.7E-09
D38	---	---	---	---	---	4.4E-05	---	---	---
Eu-152	8.1E-03	---	6.4E-04	---	---	4.0E-04	---	---	4.7E-08
Eu-154	1.1E-03	---	---	---	---	5.7E-05	---	---	---
H-3	4.6E-02	4.9E+04	1.3E+01	---	8.0E+03	5.5E+04	---	1.4E-02	3.6E-07
K-40	---	---	---	---	---	---	---	---	4.3E-07
Kr-85	---	---	---	---	---	2.5E-03	---	---	---
Mo-93	1.5E-03	1.1E-03	1.4E-03	7.5E-04	3.1E-03	1.5E-04	---	---	---
Nb-94	8.5E-05	---	---	---	---	4.4E-05	---	---	---
Ni-59	5.6E-02	---	---	---	---	3.3E-03	---	---	---
Ni-63	1.3E+02	9.6E+01	1.4E+02	6.9E+01	2.5E+02	1.2E+01	---	---	---
Np-237	---	---	---	---	---	---	---	1.0E-18	3.0E-08

--- = None

[a] This column includes radionuclides, material types, mixed activation products (MAP), and mixed fission products (MFP).

[b] Refers to waste disposed of from 1971 through September 26, 1988.

[c] Refers to waste disposed of from September 27, 1988 through 2007.

Table V-1 (Continued)
Shaft-Specific Radionuclide, Activation Product, Fission Product, and Material Type Inventories

	Waste Inventory by Disposal Shaft and Period of Disposal (Ci)								
	362	363	364	365	366	367	370	C13	C14
Constituent [a]	1988–2007 [c]	1988–2007	1988–2007	1988–2007	1988–2007	1988–2007	1988–2007	1988–2007	1988–2007
Pa-231	---	---	---	---	---	---	---	---	5.0E-08
Pb-210	---	---	---	---	---	---	---	---	2.6E-08
Pu-238	---	---	---	---	---	7.6E-04	---	7.4E-04	4.2E-04
Pu-239	1.7E-06	---	---	---	---	2.3E-03	---	2.7E-04	3.5E-04
Pu-240	---	---	---	---	---	8.6E-06	---	2.7E-04	---
Pu-242	---	---	---	---	---	2.0E-06	---	---	---
Ra-226	---	---	---	---	---	1.8E-05	---	---	3.0E-08
Sr-90	2.4E+01	---	---	---	---	6.5E-01	---	1.5E-05	---
Tc-99	1.2E-05	---	---	---	---	3.0E-08	---	---	---
Th-228	---	---	6.6E-04	---	---	---	---	---	---
Th-232	---	---	1.3E-02	---	---	---	---	1.0E-18	---
Th-88	---	---	---	---	---	---	---	---	---
U-232	---	---	---	---	---	2.0E-04	---	---	---
U-233	---	---	---	---	---	5.2E-07	---	---	---
U-235	---	---	9.3E-08	---	7.5E-06	4.1E-07	---	2.0E-07	1.1E-08
U-238	---	---	---	---	9.6E-05	1.8E-03	---	1.3E-06	4.3E-07

--- = None

[a] This column includes radionuclides, material types, mixed activation products (MAP), and mixed fission products (MFP).

[b] Refers to waste disposed of from 1971 through September 26, 1988.

[c] Refers to waste disposed of from September 27, 1988 through 2007.

LA-UR-08-06094

Approved for public release;
distribution is unlimited.

Title:	GoldSim Documentation and Data Selection for Los Alamos National Laboratory Technical Area 54, Area G Performance Assessment and Composite Analysis
Author(s):	Rob Shuman
Intended for:	U.S. Department of Energy

Form 836 (7/06)

Table of Contents

List of Figures v
List of Tables vi
List of Attachments vii
Acronyms and Abbreviations viii

1.0 Introduction 1
2.0 Model Description and Organization 3
2.1 GoldSim Modeling Basics 3
2.2 Human Exposure Pathways and Exposure Scenarios 5
2.2.1 Operational, Closure, and Active Institutional Control Periods 6
2.2.2 Passive Institutional Control Period 11
2.3 Model Organization 12
2.3.1 Area G Site Model 12
2.3.1.1 Input Data and Process Models 12
2.3.1.2 Physical Compartments—Off-Site Exposure Locations and Media 18
2.3.1.3 Physical Compartments—Disposal Facility 19
2.3.1.4 Model Documentation 21
2.3.2 Area G Intruder Model 21
2.3.2.1 Input Data and Process Models 23
2.3.2.2 Physical Compartments—Off-Site Media 25
2.3.2.3 Physical Compartments—Disposal Units 25
2.3.2.4 Model Documentation 26
2.3.3 Area G Intruder Diffusion Model 26
2.3.3.1 Input Data and Process Models 26
2.3.3.2 Physical Compartments—Off-Site Media 29
2.3.3.3 Physical Compartments—Disposal Facility 29
2.3.3.4 Model Documentation 29
2.3.4 Area G Inventory Model 30
2.3.4.1 Input Data and Process Models 30
2.3.4.2 Model Documentation 32
3.0 Modeling Approach 33
3.1 Inventory Modeling 37
3.2 Biotic Intrusion Modeling 37
3.2.1 Conceptual Model 38
3.2.2 Mathematical Model 44
3.2.2.1 Plant Intrusion 44
3.2.2.2 Animal Intrusion 51
3.3 Surface Erosion Modeling 56
3.3.1 Cover Loss 56
3.3.2 Sediment Transport 58
3.4 Human Intrusion Modeling 59
3.5 Diffusion Modeling 62
3.6 Exposure Modeling 65

3.6.1 Ingestion Exposure Route 65
3.6.2 Inhalation Exposure Route 69
3.6.3 Direct Radiation Exposure Route 69
3.7 Disposal System Configuration and Contaminant Flows 73
3.7.1 Disposal Facility Configuration and Contaminant Flows 73
3.7.2 Exposure Location and Off-Site Media Configuration and Contaminant Flows 79
3.7.3 Exposure Concentrations 83
3.7.3.1 Surface Soil, Cap, and Waste 83
3.7.3.2 Air 84
3.7.3.3 Crops 86
3.7.3.4 Animal Products 89
3.7.3.5 Groundwater 92
4.0 Input Parameter Requirements 93
5.0 Model Input Data Selection 170
5.1 Simulation Options 170
5.2 Facility Dimensions and Operations 171
5.2.1 Disposal Areas 171
5.2.2 Operational Period 174
5.2.3 Cover and Waste Configuration 175
5.2.4 Waste Emplacement Efficiency 191
5.2.5 Shaft Field Efficiency 191
5.3 Material Properties 193
5.3.1 Dry Bulk Density, Porosity, and Moisture Content 193
5.3.2 Partition Coefficients 195
5.3.3 Solubility Limits 198
5.3.4 Mass Attenuation Coefficients 199
5.3.5 Diffusion Coefficients 199
5.3.6 Radon Emanation Coefficient 205
5.3.7 Carbon-14 Gas Generation Rate 205
5.3.8 Carbon Dioxide and Methane Fractions 206
5.3.9 Organic Fraction of Carbon-14 Waste 206
5.4 Radionuclide Inventories 207
5.5 Atmospheric Transport Parameters 228
5.5.1 Dust Loading and Soil Disturbance Factor 229
5.5.2 Vertical Flux 230
5.5.3 Enhancement Factor 232
5.5.4 Dispersion Factor and Deposition Rate 234
5.6 Groundwater Transport Parameters 236
5.6.1 Area G Infiltration Rate 238
5.6.2 Contaminant Capture Fraction 238
5.6.3 Exposure Location Infiltration Rates 244
5.7 Sediment Transport Parameters 246
5.7.1 Sediment Allocation Fractions 246
5.7.2 Sediment Dispersal Fraction 253
5.7.3 Canyon Sediment Transport Rates 254

5.8 Food-Chain Transport Parameters 255
5.8.1 Crop Uptake Factor 255
5.8.2 Dry-to-Wet Weight Fraction 259
5.8.3 Translocation Factor 260
5.8.4 Agricultural Productivity 262
5.8.5 Growing Season 263
5.8.6 Plant Mass Loading Factor 265
5.8.7 Rainsplash Enhancement Factor 267
5.8.8 Plant Interception Fraction and Coefficient 268
5.8.9 Weathering Half-Life 269
5.8.10 Animal Product Transfer Factor 270
5.8.11 Animal Food, Water, and Soil Ingestion Rates 277
5.9 Biotic Intrusion Model Parameters 278
5.9.1 Time to Climax 279
5.9.2 Shape Factors 280
5.9.3 Maximum Rooting Depth 280
5.9.4 Aboveground Biomass Density 285
5.9.5 Litter Production Rate 294
5.9.6 Litter Decomposition Half-Life 298
5.9.7 Native Vegetation Plant Uptake Factor 300
5.9.8 Maximum Burrow Depth 303
5.9.9 Burrow Density 305
5.9.10 Harvester Ant Burrow Mass 309
5.9.11 Harvester Ant Colony Life Span 310
5.9.12 Pocket Gopher Soil Removal Rate 311
5.9.13 Mouse, Chipmunk, and Ground Squirrel Burrow Volume 311
5.9.14 Burrow Renewal Fraction 311
5.10 Erosion Model Parameters 312
5.10.1 Erosion Scenario 312
5.10.2 Cover Loss Functions 312
5.11 Exposure Pathway Parameters 312
5.11.1 Indoor and Outdoor Time Allotments 312
5.11.2 Excavation Occupancy Fraction 313
5.11.3 Soil Mixing Depth 313
5.11.4 Direct Radiation Shielding Factor 314
5.11.5 Inhalation Rate 314
5.11.6 Average Wind Speed 315
5.11.7 Atmospheric Mixing Height 315
5.11.8 Irrigation Rate and Fraction 315
5.11.9 Inadvertent Soil Ingestion Rate 316
5.11.10 Drinking Water Ingestion Rate 319
5.11.11 Indoor Water Usage Rate 320
5.11.12 Types of Animals Raised 320
5.11.13 Fraction of Diet Raised at Receptor Location 320
5.11.14 Crop Ingestion Rates 321

5.11.15 Animal Product Ingestion Rates 321
5.11.16 Animal Numbers 322
5.11.17 Receptor's Lot, House, and Well Dimensions 323
5.11.18 House Ventilation Rate 324
5.12 Miscellaneous Parameters 325
6.0 References 329

List of Figures

Figure 1 General Organization of the Area G Site Model 13
Figure 2 General Organization of the Area G Intruder Model 22
Figure 3 General Organization of the Area G Intruder Diffusion Model 27
Figure 4 General Organization of Area G Inventory Model 31
Figure 5 Waste Disposal Regions at Area G 34
Figure 6 Atmospheric Source Areas at Area G 36
Figure 7 Generalized Vegetative Zones of the Pajarito Plateau 40
Figure 8 Root Depth Distributions for Grasses, Forbs, and Shrubs 47
Figure 9 Root Mass Distributions for Plants with a Maximum Rooting Depth of 1.5 m 50
Figure 10 Burrow Depth Distributions for Animals with a Maximum Burrowing Depth of 3 m 55
Figure 11 Area G Sediment-Source Areas and Sediment Catchments in Habitable Canyons 60
Figure 12 Histograms of Initial Cover Depth Distribution for Waste Disposal Regions (1–6, 8) and Disposal Pits (15, 30, 31, 36–39) 176
Figure 13 Calculation of Proposed Shaft Field Area in Zone 4 192
Figure 14 Points of Maximum Exposure for Releases from Area G 237
Figure 15 Relationship between Canopy Cover and Herbage Yields 292

List of Tables

Table 1 Exposure Scenarios for the Operational, Closure, and Institutional Control Periods 8
Table 2 Elevations of Disposal Units and Depth to Regional Aquifer for the Eight Waste Disposal Regions 35
Table 3 Distribution of Small Mammals in Los Alamos County by Vegetation Overstory Type 42
Table 4 Burrow Depth Distributions for Area G Animal Species 53
Table 5 Input Data Requirements for the Area G Site Model 94
Table 6 Input Data Requirements for the Area G Intruder Model 118
Table 7 Input Data Requirements for the Area G Intruder Diffusion Model 137
Table 8 Input Data Requirements for the Area G Inventory Model 158
Table 9 Pits and Shafts Included in the Eight Waste Disposal Regions of Area G and the Region-Specific Disposal Areas 172
Table 10 Operational Periods for the Eight Waste Disposal Regions at Area G 175
Table 11 Pathway Parameter Values and Distributions Used in the Performance Assessment and Composite Analysis 178
Table 12 Distribution Coefficients and Solubility Limits 196
Table 13 Average Photon Energies and Mass Attenuation Coefficients 200
Table 14 Free-Air Diffusion Coefficients for Vapor- and Gas-Phase Radionuclides 203
Table 16 Measurement Uncertainty Factors Associated with Area G Radionuclide-Specific Inventories 212
Table 17 Radionuclide Activity Fractions for 1- to 5-Year-Old Mixed-Fission Product Waste Generated by Thermal Fission of U-235 and Pu-239 217
Table 18 Radionuclide Activity Fractions for 6- to 10-Year-Old Mixed-Fission Product Waste Generated by Thermal Fission of U-235 and Pu-239 219
Table 19 Material Type Mass Allocation Fractions for the Predominant Material Types Disposed of at Area G 220
Table 20 Point Estimates of the Mass and Activity Allocation Factors for the Predominant Material Types Disposed of at Area G 221
Table 21 Results of the Activity Fraction Evaluation for Material Type PU52 223
Table 22 Results of the Activity Fraction Evaluation for Material Type PU53 224
Table 23 Results of the Activity Fraction Evaluation for Material Type PU54 225
Table 24 Results of the Activity Fraction Evaluation for Material Type PU56 226
Table 25 Results of the Activity Fraction Evaluation for Material Type PU83 227
Table 26 Measured and Projected Flux Rates for Area G 239
Table 27 Contaminant Capture Fractions for the Area G Waste Disposal Regions 243
Table 28 Sediment Allocation Factors for the Catchment Areas in Cañada del Buey and Pajarito Canyon 247
Table 29 Sediment Allocation Fractions Averaged over Erosion Scenarios at Various Times after Facility Closure 248
Table 30 Sediment Allocation Fractions Averaged over Time after Facility Closure 251
Table 31 Size of Catchments in Cañada del Buey and Pajarito Canyon 253
Table 32 Parameter Values and Distributional Information for Plant Uptake Factors 256
Table 33 Dry-to-Wet Weight Fractions for Crops 261
Table 34 Time-to-Maturity Data for Representative Vegetables 264

Table of Contents (Continued)

Table 35 Summary of Plant Mass Loading 266
Table 36 Parameter Values and Distributional Information for Beef and Milk Transfer Factors 271
Table 37 Parameter Values and Distributions for Chicken and Egg Transfer Factors 274
Table 38 Literature-Based Rooting Depths for Grasses, Forbs, Shrubs, and Trees Growing at Los Alamos National Laboratory 282
Table 39 Measured, Estimated, and Literature-Based Plant Rooting Depths for Plants at Los Alamos National Laboratory 284
Table 40 Summary of Cover and Production Studies Used to Estimate Aboveground Biomass (early successional stages at Area G) 286
Table 41 Aboveground Production of Grasses, Forbs, and Shrubs (early successional stages of piñon-juniper cover types) 288
Table 42 Summary of Cover and Production Studies Used to Estimate Understory Biomass (Area G climax condition) 291
Table 43 Aboveground Production of Grasses, Forbs, and Shrubs in Mature Piñon-Juniper Woodlands 293
Table 44 Aboveground Biomass and Net Primary Productivity Estimates for Trees in Piñon-Juniper Woodlands 295
Table 45 Litter Decomposition Rate Constants 300
Table 46 Parameter Values and Distributional Information for Native Plant Uptake Factors 301
Table 47 Summary of Harvester Ant (*Pogonomyrmex* spp.) Colony Densities 306
Table 48 Small Mammal Densities at Area G and Background/Control Areas 307
Table 49 Summary of Harvester Ant Colony Lifetimes 310
Table 50 Water Needs of Crops 317
Table 51 Radionuclide Half-Lives and Dose Conversion Factors 326

List of Attachments

Attachment I Diffusion Model Optimization Analyses
Attachment II Development of Layer-Specific Inventories for the 1988–2004 Disposal Shafts
Attachment III Radiological Inventories for the Area G Performance Assessment and Composite Analysis
Attachment IV Plutonium Material Type Waste Spectral Data

Acronyms and Abbreviations

ACH	Air exchanges per hour
bgs	Below ground surface
CFR	Code of federal regulations
DOE	Department of Energy
EPA	U.S. Environmental Protection Agency
FEHM	Finite element heat and mass
IAEA	International Atomic Energy Agency
Laboratory	Los Alamos National Laboratory
LANL	Los Alamos National Laboratory
LLW	Low-level (radioactive) waste
MAP	Mixed-activation products
MDA	Material Disposal Area
MFP	Mixed-fission products
msl	Mean sea level
NCRP	National Council on Radiation Protection and Measurements
NRC	U.S. Nuclear Regulatory Commission
NTS	Nevada Test Site
ORNL	Oak Ridge National Laboratory
PDF	Portable document format
TA	Technical Area
TRU	Transuranic waste
USDA	US Department of Agriculture
WAC	Waste acceptance criteria

1.0 Introduction

U.S. Department of Energy (DOE) Order 435.1 (DOE, 2001a), as implemented by the *Radioactive Waste Management Manual*, (DOE, 2001b) requires that site-specific performance assessments and composite analyses be prepared for low-level radioactive waste (LLW) disposal facilities that accept waste after September 26, 1988. These assessments and analyses project the potential impacts of the buried waste on human health and safety, and are used to ensure that potential risks remain within acceptable levels. The performance assessment specifically addresses waste disposed of after September 26, 1988. The composite analysis accounts for all sources of radioactive material that may interact with a LLW disposal facility, and that contribute to any projected impacts on human health and safety.

Los Alamos National Laboratory (LANL or the Laboratory) generates radioactive waste as a result of various activities. The majority of this is LLW and is disposed of at Technical Area (TA) 54, Area G. Disposal operations began at this facility in 1957 and are projected to continue until 2044. The performance assessment and composite analysis for Area G were first issued in 1997 (Hollis et al., 1997) in compliance with DOE Order 5820.2A (DOE, 1988), the predecessor to DOE Order 435.1 (DOE, 2001a). These analyses are being revised and reissued to incorporate new knowledge about the Area G facility and site, and to update the modeling approaches used to project the long-term performance of the disposal facility.

The Area G performance assessment and composite analysis use a series of models that simulate radionuclide release, transport, and uptake in the vicinity of the disposal facility. These models have been integrated using the GoldSim™ modeling environment or platform (GoldSim, 2007a, 2007b, and 2007c); the result is four models designed to address different aspects of disposal facility performance:

- The *Area G Site Model*, which estimates the exposures received by members of the public at locations downgradient and downwind of Area G
- The *Area G Intruder Model*, which projects inadvertent intruder doses for all radionuclides except vapor- and gas-phase isotopes
- The *Area G Intruder Diffusion Model*, which addresses intruder exposures resulting from radionuclides that undergo diffusive release and transport
- The *Area G Inventory Model*, which estimates initial radionuclide inventories in the waste for input into the site and intruder models

The site model uses the initial radionuclide inventories projected by the inventory model to estimate radionuclide concentrations in various environmental media; these concentrations are used to calculate doses for exposed individuals, or receptors. The two intruder models are used to estimate exposures for persons who inadvertently intrude into the buried waste after active institutional control over the disposal site has ended; initial radionuclide inventories are also estimated using the inventory model.

This report documents the GoldSim models that were used to conduct the Area G performance assessment and composite analysis and the data that were used to implement the models. Section 2 provides a general overview of each model's structure and discusses how the various components of each model fit together. Section 3 describes the conceptual and mathematical models upon which the GoldSim models are based. Section 4 provides a complete tabulated listing of the input parameters required to implement the models. Finally, Section 5 discusses the data adopted for these parameters and how they were selected.

2.0 Model Description and Organization

A general description of the models used to conduct the Area G performance assessment and composite analysis is provided below. Insight into the GoldSim modeling environment is needed to understand how these models are organized and implemented; Section 2.1 provides information summarized from the user's guides for GoldSim (GoldSim, 2007a; 2007b) and the GoldSim contaminant transport module (GoldSim, 2007c) to address this need. The primary objective of the performance assessment and composite analysis modeling is to estimate potential exposures to persons, or receptors, exposed to contamination released from Area G. These receptors determine the transport processes, environmental media, and exposure pathways that must be addressed and thus dictate the overall structure of the models. Section 2.2 discusses the receptors included in the performance assessment and composite analysis. Finally, Section 2.3 describes the general layout of the models used to conduct the performance assessment and composite analysis.

2.1 GoldSim Modeling Basics

GoldSim represents the system being modeled using objects known as elements. These elements are used to input data into the model, perform calculations using defined inputs, and physically represent the system being modeled. To model a facility such as Area G, the species or radionuclides of interest are defined and their properties are specified. The physical components of the system (e.g., the disposal units, the atmosphere, and the regional aquifer) are represented using transport pathway elements. The system being modeled is reflected by the geometry of these transport pathway elements and the environmental media (e.g., soil, water, and air) that comprise the pathway elements. The transport pathway elements are connected to one another using mass-flux links, which define the rates at which radionuclides move from one physical compartment to another. The result is a dynamic simulation of the movement of radionuclides from the disposal units to locations that are accessible to human receptors. Contaminant concentrations projected for the various environmental media at these locations form the basis for calculating rates of radionuclide intake for the receptors and the consequent doses.

Two types of transport pathway elements are used in the Area G models, cells and external pathways. Cells are mathematically equivalent to mixing cells; contamination introduced into a cell is instantaneously and completely mixed throughout the element. A cell is defined in terms of the environmental media of which it is composed; distribution coefficients and solubility limits are used to partition radionuclides among these media. For example, cells are used in the Area G models to represent surface soils at the disposal site and at off-site exposure locations. The environmental media used to represent these soils typically include crushed tuff and water (present as soil moisture). These cells may also include the air occupying the pore space in the

soil. Distribution coefficients are used to partition radionuclides present in the surface soil among the crushed tuff and the soil moisture and, in the case of vapor- and gas-phase contaminants, the air in the pore spaces. Solubility limits may be used to place additional limits on the amount of contamination present in the soil moisture.

External pathways are modules that are linked to a GoldSim model as dynamic link libraries at the time the model is run. They are used to integrate specialized contaminant transport models, developed outside of GoldSim, with other GoldSim elements. External pathway elements are used in the Area G Site Model to simulate the groundwater transport of radionuclides from the disposal units to locations downgradient of the disposal facility. These elements accept as input the masses of radionuclides leached from the waste and transport this contamination vertically through the unsaturated zone until it reaches the regional aquifer. From that point, the contaminants are transported through the aquifer toward a domestic well downgradient of Area G. The projected quantities of radionuclides reaching the well are passed to GoldSim elements that use the information to project potential groundwater impacts.

Three types of links or transfers are used to represent the transport of contaminants between transport pathway elements. Advective mass-flux links are used to simulate the transport of contamination associated with the movement of environmental media. The media move at rates specified by the user; contaminants that are dissolved in, sorbed to, or otherwise associated with the media are transported in the process. Advective transport is normally associated with the movement of fluid such as water or air. However, it may also be used to simulate the transport of radionuclides associated with solids. For example, the GoldSim models use advective mass-flux links between cells to simulate the transport of soil by burrowing animals to the surface of the disposal facility; advective mass-flux links are also used to pass contamination to the external pathways and to receive the output from these elements.

Diffusive mass-flux links are used to transport contaminant mass through a stagnant or slowly moving fluid via the process of molecular diffusion. These links are commonly used to simulate transport between pathway elements that are not dominated by advective process. An example relevant to the Area G models includes the transport of vapor- and gas-phase radionuclides from the waste to the surface of the disposal facility.

Direct-transfer mass-flux links are used to directly move contaminant mass between transport pathway elements in situations where advective or diffusive flows are inappropriate. These links are used in the GoldSim models to simulate the uptake of radionuclides by plants growing in contaminated soils. In this instance, no fluid or solid passes from the source of contamination to the plant, and the diffusion process does not explain the contaminant transfer.

2.2 Human Exposure Pathways and Exposure Scenarios

The performance assessment and composite analysis are conducted to provide assurance that the performance objectives identified in DOE M 435.1-1 (DOE, 2001b) are satisfied. These performance objectives consist primarily of radiation dose limits for humans who are exposed to environmental media contaminated by releases from the waste disposal facility. As a result, Area G modeling efforts focused on the projection of doses to persons who may come into contact with, or otherwise be exposed to, radionuclides released from the disposal units.

Humans are exposed to radioactive media by means of different exposure pathways. Each exposure pathway includes a source or release from a source, a transport or exposure medium, a location at which the exposure occurs, and an exposure route. The actual exposure pathways that may lead to human exposures will depend upon the patterns of human activity at, and adjacent to, the disposal site. Patterns of human activity are specified using a collection of appropriate exposure pathways generally referred to as an exposure scenario.

The exposure pathways and scenarios through which people may be exposed to the radioactive waste at Area G are specific to different stages in the lifetime of the facility. Thus, to understand the basis for pathway and scenario development, it is necessary to understand these stages, which can be described as follows:

- *Operational period*, during which waste is placed in disposal pits and shafts, and interim or operational covers are placed over filled units
- *Closure period*, during which any remaining surface structures are removed from the site and all disposal units undergo final closure
- *Active institutional control period*, during which the DOE exercises control over the entire Laboratory
- *Passive institutional control period*, during which the DOE controls access to individual facilities such as Area G

The operational period is assumed to last through the year 2044. Although portions of the disposal facility will undergo final closure prior to 2044, closure of the final units receiving waste is assumed to be completed by the end of 2046. The 100-year active institutional control period starts at the end of final closure and is followed by the passive institutional control period in 2147.

It is assumed that the DOE will retain control over the entire Laboratory throughout the operational, closure, and active institutional control periods. During these periods, members of the public will be prevented from entering the disposal facility, the site will be maintained to slow the establishment of deep-rooted plants, and actions will be taken as necessary to repair any

significant damage to the cover. Although control over the entire Laboratory will cease at the end of the active institutional control period, it is assumed that the DOE will continue to exercise administrative control over individual sites such as Area G. This level of control will generally prevent people from entering the closed site; no other maintenance activities are assumed to occur during the passive institutional control period.

The level of control outlined above limits exposures during the operational, closure, and active institutional control periods to receptors who are located downwind or downgradient of the Laboratory; exposures may occur as radionuclides released from the disposal facility are transported by the prevailing winds, surface water, or groundwater to downwind or downgradient locations. The exposure pathways and scenarios modeled for these periods are discussed in Section 2.2.1. During the passive institutional control period, it is possible that potential receptors may move closer to the disposal area, perhaps as near as the Area G fence line. The possibility of inadvertent human intrusion into the facility is also considered. The exposure pathways and scenarios modeled for this period are discussed separately, in Section 2.2.2.

2.2.1 Operational, Closure, and Active Institutional Control Periods

The sources of contamination to which members of the public may be exposed will change as the site passes from the operational period to the active institutional control period. Although plants and animals may root or burrow into the buried waste and bring contamination to the surface of the disposal facility, the quantities of contamination deposited on the surface during the operational and closure periods will be small. In part, this is because the establishment of plant and animal communities at the site will be slowed, or even prevented, by ongoing operations and the closure process itself; also, any signs of significant intrusion into the waste will be remedied. The potential does exist, however, for radionuclides to be leached from the buried waste by water infiltrating through the site and for vapor- or gas-phase contaminants to diffuse from the waste and enter the atmosphere. Radioactivity leached from the waste may be transported to the regional aquifer and result in exposures to receptors downgradient of the site. Similarly, persons living downwind of Area G may be exposed to airborne contaminants transported off site by prevailing winds.

The steps taken to ensure proper facility functioning during the active institutional control period will not prevent plant roots and animal burrows from penetrating into the waste and depositing contamination on the surface. This contamination may be transported by surface runoff into the canyons adjacent to Area G; it may also be suspended and transported by the prevailing winds to locations downwind of the Laboratory. Contamination transported by surface runoff into Cañada del Buey, the drainage to the north of Area G, could expose members of the public to contamination during the active institutional control period because a portion of this canyon lies outside of the Laboratory boundary. Also, members of the public living outside the Laboratory

boundary may continue to be exposed to radionuclides discharged to the regional aquifer and to vapor- and gas-phase contaminants carried by the prevailing winds.

The exposure scenarios selected to estimate the exposures received by members of the general public are summarized in Table 1; these scenarios consider the sources of contamination discussed above. The Groundwater Resource Protection Scenario is implemented at a location 100 m (330 ft) downgradient of Area G; projected exposures are limited to the ingestion of contaminated groundwater and are used to assess compliance with groundwater protection standards. The scenario is implemented on restricted Laboratory lands because it is designed to ensure protection of the groundwater resource, regardless of whether members of the public can access the water.

The All Pathways–Groundwater Scenario is implemented at the Laboratory boundary near the town of White Rock. The receptor is assumed to receive exposures from the inhalation and ingestion of radioactivity, and from direct radiation. Radionuclides applied to the surface soil with irrigation water are suspended and inhaled by the individual during the time spent at home. Ingestion doses result from the consumption of crops irrigated with contaminated water, products from animals (e.g., beef and milk or chicken and eggs) raised by the resident, soil, and drinking water. Exposures to direct radiation from airborne contamination at the homestead and radioactivity deposited on the soil add to any internal (inhalation and ingestion) exposures.

The Atmospheric Scenario is implemented at the point of maximum atmospheric exposure outside of the Laboratory's boundaries (Table 1). The receptor inhales radioactive gases (except radon and its progeny) during the operational and closure periods; particulates resuspended from the surface of Area G and transported with the prevailing winds add to these exposures following closure. The deposition of airborne radionuclides contaminates crops grown by the individual and surface soils at the exposure location. Doses are received through the ingestion of contaminated vegetables, animal products, and soil. External exposures are received from contaminated soil surfaces and airborne radioactivity. Radon fluxes from the disposal site are projected separately.

The All Pathways–Cañada del Buey Scenario addresses exposures to receptors following the transport of contamination from Mesita del Buey to the canyon as a result of surface runoff and erosion. A person residing in the canyon is assumed to be exposed to radiation as a result of inhaling particulates suspended from contaminated soil surfaces and by ingesting contaminated crops, animal products, and soil. Exposures to direct radiation from airborne contamination at the homestead and radioactivity deposited over the resident's lot add to the internal exposures.

Table 1
Exposure Scenarios for the Operational, Closure, and Institutional Control Periods

Period and Exposure Scenario	Exposure Pathways and Routes	Receptor	Point of Exposure
Operational, Closure, and Active Institutional Control Periods			
Groundwater Resource Protection	Ingestion of drinking water	Member of the public	100 m downgradient of Area G
All Pathways—Groundwater	• Ingestion of drinking water • Ingestion of food crops irrigated with well water • Ingestion of animal products from animals raised by the receptor • Ingestion of contaminated soil • Inhalation of airborne radionuclides • Direct radiation from airborne radionuclides • Direct radiation from contaminated soils	Member of the public	LANL boundary near White Rock
Atmospheric	• Ingestion of food crops grown in contaminated soils and contaminated by airborne radionuclides • Ingestion of animal products from animals raised by the receptor • Ingestion of contaminated soil • Inhalation of airborne radionuclides • Direct radiation from airborne radionuclides • Direct radiation from contaminated soils	Member of the public	Point of maximum exposure outside of LANL boundary
All Pathways—Cañada del Buey	• Ingestion of food crops grown in contaminated soils • Ingestion of animal products from animals raised by the receptor • Ingestion of contaminated soil • Inhalation of airborne radionuclides • Direct radiation from airborne radionuclides • Direct radiation from contaminated soils	Member of the public	Cañada del Buey adjacent to Area G

Table 1 (Continued)
Exposure Scenarios for the Operational, Closure, and Institutional Control Periods

Period and Exposure Scenario	Exposure Pathways and Routes	Receptor	Point of Exposure
Passive Institutional Control Period			
Groundwater Resource Protection	Ingestion of drinking water	Member of the public	100 m downgradient of Area G
All Pathways—Groundwater	• Ingestion of drinking water • Ingestion of food crops irrigated with well water • Ingestion of animal products from animals raised by the receptor • Ingestion of contaminated soil • Inhalation of airborne radionuclides • Direct radiation from airborne radionuclides • Direct radiation from contaminated soils	Member of the public	100 m downgradient of Area G
Atmospheric	• Ingestion of food crops grown in contaminated soils and contaminated by airborne radionuclides • Ingestion of animal products from animals raised by the receptor • Ingestion of contaminated soil • Inhalation of airborne radionuclides • Direct radiation from airborne radionuclides • Direct radiation from contaminated soils	Member of the public	Point of maximum exposure outside of Area G boundary
All Pathways—Cañada del Buey	• Ingestion of food crops grown in contaminated soils • Ingestion of animal products from animals raised by the receptor • Ingestion of contaminated soil • Inhalation of airborne radionuclides • Direct radiation from airborne radionuclides • Direct radiation from contaminated soils	Member of the public	Cañada del Buey adjacent to Area G
All Pathways—Pajarito Canyon	• Ingestion of food crops grown in contaminated soils • Ingestion of animal products from animals raised by the receptor • Ingestion of contaminated soil • Inhalation of airborne radionuclides • Direct radiation from airborne radionuclides • Direct radiation from contaminated soils	Member of the public	Pajarito Canyon adjacent to Area G

Table 1 (Continued)
Exposure Scenarios for the Operational, Closure, and Institutional Control Periods

Period and Exposure Scenario	Exposure Pathways and Routes	Receptor	Point of Exposure
Passive Institutional Control Period (Continued)			
Intruder-Construction	• Inhalation of airborne radionuclides • Direct radiation from airborne radionuclides • Direct radiation from contaminated soils	Construction worker	Area G
Intruder-Agriculture	• Ingestion of food crops grown in contaminated soils • Ingestion of animal products from animals raised by the receptor • Ingestion of contaminated soil • Inhalation of airborne radionuclides • Direct radiation from airborne radionuclides • Direct radiation from contaminated soils	Agricultural intruder	Area G
Intruder–Post-Drilling	• Ingestion of food crops grown in contaminated soils • Ingestion of animal products from animals raised by the receptor • Ingestion of contaminated soil • Inhalation of airborne radionuclides • Direct radiation from airborne radionuclides • Direct radiation from contaminated soils	Post-drilling intruder	Area G

2.2.2 Passive Institutional Control Period

Radionuclide releases to groundwater and the atmosphere may continue after active institutional control has ceased and may result in exposures to the members of the public. Also, the change in the scope of DOE control will provide an opportunity for members of the public to locate immediately outside of the Area G fence line. Exposures to receptors during the passive institutional control period are projected using the exposure scenarios listed in the latter portion of Table 1. The two groundwater scenarios and the Atmospheric Scenario are functionally the same as those evaluated for the operational and active institutional control periods. The groundwater scenarios are implemented 100 m (330 ft) downgradient of Area G. The Atmospheric Scenario is implemented at the point of maximum exposure outside of the Area G fence line; radon fluxes from the disposal site are projected separately.

The All Pathways–Cañada del Buey Scenario for this period is the same as that evaluated during the active institutional control period. In addition, the loss of control over the entire Laboratory provides an opportunity for persons to reside in Pajarito Canyon, to the south of Area G. Potential exposures received by a person residing in this canyon are evaluated using the All Pathways–Pajarito Canyon Scenario. Contamination transported into the canyon with surface runoff and erosion is assumed to lead to exposures of the canyon resident via the same pathways described for the scenario in Cañada del Buey.

It is assumed that control over Area G during both active and passive institutional control periods will prevent members of the public from establishing residences over the closed pits and shafts. Nevertheless, brief lapses in custodial responsibilities after the active institutional control period may provide opportunities for inadvertent intruders to initiate on-site activities that result in exposures to radioactivity. Because these exposures may be substantial, inadvertent intruder analyses are conducted to establish concentration limits for the waste disposed of at Area G.

The performance assessment models potential exposures for the Intruder-Construction, Intruder-Agriculture, and Intruder–Post-Drilling Scenarios for the purpose of developing waste acceptance criteria (WAC) for Area G. Descriptions of these scenarios are included in the last portion of Table 1. Depending upon the scenario under consideration, exposures are received from the inhalation of airborne particulates and vapor- and gas-phase radionuclides (except radon) diffusing from the waste; the ingestion of contaminated crops, animal products, and soil; and external radiation from contaminated soils and airborne radionuclides. The primary source of contamination for the Intruder-Agriculture and Intruder–Post-Drilling Scenarios is waste brought to the surface during basement excavation and well drilling, respectively. Waste brought to the surface during basement excavation and contaminated material in the excavation itself is considered in the estimation of exposures for the Intruder-Construction Scenario. Contamination brought to the surface of the disposal facility as a result of biotic intrusion prior to the arrival of an intruder at the site may add to the intruder's exposures, as may vapor- and gas-phase radionuclides diffusing upward from the waste.

2.3 Model Organization

The Area G Site Model simulates the release and transport of radionuclides to the surface of the disposal facility and to off-site locations for all natural processes, and estimates doses for receptors at these locations. The two intruder models are used to project doses to persons who inadvertently intrude into the disposed waste after active institutional control has ended. The initial radionuclide inventories used in the three models are estimated using the inventory model. The site model is described in Section 2.3.1, followed by discussions of the intruder and intruder diffusion models in Sections 2.3.2 and 2.3.3. Section 2.3.4 describes the inventory model.

2.3.1 Area G Site Model

The general organization of the Area G Site Model is shown in Figure 1. The model is divided into three major segments. The first segment contains the elements that define the input data required to run model simulations and describe the process models used to estimate rates of radionuclide release and transport, contaminant uptake, and exposure. The second portion of the site model defines the physical compartments that are used to represent Area G and the surrounding environment. These compartments represent the disposal facility itself and the locations at which receptors are exposed to radioactive contamination. The third segment contains the model documentation.

Each of the major segments of the Area G Site Model consists of a series of GoldSim elements called containers (shown as open or closed yellow boxes in Figure 1). The containers are used to group related model input parameters, and to organize the process models, physical components, and model documentation. Within each container are the GoldSim elements that define the model; additional containers are used in many instances to further organize the model. The following sections, which describe the general layout of the different segments of the Area G Site Model, are organized in a manner consistent with Figure 1.

2.3.1.1 Input Data and Process Models

The input data and process models used in the Area G Site Model are found in this segment of the model. The input data characterize the system being modeled; the process models are used to calculate rates of contaminant transport between physical compartments and to project human exposures. The following discussion summarizes the contents of each of the containers shown in Figure 1, including input data and intermediate or calculated parameters. Complete definitions of the input parameters may be found in Section 4. The equations used to calculate intermediate parameters and to implement the process models are discussed in Section 3.

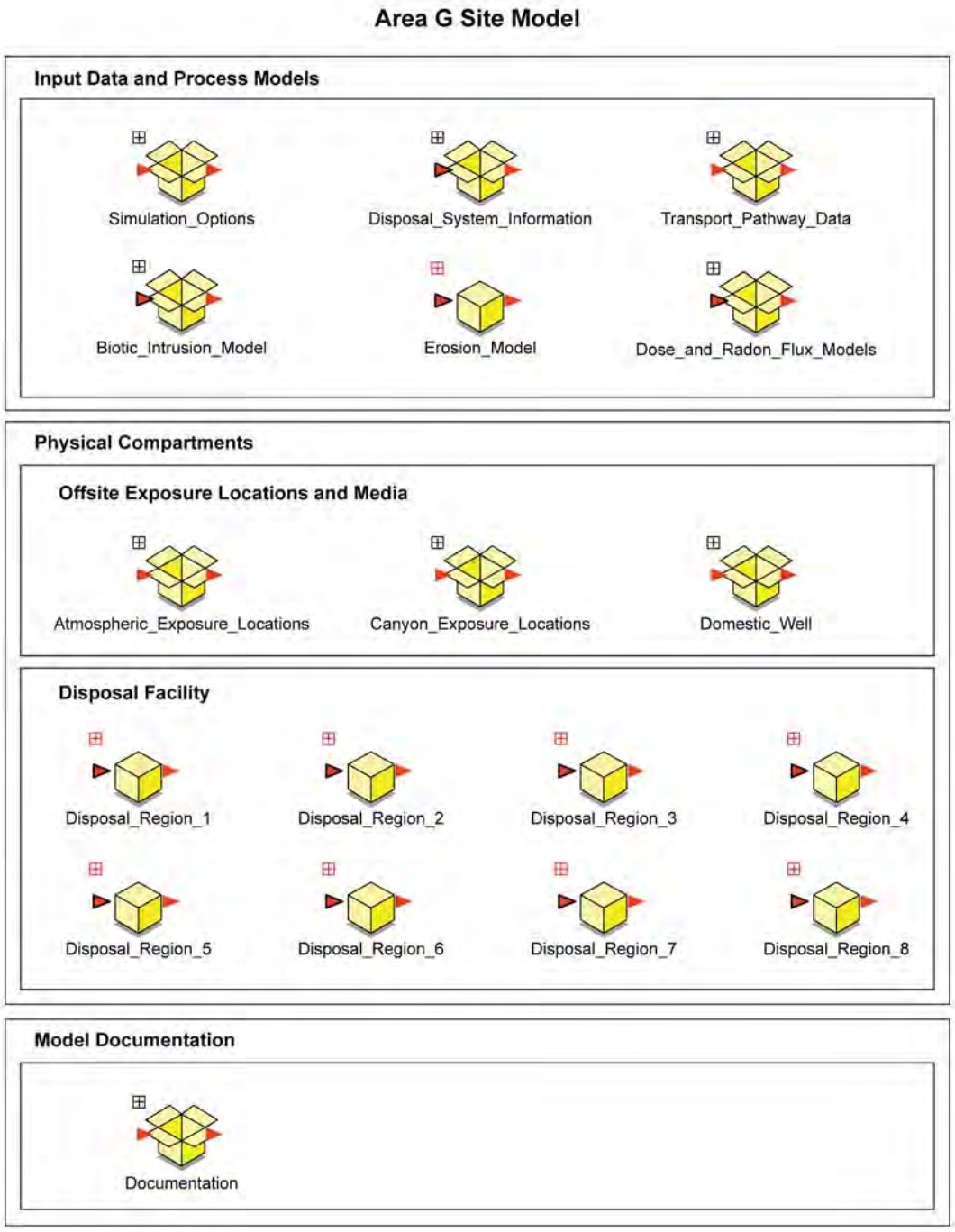

Figure 1
General Organization of the Area G Site Model

Simulation options. The Simulation_Options container includes flag variables used to control the simulation. The Analysis_Flag specifies which analysis is being conducted (i.e., the performance assessment or composite analysis). The primary distinction between the two analyses is the radioactive waste inventory used in the model simulations. The inventory corresponding to the waste disposed of after September 26, 1988 is used if the performance assessment option is selected, while waste disposed of since Area G opened is included in the composite analysis. The Diffusion_Flag indicates whether or not vapor- and gas-phase diffusion is to be included in the modeling.

Disposal system information. The Disposal_System_Information container includes data that characterize the radionuclides in the waste, the environmental media comprising the physical compartments, the disposal facility, and the waste inventory. Within this container are found the Species_and_Materials, Site_Geometry_and_Operations, and Inventory containers. The following elements are found within the Species_and_Materials container:

- A data element that specifies the half-lives of the radionuclides included in the simulation.
- A Species element that defines the element, atomic weight, and decay characteristics for each radionuclide included in the modeling.
- A Material_Properties container that organizes information about the environmental media that are used in the model. This information includes effective porosities, moisture contents, dry and bulk densities, partition coefficients, relative diffusivities, the density of water, solubility coefficients, elements defining carbon and hydrogen contents in soil and water, and elements used to model the generation of C-14 gas and the diffusion of vapor- and gas-phase contaminants.
- The environmental media (i.e., crushed tuff, waste, water, and air) that are used to define cell pathways.

As implied by its name, the Site_Geometry_and_Operations container organizes the parameters that specify key physical dimensions of the disposal units and important operational aspects of Area G. For reasons discussed in detail in Section 3, the disposal facility is divided into eight waste disposal regions. These regions are defined on the basis of the geohydrologic properties of the underlying unsaturated zone and the depths at which waste has been disposed of in the pits and shafts.

Many of the parameters included in the Site_Geometry_and_Operations container are specific to the waste disposal regions. One example is the times at which waste disposal start and stop for the eight regions. The times of disposal are used to calculate periods of disposal for the eight

regions and are used in conjunction with the closure period to estimate the total operational period for the facility. The Site_Geometry_and_Operations container holds nine additional containers; the Layer_Information container includes information used to divide the cover and waste into a series of discrete layers. The other eight disposal region-specific containers organize information about the area of each region and the initial thickness of the surface soil, cover, and waste layers.

The Inventory container includes the elements that access the initial radionuclide inventories projected by the Area G Inventory Model. Separate elements are used to define the performance assessment and composite analysis inventories; the inventory used in a given simulation is determined based on the Analysis_Flag setting.

Transport pathway data. The Transport_Pathway_Data container includes input data and calculated quantities needed to model rates of radionuclide transport. These parameters are organized in four containers labeled Atmospheric_Transport, Foodchain_Transport, Groundwater_Transport, and Sediment_Transport. The input data in the Atmospheric_Transport container characterize dust loading, particulate resuspension, wind speed at the facility, and the atmospheric mixing height; the dispersion factors and particulate deposition rates used to estimate radionuclide concentrations for the Atmospheric_Scenario receptor are included in a series of containers. The data within these containers are organized with respect to the location of the receptor.

The Foodchain_Transport container includes the input data required to estimate the rates of radionuclide uptake for crops raised by the receptors and to estimate radionuclide concentrations in animal products. The crop and animal data are organized in two containers, Plant_Data and Animal_Data. The Plant_Data container is subdivided into the Uptake_Factors and Crop_Characteristics containers. The former includes the plant-to-soil concentration factors for the crops raised by the receptors, including leafy vegetables, produce, grain, and pasture grass. Input data describing the crops are found in the Crop_Characteristics container. These parameters include dry-to-wet-weight conversion factors, translocation factors, agricultural productivities, lengths of growing seasons, and mass-loading factors. The plant interception coefficient, weathering half-life, particle size factor, and plant hydrogen and carbon fractions are also found in the container. Calculated quantities include the plant interception fractions, the weathering constant, and the areas needed to grow crops.

The Animal_Data container, located within the Foodchain_Transport container, includes data that are used to estimate radionuclide concentrations in beef, milk, chicken, and eggs. The Animal_Ingestion_Data container specifies soil, water, and forage ingestion rates for cattle, milk cows, and chickens. The Transfer_Factors container includes the transfer factors needed to

estimate radionuclide concentrations in animal products based on contaminant concentrations in the soil, water, and forage consumed by cattle, cows, and chickens.

The Groundwater_Transport container includes the input data and intermediate parameters needed to model groundwater flow in the unsaturated and saturated zones. The input data include natural rates of infiltration on Mesita del Buey, in the adjacent canyons, and at receptor locations east of Area G. The contaminant capture fraction is also included. The Flowfield element is used to structure the groundwater transport modeling.

The Sediment_Transport container includes information that is used to determine radionuclide concentrations in canyon soils, following the transport of sediments from the mesa top. The data elements specify how sediment transported from the mesa is partitioned among several catchments in Cañada del Buey and Pajarito Canyon, the areas of these catchments, the fraction of each catchment over which sediments spread upon reaching the canyon floor, and the rates of sediment transport between catchments.

Biotic intrusion model. The Biotic_Intrusion_Model container includes the input data and models used to estimate rates of radionuclide transport to the surface of Area G following penetration of the buried waste by plant roots and burrowing animals. The impacts of plants and animals change over time as the disposal site undergoes ecological succession from the grassland-dominated landscape shortly after final closure to piñon-juniper woodland. The Eco_Succession_Model container estimates the fraction of the climax condition achieved as a function of time using the user-specified Time_of_Climax parameter. The Shape_Parameters container includes coefficients that are used to estimate plant root and animal burrow distributions with depth.

The data and models used to estimate the impacts of animal intrusion on the buried waste are found in the Animal_Intrusion_Model container. The impacts of four species or categories of burrowing animals are simulated; these categories include harvester ants, pocket gophers, mice, and chipmunks and ground squirrels. The models and data used for each species or group of animals are found in their respective containers. The input data required to model the effects of intrusion are specific to the animal under consideration but include parameters such as maximum burrow depths; burrow densities, volumes, and/or masses; and burrow renewal rates. This information is used with burrow distribution functions to determine rates of soil and soil moisture transport for each animal species or group, within each waste disposal region. This taxa-specific information is used in the Animal_Soil_Transport and Animal_Water_Transport containers to determine overall soil and soil moisture transport rates for the eight waste disposal regions.

The input data and models used to simulate the intrusion of plants into the buried waste are found in the Plant_Intrusion_Model container. The impacts of plant intrusion are simulated for four plant-growth forms—grasses, forbs, shrubs, and trees. The models and data used for each growth form are found in their respective containers within the Plant_Intrusion_Model container. The data required to model the effects of plants include maximum rooting depths, aboveground biomass densities for early succession and climax conditions, litter production fractions, and plant concentration factors. These data are used in conjunction with functions that describe root distribution with depth to estimate rates of plant litter production within each waste disposal region. Litter production rates across all growth forms are calculated in the Total_Plant_Litter_Production container; they are used in the Plant_Uptake container to estimate the quantities of contamination assimilated by plants for the various waste disposal regions. The Litter_Halflife and Litter_Decay_Constant elements are used to model the incorporation of contaminated plant litter into the surface soil.

Erosion model. The Erosion_Model container includes the data and models used to estimate rates of soil loss across the closed disposal facility. The erosion rate functions are defined using a variety of elements found in the Erosion_Rates container. Included here is the Erosion_Scenario element, which specifies the conditions under which erosion is assumed to occur, and eight containers, each of which defines the rate of cover loss for a specific waste disposal region. The elements in these containers are used to define the total amount of material that has been lost due to erosion and an annual erosion rate. The results of the calculations conducted within the Erosion_Rates container are used to update the cap and waste layer thicknesses and cumulative depths to the bottoms of these layers throughout the model simulations. These calculations are organized in a series of waste-disposal-region-specific containers.

Dose and radon flux models. The Dose_and_Radon_Flux_Models container organizes the input data and models used to estimate exposures from radionuclides and the rates at which radon gas diffuses from the disposal facility. The input data are organized in two containers. The Dose_Conversion_Factors container includes the ingestion, inhalation, and direct radiation dose conversion factors for exposures to contaminated soils and air immersion. The Exposure_Pathway_Data container includes a variety of parameters required to model exposures. These include indoor and outdoor exposure times for the receptors; the inhalation rate; areas of the receptor's lot and house; and the direct radiation shielding factor for the receptor's house. Crop irrigation data are found in the Irrigation_Rates container; these data are used to calculate well pumping rates and estimate radionuclide concentrations in crops. The Ingestion_Data container includes human consumption rates of crops, animal products, soil, and water, along with expressions that estimate how much of the receptor's diet is raised at the exposure location.

The models that are used to project doses for the performance assessment and composite analysis are found in three exposure scenario containers. These containers organize the calculations that

are undertaken to estimate potential doses for the atmospheric, canyon, and groundwater-pathway-based scenarios. The dose calculations for the Atmospheric Scenario are implemented at two locations, corresponding to the points of maximum exposure before and after the end of active institutional control, while the groundwater scenarios are implemented at one location. Exposures to persons residing in the adjacent canyons are evaluated at a total of nine locations, each of which is subject to different rates of sediment transport from the mesa. The exposure concentrations used for each exposure scenario are found in the Media_Concentrations containers; the functions used to estimate receptor doses are organized by exposure route. The calculated doses are summed across exposure routes and radionuclides to provide summary doses for each scenario. Elements in the Radon_Fluxes container calculate the fluxes of Rn-220 and Rn-222 that exit the surface of the disposal facility.

2.3.1.2 Physical Compartments—Off-Site Exposure Locations and Media

This segment of the Area G Site Model includes physical representations of the exposure locations used in the modeling: Atmospheric_Exposure_Locations, Canyon_Exposure_ Locations, and the Domestic_Well. They are used to estimate exposures for the atmospheric, all pathways, and groundwater pathway scenarios.

The exposure location containers shown in Figure 1 include the transport pathway elements used by GoldSim to represent environmental media at the points of exposure. Contaminant masses and concentrations are determined for these media based on user-specified rates of inflow and outflow for each transport pathway. These masses and concentrations form the basis of the media concentrations calculated in the Dose_and_Radon_Flux_Models container and, therefore, the dose calculations.

In general, cell pathways are used to represent the different environmental media at the exposure locations. As discussed earlier, two exposure locations are considered for the Atmospheric Scenario, including the point of maximum exposure outside of the LANL boundary and the corresponding location immediately downwind of the Area G fence line; these locations are represented in the Atmospheric_Exposure_Locations container. Two cells are used to represent exposure media at each of these locations. The Exposure_Location_Soils cell represents the surface soils at a given location, an advective mass-flux link moves soil moisture from this cell to the sink element to represent the transport of contamination with water infiltrating through the receptor's lot.

A total of nine canyon locations are evaluated to estimate doses received by persons residing in Cañada del Buey and Pajarito Canyon. For each location, a cell is used to represent the canyon soils over which the receptor resides and raises crops and animals. Advective mass-flux links join these cells with the surface soils in the eight waste disposal regions on top of Mesita del Buey. These links are used to represent the movement of soils into the canyon due to surface

runoff and erosion. Links between the surface soil cells represent the transport of sediment down each canyon; links with a sink term are used to simulate the movement of radionuclides with water percolating through the receptor's lot.

A single receptor location 100 m (330 ft) downgradient of the Area G fence line is used in the site model for estimating potential groundwater pathway exposures. Four cells found in the Domestic_Well container represent the well, the surface soils at this location, and sink terms for the well water and soils for the All Pathways–Groundwater Scenario. Advective mass-flux links define the inflow of water from the regional aquifer to the well, and the outflow of water to surface soils where receptors irrigate crops. Inflows from the aquifer are ultimately proportional to the total water demands of the receptors, while outflows to the surface soils are proportional to rates of irrigation. Surface soils are subject to the aforementioned inflows of water and outflows to a sink term. The advective flow of soil moisture to the sink term represents the infiltration of water through the receptor's lot; the well sink term is used to represent water within the regional aquifer that flows past the well. Radionuclide concentrations in the water consumed by the Groundwater Resources Protection Scenario receptor are calculated directly from the aquifer-to-well advective fluxes projected by the site model; consequently, no physical representation of this receptor's well is included in the model.

Although exposures to contaminated groundwater may occur at the boundary of LANL prior to the loss of active institutional control, this exposure location is not included in the site model. This is because the results of the groundwater pathway modeling conducted in support of the performance assessment and composite analysis indicated that no radionuclides reach this location before the end of the 100-year active institutional control period. Groundwater exposures will be greatest immediately downgradient of the disposal facility following the end of active institutional control. Consequently, only a single location needs to be considered.

2.3.1.3 Physical Compartments—Disposal Facility

The eight waste disposal regions used to model the long-term performance of Area G are represented using a series of cell pathways and other GoldSim elements; these elements are organized in a series of disposal-region-specific containers. Cell pathways are used to represent the surface soil, cap material, and waste within each waste disposal region. The surface soil cells represent the uppermost portion of the cover placed over the waste; these cells are used to define radionuclide source terms for the Atmospheric, All Pathways–Cañada del Buey, and All Pathways–Pajarito Canyon Scenarios. Advective mass-flux links are used to simulate the transport of contaminants to the surface of the disposal facility by animals that penetrate into the waste, and diffusive mass-flux links account for the diffusion of vapor- and gas-phase radionuclides from the waste below. Direct transfers are used to simulate the uptake of radionuclides by plants growing over the disposal units and the deposition of these contaminants on the surface through litterfall and decay. The outflows from the surface soil cells account for

the settling and collapse of animal burrows, resuspension of particulates, transport of waterborne contaminants downward with infiltrating water, and movement of soils into Cañada del Buey and Pajarito Canyon with surface runoff; the links between the surface soil and the Sink_Onsite_Air cell found in each disposal region account for the resuspension of particulates and the diffusion of vapor- and gas-phase radionuclides from the surface of the disposal site.

The cap cells represent the cover material placed over the buried waste, less the surface soil layer. The site model uses 16 cells to represent this portion of the cover; the use of multiple cells more accurately represents the impacts of biotic intrusion on the disposal facility relative to a single layer, and more accurately models the diffusion of vapor- and gas-phase radionuclides upward from the waste. These cell pathways may be subject to inflows of infiltrating water and soil from the surface soil or cap layer above, the latter a result of burrow collapse, and to radionuclides diffusing upward from the layer below. Outflows from these cells account for the uptake of radionuclides by plants growing in the cover, soil transported by burrowing animals to the surface of Area G, soil transported downward in response to burrow collapse, the passage of infiltrating water into the underlying waste, and vapor- and gas-phase radionuclides diffusing upward. The presence or absence of many of these inflows and outflows depends upon the depth to which plants and animals penetrate into the disposal site.

The waste disposed of in each waste disposal region is represented using a series of 20 cell pathways to more accurately model vapor- and gas-phase diffusion and biotic interactions with the waste. Inventories are input directly into the waste cells over the proper period of disposal. These cells may be subject to advective inflows of infiltrating water and soil from above, representing infiltration through the site and burrow collapse, and to diffusive inflows from below. Outflows may include water infiltrating through the site, the uptake of radionuclides by plants, soil transported to the surface by burrowing animals, soil transported downward in response to burrow collapse, and vapor- and gas-phase radionuclides diffusing into the overlying layer. The presence or absence of many of these inflows and outflows depends upon the depth to which plants and animals penetrate into the disposal site.

The Plants cell found in each disposal region container represents plants growing over the disposal site that extract contamination from the cover and waste and fall to the surface as plant litter. Direct transfers account for the uptake of radionuclides by the plants and the passage of this contamination to the surface soil layer as a result of litterfall and litter decomposition.

Water exiting the bottoms of the disposal units will enter the underlying unsaturated zone; this flow is modeled using advective mass-flux links from the bottommost waste layers to the Unsaturated_Zone cell, which is located inside the disposal-region-specific container. The outflow from this cell enters an external pathway element. This element simulates the transport of waterborne contaminants vertically to the regional aquifer and horizontally to the receptor's well located

downgradient of the disposal site. The Disposed_Inventory element included in each waste disposal region container accounts for the addition of waste to the disposal units over the appropriate period of time. Waste disposal regions 1 and 8 include both pits and shafts; the addition of waste to these units is modeled separately using additional elements.

2.3.1.4 Model Documentation

All within-model documentation that is included in the site model is placed in the Documentation container. Found here are four containers labeled Model Revision Log, Model Organization, Input Parameter Requirements, and Process Model Descriptions. Double-clicking the element in the Model Revision Log container opens a Microsoft Word® file that documents the version history of the separate site and site diffusion models that were consolidated to form the Area G Site Model as well as the merged model. This history includes, for each version, the dates of model revisions, descriptions of the modifications, and the person who implemented the changes.

A figure showing the general layout of the site model is provided in the Model Organization container. Double clicking on any element in this figure provides access to the associated portion of the model. The Input Parameter Requirements container has a detailed listing of the input data required to implement the site model. Double clicking on the element in this container opens a portable document format (PDF) file that provides parameter names, descriptions, and types (i.e., scalar or vector); the units assumed by the parameters; and the input element type (i.e., data, stochastic, or lookup table).

The elements found in the Process Model Descriptions container provide access to descriptions of the conceptual and mathematical models that are used to evaluate the long-term performance of the Area G disposal facility. Double clicking on these elements opens PDF files that describe the biotic intrusion, surface erosion, and diffusion models; the exposure scenarios and equations used to estimate radiation exposures; and how the disposal facility is represented using GoldSim.

2.3.2 Area G Intruder Model

The general organization of the Area G Intruder Model is shown in Figure 2. Many aspects of the intruder model are similar to those discussed for the site model in Section 2.3.1. There are, however, differences in structure between these two models, as discussed below.

The Area G Intruder Model is divided into three major segments. The input data and the process models are contained in the first segment. The second segment includes the physical compartments used to represent the disposal pits and shafts and off-site environmental media. The Documentation container lists the different versions of the model and describes the changes that were made in conjunction with these revisions.

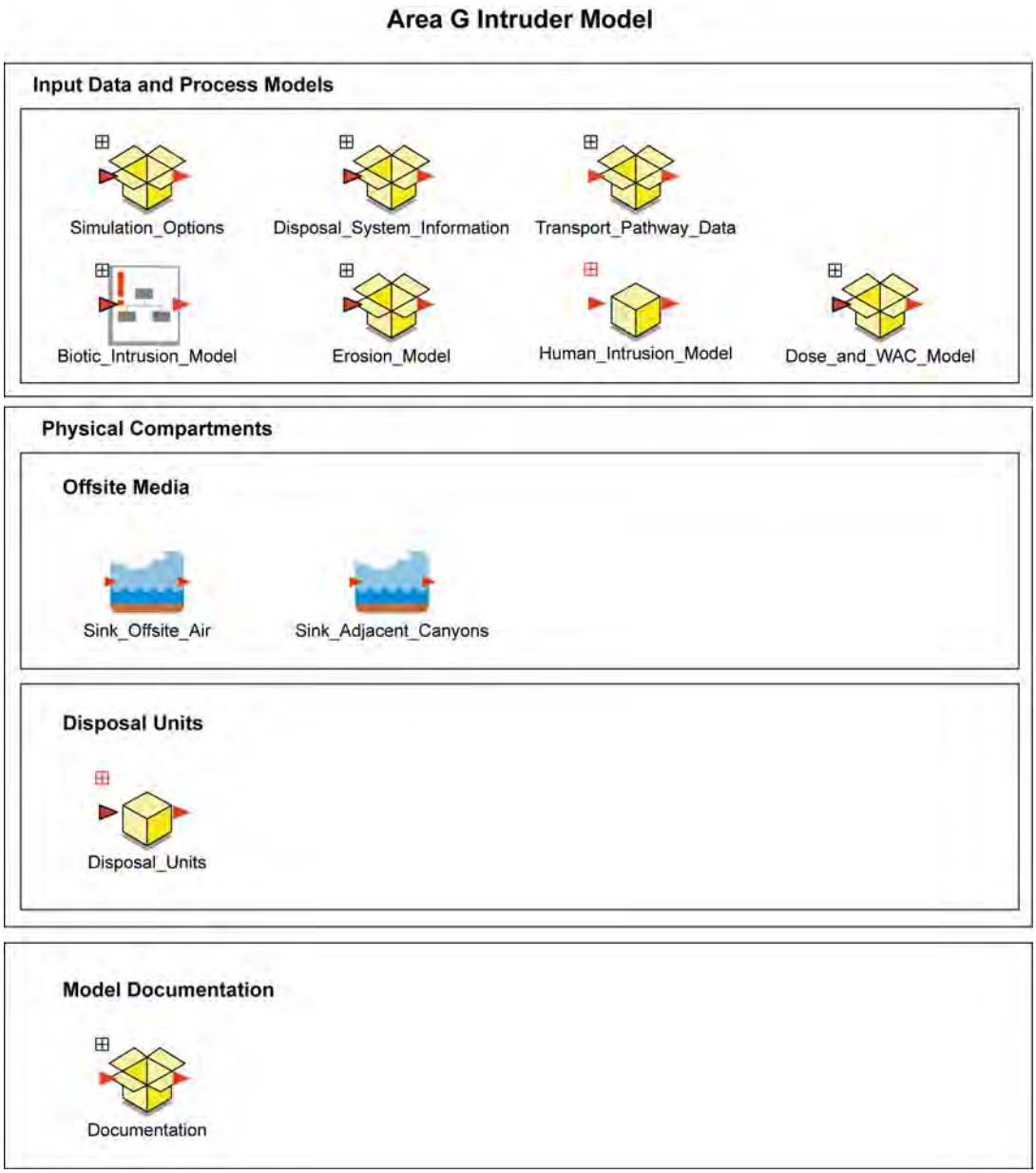

Figure 2
General Organization of the Area G Intruder Model

2.3.2.1 Input Data and Process Models

The input data and process models used in the Area G Intruder Model are found in this portion of the model. The contents of each of the containers shown in Figure 2 are discussed below. Complete definitions of the input parameters may be found in Section 4. The equations used to calculate intermediate parameters and to implement the process models are discussed in Section 3.

Simulation options. The Simulation_Options container includes three flag variables that are used in the intruder simulations. The Disposal_Unit_Flag specifies which disposal units are being considered. The intruder model addresses four sets of waste that are differentiated by the type of disposal unit and the time of disposal: waste disposed of in pits from September 27, 1988 through 2010; waste disposed of in pits from 2011 through 2044; waste disposed of in shafts from September 27, 1988 through 2015; and waste disposed of in shafts from 2016 through 2044. The Biotic_Intrusion_Flag, in conjunction with the Biota_Presence_Indicator, determines whether the effects of plant and animal intrusion into the waste prior to the arrival of the intruder are taken into account. The Inventory_Flag specifies whether the intruder simulations are being conducted using unit inventories or actual as-disposed inventories.

Disposal system information. The Disposal_System_Information container includes the data that are used to characterize the radionuclides in the waste, the materials comprising the physical compartments, the disposal system, and the waste inventory. Similar to the Area G Site Model, the Species_and_Materials container includes radionuclide decay data, a species element, a Material_Properties container, and the environmental media used in the modeling. Unlike the site model, an Attenuation_Coefficients container is found within the Material_Properties container: it contains mass and linear attenuation coefficients needed to estimate external exposures.

The Site_Geometry_and_Operations container includes elements that define the length of the active institutional control and closure periods; several elements, known as selectors, are used to identify key parameters for the disposal units specified using the Disposal_Unit_Flag. Elements found within the Layer_Information, Disposal_Pits, and Disposal_Shafts containers are used to define the operational period of each set of units; the initial thickness of the surface soil, cap, and waste layers; and the surface area of the disposal units.

The Inventory container includes several elements that access the initial radionuclide inventories projected by the Area G Inventory Model. Separate elements define the inventory for the subset of disposal units of interest; the output of these elements is used to define the waste-layer-specific inventories that are used in the modeling. The inventory used in a given simulation is determined by the setting of the Disposal_Unit_Flag. Other elements in the Inventory container specify the volume of waste for each set of disposal units and control how the input inventories are used by the intruder model.

Transport pathway data. The Transport_Pathway_Data container includes input data and calculated parameters related to atmospheric, food-chain, and groundwater transport. The Atmospheric_Transport container includes dust-loading information needed to estimate airborne radionuclide concentrations for the intruder scenarios and resuspension rate data that are used to model the transport of contamination brought to the surface by plants and animals to off-site locations. The Foodchain_Transport container includes the input data required to estimate rates of radionuclide uptake for the crops raised by the receptors and to estimate radionuclide concentrations in animal products. The types of data found in this container and the manner in which they are organized have been described with respect to the Area G Site Model. Finally, the Groundwater_Transport container includes the infiltration rate for Mesita del Buey.

Biotic intrusion model. The Biotic_Intrusion_Model container includes the input data and models that are used to estimate the impacts of biotic intrusion into the waste prior to the arrival of the inadvertent intruder. The layout of this container is similar to that discussed earlier for the site model, although there are fewer elements because the intruder model considers only a single set of disposal units at a time.

Erosion model. The amount of waste that is disturbed by human intrusion activities will be influenced by the patterns and rates of erosion at the disposal site. The erosion model implemented in the intruder model is similar to that described earlier for the site model. Fewer elements are involved, however, because the intruder model considers exposures for one set of disposal units at a time. Projected erosion rates are used to update the thicknesses of the surface soil, cap, and waste layers and to calculate the cumulative depths to the bottom of each layer.

Human intrusion model. The human intrusion model estimates the net volumes of cap material and waste that are brought to the surface of the facility as a result of basement excavation or well drilling, and the thickness of the excavated material after it has been spread across the intruder's lot. Elements needed to conduct these calculations are found here, including the dimensions of the basement and the diameter of the well casing. The model calculations are specific to the type of intrusion under consideration. The Basement_Calculations container addresses basement excavation common to the Intruder-Construction and Intruder-Agriculture Scenarios, while the Drilling_Calculations container includes calculations conducted for the Intruder–Post-Drilling Scenario.

Dose and waste acceptance criteria model. The Dose_and_WAC_Model container includes the data and functions required to estimate doses for the intruder scenarios, using radionuclide masses or concentrations projected for the pertinent physical compartments and environmental media. The projected exposures are subsequently used to calculate waste acceptance criteria for the disposal units. The input data used to conduct these calculations are organized in two containers. The Dose_Conversion_Factors container includes the ingestion, inhalation, and direct radiation dose conversion factors for exposures to contaminated soils and air immersion; external dose conversion

factors for contaminated soils are provided for two different depths of contamination. The Exposure_Pathway_Data container includes a variety of parameters required to model exposures. These include indoor and outdoor exposure times for the intruder; crop, animal product, and soil ingestion rates; inhalation rates; the area of the receptor's lot and house; the direct radiation shielding factor for the receptor's house; the soil mixing depth; and the time at which intrusion occurs. Also included are two elements that define the intruder performance objectives used to calculate the WAC.

The models used to project doses for the intruders are found in the Disposal_Unit_Doses_and_WAC container. Inside this container are found Media_Concentrations, Drilling_Intruder, Agricultural_Intruder, and Construction_Intruder containers. Elements found in the Media_Concentrations container estimate radionuclide concentrations in the cover, waste, air, plants, and animal products that are contacted or used by the intruders. The exposure calculations for the different exposure scenarios are performed using elements in the remaining containers.

Exposure-pathway-specific doses are summed to determine total radionuclide doses; doses for all radionuclides within a given decay chain are summed to determine the parent radionuclide doses. Parent doses are summed appropriately to yield the total doses for the disposal units under consideration. The peak parent doses are used to calculate the intruder-based WAC for Area G.

2.3.2.2 Physical Compartments—Off-Site Media

Cell pathways are used to represent the atmosphere downwind of the disposal facility and the canyons adjacent to Area G. Advective mass-flux links between cells used to represent the disposal facility proper and the Sink_Offsite_Air cell simulate the transport of suspended particulates with the prevailing winds. Links between the disposal facility and the Sink_Adjacent_Canyons cell are used to simulate the movement of contamination off site with surface runoff.

2.3.2.3 Physical Compartments—Disposal Units

The intruder model is designed to simulate a single set of disposal units (i.e., different subsets of pits and shafts at Area G) at a time. The Disposal_Units container includes the elements used to represent these units. Within this container, a single cell is used to represent the surface soil layer, defined as the top 1 cm (0.4 in.) of the cover. Four cells in each container are used to represent the cap (i.e., the cover less the surface soil layer) and the waste; this level of discretization is adopted to simulate the intrusive activities of plants and animals with a reasonable level of accuracy. Additional cells represent the vadose zone beneath the disposal units and native plants that inhabit the closed disposal site prior to the arrival of the intruder.

The quantities of soil, waste, and soil/waste moisture moved to the surface of the disposal facility as a result of human intrusion are calculated using the elements found in the Intrusion_Consequence container. Separate calculations are conducted for the two types of intrusion (well drilling and basement excavation); the results are used to calculate the surface soil

concentrations to which the intruder is exposed. Elements in the Cumulative_Masses container calculate the total radionuclide masses in the cover and waste as a function of time.

2.3.2.4 Model Documentation

All within-model documentation that is included in the intruder model is placed in the Documentation container. Found here is a container labeled Model Revision Log; double-clicking the element in this container opens a Microsoft Word file that documents the version history of the inventory model. This history includes, for each version, the dates of model revisions, descriptions of the modifications, and the person who implemented the changes.

2.3.3 Area G Intruder Diffusion Model

The general organization of the Area G Intruder Diffusion Model is shown in Figure 3. The model is divided into three major segments, the first of which contains input data, process models, and dose models. The second segment includes the physical compartments used to represent the disposal units at Area G and off-site environmental media. The version history of the model is provided in the Documentation container, which is shown at the bottom of Figure 3.

2.3.3.1 Input Data and Process Models

The input data and process models used in the diffusion model are found in this portion of the model. The contents of the containers shown in Figure 3 are discussed below. Complete definitions of the input parameters may be found in Section 4. The equations used to calculate intermediate parameters and to implement the process models are discussed in Section 3.

Simulation options. Six flag variables are used to control the diffusion modeling for the intruder analysis. The Intruder_Flag specifies the intruder scenario (i.e., construction, agricultural, or postdrilling) and the Disposal_Unit_Flag specifies the set of disposal units (i.e., 1988–2010 pits, 2011–2044 pits, 1988–2015 shafts, and 2016–2044 shafts) that will be addressed in the simulation. The Diffusion_Flag indicates whether or not the effects of diffusion are included in the modeling; the Biotic_Intrusion_Flag does the same with respect to plant and animal intrusion into the waste. On the basis of the intrusion flag setting, the Biota_Presence_Indicator determines when intrusive plants and animals are present at the site during the simulation. The Inventory_Flag specifies whether the intruder simulations are using unit inventories or actual as-disposed inventories. Finally, the Tritium_Package_Flag is used to indicate whether the simulation will take into account the off-gas rates of the packages used to dispose of high-activity tritium waste.

Disposal system information. The Disposal_System_Information container includes information about the radionuclides in the waste, the materials comprising the physical compartments of the model, the disposal units, and the waste inventory. The elements included in the Species_and_Materials container are similar to those found in the site and intruder models; elements needed to model diffusion within the concrete floor of the foundation of the intruder's house are the

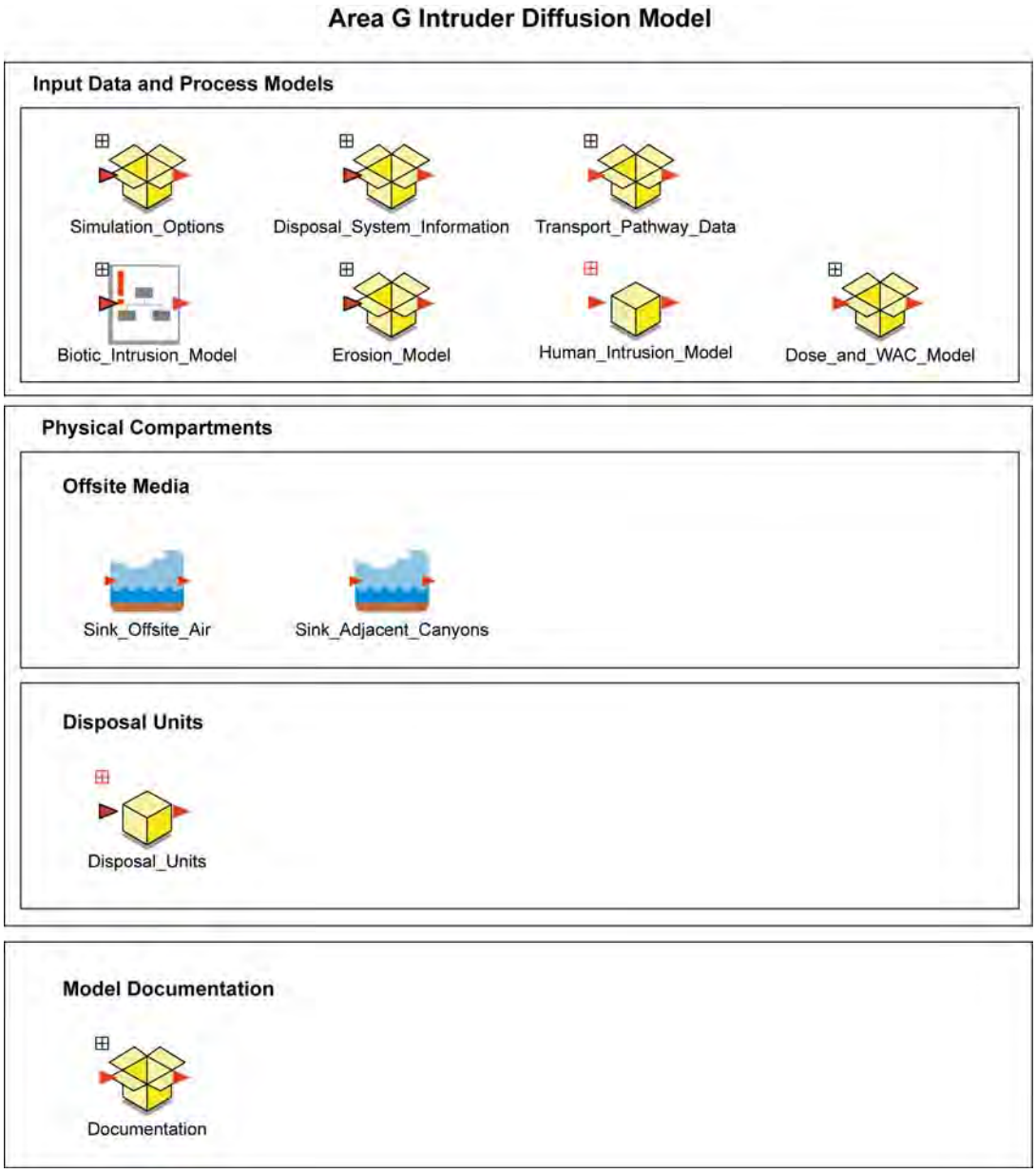

Figure 3
General Organization of the Area G Intruder Diffusion Model

notable exception. The elements included in the Site_Geometry_and_Operations container are much the same as those described for the intruder model; differences relate to the manner in which the cap, waste, and concrete foundation were discretized in the two models. Also, similar to the intruder model, the Inventory container includes elements that access the initial radionuclide inventories projected by the Area G Inventory Model; separate elements define the inventory for the different subsets of disposal units. The output of these elements is used to define waste-layer-specific inventories that are used in the modeling; other elements in the Inventory container provide the volume of waste for each set of disposal units and control how the input inventories are used by the intruder model.

Transport pathway data. The Transport_Pathway_Data container includes input data and calculated parameters needed to model rates of radionuclide transport. These parameters are organized in three containers labeled Atmospheric_Transport, Foodchain_Transport, and Groundwater_Transport. The input data found in the Atmospheric_Transport container are generally the same as those discussed for the intruder model, with the exception of the wind speed and atmospheric mixing height elements, which are used to estimate exposure concentrations for vapor- and gas-phase radionuclides above the disposal facility. The elements inside the Foodchain_Transport and Groundwater_Transport containers are the same as those found in the intruder model.

Human intrusion model. The Human_Intrusion_Model container includes elements used to calculate the net volumes of waste and cover material brought to the surface and spread over the receptor's lot. The elements included in this container are the same as those in the intruder model.

Biotic intrusion model. The Biotic_Intrusion_Model container includes the input data and models that are used to estimate the impacts of biotic intrusion into the waste prior to the arrival of the inadvertent intruder. The layout of this container is similar to that discussed earlier for the site model; fewer elements are included in the container because the intruder diffusion model considers only a single set of disposal units at a time.

Erosion model. The surface erosion model used in the intruder diffusion model is the same as that described for the intruder model. Rates of erosion are estimated and used to calculate rates of cover loss for the disposal units specified using the Disposal_Unit_Flag.

Dose model. As in the intruder model, the Dose_and_WAC_Model container includes the data and models used to estimate doses for the intruder scenarios; the results are used in the calculation of WAC for Area G. The elements used to conduct these calculations are organized in a manner similar to that described for the intruder model.

2.3.3.2 Physical Compartments—Off-Site Media

The intruder diffusion model uses a cell to represent air downwind of Area G and the canyons adjacent to the disposal facility. An advective mass-flux link is used to transport airborne contaminants from above the intruder's lot to the Sink_Offsite_Air cell; this transfer represents the transport of airborne contaminants with the prevailing winds. Transfers from the intruder's lot to the adjacent canyons represent the transport of sediment from the mesa top with surface runoff.

2.3.3.3 Physical Compartments—Disposal Facility

The cells that are used to represent the disposal facility in the intruder diffusion model are organized in a manner that is similar to that described earlier for the site model. Within the Disposal_Units container, a single cell is used to represent the surface soil layer, while 16 and 20 cells are used to represent the cap and waste, respectively. Additional cells represent the air over the disposal facility and plant litter. Unlike the site model, however, the intruder diffusion model uses several cells to represent the basement excavation, the concrete floor of the intruder's house, and the house itself. Radionuclides diffusing from the waste may travel through the cap and surface soil layer and enter the air above the site, diffuse through the concrete foundation and enter the intruder's house, or enter the basement excavation prior to construction of the house.

As discussed earlier, advective mass-flux links are used to simulate the impacts of animal intrusion into the disposal facility, while direct transfers are used to simulate the uptake of radionuclides by plants growing over the disposal units and the subsequent deposition of these contaminants on the surface through litterfall and decay. Outflows from the Surface_Soil cell account for the settling and collapse of animal burrows, resuspension of particulates, transport of waterborne contaminants downward with infiltrating water, and movement of soils into the canyons bordering Mesita del Buey. The cap and waste cells are subject to inflows of infiltrating water and soil from the layer above and to radionuclides diffusing upward from the layer below. Outflows from these cells account for soil transported by burrowing animals to the surface of Area G, soil transported downward in response to burrow collapse, the passage of infiltrating water, the diffusion of vapor- and gas-phase radionuclides, and the uptake of radionuclides by plants growing in the cover. Water exiting the bottoms of the disposal units enters the underlying unsaturated zone.

2.3.3.4 Model Documentation

All within-model documentation that is included in the intruder diffusion model is placed in the Documentation container. Found here is a container labeled Model Revision Log; double-clicking the element in this container opens a Microsoft Word file that documents the version history of the inventory model. This history includes, for each version, the dates of model revisions, descriptions of the modifications, and the person who implemented the changes.

2.3.4 Area G Inventory Model

The general organization of the Area G Inventory Model is shown in Figure 4. This model is significantly simpler than the site and intruder models as its only role is to estimate initial radionuclide inventories for the pits and shafts at Area G. The model consists of the input data and process model, and model documentation segments.

2.3.4.1 Input Data and Process Models

The input data and process models used to estimate the initial radionuclide inventories in the pits and shafts at Area G are found here. The contents of the containers shown in Figure 4 are discussed below. Complete definitions of the input parameters may be found in Section 4.

Simulation options. A series of flag variables is used to control the way inventories are projected for the four subsets of disposal units included in the intruder assessment. Found in the Depth_of_Disposal_Flags container, these elements specify whether the estimated inventories are to be homogeneously distributed throughout the pits and shafts or assigned to specific waste layers.

Species and materials. The Species_and_Materials container includes a small number of elements that identify the radionuclides for which initial inventories are estimated and define the properties of those isotopes. Elements found in the Material_Properties container are used to define decay relationships. The environmental medium (water) is included in the model by default.

Area G geometry and operations. The Area_G_Geometry_and_Operations container includes elements that define the number of layers into which the waste profile is divided and the thicknesses of those layers. Also found here are elements that assign the input radionuclide inventories to specific layers. Radionuclide inventories are distributed homogeneously throughout the waste profile or assigned to specific waste layers, depending upon the setting of the flag variables found in the Depth_of_Disposal_Flags container. The allocation factors used to distribute inventories within the waste profile are found in the Waste_Depth_Distributions container. The elements found in the Area_G_Geometry_and_Operations container are used to estimate the inadvertent intruder model inventories only and, as such, address only the waste included in the intruder dose assessment.

Inventory. The Inventory container includes the elements that are used to estimate the inventories of the radionuclides included in the performance assessment and composite analysis. The model calculates layer-specific unit inventories for the waste included in the intruder dose assessment; these calculations are found in the Unit_Inventory container. The elements found in the As-Disposed_Inventory container calculate intial inventories for various subsets of waste, including those used in the intruder analysis and the entire performance assessment and composite analysis inventories. Within the latter container, the Radionuclide_Inventories container includes point estimates of isotope-specific activities in the waste placed in the pits and shafts. The Material_Type_Inventories container includes the corresponding information for mixed-activation

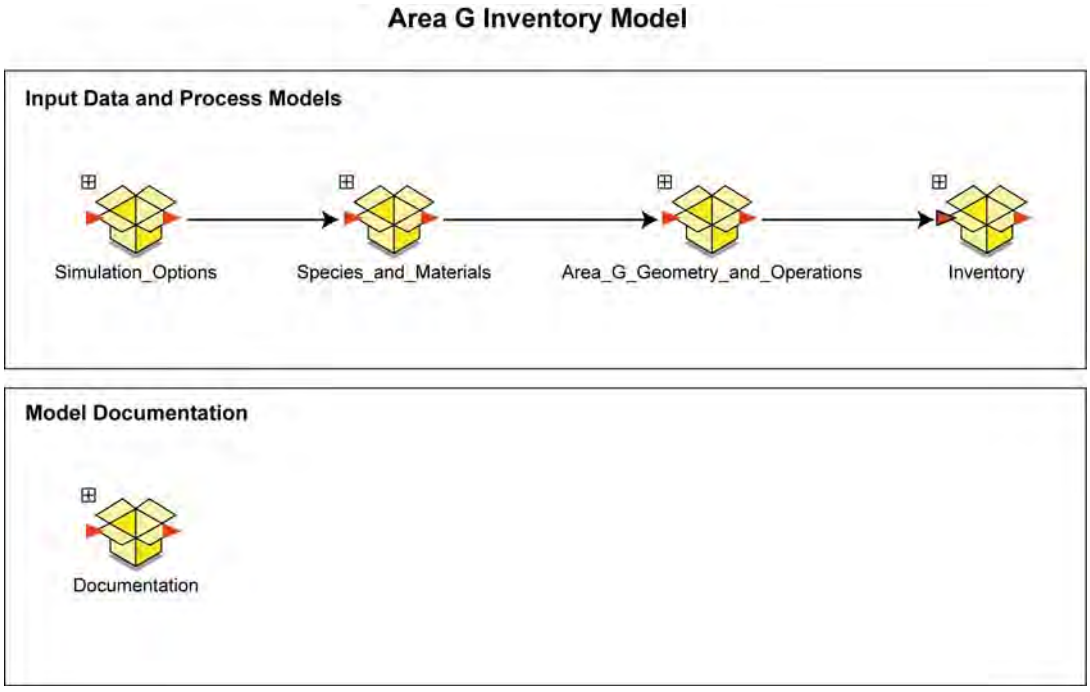

Figure 4
General Organization of Area G Inventory Model

product (MAP), mixed-fission product (MFP), and material-type waste; material types refer to specific radionuclide compositions in waste that has been disposed of at Area G. The inventories calculated for the subsets of the disposal units included in the intruder modeling are assigned to specific layers within the waste profile. Most of the remaining elements are used to estimate the uncertainties associated with the inventories, and to develop final inventories for the eight waste disposal regions and the different subsets of disposal units addressed by the intruder modeling.

2.3.4.2 Model Documentation

All within-model documentation that is included in the inventory model is placed in the Documentation container. Found here are four containers labeled Model Revision Log, Model Organization, Input Parameter Requirements, and Process Model Descriptions. Double-clicking the element in the Model Revision Log container opens a Microsoft Word file that documents the version history of the inventory model. This history includes, for each version, the dates of model revisions, descriptions of the modifications, and the person who implemented the changes.

A figure showing the general layout of the inventory model is provided in the Model Organization container. Double clicking on any element in this figure provides access to the associated portion of the model. The Input Parameter Requirements container contains a detailed listing of the input data required to implement the inventory model model. Double clicking on the element in this container opens a PDF file that provides parameter names, descriptions, and types (i.e., scalar or vector); the units assumed by the parameters; and the input element type (i.e., data, stochastic, or lookup table). The element found in the Process Model Descriptions container provides a general description of how the inventory modeling is conducted. Double clicking on this element opens a PDF file that contains this information.

3.0 Modeling Approach

The site, intruder, and intruder diffusion models described above integrate a series of submodels that are used to conduct the Area G performance assessment and composite analysis. Descriptions of the modeling conducted using these submodels are provided below. The first several sections describe the modeling that is conducted to estimate radionuclide inventories in the waste and to project rates of contaminant release, transport, and exposure. A portion of the output of this modeling defines the modes and rates of contaminant movement between the physical components that are used to represent the disposal system. The manner in which transfers between the physical components are simulated is addressed in the latter sections of the discussion.

Area G is a large, complex site. Many aspects of the facility's long-term performance are spatially dependent in response to local variations in topography and geohydrology. To more accurately model the performance of the disposal facility, the disposal site had to be divided, or discretized, into several areas. An understanding of how this was done is critical to the following discussions about models.

The primary subdivisions of the facility are referred to as waste disposal regions; these regions include various subsets of the disposal pits and shafts at Area G. Material Disposal Area G (MDA G), the portion of the facility currently receiving waste, was divided into seven disposal regions; these regions are shown in Figure 5. Disposal regions 1 and 6 each include some of the shafts in the shaft field west of pits 2 and 4, consequently the boundaries of these regions overlap. Disposal region 7 includes numerous shafts scattered among the units that make up disposal region 3 (i.e., pits 8 through 22), and thus the boundaries of these two regions also overlap. An eighth waste disposal region is used to represent the Zone 4 expansion area at Area G; it is not shown in Figure 5. The waste disposal regions were defined because the thickness of the Bandelier Tuff, which largely determines groundwater transport times, increases from east to west and because of differences in the depths of the disposal pits and shafts. Table 2 lists the elevation assigned to the bottom of the disposal units within each disposal region and the corresponding depth to the regional aquifer.

Radionuclides released from the disposal facility in the form of suspended particulates, vapors, or gases may be transported by the prevailing winds to locations downwind of the source of the airborne release. The patterns of transport and dispersal depend, in part, upon the portion of the facility from which the airborne releases originate. To better account for these dependencies, the disposal site was divided into three atmospheric source areas, as shown in Figure 6. Each source area consists of one or more of the eight waste disposal regions discussed above.

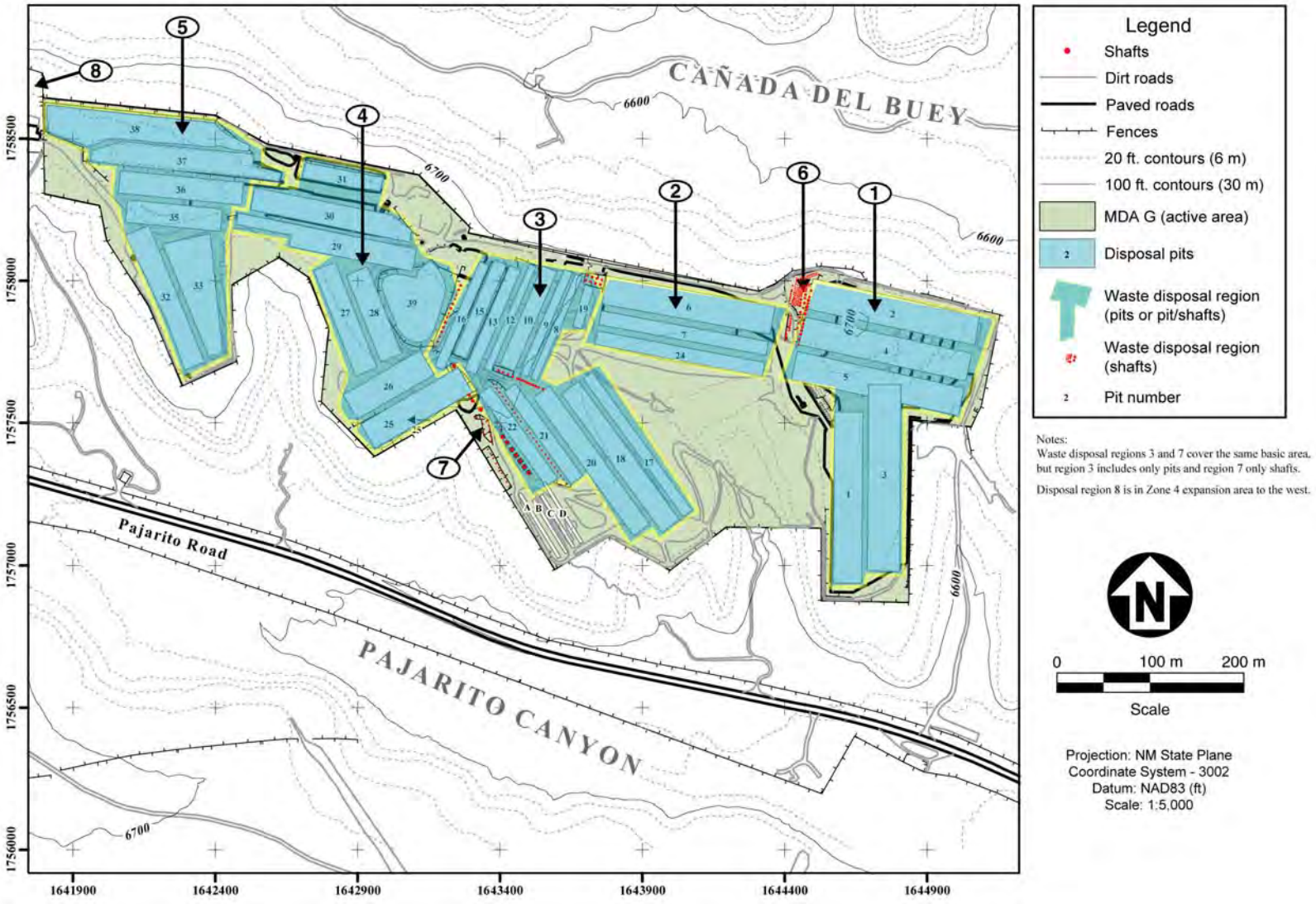

Figure 5
Waste Disposal Regions at Area G

Source: Apogen Technologies (formerly SEA)
LANL RRES Database, Map ID: 4531.021 (1) Rev . 2

Table 2
Elevations of Disposal Units and Depth to Regional Aquifer for the Eight Waste Disposal Regions

Waste Disposal Region	Elevation of Disposal Units (m above msl, from bottom of disposal units)	Depth to Regional Aquifer (m from bottom of disposal units)
1	2024	253
2	2028	257
3	2032	261
4	2036	265
5	2037	266
6	2015	244
7	2020	249
8	2038	267

msl–Mean sea level

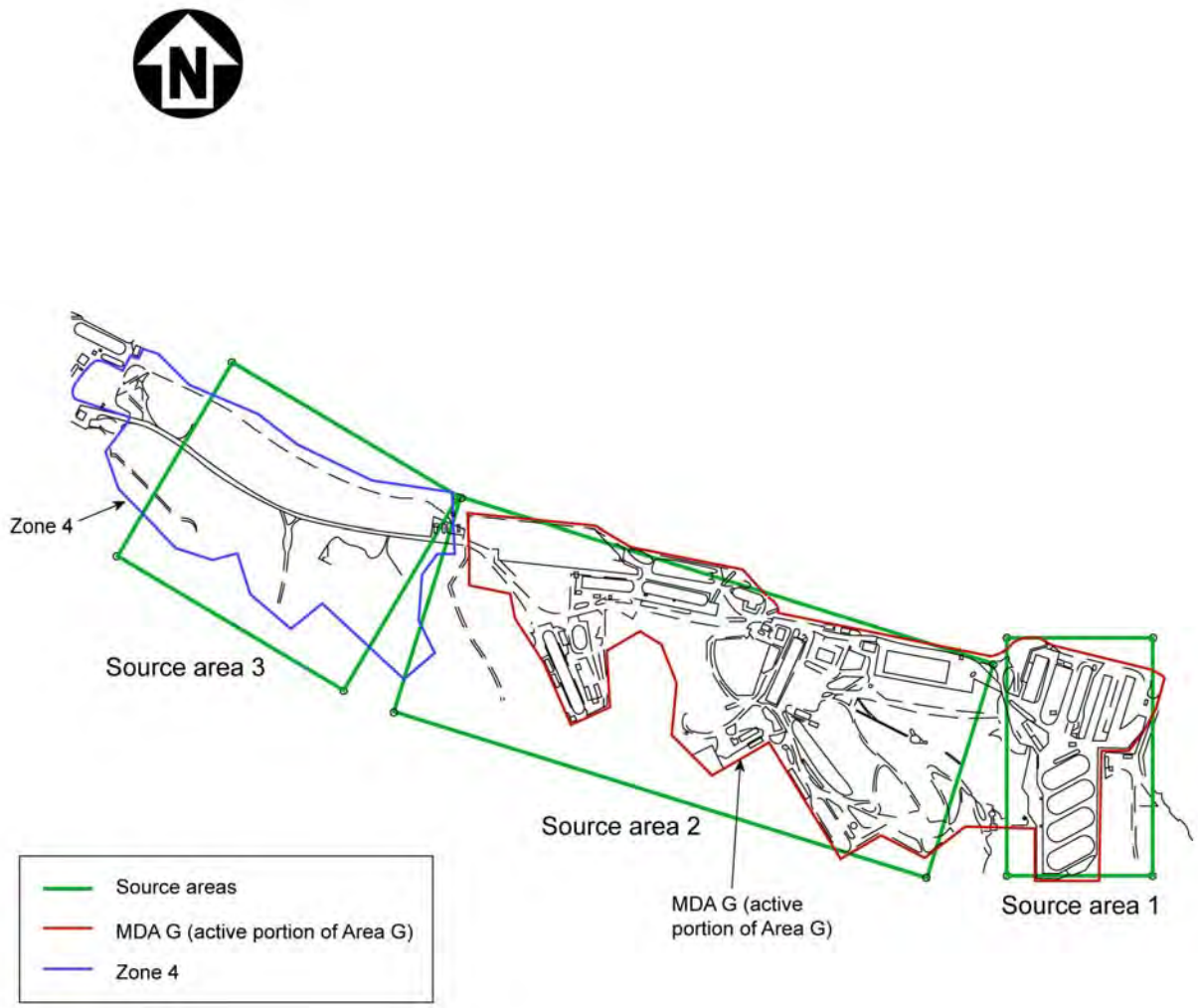

Figure 6
Atmospheric Source Areas at Area G

3.1 Inventory Modeling

The Area G Inventory Model calculates the as-disposed activities of the radionuclides placed in the pits and shafts at Area G. In general, the inventory model accepts as input point estimates of contaminant inventories on a pit- and shaft-specific basis; in some cases, inventories from multiple units are combined because the information required to allocate the waste to individual pits and shafts is unavailable. These input data are used in conjunction with information about the uncertainty associated with the point estimates to calculate the inventories that are used in the site and intruder models. Unit-specific inventories are summed appropriately to yield inventories for each of the eight waste disposal regions and for the four subsets of disposal pits and shafts included in the intruder assessment. The inventories estimated for the intruder and intruder diffusion models may be assigned to specific layers within the waste profile or assumed to be homogeneously distributed throughout the units; the inventories calculated for the site model are assumed to be homogeneously distributed throughout the units. The inventory model can also be used to define the unit inventories (i.e, inventories that are the same for all radionuclides) that are used in the intruder modeling to calculate WAC.

The point estimates of contaminant inventories that are input into the inventory model include radionuclide-specific activities and the activities associated with MAP waste, MFP waste, and waste classified by material type. A list of these material types may be found in Shuman (2008).

Several sources of uncertainty are associated with the point estimates of radionuclide activities and inventories of MAP, MFP, and material-type waste. Perhaps chief among these are the measurement and estimation techniques used to characterize the waste. The inventory calculations account for this uncertainty by using information about the potential errors to assign distributions to the user-specified inventories. Further discussion of the nature and magnitude of these errors is provided in Section 5.4 of this report. Radionuclide allocation factors are multiplied times the input inventories of MAP, MFP, and material-type waste to estimate radionuclide-specific activities; the sources of these allocation factors are also discussed in Section 5.4.

3.2 Biotic Intrusion Modeling

The biotic intrusion modeling estimates rates of radionuclide transport to the surface of Area G by plants and animals intruding into the disposed waste. The submodel evaluates the potential for plants and animals to intrude into the disposed waste and transport radioactive contamination to the surface of the disposal facility. The submodel is an adaptation of the updated biotic intrusion modeling conducted under the Area G Performance Assessment and Composite Analysis Maintenance Program (Shuman, 1999). It is used in conjunction with the site, intruder, and intruder diffusion models. A discussion of the conceptual and mathematical models upon which the biotic intrusion modeling is based is provided below.

3.2.1 Conceptual Model

The biotic intrusion submodel addresses the impacts of plant and animal intrusion into the buried waste. In terms of plants, it assumes that the roots of plants growing over the site extend into the buried waste. Radionuclides are taken up via these roots and are assimilated by the plants. Litter is formed as plants die and shed their leaves and contamination in the plant material enters the soil as the litter decomposes.

The amount of contamination deposited on the surface by plants is a function of the radionuclide concentrations in the litter and the quantity of litter generated by the plants. Radionuclide concentrations in the litter depend upon the distribution of root mass with depth and the efficiency with which radionuclides are extracted from contaminated soils by plant roots. Rates of litter production are estimated on the basis of aboveground plant yields and the fractions of these yields that fall as litter in any given year. Plant yields and litter generation fractions are specific to the plant growth forms under consideration; yields may vary over time as the disposal site undergoes ecological succession.

Animals constructing burrows for cover or as a means of foraging may also penetrate into the buried waste and bring waste contaminants to the surface of the site. This contamination is mixed with clean soil excavated from the portions of the burrows that lie above the waste, and spread over the ground surface. Over time, the burrows excavated by animals will settle or collapse, resulting in the gradual downward movement of contamination brought to the surface by animals and deposited on the ground by plants. Vertical transport of the surface contamination will be enhanced as radionuclides are transported downward with water infiltrating through the site.

The amount of contaminated soil brought to the surface by burrowing animals depends upon the distribution of burrows relative to the waste and the soil removal rates of the various species or taxa of animals. Burrow distributions are used to estimate rates of soil removal with depth; the total quantities of excavated soil are calculated using information about animal densities and life spans, and burrow renewal fractions. Many of these parameters may change over time as the composition of the animal community shifts in response to changes in the plant community.

The potential impact of biotic intrusion on the long-term integrity of Area G depends, in part, on the ecological characteristics of the site and, hence, on the plant and animal species that can reasonably be expected to inhabit it. A diverse array of plants and animals occurs in the Los Alamos region owing to the 1,500 m (5,900 ft) difference in elevation between the Rio Grande and the top of the Jemez Mountains, and to the canyon and mesa terrain (DOE, 1979). Los Alamos County has six major vegetative community types: juniper-grassland, piñon-juniper, ponderosa pine, mixed conifer, spruce-fir, and subalpine grassland. The juniper-grassland, piñon-juniper, and ponderosa pine communities predominate; each of these communities comprises about one-third of the Laboratory. Juniper-grassland extends from the Rio Grande and eastern

part of the Pajarito Plateau up to 1,700 to 1,900 m (5,600 to 6,200 ft) above mean seal level (msl) on south-facing slopes. The piñon-juniper community covers large portions of mesa tops, ranging from about 1,900 to 2,100 m (6,200 to 6,900 ft) above msl. Ponderosa pines occur at elevations from 2,100 to 2,300 m (6,900 to 7,500 ft) above msl on the western plateau (Figure 7).

Undisturbed areas on Mesita del Buey, the mesa where Area G is located, are dominated by piñon-juniper woodland. Piñon pine (*Pinus edulis*) and one-seed juniper (*Juniperus monosperma*) are the dominant tree species; common shrubs include big sagebrush (*Artemisia tridentata*), four-wing saltbush (*Atriplex canescens*), currant (*Ribes cereum*), and mountain mahogany (*Cercocarpus montanus*). Blue grama (*Bouteloua gracilis*), cryptogamic soil crust, and prickly pear cactus (*Opuntia polyacantha*) are among the most common understory plants on the mesa. Others include snakeweed (*Gutierrezia sarothrae*), pingue (*Hymenoxys richardsonii*), wild chrysanthemum (*Bahia dissecta*), leafy golden aster (*Chrysopsis filiosa*), purple horned-toothed moss (*Ceratadon purpureus*), lichen, three-awn grass (*Aristida* spp.), bottlebrush squirreltail (*Sitanion hystrix*), bluegrass (*Poa* spp.), and false tarragon (*Artemisia dracunculus*).

Waste management operations at Area G have caused a number of the native understory plants to be replaced by different species. Recently disturbed areas support goosefoot (*Chenopodium fremontii*), Russian thistle (*Salsola kali*), cutleaf evening primrose (*Oenothera caespitosa*), common sunflower (*Helianthus anuus*), and other colonizing species. Vegetation introduced as disposal units are closed consists of native grasses including blue grama, sideoats grama (*Bouteloua curtipendula*), Indian ricegrass (*Oryzopsis hymenoides*), sand dropseed (*Sporobolus cryptandrus*), sheep fescue (*Festuca ovina*), and western wheatgrass (*Agropyron smithii*), and forbs such as blue flax (*Linum perenne lewisii*) and prairie coneflower (*Ratibida columnifera*).

On the basis of the information provided above, the disposal units at Area G are expected to undergo ecological succession from their disturbed state shortly after closure to a piñon-juniper woodland climax, characteristic of the undisturbed portions of Mesita del Buey. Annual and perennial grasses and forbs will predominate when the site is in its early successional stages, becoming established as covers over disposal units are seeded and as grasses and forbs invade from surrounding areas on the mesa. Over time, shrubs and trees will take hold and become established at the site. Although some species of grasses and forbs will die out, others will continue to thrive. Given enough time, it is assumed that a condition approximating the climax piñon-juniper woodland will result.

The predominant plant communities at Area G will have a direct influence on the species of burrowing animals that occur at the site following facility closure. Several species of burrowing animals are currently found at Area G and the area surrounding the site; others may reasonably be expected to inhabit the site after widespread disturbance of the area ceases and as the site undergoes ecological succession to piñon-juniper woodland. The most prevalent of these burrowing species are expected to be harvester ants and several species of small mammals.

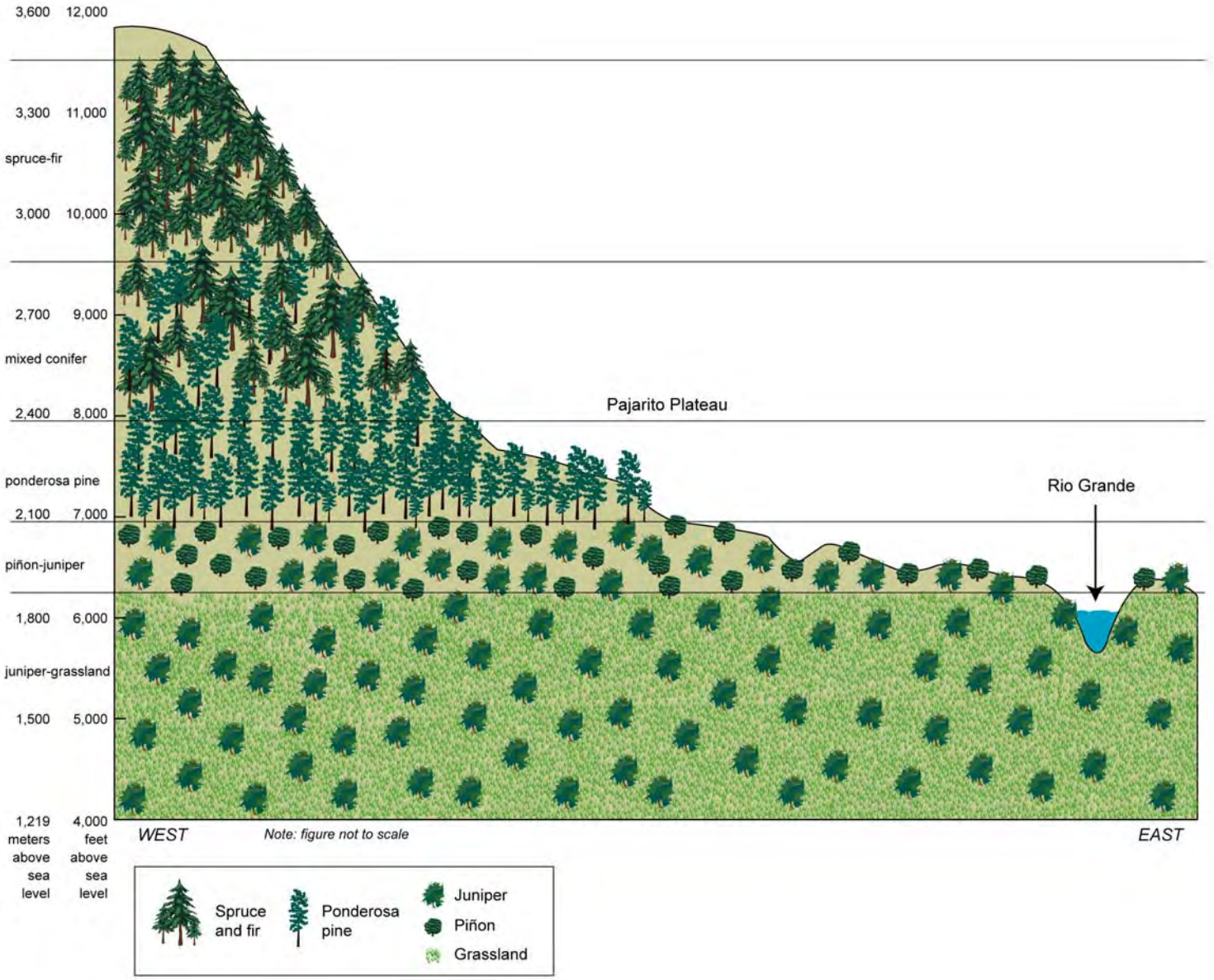

Figure 7
Generalized Vegetative Zones of the Pajarito Plateau

There are approximately 20 species of harvester ants (*Pogonomyrmex* spp.) in the southwestern U.S. The combined ranges of *Pogonomyrmex occidentalis* and *Pogonomyrmex rugosa* cover the state of New Mexico; the ants are commonly found in high grasslands and piñon-juniper woodland (Allen, 1996). Carlson and Whitford (1991) observed harvester ants (*Pogonomyrmex occidentalis*) in piñon-juniper and ponderosa pine communities near LANL. It is not surprising, then, that harvester ants have been observed in undisturbed piñon-juniper woodland on Mesita del Buey. They were also found to inhabit MDA J, 2 km (1.2 mi) west of Area G, shortly after closure of that disposal site.

A variety of species of small mammals inhabit the Laboratory and surrounding lands. Many of these species, and the habitats within which they occur, were discussed in the Los Alamos final environmental impact statement issued in 1979 (DOE, 1979). Table 3 summarizes this information, which includes the species of small mammals found in the vegetation overstory types that occur most often at the Laboratory. Area G is expected to most closely resemble the juniper-grassland shortly after closure, and the piñon-juniper woodland as it undergoes ecological succession. Deer mice (*Peromyscus maniculatus*), piñon mice (*Peromyscus truei*), woodrats (*Neotoma* spp.), and mountain cottontails (*Sylvilagus nuttalli*) are common to both of these plant communities; chipmunks (*Eutamias* spp.) are anticipated as the site passes into piñon-juniper woodland.

Trapping studies conducted at the Laboratory over the past several years have generally confirmed the small mammal distributions shown in Table 3 for the grassland and piñon-juniper woodland communities. The most commonly trapped species in disturbed areas at Area G has been the deer mouse; western harvest mice (*Reithrodontomys megalotis*), pocket gophers (*Thomomys* spp.), piñon mice, and brush mice (*Peromyscus boylei*) have also been caught (Biggs et al., 1995, 1997; Bennett et al., 1997, 1998, and 2002). The piñon mouse has been the most commonly trapped species in piñon-juniper woodland areas, although deer mice, harvest mice, brush mice, and silky pocket mice (*Perognathus flavus*) have also been caught.

Additional insight into the small mammals that may inhabit Area G following its succession to piñon-juniper woodland may be gained from a literature review. Zarn (1977) summarized the work of several investigators who characterized the species of small mammals found in piñon-juniper woodlands in Utah, western Colorado, and Arizona. Species found in those woodlands include deer mice, western harvest mice, brush mice, Great Basin pocket mice (*Perognathus parvus*), piñon mice, northern grasshopper mice (*Onychomys leucogaster*), longtail voles (*Microtus longicaudus*), Mexican voles (*Microtus mexicanus*), sagebrush voles (*Lagurus curtatus*), Great Basin kangaroo rats (*Dipodomys microps*), least chipmunks (*Eutamias minimus*), rock squirrels (*Citellus variegatus*), and several species of woodrats and lagomorphs (*Lepus* spp., *Sylvilagus* spp.).

Table 3
Distribution of Small Mammals in Los Alamos County by Vegetation Overstory Type

Vegetation Overstory Type	Approximate Elevation (m above msl)	Small Mammal Species	
Spruce-Fir	2,900–3,200	Deer mouse Northern pocket gopher Least chipmunk Montane vole	Boreal red-backed vole Tassel-eared squirrel Woodrat Shrew
Mixed Conifer	2,300–2,900	Deer mouse Northern pocket gopher Least chipmunk Montane vole	Gapper's red-backed vole Tassel-eared squirrel Woodrat Shrew
Ponderosa Pine	2,100–2,300	Deer mouse Valley pocket gopher Least chipmunk Colorado chipmunk	Pine squirrel Tassel-eared squirrel Woodrat
Piñon-Juniper	1,900–2,100	Deer mouse Piñon mouse Colorado chipmunk	Woodrat Mountain cottontail
Juniper-Grassland	1,700–1,900	Deer mouse Piñon mouse	Woodrat Mountain cottontail
Canyons		Western harvest mouse Valley pocket gopher Least chipmunk	Meadow vole Rock squirrel Mountain cottontail

Source: DOE, 1979

In a food habits study conducted in western Colorado, Haufler and Nagy (1984) found deer mice, plains pocket mice (*Perognathus flavescens*), golden-mantled ground squirrels (*Citellus lateralis*), bushytail woodrats (*Neotoma cinerea*), least chipmunks, and mountain cottontails associated with disturbed and undisturbed piñon-juniper woodlands. Smith and Urness (1984) conducted a trapping study in several habitats in southern Utah, including one piñon-juniper community. Deer mice, Great Basin pocket mice, and piñon mice were the predominant species caught; deer mice accounted for 79 percent of all trapped animals. Severson (1986) examined the effects of piñon-juniper woodland treatments on rodent abundance in southern New Mexico. White-throated woodrats (*Neotoma albigula*); brush, piñon, and southern grasshopper mice (*Onychomys torridus*); and Ord's kangaroo rat (*Dipodomys ordi*) were the most abundant species on untreated woodland.

The background information provided above was used to identify the plants and animals included in the biotic intrusion modeling. Although the general nature of the vegetative cover at Area G can be predicted for the site in its early successional stages and climax condition,

predicting the species-specific plant composition with any degree of accuracy is essentially impossible. Given this, the plant communities present at the site were identified in terms of the general growth forms present under each set of conditions, rather than on a species-specific basis. Four growth forms were identified for the modeling: annual and perennial grasses, annual and perennial forbs, shrubs (including subshrubs), and trees. The impacts of grasses, forbs, and shrubs are simulated during the early stages of site succession. Grasses and forbs are expected to be early colonizers at the site. Shrubs are expected to begin colonization of Area G within a few years after closure. Consequently, this growth form is included in the simulation of the site. Simulation of the disposal site as it passes to piñon-juniper woodland considers the impacts of trees in addition to grasses, forbs, and shrubs.

Four species or taxa of burrowing animals were selected to simulate the impacts of animal intrusion upon Area G. These include harvester ants, mice, pocket gophers, and chipmunks and ground squirrels. As mentioned earlier, harvester ants, which are found throughout much of New Mexico, have been observed at a recently closed disposal site and in piñon-juniper woodland adjacent to the disposal units at Area G. The deer mouse and a host of other mouse species have been trapped at Area G and in piñon-juniper woodland communities. Although the trapping efforts of Biggs et al. (1995 and 1997) and Bennett et al. (1997, 1998, and 2002) have indicated relatively little in the way of pocket gopher activity, these animals have been observed at Area G. Gopher mounds have been found near several disposal shafts in the past, and have been encountered in the course of conducting vegetation transects at the Laboratory (Tierney and Foxx, 1987).

Chipmunks and ground squirrels are currently uncommon at Area G, but are expected to become more common as the site passes from grassland to piñon-juniper woodland. The DOE (1979) does not include ground squirrels as potential inhabitants of the site; however, other published literature suggests species such as the rock squirrel and golden-mantled ground squirrel could take up residence at the site. The rock squirrel occurs in canyons at the Laboratory (DOE, 1979), and both of these species have been found in piñon-juniper woodland in Arizona, Colorado, and Utah. The spotted ground squirrel (*Spermophilus spilosoma*) has also been observed in the vicinity of the Laboratory; this species occurs throughout much of New Mexico but tends to inhabit grasslands on sandy soils (Streubel and Fitzgerald, 1978).

The animal species selected for the biotic intrusion modeling are expected to reasonably capture the range of species that will be present at Area G after closure, which will enable reasonably accurate projections of the potential impacts of animal intrusion. Other burrowing animals may be present at the site at various points in time, but the potential for these species to cause significant disruption of the waste is expected to be small. For example, one or more species of voles may inhabit the site, but these animals generally restrict burrowing activities to depths of 0.5 m (1.6 ft) below ground surface (bgs) or less. Although Hall (1928 and 1946, cited in CDFG, 2003) found the tunnels of the sagebrush vole as deep as 56 cm (1.8 ft), Reynolds and Laundre

(1988) found that only one of 48 burrows of the montane vole (*Microtus montanus*) extended to a depth greater than 50 cm (1.6 ft). Both of these species of voles are found in northern New Mexico. Maser et al. (1974, cited in Carroll and Genoways, 1980) found nest chambers of the sage vole that were 8 to 25 cm (0.3 to 0.8 ft) bgs, while James and Booth (1952, also cited in Carroll and Genoways, 1980) reported burrow depths of 10 to 46 cm (0.3 to 1.5 ft) bgs. Woodrats are common to New Mexico but generally live among rocks, cliffs, and vegetation, and do not establish extensive burrows for cover or foraging. While cottontail rabbits may establish burrows for cover or to give birth, these excavations are not expected to extend to great depths. For example, Ingles (1941) found desert cottontail (*Sylvilagus audubonii*) breeding burrows were 15 to 25 cm (0.5 to 0.8 ft) deep, while Orr (1940, cited in Chapman, 1975) found a maximum burrow depth of 0.6 m (2 ft) bgs for the mountain cottontail.

3.2.2 Mathematical Model

The mathematical expressions used to implement the biotic intrusion submodel are presented and discussed in the following sections. Section 3.2.2.1 describes the plant intrusion modeling and the equations used to simulate the impacts of animal intrusion are discussed in Section 3.2.2.2.

As discussed earlier, Area G is divided into eight waste disposal regions; the conditions under which biotic intrusion occurs are unique to each region. Consequently, the biotic intrusion modeling is conducted for each of these discrete locations. However, to reduce the complexity of the equations shown below, most references to specific waste disposal regions have been excluded.

3.2.2.1 Plant Intrusion

The rate at which contamination is deposited on the surface of Area G by plants is equal to the product of the litter production rate and the radionuclide concentrations in the litter. Litter production rates are calculated for the four plant growth forms included in the biotic intrusion submodel (i.e., grasses, forbs, shrubs, and trees) using the following:

$$l_{p,g,t} = (b_{a,g,e} \times (1. - f_{c,t}) + b_{a,g,c} \times f_{c,t}) \times l_{f,g} \qquad 1$$

Where

$l_{p,g,t}$ = litter production rate for plant growth form g at time t (kg/m^2/yr)
$b_{a,g,e}$ = aboveground biomass density of plant growth form g during early succession (kg/m^2)
$f_{c,t}$ = fraction of climax condition achieved at time t
$b_{a,g,c}$ = aboveground biomass density of plant growth form g under climax conditions (kg/m^2)
$l_{f,g}$ = litter production fraction for plant growth form g (yr^{-1})

The litter production fraction, $l_{f,g}$, represents the fraction of the aboveground biomass density that falls as litter during each year of the simulation.

The fraction of climax condition achieved at time t, $f_{c,t}$, is a measure of how far the site has progressed from the grassland conditions present at the time of facility closure to the piñon-juniper woodland characteristic of the expected climax condition. This fraction is estimated, based on the assumption that there is a linear transition between the condition of the disposal site at the time of final closure and the climax condition represented by piñon-juniper woodland, as follows:

$$f_{c,t} = 0.0 \qquad \text{for } t \le t_i \qquad 2$$

$$f_{c,t} = \frac{(t - t_i)}{t_c} \qquad \text{for } ti < t < t_i + t_c \qquad 3$$

$$f_{c,t} = 1.0 \qquad \text{for } t \ge t_i + t_c \qquad 4$$

Where

t = elapsed time since final closure of the disposal facility (yr)
t_i = length of institutional control period, measured from final closure of the disposal facility (yr)
t_c = length of time required to reach climax woodland condition

Maintenance activities are assumed to prevent succession toward piñon-juniper woodland throughout the active institutional control period. Site succession is assumed to start at the end of this period and to continue for a period equal to t_c, at which point the climax woodland is assumed to exist for the remainder of the simulation.

The radionuclide concentrations in the litter deposited on the surface of Area G will be proportional to the radionuclide concentrations in the soil in which the plant that produced the litter grew. The plant intrusion modeling assumes that litter is generated in proportion to the root mass found in each layer of the disposal system (i.e., the surface soil, cap, and waste layers). For example, if 50 percent of the root mass for a given growth form occurred in a given layer of the cap, 50 percent of the total litter production is assumed to have radionuclide concentrations proportional to the contaminant concentrations within that layer. Total radionuclide concentrations in the litter, then, represent the contaminant concentrations calculated for each layer of the disposal system, weighted by the root mass in each layer.

The product of the litter production rate given in Equation 1 and the fractions of the total plant root mass in the cap and waste layers yields the layer-specific litter production rates needed to

estimate the average contaminant concentrations in the litter deposited on the surface of Area G. For each growth form, root distribution functions are used to calculate the fraction of the root mass that lies between the ground surface and the bottom of each layer. The difference between the estimated fractions for a given layer and the overlying layer yields the fraction of the root mass found in the bottommost of the two layers. For instance, the fraction of the root mass that lies between the ground surface and the bottom of the first cap layer minus the corresponding fraction for the surface soil layer yields the fraction of the total root mass found in the uppermost cap layer for the growth form under consideration.

Foxx et al. (1984) conducted a comprehensive review of rooting data for species of plants that grow at LANL disposal sites and used the compiled data to develop rooting depth distributions for individual plant species. A distribution was developed for any species with at least six data points. If species-specific data were insufficient, distributions were developed on the basis of plant genera. All told, rooting depth distributions were developed for 12 species or genera of grasses, 10 species or genera of forbs, 2 species or genera of shrubs, and a single species of tree.

Least-squares regression analyses of the data developed by Foxx et al. (1984) for grasses and forbs were used to estimate composite rooting depth distributions for these two growth forms. The data used to conduct these analyses and the predicted composite distributions for grasses and forbs are shown in Figures 8a and 8b, respectively. Foxx et al. developed rooting distributions for only two species of shrubs, a number considered inadequate for estimating a composite rooting depth distribution for the growth form. Data from this study were supplemented with information from Tierney and Foxx (1987) to estimate rooting distributions for two additional shrub species, four-wing saltbush and rabbitbrush (*Chrysothamnus* spp.), which were then used in the development of the composite distribution shown in Figure 8c. Foxx et al. did not provide rooting distributions for tree species, reflecting a general lack of root distribution data for these plants. An average rooting depth of 6.4 m is cited by Foxx et al. for piñon pine; Tierney and Foxx cite estimated maximum root lengths of 1.1 to 1.3 m (3.6 to 4.3 ft) for this species. Foxx et al. cite average rooting depths ranging from 5.8 to 61 m (19 to 200 ft) for one-seed juniper, while Tierney and Foxx list a maximum root length of 1.7 m (5.6 ft).

The rooting depth distributions discussed above represent the frequencies with which plant roots penetrate to specified depths below the ground surface. As discussed earlier, plant uptake of radionuclides is assumed to be proportional to the root mass in a given layer or segment of the waste and cover. Although rooting depth frequencies and root mass distributions may be highly correlated, information in the literature suggests otherwise. For example, Jackson et al. (1996) conducted a literature review on root biomass distributions with depth. Based on that review, Jackson et al. estimated that 53, 83, and 52 percent of the total root biomass in deserts, temperate grasslands, and temperate coniferous forests, respectively, occurs within 30 cm (1 ft) of the soil surface. Looking at plant growth forms across all biomes except tundra, it was estimated that 75 percent of the root mass of grasses occurs in the top 30 cm (1 ft) of soil; the corresponding

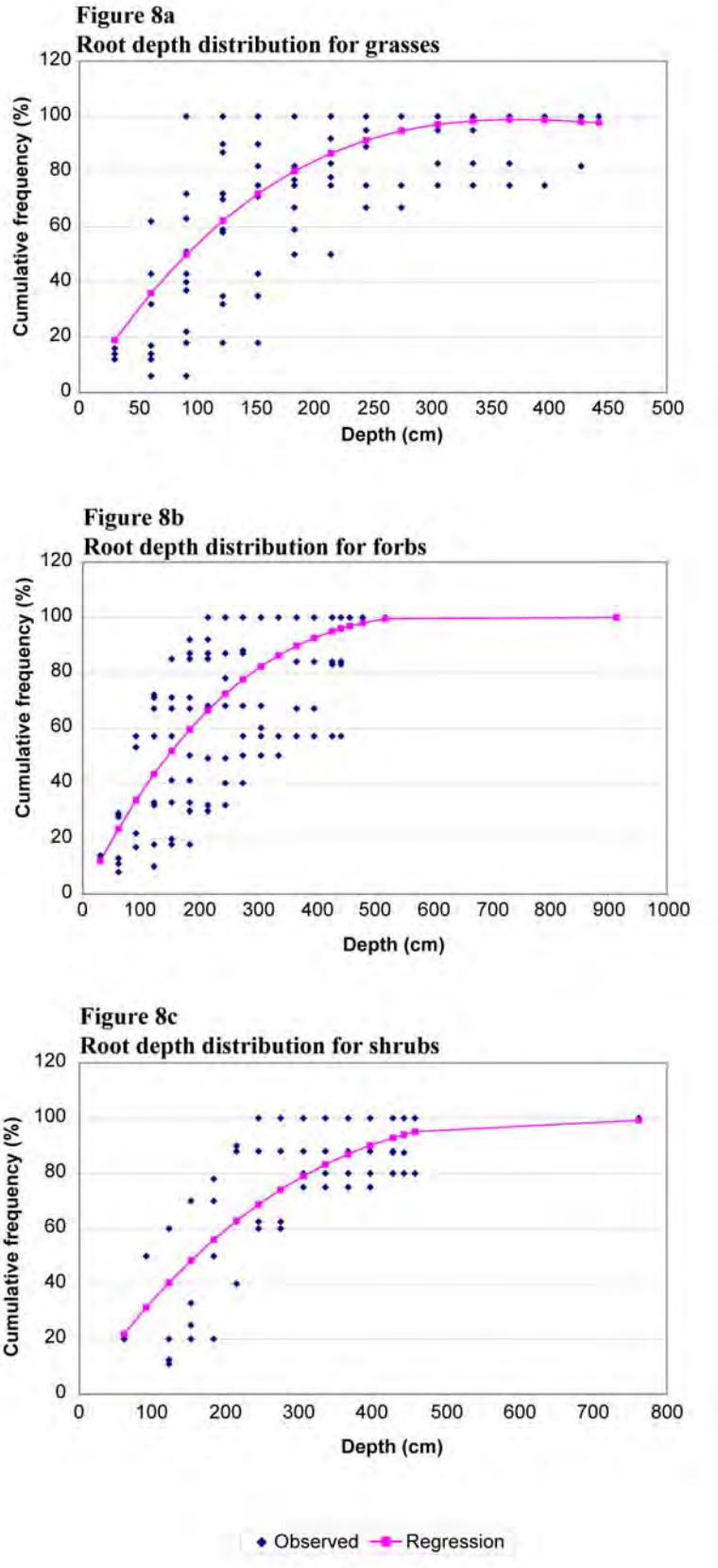

Figure 8
Root Depth Distributions for Grasses, Forbs, and Shrubs

figures for shrubs and trees are 47 and 60 percent. If the regression curves shown in Figure 8 were used to represent root mass with depth it would be concluded that less than 20 percent of the root mass of grasses, forbs, and shrubs lie within 30 cm (1 ft) of the ground surface.

The information needed to accurately characterize the distribution of root mass with depth for the grasses, forbs, shrubs, and trees that inhabit Area G is unavailable. Consequently, a series of functions was adopted to represent the distribution of root mass between the ground surface and the maximum rooting depth. This modeling was conducted using beta functions, the parameters for which were selected to evaluate a range of distribution patterns. The general form of the functions used to estimate root mass distribution with depth is:

$$R_{g,d} = B \times d^{\alpha} \times (d_{r,g,max} - d)^{\beta} \quad 5$$

Where

$R_{g,d}$ = fraction of root mass between ground surface and depth d for plant growth form g
B = beta function
d = depth (m)
α = shape factor
$d_{r,g,max}$ = maximum rooting depth of plant growth form g (m)
β = shape factor

The beta function is given by:

$$B = \frac{\Gamma(\alpha + \beta)}{\Gamma(\alpha) \times \Gamma(\beta) \times d_{r,g,max}^{\alpha+\beta}} \quad 6$$

Where

Γ = factorial of the quantities within the parentheses

The beta function can be simplified if α, one of the two shape factors, is set equal to zero, as shown in Equation 7:

$$B = \frac{1}{d_{r,g,\max}^{\alpha+\beta}} \quad 7$$

Using this formulation, the cumulative root mass distribution for a given depth, d, is given by the following:

$$R_{g,d} = 1 - \left(B \times d^{\alpha} \times (d_{r,g,\max} - d)^{\beta}\right) \quad 8$$

This is the form of the function that is implemented in the submodel. This quantity is set equal to 1.0 if the depth of interest exceeds the maximum rooting depth of the plant.

An example of the series of root mass distributions generated using the beta functions is shown in Figure 9. This figure shows the distribution curves for a plant growth form that has a maximum rooting depth of 1.5 m (4.9 ft). Similar curves are generated for alternate values of maximum rooting depth. In general, the root mass distributions estimated using this approach span the range of distributions suggested by the rooting depth frequencies discussed above and the findings of Jackson et al. (1996).

The radionuclide concentrations in the layer-specific litter fractions are determined by the rate at which plants extract contamination from the soil or waste via their roots. The uptake of radionuclides by plants is modeled in GoldSim using direct-transfer mass-flux links. These links specify the fractional rate at which radionuclides move from the soil or waste to the plant. They differ from advective mass-flux links in that only the contaminants in the soil or waste are transferred to the plants; advective mass-flux links transfer a quantity of an environmental medium (e.g., soil or water), along with whatever radionuclides it contains.

The transfer rate that is used to simulate the uptake of radionuclides by the fraction of the plant biomass that undergoes litterfall is given by the following equation:

$$p_{t,i,g,l,t} = \frac{l_{p,g,l,t} \times A_{ez} \times B_{i,c}}{A_{ez} \times t_l \times \rho} \qquad 9$$

Where

$p_{t,i,g,l,t}$ = plant transfer rate for radionuclide i in plant growth form g growing in layer l at time t (yr^{-1})
$l_{p,g,l,t}$ = litter production rate for plant growth form g growing in layer l at time t ($kg/m^2/yr$)
A_{ez} = area of disposal units over which the plants of interest are growing (m^2)
$B_{i,c}$ = soil-to-plant concentration factor for radionuclide i in crop c (Ci/kg dry weight vegetation per Ci/kg dry weight soil)
t_l = thickness of layer l (m)
ρ = bulk density of the soil or waste comprising layer l (kg/m^3)

Unlike the litter production rate included in Equation 1, the litter production rate in Equation 9 pertains only to the cover or waste layer for which the plant transfer rate is being calculated.

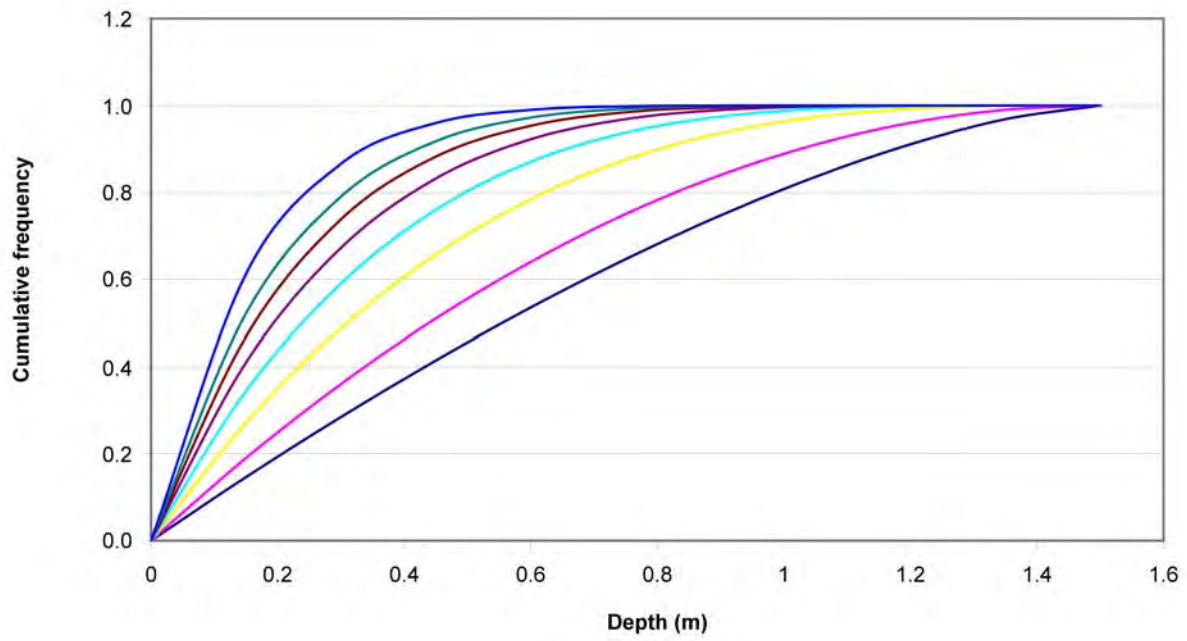

Figure 9
Root Mass Distributions for Plants with a Maximum Rooting Depth of 1.5 m

The radionuclides in the litter that falls to the ground will enter the surface soil at a rate proportional to the plant matter decomposition rate. A direct transfer mass-flux link is used to model the passage of contamination from the litter to the soil. The transfer factor used to describe this process is given by Equation 10:

$$l_t = \frac{\ln(2)}{\lambda_l} \qquad 10$$

Where

l_t = litter decomposition transfer factor (yr^{-1})
λ_l = litter decomposition half-life (yr)

The same transfer factor is used to model the decomposition of litter for all four plant growth forms included in the plant intrusion modeling.

3.2.2.2 Animal Intrusion

The animal intrusion modeling estimates the transport of contamination to the surface of Area G by harvester ants, pocket gophers, mice, and chipmunks and ground squirrels. The amount of contamination transported by these species is proportional to the amount of material excavated from the surface soil, cap, and waste layers and the radionuclide concentrations in each layer. The quantity of material excavated is estimated differently for each animal species. For harvester ants, the volume of material excavated in any given year is calculated using the following:

$$m_{s,ha,t} = (b_{d,ha,e} \times (1 - f_{c,t}) + b_{d,ha,c} \times f_{c,t}) \times b_{m,ha} \times r_{b,ha} \qquad 11$$

Where

$m_{s,ha,t}$ = rate of soil or waste excavation by harvester ants at time t (kg/ha/yr)
$b_{d,ha,e}$ = burrow density for harvester ants during early succession (ha^{-1})
$b_{d,ha,c}$ = burrow density for harvester ants under climax conditions (ha^{-1})
$b_{m,ha}$ = mass of harvester ant burrow (kg)
$r_{b,ha}$ = burrow renewal rate for harvester ants (yr^{-1})

The fraction of climax condition achieved at time t, $f_{c,t}$, is given by Equations 2 through 4. The burrow renewal rate is set equal to 1.0/yr for the first year following final closure of the disposal facility; thereafter, it is estimated as the inverse of the harvester ant colony life span.

Soil and waste excavation rates for pocket gophers are given by the following:

$$m_{s,pg,t} = (r_{r,pg,e} \times (1 - f_{c,t}) + r_{r,pg,c} \times f_{c,t}) \times r_{b,pg} \times \rho \qquad 12$$

Where

$m_{s,pg,t}$ = rate of soil or waste excavation by pocket gophers at time *t* (kg/ha/yr)
$r_{r,pg,e}$ = soil or waste removal rate during early succession (m^3/ha)
$r_{r,pg,c}$ = soil or waste removal rate under climax conditions (m^3/ha)
$r_{b,pg}$ = burrow renewal fraction for pocket gophers (yr^{-1})

Soil and waste excavation rates for mice, chipmunks, and ground squirrels are calculated as follows:

$$m_{s,a,t} = (b_{d,a,e} \times (1 - f_{c,t}) + b_{d,a,c} \times f_{c,t}) \times b_{m,a} \times r_{b,a} \times \rho \qquad 13$$

Where

$m_{s,a,t}$ = rate of soil or waste excavation by animal species *a* at time *t* (kg/ha/yr)
$b_{d,a,e}$ = burrow density for animal species *a* during early succession (ha^{-1})
$b_{d,a,c}$ = burrow density for animal species *a* under climax conditions (ha^{-1})
$b_{m,a}$ = volume of animal species' burrows (kg)
$r_{b,a}$ = burrow renewal fraction for animal species (yr^{-1})

The burrow renewal fractions in Equations 12 and 13 are set equal to 1.0/yr for the first year of the simulation following facility closure, and to the user-specified fraction thereafter.

The soil removal rates calculated for the animals are allocated among the cover and waste layers that comprise the disposal facility using burrow depth distribution functions. These functions, like the plant root-mass distributions discussed earlier, calculate the fraction of the burrow system that lies between the ground surface and the bottom of each layer. Taking the difference between the estimated fraction for a given layer and the one above it yields the fraction of the total burrow volume found in the bottommost of the two layers. For instance, if the fraction of the burrow between the ground surface and the bottom of the first waste layer is 0.9, and the corresponding fraction for the surface soil layer and entire cap is 0.8, then the fraction of the total burrow volume found in the first waste layer is 0.1.

Relatively little information is available to describe the distribution of animal burrows with depth. McKenzie et al. (1982) conducted a review of the burrowing habits of several species of harvester ants and small mammals, many of which are expected to occur at Area G. As part of that work, they estimated burrow distributions with depth; these estimates are provided in Table 4. Reynolds and Laundre (1988) examined the distribution of burrows with depth for Townsend's ground squirrel (*Spermophilus townsendii*), Ord's kangaroo rat (*Dipodomys ordii*), the deer mouse, and the montane vole. The data collected for the ground squirrel and kangaroo rat indicate that the burrows of these species are shallower than indicated by McKenzie et al. (see Table 4). However, the decrease in the fraction of the burrow system with depth was less pronounced than that suggested by the data given in McKenzie et al.

Table 4
Burrow Depth Distributions for Area G Animal Species

Animal Species	Fraction of Burrow Systems within Indicated Depth Interval				
	0–0.5 m	0.5–1.0 m	1.0–1.5 m	1.5–2.0 m	> 2.0 m
Harvester Ants	7.0E-01	1.0E-01	1.0E-01	5.0E-02	5.0E-02
Pocket Mice and Kangaroo Rats	5.0E-01	4.0E-01	5.0E-02	5.0E-02	0.0E+00
Pocket Gophers	8.5E-01	1.5E-01	0.0E+00	0.0E+00	0.0E+00
Ground Squirrels	5.0E-01	3.0E-01	1.5E-01	5.0E-02	0.0E+00

Source: McKenzie et al., 1982

The paucity of burrow depth distribution data makes it difficult to develop accurate depth distributions for the GoldSim model. Because the required information was not available, a series of burrow depth distributions was developed using beta functions. The parameters for these functions were selected to evaluate a range of burrow distribution patterns. The general form of the functions used to estimate burrow distributions with depth is as follows:

$$B_{a,d} = B \times d^{\alpha} \times (d_{b,a,\max} - d)^{\beta} \qquad 14$$

Where

$B_{a,d}$ = fraction of burrow between ground surface and depth d for animal species a
B = beta function
d = depth (m)
α = shape factor
$d_{b,a,max}$ = maximum burrowing depth of animal species a (m)
β = shape factor

The beta function is given by:

$$B = \frac{\Gamma(\alpha + \beta)}{\Gamma(\alpha) \times \Gamma(\beta) \times d_{b,a,\max}^{\alpha+\beta}} \qquad 15$$

Where

Γ = factorial of the quantities within the parentheses

Consistent with the earlier discussion about plant root-mass distributions, the beta function can be simplified to the following if α, one of the two shape factors, is set equal to zero:

$$B = \frac{1}{d_{b,a,\max}^{\alpha+\beta}} \quad 16$$

Using this formulation, the cumulative burrow distribution for a given depth, *d*, is as follows:

$$B_{a,d} = 1 - \left(B \times d^{\alpha} \times (d_{b,a,\max} - d)^{\beta}\right) \quad 17$$

This is the form of the function that is implemented in the submodel. This quantity is set to 1.0 if the depth of interest exceeds the maximum burrowing depth of the animal.

An example of the series of burrow depth distributions generated using the beta functions is shown in Figure 10. This figure shows the distribution curves for an animal species that has a maximum burrowing depth of 3.0 m (10 ft). Similar curves are generated for alternate values of maximum burrowing depth.

Multiplying the soil or waste removal rate for a given animal species by the fractions of the burrow system within the cap and waste layers yields layer-specific bulk removal rates for that material. Any radionuclides contained in the soil (or waste) will be distributed between the soil (or waste) and the moisture occupying the pores of the material. The radionuclides in the solid and liquid phases are transported separately by the GoldSim models, requiring that the bulk removal rates be allocated to the corresponding soil (or waste) and water removal rates. The equations used to calculate the soil (or waste) and water removal rates for the cap and waste layers are shown below for the harvester ant:

$$m_{ss,ha,l,t} = \frac{m_{s,ha,t} \times f_{ha,l,t} \times \rho_d}{\rho} \quad 18$$

$$m_{sm,ha,l,t} = \frac{m_{s,ha,t} \times f_{ha,l,t} \times m_s}{\rho} \quad 19$$

Where

$m_{ss,ha,l,t}$ = dry soil or waste excavation rate by harvester ants for layer *l* at time *t* (kg/ha/yr)
$f_{ha,l,t}$ = fraction of harvester ant burrow in layer *l* at time *t*
ρ_d = dry density of soil or waste (kg/m^3)
$m_{sm,ha,l,t}$ = soil or waste moisture excavation rate by harvester ants for layer *l* at time *t* (kg/ha/yr)
m_s = moisture content of soil or waste

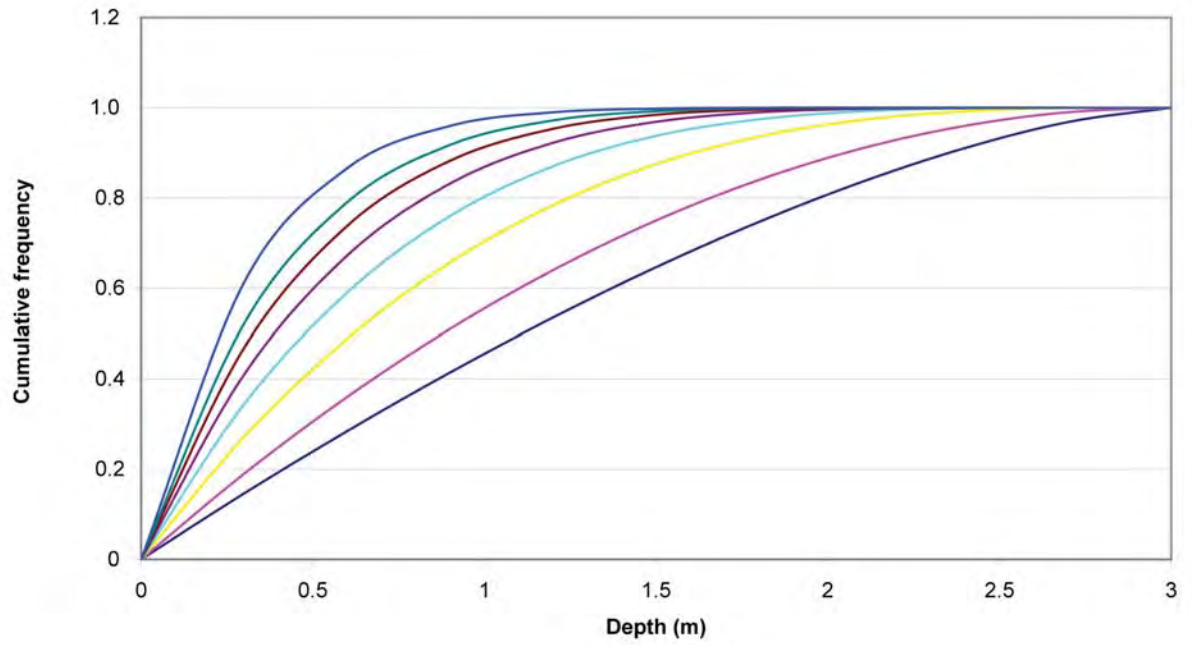

Figure 10
Burrow Depth Distributions for Animals with a Maximum Burrowing Depth of 3 m

The soil and water removal rates are summed across animal species to yield layer-specific soil and water transport rates for each of the eight waste disposal regions. The impacts of biotic intrusion are modeled in the site model throughout the simulation period. The intruder models assume native plants and animals inhabit the site and intrude into the waste until the intruder arrives at the disposal facility.

3.3 Surface Erosion Modeling

Surface erosion may have a significant impact on the long-term performance of the closed disposal facility. Erosion of the disposal site will reduce the thickness of the cover overlying the disposed waste, thereby permitting greater penetration into the waste by plants and animals and by inadvertent human intruders. The rate at which erosion occurs determines how quickly surface contamination is transported into Cañada del Buey and Pajarito Canyons and, hence, has a direct bearing on the doses projected for the canyon-resident scenarios. Finally, thinning of the cover may increase the release rates of vapor- and gas-phase contaminants.

Surface erosion modeling is conducted to project rates of cover loss at Area G and to estimate rates of sediment transport into the adjacent canyons. The erosion submodel is incorporated into the site, intruder, and intruder diffusion models. The manner in which the erosion modeling is conducted is discussed in the following sections.

3.3.1 Cover Loss

In general, patterns and rates of surface erosion at Area G are complex, due to the characteristic mesa and canyon topography of the Laboratory and the construction details of the final cover. Rates of soil loss are spatially dependent, affected by local variations in slope and drainage area, the presence of engineered features placed during cover construction, and changes in relationships between the disposal units and the underlying bedrock. Given the potential importance of surface erosion on long-term facility performance, the surface of the site was represented in three dimensions to capture this spatial dependence.

As stated earlier, Area G is represented using eight waste disposal regions. The erosion submodel estimates the cumulative soil loss within each disposal region throughout the model simulations; these losses are used to update the thickness of the surface soil, cap, and waste layers for each region. The erosion modeling yields the cumulative depths from the ground surface to the bottoms of the different layers, and the thickness of each layer.

Patterns and rates of erosion projected by the GoldSim models are based on long-term surface erosion modeling conducted using the SIBERIA computer code (Willgoose and Riley, 1998). A series of 10,000-year simulations was conducted using SIBERIA to estimate changes in cover depth over the disposal pits and/or shafts comprising each region. Separate simulations were

conducted for conditions that are expected to yield low-, moderate-, and high-erosion impacts. A detailed description of this modeling effort may be found in Wilson et al. (2005).

The SIBERIA modeling represented the disposal facility, including the disposal units and the intervening areas, using over 70,000 nodes; rates of cover loss versus time were projected for each of these nodes. The erosion submodel implemented within the GoldSim models uses the erosion calculations for these nodes to project the impacts of erosion at Area G. To illustrate, consider the disposal units in waste disposal region 1. The pits and shafts in this region are represented by approximately 4,000 nodes in the SIBERIA modeling. One of these nodes is randomly selected in the first realization of the probabilistic simulation; the initial cover thickness at that location and the projected rate at which the material is eroded are assumed to apply to all nodes within the disposal region and the performance of the facility over the 1,000-year compliance period is projected on this basis. Successive realizations are performed in which other nodes are selected to represent the disposal region and the process is repeated.

The SIBERIA modeling evaluated rates of cover loss for three scenarios under which erosional pressures were expected to vary; these are referred to as the low, moderate, and high erosion scenarios. The updated erosion modeling takes the results for these scenarios into account by assigning a likelihood of occurrence to each scenario. This distribution is sampled for each realization of the probabilistic simulation and used to determine which set of cover loss projections is adopted for each node. For example, assume moderate erosion conditions persist 80 percent of the time while conditions conducive to low and high erosion pressures each exist 10 percent of the time. In this case, the distribution of cover loss projections for the moderate erosion scenario is sampled in 80 percent of the realizations, while cover loss projections for each of the other scenarios are sampled in 10 percent of the realizations.

Projected rates of soil loss are used to reduce the thickness of the waste repository cover over time. Although actual soil loss progresses downward from the surface of the disposal facility, a different approach was adopted for the GoldSim models. Integral to this approach is the division of the cover into two components, the surface soil layer and the cap. The surface soil layer is defined as the top 1 cm (0.4 in.) of cover material; the cap represents the entire cover less this top 1 cm (0.4 in.). This division allows a more accurate estimation of the radionuclide concentrations in the material subject to resuspension and transport by surface runoff.

For modeling purposes, the surface soil layer is maintained at a constant 1 cm (0.4 in.) depth. However, this thin layer is subject to rapid erosion. To avoid the need to constantly redefine the surface layer, the GoldSim models account for the effects of erosion by replenishing it with material from the underlying cap or, if the cap has been eroded away, the waste. This is done by transporting the quantity of soil lost annually due to erosion from the surface soil layer to the

adjacent canyons and then transporting a like quantity from the cap or waste to the surface soil layer to maintain the material balance in the surface layer.

The material transferred from the cap or waste to the surface soil layer is drawn from the uppermost layer of cap (or waste) material. For example, shortly after site closure, bulk crushed tuff is transferred from cap layer 1 to the surface soil layer to simulate the loss of soil due to erosion; the thickness of the cap layer is reduced accordingly. Later, if the uppermost cap layer has been lost due to erosion, material used to replenish the surface soil layer is taken from cap layer 2 and the thickness of that layer is reduced accordingly. This process is repeated until the end of the simulation.

The origin of the cover or waste material used to replenish the surface soil layer is tracked using a series of cap-and-waste-loss fractions. The elements used for this process are found in containers specific to each waste disposal region which, in turn, are found in the Erosion_Model container. These elements determine if the soil loss for the current year of the simulation is less than the remaining cap or waste material in the uppermost layer of material. If so, the loss fraction for the cap or waste layer is set equal to 1.0, which indicates that all material used to replenish the surface soil layer originates from the uppermost cap or waste layer. This layer is then reduced in thickness and the process is repeated in the next time step of the simulation. If, however, the projected soil loss exceeds the remaining thickness of the uppermost cap or waste layer, the model transfers material from the next cap or waste layer to make up the difference and the thickness of each layer is adjusted.

Over a long enough time period, surface erosion of the disposal facility may result in the complete removal of part or all of the waste repository cover. However, because the GoldSim models become less stable when one or more of the layers used to represent the disposal system profile is completely lost, a simplification incorporated into the erosion model prevents this occurrence. Soil loss from the cap layers is assumed to continue until the total thickness of the cap reaches 1 cm (0.4 in.), after which erosion is assumed to cease for the remainder of the simulation. As a result, the minimum thickness for each cap layer is 1 cm (0.4 in.) divided by the number of cap layers. This minimum cap thickness combined with the 1 cm (0.4 in.) surface soil layer (which is held constant) results in a minimum total cover thickness of 2 cm (0.8 in.), even after complete cover loss is projected to occur. A similar approach is applied to the erosion of the waste layers; erosion is assumed to continue until 1 cm (0.4 in.) of waste remains, at which time the thickness of each waste layer is 1 cm (0.4 in.) divided by the number of waste layers.

3.3.2 Sediment Transport

In general, surface contamination transported from Area G by runoff will enter either Cañada del Buey or Pajarito Canyon, both of which are adjacent to the disposal facility. The portion of contamination allocated to each canyon will depend upon several factors including the location

of the disposal units relative to the axis of the mesa, local slope characteristics of the cover, and engineered features of the cover. Although surface erosion modeling was conducted primarily to estimate rates of cover removal, the results of this work also provide insight into spatial aspects of contaminant transport at the disposal facility.

The SIBERIA modeling results (Wilson et al., 2005) were used to estimate sediment flows into Cañada del Buey and Pajarito Canyon for the three erosion scenarios. Each canyon was divided into two or more catchments based on expected sediment transport patterns, as depicted in Figure 11. In terms of Cañada del Buey, catchment CdB1 includes the majority of the canyon that may receive contaminated sediments from Area G; catchment CdB2 lies at the east end of the disposal facility and is projected to capture sediment transported from a portion of waste disposal region 1. Pajarito Canyon was divided into seven catchments, primarily on the basis of the small drainages that transport the majority of the sediment generated on top of Mesita del Buey.

The SIBERIA model was used to estimate the quantities of sediment transported from the eight waste disposal regions to the canyon catchments. Sediment was tracked from its source on the mesa to the point at which it was transported over the edge of the mesa. The sediment was then assigned to the catchment below this point. Estimates were made of the total sediment transported from each disposal region and the sediment yield from the surface of the pits and shafts within each disposal region. Sediment transported from disposal region 7, which consists mainly of shafts scattered among the region 3 pits, was assumed to follow the paths estimated for region 3. The allocation of sediment among the nine catchments was evaluated at periods of 100, 200, 500, 1,000, 5,000, and 10,000 years after facility closure.

The results of the sediment mapping indicate that 20 to almost 100 percent of the sediment within a waste disposal region is transported to Cañada del Buey. Sediments transported from each of the waste disposal regions to Pajarito Canyon enter one to three of the catchments, depending upon the disposal region under consideration. The small drainages along the south side of the mesa tend to focus sediment flows into this canyon. Detailed results of the sediment mapping analysis are included in Section 5.7.1 of this report.

3.4 Human Intrusion Modeling

The human intrusion submodel is used to calculate the amount of cover material and waste that is excavated and spread across the receptor's lot for the Intruder-Construction, Intruder-Agriculture and Intruder–Post-Drilling Scenarios. The total volume of material brought to the surface of the disposal site as a result of basement excavation is calculated using the following equation:

$$V_b = \frac{b_d \times (b_w \times b_l + e_{w,s} \times e_{l,s} + 4 \times e_{w,0.5b} \times e_{l,0.5b})}{6} \qquad 20$$

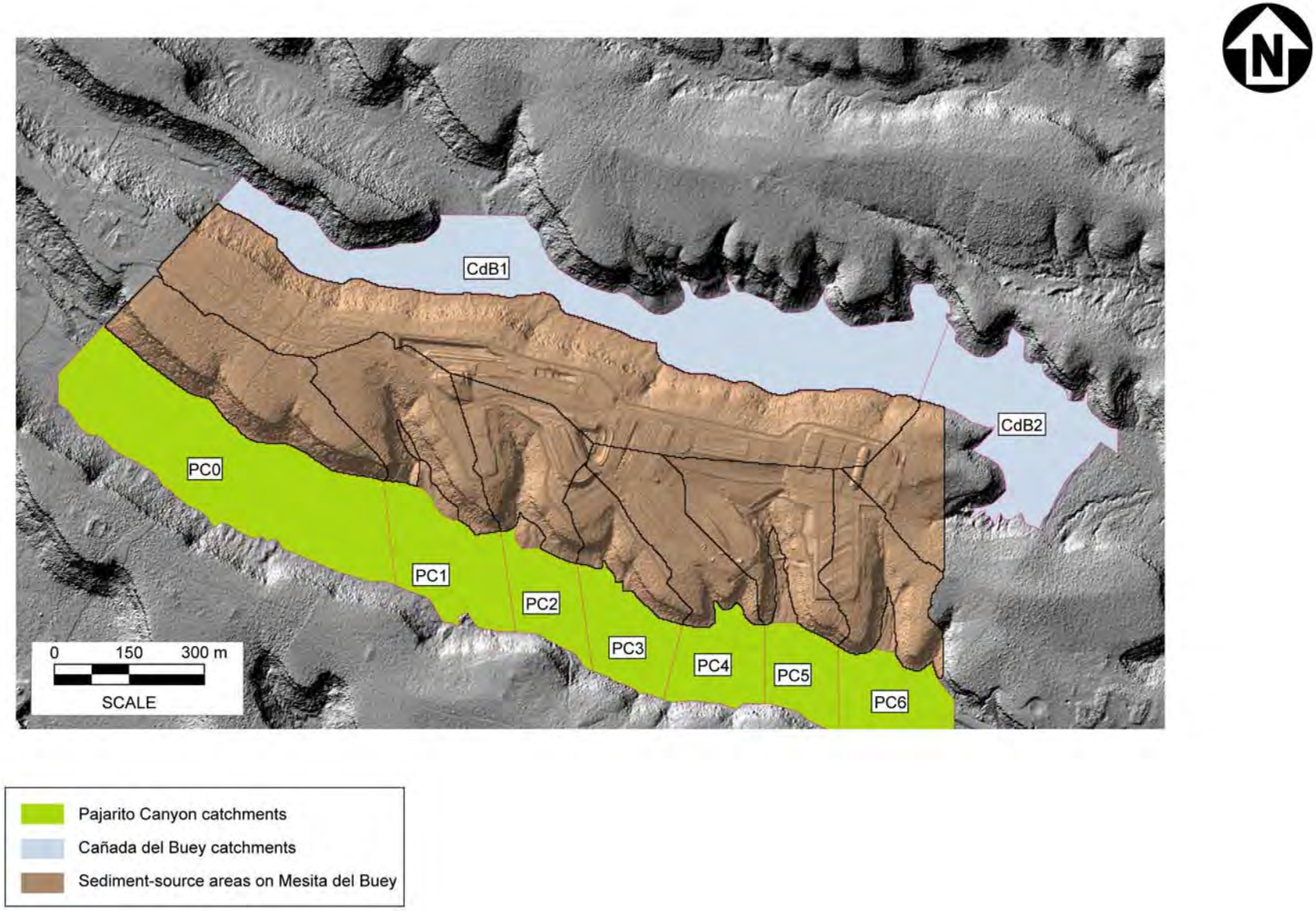

Figure 11
Area G Sediment-Source Areas and Sediment Catchments in Habitable Canyons

Where

V_b = volume of material excavated during basement construction (m^3)
b_d = depth of basement (m)
b_w = width of basement (m)
b_l = length of basement (m)
$e_{w,s}$ = width of basement excavation at ground surface (m)
$e_{l,s}$ = length of basement excavation at ground surface (m)
$e_{w,0.5b}$ = width of basement excavation at one-half of the basement depth (m)
$e_{l,0.5b}$ = length of basement excavation at one-half of the basement depth (m)

The material brought to the surface during basement excavation will include cover material and waste. Assuming the waste is a single layer of material, the volume of waste brought to the surface is calculated as follows:

$$V_{w,b} = \frac{t_w \times (b_w \times b_l + e_{w,w} \times e_{l,w} + 4 \times e_{w,0.5w} \times e_{l,0.5w})}{6} \qquad 21$$

Where

$V_{w,b}$ = volume of waste excavated during basement construction (m^3)
t_w = thickness of waste (m)
$e_{w,w}$ = width of basement excavation at cover-waste interface (m)
$e_{l,w}$ = length of basement excavation at cover-waste interface (m)
$e_{w,0.5w}$ = width of basement excavation at one-half of the waste thickness (m)
$e_{l,0.5w}$ = length of basement excavation at one-half of the waste thickness (m)

The difference between the total amount of excavated material and the amount of excavated waste is the volume of cover material excavated during basement construction.

Equation 21 is applicable only if the waste is represented by a single layer of material. In fact, the cap and waste are represented using 4 cells each in the intruder model, while the intruder model with diffusion represents the cap and waste using 16 and 20 cells, respectively. In these models, then, the volumes of material removed during basement excavation are explicitly calculated for each of the affected cap and waste layers. Although the same general equation is used to conduct these calculations, the parameters are defined in terms of the lengths and widths of the excavation at the top, midpoint, and bottom of the cap or waste layer under consideration, and the thickness of that layer.

The cover material and waste excavated during basement construction is assumed to be thoroughly mixed. A portion of the mixed material is used for backfill around the foundation of the house. The volume of this backfill is the difference between the total volume of excavated material and the product of the dimensions of the basement. The remaining material is spread over the intruder's lot. The thickness of the material over the lot is calculated as the excavation

volume less the volume of material used for backfilling, divided by the net lot area. The net lot area is the total lot size less the area of the receptor's house.

The Intruder–Post-Drilling Scenario assumes that the well that is established to supply water for domestic needs will pass through the cover, waste, and strata underlying the disposal units. The volume of waste brought to the surface during drilling is given by the following equation:

$$V_{w,d} = \pi \times r_{wc}^2 \times t_w \qquad 22$$

Where

$V_{w,d}$ = volume of waste excavated during well drilling (m^3)
r_{wc} = radius of the well casing (m)
π = the constant *pi* (3.1416)

Equation 22 is used to calculate the volume of cover material brought to the surface during drilling by substituting the cover thickness for the waste thickness. The thickness of the cover is modified over time to account for the effects of surface erosion at Area G. The well will also pass through the strata that lie between the bottom of the disposal units and the regional aquifer. Although this material will also be brought to the surface, it is ignored in terms of determining radionuclide concentrations in the surface soils to which the intruder is exposed.

3.5 Diffusion Modeling

The Area G Site and Intruder Diffusion Models estimate the rates of generation of vapor- and gas-phase radionuclides, and simulate the upward movement of the radionuclides from the disposed waste. Contamination is transported from the cover to the air above the disposal facility in the site model. The intruder diffusion model transports radionuclides to the surface of the facility, into the basement excavation, or through the floor of the concrete foundation of the intruder's house, depending upon the exposure scenario under consideration.

The diffusion of radionuclides between cells is invoked by linking the transport pathway elements with diffusive mass-flux links. The mathematical model used by GoldSim to model transport under these conditions is discussed in the user's manual for the contaminant transport module (GoldSim, 2007c).

The site and intruder diffusion models divide the cap into 16 layers and the waste into 20 layers. Dividing the cap and waste into several layers is necessary to ensure accurate estimates of the diffusion rates through these materials. Using too few layers to represent the cover and waste will artificially increase rates of transport through the disposal system, while using an excessive number of layers complicates the model and slows model execution. The level of discretization adopted for the diffusion models was determined on the basis of the analyses described in *Attachment I*.

The initial thickness of all but the uppermost cap layer is set equal to the total cover thickness divided by 16; the thickness of cap layer 1 is reduced by 1 cm (0.4 in.) to account for the presence of the surface soil layer. The initial thickness of the waste layers varies with depth. The individual thickness of the top 10 waste layers is set to either one-twentieth of the total waste thickness or 0.25 m (0.8 ft), whichever is less. The thickness of each of the bottommost 10 layers is set to one-tenth of the total waste thickness less the combined thickness of the top 10 layers. The intruder diffusion model divides the floor of the receptor's concrete foundation into 4 layers of equal thickness.

The site and intruder diffusion models simulate the movement of tritiated water vapor, C-14 gas, krypton, and radon through the disposal system. The gas-to-water partition coefficients are calculated within the models to describe how these species are allocated between their vapor or gas phase and the water occupying the pores of the cover and waste. The partition coefficient for tritium is given by the following:

$$KD_{H3,air} = \frac{VP \times M}{R \times T \times \rho_{H2O}} \qquad 23$$

Where

$KD_{H3,air}$	=	air-to-water partition coefficient for H-3
VP	=	vapor pressure of H-3 (atm)
M	=	molecular weight of water (g/mol)
R	=	ideal gas constant (atm-m^3/mol-˚K)
T	=	temperature (˚K)
ρ_{H_2O}	=	density of water (g/m^3)

C-14 (as CO_2 or CH_4), krypton, and radon will partition between air and water in the pore spaces of the cap and waste in proportion to their Henry's Law constant. The partition coefficients for these species are given by Equation 24:

$$KD_{j,air} = \frac{1}{H_j \times R \times T} \qquad 24$$

Where

$KD_{j,air}$	=	air-to-water partition coefficient for gas j
H_j	=	Henry's Law constant for gas j (mol/m^3-atm)
R	=	ideal gas constant (atm-m^3/mol-˚K)
T	=	temperature (˚K)

The diffusion coefficients used in the diffusion modeling are calculated using the empirical relationship developed by Millington (1959):

$$D_e = D_o \times \frac{p_a^{10/3}}{p^2} \qquad 25$$

Where

D_e = pore diffusion coefficient (m^2/s)
D_o = gas diffusion coefficient in free air (m^2/s)
p_a = air-filled porosity
p = effective porosity

Separate diffusion coefficients are calculated for the waste in the disposal units, the cap, and the concrete used to construct the foundation of the intruder's house. The cap and waste diffusion coefficients calculated for tritium are multiplied by a thermal gradient factor to account for the effect of thermal gradients in these materials upon the apparent rate of diffusion (Philip and DeVries, 1957); thermal gradient effects are not considered for the concrete foundation.

The diffusion coefficients estimated using Equation 25 are modified to conform to the manner in which GoldSim parameterizes the diffusion process. GoldSim requires input of unitless quantities called relative diffusivities, which it multiplies by the reference diffusivity and the available porosity, effective porosity, and tortuosity of the porous medium to yield the final effective diffusion coefficients used in the model simulations. Given this approach, the diffusion coefficients calculated above are divided by the reference diffusivity and effective porosity of the porous medium under consideration to calculate the desired relative diffusivities. The available porosity and tortuosity of the medium are both set to 1 under this modeling approach.

The amount of C-14 available for diffusion as C-14 gas is given by the product of the C-14 inventory and the organic fraction of the waste. The organic waste inventory is multiplied by a gas generation rate constant that describes the rate at which the waste biodegrades. The gas generated as a result of biodegradation is allocated to CO_2 and CH_4.

Only a portion of the radon gas generated by the decay of its long-lived parents will be available for diffusion; the rest will remain trapped within the solid waste until it decays to negligible levels. Radon gas generation rates are represented by modifying the decay characteristics of the parents of Rn-220 and Rn-222. Specifically, the fraction of time the parents of the radon isotopes decay to form radon gas is set equal to the radon emanation coefficient; during the remainder of the time, the decay of the parents forms daughters of Rn-220 and Rn-222.

3.6 Exposure Modeling

The Area G performance assessment and composite analysis project potential human exposures for the exposure scenarios described in Section 2.2.1 (Table 1). In these scenarios, the receptor is postulated to come into contact with contamination and receive doses via ingestion, inhalation, and direct radiation. The modeling that is conducted to estimate the exposures received through these routes is discussed in the following sections.

3.6.1 Ingestion Exposure Route

The performance assessment and composite analysis receptors are postulated to ingest contaminated soil, food crops, animal products, and water. In general, the ingested activity of a given radionuclide is the product of the consumption rate of the ingested item, the proportion of the total material ingested that is contaminated, and the radionuclide concentration in the soil, food, or water:

$$I_{g,m,i,t} = U_m \times f_m \times C_{m,i,t} \qquad 26$$

Where

$I_{g,m,i,t}$ = intake, through material *m*, of radionuclide *i* through time *t* (Ci/yr)
U_m = consumption rate of material *m* (kg/yr)
f_m = fraction of consumed material that is contaminated
$C_{m,i,t}$ = concentration, in material *m*, of radionuclide *i* at time *t* (Ci/kg)

The quantities of substances ingested by a receptor are given by the ingestion rates for vegetables, animal products, soil, and water. The receptors for the All Pathways–Groundwater, Atmospheric, All Pathways–Canyon, Intruder-Agriculture, and Intruder–Post-Drilling Scenarios are assumed to consume homegrown vegetables, animal products from animals raised on location, and soil. The receptor for the Groundwater Resource Protection Scenario is assumed to ingest contamination only through drinking water, while the construction intruder scenario assumes that the receptor receives contamination only from ingested soil.

The fraction of a receptor's intake of vegetables that is grown at the exposure location is defined initially from a user-specified input value. The ratio of the area available for growing crops and the area needed to raise the specified quantities of leafy vegetables, produce, and grain is then calculated using the following equation:

$$f_{cc} = \frac{A_l - A_h}{\frac{U_{lv}}{Y_{lv}} + \frac{U_p}{Y_p} + \frac{U_g}{Y_g}} \times f_{uc} \times 1 \qquad 27$$

Where

f_{cc} = crop capacity factor, or the proportion of the specified crops that can be grown on the receptor's lot
A_l = area of receptor's lot (m^2)
A_h = area of receptor's house (m^2)
U_{lv} = human consumption rate of leafy vegetables (kg/yr)
Y_{lv} = annual agricultural yield of leafy vegetables (kg/m^2 wet weight)
U_p = human consumption rate of produce (kg/yr)
Y_p = annual agricultural yield of produce (kg/m^2 wet weight)
U_g = human consumption rate of grain (kg/yr)
Y_g = annual agricultural yield of grain (kg/m^2 wet weight)
f_{uc} = user-specified fraction of crops that is grown on site
1 = constant (yr)

The crop capacity factor is set equal to the lesser of the calculated fraction or 1.0. The result is multiplied by the user-specified fraction of crops grown on site to yield the fraction used in the dose assessment. A factor of 1.0 indicates that the area required to raise the crops exists and the user-specified homegrown fraction is used in the dose calculations. Factors less than 1.0 indicate that the specified space requirements cannot be satisfied and the fraction of the receptor's intake that is contaminated is reduced.

After the area required to raise the vegetables at the receptor location is defined, the remaining portion of the receptor's lot area may be allocated for raising animals (to be consumed by the receptor). Human consumption rates of animal products are used in conjunction with crop productivities to determine the amount of land needed to raise forage for the animals. This calculation accounts for both the number of animals needed to supply the receptor's food requirements and the forage requirements of these animals. The equation used to estimate the animal forage capacity factor for cattle and cows is as follows:

$$f_{pg} = \frac{A_l - A_h - \left(\frac{U_{lv}}{Y_{lv}} + \frac{U_p}{Y_p} + \frac{U_g}{Y_g}\right) \times f_{uc} \times f_{cc} \times 1}{\frac{\left(N_{ct} \times Q_{f,ct} + N_{cw} \times Q_{f,cw}\right)}{Y_{pg}} \times 1} \qquad 28$$

Where

f_{pg} = forage capacity factor for cattle and cows, or the proportion of animals' forage requirements that can be grown on the receptor's lot
N_{ct} = number of full-time cattle equivalents required to supply the specified quantity of beef
$Q_{f,ct}$ = forage consumption rate of cattle (kg/yr dry weight)

N_{cw} = number of full-time cow equivalents required to supply the specified quantity of milk
$Q_{f,cw}$ = forage consumption rate of cows (kg/yr dry weight)
Y_{pg} = annual agricultural yield of pasture grass (kg/m^2 dry weight)
1 = constant (yr)

The numerator of Equation 28 is set to the greater of the calculated quantity or 0 m^2 (0 ft^2), and the animal forage capacity factor is set to the lesser of the calculated fraction or 1. Factors less than 1.0 indicate that the forage needed by the animals to supply the specified amounts of beef and milk cannot be grown on the land available on site. Under these conditions, portions of the animals' diet requirements are assumed to come from uncontaminated lands.

The numbers of cattle and cows required to supply the beef and milk are calculated as follows:

$$N_{ct} = \frac{U_{bf} \times f_{bf} \times 1}{w_{ct} \times r_{cl} \times f_{cb}} \quad 29$$

$$N_{cw} = \frac{U_{mk} \times f_{mk}}{y_{mk}} \quad 30$$

Where

U_{bf} = human consumption rate of beef (kg/yr)
f_{bf} = fraction of receptor-consumed beef supplied by animals raised on site
1 = constant (yr)
w_{ct} = weight of cattle at slaughter (kg)
r_{cl} = carcass-to-live-weight ratio
f_{cb} = fraction of carcass that is edible meat
U_{mk} = human consumption rate of milk (kg/yr)
f_{mk} = fraction of receptor-consumed milk supplied by animals raised on site
y_{mk} = milk production rate (kg/yr)

An equation similar to Equation 28 is used to calculate the forage capacity factor for chickens:

$$f_g = \frac{A_l - A_h - \left(\frac{U_{lv}}{Y_{lv}} + \frac{U_p}{Y_p} + \frac{U_g}{Y_g}\right) \times f_{uc} \times f_{cc} \times 1}{\frac{\left(N_{ch} \times Q_{g,ch} + N_{cl} \times Q_{g,ch}\right)}{Y_g \times d_{wg}} \times 1} \quad 31$$

Where

f_g = forage capacity factor for chickens, or the proportion of the birds' forage requirements that can be grown on the receptor's lot

N_{ch} = number of full-time equivalent chickens required to supply the specified quantity of chicken
$Q_{g,ch}$ = grain consumption rate of chickens (kg/yr dry weight)
N_{cl} = number of full-time equivalent layers required to supply the specified quantity of eggs
$d_{w,g}$ = dry-to-wet-weight fraction for grain

The numbers of chickens required to supply the chicken and eggs are calculated as follows:

$$N_{ch} = \frac{U_{ch} \times f_{ch} \times 1}{w_{ch} \times r_{cl} \times f_{cm}} \quad 32$$

$$N_{cl} = \frac{U_{eg} \times f_{eg}}{y_{eg} \times m_{eg} \times (1 - f_{sl})} \quad 33$$

Where

U_{ch} = human consumption rate of chicken (kg/yr)
f_{ch} = fraction of receptor-consumed chicken supplied by animals raised on site
1 = constant (yr)
w_{ch} = weight of chickens at slaughter (kg)
r_{cl} = ratio of ready-to-cook and live weights of chickens
f_{cm} = fraction of ready-to-cook weight of chicken that is edible meat
U_{eg} = human consumption rate of eggs (kg/yr)
f_{eg} = fraction of receptor-consumed eggs supplied by animals raised on site
y_{eg} = egg production rate of layers (kg/yr)
m_{eg} = mass of egg (kg)
f_{sl} = fraction of egg mass contributed by the shell

The doses received from the ingestion of contaminated materials are given by the following:

$$D_{g,i,m.t} = I_{g,m,i,t} \times D_{g,i} \quad 34$$

Where

$D_{g,i,m,t}$ = whole-body effective dose equivalent from the ingestion of radionuclide *i* in material *m* at time *t* (mrem/yr)
$D_{g,i}$ = ingestion dose conversion factor for radionuclide *i* (mrem/Ci).

The total dose from the ingestion of the contaminated material is the sum of the radionuclide doses. Total ingestion doses are determined by summing over all media ingested by the receptor.

3.6.2 Inhalation Exposure Route

The dose assessment includes the projection of doses due to the inhalation of radioactivity suspended in the form of particulates and released as vapors or gases. The radionuclide intake via inhalation is calculated using the following equation:

$$I_{h,i,t} = U_{air} \times t_{exp} \times C_{at,i,t} \quad 35$$

Where

$I_{h,i,t}$ = intake, through inhalation, of radionuclide i at time t (Ci/yr)
U_{air} = inhalation rate (m^3/d)
t_{exp} = time of exposure (d/yr)
$C_{at,i,t}$ = concentration, in air, of radionuclide i at time t (Ci/m^3)

The time of exposure is the sum of the time spent indoors and outdoors at the receptor location. The sum of the sampled indoor and outdoor exposure times may exceed 365 d/yr when the models are run in a probabilistic fashion; the outdoor exposure time is adjusted downward if this occurs.

The product of the inhalation intakes calculated using Equation 35 and the inhalation dose conversion factors yields the radionuclide doses due to the inhalation of contaminated air:

$$D_{h,i,t} = I_{h,i,t} \times D_{h,i} \quad 36$$

Where

$D_{h,i,t}$ = whole body effective dose equivalent from the inhalation of radionuclide i at time t (mrem/yr)
$D_{h,i}$ = inhalation dose conversion factor for radionuclide i (mrem/Ci)

The total dose from the inhalation of airborne contamination is the sum of the radionuclide doses.

3.6.3 Direct Radiation Exposure Route

All receptors included in the performance assessment and composite analysis may be exposed to direct radiation from contaminated ground surfaces. These exposures are calculated using the following:

$$D_{es,i,t} = \frac{C_{s,i,t}(f_i \times f_s + f_o) \times D_{es,i}}{\rho_s} \quad 37$$

Where

$D_{es,i,t}$ = whole-body effective dose equivalent for direct radiation from surface soil, for radionuclide i at time t (mrem/yr)

$C_{s,i,t}$ = concentration, in soil, of radionuclide *i* at time *t* (Ci/kg)
f_i = fraction of year individual spends indoors at the receptor location
f_s = shielding factor for the time spent indoors
f_o = fraction of year individual spends outdoors at the receptor location
$D_{es,i}$ = external radiation dose conversion factor for radionuclide *i* (mrem/yr/Ci/m^3)
ρ_s = bulk density of the surface soil (kg/m^3)

The dose conversion factors used to estimate direct exposures to surface soil differ depending upon the depth to which the contamination in those soils is mixed. External dose conversion factors for soil contaminated to a depth of 15 cm (6 in.) are used if the contamination is mixed to a depth of 15 cm (6 in.) or less. If the contaminant mixing depth is greater than 15 cm (6 in.), as it is for some inadvertent intruder scenarios, external dose conversion factors for soil contaminated to an infinite depth are applied.

Several other modes of external exposure exist for the inadvertent intruders. All three receptors may be exposed to direct radiation, emitted from contaminated cap material and undisturbed waste, after it travels upward through the surface soil layer. The construction intruder is subject to direct radiation from the bottom and sides of the basement excavation during the time spent in the excavation; the agricultural intruder is exposed to these same sources of radiation during the time spent inside the house, although the radiation will be attenuated by the concrete foundation.

Direct exposures received from buried waste during the time intruders spend outside are estimated as follows:

$$D_{ew,i,t} = \frac{C_{w,i,t} \times D_{es,i} \times e^{-\mu_{ls,i} * d_m}}{\rho_w} \qquad 38$$

Where

$D_{ew,i,t}$ = whole-body effective dose equivalent for direct radiation from buried waste, for radionuclide *i* at time *t* (mrem/yr)
$C_{w,i,t}$ = concentration, in waste, of radionuclide *i* at time *t* (Ci/kg)
$\mu_{ls,i}$ = linear attenuation coefficient of radionuclide *i* in soil (m^{-1})
d_m = thickness of material overlying the waste (m)
ρ_w = bulk density of waste (kg/m^3)

The linear attenuation coefficient for radionuclide *i* is given by

$$\mu_{ls,i} = \mu_{ms,i} \times \rho_s \qquad 39$$

Where

$\mu_{ms,i}$ = mass attenuation coefficient of radionuclide *i* in soil (kg/m^3)

The dose conversion factors used in Equation 38 are those for soil contaminated to an infinite depth.

Equation 38 is applied to all waste layers included in the intruder and intruder diffusion models, using layer-specific radionuclide concentrations and adjusting d_m to account for the thickness of surface soil, cap, and waste material present over each waste layer. The estimated exposures do not account for the attenuation of radiation within the waste itself.

The cap may become contaminated prior to the arrival of the intruder as a result of biotic intrusion into the waste or vapor- and gas-phase radionuclides diffusing upward from the waste. External radiation emitted from contaminants in a given layer of the cap will be attenuated by any other cap layers that lie above it as well as by the surface soil layer. The doses received from the contaminated cap layers are calculated using Equation 38, substituting the cap layer radionuclide concentrations, the appropriate d_m for each cap layer, and the bulk density of the cap material for the waste properties.

Resident intruders also may be exposed to radiation from the buried waste and contaminated cap material during the time spent indoors. For indoor exposures to occur, radiation originating in any contaminated cap or waste layer must pass through any material separating the foundation of the intruder's house from that layer and the concrete foundation itself. For example, exposure calculations for a single layer of waste account for the attenuation of the radiation as it passes through any cap material and waste that lies between the layer and the foundation and the concrete basement or slab itself. These exposures are expressed as follows:

$$D_{ew,i,t} = \frac{C_{w,i,t} \times f_i \times D_{es,i} \times e^{-\mu_{ls,i} * d_m} \times e^{-\mu_{lc,i} * d_c}}{\rho_w} \qquad 40$$

Where

$\mu_{lc,i}$ = linear attenuation coefficient of radionuclide *i* in concrete (m^{-1})
d_c = thickness of the floor of the concrete foundation (m)

The linear attenuation coefficient for radionuclide *i* in concrete is given by the following:

$$\mu_{lc,i} = \mu_{mc,i} \times \rho_c \qquad 41$$

Where

$\mu_{mc,i}$ = mass attenuation coefficient of radionuclide *i* in concrete (m^{-1})
ρ_c = bulk density of concrete (kg/m^3)

The dose conversion factors used in Equation 40 are those for soil contaminated to an infinite depth. Exposure calculations for the contaminated cap layers consider attenuation from the cap

and concrete only, and substitute cap contaminant concentrations and bulk density for the waste properties.

The material thickness used in Equations 38 and 40 will depend upon the intruder scenario under consideration, the location of the receptor, and the cap or waste source layer. For the time spent outdoors, radiation will be attenuated by any excavated material and the cap and waste layers separating the source layer from the receptor. The amount of material separating the construction and agricultural intruders from a given layer during the time spent in the excavation or inside the house will depend upon the depth of the basement excavation relative to the cap and waste layer thicknesses. For example, if the basement depth is greater than the thickness of the cover, no cap material separates the intruder from the waste. The material thickness used to estimate indoor exposures for the postdrilling intruder is the total amount of material overlying the source layer at the time of intrusion.

The construction and agricultural intruders may also be exposed to contamination in the walls of the basement excavation; such an exposure will occur while the receptor is in the excavation or the house, respectively. Potential doses for the construction intruder are calculated using the following:

$$D_{esw,i.t} = \frac{C_{sw,i,t} \times f_e \times D_{es,i}}{\rho} \qquad 42$$

Where

$D_{esw,i,t}$ = whole-body effective dose equivalent for direct radiation from the sidewall of the basement excavation, radionuclide *i* at time *t* (mrem/yr)
$C_{sw,i,t}$ = average concentration, in the exposed cap and waste layers within the basement excavation, of radionuclide *i* at time *t* (Ci/kg)
f_e = fraction of year individual spends in the basement excavation

The exposures for the agricultural intruder are calculated using the fraction of the year spent inside, rather than within the excavation, and account for the attenuation of the radiation from the walls of the excavation by the concrete foundation. The dose conversion factors used in Equation 42 are those for soil contaminated to an infinite depth.

The use of external dose conversion factors for an infinite soil medium will overstate actual exposures from the relatively thin cap and waste layers. Consequently, the dose conversion factors used in Equations 38 and 40 are adjusted before they are applied in the external exposure calculations (RAE, 1998); no such adjustment is made for the factors used in Equation 42. This adjustment is given by the following expression:

$$D_{es,i,inf} = D_{es,i,inf}(1. - e^{-\mu_{lc,i}*d_l}) \qquad 43$$

Where

$D_{es,i,inf}$ = external radiation dose conversion factor for radionuclide *i* in an infinite medium (mrem/yr/Ci/m^3)
d_l = thickness of the cap or waste layer for which exposures are being estimated (m)

Direct exposures received from immersion in airborne radioactivity are calculated using the following equation:

$$D_{ea,i,t} = C_{at,i,t} \times \left(f_i \times f_s + f_o \right) \times D_{ea,i} \qquad 44$$

Where

$D_{ea,i,t}$ = whole-body effective dose equivalent from direct radiation in air for radionuclide *i* at time *t* (mrem/yr)
$D_{ea,i}$ = air immersion dose conversion factor for radionuclide *i* (mrem/yr/Ci/m^3)

3.7 Disposal System Configuration and Contaminant Flows

As discussed earlier, transport pathway elements are used to represent the physical compartments through which radionuclides are projected to migrate in the vicinity of Area G. The elements are defined and linked with one another in a manner consistent with the conceptual model of the site. Rates of contaminant transport along the established links ultimately determine the timing and magnitude of the doses received by the various receptors. The following sections discuss the interactions among these transport pathway elements, many of which are characterized using the submodels described above. Additional submodels that are used to link the physical components of the Area G models are introduced where appropriate.

3.7.1 Disposal Facility Configuration and Contaminant Flows

The manner in which the disposal facility is represented varies across the GoldSim models. The facility configuration seen in the site model includes the disposal pits and shafts, the cover material overlying these units, the underlying unsaturated zone, and the air above the disposal facility. The intruder and intruder diffusion models do not include the unsaturated zone; only the latter model includes the air above the facility. Both intruder models include the intruder's house. The site model and the two intruder models include a Plants cell that represents plants growing on the surface of the disposal site.

The manner in which the disposal units are represented in GoldSim also depends upon the model under consideration. The site, intruder, and intruder diffusion models divide the disposal facility into surface soil, cap material, and the waste within the pits and shafts; however, there are some differences in the level of detail used by the various models. The site model and the intruder diffusion model use a single cell to represent the surface soil, while 16 and 20 cells are used to

represent the cap and waste, respectively. The cap and waste are represented using multiple layers to more accurately simulate the dynamics of contaminant transport by plants and animals and diffusive transport of vapor- and gas-phase radionuclides. The intruder model represents the cap and waste using 4 cells each; less detail is required because the model does not include vapor- and gas-phase diffusion. The intruder diffusion model uses 4 cells to represent the concrete foundation of the intruder's house.

In general, the surface soil, cap, concrete, and waste cells are defined in terms of the environmental media of which they are composed. These media are specified in the cell pathway properties dialog box under the definitions tab. The media used to define the disposal facility layers depend upon the model under consideration, but include crushed tuff, waste, concrete, water, and air. "Crushed tuff" is used to define the solids in the surface soil and cap, while "waste" is used to represent the solids in the waste layers. "Concrete" is used to represent the solid fraction of the foundation of the inadvertent intruder's house in the intruder diffusion model. "Water" represents the moisture present in the pore space of the surface soil, cap, waste, and concrete. "Air" is used to represent the air-filled pore spaces in porous media and the atmosphere above the site. To account for differences in diffusion behavior, the site and intruder diffusion models distinguish between the air that exists in the pore spaces of the cover, waste, and concrete. All media that undergo advective transport into or out of a cell must be present in that cell. Consequently, the models include crushed tuff in the waste layers and waste in the surface soil and cap layers, albeit in very small amounts.

The transport pathway elements are defined in a manner that is consistent with the geometry of the disposal site. In terms of the site model, each cell within a given waste disposal region is sized to correspond to the area of the waste disposal region that it represents; the cells in the intruder and intruder diffusion models are sized to correspond to the subset of disposal pits and shafts under consideration. The thickness of each layer or cell is defined to account for the effects of surface erosion while remaining within the boundary conditions imposed by GoldSim. As discussed earlier, the effects of surface erosion are represented in the models by maintaining a constant surface-layer thickness that is replenished with material from the cap or waste.

The quantities of environmental media in each cell are a function of the cell volumes and the properties of the materials being represented. Thus, the mass of crushed tuff in the surface soil and cap cells, waste in the waste cells, or concrete in the foundation of the intruder's house is the product of the cell volumes and the dry density of the respective medium. Very small quantities of waste occur in the surface soil and cap layers, while very small quantities of crushed tuff occur in the waste layers. These media are included for reasons discussed above; their magnitude is arbitrary. The volume of water present in the pore space of the surface soil, cap, and waste layers is equal to the volume of each cell times the moisture content of the environmental medium. In general, the volume of air in porous media is estimated as the cell volume times the

air-filled porosity. The volume of air above the disposal units in the site and intruder diffusion models is given by the product of the average annual wind speed, the square root of the area of the disposal area, and the atmospheric mixing height.

The site and intruder diffusion models place lower bounds on the volume of air in the cells that represent the surface soil layer and the layers of the cap. Modeling diffusion through very thin soil layers may lead to very high rates of diffusive transport; these rates are flagged by GoldSim as "excessive" and possibly in error. Conditions such as this occur, for instance, when cap layers erode to the minimum thickness. Increasing the amount of air in the cell increases the contaminant storage term and all but prevents the generation of "excessive transport" warnings while having no effect on the accuracy of the projected contaminant fluxes.

The source of contamination for the site, intruder, and intruder diffusion models is the waste disposed of in the waste disposal regions. The waste disposal region inventories used in the site model represent estimates of the actual quantities of material disposed of, or expected to be disposed of, in the pits and shafts at Area G; a detailed description of this waste may be found in Shuman (2008). The user has the option of using actual inventories or a unit inventory (i.e., an assumed inventory assigned to each radionuclide) when running the intruder and intruder diffusion models. The actual inventories are used to estimate doses for the disposal units under consideration; however, the calculation of WAC for a wide range of radionuclides is more easily conducted using a unit inventory because many of the contaminants encountered at Area G may not be found in a given set of disposal units. In all cases, the inventories included in the models are added to the appropriate disposal units at a uniform rate over the period of time that the units were active. For the site model, waste added to the disposal units is apportioned among each waste layer in accordance with the layer volume. The intruder models can accommodate inventories that are distributed uniformly throughout the disposal units or specific to the waste layers in the pits and shafts.

The site, intruder, and intruder diffusion models use a series of inflows and outflows to represent contaminant movement within the disposal facility and to simulate radionuclide transport beyond the pits and shafts. For the site model, the surface soil is subject to inflows from the 16 cap and 20 waste layers due to biotic intrusion into the waste. Specifically, advective mass-flux links are used to move soil from the cap and waste layers in proportion to the rates at which soil is excavated by burrowing animals. Two links are defined for each layer-to-layer transfer, representing the movement of solid media such as crushed tuff and waste as well as the transport of water, which is present in the pores of the cap material and waste. Direct-transfer mass links to and from the Plants cell account for the uptake of radionuclides by plants growing over the disposal units and the incorporation of this contamination into the surface soils following litter deposition and decay. The equations governing the transfers associated with plant and animal intrusion are provided in Sections 3.2.2.1 and 3.2.2.2, respectively.

The surface soil also receives inflows from the underlying cap layer as vapor- and gas-phase radionuclides diffuse upward from the buried waste. The diffusive mass-flux links that are used to simulate this process are specified in terms of the diffusion path lengths for the source and destination media, the porous media through which contaminants diffuse, and the area over which diffusion is taking place. The diffusion length for each medium is set to one-half of the layer's thickness. The diffusive area is set to the surface area of the layer, adjusted downward by the ratio of the air-filled porosity and the effective porosity. GoldSim assumes the effective porosity is saturated with the medium within which diffusion is taking place which, in this case, is air. In fact, water occupies some of the pore space; making the adjustment described above accounts for the presence of this moisture.

Within the site model, the surface soil layer is subject to outflows to the cap, the air over Area G, and the cells representing Cañada del Buey and Pajarito Canyon soils (found in the Canyon_Exposure_Locations container). The transfer of contamination to the cap is defined using advective flows of solids and water. Bulk soil, including solids and soil moisture, is simulated to move downward in response to the collapse and settlement of burrows constructed by animals. The rate of burrow collapse and settlement is assumed to be equal to the rate at which material is brought to the surface by the animals, resulting in no net change in the thickness of the surface soil layer. Additional water is transported from the surface soil layer to the cap to represent water percolating through the disposal site. The rate of passage between these layers is specified by the parameter MdB_Infiltration_Rate, which refers to the infiltration rate through Mesita del Buey. This rate is equal to the natural infiltration rate estimated for the disposal site.

The outflows of crushed tuff and water from the surface soil to the air over the disposal site represent the resuspension of particulates and diffusion of vapor- and gas-phase radionuclides; these releases are subsequently transported by the prevailing winds to receptor locations downwind of Area G. The on-site air cell found in each waste disposal region is defined in terms of three environmental media: air, water, and crushed tuff. Air is the primary medium; the small quantities of water and crushed tuff are included to enable the simulation of soil resuspension from the disposal site. The volumes of the materials comprising the cell are arbitrary; only the rate of particulate transfer to the cell is used in the performance modeling, and this rate is unaffected by the volumes of the materials in the cell.

Radionuclides in the surface soils at Area G are partitioned between solids and soil moisture. As discussed earlier, GoldSim models the transport of these media separately. Consequently, the Sink_Onsite_Air cell found in each disposal region has pairs of inflows to account for the "resuspension" of water and solids from the disposal units within the source area under consideration. This modeling approach is conceptually equivalent to assuming that radionuclides in the soil moisture precipitate out when the liquid is exposed to surface conditions and

evaporates. When the solids are resuspended, they carry with them all sorbed and previously soluble contaminants.

Outflows of bulk soil into Cañada del Buey and Pajarito Canyon account for the effects of surface erosion and runoff. As discussed earlier, the thickness of the cap is reduced over time to account for soil loss due to erosion. Advective mass-flux links are used to transfer bulk soil from the cap to the surface soil at rates that are consistent with the amount of soil lost due to erosion.

Advective flows into the cap and waste layers account for the movement of bulk soil downward due to burrow collapse and settlement, and the infiltration of water through the disposal site. Outflows from these cells to the surface soil layer represent the excavation of soils by burrowing animals. The flow of water through the cover and disposal units is assumed to occur under steady-state conditions, such that rates of flow are simply equal to the mesa-top infiltration rate. Direct-transfer mass links from the cap and waste cells account for the uptake of radionuclides by plants; these contaminants are deposited on the surface of the disposal facility in conjunction with litterfall and decay.

Diffusive mass-flux links are used to model the movement of vapor- and gas-phase radionuclides upward from the buried waste. With the exception of the bottommost waste layer, each cell in the site model is subject to the influx of contamination from the layer below.

Within each waste disposal region, advective flows from the bottommost waste layer account for movement of water from the bottom of the disposal units into the unsaturated zone underlying the pits and shafts. The Unsaturated_Zone cell is used to collect the output from the waste; water entering the cell immediately flows into the Finite Element Heat and Mass (FEHM) external element found in each waste disposal region. As discussed in detail in Stauffer et al. (2005), FEHM is a transfer code used to estimate rates of contaminant transport vertically through the unsaturated zone and horizontally within the regional aquifer. The FEHM elements are external one-dimensional abstractions of three-dimensional FEHM model simulations that accept infiltration rates, distribution coefficients, and radionuclide release rates from GoldSim and pass the contaminant masses crossing the groundwater compliance boundary back to GoldSim at the end of each time step. These results are subsequently used to estimate exposures for the groundwater scenarios.

The Area G Intruder Model is similar in many respects to the site model in terms of the flow of contamination among the cells representing the surface soil, cap, and waste. Advective mass-flux links are used to simulate the movement of soils by animals burrowing into the disposal site and the uptake of contamination by plants; the model does not simulate the diffusion of vapor- and gas-phase radionuclides.

The inflows and outflows found in the intruder and intruder diffusion models generally resemble one another, though there are a few differences. The intruder diffusion model explicitly models the transport of cap material and waste to the surface following human intrusion (basement excavation of well drilling); calculations conducted in the intruder model account for the impacts of human intrusion without physically moving contaminated cover material and waste. The amounts of material moved between the surface soil, cap, and waste cells by the intruder diffusion model depend upon the intruder scenario under consideration. Elements in the Intrusion_Consequences container calculate the radionuclide masses that are transferred between the cells. These calculations use the contaminant concentrations in the affected layers and the excavated quantities of cap material and waste calculated by the Human_Intrusion_Model. Material transfers are implemented using discrete change elements.

The intruder and intruder diffusion models also differ because the latter considers the transport of vapor- and gas-phase contaminants through the foundation of the intruder's house. Prior to the arrival of the intruder, vapor- and gas-phase contaminants diffuse from the waste and exit from the surface of the closed disposal facility. Once the intruder arrives, however, the pathways followed by these radionuclides change; the nature of these changes depends upon the intruder scenario under consideration. For the postdrilling scenario, a portion of the vapors and gases in the surface soil layer pass through the concrete slab of the receptor's house; the remainder diffuses into the air above the site. The contaminants passing into the house and the air are apportioned on the basis of the area of the house and the portion of the intruder's lot that is not occupied by the dwelling.

Following basement excavation and prior to pouring the foundation, a portion of the contamination diffuses into the excavation while the remainder continues upward through the cover. After the foundation has been constructed, vapor- and gas-phase radionuclides either diffuse through the concrete floor of the house or travel through the cover to the surface of the site. In either case, the relative areas of the house and the intruder's lot are used to apportion the radionuclides between the two paths.

The layer from which radionuclides diffuse into the basement excavation or the floor of the intruder's basement depends upon the depth of the cover at the time of intrusion and the depth of the basement. The intruder diffusion model calculates the cumulative depth to the bottom of each cap and waste layer at the time of intrusion, and compares this to the depth of the basement. If the bottom of the basement lies within a given cap or waste layer the diffusive species within that layer are assumed to enter the excavation or concrete.

The Area G Intruder Diffusion Model uses the House and Air_in_Excavation cells to estimate doses for the intruder scenarios. Air and water are used to define both cells; water is included only because of requirements imposed by GoldSim. The volume of air inside the house is the

product of the house area and room height; the excavation air volume is the product of the area and depth of the basement. Contaminants enter the house as vapor or gas and diffuse upward from the floor of the concrete foundation. A single advective outflow is used to simulate the passage of fresh air through the house due to ventilation; the flow rate is the product of the volume of the house and the ventilation rate. Similarly, an advective flow equal to the volume of the basement times the ventilation rate is used to simulate the renewal of air in the excavation. The air flows from the House and Air_in_Excavation cells and enters the Onsite_Air cell, which is linked to the Sink_Offsite_Air cell.

3.7.2 Exposure Location and Off-Site Media Configuration and Contaminant Flows

The Area G Site Model projects doses for off-site receptors at several exposure locations including (1) the point of maximum atmospheric exposure outside the LANL boundary and the Area G fence line, (2) several locations in Cañada del Buey and Pajarito Canyon, and (3) a domestic well 100 m (330 ft) east of the Area G fence line. Cells are used to represent relevant environmental media at these exposure locations.

The cells found inside the Atmospheric_Exposure_Locations container are used in the estimation of Atmospheric Scenario doses for the receptor at the point of maximum exposure before and after the end of active institutional control. The cells inside the LANL_Boundary container are used to represent the location of the receptor prior to the end of institutional control; these two cells represent soils at the exposure location and a sink term. The cell representing the soils is defined using water and crushed tuff; these materials represent the soil moisture and solids, respectively. The volume of water and mass of solids specified are consistent with the area of the receptor's lot, the depth to which contamination is mixed, the moisture content of the soil, and the dry density of the solids. Similarly configured cells inside the Area G_Fenceline container represent the point of maximum exposure after active institutional control has ceased.

The atmospheric transport modeling conducted within the site model is a representation of the detailed modeling conducted by Jacobson (2005). The results of complex terrain modeling are used to estimate radionuclide concentrations in air and rates of particulate deposition at the Atmospheric Scenario exposure locations. Projections of particulate deposition are used to estimate contaminant additions to the surface soils. Using discrete change elements, the appropriate radionuclide activities are added to the Exposure_Location_Soils cell. The rate of addition is given by the following equation:

$$Q_{d,i,t,j} = C_{s,i,t} \times d_{f,j} \times (A_l - A_h) \times r_{fr} \times s_{ar} \qquad 45$$

Where

$Q_{d,i,t,j}$ = quantity of radionuclide *i* deposited on surface soils at the point of maximum atmospheric exposure at time *t* for contamination originating in atmospheric source area *j* (Ci/yr)

$d_{f,j}$ = particulate deposition rate for contamination originating in atmospheric source area *j* ($kg/m^2/yr$)

A_l = area of receptor's lot (m^2)

A_h = area of receptor's house (m^2)

r_{fr} = resuspension flux ratio

s_{ar} = source area ratio

The soil concentration term in this equation ($C_{s,i,t}$) refers to radionuclide concentrations in Area G soils. Radionuclide fluxes at the exposure location are calculated for contamination originating at the three atmospheric source areas at the facility (Figure 6); these rates are summed to determine the total rate of radionuclide deposition.

The atmospheric transport modeling conducted in support of the performance assessment and composite analysis used a generic value for the particulate resuspension rate. The radionuclide deposition rates at downwind locations scale directly with the resuspension factor. Consequently, it is a simple matter to adjust the modeling results to take the actual site resuspension characteristics into account. This is done in Equation 45 using the resuspension flux ratio, which is the ratio of the actual site resuspension flux and the default resuspension flux used in the atmospheric transport modeling.

In general, particulates less than 10 μm (3.9×10^{-4} in.) in diameter will be resuspended from the surface of the disposal site; radionuclide concentrations in this resuspendable fraction will tend to be greater than those estimated by the GoldSim models for the total soil (i.e., including all size fractions). As a result, the resuspension flux input by the user is multiplied by an enhancement factor to account for differences in radionuclide concentrations among the different soil size fractions.

The modeled rates of particulate resuspension from Area G assume that all resuspended material originates from the surfaces of the disposal pits and shafts; this ignores the resuspension of uncontaminated material from portions of the site that lie between pits or near the edges of the mesa. As a result, the deposition rates projected by Jacobson (2005) were adjusted to account for the fact that the source area for modeling resuspension was smaller than the source area as shown in Figure 6. This adjustment is provided in Equation 45 by the source area ratio, which represents the surface area of the disposal units divided by the source area used in the atmospheric transport modeling.

Advective outflows of water from the soils at the Atmospheric Scenario exposure locations to the soil sink terms are used to simulate the depletion of soil contamination due to groundwater transport. Water passes out of the soil at a rate determined by the water infiltration rate at the exposure locations, carrying the soluble component of the soil contamination with it.

The canyon exposure locations found in the Area G Site Model are used to project exposures for the All Pathways–Cañada del Buey and All Pathways–Pajarito Canyon Scenarios. Cells representing the canyon soils and a sink term are used to model radionuclide concentrations at these locations. The canyon soils are defined in terms of water and crushed tuff. The volume of water is given by the product of the area over which the sediment transported from the mesa spreads within each catchment, the contaminant mixing depth, and the moisture content of the bulk soil. The product of the area of sediment dispersal, the contaminant mixing depth, and the dry density of the crushed tuff yields the mass of solids in this compartment. The area over which the sediment spreads is specific to the catchment under consideration.

The soils in Cañada del Buey and Pajarito Canyon receive advective flows of soil moisture and solids from the eight waste disposal regions. These inflows represent the transport with surface runoff of contamination deposited on the surface of Area G by plants and animals intruding into the waste. As has been discussed, separate flows are used to transport radionuclides that are soluble in the soil moisture and that are sorbed to the crushed tuff. Rates of flow are proportional to the erosion rate at the disposal site and the disposal area associated with each waste disposal region. Direct transfer links between the canyon exposure locations are used to transport sediment down Cañada del Buey and Pajarito Canyon; the flows from catchments CdB2 and PC6 (Figure 11) go to a sink term. An additional flow from each canyon soil cell accounts for the depletion of contamination by water infiltrating through the exposure location.

A single well location is used to project groundwater pathway impacts for the performance assessment and composite analysis. This well is located 100 m (330 ft) downgradient of the disposal facility boundary, and represents the exposure location for the groundwater-pathway-based scenarios after the end of the active institutional control period. As discussed earlier, persons living downgradient of Area G may receive groundwater exposures along the LANL boundary prior to the end of active institutional control. However, groundwater contaminant travel times from Area G to this boundary are such that no exposures are projected to occur within 100 years of facility closure (Stauffer et al., 2005**)**. Therefore, an exposure location along the LANL boundary is not included in the site model.

Four cells are used to represent the groundwater pathway exposure location. The first of these, the AP_Well cell, represents the receptor's well for the All Pathways–Groundwater Scenario. A second cell represents surface soils at the exposure location; the remaining two cells act as sinks for surface soil and groundwater contamination. The cell used to represent the well includes a

single material, water, and is sized to correspond to the water usage rate of the receptor. The water usage rates for the receptor include the water needed for irrigating crops, watering animals, indoor consumption, and drinking.

Advective flows between the FEHM external elements (found in the eight waste disposal region containers that comprise the disposal facility) and the AP_Well cell account for the withdrawal of water from the regional aquifer. An advective flow from the AP_Well cell to the Surface_Soil_at_100m_Well cell accounts for the application of water during irrigation of vegetable and animal forage crops. A second advective flow to the Sink_for_Well_Water cell accounts for the withdrawal of the remaining water for indoor use and personal consumption.

The FEHM external elements simulate the transport of radionuclides from the bottoms of the disposal units to the well located 100 m (330 ft) downgradient of the Area G fence line, represented by the AP_Well cell. Although these elements account for the decay and sorption characteristics of the radionuclides during transit, they are not designed to account for the effects of dilution and dispersion that occur between the point of discharge and the regional aquifer or well. Thus, using the output of these elements directly will overestimate contaminant concentrations in the water drawn from the well.

The magnitudes of the flows between the FEHM elements and the AP_Well cell are modified to account for contaminant dispersion in the regional aquifer. The flow from the FEHM element within a given waste disposal region is equal to the infiltration rate through that disposal region times the contaminant capture fraction. The contaminant capture fraction specifies the portion of the contaminant plume that reaches and is withdrawn from the well. It is largely a function of the dispersion characteristics of the aquifer between the point of contaminant discharge and the well, and the well pump rate. The approach used to define the contaminant capture fractions is described in Stauffer et al. (2005).

The cell used to represent the surface soils at the well location includes water and crushed tuff. The volume of water and mass of tuff in these cells are based on the net area of the receptor's lot (i.e., the lot area less the house area), the contaminant mixing depth, and the moisture content and dry density of the soil. The rate of water flow into the cell is the sum of the crop irrigation rates. Outflows of water to the Sink_for_Soil_Moisture cell account for the transport of radionuclides downward with water percolating through the receptor's lot.

Although several cells are used to represent the physical location of the receptor for the All Pathways–Groundwater Scenario, no physical representation of the exposure location is necessary for the Groundwater Resource Protection Scenario. Physical modeling of the exposure location is needed for the all pathways scenario to estimate contaminant concentrations in the surface soils at the receptor's residence. In contrast, the resource protection scenario addresses

the use of contaminated water only as a source of drinking water. Radionuclide concentrations in the water are calculated directly from the amount of contamination withdrawn at the well and water usage rates.

The disposal facility is the only exposure location evaluated by the intruder and intruder diffusion models; the configuration and contaminant flows within the facility have been described in Section 3.7.1. Two off-site media are included in the intruder models to simulate the transport of contamination with the prevailing winds and surface runoff. The Sink_Offsite_Air cell is defined using three materials: air, water, and crushed tuff. In the intruder model, it receives contaminants resuspended from the surface of the disposal site; this cell receives resuspended particulates and vapor- and gas-phase radionuclides diffusing from the facility in the intruder diffusion model. An advective mass-flux link is used in each model to transfer airborne radionuclides from the on-site air cell to locations downwind of the receptor. The Sink_Adjacent_Canyons cell receives contamination from the surface soil cells, representing the transport of contaminated soils into Cañada del Buey and Pajarito Canyon with surface runoff. This cell is defined in terms of two environment media, water and crushed tuff.

3.7.3 Exposure Concentrations

The doses projected for the performance assessment and composite analysis are proportional to the radionuclide concentrations in the environmental media to which the receptor is exposed. In some cases the contaminant concentrations are taken directly from the cells used to represent the exposure media; in other cases, they are calculated using contaminant masses. This section discusses how the exposure concentrations used in the dose model are defined using the GoldSim models.

3.7.3.1 Surface Soil, Cap, and Waste

A combination of approaches is used to define the radionuclide concentrations in the surface soil, cap material, and waste to which members of the public and inadvertent intruders are exposed. For the site model, surface soil concentrations are calculated similarly for exposure locations downwind and downgradient of Area G and those in the adjacent canyons. In all cases, radionuclide concentrations are calculated as the quotient of the contaminant activities and the total soil mass in the cells used to represent soils at the exposure locations. The total soil mass for the atmospheric and groundwater scenarios is given by the product of the receptor's lot size less the area occupied by the house (i.e., the net lot area), the soil mixing depth, and the soil density. Soil concentrations for the exposure locations in the canyon take into account the area within each catchment over which sediments are dispersed.

The intruder model simulates the release and transport of radionuclides resulting from biotic intrusion prior to the arrival of the intruder, but does not explicitly model the movement of contamination resulting from human intrusion. In this approach, radionuclide concentrations in surface soil are calculated by summing the contaminant activities present in the surface soil layer

at the time of intrusion and the activities brought to the surface as a result of basement excavation or well drilling. These activities are divided by the product of the net lot area, the mixing depth, and soil-density-to-yield concentrations. The mixing thickness is set equal to the greater of the thickness of the excavated material after it has been spread over the intruder's lot or a user-specified minimum mixing depth. If the minimum mixing depth is used, the calculated radionuclide concentrations take into account any contamination present in the layers within which the excavated material is mixed.

The intruder model tracks contaminant concentrations in each layer of the cap and waste. Concentrations in the layers of the cap and waste that are disturbed by the basement excavation are used to estimate average radionuclide concentrations in the side walls of the excavation. Radionuclide concentrations in the material at the bottom of the basement are set equal to those estimated for the cap or waste layer that lies at the bottom of the excavation.

In contrast to the intruder model, the intruder diffusion model explicitly models the movement of contaminants resulting from human intrusion; radionuclides are physically moved to the surface soil layer to reflect the impacts of well drilling and basement excavation. Radionuclide concentrations are calculated as the quotient of the contaminant activities in the surface soil layer and total soil mass. The total soil mass is given by the product of the net lot area, mixing depth, and soil density; as with the intruder model, the mixing depth may vary with the intruder scenario under consideration.

3.7.3.2 Air

The Atmospheric Scenario receptor is assumed to breathe airborne radioactivity transported from Area G with the prevailing winds. The general equation used to calculate contaminant concentrations in air resulting from particulate resuspension is as follows:

$$C_{at,i,t,j} = \left(\frac{\chi}{Q}\right)_j \times Q_{r,i,t,j} \qquad 46$$

Where

$C_{at,i,t,j}$ = concentration, in air, of radionuclide *i* at time *t* for contamination originating in atmospheric source area *j* (Ci/m^3)

$\left(\frac{\chi}{Q}\right)_j$ = atmospheric dispersion factor for contamination originating in atmospheric source area *j* (yr/m^3)

$Q_{r,i,t,j}$ = quantity of radionuclide *i* resuspended at time *t* from atmospheric source area *j* (Ci/yr).

Equation 46 is implemented for each of the three source areas used in the atmospheric transport modeling; the concentrations for these areas are summed to determine the exposure location concentrations due to particulate resuspension from the entire site. The dispersion factor used in the equation is one of the results from the atmospheric transport modeling that is calculated outside of the GoldSim models. The quantities of radionuclides resuspended from the surface of the disposal facility are taken directly from the fluxes projected by the site model for the mass-flux links between the Surface_Soil and the Onsite_Air sink terms for the three atmospheric source areas.

The airborne concentrations calculated above account only for the radionuclides present in the plume as it passes over the exposure location. Particulates deposited on the receptor's lot may also become suspended and add to these air concentrations. Similarly, contamination deposited on the lot of the inadvertent intruder, the receptor residing at the downgradient well location, or the receptors in Cañada del Buey and Pajarito Canyon may be resuspended, leading to inhalation exposures. Airborne radionuclide concentrations resulting from the resuspension of particulates at these receptor locations are calculated as the product of the effective dust-loading factor and the soil-contaminant concentrations. The effective dust loading for the off-site receptor is calculated using the following:

$$d_e = d \times f_d \qquad 47$$

Where

d_e = effective dust loading (kg/m^3)
d = dust loading under undisturbed conditions (kg/m^3)
f_d = human disturbance factor

The human disturbance factor, f_d, is greater than or equal to 1.0 and accounts for increases in rates of resuspension due to disturbance of the soil by humans walking over the site.

Vapor- and gas-phase radionuclides that diffuse from the site will be transported to downwind locations by the prevailing winds. Airborne concentrations of these contaminants are estimated for the Atmospheric Scenario by replacing the resuspension-based release rate in Equation 46 with the diffusive flux from the surface of each atmospheric source area. The exposure location concentrations estimated for the three atmospheric source areas are summed to estimate the air concentration due to releases from the entire site. The concentrations of vapor- and gas-phase radionuclides in the inadvertent intruder's house and in the air over the intruder's lot are taken directly from the House and Onsite_Air cells included in the intruder diffusion model.

3.7.3.3 Crops

Crops grown by the receptor may become contaminated with radionuclides due to the deposition of airborne and waterborne contaminants and as a result of root uptake of contaminants in the soil. These processes are represented using the following equation:

$$C_{c,i,t} = \left[\frac{C_{at,i,t} \times v_d \times T_c \times R_{w,c}(1.-e^{-\lambda_w * t_{g,c}})}{Y_{v,c}\lambda_w} + \frac{C_{w,i,t} \times I_r \times I_f \times T_c \times R_{w,c}(1.-e^{-\lambda_w * t_{g,c}})}{Y_{v,c}\lambda_w} + \right. \quad (48)$$

$$\left. C_{s,i,t} \times M_c \times T_c \times D_c \times p_f + C_{s,i,t} \times B_{c,i} \times D_c \right] \times e^{-\lambda * t_{h,c}}$$

Where

$C_{c,i,t}$	=	concentration, in crop *c*, of radionuclide *i* at time *t* (Ci/kg (wet weight))
$C_{at,i,t}$	=	concentration, in air, of radionuclide *i* at time *t* (Ci/m^3)
v_d	=	particulate deposition velocity (m/hr)
T_c	=	translocation factor for crop *c*
$R_{w,c}$	=	plant interception fraction of crop *c*
λ_w	=	weathering removal coefficient (hr^{-1})
$t_{g,c}$	=	growing season for crop *c* (hr)
$Y_{v,c}$	=	agricultural yield of crop *c* (kg wet weight crop/m^2)
$C_{w,i,t}$	=	concentration, in irrigation water, of radionuclide *i* at time *t* (Ci/m^3)
I_r	=	irrigation rate (m/yr)
I_f	=	fraction of year crops are irrigated
$C_{s,i,t}$	=	concentration, in soil, of radionuclide *i* at time *t* (Ci/kg dry weight soil)
M_c	=	plant mass-loading factor (Ci/kg dry weight plant per Ci/kg dry weight soil)
D_c	=	dry-to-wet weight ratio for crop *c*
p_f	=	particle size factor
$B_{c,i}$	=	soil-to-plant-concentration factor, in crop c, for radionuclide *i* (Ci/kg dry weight vegetation per Ci/kg dry weight soil)
λ	=	radioactive decay constant (hr^{-1})
$t_{h,c}$	=	delay time between crop harvest and consumption (hr)

Radionuclide concentrations in crops due to depositional processes are estimated using the first three terms in Equation 48. The first term accounts for the deposition of airborne particulates on plant surfaces as contamination is transported over the receptor's lot by prevailing winds. The second and third terms account for contamination of the plants from irrigation with contaminated water and from rainsplash, respectively. The final term in the equation accounts for root uptake of radionuclides in soil.

The plant interception fraction, $R_{w,c}$, specifies the fraction of particulates deposited on plant surfaces that is initially retained by the crops. A number of investigators have related the plant interception fraction to the agricultural productivity of the crop under consideration. This approach is implemented in the GoldSim models using the following equation (Ng et al., 1978):

$$R_{w,c} = 1.0 - e^{-\mu Y_{v,c}} \quad 49$$

Where

μ = interception coefficient (m^2/kg)

The agricultural productivity, $Y_{v,c}$, is converted to a dry weight basis before it is used in Equation 49; this is accomplished by multiplying the productivity by the dry-to-wet weight ratio for the crop under consideration.

The level of contamination in crops resulting from the use of contaminated irrigation water will depend, in part, on the mode of irrigation employed. Information provided in Peterson (1983) indicates rates of contaminant uptake when water is applied in furrows may be approximately half of those observed for spray irrigation due to the effects of soil sorption. The expression used to estimate plant assimilation of radionuclides in irrigation water is based on the assumption that spray irrigation techniques are used.

The expression used to estimate plant concentrations due to rainsplash represents a departure from the model used in the 1997 Area G performance assessment and composite analysis (Hollis et al., 1997). Those analyses used a resuspension factor approach to estimate the rates at which soil contamination was deposited on plant surfaces following the impact of raindrops on the ground surface. As discussed by Hinton (1992), this approach was not originally developed for the purposes of estimating plant concentrations. Furthermore, it is susceptible to a high level of uncertainty. Resuspension factor data are limited, and the data that do exist range over 5 to 10 orders of magnitude. Uncertainty associated with the deposition velocity, which is used to estimate the rate at which suspended particulates are deposited on plant surfaces, adds to the overall uncertainty in the projected plant concentrations.

Hinton (1992) proposed the mass-loading-factor approach as a more effective means of estimating the impacts of processes such as rainsplash. The mass-loading factor is the ratio of the radionuclide concentration on the plant to the concentration in the soil (i.e., Ci/kg dry weight plant per Ci/kg dry weight soil). Multiplying the mass-loading factor by the soil radionuclide concentrations yields an estimate of contaminant concentrations on the plant. Multiplying these surficial concentrations by the translocation factor yields internal plant concentrations. The mass-loading approach is discussed in greater detail in Hinton (1992) and Pinder and McLeod (1989).

Mass-loading factors reported in the literature have been calculated using two distinct approaches. In one approach, the factor is calculated using the contaminant concentrations in the resuspendable fraction of the soil, while in the other approach concentrations in the total soil are used. The GoldSim models are designed to accept as input the mass-loading factors for the resuspendable fraction of the soil. Given that the GoldSim-estimated soil concentrations are total

soil concentrations, these factors are multiplied by the ratio of radionuclide concentrations in the resuspendable fraction to the concentrations in the total soil. This ratio is referred to here as the particle size factor.

The soil-to-plant-uptake factors used in Equation 49 are input by the user for all radionuclides except for tritium; a specific activity model is used to estimate the concentrations of tritium in crops. Using this model, tritium concentrations in plant tissues are given by the following equation (Wood et al., 1994):

$$C_{H-3,c,t} = C_{H-3,sm,t} \times F_v^w \qquad 50$$

Where

$C_{H\text{-}3,c,t}$ = tritium concentration in crop *c* at time *t* (Ci/kg)
$C_{H\text{-}3,sm,t}$ = tritium concentration in soil moisture at time *t* (Ci/kg)
F_v^w = fraction of water in vegetation

The fraction of water in the vegetation was modified to take into account the tritium that is organically bound in the produce. This adjustment is made using the following equation (Wood et al., 1994):

$$F_v^{w2} = F_v^w + (1. - F_v^w) \times F_v^H \times 9 \qquad 51$$

Where

F_v^{w2} = effective water fraction in vegetation
F_v^H = fraction of hydrogen in vegetation
9 = coefficient to convert tritium concentration to hydrogen concentration

The quantities calculated using Equations 50 and 51 are used to estimate the plant uptake factor for tritium in a manner that is consistent with the plant uptake factors for the other radionuclides. This is accomplished using the following:

$$B_{H-3,c} = \frac{F_v^{w2}}{\theta_s \times \rho_w / \rho_{ds} \times D_c} \qquad 52$$

Where

$B_{H\text{-}3,c}$ = plant uptake factor for tritium in crop *c* (Ci/kg dry weight vegetation per Ci/kg dry weight soil)
θ_s = moisture content of soil (volume basis)
ρ_w = density of water (kg/m^3)
ρ_{ds} = density of dry soil (kg/m^3)

The actual mechanisms of plant uptake used to model receptor exposures depend upon the exposure scenario under consideration. Contamination of crops as a result of rainsplash and root uptake is considered for all receptors included in the performance assessment and composite analysis. Plant uptake due to atmospheric deposition is considered for the Atmospheric Scenario, while contamination on plants resulting from the application of contaminated irrigation water is considered for the All Pathways–Groundwater Scenario.

3.7.3.4 Animal Products

Animals raised by the receptors may ingest contaminated forage, water, and soil/grit, resulting in the contamination of animal products consumed by the individuals. For all scenarios except the Groundwater Resource Protection and Intruder-Construction Scenarios, the GoldSim models assume the receptor raises cattle and cows to supply a portion of household beef and milk, or raises chickens as a source of meat and eggs. Radionuclide concentrations in animal products are calculated using the following general expression:

$$C_{ap,i,t} = f_{i,ap}(C_{c,i,t} \times Q_c \times f_c + C_{w,i,t} \times Q_w \times f_w \times C_{s,i,t} \times Q_s \times f_s \qquad 53$$

Where

$C_{ap,i,t}$ = concentration, in animal product *ap*, of radionuclide *i* at time *t* (Ci/kg)
$f_{i,ap}$ = forage-to-animal-product transfer factor for radionuclide *i* and animal product *ap* (d/kg wet weight animal product)
$C_{c,i,t}$ = concentration, in forage crop *c*, of radionuclide *i* at time *t* (Ci/kg dry weight crop)
Q_c = animal consumption rate of forage crop *c* (kg dry weight crop/d)
f_c = fraction of consumed forage crop *c* that is contaminated
$C_{w,i,t}$ = concentration, in water, of radionuclide *i* at time *t* (Ci/kg)
Q_w = animal consumption rate of water (kg/d)
f_w = fraction of consumed water that is contaminated
Q_s = animal consumption rate of soil/grit (kg dry weight soil/d)
f_s = fraction of ingested soil/grit that is contaminated

The forage-to-animal transfer factor relates the radionuclide concentration in the animal product to the intake of contaminated media ingested by the animal. Separate transfer factors are used to project contaminant concentrations in beef, milk, chicken, and eggs. These transfer factors are assumed to apply to all ingested substances including the pasture grass consumed by cattle and cows, the grain eaten by chickens, and the water and soil/grit ingested by all classes of livestock.

The user is responsible for the entry of transfer factors for all radionuclides except tritium and C-14; specific activity models are used to estimate the concentrations of these contaminants in beef, milk, chicken, and eggs. Tritium concentrations in animal products are calculated by

correlation with the transfer of stable hydrogen to beef, milk, chicken, and eggs (ANL, 2001). In this approach, the transfer factor for tritium is given by the following equation:

$$f_{H-3,ap} = \frac{F_{H,ap}}{F_{H,c} \times Q_c + F_{H,s} \times Q_s + F_{H,w} \times Q_w} \quad 54$$

Where

$f_{H\text{-}3,ap}$ = effective tritium transfer factor for animal product *p* (d/kg)
$F_{H,ap}$ = mass fraction of stable hydrogen in animal product *ap*
$F_{H,c}$ = mass fraction of stable hydrogen in forage crop *c*
$F_{H,s}$ = mass fraction of stable hydrogen in soil
$F_{H,w}$ = mass fraction of stable hydrogen in water

The mass fraction of stable hydrogen in animal products is calculated as follows:

$$F_{H,ap} = F_{H,w} \times F_{w,ap} \quad 55$$

Where

$F_{w,ap}$ = mass water fraction in animal product *ap*

The fraction of the soil that consists of stable hydrogen is given by the following expression (ANL, 2001):

$$F_{H,s} = \frac{\left[\rho_b \times K_d + P \times R_s\right] \times F_{H,w} \times \rho_w}{\rho_b} \quad 56$$

Where

ρ_b = bulk density of soil (kg/m3)
K_d = hydrogen distribution coefficient in soil (m3/kg)
P = soil porosity
R_s = volumetric water content of soil

The first term of the expression in the brackets ($\rho_b \times K_d$) drops out when the distribution coefficient for hydrogen is zero.

The concentration of C-14 in animal products is given by the following (Napier et al., 2004):

$$C_{ap,C-14,t} = F_{ap}^{c} \times \left(\frac{C_{c,C-14,t} \times Q_c + C_{s,C-14,t} \times Q_s + C_{w,C-14,t} \times Q_w}{F_c^c \times Q_c + F_s^c \times Q_s + F_w^c \times Q_w} \right) \quad 57$$

Where

$C_{ap,C-14,t}$ = concentration, in animal product *ap*, of C-14 at time *t* (Ci/kg)
F_{ap}^{c} = fraction of animal product *ap* that is carbon (dry weight basis)
$C_{c,\,C-14,t}$ = concentration, in forage crop *c*, of C-14 at time *t* (Ci/kg dry weight)
$C_{s,\,C-14,t}$ = concentration, in soil, of C-14 at time *t* (Ci/kg dry weight)
$C_{w,C-14,t}$ = concentration, in water, of C-14 at time *t* (Ci/kg)
F_c^c = fraction of forage crop *c* that is carbon (dry weight basis)
F_s^c = fraction of soil that is carbon (dry weight basis)
F_w^c = fraction of water that is carbon

The quotient of the concentration calculated using Equation 57 and the daily animal intake of C-14 yields the effective transfer factors needed for the performance assessment and composite analysis. Given that the numerator of Equation 57 includes the animal intake, this expression simplifies to the following:

$$f_{C-14,ap} = \frac{F_{ap}^{c}}{F_c^c \times Q_c + F_s^c \times Q_s + F_w^c \times Q_w} \quad 58$$

Where

$f_{C-14,ap}$ = C-14 transfer factor for animal product *ap* (d/kg)

The radionuclide concentrations in animal products will depend upon the fraction of the animals' diets that consist of contaminated media. The fraction of forage crop *c* that is contaminated is calculated as follows:

$$f_c = \frac{(A_l - A_h - A_c) \times Y_{v,c}}{Q_c / D_c \times 365} \quad 59$$

Where

A_c = area of receptor's lot used to raise leafy vegetables, produce, and grain (m^2)
365 = 365 d

The fraction calculated using Equation 59 is also used to represent the fraction of the soil ingested by the animals that is contaminated; all water consumed by the animals is assumed to come from contaminated sources.

The sources of contamination that contribute to contaminant concentrations in animal products depend upon the exposure scenario under consideration. Animals are assumed to ingest contaminated soil and forage for all scenarios in which the receptor raises animals. The ingestion of contaminated drinking water by the animals is assumed only for the All Pathways–Groundwater Scenario.

3.7.3.5 Groundwater

The groundwater pathway receptors are assumed to use contaminated water drawn from the regional aquifer for irrigation, watering animals, and personal consumption. For a given scenario, the radionuclide concentrations in the water are calculated by dividing the annual flow from the FEHM elements to the well by the water usage rates of the receptor. Usage rates for the Groundwater Resources Protection Scenario take into account the water consumed by the individual and water needed for domestic uses (e.g., washing, food preparation, and bathing); the usage rates for the all pathways receptor are higher because they include irrigation needs.

4.0 Input Parameter Requirements

A variety of input data is required to implement the Area G Site, Intruder, Intruder Diffusion, and Inventory Models. This section provides a listing of the input parameters required to run these models. Included are the variable names used in the models, the units associated with each variable, and descriptions of the parameters. Input requirements for the Area G Site Model are provided in Table 5. The data requirements for the intruder and intruder diffusion models are listed in Tables 6 and 7, respectively. Table 8 presents the input data requirements for the Area G Inventory Model.

The majority of the data used in the Area G models are input using objects referred to in the GoldSim documentation (GoldSim, 2007a, 2007b, and 2007c) as data and stochastic elements. Data elements accept single input values, or vectors and matrices of such. Stochastic elements allow the user to represent the uncertainty inherent in a variable by designating a distribution for the parameter. These elements also allow the user to specify deterministic values for parameters that can be used when the models are run in deterministic mode.

The type of element used by the Area G models will determine the type of information required of the user. The summaries of the input data requirements provided below specify the type of element used for each parameter.

Table 5
Input Data Requirements for the Area G Site Model

Model Container/Parameter Name	Units	Parameter Description	Parameter Type	Input Element Type
Simulation_Options				
Analysis_Flag		Flag used to indicate whether the performance assessment or composite analysis is being considered. A value of 1 indicates the composite analysis inventory is included in the simulation; a value of 2 indicates the performance assessment inventory is being used.	Scalar	Data
Diffusion_Flag		Flag used to indicate whether the effects of vapor- and gas-phase diffusion are taken into account in the modeling. A value of 0 indicates that the effects of diffusion are not taken into account; a value of 1 indicates diffusive transport is modeled.	Scalar	Data
Disposal_System_Information				
Species_and_Materials				
Halflives	yr	Radionuclide half-lives	Vector (radionuclide)	Data
Material_Properties				
Air_Diffusion_Length	m	Diffusion length in air	Scalar	Data
C14_Gas_Generation_Rate	yr^{-1}	Rate constant describing the rate of C-14 gas generation due to biodegradation of organic waste	Scalar	Stochastic
CO2_Fraction		Fraction of C-14 gas generated by the biodegradation of organic waste that is carbon dioxide	Scalar	Stochastic
Density_of_Water	kg/m^3	Density of water	Scalar	Data
Organic_Waste_Fraction		Fraction of C-14 waste that is organic and susceptible to biodegradation	Scalar	Stochastic
Radon_Emanation_Coefficient		Emanation coefficient for Rn-220 and Rn-222	Scalar	Stochastic

Table 5 (Continued)
Input Data Requirements for the Area G Site Model

Model Container/Parameter Name	Units	Parameter Description	Parameter Type	Input Element Type
Soil_Carbon_Fraction		Fraction of surface soil that is carbon	Scalar	Data
Solubility_Limits	mg/L	Elemental solubility limits for crushed tuff and waste	Vector (element)	Data
Water_Carbon_Fraction		Fraction of water that is carbon	Scalar	Data
Water_Hydrogen_Fraction		Fraction of water that is hydrogen	Scalar	Data
Dry_Densities				
DD_Crushed_Tuff	kg/m^3	Dry density of crushed tuff	Scalar	Stochastic
DD_Waste	kg/m^3	Dry density of waste	Scalar	Stochastic
Moisture_Contents				
MC_Crushed_Tuff	volume basis	Moisture content of crushed tuff	Scalar	Stochastic
MC_Waste	volume basis	Moisture content of waste	Scalar	Stochastic
Effective_Porosities				
EP_Crushed_Tuff		Effective porosity of crushed tuff	Scalar	Stochastic
EP_Waste		Effective porosity of waste	Scalar	Stochastic
Partition_Coefficients				
Soil_and_Waste_Kds				
Elemental_Kds	m^3/kg	Elemental distribution coefficients for crushed tuff and waste	Vector (element)	Data
Kd_Distributions				
Ag	m^3/kg	Distribution coefficient for silver in crushed tuff and waste	Scalar	Stochastic
Am	m^3/kg	Distribution coefficient for americium in crushed tuff and waste	Scalar	Stochastic

Table 5 (Continued)
Input Data Requirements for the Area G Site Model

Model Container/Parameter Name	Units	Parameter Description	Parameter Type	Input Element Type
Ba	m^3/kg	Distribution coefficient for barium in crushed tuff and waste	Scalar	Stochastic
Cs	m^3/kg	Distribution coefficient for cesium in crushed tuff and waste	Scalar	Stochastic
Np	m^3/kg	Distribution coefficient for neptunium in crushed tuff and waste	Scalar	Stochastic
Pa	m^3/kg	Distribution coefficient for protactinium in crushed tuff and waste	Scalar	Stochastic
Pu	m^3/kg	Distribution coefficient for plutonium in crushed tuff and waste	Scalar	Stochastic
Ra	m^3/kg	Distribution coefficient for radium in crushed tuff and waste	Scalar	Stochastic
Sr	m^3/kg	Distribution coefficient for strontium in crushed tuff and waste	Scalar	Stochastic
Th	m^3/kg	Distribution coefficient for thorium in crushed tuff and waste	Scalar	Stochastic
U	m^3/kg	Distribution coefficient for uranium in crushed tuff and waste	Scalar	Stochastic
Intact_Tuff_Kds				
Elemental_Kds	m^3/kg	Elemental distribution coefficients for intact tuff	Vector (element)	Data
Kd_Distributions				
Ag	m^3/kg	Distribution coefficient for silver in intact tuff	Scalar	Stochastic
Am	m^3/kg	Distribution coefficient for americium in intact tuff	Scalar	Stochastic
Ba	m^3/kg	Distribution coefficient for barium in intact tuff	Scalar	Stochastic

Table 5 (Continued)
Input Data Requirements for the Area G Site Model

Model Container/Parameter Name	Units	Parameter Description	Parameter Type	Input Element Type
Cs	m^3/kg	Distribution coefficient for cesium in intact tuff	Scalar	Stochastic
Np	m^3/kg	Distribution coefficient for neptunium in intact tuff	Scalar	Stochastic
Pa	m^3/kg	Distribution coefficient for protactinium in intact tuff	Scalar	Stochastic
Pu	m^3/kg	Distribution coefficient for plutonium in intact tuff	Scalar	Stochastic
Ra	m^3/kg	Distribution coefficient for radium in intact tuff	Scalar	Stochastic
Sr	m^3/kg	Distribution coefficient for strontium in intact tuff	Scalar	Stochastic
Th	m^3/kg	Distribution coefficient for thorium in intact tuff	Scalar	Stochastic
U	m^3/kg	Distribution coefficient for uranium in intact tuff	Scalar	Stochastic
Air_to_Water_Coefficients				
Soil_Temperature	^oK	Temperature of the crushed tuff and waste	Scalar	Data
Tritium Coefficient				
H2O_Vapor_Pressure	atm	Vapor pressure of water at 15 ^{o} C	Scalar	Data
H2O_Molecular_Weight	g/mol	Molecular weight of water	Scalar	Data
CO2 Coefficient				
CO2_Henrys_Law_Constant	mol/L-atm	Henry's Law constant for carbon dioxide	Scalar	Data
CH4_Coefficient				
CH4_Henrys_Law_Constant	mol/L-atm	Henry's Law constant for methane	Scalar	Data
Kr_Coefficient				
Kr_Henrys_Law_ Constant	mol/L-atm	Henry's Law constant for krypton	Scalar	Data
Rn_Coefficient				
Rn_Henrys_Law_ Constant	mol/L-atm	Henry's Law constant for radon	Scalar	Data

Table 5 (Continued)
Input Data Requirements for the Area G Site Model

Model Container/Parameter Name	Units	Parameter Description	Parameter Type	Input Element Type
Relative_Diffusivities				
Free_Air_Diff_Coefficients	cm^2/s	Free-air diffusion coefficients	Vector (radionuclide)	Data
Reference_Diff_Coefficient	cm^2/s	Reference diffusion coefficient	Scalar	Data
Thermal_Gradient_Factor		Factor used to account for the effects of thermal gradients on the rate of diffusion of tritiated water vapor	Scalar	Stochastic
Site_Geometry_and_Operations				
Atmospheric_Source_Areas	m^2	Areas associated with the atmospheric transport modeling source areas	Vector (atmospheric source area)	Data
Closure_Period	yr	The length of time required to achieve final closure of the disposal facility following the end of disposal operations	Scalar	Data
End_of_Region_Disposal	yr	The last year of the simulation that waste is placed in the disposal units	Vector (disposal unit)	Data
Institutional_Control_Period	yr	The length of the institutional control period, measured from the time of facility closure	Scalar	Data
Minimum_Air_Thickness	m	Minimum air thickness in surface soil and cap cells	Scalar	Data
Start_of_Region_Disposal	yr	The first year of the simulation that waste is placed in the disposal units	Vector (disposal unit)	Data
Layer_Information				
Number_of_Cap_Layers		The number of discrete layers used to represent the cap	Scalar	Data
Number_of_Waste_Layers		The number of discrete layers used to represent the buried waste	Scalar	Data

Table 5 (Continued)
Input Data Requirements for the Area G Site Model

Model Container/Parameter Name	Units	Parameter Description	Parameter Type	Input Element Type
Waste_Region_1–Waste_Region_8				
Cover_Nodes		Number of nodes used to represent the surface of the disposal units in the erosion modeling	Scalar	Stochastic
Disposal_Unit_Area	m^2	Surface area of the disposal units	Scalar	Data
Initial_Cover_Thickness	m	Initial thickness of the cover over each node used to represent the surface of the disposal units	Scalar	Lookup Table
Surface_Soil_Thickness	m	Thickness of the surface soil layer	Vector (waste disposal region)	Data
Waste_Thickness	m	Thickness of the disposed waste	Vector (waste disposal region)	Data
Inventory				
Initial_CA_Inventory	Ci	Initial radionuclide activities in the composite analysis inventory, ordered by waste disposal region and model realization	Scalar	Spreadsheet Element
Initial_PA_Inventory	Ci	Initial radionuclide activities in the performance assessment inventory, ordered by waste disposal region and model realization	Scalar	Spreadsheet Element
Transport_Pathway_Data				
Atmospheric_Transport				
Atmospheric_Mixing_Height	m	Height to which radionuclides diffusing from the disposal site are mixed	Scalar	Data
Average_Wind_Speed	m/s	Average wind speed at Area G	Scalar	Stochastic
Default_Resuspension_Flux	$g/m^2/s$	Resuspension flux used to conduct the complex terrain atmospheric transport modeling	Scalar	Data
Dust_Loading	kg/m^3	Dust loading	Scalar	Stochastic

Table 5 (Continued)
Input Data Requirements for the Area G Site Model

Model Container/Parameter Name	Units	Parameter Description	Parameter Type	Input Element Type
Enhancement_Factor		Ratio of radionuclide concentrations in the resuspendable fraction of the soil to those in the total soil	Scalar	Stochastic
Resuspension_Flux	$g/m^2/yr$	Resuspension for particulates at Area G	Scalar	Stochastic
Soil_Disturbance_Factor		Factor by which the dust loading is increased due to human disturbance of the surface soil	Scalar	Stochastic
Particulate_Dispersion_Factors				
LANL_Boundary				
Grassland_Land_Use				
CA_Factors				
X_Q_SA1_Grassland	s/m^3	Air dispersion factor for atmospheric source area 1 and the grassland land use—composite analysis	Scalar	Stochastic
X_Q_SA2_Grassland	s/m^3	Air dispersion factor for atmospheric source area 2 and the grassland land use—composite analysis	Scalar	Stochastic
X_Q_SA3_Grassland	s/m^3	Air dispersion factor for atmospheric source area 3 and the grassland land use—composite analysis	Scalar	Stochastic
PA_Factors				
X_Q_SA1_Grassland	s/m^3	Air dispersion factor for atmospheric source area 1 and the grassland land use—performance assessment	Scalar	Stochastic
X_Q_SA2_Grassland	s/m^3	Air dispersion factor for atmospheric source area 2 and the grassland land use—performance assessment	Scalar	Stochastic
X_Q_SA3_Grassland	s/m^3	Air dispersion factor for atmospheric source area 3 and the grassland land use—performance assessment	Scalar	Stochastic

Table 5 (Continued)
Input Data Requirements for the Area G Site Model

Model Container/Parameter Name	Units	Parameter Description	Parameter Type	Input Element Type
Woodland_Land_Use				
CA_Factors				
X_Q_SA1_Woodland	s/m^3	Air dispersion factor for atmospheric source area 1 and the woodland land use—composite analysis	Scalar	Stochastic
X_Q_SA2_Woodland	s/m^3	Air dispersion factor for atmospheric source area 2 and the woodland land use—composite analysis	Scalar	Stochastic
X_Q_SA3_Woodland	s/m^3	Air dispersion factor for atmospheric source area 3 and the woodland land use—composite analysis	Scalar	Stochastic
PA_Factors				
X_Q_SA1_Woodland	s/m^3	Air dispersion factor for atmospheric source area 1 and the woodland land use—performance assessment	Scalar	Stochastic
X_Q_SA2_Woodland	s/m^3	Air dispersion factor for atmospheric source area 2 and the woodland land use—performance assessment	Scalar	Stochastic
X_Q_SA3_Woodland	s/m^3	Air dispersion factor for atmospheric source area 3 and the woodland land use—performance assessment	Scalar	Stochastic
Area_G_Fenceline				
Grassland_Land_Use				
CA_Factors				
X_Q_SA1_Grassland	s/m^3	Air dispersion factor for atmospheric source area 1 and the grassland land use—composite analysis	Scalar	Stochastic
X_Q_SA2_Grassland	s/m^3	Air dispersion factor for atmospheric source area 2 and the grassland land use—composite analysis	Scalar	Stochastic
X_Q_SA3_Grassland	s/m^3	Air dispersion factor for atmospheric source area 3 and the grassland land use—composite analysis	Scalar	Stochastic

Table 5 (Continued)
Input Data Requirements for the Area G Site Model

Model Container/Parameter Name	Units	Parameter Description	Parameter Type	Input Element Type
PA_Factors				
X_Q_SA1_Grassland	s/m^3	Air dispersion factor for atmospheric source area 1 and the grassland land use—performance assessment	Scalar	Stochastic
X_Q_SA2_Grassland	s/m^3	Air dispersion factor for atmospheric source area 2 and the grassland land use—performance assessment	Scalar	Stochastic
X_Q_SA3_Grassland	s/m^3	Air dispersion factor for atmospheric source area 3 and the grassland land use—performance assessment	Scalar	Stochastic
Woodland_Land_Use				
CA_Factors				
X_Q_SA1_Woodland	s/m^3	Air dispersion factor for atmospheric source area 1 and the woodland land use—composite analysis	Scalar	Stochastic
X_Q_SA2_Woodland	s/m^3	Air dispersion factor for atmospheric source area 2 and the woodland land use—composite analysis	Scalar	Stochastic
X_Q_SA3_Woodland	s/m^3	Air dispersion factor for atmospheric source area 3 and the woodland land use—composite analysis	Scalar	Stochastic
PA_Factors				
X_Q_SA1_Woodland	s/m^3	Air dispersion factor for atmospheric source area 1 and the woodland land use—performance assessment	Scalar	Stochastic
X_Q_SA2_Woodland	s/m^3	Air dispersion factor for atmospheric source area 2 and the woodland land use—performance assessment	Scalar	Stochastic
X_Q_SA3_Woodland	s/m^3	Air dispersion factor for atmospheric source area 3 and the woodland land use—performance assessment	Scalar	Stochastic

Table 5 (Continued)
Input Data Requirements for the Area G Site Model

Model Container/Parameter Name	Units	Parameter Description	Parameter Type	Input Element Type
Gas_Dispersion_Factors				
LANL_Boundary				
Grassland_Land_Use				
X_Q_SA1_Grassland	s/m^3	Air dispersion factor for atmospheric source area 1 and the grassland land use	Scalar	Stochastic
X_Q_SA2_Grassland	s/m^3	Air dispersion factor for atmospheric source area 2 and the grassland land use	Scalar	Stochastic
X_Q_SA3_Grassland	s/m^3	Air dispersion factor for atmospheric source area 3 and the grassland land use	Scalar	Stochastic
Area_G_Fenceline				
Grassland_Land_Use				
X_Q_SA1_Grassland	s/m^3	Air dispersion factor for atmospheric source area 1 and the grassland land use	Scalar	Stochastic
X_Q_SA2_Grassland	s/m^3	Air dispersion factor for atmospheric source area 2 and the grassland land use	Scalar	Stochastic
X_Q_SA3_Grassland	s/m^3	Air dispersion factor for atmospheric source area 3 and the grassland land use	Scalar	Stochastic
Deposition_Rates				
LANL_Boundary				
Grassland_Land_Use				
CA_Factors				
DepRate_SA1_Grassland	$g/m^2/s$	Particulate deposition rate for atmospheric source area 1 and the grassland land use—composite analysis	Scalar	Stochastic

Table 5 (Continued)
Input Data Requirements for the Area G Site Model

Model Container/Parameter Name	Units	Parameter Description	Parameter Type	Input Element Type
DepRate_SA2_Grassland	g/m²/s	Particulate deposition rate for atmospheric source area 2 and the grassland land use—composite analysis	Scalar	Stochastic
DepRate_SA3_Grassland	g/m²/s	Particulate deposition rate for atmospheric source area 3 and the grassland land use—composite analysis	Scalar	Stochastic
PA_Factors				
DepRate_SA1_Grassland	g/m²/s	Particulate deposition rate for atmospheric source area 1 and the grassland land use—performance assessment	Scalar	Stochastic
DepRate_SA2_Grassland	g/m²/s	Particulate deposition rate for atmospheric source area 2 and the grassland land use—performance assessment	Scalar	Stochastic
DepRate_SA3_Grassland	g/m²/s	Particulate deposition rate for atmospheric source area 3 and the grassland land use—performance assessment	Scalar	Stochastic
Woodland_Land_Use				
CA_Factors				
DepRate_SA1_Woodland	g/m²/s	Particulate deposition rate for atmospheric source area 1 and the woodland land use—composite analysis	Scalar	Stochastic
DepRate_SA2_Woodland	g/m²/s	Particulate deposition rate for atmospheric source area 2 and the woodland land use—composite analysis	Scalar	Stochastic
DepRate_SA3_Woodland	g/m²/s	Particulate deposition rate for atmospheric source area 3 and the woodland land use—composite analysis	Scalar	Stochastic
PA_Factors				
DepRate_SA1_Woodland	g/m²/s	Particulate deposition rate for atmospheric source area 1 and the woodland land use—performance assessment	Scalar	Stochastic
DepRate_SA2_Woodland	g/m²/s	Particulate deposition rate for atmospheric source area 2 and the woodland land use—performance assessment	Scalar	Stochastic

Table 5 (Continued)
Input Data Requirements for the Area G Site Model

Model Container/Parameter Name	Units	Parameter Description	Parameter Type	Input Element Type
DepRate_SA3_Woodland	g/m²/s	Particulate deposition rate for atmospheric source area 3 and the woodland land use—performance assessment	Scalar	Stochastic
Area_G_Fenceline				
Grassland_Land_Use				
CA_Factors				
DepRate_SA1_Grassland	g/m²/s	Particulate deposition rate for atmospheric source area 1 and the grassland land use—composite analysis	Scalar	Stochastic
DepRate_SA2_Grassland	g/m²/s	Particulate deposition rate for atmospheric source area 2 and the grassland land use—composite analysis	Scalar	Stochastic
DepRate_SA3_Grassland	g/m²/s	Particulate deposition rate for atmospheric source area 3 and the grassland land use—composite analysis	Scalar	Stochastic
PA_Factors				
DepRate_SA1_Grassland	g/m²/s	Particulate deposition rate for atmospheric source area 1 and the grassland land use—performance assessment	Scalar	Stochastic
DepRate_SA2_Grassland	g/m²/s	Particulate deposition rate for atmospheric source area 2 and the grassland land use—performance assessment	Scalar	Stochastic
DepRate_SA3_Grassland	g/m²/s	Particulate deposition rate for atmospheric source area 3 and the grassland land use—performance assessment	Scalar	Stochastic
Woodland_Land_Use				
CA_Factors				
DepRate_SA1_Woodland	g/m²/s	Particulate deposition rate for atmospheric source area 1 and the woodland land use—composite analysis	Scalar	Stochastic
DepRate_SA2_Woodland	g/m²/s	Particulate deposition rate for atmospheric source area 2 and the woodland land use—composite analysis	Scalar	Stochastic

Table 5 (Continued)
Input Data Requirements for the Area G Site Model

Model Container/Parameter Name	Units	Parameter Description	Parameter Type	Input Element Type
DepRate_SA3_Woodland	g/m²/s	Particulate deposition rate for atmospheric source area 3 and the woodland land use—composite analysis	Scalar	Stochastic
PA_Factors				
DepRate_SA1_Woodland	g/m²/s	Particulate deposition rate for atmospheric source area 1 and the woodland land use—performance assessment	Scalar	Stochastic
DepRate_SA2_Woodland	g/m²/s	Particulate deposition rate for atmospheric source area 2 and the woodland land use—performance assessment	Scalar	Stochastic
DepRate_SA3_Woodland	g/m²/s	Particulate deposition rate for atmospheric source area 3 and the woodland land use—performance assessment	Scalar	Stochastic
Foodchain_Transport				
Plant_Data				
Uptake_Factors				
Crop_GSD		Geometric standard deviation of the plant uptake factor distributions for all crops	Vector (element)	Data
Grain_GM	Ci/kg plant per Ci/kg soil (dry weight)	Geometric means of the plant uptake factor distributions for grain	Vector (element)	Data
Leafy_Vegetable_GM	Ci/kg plant per Ci/kg soil (dry weight)	Geometric means of the plant uptake factor distributions for leafy vegetables	Vector (element)	Data
PGrass_and_Native_GM	Ci/kg plant per Ci/kg soil (dry weight)	Geometric means of the plant uptake factor distributions for pasture grass and native vegetation	Vector (element)	Data
Produce_GM	Ci/kg plant per Ci/kg soil (dry weight)	Geometric means of the plant uptake factor distributions for produce	Vector (element)	Data

Table 5 (Continued)
Input Data Requirements for the Area G Site Model

Model Container/Parameter Name	Units	Parameter Description	Parameter Type	Input Element Type
Crop_Characteristics				
Particle_Size_Factor		Ratio of radionuclide concentrations in the fraction of the soil resuspended due to rainsplash to those in the total soil	Scalar	Stochastic
Plant_Carbon_Fraction		Fraction of plant that is carbon (dry weight basis)	Vector (crop)	Data
Plant_Hydrogen_Fraction		Fraction of plant that is hydrogen (dry weight basis)	Vector (crop)	Data
Plant_Interception_Coefficient	m^2/kg	Coefficient used to estimate the fraction of contamination deposited on plants that is initially retained	Scalar	Stochastic
Weathering_Halflife	d	Time required for 50 percent of the surface contamination on plants to be removed due to weathering processes	Scalar	Stochastic
Dry_to_Wet_Weight_Fractions				
DW_Grain		Dry-to-wet weight fraction for grain	Scalar	Stochastic
DW_Leafy_Vegetables		Dry-to-wet weight fraction for leafy vegetables	Scalar	Stochastic
DW_Pasture_Grass		Dry-to-wet weight fraction for pasture grass	Scalar	Stochastic
DW_Produce		Dry-to-wet weight fraction for produce	Scalar	Stochastic
Translocation_Factors				
TF_Grain		Translocation factor for grain	Scalar	Stochastic
TF_Leafy_Vegetables		Translocation factor for leafy vegetables	Scalar	Stochastic
TF_Pasture_Grass		Translocation factor for pasture grass	Scalar	Stochastic
TF_Produce		Translocation factor for produce	Scalar	Stochastic
Agricultural_Productivities				
AP_Grain	kg/m^2 (wet weight)	Agricultural productivity for grain	Scalar	Stochastic

Table 5 (Continued)
Input Data Requirements for the Area G Site Model

Model Container/Parameter Name	Units	Parameter Description	Parameter Type	Input Element Type
AP_Leafy_Vegetables	kg/m^2 (wet weight)	Agricultural productivity for leafy vegetables	Scalar	Stochastic
AP_Pasture_Grass	kg/m^2 (dry weight)	Agricultural productivity for pasture grass	Scalar	Stochastic
AP_Produce	kg/m^2 (wet weight)	Agricultural productivity for produce	Scalar	Stochastic
Growing_Season				
GS_Grain	d	Growing season for grain	Scalar	Stochastic
GS_Leafy_Vegetables	d	Growing season for leafy vegetables	Scalar	Stochastic
GS_Pasture_Grass	d	Growing season for pasture grass	Scalar	Stochastic
GS_Produce	d	Growing season for produce	Scalar	Stochastic
Mass_Loading_Factors				
MLF_Grain	g soil/g plant (dry weight)	Mass-loading factor for grain	Scalar	Stochastic
MLF_Leafy_Vegetables	g soil/g plant (dry weight)	Mass-loading factor for leafy vegetables	Scalar	Stochastic
MLF_Pasture_Grass	g soil/g plant (dry weight)	Mass-loading factor for pasture grass	Scalar	Stochastic
MLF_Produce	g soil/g plant (dry weight)	Mass-loading factor for produce	Scalar	Stochastic

Table 5 (Continued)
Input Data Requirements for the Area G Site Model

Model Container/Parameter Name	Units	Parameter Description	Parameter Type	Input Element Type
Animal_Data				
Animal_Ingestion_Data				
Cattle_and_Cows				
Cattle_Food_Ingestion	kg/d (dry weight)	Food consumption rate of cattle	Scalar	Stochastic
Cattle_Soil_Ingestion	kg/d (dry weight)	Soil consumption rate of cattle	Scalar	Stochastic
Cattle_Water_Ingestion	kg/d	Water consumption rate of cattle	Scalar	Stochastic
Cow_Food_Ingestion	kg/d (dry weight)	Food consumption rate of cows	Scalar	Stochastic
Cow_Soil_Ingestion	kg/d (dry weight)	Soil consumption rate of cows	Scalar	Stochastic
Cow_Water_Ingestion	kg/d	Water consumption rate of cows	Scalar	Stochastic
Chickens				
Chicken_Feed_Ingestion	kg/d (dry weight)	Food consumption rate of chickens	Scalar	Stochastic
Chicken_Water_Ingestion	kg/d	Water consumption rate of chickens	Scalar	Stochastic
Grit_to_Food_Ratio		Ratio of grit or soil intake to food intake for chickens	Scalar	Data
Transfer_Factors				
Beef_GM	d/kg	Geometric means of the forage-to-beef transfer factor distributions	Vector (element)	Stochastic
Beef_GSD		Geometric standard deviation of the forage-to-beef transfer factor distributions	Vector (element)	Data

Table 5 (Continued)
Input Data Requirements for the Area G Site Model

Model Container/Parameter Name	Units	Parameter Description	Parameter Type	Input Element Type
Chicken_GM	d/kg	Geometric means of the forage-to-chicken transfer factor distributions	Vector (element)	Stochastic
Chicken_GSD		Geometric standard deviation of the forage-to-chicken transfer factor distributions	Vector (element)	Data
Eggs_GM	d/kg	Geometric means of the forage-to-eggs transfer factor distributions	Vector (element)	Stochastic
Eggs_GSD		Geometric standard deviation of the forage-to-eggs transfer factor distributions	Vector (element)	Data
Milk_GM	d/kg	Geometric means of the forage-to-milk transfer factor distributions	Vector (element)	Stochastic
Milk_GSD		Geometric standard deviation of the forage-to-milk transfer factor distributions	Vector (element)	Data
H3_and_C14_Transfer_Factors				
H3_Factors				
Water_Fraction_Animal_Products		Mass water fractions of animal products	Vector (animal product)	Data
C14_Factors				
Animal_Prod_Carbon_Fraction		Carbon fractions of animal products	Vector (animal product)	Data
Groundwater_Transport				
CdB_Infiltration_Rate	m/yr	Water infiltration rate at the receptor location for the All Pathways–Cañada del Buey Scenario	Scalar	Stochastic
Contaminant_Capture_Fraction		Fraction of contaminant captured by the domestic well downgradient of Area G	Vector (waste disposal region)	Data
MdB_Infiltration_Rate	m/yr	Water infiltration rate on Mesita del Buey	Scalar	Stochastic

Table 5 (Continued)
Input Data Requirements for the Area G Site Model

Model Container/Parameter Name	Units	Parameter Description	Parameter Type	Input Element Type
PC_Infiltration_Rate	m/yr	Water infiltration rate at the receptor location for the All Pathways–Pajarito Canyon Scenario	Scalar	Stochastic
PME_Infiltration_Rate	m/yr	Water infiltration rate at the receptor location for the Atmospheric Scenario	Scalar	Stochastic
Sediment_Transport				
Catchment_Area	m^2	Area of each canyon catchment	Vector (canyon catchment)	Data
Sediment_Allocation_Factors		Fraction of contaminated sediment that is transported to each canyon catchment from each waste disposal region	Matrix (waste disposal region, canyon catchment)	Data
Sediment_Dispersal_Fraction		Fraction of canyon catchment over which sediments disperse	Scalar	Stochastic
Sediment_Transport_Rate	yr^{-1}	Rate constant describing the rate at which canyon sediments are flushed	Scalar	Stochastic
Biotic_Intrusion_Model				
Eco_Succession_Model				
Time_of_Climax	yr	Period required for disposal site to reach a piñon-juniper climax condition, measured from the time of facility closure	Scalar	Stochastic
Intrusion_Shape_Parameters				
Alpha_Shape_Factor		Shape factor used to model animal burrow and plant root distributions with depth	Scalar	Data
Beta_Shape_Factor		Shape factor used to model animal burrow and plant root distributions with depth	Scalar	Stochastic

Table 5 (Continued)
Input Data Requirements for the Area G Site Model

Model Container/Parameter Name	Units	Parameter Description	Parameter Type	Input Element Type
Animal_Intrusion_Model				
Harvester_Ants				
Burrow_Density_Grassland	ha^{-1}	Density of harvester ant burrows during early succession	Scalar	Stochastic
Burrow_Density_Woodland	ha^{-1}	Density of harvester ant burrows in the piñon-juniper climax condition	Scalar	Stochastic
Burrow_Mass	kg	Mass of soil excavated per harvester ant burrow	Scalar	Stochastic
Colony_Life_Span	yr	Life span of harvester ant colonies	Scalar	Stochastic
Maximum_Burrow_Depth	m	Maximum burrowing depth for harvester ants	Scalar	Stochastic
Pocket_Gophers				
Burrow_Renewal_Rate	yr^{-1}	Rate at which existing pocket gopher burrows are replaced with new ones	Scalar	Stochastic
Maximum_Burrow_Depth	m	Maximum burrowing depth for pocket gophers	Scalar	Stochastic
Soil_Removal_Rate_Grassland	m^3/ha	Rate of soil removal by pocket gophers during early succession	Scalar	Stochastic
Soil_Removal_Rate_Woodland	m^3/ha	Rate of soil removal by pocket gophers in the piñon-juniper climax condition	Scalar	Stochastic
Mice				
Burrow_Density_Grassland	ha^{-1}	Density of mouse burrows during early succession	Scalar	Stochastic
Burrow_Density_Woodland	ha^{-1}	Density of mouse burrows in the piñon-juniper climax condition	Scalar	Stochastic
Burrow_Renewal_Rate	yr^{-1}	Rate at which existing mouse burrows are replaced with new ones	Scalar	Stochastic
Burrow_Volume	kg	Volume of soil excavated per mouse burrow	Scalar	Stochastic

Table 5 (Continued)
Input Data Requirements for the Area G Site Model

Model Container/Parameter Name	Units	Parameter Description	Parameter Type	Input Element Type
Maximum_Burrow_Depth	m	Maximum burrowing depth for mice	Scalar	Stochastic
Chipmunks_and_Squirrels				
Burrow_Density_Grassland	ha^{-1}	Density of chipmunk and ground squirrel burrows during early succession	Scalar	Stochastic
Burrow_Density_Woodland	ha^{-1}	Density of chipmunk and ground squirrel burrows in the piñon-juniper climax condition	Scalar	Stochastic
Burrow_Renewal_Rate	yr^{-1}	Rate at which existing chipmunk and ground squirrel burrows are replaced with new ones	Scalar	Stochastic
Burrow_Volume	kg	Volume of soil excavated per chipmunk and ground squirrel burrow	Scalar	Stochastic
Maximum_Burrow_Depth	m	Maximum burrowing depth for chipmunks and ground squirrels	Scalar	Stochastic
Plant_Intrusion_Model				
Litter_Halflife	yr	Decomposition half-life of plant litter	Scalar	Stochastic
Grasses				
Biomass_Density_Grassland	kg/m^2	Aboveground biomass density of grasses during early succession	Scalar	Stochastic
Biomass_Density_Woodland	kg/m^2	Aboveground biomass density of grasses in the piñon-juniper climax condition	Scalar	Stochastic
Litter_Prod_Rate	yr^{-1}	Fraction of the aboveground biomass that falls as litter	Scalar	Stochastic
Maximum_Root_Depth	m	Maximum rooting depth of grasses	Scalar	Stochastic
Forbs				
Biomass_Density_Grassland	kg/m^2	Aboveground biomass density of forbs during early succession	Scalar	Stochastic

Table 5 (Continued)
Input Data Requirements for the Area G Site Model

Model Container/Parameter Name	Units	Parameter Description	Parameter Type	Input Element Type
Biomass_Density_Woodland	kg/m^2	Aboveground biomass density of forbs in the piñon-juniper climax condition	Scalar	Stochastic
Litter_Prod_Rate	yr^{-1}	Fraction of the aboveground biomass that falls as litter	Scalar	Stochastic
Maximum_Root_Depth	m	Maximum rooting depth of forbs	Scalar	Stochastic
Shrubs				
Biomass_Density_Grassland	kg/m^2	Aboveground biomass density of shrubs during early succession	Scalar	Stochastic
Biomass_Density_Woodland	kg/m^2	Aboveground biomass density of shrubs in the piñon-juniper climax condition	Scalar	Stochastic
Litter_Prod_Rate	yr^{-1}	Fraction of the aboveground biomass that falls as litter	Scalar	Stochastic
Maximum_Root_Depth	m	Maximum rooting depth of shrubs	Scalar	Stochastic
Trees				
Biomass_Density_Grassland	kg/m^2	Aboveground biomass density of trees during early succession	Scalar	Stochastic
Biomass_Density_Woodland	kg/m^2	Aboveground biomass density of trees in the piñon-juniper climax condition	Scalar	Stochastic
Litter_Prod_Rate	yr^{-1}	Fraction of the aboveground biomass that falls as litter	Scalar	Stochastic
Maximum_Root_Depth	m	Maximum rooting depth of trees	Scalar	Stochastic
Erosion_Model				
Erosion_Rates				
Erosion_Scenario		Probability of erosion scenario occurrence	Scalar	Stochastic

Table 5 (Continued)
Input Data Requirements for the Area G Site Model

Model Container/Parameter Name	Units	Parameter Description	Parameter Type	Input Element Type
Waste_Disposal_Region_1–Waste Disposal_Region_8				
Cover_Loss_Functions	m	Cover remaining over nodes in waste disposal region under erosion scenario *x*, at time *t*	Scalar	Lookup Table
Dose_and_Radon_Flux_Models				
Dose_Conversion_Factors				
Air_External_DCFs	mrem/yr per pCi/m^3	Dose conversion factors for direct radiation from air immersion	Vector (radionuclide)	Data
Ingestion_DCFs	mrem/pCi	Dose conversion factors for the ingestion exposure route	Vector (radionuclide)	Data
Inhalation_DCFs	mrem/pCi	Dose conversion factors for the inhalation exposure route	Vector (radionuclide)	Data
Soil_External_DCFs_15_cm	mrem/yr per pCi/m^3	Dose conversion factors for direct radiation from soils contaminated to a depth of 15 cm	Vector (radionuclide)	Data
Exposure_Pathway_Data				
Area_of_House	m^2	Area of the receptor's house	Scalar	Data
Area_of_Lot	m^2	Area of the receptor's lot	Scalar	Stochastic
Indoor_Exposure_Time	hr/d	Time spent indoors at the receptor location	Scalar	Stochastic
Inhalation_Rate	m^3/d	Inhalation rate of the receptor	Scalar	Stochastic
Outdoor_Exposure_Time	hr/d	Time spent outdoors at the receptor location	Scalar	Stochastic
Shielding_Factor		Direct radiation shielding factor for the time spent indoors	Scalar	Stochastic
Soil_Mixing_Depth	m	Contaminant mixing depth	Scalar	Data

Table 5 (Continued)
Input Data Requirements for the Area G Site Model

Model Container/Parameter Name	Units	Parameter Description	Parameter Type	Input Element Type
Ingestion_Data				
Animals_Raised		Types of animals raised by resident. A value of 0 indicates no animals are raised; a value of 1 indicates cattle and cows are raised; a value of 2 indicates chickens are raised.	Scalar	Stochastic
AP_DW_Ingestion_Rate	L/d	Drinking water ingestion rate for the All Pathways - Groundwater Scenario receptor	Scalar	Stochastic
GP_DW_Ingestion_Rate	L/d	Drinking water ingestion rate for the Groundwater Resource Protection Scenario receptor	Scalar	Data
Input_Vegetable_Fraction		User-specified fraction of the receptor's diet of leafy vegetables, produce, and grain that is grown at the receptor's location	Scalar	Stochastic
Soil_Ingestion_Rate	kg/yr (dry weight)	Rate of soil ingestion for the receptor	Scalar	Stochastic
Crop_Ingestion_Rates				
CI_Grain	kg/yr (wet weight)	Rate of ingestion of grain for the receptor	Scalar	Stochastic
CI_Leafy_Vegetables	kg/yr (wet weight)	Rate of ingestion of leafy vegetables for the receptor	Scalar	Stochastic
CI_Produce	kg/yr (wet weight)	Rate of ingestion of produce for the receptor	Scalar	Stochastic
Animal_Product_Ingestion_Rates				
API_Beef	kg/yr	Rate of ingestion of beef for the receptor	Scalar	Stochastic
API_Chicken	kg/yr	Rate of ingestion of chicken for the receptor	Scalar	Stochastic
API_Eggs	kg/yr	Rate of ingestion of eggs for the receptor	Scalar	Stochastic

Table 5 (Continued)
Input Data Requirements for the Area G Site Model

Model Container/Parameter Name	Units	Parameter Description	Parameter Type	Input Element Type
API_Milk	kg/yr	Rate of ingestion of milk for the receptor	Scalar	Stochastic
Animal_Numbers				
Cattle_Weight_at_Slaughter	kg	Weight of cattle at the time of slaughter	Scalar	Stochastic
Chicken_Weight_at_Slaughter	kg	Weight of chicken at the time of slaughter	Scalar	Stochastic
Cooked_to_Live_Ratio		Ratio of cooked weight of chicken to the live weight of the bird	Scalar	Stochastic
Cutability		Fraction of the carcass that is sold as meat	Scalar	Stochastic
Dressing_Percentage		Ratio of the carcass weight to live weight of the animal	Scalar	Stochastic
Egg_Mass	kg	Mass of egg	Scalar	Stochastic
Egg_Production_Rate	d^{-1}	Production rate of eggs by layers	Scalar	Stochastic
Meat_Fraction		Fraction of the cooked chicken that is meat	Scalar	Stochastic
Milk_Production_Rate	kg/yr	Production rate of milk by cows	Scalar	Stochastic
Shell_Fraction		Fraction of the egg mass that is contributed by the shell	Scalar	Data
Animal_Product_Fractions				
Beef		User-specified fraction of the receptor's diet of beef that is taken from animals living at the exposure location	Scalar	Stochastic
Chicken		User-specified fraction of the receptor's diet of chicken that is taken from animals living at the exposure location	Scalar	Stochastic
Eggs		User-specified fraction of the receptor's diet of eggs that is produced by animals living at the exposure location	Scalar	Stochastic
Milk		User-specified fraction of the receptor's diet of milk that is produced by animals living at the exposure location	Scalar	Stochastic

Table 6
Input Data Requirements for the Area G Intruder Model

Model Container/Parameter Name	Units	Parameter Description	Parameter Type	Input Element Type
Simulation_Options				
Intruder_Flag		Flag used to indicate which intruder scenario is being evaluated. A value of 1 indicates the Intruder–Post-Drilling Scenario is under consideration; a value of 2 indicates the Intruder-Agriculture Scenario is being modeled; a value of 3 indicates the Intruder-Construction Scenario is being assessed.	Scalar	Data
Disposal_Unit_Flag		Flag used to indicate which disposal units are being simulated. Values of 1 and 2 are input to consider the disposal pits in MDA G and the Zone 4 expansion area, respectively; values of 3 and 4 are entered to model the disposal shafts in MDA G and Zone 4, respectively.	Scalar	Data
Biotic_Intrusion_Flag		Flag used to specify if the effects of biotic intrusion will be taken into account in the intruder modeling. A value of 0 indicates that biotic intrusion will not be considered; a value of 1 specifies allows plant and animal intrusion into the disposal site prior to the time of human intrusion.	Scalar	Data
Inventory_Flag		Flag used to indicate whether unit inventories or actual pit and shaft inventories are used in the modeling. A value of 1 is input to use unit inventories; a value of 2 specifies that actual disposal unit inventories will be used.	Scalar	Data
Depth_of_Disposal_Flag		Flag used to indicate whether the input inventory will be distributed homogeneously throughout the disposal units or if waste-layer-specific inventories will be used. A value of 1 is input to use a homogeneously distributed inventory; a value of 2 specifies that waste-layer-specific inventories will be applied.	Scalar	Data

Table 6 (Continued)
Input Data Requirements for the Area G Intruder Model

Model Container/Parameter Name	Units	Parameter Description	Parameter Type	Input Element Type
Disposal_System_Information				
Species_and_Materials				
Halflives	yr	Radionuclide half-lives	Vector (radionuclide)	Data
Material_Properties				
Density_of_Water	kg/m^3	Density of water	Scalar	Data
Soil_Carbon_Fraction		Fraction of surface soil that is carbon	Scalar	Data
Water_Carbon_Fraction		Fraction of water that is carbon	Scalar	Data
Water_Hydrogen_Fraction		Fraction of water that is hydrogen	Scalar	Data
Dry_Densities				
DD_Crushed_Tuff	kg/m^3	Dry density of crushed tuff	Scalar	Stochastic
DD_Waste	kg/m^3	Dry density of waste	Scalar	Stochastic
DD_Concrete	kg/m^3	Dry density of concrete	Scalar	Stochastic
Moisture_Contents				
MC_Crushed_Tuff	(volume basis)	Moisture content of crushed tuff	Scalar	Stochastic
MC_Waste	(volume basis)	Moisture content of waste	Scalar	Stochastic
Concrete_Saturation		Saturation level of concrete	Scalar	Stochastic
Effective_Porosities				
EP_Crushed_Tuff		Effective porosity of crushed tuff	Scalar	Stochastic
EP_Waste		Effective porosity of waste	Scalar	Stochastic
EP_Concrete		Effective porosity of concrete	Scalar	Stochastic

Table 6 (Continued)
Input Data Requirements for the Area G Intruder Model

Model Container/Parameter Name	Units	Parameter Description	Parameter Type	Input Element Type
Partition_Coefficients				
Soil_and_Waste_Kds				
Elemental_Kds	m^3/kg	Elemental distribution coefficients for crushed tuff and waste	Vector (element)	Data
Kd_Distributions				
Ag	m^3/kg	Distribution coefficient for silver in crushed tuff and waste	Scalar	Stochastic
Am	m^3/kg	Distribution coefficient for americium in crushed tuff and waste	Scalar	Stochastic
Ba	m^3/kg	Distribution coefficient for barium in crushed tuff and waste	Scalar	Stochastic
Cs	m^3/kg	Distribution coefficient for cesium in crushed tuff and waste	Scalar	Stochastic
Np	m^3/kg	Distribution coefficient for neptunium in crushed tuff and waste	Scalar	Stochastic
Pa	m^3/kg	Distribution coefficient for protactinium in crushed tuff and waste	Scalar	Stochastic
Pu	m^3/kg	Distribution coefficient for plutonium in crushed tuff and waste	Scalar	Stochastic
Ra	m^3/kg	Distribution coefficient for radium in crushed tuff and waste	Scalar	Stochastic
Sr	m^3/kg	Distribution coefficient for strontium in crushed tuff and waste	Scalar	Stochastic
Th	m^3/kg	Distribution coefficient for thorium in crushed tuff and waste	Scalar	Stochastic
U	m^3/kg	Distribution coefficient for uranium in crushed tuff and waste	Scalar	Stochastic
Attenuation_Coefficients				
Soil_Mass_Atten_Coeff	cm^2/g	Mass attenuation coefficient for soil	Vector (radionuclide)	Data
Concrete_Mass_Atten_Coeff	cm^2/g	Mass attenuation coefficient for concrete	Vector (radionuclide)	Data

Table 6 (Continued)
Input Data Requirements for the Area G Intruder Model

Model Container/Parameter Name	Units	Parameter Description	Parameter Type	Input Element Type
Site_Geometry_and_Operations				
Institutional_Control_Period	yr	The length of the active institutional control period, measured from the time of facility closure	Scalar	Data
Closure_Period	yr	The length of time required to achieve final closure of the disposal facility following the end of disposal operations	Scalar	Data
Concrete_Floor_Thickness	m	The thickness of the floor of the concrete foundation of the intruder's house	Scalar	Data
Layer_Information				
Number_of_Cap_Layers		The number of discrete layers used to represent the cap	Scalar	Data
Number_of_Waste_Layers		The number of discrete layers used to represent the disposed waste	Scalar	Data
Disposal_Pits				
Pits_1988_2010				
Cover_Nodes		Number of nodes used to represent the surface of the disposal units in the erosion modeling	Scalar	Stochastic
Initial_Cover_Thickness	m	Initial thickness of the cover over each node used to represent the surface of the disposal units	Scalar	Lookup Table
Surface_Soil_Thickness	m	Thickness of the surface soil layer	Vector (waste disposal region)	Data
Waste_Thickness	m	Thickness of the disposed waste	Vector (waste disposal region)	Data
Upper_Waste_Layer_Thickness	m	Thickness of the uppermost three layers of waste	Scalar	Data
Disposal_Unit_Area	m^2	Surface area of the disposal units	Scalar	Data

Table 6 (Continued)
Input Data Requirements for the Area G Intruder Model

Model Container/Parameter Name	Units	Parameter Description	Parameter Type	Input Element Type
Start_of_Disposal	yr	The first year of the simulation that waste is placed in the disposal units	Scalar	Data
End_of_Disposal	yr	The last year of the simulation that waste is placed in the disposal units	Scalar	Data
Pits_2011_2044				
Cover_Nodes		Number of nodes used to represent the surface of the disposal units in the erosion modeling	Scalar	Stochastic
Initial_Cover_Thickness	m	Initial thickness of the cover over each node used to represent the surface of the disposal units	Scalar	Lookup Table
Surface_Soil_Thickness	m	Thickness of the surface soil layer	Vector (waste disposal region)	Data
Waste_Thickness	m	Thickness of the disposed waste	Vector (waste disposal region)	Data
Upper_Waste_Layer_Thickness	m	Thickness of the uppermost three layers of waste	Scalar	Data
Disposal_Unit_Area	m^2	Surface area of the disposal units	Scalar	Data
Start_of_Disposal	yr	The first year of the simulation that waste is placed in the disposal units	Scalar	Data
End_of_Disposal	yr	The last year of the simulation that waste is placed in the disposal units	Scalar	Data
Disposal_Shafts				
Shafts_1988_2015				
Cover_Nodes		Number of nodes used to represent the surface of the disposal units in the erosion modeling	Scalar	Stochastic
Initial_Cover_Thickness	m	Initial thickness of the cover over each node used to represent the surface of the disposal units	Scalar	Lookup Table

Table 6 (Continued)
Input Data Requirements for the Area G Intruder Model

Model Container/Parameter Name	Units	Parameter Description	Parameter Type	Input Element Type
Surface_Soil_Thickness	m	Thickness of the surface soil layer	Vector (waste disposal region)	Data
Waste_Thickness	m	Thickness of the disposed waste	Vector (waste disposal region)	Data
Upper_Waste_Layer_Thickness	m	Thickness of the uppermost three layers of waste	Scalar	Data
Disposal_Unit_Area	m^2	Surface area of the disposal units	Scalar	Data
Start_of_Disposal	yr	The first year of the simulation that waste is placed in the disposal units	Scalar	Data
End_of_Disposal	yr	The last year of the simulation that waste is placed in the disposal units	Scalar	Data
Shafts_2016_2044				
Cover_Nodes		Number of nodes used to represent the surface of the disposal units in the erosion modeling	Scalar	Stochastic
Initial_Cover_Thickness	m	Initial thickness of the cover over each node used to represent the surface of the disposal units	Scalar	Lookup Table
Surface_Soil_Thickness	m	Thickness of the surface soil layer	Vector (waste disposal region)	Data
Waste_Thickness	m	Thickness of the disposed waste	Vector (waste disposal region)	Data
Upper_Waste_Layer_Thickness	m	Thickness of the uppermost three layers of waste	Scalar	Data
Disposal_Unit_Area	m^2	Surface area of the disposal units	Scalar	Data
Start_of_Disposal	yr	The first year of the simulation that waste is placed in the disposal units	Scalar	Data
End_of_Disposal	yr	The last year of the simulation that waste is placed in the disposal units	Scalar	Data

Table 6 (Continued)
Input Data Requirements for the Area G Intruder Model

Model Container/Parameter Name	Units	Parameter Description	Parameter Type	Input Element Type
Inventory				
Initial_MDA_G_Pit_Inventory	Ci	Initial radionuclide activities in the MDA G disposal pits used from September 27, 1988 through 2010; ordered by layer-specific actual/unit inventories and model realization	Scalar	Spreadsheet Element
Initial_Zone_4_Pit_Inventory	Ci	Initial radionuclide activities in the Zone 4 disposal pits used from 2011 through 2044; ordered by layer-specific actual/unit inventories and model realization	Scalar	Spreadsheet Element
Initial_MDA_G_Shaft_Inventory	Ci	Initial radionuclide activities in the MDA G disposal shafts used from September 27, 1988 through 2015; ordered by layer-specific actual/unit inventories and model realization	Scalar	Spreadsheet Element
Initial_Zone_4_Shaft_Inventory	Ci	Initial radionuclide activities in the Zone 4 disposal shafts used from 2016 through 2044; ordered by layer-specific actual/unit inventories and model realization	Scalar	Spreadsheet Element
Waste_Disposal_Volumes				
Pit_Waste_1988_2010	m^3	Volume of waste disposed of in pits from September 27, 1988 through 2010	Scalar	Data
Pit_Waste_2011_2044	m^3	Volume of waste disposed of in pits from 2011 through 2044	Scalar	Data
Shaft_Waste_1988_2015	m^3	Volume of waste disposed of in shafts from September 27, 1988 through 2015	Scalar	Data
Shaft_Waste_2016_2044	m^3	Volume of waste disposed of in shafts from 2016 through 2044	Scalar	Data
Inventory_Multiplier		Element used to set selected radionuclide inventories to zero	Vector (radionuclide)	Data

Table 6 (Continued)
Input Data Requirements for the Area G Intruder Model

Model Container/Parameter Name	Units	Parameter Description	Parameter Type	Input Element Type
Transport_Pathway_Data				
Atmospheric_Transport				
Resident_Dust_Loading	kg/m^3	Dust loading for the Intruder–Post-Drilling and Intruder-Agriculture Scenarios	Scalar	Stochastic
Soil_Disturbance_Factor		Factor by which the dust loading is increased due to human disturbance of the surface soil	Scalar	Stochastic
Worker_Dust_Loading	kg/m^3	Dust loading for the Intruder-Construction Scenario	Scalar	Stochastic
Resuspension_Flux	$g/m^2/yr$	Resuspension for particulates at Area G	Scalar	Stochastic
Enhancement_Factor		Ratio of radionuclide concentrations in the resuspendable fraction of the soil to those in the total soil	Scalar	Stochastic
Foodchain_Transport				
Plant_Data				
Uptake_Factors				
Leafy_Vegetable_GM	Ci/kg plant per Ci/kg soil (dry weight)	Geometric means of the plant uptake factors for leafy vegetables	Vector (element)	Data
Produce_GM	Ci/kg plant per Ci/kg soil (dry weight)	Geometric means of the plant uptake factors for produce	Vector (element)	Data
Grain_GM	Ci/kg plant per Ci/kg soil (dry weight)	Geometric means of the plant uptake factors for grain	Vector (element)	Data
PGrass_and_Native_GM	Ci/kg plant per Ci/kg soil (dry weight)	Geometric means of the plant uptake factors for pasture grass and native vegetation	Vector (element)	Data

Table 6 (Continued)
Input Data Requirements for the Area G Intruder Model

Model Container/Parameter Name	Units	Parameter Description	Parameter Type	Input Element Type
Crop_GSD		Geometric standard deviation of the plant uptake factors for all crops	Scalar	Data
Crop_Characteristics				
Particle_Size_Factor		Ratio of radionuclide concentrations in the fraction of the soil resuspended due to rainsplash to those in the total soil	Scalar	Stochastic
Plant_Carbon_Fraction		Fraction of plant that is carbon (dry weight basis)	Vector (crop)	Data
Plant_Hydrogen_Fraction		Fraction of plant that is hydrogen (dry weight basis)	Vector (crop)	Data
Dry_to_Wet_Weight_Fractions				
DWW_Leafy_Vegetables		Dry-to-wet weight fraction for leafy vegetables	Scalar	Stochastic
DWW_Produce		Dry-to-wet weight fraction for produce	Scalar	Stochastic
DWW_Grain		Dry-to-wet weight fraction for grain	Scalar	Stochastic
DWW_Pasture_Grass		Dry-to-wet weight fraction for pasture grass	Scalar	Stochastic
Translocation_Factors				
TF_Leafy_Vegetables		Translocation factor for leafy vegetables	Scalar	Stochastic
TF_Produce		Translocation factor for produce	Scalar	Stochastic
TF_Grain		Translocation factor for grain	Scalar	Stochastic
TF_Pasture_Grass		Translocation factor for pasture grass	Scalar	Stochastic
Agricultural_Productivities				
AP_Leafy_Vegetables	kg/m^2 (wet weight)	Agricultural productivity for leafy vegetables	Scalar	Stochastic
AP_Produce	kg/m^2 (wet weight)	Agricultural productivity for produce	Scalar	Stochastic

Table 6 (Continued)
Input Data Requirements for the Area G Intruder Model

Model Container/Parameter Name	Units	Parameter Description	Parameter Type	Input Element Type
AP_Grain	kg/m^2 (wet weight)	Agricultural productivity for grain	Scalar	Stochastic
AP_Pasture_Grass	kg/m^2 (dry weight)	Agricultural productivity for pasture grass	Scalar	Stochastic
Mass_Loading_Factors				
MLF_Leafy_Vegetables	g soil/g plant (dry weight)	Mass-loading factor for leafy vegetables	Scalar	Stochastic
MLF_Produce	g soil/g plant (dry weight)	Mass-loading factor for produce	Scalar	Stochastic
MLF_Grain	g soil/g plant (dry weight)	Mass-loading factor for grain	Scalar	Stochastic
MLF_Pasture_Grass	g soil/g plant (dry weight)	Mass-loading factor for pasture grass	Scalar	Stochastic
Animal_Data				
Animal_Ingestion_Data				
Cattle_and_Cows				
Cattle_Food_Ingestion	kg/d (dry weight)	Food consumption rate of cattle	Scalar	Stochastic
Cow_Food_Ingestion	kg/d (dry weight)	Food consumption rate of cows	Scalar	Stochastic
Cattle_Soil_Ingestion	kg/d (dry weight)	Soil consumption rate of cattle	Scalar	Stochastic
Cow_Soil_Ingestion	kg/d (dry weight)	Soil consumption rate of cows	Scalar	Stochastic
Cattle_Water_Ingestion	kg/d	Water consumption rate of cattle	Scalar	Stochastic
Cow_Water_Ingestion	kg/d	Water consumption rate of cows	Scalar	Stochastic

Table 6 (Continued)
Input Data Requirements for the Area G Intruder Model

Model Container/Parameter Name	Units	Parameter Description	Parameter Type	Input Element Type
Chickens				
Chicken_Feed_Ingestion	kg/d (dry weight)	Food consumption rate of chickens	Scalar	Stochastic
Chicken_Water_Ingestion	kg/d	Water consumption rate of chickens	Scalar	Stochastic
Grit_to_Food_Ratio		Ratio of grit or soil intake to food intake for chickens	Scalar	Data
Transfer_Factors				
Beef_GM	d/kg	Geometric means of the forage-to-beef transfer factors	Vector (element)	Stochastic
Beef_GSD		Geometric standard deviation of the forage-to-beef transfer factors	Vector (element)	Data
Milk_GM	d/kg	Geometric means of the forage-to-milk transfer factors	Vector (element)	Stochastic
Milk_GSD		Geometric standard deviation of the forage-to-milk transfer factors	Vector (element)	Data
Chicken_GM	d/kg	Geometric means of the forage-to-chicken transfer factors	Vector (element)	Stochastic
Chicken_GSD		Geometric standard deviation of the forage-to-chicken transfer factors	Vector (element)	Data
Eggs_GM	d/kg	Geometric means of the forage-to-eggs transfer factors	Vector (element)	Stochastic
Eggs_GSD		Geometric standard deviation of the forage-to-eggs transfer factors	Vector (element)	Data
H3_and_C14_Transfer_Factors				
H3_Factors				
Water_Fraction_Animal_Products		Mass water fractions of animal products	Vector (animal product)	Data

Table 6 (Continued)
Input Data Requirements for the Area G Intruder Model

Model Container/Parameter Name	Units	Parameter Description	Parameter Type	Input Element Type
C14_Factors				
Animal_Prod_Carbon_Fraction		Carbon fractions of animal products	Vector (animal product)	Data
Groundwater_Transport				
MdB_Infiltration_Rate	m/yr	Water infiltration rate on Mesita del Buey	Scalar	Stochastic
Biotic_Intrusion_Model				
Eco_Succession_Model				
Time_of_Climax	yr	Period required for disposal site to reach a piñon-juniper climax condition, measured from the time of facility closure	Scalar	Stochastic
Intrusion_Shape_Parameters				
Alpha_Shape_Factor		Shape factor used to model animal burrow and plant root distributions with depth	Scalar	Data
Beta_Shape_Factor		Shape factor used to model animal burrow and plant root distributions with depth	Scalar	Stochastic
Animal_Intrusion_Model				
Harvester_Ants				
Maximum_Burrow_Depth	m	Maximum burrowing depth for harvester ants	Scalar	Stochastic
Burrow_Density_Grassland	ha^{-1}	Density of harvester ant burrows during early succession	Scalar	Stochastic
Burrow_Density_Woodland	ha^{-1}	Density of harvester ant burrows in the piñon-juniper climax condition	Scalar	Stochastic
Burrow_Mass	kg	Mass of soil excavated per harvester ant burrow	Scalar	Stochastic
Colony_Life_Span	yr	Life span of harvester ant colonies	Scalar	Stochastic

Table 6 (Continued)
Input Data Requirements for the Area G Intruder Model

Model Container/Parameter Name	Units	Parameter Description	Parameter Type	Input Element Type
Pocket_Gophers				
Maximum_Burrow_Depth	m	Maximum burrowing depth for pocket gophers	Scalar	Stochastic
Soil_Removal_Rate_Grassland	m^3/ha	Rate of soil removal by pocket gophers during early succession	Scalar	Stochastic
Soil_Removal_Rate_Woodland	m^3/ha	Rate of soil removal by pocket gophers in the piñon-juniper climax condition	Scalar	Stochastic
Burrow_Renewal_Rate	yr^{-1}	Rate at which existing pocket gopher burrows are replaced with new ones	Scalar	Stochastic
Mice				
Maximum_Burrow_Depth	m	Maximum burrowing depth for mice	Scalar	Stochastic
Burrow_Density_Grassland	ha^{-1}	Density of mouse burrows during early succession	Scalar	Stochastic
Burrow_Density_Woodland	ha^{-1}	Density of mouse burrows in the piñon-juniper climax condition	Scalar	Stochastic
Burrow_Volume	kg	Volume of soil excavated per mouse burrow	Scalar	Stochastic
Burrow_Renewal_Rate	yr^{-1}	Rate at which existing mouse burrows are replaced with new ones	Scalar	Stochastic
Chipmunks_and_Squirrels				
Maximum_Burrow_Depth	m	Maximum burrowing depth for chipmunks and ground squirrels	Scalar	Stochastic
Burrow_Density_Grassland	ha^{-1}	Density of chipmunk and ground squirrel burrows during early succession	Scalar	Stochastic
Burrow_Density_Woodland	ha^{-1}	Density of chipmunk and ground squirrel burrows in the piñon-juniper climax condition	Scalar	Stochastic

Table 6 (Continued)
Input Data Requirements for the Area G Intruder Model

Model Container/Parameter Name	Units	Parameter Description	Parameter Type	Input Element Type
Burrow_Volume	kg	Volume of soil excavated per chipmunk and ground squirrel burrow	Scalar	Stochastic
Burrow_Renewal_Rate	yr^{-1}	Rate at which existing chipmunk and ground squirrel burrows are replaced with new ones	Scalar	Stochastic
Plant_Intrusion_Model				
Litter_Halflife	yr	Decomposition half-life of plant litter	Scalar	Stochastic
Grasses				
Maximum_Root_Depth	m	Maximum rooting depth of grasses	Scalar	Stochastic
Biomass_Density_Grassland	kg/m^2	Aboveground biomass density of grasses during early succession	Scalar	Stochastic
Biomass_Density_Woodland	kg/m^2	Aboveground biomass density of grasses in the piñon-juniper climax condition	Scalar	Stochastic
Litter_Prod_Rate	yr^{-1}	Fraction of the aboveground biomass that falls as litter	Scalar	Stochastic
Forbs				
Maximum_Root_Depth	m	Maximum rooting depth of forbs	Scalar	Stochastic
Biomass_Density_Grassland	kg/m^2	Aboveground biomass density of forbs during early succession	Scalar	Stochastic
Biomass_Density_Woodland	kg/m^2	Aboveground biomass density of forbs in the piñon-juniper climax condition	Scalar	Stochastic
Litter_Prod_Rate	yr^{-1}	Fraction of the aboveground biomass that falls as litter	Scalar	Stochastic
Shrubs				
Maximum_Root_Depth	m	Maximum rooting depth of shrubs	Scalar	Stochastic

Table 6 (Continued)
Input Data Requirements for the Area G Intruder Model

Model Container/Parameter Name	Units	Parameter Description	Parameter Type	Input Element Type
Biomass_Density_Grassland	kg/m^2	Aboveground biomass density of shrubs during early succession	Scalar	Stochastic
Biomass_Density_Woodland	kg/m^2	Aboveground biomass density of shrubs in the piñon-juniper climax condition	Scalar	Stochastic
Litter_Prod_Rate	yr^{-1}	Fraction of the aboveground biomass that falls as litter	Scalar	Stochastic
Trees				
Maximum_Root_Depth	m	Maximum rooting depth of trees	Scalar	Stochastic
Biomass_Density_Grassland	kg/m^2	Aboveground biomass density of trees during early succession	Scalar	Stochastic
Biomass_Density_Woodland	kg/m^2	Aboveground biomass density of trees in the piñon-juniper climax condition	Scalar	Stochastic
Litter_Prod_Rate	yr^{-1}	Fraction of the aboveground biomass that falls as litter	Scalar	Stochastic
Erosion_Model				
Erosion_Rates				
Erosion_Scenario		Probability of erosion scenario occurrence	Scalar	Stochastic
Pit_1988_2010				
Cover_Loss_Functions	m	Cover remaining over nodes in waste disposal region under erosion scenario *x*, at time *t*	Scalar	Lookup Table
Pit_2011_2044				
Cover_Loss_Functions	m	Cover remaining over nodes in waste disposal region under erosion scenario *x*, at time *t*	Scalar	Lookup Table

Table 6 (Continued)
Input Data Requirements for the Area G Intruder Model

Model Container/Parameter Name	Units	Parameter Description	Parameter Type	Input Element Type
Shaft_1988_2015				
Cover_Loss_Functions	m	Cover remaining over nodes in waste disposal region under erosion scenario *x,* at time *t*	Scalar	Lookup Table
Shaft_2016_2044				
Cover_Loss_Functions	m	Cover remaining over nodes in waste disposal region under erosion scenario *x*, at time *t*	Scalar	Lookup Table
Human_Intrusion_Model				
Basement_Length	m	Length of the intruder's basement	Scalar	Data
Basement_Width	m	Width of the intruder's basement	Scalar	Data
Basement_Depth	m	Depth of the intruder's basement	Scalar	Data
Well_Casing_Diameter	m	Diameter of the well casing	Scalar	Data
Dose_and_WAC_Model				
Dose_Conversion_Factors				
Ingestion_DCFs	mrem/pCi	Dose conversion factors for the ingestion exposure route	Vector (radionuclide)	Data
Inhalation_DCFs	mrem/pCi	Dose conversion factors for the inhalation exposure route	Vector (radionuclide)	Data
Soil_External_DCFs_15_cm	mrem/yr per pCi/m^3	Dose conversion factors for direct radiation from soils contaminated to a depth of 15 cm	Vector (radionuclide)	Data
Soil_External_DCFs_Infinite	mrem/yr per pCi/m^3	Dose conversion factors for direct radiation from soils contaminated to an infinite depth	Vector (radionuclide)	Data
Air_External_DCFs	mrem/yr per pCi/m^3	Dose conversion factors for direct radiation from air immersion	Vector (radionuclide)	Data

Table 6 (Continued)
Input Data Requirements for the Area G Intruder Model

Model Container/Parameter Name	Units	Parameter Description	Parameter Type	Input Element Type
Exposure_Pathway_Data				
Minimum_Soil_Mixing_Depth	m	Contaminant mixing depth	Scalar	Data
Shielding_Factor		Direct radiation shielding factor for the time spent indoors	Scalar	Stochastic
Resident_Inhalation_Rate	m^3/d	Inhalation rate of the resident intruder	Scalar	Stochastic
Worker_Inhalation_Rate	m^3/d	Inhalation rate of the construction intruder	Scalar	Stochastic
Area_of_Lot	m^2	Area of the receptor's lot	Scalar	Stochastic
Area_of_House	m^2	Area of the receptor's house	Scalar	Data
Resident_Intruder_PO	mrem/yr	Performance objective for the postdrilling and agricultural intruders	Scalar	Data
Construction_Intruder_PO	mrem/yr	Performance objective for the construction worker	Scalar	Data
Exposure_Times				
Resident_Indoor_Exposure_Time	hr/d	Time spent inside by the resident intruder	Scalar	Stochastic
Resident_Outdoor_Exposure_Time	hr/d	Time spent outside by the resident intruder	Scalar	Stochastic
Worker_Exposure_Time	hr/d	Time spent building the house by the construction worker	Scalar	Data
Excavation_Occupancy_Factor		Fraction of time spent building the house that is spent in the bottom of the basement excavation	Scalar	Stochastic
Ingestion_Data				
Resident_Soil_Ingestion_Rate	kg/yr (dry weight)	Rate of soil ingestion for the resident intruder	Scalar	Stochastic
Worker_Soil_Ingestion_Rate	kg/yr (dry weight)	Rate of soil ingestion for the construction worker	Scalar	Stochastic

Table 6 (Continued)
Input Data Requirements for the Area G Intruder Model

Model Container/Parameter Name	Units	Parameter Description	Parameter Type	Input Element Type
Food_Ingestion_Data				
Input_Vegetable_Fraction		User-specified fraction of the receptor's diet of leafy vegetables, produce, and grain that is grown at the receptor's location	Scalar	Stochastic
Animals_Raised		The types of animals raised by the receptor to supply a portion of their diet	Scalar	Stochastic
Crop_Ingestion_Rates				
CI_Leafy_Vegetables	kg/yr (wet weight)	Rate of ingestion of leafy vegetables for the resident intruders	Scalar	Stochastic
CI_Produce	kg/yr (wet weight)	Rate of ingestion of produce for the resident intruders	Scalar	Stochastic
CI_Grain	kg/yr (wet weight)	Rate of ingestion of grain for the resident intruders	Scalar	Stochastic
Animal_Product_Ingestion_Rates				
API_Beef	kg/yr	Rate of ingestion of beef for the resident intruders	Scalar	Stochastic
API_Milk	kg/yr	Rate of ingestion of milk for the resident intruders	Scalar	Stochastic
API_Chicken	kg/yr	Rate of ingestion of chicken for the resident intruders	Scalar	Stochastic
API_Eggs	kg/yr	Rate of ingestion of eggs for the resident intruders	Scalar	Stochastic
Animal_Numbers				
Cattle_Weight_at_Slaughter	kg	Weight of cattle at the time of slaughter	Scalar	Stochastic
Dressing_Percentage		Ratio of the carcass weight to live weight of the animal	Scalar	Stochastic
Cutability		Fraction of the carcass that is sold as meat	Scalar	Stochastic
Milk_Production_Rate	kg/yr	Production rate of milk by cows	Scalar	Stochastic

Table 6 (Continued)
Input Data Requirements for the Area G Intruder Model

Model Container/Parameter Name	Units	Parameter Description	Parameter Type	Input Element Type
Chicken_Weight_at_Slaughter	kg	Weight of chicken at the time of slaughter	Scalar	Stochastic
Cook_to_Live_Ratio		Ratio of ready to cook weight of chicken to the live weight of the bird	Scalar	Stochastic
Meat_Fraction		Fraction of the cooked chicken that is meat	Scalar	Stochastic
Egg_Production_Rate	d^{-1}	Production rate of eggs by layers	Scalar	Stochastic
Egg_Mass	kg	Mass of egg	Scalar	Stochastic
Shell_Fraction		Fraction of the egg mass that is contributed by the shell	Scalar	Data
Animal_Product_Fractions				
Beef		User-specified fraction of the receptor's diet of beef that is taken from animals living at the exposure location	Scalar	Stochastic
Milk		User-specified fraction of the receptor's diet of milk that is produced by animals living at the exposure location	Scalar	Stochastic
Chicken		User-specified fraction of the receptor's diet of chicken that is taken from animals living at the exposure location	Scalar	Stochastic
Eggs		User-specified fraction of the receptor's diet of eggs that is produced by animals living at the exposure location	Scalar	Stochastic

Table 7
Input Data Requirements for the Area G Intruder Diffusion Model

Model Container/Parameter Name	Units	Parameter Description	Parameter Type	Input Element Type
Simulation_Options				
Intruder_Flag		Flag used to indicate which intruder scenario is being evaluated. A value of 1 indicates the Intruder–Post-Drilling Scenario is under consideration; a value of 2 indicates the Intruder-Agriculture Scenario is being modeled; a value of 3 indicates the Intruder-Construction Scenario is being assessed.	Scalar	Data
Disposal_Unit_Flag		Flag used to indicate which disposal units are being simulated. Values of 1 and 2 are input to consider the disposal pits in MDA G and the Zone 4 expansion area, respectively; values of 3 and 4 are entered to model the disposal shafts in MDA G and Zone 4, respectively.	Scalar	Data
Diffusion_Flag		Flag used to indicate whether the effects of vapor- and gas-phase diffusion are taken into account in the intruder modeling. A value of 0 indicates that the effects of diffusion are not taken into account; a value of 1 indicates diffusive transport is modeled.	Scalar	Data
Biotic_Intrusion_Flag		Flag used to specify if the effects of biotic intrusion will be taken into account in the intruder modeling. A value of 0 indicates that biotic intrusion will not be considered; a value of 1 specifies allows plant and animal intrusion into the disposal site prior to the time of human intrusion.	Scalar	Data
Inventory_Flag		Flag used to indicate whether unit inventories or actual pit and shaft inventories are used in the modeling. A value of 1 is input to use unit inventories; a value of 2 specifies that actual disposal unit inventories will be used.	Scalar	Data

Table 7 (Continued)
Input Data Requirements for the Area G Intruder Diffusion Model

Model Container/Parameter Name	Units	Parameter Description	Parameter Type	Input Element Type
Depth_of_Disposal_Flag		Flag used to indicate whether the input inventory will be distributed homogeneously throughout the disposal units or the waste-layer-specific inventories will be used. A value of 1 is input to use a homogeneously distributed inventory; a value of 2 specifies that waste layer specific inventories will be applied.	Scalar	Data
Tritium_Package_Flag		Flag used to indicate if off-gas rates for tritium packages will be taken into account in the modeling. A value of 0 is input to ignore the effects of off-gas rates; a value of 1 is used to consider off-gas rates for the packages.	Scalar	Data
Disposal_System_Information				
Species_and_Materials				
Halflives	yr	Radionuclide half-lives	Vector (radionuclide)	Data
Material_Properties				
Density_of_Water	kg/m^3	Density of water	Scalar	Data
Soil_Carbon_Fraction		Fraction of surface soil that is carbon	Scalar	Data
Water_Carbon_Fraction		Fraction of water that is carbon	Scalar	Data
Water_Hydrogen_Fraction		Fraction of water that is hydrogen	Scalar	Data
Air_Diffusion_Length	m	Diffusion length in air	Scalar	Data
Radon_Emanation_Coefficient		Emanation coefficient for Rn-220 and Rn-222	Scalar	Stochastic
C-14_Gas_Generation_Rate	yr^{-1}	Rate constant describing the rate of C-14 gas generation due to biodegradation of organic waste	Scalar	Stochastic
CO2_Fraction		Fraction of C-14 gas generated by the biodegradation of organic waste that is carbon dioxide	Scalar	Stochastic

Table 7 (Continued)
Input Data Requirements for the Area G Intruder Diffusion Model

Model Container/Parameter Name	Units	Parameter Description	Parameter Type	Input Element Type
Organic_Waste_Fraction		Fraction of C-14 waste that is organic and susceptible to biodegradation	Scalar	Stochastic
Dry_Densities				
DD_Crushed_Tuff	kg/m^3	Dry density of crushed tuff	Scalar	Stochastic
DD_Waste	kg/m^3	Dry density of waste	Scalar	Stochastic
DD_Concrete	kg/m^3	Dry density of concrete	Scalar	Stochastic
Moisture_Contents				
MC_Crushed_Tuff	(volume basis)	Moisture content of crushed tuff	Scalar	Stochastic
MC_Waste	(volume basis)	Moisture content of waste	Scalar	Stochastic
Concrete_Saturation		Saturation level of concrete	Scalar	Stochastic
Effective_Porosities				
EP_Crushed_Tuff		Effective porosity of crushed tuff	Scalar	Stochastic
EP_Waste		Effective porosity of waste	Scalar	Stochastic
EP_Concrete		Effective porosity of concrete	Scalar	Stochastic
Partition_Coefficients				
Soil_and_Waste_KDs				
Elemental_Kds	m^3/kg	Elemental distribution coefficients for crushed tuff, waste, and concrete	Vector (element)	Data
Kd_Distributions				
Pu	m^3/kg	Distribution coefficient for plutonium in crushed tuff, waste, and concrete	Scalar	Stochastic

Table 7 (Continued)
Input Data Requirements for the Area G Intruder Diffusion Model

Model Container/Parameter Name	Units	Parameter Description	Parameter Type	Input Element Type
Ra	m^3/kg	Distribution coefficient for radium in crushed tuff, waste, and concrete	Scalar	Stochastic
Th	m^3/kg	Distribution coefficient for thorium in crushed tuff, waste, and concrete	Scalar	Stochastic
U	m^3/kg	Distribution coefficient for uranium in crushed tuff, waste, and concrete	Scalar	Stochastic
Air_to_Water_Coefficients				
Soil_Temperature	ºK	Temperature of the cap and waste	Scalar	Stochastic
Tritium_Coefficient				
H2O_Vapor_Pressure	atm	Vapor pressure of water	Scalar	Data
H2O_Molecular_Weight	g/mol	Molecular weight of water	Scalar	Data
CO2_Coefficient				
CO2_Henry's_Law_Constant	mol/L-atm	Henry's Law constant for carbon dioxide	Scalar	Data
CH4_Coefficient				
CH4_Henrys_Law_Constant	mol/L-atm	Henry's Law constant for methane	Scalar	Data
Kr_Coefficient				
Kr_Henry's_Law_Constant	mol/L-atm	Henry's Law constant for krypton	Scalar	Data
Rn_Coefficient				
Rn_Henrys_Law_Constant	mol/L-atm	Henry's Law constant for radon	Scalar	Data
Relative_Diffusivities				
Free_Air_Diff_Coefficients	cm^2/s	Free-air diffusion coefficients	Vector (radionuclide)	Data

Table 7 (Continued)
Input Data Requirements for the Area G Intruder Diffusion Model

Model Container/Parameter Name	Units	Parameter Description	Parameter Type	Input Element Type
Thermal_Gradient_Factor		Factor used to account for the effects of thermal gradients on the rate of diffusion of tritiated water vapor	Scalar	Stochastic
Reference_Diff_Coefficient	cm^2/s	Reference diffusion coefficient	Scalar	Data
Attenuation_Coefficients				
Soil_Mass_Atten_Coeff	cm^2/g	Mass attenuation coefficient for soil	Vector (radionuclide)	Data
Concrete_Mass_Atten_Coeff	cm^2/g	Mass attenuation coefficient for concrete	Vector (radionuclide)	Data
Site_Geometry_and_Operations				
Institutional_Control_Period	yr	The length of the institutional control period, measured from the time of facility closure	Scalar	Data
Closure_Period	yr	The length of time required to achieve final closure of the disposal facility following the end of disposal operations	Scalar	Data
Minimum_Air_Thickness	cm	Minimum thickness used to calculate the amount of air in the cap cells	Scalar	Data
Concrete_Floor_Thickness	m	The thickness of the floor of the concrete foundation of the intruder's house	Scalar	Data
Number_of_Basement_Layers		The number of discrete layers used to represent the floor of the intruder's foundation	Scalar	Data
Layer_Information				
Number_of_Waste_Layers		The number of discrete layers used to represent the disposed waste	Scalar	Data
Number_of_Cap_Layers		The number of discrete layers used to represent the cap	Scalar	Data

Table 7 (Continued)
Input Data Requirements for the Area G Intruder Diffusion Model

Model Container/Parameter Name	Units	Parameter Description	Parameter Type	Input Element Type
Disposal_Pits				
Pits_1988_2010				
Cover_Nodes		Number of nodes used to represent the surface of the disposal units in the erosion modeling	Scalar	Stochastic
Initial_Cover_Thickness	m	Initial thickness of the cover over each node used to represent the surface of the disposal units	Scalar	Lookup Table
Surface_Soil_Thickness	m	Thickness of the surface soil layer	Vector (disposal region)	Data
Waste_Thickness	m	Thickness of the disposed waste	Vector (disposal region)	Data
Disposal_Unit_Area	m^2	Surface area of the disposal units	Scalar	Data
Start_of_Disposal	yr	The first year of the simulation that waste is placed in the disposal units	Scalar	Data
End_of_Disposal	yr	The last year of the simulation that waste is placed in the disposal units	Scalar	Data
Pits_2011_2044				
Cover_Nodes		Number of nodes used to represent the surface of the disposal units in the erosion modeling	Scalar	Stochastic
Initial_Cover_Thickness	m	Initial thickness of the cover over each node used to represent the surface of the disposal units	Scalar	Lookup Table
Surface_Soil_Thickness	m	Thickness of the surface soil layer	Vector (disposal region)	Data
Waste_Thickness	m	Thickness of the disposed waste	Vector (disposal region)	Data
Disposal_Unit_Area	m^2	Surface area of the disposal units	Scalar	Data

Table 7 (Continued)
Input Data Requirements for the Area G Intruder Diffusion Model

Model Container/Parameter Name	Units	Parameter Description	Parameter Type	Input Element Type
Start_of_Disposal	yr	The first year of the simulation that waste is placed in the disposal units	Scalar	Data
End_of_Disposal	yr	The last year of the simulation that waste is placed in the disposal units	Scalar	Data
Disposal_Shafts				
Shafts_1988_2015				
Cover_Nodes		Number of nodes used to represent the surface of the disposal units in the erosion modeling	Scalar	Stochastic
Initial_Cover_Thickness	m	Initial thickness of the cover over each node used to represent the surface of the disposal units	Scalar	Lookup Table
Surface_Soil_Thickness	m	Thickness of the surface soil layer	Vector (disposal region)	Data
Waste_Thickness	m	Thickness of the disposed waste	Vector (disposal region)	Data
Disposal_Unit_Area	m^2	Surface area of the disposal units	Scalar	Data
Start_of_Disposal	yr	The first year of the simulation that waste is placed in the disposal units	Scalar	Data
End_of_Disposal	yr	The last year of the simulation that waste is placed in the disposal units	Scalar	Data
Shafts_2016_2044				
Cover_Nodes		Number of nodes used to represent the surface of the disposal units in the erosion modeling	Scalar	Stochastic
Initial_Cover_Thickness	m	Initial thickness of the cover over each node used to represent the surface of the disposal units	Scalar	Lookup Table

Table 7 (Continued)
Input Data Requirements for the Area G Intruder Diffusion Model

Model Container/Parameter Name	Units	Parameter Description	Parameter Type	Input Element Type
Surface_Soil_Thickness	m	Thickness of the surface soil layer	Vector (disposal region)	Data
Waste_Thickness	m	Thickness of the disposed waste	Vector (disposal region)	Data
Disposal_Unit_Area	m^2	Surface area of the disposal units	Scalar	Data
Start_of_Disposal	yr	The first year of the simulation that waste is placed in the disposal units	Scalar	Data
End_of_Disposal	yr	The last year of the simulation that waste is placed in the disposal units	Scalar	Data
Inventory				
Initial_MDA_G_Pit_Inventory	Ci	Initial radionuclide activities in the MDA G disposal pits used from September 27, 1988 through 2010; ordered by layer-specific actual/unit inventories and model realization	Scalar	Spreadsheet Element
Initial_Zone_4_Pit_Inventory	Ci	Initial radionuclide activities in the Zone 4 disposal pits used from 2011 through 2044; ordered by layer-specific actual/unit inventories and model realization	Scalar	Spreadsheet Element
Initial_MDA_G_Shaft_Inventory	Ci	Initial radionuclide activities in the MDA G disposal shafts used from September 27, 1988 through 2015; ordered by layer-specific actual/unit inventories and model realization	Scalar	Spreadsheet Element
Initial_Zone_4_Shaft_Inventory	Ci	Initial radionuclide activities in the Zone 4 disposal shafts used from 2016 through 2010; ordered by layer-specific actual/unit inventories and model realization	Scalar	Spreadsheet Element
Waste_Disposal_Volumes				
Pit_Waste_1988_2010	m^3	Volume of waste disposed of in pits from September 27, 1988 through 2004	Scalar	Data

Table 7 (Continued)
Input Data Requirements for the Area G Intruder Diffusion Model

Model Container/Parameter Name	Units	Parameter Description	Parameter Type	Input Element Type
Pit_Waste_2011_2044	m^3	Volume of waste disposed of in pits from 2005 through 2044	Scalar	Data
Shaft_Waste_1988_2015	m^3	Volume of waste disposed of in shafts from September 27, 1988 through 2004	Scalar	Data
Shaft_Waste_2016_2044	m^3	Volume of waste disposed of in shafts from 2005 through 2044	Scalar	Data
Inventory_Multiplier		Element used to set selected radionuclide inventories to zero	Vector (radionuclide)	Data
Transport_Pathway_Data				
Atmospheric_Transport				
Resident_Dust_Loading	kg/m^3	Dust loading for the Intruder–Post-Drilling and Intruder-Agriculture Scenarios	Scalar	Stochastic
Soil_Disturbance_Factor		Factor by which the dust loading is increased due to human disturbance of the surface soil	Scalar	Stochastic
Worker_Dust_Loading	kg/m^3	Dust loading for the Intruder-Construction Scenario	Scalar	Stochastic
Resuspension_Flux	$g/m^2/yr$	Resuspension for particulates at Area G	Scalar	Stochastic
Enhancement_Factor		Ratio of radionuclide concentrations in the resuspendable fraction of the soil to those in the total soil	Scalar	Stochastic
Average_Wind_Speed	m/s	Average wind speed at Area G	Scalar	Stochastic
Atmospheric_Mixing_Height	m	Height to which radionuclides diffusing from the disposal site are mixed	Scalar	Data

Table 7 (Continued)
Input Data Requirements for the Area G Intruder Diffusion Model

Model Container/Parameter Name	Units	Parameter Description	Parameter Type	Input Element Type
Foodchain_Transport				
Plant_Data				
Uptake_Factors				
Leafy_Vegetable_GM	Ci/kg plant per Ci/kg soil (dry weight)	Geometric means of the plant uptake factors for leafy vegetables	Vector (element)	Data
Produce_GM	Ci/kg plant per Ci/kg soil (dry weight)	Geometric means of the plant uptake factors for produce	Vector (element)	Data
Grain_GM	Ci/kg plant per Ci/kg soil (dry weight)	Geometric means of the plant uptake factors for grain	Vector (element)	Data
PGrass_and_Native_GM	Ci/kg plant per Ci/kg soil (dry weight)	Geometric means of the plant uptake factors for pasture grass and native vegetation	Vector (element)	Data
Crop_GSD		Geometric standard deviation of the plant uptake factors for all crops		
Crop_Characteristics				
Particle_Size_Factor		Ratio of radionuclide concentrations in the fraction of the soil resuspended due to rainsplash to those in the total soil	Scalar	Stochastic
Plant_Carbon_Fraction		Fraction of plant that is carbon (dry weight basis)	Vector (crop)	Data
Plant_Hydrogen_Fraction		Fraction of plant that is hydrogen (dry weight basis)	Vector (crop)	Data
Dry_to_Wet_Weight_Fractions				
DWW_Leafy_Vegetables		Dry-to-wet weight fraction for leafy vegetables	Scalar	Stochastic

Table 7 (Continued)
Input Data Requirements for the Area G Intruder Diffusion Model

Model Container/Parameter Name	Units	Parameter Description	Parameter Type	Input Element Type
DWW_Produce		Dry-to-wet weight fraction for produce	Scalar	Stochastic
DWW_Grain		Dry-to-wet weight fraction for grain	Scalar	Stochastic
DWW_Pasture_Grass		Dry-to-wet weight fraction for pasture grass	Scalar	Stochastic
Translocation_Factors				
TF_Leafy_Vegetables		Translocation factor for leafy vegetables	Scalar	Stochastic
TF_Produce		Translocation factor for produce	Scalar	Stochastic
TF_Grain		Translocation factor for grain	Scalar	Stochastic
TF_Pasture_Grass		Translocation factor for pasture grass	Scalar	Stochastic
Agricultural_Productivities				
AP_Leafy_Vegetables	kg /m^2 (wet weight)	Agricultural productivity for leafy vegetables	Scalar	Stochastic
AP_Produce	kg /m^2 (wet weight)	Agricultural productivity for produce	Scalar	Stochastic
AP_Grain	kg /m^2 (wet weight)	Agricultural productivity for grain	Scalar	Stochastic
AP_Pasture_Grass	kg/m^2 (dry weight)	Agricultural productivity for pasture grass	Scalar	Stochastic
Mass_Loading_Factors				
MLF_Leafy_Vegetables	g soil/g plant (dry weight)	Mass-loading factor for leafy vegetables	Scalar	Stochastic
MLF_Produce	g soil/g plant (dry weight)	Mass-loading factor for produce	Scalar	Stochastic

Table 7 (Continued)
Input Data Requirements for the Area G Intruder Diffusion Model

Model Container/Parameter Name	Units	Parameter Description	Parameter Type	Input Element Type
MLF_Grain	g soil/g plant (dry weight)	Mass-loading factor for grain	Scalar	Stochastic
MLF_PGrass_and_Native	g soil/g plant (dry weight)	Mass-loading factor for pasture grass	Scalar	Stochastic
Animal_Data				
Animal_Ingestion_Data				
Cattle_and_Cows				
Cattle_Food_Ingestion	kg/d (dry weight)	Food consumption rate of cattle	Scalar	Stochastic
Cow_Food_Ingestion	kg/d (dry weight)	Food consumption rate of cows	Scalar	Stochastic
Cattle_Soil_Ingestion	kg/d (dry weight)	Soil consumption rate of cattle	Scalar	Stochastic
Cow_Soil_Ingestion	kg/d (dry weight)	Soil consumption rate of cows	Scalar	Stochastic
Cattle_Water_Ingestion	kg/d	Water consumption rate of cattle	Scalar	Stochastic
Cow_Water_Ingestion	kg/d	Water consumption rate of cows	Scalar	Stochastic
Chickens				
Chicken_Feed_Ingestion	kg/d (dry weight)	Food consumption rate of chickens	Scalar	Stochastic
Chicken_Water_Ingestion	kg/d	Water consumption rate of chickens	Scalar	Stochastic
Grit_to_Food_Ratio		Ratio of grit or soil intake to food intake for chickens	Scalar	Data

Table 7 (Continued)
Input Data Requirements for the Area G Intruder Diffusion Model

Model Container/Parameter Name	Units	Parameter Description	Parameter Type	Input Element Type
Transfer_Factors				
Beef_GM	d/kg	Geometric means of the forage-to-beef transfer factors	Vector (element)	Stochastic
Beef_GSD		Geometric standard deviation of the forage-to-beef transfer factors	Vector (element)	Data
Milk_GM	d/kg	Geometric means of the forage-to-milk transfer factors	Vector (element)	Stochastic
Milk_GSD		Geometric standard deviation of the forage-to-milk transfer factors	Vector (element)	Data
Chicken_GM	d/kg	Geometric means of the forage-to-chicken transfer factors	Vector (element)	Stochastic
Chicken_GSD		Geometric standard deviation of the forage-to-chicken transfer factors	Vector (element)	Data
Eggs_GM	d/kg	Geometric means of the forage-to-eggs transfer factors	Vector (element)	Stochastic
Eggs_GSD		Geometric standard deviation of the forage-to-eggs transfer factors	Vector (element)	Data
H-3_and_C-14_Transfer_Factors				
H3_Factors				
Water_Fraction_Animal_Products		Mass water fractions of animal products	Vector (animal product)	Data
C14_Factors				
Animal_Prod_Carbon_Fraction		Carbon fractions of animal products	Vector (animal product)	Data
Groundwater_Transport				
MdB_Infiltration_Rate	m/yr	Water infiltration rate on Mesita del Buey	Scalar	Stochastic

Table 7 (Continued)
Input Data Requirements for the Area G Intruder Diffusion Model

Model Container/Parameter Name	Units	Parameter Description	Parameter Type	Input Element Type
Biotic_Intrusion_Model				
Eco_Succession_Model				
Time_of_Climax	yr	Period required for disposal site to reach a piñon-juniper climax condition, measured from the time of facility closure	Scalar	Stochastic
Intrusion_Shape_Parameters				
Alpha_Shape		Shape factor used to model animal burrow and plant root distributions with depth	Scalar	Data
Beta_Shape		Shape factor used to model animal burrow and plant root distributions with depth	Scalar	Stochastic
Animal_Intrusion_Model				
Harvester_Ants				
Maximum_Burrow_Depth	m	Maximum burrowing depth for harvester ants	Scalar	Stochastic
Burrow_Density_Grassland	ha^{-1}	Density of harvester ant burrows during early succession	Scalar	Stochastic
Burrow_Density_Woodland	ha^{-1}	Density of harvester ant burrows in the piñon-juniper climax condition	Scalar	Stochastic
Burrow_Mass	kg	Mass of soil excavated per harvester ant burrow	Scalar	Stochastic
Colony_Life_Span	yr	Life span of harvester ant colonies	Scalar	Stochastic
Pocket_Gophers				
Maximum_Burrow_Depth	m	Maximum burrowing depth for pocket gophers	Scalar	Stochastic
Soil_Removal_Rate_Grassland	m^3/ha	Rate of soil removal by pocket gophers during early succession	Scalar	Stochastic

Table 7 (Continued)
Input Data Requirements for the Area G Intruder Diffusion Model

Model Container/Parameter Name	Units	Parameter Description	Parameter Type	Input Element Type
Soil_Removal_Rate_Woodland	m^3/ha	Rate of soil removal by pocket gophers in the piñon-juniper climax condition	Scalar	Stochastic
Burrow_Renewal_Rate	yr^{-1}	Rate at which existing pocket gopher burrows are replaced with new ones	Scalar	Stochastic
Mice				
Maximum_Burrow_Depth	m	Maximum burrowing depth for mice	Scalar	Stochastic
Burrow_Density_Grassland	ha^{-1}	Density of mouse burrows during early succession	Scalar	Stochastic
Burrow_Density_Woodland	ha^{-1}	Density of mouse burrows in the piñon-juniper climax condition	Scalar	Stochastic
Burrow_Volume	kg	Volume of soil excavated per mouse burrow	Scalar	Stochastic
Burrow_Renewal_Rate	yr^{-1}	Rate at which existing mouse burrows are replaced with new ones	Scalar	Stochastic
Chipmunks_and_Squirrels				
Maximum_Burrow_Depth	m	Maximum burrowing depth for chipmunks and ground squirrels	Scalar	Stochastic
Burrow_Density_Grassland	ha^{-1}	Density of chipmunk and ground squirrel burrows during early succession	Scalar	Stochastic
Burrow_Density_Woodland	ha^{-1}	Density of chipmunk and ground squirrel burrows in the piñon-juniper climax condition	Scalar	Stochastic
Burrow_Volume	kg	Volume of soil excavated per chipmunk and ground squirrel burrow	Scalar	Stochastic
Burrow_Renewal_Rate	yr^{-1}	Rate at which existing chipmunk and ground squirrel burrows are replaced with new ones	Scalar	Stochastic

Table 7 (Continued)
Input Data Requirements for the Area G Intruder Diffusion Model

Model Container/Parameter Name	Units	Parameter Description	Parameter Type	Input Element Type
Plant_Intrusion_Model				
Litter_Halflife	yr	Litter decomposition half-life	Scalar	Stochastic
Grasses				
Maximum_Root_Depth	m	Maximum rooting depth of grasses	Scalar	Stochastic
Biomass_Density_Grassland	kg/m^2	Aboveground biomass density of grasses during early succession	Scalar	Stochastic
Biomass_Density_Woodland	kg/m^2	Aboveground biomass density of grasses in the piñon-juniper climax condition	Scalar	Stochastic
Litter_Prod_Rate	yr^{-1}	Fraction of the aboveground biomass that falls as litter	Scalar	Stochastic
Forbs				
Maximum_Root_Depth	m	Maximum rooting depth of forbs	Scalar	Stochastic
Biomass_Density_Grassland	kg/m^2	Aboveground biomass density of forbs during early succession	Scalar	Stochastic
Biomass_Density_Woodland	kg/m^2	Aboveground biomass density of forbs in the piñon-juniper climax condition	Scalar	Stochastic
Litter_Prod_Rate	yr^{-1}	Fraction of the aboveground biomass that falls as litter	Scalar	Stochastic
Shrubs				
Maximum_Root_Depth	m	Maximum rooting depth of shrubs	Scalar	Stochastic
Biomass_Density_Grassland	kg/m^2	Aboveground biomass density of shrubs during early succession	Scalar	Stochastic
Biomass_Density_Woodland	kg/m^2	Aboveground biomass density of shrubs in the piñon-juniper climax condition	Scalar	Stochastic
Litter_Prod_Rate	yr^{-1}	Fraction of the aboveground biomass that falls as litter	Scalar	Stochastic

Table 7 (Continued)
Input Data Requirements for the Area G Intruder Diffusion Model

Model Container/Parameter Name	Units	Parameter Description	Parameter Type	Input Element Type
Trees				
Maximum_Root_Depth	m	Maximum rooting depth of trees	Scalar	Stochastic
Biomass_Density_Grassland	kg/m^2	Aboveground biomass density of trees during early succession	Scalar	Stochastic
Biomass_Density_Woodland	kg/m^2	Aboveground biomass density of trees in the piñon-juniper climax condition	Scalar	Stochastic
Litter_Prod_Rate	yr^{-1}	Fraction of the aboveground biomass that falls as litter	Scalar	Stochastic
Erosion_Model				
Erosion_Rates				
Erosion_Scenario		Probability of erosion scenario occurrence	Scalar	Stochastic
Pit_1988_2010				
Cover_Loss_Functions	m	Cover remaining over nodes in waste disposal region under erosion scenario *x*, at time *t*	Scalar	Lookup Table
Pit_2011_2044				
Cover_Loss_Functions	m	Cover remaining over nodes in waste disposal region under erosion scenario *x*, at time *t*	Scalar	Lookup Table
Shaft_1988_2015				
Cover_Loss_Functions	m	Cover remaining over nodes in waste disposal region under erosion scenario *x*, at time *t*	Scalar	Lookup Table
Shaft_2016_2044				
Cover_Loss_Functions	m	Cover remaining over nodes in waste disposal region under erosion scenario *x*, at time *t*	Scalar	Lookup Table

Table 7 (Continued)
Input Data Requirements for the Area G Intruder Diffusion Model

Model Container/Parameter Name	Units	Parameter Description	Parameter Type	Input Element Type
Human_Intrusion_Model				
Basement_Length	m	Length of the intruder's basement	Scalar	Data
Basement_Width	m	Width of the intruder's basement	Scalar	Data
Basement_Depth	m	Depth of the intruder's basement	Scalar	Data
Well_Casing_Diameter	m	Diameter of the well casing	Scalar	Data
Dose_and_WAC_Model				
Dose_Conversion_Factors				
Ingestion_DCFs	mrem/pCi	Dose conversion factors for the ingestion exposure route	Vector (radionuclide)	Data
Inhalation_DCFs	mrem/pCi	Dose conversion factors for the inhalation exposure route	Vector (radionuclide)	Data
Soil_External_DCFs_15_cm	mrem/yr per pCi/m^3	Dose conversion factors for direct radiation from soils contaminated to a depth of 15 cm	Vector (radionuclide)	Data
Soil_External_DCFs_Infinite	mrem/yr per pCi/m^3	Dose conversion factors for direct radiation from soils contaminated to an infinite depth	Vector (radionuclide)	Data
Air_External_DCFs	mrem/yr per pCi/m^3	Dose conversion factors for direct radiation from air immersion	Vector (radionuclide)	Data
Exposure_Pathway_Data				
Minimum_Soil_Mixing_Depth	m	Contaminant mixing depth	Scalar	Data
Shielding_Factor		Direct radiation shielding factor for the time spent indoors	Scalar	Stochastic
Resident_Inhalation_Rate	m^3/d	Inhalation rate of the resident intruder	Scalar	Stochastic
Worker_Inhalation_Rate	m^3/d	Inhalation rate of the construction intruder	Scalar	Stochastic
Ventilation_Rate	hr^{-1}	Ventilation rate of the intruder's house	Scalar	Stochastic

Table 7 (Continued)
Input Data Requirements for the Area G Intruder Diffusion Model

Model Container/Parameter Name	Units	Parameter Description	Parameter Type	Input Element Type
Room_Height	m	Height of rooms inside the intruder's house	Scalar	Data
Area_of_Lot	m^2	Area of the receptor's lot	Scalar	Stochastic
Area_of_House	m^2	Area of the receptor's house	Scalar	Data
Time_of_Intrusion	yr	Length of time before intrusion into the waste occurs, measured from the time of facility closure	Scalar	Data
Resident_Intruder_PO	mrem/yr	Performance objective for the post-drilling and agricultural intruders	Scalar	Data
Construction_Intruder_PO	mrem/yr	Performance objective for the construction worker	Scalar	Data
Exposure_Times				
Resident_Indoor_Exposure_Time	hr/d	Time spent inside by the resident intruder	Scalar	Stochastic
Resident_Outdoor_Exposure_Time	hr/d	Time spent outside by the resident intruder	Scalar	Stochastic
Worker_Exposure_Time	hr/d	Time spent building the house by the construction worker	Scalar	Data
Excavation_Occupancy_Factor		Fraction of worker exposure period spent in the bottom of the basement excavation	Scalar	Stochastic
Ingestion_Data				
Resident_Soil_Ingestion_Rate	kg/yr (dry weight)	Rate of soil ingestion for the resident intruder	Scalar	Stochastic
Worker_Soil_Ingestion_Rate	kg/yr (dry weight)	Rate of soil ingestion for the construction worker	Scalar	Stochastic
Food_Ingestion_Data				
Input_Vegetable_Fraction		User-specified fraction of the receptor's diet of leafy vegetables, produce, and grain that is grown at the receptor's location	Scalar	Stochastic

Table 7 (Continued)
Input Data Requirements for the Area G Intruder Diffusion Model

Model Container/Parameter Name	Units	Parameter Description	Parameter Type	Input Element Type
Animals_Raised		The types of animals raised by the receptor as a food source	Scalar	Stochastic
Crop_Ingestion_Rates				
CI_Leafy_Vegetables	kg/yr (wet weight)	Rate of ingestion of leafy vegetables for the resident intruders	Scalar	Stochastic
CI_Produce	kg/yr (wet weight)	Rate of ingestion of produce for the resident intruders	Scalar	Stochastic
CI_Grain	kg/yr (wet weight)	Rate of ingestion of grain for the resident intruders	Scalar	Stochastic
Animal_Product_Ingestion_Rates				
API_Beef	kg/yr	Rate of ingestion of beef for the resident intruders	Scalar	Stochastic
API_Milk	kg/yr	Rate of ingestion of milk for the resident intruders	Scalar	Stochastic
API_Chicken	kg/yr	Rate of ingestion of chicken for the resident intruders	Scalar	Stochastic
API_Eggs	kg/yr	Rate of ingestion of eggs for the resident intruders	Scalar	Stochastic
Animal_Numbers				
Cattle_Weight_at_Slaughter	kg	Weight of cattle at the time of slaughter	Scalar	Stochastic
Dressing_Percentage		Ratio of the carcass weight to live weight of the animal	Scalar	Stochastic
Cutability		Fraction of the carcass that is sold as meat	Scalar	Stochastic
Milk_Production_Rate	kg/yr	Production rate of milk by cows	Scalar	Stochastic
Chicken_Weight_at_Slaughter	kg	Weight of chicken at the time of slaughter	Scalar	Stochastic
Cook_to_Live_Ratio		Ratio of cooked weight of chicken to the live weight of the bird	Scalar	Stochastic
Meat_Fraction		Fraction of the cooked chicken that is meat	Scalar	Stochastic

Table 7 (Continued)
Input Data Requirements for the Area G Intruder Diffusion Model

Model Container/Parameter Name	Units	Parameter Description	Parameter Type	Input Element Type
Egg_Production_Rate	d^{-1}	Production rate of eggs by layers	Scalar	Stochastic
Egg_Mass	kg	Mass of egg	Scalar	Stochastic
Shell_Fraction		Fraction of the egg mass that is contributed by the shell	Scalar	Data
Animal_Product_Fractions				
Beef		User-specified fraction of the receptor's diet of beef that is taken from animals living at the exposure location	Scalar	Stochastic
Milk		User-specified fraction of the receptor's diet of milk that is produced by animals living at the exposure location	Scalar	Stochastic
Chicken		User-specified fraction of the receptor's diet of chicken that is taken from animals living at the exposure location	Scalar	Stochastic
Eggs		User-specified fraction of the receptor's diet of eggs that is produced by animals living at the exposure location	Scalar	Stochastic

Table 8
Input Data Requirements for the Area G Inventory Model

Model Container/Parameter Name	Units	Parameter Description	Parameter Type	Input Element Type
Simulation_Options				
Depth_of_Disposal_Flags				
MDA_G_Pits_Disp_Depth_Flag		Flag used to indicate whether the MDA G pit radionuclide inventories are to be distributed homogeneously throughout the disposal units or assigned to specific waste layers. A value of 1 indicates the waste will be distributed homogeneously throughout the units; a value of 2 indicates the inventories will be assigned to specific waste layers.	Scalar	Data
Zone_4_Pits_Disp_Depth_Flag		Flag used to indicate whether the Zone 4 pit radionuclide inventories are to be distributed homogeneously throughout the disposal units or assigned to specific waste layers. A value of 1 indicates the waste will be distributed homogeneously throughout the units; a value of 2 indicates the inventories will be assigned to specific waste layers.	Scalar	Data
MDA_G_Shafts_Disp_Depth_Flag		Flag used to indicate whether the MDA G shaft radionuclide inventories are to be distributed homogeneously throughout the disposal units or assigned to specific waste layers. A value of 1 indicates the waste will be distributed homogeneously throughout the units; a value of 2 indicates the inventories will be assigned to specific waste layers.	Scalar	Data
Zone_4_Shafts_Disp_Depth_Flag		Flag used to indicate whether the Zone 4 shaft radionuclide inventories are to be distributed homogeneously throughout the disposal units or assigned to specific waste layers. A value of 1 indicates the waste will be distributed homogeneously throughout the units; a value of 2 indicates the inventories will be assigned to specific waste layers.	Scalar	Data

Table 8 (Continued)
Input Data Requirements for the Area G Inventory Model

Model Container/Parameter Name	Units	Parameter Description	Parameter Type	Input Element Type
Species_and_Materials				
Halflives	yr	Radionuclide half-lives	Vector (radionuclide)	Data
Material_Properties				
C14_Gas_Generation_Rate	yr^{-1}	Rate constant describing the rate of C-14 gas generation due to biodegradation of organic waste	Scalar	Stochastic
CO2_Fraction		Fraction of C-14 gas generated by the biodegradation of organic waste that is carbon dioxide	Scalar	Stochastic
Radon_Emanation_Coefficient		Emanation coefficient for Rn-220 and Rn-222	Scalar	Stochastic
Area_G_Geometry_and_Operations				
Waste_Layer_Data				
Number_of_Waste_Layers		Number of layers used to represent the waste in the intruder model	Scalar	Data
Upper_Waste_Layer_Thickness	m	Thickness of each of the uppermost three layers of waste in the intruder model	Scalar	Data
Waste_Layer_Thickness				
Historic_Pits				
Waste_Thickness	m	Thickness of the waste in the disposal pits located in MDA G	Scalar	Data
Future_Pits				
Waste_Thickness	m	Thickness of the waste in the disposal pits located in Zone 4	Scalar	Data

Table 8 (Continued)
Input Data Requirements for the Area G Inventory Model

Model Container/Parameter Name	Units	Parameter Description	Parameter Type	Input Element Type
Historic_Shafts				
Waste_Thickness	m	Thickness of the waste in the disposal shafts located in MDA G	Scalar	Data
Future_Shafts				
Waste_Thickness	m	Thickness of the waste in the disposal shafts located in Zone 4	Scalar	Data
Waste_Depth_Distributions				
Historic_Pits				
Pre_1990_Depth_Dept_Rad		Fractions of pre-1990 radionuclide inventories in each layer of the waste profile, MDA G disposal pits.	Matrix (radionuclide, waste layer)	Data
Post_1989_Depth_Dept_Rad		Fractions of post-1989 radionuclide inventories in each layer of the waste profile, MDA G disposal pits.	Matrix (radionuclide, waste layer)	Data
Pre_1990_Depth_Dept_MT		Fractions of pre-1990 material type inventories in each layer of the waste profile, MDA G disposal pits.	Matrix (material type, waste layer)	Data
Post-1989_Depth_Dept_MT		Fractions of post-1989 material type inventories in each layer of the waste profile, MDA G disposal pits.	Matrix (material type, waste layer)	Data
Unit_Inventory_Distributions		Fractions of unit radionuclide inventories in each layer of the waste profile, MDA G disposal pits.	Matrix (radionuclide, waste layer)	Data
Future_Pits				
Pre_1990_Depth_Dept_Rad		Fractions of pre-1990 radionuclide inventories in each layer of the waste profile, Zone 4 disposal pits.	Matrix (radionuclide, waste layer)	Data
Post_1989_Depth_Dept_Rad		Fractions of post-1989 radionuclide inventories in each layer of the waste profile, Zone 4 disposal pits.	Matrix (radionuclide, waste layer)	Data
Pre_1990_Depth_Dept_MT		Fractions of pre-1990 material type inventories in each layer of the waste profile, Zone 4 disposal pits.	Matrix (material type, waste layer)	Data

Table 8 (Continued)
Input Data Requirements for the Area G Inventory Model

Model Container/Parameter Name	Units	Parameter Description	Parameter Type	Input Element Type
Post-1989_Depth_Dept_MT		Fractions of post-1989 material type inventories in each layer of the waste profile, Zone 4 disposal pits.	Matrix (material type, waste layer)	Data
Unit_Inventory_Distributions		Fractions of unit radionuclide inventories in each layer of the waste profile, Zone 4 disposal pits.	Matrix (radionuclide, waste layer)	Data
Historic Shafts				
Pre_1990_Depth_Dept_Rad		Fractions of pre-1990 radionuclide inventories in each layer of the waste profile, MDA G disposal shafts.	Matrix (radionuclide, waste layer)	Data
Post_1989_Depth_Dept_Rad		Fractions of post-1989 radionuclide inventories in each layer of the waste profile, MDA G disposal shafts.	Matrix (radionuclide, waste layer)	Data
Pre_1990_Depth_Dept_MT		Fractions of pre-1990 material type inventories in each layer of the waste profile, MDA G disposal shafts.	Matrix (material type, waste layer)	Data
Post-1989_Depth_Dept_MT		Fractions of post-1989 material type inventories in each layer of the waste profile, MDA G disposal shafts.	Matrix (material type, waste layer)	Data
Unit_Inventory_Distributions		Fractions of unit radionuclide inventories in each layer of the waste profile, MDA G disposal shafts.	Matrix (radionuclide, waste layer)	Data
Future Shafts				
Pre_1990_Depth_Dept_Rad		Fractions of pre-1990 radionuclide inventories in each layer of the waste profile, Zone 4 disposal shafts.	Matrix (radionuclide, waste layer)	Data
Post_1989_Depth_Dept_Rad		Fractions of post-1989 radionuclide inventories in each layer of the waste profile, Zone 4 disposal shafts.	Matrix (radionuclide, waste layer)	Data
Pre_1990_Depth_Dept_MT		Fractions of pre-1990 material type inventories in each layer of the waste profile, Zone 4 disposal shafts.	Matrix (material type, waste layer)	Data
Post-1989_Depth_Dept_MT		Fractions of post-1989 material type inventories in each layer of the waste profile, Zone 4 disposal shafts.	Matrix (material type, waste layer)	Data

Table 8 (Continued)
Input Data Requirements for the Area G Inventory Model

Model Container/Parameter Name	Units	Parameter Description	Parameter Type	Input Element Type
Unit_Inventory_Distributions		Fractions of unit radionuclide inventories in each layer of the waste profile, Zone 4 disposal shafts.	Matrix (radionuclide, waste layer)	Data
Inventory				
Unit_Inventory				
Radionuclide_Unit_Inventories	Ci	Unit inventory assigned to all radionuclides.	Scalar	Data
As_Disposed_Inventory				
Measurement_Errors				
Rad_Specific_Errors				
Pre_1990_Lower_Bounds		Factor used to estimate the lower bound of pre-1990 radionuclide inventories, taking into account errors introduced by measurement uncertainty	Vector (radionuclide)	Data
Pre_1990_Upper_Bounds		Factor used to estimate the upper bound of pre-1990 radionuclide inventories, taking into account errors introduced by measurement uncertainty	Vector (radionuclide)	Data
Post_1989_Lower_Bounds		Factor used to estimate the lower bound of post-1989 radionuclide inventories, taking into account errors introduced by measurement uncertainty	Vector (radionuclide)	Data
Post_1989_Upper_Bounds		Factor used to estimate the upper bound of post-1989 radionuclide inventories, taking into account errors introduced by measurement uncertainty	Vector (radionuclide)	Data
Material_Type_Errors				
Pre_1990_Lower_Bounds		Factor used to estimate the lower bound of pre-1990 material type inventories, taking into account errors introduced by measurement uncertainty	Vector (material type)	Data

Table 8 (Continued)
Input Data Requirements for the Area G Inventory Model

Model Container/Parameter Name	Units	Parameter Description	Parameter Type	Input Element Type
Pre_1990_Upper_Bounds		Factor used to estimate the upper bound of pre-1990 material type inventories, taking into account errors introduced by measurement uncertainty	Vector (material type)	Data
Post_1989_Lower_Bounds		Factor used to estimate the lower bound of post-1989 material type inventories, taking into account errors introduced by measurement uncertainty	Vector (material type)	Data
Post_1989_Upper_Bounds		Factor used to estimate the upper bound of post-1989 material type inventories, taking into account errors introduced by measurement uncertainty	Vector (material type)	Data
Radionuclide_Inventories				
Disposal_Unit_Inventories				
Disposal_Pits				
Pre_1990_PA_Pit_Activities	Ci	Point estimates of radionuclide-specific inventories in the pre-1990 performance assessment waste disposed of in pits	Matrix (radionuclide, pit number)	Data
Pre_1990_CA_Pit_Activities	Ci	Point estimates of radionuclide-specific inventories in the pre-1990 composite analysis waste disposed of in pits	Matrix (radionuclide, pit number)	Data
Post_1989_Pit_Activities	Ci	Point estimates of radionuclide-specific inventories in the post-1989 performance assessment and composite analysis waste disposed of in pits	Matrix (radionuclide, pit number)	Data
Disposal_Shafts				
Pre_1990_PA_Shaft_Activities	Ci	Point estimates of radionuclide-specific inventories in the pre-1990 performance assessment waste disposed of in shafts	Matrix (radionuclide, shaft number)	Data

Table 8 (Continued)
Input Data Requirements for the Area G Inventory Model

Model Container/Parameter Name	Units	Parameter Description	Parameter Type	Input Element Type
Pre_1990_CA_Shaft_Activities	Ci	Point estimates of radionuclide-specific inventories in the pre-1990 composite analysis waste disposed of in shafts	Matrix (radionuclide, shaft number)	Data
Post_1989_Shaft_Activities	Ci	Point estimates of radionuclide-specific inventories in the post-1989 performance assessment and composite analysis waste disposed of in shafts	Matrix (radionuclide, shaft number)	Data
Material_Type_Inventories				
Disposal_Unit_Inventories				
Disposal_Pits				
Pre_1990_PA_Pit_Activities	Ci	Point estimates of material type inventories in the pre-1990 performance assessment waste disposed of in pits	Matrix (material type, pit number)	Data
Pre_1990_CA_Pit_Activities	Ci	Point estimates of material type inventories in the pre-1990 composite analysis waste disposed of in pits	Matrix (material type, pit number)	Data
Post_1989_Pit_Activities	Ci	Point estimates of material type inventories in the post-1989 performance assessment and composite analysis waste disposed of in pits	Matrix (material type, pit number)	Data
Disposal_Shafts				
Pre_1990_PA_Shaft_Activities	Ci	Point estimates of material type inventories in the pre-1990 performance assessment waste disposed of in shafts	Matrix (material type, shaft number)	Data
Pre_1990_CA_Pit_Activities	Ci	Point estimates of material type inventories in the pre-1990 composite analysis waste disposed of in shafts	Matrix (material type, shaft number)	Data
Post_1989_Shaft_Activities	Ci	Point estimates of material type inventories in the post-1989 performance assessment and composite analysis waste disposed of in shafts	Matrix (material type, shaft number)	Data

Table 8 (Continued)
Input Data Requirements for the Area G Inventory Model

Model Container/Parameter Name	Units	Parameter Description	Parameter Type	Input Element Type
Fission_Yields				
Fraction_of_Pu239		Fraction of fission events that originate with Pu-239	Scalar	Stochastic
Age_of_MFP_Waste	yr	Age of mixed-fission product waste at the time of disposal	Scalar	Stochastic
U235_Fission_Yield		U-235 thermal fission yield as a function of waste age	Vector (radionuclide)	Data
Pu239_Fission_Yield		Pu-239 thermal fission yield as a function of waste age	Vector (radionuclide)	Data
Activation_Yields				
MAP_Allocation_Fractions		Radionuclide-specific activity fractions for mixed-activation product waste	Vector (radionuclide)	Data
Material_Type_Act_Fractions				
PU51				
Activity_Fractions		Radionuclide activity fractions in material type PU51 waste	Vector (radionuclide)	Data
PU52				
Initial_Pu238		Radionuclide activity fraction of Pu-238 in material type PU52 waste	Scalar	Stochastic
Initial_Pu239		Radionuclide activity fraction of Pu-239 in material type PU52 waste	Scalar	Stochastic
Initial_Pu240		Radionuclide activity fraction of Pu-240 in material type PU52 waste	Scalar	Stochastic
Initial_Pu241		Radionuclide activity fraction of Pu-241 in material type PU52 waste	Scalar	Stochastic

Table 8 (Continued)
Input Data Requirements for the Area G Inventory Model

Model Container/Parameter Name	Units	Parameter Description	Parameter Type	Input Element Type
Initial_Pu242		Radionuclide activity fraction of Pu-242 in material type PU52 waste	Scalar	Stochastic
PU53				
Initial_Pu238		Radionuclide activity fraction of Pu-238 in material type PU53 waste	Scalar	Stochastic
Initial_Pu239		Radionuclide activity fraction of Pu-239 in material type PU53 waste	Scalar	Stochastic
Initial_Pu240		Radionuclide activity fraction of Pu-240 in material type PU53 waste	Scalar	Stochastic
Initial_Pu241		Radionuclide activity fraction of Pu-241 in material type PU53 waste	Scalar	Stochastic
Initial_Pu242		Radionuclide activity fraction of Pu-242 in material type PU53 waste	Scalar	Stochastic
PU54				
Initial_Pu238		Radionuclide activity fraction of Pu-238 in material type PU54 waste	Scalar	Stochastic
Initial_Pu239		Radionuclide activity fraction of Pu-239 in material type PU54 waste	Scalar	Stochastic
Initial_Pu240		Radionuclide activity fraction of Pu-240 in material type PU54 waste	Scalar	Stochastic
Initial_Pu241		Radionuclide activity fraction of Pu-241 in material type PU54 waste	Scalar	Stochastic
Initial_Pu242		Radionuclide activity fraction of Pu-242 in material type PU54 waste	Scalar	Stochastic

Table 8 (Continued)
Input Data Requirements for the Area G Inventory Model

Model Container/Parameter Name	Units	Parameter Description	Parameter Type	Input Element Type
PU55				
Activity_Fractions		Radionuclide activity fractions in material type PU55 waste	Vector (radionuclide)	Data
PU56				
Initial_Pu238		Radionuclide activity fraction of Pu-238 in material type PU56 waste	Scalar	Stochastic
Initial_Pu239		Radionuclide activity fraction of Pu-239 in material type PU56 waste	Scalar	Stochastic
Initial_Pu240		Radionuclide activity fraction of Pu-240 in material type PU56 waste	Scalar	Stochastic
Initial_Pu241		Radionuclide activity fraction of Pu-241 in material type PU56 waste	Scalar	Stochastic
Initial_Pu242		Radionuclide activity fraction of Pu-242 in material type PU56 waste	Scalar	Stochastic
PU57				
Activity_Fractions		Radionuclide activity fractions in material type PU57 waste	Vector (radionuclide)	Data
PU83				
Initial_Pu238		Radionuclide activity fraction of Pu-238 in material type Pu-83 waste	Scalar	Stochastic
Initial_Pu239		Radionuclide activity fraction of Pu-239 in material type Pu-83 waste	Scalar	Stochastic
Initial_Pu240		Radionuclide activity fraction of Pu-240 in material type Pu-83 waste	Scalar	Stochastic

Table 8 (Continued)
Input Data Requirements for the Area G Inventory Model

Model Container/Parameter Name	Units	Parameter Description	Parameter Type	Input Element Type
Initial_Pu241		Radionuclide activity fraction of Pu-241 in material type Pu-83 waste	Scalar	Stochastic
Initial_Pu242		Radionuclide activity fraction of Pu-242 in material type Pu-83 waste	Scalar	Stochastic
U10				
Activity_Fractions		Radionuclide activity fractions in material type U10 waste	Vector (radionuclide)	Data
U11				
Activity_Fractions		Radionuclide activity fractions in material type U11 waste	Vector (radionuclide)	Data
U12				
Activity_Fractions		Radionuclide activity fractions in material type U12 waste	Vector (radionuclide)	Data
U35				
Activity_Fractions		Radionuclide activity fractions in material type U35 waste	Vector (radionuclide)	Data
U36				
Activity_Fractions		Radionuclide activity fractions in material type U36 waste	Vector (radionuclide)	Data
U38				
Activity_Fractions		Radionuclide activity fractions in material type U38 waste	Vector (radionuclide)	Data

Table 8 (Continued)
Input Data Requirements for the Area G Inventory Model

Model Container/Parameter Name	Units	Parameter Description	Parameter Type	Input Element Type
U39				
Activity_Fractions		Radionuclide activity fractions in material type U39 waste	Vector (radionuclide)	Data
U81				
Activity_Fractions		Radionuclide activity fractions in material type U81 waste	Vector (radionuclide)	Data
UNAT				
Activity_Fractions		Radionuclide activity fractions in material type UNAT waste	Vector (radionuclide)	Data
D38				
Activity_Fractions		Radionuclide activity fractions in material type D38 waste	Vector (radionuclide)	Data
TH88				
Activity_Fractions		Radionuclide activity fractions in material type TH88 waste	Vector (radionuclide)	Data

5.0 Model Input Data Selection

The parameters required to implement the GoldSim performance assessment and composite analysis models are described in Section 4. This section presents the input data selected for these parameters and provides the bases for the adopted values. Section 5.1 addresses the parameters used to control or define the simulations conducted in support of the performance assessment and composite analysis. Section 5.2 discusses the data used to characterize the disposal facility and describe disposal operations. The parameters used to characterize the environmental media included in the GoldSim modeling are considered in Section 5.3, while radionuclide inventories are addressed in Section 5.4. Sections 5.5 through 5.10 discuss parameters needed to conduct atmospheric transport, groundwater transport, sediment transport, food-chain transport, biotic intrusion, and surface erosion modeling, respectively. Parameters used to characterize the exposures received by members of the public and inadvertent intruders are discussed in Section 5.11, and Section 5.12 provides information about miscellaneous parameters.

The majority of the input parameters discussed below are characterized using distributions to describe the variability associated with the value; these distributions are also used to model uncertainty and sensitivity. Some of the parameters are not defined using distributions, either because it was inappropriate to do so or because the information needed to define the distributions was unavailable. Deterministic model simulations were conducted to evaluate the performance of the disposal facility well beyond the 1,000-year compliance period. Unless otherwise noted, this modeling was conducted using the medians of the parameter distributions.

5.1 Simulation Options

The Analysis_Flag, found only in the Area G Site Model, designates whether the performance assessment or composite analysis inventory is used in the model simulation. The flag was set appropriately to consider each inventory.

The Biotic_Intrusion_Flag is found in the intruder and intruder diffusion models and indicates whether the effects of biotic intrusion are taken into account when estimating exposures for members of the public and inadvertent intruders. This flag was set to 1 for all modeling, indicating the impacts of plants and animals intruding into the disposed waste were considered.

The Diffusion_Flag controls whether the effects of vapor- and gas-phase diffusion are taken into account in the site model and intruder diffusion model. This variable was set to 1 for all simulations conducted using these models, indicating that diffusive transport was taken into account. Some simulations were conducted with this variable set to 0 (no diffusion) to investigate the effects of diffusive transport on projected exposures.

The Intruder_Flag and Disposal_Unit_Flag are unique to the Area G Intruder and Intruder Diffusion Models; the former specifies the intruder scenario under consideration while the latter determines the set of pits or shafts to be evaluated. These flag variables were set appropriately to estimate exposures for the Intruder–Post-Drilling, Intruder-Agriculture, and Intruder-Construction Scenarios following intrusion into the pits and shafts.

The Depth_of_Disposal_Flag, also unique to the intruder and intruder diffusion models, was set equal to 1 for the disposal pits, causing the input inventories to be homogeneously distributed throughout the units. Values of 2 (layer-specific inventories) and 1 (uniformly distributed inventories) were used to model the 1988–2015 and 2016–2044 shafts, respectively.

The Tritium_Package_Flag is found only in the intruder diffusion model. It was set to 0 for the disposal pits, indicating that vapor-phase releases of tritium from waste packages were not limited by package off-gas rates. The flag was set to 1 for the two sets of shafts, limiting annual releases to the off-gas rate.

5.2 Facility Dimensions and Operations

Several parameters that are used in the GoldSim modeling address the layout and key operational aspects of the disposal facility. Dimensional parameters describe the physical layout of the disposal units and characterize the final covers placed over the pits and shafts. Operational parameters identify the periods over which the disposal units are active and define periods of administrative control over the facility.

5.2.1 Disposal Areas

Area G was divided into eight waste disposal regions for the modeling conducted using the site model; these disposal regions are shown in Figure 5 and information pertaining to them is summarized in Table 9. Table 9 lists the pits and shafts included in each region and shows the associated disposal area, which represents the surface area of the pits and shafts in each region. The disposal areas associated with the pits in disposal regions 1 through 5 were estimated using two approaches. In the first, the dimensions of the pits in a given region were used to calculate the pit area and the pit areas were summed to yield the region's disposal area. The second approach relied on maps of the pit locations. Coordinates along the edges of the pits were taken from these maps and used to conduct the surface erosion modeling (Wilson et al., 2005). Each pit was represented in this modeling using 6.25 m^2 (67 ft^2) cells. Multiplying the number of cells used to represent the surfaces of the pits within a region by 6.25 m^2 (67 ft^2) yields a second estimate of the pit disposal area for that region.

The two sets of estimates of the pit disposal areas differed by 7 to 21 percent; the estimates based on pit dimensions were consistently higher than those based on the map coordinates. The areas calculated on the basis of the map coordinates were, however, adopted for the performance

Table 9
Pits and Shafts Included in the Eight Waste Disposal Regions of Area G and the Region-Specific Disposal Areas

Disposal Region	Disposal Units Included in Disposal Region		Disposal Area (m^2)		
	Pits	Shafts	Pits	Shafts	All Disposal Units
1	1-5	1–33, 35–38, 40–49, 51–58, 60–69, 71–90	2.8E+04	2.8E+02	2.8E+04
2	6, 7, 24	---	1.1E+04	---	1.1E+04
3	8–10, 12, 13, 15–22	---	2.3E+04	---	2.3E+04
4	25–31, 39	---	2.5E+04	---	2.5E+04
5	32, 33, 35–38	---	2.4E+04	---	2.4E+04
6	---	34, 39, 50, 59, 70, 91–97, 99–112, 114, 115, 118–135	---	7.0E+02	7.0E+02
7	---	136–144, 147–177, 189–192, 196, 197, 206, 301, 307, 308, 309, 311, 313, 315, 317, 319, 321, 323, 325, 327, 329, 331, 333, 335, 339, 341, 343, 345, 347, 349, 351, 355, 357, 360–367, 370, C01–C14	---	2.6E+03	2.6E+03
8	Pits used for disposal from 2011 through 2044	Shafts used for disposal from 2016 through 2044	2.8E+04	1.1E+03	2.9E+04

--- = None

assessment and composite analysis for two reasons. First, the maps are generally expected to more accurately represent the extent of each disposal unit. Second, use of the map-based disposal areas is consistent with the information used to conduct the surface erosion modeling.

The pits in waste disposal region 8 have not been constructed yet, so the surface area associated with these pits was estimated using drawings developed in conjunction with the conceptual design of Zone 4 (Day et al., 2005). A second estimate of the surface area of the pits was developed using the following equation:

$$A_{d,p} = \frac{V_p}{d_p \times E_p} \qquad 60$$

Where

$A_{d,p}$ = pit disposal area (m^2)
V_p = volume of waste requiring disposal in the pits (m^3)
d_p = thickness of waste in the pits (m)
E_p = waste emplacement efficiency factor for the pits

The volume of waste requiring disposal is considered in Section 5.4. The disposal pits were assumed to be 18 m (60 ft) deep and the top 3 m (10 ft) of each unit was assumed to contain clean fill, consistent with the conceptual design for the expansion area. A waste emplacement efficiency of 50 percent was assumed; this factor is discussed below.

The disposal area estimate for the region 8 pits that was based on the conceptual drawings was almost two times greater than that calculated using Equation 60. This discrepancy occurs because the area calculated using Equation 60 does not account for that portion of the disposal units occupied by access ramps. If the ramp-occupied areas are taken into account, the two estimates of disposal area fall within 10 percent of one another. The area developed on the basis of the drawings was adopted for the performance assessment, composite analysis, and surface erosion modeling.

The process of defining the disposal areas associated with the shafts is complicated by the fact that these units have a small surface expression and are clustered in groups across the disposal facility. Consequently, a different approach was adopted for defining the shaft disposal areas. The shafts in waste disposal regions 1 and 6 are concentrated in groups referred to as shaft fields. The disposal areas for these units were estimated on the basis of the size of the shaft fields. The areas of the shafts in each disposal region were summed and these sums were divided by the shaft field efficiency factor described in Section 5.2.5 to yield the corresponding disposal area. The shafts in disposal region 7 are widely scattered among the disposal region 3 pits. The disposal area for these units was calculated as if the shafts were located in a single shaft field, as was done for the shafts in waste disposal regions 1 and 6.

The disposal area for the shafts in disposal region 8 could not be estimated using the procedure used for the shafts in regions 1 and 6 because the region 8 shafts have not been constructed. The cross-sectional area of the shafts needed to dispose of future waste was estimated as follows:

$$A_{d,s} = \frac{V_s}{d_s \times E_s \times E_f} \qquad 61$$

Where

$A_{d,s}$ = shaft disposal area (m^2)
V_s = volume of waste requiring disposal in the shafts (m^3)
d_s = thickness of waste in the shafts (m)
E_s = waste emplacement efficiency factor for the shafts
E_f = shaft field efficiency factor

It was assumed that the shafts will be 18 m (60 ft) deep and that the top 3 m (10 ft) of each unit will contain clean fill. The waste emplacement efficiency and shaft field efficiency were set equal to 50 and 11 percent, respectively; these factors are discussed in Sections 5.2.5 and 5.2.6.

The inadvertent intruder analysis estimates doses received from four subsets of the pits and shafts at Area G and calculates waste acceptance criteria for waste disposed of in the pits and shafts in MDA G. The disposal areas for the units located within MDA G were calculated in the manner described above for the waste disposal regions; these calculations yielded areas of approximately 23,700 and 1,600 m^2 (2.6×10^5 and 17,400 ft^2) for the 1988–2010 pits and 1988–2015 shafts, respectively. The modeling assumes that the pits receiving waste from 2011 through 2044 are located in the Zone 4 expansion area; the shafts that receive waste from 2016 through 2044 are also located here. The projected disposal areas for the Zone 4 disposal units are listed in Table 9 under waste disposal region 8.

5.2.2 Operational Period

The operational period covers the time during which Area G was used for the disposal of radioactive waste and, more specifically, the periods during which waste was placed in pits and shafts in each of the eight disposal regions. The operational period for Area G as a whole is 88 years; this figure is based on the fact that routine waste disposal operations began in 1959 and the assumption that final closure of the site will occur in 2046 following the end of disposal operations in Zone 4 (disposal region 8) in 2044. Table 10 summarizes the operational periods for the eight disposal regions; separate operational periods are provided for the pits and shafts in disposal regions 1 and 8. These periods are based on data provided in Shuman (2008). All waste disposed of in pits after 2010 and in shafts after 2015 is assumed to be placed in waste disposal region 8.

Table 10
Operational Periods for the Eight Waste Disposal Regions at Area G

Disposal Region	Operational Period	
	First Year of Disposal	Last Year of Disposal
1 (pits)	1959	1979
1 (shafts)	1966	1993
2	1971[a]	1976
3	1971	2007
4	1980	2007
5	1982	2010
6	1971	1998
7	1976	2015
8 (pits)	2011	2044
8 (shafts)	2016	2044

[a] *Waste was disposed of in pit 6, one of the units included in this disposal region, starting in 1970. However, the waste placed in this unit prior to 1971 was included in the waste disposal region 1 inventory.*

Four subsets of disposal units are addressed in the intruder analysis. These include pits that are active from September 27, 1988 through 2010 and from 2011 through 2044, and shafts that are active from September 27, 1988 through 2015 and from 2016 through 2044.

5.2.3 Cover and Waste Configuration

The cover and waste configuration parameters define the thickness of the cover placed over the disposal units and the thickness of the waste in these units. Current plans call for the application of a minimum of 2.5 m (8.2 ft) of cover material over all pits and shafts at Area G; a complete description of the final cover may be found in Day et al. (2005). In fact, the thickness of the final cover will be greater than 2.5 m (8.2 ft) over large portions of the disposal site because of the extensive contouring and shaping that is required to achieve the desired configuration.

As discussed in Section 3.3.1, the effects of surface erosion are modeled on a node-by-node basis for the eight waste disposal regions; the initial cover thickness at each node is required to conduct these simulations. Although the volume of data prohibits a listing of the initial cover thickness for each node overlying a disposal unit, the histograms presented in Figure 12 provide a general indication of these data for waste disposal regions 1 through 6 and 8. The shafts that comprise waste disposal region 7 are scattered among the pits assigned to disposal region 3; the distribution of initial cover was assumed to be the same for these two disposal regions. Disposal region 1 includes 5 pits and more than 80 shafts arranged in a shaft field near the west end of pits 2 and 4;

Figure 12a
Waste disposal region 1

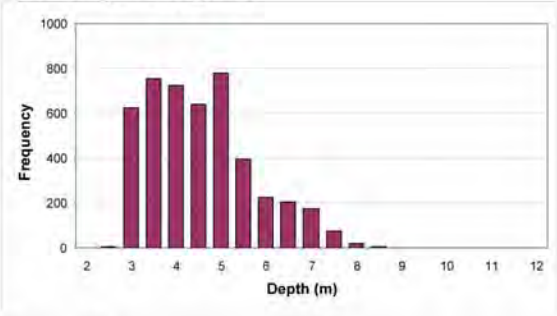

Figure 12b
Waste disposal region 2

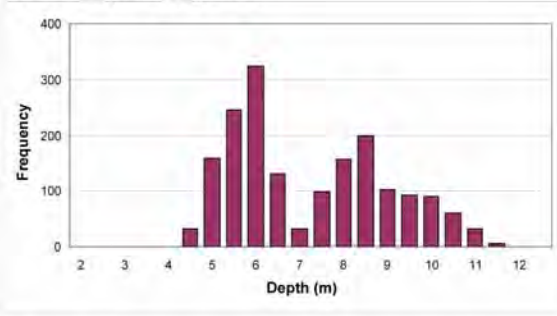

Figure 12c
Waste disposal region 3

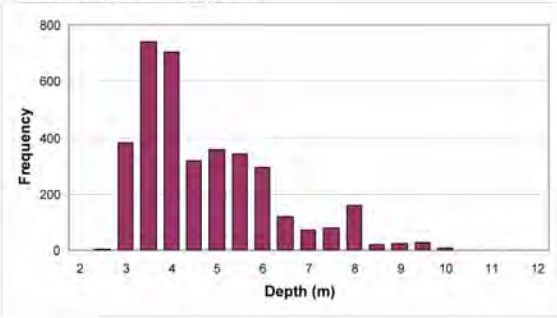

Figure 12d
Waste disposal region 4

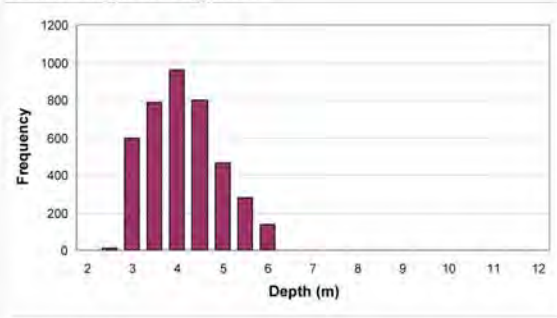

Figure 12e
Waste disposal region 5

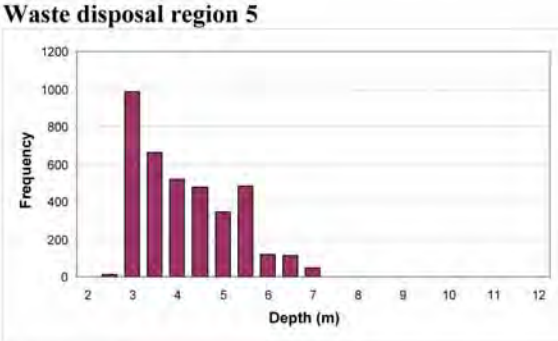

Figure 12f
Waste disposal region 6

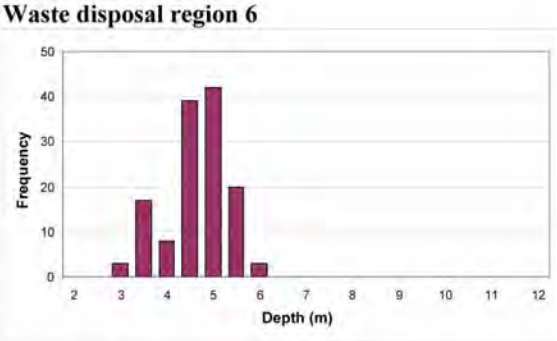

Figure 12g
Waste disposal region 8

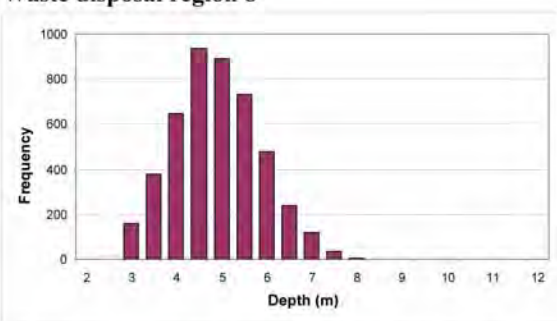

Figure 12h
Disposal pits 15, 30, 31, and 36–39

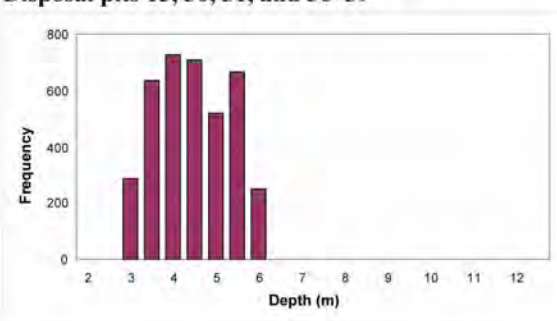

Note: Graphs shown with different ranges on vertical scales.

Figure 12
Histograms of Initial Cover Depth Distribution for Waste Disposal Regions (1–6, 8) and Disposal Pits (15, 30, 31, 36–39)

the initial cover depths for the cells overlying the pits and the shaft field were combined to develop the initial depth distribution. The distribution of cover depths shown for disposal region 6 is based on information for the shaft field located at the west end of pits 2 and 4; this shaft field actually includes disposal units belonging to disposal regions 1 and 6. The initial pit and shaft cover depths were combined to develop the distribution for waste disposal region 8 for the site model; the distribution shown in Figure 12 for this region includes the two sets of units.

The intruder modeling used initial cover thickness data for pits 15, 30, 31, and 36 through 39 to estimate exposures from waste disposed of from September 27, 1988 through 2010; the distribution of these thicknesses is included as the last histogram in Figure 12. The initial cover thicknesses over the shafts that were used for disposal from September 27, 1988 through 2015 were assumed to be the same as those shown above for waste disposal region 3; the initial cover thicknesses shown in Figure 12 for disposal region 8 address the disposal pits used from 2011 through 2044 and the shafts used for disposal from 2016 through 2044.

The thickness of the waste in the disposal pits and shafts varies among the eight disposal regions. To determine these thicknesses it is necessary to know the distance from the surface of the ground to the top of the waste, or the head space. The minimum distance to waste depends upon the operational period of the disposal unit. Although no explicit guidelines were in place when pits 1 through 4 were active, guidelines issued in subsequent years have specified minimum distances to waste ranging from 0.6 to 3 m (2 to 3.3 ft) (Koopman, 1965; LANL, 1975; LANL, 1998). Because specific knowledge of the distance to waste for the closed disposal units was not available, the waste thickness for each disposal region was estimated by subtracting 1 m (3.3 ft) from the average depth of the disposal units comprising that region; the average depth was calculated using the unit-specific depths summarized in Shuman (2008). The thickness of the waste that will be disposed of in Zone 4 units was calculated based on the assumption that all units will be 18 m (60 ft) deep with a head space of 3 m (10 ft), as specified by Day et al. (2005). Estimates of waste thickness are included in Table 11.

Waste disposal region 1 includes both pits and shafts; the average thickness of the waste in the pits is about 0.8 m (2.7 ft) greater than that in the shafts. A single waste thickness was estimated for this region by weighting the average pit and shaft waste thicknesses by the volumes of waste placed in the two types of units. Given that 99 percent of the volume of waste disposed in this region was placed in pits, the waste thickness adopted for this region was essentially the average thickness of the waste in the pits.

Table 11
Pathway Parameter Values and Distributions Used in the Performance Assessment and Composite Analysis

Parameter	Units [a]	Input Value or Distribution [b]
Site Geometry and Operations		
Waste Thickness		
Waste Disposal Region 1	m	7.7E+00
Waste Disposal Region 2	m	7.7E+00
Waste Disposal Region 3	m	7.3E+00
Waste Disposal Region 4	m	1.1E+01
Waste Disposal Region 5	m	1.4E+01
Waste Disposal Region 6	m	1.7E+01
Waste Disposal Region 7	m	1.7E+01
Waste Disposal Region 8	m	1.5E+01
1988-2010 Disposal Pits	m	1.2E+01
2011-2044 Disposal Pits	m	1.5E+01
1988-2015 Disposal Shafts	m	1.8E+01
2016-2044 Disposal Shafts	m	1.5E+01
Material Properties		
Bulk Density		
Crushed Tuff	kg/m^3 (dry weight)	N(1.4E+03, 6.9E+01)
Waste	kg/m^3 (dry weight)	N(1.4E+03, 6.9E+01)
Concrete	kg/m^3 (dry weight)	N(2.0E+03, 8.1E+01)
Porosity		
Crushed Tuff		N(4.1E-01, 3.3E-02)

--- = No distribution was defined for this parameter.

[a] *Blank cells indicate value is unitless.*

[b] *Distribution designations refer to the following distribution types: CD = cumulative distribution (cumulative probability, value),D = discrete (probability, value), LN = lognormal (geometric mean, geometric standard deviation), T = triangular (minimum, most likely, maximum), TLN = truncated lognormal distribution (geometric mean, geometric standard deviation, minimum, maximum), TN = truncated normal distribution (mean, standard deviation, minimum, maximum), U = uniform (minimum, maximum).*

[c] *The first value was used for the Intruder–Post-Drilling and Intruder-Agriculture Scenarios; the second value was used for the Intruder-Construction Scenario*

[d] *The first value represents the performance assessment; the second value the composite analysis.*

[e] *The distribution of the soil intake rate of chickens is a function of the bird's food intake rate.*

[f] *The listed mixing depth was used for the off-site exposure scenarios and the Intruder–Post-Drilling Scenario; for the Intruder-Construction and Intruder-Agriculture Scenarios the mixing depth was set equal to the thickness of the soil excavated during house construction after it was spread across the intruder's lot.*

Table 11 (Continued)
Pathway Parameter Values and Distributions Used in the Performance Assessment and Composite Analysis

Parameter	Units [a]	Input Value or Distribution [b]
Waste		N(4.1E-01, 3.3E-02)
Concrete		N(2.0E-01, 3.2E-02)
Moisture Content		
Crushed Tuff	(volume basis)	T(5.0E-02, 7.5E-02, 1.2E-01)
Waste	(volume basis)	T(5.0E-02, 7.5E-02, 1.2E-01)
Saturation Content		
Concrete	(volume basis)	U(5.0E-02, 1.5E-01)
Radon Emanation Coefficient		U(1.0E-01, 4.0E-01)
Carbon Gas Generation Rate	yr^{-1}	U(3.0E-03, 2.0E-02)
Carbon Dioxide Fraction		U(4.0E-01, 6.0E-01)
Organic Fraction of C-14 Waste		T(1.0E-02, 5.0E-02, 1.0E-01)
Atmospheric Transport Parameters		
Dust Loading		
Inadvertent Intruder	$\mu g/m^3$	LN(3.0E-08, 1.6), LN(4.5E-08, 1.6) [c]
Members of Public	$\mu g/m^3$	LN(3.0E-08, 1.6)
Vertical Flux	$g/m^2/yr$	TN(1.3E+01, 8.4E+00, 0.0E+00, 1.0E+10)
Soil Disturbance Factor		T(1.1E+00, 2.0E+00, 3.0E+00)
Enhancement Factor		T(1.0E+00, 3.0E+00, 6.0E+00)

--- = No distribution was defined for this parameter.

[a] *Blank cells indicate value is unitless.*

[b] *Distribution designations refer to the following distribution types: CD = cumulative distribution (cumulative probability, value),D = discrete (probability, value), LN = lognormal (geometric mean, geometric standard deviation), T = triangular (minimum, most likely, maximum), TLN = truncated lognormal distribution (geometric mean, geometric standard deviation, minimum, maximum), TN = truncated normal distribution (mean, standard deviation, minimum, maximum), U = uniform (minimum, maximum).*

[c] *The first value was used for the Intruder–Post-Drilling and Intruder-Agriculture Scenarios; the second value was used for the Intruder-Construction Scenario*

[d] *The first value represents the performance assessment; the second value the composite analysis.*

[e] *The distribution of the soil intake rate of chickens is a function of the bird's food intake rate.*

[f] *The listed mixing depth was used for the off-site exposure scenarios and the Intruder–Post-Drilling Scenario; for the Intruder-Construction and Intruder-Agriculture Scenarios the mixing depth was set equal to the thickness of the soil excavated during house construction after it was spread across the intruder's lot.*

Table 11 (Continued)
Pathway Parameter Values and Distributions Used in the Performance Assessment and Composite Analysis

Parameter	Units [a]	Input Value or Distribution [b]
Particulate Dispersion Factor		
Grassland Land Use		
LANL Boundary		
Atmospheric Source Area 1 Releases	s/m^3	N(1.1E-06, 1.1E-07); N(9.7E-06, 6.2E-07) [d]
Atmospheric Source Area 2 Releases	s/m^3	N(1.7E-05, 8.9E-07); N(4.5E-06, 8.5E-07) [d]
Atmospheric Source Area 3 Releases	s/m^3	N(6.3E-06, 1.5E-06); N(3.1E-06, 1.2E-06) [d]
Area G Fence Line		
Atmospheric Source Area 1 Releases	s/m^3	N(3.0E-04, 7.3E-05); N(4.3E-04, 1.2E-05) [d]
Atmospheric Source Area 2 Releases	s/m^3	N(1.1E-06, 1.4E-07); N(9.0E-06, 1.6E-06) [d]
Atmospheric Source Area 3 Releases	s/m^3	N(1.8E-04, 4.3E-05); N(3.5E-06, 1.4E-06) [d]
Woodland Land Use		
LANL Boundary		
Atmospheric Source Area 1 Releases	s/m^3	N(6.0E-07, 6.8E-08); N(3.4E-06, 2.8E-07) [d]
Atmospheric Source Area 2 Releases	s/m^3	N(1.2E-05, 8.6E-07); N(1.6E-06, 1.3E-07) [d]
Atmospheric Source Area 3 Releases	s/m^3	N(8.0E-06, 5.9E-07); 1.2E-06, 1.2E-07) [d]
Area G Fence Line		
Atmospheric Source Area 1 Releases	s/m^3	N(1.8E-07, 3.4E-08); N(2.9E-04, 1.1E-05) [d]
Atmospheric Source Area 2 Releases	s/m^3	N(6.2E-07, 8.4E-08); N(3.7E-06, 2.4E-07) [d]
Atmospheric Source Area 3 Releases	s/m^3	N(1.1E-04, 3.8E-06); N(1.6E-06, 1.7E-07) [d]
Vapor and Gas Dispersion Factors		
LANL Boundary		
Atmospheric Source Area 1 Releases	s/m^3	N(1.3E-06, 1.4E-07); N(1.3E-06, 1.4E-07) [d]
Atmospheric Source Area 2 Releases	s/m^3	N(1.8E-06, 3.7E-06); N(1.8E-06, 3.7E-06) [d]

--- = No distribution was defined for this parameter.

[a] *Blank cells indicate value is unitless.*

[b] *Distribution designations refer to the following distribution types: CD = cumulative distribution (cumulative probability, value),D = discrete (probability, value), LN = lognormal (geometric mean, geometric standard deviation), T = triangular (minimum, most likely, maximum), TLN = truncated lognormal distribution (geometric mean, geometric standard deviation, minimum, maximum), TN = truncated normal distribution (mean, standard deviation, minimum, maximum), U = uniform (minimum, maximum).*

[c] *The first value was used for the Intruder–Post-Drilling and Intruder-Agriculture Scenarios; the second value was used for the Intruder-Construction Scenario*

[d] *The first value represents the performance assessment; the second value the composite analysis.*

[e] *The distribution of the soil intake rate of chickens is a function of the bird's food intake rate.*

[f] *The listed mixing depth was used for the off-site exposure scenarios and the Intruder–Post-Drilling Scenario; for the Intruder-Construction and Intruder-Agriculture Scenarios the mixing depth was set equal to the thickness of the soil excavated during house construction after it was spread across the intruder's lot.*

Table 11 (Continued)
Pathway Parameter Values and Distributions Used in the Performance Assessment and Composite Analysis

Parameter	Units [a]	Input Value or Distribution [b]
Atmospheric Source Area 3 Releases	s/m^3	N(1.6E-05, 1.3E-06); N(1.6E-05, 1.3E-06) [d]
Area G Fence Line		
Atmospheric Source Area 1 Releases	s/m^3	N(1.4E-06, 1.7E-07); N(1.4E-06, 1.7E-07) [d]
Atmospheric Source Area 2 Releases	s/m^3	N(2.0E-04, 1.9E-05); N(2.0E-04, 1.9E-05) [d]
Atmospheric Source Area 3 Releases	s/m^3	N(2.8E-05, 1.9E-06); N(2.8E-05, 1.9E-06) [d]
Deposition Rate		
Grassland Land Use		
LANL Boundary		
Atmospheric Source Area 1 Releases	$g/m^2/s$	N(2.6E-04, 3.1E-05); N(2.7E-03, 2.5E-04) [d]
Atmospheric Source Area 2 Releases	$g/m^2/s$	N(1.3E-02; 7.3E-04); N(3.1E-03, 1.4E-04) [d]
Atmospheric Source Area 3 Releases	$g/m^2/s$	N(1.8E-03, 7.6E-04); N(8.9E-04, 3.6E-04) [d]
Area G Fence Line		
Atmospheric Source Area 1 Releases	$g/m^2/s$	N(6.9E-05, 8.6E-06); N(1.1E-01, 1.8E-02) [d]
Atmospheric Source Area 2 Releases	$g/m^2/s$	N(9.7E-04, 1.1E-04); N(5.8E-03, 2.5E-04) [d]
Atmospheric Source Area 3 Releases	$g/m^2/s$	N(5.6E-02, 2.4E-02); N(9.6E-04, 3.9E-04) [d]
Woodland Land Use		
LANL Boundary		
Atmospheric Source Area 1 Releases	$g/m^2/s$	N(3.2E-04, 3.9E-05); N(3.3E-03, 2.8E-04) [d]
Atmospheric Source Area 2 Releases	$g/m^2/s$	N(3.8E-02, 3.3E-03); N(2.8E-03, 1.2E-04) [d]
Atmospheric Source Area 3 Releases	$g/m^2/s$	N(1.0E-02, 8.8E-04); N(8.1E-04, 4.8E-05) [d]
Area G Fence Line		
Atmospheric Source Area 1 Releases	$g/m^2/s$	N(9.4E-05, 1.4E-05); N(2.9E-01, 6.6E-02) [d]
Atmospheric Source Area 2 Releases	$g/m^2/s$	N(1.7E-03, 1.3E-04); N(4.8E-03, 1.8E-04) [d]

--- = No distribution was defined for this parameter.

[a] *Blank cells indicate value is unitless.*

[b] *Distribution designations refer to the following distribution types: CD = cumulative distribution (cumulative probability, value),D = discrete (probability, value), LN = lognormal (geometric mean, geometric standard deviation), T = triangular (minimum, most likely, maximum), TLN = truncated lognormal distribution (geometric mean, geometric standard deviation, minimum, maximum), TN = truncated normal distribution (mean, standard deviation, minimum, maximum), U = uniform (minimum, maximum).*

[c] *The first value was used for the Intruder–Post-Drilling and Intruder-Agriculture Scenarios; the second value was used for the Intruder-Construction Scenario*

[d] *The first value represents the performance assessment; the second value the composite analysis.*

[e] *The distribution of the soil intake rate of chickens is a function of the bird's food intake rate.*

[f] *The listed mixing depth was used for the off-site exposure scenarios and the Intruder–Post-Drilling Scenario; for the Intruder-Construction and Intruder-Agriculture Scenarios the mixing depth was set equal to the thickness of the soil excavated during house construction after it was spread across the intruder's lot.*

Table 11 (Continued)
Pathway Parameter Values and Distributions Used in the Performance Assessment and Composite Analysis

Parameter	Units [a]	Input Value or Distribution [b]
Atmospheric Source Area 3 Releases	$g/m^2/s$	N(1.3E-01, 8.0E-03); N(9.0E-04, 6.2E-05) [d]
Groundwater Transport Parameters		
Infiltration Rate		
Mesita del Buey	cm/yr	TN(2.3E-03, 1.5E-03, 0.0E+00, 1.0E+10))
Pajarito Canyon	cm/yr	TN(4.0E+01, 2.6E-01, 0.0E+00, 1.0E+10)
Cañada del Buey	cm/yr	TN(2.2E-01, 2.7E-03, 0.0E+00, 1.0E+10)
East of Area G Fence Line	cm/yr	TN(5.0E-01, 6.4E-03, 0.0E+00, 1.0E+10)
Contaminant Capture Fraction		
Waste Disposal Region 1		4.1E-02
Waste Disposal Region 2		1.1E-01
Waste Disposal Region 3		3.6E-02
Waste Disposal Region 4		3.6E-02
Waste Disposal Region 5		5.8E-02
Waste Disposal Region 6		1.1E-01
Waste Disposal Region 7		3.6E-02
Waste Disposal Region 8		8.1E-02
Sediment Transport Parameters		
Fraction of Catchment over which Sediments Disperse		T(1.0E-01, 3.0E-01, 5.0E-01)
Canyon Sediment Transport Rate	yr^{-1}	N(5.0E-03, 1.0E-03)
Food-Chain Transport Parameters		
Dry-to-Wet Weight Fraction		
Leafy Vegetables		TN(9.8E-02, 3.4E-02, 4.8E-02, 1.7E-01)

--- = No distribution was defined for this parameter.

[a] *Blank cells indicate value is unitless.*

[b] *Distribution designations refer to the following distribution types: CD = cumulative distribution (cumulative probability, value),D = discrete (probability, value), LN = lognormal (geometric mean, geometric standard deviation), T = triangular (minimum, most likely, maximum), TLN = truncated lognormal distribution (geometric mean, geometric standard deviation, minimum, maximum), TN = truncated normal distribution (mean, standard deviation, minimum, maximum), U = uniform (minimum, maximum).*

[c] *The first value was used for the Intruder–Post-Drilling and Intruder-Agriculture Scenarios; the second value was used for the Intruder-Construction Scenario*

[d] *The first value represents the performance assessment; the second value the composite analysis.*

[e] *The distribution of the soil intake rate of chickens is a function of the bird's food intake rate.*

[f] *The listed mixing depth was used for the off-site exposure scenarios and the Intruder–Post-Drilling Scenario; for the Intruder-Construction and Intruder-Agriculture Scenarios the mixing depth was set equal to the thickness of the soil excavated during house construction after it was spread across the intruder's lot.*

Table 11 (Continued)
Pathway Parameter Values and Distributions Used in the Performance Assessment and Composite Analysis

Parameter	Units [a]	Input Value or Distribution [b]
Produce		TLN(1.3E-01, 1.1E-01, 4.1E-01)
Grain		TN(9.1E-01, 1.3E-02, 8.9E-01, 9.3E-01)
Pasture Grass		T(1.5E-01, 2.0E-01, 2.5E-01)
Translocation Factor		
Leafy Vegetables and Pasture Grass		T(8.0E-01, 9.0E-01, 1.0E+00)
Produce and Grain		T(1.0E-02, 1.0E-01, 4.0E-01)
Agricultural Productivity		
Leafy Vegetables	kg/m^2 (wet weight)	T(1.0E+00, 1.5E+00, 2.0E+00)
Produce	kg/m^2 (wet weight)	T(5.0E-01, 1.0E+00, 1.5E+00)
Grain	kg/m^2 (wet weight)	T(2.0E-01, 5.0E-01, 7.5E-01)
Pasture Grass	kg/m^2 (dry weight)	T(1.0E-01, 5.0E-01, 7.0E-01)
Growing Season		
Leafy Vegetables	d	T(4.0E+01, 6.0E+01, 1.0E+02)
Produce	d	T(4.5E+01, 8.0E+01, 1.2E+02)
Grain	d	T(7.0E+01, 1.1E+02, 1.2E+02)
Pasture Grass	d	T(3.0E+01, 4.5E+01, 6.0E+01)
Mass Loading Factors		
Leafy Vegetables	mg soil per g plant (dry weight)	TN(2.6E+02, 1.0E+02, 0.0E+00, 1.0E+04)

--- = No distribution was defined for this parameter.

[a] *Blank cells indicate value is unitless.*

[b] *Distribution designations refer to the following distribution types: CD = cumulative distribution (cumulative probability, value),D = discrete (probability, value), LN = lognormal (geometric mean, geometric standard deviation), T = triangular (minimum, most likely, maximum), TLN = truncated lognormal distribution (geometric mean, geometric standard deviation, minimum, maximum), TN = truncated normal distribution (mean, standard deviation, minimum, maximum), U = uniform (minimum, maximum).*

[c] *The first value was used for the Intruder–Post-Drilling and Intruder-Agriculture Scenarios; the second value was used for the Intruder-Construction Scenario*

[d] *The first value represents the performance assessment; the second value the composite analysis.*

[e] *The distribution of the soil intake rate of chickens is a function of the bird's food intake rate.*

[f] *The listed mixing depth was used for the off-site exposure scenarios and the Intruder–Post-Drilling Scenario; for the Intruder-Construction and Intruder-Agriculture Scenarios the mixing depth was set equal to the thickness of the soil excavated during house construction after it was spread across the intruder's lot.*

Table 11 (Continued)
Pathway Parameter Values and Distributions Used in the Performance Assessment and Composite Analysis

Parameter	Units [a]	Input Value or Distribution [b]
Produce, Grain, and Pasture Grass	mg soil per g plant (dry weight)	T(1.0E+00, 3.0E+01, 1.0E+02)
Enhancement Factor		T(1.0E+00, 1.5E+00, 2.0E+00)
Plant Interception Coefficient	m^2/kg	T(2.0E+00, 3.0E+00, 4.0E+00)
Weathering Half-Life	d	LN(1.7E+01, 1.6E+00)
Dry Matter Fraction		
Beef		3.3E-01
Milk		1.0E-01
Chicken		3.3E-01
Eggs		2.6E-01
Water Equivalent Fraction		
Beef		8.0E-01
Milk		6.7E-01
Chicken		8.0E-01
Eggs		8.4E-01
Carbon Fraction		
All Crops	(dry weight basis)	4.5E-01
Soil	(dry weight basis)	3.0E-02
Beef	(wet weight basis)	2.4E-01
Milk	(wet weight basis)	7.0E-02

--- = No distribution was defined for this parameter.

[a] *Blank cells indicate value is unitless.*

[b] *Distribution designations refer to the following distribution types: CD = cumulative distribution (cumulative probability, value),D = discrete (probability, value), LN = lognormal (geometric mean, geometric standard deviation), T = triangular (minimum, most likely, maximum), TLN = truncated lognormal distribution (geometric mean, geometric standard deviation, minimum, maximum), TN = truncated normal distribution (mean, standard deviation, minimum, maximum), U = uniform (minimum, maximum).*

[c] *The first value was used for the Intruder–Post-Drilling and Intruder-Agriculture Scenarios; the second value was used for the Intruder-Construction Scenario*

[d] *The first value represents the performance assessment; the second value the composite analysis.*

[e] *The distribution of the soil intake rate of chickens is a function of the bird's food intake rate.*

[f] *The listed mixing depth was used for the off-site exposure scenarios and the Intruder–Post-Drilling Scenario; for the Intruder-Construction and Intruder-Agriculture Scenarios the mixing depth was set equal to the thickness of the soil excavated during house construction after it was spread across the intruder's lot.*

Table 11 (Continued)
Pathway Parameter Values and Distributions Used in the Performance Assessment and Composite Analysis

Parameter	Units [a]	Input Value or Distribution [b]
Chicken	(wet weight basis)	2.0E-01
Eggs	(wet weight basis)	1.5E-01
Animal Food Ingestion Rates		
Cows	kg/d (dry weight)	T(1.0E+01, 1.6E+01, 2.5E+01)
Cattle	kg/d (dry weight)	T(7.5E+00, 1.2E+01, 1.8E+01)
Chickens	kg/d (dry weight)	T(5.0E-02, 7.0E-02, 1.5E-01)
Animal Water Ingestion Rates		
Cows	L/d	T(5.0E+01, 7.5E+01, 1.0E+02)
Cattle	L/d	T(2.0E+01, 4.0E+01, 6.0E+01)
Chickens	L/d	T(1.0E-01, 2.0E-01, 3.0E-01)
Animal Soil/Grit Ingestion Rate		
Cows and Cattle	kg/d	T(4.0E-01, 1.0E+00, 2.2E+00)
Chickens [e]	% of dry forage intake	D(1.0E+00, 2.0E-02)
Biotic Intrusion Model Parameters		
Time of Climax	yr	T(1.0E+02, 2.0E+02, 3.0E+02)
Alpha Shape Factor		0.00E+00
Beta Shape Factor		U(1.5E+00, 9.0E+00)
Maximum Rooting Depth		
Grasses	m	T(7.6E-01, 1.7E+00, 4.0E+00)

--- = No distribution was defined for this parameter.

[a] *Blank cells indicate value is unitless.*

[b] *Distribution designations refer to the following distribution types: CD = cumulative distribution (cumulative probability, value),D = discrete (probability, value), LN = lognormal (geometric mean, geometric standard deviation), T = triangular (minimum, most likely, maximum), TLN = truncated lognormal distribution (geometric mean, geometric standard deviation, minimum, maximum), TN = truncated normal distribution (mean, standard deviation, minimum, maximum), U = uniform (minimum, maximum).*

[c] *The first value was used for the Intruder–Post-Drilling and Intruder-Agriculture Scenarios; the second value was used for the Intruder-Construction Scenario*

[d] *The first value represents the performance assessment; the second value the composite analysis.*

[e] *The distribution of the soil intake rate of chickens is a function of the bird's food intake rate.*

[f] *The listed mixing depth was used for the off-site exposure scenarios and the Intruder–Post-Drilling Scenario; for the Intruder-Construction and Intruder-Agriculture Scenarios the mixing depth was set equal to the thickness of the soil excavated during house construction after it was spread across the intruder's lot.*

Table 11 (Continued)
Pathway Parameter Values and Distributions Used in the Performance Assessment and Composite Analysis

Parameter	Units [a]	Input Value or Distribution [b]
Forbs	m	T(3.0E-01, 2.4E+00, 9.1E+00)
Shrubs	m	T(1.4E+00, 2.9E+00, 9.1E+00)
Trees	m	T(2.0E+00, 6.0E+00, 1.0E+01)
Biomass Density		
Grasses—Early Succession	kg/m^2	T(2.8E-03, 5.6E-02, 1.5E-01)
Grasses—Climax Condition	kg/m^2	T(2.0E-03, 1.0E-02, 6.2E-02)
Forbs—Early Succession	kg/m^2	T(0.0E+00, 4.3E-03, 4.8E-02)
Forbs—Climax Condition	kg/m^2	T(1.0E-03, 3.5E-03, 7.7E-03)
Shrubs—Early Succession	kg/m^2	T(7.9E-04, 8.3E-03, 3.8E-02)
Shrubs—Climax Condition	kg/m^2	T(3.0E-03, 7.1E-03, 1.3E-02)
Trees	kg/m^2	T(2.3E+00, 5.3E+00, 1.2E+01)
Litter Production Fraction		
Grasses	yr^{-1}	T(3.0E-01, 6.0E-01, 1.0E+00)
Forbs	yr^{-1}	T(3.0E-01, 6.0E-01, 1.0E+00)
Shrubs	yr^{-1}	T(6.0E-02, 1.3E-01, 6.0E-01)
Trees	yr^{-1}	T(1.0E-02, 7.5E-02, 1.4E-01)
Litter Decomposition Half-Life	yr	T(1.0E+00, 20E+00, 6.0E+00)
Maximum Burrow Depth		
Harvester Ants	m	T(2.0E+00, 3.0E+00, 4.0E+00)
Mice	m	T(5.0E-01, 1.0E+00, 2.0E+00)
Pocket Gophers	m	T(5.0E-01, 1.3E+00, 2.0E+00)
Chipmunks and Ground Squirrels	m	T(5.0E-01, 1.0E+00, 2.0E+00)
Burrow Density		

--- = No distribution was defined for this parameter.

[a] *Blank cells indicate value is unitless.*

[b] *Distribution designations refer to the following distribution types: CD = cumulative distribution (cumulative probability, value),D = discrete (probability, value), LN = lognormal (geometric mean, geometric standard deviation), T = triangular (minimum, most likely, maximum), TLN = truncated lognormal distribution (geometric mean, geometric standard deviation, minimum, maximum), TN = truncated normal distribution (mean, standard deviation, minimum, maximum), U = uniform (minimum, maximum).*

[c] *The first value was used for the Intruder–Post-Drilling and Intruder-Agriculture Scenarios; the second value was used for the Intruder-Construction Scenario*

[d] *The first value represents the performance assessment; the second value the composite analysis.*

[e] *The distribution of the soil intake rate of chickens is a function of the bird's food intake rate.*

[f] *The listed mixing depth was used for the off-site exposure scenarios and the Intruder–Post-Drilling Scenario; for the Intruder-Construction and Intruder-Agriculture Scenarios the mixing depth was set equal to the thickness of the soil excavated during house construction after it was spread across the intruder's lot.*

Table 11 (Continued)
Pathway Parameter Values and Distributions Used in the Performance Assessment and Composite Analysis

Parameter	Units [a]	Input Value or Distribution [b]
Harvester Ants	ha^{-1}	TN(2.8E+01, 2.0E+01, 0.0E+00, 1.0E+03)
Mice—Early Succession	ha^{-1}	T(1.0E+01, 2.0E+01, 3.2E+01)
Mice—Climax Condition	ha^{-1}	T(1.5E+00, 7.7E+00, 8.5E+01)
Chipmunks and Ground Squirrels	ha^{-1}	T(5.0E+00, 1.5E+01, 2.5E+01)
Burrow Mass or Volume		
Harvester Ants	kg	T(2.3E+01, 3.8E+01, 6.5E+01)
Mice	m^3	T(3.0E-03, 1.4E-02, 1.0E-01)
Chipmunks and Ground Squirrels	m^3	T(8.0E-03, 2.0E-02, 7.7E-02)
Harvester Ant Colony Lifespan	yr	T(5.0E+00, 2.1E+01, 5.8E+01)
Pocket Gopher Soil Removal Rate	m^3/ha/yr	T(5.1E-01, 8.3E+00, 8.2E+01)
Burrow Renewal Fraction		
Pocket Gophers	yr^{-1}	T(7.5E-01, 8.8E-01, 1.0E+00)
Mice	yr^{-1}	T(7.5E-01, 8.8E-01, 1.0E+00)
Chipmunks and Ground Squirrels	yr^{-1}	T(5.0E-01, 7.5E-01, 1.0E+00)
Erosion Model Parameters		
Erosion Scenario		D(0.1,1,0.8,2,0.1,3)
Exposure Pathway Parameters		
Indoor Time Allotment	hr/d	CD(0.0E+00, 9.6E+00; 5.0E-02, 9.6E+00; 2.5E-01, 1.3E+01; 5.0E-01, 1.6E+01; 7.5E-01, 2.1E+01; 9.0E-01, 2.3E+01; 9.5E-01, 2.4E+01; 1.0E+00, 2.4E+01)
Outdoor Time Allotment	hr/d	CD(0.0E+00, 0.0E+00; 5.0E-02, 8.3E-02; 2.5E-01, 6.7E-01; 5.0E-01, 1.8E+00; 7.5E-01, 3.5E+00; 9.0E-01, 6.0E+00; 9.5E-01, 8.0E+00; 9.8E-01, 1.0E+01; 9.9E-01, 1.2E+01; 1.0E+01,2.2E+01)

--- = No distribution was defined for this parameter.

[a] *Blank cells indicate value is unitless.*

[b] *Distribution designations refer to the following distribution types: CD = cumulative distribution (cumulative probability, value),D = discrete (probability, value), LN = lognormal (geometric mean, geometric standard deviation), T = triangular (minimum, most likely, maximum), TLN = truncated lognormal distribution (geometric mean, geometric standard deviation, minimum, maximum), TN = truncated normal distribution (mean, standard deviation, minimum, maximum), U = uniform (minimum, maximum).*

[c] *The first value was used for the Intruder–Post-Drilling and Intruder-Agriculture Scenarios; the second value was used for the Intruder-Construction Scenario*

[d] *The first value represents the performance assessment; the second value the composite analysis.*

[e] *The distribution of the soil intake rate of chickens is a function of the bird's food intake rate.*

[f] *The listed mixing depth was used for the off-site exposure scenarios and the Intruder–Post-Drilling Scenario; for the Intruder-Construction and Intruder-Agriculture Scenarios the mixing depth was set equal to the thickness of the soil excavated during house construction after it was spread across the intruder's lot.*

Table 11 (Continued)
Pathway Parameter Values and Distributions Used in the Performance Assessment and Composite Analysis

Parameter	Units [a]	Input Value or Distribution [b]
Construction Worker Exposure Time	hr	5.0E+02
Excavation Occupancy Factor		T(0.0E+00, 1.0E-01, 2.0E-01)
Soil Mixing Depth	cm	1.5E+01 [f]
Direct Radiation Shielding Factor	---	U(2.0E-01, 6.0E-01)
Inhalation Rate		
Resident Receptors	m^3/d	T(1.3E+01, 1.5E+01, 1.7E+01)
Intruder-Construction Scenario	m^3/hr	TN(1.5E+00, 6.0E-01, 5.0E-01, 1.0E+10)
Average Wind Speed	m/s	LN(2.6E+00, 1.4E+00)
Atmospheric Mixing Height	m	2.0E+00
House Ventilation Rate	hr^{-1}	LN(4.7E-01, 2.1E+00)
Irrigation Rate		
Leafy Vegetables	cm/yr	T(1.2E+01, 4.8E+01, 8.3E+01)
Produce	cm/yr	T(2.3E+01, 7.4E+01, 1.2E+02)
Grain	cm/yr	T(3.5E+01, 6.5E+01. 8.8E+01)
Pasture Grass	cm/yr	T(4.6E+01, 8.4E+01, 1.2E+02)
Inadvertent Soil Ingestion Rate	kg/yr	LN(3.6E-02, 3.2E+00)
Drinking Water Ingestion Rate	L/d	CD(0.0E+00, 1.5E-01; 5.0E-02, 4.2E-01; 1.0E-01, 5.6E-01; 2.5E-01, 8.7E-01; 5.0E-01, 1.3E+00; 7.5E-01, 1.7E+00; 9.0E-01, 2.3E+00; 9.5E-01, 2.7E+00; 1.0E+00, 3.8E+00)
Fraction of Vegetables from Site		T(1.7E-01, 3.1E-01, 4.2E-01)
Fraction of Animal Products from Site		
Beef		T(4.0E-01, 5.0E-01, 6.0E-01)

--- = No distribution was defined for this parameter.

[a] *Blank cells indicate value is unitless.*

[b] *Distribution designations refer to the following distribution types: CD = cumulative distribution (cumulative probability, value),D = discrete (probability, value), LN = lognormal (geometric mean, geometric standard deviation), T = triangular (minimum, most likely, maximum), TLN = truncated lognormal distribution (geometric mean, geometric standard deviation, minimum, maximum), TN = truncated normal distribution (mean, standard deviation, minimum, maximum), U = uniform (minimum, maximum).*

[c] *The first value was used for the Intruder–Post-Drilling and Intruder-Agriculture Scenarios; the second value was used for the Intruder-Construction Scenario*

[d] *The first value represents the performance assessment; the second value the composite analysis.*

[e] *The distribution of the soil intake rate of chickens is a function of the bird's food intake rate.*

[f] *The listed mixing depth was used for the off-site exposure scenarios and the Intruder–Post-Drilling Scenario; for the Intruder-Construction and Intruder-Agriculture Scenarios the mixing depth was set equal to the thickness of the soil excavated during house construction after it was spread across the intruder's lot.*

Table 11 (Continued)
Pathway Parameter Values and Distributions Used in the Performance Assessment and Composite Analysis

Parameter	Units [a]	Input Value or Distribution [b]
Milk		T(1.2E-01, 1.5E-01, 1.8E-01)
Chicken		T(1.2E-01, 1.5E-01, 1.8E-01)
Eggs		T(1.6E-01, 2.0E-01, 2.4E-01)
Crop Ingestion Rates		
Leafy Vegetables	kg/yr	CD(0.0E+00, 0.0E+00; 5.0E-02, 3.2E+00; 1.0E-01, 5.2E+00; 2.5E-01, 8.6E+00; 5.0E-01, 1.3E+01; 7.5E-01, 1.9E+01; 9.0E-01, 2.6E+01; 9.5E-01, 3.1E+01; 9.9E-01, 4.3E+01; 1.0E+00, 8.4E+01)
Produce	kg/yr	CD(0.0E+00, 0.0E+00; 5.0E-02, 1.8E+01; 1.0E-01, 2.9E+01; 2.5E-01, 4.8E+01; 5.0E-01, 7.5E+01; 7.5E-01, 1.1E+02; 9.0E-01, 1.5E+02; 9.5E-01, 1.7E+02; 9.9E-01, 2.4E+02; 1.0E+00, 4.7E+02)
Grain	kg/yr	CD(0.0E+00, 0.0E+00; 1.0E-02, 1.1E+00; 5.0E-02, 1.9E+01; 1.0E-01, 2.7E+01; 2.5E-01, 4.4E+01; 5.0E-01, 6.8E+01; 7.5E-01, 9.9E+01; 9.0E-01, 1.4E+02; 9.5E-010, 1.7E+02; 9.9E-01, 2.4E+02; 1.0E+00, 5.9E+02)
Animal Product Ingestion Rates		
Beef	kg/yr	CD(0.0E+00, 0.0E+00; 1.0E-01, 1.3E+00; 2.5E-01, 6.3E+00; 5.0E-01, 1.5E+01; 7.5E-01, 2.6E+01; 9.0E-01, 4.0E+01; 9.5E-01, 5.0E+01; 9.9E-01, 7.1E+01; 1.0E+00, 1.4E+02)
Milk	L/yr	CD(0.0E+00, 0.0E+00; 5.0E-02, 2.4E+00; 1.0E-01, 6.2E+00; 2.5E-01, 2.1E+01; 5.0E-01, 5.2E+01; 7.5E-01, 9.8E+01; 9.0E-01, 1.6E+02; 9.5E-01, 2.0E+02; 9.9E-01, 3.1E+02; 1.0E+00, 7.7E+02)

--- = No distribution was defined for this parameter.

[a] *Blank cells indicate value is unitless.*

[b] *Distribution designations refer to the following distribution types: CD = cumulative distribution (cumulative probability, value),D = discrete (probability, value), LN = lognormal (geometric mean, geometric standard deviation), T = triangular (minimum, most likely, maximum), TLN = truncated lognormal distribution (geometric mean, geometric standard deviation, minimum, maximum), TN = truncated normal distribution (mean, standard deviation, minimum, maximum), U = uniform (minimum, maximum).*

[c] *The first value was used for the Intruder–Post-Drilling and Intruder-Agriculture Scenarios; the second value was used for the Intruder-Construction Scenario*

[d] *The first value represents the performance assessment; the second value the composite analysis.*

[e] *The distribution of the soil intake rate of chickens is a function of the bird's food intake rate.*

[f] *The listed mixing depth was used for the off-site exposure scenarios and the Intruder–Post-Drilling Scenario; for the Intruder-Construction and Intruder-Agriculture Scenarios the mixing depth was set equal to the thickness of the soil excavated during house construction after it was spread across the intruder's lot.*

Table 11 (Continued)
Pathway Parameter Values and Distributions Used in the Performance Assessment and Composite Analysis

Parameter	Units [a]	Input Value or Distribution [b]
Chicken	kg/yr	CD(0.0E+00, 0.0E+00; 5.0E-01, 4.7E-02; 1.0E-01, 3.5E-01; 2.5E-01, 2.3E+00; 5.0E-01, 8.0E+00; 7.5E-01, 1.9E+01; 9.0E-01, 3.3E+01; 9.5E-01, 4.2E+01; 9.9E-01, 6.4E+01; 1.0E+00, 1.3E+02)
Eggs	kg/yr	CD(0.0E+00, 0.0E+00; 7.5E-01, 1.0E+01; 9.0E-01, 2.0E+01; 9.5E-01, 2.8E+01; 9.9E-01, 4.2E+01; 1.0E+00, 1.0E+02)
Weight of Cattle at Slaughter	kg	N(5.0E+02, 2.5E+01)
Carcass-to-Live Weight Ratio for Cattle		N(6.4E-01, 2.0E-02)
Fraction of Beef Carcass Sold as Meat		N(5.0E-01, 2.4E-02)
Milk Prodction Rate of Cows	kg/yr	N(8.6E+03, 1.5E+02)
Weight of Chicken at Slaughter	kg	N(2.3E+00, 4.5E-01)
Ratio of Ready-to-Cook Chicken and Live Weight		N(7.4E-01, 4.5E-03)
Fraction of Ready-to-Cook Weight of Chicken that is Meat		5.0E-01
Egg Production Rate	yr^{-1}	N(2.6E+02, 1.3E+01)
Mass of Egg	kg	N(6.0E-02, 3.5E-03)
Fraction of Egg Mass that is Shell		5.0E-01
Area of Receptor's House	m^2	2.0E+02
Room Height	m	2.4E+00
Well Diameter	cm	2.5E+01

--- = No distribution was defined for this parameter.

[a] *Blank cells indicate value is unitless.*

[b] *Distribution designations refer to the following distribution types: CD = cumulative distribution (cumulative probability, value),D = discrete (probability, value), LN = lognormal (geometric mean, geometric standard deviation), T = triangular (minimum, most likely, maximum), TLN = truncated lognormal distribution (geometric mean, geometric standard deviation, minimum, maximum), TN = truncated normal distribution (mean, standard deviation, minimum, maximum), U = uniform (minimum, maximum).*

[c] *The first value was used for the Intruder–Post-Drilling and Intruder-Agriculture Scenarios; the second value was used for the Intruder-Construction Scenario*

[d] *The first value represents the performance assessment; the second value the composite analysis.*

[e] *The distribution of the soil intake rate of chickens is a function of the bird's food intake rate.*

[f] *The listed mixing depth was used for the off-site exposure scenarios and the Intruder–Post-Drilling Scenario; for the Intruder-Construction and Intruder-Agriculture Scenarios the mixing depth was set equal to the thickness of the soil excavated during house construction after it was spread across the intruder's lot.*

5.2.4 Waste Emplacement Efficiency

The waste emplacement efficiency is the fraction of the pit or shaft disposal capacity occupied by waste, with the remainder consisting of uncontaminated backfill. Radionuclide concentrations in the disposal units depend, in part, upon the emplacement efficiency. The waste emplacement efficiency is not directly input into the site, intruder, and intruder diffusion models but is reflected by the dimensions of the disposal pits and shafts relative to the waste volumes. The parameter was used to estimate the disposal areas of the pits and shafts in the Zone 4 expansion area. An efficiency of 0.5 was assumed for the units in this portion of Area G, based on the Zone 4 design developed by Day et al. (2005).

5.2.5 Shaft Field Efficiency

The disposal shafts at Area G are typically distributed in groups of 5 to more than 20 units; these groups are referred to as shaft fields. The shafts within the shaft fields are placed subject to minimum spacing requirements. Historically, shafts with diameters of 0.9 m (3 ft) or less had a minimum center-to-center spacing of 2.3 m (7.5 ft); larger shafts were arranged to maintain at least 5.5 m (18 ft) between centers (Kopp, 1991). The conceptual design for Zone 4 was developed based on the assumption that the sides of adjacent shafts will be separated by 3 m (10 ft).

The shaft field efficiency refers to the fractional area within a shaft field that consists of actual disposal units. It is used to define the disposal areas for the regions with shafts, and in the development of intruder dose projections and intruder-based WAC. The 1997 performance assessment (Hollis et al., 1997) estimated a shaft field efficiency factor of 0.107; this estimate is based on data representing the majority of the shafts present at Area G today. A shaft field efficiency was estimated for Zone 4 using the conceptual design developed for this area by Day et al. (2005). The design was for a single shaft field with 158 disposal shafts. These shafts included eight 6.1 m (20 ft) diameter shafts and three groups of 50 shafts with diameters of 1.2 m (4 ft), 1.8 m (6 ft), and 2.4 m (8 ft).

The shaft field efficiency for Zone 4 was estimated by dividing the combined surface area of the 158 shafts by the area of the entire shaft field. The area of the shaft field was estimated by drawing polygons around the disposal units and estimating the total area of those polygons. Figure 13 illustrates this process, depicting the expansion area shaft field and the two polygons drawn to encompass the disposal units (A and B). The total area of these polygons is approximately 5,900 m^2 (1.5 ac). Dividing this total shaft field area into the total summed area of the individual shafts yields a shaft field efficiency of 0.11.

The shaft field efficiency estimated in 1997 (Hollis et al., 1997) and that calculated for the Zone 4 expansion area are virtually identical. Given this, a single efficiency of 0.11 was adopted for this revision of the performance assessment and composite analysis. This efficiency was assumed to be constant across all disposal shafts.

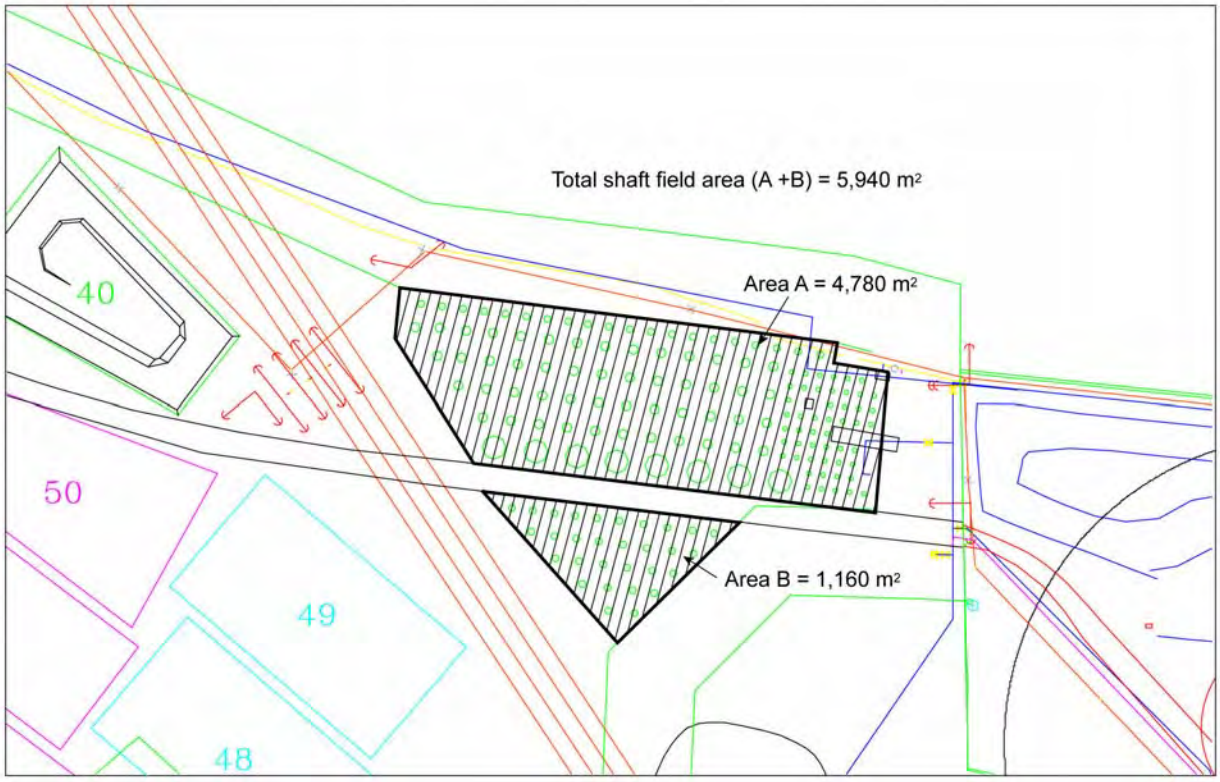

Figure 13
Calculation of Proposed Shaft Field Area in Zone 4

5.3 Material Properties

The GoldSim models simulate the release and transport of radionuclides from the disposal pits and shafts to locations accessible to the off-site receptors and inadvertent intruders. Cells are used to represent the physical media within which release and transport take place, as discussed in Section 3.6.1. Each of these cells is defined in terms of its physical dimensions and the environmental media of which it is comprised. Cells representing the buried waste, for instance, have dimensions consistent with the disposal units in which the material is disposed. Each waste cell consists of the waste itself, the water that occupies pore space in the waste, and the air that occupies the air-filled fraction of the pores. The various physical properties and parameters used to characterize these media are described below.

5.3.1 Dry Bulk Density, Porosity, and Moisture Content

Limited information is available regarding the dry bulk density of crushed tuff. In their summary of unsaturated hydraulic properties of the Bandelier Tuff, Rogers and Gallaher (1995) cite a bulk density of 1,400 kg/m^3 (87 lb/ft^3) for crushed tuff; the bulk density of Tshirege unit 2b, which forms the surface at Area G, ranged from 1,280 to 1,460 kg/m^3 (80 to 91 lb/ft^3) with a mean and median of 1,370 kg/m^3 (85 lb/ft^3). Springer (2004) reviewed matrix hydrologic properties for the Bandelier Tuff and developed distributions of unsaturated zone properties at various technical areas at the Laboratory. The density data summarized by Springer for Tshirege unit 2 at TA-54 yield mean and median densities of 1,400 kg/m^3 (87 lb/ft^3); a portion of the data evaluated for this area was common to the data evaluated by Rogers and Gallaher (1995). Finally, Abeele (1984) reported a bulk density of 1,400 kg/m^3 (87 lb/ft^3) for crushed tuff.

Information about the porosity of crushed tuff is also limited. Rogers and Gallaher (1995) cite a porosity of 0.38 for crushed tuff. A median porosity of 0.45 was found for Tshirege unit 2b; the measured values range from 0.4 to 0.74, with all but one of the measurements falling below 0.55. Springer (2004) summarized data collected from Tshirege unit 2 at TA-54 and reported porosities ranging from 0.37 to 0.46 with mean and median values of 0.41. Abeele (1984) reported a crushed tuff porosity of 0.45.

Moisture content has been measured for crushed tuff and the waste disposed of at Area G. Rogers and Gallaher (1995) cite a moisture content of 7.5 percent (volume basis) for crushed tuff. Loaiza and Vold (1995) reported measurements collected from a series of vertical boreholes located across the facility; some of these boreholes are located within disposal units or in otherwise disturbed tuff, while others occur in areas undisturbed by disposal operations. Data for the undisturbed boreholes indicate surface moisture contents ranging from 5 to 7 percent; water contents typically decreased to 1 to 2 percent at depths of 3.5 m (12 ft) or more. Moisture contents measured at disturbed locations generally ranged from 7.5 to 14 percent near the surface. The authors cite moisture content data from other studies; Abeele and Wheeler (1981)

found tuff moisture contents of 5 to 10 percent at the surface, while Abeele (1986) reported tuff moisture contents ranging from 5 to 15 percent in the upper 3 to 4.5 m (10 to 15 ft). Haagenstad (2002) reviewed moisture content data collected from pits 15, 37, and 39 and concluded the moisture content averaged 6.8 percent within 1.2 m (4 ft) of the surface, 9.5 percent at depths of 1.5 to 6.4 m (5 to 21 ft), and 10.2 percent at depths of 6.7 and 11 m (22 and 35 ft).

The bulk densities, porosities, and moisture contents adopted for the performance assessment and composite analysis are included in Table 11. The data cited by Springer (2004) for Tshirege unit 2 were used to estimate the bulk density of crushed tuff. A normal distribution with a mean and standard deviation of 1,400 and 69 kg/m^3 (87 and 4.3 lb/ft^3), respectively, was adopted for the analyses. Although the data used to define this distribution represent tuff from Tshirege unit 2 and not crushed material used for cover construction, the densities of the two materials do not appear to diverge significantly. The porosity measurements summarized by Springer (2004) for Tshirege unit 2 at TA-54 were used to estimate a distribution of porosities for the crushed tuff. A normal distribution was defined with a mean and standard deviation of 0.41 and 0.03, respectively.

The bulk density and porosity of the waste placed in the pits and shafts are unknown and are expected to be highly variable within and among units. However, 50 percent or more of the material placed in the disposal units is expected to consist of crushed tuff that has been used as backfill. Given this, along with the inability to accurately determine the properties of the waste itself, the dry bulk densities and porosities assigned to crushed tuff were also assumed to apply to the waste.

The moisture content data discussed above suggest that higher water contents exist near the surface of the disposal units than in relatively undisturbed areas. Given that the modeling focuses on the transport of radionuclides from the pits and shafts, the data for disturbed areas were relied upon to define the moisture content distribution. A triangular distribution was assumed, with minimum, most likely, and maximum values of 5, 7.5, and 12 percent (volume basis); these data were used for both crushed tuff and waste.

The material properties of the concrete used to represent the foundation of the inadvertent intruder's house could vary widely. In the absence of specific concrete-mix design specifications, it was assumed that the dry bulk density of concrete was normally distributed with a mean and standard deviation of 2,000 and 81 kg/m^3 (130 and 5.0 lb/ft^3), based on information reported by Rogers et al. (1994) for 25 samples of residential concrete. Using information for these same samples, the porosity of the material was assigned a normal distribution with mean and standard deviation of 0.2 and 0.032, respectively.

The equilibrium moisture content of the concrete used to construct the foundation of the intruder's house is expected to vary along the cross section of the member, being greatest where

the foundation contacts the underlying waste or cover. In the absence of specific information regarding this parameter, it was assumed that the saturation level of the concrete was uniformly distributed between 5 and 15 percent. Values sampled from this distribution were multiplied by the porosity of the concrete to estimate the moisture content (volume basis) of the material.

5.3.2 Partition Coefficients

Partition coefficients are used to describe the manner in which radionuclides are distributed between the liquid, solid, and gas phases of the soils and geologic materials found at Area G. Solid-to-liquid partition coefficients, or distribution coefficients, were developed for the cover material, the buried waste, and the unsaturated zone. A single set of coefficients was adopted for the cover placed over the pits and shafts and the waste placed in these units. These coefficients are based on partitioning data for tuff. Crushed tuff is the primary component of the interim and final covers and has been used historically to backfill the pits and shafts. All elements were assumed to have a partition coefficient of zero in the saturated zone. The regional aquifer lies within the poorly constrained and highly fractured Cerros del Rio basalts, conditions under which sorption is expected to be low.

The element-specific soil-to-water distribution coefficients adopted for the performance assessment and composite analysis are listed in Table 12. The sources of the coefficients are provided in the table; when available, coefficients were taken first from Longmire et al. (1996) and second from Bechtel/SAIC (2004). Longmire et al. provided coefficients for Am, Np, Pu, and U for crushed and intact tuff. These data were used to define triangular distributions for all four radionuclides. Distributions for the intact tuff were defined using the ranges as end points and the medians as the most likely values. Distribution coefficients for Am, Np, Pu, and U in crushed tuff were estimated on the basis of only two samples (Longmire et al., 1996). Given the small amount of data, triangular distributions were assumed using the reported ranges to define the end points of the distributions and the means as the most likely values. The distributions reported in Bechtel/SAIC (2004) for devitrified tuff in the unsaturated zone were used directly.

Krier et al. (1997) listed several sources of distribution coefficients for volcanic tuff; coefficients from these sources were used for elements not addressed by Longmire et al. (1996) or Bechtel/SAIC (2004). Some of the listed distribution coefficients from these sources are based on chemical similarities between elements. Baes et al. (1984) was consulted for any remaining elements that were not addressed by the sources listed above. Point estimates of the distribution coefficients were adopted for elements for which distributions could not be developed. When data specific to the material in the disposal units were unavailable, distribution coefficients for intact tuff were used for the crushed tuff.

Table 12
Distribution Coefficients and Solubility Limits

Element	Distribution Coefficient (mL/g) [a]		Solubility Limits [b] (mg/L)
	Crushed Tuff and Waste	Intact Tuff	
Ac	1.3E+02 [c]	1.3E+02 [c]	2.7E-04
Ag	T(2.7E+00, 9.0E+01, 1.0E+03) [d]	T(2.7E+00, 9.0E+01, 1.0E+03) [d]	6.0E-05
Al	1.3E+02 [c]	1.3E+02 [c]	9.4E-07
Am	T(1.6E+03, 2.1E+03, 2.6E+03) [e]	T(2.0E+02, 2.4E+03, 2.7E+04) [e]	2.9E-04
Ba	T(4.3E+02, 9.5E+02, 1.5E+03) [f]	T(4.3E+02, 9.5E+02, 1.5E+03) [f]	6.2E+00
Be	2.5E+02 [d]	2.5E+02 [d]	Not considered [g]
Bi	1.0E+02 [d]	1.0E+02 [d]	Not considered [g]
Bk	1.3E+02 [h]	1.3E+02 [h]	Not considered [g]
C	0.0E+00 [i]	0.0E+00 [i]	4.1E+00
Ca	5.0E+00 [d]	5.0E+00 [d]	Not considered [g]
Cf	1.3E+02 [c]	1.3E+02 [c]	3.0E-04
Cl	0.0E+00 [j]	0.0E+00 [j]	Very large [k]
Cm	5.0E+01 [i]	5.0E+01 [i]	3.0E-04
Co	4.5E-01 [l]	4.5E-01 [l]	1.0E-02
Cs	U(1.0E+00, 1.5E+01) [m]	U(1.0E+00, 1.5E+01) [m]	Large [k]
Eu	5.0E+01 [i]	5.0E+01 [i]	1.8E-04
Gd	5.0E+01 [n]	5.0E+01 [n]	1.9E-04
H	0.0E+00 [j]	0.0E+00[j]	Very large [k]
Ho	2.5E+02 [d]	2.5E+02 [d]	Not considered [g]
I	0.0E+00 [i]	0.0E+00 [i]	Very large [k]
K	1.5E+01 [d]	1.5E+01 [d]	Not considered [g]
Kr	NC [o]	NC [o]	Not considered [o]
Lu	5.0E+01 [n]	5.0E+01 [n]	Not considered [g]
Mo	4.0E+00 [i]	4.0E+00 [i]	Large [k]
Nb	1.0E+02 [i]	1.0E+02 [i]	1.9E-49
Nd	6.5E+02 [p]	6.5E+02 [p]	Not considered [g]
Ni	5.0E+01 [i]	5.0E+01 [i]	5.9E-01
Np	T(7.0E+01, 7.5E+00, 8.0E+00) [e]	T(1.7E-01, 2.2E+00, 3.1E+00) [e]	3.1E+01
Os	4.5E+02 [p]	4.5E+02 [p]	Not considered [g]
Pa	TN(5.50E+03, 1.50E+03, 1.00E+03, 1.00E+04) [m]	TN(5.50E+03, 1.50E+03, 1.00E+03, 1.00E+04) [m]	3.0E+01
Pb	2.5E+01 [i]	2.5E+01 [i]	3.3E-01
Pm	5.0E+01 [n]	5.0E+01 [n]	1.9E+01

See footnotes on next page

Table 12 (Continued)
Distribution Coefficients and Solubility Limits

Element	Distribution Coefficient (mL/g) [a]		Solubility Limits [b] (mg/L)
	Crushed Tuff and Waste	Intact Tuff	
Pu	T(6.5E+02, 7.1E+02, 7.7E+02) [e]	T(1.2E+00, 4.1E+00, 1.9E+01) [e]	5.6E-02
Ra	U(1.0E+02, 1.0E+03) [m]	U(1.0E+02, 1.0E+03) [m]	1.2E-05
Si	3.5E+01 [d]	3.5E+01 [d]	7.9E+00
Sm	5.0E+01 [i]	5.0E+01 [i]	1.8E-04
Sn	5.0E+01 [i]	5.0E+01 [i]	5.1E-32
Sr	U(1.0E+00, 7.0E+01) [m]	U(1.0E+00, 7.0E+01) [m]	1.2E+02
Tb	5.0E+01 [n]	5.0E+01 [n]	Not considered [g]
Tc	0.0E+00 [e]	0.0E+00 [e]	Large [k]
Th	U(1.0E+03, 1.0E+04) [m]	U(1.0E+03, 1.0E+04) [m]	4.4E-05
Ti	1.0E+03 [p]	1.0E+03 [p]	Not considered [g]
U	T(1.4E+00, 2.6E+00, 3.8E+00) [e]	T(1.4E+00, 2.4E+00, 3.5E+00) [e]	2.6E+01
Zr	5.0E+02 [i]	5.0E+02 [i]	9.1E-11

[a] *Single values indicate no distribution was identified for the element and/or parameter. Where present, the distribution designations refer to the following distribution types: T = triangular (minimum, most likely, maximum), TN = truncated normal distribution (mean, standard deviation, minimum, maximum), U = uniform (minimum, maximum)*

[b] *Source: Krier et al., 1997, unless noted otherwise*

[c] *Distribution coefficients were estimated based on chemical similarities between americium (III) and actinium (III), americium (III) and aluminum (III), and americium (III) and californium (III) (Krier et al., 1997); the listed values were taken from Wolfsberg (1980).*

[d] *Source: Thibault et al., 1990*

[e] *Source: Longmire et al., 1996*

[f] *Source: Wolfsberg, 1980*

[g] *No solubility limit was provided in Krier et al. (1997); no solubility effects were considered.*

[h] *Distribution coefficients were estimated based on assumed similarities between americium and berkelium; the listed values were taken from Wolfsberg (1980).*

[i] *Source: Brookins, 1984*

[j] *Distribution coefficients were assumed to equal zero.*

[k] *Solubility effects were not considered for elements that have solubility limits listed as large or very large.*

[l] *Source: Polzer et al., 1985*

[m] *Source: Bechtel/SAIC, 2004*

[n] *Distribution coefficients were estimated based on assumed similarities between europium, dysprosium, gadolinium, lanthanum, lutetium, promethium, and terbium, as suggested by Baes et al. (1984).*

[o] *Krypton exists as a noble gas, sorption and solubility effects were not considered.*

[p] *Source: Baes et al., 1984*

Air-to-water partition coefficients are used to simulate the diffusion of vapor- or gas-phase radionuclides including tritium, C-14, and Kr-85 and isotopes of radon. These coefficients describe how such species are allocated between their vapor or gas phase and the water occupying the pores of the cover and waste. The ratio of the vapor-to-water concentration of tritium is given by the following expression:

$$\frac{C_{H-3,v}}{C_{H-3,w}} = \frac{VP_w \times M}{R \times T \times \rho_w} \qquad 62$$

Where

$C_{H\text{-}3,v}$ = tritium concentration in water vapor (Ci/m^3)
$C_{H\text{-}3,w}$ = tritium concentration in pore water (Ci/m^3)
VP_w = vapor pressure of water (atm)
M = molecular weight of water (g/mol)
R = ideal gas constant (atm-m^3/mol-°K)
T = temperature (°K)
ρ_w = density of water (g/m^3)

Equation 62 was implemented using a water vapor pressure of 0.017 atm at 15°C (250 psi at 59ºF) (CRC, 1999), a molecular weight of water of 18 g/mol, an ideal gas constant of 8.2×10^{-5} atm-m^3/mol-°K, and a temperature of 288°K (15°C).

The air-to-water partition coefficients for C-14 gas (as CO_2 or CH_4), Kr-85, and isotopes of radon were calculated as follows:

$$K_{p,i} = \frac{1}{k_{H,i} \times R \times T} \qquad 63$$

Where

$K_{p,i}$ = air-to-water partition coefficient for radionuclide *i*
$k_{H,i}$ = Henry's Law constant for radionuclide *i* (mol/L-atm)

The Henry's Law constants for CO_2, CH_4, krypton, and radon at 288°K (15°C) and 1 atm are 0.026, 0.0011, 0.002, and 0.0068 mol/L-atm, respectively (Sander, 1999).

5.3.3 Solubility Limits

Solubility limits represent the maximum concentrations at which elements may occur in pore water within the intact or crushed tuff. The solubility limits adopted for the performance assessment and the composite analysis are included in Table 12. The data included in the table were taken from Krier et al. (1997); solubility effects were not considered for elements that were not addressed by this reference or for elements that have solubility limit values of "large" or "very large." Because

the information needed to describe the variability of these limits was lacking, no distributions were developed. Solubility effects were not considered in the intruder modeling.

5.3.4 Mass Attenuation Coefficients

Mass attenuation coefficients are used to estimate the direct radiation exposures received by the inadvertent intruder. These coefficients are a function of the energy of the radiation emitted by the radionuclide. Average photon energies were estimated using the MICROSHIELD computer code (Grove Engineering, 1996); mass attenuation coefficients for soil and concrete were calculated using the linear attenuation coefficients provided by MICROSHIELD and soil and concrete densities of 1,400 and 2,050 kg/m^3 (87 and 128 lb/ft^3) respectively. Radionuclides that were not included in MICROSHIELD or for which no photon energies were provided were assigned mass attenuation coefficients for 0.015 MeV photons. The average photon energies and the corresponding mass attenuation coefficients are listed in Table 13.

5.3.5 Diffusion Coefficients

Diffusion coefficients are used to model the vertical movement of vapor- and gas-phase radionuclides from the waste to the surface of the disposal facility. Tritiated water vapor, C-14 gas, and isotopes of krypton and radon may diffuse from the surface of the disposal site and be transported by the prevailing winds, resulting in exposures of receptors living downwind of the disposal facility. The diffusion of vapor- and gas-phase radionuclides from the waste may also expose inadvertent intruders to contamination when they are outside and in their homes.

A diffusion coefficient is specific to the radionuclide under consideration and the material through which it is moving. The diffusion modeling conducted to estimate exposures to off-site members of the public and to demonstrate compliance with radon flux performance objectives required diffusion coefficients for water vapor, C-14 as CO_2 and CH_4, Kr-85, and radon in the waste and cover. The diffusion modeling for the intruder analysis required coefficients for these same constituents in the waste, cover, and concrete floor of the receptor's house.

The gas-diffusion coefficient is typically estimated using empirical relationships; one of the more commonly used formulations is that developed by Millington (1959):

$$D_e = D_o \times \frac{p_a^{10/3}}{p^2} \qquad 64$$

Where

D_e = pore diffusion coefficient (m^2/s)
D_o = gas diffusion coefficient in free air (m^2/s)
p_a = air-filled porosity
p = effective porosity

Table 13
Average Photon Energies and Mass Attenuation Coefficients

Radionuclide	Average Photon Energy (MeV)	Mass Attenuation Coefficient (cm^2/g)	
		Soil	Concrete
Ac-227	3.2E-01	1.0E-01	1.0E-01
Ag-108m	6.4E-01	7.8E-02	7.9E-02
Al-26	1.6E+00	5.1E-02	5.1E-02
Am-241	5.9E-02	2.8E-01	2.8E-01
Am-243	1.6E-01	1.4E-01	1.4E-01
Ba-133	3.3E-01	1.0E-01	1.0E-01
Be-10	---	8.1E+00	8.1E+00
Bi-207	9.0E-01	6.5E-02	6.7E-02
Bk-247	---	8.1E+00	8.1E+00
C-14	---	8.1E+00	8.1E+00
Ca-41	---	8.1E+00	8.1E+00
Cd-113m	---	8.1E+00	8.1E+00
Cf-249	3.7E-01	9.9E-02	9.9E-02
Cf-251	1.6E-01	1.4E-01	1.4E-01
Cf-252	6.0E-02	2.7E-01	2.7E-01
Cl-36	---	8.1E+00	8.1E+00
Cm-243	2.0E-01	1.3E-01	1.3E-01
Cm-244	6.0E-02	2.7E-01	2.7E-01
Cm-245	1.1E-01	1.6E-01	1.6E-01
Cm-247	3.7E-01	9.9E-02	9.9E-02
Cm-248	6.0E-02	2.7E-01	2.7E-01
Co-60	1.3E+00	5.7E-02	5.7E-02
Cs-135	---	8.1E+00	8.1E+00
Cs-137	6.0E-01	8.1E-02	8.1E-02
Dy-154	---	8.1E+00	8.1E+00
Eu-152	1.0E+00	6.4E-02	6.4E-02
Eu-154	1.1E+00	6.1E-02	6.1E-02
Gd-148	---	8.1E+00	8.1E+00
Gd-150	---	8.1E+00	8.1E+00

--- = No average energy is provided because the radionuclide was not considered by MICROSHIELD or because photon energies were provided by the code. The mass attenuation coefficient for these radionuclides was set to the value for 0.015 MeV photons.

Table 13 (Continued)
Average Photon Energies and Mass Attenuation Coefficients

Radionuclide	Average Photon Energy (MeV)	Mass Attenuation Coefficient (cm^2/g)	
		Soil	Concrete
H-3	---	8.1E+00	8.1E+00
Hf-182	9.3E-01	6.4E-02	6.6E-02
Ho-163	---	8.1E+00	8.1E+00
Ho-166m	6.8E-01	7.5E-02	7.7E-02
I-129	3.1E-02	1.1E+00	1.1E+00
K-40	1.5E+00	5.2E-02	5.2E-02
Kr-81	3.0E-01	1.1E-01	1.1E-01
Kr-85	5.0E-01	8.7E-02	8.7E-02
La-137	---	8.1E+00	8.1E+00
Lu-176	---	8.1E+00	8.1E+00
Mo-93	1.6E-02	7.2E+00	7.2E+00
Nb-91	8.4E-02	1.9E-01	1.9E-01
Nb-92	8.5E-01	6.5E-02	6.9E-02
Nb-93m	1.6E-02	7.2E+00	7.2E+00
Nb-94	8.0E-01	6.6E-02	7.1E-02
Nd-144	---	8.1E+00	8.1E+00
Ni-59	---	8.1E+00	8.1E+00
Ni-63	---	8.1E+00	8.1E+00
Np-237	2.5E-01	1.2E-01	1.2E-01
Os-194	5.7E-01	8.3E-02	8.3E-02
Pa-231	2.5E-01	1.2E-01	1.2E-01
Pb-210	5.0E-02	3.6E-01	3.6E-01
Pd-107	---	8.1E+00	8.1E+00
Pm-145	4.3E-02	5.2E-01	5.2E-01
Pu-236	6.0E-02	2.7E-01	2.7E-01
Pu-238	6.0E-02	2.7E-01	2.7E-01
Pu-239	1.0E-01	1.7E-01	1.7E-01
Pu-240	5.0E-02	3.6E-01	3.6E-01
Pu-241	---	8.1E+00	8.1E+00
Pu-242	6.0E-02	2.7E-01	2.7E-01

--- = No average energy is provided because the radionuclide was not considered by MICROSHIELD or because photon energies were provided by the code. The mass attenuation coefficient for these radionuclides was set to the value for 0.015 MeV photons.

Table 13 (Continued)
Average Photon Energies and Mass Attenuation Coefficients

Radionuclide	Average Photon Energy (MeV)	Mass Attenuation Coefficient (cm^2/g)	
		Soil	Concrete
Pu-244	7.6E-01	6.8E-02	7.3E-02
Ra-226	1.2E+00	5.9E-02	5.9E-02
Ra-228	9.7E-01	6.4E-02	6.5E-02
Se79	---	8.1E+00	8.1E+00
Si-32	---	8.1E+00	8.1E+00
Sm-146	---	8.1E+00	8.1E+00
Sm-147	---	8.1E+00	8.1E+00
Sm-151	2.0E-02	3.5E+00	3.5E+00
Sn-121m	---	8.1E+00	8.1E+00
Sn-126	6.8E-02	2.5E-01	2.5E-01
Sr-90	---	8.1E+00	8.1E+00
Tb-157	4.2E-02	5.2E-01	5.2E-01
Tb-158	---	8.1E+00	8.1E+00
Tc-97	1.6E-02	7.1E+00	7.1E+00
Tc-99	8.0E-02	2.0E-01	2.0E-01
Th-228	1.0E+00	6.3E-02	6.3E-02
Th-229	4.1E-01	9.5E-02	9.5E-02
Th-230	7.5E-02	2.2E-01	2.2E-01
Th-232	9.2E-02	1.8E-01	1.8E-01
Ti-44	7.2E-01	7.2E-02	7.5E-02
U-232	1.0E-01	1.7E-01	1.7E-01
U-233	1.0E-01	1.7E-01	1.7E-01
U-234	7.0E-02	2.4E-01	2.4E-01
U-235	1.8E-01	1.2E-01	1.2E-01
U-236	6.0E-02	2.7E-01	2.7E-01
U-238	6.3E-01	7.8E-02	7.9E-02
Zr-93	1.6E-02	7.2E+00	7.2E+00

--- = No average energy is provided because the radionuclide was not considered by MICROSHIELD or because photon energies were provided by the code. The mass attenuation coefficient for these radionuclides was set to the value for 0.015 MeV photons.

Using an effective porosity of 0.41, a moisture content of 0.075, and the free-air diffusion coefficients listed in Table 14, the diffusion coefficients calculated for tritiated water vapor, CO_2, CH_4, Kr-85, and radon are 3.7×10^{-6}, 2.2×10^{-6}, 3.0×10^{-6}, 2.7×10^{-6}, and 1.7×10^{-6} m^2/s (4.0×10^{-5}, 2.4×10^{-5}, 3.3×10^{-5}, 2.9×10^{-5}, and 1.8×10^{-5} ft^2/s), respectively.

Table 14
Free-Air Diffusion Coefficients for Vapor- and Gas-Phase Radionuclides

Radionuclide	Diffusion Coefficient (cm^2/s)	Source
Tritium (as water vapor)	2.4E-01[a]	CRC, 1999
CO_2	1.6E-01[a]	CRC, 1999
CH_4	2.0E-01[b]	Marrero and Mason, 1972
Krypton	1.8E-01[c]	Estimated
Radon	1.1E-01[d]	Rogers and Nielson, 1991

[a] At a temperature of 293° K (20° C) and 1 atm

[b] At a temperature of 282° K (9° C) and a pressure of 1 atm

[c] The free-air diffusion coefficient for Kr-85 was estimated using the following empirical relationship:

$D_2 = D_1 \sqrt{m_2/m_1}$ where D_2 and m_2 are the free-air diffusion coefficient and molecular mass of Kr-85 and D_1 and m_1 are the corresponding quantities for Rn-222. The calculated diffusion coefficient is consistent with the coefficient of 1.5×10^{-1} cm^2/s cited in Schack-Kirchner et al., (2001) for Kr-N_2 when differences between the mass of Kr-N_2 and Kr are taken into account.

[d] At a temperature of 298° K (25° C) and a pressure of 1 atm

The quantity calculated using Equation 64 represents diffusion in a porous medium. The diffusion coefficient in the air-filled pore spaces only is given by Shan and Stephens (1995):

$$D_e = D_o \times \frac{p_a^{7/3}}{p^2} \qquad 65$$

This is the diffusion coefficient applied in the GoldSim modeling. Using the porosity, moisture content, and free-air diffusion coefficients discussed above, this equation yields diffusion coefficients that are about three times the values for the porous medium.

Rogers and Nielson (1991) reported a correlation between the diffusion coefficient of radon in soils and the saturation fraction of the soil. That correlation, which is based on 1,073 soil-diffusion coefficient measurements, is given by the following equation:

$$D_e = D_{o,Rn} \times p \times \exp(-6Sp - 6S^{14p}) \qquad 66$$

Where

$D_{o,Rn}$ = radon diffusion coefficient in air
S = volume fraction of water saturation

Using a porosity of 0.41 and a moisture content of 0.075 (volume basis) to represent the cover and waste, this equation yields a radon diffusion coefficient of 3.8×10^{-6} m^2/s (4.1×10^{-5} ft^2/s). This diffusion coefficient, which accounts for pore air-water interactions and the transfer of radon between the two phases, lies between the values calculated using Equations 64 and 65.

Philip and DeVries (1957) concluded that thermal gradients may significantly increase the apparent diffusion coefficient of water vapor in soil. Based on an "admittedly approximate" analysis, the authors concluded that the observed transfer rate of vapor may be 3.6 to 9.8 times greater than that predicted when gradients were not taken into account.

Rates of diffusion in the air-filled pore spaces of concrete can also be estimated using Equation 65. Using a concrete porosity of 0.2, a saturation level of 10 percent, and the free-air diffusion coefficients listed in Table 14, diffusion coefficients of 1.1×10^{-5}, 7.3×10^{-6}, 9.2×10^{-6}, 8.2×10^{-6}, and 5.0×10^{-6} m^2/s (2.2×10^{-5}, 1.2×10^{-5}, 1.7×10^{-5}, 1.5×10^{-5}, and 9.8×10^{-6} ft^2/s) are calculated for water vapor, CO_2, CH_4, Kr-85, and radon, respectively. These values are comparable to the coefficients estimated for diffusion in the air-filled pores in the cover and waste. Concrete diffusion coefficients for the porous media are five to six times smaller than the coefficients for the air-filled pore spaces (Equation 64).

Several studies provide additional insight into the diffusion of radon in bulk concrete. Rogers et al. (1994) summarized pore diffusion coefficients measured in six separate studies, finding coefficients that ranged from 7.0×10^{-9} to 1.7×10^{-7} m^2/s (7.5×10^{-8} to 1.8×10^{-6} ft^2/s). These investigators also conducted diffusion coefficient measurements using 25 samples of residential concretes and test cylinders of the same; diffusion coefficients for these samples ranged from 3.7×10^{-8} to 5.2×10^{-7} m^2/s (4.0×10^{-7} to 5.6×10^{-6} ft^2/s). Rogers et al. (1995) measured radon diffusion coefficients in aged residential concretes that ranged from 1.5×10^{-7} to 5.5×10^{-7} m^2/s (1.6×10^{-6} to 5.9×10^{-6} ft^2/s). Nielson et al. (1997) characterized diffusion coefficients in 12 samples of residential concrete with different configurations of cracks, pipe penetrations, cold joints, and other defects. The coefficients averaged 6.5×10^{-8} m^2/s (7.0×10^{-7} ft^2/s) over the 1,000-day study, or approximately four times greater than the pore diffusion coefficients measured in three core samples. All of these radon diffusion coefficients are similar to those estimated for porous media using the relationship developed by Millington (1959) (Equation 64).

The diffusion coefficients used to estimate radon fluxes from the site and to estimate the potential exposures received by inadvertent intruders and members of the public were calculated using Equation 65 and the free-air diffusion coefficients listed in Table 14. The calculated diffusion coefficients for tritiated water vapor in the cover and waste were multiplied by a factor to account for possible increases in the diffusion coefficient because of thermal gradients. This multiplier was assumed to have a uniform distribution and range from 3.6 to 9.8, consistent with the data reported

by Philip and DeVries (1957). The effect of thermal gradients on the diffusion of tritium was not taken into account for the 0.1 m (0.3 ft) thick concrete floor of the intruder's house.

5.3.6 Radon Emanation Coefficient

The radon emanation coefficient represents the fraction of the radon gas generated by the decay of radium precursors that enters into the pores of the waste and is available for diffusion. This coefficient is a function of many factors including the recoil energy of the radon isotope under consideration, and the pore structure and moisture content of the medium in which the gas is generated. Rogers et al. (1984) summarize emanation coefficients for several samples of uranium mill tailings; coefficients range from about 0.03 to 0.35 for very dry samples and from 0.1 to 0.4 for samples with moisture contents of about 5 percent (dry weight) or more. Yu et al. (1993) summarize emanation coefficients for several porous media of varying moisture content. The coefficients provided in the report range from 0.02 to 0.7. Values for unconsolidated soils of unknown moisture content ranged from 0.06 to 0.4; mean values for these materials ranged from 0.14 to 0.28. The U.S. Nuclear Regulatory Commission (NRC) adopted a radon emanation coefficient of 0.35 for all materials (1989). Based on these data, the emanation coefficient was assumed to be uniformly distributed, ranging from 0.1 to 0.4.

5.3.7 Carbon-14 Gas Generation Rate

The C-14 gas generation rate describes the rate at which C-14 gas is generated as a result of biodegradation of the organic fraction of the buried waste. The parameter is used to project generation rates of C-14 gas in the form of $^{14}CO_2$ and $^{14}CH_4$. Relatively little information is available to quantify organic waste biodegradation rates and, hence, gas generation rates.

The Agency for Toxic Substances and Disease Registry (ATSDR, 2001) reports that recently buried waste will generate more gas than older waste. Appreciable amounts of gas are generated within landfills 1 to 3 years after disposal, with peak generation typically occurring within 5 to 7 years of disposal. While all gas is typically generated within 20 years of disposal, gas production may continue for 50 years or more as the waste slowly degrades under anaerobic conditions. Rates of generation are generally found or assumed to be lower in arid climates, where waste moisture contents are lower. Recognizing the limitations of existing information, the U.S. Environmental Protection Agency (EPA, 2005) simulated the production of gas in a landfill gas generation model using a first-order decomposition rate equation. For generic applications, the EPA recommends generation rate constants of 0.02/yr and 0.04/yr for conventional landfills in arid and nonarid settings, respectively, and cites rate constants ranging from 0.003/yr to 0.21/yr. Environment Canada (2003) cites generation rate constants ranging from 0.006/yr to 0.024/yr as recommended values for calculating landfill emissions in Canada.

The information needed to estimate the rate at which C-14 gas will be generated in conjunction with the degradation of organic waste disposed of at Area G is unavailable. Although the EPA

(2005) suggests a rate constant of 0.02/yr for arid climates, values recommended for modeling gas generation in Canadian provinces tend to be lower. Opseth (1998) concluded that the default value cited by the EPA more nearly approximated field results for a semiarid location in Canada. The arid nature of the Laboratory and low moisture contents of the crushed tuff and waste in the disposal units at Area G suggest low rates of gas generation would prevail. Given this and the limited information summarized above, the rate constant was assumed to have a uniform distribution ranging from 0.003/yr to 0.02/yr.

5.3.8 Carbon Dioxide and Methane Fractions

The CO_2 and CH_4 fractions are used in the site and intruder diffusion models to specify the fractionation of the C-14 gas generated during biodegradation of organic waste. In general, CO_2 will be the predominant species while an adequate oxygen supply exists, and methane-producing anaerobic bacteria will dominate after the oxygen is exhausted. Typically, CO_2 accounts for 40 to 60 percent of the total gas generation on a volume basis, while 45 to 60 percent of the total gas production consists of CH_4 (ATSDR, 2001). Based on this information, the CO_2 fraction was assigned a uniform distribution ranging from 0.4 to 0.6; the CH_4 fraction was calculated as the complement of the CO_2 fraction.

5.3.9 Organic Fraction of Carbon-14 Waste

The organic fraction of the C-14 waste represents the fraction of the waste that is available for biodegradation. The organic fraction of the C-14 waste disposed of at Area G was estimated on the basis of the waste-form characteristics of the material upon which the C-14 inventory projection is based. The composite analysis inventory projection for C-14 is approximately 120 Ci (Shuman, 2005); this includes all waste that has been or is expected to be disposed of at Area G by the time the facility closes in 2044. Approximately 80 percent of the total activity of the waste was estimated on the basis of a shipment of waste generated during the decommissioning of the Omega Reactor. The waste profile for this material indicates it is combined combustible/noncombustible lab trash (waste code 19) consisting of 45 to 55 percent metal, 20 to 30 percent graphite, 15 to 25 percent concrete, and 3 to 8 percent glass /rubber/plastic/wood/herculite. Almost all of the remainder of the projected C-14 inventory consists of material classified as other combustibles (waste code 60), scrap metal (waste code 52), and combined combustible/noncombustible lab trash (waste code 19). On an activity basis, these three waste streams account for approximately 93, 5, and 2 percent of this portion of the inventory.

The 1997 performance assessment and composite analysis (Hollis et al., 1997) assumed that all of the C-14 waste identified as combustible lab trash waste (waste code 18) and 50 percent of the material identified as combined combustible/noncombustible lab trash (waste code 19) was organic. Based on the information provided above, however, it appears that less than 10 percent of waste code 19 will consist of organic material that might undergo biodegradation and generate

C-14 gas. Waste from other combustibles (waste code 60) may include organic material, but this waste accounts for only 13 percent of the total C-14 inventory.

The organic fraction of the C-14 inventory was estimated on the basis of the information provided above. The parameter was assigned a triangular distribution with minimum, most likely, and maximum values of 0, 0.05, and 0.1, respectively. The range of this distribution is consistent with the profile for the reactor waste and the contribution made by material classified as waste code 19 to the remainder of the projected inventory. This distribution was assumed to apply to all C-14 waste disposed of at Area G.

5.4 Radionuclide Inventories

The radionuclide inventories in the buried waste ultimately determine the magnitude of the projected exposures. Deterministic estimates of these inventories were developed for the performance assessment and composite analysis, based largely on information found in the LLW and transuranic (TRU) waste databases. Shuman (2008) provides a complete description of the analysis used to estimate these inventories.

The inventories that form the basis of the performance assessment and composite analysis modeling are summarized in the tables provided in *Attachment III*. These tables provide the total volumes and activities of waste included in the performance assessment and composite analysis, as well as the as-disposed radionuclide inventories. In most cases, these inventories are provided on a unit-specific basis. Existing information does not enable the allocation of the pit waste disposed of prior to 1971 to specific units; the waste that will require disposal from 2008 through 2044 also could not be allocated to specific units. The pit waste projected to be disposed of at MDA G between 2008 and 2010 was arbitrarily assigned to pit 38 and the shaft waste projected for disposal from 2008 through 2015 was assigned to disposal units in waste disposal region 7. Pit and shaft waste that will require disposal after these dates was assumed to be placed in units located in the Zone 4 expansion area.

The unit-specific radionuclide inventories presented in *Attachment III* are combined in various ways to yield the inventories needed to conduct the performance assessment and composite analysis. The inventories for the disposal units that comprise a given waste disposal region are summed to determine that region's initial inventory. For the performance assessment, these calculations consider waste disposed of since September 27, 1988; the composite analysis inventory includes all waste disposed of at Area G since the facility began operations. The disposal units that contribute to the inventory of each disposal region are listed in Table 9. Unit-specific inventories are also summed appropriately to yield the inventories needed to conduct the inadvertent intruder dose assessment. A total of four inventories are developed. Two of these address waste placed in disposal pits from September 27, 1988 through 2010 and from 2011 through 2044; the other two represent waste disposed of in shafts from September 27, 1988 through 2015 and from 2016 through 2044.

The inventory model quantifies the sources of uncertainty associated with the inventories provided in *Attachment III* to yield distributions of radionuclide inventories. In performing these calculations, a distinction is made between waste that was disposed of before and after the start of 1990 to account for differences in the magnitude of the error introduced by these uncertainties. Given this approach, the tables included in *Attachment III* distinguish between pre-1990 and post-1989 inventories, as appropriate.

Significant quantities of waste disposed of at Area G contain activation and fission product waste. Prior to the mid-1990s, the radionuclides in these wastes were often listed in terms of total activities of MAP and MFP. Similarly, the radionuclides in waste containing mixtures of plutonium, thorium, or uranium isotopes were often recorded using a series of material types. The inventory modeling conducted in support of the performance assessment and composite analysis allocates the activities associated with the MAP, MFP, and material type waste to specific radionuclides. The inventories shown in *Attachment III*, however, list MAP, MFP, and the various material types and do not assign the associated inventories to specific radionuclides. The data are presented in this manner so the uncertainties associated with the inventory projections may be evaluated in conjunction with the inventory modeling.

The activities listed in the tables in *Attachment III* represent as-disposed activities. Several radionuclides found in the waste have very short half-lives and, as a result, pose little or no risk to human health and safety and the environment. These radionuclides were eliminated from the Area G inventory and are not included in the tables. The approach used to eliminate radionuclides on the basis of their decay characteristics is discussed in Shuman (2008).

Shuman (2008) identified several sources of uncertainty that are associated with the estimated inventories. One source of uncertainty shared by all waste that has been, or will be, disposed of at Area G is introduced by the measurement and estimation techniques used to characterize the waste. The accuracy of the activity measurements and estimation techniques is influenced by the radionuclides under consideration and the disposal period. The radionuclides under consideration affect characterization efforts because the types and energies of radiation they emit make measurement more or less difficult. Furthermore, some radionuclides have strict accountability requirements, which dictate that greater effort be expended to measure or estimate the activities associated with packages of waste. The time at which the waste was characterized and disposed of is also important as both detection equipment and efforts to more accurately characterize the material placed in the disposal facility have improved over the years.

Although the errors associated with the activities that are listed in LLW and TRU waste databases cannot be determined with a high degree of accuracy, some generalities can be drawn about the source of uncertainty. The information summarized below is based on discussions with LANL personnel experienced in radiation characterization procedures and measurement

techniques (Myers, 2004). For this discussion, the radionuclides included in the Area G inventory have been divided into a number of classes or groups. These classes include pure beta emitters such as C-14, Ni-63, Sr-90 and Tc-99; strong gamma emitters such as Co-60 and Cs-137; alpha emitters such as isotopes of americium, plutonium, and uranium; and tritium.

The greatest uncertainties are expected to be associated with the measurement of the activities of the pure beta emitters. The low energy and penetrating power of beta radiation are such that detailed separation techniques must be performed before accurate assessments of the waste activity can be conducted; these techniques were seldom, if ever, performed at the Laboratory. As a result, the activities associated with these radionuclides are expected to be accurate to within an order of magnitude. Although the higher energy emissions associated with many gamma emitters should make accurate characterization an easier task, the level of accuracy for estimated activities of gamma waste disposed of prior to the 1990s is expected to be similar to that of the beta emitters. The magnitude of the errors associated with the gamma emitters decreased during the 1990s to the extent that errors currently range from ±25 to ±100 percent, depending upon the size and composition of the waste package. Small packages, low-density waste matrices, and relatively large amounts of nuclear material all contribute to low errors.

In general, greater effort has been expended on the characterization of waste contaminated with uranium and transuranics because of accountability issues. However, the concentrations of americium, plutonium, and uranium in the waste have a significant impact on the accuracy of the measured activities. Activities of these radionuclides have probably been overestimated in LLW because concentrations in this waste are low and the measurement techniques used did not have very low detection limits. For drums and boxes with detectable quantities of plutonium (i.e., about 0.5 g [0.02 oz] or more per package), errors of 20 to 30 percent are expected to apply to measurements conducted in the 1970s and 1980s. For measurements conducted in more recent years, errors of 10 to 20 percent are typical.

The ability to accurately measure quantities of uranium isotopes depends, in part, on the isotopic quantities in the waste package. Although U-235 may go undetected in drums when it is present in small quantities, generators are typically aware of drums that contain greater quantities of U-235 (e.g., 10 g [0.4 oz] or more) and measure the packages directly to determine the waste activity. Measurements of waste containing depleted uranium usually have errors of ±25 to ±100 percent, depending upon the size and composition of the package.

The error ranges discussed above for uranium and transuranics are generally applicable; however, exceptions do exist. For example, in some cases generators measured drums of TRU waste with neutron counters and used scaling factors to estimate isotopic distributions. These scaling factors were inappropriately applied to the waste in some situations, resulting in overestimates of the activities of some isotopes and underestimates of others. Am-241 activities

have been underestimated by an order of magnitude or more in a small proportion of TRU waste drums because of the misapplication of scaling factors. As mentioned earlier, U-235 in drums containing small amounts of uranium may go undetected in a small proportion of the packages.

Tritium is pure beta emitter, but it is considered separately from the other beta emitters because of its generation pattern at the Laboratory. While the low-activity tritium waste is expected to have characterization uncertainties similar to those discussed for the pure beta emitters, the high-activity tritium waste receives greater scrutiny. Estimates of the activities associated with the high-activity waste disposed of prior to the 1990s are generally expected to fall within a factor of two of the actual inventories. Improvements since that time have reduced these errors such that activity estimates are expected to be accurate to within ±25 percent.

The information summarized above was used to develop inventory distributions that address the uncertainties introduced by the characterization procedures used to estimate waste activities. The listed inventories for beta emitters were assumed to have triangular distributions with minimum and maximum values that are 0.1 and 10 times the most likely values, where the most likely values are equal to the deterministic inventory estimates. This same distribution was assigned to gamma emitters in waste buried in pits and shafts that were active prior to 1990; a triangular distribution with minimum and maximum values that are 0.5 and 2 times the most likely values was used for gamma emitters disposed of in units that started receiving waste after 1989.

Triangular distributions also were used to describe the characterization uncertainties associated with the uranium and transuranic inventories. For uranium, minimum and maximum values that are 0.25 and 2 times the most likely values were adopted. Separate distributions were developed for isotopes of americium and plutonium disposed of in units that received waste prior to 1990 and in those that became active after 1989. The minimum and maximum values of the distributions for waste placed in units active prior to this date were assigned values that are 70 and 130 percent of the most likely values. Waste disposed of in pits and shafts that became active after 1989 was assigned distributions with minimum and most likely values that are 80 and 120 percent of the most likely values. The most likely values of all of the distributions were set equal to the deterministic inventory estimates.

A triangular distribution was assigned to tritium waste disposed of in pits and shafts that were active prior to 1990; a separate distribution was adopted for tritiated waste placed in units that started receiving waste after 1989. The minimum and maximum values are 0.5 and 2 times the most likely values for the earlier waste. Minimum and maximum values that are 0.75 and 1.25 times the most likely values, respectively, were adopted for the later waste. These distributions were assigned to all tritium waste; no distinction was made between low- and high-activity waste. Although this approach ignores the higher uncertainty associated with the low-activity waste, more than 99 percent of the tritium activity included in the Area G inventory is

associated with the high-activity material. The most likely values of the tritium waste distributions were set equal to the deterministic inventory estimates.

The information required to develop distributions that describe the uncertainties associated with waste characterization was unavailable for several radionuclides, primarily alpha-emitting isotopes. All of these radionuclides were assigned triangular distributions with minimum and maximum values that are 0.1 and 10 times the most likely values. The most likely values for these radionuclides are the deterministic inventory estimates developed for the performance assessment and composite analysis (Shuman, 2008).

Table 16 summarizes the information that was used to describe the uncertainties in the radionuclide inventories arising from measurement or estimation errors. The factors by which the deterministic inventories were multiplied to estimate the minimum and maximum values of the triangular distributions are listed for each radionuclide included in the Area G inventory. Separate factors are provided for waste placed in pits and shafts that were active prior to 1990 and for material placed in disposal units that began receiving waste after 1989. As discussed earlier, the most likely values of these distributions were set equal to the deterministic inventory estimates reported in Shuman (2008).

Another source of uncertainty associated with the inventory estimates is introduced by the extrapolation process that was used to estimate the pre-1971 pit inventories and the pit and shaft inventories for waste projected to require disposal from 2008 through 2044. An extrapolation approach was used for the pre-1971 pit inventories because there were insufficient data to directly estimate these values. The pre-1971 inventory was developed, in part, by extrapolating waste data from 1971 through 1977 to the earlier period. For the future inventory, extrapolation was the only viable option. The future inventory was estimated on the basis of waste disposal data for 2000 through 2007.

The use of the extrapolation approach implicitly assumes that the composition of pre-1971 and future waste is similar to that of the waste disposed of during the periods from which the extrapolation datasets were drawn. In fact, the waste disposed of during these different time periods is expected to differ in ways that introduce errors into the inventory estimates. Pollard and Shuman (1999) found that the extrapolation approach used to establish the pre-1971 pit inventory yielded values for some radionuclides and waste streams similar to those estimated using available historical data, but projected other inventory values that were much greater than those estimated using the limited historical information. In terms of future waste, several sources of uncertainty could compromise the estimated pit and shaft inventories.

Table 16
Measurement Uncertainty Factors Associated with Area G Radionuclide-Specific Inventories

Radionuclide	Uncertainty Factor [a]	
	Waste Disposed of before 1990	Waste Disposed of after 1989
Ac-227	1.0E-01, 1.0E+01	1.0E-01, 1.0E+01
Ag-108m	1.0E-01, 1.0E+01	5.0E-01, 2.0E+00
Al-26	1.0E-01, 1.0E+01	5.0E-01, 2.0E+00
Am-241	7.0E-01, 1.3E+00	8.0E-01, 1.2E+00
Am-243	7.0E-01, 1.3E+00	8.0E-01, 1.2E+00
Ba-133	1.0E-01, 1.0E+01	5.0E-01, 2.0E+00
Be-10	1.0E-01, 1.0E+01	1.0E-01, 1.0E+01
Bi-207	1.0E-01, 1.0E+01	5.0E-01, 2.0E+00
Bk-247	1.0E-01, 1.0E+01	1.0E-01, 1.0E+01
C-14	1.0E-01, 1.0E+01	1.0E-01, 1.0E+01
Ca-41	1.0E-01, 1.0E+01	1.0E-01, 1.0E+01
Cf-249	1.0E-01, 1.0E+01	1.0E-01, 1.0E+01
Cf-251	1.0E-01, 1.0E+01	1.0E-01, 1.0E+01
Cf-252	1.0E-01, 1.0E+01	1.0E-01, 1.0E+01
Cl-36	1.0E-01, 1.0E+01	1.0E-01, 1.0E+01
Cm-243	1.0E-01, 1.0E+01	1.0E-01, 1.0E+01
Cm-244	1.0E-01, 1.0E+01	1.0E-01, 1.0E+01
Cm-245	1.0E-01, 1.0E+01	1.0E-01, 1.0E+01
Co-60	1.0E-01, 1.0E+01	5.0E-01, 2.0E+00
Cs-135	1.0E-01, 1.0E+01	1.0E-01, 1.0E+01
Cs-137	1.0E-01, 1.0E+01	5.0E-01, 2.0E+00
Eu-152	1.0E-01, 1.0E+01	5.0E-01, 2.0E+00
Eu-154	1.0E-01, 1.0E+01	5.0E-01, 2.0E+00
Gd-148	1.0E-01, 1.0E+01	1.0E-01, 1.0E+01
H-3	5.0E-01, 2.0E+00	7.5E-01, 1.3E+00
Ho-163	1.0E-01, 1.0E+01	1.0E-01, 1.0E+01
Ho-166m	1.0E-01, 1.0E+01	5.0E-01, 2.0E+00
I-129	1.0E-01, 1.0E+01	1.0E-01, 1.0E+01

[a] *The listed factors were multiplied by the deterministic estimates of the radionuclide-specific inventories to estimate minimum and maximum values of the triangular distributions used to describe the variability in the inventory estimates resulting from measurement errors.*

Table 16 (Continued)
Measurement Uncertainty Factors Associated with Area G Radionuclide-Specific Inventories

Radionuclide	Uncertainty Factor [a]	
	Waste Disposed of before 1990	Waste Disposed of after 1989
K-40	1.0E-01, 1.0E+01	1.0E-01, 1.0E+01
Kr-85	1.0E-01, 1.0E+01	1.0E-01, 1.0E+01
Lu-176	1.0E-01, 1.0E+01	1.0E-01, 1.0E+01
Mo-93	1.0E-01, 1.0E+01	1.0E-01, 1.0E+01
Nb-91	1.0E-01, 1.0E+01	1.0E-01, 1.0E+01
Nb-92	1.0E-01, 1.0E+01	5.0E-01, 2.0E+00
Nb-93m	1.0E-01, 1.0E+01	1.0E-01, 1.0E+01
Nb-94	1.0E-01, 1.0E+01	5.0E-01, 2.0E+00
Ni-59	1.0E-01, 1.0E+01	1.0E-01, 1.0E+01
Ni-63	1.0E-01, 1.0E+01	1.0E-01, 1.0E+01
Np-237	1.0E-01, 1.0E+01	1.0E-01, 1.0E+01
Np-239	1.0E-01, 1.0E+01	1.0E-01, 1.0E+01
Os-194	1.0E-01, 1.0E+01	1.0E-01, 1.0E+01
Pa-231	1.0E-01, 1.0E+01	1.0E-01, 1.0E+01
Pb-210	1.0E-01, 1.0E+01	1.0E-01, 1.0E+01
Pm-145	1.0E-01, 1.0E+01	1.0E-01, 1.0E+01
Pu-236	7.0E-01, 1.3E+00	8.0E-01, 1.2E+00
Pu-238	7.0E-01, 1.3E+00	8.0E-01, 1.2E+00
Pu-239	7.0E-01, 1.3E+00	8.0E-01, 1.2E+00
Pu-240	7.0E-01, 1.3E+00	8.0E-01, 1.2E+00
Pu-241	1.0E-01, 1.0E+01	1.0E-01, 1.0E+01
Pu-242	7.0E-01, 1.3E+00	8.0E-01, 1.2E+00
Pu-244	7.0E-01, 1.3E+00	8.0E-01, 1.2E+00
Ra-226	1.0E-01, 1.0E+01	1.0E-01, 1.0E+01
Ra-228	1.0E-01, 1.0E+01	1.0E-01, 1.0E+01
Si-32	1.0E-01, 1.0E+01	1.0E-01, 1.0E+01
Sm-151	1.0E-01, 1.0E+01	1.0E-01, 1.0E+01
Sn-121m	1.0E-01, 1.0E+01	1.0E-01, 1.0E+01

[a] *The listed factors were multiplied by the deterministic estimates of the radionuclide-specific inventories to estimate minimum and maximum values of the triangular distributions used to describe the variability in the inventory estimates resulting from measurement errors.*

Table 16 (Continued)
Measurement Uncertainty Factors Associated with
Area G Radionuclide-Specific Inventories

Radionuclide	Uncertainty Factor [a]	
	Waste Disposed of before 1990	Waste Disposed of after 1989
Sn-126	1.0E-01, 1.0E+01	1.0E-01, 1.0E+01
Sr-90	1.0E-01, 1.0E+01	1.0E-01, 1.0E+01
Tb-157	1.0E-01, 1.0E+01	1.0E-01, 1.0E+01
Tc-97	1.0E-01, 1.0E+01	1.0E-01, 1.0E+01
Tc-99	1.0E-01, 1.0E+01	1.0E-01, 1.0E+01
Th-227	1.0E-01, 1.0E+01	1.0E-01, 1.0E+01
Th-228	1.0E-01, 1.0E+01	1.0E-01, 1.0E+01
Th-229	1.0E-01, 1.0E+01	1.0E-01, 1.0E+01
Th-230	1.0E-01, 1.0E+01	1.0E-01, 1.0E+01
Th-232	1.0E-01, 1.0E+01	1.0E-01, 1.0E+01
Ti-44	1.0E-01, 1.0E+01	1.0E-01, 1.0E+01
U-232	2.5E-01, 2.0E+00	2.5E-01, 2.0E+00
U-233	2.5E-01, 2.0E+00	2.5E-01, 2.0E+00
U-234	2.5E-01, 2.0E+00	2.5E-01, 2.0E+00
U-235	2.5E-01, 2.0E+00	2.5E-01, 2.0E+00
U-236	2.5E-01, 2.0E+00	2.5E-01, 2.0E+00
U-238	2.5E-01, 2.0E+00	2.5E-01, 2.0E+00
Zr-93	1.0E-01, 1.0E+01	1.0E-01, 1.0E+01

[a] *The listed factors were multiplied by the deterministic estimates of the radionuclide-specific inventories to estimate minimum and maximum values of the triangular distributions used to describe the variability in the inventory estimates resulting from measurement errors.*

No attempt was made to quantify the uncertainties introduced by the extrapolation approach. Although the extrapolated quantities of pre-1971 waste are significantly greater than those indicated by the available disposal data, it is unclear if the disposal data address all of the waste that was placed at Area G during this period. Therefore, the assignment of any distributions to describe this uncertainty would be arbitrary at best. Only time will tell if it is appropriate to use the extrapolation process to estimate future inventories; differences between projected and actual inventories will be monitored through the disposal receipt reviews that are conducted annually under the Area G Performance Assessment and Composite Analysis Maintenance Program (LANL, 2003).

Significant quantities of waste disposed of at Area G contain activation and fission product waste. As mentioned, prior to the mid-1990s, the radionuclides in these packages were often listed in terms of total activities of MAP and MFP. One step of the inventory modeling effort was to allocate these activities to specific radionuclides so they could be considered in the performance assessment and composite analysis modeling.

The MFP waste was allocated to specific radionuclides using fission yield data published by England and Rider (1994). The estimated activities are subject to several sources of uncertainty, the most important of which include the nature of the fission reactions that generated the fission products and the age of the MFP waste at the time of disposal. In terms of the reactions responsible for the waste, it is evident that Pu-239 and U-235 fission are the primary reactions that led to the generation of the MFP waste. However, it is unclear what proportion of the waste was generated by Pu-239 fission as opposed to reactions involving U-235, and what proportion of the waste was the result of interactions with thermal (versus fast) neutrons.

Historical reviews of LANL reactor operations (e.g., Bunker, 1983; Widner et al., 2004) indicate that most reactors in operation prior to the 1990s were fueled by enriched uranium. This supports the conclusion that most fission products were the result of neutron interactions with U-235. Nevertheless, the presence of plutonium fission products is also expected. During the time MFP waste was accepted at Area G, one reactor in operation used molten plutonium as a fuel. Furthermore, plutonium fission products will occur in the waste from the uranium-based reactors as a result of interactions between fast neutrons and U-238. These plutonium fissions may represent a significant proportion of the total fission events; in commercial reactors they may account for one-third or more of the total fission events during the latter stages of operation.

It is not possible to provide a definitive assessment of the proportion of the MFP waste that was generated as a result of Pu-239 and U-235 fission events without more information. Therefore, it was assumed that as much as 30 percent of the waste was generated by Pu-239 fissions, with the remainder from U-235 fissions; the proportion of waste generated by plutonium fission events was assigned a triangular distribution with minimum, most likely, and maximum values equal to

0, 0.15, and 0.30, respectively. All fission events were assumed to result from interactions with thermal neutrons. While some fission products will result from interactions with fast neutrons, the majority of the waste will be generated by thermal fission.

The majority of the radionuclides generated by the fission process are very short-lived, with half-lives ranging from a few minutes to a few days. As a result, the radionuclides present in the MFP waste at the time of disposal will be significantly influenced by the amount of elapsed time between the fission events that generated the waste and the disposal of the waste at Area G. Although the age of the waste at the time of disposal is expected to vary, the information needed to quantify this parameter for the material placed at Area G is unavailable. Therefore, the age of the waste was assigned a triangular distribution with minimum, most likely, and maximum values of 1, 2, and 10 years.

Regression equations were developed that estimate radionuclide-specific fission yields as a function of the age of the MFP waste; the fission yield data upon which these regression equations are based are summarized in Tables 17 and 18. The activity fractions shown in these tables represent the proportions of the total MFP waste activity attributable to the listed radionuclides following thermal fission of U-235 and Pu-239. These fractions were calculated by multiplying the fission yields found in England and Rider (1994) by the radionuclide decay constants, and normalizing these activities by the total MFP activity. Only those radionuclides with activity fractions of 1.0×10^{-6} or more are included in these tables.

Fission product waste may contain several hundred different radionuclides at the time of generation. Although most of these isotopes have very short half-lives and decay to negligible levels within a few days or weeks, some may give rise to daughter products that are longer-lived than their parents. These daughter products may contribute to estimated MFP waste activities well beyond the time of generation. The contributions of any such daughter products were ignored during the development of the Area G inventory and were not evaluated quantitatively. Ignoring these radionuclides will underestimate the activities of any long-lived daughters that result from decay and will overestimate the activities of the radionuclides that were included in the final fission product allocations.

The MAP waste was allocated to specific radionuclides using information provided by a major generator of the waste. The Los Alamos Neutron Science Center (formerly the Los Alamos Meson Physics Facility) generates three major waste streams of activated waste including trash, beam-line inserts, and targets; the activity allocation factors adopted for the inventory update are based on a characterization of the trash from this facility. Although similar activated materials may occur in all three waste streams, it is unclear if the allocation factors developed for the trash accurately represent the targets and beam-line inserts.

Table 17
Radionuclide Activity Fractions for 1- to 5-Year-Old Mixed-Fission Product Waste Generated by Thermal Fission of U-235 and Pu-239

	Waste Age = 1 yr		Waste Age = 2 yr		Waste Age = 3 yr		Waste Age = 4 yr		Waste Age = 5 yr	
Radionuclide	U-235	Pu-239	U-235	Pu-239	U-235	Pu-239	U-235	Pu-239	U-235	Pu-239
Cd-115m	3.9E-06	---	---	---	---	---	---	---	---	---
Ce-141	---	4.0E-06	---	---	---	---	---	---	---	---
Ce-144	4.5E-01	2.3E-01	5.3E-01	1.9E-01	3.3E-01	1.4E-01	1.7E-01	9.0E-02	8.3E-02	5.2E-02
Cs-137	4.9E-02	7.3E-02	1.3E-01	1.4E-01	2.0E-01	2.5E-01	2.5E-01	3.8E-01	2.8E-01	5.2E-01
Eu-154	---	1.1E-05	1.3E-06	2.1E-05	1.9E-06	3.4E-05	2.3E-06	5.0E-05	2.4E-06	6.4E-05
Eu-155	1.2E-05	1.3E-04	2.9E-05	2.3E-04	3.8E-05	3.5E-04	4.3E-05	4.8E-04	4.2E-05	5.8E-04
Kr-85	5.6E-02	3.3E-03	1.5E-01	6.2E-03	2.1E-01	1.0E-02	2.5E-01	1.5E-02	2.7E-01	2.0E-02
Nb-95	2.0E-05	1.6E-05	---	---	---	---	---	---	---	---
Pm-147	---	---	---	1.1E-06		1.5E-06	---	1.8E-06	---	2.0E-06
Ru-103	8.7E-06	7.0E-05	---	---	---	---	---	---	---	---
Ru-106	1.1E-05	6.1E-01	1.6E-05	6.2E-01	1.2E-05	5.6E-01	8.1E-06	4.4E-01	4.7E-06	3.1E-01
Sb-124	1.7E-05	1.7E-05	---	---	---	---	---	---	---	---
Sb-125	1.9E-04	7.0E-04	4.2E-04	1.1E-03	5.0E-04	1.5E-03	5.0E-04	1.8E-03	4.5E-04	2.0E-03
Sm-151	---	1.6E-06	---	3.2E-06	---	5.6E-06	---	8.8E-06	---	1.2E-05
Sn-119m	1.5E-06	7.3E-06	1.8E-06	6.2E-06	1.1E-06	4.6E-06	---	3.1E-06	---	1.8E-06
Sn-121m	1.6E-05	4.6E-05	4.3E-05	9.1E-05	6.5E-05	1.6E-04	8.2E-05	2.4E-04	9.3E-05	3.4E-04
Sn-123	8.0E-03	1.6E-02	3.2E-03	4.5E-03	6.9E-04	1.1E-03	1.2E-04	2.5E-04	2.0E-05	4.9E-05
Sn-126	4.8E-06	2.8E-06	1.4E-05	5.6E-06	2.1E-05	9.9E-06	2.7E-05	1.6E-05	3.1E-05	2.2E-05
Sr-89	2.1E-02	2.8E-03	4.0E-04	3.7E-05	4.1E-06	---	---	---	---	---

--- = None

Table 17 (Continued)
Radionuclide Activity Fractions for 1- to 5-Year-Old Mixed-Fission Product Waste Generated by Thermal Fission of U-235 and Pu-239

	Waste Age = 1 yr		Waste Age = 2 yr		Waste Age = 3 yr		Waste Age = 4 yr		Waste Age = 5 yr	
Radionuclide	U-235	Pu-239	U-235	Pu-239	U-235	Pu-239	U-235	Pu-239	U-235	Pu-239
Sr-90	6.3E-02	1.2E-02	1.7E-01	2.5E-02	2.6E-01	4.2E-02	3.2E-01	6.5E-02	3.6E-01	8.8E-02
Tb-160	---	3.6E-06	---	---	---	---	---	---	---	---
Te-127m	---	2.2E-06	---	---	---	---	---	---	---	---
Te-129m	2.0E-06	1.1E-05	---	---	---	---	---	---	---	---
Y-91	6.8E-04	7.7E-04	2.5E-05	2.1E-05	---	---	---	---	---	---
Zr-95	3.5E-01	5.2E-02	1.9E-02	2.0E-03	5.5E-04	6.8E-05	1.4E-05	2.1E-06	---	---

--- = None

Table 18
Radionuclide Activity Fractions for 6- to 10-Year-Old Mixed-Fission Product Waste Generated by Thermal Fission of U-235 and Pu-239

	Waste Age = 6 yr		Waste Age = 7 yr		Waste Age = 8 yr		Waste Age = 9 yr		Waste Age = 10 yr	
Radionuclide	U-235	Pu-239	U-235	Pu-239	U-235	Pu-239	U-235	Pu-239	U-235	Pu-239
Ce-144	3.7E-02	2.7E-02	1.6E-02	1.3E-02	6.9E-03	5.7E-03	3.0E-03	2.5E-03	5.4E-04	4.5E-04
Cs-137	3.0E-01	6.4E-01	3.1E-01	7.2E-01	3.2E-01	7.7E-01	3.2E-01	8.0E-01	3.3E-01	8.3E-01
Eu-154	2.4E-06	7.4E-05	2.4E-06	7.9E-05	2.3E-06	8.0E-05	2.2E-06	7.8E-05	2.0E-06	7.2E-05
Eu-155	4.0E-05	6.3E-04	3.7E-05	6.2E-04	3.3E-05	5.9E-04	3.0E-05	5.4E-04	2.4E-05	4.4E-04
Kr-85	2.8E-01	2.3E-02	2.8E-01	2.5E-02	2.7E-01	2.6E-02	2.6E-01	2.6E-02	2.5E-01	2.5E-02
Pm-147	---	1.9E-06	---	1.7E-06	---	1.4E-06	---	1.1E-06	---	---
Ru-106	2.6E-06	2.0E-01	1.4E-06	1.2E-01	---	6.5E-02	---	3.5E-02	0.0E+00	9.6E-03
Sb-125	3.8E-04	2.0E-03	3.1E-04	1.8E-03	2.5E-04	1.5E-03	2.1E-04	1.2E-03	1.3E-04	8.1E-04
Sm-151	---	1.5E-05	---	1.7E-05	---	1.9E-05	---	2.0E-05	1.0E-06	2.1E-05
Sn-121m	1.0E-04	4.1E-04	1.0E-04	4.7E-04	1.1E-04	5.1E-04	1.1E-04	5.3E-04	1.1E-04	5.5E-04
Sn-123	3.1E-06	8.6E-06	---	1.4E-06	---	---	---	---	---	---
Sn-126	3.3E-05	2.7E-05	3.5E-05	3.1E-05	3.7E-05	3.4E-05	3.8E-05	3.6E-05	4.1E-05	3.9E-05
Sr-90	3.8E-01	1.1E-01	4.0E-01	1.2E-01	4.0E-01	1.3E-01	4.1E-01	1.3E-01	4.2E-01	1.4E-01

--- = None

Many of the radionuclides in the MAP waste are short-lived and will undergo significant decay between the time of generation and disposal. As with the MFP waste, the decay dynamics of the MAP waste will have a significant impact on the fractional abundances of radionuclides in the waste. Unfortunately, the ages of the waste at the time the allocation factors were developed and at the time it was disposed of at Area G are unknown. In the absence of this information, it was assumed these ages were the same. If this is not the case, the relative activities of the radionuclides found in the waste will be different. Without additional information, it is not possible to provide a quantitative evaluation of the uncertainties associated with the MAP waste inventory.

Several plutonium and uranium material types have been used in the past to describe the waste that has been disposed of at the Laboratory; these material types refer to specific radionuclide mixtures of plutonium and uranium isotopes. The Area G inventory includes approximately 11,000 Ci of activity reported using these material types. More than 98 percent of this activity is represented by material types PU52, PU53, PU54, PU56, and PU83, which represent various mixtures of plutonium isotopes. Material types U10, U12, and D38 are important contributors to uranium isotopic inventories, accounting for about 98 percent of the uranium-based material types. Waste was assigned to these material types based on the mass fractional contents of Pu-238, Pu-240, and U-235; the ranges in mass fractional contents upon which assignments were made are shown in Table 19. The LANL LLW and TRU waste databases used to project the Area G inventory have adopted point estimates of the mass fractional contents of these radionuclides and additional isotopes of plutonium and uranium for each material type. These mass fraction contents are listed in Table 20, along with the corresponding activity-based allocation factors.

Table 19
Material Type Mass Allocation Fractions for the Predominant Material Types Disposed of at Area G

Material Type Code	Type	Description
PU52	Pu-239	4.0 to < 7.0 % Pu-240
PU53	Pu-239	7.0 to < 10.0 % Pu-240
PU54	Pu-239	10.0 to < 13.0 % Pu-240
PU56	Pu-239	16.0 to < 20.0 % Pu-240
PU83	Pu-238	Total Pu-238
U10	U–depleted in U-235	Total U-238
U12	U–depleted in U-235	0.21 to 0.24 % U-235
D38/U15 [a]	U–depleted in U-235	0.28 to < 0.31 % U-235

[a] *Material types D38 and U15 have been used interchangeably in terms of radionuclide allocation fractions.*

Table 20
Point Estimates of the Mass and Activity Allocation Factors for the Predominant Material Types Disposed of at Area G

Material Type	Radionuclides	Fractional Abundance	
		Mass Basis	Activity Basis
PU52	Pu-238	1.0E-04	6.1E-03
	Pu-239	9.4E-01	2.1E-01
	Pu-240	6.0E-02	4.9E-02
	Pu-241	2.0E-03	7.4E-01
	Pu-242	2.0E-04	2.8E-06
PU53	Pu-238	3.0E-04	1.1E-02
	Pu-239	9.1E-01	1.2E-01
	Pu-240	8.5E-02	4.2E-02
	Pu-241	3.7E-03	8.2E-01
	Pu-242	7.1E-04	6.1E-06
PU54	Pu-238	4.6E-04	8.5E-03
	Pu-239	8.7E-01	5.9E-02
	Pu-240	1.2E-01	2.8E-02
	Pu-241	8.1E-03	9.0E-01
	Pu-242	2.2E-03	9.4E-06
PU56	Pu-238	6.1E-04	8.0E-03
	Pu-239	8.2E-01	3.9E-02
	Pu-240	1.6E-01	2.9E-02
	Pu-241	1.2E-02	9.3E-01
	Pu-242	3.5E-03	1.1E-05
PU83	Pu-238	8.7E-01	9.9E-01
	Pu-239	1.2E-01	5.0E-04
	Pu-240	1.3E-02	1.9E-04
	Pu-241	1.7E-03	1.2E-02
	Pu-242	5.3E-04	1.4E-07
U10	U-238	1.0E+00	1.0E+00
U12	U-234	2.0E-05	2.7E-01
	U-235	2.3E-03	1.0E-02
	U-238	1.0E+00	7.2E-01
D38	U-234	2.3E-05	2.9E-01
	U-235	3.0E-03	1.3E-02
	U-238	1.0E+00	6.9E-01

Using the allocation factors listed in Table 20 ignores the fact that each material type may have a range of associated radionuclide contents and, therefore, introduces uncertainty into the inventory estimates. The potential errors that may result from the use of the allocation factors were characterized for material types PU52, PU53, PU54, PU56, and PU83, which are the major contributors to the total activities of plutonium material types.

Distributions of the radionuclide-specific mass contents of the plutonium material types were estimated using spectral data collected with a high-purity germanium detector (Veilleux, 2005). Veilleux evaluated detection results for almost 3,300 drums and calculated the means, standard deviations, and medians of the mass fractions of Pu-238, Pu-239, Pu-240, Pu-241, Pu-242, and Am-241 included in each material type waste; the data used to estimate these fractions were decay-corrected to a single date. For the material types for which the sample size was large, the statistics were calculated from the distribution that included 90 percent of all assays (drums) centered at the median, to remove outliers that skewed the results. Veilleux considered this approach appropriate because the outliers are likely indicative of drums that contain mixtures of material types rather than a single material type. In cases where the sample size was small, 100 percent of the assays (drums) were used for statistical analysis.

The data presented in Veilleux (2005) were used to estimate distributions of radionuclide abundance in PU52, PU53, PU54, PU56, and PU83. For material types PU52, PU54, and PU83, the middle 90 percent of the data was used to calculate distributions of radionuclide abundance for the plutonium isotopes. Consistent with the approach adopted by Veilleux, this was done to eliminate drums that likely contained mixtures of material types. All of the assay data were used to characterize material types PU53 and PU56 because the numbers of drums sampled were small. The fractions of Am-241 in the various material type wastes were not estimated; this isotope is not addressed by the allocation fractions included in the LANL LLW and TRU waste databases. The distributions of radionuclide abundance were developed using the raw data included in Veilleux (2005), not the decay-corrected quantities; the data used in these calculations are included in *Attachment IV*.

The results of the material type evaluation are summarized in Tables 21 through 25; each table corresponds to one of the five material types listed above. The top third of each table provides descriptive statistics for the plutonium isotopes. Information needed to define cumulative distributions of radionuclide abundance for the isotopes found in each material type is provided in the middle third of the table; these data include the probability level and the corresponding radionuclide abundance. Correlations between the isotopic distributions for a given material type are provided at the bottom of each table. The cumulative distributional information and correlation coefficients estimated using the data from Veilleux (2005) were used to define input distributions for the GoldSim inventory modeling.

Table 21
Results of the Activity Fraction Evaluation for Material Type PU52

Descriptive Statistics of Activity Fraction Data					
	Radionuclide				
Statistic	Pu-238	Pu-239	Pu-240	Pu-241	Pu-242
N	1608	1608	1608	1608	1608
Mean	1.3E-02	2.5E-01	6.2E-02	6.8E-01	1.9E-05
Std Dev	8.8E-03	3.0E-02	8.5E-03	3.4E-02	3.7E-06
Median	1.1E-02	2.5E-01	6.1E-02	6.8E-01	1.8E-05
Skewness	2.9E+00	-7.0E-01	8.0E-01	5.0E-01	2.4E+00
Kurtosis	1.1E+01	4.4E-01	4.1E+00	5.9E-01	9.6E+00
Minimum	3.1E-03	1.5E-01	3.4E-02	5.6E-01	1.3E-05
Maximum	7.8E-02	3.1E-01	1.2E-01	8.0E-01	4.8E-05
Cumulative Distributions of Isotopic Activity Fractions					
Probability Level	Pu-238	Pu-239	Pu-240	Pu-241	Pu-242
0	3.1E-03	1.5E-01	3.4E-02	5.6E-01	1.3E-05
0.01	4.7E-03	1.6E-01	4.1E-02	6.1E-01	1.4E-05
0.05	6.1E-03	1.9E-01	4.9E-02	6.3E-01	1.5E-05
0.1	7.2E-03	2.0E-01	5.2E-02	6.4E-01	1.6E-05
0.25	8.9E-03	2.3E-01	5.7E-02	6.6E-01	1.7E-05
0.5	1.1E-02	2.5E-01	6.1E-02	6.8E-01	1.8E-05
0.75	1.4E-02	2.7E-01	6.6E-02	7.0E-01	2.0E-05
0.9	2.2E-02	2.8E-01	7.1E-02	7.2E-01	2.4E-05
0.95	3.2E-02	2.9E-01	7.4E-02	7.4E-01	2.7E-05
0.99	5.1E-02	3.0E-01	8.9E-02	7.7E-01	3.3E-05
1	7.8E-02	3.1E-01	1.2E-01	8.0E-01	4.8E-05
Activity Fraction Correlation Matrix					
	Radionuclide				
Radionuclide	Pu-238	Pu-239	Pu-240	Pu-241	Pu-242
Pu-238	1.0E+00				
Pu-239	-1.1E-01	1.0E+00			
Pu-240	1.4E-01	-9.7E-01	1.0E+00		
Pu-241	-6.9E-01	-1.6E-01	1.5E-01	1.0E+00	
Pu-242	-6.7E-01	-2.4E-01	2.3E-01	7.2E-01	1.0E+00

Table 22
Results of the Activity Fraction Evaluation for Material Type PU53

Descriptive Statistics of Activity Fraction Data					
	Radionuclide				
Statistic	Pu-238	Pu-239	Pu-240	Pu-241	Pu-242
N	7	7	7	7	7
Mean	1.3E-02	2.0E-01	6.8E-02	7.2E-01	3.0E-05
Std Dev	2.0E-03	6.4E-02	1.1E-02	7.0E-02	1.1E-05
Median	1.3E-02	2.2E-01	6.2E-02	7.0E-01	2.4E-05
Skewness	6.3E-01	-1.2E-01	1.9E+00	3.9E-02	5.4E-01
Kurtosis	-3.0E-01	-2.0E+00	3.7E+00	-1.7E+00	-1.3E+00
Minimum	1.1E-02	1.3E-01	6.0E-02	6.2E-01	1.6E-05
Maximum	1.6E-02	2.8E-01	9.0E-02	8.0E-01	4.7E-05
Cumulative Distributions of Isotopic Activity Fractions					
Probability Level	Pu-238	Pu-239	Pu-240	Pu-241	Pu-242
0	1.1E-02	1.3E-01	6.0E-02	6.2E-01	1.6E-05
0.01	1.1E-02	1.3E-01	6.0E-02	6.2E-01	1.6E-05
0.05	1.1E-02	1.3E-01	6.0E-02	6.3E-01	1.8E-05
0.1	1.1E-02	1.3E-01	6.1E-02	6.4E-01	2.0E-05
0.25	1.1E-02	1.5E-01	6.1E-02	6.7E-01	2.3E-05
0.5	1.3E-02	2.2E-01	6.2E-02	7.0E-01	2.4E-05
0.75	1.4E-02	2.5E-01	6.9E-02	7.8E-01	3.8E-05
0.9	1.5E-02	2.8E-01	8.0E-02	8.0E-01	4.5E-05
0.95	1.5E-02	2.8E-01	8.5E-02	8.0E-01	4.6E-05
0.99	1.6E-02	2.8E-01	8.9E-02	8.0E-01	4.6E-05
1	1.6E-02	2.8E-01	9.0E-02	8.0E-01	4.7E-05
Activity Fraction Correlation Matrix					
	Radionuclide				
Radionuclide	Pu-238	Pu-239	Pu-240	Pu-241	Pu-242
Pu-238	1.0E+00				
Pu-239	-4.0E-01	1.0E+00			
Pu-240	-3.0E-01	5.9E-01	1.0E+00		
Pu-241	3.8E-01	-9.9E-01	-6.9E-01	1.0E+00	
Pu-242	2.3E-01	-9.5E-01	-3.9E-01	9.2E-01	1.0E+00

Table 23
Results of the Activity Fraction Evaluation for Material Type PU54

Descriptive Statistics of Activity Fraction Data					
	Radionuclide				
Statistic	Pu-238	Pu-239	Pu-240	Pu-241	Pu-242
N	154	154	154	154	154
Mean	1.6E-02	2.0E-01	6.2E-02	7.2E-01	3.0E-05
Std Dev	9.6E-03	8.6E-02	1.6E-02	9.7E-02	1.4E-05
Median	1.5E-02	1.9E-01	5.7E-02	7.3E-01	2.7E-05
Skewness	2.4E+00	2.3E-01	1.2E+00	-2.4E-01	1.4E-01
Kurtosis	1.0E+01	-1.5E+00	1.5E+00	-1.4E+00	-1.6E+00
Minimum	2.5E-03	9.7E-02	3.6E-02	5.4E-01	1.1E-05
Maximum	7.6E-02	3.7E-01	1.2E-01	8.4E-01	5.4E-05
Cumulative Distributions of Isotopic Activity Fractions					
Probability Level	Pu-238	Pu-239	Pu-240	Pu-241	Pu-242
0	2.5E-03	9.7E-02	3.6E-02	5.4E-01	1.1E-05
0.01	3.0E-03	9.8E-02	4.1E-02	5.5E-01	1.1E-05
0.05	4.4E-03	1.0E-01	4.4E-02	5.7E-01	1.2E-05
0.1	6.5E-03	1.0E-01	4.6E-02	5.9E-01	1.3E-05
0.25	1.1E-02	1.1E-01	5.0E-02	6.4E-01	1.9E-05
0.5	1.5E-02	1.9E-01	5.7E-02	7.3E-01	2.7E-05
0.75	1.8E-02	2.7E-01	7.2E-02	8.2E-01	4.5E-05
0.9	2.8E-02	3.2E-01	8.4E-02	8.3E-01	4.8E-05
0.95	3.4E-02	3.4E-01	9.6E-02	8.4E-01	4.9E-05
0.99	4.6E-02	3.5E-01	1.1E-01	8.4E-01	5.3E-05
1	7.6E-02	3.7E-01	1.2E-01	8.4E-01	5.4E-05
Activity Fraction Correlation Matrix					
	Radionuclide				
Radionuclide	Pu-238	Pu-239	Pu-240	Pu-241	Pu-242
Pu-238	1.0E+00				
Pu-239	-6.8E-02	1.0E+00			
Pu-240	3.1E-05	6.2E-01	1.0E+00		
Pu-241	-3.9E-02	-9.9E-01	-7.2E-01	1.0E+00	
Pu-242	3.2E-03	-9.2E-01	-3.7E-01	8.8E-01	1.0E+00

Table 24
Results of the Activity Fraction Evaluation for Material Type PU56

Descriptive Statistics of Activity Fraction Data					
	Radionuclide				
Statistic	Pu-238	Pu-239	Pu-240	Pu-241	Pu-242
N	16	16	16	16	16
Mean	1.5E-02	1.0E-01	5.6E-02	8.3E-01	5.7E-05
Std Dev	4.3E-03	2.3E-02	9.1E-03	2.9E-02	1.4E-05
Median	1.4E-02	9.5E-02	5.8E-02	8.4E-01	5.8E-05
Skewness	1.9E+00	2.0E+00	-2.0E+00	-1.5E+00	-8.2E-01
Kurtosis	5.4E+00	3.7E+00	6.7E+00	2.6E+00	-8.2E-02
Minimum	9.5E-03	8.4E-02	2.8E-02	7.5E-01	2.9E-05
Maximum	2.8E-02	1.7E-01	7.1E-02	8.7E-01	7.6E-05
Cumulative Distributions of Isotopic Activity Fractions					
Probability Level	Pu-238	Pu-239	Pu-240	Pu-241	Pu-242
0	9.5E-03	8.4E-02	2.8E-02	7.5E-01	2.9E-05
0.01	9.6E-03	8.4E-02	3.1E-02	7.5E-01	2.9E-05
0.05	1.0E-02	8.5E-02	4.2E-02	7.7E-01	3.1E-05
0.1	1.1E-02	8.5E-02	5.0E-02	7.9E-01	3.4E-05
0.25	1.2E-02	8.7E-02	5.7E-02	8.3E-01	5.3E-05
0.5	1.4E-02	9.5E-02	5.8E-02	8.4E-01	5.8E-05
0.75	1.6E-02	1.0E-01	5.9E-02	8.4E-01	6.7E-05
0.9	1.8E-02	1.3E-01	6.2E-02	8.5E-01	7.3E-05
0.95	2.0E-02	1.5E-01	6.6E-02	8.5E-01	7.4E-05
0.99	2.6E-02	1.6E-01	7.0E-02	8.7E-01	7.5E-05
1	2.8E-02	1.7E-01	7.1E-02	8.7E-01	7.6E-05
Activity Fraction Correlation Matrix					
	Radionuclide				
Radionuclide	Pu-238	Pu-239	Pu-240	Pu-241	Pu-242
Pu-238	1.0E+00				
Pu-239	7.3E-01	1.0E+00			
Pu-240	-1.8E-01	2.0E-01	1.0E+00		
Pu-241	-6.7E-01	-9.6E-01	-4.5E-01	1.0E+00	
Pu-242	-6.8E-01	-6.9E-01	5.3E-01	4.8E-01	1.0E+00

Table 25
Results of the Activity Fraction Evaluation for Material Type PU83

Descriptive Statistics of Activity Fraction Data					
	Radionuclide				
Statistic	Pu-238	Pu-239	Pu-240	Pu-241	Pu-242
N	130	130	130	130	130
Mean	9.8E-01	1.8E-03	5.4E-04	1.6E-02	2.8E-06
Std Dev	2.6E-02	7.0E-03	1.6E-03	1.7E-02	1.6E-06
Median	9.9E-01	7.8E-04	2.7E-04	1.4E-02	2.6E-06
Skewness	-9.6E+00	1.0E+01	9.9E+00	9.3E+00	9.7E-01
Kurtosis	1.0E+02	1.1E+02	1.1E+02	9.5E+01	7.3E-01
Minimum	7.1E-01	5.0E-04	3.6E-05	6.4E-03	5.1E-07
Maximum	9.9E-01	7.7E-02	1.8E-02	2.0E-01	7.9E-06
Cumulative Distributions of Isotopic Activity Fractions					
Probability Level	Pu-238	Pu-239	Pu-240	Pu-241	Pu-242
0	7.1E-01	5.0E-04	3.6E-05	6.4E-03	5.1E-07
0.01	9.2E-01	5.4E-04	4.9E-05	9.3E-03	5.6E-07
0.05	9.8E-01	6.1E-04	7.4E-05	1.1E-02	7.1E-07
0.1	9.8E-01	6.5E-04	1.2E-04	1.2E-02	1.1E-06
0.25	9.8E-01	7.0E-04	1.9E-04	1.3E-02	1.6E-06
0.5	9.9E-01	7.8E-04	2.7E-04	1.4E-02	2.6E-06
0.75	9.9E-01	9.9E-04	4.4E-04	1.5E-02	3.6E-06
0.9	9.9E-01	1.3E-03	7.1E-04	1.6E-02	5.3E-06
0.95	9.9E-01	3.2E-03	1.1E-03	2.0E-02	6.3E-06
0.99	9.9E-01	1.8E-02	3.8E-03	5.4E-02	7.6E-06
1	9.9E-01	7.7E-02	1.8E-02	2.0E-01	7.9E-06
Activity Fraction Correlation Matrix					
	Radionuclide				
Radionuclide	Pu-238	Pu-239	Pu-240	Pu-241	Pu-242
Pu-238	1.0E+00				
Pu-239	-9.9E-01	1.0E+00			
Pu-240	-9.8E-01	9.9E-01	1.0E+00		
Pu-241	-1.0E+00	9.8E-01	9.7E-01	1.0E+00	
Pu-242	-8.4E-02	7.4E-02	1.5E-01	8.1E-02	1.0E+00

The radionuclide abundances for a given container of material type waste must, by definition, sum to 1. The sum of the abundances obtained by randomly sampling the distributions described above were centered at 1, but displayed some variation about this value. To circumvent this behavior, the inventory model calculates a scaling factor equal to the sum of the abundances for each model realization and uses the factor to scale the abundances for all radionuclides up or down so they sum to 1.

The accuracy of the distributions developed using the data from Veilleux will depend, in part, on the number of sample assays upon which they are based. For three of the material types, the number of assays ranges from 130 to more than 1,600; the sample sizes for PU53 and PU56 are much smaller, 7 and 16, respectively and thus the distributions are considerably less reliable. Nevertheless, the use of these approximations provides some insight into model sensitivity to these material types and, in so doing, helps determine if the development of more rigorous distributions is warranted.

Direct measurements of radionuclide abundance in material types U12 and D38 and the other less prevalent material types were unavailable. Consequently, the uncertainty associated with the radionuclide abundances in these material types was not modeled.

Definitions were unavailable for four material types, including GAMMA, GRALPH, GRBETA, and TRU. As a result, waste assigned these material types was excluded from the inventory characterization. This is not expected to introduce significant error into the final inventory projections because the total activity associated with all of these material types is small, approximately 1.5 Ci.

The intruder analysis was conducted to estimate exposures associated with waste disposed of since September 27, 1988 and to establish radionuclide concentration limits for waste that will be disposed of in the Zone 4 expansion area. The modeling conducted to estimate intruder exposures evaluated the uncertainties associated with the waste inventories using the approach described above. The WAC were estimated using a unit inventory for all radionuclides that were disposed of at Area G in the past, except for those that were eliminated on the basis of half-life considerations. No uncertainty was assumed to be associated with the unit inventory.

5.5 Atmospheric Transport Parameters

Atmospheric transport parameters are used to estimate concentrations of airborne radionuclides at the various off-site exposure locations and above the inadvertent intruder's lot. The distributions assigned to these parameters are included in Table 11. The information used to develop these distributions is discussed below.

5.5.1 Dust Loading and Soil Disturbance Factor

Dust loading is a measure of the particulate concentration in air, and is used to estimate airborne radionuclide concentrations above the receptor locations for the atmospheric, all pathways, and intruder scenarios. Information from the literature was used to estimate a distribution for this parameter. Baes et al. (1984) cite values for dust loading at U.S. locations that range from 3.2 to 52.4 $\mu g/m^3$ (2.0×10^{-10} to 3.3×10^{-9} lb/ft^3); the data are lognormally distributed. A default value of 15.5 $\mu g/m^3$ (9.7×10^{-10}) was adopted by Baes et al. as the geometric mean for food-chain transport modeling analyses. The National Council on Radiation Protection and Measurements (NCRP, 1984) cites dust-loading values for various suburban locations in the U.S. that range from 9 to 79 $\mu g/m^3$ (5.6×10^{-10} to 4.9×10^{-9} lb/ft^3).

Other studies provide additional insight into the appropriate magnitude of dust loading. Measurements conducted at the Idaho National Engineering and Environmental Laboratory (INEEL, 1994) from 1983 through 1990 indicated an average dust loading of 25.4 $\mu g/m^3$ (1.58×10^{-9} lb/ft^3). A decision analysis performed for a contaminated site at the DOE Nevada Test Site (NTS, 1995) adopted a dust loading of 30 $\mu g/m^3$ (1.87×10^{-9} lb/ft^3), with a geometric standard deviation of 1.6. This distribution was considered to be representative for nonurban areas of the U.S. Higher rates of resuspension may result following disturbance of the site, such as that caused by people walking over the contaminated soils. The NTS study cites data that suggest air concentrations may be 1.1 to 2.6 times greater for disturbed sites than for those in areas unaffected by humans. For screening purposes, the NCRP adopted a dust loading of 80 $\mu g/m^3$ (5.0×10^{-9} lb/ft^3) for a residential scenario that includes small-scale gardening and a value of 150 $\mu g/m^3$ (9.36×10^{-9} lb/ft^3) for a construction scenario (NCRP, 1999). Finally, Anspaugh et al. (1975) recommend a default of 100 $\mu g/m^3$ (6.24×10^{-9} lb/ft^3) in the absence of site-specific data.

A lognormal distribution was used to represent the variability of dust loading for the off-site and residential intruder exposure scenarios; this distribution was defined using a geometric mean and geometric standard deviation of 30 $\mu g/m^3$ (1.87×10^{-9} lb/ft^3) and 1.6; the geometric mean of this distribution was adopted as the point estimate. This distribution is identical to that adopted for the NTS decision analysis (NTS, 1995), and generally agrees with the other data cited. The soil disturbance factor was assigned a triangular distribution with minimum, most likely, and maximum values of 1.1, 2.0, and 3.0, also consistent with the NTS study.

To account for greater rates of resuspension that may occur during construction activities, a higher dust loading was adopted for the intruder who builds a house at Area G. In the absence of specific information, it was assumed that the mean dust loading is 1.5 times that for the members of the public and residential intruders, or 45 $\mu g/m^3$ (2.81×10^{-9} lb/ft^3). The geometric standard

deviation and distribution of soil disturbance factors were the same as those adopted for the residential intruder.

5.5.2 Vertical Flux

The vertical flux, which specifies the rate at which particulates are suspended from the surface of the disposal site, is used to define the source term for the All Pathways–Atmospheric Scenario. The vertical flux decreases with height above the site because heavier soil particles fall back to the surface due to gravity. Vertical fluxes measured 1 to 3 m (3.3 to 9.8 ft) above the surface are typically used to estimate fluxes for the smaller particulates that are susceptible to long-distance transport with the prevailing winds.

A vertical flux of 0.05 $kg/m^2/yr$ (0.01 $lb/ft^2/yr$) was adopted for the 1997 Area G performance assessment and composite analysis; this value was based on work performed by Radian (1995), which assumed that particulates are dislodged and made available for resuspension as a result of site disturbance. Specifically, it was assumed that a vehicle would be driven over the entire site once a year, on average. The estimated resuspension rate assumed that 50 percent of the site was covered by nonerodible surfaces including plants, uncontaminated roads, and buildings. Further reflection on the Radian study concluded that the assumptions upon which this vertical flux is based are not valid for the postclosure configuration of Area G, leading to possibly inaccurate estimates of the resuspension potential.

Following closure of Area G, the disposal site is expected to transition from a grassland ecosystem to a piñon-juniper woodland ecosystem. Rates of particulate resuspension at the site will vary during this transitional period. To estimate rates of resuspension during the time when the site will be primarily grassland, several sources of information were consulted. The first was a study conducted under the Area G Performance Assessment and Composite Analysis Maintenance Program in which vertical fluxes were estimated at MDA J (Whicker and Breshears, 2005). This facility, which is located about 2 km (1.2 mi) to the west of Area G on Mesita del Buey, was used for the disposal of classified material. In 2002, a final cover was applied over MDA J and the area was seeded with a mixture of native grasses. The MDA J cover is expected to resemble the conditions at Area G shortly after final closure of the facility.

Whicker and Breshears (2005) placed total suspended particulate samplers at heights of 1 and 3 m (3.3 and 9.8 ft) above MDA J. Sampling conducted over a period of 5½ months was used, in conjunction with wind and friction velocity measurements, to estimate vertical fluxes of particulates. The vertical flux approximately 2 m (6.6 ft) above the ground surface averaged 0.0017 $kg/m^2/yr$ (3.4×10^{-4} $lb/ft^2/yr$) over the 5½-month sampling period. Fluxes ranged from -0.013 to 0.015 $kg/m^2/yr$ (-0.0027 $lb/ft^2/yr$ to 0.0031 $lb/ft^2/yr$), where negative values indicate a net downward deposition (i.e., into the sampling area). The median flux of 0 $kg/m^2/yr$ indicates little, if any, net loss of soil from the area.

The vertical fluxes estimated by Whicker and Breshears (2005) may be compared to other measurements conducted in semiarid locations in the western U.S. Breshears et al. (2003) conducted vertical flux measurements over 6-to-8-month periods at several locations: a grassland adjacent to the Rocky Flats Environmental Technology site near Denver, Colorado; a shrubland near Carlsbad, New Mexico; and a forest dominated by ponderosa pine along the western edge of the Laboratory. The median vertical fluxes approximately 2 m (6.6 ft) above the ground were 0.0083, 0.015, and 0.0091 $kg/m^2/yr$ (0.0017, 0.0031, and 0.0019 $lb/ft^2/yr$) for the grassland, shrubland, and forest sites, respectively. Fluxes ranged from -0.0059 to 0.038 $kg/m^2/yr$ (-0.0012 to 7.8×10^{-4} $lb/ft^2/yr$) at the grassland site, -0.08 to 0.16 $kg/m^2/yr$ (-1.6×10^{-4} to 0.033 $lb/ft^2/yr$) within the shrubland, and -0.015 to 0.055 $kg/m^2/yr$ (-0.0031 to 0.011 $lb/ft^2/yr$) at the forest site (Whicker, 2005). The fluxes listed for the forested site were based on samplers located approximately 100 m (330 ft) from the forest canopy; vertical fluxes within the canopy would likely be smaller.

The vertical flux measurements summarized above represent the net movement of soil at the sample locations, taking into account material that is deposited on site and soil particles that are removed from the site due to resuspension. Consequently, this information is not entirely appropriate for defining the rates at which contaminated particulates are resuspended from the surface of Area G. To more accurately quantify contaminant resuspension rates it would be necessary to track the movement of soil from portions of the disposal facility that are uncontaminated and to track the movements of contaminated particulates originating over the pits and shafts.

The detailed information needed to definitively quantify the rates at which contaminated particulates are suspended from the surface of Area G is unavailable. In its absence, the data collected by Whicker and Breshears (2005) were used to estimate these resuspension rates in a manner that is expected to be reasonably conservative. Specifically, the resuspension rate was defined on the basis of the non-negative fluxes measured by the investigators, under the assumption that these fluxes represent the net removal of contaminated soils from the surface of the site. This subset of the Whicker and Breshears data indicates fluxes ranging from 0.0021 to 0.023 $kg/m^2/yr$ (4.3×10^{-4} to 0.0047 $lb/ft^2/yr$). A truncated normal distribution with a mean of 0.013 $kg/m^2/yr$ (0.0026 $lb/ft^2/yr$) and a standard deviation of 0.0084 $kg/m^2/yr$ (0.0017 $lb/ft^2/yr$) was adopted for the performance assessment and composite analysis.

The vertical flux distribution adopted for the performance assessment and composite analysis modeling represents the particulate flux at a height of 2 m (6.6 ft) above the ground surface. In contrast, the atmospheric transport modeling used a default ground-level flux. Because of uncertainties about the errors that might be introduced by applying the modeling results to the 2 m (6.6 ft) fluxes, the effects of release height on downwind concentrations were investigated. Using the CALPUFF air dispersion model (Scire et al., 2000a, 2000b), simulations were

conducted in which unit fluxes (1 g/m^2/s [0.024 lb/ft^2/s]) were assumed to occur at 2 m (6.6 ft) and ground level; simulations were conducted for releases from atmospheric source area 1 using 3 years of meteorological data (Jacobson, 2005). Dispersion factors were estimated for all cells of the atmospheric modeling domain; ratios of the factors estimated for the 2 m (6.6 ft) release height to those projected for the ground-level release results were calculated and used to compare the effects of release height on projected downwind impacts.

The release height ratios described above varied among cell locations within the atmospheric transport modeling domain and among the 3 years of meteorological data. For cells not located within the Area G boundary and atmospheric source areas, which represent about 93 percent of the total cells, the ratios ranged from 0.38 to 1.1. An average of the ratios for each cell over the 3 years yielded values that ranged from 0.38 to 0.97. Excluding several cells located just outside the boundary narrowed the range of average ratios to 0.69 to 0.97; more than 99 percent of these cells had average ratios of 0.84 and above. The calculated ratios for cells within the Area G boundary or atmospheric source areas were more variable, ranging from 0.18 to 0.99 across all locations; the flux ratios ranged from 0.42 to 0.92 when averaged over the 3 years of meteorological data.

The results summarized above indicate that treating a 2 m (6.6 ft) vertical flux as if it were a ground-level release will typically result in an overestimation of downwind air concentrations by 3 to 16 percent. Greater differences are noted at cells within or next to the fence line, probably because these are points of release (or are immediately adjacent to such) and deposition. Even at these locations, however, treating the 2 m (6.6 ft) vertical flux as a ground-level release will result in higher-than-expected downwind air concentrations. This, in combination with the fact that differences in air concentrations due to variations in release height are small for most of the receptor locations, led to the decision to treat the 2 m (6.6 ft) vertical fluxes as ground-level fluxes without any further adjustment to the flux data.

5.5.3 Enhancement Factor

The vertical flux measurements discussed above apply to the suspendable fraction of the soil, which generally includes particles with a median diameter of about 10 μm (3.9×10^{-4} in.) or less. In contrast, soil concentrations estimated using the GoldSim models are based on the total soil, including the suspendable fraction and much larger particle sizes. Because soil radionuclide concentrations are often a function of particle size, it is necessary to modify the vertical fluxes before they are used in the GoldSim models. This is done by multiplying the vertical fluxes by the enhancement factor, or enrichment ratio, which is the ratio of radionuclide concentrations in the suspendable fraction to the concentrations in the total soil.

The enhancement factor is a complex function of many parameters, including the degree of soil disturbance, the soil texture, the site vegetation, and the radionuclides under consideration. In

their plutonium resuspension studies at the Marshall Islands, Shinn et al. (1997) observed enhancement factors ranging from 0.41 in a coconut grove to 3.1 for a disturbed, bare soil. Factors less than 1 were normal for undisturbed soils, while an enhancement factor of 2.5 was estimated for a road with traffic. Shinn (1992) reported enhancement factors of 0.87 and 1.04 for Pu-239 at two NTS sites that were characterized by desert pavement and 5 to 20 percent plant cover. In the same publication, factors ranging from 0.21 to 0.79 were reported for bare cultivated fields in South Carolina and California. Disturbances such as traffic, bulldozer blading, wildfire, and freeze-thaw cycling caused enhancement factors to increase by a factor of 2.2 to 6.5. At Palomares in Spain, Shinn (2002) estimated an enhancement factor of 0.3 for undisturbed soils that had been contaminated by plutonium following a mid-air collision of U.S. military aircraft in 1966. The median aerodynamic diameters of the particles considered in these studies generally ranged from 2 to 6 μm (7.9×10^{-5} to 2.4×10^{-4} in.).

Cooper et al. (1994) reported enhancement factors for americium and plutonium as part of an investigation conducted at a former nuclear weapons testing site in Maralinga, Australia. Particle size and activity distribution data were used to estimate enhancement factors for the soil fraction that was less than 45 μm (0.0018 in.) and for the inhalable fraction, which was defined as the portion of the soil with aerodynamic diameters of 7 μm (0.0028 in.) or less. Enhancement factors ranged from 3.4 to 22.2 for the less-than-45 μm (0.0018 in.) fraction, and from 1.1 to 10.8 for the inhalable fraction. The same investigators also estimated enhancement factors for the inhalable soil fraction on the basis of artificial resuspension studies. The factors from these studies ranged from 0.3 to 32.5. Cooper et al. recommended an enhancement factor of 6 for the inhalable fraction of the soil based on the results of the field measurements and other resuspension studies.

Van Pelt and Zobeck (2005) sampled and analyzed soils, sediments in transport over eroding fields, and attic dust from a small area in the southern high plains of Texas. The results of this effort were used to estimate enrichment ratios for 13 plant nutrients and approximately 30 other trace elements. In general, enrichment ratios were less than 1 within an area characterized by 0.3 m (1 ft) high ridges that were designed to trap sediments moving as a result of creep or saltation; ratios generally ranged from 1 to 4 within a windbreak of Arizona cypress that was surrounded by a stable mowed grass surface. The investigators estimated enrichment factors for different particle-size classes of soil and for suspended sediments collected at heights of up to 1 m (3.3 ft) above the ground surface. Average enrichment ratios ranged from about 0.5 for soil particle diameters greater than 250 μm (0.0098 in.) to about 3.5 for particles with diameters less than 53 μm (0.0021 in.). The average enrichment factors for suspended sediments ranged from slightly more than 1 for collection heights of 0.2 m (0.7 ft) or less to approximately 2 for a collection height of 1 m (3.3 ft). Finally, enrichment ratios for different particle-size classes of attic dust ranged from about 2 for particle diameters greater than 53 μm (0.0021 in.) to slightly more than 6 for particles with diameters of 10 μm or less (3.9×10^{-4} in.).

It is evident from the work conducted by Cooper et al. (1994) and Van Pelt and Zobeck (2005) that the enhancement factor (or enrichment ratio) is strongly dependent upon the particle-size class under consideration. As discussed earlier, the median diameter of the suspendable soil fraction is generally expected to be on the order of 10 μm (3.9×10^{-4} in.) or less. The data reported by Cooper et al. and by Van Pelt and Zobeck for attic dust suggest average enhancement factors on the order of 6 for the smaller particles within this size fraction. Enhancement factors for slightly larger particles would appear to range from 3 to 4 based on the soil and attic dust data collected by Van Pelt and Zobeck.

The enhancement factors reported by Cooper et al. (1994) and Van Pelt and Zobeck (2005) are significantly higher than the values reported by Shinn (1992 and 2002) and Shinn et al. (1997). In most cases, the values reported by Shinn and Shinn et al. are less than 1; only the enhancement factors reported for disturbed conditions approach the Cooper et al. and Van Pelt and Zobeck values. On the basis of these variations in reported values, a triangular distribution with minimum, most likely, and maximum values of 1, 3, and 6 was used to represent the enhancement factor. All radionuclides were assigned the same enhancement factor. This distribution is consistent with the data presented by Van Pelt and Zobeck for soils and for the majority of the trace elements in smaller particle size classes of attic dust. It generally overestimates the factors reported by Shinn and Shinn et al. for undisturbed conditions, but does not capture some of the more extreme values reported by the others.

5.5.4 Dispersion Factor and Deposition Rate

The dispersion factor is defined here as the ratio of the radionuclide concentration in air at a specified location to the rate of contaminant release from the disposal site. It is used in the performance assessment and composite analysis to estimate atmospheric radionuclide concentrations downwind of Area G. The deposition rate specifies the rate at which airborne radionuclides are deposited at locations downwind of the disposal site; it is used to estimate radionuclide concentrations in plants and soil at the receptor locations. Both parameters are a function of meteorological conditions and features of the landscape.

Complex terrain atmospheric transport modeling was conducted using the CALPUFF modeling system to estimate the dispersion factors and deposition rates that were used in the performance assessment and composite analysis (Jacobson, 2005). To conduct this modeling, a 7.4 km^2 (2.8 mi^2) modeling domain was established that included the disposal site and surrounding lands. This domain was divided into 8,100 30-m^2 (320-ft^2) cells. Releases of radionuclides to the air above the site were modeled for three atmospheric source areas; these areas are shown in Figure 6 and discussed in Section 2.2. The modeling projected air concentrations and rates of deposition as a function of time for contaminants originating in each source area, at all cells or

exposure locations within the domain. A complete description of the modeling effort is provided in Jacobson (2005).

The dispersion factors and deposition rates adopted for the performance assessment and composite analysis are those associated with the points of maximum exposure outside of the DOE-controlled boundary. During the 100-year active institutional control period, this is assumed to be the Laboratory boundary; however, once the passive institutional control period begins, this boundary is assumed to coincide with the Area G fence line. The locations where maximum exposures occur outside of these boundaries will depend upon the rates at which radionuclides become airborne across the disposal facility, the dispersion patterns to which these releases are subject, and the contaminant-specific risks represented by the various isotopes.

The points of maximum exposure were identified using a screening process. A location screening value was calculated for each cell of the modeling domain as follows:

$$LSV_x = \sum_{i=1}^{3}\left[\frac{\chi}{Q_{i,x}} \times DSF_i\right] \qquad 67$$

Where

LSV_x = location screening value for grid location x

$\frac{\chi}{Q}_{i,x}$ = air dispersion factor for source area i at grid location x (s/m^3)

DSF_i = dose screening factor for source area i (mrem-m^3/yr)

In this equation, three dispersion factors for a given cell (one factor for each of the three source areas) are multiplied by the corresponding dose screening factors and the results are summed to yield an overall screening value for the cell under consideration. The dose screening factor is given by the following expression:

$$DSF_i = \sum_{j=1}^{n}\left[DCF_{inh,j} \times A_{j,i}\right] \qquad 68$$

Where

$DCF_{inh,j}$ = inhalation dose conversion factor for radionuclide j (mrem/yr per Ci/m^3)

$A_{j,i}$ = inventory of radionuclide j in source area i (Ci)

In the screening approach outlined above, effects of dispersion on exposure are accounted for using the air dispersion factor. The dispersion factors used in the screening were average values based on CALPUFF model runs using 10 years of meteorological data. The dose screening factor accounts for differences in radionuclide inventories among the three source areas and the

inhalation risk posed by each contaminant. The use of this factor implicitly assumes that releases of radionuclides to the air above the site are not isotope-specific.

Location screening values were calculated using Equations 67 and 68 for all grid or exposure locations outside the Laboratory boundary and locations outside the Area G fence line. Separate calculations were conducted for the two land uses considered in the atmospheric modeling; rangeland was used to represent the grassland-dominated site while forest was used to represent piñon-juniper woodland. For each land use, the location with the greatest screening value represents the point of maximum exposure. The dispersion factors and deposition rates for the identified points of maximum exposure were used to estimate doses for the Atmospheric Scenario.

Figure 14 shows the points of maximum exposure at or outside of the Laboratory boundary and the Area G fence line. Maximum exposure locations for particulate releases differ between the performance assessment and composite analysis, but these locations coincide for both analyses for the vapor- and gas-phase releases. For particulate releases, the points of maximum exposure outside of the LANL boundary lie to the north (performance assessment) and northeast (composite analysis) of the active portion of the disposal facility. The points of maximum exposure adjacent to the Area G fence line occur north of the Zone 4 expansion area and slightly east of the active portion of the facility for the performance assessment and composite analysis, respectively. The location outside of the LANL boundary that yields the highest exposures to vapor- and gas-phase releases lies to the north of the active portion of the disposal facility; the location along the Area G fence line is south of the facility boundary. The dispersion factors and deposition rates corresponding to the points of maximum exposure are included in Table 11; separate factors and rates are provided for the two land uses. The distributions shown are based on simulations conducted using 10 years of meteorological data.

As indicated above, Jacobson (2005) conducted two sets of CALPUFF simulations to examine the impacts of vegetation characteristics on atmospheric transport. The first of these assumed the disposal site and surrounding lands consisted of rangeland (grassland); the second assumed the region was forested (piñon-juniper woodland). The data for these two simulation sets were used as "end members" to estimate changes in atmospheric transport conditions as Area G transitions from grassland to woodland, based on the simplifying assumption that this transition is linear. For example, dispersion factors and deposition rates halfway between those listed in Table 11 were assumed to apply when the site had achieved 50 percent of the transition from grassland to woodland.

5.6 Groundwater Transport Parameters

Groundwater transport parameters include the data used to model the release and transport of radionuclides to the regional aquifer. The results of the groundwater modeling are used to determine groundwater pathway doses and to estimate rates of contaminant depletion from surface soils due to leaching. The distributions assigned to these parameters are included in Table 11: the bases of these distributions are provided below.

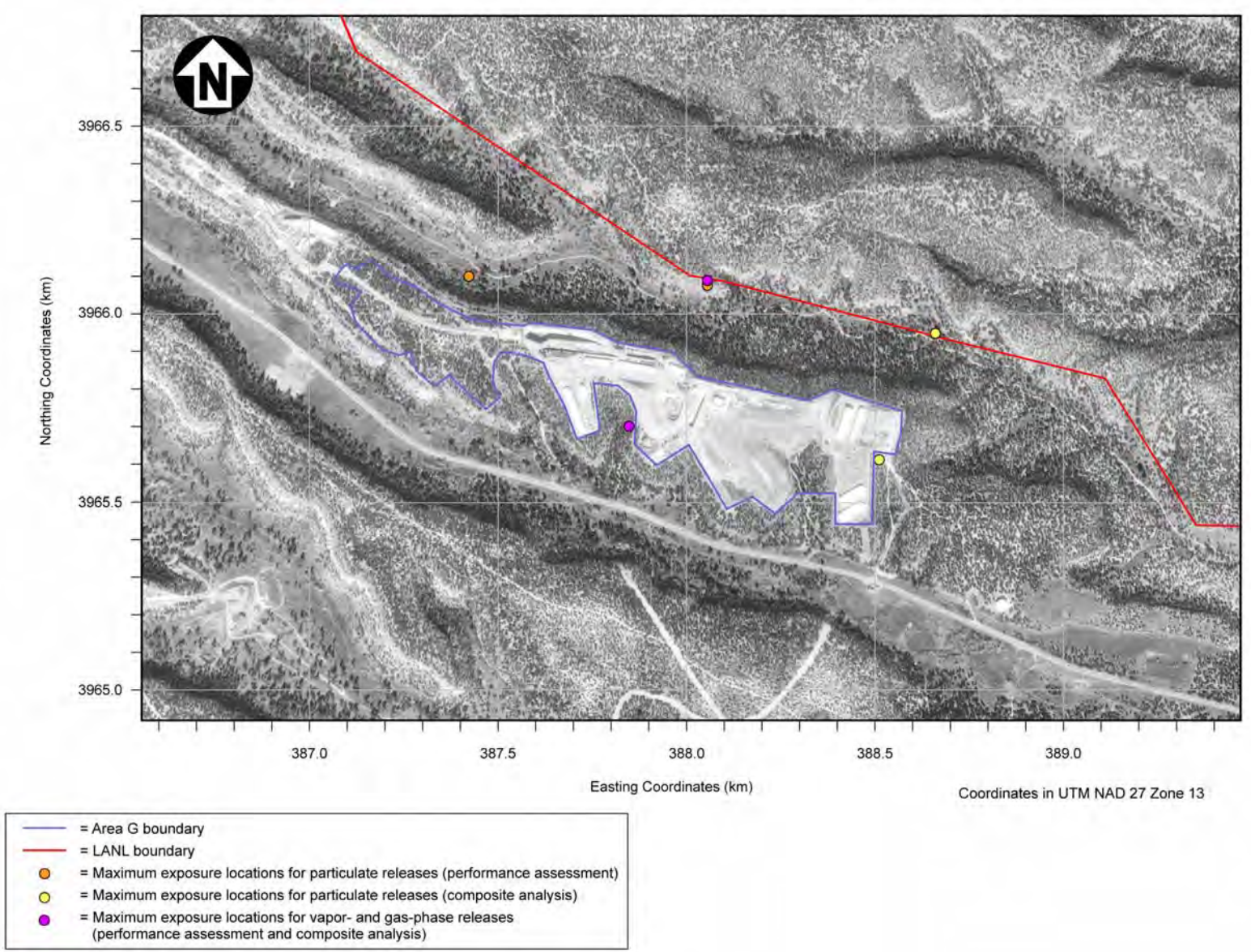

Figure 14
Points of Maximum Exposure for Releases from Area G

5.6.1 Area G Infiltration Rate

The rates at which radionuclides are leached from the waste and transported to the regional aquifer are a function of the mesa-top infiltration rate. Annual infiltration rates through the disposal site have been estimated through a variety of techniques. Newman et al. (2005) used chloride profiles to develop flux estimates through paved and unpaved portions of the disposal site. Levitt (2008) conducted numerous simulations of the near-surface water balance at Area G using the HYDRUS computer code; the results of the modeling were used to estimate rates of infiltration for the final cover proposed for the facility.

The infiltration rate distribution for Area G was developed using the results of the HYDRUS modeling, shown in Table 26. The infiltration rates shown in the table represent annual rates of infiltration over a 15-year period, whereas the performance assessment and composite analysis modeling requires infiltration rates that account for spatial and temporal variations across the disposal site over the 1,000-year compliance period. The spatially and time-averaged infiltration rate was estimated by taking the mean and standard error of the infiltration values shown in Table 26. The assumption that the mean infiltration rate is normally distributed is approximate at best, although the data shown in the table are generally symmetric.

5.6.2 Contaminant Capture Fraction

The contaminant capture fraction represents the portion of the contaminant plume intercepted by a hypothetical domestic well located downgradient of Area G. Effectively, it determines the fraction of the groundwater contamination that contributes to the exposures projected for the receptors in the Groundwater Resource Protection and All Pathways–Groundwater Scenarios.

The contaminant capture fraction is dependent on the area over which radionuclides are discharged to the aquifer, the dispersion characteristics of the aquifer, and the pumping characteristics of the well. Capture fractions were estimated for waste disposal regions 1 through 5 and 8 for a range of transverse dispersivities and well pumping rates. A complete description of this modeling is provided in Stauffer et al. (2005).

The contaminant capture fractions for the different disposal regions, transverse dispersivities, and well pumping rates are summarized in Table 27. The listed values represent the fraction of the contaminant plume that is captured by the receptor's well for the specified pumping rate. The pumping rates generally encompass the range of water usage rates expected for the receptors included in the performance assessment and composite analysis modeling.

Table 26
Measured and Projected Flux Rates for Area G

Data Source	Flux (cm/yr)	Borehole or Model Simulation	Notes
Chloride Profiles	1.0E-03	Borehole P3	---
	1.0E-02	Borehole IC2	---
	1.0E-02	Borehole J2	---
	1.0E-02	Borehole P1	---
	1.0E-02	Borehole J3	---
	1.0E-02	Borehole G1	---
	1.0E-02	Borehole IC3	---
	2.0E-02	Borehole G3	---
	2.0E-02	Borehole IC1	---
	2.0E-02	Borehole 17B	---
	2.0E-02	Borehole J1	---
	3.0E-02	Borehole IC4	---
	4.0E-02	Borehole P2	---
	6.0E-02	Borehole Pit2	---
	2.0E-01	Borehole Pit17	---
	3.0E-01	Borehole Pit24	---
	3.0E-01	Borehole 7B	---
HYDRUS Simulations	2.3E-03	RS1	3 m cover (2 m tuff-clay, 1 m tuff); 2 m rooting depth; curvilinear root distribution; tuff-clay Ksat = 1.8E-06 cm/s; tuff Ksat = 2.9E-04 cm/s; initial head = -80 m to -60 m
	3.6E-03	RS2	4 m cover (3 m tuff-clay, 1 m tuff); 2 m rooting depth; curvilinear root distribution; tuff-clay Ksat = 1.8E-06 cm/s; tuff Ksat = 2.9E-04 cm/s; initial head = -80 m to -65 m
	3.6E-03	RS3	4 m cover (2 m tuff-clay, 2 m tuff); 2 m rooting depth; curvilinear root distribution; tuff-clay Ksat = 1.8E-06 cm/s; tuff Ksat = 2.9E-04 cm/s; initial head = -80 m to -65 m
	2.2E-03	RS4	2 m cover (1 m tuff-clay, 1 m tuff); 2 m rooting depth; curvilinear root distribution; tuff-clay Ksat = 1.8E-06 cm/s; tuff Ksat = 2.9E-04 cm/s; initial head = -80 m to -75 m
	2.3E-03	RS5a	2 m cover (1 m tuff-clay, 1 m tuff); 1 m rooting depth; curvilinear root distribution; tuff-clay Ksat = 1.8E-06 cm/s; tuff Ksat = 2.9E-04 cm/s; initial head = -80 m to -75 m
	2.3E-03	RS5b	3 m cover (2 m tuff-clay, 1 m tuff); 1 m rooting depth; curvilinear root distribution; tuff-clay Ksat = 1.8E-06 cm/s; tuff Ksat = 2.9E-04 cm/s; initial head = -80 m to -60 m

Sources: Chloride profiles taken from Newman et al. (2005); HYDRUS simulation results taken from Levitt (2008).

--- = None

Table 26 (Continued)
Measured and Projected Flux Rates for Area G

Data Source	Flux (cm/yr)	Borehole or Model Simulation	Notes
HYDRUS Simulations (Continued)	3.6E-03	RS5c	4 m cover (3 m tuff-clay, 1 m tuff); 1 m rooting depth; curvilinear root distribution; tuff-clay Ksat = 1.8E-06 cm/s; tuff Ksat = 2.9E-04 cm/s; initial head = -80 m to -65 m
	1.9E-03	RS6a	2 m cover (1 m tuff-clay, 1 m tuff); 6 m rooting depth; curvilinear root distribution; tuff-clay Ksat = 1.8E-06 cm/s; tuff Ksat = 2.9E-04 cm/s; initial head = -80 m to -75 m
	2.0E-03	RS6b	3 m cover (2 m tuff-clay, 1 m tuff); 6 m rooting depth; curvilinear root distribution; tuff-clay Ksat = 1.8E-06 cm/s; tuff Ksat = 2.9E-04 cm/s; initial head = -80 m to -60 m
	2.2E-03	RS6c	4 m cover (3 m tuff-clay, 1 m tuff); 6 m rooting depth; curvilinear root distribution; tuff-clay Ksat = 1.8E-06 cm/s; tuff Ksat = 2.9E-04 cm/s; initial head = -80 m to -65 m
	2.0E-03	RS7a	2 m cover (1 m tuff-clay, 1 m tuff); 2 m rooting depth; linear root distribution; tuff-clay Ksat = 1.8E-06 cm/s; tuff Ksat = 2.9E-04 cm/s; initial head = -80 m to -75 m
	2.0E-03	RS7b	3 m cover (2 m tuff-clay, 1 m tuff); 2 m rooting depth; linear root distribution; tuff-clay Ksat = 1.8E-06 cm/s; tuff Ksat = 2.9E-04 cm/s; initial head = -80 m to -60 m
	2.1E-03	RS7c	4 m cover (3 m tuff-clay, 1 m tuff); 2 m rooting depth; linear root distribution; tuff-clay Ksat = 1.8E-06 cm/s; tuff Ksat = 2.9E-04 cm/s; initial head = -80 m to -65 m
	3.7E-02	RS8a	2 m cover (1 m tuff-clay, 1 m tuff); 2 m rooting depth; curvilinear root distribution; tuff-clay Ksat = 1.8E-06 cm/s; tuff Ksat = 2.9E-04 cm/s; initial head = -30 m; low PT
	8.4E-02	RS8b	3 m cover (2 m tuff-clay, 1 m tuff); 2 m rooting depth; curvilinear root distribution; tuff-clay Ksat = 1.8E-06 cm/s; tuff Ksat = 2.9E-04 cm/s; initial head = -25 m; low PT
	8.9E-02	RS8c	4 m cover (3 m tuff-clay, 1 m tuff); 2 m rooting depth; curvilinear root distribution; tuff-clay Ksat = 1.8E-06 cm/s; tuff Ksat = 2.9E-04 cm/s; initial head = -25 m; low PT
	3.0E-03	RS9a	2 m cover (1 m tuff-clay, 1 m tuff); 2 m rooting depth; curvilinear root distribution; tuff-clay Ksat = 1.7E-04 cm/s; tuff Ksat = 2.9E-04 cm/s; initial head = -80 m to -75 m
	3.1E-03	RS9b	3 m cover (2 m tuff-clay, 1 m tuff); 2 m rooting depth; curvilinear root distribution; tuff-clay Ksat = 1.7E-04 cm/s; tuff Ksat = 2.9E-04 cm/s; initial head = -80 m to -60 m
	5.2E-03	RS9c	4 m cover (3 m tuff-clay, 1 m tuff); 2 m rooting depth; curvilinear root distribution; tuff-clay Ksat = 1.7E-04 cm/s; tuff Ksat = 2.9E-04 cm/s; initial head = -80 m to -65 m
	1.0E-04	RS10a	2 m cover (1 m tuff-clay, 1 m tuff); 2 m rooting depth; curvilinear root distribution; tuff-clay Ksat = 6.3E-08 cm/s; tuff Ksat = 9.2E-05 cm/s; initial head = -80 m to -75 m
	1.0E-04	RS10b	3 m cover (2 m tuff-clay, 1 m tuff); 2 m rooting depth; curvilinear root distribution; tuff-clay Ksat = 6.3E-08 cm/s; tuff Ksat = 9.2E-05 cm/s; initial head = -80 m to -60 m
	2.0E-04	RS10c	4 m cover (3 m tuff-clay, 1 m tuff); 2 m rooting depth; curvilinear root distribution; tuff-clay Ksat = 6.3E-08 cm/s; tuff Ksat = 9.2E-05 cm/s; initial head = -80 m to -65 m

Sources: Chloride profiles taken from Newman et al. (2005); HYDRUS simulation results taken from Levitt (2008).

Table 26 (Continued)
Measured and Projected Flux Rates for Area G

Data Source	Flux (cm/yr)	Borehole or Model Simulation	Notes
HYDRUS Simulations (Continued)	2.3E-03	RS11a	2 m cover (1 m tuff-clay, 1 m tuff); 2 m rooting depth; curvilinear root distribution; tuff-clay Ksat = 1.8E-06 cm/s; tuff Ksat = 2.9E-04 cm/s; initial head = -80 m to -75 m; 2 x precipitation
	2.3E-03	RS11b	3 m cover (2 m tuff-clay, 1 m tuff); 2 m rooting depth; curvilinear root distribution; tuff-clay Ksat = 1.8E-06 cm/s; tuff Ksat = 2.9E-04 cm/s; initial head = -80 m to -60 m; 2 x precipitation
	3.6E-03	RS11c	4 m cover (3 m tuff-clay, 1 m tuff); 2 m rooting depth; curvilinear root distribution; tuff-clay Ksat = 1.8E-06 cm/s; tuff Ksat = 2.9E-04 cm/s; initial head = -80 m to -65 m; 2 x precipitation
	1.9E-03	RS12	2 m cover (1 m tuff-clay, 1 m tuff); 6 m rooting depth; curvilinear root distribution; tuff-clay Ksat = 1.8E-06 cm/s; tuff Ksat = 2.9E-04 cm/s; initial head = -80 m to -20 m; low PT
	1.9E-03	RS13	2 m cover (1 m tuff-clay, 1 m tuff); 6 m rooting depth; curvilinear root distribution; tuff-clay Ksat = 1.8E-06 cm/s; tuff Ksat = 2.9E-04 cm/s; initial head = -80 m to -40 m; high PT
	6.1E-01	RS14	2 m cover (1 m tuff-clay, 1 m tuff); 1 m rooting depth; curvilinear root distribution; tuff-clay Ksat = 1.8E-06 cm/s; tuff Ksat = 2.9E-04 cm/s; initial head = -40 m to -20 m; low PT
	2.3E-03	RS15a	2 m cover (1 m tuff-clay, 1 m tuff); 2 m rooting depth; curvilinear root distribution; tuff-clay Ksat = 1.8E-06 cm/s; tuff Ksat = 2.9E-04 cm/s; tuff-clay initial head = -60 m; tuff initial head = -75 m; medium PT
	2.4E-03	RS15b	3 m cover (2 m tuff-clay, 1 m tuff); 2 m rooting depth; curvilinear root distribution; tuff-clay Ksat = 1.8E-06 cm/s; tuff Ksat = 2.9E-04 cm/s; tuff-clay initial head = -75 m to -60 m; tuff initial head = -75 m; medium PT
	2.4E-03	RS15c	4 m cover (3 m tuff-clay, 1 m tuff); 2 m rooting depth; curvilinear root distribution; tuff-clay Ksat = 1.8E-06 cm/s; tuff Ksat = 2.9E-04 cm/s; tuff-clay initial head = -75 m to -65 m; tuff initial head = -75 m; medium PT
	1.9E-03	RS16a	2 m cover (1 m tuff-clay, 1 m tuff); 6 m rooting depth; linear root distribution; tuff-clay Ksat = 1.8E-06 cm/s; tuff Ksat = 2.9E-04 cm/s; tuff-clay initial head = -60 m; tuff initial head = -75 m
	1.9E-03	RS16b	3 m cover (2 m tuff-clay, 1 m tuff); 6 m rooting depth; linear root distribution; tuff-clay Ksat = 1.8E-06 cm/s; tuff Ksat = 2.9E-04 cm/s; tuff-clay initial head = -60 m; tuff initial head = -75 m
	1.9E-03	RS16c	4 m cover (3 m tuff-clay, 1 m tuff); 6 m rooting depth; linear root distribution; tuff-clay Ksat = 1.8E-06 cm/s; tuff Ksat = 2.9E-04 cm/s; tuff-clay initial head = -60 m; tuff initial head = -75 m
	1.9E-03	RS17a	2 m cover (1 m tuff-clay, 1 m tuff); 6 m rooting depth; curvilinear root distribution; tuff-clay Ksat = 1.8E-06 cm/s; tuff Ksat = 2.9E-04 cm/s; tuff-clay initial head = -60 m; tuff initial head = -75 m; medium PT
	2.0E-03	RS17b	3 m cover (2 m tuff-clay, 1 m tuff); 6 m rooting depth; curvilinear root distribution; tuff-clay Ksat = 1.8E-06 cm/s; tuff Ksat = 2.9E-04 cm/s; tuff-clay initial head = -60 m; tuff initial head = -75 m; medium PT

Sources: Chloride profiles taken from Newman et al. (2005); HYDRUS simulation results taken from Levitt (2008).

Table 26 (Continued)
Measured and Projected Flux Rates for Area G

Data Source	Flux (cm/yr)	Borehole or Model Simulation	Notes
HYDRUS Simulations (Continued)	2.1E-03	RS17c	4 m cover (3 m tuff-clay, 1 m tuff); 6 m rooting depth; curvilinear root distribution; tuff-clay Ksat = 1.8E-06 cm/s; tuff Ksat = 2.9E-04 cm/s; tuff-clay initial head = -75 m to -60 m; tuff initial head = -75 m; medium PT
	2.3E-03	92	2 m cover (1 m tuff-clay, 1 m tuff); 2 m rooting depth; curvilinear root distribution; tuff-clay Ksat = 1.8E-06 cm/s; tuff Ksat = 2.9E-04 cm/s; initial head = -75 m; topsoil and gravel layers
	2.4E-03	93	3 m cover (2 m tuff-clay, 1 m tuff); 2 m rooting depth; curvilinear root distribution; tuff-clay Ksat = 1.8E-06 cm/s; tuff Ksat = 2.9E-04 cm/s; initial head = -75 m; topsoil and gravel layers
	3.6E-03	94	4 m cover (3 m tuff-clay, 1 m tuff); 2 m rooting depth; curvilinear root distribution; tuff-clay Ksat = 1.8E-06 cm/s; tuff Ksat = 2.9E-04 cm/s; initial head = -80 m to -65 m; topsoil and gravel layers

Sources: Chloride profiles taken from Newman et al. (2005); HYDRUS simulation results taken from Levitt (2008).

Table 27
Contaminant Capture Fractions for the Area G Waste Disposal Regions

Waste Disposal Region	Transverse Dispersivity (m)	Well Pumping Rate (m^3/yr)			
		50	600	1,200	2,500
1	0	4.1E-02	4.1E-02	4.1E-02	4.1E-02
	1	1.7E-03	9.9E-03	1.9E-02	3.1E-02
	2	1.5E-03	9.2E-03	1.5E-02	2.6E-02
	5	2.0E-03	5.3E-03	1.3E-02	2.0E-02
2	0	1.1E-01	1.1E-01	1.1E-01	1.1E-01
	1	6.7E-03	2.3E-02	3.9E-02	7.1E-02
	2	5.3E-03	8.6E-03	2.2E-02	4.7E-02
	5	7.3E-04	6.7E-03	1.2E-02	2.7E-02
3	0	3.6E-02	3.6E-02	3.6E-02	3.6E-02
	1	1.2E-03	5.4E-03	9.7E-03	2.4E-02
	2	3.1E-03	2.8E-03	6.8E-03	1.4E-02
	5	3.0E-04	4.1E-03	4.2E-03	7.7E-03
4	0	3.6E-02	3.6E-02	3.6E-02	3.6E-02
	1	5.6E-04	5.0E-03	5.9E-03	1.7E-02
	2	1.0E-08	1.6E-03	5.5E-03	1.1E-02
	5	2.6E-04	2.1E-03	2.7E-03	4.8E-03
5	0	5.8E-02	5.8E-02	5.8E-02	5.8E-02
	1	1.5E-03	9.2E-03	9.3E-03	1.9E-02
	2	5.8E-04	2.0E-03	5.5E-03	1.3E-02
	5	2.8E-04	2.2E-03	1.4E-03	3.9E-03
6	0	1.1E-01	1.1E-01	1.1E-01	1.1E-01
	1	6.7E-03	2.3E-02	3.9E-02	7.1E-02
	2	5.3E-03	8.6E-03	2.2E-02	4.7E-02
	5	7.3E-04	6.7E-03	1.2E-02	2.7E-02
7	0	3.6E-02	3.6E-02	3.6E-02	3.6E-02
	1	1.2E-03	5.4E-03	9.7E-03	2.4E-02
	2	3.1E-03	2.8E-03	6.8E-03	1.4E-02
	5	3.0E-04	4.1E-03	4.2E-03	7.7E-03
8	0	2.7E-02	2.7E-02	3.2E-02	8.1E-02
	1	1.7E-03	7.3E-03	8.0E-03	2.1E-02
	2	1.0E-08	4.1E-03	4.9E-03	1.2E-02
	5	2.6E-04	1.3E-03	3.9E-03	5.1E-03

Capture fractions were not explicitly modeled for the disposal shafts in waste disposal regions 6 and 7. The former region includes shafts located near the east end of pit 6, which is located in disposal region 2; on this basis the capture fractions for regions 2 and 6 were assumed to be the same. The shafts in disposal region 7 are located among the pits over much of region 3. Therefore, the capture fractions for these shafts were assumed to be the same as those for the pits in disposal region 3.

The contaminant capture fractions are generally proportional to the north-south dimension of the disposal region. For example, the capture fractions for waste disposal region 2, the region with the smallest north-south dimension, tend to be greater than the fractions for the other regions. Within a disposal region, capture fractions tend to be inversely proportional to the transverse dispersivity, and proportional to the well pumping rate.

Contaminant capture fractions were estimated on a disposal-region-specific basis using the results summarized in Table 27. Because there were no data available to characterize the transverse dispersivity within the aquifer, it was decided to use the results for the no-dispersion case, which yields the highest capture fractions. For most of the disposal regions, the no-dispersion fractions are the same for all four pumping rates. The capture fraction for disposal region 8 increases by a factor of three as the pumping rate increases from 50 to 2,500 m^3/yr (1.3×10^4 to 6.6×10^5 gal/yr). Based on these results, the capture fractions corresponding to a well pumping rate of 2,500 m^3/yr (6.6×10^5 gal/yr) were adopted for the modeling; the variability inherent in these capture fractions was not considered in the probabilistic modeling.

5.6.3 Exposure Location Infiltration Rates

Radionuclides deposited in surface soils at the receptor locations for the atmospheric, canyon, and groundwater pathway scenarios will be depleted over time as water percolating through the exposure locations carries the contamination downward. The rate of depletion is proportional to the infiltration rate at a given location; the infiltration may represent naturally infiltrating water and irrigation water. Consequently, to model the effects of depletion, the infiltration rates at the various off-site receptor locations must be determined.

In general, infiltration rates to the east of Area G and in adjacent canyons are poorly understood. Estimates of annual infiltration in Pajarito Canyon have been made using chloride mass-balance flux data collected from regional characterization wells R-20 and R-32 (Newman et al., 2005); these data suggest rates of about 1.6 to 2.0 mm/yr (0.063 to 0.079 in./yr). Water fluxes ranging from about 35 to 60 cm/yr (14 to 24 in./yr) have been estimated at regional characterization well R-32 based on nitrate flux data and the assumption that the nitrate is anthropogenic (Newman, 2005). Nylander et al. (2003) assigned net infiltration indices to canyons at the Laboratory, taking into account the proximity of the headwaters, the existence of anthropogenic sources of water, the persistence of surface water, and observations of alluvial water. Based on the index

assigned to the portion of Pajarito Canyon that lies adjacent to Area G, an infiltration rate of 300 mm/yr (12 in./yr) was estimated. More recently, Kwicklis et al. (2005) developed an infiltration map for the Los Alamos region; rates of infiltration ranging from about 20 to 50 cm/yr (7.9 to 20 in./yr) are estimated for the canyon based on this map.

Conditions in Cañada del Buey are considerably drier than those in Pajarito Canyon; this is substantiated by the available estimates of annual infiltration rates. An infiltration rate of 1.3 mm/yr (0.050 in/yr) was estimated on the basis of chloride mass-flux data from regional characterization well R-21, while unpublished data for monitoring hole CDBM-1 indicate an upward flux of 1.8 mm/yr (0.071 in/yr) at a depth of 7.6 to 13 m (25 to 45 ft) and a downward flux of 4.4 mm/yr (0.17 in/yr) at depths between 26 and 58 m (85 and 190 ft) (Newman, 2005). Nylander et al. (2003) estimated a net infiltration rate of 1 mm/yr (0.039 in/yr) for Cañada del Buey. The infiltration map developed by Kwicklis et al. (2005) for the Pajarito Plateau indicates an infiltration rate of about 0 to 2 mm/yr (0 to 0.08 in/yr) for Cañada del Buey.

Even less information is available to characterize rates of infiltration at locations immediately east of the Area G fence line. Nylander et al. (2003) assigned an infiltration rate of 1 mm/yr (0.04 in/yr) for mesa-top locations at the Laboratory. Examination of the infiltration map of Kwicklis et al. (2005) suggests infiltration rates on the order of 0 to 10 mm/yr (0 to 0.4 in/yr).

In the absence of more definitive information, annual infiltration rates in Pajarito Canyon adjacent to Area G were assumed to range between 20 and 60 mm (0.79 to 2 in.), consistent with the nitrate data and the infiltration map developed by Kwicklis et al. (2005). Water is present in this portion of the canyon, suggesting the chloride mass-balance flux data have underestimated actual infiltration rates. The infiltration rate in Cañada del Buey, which is one of the driest canyons at the Laboratory, was assumed to range from 0 to 4.4 mm/yr (0 to 0.17 in/yr), consistent with the data summarized above. Finally, infiltration rates at exposure locations immediately east of Area G were assumed to range from 0 to 10 mm/yr (0 to 0.4 in/yr). In all cases, these ranges were assumed to represent the end points of triangular distributions; the most likely values were set equal to the midpoints of these intervals.

The modeling conducted in support of the performance assessment and composite analysis requires the average annual infiltration rate over the simulation period for each of the exposure locations. To determine this rate for a given location, sampling of the annual infiltration rate distribution was conducted, with replacement, for each year in the simulation period and the mean of these values was calculated. This process was repeated 200 times to generate a distribution of infiltration rates that represents the mean annual infiltration rate over the simulation period; the resulting distribution was used in the probabilistic modeling. This analysis yielded the distributions listed in Table 11.

The contributions of irrigation water to the depletion of contaminants in the surface soils at the exposure locations were not taken into account in the GoldSim models. The assumption was

made that most of this water would be taken up by the receptor's crops and would not contribute significantly to the downward migration of radionuclides. Thus, the infiltration rates discussed above were not modified to include the effects of irrigation.

5.7 Sediment Transport Parameters

The sediment transport parameters address the movement of sediment from the mesa top to Cañada del Buey and Pajarito Canyon and within the canyons themselves. The parameters used to characterize sediment transport are described below.

5.7.1 Sediment Allocation Fractions

Sediment generated on top of Mesita del Buey may be transported with surface runoff to Cañada del Buey to the north of Area G or Pajarito Canyon to the south. The sediment allocation fractions are used to model the movement of sediment to these canyons, including specific catchment areas within each (Figure 11). The general patterns of sediment transport projected to occur at the site have been presented and discussed in Section 3.2.

The sediment allocation fractions shown in Table 28 are average values, taking into account sediment behavior projected for the three erosion scenarios at times ranging from 100 to 10,000 years postclosure. Additional insight into the projected patterns of sediment transport at Area G is provided by the data summarized in Tables 29 and 30. Table 29 shows the allocation fractions for the waste disposal regions averaged over erosion scenarios at various times; Table 30 provides fractions averaged over time for each scenario. Together, these tables suggest that, with some exceptions, the patterns of sediment allocation are relatively constant with time and severity of erosion.

The sediment allocation fractions listed in Table 28 were used to model exposures for persons residing in Cañada del Buey and Pajarito Canyon. Although these fractions are subject to uncertainty, as indicated by the results in Tables 29 and 30, they were specified deterministically for the modeling. This approach was adopted because the model projections are not sufficiently detailed to establish the true variability inherent in the fractions or the correlations between the sediment allocations within a given waste disposal region.

The allocation fractions used in the modeling take into account erosion model projections for a period of 10,000 years following final closure of Area G. Data for projections of more than 1,000 years in the future were used to estimate the fractions because they provide insight into facility performance at times moderately greater than the compliance period. In general, allocation fractions for times up to 1,000 years postclosure fall within 20 percent of those estimated on the basis of 10,000 years.

Table 28
Sediment Allocation Factors for the Catchment Areas in Cañada del Buey and Pajarito Canyon

Waste Disposal Region	Sediment Allocation Fraction by Canyon Catchment Area								
	CdB1	CdB2	PC0	PC1	PC2	PC3	PC4	PC5	PC6
1	3.1E-01	9.9E-02	---	---	---	---	---	3.4E-01	2.5E-01
2	5.3E-01	---	---	---	---	---	---	4.7E-01	---
3	2.0E-01	---	---	---	---	1.1E-01	5.7E-01	1.3E-01	---
4	4.5E-01	---	---	---	2.6E-01	1.5E-01	1.3E-01	---	---
5	4.8E-01	---	---	2.3E-01	2.9E-01	---	---	---	---
6	9.9E-01	---	---	---	---	---	---	7.5E-03	---
7	2.0E-01	---	---	---	---	1.1E-01	5.7E-01	1.3E-01	---
8	6.6E-01	---	2.4E-01	1.0E-01	---	---	---	---	---

--- = The sediment allocation factor is zero.

Table 29
Sediment Allocation Fractions Averaged over Erosion Scenarios at Various Times after Facility Closure

Waste Disposal Region	Time (yr postclosure)	Sediment Allocation Fraction by Canyon Catchment Area (mean ± std deviation)								
		CdB1	CdB2	PC0	PC1	PC2	PC3	PC4	PC5	PC6
1	100	2.4E-01 ±8.5E-02	1.2E-01 ±4.5E-02	---	---	---	---	---	3.6E-01 ±1.3E-01	2.7E-01 ±4.9E-02
	200	2.2E-01 ±1.0E-01	9.9E-02 ±3.0E-02	---	---	---	---	---	4.5E-01 ±1.4E-01	2.3E-01 ±5.5E-02
	500	3.4E-01 ±8.8E-02	9.6E-02 ±1.1E-01	---	---	---	---	---	2.8E-01 ±1.1E-01	2.9E-01 ±9.5E-02
	1,000	3.9E-01 ±7.1E-02	5.4E-02 ±1.6E-02	---	---	---	---	---	3.4E-01 ±8.2E-02	2.1E-01 ±8.1E-02
	5,000	3.5E-01 ±1.5E-01	1.4E-01 ±2.5E-02	---	---	---	---	---	2.9E-01 ±5.6E-02	2.2E-01 ±8.8E-02
	10,000	3.2E-01 ±4.1E-01	8.3E-02 ±8.3E-02	---	---	---	---	---	2.9E-01 ±1.8E-01	3.1E-01 ±1.5E-01
2	100	5.1E-01 ±4.4E-02	---	---	---	---	---	---	4.9E-01 ±4.4E-02	---
	200	5.2E-01 ±3.9E-02	---	---	---	---	---	---	4.8E-01 ±3.9E-02	---
	500	5.4E-01 ±5.0E-02	---	---	---	---	---	---	4.6E-01 ±5.0E-02	---
	1,000	5.5E-01 ±6.1E-02	---	---	---	---	---	---	4.5E-01 ±6.1E-02	---
	5,000	5.4E-01 ±9.7E-02	---	---	---	---	---	---	4.6E-01 ±9.7E-02	---
	10,000	5.1E-01 ±1.6E-01	---	---	---	---	---	---	4.9E-01 ±1.6E-01	---
3	100	1.9E-01 ±3.2E-02	---	---	---	---	---	6.0E-01 ±3.6E-02	2.2E-01 ±4.7E-02	---
	200	1.9E-01 ±3.5E-02	---	---	---	---	6.7E-02 ±1.2E-01	5.6E-01 ±1.2E-01	1.8E-01 ±2.7E-02	---

--- = The sediment allocation fraction is zero.

Table 29 (Continued)
Sediment Allocation Fractions Averaged over Erosion Scenarios at Various Times after Facility Closure

Waste Disposal Region	Time (yr postclosure)	Sediment Allocation Fraction by Canyon Catchment Area (mean ± std deviation)								
		CdB1	CdB2	PC0	PC1	PC2	PC3	PC4	PC5	PC6
3 (Cont.)	500	1.8E-01 ±3.0E-02	---	---	---	---	2.0E-01 ±1.8E-01	4.5E-01 ±1.2E-01	1.7E-01 ±8.0E-02	---
	1,000	1.8E-01 ±8.3E-03	---	---	---	---	1.2E-01 ±2.0E-01	6.3E-01 ±2.3E-01	7.8E-02 ±6.3E-02	---
	5,000	1.9E-01 ±1.8E-02	---	---	---	---	---	7.1E-01 ±1.3E-01	1.0E-01 ±1.1E-01	---
	10,000	2.5E-01 ±4.2E-02	---	---	---	---	2.6E-01 ±2.3E-01	4.5E-01 ±2.1E-01	4.6E-02 ±6.8E-03	---
4	100	5.0E-01 ±7.8E-02	---	---	---	1.9E-01 ±5.1E-02	2.0E-01 ±2.9E-02	1.2E-01 ±4.3E-03	---	---
	200	5.0E-01 ±7.5E-02	---	---	---	2.1E-01 ±4.3E-02	2.1E-01 ±9.4E-02	8.3E-02 ±7.2E-02	---	---
	500	4.8E-01 ±5.0E-02	---	---	---	2.7E-01 ±3.1E-02	2.1E-01 ±6.8E-02	3.9E-02 ±6.8E-02	---	---
	1,000	4.7E-01 ±6.1E-02	---	---	---	2.8E-01 ±1.4E-02	1.5E-01 ±1.5E-01	9.6E-02 ±8.6E-02	---	---
	5,000	3.7E-01 ±9.0E-02	---	---	---	3.1E-01 ±1.5E-01	7.1E-03 ±8.3E-03	3.0E-01 ±2.3E-01	---	---
	10,000	4.0E-01 ±6.2E-02	---	---	---	3.1E-01 ±1.1E-01	1.3E-01 ±1.1E-01	1.6E-01 ±2.8E-01	---	---
5	100	5.4E-01 ±3.6E-02	---	---	2.1E-01 ±1.9E-02	2.5E-01 ±5.5E-02	---	---	---	---
	200	5.0E-01 ±5.4E-02	---	---	2.4E-01 ±1.5E-02	2.6E-01 ±5.8E-02	---	---	---	---
	500	4.7E-01 ±7.3E-02	---	---	2.4E-01 ±9.6E-03	2.8E-01 ±6.5E-02	---	---	---	---
	1,000	4.4E-01 ±5.3E-02	---	---	2.7E-01 ±3.6E-02	2.9E-01 ±5.1E-02	---	---	---	---

--- = The sediment allocation fraction is zero.

Table 29 (Continued)
Sediment Allocation Fractions Averaged over Erosion Scenarios at Various Times after Facility Closure

Waste Disposal Region	Time (yr postclosure)	Sediment Allocation Fraction by Canyon Catchment Area (mean ± std deviation)								
		CdB1	CdB2	PC0	PC1	PC2	PC3	PC4	PC5	PC6
5 (Cont.)	5,000	4.6E-01 ±9.2E-02	---	---	2.3E-01 ±6.9E-02	3.1E-01 ±2.4E-02	---	---	---	---
	10,000	4.8E-01 ±4.5E-02	---	---	2.0E-01 ±3.3E-02	3.3E-01 ±1.7E-02	---	---	---	---
6	100	1.0E ±00 ±0.0E ±00	---	---	---	---	---	---	---	---
	200	1.0E ±00 ±0.0E ±00	---	---	---	---	---	---	---	---
	500	1.0E ±00 ±0.0E ±00	---	---	---	---	---	---	---	---
	1,000	1.0E ±00 ±0.0E ±00	---	---	---	---	---	---	---	---
	5,000	9.8E-01 ±2.3E-02	---	---	---	---	---	---	1.6E-02 ±2.3E-02	---
	10,000	9.7E-01 ±3.8E-02	---	---	---	---	---	---	2.9E-02 ±3.8E-02	---
8	100	6.2E-01 ±3.0E-02	---	2.9E-01 ±3.7E-02	9.3E-02 ±1.7E-02	---	---	---	---	---
	200	6.3E-01 ±5.4E-02	---	2.9E-01 ±5.1E-02	8.4E-02 ±2.6E-03	---	---	---	---	---
	500	6.6E-01 ±1.4E-01	---	2.3E-01 ±1.4E-01	1.1E-01 ±1.0E-01	---	---	---	---	---
	1,000	6.9E-01 ±6.8E-02	---	2.0E-01 ±7.9E-02	1.1E-01 ±1.4E-01	---	---	---	---	---
	5,000	6.9E-01 ±5.2E-02	---	1.9E-01 ±8.4E-02	1.3E-01 ±8.5E-02	---	---	---	---	---
	10,000	6.9E-01 ±6.8E-02	---	2.4E-01 ±2.0E-02	7.3E-02 ±5.2E-02	---	---	---	---	---

--- = The sediment allocation fraction is zero.

Table 30
Sediment Allocation Fractions Averaged over Time after Facility Closure

Waste Disposal Region	Erosion Scenario	Sediment Allocation Fraction by Canyon Catchment Area (mean ± std deviation)								
		CdB1	CdB2	PC0	PC1	PC2	PC3	PC4	PC5	PC6
1	Low	3.7E-01 ±2.5E-01	9.5E-02 ±7.4E-02	---	---	---	---	3.4E-01 ±2.1E-01	1.9E-01 ±9.8E-02	---
	Moderate	2.7E-01 ±1.6E-01	1.2E-01 ±5.5E-02	---	---	---	---	3.3E-01 ±7.2E-02	2.8E-01 ±8.2E-02	---
	High	2.9E-01 ±5.7E-02	7.8E-02 ±3.8E-02	---	---	---	---	3.4E-01 ±1.5E-02	2.9E-01 ±4.4E-02	---
2	Low	5.4E-01 ±7.6E-02	---	---	---	---	---	4.6E-01 ±7.6E-02	---	---
	Moderate	5.5E-01 ±5.6E-02	---	---	---	---	---	4.5E-01 ±5.6E-02	---	---
	High	4.9E-01 ±8.2E-02	---	---	---	---	---	5.1E-01 ±8.2E-02	---	---
3	Low	1.9E-01 ±4.6E-02	---	---	---	9.0E-02 ±1.5E-01	5.9E-01 ±2.0E-01	1.3E-01 ±1.3E-01	---	---
	Moderate	1.8E-01 ±1.3E-02	---	---	---	1.8E-01 ±2.1E-01	5.2E-01 ±1.7E-01	1.2E-01 ±5.8E-02	---	---
	High	2.2E-01 ±2.7E-02	---	---	---	4.7E-02 ±1.2E-01	5.9E-01 ±1.2E-01	1.4E-01 ±6.1E-02	---	---
4	Low	4.3E-01 ±2.2E-02	---	---	3.0E-01 ±7.7E-02	1.8E-01 ±9.6E-02	9.0E-02 ±7.4E-02	---	---	---
	Moderate	4.5E-01 ±1.8E-02	---	---	2.8E-01 ±7.6E-02	2.0E-01 ±1.1E-01	6.5E-02 ±7.3E-02	---	---	---
	High	4.8E-01 ±1.4E-01	---	---	2.0E-01 ±7.7E-02	7.7E-02 ±8.2E-02	2.5E-01 ±2.3E-01	---	---	---

--- = The sediment allocation fraction is zero.

Table 30 (Continued)
Sediment Allocation Fractions Averaged over Time after Facility Closure

Waste Disposal Region	Erosion Scenario	Sediment Allocation Fraction by Canyon Catchment Area (mean ± std deviation)								
		CdB1	CdB2	PC0	PC1	PC2	PC3	PC4	PC5	PC6
5	Low	4.9E-01 ±8.2E-02	---	2.5E-01 ±3.1E-02	2.6E-01 ±6.0E-02	---	---	---	---	---
	Moderate	4.8E-01 ±5.3E-02	---	2.4E-01 ±4.1E-02	2.8E-01 ±4.6E-02	---	---	---	---	---
	High	4.7E-01 ±5.7E-02	---	2.1E-01 ±3.6E-02	3.2E-01 ±2.2E-02	---	---	---	---	---
6	Low	1.0E ±00 ±1.1E-03	---	---	---	---	---	4.6E-04 ±1.1E-03	---	---
	Moderate	1.0E ±00 ±4.5E-03	---	---	---	---	---	2.8E-03 ±4.5E-03	---	---
	High	9.8E-01 ±3.1E-02	---	---	---	---	---	1.9E-02 ±3.1E-02	---	---
8	Low	6.6E-01 ±7.0E-02	2.5E-01 ±9.5E-02	8.8E-02 ±7.2E-02	---	---	---	---	---	---
	Moderate	6.9E-01 ±9.4E-02	2.4E-01 ±7.1E-02	6.1E-02 ±2.4E-02	---	---	---	---	---	---
	High	6.3E-01 ±2.6E-02	2.1E-01 ±7.2E-02	1.5E-01 ±8.0E-02	---	---	---	---	---	---

--- = The sediment allocation fraction is zero.

5.7.2 Sediment Dispersal Fraction

The exposures projected for persons residing in Cañada del Buey and Pajarito Canyon ultimately depend upon the concentrations of radionuclides in the canyon floor soils. These concentrations, in turn, depend upon the manner in which the sediments are dispersed as they are transported to the receptor locations. Patterns of sediment dispersal are expected to be complex, affected by the spatial and temporal patterns of runoff from the disposal facility as well as the characteristics of the side slopes of the mesa and the canyon floors.

Although the SIBERIA model provided estimates of the sediment transported from the mesa top, the version of the program available at the time the modeling was conducted was incapable of modeling sediment particle paths from the mesa to the floors of Cañada del Buey and Pajarito Canyon. Consequently, the sediment dispersal fraction was estimated and applied to the modeling; the product of this factor and the catchment area (Table 31) yields the area over which contaminated sediment was assumed to spread within that catchment.

Table 31
Size of Catchments in Cañada del Buey and Pajarito Canyon

Catchment	Surface Area (m^2)
Cañada del Buey	
CdB1	1.8E+05
CdB2	7.3E+04
Pajarito Canyon	
PC0	1.4E+05
PC1	4.8E+04
PC2	2.8E+04
PC3	3.4E+04
PC4	3.1E+04
PC5	2.6E+04
PC6	3.4E+04

All sediment is assumed to be deposited on the canyon floor during the same year it is transported from the mesa top. The area over which the contaminated sediment is deposited within a given catchment could range from a small portion of the canyon to the entire canyon floor. In the absence of the information needed to define the area over which the sediments actually disperse, it was assumed that the material transported from the mesa top would cover 10 to 50 percent of each catchment. On this basis, the sediment dispersal fraction was assigned a triangular distribution with minimum, most likely, and maximum values of 0.1, 0.3, and 0.5, respectively.

Although further analysis is required to estimate suitable sediment dispersal factors, those selected for the modeling are expected to be reasonable. A portion of the sediment transported from the mesa will disperse along the slopes of the mesa, and will not reach the canyon floor until some years after it leaves the mesa top. This increase in the area of dispersal, which was not accounted for in the development of the dispersal factors, will further reduce radionuclide concentrations in the canyon soils. Also, it is considered likely that any sediment reaching the canyon floor will generally disperse over more than 10 percent of the catchment area, the lower bound of the adopted distribution.

5.7.3 Canyon Sediment Transport Rates

Sediments deposited in Cañada del Buey and Pajarito Canyon will be transported down the canyons over time. Rates of sediment transport within the canyons will depend upon various characteristics of the canyons, the frequency of flooding within the canyons, and the patterns of sediment deposition. Although a detailed evaluation of sediment transport rates within the canyons adjacent to Area G has not been undertaken, information provided by Malmon et al. (2005) provides insight into this phenomenon.

Malmon et al. (2005) modeled rates of Cs-137–contaminated sediment transport in Upper Los Alamos Canyon, between its confluence with DP Canyon and the LANL boundary, and compared the projected rates of transport to measured Cs-137 loadings in the modeled region. The modeling projected rates of transport of coarse sediments within the stream channel and fine sediments located in the floodplains adjacent to the streambed. Residence times of the coarse sediments within the stream channel were relatively short, with flushing times for the entire 5-km (3.1-mi.) reach projected to be about 20 to 25 years. In contrast, the residence time of fine sediments in the floodplains was about 60 years.

The sediment residence times projected by Malmon et al. (2005) for Upper Los Alamos Canyon are not necessarily applicable to Cañada del Buey and Pajarito Canyon, each of which is expected to be unique in terms of sediment transport. Based on field observations, it is expected that Pajarito Canyon will effectively trap sediments for long periods of time (Reneau, 2005). This is because much of the bottom of the canyon consists of large, inactive borrow pits that function as wetlands. Water spreads out into these small depressions at times of flooding, losing much of its energy and depositing sediments into heavy grasses. As a result, rates of erosion along the channel margins are expected to be small.

Sediment transport behavior in Cañada del Buey is expected to be much different than that observed in Upper Los Alamos Canyon (Malmon et al., 2005) or Pajarito Canyon (Reneau, 2005). Flow and, therefore, flooding within the canyon are infrequent. Higher sediment transmission losses are likely and the large sediment supply is expected to encourage deposition when water is flowing down the canyon. Thus, it is likely that sediment residence times within Cañada del Buey will be no shorter than those observed in Upper Los Alamos Canyon, and perhaps significantly longer.

It is reasonable to expect that contaminated sediments within Cañada del Buey and Pajarito Canyon will eventually be transported down the canyons as a result of flooding. The hypothetical canyon receptors would most likely come into contact with contamination deposited along the floodplains in these canyons. Therefore, the behavior of floodplain sediments is of most interest from the perspective of the performance assessment and composite analysis modeling. Malmon et al. (2005) found particle residence times of about 60 years over a 5 km (3.1 mi) stretch of Upper Los Alamos Canyon; this translates into flushing rate of about 0.015/yr for that segment of the canyon. As indicated above, the corresponding rates for the canyons adjacent to Area G are probably no more than this and may be much less.

The available information is not adequate for developing definitive estimates of sediment transport rates within Cañada del Buey and Pajarito Canyon. In the absence of additional information, it was assumed that the mean particle residence time in the canyons adjacent to Area G is about 200 years. This is substantially longer than the residence times estimated for Upper Los Alamos Canyon, especially considering that the canyon stretch investigated in that canyon (5 km [3.1 mi]) is about five times the lengths of the canyon reaches along Area G. Based on this assumption, a sediment transport rate of 0.005/yr was selected as the mean of a normal distribution; the coefficient of variation of this distribution was assumed to be 0.2.

5.8 Food-Chain Transport Parameters

Food-chain transport parameters were used to estimate radionuclide concentrations in crops and animals raised by a receptor as food sources. The point estimates and distributions used to describe these parameters and the information on which these data were based, are discussed below.

5.8.1 Crop Uptake Factor

The plant uptake factors for vegetable crops are used to model root uptake of radionuclides from contaminated soils. Compilations of uptake factors have been published by Baes et al. (1984), the International Atomic Energy Agency (IAEA, 1994), the NCRP (1999), Napier et al. (2004), and the NRC (1992), among others. The uptake factors for many elements included in these syntheses come from the same original sources.

The plant uptake factors compiled by Napier et al. (2004) were adopted for the performance assessment and composite analysis; these factors are listed in Table 32. This source was selected because it addresses a comprehensive list of elements and draws on more recent data than some of the other compilations. Napier et al. (2004) provide uptake factors for leafy vegetables, root vegetables, and grain. The factors provided for leafy vegetables and grain were used to estimate contaminant concentrations in those crops, while the factors for root vegetables were used to model plant uptake in all other produce.

Table 32
Parameter Values and Distributional Information for Plant Uptake Factors

Element	Leafy Vegetables and Pasture Grass (dry weight)		Produce (dry weight)		Grain (dry weight)	
	Geometric Mean	Geometric Standard Deviation	Geometric Mean	Geometric Standard Deviation	Geometric Mean	Geometric Standard Deviation
Ac	4.7E-04	3.5E+00	3.5E-04	3.5E+00	2.2E-05	3.5E+00
Ag	2.7E-04	3.5E+00	1.3E-03	3.5E+00	2.5E-01	3.5E+00
Al [a]	4.0E-03	3.5E+00	4.0E-04	3.5E+00	4.0E-04	3.5E+00
Am	4.7E-04	3.5E+00	3.5E-04	3.5E+00	2.2E-05	3.5E+00
Ba	1.5E-01	3.5E+00	1.5E-02	3.5E+00	1.5E-02	3.5E+00
Be	1.0E-02	3.5E+00	1.5E-03	3.5E+00	2.0E-03	3.5E+00
Bi	5.0E-01	3.5E+00	5.0E-01	3.5E+00	5.0E-01	3.5E+00
Bk [b]	4.7E-04	3.5E+00	3.5E-04	3.5E+00	2.2E-05	3.5E+00
C	7.0E-01	3.5E+00	7.0E-01	3.5E+00	7.0E-01	3.5E+00
Ca	3.5E+00	3.5E+00	3.5E-01	3.5E+00	3.5E-01	3.5E+00
Cf	4.7E-04	3.5E+00	3.5E-04	3.5E+00	2.2E-05	3.5E+00
Cl	7.0E+01	3.5E+00	7.0E+01	3.5E+00	7.0E+01	3.5E+00
Cm	7.7E-04	3.5E+00	4.3E-04	3.5E+00	2.1E-05	3.5E+00
Co	2.3E-01	3.5E+00	6.7E-02	3.5E+00	3.7E-03	3.5E+00
Cs	4.6E-01	3.5E+00	1.3E-01	3.5E+00	2.6E-02	3.5E+00
Eu	2.0E-02	3.5E+00	2.0E-02	3.5E+00	2.0E-02	3.5E+00
Gd	2.0E-02	3.5E+00	2.0E-02	3.5E+00	2.0E-02	3.5E+00

Source: Napier et al. (2004) unless otherwise indicated

--- = Element exists solely as a gas and was ignored in terms of food-chain transport

[a] Uptake factors for Al were set equal to the corresponding factors for Ga, In, and Tl.

[b] Uptake factors for Bk were set equal to the values for Am.

[c] Plant uptake factors for tritium were estimated using specific activity models. See discussion in text.

[d] Uptake factors for Lu were set equal to the corresponding factors for Eu, Gd, and Ti.

[e] Uptake factors for Ti were set equal to the corresponding factors for Hf and Zr.

Table 32 (Continued)
Parameter Values and Distributional Information for Plant Uptake Factors

Element	Leafy Vegetables and Pasture Grass (dry weight)		Produce (dry weight)		Grain (dry weight)	
	Geometric Mean	Geometric Standard Deviation	Geometric Mean	Geometric Standard Deviation	Geometric Mean	Geometric Standard Deviation
H [c]	---	---	---	---	---	---
Ho	2.0E-02	3.5E+00	2.0E-02	3.5E+00	2.0E-02	3.5E+00
I	4.0E-02	3.5E+00	4.0E-02	3.5E+00	4.0E-02	3.5E+00
K	1.0E+00	3.5E+00	5.5E-01	3.5E+00	5.5E-01	3.5E+00
Kr	---	---	---	---	---	---
Lu [d]	2.0E-02	3.5E+00	2.0E-02	3.5E+00	2.0E-02	3.5E+00
Mo	8.0E-01	3.5E+00	8.0E-01	3.5E+00	8.0E-01	3.5E+00
Nb	2.5E-02	3.5E+00	2.5E-02	3.5E+00	2.5E-02	3.5E+00
Nd	2.0E-02	3.5E+00	2.0E-02	3.5E+00	2.0E-02	3.5E+00
Ni	2.8E-01	3.5E+00	6.0E-02	3.5E+00	3.0E-02	3.5E+00
Np	3.2E-02	3.5E+00	1.3E-02	3.5E+00	2.7E-03	3.5E+00
Os	1.5E-02	3.5E+00	3.5E-03	3.5E+00	3.5E-03	3.5E+00
Pa	4.7E-04	3.5E+00	3.5E-04	3.5E+00	2.2E-05	3.5E+00
Pb	1.0E-02	3.5E+00	6.0E-03	3.5E+00	4.7E-03	3.5E+00
Pm	2.0E-02	3.5E+00	2.0E-02	3.5E+00	2.0E-02	3.5E+00
Pu	6.0E-05	3.5E+00	1.1E-03	3.5E+00	8.6E-06	3.5E+00
Ra	4.9E-02	3.5E+00	2.0E-03	3.5E+00	1.2E-03	3.5E+00

Source: Napier et al. (2004) unless otherwise indicated

--- = Element exists solely as a gas and was ignored in terms of food-chain transport

[a] Uptake factors for Al were set equal to the corresponding factors for Ga, In, and Tl.

[b] Uptake factors for Bk were set equal to the values for Am.

[c] Plant uptake factors for tritium were estimated using specific activity models. See discussion in text.

[d] Uptake factors for Lu were set equal to the corresponding factors for Eu, Gd, and Ti.

[e] Uptake factors for Ti were set equal to the corresponding factors for Hf and Zr.

Table 32 (Continued)
Parameter Values and Distributional Information for Plant Uptake Factors

Element	Leafy Vegetables and Pasture Grass (dry weight)		Produce (dry weight)		Grain (dry weight)	
	Geometric Mean	Geometric Standard Deviation	Geometric Mean	Geometric Standard Deviation	Geometric Mean	Geometric Standard Deviation
Si	3.5E-01	3.5E+00	7.0E-02	3.5E+00	7.0E-02	3.5E+00
Sm	2.0E-02	3.5E+00	2.0E-02	3.5E+00	2.0E-02	3.5E+00
Sn	3.0E-02	3.5E+00	6.0E-03	3.5E+00	6.0E-03	3.5E+00
Sr	3.0E+00	3.5E+00	5.0E-01	3.5E+00	2.1E-01	3.5E+00
Tb	2.0E-02	3.5E+00	2.0E-02	3.5E+00	2.0E-02	3.5E+00
Tc	2.1E+02	3.5E+00	2.4E-01	3.5E+00	7.3E-01	3.5E+00
Th	1.8E-03	3.5E+00	3.3E-04	3.5E+00	3.4E-05	3.5E+00
Ti [e]	1.0E-03	3.5E+00	1.0E-03	3.5E+00	1.0E-03	3.5E+00
U	8.3E-03	3.5E+00	1.2E-02	3.5E+00	1.3E-03	3.5E+00
Zr	1.0E-03	3.5E+00	1.0E-03	3.5E+00	1.0E-03	3.5E+00

Source: Napier et al. (2004) unless otherwise indicated

--- = Element exists solely as a gas and was ignored in terms of food-chain transport

[a] Uptake factors for Al were set equal to the corresponding factors for Ga, In, and Tl.

[b] Uptake factors for Bk were set equal to the values for Am.

[c] Plant uptake factors for tritium were estimated using specific activity models. See discussion in text.

[d] Uptake factors for Lu were set equal to the corresponding factors for Eu, Gd, and Ti.

[e] Uptake factors for Ti were set equal to the corresponding factors for Hf and Zr.

Baes et al. (1984) conducted an extensive literature review of uptake factors and found that these parameters were generally lognormally distributed. Geometric means and standard deviations were estimated for the elements with sufficient data, and the geometric means of the distributions were generally adopted as the best estimates of plant uptake. Based on this work, the values taken from Napier et al. (2004) were assumed to represent geometric means of the lognormal distributions used in the uncertainty analyses. Sufficient data to define element-specific geometric standard deviations for these distributions were not found; consequently, a standard deviation of 3.5 was assumed for all plant uptake distributions except tritium (see below). This value is the approximate average of the standard deviations reported by Baes et al. for those elements whose distributions could be estimated.

The geometric standard deviation of 3.5 adopted for the plant uptake distributions is also consistent with other information in the literature. The NCRP (1999) adopted geometric standard deviations ranging from 2.5 to 3.0 to estimate soil-screening criteria. Sheppard and Evenden (1997) list appropriate geometric standard deviations for stochastic evaluations of plant uptake ranging from 1.5 to 5.7, depending upon available site and crop information. A geometric standard deviation of 3.3 is considered appropriate when information exists about the crop type but not about the site or soil characteristics. Finally, a geometric standard deviation of 3.5 is equal to the value cited by the NCRP (1984) for cesium in food and forage crops, but less than the cited NCRP value of 4.1 for strontium.

Napier et al. (2004) did not provide plant uptake factors for some of the elements in the performance assessment and composite analysis, including aluminum, berkelium, lutetium, titanium, and hydrogen. Plant uptake factors for four of these elements were assigned values common to other elements in the same groups. The factors for aluminum were set equal to thevalues for gallium, indium, and thallium, while uptake factors for berkelium were set equal to those for americium. The uptake factors for lutetium were set equal to the values provided for europium, gadolinium, and terbium. Finally, the plant uptake factors for titanium were set equal to the factors given for hafnium and zirconium.

Plant concentrations of hydrogen as tritium were estimated using the specific activity model described in Section 3.7.3.3. Implementation of this model required information about the fraction of water in the vegetation and the fraction of hydrogen in plants. The water fraction was estimated using the dry-to-wet weight fractions discussed below. The fraction of hydrogen in plants was assumed to be 0.062 (dry weight basis) for all crops (Napier et al., 1988).

5.8.2 Dry-to-Wet Weight Fraction

Dry-to-wet weight fractions are used to convert plant uptake factors and forage intake rates from a dry-to-wet weight basis. Point estimates and distributions were defined for these fractions using moisture content data from Baes et al. (1984) and the EPA (1997) for various species of leafy

vegetables, produce, and grain; these data are summarized in Table 33. Crop-specific data were used to define the distributions shown in Table 11 for the various crop categories or types.

Peterson (1983) provides fresh-to-dry weight ratios for forage of 4.44, 5.0, 5.5, and 4.2 for alfalfa, clover, grass, and silage, respectively. These data indicate dry-to-wet weight fractions ranging from 0.18 to 0.24. Data cited in IAEA Technical Report 364 (1994) include dry-to-wet weight fractions of 0.19 and 0.1 for alfalfa and grass, respectively. Because no additional information was available, a value of 0.2 was adopted as the most likely value of a triangular distribution for the forage eaten by cows and cattle. Minimum and maximum values were assumed to be 0.15 and 0.25, respectively. The point estimate and distribution for the dry-to-wet weight fraction for grain (Table 11) were used to define the dry-to-wet weight fraction for the feed consumed by chickens.

5.8.3 Translocation Factor

Translocation factors describe the portion of the contamination deposited on the exterior of the crops that passes into the plant tissues and becomes assimilated. Limited data exist to develop distributions of the crop-specific factors. The NCRP (1984) cites default values of 1.0 and 0.1 for leafy vegetables and other produce, respectively. Ng et al. (1978) list translocation factors for various crops and radionuclides. The maximum translocation factor listed for produce (excluding fruit) and grain is 0.36; data provided for leafy vegetables are limited to cabbage, which has a translocation factor as high as 0.12, depending upon the radionuclide under consideration. The factors for cabbage are significantly lower than the default value of 1.0 recommended for leafy vegetables by the NCRP (1984). Ng et al. (1978) assigned a translocation factor of 1.0 to all radionuclides for hay and other types of animal forage and feed. Hinton (1994), cited by the Oak Ridge National Laboratory guidance (ORNL, 1999), provided translocation factors for cesium,strontium, iodine, and plutonium in winter barley and wheat, root vegetables, other vegetables, and fruits. With the exception of potatoes, which had a translocation factor of 0.5, all crops had factors less than or equal to 0.02.

On the basis of the data provided above, the translocation factor for leafy vegetables was assigned a point estimate of 1.0 for use in the deterministic modeling. The parameter was assigned a triangular distribution with minimum, most likely, and maximum values of 0.8, 0.9, and 1.0. This distribution ignores the very low translocation factor estimated for cabbage by Ng et al. (1978), but considers reduced rates of assimilation by the plants. The same deterministic value and distribution were assumed to apply to pasture grass grown for animal consumption. The translocation factors for produce and grain were also assumed to have a triangular distribution with minimum, most likely, and maximum values of 0.01, 0.1, and 0.4, respectively. The end points of the distribution roughly coincide with the data discussed above.

Table 33
Dry-to-Wet Weight Fractions for Crops

Crop	Dry-To-Wet Weight Fraction	Crop	Dry-to-Wet Weight Fraction
Leafy Vegetables			
Alfalfa Sprouts	8.9E-02	Green onions	1.2E-01
Beets—Greens	7.9E-02	Kale	1.6E-01
Broccoli	9.7E-02 [a]	Leeks	1.7E-01
Brussels Sprouts	1.5E-01 [a]	Lettuce	4.8E-02 [a]
Cabbage	8.4E-02 [a]	Mung bean sprouts	9.6E-02
Cauliflower	8.0E-02 [a]	Mustard greens	9.2E-02
Celery	5.8E-02 [a]	Parsley	1.2E-01
Collards	6.1E-02	Rhubarb	6.4E-02
Cress	1.1E-01 [a]	Spinach	7.9E-02 [a]
Dandelion Greens	1.4E-01	Swiss chard	7.3E-02
Endive	6.2E-02	Turnips—tops	8.9E-02
Escarole	1.3E-01		
Produce			
Asparagus	7.4E-02 [a]	Parsnips	2.0E-01
Beans - Lima	3.0E-01	Peas	2.6E-01
Beans—Snap, Italian, Green, Yellow	1.0E-01 [a]	Peppers—sweet	7.2E-02
Beets	1.3E-01	Potatoes	1.9E-01 [a]
Carrots	1.2E-01 [a]	Pumpkin	8.4E-02
Chili Peppers	1.2E-01	Radishes—roots	5.2E-02
Corn - Sweet	2.5E-01 [a]	Rutabaga	1.0E-01
Cucumbers	3.9E-02 [a]	Shallots	2.0E-01
Eggplant	7.7E-02 [a]	Soybeans	3.1E-01
Garlic	4.1E-01	Squash	8.6E-02 [a]
Kohlrabi	9.0E-02	Sugar beet	1.6E-01
Lentils - Whole	3.3E-01	Sweet potato	2.9E-01 [a]
Mushrooms	8.2E-02	Tomatoes	6.0E-02 [a]
Okra	1.0E-01	Turnips—roots	8.1E-02
Onions	1.1E-01 [a]		
Grain			
Barley	8.9E-01 [a]	Rye	8.9E-01 [a]
Corn—Grain, Bran	9.2E-01 [a]	Sorghum (incl. milo)	9.1E-01
Millet	9.1E-01	Soybean	9.3E-01
Oats	9.2E-01 [a]	Wheat	8.9E-01 [a]

Sources: Baes et el., (1984) and EPA (1997)

[a] *Listed values represent mean values for the crop.*

5.8.4 Agricultural Productivity

Crop productivities are used to model radionuclide concentrations in vegetable and forage crops due to atmospheric deposition. Baes et al. (1984) provide maps of the U.S. showing ranges of productivities for various crops in northern New Mexico. The fresh weight productivities range from 0.5 to 1.5 kg/m^2 (0.1 to 0.3 lb/ft^2) for leafy vegetables and protected produce, 0.1 to 1.5 kg/m^2 (0.02 to 0.3 lb/ft^2) for exposed produce, and 0.1 to 0.2 kg/m^2 (0.02 to 0.04 lb/ft^2) for grain. NCRP Report 76 (1984) cites default values of 2 kg/m^2 (0.4 lb/ft^2) for produce and leafy vegetables and 0.6 kg/m^2 (0.1 lb/ft^2) for other aboveground vegetables; all productivities are given in terms of fresh weight. Ng et al. (1982) provide yields for various crops in Georgia and South Carolina. The average yields by vegetation class are 1.35 (one observation), 0.64, and 0.17 kg/m^2 (0.3, 0.1, and 0.03 lb/ft^2) (fresh weight) for leafy vegetables, produce, and grain, respectively. The RESRAD computer code (ANL, 2001) uses default values of 1.5 kg/m^2 (0.3 lb/ft^2) (fresh weight) for leafy vegetables, and 0.7 kg/m^2 (0.14 lb/ft^2) (fresh weight) for fruit, other vegetables, and grain. Oak Ridge National Laboratory guidance on risk assessment (ORNL, 1999) adopts fresh weight productivities of 2.0 kg/m^2 (0.4 lb/ft^2) for leafy vegetables (taken from NCRP, 1984), 0.62 kg/m^2 (0.13 lb/ft^2) for nonleafy vegetables, and 0.67 kg/m^2 (0.14 lb/ft^2) for root vegetables for DOE sites in Portsmouth, Ohio and Paducah, Kentucky. The ORNL report cites a range of 0.112 to 1.12 kg/m^2 (0.02 to 0.2 lb/ft^2) for leafy vegetables and 0.224 to 1.12 kg/m^2 (0.04 to 0.2 lb/ft^2) for root vegetables in the Paducah area.

NCRP Report 76 (1984) cites crop yields of 0.7 kg/m^2 (0.14 lb/ft^2) (fresh weight) and 0.3 kg/m^2 (0.06 lb/ft^2) (dry weight) for pasture vegetation, while Ng et al. (1978) provide a yield for hay of 0.5 kg/m^2 (0.1 lb/ft^2) (dry weight). ORNL risk assessment guidance (1999) provides dry weight yields for pasture grass, citing a range of 0.112 to 0.225 kg/m^2 (0.023 to 0.046 lb/ft^2) for the Paducah, Kentucky and Portsmouth, Ohio areas. Baes et al. (1984) provide estimates of yield for hay in northern New Mexico ranging from 0.3 to 0.6 kg/m^2/yr (0.06 to 0.12 lb/ft^2) (dry weight). The U.S. Department of Agriculture (USDA, 2004a) provides commercial yields for alfalfa, alfalfa mixtures, and other types of hay. The annual yield of alfalfa and alfalfa mixtures in New Mexico averaged about 1.1 kg/m^2 (0.22 lb/ft^2) (dry weight) between 2001 and 2003, while the annual yield of all other types of hay was about 0.5 kg/m^2 (0.1 lb/ft^2) (dry weight).

Triangular distributions were used to describe crop productivities for the performance assessment and composite analysis. The distributions use minimum, most likely, and maximum values of 1.0, 1.5, and 2.0 kg/m^2 (0.2, 0.3. and 0.4 lb/ft^2) for leafy vegetables; 0.5, 1.0, and 1.5 kg/m^2 (0.1, 0.2, and 0.3 lb/ft^2) for produce; and 0.2, 0.5, and 0.75 kg/m^2 (0.04, 0.1, 0.15 lb/ft^2) for grain. These values, all of which are given in terms of fresh weight, generally encompass the observations discussed above. The distribution for pasture grass productivity was defined using the data cited above for pasture grass and hay; minimum, most likely, and maximum values of 0.1, 0.5, and 0.7 kg/m^2 (0.02, 0.1, and 0.14 lb/ft^2) (dry weight) were assumed.

5.8.5 Growing Season

Radionuclides deposited on plant surfaces will be depleted throughout the growing season as a result of weathering. The length of the growing season will vary with the crop under consideration and the conditions under which the crops are grown. Ng et al. (1978) adopted a 3-month (2,190-hour) growing season to model food-chain transport at the DOE Savannah River Site. Regulatory Guide 1.109 (NRC, 1977) suggests a growing season of 1,440 hours for vegetables, produce, and grain, and 720 hours for forage. The value for forage is based on the average time between successive grazing episodes by cattle. The RESRAD computer code (ANL, 2001) adopts a default growing season of 1,490 hours for fruits, vegetables, and grain, and 2,190 hours for leafy vegetables. Baes et al. (1984) indicate that the average time between successive hay harvests is 1,440 hours.

Time-to-maturity data for vegetables provide additional information about the periods of time crops may be exposed to contaminant releases. Table 34 summarizes representative maturity times for a variety of leafy vegetables, produce, and grain. On the basis of these data, maturity times for leafy vegetables range from 40 to 120 days; the median of the midpoints of the ranges listed in the table is about 60 days. The maturity times for produce range from 46 to 150 days, while a limited amount of information for grain indicates a time to maturity ranging from 70 to 120 days. Median growing seasons for produce and grain, calculated using the midpoints of the listed ranges, are 80 and 110 days, respectively.

The time-to-maturity data provided in Table 34 played a key role in the development of distributions of growing seasons for vegetables. A triangular distribution was defined for leafy vegetables using minimum, most likely, and maximum values of 40, 60, and 100 days. The endpoints are reasonable estimates of the ranges listed for individual crops. The most likely value of 60 days is representative of the midpoints of the individual crop ranges and agrees with guidance in Regulatory Guide 1.109 (NRC, 1977). The growing season for produce was assumed to have minimum, most likely, and maximum values of 45, 80, and 120 days, respectively. The most likely value of the triangular distribution defined for the growing season of grain was set equal to 110 days, while the minimum and maximum values were assumed to be 70 and 120 days, respectively. The distributions for produce and grain generally conform to the time to maturity data listed in Table 34, and bracket the 3-month period adopted by Ng et al. (1978). The triangular distribution defined for pasture grass has minimum and maximum values of 30 and 60 days, consistent with data found in NRC (1977) and Baes et al. (1984). The midpoint of this range was adopted as the most likely value.

Table 34
Time-to-Maturity Data for Representative Vegetables

Crop Type/Crop	Time to Harvest or Maturity (d)	Source
Leafy Vegetables		
Beet greens	50	Lerner and Dana, 2001
Cabbage	62–120 [a]	LSU, 2003; CUCES, 1999; TAMU, 2001; Smith, 1995
Collards	60–85	Lerner and Dana, 2001; LSU, 2003; TAMU, 2001; CUCES, 1999
Endive	85–100	Lerner and Dana, 2001; TAMU, 2001
Kale	50–60	Lerner and Dana, 2001; TAMU, 2001; CUCES, 1999
Lettuce	40–80	LSU, 2003; CUCES, 1999
Lettuce, leaf	40–50	Lerner and Dana, 2001; TAMU, 2001; Smith, 1995
Lettuce, other [b]	30–85	TAMU, 2001; CUCES, 1999; Smith, 1995
Mustard	35–60	Lerner and Dana, 2001; LSU, 2003; TAMU, 2001; CUCES, 1999; Smith, 1995
Spinach	35–75	Lerner and Dana, 2001; LSU, 2003; TAMU, 2001; CUCES, 1999; Smith, 1995
Swiss chard	45–60	Lerner and Dana, 2001; LSU, 2003; TAMU, 2001
Turnip greens	40	Lerner and Dana, 2001
Produce		
Beans [c]	46–90	CUCES, 1999; LSU, 2003; TAMU, 2001; Smith, 1995
Beets	50–80	CUCES, 1999; LSU, 2003; TAMU, 2001; Smith, 1995
Carrots	50–95	CUCES, 1999; LSU, 2003; TAMU, 2001; Smith, 1995
Corn	64–100	CUCES, 1999; LSU, 2003; TAMU, 2001; Smith, 1995
Cucumbers	48–72	CUCES, 1999; LSU, 2003; TAMU, 2001; Smith, 1995
Eggplant	60–85 [a]	CUCES, 1999; LSU, 2003; TAMU, 2001; Smith, 1995
Onions, bulb	85–150	CUCES, 1999; LSU, 2003; TAMU, 2001; Smith, 1995
Peas	58–85	CUCES, 1999; LSU, 2003; TAMU, 2001; Smith, 1995
Peppers, hot and sweet	60–80 [a]	CUCES, 1999; LSU, 2003; TAMU, 2001; Smith, 1995
Potatoes	90–120 [a]	CUCES, 1999; LSU, 2003; TAMU, 2001; Smith, 1995
Potatoes, Irish	90–120	CUCES, 1999; LSU, 2003
Pumpkins	90–120	LSU, 2003; TAMU, 2001; Smith, 1995
Squash, summer	40–120	CUCES, 1999; LSU, 2003; TAMU, 2001; Smith, 1995
Squash, winter	50–120	CUCES, 1999; TAMU, 2001; Smith, 1995
Tomatoes	70–100 [a]	CUCES, 1999; LSU, 2003; TAMU, 2001; Smith, 1995
Turnips	40–75	CUCES, 1999; LSU, 2003; TAMU, 2001; Smith, 1995
Grain		
Millet	70–90	Croissant and Echols, 1998
Oats	100–120	Croissant and Echols, 1998
Wheat	110–120	Croissant and Echols, 1998

[a] *Plants may be started from transplants.*

[b] *Types of lettuce include head, butterhead, and cos.*

[c] *Includes snap, pole, half-runner, lima, pole lima, and edible soybeans.*

5.8.6 Plant Mass Loading Factor

Plant mass-loading factors are used to estimate rates of radionuclide deposition on plant surfaces due to rainsplash. Estimates of mass-loading factors taken from several investigations are summarized in Table 35. Most of this information comes from Hinton (1992) and Pinder and McLeod (1989); original references for the data are included in the table. These factors are given in terms of concentration, rather than inventory. Pinder and McLeod (1989) discuss the fact that estimating concentration-based factors is complicated by plant biomass and canopy structure. The inventory-based factors are expected to be less variable and, therefore, preferable for use in dose assessment models. However, the data required to estimate the plant-loading factor on an inventory basis for the studies cited in the table are generally unavailable.

Concentration-based mass-loading factors were used for the performance assessment and composite analysis. The distribution for leafy vegetables was based on the information provided in Pinder and McLeod (1989) for lettuce. A normal distribution with a mean and standard error of 260 and 100 mg soil/g plant (0.24 and 0.09 lb soil/lb plant) (dry weight), respectively, was adopted for the uncertainty analysis; the distribution was truncated to prevent the occurrence of negative values of the parameter. The mass-loading factors range from about 1 to 210 mg soil/g plant (9×10^{-4} to 0.19 lb soil/lb plant) (dry weight) for the nonleafy vegetables included in Table 35. The factors for all crops except squash are 60 mg soil/g plant (0.06 lb soil/lb plant) (dry weight) or less. The higher mass loading observed for squash pertains only to the lower portions of the plant; factors based on the entire plant will be significantly smaller. Based on this information, a point estimate of 30 mg soil/g plant (0.03 lb soil/lb plant) (dry weight) was adopted for the performance assessment and composite analysis. A triangular distribution was assumed to apply, and was defined using minimum, most likely, and maximum values of 1, 30, and 100 mg soil/g plant (9×10^{-4}, 0.03, and 0.09 lb soil/lb plant) (dry weight).

The mass-loading factors listed for pasture grass in Table 35 range from less than 1 to 500 mg soil/g plant ($9 \times 10^{-4}$to 0.47 lb soil/lb plant) (dry weight). However, the distribution adopted for the nonleafy vegetables was applied to animal forage as well. This distribution is a conservative representation of data presented in Hinton et al. (1995) and Pinder et al. (1991) and omits from consideration data that pertain to conditions that are not expected to exist at Area G or the receptor locations. For example, the mass-loading factors developed by Beresford and Howard (1991) and Oughton (1990) are considered to be indicative of extreme conditions (Hinton, 1992). Also ignored is the mass loading of almost 250 mg soil/g plant (0.23 lb soil/lb plant) (dry weight) that was estimated by Arthur and Alldredge (1982); this value pertained to a single sample, mass loadings for 25 other samples were several times smaller. Finally, some of the higher mass loadings listed in Table 35 for pasture grass were estimated using techniques that will tend to overestimate mass loadings for the suspendable portion of the soil (Pinder et al., 1991).

Table 35
Summary of Plant Mass Loading

Crop	Location	Mass-Loading Factor (mg soil/g dry vegetation)	Reference [a]
Bush Beans	New Mexico	3.0E+01–6.0E+01	White et al., 1981
Broccoli	South Carolina	1.0E+01 ± 8.1E+00 [b]	McLeod et al., 1984a
Cabbage	South Carolina	1.1E+00 ± 1.1E+00	McLeod et al., 1984a
Corn	South Carolina	1.7E+00; 1.4E+00 [c]	Pinder and McLeod, 1989
Lettuce	South Carolina	2.6E+02 ± 1.0E+02 [b]	McLeod et al., 1984a
Soybean	South Carolina	8.4E+00; 2.1E+00 [b]	Pinder and McLeod, 1989
Squash	New Mexico	1.4E+02–2.1E+02 [d]	White et al., 1981
		3.0E+01–4.0E+01 [e]	White et al., 1981
Sunflower	South Carolina	2.6E+00 ± 9.0E-01 [b]	Pinder and McLeod, 1989
Tobacco	South Carolina	2.1E+00 ± 6.0E-01 [b]	McLeod et al., 1984b
Tomatoes	New Mexico	1.7E+01 [f]	Dreicer et al., 1984
		3.0E+01 [g]	Dreicer et al., 1984
Turnips	South Carolina	3.2E+01 ± 1.1E+01 [b]	McLeod et al., 1984a
Wheat	South Carolina	4.3E+00; 4.8E+00 [c]	Pinder and McLeod, 1989
Pasture	Sellafield, UK	7.0E+01	Green and Dodd, 1988
Pasture	Sellafield, UK	1.8E+02	Beresford and Howard, 1991
		3.0E+01 [h]	
		3.0E+02 [i]	
Pasture	Norway	<1.0E+00 [h]	Oughton, 1990
	Byelorussia	3.0E+02–5.0E+02	
Pasture	Colorado	1.8E+01 ± 4.8E+01 [j]	Arthur and Alldredge, 1982
Pasture	Sellafield, UK	5.0E+01–2.0E+02	Summerling et al., 1984
Pasture	South Carolina	9.0E+00 ± 1.7E+00 [b]	Pinder et al., 1991
Pasture	Kloten, Switzerland	7.0E+00 ± 1.1E+00 [b]	Hinton et al., 1995
Sagebrush	Wyoming	2.4E+01	Skinner, 1982

[a] *Many of the cited data were taken from Hinton (1992) and Pinder and McLeod (1989). The references listed in the table are the original references for each investigation.*

[b] *Measurement represents mean ± standard error.*

[c] *First value represents the mean mass loading factor across all sampling times; second value represents the mean at the time of harvest.*

[d] *Mass loading factor pertains to plant heights of 0.2 m or less.*

[e] *Mass loading factor pertains to plant heights greater than 0.2 m.*

[f] *Mass loading factor pertains to particle sizes less than 0.53 μm.*

[g] *Mass loading factor pertains to particle sizes less than 100 μm.*

[h] *Measurements were taken in summer.*

[i] *Measurements were taken in winter.*

[j] *Measurement represents mean ± standard deviation.*

5.8.7 Rainsplash Enhancement Factor

The plant mass-loading factors discussed above are defined in terms of the suspendable fraction of the soil. In contrast, the soil concentrations estimated using the GoldSim models are based on the total soil; concentrations are not calculated as a function of soil particle size. Given this difference, it is necessary to modify the mass-loading factors discussed above before they are applied in the GoldSim models. This is done by multiplying the mass-loading factors by the rainsplash enhancement factor (the ratio of radionuclide concentrations in the suspendable fraction to the concentrations in the total soil).

In terms of mass loading on plants, the suspendable fraction is typically defined as particles less than or equal to 125 μm (0.0049 in.) in diameter; soil particles of this size may be readily suspended by wind and rainsplash and appear to be preferentially retained on plant surfaces (Dreicer et al., 1984 and Wallwork-Barber and Hakonson, 1981, as cited in Pinder and McLeod, 1989). Because radionuclide concentrations in soil tend to increase with decreasing soil particle size (Livens and Baxter, 1988), the enhancement factor for the suspendable fraction tends to be greater than 1.0. Pinder and McLeod (1989) found Pu-238 concentrations in the suspendable soil fraction to be 1.5 times the concentrations in the total soil. Similarly, Pu-238 concentrations in soil particles less than or equal to 100 μm in diameter were found by White et al. (1981) to be 1.7 times the concentrations in the total soil.

Livens and Baxter (1988) examined radionuclide concentrations in four West Cumbrian (England) soils as a function of particle size; the radionuclides evaluated included Am-241, Cs-137, Ru-106, Pu-238, and Pu-239/240. The results of this investigation were used to estimate the enhancement factor for soil particles less than 125 μm (0.0049 in.) in diameter. The factors for a sandy soil were greatest, ranging from 4.5 to 6.7 across the radionuclides evaluated. Factors for a gley soil (which develop in areas of poor drainage) ranged from 0.74 to 2.1; the factors for woodland and pasture soils ranged from 1.7 to 1.9 and 1.3 to 1.4, respectively. The higher factors for the sand were thought to be due to the very small fraction of fine material (i.e., < 32 μm [0.001 in.] in diameter) and the low radionuclide uptake capacity of the predominant quartz fraction.

Nyhan et al. (1976a, 1976b) provide additional insight into the distribution of radionuclides as a function of soil particle size. In one study, alluvial soils from three liquid effluent discharge areas at LANL were sampled and used to determine Pu-238 and Pu-239/240 concentrations as a function of particle size (Nyhan et al., 1976a). Radionuclide concentrations in soil particles less than 53 μm (0.021 in.) in diameter were approximately 10 times the concentrations in the 2 to 23 μm (7.9×10^{-5} to 9.0×10^{-5} in.) diameter fraction; a similar relationship was evident for 53 to 105 μm (0.021 to 0.041 in.) diameter soil particles relative to the 2 to 23 μm (7.9×10^{-5} to 9.0×10^{-5} in.) diameter fraction. Nyhan et al. (1976b) examined the distribution of Pu-239/240 as a function of particle size in soils collected downwind of the Trinity Site in New Mexico. In

several instances the concentrations on particle sizes of 105 μm (0.041 in.) or less were greater than those in larger size classes, although exceptions were observed. In both of these studies, however, contaminant concentrations in the suspendable fractions were less than those in the total soil, yielding enhancement factors less than 1.0.

The data summarized above present a mixed picture with respect to the magnitude of the enhancement factor. In the absence of definitive information it was decided to assign this parameter a triangular distribution with minimum, most likely, and maximum values of 1.0, 1.5, and 2.0, respectively. This distribution generally encompasses the data discussed by Pinder and McLeod (1989), White et al. (1981), and Livens and Baxter (1988), but ignores the possibility raised by Nyhan et al. (1976a, 1976b) that enhancement factors may be less than 1.0 under some conditions.

5.8.8 Plant Interception Fraction and Coefficient

The plant interception fraction specifies the fraction of particulates deposited on plant surfaces that is initially retained by the crops. The NCRP (1984) cites default values of 0.20 and 0.25 for the interception fraction for vegetable crops and pasture grass, respectively, while the RESRAD code (ANL, 2001) uses 0.25 as a default value for all vegetation types. Miller (1980) reviewed a number of studies and found interception fractions for pasture grass ranging from 0.02 to 0.82 for wet and dry deposition. Interception fractions following the dry deposition of particulates ranged from 0.06 to 1.2 for peanut, squash, soybean, and sorghum plants; the majority of the values were 0.49 or less. The values greater than 1 were attributed to the bush-like form of the plants in combination with the experimental methods used to estimate interception fraction.

The GoldSim models estimate the plant interception fraction as a function of agricultural productivity using Equation 49 (Section 3.6.3.3). This equation was taken from Ng et al. (1978), who adopted a value of 3.0 m^2/kg for the interception coefficient, μ. Using this coefficient, the ranges of agricultural productivities discussed above, and the best estimates of dry-to-wet weight fractions provided earlier yields plant interception factors of about 0.2 to 0.4 for leafy vegetables and produce, 0.4 to 0.9 for grain, and 0.3 to 0.9 for pasture grass.

Peterson (1983) provides interception fractions for four grasses exposed to simulated fallout particles; these fractions range from 0.69 to 0.82 for vegetative productivities of 0.4 to 0.8 kg/m^2 (0.08 to 0.16 lb/ft^2) (dry weight). Peterson also cites work performed by Chamberlain (1970) who relates the interception fraction to the dry forage density using an equation similar in form to that developed by Ng et al. (1978). Values for the interception coefficient were found to range from 2.3 to 3.3 m^2/kg (11.2 to 16.1 ft^2/lb) for various forage crops. Other investigations cited in Peterson had values of μ ranging from 1.3 to 18.2 m^2/kg (6.4 to 89 ft^2/lb) for common varieties of leafy vegetables, produce, and grass. Pinder et al. (1988) estimated the interception coefficient for grass canopies using data collected by other investigators. A value of 2.9 m^2/kg (14.2 ft^2/lb)

was estimated when the data from several studies were combined; estimates of the interception coefficient for the individual studies ranged from 2.3 to 3.3 m^2/kg (11.2 to 16.1 ft^2/lb).

Baes et al. (1984) used models to estimate interception fractions as a function of vegetation coverage and productivity. One model estimates interception fractions for leafy vegetables on the basis of the ground surface area covered by vegetation. This model was used to predict time weighted average and maximum interception fractions of 0.15 and 0.39, respectively. These values account for the change in plant coverage with growth, and are weighted to address a range of leafy vegetables. When the same general approach was applied to exposed produce (i.e., three types of fruit grown on trees, snap beans, and tomatoes), an interception fraction of 0.052 was estimated. Baes et al. (1984) also developed equations similar in form to Equation 49 and used data collected by Hoffman and Baes (1979) to estimate an interception coefficient of 2.88 m^2/kg (14.1 ft^2/lb) for pasture grass on a dry weight basis. Interception coefficients of 0.085 and 0.032 m^2/kg (0.4 to 0.16 ft^2/lb) (wet weight basis) were estimated for leafy vegetables and exposed produce, respectively, based on alternate sources of data. When these coefficients are applied to the ranges of agricultural productivities discussed in Section 5.8.4, the resulting interception fractions range from about 0.1 to 0.2 for leafy vegetables and 0.05 or less for exposed produce.

Interception coefficients are provided in IAEA (1994) for grass, wheat, and corn, taking into account several particle types and sizes. Mean coefficients range from 0.24 to 3.6 m^2/kg (1.2 to 17.6 ft^2/lb) for productivities expressed on a dry weight basis, and from 0.46 to 9.6 m^2/kg (2.2 to 47 ft^2/lb) for use with wet weight productivities.

The data cited above indicate a wide range of interception fractions and coefficients for pasture grass and food crops, both within and between studies. An interception coefficient of 3.0 m^2/kg (14.7 ft^2/lb) was selected for use with productivities stated in terms of dry weight. This value was assumed to be the most likely value in a triangular distribution ranging from 2.0 to 4.0 m^2/kg (9.8 to 19.6 ft^2/lb), which is generally consistent with the information cited above.

5.8.9 Weathering Half-Life

The weathering half-life is the time needed to remove 50 percent of the contamination deposited on plant surfaces due to processes such as wind removal and washoff. Regulatory Guide 1.109 (NRC, 1977) assumes a weathering half-life of 14 days, a value that is frequently used as a default for radiological risk assessments. Miller and Hoffman (1982; cited in NCRP, 1984) indicate that weathering half-lives range from 4.5 to 34 days, depending upon the radionuclide and vegetation under consideration. Data provided for particulates on herbaceous vegetation indicate a median and mean of 17 and 19 days, respectively, and a geometric standard deviation of 1.6. Peterson (1983) discusses weathering half-lives due to wind that range from 1 to 23 days

and half-lives due to washoff that range from 6 to 56 days, depending upon rainfall. Measured effective half-lives ranged from 2.7 to more than 30 days on various plant types.

The data reported by Miller and Hoffman (1982) for particulates were used to define the weathering half-life for the performance assessment and composite analysis. A best estimate of 17 days was adopted. This value was set equal to the geometric mean of a lognormal distribution having a geometric standard deviation of 1.6.

5.8.10 Animal Product Transfer Factor

Transfer factors for beef, milk, chicken, and eggs represent the fraction of the daily elemental intake in food that is transferred to a volume or mass of the food product. These factors were used in the performance assessment and composite analysis to estimate radionuclide concentrations in animal products resulting from the ingestion of contaminated forage or feed, water, and soil or grit. Several compilations of transfer factors exist in the literature, including those found in Baes et al. (1984), IAEA (1994), Napier et al. (2004), NCRP Report 129 (1999), and the NRC's Regulatory Guide 1.109 (1977). Many of the factors included in these compilations come from the same original sources; the authors have made various assumptions to estimate transfer factors for elements for which data are unavailable.

The transfer factors for beef and milk found in Napier et al. (2004) were adopted as point estimates of these parameters for the performance assessment and composite analysis. This source addresses a comprehensive list of elements and draws on more recent data than some of the other compilations. While NCRP Report 129 (1999) is of a similar vintage, the transfer factors included in that reference were selected in a more conservative manner to serve as screening values. In fact, the majority of the transfer factors listed in that report are greater than those found in two or more of the other compilations.

The beef and milk transfer factors adopted from Napier et al. (2004) were used to represent the geometric means of lognormal distributions (Table 36). Geometric standard deviations of 3.0 and 2.5 were adopted for the beef and milk transfer factors, respectively. These values are consistent with the maximum standard deviations adopted by the NCRP (1999) and other sources of data. The NCRP used geometric standard deviations ranging from 1.2 to 2.8 for beef and from 1.6 to 2.5 for milk. NCRP Report 76 (1984) noted that, in general, the variability of beef transfer factors derived from stable element concentrations in unassociated meat and vegetation is characterized by geometric standard deviations ranging from 1.3 to 3.8. The NCRP report cites a study by Little (1979), who found transfer factors for cesium in beef to be lognormally distributed, with a geometric standard deviation of 2.3. Hoffman (1979), also cited in the NCRP report, found that milk transfer factors for strontium, iodine, and cesium were lognormally distributed, and had geometric standard deviations of 1.6 to 1.8.

Table 36
Parameter Values and Distributional Information for Beef and Milk Transfer Factors

Element	Forage-to-Beef Transfer Factor (d/kg)		Forage-to-Milk Transfer Factor (d/kg)	
	Geometric Mean	Geometric Standard Deviation	Geometric Mean	Geometric Standard Deviation
Ac	4.0E-04	3.0E+00	2.0E-05	2.5E+00
Ag	3.0E-03	3.0E+00	5.0E-05	2.5E+00
Al [a]	4.0E-02	3.0E+00	2.0E-03	2.5E+00
Am	4.0E-05	3.0E+00	1.5E-06	2.5E+00
Ba	2.0E-04	3.0E+00	4.8E-04	2.5E+00
Be	1.0E-03	3.0E+00	9.0E-07	2.5E+00
Bi	4.0E-04	3.0E+00	5.0E-04	2.5E+00
Bk [b]	4.0E-05	3.0E+00	1.5E-06	2.5E+00
C [c]	---	---	---	---
Ca	2.0E-03	3.0E+00	3.0E-03	2.5E+00
Cf	4.0E-05	3.0E+00	1.5E-06	2.5E+00
Cl	2.0E-02	3.0E+00	1.7E-02	2.5E+00
Cm	4.0E-05	3.0E+00	2.0E-05	2.5E+00
Co	1.0E-02	3.0E+00	3.0E-04	2.5E+00
Cs	5.0E-02	3.0E+00	7.9E-03	2.5E+00
Eu	2.0E-05	3.0E+00	3.0E-05	2.5E+00
Gd	2.0E-05	3.0E+00	3.0E-05	2.5E+00
H [c]	---	---	---	---
Ho	2.0E-05	3.0E+00	3.0E-05	2.5E+00
I	4.0E-02	3.0E+00	9.0E-03	2.5E+00
K	2.0E-02	3.0E+00	7.2E-03	2.5E+00
Kr	NA	NA	NA	NA
Lu [d]	2.0E-05	3.0E+00	3.0E-05	2.5E+00
Mo	1.0E-03	3.0E+00	1.7E-03	2.5E+00
Nb	3.0E-07	3.0E+00	4.1E-07	2.5E+00

Source: Napier et al. (2004)

NA = Not applicable; element exists solely as a gas and was ignored in terms of food-chain transport.

[a] Transfer factors for Al were set equal to the maximum of the factors for Ga, In, and Tl.

[b] Transfer factors for Bk were set equal to the factors for Am.

[c] Transfer factors for C and H were estimated using specific activity models; see discussion in text.

[d] Transfer factors for Lu were set equal to the corresponding factors for Gd, Eu, and Tb.

[e] Transfer factors for Ti were set equal to the maximum of the factors for Hf and Zr.

Table 36 (Continued)
Parameter Values and Distributional Information for Beef and Milk Transfer Factors

Element	Forage-to-Beef Transfer Factor (d/kg)		Forage-to-Milk Transfer Factor (d/kg)	
	Geometric Mean	Geometric Standard Deviation	Geometric Mean	Geometric Standard Deviation
Nd	2.0E-05	3.0E+00	3.0E-05	2.5E+00
Ni	5.0E-03	3.0E+00	1.6E-02	2.5E+00
Np	1.0E-03	3.0E+00	5.0E-06	2.5E+00
Os	4.0E-01	3.0E+00	5.0E-03	2.5E+00
Pa	4.0E-05	3.0E+00	5.0E-06	2.5E+00
Pb	4.0E-04	3.0E+00	2.6E-04	2.5E+00
Pm	2.0E-05	3.0E+00	3.0E-05	2.5E+00
Pu	1.0E-05	3.0E+00	1.1E-06	2.5E+00
Ra	9.0E-04	3.0E+00	1.3E-03	2.5E+00
Si	4.0E-05	3.0E+00	2.0E-05	2.5E+00
Sm	2.0E-05	3.0E+00	3.0E-05	2.5E+00
Sn	8.0E-02	3.0E+00	1.0E-03	2.5E+00
Sr	8.0E-03	3.0E+00	2.8E-03	2.5E+00
Tb	2.0E-05	3.0E+00	3.0E-05	2.5E+00
Tc	1.0E-04	3.0E+00	1.4E-04	2.5E+00
Th	4.0E-05	3.0E+00	5.0E-06	2.5E+00
Ti [e]	1.0E-03	3.0E+00	5.5E-07	2.5E+00
U	3.0E-04	3.0E+00	4.0E-04	2.5E+00
Zr	1.0E-06	3.0E+00	5.5E-07	2.5E+00

Source: Napier et al. (2004)

NA = Not applicable; element exists solely as a gas and was ignored in terms of food-chain transport.

[a] *Transfer factors for Al were set equal to the maximum of the factors for Ga, In, and Tl.*

[b] *Transfer factors for Bk were set equal to the factors for Am.*

[c] *Transfer factors for C and H were estimated using specific activity models; see discussion in text.*

[d] *Transfer factors for Lu were set equal to the corresponding factors for Gd, Eu, and Tb.*

[e] *Transfer factors for Ti were set equal to the maximum of the factors for Hf and Zr.*

There is considerably less information available to characterize transfer factors for chicken and eggs. Perhaps the most complete compilation is found in Napier et al. (2004); this reference was used to define transfer factors for most elements. The point estimates found in this report were adopted as the geometric means of lognormal distributions. The geometric standard deviations of these distributions were estimated based on the assumption that the first and ninety-ninth percentiles were 0.1 and 10 times the mean values. The implied ranges are generally consistent with, or greater than, those indicated for selected elements in the IAEA report (1994). The chicken and egg transfer factors used in the performance assessment and composite analysis are summarized in Table 37.

Animal product transfer factors were not included in Napier et al. (2004) for seven elements included in the performance assessment and composite analysis. These elements were aluminum, berkelium, krypton, lutetium, titanium, hydrogen, and carbon. Transfer factors for aluminum were set equal to the maximum factors for other elements in the same group, including gallium, indium, and thallium; the transfer factors for berkelium were set equal to those for americium. Krypton exists solely as a gas and was ignored in terms of food-chain transport. The animal-product transfer factors for lutetium were set equal to those for gadolinium, europium, and terbium, while the factors for titanium were assumed to be equal to the maximum of the factors listed for hafnium and zirconium.

Transfer factors for hydrogen, as H-3, and carbon, as C-14, were estimated using specific activity models. The animal product information needed to estimate the tritium transfer factors were taken from Napier et al. (1988). The water fractions of beef, milk, chicken, and eggs were set equal to 0.6, 0.88, 0.7, and 0.75, respectively. The fractional contents of hydrogen and carbon in several substances were needed to implement the specific activity models. The hydrogen fraction of water was set to 0.11 while the carbon fraction of all crops, including the pasture grass consumed by cows and cattle and the grain consumed by chickens, is 0.45 (dry weight basis). The carbon fraction of soil was set to 0.03 and that of water was set to 2.0×10^{-5}. The fractions of beef, milk, chicken, and eggs that are carbon are 0.6, 0.58, 0.67, and 0.6 (dry weight basis), respectively.

Table 37
Parameter Values and Distributions for Chicken and Egg Transfer Factors

Element	Forage-to-Chicken Transfer Factor (d/kg)		Forage-to-Egg Transfer Factor (d/kg)	
	Deterministic Value	Distribution [a]	Deterministic Value	Distribution [a]
Ac	6.0E-03	6.0E-04, 6.0E-03, 6.0E-02	4.0E-03	4.0E-04, 4.0E-03, 4.0E-02
Ag	2.0E+00	2.0E-01, 2.0E+00, 2.0E+01	5.0E-01	5.0E-02, 5.0E-01, 5.0E+00
Al [b]	8.0E-01	8.0E-02, 8.0E-01, 8.0E+00	1.0E+00	1.0E-01, 1.0E+00, 1.0E+01
Am	6.0E-03	6.0E-04, 6.0E-03, 6.0E-02	4.0E-03	4.0E-04, 4.0E-03, 4.0E-02
Ba	9.0E-03	9.0E-04, 9.0E-03, 9.0E-02	9.0E-01	9.0E-02, 9.0E-01, 9.0E+00
Be	4.0E-01	4.0E-02, 4.0E-01, 4.0E+00	2.0E-02	2.0E-03, 2.0E-02, 2.0E-01
Bi	9.8E-02	9.8E-03, 9.8E-02, 9.8E-01	2.6E-01	2.6E-02, 2.6E-01, 2.6E+00
Bk [c]	6.0E-03	6.0E-04, 6.0E-03, 6.0E-02	4.0E-03	4.0E-04, 4.0E-03, 4.0E-02
C [d]	---	---	---	---
Ca	4.0E-02	4.0E-03, 4.0E-02, 4.0E-01	4.0E-01	4.0E-02, 4.0E-01, 4.0E+00
Cf	6.0E-03	6.0E-04, 6.0E-03, 6.0E-02	4.0E-03	4.0E-04, 4.0E-03, 4.0E-02
Cl	3.0E-02	3.0E-03, 3.0E-02, 3.0E-01	2.7E+00	2.7E-01, 2.7E+00, 2.5E+01
Cm	6.0E-03	6.0E-04, 6.0E-03, 6.0E-02	4.0E-03	4.0E-04, 4.0E-03, 4.0E-02
Co	2.0E+00	2.0E-01, 2.0E+00, 2.0E+01	1.0E-01	1.0E-02, 1.0E-01, 1.0E+00
Cs	3.0E+00	3.0E-01, 3.0E+00, 3.0E+01	4.0E-01	4.0E-02, 4.0E-01, 4.0E+00
Eu	2.0E-03	2.0E-04, 2.0E-03, 2.0E-02	4.0E-05	4.0E-06, 4.0E-05, 4.0E-04

Source: Napier et al. (2004)

NA = Not applicable; element exists solely as a gas and was ignored in terms of food-chain transport.

[a] Distribution designations are triangular; values represent minimum, most likely, maximum.

[b] Transfer factors for Al were set equal to the maximum of the factors for Ga, In, and Tl.

[c] Transfer factors for Bk were set equal to the factors for Am.

[d] Transfer factors for C and H were estimated using specific activity models; see discussion in text.

[e] Transfer factors for Lu were set equal to the corresponding factors for Gd, Eu, and Tb.

[f] Transfer factors for Ti were set equal to the maximum of the factors for Hf and Zr.

Table 37 (Continued)
Parameter Values and Distributions for Chicken and Egg Transfer Factors

Element	Forage-to-Chicken Transfer Factor (d/kg)		Forage-to-Egg Transfer Factor (d/kg)	
	Deterministic Value	Distribution [a]	Deterministic Value	Distribution [a]
Gd	2.0E-03	2.0E-04, 2.0E-03, 2.0E-02	4.0E-05	4.0E-06, 4.0E-05, 4.0E-04
H [d]	---	---	---	---
Ho	2.0E-03	2.0E-04, 2.0E-03, 2.0E-02	4.0E-05	4.0E-06, 4.0E-05, 4.0E-04
I	5.0E-02	5.0E-03, 5.0E-02, 5.0E-01	3.0E+00	3.0E+00, 3.0E+00, 2.5E+01
K	4.0E-01	4.0E-02, 4.0E-01, 4.0E+00	1.0E+00	1.0E-01, 1.0E+00, 1.0E+01
Kr	NA	NA	NA	NA
Lu [e]	2.0E-03	2.0E-04, 2.0E-03, 2.0E-02	4.0E-05	4.0E-06, 4.0E-05, 4.0E-04
Mo	1.8E-01	1.8E-02, 1.8E-01, 1.8E+00	9.0E-01	9.0E-02, 9.0E-01, 9.0E+00
Nb	3.0E-04	3.0E-05, 3.0E-04, 3.0E-03	1.0E-03	1.0E-04, 1.0E-03, 1.0E-02
Nd	2.0E-03	2.0E-04, 2.0E-03, 2.0E-02	4.0E-05	4.0E-06, 4.0E-05, 4.0E-04
Ni	1.0E-03	1.0E-04, 1.0E-03, 1.0E-02	1.0E-01	1.0E-02, 1.0E-01, 1.0E+00
Np	6.0E-03	6.0E-04, 6.0E-03, 6.0E-02	4.0E-03	4.0E-04, 4.0E-03, 4.0E-02
Os	8.4E-02	8.4E-03, 8.4E-02, 8.4E-01	7.1E-02	7.1E-03, 7.1E-02, 7.1E-01
Pa	6.0E-03	6.0E-04, 6.0E-03, 6.0E-02	4.0E-03	4.0E-04, 4.0E-03, 4.0E-02
Pb	8.0E-01	8.0E-02, 8.0E-01, 8.0E+00	1.0E+00	1.0E-01, 1.0E+00, 1.0E+01
Pm	2.0E-03	2.0E-04, 2.0E-03, 2.0E-02	2.0E-02	2.0E-03, 2.0E-02, 2.0E-01

Source: Napier et al. (2004)

NA = Not applicable; element exists solely as a gas and was ignored in terms of food-chain transport.

[a] Distribution designations are triangular; values represent minimum, most likely, maximum.

[b] Transfer factors for Al were set equal to the maximum of the factors for Ga, In, and Tl.

[c] Transfer factors for Bk were set equal to the factors for Am.

[d] Transfer factors for C and H were estimated using specific activity model;, see discussion in text.

[e] Transfer factors for Lu were set equal to the corresponding factors for Gd, Eu, and Tb.

[f] Transfer factors for Ti were set equal to the maximum of the factors for Hf and Zr.

Table 37 (Continued)
Parameter Values and Distributions for Chicken and Egg Transfer Factors

Element	Forage-to-Chicken Transfer Factor (d/kg)		Forage-to-Egg Transfer Factor (d/kg)	
	Deterministic Value	Distribution [a]	Deterministic Value	Distribution [a]
Pu	3.0E-03	3.0E-04, 3.0E-03, 3.0E-02	5.0E-04	5.0E-05, 5.0E-04, 5.0E-03
Ra	3.0E-02	3.0E-03, 3.0E-02, 3.0E-01	3.1E-01	3.1E-02, 3.1E-01, 3.1E+00
Si	8.0E-01	8.0E-02, 8.0E-01, 8.0E+00	1.0E+00	1.0E-01, 1.0E+00, 1.0E+01
Sm	2.0E-03	2.0E-04, 2.0E-03, 2.0E-02	4.0E-05	4.0E-06, 4.0E-05, 4.0E-04
Sn	8.0E-01	8.0E-02, 8.0E-01, 8.0E+00	1.0E+00	1.0E-01, 1.0E+00, 1.0E+01
Sr	8.0E-02	8.0E-03, 8.0E-02, 8.0E-01	2.0E-01	2.0E-02, 2.0E-01, 2.0E+00
Tb	2.0E-03	2.0E-04, 2.0E-03, 2.0E-02	4.0E-05	4.0E-06, 4.0E-05, 4.0E-04
Tc	3.0E-02	3.0E-03, 3.0E-02, 3.0E-01	3.0E+00	3.0E-01, 3.0E+00, 2.5E+01
Th	6.0E-03	6.0E-04, 6.0E-03, 6.0E-02	4.0E-03	4.0E-04, 4.0E-03, 4.0E-02
Ti [f]	6.0E-05	6.0E-06, 6.0E-05, 6.0E-04	2.0E-04	2.0E-05, 2.0E-04, 2.0E-03
U	1.0E+00	1.0E-01, 1.0E+00, 1.0E+01	1.0E+00	1.0E-01, 1.0E+00, 1.0E+01
Zr	6.0E-05	6.0E-06, 6.0E-05, 6.0E-04	2.0E-04	2.0E-05, 2.0E-04, 2.0E-03

Source: Napier et al. (2004)

NA = Not applicable; element exists solely as a gas and was ignored in terms of food-chain transport.

[a] Distribution designations are triangular; values represent minimum, most likely, maximum.

[b] Transfer factors for Al were set equal to the maximum of the factors for Ga, In, and Tl.

[c] Transfer factors for Bk were set equal to the factors for Am.

[d] Transfer factors for C and H were estimated using specific activity model;, see discussion in text.

[e] Transfer factors for Lu were set equal to the corresponding factors for Gd, Eu, and Tb.

[f] Transfer factors for Ti were set equal to the maximum of the factors for Hf and Zr.

5.8.11 Animal Food, Water, and Soil Ingestion Rates

Radionuclide concentrations in meat, milk, chicken, and eggs are proportional to the amount of contaminated material ingested by the respective animals. Cows and cattle were assumed to ingest forage crops (e.g., pasture grass) grown in contaminated soils, water drawn from the regional aquifer, and soil; chickens were assumed to eat contaminated feed, water, and grit. In terms of cow and cattle food consumption rates, Regulatory Guide 1.109 (NRC, 1977) lists a value of 50 kg/d (110 lb/d) (fresh weight), while the RESRAD code (ANL, 2001) uses default values of 55 and 68 kg/d (120 and 150 lb/d) for cows and cattle, respectively. NCRP Report 76 (1984) lists estimates of 16 and 12 kg/d (35 and 26 lb/d) (dry weight) for cows and cattle, respectively. Values tabulated by the IAEA (1994) include a default ingestion rate of 16.1 kg/d (35 lb/d) (dry weight) for cows, with a range of 10 to 25 kg/d (22 to 55 lb/d). A default value of 7.2 kg/d (16 lb/d) (dry weight) is given by the IAEA for 500 kg (1,100 lb) cattle, with a range of 5 to 10 kg/d (11 to 22 lb/d). A daily intake rate (dry weight) of 2.5 to 3 percent of the animal's live weight is commonly used to estimate range requirements for cows and cattle (e.g., Lyons et al., 1999; Pratt and Rasmussen, 2001). Assuming an average animal weight of 600 kg (1,300 lb), these percentages yield intake rates ranging from 15 to 18 kg/d (33 to 40 lb/d) (dry weight).

The forage intake rates provided by the IAEA (1994) for cows were adopted for the performance assessment and composite analysis. The value of 16 kg/d (35 lb/d) (dry weight) was used in the deterministic modeling, while the range was used to define the end points of a triangular distribution. The intake rates listed in IAEA (1994) for cattle appear to be low in comparison to the other sources cited above. Consequently, the value of 12 kg/d (26 lb/d) (dry weight) reported by the NCRP (1984) was adopted for the deterministic modeling. A triangular distribution with minimum and maximum values of 7.5 and 18 kg/d (16 and 40 lb/d) (dry weight) was assumed for this parameter; this range is generally consistent with the information cited above.

Regulatory Guide 1.109 (NRC, 1977) estimates rates of water intake for cows and cattle at 60 and 50 L/d (15 and 13 gal/d), respectively. The RESRAD computer code (ANL, 2001) uses the NRC value for cattle as a default, but assumes 160 L/d (40 gal/d) for cows. This value for cows includes a base consumption rate of 50 L/d (13 gal/d) and water required to produce approximately 40 L (10 gal) of milk per day. Ng et al. (1978) adopt water consumption rates of 60 and 38 L/d (15 and 10 gal/d) for cows and cattle, respectively. Oak Ridge National Laboratory risk assessment guidance (ORNL, 1999) cites default values of 75 L/d (20 gal/d) for cows and 50 L/d (13 gal/d) for cattle, while the IAEA (1994) lists ranges of 50 to 100 L/d (13 to 26 gal/d) for cows and 20 to 60 L/d (5 to 15 gal/d) for beef cattle. Based on this information, triangular distributions were adopted to define water intake rates. The water consumption rate for cows was defined using minimum and maximum values of 50 and 100 L/d (13 and 26 gal/d), while corresponding values of 20 and 60 L/d (5 and 15 gal/d) were adopted for cattle. These values approximate the ranges of the data listed above, but exclude the additional intake used by

the RESRAD code to account for milk production. The midpoints of these ranges were used to define the most likely values of the distributions.

Oak Ridge National Laboratory risk assessment guidance (ORNL, 1999) cites a number of studies concerned with rates of soil ingestion by cows and cattle. Smith (1977) estimates an ingestion rate of 0.25 to 0.5 kg/d (0.55 to 1.1 lb/d) for cattle; McKone and Ryan (1989) summarize six studies and report mean ingestion rates of 0.39 and 0.41 kg/d (0.86 to 0.90 lb/d) for cattle and cows, respectively. Zach and Mayoh (1984) suggest that soil ingestion rates may range from 0.1 to 2.2 kg/d (0.2 to 5 lb/d), while Mayland et al. (1977) report rates of 0.73 and 0.99 kg/d (1.6 to 2.2 lb/d) in June and August, respectively. The ORNL guidance notes that soil ingestion rates for cows and cattle are generally assigned default values of 1 kg/d (2.2 lb/d), while the RESRAD code (ANL, 2001) uses a default soil ingestion rate of 0.5 kg/d (1.1 lb/d). Studies cited in IAEA (1994) add to this information. Healy (1968) quoted soil intake equivalent to 4-to-8 percent of herbage intake, while Beresford and Howard (1991) gave intake rates ranging from 2 to 4 percent. Based on work conducted by Zach and Mayoh (1984) and Green and Dodd (1988), the IAEA report suggests a soil intake rate equal to 6 percent of forage intake (dry weight) for grazing cattle. Using the point estimates adopted above for food intake (i.e., 16.1 and 12 kg/d [35 and 25 lb/d] [dry weight] for cows and cattle, respectively), a soil intake rate of 6 percent represents soil ingestion rates of about 1 and 0.7 kg/d (2.2 and 1.5 lb/d).

A single distribution based on the data cited above was used to describe soil ingestion for cows and cattle. The distribution was assumed to be triangular with minimum, most likely, and maximum values of 0.4, 1.0, and 2.2 kg/d (0.9, 2.2, and 5 lb/d).

Limited information exists with respect to food, water, and soil ingestion rates for chickens. The IAEA report (1994) lists an expected food intake rate of 0.1 kg/d (0.2 lb/d) (dry weight) for laying hens, with a range of 0.07 to 0.15 kg/d (0.15 to.33 lb/d) (dry weight). Food intake rates for chickens include an expected value of 0.07 kg/d (0.15 lb/d) (dry weight) and a range of 0.05 to 0.15 kg/d (0.11 to 0.33 lb/d) (dry weight). These data were used to define a triangular distribution with minimum, most likely, and maximum values of 0.05, 0.07, and 0.15 kg/d (0.11, 0.15, and 0.33 lb/d) (dry weight). Water intake rates ranging from 0.1 to 0.3 L/d (0.03 to 0.08 gal/d) for laying hens and chickens are listed in IAEA (1994). These values were used to define the end points of a triangular distribution; the most likely value of this distribution was set to 0.2 L/d (0.05 gal/d). In a study cited by the ORNL guidance report (1999), 2 percent grit by weight in the diet is thought to be optimum for digestion in chickens (NRC, 1994). Therefore, grit intake was estimated by multiplying the food intake by 0.02.

5.9 Biotic Intrusion Model Parameters

The biotic intrusion modeling conducted in support of the performance assessment and composite analysis considers the potential for plants and animals to intrude into the disposed

waste and, subsequently, to transport radioactive contamination to the surface of the disposal facility. A variety of parameters are required to simulate rates of intrusion into the waste by the plant and animal communities inhabiting the closed site. The sources of information used to develop point estimates and distributions for these parameters are discussed below.

5.9.1 Time to Climax

The potential impacts of biotic intrusion depend upon the plant and animal communities present at the site. These communities are expected to change over time as the site transitions from a landscape dominated by grasses and forbs at the time of closure to piñon-juniper woodland that is characteristic of the undisturbed portions of Area G. The time required for the site to transition to a fully functioning piñon-juniper woodland community is referred to here as the time to climax.

The length of time required for the site to pass from the early stages of succession to a climax condition depends upon conditions at the disposal site, many of which are difficult to predict with certainty. However, information gathered by Arnold et al. (1964) provides some insight into the temporal aspects of succession in these communities. These investigators compared transect measurements from burned areas to measurements taken in adjacent unburned piñon-juniper stands at three locations in northern Arizona. Measurements were taken in 1954, approximately 70 to 90 years after the fires had occurred. At a site that had been burned about 80 years prior, tree canopy intercept was about 0.1 percent of that in the adjacent unburned areas; intercepts of mid-grasses and shrub cover were 2.8 and 5.8 times greater in the burned area than in the adjacent mature woodland. Tree cover in 70- and 90-year-old burns was 12 and 15 percent of the cover measured in adjacent unburned communities, while grasses and shrubs were still much more abundant in the burned areas.

Based on the data from Arnold et al. (1964), it appears that considerably more than 100 years will be required to establish mature piñon-juniper woodland at Area G. This conclusion is supported by published studies and informal analyses specific to Area G. Tress and Klopatek (1987) estimated the rate of succession in piñon-juniper woodlands in north-central Arizona based on several postfire communities. Based on crown cover estimates, it was estimated that slightly more than 200 years would be required for the community to return to pre-burn conditions. Longer periods of time for recovery were indicated by other measures of community structure. Ludwig et al. (1977, cited in Schott and Pieper, 1987) evaluated rates of recovery for northern New Mexico piñon-juniper communities that had been bulldozed and estimated that full recovery of the tree canopy would require at least 100 years.

Koniak (1985) examined vegetation recovery in burned piñon-juniper woodlands located in Nevada and California. Trees began to recolonize the sites 20 to 30 years after the fires, but cover was still minimal after 60 years. Work cited by Koniak suggests that trees will rapidly increase in density and cover from this point onward, and will dominate the sites within 100 to 150 years after

burning. Barney and Frischknecht (1974) examined postfire vegetation changes in the piñon-juniper type of west-central Utah. They found tree density (numbers) was greater in 86-year-old burn areas than in areas that had been undisturbed for more than 100 years. However, crown cover and basal area in the 86-year-old burns were about 50 and 25 percent, respectively, of the corresponding quantities in the 100-year-old-plus communities. Miller and Tausch (2001) cite information indicating tree densities in northern Arizona piñon-juniper woodlands have increased significantly in the past 100 to 200 years, even in stands with trees in excess of 300 years old. These results suggest the transition to climax woodland requires from 100 to several hundred years to complete. Consistent with these observations, Grier et al. (1992) observed tree canopy cover in a 350-year-old piñon juniper woodland in northern Arizona that was about twice the cover estimated for a 90-year-old woodland. Finally, Gallegos (1999) simulated the passage of Area G to piñon-juniper woodland for a preliminary assessment of surface erosion rates at the site. The initial appearance of trees at the site varied for different parts of the site. Trees were projected to appear in areas adjacent to the disposal pits first, showing up 30 to 40 years after closure. The appearance of trees over closed pits was projected to require 40 to 50 years. Much longer periods of time will be required for trees to fully populate the site.

Based on the information summarized above, it appears the time at which climax will likely be attained may be in the range of 100 to several hundred years. On this basis, a triangular distribution was developed to define the time to climax. Minimum, most likely, and maximum values of 100, 200, and 300 years were adopted, values which are in general agreement with the cited studies.

5.9.2 Shape Factors

The functions used to define the distributions of root mass and burrows with depth are series of curves defined using beta distributions (see Section 3.1.2). The shape of these functions is determined by the shape factors. For both sets of curves, the alpha-shape factor is assigned a constant value of zero while the beta-shape factor is assigned a uniform distribution that ranges from 1.5 to 9.

5.9.3 Maximum Rooting Depth

Plant root distributions estimate the mass of plant roots as a function of depth below the ground surface. These distributions are used to estimate the portions of the plant root systems that penetrate into the disposed waste; the amount of contamination deposited on the surface of disposal site due to litterfall is ultimately determined by the fraction of the root system contacting the waste. Maximum rooting depths are used in conjunction with root distribution functions to model the root distributions for grasses, forbs, shrubs, and trees.

Foxx et al. (1984) reviewed the rooting characteristics of native and crop plants within the U.S., focusing their efforts on 53 species of plants found on LLW disposal sites at the Laboratory. Based on this review, they constructed a database of plant rooting depths, and used this

information to estimate rooting depth distributions for individual plant species. Table 38 summarizes the rooting depths estimated by Foxx et al. for a variety of grasses, forbs, shrubs, and trees. Measurements of plant rooting depths taken at the Laboratory are provided in Tierney and Foxx (1987); these data are summarized in Table 39 along with other literature-based rooting depths given in Tierney and Foxx. More recently, Canadell et al. (1996) and Jackson et al. (1999) conducted literature reviews and measured maximum rooting depths. With few exceptions, the maximum rooting depths reported by these investigators for the plant species that inhabit LANL disposal sites are within the rooting depth ranges developed by Foxx et al. (1984).

The rooting data reported by Foxx et al. (1984) and Tierney and Foxx (1987) were used to develop distributions of maximum rooting depths for grasses, forbs, and shrubs. In general, minimum and maximum values of triangular distributions were defined using the rooting depth ranges reported for each growth form; the medians of the datasets were used to define the most likely values. For the distribution of maximum rooting depth in grasses, this approach yields minimum, most likely, and maximum values of 0.76, 1.7, and 4.0 m (2.5, 5.6, and 13 ft), respectively. The corresponding values for forbs are 0.3, 2.4, and 9.1 m (1.0, 7.9, and 30 ft) and those for shrubs are 1.4, 2.9, and 9.1 m (4.6, 9.5, and 30 ft). The rooting depth data for alfalfa were modified prior to defining the distribution for forbs. Specifically, the two highest rooting depths reported for this species (i.e., 19 and 39 m (62 and 130 ft) were eliminated, leaving a maximum rooting depth of 9.1 m (30 ft) for the species. The eliminated data were from plants associated with mine shafts, which represent conditions that are not relevant to Area G.

Relatively few data exist to define the distribution of maximum rooting depths for trees. Information provided by Foxx et al. (1984) and Tierney and Foxx (1987) suggest maximum depths are generally about 6 m (20 ft) for piñon pine and one-seed juniper. Although Foxx et al. (1984) found a rooting depth of 61 m (200 ft) for juniper, Tierney and Foxx (1987) estimated rooting depths of 1.1 to 1.7 m (3.6 to 5.6 ft) for three species of pine and juniper trees. For modeling purposes, a triangular distribution was defined using minimum, most likely, and maximum values of 2, 6, and 10 m (6.6, 20, and 33 ft), respectively. The range of the distribution generally coincides with the cited data and with estimates of maximum rooting depths for *Pinus* spp. (e.g., Canadell et al., 1996), but omits the extreme rooting depth noted by Foxx et al. (1984). The most likely value is approximately equal to the rooting depths of 5.8 and 6.4 m (19 and 21 ft) cited in Foxx et al. (1984) for the one-seed juniper and the 6.4 m (21 ft) rooting depth cited by the same authors for piñon pine.

Table 38
Literature-Based Rooting Depths for Grasses, Forbs, Shrubs, and Trees Growing at Los Alamos National Laboratory

Growth Form and Common Name	Scientific Name	Rooting Depth (cm)	
		Average	Range
Grasses			
Blue Grama	*Bouteloua gracilis*	1.2E+02	3.8E+01–4.0E+02
Bluegrass	*Poa* spp.	8.8E+01	3.5E+01–2.1E+02
Brome Grass	*Bromus inermis*	2.0E+02	1.7E+02–2.3E+02
Buffalo Grass	*Buchloe dactyloides*	1.6E+02	4.6E+01–2.1E+02
Downy Chess	*Bromus tectorum*	7.0E+01	3.0E+01–1.1E+02
Fescue	*Festuca* spp.	7.8E+01	5.0E+00–1.5E+02
Indian Rice Grass	*Oryzopsis hymenoides*	8.4E+01	4.5E+01–1.2E+02
June Grass	*Koeleria cristata*	5.8E+01	3.0E+01–7.6E+01
Little Bluestem	*Andropogon scoparius*	1.7E+02	7.1E+01–2.7E+02
Mountain Muhly	*Muhlenbergia montana*	9.1E+01	2.0E+01–1.4E+02
Needle-and-Thread	*Stipa comata*	1.1E+02	6.3E+01–1.7E+02
Sand Dropseed	*Sporobolus crypandrus*	9.9E+01	9.1E+01–1.2E+02
Sideoats Grama	*Bouteloua curtipendula*	2.2E+02	7.6E+01–4.0E+02
Three-Awn	*Aristida* spp.	1.1E+02	7.6E+01–1.5E+02
Western Wheatgrass	*Agropyron smithii*	1.5E+02	6.8E+01–3.1E+02
Forbs			
Alfalfa	*Medicago sativa*	6.9E+02	3.8E+01–3.9E+03
Aster	*Aster* spp.	1.5E+02	1.5E+01–3.4E+02
Blazing Star	*Mentzelia* spp.	5.8E+01	1.1E+01–1.5E+02
Buckwheat	*Erigonum* spp.	1.7E+02	6.4E+01–3.1E+02
Cinquefoil	*Potentilla* spp.	1.1E+02	5.3E+01–2.3E+02
Estafiata	*Artemisia frigida*	1.0E+02	4.6E+01–2.4E+02
Evening Primrose	*Oenothera* spp.	2.1E+02	5.3E+01–3.1E+02
False Tarragon	*Artemisia dracunculus*	2.1E+02	---
Gayfeather	*Liatris punctata*	3.1E+02	1.2E+02–4.8E+02
Globe Mallow	*Spheralcea* spp.	2.6E+02	8.0E+01–4.0E+02
Goldenaster	*Chrysopsis villosa*	2.8E+02	1.3E+02–4.0E+02
Goldenrod	*Solidago* spp.	2.6E+02	1.1E+02–3.4E+02
Goldenweed	*Haplopappus* spp.	2.9E+02	1.1E+02–5.2E+02
Groundsel	*Senecio* spp.	1.1E+02	3.0E+01–1.5E+02

Source: Foxx et al., 1984

--- = Only one rooting depth was provided; as a result no range is specified.

Table 38 (Continued)
Literature-Based Rooting Depths for Grasses, Forbs, Shrubs, and Trees Growing at Los Alamos National Laboratory

Growth Form and Common Name	Scientific Name	Rooting Depth (cm)	
		Average	Range
Indian Paintbrush	*Castilleja* spp.	2.8E+01	2.5E+01–3.0E+01
Lamb's Quarter	*Chenopodium album*	1.2E+02	---
Penstemon	*Penstemon* spp.	1.3E+02	3.6E+01–3.1E+02
Pigweed	*Amaranthus* spp.	1.0E+02	1.0E+01–2.4E+02
Pingue	*Hymenoxys richardsonii*	9.0E+01	---
Prairie Clover	*Petalostemon* spp.	1.7E+02	8.5E+01–2.1E+02
Puccoon	*Lithospermum* spp.	2.2E+02	1.8E+02–3.1E+02
Russian Thistle	*Salsola kali var tenuifolia*	6.7E+01	---
Summer Cypress	*Kochia scoparia*	2.0E+02	---
Sweetclover	*Melilotus* spp.	1.3E+02	8.5E+01–1.5E+02
Vetch	*Vicia* spp.	8.0E+01	2.0E+01–1.4E+02
Yucca	*Yucca* spp.	1.1E+02	3.0E+01–2.1E+02
Shrubs and Subshrubs			
Apache Plum	*Fallugia paradoxa*	1.2E+02	6.0E+01–1.4E+02
Big Sagebrush	*Artemisia tridentate*	2.5E+02	1.1E+02–9.1E+02
Chamisa	*Chrysothamnus nauseosus*	2.9E+02	1.0E+02–4.6E+02
Four-Wing Saltbush	*Atriplex canescens*	3.9E+02	1.1E+02–7.6E+02
Gambel's Oak	*Quercus gambelli*	2.4E+02	8.0E+01–4.0E+02
Mountain Mahogany	*Cercocarpus montanus*	1.1E+02	4.0E+01–1.5E+02
Snakeweed	*Gutierrezia* spp.	1.2E+02	5.1E+01–2.4E+02
Wild rose	*Rosa* spp.	3.9E+02	9.1E+01–6.4E+02
Trees			
Elm	*Ulmus pumila*	1.3E+02	---
One-Seed Juniper	*Juniperus monosperma*	2.4E+03	5.8E+02–6.1E+03
Piñon Pine	*Pinus edulis*	6.4E+02	---
Ponderosa Pine	*Pinus ponderosa*	4.5E+02	1.0E+01–2.4E+03

Source: Foxx et al., 1984

--- = Only one rooting depth was provided; as a result no range is specified.

Table 39
Measured, Estimated, and Literature-Based Plant Rooting Depths for Plants at Los Alamos National Laboratory

Growth Form and Common Name	Scientific Name	Rooting Depth Ranges(cm)		
		Measured	Estimated [a]	Literature-Based
Grasses				
Blue Grama	*Bouteloua gracilis*	5.3E+01–5.8E+01	---	3.8E+01–4.0E+02
Forbs				
Mullein	*Verbascum thapsus*	2.8E+01–4.2E+01	---	NA
Narrowleaf Yucca	*Yucca angustissima*	2.0E+01	---	4.0E+01–1.5E+02
Prickly pear	*Opuntia polyacantha*	8.0E+00–2.8E+01	---	2.0E+00–3.7E+02
Sunflower	*Helianthus petiolaris*	4.0E+01–4.5E+01	---	NA
Shrubs and Subshrubs				
Apache Plum	*Fallugia paradoxa*	6.0E+01–1.3E+02	1.7E+02–2.9E+02	NA
Big Sagebrush	*Artemisia tridentata*	1.0E+01–1.5E+02	1.3E+02–1.8E+02	1.1E+02–9.1E+02
Chamisa	*Chrysothamnus nauseosus*	1.0E+02–1.8E+02	1.4E+02–2.1E+02	1.0E+02–4.6E+02
Four-Wing Saltbush	*Atriplex canescens*	6.0E+01–1.1E+02	1.9E+02–2.2E+02	8.0E+01–7.6E+02
Mountain Mahogany	*Cercocarpus montanus*	4.0E+01 [b]	5.0E+01 [b]	4.0E+01–1.5E+02
New Mexico Locust	*Robinia neomexicana*	1.0E+02–1.4E+02	---	NA
Oak	*Quercus* spp.	4.5E+01–1.0E+02	1.5E+02–3.2E+02	8.0E+01–4.0E+02
Snakeweed	*Gutierrezia sarothrae*	6.0E+01–1.3E+02	1.7E+02–2.9E+02	5.1E+01–2.4E+02
Squawberry	*Rhus trilobata*	1.5E+02–1.7E+02	2.1E+02–2.3E+02	NA
Wax Currant	*Ribes cereum*	7.0E+01–1.5E+02	8.0E+01–2.9E+02	NA
Trees				
One-Seed Juniper	*Juniperus monosperma*	1.5E+02 [b]	1.7E+02 [b]	5.8E+02–6.1E+03
Piñon Pine	*Pinus edulis*	3.0E+01–6.0E+01	1.1E+02–1.3E+02	NA
Ponderosa Pine	*Pinus ponderosa*	1.3E+02–1.5E+02	1.5E+02–1.6E+02	1.0E+01–2.4E+03

Source: Tierney and Foxx (1987)

--- = Indicates no root depths were estimated for the species.

NA = Not applicable; no range in rooting depths was reported.

[a] *Estimated root lengths are provided for roots that broke during excavation and roots that could not be completely excavated due to safety considerations and/or the soil profile.*

[b] *No range is provided either because all root length measurements were the same length or because only a single measurement of root length was collected.*

5.9.4 Aboveground Biomass Density

Litter generated by leaf fall and plant death contributes to soil formation as the organic matter decays; radionuclides that are assimilated by the plants will also enter into the soil. The rate at which organic material is added to surface soils is a function of the aboveground biomass of the plant and the fraction of this biomass that becomes litter. Estimates of aboveground biomass were developed using growth-form-specific information in the literature; these estimates addressed the site during early succession and after the piñon-juniper climax condition was attained. The studies upon which these estimates are based are discussed below.

Estimates of understory biomass for the early successional stages at Area G were based on information from several different sites. These sites included piñon-juniper woodlands that had been disturbed by fire or physical means, piñon-juniper grasslands, and areas adjacent to mature woodlands. Although the conditions at Area G are not expected to exactly coincide with the conditions at any one of these sites, understory production data obtained from these communities are expected to provide reasonable estimates of conditions at the disposal site.

Direct measurements of aboveground production of grasses, forbs, and shrubs were found for a number of sites in the western U.S.; those used to develop biotic intrusion modeling data are summarized in Table 40. Clary (1989) evaluated the production of grasses, forbs, and shrubs on areas that had been disturbed by chaining and cabling 2 to 30 years prior. The treated areas were reseeded with a mix of grass and forb species after chaining or cabling; seeding would also be undertaken at Area G after the final cover was constructed. Average yields across the four sites and the 4 years in which measurements were conducted were 570 kg/ha (510 lb/ac) for grasses, 33 kg/ha (30 lb/ac) for forbs, and 76 kg/ha (70 lb/ac) for shrubs. Clary (1971) evaluated understory production prior to and following the cabling of piñon-juniper woodland located in northern Arizona. Yields of grasses, forbs, and shrubs averaged 250, 480, and 380 kg/ha (220, 425, and 340 lb/ac), respectively, 4 to 11 years after cabling and seeding had occurred.

Dwyer and Pieper (1967) measured production of grasses and forbs in burned and unburned areas on piñon-juniper rangeland in south-central New Mexico. The unburned area was largely free of trees and, as such, was considered to be a reasonable approximation of Area G in its early successional stages. The data for the site, collected over a 3-year period, indicated an average production of about 890 kg/ha (800 lb/ac) for grasses and 140 kg/ha (125 lb/ac) for forbs.

Additional work conducted by Pieper (1968) in south-central New Mexico examined the effects of grazing on herbage production in piñon-juniper grasslands. Aboveground production ranged from 680 to 730 kg/ha (600 to 650 lb/ac) on two open grassland areas that were protected from grazing; grass production on two grazed areas ranged from 330 to 620 kg/ha (290 to 550 lb/ac). The basal cover was 9.4 to 12 percent at the two ungrazed sites, and 9.6 to 14 percent at the sites that had been grazed. Grasses accounted for 81 to 98 percent of the total plant cover. O'Rourke and Ogden (1969) evaluated

Table 40
Summary of Cover and Production Studies Used to Estimate Aboveground Biomass (early successional stages at Area G)

Community Characteristics	Reference	Cover (%)			Aboveground Production (kg/ha)		
		Grasses	Forbs	Shrubs	Grasses	Forbs	Shrubs
Piñon-Juniper Woodland in Central Utah (4 sites)	Clary, 1989	---	---	---	2.9E+02–7.7E+02	0–1.0E+02	7.9E+00–1.8E+02
Piñon-Juniper Woodland in Northern Arizona (4 plots, 4–11 years after cabling and seeding)	Clary, 1971	---	---	---	2.5E+02 (avg.)	4.8E+02 (avg.)	3.8E+02 (avg.)
Piñon-Juniper Woodland in Arizona (22 plots)	Clary and Jameson, 1981	---	---	---	1.1E+03 (avg.)	2.8E+02 (avg.)	1.1E+02 (avg.)
Piñon-Juniper Rangeland in South-Central New Mexico (3 transects)	Dwyer and Pieper, 1967	1.3E+01–2.7E+01	1.7E-01–8.7E-01	NA	8.1E+02–1.0E+03	7.1E+02–2.4E+03	NA
Piñon-Juniper Rangeland in South-Central New Mexico (2 ungrazed sites)	Pieper, 1968	7.6E+00–1.1E+01, (basal cover)	3.0E-01–1.8E+00	NA	6.8E+02 and 7.3E+02 (total herbage)		
(2 grazed sites)		9.2E+00–1.4E+01 (basal cover)			3.3E+02 and 6.2E+03 (total herbage)		
Piñon-Juniper Woodland in Northern Arizona	O'Rourke and Ogden, 1969	1.4E+01–2.4E+01 (perennial basal cover) 1.0E+00–1.4E+01 (annual basal cover)	1.2E+00–5.6E+00	Statistically similar to cover for woodland (3.0E-01–2.1E+00)	2.8E+01–3.9E+03 (perennial grasses)	NA	NA
Grasslands Surrounding Piñon-Juniper Woodlands in Arizona (sites without trees)	Arnold et al., 1964	3.7E+00 (mean basal cover)	5.0E-01 (mean basal cover)	3.9E+00 (mean canopy cover)	7.0E+02		
Piñon-Juniper Rangeland in South-Central New Mexico	Pieper, 1990	---	---	---	9.0E+02–1.1E+03 (areas with 10% tree cover; three species of grass accounted for 7.0E+02–8.5E+02 kg/ha of this amount)		
Piñon-Juniper Woodland Sites Converted to Grassland (5 sites)	Aro, 1971	---	---	---	5.6E+02–1.5E+03	NA	NA

--- = Measurements were not performed.

NA = Not applicable; growth form was not considered in the study.

the effects of piñon-juniper control on herbage (i.e., grasses and forbs) production at four woodland sites in north-central Arizona. The 2-year study included measurements of mean basal cover of grass, forbs, and shrubs in areas that had been cleared of trees 4 to 5 years prior and grazed for a total of 4 months over a 2-year period; perennial grass production was also measured. Perennial grass cover ranged from 14 to 24 percent, cover for annual grasses ranged from 1 to 14 percent over the four sites. The mean basal cover for forbs ranged from 1.2 to 5.6 percent while the cover for shrubs ranged from 0.3 to 2.1 percent. Total production of perennial grasses ranged from 28 to 390 kg/ha (25 to 350 lb/ac).

Aro (1971) evaluated the effectiveness of converting piñon-juniper woodland to grassland using a variety of techniques, including chaining, chaining followed by windrowing, and fire. Approximately 50 sites that had undergone tree removal prior to 1963 were examined; among the data collected at these sites were yields of grasses. A yield of 560 kg/ha (500 lb/ac) was observed at one site in Colorado following chaining, while yields at sites that had been windrowed ranged from 560 to over 1,100 kg/ha (500 to over 980 lb/ac). Yields at three sites that had been burned ranged from 560 to over 1,450 kg/ha (500 to over 1,300 lb/ac).

Arnold et al. (1964) developed estimates of total herbage yields for piñon-juniper woodlands as a function of tree canopy intercept. Yields were about 700 kg/ha (625 lb/ac) of air-dry vegetation in areas that were free of trees, but dropped to about 400 kg/ha (350 lb/ac) for areas with 10 percent tree canopy cover. Pieper (1990) conducted an analysis similar to that of Arnold et al. for piñon-juniper woodland in south-central New Mexico. A yield of about 1,060 kg/ha (945 lb/ac) of grasses and forbs was predicted for areas without trees; production was estimated to decrease to 900 kg/ha (800 lb/ac) for areas with tree cover of 10 percent. Three species of grass accounted for 80 percent of the total production, with other grasses and forbs accounting for the remainder. Clary and Jameson (1981) measured production in piñon-juniper woodland, before and after overstory removal, on 22 plots at 11 sites. Production of grasses, forbs, and shrubs was measured 4, 6, and 8 years after vegetation was killed by girdling and sawing the trees and through herbicide use. Production of grasses averaged 1,050 kg/ha (935 lb/ac) over the 3 years of measurements, while forbs and shrub production averaged 275 and 114 kg/ha (250 and 100 lb/ac), respectively.

The studies summarized above were used to develop distributions of aboveground biomass for grasses, forbs, and shrubs for Area G while it is in the early stages of succession; Table 41 lists the data adopted from these investigations. Pieper's 1968 production estimates were divided between grasses and forbs based on percent cover of each growth form, while his 1990 estimate for "other grasses and forbs" was assumed to represent forbs. The median of each growth form's production data was used to define the most likely values of the triangular distributions, while the minimum and maximum values were defined using the ranges. The distributions of aboveground biomass are summarized in Table 11. The sum of the median grass and forbs production data is less than the overall production estimates of 700 and 1,060 kg/ha (625 and 945 lb/ac) reported by Arnold et al. (1964) and Pieper (1990), respectively.

Table 41
Aboveground Production of Grasses, Forbs, and Shrubs
(early successional stages of piñon-juniper cover types)

Study	Aboveground Production (kg/ha, dry weight)		
	Grasses	Forbs	Shrubs
Clary, 1989			
Church Hills Site—1982	3.9E+02	9.5E+01	1.8E+02
Church Hills Site—1985	4.3E+02	1.0E+02	8.5E+01
Clay Springs Site—1980	2.9E+02	3.7E+01	7.5E+01
Clay Springs—1985	4.9E+02	2.0E+01	2.0E+01
Eight Mile Site No. 1—1980			
Side Slope	7.7E+02	3.4E+00	1.3E+01
Ridge Crest	4.1E+02	1.5E+01	8.6E+01
Eight Mile Site No. 1—1982			
Side Slope	5.6E+02	1.1E+00	2.4E+01
Ridge Crest	4.1E+02	3.8E+01	1.1E+02
Eight Mile Site No. 1—1985			
Side Slope	7.1E+02	0.0E+00	7.9E+00
Ridge Crest	5.5E+02	1.5E+01	5.8E+01
Eight Mile Site No. 2—1980			
Side Slope	6.3E+02	1.7E+01	4.5E+01
Ridge Crest	5.7E+02	1.6E+01	4.2E+01
Eight Mile Site No. 1—1981			
Side Slope	6.9E+02	4.7E+01	1.2E+02
Ridge Crest	7.7E+02	1.9E+01	1.2E+02
Eight Mile Site No. 1—1985			
Side Slope	7.6E+02	8.6E+01	1.5E+02
Ridge Crest	6.7E+02	2.2E+01	8.1E+01
Clary, 1971	2.5E+02	4.8E+02	3.8E+02
Dwyer and Pieper, 1967			
Unburned Site—1964	8.1E+02	7.1E+01	---
Unburned Site—1965	1.0E+03	2.4E+02	---
Unburned Site—1966	8.5E+02	1.1E+02	---

--- = Indicates no estimate of production was available for growth form.

[a] *Production was presented in the report as total herbage (i.e., grass and forbs) production. These yields were divided between grasses and forbs based on percent cover.*

Table 41 (Continued)
Aboveground Production of Grasses, Forbs, and Shrubs
(early successional stages of piñon-juniper cover types)

Study	Aboveground Production (kg/ha, dry weight)		
	Grasses	Forbs	Shrubs
Pieper, 1968			
Loamy Bottomland—Ungrazed	6.2E+02[a]	6.0E+01 [a]	---
Loamy Upland - Ungrazed	5.9E+02[a]	1.4E+02 [a]	---
O'Rourke and Ogden, 1969			
Boundary Site—1961	2.0E+02	---	---
Boundary Site—1962	1.8E+02	---	---
Ryan Site—1961	2.8E+01	---	---
Ryan Site—1962	1.3E+02	---	---
Second Site—1961	2.0E+02	---	---
Second Site—1962	2.2E+02	---	---
Chevelon Site—1961	3.9E+02	---	---
Chevelon Site—1962	3.9E+02	---	---
Pieper, 1990	8.5E+02	2.1E+02	---
Clary and Jameson, 1981	1.1E+03	2.8E+02	1.1E+02
Aro, 1971			
Colorado Site	5.6E+02	---	---
Windrowed Site No. 1	5.6E+02	---	---
Windrowed Site No. 2	1.1E+03	---	---
Fire Site No. 1	5.6E+02	---	---
Fire Site No. 2	6.7E+02	---	---
Fire Site No. 3	1.5E+03	---	---

--- = Indicates no estimate of production was available for growth form.

[a] *Production was presented in the report as total herbage (i.e., grass and forbs) production. These yields were divided between grasses and forbs based on percent cover.*

Biomass estimates for grasses, forbs, and shrubs in the mature piñon-juniper woodland were developed in a manner similar to that described above for the disturbed site. The data used to generate these estimates are summarized in Table 42, which includes a description of the sites that were investigated and a summary of the production and cover information that was taken from the reports. Some of these studies provide direct estimates of understory production in the mature woodland. Clary (1971) studied the effects of tree removal on herbage yields in piñon-juniper woodlands in northern Arizona. Herbage yields of grasses, forbs, and shrubs averaged 71, 77, and 100 kg/ha/yr (63, 68, and 90 lb/ac), respectively, in areas where no trees were removed. In other work, Clary (1989) reported yields ranging from 20 to 140 kg/ha (20 to 125 lb/ac) for grasses, 10 to 45 kg/ha (9 to 40 lb/ac) for forbs, and 30 to 130 kg/ha (26 to 115 lb/ac) for shrubs in mature piñon-juniper woodlands in central Utah. Clary and Jameson (1981) measured production in piñon-juniper woodland on 22 plots at 11 sites, piñon-juniper crown cover ranged from 0 to 43 percent with a median value of about 17 percent. Production of grasses, forbs, and shrubs averaged 100, 46, and 216 kg/ha (90, 40, and 190 lb/ac), respectively, at these locations.

Pieper (1968) estimated total herbage production and cover in piñon-juniper rangeland located in south-central New Mexico. Aboveground production was 630 kg/ha (560 lb/ac) at an ungrazed piñon-juniper community with grass understory, while production on a grazed site was 530 kg/ha 470 lb/ac). Grasses accounted for about 98 percent of the total vegetation at both sites. O'Rourke and Ogden (1969) measured the basal cover of grass, forbs, and shrubs at four undisturbed woodland sites in north-central Arizona; the canopy cover of trees and perennial grass production were also evaluated. Perennial grass cover ranged from 8 to 21 percent over the 2-year study, while the cover for annual grasses ranged from 0 to 0.3 percent. The mean basal cover for shrubs ranged from 0.3 to 2.1 percent and the canopy cover for trees ranged from 13 to 44 percent. Total production of perennial grasses ranged from about 60 to 230 kg/ha (53 to 200 lb/ac).

Aro (1971) measured grass yields of about 110 kg/ha (100 lb/ac) at two sites prior to their conversion from woodland to grassland, and approximately 30 and 220 kg/ha (26 and 195 lb/ac) at two other pretreatment sites. As discussed earlier, Arnold et al. (1964) developed a relationship between total herbage yield and tree canopy intercept (shown in Figure 15a). Clary (1971) developed a similar relationship between tree cover and total understory production (i.e., grasses, forbs, and shrubs) in his work in northern Arizona (Figure 15b); Pieper (1990) related canopy cover to total herbage production for woodlands in New Mexico (Figure 15c).

The production data of Clary (1971, 1989), Clary and Jameson (1981), Pieper (1968), O'Rourke and Ogden (1969), and Aro (1971) were used to generate distributions for aboveground production for grasses, forbs, and shrubs in mature piñon-juniper woodland. Table 43 lists the data estimated on the basis of these studies. Pieper's production estimates for ungrazed sites were divided between grasses and forbs based on the percent cover measurements provided in that study. Perennial grass

Table 42
Summary of Cover and Production Studies Used to Estimate Understory Biomass (Area G climax condition)

Community Characteristics	Reference	Cover (%)				Aboveground Production (kg/ha)		
		Grasses	Forbs	Shrubs	Trees	Grasses	Forbs	Shrubs
Piñon-Juniper Woodland in Northern Arizona (4 plots)	Clary, 1971	---	---	---	1.0E+01–4.5E+01 (crown cover)	7.1E+01 (4-year avg.)	7.7E+01 (4-year avg)	1.0E+02 (4-year avg.)
Piñon-Juniper Woodland in Central Utah (2 sites)	Clary, 1989	---	---	---	---	2.0E+01–1.4E+02	1.0E+01–4.5E+01	3.0E+01–1.3E+02
Piñon-Juniper Woodland in Arizona (22 plots)	Clary and Jameson, 1981	---	---	---	0E+00–4.3E+01 (crown cover)	1.0E+02 (avg)	4.6E+01 (avg)	7.0E+01 (avg)
Piñon-Juniper Rangeland in South-Central New Mexico (grazed and ungrazed sites)	Pieper, 1968	1.2E+01–1.8E+01 (basal cover)	1.3E+00–1.7E+00 (basal cover for forbs and other vegetation)			5.3E+02 (total herbage, grazed site) 6.3E+02 (total herbage, ungrazed site)		
Piñon-Juniper Woodland in North-Central Arizona (4 sites)	O'Rourke and Ogden, 1969	8.0E+00–2.2E+01 (perennial basal cover) 1E+00–2E+00 (annual basal cover)	0E+00–0.3E+00 (mean basal cover)	0.3E+00–2.1E+00 (mean basal cover)	1.3E+01–4.4E+01 (mean crown cover)	6.0E+01–2.3E+02 (perennial grasses)	NA	NA
Piñon-Juniper Woodland Sites, Western U.S. (4 sites)	Aro, 1971	---	---	---	---	3.0E+01–2.2E+02	NA	NA
Piñon-Juniper Woodland Communities in Northern Arizona	Arnold et al., 1964	---	---	---	---	Estimates of total herbage production as a function of tree canopy cover		

--- = Cover measurements were not performed. *NA = Not applicable; growth-form was not considered in the study.*

Figure 15a. Relationship between air-dry herbage yield to percent intercept of overstory juniper and piñon (adapted from Arnold et al., 1964)

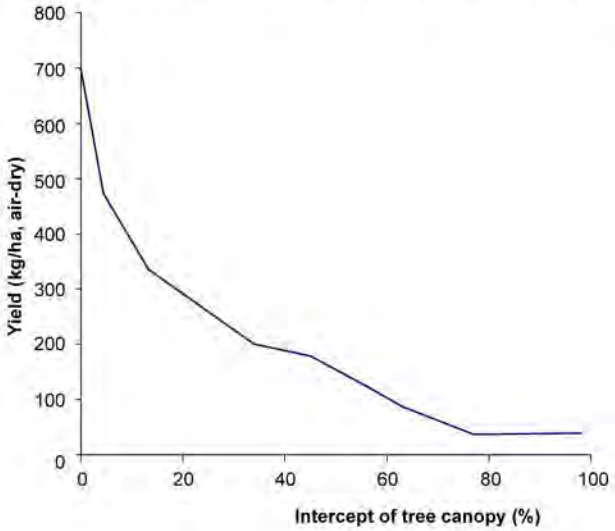

Figure 15b. Relationship of total understory yields to percent crown cover of intact overstory (adapted from Clary, 1971)

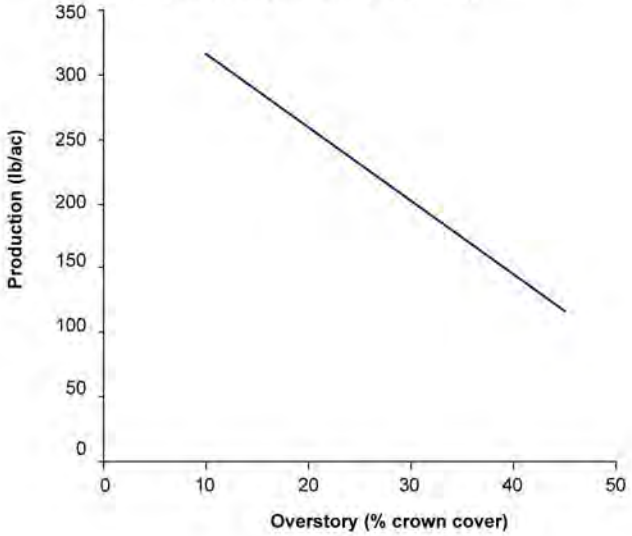

Figure 15c. Relationship between canopy cover and total herbage biomass. (adapted from Pieper, 1990)

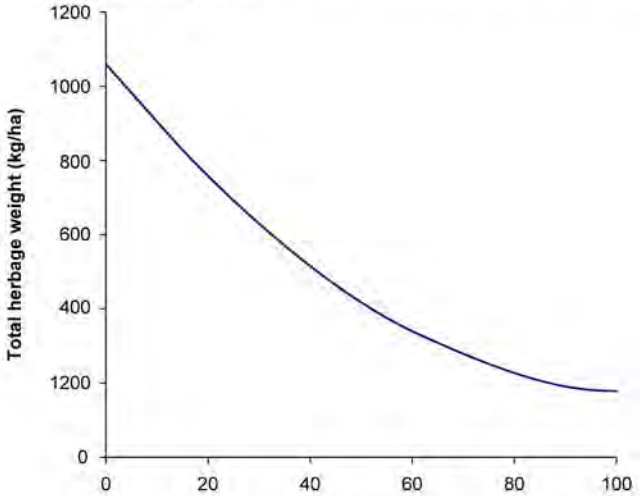

Figure 15
Relationship between Canopy Cover and Herbage Yields

Table 43
Aboveground Production of Grasses, Forbs, and Shrubs in Mature Piñon-Juniper Woodlands

Study	Aboveground Production (kg/ha, dry weight)		
	Grasses	Forbs	Shrubs
Clary, 1971	7.1E+01	7.7E+01	1.0E+02
Clary, 1989			
Church Hills Site—1980	4.7E+01	4.5E+01	5.7E+01
Church Hills Site—1982	1.4E+02	1.6E+01	1.3E+02
Church Hills Site—1985	7.7E+01	3.5E+01	7.2E+01
Clay Springs Site—1980	2.0E+01	1.0E+01	3.0E+01
Clary and Jameson, 1981	1.0E+02	4.6E+01	7.0E+01
Pieper, 1968	6.2E+02	1.1E+01	---
O'Rourke and Ogden, 1969			
Boundary Site—1961	2.5E+02	---	---
Boundary Site—1962	1.7E+02	---	---
Ryan Site—1961	9.8E+01	---	---
Ryan Site—1962	2.1E+02	---	---
Second Site—1961	1.0E+02	---	---
Second Site—1962	6.7E+01	---	---
Chevelon Site—1961	1.6E+02	---	---
Chevelon Site—1962	9.4E+01	---	---
Aro, 1971			
Colorado Site	2.8E+01	---	---
Fire Site No. 1	1.1E+02	---	---
Fire Site No. 2	1.1E+02	---	---
Fire Site No. 3	2.2E+02	---	---

--- = No production measurements were conducted for the indicated growth form.

production data provided by O'Rourke and Ogden were adjusted upward to account for the contributions from annual grasses. The most likely values of the triangular distributions were defined using the medians of the growth-form production data; minimum and maximum values were defined on the basis of the ranges. The biomass distributions are summarized in Table 11. The median productivities suggest a woodland community with crown cover of approximately 30 to 45 percent based on the relationships developed by Arnold et al. (1964) and Clary (1971) (Figure 15a and 15b). This is consistent with work by Padien and Lajtha (1992) that suggests the total canopy cover at Area G may be about 37 to 50 percent after the site has transitioned to a piñon-juniper community. In contrast, the median productivities suggest a woodland canopy cover of approximately 85 percent based on the relationship developed by Pieper (1990) (Figure 15c).

Limited information exists with respect to the aboveground biomass of trees in piñon-juniper woodlands. Grier et al. (1992) estimated aboveground biomass and aboveground net productivity for 90- and 350-year-old piñon-juniper communities in northern Arizona. Tree biomass was estimated using regression equations developed from destructive analysis of the two tree species, taking into account the full diameter range of trees found at the study sites. Net productivity was estimated as the sum of the annual biomass increment and litterfall.

The estimates developed by Grier et al. (1992) are summarized in Table 44. Total tree biomass of the 350-year-old woodland was 2.3 times greater than that estimated for the 90-year-old stand. These biomass estimates fall at the low end of the range reported for piñon-juniper woodlands in other regions. Meeuwig (1979), cited in Grier et al., reported aboveground biomass for Great Basin woodlands consisting of singleleaf piñon (*Pinus monophylla*) and Utah juniper (*Juniperus osteosperma*) ranging from 60 to 121 Mg/ha (27 to 54 T/ac). The oldest trees in these stands were about 320 and 260 years old, respectively. Grier et al. observed that the productivities measured in the northern Arizona piñon-juniper communities are also low compared to most other forests and woodlands in North America. Though limited in nature, the information provided in Grier et al. was used to develop the distribution for aboveground biomass in trees. A triangular distribution was assumed and assigned minimum and maximum values of 2.3×10^4 and 1.2×10^5 kg/ha (2.0×10^4 and 1.1×10^5 lb/ac), respectively. These values represent the tree biomass estimated by Grier et al. for the young piñon-juniper stand and the maximum biomass reported by Meeuwig. The biomass estimate developed by Grier et al. for the mature woodland, 5.3×10^4 kg/ha (4.7×10^4 lb/ac), was adopted for the most likely value.

5.9.5 Litter Production Rate

The litter production rate is defined as the fraction of the aboveground biomass that dies and falls to the ground surface on an annual basis. Insight into the litter production rates of grasses and forbs may be gained by using the biomass distribution data collected by Grier et al. (1992) and Cox (1984). Grier et al. measured biomass distribution in young and mature stands of piñon-juniper in north-central Arizona. Those investigators found that standing dead material accounted

Table 44
Aboveground Biomass and Net Primary Productivity Estimates for Trees in Piñon-Juniper Woodlands

Component	90-Year-Old Stand			350-Year-Old Stand		
	Piñon Pine	Juniper	Total	Piñon Pine	Juniper	Total
Biomass (Mg/ha, dry weight)						
Canopy						
Foliage	2.7E+00	1.7E+00	4.4E+00	2.4E+00	3.3E+00	5.7E+00
Foliage-Bearing Twigs	1.6E+00	1.6E-01	1.7E+00	1.0E+00	4.1E-01	1.4E+00
Living Branches (incl. bark)	6.5E+00	4.2E+00	1.1E+01	1.3E+01	1.5E+01	2.9E+01
Dead Branches	6.9E-01	2.7E-01	9.6E-01	2.2E+00	1.4E+00	3.5E+00
Stem (wood and bark)	3.4E+00	1.5E+00	4.9E+00	7.2E+00	6.5E+00	1.4E+01
Total	1.5E+01	7.9E+00	2.3E+01	2.6E+01	2.7E+01	5.3E+01
Productivity (Mg/ha/yr, dry weight)						
Biomass Increment						
Living Wood	2.0E-01	5.0E-02	2.5E-01	3.2E-01	1.1E-01	4.3E-01
Attached Dead Material	2.0E-02	Trace	2.0E-02	7.0E-02	1.0E-02	8.0E-02
Bark	4.0E-02	1.0E-02	5.0E-02	6.0E-02	2.0E-02	8.0E-02
Foliage Production	7.0E-01	4.5E-01	1.2E+00	9.0E-01	8.2E-01	1.7E+00
Total			1.5E+00			2.3E+00
Litterfall			3.0E-02			5.0E-02

Source: Grier et al. (1992)

for approximately 40 percent of the interspace (i.e., between trees) vegetation biomass during the growing season; the dominant species growing in these areas was blue grama (*Bouteloua gracilis*), a perennial grass. Cox (1984) found that standing dead matter accounted for at least 26 to 72 percent of the biomass in a perennial grassland community in southeast Arizona. Sims and Singh (1978) evaluated mass transfers among various biotic compartments for 10 North American grasslands; one such transfer was the passage, during the growing season, of live material to standing dead material. The results of the study indicated that 2 to 100 percent of the live matter was incorporated into the standing dead compartment.

Scurlock et al. (2003) summarized biomass data collected from 31 grassland sites located around the world. Eight of the sites are in the U.S. and include a high mountain meadow, dry and humid temperate steppes, and a subtropical semidesert steppe. The data collected for all but the high mountain meadow were used to estimate the fraction of the aboveground biomass consisting of dead material. Fractions for these seven sites ranged from 0.0 to 1.0, with a median fraction of about 0.5; similar results were observed for the dry temperate steppes, which are expected to have vegetation most like that at Area G shortly after closure.

The data for standing dead matter cited above may be used to estimate rates of litter production for grasses and forbs if it is assumed that the subject woodland and grassland communities have been under steady-state conditions and that all aboveground biomass has died each year. Under these conditions, the litter production rate may be estimated as the complement of the fraction of the aboveground biomass that is standing dead matter. Using this approach, litter production rates of 0.28/yr to 0.74/yr are estimated using the data of Cox (1984), while a rate of 0.6/yr is calculated using the data from Grier et al. (1992). The data of Scurlock et al. (2003) yield litter production rates that range from 0/yr to 1.0/yr, with a median production rate of 0.5/yr. Sims and Singh (1978) indicate litter production rates of 0/yr to 0.98/yr.

Other estimates of litter production rates may be developed using biomass accumulation ratios. This ratio is the dry weight biomass divided by the annual net primary productivity. Whittaker (1975) provides ranges of the accumulation ratio (for aboveground parts of plants) for different terrestrial communities; normal ranges are from 2 to 10 in the desert, 1 to 3 in grasslands, 3 to 12 in shrublands, 10 to 30 in woodlands, and 20 to 50 in mature forests. Assuming the plant community is under steady-state conditions, the inverse of these ratios estimates the fraction of the aboveground biomass that goes into annual litter production. Using this approach and the data provided by Whittaker for grasslands, it is estimated that 33 to 100 percent of the aboveground biomass of grasses and forbs will enter into annual litter production. Separately, Rodin and Bazilevich (1967, cited in Strojan et al., 1979) note that 45 to 60 percent of the aboveground and belowground biomass in grasslands becomes litter each year.

The litter production rate for grasses and forbs was assigned a triangular distribution using the data summarized above. The minimum and maximum values of the distribution were set to 0.3/yr and 1.0/yr, and the most likely value was set to 0.6/yr. The range of this distribution is consistent with the rates estimated using the data from Cox (1984) and the biomass accumulation ratios published by Whittaker (1975), but it does not capture the low end of the distribution indicated using the data published by Scurlock et al. (2003) and Sims and Singh (1978). The most likely value of 0.6/yr is consistent with the findings of Grier et al. (1992) and Rodin and Bazilevich (1967). The same distribution was assumed to apply to grasses and forbs in the grassland and piñon-juniper woodland communities.

Litter production in shrubs has been investigated on a number of occasions. Strojan et al. (1979) collected litter from six shrub species in the northern Mojave Desert. Their results indicate that 7 to 83 percent of live aboveground biomass was shed annually as litter; the fraction of aboveground biomass going to litter was typically less than 60 percent. These investigators cite results from Charley and Cowling (1968) who estimated that approximately 46 percent of the aboveground biomass of bladder saltbush was converted to litter. West (1985) examined litter production in three species of shrubs found in northwestern Utah, the Great Basin sagebrush, shadscale, and white sage. Litterfall was found to average 10, 38, and 63 percent of the midsummer aboveground biomass.

Parmenter et al. (1987) cite studies conducted by West and Gunn (1974) and Mack (1977) that indicate 5.8 to 13.4 percent of the aboveground biomass of sagebrush in the Great Basin desert is converted to litter annually. Biomass accumulation ratios for shrublands may be used in the manner described above for grasslands to arrive at additional estimates of litter production rates. Using the data published by Whittaker (1975) suggests that 8 to 33 percent of the aboveground biomass of shrubs will enter into annual litter production.

The data cited above were used to construct a triangular distribution for the shrub litter production rate. The minimum and maximum values of the distribution were set to 0.06/yr and 0.60/yr; this range generally agrees with the data summarized above. The most likely value was set to 0.13/yr, which is equivalent to the litter production fraction observed by Mack (1977) and is the inverse of the midpoint of the bioaccumulation ratios cited by Whittaker (1975).

As discussed earlier, Grier et al. (1992) estimated aboveground biomass, net productivity, and litterfall for young and mature stands of piñon-juniper. The litter production rates estimated by Grier et al. are approximately 0.1 percent of the aboveground biomass estimates for the two woodland communities (see Table 44). This relative rate of production cannot be compared to data for other piñon-juniper woodlands because no such data were found. Nevertheless, it appears this production rate is significantly smaller than rates indicated for other forest communities. This conclusion is based on several lines of evidence.

Hinesley et al. (1991) measured litter production in four stands of oak-hickory-pine forests in northern Mississippi. Annual litter production ranged from 3 to 6.5 percent of the tree biomass, and was highest in the stands that were predominantly pine. Rodin and Bazilevich (1967, cited in Strojan et al., 1979) note that 1 to 4 percent of forest biomass is shed as litter. Whittaker (1975) reported that litter production in a young mixed deciduous forest in the northeastern U.S. was approximately 3.7 percent of the aboveground biomass. Whittaker also reported a range of biomass accumulation ratios of 10 to 30 for aboveground parts of plants in woodlands. These ratios are largely determined by the presence of trees in the communities. If it is assumed that these ratios remain relatively constant over time, taking the inverse of the ratios yields estimates of the portion of the biomass that goes into litter production each year. This calculation yields annual litter generation rates that are 3 to 10 percent of the aboveground biomass.

An indirect method of estimating the litter production fraction for trees considers the relative contributions of foliage to aboveground biomass and litter. Ricklefs (1979) reported that leaves comprise between 1 and 10 percent of the aboveground biomass of forests; evergreen forests tended to occupy the high end of this range. Grier et al. (1992) found that leaves were 11 and 19 percent of the total aboveground tree biomass in the two piñon-juniper woodlands they studied. In terms of litter, Williams and Gray (1974) indicate that leaf material accounts for approximately 70 percent of forest litter in gymnosperms.

Using an assumed lifetime for leaf material, the data cited above can be used to estimate litter production fractions. For example, using a life span of 3 years for the leaf material and the data from Grier et al. (1992), it is estimated that 3.7 to 6.3 percent of the aboveground tree biomass falls as leaf litter in a given year. However, if this litter comprises only 70 percent of the annual litterfall, as indicated by Williams and Gray (1974), the total annual litter production factor is around 5 to 9 percent. Annual litter production fractions ranging from 8 to 14 percent are estimated for a leaf material life span of 2 years, while fractions ranging from 4 to 7 percent are estimated using a leaf life span of 4 years.

The information provided above suggests annual litter production in coniferous forests may be about 1 to 14 percent of the aboveground biomass, much higher than the litter production fractions estimated by Grier et al. (1992). In the absence of data needed to confirm the results of Grier et al. (1992), the 1 to 14 percent range was used to define the distribution for the parameter. A triangular distribution was defined with minimum, most likely, and maximum values of 0.01/yr, 0.075/yr, and 0.14/yr.

5.9.6 Litter Decomposition Half-Life

The rate at which litter decays to form soil will depend upon the climatic conditions under which decomposition occurs and the nature of the plant material. In general, rates of decomposition typically rise with increased temperature and moisture. For example, rates of decomposition tend

to be greater in warm, moist tropical forests than in a more temperate, arid environment such as that found at LANL. In terms of plant characteristics, wood is more resistant to decay than leaves, while evergreen leaves generally decompose more slowly than deciduous leaves. Based on these generalizations, it is reasonable to expect that litter from grasses and forbs will tend to decompose relatively quickly, while litter produced from shrubs and trees will take longer to decay.

Whittaker (1975) discusses litter decay in terms of the decomposition half-life, or the time needed for half of the original dry mass of litter to decompose. Half-lives for litter in grasslands, boreal conifer forests, and temperate deciduous forests were estimated at 2.8, 7.0, and 1.0 years, respectively. Koukoura et al. (2003) evaluated rates of litter decomposition in semiarid grassland in northern Greece. Rates of decay were characterized for three perennial grasses and an annual legume; separate estimates were developed for leaves and stems. The rate constants estimated for leaves indicated litter half-lives ranging from 1.0 to 1.8 years, while the data collected for the stems yielded half-lives ranging from 2.2 to 2.8 years. Shariff et al. (1994) reported average annual litter decomposition rates of 12 to 22 percent for ungrazed arid grassland in North Dakota, yielding decomposition half-lives of around 3 to 6 years. Millar (1974) cites work by others in which 10 or more years were required for *Pinus* needles to reach the humus layer of the soil.

Murphy et al. (1998) examined rates of litter decomposition at five sites along an elevational gradient in northern Arizona. These sites include Great Basin Desert scrub, piñon-juniper woodland, ponderosa pine forest, and transition zones between these communities. Litter decomposition rates were measured for leaf litter collected from ponderosa pine, piñon pine, one-seed juniper, and blue grama grass; and for leaves and stems from snakeweed. Based on these measurements, the investigators calculated annual decomposition rate constants for each species. Separate constants were estimated for the first and second years of the 2-year study.

The litter decomposition constants estimated by Murphy et al. (1998) for the five study sites are summarized in Table 45. Decomposition was greatest in the first year, as litter with the most favorable decay characteristics was consumed. Decay of more recalcitrant litter components proceeded at slower rates. If the rate of decay is assumed to remain constant over time, the rate constants for the first year of the study infer a litter half-life of 1.7 years for snakeweed, 2 years for blue grama, and 3.3 years for piñon and juniper trees (averaged over the two species). Similarly, if the rate constants for the second year were assumed to be constant, litter half-lives for the shrub, grass, and tree species are 2.8, 5.4, and 4.7 years, respectively. Even longer half-lives may be anticipated for the more substantial woody litter from mature shrubs and trees.

The data cited above suggest that litter generated from grasses, forbs, and the leaves of shrubs may require a minimum of 5 to 10 years to fully decompose, while the leaf material from piñon pine and juniper may require 15 years or more to fully decay. The time required for the woody litter from shrubs and trees may require longer still. A single, triangular distribution was adopted to describe the

litter half-life for all growth forms. This distribution was assigned minimum, most likely, and maximum values of 1, 2, and 6 years, respectively.

Table 45
Litter Decomposition Rate Constants

Plant Species	Decomposition Rate Constant (/yr)	
	First Year	Second Year
Snakeweed	-4.2E-01	-2.5E-01
Blue Grama	-3.4E-01	-1.3E-01
One-Seed Juniper	-2.2E-01	-1.5E-01
Piñon Pine	-2.0E-01	-1.5E-01
Ponderosa Pine	-2.2E-01	-1.3E-01

Source: Murphy et al. (1998)

5.9.7 Native Vegetation Plant Uptake Factor

The radionuclide plant uptake factors characterize the extent to which contaminants in the waste are taken up by the roots of native vegetation growing at Area G. Authors such as Baes et al. (1984) suggest applying plant uptake factors for leafy vegetables to fresh forage such as grass; however, other information indicates that plant uptake factors for native plants may be greater than those observed for agricultural crops. Sheppard and Evenden (1997) have shown that native plants have higher cesium uptake factors than agricultural crops. Wirth (1999) compared uptake factors for plants growing in arid and semiarid climates to those for agricultural crops and found native species had mean uptake factors that were one to two times greater than those for crops.

There are relatively few data available to characterize plant uptake for native species. Given this, the plant uptake factors provided in NCRP Report 129 (1999) for grass and fodder were adopted for the biotic intrusion modeling. Uptake factors for leafy vegetables were taken from Napier et al. (2004) for elements that were not included in the NCRP report; the factor for tritium was estimated using the specific activity model described earlier. In adopting this approach, it was assumed that patterns of plant uptake in grasses will more nearly approximate those in native vegetation, relative to agricultural crops. These factors are typically larger than those adopted for agricultural crops and generally agree with the plant uptake factors reported by Wirth (1999) for selected elements. These values, shown in Table 46, were assumed to represent the geometric means of lognormal distributions. A geometric standard deviation of 3.5 was assumed for all elements, consistent with the geometric standard deviation selected for the lognormal distributions of uptake factors for crops.

Table 46
Parameter Values and Distributional Information for Native Plant Uptake Factors

Element	Geometric Mean [a]	Geometric Standard Deviation
Ac	4.0E-03	3.5E+00
Ag	1.0E-01	3.5E+00
Al	2.0E-02	3.5E+00
Am	4.0E-03	3.5E+00
Ba	1.0E-01	3.5E+00
Be	2.0E-02	3.5E+00
Bi	5.0E-01	3.5E+00
Bk	4.0E-03	3.5E+00
C	7.0E-01 [b]	3.5E+00
Ca	5.0E+00	3.5E+00
Cf	4.0E-03	3.5E+00
Cl	1.0E+02	3.5E+00
Cm	4.0E-03	3.5E+00
Co	2.0E+00	3.5E+00
Cs	2.0E-01	3.5E+00
Eu	5.0E-02	3.5E+00
Gd	5.0E-02	3.5E+00
H [c]	---	---
Ho	5.0E-02	3.5E+00
I	1.0E-01	3.5E+00
K	3.0E+00	3.5E+00
Kr [d]	---	---
Lu	1.5E-02	3.5E+00
Mo	4.0E-01	3.5E+00
Nb	1.0E-01	3.5E+00
Nd	5.0E-02	3.5E+00
Ni	1.0E+00	3.5E+00
Np	1.0E-01	3.5E+00
Os	2.0E-01	3.5E+00
Pa	5.0E-02	3.5E+00
Pb	9.0E-02	3.5E+00
Pm	5.0E-02	3.5E+00
Pu	1.0E-03	3.5E+00
Ra	2.0E-01	3.5E+00

[a] Source: NCRP (1999) except as noted

[b] Source: Napier et al. (2004)

[c] Plant uptake factors for tritium were estimated using a specific activity models; see discussion in text.

[d] Element exists solely as a gas and was ignored in terms of food-chain transport.

Table 46
Parameter Values and Distributional Information for Native Plant Uptake Factors

Element	Geometric Mean [a]	Geometric Standard Deviation
Se	5.0E-01	3.5E+00
Si	1.0E-01	3.5E+00
Sm	5.0E-02	3.5E+00
Sn	1.0E+00	3.5E+00
Sr	4.0E+00	3.5E+00
Tb	5.0E-02	3.5E+00
Tc	4.0E+01	3.5E+00
Th	1.0E-03	3.5E+00
Ti	5.0E-03	3.5E+00
U	1.0E-01	3.5E+00
Zr	5.0E-03	3.5E+00

[a] Source: NCRP (1999) except as noted

[b] Source: Napier et al. (2004)

[c] Plant uptake factors for tritium were estimated using a specific activity models; see discussion in text.

[d] Element exists solely as a gas and was ignored in terms of food-chain transport.

5.9.8 Maximum Burrow Depth

Maximum burrowing depths for harvester ants, various species of mice, pocket gophers, chipmunks, and ground squirrels are used to model burrow distributions with depth for these species. Limited information exists on the burrowing habits of animals; several studies relevant to the performance assessment and composite analysis are summarized below.

McKenzie et al. (1982) provide burrow distributions with depth for several species of burrowing animals. These data suggest a maximum burrowing depth of more than 2 m (6.6 ft) for harvester ants. Jensen and Hooten (2000) summarized burrowing depths of ant species inhabiting the transition desert and piñon-juniper communities at the Nevada Test Site. Those investigators noted that colonies of *Pogonomyrmex rugosa* have been observed to extend 3 to 4 m (9.8 to 13 ft) bgs (Wheeler and Wheeler, 1986), while colonies of *P. occidentalis* and *P. salinus* have been found to a depth of 2.7 m (8.8 ft) (Lavigne, 1969; Fitzner et al., 1979). All three of these species of ants occur in New Mexico.

Many species of mice use burrows abandoned by other species; others excavate new burrows. For example, silky pocket mice have been observed to use the abandoned burrows of kangaroo rats and pocket gophers (Best and Skupsi, 1994). Other species, such as the western harvest mouse, commonly build nests on the ground surface as well as nesting in burrows (Webster and Jones, 1982). Brush, deer, and piñon mice build their nests in a variety of locations including abandoned burrows, hollow branches, logs, rock crevices, and at the base of shrubs.

Mouse burrows generally extend to moderate depths. Best and Skupsi (1994) provide data suggesting the nests of the silky pocket mouse are generally 40 cm (16 in.) or less from the ground surface. MacMahon (1985) indicates that the burrows of this species are generally not more than 10 cm (3.9 in.) deep. A burrow excavated by a hispid pocket mouse (*Chaetodipus hispidus)* in Texas extended to a depth of about 40 cm (16 in.) (Davis and Schmidley, 1997); this species occurs in southern New Mexico. Reynolds and Laundre (1988) characterized the distribution of deer mouse burrows, finding that none of the 43 burrows examined extended deeper than 50 cm (20 in.). Winter burrows of the Great Basin pocket mouse have been noted to extend up to 1.8 m (2.6 ft) (Whitaker, 1980); Suter et al. (1993) and Cline et al. (1982, cited in Hakonson, 2002) list maximum depths of 1.4 and 1.9 m (4.6 and 6.2 ft), respectively, for this species. McKenzie et al. (1982) list a maximum burrowing depth of 2 m (6.6 ft) for pocket mice and kangaroo rats. Cline et al. (1982, cited in Hakonson, 2002) list a burrowing depth of 52 to 62 cm (20 to 24 in.) for the little pocket mouse (*Perognathus longmembris*).

Information cited by Gonzales et al. (2000) indicates that the deeper portions of pocket gopher burrow systems typically occur at 0.5 to 1.5 m (1.6 to 4.9 ft) bgs. Some observations exist on the depth of burrowing in pocket gophers that are specific to LANL. Tierney and Foxx (1987) observed gopher burrows at depths of 95 to 110 cm (37 to 43 in.) during the excavation of plant

roots. Gonzales et al. (1995) evaluated the impacts of pocket gopher burrowing on erosion using simulated waste covers. Pocket gopher activity extended to a depth of 1.5 m (4.9 ft) in that study. Results from a study conducted by Hakonson et al. (1982) indicate that gophers had not penetrated into waste below a 1.25-m (4.1-ft) cover over a 4-year period. McKenzie et al. (1982) list a maximum burrowing depth of 1 m (3.3 ft) for pocket gophers; Cline et al. (1982, cited in Hakonson, 2002) list burrowing depths ranging from 5 to 35 cm (2 to 14 in.) for valley and northern pocket gophers (*Thomomys bottae* and *T. talpoides*, respectively). In a summary of maximum reported burrow depths, Suter et al. (1993) list a burrowing depth in excess of 1 m (3.3 ft) for the northern pocket gopher, while Miller (1957, cited in Hakonson, 2002) reported a burrowing depth of 2 m (6.6 ft) for the valley gopher. Anderson (1980) noted that the nesting galleries of the northern pocket gopher may range from 1 to 3 m (3.3 to 9.8 ft) deep.

Kawamichi (1989) examined the burrow structure of Siberian chipmunks (*Eutamias sibiricus*) as a function of season. The deepest burrows were excavated when the animals were preparing to hibernate. These burrows averaged 79 to 83 cm (31 to 33 in.) in depth, and extended as deep as 107 cm (3.5 ft). Sources cited in Gano and States (1982) indicate that the burrows of the eastern chipmunk (*Tamias striatus*) and western species of chipmunks (*Eutamias* spp.) generally extend to depths of 30 to 40 cm (12 to 16 in.). Suter et al. (1993) list a maximum burrowing depth of 1 m (3.3 ft) for the eastern chipmunk.

The nesting burrows of thirteen-lined ground squirrels extended to an average depth of 24 cm (9.5 in.) in Oklahoma (Hoffmeister, 1986, cited in SLTERP, 2003); in Texas, burrows extended to depths of 10 to 115 cm (3.9 to 45 in.) (Davis, 1974, cited in SLTERP, 2003). Oaks et al. (1987) cite studies that found rock squirrel burrowing depths ranging from 0.3 to 1 m (1 to 3.3 ft). The white-tailed antelope squirrel often uses abandoned burrows, and animals have been observed using burrows with depths ranging from 25 to 66 cm (9.8 to 26 in.) (Belk and Smith, 1991). Golden-mantled ground squirrels often dig their own burrows; Bartels and Thompson (1993) cite studies in which burrow depths ranged up to 90 cm (2.9 ft). Reynolds and Laundre (1988) reported a maximum burrowing depth of approximately 1.3 m (4.3 ft) for the Townsend's ground squirrel (*Spermophilus townsendii*) in southeastern Idaho. McKenzie et al. (1982) report a maximum burrowing depth of 2 m (6.6 ft) for ground squirrels, based on data for the Mohave (*Citellus mohavensis*), Townsend's, thirteen-lined, Columbian (*Citellus columbianus*), Franklin (*Citellus franklini*), and Californian (*Citellus beecheyi*) ground squirrels.

Although the burrowing depth data are admittedly sparse, the studies summarized above were used to estimate parameter distributions for the performance assessment and composite analysis. Triangular distributions were assumed in all cases. Minimum, most likely, and maximum values of 2, 3, and 4 m (6.6, 9.8, and 13 ft) were adopted to describe the maximum burrowing depth of harvester ants. The range of these data approximately bounds the observations summarized in

Jensen and Hooten (2000) for *Pogonomyrmex* spp.; the midpoint of this range was assumed to be the most likely value.

The use of the deer mouse as a surrogate for all mouse species that may inhabit the closed disposal site complicates the development of distributions for burrowing depth. The information cited above suggests the species present during the early successional stages will likely burrow to depths of about 50 cm (20 in.) or less. Although some species of pocket mice may burrow to depths as great as 1.5 to 2 m (4.9 to 6.6 ft), these species are not expected to occur in great numbers at Area G. On the basis of available data, a distribution with minimum, most likely, and maximum values of 0.5, 1, and 2 m (1.6, 3.3, and 6.6 ft) was assumed for the performance assessment and composite analysis. This distribution was assumed to apply to all mouse species inhabiting the site, from the early successional stages to the piñon-juniper climax condition.

Minimum, most likely, and maximum values of the burrowing depth of pocket gophers are 0.5, 1.25, and 2 m (1.6, 4.1, and 6.6 ft), respectively. The minimum value is generally consistent with the observations of Gonzales et al. (2000) and Cline et al. (1982, as cited in Hakonson (2002); the maximum value bounds all but one of the observations discussed above. The most likely value—the midpoint of this range—is generally consistent with observed gopher burrowing depths at LANL.

The distribution of maximum burrowing depth for chipmunks and ground squirrels was described using minimum, most likely, and maximum values of 0.5, 1, and 2 m (1.6, 4.1, and 6.6 ft), respectively. These values generally coincide with the range of burrow depths discussed above, although many of the species of ground squirrels discussed are not expected to occur at the closed disposal site.

5.9.9 Burrow Density

Burrow densities are used in conjunction with estimates of the amount of soil excavated per burrow and with burrow renewal fractions to calculate the annual mass of soil excavated by ants, mice, chipmunks, and ground squirrels. The burrow density for harvester ants was set equal to colony density. Numerous estimates of colony density are found in the literature for harvester ants of the genus Pogonomyrmex; Table 47 summarizes several of these. These data were used to construct a normal distribution with a mean and standard deviation of 28.3 and 20.2 colonies/ha (11.5 and 8.2 colonies/ac), respectively. Harvester ants are assumed to be present at the disposal site during early succession and after the site transitions to piñon-juniper woodland. The same distribution of colony density was used throughout the simulation period.

Data describing burrow densities for mice, chipmunks, and ground squirrels are generally lacking. In lieu of this information, it was assumed that the burrow densities of these species were equivalent to animal densities. This approach may be quite conservative, depending upon when estimates of animal densities are collected. For example, densities of many species will be

Table 47
Summary of Harvester Ant (*Pogonomyrmex* spp.) Colony Densities

Colony Density (ha^{-1})	Species, Habitat, and Comments	Reference
7.2E+01	*P. occidentalis*; shortgrass prairie; average over 15-yr study	Keeler, 1993
2.3E+01 ± 9.0E+00	*P. occidentalis*; shortgrass prairie; ungrazed; mean ± std dev.	Rogers and Lavigne, 1974
2.8E+01 ± 1.6E+01	*P. occidentalis*; shortgrass prairie; light grazing; mean ± std dev.	Rogers and Lavigne, 1974
3.1E+01 ± 9.0E+00	*P. occidentalis*; shortgrass prairie; moderate grazing; mean ± std dev.	Rogers and Lavigne, 1974
3.0E+00 ± 4.0E+00	*P. occidentalis*; shortgrass prairie; heavy grazing; mean ± std dev.	Rogers and Lavigne, 1974
3.0E+01–4.3E+01	*P. occidentalis*; sagebrush/wheatgrass dominant; lightly grazed, recent burns; range	Clark and Comanor, 1975 [a]
2.5E+01	*P. occidentalis*; grassland; moderate grazing	Coffin and Lauenroth, 1988 [a]
3.1E+01	*P. occidentalis*; grassland; light grazing	Coffin and Lauenroth, 1990 [a]
1.7E+01	*P. occidentalis*; piñon-juniper woodland	Carlson and Whitford, 1991
1.4E+01	*P. occidentalis*; ponderosa pine community	Carlson and Whitford, 1991
4.0E+01	*P. occidentalis*; grass-shrub community	Mandel and Sorenson, 1982 [b]
4.5E+01	*P. occidentalis*; shrubland	Cole et al., 2001
3.1E+00; 4.5E+00	*P. rugosus*, *P. babatus*, *P. occidentalis*; shortgrass prairie; w/ and w/o prairie dogs	Kretzer and Cully, 2001
1.6E+01; 1.0E+00–3.6E+01	*P. occidentalis*; pasture; light grazing; mean and range	Crist and Wiens, 1996 [c]
9.0E+00; 0.0E+00–5.0E+01	*P. occidentalis*; pasture; moderate grazing; mean and range	Crist and Wiens, 1996 [c]
5.8E+00; 0.0E+00–1.3E+01	*P. occidentalis*; pasture; heavy grazing; mean and range	Crist and Wiens, 1996 [c]
1.8E+01	*P.* spp.	Scott, 1951 [d]
2.8E+01	*P. owyheei*; sagebrush steppe	Soule and Knapp, 1996
4.0E+01	*P. owyheei*; saltbush and halogeton dominant; "misused/depleted"	Sharp and Barr, 1960 [a]
9.0E+00	*P. owyheei*; saltbush dominant; "vigorous stand"	Sharp and Barr, 1960 [a]
1.2E+01	*P. owyheei*; shadscale dominant	Sharp and Barr, 1960 [a]
4.9E+01–7.4E+01	*P. owyheei*; cheatgrass dominant; range	Willard and Crowell, 1965 [a]
4.0E+01	*P. owyheei*; mixed sagebrush/greasewood association; mean density	Porter and Jorgensen, 1988
3.2E+01	*P. owyheei*; shrubland/grassland	Johnson et al., 1938 [e]
8.0E+01, 5.7E+01	*P. owyheei*; shrubland/grassland; 1962 and 1974 measurements	Sneva, 1979
6.0E+00–2.1E+01	*P. rugosus*; Chihuahuan desert; range	Whitford and DiMarco, 1995 [f]
2.2E+01	*P. rugosus*; shrubland community	Lei, 2000
0.0E+00–1.6E+02 [g]	*P. salinus*; range over seven vegetation communities	Blom et al., 1991

[a] Cited in Soule and Knapp, 1996
[b] Cited in Carlson and Whitford, 1991
[c] Cited in Peters et al., 2002
[d] Cited in MAFES, 1999
[e] Cited in Sneva, 1979
[f] Cited in Lobry de Bruyn, 1999
[g] Colony densities for all but one sample plot ranged from 0.0E+00 to 6.9E+01 colonies/ha.

greatest during the breeding season, while the young of the year still reside with or near their parents. Assuming that burrow density is equal to the animal density during these times may result in significant overestimation of the actual number of burrows present. Nevertheless, few alternatives to this approach exist.

Estimates of mouse densities at Area G took into account the trapping data of Biggs et al. (1995 and 1997) and Bennett et al. (1997, 1998, and 2002), as well as density estimates from the literature. Biggs et al. and Bennett et al. trapped small mammals at two waste disposal sites within Area G and in undisturbed piñon-juniper woodlands from 1994 through 1998. Estimates of total animal densities at these sites are summarized in Table 48.

Table 48
Small Mammal Densities at Area G and Background/Control Areas

Site Name	Site Number [a]	Animal Density (individuals /ha)					Mean Density (individuals/ha)
		1994	1995	1996	1997	1998	
Waste Burial Site	5	2.4E+01	3.2E+01	2.3E+01	1.0E+01	1.7E+01	2.1E+01
Waste Burial Site	7	2.1E+01	1.4E+01	1.1E+01	2.0E+01	ND	1.6E+01
Control Site	8	3.3E+00	---	1.5E+00	7.7E+00	3.1E+01	1.1E+01
Background Site	9	ND	8.7E+00	ND	4.9E+00	8.5E+01	3.3E+01

Source: Biggs et al. (1995, 1997) and Bennett et al. (1997, 1998, and 2002)

ND = No data

--- = No animals were captured at the site.

[a] Site number, as assigned for the 1997 trapping effort. The characteristics of these sites are provided in the text.

The vast majority of the animals trapped at the two waste sites were deer mice; the densities observed at these sites generally coincide with deer mouse densities noted in the literature. For example, Burt and Grossenheider (1976) note that summertime densities of 25 to 37 animals/ha (10 to 15 animals/ac) are high. Data summarized in EPA (1993b) include summertime and winter densities ranging from 12.8 to 22.4 and 3.4 to 8.4 animals/ha (5.2 to 9 and 1.4 to 3.4 animals/ac), respectively, in a subalpine meadow in Utah (Cranford, 1984). Additional citations in EPA (1993b) indicate densities ranging from 12.7 to 45.5 animals/ha (5.1 to 18.4 animals/ac) in burnt slash in British Columbia, a range of 3.9 to 28 animals/ha (1.6 to 11.3 animals/ac) was observed in understory along a river in Montana. Smith and Urness (1984) observed mean deer mouse densities ranging from 6.7 to 24.2 animals/ha (2.7 to 9.8 animals/ac) in sagebrush and crested wheatgrass communities in Utah; a range of 7.2 to 28 animals/ha (2.9 to 11.3 animals/ac) was found in the transitional zone between these communities. Banfield (1974; cited in Nowak, 2003) reported that the densities of deer mice generally range from about 1 to 25 animals/ha (0.4 to 10 animals/ac). Densities of this species in Kansas ranged from 4 animals/ha (1.6 animals/ac) in weedy areas during

the spring and summer to about 19 animals/ha (7.7 animals/ac) in a bluestem grass community during the fall (Hansen and Fleharty, 1974). Finally, Verner and Boss (1980) reported densities of up to 10 to 25 animals/ha (4 to 10 animals/ac) in the Sierra Nevada of California.

The majority of the small mammals trapped by Biggs et al. (1995 and 1997) and Bennett et al. (1997, 1998, and 2002) at the piñon-juniper woodland sites were piñon mice, although deer mice, harvester mice, brush mice, and silky pocket mice were also caught. The mean animal densities estimated for these sites ranged from 1.5 to 85 animals/ha (0.6 to 34 animals/ac), respectively. The densities observed in 1998, the last year for which trapping data are available, were 4 to 10 times greater than densities measured at the two control sites between 1994 and 1997. The reason for this rise was attributed to increases in moisture that, in turn, led to greater food supplies and increased cover availability (Bennett et al., 2002).

Estimates of mouse species other than deer mice are also available in the literature. Brant (1962, cited in CDFG, 2003) and Meserve (1977, cited in CDFG, 2003) found densities of the western harvest mouse ranging from 2.5 to 123 animals/ha (1 to 50 animals/ac) in California coastal scrub communities. Gray (1943; cited in Webster and Jones, 1982) observed a western harvest mouse density of 11.9 animals/ha (4.8 animals/ac) in a sagebrush community in Washington. Whitford (1976, cited in Webster and Jones, 1982) found densities of 4 to 60 animals/ha (1.6 to 24 animals/ac) for this species in New Mexico; the latter density was observed when ground vegetation became dense following September rains. Merritt (1974, cited in Verner and Boss, 1980) reported densities of piñon mice ranging from 2.5 animals/ha (1 animals/ac) in oak-bay woodland to 86 animals/ha (35 animals/ac) in chaparral. Storer et al. (1944, cited in CDFG, 2003) observed densities ranging from 2 to 17.3 animals/ha (1 to 7 animals/ac) for resident brush mice in the Sierra Nevada of California. Best and Skupsi (1994) summarized information regarding silky pocket mouse densities. While most densities were less than 8 animals/ha (3 animals/ac), Whitford (1976, cited in Webster and Jones, 1982) reported a density of 13 animals/ha (5 animals/ac) and Britt (1972) observed densities ranging from 20.8 to 53 animals/ha (8.4 to 21 animals/ac) at sites in New Mexico.

The density estimates for mouse species summarized above are in general agreement with those estimated by Biggs et al. (1995 and 1997) and Bennett et al. (1997, 1998, and 2002) Consequently, the data from these investigators' trapping studies were used to develop point estimates and distributions for the performance assessment and composite analysis. Densities estimated for the disposal units were used to represent the site during early succession, while densities reported for piñon-juniper woodland were used to represent the climax condition. Mouse densities within each community were assumed to be normally distributed with mean densities equal to the overall average densities. The standard deviations of these distributions were defined using a coefficient of variation of 0.25, which is generally consistent with the variability observed in the density estimates.

Chipmunks and ground squirrels are assumed to be present only in piñon-juniper woodland; these species have not been trapped at or near the disposal units at Area G, but are common inhabitants of mature woodlands. Limited information is available regarding the densities of chipmunks. Burt and Grossenheider (1976) cite densities of 5 to 10 animals/ha (2 to 4 animals/ac) for the eastern chipmunk (*Tamias striatus*). Rosenberg and Anthony (1993) found densities of the Townsend's chipmunk (*Eutamis townsendii*) ranged from 1.9 to 7.7 animals/ha (0.8 to 3.1 animals/ac) during the autumn and spring in second- and old-growth forests in western Oregon. Goodwin and Hungerford (1979, cited in CDFG, 2003) estimated densities of golden-mantled ground squirrels at 0.6 animals/ha (0.2 animals/ac) in dense stands of ponderosa pine in Arizona, and about 0.1 animals/ha (0.04 animals/ac) in open stands. Verner and Boss (1980) provide density estimates of 1 to 3 animals/ha (0.4 to 1.2 animals/ac) for this species. Johnson (1981, cited in Oaks et al., 1987) reported a springtime density of 13 animals/ha (5.3 animals/ac) for the rock squirrel in Texas; Juelson (1970, cited in Oaks et al., 1987) reported densities of 2 and 5.7 animals/ha (0.8 and 2 animals/ac) for marginal and good habitat, respectively. McKenzie et al. (1982) summarized the work of several investigators, and reported a mean density of 25 animals/ha (10 animals/ac) for several species of ground squirrels; densities ranged from 5.7 to 74 animals/ha (2.3 to 30 animals/ac). Only one of the four species upon which these estimates are based, the thirteen-lined ground squirrel, occurs in New Mexico. Streubel and Fitzgerald (1978) provided several density estimates for the thirteen-lined ground squirrel. These include values of 2.5 to 5.0 animals/ha (1 to 2 animals/ac) in the spring and 24.6 animals/ha (10 animals/ac) following the emergence of young (Rongstad, 1965); 18 animals/ha (7 animals/ac) on grazed prairie in Colorado (Mitchell, 1972); and 4.5 animals/ha (1.8 animals/ac) on ungrazed prairie in Colorado (Grant, 1972).

The point estimate and distribution of chipmunk/ground squirrel density were determined using the information summarized above. Density estimates for species that may be found at Area G appear to be less than the mean and maximum densities listed in McKenzie et al. (1982). Taking this into account, a triangular distribution was defined using minimum, most likely, and maximum values of 5, 15, and 25 animals/ha (2, 6, and 10 animals/ac), respectively.

5.9.10 Harvester Ant Burrow Mass

Limited information exists on the mass of soil excavated by harvester ant colonies. Rogers and Lavigne (1974) estimated that an average of 2.8 kg (6.2 lb) of soil was excavated by harvester ant colonies in northeastern Colorado. Using this mass and the maximum colony density observed by the investigators, the total amount of soil excavated is approximately 87 kg/ha (77 lb/ac). Carlson and Whitford (1991) estimated that the average mass of ant mounds in piñon-juniper woodlands near Los Alamos was 38 ± 4.8 kg (84 ± 4.38 lb), while the mass of mounds in a ponderosa pine community averaged 48 ± 5.5 kg (105 ± 12.1 lb); information regarding the range of mound sizes was not provided. The total amount of soil removed in the two

communities was about 650 kg/ha (580 lb/ac). Cole (1994) used measurements of harvester ant mounds in Colorado shrubland to estimate the volume of soil brought to the surface. The mean volume of 53 mounds was estimated to be 0.039 m^3 (1.4 ft^3). Assuming a bulk density of 1300 kg/m^3 (80 lb/ft^3), this volume represents about 50 kg (110 lb) of soil per mound. Mandel and Sorenson (1982) reported an average mound volume of 0.32 m^3 (11.3 ft^3) for work conducted in Colorado, this volume represents a mass of about 42 kg (92 lb) if the bulk density of the material is 1,300 kg/m^3 (80 lb/ft^3).

Given the limited amount of information on harvester ant burrow mass, the work conducted by Carlson and Whitford (1991) was relied upon to estimate a distribution for the parameter. Minimum and maximum values of a triangular distribution were defined using the approximate lower bound of the mound mass at the piñon-juniper study site (i.e., 23 kg [50 lb]) and the approximate upper bound of the mound mass at the ponderosa pine study site (i.e., 65 kg [143 lb]). The mean mound mass of 38 kg (84 lb) observed for the piñon-juniper study site was adopted as the most likely value and the point estimate for the deterministic modeling.

5.9.11 Harvester Ant Colony Life Span

The proportion of burrows established by harvester ants each year will depend upon the life span of the individual colonies and whether the number of colonies at Area G is increasing, decreasing, or remaining constant. Information from the literature indicates life spans for harvester ant colonies range from 5 to 58 years under a variety of conditions. These data, summarized in Table 49, were used to construct a triangular distribution for colony life span, using the range of lifetimes noted above to define the minimum and maximum values. The most likely value of the distribution was set to 21 years, the median of the data listed in the table.

Table 49
Summary of Harvester Ant Colony Lifetimes

Species	Colony Lifetime (yr)	Reference
Unknown	5.0E+00–3.0E+01	Various [a]
Pogonomyrmex owyheei	1.4E+01, 1.5E+01	Porter and Jorgensen, 1988
P. owyheei	1.4E+01, 2.8E+01, 3.0E+01	Sharp and Barr, 1960[a]
P. occidentalis	2.9E+01–5.8E+01	Coffin and Lauenroth, 1990[b]
P. occidentalis	2.1E+01–4.4E+01	Keeler, 1993
P. barbatus	1.5E+01–2.0E+01	Gordon, 1991[c]

[a] *Cited in Porter and Jorgensen, 1988*
[b] *Cited in Keeler, 1993*
[c] *Cited in Barton et al., 2002*

5.9.12 Pocket Gopher Soil Removal Rate

Hakonson (2002) and McKenzie et al. (1982) cite several references in which estimates of the soil removal rate of pocket gophers are found. Hakonson (2002) cites the work of Mielke (1977) and Spencer et al. (1985), stating that the amount soil brought to the surface by gophers ranges from 16 to 103 T/ha/yr (7.2 to 46 t/ac/yr). Hakonson et al. (1982) examined soil excavation rates by pocket gophers on a LLW disposal site at LANL. Over the 401-day study, the animals excavated soil at a rate of about 11 T/ha/yr (5 t/ac/yr), or about 8.3 m^3/ha/yr (120 ft^3/ac/yr) of material. McKenzie et al. (1982) estimate that the volume of soil excavated annually by pocket gophers ranges from 0.51 to almost 82 m^3/ha (7.3 to almost 1,200 ft^3/ac), based on numerous references in the literature. They list a mean soil volume of 8.3 m^3/ha (120 ft^3/ac), which was the volume of soil brought to the surface in the study conducted by Hakonson et al. (1982).

A triangular distribution was developed for the pocket gopher soil removal rate based on the information provided in McKenzie et al. (1982). The minimum, most likely, and maximum values were set equal to 0.51, 8.3, and 82 m^3/ha/yr (7.3, 120, and 1,170 ft^3/ac/yr), respectively.

Pocket gophers are expected to reside at Area G as long as the site is in a relatively disturbed condition. Visual observations at the site indicate the species prefers disturbed areas; the animals are generally less common in piñon-juniper woodland. Where pocket gophers do occur in the woodland habitat, they tend to occur either in very limited areas or in disturbed areas such as those that occur along the sides of roads. Based on these observations and general information about habitat preference, the pocket gopher was not assumed to be present at Area G after it undergoes succession to piñon-juniper woodland. Consistent with this assumption, the soil removal rate for the species at the climax site was set to zero.

5.9.13 Mouse, Chipmunk, and Ground Squirrel Burrow Volume

McKenzie et al. (1982) summarize information about the burrow volumes of selected small mammal species. Minimum, mean, and maximum volumes of 0.003, 0.014, and 0.001 m^3 (0.1, 0.5, and 0.04 ft^3) are listed for pocket mice and kangaroo rats; these values were used to define a triangular distribution that was applied to all mouse species. The minimum, mean, and maximum burrow volumes listed for ground squirrels (i.e., 0.008, 0.02, and 0.0772 m^3 [0.3, 0.7, and 2.7 ft^3]) were used to define the distribution for chipmunks and ground squirrels.

5.9.14 Burrow Renewal Fraction

The burrow renewal fraction is the ratio of new burrows constructed each year to the number of burrows constructed by animals in their first year at the closed site. This fraction is used to adjust the annual soil removal rates for pocket gophers, mice, and chipmunks. Distributions for the renewal fractions for these species were defined using data taken from McKenzie et al. (1982), who found renewal fractions ranging from 0.5 to 1.0 for ground squirrels, 0.75 to 1.0 for pocket

mice and kangaroo rates, and 0.75 to 1.0 for pocket gophers. These ranges were used to define the minimum and maximum values of triangular distributions; the midpoints of these ranges were adopted as the most likely values. The distribution for ground squirrels was adopted for chipmunks, while the distribution for pocket mice and kangaroo rats was assumed to apply to all species of mice inhabiting Area G.

5.10 Erosion Model Parameters

Erosion model parameters are used to estimate rates of surface erosion across the disposal site. The effect of surface erosion on facility performance is twofold. First, the rate at which the cover erodes will influence the degree to which plant roots and animal burrows extend into the waste, and will determine the amount of waste excavated during inadvertent human intrusion. Second, contamination deposited on the surface of Area G by the plants and animals that penetrate into the waste will be transported into the adjacent canyons by surface runoff. The parameters used to characterize the impacts of surface erosion are discussed below.

5.10.1 Erosion Scenario

As discussed earlier, the erosion modeling conducted using SIBERIA projected rates of cover loss under three erosion scenarios. The erosion scenario parameter specifies the probability of occurrence of these scenarios and is used to determine how the cover loss functions are sampled for the eight waste disposal regions. As shown in Table 11, the low, moderate, and high erosion scenarios are assumed to have probabilities of occurrence of 0.1, 0.8, and 0.1, respectively.

5.10.2 Cover Loss Functions

The cover loss functions specify the amount of cover remaining over the disposal units in the eight waste disposal regions. For each region, cover depths are provided as a function of time for all nodes used to represent the disposal units within that region; separate cover loss functions are defined for the low, moderate, and high erosion scenarios. Approximately 4 million data points are used to define the cover loss behavior at Area G over the 1,000-year compliance period; the sheer volume of this information prohibits its reproduction in this report.

5.11 Exposure Pathway Parameters

Exposure pathway parameters define the receptor activities and intakes necessary to estimate doses for the exposure scenarios included in the performance assessment and composite analysis. The data used to describe these parameters are included in Table 11; the information upon which the selected data are based is discussed below.

5.11.1 Indoor and Outdoor Time Allotments

The indoor and outdoor time allotments define the time spent by the receptor indoors and outdoors at the receptor location. The time allotments sum to 24 hr/d or less; if less, it is assumed

that any additional time is spent at uncontaminated locations. The NRC (1986) and NCRP (1999) adopted nominal values of 12 hr/d for the time spent indoors by a resident at a contaminated site; a period of 4.9 hr/d is adopted by the NRC (1986) for the time spent outdoors while the NCRP (1999) adopted a value that is almost twice that for their screening assessment. The RESRAD code (ANL, 2001) uses default average indoor and outdoor exposure times of 12 and 6 hr/d, respectively, while values of 13.2 and 4.7 hr/d were used for a residential scenario in a decommissioning study (NRC, 1992). The Exposure Factors Handbook (EPA, 1997) provides distributions of time spent inside and outside of a residence for various segments of the population.

A total exposure period of 500 hours was adopted for the Intruder-Construction Scenario (NRC, 1986); it was assumed that all of this time was spent outdoors. Information in the Exposure Factors Handbook (EPA, 1997) was used to define distributions of occupancy times for the residential intruder and off-site exposure scenarios; these distributions were based on occupancy times averaged over all segments of the population. The distribution for indoor occupancy time was truncated at the fifth percentile value to ensure a nominal amount of time was spent inside at the point of exposure. Outdoor exposure times were adjusted as necessary to assure that the sum of the indoor and outdoor exposure times did not exceed 24 hr/d.

5.11.2 Excavation Occupancy Fraction

The severity of the external exposures projected for the Intruder-Construction Scenario will depend upon the location of the receptor relative to the waste. In many cases, rates of exposure will be greatest during the time spent in the basement excavation because the amount of shielding between the receptor and the waste will be at a minimum at this location. Given this, the NRC (1986) assumed that the entire exposure period was spent in the excavation. It is more realistic to expect that a person will spend considerably less than the total construction time at the bottom of the basement excavation. Consistent with this expectation, the excavation occupancy factor was assigned a triangular distribution with minimum, most likely, and maximum values of 0, 0.1, and 0.2, respectively.

5.11.3 Soil Mixing Depth

As its name implies, this parameter specifies the depth to which surface soils are mixed at the receptor locations. The soil mixing depth was set to 15 cm (6 in.) for all off-site receptor locations, for both the deterministic and probabilistic modeling. This value was selected based on the assumption that soils will be plowed or otherwise mixed to this depth during construction of the residence and the establishment of a garden. The same mixing depth was applied to the Intruder–Post-Drilling Scenario. The soil mixing depth for the Intruder-Construction and Intruder-Agriculture Scenarios was set equal to the volume of soil excavated during house construction divided by the net area of the intruder's lot.

5.11.4 Direct Radiation Shielding Factor

The direct radiation shielding factor is used to describe the attenuation of direct radiation during the time spent inside; it represents the fraction of the radiation that passes through the structure in which the receptor resides. The RESRAD code (ANL, 2001) uses a default shielding factor of 0.7 for time spent indoors. The NRC's Regulatory Guide 1.109 (1977) suggests using this value for the maximally exposed individual and a value of 0.5 for the general population for the entire time spent at the site. NCRP Report 129 (1999) compiles shielding factors for the time spent inside a variety of buildings. Shielding factors cited in the NCRP report include 0.02 to 0.5 for prefabricated housing; 0.25 for a single family, two-story house; 0.40 for light construction; 0.23 to 0.43 for wood-frame, one-story houses; 0.07 ± 0.06 for brick houses; 0.13 ± 0.06 for wood houses; and most likely values ranging from 0.02 to 0.4 for residential structures. The magnitude of the shielding factor will partially depend upon the energies of the photons emitted by the radionuclides of interest. The NCRP (1999) used a shielding factor for radionuclides with the highest energy photons that ranged from about 0.2 to 0.6 for the development of soil screening criteria; shielding factors for radionuclides with the lowest emission energies ranged from 0.004 to 0.16. NCRP Report 76 (1984) suggests the shielding factors are uniformly distributed.

The direct shielding factor was assigned a uniform distribution ranging from 0.2 to 0.6. This distribution is consistent with the range adopted by the NCRP (1999) for high-energy photons and generally coincides with the building-specific data summarized above; the shape of the distribution is consistent with NCRP Report 76 (1984).

5.11.5 Inhalation Rate

The inhalation rate is used to estimate the intake of contamination from breathing airborne radioactivity. Recommended mean inhalation rates for adults have typically been about 20 m^3/d (700 ft^3/d). The International Commission on Radiation Protection adopted values of 21 and 23 m^3/d (740 and 810 ft^3/d) for women and men, respectively (ICRP, 1975, cited in NCRP, 1984); the average of these values was used in Regulatory Guide 1.109 (NRC, 1977) and the Part 61 Impacts Analysis (NRC, 1986). NCRP Report 129 (1999) reports a value of 22 m^3/d (775 ft^3/d) adopted by the United Nations Scientific Committee on the Effects of Atomic Radiation (UNSCEAR, 1993) and a range of 16 to 20 m^3/d (565 to 700 ft^3/d) cited in ICRP Publication 66 (1994). The EPA (1997) recommended lower average inhalation rates of 11.3 and 15.2 m^3/d (400 and 540 ft^3/d) for women and men, respectively.

The data provided by the EPA (1997) suggest that inhalation rates of about 20 m^3/d (700 ft^3/d) will overstate actual air intake rates for the average individual. Consequently, the performance assessment and composite analysis modeling adopted inhalation rates that are expected to more realistically represent long-term average inhalation rates. The deterministic evaluation used an inhalation rate of 15.2 m^3/d (540 ft^3/d), which is the average inhalation rate cited by the EPA

(1997) for adult men. The range of average inhalation rates for adult men is from 13 to 17 m^3/d (460 to 600 ft^3/day), depending upon the age class of the individual. A triangular distribution was defined for the average inhalation rate using these values; this distribution has minimum, most likely, and maximum values of 13, 15.2, and 17 m^3/d (460, 540, 600 ft^3/d), respectively.

It is reasonable to expect that the intruder homebuilder will achieve a higher level of activity than members of the public and residential intruders addressed by the other exposure scenarios. For the Intruder-Construction Scenario, then, an hourly inhalation rate of 1.5 m^3/hr (53 ft^3/hr) was adopted; this value is the mean inhalation rate cited for outdoor workers by the EPA (1997) for moderate activity levels. Inhalation data cited by the EPA for various classes of workers had coefficients of variation of approximately 0.4. This coefficient was applied to the inhalation rate adopted for the intruder analysis to arrive at a standard deviation of 0.6 m^3/hr (21 ft^3/hr). The distribution was truncated at 0.5 m^3/hr (18 ft^3/hr), which is the approximate mean inhalation rate cited in the Exposure Factors Handbook (EPA, 1997) for adults at rest.

5.11.6 Average Wind Speed

The average wind speed is used to model inadvertent intruder exposures to vapor- and gas-phase radionuclides diffusing from Area G. Meteorological monitoring is conducted across the Laboratory; one of the monitoring towers used to collect these measurements is located at TA-54, to the east of Area G. Average daily wind speed data for this tower (Rishel et al., 2003) were used to define the distribution for this parameter. Data collected from January 1992 through April 2005 at a height of 12 m (39 ft) above the ground are lognormally distributed and exhibit a geometric mean and standard deviation of 2.7 m/s (8.7 ft/s) and 1.4, respectively.

5.11.7 Atmospheric Mixing Height

Atmospheric mixing height refers to the height at which airborne radionuclides are mixed above the disposal site. It is used in the intruder diffusion model to define a dilution volume for vapor- and gas-phase radionuclides that are inhaled by the receptor. A mixing height of 2 m (6.6 ft) was used in the intruder modeling, consistent with the value used in RESRAD (Yu et al., 1993).

5.11.8 Irrigation Rate and Fraction

The irrigation rate and fraction of the year crops are irrigated are used to estimate radionuclide concentrations in plants due to wet deposition. The rate of irrigation will depend on the crops being grown, the nature of the soil in which the crops are grown, and site meteorological conditions. The 1997 performance assessment and composite analysis assumed an irrigation rate of 5 to 18 cm/wk (2 to 7 in./wk) for all but the last 2 weeks of the growing season. Using the point estimates of the growing seasons discussed earlier and an application rate of 12 cm/wk (5 in./wk) over the periods indicated yields irrigation rates ranging from about 80 to 160 cm/yr (30 to 60 in./yr).

A reevaluation of irrigation rates indicates that the annual rates estimated above may overestimate actual watering rates. Baes et al. (1984) estimated annual irrigation rates of 40 to 70 cm/yr (16 to 27 in./yr) in the general vicinity of Los Alamos, based on data taken from the 1974 Census of Agriculture. The 1998 and 2003 Farm and Ranch Irrigation Surveys (USDA, 1999 and 2004b) provide total irrigated acres and quantities of water applied to such on a state-by-state basis. The data for New Mexico indicate an annual irrigation rate of about 72 cm/yr (28 in./yr), which falls at the high end of the range cited by Baes et al. (1984).

Data from the 2003 Farm and Ranch Irrigation Survey (USDA, 2004b) attest to the crop-specific nature of irrigation needs. Annual irrigation rates for lettuce and beans are about 12 and 60 cm (5 and 24 in.), respectively, while rates for various grains range from about 40 to 60 cm per season (16 to 24 in. per season); 70 to 100 cm (27 to 40 in.) of water is applied through irrigation for various varieties of corn. An average of 85 cm (34 in.) is applied to alfalfa and alfalfa mixtures, while pasture and all other hay receive about 60 cm (24 in.) of water through irrigation.

Additional insight into irrigation needs may be gained through an examination of the water needs of various crops. Table 50 summarizes estimates of these needs for several crops. The irrigation application rates are a function of the crop's water needs and the efficiency of the irrigation system, defined here as the ability of the irrigation system to apply water equally across the area under cultivation. Although large-scale sprinkler-based irrigation systems may have efficiencies ranging from about 50 to 90 percent (e.g., Martin, 2000), the efficiency of concern is the homeowner's system of watering crops. For modeling purposes, it was assumed that this efficiency was 75 percent. On this basis, the water needs listed in Table 50 may be multiplied by 1.3 to estimate the corresponding irrigation water application rates; these rates assume that natural precipitation makes no significant contribution to the water needs of the plants.

The irrigation data discussed above were used to estimate distributions for the performance assessment and composite analysis modeling. Irrigation data were grouped by crop type (i.e., leafy vegetables, produce, grain, and pasture grass) and used to define triangular distributions of water application rates; these distributions are summarized in Table 11. The most likely values were estimated as the average of the listed seasonal water application rates; in cases where ranges of application rates were given, the midpoints were used in these calculations. The minimum and maximum values were defined on the basis of the ranges of application rates.

5.11.9 Inadvertent Soil Ingestion Rate

The soil ingestion rate is used to estimate doses for receptors who inadvertently ingest small quantities of contaminated soil. The Exposure Factors Handbook (EPA, 1997) cites several studies that examined rates of inadvertent soil ingestion. Hawley (1985) suggests adult soil ingestion rates of 480 mg/d (0.017 oz/d) during outdoor activities, 0.56 to 110 mg/d (2×10^{-5} to 0.004 oz/d) of house dust during indoor activities, and an annual average of 60.5 mg/d (0.002 oz/d). Krablin (1989)

Table 50
Water Needs of Crops

Crop	Seasonal Water Needs (cm)				
	Eastern Colorado [a]	Western Colorado [a]	Generic Estimates [b]	Eastern Oregon [c]	Southwestern U.S. [d]
Alfalfa and Alfalfa Mixtures	7.6E+01–9.9E+01	3.3E+01–9.2E+01	8.0E+01–1.6E+02	1.1E+02	2.0E+02
All Other Hay	---	---	---	---	---
Barley/Oats/Wheat	---	---	4.5E+01–6.5E+01	---	---
Beans	---	---	3.0E+01–5.0E+01	6.1E+01	---
Beans—Dry, Edible	4.0E+01–4.9E+01	5.1E+01	---	---	---
Broccoli	---	---	---	---	5.0E+01
Cabbage	---	---	3.5E+01–5.0E+01	---	---
Cauliflower	---	---	---	---	4.7E+01
Corn—Grain, Seed	5.2E+01–7.0E+01	6.4E+01	---	---	---
Corn—Silage	4.6E+01–6.2E+01	4.1E+01–5.8E+01	---	---	---
Corn—Sweet	5.2E+01–5.8E+01	---	---	---	5.0E+01
Corn—Field	---	---	---	7.6E+01	---
Grain—Small (oats, rye)	---	---	---	---	---
Grain—Spring (barley, wheat)	2.7E+01–3.9E+01	2.9E+01–5.0E+01	---	---	---
Lettuce and Romaine	---	---	---	---	2.2E+01
Onions	---	---	3.5E+01–5.5E+01	8.1E+01	5.9E+01

--- = Crop was not addressed by source.

[a] Broner and Schneekloth, 2003

[b] Brouwer and Heibloem, 1986

[c] Jensen and Shock, 2001

[d] Erie et al., 1982

Table 50 (Continued)
Water Needs of Crops

Crop	Seasonal Water Needs (cm)				
	Eastern Colorado [a]	Western Colorado [a]	Generic Estimates [b]	Eastern Oregon [c]	Southwestern U.S. [d]
Pastureland, All Types	6.6E+01–8.7E+01	3.5E+01–8.5E+01	---	9.1E+01	---
Peas	---	---	3.5E+01–5.0E+01	---	---
Peppers	---	---	6.0E+01–9.0E+01	---	---
Potatoes	7.1E+01	4.2E+01	5.0E+01–7.0E+01	7.6E+01	---
Sorghum, Grain	4.1E+01–5.8E+01	---	---	---	---
Sorghum/Millet	---	---	4.5E+01–6.5E+01	---	---
Soybean	---	---	4.5E+01–7.0E+01	---	---
Tomatoes	---	---	4.0E+01–8.0E+01	---	---
Vegetables—Small	4.5E+01–5.6E+01	1.7E+01–4.6E+01	---	---	---
Wheat—Grain, Seed, Winter, Spring	3.6E+01–4.9E+01	4.7E+01–5.1E+01	---	6.6E+01	6.6E+01

--- = Crop was not addressed by source.

[a] *Broner and Schneekloth, 2003*

[b] *Brouwer and Heibloem, 1986*

[c] *Jensen and Shock, 2001*

[d] *Erie et al., 1982*

indicates a soil ingestion rate of 10 mg/d (3.5×10^{-4} oz/d) for adults, while Calabrese et al. (1990) estimated a range of 30 to 100 mg/d (0.001 to 0.0035 oz/d) for adults. The EPA (1997) recommends a central estimate of 50 mg/d (0.0017 oz/d) for adults, but gives this value a low confidence rating. A median soil ingestion rate of 200 mg/d (0.007 oz/d) for both children and adults was adopted for work performed by the Risk Assessment Corporation (RAC, 1999) at Rocky Flats in Colorado. A lognormal distribution was defined using this value and a geometric standard deviation of 2.2. Simon (1998) conducted an exhaustive review of soil ingestion data for humans and estimated distributions for a variety of conditions. A geometric mean of 100 mg/d (0.0035 oz/d) was assigned for adults in rural residential lifestyles in heavily vegetated (i.e., forests and fields) areas and for occupations at construction sites; a geometric mean of 200 mg/d (0.007 oz/d) was estimated for a rural residential lifestyle in a sparsely vegetated area. A geometric standard deviation of 3.2 was adopted for all three scenarios. The NCRP (1999) adopted inadvertent soil ingestion rates of 50 and 100 mg/d (0.0017 to 0.0035 oz/d) for receptors in rural settings with heavy and sparse vegetation, respectively, while a value of 100 mg/d (0.0035 oz/d) was used for a construction scenario. The NCRP report noted the need to "have wide uncertainty distributions that allow for high values to occur with finite probability." Towards this end, a geometric standard deviation of 3.2 was adopted for the purpose of developing soil screening limits.

A soil ingestion rate of 100 mg/d (0.0035 oz/d) was used to conduct the deterministic modeling for all exposure scenarios. This value is consistent with estimates for construction site exposures cited above and equals or exceeds the ingestion rates provided for rural lifestyles in areas with heavy vegetation. A lognormal distribution was used to describe soil ingestion rates, and was defined using a geometric mean and standard deviation of 100 mg/d (0.0035 oz/d) and 3.2, respectively. The standard deviation is the same as that applied by Simon (1998) and the NCRP (1999).

5.11.10 Drinking Water Ingestion Rate

The drinking water rate is used to estimates doses for the Groundwater Resource Protection and All Pathways–Groundwater Scenarios. The Exposure Factors Handbook (EPA, 1997) discusses rates of tap water consumption at length, and suggests distributional informational. New Mexico drinking water regulations adopt the majority of 40 CFR Part 141 (EPA, 2000); this regulation prescribes the use of a drinking water ingestion rate of 2 L/d (0.5 gal/d) to demonstrate compliance with the CFR requirements. Consequently, this ingestion rate was used to model exposures for the Groundwater Resource Protection Scenario and no distribution of this rate was considered in the probabilistic modeling. Information for adults aged 20 through 64 was used to define the distribution of ingestion rates for the All Pathways–Groundwater Scenario; this distribution is included in Table 11.

5.11.11 Indoor Water Usage Rate

The indoor water usage rate specifies the amount of water used by the groundwater pathway receptors for personal needs such as food preparation, clothes washing, and bathing. This quantity is used in conjunction with other information to estimate the well pumping rate for the Groundwater Resource Protection and All Pathways–Groundwater Scenarios.

The EPA (2002) has summarized several studies that monitored water usage in suburban households in the U.S. These studies, which lasted as long as 3 months, found average daily usage rates ranged from 0.2 to 0.3 m^3 (50 to 70 gal) per person. Data collected by Mayer et al. (1999) from 1,188 households in 12 cities across the country showed daily per capita indoor water use was lognormally distributed with a median usage rate of about 0.23 m^3 (60 gal). Using these data, a distribution of indoor water usage rates was estimated, with the geometric mean set to the median reported by Mayer et al. The geometric standard deviation was set to 1.49 to yield a distribution that generally resembled that reported by the investigators.

5.11.12 Types of Animals Raised

The receptors for all but the Groundwater Resource Protection and the Intruder-Construction Scenarios are exposed to radiation through the intake of contaminated vegetables and animal products. In terms of animal product intake, it was assumed that the receptors raise cattle and cows to supply a portion of their beef and milk intake, or chickens to supply meat and eggs. The probabilities of raising cattle and cows or of raising chickens were assumed to be equal; the deterministic modeling was based on the assumption that cattle and cows were raised by the receptors.

5.11.13 Fraction of Diet Raised at Receptor Location

Most of the receptors included in the performance assessment and composite analysis are assumed to raise a portion of their diet at the exposure location. The Exposure Factors Handbook (EPA, 1997) provides estimates of the fraction of the vegetable diet grown by households that garden and those that farm. In terms of gardening households, the report cites a range of 0.106 to 0.233 for exposed, protected, and root vegetables, and a fraction of 0.173 averaged over all crops. A range of 0.173 to 0.42 for exposed, protected, and root vegetables was found for households that farm; averaging over all vegetables yielded a fraction of 0.308. The range and mean for households that farm were adopted for the modeling; these data were used to construct a triangular distribution.

The EPA (1997) also provides data for the fraction of animal product intake that is home-produced. For households that raise animals, the fractions given for beef, total dairy, chicken, and eggs are 0.48, 0.21, 0.15, and 0.21, respectively; the corresponding fractions for households that farm are 0.49, 0.25, 0.16, and 0.15. These data were used to develop triangular distributions

for each animal product. It was assumed that the receptors raised enough animals to provide 50 and 25 percent of the beef and milk they consumed, respectively. Similarly, the individuals were assumed to raise enough chickens to provide 15 and 20 percent of the chicken and eggs they consumed. Triangular distributions were defined for all four parameters based on the assumption that the fractions varied over a range of ± 20 percent.

The diet fractions sampled from the distributions described above were adjusted downward if the areas required to raise the crops or animals exceeded the available area at the receptor location. The portion of the receptor's lot that was available for the production of food was first allocated to vegetable crops; any remaining area was assumed to be available for raising animals.

5.11.14 Crop Ingestion Rates

The doses received from the consumption of contaminated crops are directly proportional to the ingestion rates of those foods. The RESRAD code (ANL, 2001) uses default ingestion rates of 14 kg/yr (30 lb/yr) for leafy vegetables and 160 kg/yr (350 lb/yr) for fruit, other vegetables, and grain. Data provided in the NRC's Regulatory Guide 1.109 (NRC, 1977) indicate a consumption rate for the average adult of 190 kg/yr (420 lb/yr) for fruit, vegetables, and grain; 520 kg/yr (1,150 lb/yr) is listed for the maximally exposed individual. The NRC (1992) adopted an average consumption rate of 177 kg/yr (390 lb/yr) for fruit, vegetables, and grain to estimate doses from residual contamination following facility decommissioning; essentially the same rate is provided by Yang and Nelson (1986). Data adapted from Rupp (1980) indicate a best estimate of 170 kg/yr (375 lb/yr) for the consumption of fruit, vegetables, and grain by persons older than 18.

The Exposure Factors Handbook (EPA, 1997) includes a large amount of information on vegetable consumption rates; data contained in this report for adults aged 20 to 75 were used to develop the distributions shown in Table 11. The data used to estimate consumption rates were provided in terms of grain and total vegetables. It was assumed that 85 percent of the listed consumption rates for vegetables other than grain consisted of produce, while the remaining 15 percent consisted of leafy vegetables. This allocation is consistent with the per capita intake data provided in the Exposure Factors Handbook for different food classes. All consumption rates were given in terms of daily intake per unit body mass; these rates were converted to total daily intakes by multiplying them by an adult body mass of 71.8 kg (160 lb) (EPA, 1997).

5.11.15 Animal Product Ingestion Rates

Ingestion rates for beef, milk, chicken, and eggs are used to estimate doses for the off-site receptors and two of the intruder scenarios. For the average adult, Regulatory Guide 1.109 (NRC, 1977) lists ingestion rates of 95 kg/yr (210 (lb/yr) for meat and poultry, and 110 L/yr (30 gal/yr) for milk; the maximum exposed adult is assumed to consume 110 kg/yr (240 lb/yr) of meat and poultry and 310 L/yr (80 gal/yr) of milk. RESRAD (ANL, 2001) uses a meat and poultry consumption rate of 63 kg/yr (140 lb/yr), and a value of 92 L/yr (25 gal/yr) for milk.

Rupp (1980) lists average adult consumption rates of 31 kg/yr, 9.5 kg/yr, 95 L/yr, and 15 kg/yr (68 lb/yr, 21 lb/yr, 25 gal/yr, and 33 lb/yr) for beef, poultry, milk, and eggs, respectively. Yang and Nelson (1986) list rates of 32 kg/yr, 11 kg/yr, 92 L/yr, and 9.8 kg/yr (70 lb/yr, 24 lb/yr, 24 gal/yr, and 22 lb/yr) for beef, poultry, milk, and eggs, respectively, while the NRC (1992) adopts values of 59 kg/yr, 9 kg/yr, 100 L/yr, and 10 kg/yr (130 lb/yr, 20 lb/yr, 26 gal/yr, and 22 lb/yr) for these same food products.

The EPA's Exposure Factors Handbook (EPA, 1997) contains consumption data for beef, poultry, eggs, and dairy products for various age groups. Using this information, distributions of consumption rates were calculated for persons 20 years and older; these distributions were adopted for the performance assessment and composite analysis modeling. The calculations used an adult body mass of 71.8 kg (160 lb), assumed that the consumption rates listed for poultry represented chicken, and assumed that 80 percent of the dairy intake consisted of milk.

5.11.16 Animal Numbers

The fraction of a receptor's diet that comes from home-raised animals will be influenced by the number of animals that are required to supply the food. Simply put, as the numbers of animals required to provide the receptor's food increases, the likelihood that the receptor will have the necessary land to raise the cattle, cows, or chickens decreases. Estimates of the number of animals needed to supply the specified food requirements depend on various animal production parameters.

The numbers of cattle and chickens required to supply the specified quantities of beef and chicken depend upon the live weights of the animals at the time they are killed and the fractions of the live weights represented by edible meat. The live weights of the cattle at the time of slaughter were assumed to average 500 kg (1,100 lb); this weight is consistent with the animal forage consumption rate selected for the modeling and generally agrees with average live weights reported in USDA (2005a). A standard deviation of 25 kg (55 lb) was adopted based on an assumed coefficient of variation of 5 percent. The fraction of the animal's live weight that consists of meat was estimated as the product of the carcass-to-live weight ratio, or dressing percentage, and the cutability index, which represents the fraction of the carcass with saleable retail meat. The dressing percentage was assumed to be normally distributed with a mean and standard deviation of 0.64 and 0.02, based on data provided by the University of Nebraska Cooperative Extension (UNCE, 2001) and Harris et al. (1997). The cutability index was assumed to be normally distributed with a mean and standard deviation of 0.5 and 0.024, based on information provided by UNCE and May et al. (2000).

The number of chickens necessary to provide the specified food requirements of the receptor is estimated using data for various meat-type chickens. The USDA (2004a) reported an average live weight of 2.4 kg (5.2 lb) for young chickens at the time of slaughter. This is approximately the midpoint of the average live weights provided by Skinner and Sunde (1983) for Cornish game hens

(0.8 kg [1.8 lb]), broilers/fryers (1.8 kg [4 lb]), and roasters (3.6 kg [8 lb]). Using this information, the live weights of the birds at the time of slaughter were assumed to be normally distributed with a mean and standard deviation of 2.3 and 0.45 kg (5.0 and 1.0 lb), respectively. The standard deviation was selected so the distribution ranged approximately from 0.9 to 3.6 kg (2 to 8 lb).

The ratio of the ready-to-cook and live weight production data provided in USDA (2004a) was used to estimate a ready-to-cook weight fraction for chickens. Based on monthly data for 2000 through 2002, a mean and standard deviation of 0.74 and 0.0045 were calculated. In the absence of specific information on the fraction of the ready-to-cook carcass that is meat, a fraction of 0.5 was assumed.

The number of milk cows required to supply the specified milk intakes is directly dependent upon the milk production rate of the animals. This rate was assumed to be normally distributed with a mean of 8,600 kg/yr (1.9×10^4 lb/yr), consistent with data found in USDA (2005b). Information needed to describe the variability associated with this value was not found; in its absence a standard deviation of 150 kg/yr (330 lb/yr) was selected, which yields production rates that generally span the range of those projected using the minimum and maximum mean monthly milk production rates.

An egg production rate of 260 eggs/yr (USDA, 2005c) was used to estimate the number of layers required to meet the specified intake. In the absence of information needed to characterize the variability of egg production, a coefficient of variation of 5 percent was assumed. This assumption results in a distribution that approximately spans the average rates given for 42 states. The USDA (1995) provides data for weight classes of shell eggs; the minimum egg mass for medium, large, extra large, and jumbo eggs ranges from approximately 0.05 to 0.07 kg (0.11 to 0.16 lb). Using these data, a normal distribution of egg mass was developed with a mean and standard deviation of 0.06 and 0.0035 kg (0.13 and 0.0078 lb). The mean of the distribution was estimated as the midpoint of the minimum mass for large and extra large eggs and the standard deviation was selected so that the distribution generally ranged over the minimum egg masses provided above. The shell of the egg was assumed to contribute 10 percent of the total mass.

5.11.17 Receptor's Lot, House, and Well Dimensions

All of the off-site receptors are assumed to take up residence downwind or downgradient of the disposal facility. The 200 m^2 (2,200 ft^2) house is assumed to sit on a 2,300 m^2 (2.5×10^4 ft^2) lot, leaving as much as 2,100 m^2 (2.3×10^4 ft^2) for raising crops and animals; the same house and lot dimensions are used for the intruder analysis. The well drilled through the disposal site under the Intruder–Post-Drilling Scenario is assumed to be 25 cm (10 in.) in diameter.

5.11.18 House Ventilation Rate

The ventilation rate of the intruder's house specifies the frequency with which air inside the dwelling is replaced with fresh air. The parameter is used to estimate doses received by the receptor from the inhalation of vapor- and gas-phase radionuclides during the time spent indoors. The EPA (1997) cites several studies that address air exchange rates in domestic dwellings. Nazaroff et al. (1988) evaluated the data collected by other investigators. Air exchange rates in low-income houses with a median age of 45 years had a geometric mean and standard deviation of 0.90 ± 2.13 air exchanges per hour (ACH). Measurements taken during the heating season in 312 houses with a median age of 10 years indicated a geometric mean and standard deviation of 0.53 ± 1.71 ACH.

Versar (1990) provides distributional information for air exchange rates in houses in several states; air exchange measurements were generally taken during the cooler months at most locations, although some summertime data are included. In general, the mean air exchange rate ranged from 0.22 to 0.9; the means for three locations exceeded 1.0 and measurements at two of these locations were conducted in midsummer, when windows would most likely be open. Koontz and Rector (1995) evaluated data from numerous studies and estimated air exchange rates for different segments of the U.S. (i.e., west, north-central, northeast, and south). Data from each state were weighted to compensate for imbalances in locations where measurements were taken. For the west region, the air exchange rate had a geometric mean and standard deviation of 0.47 ± 2.11 ACH.

Using essentially the same data as Koontz and Rector, but without the compensating weights, Murray and Burmaster (1995) developed estimates of air exchange rates for different climate regions (i.e., coldest, colder, warmer, and warmest) and seasons. The regions were defined on the basis of heating degree days; seasons were defined as 3-month intervals, beginning with December, January, and February for winter. Using a base temperature of 18°C (65°F), the annual heating degree days for Los Alamos is approximately 6,400 (WRCC, 2005), qualifying the site for inclusion in the colder climate region. Mean air exchange rates for this region range from 0.35 in the fall to 1.3 in the summer.

The ventilation rate adopted for the performance assessment and composite analysis was based on the results for the western region cited by Koontz and Rector (1995). This distribution generally agrees with the seasonal data provided by Murray and Burmaster (1995) and is consistent with the data for newer houses found in Nazaroff et al. (1988).

Information needed to characterize air exchange rates during the time spent by the construction worker within the basement excavation was not found. In the absence of the necessary data, the air exchange rate for the excavation was assumed to be the same as that described above for the intruder's house.

5.12 Miscellaneous Parameters

Table 51 presents the radionuclide half-lives and dose conversion factors used in the GoldSim modeling. The radionuclides found in the table include all isotopes for which radionuclide inventories were developed or that were explicitly included in decay and ingrowth calculations. In general, daughter products with half-lives of less than 1 year were assumed to be in secular equilibrium with their parents. The half-lives included in Table 51 were taken from KAPL (2002).

The dose conversion factors used in the performance assessment and composite analysis were taken from federal guidance reports 11 and 12 (EPA, 1988, 1993a). The factors listed in Table 51 represent those of the parent radionuclides and any daughters assumed to be in secular equilibrium with those isotopes.

Table 51
Radionuclide Half-Lives and Dose Conversion Factors

Radionuclide	Half-Life (yr)	Ingestion (mrem/pCi)	Inhalation (mrem/pCi)	Direct Radiation (mrem-m³/yr-pCi)		
				15 cm Depth	Infinite Depth	Air Immersion
Ac-227	2.2E+01	1.5E-02	6.7E+00	1.2E-06	1.3E-06	2.2E-03
Ag-108m	4.2E+02	7.6E-06	2.8E-04	5.4E-06	6.1E-06	9.2E-03
Al-26	7.1E+05	1.5E-05	8.0E-05	9.0E-06	1.1E-05	1.6E-02
Am-241	4.3E+02	3.6E-03	4.4E-01	2.7E-08	2.7E-08	9.6E-05
Am-243	7.4E+03	3.6E-03	4.4E-01	5.4E-07	5.6E-07	1.2E-03
Ba-133	1.1E+01	3.4E-06	7.8E-06	1.2E-06	1.2E-06	2.1E-03
Be-10	1.5E+06	4.7E-06	3.5E-04	6.6E-10	6.7E-10	1.3E-06
Bi-207	3.2E+01	5.5E-06	2.0E-05	5.1E-06	5.9E-06	8.8E-03
Bk-247	1.4E+03	4.7E-03	5.7E-01	2.6E-07	2.7E-07	5.5E-04
C-14	5.7E+03	2.1E-06	2.1E-06	8.4E-12	8.4E-12	2.6E-08
Ca-41	1.0E+05	1.3E-06	1.3E-06	0.0E+00	0.0E+00	0.0E+00
Cd-113m	1.4E+01	1.6E-04	1.5E-03	4.0E-10	4.1E-10	8.1E-07
Cf-249	3.5E+02	4.7E-03	5.8E-01	1.1E-06	1.2E-06	1.8E-03
Cf-251	9.0E+02	4.8E-03	5.9E-01	3.2E-07	3.3E-07	6.5E-04
Cf-252	2.6E+00	1.1E-03	1.6E-01	1.1E-10	1.1E-10	5.9E-07
Cl-36	3.0E+05	3.0E-06	2.2E-05	1.4E-09	1.5E-09	2.6E-06
Cm-243	2.9E+01	2.5E-03	3.1E-01	3.5E-07	3.6E-07	6.9E-04
Cm-244	1.8E+01	2.0E-03	2.5E-01	7.9E-11	7.9E-11	5.7E-07
Cm-245	8.5E+03	3.7E-03	4.6E-01	2.1E-07	2.1E-07	4.6E-04
Cm-247	1.6E+07	3.4E-03	4.1E-01	1.1E-06	1.2E-06	1.9E-03
Cm-248	3.5E+05	1.4E-02	1.7E+00	5.5E-11	5.5E-11	4.0E-07
Co-60	5.3E+00	2.7E-05	2.2E-04	8.5E-06	1.0E-05	1.5E-02
Cs-135	2.3E+06	7.1E-06	4.6E-06	2.4E-11	2.4E-11	6.6E-08
Cs-137	3.0E+01	5.0E-05	3.2E-05	1.9E-06	2.1E-06	3.2E-03
Dy-154	3.0E+06	0.0E+00	0.0E+00	0.0E+00	0.0E+00	0.0E+00
Eu-152	1.4E+01	6.5E-06	2.2E-04	3.8E-06	4.4E-06	6.6E-03
Eu-154	8.6E+00	9.5E-06	2.9E-04	4.1E-06	4.8E-06	7.2E-03
Gd-148	7.5E+01	2.2E-04	3.3E-01	0.0E+00	0.0E+00	0.0E+00
Gd-150	1.8E+06	0.0E+00	0.0E+00	0.0E+00	0.0E+00	0.0E+00

Table 51 (Continued)
Radionuclide Half-Lives and Dose Conversion Factors

Radionuclide	Half-Life (yr)	Ingestion (mrem/pCi)	Inhalation (mrem/pCi)	Direct Radiation (mrem-m^3/yr-pCi)		
				15 cm Depth	Infinite Depth	Air Immersion
H-3	1.2E+01	6.4E-08	6.4E-08	0.0E+00	0.0E+00	0.0E+00
Hf-182	9.0E+06	2.2E-05	3.4E-03	5.0E-06	5.7E-06	8.8E-03
Ho-163	4.6E+03	0.0E+00	0.0E+00	0.0E+00	0.0E+00	0.0E+00
Ho-166m	1.2E+03	8.1E-06	7.7E-04	5.7E-06	6.4E-06	9.9E-03
I-129	1.6E+07	2.8E-04	1.7E-04	8.1E-09	8.1E-09	4.4E-05
K-40	1.3E+09	1.9E-05	1.2E-05	5.3E-07	6.5E-07	9.4E-04
Kr-81	2.3E+05	0.0E+00	0.0E+00	1.8E-08	1.9E-08	3.1E-05
Kr-85	1.1E+01	0.0E+00	0.0E+00	8.1E-09	8.9E-09	1.4E-05
La-137	6.0E+04	4.6E-07	8.8E-05	8.8E-09	8.8E-09	4.7E-05
Lu-176	3.8E+10	7.3E-06	6.6E-04	1.5E-06	1.6E-06	2.7E-03
Mo-93	3.5E+03	1.3E-06	2.8E-05	3.7E-10	3.7E-10	2.9E-06
Nb-91	7.0E+02	0.0E+00	0.0E+00	0.0E+00	0.0E+00	0.0E+00
Nb-92	3.5E+07	0.0E+00	0.0E+00	0.0E+00	0.0E+00	0.0E+00
Nb-93m	1.6E+01	5.2E-07	2.9E-05	6.5E-11	6.5E-11	5.2E-07
Nb-94	2.0E+04	7.1E-06	4.1E-04	5.3E-06	6.1E-06	9.0E-03
Nd-144	2.4E+15	0.0E+00	0.0E+00	0.0E+00	0.0E+00	0.0E+00
Ni-59	7.6E+04	2.1E-07	1.3E-06	0.0E+00	0.0E+00	0.0E+00
Ni-63	1.0E+02	5.8E-07	3.1E-06	0.0E+00	0.0E+00	0.0E+00
Np-237	2.1E+06	4.4E-03	5.4E-01	6.5E-07	6.9E-07	1.2E-03
Os-194	6.0E+00	1.6E-05	6.7E-04	3.1E-07	3.4E-07	5.3E-04
Pa-231	3.3E+04	1.1E-02	1.3E+00	1.1E-07	1.2E-07	2.0E-04
Pb-210	2.2E+01	7.3E-03	2.3E-02	3.7E-09	3.8E-09	1.0E-05
Pd-107	6.5E+06	1.5E-07	1.3E-05	0.0E+00	0.0E+00	0.0E+00
Pm-145	1.8E+01	4.7E-07	3.0E-05	1.8E-08	1.8E-08	8.3E-05
Pu-236	2.9E+00	1.2E-03	1.4E-01	1.4E-10	1.4E-10	7.4E-07
Pu-238	8.8E+01	3.2E-03	3.9E-01	9.4E-11	9.5E-11	5.7E-07
Pu-239	2.4E+04	3.5E-03	4.3E-01	1.8E-10	1.8E-10	5.0E-07
Pu-240	6.6E+03	3.5E-03	4.3E-01	9.2E-11	9.2E-11	5.5E-07
Pu-241	1.4E+01	6.8E-05	8.3E-03	3.7E-12	3.7E-12	8.5E-09

Table 51 (Continued)
Radionuclide Half-Lives and Dose Conversion Factors

Radionuclide	Half-Life (yr)	Ingestion (mrem/pCi)	Inhalation (mrem/pCi)	Direct Radiation (mrem-m³/yr-pCi)		
				15 cm Depth	Infinite Depth	Air Immersion
Pu-242	3.8E+05	3.4E-03	4.1E-01	8.0E-11	8.0E-11	4.7E-07
Pu-244	8.0E+07	3.3E-03	4.0E-01	1.1E-06	1.3E-06	1.9E-03
Ra-226	1.6E+03	1.3E-03	8.6E-03	5.9E-06	7.0E-06	1.0E-02
Ra-228	5.8E+00	1.4E-03	5.1E-03	3.2E-06	3.7E-06	5.6E-03
Se-79	2.9E+05	8.7E-06	9.8E-06	1.2E-11	1.2E-11	3.5E-08
Si-32	1.6E+02	1.1E-05	1.0E-03	7.0E-09	7.4E-09	1.2E-05
Sm-146	1.0E+08	2.0E-04	8.3E-02	0.0E+00	0.0E+00	0.0E+00
Sm-147	1.1E+11	1.9E-04	7.5E-02	0.0E+00	0.0E+00	0.0E+00
Sm-151	9.0E+01	3.9E-07	3.0E-05	6.2E-13	6.2E-13	4.2E-09
Sn-121m	4.4E+01	1.6E-06	1.2E-05	1.2E-09	1.2E-09	7.0E-06
Sn-126	2.3E+05	1.9E-05	1.0E-04	9.2E-08	9.2E-08	2.5E-04
Sr-90	2.9E+01	1.5E-04	1.3E-03	1.4E-08	1.5E-08	2.3E-05
Tb-157	7.0E+01	1.2E-07	9.2E-06	1.8E-09	1.8E-09	7.9E-06
Tb-158	1.8E+02	4.4E-06	2.6E-04	2.6E-06	3.0E-06	4.5E-03
Tc-97	4.2E+06	1.7E-07	9.9E-07	5.1E-10	5.1E-10	3.9E-06
Tc-99	2.1E+05	1.5E-06	8.3E-06	7.8E-11	7.8E-11	1.9E-07
Th-228	1.9E+00	8.1E-04	3.4E-01	5.1E-06	6.4E-06	9.4E-03
Th-229	7.3E+03	4.0E-03	2.2E+00	9.2E-07	1.0E-06	1.7E-03
Th-230	7.5E+04	5.5E-04	3.3E-01	7.5E-10	7.6E-10	2.0E-06
Th-232	1.4E+10	2.7E-03	1.6E+00	3.2E-10	3.3E-10	1.0E-06
Ti-44	6.0E+01	2.5E-05	1.0E-03	7.4E-06	8.5E-06	1.3E-02
U-232	7.0E+01	1.3E-03	6.6E-01	5.6E-10	5.6E-10	1.7E-06
U-233	1.6E+05	2.9E-04	1.4E-01	8.5E-10	8.7E-10	1.9E-06
U-234	2.5E+05	2.8E-04	1.3E-01	2.5E-10	2.5E-10	8.9E-07
U-235	7.0E+08	2.7E-04	1.2E-01	4.6E-07	4.7E-07	9.0E-04
U-236	2.3E+07	2.7E-04	1.3E-01	1.3E-10	1.3E-10	5.9E-07
U-238	4.5E+09	2.7E-04	1.2E-01	7.4E-08	8.3E-08	1.4E-04
Zr-93	1.5E+06	1.7E-06	3.2E-04	0.0E+00	0.0E+00	0.0E+00

6.0 References

Abeele, W.V., 1984, *Geotechnical Aspects of Hackroy Sandy Loam and Crushed Tuff*, Los Alamos National Laboratory Report LA-9916-MS.

Abeele, W.V., 1986, *Determination of Hydraulic Conductivity in Crushed Bandelier Tuff*, Los Alamos Scientific Laboratory Report LA-8147-MS.

Abeele, W.V. and M.L. Wheeler, 1981, *Geohydrology of Bandelier Tuff*, Los Alamos National Laboratory Report LA-8962-MS.

Allen, E.J., 1996, "Harvester Ants: Specialists in Plant Seeds," *New Mexico Wildlife*, Vol. 41, No. 1, pp. 22–23.

Anderson, G.G., 1980, *Rodent Control on Agricultural Land in British Columbia*, Province of British Columbia, Ministry of Agriculture, Victoria.

ANL, 2001, *User's Manual for RESRAD Version 6*, Argonne National Laboratory Report ANL/EAD-4, July.

Anspaugh, L.R., J.H. Shinn, P.L. Phelps, and N.C. Kennedy, 1975, "Resuspension and Redistribution of Plutonium in Soils," *Health Physics*, Vol. 29, pp. 571–582.

Arnold, J. F., D.A. Jameson, and E.H. Reid, 1964, *The Piñon-Juniper Type of Arizona: Effects of Grazing, Fire, and Tree Control*, U.S. Department of Agriculture, Forest Service, Production Research Report No. 84, September.

Aro, R.S., 1971, "Evaluation of Piñon-Juniper Conversion to Grassland," *J. Range Manage.*, Vol. 24, 188–197.

Arthur, W.J., III and A.W. Alldredge, 1982, "Importance of Plutonium Contamination on Vegetation Surfaces at Rocky Flats, CO," *Environ. Exp. Botany*, Vol. 22, pp. 33–38.

ATSDR, 2001, *Landfill Gas Primer—An Overview for Environmental Health Professionals*, Department of Human Health and Services, Agency for Toxic Substances and Disease Registry, November.

Baes, C.F. III, R.D. Sharp, A.L. Sjoreen, and R.W. Shor, 1984, *A Review and Analysis of Parameters for Assessing Transport of Environmentally Released Radionuclides through Agriculture*, Oak Ridge National Laboratory, ORNL-5786, September.

Banfield, A.W.F., 1974, *The Mammals of Canada*," University of Toronto Press, Toronto.

Barney, M.A. and N.C. Frischknecht, 1974, "Vegetation Changes Following Fire in the Piñon-Juniper Type of West-Central Utah," *J. of Range Manage.*, Vol. 27, No. 2, pp. 91–96.

Bartels, M.A. and D.P. Thompson, 1993, "Mammalian Species—*Spermophilus lateralis*," *The Society of Mammalogists*, No. 440, April.

Barton, K.E., N.J. Sanders, and D.M. Gordon, 2002, "The Effects of Proximity and Colony Age on Interspecific Interference Competition between the Desert Ants *Pogonomyrmex barbatus* and *Aphaenogaster cockerelli*," *American Midland Naturalist*, Vol. 148, pp. 376–382.

Bechtel/SAIC, 2004, *Radionuclide Transport Models under Ambient Conditions*, prepared for U.S. Department of Energy, Office of Civilian Radioactive Waste Management, by Bechtel SAIC Company, DOC.20041101.0002, October.

Belk, M.C. and H.D. Smith, 1991, "Mammalian Species—*Ammospermophilus luecurus*," *The Society of Mammalogists* No. 368, April.

Bennett, K., J. Biggs, and P. Fresquez, 1997, *Radionuclide Contaminant Analysis of Small Mammals at Area G, TA-54, Los Alamos National Laboratory, 1995*, Los Alamos National Laboratory Report LA-13242-MS, January.

Bennett, K., J. Biggs, and P. Fresquez, 1998, *Radionuclide Contaminant Analysis of Small Mammals at Area G, Technical Area 54, G 1997 (with cumulative summary 1994–1997)*, Los Alamos National Laboratory Report LA-13517-MS, December.

Bennett, K.D., R.J. Robinson, and P.R. Fresquez, 2002, *Radionuclide Contaminant Analysis of Small Mammals at Area G, Technical Area 54, 1998 (with cumulative summary 1994–1998)*, Los Alamos National Laboratory Report LA-13874-MS, January.

Beresford, N.A. and B.J. Howard, 1991, "The Importance of Soil Adhered to Vegetation as a Source of Radionuclides Ingested by Grazing Animals," *Sci. Total Environ.*,Vol. 107, pp. 237–254.

Best, T.L. and M.P. Skupsi, 1994, "Mammalian Species—*Perognathus flavus*," *The Society of Mammalogists*, No. 471, December.

Biggs, J.R., K.D. Bennett, and P.R. Fresquez, 1995, *Radionuclide Contaminant Analysis of Small Mammals at Area G, TA-54, 1994*," Los Alamos National Laboratory Report LA-13015-MS, September.

Biggs, J.R., K.D. Bennett, and P.R. Fresquez, 1997, *Radionuclide Contaminant Analysis of Small Mammals at Area G, Technical Area 54, 1996 (with cumulative summary for 1994-1995)*, Los Alamos National Laboratory Report LA-13345-MS, July.

Blom, P.E., W.H. Clark, and J.B. Johnson, 1991, "Colony Densities of the Seed Harvesting Ant *Pogonomyrmex salinus* in Seven Plant Communities on the Idaho National Engineering Laboratory," *Journal of the Idaho Academy of Science*, Vol. 27, No. 1, pp. 28–36.

Brant, D.H., 1962, "Measures of the Movements and Population Densities of Small Rodents," *Univ. Calif. Publ. Zool.* Vol. 62, pp. 105–184.

Breshears, D.D., J.J. Whicker, M.P. Johansen, and J.E. Pinder, 2003, "Wind and Water Erosion and Transport in Semi-Arid Shrubland, Grassland, and Forest Ecosystems: Quantifying Dominance of Horizontal Wind-Driven Transport," *Earth Surface Processes and Landforms,* Vol. 28, pp. 1,189–1,209.

Britt, L.G., 1972, "Some Aspects of the Ecology of *Perognathus flavus*, *Dipodomys ordi*, and *Dipodomys merriami*," Ph.D. dissertation, University of New Mexico, Albuquerque.

Broner, I. and J. Schneekloth, 2003, *Seasonal Water Needs and Opportunities for Limited Irrigation for Colorado Crops*, Colorado State University Cooperative Extension Crop Series Irrigation No. 4.718, Colorado State University, Fort Collins, CO. <http://www.ext.colostate.edu /pubs/crops/04718.html>.

Brookins, D.G., 1984, *Geochemical Aspects of Radioactive Waste Disposal*, Springer-Verlag, New York.

Brouwer, C. and M. Heibloem, 1986, *Irrigation Water Needs, Training Manual No. 3*, Land and Water Development Division, Food and Agriculture Organization of the United Nations, Rome, Italy.

Bunker, M.E., 1983, "Early Reactors," *Los Alamos Science*, Vol. Winter/Spring.

Burt, W.H. and R.P. Grossenheider, 1976, *Mammals*, Houghton Mifflin, New York.

Calabrese, E.J., E.J. Stanek, C.E. Gilbert, and R.M. Barnes, 1990, "Preliminary Adult Soil Ingestion Estimates; Results of a Pilot Study," *Regul. Toxicol. Pharmacol.*, Vol. 12, pp. 88–95.

Canadell, J., R.B. Jackson, J.B. Ehleringer, H.A. Mooney, O.E. Sala, and E.D. Schulze, 1996, "Maximum Rooting Depth of Vegetation Types at the Global Scale," *Oecologia,* Vol. 108, pp. 583–595.

Carlson, S.R. and W.G. Whitford, 1991, "Ant Mound Influence on Vegetation and Soil in a Semiarid Mountain Ecosystem," *American Midland Naturalist,* Vol. 126, No. 1, pp. 125–139.

Carroll, L.E. and H.H. Genoways, 1980, "Mammalian Species—*Lagurus curtatus*," *The American Society of Mammalogists* No. 124, April.

CDFG, 2003, *California Wildlife Habitat Relationships System*, California Department of Fish and Game, Wildlife and Habitat Data Analysis Branch, <http://www.dfg.ca.gov/ whdab/html/cwhr.html>.

Chamberlain, A.C., 1970, "Interception and Retention of Radioactive Aerosols by Vegetation," *Atmospheric Environment,* Vol. 4, pp. 57–63.

Chapman, J.A., 1975, "Mammalian Species—*Sylvilagus nuttalli*," *American Society of Mammalogists,* No. 56, November.

Charley, J.L. and S.W. Cowling, 1968, "Changes in Soil Nutrient Status Resulting from Overgrazing and their Consequences in Plant Communities of Semiarid Areas," *Proceedings of the Ecological Society of Australia*, Vol. 3, pp. 28–38.

Clark, W.H. and P.L. Comanor, 1975, "Removal of Annual Plants from the Desert Ecosystem by Western Harvester Ants, *Pogonomyrmex occidentalis*," *Env. Entomol.*, Vol. 4, pp. 52–56.

Clary, W.P., 1971, "Effects of Utah Juniper Removal on Herbage Yields from Springerville Soils," *J. Range Manage.*, Vol. 24, pp. 373–378.

Clary, W.P., 1989, *Test of RPA Production Coefficients and Local Assumptions for the Piñon-Juniper Ecosystem in Central Utah*, U.S. Forest Service, Intermountain Research Station, Research Paper INT-403, May.

Clary, W.P. and D.A. Jameson, 1981, "Herbage Production Following Tree and Shrub Removal in the Piñon-Juniper Type of Arizona," *J. Range Manage.*, Vol. 34, No. 2, pp. 109–113.

Cline J.F., D.A. Cataldo, W.E. Skiens, and K.A. Gado, 1982, *Long Term Biobarriers to Plant and Animal Intrusion of Uranium Tailings*, Pacific Northwest Laboratory Report PNL-4340, September.

Coffin, D.P., and W.K. Lauenroth, 1988, "The Effects of Disturbance Size and Frequency on a Shortgrass Plant Community," *Ecology*, Vol. 69, pp. 1609–1617.

Coffin, D.P. and W.K. Lauenroth, 1990, "Vegetation Associated with Nest Sites of Western Harvester Ants (*Pogonomyrmex occidentalis Cresson*) in a Semiarid Grassland," *American Midland Naturalist,* Vol. 123, pp. 226–235.

Cole, B.J., 1994, "Nest Architecture in the Western Harvester Ant, *Pogonomyrmex occidentalis* (Cresson)," *Ins. Soc.*, Vol. 41, pp. 401–410.

Cole, B.J., K. Haight, and D.C. Wiernasz, 2001, "Distribution of *Myrmecocystus mexicanus* (Hymenoptera: Formicidae): Association with *Pogonomyrmex occidentalis* (Hymenoptera: Formicidae)," *Ann. Entomol. Soc. Am.*, Vol. 94, No. 1, pp. 59–63.

Cooper, M.B., P.A. Burn, B.L. Tracy, M.J. Wilks, and G.A. Williams., 1994, "Characterization of Plutonium Contamination at the Former Nuclear Weapons Testing Range at Maralinga in South Australia," *J. Radioanalytical and Nuclear Chemistry*, Vol. 177, No. 1, pp. 161–184.

Cox, J.R., 1984, "Shoot Production and Biomass Transfer of Big Sacaton [*Sporobolus wrightii*]," *J. Range Manage.*, Vol. 34, No. 7, pp. 377–380.

Cranford, J. A., 1984, "Population Ecology and Home Range Utilizations of Two Subalpine Meadow Rodents (*Microtus longicaudus* and *Peromyscus maniculatus*)," in *Winter Ecology of Small Mammals:* v. 10, J.F. Merrit, ed., Spec. Publ. Carnegie Mus. Nat. Hist.

CRC, 1999, *CRC Handbook of Chemistry and Physics*, 79th Edition, CRC Press.

Crist, T. O. and J. A. Wiens, 1996, "The Distribution of Ant Colonies in a Semiarid Landscape: Implications for Community and Ecosystem Processes." *Oikos,* Vol. 76, pp. 301–311.

Croissant, R.L. and J.W. Echols, 1998, *Planting Guide for Field Crops*, Colorado State University Cooperative Extension Report No. 103.

CUCES, 1999, *Planning a Garden*, Clemson University Cooperative Extension Service, Home & Garden Information Center Report HGIC 1256.

Davis, W.B., 1974, *The Mammals of Texas*, Texas Parks and Wildlife Department, Bulletin 41, pp. 146–148.

Davis, W.B. and D.J. Schmidly, 1997, "Mammals of Texas—Online Edition," <www.nsrl.ttu.edu/tmot1/Default.htm> (2002).

Day, M.S., C.K. Anderson, and C.D. Pedersen, 2005, *Conceptual Design of the Earthen Cover for at Los Alamos National Laboratory Technical Area 54, Material Disposal Area G*, URS Corporation Report to LANL, Los Alamos National Laboratory Report LA-UR-05-7394, September.

DOE, 1979, *Final Environmental Impact Statement, Los Alamos National Laboratory Site, Los Alamos, New Mexico*, U.S. Department of Energy Report DOE/EIS-0018, December 1979.

DOE, 1988, *Radioactive Waste Management*, U.S. Department of Energy Order 5820.2A, September 26.

DOE, 2001a, *Radioactive Waste Management*, U.S. Department of Energy Order DOE O 435.1 (change 1 to document issued July 9, 1999), August 28.

DOE, 2001b, *Radioactive Waste Management Manual*, U.S. Department of Energy Report DOE M 435.1-1 (change 1 to document approved on July 9, 1999), June 19.

Dreicer, M., T.E. Hakonson, G.C. White, and F.W. Whicker, 1984, "Rainsplash as a Mechanism for Soil Contamination of Plant Surfaces," *Health Phys.,* Vol. 46, pp. 177–187.

Dwyer, D.D. and R.D. Pieper, 1967, "Fire Effects on Blue Grama-Piñon-Juniper Rangeland in New Mexico," *J. Range Manage.*, Vol. 20, pp. 359–362.

England, T.R. and B.F. Rider, 1994, *Evaluation and Compilation of Fission Product Yields 1993*, Los Alamos National Laboratory Report LA-UR-94-3106, October.

Environment Canada, 2003, *Landfill Gas Capture and Combustion Quantification Protocol*, Environment Canada, <http://www.ec.gc.ca/pdb/ghg/lfg_protocol_e.cfm>.

EPA, 1988, *Limiting Values of Radionuclide Intake and Air Concentration and Dose Conversion Factors for Inhalation, Submersion, and Ingestion*," U.S. Environmental Protection Agency, Federal Guidance Report 11.

EPA, 1993a, *External Exposure to Radionuclides in Air, Water, and Soil*, U.S. Environmental Protection Agency Federal Guidance Report 12, EPA 402-R-93-081, September.

EPA, 1993b, *Wildlife Exposure Factors Handbook, Appendix: Literature Review Database Volume II of II*, U.S. Environmental Protection Agency Report EPA/600/R93-187, December.

EPA, 1997, *Exposure Factors Handbook*, U.S. Environmental Protection Agency, EPA/600/P-95/002Fa, August.

EPA, 2000, "Part II, Environmental Protection Agency, 40 CFR Parts 9, 141, and 142, National Primary Drinking Water Regulations; Radionuclides; Final Rule," Federal Register, Vol. 65, No. 236, pp. 76708–76753, December 7, <http://www.epa.gov/fedrgstr/EPA-GENERAL/2000/December/Day-07/g30421.pdf>.

EPA, 2002, *Onsite Wastewater Treatment Systems Manual*, U.S. Environmental Protection Agency, EPA/625/R-00/008, February.

EPA, 2005, *Landfill Gas Emissions (LandGEM) Version 3.02 User's Guide*, U.S. Environmental Protection Agency, EPA-600/R-05/47, May.

Erie, L.J., O.F. French, D.A. Bucks, and K. Harris, 1982, *Consumptive Use of Water by Major Crops in the Southwestern United States*, U.S. Department of Agriculture, Agricultural Research Service, Conservation Research Report Number 29, 40 p.

Fitzner, R.E., K.A. Gano, W.H. Rickard and L.E. Rogers, 1979, *Characterization of the Hanford 300 Area Burial Grounds, Task IV—Biological Transport*, Pacific Northwest Laboratory Report PNL-2774.

Foxx, T.S., G.D. Tierney, and J.M. Williams, 1984, *Rooting Depths of Plants on Low-Level Waste Disposal Sites*, Los Alamos National Laboratory Report LA-10253-MS, November.

Gallegos, A.F., 1999, *Surface Erosion Study of Several TRU Mixed Waste Pits at MDA G at LANL*, Los Alamos National Laboratory.

Gano, K.A., and J.B. States, 1982, *Habitat Requirements and Burrowing Depths of Rodents in Relation to Shallow Waste Burial Sites*," Pacific Northwest Laboratory Report PNL-4140, May.

GoldSim, 2007a, *User's Guide—GoldSim Probabilistic Simulation Environment,Volume 1 of 2, Version 9.60*, GoldSim Technology Group, March.

GoldSim, 2007b, *User's Guide—GoldSim Probabilistic Simulation Environment,Volume 2 of 2, Version 9.60*, GoldSim Technology Group, March.

GoldSim, 2007c, *User's Guide—GoldSim Contaminant Transport Module, Version 4.20*, GoldSim Technology Group, March.

Gonzales, G.J., M.T. Saladen, T.E. Hakonson, 1995, "Effects of Pocket Gopher Burrowing on Cesium-133 Distribution on Engineered Test Plots," *J. of Env. Qual.*, Vol. 24, pp. 1,056–1,062.

Gonzales, G.J., R.L. Budd, P.R. Fresquez, and R.J. Wechsler, 2000, *Source Document: The Relationship Between Pocket Gophers (Thomomys bottae) and the Distribution of Buried Radioactive Waste at the Los Alamos National Laboratory*, Los Alamos National Laboratory Report LA-13719-MS, July.

Goodwin, J.G., Jr., and C.R. Hungerford, 1979, *Rodent Population Densities and Food Habits in Arizona Ponderosa Pine Forests*, USDA, For. Serv., Rocky Mtn. For. and Range Exp. Sta. Res. Pap. RM-214.

Gordon, D.M., 1991, "Behavioral Flexibility and the Foraging Ecology of Seed-Eating Ants," *Am. Nat.*, Vol. 138, pp. 379–411.

Grant, W.E., 1972, *Small Mammal Studies on the Pawnee Site During the 1971 Field Season*, U.S. IBP Grassland Biome Tech. Rep., Colorado State Univ., Fort Collins.

Gray, J.A., Jr., 1943, "Rodent Populations in the Sagebrush Desert of the Yakima Valley, Washington," *J. Mamm.*, Vol. 24, pp. 191–193.

Green, N. and N.J. Dodd, 1988, "The Uptake of Radionuclides from Inadvertent Consumption of Soil by Grazing Animals," *Sci. Total Environ.*, Vol. 69, pp. 367–377.

Grier, C.C., K.J. Elliott, and D.G. McCullough, 1992, "Biomass Distribution and Productivity of *Pinus edulis–Juniperus monosperma* Woodlands of North-Central Arizona," *Forest Ecology and Management*, Vol. 50, pp. 331–350.

Grove Engineering, 1996, *MICROSHIELD Version 5 User's Manual*, October 1996.

Haagenstad, M.P., 2002, "Stochastic Groundwater Flow and Transport Models Using GoldSim; A Thesis," New Mexico Highlands University Research Publication, Las Vegas, New Mexico.

Hakonson, T.E., 2002, *Review of Sandia National Laboratories/New Mexico Evapotranspiration Cap Closure Plans for the Mixed Waste Landfill*, Environmental Evaluation Services, February.

Hakonson, T.E., J.L. Martinez, and G.C. White, 1982, "Disturbance of a Low-Level Waste Burial Site Cover by Pocket Gophers," *Health Physics*, Vol. 42, No. 6, pp. 871–873.

Hall, E.R., 1928, "Notes of the Life History of the Sagebrush Meadow Mouse (*Lagurus*)," *J. Mammal.*, Vol. 9, pp. 201–204.

Hall, E.R., 1946, *Mammals of Nevada*, Univ. California Press, Berkeley.

Hansen, C.M. and E. D. Fleharty, 1974, "Structural Ecological Parameters of a Population of *Peromyscus maniculatus* in West-Central Kansas," *Southwestern Natur.*, Vol. 19, pp. 293–303.

Harris, J.J., D.K. Lunt, S.B. Smith, W.L. Mies, D.S. Hale, M. Koohmaraie, and J.W. Savell, 1997, "Live Animal Performance, Carcass Traits, and Meat Palatability of Calf- and Yearling-Fed Cloned Steers," *J. Anim. Sci.*, Vol. 75, pp. 986–992.

Haufler, J.B., and J.G. Nagy, 1984, "Summer Food Habits of a Small Mammal Community in the Piñon-Juniper Ecosystem," *Great Basin Naturalist*, Vol. 44, No. 1, pp. 145–150.

Hawley, J.K., 1985, "Assessment of Health Risk from Exposure to Contaminated Soil," *Risk Analysis*, Vol. 5, pp. 289–302.

Healy, W.B., 1968, "Ingestion of Soil by Dairy Cows," *N. Z. J. Agric. Res.*, Vol. 11, pp. 487–499.

Hinesley, L.E., L.E. Nelson, and G.L. Switzer, 1991, "Weight and Nutrient Content of Litter During Secondary Succession on Well-Drained Uplands of the East Gulf Coastal Plain in Mississippi," *Can. J. For. Res.*, Vol. 21, pp. 848–857.

Hinton, T.G., 1992, "Contamination of Plants by Resuspension: A Review, with Critique of Measurement Methods," *The Science of the Total Environment*, Vol. 121, pp. 177–193.

Hinton, T.G., 1994, "Sensitivity Analysis of ECOSYS-87: An Emphasis on the Ingestion Pathway as a Function of Radionuclide and Type of Deposition," *Health Physics*, Vol. 66, No. 5, pp. 513–531.

Hinton, T.G., J.M. Stoll, and L. Tobler, 1995, "Soil Contamination of Plant Surfaces from Grazing and Rainfall Interactions," *J. Environ. Radioactivity*, Vol. 29, No. 1, pp. 11–26.

Hoffman, F.O., 1979, "The Coefficient for the Transfer of Radionuclides from Animal Intake to Milk, F_M," in *A Statistical Analysis of Selected Parameters for Prediction of Food Chain Transport and Internal Dose of Radionuclides*, F.O. Hoffman and C.F. Baes, eds., NUREG/CR-1004.

Hoffman, F. O. and C. F. Baes, III (eds.), 1979, *A Statistical Analysis of Selected Parameters for Predicting Food Chain Transport and Internal Dose of Radionuclides, Final Report*, Oak Ridge National Laboratory Report ORNL/NUREG/TM-282.

Hoffmeister, D.F., 1986, *Mammals of Arizona*, University of Arizona Press, Tucson.

Hollis, D., E. Vold, R. Shuman, K. Birdsell, K. Bower, W. Hansen, D. Krier, P. Longmire, B. Newman, D. Rogers, E. Springer, 1997, *Performance Assessment and Composite Analysis for the Los Alamos National Laboratory Disposal Area G*, Los Alamos National Laboratory Report LA-UR-97-85, Report-54G-013, March.

IAEA, 1994, *Handbook of Parameter Values for the Prediction of Radionuclide Transfer in Temperate Environments*, International Atomic Energy Agency, Technical Report Series No. 364, Vienna, Austria.

ICRP, 1975, *Report of the Task Group on Reference Man*, International Commission on Radiation Protection Publication 23.

ICRP, 1994, *Human Respiratory Tract Model for Radiological Protection*, International Commission on Radiation Protection Publication 66.

INEEL, 1994, *Radioactive Waste Management Complex Low-Level Waste Radiological Performance Assessment*, Idaho National Engineering and Environmental Laboratory Report EGG-WM-8773, May.

Ingles, L.D., 1941, "Natural History of the Audubon Cottontail," *J. Mammal.*, Vol. 22, No. 3, pp. 227–250.

Jackson, R.B., J. Canadell, J.R. Ehleringer, H.A. Mooney, O.E. Sala, and E.D. Schulze, 1996, "A Global Analysis of Root Distributions for Terrestrial Biomes," *Oecologia*, Vol. 108, pp. 389–411.

Jackson, R.B., L.A. Moore, W.A. Hoffmann, W.T. Pockman, and C.R. Linder, 1999, "Ecosystem Rooting Depth Determined with Caves and DNA," *Proc. Nat. Acad. Sci.*, Vol. 96, pp. 11,387–11,392.

Jacobson, K.W., 2005, *Air Dispersion Analysis for Los Alamos National Laboratory Technical Area 54, Material Disposal Area G*, Los Alamos National Laboratory Report LA-UR-05-7232, September.

James, W.B. and E.S. Booth, 1952, "Biology and Life History of the Sagebrush Vole," Walla Walla College Publ., *Dept. Biol. Sci*., Vol. 1, pp. 23–43.

Jensen, L. and C.C. Shock, 2001 Strategies for Reducing Irrigation Water Use, Oregon State University Extension, Corvallis OR, EM8783 <http://eesc.orst.edu/agcomwebfile/EdMat /html /EM/EM8783/em8783.html>.

Jensen, P. and M.M. Hooten, 2000, *Burrowing Depths of Ant Species of the Transition Desert and Piñon-Juniper Plant Communities of the Nevada Test Site*, Neptune and Co., Inc. Document No. 05100-02.

Johnson, K., 1981, "Social Organization in a Colony of Rock Squirrels (*Spermophilus variegatus*, Sciuridae)," *Southwestern Nat.*, Vol. 26, pp. 237–242.

Johnson, et al., 1938, "The Influence of the Harvester Ant *(Pogomyrmex occidentalis* Cress), upon Range Vegetation," Unpub. Rep. Squaw Butte Oregon Agr. Exp. Sta.

Juelson, T.C., 1970, "A Study of the Ecology and Ethology of the Rock Squirrel *Spemophilus variegatus* (Erxleben) in Northern Utah," unpublished Ph.D. dissertation, Univ. Utah, Salt Lake City.

KAPL, 2002, *Nuclides and Isotopes, Chart of the Nuclides, 16th Edition*, Knolls Atomic Power Laboratory, Baum, E.M., H.D. Knox, and T.R. Miller, eds.

Kawamichi, 1989, "Nest Structure Dynamics and Seasonal Use of Nests by Siberian Chipmunks (*Eutamias sibiricus*)," *J. Mammal.*, Vol. 70, No. 1, pp. 44–57.

Keeler, K.H., 1993, "Fifteen Years of Colony Dynamics in *Pogonomyrmex Occidentialis*: The Western Harvester Ant, in Western Nebraska," *The Southwestern Naturalist*, Vol. 38, No. 3, pp. 286–289.

Koniak, S., 1985, "Succession in Piñon-Juniper Woodlands Following Wildfire in the Great Basin," *Great Basin Naturalist*, Vol. 45, No. 3, pp. 556–566.

Koontz, M.D., and H.E. Rector, 1995, *Estimation of Distributions for Residential Air Exchange Rates*, U.S. Environmental Protection Agency Contract No. 68-D9-0166, Work Assignment No. 3-19, U.S. Environmental Protection Agency, Office of Pollution Prevention and Toxics, Washington, D.C.

Koopman, 1965, Memorandum from F.C. Koopman, US Dept of the Interior Geological Survey, to Salvatore E. Russo, Engineering 3, LASL, June 30.

Kopp, B., 1991, Personal communication between B. Kopp, Los Alamos National Laboratory, and R. Shuman, Rogers and Associates Engineering Corporation.

Koukoura, Z., A.P. Mamolos, and K.L. Kalburtji, 2003, "Decomposition of Dominant Plant Species Litter in a Semiarid Grassland," *Applied Soil Ecology*, Vol. 23, pp. 13–23.

Krablin, R., 1989, Personal communication with Jonathan Z. Cannon concerning soil ingestion rates, Denver, CO, Arco Coal Co, October 13.

Kretzer, J.E. and J.F. Cully, Jr., 2001, "Prairie Dog Effects on Harvester Ant Species Diversity and Density," *J. Range Manage.*, Vol. 54, pp. 11–14.

Krier, D., P.A. Longmire, R.H. Gilkeson, and H.J. Turin, 1997, *Geologic, Geohydrologic, and Geochemical Data Summary of Material Disposal Area G, Technical Area 54, Los Alamos National Laboratory*, Los Alamos National Laboratory Report LA-UR-95-2696, February.

Kwicklis, E., M. Witkowski, K. Birdsell, B. Newman, and D. Walther, 2005, "Development of an Infiltration Map for the Los Alamos Area, New Mexico," *Vadose Zone Journal*, Vol. 4, pp. 672–693).

LANL, 1975, Memorandum "Solid Radioactive Waste Disposal Guidelines" from L.J. Johnson, H8-WM-461 at LASL, to Distribution. April 24.

LANL, 1998, *Material Disposal Unit Design, Construction, Use, and Closure*, Los Alamos National Laboratory Report, Draft DOP-54G-013, Rev. 1, August.

LANL, 2003, *Performance Assessment and Composite Analysis Maintenance Program Plan for MDA G—2003*, Los Alamos National Laboratory Report LA-UR-03-3472.

Lavigne, R.J, 1969, "Bionomics and Nest Structure of *Pogonomyrmex occidentalis* (Hymenoptera: Formicidae)," *Ann. Ent. Soc. Am.*, Vol. 62, pp. 1,166–1,175.

Lei, S.A., 2000, "Ecological Impacts of Seed Harvester Ants on Soil Attributes in a *Larrea*-Dominated Shrubland," *Western North Am. Nat.*, Vol. 60, No. 4, pp. 439–444.

Lerner, B.R. and M.N. Dana, 2001, *Leafy Greens for the Home Garden*, Purdue University Cooperative Extension Service, HO-29-W, April.

Levitt, D.G., 2008, Modeling of an Evapotranspiration Cover for the Groundwater Pathway at Los Alamos National Laboratory Technical Area 54, Area G, Los Alamos National Laboratory Report LA-UR-08-5468.

Little, C.A., 1979, "The Coefficient for the Transfer of Radionuclides from Animal Intake to Meat, F_f," In *A Statistical Analysis of Selected Parameters for Predicting Food Chain Transport and Internal Dose of Radionuclides*, Hoffman, F.O. and C.F. Baes, III, eds., Oak Ridge National Laboratory Report ORNL/NUREG/TM-282.

Livens, F.R. and M.S. Baxter, 1988, "Particle Size and Radionuclide Levels in Some West Cumbrian Soils," *Sci. Tot. Environ.*, Vol. 70, pp. 1–17.

Loaiza, D. and E. Vold, 1995, *Moisture Profiles Measured in Subsurface Monitor Holes at the Los Alamos LLRW Disposal Site*, Los Alamos National Laboratory Report LA-UR-95-1922.

Lobry de Bruyn, L.A., 1999, "Ants as Bioindicators of Soil Function in Rural Environments," *Agriculture, Ecosystems and Environment*, Vol. 74, pp. 425–441.

Longmire, P., C.R. Cotter, I.R. Triay, J.J. Kitten, C. Hall, J. Bentley, D. Hollis, and A.I. Adams, 1996, *Batch Sorption Results for Americium, Neptunium, Plutonium, Technetium, and Uranium Transport through the Bandelier Tuff, Los Alamos, New Mexico*, Los Alamos National Laboratory Report LA-UR-96-4716.

LSU, 2003, *Louisiana Vegetable Planting Guide*, Louisiana State University Agricultural Center, Publication 1980, April.

Ludwig, J.L., W.G. Whitford, A.B. Rodney, and R.E. Grieve, 1977, "An Evaluation of Transmission Line Construction on Piñon-Juniper Wood-Land and Grassland Communities in New Mexico," *J. Environ. Manage.*, Vol. 5, pp. 127–137.

Lyons, R.K., R. Machen, and T.D.A. Forbes, 1999, *Understanding Forage Intake in Range Animals*, Texas Agricultural Extension Service publication L-5152, January 1999.

Mack, R.N., 1977, "Mineral Return via the Litter of *Artemisia tridentata*," *American Midland Naturalist*, Vol. 97, pp. 189–197.

MacMahon, J.A., 1985, *The Audubon Society Nature Guides: Deserts*, Alfred A. Knopf, New York.

MAFES, 1999, *Impact of Imported Fire Ants on Mississippi*, Mississippi Agricultural and Forestry Experiment Station, Technical Bulletin 223, May.

Malmon, D.V., S.L. Reneau, T. Dunne, D. Katzman, and P.G. Drakos, 2005, "Influence of Sediment Storage on Downstream Delivery of Contaminated Sediment," *Water Resour. Res*., Vol. 41, W05008.

Mandel, R.D. and C.J. Sorenson, 1982, "The Role of the Western Harvester Ant (*Pogonomyrmex occidentalis*) in Soil Formation," *Soil Sci. Soc. Am. J*., Vol. 46, pp. 785–788.

Marrero, T.R. and E.A. Mason, 1972,"Gaseous Diffusion Coefficients," *J. Phys. Chem. Ref. Data*, Vol. 1, pp. 3–118.

Martin, E.C., 2000, *Determining the Amount of Irrigation Water Applied to a Field*, Univ of Arizona, Cooperative Extension, Arizona Water Series, No. 29, AZ1157.

Maser, C., E.W. Hammer, C. Brown, R.E. Lewis, R.L. Rausch, and M.L. Johnson., 1974, "The Sage Vole, *Lagurus curtatus* (Cope, 1868)," In Crooked River National Grassland, Jefferson County, Oregon: A Contribution to its Life History and Ecology, *Saugetierk. Mitt.*, Vol. 22, pp. 193–222.

May, S.G., W.L. Mies, J.W. Edwards, J.J. Harris, J.B. Morgan, R.P. Garrett, F.L. Williams, J.W. Wise, H.R. Cross, and J.W. Savell, 2000, "Using Live Estimates and Ultrasound Measurements to Predict Beef Carcass Cutability," *J. Anim. Sci.*, Vol. 78, pp. 1,255–1,261.

Mayer, P.W., W.B. DeOreo, E.M. Opitz, J.C. Kiefer, W.Y. Davis, B. Dziegielewski, and J.O. Nelson., 1999, *Residential End Uses of Water*, Report to AWWA Research Foundation and American Water Works Association (AWWA), Denver, CO.

Mayland, H.F., G.E. Shewmaker, and R.C. Bull, 1977, "Soil Ingestion by Cattle Grazing Crested Wheatgrass," *J. of Range Manage.*, Vol. 30, pp. 264–265.

McKenzie, D.H., L.L. Cadwell, L.E. Eberhardt, W.E. Kennedy, Jr., R.A. Peloquin, and M.A. Simmons, M.A., 1982, *Relevance of Biotic Pathways to the Long-Term Regulation of Nuclear Waste Disposal*, prepared by Pacific Northwest Laboratory for the U.S. Nuclear Regulatory Commission, NUREG/CR-2675, Volume 2, October.

McKone, T.E. and P.B. Ryan, 1989, "Human Exposures to Chemicals through Food Chains: An Uncertainty Analysis," *Environ. Sci. Technol.*, Vol. 23, pp. 1,154–1,163.

McLeod, K.W., J.J. Alberts, D.C. Adriano, and J.E. Pinder III, 1984a, "Plutonium Contents of Broadleaf Vegetable Crops Grown Near a Nuclear Fuel Chemical Separations Facility," *Health Phys.*, Vol. 46, pp. 261–267.

McLeod, K.W., J.E. Pinder III, and J.R. Watts, Jr., 1984b, "Contribution of a Nuclear Fuel Chemical Separations Facility to the Plutonium Content of a Tobacco Crop," *Health Phys.*, Vol. 46, pp. 1,205–1,211.

Meeuwig, R.O., 1979, *Growth Characteristics of Piñon-Juniper Stands in the Western Great Basin*, U.S. Dept. Agriculture Forest Service Paper INT-238.

Merritt, J.F., 1974, "Factors Influencing the Local Distribution of *Peromyscus californicus* in Northern California," *J. Mammal.*, Vol. 55, pp. 102–114.

Meserve, P.L., 1977, "Three-Dimensional Home Ranges of Cricetid Rodents," *J. Mammal.*, Vol. 58, pp. 549–558.

Mielke, H.W., 1977, "Mound Building by Pocket Gophers (Geomyidae): Their Impact on Soils and Vegetation in North America," *J. of Biogeography*, Vol. 4, pp. 171–180.

Millar, C.S., 1974, "Decomposition of Coniferous Leaf Litter," In *Biology of Plant Litter Decomposition, Volume II*, Dickinson, C.H. and G.J.F. Pugh, eds., Academic Press, London.

Miller, C.W., 1980, "An Analysis of Measured Values for the Fraction of a Radioactive Aerosol Intercepted by Vegetation," *Health Physics*, Vol. 38, pp. 705–712.

Miller, C.W. and F.O. Hoffman, 1982, "An Analysis of Reported Values of the Environmental Half-Times for Radionuclides Deposited on the Surfaces of Vegetation," in *Environmental Migration of Long-Lived Radionuclides*, International Atomic Energy Agency, IAEA-STI/PUB/597.

Miller, M.A. 1957, "Burrows of the Sacramento Valley Pocket Gopher in Flood-Irrigated Alfalfa Fields," *Hilgardia*, Vol. 26, pp. 431–452.

Miller, R.F. and R.J. Tausch, 2001, *The Role of Fire in Juniper and Piñon Woodlands: A Descriptive Analysis*, Tall Timbers Research Station Miscellaneous Publication No. 11, pp. 15–30.

Millington, R.J., 1959, "Gas Diffusion in Porous Media," *Science*, Vol. 130, pp.100–102.

Mitchell, R.S., 1972, *Small Rodents of the Flood Plain of the South Platte River at the Proposed Narrows Reservoir Site*, M.A. thesis, Univ. Northern Colorado, Greeley.

Murphy, K.L., J.M. Klopatek, and C.C. Klopatek, 1998, "The Effects of Litter Quality and Climate on Decomposition along an Elevational Gradient," *Ecological Applications*, Vol. 8, No. 4, pp. 1,061–1,071.

Murray, D.M. and D.E. Burmaster, 1995, "Residential Air Exchange Rates in the United States: Empirical and Estimated Parametric Distribution by Season and Climatic Region," *Risk Analysis*, Vol. 15, No. 4, pp. 459–465.

Myers, S., 2004, E-mail from Steve Myers, LANL Nuclear Waste and Infrastructure Services — Solid Waste Operations, to Rob Shuman, URS Corporation, regarding measurement errors, June 15.

Napier, B.A., R.A. Peloquin, D. L. Strenge, and J. V. Ramsdell, 1988, *GENII—The Hanford Environmental Radiation Dosimetry Software System*, Pacific Northwest Laboratory Report PNL-6584.

Napier, B.A., D.L. Strenge, J.V. Ramsdell, Jr., P.W. Eslinger, and C.J. Fosmire, 2004, GENII Version 2 Software Design Document, PNNL-14584, Pacific Northwest National Laboratory.

Nazaroff, W.W., B.A. Moed, and R.G. Sextro, 1988, "Radon Entry via Potable Water," In *Radon and Its Decay Products in Indoor Air*, Nazaroff, W.W. and A.V. Nero, eds., John Wiley and Sons, NY. pp. 131–157.

NCRP, 1984, *Radiological Assessment: Predicting the Transport, Bioaccumulation, and Uptake by Man of Radionuclides Released to the Environment*, National Council on Radiation Protection and Measurements, Report No. 76, March.

NCRP, 1999, *Recommended Screening Limits for Contaminated Surface Soil and Review of Factors Relevant to Site-Specific Studies*, National Council on Radiation Protection and Measurements, Report No. 129.

Newman, B.D., 2005, Personal communication from B. Newman, Los Alamos National Laboratory, to R. Shuman, URS Corporation, May, 6.

Newman, B.D., M. Gard, D. Counce, E. Kluk, L. Martinez, D. Newell, J. Salazar, 2005, *Spatial Variation in Near-Surface Hydrologic Behavior at Los Alamos National Laboratory Technical Area 54, Material Disposal Area G*, Los Alamos National Laboratory Report LA-UR-05-6898, September.

Ng, Y.C., W.D. Phillips, Y.E. Ricker, and R.K. Tandy, 1978, *Methodology for Assessing Dose Commitment to Individuals and to the Population from Ingestion of Terrestrial Foods Contaminated by Emissions from a Nuclear Fuel Reprocessing Plant at the Savannah River Plant*, Lawrence Livermore Laboratory, UCID-17743, March.

Ng, Y.C., C. Colsher, and S.E. Thompson, 1982, *Transfer Coefficients for Assessing Dose from Radionuclides in Meat and Eggs*, U.S. Nuclear Regulatory Commission, NUREG/CR-2976.

Nielson, K.K., V.C. Rogers, R.B. Holt, T.D. Pugh, W.A. Grondzik, and R.J. de Meijer, 1997, "Radon Penetration of Concrete Slab Cracks, Joints, Pipe Penetrations, and Sealants," *Health Physics*, Vol. 73, pp. 668–678.

Nowak, R.M., 2003, *Walker's Mammals of the World Online*, Johns Hopkins University Press, Baltimore.

NRC, 1977, *Regulatory Guide 1.109, Calculation of Annual Doses to Man from Routine Release of Effluents for the Purpose of Evaluating Compliance with 10 CRR Part 50, Appendix I*, U.S. Nuclear Regulatory Commission, Revision 1, October.

NRC, 1986, *Update of Part 61 Impacts Analysis Methodology, Methodology Report*, U.S. Nuclear Regulatory Commission, NUREG/CR-4370, Vol. 1, January.

NRC, 1989, *Regulatory Guide 3.64, Calculation of Radon Flux Attenuation by Earthen Uranium Mill Tailings Covers*, U.S. Nuclear Regulatory Commission, June.

NRC, 1992, *Residual Radioactive Contamination from Decommissioning—Technical Basis for Translating Contamination Levels to Annual Total Effective Dose Equivalent: Final Report*, prepared by Pacific Northwest Laboratory for the U.S. Nuclear Regulatory Commission, NUREG/CR-5512, October.

NRC, 1994, *Nutrient Requirements of Poultry*, Eighth Revised Edition, National Research Council, National Academy Press, Washington, D.C.

NTS, 1995, *Cost/Risk/Benefit Analysis of Alternative Cleanup Requirements for Plutonium-Contaminated Soils on and near the Nevada Test Site*, DOE/NV-399, May.

Nyhan, J.W., F.R. Miera, and R.J. Peters, R. J 1976a, "Distribution of Plutonium in Soil Particle Size Fractions of Liquid Effluent-Receiving Areas at Los Alamos," *J. Environ. Qual.*, Vol. 5, No. 1, pp. 50–56.

Nyhan, J.W., F.R. Micra, Jr., and R.E. Neher., 1976b, "Distribution of Plutonium in Trinity Soils after 28 Years," *J. Environ. Qual.*, Vol. 5, No. 1, pp. 431–437.

Nylander, C.L, K.A. Bitner, G. Cole, E.H. Keating, S. Kinkead, P. Longmire, B. Robinson, D.B. Rogers, and D. Vaniman, 2003, *Groundwater Annual Status Report for Fiscal Year 2002*, Los Alamos National Laboratory Report LA-UR-03-0244.

O'Rourke, J.T. and P.R. Ogden, 1969, "Vegetative Response Following Piñon-Juniper Control in Arizona," *J. Range Manage.*, Vol. 22, No. 6, pp. 416–418.

Oaks, E.C., P.J. Young, and G.L. Kirkland, Jr., 1987, "Mammalian Species—*Spermophilus variegatus*," *The Society of Mammalogists* No. 272, February.

Opseth, D.A., 1998, *Landfill Gas Generation at a Semi-Arid Landfill*, Thesis, University of Regina, Regina, Saskatchewan, Canada, December.

ORNL, 1999, *Guidance for Conducting Risk Assessments and Related Risk Activities for the DOE-ORO Environmental Management Program*, Oak Ridge National Laboratory, BJC/OR-271, April.

Orr, R.T., 1940, "The Rabbits of California," *Occas. Papers California Acad. Sci.,* Vol. 17, pp. 1–227.

Oughton, D.H., 1990, "Radiocesium Association with Soil Components: The Application of a Sequential Extraction Technique," In *International Union of Radioecologists VIIth Report of the Working Group Soil-to-Plant Transfer Factors*, M.J. Frissel ed., Uppsala, Sweden, September.

Padien, D.J. and K. Lajtha, 1992, "Plant Spatial Pattern and Nutrient Distribution in Piñon-Juniper Woodlands along an Elevational Gradient in Northern New Mexico," *Int. J. Plant Sci*., Vol. 153, No. 3, pp. 425–433.

Parmenter, R.R., M.R. Mesch, and J.A. Macmahon, 1987, "Shrub Litter Production in a Sagebrush-Steppe Ecosystem: Rodent Population Cycles as a Regulating Factor," *J. Range Manage.*, Vol. 40, No. 1, pp. 50–54.

Peters, D.P.C., W.K. Lauenroth, and I.C. Burke, 2002, "The Role of Disturbances in Shortgrass Steppe Community and Ecosystem Dynamics," In *Ecology of the Shortgrass Steppe: Perspectives from Long-Term Research*, Lauenroth, W.K. and I.C. Burke, eds., Oxford Press, in press.

Peterson, J.T., Jr., 1983, "Terrestrial and Aquatic Food Chain Pathways," in *Radiological Risk Assessment, A Textbook on Environmental Dose Analysis*, Till, J.E. and H.R. Meyer, eds., NUREG/CR-3332.

Philip, J.R. and D.A. DeVries, 1957, "Moisture Movement in Porous Materials under Temperature Gradients," Trans., *Amer. Geophys. Union*, Vol. 38, No. 2, pp. 222–232.

Pieper, R.D., 1968, "Comparison of Vegetation on Grazed and Ungrazed Piñon-Juniper Grassland Sites in Southcentral New Mexico," *J. Range Manage.*, Vol. 21, pp.51–53.

Pieper, R.D., 1990, "Overstory-Understory Relations in Piñon-Juniper Woodlands in New Mexico," *J. Range Manage.*, Vol. 43, No. 5, pp. 413–415.

Pinder, J.E., III, T.G. Ciravolo, and J.W. Bowling, 1988, "The Interrelationships Among Plant Biomass, Plant Surface Area and the Interception of Particulate Deposition by Grasses," *Health Physics*, Vol. 55, No. 1, pp. 51–58.

Pinder, J.E., and K.W. McLeod, 1989, Mass Loading of Soil Particles on Plant Surfaces," *Health Physics*, Vol. 57, No. 6, pp. 935–942.

Pinder, J.E., III, K.W. McLeod, R.F. Lide, and K.C. Sherrod, 1991, "Mass Loading of Soil Particles on a Pasture Grass," *J. Environ. Radioactivity*, Vol. 13, pp. 341–354.

Pollard, C.G. and R. Shuman, 1999, *Evaluation of Pre-1971 Radioactive Waste Disposal Data for TA-54 MDA G*, Rogers and Associates Engineering Corporation Report RAE-9629/3005-3, December.

Polzer, W.L., et al., 1985, *Equilibrium Sorption of Cobalt, Cesium, and Strontium on Bandelier Tuff: Analysis of Alternative Mathematical Modeling*, Los Alamos National Laboratory Report LA-UR-85-785.

Porter, S.D. and C.D. Jorgensen, 1988, "Longevity of Harvester Ant Colonies in Southern Idaho," *J. Range Manage.*, Vol. 41, No. 2, pp. 104–107.

Pratt, M. and G.A. Rasmussen, 2001, *Determining Your Stocking Rate*, Utah State University Extension Range Management Fact Sheet NR/RM/04, May.

RAC, 1999, *Final Report, Task 3: Inputs and Assumptions, Radionuclide Soil Action Level Oversight Panel*, Risk Assessment Corporation, RAC Report No. 15-RSALOP-RFSAL-1999-FINAL, October.

Radian, 1995, *Air Quality Impacts Analysis for Area G*, Final Report 4/4 from Radian to CST-14, Los Alamos National Laboratory under DOE subcontract 6345L0013-31.

RAE, 1998, *User's Guide for PRESTO-EPA-CLNCPG/CLNPOP Operation System*, Rogers and Associates Engineering Corporation report RAE-9535/14-1, September.

Reneau, S., 2005, Personal communication (e-mail) from Steven Reneau, Los Alamos National Laboratory, to Rob Shuman, URS Corporation, September 16.

Reynolds, T.D. and J.W. Laundre, 1988, "Vertical Distribution of Soil Removed by Four Species of Burrowing Rodents in Disturbed and Undisturbed Soils," *Health Physics*, Vol. 54, No. 4, pp. 445–450.

Ricklefs, R.E., 1979, *Ecology*, Second Edition, Chiron Press, New York.

Rishel, J., S.D. Johnson, H.D. Holt, and W.A. Olsen, 2003, *Meteorological Monitoring at Los Alamos*, Los Alamos National Laboratory Report LA-UR-03-8097.

Rodin, L.E. and N.I. Bazilevich, 1967, *Production and Mineral Cycling in Terrestrial Vegetation*, English Translation, G.E. Fogg, ed., Oliver and Boyd, Edinburgh, Scotland and London, England.,

Rogers, D.B. and B.M. Gallaher, 1995, *The Unsaturated Hydraulic Characteristics of the Bandelier Tuff*, Los Alamos National Laboratory Report LA-12968-MS, September.

Rogers, L.E. and R.J. Lavigne, 1974, "Environmental Effects of Western Harvester Ants on the Shortgrass Plains Ecosystem," *Environmental Entomology*, Vol. 3, No. 6, pp. 994–997.

Rogers, V.C., K.K. Nielson, and D.R. Kalkwarf, 1984, *Radon Attenuation Handbook for Uranium Mill Tailings Cover Design*, U.R. Nuclear Regulatory Commission Report NUREG/CR-3533, April.

Rogers, V.C. and K.K. Nielson, 1991, Correlations for Predicting Air Permeabilities and 222Rn Diffusion Coefficients of Soils, *Health Physics*, Vol. 61, No. 2, pp. 225–230.

Rogers, V.C., K.K. Nielson, R.B. Holt, and R. Snoddy., 1994, "Radon Diffusion Coefficients for Residential Concretes," *Health Physics*, Vol. 67, No. 3, pp. 261–265.

Rogers, V.C., K.K. Nielson, and R.B. Holt, 1995, "Radon Diffusion Coefficients for Aged Residential Concretes," *Health Physics*, Vol. 68, No. 6, pp. 832–834.

Rongstad, O.J., 1965, "A Life History Study of Thirteen-Lined Ground Squirrels in Southern Wisconsin," *J. Mamm.*, Vol. 46, pp. 76–87.

Rosenberg, D.K. and R.G. Anthony, 1993, "Differences in Townsend's Chipmunk Populations Between Second- and Old-Growth Forest in Western Oregon," *J. Wildlife Manage.*, Vol. 57, No. 2, pp. 365–373.

Rupp, E.M., 1980, "Age Dependent Values of Dietary Intake for Assessing Human Exposures to Environmental Pollutants," *Health Physics*, Vol. 39, pp. 151.

Sander, R., 1999, "Compilation of Henry's Law Constants for Inorganic and Organic Species of Potential Importance in Environmental Chemistry," Air Chemistry Department Max-Planck Institute of Chemistry, Version 3 <http://www.mpch-mainz.mpg.de/~sander/res/henry.html> (April 8, 1999).

Schack-Kirchner, H., T.V. Gaertig, K. Wilpert, and E.E. Hildebrand, 2001, "A Modified McIntyre and Phillip Approach to Measure Top Soil Gas Diffusivity in International Telecommunication Union," *J. Plant Nutr. Soil Sci.*, Vol. 164, pp. 253–258.

Schott, M.R. and R.D. Pieper, 1987, "Succession of Piñon-Juniper Communities after Mechanical Disturbance in Southcentral New Mexico," *J. Range Manage.*, Vol. 40, No. 1, pp. 88–94.

Scire, J.S., D. G. Stimanitis., and R.J. Yamartino, 2000a, *A Users Guide for the CALPUFF Dispersion Mode (Version 5)*, Earth Tech. Inc., Concord, Massachusetts, January.

Scire, J.S., F.R. Robe, M.E. Fernau and R.J. Yamartino, 2000b, *A User's Guide for the CALMET Meteorological Model (Version 5)*, Earth Tech, Inc., Concord, Massachusetts.

Scott, H.W., 1951, "The Geological Work of the Mound-Building Ants in Western United States," *J. Geol.*, Vol. 59, pp. 173–175.

Scurlock, J.M.O., K.R. Johnson, and R.J. Olson, 2003, *NPP Grassland: NPP Estimates from Biomass Dynamics for 31 Sites, 1948-1994*, Dataset available on-line [http://www.daac.ornl.gov] from Oak Ridge National Laboratory Distributed Active Archive Center, Oak Ridge, TN.

Severson, K.E., 1986, "Small Mammals in Modified Piñon-Juniper Woodlands, New Mexico," *J. Range Manage.*, Vol. 39, No. 1, pp. 31–34.

Shan, C. and D. Stephens, 1995, "An Analytical Solution for Vertical Transport of Volatile Chemicals in the Vadose Zone," *J. Contaminant Hydrology*, Vol. 18, pp. 259–277.

Shariff, A.R., M.E. Biondini, and C.E. Grygiel, 1994, "Grazing Intensity Effects on Litter Decomposition and Soil Nitrogen Mineralization," *J. Range Manage.*, Vol. 47, No. 6, pp. 444–449.

Sharp, L.E., and W.F. Barr, 1960, "Preliminary Investigations of Harvester Ants on Southern Idaho Rangelands," *J. Range Manage.*, Vol. 13, pp. 131–134.

Sheppard, S.C. and W.G. Evenden, 1997, "Variation in Transfer Factors for Stochastic Models: Soil-to-Plant Transfer," *Health Physics*, Vol. 72, No. 5, pp. 727–733.

Shinn, J.H., 1992, "Enhancement Factors for Resuspended Aerosol Radioactivity: Effects of Topsoil Disturbance," In *Precipitation Scavenging and Atmosphere-Surface Exchange, Volume 3*, Schwartz, S.E. and W.G.N. Slinn, eds., Hemisphere Publishing Corp., Washington, Philadelphia, and London.

Shinn, J.H., 2002, *Complementary Pu Resuspension Study at Palomares, Spain*, Lawrence Livermore National Laboratory Report UCRL-ID-150980.

Shinn, J.H., D.N. Homan, and W.L. Robison, 1997, "Resuspension Studies in the Marshall Islands," *Health Physics*, Vol. 73, pp. 248–257.

Shuman, R., 1999, *An Evaluation of the Potential Impacts of Plant and Animal Intrusion into Disposed Waste at TA-54, MDA G*, Rogers and Associates Engineering Corporation, RAE-9629/3005-1, April.

Shuman, R., 2008, *Radioactive Waste Inventory for Los Alamos National Laboratory Technical Area 54, Area G*, Los Alamos National Laboratory Report LA-UR-08-06107, September.

Simon, S.L., 1998, "Soil Ingestion by Humans: A Review of History, Data, and Etiology with Application to Risk Assessment of Radioactively Contaminated Soil," *Health Physics*, Vol. 74, No. 6, pp. 647–672.

Sims, P.L. and J.S. Singh, 1978, "The Structure and Function of Ten Western North American Grasslands; IV Compartmental Transfers and Energy Flow Within the Ecosystem," *Journal of Ecology*, Vol. 66, pp. 983–1,009.

Skinner, D.J., 1982, *^{226}Ra Contamination of Soil and Foliage as a Function of Distance Downwind from Uranium Mill Tailings*, M.S. Thesis, Colorado State Univ., Fort Collins.

Skinner, J.L. and M.L. Sunde, 1983, *Raising Meat-Type Chickens*, University of Wisconsin Cooperative Extension Service publication A3225.

SLTERP, 2003, *Sevilleta Long-Term Ecological Research Program*, University of New Mexico, <http://sevilleta.unm.edu/data/species/>.

Smith, C.B. and P.J. Urness, 1984, "Small Mammal Abundance on Native and Improved Foothill Ranges, Utah," *J. Range Manage.*, Vol. 37, No. 4, pp. 353–357.

Smith, D.D., 1977, "Grazing Studies on a Contaminated Range of the Nevada Test Site," In *Environmental Plutonium on the Nevada Test Site and Environs*, ERDA Report NVO-171, Nevada Operations Office, NTIS.

Smith, R.C., 1995, *Vegetable Maturity Dates, Yields and Storage*, North Dakota State University Extension Service publication H-912, April.

Sneva, F.A., 1979, "The Western Harvester Ants: Their Density and Hill Size in Relation to Herbaceous Productivity and Big Sagebrush Cover," *J. Range Manage.*, Vol. 32, No. 1, pp. 46–47.

Soule, P.T. and P.A. Knapp, 1996, "The Influence of Vegetation Removal of by Western Harvester Ants (*Pogonomyrmex owyheei*) in a Relict Area of Sagebrush-Steppe in Central Oregon," *American Midland Naturalist*, Vol. 136, No. 2, pp. 336–345.

Spencer, S.R., G.N. Cameron, B.D. Eshelman, L.C. Cooper, and L.R. Williams, 1985, "Influence of Pocket Gopher Mounds on a Texas Coastal Prairie," *Oecologia*, Vol. 66, pp.111–115.

Springer, E.P., 2004, *Statistical Exploration of Matrix Hydrologic Properties for the Bandelier Tuff, Los Alamos, New Mexico*, Los Alamos National Laboratory Report LA-UR-04-2830.

Stauffer, P.H., H.S. Viswanathan, B.A. Robinson, C.W. Gable, G.L. Cole, D.E. Broxton, E.P. Springer, T.G. Schofield, 2005, *Groundwater Pathway Model for the Los Alamos National Laboratory Technical Area 54, Material Disposal Area G*, Los Alamos National Laboratory Report LA-UR-05-7393, September.

Storer, T.I., F.C. Evans, and F.G. Palmer, 1944, "Some Rodent Populations in the Sierra Nevada of California," *Ecol. Monogr.*, Vol. 14, pp. 166–192.

Streubel, D.P. and J.P. Fitzgerald, 1978, "Mammalian Species—*Spermophilus tridecemlineatus*," *The Society of Mammalogists* No. 103, September.

Strojan, C.L., F.B. Turner, and R. Castetter, 1979, "Litter Fall from Shrubs in the Northern Mojave Desert," *Ecology*, Vol. 60, No. 5, pp. 891–900.

Summerling, T.J., N.J. Dodd, and N. Green, 1984, "The Transfer of ^{90}Sr and ^{137}Cs to Milk in a Dairy Herd Grazing Near a Major Nuclear Installation," *Sci. Total. Environ.*, Vol. 34, pp. 57–72.

Suter, G.W., R.J. Luxmoore, and E.D. Smith, 1993, "Compacted Soil Barriers at Abandoned Landfill Sites are Likely to Fail in the Long Term," *J. Environ. Qual.*, Vol. 22, pp. 217–226.

TAMU, 2001, *Vegetable Grower's Handbook*, Web Edition, Texas A&M University, Texas Agricultural Extension Service, January, <http://aggie-horticulture.tamu.edu/extension/veghandbook/index.html>.

Thibault, D.H., M.I. Sheppard, and P.A. Smith, 1990, *A Critical Compilation and Review of Default Soil Solid/Liquid Partition Coefficients, K_d, for use in Environmental Assessments*, Atomic Energy of Canada Limited Report AECL-10125, March.

Tierney, G.D., and T.S. Foxx, 1987, *Root Lengths of Plants on Los Alamos National Laboratory Lands*," Los Alamos National Laboratory Report LA-10865-MS, January.

Tress, J.A. Jr. and J.M. Klopatek, 1987, "Successional Changes in Community Structure of Piñon-Juniper Woodlands on North-Central Arizona," in *Proceedings—Piñon-Juniper Conference*, U.S. Dept. Agriculture Forest Service, Intermountain Research Station, General Technical Report INT-215, January.

UNCE, 2001, *Understanding Beef Carcass Contest Information*, University of Nebraska Cooperative Extension, G01-1431-A.

UNSCEAR, 1993, *Sources and Effects of Ionizing Radiation*, United Nations Scientific Committee of the Effects of Atomic Radiation, report to the General Assembly, Publication E.94.IX.2.

USDA, 1995, *United States Standards, Grades, and Weight Classes for Shell Eggs*, U.S. Agriculture Department, Agricultural Marketing Service AMS-56, April.

USDA, 1999, *Farm and Ranch Irrigation Survey (1998), Volume 3*, 1997 Census of Agriculture, U.S. Department of Agriculture.

USDA, 2004a, *Agricultural Statistics 2004*, National Agricultural Statistics Service, U.S. Department of Agriculture.

USDA, 2004b, *Farm and Ranch Irrigation Survey (2003), Volume 3*, Special Studies, Part 1, 2002 Census of Agriculture, U.S. Department of Agriculture, November.

USDA, 2005a, *Livestock Slaughter*, National Agricultural Statistics Service, U.S. Department of Agriculture, May.

USDA, 2005b, *Milk Production*, National Agricultural Statistics Service, U.S. Department of Agriculture, May.

USDA, 2005c, *Chickens and Eggs—2004 Summary, February 2005*, National Agricultural Statistics Service, U.S. Department of Agriculture, Pou 2-4 (05).

Van Pelt, R.S. and T.M. Zobeck, 2005, "Chemical Constituents of Fugitive Dust," In review, *Environmental Management and Assessment.*

Veilleux, J.M., 2005, *Determination of Plutonium Mass Fractions and Uncertainties from Waste Assay Measurements*, Los Alamos National Laboratory Report LA-UR-05-8922, November.

Verner, J. and A.S. Boss, 1980, *California Wildlife and Their Habitats: Western Sierra Nevada*, Pacific Southwest Forest and Range Experimental Station, General Technical Report PSW-37, Berkeley.

Versar, 1990, *Database of Perfluorocarbon Tracer (PFT) Ventilation Measurements: Description and User's Manual*, U.S. Environmental Protection Agency Contract No. 68-02-4254, Task No. 39. Washington, D.C., U.S. Environmental Protection Agency, Office of Toxic Substances.

Wallwork-Barber, M.K. and T.E. Hakonson, 1981, *Accumulation and Retention of Soil Particles on Plants in Environmental Surveillance at Los Alamos During 1980*, Los Alamos National Laboratory Report LA-8810-ENV.

Webster, W.D. and J.K. Jones Jr., 1982, "Mammalian Species—*Reithrodontomys megalotis*," *The Society of Mammalogists* No. 167, May.

West, N.E., 1985, "Aboveground Litter Production of Three Temperate Semidesert Shrubs," *American Midland Naturalist,* Vol. 113, No. 1, pp. 158–169.

West, N.E. and C. Gunn, 1974, *Phenology, Productivity and Nutrient Dynamics of Some Cool Desert Shrubs,* U.S./ IBP Desert Biome Res. Memo. 74-7.

Wheeler, G.C. and J.N. Wheeler, 1986, *The Ants of Nevada*, Natural History Museum of Los Angeles County, Los Angeles, California.

Whicker, J.J., 2005, Personal Communication from J. Whicker, Los Alamos National Laboratory, to R. Shuman, URS Corporation, January 3.

Whicker, J.J. and D.D. Breshears, 2005, *Assessing Wind Erosion as a Contaminant Transport Mechanism for Los Alamos National Laboratory Technical Area 54, Material Disposal Area G*, Los Alamos National Laboratory Report LA-UR-05-5371, September.

Whitaker, J.O., Jr., 1980, *National Audubon Society Field Guide to North American Mammals,* Alfred A. Knopf, Inc., New York.

White, G.C., T.E. Hakonson, and A.J. Ahlquist, 1981, "Factors Affecting Radionuclide Availability to Vegetables Grown at Los Alamos," *Journal of Environmental Quality*, Vol. 10, pp. 294–299.

Whitford, W.G., 1976, "Temporal Fluctuations in Density and Diversity of Desert Rodent Populations," *J. Mamm.*, Vol. 57, pp. 351–369.

Whitford, W.G. and DiMarco, R., 1995, "Variability in Soils and Vegetation Associated with Harvester Ant (*Pogonomyrmex rugosus*) Nests in Chihuahuan Desert Watershed," *Biol. Fertility of Soils,* Vol. 20, pp.169–173.

Whittaker, R.H., 1975, *Communities and Ecosystems*, MacMillan Publishing Co., New York.

Widner, T., J. Shonka, S. Flack, J. O'Brien, R. Burns, J. Buddenbaum, D. Shonka, et al., 2004, *Draft Interim Report of the Los Alamos Historical Document Retrieval and Assessment (LAHDRA) Project*, prepared by individuals from ENSR Corporation, Shonka Research Associates, Inc., and ChemRisk, Inc. for the Centers for Disease Control and Prevention, March.

Willard, J.R. and H.H. Crowell, 1965, "Biological Activities of the Harvester Ant, *Pogonomyrmex owyheei*, in Central Oregon," *J. Econ. Entomol,* Vol. 58, pp. 484–489.

Willgoose, G.R. and S. Riley, 1998, "The Long Term Stability of Engineered Landforms of the Ranger Uranium Mine, Northern Territory, Australia: Application of a Catchment Evolution Model," *Earth Surf. Process. Landf.*, Vol. 23, No. 3, pp. 237–259.

Williams, S.T. and T.R.G. Gray, 1974, "Decomposition of Litter on the Soil Surface," In *Biology of Plant Litter Decomposition, Volume II,* Dickinson, C.H. and G.J.F. Pugh, eds., Academic Press, London.

Wilson, J.C.J., K.J. Crowell, and L.J. Lane, 2005, *Surface Erosion Modeling for the Repository Waste Cover at Los Alamos National Laboratory Technical Area 54, Material Disposal Area G*, Los Alamos National Laboratory Report LA-UR-05-7771, September.

Wirth, S., 1999, *Modeling the Potential Biological Effects on the Performance of TRU Waste Buried in GCD Boreholes at the Nevada Test Site*, IT Corporation Report, February.

Wolfsberg, K., 1980, "Sorptive Properties of Tuff and Nuclide Transport and Retardation," pp. 39–48 In *Evaluation of Tuff as a Medium for a Nuclear Waste Repository: Interim Status Report on the Properties of Tuff*, Sandia National Laboratory Report SAND80-1464, July.

Wood, M.I., R. Khaleel, P.D. Rittman, A.H. Lu, S.H. Finfrock, R.J. Serne, K.J. Cantrell, and T.H. DeLorenzo., 1994, *Performance Assessment for the Disposal of Low-Level Waste in the 200 West Area Burial Grounds*, Westinghouse Hanford Company, WHC-EP-0645, November.

WRCC, 2005, Western Regional Climate Center, Reno, NV, <www.wrcc.dri.edu>.

Yang, Y. and C.B. Nelson, 1986, "An Estimation of Daily Food Usage Factors for Assessing Radionuclide Intakes in the U.S. Population," *Health Physics*, Vol. 50, No. 2, pp. 245–257.

Yu, C., C. Loureiro, J.-J. Cheng, L.G. Jones, Y.Y. Wang, Y.P. Chia, and E. Faillace, 1993, *Data Collection Handbook to Support Modeling Impacts of Radioactive Material in Soil*, Environmental Assessment and Information Sciences Division Argonne National Laboratory, Argonne, Illinois, April.

Zach, R. and K.R. Mayoh, 1984, "Soil Ingestion by Cattle: A Neglected Pathway," *Health Physics*, Vol. 46, No. 2, pp. 426–431.

Zarn, M., 1977, *Ecological Characteristics of Piñon-Juniper Woodlands on the Colorado Plateau, A Literature Survey*, U.S. Department of the Interior—Bureau of Land Management, Technical Note, December.

Attachment I
Diffusion Model Optimization Analyses

I.1 Introduction

The diffusion modeling conducted in support of the Area G performance assessment and composite analysis represents the disposal site using cell pathway elements. Diffusive flux links between these cells simulate the transport of vapor- and gas-phase radionuclides from the buried waste to the surface of the disposal facility and into the house of the inadvertent intruder. The accuracy of the diffusive fluxes projected using GoldSim is significantly influenced by the manner in which the systems being modeled are represented. In general, the accuracy of the diffusion solution improves as the numbers of cells used to represent the waste, cover, and concrete foundation increase. The diffusion model optimization analysis was undertaken to identify a level of discretization that yields reasonably accurate estimates of diffusive fluxes while minimizing model complexity and the computer resources required for running the models. The analyses conducted in support of the development of the site and intruder diffusion models are discussed below.

I.2 Site Diffusion Model

The level of discretization required for modeling diffusive releases from the surface of the disposal site depends on several factors including the system being modeled, the magnitude of the gaseous diffusion coefficients, and the half-lives of the radionuclides undergoing diffusion. The analysis for the disposal site projected fluxes for disposal units with a 15 m (49 ft) layer of waste overlain by a 4.5 m (15 ft) cover. The waste layer thickness is representative of the deepest disposal pits and shafts excavated at Area G; the 4.5 m (15 ft) cover is approximately equal to the mean initial cover depth across all disposal units at the facility.

The diffusion model was used to estimate rates of release of tritiated water vapor, C-14 gas, Kr-81, Kr-85, Rn-220, and Rn-222 from the disposal facility. The modeling was conducted using unit inventories for all vapor- and gas-phase radionuclides except radon; Rn-220 and Rn-222 inventories were represented by assigning unit inventories to Ra-226 and Th-232, the long-lived parents that give rise to these daughter products. The entire inventories of C-14, Kr, and Rn were assumed to be present in the form of gas, and were forced into the air-filled pore space using high air-to-water partition coefficients. H-3 was modeled to partition between water and air based on the vapor pressure of the species. The partition coefficient is given by:

$$KD_{H3,air} = \frac{VP \times M}{R \times T \times \rho_{H2O}} \qquad 1$$

Where

$KD_{H3,air}$ = air:water partition coefficient for H-3
VP = vapor pressure of H-3 (atm)

M = molecular weight of water (g/mol)
R = ideal gas constant (atm-m^3/mol-^oK)
T = temperature (^oK)
ρ_{H2O} = density of water (g/m^3)

Rates of release were projected for two diffusion coefficients: 0.01 and 0.1 cm^2/s (0.0016 and 0.016 $in.^2$/s). In general, these coefficients are expected to encompass the effective diffusion coefficients observed in the cover and the waste.

The initial modeling evaluated the sensitivity of the diffusion modeling to diffusion length in air above the site. For this analysis, the cover and waste were divided into 52 layers of equal thickness. Diffusive fluxes were projected using an effective diffusion coefficient of 0.01 cm^2/s (0.0016 $in.^2$/s) and air diffusion lengths ranging from 1×10^{-4} to 1 m (3.3×10^{-4} to 3.3 ft). The results of these calculations are provided in Table I-1, with the projected peak fluxes shown as a function of air diffusion length. Projected peak fluxes increase for all radionuclides as the diffusion length is decreased from 1 m (3.3 ft); fluxes appear to have stabilized at diffusion lengths of 0.5 cm (0.2 in.) or less. On the basis of these results, an air diffusion length of 0.5 cm (0.2 in.) was adopted for all subsequent modeling analyses.

The sensitivity of the diffusion model to the level of discretization of the disposal system was evaluated by dividing the cover and waste into various numbers of layers, running the diffusion model, and observing the degree to which the projected fluxes converged. Table I-2 summarizes the results of this effort when an effective diffusion coefficient of 0.01 cm^2/s (0.0016 $in.^2$/s) was applied. The information in the upper half of the table shows the effect of dividing the cover into additional layers while representing the waste using a single layer. Fluxes of all radionuclides except Rn-220 were reasonably stable when the cover is divided into 16 or more layers. Increasing the level of discretization of the waste in conjunction with the cover yielded higher flux estimates for all radionuclides; these results are shown in the lower portion of Table I-2. Dividing the cover and waste zones into 16 or more layers of equal thickness yielded stable peak fluxes for C-14, H-3, krypton, and Rn-222; the projected fluxes of Rn-220 declined to zero as the number of cover and waste layers was increased.

Table I-3 summarizes the effect of cover and model discretization for an effective diffusion coefficient of 0.1 cm^2/s (0.016 $in.^2$/s). In general, stable peak fluxes were achieved at lower levels of discretization of the cover and waste. The upper half of the table indicates that dividing the cover into four or more layers while representing the waste by a single layer results in relatively stable fluxes for all radionuclides except Rn-220. When the lower diffusion coefficient was applied, the cover had to be divided into 16 layers to achieve a similar level of stability. A similar pattern was noted when the cover and waste were discretized simultaneously. Stable peak fluxes were observed when the cover and waste were divided into 12 or more layers; a comparable level of stability occurred for the lower diffusion coefficient with 16 or more layers.

Table I-1
Projected Peak Fluxes as a Function of Diffusion Length in Air (effective diffusion coefficient = 0.01 cm^2/s)

Air Diffusion Length (m)	Peak Flux ($pCi/m^2/s$)					
	C-14	H-3	Kr-81	Kr-85	Rn-220	Rn-222
1.0E+00	2.7E+00	3.0E-10	2.7E+00	2.6E+00	0.0E+00	5.7E-01
5.0E-01	2.7E+00	4.3E-10	2.7E+00	2.6E+00	0.0E+00	6.5E-01
1.0E-01	2.8E+00	6.4E-10	2.8E+00	2.7E+00	0.0E+00	7.4E-01
5.0E-02	2.8E+00	6.8E-10	2.8E+00	2.7E+00	0.0E+00	7.5E-01
1.0E-02	2.8E+00	7.1E-10	2.8E+00	2.7E+00	0.0E+00	7.6E-01
5.0E-03	2.8E+00	7.2E-10	2.8E+00	2.7E+00	0.0E+00	7.6E-01
1.0E-03	2.8E+00	7.2E-10	2.8E+00	2.7E+00	0.0E+00	7.6E-01
5.0E-04	2.8E+00	7.2E-10	2.8E+00	2.7E+00	0.0E+00	7.6E-01
1.0E-04	2.8E+00	7.2E-10	2.8E+00	2.7E+00	0.0E+00	7.6E-01

Table I-2
Projected Peak Fluxes as a Function of Cover and Waste Discretization (effective diffusion coefficient = 0.01 cm^2/s)

No. of Cover/Waste Layers	Peak Flux ($pCi/m^2/s$)					
	C-14	H-3	Kr-81	Kr-85	Rn-220	Rn-222
1/1	2.3E+00	8.0E-07	2.3E+00	2.2E+00	9.7E-05	4.8E-01
2/1	2.3E+00	4.8E-08	2.3E+00	2.2E+00	2.1E-08	3.0E-01
3/1	2.3E+00	7.8E-09	2.3E+00	2.2E+00	1.2E-11	2.5E-01
4/1	2.3E+00	2.3E-09	2.3E+00	2.2E+00	1.3E-14	2.3E-01
8/1	2.3E+00	2.3E-10	2.3E+00	2.2E+00	1.1E-24	2.1E-01
12/1	2.3E+00	1.1E-10	2.3E+00	2.2E+00	5.9E-33	2.1E-01
16/1	2.3E+00	8.4E-11	2.3E+00	2.2E+00	4.7E-40	2.1E-01
20/1	2.3E+00	7.2E-11	2.3E+00	2.2E+00	0.0E+00	2.1E-01
24/1	2.3E+00	6.6E-11	2.3E+00	2.2E+00	0.0E+00	2.1E-01
1/1	2.3E+00	8.0E-07	2.3E+00	2.2E+00	9.7E-05	4.8E-01
2/2	2.6E+00	8.4E-08	2.6E+00	2.6E+00	3.7E-08	4.9E-01
3/3	2.7E+00	2.0E-08	2.7E+00	2.6E+00	2.9E-11	5.4E-01
4/4	2.8E+00	7.3E-09	2.8E+00	2.7E+00	4.2E-14	5.9E-01
8/8	2.8E+00	1.3E-09	2.8E+00	2.7E+00	6.9E-24	6.9E-01
12/12	2.8E+00	8.6E-10	2.8E+00	2.7E+00	5.6E-32	7.3E-01
16/16	2.8E+00	7.5E-10	2.8E+00	2.7E+00	5.9E-39	7.4E-01
20/20	2.8E+00	7.2E-10	2.8E+00	2.7E+00	0.0E+00	7.5E-01
32/32	2.8E+00	7.1E-10	2.8E+00	2.7E+00	0.0E+00	7.6E-01
40/40	2.8E+00	7.1E-10	2.8E+00	2.7E+00	0.0E+00	7.6E-01
48/48	2.8E+00	7.2E-10	2.8E+00	2.7E+00	0.0E+00	7.6E-01
52/52	2.8E+00	7.2E-10	2.8E+00	2.7E+00	0.0E+00	7.6E-01

Table I-3
Projected Peak Fluxes as a Function of Cover and Waste Discretization (effective diffusion coefficient of 0.1 cm^2/s)

No. of Cover/Waste Layers	Peak Flux ($pCi/m^2/s$)					
	C-14	H-3	Kr-81	Kr-85	Rn-220	Rn-222
1/1	6.1E+00	7.6E-05	6.1E+00	6.0E+00	9.6E-03	1.9E+01
2/1	6.1E+00	3.2E-05	6.1E+00	6.0E+00	2.1E-05	1.9E+01
3/1	6.1E+00	2.3E-05	6.1E+00	6.0E+00	1.2E-07	1.9E+01
4/1	6.1E+00	2.1E-05	6.1E+00	6.0E+00	1.2E-09	1.9E+01
8/1	6.1E+00	1.8E-05	6.1E+00	6.0E+00	9.7E-16	1.9E+01
12/1	6.1E+00	1.8E-05	6.1E+00	6.0E+00	4.1E-20	1.9E+01
16/1	6.1E+00	1.8E-05	6.1E+00	6.0E+00	2.0E-23	1.9E+01
20/1	6.1E+00	1.8E-05	6.1E+00	6.0E+00	5.6E-26	1.9E+01
24/1	6.1E+00	1.8E-05	6.1E+00	6.0E+00	5.3E-28	1.9E+01
1/1	6.1E+00	7.6E-05	6.1E+00	6.0E+00	9.6E-03	1.9E+01
2/2	6.2E+00	5.5E-05	6.2E+00	6.1E+00	3.6E-05	2.6E+01
3/3	6.2E+00	5.5E-05	6.2E+00	6.1E+00	2.9E-07	2.9E+01
4/4	6.2E+00	5.8E-05	6.2E+00	6.1E+00	4.1E-09	3.0E+01
8/8	6.2E+00	7.3E-05	6.2E+00	6.1E+00	6.2E-15	3.1E+01
12/12	6.2E+00	8.0E-05	6.2E+00	6.1E+00	3.9E-19	3.2E+01
16/16	6.2E+00	8.3E-05	6.2E+00	6.1E+00	2.5E-22	3.2E+01
20/20	6.2E+00	8.5E-05	6.2E+00	6.1E+00	8.5E-25	3.2E+01
32/32	6.2E+00	8.6E-05	6.2E+00	6.1E+00	1.5E-29	3.2E+01
40/40	6.2E+00	8.7E-05	6.2E+00	6.1E+00	2.0E-31	3.2E+01
48/48	6.2E+00	8.7E-05	6.2E+00	6.1E+00	1.1E-32	3.2E+01
52/52	6.2E+00	8.7E-05	6.2E+00	6.1E+00	3.6E-33	3.2E+01

The results shown in the lower halves of Tables I-2 and I-3 were generated by using equal numbers of cover and waste layers, where the layer thicknesses in each component of the disposal unit were uniform. As suggested by the results, however, the degrees to which the cover and waste must be discretized to achieve stable diffusion fluxes are not the same; this is due to the different thicknesses of the cover and disposed waste. Additionally, it was found that the stability of the flux projections is most sensitive to discretization in the boundary regions in the disposal system, such as the boundary between the cover and waste zones. Given these findings, an effort was made to optimize the discretization of the disposal system for diffusion modeling. The goal of this optimization effort was to accurately project rates of diffusion from the disposal system while minimizing model complexity.

The optimization analysis was conducted using a 15 m (49 ft) thick waste zone, a 4.5 m (15 ft) thick cover zone, and a diffusion coefficient of 0.01 cm^2/s (0.0016 $in.^2/s$). The diffusion length in the air above the disposal site was set equal to 0.5 cm (0.2 in.). Using these conditions, fluxes from the disposal system were projected at various levels of discretization. The results were compared to the fluxes obtained when the cover and waste zones were represented by 52 layers each. The configurations evaluated divided the cover into 8 to 16 layers and the waste into 12 to 28 layers. The cover was divided into layers of equal thickness in all configurations. The uppermost 6 to 14 layers used to represent the waste were each assigned a thickness of 0.25 m (0.82 ft); the other layers were equally spaced to account for the remainder of the waste. For example, in the case where the waste was divided into 16 layers, each of the topmost 8 layers was assigned a thickness of 0.25 m (0.82 ft) while each of the bottommost 8 layers was assigned a thickness of 1.6 m (5.4 ft), for a total waste thickness of 15 m (49 ft).

The results of the optimization analysis are summarized in Table I-4. The topmost row of this table shows the peak fluxes projected with the cover and waste zones divided into 52 layers; subsequent rows show the fluxes projected using lower levels of discretization. The fluxes of C-14 gas, krypton, and Rn-222 are relatively stable for most, if not all, of the listed cover and waste configurations. Stable tritium fluxes similar to the results shown in the topmost row were not attained until the cover and waste were divided into 16 or more layers. Projected fluxes of Rn-220 are generally stable for a given cover configuration; but these fluxes vary widely across configurations and are greater than the projections shown in the topmost row. The fluxes of this radionuclide are highly sensitive to the model configuration because of the very short half-life of the isotope (55 s). Because of the way in which GoldSim models gas diffusion, increasing the number of cover and waste layers in the model effectively increases the distance the gas must diffuse to reach the surface of the disposal site. The additional travel time allows the radionuclide to undergo significantly more radioactive decay before reaching the ground surface, resulting in much smaller fluxes.

Table I-4
Projected Peak Fluxes as a Function of Discretization for the Optimization Analysis
(effective diffusion coefficient = 0.01 cm^2/s)

No. of Cover/Waste Layers	Peak Flux ($pCi/m^2/s$)					
	C-14	H-3	Kr-81	Kr-85	Rn-220	Rn-222
52/52	2.8E+00	7.2E-10	2.8E+00	2.7E+00	0.0E+00	7.6E-01
8/12	2.8E+00	4.2E-09	2.8E+00	2.7E+00	6.7E-23	8.7E-01
8/16	2.8E+00	4.2E-09	2.8E+00	2.8E+00	6.7E-23	8.8E-01
8/20	2.8E+00	4.2E-09	2.8E+00	2.8E+00	6.7E-23	8.8E-01
8/24	2.8E+00	4.2E-09	2.8E+00	2.8E+00	6.7E-23	8.8E-01
8/28	2.8E+00	2.6E-09	2.8E+00	2.7E+00	2.1E-23	7.8E-01
12/12	2.8E+00	1.3E-09	2.8E+00	2.7E+00	1.4E-31	7.6E-01
12/16	2.8E+00	1.9E-09	2.8E+00	2.7E+00	3.6E-31	8.3E-01
12/20	2.8E+00	1.9E-09	2.8E+00	2.7E+00	3.6E-31	8.3E-01
12/24	2.8E+00	1.9E-09	2.8E+00	2.7E+00	3.6E-31	8.3E-01
12/28	2.8E+00	1.9E-09	2.8E+00	2.7E+00	3.6E-31	8.4E-01
16/12	2.8E+00	1.2E-09	2.8E+00	2.7E+00	2.3E-38	7.9E-01
16/16	2.8E+00	1.0E-09	2.8E+00	2.7E+00	1.3E-38	7.6E-01
16/20	2.8E+00	1.0E-09	2.8E+00	2.7E+00	1.3E-38	7.7E-01
16/24	2.8E+00	1.0E-09	2.8E+00	2.7E+00	1.3E-38	7.7E-01
16/28	2.8E+00	1.0E-09	2.8E+00	2.7E+00	1.3E-38	7.7E-01

A similar optimization procedure was repeated using an effective diffusion coefficient of 0.1 cm^2/s (0.016 $in.^2/s$) for all radionuclides; the results of this analysis are summarized in Table I-5. As was the case when smaller diffusion coefficients were used, the fluxes of C-14, krypton, and Rn-222 are stable for all of the listed cover and waste configurations. Stable fluxes of tritium comparable to the flux projection for the configuration with 52 cover and waste layers are observed when the cover and waste are divided into 16 or more layers. Projected fluxes of Rn-220 vary widely across configurations and are greater than those projected using the model with 52 cover and waste layers.

The cover and waste layer divisions shown in Tables I-4 and I-5 are only a few of the countless configurations possible. However, on the basis of the results discussed above, a diffusion model employing one surface soil layer, 16 cap layers, and 20 waste layers was adopted for modeling releases from the disposal facility. The cap layer was divided into equal increments. The topmost 10 layers of the waste were assigned a thickness of 0.25 m (0.82 ft) each. The bottom 10 layers were divided equally to represent the remainder of the waste.

As discussed above, the diffusion model optimization analyses were conducted using a cover thickness of 4.5 m (15 ft) and a waste thickness of 15 m (49 ft). This cover thickness is approximately equal to the mean initial cover thickness over all of the pits and shafts at Area G; however, initial cover depths vary widely over the site within and between the waste disposal regions (see Figure 16 of main report). Furthermore, cover depths will change over time due to the effects of surface erosion. Variations in the waste thickness are also seen.

Although the diffusion model used to represent the disposal site is expected to provide reasonably accurate results, additional testing would be required to verify this for the ranges of cover and waste thickness seen at Area G A level of accuracy equal to or better than that indicated above would be realized for all cover and waste thicknesses less than those used in the optimization analysis. While inaccuracies may exist when the model is used to estimate rates of diffusion for thicker covers, the tendency will be to overestimate diffusive fluxes at the surface of the disposal facility.

Table I-5
Projected Peak Fluxes as a Function of Discretization for the Optimization Analysis
(effective diffusion coefficient =0.1 cm^2/s)

No. of Cover/Waste Layers	Peak Flux ($pCi/m^2/s$)					
	C-14	H-3	Kr-81	Kr-85	Rn-220	Rn-222
52/52	6.2E+00	8.7E-05	6.2E+00	6.1E+00	3.6E-33	3.2E+01
8/12	6.2E+00	1.0E-04	6.2E+00	6.1E+00	5.5E-14	3.3E+01
8/16	6.2E+00	1.1E-04	6.2E+00	6.1E+00	5.5E-14	3.3E+01
8/20	6.2E+00	1.1E-04	6.2E+00	6.1E+00	5.5E-14	3.3E+01
8/24	6.2E+00	1.1E-04	6.2E+00	6.1E+00	5.5E-14	3.3E+01
8/28	6.2E+00	8.9E-05	6.2E+00	6.1E+00	1.8E-14	3.2E+01
12/12	6.2E+00	8.8E-05	6.2E+00	6.1E+00	9.7E-19	3.2E+01
12/16	6.2E+00	9.8E-05	6.2E+00	6.1E+00	2.3E-18	3.3E+01
12/20	6.2E+00	9.8E-05	6.2E+00	6.1E+00	2.3E-18	3.3E+01
12/24	6.1E+00	9.8E-05	6.2E+00	6.1E+00	2.3E-18	3.3E+01
12/28	6.2E+00	9.8E-05	6.2E+00	6.1E+00	2.3E-18	3.3E+01
16/12	6.2E+00	9.3E-05	6.2E+00	6.1E+00	9.2E-22	3.2E+01
16/16	6.2E+00	8.8E-05	6.2E+00	6.1E+00	5.5E-22	3.2E+01
16/20	6.2E+00	8.8E-05	6.2E+00	6.1E+00	5.5E-22	3.2E+01
16/24	6.2E+00	8.8E-05	6.2E+00	6.1E+00	5.5E-22	3.2E+01
16/28	6.2E+00	8.8E-05	6.2E+00	6.1E+00	5.5E-22	3.2E+01

I.3 Intruder Diffusion Model

The inadvertent intruder scenarios consider potential exposures to persons constructing or residing in houses located on top of the disposal units. These individuals may be exposed to vapor- and gas-phase radionuclides that diffuse from the surface of the site and enter their homes. The magnitude of the exposures received by the intruders will be specific to the scenario under consideration because of differences in the exposure geometry. The excavation of a 3-m (10-ft) basement may or may not extend into the disposed waste, depending upon the initial cover thickness and the amount of erosion that has occurred prior to the arrival of the intruder. If the cover thickness at the time of intrusion is 3 m (10 ft) or less, a person building the house may be exposed to radionuclides diffusing directly from the waste, through the concrete foundation, and through the cover overlying the waste; the actual exposures received will depend upon the stage of construction and where the individual is located.

Living in a house with a full foundation, an agricultural intruder will be separated from the waste by the floor of the concrete foundation and any cover material that separates the foundation and the waste. Radionuclides diffusing through the concrete will lead to exposures during the time spent indoors. The receptor evaluated using the Intruder–Post-Drilling Scenario lives in a house that is built on a 10-cm (4-in.) concrete slab at the surface of the site. In this case, exposures may occur after radionuclides diffusing from the waste pass through the cover and the concrete slab upon which the house is built. The agricultural and drilling intruders may also be exposed to vapor- and gas-phase contaminants that diffuse from the surface of the disposal facility during time spent outdoors.

The level of discretization required to accurately project diffusive releases for the intruder scenarios was determined using the results of the site diffusion model analysis and additional modeling. The results of the modeling for the disposal site indicate that 16 cover layers and 20 waste layers yield stable diffusion flux estimates. This level of discretization was used to model releases during the time spent by the intruders outside of the house and to model the transport of radionuclides from the waste to the concrete slab upon which the house of the post-drilling intruder sits. The concrete floor of the foundation of the house was modeled using different numbers of layers to determine the level of discretization required to obtain stable fluxes. The additional modeling analyses were conducted using effective diffusion coefficients of 0.1 and 0.01 cm^2/s (0.016 and 0.0016 $in.^2/s$) for the cover and waste; the diffusion coefficients of the concrete foundation were assumed to be equal to and 10 percent of the cover and waste coefficients. An air diffusion length of 0.5 cm (0.2 in.) was used for all optimization model runs.

The optimization analysis was conducted for the exposure geometry pertaining to the Intruder–Post-Drilling Scenario, including a 15 m (49 ft) waste layer, 4.5 m (15 ft) of cover material, and

a 10 cm (4 in.) thick slab of concrete used to represent the floor of the house. The peak fluxes projected using cover and waste diffusion coefficients of 0.01 cm^2/s (0.0016 $in.^2/s$) are shown in Table I-6. The fluxes shown in the upper half of the table were projected using an effective diffusion coefficient of 0.01 cm^2/s (0.0016 $in.^2/s$) for the 10 cm (4 in.) concrete slab, while the results in the lower half of the table are based on a concrete diffusion coefficient of 0.001 cm^2/s (1.6×10^{-4} $in.^2/s$). The projected fluxes are generally unaffected by the degree to which the concrete slab is discretized for either concrete diffusion coefficient; the fluxes projected for Rn-220 are the lone exception. The results shown in Table I-7 reveal the same outcome when the effective diffusion coefficients for the cover and waste are set equal to 0.1 cm^2/s (0.016 $in.^2/s$).

Based on the results shown above, a diffusion model with four concrete layers, one surface soil layer, 16 cap layers, and 20 waste layers was used to model exposures for the inadvertent intruder scenarios. The concrete and cap layers were divided into equal increments. The topmost 10 layers of the waste were assigned a thickness of 0.25 m (0.82 ft) each. The bottom 10 layers were divided equally to represent the remainder of the waste.

The diffusion model adopted for the intruder analysis is expected to provide reasonably accurate projections of diffusive fluxes at the surface of the disposal facility and in the intruder's house. Additional testing would be required to verify this for the ranges of cover and waste thickness seen at Area G. A level of accuracy equal to or better than that indicated above is expected for all cover and waste thicknesses that are less than those used in the optimization analysis; the model may overestimate diffusive fluxes for covers substantially thicker than 4.5 m (15 ft).

Table I-6
Optimization Analysis Results for the Intruder-Post-Drilling Scenario Exposure Geometry
(cover and waste diffusion coefficients = 0.01 cm^2/s)

No. of Concrete/Cover/Waste Layers	Peak Flux ($pCi/m^2/s$)					
	C-14	H-3	Kr-81	Kr-85	Rn-220	Rn-222
Concrete Diffusion Coefficient = 10^{-2} cm^2/s						
1/16/20	2.8E+00	7.7E-10	2.8E+00	2.7E+00	7.5E-40	8.0E-01
2/16/20	2.8E+00	7.7E-10	2.8E+00	2.7E+00	3.5E-40	7.1E-01
3/16/20	2.8E+00	7.7E-10	2.8E+00	2.7E+00	2.6E-40	7.1E-01
4/16/20	2.8E+00	7.7E-10	2.8E+00	2.7E+00	2.2E-40	7.1E-01
6/16/20	2.8E+00	7.7E-10	2.8E+00	2.7E+00	2.0E-40	7.1E-01
8/16/20	2.8E+00	7.7E-10	2.8E+00	2.7E+00	1.9E-40	7.1E-01
Concrete Diffusion Coefficient = 10^{-3} cm^2/s						
1/16/20	2.5E+00	2.3E-10	2.5E+00	2.4E+00	2.5E-41	4.1E-01
2/16/20	2.5E+00	2.3E-10	2.5E+00	2.4E+00	2.7E-42	4.1E-01
3/16/20	2.5E+00	2.3E-10	2.5E+00	2.4E+00	5.7E-43	4.1E-01
4/16/20	2.5E+00	2.3E-10	2.5E+00	2.4E+00	1.9E-43	4.1E-01
6/16/20	2.5E+00	2.3E-10	2.5E+00	2.4E+00	3.8E-44	4.1E-01
8/16/20	2.5E+00	2.3E-10	2.5E+00	2.4E+00	3.8E-44	4.1E-01

Table I-7
Optimization Analysis Results for the Intruder-Post-Drilling Scenario Exposure Geometry
(cover and waste diffusion coefficients = 0.1 cm^2/s)

No. of Concrete/Cover/Waste Layers	Peak Flux ($pCi/m^2/s$)					
	C-14	H-3	Kr-81	Kr-85	Rn-220	Rn-222
Concrete Diffusion Coefficient = 10^{-2} cm^2/s						
1/16/20	6.2E+00	7.9E-05	6.2E+00	6.1E+00	1.7E-22	3.1E+01
2/16/20	6.2E+00	7.9E-05	6.2E+00	6.1E+00	1.6E-22	3.1E+01
3/16/20	6.2E+00	7.9E-05	6.2E+00	6.1E+00	1.6E-22	3.1E+01
4/16/20	6.2E+00	7.9E-05	6.2E+00	6.1E+00	1.6E-22	3.1E+01
6/16/20	6.2E+00	7.9E-05	6.2E+00	6.1E+00	1.6E-22	3.1E+01
8/16/20	6.2E+00	7.9E-05	6.2E+00	6.1E+00	1.6E-22	3.1E+01
Concrete Diffusion Coefficient = 10^{-3} cm^2/s						
1/16/20	6.1E+00	4.0E-05	6.1E+00	6.1E+00	9.5E-24	2.5E+01
2/16/20	6.1E+00	4.0E-05	6.1E+00	6.1E+00	5.9E-24	2.5E+01
3/16/20	6.1E+00	4.0E-05	6.1E+00	6.1E+00	4.8E-24	2.5E+01
4/16/20	6.1E+00	4.0E-05	6.1E+00	6.1E+00	4.4E-24	2.5E+01
6/16/20	6.1E+00	4.0E-05	6.1E+00	6.1E+00	4.0E-24	2.5E+01
8/16/20	6.1E+00	4.0E-05	6.1E+00	6.1E+00	3.9E-24	2.5E+01

Attachment II
Development of Layer-Specific Inventories for the 1988–2007 Disposal Shafts

1.0 Introduction

The Area G performance assessment projects exposures for the Intruder-Construction, Intruder-Agriculture, and Intruder-Post-Drilling Scenarios. Preliminary modeling results indicate that the peak mean doses projected for all three intruder scenarios fall well within acceptable limits for the disposal pits. In contrast, assumptions made about how the waste is distributed within the disposal shafts significantly affect the ability of the disposal facility to comply with the intruder performance objectives. Distributing the waste uniformly throughout the waste profile results in peak mean exposures that were close to or greater than acceptable limits for the agricultural intruder scenario.

The Intruder-Construction Scenario is based on the premise that a person builds a house over the disposal units at Area G, while the Intruder-Agriculture Scenario considers exposures received by a person who lives in that house. A major source of contamination for these scenarios is waste that is contacted and/or brought to the ground surface as a result of excavating a 3-m (9.8-ft) basement; the receptors may be exposed to additional contamination transported by plants and animals prior to the intruder's arrival at the site. Waste disposed of at depths that exceed the depth of the basement, the rooting depths of plants, and the burrowing depths of animals will remain undisturbed and exposures received by the agricultural and construction intruders will be small. Given the dependence of the intruder doses for these scenarios on depth of waste disposal and the magnitude of the agricultural intruder doses relative to the performance objectives, efforts were made to better represent the actual distribution of waste within the shafts.

This report documents the depth-of-disposal evaluation. The approach used to classify the waste with respect to placement depth is described in Section 2; the results of the analysis are presented and discussed in Section 3.

2.0 Approach

Over 160 radionuclides were disposed of in the disposal shafts between September 27, 1988 and 2007. The majority of these are short-lived isotopes that pose little risk to an intruder because they decay to negligible levels prior to the individual's arrival at the closed disposal facility. Of the remainder, only a small number make significant contributions to the doses projected for the agricultural intruder. To illustrate, preliminary modeling indicates that eight radionuclides in disposal shafts contribute 1 percent or more to the peak mean dose projected for this receptor: Ag-108m, C-14, Cs-137, H-3, Ni-63, Ra-226, Sr-90, and Th-232. Consequently, the disposal depth evaluation focused on these eight radionuclides.

The disposal records were collected for all waste that was placed in shafts from September 27, 1988 through December 31, 2007, and that contains the radionuclides listed above; these data are compiled in Table II-1. Examination of these data reveals that most of the total inventory of each critical radionuclide resides in a small number of waste containers. Table II-2 provides disposal data for the waste packages that hold 1 percent or more of the total inventory of each radionuclide.

The information provided in Table II-2 was used to identify the waste containers most likely to impact intruder doses; these containers were the focus of the depth-of-disposal analysis. With the exception of H-3, the containers listed in the table account for 97 percent or more of the total inventory of each critical radionuclide, and thus the depth analysis for all of the radionuclides except tritium was limited to these packages. Because the containers listed in Table II-2 account for only 83 percent of the total inventory of tritium, the depth-of-disposal analysis for this radionuclide was expanded to consider all containers that contributed 0.1 percent or more of the total H-3 inventory placed in the shafts. Together, these containers accounted for more than 95 percent of the total tritium inventory. The waste containers included in the depth-of-disposal analysis for H-3 are listed in Table II-3.

The placement depths for the containers listed in Tables II-2 and II-3 were estimated using several approaches. In many cases, the depth from the ground surface to the top of the waste container or the overlying fill was measured following the placement of the waste and these measurements could be used directly to characterize placement depth. However, measurements of depth of placement were unavailable for about 60 percent of the waste containers of interest. For many of these containers, placement depths could be bounded using the depths of disposal recorded for later waste packages disposed of in the same shafts (i.e., above the containers of interest). The placement depths of other containers were estimated on the basis of the total depths of the shafts and the sequence of container placement within those units. For example, the depth of placement of the first container disposed of in a shaft can be reasonably bounded if the depth of the shaft and the height of the package are known. Finally, visual inspections of selected shafts were conducted when other sources of information were not adequate for characterizing container placement depths.

The depths of disposal were categorized in terms of two depth intervals. Specifically, waste was assigned either to the top 1.5 m (4.9 ft) of the waste profile within the disposal shaft or to the portion of the profile below 1.5 m (4.9 ft). As stated above, the depths to the tops of waste containers were measured from the ground surface. To determine the locations of containers within the waste profile, it was necessary to restate these measurements in terms of their depths from the top of the waste column. This was done by subtracting 3 m (9.8 ft) from the ground-surface-to-waste depths; thus, the depth of placement relative to the top of the waste was estimated as the difference between measured depth values and 3 m (9.8 ft).

Table II- 1
Disposal Data for Waste Containing Critical Radionuclides

Disposal Date	Container-Item ID	Shaft No.	Radionuclide	Activity (Ci)
13-Dec-88	S880453-522167	141	Sr-90	1.0E+00
12-Jan-89	S890123-523464	155	C-14	8.9E-03
12-Jan-89	S890120-522556	155	H-3	2.0E-02
12-Jan-89	S890122-526249	155	H-3	4.8E+03
12-Jan-89	S890124-523609	155	H-3	5.5E+03
12-Jan-89	S890125-522908	155	H-3	4.3E+04
12-Jan-89	S890121-522808	155	H-3	2.5E+03
7-Apr-89	S893507-522401	137	H-3	1.0E-02
7-Apr-89	S893506-522367	155	H-3	1.1E+01
7-Apr-89	S893505-522694	155	H-3	1.0E+00
7-Apr-89	S891537-522804	155	H-3	5.0E+02
7-Apr-89	S891535-523123	155	H-3	2.0E+00
7-Apr-89	S891536-523567	155	H-3	8.2E+01
7-Apr-89	S891532-522783	155	H-3	9.5E+01
7-Apr-89	S892073-522448	159	H-3	3.6E+00
7-Apr-89	S891538-523369	159	H-3	5.0E+00
8-May-89	S892166-522625	137	H-3	1.2E-05
30-May-89	S892169-522750	137	H-3	1.1E-05
18-Sep-89	S891541-522380	158	H-3	1.1E+04
16-Oct-89	S893914-522817	141	Ra-226	1.5E-05
27-Nov-89	S893139-523470	137	H-3	5.0E+01
27-Nov-89	S894114-523403	158	H-3	1.1E+02
27-Feb-90	S900020-523892	22	Sr-90	5.0E-04
16-Mar-90	S902455-526280	22	Cs-137	9.0E-04
25-May-90	S902726-523907	141	Cs-137	1.1E-02
25-May-90	S902983-524036	22	Sr-90	2.4E-06
28-Jun-90	S900119-524316	160	H-3	1.0E-01

Table II-1 (Continued)
Disposal Data for Waste Containing Critical Radionuclides

Disposal Date	Container-Item ID	Shaft No.	Radionuclide	Activity (Ci)
13-Aug-90	S903359-524016	141	Sr-90	4.0E+00
7-Nov-90	S900163-526292	137	H-3	1.3E+00
13-Nov-90	S902418-523815	158	H-3	1.1E+02
25-Feb-91	S910637-526411	137	H-3	1.0E+00
25-Feb-91	S910635-526413	158	H-3	4.3E+01
1-Apr-91	S910586-526527	124	Th-232	1.0E-04
1-Apr-91	S911252-526528	124	Th-232	1.0E-04
1-Apr-91	S911154-526529	124	Th-232	2.0E-04
5-Sep-91	S911407-526980	C13	Cs-137	4.4E-06
5-Sep-91	S911408-526983	C13	Cs-137	4.4E-06
5-Sep-91	S911412-526984	C13	Cs-137	4.4E-06
5-Sep-91	S911413-527355	C13	Cs-137	4.4E-06
12-Mar-92	L92000134-500118	137	H-3	1.0E-01
12-Mar-92	L92000135-500119	137	H-3	1.0E-01
12-Mar-92	L92000136-500120	137	H-3	1.0E-01
12-Mar-92	L92000137-500227	137	H-3	1.0E-01
12-Mar-92	L92000138-500229	137	H-3	1.0E-01
12-Mar-92	L92000139-500225	137	H-3	1.0E-01
12-Mar-92	L92000140-500121	137	H-3	1.0E-01
12-Mar-92	L92000142-500122	137	H-3	1.0E-01
12-Mar-92	L92000143-500399	137	H-3	1.0E-01
12-Mar-92	L92000144-500228	137	H-3	1.0E-01
12-Mar-92	L92000145-500123	137	H-3	1.0E-01
12-Mar-92	L92000146-500124	137	H-3	1.0E-01
12-Mar-92	L92000147-500488	137	H-3	1.0E-01
12-Mar-92	L92000148-500226	137	H-3	1.0E-01
12-Mar-92	L92000149-500125	137	H-3	1.0E-01
12-Mar-92	L92000150-500126	137	H-3	1.0E-01
7-May-92	L92000235-500372	137	H-3	1.0E-01

Table II-1 (Continued)
Disposal Data for Waste Containing Critical Radionuclides

Disposal Date	Container-Item ID	Shaft No.	Radionuclide	Activity (Ci)
7-May-92	L92000237-500178	137	H-3	1.0E-01
7-May-92	L92000238-500177	137	H-3	1.0E-01
7-May-92	L92000240-500188	137	H-3	1.0E-01
7-May-92	L92000241-500187	137	H-3	1.0E-01
7-May-92	L92000242-500219	137	H-3	1.0E-01
7-May-92	L92000243-500218	137	H-3	1.0E-01
7-May-92	L92000245-500175	137	H-3	1.0E-01
7-May-92	L92000246-500174	137	H-3	1.0E-01
7-May-92	L92000251-500171	137	H-3	1.0E-01
7-May-92	L92000252-500172	137	H-3	1.0E-01
7-May-92	L92000253-500182	137	H-3	1.0E-01
7-May-92	L92000254-500220	137	H-3	1.0E-01
7-May-92	L92000255-500221	137	H-3	1.0E-01
3-Sep-92	L92000236-500179	137	H-3	1.0E-01
3-Sep-92	L92000244-500217	137	H-3	1.0E-01
3-Sep-92	L92000247-500173	137	H-3	1.0E-01
21-Sep-92	L92000741-528951	301	Cs-137	6.7E+01
29-Sep-92	L92000673-500481	C13	Cs-137	9.9E-07
22-Feb-93	L93000078-529200	301	Cs-137	7.9E-06
22-Feb-93	L93000078-529200	301	Sr-90	3.6E-03
4-Mar-93	L93000093-529213	301	Sr-90	1.9E-01
17-Mar-93	L93000141-529261	301	Ra-226	2.0E-07
27-May-93	L93000176-529440	22	C-14	2.7E-09
27-May-93	L93000176-529440	22	Cs-137	2.0E-06
27-May-93	L93000180-529291	22	Cs-137	7.8E-07
27-May-93	L93000181-529288	22	Ni-63	3.0E-05
27-May-93	L93000176-529440	22	Sr-90	2.2E-04
27-May-93	L93000178-529290	22	Th-232	2.2E-06
9-Aug-93	L93000139-529257	158	H-3	5.0E+02

Table II-1 (Continued)
Disposal Data for Waste Containing Critical Radionuclides

Disposal Date	Container-Item ID	Shaft No.	Radionuclide	Activity (Ci)
11-Aug-93	L93000924-529545	158	H-3	7.0E+01
11-Aug-93	L93000922-530200	160	H-3	7.0E+02
11-Aug-93	L93000923-530201	161	H-3	2.2E+02
22-Sep-93	L93000651-529719	161	H-3	9.6E+02
10-Nov-93	L93000824-529871	136	H-3	5.0E-02
15-Mar-94	L94000135-530110	C13	H-3	1.4E-05
7-Jun-94	L94000230-530199	161	H-3	9.7E+02
7-Jun-94	L94000228-530198	161	H-3	6.8E+02
7-Jun-94	L94000229-531225	161	H-3	5.0E+01
30-Jun-94	L94000445-530809	131	Cs-137	1.5E+01
7-Oct-94	L94000620-530957	197	Cs-137	4.5E-01
14-Oct-94	L94000484-530844	C13	H-3	1.4E-02
14-Oct-94	L94000515-530866	147	Th-232	6.5E-06
14-Oct-94	L94000524-530871	147	Th-232	4.0E-06
4-Nov-94	L94000759-529698	131	Cs-137	1.0E-01
20-Jan-95	L94000845-531302	C13	H-3	1.0E-09
17-Feb-95	L94000599-530943	136	H-3	2.0E+01
17-May-95	L95049714-2010397	162	H-3	1.7E+05
17-May-95	L95049715-2010398	162	H-3	1.3E+05
30-Jun-95	L95051327-2011497	171	H-3	5.8E-04
30-Jun-95	L95051328-2011498	171	H-3	5.8E-04
9-Aug-95	L95053058-2037996	136	H-3	2.3E+02
9-Aug-95	L95053068-2037999	136	H-3	6.8E+02
26-Sep-95	L95056351-2023593	162	H-3	5.5E+04
29-Apr-96	L96065300-2010349	137	H-3	3.9E-03
29-Apr-96	L96065304-2010351	137	H-3	5.2E-03
29-Apr-96	L96065303-2010350	137	H-3	5.5E-03
29-Apr-96	L96065302-2010348	137	H-3	5.8E-03
29-Apr-96	L96065306-2010353	137	H-3	9.0E-03

Table II-1 (Continued)
Disposal Data for Waste Containing Critical Radionuclides

Disposal Date	Container-Item ID	Shaft No.	Radionuclide	Activity (Ci)
29-Apr-96	L96065305-2010352	137	H-3	1.1E-01
29-Apr-96	L96065301-2010347	137	H-3	6.2E+00
29-Apr-96	L96065299-2010346	137	H-3	6.3E+00
8-May-96	L96063716-5001784	144	Cs-137	1.7E-01
10-Jun-96	L96068594-2057879	C13	Cs-137	1.9E-06
10-Jun-96	L96068595-2057884	C13	Cs-137	5.5E-06
10-Jun-96	L96068594-2057879	C13	H-3	5.5E-12
10-Jun-96	L96068595-2057884	C13	H-3	5.5E-12
10-Jun-96	L96068594-2057879	C13	Sr-90	3.7E-06
10-Jun-96	L96068595-2057884	C13	Sr-90	1.1E-05
11-Jun-96	L96067978-2033108	301	Ra-226	4.9E-01
11-Jun-96	L96067977-2033113	301	Ra-226	5.5E-02
14-Jun-96	L96068794-2036188	144	Ag-108m	1.3E-03
17-Jun-96	L96068998-2036187	144	Ag-108m	3.6E-03
1-Jul-96	L96069149-2013966	136	H-3	9.0E+00
1-Jul-96	L96069150-2013967	136	H-3	9.0E+00
1-Jul-96	L96069151-2013968	136	H-3	9.0E+00
1-Jul-96	L96069152-2013969	136	H-3	9.0E+00
1-Jul-96	L96069153-2013970	136	H-3	9.0E+00
1-Jul-96	L96069154-2013971	136	H-3	9.0E+00
1-Jul-96	L96069155-2026702	136	H-3	9.0E+00
1-Jul-96	L96069156-2026576	136	H-3	9.0E+00
1-Jul-96	L96069157-2026577	136	H-3	9.0E+00
31-Jul-96	L96070976-2058097	136	H-3	1.0E+02
31-Jul-96	L96070978-2058098	136	H-3	1.0E+02
31-Jul-96	L96070979-2058099	136	H-3	1.0E+02
31-Jul-96	L96070980-2058100	136	H-3	1.0E+02
31-Jul-96	L96070981-2058101	136	H-3	1.0E+02
31-Jul-96	L96070982-2058102	136	H-3	1.0E+02

Table II-1 (Continued)
Disposal Data for Waste Containing Critical Radionuclides

Disposal Date	Container-Item ID	Shaft No.	Radionuclide	Activity (Ci)
31-Jul-96	L96070983-2058103	136	H-3	1.0E+02
31-Jul-96	L96070984-2058104	136	H-3	1.0E+02
13-Aug-96	L96066837-2032960	147	Cs-137	1.0E-05
13-Aug-96	L96067342-2010197	147	Cs-137	5.0E-06
13-Aug-96	L96065213-2043757	147	H-3	2.6E-10
13-Aug-96	L96070837-2058135	147	H-3	4.5E-03
13-Aug-96	L96070838-2058136	147	H-3	6.8E-03
13-Aug-96	L96070839-2058137	147	H-3	6.8E-03
13-Aug-96	L96070840-2058138	147	H-3	6.8E-03
13-Aug-96	L96070841-2058139	147	H-3	6.8E-03
13-Aug-96	L96066837-2032960	147	Th-232	1.9E-07
13-Aug-96	L96067342-2010199	147	Th-232	5.0E-12
13-Aug-96	L95061111-2034624	C13	Th-232	2.5E-19
13-Aug-96	L95061111-2034624	C13	Th-232	2.5E-19
13-Aug-96	L95061111-2034624	C13	Th-232	5.0E-19
30-Sep-97	L97096618-2088682	144	Ra-226	5.0E-02
30-Sep-97	L97096618-2088682	144	Sr-90	5.6E+01
1-Oct-97	L97095087-2072222	339	H-3	5.3E+04
1-Oct-97	L97095088-2072221	339	H-3	7.7E+04
3-Oct-97	L97077952-2062536	144	Cs-137	1.0E-09
3-Oct-97	L97077952-2062536	144	H-3	1.0E-09
3-Oct-97	L97077952-2062536	144	Th-232	1.0E-09
8-Oct-97	L97096768-2075251	144	Cs-137	1.5E-02
22-Oct-97	L96072211-2047307	C13	Cs-137	2.1E-08
26-Jun-98	L98105432-2088731	308	Ra-226	2.0E-09
26-Jun-98	L98105432-2088731	308	Ra-226	2.0E-09
26-Jun-98	L98105432-2088731	308	Ra-226	4.1E-09
26-Jun-98	L98105432-2088731	308	Th-232	2.2E-09
26-Jun-98	L98105432-2088731	308	Th-232	2.2E-09

Table II-1 (Continued)
Disposal Data for Waste Containing Critical Radionuclides

Disposal Date	Container-Item ID	Shaft No.	Radionuclide	Activity (Ci)
26-Jun-98	L98105432-2088731	308	Th-232	4.4E-09
29-Oct-98	L98109894-2099042	308	Th-232	3.6E-03
29-Oct-98	L98109896-2099044	308	Th-232	3.7E-03
29-Oct-98	L98109897-2099045	308	Th-232	3.7E-03
29-Oct-98	L98109886-2099034	308	Th-232	3.8E-03
29-Oct-98	L98109889-2099037	308	Th-232	3.8E-03
29-Oct-98	L98109887-2099035	308	Th-232	4.1E-03
29-Oct-98	L98109903-2099051	308	Th-232	4.4E-03
29-Oct-98	L98109899-2099047	308	Th-232	4.9E-03
29-Oct-98	L98109902-2099050	308	Th-232	5.5E-03
29-Oct-98	L98109908-2099062	308	Th-232	4.2E-03
29-Oct-98	L98109907-2099061	308	Th-232	7.6E-03
29-Oct-98	L98109906-2099060	308	Th-232	1.6E-02
29-Oct-98	L98109916-2099070	308	Th-232	2.2E-03
4-Feb-99	L98109888-2099036	197	Th-232	2.6E-03
4-Feb-99	L98109895-2099043	197	Th-232	3.0E-03
4-Feb-99	L98109901-2099049	197	Th-232	3.4E-03
4-Feb-99	L98109891-2099039	197	Th-232	3.5E-03
4-Feb-99	L98109900-2099048	197	Th-232	3.6E-03
4-Feb-99	L98109893-2099041	197	Th-232	3.7E-03
4-Feb-99	L98109885-2099033	197	Th-232	3.8E-03
4-Feb-99	L98109892-2099040	197	Th-232	3.8E-03
4-Feb-99	L98109898-2099046	197	Th-232	3.8E-03
4-Feb-99	L98109890-2099038	197	Th-232	3.9E-03
4-Feb-99	L98109915-2099069	197	Th-232	8.7E-04
4-Feb-99	L98109910-2099064	197	Th-232	2.2E-03
4-Feb-99	L98109914-2099068	197	Th-232	2.3E-03
4-Feb-99	L98109911-2099065	197	Th-232	2.5E-03
4-Feb-99	L98109909-2099063	197	Th-232	2.8E-03

Table II-1 (Continued)
Disposal Data for Waste Containing Critical Radionuclides

Disposal Date	Container-Item ID	Shaft No.	Radionuclide	Activity (Ci)
4-Feb-99	L98109912-2099066	197	Th-232	3.7E-03
4-Feb-99	L98109904-2099052	197	Th-232	4.5E-03
4-Feb-99	L98109913-2099067	197	Th-232	5.9E-03
4-Feb-99	L98109905-2099059	197	Th-232	2.8E-02
4-Feb-99	L98109917-2099071	197	Th-232	2.3E-02
6-Apr-99	L99114245-2097060	339	C-14	1.1E-06
6-Apr-99	L99114245-2097060	339	Cs-137	8.9E-04
6-Apr-99	L99114245-2097060	339	Ra-226	1.7E-01
6-Apr-99	L99114245-2097060	339	Sr-90	6.2E-03
6-Apr-99	L99114245-2097060	339	Th-232	4.5E-07
22-Apr-99	L99112392-2110592	163	H-3	4.0E+02
22-Apr-99	L99112399-2110599	163	H-3	4.2E+02
22-Apr-99	L99112393-2110593	163	H-3	4.3E+02
22-Apr-99	L99112400-2110600	163	H-3	4.4E+02
22-Apr-99	L99112395-2110595	163	H-3	4.4E+02
22-Apr-99	L99112394-2110594	163	H-3	4.5E+02
22-Apr-99	L99112397-2110597	163	H-3	4.5E+02
22-Apr-99	L99112396-2110596	163	H-3	4.7E+02
22-Apr-99	L99112398-2110598	163	H-3	4.7E+02
22-Apr-99	L99112402-2110602	163	H-3	4.7E+02
22-Apr-99	L99112401-2110601	164	H-3	4.4E+02
22-Apr-99	L99112403-2110603	164	H-3	4.8E+02
22-Apr-99	L99115423-2043225	164	H-3	4.5E+01
22-Apr-99	L99115424-2043226	164	H-3	4.5E+01
22-Apr-99	L99115425-2058801	164	H-3	4.5E+01
22-Apr-99	L99115426-2058872	164	H-3	4.5E+01
22-Apr-99	L99115427-2080011	164	H-3	4.5E+01
4-May-99	L99114445-2096734	339	Ra-226	3.6E-06
4-May-99	L99114445-2096734	339	Sr-90	6.0E-07

Table II-1 (Continued)
Disposal Data for Waste Containing Critical Radionuclides

Disposal Date	Container-Item ID	Shaft No.	Radionuclide	Activity (Ci)
15-Jul-99	L99116048-2144000	339	H-3	9.3E-06
27-Jul-99	L99117197-2058887	163	H-3	3.6E+02
27-Jul-99	L99117198-2058888	164	H-3	3.8E+02
27-Jul-99	L99117243-2042297	164	H-3	4.3E+02
27-Jul-99	L99117241-2042295	164	H-3	4.4E+02
27-Jul-99	L99117374-2042303	164	H-3	4.5E+02
27-Jul-99	L99117201-2058874	164	H-3	4.9E+02
27-Jul-99	L99117196-2058884	164	H-3	4.4E+02
27-Jul-99	L99117377-2042306	165	H-3	3.2E+02
27-Jul-99	L99117376-2042305	165	H-3	3.9E+02
27-Jul-99	L99117378-2042307	165	H-3	4.5E+02
27-Jul-99	L99117242-2042296	165	H-3	4.7E+02
27-Jul-99	L99117240-2042294	165	H-3	4.7E+02
27-Jul-99	L99117239-2042293	165	H-3	4.7E+02
27-Jul-99	L99117375-2042304	165	H-3	4.8E+02
7-Oct-99	L99117194-2042309	165	H-3	2.5E+02
7-Oct-99	L99121101-2042628	165	H-3	3.1E+02
7-Oct-99	L99120849-2042459	165	H-3	3.9E+02
7-Oct-99	L99121104-2042631	165	H-3	4.7E+02
7-Oct-99	L99121103-2042630	165	H-3	4.9E+02
7-Oct-99	L99120848-2042639	165	H-3	1.1E+03
7-Oct-99	L99117193-2042299	169	H-3	2.7E+02
7-Oct-99	L99121082-2042437	169	H-3	3.4E+02
7-Oct-99	L99121098-2042625	169	H-3	3.6E+02
7-Oct-99	L99121100-2042627	169	H-3	3.8E+02
7-Oct-99	L99120263-2042642	169	H-3	4.4E+02
7-Oct-99	L99120262-2042641	169	H-3	4.6E+02
7-Oct-99	L99121099-2042626	169	H-3	4.7E+02
7-Oct-99	L99121102-2042629	169	H-3	4.8E+02

Table II-1 (Continued)
Disposal Data for Waste Containing Critical Radionuclides

Disposal Date	Container-Item ID	Shaft No.	Radionuclide	Activity (Ci)
9-Dec-99	L99120851-2042457	351	H-3	9.6E+01
9-Dec-99	L99120850-2042458	351	H-3	8.7E+02
9-Dec-99	L99120862-2042456	351	H-3	8.9E+02
9-Dec-99	L99120863-2042455	351	H-3	3.7E+02
1-Jan-00	L99121791-2042620	339	H-3	4.3E-03
25-Jan-00	L99122700-2042611	351	H-3	2.4E+03
25-Jan-00	L99122703-2042614	351	H-3	2.5E+03
25-Jan-00	L99122702-2042615	351	H-3	2.6E+03
25-Jan-00	L99122701-2042613	351	H-3	3.2E+03
25-Jan-00	L99122704-2042612	351	H-3	5.1E+03
9-Mar-00	L99122341-2042604	349	H-3	1.3E+02
9-Mar-00	L00125845-2042605	349	H-3	3.3E+02
9-Mar-00	L99122336-2042600	349	H-3	4.1E+02
9-Mar-00	L99122346-2042598	349	H-3	4.8E+02
9-Mar-00	L99122337-2042601	349	H-3	1.8E+03
9-Mar-00	L99122338-2042602	349	H-3	2.4E+03
9-Mar-00	L99122343-2042606	351	H-3	1.0E+02
9-Mar-00	L99122347-2042599	351	H-3	3.7E+02
23-Mar-00	L00125886-2097239	357	Cs-137	3.2E-01
23-Mar-00	L00125886-2097239	357	Sr-90	3.2E-01
16-Jun-00	L00126598-2152276	349	H-3	2.0E+02
16-Jun-00	L00126599-2152277	349	H-3	2.8E+02
16-Jun-00	L00126595-2152273	349	H-3	2.9E+02
16-Jun-00	L00126596-2152274	349	H-3	3.4E+02
16-Jun-00	L00126597-2152275	349	H-3	3.4E+02
16-Jun-00	L00127041-2174951	349	H-3	3.4E+02
16-Jun-00	L00127046-2174955	349	H-3	3.9E+02
16-Jun-00	L00127044-2174953	349	H-3	4.1E+02
16-Jun-00	L00126589-2042443	349	H-3	4.1E+02

Table II-1 (Continued)
Disposal Data for Waste Containing Critical Radionuclides

Disposal Date	Container-Item ID	Shaft No.	Radionuclide	Activity (Ci)
16-Jun-00	L00126593-2042447	349	H-3	4.1E+02
16-Jun-00	L00126586-2042442	349	H-3	4.1E+02
16-Jun-00	L00127043-2174952	349	H-3	4.1E+02
16-Jun-00	L00126594-2152272	349	H-3	4.2E+02
16-Jun-00	L00126590-2042444	349	H-3	4.3E+02
16-Jun-00	L00127045-2174954	349	H-3	4.7E+02
16-Jun-00	L00127047-2174956	349	H-3	4.7E+02
16-Jun-00	L00126591-2042445	349	H-3	4.7E+02
16-Jun-00	L00126592-2042446	349	H-3	4.7E+02
8-Mar-01	L00131634-2180620	161	H-3	2.2E+02
8-Mar-01	L00131638-2058882	161	H-3	3.0E+02
8-Mar-01	L00131637-2058885	161	H-3	3.7E+02
8-Mar-01	L00131632-2180619	161	H-3	3.9E+02
8-Mar-01	L00131639-2058879	161	H-3	4.5E+02
10-May-01	L01136820-2192581	355	H-3	3.5E+01
10-May-01	L01136823-2192584	355	H-3	3.5E+01
10-May-01	L01136825-2192586	355	H-3	3.5E+01
10-May-01	L01136828-2192589	355	H-3	3.5E+01
10-May-01	L01136818-2192579	357	H-3	3.5E+01
10-May-01	L01136819-2192580	357	H-3	3.5E+01
10-May-01	L01136821-2192582	357	H-3	3.5E+01
10-May-01	L01136822-2192583	357	H-3	3.5E+01
10-May-01	L01136824-2192585	357	H-3	3.5E+01
10-May-01	L01136826-2192587	357	H-3	3.5E+01
10-May-01	L01136827-2192588	357	H-3	3.5E+01
10-May-01	L01136829-2192590	357	H-3	3.5E+01
14-Jun-01	L01136482-2160417	355	H-3	1.7E+01
15-Aug-01	L01138368-2185623	355	H-3	3.8E-08
28-Sep-01	L01142533-2197862	C14	Cs-137	2.5E-10

Table II-1 (Continued)
Disposal Data for Waste Containing Critical Radionuclides

Disposal Date	Container-Item ID	Shaft No.	Radionuclide	Activity (Ci)
28-Sep-01	L01142532-2197859	C14	Cs-137	3.2E-10
28-Sep-01	L01142529-2197719	C14	Cs-137	1.1E-09
28-Sep-01	L01142530-2197720	C14	Cs-137	1.2E-09
28-Sep-01	L01142531-2197721	C14	Cs-137	1.8E-09
28-Sep-01	L01142533-2197862	C14	Ra-226	1.6E-09
28-Sep-01	L01142532-2197859	C14	Ra-226	2.0E-09
28-Sep-01	L01142529-2197719	C14	Ra-226	6.8E-09
28-Sep-01	L01142530-2197720	C14	Ra-226	7.8E-09
28-Sep-01	L01142531-2197721	C14	Ra-226	1.2E-08
18-Oct-01	L01142863-2165217	355	Cs-137	2.4E-03
23-Oct-01	L01143715-2210006	166	H-3	8.0E+00
23-Oct-01	L01143714-2210005	347	H-3	1.0E+00
23-Oct-01	L01143709-2210000	347	H-3	2.0E+00
23-Oct-01	L01143710-2210001	347	H-3	3.0E+00
23-Oct-01	L01143711-2210002	347	H-3	8.0E+00
23-Oct-01	L01143712-2210003	347	H-3	9.0E+00
23-Oct-01	L01143699-2210017	347	H-3	1.2E+01
23-Oct-01	L01143707-2210014	347	H-3	2.7E+01
23-Oct-01	L01143716-2210007	347	H-3	2.7E+01
23-Oct-01	L01143708-2210015	347	H-3	5.6E+01
23-Oct-01	L01143698-2210016	347	H-3	6.3E+01
23-Oct-01	L01143701-2210008	347	H-3	7.4E+01
23-Oct-01	L01143702-2210009	347	H-3	9.6E+01
23-Oct-01	L01143703-2210010	347	H-3	1.9E+02
23-Oct-01	L01143704-2210011	347	H-3	1.9E+02
23-Oct-01	L01143705-2210012	347	H-3	1.9E+02
23-Oct-01	L01143706-2210013	347	H-3	1.9E+02
23-Oct-01	L01143700-2210018	347	H-3	3.2E+02
23-Oct-01	L01143713-2210004	347	H-3	3.8E+02

Table II-1 (Continued)
Disposal Data for Waste Containing Critical Radionuclides

Disposal Date	Container-Item ID	Shaft No.	Radionuclide	Activity (Ci)
24-Oct-01	L01143676-2209990	166	H-3	3.3E+03
24-Oct-01	L01143683-2209997	166	H-3	1.4E+04
24-Oct-01	L01143694-2209980	166	H-3	1.8E+04
24-Oct-01	L01143717-2209998	166	H-3	1.8E+04
24-Oct-01	L01143684-2209986	166	H-3	2.3E+04
24-Oct-01	L01143693-2209979	166	H-3	2.7E+04
24-Oct-01	L01143677-2209991	166	H-3	4.3E+04
24-Oct-01	L01143691-2209985	167	H-3	1.3E+04
24-Oct-01	L01143692-2209978	167	H-3	1.4E+04
24-Oct-01	L01143689-2209983	167	H-3	1.5E+04
24-Oct-01	L01143686-2209988	167	H-3	1.5E+04
24-Oct-01	L01143690-2209984	167	H-3	1.6E+04
24-Oct-01	L01143685-2209987	167	H-3	2.3E+04
24-Oct-01	L01143682-2209996	167	H-3	5.1E+04
24-Oct-01	L01143688-2209982	168	H-3	1.1E+03
24-Oct-01	L01143680-2209994	168	H-3	2.2E+03
24-Oct-01	L01143679-2209993	168	H-3	5.4E+03
24-Oct-01	L01143681-2209995	168	H-3	1.4E+04
24-Oct-01	L01143695-2209981	168	H-3	1.8E+04
24-Oct-01	L01143718-2209999	168	H-3	2.7E+04
24-Oct-01	L01143678-2209992	168	H-3	2.7E+04
24-Oct-01	L01143687-2209989	170	H-3	1.4E+04
14-Feb-02	L01142601-2190035	339	H-3	3.1E+02
14-Feb-02	L01142416-2192739	339	H-3	3.4E+02
14-Feb-02	L01142602-2190036	339	H-3	3.6E+02
14-Feb-02	L01142598-2190032	339	H-3	3.7E+02
14-Feb-02	L01142599-2190033	339	H-3	4.4E+02
14-Feb-02	L01142600-2190034	339	H-3	4.8E+02
3-Apr-02	L02146222-2210050	345	H-3	8.5E+01

Table II-1 (Continued)
Disposal Data for Waste Containing Critical Radionuclides

Disposal Date	Container-Item ID	Shaft No.	Radionuclide	Activity (Ci)
3-Apr-02	L01143851-2209818	345	H-3	3.8E+02
3-Apr-02	L02146485-2210055	345	H-3	4.6E+02
2-Jul-02	L02150024-2218970	345	H-3	1.5E+00
2-Jul-02	L02150025-2218971	345	H-3	1.9E+02
2-Jul-02	L02150027-2218973	345	H-3	4.0E+02
2-Jul-02	L02150026-2218972	345	H-3	4.4E+02
2-Jul-02	L02150023-2218969	345	H-3	4.6E+02
17-Jul-02	L02149548-2152231	351	H-3	3.0E+00
17-Jul-02	L02149549-2152223	351	H-3	3.0E+02
17-Jul-02	L02149550-2152226	351	H-3	3.2E+02
17-Jul-02	L02151227-2229810	345	Th-232	4.0E-08
16-Oct-02	L02153538-2220115	343	H-3	5.5E-04
16-Oct-02	L02153539-2220116	343	H-3	5.5E-04
16-Oct-02	L02153538-2220115	343	H-3	5.5E-04
16-Oct-02	L02153539-2220116	343	H-3	5.5E-04
16-Oct-02	L02153538-2220115	343	H-3	1.1E-03
16-Oct-02	L02153539-2220116	343	H-3	1.1E-03
19-Nov-02	L02152167-2218930	343	H-3	1.9E+02
19-Nov-02	L02153586-2220167	343	H-3	1.9E+02
19-Nov-02	L02153728-2241636	343	H-3	3.5E+02
19-Nov-02	L02153588-2220169	343	H-3	3.6E+02
19-Nov-02	L02153587-2220168	343	H-3	3.8E+02
29-Jan-03	L02152798-2218985	343	C-14	7.6E-02
19-Feb-03	L03157462-2241405	362	Ni-63	1.2E+02
20-Feb-03	L03157800-2268806	170	H-3	2.1E+04
20-Feb-03	L03157433-2268807	170	H-3	5.9E+04
20-Feb-03	L03157434-2268808	333	H-3	1.9E+04
20-Feb-03	L03157802-2268810	333	H-3	6.0E+04
20-Feb-03	L03157801-2268809	333	H-3	8.7E+04

Table II-1 (Continued)
Disposal Data for Waste Containing Critical Radionuclides

Disposal Date	Container-Item ID	Shaft No.	Radionuclide	Activity (Ci)
20-Feb-03	L03157386-2268804	333	H-3	8.4E+02
20-Feb-03	L03157387-2268805	333	H-3	5.0E+03
20-Feb-03	L03157385-2268803	333	H-3	1.5E+04
20-Feb-03	L03157761-2268811	335	H-3	2.3E+04
25-Feb-03	L03158115-2220828	361	C-14	1.7E-03
25-Feb-03	L03158115-2220828	361	Ni-63	7.3E+01
27-Feb-03	L03158263-2220827	360	Ni-63	7.2E+01
27-Feb-03	L03158263-2220827	360	Ni-63	7.2E+01
27-Feb-03	L03158263-2220827	360	Ni-63	1.4E+02
6-Mar-03	L03158537-2220824	363	C-14	1.6E+01
6-Mar-03	L03158537-2220824	363	Ni-63	9.6E+01
11-Mar-03	L03158802-2241404	365	Ni-63	6.9E+01
13-Mar-03	L03158958-2241399	367	Ni-63	1.2E+01
18-Mar-03	L03159032-2220825	364	C-14	7.4E-03
18-Mar-03	L03159032-2220825	364	Ni-63	1.4E+02
26-Mar-03	L03157377-2245203	331	H-3	3.5E+01
26-Mar-03	L03157378-2245204	331	H-3	3.5E+01
26-Mar-03	L03156866-2241726	331	H-3	4.6E+02
26-Mar-03	L03157375-2245201	341	H-3	3.5E+01
26-Mar-03	L03157376-2245202	341	H-3	3.5E+01
26-Mar-03	L03157379-2245205	341	H-3	3.5E+01
26-Mar-03	L03156864-2245198	341	H-3	1.1E+02
26-Mar-03	L03156862-2241730	341	H-3	1.5E+02
26-Mar-03	L03156863-2241728	341	H-3	1.5E+02
26-Mar-03	L03156865-2241729	341	H-3	2.2E+02
26-Mar-03	L03156861-2241731	341	H-3	2.6E+02
26-Mar-03	L02154821-2241699	341	H-3	2.8E+02
26-Mar-03	L03156860-2241724	341	H-3	3.0E+02
26-Mar-03	L02154816-2241657	341	H-3	3.5E+02

Table II-1 (Continued)
Disposal Data for Waste Containing Critical Radionuclides

Disposal Date	Container-Item ID	Shaft No.	Radionuclide	Activity (Ci)
26-Mar-03	L02154814-2241655	341	H-3	3.5E+02
26-Mar-03	L03157069-2268802	341	H-3	3.7E+02
26-Mar-03	L02154815-2241656	341	H-3	3.7E+02
26-Mar-03	L03157098-2268801	341	H-3	4.0E+02
26-Mar-03	L03156867-2241727	341	H-3	4.7E+02
26-Mar-03	L02154991-2189525	341	Th-232	1.2E-05
26-Mar-03	L02154991-2189525	341	Th-232	1.2E-05
26-Mar-03	L02154991-2189525	341	Th-232	2.4E-05
27-Mar-03	L03159190-2241400	366	Ag-108m	4.4E+00
27-Mar-03	L03159190-2241400	366	C-14	8.9E-05
27-Mar-03	L03159190-2241400	366	H-3	8.0E+03
27-Mar-03	L03159190-2241400	366	Ni-63	2.5E+02
8-Apr-03	L03159849-2248172	360	Ni-63	3.8E+01
10-Apr-03	L03159850-2248175	360	Ni-63	4.5E+01
15-Apr-03	L03160089-2250140	360	Ni-63	6.1E-01
17-Apr-03	L03160088-2250141	360	C-14	1.0E-02
17-Apr-03	L03160088-2250141	360	Ni-63	4.2E+00
22-Apr-03	L03160219-2250139	360	C-14	6.0E-04
22-Apr-03	L03160219-2250139	360	Ni-63	3.6E-01
23-Apr-03	L03160220-2250142	361	Ni-63	3.2E+00
26-Jun-03	L03160127-2269096	331	H-3	3.5E+00
26-Jun-03	L03159474-2269084	331	H-3	8.1E+02
26-Jun-03	L03160627-2269094	331	H-3	7.4E+00
26-Jun-03	L03160631-2152267	331	H-3	4.9E+01
26-Jun-03	L03160126-2269095	331	H-3	2.5E+02
6-Aug-03	L02154749-2241670	329	H-3	4.7E+02
6-Aug-03	L02154753-2241668	329	H-3	4.7E+02
6-Aug-03	L02154751-2241666	329	H-3	4.8E+02
6-Aug-03	L02154750-2241665	329	H-3	4.8E+02

Table II-1 (Continued)
Disposal Data for Waste Containing Critical Radionuclides

Disposal Date	Container-Item ID	Shaft No.	Radionuclide	Activity (Ci)
6-Aug-03	L02154770-2241671	329	H-3	4.9E+02
6-Aug-03	L02154746-2241669	329	H-3	5.0E+02
6-Aug-03	L02154752-2241667	329	H-3	5.0E+02
6-Aug-03	L02154721-2241659	329	H-3	6.8E+02
6-Aug-03	L02154720-2241658	329	H-3	9.7E+01
10-Sep-03	L03166514-2220653	329	H-3	3.9E+01
10-Sep-03	L03166515-2220654	329	H-3	5.2E+01
10-Sep-03	L03162840-2277647	329	H-3	7.4E+00
1-Oct-03	L03166541-2220655	327	H-3	3.6E+01
1-Oct-03	L03166540-2220736	327	H-3	7.9E+01
1-Oct-03	L03166681-2220749	327	H-3	9.0E+01
1-Oct-03	L03166550-2220734	327	H-3	1.1E+02
1-Oct-03	L03166549-2220735	327	H-3	1.7E+02
1-Oct-03	L03166677-2220740	327	H-3	1.9E+02
1-Oct-03	L03166678-2220745	327	H-3	1.9E+02
1-Oct-03	L03166549-2220735	327	H-3	1.7E+02
1-Oct-03	L03166677-2220740	327	H-3	1.9E+02
1-Oct-03	L03166678-2220745	327	H-3	1.9E+02
1-Oct-03	L03166681-2220749	327	H-3	9.0E+01
1-Oct-03	L03166541-2220655	327	H-3	3.6E+01
1-Oct-03	L03166540-2220736	327	H-3	7.9E+01
1-Oct-03	L03166550-2220734	327	H-3	1.1E+02
1-Oct-03	L03166679-2220744	329	H-3	1.9E+02
1-Oct-03	L03166898-2220746	329	H-3	3.1E+02
1-Oct-03	L03166899-2220747	329	H-3	3.1E+02
1-Oct-03	L03166679-2220744	329	H-3	1.9E+02
1-Oct-03	L03166898-2220746	329	H-3	3.1E+02
1-Oct-03	L03166899-2220747	329	H-3	3.1E+02
17-Dec-03	L03166836-2220751	327	H-3	5.9E+01

Table II-1 (Continued)
Disposal Data for Waste Containing Critical Radionuclides

Disposal Date	Container-Item ID	Shaft No.	Radionuclide	Activity (Ci)
11-Mar-04	L04170012-2205574	327	H-3	9.7E+00
11-Mar-04	L04170013-2205575	327	H-3	9.7E+00
11-Mar-04	L04170014-2214332	327	H-3	1.0E+01
20-May-04	L04170720-2286545	C14	Ag-108m	9.0E-09
20-May-04	L03169683-2236787	323	Cs-137	3.4E-08
20-May-04	L03169389-2287263	323	H-3	2.3E+02
20-May-04	L03169390-2287269	323	H-3	2.5E+02
20-May-04	L03169391-2287268	323	H-3	1.1E+02
20-May-04	L04169714-2287270	323	H-3	1.1E+02
20-May-04	L04169744-2287276	323	H-3	1.1E+02
20-May-04	L04171151-2287338	323	H-3	4.4E+01
20-May-04	L04172462-2287356	323	H-3	1.6E+02
20-May-04	L03164153-2277708	C14	H-3	3.3E-07
17-Feb-05	L04172457-2289617	362	Cs-137	2.3E-06
19-Apr-05	L05176986-2306616	321	Cs-137	4.0E-08
19-Apr-05	L04171587-2287341	321	H-3	9.0E+00
19-Apr-05	L05178620-2335530	321	H-3	3.6E+02
19-Apr-05	L05178621-2335531	321	H-3	3.0E+02
19-Apr-05	L05178622-2335532	321	H-3	2.3E+02
19-Apr-05	L05178618-2335528	321	H-3	3.1E+02
19-Apr-05	L05178619-2335529	321	H-3	3.8E+02
13-May-05	L04176497-2287277	317	H-3	1.1E+02
13-May-05	L04172271-2287352	317	H-3	4.5E+02
13-May-05	L04173418-2287370	317	H-3	4.8E+02
13-May-05	L04174654-2304707	317	H-3	4.6E+02
13-May-05	L04173119-2287361	317	H-3	9.2E+01
13-May-05	L04173120-2287362	317	H-3	9.2E+01
13-May-05	L04172270-2287342	317	H-3	1.8E+02
13-May-05	L04171697-2287353	317	H-3	2.4E+02

Table II-1 (Continued)
Disposal Data for Waste Containing Critical Radionuclides

Disposal Date	Container-Item ID	Shaft No.	Radionuclide	Activity (Ci)
13-May-05	L05178609-2313051	319	H-3	7.0E+03
13-May-05	L05178610-2313052	319	H-3	2.8E+04
13-May-05	L05178611-2313053	319	H-3	3.2E+04
13-May-05	L05178614-2313050	319	H-3	2.3E+04
13-May-05	L05178612-2313048	319	H-3	2.4E+04
13-May-05	L05178613-2313049	319	H-3	3.3E+04
18-Jul-05	L05180108-10011018	317	Ag-108m	2.0E-05
18-Jul-05	L05180109-10011017	317	C-14	9.1E-07
18-Jul-05	L05180108-10011018	317	Cs-137	1.4E-01
18-Jul-05	L05180109-10011017	317	Cs-137	6.0E-07
18-Jul-05	L05180109-10011017	317	H-3	3.0E-09
18-Jul-05	L05180108-10011018	317	Ra-226	1.8E-09
18-Jul-05	L05180109-10011017	317	Sr-90	3.4E-05
26-Jul-05	L04172790-2287347	C14	H-3	3.4E-08
11-Aug-05	L05180419-10004344	317	Cs-137	1.9E-04
16-Sep-05	L05181046-10011019	362	C-14	9.1E-03
16-Sep-05	L05181236-10011027	362	Cs-137	2.7E-02
16-Sep-05	L05181236-10011028	362	Cs-137	2.7E-02
16-Sep-05	L05181046-10011019	362	H-3	4.6E-02
16-Sep-05	L05181046-10011019	362	Ni-63	7.0E+00
16-Sep-05	L05181236-10011027	362	Sr-90	1.2E+01
16-Sep-05	L05181236-10011028	362	Sr-90	1.2E+01
22-Sep-05	L05180106-2329822	317	Ni-63	4.1E+00
27-Sep-05	L05181624-2329823	317	Ni-63	5.8E+00
20-Oct-05	L05181861-10019025	315	Cs-137	3.6E-02
20-Oct-05	L05181862-10019026	315	Cs-137	3.6E-02
20-Oct-05	L05181876-10019029	317	Cs-137	1.7E-05
20-Oct-05	L05181867-10019030	317	Cs-137	6.3E-05
20-Oct-05	L05181862-10019026	315	H-3	1.1E-04

Table II-1 (Continued)
Disposal Data for Waste Containing Critical Radionuclides

Disposal Date	Container-Item ID	Shaft No.	Radionuclide	Activity (Ci)
20-Oct-05	L05181861-10019025	315	H-3	1.1E-04
20-Oct-05	L05181880-10019028	317	Ra-226	3.0E-03
20-Oct-05	L05181876-10019029	317	Ra-226	3.9E-03
20-Oct-05	L05181867-10019030	317	Ra-226	2.7E-03
20-Oct-05	L05181861-10019025	315	Sr-90	3.4E-02
20-Oct-05	L05181862-10019026	315	Sr-90	3.4E-02
20-Oct-05	L05181876-10019029	317	Sr-90	1.0E-03
16-Feb-06	L05183139-2336227	313	H-3	4.2E+02
16-Feb-06	L05183140-2336228	313	H-3	5.0E+02
16-Feb-06	L05183156-2336222	313	H-3	4.4E+02
16-Feb-06	L05183158-2336224	313	H-3	4.8E+02
16-Feb-06	L05183159-2336225	313	H-3	4.9E+02
16-Feb-06	L05183157-2336223	313	H-3	4.3E+02
16-Feb-06	L05183160-2336226	313	H-3	4.2E+02
16-Feb-06	L06183254-2336232	313	H-3	4.8E+02
16-Feb-06	L06183252-2336230	313	H-3	4.8E+02
16-Feb-06	L06183253-2336231	313	H-3	4.8E+02
16-Feb-06	L05182079-10003691	313	Sr-90	4.0E-06
16-Feb-06	L05182079-10003692	313	Sr-90	4.0E-06
24-May-06	L06186548-2336392	309	H-3	5.3E+04
24-May-06	L06186545-2336389	311	H-3	4.6E+04
24-May-06	L06184750-2336313	311	H-3	3.2E+01
24-May-06	L06184750-2336333	311	H-3	3.2E+01
24-May-06	L06186237-2336397	311	H-3	4.9E+02
24-May-06	L06186236-2336396	311	H-3	4.9E+02
24-May-06	L06186546-2336390	363	H-3	4.9E+04
24-May-06	L06186547-2336391	367	H-3	5.3E+04
24-May-06	L06186551-2336407	311	H-3	3.6E+03
24-May-06	L05179632-2335968	311	H-3	2.3E+02

Table II-1 (Continued)
Disposal Data for Waste Containing Critical Radionuclides

Disposal Date	Container-Item ID	Shaft No.	Radionuclide	Activity (Ci)
8-Aug-06	L06187451-10039389	367	Ag-108m	9.8E-05
8-Aug-06	L06187451-10039389	367	Cs-137	4.5E-05
8-Aug-06	L06187135-2336453	367	Cs-137	1.0E-02
8-Aug-06	L06187456-10039384	367	Cs-137	1.0E-01
8-Aug-06	L06187456-10039384	367	H-3	4.5E-04
8-Aug-06	L06187455-10039388	367	Ni-63	5.7E-02
8-Aug-06	L06187135-2336453	367	Ra-226	1.8E-05
8-Aug-06	L06187451-10039389	367	Sr-90	6.1E-07
8-Aug-06	L06187456-10039384	367	Sr-90	2.8E-02
22-Aug-06	L06187449-2336592	309	H-3	3.4E+02
12-Sep-06	L06187941-10052704	367	C-14	4.4E-03
12-Sep-06	L06187941-10052704	367	H-3	1.8E-03
12-Sep-06	L06187941-10052704	367	Ni-63	4.1E-01
19-Sep-06	L06187593-2336629	367	H-3	7.6E+01
19-Sep-06	L06187594-2336630	367	H-3	1.4E+02
19-Sep-06	L06187595-2336631	367	H-3	6.0E+01
19-Sep-06	L06187834-2336729	367	H-3	8.0E+00
19-Sep-06	L06186504-10019034	367	Cs-137	8.0E-04
19-Sep-06	L06186506-10019035	367	Cs-137	5.8E-02
19-Sep-06	L06186506-10019035	367	Sr-90	2.5E-02
19-Sep-06	L06186503-10019032	367	Sr-90	6.0E-01
10-Oct-06	L06187412-2287273	367	Cs-137	1.3E-02
10-Oct-06	L06187929-10042149	367	H-3	1.2E+00
10-Oct-06	L06187929-10042154	367	H-3	1.2E+00
10-Oct-06	L06187929-10042150	367	H-3	1.2E+00
10-Oct-06	L06187869-10005839	367	Ra-226	1.5E-08
10-Oct-06	L06187870-10005840	367	Ra-226	1.5E-08
10-Oct-06	L06187871-10005841	367	Ra-226	1.5E-08
10-Oct-06	L06187868-10005838	367	Ra-226	1.5E-08

Table II-1 (Continued)
Disposal Data for Waste Containing Critical Radionuclides

Disposal Date	Container-Item ID	Shaft No.	Radionuclide	Activity (Ci)
10-Oct-06	L06187867-10005837	367	Ra-226	1.5E-08
10-Oct-06	L06187866-10005836	367	Ra-226	1.5E-08
12-Dec-06	L06188746-2333556	367	H-3	1.3E+02
12-Dec-06	L06188745-2333555	367	H-3	9.6E+02
1-Mar-07	L07190166-10047128	367	H-3	5.6E+02
1-Mar-07	L06187985-10047130	367	H-3	1.4E+02
1-Mar-07	L06187984-10047129	367	H-3	3.4E+02
1-Mar-07	L06187986-10047131	367	H-3	1.4E+02
12-Apr-07	L05180717-10005702	364	H-3	4.2E+00
12-Apr-07	L05180718-10005701	364	H-3	5.6E+00
12-Apr-07	L05180716-10005703	364	H-3	3.0E+00

Table II- 2
Disposal Data for Waste Containers that Account for 1 Percent or More of the Total Critical Radionuclide Inventories

Radionuclide	Disposal Date	Container-Item ID	Shaft No.	Activity (Ci)	Percent of Total Inventory
Ag-108m	27-Mar-03	L03159190-2241400	366	4.4E+00	100
C-14	6-Mar-03	L03158537-2220824	363	1.6E+01	99
Cs-137	30-Jun-94	L94000445-530809	131	1.5E+01	17
	21-Sep-92	L92000741-528951	301	6.7E+01	81
H-3	12-Jan-89	S890125-522908	155	4.3E+04	3
	17-May-95	L95049714-2010397	162	1.7E+05	10
	17-May-95	L95049715-2010398	162	1.3E+05	8
	26-Sep-95	L95056351-2023593	162	5.5E+04	3
	24-Oct-01	L01143694-2209980	166	1.8E+04	1
	24-Oct-01	L01143717-2209998	166	1.8E+04	1
	24-Oct-01	L01143684-2209986	166	2.3E+04	1
	24-Oct-01	L01143693-2209979	166	2.7E+04	2
	24-Oct-01	L01143677-2209991	166	4.3E+04	3
	24-Oct-01	L01143685-2209987	167	2.3E+04	1
	24-Oct-01	L01143682-2209996	167	5.1E+04	3
	24-Oct-01	L01143695-2209981	168	1.8E+04	1
	24-Oct-01	L01143718-2209999	168	2.7E+04	2
	24-Oct-01	L01143678-2209992	168	2.7E+04	2
	20-Feb-03	L03157800-2268806	170	2.1E+04	1
	20-Feb-03	L03157433-2268807	170	5.9E+04	3
	24-May-06	L06186548-2336392	309	5.3E+04	3
	24-May-06	L06186545-2336389	311	4.6E+04	3
	13-May-05	L05178610-2313052	319	2.8E+04	2
	13-May-05	L05178611-2313053	319	3.2E+04	2
	13-May-05	L05178614-2313050	319	2.3E+04	1
	13-May-05	L05178612-2313048	319	2.4E+04	1

Table II-2 (Continued)
Disposal Data for Waste Containers that Account for 1 Percent or More of the Total Critical Radionuclide Inventories

Radionuclide	Disposal Date	Container-Item ID	Shaft No.	Activity (Ci)	Percent of Total Inventory
H-3 (Continued)	13-May-05	L05178613-2313049	319	3.3E+04	2
	20-Feb-03	L03157434-2268808	333	1.9E+04	1
	20-Feb-03	L03157802-2268810	333	6.0E+04	4
	20-Feb-03	L03157801-2268809	333	8.7E+04	5
	20-Feb-03	L03157761-2268811	335	2.3E+04	1
	1-Oct-97	L97095087-2072222	339	5.3E+04	3
	1-Oct-97	L97095088-2072221	339	7.7E+04	5
	24-May-06	L06186546-2336390	363	4.9E+04	3
	24-May-06	L06186547-2336391	367	5.3E+04	3
Ni-63	27-Feb-03	L03158263-2220827	360	7.2E+01	6
	27-Feb-03	L03158263-2220827	360	7.2E+01	6
	27-Feb-03	L03158263-2220827	360	1.4E+02	12
	10-Apr-03	L03159850-2248175	360	4.5E+01	4
	8-Apr-03	L03159849-2248172	360	3.8E+01	3
	25-Feb-03	L03158115-2220828	361	7.3E+01	6
	19-Feb-03	L03157462-2241405	362	1.2E+02	10
	6-Mar-03	L03158537-2220824	363	9.6E+01	8
	18-Mar-03	L03159032-2220825	364	1.4E+02	12
	11-Mar-03	L03158802-2241404	365	6.9E+01	6
	27-Mar-03	L03159190-2241400	366	2.5E+02	22
	13-Mar-03	L03158958-2241399	367	1.2E+01	1
Ra-226	30-Sep-97	L97096618-2088682	144	5.0E-02	6
	11-Jun-96	L96067978-2033108	301	4.9E-01	64
	11-Jun-96	L96067977-2033113	301	5.5E-02	7
	6-Apr-99	L99114245-2097060	339	1.7E-01	22
Sr-90	13-Dec-88	S880453-522167	141	1.0E+00	1
	13-Aug-90	S903359-524016	141	4.0E+00	5

Table II-2 (Continued)
Disposal Data for Waste Containers that Account for 1 Percent or More of the Total Critical Radionuclide Inventories

Radionuclide	Disposal Date	Container-Item ID	Shaft No.	Activity (Ci)	Percent of Total Inventory
Sr-90 (Continued)	30-Sep-97	L97096618-2088682	144	5.6E+01	65
	16-Sep-05	L05181236-10011027	362	1.2E+01	14
	16-Sep-05	L05181236-10011028	362	1.2E+01	14
Th-232	4-Feb-99	L98109888-2099036	197	2.6E-03	1
	4-Feb-99	L98109895-2099043	197	3.0E-03	2
	4-Feb-99	L98109901-2099049	197	3.4E-03	2
	4-Feb-99	L98109891-2099039	197	3.5E-03	2
	4-Feb-99	L98109900-2099048	197	3.6E-03	2
	4-Feb-99	L98109893-2099041	197	3.7E-03	2
	4-Feb-99	L98109885-2099033	197	3.8E-03	2
	4-Feb-99	L98109892-2099040	197	3.8E-03	2
	4-Feb-99	L98109898-2099046	197	3.8E-03	2
	4-Feb-99	L98109890-2099038	197	3.9E-03	2
	4-Feb-99	L98109910-2099064	197	2.2E-03	1
	4-Feb-99	L98109914-2099068	197	2.3E-03	1
	4-Feb-99	L98109911-2099065	197	2.5E-03	1
	4-Feb-99	L98109909-2099063	197	2.8E-03	2
	4-Feb-99	L98109912-2099066	197	3.7E-03	2
	4-Feb-99	L98109904-2099052	197	4.5E-03	2
	4-Feb-99	L98109913-2099067	197	5.9E-03	3
	4-Feb-99	L98109905-2099059	197	2.8E-02	15
	4-Feb-99	L98109917-2099071	197	2.3E-02	13
	29-Oct-98	L98109894-2099042	308	3.6E-03	2
	29-Oct-98	L98109896-2099044	308	3.7E-03	2
	29-Oct-98	L98109897-2099045	308	3.7E-03	2
	29-Oct-98	L98109886-2099034	308	3.8E-03	2
	29-Oct-98	L98109889-2099037	308	3.8E-03	2

Table II-2 (Continued)
Disposal Data for Waste Containers that Account for 1 Percent or More of the Total Critical Radionuclide Inventories

Radionuclide	Disposal Date	Container-Item ID	Shaft No.	Activity (Ci)	Percent of Total Inventory
Th-232 (Continued)	29-Oct-98	L98109887-2099035	308	4.1E-03	2
	29-Oct-98	L98109903-2099051	308	4.4E-03	2
	29-Oct-98	L98109899-2099047	308	4.9E-03	3
	29-Oct-98	L98109902-2099050	308	5.5E-03	3
	29-Oct-98	L98109908-2099062	308	4.2E-03	2
	29-Oct-98	L98109907-2099061	308	7.6E-03	4
	29-Oct-98	L98109906-2099060	308	1.6E-02	9
	29-Oct-98	L98109916-2099070	308	2.2E-03	1

Table II- 3
Disposal Data for Tritium Waste Containers Included in the Depth-of-Disposal Analysis

Disposal Date	Container-Item ID	Shaft No.	Activity (Ci)
12-Jan-89	S890122-526249	155	4.8E+03
12-Jan-89	S890124-523609	155	5.5E+03
12-Jan-89	S890125-522908	155	4.3E+04
12-Jan-89	S890121-522808	155	2.5E+03
18-Sep-89	S891541-522380	158	1.1E+04
17-May-95	L95049714-2010397	162	1.7E+05
17-May-95	L95049715-2010398	162	1.3E+05
26-Sep-95	L95056351-2023593	162	5.5E+04
24-Oct-01	L01143676-2209990	166	3.3E+03
24-Oct-01	L01143683-2209997	166	1.4E+04
24-Oct-01	L01143694-2209980	166	1.8E+04
24-Oct-01	L01143717-2209998	166	1.8E+04
24-Oct-01	L01143684-2209986	166	2.3E+04
24-Oct-01	L01143693-2209979	166	2.7E+04
24-Oct-01	L01143677-2209991	166	4.3E+04
24-Oct-01	L01143691-2209985	167	1.3E+04
24-Oct-01	L01143692-2209978	167	1.4E+04
24-Oct-01	L01143689-2209983	167	1.5E+04
24-Oct-01	L01143686-2209988	167	1.5E+04
24-Oct-01	L01143690-2209984	167	1.6E+04
24-Oct-01	L01143685-2209987	167	2.3E+04
24-Oct-01	L01143682-2209996	167	5.1E+04
24-Oct-01	L01143680-2209994	168	2.2E+03
24-Oct-01	L01143679-2209993	168	5.4E+03
24-Oct-01	L01143681-2209995	168	1.4E+04
24-Oct-01	L01143695-2209981	168	1.8E+04
24-Oct-01	L01143718-2209999	168	2.7E+04
24-Oct-01	L01143678-2209992	168	2.7E+04
20-Feb-03	L03157800-2268806	170	2.1E+04

Table II-3 (Continued)
Disposal Data for Tritium Waste Containers Included in the Depth-of-Disposal Analysis

Disposal Date	Container-Item ID	Shaft No.	Activity (Ci)
24-Oct-01	L01143687-2209989	170	1.4E+04
20-Feb-03	L03157433-2268807	170	5.9E+04
24-May-06	L06186548-2336392	309	5.3E+04
24-May-06	L06186545-2336389	311	4.6E+04
24-May-06	L06186551-2336407	311	3.6E+03
13-May-05	L05178609-2313051	319	7.0E+03
13-May-05	L05178610-2313052	319	2.8E+04
13-May-05	L05178611-2313053	319	3.2E+04
13-May-05	L05178614-2313050	319	2.3E+04
13-May-05	L05178612-2313048	319	2.4E+04
13-May-05	L05178613-2313049	319	3.3E+04
20-Feb-03	L03157434-2268808	333	1.9E+04
20-Feb-03	L03157802-2268810	333	6.0E+04
20-Feb-03	L03157801-2268809	333	8.7E+04
20-Feb-03	L03157387-2268805	333	5.0E+03
20-Feb-03	L03157385-2268803	333	1.5E+04
20-Feb-03	L03157761-2268811	335	2.3E+04
1-Oct-97	L97095087-2072222	339	5.3E+04
1-Oct-97	L97095088-2072221	339	7.7E+04
9-Mar-00	L99122337-2042601	349	1.8E+03
9-Mar-00	L99122338-2042602	349	2.4E+03
25-Jan-00	L99122700-2042611	351	2.4E+03
25-Jan-00	L99122703-2042614	351	2.5E+03
25-Jan-00	L99122702-2042615	351	2.6E+03
25-Jan-00	L99122701-2042613	351	3.2E+03
25-Jan-00	L99122704-2042612	351	5.1E+03
24-May-06	L06186546-2336390	363	4.9E+04
27-Mar-03	L03159190-2241400	366	8.0E+03
24-May-06	L06186547-2336391	367	5.3E+04

3.0 Results

The depths of disposal for the waste containers of interest that had recorded placement depths are summarized in Table II-4. Consistent with the discussion in Section 2.0, the containers with measured depths of 4.5 m (14.8 ft) or more below ground level were assigned to the lower portion of the waste profile while containers with disposal depths that were less than this were assigned to the top 1.5 m (4.9 ft) of the waste profile. Only three containers of interest are located within the upper portion of the waste profile; these are listed in bold in Table II-4.

Table II-5 lists the disposal depth data for waste packages placed in shafts with containers of interest; the containers of interest are listed in bold. Several steps were taken to reduce the amount of data included in the table. The shafts with no disposal depth data and those that received only containers of interest are excluded from the table. Also, if the data in Table II-4 can be used to directly characterize the depth of disposal for the containers of interest in a given shaft, that shaft is excluded from Table II-5. If a shaft contains many waste packages, disposal depth information is listed for ranges of containers and only a representative number of packages that were disposed of after the last container of interest was placed are included.

The information included in Table II-5 can be used to assign depths of placement for some of the waste containers of interest. For example, the depth of disposal listed for container-item L07189457-10031004, disposed of in shaft 333, indicates that all containers of interest lie in the lower portion of the waste profile. A similar conclusion can be reached with respect to container-items L97095088-2072221 and L97095087-2072222 in shaft 339, L03157462-2241405 in shaft 362, L03159190-2241400 in shaft 366, and L03158958-2241399 in shaft 367, using the disposal depth information for waste that was placed in the shafts after these wastes. Conversely, the information included in Table II-5 indicates that the containers of interest in shaft 197 were placed in the upper portion of the waste profile. There is insufficient information in Table II-5 to assign depths of disposal for the other containers of interest.

The depths to the topmost containers in open shafts, or to the tuff backfill that was placed over the containers, are measured periodically as a means of estimating remaining disposal capacity. Measurements taken in August 2005 provide information about some of the containers of interest for which depths of disposal have not yet been determined; these depths are summarized in Table II-6. Although these measurements may not represent the actual depths to the containers of interest, they can be used to estimate the minimum depths to these packages. The results in the table indicate that all waste containers of interest in shafts 170, 301, 335, 364, and 365 may be assigned to the lower portion of the waste profile.

Table II-4
Direct Measurements of Disposal Depth

Shaft	Disposal Date	Container-Item ID	Depth to Top of Disposal Container (m) [a]
144	30-Sep-97	L97096618-2088682	11.9
166	24-Oct-01	L01143676-2209990	9.9
166	24-Oct-01	L01143683-2209997	11.9
166	24-Oct-01	L01143694-2209980	7.8
166	24-Oct-01	L01143717-2209998	15.6
166	24-Oct-01	L01143684-2209986	13.8
166	24-Oct-01	L01143693-2209979	5.6
166	**24-Oct-01**	**L01143677-2209991**	**3.5**
167	24-Oct-01	L01143691-2209985	10.5
167	24-Oct-01	L01143692-2209978	16.3
167	24-Oct-01	L01143689-2209983	6.4
167	24-Oct-01	L01143686-2209988	12.6
167	24-Oct-01	L01143690-2209984	8.4
167	24-Oct-01	L01143685-2209987	14.3
167	24-Oct-01	L01143682-2209996	4.5
168	24-Oct-01	L01143680-2209994	16.2
168	24-Oct-01	L01143679-2209993	8.4
168	24-Oct-01	L01143681-2209995	6.4
168	**24-Oct-01**	**L01143695-2209981**	**4.4**
168	24-Oct-01	L01143718-2209999	12.3
168	24-Oct-01	L01143678-2209992	10.4
170	24-Oct-01	L01143687-2209989	16.7
311	24-May-06	L06186545-2336389	5.5
311	24-May-06	L06186551-2336407	5.5
319	13-May-05	L05178609-2313051	5.8

***Bold** type indicates a container of interest that resides in the upper portion of the waste profile.*

[a] *Disposal depths are measured from the ground surface to the top of the waste containers; the depth of disposal relative to the top of the waste was estimated as the listed depth less 3 m (9.8 ft).*

Table II-4 (Continued)
Direct Measurements of Disposal Depth

Shaft	Disposal Date	Container-Item ID	Depth to Top of Disposal Container (m) [a]
319	13-May-05	L05178610-2313052	11.3
319	13-May-05	L05178611-2313053	8.5
319	13-May-05	L05178614-2313050	3.0
319	13-May-05	L05178612-2313048	11.3
319	13-May-05	L05178613-2313049	14.0
333	20-Feb-03	L03157434-2268808	12.9
339	6-Apr-99	L99114245-2097060	19.2
349	9-Mar-00	L99122337-2042601	14.6
349	9-Mar-00	L99122338-2042602	14.6
351	25-Jan-00	L99122700-2042611	6.6
351	25-Jan-00	L99122703-2042614	8.4
351	25-Jan-00	L99122702-2042615	7.5
351	25-Jan-00	L99122701-2042613	10.4
351	25-Jan-00	L99122704-2042612	9.4
360	27-Feb-03	L03158263-2220827	16.6
360	8-Apr-03	L03158849-2248172	14.1
360	10-Apr-03	L03159850-2248175	11.5
362	16-Sep-05	L05181236-10011027	5.2
362	16-Sep-05	L05181236-10011028	5.2
363	6-Mar-03	L033158537-2220824	17.8

***Bold** type indicates a container of interest that resides in the upper portion of the waste profile.*

[a] *Disposal depths are measured from the ground surface to the top of the waste containers; the depth of disposal relative to the top of the waste was estimated as the listed depth less 3 m (9.8 ft).*

Table II-5
Disposal Depths for Waste Containers Placed in Selected Shafts

Shaft	Disposal Date	Container-Item ID	Depth to Top of Disposal Container (m) [a]
131	5-Mar-92 – 27-Jun-94	Various	---
131	30-Jun-94	L94000445-530809	---
131	27-Jul-94 – 26-Jul-95	Various	---
131	19-May-98	L98104604-2113234	3.0
131	20-May-98	L98104552-2113236	2.4
197	27-Oct-93 – 13-Jan-97	Various	---
197	15-Jan-98	L97099821-2066176	4.3
197	15-Jan-98	L97099817-2066175	4.3
197	24-Mar-98	L98102327-2046467	4.3
197	24-Mar-98	L98102326-2046466	4.3
197	24-Mar-98	L98102325-2046465	4.3
197	4-Feb-99	Various	---
197	4-Feb-99	L98109917-2099071	---
197	4-Feb-99	L98109914-2099068	---
197	4-Feb-99	L98109913-2099067	---
197	4-Feb-99	L98109912-2099066	---
197	4-Feb-99	L98109911-2099065	---
197	4-Feb-99	L98109910-2099064	---
197	4-Feb-99	L98109909-2099063	---
197	4-Feb-99	L98109905-2099059	---
197	4-Feb-99	L98109904-2099052	---
197	4-Feb-99	L98109901-2099049	---
197	4-Feb-99	L98109900-2099048	---
197	4-Feb-99	L98109898-2099046	---
197	4-Feb-99	L98109895-2099043	---

--- = Indicates that depth of disposal information is unavailable.

***Bold** type indicates the package is a container of interest.*

[a] *Disposal depths are measured from the ground surface to the top of the waste containers; the depth of disposal relative to the top of the waste was estimated as the listed depth less 3 m (9.8 ft).*

Table II-5 (Continued)
Disposal Depths for Waste Containers Placed in Selected Shafts

Shaft	Disposal Date	Container-Item ID	Depth to Top of Disposal Container (m) [a]
197	4-Feb-99	L98109893-2099041	---
197	4-Feb-99	L98109892-2099040	---
197	4-Feb-99	L98109891-2099039	---
197	4-Feb-99	L98109890-2099038	---
197	4-Feb-99	L98109888-2099036	---
197	4-Feb-99	L98109885-2099033	---
308	18-Mar-94	L93000807-529862	---
308	26-Jun-98	L98105432-2088731	16.2
308	29-Oct-98	L98109916-2099070	---
308	29-Oct-98	L98109908-2099062	---
308	29-Oct-98	L98109907-2099061	---
308	29-Oct-98	L98109906-2099060	---
308	29-Oct-98	L98109903-2099051	---
308	29-Oct-98	L98109902-2099050	---
308	29-Oct-98	L98109899-2099047	---
308	29-Oct-98	L98109897-2099045	---
308	29-Oct-98	L98109896-2099044	---
308	29-Oct-98	L98109894-2099042	---
308	29-Oct-98	L98109889-2099037	---
308	29-Oct-98	L98109887-2099035	---
308	29-Oct-98	L98109886-2099034	---
333	20-Feb-03	L03157802-2268810	---
333	20-Feb-03	L03157801-2268809	---
333	20-Feb-03	L03157434-2268808	12.9
333	20-Feb-03	L03157387-2268805	---
333	20-Feb-03	L03157386-2268804	---

--- = Indicates that depth of disposal information is unavailable.

Bold *type indicates the package is a container of interest.*

[a] *Disposal depths are measured from the ground surface to the top of the waste containers; the depth of disposal relative to the top of the waste was estimated as the listed depth less 3 m (9.8 ft).*

Table II-5 (Continued)
Disposal Depths for Waste Containers Placed in Selected Shafts

Shaft	Disposal Date	Container-Item ID	Depth to Top of Disposal Container (m) [a]
333	20-Feb-03	L03157385-2268803	---
333	11-Jan-07	L07189457-10031004	12.1
333	1-Feb-07	L07189634-10031005	11.3
333	8-Mar-07	L07190317-10031006	10.1
333	29-Mar-07	L07190552-10031007	8.3
333	19-Apr-07	L07190645-10031008	7.0
333	10-May-07	L07191052-10031009	4.6
333	17-May-07	L07191103-10031010	4.0
333	14-Jun-07	L07191500-10031011	---
339	**1-Oct-97**	**L97095088-2072221**	---
339	**1-Oct-97**	**L97095087-2072222**	---
339	6-Apr-99	L99114245-2097061	19.2
339	**6-Apr-99**	**L99114245-2097060**	**19.2**
339	27-Apr-99	L99115436-2096367	13.1
339	27-Apr-99	L99115435-2096366	13.1
339	27-Apr-99	L99115434-2098369	13.1
339	27-Apr-99	L99115433-2098368	13.1
339	27-Apr-99	L99115432-2098367	13.1
339	27-Apr-99	L99115431-2098366	13.1
339	27-Apr-99	L99115430-2098365	13.1
339	27-Apr-99	L99115429-2098364	13.1
362	**19-Feb-03**	**L03157462-2241405**	---
362	**16-Sep-05**	**L05181236-10011027**	**5.2**
362	**16-Sep-05**	**L05181236-10011028**	**5.2**
366	**27-Mar-03**	**L03159190-2241400**	---
366	30-May-06	L06184324-10025812	12.1

--- = Indicates that depth of disposal information is unavailable.

***Bold** type indicates the package is a container of interest.*

[a] *Disposal depths are measured from the ground surface to the top of the waste containers; the depth of disposal relative to the top of the waste was estimated as the listed depth less 3 m (9.8 ft).*

Table II-5 (Continued)
Disposal Depths for Waste Containers Placed in Selected Shafts

Shaft	Disposal Date	Container-Item ID	Depth to Top of Disposal Container (m) [a]
366	30-May-06	L06184325-10025813	12.1
367	13-Mar-03	L03158958-2241399	---
367	24-May-06	L06186547-2336391	18.1
367	8-Aug-06	L06187457-10039385	16.6
367	8-Aug-06	L06187456-10039384	16.6
367	8-Aug-06	L06187455-10039387	16.6
367	8-Aug-06	L06187454-10039383	16.6
367	8-Aug-06	L06187453-10039390	16.6
367	8-Aug-06	L06187451-10039389	16.6
367	8-Aug-06	L06187450-10039386	16.6
367	8-Aug-06	L06187135-2336453	16.6

--- = Indicates that depth of disposal information is unavailable.

***Bold** type indicates the package is a container of interest.*

[a] *Disposal depths are measured from the ground surface to the top of the waste containers; the depth of disposal relative to the top of the waste was estimated as the listed depth less 3 m (9.8 ft).*

Table II- 6
Summary of August 2005 Measurements of Remaining Depths in Selected Shafts

Shaft	Depth to Uppermost Container or Backfill (m)
170	12.5
301	6.1
335	9.1
364	9.1
365	19.8

Strong inferences may be made about the depths of disposal for several containers on the basis of the depths of the shafts in which they were placed and the dates of placement relative to other packages in those shafts. Table II-7 summarizes the information used to make these inferences; the containers of interest are listed in bold. The conclusions reached on the basis of these data are provided in the following paragraphs.

Shaft 155 contains four containers of interest with tritium activities ranging from 2,500 to 5,500 Ci; these were among the first six containers placed in the 20-m (65-ft) deep disposal unit. This waste was disposed of in 1989, when it was common practice to place high-activity tritium in 0.057- and 0.114-m^3 (15- and 30-gal) containers that were subsequently placed in 0.21 m^3 (55-gal) drums. The 0.21m^3 (55-gal) drums are approximately 0.91 m (3 ft) tall. Assuming the drums were stacked upon one another in the 0.91-m (3-ft) diameter shaft, the top of these six containers would lie approximately 14 m (45 ft) from the ground surface. Therefore, all containers of interest reside in the lower waste profile.

The container of interest in shaft 158 was the first package placed in the 13.7 m (45 ft) deep disposal unit. This waste was disposed of in 1989, when it was common practice to place high-activity tritium in 0.057- and 0.114-m^3 (15- and 30-gal) containers that were subsequently placed in 0.21 m^3 (55-gal) drums. Clearly, this waste resides in the lower portion of the waste profile.

The three containers of interest in shaft 162 contained 55,000 to 166,000 Ci of tritium at the time of disposal; the containers were the first placed in the unit. This waste was packaged in stainless steel containers that were subsequently placed in "torpedo tubes" that were on the order of 2.4 to 3 m (8 to 10 ft) tall and about 0.91 m (3 ft) in diameter; these tubes were designed to be stacked directly upon one another. Following placement of these tubes in the 18-m (60-ft) deep shaft, the top of this waste would lie at least 9.1 m (30 ft) below the surface of the ground, placing it in the lower portion of the waste profile.

Thirteen containers of interest were disposed of in shaft 308, all of which contained Th-232. Ten containers were disposed of in the 20-m (65-ft) deep, 1.5-m (5-ft) diameter shaft prior to these containers; the last of these containers was placed in June of 1998. The distance to the top of the waste was measured after the first 10 containers were placed in the shaft and found to be 16 m (53 ft). Disposal records for these containers indicate the waste was placed in 0.11- and 0.21-m^3 (30- and 55-gal) drums. Based on the approximate heights of these containers (0.91 m (3 ft) or less) and the shaft depth occupied by the packages, it appears that containers were packed side-by-side within the shaft. Of the 13 containers of interest, 12 are 0.21-m^3 (55-gal) drums and 1 is a 0.32-m^3 (85-gal) drum. Assuming these drums were packed in a manner similar to the first 10 containers, the waste of concern is expected to occupy less than 5 m (16 ft) of shaft space, placing the waste in the lower portion of the waste profile.

Table II- 7
Disposal Data for Selected Waste Containers and Shaft Depths

Shaft	Disposal Date	Container-Item ID	Shaft Depth (m) [a]
155	12-Jan-89	S890125-522908	19.8
155	12-Jan-89	S890124-523609	
155	12-Jan-89	S890123-523464	
155	12-Jan-89	S890122-526249	
155	12-Jan-89	S890121-522808	
155	12-Jan-89	S890120-522556	
155	7-Apr-89	S893506-522367	
155	7-Apr-89	S893505-522694	
155	7-Apr-89	S891537-522804	
155	7-Apr-89	S891536-523567	
155	7-Apr-89	S891535-523123	
155	7-Apr-89	S891532-522783	
158	18-Sep-89	S891541-522380	13.7
158	27-Nov-89	S894114-523403	
158	13-Nov-90	S902418-523815	
158	25-Feb-91	S910635-526413	
158	9-Aug-93	L93000139-529257	
158	11-Aug-93	L93000924-529545	
162	17-May-95	L95049715-2010398	18.3
162	17-May-95	L95049714-2010397	
162	26-Sep-95	L95056351-2023593	
308	18-Mar-94	L93000807-529862	19.8
308	26-Jun-98	L98105432-2088731	
308	29-Oct-98	L98109916-2099070	
308	29-Oct-98	L98109908-2099062	
308	29-Oct-98	L98109907-2099061	
308	29-Oct-98	L98109906-2099060	

*-**Bold** font indicates package is a container of interest.*

Table II-7 (Continued)
Disposal Data for Selected Waste Containers and Shaft Depths

Shaft	Disposal Date	Container-Item ID	Shaft Depth (m) [a]
308 (continued)	29-Oct-98	L98109903-2099051	
308	29-Oct-98	L98109902-2099050	
308	29-Oct-98	L98109899-2099047	
308	29-Oct-98	L98109897-2099045	
308	29-Oct-98	L98109896-2099044	
308	29-Oct-98	L98109894-2099042	
308	29-Oct-98	L98109889-2099037	
308	29-Oct-98	L98109887-2099035	
308	29-Oct-98	L98109886-2099034	
361	25-Feb-03	L03158115-2220828	19.2
361	23-Apr-03	L03160220-2250142	
361	16-Feb-05	L04172455-2289616	

Bold font indicates the package is a container of interest.

Similar to the situation noted above for shaft 158, the waste container of interest in shaft 361 was the first container placed in the 19.2-m (63-ft) unit. The container is a liner that stands 1.9 m (6.2 ft) tall and is about 1.5 m (5.1 ft) in diameter. Assuming the package was placed on end in the 1.8 m (6 ft) diameter shaft, the top of the container would lie about 17.3 m (56.8 ft) below the surface of the disposal site after placement and, as a result, can be assigned to the lower portion of the waste profile.

There is not enough information available to assign a depth of disposal for the containers of interest that were disposed of in shafts 131 and 141. In terms of shaft 131, information for other containers in this unit indicate that the container of interest was placed at least 3.1 m (10 ft) down from the surface. However, a definitive assignment of the disposal depth cannot be made in the absence of information about the packing arrangement of the containers placed in the unit after the container of interest but before the containers for which depth of disposal data are available. It is expected that container-item S880453-522167 resides in the lower portion of the waste profile in shaft 141 because it was one of the first containers placed in the disposal unit. The other container-item of interest in this unit, S903359-524016, may very well reside in the upper portion of the waste. Without more definitive information, however, neither container can be confidently assigned a depth of disposal.

The final results of the depth-of-disposal evaluation are summarized in Table II-8. For each of the containers of interest, the table indicates the shaft in which disposal took place, date of disposal, container and item identification numbers, and depth to the top of the package (where available); the positions of the containers within the waste profile and the rationale for these assignments are also provided. Containers assigned to the lower waste profile are those that lie at least 1.5 m (4.9 ft) below the top of the waste and 4.5 m (14.8 ft) below ground surface.

As discussed above, there was insufficient information to assign depths of disposal for three containers of interest. Lacking such data, the waste in these containers is assumed to be homogeneously distributed throughout the disposal units. The radionuclides that made small contributions to the projected intruder doses and were, therefore, not included in the depth-of-disposal evaluation were also assumed to be homogeneously distributed within the waste profile.

Table II- 8
Summary of the Depth-of-Disposal Evaluation

Shaft	Disposal Date	Container-Item ID	Depth to Top of Disposal Container (m) [a]	Assigned Position Within Waste Profile	Rationale for Assignment
131	30-Jun-94	L94000445-530809	---	Uniformly distributed throughout waste profile	Insufficient data to assign container to upper or lower waste profile
141	13-Dec-88	S880453-522167	---	Uniformly distributed throughout waste profile	Insufficient data to assign container to upper or lower waste profile
141	13-Aug-90	S903359-524016	---	Uniformly distributed throughout waste profile	Insufficient data to assign container to upper or lower waste profile
144	30-Sep-97	L97096618-2088682	11.9	Lower waste profile	Direct measurement of depth of disposal
155	12-Jan-89	S890122-526249	---	Lower waste profile	Four of bottom-most six containers in 19.8 m deep shaft.
155	12-Jan-89	S890124-523609	---	Lower waste profile	Four of bottom-most six containers in 19.8 m deep shaft.
155	12-Jan-89	S890125-522908	---	Lower waste profile	Four of bottom-most six containers in 19.8 m deep shaft.
155	12-Jan-89	S890121-522808	---	Lower waste profile	Four of bottom-most six containers in 19.8 m deep shaft.
158	18-Sep-89	S891541-522380	---	Lower waste profile	Bottom-most container in 13.7 m deep shaft.
162	17-May-95	L95049714-2010397	---	Lower waste profile	Bottom-most container in 18.3 m deep shaft.
162	17-May-95	L95049715-2010398	---	Lower waste profile	Bottom-most container in 18.3 m deep shaft.
162	26-Sep-95	L95056351-2023593	---	Lower waste profile	Bottom-most container in 18.3 m deep shaft.
166	24-Oct-01	L01143676-2209990	9.9	Lower waste profile	Direct measurement of depth of disposal
166	24-Oct-01	L01143683-2209997	11.9	Lower waste profile	Direct measurement of depth of disposal
166	24-Oct-01	L01143694-2209980	7.8	Lower waste profile	Direct measurement of depth of disposal
166	24-Oct-01	L01143717-2209998	15.6	Lower waste profile	Direct measurement of depth of disposal

--- Indicates that depth-of-disposal information is unavailable.

[a] Disposal depths are measured from the ground surface to the top of the waste containers; the depth of disposal relative to the top of the waste was estimated as the listed depths less 3 m (9.8 ft).

Table II-8 (Continued)
Summary of the Depth-of-Disposal Evaluation

Shaft	Disposal Date	Container-Item ID	Depth to Top of Disposal Container (m) [a]	Assigned Position Within Waste Profile	Rationale for Assignment
166	24-Oct-01	L01143684-2209986	13.8	Lower waste profile	Direct measurement of depth of disposal
166	24-Oct-01	L01143693-2209979	5.6	Lower waste profile	Direct measurement of depth of disposal
166	24-Oct-01	L01143677-2209991	3.5	Lower waste profile	Direct measurement of depth of disposal
167	24-Oct-01	L01143691-2209985	10.5	Lower waste profile	Direct measurement of depth of disposal
167	24-Oct-01	L01143692-2209978	16.3	Lower waste profile	Direct measurement of depth of disposal
167	24-Oct-01	L01143689-2209983	6.4	Lower waste profile	Direct measurement of depth of disposal
167	24-Oct-01	L01143686-2209988	12.6	Lower waste profile	Direct measurement of depth of disposal
167	24-Oct-01	L01143690-2209984	8.4	Lower waste profile	Direct measurement of depth of disposal
167	24-Oct-01	L01143685-2209987	14.3	Lower waste profile	Direct measurement of depth of disposal
167	24-Oct-01	L01143682-2209996	4.5	Lower waste profile	Direct measurement of depth of disposal
168	24-Oct-01	L01143680-2209994	16.2	Lower waste profile	Direct measurement of depth of disposal
168	24-Oct-01	L01143679-2209993	8.4	Lower waste profile	Direct measurement of depth of disposal
168	24-Oct-01	L01143681-2209995	6.4	Lower waste profile	Direct measurement of depth of disposal
168	24-Oct-01	L01143695-2209981	4.4	Lower waste profile	Direct measurement of depth of disposal
168	24-Oct-01	L01143718-2209999	12.3	Lower waste profile	Direct measurement of depth of disposal
168	24-Oct-01	L01143678-2209992	10.4	Lower waste profile	Direct measurement of depth of disposal
170	24-Oct-01	L01143687-2209989	16.7	Lower waste profile	Direct measurement of depth of disposal
170	20-Feb-03	L03157800-2268806	---	Lower waste profile	2005 measurement of depth to waste surface

--- Indicates that depth-of-disposal information is unavailable.

[a] Disposal depths are measured from the ground surface to the top of the waste containers; the depth of disposal relative to the top of the waste was estimated as the listed depths less 3 m (9.8 ft).

Table II-8 (Continued)
Summary of the Depth-of-Disposal Evaluation

Shaft	Disposal Date	Container-Item ID	Depth to Top of Disposal Container (m) [a]	Assigned Position Within Waste Profile	Rationale for Assignment
170	20-Feb-03	L03157433-2268807	---	Lower waste profile	2005 measurement of depth to waste surface
197	4-Feb-99	L98109888-2099036	---	Upper waste profile	Depth of disposal of waste placed prior to containers of interest
197	4-Feb-99	L98109895-2099043	---	Upper waste profile	Depth of disposal of waste placed prior to containers of interest
197	4-Feb-99	L98109901-2099049	---	Upper waste profile	Depth of disposal of waste placed prior to containers of interest
197	4-Feb-99	L98109891-2099039	---	Upper waste profile	Depth of disposal of waste placed prior to containers of interest
197	4-Feb-99	L98109900-2099048	---	Upper waste profile	Depth of disposal of waste placed prior to containers of interest
197	4-Feb-99	L98109893-2099041	---	Upper waste profile	Depth of disposal of waste placed prior to containers of interest
197	4-Feb-99	L98109885-2099033	---	Upper waste profile	Depth of disposal of waste placed prior to containers of interest
197	4-Feb-99	L98109892-2099040	---	Upper waste profile	Depth of disposal of waste placed prior to containers of interest
197	4-Feb-99	L98109898-2099046	---	Upper waste profile	Depth of disposal of waste placed prior to containers of interest
197	4-Feb-99	L98109890-2099038	---	Upper waste profile	Depth of disposal of waste placed prior to containers of interest

--- Indicates that depth-of-disposal information is unavailable.

[a] Disposal depths are measured from the ground surface to the top of the waste containers; the depth of disposal relative to the top of the waste was estimated as the listed depths less 3 m (9.8 ft).

Table II-8 (Continued)
Summary of the Depth-of-Disposal Evaluation

Shaft	Disposal Date	Container-Item ID	Depth to Top of Disposal Container (m) [a]	Assigned Position Within Waste Profile	Rationale for Assignment
197	4-Feb-99	L98109910-2099064	---	Upper waste profile	Depth of disposal of waste placed prior to containers of interest
197	4-Feb-99	L98109914-2099068	---	Upper waste profile	Depth of disposal of waste placed prior to containers of interest
197	4-Feb-99	L98109911-2099065	---	Upper waste profile	Depth of disposal of waste placed prior to containers of interest
197	4-Feb-99	L98109909-2099063	---	Upper waste profile	Depth of disposal of waste placed prior to containers of interest
197	4-Feb-99	L98109912-2099066	---	Upper waste profile	Depth of disposal of waste placed prior to containers of interest
197	4-Feb-99	L98109904-2099052	---	Upper waste profile	Depth of disposal of waste placed prior to containers of interest
197	4-Feb-99	L98109913-2099067	---	Upper waste profile	Depth of disposal of waste placed prior to containers of interest
197	4-Feb-99	L98109905-2099059	---	Upper waste profile	Depth of disposal of waste placed prior to containers of interest
197	4-Feb-99	L98109917-2099071	---	Upper waste profile	Depth of disposal of waste placed prior to containers of interest
301	21-Sep-92	L92000741-528951	---	Lower waste profile	2005 measurement of depth to waste surface
301	11-Jun-96	L96067978-2033108	---	Lower waste profile	2005 measurement of depth to waste surface
301	11-Jun-96	L96067977-2033113	---	Lower waste profile	2005 measurement of depth to waste surface

--- Indicates that depth-of-disposal information is unavailable.

[a] Disposal depths are measured from the ground surface to the top of the waste containers; the depth of disposal relative to the top of the waste was estimated as the listed depths less 3 m (9.8 ft).

Table II-8 (Continued)
Summary of the Depth-of-Disposal Evaluation

Shaft	Disposal Date	Container-Item ID	Depth to Top of Disposal Container (m) [a]	Assigned Position Within Waste Profile	Rationale for Assignment
308	29-Oct-98	L98109894-2099042	---	Lower waste profile	Depth measurement for prior waste; assumption about packing efficiency
308	29-Oct-98	L98109896-2099044	---	Lower waste profile	Depth measurement for prior waste; assumption about packing efficiency
308	29-Oct-98	L98109897-2099045	---	Lower waste profile	Depth measurement for prior waste; assumption about packing efficiency
308	29-Oct-98	L98109886-2099034	---	Lower waste profile	Depth measurement for prior waste; assumption about packing efficiency
308	29-Oct-98	L98109889-2099037	---	Lower waste profile	Depth measurement for prior waste; assumption about packing efficiency
308	29-Oct-98	L98109887-2099035	---	Lower waste profile	Depth measurement for prior waste; assumption about packing efficiency
308	29-Oct-98	L98109903-2099051	---	Lower waste profile	Depth measurement for prior waste; assumption about packing efficiency
308	29-Oct-98	L98109899-2099047	---	Lower waste profile	Depth measurement for prior waste; assumption about packing efficiency
308	29-Oct-98	L98109902-2099050	---	Lower waste profile	Depth measurement for prior waste; assumption about packing efficiency
308	29-Oct-98	L98109908-2099062	---	Lower waste profile	Depth measurement for prior waste; assumption about packing efficiency
308	29-Oct-98	L98109907-2099061	---	Lower waste profile	Depth measurement for prior waste; assumption about packing efficiency

--- Indicates that depth-of-disposal information is unavailable.

[a] Disposal depths are measured from the ground surface to the top of the waste containers; the depth of disposal relative to the top of the waste was estimated as the listed depths less 3 m (9.8 ft).

Table II-8 (Continued)
Summary of the Depth-of-Disposal Evaluation

Shaft	Disposal Date	Container-Item ID	Depth to Top of Disposal Container (m) [a]	Assigned Position Within Waste Profile	Rationale for Assignment
308	29-Oct-98	L98109906-2099060	---	Lower waste profile	Depth measurement for prior waste; assumption about packing efficiency
308	29-Oct-98	L98109916-2099070	---	Lower waste profile	Depth measurement for prior waste; assumption about packing efficiency
309	24-May-06	L06186548-2336392	18.9	Lower waste profile	Direct measurement of depth of disposal
311	24-May-06	L06186545-2336389	5.5	Lower waste profile	Direct measurement of depth of disposal
311	24-May-06	L06186551-2336407	5.5	Lower waste profile	Direct measurement of depth of disposal
319	13-May-05	L05178609-2313051	5.8	Lower waste profile	Direct measurement of depth of disposal
319	13-May-05	L05178610-2313052	11.3	Lower waste profile	Direct measurement of depth of disposal
319	13-May-05	L05178611-2313053	8.5	Lower waste profile	Direct measurement of depth of disposal
319	13-May-05	L05178614-2313050	3.0	Upper waste profile	Direct measurement of depth of disposal
319	13-May-05	L05178612-2313048	11.3	Lower waste profile	Direct measurement of depth of disposal
319	13-May-05	L05178613-2313049	14.0	Lower waste profile	Direct measurement of depth of disposal
333	20-Feb-03	L03157434-2268808	12.9	Lower waste profile	Direct measurement of depth of disposal
333	20-Feb-03	L03157802-2268810	---	Lower waste profile	Direct measurement of depth of disposal for waste disposed of at later date
333	20-Feb-03	L03157801-2268809	---	Lower waste profile	Direct measurement of depth of disposal for waste disposed of at later date
333	20-Feb-03	L03157387-2268805	---	Lower waste profile	Direct measurement of depth of disposal for waste disposed of at later date

--- Indicates that depth-of-disposal information is unavailable.

[a] Disposal depths are measured from the ground surface to the top of the waste containers; the depth of disposal relative to the top of the waste was estimated as the listed depths less 3 m (9.8 ft).

Table II-8 (Continued)
Summary of the Depth-of-Disposal Evaluation

Shaft	Disposal Date	Container-Item ID	Depth to Top of Disposal Container (m) [a]	Assigned Position Within Waste Profile	Rationale for Assignment
333	20-Feb-03	L03157385-2268803	---	Lower waste profile	Direct measurement of depth of disposal for waste disposed of at later date
335	20-Feb-03	L03157761-2268811	---	Lower waste profile	2005 measurement of depth to waste surface
339	1-Oct-97	L97095087-2072222	---	Lower waste profile	Direct measurement of depth of disposal for waste disposed of at later date
339	1-Oct-97	L97095088-2072221	---	Lower waste profile	Direct measurement of depth of disposal for waste disposed of at later date
339	6-Apr-99	L99114245-2097060	19.2	Lower waste profile	Direct measurement of depth of disposal
349	9-Mar-00	L99122337-2042601	14.6	Lower waste profile	Direct measurement of depth of disposal
349	9-Mar-00	L99122338-2042602	14.6	Lower waste profile	Direct measurement of depth of disposal
351	25-Jan-00	L99122700-2042611	6.6	Lower waste profile	Direct measurement of depth of disposal
351	25-Jan-00	L99122703-2042614	8.4	Lower waste profile	Direct measurement of depth of disposal
351	25-Jan-00	L99122702-2042615	7.5	Lower waste profile	Direct measurement of depth of disposal
351	25-Jan-00	L99122701-2042613	10.4	Lower waste profile	Direct measurement of depth of disposal
351	25-Jan-00	L99122704-2042612	9.4	Lower waste profile	Direct measurement of depth of disposal
360	27-Feb-03	L03158263-2220827	16.6	Lower waste profile	Direct measurement of depth of disposal
360	8-Apr-03	L03159849-2248172	14.1	Lower waste profile	Direct measurement of depth of disposal
360	10-Apr-03	L03159850-2248175	11.5	Lower waste profile	Direct measurement of depth of disposal
361	25-Feb-03	L03158115-2220828	---	Lower waste profile	Bottom-most container in 19.2 m deep shaft.

--- Indicates that depth-of-disposal information is unavailable.

[a] Disposal depths are measured from the ground surface to the top of the waste containers; the depth of disposal relative to the top of the waste was estimated as the listed depths less 3 m (9.8 ft).

Table II-8 (Continued)
Summary of the Depth-of-Disposal Evaluation

Shaft	Disposal Date	Container-Item ID	Depth to Top of Disposal Container (m) [a]	Assigned Position Within Waste Profile	Rationale for Assignment
362	19-Feb-03	L03157462-2241405	---	Lower waste profile	Direct measurement of depth of disposal for waste disposed of at later date
362	16-Sep-05	L05181236-10011027	5.2	Lower waste profile	Direct measurement of depth of disposal
362	16-Sep-05	L05181236-10011028	5.2	Lower waste profile	Direct measurement of depth of disposal
363	6-Mar-03	L03158537-2220824	---	Lower waste profile	Direct measurement of depth of disposal
364	18-Mar-03	L03159032-2220825	---	Lower waste profile	2005 measurement of depth to waste surface
365	11-Mar-03	L03158802-2241404	---	Lower waste profile	2005 measurement of depth to waste surface
366	27-Mar-03	L03159190-2241400	---	Lower waste profile	Direct measurement of depth of disposal for waste disposed of at later date
367	13-Mar-03	L03158958-2241399	---	Lower waste profile	Direct measurement of depth of disposal for waste disposed of at later date
367	24-May-06	L06186547-2336391	1.8	Lower waste profile	Direct measurement of depth of disposal

--- Indicates that depth-of-disposal information is unavailable.

[a] Disposal depths are measured from the ground surface to the top of the waste containers; the depth of disposal relative to the top of the waste was estimated as the listed depths less 3 m (9.8 ft).

Attachment III
Radiological Inventories for the Area G Performance Assessment and Composite Analysis

This attachment summarizes the waste inventories used to conduct the Area G performance assessment and composite analysis. A detailed accounting of how these inventories were developed is provided in Shuman (2008). Table III-1 lists the total volumes and activities of waste placed in the disposal pits and shafts from the start of operations through the end of 2007; this was the last year for which disposal data were available at the time the inventory projections were developed. In most cases, these inventories are provided on a unit-specific basis. Existing information does not enable the allocation of the pit waste disposed of prior to 1971 to specific units; consequently, this waste is simply assigned to "Pits 1–5."

The waste inventories that are projected to require disposal in the pits and shafts from 2008 through 2044 are summarized in Table III-2. The waste placed in pits from 2008 through 2010 and the waste placed in shafts from 2008 through 2015 is expected to be disposed of in MDA G; waste disposed of after these dates will be placed in the Zone 4 expansion area.

The disposal-unit-specific radionuclide inventories for the pits and shafts are listed in Tables III-3 through III-6. Table III-3 and III_4 address the pit inventories disposed of from the start of operations through 2007 and from 2008 through 2044, respectively. The waste disposed of in pits prior to 1971 is assigned to pits 1 through 5 in Table III-3 because unit-specific assignments were not possible. The pit waste projected to be disposed of from 2008 through 2044 (Table III-4) is divided between the pits used from 2008 through 2010 and those receiving waste from 2011 through 2044. The shaft inventories for waste disposed of from the start of operations through 2007 are provided in Table III-5. Table III-6 presents the shaft inventories for the units that receive waste from 2008 through 2015 and from 2016 through 2044.

As noted above, the radionuclide inventories listed in Tables III-3 through III-6 are divided into various time periods. The inventories listed for all periods are included in the composite analysis; waste disposed of after September 26, 1988 is included in the performance assessment. The inventory modeling conducted in support of the performance assessment and composite analysis makes a distinction between waste disposed of prior to 1990 and waste disposed of after 1989 when characterizing the uncertainties associated with the radionuclide inventories. The tables distinguish between these time periods as appropriate.

Table III-1
Disposal-Unit-Specific Inventories for Waste Disposed of at Area G from the Start of Operations Through 2007

Disposal Unit	Pre-1971		1971 Through September 26, 1988		September 27, 1988 Through 2007	
	Volume (m^3)	Activity (Ci)	Volume (m^3)	Activity (Ci)	Volume (m^3)	Activity (Ci)
Pits 1–5	4.9E+04	1.8E+04	---	---	---	---
Pit 5	---	---	5.6E+02	2.6E+02	---	---
Pit 6	---	---	5.5E+03	1.9E+02	---	---
Pit 7	---	---	3.3E+03	2.1E+01	---	---
Pit 8	---	---	1.8E+03	2.1E+01	---	---
Pit 9	---	---	4.8E+00	1.2E+00	---	---
Pit 10	---	---	3.1E+03	6.8E+03	---	---
Pit 12	---	---	1.8E+03	3.5E-01	---	---
Pit 13	---	---	1.5E+03	2.1E+00	---	---
Pit 15	---	---	---	---	6.6E+03	2.1E+02
Pit 16	---	---	1.7E+03	1.9E+00	---	---
Pit 17	---	---	3.8E+03	7.0E-02	---	---
Pit 18	---	---	9.6E+03	3.0E+04	---	---
Pit 19	---	---	5.5E+01	3.0E-01	---	---
Pit 20	---	---	1.1E+04	6.4E+00	---	---
Pit 21	---	---	2.8E+03	5.5E-01	---	---
Pit 22	---	---	2.9E+03	6.0E+02	---	---
Pit 24	---	---	5.6E+03	1.4E+01	---	---
Pit 25	---	---	4.6E+03	3.7E+02	---	---
Pit 26	---	---	3.8E+03	1.2E+02	---	---
Pit 27	---	---	6.1E+03	1.9E+02	---	---
Pit 28	---	---	3.6E+03	1.3E+03	---	---
Pit 29	---	---	8.0E+03	2.3E+03	---	---

--- = None

Table III-1
Disposal-Unit-Specific Inventories for Waste Disposed of at Area G from the Start of Operations Through 2007

	Pre-1971		1971 Through September 26, 1988		September 27, 1988 Through 2007	
Disposal Unit	Volume (m^3)	Activity (Ci)	Volume (m^3)	Activity (Ci)	Volume (m^3)	Activity (Ci)
Pit 30	---	---	---	---	1.0E+04	3.7E+01
Pit 31	---	---	---	---	3.7E+03	8.5E-01
Pit 32	---	---	4.8E+03	1.6E+02	8.5E+00	0.0E+00
Pit 33	---	---	6.6E+03	5.3E+01	---	---
Pit 35	---	---	2.9E+03	8.0E+01	---	---
Pit 36	---	---	3.0E+03	3.7E+01	1.1E+03	1.9E+00
Pit 37	---	---	---	---	2.2E+04	8.9E+02
Pit 38	---	---	---	---	2.0E+04	2.3E+03
Pit 39	---	---	---	---	2.5E+04	2.3E+01
Shaft 1	1.8E+00	3.2E+02	---	---	---	---
Shaft 2	1.2E+00	1.2E+03	---	---	---	---
Shaft 3	1.1E+00	2.2E+02	---	---	---	---
Shaft 4	1.3E+00	1.1E+01	---	---	---	---
Shaft 5	8.4E-01	2.5E+01	---	---	---	---
Shaft 6	5.8E-01	3.0E+02	---	---	---	---
Shaft 7	1.6E+00	5.2E+03	---	---	---	---
Shaft 8	3.0E+00	3.0E+00	---	---	---	---
Shaft 9	2.0E+00	5.6E+00	---	---	---	---
Shaft 10	1.5E+00	1.0E+00	---	---	---	---
Shaft 11	2.0E+00	3.1E+00	---	---	---	---
Shaft 12	2.3E+00	5.6E+01	---	---	---	---
Shaft 13	3.4E+00	5.0E+01	---	---	---	---
Shaft 14	7.6E-01	5.9E+00	---	---	---	---
Shaft 15	1.4E-01	1.8E+04	---	---	---	---

--- = *None*

Table III-1
Disposal-Unit-Specific Inventories for Waste Disposed of at Area G from the Start of Operations Through 2007

	Pre-1971		1971 Through September 26, 1988		September 27, 1988 Through 2007	
Disposal Unit	Volume (m^3)	Activity (Ci)	Volume (m^3)	Activity (Ci)	Volume (m^3)	Activity (Ci)
Shaft 16	1.1E-01	1.8E+04	---	---	---	---
Shaft 17	1.5E-01	2.1E+04	2.9E-02	4.9E+00	---	---
Shaft 18	1.5E-01	5.2E+01	1.7E-01	3.8E+01	---	---
Shaft 19	---	---	7.6E-02	1.5E-01	---	---
Shaft 20	---	---	7.6E-02	3.2E-02	---	---
Shaft 21	---	---	3.8E-03	9.5E-06	---	---
Shaft 22	---	---	6.4E-02	4.9E+02	1.3E-01	1.5E+00
Shaft 23	---	---	2.8E-02	5.6E+02	---	---
Shaft 24	1.2E+00	2.6E+00	6.2E-01	0.0E+00	---	---
Shaft 25	9.6E-01	4.4E+01	2.8E-01	0.0E+00	---	---
Shaft 26	1.6E+00	2.8E+00	---	---	---	---
Shaft 27	3.6E-01	1.0E+02	---	---	---	---
Shaft 28	8.4E-01	2.7E+02	---	---	---	---
Shaft 29	6.7E-01	2.5E+01	8.8E-02	2.5E-02	---	---
Shaft 30	2.4E-01	7.3E+01	2.6E-01	1.0E+01	---	---
Shaft 31	5.4E-01	7.5E-03	7.9E-01	4.3E+00	---	---
Shaft 32	2.8E-01	6.2E-03	1.4E+00	1.7E+00	---	---
Shaft 33	2.7E-01	7.4E+01	2.4E-01	1.7E+01	---	---
Shaft 34	1.1E+01	0.0E+00	1.5E+01	0.0E+00	---	---
Shaft 35	---	---	2.7E+00	3.5E+01	---	---
Shaft 36	1.8E+00	0.0E+00	7.9E-01	1.2E+02	---	---
Shaft 37	1.8E+00	0.0E+00	3.8E+00	0.0E+00	---	---
Shaft 38	1.8E+00	0.0E+00	1.1E-01	1.2E-02	---	---
Shaft 39	9.3E-01	5.7E+02	1.5E+01	8.2E+03	---	---

--- = None

Table III-1
Disposal-Unit-Specific Inventories for Waste Disposed of at Area G from the Start of Operations Through 2007

	Pre-1971		1971 Through September 26, 1988		September 27, 1988 Through 2007	
Disposal Unit	Volume (m^3)	Activity (Ci)	Volume (m^3)	Activity (Ci)	Volume (m^3)	Activity (Ci)
Shaft 40	---	---	1.1E+00	2.1E+01	---	---
Shaft 41	---	---	2.3E+00	3.0E+01	---	---
Shaft 42	---	---	1.8E+00	1.3E+01	---	---
Shaft 43	---	---	1.5E+00	1.3E+01	---	---
Shaft 44	---	---	1.7E+00	4.7E+01	---	---
Shaft 45	---	---	1.8E+00	1.2E+02	---	---
Shaft 46	---	---	1.8E+00	2.9E+00	---	---
Shaft 47	---	---	1.0E+00	1.1E+01	---	---
Shaft 48	---	---	1.1E+00	2.0E+01	---	---
Shaft 49	---	---	7.9E-01	2.9E+00	---	---
Shaft 50	---	---	1.9E+01	2.9E+04	---	---
Shaft 51	---	---	3.6E-01	3.6E+02	---	---
Shaft 52	---	---	3.1E-01	1.6E+02	---	---
Shaft 53	---	---	8.3E-01	1.1E+02	---	---
Shaft 54	---	---	4.5E-01	1.9E+02	---	---
Shaft 55	---	---	1.4E+00	5.1E+01	---	---
Shaft 56	---	---	7.5E-01	2.7E+01	---	---
Shaft 57	---	---	3.1E-01	7.5E+00	---	---
Shaft 58	---	---	3.6E+00	2.3E+02	---	---
Shaft 59	---	---	5.4E+00	2.3E+03	---	---
Shaft 60	---	---	3.2E+01	0.0E+00	---	---
Shaft 61	---	---	4.4E+00	5.0E+00	---	---
Shaft 62	---	---	3.5E+00	1.0E-03	---	---
Shaft 63	---	---	2.3E+00	2.0E-01	---	---
Shaft 64	---	---	1.1E+00	1.9E-02	---	---

--- = *None*

Table III-1
Disposal-Unit-Specific Inventories for Waste Disposed of at Area G from the Start of Operations Through 2007

	Pre-1971		1971 Through September 26, 1988		September 27, 1988 Through 2007	
Disposal Unit	Volume (m^3)	Activity (Ci)	Volume (m^3)	Activity (Ci)	Volume (m^3)	Activity (Ci)
Shaft 65	---	---	3.9E+00	1.6E+01	---	---
Shaft 66	---	---	6.5E-01	2.0E-03	---	---
Shaft 67	---	---	1.3E+00	4.4E+01	---	---
Shaft 68	---	---	9.0E-01	1.0E+02	---	---
Shaft 69	---	---	5.7E-01	2.1E-03	---	---
Shaft 70	---	---	2.6E+01	0.0E+00	---	---
Shaft 71	---	---	8.8E-01	5.2E+01	---	---
Shaft 72	---	---	2.8E+00	4.8E+01	---	---
Shaft 73	---	---	3.4E-01	1.5E+02	---	---
Shaft 74	---	---	9.3E-01	1.6E+02	---	---
Shaft 75	---	---	9.2E-01	7.9E+01	---	---
Shaft 76	---	---	8.1E-01	1.4E+02	---	---
Shaft 77	---	---	3.4E-01	4.7E+02	---	---
Shaft 78	---	---	1.3E+00	4.7E+01	---	---
Shaft 79	---	---	3.4E-01	1.9E+02	---	---
Shaft 80	---	---	1.2E+00	3.1E+01	---	---
Shaft 81	---	---	9.9E-01	3.0E-03	---	---
Shaft 82	---	---	6.9E-01	3.7E+01	---	---
Shaft 83	---	---	1.3E+00	1.7E+01	---	---
Shaft 84	---	---	4.9E-01	5.5E+01	---	---
Shaft 85	---	---	5.1E-01	5.8E+01	---	---
Shaft 86	---	---	6.2E-01	1.0E+03	---	---
Shaft 87	---	---	6.1E-01	8.8E+01	---	---
Shaft 88	---	---	5.0E-01	4.1E+01	---	---
Shaft 89	---	---	8.1E-01	1.9E+01	---	---

--- = None

Table III-1
Disposal-Unit-Specific Inventories for Waste Disposed of at Area G from the Start of Operations Through 2007

	Pre-1971		1971 Through September 26, 1988		September 27, 1988 Through 2007	
Disposal Unit	Volume (m^3)	Activity (Ci)	Volume (m^3)	Activity (Ci)	Volume (m^3)	Activity (Ci)
Shaft 90	---	---	9.1E-01	3.5E+02	---	---
Shaft 91	---	---	2.1E+00	3.2E+01	---	---
Shaft 92	---	---	3.7E+00	3.9E+01	---	---
Shaft 93	---	---	7.5E+00	6.3E+02	---	---
Shaft 94	---	---	2.7E+00	3.5E+03	---	---
Shaft 95	---	---	4.1E+00	2.1E+02	---	---
Shaft 96	---	---	1.2E+01	4.4E+00	---	---
Shaft 97	---	---	6.8E+00	1.4E+02	---	---
Shaft 99	---	---	5.6E+00	1.4E+01	---	---
Shaft 100	---	---	1.7E+00	3.7E+02	---	---
Shaft 101	---	---	2.5E+00	1.2E+01	---	---
Shaft 102	---	---	5.2E+00	3.4E+02	---	---
Shaft 103	---	---	4.8E+00	5.2E+01	---	---
Shaft 104	---	---	4.3E+00	1.8E-01	---	---
Shaft 105	---	---	5.6E+00	1.8E-03	---	---
Shaft 106	---	---	2.1E+00	9.4E+01	---	---
Shaft 107	---	---	1.4E+00	7.4E+02	---	---
Shaft 108	---	---	6.5E+00	4.3E+02	---	---
Shaft 109	---	---	2.3E+00	2.1E+01	---	---
Shaft 110	---	---	3.6E+00	4.6E+02	---	---
Shaft 111	---	---	3.8E+00	5.8E+01	---	---
Shaft 112	---	---	4.2E+00	2.6E+02	---	---
Shaft 114	---	---	2.8E+01	5.3E+02	---	---
Shaft 115	---	---	1.5E+01	9.2E-01	---	---
Shaft 118	---	---	1.3E+01	0.0E+00	---	---

--- = None

Table III-1
Disposal-Unit-Specific Inventories for Waste Disposed of at Area G from the Start of Operations Through 2007

	Pre-1971		1971 Through September 26, 1988		September 27, 1988 Through 2007	
Disposal Unit	Volume (m^3)	Activity (Ci)	Volume (m^3)	Activity (Ci)	Volume (m^3)	Activity (Ci)
Shaft 119	---	---	1.6E+01	1.4E+00	---	---
Shaft 120	---	---	1.5E+01	6.3E+02	---	---
Shaft 121	---	---	6.9E+00	4.1E-04	---	---
Shaft 122	---	---	7.3E+00	2.6E+03	---	---
Shaft 123	---	---	1.5E+01	9.3E-01	---	---
Shaft 124	---	---	1.1E+01	1.1E-02	3.0E+00	1.0E+00
Shaft 125	---	---	1.7E+01	1.2E+01	---	---
Shaft 126	---	---	2.2E+01	7.0E+02	---	---
Shaft 127	---	---	1.4E+01	1.3E+00	---	---
Shaft 128	---	---	1.2E+01	4.5E-03	---	---
Shaft 129	---	---	3.8E+00	9.3E+02	---	---
Shaft 130	---	---	3.1E+01	3.6E+01	---	---
Shaft 131	---	---	3.6E+00	1.9E+01	9.0E+00	2.1E+03
Shaft 132	---	---	4.5E+00	4.3E-05	1.3E+01	1.0E-05
Shaft 133	---	---	2.7E+00	3.4E+03	---	---
Shaft 134	---	---	6.8E+00	2.5E+00	---	---
Shaft 135	---	---	6.2E+00	0.0E+00	---	---
Shaft 136	---	---	6.1E+00	3.7E+03	3.2E+00	1.8E+03
Shaft 137	---	---	3.8E+00	1.5E+00	1.5E+01	6.8E+01
Shaft 138	---	---	5.4E+00	0.0E+00	---	---
Shaft 139	---	---	8.0E+00	8.7E+02	7.9E-01	6.0E+01
Shaft 140	---	---	8.9E+00	1.0E-03	1.6E+01	0.0E+00
Shaft 141	---	---	---	---	9.2E+00	1.8E+03
Shaft 142	---	---	---	---	3.2E+00	3.8E+02
Shaft 143	---	---	---	---	9.4E+00	3.2E+03

--- = None

Table III-1
Disposal-Unit-Specific Inventories for Waste Disposed of at Area G from the Start of Operations Through 2007

	Pre-1971		1971 Through September 26, 1988		September 27, 1988 Through 2007	
Disposal Unit	Volume (m^3)	Activity (Ci)	Volume (m^3)	Activity (Ci)	Volume (m^3)	Activity (Ci)
Shaft 144	---	---	---	---	8.8E+00	6.0E+03
Shaft 147	---	---	---	---	9.5E+00	1.9E+01
Shaft 148	---	---	---	---	7.9E+00	3.0E-02
Shaft 149	---	---	---	---	9.1E+00	2.0E+03
Shaft 150	---	---	1.8E+01	1.6E+05	---	---
Shaft 151	---	---	2.0E+01	1.4E+05	---	---
Shaft 152	---	---	4.2E+00	4.3E+04	---	---
Shaft 153	---	---	3.1E+00	2.6E+04	---	---
Shaft 154	---	---	5.5E+00	3.2E+05	---	---
Shaft 155	---	---	1.0E+00	5.5E+03	2.7E+00	5.7E+04
Shaft 156	---	---	1.7E+00	3.7E+04	---	---
Shaft 157	---	---	2.5E+00	2.4E+04	---	---
Shaft 158	---	---	---	---	2.2E+00	1.2E+04
Shaft 159	---	---	---	---	3.2E-01	8.6E+00
Shaft 160	---	---	---	---	2.5E+00	7.0E+02
Shaft 161	---	---	---	---	3.7E+00	4.6E+03
Shaft 162	---	---	---	---	1.6E+00	3.6E+05
Shaft 163	---	---	---	---	3.5E+00	4.8E+03
Shaft 164	---	---	---	---	3.4E+00	3.8E+03
Shaft 165	---	---	---	---	2.7E+00	6.0E+03
Shaft 166	---	---	---	---	2.6E+00	1.5E+05
Shaft 167	---	---	---	---	2.4E+00	1.5E+05
Shaft 168	---	---	---	---	2.4E+00	9.5E+04
Shaft 169	---	---	---	---	1.7E+00	3.2E+03
Shaft 170	---	---	---	---	9.5E-01	9.4E+04

--- = None

Table III-1
Disposal-Unit-Specific Inventories for Waste Disposed of at Area G from the Start of Operations Through 2007

	Pre-1971		1971 Through September 26, 1988		September 27, 1988 Through 2007	
Disposal Unit	Volume (m^3)	Activity (Ci)	Volume (m^3)	Activity (Ci)	Volume (m^3)	Activity (Ci)
Shaft 171	---	---	---	---	5.0E+00	1.7E-03
Shaft 172	---	---	---	---	8.3E+00	3.5E-02
Shaft 173	---	---	---	---	3.7E+00	1.2E-06
Shaft 174	---	---	---	---	6.2E+00	9.1E-02
Shaft 175	---	---	---	---	2.3E+00	0.0E+00
Shaft 176	---	---	---	---	6.0E+00	7.1E-02
Shaft 177	---	---	---	---	9.4E+00	1.7E-01
Shaft 189	---	---	4.9E+01	1.0E+02	---	---
Shaft 190	---	---	3.1E+01	8.8E+02	---	---
Shaft 191	---	---	3.9E+01	1.4E+02	---	---
Shaft 192	---	---	4.4E+01	7.8E+02	---	---
Shaft 196	---	---	---	---	5.8E+01	2.7E+03
Shaft 197	---	---	---	---	4.0E+01	2.2E+04
Shaft 206	---	---	4.5E-01	4.5E-05	---	---
Shaft 301	---	---	---	---	6.4E-01	1.8E+02
Shaft 307	---	---	---	---	3.4E+00	1.9E+02
Shaft 308	---	---	---	---	2.9E+00	6.7E-02
Shaft 309	---	---	---	---	2.0E+00	5.4E+04
Shaft 311	---	---	---	---	3.4E+00	5.1E+04
Shaft 313	---	---	---	---	4.3E+00	4.6E+03
Shaft 315	---	---	---	---	3.1E+00	5.4E+01
Shaft 317	---	---	---	---	3.2E+00	2.2E+03
Shaft 319	---	---	---	---	8.0E+00	1.5E+05
Shaft 321	---	---	---	---	2.7E+00	1.7E+03
Shaft 323	---	---	---	---	3.1E+00	1.0E+03

--- = *None*

Table III-1
Disposal-Unit-Specific Inventories for Waste Disposed of at Area G from the Start of Operations Through 2007

	Pre-1971		1971 Through September 26, 1988		September 27, 1988 Through 2007	
Disposal Unit	Volume (m^3)	Activity (Ci)	Volume (m^3)	Activity (Ci)	Volume (m^3)	Activity (Ci)
Shaft 325	---	---	---	---	2.1E+00	3.1E-05
Shaft 327	---	---	---	---	4.9E+00	9.6E+02
Shaft 329	---	---	---	---	3.7E+00	5.1E+03
Shaft 331	---	---	---	---	2.9E+00	1.7E+03
Shaft 333	---	---	---	---	2.5E+00	1.9E+05
Shaft 335	---	---	---	---	1.4E+00	2.3E+04
Shaft 339	---	---	---	---	5.4E+00	1.3E+05
Shaft 341	---	---	---	---	6.2E+00	3.9E+03
Shaft 343	---	---	---	---	6.0E+00	1.5E+03
Shaft 345	---	---	---	---	4.1E+00	2.4E+03
Shaft 347	---	---	---	---	3.8E+00	1.8E+03
Shaft 349	---	---	---	---	5.0E+00	1.2E+04
Shaft 351	---	---	---	---	6.8E+00	1.9E+04
Shaft 355	---	---	---	---	4.9E+00	1.9E+02
Shaft 357	---	---	---	---	5.5E+00	4.7E+02
Shaft 360	---	---	---	---	1.9E+01	1.1E+03
Shaft 361	---	---	---	---	2.4E+01	5.6E+02
Shaft 362	---	---	---	---	2.2E+01	4.5E+02
Shaft 363	---	---	---	---	3.4E+00	4.9E+04
Shaft 364	---	---	---	---	6.2E+00	3.7E+02
Shaft 365	---	---	---	---	3.1E+00	1.8E+02
Shaft 366	---	---	---	---	8.2E+00	1.0E+04
Shaft 367	---	---	---	---	1.2E+01	5.5E+04
Shaft 370	---	---	---	---	5.0E-01	1.1E+01
Shaft C01	---	---	6.2E+00	0.0E+00	---	---

--- = None

Table III-1
Disposal-Unit-Specific Inventories for Waste Disposed of at Area G from the Start of Operations Through 2007

	Pre-1971		1971 Through September 26, 1988		September 27, 1988 Through 2007	
Disposal Unit	Volume (m^3)	Activity (Ci)	Volume (m^3)	Activity (Ci)	Volume (m^3)	Activity (Ci)
Shaft C02	---	---	1.0E+01	0.0E+00	---	---
Shaft C03	---	---	9.6E+00	0.0E+00	---	---
Shaft C04	---	---	1.1E+01	0.0E+00	---	---
Shaft C05	---	---	7.3E+00	0.0E+00	---	---
Shaft C06	---	---	1.3E+01	0.0E+00	---	---
Shaft C07	---	---	1.4E+01	0.0E+00	---	---
Shaft C08	---	---	1.4E+01	0.0E+00	---	---
Shaft C09	---	---	1.1E+01	0.0E+00	---	---
Shaft C10	---	---	1.5E+01	0.0E+00	---	---
Shaft C11	---	---	1.3E+01	0.0E+00	1.0E+00	0.0E+00
Shaft C12	---	---	1.6E+01	0.0E+00	3.7E-01	0.0E+00
Shaft C13	---	---	2.9E+00	0.0E+00	2.8E+01	1.5E-02
Shaft C14	---	---	---	---	2.4E+00	9.2E-04

--- = None

--- = None

Table III-2
Estimated Inventories for Waste Projected to Be Disposed of at Area G from 2008 Through 2044

	Pits		Shafts	
Disposal Period	Volume (m^3)	Activity (Ci)	Volume (m^3)	Activity (Ci)
2008–2010	4.5E+04	3.9E+01	---	---
2011–2044	1.2E_05	3.5E+02	---	---
2008–2015	---	---	2.2E+02	3.3E+05
2016–2044	---	---	8.1E+02	6.5E+05

--- = None

Table III-3
Radionuclide and Material Type Inventories, by Disposal Pit, for the Area G Performance Assessment

	Waste Inventory by Disposal Pit and Period of Disposal (Ci)											
	1–5	5	6	7	8	9	10	12	13	15	16	17
Constituent [a]	Pre-1971	1971–1988 [b]	1971–1988	1971–1988	1971–1988	1971–1988	1971–1988	1971–1988	1971–1988	1990–2007	1971–1988	1971–1988
Ac-227	8.6E-01	---	---	---	---	---	---	---	---	---	---	7.0E-02
Ag-108m	---	---	---	---	---	---	---	---	---	1.1E-04	---	---
Am-241	2.4E+03	---	---	1.3E-01	9.7E-01	---	1.0E-03	---	---	1.7E-01	---	---
Am-243	---	---	---	---	---	---	---	---	---	1.3E-05	---	---
Ba-133	---	---	---	---	---	---	---	---	---	6.2E-06	---	---
Bk-249	1.6E-03	---	---	---	---	---	---	---	---	---	---	---
C-14	---	---	---	---	---	---	9.0E-07	---	---	5.2E-07	---	---
Cf-249	2.4E-03	---	---	---	---	---	---	---	---	4.3E-07	---	---
Cf-251	2.7E-03	---	---	---	---	---	---	---	---	---	---	---
Cf-252	1.5E-02	---	---	8.6E-03	---	---	8.0E-06	---	---	---	---	---
Cm-242	1.8E-03	---	---	---	---	---	---	---	---	---	---	---
Cm-243	---	---	---	---	---	---	---	---	---	7.2E-07	---	---
Cm-244	1.7E-03	---	---	---	---	---	---	---	---	---	---	---
Co-60	---	---	---	---	---	---	1.6E-02	---	---	2.4E+00	---	---
Cs-135	---	---	---	---	---	---	---	---	---	5.9E-07	---	---
Cs-137	2.6E-01	---	---	---	---	---	1.5E-03	---	---	1.0E+00	---	---
D38	---	---	---	---	---	---	---	---	---	4.1E-01	---	---
Eu-152	---	---	---	---	---	---	---	---	---	2.7E-03	---	---
Eu-154	---	---	---	---	---	---	---	---	---	2.1E-06	---	---
H-3	2.7E+00	---	---	---	---	---	6.1E+03	---	5.0E-01	1.5E+02	---	---
Ho-166m	---	---	---	---	---	---	---	---	---	6.2E-06	---	---

--- = None

[a] This column includes radionuclides, material types, mixed-activation products (MAP), and mixed-fission products (MFP).

[b] Refers to waste disposed of from 1971 through September 26, 1988.

Table III-3 (Continued)
Radionuclide and Material Type Inventories, by Disposal Pit, for the Area G Performance Assessment

	Waste Inventory by Disposal Pit and Period of Disposal (Ci)											
	1–5	5	6	7	8	9	10	12	13	15	16	17
Constituent [a]	Pre-1971	1971–1988 [b]	1971–1988	1971–1988	1971–1988	1971–1988	1971–1988	1971–1988	1971–1988	1990–2007	1971–1988	1971–1988
I-129	---	---	---	---	---	---	---	---	---	1.0E-06	---	---
K-40	---	---	---	---	---	---	---	---	---	3.3E-04	---	---
Kr-85	1.7E-03	---	---	---	---	---	---	---	---	2.2E-06	---	---
MAP	3.6E-01	---	---	5.4E-02	---	---	7.6E+02	---	3.6E-02	---	1.2E-01	---
MFP	1.0E+03	---	---	4.7E-02	---	1.0E+00	5.1E-02	8.0E-03	1.5E-02	---	---	---
Nb-94	---	---	---	---	---	---	---	---	---	1.7E-05	---	---
Ni-59	---	---	---	---	---	---	---	---	---	6.1E-06	---	---
Ni-63	---	---	---	---	---	---	---	---	---	5.5E-04	---	---
Np-237	4.0E-03	---	---	---	---	---	---	---	---	1.1E-04	---	---
Pa-231	---	---	---	---	---	---	---	---	---	1.0E-09	---	---
Po-210	1.9E-03	---	---	---	---	---	---	---	---	1.6E-01	---	---
Pu-238	3.8E+03	2.6E+02	1.8E+02	2.0E+01	1.6E+01	1.8E-01	2.2E-02	2.7E-01	---	1.2E+00	---	---
Pu-239	1.7E+02	---	3.8E+00	4.3E-01	3.5E+00	---	5.2E-02	7.1E-02	---	9.7E-01	---	---
Pu-240	4.0E+00	---	---	---	---	---	---	---	---	6.9E-02	---	---
Pu-241	---	---	---	---	---	---	---	---	---	1.2E+00	---	---
Pu-242	---	---	---	---	---	---	---	---	---	5.1E-04	---	---
Pu51	1.6E+00	---	---	---	---	---	---	---	---	---	---	---
PU52	7.7E+03	---	---	2.4E-03	---	---	1.3E-02	2.1E-04	---	---	---	---
PU53	2.5E+02	---	---	---	---	---	---	---	---	---	---	---
PU54	1.1E+03	---	---	---	---	---	---	---	---	---	---	---
PU55	6.8E+01	---	---	---	---	---	---	---	---	---	---	---
PU56	1.2E+03	---	---	---	---	---	---	---	---	---	---	---

--- = None

[a] This column includes radionuclides, material types, mixed-activation products (MAP), and mixed-fission products (MAP).

[b] Refers to waste disposed of from 1971 through September 26, 1988.

Table III-3 (Continued)
Radionuclide and Material Type Inventories, by Disposal Pit, for the Area G Performance Assessment

	Waste Inventory by Disposal Pit and Period of Disposal (Ci)											
	1–5	5	6	7	8	9	10	12	13	15	16	17
Constituent [a]	Pre-1971	1971–1988 [b]	1971–1988	1971–1988	1971–1988	1971–1988	1971–1988	1971–1988	1971–1988	1990–2007	1971–1988	1971–1988
PU57	7.1E+01	---	---	---	---	---	---	---	---	---	---	---
PU83	5.0E+02	---	---	---	---	---	2.0E-04	---	---	---	---	---
Ra-226	---	---	---	---	---	---	9.9E-02	---	---	7.7E-02	---	---
Ra-228	---	---	---	---	---	---	---	---	---	1.9E-04	---	---
Si-32	---	---	---	---	---	---	---	---	---	1.2E-05	---	---
Sm-151	---	---	---	---	---	---	---	---	---	---	---	---
Sn-126	---	---	---	---	---	---	---	---	---	1.9E-06	---	---
Sr-90	2.9E-01	---	---	---	---	---	2.1E-01	---	---	5.1E-02	---	---
Tb-157	---	---	---	---	---	---	---	---	---	4.5E-08	---	---
Tc-99	---	---	---	---	---	---	---	---	---	9.9E-03	---	---
Th-228	---	---	---	---	---	---	---	---	---	4.9E-04	---	---
Th-229	---	---	---	---	---	---	---	---	---	6.9E-05	---	---
Th-230	1.6E+01	---	---	---	---	---	---	---	---	2.2E-08	---	---
Th-232	---	---	---	---	---	---	4.4E-04	---	---	1.6E-02	---	---
TH88	1.9E-03	---	---	---	3.3E-05	---	---	---	---	---	6.5E-04	---
Ti-44	---	---	---	---	---	---	---	---	---	3.8E-04	---	---
U10	8.8E-01	---	---	---	---	---	---	---	---	---	5.1E-01	---
U12	7.9E+00	---	---	---	---	---	3.0E-01	---	4.6E-01	---	4.3E-01	---
U-232	---	---	---	---	---	---	---	---	---	1.8E-08	---	---
U-233	6.1E+00	---	---	---	---	---	1.9E-05	---	---	7.5E-03	---	---
U-234	---	---	---	---	---	---	---	---	---	1.4E-01	---	---
U-235	3.7E-01	4.9E-03	---	1.6E-03	---	---	7.9E-03	---	1.1E-05	1.6E-02	3.9E-02	---

--- = None

[a] This column includes radionuclides, material types, mixed-activation products (MAP), and mixed-fission products (MAP).

[b] Refers to waste disposed of from 1971 through September 26, 1988.

Table III-3 (Continued)
Radionuclide and Material Type Inventories, by Disposal Pit, for the Area G Performance Assessment

	Waste Inventory by Disposal Pit and Period of Disposal (Ci)											
	1–5	5	6	7	8	9	10	12	13	15	16	17
Constituent [a]	Pre-1971	1971–1988 [b]	1971–1988	1971–1988	1971–1988	1971–1988	1971–1988	1971–1988	1971–1988	1990–2007	1971–1988	1971–1988
U-236	---	---	---	---	---	---	6.3E-08	---	---	3.2E-05	---	---
U-238	4.3E+00	1.6E-04	---	---	---	---	1.5E+00	---	1.1E+00	5.5E+00	8.0E-01	---
U38	2.3E-02	---	---	---	---	---	---	---	---	---	1.3E-02	---
U81	4.7E-03	---	---	---	---	---	---	---	---	---	---	---
Zr-93	---	---	---	---	---	---	---	---	---	2.0E-08	---	---

--- = None

[a] This column includes radionuclides, material types, mixed-activation products (MAP), and mixed-fission products (MAP).

[b] Refers to waste disposed of from 1971 through September 26, 1988.

Table III-3 (Continued)
Radionuclide and Material Type Inventories, by Disposal Pit, for the Area G Performance Assessment

Constituent [a]	Waste Inventory by Disposal Pit and Period of Disposal (Ci)										
	18	19	20	21	22	24	25	26	27	28	29
	1971–1988 [b]	1971–1988	1971–1988	1971–1988	1971–1988	1971–1988	1971–1988	1971–1988	1971–1988	1971–1988	1971–1988
Am-241	3.3E-01	---	1.0E-01	---	1.7E-01	---	3.1E-03	1.4E+01	8.6E-06	3.0E-06	3.2E+00
C-14	2.0E-06	---	---	---	---	---	---	---	---	---	2.1E-01
Cf-249	---	---	4.1E-04	---	---	---	---	---	---	---	---
Cf-251	---	---	1.6E-03	---	---	---	---	---	---	---	---
Co-60	1.1E+03	---	---	---	---	2.0E-03	1.2E+02	1.0E+00	2.0E-03	---	8.0E-03
Cs-135	---	---	---	---	---	---	---	---	---	---	---
Cs-137	---	---	---	---	---	1.5E-01	2.0E+02	---	2.0E-06	---	8.8E+02
H-3	1.0E+01	---	6.0E-01	---	5.0E-05	5.0E-01	5.0E+01	3.0E-03	1.1E+02	1.2E+03	5.8E-01
Kr-85	---	---	---	---	1.0E-03						
MAP	5.2E+00	---	---	---	3.2E-01	8.3E-01	1.0E+00	9.6E+01	8.0E+01	1.3E+02	4.8E+00
MFP	1.2E+00	3.0E-01	6.5E-02	---	6.0E+02	---	1.2E+00	5.7E-01	3.2E-02	---	1.7E+01
Np-237	---	---	---	---	---	---	---	---	---	---	7.0E-07
Pu-238	1.2E+00	---	4.4E+00	---	4.5E-01	---	1.2E-03	8.2E-01	4.8E-02	3.2E-01	1.5E+00
Pu-239	1.0E+00	---	1.2E+00	---	1.3E+00	---	5.3E-02	2.7E+00	5.7E-01	2.4E-01	5.7E-01
Pu-240	---	---	---	---	---	---	5.0E-07	---	---	---	---
Pu-241	---	---	---	---	---	---	---	---	---	---	5.8E-06
PU52	4.1E-02	---	1.1E-02	---	2.5E-02	---	9.5E-03	2.8E-01	1.4E-02	1.3E-02	6.8E-01
PU53	---	---	---	---	---	---	---	---	---	---	3.7E-04
PU54	---	---	---	---	---	---	---	---	---	---	1.3E-01
PU83	4.9E-04	---	3.5E-03	---	5.3E-03	---	3.8E-04	3.0E-05	1.6E-03	7.1E-05	2.1E-03

--- = None

[a] This column includes radionuclides, material types, mixed-activation products (MAP), and mixed-fission products (MAP).

[b] Refers to waste disposed of from 1971 through September 26, 1988.

Table III-3 (Continued)
Radionuclide and Material Type Inventories, by Disposal Pit, for the Area G Performance Assessment

	Waste Inventory by Disposal Pit and Period of Disposal (Ci)										
	18	19	20	21	22	24	25	26	27	28	29
Constituent [a]	1971–1988 [b]	1971–1988	1971–1988	1971–1988	1971–1988	1971–1988	1971–1988	1971–1988	1971–1988	1971–1988	1971–1988
Ra-226	---	---	---	---	---	---	---	---	9.7E-02	---	---
Sr-90	1.0E+00	---	---	---	---	1.7E-01	1.1E-02	1.0E-01	2.1E-03	---	1.4E+03
Th-230	---	---	---	---	---	9.5E+00	---	---	---	---	---
Th-232	8.7E-04	---	---	---	---	---	---	---	---	---	4.9E-05
TH88	---	---	---	---	---	4.4E-04	---	---	---	2.3E-02	---
U10	---	---	---	---	---	5.0E-09	---	---	---	---	---
U11	---	---	---	---	---	---	---	---	---	---	1.3E-01
U12	5.7E-01	---	---	3.8E-01	1.8E-01	3.2E+00	1.0E-01	---	1.7E-01	---	---
U-233	---	---	---	---	---	---	---	---	---	---	1.9E-02
U-235	9.4E-03	---	4.7E-04	1.7E-01	5.8E-04	1.9E-03	9.9E-03	1.5E-01	6.1E-03	8.0E-03	2.4E-01
U-238	1.9E+00	---	---	1.8E-03	4.7E-01	1.1E-01	1.2E+00	1.1E-01	7.4E-01	5.2E-01	8.2E-01
U35	---	---	---	---	---	---	---	---	4.9E-04	---	---
U36	---	---	---	---	---	---	---	---	2.2E-05	---	---
U38	1.3E-03	---	---	---	---	7.5E-04	---	---	1.5E-03	---	1.1E-02
U81	---	---	---	---	2.8E-03	---	---	---	---	---	---

--- = None

[a] This column includes radionuclides, material types, mixed-activation products (MAP), and mixed-fission products (MAP).

[b] Refers to waste disposed of from 1971 through September 26, 1988.

Table III-3 (Continued)
Radionuclide and Material Type Inventories, by Disposal Pit, for the Area G Performance Assessment

Constituent [a]	Waste Inventory by Disposal Pit and Period of Disposal (Ci)											
	30		31	32		33	35	36		37	38	39
	1988–1989	1990–2007	1990–2007	1971–1988 [b]	1990–2007	1971–1988	1971–1988	1971–1988	1988–1989	1990–2007	1990 – 2007	1990–2007
Ac-227	---	---	---	---	---	---	---	---	---	3.7E-06	1.4E-05	---
Ag-108m	---	---	---	---	---	---	---	---	---	---	1.3E-05	4.9E-05
Al-26	---	---	---	---	---	---	---	---	---	2.6E-04	2.7E-07	---
Am-241	1.9E-03	2.6E-02	1.3E-01	2.2E+00	---	1.9E+00	4.3E-01	1.3E-01	1.2E-04	3.7E-01	6.6E+00	7.3E-01
Am-243	---	---	---	---	---	---	---	---	---	2.5E-05	8.5E-03	1.3E-06
Ba-133	---	---	---	---	---	---	---	---	---	1.3E-03	6.9E-01	1.6E-06
Be-10	---	---	---	---	---	---	---	---	---	---	4.6E-03	---
Bi-207	---	---	---	---	---	---	---	---	---	2.0E-05	1.5E-02	7.4E-05
Bk-247	---	---	---	---	---	---	---	---	---	5.4E-08	2.3E-07	---
C-14	2.0E-09	---	6.8E-09	1.5E-06	---	1.5E-02	---	---	---	1.7E-02	3.3E+00	4.8E-05
Ca-41	---	---	---	---	---	---	---	---	---	---	2.7E-01	---
Cf-249	---	---	---	---	---	---	---	---	---	---	1.0E-04	---
Cf-252	---	---	---	---	---	---	---	---	---	1.4E-05	5.6E-06	---
Cl-36	---	---	---	---	---	---	---	---	---	3.7E-04	1.8E-02	---
Cm-243	---	---	---	---	---	---	---	---	---	---	4.1E-05	---
Cm-244	---	---	---	---	---	---	---	---	---	---	2.8E-03	---
Cm-245	---	---	---	---	---	---	---	---	---	---	4.6E-05	---
Cm-248	---	---	---	---	---	---	---	---	---	---	4.5E-07	---
Co-60	7.5E-01	2.1E-03	3.7E-05	1.0E-02	---	5.0E-02	---	1.0E-04	3.2E-01	6.9E+00	2.8E+01	6.0E+00
Cs-135	---	---	---	---	---	---	---	---	---	7.0E-08	3.2E-05	1.0E-04
Cs-137	1.7E+00	4.0E-02	2.8E-01	7.2E-03	---	1.5E+00	---	1.4E-03	3.0E-01	4.0E-01	1.9E+00	2.2E-01
D38	---	---	6.6E-03	---	---	---	---	---	---	3.0E-02	8.7E+00	1.9E-01
Eu-152	---	---	---	---	---	---	---	---	2.9E-02	5.8E-07	3.9E-01	1.2E-02

[a] *This column includes radionuclides, material types, mixed-activation products (MAP), and mixed-fission products (MFP).*

Table III-3 (Continued)
Radionuclide and Material Type Inventories, by Disposal Pit, for the Area G Performance Assessment

	Waste Inventory by Disposal Pit and Period of Disposal (Ci)											
	30		31	32		33	35	36		37	38	39
Constituent [a]	1988–1989	1990–2007	1990–2007	1971–1988 [b]	1990–2007	1971–1988	1971–1988	1971–1988	1988–1989	1990–2007	1990 – 2007	1990–2007
Eu-154	---	---	---	---	---	---	---	---	---	1.0E-06	5.2E-02	1.2E-04
Gd-148	---	---	---	---	---	---	---	---	---	---	---	1.0E-05
H-3	4.8E-01	3.8E-01	1.8E-02	1.5E+00	---	4.0E+00	1.2E+00	3.0E+01	2.9E-01	7.5E+02	2.2E+03	4.1E+00
Ho-163	---	---	---	---	---	---	---	---	---	8.3E-01	8.3E-02	---
Ho-166m	---	---	---	---	---	---	---	---	---	---	1.4E-03	---
I-129	---	---	---	---	---	---	---	---	---	---	2.9E-05	1.1E-06
K-40	---	---	1.5E-03	---	---	---	---	---	---	1.5E-01	1.2E-01	2.4E-04
Kr-85	4.3E-02	---	---	---	---	---	---	1.4E-06	---	6.7E-04	2.9E-03	5.7E-08
Lu-176	---	---	---	---	---	---	---	---	---	---	1.7E-06	---
MAP	7.7E+00	2.3E-01	1.0E-07	2.0E+01	---	3.0E+01	6.8E+01	4.0E+00	8.8E-01	4.1E+00	---	---
MFP	5.9E+00	1.1E+01	1.9E-05	2.1E+00	---	1.2E+01	8.6E+00	1.2E+00	1.0E-02	6.1E-01	---	---
Mo-93	---	---	---	---	---	---	---	---	---	---	2.0E-05	---
Nb-91	---	---	---	---	---	---	---	---	---	---	1.2E-05	---
Nb-92	---	---	---	---	---	---	---	---	---	---	3.0E-06	---
Nb-93m	---	---	---	---	---	---	---	---	---	---	1.0E-03	---
Nb-94	---	---	---	---	---	---	---	8.0E-06	---	2.5E-02	1.5E-02	1.0E-05
Nd-144	---	---	---	---	---	---	---	---	---	---	---	1.0E-08
Ni-59	---	---	---	---	---	---	---	---	---	2.1E-03	1.8E-03	2.4E-03
Ni-63	---	1.0E-05	---	---	---	---	---	---	---	5.6E-03	2.0E+00	5.1E-04
Np-237	---	---	---	---	---	---	---	---	---	1.1E-05	4.2E-03	6.3E-04
Os-194	---	---	---	---	---	---	---	---	---	---	1.3E-07	---
Pa-231	---	---	---	---	---	---	---	---	---	1.0E-08	2.4E-05	1.8E-05
Pb-210	---	---	2.8E-03	---	---	---	---	---	---	9.6E-03	3.3E-03	9.0E-02

[a] *This column includes radionuclides, material types, mixed-activation products (MAP), and mixed-fission products (MFP).*

Table III-3 (Continued)
Radionuclide and Material Type Inventories, by Disposal Pit, for the Area G Performance Assessment

	Waste Inventory by Disposal Pit and Period of Disposal (Ci)											
	30		31	32		33	35	36		37	38	39
Constituent [a]	1988–1989	1990–2007	1990–2007	1971–1988 [b]	1990–2007	1971–1988	1971–1988	1971–1988	1988–1989	1990–2007	1990 – 2007	1990–2007
Pm-145	---	---	---	---	---	---	---	---	---	1.0E-01	1.0E-02	---
Pu-236	---	---	---	---	---	---	---	---	---	---	1.0E-09	---
Pu-238	1.6E+00	2.1E-02	3.5E-02	1.5E+00	---	5.9E-02	3.1E-01	8.5E-02	1.0E-09	1.1E+00	8.6E+00	1.9E+00
Pu-239	1.2E-01	4.2E-02	2.0E-01	3.6E+00	---	2.2E+00	9.3E-01	3.9E-01	3.8E-03	3.1E+00	1.0E+01	1.5E+00
Pu-240	---	---	4.3E-03	2.7E-05	---	---	---	---	---	2.4E-02	1.7E-01	2.6E-01
Pu-241	---	---	5.6E-02	---	---	---	---	---	---	2.9E-01	6.1E-01	6.1E-01
Pu-242	---	---	2.3E-07	---	---	---	---	7.8E-06	---	8.0E-07	5.8E-03	7.2E-06
Pu-244	---	---	---	---	---	---	---	---	---	---	3.5E-06	---
PU52	4.5E-01	1.4E-01	---	1.6E-01	---	1.1E-01	5.1E-01	4.1E-01	4.4E-02	4.4E+00	---	1.6E-01
PU53	---	---	---	---	---	---	---	---	---	---	---	---
PU54	---	---	---	2.0E-02	---	---	---	---	---	---	---	---
PU83	---	---	---	1.1E-05	---	1.3E-03	1.3E-04	---	---	---	---	---
Ra-226	---	1.0E-03	2.3E-03	1.0E-05	---	---	---	---	---	2.8E-02	1.5E-02	1.3E-03
Ra-228	---	---	3.7E-03	---	---	2.1E-01	---	---	---	5.9E-03	7.5E-03	1.7E-02
Si-32	---	---	---	---	---	---	---	---	---	---	1.6E-05	1.1E-07
Sm-151	---	---	9.0E-10	---	---	---	---	---	---	---	2.5E-09	---
Sn-126	---	---	---	---	---	---	---	---	---	---	---	8.5E-07
Sr-90	1.1E-01	2.2E-02	1.0E-01	1.3E-03	---	1.2E-01	---	---	---	1.2E-01	2.3E+00	7.8E-02
Tc-97	---	---	---	---	---	---	---	---	---	2.1E-06	2.0E-08	7.0E-09
Tc-99	---	8.3E-09	9.6E-06	---	---	---	---	---	---	9.9E-03	2.8E-01	2.8E-02
Th-228	---	1.0E-06	3.3E-07	---	---	---	---	---	---	1.1E-03	5.7E-04	4.4E-05
Th-229	---	---	---	---	---	---	---	---	---	4.0E-05	2.7E-04	4.8E-07
Th-230	---	---	---	2.6E-09	---	---	---	---	---	5.0E-07	1.2E-03	5.2E-07

[a] *This column includes radionuclides, material types, mixed-activation products (MAP), and mixed-fission products (MFP).*

Table III-3 (Continued)
Radionuclide and Material Type Inventories, by Disposal Pit, for the Area G Performance Assessment

	Waste Inventory by Disposal Pit and Period of Disposal (Ci)											
	30		31	32		33	35	36		37	38	39
Constituent [a]	1988–1989	1990–2007	1990–2007	1971–1988 [b]	1990–2007	1971–1988	1971–1988	1971–1988	1988–1989	1990–2007	1990 – 2007	1990–2007
Th-232	1.1E-05	---	3.0E-06	1.0E-09	---	---	---	---	---	1.6E-02	2.9E-01	1.4E-03
TH88	3.7E-02	---	---	---	---	2.6E-03	---	---	---	2.0E-09	---	---
Ti-44	---	---	---	---	---	---	---	---	---	3.0E-05	2.2E-03	---
U(NAT)	---	---	---	---	---	---	---	---	---	---	6.4E-05	---
U11	---	---	---	2.4E-02	---	---	---	---	---	8.7E-06	---	---
U12	---	---	---	---	---	2.4E-03	---	---	---	---	---	---
U-232	---	---	---	---	---	---	---	---	---	3.4E-05	3.2E-04	5.2E-04
U-233	---	---	---	---	---	---	---	---	---	2.3E-03	6.2E-02	5.4E-04
U-234	---	1.5E-04	1.2E-03	---	---	---	---	---	---	3.5E-01	2.7E-01	2.9E-01
U-235	1.9E-01	3.2E-01	7.2E-04	2.9E-03	---	1.1E-02	1.2E-03	4.8E-02	4.2E-09	2.9E-01	2.8E-02	1.9E-02
U-236	---	---	---	---	---	---	---	---	---	3.1E-05	3.6E-03	1.3E-07
U-238	1.4E+00	2.1E+00	1.7E-03	3.9E-01	---	7.6E-01	1.6E-01	3.1E-03	6.5E-02	9.6E-01	9.1E-01	8.3E-01
U38	3.0E-02	---	---	1.6E-02	---	---	---	8.2E-04	---	2.0E-02	---	---
U39	---	---	---	---	---	---	---	---	---	3.1E-03	---	---
U81	---	3.5E-06	---	---	---	---	---	---	---	5.7E-04	---	---

[a] *This column includes radionuclides, material types, mixed-activation products (MAP), and mixed-fission products (MFP).*

Table III- 4
Future Radionuclide and Material Type Inventories, by Disposal Pit, for the Area G Performance Assessment

Constituent a	Future Waste Inventory by Period of Disposal (Ci)	
	2008–2010 Pits	2011–2044 Pits
Ac-227	5.3E-06	6.0E-05
Ag-108m	4.7E-06	5.3E-05
Al-26	1.0E-07	1.1E-06
Am-241	1.8E+00	1.3E+01
Am-243	3.1E-03	3.5E-02
Ba-133	2.6E-01	2.9E+00
Bi-207	5.7E-03	6.5E-02
C-14	9.6E-04	1.1E-02
Cf-249	3.8E-05	4.3E-04
Cm-243	4.1E-06	4.6E-05
Cm-244	1.1E-03	1.2E-02
Cm-245	1.7E-05	2.0E-04
Cm-248	1.7E-07	1.9E-06
Co-60	7.9E+00	6.7E+01
Cs-135	6.1E-07	6.9E-06
Cs-137	8.3E-01	4.0E+00
D38	2.3E+00	2.6E+01
Eu-152	1.8E-02	1.8E-01
Eu-154	2.5E-04	2.8E-03
H-3	2.5E+00	1.7E+01
Ho-166m	5.3E-04	6.0E-03
I-129	1.2E-05	1.3E-04
K-40	3.0E-01	5.5E-01
Kr-85	3.8E-05	4.3E-04
Mo-93	7.5E-06	8.5E-05
Nb-91	4.3E-06	4.9E-05
Nb-92	1.1E-06	1.3E-05
Nb-93m	3.9E-04	4.4E-03
Nb-94	5.6E-03	6.4E-02

[a] *This column includes radionuclides, material types, mixed-activation products (MAP), and mixed-fission products (MFP).*

Table III-4 (Continued)
Future Radionuclide and Material Type Inventories, by Disposal Pit, for the Area G Performance Assessment

Constituent a	Future Waste Inventory by Period of Disposal (Ci)	
	2008–2010 Pits	2011–2044 Pits
Nd-144	3.7E-09	4.2E-08
Ni-59	2.7E-06	3.0E-05
Ni-63	7.7E-02	8.7E-01
Np-237	1.6E-03	1.8E-02
Os-194	4.9E-08	5.5E-07
Pa-231	9.0E-06	1.0E-04
Pb-210	3.0E-02	5.5E-02
Pm-145	3.7E-09	4.2E-08
Pu-236	3.7E-10	4.2E-09
Pu-238	2.1E+00	2.0E+01
Pu-239	2.9E+00	1.5E+01
Pu-240	3.9E-01	9.1E-01
Pu-241	4.4E-01	4.4E+00
Pu-242	2.1E-03	2.4E-02
Pu-244	1.3E-06	1.5E-05
Ra-226	9.8E-02	2.2E-01
Ra-228	3.9E-02	7.5E-02
Si-32	6.2E-06	7.1E-05
Sm-151	2.0E-09	1.2E-08
Sr-90	9.7E-01	8.9E+00
Tb-157	1.7E-08	1.9E-07
Tc-97	7.5E-09	8.5E-08
Tc-99	2.2E-02	2.5E-01
Th-228	3.0E-04	2.7E-03
Th-229	1.1E-04	1.3E-03
Th-230	5.4E-05	3.6E-04
Th-232	6.8E-04	7.4E-03
Ti-44	9.8E-04	1.1E-02
U(NAT)	2.4E-05	2.7E-04
U-232	1.4E-05	1.6E-04

[a] *This column includes radionuclides, material types, mixed-activation products (MAP), and mixed-fission products (MFP).*

Table III-4 (Continued)
Future Radionuclide and Material Type Inventories, by Disposal Pit, for the Area G Performance Assessment

Constituent a	Future Waste Inventory by Period of Disposal (Ci)	
	2008–2010 Pits	2011–2044 Pits
U-233	7.3E-02	1.7E-01
U-234	4.2E-01	1.2E+00
U-235	2.6E-02	7.8E-02
U-236	3.8E-03	7.4E-03
U-238	4.3E-01	2.1E+00

[a] *This column includes radionuclides, material types, mixed-activation products (MAP), and mixed-fission products (MFP).*

Table III-5
Radionuclide and Material Type Inventories, by Disposal Shaft, for the Area G Performance Assessment

	Waste Inventory by Disposal Shaft and Period of Disposal (Ci)											
	1	2	3	4	5	6	7	8	9	10	11	12
Constituent [a]	Pre-1971	Pre-1971	Pre-1971	Pre-1971	Pre-1971	Pre-1971	Pre-1971	Pre-1971	Pre-1971	Pre-1971	Pre-1971	Pre-1971
Am-243	---	---	---	---	---	---	---	---	---	---	---	2.0E-02
Cf-252	---	---	---	---	---	---	4.0E+00	---	---	---	---	---
Cm-244	---	---	---	2.3E-04	---	---	---	---	---	---	---	---
Co-60	6.0E+00	9.0E+00	---	5.0E-01	---	---	---	---	1.2E-01	---	---	---
Cs-137	---	---	---	5.0E-01	---	---	---	---	1.2E-01	---	---	---
D38	---	---	1.1E-05	---	---	---	---	---	---	---	---	---
Eu-152	---	---	---	---	---	---	---	---	1.2E-01	---	---	---
H-3	1.5E+02	---	---	---	1.0E-01	3.0E+02	5.2E+03	---	---	---	---	1.9E+01
MAP	2.0E+00	5.0E-01	8.0E-01	7.0E+00	---	---	---	3.0E+00	5.0E+00	---	2.0E+00	6.0E+00
MFP	1.6E+02	1.2E+03	2.2E+02	3.0E+00	2.5E+01	---	1.9E+01	---	---	1.0E+00	1.0E+00	3.1E+01
Np-237	1.4E-04	---	---	4.2E-06	---	---	---	---	---	---	---	---
Pu-238	---	---	---	---	---	---	3.9E-02	---	---	---	---	---
Pu-239	6.2E-02	---	9.1E+00	6.5E-03	3.1E-02	---	4.7E-04	---	5.1E-04	---	1.2E-01	6.8E-04
Pu-240	---	---	---	6.7E-04	---	---	---	---	1.3E-04	---	---	3.4E-02
Pu-241	---	---	---	5.2E-03	---	---	---	---	2.1E-04	---	---	---
Sr-90	1.0E+00	---	---	---	---	---	---	---	---	---	---	---
Th-230	---	---	---	5.7E-04	---	---	---	---	---	---	---	---
Th-232	---	---	---	---	---	---	---	1.7E-05	---	---	---	---
U-233	---	1.5E+00	---	3.1E-03	---	---	7.2E-05	---	1.3E-06	---	---	---
U-234	---	---	---	7.8E-06	---	---	---	---	---	---	---	---
U-235	5.5E-04	3.3E-04	5.0E-05	1.0E-03	1.1E-06	2.0E-03	5.0E-06	---	4.0E-08	2.8E-04	9.7E-04	1.4E-03
U-236	---	---	---	9.7E-08	---	---	---	---	2.1E-08	---	---	---

--- = None

[a] *This column includes radionuclides, material types, mixed activation products (MAP), and mixed fission products (MFP).*

Table III-5 (Continued)
Radionuclide and Material Type Inventories, by Disposal Shaft, for the Area G Performance Assessment

	Waste Inventory by Disposal Shaft and Period of Disposal (Ci)										
	13	14	15	16	17		18		19	20	21
Constituent [a]	Pre-1971	Pre-1971	Pre-1971	Pre-1971	Pre-1971	1971–1988 [b]	Pre-1971	1971–1988	1971–1988	1971–1988	1971–1988
Cf-252	---	---	---	---	---	---	---	---	---	---	9.5E-06
Co-60	2.2E+00	---	---	---	---	---	---	---	---	---	---
H-3	8.7E-04	---	1.8E+04	1.8E+04	2.0E+04	---	---	---	---	---	---
MAP	1.3E+00	---	---	---	---	---	3.0E+01	5.0E-02	---	---	---
MFP	4.5E+01	5.9E+00	4.0E+00	---	4.0E+02	7.7E-01	2.2E+01	3.7E+01	1.5E-01	3.2E-02	---
Pu-238	4.3E-01	---	---	---	---	---	---	2.4E-01	---	---	---
Pu-239	8.7E-01	---	---	---	---	1.9E-01	---	6.1E-07	---	---	---
Ra-226	1.0E-01	---	---	---	---	---	---	---	---	---	---
U-233	---	---	---	---	---	4.0E+00	---	---	---	---	---
U-235	2.3E-03	3.5E-05	---	---	6.3E-07	2.3E-05	---	---	2.3E-05	---	---
U-238	---	---	---	---	---	---	---	3.3E-04	---	---	---

--- = None

[a] This column includes radionuclides, material types, mixed activation products (MAP), and mixed fission products (MFP).

[b] Refers to waste disposed of from 1971 through September 26, 1988.

Table III-5 (Continued)
Radionuclide and Material Type Inventories, by Disposal Shaft, for the Area G Performance Assessment

Constituent [a]	Waste Inventory by Disposal Shaft and Period of Disposal (Ci)											
	22		23	24	25	26	27	28	29		30	
	1971–1988 [b]	1988–2007 [c]	1971–1988	Pre-1971	Pre-1971	Pre-1971	Pre-1971	Pre-1971	Pre-1971	1971–1988	Pre-1971	1971–1988
Am-241	---	5.0E-07	---	---	---	---	---	---	---	---	---	---
Ba-133	---	2.5E-04	---	---	---	---	---	---	---	---	---	---
C-14	---	2.7E-09	---	---	---	---	---	---	---	---	---	---
Co-60	4.9E+02	1.5E+00	5.2E+02	---	---	---	---	---	---	---	---	---
Cs-137	---	9.0E-04	4.2E+01	---	---	5.5E-03	---	---	---	---	---	---
D38	---	---	---	---	2.4E-05	2.4E-05	---	---	---	---	---	---
Eu-152	---	7.5E-09	---	---	---	---	---	---	---	---	---	---
Kr-85	---	1.0E-03	---	---	---	---	---	---	---	---	---	---
MAP	---	---	---	2.4E+00	5.7E+00	---	2.0E-01	1.4E+01	---	2.5E-02	1.0E-01	2.0E-01
MFP	---	---	---	1.7E-01	3.9E+01	2.7E+00	9.5E+01	2.6E+02	2.5E+01	---	7.2E+01	1.0E+01
Ni-63	---	3.0E-05	---	---	---	---	---	---	---	---	---	---
Pb-210	---	2.3E-09	---	---	---	---	---	---	---	---	---	---
Pu-239	---	4.1E-05	---	---	---	---	5.9E+00	---	---	---	3.4E-01	---
Pu-242	---	---	---	---	---	1.2E-04	---	---	---	---	---	---
Sr-90	---	7.3E-04	---	---	---	1.0E-01	---	---	---	---	---	---
Th-232	---	2.2E-06	---	---	---	---	---	---	---	---	---	---
U-233	---	---	---	---	1.9E-05	---	---	---	---	---	---	---
U-235	---	5.2E-05	---	1.1E-03	9.1E-04	4.4E-04	---	5.7E-04	6.1E-04	---	---	---
U-238	---	5.0E-07	---	---	---	---	---	---	---	---	---	---

--- = None

[a] This column includes radionuclides, material types, mixed activation products (MAP), and mixed fission products (MFP).

[b] Refers to waste disposed of from 1971 through September 26, 1988.

[c] Refers to waste disposed of from September 27, 1988 through 2007.

Table III-5 (Continued)
Radionuclide and Material Type Inventories, by Disposal Shaft, for the Area G Performance Assessment

Constituent [a]	Waste Inventory by Disposal Shaft and Period of Disposal (Ci)											
	31		32		33		35	36	38	39		40
	Pre-1971	1971–1988 [b]	Pre-1971	1971–1988	Pre-1971	1971–1988	1971–1988	1971–1988	1971–1988	Pre-1971	1971–1988	1971–1988
D38	1.9E-06	---	---	---	---	---	---	---	---	---	---	---
H-3	---	---	---	---	---	---	3.9E-02	---	---	5.7E+02	8.2E+03	---
MAP	---	---	---	5.6E-01	---	---	---	---	1.2E-02	2.0E-03	---	4.8E-01
MFP	1.0E-03	---	---	1.1E+00	6.4E+01	1.6E+01	3.5E+01	1.2E+02	---	---	---	2.0E+01
Pu-238	---	---	---	---	5.1E+00	---	---	---	---	---	---	---
Pu-239	6.2E-03	---	6.2E-03	9.1E-03	4.3E+00	9.6E-01	---	---	---	---	---	---
Th-232	---	---	---	1.0E-02	---	---	---	---	---	---	---	---
U-235	3.2E-04	---	---	2.4E-05	2.7E-05	1.7E-05	---	---	---	---	---	---
U-238	1.3E-06	4.3E+00	---	1.0E-04	---	---	---	---	---	---	---	5.4E-02

--- = None

[a] This column includes radionuclides, material types, mixed activation products (MAP), and mixed fission products (MFP).

[b] Refers to waste disposed of from 1971 through September 26, 1988.

Table III-5 (Continued)
Radionuclide and Material Type Inventories, by Disposal Shaft, for the Area G Performance Assessment

Constituent [a]	Waste Inventory by Disposal Shaft and Period of Disposal (Ci)											
	41	42	43	44	45	46	47	48	49	50	51	52
	1971–1988 [b]	1971–1988	1971–1988	1971–1988	1971–1988	1971–1988	1971–1988	1971–1988	1971–1988	1971–1988	1971–1988	1971–1988
Cf-252	---	---	---	---	5.4E+01	---	1.6E+00	---	---	---	4.7E-05	---
Co-60	---	---	---	---	---	---	---	---	---	---	---	1.5E-02
H-3	1.0E+01	---	7.0E+00	3.0E-03	3.7E-02	---	1.4E+00	---	---	2.9E+04	---	---
MAP	2.0E+01	4.4E-01	4.1E-01	---	2.0E+01	5.0E-01	1.0E-03	1.2E+01	1.0E+00	1.5E+01	1.1E-01	4.0E-02
MFP	---	1.2E+01	4.4E+00	4.0E+01	4.0E+01	1.8E+00	7.2E+00	7.7E+00	1.2E+00	1.5E-01	2.3E+02	1.5E+02
Pu-238	---	---	3.0E-04	---	---	5.4E-01	---	---	---	---	---	---
Pu-239	---	6.2E-02	2.5E-01	6.6E+00	4.1E+00	4.7E-02	3.2E-01	5.1E-01	6.7E-01	---	9.7E+00	3.4E+00
Pu-241	---	---	7.3E-01	---	---	---	---	---	---	---	---	---
U10	---	---	---	---	---	---	---	---	---	---	1.8E-05	---
U12	---	---	---	---	---	---	---	5.6E-05	5.6E-05	4.6E-02	---	---
U-232	---	---	---	---	---	---	---	---	---	---	---	2.1E-01
U-233	---	---	6.2E-05	---	---	---	---	---	---	---	---	---
U-234	---	---	---	---	---	---	---	---	---	---	---	---
U-235	2.2E-03	---	4.6E-04	2.4E-04	1.2E-04	---	1.5E-05	1.5E-05	---	---	1.7E-03	7.6E-05
U-236	---	---	---	---	---	---	---	---	---	---	2.5E-05	---
U-238	---	1.7E-05	9.8E-04	2.4E-04	8.2E-04	---	---	---	---	5.1E-05	1.0E-05	3.3E-04

--- = None

[a] This column includes radionuclides, material types, mixed activation products (MAP), and mixed fission products (MFP).

[b] Refers to waste disposed of from 1971 through September 26, 1988.

Table III-5 (Continued)
Radionuclide and Material Type Inventories, by Disposal Shaft, for the Area G Performance Assessment

Constituent [a]	Waste Inventory by Disposal Shaft and Period of Disposal (Ci)											
	53	54	55	56	57	58	59	61	62	63	64	65
	1971–1988 [b]	1971–1988	1971–1988	1971–1988	1971–1988	1971–1988	1971–1988	1971–1988	1971–1988	1971–1988	1971–1988	1971–1988
Am-241	---	3.4E-03	---	---	3.5E-02	---	---	---	---	---	---	---
Am-243	---	---	---	---	---	---	---	---	---	---	---	1.1E-05
Cm-244	---	---	---	---	---	---	---	---	---	---	---	2.3E-04
H-3	2.0E+00	---	---	---	---	---	2.3E+03	---	---	---	---	---
MAP	5.0E-04	---	---	---	1.2E-04	2.3E+02	---	---	---	---	---	2.4E-02
MFP	1.1E+02	1.9E+02	5.0E+01	1.1E+01	7.5E+00	2.8E+00	---	5.0E+00	---	---	---	1.6E+01
Pu-238	---	---	---	---	---	---	---	---	1.0E-03	---	2.0E-03	4.1E-03
Pu-239	1.8E+00	4.5E+00	1.0E+00	---	---	6.9E-02	---	6.1E-06	6.1E-08	---	2.0E-03	1.1E-03
Pu-242	---	---	---	---	---	---	---	---	---	---	---	3.1E-07
PU52	---	---	---	1.5E+01	---	---	---	---	---	---	---	---
Ra-226	---	3.6E-04	---	---	---	---	---	---	---	---	---	---
Th-232	---	---	---	---	---	---	---	4.7E-04	---	---	---	---
U12	---	---	---	---	---	---	---	---	---	1.9E-01	1.3E-02	---
U-233	1.9E-02	---	---	---	---	---	---	---	---	---	---	---
U-234	---	---	---	---	---	---	---	---	---	---	---	1.4E-06
U-235	2.8E-04	6.4E-04	1.3E-04	---	---	3.1E-04	---	---	---	5.0E-04	---	3.5E-04
U-238	5.7E-06	4.5E-04	3.0E-04	---	---	2.3E-03	---	---	---	1.0E-06	1.7E-04	2.1E-01
U81	---	---	---	---	---	---	---	---	---	1.8E-02	---	---

--- = None

[a] This column includes radionuclides, material types, mixed activation products (MAP), and mixed fission products (MFP).

[b] Refers to waste disposed of from 1971 through September 26, 1988.

Table III-5 (Continued)
Radionuclide and Material Type Inventories, by Disposal Shaft, for the Area G Performance Assessment

Constituent [a]	Waste Inventory by Disposal Shaft and Period of Disposal (Ci)											
	66	67	68	69	71	72	73	74	75	76	77	78
	1971–1988 [b]	1971–1988	1971–1988	1971–1988	1971–1988	1971–1988	1971–1988	1971–1988	1971–1988	1971–1988	1971–1988	1971–1988
Am-241	---	---	---	---	---	---	---	---	---	3.4E-08	---	---
Cf-252	---	---	---	---	---	---	---	---	---	2.7E-07	---	1.1E-06
Cm-244	---	---	---	---	---	---	---	---	3.0E-03	---	---	---
Co-60	---	---	---	---	---	1.0E+00	---	---	---	---	---	---
H-3	---	1.0E-02	---	---	---	1.0E-01	---	---	---	---	---	---
MAP	---	4.7E-04	8.3E-02	---	5.0E-01	4.0E-01	2.0E-01	1.3E+01	1.7E+00	1.4E+01	4.4E+01	2.0E-01
MFP	---	4.1E+01	1.0E+02	---	4.4E+01	4.6E+01	1.5E+02	1.5E+02	7.6E+01	1.1E+02	4.3E+02	4.5E+01
Np-237	---	---	---	---	---	---	---	---	---	7.0E-05	---	---
Pu-238	1.0E-03	---	---	---	1.0E-07	5.0E-03	---	---	---	---	---	---
Pu-239	---	2.7E+00	3.5E+00	---	3.8E+00	2.3E-01	1.3E+00	1.9E+00	1.4E+00	1.0E+01	6.5E-01	1.4E+00
PU52	---	---	---	---	3.8E+00	---	---	---	---	---	---	---
U10	---	---	---	---	---	---	---	---	---	---	---	3.0E-03
U12	---	---	---	2.0E-06	---	---	---	---	---	---	---	---
U-233	---	---	---	---	---	2.0E-03	---	---	---	---	---	---
U-234	---	---	---	---	---	---	---	---	---	4.3E-07	---	---
U-235	---	2.4E-05	3.8E-04	---	5.7E-05	4.6E-05	1.8E-04	3.3E-04	4.6E-05	5.8E-05	1.5E-04	1.7E-04
U-238	---	---	1.5E-06	---	---	---	---	---	---	8.0E-05	---	8.3E-04
U38	---	---	---	2.1E-03	---	7.6E-03	7.6E-03	2.0E-07	---	---	---	---
U81	---	---	---	---	---	---	---	1.5E-04	---	---	---	---

--- = None

[a] This column includes radionuclides, material types, mixed activation products (MAP), and mixed fission products (MFP).

[b] Refers to waste disposed of from 1971 through September 26, 1988.

Table III-5 (Continued)
Radionuclide and Material Type Inventories, by Disposal Shaft, for the Area G Performance Assessment

Constituent [a]	Waste Inventory by Disposal Shaft and Period of Disposal (Ci)											
	79	80	81	82	83	84	85	86	87	88	89	90
	1971–1988 [b]	1971–1988	1971–1988	1971–1988	1971–1988	1971–1988	1971–1988	1971–1988	1971–1988	1971–1988	1971–1988	1971–1988
C-14	---	1.0E-02	---	---	---	---	---	---	---	---	---	---
Cm-244	---	1.8E-01	---	---	---	---	---	---	---	---	---	---
Co-60	1.0E-03	2.9E-03	---	---	---	---	---	---	---	---	---	---
Cs-137	---	5.0E-03	---	---	---	---	---	---	---	---	---	---
H-3	---	---	---	---	5.0E-07	---	---	---	---	---	---	---
Kr-85	---	---	---	---	---	---	---	---	---	---	---	---
MAP	1.0E+01	---	---	---	---	---	---	2.0E-01	---	---	---	---
MFP	1.5E+02	---	---	1.4E+01	1.0E+01	4.4E+01	5.6E+01	1.0E+03	8.8E+01	3.8E+01	1.9E+01	3.5E+02
Np-237	---	---	---	---	7.1E-06	---	---	---	---	---	---	---
Pu-238	1.7E-01	---	3.0E-03	---	1.0E-03	---	---	---	1.0E-03	1.0E-04	1.1E-04	1.0E-04
Pu-239	2.5E+00	---	---	4.3E+00	6.7E+00	1.5E+00	1.9E+00	1.1E+00	6.3E-02	2.6E+00	1.6E-01	9.3E-02
PU52	2.1E+01	---	---	1.9E+01	---	9.7E+00	---	---	---	---	---	3.1E-01
Sr-90	4.9E-08	---	---	---	---	---	---	---	---	---	---	---
Th-88	---	3.3E-03	---	---	---	---	---	---	---	---	---	---
U12	---	---	---	---	---	---	---	6.7E-04	---	---	---	2.8E-03
U-233	---	---	---	---	9.7E-04	---	---	---	---	---	---	---
U-234	3.1E-06	---	---	---	---	---	---	---	---	---	---	---
U-235	2.3E-04	8.1E-06	---	4.0E-08	6.9E-04	1.5E-04	9.9E-05	1.6E-04	8.8E-06	2.8E-07	2.3E-05	1.3E-05
U-238	7.5E-04	9.3E-06	3.3E-05	3.3E-05	6.8E-05	---	---	---	---	---	---	---
U38	2.1E-02	---	---	---	---	---	---	3.9E-06	---	---	---	---

--- = None

[a] This column includes radionuclides, material types, mixed activation products (MAP), and mixed fission products (MFP).

[b] Refers to waste disposed of from 1971 through September 26, 1988.

Table III-5 (Continued)
Radionuclide and Material Type Inventories, by Disposal Shaft, for the Area G Performance Assessment

Constituent [a]	Waste Inventory by Disposal Shaft and Period of Disposal (Ci)											
	91	92	93	94	95	96	97	99	100	101	102	103
	1971–1988 [b]	1971–1988	1971–1988	1971–1988	1971–1988	1971–1988	1971–1988	1971–1988	1971–1988	1971–1988	1971–1988	1971–1988
Am-241	---	---	---	1.0E-04	---	---	1.0E-06	---	---	---	---	1.2E-05
C-14	---	---	---	---	---	---	---	---	---	---	---	5.0E-04
Co-60	---	---	1.0E-03	1.5E+02	---	---	1.0E+02	1.2E+01	---	---	3.3E+02	3.0E-06
Cs-137	---	---	---	2.0E-03	---	---	1.0E-04	---	---	---	1.0E-03	8.7E-08
H-3	---	---	1.0E-06	---	---	---	1.0E+01	---	---	---	---	---
MAP	---	3.3E+00	2.1E+01	3.4E+03	---	4.0E+00	2.5E-01	2.0E+00	3.7E+02	---	8.0E-01	5.2E+01
MFP	2.5E+01	3.6E+01	6.1E+02	4.4E+01	2.1E+02	2.5E-01	2.6E+01	---	---	1.2E+01	7.0E+00	---
Pu-238	2.0E-04	3.0E-05	6.0E-05	3.0E-05	7.5E-05	---	7.5E-05	2.1E-04	---	6.0E-05	1.5E-05	---
Pu-239	2.6E-04	3.0E-05	6.0E-05	3.0E-05	7.5E-05	---	1.1E-03	2.1E-04	---	6.0E-05	1.5E-05	---
PU52	7.3E+00	---	---	---	---	---	---	---	---	---	---	---
Ra-226	---	---	4.4E-05	---	---	---	2.0E-03	---	---	---	2.5E+00	---
Sr-90	---	---	---	5.0E-02	---	---	---	---	---	---	---	---
Th-232	---	3.7E-03	---	---	---	---	---	---	---	---	---	---
U12	---	5.4E-03	1.0E-01	---	---	---	---	---	---	---	6.0E-06	---
U-235	---	5.6E-02	---	---	---	1.0E-09	---	---	---	3.0E-05	3.6E-04	1.3E-03
U-238	2.2E-04	---	2.2E-02	---	---	1.0E-01	1.8E-03	2.0E-03	---	1.3E-04	---	3.3E-07

--- = None

[a] This column includes radionuclides, material types, mixed activation products (MAP), and mixed fission products (MFP).

[b] Refers to waste disposed of from 1971 through September 26, 1988.

Table III-5 (Continued)
Radionuclide and Material Type Inventories, by Disposal Shaft, for the Area G Performance Assessment

Constituent [a]	Waste Inventory by Disposal Shaft and Period of Disposal (Ci)											
	104	105	106	107	108	109	110	111	112	114	115	119
	1971–1988 [b]	1971–1988	1971–1988	1971–1988	1971–1988	1971–1988	1971–1988	1971–1988	1971–1988	1971–1988	1971–1988	1971–1988
Am-241	---	1.0E-03	---	---	---	---	---	---	---	---	---	---
C-14	1.1E-01	---	---	---	1.0E-03	---	---	1.0E-06	---	1.0E+00	---	---
Cf-252	---	---	---	---	---	---	---	---	5.6E-04	---	---	---
Cm-244	---	---	---	---	---	---	---	---	5.0E-05	---	---	---
Co-60	---	---	---	---	4.3E+02	---	---	---	---	---	---	---
Cs-137	---	---	---	---	---	---	1.1E-02	---	5.0E-06	---	---	---
H-3	---	---	---	1.0E-06	1.0E-03	---	1.0E-09	---	---	5.1E-01	4.0E-01	---
Kr-85	---	---	---	---	---	---	---	---	---	9.0E-05	---	---
MAP	---	---	---	---	---	5.0E-01	1.0E-09	2.5E+00	---	5.3E+02	---	---
MFP	---	---	9.4E+01	7.4E+02	---	2.0E+01	4.6E+02	5.5E+01	2.6E+02	---	---	---
Ni-63	---	---	---	---	---	---	---	---	---	3.2E-04	---	---
Pu-238	---	2.4E-04	6.0E-05	3.0E-05	1.5E-04	6.0E-05	6.0E-05	1.0E-04	6.0E-05	1.5E-05	---	---
Pu-239	---	2.4E-04	5.5E-05	3.0E-05	1.5E-04	6.0E-05	6.2E-02	1.1E-04	6.0E-05	1.5E-05	---	---
Ra-226	---	---	---	---	---	---	1.0E-04	---	---	---	---	---
Sr-90	---	---	1.0E-03	---	2.0E-03	---	---	---	4.2E-02	---	---	---
Th-232	---	---	---	---	---	---	---	---	---	---	6.5E-04	2.2E-04
Th-88	---	---	---	---	---	---	---	---	---	---	---	2.7E-06
U12	6.4E-02	---	---	---	---	---	---	---	---	---	---	8.0E-01
U-235	---	---	---	---	1.1E-05	---	8.8E-06	4.0E-06	2.1E-07	1.0E-09	---	1.8E-03
U-238	---	---	---	6.7E-04	---	---	6.7E-03	4.3E-03	2.4E-02	1.0E-03	5.2E-01	6.3E-01
U81	---	---	---	---	---	---	---	---	---	---	4.5E-03	---

--- = None

[a] This column includes radionuclides, material types, mixed activation products (MAP), and mixed fission products (MFP).

[b] Refers to waste disposed of from 1971 through September 26, 1988.

Table III-5 (Continued)
Radionuclide and Material Type Inventories, by Disposal Shaft, for the Area G Performance Assessment

Constituent [a]	Waste Inventory by Disposal Shaft and Period of Disposal (Ci)											
	120	121	122	123	124		125	126	127	128	129	130
	1971–1988 [b]	1971–1988	1971–1988	1971–1988	1971–1988	1990–2007	1971–1988	1971–1988	1971–1988	1971–1988	1971–1988	1971–1988
Am-241	2.6E-04	---	---	---	---	---	---	---	---	---	---	---
Co-60	---	---	2.3E+02	---	1.1E-02	---	---	5.1E-01	---	---	8.1E+01	---
Cs-137	1.5E-02	---	5.0E-03	---	---	---	---	---	---	---	---	---
H-3	1.3E+01	---	---	---	3.0E-07	---	---	---	---	---	---	---
Kr-85	3.6E-04	---	---	---	---	---	---	---	---	---	---	---
MAP	6.2E+02	---	2.0E+03	---	---	1.0E+00	1.1E+01	6.2E+02	---	---	1.4E+02	3.4E+01
MFP	---	---	3.5E+02	---	---	---	---	7.1E+01	---	---	2.2E+02	---
Ni-63	1.5E-07	---	---	---	---	---	---	---	---	---	---	---
Pu-238	---	1.0E-04	6.0E-05	---	---	---	---	---	---	1.7E-05	---	---
Pu-239	---	1.0E-04	7.3E-05	---	---	---	---	---	---	6.1E-08	---	5.8E-08
PU54	---	---	---	---	2.0E-08	---	---	---	---	---	---	---
Ra-226	5.1E-03	---	---	---	---	---	---	---	---	---	---	---
Sr-90	1.8E-04	---	---	---	---	---	---	---	---	---	---	---
Th-232	---	---	---	---	---	4.0E-04	---	---	---	---	---	---
Th-88	---	---	2.1E-06	---	---	---	7.6E-04	---	---	---	---	---
U12	---	---	---	6.4E-02	---	---	3.8E-01	---	---	---	---	---
U-235	---	3.0E-06	2.1E-06	---	---	1.0E-05	---	3.2E-12	---	---	---	9.1E-01
U-238	---	9.5E-05	4.0E-05	8.7E-01	---	---	5.7E-01	9.8E-02	1.3E+00	---	---	8.5E-01

--- = None

[a] This column includes radionuclides, material types, mixed activation products (MAP), and mixed fission products (MFP).

[b] Refers to waste disposed of from 1971 through September 26, 1988.

Table III-5 (Continued)
Radionuclide and Material Type Inventories, by Disposal Shaft, for the Area G Performance Assessment

Constituent [a]	Waste Inventory by Disposal Shaft and Period of Disposal (Ci)													
	131		132		133	134	136		137			139		
	1971–1988 [b]	1990–2007	1971–1988	1990–2007	1971–1988	1971–1988	1971–1988	1990–2007	1971–1988	1988–1989	1990–2007	1971–1988	1988–1989	1990–2007
Co-60	---	7.6E+01	---	---	2.2E+02	---	---	---	---		---	2.6E+02	---	6.0E-02
Cs-137	---	1.5E+01	---	---	---	---	---	---	---		---	---		---
Eu-152	---	1.9E-03	---	---	---	---	---	---	---		---	---		---
Eu-154	---	9.7E-02	---	---	---	---	---	---	---		---	---		---
H-3	---	---	---	---	---	---	3.7E+03	1.8E+03	1.5E+00	5.0E+01	1.8E+01	---		---
MAP	1.9E+01	1.0E-02	---	---	3.1E+03	---	---	---	---		---	5.3E+02	2.0E+00	---
MFP	---	---	---	---	8.3E+01	2.5E+00	---	---	---		---	1.0E+01	5.8E+01	---
Nb-92	---	4.0E-03	---	---	---	---	---	---	---		---	---		---
Pu-238	---	---	---	1.0E-05	---	---	---	---	---		---	---		---
Pu-239	---	---	---	2.0E-09	---	---	---	---	---		---	---		---
Sn-126	---	2.4E-02	---	---	---	---	---	---	---		---	---		---
U-238	3.3E-07	---	4.3E-05	1.0E-09	---	---	---	---	---		---	---		---

--- = None

[a] This column includes radionuclides, material types, mixed activation products (MAP), and mixed fission products (MFP).

[b] Refers to waste disposed of from 1971 through September 26, 1988.

Table III-5 (Continued)
Radionuclide and Material Type Inventories, by Disposal Shaft, for the Area G Performance Assessment

Constituent [a]	Waste Inventory by Disposal Shaft and Period of Disposal (Ci)												
	140	141		142	143	144	147	148	149	150	151	152	153
	1971–1988 [b]	1988–1989	1990–2007	1990–2007	1990–2007	1990–2007	1990–2007	1990–2007	1990–2007	1971–1988	1971–1988	1971–1988	1971–1988
Ag-108m	---	---	---	---	---	4.9E-03	---	---	---	---	---	---	---
Am-241	---	---	---	---	6.7E-04	2.1E-03	6.0E-06	---	3.6E-04	---	---	---	---
Am-243	---	---	---	---	---	1.0E-09	---	---	---	---	---	---	---
Ba-133	---	---	---	---	---	---	1.3E-03	---	---	---	---	---	---
Bi-207	---	---	---	---	---	5.0E-05	---	---	---	---	---	---	---
Cf-252	---	---	---	---	---	2.7E-08	---	---	---	---	---	---	---
Cm-244	---	---	---	---	---	---	4.0E-09	---	---	---	---	---	---
Co-60	---	3.0E-01	4.7E+01	4.1E+01	4.0E+01	1.2E+01	6.0E-02	---	6.3E-01	---	---	---	---
Cs-137	---	---	1.1E-02	---	---	1.8E-01	1.5E-05	---	---	---	1.0E-03	---	---
D38	---		---	---	---	2.9E-04	---	---	---	---	---	---	---
Eu-152	---		---	---	---	6.4E-05	5.5E-08	---	---	---	---	---	---
H-3	---		---	---	---	1.0E-09	3.2E-02	---	---	1.6E+05	1.4E+05	4.3E+04	2.6E+04
MAP	1.0E-03	1.5E+03	1.4E+02	1.4E+02	1.2E+03	---	---	1.0E-07	5.5E+02	---	1.0E-03	---	---
MFP	---	2.1E+00	---	---	---	---	---	---	---	---	---	---	---
Ni-63	---	---	---	---	---	---	---	---	---	---	4.0E-03	---	---
Np-237	---	---	---	---	---	1.0E-09	---	---	---	---	---	---	---
Pu-238	---	---	---	---	6.7E-04	1.8E-02	---	---	3.6E-04	---	---	---	---
Pu-239	---	---	---	---	6.7E-04	8.8E-04	1.1E-06	2.2E-05	3.6E-04	---	---	---	---
Pu-240	---	---	---	---	---	9.3E-04	---	---	---	---	---	---	---
Pu-241	---	---	---	---	---	3.7E-02	---	---	---	---	---	---	---
Pu-242	---	---	---	---	---	1.0E-09	---	---	---	---	---	---	---

--- = None

[a] This column includes radionuclides, material types, mixed activation products (MAP), and mixed fission products (MFP).

[b] Refers to waste disposed of from 1971 through September 26, 1988.

Table III-5 (Continued)
Radionuclide and Material Type Inventories, by Disposal Shaft, for the Area G Performance Assessment

	Waste Inventory by Disposal Shaft and Period of Disposal (Ci)												
	140	141		142	143	144	147	148	149	150	151	152	153
Constituent [a]	1971–1988 [b]	1988–1989	1990–2007	1990–2007	1990–2007	1990–2007	1990–2007	1990–2007	1990–2007	1971–1988	1971–1988	1971–1988	1971–1988
PU52	---	---	---	---	---	---	---	---	---	---	5.4E-09	---	---
Ra-226	---	1.5E-05	---	---	---	5.0E-02	---	---	---	---	---	---	---
Sr-90	---	1.0E+00	4.0E+00	---	---	5.6E+01	---	---	---	---	---	---	---
Th-232	---	---	---	---	---	1.0E-09	1.1E-05	---	---	---	---	---	---
U-233	---	---	---	---	---	---	1.6E-06	---	---	---	---	---	---
U-234	---	---	---	---	---	2.8E-07	1.4E-02	---	---	---	---	---	---
U-235	---	---	---	---	6.7E-04	1.0E-09	1.2E-04	---	3.6E-04	---	---	---	---
U-238	1.0E-06	---	---	9.5E-02	6.7E-04	1.0E-09	8.3E-02	---	3.6E-04	---	---	1.5E-05	---

--- = None

[a] *This column includes radionuclides, material types, mixed activation products (MAP), and mixed fission products (MFP).*

[b] *Refers to waste disposed of from 1971 through September 26, 1988.*

Table III-5 (Continued)
Radionuclide and Material Type Inventories, by Disposal Shaft, for the Area G Performance Assessment

	Waste Inventory by Disposal Shaft and Period of Disposal (Ci)												
	154	155		156	157	158		159	160	161	162	163	164
Constituent [a]	1971–1988 [b]	1971–1988	1988–1989	1971–1988	1971–1988	1988–1989	1990-2007	1988–1989	1990–2007	1990–2007	1990–2007	1990–2007	1988–2007
C-14	---	---	8.9E-03	---	---	---		---	---	---	---	---	---
H-3	3.2E+05	5.5E+03	5.7E+04	3.7E+04	2.4E+04	1.1E+04	7.2E+02	8.6E+00	7.0E+02	4.6E+03	3.6E+05	4.8E+03	3.8E+03
Pu-239	---	---	---	---	---	---		---	---	---	---	4.6E-07	---
PU52	---	---	---	---	---	---	5.7E-02	---	---	---	---	---	---

--- = None

[a] This column includes radionuclides, material types, mixed activation products (MAP), and mixed fission products (MFP).

[b] Refers to waste disposed of from 1971 through September 26, 1988.

Table III-5 (Continued)
Radionuclide and Material Type Inventories, by Disposal Shaft, for the Area G Performance Assessment

Constituent [a]	Waste Inventory by Disposal Shaft and Period of Disposal (Ci)											
	165	166	167	168	169	170	171	172	173	174	176	177
	1990–2007	1990–2007	1990–2007	1990–2007	1990–2007	1990–2007	1990–2007	1990–2007	1990–2007	1990–2007	1990–2007	1990–2007
Am-241	---	---	---	---	---	---	---	2.3E-02	1.9E-08	1.0E-02	8.3E-03	2.8E-02
H-3	6.0E+03	1.5E+05	1.5E+05	9.5E+04	3.2E+03	9.4E+04	1.2E-03	---	---	---	---	---
Pu-238	---	---	---	---	---	---	---	3.8E-03	6.4E-09	6.8E-02	5.0E-02	1.1E-01
Pu-239	---	---	---	---	---	---	---	8.2E-03	1.7E-08	1.2E-02	1.3E-02	3.1E-02
U-235	---	---	---	---	---	---	---	6.0E-05	1.8E-07	2.1E-05	5.1E-06	4.2E-05
U-238	---	---	---	---	---	---	1.7E-05	2.0E-09	1.0E-06	---	---	3.8E-07

--- = None

[a] *This column includes radionuclides, material types, mixed activation products (MAP), and mixed fission products (MFP).*

Table III-5 (Continued)
Radionuclide and Material Type Inventories, by Disposal Shaft, for the Area G Performance Assessment

Constituent [a]	Waste Inventory by Disposal Shaft and Period of Disposal (Ci)											
	189	190	191	192	196		197	206	301	307	308	309
	1971–1988 [b]	1971–1988	1971–1988	1971–1988	1988–1989	1990–2007	1990–2007	1971–1988	1990–2007	1990–2007	1990–2007	1990–2007
Am-241	---	---	---	---	---	---	---	---	1.0E-05	---	---	1.0E-04
Ba-133	---	---	---	---	---	---	---	---	2.6E-06	---	---	---
Bi-207	---	---	---	---	---	---	---	---	4.0E-06	---	---	---
Cf-252	---	---	---	---	---	---	---	---	4.5E-08	---	---	---
Co-60	---	1.1E-05	---	---	7.0E-01	1.6E+02	3.6E+02	---	1.2E+02	1.7E+02	---	---
Cs-135	---	---	---	---	---	---	4.5E-06	---	---	---	---	---
Cs-137	---	---	---	---	---	---	4.5E-01	---	6.7E+01	---	---	---
D38	---	---	---	---	---	---	4.4E-01	---	---	---	4.5E-07	---
Eu-152	---	---	---	---	---	---	---	---	3.4E-04	---	---	---
Eu-154	---	---	---	---	---	---	---	---	5.5E-10	---	---	---
H-3	---	---	---	---	---	---	---	---	---	---	---	5.3E+04
Ho-163	---	---	---	---	---	---	7.0E-02	---	---	---	---	---
MAP	1.0E+02	8.8E+02	1.4E+02	7.8E+02	1.2E+02	1.9E+03	---	---	---	---	---	---
Pu-238	---	---	---	---	---	---	---	1.5E-05	---	---	---	---
Pu-239	---	---	---	---	---	---	---	1.5E-05	---	---	---	6.0E-04
Ra-226	---	---	---	---	---	---	---	---	5.5E-01	---	8.2E-09	---
Sr-90	---	---	---	---	---	---	---	---	1.9E-01	---	---	---
Th-228	---	---	---	---	---	---	---	---	---	---	1.3E-09	---
Th-229	---	---	---	---	---	---	---	---	5.4E-08	---	---	---
Th-232	---	---	---	---	---	---	1.1E-01	---	---	---	6.7E-02	---
U-235	---	---	---	---	---	---	---	---	---	---	1.4E-09	1.1E-05
U-238	---	---	---	---	---	2.5E-02	---	---	---	---	8.9E-07	1.0E-03

--- = None

[a] This column includes radionuclides, material types, mixed activation products (MAP), and mixed fission products (MFP).

[b] Refers to waste disposed of from 1971 through September 26, 1988.

Table III-5 (Continued)
Radionuclide and Material Type Inventories, by Disposal Shaft, for the Area G Performance Assessment

	Waste Inventory by Disposal Shaft and Period of Disposal (Ci)											
	311	313	315	317	319	321	323	325	327	329	331	333
Constituent [a]	1990–2007	1990–2007	1990–2007	1990–2007	1990–2007	1990–2007	1990–2007	1990–2007	1990–2007	1990–2007	1990–2007	1990–2007
Ag-108m	---	---	---	2.0E-05	---	---	---	---	---	---	---	---
Am-241	---	---	1.1E-07	9.0E-05	---	3.0E-07	2.6E-07	9.4E-08	2.1E-06	---	3.3E-06	---
Ba-133	---	---	---	5.8E-06	---	5.1E-10	---	---	5.3E-06	---	---	---
C-14	---	---	---	9.1E-07	---	---	---	---	---	---	---	---
Cf-252	---	---	---	1.8E-06	---	---	---	---	---	---	---	---
Cl-36	---	---	---	1.0E-08	---	---	---	---	---	---	---	---
Co-60	---	6.1E-03	8.8E-01	6.2E+00	---	---	1.7E-02	---	1.4E-06	---	7.8E-03	---
Cs-137	---	---	7.1E-02	1.4E-01	---	4.0E-08	3.4E-08	---	---	---	---	---
D38	---	---	---	---	5.0E-02	---	3.8E-09	---	---	---	7.0E-05	---
Eu-152	---	---	---	1.0E-05	---	---	---	---	---	---	---	---
H-3	5.1E+04	4.6E+03	2.1E-04	2.1E+03	1.5E+05	1.6E+03	1.0E+03	---	9.6E+02	5.1E+03	1.6E+03	1.9E+05
I-129	---	---	---	3.0E-08	---	---	---	---	---	---	---	---
Kr-85	---	---	5.4E-03	---	---	---	---	---	---	---	---	---
Nb-91	---	9.4E-03	---	---	---	---	---	---	---	---	---	---
Nb-93m	---	---	---	2.2E+00	---	---	---	---	---	---	---	---
Nb-94	---	---	---	9.2E-07	---	---	---	---	---	---	---	---
Ni-59	---	---	---	2.0E-07	---	---	---	---	---	---	---	---
Ni-63	---	---	---	9.9E+00	---	---	---	---	---	---	---	---
Pa-231	---	---	---	2.7E-03	---	---	---	---	---	---	---	---
Pu-238	---	---	1.2E-04	2.0E-08	---	7.1E-05	2.1E-04	---	1.1E-03	---	1.2E-03	---

--- = None

[a] *This column includes radionuclides, material types, mixed activation products (MAP), and mixed fission products (MFP).*

Table III-5 (Continued)
Radionuclide and Material Type Inventories, by Disposal Shaft, for the Area G Performance Assessment

	Waste Inventory by Disposal Shaft and Period of Disposal (Ci)											
	311	313	315	317	319	321	323	325	327	329	331	333
Constituent [a]	1990–2007	1990–2007	1990–2007	1990–2007	1990–2007	1990–2007	1990–2007	1990–2007	1990–2007	1990–2007	1990–2007	1990–2007
Pu-239	---	---	1.5E-04	3.0E-07	---	6.5E-05	1.9E-04	3.1E-05	8.6E-04	---	9.1E-04	---
Ra-226	---	---	---	9.6E-03	---	---	---	---	---	---	---	---
Sr-90	---	8.0E-06	6.9E-02	1.0E-03	---	---	---	---	---	---	---	---
Tc-99	---	---	---	3.0E-08	---	---	---	---	---	---	---	---
Th-228	---	---	---	5.7E-08	---	---	---	---	---	---	---	---
Th-230	---	---	---	1.1E-08	---	---	---	---	---	---	---	---
Ti-44	---	---	2.0E-02	---	---	---	---	---	---	---	---	---
U-234	---	---	4.9E-01	---	---	---	---	---	---	---	---	---
U-235	---	3.8E-07	2.7E-02	---	---	4.1E-08	1.9E-08	---	8.5E-08	---	7.7E-08	---
U-238	4.4E-04	1.0E-05	2.2E-02	1.7E-05	---	1.0E-04	8.3E-07	---	6.1E-06	---	6.8E-03	---

--- = None

[a] *This column includes radionuclides, material types, mixed activation products (MAP), and mixed fission products (MFP).*

Table III-5 (Continued)
Radionuclide and Material Type Inventories, by Disposal Shaft, for the Area G Performance Assessment

Constituent [a]	Waste Inventory by Disposal Shaft and Period of Disposal (Ci)											
	335	339	341	343	345	347	349	351	355	357	360	361
	1990–2007	1990–2007	1990–2007	1990–2007	1990–2007	1990–2007	1990–2007	1990–2007	1990–2007	1990–2007	1990–2007	1990–2007
Ac-227	---	5.3E-07	---	---	---	---	---	---	---	---	---	---
Am-241	---	3.7E-08	7.2E-06	1.1E-06	9.3E-08	---	---	---	2.3E-07	5.6E-07	---	1.2E-06
Ba-133	---	6.6E-06	---	---	---	---	---	---	---	---	---	---
C-14	---	1.1E-06	---	7.6E-02	---	---	---	---	---	---	1.1E-02	1.7E-03
Cl-36	---	9.9E-09	---	---	---	---	---	---	---	---	---	---
Co-60	---	1.2E-02	---	1.5E-02	1.5E-04	8.4E-01	---	---	6.5E-01	1.8E+02	4.7E+02	7.3E+01
Cs-137	---	8.9E-04	---	---	---	---	---	---	2.4E-03	3.2E-01	---	---
D38	---	---	1.3E-02	1.6E-01	6.0E-02	---	---	4.8E-01	6.7E-01	5.6E-01	---	---
Eu-152	---	5.1E-07	---	---	---	---	---	---	---	---	---	---
Eu-154	---	1.2E-06	---	---	---	---	---	---	---	---	---	---
Gd-148	---	7.7E-09	---	---	---	---	---	---	---	---	---	---
H-3	2.3E+04	1.3E+05	3.9E+03	1.5E+03	2.4E+03	1.8E+03	1.2E+04	1.9E+04	1.6E+02	2.8E+02	---	---
Mo-93	---	---	---	---	---	---	---	---	---	---	5.1E-03	---
Ni-59	---	---	---	---	---	---	---	---	---	---	2.5E+00	
Ni-63	---	---	---	---	---	---	---	---	---	---	3.8E+02	7.6E+01
Pu-238	---	3.6E-11	2.6E-03	8.0E-04	---	---	---	---	3.4E-06	3.9E-04	---	---
Pu-239	---	5.2E-07	2.0E-03	7.2E-04	---	---	---	---	1.7E-07	9.6E-04	---	1.8E-06
Ra-226	---	1.7E-01	---	---	---	---	---	---	---	---	---	---
Sr-90	---	6.2E-03	---	---	---	---	---	---	---	3.2E-01	---	---
Tc-99	---	1.0E-08	---	---	---	---	---	---	---	---	---	---

--- = None

[a] *This column includes radionuclides, material types, mixed activation products (MAP), and mixed fission products (MFP).*

Table III-5 (Continued)
Radionuclide and Material Type Inventories, by Disposal Shaft, for the Area G Performance Assessment

	Waste Inventory by Disposal Shaft and Period of Disposal (Ci)											
	335	339	341	343	345	347	349	351	355	357	360	361
Constituent [a]	1990–2007	1990–2007	1990–2007	1990–2007	1990–2007	1990–2007	1990–2007	1990–2007	1990–2007	1990–2007	1990–2007	1990–2007
Th-228	---	1.5E-06	2.5E-05	---	---	---	---	---	---	---	---	---
Th-230	---	5.3E-09	---	---	---	---	---	---	---	---	---	---
Th-232	---	4.5E-07	4.8E-05	---	4.0E-08	---	---	---	---	---	---	---
U(NAT)	---	---	---	---	---	---	---	1.8E-01	---	---	---	---
U-233	---	5.8E-04	---	---	---	---	---	---	---	---	---	---
U-234	---	---	---	---	---	---	---	---	3.7E-08	2.0E-03	---	---
U-235	---	---	1.5E-07	6.3E-08	---	---	---	4.4E-07	3.5E-09	6.0E-05	---	---
U-236	---	---	---	---	---	---	---	---	---	3.8E-06	---	---
U-238	---	7.7E-06	1.0E-02	3.8E-06	5.0E-06	---	---	2.7E-05	2.0E-01	1.1E-06	---	---

--- = None

[a] *This column includes radionuclides, material types, mixed activation products (MAP), and mixed fission products (MFP).*

Table III-5 (Continued)
Radionuclide and Material Type Inventories, by Disposal Shaft, for the Area G Performance Assessment

	Waste Inventory by Disposal Shaft and Period of Disposal (Ci)								
	362	363	364	365	366	367	370	C13	C14
Constituent [a]	1990–2007	1990–2007	1990–2007	1990–2007	1990–2007	1990–2007	1990–2007	1990–2007	1990–2007
Ag-108m	---	---	---	---	4.4E+00	9.8E-05	---	---	9.0E-09
Am-241	1.2E-06	---	2.0E-06	---	---	2.4E-01	---	8.6E-05	1.5E-04
Am-243	---	---	---	---	---	---	---	1.0E-18	---
Ba-133	1.0E-03	---	1.0E-06	---	---	2.4E-04	---	---	---
Bi-207	---	---	1.6E-06	---	---	4.8E-06	---	---	---
C-14	9.1E-03	1.6E+01	7.4E-03	---	8.9E-05	4.4E-03	---	---	---
Cf-252	---	---	7.7E-06	---	---	---	---	---	---
Cl-36	1.9E-04	---	---	---	---	6.5E-05	---	---	---
Cm-244	---	---	2.0E-03	---	---	1.6E-04	---	---	---
Co-60	1.8E+02	1.1E+02	1.6E+02	7.9E+01	7.7E+02	1.7E+01	4.2E+00	---	3.1E-06
Cs-137	5.4E-02	---	2.2E-07	---	---	1.8E-01	---	2.6E-05	4.7E-09
D38	---	---	---	---	---	4.4E-05	---	---	---
Eu-152	8.1E-03	---	6.4E-04	---	---	4.0E-04	---	---	4.7E-08
Eu-154	1.1E-03	---	---	---	---	5.7E-05	---	---	---
H-3	4.6E-02	4.9E+04	1.3E+01	---	8.0E+03	5.5E+04	---	1.4E-02	3.6E-07
K-40	---	---	---	---	---	---	---	---	4.3E-07
Kr-85	---	---	---	---	---	2.5E-03	---	---	---
Mo-93	1.5E-03	1.1E-03	1.4E-03	7.5E-04	3.1E-03	1.5E-04	---	---	---
Nb-94	8.5E-05	---	---	---	---	4.4E-05	---	---	---
Ni-59	5.6E-02	---	---	---	---	3.3E-03	---	---	---
Ni-63	1.3E+02	9.6E+01	1.4E+02	6.9E+01	2.5E+02	1.2E+01	---	---	---
Np-237	---	---	---	---	---	---	---	1.0E-18	3.0E-08
Pa-231	---	---	---	---	---	---	---	---	5.0E-08

--- = None

[a] *This column includes radionuclides, material types, mixed activation products (MAP), and mixed fission products (MFP).*

Table III-5 (Continued)
Radionuclide and Material Type Inventories, by Disposal Shaft, for the Area G Performance Assessment

	Waste Inventory by Disposal Shaft and Period of Disposal (Ci)								
	362	363	364	365	366	367	370	C13	C14
Constituent [a]	1990–2007	1990–2007	1990–2007	1990–2007	1990–2007	1990–2007	1990–2007	1990–2007	1990–2007
Pb-210	---	---	---	---	---	---	---	---	2.6E-08
Pu-238	---	---	---	---	---	7.6E-04	---	7.4E-04	4.2E-04
Pu-239	1.7E-06	---	---	---	---	2.3E-03	---	2.7E-04	3.5E-04
Pu-240	---	---	---	---	---	8.6E-06	---	2.7E-04	---
Pu-242	---	---	---	---	---	2.0E-06	---	---	---
Ra-226	---	---	---	---	---	1.8E-05	---	---	3.0E-08
Sr-90	2.4E+01	---	---	---	---	6.5E-01	---	1.5E-05	---
Tc-99	1.2E-05	---	---	---	---	3.0E-08	---	---	---
Th-228	---	---	6.6E-04	---	---	---	---	---	---
Th-232	---	---	1.3E-02	---	---	---	---	1.0E-18	---
Th-88	---	---	---	---	---	---	---	---	---
U-232	---	---	---	---	---	2.0E-04	---	---	---
U-233	---	---	---	---	---	5.2E-07	---	---	---
U-235	---	---	9.3E-08	---	7.5E-06	4.1E-07	---	2.0E-07	1.1E-08
U-238	---	---	---	---	9.6E-05	1.8E-03	---	1.3E-06	4.3E-07

--- = None

[a] *This column includes radionuclides, material types, mixed activation products (MAP), and mixed fission products (MFP).*

Table III-6
Future Radionuclide and Material Type Inventories, by Disposal Shaft, for the Area G Performance Assessment

Constituent [a]	Future Waste Inventory by Period of Disposal (Ci)	
	2008–2015	2016–2044
Ag-108m	9.0E-09	3.3E-08
Am-241	2.7E-04	9.7E-04
Bi-207	1.6E-06	5.7E-06
C-14	7.6E-02	2.8E-01
Cf-252	7.7E-06	2.8E-05
Cm-244	2.0E-03	7.3E-03
Co-60	8.3E+00	3.0E+01
Cs-137	4.2E-01	1.5E+00
D38	1.5E+00	5.5E+00
Eu-152	6.4E-04	2.3E-03
H-3	3.3E+05	6.5E+05
K-40	4.3E-07	1.5E-06
Kr-85	7.9E-03	2.9E-02
Nb-91	9.4E-03	3.4E-02
Nb-93m	2.2E+00	8.1E+00
Ni-63	9.9E+00	3.6E+01
Np-237	3.0E-08	1.1E-07
Pa-231	5.0E-08	1.8E-07
Pb-210	2.6E-08	9.5E-08
Pu-238	7.6E-03	2.8E-02
Pu-239	7.0E-03	2.5E-02
Ra-226	1.8E-05	6.6E-05
Sr-90	3.9E-01	1.4E+00
Th-228	6.9E-04	2.5E-03
Th-232	1.3E-02	4.7E-02
Ti-44	2.0E-02	7.1E-02
U(NAT)	1.8E-01	6.5E-01
U-234	4.9E-01	1.8E+00
U-235	2.7E-02	9.8E-02
U-236	3.8E-06	1.4E-05
U-238	2.4E-01	8.9E-01

[a] *This column includes radionuclides, material types, mixed-activation products (MAP), and mixed-fission products (MFP).*

Attachment IV
Plutonium Material Type Waste Spectral Data

This attachment summarizes the data used to develop distributions of radionuclide activity fractions for material types PU52, PU53, PU54, PU56, and PU83. These data, taken from Veilleux (2005), were estimated using spectral information collected from almost 3,300 drums of waste using a high-purity germanium detector. Some data were removed from the analysis in an attempt to eliminate drums of waste that contained mixtures of material types. A discussion of the manner in which the analysis was conducted is provided in Section 5.4 of the main report.

Table IV-1
Sample Data Used to Estimate Radionuclide Activity Fraction Distributions in Plutonium Material Types

Material Type	Drum ID	Pu238	Pu239	Pu240	Pu241	Pu242
PU52	52007	2.28E-04	9.39E-01	5.88E-02	1.43E-03	9.46E-05
	52015	6.40E-05	9.36E-01	6.26E-02	1.32E-03	9.39E-05
	52032	1.28E-04	9.38E-01	6.04E-02	1.56E-03	2.62E-04
	52033	1.60E-04	9.40E-01	5.87E-02	1.38E-03	9.10E-05
	52034	9.80E-05	9.41E-01	5.80E-02	1.14E-03	7.44E-05
	52039	7.31E-05	9.09E-01	8.87E-02	2.02E-03	2.15E-04
	52040	1.62E-04	9.35E-01	6.37E-02	1.50E-03	1.09E-04
	52045	9.90E-05	9.33E-01	6.59E-02	1.39E-03	1.04E-04
	52048	1.04E-04	9.36E-01	6.20E-02	1.39E-03	9.75E-05
	52049	1.41E-04	9.19E-01	7.87E-02	1.49E-03	1.38E-04
	52059	9.55E-05	9.40E-01	5.86E-02	1.43E-03	9.40E-05
	52060	1.45E-04	9.31E-01	6.71E-02	1.46E-03	1.12E-04
	52061	1.36E-04	9.38E-01	5.99E-02	1.68E-03	1.14E-04
	52062	8.57E-05	9.32E-01	6.64E-02	1.62E-03	1.24E-04
	52082	6.38E-05	9.20E-01	7.79E-02	1.47E-03	1.35E-04
	52083	8.71E-05	9.39E-01	5.91E-02	1.37E-03	9.12E-05
	52088	8.85E-05	9.38E-01	6.03E-02	1.43E-03	9.74E-05
	52092	1.44E-04	9.41E-01	5.69E-02	1.48E-03	9.45E-05
	52095	1.85E-04	9.37E-01	6.13E-02	1.46E-03	1.02E-04
	52096	1.39E-04	9.39E-01	5.92E-02	1.47E-03	9.83E-05
	52100	1.25E-04	9.34E-01	6.44E-02	1.41E-03	1.03E-04
	52103	1.03E-04	9.36E-01	6.27E-02	1.45E-03	1.03E-04
	52108	1.11E-04	9.40E-01	5.80E-02	1.72E-03	1.12E-04
	52113	1.58E-04	9.31E-01	6.65E-02	1.73E-03	1.32E-04
	52116	1.07E-04	9.38E-01	6.01E-02	1.35E-03	9.16E-05
	52117	1.41E-04	9.39E-01	5.87E-02	1.65E-03	1.09E-04
	52120	1.59E-04	9.37E-01	6.15E-02	1.46E-03	1.02E-04
	52124	1.93E-04	9.27E-01	7.09E-02	1.82E-03	1.49E-04
	52128	1.36E-04	9.33E-01	6.48E-02	1.67E-03	1.23E-04
	52134	1.52E-04	9.39E-01	5.89E-02	1.48E-03	9.79E-05
	52135	1.20E-04	9.35E-01	6.31E-02	1.68E-03	1.20E-04
	52142	2.20E-04	9.42E-01	5.63E-02	1.61E-03	1.02E-04

Table IV-1 (Continued)
Sample Data Used to Estimate Radionuclide Activity Fraction Distributions in Plutonium Material Types

Material Type	Drum ID	Pu238	Pu239	Pu240	Pu241	Pu242
PU52 (Cont.)	52145	1.12E-04	9.42E-01	5.69E-02	1.20E-03	7.67E-05
	52147	7.70E-05	9.47E-01	5.16E-02	1.63E-03	9.32E-05
	52148	8.96E-05	9.32E-01	6.62E-02	1.46E-03	1.11E-04
	52150	1.16E-04	9.35E-01	6.28E-02	1.61E-03	1.15E-04
	52151	1.55E-04	9.37E-01	6.06E-02	1.70E-03	1.17E-04
	52154	1.21E-04	9.39E-01	5.91E-02	1.49E-03	9.89E-05
	52156	1.81E-04	9.40E-01	5.76E-02	1.66E-03	1.08E-04
	52157	1.30E-04	9.39E-01	5.90E-02	1.55E-03	1.03E-04
	52158	3.16E-04	9.23E-01	7.44E-02	1.75E-03	1.52E-04
	52190	1.88E-04	9.23E-01	7.50E-02	1.82E-03	1.59E-04
	52191	1.74E-04	9.40E-01	5.85E-02	1.53E-03	1.01E-04
	52193	1.44E-04	8.99E-01	9.97E-02	1.47E-03	1.80E-04
	52198	2.90E-04	9.45E-01	5.30E-02	1.96E-03	1.16E-04
	52320	2.02E-04	9.30E-01	6.85E-02	1.30E-03	1.02E-04
	52322	1.44E-04	9.33E-01	6.52E-02	1.57E-03	1.17E-04
	52323	1.10E-04	9.39E-01	5.90E-02	1.33E-03	8.81E-05
	52324	1.14E-04	8.97E-01	1.01E-01	1.12E-03	1.40E-04
	52326	3.61E-04	9.30E-01	6.76E-02	1.79E-03	1.39E-04
	52327	1.17E-04	9.32E-01	6.62E-02	1.44E-03	1.09E-04
	52329	9.92E-05	9.40E-01	5.86E-02	1.21E-03	7.96E-05
	52332	1.37E-04	9.40E-01	5.81E-02	1.57E-03	1.03E-04
	52336	1.16E-04	9.40E-01	5.86E-02	1.35E-03	8.93E-05
	52337	1.11E-04	9.37E-01	6.10E-02	1.43E-03	9.89E-05
	52339	1.23E-04	9.39E-01	5.92E-02	1.43E-03	9.55E-05
	52341	1.47E-04	9.34E-01	6.45E-02	1.53E-03	1.13E-04
	52344	1.42E-04	9.42E-01	5.63E-02	1.33E-03	8.38E-05
	52345	1.93E-04	9.37E-01	6.12E-02	1.53E-03	1.06E-04
	52346	1.29E-04	9.31E-01	6.78E-02	1.39E-03	1.09E-04
	52347	1.28E-04	9.39E-01	5.89E-02	1.46E-03	9.66E-05
	52351	1.60E-04	9.38E-01	6.06E-02	1.49E-03	1.02E-04
	52357	1.42E-04	9.26E-01	7.25E-02	1.47E-03	1.23E-04
	52358	1.44E-04	9.40E-01	5.85E-02	1.61E-03	1.06E-04
	52361	1.56E-04	9.36E-01	6.22E-02	1.71E-03	1.21E-04
	52363	1.40E-04	9.35E-01	6.32E-02	1.30E-03	9.37E-05

Table IV-1 (Continued)
Sample Data Used to Estimate Radionuclide Activity Fraction Distributions in Plutonium Material Types

Material Type	Drum ID	Pu238	Pu239	Pu240	Pu241	Pu242
PU52 (Cont.)	52364	1.10E-04	9.30E-01	6.77E-02	1.88E-03	1.46E-04
	52365	7.82E-05	9.32E-01	6.61E-02	1.43E-03	1.08E-04
	52374	1.15E-04	9.41E-01	5.78E-02	1.40E-03	9.10E-05
	52375	8.66E-05	9.49E-01	4.87E-02	1.86E-03	1.00E-04
	52377	1.95E-04	9.34E-01	6.44E-02	1.65E-03	1.21E-04
	52378	6.35E-05	9.25E-01	7.29E-02	1.77E-03	1.50E-04
	52379	1.86E-04	9.41E-01	5.73E-02	1.91E-03	1.23E-04
	52380	9.36E-05	9.32E-01	6.58E-02	1.57E-03	1.18E-04
	52381	1.83E-04	9.39E-01	5.95E-02	1.46E-03	9.82E-05
	52382	8.47E-05	9.35E-01	6.31E-02	1.26E-03	8.99E-05
	52383	1.59E-04	9.34E-01	6.39E-02	1.70E-03	1.24E-04
	52385	1.55E-04	9.36E-01	6.25E-02	1.68E-03	1.20E-04
	52386	1.24E-04	9.34E-01	6.48E-02	1.36E-03	1.00E-04
	52389	1.58E-04	9.50E-01	4.85E-02	1.53E-03	8.18E-05
	52392	1.23E-04	9.36E-01	6.24E-02	1.56E-03	1.11E-04
	52394	1.77E-04	9.47E-01	5.09E-02	1.53E-03	8.64E-05
	52407	1.25E-04	9.39E-01	5.95E-02	1.56E-03	1.05E-04
	52408	1.26E-04	9.37E-01	6.13E-02	1.57E-03	1.09E-04
	52413	1.63E-04	9.29E-01	6.92E-02	1.38E-03	1.10E-04
	52416	5.82E-05	9.34E-01	6.47E-02	1.56E-03	1.15E-04
	52420	1.18E-04	9.39E-01	5.93E-02	1.27E-03	8.46E-05
	52421	1.18E-04	9.49E-01	4.83E-02	2.00E-03	1.06E-04
	52422	1.71E-04	9.41E-01	5.74E-02	1.57E-03	1.01E-04
	52424	1.10E-04	9.33E-01	6.57E-02	1.44E-03	1.08E-04
	52425	1.53E-04	9.27E-01	7.14E-02	1.71E-03	1.41E-04
	52426	1.29E-04	9.37E-01	6.08E-02	1.45E-03	1.00E-04
	52431	2.09E-04	9.35E-01	6.34E-02	1.74E-03	1.25E-04
	52437	1.25E-04	9.30E-01	6.81E-02	1.47E-03	1.15E-04
	52438	3.02E-04	9.37E-01	6.07E-02	1.72E-03	1.18E-04
	52439	1.27E-04	9.41E-01	5.73E-02	1.52E-03	9.75E-05
	52441	1.47E-04	9.43E-01	5.49E-02	1.47E-03	8.99E-05
	52442	1.94E-04	9.37E-01	6.13E-02	1.52E-03	1.05E-04
	52445	1.35E-04	9.34E-01	6.44E-02	1.34E-03	9.80E-05
	52449	1.07E-04	9.25E-01	7.31E-02	1.58E-03	1.34E-04

Table IV-1 (Continued)
Sample Data Used to Estimate Radionuclide Activity Fraction Distributions in Plutonium Material Types

Material Type	Drum ID	Pu238	Pu239	Pu240	Pu241	Pu242
PU52 (Cont.)	52450	6.66E-05	9.33E-01	6.45E-02	2.04E-03	1.50E-04
	52451	1.15E-04	9.37E-01	6.10E-02	1.43E-03	9.86E-05
	52452	2.07E-04	9.46E-01	5.22E-02	1.74E-03	1.01E-04
	52458	1.23E-04	9.33E-01	6.50E-02	1.41E-03	1.04E-04
	52462	1.40E-04	9.36E-01	6.20E-02	1.58E-03	1.11E-04
	52463	2.22E-04	9.34E-01	6.35E-02	2.02E-03	1.46E-04
	52464	2.07E-04	9.31E-01	6.73E-02	1.66E-03	1.28E-04
	52467	1.41E-04	9.35E-01	6.30E-02	1.48E-03	1.06E-04
	52474	1.98E-04	9.35E-01	6.25E-02	1.66E-03	1.18E-04
	52475	1.18E-04	9.38E-01	6.04E-02	1.36E-03	9.25E-05
	52493	2.29E-04	9.32E-01	6.61E-02	1.74E-03	1.31E-04
	52498	1.61E-04	9.35E-01	6.25E-02	1.86E-03	1.32E-04
	52527	1.52E-04	9.39E-01	5.90E-02	1.44E-03	9.54E-05
	52531	2.77E-04	9.39E-01	5.91E-02	1.66E-03	1.11E-04
	52534	1.30E-04	9.36E-01	6.21E-02	1.76E-03	1.24E-04
	52535	1.18E-04	9.38E-01	6.08E-02	1.39E-03	9.56E-05
	52538	1.07E-04	9.43E-01	5.56E-02	1.55E-03	9.61E-05
	52541	8.43E-05	9.41E-01	5.77E-02	1.56E-03	1.01E-04
	52542	1.71E-04	9.47E-01	5.08E-02	1.50E-03	8.46E-05
	52544	1.45E-04	9.28E-01	6.94E-02	1.93E-03	1.55E-04
	52548	1.85E-04	9.31E-01	6.72E-02	1.68E-03	1.29E-04
	52549	1.45E-04	9.39E-01	5.94E-02	1.39E-03	9.28E-05
	52553	1.58E-04	9.35E-01	6.34E-02	1.71E-03	1.23E-04
	52554	1.62E-04	9.31E-01	6.74E-02	1.64E-03	1.27E-04
	52555	1.58E-04	9.34E-01	6.34E-02	1.92E-03	1.39E-04
	52556	1.12E-04	9.38E-01	6.07E-02	1.42E-03	9.75E-05
	52557	1.33E-04	9.35E-01	6.30E-02	1.47E-03	1.05E-04
	52560	9.30E-05	9.33E-01	6.53E-02	1.56E-03	1.16E-04
	52565	1.02E-04	9.37E-01	6.10E-02	1.44E-03	9.96E-05
	52566	1.46E-04	9.33E-01	6.54E-02	1.81E-03	1.36E-04
	52569	1.73E-04	9.36E-01	6.22E-02	1.76E-03	1.24E-04
	52570	1.40E-04	9.35E-01	6.32E-02	1.63E-03	1.17E-04
	52576	1.44E-04	9.41E-01	5.68E-02	1.69E-03	1.08E-04
	52579	1.24E-04	9.37E-01	6.11E-02	1.64E-03	1.14E-04

Table IV-1 (Continued)
Sample Data Used to Estimate Radionuclide Activity Fraction Distributions in Plutonium Material Types

Material Type	Drum ID	Pu238	Pu239	Pu240	Pu241	Pu242
PU52 (Cont.)	52580	3.05E-04	9.21E-01	7.64E-02	1.85E-03	1.66E-04
	52581	1.29E-04	9.38E-01	6.05E-02	1.65E-03	1.13E-04
	52582	2.37E-04	9.34E-01	6.40E-02	1.26E-03	9.20E-05
	52588	5.86E-04	9.21E-01	7.58E-02	2.09E-03	1.86E-04
	52589	3.39E-04	9.36E-01	6.19E-02	1.88E-03	1.32E-04
	52590	1.12E-04	9.40E-01	5.82E-02	1.50E-03	9.80E-05
	52591	1.36E-04	9.34E-01	6.47E-02	1.39E-03	1.03E-04
	52646	3.27E-04	9.51E-01	4.75E-02	1.36E-03	7.12E-05
	52653	3.21E-04	9.32E-01	6.56E-02	1.72E-03	1.29E-04
	52662	5.24E-04	9.28E-01	6.99E-02	1.53E-03	1.23E-04
	52663	3.00E-04	9.42E-01	5.58E-02	1.72E-03	1.08E-04
	52665	2.59E-04	9.43E-01	5.46E-02	1.75E-03	1.07E-04
	52678	7.27E-04	9.38E-01	5.97E-02	1.36E-03	9.14E-05
	52801	1.66E-04	9.35E-01	6.36E-02	1.58E-03	1.14E-04
	52804	1.30E-04	9.36E-01	6.25E-02	1.45E-03	1.03E-04
	52806	1.37E-04	9.35E-01	6.28E-02	1.67E-03	1.19E-04
	52807	1.02E-04	9.35E-01	6.31E-02	1.56E-03	1.12E-04
	52808	1.45E-04	9.34E-01	6.44E-02	1.55E-03	1.13E-04
	52810	2.12E-04	9.44E-01	5.42E-02	1.19E-03	7.21E-05
	52814	6.08E-05	9.36E-01	6.23E-02	1.40E-03	9.92E-05
	52815	1.15E-04	9.38E-01	6.04E-02	1.36E-03	9.26E-05
	52820	1.81E-04	9.40E-01	5.77E-02	1.59E-03	1.03E-04
	52823	1.94E-04	9.37E-01	6.10E-02	1.47E-03	1.01E-04
	52827	7.54E-04	9.27E-01	7.00E-02	2.07E-03	1.67E-04
	52829	1.07E-04	9.41E-01	5.71E-02	1.63E-03	1.04E-04
	52831	1.38E-04	9.39E-01	6.00E-02	1.30E-03	8.78E-05
	52833	9.76E-05	9.43E-01	5.58E-02	1.30E-03	8.11E-05
	52834	1.43E-04	9.36E-01	6.27E-02	1.38E-03	9.82E-05
	52835	1.58E-04	9.35E-01	6.35E-02	1.42E-03	1.02E-04
	52837	1.38E-04	9.33E-01	6.53E-02	1.64E-03	1.22E-04
	52839	3.20E-04	9.45E-01	5.31E-02	1.81E-03	1.07E-04
	52844	1.66E-04	9.49E-01	4.94E-02	1.39E-03	7.59E-05
	52845	1.17E-04	9.37E-01	6.17E-02	1.48E-03	1.03E-04
	52848	2.30E-04	9.37E-01	6.11E-02	1.48E-03	1.03E-04

Table IV-1 (Continued)
Sample Data Used to Estimate Radionuclide Activity Fraction Distributions in Plutonium Material Types

Material Type	Drum ID	Pu238	Pu239	Pu240	Pu241	Pu242
PU52 (Cont.)	52853	1.09E-04	9.38E-01	5.98E-02	1.76E-03	1.19E-04
	52855	2.16E-04	9.38E-01	6.01E-02	1.91E-03	1.30E-04
	52858	2.36E-04	9.31E-01	6.69E-02	1.43E-03	1.10E-04
	52861	4.94E-04	9.27E-01	6.99E-02	1.93E-03	1.56E-04
	52862	1.30E-04	9.45E-01	5.31E-02	1.45E-03	8.58E-05
	52864	1.13E-04	9.31E-01	6.70E-02	1.42E-03	1.09E-04
	52869	1.35E-04	9.40E-01	5.87E-02	1.47E-03	9.72E-05
	52870	1.56E-04	9.47E-01	5.16E-02	1.45E-03	8.32E-05
	52871	1.48E-04	9.37E-01	6.08E-02	1.48E-03	1.02E-04
	52874	1.48E-04	9.41E-01	5.73E-02	1.18E-03	7.59E-05
	52875	7.31E-05	9.27E-01	7.17E-02	1.55E-03	1.28E-04
	52879	9.93E-05	9.32E-01	6.56E-02	1.56E-03	2.38E-04
	52880	9.16E-05	9.37E-01	6.17E-02	1.30E-03	9.07E-05
	52884	1.09E-04	9.40E-01	5.81E-02	1.42E-03	9.29E-05
	52890	1.86E-04	9.37E-01	6.13E-02	1.49E-03	1.03E-04
	52893	1.32E-04	9.39E-01	5.92E-02	1.29E-03	8.62E-05
	52898	1.99E-04	9.37E-01	6.15E-02	1.37E-03	9.51E-05
	52917	1.56E-04	9.36E-01	6.26E-02	1.53E-03	1.09E-04
	52920	1.63E-04	9.36E-01	6.24E-02	1.49E-03	1.05E-04
	52921	8.95E-05	9.37E-01	6.15E-02	1.41E-03	9.83E-05
	52923	8.02E-05	9.40E-01	5.85E-02	1.30E-03	8.56E-05
	52924	2.13E-04	9.35E-01	6.27E-02	1.53E-03	1.09E-04
	52925	1.61E-04	9.40E-01	5.82E-02	1.41E-03	9.20E-05
	52928	1.58E-04	9.33E-01	6.49E-02	1.62E-03	1.20E-04
	52933	1.11E-04	9.40E-01	5.83E-02	1.52E-03	9.96E-05
	52934	6.16E-05	9.25E-01	7.30E-02	1.58E-03	1.34E-04
	52935	9.09E-05	9.43E-01	5.59E-02	1.30E-03	8.14E-05
	52939	1.29E-04	9.36E-01	6.23E-02	1.34E-03	9.47E-05
	52942	1.09E-04	9.37E-01	6.14E-02	1.30E-03	9.05E-05
	52945	3.83E-04	9.28E-01	7.04E-02	1.36E-03	1.11E-04
	52954	1.15E-04	9.36E-01	6.27E-02	1.39E-03	9.87E-05
	52955	2.19E-04	9.29E-01	6.86E-02	2.32E-03	1.84E-04
	52961	1.24E-04	9.30E-01	6.80E-02	1.61E-03	1.26E-04
	52963	5.77E-05	9.28E-01	7.07E-02	1.52E-03	1.24E-04

Table IV-1 (Continued)
Sample Data Used to Estimate Radionuclide Activity Fraction Distributions in Plutonium Material Types

Material Type	Drum ID	Pu238	Pu239	Pu240	Pu241	Pu242
PU52 (Cont.)	52966	1.45E-04	9.39E-01	5.94E-02	1.59E-03	1.06E-04
	52967	1.47E-04	9.36E-01	6.17E-02	1.55E-03	1.08E-04
	52972	1.14E-04	9.31E-01	6.76E-02	1.39E-03	1.08E-04
	52975	2.70E-04	9.48E-01	4.93E-02	1.97E-03	1.07E-04
	52976	2.64E-04	9.21E-01	7.63E-02	2.13E-03	1.91E-04
	52977	1.07E-04	9.42E-01	5.66E-02	1.56E-03	9.92E-05
	52984	1.24E-04	9.38E-01	6.08E-02	1.43E-03	9.84E-05
	52986	9.27E-05	9.37E-01	6.16E-02	1.42E-03	9.92E-05
	52987	1.43E-04	9.37E-01	6.15E-02	1.36E-03	9.47E-05
	52988	1.87E-04	9.35E-01	6.34E-02	1.63E-03	1.17E-04
	52998	1.61E-04	9.34E-01	6.46E-02	1.43E-03	1.05E-04
	53005	1.04E-04	9.37E-01	6.17E-02	1.47E-03	1.03E-04
	53006	1.20E-04	9.39E-01	5.93E-02	1.45E-03	9.65E-05
	53007	1.22E-04	9.38E-01	6.08E-02	1.42E-03	9.74E-05
	53013	9.83E-05	9.40E-01	5.80E-02	1.51E-03	9.83E-05
	53019	1.03E-04	9.39E-01	5.90E-02	1.34E-03	8.90E-05
	53023	1.56E-04	9.35E-01	6.35E-02	1.59E-03	1.15E-04
	53024	1.57E-04	9.35E-01	6.28E-02	2.07E-03	1.48E-04
	53025	1.29E-04	9.38E-01	6.00E-02	1.33E-03	9.01E-05
	53031	1.44E-04	9.37E-01	6.15E-02	1.45E-03	1.01E-04
	53032	1.11E-04	9.37E-01	6.09E-02	1.44E-03	9.89E-05
	53036	2.22E-04	9.23E-01	7.44E-02	2.07E-03	1.80E-04
	53038	1.06E-04	9.40E-01	5.80E-02	1.52E-03	9.91E-05
	53039	2.47E-04	9.38E-01	5.98E-02	1.85E-03	1.25E-04
	53041	1.22E-04	9.39E-01	5.91E-02	1.58E-03	1.05E-04
	53042	1.76E-04	9.29E-01	6.89E-02	1.41E-03	1.12E-04
	53043	1.35E-04	9.32E-01	6.61E-02	1.51E-03	1.14E-04
	53046	9.61E-05	9.41E-01	5.68E-02	1.57E-03	1.00E-04
	53055	1.41E-04	9.39E-01	5.92E-02	1.52E-03	1.01E-04
	53062	1.30E-04	9.39E-01	5.96E-02	1.41E-03	9.50E-05
	53064	1.30E-04	9.36E-01	6.20E-02	1.39E-03	9.79E-05
	53068	1.14E-04	9.35E-01	6.36E-02	1.46E-03	1.05E-04
	53070	9.74E-05	9.42E-01	5.67E-02	1.45E-03	9.18E-05
	53071	1.15E-04	9.40E-01	5.78E-02	1.55E-03	1.01E-04

Table IV-1 (Continued)
Sample Data Used to Estimate Radionuclide Activity Fraction Distributions in Plutonium Material Types

Material Type	Drum ID	Pu238	Pu239	Pu240	Pu241	Pu242
PU52 (Cont.)	53074	4.35E-04	9.39E-01	5.87E-02	1.35E-03	8.92E-05
	53075	1.11E-04	9.38E-01	6.01E-02	1.40E-03	9.51E-05
	53088	1.74E-04	9.33E-01	6.50E-02	1.69E-03	1.26E-04
	53089	1.68E-04	9.36E-01	6.16E-02	1.64E-03	1.14E-04
	53100	1.20E-04	9.29E-01	6.89E-02	1.83E-03	1.45E-04
	53108	1.30E-04	9.33E-01	6.50E-02	1.69E-03	1.25E-04
	53116	1.01E-04	9.44E-01	5.43E-02	1.41E-03	8.52E-05
	53117	1.38E-04	9.39E-01	5.89E-02	1.48E-03	9.79E-05
	53118	1.13E-04	9.42E-01	5.61E-02	1.26E-03	7.89E-05
	53121	1.53E-04	9.33E-01	6.56E-02	1.61E-03	1.20E-04
	53127	1.40E-04	9.47E-01	5.15E-02	1.55E-03	8.84E-05
	53128	1.46E-04	9.28E-01	6.98E-02	1.48E-03	1.19E-04
	53130	1.48E-04	9.37E-01	6.12E-02	1.44E-03	9.95E-05
	53131	3.24E-04	9.25E-01	7.26E-02	2.06E-03	1.74E-04
	53133	1.24E-04	9.35E-01	6.32E-02	1.27E-03	9.11E-05
	53134	1.32E-04	9.37E-01	6.13E-02	1.51E-03	1.05E-04
	53139	1.44E-04	9.28E-01	7.05E-02	1.65E-03	1.35E-04
	53143	1.50E-04	9.39E-01	5.95E-02	1.46E-03	9.79E-05
	53145	1.06E-04	9.35E-01	6.33E-02	1.49E-03	1.07E-04
	53146	1.29E-04	9.35E-01	6.30E-02	1.40E-03	1.00E-04
	53151	1.03E-04	9.39E-01	5.93E-02	1.37E-03	9.15E-05
	53153	2.85E-04	9.36E-01	6.17E-02	1.50E-03	1.05E-04
	53157	1.34E-04	9.37E-01	6.09E-02	1.81E-03	1.25E-04
	53158	1.07E-04	9.37E-01	6.14E-02	1.39E-03	9.68E-05
	53165	1.49E-04	9.39E-01	5.94E-02	1.29E-03	8.63E-05
	53169	1.12E-04	9.34E-01	6.44E-02	1.45E-03	1.07E-04
	53172	1.96E-04	9.40E-01	5.85E-02	1.47E-03	9.67E-05
	53173	1.30E-04	9.39E-01	5.88E-02	1.80E-03	1.19E-04
	53175	9.62E-05	9.44E-01	5.46E-02	1.58E-03	9.64E-05
	53176	1.23E-04	9.39E-01	5.98E-02	1.45E-03	9.79E-05
	53181	9.61E-05	9.38E-01	6.02E-02	1.50E-03	1.02E-04
	53184	1.38E-04	9.38E-01	6.06E-02	1.47E-03	1.00E-04
	53190	1.10E-04	9.39E-01	5.94E-02	1.45E-03	9.70E-05
	53197	1.18E-04	9.36E-01	6.19E-02	1.68E-03	1.18E-04

Table IV-1 (Continued)
Sample Data Used to Estimate Radionuclide Activity Fraction Distributions in Plutonium Material Types

Material Type	Drum ID	Pu238	Pu239	Pu240	Pu241	Pu242
PU52 (Cont.)	53198	9.80E-05	9.30E-01	6.82E-02	1.42E-03	1.11E-04
	53199	9.61E-04	9.20E-01	7.71E-02	1.62E-03	1.46E-04
	53202	1.67E-04	9.39E-01	5.95E-02	1.48E-03	9.96E-05
	53207	9.67E-05	9.32E-01	6.59E-02	1.40E-03	1.06E-04
	53212	1.07E-04	9.36E-01	6.24E-02	1.52E-03	1.08E-04
	53213	1.60E-04	9.47E-01	5.08E-02	1.65E-03	9.29E-05
	53214	1.36E-04	9.36E-01	6.27E-02	1.50E-03	1.07E-04
	53221	1.26E-04	9.37E-01	6.15E-02	1.38E-03	9.59E-05
	53227	1.77E-04	9.35E-01	6.34E-02	1.51E-03	1.09E-04
	53230	1.05E-04	9.36E-01	6.24E-02	1.45E-03	1.03E-04
	53237	1.45E-04	9.39E-01	5.90E-02	1.71E-03	1.14E-04
	53239	1.05E-04	9.38E-01	6.05E-02	1.30E-03	8.88E-05
	53245	1.33E-04	9.32E-01	6.61E-02	1.34E-03	1.01E-04
	53247	1.58E-04	9.38E-01	6.07E-02	1.27E-03	8.71E-05
	53251	1.18E-04	9.36E-01	6.20E-02	1.63E-03	1.15E-04
	53300	6.20E-05	9.44E-01	5.44E-02	1.64E-03	9.98E-05
	53309	1.01E-04	9.37E-01	6.12E-02	1.45E-03	1.00E-04
	53312	1.37E-04	9.36E-01	6.26E-02	1.66E-03	1.18E-04
	53317	1.56E-04	9.34E-01	6.40E-02	1.35E-03	9.85E-05
	53320	1.37E-04	9.43E-01	5.49E-02	1.42E-03	8.72E-05
	53323	1.77E-04	9.31E-01	6.70E-02	1.69E-03	1.30E-04
	53324	1.16E-04	9.37E-01	6.15E-02	1.43E-03	9.98E-05
	53330	1.13E-04	9.37E-01	6.13E-02	1.43E-03	9.92E-05
	53332	1.97E-04	9.24E-01	7.46E-02	1.53E-03	1.33E-04
	53335	2.49E-04	9.15E-01	8.26E-02	2.28E-03	2.24E-04
	53339	1.78E-04	9.35E-01	6.26E-02	1.82E-03	1.29E-04
	53342	2.38E-04	9.34E-01	6.44E-02	1.59E-03	1.17E-04
	53344	9.08E-05	9.40E-01	5.87E-02	1.54E-03	1.02E-04
	53346	8.50E-05	9.44E-01	5.43E-02	1.46E-03	8.86E-05
	53348	1.06E-04	9.43E-01	5.54E-02	1.50E-03	9.28E-05
	53362	1.09E-04	9.38E-01	6.05E-02	1.37E-03	9.35E-05
	53364	9.87E-05	9.34E-01	6.47E-02	1.53E-03	1.13E-04
	53365	1.73E-04	9.42E-01	5.65E-02	1.44E-03	9.11E-05
	53366	1.20E-04	9.36E-01	6.26E-02	1.30E-03	9.26E-05

Table IV-1 (Continued)
Sample Data Used to Estimate Radionuclide Activity Fraction Distributions in Plutonium Material Types

Material Type	Drum ID	Pu238	Pu239	Pu240	Pu241	Pu242
PU52 (Cont.)	53367	3.58E-04	9.30E-01	6.76E-02	1.87E-03	1.45E-04
	53377	1.35E-04	9.40E-01	5.79E-02	1.46E-03	9.52E-05
	53379	1.34E-04	9.40E-01	5.85E-02	1.32E-03	8.72E-05
	53381	1.23E-04	9.37E-01	6.18E-02	1.43E-03	9.99E-05
	53385	1.24E-04	9.35E-01	6.35E-02	1.75E-03	1.26E-04
	53386	1.15E-04	9.25E-01	7.33E-02	1.49E-03	1.27E-04
	53387	9.40E-05	9.41E-01	5.79E-02	1.41E-03	9.17E-05
	53388	1.19E-04	9.38E-01	6.04E-02	1.42E-03	9.65E-05
	53389	2.20E-04	9.30E-01	6.73E-02	1.99E-03	1.54E-04
	53390	2.01E-04	9.28E-01	7.04E-02	1.71E-03	1.39E-04
	53392	8.85E-05	9.38E-01	5.99E-02	1.74E-03	1.18E-04
	53394	9.98E-05	9.35E-01	6.36E-02	1.46E-03	1.06E-04
	53396	1.36E-04	9.41E-01	5.77E-02	1.45E-03	9.41E-05
	53399	1.56E-04	9.41E-01	5.70E-02	1.51E-03	9.67E-05
	53400	1.79E-04	9.34E-01	6.36E-02	1.76E-03	1.27E-04
	53401	1.11E-04	9.32E-01	6.66E-02	1.56E-03	1.19E-04
	53409	1.76E-04	9.37E-01	6.10E-02	1.87E-03	1.29E-04
	53418	1.70E-04	9.31E-01	6.75E-02	1.59E-03	1.23E-04
	53421	1.38E-04	9.38E-01	6.04E-02	1.42E-03	9.70E-05
	53423	1.14E-04	9.29E-01	6.95E-02	1.42E-03	1.13E-04
	53429	7.26E-05	9.37E-01	6.14E-02	1.39E-03	9.66E-05
	53430	1.01E-04	9.37E-01	6.12E-02	1.50E-03	1.04E-04
	53431	1.25E-04	9.35E-01	6.35E-02	1.46E-03	1.06E-04
	53433	1.56E-04	9.34E-01	6.38E-02	1.46E-03	1.06E-04
	53435	2.00E-04	9.35E-01	6.26E-02	1.59E-03	1.13E-04
	53438	1.03E-04	9.42E-01	5.61E-02	1.50E-03	9.41E-05
	53439	1.48E-04	9.36E-01	6.22E-02	1.39E-03	9.78E-05
	53442	1.09E-04	9.41E-01	5.75E-02	1.38E-03	8.87E-05
	53446	1.78E-04	9.36E-01	6.15E-02	1.88E-03	1.31E-04
	53447	1.05E-04	9.41E-01	5.70E-02	1.44E-03	9.22E-05
	53449	1.89E-04	9.36E-01	6.22E-02	1.57E-03	1.11E-04
	53450	8.53E-05	9.42E-01	5.61E-02	1.39E-03	8.74E-05
	53451	1.21E-04	9.37E-01	6.14E-02	1.60E-03	1.12E-04
	53456	3.44E-04	9.23E-01	7.50E-02	1.83E-03	1.60E-04

Table IV-1 (Continued)
Sample Data Used to Estimate Radionuclide Activity Fraction Distributions in Plutonium Material Types

Material Type	Drum ID	Pu238	Pu239	Pu240	Pu241	Pu242
PU52 (Cont.)	53460	1.46E-04	9.41E-01	5.66E-02	1.64E-03	1.04E-04
	53462	1.73E-04	9.42E-01	5.64E-02	1.62E-03	1.03E-04
	53464	1.22E-04	9.34E-01	6.47E-02	1.42E-03	1.05E-04
	53467	4.13E-04	9.28E-01	6.85E-02	2.56E-03	2.03E-04
	53472	2.08E-04	9.35E-01	6.28E-02	1.71E-03	1.22E-04
	53473	6.69E-05	9.49E-01	4.95E-02	1.69E-03	9.22E-05
	53475	1.44E-04	9.44E-01	5.47E-02	1.47E-03	8.96E-05
	53476	8.22E-05	9.42E-01	5.64E-02	1.37E-03	8.63E-05
	53478	1.83E-04	9.31E-01	6.66E-02	1.86E-03	1.42E-04
	53481	1.17E-04	9.33E-01	6.54E-02	1.47E-03	1.09E-04
	53483	1.50E-04	9.34E-01	6.41E-02	1.55E-03	1.13E-04
	53484	1.40E-04	9.39E-01	5.89E-02	1.61E-03	1.07E-04
	53486	1.35E-04	9.35E-01	6.33E-02	1.47E-03	1.06E-04
	53488	1.37E-04	9.37E-01	6.08E-02	1.46E-03	1.00E-04
	53490	2.30E-04	9.25E-01	7.26E-02	1.83E-03	1.55E-04
	53491	2.41E-04	9.40E-01	5.83E-02	1.51E-03	9.87E-05
	53492	9.40E-05	9.39E-01	5.90E-02	1.70E-03	1.13E-04
	53505	7.40E-05	9.34E-01	6.48E-02	1.26E-03	9.28E-05
	53507	2.92E-04	9.33E-01	6.50E-02	1.62E-03	1.20E-04
	53508	2.53E-04	9.07E-01	9.05E-02	2.33E-03	2.55E-04
	53517	1.38E-04	9.38E-01	6.00E-02	1.56E-03	1.05E-04
	53520	1.43E-04	9.38E-01	6.04E-02	1.41E-03	9.66E-05
	53527	1.36E-04	9.38E-01	6.02E-02	1.55E-03	1.05E-04
	53533	1.57E-04	9.34E-01	6.40E-02	1.58E-03	1.15E-04
	53536	1.25E-04	9.40E-01	5.85E-02	1.60E-03	1.05E-04
	53538	8.22E-04	9.33E-01	6.38E-02	2.00E-03	1.46E-04
	53541	1.36E-04	9.43E-01	5.56E-02	1.37E-03	8.50E-05
	53544	1.35E-04	9.33E-01	6.49E-02	1.61E-03	1.20E-04
	53547	1.35E-04	9.37E-01	6.15E-02	1.46E-03	1.02E-04
	53548	1.88E-04	9.17E-01	8.01E-02	2.21E-03	2.10E-04
	53550	1.44E-04	9.37E-01	6.12E-02	1.44E-03	1.00E-04
	53554	1.56E-04	9.37E-01	6.14E-02	1.48E-03	1.03E-04
	53555	1.83E-04	9.27E-01	7.09E-02	1.84E-03	1.51E-04
	53557	1.26E-04	9.36E-01	6.24E-02	1.38E-03	9.76E-05

Table IV-1 (Continued)
Sample Data Used to Estimate Radionuclide Activity Fraction Distributions in Plutonium Material Types

Material Type	Drum ID	Pu238	Pu239	Pu240	Pu241	Pu242
PU52 (Cont.)	53564	5.12E-04	9.32E-01	6.51E-02	1.86E-03	1.38E-04
	53570	1.23E-04	9.40E-01	5.86E-02	1.50E-03	9.89E-05
	53572	1.19E-04	9.39E-01	5.92E-02	1.38E-03	9.20E-05
	53577	8.12E-05	9.43E-01	5.49E-02	1.50E-03	9.19E-05
	53581	1.02E-04	9.33E-01	6.52E-02	1.32E-03	9.86E-05
	53582	1.16E-04	9.34E-01	6.39E-02	1.53E-03	1.11E-04
	53583	2.75E-04	9.40E-01	5.68E-02	2.44E-03	1.56E-04
	53590	1.12E-04	9.36E-01	6.19E-02	1.56E-03	1.10E-04
	53591	9.75E-05	9.37E-01	6.16E-02	1.71E-03	1.19E-04
	53592	1.27E-04	9.34E-01	6.40E-02	1.41E-03	1.03E-04
	53598	1.30E-04	9.37E-01	6.14E-02	1.62E-03	1.13E-04
	53599	1.39E-04	9.34E-01	6.47E-02	1.43E-03	1.06E-04
	53611	1.35E-04	9.35E-01	6.33E-02	1.53E-03	1.10E-04
	53612	1.96E-04	9.33E-01	6.48E-02	1.52E-03	1.12E-04
	53616	1.77E-04	9.43E-01	5.55E-02	1.67E-03	1.04E-04
	53624	1.27E-04	9.38E-01	6.01E-02	1.58E-03	1.07E-04
	53625	2.26E-04	9.21E-01	7.66E-02	1.92E-03	1.73E-04
	53636	1.20E-04	9.37E-01	6.11E-02	1.36E-03	9.40E-05
	53638	1.47E-04	9.37E-01	6.07E-02	1.67E-03	1.15E-04
	53641	1.85E-04	9.34E-01	6.43E-02	1.80E-03	1.32E-04
	53643	1.31E-04	9.40E-01	5.88E-02	1.43E-03	9.46E-05
	53644	1.22E-04	9.36E-01	6.29E-02	1.31E-03	9.34E-05
	53647	1.32E-04	9.38E-01	6.04E-02	1.51E-03	1.03E-04
	53648	1.74E-04	9.34E-01	6.41E-02	1.66E-03	1.21E-04
	53652	2.27E-04	9.16E-01	8.11E-02	2.07E-03	1.99E-04
	53665	1.01E-04	9.39E-01	5.93E-02	1.59E-03	1.07E-04
	53667	4.49E-04	9.26E-01	7.12E-02	1.98E-03	1.63E-04
	53668	1.16E-04	9.39E-01	5.96E-02	1.25E-03	8.38E-05
	53799	8.59E-05	9.27E-01	7.14E-02	1.35E-03	1.11E-04
	53876	2.08E-04	9.35E-01	6.30E-02	1.71E-03	1.23E-04
	53901	1.57E-04	9.39E-01	5.94E-02	1.37E-03	9.15E-05
	53902	9.35E-05	9.32E-01	6.66E-02	1.38E-03	1.05E-04
	53903	1.44E-04	9.33E-01	6.55E-02	1.39E-03	1.04E-04
	53904	1.02E-04	9.36E-01	6.24E-02	1.40E-03	9.88E-05

Table IV-1 (Continued)
Sample Data Used to Estimate Radionuclide Activity Fraction Distributions in Plutonium Material Types

Material Type	Drum ID	Pu238	Pu239	Pu240	Pu241	Pu242
PU52 (Cont.)	53905	1.64E-04	9.37E-01	6.17E-02	1.42E-03	9.92E-05
	53906	2.16E-04	9.31E-01	6.70E-02	1.66E-03	1.27E-04
	53907	1.46E-04	9.40E-01	5.86E-02	1.63E-03	1.07E-04
	53912	2.79E-04	9.39E-01	5.89E-02	1.63E-03	1.08E-04
	53916	1.33E-04	9.40E-01	5.84E-02	1.37E-03	9.00E-05
	53917	1.29E-04	9.32E-01	6.68E-02	1.42E-03	1.08E-04
	53918	1.53E-04	9.36E-01	6.21E-02	1.55E-03	1.09E-04
	53920	1.80E-04	9.26E-01	7.21E-02	1.43E-03	1.19E-04
	53922	2.13E-04	8.95E-01	1.03E-01	1.59E-03	2.03E-04
	53928	1.29E-04	9.43E-01	5.51E-02	1.51E-03	9.30E-05
	53930	8.96E-05	9.30E-01	6.83E-02	1.12E-03	8.79E-05
	53931	1.96E-04	9.23E-01	7.43E-02	1.98E-03	1.71E-04
	53933	1.38E-04	9.38E-01	5.98E-02	1.54E-03	1.04E-04
	53937	1.26E-04	9.35E-01	6.38E-02	1.45E-03	1.05E-04
	53941	1.34E-04	9.36E-01	6.20E-02	1.52E-03	1.07E-04
	53943	6.52E-04	9.42E-01	5.56E-02	1.50E-03	9.30E-05
	53944	4.92E-04	9.11E-01	8.71E-02	1.55E-03	1.61E-04
	53948	1.12E-04	9.37E-01	6.19E-02	1.34E-03	9.40E-05
	53950	1.21E-04	9.39E-01	5.98E-02	1.38E-03	9.30E-05
	53952	9.71E-05	9.34E-01	6.46E-02	1.40E-03	1.03E-04
	53954	2.09E-04	9.19E-01	7.89E-02	2.15E-03	2.00E-04
	53955	1.88E-04	9.38E-01	6.01E-02	1.38E-03	9.35E-05
	53958	9.49E-05	9.36E-01	6.27E-02	1.45E-03	1.03E-04
	53960	1.68E-04	9.30E-01	6.78E-02	1.59E-03	1.24E-04
	53961	1.57E-04	9.38E-01	6.00E-02	1.48E-03	9.99E-05
	53962	1.46E-04	9.42E-01	5.62E-02	1.51E-03	9.52E-05
	53965	1.39E-04	9.42E-01	5.61E-02	1.40E-03	8.76E-05
	53966	1.37E-04	9.32E-01	6.68E-02	1.34E-03	1.03E-04
	53971	1.72E-04	9.23E-01	7.51E-02	1.95E-03	1.71E-04
	53972	1.16E-04	9.37E-01	6.20E-02	1.21E-03	8.54E-05
	53976	1.29E-04	9.39E-01	5.91E-02	1.48E-03	9.86E-05
	53977	1.66E-04	9.37E-01	6.12E-02	1.51E-03	1.05E-04
	53978	1.56E-04	9.37E-01	6.18E-02	1.28E-03	8.93E-05
	53981	1.53E-04	9.37E-01	6.15E-02	1.41E-03	9.85E-05

Table IV-1 (Continued)
Sample Data Used to Estimate Radionuclide Activity Fraction Distributions in Plutonium Material Types

Material Type	Drum ID	Pu238	Pu239	Pu240	Pu241	Pu242
PU52 (Cont.)	53982	1.27E-04	9.36E-01	6.23E-02	1.38E-03	9.74E-05
	53992	1.10E-04	9.38E-01	6.09E-02	1.33E-03	9.13E-05
	53994	3.75E-04	9.32E-01	6.59E-02	1.52E-03	1.15E-04
	53996	1.91E-04	9.23E-01	7.52E-02	1.93E-03	1.69E-04
	53997	1.88E-04	9.24E-01	7.34E-02	1.79E-03	1.53E-04
	53998	9.05E-05	9.39E-01	5.98E-02	1.38E-03	9.31E-05
	54120	1.53E-04	9.36E-01	6.18E-02	1.58E-03	1.11E-04
	54122	8.41E-05	9.36E-01	6.25E-02	1.43E-03	1.01E-04
	54123	1.31E-04	9.39E-01	5.89E-02	1.56E-03	1.03E-04
	54125	1.51E-04	9.04E-01	9.37E-02	1.60E-03	1.82E-04
	54131	1.29E-04	9.37E-01	6.14E-02	1.45E-03	1.01E-04
	54132	8.99E-05	9.35E-01	6.36E-02	1.56E-03	1.13E-04
	54141	1.37E-04	9.36E-01	6.19E-02	1.44E-03	1.01E-04
	54143	2.11E-04	9.33E-01	6.42E-02	2.14E-03	1.57E-04
	54146	2.38E-04	9.33E-01	6.46E-02	2.08E-03	1.53E-04
	54150	1.23E-04	9.34E-01	6.44E-02	1.47E-03	1.08E-04
	54151	1.43E-04	9.32E-01	6.61E-02	1.58E-03	1.19E-04
	54155	1.33E-04	9.39E-01	5.90E-02	1.36E-03	9.05E-05
	54160	8.98E-05	9.41E-01	5.72E-02	1.47E-03	9.45E-05
	54161	6.55E-05	9.39E-01	5.90E-02	1.51E-03	1.00E-04
	54163	1.29E-04	9.37E-01	6.11E-02	1.70E-03	1.18E-04
	54168	1.75E-04	9.36E-01	6.24E-02	1.49E-03	1.05E-04
	54170	2.06E-04	9.36E-01	6.23E-02	1.56E-03	1.10E-04
	54172	1.47E-04	9.38E-01	6.02E-02	1.45E-03	9.83E-05
	54176	1.44E-04	9.36E-01	6.27E-02	1.48E-03	1.06E-04
	54180	1.10E-04	9.27E-01	7.13E-02	1.76E-03	1.45E-04
	54181	1.33E-04	9.38E-01	6.04E-02	1.51E-03	1.03E-04
	54185	1.49E-04	9.36E-01	6.25E-02	1.45E-03	1.03E-04
	54188	1.03E-04	9.35E-01	6.36E-02	1.41E-03	1.02E-04
	54192	1.45E-04	9.29E-01	6.97E-02	1.42E-03	1.14E-04
	54193	1.69E-04	9.30E-01	6.80E-02	1.58E-03	1.23E-04
	54195	8.33E-05	9.20E-01	7.79E-02	1.41E-03	1.29E-04
	54197	1.52E-04	9.39E-01	5.88E-02	1.49E-03	9.87E-05
	54198	9.30E-05	9.46E-01	5.20E-02	1.50E-03	8.63E-05

Table IV-1 (Continued)
Sample Data Used to Estimate Radionuclide Activity Fraction Distributions in Plutonium Material Types

Material Type	Drum ID	Pu238	Pu239	Pu240	Pu241	Pu242
PU52 (Cont.)	54302	3.64E-04	9.36E-01	6.21E-02	1.57E-03	1.11E-04
	54304	2.37E-04	9.31E-01	6.74E-02	1.36E-03	1.05E-04
	54308	1.17E-04	9.36E-01	6.21E-02	1.51E-03	1.06E-04
	54309	2.20E-04	9.27E-01	7.08E-02	1.56E-03	1.28E-04
	54313	2.66E-04	9.32E-01	6.54E-02	1.72E-03	1.29E-04
	54314	1.58E-04	9.34E-01	6.39E-02	1.58E-03	1.15E-04
	54315	9.58E-05	9.38E-01	5.97E-02	1.76E-03	1.19E-04
	54317	1.83E-04	9.36E-01	6.23E-02	1.63E-03	1.15E-04
	54321	2.25E-04	9.33E-01	6.51E-02	1.61E-03	1.20E-04
	54324	3.59E-04	9.37E-01	6.10E-02	1.66E-03	1.15E-04
	54327	2.63E-04	9.34E-01	6.43E-02	1.61E-03	1.18E-04
	54328	2.12E-04	9.34E-01	6.46E-02	1.49E-03	1.09E-04
	54330	2.12E-04	9.43E-01	5.49E-02	1.48E-03	9.09E-05
	54331	3.74E-04	9.49E-01	4.93E-02	1.66E-03	9.04E-05
	54335	1.55E-04	9.29E-01	6.87E-02	1.56E-03	1.24E-04
	54340	7.09E-05	9.47E-01	5.12E-02	1.65E-03	9.37E-05
	54345	3.03E-04	9.09E-01	8.97E-02	1.17E-03	1.27E-04
	54354	1.65E-04	9.31E-01	6.75E-02	1.66E-03	1.29E-04
	54357	2.30E-04	9.30E-01	6.82E-02	1.33E-03	1.04E-04
	54358	4.30E-04	9.28E-01	6.99E-02	1.35E-03	1.08E-04
	54360	1.45E-04	9.32E-01	6.62E-02	1.67E-03	1.27E-04
	54365	1.42E-04	9.15E-01	8.31E-02	1.97E-03	1.94E-04
	54370	1.21E-04	9.40E-01	5.85E-02	1.58E-03	1.04E-04
	54372	1.54E-04	9.36E-01	6.25E-02	1.56E-03	1.11E-04
	54377	1.32E-04	9.38E-01	6.01E-02	1.34E-03	9.07E-05
	54382	1.46E-04	9.38E-01	6.03E-02	1.56E-03	1.07E-04
	54384	7.23E-05	9.39E-01	5.89E-02	1.60E-03	1.06E-04
	54388	2.00E-04	9.38E-01	6.01E-02	1.40E-03	9.48E-05
	54391	1.03E-04	9.43E-01	5.54E-02	1.50E-03	9.29E-05
	54392	1.69E-04	9.40E-01	5.84E-02	1.38E-03	9.07E-05
	54400	2.37E-04	9.42E-01	5.65E-02	1.58E-03	1.00E-04
	54401	8.36E-05	9.13E-01	8.56E-02	1.62E-03	1.66E-04
	54402	2.27E-04	9.16E-01	8.15E-02	2.43E-03	2.35E-04
	54406	1.40E-04	9.39E-01	5.88E-02	1.63E-03	1.08E-04

Table IV-1 (Continued)
Sample Data Used to Estimate Radionuclide Activity Fraction Distributions in Plutonium Material Types

Material Type	Drum ID	Pu238	Pu239	Pu240	Pu241	Pu242
PU52 (Cont.)	54411	1.75E-04	9.41E-01	5.78E-02	1.32E-03	8.58E-05
	54414	6.94E-05	9.32E-01	6.70E-02	1.25E-03	9.56E-05
	54421	6.61E-04	8.93E-01	1.05E-01	1.78E-03	2.32E-04
	54431	1.74E-04	9.29E-01	6.96E-02	1.54E-03	1.24E-04
	54440	1.59E-04	9.29E-01	6.89E-02	1.58E-03	1.26E-04
	54441	5.98E-04	9.04E-01	9.31E-02	2.33E-03	2.64E-04
	54443	1.25E-04	9.37E-01	6.12E-02	1.37E-03	9.47E-05
	54448	1.36E-04	9.38E-01	6.02E-02	1.31E-03	8.91E-05
	54449	9.61E-05	9.37E-01	6.13E-02	1.69E-03	1.18E-04
	54453	1.47E-04	9.46E-01	5.23E-02	1.44E-03	8.35E-05
	54456	1.86E-04	9.33E-01	6.56E-02	1.53E-03	1.15E-04
	54458	1.81E-04	9.35E-01	6.27E-02	1.64E-03	1.17E-04
	54459	2.22E-04	9.47E-01	5.09E-02	1.43E-03	8.05E-05
	54460	3.51E-04	9.41E-01	5.71E-02	1.14E-03	7.27E-05
	54461	7.81E-05	9.27E-01	7.09E-02	1.56E-03	1.28E-04
	54462	1.60E-04	9.42E-01	5.50E-02	2.31E-03	1.42E-04
	54463	1.63E-04	9.36E-01	6.26E-02	1.44E-03	1.02E-04
	54465	1.11E-04	9.31E-01	6.71E-02	1.50E-03	1.16E-04
	54471	4.67E-04	9.28E-01	6.95E-02	2.21E-03	1.78E-04
	54472	1.73E-04	9.26E-01	7.24E-02	1.59E-03	1.33E-04
	54474	6.51E-04	9.29E-01	6.81E-02	1.70E-03	1.33E-04
	54475	2.13E-04	9.19E-01	7.92E-02	1.79E-03	1.67E-04
	54481	1.24E-04	9.36E-01	6.19E-02	1.52E-03	1.07E-04
	54483	1.44E-04	9.38E-01	6.08E-02	1.31E-03	8.99E-05
	54486	1.62E-04	9.36E-01	6.25E-02	1.47E-03	1.04E-04
	54487	1.51E-04	9.36E-01	6.20E-02	1.44E-03	1.01E-04
	54489	1.20E-04	9.40E-01	5.88E-02	1.40E-03	9.27E-05
	54493	1.64E-04	9.41E-01	5.73E-02	1.41E-03	9.10E-05
	54496	1.69E-04	9.37E-01	6.13E-02	1.57E-03	1.09E-04
	54497	2.01E-04	9.37E-01	6.12E-02	1.75E-03	1.21E-04
	54498	1.54E-04	9.39E-01	5.91E-02	1.84E-03	1.23E-04
	54499	1.26E-04	9.35E-01	6.34E-02	1.24E-03	8.93E-05
	54500	1.27E-04	9.32E-01	6.60E-02	1.39E-03	1.05E-04
	54501	2.81E-04	9.34E-01	6.40E-02	1.42E-03	1.04E-04

Table IV-1 (Continued)
Sample Data Used to Estimate Radionuclide Activity Fraction Distributions in Plutonium Material Types

Material Type	Drum ID	Pu238	Pu239	Pu240	Pu241	Pu242
PU52 (Cont.)	54503	1.27E-04	9.36E-01	6.22E-02	1.56E-03	1.10E-04
	54504	1.03E-03	9.21E-01	7.56E-02	2.43E-03	2.15E-04
	54506	1.32E-04	9.35E-01	6.30E-02	1.47E-03	1.05E-04
	54507	1.78E-04	9.15E-01	8.27E-02	2.28E-03	2.24E-04
	54510	6.21E-04	9.30E-01	6.73E-02	2.16E-03	1.67E-04
	54511	1.58E-04	9.41E-01	5.74E-02	1.37E-03	8.86E-05
	54518	4.66E-04	9.37E-01	6.02E-02	2.04E-03	1.39E-04
	54521	1.24E-04	9.34E-01	6.48E-02	1.41E-03	1.04E-04
	54522	1.69E-04	9.32E-01	6.55E-02	1.71E-03	1.28E-04
	54526	1.61E-04	9.37E-01	6.16E-02	1.37E-03	9.53E-05
	54528	1.28E-04	9.35E-01	6.31E-02	1.49E-03	1.06E-04
	54532	1.18E-04	9.37E-01	6.16E-02	1.35E-03	9.38E-05
	54533	1.33E-04	9.39E-01	5.98E-02	1.50E-03	1.01E-04
	54543	8.41E-04	9.28E-01	6.99E-02	1.61E-03	1.30E-04
	54544	1.98E-04	9.31E-01	6.68E-02	2.17E-03	1.66E-04
	54545	2.79E-04	9.35E-01	6.26E-02	1.70E-03	1.21E-04
	54548	1.83E-04	9.40E-01	5.82E-02	1.86E-03	1.22E-04
	54551	1.28E-04	9.44E-01	5.36E-02	1.74E-03	1.04E-04
	54552	1.07E-04	9.29E-01	6.93E-02	1.45E-03	1.16E-04
	54556	1.26E-04	9.38E-01	5.98E-02	1.49E-03	1.01E-04
	54557	1.61E-04	9.38E-01	5.96E-02	1.96E-03	1.32E-04
	54558	1.71E-04	9.29E-01	6.96E-02	1.62E-03	1.30E-04
	54563	3.68E-04	9.38E-01	5.95E-02	2.22E-03	1.49E-04
	54566	1.11E-04	9.42E-01	5.69E-02	1.28E-03	8.17E-05
	54574	9.43E-05	9.46E-01	5.24E-02	1.88E-03	1.10E-04
	54578	6.49E-05	9.16E-01	8.20E-02	1.49E-03	1.45E-04
	54588	1.22E-04	9.35E-01	6.31E-02	1.42E-03	1.02E-04
	54594	1.47E-04	9.39E-01	5.97E-02	1.41E-03	9.50E-05
	54595	2.19E-04	9.35E-01	6.25E-02	1.67E-03	1.18E-04
	54654	1.20E-04	9.39E-01	5.97E-02	1.43E-03	9.66E-05
	54658	1.71E-04	9.38E-01	6.01E-02	1.58E-03	1.08E-04
	54660	2.99E-04	9.31E-01	6.67E-02	1.96E-03	1.50E-04
	54661	3.90E-04	8.94E-01	1.04E-01	1.41E-03	1.82E-04
	54665	1.13E-04	9.38E-01	6.01E-02	1.28E-03	8.70E-05

Table IV-1 (Continued)
Sample Data Used to Estimate Radionuclide Activity Fraction Distributions in Plutonium Material Types

Material Type	Drum ID	Pu238	Pu239	Pu240	Pu241	Pu242
PU52 (Cont.)	54666	2.95E-04	9.22E-01	7.51E-02	2.18E-03	1.91E-04
	54671	9.33E-05	9.42E-01	5.61E-02	1.41E-03	8.89E-05
	54674	2.22E-04	9.38E-01	5.96E-02	1.64E-03	1.10E-04
	54675	1.11E-04	9.39E-01	5.99E-02	1.24E-03	8.41E-05
	54676	1.76E-04	9.38E-01	5.99E-02	1.70E-03	1.15E-04
	54678	5.06E-04	9.36E-01	6.15E-02	2.04E-03	1.42E-04
	54684	1.33E-04	9.30E-01	6.84E-02	1.53E-03	1.20E-04
	54686	1.55E-04	9.35E-01	6.37E-02	1.36E-03	9.87E-05
	54687	1.18E-04	9.41E-01	5.76E-02	1.62E-03	1.05E-04
	54689	1.38E-04	9.40E-01	5.80E-02	1.68E-03	1.09E-04
	54690	1.25E-04	9.39E-01	5.94E-02	1.62E-03	1.09E-04
	54693	1.37E-04	9.37E-01	6.13E-02	1.47E-03	1.02E-04
	54694	1.34E-04	9.39E-01	5.95E-02	1.64E-03	1.10E-04
	54697	1.37E-04	9.38E-01	5.99E-02	1.64E-03	1.11E-04
	54702	2.95E-04	9.10E-01	8.75E-02	1.79E-03	1.88E-04
	54703	1.42E-04	9.03E-01	9.44E-02	1.82E-03	2.10E-04
	54704	2.30E-04	9.34E-01	6.30E-02	2.69E-03	1.93E-04
	54705	1.33E-04	9.37E-01	6.09E-02	1.42E-03	9.75E-05
	54709	1.68E-04	9.37E-01	6.17E-02	1.39E-03	9.70E-05
	54711	9.69E-05	9.38E-01	6.02E-02	1.29E-03	8.78E-05
	54712	1.13E-04	9.33E-01	6.48E-02	1.55E-03	1.15E-04
	54713	1.71E-04	9.50E-01	4.80E-02	1.68E-03	8.86E-05
	54714	3.95E-04	9.12E-01	8.54E-02	1.80E-03	1.83E-04
	54715	1.26E-04	9.37E-01	6.10E-02	1.51E-03	1.04E-04
	54716	1.93E-04	9.34E-01	6.39E-02	1.74E-03	1.27E-04
	54717	1.69E-04	9.35E-01	6.34E-02	1.52E-03	1.09E-04
	54718	5.27E-04	9.34E-01	6.28E-02	2.28E-03	1.63E-04
	54722	1.71E-04	9.38E-01	5.97E-02	2.00E-03	1.35E-04
	54725	1.29E-04	9.40E-01	5.75E-02	2.09E-03	1.35E-04
	54742	1.36E-04	9.37E-01	6.08E-02	1.61E-03	1.10E-04
	54745	1.39E-04	9.38E-01	6.05E-02	1.36E-03	9.27E-05
	54749	1.40E-04	9.40E-01	5.87E-02	1.47E-03	9.69E-05
	54757	1.42E-04	9.33E-01	6.47E-02	1.76E-03	1.30E-04
	54761	1.33E-04	9.35E-01	6.29E-02	1.46E-03	1.04E-04

Table IV-1 (Continued)
Sample Data Used to Estimate Radionuclide Activity Fraction Distributions in Plutonium Material Types

Material Type	Drum ID	Pu238	Pu239	Pu240	Pu241	Pu242
PU52 (Cont.)	54772	3.04E-04	9.37E-01	6.10E-02	1.61E-03	1.11E-04
	54785	1.32E-04	9.38E-01	5.98E-02	1.80E-03	1.22E-04
	54789	1.90E-04	9.34E-01	6.39E-02	1.45E-03	1.06E-04
	54801	1.65E-04	9.28E-01	7.01E-02	1.50E-03	1.21E-04
	54803	1.58E-04	9.42E-01	5.65E-02	1.51E-03	9.55E-05
	54807	2.18E-04	9.40E-01	5.80E-02	1.75E-03	1.15E-04
	54809	1.53E-04	9.42E-01	5.58E-02	1.68E-03	1.05E-04
	54811	1.09E-04	9.35E-01	6.34E-02	1.32E-03	9.51E-05
	54813	9.99E-05	9.42E-01	5.66E-02	1.40E-03	8.86E-05
	54814	1.13E-04	9.36E-01	6.24E-02	1.48E-03	1.05E-04
	54824	3.86E-04	9.16E-01	8.18E-02	1.66E-03	1.61E-04
	54825	9.62E-05	9.32E-01	6.67E-02	1.49E-03	1.14E-04
	54828	1.21E-04	9.08E-01	8.95E-02	2.39E-03	2.58E-04
	54829	6.56E-05	9.37E-01	6.22E-02	1.18E-03	8.29E-05
	54837	2.68E-04	9.17E-01	8.03E-02	2.21E-03	2.10E-04
	54843	1.20E-04	9.38E-01	6.00E-02	1.63E-03	1.11E-04
	54844	1.17E-04	9.36E-01	6.25E-02	1.64E-03	1.16E-04
	54845	1.19E-04	9.37E-01	6.11E-02	1.49E-03	1.03E-04
	54846	1.19E-04	9.38E-01	6.02E-02	1.45E-03	9.82E-05
	54848	1.19E-04	9.42E-01	5.66E-02	1.49E-03	9.45E-05
	54861	1.20E-04	9.45E-01	5.27E-02	1.64E-03	9.59E-05
	54866	3.13E-04	9.51E-01	4.70E-02	1.68E-03	8.68E-05
	54870	3.53E-04	9.37E-01	6.07E-02	1.72E-03	1.18E-04
	54883	1.11E-04	9.38E-01	6.02E-02	1.48E-03	1.00E-04
	54887	1.15E-04	9.40E-01	5.85E-02	1.47E-03	9.69E-05
	54888	1.64E-04	9.36E-01	6.24E-02	1.50E-03	1.06E-04
	54898	5.28E-04	9.37E-01	6.04E-02	1.62E-03	1.11E-04
	54905	1.52E-04	9.30E-01	6.80E-02	1.58E-03	1.23E-04
	54910	1.54E-04	9.27E-01	7.14E-02	1.45E-03	1.20E-04
	54914	7.38E-05	9.38E-01	6.04E-02	1.68E-03	1.15E-04
	54915	1.48E-04	9.41E-01	5.70E-02	1.88E-03	1.20E-04
	54924	1.36E-04	9.42E-01	5.58E-02	1.75E-03	1.10E-04
	54939	8.88E-05	9.24E-01	7.45E-02	1.61E-03	1.39E-04
	54940	5.84E-05	9.19E-01	7.90E-02	1.69E-03	1.57E-04

Table IV-1 (Continued)
Sample Data Used to Estimate Radionuclide Activity Fraction Distributions in Plutonium Material Types

Material Type	Drum ID	Pu238	Pu239	Pu240	Pu241	Pu242
PU52 (Cont.)	54943	5.72E-05	9.49E-01	4.94E-02	1.69E-03	9.24E-05
	54945	3.19E-04	9.22E-01	7.55E-02	1.88E-03	1.66E-04
	54956	1.65E-04	9.31E-01	6.67E-02	1.61E-03	1.23E-04
	54958	7.84E-05	9.39E-01	5.99E-02	1.37E-03	9.25E-05
	54959	9.89E-05	9.09E-01	8.93E-02	1.58E-03	1.70E-04
	54961	2.45E-04	9.51E-01	4.65E-02	1.94E-03	9.91E-05
	54966	1.73E-04	9.41E-01	5.74E-02	1.60E-03	1.03E-04
	54971	1.34E-04	9.41E-01	5.72E-02	1.56E-03	9.99E-05
	54978	7.74E-05	9.29E-01	6.88E-02	1.49E-03	1.18E-04
	54992	1.28E-04	9.34E-01	6.38E-02	1.59E-03	1.16E-04
	54994	1.12E-04	9.37E-01	6.14E-02	1.44E-03	1.00E-04
	55127	1.49E-04	9.37E-01	6.07E-02	1.57E-03	1.08E-04
	55148	1.14E-04	9.42E-01	5.60E-02	1.58E-03	9.88E-05
	55165	4.29E-04	8.96E-01	1.02E-01	1.68E-03	2.13E-04
	55168	6.02E-05	9.45E-01	5.33E-02	1.52E-03	8.99E-05
	55169	1.21E-04	9.40E-01	5.80E-02	1.52E-03	9.93E-05
	55175	1.11E-04	9.31E-01	6.77E-02	1.58E-03	1.23E-04
	55177	1.42E-04	9.38E-01	6.04E-02	1.47E-03	1.01E-04
	55179	1.54E-04	9.28E-01	6.97E-02	1.63E-03	1.31E-04
	55180	1.32E-04	9.38E-01	6.02E-02	1.46E-03	9.92E-05
	55183	1.49E-04	9.38E-01	6.00E-02	1.68E-03	1.14E-04
	55200	1.31E-04	9.43E-01	5.52E-02	1.61E-03	9.91E-05
	55201	9.93E-05	9.37E-01	6.13E-02	1.48E-03	1.03E-04
	55203	1.08E-04	9.39E-01	5.95E-02	1.29E-03	8.65E-05
	55213	1.19E-04	9.39E-01	6.01E-02	1.21E-03	8.20E-05
	55219	1.25E-04	9.33E-01	6.52E-02	1.41E-03	1.05E-04
	55220	1.33E-04	9.33E-01	6.53E-02	1.53E-03	1.14E-04
	55222	2.04E-04	9.34E-01	6.45E-02	1.47E-03	1.08E-04
	55226	4.51E-04	9.34E-01	6.35E-02	1.68E-03	1.21E-04
	55232	1.63E-04	9.32E-01	6.66E-02	1.52E-03	1.16E-04
	55233	2.02E-04	9.37E-01	6.14E-02	1.76E-03	1.22E-04
	55234	9.83E-05	9.45E-01	5.37E-02	1.46E-03	8.75E-05
	55239	1.56E-04	9.40E-01	5.86E-02	1.49E-03	9.86E-05
	55244	2.63E-04	9.28E-01	6.97E-02	1.86E-03	1.50E-04

Table IV-1 (Continued)
Sample Data Used to Estimate Radionuclide Activity Fraction Distributions in Plutonium Material Types

Material Type	Drum ID	Pu238	Pu239	Pu240	Pu241	Pu242
PU52 (Cont.)	55246	1.79E-04	9.36E-01	6.24E-02	1.61E-03	1.14E-04
	55247	3.59E-04	9.22E-01	7.52E-02	2.23E-03	1.96E-04
	55249	2.40E-04	9.38E-01	6.04E-02	1.58E-03	1.08E-04
	55250	2.15E-04	9.43E-01	5.52E-02	1.71E-03	1.06E-04
	55261	1.17E-04	9.41E-01	5.68E-02	1.63E-03	1.04E-04
	55263	5.13E-04	9.41E-01	5.69E-02	1.65E-03	1.06E-04
	55267	1.34E-04	9.40E-01	5.85E-02	1.62E-03	1.07E-04
	55268	2.07E-04	9.43E-01	5.57E-02	1.38E-03	8.60E-05
	55272	2.17E-04	9.37E-01	6.15E-02	1.43E-03	9.93E-05
	55273	1.83E-04	9.31E-01	6.68E-02	1.47E-03	1.13E-04
	55275	1.60E-04	9.35E-01	6.33E-02	1.72E-03	1.24E-04
	55278	1.20E-04	9.34E-01	6.47E-02	1.52E-03	1.12E-04
	55279	1.27E-04	9.34E-01	6.43E-02	1.55E-03	1.14E-04
	55281	1.70E-04	9.36E-01	6.22E-02	1.50E-03	1.06E-04
	55288	1.75E-04	9.27E-01	7.14E-02	1.56E-03	1.29E-04
	55292	6.02E-04	9.35E-01	6.17E-02	2.22E-03	1.56E-04
	55294	1.15E-04	9.38E-01	6.06E-02	1.62E-03	1.11E-04
	55297	1.36E-04	9.34E-01	6.44E-02	1.53E-03	1.12E-04
	55299	1.32E-04	9.36E-01	6.24E-02	1.62E-03	2.94E-04
	55426	1.29E-04	9.41E-01	5.77E-02	1.51E-03	9.79E-05
	55428	1.54E-04	9.37E-01	6.14E-02	1.60E-03	1.12E-04
	55429	7.43E-04	9.37E-01	5.95E-02	2.43E-03	1.64E-04
	55430	2.54E-04	9.28E-01	7.01E-02	1.94E-03	1.58E-04
	55433	1.17E-04	9.38E-01	6.05E-02	1.58E-03	1.08E-04
	55436	3.22E-04	9.19E-01	7.77E-02	2.44E-03	2.23E-04
	55445	1.82E-04	9.39E-01	5.92E-02	1.83E-03	1.22E-04
	55457	1.70E-04	9.32E-01	6.62E-02	1.55E-03	1.17E-04
	55467	4.34E-04	9.50E-01	4.84E-02	1.39E-03	7.42E-05
	55468	1.18E-04	9.39E-01	5.97E-02	1.51E-03	1.02E-04
	55470	1.87E-04	9.37E-01	6.14E-02	1.60E-03	1.11E-04
	55478	7.63E-05	9.41E-01	5.76E-02	1.46E-03	9.45E-05
	55479	1.57E-04	9.35E-01	6.33E-02	1.58E-03	1.14E-04
	55480	1.09E-04	9.38E-01	6.03E-02	1.55E-03	1.06E-04
	55482	1.59E-04	9.31E-01	6.76E-02	1.61E-03	1.25E-04

Table IV-1 (Continued)
Sample Data Used to Estimate Radionuclide Activity Fraction Distributions in Plutonium Material Types

Material Type	Drum ID	Pu238	Pu239	Pu240	Pu241	Pu242
PU52 (Cont.)	55484	1.76E-04	9.34E-01	6.47E-02	1.25E-03	9.18E-05
	55486	2.55E-04	9.37E-01	6.14E-02	1.54E-03	1.07E-04
	55489	1.17E-04	9.38E-01	6.07E-02	1.60E-03	1.10E-04
	55496	9.65E-05	9.43E-01	5.55E-02	1.52E-03	9.41E-05
	55501	6.01E-05	9.28E-01	6.93E-02	2.45E-03	1.96E-04
	55508	1.19E-04	9.32E-01	6.59E-02	1.63E-03	1.22E-04
	55510	1.61E-04	9.35E-01	6.35E-02	1.37E-03	9.92E-05
	55511	1.57E-04	9.39E-01	5.91E-02	1.58E-03	1.05E-04
	55512	2.24E-04	9.49E-01	4.84E-02	1.79E-03	9.53E-05
	55528	5.82E-04	9.26E-01	7.14E-02	1.83E-03	1.52E-04
	55559	2.20E-04	9.46E-01	5.23E-02	1.57E-03	9.13E-05
	55560	2.93E-04	9.28E-01	7.00E-02	1.67E-03	1.35E-04
	55591	4.45E-04	9.40E-01	5.80E-02	1.63E-03	1.07E-04
	55609	2.32E-04	9.34E-01	6.43E-02	1.72E-03	1.26E-04
	55613	1.45E-04	9.37E-01	6.09E-02	1.56E-03	1.07E-04
	55621	1.46E-04	9.31E-01	6.68E-02	1.66E-03	1.27E-04
	55624	1.35E-04	9.38E-01	6.03E-02	1.64E-03	1.12E-04
	55626	1.92E-04	9.18E-01	8.00E-02	2.04E-03	1.92E-04
	55632	1.29E-04	9.37E-01	6.11E-02	1.35E-03	9.34E-05
	55633	1.74E-04	9.21E-01	7.74E-02	1.34E-03	1.21E-04
	55642	7.74E-05	9.30E-01	6.88E-02	1.52E-03	1.20E-04
	55656	8.38E-05	9.34E-01	6.41E-02	1.56E-03	1.14E-04
	55657	2.14E-04	8.97E-01	1.01E-01	1.72E-03	2.16E-04
	55660	1.37E-04	9.37E-01	6.08E-02	1.55E-03	1.06E-04
	55687	2.16E-04	9.29E-01	6.93E-02	1.38E-03	1.10E-04
	55808	2.44E-04	9.37E-01	6.13E-02	1.42E-03	9.84E-05
	55818	1.83E-04	9.33E-01	6.54E-02	1.28E-03	9.54E-05
	55851	3.47E-04	9.34E-01	6.35E-02	1.82E-03	1.31E-04
	55860	4.10E-04	9.32E-01	6.57E-02	1.55E-03	1.16E-04
	55864	4.13E-04	9.35E-01	6.26E-02	1.58E-03	1.13E-04
	55876	4.70E-04	9.39E-01	5.92E-02	1.51E-03	1.01E-04
	55881	3.69E-04	9.27E-01	7.04E-02	2.01E-03	1.64E-04
	55882	1.04E-04	9.40E-01	5.77E-02	1.63E-03	2.78E-04
	55886	1.43E-04	9.38E-01	6.04E-02	1.44E-03	9.82E-05

Table IV-1 (Continued)
Sample Data Used to Estimate Radionuclide Activity Fraction Distributions in Plutonium Material Types

Material Type	Drum ID	Pu238	Pu239	Pu240	Pu241	Pu242
PU52 (Cont.)	55918	3.14E-04	9.19E-01	7.93E-02	1.48E-03	1.38E-04
	55928	1.22E-04	9.23E-01	7.52E-02	1.38E-03	1.21E-04
	55937	2.51E-04	9.31E-01	6.67E-02	1.64E-03	1.26E-04
	55953	1.89E-04	9.41E-01	5.67E-02	1.57E-03	9.98E-05
	55955	6.31E-04	9.32E-01	6.64E-02	1.26E-03	9.60E-05
	55960	2.26E-04	9.24E-01	7.41E-02	1.79E-03	1.54E-04
	55969	1.82E-04	9.40E-01	5.85E-02	1.56E-03	1.03E-04
	55972	3.31E-04	9.31E-01	6.76E-02	1.17E-03	9.08E-05
	55978	9.15E-04	9.33E-01	6.46E-02	1.57E-03	1.16E-04
	55985	5.90E-04	9.29E-01	6.90E-02	1.46E-03	1.16E-04
	56004	1.23E-04	9.32E-01	6.64E-02	1.37E-03	1.04E-04
	56009	1.58E-04	9.32E-01	6.60E-02	1.63E-03	1.23E-04
	56016	2.34E-04	9.35E-01	6.35E-02	1.52E-03	1.10E-04
	56023	2.12E-04	9.39E-01	5.90E-02	1.56E-03	1.04E-04
	56028	1.27E-04	9.38E-01	6.01E-02	1.41E-03	9.55E-05
	56037	5.72E-04	9.38E-01	5.99E-02	1.50E-03	1.01E-04
	56077	8.19E-05	9.17E-01	8.13E-02	1.72E-03	1.65E-04
	56088	2.97E-04	9.38E-01	5.97E-02	1.44E-03	9.72E-05
	56092	6.87E-04	9.51E-01	4.61E-02	1.80E-03	9.12E-05
	56117	2.73E-04	9.38E-01	6.05E-02	1.47E-03	1.01E-04
	56127	3.24E-04	9.40E-01	5.86E-02	1.28E-03	8.45E-05
	56131	3.52E-04	9.23E-01	7.48E-02	1.76E-03	1.54E-04
	56133	3.12E-04	9.33E-01	6.49E-02	1.72E-03	1.28E-04
	56145	2.91E-04	9.35E-01	6.33E-02	1.54E-03	1.11E-04
	56148	4.48E-04	9.33E-01	6.48E-02	1.79E-03	1.33E-04
	56151	3.01E-04	9.31E-01	6.72E-02	1.42E-03	1.10E-04
	56157	6.43E-05	9.37E-01	6.15E-02	1.70E-03	1.19E-04
	56188	3.59E-04	9.22E-01	7.56E-02	2.26E-03	2.00E-04
	56190	9.87E-05	9.37E-01	6.13E-02	1.50E-03	1.04E-04
	56210	1.33E-04	9.29E-01	6.97E-02	1.52E-03	1.22E-04
	56264	2.69E-04	9.21E-01	7.70E-02	1.70E-03	1.54E-04
	56270	3.31E-04	9.34E-01	6.38E-02	1.90E-03	1.38E-04
	56273	1.34E-04	9.43E-01	5.56E-02	1.55E-03	9.62E-05
	56274	1.97E-04	9.23E-01	7.43E-02	2.07E-03	1.79E-04

Table IV-1 (Continued)
Sample Data Used to Estimate Radionuclide Activity Fraction Distributions in Plutonium Material Types

Material Type	Drum ID	Pu238	Pu239	Pu240	Pu241	Pu242
PU52 (Cont.)	56279	1.95E-04	9.32E-01	6.62E-02	1.37E-03	1.04E-04
	56280	2.57E-04	9.30E-01	6.82E-02	1.91E-03	1.50E-04
	56287	8.80E-04	9.36E-01	6.12E-02	1.53E-03	1.06E-04
	56292	1.66E-04	9.44E-01	5.35E-02	2.05E-03	1.22E-04
	56302	6.98E-04	9.34E-01	6.34E-02	1.53E-03	1.10E-04
	56322	1.55E-04	9.38E-01	6.05E-02	1.63E-03	1.12E-04
	56323	1.52E-04	9.34E-01	6.48E-02	1.30E-03	9.57E-05
	56335	1.61E-04	9.34E-01	6.41E-02	1.52E-03	1.11E-04
	56339	1.20E-04	9.28E-01	6.99E-02	1.57E-03	1.27E-04
	56343	1.63E-04	9.39E-01	5.94E-02	1.76E-03	1.18E-04
	56351	2.24E-04	9.47E-01	5.12E-02	1.58E-03	8.98E-05
	56352	1.06E-04	9.43E-01	5.49E-02	1.65E-03	1.01E-04
	56356	1.01E-04	9.36E-01	6.19E-02	1.55E-03	1.09E-04
	56371	1.28E-04	9.37E-01	6.08E-02	1.55E-03	1.07E-04
	56377	2.78E-04	9.27E-01	7.06E-02	1.57E-03	1.28E-04
	56383	8.71E-04	9.41E-01	5.70E-02	1.48E-03	9.51E-05
	56387	3.31E-04	9.36E-01	6.23E-02	1.36E-03	9.58E-05
	56393	6.44E-04	9.39E-01	5.84E-02	1.61E-03	1.06E-04
	56535	2.68E-04	9.37E-01	6.12E-02	1.71E-03	1.19E-04
	56540	8.77E-04	9.35E-01	6.14E-02	2.23E-03	1.56E-04
	56548	1.41E-04	9.45E-01	5.37E-02	1.32E-03	7.89E-05
	56549	4.49E-04	9.37E-01	6.08E-02	1.55E-03	1.07E-04
	56550	4.99E-04	9.34E-01	6.39E-02	1.74E-03	1.27E-04
	56551	1.79E-04	9.42E-01	5.66E-02	1.45E-03	9.18E-05
	56570	1.10E-04	9.43E-01	5.55E-02	1.40E-03	8.68E-05
	56571	3.04E-04	9.41E-01	5.70E-02	1.49E-03	9.56E-05
	56574	6.98E-04	9.21E-01	7.65E-02	1.85E-03	1.66E-04
	56578	1.40E-04	9.41E-01	5.73E-02	1.50E-03	9.67E-05
	56600	8.45E-05	9.28E-01	7.04E-02	1.59E-03	1.29E-04
	56611	3.02E-04	9.40E-01	5.83E-02	1.39E-03	9.11E-05
	56625	1.09E-04	9.15E-01	8.36E-02	1.59E-03	1.58E-04
	56626	1.89E-04	9.39E-01	5.92E-02	1.55E-03	1.04E-04
	56628	2.08E-04	9.37E-01	6.06E-02	1.79E-03	1.23E-04
	56636	2.03E-04	9.38E-01	6.01E-02	1.66E-03	1.13E-04

Table IV-1 (Continued)
Sample Data Used to Estimate Radionuclide Activity Fraction Distributions in Plutonium Material Types

Material Type	Drum ID	Pu238	Pu239	Pu240	Pu241	Pu242
PU52 (Cont.)	56639	2.46E-04	9.26E-01	7.19E-02	1.71E-03	1.43E-04
	56640	1.95E-04	9.31E-01	6.70E-02	1.69E-03	1.30E-04
	56653	2.23E-04	9.32E-01	6.61E-02	1.32E-03	9.95E-05
	56659	2.16E-04	9.16E-01	8.25E-02	1.53E-03	1.50E-04
	56668	3.44E-04	9.27E-01	7.03E-02	2.36E-03	1.92E-04
	56685	1.33E-04	9.35E-01	6.30E-02	1.70E-03	1.22E-04
	56805	1.75E-04	9.37E-01	6.10E-02	1.31E-03	9.06E-05
	56809	1.42E-04	9.26E-01	7.19E-02	1.42E-03	1.18E-04
	56825	4.30E-04	9.31E-01	6.63E-02	1.79E-03	1.36E-04
	56832	1.63E-04	9.31E-01	6.73E-02	1.49E-03	1.15E-04
	56842	4.49E-04	9.33E-01	6.52E-02	1.52E-03	1.14E-04
	56861	2.15E-04	9.32E-01	6.62E-02	1.42E-03	1.07E-04
	56863	1.68E-04	9.42E-01	5.61E-02	1.20E-03	7.53E-05
	56866	4.87E-04	9.51E-01	4.66E-02	1.58E-03	8.09E-05
	56872	1.70E-04	9.37E-01	6.18E-02	1.40E-03	9.80E-05
	56882	2.79E-04	9.48E-01	4.96E-02	1.80E-03	9.86E-05
	56883	3.55E-04	9.06E-01	9.20E-02	1.75E-03	1.95E-04
	56886	2.22E-04	9.16E-01	8.19E-02	2.13E-03	2.07E-04
	56893	5.91E-04	9.34E-01	6.33E-02	1.61E-03	1.16E-04
	56898	2.03E-04	9.38E-01	5.99E-02	1.57E-03	1.06E-04
	56902	1.02E-03	9.38E-01	5.96E-02	1.64E-03	1.11E-04
	56907	2.83E-04	9.41E-01	5.70E-02	1.20E-03	7.65E-05
	56911	1.66E-04	9.34E-01	6.45E-02	1.22E-03	8.94E-05
	56915	6.97E-04	9.27E-01	7.03E-02	2.08E-03	1.69E-04
	56964	3.05E-04	9.38E-01	6.01E-02	1.48E-03	1.01E-04
	57057	1.64E-04	9.38E-01	6.05E-02	1.20E-03	8.20E-05
	57077	5.08E-04	9.35E-01	6.22E-02	1.91E-03	1.35E-04
	57110	2.47E-04	9.30E-01	6.78E-02	1.90E-03	1.48E-04
	57116	1.91E-04	9.47E-01	5.15E-02	1.68E-03	9.62E-05
	57129	1.53E-04	9.34E-01	6.37E-02	1.66E-03	1.21E-04
	57143	1.22E-04	9.39E-01	5.95E-02	1.63E-03	1.10E-04
	57185	1.60E-04	9.42E-01	5.57E-02	1.80E-03	1.12E-04
	57389	1.45E-04	9.42E-01	5.69E-02	1.29E-03	8.21E-05
	57397	1.22E-04	9.28E-01	7.07E-02	1.17E-03	9.56E-05

Table IV-1 (Continued)
Sample Data Used to Estimate Radionuclide Activity Fraction Distributions in Plutonium Material Types

Material Type	Drum ID	Pu238	Pu239	Pu240	Pu241	Pu242
PU52 (Cont.)	57717	1.55E-04	9.42E-01	5.62E-02	1.74E-03	1.10E-04
	57724	5.94E-04	9.20E-01	7.75E-02	1.77E-03	1.61E-04
	57726	3.01E-04	9.23E-01	7.48E-02	1.80E-03	1.57E-04
	57730	1.45E-04	9.39E-01	5.87E-02	1.65E-03	1.09E-04
	57739	2.77E-04	9.35E-01	6.31E-02	1.52E-03	1.09E-04
	57749	2.18E-04	9.41E-01	5.66E-02	1.88E-03	1.19E-04
	57751	2.21E-04	9.39E-01	5.90E-02	1.53E-03	1.02E-04
	57752	5.20E-04	9.30E-01	6.80E-02	1.76E-03	1.38E-04
	57758	5.71E-04	9.31E-01	6.65E-02	1.38E-03	1.05E-04
	57761	3.07E-04	9.33E-01	6.46E-02	1.52E-03	1.12E-04
	57772	2.64E-04	9.31E-01	6.71E-02	1.75E-03	3.11E-04
	57936	1.43E-04	9.37E-01	6.13E-02	1.54E-03	1.07E-04
	57937	1.83E-04	9.35E-01	6.24E-02	1.80E-03	1.28E-04
	57938	5.65E-04	9.32E-01	6.50E-02	1.99E-03	1.48E-04
	57939	1.31E-04	9.40E-01	5.84E-02	1.51E-03	9.91E-05
	57945	3.20E-04	9.34E-01	6.42E-02	1.69E-03	1.24E-04
	57947	2.29E-04	9.38E-01	6.01E-02	1.73E-03	1.18E-04
	57948	1.66E-04	9.37E-01	6.13E-02	1.65E-03	1.15E-04
	57949	4.47E-04	9.31E-01	6.72E-02	1.58E-03	1.22E-04
	57951	1.74E-04	9.36E-01	6.17E-02	1.68E-03	1.18E-04
	57954	3.89E-04	9.37E-01	6.10E-02	1.50E-03	1.04E-04
	57957	2.38E-04	9.26E-01	7.18E-02	1.47E-03	1.23E-04
	57958	2.85E-04	9.39E-01	5.86E-02	1.60E-03	1.06E-04
	57961	2.57E-04	9.43E-01	5.53E-02	1.66E-03	1.03E-04
	57962	1.53E-04	9.39E-01	5.95E-02	1.46E-03	9.82E-05
	57966	2.89E-04	9.39E-01	5.86E-02	1.60E-03	1.06E-04
	57967	7.64E-04	9.27E-01	7.01E-02	1.93E-03	1.56E-04
	57968	1.79E-04	9.39E-01	5.97E-02	1.36E-03	9.16E-05
	57975	1.87E-04	9.41E-01	5.68E-02	1.57E-03	9.98E-05
	57976	1.52E-04	9.37E-01	6.15E-02	1.63E-03	1.13E-04
	57979	2.03E-04	9.34E-01	6.38E-02	1.66E-03	1.21E-04
	57986	3.22E-04	9.34E-01	6.33E-02	1.71E-03	1.23E-04
	57995	1.09E-04	9.43E-01	5.52E-02	1.33E-03	8.21E-05
	58003	2.66E-04	9.38E-01	6.01E-02	1.70E-03	1.57E-04

Table IV-1 (Continued)
Sample Data Used to Estimate Radionuclide Activity Fraction Distributions in Plutonium Material Types

Material Type	Drum ID	Pu238	Pu239	Pu240	Pu241	Pu242
PU52 (Cont.)	58004	1.61E-04	9.39E-01	5.94E-02	1.51E-03	2.02E-04
	58009	7.58E-04	9.38E-01	5.84E-02	2.37E-03	1.56E-04
	58011	7.15E-04	9.11E-01	8.54E-02	2.85E-03	2.92E-04
	58012	2.57E-04	9.46E-01	5.23E-02	1.68E-03	9.77E-05
	58016	2.64E-04	9.41E-01	5.69E-02	1.55E-03	1.86E-04
	58018	1.49E-04	9.24E-01	7.36E-02	1.63E-03	1.40E-04
	58022	4.79E-04	9.40E-01	5.78E-02	2.04E-03	1.33E-04
	58023	1.21E-04	9.43E-01	5.55E-02	1.33E-03	8.23E-05
	58024	1.31E-04	9.38E-01	6.00E-02	1.51E-03	1.02E-04
	58029	1.38E-04	9.41E-01	5.77E-02	1.50E-03	9.69E-05
	58040	1.10E-04	9.37E-01	6.09E-02	1.45E-03	9.95E-05
	58047	3.32E-04	9.33E-01	6.50E-02	1.88E-03	1.40E-04
	58048	1.01E-04	9.39E-01	6.00E-02	1.22E-03	8.26E-05
	58056	1.47E-04	9.32E-01	6.57E-02	1.64E-03	1.23E-04
	58060	2.40E-04	9.33E-01	6.47E-02	1.82E-03	1.34E-04
	58061	1.33E-04	9.38E-01	6.01E-02	1.62E-03	1.10E-04
	58070	2.24E-04	9.36E-01	6.20E-02	1.57E-03	1.10E-04
	58076	1.22E-04	9.42E-01	5.67E-02	1.49E-03	9.43E-05
	58077	3.00E-04	9.30E-01	6.74E-02	1.90E-03	1.47E-04
	58083	1.29E-04	9.39E-01	5.91E-02	1.38E-03	9.22E-05
	58086	1.71E-04	9.40E-01	5.74E-02	1.92E-03	1.24E-04
	58089	1.90E-04	9.36E-01	6.19E-02	1.42E-03	9.93E-05
	58090	3.13E-04	9.29E-01	6.86E-02	2.14E-03	1.69E-04
	58094	1.54E-04	9.42E-01	5.54E-02	1.77E-03	2.40E-04
	58098	2.44E-04	9.19E-01	7.81E-02	2.59E-03	2.38E-04
	58107	1.48E-04	9.39E-01	5.89E-02	1.56E-03	1.04E-04
	58113	1.26E-04	9.36E-01	6.22E-02	1.48E-03	1.04E-04
	58127	3.16E-04	9.42E-01	5.64E-02	1.63E-03	1.03E-04
	58132	1.48E-04	9.38E-01	6.03E-02	1.31E-03	8.90E-05
	58136	1.29E-04	9.37E-01	6.16E-02	1.41E-03	9.87E-05
	58138	1.29E-04	9.39E-01	5.92E-02	1.27E-03	8.49E-05
	58139	1.63E-04	9.38E-01	6.00E-02	1.41E-03	9.57E-05
	58141	1.38E-04	9.37E-01	6.16E-02	1.57E-03	1.10E-04
	58142	7.46E-05	9.34E-01	6.49E-02	1.32E-03	9.78E-05

Table IV-1 (Continued)
Sample Data Used to Estimate Radionuclide Activity Fraction Distributions in Plutonium Material Types

Material Type	Drum ID	Pu238	Pu239	Pu240	Pu241	Pu242
PU52 (Cont.)	58143	1.32E-04	9.38E-01	6.04E-02	1.63E-03	1.11E-04
	58152	9.59E-05	9.38E-01	6.01E-02	1.53E-03	1.04E-04
	58154	1.31E-04	9.40E-01	5.87E-02	1.21E-03	8.01E-05
	58159	1.34E-04	9.37E-01	6.16E-02	1.57E-03	1.10E-04
	58162	1.75E-04	9.35E-01	6.36E-02	1.40E-03	1.01E-04
	58175	1.86E-04	9.36E-01	6.14E-02	1.95E-03	1.36E-04
	58186	6.67E-05	9.40E-01	5.85E-02	1.66E-03	1.09E-04
	58187	1.35E-04	9.40E-01	5.80E-02	1.65E-03	1.08E-04
	58188	1.36E-04	9.39E-01	5.93E-02	1.45E-03	9.72E-05
	58192	1.22E-04	9.34E-01	6.46E-02	1.41E-03	1.04E-04
	58198	1.15E-04	9.36E-01	6.21E-02	1.36E-03	9.58E-05
	58199	1.68E-04	9.01E-01	9.62E-02	2.24E-03	2.64E-04
	58346	1.29E-04	9.39E-01	5.90E-02	1.30E-03	8.62E-05
	58362	9.74E-05	9.42E-01	5.65E-02	1.16E-03	7.32E-05
	58366	1.85E-04	9.31E-01	6.76E-02	1.56E-03	1.21E-04
	58367	4.43E-04	9.39E-01	5.86E-02	1.62E-03	1.07E-04
	58376	9.71E-05	9.40E-01	5.82E-02	1.33E-03	8.69E-05
	58388	2.54E-04	9.40E-01	5.87E-02	1.30E-03	8.60E-05
	58393	1.84E-04	9.37E-01	6.13E-02	1.58E-03	1.10E-04
	58394	1.31E-04	9.37E-01	6.17E-02	1.49E-03	1.04E-04
	58834	7.64E-05	9.31E-01	6.76E-02	1.52E-03	1.18E-04
	58836	1.20E-04	9.41E-01	5.77E-02	1.46E-03	9.47E-05
	58839	2.90E-04	9.27E-01	7.01E-02	2.15E-03	1.75E-04
	58850	7.40E-04	9.20E-01	7.79E-02	1.36E-03	1.24E-04
	59005	3.30E-04	9.05E-01	9.16E-02	2.64E-03	2.94E-04
	59007	6.74E-05	9.43E-01	5.54E-02	1.38E-03	8.55E-05
	59012	1.56E-04	9.49E-01	4.92E-02	1.29E-03	6.97E-05
	59015	2.12E-04	9.35E-01	6.37E-02	1.29E-03	9.32E-05
	59018	3.03E-04	9.25E-01	7.24E-02	1.98E-03	1.67E-04
	59022	1.95E-04	9.39E-01	5.94E-02	1.28E-03	8.60E-05
	59023	2.98E-04	8.95E-01	1.02E-01	2.13E-03	2.69E-04
	59027	3.11E-04	9.36E-01	6.18E-02	1.77E-03	1.24E-04
	59031	1.79E-04	9.40E-01	5.89E-02	1.25E-03	8.30E-05
	59036	6.44E-04	9.38E-01	5.96E-02	2.03E-03	1.37E-04

Table IV-1 (Continued)
Sample Data Used to Estimate Radionuclide Activity Fraction Distributions in Plutonium Material Types

Material Type	Drum ID	Pu238	Pu239	Pu240	Pu241	Pu242
PU52 (Cont.)	59037	3.51E-04	9.41E-01	5.72E-02	1.74E-03	1.12E-04
	59045	8.88E-05	9.37E-01	6.13E-02	1.38E-03	9.56E-05
	59049	7.46E-05	9.37E-01	6.13E-02	1.70E-03	1.18E-04
	59052	1.81E-04	9.39E-01	5.93E-02	1.45E-03	9.72E-05
	59058	1.07E-04	9.32E-01	6.65E-02	1.34E-03	1.02E-04
	59060	2.25E-04	9.25E-01	7.28E-02	2.00E-03	1.70E-04
	59062	1.29E-04	9.39E-01	5.95E-02	1.35E-03	9.02E-05
	59064	1.27E-04	9.36E-01	6.22E-02	1.28E-03	9.01E-05
	59065	2.28E-04	9.22E-01	7.59E-02	1.50E-03	1.33E-04
	59067	1.29E-04	9.33E-01	6.51E-02	1.30E-03	9.66E-05
	59075	2.71E-04	9.43E-01	5.54E-02	1.58E-03	9.78E-05
	59076	3.36E-04	9.31E-01	6.67E-02	1.83E-03	1.40E-04
	59077	3.04E-04	9.27E-01	7.06E-02	1.86E-03	1.52E-04
	59081	1.30E-04	9.44E-01	5.50E-02	1.27E-03	7.82E-05
	59083	5.11E-04	9.34E-01	6.44E-02	1.30E-03	9.53E-05
	59085	1.15E-04	9.40E-01	5.86E-02	1.30E-03	8.58E-05
	59086	1.24E-04	9.39E-01	5.91E-02	1.33E-03	8.83E-05
	59088	1.11E-04	9.44E-01	5.48E-02	1.39E-03	8.47E-05
	59092	1.19E-04	9.37E-01	6.18E-02	1.25E-03	8.72E-05
	59102	1.72E-04	9.29E-01	6.88E-02	1.68E-03	1.33E-04
	59105	1.28E-04	9.37E-01	6.09E-02	1.36E-03	9.35E-05
	59108	1.75E-04	9.30E-01	6.84E-02	1.41E-03	1.11E-04
	59109	1.36E-04	9.32E-01	6.64E-02	1.48E-03	1.13E-04
	59110	1.32E-04	9.37E-01	6.17E-02	1.35E-03	9.40E-05
	59111	1.32E-04	9.38E-01	5.99E-02	1.59E-03	1.07E-04
	59114	5.20E-04	9.39E-01	5.85E-02	1.69E-03	1.11E-04
	59116	3.59E-04	9.38E-01	5.99E-02	1.88E-03	1.28E-04
	59117	1.22E-04	9.37E-01	6.13E-02	1.43E-03	9.91E-05
	59118	1.05E-04	9.35E-01	6.39E-02	1.19E-03	8.61E-05
	59121	8.94E-05	9.40E-01	5.83E-02	1.46E-03	9.55E-05
	59123	1.77E-04	9.18E-01	7.93E-02	1.82E-03	1.71E-04
	59127	3.02E-04	9.18E-01	7.91E-02	1.98E-03	1.85E-04
	59128	8.91E-05	9.23E-01	7.53E-02	1.25E-03	1.10E-04
	59129	1.36E-04	9.38E-01	6.03E-02	1.51E-03	1.03E-04

Table IV-1 (Continued)
Sample Data Used to Estimate Radionuclide Activity Fraction Distributions in Plutonium Material Types

Material Type	Drum ID	Pu238	Pu239	Pu240	Pu241	Pu242
PU52 (Cont.)	59139	6.68E-05	9.32E-01	6.69E-02	1.32E-03	1.02E-04
	59141	3.68E-04	9.23E-01	7.53E-02	1.40E-03	1.23E-04
	59142	2.51E-04	9.09E-01	8.78E-02	2.49E-03	2.63E-04
	59155	1.14E-04	9.38E-01	6.05E-02	1.53E-03	1.05E-04
	59156	1.15E-04	9.41E-01	5.71E-02	1.49E-03	9.54E-05
	59159	1.05E-04	9.40E-01	5.88E-02	1.27E-03	8.40E-05
	59160	1.02E-04	9.38E-01	6.02E-02	1.30E-03	8.81E-05
	59162	1.14E-04	9.35E-01	6.36E-02	1.32E-03	9.57E-05
	59164	1.16E-04	9.38E-01	6.04E-02	1.48E-03	1.01E-04
	59167	1.23E-04	9.38E-01	6.05E-02	1.60E-03	1.10E-04
	59174	1.60E-04	9.31E-01	6.70E-02	1.56E-03	1.20E-04
	59181	1.48E-04	9.36E-01	6.24E-02	1.51E-03	1.07E-04
	59182	1.18E-04	9.37E-01	6.12E-02	1.31E-03	9.10E-05
	59183	1.07E-04	9.34E-01	6.40E-02	1.68E-03	1.22E-04
	59190	1.83E-04	9.36E-01	6.23E-02	1.40E-03	9.91E-05
	59191	7.30E-05	9.34E-01	6.49E-02	1.31E-03	9.68E-05
	59195	2.69E-04	9.26E-01	7.15E-02	1.79E-03	1.49E-04
	59199	6.72E-05	9.20E-01	7.77E-02	1.64E-03	1.50E-04
	59288	1.62E-04	9.34E-01	6.43E-02	1.53E-03	1.12E-04
	59289	7.83E-05	9.36E-01	6.24E-02	1.44E-03	1.02E-04
	59292	2.17E-04	9.35E-01	6.26E-02	2.45E-03	1.75E-04
	59294	1.64E-04	9.40E-01	5.83E-02	1.43E-03	9.37E-05
	59298	1.53E-04	9.37E-01	6.11E-02	1.31E-03	9.07E-05
	59299	1.86E-04	9.38E-01	6.00E-02	1.65E-03	1.12E-04
	59300	1.44E-04	9.38E-01	6.06E-02	1.55E-03	1.06E-04
	59302	5.23E-04	9.24E-01	7.32E-02	2.22E-03	1.89E-04
	59306	1.16E-04	9.40E-01	5.80E-02	1.36E-03	8.87E-05
	59307	1.21E-04	9.39E-01	5.95E-02	1.38E-03	9.25E-05
	59308	1.43E-04	9.37E-01	6.18E-02	1.46E-03	1.02E-04
	59309	1.21E-04	9.39E-01	5.94E-02	1.37E-03	9.17E-05
	59313	1.70E-04	9.43E-01	5.53E-02	1.42E-03	8.78E-05
	59314	2.21E-04	9.42E-01	5.61E-02	1.76E-03	1.11E-04
	59319	1.15E-04	9.36E-01	6.23E-02	1.29E-03	9.08E-05
	59320	2.37E-04	9.37E-01	6.07E-02	1.55E-03	1.06E-04

Table IV-1 (Continued)
Sample Data Used to Estimate Radionuclide Activity Fraction Distributions in Plutonium Material Types

Material Type	Drum ID	Pu238	Pu239	Pu240	Pu241	Pu242
PU52 (Cont.)	59323	1.15E-04	9.37E-01	6.13E-02	1.22E-03	8.49E-05
	59333	1.97E-04	8.97E-01	1.01E-01	1.62E-03	2.01E-04
	59336	2.42E-04	9.43E-01	5.55E-02	1.46E-03	9.06E-05
	59338	1.29E-04	9.39E-01	5.98E-02	1.29E-03	8.73E-05
	59346	1.67E-04	9.42E-01	5.69E-02	1.29E-03	8.23E-05
	59347	2.22E-04	9.38E-01	6.01E-02	1.36E-03	9.23E-05
	59351	6.56E-05	9.26E-01	7.20E-02	1.64E-03	1.37E-04
	59365	1.01E-04	9.36E-01	6.27E-02	1.33E-03	9.46E-05
	59376	1.55E-04	9.35E-01	6.30E-02	1.34E-03	9.55E-05
	59377	1.81E-04	9.38E-01	6.01E-02	1.22E-03	8.28E-05
	59379	1.70E-04	9.44E-01	5.41E-02	1.38E-03	8.29E-05
	59381	4.54E-04	9.30E-01	6.80E-02	1.89E-03	1.47E-04
	59385	4.27E-04	9.35E-01	6.31E-02	1.51E-03	1.08E-04
	59387	5.84E-04	9.47E-01	5.07E-02	1.38E-03	7.74E-05
	59394	1.30E-04	9.36E-01	6.22E-02	1.22E-03	8.57E-05
	59404	1.54E-04	9.38E-01	6.01E-02	1.39E-03	9.41E-05
	59406	1.05E-04	9.39E-01	5.98E-02	1.21E-03	8.15E-05
	59411	1.39E-04	9.39E-01	5.95E-02	1.43E-03	9.62E-05
	59426	8.43E-04	9.23E-01	7.35E-02	2.09E-03	1.79E-04
	59436	1.11E-04	9.40E-01	5.89E-02	1.20E-03	7.92E-05
	59438	2.35E-04	9.44E-01	5.43E-02	1.26E-03	7.63E-05
	59444	1.19E-04	9.36E-01	6.23E-02	1.32E-03	9.33E-05
	59448	1.38E-04	9.50E-01	4.83E-02	1.44E-03	7.65E-05
	59449	8.62E-05	9.42E-01	5.64E-02	1.47E-03	9.28E-05
	59481	8.47E-05	9.28E-01	7.04E-02	1.26E-03	1.03E-04
	59485	3.20E-04	9.25E-01	7.22E-02	1.98E-03	1.66E-04
	59716	1.41E-04	9.36E-01	6.23E-02	1.47E-03	1.04E-04
	59721	4.19E-04	9.14E-01	8.26E-02	2.48E-03	2.43E-04
	59734	2.80E-04	9.43E-01	5.53E-02	1.37E-03	8.50E-05
	59739	1.43E-04	9.37E-01	6.18E-02	1.33E-03	9.29E-05
	59743	1.87E-04	9.38E-01	6.00E-02	1.43E-03	9.70E-05
	59749	1.28E-04	9.37E-01	6.17E-02	1.39E-03	9.70E-05
	59751	1.08E-04	9.35E-01	6.32E-02	1.28E-03	9.20E-05
	59757	4.82E-04	9.34E-01	6.38E-02	1.80E-03	1.31E-04

Table IV-1 (Continued)
Sample Data Used to Estimate Radionuclide Activity Fraction Distributions in Plutonium Material Types

Material Type	Drum ID	Pu238	Pu239	Pu240	Pu241	Pu242
PU52 (Cont.)	59766	2.02E-04	9.39E-01	5.96E-02	1.22E-03	8.17E-05
	59781	2.20E-04	9.35E-01	6.32E-02	1.53E-03	1.10E-04
	59782	8.18E-04	9.42E-01	5.53E-02	1.57E-03	9.69E-05
	59783	1.70E-04	9.42E-01	5.68E-02	1.36E-03	8.68E-05
	60401	6.66E-05	9.27E-01	7.10E-02	1.63E-03	1.34E-04
	60402	1.36E-04	9.34E-01	6.39E-02	1.41E-03	1.03E-04
	60405	1.81E-04	9.36E-01	6.18E-02	1.48E-03	1.04E-04
	60408	1.08E-04	9.31E-01	6.73E-02	1.40E-03	1.08E-04
	60410	2.31E-04	9.27E-01	6.97E-02	2.64E-03	2.13E-04
	60411	2.03E-04	9.27E-01	7.08E-02	1.60E-03	1.31E-04
	60413	1.14E-04	9.36E-01	6.26E-02	1.35E-03	9.60E-05
	60414	1.17E-04	9.41E-01	5.76E-02	1.29E-03	8.34E-05
	60415	1.38E-04	9.39E-01	5.97E-02	1.47E-03	9.90E-05
	60418	1.55E-04	9.25E-01	7.24E-02	1.84E-03	1.55E-04
	60420	1.96E-04	9.34E-01	6.40E-02	2.11E-03	1.54E-04
	60421	1.30E-04	9.37E-01	6.10E-02	1.32E-03	9.08E-05
	60422	7.10E-05	9.36E-01	6.22E-02	1.33E-03	9.37E-05
	60423	1.53E-04	9.43E-01	5.50E-02	1.98E-03	1.22E-04
	60426	1.11E-04	9.38E-01	6.06E-02	1.36E-03	9.31E-05
	60429	1.21E-04	9.33E-01	6.48E-02	1.63E-03	1.21E-04
	60432	1.09E-04	9.32E-01	6.62E-02	1.33E-03	1.01E-04
	60433	9.81E-05	9.38E-01	6.07E-02	1.29E-03	8.83E-05
	60435	1.68E-04	9.35E-01	6.27E-02	1.87E-03	1.33E-04
	60437	1.01E-04	9.38E-01	6.02E-02	1.20E-03	8.16E-05
	60438	1.36E-04	9.38E-01	6.10E-02	1.22E-03	8.40E-05
	60453	3.89E-04	9.19E-01	7.82E-02	2.36E-03	2.17E-04
	60470	1.41E-04	9.32E-01	6.64E-02	1.68E-03	1.27E-04
	60471	9.42E-05	9.39E-01	5.93E-02	1.31E-03	8.74E-05
	60474	1.42E-04	9.42E-01	5.66E-02	1.39E-03	8.82E-05
	60475	9.57E-04	9.38E-01	5.93E-02	1.71E-03	1.15E-04
	60476	4.21E-04	9.41E-01	5.67E-02	1.58E-03	1.00E-04
	60480	2.35E-04	9.30E-01	6.82E-02	1.78E-03	1.39E-04
	60481	2.47E-04	9.32E-01	6.66E-02	1.53E-03	1.17E-04
	60483	2.57E-04	9.32E-01	6.44E-02	2.74E-03	2.02E-04

Table IV-1 (Continued)
Sample Data Used to Estimate Radionuclide Activity Fraction Distributions in Plutonium Material Types

Material Type	Drum ID	Pu238	Pu239	Pu240	Pu241	Pu242
PU52 (Cont.)	60484	9.08E-05	9.41E-01	5.79E-02	1.32E-03	8.57E-05
	60486	6.96E-05	9.41E-01	5.74E-02	1.14E-03	7.31E-05
	60488	1.55E-04	9.33E-01	6.50E-02	1.48E-03	1.10E-04
	60490	2.63E-04	9.28E-01	6.90E-02	2.75E-03	2.19E-04
	60493	1.36E-04	9.47E-01	5.11E-02	1.46E-03	8.26E-05
	60494	1.28E-04	9.38E-01	6.05E-02	1.55E-03	1.06E-04
	60495	1.68E-04	9.38E-01	6.01E-02	1.38E-03	9.37E-05
	60496	1.45E-04	9.39E-01	5.90E-02	1.38E-03	9.17E-05
	60497	1.36E-04	9.36E-01	6.22E-02	1.54E-03	1.08E-04
	60701	7.56E-05	9.41E-01	5.78E-02	1.39E-03	9.02E-05
	60706	1.14E-04	9.40E-01	5.83E-02	1.24E-03	8.11E-05
	60707	2.22E-04	9.27E-01	7.04E-02	1.95E-03	1.58E-04
	60712	5.64E-04	9.37E-01	6.06E-02	1.32E-03	9.07E-05
	60714	1.34E-04	9.44E-01	5.44E-02	1.60E-03	9.72E-05
	60715	1.05E-04	9.43E-01	5.56E-02	1.16E-03	7.21E-05
	60716	2.17E-04	9.29E-01	6.76E-02	2.72E-03	2.11E-04
	60718	5.23E-04	9.37E-01	6.10E-02	1.22E-03	8.44E-05
	60722	2.45E-04	9.27E-01	6.93E-02	2.75E-03	2.20E-04
	60725	1.82E-04	9.30E-01	6.72E-02	2.09E-03	1.61E-04
	60726	1.13E-04	9.38E-01	5.99E-02	1.47E-03	9.95E-05
	60727	9.86E-05	9.39E-01	5.98E-02	1.26E-03	8.52E-05
	60734	1.17E-04	9.38E-01	6.05E-02	1.32E-03	9.02E-05
	60798	1.22E-04	9.36E-01	6.24E-02	1.36E-03	9.64E-05
	60800	1.12E-04	9.36E-01	6.20E-02	1.35E-03	9.50E-05
	60803	3.72E-04	9.17E-01	7.98E-02	2.57E-03	2.42E-04
	60804	1.72E-04	9.41E-01	5.71E-02	1.32E-03	8.44E-05
	60805	1.42E-04	9.44E-01	5.44E-02	1.25E-03	7.54E-05
	60809	7.89E-05	9.36E-01	6.25E-02	1.52E-03	1.08E-04
	60899	1.41E-04	9.37E-01	6.12E-02	1.29E-03	8.92E-05
	60908	1.53E-04	9.43E-01	5.53E-02	1.34E-03	8.25E-05
	60909	2.09E-04	9.35E-01	6.23E-02	2.22E-03	1.57E-04
	60910	1.25E-04	9.35E-01	6.38E-02	1.34E-03	9.72E-05
	60943	9.78E-05	9.45E-01	5.37E-02	1.27E-03	7.56E-05
	61017	1.24E-04	9.37E-01	6.10E-02	1.55E-03	1.07E-04

Table IV-1 (Continued)
Sample Data Used to Estimate Radionuclide Activity Fraction Distributions in Plutonium Material Types

Material Type	Drum ID	Pu238	Pu239	Pu240	Pu241	Pu242
PU52 (Cont.)	61027	1.30E-04	9.33E-01	6.50E-02	1.52E-03	1.13E-04
	61031	1.46E-04	9.43E-01	5.50E-02	1.40E-03	8.61E-05
	61069	1.35E-04	9.39E-01	5.93E-02	1.42E-03	9.51E-05
	61073	2.49E-04	9.14E-01	8.41E-02	1.69E-03	1.69E-04
	61086	1.37E-04	9.39E-01	6.01E-02	1.10E-03	7.43E-05
	61116	1.94E-04	9.23E-01	7.42E-02	1.93E-03	1.67E-04
	s793764	2.15E-04	9.18E-01	8.00E-02	1.88E-03	1.77E-04
	s793774	1.84E-04	9.20E-01	7.73E-02	2.03E-03	1.85E-04
	s794446	5.81E-04	9.31E-01	6.69E-02	1.72E-03	1.32E-04
	s802578	5.55E-04	9.05E-01	9.14E-02	2.87E-03	3.19E-04
	s802737	6.35E-04	9.30E-01	6.73E-02	2.14E-03	1.66E-04
	s802804	5.86E-04	9.38E-01	5.84E-02	2.57E-03	1.69E-04
	s805270	1.00E-04	9.42E-01	5.69E-02	1.10E-03	7.00E-05
	s805273	1.20E-04	9.33E-01	6.59E-02	1.21E-03	9.10E-05
	s805291	1.35E-04	9.37E-01	6.20E-02	1.19E-03	8.33E-05
	s811706	1.56E-04	9.43E-01	5.60E-02	1.17E-03	7.36E-05
	s811715	2.23E-04	9.25E-01	7.30E-02	1.90E-03	1.61E-04
	s811732	1.60E-04	9.39E-01	5.95E-02	1.09E-03	7.28E-05
	s811783	2.07E-04	9.49E-01	4.97E-02	1.36E-03	7.46E-05
	s813211	5.71E-05	9.40E-01	5.88E-02	1.24E-03	8.20E-05
	s813218	1.58E-04	9.31E-01	6.76E-02	1.36E-03	1.05E-04
	s813222	1.30E-04	9.35E-01	6.35E-02	1.28E-03	9.26E-05
	s813353	3.83E-04	9.45E-01	5.31E-02	1.75E-03	1.04E-04
	s813587	1.74E-04	9.27E-01	7.10E-02	1.33E-03	1.09E-04
	s813605	1.25E-04	9.33E-01	6.51E-02	1.38E-03	1.02E-04
	s813650	2.77E-04	9.10E-01	8.63E-02	2.75E-03	2.85E-04
	s813684	8.73E-04	9.32E-01	6.43E-02	2.56E-03	1.88E-04
	s814954	7.21E-05	9.41E-01	5.77E-02	1.55E-03	1.00E-04
	s815038	3.00E-04	9.41E-01	5.67E-02	1.56E-03	9.92E-05
	s815128	1.69E-04	9.23E-01	7.49E-02	2.02E-03	1.77E-04
	s815135	1.44E-04	9.31E-01	6.79E-02	1.14E-03	8.90E-05
	s816659	1.37E-04	9.38E-01	6.07E-02	1.09E-03	7.49E-05
	s816706	1.15E-04	9.38E-01	6.03E-02	1.14E-03	7.75E-05
	s816757	1.04E-04	9.37E-01	6.19E-02	1.26E-03	8.83E-05

Table IV-1 (Continued)
Sample Data Used to Estimate Radionuclide Activity Fraction Distributions in Plutonium Material Types

Material Type	Drum ID	Pu238	Pu239	Pu240	Pu241	Pu242
PU52 (Cont.)	s816870	6.68E-04	9.47E-01	4.98E-02	2.07E-03	1.14E-04
	s816892	1.13E-04	9.41E-01	5.71E-02	1.46E-03	9.34E-05
	s818253	1.00E-04	9.37E-01	6.19E-02	1.23E-03	8.61E-05
	s818278	1.13E-04	9.38E-01	6.05E-02	1.26E-03	8.64E-05
	s818279	1.37E-04	9.38E-01	6.01E-02	1.39E-03	9.45E-05
	s818280	1.09E-04	9.36E-01	6.29E-02	1.36E-03	9.73E-05
	s818281	1.22E-04	9.35E-01	6.30E-02	1.33E-03	9.52E-05
	s818295	1.27E-04	9.38E-01	6.10E-02	1.14E-03	7.87E-05
	s818296	1.24E-04	9.39E-01	5.92E-02	1.45E-03	9.65E-05
	s818297	1.34E-04	9.33E-01	6.56E-02	1.10E-03	8.25E-05
	s818308	1.71E-04	9.37E-01	6.13E-02	1.26E-03	8.76E-05
	s818310	1.65E-04	9.38E-01	6.05E-02	1.40E-03	9.61E-05
	s818424	8.65E-05	9.29E-01	6.95E-02	1.56E-03	1.25E-04
	s822692	1.57E-04	9.23E-01	7.50E-02	1.85E-03	1.62E-04
	s822797	5.59E-04	9.10E-01	8.65E-02	2.64E-03	2.74E-04
	s822821	8.94E-04	9.49E-01	4.78E-02	2.17E-03	1.14E-04
	s822870	9.46E-05	9.32E-01	6.61E-02	1.25E-03	9.45E-05
	s823201	6.14E-05	9.36E-01	6.20E-02	1.49E-03	1.05E-04
	s823219	1.65E-04	9.42E-01	5.68E-02	1.23E-03	7.79E-05
	s824093	9.46E-04	9.19E-01	7.85E-02	1.14E-03	1.05E-04
	s824096	8.88E-05	9.36E-01	6.22E-02	1.17E-03	8.27E-05
	s824109	1.09E-04	9.34E-01	6.43E-02	1.19E-03	8.71E-05
	s824134	2.80E-04	9.50E-01	4.86E-02	1.44E-03	7.70E-05
	s824149	1.62E-04	9.38E-01	6.03E-02	1.25E-03	8.52E-05
	s824175	1.02E-04	9.41E-01	5.75E-02	1.23E-03	7.93E-05
	s824190	6.36E-05	9.42E-01	5.65E-02	1.33E-03	8.44E-05
	s824206	1.12E-04	9.41E-01	5.80E-02	1.26E-03	8.20E-05
	s824436	1.04E-04	9.30E-01	6.87E-02	1.40E-03	1.10E-04
	s824480	8.71E-05	9.42E-01	5.69E-02	1.31E-03	8.36E-05
	s824489	1.48E-04	9.31E-01	6.77E-02	1.28E-03	9.97E-05
	s824499	6.28E-05	8.92E-01	1.07E-01	1.58E-03	2.11E-04
	s824554	7.42E-05	9.22E-01	7.66E-02	1.43E-03	1.29E-04
	s824563	1.23E-04	9.29E-01	6.91E-02	1.34E-03	1.07E-04
	s824569	1.97E-04	9.35E-01	6.30E-02	1.49E-03	1.06E-04

Table IV-1 (Continued)
Sample Data Used to Estimate Radionuclide Activity Fraction Distributions in Plutonium Material Types

Material Type	Drum ID	Pu238	Pu239	Pu240	Pu241	Pu242
PU52 (Cont.)	s824570	1.05E-04	9.35E-01	6.39E-02	1.30E-03	9.42E-05
	s824585	1.64E-04	9.27E-01	7.16E-02	1.33E-03	1.10E-04
	s824609	1.14E-04	9.18E-01	8.03E-02	1.34E-03	1.27E-04
	s824648	8.14E-05	9.36E-01	6.26E-02	1.23E-03	8.70E-05
	s824656	6.29E-04	9.38E-01	5.92E-02	2.21E-03	1.48E-04
	s824668	1.36E-04	9.37E-01	6.10E-02	1.27E-03	8.75E-05
	s824968	7.97E-05	9.40E-01	5.87E-02	1.27E-03	8.42E-05
	s825035	1.07E-04	9.30E-01	6.87E-02	1.32E-03	1.04E-04
	s825036	1.29E-04	9.32E-01	6.60E-02	1.30E-03	9.84E-05
	s825708	1.84E-04	9.16E-01	8.19E-02	2.11E-03	2.04E-04
	s825709	6.92E-05	9.34E-01	6.43E-02	1.32E-03	9.64E-05
	s825711	2.27E-04	9.33E-01	6.54E-02	1.09E-03	8.11E-05
	s825753	2.74E-04	9.21E-01	7.62E-02	2.20E-03	1.97E-04
	s825903	1.46E-04	9.16E-01	8.19E-02	1.41E-03	1.37E-04
	s832212	9.04E-05	9.30E-01	6.82E-02	1.18E-03	9.24E-05
	s832269	1.06E-04	9.37E-01	6.19E-02	1.23E-03	8.65E-05
	s832327	1.15E-04	9.47E-01	5.13E-02	1.17E-03	6.66E-05
	s832356	1.27E-04	9.29E-01	6.96E-02	1.42E-03	1.14E-04
	s832359	1.74E-04	9.22E-01	7.66E-02	1.36E-03	1.22E-04
	s832364	1.11E-04	9.33E-01	6.57E-02	1.34E-03	1.00E-04
	s832369	1.84E-04	9.15E-01	8.26E-02	2.00E-03	1.96E-04
	s832405	2.08E-04	9.23E-01	7.46E-02	1.70E-03	1.48E-04
	s832432	4.05E-04	9.41E-01	5.71E-02	1.09E-03	7.00E-05
	s832506	2.54E-04	9.29E-01	6.80E-02	2.83E-03	2.22E-04
	s832508	2.04E-04	9.06E-01	9.17E-02	2.27E-03	2.53E-04
	s832572	2.24E-04	9.16E-01	8.16E-02	2.29E-03	2.21E-04
	s832589	9.36E-05	9.31E-01	6.71E-02	1.35E-03	1.04E-04
	s832603	1.30E-04	9.14E-01	8.36E-02	2.02E-03	2.01E-04
	s832606	1.78E-04	9.38E-01	6.03E-02	1.42E-03	9.66E-05
	s833094	1.05E-04	9.36E-01	6.30E-02	1.16E-03	8.30E-05
	s833227	1.52E-04	9.21E-01	7.70E-02	1.78E-03	1.60E-04
	s833311	7.19E-05	9.36E-01	6.31E-02	1.19E-03	8.55E-05
	s833345	1.82E-04	9.30E-01	6.78E-02	2.13E-03	1.66E-04
	s833408	2.69E-04	9.48E-01	5.06E-02	1.49E-03	8.35E-05

Table IV-1 (Continued)
Sample Data Used to Estimate Radionuclide Activity Fraction Distributions in Plutonium Material Types

Material Type	Drum ID	Pu238	Pu239	Pu240	Pu241	Pu242
PU52 (Cont.)	s833450	1.03E-04	9.37E-01	6.14E-02	1.22E-03	8.50E-05
	s833452	9.03E-05	9.39E-01	5.95E-02	1.22E-03	8.19E-05
	s833539	2.54E-04	9.21E-01	7.64E-02	2.06E-03	1.85E-04
	s833823	1.73E-04	9.34E-01	6.40E-02	1.58E-03	1.15E-04
	s833866	1.88E-04	9.38E-01	6.07E-02	1.29E-03	8.86E-05
	s833879	1.19E-04	9.25E-01	7.34E-02	1.28E-03	1.09E-04
	s833942	1.09E-04	9.43E-01	5.52E-02	1.14E-03	7.06E-05
	s834415	2.36E-04	9.12E-01	8.53E-02	2.16E-03	2.20E-04
	s834425	1.54E-04	9.32E-01	6.66E-02	1.28E-03	9.72E-05
	s834427	1.55E-04	8.98E-01	9.94E-02	2.20E-03	2.69E-04
	s834447	2.20E-04	9.42E-01	5.62E-02	1.68E-03	1.06E-04
	s834451	1.40E-04	9.07E-01	9.04E-02	2.61E-03	2.85E-04
	s834457	1.46E-04	9.29E-01	6.96E-02	1.50E-03	1.21E-04
	s834481	1.41E-04	9.36E-01	6.28E-02	1.39E-03	9.95E-05
	s834535	1.35E-04	9.31E-01	6.72E-02	1.47E-03	1.13E-04
	s834584	1.32E-04	9.47E-01	5.14E-02	1.14E-03	6.48E-05
	s834609	8.24E-04	8.91E-01	1.06E-01	1.89E-03	2.50E-04
	s834628	1.37E-04	9.27E-01	7.13E-02	1.56E-03	1.29E-04
	s834630	2.49E-04	9.21E-01	7.65E-02	2.33E-03	2.09E-04
	s834670	2.51E-04	9.37E-01	6.11E-02	1.81E-03	1.25E-04
	s834683	1.05E-04	9.10E-01	8.82E-02	1.23E-03	1.30E-04
	s835353	2.37E-04	9.18E-01	8.00E-02	2.00E-03	1.89E-04
	s835369	6.40E-05	9.42E-01	5.59E-02	1.57E-03	9.85E-05
	s835419	2.60E-04	9.37E-01	6.14E-02	1.68E-03	1.17E-04
	s835431	2.73E-04	9.22E-01	7.59E-02	1.61E-03	1.43E-04
	s835433	4.19E-04	9.07E-01	9.06E-02	1.35E-03	1.47E-04
	s841248	1.44E-04	9.27E-01	7.17E-02	1.38E-03	1.15E-04
	s841277	9.87E-05	9.40E-01	5.84E-02	1.25E-03	8.18E-05
	s841298	1.03E-03	9.20E-01	7.62E-02	2.35E-03	2.10E-04
	s841331	8.52E-05	9.35E-01	6.37E-02	1.40E-03	1.01E-04
	s841339	5.72E-04	9.28E-01	6.99E-02	1.54E-03	1.25E-04
	s841623	3.65E-04	9.25E-01	7.31E-02	1.32E-03	1.12E-04
	s842309	2.43E-04	9.11E-01	8.59E-02	2.30E-03	2.37E-04
	s842314	2.73E-04	9.28E-01	6.93E-02	1.85E-03	1.48E-04

Table IV-1 (Continued)
Sample Data Used to Estimate Radionuclide Activity Fraction Distributions in Plutonium Material Types

Material Type	Drum ID	Pu238	Pu239	Pu240	Pu241	Pu242
PU52 (Cont.)	s842350	1.40E-04	9.33E-01	6.49E-02	1.41E-03	1.04E-04
	s842363	2.02E-04	9.25E-01	7.35E-02	1.49E-03	1.28E-04
	s842389	1.29E-04	9.36E-01	6.27E-02	1.33E-03	9.49E-05
	s842404	1.76E-04	9.21E-01	7.65E-02	1.87E-03	1.67E-04
	s842421	1.55E-04	9.32E-01	6.58E-02	1.52E-03	1.15E-04
	s842424	2.37E-04	9.14E-01	8.35E-02	2.07E-03	2.06E-04
	s842435	1.10E-04	9.33E-01	6.56E-02	1.45E-03	1.09E-04
	s842441	8.77E-05	9.34E-01	6.49E-02	1.34E-03	9.91E-05
	s842492	2.42E-04	9.30E-01	6.82E-02	1.56E-03	1.23E-04
	s842515	2.13E-04	9.24E-01	7.38E-02	1.86E-03	1.59E-04
	s842525	1.51E-04	9.37E-01	6.10E-02	1.55E-03	1.07E-04
	s842533	8.00E-04	8.94E-01	1.03E-01	1.27E-03	1.62E-04
	s842557	6.10E-04	9.23E-01	7.44E-02	2.20E-03	1.91E-04
	s842561	2.60E-04	9.48E-01	5.01E-02	1.85E-03	1.03E-04
	s842562	1.21E-04	9.35E-01	6.36E-02	1.26E-03	9.10E-05
	s842568	1.67E-04	9.28E-01	7.01E-02	1.62E-03	1.31E-04
	s842570	1.35E-04	9.27E-01	7.15E-02	1.44E-03	1.19E-04
	s843557	2.65E-04	9.07E-01	9.05E-02	2.34E-03	2.56E-04
	s843570	1.49E-04	9.31E-01	6.74E-02	1.37E-03	1.06E-04
	s843596	2.59E-04	9.32E-01	6.60E-02	2.10E-03	1.59E-04
	s843598	1.00E-03	9.22E-01	7.47E-02	1.71E-03	1.49E-04
	s843608	2.14E-04	9.15E-01	8.32E-02	1.54E-03	1.52E-04
	s844234	8.99E-05	9.19E-01	7.92E-02	1.34E-03	1.25E-04
	s844282	1.79E-04	9.22E-01	7.55E-02	1.94E-03	1.71E-04
	s844287	1.66E-04	9.27E-01	7.11E-02	1.56E-03	1.28E-04
	s844295	3.79E-04	9.30E-01	6.73E-02	1.76E-03	1.36E-04
	s844302	1.38E-04	9.19E-01	7.87E-02	2.12E-03	1.97E-04
	s844303	3.10E-04	9.32E-01	6.55E-02	2.17E-03	1.63E-04
	s844320	5.91E-05	9.34E-01	6.50E-02	1.30E-03	9.61E-05
	s844589	7.56E-04	9.07E-01	8.97E-02	2.35E-03	2.55E-04
	s844604	2.15E-04	9.20E-01	7.82E-02	1.85E-03	1.70E-04
	s844655	8.87E-05	9.39E-01	5.93E-02	1.34E-03	8.93E-05
	s844711	1.31E-04	9.34E-01	6.43E-02	1.21E-03	8.87E-05
	s844714	1.06E-04	9.40E-01	5.86E-02	1.20E-03	7.93E-05

Table IV-1 (Continued)
Sample Data Used to Estimate Radionuclide Activity Fraction Distributions in Plutonium Material Types

Material Type	Drum ID	Pu238	Pu239	Pu240	Pu241	Pu242
PU52 (Cont.)	s844720	8.90E-05	9.34E-01	6.40E-02	1.34E-03	9.75E-05
	s844945	1.40E-04	9.30E-01	6.86E-02	1.59E-03	1.26E-04
	s845008	9.63E-05	9.32E-01	6.63E-02	1.19E-03	9.02E-05
	s845035	7.01E-05	9.41E-01	5.76E-02	1.29E-03	8.35E-05
	s845051	2.39E-04	9.34E-01	6.42E-02	1.51E-03	1.10E-04
	s845064	1.76E-04	9.40E-01	5.81E-02	1.17E-03	7.63E-05
	s845101	1.08E-04	9.34E-01	6.40E-02	1.43E-03	1.04E-04
	s845105	8.49E-05	9.38E-01	6.07E-02	1.26E-03	8.62E-05
	s845107	3.06E-04	9.17E-01	8.17E-02	1.39E-03	1.35E-04
	s845119	1.37E-04	9.37E-01	6.20E-02	1.26E-03	8.88E-05
	s845129	3.54E-04	9.27E-01	7.08E-02	1.78E-03	1.46E-04
	s845178	6.45E-05	9.42E-01	5.69E-02	1.16E-03	7.36E-05
	s845192	2.33E-04	9.38E-01	6.07E-02	1.28E-03	8.77E-05
	s845194	1.42E-04	9.28E-01	6.97E-02	1.52E-03	1.22E-04
	s845196	1.42E-04	9.33E-01	6.54E-02	1.34E-03	1.00E-04
	s845202	2.14E-04	9.32E-01	6.62E-02	1.81E-03	1.37E-04
	s845329	1.99E-04	9.13E-01	8.47E-02	1.89E-03	1.91E-04
	s845372	9.18E-04	9.31E-01	6.53E-02	2.36E-03	1.77E-04
	s846001	8.78E-05	9.49E-01	4.98E-02	1.39E-03	7.63E-05
	s846003	1.58E-04	9.26E-01	7.18E-02	1.61E-03	1.34E-04
	s846017	1.89E-04	9.25E-01	7.29E-02	1.71E-03	1.45E-04
	s846041	1.32E-04	9.37E-01	6.14E-02	1.37E-03	9.55E-05
	s846079	1.12E-04	9.35E-01	6.35E-02	1.37E-03	9.86E-05
	s846115	1.35E-04	9.35E-01	6.30E-02	1.47E-03	1.05E-04
	s846170	1.88E-04	9.37E-01	6.17E-02	1.47E-03	1.03E-04
	s846576	4.12E-04	9.05E-01	9.25E-02	2.02E-03	2.27E-04
	s846715	1.22E-04	9.40E-01	5.88E-02	1.22E-03	8.11E-05
	s846716	1.30E-04	9.32E-01	6.68E-02	1.40E-03	1.07E-04
	s851217	9.55E-05	9.01E-01	9.75E-02	1.46E-03	1.74E-04
	s851431	1.42E-04	9.36E-01	6.26E-02	1.35E-03	9.58E-05
	s851503	1.35E-04	9.34E-01	6.40E-02	1.54E-03	1.12E-04
	s851540	1.58E-04	9.37E-01	6.12E-02	1.28E-03	8.84E-05
	s851611	5.92E-04	9.34E-01	6.42E-02	1.60E-03	1.17E-04
	s851705	1.32E-04	9.36E-01	6.20E-02	1.81E-03	1.27E-04

Table IV-1 (Continued)
Sample Data Used to Estimate Radionuclide Activity Fraction Distributions in Plutonium Material Types

Material Type	Drum ID	Pu238	Pu239	Pu240	Pu241	Pu242
PU52 (Cont.)	s851715	1.08E-04	9.30E-01	6.79E-02	1.45E-03	1.13E-04
	s851717	1.16E-04	9.42E-01	5.67E-02	1.24E-03	7.89E-05
	s851765	7.19E-04	9.47E-01	5.07E-02	1.38E-03	7.74E-05
	s851773	1.13E-04	9.44E-01	5.42E-02	1.55E-03	9.37E-05
	s851775	1.21E-04	9.38E-01	6.09E-02	1.26E-03	8.67E-05
	s851780	1.62E-04	9.25E-01	7.29E-02	1.55E-03	1.31E-04
	s851796	1.74E-04	9.31E-01	6.66E-02	1.64E-03	1.25E-04
	s851815	1.01E-04	9.29E-01	6.93E-02	1.25E-03	1.00E-04
	s851853	1.34E-04	9.35E-01	6.37E-02	1.50E-03	1.09E-04
	s851871	9.87E-05	9.40E-01	5.82E-02	1.50E-03	9.84E-05
	s852502	1.24E-04	9.24E-01	7.44E-02	1.71E-03	1.48E-04
	s852514	3.14E-04	9.15E-01	8.18E-02	2.49E-03	2.42E-04
	s852517	1.01E-04	9.35E-01	6.39E-02	1.42E-03	1.03E-04
	s852898	2.77E-04	9.35E-01	6.35E-02	1.48E-03	1.07E-04
	s852904	1.08E-04	9.46E-01	5.21E-02	1.33E-03	7.70E-05
	s852919	1.32E-04	9.32E-01	6.63E-02	1.55E-03	1.18E-04
	s852920	1.04E-04	9.43E-01	5.51E-02	1.35E-03	8.32E-05
	s852921	2.46E-04	9.30E-01	6.85E-02	1.42E-03	1.12E-04
	s852969	6.81E-04	9.47E-01	5.02E-02	2.00E-03	1.11E-04
	s852993	6.53E-04	8.98E-01	9.94E-02	1.84E-03	2.25E-04
	s852995	1.23E-04	9.30E-01	6.87E-02	1.52E-03	1.20E-04
	s853008	2.43E-04	9.34E-01	6.36E-02	1.54E-03	1.12E-04
	s853276	2.33E-04	9.41E-01	5.61E-02	2.19E-03	1.37E-04
	s853283	1.94E-04	9.27E-01	7.06E-02	2.08E-03	1.70E-04
	s853285	1.09E-04	9.28E-01	7.06E-02	1.46E-03	1.19E-04
	s853286	1.69E-04	9.25E-01	7.26E-02	1.70E-03	1.43E-04
	s853292	2.65E-04	9.35E-01	6.28E-02	1.58E-03	1.12E-04
	s853293	2.00E-04	9.35E-01	6.35E-02	1.44E-03	1.04E-04
	s853325	1.08E-04	9.39E-01	5.93E-02	1.46E-03	9.73E-05
	s853351	1.88E-04	9.30E-01	6.82E-02	1.93E-03	1.52E-04
	s853457	1.52E-04	9.39E-01	5.90E-02	1.75E-03	1.16E-04
	s853467	1.77E-04	9.36E-01	6.15E-02	1.69E-03	1.18E-04
	s853468	7.96E-05	9.28E-01	7.07E-02	1.47E-03	1.20E-04
	s853483	1.41E-04	9.30E-01	6.88E-02	1.36E-03	1.07E-04

Table IV-1 (Continued)
Sample Data Used to Estimate Radionuclide Activity Fraction Distributions in Plutonium Material Types

Material Type	Drum ID	Pu238	Pu239	Pu240	Pu241	Pu242
PU52 (Cont.)	s853556	1.95E-04	9.33E-01	6.50E-02	2.10E-03	1.56E-04
	s853563	1.47E-04	9.37E-01	6.04E-02	2.05E-03	1.40E-04
	s853568	9.75E-05	9.28E-01	7.00E-02	1.39E-03	1.13E-04
	s853623	7.54E-05	9.40E-01	5.83E-02	1.52E-03	1.00E-04
	s853630	1.85E-04	9.32E-01	6.66E-02	1.28E-03	9.78E-05
	s853631	2.10E-04	9.14E-01	8.31E-02	2.59E-03	2.56E-04
	s853652	2.32E-04	9.30E-01	6.70E-02	2.73E-03	2.10E-04
	s853653	3.26E-04	9.04E-01	9.26E-02	2.59E-03	2.92E-04
	s853710	6.47E-05	9.38E-01	5.99E-02	1.60E-03	1.08E-04
	s853713	9.10E-05	9.36E-01	6.21E-02	1.25E-03	8.77E-05
	s853726	1.43E-04	9.32E-01	6.61E-02	1.60E-03	1.21E-04
	s853735	1.25E-04	9.33E-01	6.50E-02	1.66E-03	1.24E-04
	s853736	6.98E-05	9.34E-01	6.43E-02	1.52E-03	1.11E-04
	s853742	3.66E-04	9.28E-01	6.97E-02	1.42E-03	1.14E-04
	s853743	8.17E-05	9.29E-01	6.98E-02	1.33E-03	1.07E-04
	s853744	2.47E-04	9.37E-01	6.09E-02	1.67E-03	1.15E-04
	s853776	1.23E-04	9.34E-01	6.47E-02	1.40E-03	1.03E-04
	s853808	1.25E-04	9.36E-01	6.22E-02	1.47E-03	1.04E-04
	s853809	8.65E-05	9.28E-01	7.01E-02	1.36E-03	1.10E-04
	s853810	3.26E-04	8.97E-01	1.01E-01	1.29E-03	1.61E-04
	s853811	1.03E-04	9.40E-01	5.89E-02	1.43E-03	9.46E-05
	s853813	1.16E-04	9.33E-01	6.50E-02	1.92E-03	1.43E-04
	s853821	4.32E-04	9.32E-01	6.49E-02	2.50E-03	1.86E-04
	s853825	2.25E-04	9.21E-01	7.56E-02	2.51E-03	2.22E-04
	s853828	1.39E-04	9.35E-01	6.29E-02	1.34E-03	9.60E-05
	s853847	2.18E-04	9.25E-01	7.25E-02	2.10E-03	1.77E-04
	s853867	8.73E-05	9.42E-01	5.61E-02	1.32E-03	8.26E-05
	s853879	2.87E-04	9.25E-01	7.27E-02	2.16E-03	1.82E-04
	s853888	1.30E-04	9.36E-01	6.27E-02	1.47E-03	1.05E-04
	s853893	6.90E-05	9.38E-01	6.02E-02	1.35E-03	9.18E-05
	s853902	2.15E-04	9.42E-01	5.52E-02	2.83E-03	1.75E-04
	s854594	9.27E-05	9.27E-01	7.11E-02	1.52E-03	1.25E-04
	s854597	2.35E-04	9.22E-01	7.59E-02	2.08E-03	1.84E-04
	s854602	3.70E-04	9.35E-01	6.37E-02	1.31E-03	9.52E-05

Table IV-1 (Continued)
Sample Data Used to Estimate Radionuclide Activity Fraction Distributions in Plutonium Material Types

Material Type	Drum ID	Pu238	Pu239	Pu240	Pu241	Pu242
PU52 (Cont.)	s854640	3.22E-04	9.29E-01	6.90E-02	1.62E-03	1.29E-04
	s854657	9.59E-05	9.41E-01	5.75E-02	1.28E-03	8.25E-05
	s854660	7.30E-05	9.29E-01	6.98E-02	1.15E-03	9.27E-05
	s855155	9.41E-05	9.29E-01	6.92E-02	1.19E-03	9.47E-05
	s855182	2.29E-04	9.31E-01	6.60E-02	2.58E-03	1.95E-04
	s855184	2.29E-04	9.14E-01	8.44E-02	1.53E-03	1.54E-04
	s855189	1.99E-04	9.23E-01	7.51E-02	2.02E-03	1.77E-04
	s855190	1.16E-04	9.36E-01	6.26E-02	1.62E-03	1.15E-04
	s855215	1.67E-04	9.30E-01	6.83E-02	1.39E-03	1.09E-04
	s855232	2.61E-04	9.41E-01	5.76E-02	1.50E-03	9.70E-05
	s855242	1.74E-04	9.40E-01	5.87E-02	1.35E-03	8.94E-05
	s855260	2.91E-04	9.31E-01	6.71E-02	1.27E-03	9.75E-05
	s855282	1.17E-04	9.27E-01	7.13E-02	1.36E-03	1.12E-04
	s855285	8.06E-05	9.36E-01	6.25E-02	1.54E-03	1.09E-04
	s855304	6.05E-05	9.33E-01	6.58E-02	1.42E-03	1.07E-04
	s855509	5.92E-05	9.26E-01	7.29E-02	1.38E-03	1.16E-04
	s855546	2.01E-04	9.41E-01	5.78E-02	1.16E-03	7.55E-05
	s855547	2.41E-04	9.32E-01	6.60E-02	1.82E-03	1.38E-04
	s855548	1.10E-04	9.42E-01	5.63E-02	1.16E-03	7.33E-05
	s855549	1.54E-04	9.27E-01	7.01E-02	2.04E-03	1.65E-04
	s855554	1.55E-04	9.13E-01	8.48E-02	1.49E-03	1.51E-04
	s855620	1.07E-04	9.35E-01	6.42E-02	1.12E-03	8.14E-05
	s855626	1.55E-04	9.38E-01	6.04E-02	1.62E-03	1.10E-04
	s855629	2.08E-04	9.12E-01	8.57E-02	2.15E-03	2.21E-04
	s855640	9.72E-05	9.37E-01	6.13E-02	1.20E-03	8.33E-05
	s855692	6.92E-05	9.30E-01	6.82E-02	1.21E-03	9.43E-05
	s855693	3.65E-04	9.38E-01	6.01E-02	1.22E-03	8.28E-05
	s855695	1.04E-04	9.37E-01	6.15E-02	1.52E-03	1.06E-04
	s855790	2.09E-04	9.37E-01	6.11E-02	1.87E-03	1.30E-04
	s855813	1.96E-04	9.21E-01	7.65E-02	2.14E-03	1.92E-04
	s855835	7.02E-05	9.11E-01	8.78E-02	1.21E-03	1.27E-04
	s855836	1.60E-04	9.44E-01	5.38E-02	1.51E-03	9.03E-05
	s855859	1.77E-04	9.37E-01	6.09E-02	1.93E-03	1.33E-04
	s855884	2.34E-04	9.41E-01	5.66E-02	2.05E-03	1.30E-04

Table IV-1 (Continued)
Sample Data Used to Estimate Radionuclide Activity Fraction Distributions in Plutonium Material Types

Material Type	Drum ID	Pu238	Pu239	Pu240	Pu241	Pu242
PU52 (Cont.)	s855885	3.16E-04	9.19E-01	7.91E-02	1.61E-03	1.50E-04
	s855898	2.06E-04	9.34E-01	6.35E-02	2.21E-03	1.60E-04
	s855906	1.60E-04	9.18E-01	7.97E-02	1.86E-03	1.75E-04
	s855910	1.84E-04	9.38E-01	6.04E-02	1.69E-03	1.16E-04
	s855922	6.98E-04	9.32E-01	6.53E-02	1.52E-03	1.13E-04
	s855926	1.18E-04	9.35E-01	6.32E-02	1.93E-03	1.38E-04
	s856118	1.80E-04	9.29E-01	6.89E-02	1.52E-03	1.21E-04
	s856119	9.41E-05	9.41E-01	5.73E-02	1.48E-03	9.51E-05
	s856121	1.81E-04	9.42E-01	5.60E-02	1.58E-03	9.92E-05
	s860052	1.55E-04	9.31E-01	6.71E-02	1.83E-03	1.41E-04
	s860057	1.94E-04	9.14E-01	8.34E-02	2.12E-03	2.11E-04
	s860110	1.13E-04	9.41E-01	5.76E-02	1.52E-03	9.82E-05
	s860111	1.86E-04	9.32E-01	6.54E-02	2.24E-03	1.68E-04
	s860142	2.40E-04	9.34E-01	6.32E-02	2.52E-03	1.82E-04
	s860173	2.02E-04	9.32E-01	6.59E-02	1.47E-03	1.11E-04
	s860175	1.92E-04	9.26E-01	7.17E-02	1.73E-03	1.44E-04
	s860184	8.58E-05	9.39E-01	5.96E-02	1.44E-03	9.66E-05
	s861727	2.50E-04	9.37E-01	6.15E-02	1.62E-03	1.13E-04
	s861728	2.22E-04	9.32E-01	6.60E-02	1.78E-03	1.34E-04
	s861729	1.60E-04	9.33E-01	6.49E-02	1.84E-03	1.36E-04
	s861734	1.53E-04	9.30E-01	6.87E-02	1.51E-03	1.19E-04
	s861738	1.77E-04	9.32E-01	6.70E-02	1.14E-03	8.73E-05
	s861742	1.97E-04	9.24E-01	7.38E-02	1.70E-03	1.46E-04
	s861744	1.71E-04	9.31E-01	6.70E-02	1.80E-03	1.39E-04
	s861750	1.52E-04	9.41E-01	5.76E-02	1.39E-03	9.00E-05
	s861756	7.30E-05	9.31E-01	6.76E-02	1.45E-03	1.12E-04
	s861770	1.23E-04	9.37E-01	6.18E-02	1.38E-03	9.64E-05
	s861774	1.32E-04	9.36E-01	6.23E-02	1.36E-03	9.62E-05
	s861777	1.29E-04	9.25E-01	7.36E-02	1.49E-03	1.28E-04
	s861780	1.63E-04	9.29E-01	6.91E-02	1.73E-03	1.38E-04
	s861784	1.30E-04	9.27E-01	7.00E-02	2.47E-03	2.00E-04
	s861785	1.69E-04	9.48E-01	4.99E-02	1.84E-03	1.01E-04
	s861788	1.25E-04	9.37E-01	6.11E-02	1.82E-03	1.26E-04
	s861965	1.10E-04	9.39E-01	5.95E-02	1.31E-03	8.80E-05

Table IV-1 (Continued)
Sample Data Used to Estimate Radionuclide Activity Fraction Distributions in Plutonium Material Types

Material Type	Drum ID	Pu238	Pu239	Pu240	Pu241	Pu242
PU52 (Cont.)	s861966	7.87E-05	9.33E-01	6.57E-02	1.47E-03	1.11E-04
	s861967	2.77E-04	9.46E-01	5.19E-02	1.44E-03	8.31E-05
	s861970	8.14E-05	9.03E-01	9.50E-02	1.42E-03	1.64E-04
	s861971	2.64E-04	9.18E-01	7.98E-02	1.83E-03	1.72E-04
	s861979	1.39E-04	9.38E-01	5.99E-02	1.93E-03	1.31E-04
	s861981	1.25E-04	9.37E-01	6.15E-02	1.50E-03	1.04E-04
	s861989	1.25E-04	9.28E-01	7.00E-02	1.60E-03	1.30E-04
	s862012	2.31E-04	9.28E-01	6.92E-02	2.15E-03	1.72E-04
	s862014	1.43E-04	9.32E-01	6.66E-02	1.56E-03	1.19E-04
	s862017	1.62E-04	9.41E-01	5.68E-02	1.55E-03	9.88E-05
	s862054	2.40E-04	9.34E-01	6.43E-02	1.45E-03	1.06E-04
	s862084	1.10E-04	9.31E-01	6.68E-02	1.85E-03	1.42E-04
	s862085	9.41E-05	9.29E-01	6.83E-02	2.11E-03	1.66E-04
	s862086	3.80E-04	9.23E-01	7.49E-02	1.99E-03	1.74E-04
	s862095	1.13E-04	9.35E-01	6.33E-02	1.61E-03	1.16E-04
	s862251	1.24E-04	9.35E-01	6.32E-02	1.35E-03	9.71E-05
	s862269	1.30E-04	9.18E-01	7.94E-02	1.90E-03	1.78E-04
	s862272	1.63E-04	9.31E-01	6.75E-02	1.22E-03	9.48E-05
	s862276	1.45E-04	9.32E-01	6.58E-02	1.46E-03	1.10E-04
	s862277	1.42E-04	9.23E-01	7.53E-02	1.82E-03	1.60E-04
	s862279	2.73E-04	9.51E-01	4.65E-02	2.07E-03	1.06E-04
	s862282	1.48E-04	9.28E-01	7.03E-02	1.79E-03	1.45E-04
	s862302	9.61E-05	9.26E-01	7.21E-02	1.73E-03	1.44E-04
	s862316	3.67E-04	9.29E-01	6.83E-02	2.23E-03	1.76E-04
	s862375	1.03E-04	9.34E-01	6.42E-02	1.83E-03	1.34E-04
	s862383	6.44E-05	9.46E-01	5.24E-02	1.20E-03	6.95E-05
	s862412	1.54E-04	9.40E-01	5.85E-02	1.51E-03	9.95E-05
	s862451	3.18E-04	9.21E-01	7.62E-02	2.24E-03	2.00E-04
	s862457	8.15E-05	9.33E-01	6.52E-02	1.27E-03	9.45E-05
	s862471	1.04E-04	9.37E-01	6.14E-02	1.29E-03	8.96E-05
	s862473	9.30E-05	9.38E-01	6.04E-02	1.38E-03	9.39E-05
	s862523	1.11E-04	9.42E-01	5.66E-02	1.35E-03	8.57E-05
	s862896	1.22E-04	9.34E-01	6.41E-02	1.55E-03	1.13E-04
	s862915	1.03E-04	9.38E-01	6.03E-02	1.31E-03	8.89E-05

Table IV-1 (Continued)
Sample Data Used to Estimate Radionuclide Activity Fraction Distributions in Plutonium Material Types

Material Type	Drum ID	Pu238	Pu239	Pu240	Pu241	Pu242
PU52 (Cont.)	s862921	7.77E-05	9.39E-01	5.92E-02	1.16E-03	7.75E-05
	s862927	1.17E-04	9.44E-01	5.42E-02	1.54E-03	9.31E-05
	s862970	7.01E-05	9.33E-01	6.49E-02	1.42E-03	1.05E-04
	s863010	1.21E-04	9.37E-01	6.11E-02	1.24E-03	8.57E-05
	s863031	9.61E-05	9.34E-01	6.41E-02	1.71E-03	1.25E-04
	s863625	1.05E-04	9.41E-01	5.72E-02	1.38E-03	8.86E-05
	s863639	1.24E-04	9.18E-01	7.94E-02	1.80E-03	1.69E-04
	s863731	3.22E-04	9.31E-01	6.68E-02	1.77E-03	1.36E-04
	s863741	1.50E-04	9.37E-01	6.08E-02	1.60E-03	1.10E-04
	s863746	1.33E-04	9.35E-01	6.33E-02	1.65E-03	1.19E-04
	s864217	1.55E-04	9.25E-01	7.29E-02	1.60E-03	1.36E-04
	s864237	6.35E-05	9.38E-01	6.08E-02	1.34E-03	9.23E-05
	s864239	2.89E-04	9.02E-01	9.42E-02	2.84E-03	3.27E-04
	s864242	9.85E-05	9.40E-01	5.89E-02	1.36E-03	9.04E-05
	s864245	1.55E-04	9.34E-01	6.43E-02	1.72E-03	1.26E-04
	s864250	1.96E-04	9.22E-01	7.63E-02	1.79E-03	1.60E-04
	s864251	1.30E-04	9.28E-01	7.01E-02	1.75E-03	1.42E-04
	s864262	1.14E-04	9.31E-01	6.64E-02	2.05E-03	1.56E-04
	s864265	2.87E-04	9.20E-01	7.70E-02	2.17E-03	1.96E-04
	s864266	1.46E-04	9.40E-01	5.79E-02	1.45E-03	9.45E-05
	s864300	9.10E-05	9.39E-01	5.90E-02	1.49E-03	9.87E-05
	s864310	2.77E-04	9.33E-01	6.47E-02	2.13E-03	1.58E-04
	s864320	7.87E-05	9.42E-01	5.64E-02	1.49E-03	9.38E-05
	s864321	9.44E-05	9.45E-01	5.38E-02	1.46E-03	8.72E-05
	s864334	2.57E-04	9.16E-01	8.10E-02	2.42E-03	2.32E-04
	s864341	1.30E-04	9.18E-01	8.01E-02	1.65E-03	1.56E-04
	s864344	1.34E-04	9.38E-01	6.08E-02	1.27E-03	8.75E-05
	s864345	4.23E-04	9.08E-01	8.98E-02	1.99E-03	2.16E-04
	s864349	1.05E-04	8.98E-01	1.00E-01	1.42E-03	1.75E-04
	s864363	6.88E-05	9.47E-01	5.12E-02	1.49E-03	8.45E-05
	s864534	8.95E-05	9.31E-01	6.60E-02	2.65E-03	2.01E-04
	s864538	1.95E-04	9.29E-01	6.86E-02	1.78E-03	1.40E-04
	s864559	1.66E-04	9.33E-01	6.51E-02	1.47E-03	1.09E-04
	s864619	5.92E-04	9.27E-01	7.04E-02	2.06E-03	1.67E-04

Table IV-1 (Continued)
Sample Data Used to Estimate Radionuclide Activity Fraction Distributions in Plutonium Material Types

Material Type	Drum ID	Pu238	Pu239	Pu240	Pu241	Pu242
PU52 (Cont.)	s864622	5.22E-04	9.14E-01	8.30E-02	2.69E-03	2.66E-04
	s864634	1.92E-04	9.35E-01	6.26E-02	1.64E-03	1.16E-04
	s864641	1.02E-04	9.40E-01	5.87E-02	1.38E-03	9.10E-05
	s864643	1.36E-04	9.36E-01	6.20E-02	1.41E-03	9.91E-05
	s864673	1.38E-04	9.34E-01	6.39E-02	1.66E-03	1.21E-04
	s864676	2.44E-04	9.41E-01	5.76E-02	1.44E-03	9.33E-05
	s864677	1.29E-04	9.39E-01	5.92E-02	1.40E-03	9.37E-05
	s864678	1.52E-04	9.38E-01	6.04E-02	1.47E-03	1.01E-04
	s864679	1.31E-04	9.35E-01	6.35E-02	1.36E-03	9.79E-05
	s864688	9.18E-05	9.36E-01	6.19E-02	1.50E-03	1.05E-04
	s865295	1.99E-04	9.31E-01	6.67E-02	2.01E-03	1.54E-04
	s865296	1.22E-04	9.36E-01	6.23E-02	1.58E-03	1.12E-04
	s865298	1.26E-04	9.33E-01	6.54E-02	1.58E-03	1.18E-04
	s865302	1.07E-04	9.38E-01	5.99E-02	1.53E-03	1.03E-04
	s865308	9.46E-05	9.37E-01	6.10E-02	1.36E-03	9.36E-05
	s865320	1.86E-04	9.28E-01	7.02E-02	1.88E-03	1.53E-04
	s870002	1.71E-04	9.33E-01	6.44E-02	1.82E-03	1.34E-04
	s870007	2.53E-04	9.05E-01	9.13E-02	2.70E-03	2.99E-04
	s870008	2.30E-04	9.30E-01	6.80E-02	1.86E-03	1.45E-04
	s870017	2.57E-04	9.24E-01	7.37E-02	1.92E-03	1.65E-04
	s870024	2.42E-04	9.31E-01	6.69E-02	2.04E-03	1.57E-04
	s870025	1.37E-04	9.41E-01	5.73E-02	1.67E-03	1.08E-04
	s870028	1.35E-04	9.34E-01	6.37E-02	1.63E-03	1.18E-04
	s870036	1.37E-04	9.42E-01	5.60E-02	1.40E-03	8.78E-05
	s870037	1.39E-04	9.35E-01	6.26E-02	1.64E-03	1.17E-04
	s870048	1.39E-04	9.36E-01	6.21E-02	1.57E-03	1.10E-04
	s870109	1.47E-04	9.43E-01	5.56E-02	1.38E-03	8.60E-05
	s870113	4.94E-04	9.29E-01	6.90E-02	1.23E-03	9.80E-05
	s870118	2.88E-04	9.43E-01	5.38E-02	2.58E-03	1.55E-04
	s870121	2.57E-04	9.25E-01	7.19E-02	2.39E-03	2.00E-04
	s870144	1.83E-04	9.36E-01	6.16E-02	1.70E-03	1.19E-04
	s870145	1.14E-04	9.35E-01	6.28E-02	1.64E-03	1.17E-04
	s870154	1.04E-04	9.39E-01	5.95E-02	1.37E-03	9.21E-05
	s870182	2.30E-04	9.15E-01	8.31E-02	1.91E-03	1.89E-04

Table IV-1 (Continued)
Sample Data Used to Estimate Radionuclide Activity Fraction Distributions in Plutonium Material Types

Material Type	Drum ID	Pu238	Pu239	Pu240	Pu241	Pu242
PU52 (Cont.)	s870183	4.97E-04	9.51E-01	4.66E-02	1.76E-03	9.00E-05
	s870195	7.29E-05	9.42E-01	5.69E-02	1.15E-03	7.31E-05
	s870196	8.66E-05	9.42E-01	5.67E-02	1.14E-03	7.25E-05
	s870219	7.41E-05	9.41E-01	5.75E-02	1.22E-03	7.85E-05
	s870224	1.16E-04	9.37E-01	6.14E-02	1.34E-03	9.31E-05
	s870247	1.46E-04	9.41E-01	5.77E-02	1.54E-03	9.97E-05
	s870249	4.76E-04	8.96E-01	1.01E-01	2.16E-03	2.70E-04
	s870253	1.37E-04	9.37E-01	6.12E-02	1.45E-03	1.01E-04
	s870263	1.49E-04	9.29E-01	6.89E-02	1.44E-03	1.14E-04
	s870302	1.39E-04	9.39E-01	5.90E-02	1.63E-03	1.09E-04
	s870303	1.39E-04	9.32E-01	6.62E-02	1.71E-03	1.30E-04
	s870306	4.06E-04	9.33E-01	6.49E-02	1.71E-03	1.27E-04
	s870313	1.15E-04	9.24E-01	7.45E-02	1.59E-03	1.38E-04
	s870318	1.40E-04	9.34E-01	6.42E-02	1.52E-03	1.11E-04
	s870319	1.36E-04	9.14E-01	8.31E-02	2.08E-03	2.06E-04
	s870322	1.08E-04	9.37E-01	6.16E-02	1.40E-03	9.78E-05
	s870325	1.66E-04	9.41E-01	5.70E-02	1.39E-03	8.89E-05
	s870339	3.11E-04	9.24E-01	7.28E-02	2.34E-03	1.98E-04
	s870342	1.68E-04	9.38E-01	6.04E-02	1.83E-03	1.25E-04
	s870350	1.69E-04	9.33E-01	6.53E-02	1.73E-03	1.29E-04
	s870355	1.38E-04	9.36E-01	6.22E-02	1.50E-03	1.06E-04
	s870357	1.13E-04	9.34E-01	6.42E-02	1.29E-03	9.42E-05
	s870422	1.39E-04	9.38E-01	5.99E-02	1.49E-03	1.01E-04
	s870458	1.27E-04	9.40E-01	5.83E-02	1.39E-03	9.13E-05
	s870466	1.35E-04	9.38E-01	5.99E-02	1.41E-03	9.55E-05
	s871820	1.13E-04	9.36E-01	6.23E-02	1.69E-03	1.19E-04
	s871824	1.34E-04	9.34E-01	6.40E-02	1.46E-03	1.06E-04
	s871845	1.14E-04	9.37E-01	6.10E-02	1.47E-03	1.02E-04
	s871851	1.76E-04	9.46E-01	5.19E-02	1.59E-03	9.16E-05
	s871852	1.17E-04	9.31E-01	6.69E-02	1.51E-03	1.16E-04
	s871884	1.53E-04	9.35E-01	6.34E-02	1.48E-03	1.07E-04
	s871891	1.78E-04	9.35E-01	6.34E-02	1.44E-03	1.04E-04
	s871892	1.99E-04	9.26E-01	7.16E-02	1.57E-03	1.30E-04
	s871893	1.95E-04	9.31E-01	6.74E-02	1.30E-03	1.00E-04

Table IV-1 (Continued)
Sample Data Used to Estimate Radionuclide Activity Fraction Distributions in Plutonium Material Types

Material Type	Drum ID	Pu238	Pu239	Pu240	Pu241	Pu242
PU52 (Cont.)	s871898	1.34E-04	9.36E-01	6.27E-02	1.52E-03	1.08E-04
	s871913	3.01E-04	9.41E-01	5.70E-02	1.60E-03	1.02E-04
	s871916	1.77E-04	9.32E-01	6.58E-02	1.56E-03	1.17E-04
	s873571	1.27E-04	9.37E-01	6.11E-02	1.47E-03	1.01E-04
	s883110	1.33E-04	9.40E-01	5.86E-02	1.35E-03	8.89E-05
	s883126	9.90E-05	9.30E-01	6.82E-02	1.55E-03	1.22E-04
	s883138	1.66E-04	9.32E-01	6.64E-02	1.68E-03	1.28E-04
	s883145	1.49E-04	9.37E-01	6.11E-02	1.51E-03	1.04E-04
	s890337	1.39E-04	9.41E-01	5.69E-02	2.02E-03	1.29E-04
	S910759	1.16E-04	9.38E-01	6.03E-02	1.29E-03	8.78E-05
	S910797	1.05E-04	9.39E-01	5.93E-02	1.33E-03	8.86E-05
	S911201	1.38E-04	9.34E-01	6.47E-02	1.45E-03	1.07E-04
PU53	59050	1.99E-04	9.19E-01	7.91E-02	1.65E-03	1.53E-04
	59378	1.97E-04	9.23E-01	7.49E-02	1.73E-03	1.51E-04
	s793747	3.24E-04	9.03E-01	9.38E-02	2.52E-03	2.88E-04
	s793748	2.66E-04	8.84E-01	1.12E-01	3.23E-03	4.58E-04
	s802790	3.44E-04	8.78E-01	1.18E-01	3.36E-03	5.13E-04
	s860059	1.28E-04	9.17E-01	8.11E-02	1.23E-03	1.18E-04
	s870180	1.36E-04	9.42E-01	5.67E-02	1.35E-03	8.59E-05
PU54	52119	6.16E-04	9.04E-01	9.33E-02	2.26E-03	2.57E-04
	52355	5.68E-04	8.77E-01	1.18E-01	4.25E-03	6.47E-04
	52360	5.16E-04	8.80E-01	1.14E-01	4.49E-03	6.56E-04
	52371	4.34E-04	8.85E-01	1.09E-01	4.42E-03	6.13E-04
	52372	4.93E-04	8.82E-01	1.12E-01	4.59E-03	6.56E-04
	52373	5.09E-04	8.75E-01	1.20E-01	4.31E-03	6.70E-04
	52404	5.28E-04	8.83E-01	1.11E-01	4.39E-03	6.22E-04
	52405	4.17E-04	8.83E-01	1.12E-01	4.24E-03	6.04E-04
	52526	4.73E-04	8.81E-01	1.14E-01	4.27E-03	6.24E-04
	52545	5.54E-04	8.83E-01	1.12E-01	4.47E-03	6.38E-04
	52559	3.53E-04	8.84E-01	1.11E-01	4.14E-03	5.83E-04
	53663	4.62E-04	8.83E-01	1.12E-01	3.92E-03	5.60E-04
	53910	2.42E-04	8.99E-01	9.82E-02	2.59E-03	3.13E-04
	53969	4.77E-04	8.83E-01	1.11E-01	4.32E-03	6.15E-04
	54555	5.41E-04	8.86E-01	1.09E-01	4.19E-03	5.75E-04

Table IV-1 (Continued)
Sample Data Used to Estimate Radionuclide Activity Fraction Distributions in Plutonium Material Types

Material Type	Drum ID	Pu238	Pu239	Pu240	Pu241	Pu242
PU54 (Cont.)	55971	2.58E-04	8.81E-01	1.14E-01	3.96E-03	5.77E-04
	57543	3.29E-04	8.98E-01	9.68E-02	3.99E-03	4.76E-04
	59269	9.33E-05	9.37E-01	6.15E-02	9.62E-04	6.68E-05
	60729	5.05E-04	8.76E-01	1.19E-01	4.13E-03	6.35E-04
	s793732	2.08E-04	9.13E-01	8.52E-02	1.76E-03	1.79E-04
	s793734	4.87E-05	9.17E-01	8.10E-02	1.53E-03	1.46E-04
	s793754	4.19E-04	8.77E-01	1.18E-01	4.14E-03	6.32E-04
	s793756	6.25E-04	8.85E-01	1.10E-01	3.98E-03	5.54E-04
	s794436	4.40E-04	8.78E-01	1.17E-01	3.94E-03	5.92E-04
	s794452	2.74E-04	8.86E-01	1.10E-01	3.78E-03	5.26E-04
	s802584	4.17E-04	9.35E-01	6.20E-02	2.33E-03	1.64E-04
	s802603	1.04E-04	9.34E-01	6.50E-02	1.07E-03	7.91E-05
	s802630	1.73E-04	8.78E-01	1.19E-01	2.77E-03	4.26E-04
	s802648	1.29E-04	9.29E-01	6.91E-02	1.42E-03	1.13E-04
	s802652	4.65E-04	8.74E-01	1.20E-01	4.26E-03	6.68E-04
	s802670	6.84E-05	9.33E-01	6.51E-02	1.37E-03	1.02E-04
	s802691	9.67E-05	9.18E-01	7.87E-02	3.39E-03	3.15E-04
	s802692	3.73E-04	8.87E-01	1.09E-01	3.64E-03	5.01E-04
	s802704	3.72E-04	8.95E-01	1.01E-01	3.23E-03	4.07E-04
	s802705	3.66E-04	8.74E-01	1.22E-01	3.73E-03	5.90E-04
	s802711	5.98E-04	9.16E-01	8.07E-02	2.67E-03	2.56E-04
	s802722	1.56E-04	8.60E-01	1.36E-01	2.89E-03	5.28E-04
	s802773	4.05E-04	8.91E-01	1.04E-01	3.92E-03	5.10E-04
	s802780	5.65E-05	9.33E-01	6.55E-02	1.27E-03	9.47E-05
	s802781	1.63E-04	9.49E-01	4.92E-02	1.21E-03	6.55E-05
	s802908	9.09E-04	8.89E-01	1.09E-01	1.07E-03	1.47E-04
	s802925	1.75E-04	9.39E-01	5.97E-02	1.04E-03	7.02E-05
	s802929	4.33E-04	8.77E-01	1.18E-01	4.24E-03	6.47E-04
	s802934	2.36E-04	9.36E-01	6.28E-02	1.21E-03	8.63E-05
	s802949	3.82E-04	8.73E-01	1.22E-01	3.92E-03	6.25E-04
	s802962	4.62E-05	9.50E-01	4.85E-02	1.47E-03	7.84E-05
	s803029	3.57E-05	9.13E-01	8.56E-02	1.35E-03	1.38E-04
	s803085	4.26E-04	8.78E-01	1.17E-01	3.75E-03	5.66E-04
	s803101	8.62E-04	9.21E-01	7.55E-02	2.40E-03	2.12E-04

Table IV-1 (Continued)
Sample Data Used to Estimate Radionuclide Activity Fraction Distributions in Plutonium Material Types

Material Type	Drum ID	Pu238	Pu239	Pu240	Pu241	Pu242
PU54 (Cont.)	s803161	1.55E-04	9.25E-01	7.32E-02	1.50E-03	1.28E-04
	s803162	2.85E-04	9.26E-01	7.12E-02	2.40E-03	1.98E-04
	s803205	4.00E-04	9.23E-01	7.50E-02	1.12E-03	9.78E-05
	s803612	4.55E-04	8.66E-01	1.29E-01	3.74E-03	6.40E-04
	s804912	3.02E-04	9.16E-01	8.23E-02	1.11E-03	1.08E-04
	s804915	3.28E-04	9.48E-01	5.09E-02	1.15E-03	6.47E-05
	s804978	9.69E-05	9.49E-01	4.98E-02	1.03E-03	5.67E-05
	s805000	1.34E-04	9.25E-01	7.32E-02	1.16E-03	9.85E-05
	s805264	4.38E-04	8.65E-01	1.30E-01	3.44E-03	5.94E-04
	s811619	8.02E-04	8.70E-01	1.24E-01	3.86E-03	6.30E-04
	s811666	6.72E-05	9.49E-01	4.98E-02	1.08E-03	5.92E-05
	s811703	4.65E-04	8.85E-01	1.10E-01	4.11E-03	5.72E-04
	s811745	3.03E-04	9.25E-01	7.34E-02	1.04E-03	8.90E-05
	s811756	5.55E-04	8.76E-01	1.18E-01	4.40E-03	6.72E-04
	s811766	2.35E-05	9.52E-01	4.67E-02	8.71E-04	4.45E-05
	s811772	6.03E-05	9.09E-01	8.97E-02	1.32E-03	1.42E-04
	s811817	1.64E-04	9.34E-01	6.44E-02	1.10E-03	8.05E-05
	s811818	1.48E-04	9.14E-01	8.44E-02	1.10E-03	1.10E-04
	s811902	2.77E-04	9.51E-01	4.76E-02	9.88E-04	5.16E-05
	s811903	1.25E-04	9.22E-01	7.70E-02	8.96E-04	8.06E-05
	s811915	3.34E-04	9.13E-01	8.46E-02	1.63E-03	1.64E-04
	s813295	3.25E-04	9.41E-01	5.75E-02	9.95E-04	6.42E-05
	s813303	1.17E-04	9.54E-01	4.45E-02	1.31E-03	6.39E-05
	s813345	6.32E-04	9.18E-01	7.97E-02	1.74E-03	1.64E-04
	s813368	4.73E-05	9.30E-01	6.84E-02	1.66E-03	1.31E-04
	s813376	2.47E-04	9.25E-01	7.29E-02	1.27E-03	1.07E-04
	s813407	1.28E-04	8.92E-01	1.07E-01	1.13E-03	1.52E-04
	s813451	4.78E-05	9.22E-01	7.64E-02	1.76E-03	1.58E-04
	s813455	1.63E-04	9.51E-01	4.75E-02	1.03E-03	5.38E-05
	s813594	9.59E-05	9.38E-01	6.04E-02	1.43E-03	9.74E-05
	s813618	2.25E-04	9.24E-01	7.33E-02	2.25E-03	1.92E-04
	s813659	1.65E-04	9.31E-01	6.78E-02	1.41E-03	1.10E-04
	s813671	3.99E-05	9.52E-01	4.68E-02	1.02E-03	5.24E-05
	s814852	3.27E-04	9.17E-01	8.06E-02	1.71E-03	1.63E-04

Table IV-1 (Continued)
Sample Data Used to Estimate Radionuclide Activity Fraction Distributions in Plutonium Material Types

Material Type	Drum ID	Pu238	Pu239	Pu240	Pu241	Pu242
PU54 (Cont.)	s815106	1.86E-04	9.49E-01	5.00E-02	1.14E-03	6.31E-05
	s815136	1.35E-04	9.12E-01	8.64E-02	1.29E-03	1.33E-04
	s815141	3.39E-04	8.82E-01	1.13E-01	3.68E-03	5.33E-04
	s815159	2.89E-04	9.56E-01	4.24E-02	1.28E-03	5.90E-05
	s816447	1.37E-04	9.06E-01	9.17E-02	1.58E-03	1.75E-04
	s816471	5.00E-05	9.46E-01	5.34E-02	9.01E-04	5.34E-05
	s816661	2.12E-04	9.54E-01	4.50E-02	1.13E-03	5.55E-05
	s816675	2.10E-04	9.18E-01	7.97E-02	1.53E-03	1.43E-04
	s816722	2.23E-04	8.74E-01	1.23E-01	2.40E-03	3.83E-04
	s816735	1.01E-04	9.46E-01	5.25E-02	1.03E-03	5.98E-05
	s816740	1.08E-04	9.43E-01	5.54E-02	1.28E-03	7.90E-05
	s816811	8.73E-05	9.26E-01	7.28E-02	9.12E-04	7.70E-05
	s816855	1.75E-04	9.32E-01	6.57E-02	1.72E-03	1.29E-04
	s816880	6.12E-05	9.44E-01	5.54E-02	9.44E-04	5.84E-05
	s816897	2.00E-04	9.34E-01	6.45E-02	1.04E-03	7.62E-05
	s816932	2.92E-04	9.30E-01	6.83E-02	1.56E-03	1.23E-04
	s816934	1.64E-04	9.26E-01	7.20E-02	1.36E-03	1.13E-04
	s817485	4.15E-04	9.40E-01	5.79E-02	1.48E-03	9.61E-05
	S818268	2.75E-04	9.36E-01	6.20E-02	1.71E-03	1.21E-04
	s818372	1.43E-04	9.54E-01	4.39E-02	1.55E-03	7.43E-05
	s818381	2.09E-04	9.48E-01	5.04E-02	1.62E-03	9.05E-05
	s822716	1.05E-04	9.33E-01	6.58E-02	1.09E-03	8.17E-05
	s822719	1.20E-04	9.09E-01	8.94E-02	1.07E-03	1.15E-04
	s822788	1.47E-04	9.22E-01	7.63E-02	1.46E-03	1.30E-04
	s822803	3.13E-04	9.12E-01	8.53E-02	2.59E-03	2.64E-04
	s822804	2.52E-04	9.17E-01	8.19E-02	1.07E-03	1.04E-04
	s822987	3.93E-04	9.49E-01	4.96E-02	9.03E-04	4.94E-05
	s823003	4.79E-04	8.81E-01	1.14E-01	4.26E-03	6.23E-04
	s823005	4.33E-04	9.01E-01	9.43E-02	3.72E-03	4.30E-04
	s823228	4.40E-04	8.81E-01	1.14E-01	4.09E-03	5.97E-04
	s824059	5.38E-04	8.78E-01	1.17E-01	4.06E-03	6.11E-04
	s824106	1.55E-04	9.47E-01	5.14E-02	1.56E-03	8.90E-05
	s824588	1.75E-04	9.48E-01	5.06E-02	1.41E-03	7.87E-05
	s824641	1.13E-04	9.49E-01	4.98E-02	1.20E-03	6.61E-05

Table IV-1 (Continued)
Sample Data Used to Estimate Radionuclide Activity Fraction Distributions in Plutonium Material Types

Material Type	Drum ID	Pu238	Pu239	Pu240	Pu241	Pu242
PU54 (Cont.)	s824651	4.40E-04	8.93E-01	1.03E-01	3.81E-03	4.88E-04
	s825724	4.13E-04	9.34E-01	6.36E-02	1.57E-03	1.14E-04
	s825761	5.00E-04	9.26E-01	7.06E-02	2.67E-03	2.18E-04
	s832253	2.20E-04	9.19E-01	7.93E-02	1.42E-03	1.32E-04
	s832426	2.48E-04	8.89E-01	1.08E-01	2.94E-03	3.98E-04
	s832540	1.60E-04	8.93E-01	1.05E-01	1.89E-03	2.48E-04
	s833435	1.17E-04	9.29E-01	6.94E-02	1.65E-03	1.32E-04
	s833836	6.29E-05	9.49E-01	4.98E-02	1.47E-03	8.07E-05
	s833869	3.87E-04	8.81E-01	1.13E-01	4.28E-03	6.20E-04
	s834436	2.56E-04	8.83E-01	1.12E-01	4.29E-03	6.14E-04
	s834516	1.08E-04	9.28E-01	7.00E-02	1.59E-03	1.29E-04
	s834751	3.06E-04	9.18E-01	7.97E-02	2.16E-03	2.03E-04
	s835414	3.36E-04	8.79E-01	1.15E-01	4.15E-03	6.16E-04
	s835415	9.85E-04	8.96E-01	9.93E-02	3.70E-03	4.56E-04
	s842177	1.32E-04	9.14E-01	8.39E-02	1.80E-03	1.80E-04
	s842374	2.96E-04	9.35E-01	6.20E-02	2.07E-03	1.46E-04
	s844228	5.42E-04	8.77E-01	1.18E-01	4.32E-03	6.60E-04
	s844606	4.45E-04	8.79E-01	1.17E-01	3.56E-03	5.36E-04
	s844666	1.21E-03	8.88E-01	1.06E-01	4.31E-03	5.76E-04
	s845002	3.41E-04	8.92E-01	1.04E-01	3.46E-03	4.49E-04
	s845237	4.08E-04	8.77E-01	1.18E-01	3.53E-03	5.38E-04
	s845241	3.33E-04	8.97E-01	9.81E-02	4.23E-03	5.13E-04
	s845272	5.26E-04	8.79E-01	1.15E-01	4.06E-03	6.02E-04
	s845360	4.49E-04	8.95E-01	1.01E-01	3.12E-03	3.93E-04
	s846661	1.49E-04	9.03E-01	9.26E-02	3.64E-03	4.11E-04
	s852944	8.92E-04	9.43E-01	5.41E-02	2.19E-03	1.33E-04
	s853739	3.91E-04	8.87E-01	1.08E-01	4.52E-03	6.15E-04
	s853812	4.24E-04	9.00E-01	9.62E-02	3.25E-03	3.85E-04
	s860015	5.80E-04	8.77E-01	1.17E-01	4.28E-03	6.49E-04
	s860166	2.67E-04	9.00E-01	9.70E-02	2.49E-03	2.97E-04
	s861740	6.28E-04	8.88E-01	1.07E-01	4.21E-03	5.68E-04
	s862242	6.36E-04	8.80E-01	1.14E-01	4.33E-03	6.35E-04
	s862249	9.54E-04	9.14E-01	8.02E-02	4.02E-03	3.83E-04
	s863680	5.45E-04	8.77E-01	1.18E-01	4.24E-03	6.46E-04

Table IV-1 (Continued)
Sample Data Used to Estimate Radionuclide Activity Fraction Distributions in Plutonium Material Types

Material Type	Drum ID	Pu238	Pu239	Pu240	Pu241	Pu242
PU54 (Cont.)	s864258	5.22E-04	8.83E-01	1.11E-01	4.64E-03	6.55E-04
	s870244	1.28E-04	9.41E-01	5.75E-02	1.29E-03	8.30E-05
	S910739	5.10E-04	8.82E-01	1.13E-01	4.09E-03	5.88E-04
PU56	59172	3.05E-04	8.54E-01	1.41E-01	4.46E-03	8.55E-04
	60498	4.42E-04	8.46E-01	1.48E-01	4.41E-03	9.06E-04
	60700	4.92E-04	8.29E-01	1.64E-01	4.75E-03	1.13E-03
	60986	5.91E-04	8.63E-01	1.31E-01	4.66E-03	8.15E-04
	s824083	4.99E-04	8.41E-01	1.52E-01	5.01E-03	1.07E-03
	s824199	3.27E-04	8.60E-01	1.35E-01	4.16E-03	7.56E-04
	s824412	6.59E-04	9.12E-01	8.08E-02	5.58E-03	5.39E-04
	s824420	4.29E-04	8.35E-01	1.59E-01	4.99E-03	1.13E-03
	s832352	3.28E-04	8.58E-01	1.36E-01	4.31E-03	7.93E-04
	s833034	4.70E-04	8.71E-01	1.23E-01	4.89E-03	7.90E-04
	s834450	4.00E-04	8.46E-01	1.48E-01	4.71E-03	9.65E-04
	s835351	3.91E-04	8.55E-01	1.41E-01	3.46E-03	6.61E-04
	s842466	4.09E-04	8.99E-01	9.72E-02	2.95E-03	3.52E-04
	s844278	4.47E-04	8.66E-01	1.28E-01	4.01E-03	6.82E-04
	s844280	5.20E-04	8.34E-01	1.59E-01	5.04E-03	1.14E-03
	s854579	5.51E-04	9.12E-01	8.46E-02	2.47E-03	2.50E-04
PU83	52660	8.47E-01	1.43E-01	7.90E-03	1.35E-03	5.20E-04
	52675	7.32E-01	2.53E-01	1.21E-02	1.97E-03	3.70E-04
	52677	8.21E-01	1.62E-01	1.47E-02	1.67E-03	9.33E-04
	54696	7.84E-01	1.73E-01	3.93E-02	1.78E-03	2.32E-03
	54698	6.36E-01	3.34E-01	2.69E-02	2.23E-03	5.34E-04
	55173	8.59E-01	1.36E-01	2.38E-03	2.10E-03	2.68E-04
	55401	8.55E-01	1.20E-01	2.03E-02	1.81E-03	2.55E-03
	55402	7.97E-01	1.79E-01	2.10E-02	2.07E-03	1.35E-03
	55416	3.03E-02	9.10E-01	5.83E-02	1.42E-03	9.96E-05
	55419	4.93E-01	4.55E-01	5.16E-02	7.65E-04	1.90E-04
	55499	8.09E-01	1.71E-01	1.67E-02	2.02E-03	1.15E-03
	55500	7.93E-01	1.67E-01	3.58E-02	1.90E-03	2.44E-03
	55505	8.17E-01	1.67E-01	1.33E-02	1.85E-03	8.77E-04
	55531	8.36E-01	1.58E-01	3.39E-03	1.83E-03	2.46E-04
	55568	7.70E-01	2.00E-01	2.64E-02	1.97E-03	1.29E-03

Table IV-1 (Continued)
Sample Data Used to Estimate Radionuclide Activity Fraction Distributions in Plutonium Material Types

Material Type	Drum ID	Pu238	Pu239	Pu240	Pu241	Pu242
PU83 (Cont.)	55574	8.06E-01	1.81E-01	1.06E-02	1.73E-03	5.56E-04
	55575	8.27E-01	1.63E-01	7.94E-03	1.94E-03	5.79E-04
	55584	8.17E-01	1.64E-01	1.56E-02	1.83E-03	1.05E-03
	55587	7.90E-01	1.91E-01	1.59E-02	1.70E-03	7.30E-04
	55593	5.26E-01	4.43E-01	2.90E-02	1.81E-03	2.65E-04
	55598	8.26E-01	1.52E-01	1.82E-02	1.78E-03	1.40E-03
	55614	8.18E-01	1.73E-01	6.79E-03	1.84E-03	4.18E-04
	55667	1.65E-01	7.88E-01	4.60E-02	1.48E-03	1.09E-04
	55671	7.93E-01	1.89E-01	1.53E-02	1.91E-03	8.09E-04
	55691	8.26E-01	1.62E-01	9.36E-03	1.97E-03	6.97E-04
	55692	8.23E-01	1.55E-01	1.82E-02	1.86E-03	1.39E-03
	55694	8.06E-01	1.74E-01	1.70E-02	1.88E-03	1.04E-03
	55713	3.42E-01	6.02E-01	5.30E-02	2.73E-03	3.97E-04
	55803	8.10E-01	1.77E-01	1.02E-02	1.80E-03	5.78E-04
	55804	7.34E-01	2.51E-01	1.19E-02	1.93E-03	3.63E-04
	55811	8.28E-01	1.50E-01	1.83E-02	1.93E-03	1.55E-03
	55823	8.07E-01	1.78E-01	1.25E-02	1.81E-03	7.08E-04
	55824	7.88E-01	2.05E-01	4.73E-03	1.98E-03	2.21E-04
	55827	8.19E-01	1.67E-01	1.16E-02	1.91E-03	7.86E-04
	55833	7.67E-01	2.12E-01	1.88E-02	1.74E-03	7.22E-04
	55840	1.48E-01	8.03E-01	4.75E-02	1.48E-03	1.09E-04
	55845	8.12E-01	1.62E-01	2.25E-02	1.86E-03	1.59E-03
	55858	8.18E-01	1.52E-01	2.65E-02	1.78E-03	2.03E-03
	55866	8.13E-01	1.69E-01	1.48E-02	1.93E-03	9.86E-04
	55872	8.11E-01	1.77E-01	9.31E-03	1.82E-03	5.34E-04
	55880	8.08E-01	1.77E-01	1.22E-02	2.04E-03	7.86E-04
	55884	8.28E-01	1.53E-01	1.61E-02	1.91E-03	1.31E-03
	55889	7.71E-01	2.15E-01	1.18E-02	1.68E-03	4.26E-04
	55896	6.91E-01	2.84E-01	2.33E-02	1.88E-03	5.40E-04
	55897	8.29E-01	1.58E-01	1.09E-02	1.79E-03	7.82E-04
	55912	7.96E-01	1.97E-01	5.58E-03	1.73E-03	2.48E-04
	55965	7.86E-01	1.76E-01	3.39E-02	2.11E-03	2.29E-03
	55974	8.29E-01	1.66E-01	3.53E-03	1.68E-03	2.15E-04
	55987	7.85E-01	1.92E-01	2.07E-02	1.78E-03	9.92E-04

Table IV-1 (Continued)
Sample Data Used to Estimate Radionuclide Activity Fraction Distributions in Plutonium Material Types

Material Type	Drum ID	Pu238	Pu239	Pu240	Pu241	Pu242
PU83 (Cont.)	56012	7.12E-01	2.67E-01	1.85E-02	2.14E-03	5.51E-04
	56018	8.20E-01	1.50E-01	2.58E-02	1.59E-03	1.81E-03
	56020	8.17E-01	1.63E-01	1.75E-02	1.81E-03	1.19E-03
	56022	8.05E-01	1.65E-01	2.58E-02	2.04E-03	1.92E-03
	56044	8.23E-01	1.58E-01	1.58E-02	1.80E-03	1.13E-03
	56084	8.42E-01	1.51E-01	4.82E-03	1.87E-03	3.92E-04
	56153	8.28E-01	1.50E-01	1.84E-02	1.91E-03	1.55E-03
	56164	7.53E-01	2.21E-01	2.35E-02	1.85E-03	8.86E-04
	56165	7.87E-01	1.76E-01	3.30E-02	1.95E-03	2.07E-03
	56173	8.11E-01	1.77E-01	9.05E-03	1.88E-03	5.37E-04
	56175	8.36E-01	1.57E-01	4.65E-03	1.96E-03	3.67E-04
	56178	8.01E-01	1.85E-01	1.12E-02	1.81E-03	5.88E-04
	56181	7.51E-01	2.12E-01	3.35E-02	1.75E-03	1.30E-03
	56198	8.36E-01	1.36E-01	2.40E-02	1.86E-03	2.41E-03
	56202	7.83E-01	1.94E-01	1.97E-02	1.88E-03	9.77E-04
	56207	8.28E-01	1.60E-01	9.59E-03	1.67E-03	6.18E-04
	56213	7.95E-01	1.82E-01	1.99E-02	1.76E-03	1.05E-03
	56257	8.32E-01	1.49E-01	1.48E-02	2.01E-03	1.33E-03
	56267	8.03E-01	1.78E-01	1.66E-02	1.91E-03	9.99E-04
	56282	6.34E-01	3.28E-01	3.54E-02	1.95E-03	6.38E-04
	56294	8.11E-01	1.70E-01	1.66E-02	1.81E-03	1.04E-03
	56299	7.99E-01	1.85E-01	1.33E-02	1.91E-03	7.33E-04
	56303	7.50E-01	2.12E-01	3.48E-02	1.73E-03	1.32E-03
	56317	7.70E-01	1.76E-01	4.97E-02	1.70E-03	2.70E-03
	56321	7.70E-01	2.23E-01	4.31E-03	2.18E-03	1.87E-04
	56324	8.34E-01	1.53E-01	9.54E-03	1.83E-03	7.34E-04
	56554	7.10E-01	2.43E-01	4.47E-02	1.44E-03	1.09E-03
	56566	8.37E-01	1.52E-01	9.03E-03	1.84E-03	7.17E-04
	56569	8.23E-01	1.63E-01	1.17E-02	1.81E-03	7.96E-04
	56575	8.18E-01	1.61E-01	1.80E-02	1.92E-03	1.33E-03
	56603	7.97E-01	1.83E-01	1.68E-02	1.80E-03	8.96E-04
	56638	3.15E-01	6.43E-01	3.84E-02	2.74E-03	2.53E-04
	56641	7.78E-01	2.10E-01	1.01E-02	1.60E-03	3.64E-04
	56642	8.25E-01	1.56E-01	1.64E-02	1.96E-03	1.32E-03

Table IV-1 (Continued)
Sample Data Used to Estimate Radionuclide Activity Fraction Distributions in Plutonium Material Types

Material Type	Drum ID	Pu238	Pu239	Pu240	Pu241	Pu242
PU83 (Cont.)	56670	6.51E-01	3.16E-01	3.04E-02	1.80E-03	5.44E-04
	56673	8.19E-01	1.65E-01	1.35E-02	1.93E-03	9.54E-04
	56679	8.32E-01	1.62E-01	4.53E-03	1.93E-03	3.34E-04
	56815	8.57E-01	1.27E-01	1.34E-02	1.63E-03	1.35E-03
	56870	8.15E-01	1.66E-01	1.64E-02	1.79E-03	1.07E-03
	56879	8.29E-01	1.56E-01	1.23E-02	1.86E-03	9.40E-04
	56897	8.27E-01	1.65E-01	5.95E-03	1.90E-03	4.14E-04
	57025	7.53E-01	2.16E-01	2.98E-02	1.19E-03	7.57E-04
	57140	8.37E-01	1.30E-01	2.74E-02	1.82E-03	2.91E-03
	57212	8.39E-01	1.38E-01	1.95E-02	1.82E-03	1.86E-03
	57214	7.70E-01	1.98E-01	2.98E-02	1.57E-03	1.19E-03
	57218	7.23E-01	2.53E-01	2.18E-02	1.71E-03	5.81E-04
	60465	7.63E-01	2.10E-01	2.36E-02	2.17E-03	1.16E-03
	s816347	7.65E-01	2.12E-01	2.06E-02	1.90E-03	8.66E-04
	s822811	7.52E-01	2.09E-01	3.70E-02	1.35E-03	1.14E-03
	s834538	7.74E-01	1.92E-01	3.07E-02	1.99E-03	1.65E-03
	s834568	7.34E-01	2.43E-01	2.11E-02	1.45E-03	5.14E-04
	s841258	8.28E-01	1.52E-01	1.75E-02	1.73E-03	1.31E-03
	s843805	7.94E-01	2.01E-01	2.91E-03	2.52E-03	1.81E-04
	s845216	8.02E-01	1.78E-01	1.68E-02	2.06E-03	1.08E-03
	s853476	7.43E-01	2.09E-01	4.51E-02	1.74E-03	1.79E-03
	s853478	8.14E-01	1.67E-01	1.62E-02	1.99E-03	1.15E-03
	s853885	8.18E-01	1.58E-01	2.01E-02	2.05E-03	1.63E-03
	s860007	8.31E-01	1.43E-01	2.18E-02	1.96E-03	2.08E-03
	s861821	8.17E-01	1.67E-01	1.31E-02	2.16E-03	1.01E-03
	s861822	7.31E-01	2.34E-01	3.28E-02	1.65E-03	9.80E-04
	s862246	8.10E-01	1.75E-01	1.22E-02	1.99E-03	7.90E-04
	s862377	8.04E-01	1.86E-01	7.16E-03	1.98E-03	4.07E-04
	s862968	8.11E-01	1.72E-01	1.47E-02	1.88E-03	9.27E-04
	s864244	8.28E-01	1.57E-01	1.16E-02	1.89E-03	8.81E-04
	s864541	7.73E-01	2.17E-01	7.86E-03	1.58E-03	2.61E-04
	s864544	4.75E-01	4.69E-01	5.51E-02	5.13E-04	1.28E-04
	s870370	8.15E-01	1.71E-01	1.11E-02	1.97E-03	7.42E-04
	s870372	8.11E-01	1.66E-01	1.96E-02	1.94E-03	1.37E-03

Table IV-1 (Continued)
Sample Data Used to Estimate Radionuclide Activity Fraction Distributions in Plutonium Material Types

Material Type	Drum ID	Pu238	Pu239	Pu240	Pu241	Pu242
PU83 (Cont.)	s870375	7.51E-01	2.05E-01	4.06E-02	1.86E-03	1.79E-03
	s870395	8.24E-01	1.64E-01	9.72E-03	1.97E-03	7.08E-04
	s870461	8.19E-01	1.61E-01	1.70E-02	1.89E-03	1.23E-03
	s870463	8.27E-01	1.57E-01	1.34E-02	1.98E-03	1.07E-03
	s870481	7.76E-01	1.89E-01	3.17E-02	1.97E-03	1.74E-03
	s870486	7.52E-01	2.09E-01	3.61E-02	1.53E-03	1.25E-03
	s872471	7.51E-01	2.32E-01	1.46E-02	1.31E-03	3.54E-04
	s882087	5.46E-01	4.18E-01	3.36E-02	1.93E-03	3.68E-04
	S910737	8.08E-01	1.72E-01	1.64E-02	1.90E-03	1.05E-03
	S910762	6.96E-01	2.57E-01	4.44E-02	1.81E-03	1.21E-03
	S910765	8.19E-01	1.63E-01	1.45E-02	1.98E-03	1.07E-03
	S910795	7.06E-01	2.61E-01	3.00E-02	1.86E-03	8.11E-04
	S910796	7.33E-01	2.51E-01	1.38E-02	1.81E-03	3.95E-04

LA-UR-08-06109

Approved for public release;
distribution is unlimited.

Title:	Radiological Dose Assessment for Los Alamos National Laboratory Technical Area 54, Area G Performance Assessment and Composite Analysis
Author(s):	Rob Shuman
Intended for:	U.S. Department of Energy

Form 836 (7/06)

Table of Contents

List of Figures iii
List of Tables iv
List of Attachments v
Acronyms and Abbreviations vi

1.0 Introduction 1
1.1 Public Protection Performance Objectives 2
1.2 Groundwater Protection Performance Objectives 3
1.3 Inadvertent Intruder and Composite Analysis Performance Objectives 6
2.0 Dose Assessment Methodology 7
2.1 Human Exposure Pathways and Scenarios 7
2.1.1 Operational, Closure, and Active Institutional Control Periods 8
2.1.2 Passive Institutional Control Period 15
2.2 Modeling Approach and Input Data 22
2.2.1 Model Configuration and Implementation 22
2.2.1.1 Disposal Facility Characteristics and Radionuclide Inventory 22
2.2.1.2 Radionuclide Release Mechanisms and Transport Pathways 26
2.2.1.3 Exposure Estimates and Waste Acceptance Criteria Calculations 30
2.2.2 Alternate Source Analysis 32
3.0 Performance Assessment and Composite Analysis Dose Projections 34
3.1 Performance Assessment Projections 34
3.1.1 Groundwater Scenarios 35
3.1.1.1 Groundwater Resource Protection Scenario 35
3.1.1.2 All Pathways–Groundwater Scenario 35
3.1.2 Atmospheric Scenario 38
3.1.3 All Pathways–Canyon Scenarios 42
3.2 Composite Analysis Projections 46
3.2.1 All Pathways–Groundwater Scenario 46
3.2.2 Atmospheric Scenario 46
3.2.3 All Pathways–Canyon Scenarios 50
3.2.4 Alternate Source Evaluation 57
3.2.4.1 Alternate Source Descriptions 57
3.2.4.2 Alternate Source Interactions 65
4.0 Intruder Dose Projections and Intruder-Based Waste Acceptance Criteria 75
4.1 Intruder Exposure Projections 75
4.2 Intruder-Based Waste Acceptance Criteria 81
4.3 Comparison of 1997 and 2008 Waste Acceptance Criteria 93
4.3.1 Intruder–Post-Drilling Scenario 97
4.3.2 Intruder-Agriculture Scenario 111
5.0 Uncertainty and Sensitivity 115
5.1 Performance Assessment and Composite Analysis Uncertainty and Sensitivity 115
5.1.1 Sensitivity Analysis 115
5.1.1.1 Performance Assessment 115

5.1.1.2 Composite Analysis 119
5.1.2 Additional Sources of Uncertainty 121
5.1.2.1 Key Assumptions 121
5.1.2.2 Saturated Hydraulic Conductivity 123
5.1.2.3 Sediment Transport and Canyon Interactions 126
5.1.2.4 Short-Term Moisture Conditions 127
5.1.2.5 Effects of Waste Form and Packaging 127
5.1.2.6 Spatial Dependencies of Long-Term Performance 128
5.2 Inadvertent Intruder Analysis 128
6.0 References 133

List of Figures

Figure 1 Waste Disposal Regions at Area G 25
Figure 2 Deterministic Dose Projections for the Groundwater Resource Protection Scenario 36
Figure 3 Deterministic Dose Projections for the All Pathways– Groundwater Scenario (performance assessment) 37
Figure 4 Deterministic Dose Projections for the Atmospheric Scenario (performance assessment) 39
Figure 5 Probabilistic Dose Projections for the Atmospheric Scenario (performance assessment) 40
Figure 6 Mean Radionuclide Exposures for the Atmospheric Scenario at the Area G Fence Line Location (performance assessment) 41
Figure 7 Deterministic Dose Projections for the All Pathways–Canyon Scenarios (performance assessment) 43
Figure 8 Probabilistic Dose Projections for the All Pathways–Cañada del Buey Scenario (performance assessment) 45
Figure 9 Mean Radionuclide Doses for the All Pathways–Cañada del Buey Scenario within Catchment CdB2 (performance assessment) 47
Figure 10 Deterministic Dose Projections for the All Pathways–Groundwater Scenario (composite analysis) 48
Figure 11 Deterministic Dose Projections for the Atmospheric Scenario (composite analysis) 49
Figure 12 Probabilistic Dose Projections for the Atmospheric Scenario (composite analysis) 51
Figure 13 Mean Radionuclide Exposures for the Atmospheric Scenario at the Area G Fence Line Exposure Location (composite analysis) 52
Figure 14 Deterministic Dose Projections for the All Pathways–Canyon Scenarios (composite analysis) 53
Figure 15 Probabilistic Dose Projections for the All Pathways–Pajarito Canyon Scenario (composite analysis) 55
Figure 16 Mean Radionuclide Exposures for the All Pathways–Pajarito Canyon Scenario within Catchment PC5 (composite analysis) 56
Figure 17 Generalized Stratigraphic Relationships of the Pajarito Plateau 71
Figure 18 Location of Alternate Contamination Sources and Generalized Water-Level Contours on the Top of the Regional Aquifer 73

List of Tables

Table 1 Derived Concentrations of Beta and Photon Emitters in Drinking Water Yielding an Annual Total Body or Critical Organ Dose of 4 mrem/yr 4
Table 2 Off-Site Exposure Scenarios for the Area G Performance Assessment and Composite Analysis 10
Table 3 Inadvertent Intruder Exposure Scenarios Evaluated for Inclusion in the Area G Intruder Assessment 17
Table 4 Projected Radon Fluxes for the Eight Waste Disposal Regions 42
Table 5 Probabilistic Dose Projections for the All Pathways–Canyon Scenarios (performance assessment) 44
Table 6 Probabilistic Dose Projections for the All Pathways–Canyon Scenarios (composite analysis) 54
Table 7 Estimates of Radionuclide Inventories at the Material Disposal Areas Included in the Alternate Source Evaluation 58
Table 8 Estimates of Radionuclide Inventories at Material Disposal Area C 61
Table 9 Summary of Radionuclide Inventories at the MDAs Included in the Alternate Source Evaluation 66
Table 10 Comparison of Air Dispersion Factors for Releases from Alternate Source Material Disposal Areas 69
Table 11 Comparison of Intruder Dose Projections with and without the Effects of Radon Diffusion 76
Table 12 Probabilistic Doses for the Inadvertent Intruder Exposure Scenarios 78
Table 13 Intruder-Based Waste Acceptance Criteria for the Disposal Pits at MDA G 82
Table 14 Intruder-Based Waste Acceptance Criteria for the Disposal Shafts at MDA G 85
Table 15 Final Waste Acceptance Criteria for the Disposal Pits and Shafts at MDA G 90
Table 16 Comparison of the 1997/1999 and 2008 WAC for MDA G 94
Table 17 Comparison of the 1999 and 2008 Disposal Pit Waste Acceptance Criteria (Intruder–Post-Drilling Scenario) 98
Table 18 Summary of Input Data Used in the 1997/1999 WAC Development Effort and the Deterministic Values Adopted for the 2008 WAC Development Effort 101
Table 19 Comparison of the 1997 and 2008 Disposal Shaft Waste Acceptance Criteria (Intruder-Agriculture Scenario) 112
Table 20 Rank Correlation Coefficients for Selected Performance Assessment Exposure Scenarios 116
Table 21 Rank Correlation Coefficients for Radon Flux from Waste Disposal Region 7 118
Table 22 Rank Correlation Coefficients for Selected Composite Analysis Exposure Scenarios 120
Table 23 Field Measurements of Saturated Hydraulic Conductivity at MDA J 124
Table 24 Rank Correlation Coefficients for Selected Intruder Exposure Scenarios 131

List of Attachments

I Groundwater Pathway Screening Approach and Results

Acronyms and Abbreviations

ALARA	As low as reasonably achievable
bgs	Below ground surface
CFR	Code of Federal Regulations
D&D	Decontamination and decommissioning
DOE	U.S. Department of Energy
DSA	Documented Safety Analysis
ER	Environmental restoration
FEHM	Finite Element Heat and Mass
Laboratory	Los Alamos National Laboratory
LANL	Los Alamos National Laboratory
LLW	Low-level radioactive waste
MAP	Mixed-activation products
MDA	Material Disposal Area
MFP	Mixed-fission products
PRS	Potential release site
RCRA	Resource Conservation and Recovery Act
RFI	RCRA Facilities Investigation
TA	Technical Area
WAC	Waste acceptance criteria

1.0 Introduction

The Los Alamos National Laboratory (LANL or the Laboratory) generates radioactive waste as a result of various activities. Operational waste is generated at the Laboratory from a wide variety of research and development activities including nuclear weapons development, energy production, and medical research. Environmental restoration (ER) and decontamination and decommissioning (D&D) waste is generated as contaminated sites and facilities at LANL undergo cleanup or remediation. The majority of this waste is low-level radioactive waste (LLW) and is disposed of at Technical Area (TA) 54, Area G.

U.S. Department of Energy (DOE) Order 435.1 (DOE, 2001a) requires that radioactive waste be managed in a manner that protects worker and public health and safety, and the environment. To comply with this order, DOE field sites must prepare and maintain site-specific radiological performance assessments for LLW disposal facilities that accept waste after September 26, 1988. Furthermore, composite analyses must be conducted for disposal facilities that receive waste after September 26, 1988. The composite analysis accounts for the cumulative impacts of all waste that has been (or will be) disposed of at the facilities and other sources of radioactive material that may interact with the disposal facilities.

In compliance with DOE Order 5820.2A (DOE, 1988a), the predecessor to Order 435.1, LANL issued the Area G performance assessment and composite analysis in 1997 (Hollis et al., 1997). The 1997 analyses are being revised to incorporate new knowledge about the Area G facility and site, and to update the modeling approaches used to project the long-term performance of the disposal facility. This report documents the evaluation of the long-term radiological impacts associated with the disposal of radioactive waste at Area G.

A radiological dose assessment is an integral part of the performance assessment and composite analysis. It estimates the potential exposures that may be received by persons coming into contact with the radioactive waste placed in the disposal facility. The projected doses are compared to DOE performance objectives to assess facility compliance with Order 435.1, and are used to develop waste acceptance criteria (WAC) for the disposal facility. Sections 1.1 and 1.2 discuss the DOE performance objectives for the protection of the public and groundwater resources. Section 1.3 provides additional performance objectives that establish limits for inadvertent intruders and the composite analysis. A series of exposure scenarios was used to demonstrate compliance with the established performance objectives. These scenarios are discussed in Section 2, which also describes the methods used to conduct the radiological dose assessment for the Area G performance assessment and composite analysis. The results of the analyses that were conducted to estimate impacts for members of the public are presented and

discussed in Section 3; Section 4 discusses the results of the intruder analysis. An evaluation of the uncertainties associated with the projected impacts is provided in Section 5.

1.1 Public Protection Performance Objectives

In accordance with DOE Order 435.1 (DOE, 2001a), the long-term performance of an LLW disposal facility is evaluated through a series of performance objectives. These criteria, provided in DOE M 435.1 (DOE, 2001b), are designed to ensure the health and safety of the public, protect groundwater resources, safeguard persons who may inadvertently intrude into the buried waste, and maintain radiation doses from DOE facilities at levels that are as low as reasonably achievable (ALARA).

The performance objectives pertinent to the protection of the public, as stated in DOE M 435.1 (DOE, 2001b), include the following:

- Dose to representative members of the public shall not exceed 25 mrem in a year total effective dose equivalent from all exposure pathways, excluding the dose from radon and its progeny in air.
- Dose to representative members of the public via the air pathway shall not exceed 10 mrem in a year total effective dose equivalent, excluding the dose from radon and its progeny.
- Release of radon shall be less than an average flux of 20 pCi/m^2/s at the surface of the disposal facility. Alternatively, a limit of 0.5 pCi/L of radon in air may be applied at the boundary of the facility.

The all pathways performance objective addresses exposures that may be received from any and all modes of exposure, including exposures from airborne contaminants (except radon and its progeny). Compliance with this performance objective is to be demonstrated over a period of 1,000 years following closure of the disposal facility, at the point of maximum exposure that is accessible to members of the public. An evaluation of potential exposures beyond the period of compliance is to be conducted to provide increased confidence in the long-term performance of the disposal facility.

The air pathway performance objective is found in the National Emissions Standards for Hazardous Air Pollutants (40 Code of Federal Regulations [CFR] 61, Subpart H [EPA, 2004]). It requires that exposures from sources of airborne radioactivity at DOE facilities result in a dose of 10 mrem/yr or less, excluding the contributions of radon and its progeny. Compliance with this criterion is to be demonstrated at the point of maximum exposure that is accessible to members of the public for a period of 1,000 years following facility closure.

Releases of radon gas (i.e., Rn-220 and Rn-222) are subject to requirements in 40 CFR 61, Subpart Q (EPA, 1989 [as amended in 2000]), which limit releases to an average flux of 20 $pCi/m^2/s$ at the surface of the disposal facility. An incremental increase in the air concentration of radon of 0.5 pCi/L at the point of assessment may also be used to demonstrate compliance with the radon performance objective. Compliance must be demonstrated for a period of 1,000 years following closure of the disposal facility.

1.2 Groundwater Protection Performance Objectives

The performance assessment must also include an evaluation of impacts to groundwater resources (DOE, 2001b). Potential impacts to groundwater are to be assessed on a site-specific basis in accordance with a hierarchical set of criteria. In general, these criteria require that the LLW disposal site comply with any applicable state or local law, regulation, or other legally applicable requirement for water resource protection. Potential impacts are to be evaluated at the point of highest groundwater concentration outside of a 100 m (330 ft) buffer zone for a period of 1,000 years following facility closure.

The performance objectives that were adopted to evaluate potential impacts to groundwater resources at Area G are based on the drinking water regulations of New Mexico (NMEIB, 2002). These regulations incorporate the requirements set forth in the Safe Drinking Water Act, as codified in 40 CFR 141 (EPA, 2000). The standards in 40 CFR 141 that are relevant to the radiological performance assessment and composite analysis include maximum concentration limits for Ra-226, Ra-228, uranium, and gross alpha activity, as well as for beta particle and photon radioactivity. The specific requirements, as stated in 40 CFR 141, include:

- 141.66(a)—The maximum contaminant level for combined radium-226 and radium-228 is 5 pCi/L.
- 141.66(b)—The maximum contaminant level for gross alpha particle activity (including radium-226 but excluding radon and uranium) is 15 pCi/L.
- 141.66(c)—The average annual concentration of beta particle and photon radioactivity from man-made radionuclides in drinking water must not produce an annual dose equivalent to the total body or any internal organ greater than 4 mrem/yr.
- 141.66(e)—The maximum contaminant level for uranium is 30 µg/L (30 ppb).

The concentrations of radionuclides causing an annual dose equivalent of 4 mrem to the total body or organ have been published in EPA (2002); these concentrations are summarized in Table 1.

Table 1
Derived Concentrations of Beta and Photon Emitters in Drinking Water Yielding an Annual Total Body or Critical Organ Dose of 4 mrem/yr

Radionuclide	Concentration (pCi/L)	Radionuclide	Concentration (pCi/L)	Radionuclide	Concentration (pCi/L)
Ag-105	3.0E+02	Co-58	3.0E+02	Hg-203	6.0E+01
Ag-110m	9.0E+01	Co-58m	9.0E+03	Ho-166	9.0E+01
Ag-111	1.0E+02	Co-60	1.0E+02	I-126	3.0E+00
As-73	1.0E+03	Cr-51	6.0E+03	I-129	1.0E+00
As-74	1.0E+02	Cs-131	2.0E+04	I-131	3.0E+00
As-76	6.0E+01	Cs-134	8.0E+01	I-132	9.0E+01
As-77	2.0E+02	Cs-134m	2.0E+04	I-133	1.0E+01
Au-196	6.0E+02	Cs-135	9.0E+02	I-134	1.0E+02
Au-198	1.0E+02	Cs-136	8.0E+02	I-135	3.0E+01
Au-199	6.0E+02	Cs-137	2.0E+02	In-113m	3.0E+03
Ba-131	6.0E+02	Cu-64	9.0E+02	In-114m	6.0E+01
Ba-140	9.0E+01	Dy-165	1.0E+03	In-115	3.0E+02
Be-7	6.0E+03	Dy-166	1.0E+02	In-115m	1.0E+03
Bi-206	1.0E+02	Er-169	3.0E+02	Ir-190	6.0E+02
Bi-207	2.0E+02	Er-171	3.0E+02	Ir-192	1.0E+02
Bk-249	2.0E+03	Eu-152	2.0E+02	Ir-194	9.0E+01
Br-82	1.0E+02	Eu-154	6.0E+01	K-42	9.0E+02
C-14	2.0E+03	Eu-155	6.0E+02	La-140	6.0E+01
Ca-45	1.0E+01	F-18	2.0E+03	Lu-177	3.0E+02
Ca-47	8.0E+01	Fe-55	2.0E+03	Mn-52	9.0E+01
Cd-109	6.0E+02	Fe-59	2.0E+02	Mn-54	3.0E+02
Cd-115	9.0E+01	Ga-72	1.0E+02	Mn-56	3.0E+02
Cd-115m	9.0E+01	Gd-153	6.0E+02	Mo-99	6.0E+02
Ce-141	3.0E+02	Gd-159	2.0E+02	Na-22	4.0E+02
Ce-143	1.0E+02	Ge-71	6.0E+03	Na-24	6.0E+02
Ce-144	3.0E+01	H-3	2.0E+04	Nb-93m	1.0E+03
Cl-36	7.0E+02	Hf-181	2.0E+02	Nb-95	3.0E+02
Cl-38	1.0E+03	Hg-197	9.0E+02	Nb-97	3.0E+03
Co-57	1.0E+03	Hg-197m	6.0E+02	Nd-147	2.0E+02

Source: EPA, 2002

Table 1 (Continued)
Derived Concentrations of Beta and Photon Emitters in Drinking Water Yielding an Annual Total Body or Critical Organ Dose of 4 mrem/yr

Radionuclide	Concentration (pCi/L)	Radionuclide	Concentration (pCi/L)	Radionuclide	Concentration (pCi/L)
Nd-149	9.0E+02	Ru-106	3.0E+01	Te-129m	9.0E+01
Ni-59	3.0E+02	Ru-97	1.0E+03	Te-131m	2.0E+02
Ni-63	5.0E+01	S-35 (inorg.)	5.0E+02	Te-132	9.0E+01
Ni-65	3.0E+02	Sb-122	9.0E+01	Tl-200	1.0E+03
Np-239	3.0E+02	Sb-124	6.0E+01	Tl-201	9.0E+02
Os-185	2.0E+02	Sb-125	3.0E+02	Tl-202	3.0E+02
Os-191	6.0E+02	Sc-46	1.0E+02	Tl-204	3.0E+02
Os-191m	9.0E+03	Sc-47	3.0E+02	Tm-170	1.0E+02
Os-193	2.0E+02	Sc-48	8.0E+01	Tm-171	1.0E+03
P-32	3.0E+01	Se-75	9.0E+02	V-48	9.0E+01
Pa-230	6.0E+02	Si-31	3.0E+03	W-181	1.0E+03
Pa-233	3.0E+02	Sm-151	1.0E+03	W-185	3.0E+02
Pb-203	1.0E+03	Sm-153	2.0E+02	W-187	2.0E+02
Pd-103	9.0E+02	Sn-113	3.0E+02	Y-90	6.0E+01
Pd-109	3.0E+02	Sn-125	6.0E+01	Y-91	9.0E+01
Pm-147	6.0E+02	Sr-85	9.0E+02	Y-91m	9.0E+03
Pm-149	1.0E+02	Sr-85 m	2.0E+04	Y-92	2.0E+02
Pr-142	9.0E+01	Sr-89	2.0E+01	Y-93	9.0E+01
Pr-143	1.0E+02	Sr-90	8.0E+00	Yb-175	3.0E+02
Pt-191	3.0E+02	Sr-91	2.0E+02	Zn-65	3.0E+02
Pt-193	3.0E+03	Sr-92	2.0E+02	Zn-69	6.0E+03
Pt-193m	3.0E+03	Ta-182	1.0E+02	Zn-69m	2.0E+02
Pt-197	3.0E+02	Tb-160	1.0E+02	Zr-93	2.0E+03
Pt-197m	3.0E+03	Tc-96	3.0E+02	Zr-95	2.0E+02
Pu-241	3.0E+02	Tc-96m	3.0E+04	Zr-97	6.0E+01
Rb-86	6.0E+02	Tc-97	6.0E+03	Yb-175	3.0E+02
Rb-87	3.0E+02	Tc-97m	1.0E+03	Zn-65	3.0E+02
Re-186	3.0E+02	Tc-99	9.0E+02	Zn-69	6.0E+03
Re-187	9.0E+03	Tc-99m	2.0E+04	Zn-69m	2.0E+02
Re-188	2.0E+02	Te-125m	6.0E+02	Zr-93	2.0E+03
Rh-103m	3.0E+04	Te-127	9.0E+02	Zr-95	2.0E+02
Rh-105	3.0E+02	Te-127m	2.0E+02	Zr-97	6.0E+01

Source: EPA, 2002

1.3 Inadvertent Intruder and Composite Analysis Performance Objectives

To satisfy DOE requirements for performance assessments, LANL is required to evaluate the potential exposures received by persons who inadvertently intrude into the buried waste. As discussed in more detail in Section 2.1, institutional controls over the disposal facility are assumed to prevent intrusion from occurring for a minimum of 100 years after facility closure. Projected intruder exposures are subject to chronic and acute dose limits of 100 and 500 mrem/yr, respectively, excluding contributions of radon in air. The results of the intruder analysis are also to be used to develop limits or WAC for the disposal facility. Potential intruder exposures are to be projected for a period of 1,000 years following closure of the disposal facility.

The composite analysis accounts for the cumulative impacts of all waste that has been (or will be) disposed of at Area G and other sources of radioactivity at the Laboratory that may interact with releases from the disposal facility. Like the performance assessment, the compliance period for the composite analysis is 1,000 years following closure of the disposal facility. Potential exposures are to be evaluated at the point(s) of maximum exposure accessible to members of the public over this period.

The performance objective for the composite analysis is the DOE's primary dose limit of 100 mrem/yr (DOE, 1993). A dose constraint of 30 mrem/yr is adopted to ensure that any exposures received in conjunction with the disposal facility do not constitute an extraordinary portion of the primary dose limit. If the doses projected for the composite analysis exceed the primary dose limit, mitigating actions must be taken before the dose limit is exceeded. The air pathway performance objective of 10 mrem/yr from all sources of airborne radioactivity at the Laboratory, discussed in Section 1.1, also applies to the composite analysis.

DOE also requires a demonstration that disposal is conducted in a manner that maintains releases to the environment ALARA. This performance objective is not addressed in this report.

2.0 Dose Assessment Methodology

The primary objective of the performance assessment and composite analysis modeling is to estimate potential doses to persons exposed to contamination released from Area G. Assumptions made about these persons, or receptors, define the transport processes, environmental media, and exposure pathways that must be addressed and, as such, dictate the overall approach adopted for the dose assessment. Section 2.1 discusses the exposure pathways and scenarios used in the dose assessment. The models and information used to estimate the potential doses received by these receptors and the methods used to estimate WAC for the disposal facility are discussed in Section 2.2. The approach adopted to estimate radon fluxes from the disposal site is also described.

2.1 Human Exposure Pathways and Scenarios

The means through which humans may be exposed to radioactive materials are called exposure pathways. Each exposure pathway includes a source or release from a source, a transport or exposure medium, a location at which the exposure occurs, and an exposure route. The actual exposure pathways that may lead to human exposures will depend upon the patterns of human activity at, and adjacent to, the disposal site. Patterns of human activity may be specified by using a collection of appropriate exposure pathways, which is generally referred to as an exposure scenario.

The exposure pathways and scenarios through which people may be exposed to radioactive waste that has been disposed of at Area G are specific to the period of the facility's lifetime. Thus, to understand the basis for pathway and scenario development, it is necessary to understand the stages of the disposal facility's lifetime. These stages are as follows:

- *Operational period*. This is defined as the period during which waste is placed in disposal pits and shafts. Operations at Area G began in 1957 with the disposal of nonroutine waste. Routine waste disposal began in 1959 and is assumed to continue through the year 2044.

- *Closure period.* During this period, the final pits and shafts are closed and any remaining surface structures are removed from the site; it is assumed that final site closure will require a period of 2 years (2045 and 2046) to complete.

- *Active institutional control period*. This period is characterized by continuing DOE control over the entire Laboratory. Consistent with DOE M 435.1 (DOE, 2001b), this period is assumed to last 100 years, extending from 2047 through 2146.

- *Passive institutional control period*. The DOE control shifts from the entire Laboratory to specific high-risk facilities such as Area G during this time. This period is assumed to last until the disposal facility no longer poses a risk to human health and safety and the environment.

DOE is assumed to retain control over the entire Laboratory throughout the operational, closure, and active institutional control periods. During this time, members of the public will be prevented from entering Area G, the site will be maintained to slow the establishment of deep-rooted plants, and actions will be taken as necessary to repair any significant damage to the cover. Although control over the entire Laboratory is assumed to cease at the end of the active institutional control period, it is expected that DOE will continue to exercise administrative control over individual sites such as Area G. This level of control will generally prevent members of the public from residing within the closed site, but it is assumed that no maintenance activities will be undertaken.

The level of control outlined above limits exposures during the operational, closure, and active institutional control periods to members of the public who are located downwind or downgradient of the Laboratory, following the transport of contaminant releases with the prevailing winds, surface water, or groundwater. Receptors may move closer to the closed disposal facility during the passive institutional control period, including to locations immediately outside of the Area G fence line. Inadvertent intrusion into the facility is assumed to be prevented as long as the DOE maintains active institutional control over the site. Although it is generally expected that all persons will be prevented from occupying the site during the passive institutional control period, it is conceivable that a temporary lapse in control could provide an opportunity for persons to arrive at the disposal site and inadvertently intrude into the buried waste. This is the basis for the inadvertent intruder analysis. The exposure pathways and scenarios used to estimate the potential exposures received by members of the public and inadvertent intruders during these periods are discussed in the following sections.

2.1.1 Operational, Closure, and Active Institutional Control Periods

The sources of contamination that may result in human exposure will change as the site passes from the operational period to the active institutional control period. Plants and animals may root or burrow into the buried waste and bring contamination to the surface of the disposal facility during all phases; however, the quantities of contamination deposited on the surface during the operational and closure periods will tend to be small. The establishment of plant and animal communities at the site will be slowed or prevented by ongoing operations and closure activities, and any signs of significant intrusion into the waste will be remedied quickly. Radionuclides may be leached from the buried waste by water infiltrating through the site and may then be transported to the regional aquifer, exposing persons who use this water downgradient of the Laboratory to contamination. Similarly, vapor- or gas-phase contaminants may diffuse from the

waste and enter the atmosphere, exposing persons living downwind of LANL to airborne contaminants that have been transported by the prevailing winds.

Although steps will be taken to ensure proper facility functioning during the active institutional control period, these actions may not prevent plant roots and animal burrows from penetrating into the waste and depositing contamination on the surface. Contamination may be suspended and transported by prevailing winds to locations downwind of the Laboratory and transported to canyons adjacent to Area G by surface runoff. Receptors in areas downwind of the Laboratory or in Cañada del Buey, part of which lies outside the Laboratory, may be exposed to radiation. Members of the public living outside the Laboratory boundary may continue to be exposed to radionuclides discharged to the regional aquifer and to vapor- and gas-phase contaminants diffusing from the disposal facility.

The exposure scenarios selected for the performance assessment and composite analysis take into account the sources of contamination discussed above; these scenarios are summarized in Table 2. The Groundwater Resource Protection Scenario is implemented at a location 100 m (330 ft) downgradient of Area G; projected exposures are limited to the ingestion of contaminated groundwater and are used to assess compliance with the groundwater protection standards discussed in Section 1.2. The scenario is implemented on restricted Laboratory lands because it is designed to ensure protection of the groundwater resource, regardless of whether members of the public can access the water.

The All Pathways–Groundwater Scenario is implemented at the Laboratory boundary near the town of White Rock. The receptor is assumed to receive exposures from the inhalation and ingestion of radioactivity, and from direct radiation. Radionuclides deposited on the surface soil with irrigation water are suspended and inhaled by the individual during the time spent at home. Ingestion doses result from the consumption of crops irrigated with contaminated water, animal products (e.g., beef and milk or chicken and eggs) from animals raised on location, soil, and drinking water. Exposures to direct radiation from airborne contamination at the homestead and radioactivity deposited on the soil add to the internal exposures.

The Atmospheric Scenario is implemented at the point of maximum atmospheric exposure outside of the Laboratory's boundaries. During the operational and closure periods, the receptor inhales radioactive gases (excluding radon and its progeny, which are modeled separately); following closure, contaminated particulates resuspended from the surface of Area G and transported with the prevailing winds add to these exposures. The deposition of airborne radionuclides contaminates crops grown by the individual and surface soils at the exposure location. Doses are received through the ingestion of contaminated vegetables, animal products, and soil. External exposures are received from contaminated soil surfaces and airborne radioactivity. Radon fluxes from the disposal site are projected separately.

Table 2
Off-Site Exposure Scenarios for the Area G Performance Assessment and Composite Analysis

Period and Exposure Scenario	Exposure Pathways and Routes	Point of Exposure
Operational, Closure, and Active Institutional Control Periods		
Groundwater Resource Protection [a]	Ingestion of drinking water	100 m downgradient of Area G
All Pathways–Groundwater	• Ingestion of drinking water • Ingestion of food crops grown in contaminated soils and irrigated with well water • Ingestion of animal products from animals raised by the receptor • Ingestion of contaminated soil • Inhalation of airborne radionuclides • Direct radiation from airborne radionuclides • Direct radiation from contaminated soils	LANL boundary near White Rock
Atmospheric	• Ingestion of food crops grown in contaminated soils and contaminated by airborne radionuclides • Ingestion of animal products from animals raised by the receptor • Ingestion of contaminated soil • Inhalation of airborne radionuclides • Direct radiation from airborne radionuclides • Direct radiation from contaminated soils	Point of maximum exposure outside of LANL boundary
All Pathways–Cañada del Buey	• Ingestion of food crops grown in contaminated soils • Ingestion of animal products from animals raised by the receptor • Ingestion of contaminated soil • Inhalation of airborne radionuclides • Direct radiation from airborne radionuclides • Direct radiation from contaminated soils	Cañada del Buey adjacent to Area G

[a] *This scenario was evaluated only for the performance assessment.*

Table 2 (Continued)
Off-Site Exposure Scenarios for the Area G Performance Assessment and Composite Analysis

Period and Exposure Scenario	Exposure Pathways and Routes	Point of Exposure
Passive Institutional Control Period		
Groundwater Resource Protection [a]	Ingestion of drinking water	100 m downgradient of Area G
All Pathways–Groundwater	• Ingestion of drinking water • Ingestion of food crops grown in contaminated soils and irrigated with well water • Ingestion of animal products from animals raised by the receptor • Ingestion of contaminated soil • Inhalation of airborne radionuclides • Direct radiation from airborne radionuclides • Direct radiation from contaminated soils	100 m downgradient of Area G
Atmospheric	• Ingestion of food crops grown in contaminated soils and contaminated by airborne radionuclides • Ingestion of animal products from animals raised by the receptor • Ingestion of contaminated soil • Inhalation of airborne radionuclides • Direct radiation from airborne radionuclides • Direct radiation from contaminated soils	Point of maximum exposure outside of Area G boundary
All Pathways–Cañada del Buey	• Ingestion of food crops grown in contaminated soils • Ingestion of animal products from animals raised by the receptor • Ingestion of contaminated soil • Inhalation of airborne radionuclides • Direct radiation from airborne radionuclides • Direct radiation from contaminated soils	Cañada del Buey adjacent to Area G

[a] *This scenario was evaluated only for the performance assessment.*

Table 2 (Continued)
Off-Site Exposure Scenarios for the Area G Performance Assessment and Composite Analysis

Period and Exposure Scenario	Exposure Pathways and Routes	Point of Exposure
All Pathways–Pajarito Canyon	• Ingestion of food crops grown in contaminated soils • Ingestion of animal products from animals raised by the receptor • Ingestion of contaminated soil • Inhalation of airborne radionuclides • Direct radiation from airborne radionuclides • Direct radiation from contaminated soils	Pajarito Canyon adjacent to Area G

[a] *This scenario was evaluated only for the performance assessment.*

The All Pathways–Cañada del Buey Scenario estimates potential doses resulting from the transport of contamination from Mesita del Buey to the canyon due to surface runoff and erosion. A person residing in the canyon is assumed to be exposed to radiation as a result of inhaling particulates suspended from contaminated soil surfaces and by way of ingesting contaminated crops, animal products, and soil. Exposures to direct radiation from airborne contamination at the homestead and radioactivity deposited over the resident's lot add to the internal exposures.

The locations used to project doses for the off-site exposure scenarios are consistent with DOE restrictions on public access, hydrologic and atmospheric conditions, and land-use patterns in the vicinity of Area G. As discussed earlier, the DOE is expected to retain control of the entire Laboratory during the operational, closure, and active institutional control periods and thus prevent the establishment of a residence or well any closer to the disposal facility than Cañada del Buey to the north of Area G or the area immediately adjacent to White Rock. The area around White Rock lies along the prevailing groundwater flow path and is the first location at which groundwater contaminated by releases from Area G could be used while restrictions on Laboratory access are in place. Establishment of a well at this location is possible since the LANL boundary currently runs along the western edge of town.

The exposures modeled at the point of maximum atmospheric exposure account for the prevailing meteorological conditions, the complex terrain, and the demographics in the vicinity of Area G. The receptor location in Cañada del Buey is the closest point to the disposal facility that members of the public can take up residence while DOE maintains control over the Laboratory. Although no residences currently exist in the canyon, inclusion of the All Pathways–Cañada del Buey scenario addresses this future possibility.

The assessment of exposures to members of the public at the locations identified in Table 2 is expected to provide reasonably conservative estimates of potential exposures during the operational, closure, and active institutional control periods. As stated earlier, the location near White Rock is the first point where regular usage of water drawn from the regional aquifer is possible. Consequently, any exposures from the use of contaminated groundwater are expected to be greatest at this location. Groundwater pathway doses at locations farther downgradient of Area G will diminish as the concentrations of groundwater contamination abate due to dilution and dispersion. By definition, the location of maximum atmospheric exposure will bound doses to off-site individuals following airborne releases from the disposal facility. Finally, during the operational, closure, and active institutional control periods, Cañada del Buey will be the closest receptor location subject to potential impacts from contamination transported by surface runoff from Area G.

Groundwater may occur at the Laboratory in the alluvium in canyon bottoms, as zones of perched groundwater, and in the regional aquifer. The source of water used by a member of the

public will directly influence the magnitude of any doses received from contaminated groundwater. Therefore, the water source selected for the performance assessment and composite analysis is a significant aspect of the dose assessment.

The groundwater source used to estimate groundwater pathway exposures must meet three conditions. First, the potential for the groundwater source to be contaminated by radionuclides leached from the disposal facility must exist. Second, the groundwater must be of adequate quality and quantity to meet the user's needs. Finally, the source must be accessible to the individual during the operational, closure, and active institutional control periods.

The water percolating through the disposal facility is expected to flow vertically until it contacts the regional aquifer. Alluvial water in Pajarito Canyon and Cañada del Buey may become contaminated if radionuclides deposited on the surface of the disposal facility are transported into the canyons with surface runoff. No contamination of canyon alluvial waters is anticipated from radionuclides leached from the waste and transported downward with the water percolating through the disposal site. Zones of perched water may be present in the canyons and may become contaminated as radioactivity in the alluvium is transported downward; perched groundwater has not been observed below the surface of Mesita del Buey (LANL, 1998, as cited in LANL, 2001).

In terms of water quality and supply characteristics, there is no evidence that zones of perched water in the vicinity of Area G are capable of meeting an individual's water needs. Similarly, the alluvial waters in Pajarito Canyon and Cañada del Buey are not expected to be capable of supporting average household use. The alluvial water in Pajarito Canyon, which is a more substantial source of water than Cañada del Buey, would generally be pumped dry by a household well during most seasons of the year. Adequate water may be available in the canyons for short periods of time following spring snowmelt and in summer thunderstorms. However, the only reliable source of water capable of meeting the quality and quantity needs of a resident is the regional aquifer.

During the operational, closure, and active institutional control periods, off-site residents will have limited access to groundwater from alluvial and perched zone sources. Any such sources within Pajarito Canyon near Area G will be inaccessible because of DOE land use restrictions; access may be available near the town of White Rock, approximately 2 km (1.2 mi.) downstream. The limited quantity of alluvial and perched groundwater within Cañada del Buey will be accessible to individuals throughout these periods because the border of LANL and San Ildefonso lands cuts through this canyon.

On the basis of the information presented above, the regional aquifer was selected as the source of water for the Groundwater Resource Protection and All Pathways–Groundwater Scenarios.

Although alluvial and perched groundwater in Cañada del Buey is accessible in some areas and may be contaminated with radionuclides transported with surface runoff, it is not capable of meeting year-round household water needs. The regional aquifer may be contaminated by releases from Area G, is capable of meeting the off-site receptor's water needs, and is accessible to members of the public during the operational, closure, and active institutional control periods.

The potential exists for a member of the public to be exposed to radionuclides that have been released from Area G to surface waters adjacent to, and downgradient of, Mesita del Buey. Surface runoff from the mesa may result in contaminated flows in Pajarito Canyon and Cañada del Buey. Separately, contaminated groundwater in the regional aquifer may eventually discharge to the Rio Grande, approximately 5 km (3.1 mi) downgradient of Area G.

Exposures resulting from the use of contaminated surface water during the operational, closure, and active institutional control periods were not considered in the Area G dose assessment. Surface flows within Cañada del Buey will be infrequent at best, and involve small amounts of water. Furthermore, active controls over the disposal site during these periods are expected to prevent significant transfers of contamination into the canyon via surface runoff. Surface waters within Pajarito Canyon will be inaccessible due to DOE land use restrictions. Projected exposures resulting from the use of contaminated surface water from the Rio Grande will be bounded by doses resulting from the use of contaminated water drawn from the regional aquifer. Radionuclide concentrations in the river will be lower than concentrations in the aquifer because of dispersive effects that occur within the aquifer during transport and because releases will be diluted in the river. Consequently, the potential doses resulting from the use of surface water will be lower than the exposures received from the use of groundwater closer to the disposal facility.

2.1.2 Passive Institutional Control Period

Radionuclide releases to groundwater and the atmosphere may continue after active institutional control ends and may result in exposures to the members of the public. The change in DOE control from the entire Laboratory to individual sites such as Area G will provide an opportunity for members of the public to locate immediately outside of the Area G fence line. Exposures to these receptors are projected using the exposure scenarios listed in the latter portion of Table 2 (under the banner row titled "Passive Institutional Control Period"). The groundwater scenarios and the Atmospheric Scenario are functionally the same as those evaluated for the operational, closure, and institutional control periods. Both the Groundwater Resource Protection and All Pathways–Groundwater Scenarios are implemented 100 m (330 ft) downgradient of Area G. The Atmospheric Scenario is implemented at the point of maximum exposure outside of the Area G boundary; radon fluxes from the disposal site are projected separately.

The All Pathways–Cañada del Buey and All Pathways–Pajarito Canyon Scenarios address exposures to receptors following the transport of contamination from Mesita del Buey to the

canyons due to surface runoff and erosion. Exposure to a receptor in Cañada del Buey is considered prior to the end of active institutional control because part of the canyon is outside of DOE control during that time; however, it is assumed that no residences will be established in Pajarito Canyon until after the end of active institutional control.

The source of groundwater for the Groundwater Resource Protection and All Pathways–Groundwater Scenarios is assumed to be the regional aquifer. While Pajarito Canyon is much wetter than Cañada del Buey, the alluvial groundwater is still not plentiful enough to meet domestic household needs. Exposures resulting from the use of contaminated surface water during the passive institutional control period are not considered. Concentrations of soluble radionuclides in the stream in Pajarito Canyon are expected to be small, and flow within the stream is not sufficient to supply water needs on a permanent basis. Radionuclide concentrations in the regional aquifer are expected to exceed those encountered in the Rio Grande for the reasons discussed above.

As mentioned, the DOE is expected to maintain control of Area G throughout the 1,000-year compliance period, thereby preventing people from taking up residence over the closed disposal pits and shafts. However, if DOE control lapses for a short period of time (e.g., 1 or 2 years), an inadvertent intruder may arrive at the site and become exposed to radiation. The intruder analysis was conducted to assess the potential exposures received by an intruder and to develop WAC that will protect the individual if this chain of events occurs.

Five intruder exposure scenarios were evaluated for inclusion in the intruder dose assessment; these are summarized in Table 3. This table briefly describes the activities that are assumed to occur, lists the period of time each intruder is exposed to radioactivity, and summarizes the potential routes of exposure. The exposure scenarios are the same as those evaluated for the 1997 Area G Performance Assessment and generally resemble those used by the U.S. Nuclear Regulatory Commission in support of 10 CFR Part 61 (NRC, 1986).

The Intruder-Construction and Intruder-Agriculture Scenarios are based on the assumption that an individual arrives at Area G and decides to establish a residence over one or more of the closed disposal units. The house includes a full basement, which extends to a depth of 3 m (9.8 ft) below the ground surface (bgs). Any waste brought to the surface during basement excavation is spread over the homeowner's lot. The Intruder-Construction Scenario projects exposures received by the builder during construction, while the Intruder-Agriculture Scenario estimates the doses for a person living in the completed house.

Table 3
Inadvertent Intruder Exposure Scenarios Evaluated for Inclusion in the Area G Intruder Assessment

Exposure Scenario	Scenario Description	Period of Exposure (hr/yr)	Exposure Routes
Intruder-Construction	An individual arrives at the disposal site and constructs a house over the closed disposal units. Radioactivity brought to the surface during basement excavation is spread over the house lot.	500	• Inhalation of airborne radionuclides • Ingestion of contaminated soils • Direct radiation from airborne contaminants and contaminated soils
Intruder-Agriculture	The intruder resides in a house constructed over the closed disposal units. The person works away from the house during the day and spends time raising crops and animals to provide foodstuffs for personal consumption. Crops and forage crops for animals are grown in contamination brought to the surface during basement excavation.	7,100 [a]	• Ingestion of contaminated crops, animal products (e.g., milk and beef or chicken and eggs), and soil • Inhalation of airborne contaminants • Direct radiation from airborne radionuclides and contaminated soils
Intruder–Post-Drilling	An individual resides in a house constructed over the closed disposal units. The person works away from the house during the day and spends time raising crops and animals to provide foodstuffs for personal consumption. Crops and forage crops for animals are grown in contamination brought to the surface during well drilling.	7,100 [a]	• Ingestion of contaminated crops, animal products (e.g., milk and beef or chicken and eggs), and soil • Inhalation of airborne contaminants • Direct radiation from airborne radionuclides and contaminated soils
Intruder-Drilling	A local well driller is contracted to drill a well through the closed disposal units. Radioactivity brought to the surface with the drill cuttings is spread over a limited area around the drill rig.	100 or less [b]	• Inhalation of airborne radionuclides • Ingestion of contaminated soils • Direct radiation from air immersion and contaminated drill cuttings
Intruder-Discovery	An individual arrives at the disposal site to construct a house. The person encounters an intact barrier, stabilized waste, or a waste package in the course of excavating a basement; determines that the site was used for radioactive waste disposal; and abandons all efforts.	6	• Inhalation of airborne radionuclides • Ingestion of contaminated soils • Direct radiation from airborne contaminants and contaminated soils

[a] A distribution of exposure times is used in the intruder analysis; the value listed is approximately equal to the sum of the mean indoor and outdoor exposure times.

[b] The time required to drill the well is specific to the area geology and depth of the well.

The homebuilder may be exposed to contamination through several exposure routes. Contaminated soils suspended during construction may be inhaled by the worker; vapor- and gas-phase radionuclides diffusing upward from the waste may also be subject to inhalation. The individual is assumed to inadvertently ingest contaminated soils during the construction process. Finally, exposures to direct radiation may result from immersion in airborne radionuclides, both as particulates and vapor- or gas-phase species, and from exposure to the waste and the material excavated during construction. The magnitude of the exposures received will depend, in part, on the length of time the receptor spends in the excavation as opposed to on the surface of the disposal site or inside the house.

Several exposure routes may contribute to the doses received by the agricultural intruder. Radionuclides suspended from the surface of the intruder's lot and contaminants diffusing from the surface of the site or into the receptor's home may result in inhalation exposures. The individual is assumed to raise vegetable crops for home consumption, and to raise forage crops for animals that supply the household with beef and milk or chicken and eggs. The dose received by the intake of contaminated soil will add to the ingestion exposure. Finally, the intruder is subject to direct radiation from the contaminated soils spread over his or her lot and from airborne radionuclides.

The Intruder–Post-Drilling Scenario also considers the exposures received by a person who lives in a house built over the disposal facility. Unlike the agricultural intruder scenario, the house is assumed to be built at grade on a concrete slab, rather than a full foundation. While this construction technique avoids the excavation of buried waste, it is assumed that contamination is brought to the surface in the course of drilling a well for domestic use. This contamination is assumed to be spread over the homeowner's lot. Routes of exposure for this intruder are the same as those outlined above for the Intruder-Agriculture Scenario.

The Intruder-Drilling Scenario evaluates the potential exposures received by a member of the crew responsible for drilling the domestic well through the closed disposal units. Contaminated cuttings brought to the surface during drilling may result in exposures to the crew. The Intruder-Discovery Scenario represents an aborted attempt to build a house over the closed disposal units. It is assumed that an individual arrives at the site to begin construction, but abandons efforts when waste or a waste package is encountered.

The routes through which members of a drilling crew or a prospective homebuilder may be exposed to radiation are limited to the inhalation of airborne radionuclides (i.e., suspended particulates, vapors, and gases), the incidental ingestion of contaminated soil and waste, and direct radiation from airborne radionuclides or contaminated soil and waste. The exposures received by the drilling crew member may be moderated because of the high moisture content of

the drill cuttings. The moisture may reduce the rate at which radionuclides are resuspended and thereby limit driller exposure from inhalation, air immersion, and possibly soil ingestion.

The intruder scenario yielding the highest doses will result in the most restrictive radionuclide concentration limits. Although all the scenarios listed in Table 3 could be included in the intruder assessment, it is more efficient to eliminate scenarios that clearly do not result in significant exposures. Toward this end, the intruder scenarios were evaluated in terms of their expected impact, and the scenarios with the greatest potential doses were identified.

The magnitude of the exposure received by an intruder is a function of the length of exposure to the contaminated media, the radionuclide concentrations in these media, and the extent to which the individual uses the contaminated resources. The two resident scenarios—the Intruder–Post-Drilling and Intruder-Agriculture Scenarios—assume the same period of exposure. The homebuilder in the Intruder-Construction Scenario is assumed to be exposed to contamination for a significantly longer period of time than the receptors for the Intruder-Discovery and Intruder-Drilling Scenarios. However, the times of exposure for all three of these intruders are much smaller than those associated with the resident intruder scenarios.

The two resident intruder scenarios differ in terms of the radionuclide concentrations in the media contacted by the individuals. If the basement excavation exceeds the thickness of the waste cover depth, the quantities of waste brought to the surface during basement excavation will generally exceed those brought to the surface with drill cuttings. Under these conditions, the agricultural intruder will be exposed to higher radionuclide concentrations in surface soils. If, however, the thickness of the cover at the time of intrusion is greater than the assumed basement depth of 3 m (9.8 ft), no waste will be brought to the surface during construction of the house. In this case, radionuclide concentrations in surface soils will be greatest for the postdrilling intruder. Concentrations of vapor- and gas-phase radionuclides in the agricultural intruder's house may be greater than those projected for the postdrilling intruder because the distance these contaminants must diffuse before entering the house is shorter.

The radionuclide concentrations encountered by the homebuilder, the intruder who abandons construction when waste is encountered, and members of the drilling crew may be greater than those encountered by the resident intruders, at least for a portion of the exposure time. If the depth of the basement excavation exceeds the cover depth, the homebuilder may come into contact with undiluted waste during the time spent in the basement excavation; contaminant concentrations during the time spent on the surface are assumed to be the same as those used to model exposures for the agricultural intruder. The receptor for the Intruder-Discovery Scenario may contact the waste during exploratory activities; the drilling crew may also come in contact with undiluted waste.

The resource utilization patterns are identical for the agricultural and postdrilling intruder scenarios. Rates of resource utilization for both of these receptors are higher than the rates corresponding to the homebuilder, the person who abandons construction efforts, and the well driller.

When the concentrations of radioactivity encountered, the times of exposure, and the level of resource utilization are taken into consideration, potential exposures are expected to be greatest for the agricultural intruder. Consequently, this scenario was included in the intruder analysis. The period of time the construction worker is exposed to contamination is much shorter than the agricultural intruder's exposure period; however, it was not clear, based on the preliminary evaluation, whether closer contact with the waste might result in higher exposures of the homebuilder in some situations. Thus, the Intruder-Construction Scenario was also included in the intruder assessment.

From all appearances, the exposures received by the postdrilling intruder should be significantly smaller than those estimated for the agricultural intruder, and possibly less than those estimated for the construction worker. However, if the waste remains undisturbed by the construction of the house (because the thickness of the cover is greater than the depth of the basement), potential exposures will be greater for the postdrilling intruder than for the agricultural intruder. The Intruder–Post-Drilling Scenario was also included in the inadvertent intruder analysis because neither the Intruder-Agriculture nor Intruder-Construction Scenarios adequately address the potential risk posed by waste disposed of at depth.

The Intruder-Discovery and Intruder-Drilling Scenarios were excluded from the intruder analysis. The receptor for the discovery scenario has the shortest exposure time of all the intruders and will contact contaminant concentrations similar to those encountered by the construction worker during basement excavation. Since the potential exposures will be greater for the construction worker (and will lead to more restrictive WAC), the Intruder-Discovery Scenario was not evaluated.

The radionuclide concentrations to which members of the drilling crew may be exposed will probably be greater than those encountered by the postdrilling resident. However, because the maximum exposure time for the well driller is about 3 percent of the exposure time for the postdrilling intruder, the driller is expected to receive much smaller exposures than the postdrilling intruder. In addition, the saturated nature of the drill cuttings will tend to minimize the potential for exposure of the crew. On this basis, then, the Intruder-Drilling Scenario was excluded from the intruder analysis.

The time at which the intruder scenarios are considered to be feasible may have significant effects on the projected doses. In general, intrusion into the waste is considered feasible at any time following the 100-year active institutional control period as long as the waste has

decomposed sufficiently to resemble ordinary soil and no barriers to intrusion are encountered. If the intruder encounters intact waste packages, stabilized waste (e.g., grout), or engineered barriers (e.g., concrete caps on disposal shafts), it is assumed that the person will stop all intrusive activities and leave the site.

It is assumed that, beyond the 100-year active institutional control period, conditions will not prevent intrusion into the disposal pits and shafts. The waste disposed of at Area G generally consists of bulk material generated from remediation and decommissioning efforts at the Laboratory, and routine operational waste; operational waste destined for the pits has been placed in metal containers since the mid-1990s while almost all waste placed in shafts since 1988 has been containerized. No impediments to intrusion into the bulk waste exist. While intact, the metal containers used in the disposal of routine operational waste may resist intrusion attempts, but their actual lifetimes under the disposal conditions at Area G are not known. Consequently, it is assumed that these containers do not limit the potential for intrusion into the waste. In terms of waste form, metals and stabilized waste may be recognizable after 100 years of burial. Once again, however, the rate at which these materials will degrade to forms that are indistinguishable from the remainder of the material in the disposal units is unknown. Lacking this information, it is assumed that these waste forms do not prevent intrusion. The other forms of waste disposed of in the pits and shafts (e.g., cellulosics, sludges, animal tissues, and filters) may be totally unrecognizable as waste within 100 years of closure of the disposal facility. Intrusion into the disposal pits and shafts is not assumed to be limited by the presence of engineered barriers because no such features are included in the facility's final closure configuration.

As discussed earlier, the basis for projecting intruder exposures and establishing intruder-based WAC is that the DOE may experience a temporary lapse in control that allows persons to arrive at the disposal site and inadvertently intrude into the buried waste. The period of time that hypothetical intruders occupy the site must be established in order to compare the projected exposures to the appropriate intruder performance objectives and to calculate radionuclide concentration limits. The NRC defines acute exposure events as those that occur for less than 1 year (NRC, 1986). On this basis, then, the Intruder-Construction scenario constitutes an acute exposure, and is subject to the acute intruder dose limit of 500 mrem/yr. Although it is unclear how long a temporary lapse in the DOE's control over the site may last, it is assumed that the resident intruders will occupy the site for a year or more. Consequently, these scenarios constitute chronic exposures that are subject to the chronic intruder performance objective of 100 mrem/yr.

The intruder exposure scenarios used to develop WAC should be placed in proper perspective with respect to current land use patterns and the need to demonstrate compliance with DOE performance objectives. The exposure scenarios were selected to provide reasonably conservative estimates of the potential exposures that may result from the waste disposed of at

Area G in the event that DOE control over the facility lapses for a brief period of time. To the extent that the scenarios represent more intensive use of potentially contaminated resources than might actually occur, the calculated doses are expected to provide additional assurance that the disposal system will perform at least as well as projected.

2.2 Modeling Approach and Input Data

Four models were used to simulate the long-term performance of Area G and to estimate potential impacts to human health and safety; these models were developed using the GoldSim™ modeling environment or platform (GoldSim, 2007a, 2007b, and 2007c). Briefly, the Area G Site Model simulates the release and transport of radionuclides to the surface of the disposal facility and to off-site locations for all natural processes. The Area G Intruder Model projects doses and estimates intruder-based WAC for all radionuclides except vapor- and gas-phase isotopes and radionuclides that decay to form such; the Area G Intruder Diffusion Model estimates doses and WAC for radionuclides subject to diffusive releases and transport and the parents of such. The Area G Inventory Model calculates the initial radionuclide inventories that are used in the site, intruder, and intruder diffusion models. The GoldSim models used to conduct the performance assessment and composite analysis have been fully documented in Shuman (2008a), which includes a detailed description of the models, the mathematical bases of the models, and the data used to conduct the simulations.

This section presents the approach that was used for modeling. Section 2.2.1 briefly describes the models used to conduct the dose assessment, drawing on the information found in Shuman (2008a), and discusses the manner in which the models were implemented. As discussed earlier, field sites that are required to conduct a composite analysis must consider the cumulative impacts of LLW disposal facilities and other sources of radioactivity that could interact with releases from these facilities. Consistent with this requirement, the composite analysis includes all waste disposed of at Area G and evaluates the potential impacts of other sources of radioactivity at the Laboratory. Section 2.2.2 describes the approach adopted for this alternate source analysis.

2.2.1 Model Configuration and Implementation

The general modeling approach used to estimate doses and calculate intruder-based WAC is described below, focusing on the how the GoldSim models were implemented. Section 2.2.1.1 discusses the radionuclide inventories adopted for the dose assessment, while Section 2.2.1.2 discusses the release and transport pathways relevant to Area G. Information concerning the manner in which the exposure scenarios were modeled is found in Section 2.2.1.3.

2.2.1.1 Disposal Facility Characteristics and Radionuclide Inventory

The performance assessment and composite analysis address different portions of the waste that have been disposed of at Area G since the facility opened in 1957. The performance assessment

addresses the waste disposed of after September 26, 1988, and the waste expected to require disposal through the end of disposal operations, which is assumed to occur in 2044. The inventory for the composite analysis includes all waste disposed of at Area G since the facility opened and any waste requiring disposal in the future.

Two major types of disposal units are used at Area G: pits and shafts. The vast majority of the waste is placed in disposal pits, which are large, generally rectangular units excavated using heavy equipment. Pit disposal began in the second quarter of 1957, when nonroutine waste was placed in pit 1. Prior to the mid-1990s, the majority of the waste disposed of in the pits was placed in lifts, separated by layers of uncontaminated crushed tuff. Current operational procedures require that waste other than bulk soils and debris be placed in metal containers prior to disposal. Bulk materials are placed directly in the disposal pits, and may be used to fill void spaces between and within waste containers.

Disposal shafts have been used at Area G since 1966. A regulatory requirement for some types of waste, shafts are used to provide additional shielding of waste with high external radiation levels, to facilitate placement using remote handling techniques, and to accommodate special packaging requirements. The shafts are drilled using augers; shaft diameters generally range from 0.3 to 4.9 m (1 to 16 ft). Waste packages are lowered into the shafts and stacked on top of one another. Crushed tuff may be added as backfill around the waste packages, thereby reducing void spaces in the disposal units.

Area G consists of Material Disposal Area (MDA) G, the portion of the site currently receiving waste, and the Zone 4 expansion area, located immediately west of MDA G. Estimates of the volumes and activities of waste that have been, or will be, disposed of in these portions of the facility have been prepared. Separate radiological inventories have been developed for the performance assessment and composite analysis. Each of these inventories addresses different periods of disposal and the waste placed in the pits and shafts. Distinctions between the times and modes of disposal were made to allow demonstration of compliance with the performance assessment and composite analysis performance objectives and to better understand the uncertainties associated with the inventory projections. A complete description of the methods used to estimate these inventories is available in Shuman (2008b).

The inventory projections estimate that more than 240 radionuclides have been disposed of at Area G. Many of these radionuclides are short-lived and pose little or no risk to human health and safety or the environment. Given this, radionuclides with half-lives of 5 years or less were generally excluded from the inventories used to conduct the performance assessment and composite analysis modeling. Short-lived radionuclides that are daughters of long-lived parents were accounted for through the modeling of radioactive decay and ingrowth; short-lived radionuclides that give rise to potentially significant activities of long-lived daughters were maintained in the performance

assessment and composite analysis inventories. Shuman (2008b) details the approach used to exclude contaminants from the modeling on the basis of decay characteristics.

Current plans call for the disposal of waste in the pits and shafts in MDA G through 2010 and 2015, respectively; pits and shafts established in the expansion area will receive waste thereafter. It is anticipated that the waste included in the performance assessment and composite analysis inventories will be disposed of in more than 40 pits and 200 shafts by the time Area G closes in 2044. The nature of these units and their locations within the disposal facility influence the modeling conducted to project the long-term performance of Area G. Because of this, the disposal facility was divided into eight smaller areas referred to as waste disposal regions. The portion of the site occupied by MDA G is divided into seven regions as shown in Figure 1. An eighth waste disposal region is used to represent the Zone 4 expansion area at Area G; this region is not shown in the figure. Disposal regions 2 through 5 consist exclusively of pits and regions 6 and 7 include only shafts; disposal regions 1 and 8 include both pits and shafts.

The basis for defining the waste disposal regions is discussed later in this report. From an inventory perspective, however, dividing the site into smaller regions required development of performance assessment and composite analysis inventories specific to these regions. This was done by summing the inventories over the disposal units located in each disposal region. Separate inventories were developed for the waste addressed by the performance assessment and composite analysis.

The radionuclides disposed of at Area G will undergo radioactive decay and ingrowth over time; accounting for these processes is an important aspect of the performance assessment and composite analysis modeling. Patterns of decay and ingrowth are influenced by the disposal history of the waste. To minimize the need for detailed accounting of disposal dates, all waste disposed of within a waste disposal region was assumed to be placed in the disposal units at a uniform rate over the period of time those units were active.

The radionuclide concentrations in the buried waste will depend, in part, upon the waste emplacement efficiency. The emplacement efficiency is defined as the fraction of the disposal capacity that is occupied by waste; the remainder of the disposal unit is assumed to contain uncontaminated fill. The site, intruder, and intruder models use the disposal area and waste thickness for each waste disposal region to account for the dilution of the waste with uncontaminated backfill.

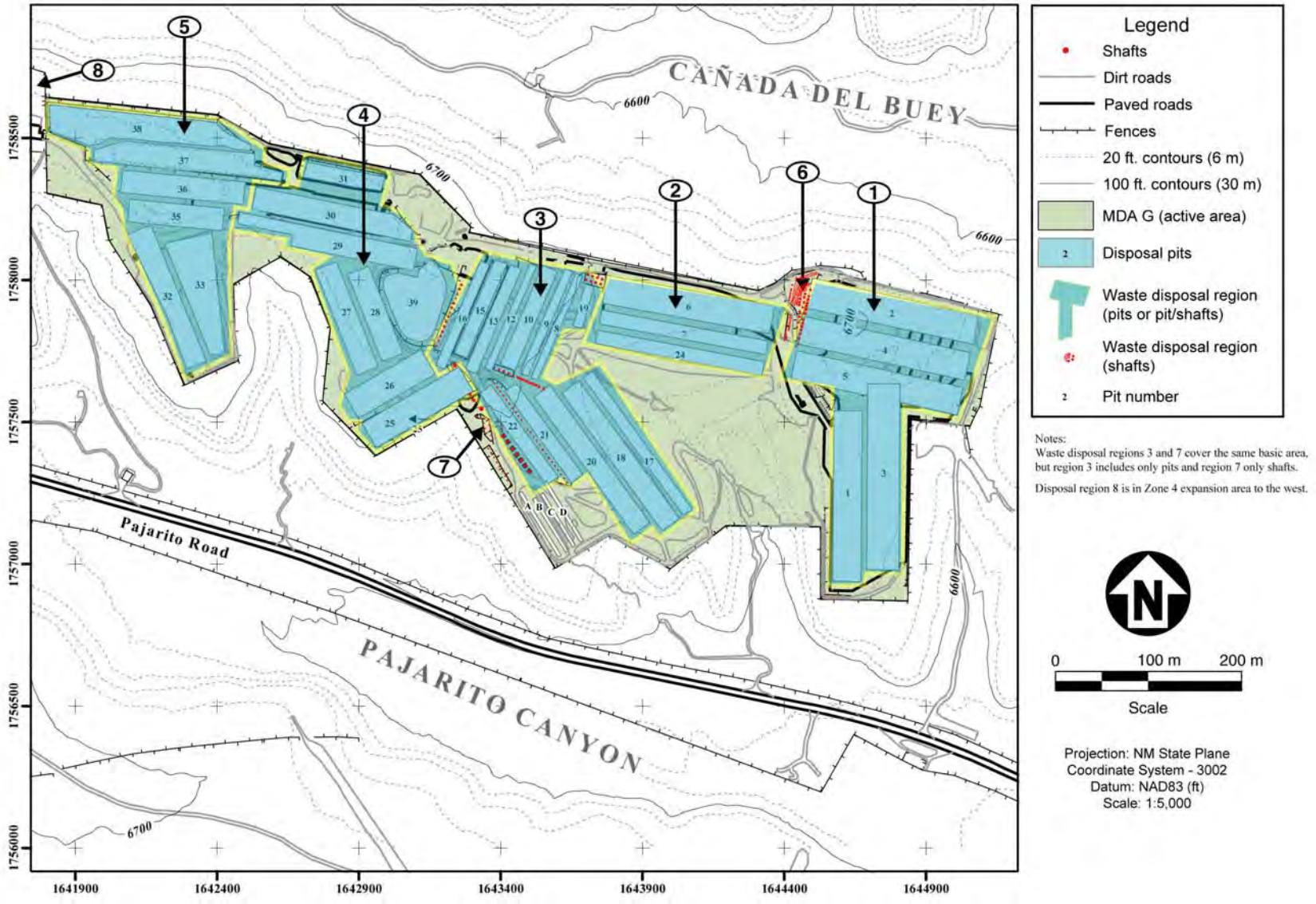

Figure 1
Waste Disposal Regions at Area G

Source: Apogen Technologies (formerly SEA)
LANL RRES Database, Map ID: 4531.021 (1) Rev. 2

The radionuclide concentrations estimated for the disposal shafts also take into consideration what is referred to as the shaft field efficiency. Shafts are relatively small, discrete units that are generally arranged in groups referred to as shaft fields; a single shaft field typically contains a handful to tens of disposal units. Shafts within a shaft field are required to be placed a minimum distance apart from one another, generally on the order of 2 to 5 m (6.6 to 16 ft). As a result, approximately 10 percent of the surface area of the shaft field consists of disposal units, the remainder consisting of undisturbed portions of the disposal site. Radionuclide concentrations in the shafts are calculated on a shaft-field basis, taking the effects of unit placement into account.

The modeling conducted to estimate doses for members of the public uses the entire performance assessment and composite analysis inventories. The intruder analysis considers subsets of the performance assessment inventory; the performance assessment inventory was divided into time-specific segments to enable the development of WAC specific to the disposal pits and shafts located in MDA G.

The inventories in the disposal pits and shafts were assumed to be uniformly distributed throughout the units for the modeling that estimated exposures for members of the public. This same approach was used to model the exposures received by any intruders who disturb the waste disposed of in the 1988–2010 pits, 2011–2044 pits, or 2016–2044 shafts. Preliminary modeling indicated that the projected exposures for the 1988–2015 shafts under the agricultural intruder scenario would be approximately equal to or greater than the 100 mrem/yr chronic dose objective if the radionuclides in the waste were homogeneously mixed throughout the disposal units. Consequently, the depth at which critical radionuclides are disposed of within these units was evaluated to ensure that the projected inventory for these units was disposed of in a safe manner. The approach used to conduct the depth-of-disposal evaluation is described in Shuman (2008a); the results of the analysis were used to model the exposures that would result from intrusion into the 1988–2015 shafts.

2.2.1.2 Radionuclide Release Mechanisms and Transport Pathways

Radionuclides in the waste disposed of at Area G may be released to the environment as a result of biotic intrusion, contaminant leaching, vapor- and gas-phase diffusion, and human intrusion. Transport of these releases may result in the contamination of ground and surface waters, surface soils, biota, and air. This section summarizes the release and transport pathways included in the performance assessment and composite analysis modeling. Detailed descriptions of the manner in which these processes were modeled may be found in Shuman (2008a).

Release Mechanisms

Biotic intrusion is a potentially significant mechanism through which radionuclides may be transported to the surface of the disposal facility. Native vegetation growing over the site may extend into the waste and assimilate radionuclides in the waste, depositing contamination on the

surface of the site when plant litter falls to the ground and decays. Animals inhabiting the disposal site may burrow into the waste, displacing contaminated material to the surface of the site. Over time, contamination deposited on the ground may be mixed over the interval occupied by animal burrows as the burrows collapse.

The GoldSim models project rates of radionuclide release due to biotic intrusion, taking into account temporal changes in the plant and animal communities that may occur as a result of ecological succession. Rates of radionuclide uptake are estimated for four plant growth forms (i.e., grasses, forbs, shrubs, and trees) and used to determine the rates at which contaminants enter the surface soil following litterfall and litter decomposition. The quantities of waste displaced by four taxa of burrowing animals (i.e., harvester ants, pocket gophers, mice, and chipmunks and ground squirrels) are projected and factored into estimates of contaminant concentration in surface soils.

Rates of radionuclide release due to leaching are proportional to the rate of infiltration through the disposal units and inversely proportional to the contaminant-specific soil-to-water partition coefficients. The modeling conducted in support of the performance assessment and composite analysis is based on the assumption that steady-state flow conditions exist within the disposal units; rates of infiltration in this region were estimated on the basis of work conducted by Newman et al. (2005) and Levitt (2008). Radionuclides were assumed to partition between pore moisture and the solid fraction of the waste; partition coefficients for crushed tuff—the material used as backfill in the pits and shafts—were used to estimate contaminant concentrations in the pore water. Rates of leaching from the waste were assumed to be unaffected by the presence of waste containers, which may limit contact between the waste and infiltrating water while they are intact, or the form of the waste (e.g., activated metals or other bulk-contaminated media).

A small number of the contaminants included in the performance assessment and composite analysis exist in a vapor or gaseous phase: these include tritiated water vapor, C-14 gas, and isotopes of krypton and radon. Such radionuclides may diffuse upward from the buried waste and exit from the surface of the facility; diffusive releases may enter the basement excavation or the house of the resident intruder as well. The Area G Site and Intruder Diffusion Models estimate rates of diffusive release from the buried waste differently depending upon the radionuclide under consideration. Quantities of tritiated water vapor present in the waste are estimated on the basis of water vapor pressure, while C-14 gas is generated when the organic fraction of the C-14 waste biodegrades to form carbon dioxide and methane. Concentrations of krypton gas in the air-filled pore spaces of the waste are estimated using an air-to-water partition coefficient. A similar approach is taken for Rn-222 and Rn-220 following the generation of these isotopes through the decay of Ra-226 and Th-228, respectively.

Human activity may also release radionuclides to the surface. The amount of contamination brought to the surface of the disposal facility as a result of human intrusion depends upon the intruder scenario under consideration and the thickness of the cover at the time of intrusion. During construction, for example, excavation of the basement will result in waste being transported to the surface of the facility only if the assumed depth of the basement (3 m [9.8 ft]), exceeds the cover thickness. Establishment of a domestic well at the site will result in surface contamination regardless of the cover depth. The radionuclide concentrations in the surface soils resulting from these human activities are estimated based on the assumption that the excavated material is spread evenly across the intruder's net lot area (i.e., the area of the lot minus the area occupied by the house).

With one exception, the rates of release via the mechanisms outlined above were assumed to be unaffected by the presence of waste containers or the form of the waste (e.g., activated metals or other bulk-contaminated media). This approach overlooks the fact that intact containers may limit contact between the waste and plants, animals, and infiltrating water, and may slow the release of vapor- or gas-phase radionuclides. The potential impact of container performance on vapor-phase tritium releases was investigated as part of the intruder analysis for the disposal shafts. The containers used to dispose of high-activity tritium waste in these units are subject to WAC that prescribe maximum off-gas rates (LANL, 2008); exposures for the intruders were evaluated taking these release limits into account.

Transport Pathways

Radionuclides may be transported from the point of release through a number of transport pathways. Contaminants leached from the waste will be transported vertically through the unsaturated zone with infiltrating water, eventually discharging to the regional aquifer under the Laboratory. Contamination entering the aquifer will be transported horizontally to locations downgradient of Area G, where it may intersect groundwater wells. Stauffer et al. (2005) modeled groundwater flow and contaminant transport in support of the performance assessment and composite analysis. This analysis relied on the Finite Element Heat and Mass (FEHM) computer code to construct three-dimensional groundwater models and to develop one-dimensional abstractions of these models. The one-dimensional abstractions are incorporated into the GoldSim site model and used to project rates of contaminant discharge to a well located 100 m (330 ft) downgradient of the Area G fence line.

The rates at which radionuclides are transported to the regional aquifer are strongly influenced by the geohydrologic properties of the unsaturated zone underlying the pits and shafts. Changes in these properties along the east-west axis of the disposal site have substantial effects on contaminant transport behavior. The waste disposal regions described earlier are used to represent the spatial variability in the geohydrologic properties of the unsaturated zone. Dividing

the site into waste disposal regions also allows differences in the depth of disposal in the pits and shafts to be modeled.

Most of the radionuclides included in the performance assessment and composite analysis will be present in the regional aquifer in negligible quantities, if at all, and thus will not pose a health threat to persons using water contaminated by Area G releases. A screening evaluation was conducted to identify all such radionuclides, which were then eliminated from the groundwater transport modeling. The two-step process took into account the risk posed by the contaminants under conservative release conditions and radionuclide travel times to a well immediately downgradient of Area G. A detailed description of the screening evaluation is provided in *Attachment I.*

Contamination deposited on the surface of the disposal facility is subject to resuspension and transport to downwind locations by the prevailing site winds and to transport into the canyons adjacent to Area G by surface runoff. Rates of particulate resuspension were estimated on the basis of work conducted by Whicker and Breshears (2005). These resuspension rates, in conjunction with the radionuclide concentrations in surface soils projected by the GoldSim models, were used to estimate contaminant fluxes from the surface of the disposal facility. Contaminant concentrations in air and surface soils were estimated for locations downwind of Area G using dispersion factors and deposition rates projected by the atmospheric transport modeling conducted by Jacobson (2005).

The transport of vapor- and gas-phase radionuclides from the waste to the surface of the disposal facility was modeled using the diffusion modeling capabilities of GoldSim. Contaminants exiting from the surface of the facility will be transported downwind with the prevailing winds. Concentrations of these contaminants in the air at potential downwind receptor locations were estimated on the basis of the atmospheric transport modeling (Jacobson, 2005). Modeling of the diffusion of vapor- and gas-phase radionuclides into the basement excavation and the house of the residential intruder relied on the diffusion modeling capabilities of GoldSim.

Contaminated surface soils may be transported into Cañada del Buey and Pajarito Canyon by the prevailing winds and surface runoff. Work conducted by Whicker and Breshears (2005) indicated no net loss of cover under conditions similar to those expected at Area G following closure of the disposal facility. Work conducted by Wilson et al. (2005) projected spatially variable rates of erosion due to surface runoff, and estimated rates and patterns of sediment transport into the canyons. The results of this effort were used to model the transport of radionuclides from the mesa top and subsequent contamination of potential receptor locations within Pajarito Canyon and Cañada del Buey.

Surface erosion at Area G will gradually reduce the thickness of the cover placed over the disposal units. The loss of cover may provide greater opportunities for plant roots and animal burrows to penetrate into the waste. As the cover thins, greater proportions of the plant roots and animal burrows will contact the waste, bringing larger amounts of contamination to the surface of the facility. Higher contaminant concentrations in the surface soils at Area G may result in higher radionuclide concentrations at downwind locations and at receptor locations within the adjacent canyons. The surface erosion modeling results of Wilson et al. (2005) were used to account for the effects of cover loss on the impacts of biotic intrusion and vapor- and gas-phase diffusion; projected rates of cover loss were also taken into account when estimating the impacts of human intrusion.

As indicated earlier, the primary radionuclide release mechanism for the intruder modeling is expected to be the deposition of waste on the surface of the disposal facility during basement excavation and well drilling. However, the release and transport of radionuclides prior to the arrival of the intruder may influence the projected intruder exposures. For example, contamination deposited on the surface of the disposal facility by plants and animals may add to the exposures received from waste excavated as a result of human activities. In cases where the cover depth is greater than 3 m (9.8 ft) at the time of intrusion, the exposures received by the construction or agricultural intruders may be determined largely by the contaminants transported up into the cover as a result of biotic intrusion. Consequently, the intruder models simulate the effects of biotic intrusion up to the time at which humans arrive at the facility.

2.2.1.3 Exposure Estimates and Waste Acceptance Criteria Calculations

Several exposure scenarios were used to evaluate the risk posed by the disposal of radioactive waste at Area G to members of the public, and to project doses for the inadvertent intruder. These scenarios and the exposure pathways included in each are discussed in Section 2.2. The models and data used to estimate the potential exposures are described in Shuman (2008a).

The site model was implemented in deterministic and probabilistic fashions to project potential exposures for members of the public. Deterministic simulations were conducted to gain insight into the long-term performance of the disposal facility, well beyond the 1,000-year compliance period. A simulation period of 100,000 years was used for the groundwater pathway-based scenarios and a 50,000-year period was modeled for the Atmospheric and All Pathways–Canyon Scenarios. The probabilistic modeling was used to simulate facility performance and project potential exposures over the 1,000-year compliance period.

Preliminary modeling of the groundwater pathway exposures indicated that most radionuclides included in the Area G inventory arrive at the downgradient well long after the 1,000-year compliance period. To focus the modeling on those contaminants that pose a potentially significant risk to groundwater users during the compliance period, many of the 19 contaminants

initially included in the groundwater transport modeling were excluded from the probabilistic modeling. The radionuclides selected for exclusion were identified using a 50-realization probabilistic simulation; potential doses were projected for the All Pathways–Groundwater Scenario over a period of 1,000 years using the composite analysis inventory. Contaminants that did not reach the aquifer during the compliance period or contributed less than 1 percent of the peak mean dose projected for this period were excluded from the final probabilistic analysis.

A portion of the radon diffusing upward from the waste will decay prior to exiting from the surface of the disposal facility. The daughter products will be deposited at the site of decay and may constitute a source of contamination for persons living downwind of the disposal facility or in the adjacent canyons. In general, the only impacts of radon diffusion that need be considered are those associated with Rn-222. The decay products of this isotope include relatively long-lived Pb-210, which will persist in the environment for some time. All daughter products of Rn-220 have half-lives of hours or less and will quickly decay to negligible levels. The potential impacts of Rn-222 diffusion on projected exposures were taken into account.

The intruder and intruder diffusion models were applied in a probabilistic fashion to project potential exposures and to calculate intruder-based WAC. Intruder doses were projected separately for the pit inventories disposed of from September 27, 1988 through 2010, the shaft inventories disposed of from September 27, 1988 through 2015, and the pit and shaft inventories disposed of between the end of each of these periods and 2044. Waste acceptance criteria were calculated for waste disposed of in the pits and shafts in MDA G; this portion of the facility is assumed to receive all pit waste through 2010 and all shaft waste through 2015.

The exposures projected for the inadvertent intruders are influenced by the locations of the pits and shafts within the disposal facility. The amount of cover placed over the site at the time of final closure will vary spatially in response to the contouring conducted to achieve the final cover characteristics; rates of erosion will also vary spatially. These factors ultimately determine how much cover exists over the disposal units at the time of human intrusion and, therefore, how much of the waste is disturbed by the intrusive activities.

The waste disposed of in pits since 1988 has been placed in units 15, 30, 31, and 36 through 39; these units are located in waste disposal regions 3, 4, and 5 (Figure 1). Waste placed in pits through 2010 is expected to be disposed of in MDA G; for modeling purposes, this waste was assumed to be placed in pit 38. The intruder analysis for the 1988–2010 waste was conducted using the initial cover thicknesses and erosion rates estimated for the specific pits in which the waste was placed. Waste disposed of in pits from 2011 through 2044 is expected to be placed in the Zone 4 expansion area; the cover and erosion characteristics of waste disposal region 8 were used to model intruder exposures for this waste.

Waste disposed of in shafts since 1988 has been placed in units located in disposal region 6 (Figure 1), near the east end of the facility, and in region 7, in the center of MDA G; most waste has been placed in shafts located in disposal region 7. The cover thicknesses and erosion rates projected for waste disposal region 7 formed the basis of the intruder modeling for the 1988–2015 shaft waste; the Zone 4 cover and erosion characteristics were used to evaluate the 2016 through 2044 waste.

Preliminary modeling was conducted to determine if the redistribution of radionuclides resulting from radon diffusion had any impacts on the exposures estimated for the three intruder scenarios. A series of 50-realization probabilistic simulations was conducted in which intruder doses were calculated with and without the effects of radon diffusion; these simulations addressed the waste placed in pits from 1988 through 2010 and in shafts from 1988 through 2015 as well as the waste placed in pits and shafts after these periods. The results of this modeling were used to configure the full probabilistic assessment of intruder doses.

The intruder and intruder diffusion models were used to calculate WAC for all radionuclides considered in the development of the performance assessment inventory, except for those eliminated on the basis of half-life. This modeling yielded distributions of radionuclide-specific doses for the disposal units under consideration and distributions of corresponding WAC. The final concentration limits adopted for the disposal units are the mean or median values of the WAC distributions, whichever are more restrictive.

The results of the probabilistic modeling were used to conduct sensitivity analyses. These analyses provide a means for identifying the sources of significant uncertainty associated with the projected impacts, helping to focus future research and development and modeling efforts on facility characteristics and site processes that are most important to the long-term performance of Area G. Model sensitivity was evaluated using rank correlation coefficients calculated within the GoldSim models. Analyses were performed for a subset of the exposure scenarios included in Tables 2 and 3; these scenarios were selected on the basis of the impacts projected for each.

2.2.2 Alternate Source Analysis

The composite analysis must consider alternate sources of contamination that may add to exposures resulting from Area G releases. The first step in the alternate source analysis was to locate other potentially significant contaminant sources at the Laboratory. A source was considered a viable candidate for inclusion in the analysis if its radionuclide inventories are similar in scale to those at Area G, or if it is in close proximity to Area G or the area affected by potential releases from Area G.

Once the alternate sources were identified, the potential for significant interaction between releases from these sources and from Area G was evaluated. In most cases, interaction requires

the release of contaminants from the alternate sources and the subsequent transport of this contamination to locations downwind or downgradient of Area G. Radionuclides released to, or otherwise present in, Cañada del Buey and Pajarito Canyon may also interact with releases from the disposal facility, if they are discharged or transported to locations adjacent to Area G.

Modeling conducted in support of the performance assessment and composite analysis was used to estimate the potential for interaction between contaminants released to the atmosphere or groundwater from alternate sources and from Area G. Atmospheric transport modeling (Jacobson, 2005) considered whether airborne releases from alternate sources might add to the exposures estimated for members of the public living downwind of Area G. The groundwater flow and transport modeling conducted by Stauffer et al. (2005) provided information that was used to assess the potential for significant interaction from a groundwater pathway perspective. The potential significance of interactions between canyon contamination from other sources and releases to Cañada del Buey and Pajarito Canyon from Area G was evaluated using information about the types of discharges that enter the canyons and sampling results for canyon sediments.

3.0 Performance Assessment and Composite Analysis Dose Projections

The dose projections for members of the public living in the vicinity of Area G are presented below. Section 3.1 presents and discusses the doses projected using the Area G performance assessment inventory; exposure estimates for the composite analysis are presented in Section 3.2. Both deterministic and probabilistic dose projections are provided.

The deterministic modeling was conducted to provide general insight into the performance of the disposal facility well past the 1,000-year compliance period. The results of this modeling provide an indication of the spatial and temporal aspects of radionuclide release and transport over the simulation periods shown, but the magnitudes of the projected exposures should be used with caution. The input data used in this modeling are almost exclusively the median values of the distributions adopted for stochastic parameters. An important aspect of the long-term performance of the disposal facility is the thickness of the cover over the disposal units and the rate(s) at which cover is lost due to surface erosion. For the deterministic modeling, median values of initial cover thickness were adopted for the different waste disposal regions, and cover loss functions estimated for the locations with those initial thicknesses were used to simulate the impacts of erosion. Exposures projected on the basis of these data do not necessarily represent the most likely doses, nor do they necessarily bound likely exposures. Full probabilistic modeling is required to estimate doses that are statistically meaningful.

The probabilistic modeling results are provided in terms of dose distributions. Information is presented throughout the following discussion to provide an indication of the nature of the projected distributions.

3.1 Performance Assessment Projections

The exposure scenarios discussed in Section 2.1 address potential exposures received by persons living downgradient of the disposal facility, at the point(s) of maximum atmospheric exposure, and in the canyons adjacent to Area G. The dose projections for the performance assessment are organized in terms of these exposure locations. Section 3.1.1 presents and discusses dose estimates for members of the public exposed to contaminated groundwater, while Section 3.1.2 addresses potential exposures of persons living downwind of the site and fluxes of radon gas from the disposal facility. The discussion is concluded in Section 3.1.3, with the presentation of exposure projections for persons living in Cañada del Buey and Pajarito Canyon.

3.1.1 Groundwater Scenarios

The potential impacts of radionuclides released from Area G and discharged to the regional aquifer were evaluated using the Groundwater Resource Protection Scenario and the All Pathways–Groundwater Scenario. The doses projected for these exposure scenarios are presented below.

3.1.1.1 Groundwater Resource Protection Scenario

Deterministic and probabilistic analyses were conducted to estimate the potential impacts of radionuclides discharged to the regional aquifer on persons who rely upon that aquifer as a source of drinking water. The deterministic analysis simulated facility performance over a period of 100,000 years to provide insight into facility performance well beyond the 1,000-year compliance period.

The results of the deterministic simulation are shown in Figure 2; the doses shown in the figure correspond to a location 100 m (330 ft) east of the Area G fence line. Annual doses peak about 46,000 years after facility closure, reaching a maximum of 0.0058 mrem/yr; C-14 is the sole contributor to this exposure. No other radionuclides are projected to reach the receptor's well during the 100,000-year period.

A screening analysis was conducted to limit the number of radionuclides included in the probabilistic modeling to those that would make a meaningful contribution to exposures during the 1,000-year compliance period. The results of this 50-realization probabilistic evaluation indicated that no radionuclides would reach the well located 100 m (330 ft) east of Area G during this period. Consequently, a probabilistic assessment of the exposures for the groundwater protection scenario was not conducted.

3.1.1.2 All Pathways–Groundwater Scenario

The deterministic modeling results for the All Pathways–Groundwater Scenario are shown in Figure 3. The doses shown in the figure correspond to the point of maximum groundwater exposure 100 m (330 ft) east of the Area G fence line. The receptor near the town of White Rock was not projected to be exposed to contaminated groundwater during the operational, closure, and active institutional control periods because of very long groundwater travel times to this location. The projected peak exposure, which occurs 46,000 years after facility closure, is 0.0062 mrem/yr; C-14 concentrations in the regional aquifer decline thereafter. No other radionuclides are projected to discharge to the regional aquifer within 100,000 years of facility closure. The doses are dominated by the ingestion of contaminated crops and animal products raised by the receptor, with the ingestion of contaminated drinking water making a smaller contribution. The screening analysis indicated that no radionuclides will reach the receptor's well during the 1,000-year compliance period. Therefore, no probabilistic modeling results are provided for this scenario.

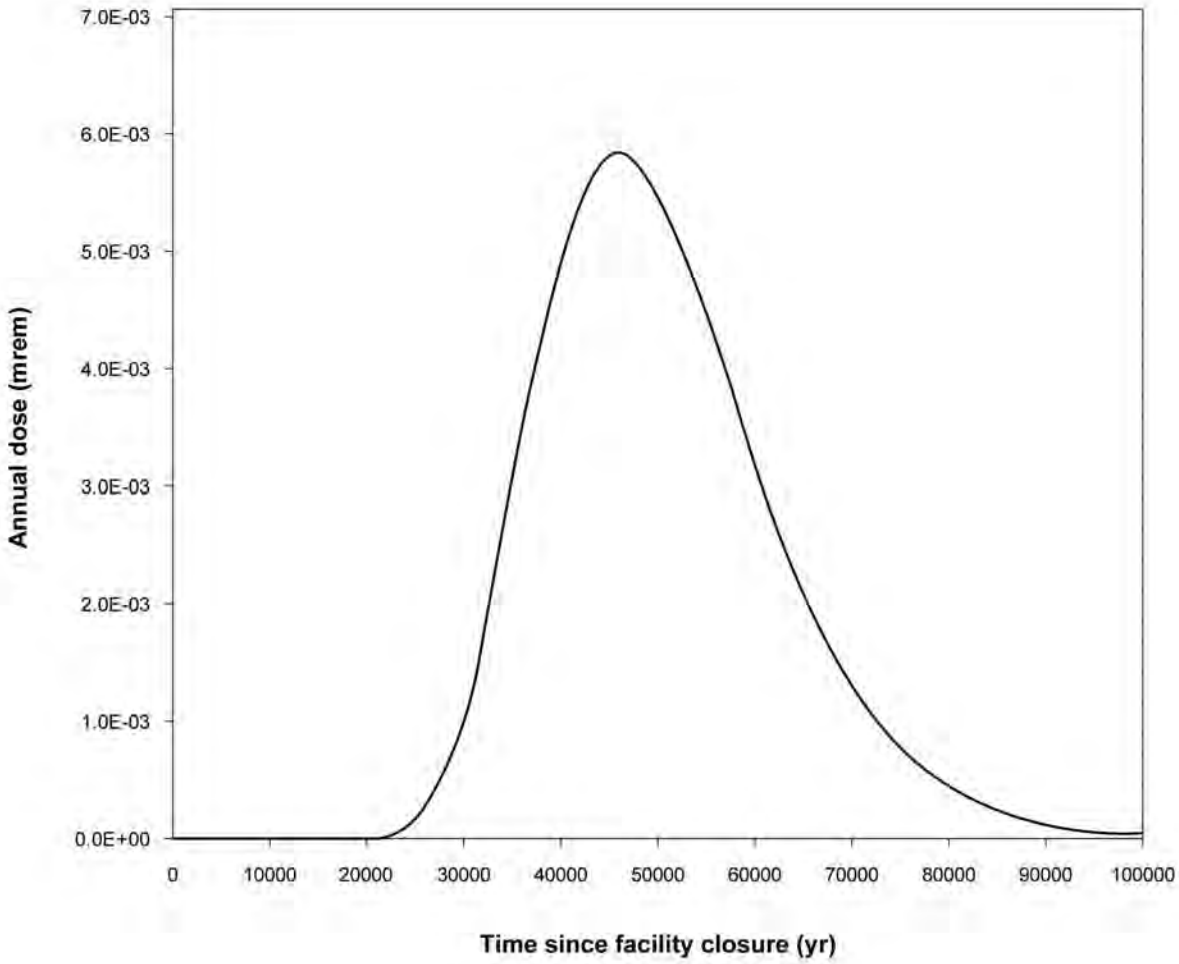

Figure 2
Deterministic Dose Projections for the Groundwater Resource Protection Scenario

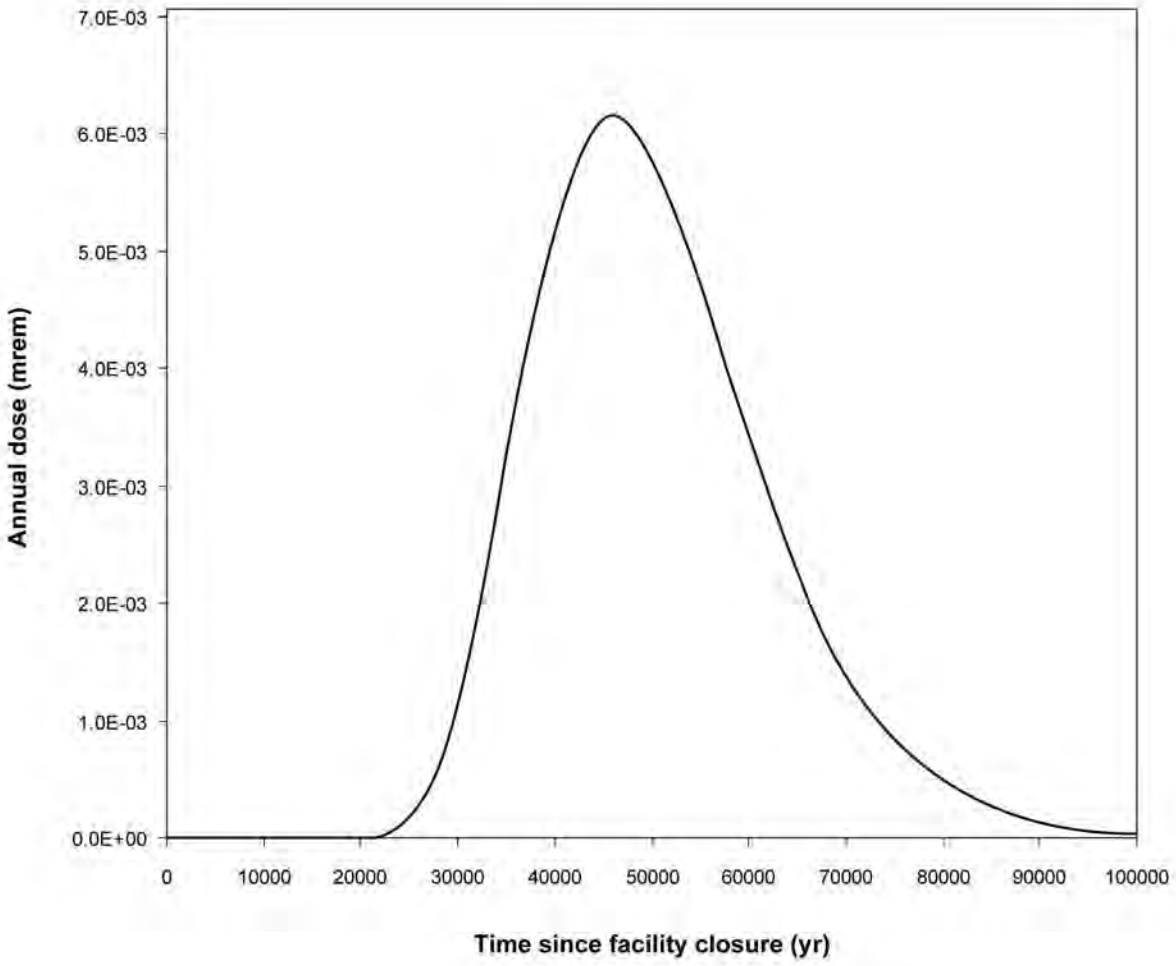

Figure 3
Deterministic Dose Projections for the All Pathways–Groundwater Scenario (performance assessment)

3.1.2 Atmospheric Scenario

The deterministic modeling results for the Atmospheric Scenario are shown in Figure 4 for 50,000 years following site closure, the period for which surface erosion modeling was conducted. The projected downwind exposures at the LANL boundary are greatest early in the simulation period and are the result of tritiated water vapor diffusing from the disposal facility. A peak exposure of 0.25 mrem/yr is projected to occur and results almost entirely from inhaling airborne tritium. Following an initial peak due to tritium releases, the exposures projected for the Area G fence line exposure location increase throughout the simulation. The peak exposure of 0.032 mrem/yr is dominated by exposures to Ac-227, K-40, Pa-231, Pb-210, Ra-226, and U-238; the projected exposures result primarily from the ingestion of crops grown in contaminated soils and direct radiation from these soils.

Figure 5 shows probabilistic model projections for the Atmospheric Scenario. The mean doses projected for the receptor at the LANL boundary reach a maximum of 0.18 mrem/yr about 60 years after the start of disposal operations at Area G (Figure 5a). This exposure is due to the inhalation of tritiated water vapor that diffuses upward from the site and is transported with the prevailing winds. The exposures to tritium decrease rapidly as the inventory of the radionuclide is depleted and the isotope undergoes radioactive decay. The exposures projected for the other radionuclides in the waste increase slowly over the time, reaching a peak mean exposure of 0.0055 mrem/yr at the end of the 1,000-year compliance period. The exposures projected for the LANL boundary receptor are less than the 10 mrem/yr performance objective that applies to all airborne releases from the Laboratory.

The exposures projected for the receptor at the Area G fence line (Figure 5b) decrease initially as exposures from vapor- and gas-phase radionuclides wane. The projected doses increase throughout the latter portion of the compliance period, however, reaching a peak mean dose of 0.014 mrem/yr at the end of the period. The radionuclides that make major contributions to the projected exposures are shown in Figure 6. K-40 is responsible for 79 percent of the projected peak mean exposure; Pb-210, U-234, and U-238 contribute another 16 percent of the total. The primary exposure pathways for the fence line receptor are the ingestion of contaminated crops and animal products, and direct radiation from soils; these account for about 90 percent of the peak mean exposure. All of the projected mean exposures are much less than the 10 mrem/yr performance objective that applies to airborne releases.

The radon fluxes projected for the eight waste disposal regions are summarized in Table 4. The peak mean fluxes range from about 1.8×10^{-6} pCi/m^2/s for disposal region 1 to 14 pCi/m^2/s for region 7; fluxes for all disposal regions are less than the flux objective of 20 pCi/m^2/s. The radon fluxes projected for the different waste disposal regions yield a site-wide peak mean flux of 0.43 pCi/m^2/s; this peak occurs at about the time disposal at Area G ceases.

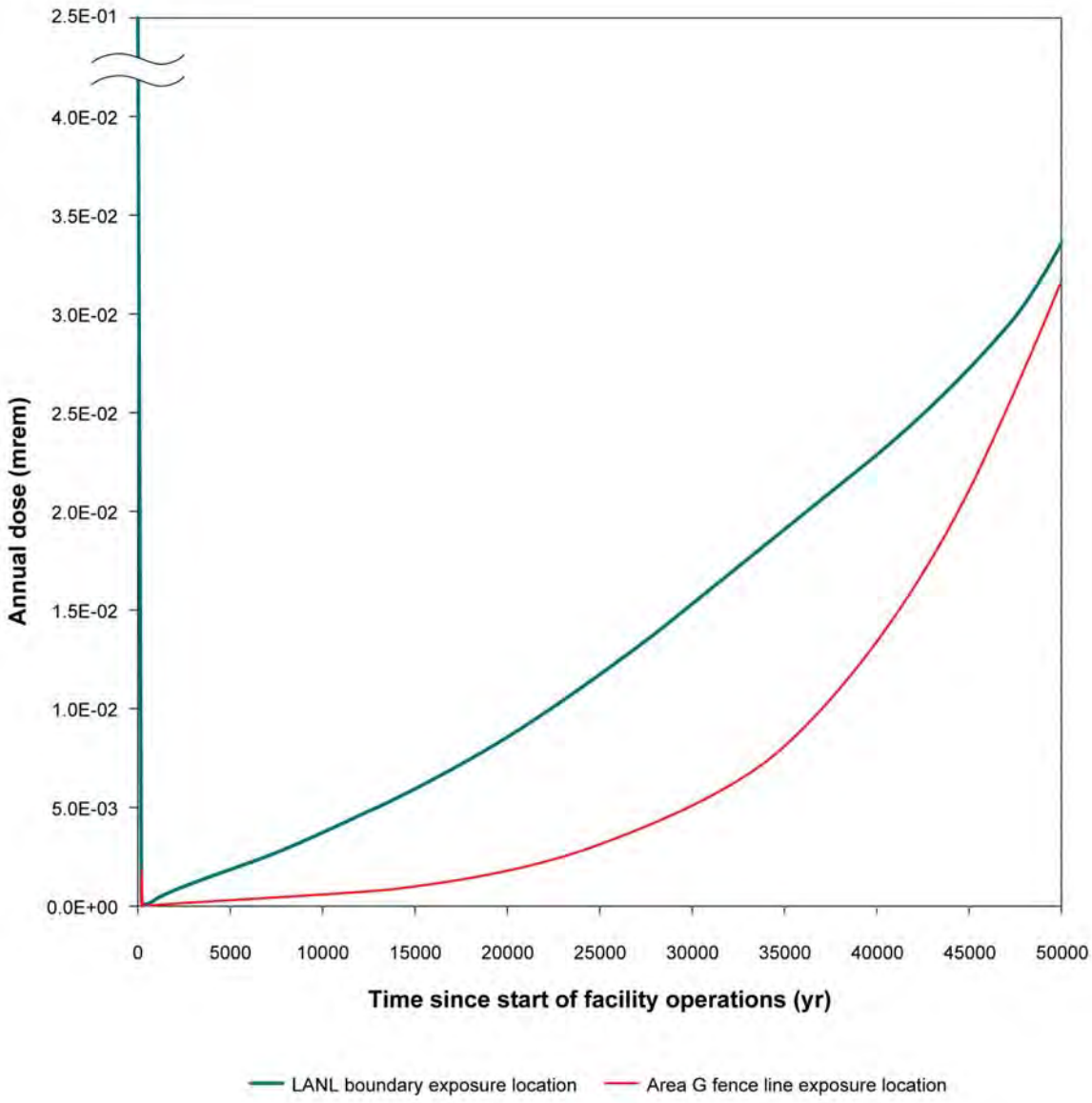

Figure 4
Deterministic Dose Projections for the Atmospheric Scenario (performance assessment)

Figure 5a. LANL boundary exposure location

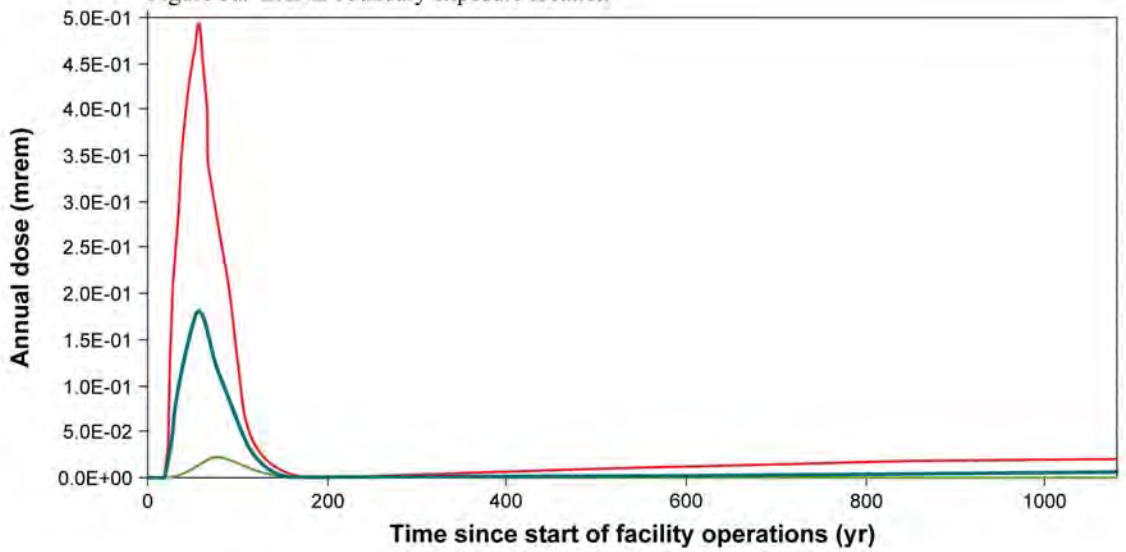

Figure 5b. Area G fence line exposure location

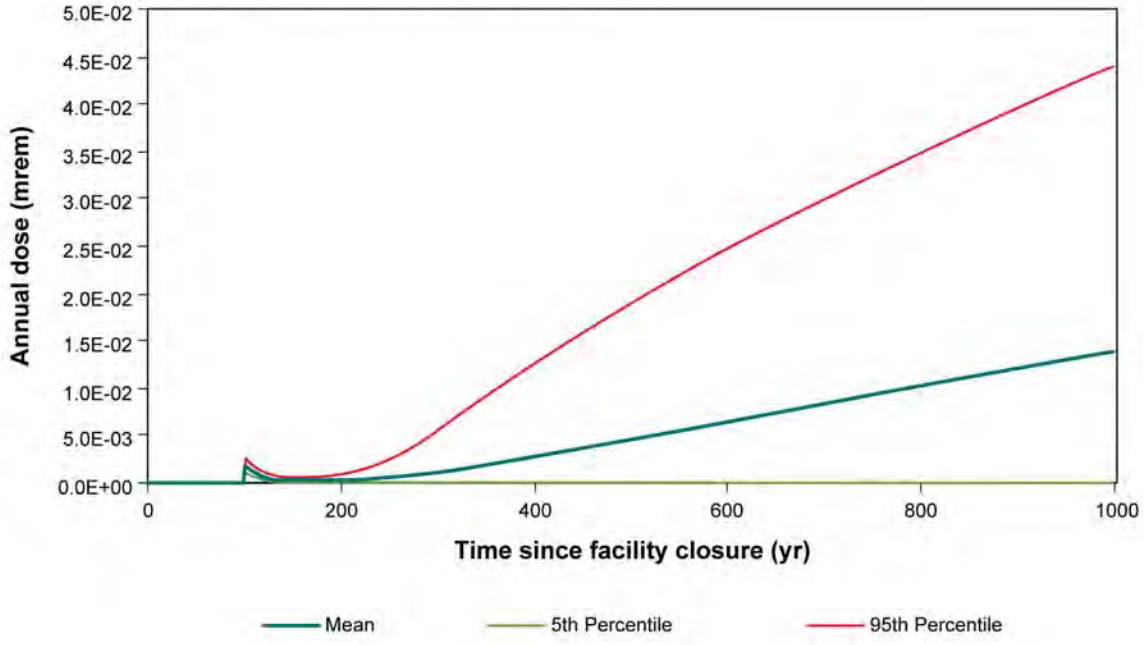

Figure 5
Probabilistic Dose Projections for the Atmospheric Scenario (performance assessment)

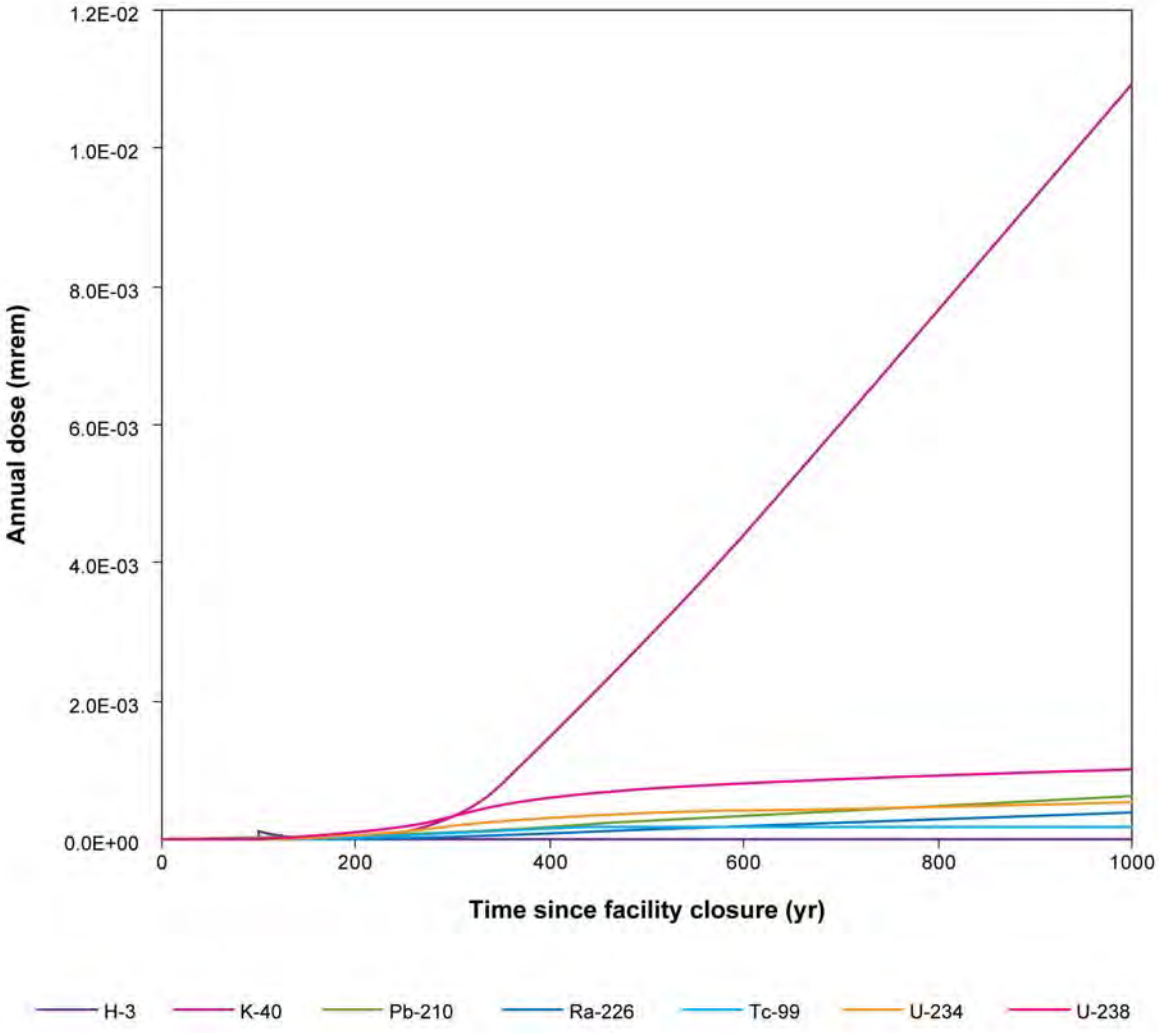

Figure 6
Mean Radionuclide Exposures for the Atmospheric Scenario at the Area G Fence Line Location (performance assessment)

Table 4
Projected Radon Fluxes for the
Eight Waste Disposal Regions

Waste Disposal Region	Projected Radon Flux (pCi/m^2/s)		
	Mean	5th Percentile	95th Percentile
1	1.8E-06	3.3E-13	7.3E-06
2	---	---	---
3	3.5E-01	3.6E-02	1.0E+00
4	3.9E-02	2.1E-03	1.2E-01
5	5.0E-01	5.1E-02	1.5E+00
6	3.5E-03	6.8E-11	1.4E-02
7	1.4E+01	1.1E+00	4.3E+01
8	3.3E-01	4.5E-02	9.4E-01

--- = None of the performance assessment inventory was disposed of in this waste disposal region.

3.1.3 All Pathways–Canyon Scenarios

Doses received by persons residing in the canyons adjacent to Area G were projected for two locations in Cañada del Buey and seven locations in Pajarito Canyon. Figure 7 shows the deterministic modeling results for these locations over a period of 50,000 years, the period for which surface erosion modeling was conducted. The doses projected for all locations behave similarly, reaching maximum values at the end of the simulation period. Peak annual doses range from 0.013 to 0.35 mrem among the nine receptor locations. Ac-227, K-40, Pa-231, Pb-210, Ra-226, and U-238 make significant contributions to the projected exposures for one or more exposure locations. Important exposure pathways include the ingestion of contaminated crops and direct radiation from radionuclides in the canyon soils.

The probabilistic doses for the canyon scenario are summarized in Table 5. The projected doses for catchments CdB1 and CdB2 are shown in Figure 8; these catchments yielded the highest peak mean doses among the nine canyon locations, with peak exposures projected at approximately 20 and 1,000 years after facility closure, respectively. Tritium is responsible for the peak mean exposure projected for catchment CdB1. In this case, tritiated water vapor diffuses upward from the waste and contaminates surface soils at Area G; the contaminated soils are subsequently transported into Cañada del Buey. The radionuclides that make significant contributions to the doses projected for the receptor in catchment CdB2 are Cl-36, K-40, Pb-210, Ra-226, and U-238; these isotopes

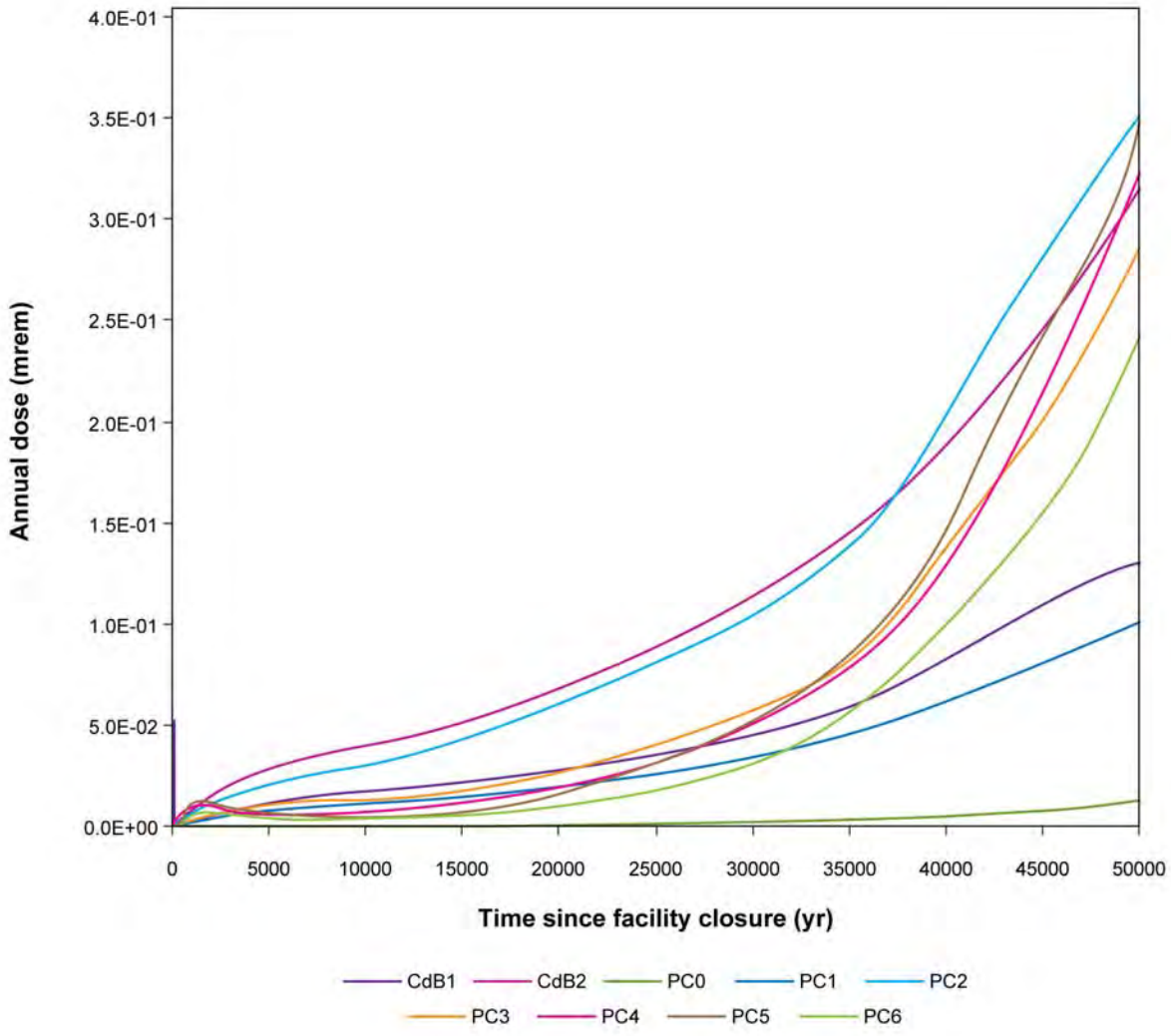

Figure 7
Deterministic Dose Projections for the All Pathways–Canyon Scenarios (performance assessment)

Table 5
Probabilistic Dose Projections for the All Pathways–
Canyon Scenarios (performance assessment)

Exposure Location (Catchment)	Projected Dose (mrem/yr)			Time of Peak Exposure (yr postclosure)
	Mean	5th Percentile	95th Percentile	
CdB1	2.3E+00	8.3E-04	1.3E+01	20
CdB2	4.1E-01	8.1E-05	1.3E+00	1,000
PC0	1.3E-02	9.9E-07	3.3E-02	808
PC1	8.8E-02	2.2E-05	2.7E-01	868
PC2	1.9E-01	3.4E-05	6.8E-01	960
PC3	1.1E-01	7.9E-05	5.0E-01	1,000
PC4	3.3E-01	2.5E-04	1.5E+00	904
PC5	3.6E-01	1.2E-04	1.6E+00	1,000
PC6	1.9E-01	1.9E-05	8.2E-01	1,000

Figure 8a. Projected doses for catchment CdB1

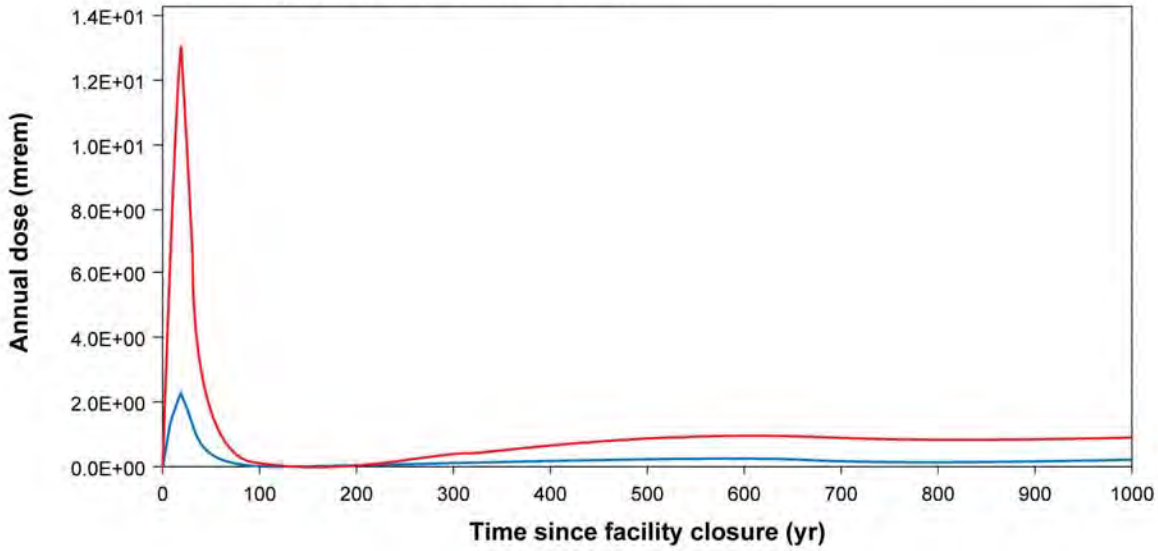

Figure 8b. Projected doses for catchment CdB2

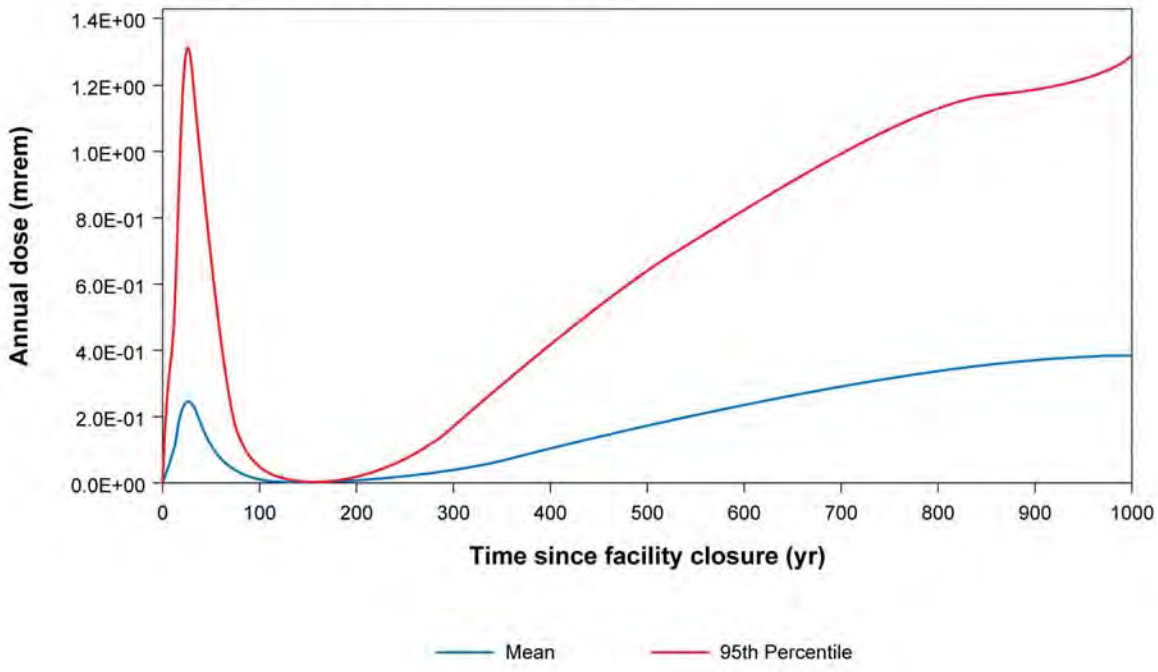

Figure 8
Probabilistic Dose Projections for the All Pathways–Cañada del Buey Scenario (performance assessment)

account for about 90 percent of the peak exposure. Radionuclide-specific contributions to the mean dose over time are shown for catchment CdB2 in Figure 9. Important exposure pathways include the ingestion of crops, beef, and milk at CdB1; these same pathways and direct radiation from contaminated soils account for the major portion of the peak dose at catchment CdB2. The peak mean doses projected for the canyon residents are 0.05 to 9 percent of the 25 mrem/yr all-pathways performance objective.

3.2 Composite Analysis Projections

The dose projections for the composite analysis are presented below. Section 3.2.1 presents and discusses the dose estimates for the All Pathways–Groundwater Scenario, and Section 3.2.2 considers the exposures projected for the Atmospheric Scenario. The exposures projected for persons residing in Cañada del Buey and Pajarito Canyon are discussed in Section 3.2.3. The potential impacts of alternate sources of contamination on the receptors represented using these exposure scenarios are discussed in Section 3.2.4.

3.2.1 All Pathways–Groundwater Scenario

The deterministic modeling results for the All Pathways–Groundwater Scenario are shown in Figure 10. The deterministic doses peak at 0.025 mrem/yr approximately 43,000 years after facility closure; exposures at this time are due solely to C-14 that is leached from the waste and transported to the compliance well. The ingestion of crops and animal products raised by the receptor make the largest contributions to the peak dose in terms of exposure pathways. No other radionuclides are projected to discharge to the regional aquifer within 100,000 years of facility closure.

The probabilistic modeling projected that no radionuclides would discharge to the regional aquifer during the 1,000-year compliance period. Therefore, no exposures were projected for the individual residing 100 m (330 ft) downgradient of the Area G fence line.

3.2.2 Atmospheric Scenario

Figure 11 shows the composite analysis doses for the Atmospheric Scenario based on the deterministic modeling. The results shown in this figure are for receptors residing at the LANL boundary (Figure 11a) and the Area G fence line (Figure 11b). The peak exposure for the receptor at the LANL boundary is projected to occur while the facility is still receiving waste; tritiated water vapor diffusing from the site is responsible for the 0.28 mrem/yr dose. Exposures from the other radionuclides in the inventory increase slowly throughout the 50,000-year period as the cover thins and plants and animals inhabiting the site gain greater access to the waste. The exposures projected for the fence line receptor increase throughout much of the 50,000-year period, reaching a maximum of 0.70 mrem/yr. Ac-227, Pa-231, Pb-210, Pu-239, Ra-226, and Sn-126 are among the major contributors to the peak dose; the exposures for this receptor are due largely to the ingestion of contaminated crops, inhalation, and direct radiation from soils.

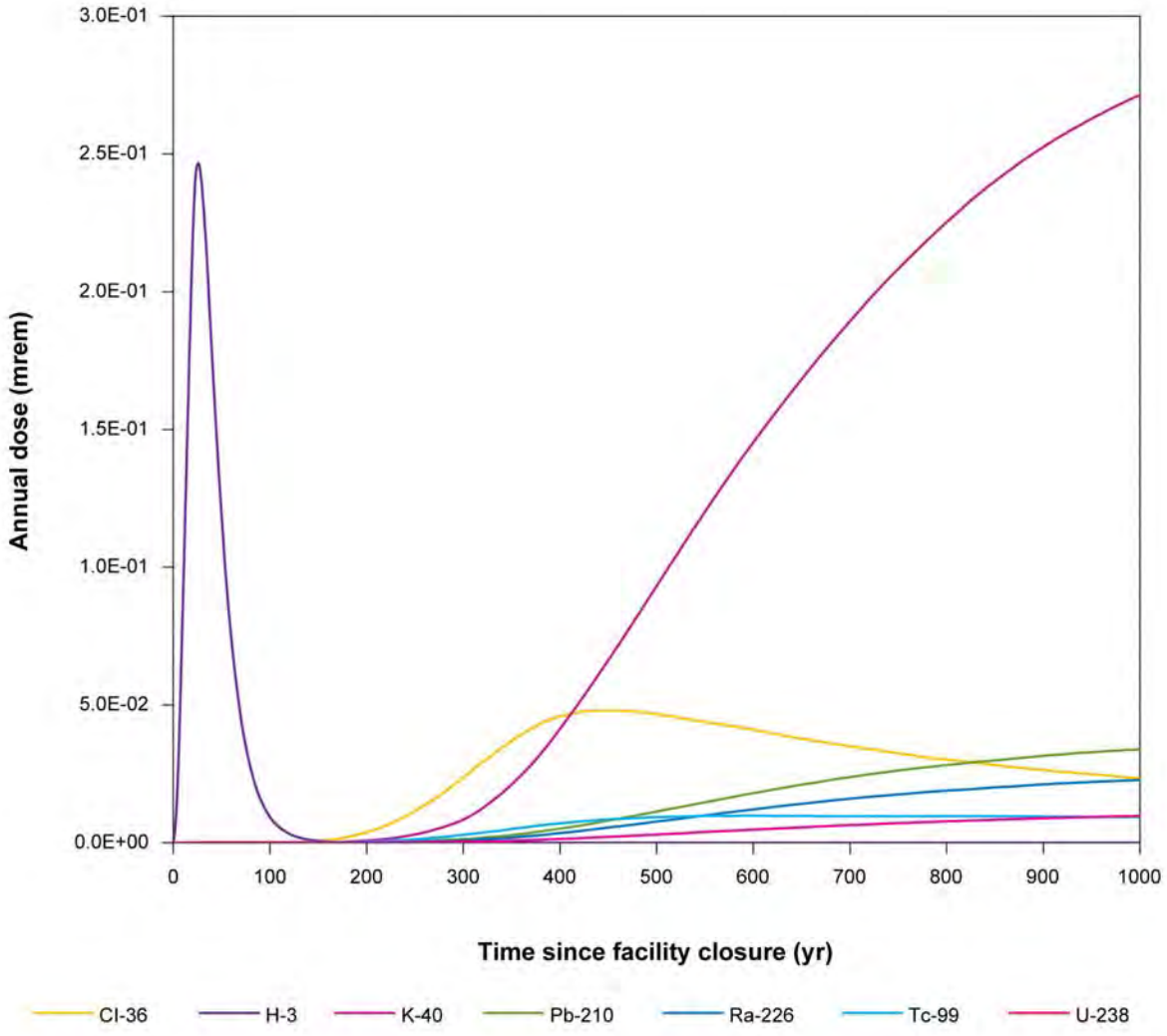

Figure 9
Mean Radionuclide Doses for the All Pathways–Cañada del Buey Scenario within Catchment CdB2 (performance assessment)

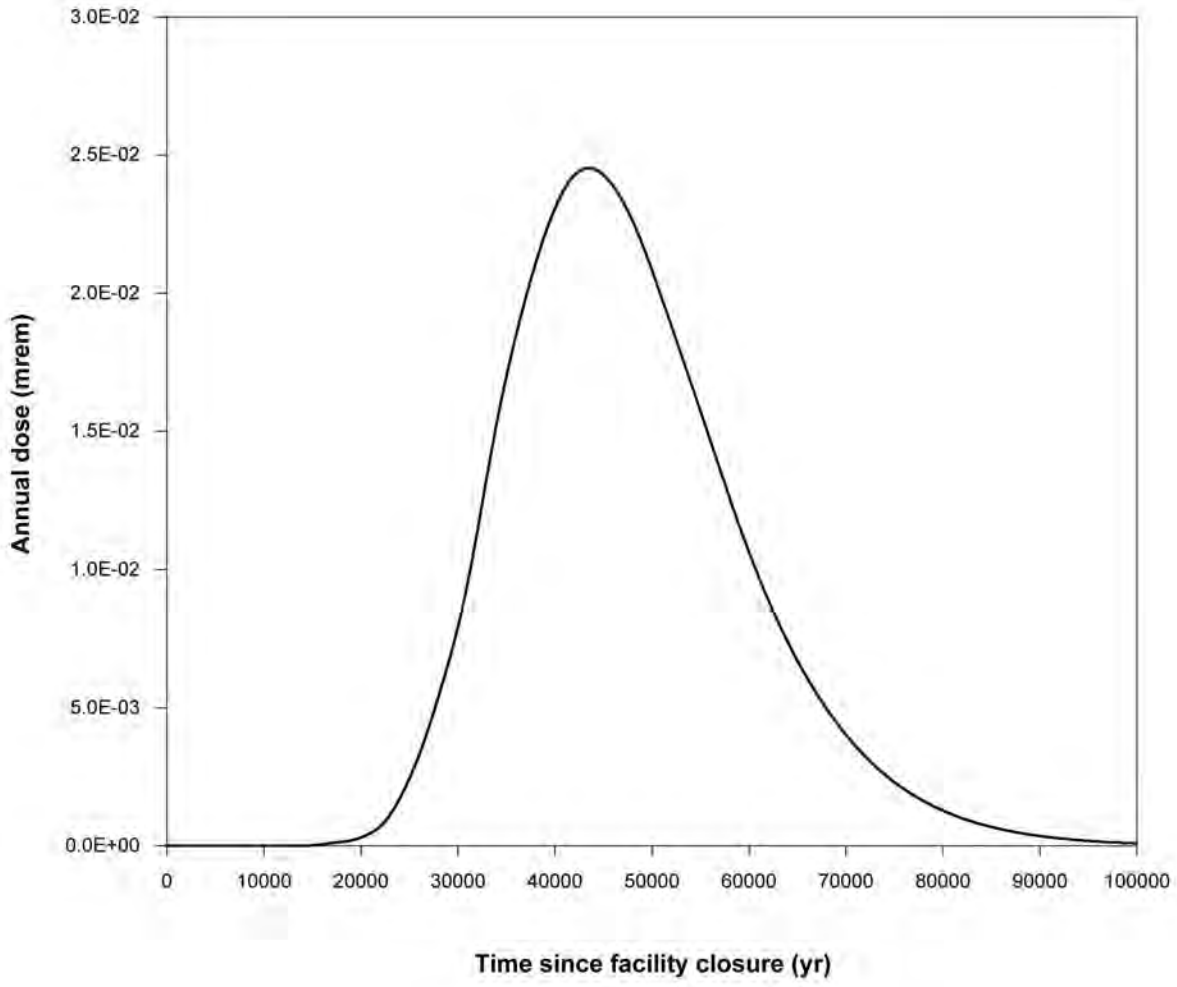

Figure 10
Deterministic Dose Projections for the All Pathways–Groundwater Scenario (composite analysis)

Figure 11a. LANL boundary exposure location

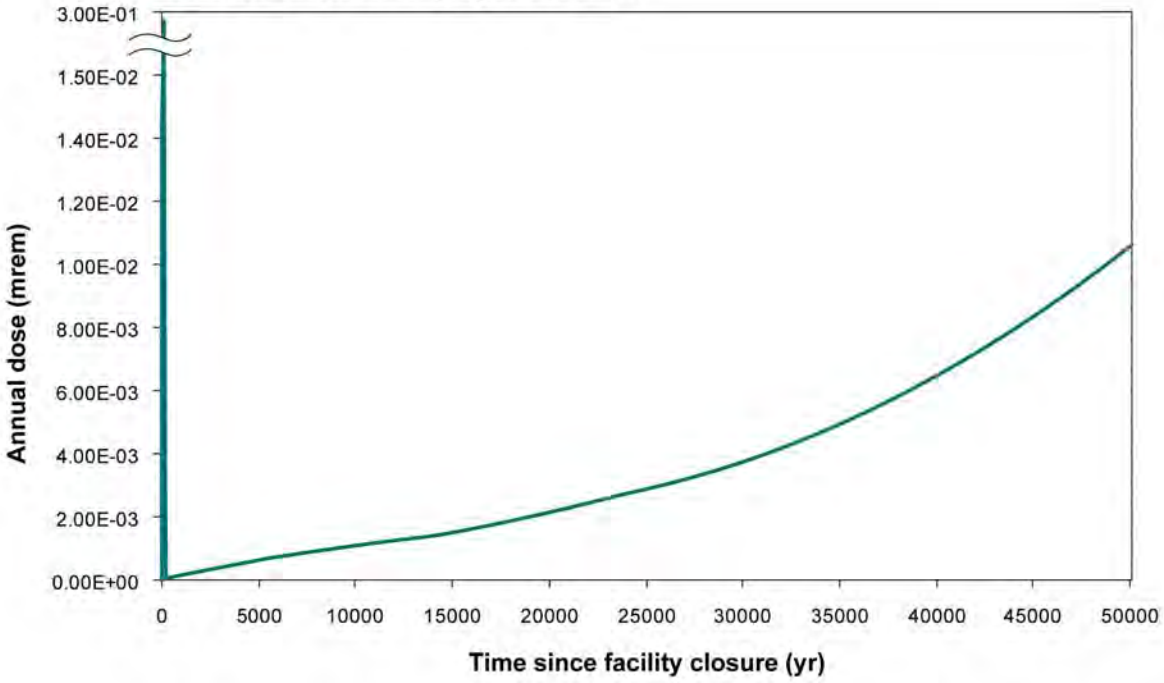

Figure 11b. Area G fence line exposure location

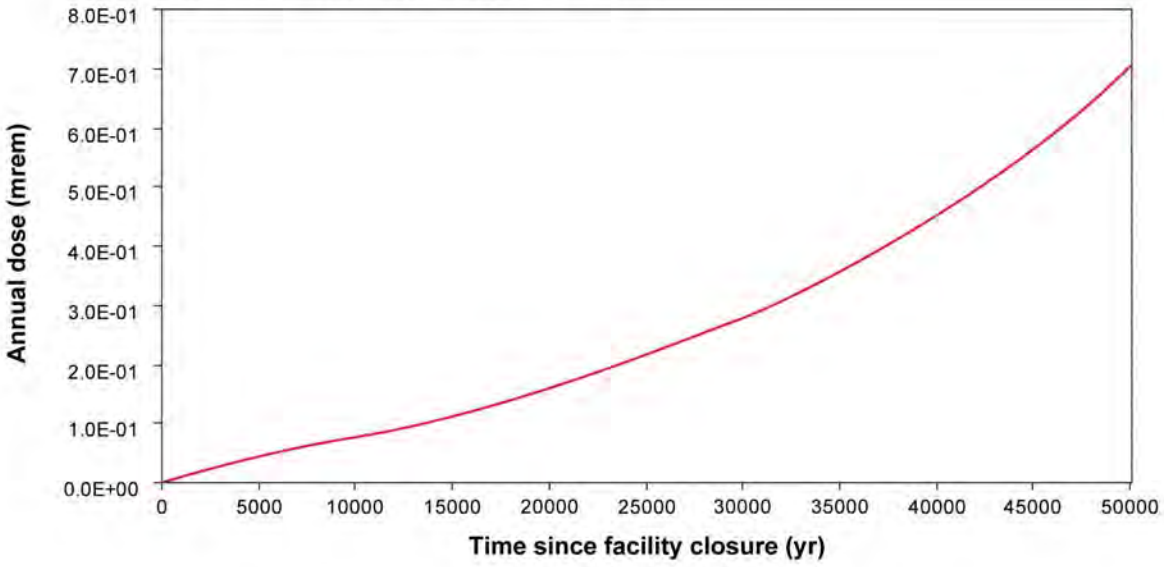

Figure 11
Deterministic Dose Projections for the Atmospheric Scenario (composite analysis)

The probabilistic model projections for the Atmospheric Scenario are shown in Figure 12. The peak mean dose for the receptor at the LANL boundary is 0.23 mrem/yr (Figure 12a); it is due entirely to tritium vapor diffusing from the surface of the disposal facility and traveling downwind with the prevailing winds. The peak exposure is projected to occur in about 2015, while the disposal facility is still in its operational phase. Much smaller doses are projected to occur later, in response to the resuspension of contaminated soils from the surface of Area G; particulate releases yield a dose of 0.0081 mrem/yr at the end of the 1,000-year compliance period. All of the projected mean exposures are much less than the 10 mrem/yr performance objective that applies to airborne releases.

The exposures projected for the receptor at the Area G fence line increase throughout much of the compliance period, reaching a peak mean dose of 0.64 mrem/yr (Figure 12b). Two important contributors to the exposures projected for this location are Pb-210 and Ra-226, which account for 42 and 22 percent of the peak mean dose, respectively. Together, Am-241, Pu-239, and Pu-240 contribute about 32 percent of the peak mean exposure. Figure 13 illustrates the contributions made by various radionuclides to the projected receptor exposures at the fence line location. The primary exposure pathways for the fence line receptor are the ingestion of contaminated crops, inhalation, and direct radiation from soils; these account for 63, 14, and 13 percent of the peak mean exposures, respectively. The peak mean dose projected for the fence line receptor is about 6 percent of the 10 mrem/yr performance objective.

3.2.3 All Pathways–Canyon Scenarios

The deterministic composite analysis doses projected for the Cañada del Buey and Pajarito Canyon receptors over a 50,000-year period are shown in Figure 14. The doses projected for the nine exposure locations behave similarly, reaching maxima at the end of the simulation period. Peak annual doses range from 0.017 to 1.2 mrem among the nine receptor locations. Ac-227, K-40, Pa-231, Pb-210, Pu-239, Ra-226, and U-238 make significant contributions to the projected exposures for one or more exposure locations; the ingestion of contaminated crops and direct radiation from contaminated soils make significant contributions to the peak mean doses.

The probabilistic doses for the canyon scenarios are summarized in Table 6. The projected doses for catchments PC5 and PC6 are shown in Figure 15; these catchments yielded the highest peak mean doses among the nine canyon locations. The mean dose at the former location reaches a peak value about 230 years after Area G undergoes final closure (Figure 15a); the mean dose for catchment PC6 displays an intermediate peak about 230 years after facility closure but reaches a maximum at the end of the compliance period (Figure 15b). Sr-90 accounts for more than 97 percent of the peak mean exposure projected for catchment PC5. Pb-210 and Ra-226 account for 78 percent of the peak mean dose projected for catchment PC6; a total of 17 percent of the projected exposure comes from Pu-239 and Am-241. Changes in radionuclide contributions to the projected exposures over time are shown in Figure 16 for catchment PC5; a similar pattern is seen for catchment PC6. The peak mean exposure estimated for the receptor in catchment PC5 is due almost entirely to the ingestion

Figure 12a. LANL boundary exposure location

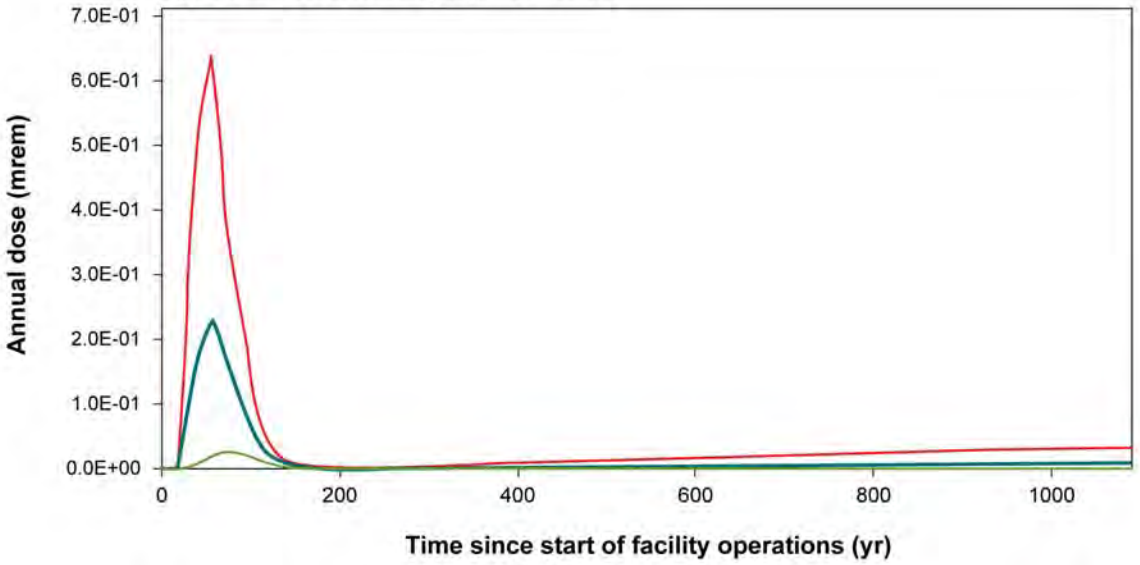

Figure 12b. Area G fence line exposure location

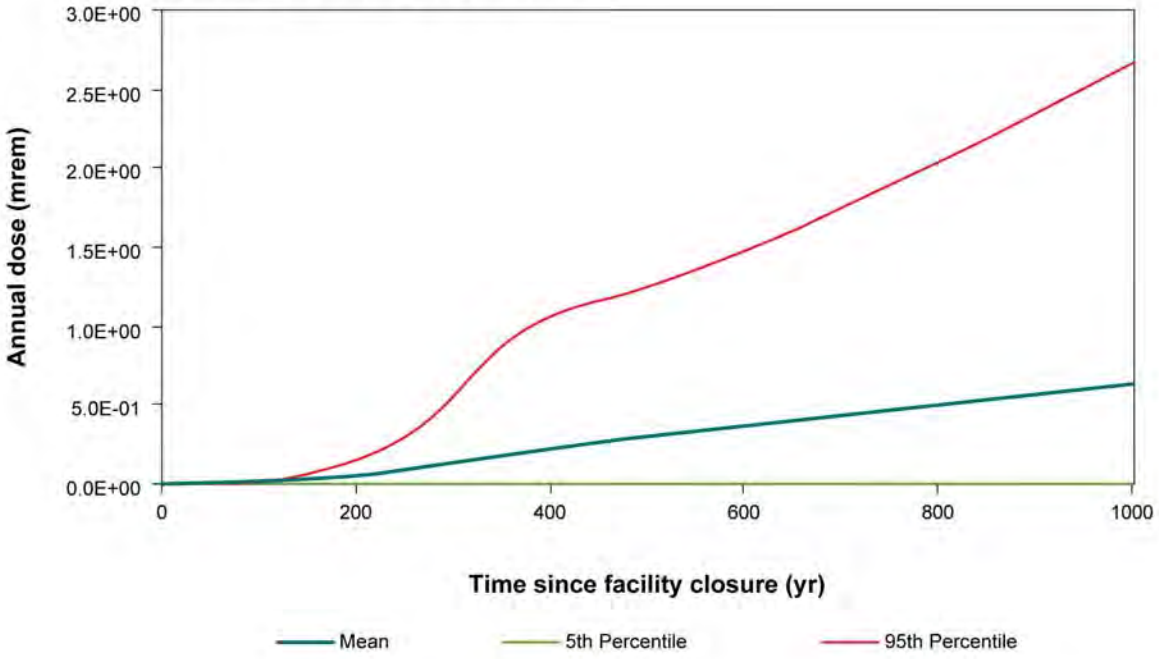

Figure 12
Probabilistic Dose Projections for the Atmospheric Scenario (composite analysis)

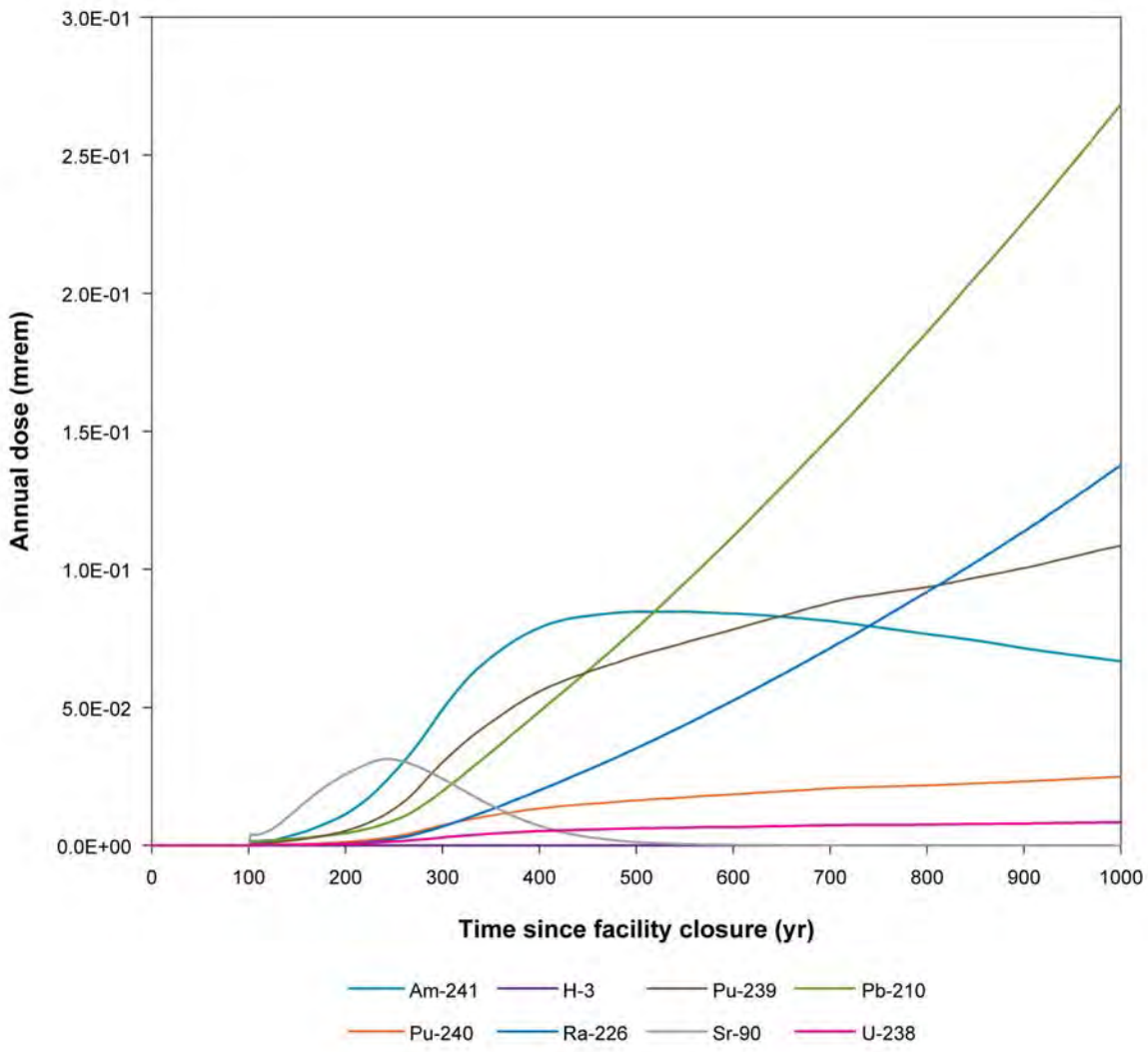

Figure 13
Mean Radionuclide Exposures for the Atmospheric Scenario at the Area G Fence Line Exposure Location (composite analysis)

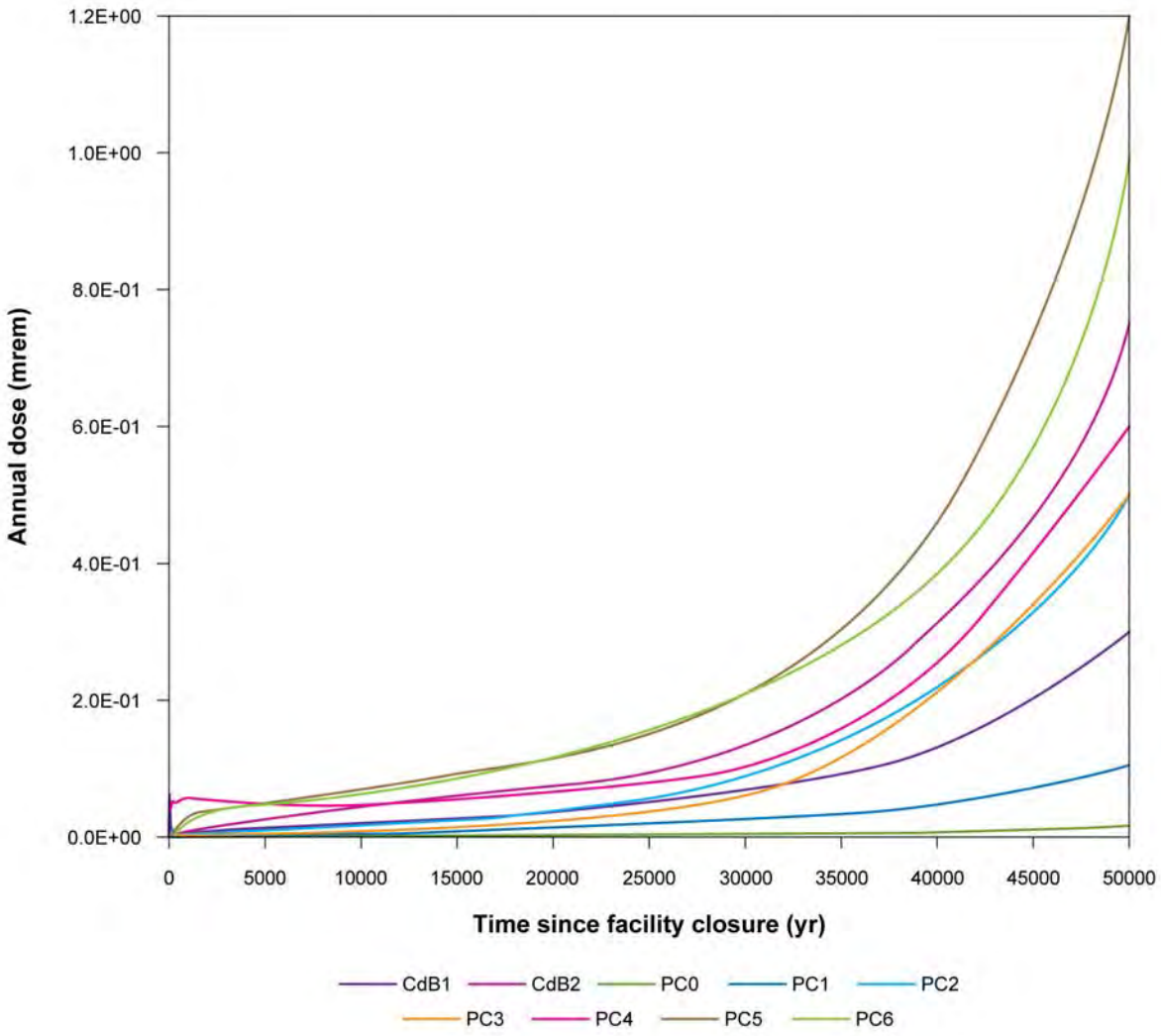

Figure 14
Deterministic Dose Projections for the All Pathways–Canyon Scenarios (composite analysis)

Table 6
Probabilistic Dose Projections for the All Pathways–Canyon Scenarios (composite analysis)

Catchment	Projected Peak Dose (mrem/yr)			Time of Peak Exposure (yr postclosure)
	Mean	5th Percentile	95th Percentile	
CdB1	2.2E+00	2.7E-03	1.4E+01	20
CdB2	2.1E+00	1.7E-03	1.0E+01	1,000
PC0	1.4E-02	7.9E-07	3.4E-02	700
PC1	9.3E-02	2.3E-05	2.6E-01	724
PC2	4.4E-01	4.3E-05	2.8E-01	196
PC3	4.2E-01	8.4E-05	2.0E-01	196
PC4	1.2E+00	2.4E-04	4.4E-01	196
PC5	4.4E+00	7.9E-04	8.7E-01	232
PC6	3.6E+00	1.4E-03	1.5E+01	1,000

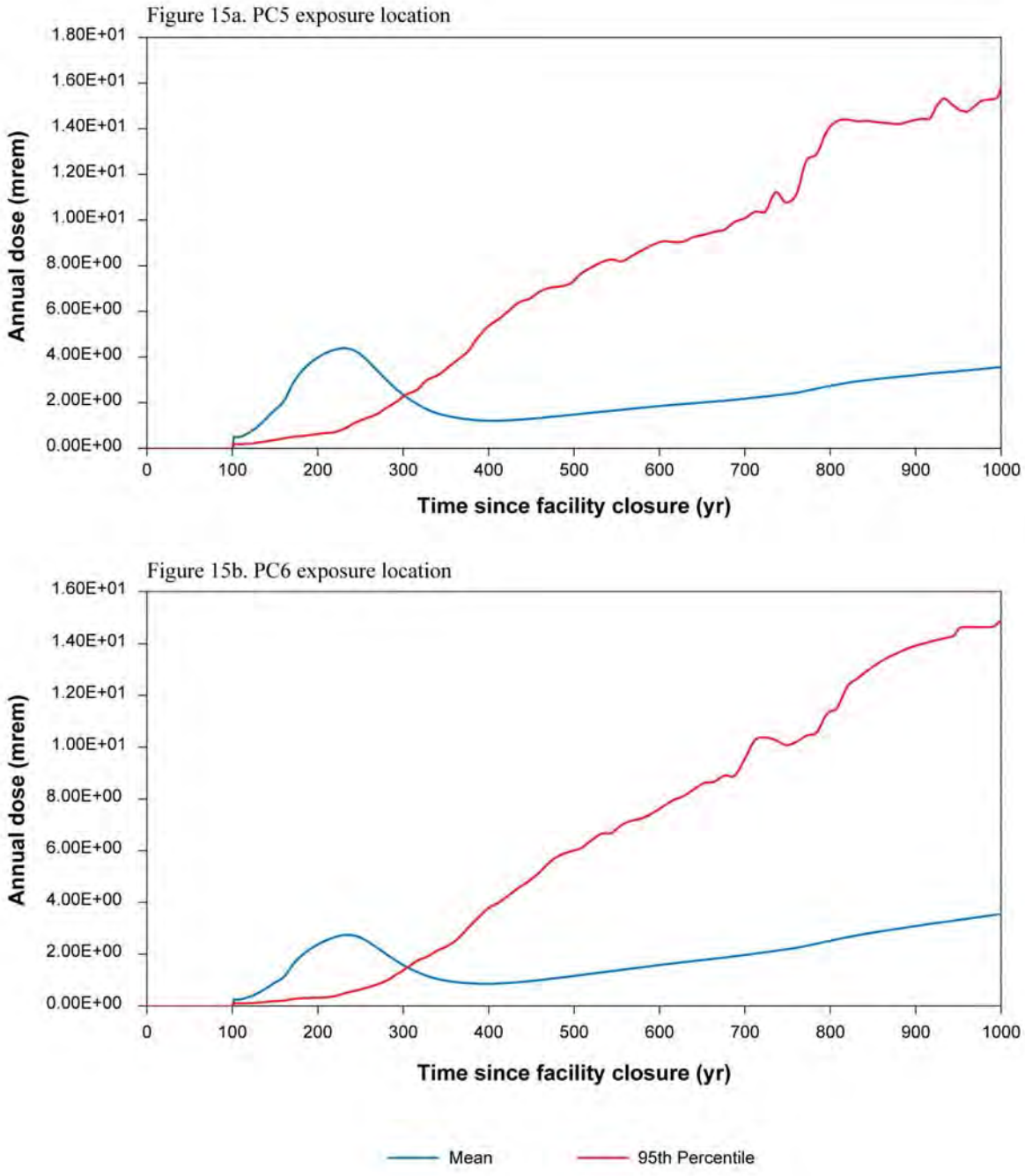

Figure 15
Probabilistic Dose Projections for the All Pathways–Pajarito Canyon Scenario (composite analysis)

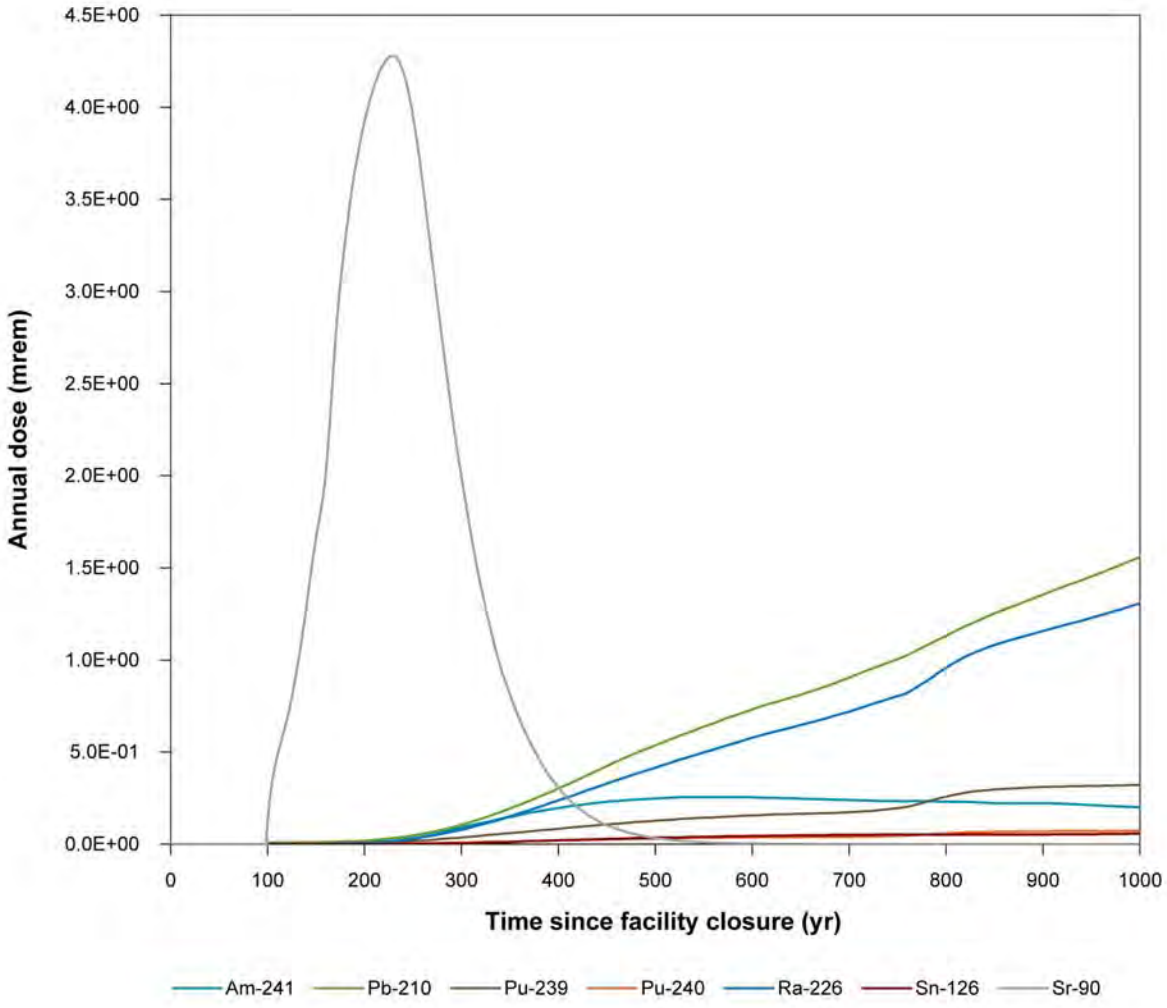

Figure 16
Mean Radionuclide Exposures for the All Pathways–Pajarito Canyon Scenario within Catchment PC5 (composite analysis)

of contaminated crops, beef, and milk; the ingestion of vegetables grown in, and direct radiation from, contaminated soils account for about 84 percent of the peak mean dose projected for catchment PC6. The peak mean exposures projected for all nine canyon exposure locations are less than the 100 mrem/yr primary dose limit and the 30 mrem/yr dose constraint.

Examination of Figure 15 reveals that the mean doses projected for catchments PC5 and PC6 exceed the ninety-fifth percentile exposures for a period of about 200 years following facility closure. This behavior is an outcome of the distribution selected to model Sr-90 uptake by native vegetation growing over the closed disposal facility. Large values are sampled from the distribution in a small fraction of the model realizations, yielding large Sr-90 concentrations in the surface soils at Area G and large exposures for the canyon residents. These doses are great enough to significantly elevate the mean exposure estimated for all 1,000 realizations.

3.2.4 Alternate Source Evaluation

Several sources of contamination at the Laboratory were identified for consideration in the alternate source analysis. These sources include MDAs A, AB, B, C, H, J, L, and T; Cañada del Buey; and Pajarito Canyon. The MDAs were included either because they were used to dispose of potentially large quantities of radioactive waste, are highly contaminated, or are located near Area G. All of these facilities are located on mesas. The two canyons were included in the alternate source evaluation because they are adjacent to Area G and have received discharges of waste in the past or are otherwise contaminated.

Brief descriptions of the alternate sources of contamination are provided in Section 3.2.4.1; the summaries draw on information presented in the 1997 performance assessment and composite analysis (Hollis et al., 1997) and additional sources where appropriate. The potential for interaction between these sources and releases from Area G is discussed in Section 3.2.4.2.

3.2.4.1 Alternate Source Descriptions

Material Disposal Area A. This disposal area is located at TA-21, approximately 6.7 km (4.2 mi) north-northwest of Area G, and occupies 5,060 m^2 (1.25 ac). Pits were excavated to a depth of about 4 m (13 ft) at the east end of the facility in late 1944 or early 1945 and used to dispose of solid waste with alpha contamination and small amounts of beta and gamma contamination. Approximately 1,020 m^3 (3.6×10^4 ft^3) of waste was disposed of in the pits. Incomplete information in Rogers (1977) indicates the principal alpha contamination was an unnamed long-lived radionuclide or short-lived polonium, with possible trace amounts of Pu-239.

Two underground tanks were built in 1945 and used to store approximately 185 m^3 (4.9×10^4 gal) of a sodium hydroxide solution that contained 334 g (0.74 lb) of Pu-239 (approximately 21 Ci) at the time of emplacement in or about 1947 (LANL, 1971). The liquid from these tanks was recovered, treated, and solidified in cement in 1975. The contaminated cement was buried at

Table 7
Estimates of Radionuclide Inventories at the Material Disposal Areas Included in the Alternate Source Evaluation

Material Disposal Area	Radionuclide	Inventory (Ci)
MDA A	Am-241	6.1E+00
	Pu-238	2.7E-01
	Pu-239	5.4E+01
	Pu-241	7.9E+01
	U-235	1.4E-03
MDA AB	Am-241	5.3E+02
	Pu-239	2.4E+03
	Pu-240	5.1E+02
	Pu-241	2.5E+03
	U-235	2.0E-01
	U-238	5.7E-02
MDA B	Cs-134	5.5E-03
	Pu-239	6.2E+00
	Sr-90	2.9E-01
	Th-228	1.8E-01
MDA H	Am-241	5.0E-06
	H-3	2.4E+02
	Pu (total)	---
	Pu-238	2.5E-02
	Pu-240	1.6E-03
	Pu-241	5.0E-05
	U (total)	---
	U-234	2.6E+01
	U-235	1.4E+01
	U-236	5.7E-01
	U-238	3.5E+01
MDA T	Am-241	3.7E+03
	H-3	---
	MFP	---
	Pu (undifferentiated)	9.8E+00
	Pu-238	3.1E+01
	Pu-239	1.5E+02
	Pu-241	3.7E+04
	U-233	6.9E+00

--- = No inventory included for this radionuclide. *MFP = Mixed-fission products*

Source: LANL, 2007a

MDA A for several years, but was retrieved in the late 1980s and moved to pit 29 at Area G. Estimates of the residual radionuclide inventories in the two tanks are provided in the LANL Documented Safety Analysis (DSA) (LANL, 2007a); these estimates are included in Table 7.

In 1969, a 9 m (30 ft) deep pit was excavated at MDA A for the disposal of U-235, Pu-238, and Pu-239 contaminated building debris from demolition work at TA-21. Estimates of the inventories in this pit are unavailable; however, the activities of these radionuclides are expected to be significantly smaller than the corresponding activities at Area G.

Material Disposal Area AB. Material Disposal Area AB is located at TA-49, which is about 5 km (3 mi) west-southwest of Area G. It was used for belowground hydronuclear experiments in 1960 and 1961. Experiments were conducted in shafts and chambers at depths between 18 and 24 m (60 and 80 ft). The total volume of contaminated tuff has been estimated at about 3×10^4 m^3 (1×10^6 ft^3) (LANL, 1995). Estimates of the radiological inventories at MDA AB are included in Table 7.

Material Disposal Area B. Like MDA A, this disposal area is located at TA-21. It occupies approximately 2.4×10^4 m^2 (6.0 ac), and was probably the first common solid-waste burial site for the Laboratory (Rogers, 1977). Engineering drawings show that MDA B is a single large pit, but other evidence indicates that several pits were excavated. Solid waste was disposed of at MDA B between 1947 and 1950. The radiological inventory includes "plutonium, polonium, uranium, americium, curium, RaLa [radioactive lanthanum], actinium" (LANL, 1952). The disposal capacity of the MDA B pits is estimated to be about 2.1×10^4 m^3 (7.6×10^5 ft^3); the LANL DSA (LANL, 2007a) estimates of the radionuclide inventories at MDA B are included in Table 7.

In 1984, MDA B was resurfaced with a variety of cover systems during a pilot study conducted in support of the National Low Level Waste Management Program and the EPA's Land Pollution Control Division, Contaminant Branch. At present, the MDA B surface incorporates several variations of a nominal 1 m (3.3 ft) thick crushed-tuff cover overlying the original crushed-tuff cover. Variations include cobble and gravel biobarriers between the old and new covers, as well as shrub, grass, and gravel-mulch surface treatments. The total cover thickness at MDA B is nominally 2 m (6.6 ft).

Material Disposal Area C. Located at TA-50 on a mesa about 6.7 km (4 mi) northwest of Area G, MDA C occupies about 4.9×10^4 m^2 (12 ac). Radioactive and hazardous waste was disposed of in 6 pits and 107 shafts at MDA C between 1948 and 1965. The average depth of the disposal pits is 6 m (20 ft) and the average depth of the shafts is about 5 m (16 ft). The pits were filled between 1948 and 1959 and the shafts were filled between 1958 and 1965. Logbooks were used to record general information about the waste disposals after 1954; records prior to 1954 are incomplete (Rogers, 1977).

Estimates of the total radiological inventory at MDA C are 196 Ci in pits and 4.9×10^4 Ci in shafts. Rogers (1977) provides preliminary estimates of radionuclide-specific inventories decay-corrected to January 1, 1973. The pits contain 25 Ci of uranium (including U-234, U-235, U-236, and U-238), 26 Ci of Pu-239, and 149 Ci of Am-241. The shafts are estimated to contain 4.9×10^4 Ci of H-3, 40 Ci of Na-22, 20 Ci of Co-60, 31 Ci of Sr-90/Y-90, 1 Ci of Ra-226, 5 Ci of U-233, less than 0.1 Ci of uranium (including U-234, U-235, U-236, and U-238), 50 Ci of fission products, and 200 Ci of induced activity.

Estimates of the radionuclide inventories disposed of at MDA C were developed in conjunction with the investigation report issued in 2006 (LANL, 2006); these updated inventory estimates are presented in Table 8 along with the inventories for this MDA that were included in the LANL DSA (LANL, 2007a). The 2006 investigation report lists inventories for several radionuclides that are not included in the DSA inventory for this MDA. The 2006 investigation report inventories are typically higher than the DSA inventories for radionuclides that are common to both efforts; exceptions include the inventories for Am-241 and Ra-226.

Material Disposal Area H. This MDA is located at TA-54, about 2 km (1.2 mi) northwest of Area G; the site is approximately 1,300 m^2 (0.3 ac) in area and contains nine inactive shafts. The facility served as the Laboratory's primary disposal area for solid classified waste from 1960 to 1986. The waste in all but one shaft is covered with 0.9 m (3 ft) of concrete placed over 0.9 m (3 ft) of crushed tuff; the waste in the remaining shaft is covered with 1.8 m (6 ft) of concrete. The majority of the waste disposed of at MDA H was nonhazardous classified waste; some of the material was contaminated with radionuclides at the time of disposal. Estimates of the radiological inventory are reported in LANL (2003a) and include 3.5 to 106 Ci of H-3, as much as 284.5 Ci of uranium (best estimate is 94.2 Ci), and a maximum of 0.014 Ci of plutonium. More recently, estimates of the radionuclide inventories at MDA H were published in the LANL DSA; these inventories are included in Table 7.

Material Disposal Area J. This site is located west of Area G at TA-54, between MDAs H and L. The 1.1×10^4 m^2 (2.7 ac) facility was used for the disposal of administratively controlled waste, for surface storage of nonfriable asbestos, and for land-farming (aeration) of petroleum-contaminated soils (LANL, 1999). The administratively controlled waste includes classified items such as safes with secured locks, objects with classified shapes, scrap equipment, treated sand from barium sand treatment operations at MDA L, and empty containers; equipment, asbestos, and residual amounts of hazardous waste were also discarded during early operations. Waste was disposed of in six pits and four shafts starting in 1961; the facility underwent final closure in 2002. No radioactive waste was disposed of at MDA J (LANL, 2002a).

Table 8
Estimates of Radionuclide Inventories at Material Disposal Area C

Radionuclide	Inventory (Ci)	
	Investigation Report (LANL, 2006)	LANL DSA (LANL, 2007a)
Ac-227	1.8E+00	---
Al-26	1.4E+02	---
Am-241	4.5E+01	1.5E+02
Cf-249	6.4E-04	---
Cf-251	2.5E-03	---
Cf-252	1.3E-02	---
Cl-36	5.0E-02	---
Co-60	1.9E+02	2.4E+00
Cs-137	1.5E+03	---
Eu-154	5.9E-02	---
H-3	6.1E+04	2.0E+04
Kr-85	2.1E+02	---
Na-22	---	5.8E-01
Np-237	2.9E-04	---
Pu-238	4.0E+03	2.6E+01
Pu-239	1.7E+03	---
Pu-240	4.3E+02	---
Pu-241	7.5E+03	1.5E+03
Pu-242	4.5E-02	---
Ra-226	7.0E-01	1.0E+00
Sm-151	7.9E-03	---
Sn-121m	4.9E-01	---
Sn-126	5.6E-02	---
Sr-90	1.1E+03	2.1E+01
Tc-99	7.1E-05	---
Th-230	1.5E+01	---
Th-232	7.5E-01	---
U (total)	1.2E+02[g]	2.5E+01
U-233	7.0E+00	5.0E+00
U-234	1.9E+01	---
U-235	8.1E+01	---
U-236	2.5E-01	---
U-238	1.2E+01	---
Zr-93	1.3E-01	---

--- = No inventory included for this radionuclide.

Material Disposal Area L. Located immediately west of Area G at TA-54, this 1.0×10^4 m^2 (2.5 ac) site was used for the disposal of Laboratory-generated hazardous (nonradioactive) wastes until 1985. It is presently used for hazardous waste storage and treatment permitted under the Resource Conservation and Recovery Act (RCRA), and for mixed waste storage under interim status authority. Waste was disposed of in 1 pit, 3 surface impoundments, and 34 shafts; all of these units were used for the disposal of uncontained or packaged liquid wastes. Waste was placed in the pit to within 0.9 m (3 ft) of the ground surface and covered with crushed tuff; the 3 surface impoundments were also covered with crushed tuff. The filled shafts were covered with 0.9 m (3 ft) of concrete. No radioactive contaminants are included in the disposal records for MDA L (LANL, 2005a).

Material Disposal Area T. This facility is located at TA-21, along with MDAs A and B. Material Disposal Area T includes four 1.2 m (3.9 ft) deep absorption beds where radioactive liquid waste from the plutonium processing laboratories at TA-21 was disposed of between 1945 and 1952. In 1952, a liquid-waste treatment plant was installed to remove plutonium and other radionuclides. The absorption beds received relatively small quantities of LLW until 1967, when a new liquid-waste treatment process was initiated. Between 1968 and 1975, treated liquid waste was mixed with cement and pumped into 4.6 to 19.8 m (15 to 65 ft) deep shafts at MDA T for disposal. After 1975, the cement paste was poured into corrugated metal pipes, and retrievably buried at MDA T. There were 62 shafts at MDA T used for the permanent disposal of cement-treated liquid waste.

Approximately 6.9×10^4 m^3 (1.8×10^7 gal) of liquid waste was disposed of in the MDA T absorption beds between 1945 and 1967. The absorption beds contained 4 Ci of H-3 and 10 Ci of Pu-239 as of January 1973 (Rogers, 1977); the disposal shafts contained 7 Ci of U-233, 47 Ci of Pu-238, 191 Ci of Pu-239, 3,761 Ci of Am-241, and 3 Ci of mixed fission products. The total volume of cement paste permanently disposed of in shafts at MDA T was 3,500 m^3 (1.2×10^5 ft^3). Estimates of radionuclide inventories at MDA T taken from the LANL DSA (LANL, 2007a) are summarized in Table 7; all but the undifferentiated plutonium was disposed of in the shafts.

Cañada del Buey. This canyon has been used as a buffer zone for disposal areas at TA-54, including Area G, and, to a lesser extent for liquid waste disposal. The earliest discharges to the canyon were associated with outfalls, surface runoff, and dispersion from firing sites located at the former TA-4, a site that is now located partially within the boundaries of TA-52 (LANL, 1999). Additional discharges began with the expansion of Laboratory operations to new sites from the 1950s through the 1990s, specifically at TA-46, TA-51, TA-52, and TA-54. The following information about discharges to the canyon is taken from the RCRA facility investigation (RFI) work plan prepared for Cañada del Buey (LANL, 1999).

The majority of the potential release sites (PRSs) at TA-46 that are located within the Cañada del Buey watershed were recommended for RCRA Phase I investigations; radioactive contaminants such as Am-241, Cs-137, Pu-238, Pu-239/240, U-234, U-235, U-238, and Th-230 may occur at these sites. Soil samples collected below the outfalls and drainages associated with some of these PRSs have found elevated levels of many of these contaminants. "No further action" was recommended for four of the five PRSs at TA-51 and the fifth PRS underwent a Phase I investigation to confirm the absence of a release associated with a septic system. Potential release sites located within the Cañada del Buey watershed at TA-52 have been recommended for no further action. One of the three PRSs at the former TA-4 has been recommended for no further action and the other two have undergone RCRA Phase I investigations. Surface and subsurface soil samples collected in 1995 at these sites had concentrations of Pu-238 and Pu-239 that were above background.

A number of PRSs are associated with TA-54. Three of these, at TA-54 West, are septic systems that do not appear to have received radioactive contamination; three others were recommended for no further action. A total of 24 PRSs associated with Area G contain various groups of pits and shafts. In association with an RFI analysis of sediment channel pathways from Area G and MDAs H, J, and L, 47 sediment samples were collected from six drainage channels that enter Cañada del Buey (LANL, 1996). The associated report concluded that unacceptable risk from radionuclides is unlikely and recommended no further evaluation or remediation of drainage channels adjacent to Area G. Other assessments conducted at the drainage channels that lead from MDAs J and L to Cañada del Buey reached similar conclusions. Potential releases from MDA H were not evaluated because this site is associated with the Pajarito Canyon watershed.

Routine sampling of canyon sediments at the Laboratory includes several locations near Area G in Cañada del Buey and Pajarito Canyon. From 2001 through 2003, Pu-238 and Pu-239/240 were detected at levels greater than background within Cañada del Buey at the east end of Area G (LANL, 2002b, 2004a, and 2004b). Sampling conducted in 2006 also found elevated radionuclide concentrations in sediments (LANL, 2007b).

Pajarito Canyon. Pajarito Canyon has been the location of the Los Alamos Critical Experiments Facility at TA-18; areas within this watershed have also been used for surface and subsurface disposal areas and as a buffer zone for mesa-top firing activities (LANL, 1998). The canyon has been used for liquid waste disposal since the Laboratory began operation in 1943. Early discharges to the canyon were associated with outfalls, surface runoff, and dispersion from firing sites. Additional discharges began during the 1950s and continued through the 1970s as Laboratory operations expanded to new sites, specifically TA-3, TA-36, TA-40, TA-48, and TA-59. Discharges to the canyon have decreased as firing sites in the watershed have become inactive; many of the outfalls have also become inactive or have been rerouted. The information

about discharges to the canyon that follows is taken from the RFI work plan prepared for Pajarito Canyon (LANL, 1998).

Several PRSs exist along the length of Pajarito Canyon that falls within Laboratory lands; investigations into these sites have focused on contaminants of potential concern including plutonium, thorium, and uranium. Routine sampling of sediments within the canyon has occurred at several locations on Laboratory lands. Six of these locations correspond to ephemeral tributary channels from Area G, at the foot of Mesita del Buey. Sampling results for 1982 through 1996 indicate average concentrations of Pu-238 and Pu-239/240 that are 2.5 and 2.8 times background levels (0.06 to 0.068 pCi/g), respectively. These results were considered indicative of residual contamination from the mesa as opposed to releases from the pits and shafts.

Supplemental surveillance data were collected in 1993, 1994, and 1995 and incorporated into an RFI for the channel sediment pathway in Cañada del Buey and Pajarito Canyon (LANL, 1996). Sediment samples were collected from several drainage channels associated with Area G, including depositional areas on the canyon floor. The results indicated that several radionuclides, including Am-241, Cs-137, Co-60, H-3, Pu-239/240, Po-210, Sr-90/Y-90, Tc-99, and U-235, were present at levels in excess of background. Contaminant concentrations were less than soil screening values and it was concluded that unacceptable risks from radionuclides in canyon sediments were unlikely. Sediment samples collected from a drainage channel entering the canyon from MDA H were also considered in the sediment pathway RFI (LANL, 1996). No radionuclides were present at levels greater than background. Sediments eroded from MDAs L and J are transported into Cañada del Buey.

More recent sediment sampling at the locations along the south side of Area G indicates concentrations of some radionuclides in excess of background or fallout levels. For example, surveillance data for 2001 (LANL, 2002b) indicated concentrations of Am-241, Pu-238, and Pu-239/240 that were 6 to 150 times background levels; tritium was also detected in significant quantities. During 2002 and 2003, Am-241, Pu-238, and Pu-239/240 were found at concentrations greater than background in the vicinity of Area G (LANL, 2004a and 2004b). These elevated levels have proved persistent; concentrations of Am-241, Pu-238, and Pu-239/240 were elevated in sediment samples collected in 2006 from channels draining Area G (LANL, 2007b).

Other canyons. In addition to Cañada del Buey and Pajarito Canyon, other canyons have been contaminated as a result of Laboratory operations. These include Pueblo and Los Alamos Canyons, which have received liquid effluent discharges from nuclear materials processing, and Mortandad Canyon, which has been contaminated in conjunction with liquid waste treatment activities. In general, the probability that contaminants discharged to canyons other than Cañada del Buey and Pajarito Canyon will interact with releases from Area G is small. However, groundwater transport

modeling has indicated that, under some water supply well pumping scenarios, small portions of discharges to Mortandad Canyon that reach the regional aquifer could migrate towards Area G and possibly interact with groundwater releases from the disposal facility (Birdsell, 2005).

3.2.4.2 Alternate Source Interactions

The potential for significant interactions between alternate sources of radioactive contamination at the Laboratory and releases from Area G were evaluated using three criteria:

- The magnitude of radionuclide inventories
- The potential for contaminant releases and the magnitude of any such releases
- The potential for the transport of significant quantities of contamination to the exposure locations included in the Area G composite analysis during the 1,000-year compliance period

If radionuclide inventories or contaminant release rates for the alternate sources are low compared to those projected for Area G, there is little likelihood that significant interactions will occur. Likewise, the risk posed by alternate sources to the receptors included in the composite analysis will be low as long as contaminants released from the other sources are not transported to the exposure locations associated with Area G or undergo significant dilution before reaching these locations.

Table 9 compares the radiological inventory estimates provided for the MDAs in the LANL DSA (LANL, 2007a) to the radionuclide inventories projected for the Area G composite analysis; short-lived radionuclides are excluded from the table. Generally speaking, the Area G inventories are substantially greater than the inventories listed for the MDAs. Exceptions are as follows:

- MDA AB Pu-239 and Pu-240 inventories are 11 to 14 percent greater than their Area G counterparts.
- MDA B Th-228 inventory is about 20 times that projected for Area G.
- MDA H U-234, U-235 and U-236 inventories are 1.1, 3.3, and 38 times the corresponding Area G inventories.
- MDA T Am-241 and Pu-241 inventories are 54 percent and 4.5 times greater than the Area G activities.

Also, although the DSA inventory estimates for MDA C are less than the corresponding Area G activities, the inventories projected for U-235 and U-236 in the MDA C investigation report are about 20 and 16 times greater than the corresponding Area G inventories.

Table 9
Summary of Radionuclide Inventories at the MDAs
Included in the Alternate Source Evaluation

Radionuclide	Disposal Area [a]						
	Area G [b]	MDA A	MDA AB	MDA B	MDA C [b]	MDA H	MDA T [b]
Am-241	2.4E+03	6.1E+00	5.3E+02	---	1.5E+02	5.0E-06	3.7E+03
Co-60	8.0E+03 [c]	---	---	---	2.4E+00	---	---
H-3	3.5E+06	---	---	---	2.0E+04	2.4E+02	
Pu (undifferentiated)	1.6E+04 [d,e]	---	---	---	---		9.8E+00
Pu-238	4.9E+03 [e]	2.7E-01	---	---		2.5E-02	3.1E+01
Pu-239	2.1E+03 [e]	5.4E+01	2.4E+03	6.2E+00	---	---	1.5E+02
Pu-240	4.6E+02 [e]		5.1E+02			1.6E-03	
Pu-241	8.2E+03 [e]	7.9E+01	2.5E+03		1.5E+03	5.0E-05	3.7E+04
Ra-226	4.0E+00	---	---	---	1.0E+00	---	---
Sr-90	3.3E+03 [f]	---	---	2.9E-01	2.1E+01	---	---
Th-228	9.1E-03			1.8E-01			
U	1.3E+02 [e,g]	---	---	---	2.5E+01		---
U-233	1.2E+01	---	---	---	5.0E+00	---	6.9E+00
U-234	2.4E+01 [e]					2.6E+01	
U-235	4.0E+00 [e]	1.4E-03	2.0E-01	---	---	1.4E+01	---
U-236	1.6E-02 [e]					5.7E-01	
U-238	8.6E+01 [e]		5.7E-02			3.5E+01	

--- None reported

Source: LANL (2007a)

[a] No radioactive waste inventories are expected to reside in MDAs J and L.

[b] Includes pit and shaft waste inventories.

[c] Listed activity includes the mixed-activation product waste assigned to Co-60.

[d] Includes total activity of all plutonium isotopes.

[e] Listed activity includes the material type waste activity assigned to isotope.

[f] Listed activity includes the mixed fission product waste activity assigned to Sr-90.

[g] Includes total activity of all uranium isotopes.

On the basis of the comparison of the LANL DSA and Area G activities, all disposal areas except MDAs AB, H, and T were excluded from further consideration in the alternate source analysis. Although the Th-228 inventory for MDA B was greater than that for Area G, this radionuclide has a short half-life (1.9 yr) and, therefore, has little impact on the long-term performance of the disposal facilities. The inventory estimates provided in the MDA C investigation report are expected to be approximate at best. Nevertheless, this MDA was added to the list of MDAs carried through the alternate source evaluation.

The primary release mechanisms for radionuclides disposed of at MDAs AB, C, H, and T are similar to those evaluated for Area G. Plants whose roots penetrate into the buried waste or zone of contamination may deposit radionuclides on the surface of the facility following litterfall and decay. Similarly, animals whose burrows extend into the contamination may transport contamination to the ground surface. Water infiltrating through the disposal areas may leach radionuclides and transport them to the regional aquifer. Finally, vapor- and gas-phase radionuclides may diffuse upward from the waste, exiting from the surface of the facility.

The potential for releases to occur as a result of biotic intrusion is primarily a function of the depth of the cover over the waste or zone of contamination and the presence of barriers to root and burrow penetration. Based on the information given above, the transport of contamination to the surface of the facility by plants and animals cannot be ruled out for MDAs C and T. If the units at these facilities were closed on an interim basis in a fashion similar to that observed at Area G, existing cover depths at MDA T are expected to be about 2 m (6.6 ft) or less. This is less than the rooting and burrowing depths considered in the biotic intrusion modeling conducted for Area G. However, the shafts at MDA C were closed by filling the units with crushed tuff and concrete, while the majority of the waste (on an activity basis) disposed of at MDA T exists as a cement paste. The use of concrete for shaft closure and the cement waste form could reduce plant and animal interactions with the material.

Biotic intrusion is not generally expected to provide a viable release mechanism for the contamination at MDA AB and the waste disposed of at MDA H. The zone of contamination at the former site is 18 to 24 m (60 to 80 ft) bgs, well below the maximum plant rooting and animal burrowing depths identified for the Area G composite analysis. The disposal shafts at MDA H have been covered with a total of 1.8 m (6.6 ft) of cover material, including 0.9 to 1.8 m (3 to 6 ft) of concrete. The presence of the concrete is expected to largely exclude plants and animals from the waste, although some intrusion into the waste cannot be ruled out. The Corrective Measures Study for MDA H (LANL, 2003a) recommended a closure alternative that includes placement of an engineered cover over the concrete/tuff caps, further reducing the likelihood of significant intrusion into the waste in the future.

The potential for releases of radionuclides due to leaching at MDAs AB, C, H, and T may or may not resemble that projected for Area G. Wet conditions have existed at MDA AB in the past because portions of the site were paved with asphalt; the elevated asphalt pad inhibited evapotranspiration and caused surface water to accumulate because of damming. Monitoring at MDA AB in areas affected by the asphalt pad revealed elevated moisture to depths of about 18 m (60 ft) bgs (Birdsell et al., 2005). However, the pad at MDA AB has been removed and moisture contents are projected to return to background levels over several years. Elevated moisture contents may persist for some time at depths of 12 to 18 m (40 to 60 ft) bgs, but it is unclear whether this additional moisture will result in more rapid leaching of the contamination found at depths of 18 to 24 m (60 to 80 ft) bgs.

The hydrologic conditions at Area G and MDA H are expected to be similar; wetter conditions may exist at MDA C due to moderately higher rates of precipitation. Hydrologic conditions at MDA T are expected to be more severe than those at Area G for two reasons. First, MDA T receives higher annual average precipitation. Second, rates of water infiltration through the absorption beds at MDA T were considerably higher than background or natural rates during the 22 years that liquid waste was disposed of at this facility. However, the Am-241 and Pu-241 that have been identified as the critical radionuclides at this facility were disposed of in shafts, which did not receive liquid waste. Birdsell et al. (2005) note that data collected beneath the absorption beds show evidence of fracture flow, while data collected from boreholes adjacent to the beds do not. These results suggest the effects of liquid discharges may have been reasonably contained within the absorption beds.

Although the potential for vapor-and gas-phase radionuclides to diffuse from the waste disposed of at the alternate MDAs exists, the magnitude of any such release is expected to be small. None of the radionuclides present at MDAs AB, C, H, or T at elevated levels (Table 9) exist as a vapor or gas. Although radon gas may be generated from the uranium disposed of at MDA H, the amount of radon that will be generated over the 1,000-year compliance period will be small because the half-lives of the uranium isotopes are large, leading to small generation rates of radon. Therefore, any diffusive releases from these facilities will be low compared to those from Area G.

Releases from the alternate source MDAs must be transported to locations downwind and downgradient of Area G in order to significantly contribute to the exposures estimated in Sections 3.2.1 and 3.2.2. Atmospheric transport modeling by Jacobson (2005) projected particulate air concentrations at locations downwind of Area G for releases from MDAs A, AB, B, C, and T. Model simulations were conducted using meteorological data for 2001 and a land use type of rangeland across the model domain. A complete description of the modeling effort is available in Jacobson (2005).

The results of the atmospheric transport modeling are summarized in Table 10 for MDAs AB, C, and T. This table compares the projected air dispersion factors for unit releases from

Area G and the MDAs at receptor locations in the vicinity of Area G. Examination of these results reveals that the air dispersion factors for MDAs AB, C, and T are less than 1 percent of those estimated for releases from Area G. In other words, for a given release rate, concentrations of airborne contaminants originating at MDAs AB, C, and T will be less than 1 percent of those resulting from the same releases at Area G.

Table 10
Comparison of Air Dispersion Factors for
Releases from Alternate Source Material Disposal Areas

UTM Grid Coordinates (m) of Exposure Location		Air Dispersion Factor by Release Location (s/m^3)			
Easting	Northing	Source Area 1 Area G	MDA AB	MDA C	MDA T
388567	3965965	8.9E-06	5.1E-08	6.0E-08	6.7E-08
388586	3965960	9.3E-06	5.0E-08	5.9E-08	6.7E-08
388606	3965955	9.7E-06	5.0E-08	5.9E-08	6.6E-08
388625	3965950	9.6E-06	5.0E-08	5.8E-08	6.6E-08
388644	3965945	9.9E-06	4.9E-08	5.8E-08	6.5E-08
388664	3965940	9.5E-06	4.9E-08	5.7E-08	6.4E-08
388683	3965935	9.6E-06	4.9E-08	5.7E-08	6.4E-08
388703	3965931	9.4E-06	4.8E-08	5.7E-08	6.3E-08
388722	3965926	9.4E-06	4.8E-08	5.6E-08	6.3E-08
388741	3965921	9.1E-06	4.7E-08	5.6E-08	6.2E-08

Source: Jacobson (2005)

Atmospheric transport modeling of the alternate source MDAs did not consider the dispersion characteristics of particulate releases from MDA H or the dispersion of vapor- and gas-phase releases from any of the MDAs. For a given release, downwind concentrations of particulates originating at MDA H should be approximately similar to those estimated for releases from Area G. The relative dispersion characteristics of vapor- and gas-phase releases from the various MDAs are generally expected to resemble those shown in Table 10 for particulate releases.

Modeling of the transport of groundwater contaminants from the alternate source MDAs to locations downgradient of Area G was not conducted. However, various lines of evidence were used to estimate the potential for interactions between contaminant plumes from these facilities and releases from Area G during the compliance period, as discussed below.

Interactions between groundwater contaminant plumes originating at MDAs AB, C, H, and T and releases from Area G may occur during the compliance period if two conditions are satisfied. First, radionuclides released from the MDAs must discharge to the regional aquifer within 1,000 years of the closure of Area G. Second, the groundwater flowpaths in the aquifer beneath the alternate source MDAs must intersect with contaminant plumes from Area G.

The groundwater flow and transport modeling conducted in support of the performance assessment and composite analysis (Stauffer et al., 2005) projected groundwater travel times to a domestic well 100 m (330 ft) downgradient of Area G ranging from about 1,000 years to more than 10,000 years, depending upon the infiltration rate and location of the disposal units where the release occurs. Using the infiltration rate estimated for the final cover at Area G, the probabilistic modeling conducted using the Area G Site Model projected that no radionuclides will arrive at the compliance well within the 1,000-year compliance period.

The groundwater travel times (to the compliance well) estimated by Stauffer et al. (2005) are determined by the rate at which water passes through the Bandelier Tuff; travel times through the Cerros del Rio basalts and the regional aquifer are relatively rapid and do not add significantly to the overall travel time. Stratigraphic comparisons across the Laboratory indicate that the thickness of the Bandelier Tuff generally increases from east to west; Figure 17 illustrates this trend. This suggests that groundwater travel times at MDAs AB, C, and T may be greater than those estimated for Area G. Given the proximity of Area G and MDA H, relatively little difference in travel time is expected for groundwater contamination from these facilities.

The comparison of relative travel times to the aquifer, based on stratigraphy, is expected to be valid if the hydrologic conditions, most notably rates of infiltration through the disposal units, are similar at the various facilities. Rates of infiltration at MDA H are generally expected to be similar to those modeled by Stauffer et al. (2005). As discussed earlier, this may not be the case with respect to MDAs AB, C, and T. However, although wet conditions have prevailed at MDA AB in the past, it is not clear that the additional moisture observed at depths of 12 to 18 m (40 to 60 ft) bgs will yield faster rates of contaminant travel to the regional aquifer now that the pads have been removed. Although the average precipitation rate at MDA C may be moderately higher than that at Area G, the two locations are not expected to have significantly different infiltration rates. Neither disposal facility received liquid waste during its operational history or was otherwise exposed to long periods of elevated moisture. In terms of MDA T, the effects of liquid discharges to the absorption beds do not appear to have affected the disposal shafts that received the large quantities of Am-241 and Pu-241.

Based on the preceding discussion, no significant releases of uranium from MDA H are expected to discharge to the regional aquifer during the 1,000-year compliance period. Deterministic modeling for Area G suggests that radionuclides other than C-14 will require more than 100,000 years to reach

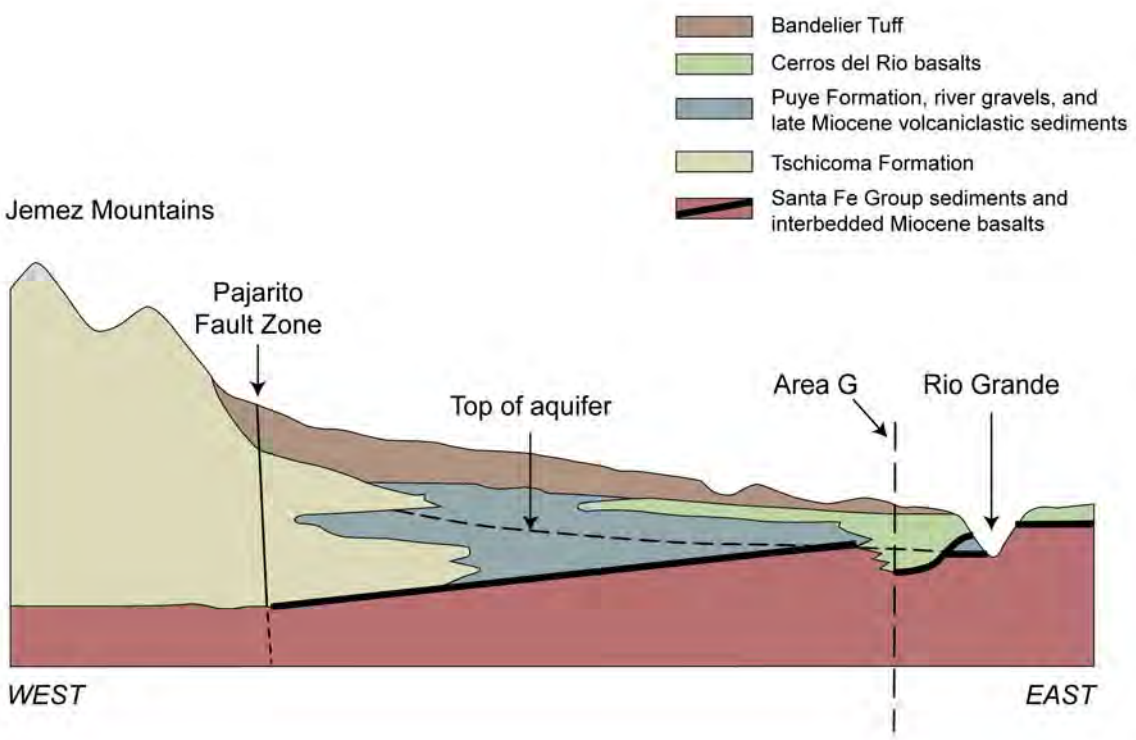

Figure 17
Generalized Stratigraphic Relationships of the Pajarito Plateau

Source: Adapted from Hollis et al., (1997) with input from Stauffer (2005) and Broxton (2005)

the aquifer beneath the disposal facility. Available data also indicate that releases from MDAs AB, C, and T are unlikely to reach the aquifer during the composite analysis compliance period. If the infiltration rates at MDAs AB, C, and T are at all similar to those at Area G, the critical radionuclides at these sites will require thousands or tens of thousands of years to reach the regional aquifer.

Some, but not all, of any contamination discharged to the regional aquifer from MDAs AB, C, H, and T may intersect with contaminant plumes from Area G. Figure 18 indicates the general flow paths of the regional aquifer beneath the Laboratory and the approximate locations of MDAs AB, C, H, and T and Area G. Based on the information provided in this figure, the aquifer flow paths beneath MDAs AB, C, and T appear to parallel the flow path below Area G. MDA H lies on the same aquifer flow path as Area G, and any contaminant discharges to the aquifer from MDA H are expected to interact directly with releases from Area G.

The information summarized in Section 3.2.4.1 suggests that Area G is the primary source of contamination in the portions of Cañada del Buey and Pajarito Canyon that could affect the receptors considered in the performance assessment and composite analysis. As discussed, it is likely that radionuclides detected in the canyon sediments are related to residual contamination rather than releases from the pits and shafts. The release of residual contamination to Cañada del Buey and Pajarito Canyon should decrease as Area G undergoes closure and the final cover is applied across the facility. After closure, any contamination in the canyons is expected to result primarily from releases from the disposal facility. Thus, no significant interactions between canyon contamination from other sources at the Laboratory and Area G are anticipated. This conclusion may change if unforeseen releases to the canyons occur.

Some groundwater transport modeling has indicated that, under certain supply well pumping scenarios, small amounts of contamination released to Mortandad Canyon could discharge to the regional aquifer and intersect groundwater releases from Area G (Birdsell, 2005). Although theoretically possible, the likelihood of such interaction is small because water-supply pumping has had little effect on water levels to date. Any contaminants that arrive at the aquifer will tend to follow the water table gradient; this gradient is almost due east below Mortandad Canyon and to the southeast at Area G.

In summary, the findings of the alternate source evaluation are as follows:

- Radionuclide inventories at most MDAs are significantly smaller than the corresponding inventories at Area G. Possible exceptions include Pu-239 and Pu-240 at MDA AB; U-235 and U-236 at MDA C; U-234, U-235, and U-236 at MDA H; and Am-241 and Pu-241 at MDA T. On a radionuclide-specific basis, this means that potential exposures resulting from releases at the MDAs will generally be much lower than the contaminant-specific exposures projected for Area G. Divergences between the

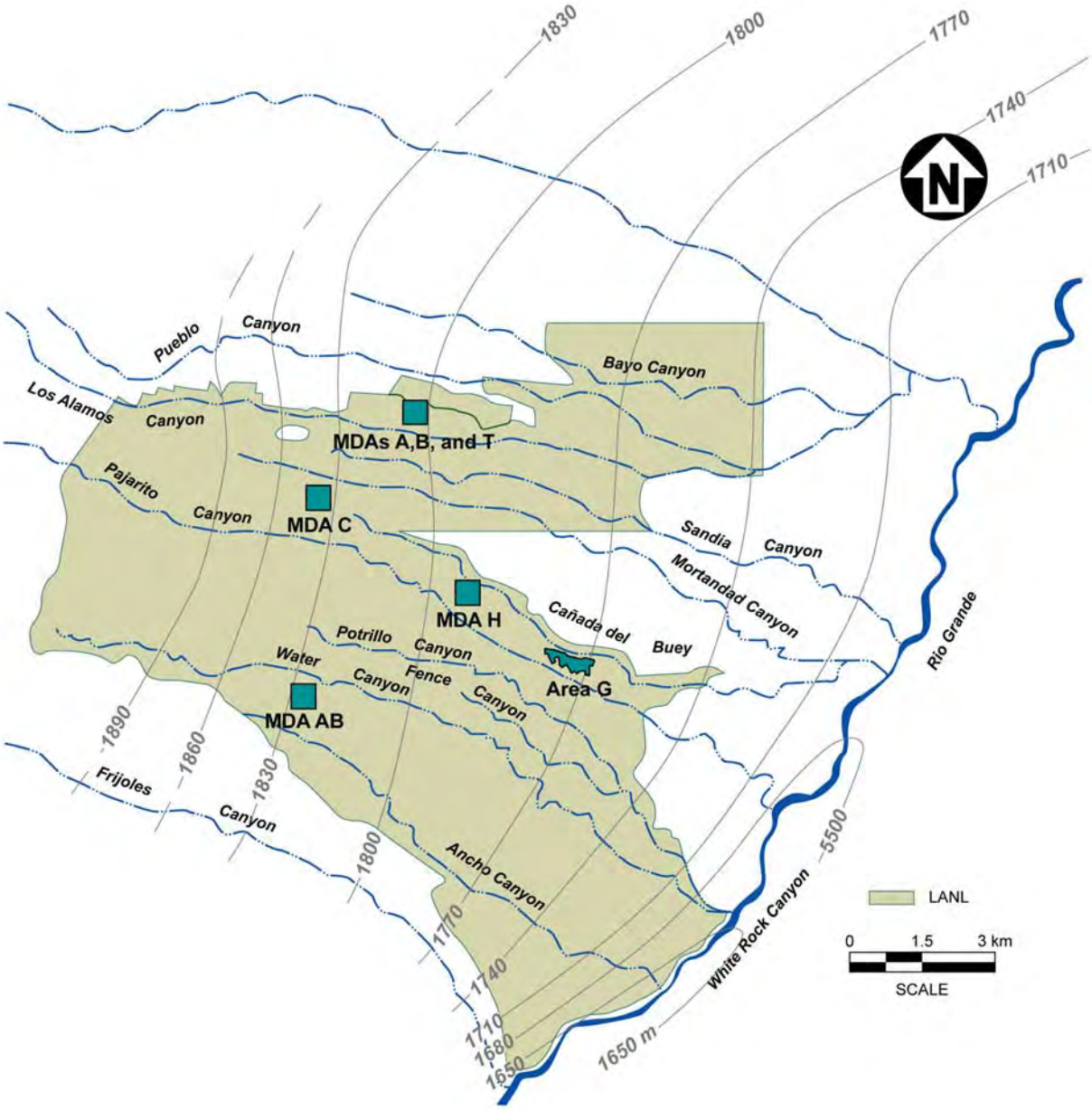

Figure 18
Location of Alternate Contamination Sources and Generalized Water-Level Contours on the Top of the Regional Aquifer

exposures projected for the alternate source MDAs and Area G will be even greater when the cumulative exposures from all radionuclides are considered because Area G is the only source under consideration that has large inventories of several radionuclides.

- The likelihood of radionuclide releases due to biotic intrusion at MDAs AB and H is expected to be smaller than that at Area G; the impacts of biotic intrusion on the waste disposed of at MDA C and in the shafts at MDA T may be similar to those projected for Area G. Elevated moisture contents that could result in increased leaching have been observed at MDAs AB and T in the past, but it is not clear that these conditions will affect the waste containing the critical radionuclides at these sites. Hydrologic conditions at Area G and MDAs C and H are probably similar.

- On a relative basis, airborne concentrations of contaminants released from MDAs AB, C, and T will be diluted by a factor of 100 or more at the exposure locations downwind of Area G. Contaminant releases from Area G and MDA H are expected to disperse in a similar manner.

- Releases of critical radionuclides from MDAs AB, C, H, and T are generally expected to discharge to the regional aquifer long after the 1,000-year compliance period. It is not clear that contaminants discharged to the aquifer below MDAs AB, C, and T will intersect contaminant plumes that originate at Area G.

- The major source of contamination in the canyons adjacent to Area G is expected to be the disposal facility itself.

Based on these findings, the potential for significant interaction between the releases from Area G and discharges from other facilities at the Laboratory is expected to be low. This conclusion should be verified as further information about alternate sources of radioactivity at the Laboratory becomes available.

The alternate source evaluation does not address releases from facilities that are currently operating at LANL. The composite analysis focuses on the long-term performance of Area G after the facility undergoes final closure. It is assumed that the facilities that are currently operating and that may pose a current-day risk to human health and safety will not be operating over most, if not all, of the 1,000-year compliance period that starts when the final closure of Area G is complete. The impacts of present-day radionuclide releases on persons living in the vicinity of LANL are evaluated as part of the Laboratory's ongoing environmental surveillance program; results such as those presented in LANL (2007b) indicate that the Laboratory's current operations pose little or no risk to members of the public.

4.0 Intruder Dose Projections and Intruder-Based Waste Acceptance Criteria

This section presents the doses projected for the inadvertent intruder scenarios and the WAC developed on the basis of these exposures. Section 4.1 summarizes the projected exposures for the different subsets of the performance assessment inventory and intruder scenarios. The intruder-based WAC are presented in Section 4.2, and Section 4.3 compares these limits to those developed in conjunction with the 1997 performance assessment.

4.1 Intruder Exposure Projections

As discussed in Section 2.2.1, preliminary modeling was conducted to determine the need for considering the effects of radon diffusion when estimating the total intruder exposures from the different subsets of waste. The results of this analysis are summarized in Table 11, which shows projected exposures for selected parent radionuclides that eventually decay to form Rn-220 or Rn-222. This table shows two sets of results, one that includes the effects of diffusion and one that excludes these effects. The doses shown in the table are the peak mean exposures projected for each parent radionuclide, including contributions from all daughter products, assuming intrusion occurs at the end of the 100-year active institutional control period.

The results shown in Table 11 indicate that the diffusion of Rn-220 has little or no effect on the doses projected for its longer-lived parents (i.e., Th-232, Ra-228, and Th-228); doses projected for the parent radionuclides are the same whether or not diffusion is considered. These results are not surprising because Rn-220 is very short-lived and decays to form very short-lived daughters.

In contrast, the effects of radon diffusion on intruder exposures are apparent for some radionuclides that decay to form Rn-222 under certain circumstances. For example, depending upon the disposal units and intruder scenario under consideration, the peak mean Ra-226 dose increases 1.1 to 14 times when the effects of radon diffusion are included. The peak mean exposures projected for Th-230 tend to be affected by diffusion in a similar fashion, but the effects are negligible from the perspective of overall intruder exposures because the doses from this radionuclide are small. The projected exposures for U-234 are little affected by radon diffusion. Based on these results, the intruder exposures for tritium, C-14, Kr-85, and Ra-226 were projected using the intruder diffusion model, while doses for all remaining radionuclides were modeled using the intruder model.

Table 11
Comparison of Intruder Dose Projections with and without the Effects of Radon Diffusion

Parent Radionuclide by Exposure Scenario	Peak Mean Dose (mrem/yr)							
	Diffusive Effects Included				Diffusive Effects Excluded			
	1988–2010 Pits	2011–2044 Pits	1988–2015 Shafts	2016–2044 Shafts	1988–2010 Pits	2011–2044 Pits	1988–2015 Shafts	2016–2044 Shafts
Postdrilling Intruder								
U-234	6.7E-04	8.5E-04	3.7E-02	4.8E-02	6.6E-04	8.5E-04	3.7E-02	4.8E-02
Th-230	1.6E-05	1.6E-06	4.9E-09	---	2.3E-06	3.2E-07	3.9E-09	---
Ra-226	5.4E-02	2.4E-02	2.6E+00	3.9E-04	4.0E-03	2.6E-03	2.0E+00	2.3E-04
Th-232	4.2E-03	5.9E-05	4.1E-01	1.2E-01	4.2E-03	5.9E-05	4.1E-01	1.2E-01
Ra-228	2.4E-11	6.8E-10	---	---	2.4E-11	6.8E-10	---	---
Th-228	9.2E-23	1.1E-22	1.5E-20	3.8E-20	9.2E-23	1.1E-22	1.5E-20	3.8E-20
Agricultural Intruder								
U-234	8.2E-04	2.5E-04	7.7E-02	8.1E-01	8.1E-04	2.5E-04	7.6E-02	8.1E-01
Th-230	1.8E-04	1.0E-05	6.4E-08	---	1.5E-04	9.1E-06	5.3E-08	---
Ra-226	5.3E-01	1.9E-01	7.0E-01	1.8E-02	4.9E-01	1.7E-01	4.0E-01	1.6E-02
Th-232	6.5E-01	7.0E-03	8.0E+01	1.5E+01	6.5E-01	7.0E-03	8.0E+01	1.5E+01
Ra-228	7.5E-09	5.4E-08	---	---	7.5E-09	5.4E-08	---	---
Th-228	3.0E-20	8.7E-21	5.7E-19	7.3E-18	3.0E-20	8.7E-21	5.7E-19	7.3E-18
Construction Intruder								
U-234	6.3E-04	6.4E-04	3.6E-02	1.8E-01	6.3E-04	6.4E-04	3.6E-02	1.8E-01
Th-230	7.0E-06	8.6E-07	7.5E-09	---	4.6E-06	5.7E-07	6.7E-09	---
Ra-226	2.1E-02	1.1E-02	4.7E-01	9.0E-04	1.3E-02	7.7E-03	3.3E-02	7.7E-04
Th-232	1.8E-02	3.2E-04	5.7E+00	7.6E-01	1.8E-02	3.2E-04	5.7E+00	7.6E-01
Ra-228	1.9E-10	2.0E-09	---	---	1.9E-10	2.0E-09	---	---
Th-228	7.6E-22	3.4E-22	2.9E-20	3.2E-19	7.6E-22	3.4E-22	2.9E-20	3.2E-19

-- = Radionuclide was not included in the inventory.

The projected dose distributions for the Intruder-Construction, Intruder-Agriculture, and Intruder–Post-Drilling exposure scenarios are summarized in Table 12; exposures are provided for each subset of the performance assessment inventory discussed earlier. The distributional information included in the table includes the mean, fifth percentile, and ninety-fifth percentile exposures; results for nondiffusive contaminants and radionuclides whose impacts are influenced by the effects of diffusion (i.e., tritium, C-14, Kr-85, and Ra-226) are provided for each exposure scenario.

The peak mean doses for the 1988–2010 disposal pits range from 0.49 to 3.7 mrem/yr for the radionuclides that are unaffected by diffusive releases; the exposures projected for H-3, C-14, Kr-85, and Ra-226 range from 0.04 to 0.47 mrem/yr. The corresponding ranges for the 2011–2044 pits are 0.021 to 0.60 mrem/yr and 0.0069 to 0.097 mrem/yr. The radionuclides making significant contributions to the doses projected for the three receptors include Cl-36, K-40, Pu-239, Ra-226, Tc-99, and U-238, depending upon the disposal units and exposure scenario under consideration. The exposures projected for the agricultural and postdrilling intruders are largely the result of the ingestion of contaminated crops and animal products and direct radiation from contaminated soils; the exposures for the homebuilder result primarily from the ingestion of soil, inhalation, and direct radiation from contaminated soils.

The exposures projected for the disposal pits under the three intruder scenarios are of a similar magnitude, despite the fact that excavation of the basement brings significantly more material to the surface than does well drilling. This is because of the thickness of the cover placed over the disposal units relative to the depth of disturbance associated with the different intruder scenarios. The initial cover thickness over the 1988–2010 disposal pits ranges from 2.5 to 6 m (8.2 to 19.6 ft) and has a median value of 4.2 m (13.7 ft); the initial cover thickness is greater than 3 m (9.8 ft) for 92 percent of the nodes used to represent the pits. Setting aside the effects of surface erosion for a moment, this means that in 92 percent of the model realizations the waste is undisturbed by the excavation of a 3 m (9.8 ft) basement and no contamination is brought to the surface as a result of human activities. A similar set of circumstances is seen for the 2011–2044 pits; the initial cover thickness over these units is less than 3 m (9.8 ft) in only 2 percent of the model realizations. In contrast, drilling a well through the pits brings contamination to the surface of the facility in all model realizations.

Projected exposures change over time in response to the decay of shorter-lived radionuclides, continued penetration into the waste by plants and animals inhabiting the site, and thinning of the cover due to erosion. In terms of the 1988–2010 pits, the peak mean exposures projected for the construction, agricultural, and postdrilling scenarios occur 100, 740, and 620 years after facility closure. The peak exposures for all three scenarios occur at the end of the 1,000-year compliance period for the 2011–2044 disposal pits.

Table 12
Probabilistic Doses for the Inadvertent Intruder Exposure Scenarios

Disposal Units	Exposure Scenario	Projected Dose (mrem/yr)					
		Mean		5th Percentile		95th Percentile	
		Nondiffusive Radionuclides	Diffusive Radionuclides	Nondiffusive Radionuclides	Diffusive Radionuclides	Nondiffusive Radionuclides	Diffusive Radionuclides
1988–2010 Pits	Construction	4.9E-01	4.0E-02	1.5E-09	5.6E-04	2.6E+00	1.7E-01
	Agriculture	3.7E+00	4.7E-01	1.5E-05	3.4E-03	2.1E+01	3.5E+00
	Postdrilling	3.3E+00	2.5E-01	1.8E-01	4.8E-03	1.2E+01	1.1E+00
2011–2044 Pits	Construction	2.1E-02	6.9E-03	3.5E-12	1.3E-04	2.7E-02	2.7E-02
	Agriculture	3.6E-01	9.7E-02	2.1E-10	8.8E-04	1.4E+00	2.3E-01
	Postdrilling	6.0E-01	9.2E-02	8.7E-02	1.7E-03	1.5E+00	2.4E-01
1988–2015 Shafts	Construction	4.5E+00	5.2E-01	5.0E-17	1.1E-02	3.0E+01	2.1E+00
	Agriculture	8.4E+01	5.8E+00	1.4E-15	3.0E-01	5.5E+02	1.9E+01
	Postdrilling	6.4E+00	4.5E+00	1.7E+00	1.5E+00	1.8E+01	9.6E+00
2016–2044 Shafts	Construction	1.5E+00	9.7E-01	6.4E-04	1.9E-01	5.2E+00	2.3E+00
	Agriculture	2.6E+01	2.3E+01	3.7E-02	5.9E+00	8.6E+01	5.6E+01
	Postdrilling	4.3E-01	2.7E+00	1.3E-01	1.2E+00	1.0E+00	4.8E+00

The agricultural intruder doses shown in Table 12 for waste disposed of in pits from 1988 through 2010 and from 2011 through 2044 are less than the exposures projected for the historical and future pits in conjunction with the 1997 performance assessment (Hollis et al., 1997). The 1997 analysis projected peak agricultural intruder doses of about 30 mrem/yr for both the 1988–1995 and 1996–2044 pits. Several differences exist between the earlier, deterministic modeling and the current intruder dose assessment; however, the decrease in the projected exposures for the agricultural intruder is primarily a reflection of the placement of additional cover over the disposal units. The 1997 assessment included 1 to 2 m (3.3 to 6.6 ft) of cover over the pits; 2.5 m (8.2 ft) or more exists over the 1988–2010 and 2011–2044 pits, as modeled here.

The 1997 performance assessment did not estimate the exposures received by the construction and postdrilling intruders following disturbance of the disposal pits. Dose projections for the postdrilling scenario were, however, estimated by Shuman (1999). The peak mean dose projected for the postdrilling intruder living over the 2011–2044 pits is greater than the dose of 0.3 mrem/yr projected for the 1996–2044 pits by Shuman. This increase is due to differences in the models and data used in the two analyses.

The peak mean exposures calculated for the waste disposed of in shafts from 1988 through 2015 range from 4.5 to 84 mrem/yr for radionuclides that are unaffected by diffusion and 0.52 to 5.8 mrem/yr for H-3, C-14, Kr-85, and Ra-226. Total peak mean doses representing the sum of these results range from 5.1 to 89 mrem/yr. Th-232 accounts for 92 and 87 percent of the peak mean doses for the construction and agricultural intruders, respectively; Ra-226 is the other major contributor to the projected exposures for these intruders. Important radionuclides for the postdrilling scenario include Ag-108m, C-14, Cs-137, H-3, Ni-63, Ra-226, and Sr-90; these isotopes account for almost 95 percent of the peak exposure. The ingestion of crops and animal products, and direct radiation from contaminated soils are the exposure pathways that contribute most to the postdrilling intruder dose; the ingestion of crops and direct radiation from contaminated soils are the major contributors to the projected agricultural intruder dose. Inhalation, the ingestion of contaminated soils, and direct radiation are the pathways making the largest contributions to the peak mean dose for the construction worker.

The peak mean exposures projected for the waste disposed of in shafts from 2016 through 2044 range from 0.43 to 26 mrem/yr for radionuclides that are unaffected by diffusion and from 0.97 to 23 mrem/yr for tritium, C-14, Kr-85, and Ra-226; summing these results yields total peak mean doses of 2.5 to 49 mrem/yr. Tritium accounts for 39 to 86 percent of the peak mean doses projected for the three intruder scenarios; the sum of the exposures estimated for Sr-90 and Th-232 account for 9 and 43 percent of the postdrilling and agricultural doses, respectively; Cs-137, Th-232, U-234, and U-238 account for 57 percent of the construction intruder's peak dose. Inhalation of tritium, and the ingestion of crops and animal products are the major exposure pathways for the postdrilling intruder; the same pathways plus direct radiation from contaminated soils play a major role in the exposures

estimated for the agricultural intruder. The inhalation of resuspended soil and tritium, direct radiation from contaminated soils, and ingestion of soil all make significant contributions to the peak mean dose projected for the construction intruder.

The dose projections provided in Table 12 for the 1988–2015 and 2016–2044 shafts take into account the packaging requirements for containers of high-activity tritium waste. Waste acceptance criteria for tritium disposal at Area G impose off-gas limits on the containers used to dispose of the waste (LANL, 2008). For waste packages with a tritium concentration of 10 Ci/m^3 of waste to 500 Ci per package, the stainless steel containers in which the waste is placed must limit the annual off-gas rate to 0.01/yr or less; containers with 500 to 100,000 Ci of tritium per package must meet an off-gas requirement of no more than 1×10^{-4}/yr. Based on these requirements, the effects of limiting off-gas rates to 0.01/yr were simulated in the modeling for the 1988–2015 and 2016–2044 shafts.

The use of the higher of the two off-gas rates is expected to yield conservative results in terms of the overall release of tritium. That is because most waste packages disposed of to date have contained more than 500 Ci of tritium, making them subject to the more restrictive off-gas limits. For example, about 96 percent of the tritium waste activity disposed of in shafts from September 27, 1988 through 2007 was packaged in containers that contained at least 500 Ci. It is anticipated that a similar pattern of disposal will occur in the future.

The magnitude of the tritium container off-gas rate has a significant impact on the doses projected for the 2016–2044 disposal shafts. Tritium contributes about 47 percent (23 mrem) to the peak annual dose (49 mrem) calculated for these units under the agricultural intruder scenario when an off-gas rate of 0.01/yr is assumed. If this rate is decreased to 0.0001/yr, the peak mean tritium dose drops to less than 0.5 mrem/yr. On this basis alone, the peak mean dose for the scenario declines approximately 50 percent if the more restrictive off-gas rate is applied. Tritium did not make a significant contribution to the peak mean dose calculated for the 1988–2015 shafts under the agricultural intruder scenario. Therefore, the off-gas rate used in the modeling is less important for these disposal units.

The projected doses for the two sets of disposal shafts are significantly higher than those estimated for the pits. This is because higher activity waste has been placed in the shafts and because the average cover thickness over the shafts is less than that of the pits.

The agricultural intruder doses projected for the waste disposed of in shafts are substantially higher than those estimated in conjunction with the 1997 performance assessment. In the earlier assessment, a peak dose of 22 mrem/yr was estimated for the disposal units that were active from 1988 through 1995. This is only about 24 percent of the total dose determined by the GoldSim modeling for the 1988–2015 shafts. Much of the reason these estimates differ is because of the

Th-232 inventories used in the two analyses. The 1997 modeling was based on a Th-232 inventory of 4.1 x 10^{-4} Ci, which was assumed to be distributed uniformly throughout the disposal shafts. In contrast, the current intruder analysis uses a mean Th-232 inventory of 0.74 Ci and assumes that more than half of the inventory is in the upper 1.5 m (4.9 ft) of the waste profile. As a result, higher concentrations of Th-232 are brought to the surface during basement excavation, leading to higher exposures for the receptor.

The peak agricultural intruder dose projected for waste disposed of in the 2016–2044 shafts is about 4 times greater than the peak dose of 12 mrem/yr that was estimated in 1997 for waste disposed of from 1996 through 2044. Part of the difference in these doses stems from different assumptions about when intrusion might occur: the 1997 modeling assumed that concrete caps placed over the disposal shafts would prevent intrusion into the waste for 300 years after facility closure but the current assessment assumes intrusion could take place any time after the 100-year active institutional control period ends. The extra 200-year delay in intrusion assumed for the 1997 modeling allows for additional decay; if this delay had been assumed in the current modeling it would have decreased the peak mean dose for the agricultural intruder by about 57 percent. Other factors that contribute to the disparity between the two modeling efforts include differences in the radionuclide inventories used, the closure configuration of the disposal facility, and the projected impacts of biotic intrusion and surface erosion on the disposal units.

The peak postdrilling dose estimated for the 2016-2044 shafts is about 10 percent of the peak dose projected for the 1996-2044 waste by Shuman (1999) using the 1997 performance assessment methodology; both of these doses pertain to intrusion at the end of the 100-year active institutional control period. Differences in inventories and assumptions about off-gas rates are major factors contributing to this disparity.

All of the peak intruder doses projected by the current modeling effort for the disposal pits and shafts at Area G are lower than the chronic and acute intruder performance objectives (100 and 500 mrem/yr, respectively). In terms of the pits, none of the peak mean exposures exceeds 4.1 percent of the respective limits. The peak mean doses projected for the shafts under the construction scenario are 1 percent or less of the 500 mrem/yr acute dose limit, while the exposures projected for the postdrilling intruder range from 3 to 11 percent of the chronic limit. Finally, the peak mean doses received by the agricultural intruder from waste disposed of in the 1988–2015 and 2016–2044 shafts are 89 and 49 percent of the dose objective, respectively.

4.2 Intruder-Based Waste Acceptance Criteria

The intruder-based WAC developed for the disposal pits and shafts in MDA G are summarized in Tables 13 and 14, respectively. Separate criteria are listed for the three exposure scenarios, based on exposures during the 1,000-year compliance period. Limits were estimated for radionuclides that may exist in a vapor or gas phase, or give rise to such, using the intruder and

Table 13
Intruder-Based Waste Acceptance Criteria for the Disposal Pits at MDA G

Radionuclide	Waste Acceptance Criteria (Ci/m^3)		
	Intruder-Construction Scenario	Intruder-Agriculture Scenario	Intruder–Post-Drilling Scenario
Ac-227	3.4E+06	8.4E+04	1.8E+00
Ag-108m	1.1E+02	2.4E+00	6.8E-02
Al-26	2.0E+01	1.9E-01	3.1E-02
Am-241	2.6E+04	5.0E+02	1.2E-01
Am-243	3.3E+03	8.4E+01	7.9E-02
Ba-133	6.1E+08	1.6E+07	4.2E+03
Be-10	1.2E+06	1.9E+04	4.8E+01
Bi-207	5.6E+03	9.7E+01	1.4E+00
Bk-247	4.7E+03	1.0E+02	7.2E-02
C-14	4.2E+02	1.8E+00	1.3E+00
Ca-41	2.8E+04	8.3E+00	2.2E+00
Cf-249	3.2E+03	6.3E+01	7.6E-02
Cf-251	6.3E+03	1.2E+02	7.2E-02
Cf-252	3.0E+08	5.1E+06	3.2E+03
Cl-36	3.3E+02	2.4E-03	1.2E-03
Cm-243	3.8E+06	7.8E+04	3.7E+00
Cm-244	1.2E+07	2.5E+05	2.0E+01
Cm-245	5.6E+03	1.1E+02	8.4E-02
Co-60	1.9E+10	2.0E+08	6.1E+06
Cs-135	1.3E+05	2.3E+02	4.4E+00
Cs-137	6.0E+04	1.1E+03	3.9E+00
Eu-152	4.0E+06	3.2E+04	1.6E+02
Eu-154	2.1E+08	1.4E+06	9.8E+03
Gd-148	2.3E+05	4.4E+03	1.8E+00
H-3	5.8E+04	4.9E+02	2.1E+03
Ho-163	---	---	---
Ho-166m	7.7E+01	1.6E+00	5.7E-02
I-129	8.6E+03	2.2E+01	1.8E-01

--- = Concentration limits could not be calculated due to the lack of dose conversion factors for the radionuclide.

Table 13 (Continued)
Intruder-Based Waste Acceptance Criteria for the Disposal Pits at MDA G

Radionuclide	Waste Acceptance Criteria (Ci/m^3)		
	Intruder-Construction Scenario	Intruder-Agriculture Scenario	Intruder–Post-Drilling Scenario
K-40	1.5E+01	1.1E-01	6.3E-02
Kr-85	7.0E+17	4.1E+15	2.2E+15
Lu-176	3.0E+03	9.9E+01	1.9E-01
Mo-93	1.5E+05	1.1E+02	3.7E+00
Nb-91	---	---	---
Nb-92	---	---	---
Nb-93m	2.1E+11	1.5E+09	1.3E+05
Nb-94	2.6E+01	4.9E-01	4.9E-02
Nd-144	---	---	---
Ni-59	7.6E+05	1.8E+03	1.0E+02
Ni-63	7.7E+06	1.8E+04	2.0E+02
Np-237	1.3E+02	2.0E+00	3.6E-02
Os-194	9.5E+11	1.1E+10	1.3E+07
Pa-231	4.7E+01	1.1E+00	9.9E-03
Pb-210	2.9E+06	3.0E+04	3.2E+00
Pm-145	3.8E+09	1.2E+08	5.1E+03
Pu-236	5.3E+03	4.2E+01	1.7E+00
Pu-238	5.8E+05	1.3E+04	3.4E-01
Pu-239	3.1E+04	6.6E+02	9.5E-02
Pu-240	3.5E+04	7.5E+02	9.6E-02
Pu-241	7.5E+05	1.5E+04	3.4E+00
Pu-242	3.3E+04	7.0E+02	9.9E-02
Pu-244	1.6E+03	2.3E+01	6.7E-02
Ra-226	5.6E-01	2.1E-02	1.6E-02
Ra-228	1.4E+10	1.5E+08	7.7E+05
Si-32	6.1E+05	3.7E+03	8.6E+00
Sm-146	9.1E+03	8.3E+01	5.7E-01
Sm-151	3.4E+08	2.0E+06	1.2E+03
Sn-121m	1.5E+07	1.2E+05	5.0E+02

--- = Concentration limits could not be calculated because no dose conversion factor was found for the radionuclide.

Table 13 (Continued)
Intruder-Based Waste Acceptance Criteria for the Disposal Pits at MDA G

Radionuclide	Waste Acceptance Criteria (Ci/m^3)		
	Intruder-Construction Scenario	Intruder-Agriculture Scenario	Intruder–Post-Drilling Scenario
Sn-126	5.4E+02	8.4E+00	8.1E-01
Sr-90	6.5E+05	4.3E+02	2.2E+00
Tb-157	4.7E+07	1.3E+06	6.3E+02
Tc-97	3.5E+03	1.7E+00	7.6E-01
Tc-99	3.2E+03	2.1E-01	9.1E-02
Th-228	2.3E+25	1.3E+23	5.4E+20
Th-229	3.2E+03	7.0E+01	5.5E-02
Th-230	1.2E+00	4.3E-02	3.5E-02
Th-232	6.4E+01	8.6E-01	2.0E-02
Ti-44	1.1E+04	1.8E+02	2.4E-01
U-232	8.5E+02	1.2E+01	1.6E-01
U-233	9.9E+02	1.8E+01	2.7E-01
U-234	1.7E+02	5.8E+00	5.3E-01
U-235	3.4E+02	9.1E+00	1.8E-01
U-236	2.6E+03	5.3E+01	6.2E-01
U-238	8.8E+02	1.3E+01	5.3E-01
Zr-93	4.4E+06	4.6E+04	8.6E+01

--- = Concentration limits could not be calculated because no dose conversion factor was found for the radionuclide.

Table 14
Intruder-Based Waste Acceptance Criteria for the Disposal Shafts at MDA G

Radionuclide	Waste Acceptance Criteria (Ci/m^3)		
	Intruder-Construction Scenario	Intruder-Agriculture Scenario	Intruder–Post-Drilling Scenario
Ac-227	1.3E+11	2.6E+09	2.1E+01
Ag-108m	4.3E+06	8.0E+04	8.7E-01
Al-26	3.4E+05	3.7E+03	4.2E-01
Am-241	5.0E+08	1.1E+07	1.4E+00
Am-243	1.2E+08	2.6E+06	9.8E-01
Ba-133	1.8E+13	5.1E+11	4.2E+04
Be-10	2.4E+10	3.0E+08	6.4E+02
Bi-207	1.5E+08	2.6E+06	1.6E+01
Bk-247	1.5E+08	2.6E+06	8.8E-01
C-14	1.5E+04	5.4E+01	2.2E+01
Ca-41	4.2E+08	1.6E+05	6.9E+01
Cf-249	2.1E+08	4.6E+06	9.2E-01
Cf-251	2.2E+08	3.6E+06	8.9E-01
Cf-252	6.7E+12	8.8E+10	4.0E+04
Cl-36	3.7E+06	2.6E+01	1.2E-01
Cm-243	1.3E+11	2.7E+09	4.3E+01
Cm-244	1.9E+11	3.7E+09	2.3E+02
Cm-245	1.7E+08	3.2E+06	1.0E+00
Co-60	3.6E+14	4.3E+12	4.8E+07
Cs-135	2.4E+09	5.5E+06	6.8E+01
Cs-137	2.4E+09	4.9E+07	4.4E+01
Eu-152	1.2E+11	1.7E+09	1.6E+03
Eu-154	5.5E+12	6.7E+10	9.1E+04
Gd-148	5.3E+09	9.5E+07	2.2E+01
H-3	5.5E+06	4.5E+04	1.1E+05
Ho-163	---	---	---
Ho-166m	3.1E+06	6.6E+04	7.3E-01
I-129	1.2E+08	2.8E+05	2.5E+00

--- = Concentration limits could not be calculated due to the lack of dose conversion factors for the radionuclide.

NA = No exposures were projected to occur; therefore no concentration limit is listed.

Table 14 (Continued)
Intruder-Based Waste Acceptance Criteria for the Disposal Shafts at MDA G

Radionuclide	Waste Acceptance Criteria (Ci/m^3)		
	Intruder-Construction Scenario	Intruder-Agriculture Scenario	Intruder–Post-Drilling Scenario
K-40	4.4E+05	3.1E+03	2.0E+00
Kr-85	NA	NA	4.6E+06
Lu-176	6.1E+07	2.0E+06	2.5E+00
Mo-93	3.7E+09	2.3E+06	6.2E+01
Nb-91	---	---	---
Nb-92	---	---	---
Nb-93m	2.2E+15	2.2E+13	1.4E+06
Nb-94	9.6E+05	1.9E+04	7.0E-01
Nd-144	---	---	---
Ni-59	1.8E+10	3.1E+07	2.3E+03
Ni-63	1.9E+11	3.4E+08	2.7E+03
Np-237	4.1E+06	5.6E+04	5.3E-01
Os-194	3.3E+16	6.4E+14	1.0E+08
Pa-231	1.8E+06	3.6E+04	1.3E-01
Pb-210	4.4E+10	3.3E+08	3.6E+01
Pm-145	3.6E+13	1.1E+12	5.5E+04
Pu-236	5.8E+08	9.1E+06	1.8E+00
Pu-238	2.2E+09	1.5E+05	4.0E+00
Pu-239	7.8E+08	1.3E+07	1.2E+00
Pu-240	8.4E+08	1.4E+07	1.2E+00
Pu-241	1.5E+10	3.2E+08	4.1E+01
Pu-242	8.0E+08	1.3E+07	1.2E+00
Pu-244	6.5E+07	7.7E+05	8.3E-01
Ra-226	7.2E+00	9.2E-02	1.9E-01
Ra-228	4.1E+14	5.5E+12	6.1E+06
Si-32	1.1E+10	7.0E+07	1.1E+02
Sm-146	1.4E+08	1.9E+06	7.9E+00
Sm-151	4.6E+12	3.4E+10	1.4E+04
Sn-121m	2.2E+11	1.9E+09	6.1E+03

--- = Concentration limits could not be calculated because no dose conversion factor was found for the radionuclide.

NA = No exposures were projected to occur; therefore no concentration limit is listed.

Table 14 (Continued)
Intruder-Based Waste Acceptance Criteria for the Disposal Shafts at MDA G

Radionuclide	Waste Acceptance Criteria (Ci/m^3)		
	Intruder-Construction Scenario	Intruder-Agriculture Scenario	Intruder–Post-Drilling Scenario
Sn-126	1.5E+07	2.1E+05	1.9E+01
Sr-90	6.5E+09	4.4E+06	2.6E+01
Tb-157	9.7E+11	2.5E+10	7.6E+03
Tc-97	4.6E+07	2.3E+04	5.2E+01
Tc-99	4.2E+07	2.7E+03	6.2E+00
Th-228	7.7E+27	5.3E+27	1.3E+21
Th-229	2.0E+08	4.9E+06	6.8E-01
Th-230	1.4E+02	2.3E-01	4.3E-01
Th-232	1.5E+06	2.4E+04	2.5E-01
Ti-44	6.7E+08	1.1E+07	2.8E+00
U-232	2.5E+07	3.9E+05	1.9E+00
U-233	3.6E+07	6.8E+05	3.7E+00
U-234	2.5E+05	4.3E+01	7.6E+00
U-235	1.0E+07	2.6E+05	2.5E+00
U-236	6.6E+07	1.1E+06	8.9E+00
U-238	3.1E+07	2.5E+04	7.5E+00
Zr-93	7.4E+10	9.1E+08	1.1E+03

--- = Concentration limits could not be calculated because no dose conversion factor was found for the radionuclide.

NA = No exposures were projected to occur; therefore no concentration limit is listed.

intruder diffusion models (i.e., with and without the effects of diffusion). With the exception of Kr-85, which exists only as a gas, the smaller of the limits calculated for each radionuclide was adopted as the final criterion for that contaminant. The limits included in the tables were not adjusted to reflect or account for the specific activities of the isotopes.

The limits included in the tables are the lesser of the medians and means of the estimated distributions; since projected distributions of the WAC are generally skewed to the right, the median values tend to be most limiting. Concentration limits are not listed for five of the radionuclides included in the tables; limits for four of these could not be estimated because federal guidance reports 11 and 12 (EPA, 1988 and 1993) do not list dose conversion coefficients for these isotopes.

The depth at which waste is placed in the disposal pits and shafts will have a significant effect on the magnitude of the projected intruder doses and, therefore, the WAC. The WAC calculated for the pits in MDA G are based on the assumption that waste will be uniformly distributed throughout the waste profile, consistent with disposal practices in MDA G. The surface erosion modeling estimated the top of the waste profile, or waste elevation, for the disposal shafts in MDA G. The WAC listed in Table 14 for the 1988–2015 shafts assume the waste placed in these units is an additional 1.5 m (4.9 ft) below the waste elevation established for the erosion modeling. Placing additional restrictions on the minimum depth of disposal allows the disposal of waste with higher radionuclide concentrations.

Examination of Table 13 reveals that, on the whole, the WAC for the disposal pits are lowest for the Intruder–Post-Drilling Scenario. The significantly higher limits calculated for most radionuclides using the construction and agricultural intruder scenarios reflect the thickness of the cover placed over the disposal units relative to the depth of disturbance associated with the different intruder scenarios. As discussed earlier, the excavation of a basement does not disturb the waste in most model realizations. In contrast, drilling a well through the pits brings contamination to the surface of the facility in all model realizations.

Only small amounts of contamination are brought to the surface of the disposal facility in cases where the waste is undisturbed by the excavation of the basement. Plants penetrating the waste with their roots deposit contamination at the surface through litterfall and litter decomposition. Although animals may burrow into the waste and also transport radionuclides to the ground surface, the maximum burrowing depths of the species or taxa included in the modeling are less than the median value of the cover thickness distribution. Therefore, animal intrusion into the waste plays a relatively minor role. In any event, only small amounts of contamination reach the surface by the time an intruder arrives at the site to excavate the basement, resulting in very low doses for the construction worker and agricultural intruder. Consequently, the WAC based on these scenarios are high compared to those estimated for the postdrilling scenario.

As discussed, the distribution of initial cover thicknesses indicates that, in about 8 percent of the model realizations, cover depth will be less than 3 m (9.8 ft) and, therefore, prone to disturbance

during basement excavation. This percentage may increase because of the effects of surface erosion. That is, sampled cover depths equal to or greater than 3 m (9.8 ft) may be eroded to depths of less than 3 m (9.8 ft) by the time the intruder arrives at the disposal site. Under these conditions, basement excavation will expose waste and contamination will be brought to the surface. In most cases, however, the waste will not be disturbed by the excavation of the basement and exposures received by the construction and agricultural intruders will be low.

The WAC listed in Table 13 for H-3 are lowest for the agricultural intruder. The diffusion of this species upward from the waste to locations accessible to the agricultural intruder results in higher exposures for this intruder than for the postdrilling intruder, despite the fact that greater amounts of contamination are generally excavated during the drilling of the well.

Projected exposures for the agricultural and postdrilling intruders yield the most restrictive WAC for the disposal shafts (Table 14). The doses projected for the postdrilling intruder prove most restrictive for all but three of the radionuclides because the agricultural intruder has little or no direct contact with the waste. The radionuclides for which the agricultural intruder doses are most limiting are H-3, Ra-226, and Th-230. These radionuclides diffuse upward, or have daughters that diffuse upward, from the waste, making them more accessible to the agricultural intruder.

The postdrilling WAC listed in Table 14 for the disposal shafts are typically about an order of magnitude greater than the corresponding criteria for the pits (Table 13). This difference is primarily the result of how the shafts were represented in the modeling. In general, the disposal shafts are placed in groups referred to as shaft fields. Approximately 11 percent of the surface area of these shaft fields is expected to be occupied by disposal units (Shuman, 2008a). Given the spacing of the shafts within the shaft field, the well drilling crew has approximately a one-in-nine chance of contacting waste during the establishment of the postdrilling intruder's well. This likelihood of contacting the waste is taken into account in the WAC calculations by effectively reducing the radionuclide concentrations in the waste by a factor of 9.

Vapor- and gas-phase diffusion has a significant effect on the shaft WAC for tritium and C-14. The diffusion of tritiated water vapor and C-14 gas adds significantly to the construction and agricultural intruder doses, resulting in more restrictive WAC. The exposure received from these radionuclides by the postdrilling intruder is relatively unaffected by vapor- and gas-phase diffusion. The generation and diffusion of radon gas have significant impacts on the doses projected for some of the parents that count Rn-222 among their decay products.

The final intruder-based WAC may be identified for MDA G using the results summarized in Tables 13 and 14. These criteria, shown in Table 15, represent the most restrictive limits across all intruder scenarios and times of intrusion; the limits were not adjusted to reflect or account for the specific activities of the isotopes.

Table 15
Final Waste Acceptance Criteria for the Disposal Pits and Shafts at MDA G

Radionuclide	Disposal Pits		Disposal Shafts	
	Limit (Ci/m^3)	Limiting Scenario	Limit (Ci/m^3)	Limiting Scenario
Ac-227	1.8E+00	Post-Drilling	2.1E+01	Post-Drilling
Ag-108m	6.8E-02	Post-Drilling	8.7E-01	Post-Drilling
Al-26	3.1E-02	Post-Drilling	4.2E-01	Post-Drilling
Am-241	1.2E-01	Post-Drilling	1.4E+00	Post-Drilling
Am-243	7.9E-02	Post-Drilling	9.8E-01	Post-Drilling
Ba-133	4.2E+03	Post-Drilling	4.2E+04	Post-Drilling
Be-10	4.8E+01	Post-Drilling	6.4E+02	Post-Drilling
Bi-207	1.4E+00	Post-Drilling	1.6E+01	Post-Drilling
Bk-247	7.2E-02	Post-Drilling	8.8E-01	Post-Drilling
C-14	1.3E+00	Post-Drilling	2.2E+01	Post-Drilling
Ca-41	2.2E+00	Post-Drilling	6.9E+01	Post-Drilling
Cf-249	7.6E-02	Post-Drilling	9.2E-01	Post-Drilling
Cf-251	7.2E-02	Post-Drilling	8.9E-01	Post-Drilling
Cf-252	3.2E+03	Post-Drilling	4.0E+04	Post-Drilling
Cl-36	1.2E-03	Post-Drilling	1.2E-01	Post-Drilling
Cm-243	3.7E+00	Post-Drilling	4.3E+01	Post-Drilling
Cm-244	2.0E+01	Post-Drilling	2.3E+02	Post-Drilling
Cm-245	8.4E-02	Post-Drilling	1.0E+00	Post-Drilling
Co-60	6.1E+06	Post-Drilling	4.8E+07	Post-Drilling
Cs-135	4.4E+00	Post-Drilling	6.8E+01	Post-Drilling
Cs-137	3.9E+00	Post-Drilling	4.4E+01	Post-Drilling
Eu-152	1.6E+02	Post-Drilling	1.6E+03	Post-Drilling
Eu-154	9.8E+03	Post-Drilling	9.1E+04	Post-Drilling
Gd-148	1.8E+00	Post-Drilling	2.2E+01	Post-Drilling
H-3	4.9E+02	Agriculture	4.5E+04	Agricultural
Ho-163	---	---	---	---
Ho-166m	5.7E-02	Post-Drilling	7.3E-01	Post-Drilling
I-129	1.8E-01	Post-Drilling	2.5E+00	Post-Drilling

--- = Concentration limits could not be calculated due to the lack of dose conversion factors for the radionuclide.

Table 15 (Continued)
Final Waste Acceptance Criteria for the Disposal Pits and Shafts at MDA G

Radionuclide	Disposal Pits		Disposal Shafts	
	Limit (Ci/m^3)	Limiting Scenario	Limit (Ci/m^3)	Limiting Scenario
K-40	6.3E-02	Post-Drilling	2.0E+00	Post-Drilling
Kr-85	2.2E+15	Post-Drilling	4.6E+06	Post-Drilling
Lu-176	1.9E-01	Post-Drilling	2.5E+00	Post-Drilling
Mo-93	3.7E+00	Post-Drilling	6.2E+01	Post-Drilling
Nb-91	---	---	---	---
Nb-92	---	---	---	---
Nb-93m	1.3E+05	Post-Drilling	1.4E+06	Post-Drilling
Nb-94	4.9E-02	Post-Drilling	7.0E-01	Post-Drilling
Nd-144	---	---	---	---
Ni-59	1.0E+02	Post-Drilling	2.3E+03	Post-Drilling
Ni-63	2.0E+02	Post-Drilling	2.7E+03	Post-Drilling
Np-237	3.6E-02	Post-Drilling	5.3E-01	Post-Drilling
Os-194	1.3E+07	Post-Drilling	1.0E+08	Post-Drilling
Pa-231	9.9E-03	Post-Drilling	1.3E-01	Post-Drilling
Pb-210	3.2E+00	Post-Drilling	3.6E+01	Post-Drilling
Pm-145	5.1E+03	Post-Drilling	5.5E+04	Post-Drilling
Pu-236	1.7E+00	Post-Drilling	1.8E+00	Post-Drilling
Pu-238	3.4E-01	Post-Drilling	4.0E+00	Post-Drilling
Pu-239	9.5E-02	Post-Drilling	1.2E+00	Post-Drilling
Pu-240	9.6E-02	Post-Drilling	1.2E+00	Post-Drilling
Pu-241	3.4E+00	Post-Drilling	4.1E+01	Post-Drilling
Pu-242	9.9E-02	Post-Drilling	1.2E+00	Post-Drilling
Pu-244	6.7E-02	Post-Drilling	8.3E-01	Post-Drilling
Ra-226	1.6E-02	Post-Drilling	9.2E-02	Agricultural
Ra-228	7.7E+05	Post-Drilling	6.1E+06	Post-Drilling
Si-32	8.6E+00	Post-Drilling	1.1E+02	Post-Drilling
Sm-146	5.7E-01	Post-Drilling	7.9E+00	Post-Drilling
Sm-151	1.2E+03	Post-Drilling	1.4E+04	Post-Drilling

--- = Concentration limits could not be calculated because no dose conversion factor was found for the radionuclide.

Table 15 (Continued)
Final Waste Acceptance Criteria for the Disposal Pits and Shafts at MDA G

Radionuclide	Disposal Pits		Disposal Shafts	
	Limit (Ci/m^3)	Limiting Scenario	Limit (Ci/m^3)	Limiting Scenario
Sn-121m	5.0E+02	Post-Drilling	6.1E+03	Post-Drilling
Sn-126	8.1E-01	Post-Drilling	1.9E+01	Post-Drilling
Sr-90	2.2E+00	Post-Drilling	2.6E+01	Post-Drilling
Tb-157	6.3E+02	Post-Drilling	7.6E+03	Post-Drilling
Tc-97	7.6E-01	Post-Drilling	5.2E+01	Post-Drilling
Tc-99	9.1E-02	Post-Drilling	6.2E+00	Post-Drilling
Th-228	5.4E+20	Post-Drilling	1.3E+21	Post-Drilling
Th-229	5.5E-02	Post-Drilling	6.8E-01	Post-Drilling
Th-230	3.5E-02	Post-Drilling	2.3E-01	Agricultural
Th-232	2.0E-02	Post-Drilling	2.5E-01	Post-Drilling
Ti-44	2.4E-01	Post-Drilling	2.8E+00	Post-Drilling
U-232	1.6E-01	Post-Drilling	1.9E+00	Post-Drilling
U-233	2.7E-01	Post-Drilling	3.7E+00	Post-Drilling
U-234	5.3E-01	Post-Drilling	7.6E+00	Post-Drilling
U-235	1.8E-01	Post-Drilling	2.5E+00	Post-Drilling
U-236	6.2E-01	Post-Drilling	8.9E+00	Post-Drilling
U-238	5.3E-01	Post-Drilling	7.5E+00	Post-Drilling
Zr-93	8.6E+01	Post-Drilling	1.1E+03	Post-Drilling

--- = Concentration limits could not be calculated because no dose conversion factor was found for the radionuclide.

4.3 Comparison of 1997 and 2008 Waste Acceptance Criteria

Table 16 compares the final WAC presented in Table 15 to the WAC developed in conjunction with the 1997 performance assessment; only those radionuclides common to the two efforts are included. Separate comparisons are provided for the pits and shafts. The 1997 pit limits represent the most restrictive criteria estimated on the basis of the Intruder–Post-Drilling and Intruder-Agriculture Scenarios; the former limits are provided in Shuman (1999) while the limits for the agricultural intruder are taken from Hollis et al. (1997). The 1997 limits for the shafts include two sets of criteria to address different depths of disposal.

The 2008 intruder-based WAC for the disposal pits are significantly higher than the limits calculated in conjunction with the 1997 performance assessment for all radionuclides except tritium. Although several differences exist in the models and data used to calculate the two sets of WAC, the primary reason for this difference is the amount of cover placed over the disposal units. Whereas the earlier limits are based on an initial cover thickness of 2 m (8.2 ft), the 2008 analysis considers initial cover depths ranging from 2.5 to 6.0 m (8.2 to 20 ft), with a median thickness of 4.2 m (14 ft). The additional cover all but eliminates contact with the waste during basement excavation, resulting in low exposures to the intruder and higher WAC. The much lower concentration limit calculated for tritium in the 2008 analysis is due, in large measure, to differences in diffusion models.

The WAC calculated in 2008 for the disposal shafts are greater than the 1997 disposal-at-any-depth limits for some radionuclides and lower for others. In most cases, the radionuclides with 2008 limits that are much lower than, or similar to, the 1997 limits are short-lived. The 2008 limits for these radionuclides would be substantially higher if it was assumed that intrusion occurred 300 years after facility closure, as was assumed for the 1997 analysis. The 2008 limits for most long-lived radionuclides are significantly greater than their 1997 counterparts, reflecting differences in the initial cover thickness placed over the disposal units and the distribution of waste within the units. The 2008 limit for H-3 is much lower than the 1997 limit due to differences in the time of intrusion and differences in diffusion models.

The 2008 WAC for the disposal shafts are lower than about half of the disposal-at-depth limits calculated in conjunction with the 1997 performance assessment (Table 16). The limits for 22 of the 28 radionuclides that are common to both sets of criteria differ by a factor of 5 or less. Many of these differences, as well as those noted earlier, result from differences in the models and data used to project intruder exposures in 1997 and 2008. To illustrate some of these differences, the concentration limits for selected radionuclides are compared below. These comparisons examine the criteria calculated on the basis of the postdrilling scenario for the disposal pits and the agricultural scenario for the disposal shafts.

Table 16
Comparison of the 1997/1999 and 2008 WAC for MDA G

Radionuclide	Disposal Pits		Disposal Shafts		
			1997 WAC		
	1997 WAC [a]	2008 WAC	Disposal at any Depth [a,b]	Disposal at Depth [c]	2008 WAC
Ac-227	5.1E-03	1.8E+00	---	---	2.1E+01
Ag-108m	3.5E-04	6.8E-02	---	---	8.7E-01
Al-26	1.0E-04	3.1E-02	---	---	4.2E-01
Am-241	2.3E-03	1.2E-01	3.7E-02	2.7E+00	1.4E+00
Am-243	1.1E-03	7.9E-02	---	---	9.8E-01
Ba-133	7.3E+01	4.2E+03	1.9E+11	9.2E+04	4.2E+04
Bi-207	3.3E-03	1.4E+00	3.7E+00	4.4E+00	1.6E+01
Bk-247	2.7E-03	7.2E-02	---	---	8.8E-01
C-14	2.8E-03	1.3E+00	2.1E-01	2.1E+01	2.2E+01
Cf-252	1.1E+02	3.2E+03	8.8E+02	8.7E+04	4.0E+04
Cl-36	1.3E-04	1.2E-03	---	---	1.2E-01
Co-60	5.1E+02	6.1E+06	1.6E+15	6.9E+05	4.8E+07
Cs-135	1.2E-01	4.4E+00	2.3E+00	2.3E+02	6.8E+01
Cs-137	9.2E-03	3.9E+00	1.1E+01	1.2E+01	4.4E+01
Eu-152	2.0E-01	1.6E+02	1.2E+05	2.7E+02	1.6E+03
Eu-154	4.4E-02	9.8E+03	2.9E+03	5.9E+01	9.1E+04
Gd-148	1.3E-02	1.8E+00	---	---	2.2E+01
H-3	3.4E+04	4.9E+02	1.2E+09	1.6E+04	4.5E+04

--- = Not included in the 1999 shaft WAC effort.

[a] Source: Hollis et al., 1997

[b] Corresponds to the concentration limits developed on the basis of the Intruder-Agriculture Scenario; intrusion into the shafts is assumed to be feasible 300 years after facility closure.

[c] Corresponds to the concentration limits developed on the basis of the Intruder–Post-Drilling Scenario (Shuman, 1999); intrusion is assumed to be feasible 100 years after facility closure.

Table 16 (Continued)
Comparison of the 1997/1999 and 2008 WAC for MDA G

Radionuclide	Disposal Pits		Disposal Shafts		
			1997 WAC		
	1997 WAC [a]	2008 WAC	Disposal at any Depth [a,b]	Disposal at Depth [c]	2008 WAC
I-129	1.8E-03	1.8E-01	---	---	2.5E+00
K-40	1.1E-03	6.3E-02	---	---	2.0E+00
Kr-85	3.1E+02	2.2E+15	1.3E+09	4.0E+05	4.6E+06
Mo-93	1.2E-01	3.7E+00	---	---	6.2E+01
Nb-92	1.8E-04	---	2.0E-03	2.4E-01	---
Nb-94	1.8E-04	4.9E-02	---	---	7.0E-01
Ni59	2.3E+00	1.0E+02	---	---	2.3E+03
Ni-63	2.2E+00	2.0E+02	1.6E+03	3.5E+04	2.7E+03
Np-237	3.7E-04	3.6E-02	---	---	5.3E-01
Pa-231	1.4E-04	9.9E-03	---	---	1.3E-01
Pb-210	2.5E-02	3.2E+00	4.0E+02	4.4E+01	3.6E+01
Pm-145	3.8E+00	5.1E+03	1.5E+05	5.8E+03	5.5E+04
Pu-238	6.8E-03	3.4E-01	3.7E-01	7.5E+00	4.0E+00
Pu-239	2.2E-03	9.5E-02	2.6E-02	2.5E+00	1.2E+00
Pu-240	2.3E-03	9.6E-02	2.6E-02	2.5E+00	1.2E+00
Pu-241	7.4E-02	3.4E+00	1.0E+00	7.5E+01	4.1E+01
Pu-242	2.3E-03	9.9E-02	2.7E-02	2.7E+00	1.2E+00
Ra-226	1.2E-04	1.6E-02	1.7E-03	1.7E-01	9.2E-02

--- = Not included in the 1999 shaft WAC effort.

[a] Source: Hollis et al., 1997

[b] Corresponds to the concentration limits developed on the basis of the Intruder-Agriculture Scenario; intrusion into the shafts is assumed to be feasible 300 years after facility closure.

[c] Corresponds to the concentration limits developed on the basis of the Intruder–Post-Drilling Scenario (Shuman, 1999); intrusion is assumed to be feasible 100 years after facility closure.

Table 16 (Continued)
Comparison of the 1997/1999 and 2008 WAC for MDA G

Radionuclide	Disposal Pits		Disposal Shafts		
			1997 WAC		
	1997 WAC [a]	2008 WAC	Disposal at any Depth [a,b]	Disposal at Depth [c]	2008 WAC
Sm-146	1.3E-02	5.7E-01	---	---	7.9E+00
Sm-151	3.1E+01	1.2E+03	---	---	1.4E+04
Sr-90	1.5E-02	2.2E+00	3.9E+01	2.6E+01	2.6E+01
Tb-157	5.0E-01	6.3E+02	---	---	7.6E+03
Tc-97	7.2E-02	7.6E-01	---	---	5.2E+01
Tc-99	1.3E-02	9.1E-02	---	---	6.2E+00
Th-229	4.8E-04	5.5E-02	5.6E-03	5.7E-01	6.8E-01
Th-230	3.1E-04	3.5E-02	---	---	2.3E-01
Th-232	9.9E-05	2.0E-02	1.1E-03	1.3E-01	2.5E-01
Ti-44	8.8E-04	2.4E-01	---	---	2.8E+00
U-232	5.5E-04	1.6E-01	---	---	1.9E+00
U-233	3.2E-03	2.7E-01	---	---	3.7E+00
U-234	7.4E-03	5.3E-01	9.5E-02	9.5E+00	7.6E+00
U-235	1.5E-03	1.8E-01	1.7E-02	1.8E+00	2.5E+00
U-236	8.8E-03	6.2E-01	1.2E-01	1.1E+01	8.9E+00
U-238	5.7E-03	5.3E-01	7.0E-02	7.4E+00	7.5E+00
Zr-93	8.5E-01	8.6E+01	---	---	1.1E+03

--- = Not included in the 1999 shaft WAC effort.

[a] Source: Hollis et al., 1997

[b] Corresponds to the concentration limits developed on the basis of the Intruder-Agriculture Scenario; intrusion into the shafts is assumed to be feasible 300 years after facility closure.

[c] Corresponds to the concentration limits developed on the basis of the Intruder–Post-Drilling Scenario (Shuman, 1999); intrusion is assumed to be feasible 100 years after facility closure.

The comparisons evaluate the limits calculated for six radionuclides, including Am-241, Cs-137, Pu-239, Sr-90, Tc-99, and U-238. These isotopes were selected because they exhibit a range of behaviors and because they have been disposed of at Area G in relatively large quantities. Additional comparisons were conducted for radionuclides that may exist in a vapor or gas phase. Comparisons of WAC calculated on the basis of the Intruder-Construction Scenario were not possible because the 1997 performance assessment did not consider this receptor.

The 2008 intruder analysis evaluated the potential exposures received by the receptors using probabilistic models; the 1999 analysis used deterministic models. To compare the two modeling efforts, it was necessary to run the GoldSim models in a deterministic mode. Implementing the GoldSim models in this manner yields doses and WAC different from those projected by the models when they are applied probabilistically. For this and other reasons, the comparisons that follow are conducted in relative terms.

4.3.1 Intruder–Post-Drilling Scenario

Table 17 compares the 2008 WAC that were calculated for the disposal pits on the basis of the Intruder–Post-Drilling Scenario to those published in 1999 by Shuman; only radionuclides that were common to both evaluations are listed. Examination of these results indicates that the criteria differ by less than a factor of 4 for about 80 percent of the radionuclides included in the table. For example, while the 1999 and 2008 concentration limits for I-129 and Np-237 are nearly the same, the 2008 limit for Am-241 is about one-half of the value calculated in 1999. Limits for C-14 and Eu-154 differ by factors of 340 and 1,700, respectively.

In general, the comparisons of the two sets of WAC were made by modifying the input data used in the 1999 modeling effort to more closely resemble the data used in the 2008 GoldSim modeling. Nevertheless, some modifications of the 2008 intruder model were needed to conduct the comparisons, as discussed below.

The 2008 Area G Intruder Model provides more options for evaluating intruder impacts than does the model used in 1999. For example, the 2008 model estimates the impacts of differential rates of erosion across the disposal site and provides options for estimating exposures associated with the consumption of different combinations of animal products (e.g., beef and milk or chicken and eggs). The 1999 model assumed a constant rate of erosion across the disposal site and did not consider the ingestion of animal products when estimating intruder exposures.

Variations in how the two models operate complicate the comparison of the two WAC development efforts. Consequently, for the benchmarking process, the 2008 model was modified to estimate the impacts of surface erosion in a manner that more nearly resembles the way in which the 1999 modeling was conducted. Specifically, the 2008 model was configured to apply a uniform rate of surface erosion across the disposal site; the erosion rate adopted for the modeling

Table 17
Comparison of the 1999 and 2008 Disposal Pit
Waste Acceptance Criteria (Intruder–Post-Drilling Scenario)

Radionuclide	Waste Acceptance Criteria (Ci/m^3)	
	1999 Criteria	2008 Criteria
Ac-227	5.4E-01	1.8E+00
Ag-108m	4.3E-02	6.8E-02
Al-26	1.3E-02	3.1E-02
Am-241	2.4E-01	1.2E-01
Am-243	1.2E-01	7.9E-02
Ba-133	8.7E+03	4.2E+03
Bi-207	4.2E-01	1.4E+00
Bk-247	2.9E-01	7.2E-02
C-14	3.8E-03	1.3E+00
Cf-252	1.1E+04	3.2E+03
Cl-36	1.4E-02	1.2E-03
Co-60	6.5E+04	6.1E+06
Cs-135	1.3E+01	4.4E+00
Cs-137	1.1E+00	3.9E+00
Eu-152	2.5E+01	1.6E+02
Eu-154	5.6E+00	9.8E+03
Gd-148	1.3E+00	1.8E+00
H-3	3.5E+04	2.1E+03
I-129	1.9E-01	1.8E-01
K-40	1.3E-01	6.3E-02
Kr-85	3.8E+04	2.2E+15
Mo-93	1.2E+01	3.7E+00
Nb-92	2.2E-02	---
Nb-94	2.2E-02	4.9E-02
Ni-59	2.4E+02	1.0E+02
Ni-63	2.3E+02	2.0E+02
Np-237	4.0E-02	3.6E-02
Pa-231	1.6E-02	9.9E-03

--- = The lack of dose conversion factors in EPA federal guidance reports (1988, 1993) prevented the calculation of a radionuclide concentration limit.

Table 17 (Continued)
Comparison of the 1999 and 2008 Disposal Pit
Waste Acceptance Criteria (Intruder–Post-Drilling Scenario)

Radionuclide	Waste Acceptance Criteria (Ci/m^3)	
	1999 Criteria	2008 Criteria
Pb-210	2.7E+00	3.2E+00
Pm-145	4.0E+02	5.1E+03
Pu-238	7.2E-01	3.4E-01
Pu-239	2.4E-01	9.5E-02
Pu-240	2.4E-01	9.6E-02
Pu-241	7.8E+00	3.4E+00
Pu-242	2.5E-01	9.9E-02
Ra-226	1.5E-02	1.6E-02
Si-32	4.6E+00	8.6E+00
Sm-151	3.2E+03	1.2E+03
Sr-90	1.6E+00	2.2E+00
Tb-157	5.3E+01	6.3E+02
Tc-97	7.6E+00	7.6E-01
Tc-99	1.4E+00	9.1E-02
Th-229	5.3E-02	5.5E-02
Th-230	3.6E-02	3.5E-02
Th-232	1.2E-02	2.0E-02
Ti-44	1.1E-01	2.4E-01
U-232	6.8E-02	1.6E-01
U-233	3.5E-01	2.7E-01
U-234	7.9E-01	5.3E-01
U-235	1.6E-01	1.8E-01
U-236	9.4E-01	6.2E-01
U-238	6.4E-01	5.3E-01
Zr-93	9.1E+01	8.6E+01

--- = The lack of dose conversion factors in EPA federal guidance reports (1988, 1993) prevented the calculation of a radionuclide concentration limit.

is the same as that used in the 1999 modeling. While the 1999 modeling did not consider exposures following the intake of contaminated animal products, the ingestion of beef and milk were included in the 2008 model runs that were conducted in support of the comparisons reported below. This ingestion pathway may contribute significantly to the projected intruder exposures for some radionuclides; as such, including it in the comparison of the WAC was considered appropriate.

The intruder exposures estimated for Am-241, Cs-137, Pu-239, Sr-90, Tc-99, and U-238 depend upon numerous general parameters that are common to all of the isotopes as well as several parameters that are radionuclide-specific. The parameters required for the two modeling efforts and the input data used to describe the general parameters are compared in Table 18; the sources of radionuclide-specific input data are also included. The data listed for the 1997 and 1999 WAC development efforts represent the actual input data used in those evaluations. The data listed for the 2008 WAC development effort represent the data used to conduct the modeling for nonstochastic parameters and point estimates for the parameters that are described by distributions.

Examination of Table 18 indicates that several parameters are common to the two analyses, and highlights other parameters that are unique to one of the two assessments. Parameters may be unique to one of the intruder assessments for several reasons. First, although the disposal systems being modeled are similar, the parameters required to represent them may differ because of the different modeling approaches. An example of this is seen with respect to the material properties data. The approach used to estimate the 1997 and 1999 WAC required characterization of the cover and waste only in terms of their bulk densities. In contrast, the GoldSim model represents the cover and waste in terms of the environmental media that comprise these features, including the dry solids and the water that occupies the pore spaces. As a result, additional material properties (e.g., porosity and moisture content) are needed to define the nature of the cover and waste for the GoldSim model.

Parameters may also be unique to one or the other approach because radionuclide transport mechanisms are modeled differently in the two efforts. For example, while both modeling efforts considered the deposition of contaminants on plant surfaces due to rainsplash, different approaches were used to model this process. The earlier intruder analysis used a resuspension factor approach to model the deposition of particulates on plants. In contrast, the updated intruder assessment used a mass-loading factor approach to simulate the impacts of rainsplash This difference explains why the input of a resuspension factor, a deposition velocity, mass-loading factors, and a particle size factor is required for one modeling effort but not the other.

Finally, input parameters may be unique to one of the intruder analyses because of differences in the transport pathways considered. The development of the 2008 WAC considered potential doses received by an intruder who ingests animal products (i.e., beef and milk or chicken and eggs) from.

Table 18
Summary of Input Data Used in the 1997/1999 WAC Development Effort and the Deterministic Values Adopted for the 2008 WAC Development Effort

Parameter	Units	Input Data	
		1997 and 1999 Analyses	2008 Analyses
Material Properties			
Cover/Waste Bulk Density	kg/m^3	1.3E+03	1.4E+03 [a]
Cover/Waste Bulk Porosity	---	NA	4.1E-01
Cover/Waste Moisture Content	% (volume basis)	NA	7.5E-02
Density of Water	kg/m^3	NA	1.0E+03
Soil Carbon Fraction	---	NA	3.0E-02
Water Carbon Fraction	---	NA	2.0E-05
Water Hydrogen Fraction	---	NA	1.1E-01
Facility and Operations Parameters			
Period of Facility Operation	yr	4.9E+01	2.3E+01
Closure Period	yr	2.0E+00	2.0E+00
Institutional Control Period	yr	1.0E+02	1.0E+02
Disposal Unit Length	m	1.4E+02/1.5E+01 [b]	1.5E+02
Disposal Unit Width	m	1.4E+02/1.5E+01 [b]	1.5E+02
Disposal Unit Area	m^2	NA	2.4E+04

--- = Unitless

NA = Indicates that the parameter was not used in the modeling effort.

[a] *The listed density is the dry bulk density of the solids comprising the cover and waste.*

[b] *The first value listed applies to the disposal pits, while the second value applies to the shafts.*

[c] *The first value listed applies to the Intruder–Post-Drilling Scenario, while the second value applies to the Intruder-Agriculture Scenario. These values are directly entered into the 1997/1999 models; the mixing depth for the postdrilling scenario is entered into the GoldSim models, while the mixing depth for the agricultural intruder scenario is calculated.*

[d] *The modeling used to establish the 2008 WAC used spatially dependent surface erosion rates.*

[e] *The dust loading is multiplied by the soil disturbance factor to yield the dust loading used to estimate intruder exposures.*

[f] *While the radionuclide-specific data used in the WAC development efforts are not listed, references for this information are provided to illustrate the use of different sources of data.*

Table 18 (Continued)
Summary of Input Data Used in the 1997/1999 WAC Development Effort and the Deterministic Values Adopted for the 2008 WAC Development Effort

Parameter	Units	Input Data	
		1997 and 1999 Analyses	2008 Analyses
Cover Thickness	m	2.0E+00	3.6E+00
Waste Thickness	m	1.5E+01/1.6E+01 [b]	1.2E+01
Soil Mixing Depth	m	1.5E-01/2.9E-01 [c]	1.5E-01/2.9E-01 [d]
Volume of Disposed Waste	m^3	1.4E+05/1.4E+03 [b]	1.3E+05
Waste Emplacement Efficiency	---	5.0E-01/4.2E-01 [b]	NA
Erosion/Atmospheric Pathway Parameters			
Surface Erosion Rate	m/yr	4.0E-07	Various [d]
Dust Loading	kg/m^3	1.0E-07	3.0E-08 [e]
Soil Disturbance Factor	---	NA	2.0E+00
Resuspension Factor	m^{-1}	1.0E-09	N/A
Resuspension Flux	$g/m^2/yr$	NA	1.3E+01
Enhancement Factor	---	NA	3.0E+00
Deposition Velocity	m/s	1.0E-03	NA
Foodchain Parameters			
Vegetation Weathering Removal Constant	hr^{-1}	2.1E-03	NA
Vegetation Translocation Factor			

--- = Unitless

NA = Indicates that the parameter was not used in the modeling effort.

[a] *The listed density is the dry bulk density of the solids comprising the cover and waste.*

[b] *The first value listed applies to the disposal pits, while the second value applies to the shafts.*

[c] *The first value listed applies to the Intruder–Post-Drilling Scenario, while the second value applies to the Intruder-Agriculture Scenario. These values are directly entered into the 1997/1999 models; the mixing depth for the postdrilling scenario is entered into the GoldSim models, while the mixing depth for the agricultural intruder scenario is calculated.*

[d] *The modeling used to establish the 2008 WAC used spatially dependent surface erosion rates.*

[e] *The dust loading is multiplied by the soil disturbance factor to yield the dust loading used to estimate intruder exposures.*

[f] *While the radionuclide-specific data used in the WAC development efforts are not listed, references for this information are provided to illustrate the use of different sources of data.*

Table 18 (Continued)
Summary of Input Data Used in the 1997/1999 WAC Development Effort and the Deterministic Values Adopted for the 2008 WAC Development Effort

Parameter	Units	Input Data	
		1997 and 1999 Analyses	2008 Analyses
Leafy Vegetables	---	1.0E+00	1.0E+00
All Other Food Crops	---	1.0E-01	NA
Produce	---	NA	1.0E-01
Grain	---	NA	1.0E-01
Pasture Grass	---	NA	1.0E+00
Agricultural Productivity (wet weight)			
Leafy Vegetables	kg/m^2	2.0E+00	1.5E+00
Produce	kg/m^2	2.0E+00	1.0E+00
All Other Food Crops	kg/m^2	6.0E-01	NA
Grain	kg/m^2	NA	5.0E-01
Pasture Grass	kg/m^2	NA	2.5E+00
Dry-to-Wet-Weight Fraction			
Leafy Vegetables	---	1.0E-01	9.8E-02
All Other Food Crops	---	4.3E-01	NA
Produce	---	NA	1.3E-01

--- = Unitless

NA = Indicates that the parameter was not used in the modeling effort.

[a] *The listed density is the dry bulk density of the solids comprising the cover and waste.*

[b] *The first value listed applies to the disposal pits, while the second value applies to the shafts.*

[c] *The first value listed applies to the Intruder–Post-Drilling Scenario, while the second value applies to the Intruder-Agriculture Scenario. These values are directly entered into the 1997/1999 models; the mixing depth for the postdrilling scenario is entered into the GoldSim models, while the mixing depth for the agricultural intruder scenario is calculated.*

[d] *The modeling used to establish the 2008 WAC used spatially dependent surface erosion rates.*

[e] *The dust loading is multiplied by the soil disturbance factor to yield the dust loading used to estimate intruder exposures.*

[f] *While the radionuclide-specific data used in the WAC development efforts are not listed, references for this information are provided to illustrate the use of different sources of data.*

Table 18 (Continued)
Summary of Input Data Used in the 1997/1999 WAC Development Effort and the Deterministic Values Adopted for the 2008 WAC Development Effort

Parameter	Units	Input Data	
		1997 and 1999 Analyses	2008 Analyses
Grain	---	NA	9.1E-01
Pasture Grass	---	NA	2.0E-01
Growing Season			
Leafy Vegetables	hr	1.4E+03	NA
Other Vegetation	hr	1.4E+03	NA
Mass Loading Factor			
Leafy Vegetables	---	NA	2.6E-01
Produce	---	NA	3.0E-02
Grain	---	NA	3.0E-02
Pasture Grass	---	NA	3.0E-02
Plant Interception Factors			
Leafy Vegetables	---	2.5E-01	NA
Produce	---	2.5E-01	NA
Grain	---	2.5E-01	NA
Plant Carbon Fraction (dry-weight basis)	---	NA	4.5E-01
Plant Hydrogen Fraction (dry-weight basis)	---	NA	6.2E-02

--- = Unitless

NA = Indicates that the parameter was not used in the modeling effort.

[a] *The listed density is the dry bulk density of the solids comprising the cover and waste.*

[b] *The first value listed applies to the disposal pits, while the second value applies to the shafts.*

[c] *The first value listed applies to the Intruder–Post-Drilling Scenario, while the second value applies to the Intruder-Agriculture Scenario. These values are directly entered into the 1997/1999 models; the mixing depth for the postdrilling scenario is entered into the GoldSim models, while the mixing depth for the agricultural intruder scenario is calculated.*

[d] *The modeling used to establish the 2008 WAC used spatially dependent surface erosion rates.*

[e] *The dust loading is multiplied by the soil disturbance factor to yield the dust loading used to estimate intruder exposures.*

[f] *While the radionuclide-specific data used in the WAC development efforts are not listed, references for this information are provided to illustrate the use of different sources of data.*

Table 18 (Continued)
Summary of Input Data Used in the 1997/1999 WAC Development Effort and the Deterministic Values Adopted for the 2008 WAC Development Effort

Parameter	Units	Input Data	
		1997 and 1999 Analyses	2008 Analyses
Particle Size Factor	---	NA	1.5E+00
Animal Food Consumption Rate			
Cattle	kg/d (dry weight)	NA	1.2E+01
Cows	kg/d (dry weight)	NA	1.6E+01
Animal Soil Consumption Rate	kg/d (dry weight)	NA	1.0E+00
Animal Water Consumption Rate			
Cattle	kg/d	NA	4.0E+01
Cows	kg/d	NA	7.5E+01
Animal Product Water Fractions			
Beef	---	NA	6.0E-01
Milk	---	NA	8.8E-01
Animal Product Carbon Fractions (dry-weight basis)			
Beef	---	NA	6.0E-01
Milk	---	NA	5.8E-01
Intrusion Parameters			
Area of intruder's Lot	m^2	2.3E+03	2.3E+03

--- = Unitless

NA = Indicates that the parameter was not used in the modeling effort.

[a] *The listed density is the dry bulk density of the solids comprising the cover and waste.*

[b] *The first value listed applies to the disposal pits, while the second value applies to the shafts.*

[c] *The first value listed applies to the Intruder–Post-Drilling Scenario, while the second value applies to the Intruder-Agriculture Scenario. These values are directly entered into the 1997/1999 models; the mixing depth for the postdrilling scenario is entered into the GoldSim models, while the mixing depth for the agricultural intruder scenario is calculated.*

[d] *The modeling used to establish the 2008 WAC used spatially dependent surface erosion rates.*

[e] *The dust loading is multiplied by the soil disturbance factor to yield the dust loading used to estimate intruder exposures.*

[f] *While the radionuclide-specific data used in the WAC development efforts are not listed, references for this information are provided to illustrate the use of different sources of data.*

Table 18 (Continued)
Summary of Input Data Used in the 1997/1999 WAC Development Effort and the Deterministic Values Adopted for the 2008 WAC Development Effort

Parameter	Units	Input Data	
		1997 and 1999 Analyses	2008 Analyses
Area of Intruder's House	m^2	2.0E+02	2.0E+02
Well Casing Diameter	m	2.5E-01	2.5E-01
Depth of Basement	m	3.0E+00	3.0E+00
Length of Basement Excavation			
Bottom of Excavation	m	2.0E+01	2.0E+01
Top of Excavation	m	2.6E+01	2.6E+01
Width of Basement Excavation			
Bottom of Excavation	m	1.0E+01	1.0E+01
Top of Excavation	m	1.6E+01	1.6E+01
Thickness of Concrete Floor of Foundation	m	NA	1.0E-01
Time Allotments			
Outside of House	hr	1.8E+03	6.4E+02
Inside House	hr	4.4E+03	6.0E+03
House Shielding Factor for Direct Radiation	---	7.0E-01	4.0E-01

--- = Unitless

NA = Indicates that the parameter was not used in the modeling effort.

[a] *The listed density is the dry bulk density of the solids comprising the cover and waste.*

[b] *The first value listed applies to the disposal pits, while the second value applies to the shafts.*

[c] *The first value listed applies to the Intruder–Post-Drilling Scenario, while the second value applies to the Intruder-Agriculture Scenario. These values are directly entered into the 1997/1999 models; the mixing depth for the postdrilling scenario is entered into the GoldSim models, while the mixing depth for the agricultural intruder scenario is calculated.*

[d] *The modeling used to establish the 2008 WAC used spatially dependent surface erosion rates.*

[e] *The dust loading is multiplied by the soil disturbance factor to yield the dust loading used to estimate intruder exposures.*

[f] *While the radionuclide-specific data used in the WAC development efforts are not listed, references for this information are provided to illustrate the use of different sources of data.*

Table 18 (Continued)
Summary of Input Data Used in the 1997/1999 WAC Development Effort and the Deterministic Values Adopted for the 2008 WAC Development Effort

Parameter	Units	Input Data	
		1997 and 1999 Analyses	2008 Analyses
Intruder Intake Parameters			
Ingestion Rates			
Leafy Vegetables	kg/yr	1.7E+01	1.5E+01
Other (protected, fruit, etc.)	kg/yr	9.1E+01	8.5E+01
Grain	kg/yr	7.4E+01	7.9E+01
Meat	kg/yr	NA	1.9E+01
Milk	kg/yr	NA	7.4E+01
Soil	kg/yr	3.7E-02	3.7E-02
Fraction of Food Eaten Grown On-Site	---	5.0E-01	Initially set to 0.3, adjusted to account for the area available to raise crops and animals.
Inhalation Rate	m^3/yr	8.0E+03	5.6E+03
Radionuclide-Specific Parameters [f]			
Half-Lives	yr	RHHB, 1970	KAPL, 2002
Initial Inventories	Ci	Projected disposal unit inventories used for analysis	1.0E+06 for all parent radionuclides

--- = Unitless

NA = Indicates that the parameter was not used in the modeling effort.

[a] *The listed density is the dry bulk density of the solids comprising the cover and waste.*

[b] *The first value listed applies to the disposal pits, while the second value applies to the shafts.*

[c] *The first value listed applies to the Intruder–Post-Drilling Scenario, while the second value applies to the Intruder-Agriculture Scenario. These values are directly entered into the 1997/1999 models; the mixing depth for the postdrilling scenario is entered into the GoldSim models, while the mixing depth for the agricultural intruder scenario is calculated.*

[d] *The modeling used to establish the 2008 WAC used spatially dependent surface erosion rates.*

[e] *The dust loading is multiplied by the soil disturbance factor to yield the dust loading used to estimate intruder exposures.*

[f] *While the radionuclide-specific data used in the WAC development efforts are not listed, references for this information are provided to illustrate the use of different sources of data.*

Table 18 (Continued)
Summary of Input Data Used in the 1997/1999 WAC Development Effort and the Deterministic Values Adopted for the 2008 WAC Development Effort

Parameter	Units	Input Data	
		1997 and 1999 Analyses	2008 Analyses
Dose Conversion Factors			
Ingestion	mrem/pCi	DOE, 1988b; EPA, 1988 for values not found in DOE, 1988b.	EPA, 1988
Inhalation	mrem/pCi	DOE, 1988b; EPA, 1988 for values not found in DOE, 1988b.	EPA, 1988
Direct Radiation from Soil	mrem/yr per pCi/m^3	Estimated using MICROSHIELD (Grove Engineering, 1992)	EPA, 1993
Air Immersion	mrem/yr per pCi/m^3	DOE, 1988c; EPA, 1993 for values not found in DOE, 1988c.	EPA, 1993
Soil-to-Water Distribution Coefficients	m^3/kg	NA	Various sources
Soil Mass Attenuation Coefficients	cm^2/g	NA	RHHB, 1970
Plant-Uptake Factors	---	Baes et al., 1984; Sheppard et al., 1991 for carbon; specific activity model for hydrogen	Napier et al., 2004; specific activity model for hydrogen
Animal Transfer Factors	d/kg	NA	Napier et al., 2004; specific activity models for carbon and hydrogen

--- = Unitless

NA = Indicates that the parameter was not used in the modeling effort.

[a] *The listed density is the dry bulk density of the solids comprising the cover and waste.*

[b] *The first value listed applies to the disposal pits, while the second value applies to the shafts.*

[c] *The first value listed applies to the Intruder–Post-Drilling Scenario, while the second value applies to the Intruder-Agriculture Scenario. These values are directly entered into the 1997/1999 models; the mixing depth for the postdrilling scenario is entered into the GoldSim models, while the mixing depth for the agricultural intruder scenario is calculated.*

[d] *The modeling used to establish the 2008 WAC used spatially dependent surface erosion rates.*

[e] *The dust loading is multiplied by the soil disturbance factor to yield the dust loading used to estimate intruder exposures.*

[f] *While the radionuclide-specific data used in the WAC development efforts are not listed, references for this information are provided to illustrate the use of different sources of data.*

animals raised at the exposure location. In contrast, the WAC developed in 1997 and 1999 did not consider this pathway, based on the assumption that animals would be range-fed in uncontaminated areas. Inclusion of the consumption of animal products requires the input of several additional input parameters such as the consumption rates of animal products by humans; animal food, soil, and water ingestion rates; and animal product transfer factors.

The impact that using different input data and models has upon the calculated WAC will depend upon the radionuclide under consideration. The 1999 and 2008 postdrilling concentration limits for Am-241 differ, in part, because of the manner in which the contamination of crops due to rainsplash was modeled. The significance of this difference may be appreciated by comparing the exposure pathway contributions to the peak intruder doses projected using the 1999 model and the deterministic implementation of the Area G Intruder Model. Fifty-four percent of the peak dose projected for Am-241 in the 1999 WAC analysis resulted from the inhalation of airborne contaminants; the ingestion of contaminated soil and food accounted for 30 and 12 percent of the peak dose, respectively. In contrast, 80 percent of the peak dose estimated using the GoldSim model in its deterministic form results from the ingestion of contaminated crops, while the inhalation and soil ingestion pathways account for 8 and 10 percent of the total, respectively.

As indicated earlier, the deposition of contaminants on plant surfaces due to rainsplash was modeled using a resuspension factor approach for the 1997 and 1999 WAC development efforts. A reexamination of that approach concluded that using the mass-loading approach to estimate the impacts of rainsplash may yield more accurate estimates of radionuclide concentrations in plants, especially for radionuclides with small root-uptake factors such as Am-241. Hinton (1992) reviewed methods used to estimate plant contamination due to particulate resuspension and concluded that the magnitude of the uncertainty associated with the mass-loading approach was orders of magnitude less than that associated with the resuspension factor approach. Hansen (1995) estimated effective plant-uptake factors for plutonium, an element that, like americium, is typically characterized by low root-uptake factors; these effective factors took into account rates of contaminant uptake via the roots of the plants and the effects of rainsplash. The estimated factors were significantly higher than those estimated for the 1997 and 1999 WAC efforts, when the effects of rainsplash were estimated using the resuspension factor approach. The mass-loading approach to estimating plant loading due to rainsplash yields much higher rates of effective plant uptake that more closely resemble the results presented by Hansen.

The effect that the adoption of the mass-loading approach has on projected postdrilling intruder exposures was estimated by developing effective plant-uptake factors and using those factors in the 1999 model. The effective uptake factors were developed using the GoldSim model and account for root uptake and contamination due to rainsplash, where the rainsplash component is estimated using the mass-loading approach. Accounting only for the differences in plant uptake

causes the 1999 model to project a significantly higher projected peak dose for Am-241, and a radionuclide concentration limit that is 20 percent of the postdrilling limit estimated in 1999.

Variations in the remaining input parameters account for the difference that exists between the two Am-241 concentration limits once the rainsplash model divergence is taken into account. This was confirmed by revising the input parameters in the 1999 model to reflect the input data used in the 2008 GoldSim modeling. With the exception of the external radiation dose conversion factors for soils, all parameters common to the two modeling efforts were modified. The dose conversion factors were not altered because the two models estimate external exposures from contaminated soils in different ways, making it inappropriate to share these data between the two efforts. Also, slight changes were made to the formulas used in the 1999 model to estimate radionuclide concentrations in crops to incorporate crop-specific dry-to-wet weight fractions. Upon making these changes, a radionuclide concentration limit of 0.15 Ci/m^3 was calculated using the 1999 modeling methodology. This is equal to the value that was calculated for Am-241 using deterministic values in the GoldSim model.

The 2008 concentration limit calculated for Cs-137 is about 3.5 times greater than that calculated in 1999 (Table 17). Updating the 1999 model to reflect the 2008 data and using the direct exposure dose conversion factor from the GoldSim model yields a limit that is about 10 percent greater than that calculated with the GoldSim intruder model in the deterministic mode. This difference is due largely to the fact that, unlike the 1999 model, the 2008 model includes exposures from the ingestion of beef and milk. When this difference is considered, the resultant Cs-137 limits differ by less than 5 percent.

A comparison of the concentration limits estimated for Pu-239 and an examination of the results responsible for the observed difference yields conclusions similar to those reached for Am-241. The inhalation of suspended particulates accounts for 63 percent of the peak dose estimated for the 1999 effort; soil and crop ingestion account for 34 and 3 percent of the total, respectively. In contrast, the ingestion of contaminated crops is responsible for 81 percent of the peak postdrilling dose estimated using the GoldSim model in its deterministic form; the inhalation of airborne particulates and ingestion of soil account for about 8 and 10 percent of the peak exposure, respectively. Inserting effective plant-uptake factors into the 1999 modeling methodology to account for the revised rainsplash modeling approach and updating the other input data used in 1999 yields a concentration limit for Pu-239 essentially equal to that calculated using the GoldSim intruder model in its deterministic form.

The postdrilling WAC estimated for Sr-90 using the probabilistic GoldSim models is 40 percent greater than the limit calculated in 1999 (Table 17). While the ingestion of crops accounts for practically all of the exposures projected for the 1999 effort, it accounts for only 52 percent of the peak dose projected using the GoldSim intruder model in its deterministic form. The

ingestion of beef and milk accounts for 47 percent of the peak exposure calculated using the deterministic 2008 model; these exposure pathways were not considered in the 1999 analysis. Revising the data used in the 1999 analysis to make them consistent with the 2008 WAC development effort yields a Sr-90 concentration limit that is almost twice the deterministic limit calculated using GoldSim. This difference is due almost entirely to the inclusion of the beef and milk ingestion pathways in the 2008 modeling.

The 2008 Tc-99 concentration limit is 7 percent of the limit estimated for the 1999 postdrilling WAC analysis (Table 17). The primary difference between the two analyses lies in the root-uptake factors used for modeling. The uptake factor used in the 2008 revision for leafy vegetables is more than 20 times greater than the value used in 1999; the factors for produce and grain are about 15 and 50 percent of the values used in 1999, respectively. Accounting for these differences and updating the data used in the earlier modeling effort yields WAC for Tc-99 that are essentially equal.

The 2008 concentration limit for U-238 is about 83 percent of the limit estimated in 1999. U-238 is another example of a radionuclide with a low plant-uptake factor. Inserting effective plant-uptake factors in the 1999 model and updating the rest of that model's data yields concentration limits that are consistent across the two WAC development efforts.

As discussed, most of the 2008 WAC fall within a factor of 4 of the 1999 values. One of the more notable exceptions is the concentration limit for Eu-154; the 2008 limit for Eu-154 is more than 1,700 times its 1999 counterpart. The reason for this uncharacteristically large disparity lies in the half-lives used in the two modeling efforts. The half-life adopted for Eu-154 in the 2008 analysis is about half of the value used in 1999. Reducing the half-life results in a substantially smaller dose at the time intrusion into the waste occurs, yielding a significantly higher concentration limit. Taking only the half-life differences into account, the concentration limits calculated for Eu-154 differ by a factor of 1.3.

4.3.2 Intruder-Agriculture Scenario

The radionuclide concentration limits calculated for the disposal shafts on the basis of the agricultural intruder scenario are compared to the WAC developed in 1997 in Table 19; only those radionuclides common to the 1997 and 2008 evaluations are included. The 2008 limits for most radionuclides are significantly greater than the criteria calculated in 1997. This is because the assumed placement depth for the waste in the 2008 analysis is significantly greater than that assumed in 1997. For the 2008 modeling, the median distance between the ground surface and the top of the waste is almost 6.0 m (19 ft) in the 1988–2016 shafts; the 1997 analysis assumed 2 m (6.6 ft) of cover would separate the waste from the surface of the disposal facility.

Table 19
Comparison of the 1997 and 2008 Disposal Shaft
Waste Acceptance Criteria (Intruder-Agriculture Scenario)

Radionuclide	Waste Acceptance Criteria (Ci/m^3)	
	1997 Criteria	2008 Criteria
Am-241	3.7E-02	1.1E+07
Ba-133	1.9E+11	5.1E+11
Bi-207	3.7E+00	2.6E+06
C-14	2.1E-01	5.4E+01
Cf-252	8.8E+02	8.8E+10
Co-60	1.6E+15	4.3E+12
Cs-135	2.3E+00	5.5E+06
Cs-137	1.1E+01	4.9E+07
Eu-152	1.2E+05	1.7E+09
Eu-154	2.9E+03	6.7E+10
H-3	1.2E+09	4.5E+04
Kr-85	1.3E+09	NA
Nb-92	2.0E-03	---
Ni-63	1.6E+03	3.4E+08
Pb-210	4.0E+02	3.3E+08
Pm-145	1.5E+05	1.1E+12
Pu-238	3.7E-01	1.5E+05
Pu-239	2.6E-02	1.3E+07
Pu-240	2.6E-02	1.4E+07
Pu-241	1.0E+00	3.2E+08
Pu-242	2.7E-02	1.3E+07
Ra-226	1.7E-03	9.2E-02
Sr-90	3.9E+01	4.4E+06
Th-229	5.6E-03	4.9E+06
Th-232	1.1E-03	2.4E+04
U-234	9.5E-02	4.3E+01
U-235	1.7E-02	2.6E+05
U-236	1.2E-01	1.1E+06
U-238	7.0E-02	2.5E+04

--- = The lack of dose conversion factors in EPA (1988, 1993) prevented the calculation of a radionuclide concentration limit.

NA = No exposures were projected to occur; therefore no concentration limit is listed.

The agricultural intruder limits calculated in 1997 and 2008 are fundamentally different with respect to assumptions regarding the time at which intrusion into the shafts occurs. In 1997, concrete caps were routinely placed over the shafts when the units underwent interim closure. The 1997 performance assessment assumed those caps would remain in place when the facility underwent final closure. In terms of the intruder analysis, it was assumed the concrete caps would prevent persons from excavating a basement over the waste for 300 years following final closure of the facility. Concrete caps are no longer planned for incorporation into the final cover. Given this, the 2008 WAC development effort was based on the assumption that intrusion into the disposal units was possible at the end of the 100-year active institutional control period. Reducing the time of first intrusion from 300 to 100 years after final site closure has profound effects on the WAC. Radionuclides with short-to-moderate half-lives will be present in much higher concentrations at 100 years postclosure, resulting in greater potential exposures to intruders. These higher doses will, in turn, result in significantly smaller concentration limits for the affected isotopes.

For benchmarking purposes, adjustments were made to the 1997 and 2008 models to account for differences in the depth to waste at the time of intrusion. Specifically, the initial cover thickness in the GoldSim model was set so the depth to the waste was 2 m (6.6 ft), and the time of intrusion was set to 100 years after final closure in the 1997 model. The differences remaining between the two sets of shaft WAC, after accounting for variations in the time of intrusion and cover thickness, are largely attributable to the factors discussed in Section 4.3.1 for the disposal pits.

A few radionuclides included in the WAC development effort may exist as a vapor or gas. For example, tritium will partition between liquid water and water vapor within the waste, while some or all of the C-14 and isotopes of krypton will exist as gas. These species may diffuse upward from the waste and enter into the intruder's house or diffuse from the surface of the disposal facility. Such releases may result in inhalation or air immersion doses, adding to other exposures received by the intruder.

The effects of diffusion are evident in the tritium and C-14 WAC developed for the disposal shafts on the basis of the agricultural intruder scenario. As shown in Table 19, the 2008 tritium concentration limit is significantly lower than that estimated in 1999; the 2008 C-14 limit is significantly higher than the earlier value. Some of the reasons for the difference noted for tritium are discussed below.

The 1997 concentration limit for tritium is about 28,000 times greater than its 2008 counterpart. This disparity is due, in large part, to the time at which intrusion was assumed to occur. The 1997 WAC developed for the shafts on the basis of the agricultural intruder scenario assumed that the presence of concrete caps over the disposal units would prevent intrusion into the waste for a period of 300 years following facility closure; no such assumption was made for the 2008

intruder analysis. Differences in the time of intrusion leads to significant differences in the WAC estimated for tritium. For example, the 1997 tritium concentration limit would decrease by a factor of about 8×10^4 if intrusion was assumed to be feasible at the end of the 100-year active institutional control period. Taking differences in the time of intrusion into account, the 1997 limit is approximately one-third of the 2008 limit. The 2008 analysis assumed that the disposal containers in which the high-activity tritium waste is placed limit vapor-phase releases to 0.01 of the inventory annually; no credit was taken for container performance in the 1997 analysis. If the same approach had been used in both WAC development efforts, the 1997 limit for tritium would be significantly greater than the 2008 limit.

Putting aside the effects of container performance, the difference in the 1997 and 2008 tritium limits reflects differences in the diffusion models used in the two analyses. The diffusion model used in 1997 considers steady-state diffusion through an infinite medium (i.e., the concrete floor of the intruder's house), with a constant source of contamination on one side of that medium. Under these conditions, the concentration gradient driving the diffusion is created by small differences in tritium concentrations that form as a result of radioactive decay. The small gradient results in minor diffusive fluxes through the concrete.

The diffusion model used in the 2008 WAC development effort takes a distinctly different approach to modeling the passage of tritiated water vapor into the intruder's house. Diffusion is modeled through finite thicknesses of waste, cover, and concrete, and the tritium inventory is depleted over time as diffusion progresses and as radioactive decay takes its toll. At the time of intrusion, a gradient exists between the contaminated cover or waste and the initially uncontaminated concrete foundation upon which the house rests; contamination entering the house is removed in proportion to the ventilation rate of the building. Because of this, and the fact that the concrete is modeled as a finite medium, a larger concentration gradient exists across the foundation and the rate of entry of tritium into the house is increased. As a result, when container performance is ignored, the intruder exposures projected using GoldSim are greater than those estimated using the 1997 model and the corresponding concentration limit is less.

5.0 Uncertainty and Sensitivity

The doses and radon fluxes discussed in Sections 3 and 4 are subject to several sources of uncertainty. These uncertainties may be categorized as improper parameter estimation, improper model formulation, and stochastic effects due to random measurement and sampling errors and natural variation (Hoffman and Gardner, 1983). The first two categories may be especially significant when models and data are used for conditions for which they were not intended. Uncertainties introduced by parameter variability may be addressed using stochastic models such as those developed for the performance assessment and composite analysis.

Several sources of uncertainty associated with the performance assessment and composite analysis modeling are discussed below. The results of this evaluation and the output from the GoldSim modeling are used to identify processes and parameters that significantly influence the impacts that Area G is projected to have on human health and safety and the environment. This discussion is organized in terms of the modeling conducted to project performance assessment and composite analysis exposures for members of the public and the evaluations used to estimate inadvertent intruder exposures.

5.1 Performance Assessment and Composite Analysis Uncertainty and Sensitivity

The probabilistic modeling conducted using the GoldSim models provides insight into the uncertainties introduced by parameter variability. These results may be used to identify the site characteristics and processes to which the long-term performance of the disposal facility is most responsive. The results of the sensitivity analysis conducted for the performance assessment and composite analysis are presented in Section 5.1.1. Several other sources of uncertainty were not explicitly represented in the modeling; some of these are discussed in Section 5.1.2.

5.1.1 Sensitivity Analysis

Separate sensitivity analyses were conducted for the performance assessment and composite analysis. The results of these evaluations are presented in Section 5.1.1.1 and 5.1.1.2.

5.1.1.1 Performance Assessment

Model sensitivities were evaluated for the Atmospheric Scenario and the All Pathways–Cañada del Buey Scenario within catchments CdB1 and CdB2. An additional analysis examined the sensitivity of the projected radon fluxes in waste disposal region 7. The fact that no exposures were projected to occur for the Groundwater Resource Protection and All Pathways–Groundwater Scenarios eliminated the need to evaluate model sensitivities for these scenarios.

Sensitivity analysis results for the two exposure scenarios are summarized in Table 20. This table includes the five parameters that had the highest absolute values of the Spearman rank correlation

Table 20
Rank Correlation Coefficients for Selected Performance Assessment Exposure Scenarios

Exposure Scenario	Exposure Location	Model Parameter	Rank Correlation Coefficient
Atmospheric	LANL boundary	Moisture content of crushed tuff	-4.6E-01
		Moisture content of waste	-4.6E-01
		Thermal gradient factor	4.3E-01
		Indoor exposure time	2.6E-01
		Dispersion factor for atmospheric source area 2	2.0E-01
	Area G fence line	Maximum rooting depth of trees	5.4E-01
		Root-mass-distribution beta-shape factor	-4.8E-01
		Particulate resuspension flux	2.6E-01
		Aboveground biomass density of trees in piñon-juniper woodland	1.5E-01
		Plant-uptake factor of potassium in native vegetation	1.3E-01
All Pathways–Cañada del Buey	Catchment CdB1	Surface erosion scenario	4.8E-01
		Sediment dispersal factor	-1.9E-01
		Moisture content of crushed tuff	-1.8E-01
		Moisture content of waste	-1.8E-01
		Thermal gradient factor	1.5E-01
	Catchment CdB2	Maximum rooting depth of trees	5.6E-01
		Root-mass-distribution beta-shape factor	-4.9E-01
		Plant litter production factor for trees	1.7E-01
		Aboveground biomass density of trees in piñon-juniper woodland	1.7E-01
		Plant-uptake factor of potassium in native vegetation	1.5E-01

coefficient. The rank correlation coefficient is a nonparametric method to delineate relationships between random variables, in this case the projected doses and the stochastic parameters used in their estimation.

The sensitivity analysis results for the Atmospheric Scenario indicate that the parameters to which the projected peak mean doses are correlated differ between the two exposure locations. The peak exposure projected for the receptor at the LANL boundary is due almost entirely to tritium diffusing from the disposal site. The first three parameters listed in Table 20 for this scenario affect the magnitude of the diffusion coefficient of the water vapor and, therefore, the rates at which the contaminant is released to the atmosphere. The moisture contents of the crushed tuff and waste are inversely correlated to the projected exposure because the diffusion coefficient of water vapor decreases as more of the pore space of these media is occupied by water. The diffusion coefficient of vapor-phase tritium is multiplied by the thermal gradient factor to account for the effects of thermal gradients in the waste and cover on rates of diffusion. The indoor exposure time is directly proportional to how long the receptor is exposed to the airborne vapor at the LANL boundary. The dispersion factor affects the concentration of tritiated water vapor at the exposure location; a higher factor implies a higher concentration of airborne tritium. The dispersion factor for atmospheric source area 2 is important because a major portion of the tritium inventory resides in this part of Area G.

All of the parameters listed in Table 20 for the Atmospheric Scenario at the Area G fence line influence the rates at which contaminants are either deposited on the surface by plants growing over the disposal facility or resuspended for transport downwind of the site. Three of the parameters (the beta-shape factor used to describe root mass distributions with depth, the maximum rooting depth of trees, and the aboveground biomass density of trees) influence the degree to which plant roots penetrate into the waste and deposit contamination on the soil surface. Doses are inversely proportional to the shape factor because larger values of the parameter predict that a greater proportion of the total root mass lies close to the surface; fewer roots are likely to extend into the waste as a result. The plant-uptake factor for potassium in native vegetation controls the rate of K-40 assimilation by plants; this isotope is one of the major contributors to the peak mean dose. Finally, the projected exposures are sensitive to the particulate resuspension flux as this parameter determines the rate at which contamination deposited on the surface of Area G is entrained by the prevailing winds.

The peak mean dose projected for the All Pathways–Canyon Scenario within catchment CdB1 is dominated by exposures to tritium; a portion of the tritium diffusing upward from the waste partitions into the liquid phase of the surface soils and acts as a source of contamination for the canyon resident. Three of the parameters included in Table 20 affect the rates at which tritiated water vapor diffuses from the waste and, therefore, the level of contamination in the surface soils. The erosion scenario is a parameter used in the GoldSim modeling to evaluate the impacts of low,

moderate, and high erosion on facility performance. As the scenario index increases so too does the rate of erosion, causing greater cover loss and, ultimately, increased exposures to the canyon resident. The sediment dispersal factor is used to control the area over which the sediments eroded from Area G are dispersed within catchment CdB1; the dispersal area increases as the value of the factor rises, yielding lower soil concentrations of tritium and smaller exposures.

The results of the sensitivity analysis for the exposures projected for the canyon resident in catchment CdB2 indicate the importance of plant intrusion into the waste. Four of the five parameters relate to the distribution of tree roots with depth and the plants' litter production capacity. The plant-uptake factor for potassium influences the degree to which K-40 is assimilated by plants growing over the disposal site; K-40 is a major contributor to the doses projected for the resident in catchment CdB2.

The sensitivity of radon flux to the site diffusion model input parameters was evaluated using the model projections for waste disposal region 7, the region yielding the highest flux for the performance assessment inventory. Table 21 shows the results of this analysis, which indicate that the fluxes are most sensitive to the inventory of Ra-226. The radon-emanation coefficient specifies how much of the generated radon enters the air-filled pore spaces within the waste and, therefore, the amount of gas available for diffusion. The moisture contents of the crushed tuff and waste influence the magnitude of the radon diffusion coefficients used in the modeling.

Table 21
Rank Correlation Coefficients for Radon Flux from Waste Disposal Region 7

Model Parameter	Rank Correlation Coefficient
Ra-226 Inventory	7.1E-01
Radon Emanation Coefficient	3.8E-01
Moisture Content of Crushed Tuff	-1.5E-01
Moisture Content of Waste	-1.5E-01
Cover Node	-7.5E-02

The final parameter listed in Table 21, the cover node, highlights the relationship between cover thickness and radon flux. The surface erosion modeling conducted in support of the performance assessment and composite analysis divided or discretized the cover overlying the disposal units into a series of 6.25-m^2 (67-ft^2) nodes. Each node is characterized by an initial cover thickness and soil loss function. The site model randomly selects a node at the start of each realization of the probabilistic simulation and uses the corresponding cover thickness and cover loss function to project facility performance over the 1,000-year compliance period. Selecting a cover node

that has a relatively high initial cover thickness and a slow erosion rate will tend to yield lower radon fluxes than will a node with a thin initial cover and high rate of erosion.

The nodes used to represent the disposal site are sequentially numbered; the cover node element identified in the sensitivity analysis is simply a distribution of those numbers. The numbers of the nodes are assigned in a random manner and do not systematically increase or decrease with the initial cover thickness. Because of this, the correlation between the peak mean dose and the cover node is low.

Several parameters that have no apparent effect on the radon fluxes projected for waste disposal region 7 were identified as potentially important by the sensitivity analysis. Examples include plant uptake factors and transfer factors for various radionuclides, plant biomass and animal burrow characteristics at Area G, and sediment transport rates for selected contaminants. These parameters do not affect the rates of generation of radon or the diffusion characteristics of the gas and, therefore, the projected fluxes. Consequently, these results are considered spurious and are not included in Table 21.

5.1.1.2 Composite Analysis

Sensitivity analyses were conducted using the site model results for the Atmospheric and All Pathways–Canyon Scenarios. The analysis for the All Pathways–Canyon Scenario considered the exposures for the receptors within catchments PC5 and PC6, the locations with the highest peak mean doses of the nine canyon locations included in the dose assessment. The results of the sensitivity analysis are summarized in Table 22. This table includes the five parameters with the highest absolute values of the Spearman rank correlation coefficient.

The results of the sensitivity analysis for the Atmospheric Scenario receptor at the LANL boundary are the same as those discussed above for the performance assessment. Three of the five parameters control rates of tritium diffusion from the site, while the other two define the length of exposure and airborne concentrations over the receptor's residence. In terms of the exposures projected for the individual at the Area G fence line, it is clear that trees play a major role in the release of contamination to the surface environment. Three of the listed parameters influence the degree to which tree roots penetrate into the waste and deposit contaminated litter on the surface of the disposal site. The resuspension flux at Area G affects the rate at which contamination deposited on the surface of the facility is released to the atmosphere and transported downwind. The initial inventory of Th-230 in the pre-1971 disposal pits is important because it is a source of Ra-226 and Pb-210, two of the major contributors to the peak mean exposure.

Table 22
Rank Correlation Coefficients for Selected Composite Analysis Exposure Scenarios

Exposure Scenario	Exposure Location	Model Parameter	Rank Correlation Coefficient
Atmospheric	LANL boundary	Moisture content of crushed tuff	-4.6E-01
		Moisture content of waste	-4.6E-01
		Thermal gradient factor	4.3E-01
		Indoor exposure time	2.6E-01
		Dispersion factor for atmospheric source area 2	2.0E-01
	Area G fence line	Root-mass-distribution beta-shape factor	-4.7E-01
		Maximum rooting depth of trees	4.6E-01
		Particulate resuspension flux	3.0E-01
		Initial inventory of Th-230 in pre-1971 disposal pits	1.7E-01
		Aboveground biomass density of trees in piñon-juniper woodland	1.5E-01
All Pathways–Pajarito Canyon	Catchment PC5	Root-mass-distribution beta-shape factor	-3.7E-01
		Maximum rooting depth of trees	3.4E-01
		Erosion scenario	2.9E-01
		Plant-uptake factor of strontium in native vegetation	1.9E-01
		Ingestion rate of grain	1.5E-01
	Catchment PC6	Maximum rooting depth of trees	5.0E-01
		Root-mass-distribution beta-shape factor	-4.1E-01
		Plant-uptake factor of radium in native vegetation	2.2E-01
		Initial inventory of Th-230 in pre-1971 disposal pits	1.7E-01
		Erosion scenario	1.7E-01

Four of the parameters to which the canyon exposures in catchments PC5 and PC6 are most sensitive influence the amount of contamination taken up by deep-rooting trees. Two of these affect the distribution of root mass with depth, while the plant uptake factors control the rates of Sr-90 and Ra-226 assimilation by plants; these radionuclides are major contributors to the peak mean exposures projected for the different catchments. The dose projections for the two locations are also sensitive to the erosion scenario, because of the effect this parameter has on the rate of soil loss. The ingestion rate of grain is important for catchment PC5 because this exposure route is an important contributor to the projected doses. The initial Th-230 inventory in the pre-1971 disposal pits is important for catchment PC6 because it is a source of Ra-226 and Pb-210, the two radionuclides that make the greatest contributions to the projected peak mean dose.

5.1.2 Additional Sources of Uncertainty

The sensitivity analyses conducted in support of the performance assessment and composite analysis are useful for evaluating the effects of parameter variability on the dose and radon flux projections. However, several additional sources of uncertainty are associated with the results provided in Section 4 of this report. Some of these are discussed in the following sections.

5.1.2.1 Key Assumptions

The performance assessment and composite analysis are based on several key assumptions. The first of these pertains to the level of control exerted over the disposal facility after final closure. The analyses are based on the assumption that the DOE will actively maintain the disposal facility for a period of 100 years following closure, during which time efforts will be made to prevent the establishment of deep-rooting trees at the site and to limit significant erosion of the cover placed over the disposal pits and shafts.

The doses projected for the Atmospheric Scenario at the Area G fence line and for the All Pathways–Canyon Scenarios at most exposure locations are dominated by exposures to contaminated soils that are suspended from the disposal site and transported with the prevailing winds, and to contaminated sediments transported with surface runoff into Cañada del Buey and Pajarito Canyon. In many cases, the contamination responsible for these exposures is deposited on the surface of the disposal facility by plants and animals intruding into the waste. Logically, then, any controls on the establishment of deep-rooting plants at the site could be viewed as having a potentially significant impact on the exposures projected for these scenarios. This hypothesis is supported by the results of the sensitivity analysis, which indicate that the doses projected for many receptor locations are highly correlated with the abundance and rooting characteristics of trees.

Nevertheless, modeling results suggest that the control of deep-rooting species of plants by the DOE during the active institutional control period will have a limited impact on the doses projected for the downwind and canyon receptors. For example, the composite analysis exposures projected for the fence line location increase slowly over the latter portions of the compliance period, with the highest doses occurring at the end of the 1,000-year compliance period. Earlier establishment of deep-rooted trees at the closed facility will cause exposures to increase sooner. However, the rate of increase during the latter stages of the compliance period is expected to be similar to that indicated by the GoldSim modeling. If this is the case, the peak mean exposures will likely increase 10 to 15 percent if the DOE fails to prevent the site from transitioning to piñon-juniper woodland during the active institutional control period.

A similar pattern is observed for the exposures projected for the canyon residents in catchments CdB2, PC0, PC1, and PC6. In each case, the projected exposures for most radionuclides increase slowly over long periods of time suggesting the earlier presence of trees will only cause

moderate increases in dose. In some cases, Sr-90 taken up by plants and deposited on the surface of the disposal facility makes an important contribution to the exposures projected for the canyon receptors. Sr-90 has a relatively short half-life and is, therefore, more influenced by the time required for deep-rooted vegetation to become established at the closed site. Earlier establishment of trees could result in significantly higher doses from this isotope, perhaps as much as three times higher. That said, the total exposures received by the receptors are expected to remain well within the 30 mrem/yr dose constraint that applies to the canyon scenario.

It is also assumed that the DOE will prevent any significant erosion of the closed site during the active institutional control period. However, the surface erosion rate modeling did not project any significant rates of soil loss during this period and erosion was allowed to proceed unimpeded. Although prevention of all soil loss for a period of 100 years would help minimize plant root penetration of the waste, any resulting reductions in projected exposures are expected to be less than 10 percent. That aside, it is unrealistic to expect that all soil loss could be prevented.

The long-term performance modeling is based on the assumption that there will be no significant climatic changes during the period of performance. Should climatic changes occur, many aspects of the facility's performance could be affected. A wetter climate would likely result in increased rates of infiltration through the disposal units with subsequent elevated rates of radionuclide leaching from the waste and reduced groundwater travel times to the regional aquifer; both of these effects could increase the potential for exposures to persons who use groundwater resources downgradient of Area G. Additional moisture could result in different plant and animal communities at the site, possibly altering the impacts of biotic intrusion on facility performance. On the other hand, drier conditions would likely result in reduced rates of contaminant leaching and longer groundwater travel times, ensuring little or no risk of exposure to groundwater users. Again, shifts in the plant and animal communities may occur, influencing the degree to which biotic intrusion impacts the site.

Subsidence of incompletely filled disposal units is not explicitly modeled nor is it assumed to impact the long-term performance of the disposal facility. Although the potential for subsidence may be real, it is assumed that efforts will be taken to minimize or eliminate this potential by the time the facility undergoes final closure. If subsidence does occur, the potential impacts on facility performance will depend upon what disposal units are impacted and the degree to which the integrity of the affected pits and shafts is undermined. In general, however, subsidence could lead to greater rates of infiltration through the waste, faster contaminant travel times to the regional aquifer, and increased access to the waste by plants and animals inhabiting the site; under extreme circumstances waste could, conceivably, be exposed.

Isolated incidences of subsidence have been observed at Area G. Most of these have consisted of small holes developing next to several disposal shafts. However, more significant subsidence

events have been also been observed. In 2004, a 1 to 1.5 m (3.3 to 5 ft) diameter hole of unknown depth developed in a portion of pit 15. Pit 15 was dedicated to the disposal of waste packaged in metal and wood containers of various proportions; comparisons of the volumes of waste placed in these containers and the capacities of the packages suggest that many of these containers were incompletely filled. Also in 2004, a 1 to 1.5 m (3.3 to 5 ft) diameter hole of unknown depth developed between pits 32 and 33; these pits received mostly uncontainerized waste in the mid-1980s. In 2005, subsidence occurred over an area of approximately 50 m^2 (500 ft^2) within pit 9; the maximum depth of the depression was about 0.6 m (2 ft). This pit contains retrievably stored transuranic waste that was packaged in wooden boxes and metal drums to facilitate its retrieval. Finally, a 1 to 1.5 m (3.3 to 5 ft) diameter hole of unknown depth developed in pit 31 in 2005. This pit, which underwent interim closure in 2005, received both containerized and bulk (uncontainerized) waste (French, 2005).

Inspections are conducted annually to identify and correct the impacts of any subsidence events. Other options, including dynamic compaction of selected disposal units, have also been considered by Laboratory personnel for addressing subsidence issues at Area G. To the extent that such options are successful, the long-term performance of Area G is not expected to be substantially undermined by subsidence. It is on this basis that the long-term performance modeling was conducted.

5.1.2.2 Saturated Hydraulic Conductivity

The material properties of the cover and bedrock are critical in terms of the long-term erosion and infiltration behavior of the final cover. An important parameter for both processes is the saturated hydraulic conductivity of the bentonite/crushed tuff layer. The surface erosion and infiltration modeling relied on different literature-based estimates of this parameter. The SIBERIA modeling (Wilson et al., 2005) adopted a saturated hydraulic conductivity of 11 mm/hr (0.43 in./hr); this value is significantly greater than the value of 0.065 mm/hr (0.0026 in./hr) adopted as the base-case condition for the infiltration modeling (Levitt, 2008).

The hydraulic conductivity values used in the surface erosion modeling were taken from literature values (Nyhan et al., 1993; Charman and Murphy, 1992) for actual soils with the same texture (i.e., the same proportions of sand, silt and clay) as that for the proposed cover. The infiltration calculations used an estimated hydraulic conductivity for a 6 percent bentonite/crushed tuff mixture; this estimate was based on a linear regression fit between the measured hydraulic conductivity of pure crushed tuff and the value reported in Nyhan et al. (1997) for a 10 percent bentonite/tuff mixture. Both sets of values have limitations. The values representing actual soils reflect the fact that these soils have developed, over a long period of time, a structure with a hierarchy of pores and water pathways. This type of soil structure may develop at Area G, but it may require many years after the placement of the final cover to do so. On the other hand, the hydraulic conductivity of crushed tuff/bentonite that was used for the

infiltration modeling assumes the material is homogeneous, with none of the characteristics that may develop near the surface of the disposal site as a result of biotic activities such as root growth or the burrowing activities of insects or animals.

The uncertainty about the saturated hydraulic conductivity characteristics of the cover material is a potentially significant source of error in the surface erosion modeling. If the actual hydraulic conductivity values are lower than the values adopted for the modeling, the SIBERIA runoff rates—and subsequent erosion—will be higher than predicted; rates of infiltration will tend to decline. Given higher saturated hydraulic conductivities, rates of erosion will decrease while the amount of water passing through the disposal units will rise. As discussed earlier, increases in rates of infiltration may result in greater leaching of the waste and faster contaminant travel times to the compliance well.

Field and laboratory data provide additional insight into the values used to characterize the saturated hydraulic conductivity of the cover material at Area G. Field measurements of saturated hydraulic conductivity were collected as a function of depth below the surface at MDA J, a disposal site located 2 km (1.2 mi) west of Area G that underwent final closure in 2002 (Apogen, 2006). At each of three locations, measurements were collected at the soil surface, at 15 cm (6 in.) bgs, and at the top of a bentonite/tuff infiltration layer found at depths ranging from 23 to 28 cm (9 to 11 in.) bgs. Although the cover at MDA J differs from that assumed for Area G, the properties of the surface soils and bentonite/tuff layers are expected to be similar. The results of the field measurements are summarized in Table 23.

Table 23
Field Measurements of Saturated Hydraulic Conductivity at MDA J

Sample Hole	Sample Depth	Saturated Hydraulic Conductivity (mm/hr)
1	Surface	9.3E+00
	15 cm	8.5E+00
	25 cm [a]	4.9E-02
2	Surface	1.0E+01
	15 cm	8.1E+00
	28 cm [a]	1.5E-01
3	Surface	2.4E+00
	15 cm	2.4E+00
	23 cm [a]	2.6E-01

Source: Apogen, 2006

[a] *Sample was collected at the top of the bentonite/crushed tuff infiltration layer.*

The field measurements at MDA J indicate that the saturated hydraulic conductivity decreases with depth from the topsoil layer to the bentonite/tuff infiltration layer. The average conductivity for the surface and at a 15 cm (6 in.) depth in sample hole 1 is about 180 times that measured in the infiltration layer, while the average conductivities measured at the surface and at a depth of 15 cm (6 in.) in holes 2 and 3 are 62 and 9 times greater than the corresponding infiltration layer values. The mean conductivity for all three sample holes at the surface and at a 15 cm (6 in.) depth is 6.8 mm/hr (0.27 in./hr), or about 45 times the mean conductivity of 0.15 mm/hr (0.0059 in./hr) found for the infiltration layer.

The decrease in saturated conductivity with depth observed at MDA J is a direct reflection of the materials comprising the surface and infiltration layers of the final cover. The topsoil layer is much less compacted than the bentonite/tuff infiltration layer and, therefore, is more permeable to water. The presence of plant roots and insect and animal burrows in the cover may enhance the conductivity of the cover. Although these effects may reasonably be expected to be greatest near the surface of the site, measurements needed to differentiate between the relative influence of roots and burrows on the two layers were not collected.

On the basis of the findings at MDA J, the saturated hydraulic conductivity used for the erosion modeling should be representative of the surface of the cover at Area G. The conductivity measurements for the surface of MDA J average 7.3 mm/hr (0.29 in./hr); the measurements at 15 cm (6 in.) bgs are functionally the same and average 6.3 mm/hr (0.25 in./hr) across the three holes. These measurements compare favorably with the value of 11 mm/hr (0.43 in./hr) used in the SIBERIA modeling. In terms of infiltration characteristics, the 6 percent bentonite/tuff layer included in the final cover design for Area G is generally expected to have the greatest impact on rates of infiltration through the disposal units. The average saturated hydraulic conductivity measured for the infiltration layer at MDA J is 0.15 mm/hr (0.0059 in./hr); this value is similar to the average conductivity of 0.14 mm/hr (0.0055 in./hr) measured in four holes in 2003 (LANL, 2003b), shortly after the cover was placed over the disposal facility. These values are 2.1 to 2.3 times greater than the value of 0.065 mm/hr (0.0026 in./hr) adopted for the base-case HYDRUS simulations.

Laboratory measurements of hydraulic conductivity were conducted on replicate samples of crushed tuff with 6 and 8 percent bentonite (DBS&A, 2006). The average saturated hydraulic conductivity of the two 6 percent bentonite/tuff samples was 0.099 mm/hr (0.0039 in./hr); the corresponding value for the two 8 percent bentonite/tuff samples was 0.038 mm/hr (0.0015 in./hr). The mean conductivity for the 6 percent mixture is 1.5 times greater than the value used for the HYDRUS modeling, while the mean for the 8 percent mixture is about 60 percent of the value used in HYDRUS. The fact that the conductivity measured for the 6 percent mixture is higher than the modeled value may result, in part, from the fact that the laboratory samples were less compacted than the samples upon which the HYDRUS model value was based. The mean bulk density of all four laboratory samples was 1,250 kg/m^3 (78 lb/ft^3), or

about 90 percent of the 1,400 kg/m^3 (87 lb/ft^3) bulk density typical of the mixtures upon which the conductivity used in the HYDRUS infiltration modeling was based.

Based on the preceding discussion, the use of two distinct saturated hydraulic conductivities for the erosion and infiltration modeling appears warranted. The higher value used for the SIBERIA modeling addresses the properties of the surface soils expected at Area G and is consistent with measurements conducted for surface soil at MDA J. It remains to be seen, however, if the conductivity of the bentonite/tuff layer at Area G will increase over time as the surface soil erodes and plant roots and insect and animal burrows penetrate further into the material. The measurements collected at MDA J indicate that no significant changes in the conductivity of the bentonite/tuff layer have occurred since the disposal site was covered, but only 4 years had passed between the time the cover was applied and the time the measurements were taken.

The use of a much lower hydraulic conductivity for the infiltration modeling is consistent with the expectation that the bentonite/tuff layer will exert a major influence on rates of water infiltration through the cover at Area G. The values used in the HYDRUS modeling are generally consistent with the values measured at MDA J and in the laboratory.

5.1.2.3 Sediment Transport and Canyon Interactions

The exposures projected for the All Pathways–Cañada del Buey and All Pathways–Pajarito Canyon Scenarios result from the transport of contaminated sediments into the canyons adjacent to Area G. Sediments transported to the edge of the mesa were allocated among several drainages or catchments within the two canyons in an attempt more accurately estimate contaminant concentrations on the canyon floors. Nevertheless, the projected sediment paths and radionuclide concentrations are subject to a large amount of uncertainty.

The SIBERIA model does not allow particle tracking or sediment-packet tracking, which means the model cannot determine if contaminated particles reaching the edge of the mesa will become trapped within the rock armor or migrate over the mesa edge to a downhill location. Because of this limitation, the modeling conducted in support of the performance assessment and composite analysis assumed that all sediments reaching the edge of the mesa were transported over the edge and migrated immediately to the canyon floors. This approach is expected to be conservative in terms of the exposures received by persons living in the canyon because a portion of the sediments would probably require longer periods of time to reach the canyon floors.

Sediments transported from the mesa top will disperse over some portion of the canyon floor in Cañada del Buey and Pajarito Canyon. Lacking specific information about how sediment dispersal will evolve, it was assumed that the material will spread over 10 to 50 percent of the area of a given catchment. Dispersal over smaller areas will result in doses that are larger than projected; the reverse will be true if the area of dispersal is larger.

As modeled, the sediments reaching the canyon floors are assumed to be slowly transported down Cañada del Buey and Pajarito Canyon in response to flooding events. Information about sediment transport rates has been collected within some canyons at the Laboratory, but no direct estimates of sediment transport within Cañada del Buey and Pajarito Canyon exist. Although rates of transport are assumed to be slow within these canyons, the 200-year residence time upon which the modeled rates are based is still highly uncertain. Shorter residence times will result in lower exposures than those projected for the canyon residents. If however, sediment transport rates are substantially lower than assumed, exposures could rise significantly over long periods of time.

5.1.2.4 Short-Term Moisture Conditions

Several surface structures have been constructed at Area G in support of waste management operations at that facility. These structures include asphalt pads, the presence of which has been shown to result in elevated moisture contents in nearby areas and subsurface soils. These pads inhibit the removal of water through evapotranspiration and often focus runoff to small portions of the site. The result is increased fluxes of water: Newman et al. (2005) compared moisture contents in boreholes drilled in paved and unpaved portions of Area G and found that moisture contents and fluxes in the former were significantly higher than those in unpaved portions of the site. Birdsell et al. (2005) found that runoff focused by an asphalt pad at Area G resulted in a transient ponded condition near a borehole. Periodic monitoring of water content in the borehole revealed increasing water contents to a depth of 24 m (80 ft) bgs within 10 years of when the borehole was established.

Elevated moisture conditions and corresponding increases in rates of infiltration that persist over time will have obvious effects on the rates at which contaminants are leached from the waste and transported to the regional aquifer. However, evidence from MDA AB suggests that moisture contents will gradually return to natural levels once the asphalt pads are removed (Birdsell et al., 2005). Thus, the long-term impacts of these pads will depend on the length of the period they are in place as well as flow conditions specific to each pad.

5.1.2.5 Effects of Waste Form and Packaging

The waste disposed of at Area G has assumed a wide variety of chemical and physical forms. Packaging of this waste has ranged from nonexistent to metal containers. Despite this, the modeling conducted in support of the performance assessment and composite analysis is based on the simplifying assumption that all waste radionuclides are in equilibrium with the crushed tuff backfill as soon as the waste is placed in the disposal units.

Simplifying the effects of waste form and packaging in this manner may provide estimates of radionuclide release in excess of what will actually occur. For example, plants will be unable to assimilate contaminants in solidified waste (e.g., concrete), sealed sources, and activated metals until those matrices degrade. The radionuclides in these wastes will also be resistant to transport

to the surface of the facility by burrowing animals and contaminant leaching. Likewise, as long as metal containers remain intact, the impacts of biotic intrusion and contaminant leaching may be limited. Understanding the overall effect of waste form and packaging on the doses projected for the performance assessment and composite analysis will require a detailed investigation of the distributions of the critical radionuclides among the various forms and package types.

5.1.2.6 Spatial Dependencies of Long-Term Performance

Several aspects of the long-term performance modeling conducted in support of the performance assessment and composite analysis are spatially variable across the facility. In response to this, the facility was divided into eight waste disposal regions to account for variations in groundwater flow and transport behavior. The erosion modeling estimates rates of cover loss taking into account the locations of the disposal units and variations in cover thickness and slope. Accounting for the spatial variability in site conditions is expected to provide a more accurate representation of facility performance.

The spatial dependencies of facility performance make it clear that the manner in which the facility is operated, maintained, and closed need to be carefully considered. As an example, the groundwater transport modeling conducted by Stauffer et al. (2005) indicates that groundwater travel times to the compliance well generally increase from the eastern edge of Area G to the western boundary; travel times for releases from waste disposal regions 1 and 8 may differ by hundreds to thousands of years depending upon the rate at which water infiltrates through the site. In this instance, the placement of large inventories of highly mobile radionuclides in the easternmost disposal units could have more serious consequences than placing the same waste in pits and shafts in the western portion of the facility. Alternatively, the surface erosion modeling conducted using SIBERIA (Wilson et al., 2005) generally indicates more severe erosion pressures exist along the edges of the mesa; information of this nature should be used to intelligently site future disposal units.

5.2 Inadvertent Intruder Analysis

The distributional information provided in Table 12 provides insight into the uncertainty associated with the projected intruder doses. In terms of the doses for radionuclides that are unaffected by diffusion, the variability associated with the construction and agricultural intruder exposures is significantly greater than that observed for the postdrilling intruder doses. The greater variability noted for the former scenarios is an indication of the impact that the thickness of the cover placed over the pits and shafts has upon the projected impacts. As discussed earlier, the distributions of initial cover thickness over many of the disposal units are such that the excavation of a basement is not projected to contact the waste in a large number of model realizations. In terms of the disposal pits, the waste will remain undisturbed by basement excavation in about 90 percent or more of the model realizations. Contact with the 1988–2015

shaft waste during basement excavation will occur about 10 percent of the time and contact with the 2016–2044 shaft waste will occur about 50 percent of the time.

Failure to contact the waste during basement excavation does not prevent exposures of the construction and agricultural intruders; plants and animals may transport contaminants to portions of the cover that are disturbed during excavation and vapor- and gas-phase radionuclides may diffuse upward. However, the intruders are exposed to significantly smaller concentrations of contamination under these conditions, relative to the contaminant concentrations encountered when the basement extends into the waste. Because of this, a wide range in the projected exposures is observed, as witnessed by the statistics shown in Table 12. The variability in the exposures projected for the postdrilling intruder is much smaller because contact with the waste occurs in all model realizations. In this situation, similar amounts of waste are brought to the surface in all realizations, resulting in narrower distributions of dose.

The variability inherent in the doses projected for vapor- and gas-phase radionuclides tends to be less than that for contaminants that are unaffected by diffusion. Diffusion through the cover and waste makes vapor- and gas-phase contaminants accessible to the intruders over the range of cover depths modeled. More stable contaminant concentrations result between model realizations, leading to less variable dose estimates.

The inadvertent intruder exposures projected for the disposal pits are based on average radionuclide concentrations in the buried waste. Radionuclide concentrations are averaged over the units used from September 27, 1988 through 2010 and from 2011 through 2044. Depth-dependent inventories are used to model exposures from the 1988–2015 shafts, but these inventories are averaged over discrete depth intervals; the waste in the 2016–2044 shafts is uniformly distributed throughout the disposal units. Radionuclide concentrations in all shafts are further modified to account for the discrete nature of these units and their spatial distribution within the shaft fields. Using spatially averaged inventories all but ensures that the projected doses will not equal the doses received if human intrusion actually occurred. However, this approach takes into account the fact that a person arriving at the site could excavate a basement or drill a well at countless locations at the site. Using average waste concentrations functionally weights the likelihood that the individual will decide to intrude into waste that contains higher or lower than average radionuclide concentrations.

It is assumed that intrusion may occur at any time following the end of active institutional control over the site. This assumption, in conjunction with the degree of disturbance assumed, is expected to result in reasonably conservative estimates of potential intruder impacts. Use of the site for nonresidential activities (e.g., hunting or other forms of recreation) will result in little or no disruption of the waste and, consequently, significantly lower exposures. As shown by the

results of the agricultural and postdrilling intruder scenarios, impacts may vary significantly for resident intruders, depending upon the type of construction undertaken.

Sensitivity analyses were conducted for the agricultural and postdrilling intruder scenarios in conjunction with the 1988–2010 pits and 1988–2015 shafts. These scenarios address two distinct types or degrees of intrusion into the waste, one in which large quantities of material are excavated from shallow depths (basement excavation) and one in which smaller amounts of material are removed throughout the cover and waste profile (well drilling). These disposal units were chosen for consideration because they yielded higher doses than the pits and shafts in the Zone 4 expansion area.

The results of the sensitivity analysis are summarized in Table 24. This table includes the five parameters that had the highest absolute values of the Spearman rank correlation coefficient. For the 1988–2010 disposal pits, the doses projected for the agricultural intruder using the intruder model are correlated with two parameters that determine the degree to which plants intrude into the waste prior to the intruder's arrival: root depth and the beta shape factor for root-mass distribution. Greater penetration of the waste occurs as the maximum root depth of the trees increases; the trees deposit higher radionuclide activities on the surface of the facility prior to the arrival of the intruder and radionuclide concentrations in the material brought to the surface during basement excavation increase. The intruder doses are inversely proportional to the shape factor. Larger values of the parameter predict that a greater proportion of the total root mass lies close to the surface; less contamination is brought to the surface as a result. The third parameter listed in Table 24, the cover node, relates to the initial cover thicknesses and erosion loss functions that are used in the modeling. In addition to affecting how deeply tree roots extend into the waste, these factors determine how far the basement of the intruder's house extends into the waste and, therefore, how much contamination is brought to the surface. The last two parameters in the table affect how much Cl-36 is assimilated by trees growing over the closed disposal site and to what degree the milk consumed by the intruder is contaminated with Pu-239. Both of these radionuclides are important contributors to the projected peak mean dose.

The sensitivity analysis for the intruder diffusion model indicates that the peak mean dose estimated for the agricultural intruder who accesses waste in the 1988–2010 pits is most sensitive to the Ra-226 inventory in these pits. Similar to the intruder model, two parameters control the distribution of tree roots in the waste: the maximum rooting depth of trees and the beta shape factor. The cover node parameter reflects the importance of the initial cover thickness over the waste and the rate at which the cover is eroded over extended periods of time. The peak mean dose is also sensitive to the radon emanation coefficient. Pb-210, a daughter of Ra-226, is a major contributor to the peak exposure projected for the intruder. The surface soils over the intruder's lot become contaminated with Pb-210 following the diffusion of Rn-222 upward from the waste; the magnitude of the projected radon flux is determined, in part, by the radon-emanation coefficient.

Table 24
Rank Correlation Coefficients for Selected Intruder Exposure Scenarios

Waste Disposal Units and Exposure Scenario	Intruder Model		Intruder Diffusion Model	
	Model Parameter	Rank Correlation Coefficient	Model Parameter	Rank Correlation Coefficient
1988–2010 Disposal Pits				
Intruder-Agriculture Scenario	Maximum rooting depth of trees	4.2E-01	Ra-226 waste inventory in 1988–2015 pits	3.6E-01
	Root-mass-distribution beta-shape factor	-3.1E-01	Cover node	-2.3E-01
	Cover node	-2.4E-01	Radon emanation coefficient	1.6E-01
	Plant uptake factor of chloride in native vegetation	1.5E-01	Root-mass-distribution beta-shape factor	-1.5E-01
	Milk transfer factor for plutonium	1.1E-01	Maximum rooting depth of trees	1.5E-01
Intruder–Post-Drilling Scenario	Maximum rooting depth of trees	4.3E-01	Ra-226 waste inventory in 1988–2015 pits	4.2E-01
	Root-mass-distribution beta-shape factor	-4.1E-01	Root-mass-distribution beta-shape factor	3.9E-01
	Ingestion rate of grain	2.2E-01	Maximum rooting depth of trees	3.3E-01
	Plant uptake factor of chloride in native vegetation	1.6E-01	Ingestion rate of grain	2.0E-01
	Fractions of vegetables grown by intruder	1.2E-01	Cover node	-1.7E-01
1988–2015 Disposal Shafts				
Intruder-Agriculture Scenario	Cover node	-1.9E-01	Ra-226 waste inventory in 1988–2015 shafts	5.8E-01
	Maximum rooting depth of trees	1.4E-01	Radon-emanation coefficient	3.0E-01
	Indoor exposure time	8.6E-02	Ingestion rate of grain	2.1E-01
	Dry-to-wet weight fraction for produce	-8.3E-02	Fraction of vegetables grown by intruder	1.4E-01
	Root-mass-distribution beta-shape factor	-8.0E-02	Plant-uptake factor of lead in grain	1.4E-01
Intruder–Post-Drilling Scenario	Animals raised	-4.4E-01	Ra-226 waste inventory in 1988–2015 shafts	6.5E-01
	Sr-90 waste inventory in 2005–2044 shafts	3.4E-01	Ingestion rate of grain	3.4E-01
	Plant-uptake factor of strontium in grain	2.7E-01	Fraction of vegetables grown by intruder	2.4E-01
	Ingestion rate of grain	2.1E-01	Animals raised by intruder	-2.4E-01
	Plant-uptake factor of strontium in pasture grass and native vegetation	2.1E-01	Plant-uptake factor of carbon in grain	1.6E-01

--- = Sensitivity analysis did not address intruder diffusion dose projections for this exposure scenario.

The sensitivity analysis results for the postdrilling intruder with respect to the 1988–2010 pits are similar to those for the agricultural intruder. The intruder model projections are sensitive to the root-mass distribution of trees with depth and the rate at which Cl-36 is assimilated by the trees. The quantity of the intruder's diet that comes from growing crops on the receptor's lot and the rate at which grain is consumed also affect the results for this model; the ingestion of crops makes a significant contribution to the peak mean dose projected for the intruder. The peak mean dose projected by the intruder diffusion model for the postdrilling scenario is most sensitive to the Ra-226 inventory in the disposal pits. Three parameters control the distribution of tree roots in the waste; these include the maximum rooting depth of trees, the beta shape factor, and the cover node parameter. The ingestion rate of grain influences how much contaminated food is consumed by the intruder.

The agricultural intruder exposures projected in conjunction with the 1988–2015 shafts using the intruder model are correlated with three parameters that determine the extent to which plant roots penetrate the buried waste: the cover node parameter, the maximum rooting depth of trees, and the beta-shape factor. The indoor exposure time and the wet-to-dry weight fraction for produce affect the magnitudes of the exposures received through direct radiation and crop ingestion; these exposure pathways are responsible for most of the projected peak mean dose. The sensitivity analysis identified two spurious parameters that are used to model radionuclide concentrations in crops for two isotopes that did not contribute to the projected exposures; these parameters are excluded from the table.

The agricultural intruder diffusion model projections for the 1988–2015 shafts are highly correlated to the inventory of Ra-226 and the radon-emanation coefficient. The remaining parameters listed in Table 24 relate to the intake of vegetables contaminated with Pb-210; the ingestion of contaminated crops is an important contributor to the peak mean exposure. The parameters specify how much grain is consumed by the individual, the fraction of the receptor's crops raised in contaminated soils, and the rate at which lead is assimilated by food crops.

The postdrilling intruder doses projected by the intruder model in conjunction with the 1988–2015 shafts are strongly correlated to the inventory of Sr-90, the parameters that determine Sr-90 concentrations in various foodstuffs, and the quantity of food consumed. The correlation between the projected exposures and the type of animal raised by the intruder reflects the fact that much higher Sr-90 doses result from the consumption of beef and milk than from the ingestion of chicken and eggs. The doses projected for this scenario using the intruder diffusion model are sensitive to the Ra-226 inventory in the shafts and to several factors that determine the types and amounts of contaminated foodstuffs that are consumed by the receptor. These parameters include how much grain is consumed, the fraction of the intruder's food that is grown on site, the types of animal products consumed by the intruder (i.e., beef and milk or chicken and eggs), and the plant uptake factor for carbon in grain.

6.0 References

Apogen. 2006, *Field Saturated Hydraulic Conductivity Investigation of Engineered Pit Cover Soils at Los Alamos National Laboratory, Material Disposal Area J*, Los Alamos report LA-UR-06-8746, November.

Baes, C.F., III, R.D. Sharp, A.L. Sjoreen, and R.W. Shor, 1984, *A Review and Analysis of Parameters for Assessing Transport of Environmentally Released Radionuclides through Agriculture*, Oak Ridge National Laboratory, ORNL-5786, September.

Birdsell, K., 2005, Personal communication from Kay Birdsell, Los Alamos National Laboratory, to Rob Shuman, URS Corporation, October 26.

Birdsell, K.H., B.D. Newman, D.E. Broxton, and B.A. Robinson, 2005, "Conceptual Models of Vadose Zone Flow and Transport beneath the Pajarito Plateau, Los Alamos, New Mexico," *Vadose Zone Journal*, Vol. 4, pp. 620–636.

Broxton, D.E., 2005, Personal communication between Dave Broxton, LANL EES-6, and Phil Stauffer, LANL EES-6, October.

Charman, P.E.V. and B.W. Murphy, 1992, *Soils—Their Properties and Management, A Soil Conservation Handbook for New South Wales*, Sydney University Press, ISBN 042 4001837, 363 pp.

DBS&A (Daniel B. Stephens & Associates, Inc.), 2006 Laboratory Report for Los Alamos National Laboratory, Request No. 4526S, April 25.

DOE, 1988a, *Radioactive Waste Management*, U.S. Department of Energy Order 5820.2A, September 26.

DOE, 1988b, *Internal Dose Conversion Factors for Calculation of Dose to the Public*, U.S. DOE, DOE/EH-0071, July 1988.

DOE, 1988c, *External Dose-Rate Conversion Factors for Calculation of Dose to the Public*, DOE/EH-0070, July 1988.

DOE, 1993, *Radiation Protection of the Public and the Environment*, U.S. Department of Energy Order 5400.5, Change 2, January 7

DOE, 2001a, *Radioactive Waste Management*, U.S. Department of Energy Order 435.1 (change order to DOE O 435.1 of July 1999), August 28.

DOE, 2001b, *Radioactive Waste Management Manual*, U.S. Department of Energy Report DOE M 435.1-1 (change 1 to document approved on July 9, 1999), June 19.

EPA, 1988, *Limiting Values of Radionuclide Intake and Air Concentration and Dose Conversion Factors for Inhalation, Submersion, and Ingestion*, U.S. Environmental Protection Agency Federal Guidance Report 11, EPA 520/1-88-020, September.

EPA, 1989, Code of Federal Regulations, 40 CFR 61.192 Subpart Q, *National Emission Standards for Radon Emissions from Department of Energy Facilities*, (published in Federal Register Vol. 54, p. 51701, December 15 1989 and amended in Vol. 65, p. 62158, October 17, 2000), <http://www.access.gpo.gov/nara/cfr/waisidx_04/40cfr61_04.html >).

EPA, 1993, *External Exposure to Radionuclides in Air, Water, and Soil*, U.S. Environmental Protection Agency Federal Guidance Report 12, EPA 402-R-93-081, September.

EPA, 2000, "Part II, Environmental Protection Agency, 40 CFR Parts 9, 141, and 142, National Primary Drinking Water Regulations; Radionuclides; Final Rule," *Federal Register*, Vol. 65, No. 236, pp. 76708–76753, December 7, <http://www.epa.gov/fedrgstr/EPA-GENERAL/2000/December/Day-07/g30421.pdf>.

EPA, 2002, *Final Implementation Guidance for Radionuclides*, United States Environmental Protection Agency, EPA 816-F-00-002, March.

EPA, 2004, Code of Federal Regulations, 40 CFR 61.93 Subpart H, "National Emission Standards for Hazardous Air Pollutants; National Emission Standards for Emissions of Radionuclides Other than Radon from Department of Energy Facilities," *Federal Register*, Vol. 69, No. 116, p. 33865, June 2004, <http://www.epa.gov/fedrgstr/EPA-AIR/2004/June/Day-17/a13679.htm>.

French, S.B., 2005, Personal communication between Sean French, Los Alamos National Laboratory, and Rob Shuman, URS Corporation, October 24.

GoldSim, 2007a, *User's Guide—GoldSim Probabilistic Simulation Environment,Volume 1 of 2, Version 9.60*, GoldSim Technology Group, March.

GoldSim, 2007b, *User's Guide—GoldSim Probabilistic Simulation Environment,Volume 2 of 2, Version 9.60*, GoldSim Technology Group, March.

GoldSim, 2007c, *User's Guide—GoldSim Contaminant Transport Module, Version 4.20*, GoldSim Technology Group, March.

Grove Engineering, 1992, *MICROSHIELD Version 4, User's Manual*, Grove Engineering, Inc.

Hansen, W.R., 1995, Personal communication from W.R. Hansen, Los Alamos National Laboratory, to Rob Shuman, Rogers and Associates Engineering Corporation, Inc., May 23.

Hinton, T.G. 1992, "Contamination of Plants by Resuspension: A Review, with Critique of Measurement Methods," *The Science of the Total Environment,* Vol. 121, pp. 177-193.

Hoffman, F.O. and R.H. Gardner, 1983, "Evaluation of Uncertainties in Radiological Assessment Models," In *Radiological Assessment — A Textbook on Environmental Dose*

Analysis, Till, J.E. and H.R. Meyer, eds., prepared for the U.S. Nuclear Regulatory Commission, NUREG/CR-3332, September.

Hollis, D., E. Vold, R. Shuman, K. Birdsell, K. Bower, W. Hansen, D. Krier, P. Longmire, B. Newman, D. Rogers, E. Springer, 1997, *Performance Assessment and Composite Analysis for the Los Alamos National Laboratory Disposal Area G*, Los Alamos National Laboratory Report LA-UR-97-85, Report-54G-013, March.

Jacobson, K.W., 2005, *Air Dispersion Analysis for Los Alamos National Laboratory Technical Area 54, Material Disposal Area G*, Los Alamos National Laboratory Report LA-UR-05-7232, September.

KAPL, 2002, *Nuclides and Isotopes, Chart of the Nuclides, 16th Edition*, Knolls Atomic Power Laboratory, Baum, E.M., H.D. Knox, and T.R. Miller, eds.

LANL, 1952, Los Alamos National Laboratory Internal Memorandum from Dean Meyer to Salvatore Russo, Subject: "Location of Contaminated Waste Burial Pits," January 31, 1952.

LANL, 1971, Los Alamos Scientific Laboratory internal memorandum from W.B. Gibson to W.J. Maramam, Subject: General's Tanks–Memo from Dean D. Meyer, December 3.

LANL, 1995, *Installation Work Plan for Environmental Restoration*, Los Alamos National Laboratory ER Project Report LA-UR-95-4048.

LANL, 1996, *RFI Report for Channel Sediment Pathways from MDAs G, H, J, and L, TA-54: Field Unit 5 Environmental Restoration Project*, Los Alamos National Laboratory Report LA-UR-96-110, February.

LANL, 1998, *Work Plan for Pajarito Canyon: Environmental Restoration Project*, Los Alamos National Laboratory Report LA-UR-98-2550, September.

LANL, 1999, *Work Plan for Sandia Canyon and Cañada del Buey: Environmental Restoration Project September 1999*, Los Alamos National Laboratory Report LA-UR-99-3610, September.

LANL, 2001, *RFI Report for Material Disposal Area H at Technical Area 54*, Los Alamos National Laboratory Report LA-UR-01-1208, May.

LANL, 2002a, *TA-54 Area J Closure Certification Report*, Los Alamos National Laboratory Report LA-UR-02-6548.

LANL, 2002b, *Environmental Surveillance at Los Alamos during 2001*, Los Alamos National Laboratory Report LA-13979-ENV, September.

LANL, 2003a, *Corrective Measures Study Report for Material Disposal Area H, Solid Waste Management Unit 54-004, at Technical Area 54*, Risk Reduction and Environmental Stewardship Division–Remediation Program, Los Alamos National Laboratory Report LA-UR-03-3354, May.

LANL, 2003b, *Measurements of Field Saturated Hydraulic Conductivity of an Engineered Soil at Los Alamos National Laboratory's Technical Area 54, Material Disposal Area J*, Los Alamos National Laboratory report LA-UR-04-0325.

LANL, 2004a, *Environmental Surveillance at Los Alamos during 2002*, Los Alamos National Laboratory Report LA-14085-ENV, January.

LANL, 2004b, *Environmental Surveillance at Los Alamos during 2003*, Los Alamos National Laboratory Report LA-14162-ENV, September.

LANL, 2005a, *Investigation Report for MDA L*, Los Alamos National Laboratory Report LA-UR-05-5777, September.

LANL, 2005b, *Conceptual Design of Zone 4 Disposal Units at Los Alamos National Laboratory Technical Area 54, Material Disposal Area G*, Los Alamos National Laboratory Report LA-UR-05-6899, September.

LANL, 2006, *Investigation Report for Material Disposal Area C, Solid Waste Management Unit 50-009, at Technical Area 50*, Los Alamos National Laboratory Report LA-UR-06-8096, December.

LANL, 2007a, *Documented Safety Analysis for Surveillance and Maintenance of Nuclear Environmental Sites at Los Alamos National Laboratory, Los Alamos National Laboratory Report NES-ABD-0101*, Revision 1.0, June.

LANL, 2007b, *Environmental Surveillance at Los Alamos During 2006*, Los Alamos National Laboratory Report LA-14341-ENV, September.

LANL, 2008, *LANL Waste Acceptance Criteria*, Los Alamos National Laboratory Procedure No. P930-1, Rev. 0, Issued June 5.

Levitt, D.G., 2008, Modeling of an Evapotranspiration Cover for the Groundwater Pathway at Los Alamos National Laboratory Technical Area 54, Area G, Los Alamos National Laboratory Report LA-UR-08-5468, August.

Napier, B.A., D.L. Strenge, J.V. Ramsdell, Jr., P.W. Eslinger, and C.J. Fosmire., 2004, *GENII Version 2 Software Design Document*, PNNL-14584, Pacific Northwest National Laboratory.

Newman, B., M. Gard, D. Counce, E. Kluk, L. Martinez, D. Newell, J. Salazar, 2005, *Spatial Variation in Near-Surface Hydrologic Behavior at Los Alamos National Laboratory Technical Area 54, Material Disposal Area G*, Los Alamos National Laboratory Report LA-UR-05-6898, September.

NMEIB, 2002, *Drinking Water*, New Mexico Environmental Improvement Board, 20.7.10 NMAC (12/4/02 as amended through 9/1/2005).

NRC, 1986, *Update of Part 61 Impacts Analysis Methodology, Methodology Report*, U.S. Nuclear Regulatory Commission, NUREG/CR-4370, Vol. 1, January

Nyhan, J.W., G.J. Langhorst, C.E. Martin, J.L. Martinez, and T.G. Schofield, 1993, "Field Studies of Engineered Barriers for Closure of Low Level Radioactive Waste Landfills at Los Alamos, New Mexico, USA," *Proceedings of the International Conf. on Nuclear Waste Management and Environmental Restoration*, (P.E. Ahlstroem, C.C. Chapman, R. Kohout, and J. Marek, eds.), Am. Soc. of Mechanical Engineers, pp. 255–266.

Nyhan, J.W., T.G. Schofield, and R.H. Starmer, 1997, "A Water Balance Study of Four Landfill Cover Designs Varying in Slope for Semiarid Regions," *Journal of Environmental Quality*, Vol. 26, pp. 1385–1392.

RHHB, 1970, *Radiological Health Handbook*, U.S. Dept of Health, Education, and Welfare, January.

Rogers, M.A., 1977, *History and Environmental Setting of LASL Near-Surface Land Disposal Facilities for Radioactive Wastes (Areas A, B, C, D, E, F, G, and T)*, Los Alamos Scientific Laboratory Report LA-6848-MN, Vol. 1, June.

Sheppard, M.I., S.C. Sheppard, and B.D. Amiro, 1991, "Mobility and Plant Uptake of Inorganic ^{14}C and ^{14}C-Labelled PCB in Soils of High and Low Retention," *Health Physics, Vol.* 61, No. 4, pp. 481–492.

Shuman, R., 1999, *An Evaluation of the Potential Impacts of Plant and Animal Intrusion into Disposed Waste at TA-54, MDA G*, Rogers and Associates Engineering Corporation, RAE-9629/3005-1, April.

Shuman, R., 2008a, *GoldSim Model Documentation and Data Selection for Los Alamos National Laboratory Technical Area 54, Area G Performance Assessment and Composite Analysis*, Los Alamos National Laboratory Report , Los Alamos National Laboratory Report LA-UR-08-06094, September.

Shuman, R. 2008b, *Radioactive Waste Inventory for Los Alamos National Laboratory Technical Area 54, Area G*, Los Alamos National Laboratory Report LA-UR-08-06107, September.

Stauffer, P.H., 2005, Personal communication from Phil Stauffer, LANL EES-6, to Konnie Andrews, Shaw Environmental, October 13.

Stauffer, P.H., H.S. Viswanathan, B.A. Robinson, C.W. Gable, G.L. Cole, D.E. Broxton, E.P. Springer, T.G. Schofield, 2005, *Groundwater Pathway Model for the Los Alamos National Laboratory Technical Area 54, Material Disposal Area G*, Los Alamos National Laboratory Report LA-UR-05-7393, September.

Whicker, J.J. and D.D. Breshears, 2005, *Assessing Wind Erosion as a Contaminant Transport Mechanism for Los Alamos National Laboratory Technical Area 54, Material Disposal Area G*, Los Alamos National Laboratory Report LA-UR-05-5371, September.

Wilson, J.C.J., K.J. Crowell, and L.J. Lane, 2005, *Surface Erosion Modeling for the Repository Waste Cover at Los Alamos National Laboratory Technical Area 54, Material Disposal Area G*, Los Alamos National Laboratory Report LA-UR-05-7771, September.

Attachment I
Groundwater Pathway Screening Approach and Results

I.1 Introduction

The majority of the radionuclides included in the Area G inventory will not pose a threat to persons using water contaminated by the release of radionuclides from the disposal facility. To minimize the complexity of the groundwater models and to streamline model computations, the noncritical radionuclides were identified and excluded from the groundwater pathway analysis. The screening approach that was used to exclude radionuclides from the groundwater pathway analysis and the results of this evaluation are discussed below.

I.2 Screening Methodology

The risk posed to persons using water that is contaminated by releases from Area G is directly proportional to the radionuclide concentrations in the regional aquifer. These concentrations, in turn, depend upon the radionuclide inventories in the pits and shafts, the rates at which the contaminants are leached from the waste, the degree to which the leached radionuclides decay prior to discharge to the regional aquifer, and the volume of water within which the radionuclides entering the aquifer are diluted. These dependencies formed the basis of the screening approach that was used to limit the number of contaminants included in the groundwater modeling analysis.

The first screen applied to the Area G inventory examined the potential for unacceptable impacts under conservative release conditions. For this screen, it was assumed that all radionuclides present in the waste entered into the soil moisture and were transported immediately to the regional aquifer. It was assumed that the leachate would be diluted in the regional aquifer and that water drawn from the aquifer would be consumed by a person at the rate of 2 L/d (0.53 gal/d). Radionuclide-specific doses were estimated for the hypothetical receptor and compared to a dose limit of 4 mrem/yr. All radionuclides for which the estimated dose was less than 4 mrem/yr were eliminated from the groundwater pathway modeling; contaminants with doses greater than 4 mrem/yr were carried forward in the screening process.

The maximum leachate concentrations were calculated as the quotient of the radionuclide concentrations in the disposed waste and the volume of moisture in the pit and shaft waste; a moisture content of 0.075 (volume basis) was adopted for the screening based on moisture contents measured in disposal units at Area G (see Section 5 of Shuman, 2008). The inventories used in these calculations were those estimated for the composite analysis and, as such, represent all waste that has been, and is projected to be, disposed of at Area G. The volume of water in which these inventories were dissolved was estimated by multiplying the total waste volume by the volume-based moisture content of the material. Leachate discharged to the regional aquifer will be diluted with clean water prior to the withdrawal of the contaminated water via a domestic well. This dilution volume was estimated as the product of the area of the disposal units in which the waste is disposed of at Area G and the casing length of the domestic well (10 m [33 ft]).

Several radionuclides included in the Area G inventory are parents of radioactive-decay chains. To project drinking water doses for these radionuclides, it was necessary to make assumptions about the extent to which daughter ingrowth occurred for these constituents. Consequently, all short-lived daughters of long-lived parents were assumed to be in secular equilibrium with their parents. Long-lived daughters of short-lived parents were assumed to be present at a fraction of the parents' inventory that was equal to the ratio of the parents' and daughters' half-lives. Long-lived daughters of long-lived parents were assumed to be present at the maximum activity achieved during 10,000 years of ingrowth.

The time required for water exiting the pits and shafts to reach the regional aquifer is on the order of thousands of years. Many of the radionuclides leached from the waste will decay to negligible levels by the time they discharge to the aquifer, rendering them harmless to persons using the water. Given this, the decay characteristics of the radionuclides that were not excluded from the groundwater pathway modeling on the basis of the first screen were evaluated relative to the time required to transport releases from the pits and shafts to the aquifer.

The screening conducted on the basis of travel times to the regional aquifer was conducted in two steps. The first step compared the estimated groundwater travel time, from the base of the disposal units to the aquifer, to the half-lives of the radionuclides. If the ratio of groundwater travel time to a radionuclide's half-life was greater than 10, the contaminant was excluded from further consideration. The second step compared contaminant travel times to radionuclide half-lives; if the ratios of the contaminant travel times and half-lives were equal to or greater than 10, the constituents were excluded from the performance assessment and composite analysis groundwater modeling.

Particle tracking using the FEHM model was used to estimate the groundwater travel times. These times will depend upon the rate at which water infiltrates through the disposal site. For screening purposes, an infiltration rate of 0.1 mm/yr (0.039 in./yr) was assumed; this rate functionally bounds the infiltration rates projected for the final cover configuration that was adopted for the performance assessment and composite analysis. Based on this infiltration rate, a distribution of travel times ranging from approximately 23,000 to 100,000 years was projected; a travel time of 23,000 years was adopted for screening purposes.

The contaminant travel time is given by

$$CT_i = \frac{GT \times Kd_i \times \rho}{p} \qquad 1$$

Where

CT_i = contaminant travel time for radionuclide i (yr)

GT = groundwater travel time (yr)
Kd_i = distribution coefficient for radionuclide i (m^3/kg)
ρ = bulk density of unsaturated zone (kg/m^3)
p = effective porosity of unsaturated zone

The unsaturated zone distribution coefficients that were used to estimate contaminant travel times were selected on the basis of several sources of information about devitrified tuffs and, when necessary, other soils; these data are summarized in Table I-1. The minimum values found in these sources were used to conduct the groundwater pathway screening. A bulk density of 1,400 kg/m^3 (87 lb/ft^3) and an effective porosity of 0.4 were adopted for the contaminant travel time calculations, consistent with the data discussed in Section 5 of Shuman (2008).

I.3 Screening Results

The results of the screening analyses are summarized in Tables I-2 through I-4. Table I-2 summarizes the results of the leachate screen; it provides the total inventory for each parent radionuclide, the corresponding maximum aquifer concentration, and the projected drinking water dose. The final column in the table gives the ratios of the projected doses to the dose objective of 4 mrem/yr; the projected doses for several radionuclides are zero because ingestion dose conversion factors were unavailable. Radionuclides with ratios equal to or greater than 1.0 were carried forward in the screening process; all other radionuclides were excluded from the groundwater pathway modeling. Examination of these results reveals that more than half of the radionuclides listed in the final Area G inventory were excluded on the basis of this screen.

Table I-3 summarizes the results of the screen based on groundwater travel times, listing the parent radionuclides, their half-lives, and the ratios of the groundwater travel time to these half-lives. The corresponding results for the screen based on contaminant travel time are provided in Table I-4. As discussed earlier, all radionuclides for which the calculated ratios were 10 or greater were excluded from the groundwater pathway analyses. Nineteen radionuclides were excluded from further consideration based on the groundwater travel time screen; an additional four radionuclides were eliminated based on contaminant travel times.

Four of the radionuclides eliminated on the basis of the travel time screens bear special mention. Pu-238 and Pu-241 are short-lived relative to the groundwater travel time of 3,500 years and decay to negligible levels by the time they reach the aquifer. However, these isotopes decay to form long-lived daughters (U-234 and Np-237, respectively) that may still pose a risk to persons using contaminated groundwater. Consequently, U-234 and Np-237 were not eliminated on the basis of the travel time screens. A similar situation is seen for Am-241 and Am-243 and the results of the contaminant travel time-based screens. Although these radionuclides were eliminated from further consideration, their long-lived daughters (Np-237 and Pu-239, respectively) were not.

Table I-1
Distribution Coefficients Used for the Groundwater Pathway Screening Process

Element	Distribution Coefficients (mL/g)			
	Bechtel/SAIC, 2004	Longmire et al., 1996	Various Sources	Value Adopted for Screening
Ag	NA	NA	2.7E+00 – 1.0E+03 [a]	2.7E+00
Am	1.0E+03 – 1.0E+04	2.0E+02 -2.7E+04	NA	2.0E+02
C	NA	NA	0.0E+00 [b]	0.0E+00
Cf	NA	NA	8.2E+00 – 3.0E+05 [c]	8.2E+00
K	NA	NA	2.0E+00 – 9.0E+00 [d]; 1.5E+01 [a]	2.0E+00
Np	0.0E+00 – 6.0E+00	1.7E-01 – 3.1E+00	NA	0.0E+00
Pa	1.0E+03 – 1.0E+04	NA	1.0E+02 [b]	1.0E+02
Pu	1.0E+01 - 2.0E+02	1.2E+00 – 1.9E+01	NA	1.2E+00
Ra	1.0E+02 – 1.0E+03	NA	5.7E+01 – 2.1E+04 [a]	5.7E+01
Th	1.0E+03 – 1.0E+04	NA	2.1E+02 – 1.5E+05 [a]	2.1E+02
U	0.0E+00 – 4.0E+00	1.4E+00 - 3.4E+00	NA	0.0E+00

NA = Not applicable

[a] Listed values are based on data provided for sand by Thibault et al. (1990).

[b] Listed values are based on data provided for tuff by Brookins (1984).

[c] The distribution coefficient for californium was assumed to be equal to that of americium; the data listed in the table were taken from Thibault et al.(1990).

[d] Listed values were cited by Baes et al. (1984) for agricultural soils.

Table I-2
Screening Results for the Inventory-Based Screen

Parent Radionuclide	Inventory (Ci)	Aquifer Concentration (Ci/m^3)	Projected Dose (mrem/yr)	Ratio of Dose to Acceptable Limit
Ac-227	9.3E-01	6.2E-07	6.3E+03	1.7E+03
Ag-108m	4.4E+00	2.9E-06	1.6E+01	4.1E+00
Al-26	2.6E-04	1.7E-10	1.8E-03	4.6E-04
Am-241	2.4E+03	1.6E-03	4.2E+06	1.1E+06
Am-243	6.7E-02	4.4E-08	1.2E+02	3.4E+01
Ba-133	3.9E+00	2.6E-06	6.4E+00	1.6E+00
Be-10	4.6E-03	3.0E-09	1.0E-02	2.6E-03
Bi-207	8.6E-02	5.7E-08	2.3E-01	5.7E-02
Bk-247	2.8E-07	1.9E-13	6.4E-04	1.7E-04
C-14	2.1E+01	1.4E-05	2.1E+01	5.3E+00
Ca-41	2.7E-01	1.8E-07	1.7E-01	4.2E-02
Cf-249	3.4E-03	2.3E-09	7.8E+00	2.0E+00
Cf-251	4.3E-03	2.9E-09	1.0E+01	2.5E+00
Cf-252	5.9E+01	3.9E-05	3.1E+04	7.8E+03
Cl-36	1.8E-02	1.2E-08	2.7E-02	6.6E-03
Cm-243	9.2E-05	6.1E-11	1.1E-01	2.8E-02
Cm-244	2.2E-01	1.4E-07	2.1E+02	5.3E+01
Cm-245	2.6E-04	1.7E-10	4.7E-01	1.4E-01
Cm-248	2.5E-06	1.7E-12	2.0E+00	5.1E-01
Co-60	8.0E+03	5.3E-03	1.0E+05	2.6E+04
Cs-135	1.5E-04	9.7E-11	5.0E-04	1.2E-04
Cs-137	2.8E+03	1.9E-03	6.8E+04	1.7E+04
Eu-152	7.7E-01	5.1E-07	2.4E+00	6.1E-01
Eu-154	2.0E-01	1.4E-07	9.4E-01	2.4E-01
Gd-148	1.0E-05	6.6E-12	1.1E-03	2.6E-04
H-3	3.5E+06	2.3E+00	1.1E+05	2.7E+04
Ho-163	9.8E-01	6.5E-07	0.0E+00	0.0E+00
Ho-166m	8.0E-03	5.3E-09	3.1E-02	7.8E-03
I-129	1.7E-04	1.2E-10	2.3E-02	5.8E-03

Table I-2 (Continued)
Screening Results for the Inventory-Based Screen

Parent Radionuclide	Inventory (Ci)	Aquifer Concentration (Ci/m^3)	Projected Dose (mrem/yr)	Ratio of Dose to Acceptable Limit
K-40	1.1E+00	7.4E-07	1.0E+01	2.5E+00
Kr-85	1.5E+03	9.8E-04	0.0E+00	0.0E+00
Lu-176	1.7E-06	1.1E-12	6.0E-06	1.5E-06
Mo-93	1.3E-02	8.7E-09	8.6E-03	3.0E-03
Nb-91	5.3E-02	3.5E-08	0.0E+00	0.0E+00
Nb-92	4.0E-03	2.7E-09	0.0E+00	0.0E+00
Nb-93m	1.3E+01	8.3E-06	3.2E+00	7.9E-01
Nb-94	1.1E-01	7.3E-08	3.8E-01	9.5E-02
Nd-144	5.6E-08	3.7E-14	0.0E+00	0.0E+00
Ni-59	2.6E+00	1.7E-06	2.6E-01	6.5E-02
Ni-63	1.2E+03	8.0E-04	3.4E+02	8.4E+01
Np-237	2.9E-02	1.9E-08	6.2E+01	1.6E+01
Os-194	7.3E-07	4.8E-13	3.9E-06	9.6E-07
Pa-231	2.9E-03	1.9E-09	1.5E+01	8.8E+00
Pb-210	3.5E-01	2.3E-07	9.2E+02	3.1E+02
Pm-145	1.1E-01	7.3E-08	2.5E-02	6.3E-03
Pu-236	5.6E-09	3.7E-15	3.2E-06	8.5E-07
Pu-238	4.9E+03	3.2E-03	7.5E+06	1.9E+06
Pu-239	2.1E+03	1.4E-03	3.6E+06	8.9E+05
Pu-240	4.6E+02	3.1E-04	7.9E+05	2.0E+05
Pu-241	8.2E+03	5.4E-03	2.7E+05	1.9E+05
Pu-242	8.2E-02	5.4E-08	1.3E+02	3.3E+01
Pu-244	2.0E-05	1.3E-11	3.2E-02	1.3E-02
Ra-226	4.0E+00	2.7E-06	2.6E+03	4.2E+03
Ra-228	3.6E-01	2.4E-07	2.5E+02	9.8E+01
Si-32	1.0E-04	6.9E-11	1.1E-04	2.8E-05
Sm-151	5.7E-03	3.8E-09	1.1E-03	2.7E-04
Sn-121m	6.0E-01	4.0E-07	4.5E-01	1.1E-01
Sn-126	1.7E-01	1.1E-07	1.6E+00	4.0E-01
Sr-90	3.3E+03	2.2E-03	2.3E+05	6.1E+04

Table I-2 (Continued)
Screening Results for the Inventory-Based Screen

Parent Radionuclide	Inventory (Ci)	Aquifer Concentration (Ci/m^3)	Projected Dose (mrem/yr)	Ratio of Dose to Acceptable Limit
Tb-157	2.5E-07	1.7E-13	1.5E-08	3.8E-09
Tc-97	2.2E-06	1.5E-12	1.9E-07	4.6E-08
Tc-99	6.0E-01	4.0E-07	4.2E-01	1.1E-01
Th-228	9.1E-03	6.0E-09	1.7E+00	8.9E-01
Th-229	1.8E-03	1.2E-09	3.0E+00	8.6E-01
Th-230	2.6E+01	1.7E-05	6.8E+03	2.6E+04
Th-232	6.6E-01	4.4E-07	8.8E+02	4.0E+02
Ti-44	1.2E-01	8.2E-08	1.4E+00	3.7E-01
U-232	2.2E-01	1.4E-07	1.4E+02	5.5E+01
U-233	1.2E+01	7.9E-06	1.7E+03	3.9E+03
U-234	2.4E+01	1.6E-05	3.3E+03	2.7E+03
U-235	4.0E+00	2.7E-06	5.2E+02	2.5E+03
U-236	1.6E-02	1.0E-08	2.0E+00	5.1E-01
U-238	8.6E+01	5.7E-05	1.1E+04	3.0E+03
Zr-93	2.0E-08	1.3E-14	1.6E-08	5.3E-09

Table I-3
Screening Results for the Groundwater Travel Time-Based Screen

Radionuclide	Half-Life (yr)	Ratio of Groundwater Travel Time to Half-Life
Ac-227	2.2E+01	1.1E+03
Ag-108m	4.2E+02	5.5E+01
Am-241	4.3E+02	5.3E+01
Am-243	7.4E+03	3.1E+00
Ba-133	1.1E+01	2.2E+03
C-14	5.7E+03	4.0E+00
Cf-249	3.5E+02	6.6E+01
Cf-251	9.0E+02	2.6E+01
Cf-252	2.6E+00	8.7E+03
Cm-244	1.8E+01	1.3E+03
Co-60	5.3E+00	4.4E+03
Cs-137	3.0E+01	7.6E+02
H-3	1.2E+01	1.9E+03
K-40	1.3E+09	1.8E-05
Ni-63	1.0E+02	2.3E+02
Np-237	2.1E+06	1.1E-02
Pa-231	3.3E+04	7.0E-01
Pb-210	2.2E+01	1.0E+03
Pu-238	8.8E+01	2.6E+02
Pu-239	2.4E+04	9.5E-01
Pu-240	6.6E+03	3.5E+00
Pu-241	1.4E+01	1.6E+03
Pu-242	3.8E+05	6.1E-02
Ra-226	1.6E+03	1.4E+01
Ra-228	5.8E+00	4.0E+03
Sr-90	2.9E+01	8.0E+02
Th-230	7.5E+04	3.1E-01
Th-232	1.4E+10	1.6E-06
U-232	7.0E+01	3.3E+02
U-233	1.6E+05	1.4E-01
U-234	2.5E+05	9.3E-02
U-235	7.0E+08	3.3E-05
U-238	4.5E+09	5.1E-06

Table I-4
Screening Results for the Contaminant Travel Time-Based Screen

Radionuclide	Half-Life (yr)	Ratio of Contaminant Travel Time to Half-Life
Am-243	7.4E+03	2.1E+03
C-14	5.7E+03	4.0E+00
K-40	1.3E+09	1.4E-04
Np-237	2.1E+06	1.1E-02
Pa-231	3.3E+04	2.4E+02
Pu-239	2.4E+04	5.0E+00
Pu-240	6.6E+03	1.8E+01
Pu-242	3.8E+05	3.2E-01
Th-230	7.5E+04	2.2E+02
Th-232	1.4E+10	1.2E-03
U-233	1.6E+05	1.4E-01
U-234	2.5E+05	9.3E-02
U-235	7.0E+08	3.3E-05
U-238	4.5E+09	5.1E-06

The radionuclides that were eliminated from the groundwater pathway analysis on the basis of the screening process are summarized in Table I-5. A total of 41 radionuclides were excluded from further consideration on the basis of the leachate screen, another 22 radionuclides were excluded on the basis of travel time considerations. On the basis of the screening, 10 radionuclides were identified for inclusion in the groundwater modeling; these constituents are shown in the last column of the table. Long-lived daughters of these radionuclides were included in the model simulations as appropriate.

The objective of the screening process was to eliminate radionuclides that pose little or no threat to members of the public that use water contaminated by releases from Area G. The elimination of these radionuclides provided an opportunity to reduce the complexity of the groundwater models used to project potential impacts and to streamline model computations. Nevertheless, care was taken to conduct the screening process in a conservative manner to minimize the possibility of overlooking radionuclides that pose a potentially significant risk. The conservative nature of the screening process is discussed in the following paragraphs.

The leachate screen used estimates of drinking water doses to limit the number of radionuclides included in the groundwater pathway modeling. For several reasons, the calculated doses are expected to provide conservative estimates of any exposures that may be realized. First, the actual leachate concentrations for most radionuclides in the disposal units will be much less than those estimated for purposes of screening. The calculations outlined above implicitly assume that all radionuclides are leached instantly from the waste and enter into the pore fluids of the waste. In fact, radionuclides will partition between the solid and liquid phases of the waste in proportion to their distribution coefficients. Ignoring this partitioning behavior will overestimate leachate concentrations for all radionuclides with distribution coefficients greater than zero. Second, reductions in concentration due to dispersion and dilution are underestimated by the screening approach. Releases from the waste will be dispersed as they are transported in the unsaturated and saturated zones, and diluted in the deep aquifer prior to reaching the well. Although a moderate degree of dilution was assumed in the screen, dispersive effects were not considered. Finally, the drinking water dose calculations are based on maximum concentrations of the parent and all daughter radionuclides over a period of 10,000 years. In actuality, the maximum concentrations of the parents oftentimes will not coincide with maximum daughter radionuclide levels.

Table I-5
Summary of the Groundwater Pathway Screening Process

Radionuclide	Basis of Elimination [a]			Included in Groundwater Modeling [b]
	Leachate Screen	Groundwater Travel Time Screen	Contaminant Travel Time Screen	
Ac-227	---	X	---	---
Ag-108m	---	X	---	---
Al-26	X	---	---	---
Am-241	---	X	---	---
Am-243	---	---	X	---
Ba-133	---	X	---	---
Be-10	X	---	---	---
Bi-207	X	---	---	---
Bk-247	X	---	---	---
C-14	---	---	---	X
Ca-41	X	---	---	ere---
Cf-249	---	X	---	---
Cf-251	---	X	---	---
Cf-252	---	X	---	---
Cl-36	X	---	---	---
Cm-243	X	---	---	---
Cm-244	---	X	---	---
Cm-245	X	---	---	---
Cm-248	X	---	---	---
Co-60	---	X	---	---
Cs-135	X	---	---	---
Cs-137	---	X	---	---
Eu-152	X	---	---	---
Eu-154	X	---	---	---
Gd-148	X	---	---	---
H-3	---	X	---	---

--- = None

[a] Radionuclides marked with an X were eliminated from the groundwater pathway modeling on the basis of the indicated screen.

[b] Radionuclides marked with an X were included in the groundwater pathway modeling.

[c] One or more long-lived daughters of the radionuclide were not eliminated from the groundwater pathway modeling.

Table I-5 (Continued)
Summary of the Groundwater Pathway Screening Process

Radionuclide	Basis of Elimination [a]			Included in Groundwater Modeling [b]
	Leachate Screen	Groundwater Travel Time Screen	Contaminant Travel Time Screen	
Ho-163	X	---	---	---
Ho-166m	X	---	---	---
I-129	X	---	---	---
K-40	---	---	---	X
Kr-85	X	---	---	---
Lu-176	X	---	---	---
Mo-93	X	---	---	---
Nb-91	X	---	---	---
Nb-92	X	---	---	---
Nb-93m	X	---	---	---
Nb-94	X	---	---	---
Nd-144	X	---	---	---
Ni-59	X	---	---	---
Ni-63	---	X	---	---
Np-237	---	---	---	X
Os-194	X	---	---	---
Pa-231	---	---	X	---
Pb-210	---	X	---	---
Pm-145	X	---	---	---
Pu-236	X	---	---	---
Pu-238	---	X	---	---
Pu-239	---	---	---	X
Pu-240	---	---	X	---
Pu-241	---	X	---	---
Pu-242	---	---	---	X
Pu-244	X	---	---	---

--- = None

[a] Radionuclides marked with an X were eliminated from the groundwater pathway modeling on the basis of the indicated screen.

[b] Radionuclides marked with an X were included in the groundwater pathway modeling.

[c] One or more long-lived daughters of the radionuclide were not eliminated from the groundwater pathway modeling.

Table I-5 (Continued)
Summary of the Groundwater Pathway Screening Process

Radionuclide	Basis of Elimination [a]			Included in Groundwater Modeling [b]
	Leachate Screen	Groundwater Travel Time Screen	Contaminant Travel Time Screen	
Ra-226	---	X	---	---
Ra-228	---	X	---	---
Si-32	X	---	---	---
Sm-151	X	---	---	---
Sn-121m	X	---	---	---
Sn-126	X	---	---	---
Sr-90	---	X	---	---
Tb-157	X	---	---	---
Tc-97	X	---	---	---
Tc-99	X	---	---	---
Th-228	X	---	---	---
Th-229	X	---	---	---
Th-230	---	---	X	---
Th-232	---	---	---	X
Ti-44	X	---	---	---
U-232	---	X	---	---
U-233	---	---	---	X
U-234	---	---	---	X
U-235	---	---	---	X
U-236	X	---	---	---
U-238	---	---	---	X
Zr-93	X	---	---	---

--- = None

[a] Radionuclides marked with an X were eliminated from the groundwater pathway modeling on the basis of the indicated screen.

[b] Radionuclides marked with an X were included in the groundwater pathway modeling.

[c] One or more long-lived daughters of the radionuclide were not eliminated from the groundwater pathway modeling.

The leachate screen examines the potential consequences of groundwater releases on a radionuclide-by-radionuclide basis. This approach may overlook radionuclides that do not result in significant drinking water doses on their own, but that are important in terms of their contribution to the cumulative dose received from water contaminated with multiple radionuclides. In fact, this potential oversight does not appear to be significant in terms of the screening calculations. The cumulative annual dose of all radionuclides screened from the performance assessment and composite analysis on the basis of drinking water doses is approximately 21 mrem. To the extent that doses for the screened radionuclides will not coincide, and given the level of conservatism built into the screening approach (see discussion above), the contribution of the screened radionuclides to the cumulative groundwater dose is expected to be negligible.

The travel-time-based screens applied to the Area G inventory are also expected to conservatively represent the potential threat posed by the waste radionuclides. This is largely because the travel times used in the screens are likely conservative estimates of the actual travel times. The groundwater travel time used in these screens represents a minimum travel time for an infiltration rate that bounds those rates projected for the final cover that was adopted for the performance assessment and composite analysis; the contaminant travel times were estimated using minimum values of distribution coefficients. If more realistic values of groundwater travel time and distribution coefficients were used, much longer travel times would have been projected, possibly resulting in the exclusion of additional radionuclides from the groundwater pathway analyses.

I.4 References

Baes, C.F. III, R.D. Sharp, A.L. Sjoreen, and R.W. Shor, 1984, *A Review and Analysis of Parameters for Assessing Transport of Environmentally Released Radionuclides through Agriculture*, Oak Ridge National Laboratory, ORNL-5786, September.

Bechtel/SAIC, 2004, *Radionuclide Transport Models Under Ambient Conditions*, prepared for U.S. Department of Energy, Office of Civilian Radioactive Waste Management, by Bechtel SAIC Company, DOC.20041101.0002, October.

Brookins, D.G., 1984, *Geochemical Aspects of Radioactive Waste Disposal*, Springer-Verlag, New York.

Longmire, P., C.R. Cotter, I.R. Triay, J.J. Kitten, C. Hall, J. Bentley, D. Hollis, and A.I. Adams, 1996, *Batch Sorption Results for Americium, Neptunium, Plutonium, Technetium, and Uranium Transport through the Bandelier Tuff, Los Alamos, New Mexico*, Los Alamos National Laboratory Report LA-UR-96-4716.

Shuman, R., 2008, *GoldSim Model Documentation and Data Selection for Los Alamos National Laboratory Technical Area 54, Material Disposal Area G Performance Assessment and Composite Analysis*, Los Alamos National Laboratory Report LA-UR-08-06094, September.

Thibault, D.H., M.I. Sheppard, and P.A. Smith, 1990, *A Critical Compilation and Review of Default Soil Solid/Liquid Partition Coefficients, K_d, for use in Environmental Assessments*, Atomic Energy of Canada Limited Report AECL-10125, March.

LA-UR-08-06108

Approved for public release;
distribution is unlimited.

Title:	As Low As Reasonably Achievable (ALARA) Analysis for Los Alamos National Laboratory Technical Area 54, Area G Performance Assessment and Composite Analysis
Author(s):	Rob Shuman
Intended for:	U.S. Department of Energy

Form 836 (7/06)

Table of Contents

List of Figures i
List of Tables i
Acronyms and Abbreviations ii

1.0 Introduction 1
2.0 ALARA Analysis Approach 3
2.1 Background and Assumptions 3
2.2 Final Closure Configurations 4
2.3 Modeling Approach 5
2.4 Input Data 7
2.4.1 Performance Modeling Data 7
2.4.2 Cost and Impact Data 24
3.0 Results 28
4.0 References 30

List of Figures

Figure 1 Population Data Array within 80-km Radius of Area G 9
Figure 2 Sediment Catchments in Habitable Canyon Bottoms Adjacent to Area G 22

List of Tables

Table 1 2002 Population within 80 km of Area G 10
Table 2 Dispersion Factors and Particulate Deposition Rates for the ALARA Analysis 11
Table 3 Size of Catchments in Cañada del Buey and Pajarito Canyon 23
Table 4 Cost Estimates for Closure of MDA G 25
Table 5 Annual Maintenance Costs for MDA J 27
Table 6 Collective Doses Estimated for the Area G ALARA Analysis 28
Table 7 Health Detriment and Closure Strategy Implementation Costs for the Area G ALARA Analysis 28

Acronyms and Abbreviations

ALARA	As low as reasonably achievable
DOE	U.S. Department of Energy
Laboratory	Los Alamos National Laboratory
LANL	Los Alamos National Laboratory
LLW	Low-level radioactive waste
MDA	Material Disposal Area
TA	Technical Area
TDR	Time domain reflectometry

1.0 Introduction

The Los Alamos National Laboratory (LANL or the Laboratory) generates radioactive waste as a result of various activities. Operational waste is generated at the Laboratory from a wide variety of research and development activities including nuclear weapons development, energy production, and medical research. Environmental restoration and decontamination and decommissioning waste is generated as contaminated sites and facilities at LANL undergo cleanup or remediation. The majority of this waste is low-level radioactive waste (LLW) and is disposed of at the Technical Area (TA) 54, Area G disposal facility.

U.S. Department of Energy (DOE) Order 435.1 (DOE, 2001) requires that radioactive waste be managed in a manner that protects worker and public health and safety, and the environment. To comply with this order, DOE field sites must prepare and maintain site-specific radiological performance assessments for LLW disposal facilities that accept waste after September 26, 1988. Furthermore, sites are required to conduct composite analyses for disposal facilities that receive waste after September 26, 1988. The composite analysis accounts for the cumulative impacts of all waste that has been (or will be) disposed of at the facilities and other sources of radioactive material that may interact with the disposal facilities.

A radiological dose assessment is an integral part of the performance assessment and composite analysis. It estimates the potential exposures that may be received by persons coming into contact with the radioactive waste placed in the disposal facility. The projected doses are compared to DOE performance objectives to assess facility compliance with Order 435.1. One of these performance objectives requires that projected releases of radionuclides to the environment be maintained as low as reasonably achievable (ALARA).

A detailed discussion of the ALARA process may be found in draft DOE guidance (DOE, 1997). That document defines the process as:

> . . . a logical procedure for evaluating alternative operations, processes, and other measures, designed to reduce exposures to radiation and emissions of radioactive material into the environment, taking into account societal, environmental, technological, economic, practical, and public policy considerations to make a judgment concerning the optimum level of public health protection.

The process is a decision-making tool that is used to maximize the benefits of efforts taken to protect members of the public from DOE activities that may result in the release of radiation. The optimum radiation protection program is one in which the cost of radiological protection plus the cost of the detriment are minimal.

A key component of the ALARA process is the cost-benefit analysis of the activity under evaluation. The cost-benefit analysis is used to estimate the effectiveness of different radiation protection systems. This is accomplished by estimating the health and nonhealth detriments associated with each system, assigning costs to these detriments, and adding these costs to the costs associated with implementing each system. As indicated above, the radiation protection system that has the lowest total associated cost is generally considered to be optimal.

With respect to the Area G performance assessment and composite analysis, the ALARA process provides the means for identifying effective closure options or strategies for the disposal facility. In this application, the radiation protection systems refer to different final closure configurations for the facility. The potential detriment to members of the public is estimated for each candidate closure option and assigned a cost. This cost is added to the cost of implementing the closure option to arrive at a total cost of the closure strategy. By definition, the closure option with the smallest total cost is the optimum system.

This report describes the ALARA process that was undertaken in conjunction with the Area G performance assessment and composite analysis. Section 2 describes the approach used to conduct the ALARA analysis, including a discussion of the closure options that were considered and the models and data that were used to perform the assessment. The results of the analysis are presented in Section 3.

2.0 ALARA Analysis Approach

The general approach adopted for the Area G ALARA analysis is presented in this section. Section 2.1 discusses some of the general characteristics of ALARA analyses and outlines the assumptions upon which the evaluation is based. Section 2.2 describes the different closure options that are included in the ALARA process. Sections 2.3 and 2.4 discuss the models and input data that were used to conduct the analysis, respectively.

2.1 Background and Assumptions

The Area G performance assessment and composite analysis estimate doses received by members of the public who are exposed to radionuclides released from the disposal facility. Exposures are estimated using a series of exposure scenarios, each of which addresses different radionuclide release and transport processes. In general, the scenarios project doses for persons expected to receive the greatest exposures for each release and transport pathway. The projected doses are compared to performance objectives to determine if the disposal facility is in compliance with DOE orders.

The ALARA analysis for Area G differs from the performance assessment and composite analysis insofar as it is based on the total health detriment to the exposed population. The collective dose that describes this detriment is the product of the individual dose rate, the number of persons that are exposed, and the period over which the exposure occurs. Although simple in theory, the collective dose needs to account for the exposure conditions and population size over the area of exposure, as well as how these factors change over time. Unlike the individual doses projected for the performance assessment and composite analysis, there are no promulgated limits for the collective dose. However, it is necessary to comply with individual dose limits at all times.

The period over which the collective dose is integrated will have a profound effect on the results of ALARA analyses. Although the exposure period for short-term releases may be readily defined, this period is much harder to define for a situation in which long-lived radionuclides are released into the environment over hundreds to thousands of years. Under these conditions, exposures may occur over several generations, during which population densities and distributions may change substantially. In its draft guidance on the ALARA process (DOE, 1997), the DOE states that quantitative comparisons should typically consider periods of a few hundred years or less, and that periods of more than 1,000 years should not be used. This guidance document also discusses how the probability of occurrence of exposure scenarios can be used in conjunction with the integration of doses over time. For example, it may be reasonable to weight doses projected for the near-term more heavily than doses that are projected to occur far into the future.

Another complicating factor associated with activities that pose long-term risks to members of the public is the discounting of costs for reducing health detriments that are projected to occur hundreds or thousands of years in the future. Draft DOE guidance (DOE, 1997) notes that it is rational from an economics standpoint to discount cost estimates for projected health effects that are centuries in the future. However, using any finite discounting will cause the present worth to be a very small fraction of the cost of the future impact. Because of this and the level of uncertainty associated with long-range dose projections, the DOE concludes that quantitative ALARA analyses should be limited to a few hundred years.

The nature of the risks posed by the waste disposed of at Area G requires that hard decisions be made regarding the period of integration and the issue of cost discounting. Modeling of the facility indicates that some of the risks posed by the site increase throughout the 1,000-year compliance period due to the release of long-lived radionuclides. Thus, limiting the ALARA analysis to the first few hundred years, as suggested by the draft DOE guidance, will fail to capture the greatest potential risks posed by the disposal facility. On the other hand, it is not prudent to assume that doses hundreds of years into the future are as certain as those projected for times shortly after Area G is closed.

The preceding discussion suggests that any approach used to deal with integration periods and cost discounting is open to criticism. A moderate period of integration (300 years) and no cost discounting were selected for use in conducting the ALARA analysis for the Area G performance assessment and composite analysis. Although this approach does not address the most severe risks posed by the site, it also does not weight the importance of future exposures through considerations of scenario probability and cost discounting. Overall, this approach is generally consistent with DOE guidance.

The discussion of the detriments associated with the different closure options for Area G has, to this point, focused on health detriments. In fact, nonhealth detriments such as increased risks in industrial safety, comfort considerations, and political factors may also be associated with the different options. In general, such detriments are difficult to express in monetary terms and do not have a linear relationship to the collective dose. For these reasons, the Area G ALARA analysis does not address the nonhealth detriments associated with the various closure options.

2.2 Final Closure Configurations

The ALARA analysis evaluates the effectiveness of three closure strategies. The first of these, referred to as the Base-Case Scenario, considers the facility configuration used as the basis for the performance assessment and composite analysis modeling. This scenario assumes that the final cover configuration described in Day et al. (2005) is applied to the site at the time of final closure. The DOE is assumed to maintain active institutional control over the site for a period of 100 years following facility closure, during which time actions are taken to prevent the

establishment of deep-rooted trees, prevent serious erosion, and exclude persons from establishing residences over the site. In the passive institutional control period that follows, the DOE is assumed to take only those actions necessary to prevent human habitation of the site.

The first closure alternative to the Base-Case Scenario is referred to as the Extended Control Option. It is similar to the base-case condition insofar as it assumes that the same cover configuration exists at the time of closure. The option differs, however, in the level of maintenance that is assumed to occur during the 1,000-year compliance period. In essence, active institutional control over the site is assumed to exist throughout this period. In addition to the actions described for the base-case condition, it is assumed that the establishment of shrubs is prevented through annual mowing of the site. Furthermore, inhabitance of the site by burrowing animals is assumed to be discouraged by conducting periodic trapping campaigns, poisoning, and destroying surface manifestations of burrows. This option is evaluated because biotic intrusion into the waste represents a potentially important mechanism of radionuclide release at Area G.

The second alternative closure strategy is referred to as the Biobarrier Option. As its name implies, this option assumes the incorporation of a biobarrier into the final cover placed over the pits and shafts and evaluates its effectiveness in minimizing biotic intrusion into the waste relative to reliance on total cover depth. The level of DOE control over the site is assumed to be the same as that described for the Base-Case Scenario.

2.3 Modeling Approach

The Area G performance assessment and composite analysis estimate the potential doses received by persons living in the vicinity of the disposal facility following the end of operations. Radiation doses are projected for the Atmospheric, All Pathways–Cañada del Buey, All Pathways–Pajarito Canyon, Groundwater Resource Protection, and All Pathways–Groundwater Scenarios. Complete descriptions of these scenarios may be found in Shuman (2008a). In addition, for the purpose of establishing waste acceptance criteria for the disposal facility, doses are projected for persons who inadvertently intrude into the waste.

The Area G ALARA analysis is used to estimate total costs associated with each closure strategy on the basis of the Atmospheric, All Pathways–Cañada del Buey, and All Pathways–Pajarito Canyon Scenarios. The alternative closure options outlined above are not expected to influence the rate at which radionuclides are leached from the waste or transported to the groundwater pathway receptor's well downgradient of Area G. Furthermore, the groundwater modeling conducted in support of the performance assessment and composite analysis indicated that it would require in excess of 1,000 years for radionuclides to be leached from the waste and discharge to the regional aquifer. Therefore, the ALARA analysis does not address the collective exposure of groundwater users. The inadvertent intruder scenarios are conducted primarily to

establish waste acceptance criteria, as opposed to projecting health detriment. Consequently, these scenarios were also excluded from the ALARA analysis.

The model used to conduct the Area G ALARA analysis is substantially the same as that used to estimate individual doses for the performance assessment and composite analysis. The Area G Site Model was used to estimate the potential risks posed by the disposal facility to off-site receptors; a detailed description of the model may be found in Shuman (2008b). To project collective doses and calculate total costs associated with the different closure options, the ALARA analysis uses a modified version of the site model that allows estimation of radionuclide concentrations at locations within 80 km of Area G.

The ALARA analysis does not address Atmospheric Scenario exposures projected to occur due to the release of tritiated water vapor, C-14 gas, and Kr-85. The release and transport of these contaminants are not expected to be influenced by the different closure options included in the analysis. Therefore, the collective impact of these radionuclides will not be a discriminating factor among the closure alternatives.

The ALARA analysis for the Atmospheric Scenario estimates the collective dose for all persons living within 80 km (50 mi) of Area G. This is accomplished by assigning the population surrounding the disposal facility to a discrete number of locations. The GoldSim™ model estimates radionuclide concentrations in air and surface soils at each location. These concentrations are weighted by the location-specific populations and used to estimate the collective dose.

A portion of the particulates transported downwind will be deposited on the surface soil at each location. Rates of deposition at each receptor location are explicitly modeled using GoldSim; radionuclide concentrations in the soils at the locations are calculated as the quotient of the contaminant masses projected by GoldSim and the volume of affected soil. These concentrations are multiplied by the population size at each location to estimate population-weighted radionuclide concentrations. Radionuclide concentrations in the off-site soils increase as particulates are deposited over successive years; soil inventories are depleted by radioactive decay and leaching from water that infiltrates through soils at the exposure locations.

The ALARA analysis performed for the All Pathways–Cañada del Buey and All Pathways–Pajarito Canyon Scenarios estimates the collective dose for all persons living adjacent to Area G in these canyons. Radionuclide concentrations in canyon soils and air are estimated in the same manner as that used in the Area G Site Model (Shuman, 2008a). The only difference between the ALARA analysis and site models is the fact that the individual doses estimated by the former are multiplied by the canyon population and integrated over time.

The rates at which radionuclides are released and transported from Area G will be influenced by the closure strategy implemented at the facility. Modifications are made to the base-case condition model to estimate these impacts for the ALARA analysis. The assumptions upon which the modeling of the closure alternatives are based are discussed below.

The Extended Control Option assumes the closed disposal site is mowed annually throughout the 1,000-year compliance period. Mowing prevents the establishment of shrubs and trees, effectively maintaining the site in a grassland-dominated community. For comparison, the establishment of trees is assumed to be prevented during the 100-year active institutional control period under the base-case condition, after which the site is assumed to transition from a grassland-dominated landscape to piñon-juniper woodland. Efforts are also made under the Extended Control Option to prevent burrowing animals from inhabiting the closed site. From a modeling standpoint, the impact of annual mowing is simulated using a number of assumptions regarding plant growth. Grasses and forbs are assumed to be present at biomass densities characteristic of early successional stages throughout the 1,000-year compliance period, while shrubs and trees are assumed to be absent. Reduced populations of the burrowing animals are assumed to be present, as eradication efforts may not be completely effective. Animals that inhabit the site are assumed to be characteristic of a grassland community, consistent with the controls on plant colonization.

The Biobarrier Option assumes a biobarrier is incorporated into the final cover design, thereby limiting the impacts of plant and animal intrusion on facility performance. The level of DOE control over the site is assumed to be the same as that described for base-case conditions. The effects of excluding roots and burrows from the waste are approximated by reducing plant biomass densities and burrow densities in proportion to the assumed effectiveness of the biobarrier, while maintaining the same rooting and burrowing distributions with depth. Although this approach is only an approximation of the actual effects of a biobarrier, it is expected to provide a reasonable level of accuracy for the ALARA analysis. Successional changes in the plant and animal communities at the site are assumed to proceed unimpeded.

2.4 Input Data

A variety of input data are required to conduct the Area G ALARA analysis. These include parameters needed to model the performance of the disposal facility and information used to associate costs to estimated impacts. These data are discussed below.

2.4.1 Performance Modeling Data

The majority of the input data are identical to those used to conduct the performance assessment and composite analysis modeling; these data are provided in Shuman (2008b). This section discusses the input data requirements that are specific to the ALARA analysis model.

The data required for the Atmospheric Scenario ALARA analysis include location-specific populations, dispersion factors, and deposition fluxes. These data were taken from work conducted by Jacobson (2005) in support of the performance assessment and composite analysis. Jacobson modeled particulate concentrations in air and soil deposition rates up to 80 km (50 mi) from Area G, and used those results in conjunction with regional population data to estimate the impacts of releases from Area G on surrounding populations. The population distribution used by Jacobson is shown in Figure 1; population data are summarized in Table 1.

The atmospheric transport modeling conducted in support of the performance assessment and composite analysis divides the disposal facility into three atmospheric source areas; releases from each portion of the site were modeled separately. The transport modeling conducted for the ALARA analysis adopted this same approach. Dispersion factors and particulate deposition rates were calculated for each population location shown in Table 1; separate factors were estimated for the three atmospheric source areas. These data are summarized in Table 2.

The ALARA analysis for the Atmospheric Scenario considers exposures to members of the public over a period of 300 years following facility closure. Given this long period of time, it is reasonable to expect that the size and distribution of the regional population will change during the period of analysis, thereby affecting the collective dose calculations. Having said this, it is almost impossible to predict how populations will change over time. Consequently, it is assumed for the ALARA analysis that the location-specific population grows at an average rate of 1 percent per year; this value is in excess of the long-term growth rate of about 0.5 percent suggested by University of New Mexico Bureau of Business and Economic Research (BBER, 2005).

The input data used for the All Pathways–Cañada del Buey and All Pathways–Pajarito Canyon Scenarios are identical to those used for this scenario in the Area G Site Model, except for the population assigned to the canyons adjacent to Area G. Estimating potential canyon populations is difficult at best. No one currently resides in Cañada del Buey, part of which lies outside of Laboratory lands; DOE control over LANL prevents people from taking up residence within Pajarito Canyon.

In the absence of information required to define current or future populations within the canyons, conservative estimates were developed on the basis of the habitable area within each canyon. The habitable area is defined here as portions of the canyon floor with slopes of 10 percent or less that do not extend into the small drainages that occur along the edges of Mesita del Buey. These regions are depicted in Figure 2; the area within each canyon is divided into a number of catchments which were used to estimate exposure concentrations for the performance assessment and composite analysis. The areas associated with these catchments are summarized in Table 3.

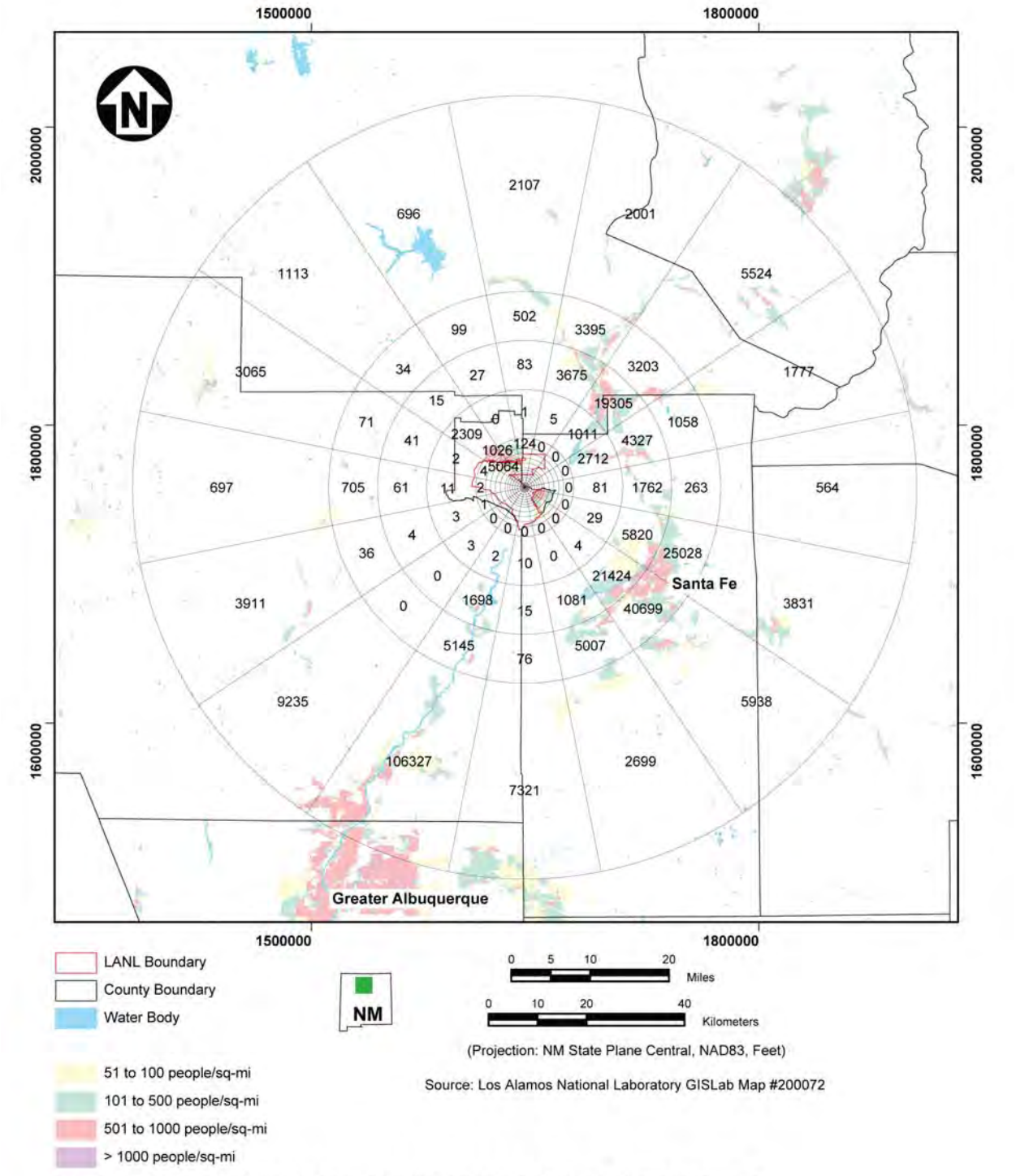

Entire Model Rings at .2, .4, .6, .8, 1, 1.5, 2, 2.5, 3, 3.5, 4, 5, 6, 7, 8, 10, 20, 30, 40, and 80 kilometers.

Note: Populations for grid sectors within first 8 km of Area G not shown because of space; this includes populations for White Rock and some portions of Los Alamos.

Figure 1
Population Data Array within 80-km Radius of Area G

Table 1
2002 Population within 80 km of Area G

Direction	Population by Distance (km) and Direction from Area G												
	0–2.5 [a]	2.5–3.0	3.0–3.5	3.5–4.0	4.0–5.0	5.0–6.0	6.0–7.0	7.0–8.0	8.0–10	10–20	20–30	30–40	40–80
N	0E+00	0E+00	0E+00	0E+00	1.0E+01	7.3E+01	7.2E+01	1.5E+02	1.2E+02	1.0E+00	8.3E+01	5.0E+02	2.1E+03
NNW	0E+00	0E+00	0E+00	0E+00	4.6E+01	1.4E+02	7.0E+03	8.9E+02	1.0E+03	0E+00	2.7E+01	9.9E+01	7.0E+02
NW	0E+00	0E+00	0E+00	0E+00	0E+00	0E+00	2.3E+02	1.8E+03	5.0E+03	2.3E+03	1.5E+01	3.4E+01	1.1E+03
WNW	0E+00	0E+00	0E+00	0E+00	0E+00	0E+00	0E+00	0E+00	0E+00	3.0E+00	4.1E+01	7.1E+01	3.1E+03
W	0E+00	0E+00	0E+00	0E+00	0E+00	0E+00	0E+00	1E+00	2E+01	1.0E+01	6.1E+01	7.1E+03	7.0E+02
WSW	0E+00	0E+00	0E+00	0E+00	0E+00	0E+00	0E+00	1E+00	1E+01	3E+00	4E+00	3.6E+01	3.9E+03
SW	0E+00	0E+00	0E+00	0E+00	0E+00	0E+00	0E+00	0E+00	0E+00	3E+00	0E+00	0E+00	9.2E+03
SSW	0E+00	0E+00	0E+00	0E+00	0E+00	1.3E+01	9E+00	1.0E+00	0E+00	2E+00	1.7E+03	5.2E+03	1.1E+05
S	0E+00	0E+00	0E+00	0E+00	0E+00	0E+00	0E+00	0E+00	0E+00	1.0E+01	1.5E+01	7.6E+01	7.3E+03
SSE	3E+00	1.6E+01	2.1E+01	2.6E+01	5.6E+01	4.3E+01	2.7E+01	0E+00	0E+00	0E+00	1.1E+03	5.0E+03	2.7E+03
SE	1.1E+02	1.6E+02	1.3E+02	1.4E+02	2.0E+02	8.1E+01	9E+00	0E+00	0E+00	4E+00	2.1E+04	4.1E+04	5.9E+03
ESE	2.6E+02	4.4E+02	6.9E+02	1.3E+03	1.7+03	1.2E+03	3E+00	0E+00	0E+00	3E+00	5.8E+03	2.5E+04	3.8E+03
E	0E+00	5E+00	1.8E+02	2.6E+03	6.0E+02	5.2E+01	6E+00	0E+00	0E+00	8.1E+01	1.8E+03	2.6E+02	5.6E+02
ENE	0E+00	0E+00	0E+00	0E+00	0E+00	0E+00	0E+00	0E+00	0E+00	2.7E+03	4.3E+03	1.1E+03	1.8E+03
NE	0E+00	0E+00	0E+00	0E+00	0E+00	0E+00	0E+00	1E+00	0E+00	1.0E+03	1.9E+04	3.2E+03	5.5E+03
NNE	0E+00	0E+00	0E+00	0E+00	0E+00	0E+00	0E+00	0E+00	0E+00	5E+00	3.7E+03	3.4E+03	2.0E+03

[a] *The 2000 census showed no persons living at a distance of 0 to 2.0 km from Area G.*

Table 2
Dispersion Factors and Particulate Deposition Rates for the ALARA Analysis

Direction	Radial Distance from Area G (km)	Atmospheric Source Area 1		Atmospheric Source Area 2		Atmospheric Source Area 3	
		Dispersion Factor (s/m^3)	Particulate Deposition Rate ($g/m^2/s$)	Dispersion Factor (s/m^3)	Particulate Deposition Rate ($g/m^2/s$)	Dispersion Factor (s/m^3)	Particulate Deposition Rate ($g/m^2/s$)
N	0.0 to 2.5	1.1E-07	1.3E-04	1.3E-07	5.1E-04	7.9E-08	2.0E-04
	2.5 to 3.0	6.6E-08	8.0E-05	7.8E-08	3.2E-04	4.9E-08	1.3E-04
	3.0 to 3.5	4.1E-08	5.2E-05	4.9E-08	2.1E-04	3.1E-08	8.3E-05
	3.5 to 4.0	2.5E-08	3.4E-05	2.4E-08	1.3E-04	2.0E-08	5.5E-05
	4.0 to 5.0	1.2E-08	1.8E-05	1.4E-08	7.2E-05	1.4E-08	3.2E-05
	5.0 to 6.0	5.4E-09	8.0E-06	5.5E-09	3.0E-05	6.4E-09	1.5E-05
	6.0 to 7.0	1.8E-09	3.1E-06	1.9E-09	1.1E-05	2.1E-09	5.5E-06
	7.0 to 8.0	9.3E-10	1.2E-06	9.6E-10	4.3E-06	9.3E-10	2.1E-06
	8.0 to 10	5.9E-10	3.8E-07	1.0E-09	1.9E-06	6.3E-10	6.4E-07
	10 to 20	2.1E-10	1.1E-07	2.0E-10	3.9E-07	2.1E-10	1.9E-07
	20 to 30	1.5E-10	8.5E-08	1.6E-10	3.1E-07	1.5E-10	1.6E-07
	30 to 40	2.1E-10	1.5E-07	1.7E-10	3.6E-07	1.6E-10	1.9E-07
	40 to 80	2.0E-11	3.0E-08	1.8E-11	1.0E-07	1.8E-11	4.6E-08
NNW	0.0 to 2.5	2.1E-07	2.3E-04	2.1E-07	6.4E-04	2.4E-07	3.8E-04
	2.5 to 3.0	1.5E-07	1.5E-04	1.3E-07	4.3E-04	1.5E-07	2.5E-04
	3.0 to 3.5	9.0E-08	1.0E-04	8.2E-08	2.9E-04	1.0E-07	1.7E-04
	3.5 to 4.0	5.1E-08	6.7E-05	4.9E-08	2.0E-04	6.4E-08	1.2E-04
	4.0 to 5.0	3.4E-08	4.0E-05	3.2E-08	1.2E-04	3.2E-08	6.4E-05
	5.0 to 6.0	1.3E-08	1.7E-05	1.0E-08	4.7E-05	1.5E-08	2.9E-05

Table 2 (Continued)
Dispersion Factors and Particulate Deposition Rates for the ALARA Analysis

Direction	Radial Distance from Area G (km)	Atmospheric Source Area 1		Atmospheric Source Area 2		Atmospheric Source Area 3	
		Dispersion Factor (s/m^3)	Particulate Deposition Rate ($g/m^2/s$)	Dispersion Factor (s/m^3)	Particulate Deposition Rate ($g/m^2/s$)	Dispersion Factor (s/m^3)	Particulate Deposition Rate ($g/m^2/s$)
NNW (Cont.)	6.0 to 7.0	6.4E-09	6.9E-06	5.3E-09	1.9E-05	4.9E-09	1.1E-05
	7.0 to 8.0	3.5E-09	2.6E-06	3.4E-09	7.8E-06	3.2E-09	4.4E-06
	8.0 to 10	2.3E-09	9.5E-07	2.0E-09	2.8E-06	2.4E-09	1.7E-06
	10 to 20	7.9E-10	3.6E-07	7.2E-10	1.1E-06	7.0E-10	4.9E-07
	20 to 30	5.8E-10	2.9E-07	5.5E-10	9.2E-07	3.8E-10	2.7E-07
	30 to 40	1.1E-10	6.7E-08	1.2E-10	3.1E-07	2.8E-10	3.1E-07
	40 to 80	3.0E-11	2.5E-08	3.1E-11	8.9E-08	3.2E-11	4.3E-08
NW	0.0 to 2.5	2.8E-07	2.1E-04	2.1E-07	5.2E-04	3.6E-07	3.8E-04
	2.5 to 3.0	1.6E-07	1.3E-04	1.3E-07	3.5E-04	2.2E-07	2.5E-04
	3.0 to 3.5	1.5E-07	1.0E-04	1.2E-07	2.6E-04	1.5E-07	1.7E-04
	3.5 to 4.0	9.6E-08	6.7E-05	7.7E-08	1.8E-04	9.2E-08	1.1E-04
	4.0 to 5.0	4.4E-08	3.5E-05	3.7E-08	9.5E-05	3.9E-08	5.7E-05
	5.0 to 6.0	1.8E-08	1.5E-05	2.1E-08	4.4E-05	2.4E-08	2.8E-05
	6.0 to 7.0	1.2E-08	7.0E-06	1.0E-08	1.9E-05	1.2E-08	1.2E-05
	7.0 to 8.0	7.6E-09	3.3E-06	6.3E-09	8.5E-06	7.1E-09	5.6E-06
	8.0 to 10	5.7E-09	1.7E-06	4.4E-09	4.6E-06	4.5E-09	2.3E-06
	10 to 20	2.3E-09	7.2E-07	2.5E-09	2.8E-06	1.8E-09	9.6E-07
	20 to 30	4.9E-10	1.8E-07	4.9E-10	6.6E-07	5.8E-10	3.9E-07
	30 to 40	4.4E-11	3.2E-08	4.4E-11	1.1E-07	4.8E-11	5.5E-08

Table 2 (Continued)
Dispersion Factors and Particulate Deposition Rates for the ALARA Analysis

Direction	Radial Distance from Area G (km)	Atmospheric Source Area 1		Atmospheric Source Area 2		Atmospheric Source Area 3	
		Dispersion Factor (s/m^3)	Particulate Deposition Rate ($g/m^2/s$)	Dispersion Factor (s/m^3)	Particulate Deposition Rate ($g/m^2/s$)	Dispersion Factor (s/m^3)	Particulate Deposition Rate ($g/m^2/s$)
NW (Cont.)	40 to 80	5.9E-12	7.0E-09	5.5E-12	2.3E-08	6.0E-12	1.2E-08
WNW	0.0 to 2.5	3.2E-07	1.5E-04	2.2E-07	3.9E-04	3.1E-07	2.6E-04
	2.5 to 3.0	2.2E-07	9.9E-05	1.5E-07	2.7E-04	1.9E-07	1.7E-04
	3.0 to 3.5	1.4E-07	6.5E-05	1.0E-07	1.8E-04	1.3E-07	1.1E-04
	3.5 to 4.0	7.9E-08	4.1E-05	6.3E-08	1.2E-04	1.0E-07	8.0E-05
	4.0 to 5.0	3.3E-08	2.0E-05	2.8E-08	5.7E-05	5.4E-08	4.3E-05
	5.0 to 6.0	2.3E-08	1.0E-05	1.4E-08	2.5E-05	2.3E-08	1.8E-05
	6.0 to 7.0	8.7E-09	4.1E-06	7.0E-09	1.1E-05	6.0E-09	6.1E-06
	7.0 to 8.0	1.1E-08	3.7E-06	1.0E-08	1.2E-05	4.9E-09	3.4E-06
	8.0 to 10	2.7E-09	7.8E-07	5.8E-09	5.9E-06	7.1E-09	3.3E-06
	10 to 20	1.8E-09	4.9E-07	1.8E-09	1.8E-06	1.9E-09	8.7E-07
	20 to 30	1.9E-10	7.8E-08	1.7E-10	2.5E-07	2.0E-10	1.4E-07
	30 to 40	2.0E-11	1.6E-08	1.9E-11	5.5E-08	2.5E-11	3.0E-08
	40 to 80	2.6E-12	3.0E-09	2.3E-12	9.7E-09	2.4E-12	4.8E-09
W	0.0 to 2.5	3.0E-07	1.2E-04	2.2E-07	3.3E-04	2.2E-07	1.8E-04
	2.5 to 3.0	1.6E-07	7.2E-05	1.3E-07	2.1E-04	1.7E-07	1.3E-04
	3.0 to 3.5	9.0E-08	4.6E-05	7.2E-08	1.3E-04	1.3E-07	9.0E-05
	3.5 to 4.0	8.3E-08	3.5E-05	5.3E-08	9.0E-05	8.0E-08	5.9E-05
	4.0 to 5.0	4.2E-08	1.8E-05	4.1E-08	5.8E-05	3.3E-08	2.8E-05

Table 2 (Continued)
Dispersion Factors and Particulate Deposition Rates for the ALARA Analysis

Direction	Radial Distance from Area G (km)	Atmospheric Source Area 1		Atmospheric Source Area 2		Atmospheric Source Area 3	
		Dispersion Factor (s/m^3)	Particulate Deposition Rate ($g/m^2/s$)	Dispersion Factor (s/m^3)	Particulate Deposition Rate ($g/m^2/s$)	Dispersion Factor (s/m^3)	Particulate Deposition Rate ($g/m^2/s$)
W (Cont.)	5.0 to 6.0	3.0E-08	1.1E-05	2.4E-08	3.0E-05	2.6E-08	1.7E-05
	6.0 to 7.0	1.9E-08	6.0E-06	1.6E-08	1.8E-05	1.8E-08	9.6E-06
	7.0 to 8.0	1.4E-08	4.2E-06	1.2E-08	1.2E-05	1.3E-08	6.1E-06
	8.0 to 10	1.0E-08	3.2E-06	9.1E-09	1.1E-05	9.0E-09	4.2E-06
	10 to 20	6.8E-10	2.0E-07	7.3E-10	7.9E-07	8.2E-10	4.0E-07
	20 to 30	1.2E-10	5.1E-08	1.1E-10	1.7E-07	1.6E-10	1.0E-07
	30 to 40	1.7E-11	1.3E-08	1.7E-11	4.7E-08	1.9E-11	2.4E-08
	40 to 80	3.1E-12	2.8E-09	2.9E-12	9.3E-09	2.9E-12	4.5E-09
WSW	0.0 to 2.5	2.8E-07	1.1E-04	2.3E-07	3.5E-04	2.4E-07	1.8E-04
	2.5 to 3.0	1.8E-07	7.1E-05	1.5E-07	2.2E-04	1.8E-07	1.3E-04
	3.0 to 3.5	1.3E-07	4.9E-05	1.0E-07	1.5E-04	1.3E-07	8.8E-05
	3.5 to 4.0	9.9E-08	3.6E-05	7.0E-08	1.0E-04	8.3E-08	5.9E-05
	4.0 to 5.0	6.9E-08	2.3E-05	4.8E-08	6.4E-05	5.1E-08	3.4E-05
	5.0 to 6.0	3.7E-08	1.1E-05	3.0E-08	3.4E-05	3.4E-08	1.9E-05
	6.0 to 7.0	8.6E-09	3.1E-06	1.5E-08	1.5E-05	2.2E-08	1.0E-05
	7.0 to 8.0	8.0E-09	2.1E-06	6.2E-09	6.2E-06	1.0E-08	4.5E-06
	8.0 to 10	6.1E-09	1.3E-06	7.6E-09	6.9E-06	5.5E-09	2.2E-06
	10 to 20	3.1E-09	9.9E-07	2.2E-09	2.3E-06	2.7E-09	1.4E-06
	20 to 30	1.2E-10	5.4E-08	1.3E-10	2.0E-07	1.3E-10	1.0E-07

Table 2 (Continued)
Dispersion Factors and Particulate Deposition Rates for the ALARA Analysis

Direction	Radial Distance from Area G (km)	Atmospheric Source Area 1		Atmospheric Source Area 2		Atmospheric Source Area 3	
		Dispersion Factor (s/m^3)	Particulate Deposition Rate ($g/m^2/s$)	Dispersion Factor (s/m^3)	Particulate Deposition Rate ($g/m^2/s$)	Dispersion Factor (s/m^3)	Particulate Deposition Rate ($g/m^2/s$)
WSW (Cont.)	30 to 40	3.0E-11	1.9E-08	3.1E-11	6.7E-08	3.4E-11	3.3E-08
	40 to 80	9.4E-12	5.6E-09	8.9E-12	1.9E-08	8.4E-12	9.2E-09
SW	0.0 to 2.5	2.9E-07	9.0E-05	2.5E-07	3.1E-04	2.9E-07	1.6E-04
	2.5 to 3.0	1.7E-07	5.4E-05	1.5E-07	2.0E-04	2.2E-07	1.2E-04
	3.0 to 3.5	1.2E-07	3.9E-05	8.9E-08	1.2E-04	1.4E-07	7.7E-05
	3.5 to 4.0	1.1E-07	3.1E-05	7.9E-08	9.6E-05	8.4E-08	4.8E-05
	4.0 to 5.0	7.4E-08	2.0E-05	6.4E-08	7.0E-05	3.3E-08	2.3E-05
	5.0 to 6.0	4.3E-08	1.2E-05	3.7E-08	3.7E-05	3.3E-08	1.6E-05
	6.0 to 7.0	2.4E-08	5.9E-06	2.3E-08	2.0E-05	2.5E-08	1.1E-05
	7.0 to 8.0	7.0E-09	1.7E-06	7.6E-09	7.0E-06	1.5E-08	6.0E-06
	8.0 to 10	1.9E-09	5.1E-07	1.5E-09	1.5E-06	3.2E-09	1.3E-06
	10 to 20	4.1E-09	1.0E-06	3.7E-09	3.3E-06	3.6E-09	1.5E-06
	20 to 30	6.6E-10	1.7E-07	6.4E-10	6.2E-07	7.5E-10	3.3E-07
	30 to 40	1.2E-10	3.8E-08	1.2E-10	1.4E-07	1.3E-10	6.6E-08
	40 to 80	5.7E-11	1.5E-08	5.2E-11	4.9E-08	5.6E-11	2.5E-08
SSW	0.0 to 2.5	4.7E-07	1.1E-04	4.0E-07	3.9E-04	4.6E-07	1.9E-04
	2.5 to 3.0	2.9E-07	7.1E-05	2.6E-07	2.5E-04	3.0E-07	1.3E-04
	3.0 to 3.5	1.5E-07	3.9E-05	1.6E-07	1.6E-04	2.0E-07	8.6E-05
	3.5 to 4.0	1.2E-07	3.1E-05	8.5E-08	9.4E-05	1.3E-07	5.6E-05

Table 2 (Continued)
Dispersion Factors and Particulate Deposition Rates for the ALARA Analysis

Direction	Radial Distance from Area G (km)	Atmospheric Source Area 1		Atmospheric Source Area 2		Atmospheric Source Area 3	
		Dispersion Factor (s/m^3)	Particulate Deposition Rate ($g/m^2/s$)	Dispersion Factor (s/m^3)	Particulate Deposition Rate ($g/m^2/s$)	Dispersion Factor (s/m^3)	Particulate Deposition Rate ($g/m^2/s$)
SSW (Cont.)	4.0 to 5.0	9.8E-08	2.3E-05	9.0E-08	8.3E-05	8.2E-08	3.5E-05
	5.0 to 6.0	5.0E-08	1.1E-05	4.8E-08	4.3E-05	1.6E-08	9.2E-06
	6.0 to 7.0	3.1E-08	7.0E-06	2.9E-08	2.5E-05	2.8E-08	1.1E-05
	7.0 to 8.0	1.2E-08	2.8E-06	8.6E-09	8.3E-06	2.0E-08	7.8E-06
	8.0 to 10	1.4E-08	2.9E-06	1.2E-08	9.4E-06	6.8E-09	2.6E-06
	10 to 20	3.5E-09	8.6E-07	2.9E-09	2.5E-06	2.8E-09	1.2E-06
	20 to 30	1.9E-09	4.4E-07	1.6E-09	1.4E-06	1.6E-09	6.2E-07
	30 to 40	7.1E-10	2.1E-07	7.3E-10	9.5E-07	7.8E-10	4.5E-07
	40 to 80	8.8E-11	2.2E-08	7.7E-11	7.3E-08	6.5E-11	2.9E-08
S	0.0 to 2.5	5.7E-07	1.4E-04	5.9E-07	5.2E-04	4.9E-07	2.2E-04
	2.5 to 3.0	3.7E-07	9.4E-05	4.0E-07	3.5E-04	3.4E-07	1.5E-04
	3.0 to 3.5	2.2E-07	5.9E-05	2.5E-07	2.3E-04	2.3E-07	1.0E-04
	3.5 to 4.0	1.2E-07	3.6E-05	1.6E-07	1.5E-04	1.5E-07	6.6E-05
	4.0 to 5.0	5.6E-08	1.7E-05	7.0E-08	7.3E-05	7.7E-08	3.7E-05
	5.0 to 6.0	5.0E-08	1.3E-05	3.6E-08	3.6E-05	4.1E-08	1.9E-05
	6.0 to 7.0	2.8E-08	6.8E-06	1.6E-08	1.7E-05	1.3E-08	6.8E-06
	7.0 to 8.0	1.7E-08	3.9E-06	2.0E-08	1.7E-05	1.7E-08	7.2E-06
	8.0 to 10	5.4E-09	1.4E-06	4.8E-09	4.8E-06	8.2E-09	3.3E-06
	10 to 20	4.4E-09	1.0E-06	4.4E-09	4.0E-06	4.1E-09	1.7E-06

Table 2 (Continued)
Dispersion Factors and Particulate Deposition Rates for the ALARA Analysis

Direction	Radial Distance from Area G (km)	Atmospheric Source Area 1		Atmospheric Source Area 2		Atmospheric Source Area 3	
		Dispersion Factor (s/m^3)	Particulate Deposition Rate ($g/m^2/s$)	Dispersion Factor (s/m^3)	Particulate Deposition Rate ($g/m^2/s$)	Dispersion Factor (s/m^3)	Particulate Deposition Rate ($g/m^2/s$)
S (Cont.)	20 to 30	1.6E-09	4.1E-07	1.2E-09	1.1E-06	1.2E-09	5.3E-07
	30 to 40	1.1E-09	3.6E-07	1.1E-09	1.2E-06	1.0E-09	5.3E-07
	40 to 80	3.2E-11	1.4E-08	2.7E-11	4.4E-08	3.0E-11	2.3E-08
SSE	0.0 to 2.5	2.1E-07	8.5E-05	4.8E-07	5.3E-04	3.2E-07	1.8E-04
	2.5 to 3.0	2.2E-07	7.2E-05	3.4E-07	3.7E-04	1.9E-07	1.1E-04
	3.0 to 3.5	1.3E-07	4.7E-05	1.5E-07	2.0E-04	1.4E-07	8.2E-05
	3.5 to 4.0	7.5E-08	3.0E-05	8.2E-08	1.2E-04	9.4E-08	5.6E-05
	4.0 to 5.0	4.4E-08	1.8E-05	7.4E-08	9.0E-05	4.7E-08	3.0E-05
	5.0 to 6.0	1.8E-08	8.0E-06	2.9E-08	3.9E-05	1.7E-08	1.3E-05
	6.0 to 7.0	8.3E-09	3.7E-06	1.2E-08	1.8E-05	1.0E-08	6.6E-06
	7.0 to 8.0	9.1E-09	2.8E-06	7.4E-09	9.4E-06	5.9E-09	3.4E-06
	8.0 to 10	6.5E-09	1.7E-06	6.8E-09	6.6E-06	5.8E-09	2.6E-06
	10 to 20	3.2E-09	1.1E-06	3.4E-09	4.0E-06	3.0E-09	1.6E-06
	20 to 30	1.7E-09	5.5E-07	2.0E-09	2.0E-06	1.6E-09	7.8E-07
	30 to 40	7.1E-10	2.4E-07	8.2E-10	1.1E-06	7.2E-10	4.3E-07
	40 to 80	3.5E-11	2.0E-08	3.5E-11	7.2E-08	3.6E-11	3.6E-08
SE	0.0 to 2.5	1.2E-07	5.3E-05	2.5E-07	3.4E-04	1.5E-07	9.6E-05
	2.5 to 3.0	7.3E-08	3.4E-05	1.4E-07	2.0E-04	4.7E-08	4.8E-05
	3.0 to 3.5	4.6E-08	2.2E-05	8.5E-08	1.3E-04	5.8E-08	4.2E-05

Table 2 (Continued)
Dispersion Factors and Particulate Deposition Rates for the ALARA Analysis

Direction	Radial Distance from Area G (km)	Atmospheric Source Area 1		Atmospheric Source Area 2		Atmospheric Source Area 3	
		Dispersion Factor (s/m^3)	Particulate Deposition Rate ($g/m^2/s$)	Dispersion Factor (s/m^3)	Particulate Deposition Rate ($g/m^2/s$)	Dispersion Factor (s/m^3)	Particulate Deposition Rate ($g/m^2/s$)
SE (Cont.)	3.5 to 4.0	3.7E-08	1.7E-05	5.4E-08	8.4E-05	3.4E-08	2.7E-05
	4.0 to 5.0	1.5E-08	8.3E-06	2.7E-08	4.7E-05	1.3E-08	1.3E-05
	5.0 to 6.0	6.4E-09	3.8E-06	9.8E-09	2.0E-05	5.8E-09	6.1E-06
	6.0 to 7.0	5.3E-09	2.3E-06	7.2E-09	1.1E-05	3.9E-09	3.3E-06
	7.0 to 8.0	2.3E-09	1.0E-06	2.6E-09	4.7E-06	2.2E-09	1.7E-06
	8.0 to 10	1.5E-09	5.9E-07	1.5E-09	2.3E-06	1.1E-09	8.2E-07
	10 to 20	5.1E-10	2.3E-07	4.2E-10	7.2E-07	4.1E-10	3.2E-07
	20 to 30	2.9E-10	1.3E-07	2.5E-10	4.2E-07	2.3E-10	1.9E-07
	30 to 40	1.3E-10	7.5E-08	1.3E-10	2.7E-07	1.2E-10	1.3E-07
	40 to 80	2.8E-11	2.6E-08	3.3E-11	1.1E-07	3.2E-11	5.0E-08
ESE	0.0 to 2.5	6.9E-08	3.3E-05	1.3E-07	2.0E-04	5.2E-08	5.1E-05
	2.5 to 3.0	4.2E-08	2.0E-05	7.2E-08	1.2E-04	3.8E-08	3.3E-05
	3.0 to 3.5	1.6E-08	1.1E-05	4.2E-08	7.1E-05	2.3E-08	2.1E-05
	3.5 to 4.0	1.1E-08	7.3E-06	1.8E-08	3.9E-05	1.3E-08	1.4E-05
	4.0 to 5.0	5.7E-09	4.0E-06	9.7E-09	2.2E-05	6.0E-09	7.2E-06
	5.0 to 6.0	3.1E-09	2.1E-06	4.6E-09	1.1E-05	2.6E-09	3.5E-06
	6.0 to 7.0	1.7E-09	1.1E-06	2.0E-09	5.3E-06	1.5E-09	1.9E-06
	7.0 to 8.0	9.8E-10	6.3E-07	1.1E-09	2.9E-06	1.4E-09	1.3E-06
	8.0 to 10	4.8E-10	3.1E-07	5.7E-10	1.4E-06	4.6E-10	5.3E-07

Table 2 (Continued)
Dispersion Factors and Particulate Deposition Rates for the ALARA Analysis

Direction	Radial Distance from Area G (km)	Atmospheric Source Area 1		Atmospheric Source Area 2		Atmospheric Source Area 3	
		Dispersion Factor (s/m^3)	Particulate Deposition Rate ($g/m^2/s$)	Dispersion Factor (s/m^3)	Particulate Deposition Rate ($g/m^2/s$)	Dispersion Factor (s/m^3)	Particulate Deposition Rate ($g/m^2/s$)
ESE (Cont.)	10 to 20	1.8E-10	1.2E-07	1.8E-10	4.2E-07	1.4E-10	1.8E-07
	20 to 30	6.8E-11	6.2E-08	6.7E-11	2.2E-07	6.4E-11	1.0E-07
	30 to 40	4.0E-11	3.9E-08	3.6E-11	1.3E-07	3.6E-11	6.2E-08
	40 to 80	1.2E-11	1.3E-08	1.3E-11	4.9E-08	1.3E-11	2.3E-08
E	0.0 to 2.5	3.9E-08	2.4E-05	5.1E-08	1.3E-04	4.2E-08	4.1E-05
	2.5 to 3.0	1.9E-08	1.4E-05	3.2E-08	7.4E-05	2.6E-08	2.5E-05
	3.0 to 3.5	1.4E-08	9.0E-06	2.2E-08	4.6E-05	1.0E-08	1.4E-05
	3.5 to 4.0	9.0E-09	6.7E-06	1.3E-08	2.9E-05	7.1E-09	9.3E-06
	4.0 to 5.0	3.9E-09	3.1E-06	5.0E-09	1.5E-05	4.6E-09	6.0E-06
	5.0 to 6.0	2.5E-09	1.7E-06	3.5E-09	8.3E-06	2.5E-09	2.9E-06
	6.0 to 7.0	1.1E-09	8.5E-07	1.6E-09	4.0E-06	1.4E-09	1.5E-06
	7.0 to 8.0	6.2E-10	4.9E-07	1.1E-09	2.3E-06	7.3E-10	8.6E-07
	8.0 to 10	3.1E-10	2.4E-07	3.7E-10	9.9E-07	3.4E-10	4.0E-07
	10 to 20	9.5E-11	8.5E-08	9.4E-11	3.0E-07	9.7E-11	1.4E-07
	20 to 30	4.2E-11	4.8E-08	4.2E-11	1.7E-07	3.9E-11	7.7E-08
	30 to 40	2.0E-11	2.6E-08	2.0E-11	9.1E-08	2.0E-11	4.2E-08
	40 to 80	6.1E-12	7.3E-09	6.1E-12	2.7E-08	6.1E-12	1.2E-08
ENE	0.0 to 2.5	2.8E-08	2.1E-05	4.9E-08	1.2E-04	4.2E-08	3.9E-05
	2.5 to 3.0	2.0E-08	1.3E-05	3.1E-08	6.7E-05	2.3E-08	2.2E-05

Table 2 (Continued)
Dispersion Factors and Particulate Deposition Rates for the ALARA Analysis

Direction	Radial Distance from Area G (km)	Atmospheric Source Area 1		Atmospheric Source Area 2		Atmospheric Source Area 3	
		Dispersion Factor (s/m^3)	Particulate Deposition Rate ($g/m^2/s$)	Dispersion Factor (s/m^3)	Particulate Deposition Rate ($g/m^2/s$)	Dispersion Factor (s/m^3)	Particulate Deposition Rate ($g/m^2/s$)
ENE (Cont.)	3.0 to 3.5	1.3E-08	8.5E-06	2.0E-08	4.2E-05	1.2E-08	1.4E-05
	3.5 to 4.0	8.7E-09	5.9E-06	8.1E-09	2.3E-05	6.7E-09	8.5E-06
	4.0 to 5.0	3.4E-09	2.9E-06	4.3E-09	1.2E-05	3.7E-09	4.7E-06
	5.0 to 6.0	1.7E-09	1.4E-06	2.2E-09	6.0E-06	1.6E-09	2.2E-06
	6.0 to 7.0	8.2E-10	7.5E-07	1.0E-09	3.0E-06	9.7E-10	1.2E-06
	7.0 to 8.0	5.3E-10	4.3E-07	6.5E-10	1.7E-06	5.0E-10	6.9E-07
	8.0 to 10	2.5E-10	2.2E-07	2.9E-10	8.1E-07	2.7E-10	3.4E-07
	10 to 20	6.9E-11	7.2E-08	6.8E-11	2.5E-07	6.6E-11	1.2E-07
	20 to 30	3.3E-11	4.2E-08	3.3E-11	1.5E-07	3.2E-11	6.8E-08
	30 to 40	1.7E-11	2.3E-08	1.6E-11	8.1E-08	1.6E-11	3.7E-08
	40 to 80	4.1E-12	5.2E-09	4.1E-12	1.9E-08	4.1E-12	9.0E-09
NE	0.0 to 2.5	3.2E-08	2.6E-05	5.3E-08	1.6E-04	4.9E-08	4.8E-05
	2.5 to 3.0	2.2E-08	1.6E-05	3.4E-08	8.8E-05	1.6E-08	2.5E-05
	3.0 to 3.5	1.4E-08	1.0E-05	2.2E-08	5.3E-05	1.0E-08	1.6E-05
	3.5 to 4.0	9.1E-09	6.9E-06	9.7E-09	3.0E-05	7.5E-09	1.0E-05
	4.0 to 5.0	3.1E-09	3.5E-06	4.1E-09	1.5E-05	4.2E-09	5.7E-06
	5.0 to 6.0	1.7E-09	1.8E-06	2.0E-09	7.1E-06	1.4E-09	2.6E-06
	6.0 to 7.0	9.6E-10	8.6E-07	1.1E-09	3.5E-06	8.4E-10	1.4E-06
	7.0 to 8.0	6.7E-10	4.8E-07	6.7E-10	1.8E-06	6.0E-10	7.6E-07

Table 2 (Continued)
Dispersion Factors and Particulate Deposition Rates for the ALARA Analysis

Direction	Radial Distance from Area G (km)	Atmospheric Source Area 1		Atmospheric Source Area 2		Atmospheric Source Area 3	
		Dispersion Factor (s/m^3)	Particulate Deposition Rate ($g/m^2/s$)	Dispersion Factor (s/m^3)	Particulate Deposition Rate ($g/m^2/s$)	Dispersion Factor (s/m^3)	Particulate Deposition Rate ($g/m^2/s$)
NE (Cont.)	8.0 to 10	3.1E-10	2.2E-07	3.8E-10	8.7E-07	3.5E-10	3.8E-07
	10 to 20	6.7E-11	7.1E-08	6.6E-11	2.5E-07	6.2E-11	1.1E-07
	20 to 30	3.3E-11	4.5E-08	3.1E-11	1.5E-07	3.0E-11	7.1E-08
	30 to 40	2.1E-11	2.9E-08	2.0E-11	1.0E-07	1.9E-11	4.6E-08
	40 to 80	5.8E-12	7.3E-09	5.7E-12	2.6E-08	5.7E-12	1.2E-08
NNE	0.0 to 2.5	3.8E-08	4.8E-05	5.3E-08	2.7E-04	6.3E-08	9.3E-05
	2.5 to 3.0	2.4E-08	2.8E-05	3.4E-08	1.6E-04	4.0E-08	5.6E-05
	3.0 to 3.5	1.6E-08	1.7E-05	2.2E-08	9.3E-05	2.6E-08	3.5E-05
	3.5 to 4.0	1.1E-08	1.1E-05	1.4E-08	5.7E-05	1.5E-08	2.2E-05
	4.0 to 5.0	5.9E-09	6.1E-06	5.5E-09	2.7E-05	6.7E-09	1.1E-05
	5.0 to 6.0	2.5E-09	2.6E-06	2.2E-09	1.1E-05	2.4E-09	4.6E-06
	6.0 to 7.0	1.5E-09	1.3E-06	1.6E-09	5.3E-06	1.7E-09	2.2E-06
	7.0 to 8.0	6.1E-10	5.7E-07	6.9E-10	2.3E-06	6.6E-10	1.0E-06
	8.0 to 10	3.0E-10	2.4E-07	3.3E-10	8.8E-07	5.1E-10	4.9E-07
	10 to 20	9.6E-11	8.4E-08	1.3E-10	3.7E-07	1.3E-10	1.7E-07
	20 to 30	5.5E-11	5.4E-08	6.5E-11	2.2E-07	4.2E-11	8.4E-08
	30 to 40	4.4E-11	4.8E-08	4.2E-11	1.7E-07	3.9E-11	7.6E-08
	40 to 80	1.9E-11	1.9E-08	1.7E-11	6.2E-08	1.5E-11	2.8E-08

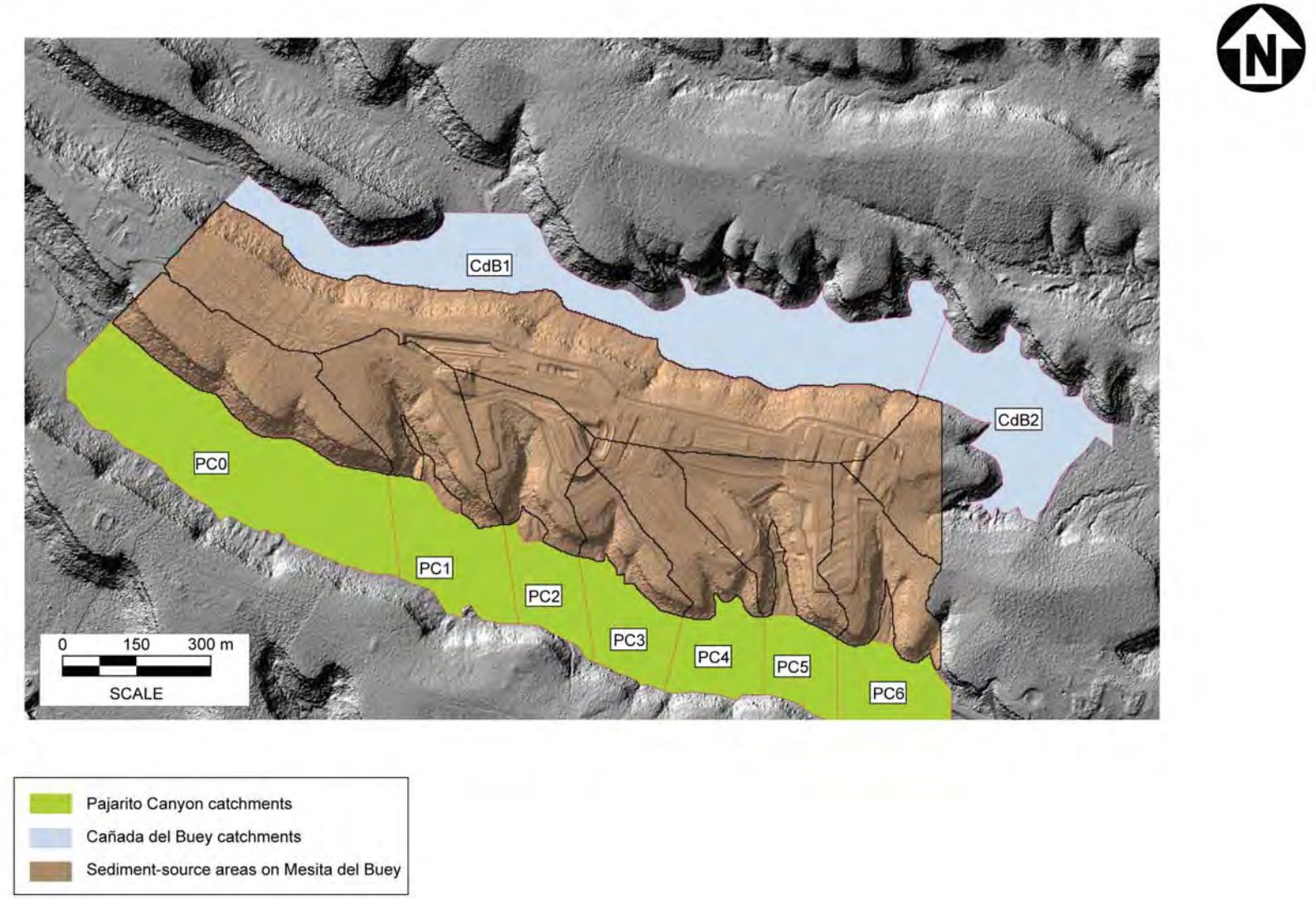

Figure 2
Sediment Catchments in Habitable Canyon Bottoms Adjacent to Area G

Table 3
Size of Catchments in Cañada del Buey and Pajarito Canyon

Catchment	Surface Area (m^2)
Cañada del Buey	
CdB1	1.8E+05
CdB2	7.3E+04
Pajarito Canyon	
PC0	1.4E+05
PC1	4.8E+04
PC2	2.8E+04
PC3	3.4E+04
PC4	3.1E+04
PC5	2.6E+04
PC6	3.4E+04

A conservative approach to defining the population within each catchment is to assume that the portion of each area that is contaminated as a result of sediment transport from Area G is fully populated. Dividing the area over which contamination disperses by the area of the receptor's lot yields an estimate of the number of people living in that portion of the canyon. These calculations were performed using a lot size of 2,300 m^2 (0.6 ac), the same value used in the performance assessment and composite analysis modeling.

The closure options outlined above will affect the long-term performance of the disposal facility in one manner or another. The Base-Case Scenario assumes the facility will operate as projected for the performance assessment and composite analysis. Under the Extended Control Option, it is assumed that annual mowing prevents the establishment of all shrubs and trees at the site, thus aboveground biomass densities of these growth forms are set to zero. Pest control is assumed to be partially ineffective; animal and burrow densities at the site are assumed to range from 10 to 30 percent of the values expected in the absence of eradication measures, with a most likely value of 20 percent. As stated earlier, the animals inhabiting the site are assumed to be those characteristic of the grassland community. Placement of a biobarrier within the final cover under the Biobarrier Option is generally assumed to limit plant root and animal burrow penetration to 2 m (6.6 ft) from the ground surface. Recognizing that the barrier will probably be less than 100 percent effective, 10 to 30 percent of the plants and animals inhabiting the site were assumed to root and burrow to their unrestricted depths. This triangular distribution was assigned a most likely value of 20 percent.

The closure strategies evaluated by the ALARA analysis were assumed to apply to the entire disposal facility. On this basis, the analysis was conducted using the composite analysis inventory, which includes all waste projected to be disposed of at Area G. Probabilistic assessments of the impacts of this inventory on the downwind and canyon receptors were estimated using simulations consisting of 100 realizations each.

2.4.2 Cost and Impact Data

The ALARA process is a decision-making tool that aims to maximize the total benefits of the radiological protection provisions for DOE activities likely to expose members of the public to ionizing radiation (DOE, 1997). In general, the process identifies the costs associated with protection provisions and the detriment caused by the activity, and then optimizes these costs to determine how best to manage the activity responsible for the exposure. As discussed earlier, the closure option with the lowest total cost is generally considered to be the optimum strategy.

The detriment associated with an activity includes health and nonhealth components. The ALARA analysis conducted for the Area G performance assessment and composite analysis focused on the health detriment as this is directly, and linearly, related to the dose projections for the disposal facility. The fact that costs associated with nonhealth detriments may not be related to the collective dose makes their inclusion difficult at best. Although the nonhealth aspect is not addressed, it may require consideration at some point in time.

The magnitude of the health detriment of an activity is generally estimated in terms of collective dose to the exposed population. For the ALARA process, the monetary equivalent value of the collective dose must be established so that it can be compared to costs associated with actions designed to reduce exposures. In its guidance for conducting composite analyses (DOE, 1996), the DOE recommends using a monetary equivalent value of $1,000 to $10,000 per person-rem for converting collective dose to dollars. Since that time, however, the department has adopted a range of $1,000 to $6,000 per person-rem, with a nominal value of $2,000 (DOE, 1997).

The collective dose is calculated as the product of the average dose, the number of exposed persons, and the time over which doses are integrated. The DOE has suggested the use of a “few hundred years, or less” as a suitable period of integration in cases where chronic exposures to long-lived radionuclides are concerned (DOE, 1996 and 1997). In any event, the DOE indicates that periods beyond 1,000 years should not be used in the ALARA analysis. As discussed earlier, collective doses were calculated in the Area G ALARA analysis using an integration period of 300 years.

The Base-Case Scenario and the two closure alternatives have associated design and implementation costs. Cost estimates for the Base-Case Scenario are based on those developed in support of the final closure of Material Disposal Area (MDA) G, the portion of Area G that is currently accepting waste. Site closure is assumed to occur in three phases; the costs associated with these phases are summarized in Table 4. This table lists costs that reflect the design and placement of a 2.4 m (8 ft)

Table 4
Cost Estimates for Closure of MDA G

Phase	Cost ($)	Comments
Phase 1		
Design Activities	1,041,645	Includes all design activities for the cap/cover, fencing, and time domain reflectometry (TDR) system.
1.1 Mobilization/Demobilization	35,490	Mobilize and demobilize personnel and equipment for clearing, grubbing, excavation, grading, drilling, and hauling.
1.2 Fence Removal and Site Preparation	290,129	Includes removal of existing security fence, and site clearing and grubbing. Removal and disposal of 910 m of fencing and existing gate.
1.3 Regrading, Evapotranspiration Cover, and Revegetation	16,290,799	Apply a total of 2.4 m of cover material over the area of 14 ha. Add a thin layer of gravel for erosion control after reseeding with native plants and grasses. Task involves mechanical cobble placement, spreading and fine grading of topsoil, watering (dust abatement) and watering of planted area for vegetation germination at approved levels.
1.4 Installation of New Fencing	210,240	Install 1,600 m of security fencing to replace aged fencing on-site.
1.5 Installation of Time Domain Reflectometry (TDR) System	891,652	Install TDR system to allow for postclosure monitoring.
1.6 Health and Safety	128,389	Develop and implement a health and safety plan.
1.7 Completion Report	37,913	Prepare a completion report at end of the construction phase.
1.8 O&M for Phase 1	125,526	Includes operations and maintenance for Phase 1.
Phase 1 Total	19,051,783	
Phase 2		
ER Design Activities	1,121,749	Includes all design activities for the cap/cover, fencing, and TDR system.
2.1 Mobilization/Demobilization	35,490	Mobilize and demobilize personnel and equipment for clearing, grubbing, excavation, grading, drilling, and hauling.
2.2 Fence Removal and Site Preparation	251,834	Includes removal of existing security fence, and site clearing and grubbing. Removal and disposal of 910 m of fencing and existing gate.
2.3 Regrading, Evapotranspiration Cover, and Revegetation	18,406,569	Apply a total of 2.4 m of cover material over the area of 12 ha. Add a thin layer of gravel for erosion control after reseeding with native plants and grasses. Task involves mechanical cobble placement, spreading and fine grading of topsoil, watering (dust abatement) and watering of planted area for vegetation germination at approved levels.

Source: Adapted from information provided by Moran, 2005

Table 4 (Continued)
Cost Estimates for Closure of the Active Portion of MDA G

Phase	Cost ($)	Comments
2.4 Installation of New Fencing	150,310	Install 1,600 m of security fencing to replace aged fencing on-site.
2.5 Installation of TDR System	786,751	Install TDR system to allow for postclosure monitoring.
2.6 Health and Safety	96,292	Develop and implement Health and Safety Plan.
2.7 Completion Report	37,913	Prepare a completion report at end of the construction phase.
2.8 O&M for Phase 2	124,424	Includes operations and maintenance for Phase 2.
Phase 2 Total	21,011,332	
Phase 3		
Design Activities	500,397	Includes all design activities for the cap/cover, fencing, and TDR system.
3.1 Mobilization/Demobilization	35,490	Mobilize and demobilize personnel and equipment for clearing, grubbing, excavation, grading, drilling, and hauling.
3.2 Fence Removal and Site Preparation	167,686	Includes removal of existing security fence, and site clearing and grubbing. Removal and disposal of 910 m of fencing and existing gate.
3.3 Regrading, Evapotranspiration Cover, and Revegetation	7,901,813	Apply a total of 2.4 m of cover material over the area of 6.5 ha. Add a thin layer of gravel for erosion control after reseeding with native plants and grasses. Task involves mechanical cobble placement, spreading and fine grading of topsoil, watering (dust abatement) and watering of planted area for vegetation germination at approved levels.
3.4 Installation of New Fencing	146,301	Install 1,600 m of security fencing to replace aged fencing on-site.
3.5 Installation of TDR System	419,601	Install TDR system to allow for postclosure monitoring.
3.6 Health and Safety	96,292	Develop and implement Health and Safety Plan.
3.7 Completion Report	37,913	Prepare a completion report at end of the construction phase.
3.8 O&M for Phase 3	120,565	Includes operations and maintenance for Phase 3.
Phase 3 Total	*9,426,058*	
Infrastructure	702,093	Includes infrastructure requirements, including roads, water, and electrical service.
Grand Total	50,191,266	

Source: Adapted from information provided by Moran, 2005

cover over an area of 32 ha (80 ac). Although the amount of cover placed over the site will vary in accordance with the cover design developed by Day et al. (2005), the costs estimated for the 2.4 m (8 ft) cover were adopted for the active portion of the site.

The costs listed in Table 4 do not address the design and placement of a final cover over the 12 ha (30 ac) Zone 4 expansion area. The closure costs associated with this portion of the site were estimated by scaling the costs for MDA G. For items whose costs are related to the size of the site (e.g., installation of the cover), estimates of the average cost per unit area were developed using the costs for the three closure phases included in Table 4. Costs that are constant regardless of the size of the site were applied directly to the Zone 4 expansion area. On this basis, the total cost associated with the closure of the expansion area was estimated to be about $19 million.

The cost of actively maintaining Area G under the Extended Control Option was estimated using information for MDA J, a 2.1 ha (5.3 ac) disposal area just west of Area G; these costs are summarized in Table 5. The costs were scaled upward to reflect maintenance of the 45 ha (110 ac) at Area G. A total annual maintenance cost of $560,000 was estimated.

Table 5
Annual Maintenance Costs for MDA J

Maintenance Activity	Annual Cost ($)
Mowing and weeding	18,000.00
Pest control	6,500.00
Fence repair	2,500.00

Source: French, 2005

The cost of substituting a 20 cm (7.9 in.) gravel biobarrier was estimated in a manner consistent with the cost data presented in Table 4. This modification was estimated to add $1 million to the cost of the cover used to model the Base-Case Scenario.

The costs estimated above are uncertain. For the purposes of the ALARA analysis all of these costs were assumed to be normally distributed with a coefficient of variation of 5 percent.

3.0 Results

The results of the ALARA analysis are summarized in Tables 6 and 7. Table 6 summarizes the mean collective population doses for the Atmospheric and All Pathways–Canyon Scenarios, integrated over 300 years. The doses listed for the canyon scenario include all persons living in both canyons. Table 7 summarizes the costs associated with the projected health impacts and implementation of each closure strategy.

Table 6
Collective Doses Estimated for the Area G ALARA Analysis

Closure Strategy	Mean Collective Dose (person-rem)	
	Atmospheric Scenario	All Pathways–Canyon Scenario
Base-Case Scenario	1.1E-01	2.9E+00
Extended Control Option	3.2E-02	2.3E+00
Biobarrier Option	4.6E-02	2.2E+00

Table 7
Health Detriment and Closure Strategy
Implementation Costs for the Area G ALARA Analysis

Exposure Scenario and Closure Strategy	Mean Cost ($)		
	Health Detriment	Strategy Implementation	Total
Atmospheric Scenario			
Base-Case Scenario	3.3E+02	6.9E+07	6.9E+07
Extended Control Option	1.1E+02	2.4E+08	2.4E+08
Biobarrier Option	1.4E+02	6.9E+07	6.9E+07
All Pathways–Canyon Scenario			
Base-Case Scenario	7.1E+03	6.9E+07	6.9E+07
Extended Control Option	5.0E+03	2.4E+08	2.4E+08
Biobarrier Option	4.8E+03	6.9E+07	6.9E+07

Examination of the results in Table 6 indicates that the collective doses over the 300-year integration period are small and similar among the three closure strategies. Although the exposed population for the Atmospheric Scenario is orders of magnitude greater than the total canyon population, the collective dose for the latter is larger. The costs associated with the projected doses are small compared to the costs associated with implementing the three closure alternatives (Table 7). For example, the health detriment costs for the Base-Case Scenario are about 0.01 percent of the total cost projected for the All Pathways–Canyon Scenario.

The costs associated with the Base-Case Scenario and the Biobarrier Option are essentially the same, reflecting the small cost of installing a biobarrier during facility closure. The mean cost of the Extended Control Option is significantly higher than the costs of the other closure strategies because of the expense of continued active maintenance of the site.

The results shown in Table 6 indicate that the collective doses projected for the Atmospheric and All Pathways–Canyon Scenarios are very small. For the three closure strategies examined here, these doses are ALARA insofar as the implementation costs of these strategies far exceed the costs associated with the health detriments (Table 7). This conclusion is consistent with the guidance offered by the DOE on ALARA analyses (DOE, 1997).

The fact that the total cost of the Base-Case Scenario closure strategy is dominated by implementation expenses suggests that an evaluation of more cost-effective ways of closing the disposal facility may be in order. That is, from an ALARA standpoint, the development of less expensive strategies may be called for as long as the associated collective health impacts of such strategies are not substantially greater than those estimated here. Any such strategy will, of course, need to comply with all individual dose limits no matter what the cost.

The ALARA analysis performed here was conducted using an integration period of 300 years and did not discount costs or consider the probability of scenarios occurring far in the future. Although different sets of assumptions regarding these aspects of the analysis would yield different results, the costs associated with health detriment are expected to remain a small proportion of the total closure strategy cost. Furthermore, the relative cost-effectiveness of the three strategies is not expected to change. Finally, the same general trends noted here are expected to apply if the performance assessment inventory is substituted for the composite analysis inventory used in the ALARA analysis.

4.0 References

BBER, 2005, The Bureau of Business and Economic Research, University of New Mexico, "Data Bases on our Web Site," <www.unm.edu/~bber/demo/table2.xls>.

Day, M.S., C.K. Anderson, and C.D. Pedersen, 2005, *Conceptual Design of the Earthen Cover for at Los Alamos National Laboratory Technical Area 54, Material Disposal Area G*, Los Alamos National Laboratory Report LA-UR-05-7394, September.

DOE, 1996, *Guidance for a Composite Analysis of the Impact of Interacting Source Terms on the Radiological Protection of the Public from DOE LLW Disposal Facilities*, U.S. Department of Energy, April 1996.

DOE, 1997, *Applying the ALARA Process for Radiation Protection of the Public and Environmental Compliance with 10 CFR Part 834 and DOE 5400.5 ALARA Program Requirements, Volume 1—Discussion*, U.S. Department of Energy, DOE-STD-ALARA1 Draft, April.

DOE, 2001, *Radioactive Waste Management*, U.S. Department of Energy Order DOE O 435.1 (change order to DOE O 435.1 of July 1999), August 28.

French, S.B., 2005, Personal communication between Sean French, Los Alamos National Laboratory, and Rob Shuman, URS Corporation, October 24.

Jacobson, K.W., 2005, *Air Dispersion Analysis for Los Alamos National Laboratory Technical Area 54, Material Disposal Area G*, Los Alamos National Laboratory Report LA-UR-05-7232, September.

Moran, M., 2005, Personal communication between M. Moran, Los Alamos National Laboratory, and Rob Shuman, URS Corporation, September 29.

Shuman, R., 2008a, *Radiological Dose Assessment for Los Alamos National Laboratory Technical Area 54, Area G Performance Assessment and Composite Analysis*, Los Alamos National Laboratory Report LA-UR-08-06109, September.

Shuman, R., 2008b, *GoldSim Model Documentation and Data Selection for Los Alamos National Laboratory Technical Area 54, Area G Performance Assessment and Composite Analysis*, Los Alamos National Laboratory Report LA-UR-08-06094, September.